DOI: 10.1007/s00259-023-06333-x

EANM'23

Annual Congress of the
European Association of Nuclear Medicine
September 9–13, 2023
Vienna, Austria

Abstracts

European Journal of Nuclear Medicine and
Molecular Imaging (2023) 50 (Suppl 1): S1–S898

This supplement was not sponsored by outside commercial interests. It was funded entirely by the association's own resources.

Words of Welcome S3

Programme at a Glance S4

Oral Sessions S7

e-Poster Presentation Sessions S209

e-Posters S431

Authors Index S840

EANM'24 S897

EANM Clubbing hosted by EARL S898

Dear colleagues,

It is my great honour to invite you to the 36th Annual EANM Congress on behalf of the European Association of Nuclear Medicine. This year's event will be held in Vienna from September 9–13.

We are able to meet in person again for this edition of the EANM Congress, meaning we will enjoy the fantastic science and face-to-face interchange the occasion offers while also continuing to bolster our growth as a specialist community.

Our present is bright, and our future is even more promising. Our relevance for diagnostics and therapy continues to increase, new tools and tracers have been established, and ongoing research and innovation are consistently providing fresh solutions for validation and testing. The number of joint projects with other disciplines and societies continues to grow, with more and more communities recognising the important help that nuclear medicine can provide their patients and in answering their questions. This is the main reason for the unusual date of this year's EANM Congress, as we wanted to avoid clashing with another major event that many of our participants and industry partners will also want to attend. We plan to return to our usual mid-October dates in 2024.

The number of visitors to the Congress continues to rise year after year, with the 2022 edition of the event welcoming an unprecedented 7000 participants. The many innovative features you discovered and liked in Barcelona last year will be present once more, including sessions specifically devoted to exchange and discussion. Please prepare your questions across the year and get ready to challenge our experts during the congress! We want to make sure that you return home with input and suggestions that allow each and every one of you to contribute to the success of our field in your daily work.

Needless to say, we should not simply sit back and enjoy our success. We must continue to provide convincing evidence of the positive impact our chosen field has in a complex world of limited resources, meaning we should constantly strive for a more efficient, accessible and sustainable nuclear medicine. This year's scientific programme will help you deal with such issues thanks to superb material combined with multidisciplinary sessions. And as we know that fun helps foster collaboration and cooperation, and some will also be uniquely entertaining. On top of this, we hope you will provide numerous contributions and plenty of input via the abstract submission portal, which is now open. Share your work with the nuclear medicine community!

We have prepared content that will maximise opportunities for exchange and networking for all those who travel to Vienna for EANM'23. On the other hand, we still want to reach as large an audience as possible, just as virtual congresses have done, including anyone that cannot make it to Vienna for this year's congress. For this reason, selected content will also be made available online and will remain accessible afterwards so that everyone can benefit from it in a way which fits around each individual's schedule.

In summary, we are working to provide you all with a special, first-rate Congress tailored to your needs and wishes. Join us and savour every moment of it!

Valentina Garibotto
EANM Congress Chair 2023–2025

Saturday, September 09, 2023

Location/ Time	Hall A				Location/ Time
08:00–08:30					08:00–08:30
08:30–09:00					08:30–09:00
09:00–09:30					09:00–09:30
09:30–10:00					09:30–10:00
10:00–10:30					10:00–10:30
10:30–11:00					10:30–11:00
11:00–11:30		Advisory Council Meeting (11:00–13:00) (Room 1.86)			11:00–11:30
11:30–12:00					11:30–12:00
12:00–12:30					12:00–12:30
12:30–13:00					12:30–13:00
13:00–13:30					13:00–13:30
13:30–14:00					13:30–14:00
14:00–14:30			Delegates' Assembly (14:00–16:00) (Hall F2)	Committee Meetings (14:00–17:45) (Room 1.86)	14:00–14:30
14:30–15:00					14:30–15:00
15:00–15:30					15:00–15:30
15:30–16:00					15:30–16:00
16:00–16:30					16:00–16:30
16:30–17:00					16:30–17:00
17:00–17:30					17:00–17:30
17:30–18:00					17:30–18:00
18:00–18:30	Opening Ceremony including Awards Ceremony (18:00–18:35)				18:00–18:30
18:30–19:00	101 Plenary 1 Highlights Lecture (18:35–19:35)				19:30–20:30
20:30–21:00	Welcome Reception (19:45–21:45)				20:30–21:00
21:00–21:30					21:00–21:30
21:30–22:00					21:30–22:00

Sunday, September 10, 2023

Location/ Time	Hall A	Hall D – Arena	Hall E1	Hall E2	Hall B	Hall C	Hall F1	Hall F2	Hall G2	Hall K	Hall G1	Location/ Time
	LIVE STREAM									LIVE STREAM		
08:00–08:30	201 CME 1 Inflammation & Infection Committee Infection and Inflammation – New Guidelines	202 Special Track Cardiovascular Committee Debate: Myocardial Perfusion Imaging after ISCHEMIA Trial	203 LIPS Interactive Session Oncology & Theranostics Committee Novelties in Radionuclide Therapy	204 M2M Track TROP Session Radiopharmaceutical Sciences + Translational Molecular Imaging & Therapy Committee At the Nucleus: Radionuclide Production	205 Cutting Edge Science Track TROP Session Physics Committee Quality Control, Performance, Standardisation	206 Clinical Oncology Track TROP Session Oncology & Theranostics Committee Prostate Cancer Staging	207 Featured Session Neuroimaging Committee Methods in NeuroImaging: Spotlight on Brain Connectivity	208 TROP Session Paediatrics Committee Paediatric PET/CT & PET/MR	209 e-Poster Presentations Session 1 Oncology & Theranostics Committee Neuroendocrine tumours and Gynaecological Malignancies	210 Technologists' Track Opening CTE 1 Technologists Committee / SNMMI Technologists' Guide launch – Gastro Intestinal Molecular Imaging Studies	Members' Assembly (08:00–11:00)	08:00–08:30
08:30–09:00												08:30–09:00
09:00–09:30												09:00–09:30
09:30–10:00												09:30–10:00
10:00–10:30	301 CME 2 Translational Molecular Imaging & Therapy + Oncology & Theranostics + Radiopharmaceutical Sciences Committee FAP – Moving Towards Therapy	302 Special Track Thyroid Committee Challenge the Expert: Integrated Diagnostics of Thyroid Disease	303 LIPS Interactive Session Radiation Protection + Physics Committee / EFOMP Careers in Radiation Protection	304 M2M Track TROP Session Radiopharmaceutical Sciences + Translational Molecular Imaging & Therapy Committee Validating Methodology: In Vitro and in Vivo Models	305 Cutting Edge Science Track Featured Session Physics Committee Radiomics	306 Clinical Oncology Track Featured Session Oncology & Theranostics Committee Hematological Disease	307 TROP Session Neuroimaging Committee Amyloid, Tau and More in Neurodegenerative Disorders	308 Joint Symposium 1 Cardiovascular + Inflammation & Infection Committee / EANM PET in Valvular Diseases – All In!	309 e-Poster Presentations Session 2 Paediatrics Committee Paediatric Nuclear Medicine & Adults General Nuclear Medicine	310 Technologists' Track CTE 2 Technologists Committee Head and Neck Molecular Imaging – Updates and Perspectives		10:00–10:30
10:30–11:00												10:30–11:00
11:00–11:30												11:00–11:30
11:30–12:00	401 Plenary 2 incl. Marie Curie New Imaging Techniques – Jump Aboard or Watch and Wait											11:30–12:00
12:00–12:30												12:00–12:30
12:30–13:00												12:30–13:00
13:00–13:30												13:00–13:30
13:30–14:00	Lunch Break			Satellite Symposium	Satellite Symposium	Satellite Symposium	Satellite Symposium	Satellite Symposium		Satellite Symposium	Satellite Symposium	13:30–14:00
14:00–14:30												14:00–14:30
14:30–15:00												14:30–15:00
15:00–15:30	501 CME 3 Cardiovascular Committee Nuclear Imaging in Cardiac Amyloidosis – What Else?	502 Special Track Oncology & Theranostics Committee Challenge the Expert: Risk in Diagnostic and Therapeutic Nuclear Medicine	503 LIPS Interactive Session Thyroid Committee Rational Use of PET/CT with 18F-FDG in DTC	504 M2M Track TROP Session Radiopharmaceutical Sciences + Translational Molecular Imaging & Therapy Committee Radioligand Therapy - New and Old Targets	505 Cutting Edge Science Track TROP Session Dosimetry Committee From Cells to Human via the Fish	506 Clinical Oncology Track TROP Session Oncology & Theranostics Committee Gastrointestinal Malignancies	507 TROP Session Paediatrics Committee Adults General Nuclear Medicine	508 Joint Symposium 2 Oncology & Theranostics Committee / EORTC Nuclear Medicine Imaging of the Immune System	509 e-Poster Presentations Session 3 Inflammation & Infection Committee More on Infection and Inflammation Imaging	510 Technologists' Track Oral Presentations 1 Technologists Committee SPECT-CT in Diagnosis and Therapy	511 Theranostics Track Featured Session Oncology & Theranostics Committee / EARL Old but Novel Techniques	15:00–15:30
15:30–16:00												15:30–16:00
16:00–16:30												16:00–16:30
16:30–17:00	601 CME 4 Oncology & Theranostics Committee Update in Multiple Myeloma	602 Special Track Dosimetry Committee Challenge the Expert: Dosimetry Live	603 LIPS Interactive Session Oncology & Theranostics Committee Residents for Residents	604 M2M Track TROP Session Radiopharmaceutical Sciences + Translational Molecular Imaging & Therapy Committee Novel Imaging Targets in Oncology	605 Cutting Edge Science Track TROP Session Physics Committee Segmentation and Denoising	606 Clinical Oncology Track TROP Session Oncology & Theranostics Committee Neuroendocrine tumours Treatment	607 TROP Session Cardiovascular Committee Functional Imaging, Plaque and Total-Body PET	608 TROP Session Inflammation & Infection Committee Infection and Inflammation Imaging: New Frontiers	609 e-Poster Presentations Session 4 Thyroid Committee Thyroid and Parathyroid Disease	610 Technologists' Track CTE 3 Technologists Committee Patient Care in Nuclear Medicine	611 Special Symposium 1 EANM / EARL Harmonisation and Accreditation accelerate Research and Clinical Translation	16:30–17:00
17:00–17:30												17:00–17:30
17:30–18:00												17:30–18:00
18:00–18:30												18:00–18:30

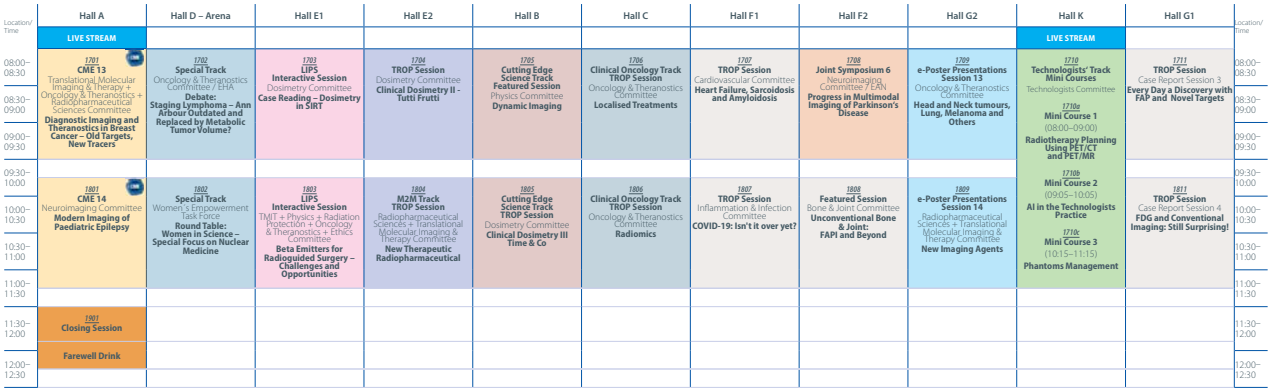
Monday, September 11, 2023

Location/Time	Hall A	Hall D – Arena	Hall E1	Hall E2	Hall B	Hall C	Hall F1	Hall F2	Hall G2	Hall K	Hall G1	Location/Time
	LIVE STREAM									LIVE STREAM		
08:00–08:30	701 CME 5 Oncology & Theranostics Committee **Will the Microenvironment Become Even More Important in Nuclear Medicine?**	702 Special Track Neuroimaging Committee **Debate: What is the Best Tracer for Molecular Brain Tumour Imaging?**	703 LIPS Interactive Session Cardiovascular Committee **Challenges in MBF Quantification with PET and SPECT**	704 M2M Track TROP Session Radiopharmaceutical Sciences + Translational Molecular Imaging & Therapy Committee **Imaging Inflammatory Processes in Cardiovascular Diseases**	705 Cutting Edge Science Track Featured Session Physics Committee **Imaging Guided Surgery**	706 Clinical Oncology Track TROP Session Oncology & Theranostics Committee **Neuroendocrine tumours - Diagnosis**	707 TROP Session Paediatrics Committee **Neuroblastoma & Non-PET Paediatric Studies**	708 Special Symposium 2 Inflammation & Infection Committee **Usefulness of PET in the Evaluation of Inflammatory Rheumatisms**	709 e-Poster Presentations Session 5 Physics Committee **SPECT/CT, PET/CT, PET/MR Quantitating Imaging**	710 Technologists' Track Oral Presentations 2 Technologists Committee **All about PET-CT!**	711 Theranostics Track TROP Session Oncology & Theranostics Committee **What's New in Prostate Cancer?**	08:00–08:30
08:30–09:00												08:30–09:00
09:00–09:30												09:00–09:30
09:30–10:00	801 CME 6 Dosimetry Committee **Understanding Radiobiology for Dosimetry-guided Molecular Radiotherapy**	802 Special Track Translational Molecular Imaging & Therapy + Oncology & Theranostics + Radiopharmaceutical Sciences Committee **Round Table: Dialogue with the Treating Physician**	803 LIPS Interactive Session Neuroimaging + Cardiovascular + Inflammation & Infection Committee **Molecular Imaging to Solve the Problem of Long COVID**	804 M2M Track TROP Session Radiopharmaceutical Sciences + Translational Molecular Imaging & Therapy Committee **TME and Therapy: Direct Targeting and Secondary Effects**	805 Cutting Edge Science Track TROP Session Physics Committee **Image Reconstruction and Data Corrections**	806 Clinical Oncology Track Featured Session Oncology & Theranostics Committee **FAP Imaging**	807 TROP Session Cardiovascular Committee **Clinical Perfusion Imaging with PET**	808 Featured Session Thyroid Committee **Iodine-131 Therapy and Beyond in differentiated Thyroid Cancer**	809 e-Poster Presentations Session 6 Oncology & Theranostics Committee **Prostate Cancer**	810 Technologists' Track CTE 4 Technologists Committee **Prostate Cancer Theranostics**	811 Special Symposium 3 EANM / EJNMMI **You, the EANM and the EJNMMI**	09:30–10:00
10:00–10:30												10:00–10:30
10:30–11:00												10:30–11:00
11:00–11:30												11:00–11:30
11:30–12:00	901 Plenary 3 **Radiotheranostics: What's New?**											11:30–12:00
12:00–12:30												12:00–12:30
12:30–13:00												12:30–13:00
13:00–13:30	Lunch Break			Satellite Symposium	Satellite Symposium	Satellite Symposium	Satellite Symposium	Satellite Symposium		Satellite Symposium		13:00–13:30
13:30–14:00												13:30–14:00
14:00–14:30												14:00–14:30
14:30–15:00												14:30–15:00
15:00–15:30	1001 CME 7 Thyroid + Dosimetry Committee **New NM Guidelines of Benign Thyroid Disease**	1002 Special Track **EANM Sanjiv Sam Gambhir Award – Compete and Win!**	1003 LIPS Interactive Session Inflammation & Infection Committee **Tips and Tricks in the Study of Prosthesis Infection**	1004 M2M Track TROP Session Radiopharmaceutical Sciences + Translational Molecular Imaging & Therapy Committee **New Roads towards FAP-directed Theranostics**	1005 Cutting Edge Science Track TROP Session Dosimetry Committee **Clinical Dosimetry I 177Lu / 225Ac and 161Tb RLT**	1006 Clinical Oncology Track Featured Session Oncology & Theranostics Committee **Melanoma**	1007 TROP Session Neuroimaging Committee **Imaging Neurotransmission in Movement Disorders**	1008 Joint Symposium 3 Translational Molecular Imaging & Therapy Committee + Oncology & Theranostics + Physics / EAU **Metastases Directed Prostate Cancer Surgery - Translational Challenges and Possibilities**	1009 e-Poster Presentations Session 7 Cardiovascular Committee **Cardiovascular Imaging e-Posters**	1010 Technologists' Track Technologists' e-Poster Presentations Session Technologists Committee **Techs' e-Posters**	1011 TROP Session Case Report Session 1 **Learning from Single Cases in Theranostics**	15:00–15:30
15:30–16:00												15:30–16:00
16:00–16:30												16:00–16:30
16:30–17:00	1101 CME 8 Oncology & Theranostics Committee **Assessing Response to Peptide Receptor Radionuclide Therapy in Patients with Neuroendocrine Tumors**	1102 Special Track Physics Committee **Debate: AI in Nuclear Medicine: Fear or Embrace?**	1103 LIPS Interactive Session Cardiovascular Committee **Stiff to Sweet - Infiltration and Inflammation**	1104 M2M Track TROP Session Radiopharmaceutical Sciences + Translational Molecular Imaging & Therapy Committee **Efficient Radiolabelling: Key for Clinical Translation**	1105 Cutting Edge Science Track TROP Session Radiation Protection Committee **Current issues of Radiation Protection**	1106 Clinical Oncology Track TROP Session Oncology & Theranostics Committee **Prostate Cancer Biochemical Recurrence**	1107 TROP Session Inflammation & Infection Committee **Vasculitis and Endocarditis: Current and New Evidence**	1108 TROP Session Thyroid Committee **Iodine-131 Therapy in Differentiated Thyroid Cancer: Present and Future Perspective**	1109 e-Poster Presentations Session 8 Neuroimaging Committee **E-Poster Neurology: It's in the Brain!**	1110 Technologists' Track CTE 5 Technologists Committee **Cardiac Inflammatory Disease**	1111 TROP Session Case Report Session 2 **Successful Molecular Targeting in Oncology**	16:30–17:00
17:00–17:30												17:00–17:30
17:30–18:00												17:30–18:00
18:00–18:30												18:00–18:30

Tuesday, September 12, 2023

Location/Time	Hall A	Hall D – Arena	Hall E1	Hall E2	Hall B	Hall C	Hall F1	Hall F2	Hall G2	Hall K	Hall G1	Location/Time
	LIVE STREAM									LIVE STREAM		
08:00–08:30	1201 CME 9 Bone & Joint + Physics Committee **Current Bone SPECT/CT (including 360 CZT)**	1202 Special Track Radiation Protection Committee **Round Table: Establishing and Running a Theranostics Center in a Clinical Setting**	1203 LIPS Interactive Session Paediatrics Committee **Paediatric Nephro-Urology – Beyond Hydro-Nephrosis**	1204 M2M Track TROP Session Radiopharmaceutical Sciences + Translational Molecular Imaging & Therapy Committee **Imaging the Brain from all Angles**	1205 Cutting Edge Science Track TROP Session Physics Committee **Total Body PET Methods**	1206 Clinical Oncology Track TROP Session Oncology & Theranostics Committee **Gynaecological Malignancies**	1207 Featured Session Neuroimaging Committee **Breadth of Tracers and Approaches in Neuro-Oncology**	1208 Joint Symposium 4 Dosimetry Committee / ESTRO **Dosimetry in Different Modalities - Where We Are and Where We Want To Be**	1209 e-Poster Presentations Session 9 Physics Committee **Artificial Intelligence and Radiomics**	1210 Technologists' Track CTE 6 Technologists Committee **Extravasation Incidents Management**	1211 Special Symposium 4 **Lung Scintigraphy for Pulmonary Embolism Diagnosis and long term Management**	08:00–08:30
08:30–09:00												08:30–09:00
09:00–09:30												09:00–09:30
09:30–10:00	1301 CME 10 Radiation Protection + Paediatrics Committee + Women's Empowerment Task Force **Radiation Protection in Motherhood and Childhood – What is so Special?**	1302 Special Track Physics + Oncology & Theranostics Committee **Debate: Whole Body Parametric Imaging**	1303 LIPS Interactive Session Neuroimaging Committee **The Sunrise of Alpha-Synuclein in vivo Brain Imaging**	1304 M2M Track TROP Session Radiopharmaceutical Sciences + Translational Molecular Imaging & Therapy Committee **Emerging Theranostic Concepts**	1305 Cutting Edge Science Track TROP Session Physics Committee **Quantitative SPECT/CT Imaging**	1306 Clinical Oncology Track TROP Session Oncology & Theranostics Committee **Lung**	1307 TROP Session Cardiovascular Committee **Plaque, Fibrosis and Cardio-Oncology**	1308 TROP Session Thyroid Committee **18F-FDG and Novel Tracers in the Diagnostic Management of Patients with Thyroid Cancers**	1309 e-Poster Presentations Session 10 Oncology & Theranostics Committee **Haematological and Abdominal Malignancies / localised Treatments**	1310 Technologists' Track Oral Presentations 3 Technologists Committee **NM Technologists: Competencies and Training**	1311 Theranostic's Track Oncology & Theranostics Committee **What's New in Neuroendocrine tumours?**	09:30–10:00
10:00–10:30												10:00–10:30
10:30–11:00												10:30–11:00
11:00–11:30												11:00–11:30
11:30–12:00	1401 Plenary 4 **Diagnostic Imaging: Proven Beyond Doubt?**											11:30–12:00
12:00–12:30												12:00–12:30
12:30–13:00												12:30–13:00
13:00–13:30	Lunch Break			Satellite Symposium	Satellite Symposium	Satellite Symposium	Satellite Symposium	Satellite Symposium		Satellite Symposium	Satellite Symposium	13:00–13:30
13:30–14:00												13:30–14:00
14:00–14:30												14:00–14:30
14:30–15:00												14:30–15:00
15:00–15:30	1501 CME 11 Paediatrics Committee **Pediatric Lymphoma and Update on FDG**	1502 Special Track Neuroimaging Committee **Challenge the Expert: Amyloid vs Tau PET - Which Is First in suspected Alzheimer Patients? Germany versus Italy**	1503 LIPS Interactive Session Bone & Joint Committee **Pitfalls and Common Bony Findings in PET-CT/MRI using Novel Tracers**	1504 M2M Track TROP Session Radiopharmaceutical Sciences + Translational Molecular Imaging & Therapy Committee **Imaging the Components of the TME**	1505 Cutting Edge Science Track TROP Session Physics Committee **AI Methods and Applications**	1506 Clinical Oncology Track TROP Session Oncology & Theranostics Committee **Prostate Cancer Treatment**	1507 TROP Session Cardiovascular Committee **Perfusion**	1508 Joint Symposium 5 Oncology & Theranostics Committee / EANM **Prostate Cancer Theranostics: Where Do We Go?**	1509 e-Poster Presentations Session 11 Radiopharmaceutical Sciences + Translational Molecular Imaging & Therapy Committee **Novel Therapeutic Approaches**	1510 Technologists' Track CTE 7 Technologists & Thyroid Committee **Molecular Thyroid Imaging - Qualitative and Quantitative Approaches**	1511 EU Policy Symposium 1 Policy & Regulatory Affairs Committee **Supply & Shortages of Radiopharmaceuticals**	15:00–15:30
15:30–16:00												15:30–16:00
16:00–16:30												16:00–16:30
16:30–17:00	1601 CME 12 Physics + Oncology & Theranostics + Translational Molecular Imaging & Therapy + Technologists Committee **Long Axial Field-of-View PET Scanners – A Copernical Revolution**	1602 Special Track Bone & Joint + Cardiovascular Committee **Debate: NaF PET in Cardiology and MSK: Pro or Cons?**	1603 LIPS Interactive Session Neuroimaging + Inflammation & Infection Committee **The Role of FDG PET in the Diagnosis of Auto-Immune Encephalitis**	1604 M2M Track TROP Session Radiopharmaceutical Sciences + Translational Molecular Imaging & Therapy Committee **Understanding and Improving RLT**	1605 Cutting Edge Science Track TROP Session Physics Committee **Data Analysis**	1606 Clinical Oncology Track TROP Session Oncology & Theranostics Committee **Head and Neck Imaging**	1607 TROP Session Neuroimaging Committee **New PET Tracers for Brain Imaging**	1608 TROP Session Thyroid Committee **Nuclear Medicine Imaging in Thyroid and Parathyroid Disorders**	1609 e-Poster Presentations Session 12 Dosimetry Committee **Dosimetry Simphony**	1610 Technologists' Track CTE 8 Technologists Committee **Gynaecological Studies**	1611 EU Policy Symposium 2 Policy & Regulatory Affairs Committee **Regulatory Challenges of Radiopharmaceuticals**	16:30–17:00
17:00–17:30												17:00–17:30
17:30–18:00												17:30–18:00
18:00–18:30												18:00–18:30

Wednesday, September 13, 2023



Oral Sessions

OC

Saturday, September 9, 2023, 18:00 - 18:35
Hall A

Opening Ceremony including Awards Ceremony

OP-001
Opening Ceremony including Awards Ceremony
V. Garibotto;
University Hospitals and University of Geneva, Geneva, SWITZERLAND.

101

Saturday, September 9, 2023, 18:35 - 19:35
Hall A

Plenary 1: Highlights Lecture

OP-002
Highlight Lecture
S. Veldhuijzen van Zanten;
Erasmus Medical Center, Amsterdam, NETHERLANDS.

OP-003
Highlight Lecture
S. Morbelli;
San Martino Hospital, University of Genoa, Genoa, ITALY.

OP-004
Highlight Lecture
D. Kersting;
University Hospital, Essen, Department of Nuclear Medicine, Essen, GERMANY.

OP-005
Highlight Lecture
H. Verberne;
University of Amsterdam, NETHERLANDS.

201

Sunday, September 10, 2023, 08:00 - 09:30
Hall A

CME 1 - Inflammation & Infection Committee: Infection and Inflammation - New Guidelines

OP-006
New Guidelines about Infection
G.Abikhzer;
Nuclear Medicine, Jewish General Hospital, Quebec, CANADA.

OP-007
New Guidelines about Inflammation
O. Gheysens;
Nuclear Medicine Department, Cliniques Universitaires Saint-Luc, Université Catholique de Louvain, Brussels, BELGIUM.

OP-008
FUO Guidelines
D. Albano;
Nuclear Medicine Department, Università degli Studi di Brescia, ASST Spedali Civili of Brescia, Brescia, ITALY .

OP-009
Diabetic Foot Guidelines
R. Chakravartthy;
Nuclear Medicine department, Kings College London Hospital Trust, Shrewsbury, UNITED KINGDOM .

202

Sunday, September 10, 2023, 08:00 - 09:30
Hall D (Arena)

Debate 1 - Cardiovascular Committee: Myocardial Perfusion Imaging after ISCHEMIA

OP-010
Anatomical imaging with coronary CTA is all I need!
A. Rossi;
UniversityHospital of Zurich, Zurich, SWITZERLAND.

OP-011
Myocardial perfusion imaging: let's go with the flow!
M. Mallah;
Houston Methodist Academic Institute, Houston, UNITED STATES OF AMERICA.

OP-012
Debate

203

Sunday, September 10, 2023, 08:00 - 09:30
Hall E1

LIPS Session 1 - Oncology & Theranostics Committee: Novelties in Radionuclide Therapy

OP-013
Emerging radiopharmaceuticals in radionuclide therapy
L. Unterrainer;
LMU Munich, Department of Nuclear Medicine, Munich, GERMANY.

OP-014
Intra-arterial Peptide Receptor Radionuclide Therapy
A. Braat;
UniversityMedical Center Utrecht, Department of Radiology and Nuclear Medicine, Utrecht, GERMANY.

OP-015
Pancreatic cancer treatment with P-32
Z. Win;
Imperial College Healthcare NHS Trust Hammersmith, St Mary's and Charing Cross Hospitals, Department of Nuclear Medicine, London, UNITED KINGDOM.

204

Sunday, September 10, 2023, 8:00 AM - 9:30 AM
Hall E2

M2M Track - TROP Session: Translational Molecular Imaging & Therapy Committee + Radiopharmaceutical Sciences Committee: At the Nucleus: Radionuclide Production

OP-016

Terbium-149 production: a pragmatic view of its clinical potential

N. van der Meulen[1], *P. V. Grundler*[1], *Z. Talip*[1], *C. Favaretto*[1], *C. C. Hillhouse*[1], *U. Koester*[2], *K. Johnston*[3], *R. Schibli*[1], *R. Eichler*[1], *C. Mueller*[1];
[1]*Paul Scherrer Institut, Villigen, SWITZERLAND,*
[2]*ILL, Grenoble, FRANCE,* [3]*CERN, Geneva, SWITZERLAND.*

Aim/Introduction: Terbium-149 was proposed as an attractive candidate for Targeted Alpha Therapy (TAT) in the late 1990's [1], due to its favourable physical decay properties ($T_{1/2}$ = 4.1 h, E_{α} = 3.97 MeV, 16.7 %; $E_{\beta+\ mean}$ = 720 keV, 7.11%) [2]. While preclinical studies demonstrated its potential for therapeutic purposes [3-5], it was also shown that it could be used for positron emission tomography [4]. ***Materials and Methods:*** Terbium-149 was produced at ISOLDE/CERN via spallation of a tantalum target using high-energy (1.4 GeV) protons, followed by resonant ionization of spallation products and online mass separation. The mass 149 isobars were implanted in a zinc-coated gold foil and shipped to Paul Scherrer Institute for processing. Terbium-149 was separated from its isobaric impurities, as well as the ion-implantation matrix, using cation exchange and extraction chromatography, employing an optimized process to that previously reported [5]. The quality of the radionuclide produced was assessed by means of radiolabelling and ICP-MS measurements. ***Results:*** Up to 450 MBq terbium-149 was collected daily and transported, with ~200 MBq activity received at PSI. The four-hour radiochemical separation process resulted in ~100 MBq obtained as final product. The radiochemical purity of the final product formulated in 1 mL 0.05 HCl was 99.8%. Quality control was performed using DOTATATE, which was successfully labelled at molar activities up to 20 MBq/nmol with >99% radiochemical purity - three times better than previously achieved [5]. The chemical purity was further proved by ICP-MS measurements, showing lead, copper, iron and zinc in ppb levels. ***Conclusion:*** Preclinical data using terbium-149 has indicated great potential towards TAT. The chemical separation procedure has steadily improved over the years, such that the quality of product can ensure more efficient labelling of small molecules. While only CERN/ISOLDE currently produces this radionuclide (where one has to lobby for beam time for one-to-two weeks' collection per year), CERN/MEDICIS is currently developing efficient methods to do so as well. The interest in the radionuclide remains high, with governments in Switzerland (IMPACT project) and Belgium (MYRRHA) having approved grants to fund facilities to upscale and produce large activities of terbium-149, amongst other interesting radionuclides, towards medical research and potential clinical application. ***References:*** [1] Allen. Australasian Radiology 1999, 43:480. [2] Singh & Chen. Nuclear Dataa Sheets 2022, 185:2 [3] Beyer et al. Radiochim Acta 2002, 90:247. [4] Müller et al. EJNMMI Radiopharm Chem 2016, 1:5. [5] Umbricht et al. Sci Rep 2019, 9:17800.

OP-017

Small-scale production of ^{161}Tb for preclinical studies

M. Skálová*, J. Kozempel, M. Vlk, K. Ondrák Fialová, L. Ondrák;*
Department of Nuclear Chemistry, Faculty of Nuclear Sciences and Physical Engineering, Czech Technical University in Prague, Prague, CZECH REPUBLIC.

Aim/Introduction: Terbium-161 is promising theranostic radionuclide thanks to its good decay characteristics, i.e. its half-life of 6,89 d and emission of soft β^- particles with $E_{\beta max}$ of 593 keV together with several conversion and Auger-Meitner secondary low energy electrons that contribute to the enhancement of the therapeutic effect. It also emits γ radiation with energy 74 keV, suitable for SPECT imaging and therapy follow-up monitoring. The most convenient method for no-carrier-added ^{161}Tb production is the nuclear reactor irradiation of enriched ^{160}Gd using indirect route of ^{160}Gd(n,γ)^{161}Gd → ^{161}Tb. The most common method used for separation of the prepared ^{161}Tb from the bulk irradiated target is cation exchange chromatography with the 2-hydroxy-butyric acid. This method was implemented in small-scale production of this theranostic nuclide. ***Materials and Methods:*** The ^{161}Tb was produced by the irradiation of highly enriched ^{160}Gd (98,6 %) in the form of oxide or nitrate in the nuclear reactor LVR-15 (CV Řež, Czech rep.). The separation was performed using cation exchange chromatography on Dowex 50W×8 resin with α-hydroxyisobutyric acid as co-eluent. Different dimensions of glass chromatography columns were tested with respect to the target mass. The finally separated and purified ^{161}Tb was formulated to 0.05 M HCl in the form of terbium chloride. The radionuclidic purity of prepared ^{161}Tb was verified by gamma spectrometry on an HPGe detector, chemical purity was estimated by ICP-MS. Further, the labelling test with DOTA was performed to assess overall sample purity. ***Results:*** The ^{161}Tb was successfully prepared with the highest amounts of up to 13 GBq and the highest activities of purified ^{161}Tb samples reached almost 12 GBq (EOB). Dowex 50W×8 resin with 200-400 mesh size proved to be significantly better for both separation and purification process compared to higher granulosity sample. The radionuclidic purity of ^{161}Tb was higher than 99,999 %, specific activity typically higher than 15 GBq/μg. ***Conclusion:*** Pure ^{161}Tb samples for preclinical studies could be prepared reliably in a small scale by neutron irradiation of highly enriched ^{160}Gd targets with subsequent separation and purification on a laboratory scale. Further method development and automation would enable wider availability of ^{161}Tb for our studies. This work was supported by the project "Efficient Low-Energy Electron Cancer Therapy with Terbium-161" granted by the Norway and Technology Agency of the Czech Republic within the KAPPA Programme (grant No.: TO01000074). ***References:*** Gracheva, N., Müller, C., Talip, Z. et al. EJNMMI radiopharm. chem. 4, 12 (2019).

OP-018

Separation and Purification of ^{225}Ac for Targeted Alpha Therapy Radiopharmaceuticals

E. Yalcintas Bethune*, J. F. Camacaro, S. Chatterjee, C. P. Dunckley, H. A. Fitzgerald, E. Harman, A. L. Lakes, Z. Liao, L. M. Lilley, R. C. Ludwig, K. M. McBride, A. Younes;*
TerraPower LLC, Bellevue, WA, UNITED STATES OF AMERICA.

Aim/Introduction: In this work, we present the separation and purification of ^{225}Ac from its highly radioactive and chemically variable source. ^{225}Ac is a unique relatively short-lived ($t_{1/2}$ = 9.92 days) actinide that decays via four alpha particles, which makes it an attractive candidate for development of targeted alpha therapy

radiopharmaceuticals. Currently the world's supply of ^{225}Ac cannot fulfill the needs of large-scale clinical trials or patient treatments. The most direct and radio-isotopically pure route to obtain ^{225}Ac is routinely harvesting from its long-lived ($t_{1/2}$ = 7932 y) parent ^{229}Th after it has naturally decayed to ^{225}Ac via ^{225}Ra. We are working with a U.S. federal contractor to recover ^{229}Th from ^{233}U stockpiles that would otherwise be irretrievably converted into final disposal form as a radioactive waste. ***Materials and Methods:*** The ^{229}Th source in our facility contains a certain amount of the highly radioactive ^{228}Th, which poses unique radiological challenges with handling this material. ^{225}Ac production from this source requires development in three areas: i. consistent separation and purification of ^{229}Th from its stable metal, uranic, and transuranic impurities; ii. separating ^{225}Ac from ^{229}Th and ^{225}Ra parents while preserving them for later ^{225}Ac in-growth; and iii. improving analytical methods to verify the high-grade ^{225}Ac product. Chemical treatment and separation routes for purifying initial ^{229}Th material must be tailored to the specific impurities of each batch received. The current processing scheme for routine isolation of ^{225}Ac is based on an anion exchange separation of ^{225}Ac/^{225}Ra from ^{229}Th, where Th is retained on the anion exchange resin as the $[Th(NO_3)_6]^{2-}$ anion. The ^{225}Ac/^{225}Ra separation is achieved through extraction chromatography using a UTEVA resin, followed by DGA resin and prefilter resins. Aliquots collected after each separation step and from the final ^{225}Ac product have been analyzed by analytical methods, including HPGe, alpha spectroscopy, ICP-MS, and iTLC, to confirm that the ^{225}Ac yield is as expected, there is no Th and ^{225}Ra breakthrough, stable impurities are at the limit of detection, and high radiolabeling yield is achieved. ***Results:*** Our current method shows an excellent process yield of 98% for recovery of carrier-free ^{225}Ac based on theoretical decay of ^{229}Th. ***Conclusion:*** By setting up multiple ^{229}Th generators operated in parallel, we seek to provide increased, stable supply of clinical grade ^{225}Ac and thereby support radiopharmaceutical drug development to enable widespread treatment of cancer patients via ^{225}Ac based targeted alpha therapy.

OP-019

Cyclotron based production of ^{64}Cu/^{67}Cu diagnostic and theragnostic pair

J. Lee, *J. Park;*
Korea Atomic Energy Research Institute, Jeollabuk-do Jeongeup-si, KOREA, REPUBLIC OF.

Aim/Introduction: Copper-64 (^{64}Cu) and Copper-67 (^{67}Cu) are two important isotopes of copper with significant importance in various fields such as nuclear medicine, radiopharmaceuticals and cancer therapy. The production of ^{64}Cu and ^{67}Cu requires specialized facilities and expertise, as well as careful handling of radioactive materials. However, despite these challenges, their potential applications in medical imaging and cancer therapy make them an important focus of research and development in the nuclear medicine field. In this study, we aim to discuss the research results on target preparation, proton beam irradiation, chemical separation, and quality control for the production of ^{64}Cu and ^{67}Cu. ***Materials and Methods:*** This study focuses on the production of radioisotopes, specifically ^{64}Cu and ^{67}Cu, through the proton beam irradiation process of electrodeposited targets of ^{64}Ni and ^{70}Zn. To enhance target cooling and increase production efficiency, a tilted target and a backside water cooling system were employed. The radioactive copper obtained from the target materials was purified through a solid-phase separation method to remove impurities and recover the target material. Quality control measures were taken to verify the radionuclidic purity and impurity metal content of ^{64}Cu and ^{67}Cu. ***Results:*** We used an electrodeposition method to uniformly distribute ^{64}Ni and ^{70}Zn onto a gold-coated copper and silver backing material, respectively, on a 5-degree tilted target optimized for proton beam irradiation efficiency. The target was then irradiated with proton beams at cumulative currents of 90 and 1200 uAh, and incident energies of 11 and 17.7 MeV, producing ^{64}Cu and ^{67}Cu at yields of 28.5 MBq/μAh and 0.58 MBq/μAh, respectively. We recovered over 98% of the irradiated target using a self-developed target dissolution device. The ^{64}Cu and ^{67}Cu were then chemically separated using an anion exchange resin and a copper selective resin, achieving a separation efficiency of >98%. Finally, quality control was performed through the evaluation of radionuclidic purity and impurity metal content, confirming results of >99.9% radionuclidic purity and <1 ppm impurity metal content. ***Conclusion:*** We produced pair-radioisotopes ^{64}Cu and ^{67}Cu with high yields and radioisotope purity using RFT-30 cyclotron, equipment, and chemicals. The electrodeposited targets provided advantages for beam irradiation and maximum irradiation area. We achieved >98% separation efficiency using ZR cartridges and resins. The final product was prepared under mild reaction conditions, and quality control ensured >99% radioisotope purity and <1 ppm metallic impurity content. Automation for separating apparatus is being studied for mass production.

OP-020

Production of Lanthanum-133 via the^{134}Ba(p,2n)^{133}La Nuclear Reaction with High Radionuclide Purity for Theranostic Purposes

S. Brühlmann[1,2], *M. Kreller*[1], *H. Pietzsch*[1], *K. Kopka*[1,2], *C. Mamat*[1,2], *M. Walther*[1], *F. Reissig*[1];
[1]*Helmholtz-Zentrum Dresden-Rossendorf, Dresden, GERMANY,*
[2]*Technische Universität Dresden, Dresden, GERMANY.*

Aim/Introduction: Actinium-225 has gained great importance in Targeted Alpha Therapy (TAT) due to its suitable physical and chemical properties. In past years, studies using ^{225}Ac-PSMA-617 have shown promising results [1], however, the macropa chelator has proven more beneficial properties regarding labelling and stability in vivo as compared with DOTA. While ^{68}Ga has been used for DOTA-based radioconjugates, the macropa chelator lacks an imaging radionuclide counterpart. For this purpose, the β^+-emitter ^{133}La is an attractive candidate due to its physical properties and similar to ^{225}Ac coordination chemistry. Following our recent publication [2], further optimization of the production of ^{133}La with high radionuclidic purity (RNP) for theranostic purposes is presented. ***Materials and Methods:*** Lanthanum-133 was produced via the ^{134}Ba(p,2n)^{133}La nuclear reaction. Proton irradiation (19 MeV, 35 μA, 30 min) was performed using the HZDR TR-FLEX (ACSI) cyclotron on silver discs filled with 25 mg of $[^{134}Ba]BaCO_3$ capped with a 25 μm aluminum foil. The solid target was opened and the powder dissolved in 2 mL of 1 M HNO_3. A one-step separation was carried out with a branched DGA resin cartridge after testing other resins. The ^{134}Ba-containing fractions were collected and recycled through $[^{134}Ba]BaCO_3$ precipitation. Test radiolabelling of macropa-derived PSMA conjugates previously published by our group was performed in the MBq/nmol range [3]. ***Results:*** Lanthanum-133 yields of ca. 1.8 GBq for the described targets were reached at end of bombardment (EOB), accounting for about 65 % of the theoretical yield. After radiochemical separation, 1.2 GBq ^{133}La were collected in 1 mL of

0.05 M HCl ready to label, with a RNP over 99.5 %. Further studies showed no detriment of the RNP by 21 MeV proton irradiation, thus being feasible irradiation of larger targets (prior thermal studies). Furthermore, quantitative radiolabeling was achieved with ligand concentrations down to 300 MBq/nmol. ***Conclusion:*** Lanthanum-133 of high RNP was produced for the first time. Considering future medical demands, the scale up to radioactivity amounts that are needed for clinical application purposes could be achieved by increasing the irradiation time. Alternatively, irradiation with higher currents or of thicker targets could also lead to higher activities. Based on these results, our group will attempt to establish a diagnostic platform for ^{225}Ac-TAT based on ^{133}La-macropa radioconjugates instead of the conventional ^{68}Ga-DOTA application. ***References:*** [1] Kratochwil et al., J. Nucl. Med. 2016, 57, 1941-1944 [2] Brühlmann et al., Pharmaceuticals 2022, 15, 1167. [3] Reissig et al., Cancers 2021, 13, 1974.

OP-021

Neutron Capture-Based Production via Power Reactor and Potential Market Penetration

C. Horne[1], *J. Quirt*[1], *M. Flagg*[2];
[1]*Laurentis Energy Partners (subsidiary of Ontario Power Generation), Pickering, ON, CANADA,*
[2]*BWXT Medical, Kanata, ON, CANADA.*

Aim/Introduction: This paper discusses non-proprietary aspects of neutron capture-based Mo99 production through a commercial CAndU reactor in Ontario, Canada and potential future market possibilities. ***Materials and Methods:*** Historically, the production of Molybdenum-99 (Mo99) via neutron capture has been limited, stemming from lower reaction efficiencies and extraction capacities based on low specific activity. A breakthrough in technetium generator technology, developed by BWX Technologies (BWXT) in the United States, has regained attention as a viable method for high-volume uranium-based Mo99 production. Through a partnership with Laurentis Energy Partners of Canada, a commercial CAndU (Canadian Atomic Natural Deuterium Uranium) nuclear reactor near Toronto, Canada, will generate Mo99 via neutron capture with subsequent processing at a local BWXT facility - both technologies being a first of a kind in the industry. Given the scale of power reactors, additional operating and safety considerations beyond those incorporated in research reactors will be required for the production and handling of Mo99 ***Results:*** The Mo99 Target Delivery System has been successfully installed and commissioned at low power and 100% power levels. ***Conclusion:*** Initial tests of Mo99 targets analyzed have been promising and allows for numerous possibilities of new isotope irradiations, as well as expansion to other CAndU reactors around the world.

OP-022

Testing new resins for ^{225}Ac separation

O. Lebeda[1], *K. Ondrák Fialová*[1], *L. Ondrák*[1], *S. Happel*[2], *J. Ráliš*[1], *M. Kleinová*[1], *I. Dovhyi*[2];
[1]*Nuclear Physics Institute of the CAS, Husinec-Rez, CZECH REPUBLIC,* [2]*TRISKEM International, Bruz, FRANCE.*

Aim/Introduction: All the ways for production of ^{225}Ac in relevant amounts require its separation, concentration and conversion to chloride. Development of a suitable separation tool that may undertake efficiently these tasks is naturally highly desirable. We have, therefore, determined mass distribution coefficient DW and elution profiles for ^{225}Ac of recently designed resins TK221 and TK222 in nitric and hydrochloric acids. Although these resins have been characterized with respect to the uptake of many stable elements, very little is known about actinium behaviour on them. ***Materials and Methods:*** TK221 and TK222 (50-100 µm) were synthesized in TRISKEM. The DW was determined by 1 hour long shaking of 50 mg of a given resin with 5 ml of ^{225}Ac (25 kBq) solution in HCl or HNO_3 with molarities ranging between 0.01M and 10M. The mass distribution coefficient was deduced from the activity drop in filtered supernatant (1 µm glass fiber) compared to the initial ^{225}Ac solution measured in an automated gamma counter equipped with well-type NaI(Tl) detector. Elution profile of ^{225}Ac was determined on 2 ml columns filled with a given resin. Loading and rinsing of ^{225}Ac (1 MBq) in optimal molarity HNO_3 was followed by elution of actinium into diluted HCl or HNO_3. Activity of the resulting fractions was measured either on an automated gamma counter equipped with well-type NaI(Tl) detector or on gamma-ray spectrometer with HPGe detector. ***Results:*** The DW values show high affinity of ^{225}Ac to both resins in wide range of nitric acid concentrations. The affinity in hydrochloric acid dropped significantly with maximum shifted towards high acid concentrations. Diluted hydrochloric acid releases rapidly ^{225}Ac from both resins after its loading in diluted or medium concentrated nitric acid. Elution of ^{225}Ac from the resins into diluted nitric acid is also possible, the process is, however, very slow. ***Conclusion:*** The resins TK221 and TK222 have been characterized and its suitability for ^{225}Ac separation/concentration/re-salting was tested. The obtained data clearly demonstrate that both resins have very favourable properties regarding efficient concentration of ^{225}Ac from large volumes nitric acid solutions and elution into very small volumes of diluted hydrochloric acid. The TK221 obviously allows for extraction of ^{225}Ac even from diluted nitric acid and its rapid conversion to chloride. The TK222 resin seems to be slightly superior to the TK221 regarding the elution volume.

OP-023

Production of gallium-68 using IBA and GE liquid target system - comparison and optimization

A. Uhlending, *V. Hugenberg;*
Institute of Radiology, Nuclear Medicine and Molecular Imaging, Heart and Diabetes Center North Rhin, Bad Oeynhausen, GERMANY.

Aim/Introduction: The increasing demand for ^{68}Ga-labelled radiotracers requires a secure supply of the nuclide gallium-68. A reliable method represents the cyclotron production of gallium-68 from liquid target. We have set Gallium-68-liquid target systems for our two cyclotrons (IBA 18/9 and GE PETtrace). The aim is the comparison and optimization both for a reliable ^{68}Ga radiotracer production. ***Materials and Methods:*** For the production both cyclotrons are equipped with cooled niobium liquid targets and enriched zinc-68 nitrate solution was irradiate for 60 min. Differences between IBA and GE system exist in niobium target design, helium-cooling, degrading foils, target volumes and the post-processing. The IBA post-processing of the irradiated solution is accomplished via cation and anion exchange cartridges. The GE post-processing is performed using a 2-column solid phase method. Peptide labeling is performed on a cassette-based automated synthesis module. Quality control of [^{68}Ga]$GaCl_3$ and ^{68}Ga-labelled peptides were carried out according to Ph. Eur. ***Results:*** Post-processing of the irradiated gallium-68 solution vary in the choice of cartridges and the used solutions. While the IBA method is based on cation and anion exchange cartridges using a combination of concentrated acid and organic solvent solutions, the GE process is based on a two-column approach using a ZR

resin and a TK200 resin, diluted acids and saline solutions. We optimized both systems by using larger capacity cartridges and additional rinsing steps. Quality control of the obtained [^{68}Ga] $GaCl_3$ solution revealed reproducible low zinc concentrations >0.2 mg/mL for both processes. In comparison to the volume the target yields are the same. Due to the larger volume of the IBA target produced more activity. Peptide labeling was successfully accomplished and improved by additional rinsing steps and the addition of sodium ascorbate to the reaction mixture. ***Conclusion:*** The routine production of gallium-68 via cyclotron using liquid targets from IBA and GE has been successfully implemented into the routine production of ^{68}Ga-labelled radiotracers. Both systems reveal their advantages, while the IBA system due to the larger volume gives higher yields. In comparison to the volume the target yields are the same. The advantages of the GE system are no helium-cooling and less aggressive chemicals. ***References:*** Alves et al., (2018), Instruments, 2, 17. [2] Alves et al., (2017), J Label Compd Rad, 60, Sl611., Rodnick et al. EJNMMI Radiopharmacy and Chemistry (2020)

OP-024

Radium targets for cyclotron production of Ac-225 in view of targeted alpha therapy

A. Kellerbauer[1], *R. Malmbeck*[1], *C. De Almeida Carrapiço*[1], *E. Jajcisinova*[1,2], *Rachel Eloirdi*[1], *Ondrej Lebeda*[3], *Alfred Morgenstern*[1]; *[1]European Commission, Joint Research Centre, Karlsruhe, GERMANY, [2]KU Leuven, Leuven, BELGIUM, [3]Nuclear Physics Institute of the CAS, Řež, CZECH REPUBLIC.*

Aim/Introduction: Targeted alpha therapy using the radionuclide Ac-225 has shown remarkable benefit in clinical trials to patients suffering from various cancer types. Currently most Ac-225 is produced from a few sources of Th-229 existing worldwide. However, the total amount available is only sufficient for a few thousand patient doses. Given a projected demand that is several orders of magnitude higher, alternative paths for the production of Ac-225 must be developed. We have been investigating the route using the Ra-226(p,2n)Ac-225 reaction. It is particularly attractive due to its large cross-section near 17 MeV proton energy and because it can be readily employed at a large number of cyclotron facilities. The excitation function of this reaction has been previously measured by us for a few energies [1], but discrepancies with calculations remain. Hence, new irradiation experiments are required to improve the knowledge of the excitation function to support the industrial production of Ac-225 via this route. ***Materials and Methods:*** We have built a new electrodeposition setup to deposit homogeneous layers of Ra-226 on various substrates. The process is based on a mixed organic/aqueous solution and a custom-built electroplating cell using a platinum electrode and a high-voltage power supply. ***Results:*** A number of radium targets have been produced and examined to quantitatively determine the deposition efficiency as well as the homogeneity of deposition, which is crucial for highly precise cross-section measurements. ***Conclusion:*** In this talk, we will describe our electrodeposition setup and process, and report on the properties of the prepared Ra-226 targets. ***References:*** [1] C. Apostolidis et al., Appl. Rad. Isot. 62 (2005) 383

205

Sunday, September 10, 2023, 8:00 AM - 9:30 AM
Hall B

Cutting Edge Science Track - TROP Session: Quality Control, Performance, Standardisation

OP-025

An academic/industrial PET raw data standardisation initiative

K. Thielemans[1], *A. L. Kesner*[2], *E. Asma*[3], *J. Cabello*[4], *M. J. Cook*[5], *M. Hansen*[6], *J. Jones*[4], *N. A. Karakatsanis*[7], *E. K. Leung*[8], *P. Markiewicz*[9], *S. Prevrhal*[10], *A. Rahmim*[11], *B. Saboury*[12], *J. Stairs*[6], *S. Stute*[13], *H. Tashima*[14], *G. Wells*[15];
[1]Institute of Nuclear Medicine, London, UNITED KINGDOM, [2]Memorial Sloan Kettering Cancer Center, New York, NY, UNITED STATES OF AMERICA, [3]Canon Medical Research UNITED STATES OF AMERICA, Vernon Hills, IL, UNITED STATES OF AMERICA, [4]Siemens Medical Solutions UNITED STATES OF AMERICA, Inc, Knoxville, TN, UNITED STATES OF AMERICA, [5]GE HealthCare, Waukesha, IL, UNITED STATES OF AMERICA, [6]Microsoft Research, Redmond, WA, UNITED STATES OF AMERICA, [7]Weill Cornell Medical College, Cornell University, New York, NY, UNITED STATES OF AMERICA, [8]UIH America, Inc., Houston, TX, UNITED STATES OF AMERICA, [9]University College London, London, UNITED KINGDOM, [10]Philips Research, Hamburg, GERMANY, [11]University of British Columbia, Vancouver, BC, CANADA, [12]National Institutes of Health (NIH) - Clinical Center, Bethesda, MD, UNITED STATES OF AMERICA, [13]Nantes University Hospital, CRCI2NA, Nantes, FRANCE, [14]National Institutes for Quantum Science and Technology, Chiba, JAPAN, [15]University of Ottawa Heart Institute, Ottawa, ON, CANADA.

Aim/Introduction: As the capabilities of computer hardware and software progresses, the importance of standardised data is becoming more relevant. In current PET practice, raw acquisition data are recorded in an intermediate listmode format before vendors apply the necessary processing to deliver standard, sharable, PET DICOM images. However, all current vendor formats differ, to accommodate different architectures and processing strategies. Our goals are to define an open, extendable, standardised and vendor-agnostic description of PET listmode and associated data; define a standard for storage and transmission of that data; and develop a standardised description of software to access and manipulate the standardised data, as well as prototype software. Such a standard will facilitate a new paradigm for PET innovation, including new opportunities for inter-scanner and inter-vendor harmonization and AI applications, and aide in development of advances in novel PET applications and analysis tools. ***Materials and Methods:*** An international working group comprised of PET imaging experts from academia and industry was formed in 2022 to establish a pathway for building the new standard format. This includes establishing the key informational elements to include in the standard, data container formats, and integration initiatives. All portions of the format, tools for accessing the data in the standardised format, and example data will be made open source and publicly available. ***Results:*** The initiative's "Data Elements" subgroup has defined a content description that is compatible with most major PET vendors. The content includes coincidence recording, scanner geometry, data corrections, normalisation, and concurrent physiologic signals. The "Container" subgroup has developed a meta-language called Yardl for defining data structure and protocols for accessing,

transferring, and storing data. The meta-language approach and associated tooling are also applicable to other modalities and are, for example, under consideration for a revision of the ISMRM Raw Data standard. A prototype of the meta-language standard definition and software for processing it into C++ subroutines are available in open source on GitHub. ***Conclusion:*** The PET standardisation initiative is being pursued as an opportunity for academia and industry to cooperatively expand the capacity of the future PET field, ensuring that we are able to build modern applications that make the most of PET clinical and preclinical data. The effort is ongoing, and we welcome interest, feedback, and support from the greater community.

OP-026

A reference-free PET quality metric using multi-scale sharpness index

F. Moradi[1], *P. Gurunath Bharathi*[1], *M. Khalighi*[1], *K. Su*[2], *M. Spangler-Bickell*[2];
[1]*Stanford University, Stanford, CA, UNITED STATES OF AMERICA,* [2]*GE Healthcare, Waukesha, WI, UNITED STATES OF AMERICA.*

Aim/Introduction: Spatial resolution is critical in medical imaging. Detectability and accurate characterization of small lesions on PET are affected by actual (as opposed to nominal) resolution, which depend on positron range, instrumentation, reconstruction algorithm, post-reconstruction filtering/noise-reduction, and patient factors such as motion blur. Here we a propose a framework for assessing and quantifying image resolution and sharpness directly from actual patient FDG PET images, for which spatial features are not a priori known and images are subject to inherent complex non-uniform noise different from phantom studies. ***Materials and Methods:*** Fifty-two patients underwent standard of care oncologic FDG PET using a GE Discovery MI PET/CT scanner. Images (70 cm FOV, 256x256) were reconstructed reconstructed using Time-Of-Flight Block-Sequential Regularized Expectation Maximization (BSREM) using a range of β (400-1200) and time per bed (60s - 360s). We measured perceived sharpness of each scan using a 5-point Likert scale, blinded to reconstruction method/β. Images were cropped to 128x128 (to reduce empty area) and sharpness index (based on phase-coherence)[1] was calculated on each image and its scaled down versions (1/2, 1/4, 1/8, and 1/16th for size, 1/2, 1/3, and 1/4 SUV gamma scale). Together, these values provide a multiscale representation of sharpness for each image. We used logistic regression with 13-fold cross validation to explore the relationship between this multiscale representation and reconstruction parameter β. ***Results:*** For axial PET images, sharpness indices inversely correlated with β with some dependence on image noise (a function of acquisition time per bed) and values were not directly comparable across axial slices and different patients. Highest values were observed in areas of very high contrast (e.g., slices containing urinary activity in kidneys or bladder). However, a logistic regression model based on multiscale sharpness index for each image correlated strongly with β (cross-validated R^2=0.82) and was robust to noise and consistent across body position and patients (cross-validated R^2=0.91). ***Conclusion:*** Multiscale sharpness index provides a useful representation and can be used to derive a spatial resolution/sharpness image quality metric for PET without the need for a reference image or explicit assumptions about spatial features. ***References:*** G. Blanchet and L. Moisan, "An explicit sharpness index related to global phase coherence," 2012 IEEE International Conference on Acoustics, Speech and Signal Processing (ICASSP), Kyoto, Japan, 2012, pp. 1065-1068.

OP-027

Mitigating SUV Uncertainties Using Total Body PET Imaging

C. L. C. Smith[1,2], *G. J. C. Zwezerijnen*[1,2], *M. den Hollander*[1], *J. Weijland*[1], *M. Yaqub*[1,2], *R. Boellaard*[1,2];
[1]*Amsterdam UMC location Vrije Universiteit Amsterdam, Department of Radiology and Nuclear Medicine, Boelelaan 1117, Amsterdam, NETHERLANDS,* [2]*Cancer Center Amsterdam, Imaging and Biomarkers, Amsterdam, NETHERLANDS.*

Aim/Introduction: Standardized uptake values (SUV) are commonly used as a quantitative assessment of lesion uptake in ^{18}F-FDG PET/CT studies. However, SUVs may suffer from several uncertainties and errors. Long-axial field-of-view PET/CT systems enable image-based quality control (QC) by deriving ^{18}F-FDG activity and patient weight from a total body (TB) ^{18}F-FDG PET image. In this study, we aimed to develop image-based QC to reduce errors and mitigate SUV uncertainties. ***Materials and Methods:*** First, three phantoms were scanned to verify scanner calibration accuracy. Thereafter, 25 out of 81 patients were used as training dataset. Patients were accurately weighed on the day of the PET/CT study to determine if patient weight could be obtained from a TB and half-body (HB) ^{18}F-FDG PET image. In addition, we developed an algorithm to derive the injected ^{18}F-FDG activity from these scans. Finally, the other 56 patients were used as test dataset to study the agreement of image-derived activity and weight with reported ^{18}F-FDG activity and weight. Moreover, we studied the impact of image-based values on the precision of liver SUVmean and lesion SUVpeak. ***Results:*** Reported activity and image-derived activity from the phantoms agreed within 5.8%. The training data showed that ^{18}F-FDG activity and patient weight significantly predicted reported injected activity (r = 0.999) and weight (r = 0.999). The test dataset showed that ^{18}F-FDG activity and patient weight can be accurately derived within 4.8% and 3.2% from TB ^{18}F-FDG PET images and within 4.9% and 3.1% from HB ^{18}F-FDG PET images, respectively. In addition, liver and lesion SUV variability decreased when image-derived values were used instead of reported values. ***Conclusion:*** Both HB and TB ^{18}F-FDG PET images can be used to derive ^{18}F-FDG activity and patient weight accurately. Furthermore, image-derived values increased liver SUV precision and corrected lesion SUV errors. Therefore, calculating SUVs based on image-derived information may be a good approach to correct for data entry or measurement errors. Image-derived values should be included as QC to generate a more reliable and reproducible quantitative uptake measurement.

OP-028

Calibration Procedures for Radionuclide Calibrators to Achieve Traceable Activity Measurements for Lu-177

V. Reijonen[1], *P. Toroi*[2], *M. Tenhunen*[1];
[1]*Comprehensive Cancer Center, Helsinki University Hospital, Helsinki, FINLAND,* [2]*STUK - Radiation and Nuclear Safety Authority, Helsinki, FINLAND.*

Aim/Introduction: The number of lutetium-177-based radiopharmaceutical treatments is increasing. The activity of the radiopharmaceutical (treatment dose) is measured with a radionuclide calibrator (RC). This measurement result needs to be traceable and accurate. The aim is to establish calibration procedures for Lu-177 settings of RCs in Finland. ***Materials and Methods:*** Two no-carrier-added Lu-177-chloride samples from an isotope technology provider were used: 1. Lu-177 standard sample (1.00 ml liquid, 10 ml P6-vial, ~1 GBq), and 2. Lu-177 technical sample (0.38 ml liquid, 3 ml V-vial, ~15 GBq). The sample

1 was used for calibration and the sample 2 to perform linearity check covering the scale of activity used in patient treatments. The sample 1 was provided with a calibration certificate stating activity, with relative uncertainty of 3% and traceability to an accredited laboratory using liquid scintillation counting. The reference activity of the sample 2 was defined by the provider with their RC. Repeated measurements were performed over a period of month with a secondary standard radionuclide calibrator (SSRNC) as well as six RCs from four manufacturers A-D: A1-A3 and B1 (new, with factory dial settings), C1 (five years old), and D1 (12 years old). Additional measurements were performed to determine the impact of the container type. ***Results:*** The activity measured with the SSRNC and given in the sample 1 certificate agreed within 0.2%. However, the activity of the sample 2 differed by -9.0% from the provider's reference data. For the RCs A1-A3, the activity reading of the sample 1 differed initially by +5.4%, +5.0%, and +5.8%. For the RCs B1, C1 and D1, the differences were -1.1%, +0.4%, and -3.1%, respectively. The Lu-177 dial setting of each calibrator was then tuned to match the calibration certificate reference value. During the following weeks, the linearity of all the RCs was excellent, and for the sample 1 differences in measured activity were on average 0.3% for all calibrators. However, measuring the sample 2 indicated an average difference of -7.2% compared to the provider's reference information, which is consistent with the results received with the SSRNC. According to our additional measurements, the difference in measuring geometry does not explain this discrepancy. ***Conclusion:*** Based on the SSRNC results it could be used as a reference standard for Lu-177 calibrations of RCs. Significant differences between RC models with factory dial settings were found, and thus calibration is strongly recommended. Regular verification is also needed.

OP-029

Accuracy of absolute quantification for high count rate holmium-166 SPECT/CT

L. E. L. Westlund Gotby[1], *D. Lobeek*[1], *J. Roosen*[1], *M. de Bakker*[1], *M. W. Konijnenberg*[1,2], *J. F. W. Nijsen*[1];
[1]*Department of Medical Imaging, Radboud University Medical Center, Nijmegen, NETHERLANDS,* [2]*Department of Radiology and Nuclear Medicine, Erasmus Medical Center, Rotterdam, NETHERLANDS.*

Aim/Introduction: Personalization of transarterial radioembolization with holmium-166 (^{166}Ho) microspheres could benefit from dosimetric information during or shortly after the therapy has been administered, and quantitative SPECT/CT imaging at high count rates is therefore desired. We aim to characterize the performance of a proprietary absolute quantification method and compare it with conventional relative quantification. ***Materials and Methods:*** A Jaszczak phantom with six fillable, spherical inserts (0.5, 2.0, 4.0, 8.0, 16.0, and 113mL) was filled with ^{166}Ho-chloride. A 10:1 sphere-to-background activity concentration ratio was used (3.94:0.39MBq/ml at first scan). The phantom was imaged using a Symbia Intevo Bold (Siemens Healthineers) at 14 timepoints (activity range 3260-64MBq). Data were acquired with a photon peak window at 81keV (15% width), two adjacent scatter windows (8% width), 20s per projection, 2x60 projections, and medium energy low penetration collimators. Additionally the scanner was equipped with proprietary absolute quantification software (Broad Quantification) including an algorithm meant to improve the detector response at high count rates (TrueCalc). The data were reconstructed using both an ordered subset conjugate gradient method (OSCG; xSPECT reconstruction, 24 iterations 1 subset, 15mm post-reconstruction filtering) as well as an 3D ordered subset expectation maximization method (OSEM3D; Flash3D reconstruction, 10 iterations 8 subsets, no post-reconstruction filtering), both methods applying triple energy window scatter correction. Calibration of the OSCG method had been carried out prior to the experiment, enabling absolute quantification of the reconstructed images. The images derived from the OSEM3D method were quantified by applying a conversion factor based on the mean of the measured count rate density, and the known mean activity concentration in the phantom (relative quantification). The performance of the quantification was evaluated based on percentage recovered activity in the whole phantom (OSCG only) and the activity concentration recovery coefficient (ACRC). ***Results:*** The whole phantom percentage recovered activity ranged from 56% (highest activity) to 97% (lowest activity). The ACRC for the four largest spheres were consistently higher for OSEM3D than for OSCG. For the largest sphere, the ACRC range was 0.77-0.86 for OSEM3D and 0.36-0.74 for OSCG. The two smallest spheres were not detectable with either of the reconstruction methods. The range of ACRC in a volume-of-interest in the homogeneous background was 1.08-1.26 for OSEM3D and 0.73-1.11 for OSCG. ***Conclusion:*** The relatively quantified images had a higher ACRC for the detectable spheres than the images utilizing absolute quantification. The absolute quantification method underestimated the activity concentration at high count rates.

OP-030

Design and Development of a Phantom for Commissioning and Quality Assurance of Intraoperative Gamma Probes

A. Stapleton*, O. Berry, J. Grey, R. Harding, L. McKinley, E. Norman; Royal Surrey County Hospital, Guildford, UNITED KINGDOM.*

Aim/Introduction: Intraoperative gamma probes are used for the localisation of areas of radiopharmaceutical uptake in vivo to support effective surgical procedures such as sentinel lymph node removal. As for all Nuclear Medicine equipment, these systems should undergo commissioning for performance characterisation and assessment against the manufacturer's specification. Similarly, continuing quality assurance ensures their fitness for purpose when in clinical use and following repair. NEMA NU-3 2004 provides guidance for appropriate testing on such equipment, however no commercial solutions exist to enable reproducible measurements to be made for the recommended tests on these probes. This work describes the design and development of a phantom able to support these commissioning and quality assurance tests. ***Materials and Methods:*** The test phantom comprises of: a tank to enable tests to be performed both in a scatter medium and in air; two radioactive source holders which allow the straightforward completion of angular and spatial resolution measurements; and a gamma probe holder with inserts allowing for different probe end dimensions including with and without collimators. The source holders have adapters to hold either sealed or unsealed radioactive sources. The unsealed radioactive source option comprises a small fillable sphere, typically to be used with Tc-99m or other clinically appropriate isotopes. Optionally, the sealed source holder can be deployed which securely holds radioactive pen sources including Co-57 pens. ***Results:*** The phantom has been used in the testing of multiple intraoperative gamma probes following the NEMA NU-3 guidance. The phantom enables straightforward performance of the following tests using sealed and unsealed sources: sensitivity in air; sensitivity in scatter; spatial resolution in a scatter medium;

volume sensitivity to distributed activity in a scatter; short-term sensitivity stability; count rate capability in a scatter medium; and angular resolution in a scatter medium. ***Conclusion:*** The phantom developed allows for simple and reproducible measurements for commissioning, post repair testing, and ongoing quality assurance. ***References:*** NEMA NU 3-2004 Performance Measurements and Quality Control Guidelines for Non-Imaging Intraoperative Gamma Probes Radioactive Sample Counting Principles and Practice (Institute of Physics Publishing, 2022) by Sofia Michopoulou (Editor) et al.

OP-031

Design and manufacture of a 3D printed phantom for PET quality control

J. Robinson[1,2], *D. Rushforth*[1,2], *I. Murray*[1,2], *G. Flux*[1,2], *J. Gear*[1,2];
[1]*The Royal Marsden NHS Foundation Trust, Sutton, UNITED KINGDOM,* [2]*The Institute of Cancer Research, London, UNITED KINGDOM.*

Aim/Introduction: Complex analysis of PET scanner performance typically requires time-consuming phantom preparation, with the filling of multiple compartments with different activity concentrations. Mistakes made during this stage can necessitate repeat scans, potentially increasing system downtime. Long-lived, sealed phantoms can also be used, but are only available with uniform activity distributions, limiting evaluation to measurement of SUV or uniformity. It has been proposed to incorporate radioisotopes into the resin material of 3D printers, facilitating the production of complex designs for more sophisticated analysis. This project aimed to demonstrate this possibility by producing a lesion detection phantom with associated software for PET QC and system benchmarking. ***Materials and Methods:*** Phantom design was developed based on analysis of existing phantoms, alongside clinical PET data, such that it would test PET scanners in a clinically relevant manner, using a design which introduces performance tests not currently possible using commercially available phantoms.Simulated PET data was created, by applying Gaussian blur, pixel resampling and adding noise to the digital data. Iterations of the simulated images were used to optimise the ideal range of insert sizes and contrast ratios. After finalising the design, 80MBq 89Zr was added to the support resin of an Objet30-Pro 3D-printer and printed alongside the build resin to create the desired activity geometry. The phantom (110mm length, 140mm diameter) contained 40 radioactive cylinders ranging from 1.3 to 13.9mm in diameter. The background to insert activity concentration varied down the phantom at ratios of 3:2, 2:1, 4:1, 8:1 and 1:0.Imaging was performed using a list mode acquisition on a 128-slice PET/CT scanner. Reconstructions were performed for acquisition durations from 3s to 1h, with and without partial-volume correction. Dedicated software was developed to conduct ROC analysis and calculate AUCs to quantify image quality. ***Results:*** The phantom took 94 hours to print with suitable print quality and matching the original design specification. 89Zr remained uniformly distributed within the resin. Visual inspection of the images highlighted significant differences between the images reconstructed with different parameters. Quantitative analysis showed AUC to increase with acquisition duration, ranging from 0.60 to 0.92. Reconstructions with partial-volume corrections produced higher AUC than those without for acquisitions up to 2 minutes, with a maximum improvement in AUC of 8.5%. Beyond 2 minutes, images without partial-volume correction had consistently higher AUCs. ***Conclusion:*** Radioactive 3D printing is a promising tool and could be utilised for the manufacture of PET QC phantoms.

OP-032

Automatic trending and analysis of SPECT daily quality control data with optical character recognition AI

T. Pan*, S. Ding, O. Mawlawi;*
The University of Texas, M.D. Anderson Cancer Center, Houston, TX, UNITED STATES OF AMERICA.

Aim/Introduction: We have developed a QC server with an optical character recognition (OCR) AI system to store and trend the intrinsic/extrinsic uniformities and center of rotation (COR) metrics reported daily and weekly on the 13 SPECT/CT scanners. The aims are to improve the efficiency of daily/weekly QC review, and to provide trending, storage and auditing of the SPECT QC data on a large hospital network. ***Materials and Methods:*** A SPECT QC server has been designed and implemented to automatically query QC data of 13 SPECT/CT scanners of various models across multiple campuses on our hospital network. The data are sorted according to extrinsic uniformity (daily), intrinsic uniformity (weekly), COR (weekly) and bar pattern (weekly). All the reported QC values of integral/differential uniformities of central FOV (CFOV) and useful FOV (UFOV), COR, axial shift and back projection angle are extracted from the screen captured QC images by an OCR AI system and compared with the manufacturer specifications automatically. Our AI system utilizes deep learning models, including residual network, visual geometry group 16, connectionist temporal classification, which are designed for efficiency and accuracy while minimizing computational requirement. The QC results are viewable on the server webpage by a computer or mobile device such as iPad or iPhone. The QC server is built on a computer with the open-source software Ubuntu, Python, and Dicom toolkit. ***Results:*** QC review is more efficient on the new server with an OCR AI than our previous manual QC review on the hospital PACS. The major improvements are (1) automatic query of the QC data from the scanners (2) automatic extraction of the QC results by the OCR AI compared with the vendor's specification, and (3) trending and documentation of scanner and service issues including artifact floods can also be captured on the server for follow-up. ***Conclusion:*** We have developed a SPECT QC server with an OCR AI system to increase efficiency of QC review of 13 SPECT/CT scanners on a large hospital network. ***References:*** Shi B, Bai X and Yao C. "An End-to-End Trainable Neural Network for Image-Based Sequence Recognition and Its Application to Scene Text Recognition." IEEE Transactions on Pattern Analysis and Machine Intelligence 39 (2015): 2298-2304.

OP-033

AI-Based Automatic Positioning in a Digital-BGO PET/CT Scanner: Efficacy and Impact

J. Kennedy[1,2], *T. Palchan-Hazan*[1], *Z. Keidar*[1,2];
[1]*Rambam - Health Care Campus, Haifa, ISRAEL,* [2]*Ruth and Bruce Rappaport Faculty of Medicine, Technion–Israel Institute of Technology, Haifa, ISRAEL.*

Aim/Introduction: A recently released digital solid-state positron emission tomography/x-ray CT (PET/CT) scanner with bismuth germanate (BGO) scintillators coupled to silicon photomultipliers provides an artificial intelligence (AI) based system for automatic patient positioning. The efficacy of this digital-BGO system in patient placement at the isocenter and its impact on image quality and radiation exposure was evaluated. ***Materials and Methods:*** A new digital-BGO PET/CT with a 32 cm axial field of view (FOV) and AI-based auto-positioning was compared (χ^2, t-tests) to a solid-state lutetium oxyorthosilicate (digital-LSO) PET/CT with manual positioning (n=432 and 343 studies each, respectively). The digital-BGO system results were split into two

groups: before (n=292) and after (n=140) a recalibration of the auto-positioning camera. To measure the transverse displacement of the patient center from the scanner isocenter, CT slices covering 30 cm axially below the diaphragm were retrospectively selected and automatically analyzed using in-house software. Noise was measured as the coefficient of variance of absolute HU (Hounsfield units) above HU_{air} within a 25 mm circular region-of-interest in a homogenous region of the liver. Radiation exposure was recorded as dose-length product (DLP). The isocenter displacement measurement was validated by the precise placement of a cylindrical phantom at 13 positions throughout the transverse FOV. ***Results:*** The phantom validation study gave <1mm error in isocenter displacement measurements. Patient isocenter displacement was biased 1.83±1.86 cm (mean±standard deviation) in the posterior direction for the digital-BGO and 2.02±1.81 cm for the digital-LSO (p=0.007). Left lateral displacements were −0.26±1.06 cm and 0.80±1.43 cm respectively (p<0.001). The average total isocenter displacement was 2.68±1.47 cm for the digital-BGO before recalibration, compared to 2.77±1.31 cm (no significant difference) for the digital-LSO. After recalibration, the digital-BGO isocenter displacement improved to 1.93±1.63 cm (p<0.001) and was superior to the digital-LSO (p<0.001). Also, after recalibration, 26% (36/140) of the studies had isocenter displacements >2.5cm for the digital-BGO, which was significantly better than the 49% (142/292, p<0.001) before recalibration or the 56% (191/343, p<0.001) for the digital-LSO. On average, image quality was superior for non-obese patients (BMI<30 kg/m^2) with arms up who were most closely aligned with the isocenter: noise increased by 3.3±0.1% for every 1 cm increase in isocenter displacement. DLP increased by 177±10 Gy·cm for every 1 cm increase in anterior isocenter displacement. ***Conclusion:*** AI-based automatic positioning in a digital-BGO PET/CT scanner significantly improves patient placement with respect to the isocenter, thereby improving image quality and ensuring proper radiation exposure.

206

Sunday, September 10, 2023, 8:00 AM - 9:30 AM

Hall C

Clinical Oncology Track - TROP Session: Prostate Cancer Staging

OP-034

Association of aggressive prostate cancer features on whole-mount pathology with quantitative measures on PSMA PET

I. Sonni[1,2], *D. H. Kim*[1], *A. Ter-Pogosyan*[1], *T. Grogan*[1], *N. Barroso*[1], *P. Ahuja*[1], *J. Calais*[1], *A. Sisk*[1], *S. Raman*[1];
[1]*University of California, Los Angeles, Los Angeles, CA, UNITED STATES OF AMERICA,* [2]*Università Magna Graecia, Catanzaro, ITALY.*

Aim/Introduction: Two distinct morphologic entities of prostate cancer (PC), the intraductal carcinoma (IDC) and the large cribriform growth pattern, are associated to more aggressive disease, high Gleason scores, advanced tumor stage, biochemical relapse, and distant metastasis. Predicting the presence of these pathology features could be of significant help in case whole-mount pathology (WMHP) is unavailable. The goal of this analysis was to assess the distribution of quantitative PSMA-PET parameters in lesions with and without cribriform/IDC patterns on pathology. We assessed the ability of pre-surgical PSMA-PET metrics to predict the presence of aggressive pathology features. ***Materials and Methods:*** With IRB approval and HIPAA compliance, we derived a study cohort of all PC patients who underwent 68Ga-PSMA-11 PET/CT (PSMA-PET) within 3 months of robotic radical prostatectomy (RALP) and WMHP and description of presence/absence of cribriform/IDC pattern between 05/2019 and 08/2022.A board-certified nuclear medicine physician contoured all PC lesions on PSMA-PET, matching each lesion with WMHP. PSMA-PET metrics (SUVmax, SUVmean, total lesion activity - TLA) were extracted for the image analysis.The analysis only included true positive lesions that were categorized as: (a) cribriform+/IDC- (b) cribriform+/IDC+, (c) cribriform-/IDC-. One way-ANOVA Welch test was used to identify differences among the imaging parameters in the three groups. The area under the curve (AUC) from ROC analysis was used to assess the ability to predict presence of cribriform and/or IDC pattern on pathology based on imaging parameters on PSMA-PET. ***Results:*** The study cohort comprised 77 patients (median age at time of RALP: 64±6.95 years), and 82 lesions on WMHP. The serum PSA levels at time of RALP was 9.07 ng/ml ± 5.8. On WMHP, cribriform+/IDC- was described in 21/83 lesions, cribriform+/IDC+ in 41/83 lesions, cribriform-/IDC- in 20/83 lesions. The SUVmean and TLA were statistically different among the three groups (p=0.003 and 0.039), whereas SUVmax was not (p=0.062). In the cribriform+/IDC-, cribriform+/IDC+, and cribriform-/IDC- group, average (SD) SUVmean was 6.7 (4.1), 5.9 (2.7), 4.5 (1), SUVmax was 13.7 (8.4), 11.7 (6.9), and 9.3 (4.1), and TLA was 27.1 (26), 53.8 (68.5), and 21.7 (26), respectively. AUC showed that SUVmean predicts the presence of features of aggressive PC on WMHP with 67% accuracy (p=0.03). ***Conclusion:*** SUVmean was significantly lower in cribriform-/IDC- lesions, TLA was significantly higher in cribriform+/IDC+ lesions. SUVmean on PSMA PET predicted aggressive pathology with moderate AUC on ROC analysis.

OP-035

The role of PSMA PET/CT in the diagnosis of clinically significant prostate cancer

A. Kibar[1], *O. E. Sahin*[1], *S. Asa*[1], *M. Demirbilek*[2], *S. Bilgic*[3], *B. Onal*[2], *L. Kabasakal*[1];
[1]*Istanbul University-Cerrahpasa, Cerrahpasa Faculty of Medicine, Department of Nuclear Medicine, Istanbul, TÜRKIYE,* [2]*Istanbul University-Cerrahpasa, Cerrahpasa Faculty of Medicine, Department of Urology, Istanbul, TÜRKIYE,* [3]*Sirnak State Hospital, Department of Nuclear Medicine, Sirnak, TÜRKIYE.*

Aim/Introduction: Follow-up of patients reported as Gleason 3+3 prostate cancer as a result of prostate biopsy is a controversial issue. It is an important decision which patients should be actively monitored and which should be referred for surgery. In our study, we wanted to investigate the guiding role of PSMA PET/CT imaging performed on patients whose prostate biopsy results were reported as Gleason 3+3, in the diagnosis of clinically important prostate cancer (ISUP 2 and above). ***Materials and Methods:*** 76 patients who were reported as Gleason 3+3 prostate cancer as a result of TRUS biopsy and who were operated afterwards, mostly due to abnormal MRI findings, were selected. Of these patients, 44 had PSMA PET/CT, 68 had MRI, 36 had both imaging. Patients who had Ga-68 PSMA PET imaging were classified according to their PRIMARY scores(1). They were divided into two groups as PRIMARY 1-2 (negative) and PRIMARY 3-4-5 (positive). Patients with MRI imaging were divided into two groups as those with PIRADS 1-2 (negative) and those with PIRADS 3-4-5 (positive).

The operation results of these groups (ISUP 1 vs >ISUP 2) were compared. ***Results:*** 15 patients were classified as PRIMARY 1-2 and 29 patients were classified as PRIMARY 3-4-5. The sensitivity, specificity, positive predictive value and negative predictive value were 80.77%, 55.56%, 72.41%, 66.67%, respectively. 54 patients were classified as PIRADS 1-2 and 14 patients were classified as PIRADS 3-4-5. The sensitivity, specificity, positive predictive value and negative predictive value were 83.33%, 26.92%, 64.81%, 50%, respectively. In 36 patients who underwent both PSMA PET and MR imaging; the sensitivity, specificity, positive predictive value and negative predictive value of PSMA PET were 76.19%, 60%, 72.73%, 64.29%, and MRI were 90.48%, 20%, 61.29%, 60%, respectively. Also, according to independent samples t-test, while PSMA PET can predict clinically important prostate cancer significantly, while MRI can not (P values: 0.0032 and 0.392 respectively). ***Conclusion:*** Ga-68 PSMA PET/CT can be an important guide, mostly because of its high positive predictive value, in diagnosing clinically important prostate cancer in patients with Gleason 3+3 as a result of biopsy and helps in deciding for follow-up or operation. In our study, PSMA PET's positive predictive value, negative predictive value and specificity were found to be higher than MRI. ***References:*** 1) Emmett L, Papa N, Buteau J, et al. The PRIMARY Score: Using Intraprostatic 68Ga-PSMA PET/CT Patterns to Optimize Prostate Cancer Diagnosis. J Nucl Med. 2022;63(11):1644-1650. doi:10.2967/jnumed.121.263448

OP-036

In-depth analysis of PSMA PET/CT and mpMRI discrepancies in prostate cancer detection with histopathology gold standard

I. Sonni[1,2], *S. Doddipalli*[1], *M. Deol*[1], *D. Ban*[1], *H. Kim*[1], *T. Grogan*[1], *N. Barroso*[1], *P. Ahuja*[1], *Y. Zong*[1], *A. Sisk*[1], *J. Calais*[1], *R. Reiter*[1], *S. Raman*[1];
[1]*University of California, Los Angeles, Los Angeles, CA, UNITED STATES OF AMERICA,* [2]*Università Magna Graecia, Catanzaro, ITALY.*

Aim/Introduction: Multiparametric MRI (mpMRI) and PSMA-PET provide complementary information in the pre-surgical evaluation of patients with prostate cancer (PCa). The aim of this analysis was to evaluate the factors associated with PSMA-PET and MRI agreement/disagreement with each other and with gold standard histopathology. ***Materials and Methods:*** All patients who underwent radical prostatectomy (RP), pre-surgical PSMA-PET, and mpMRI were screened for this study. Included patients had two imaging scans done <3 months from each other, and whole mount histopathology (WMHP) slides available, with ISUP grade group (GG) classification. Two nuclear medicine physicians and 2 radiologists manually contoured PCa lesions on PSMA-PET and mpMRI, respectively. A consensus read was done with a third reader for each modality, and a majority rule was applied (2:1). Quantitative measures were extracted on a lesion-basis (SUVmean, SUVmax, tumor volume). A PET/MRI fusion was obtained, and agreement/disagreement was assessed visually, based on the overlapping lesion contours. WMHP slides were used to establish the agreement/disagreement between imaging-identified lesions and WMHP. One-way ANOVA and ROC analysis were used to assess differences among groups and accuracy in predicting agreement/disagreement. ***Results:*** The cohort included 114 patients, and 175 pathology lesions were identified (ISUP 3, n=22; ISUP>3, n=153). PSMA-PET and mpMRI identified 170 and 136 lesions, respectively. Sensitivity for ISUP>3 lesions was 80% and 87% for mpMRI and PSMA-PET, respectively. 117/153 (76%) ISUP>3lesions were correctly identified and 15/153 (10%) missed by both imaging modalities, respectively. 5/153 (3%) were correctly identified by mpMRI and missed by PSMA-PET, 16/153 (10%) were correctly identified by PSMA-PET and missed by mpMRI. Lesion's ISUP GG and size on pathology were significantly lower in PET- compared to PET+, and in mpMRI- compared to mpMRI+ lesions. Lesion's ISUP GG and size were significantly correlated to PSMA-PET and MRI agreement, whereas PSMA-PET metrics were not. SUVmax, SUVmean, and tumor volume on PSMA-PET were significantly higher in true positive (TP), compared to false positive (FP) lesions on PSMA-PET. ROC curve analysis showed that an SUVmax of 5.17, SUVmean of 4.67 and a tumor volume of 0.54 on PSMA-PET accurately discriminated a TP from a FP finding (AUC 0.85, 0.82 and 0.78, respectively). ***Conclusion:*** Higher SUVmax, SUVmean and tumor volume on PSMA-PET were associated with a TP finding on PSMA-PET, higher ISUP grade group and size on pathology were associated with a TP finding on both PSMA-PET and mpMRI, and with agreement between PSMA-PET and mpMRI.

OP-037

Baseline PSMA PET-CT is prognostic for treatment failure in men with intermediate-to-high risk prostate cancer: 54 months follow-up of the proPSMA randomised trial

M. Hofman[1], *V. Kasivisvanathan*[1], *E. Link*[1], *N. Lawrentschuk*[1], *J. O'Brien*[1], *J. P. Buteau*[1], *M. Roberts*[2], *R. Francis*[3], *C. Tang*[4], *I. Vela*[5], *P. Thomas*[6], *N. Rutherford*[7], *J. M. Martin*[6], *M. Frydenberg*[8], *R. Shakher*[9], *L. Wong*[10], *K. Taubman*[11], *S. Lee*[12], *E. Hsiao*[13], *M. Nottage*[14], *I. Kirkwood*[15], *A. Iravani*[1], *S. Williams*[1], *D. Murphy*[1];
[1]*Peter MacCallum Cancer Centre, Melbourne, AUSTRALIA,* [2]*Royal Brisbane and Women's Hospital, Brisbane, AUSTRALIA,* [3]*The University of Western Australia, Perth, AUSTRALIA,* [4]*Sir Charles Gairdner Hospital, Perth, AUSTRALIA,* [5]*Princess Alexandra Hospital, Brisbane, AUSTRALIA,* [6]*Royal Brisbane and Women's Hospital, Brisbane, AUSTRALIA,* [7]*Hunter New England Health, Newcastle, AUSTRALIA,* [8]*Monash University, Melbourne, AUSTRALIA,* [9]*1Monash Health Imaging, Melbourne, AUSTRALIA,* [10]*St Vincent's Health Melbourne, Melbourne, AUSTRALIA,* [11]*St Vincent's Health, Melbourne, AUSTRALIA,* [12]*Austin Health, Melbourne, AUSTRALIA,* [13]*Royal North Shore Hospital, Sydney, AUSTRALIA,* [14]*Dr Jones and Partners Medical Imaging, Adelaide, AUSTRALIA,* [15]*Royal Adelaide Hospital, Adelaide, AUSTRALIA.*

Aim/Introduction: The proPSMA randomised controlled trial demonstrated the superior accuracy of PSMA PET-CT over conventional imaging for detecting nodal and distant metastatic disease in prostate cancer[1]. However, the clinical implications of PET findings remain unclear. This pre-specified secondary objective evaluates the prognostic value of PET-detected nodal involvement in patients without distant metastases using baseline ^{68}Ga-PSMA-11 PET-CT. ***Materials and Methods:*** Patients with intermediate-to-high risk prostate cancer (ISUP grade group 3-5, PSA ≥20 ng/ml or clinical stage ≥T3) received PSMA PET-CT as first or second-line imaging. Patients without distant metastatic disease (M0) were grouped based on PSMA PET-CT nodal status (N0 or N1) and monitored for up to 54 months. Treatment failure was defined by biochemical failure (PSA >0.2ng/ml after surgery or rise by 2ng/ml above nadir after radiotherapy), initiation of salvage therapy, or development of distant metastatic disease. Kaplan-Meier curves were used to estimate freedom from treatment failure based on PET-CT and CT/bone scan classifications for N0 and N1 cancer. Cox proportional hazards were employed to calculate hazard ratios (HR) for freedom from treatment failure. Clinical trial registry: ANZCTR12617000005358. ***Results:*** Among 302 patients randomised across 10 sites, 294 underwent a PSMA PET-CT. 251 patients with M0 disease and median follow-up

of 41.0 (95%CI 40.1-41.9) months were included in this analysis. Patients were treated with curative-intent surgery or radiotherapy with or without androgen deprivation. During follow-up, biochemical failure alone occurred in 48/251 (19%) patients, salvage therapy commenced in 57/251 (23%) and development of distant metastatic disease in 13/251 (5%) during follow-up. PSMA-PET defined N0M0 patients had longer freedom from treatment failure than N1M0 patients, with a HR of 2.1 (95%CI 1.2-3.7), p=0.01. At 3 years, 70% (95%CI 64 - 76) with N0M0 versus 46% (95%CI 26 - 64) with N1M0 remained free from treatment failure. CT and bone scan defined N1M0 versus N0M0 was not prognostic (HR 0.6, 95%CI 0.1-2.4, p=0.45). ***Conclusion:*** For patients with intermediate-to-high risk prostate cancer and no distant metastases, PSMA PET-CT regional nodal status is prognostic for medium-term oncologic outcomes, outperforming conventional imaging in identifying patients at higher risk of treatment failure.
References: [1] Lancet. 2020 Apr 11;395(10231):1208-1216. doi: 10.1016/S0140-6736(20)30314-7.

OP-038

Radio-guided surgery with DROP-IN beta probe for 68Ga-PSMA, in high-risk prostate cancer patients eligible for robotic-assisted radical prostatectomy.

F. Ceci[1], *F. Collamati*[2], *S. Luzzago*[3], *F. A. Mistretta*[3], *L. Muraglia*[1], *G. Renne*[4], *R. Mirabelli*[2], *S. Morganti*[5], *O. De Cobelli*[3], *N. Fusco*[4], *G. Musi*[3];
[1]*Division of Nuclear Medicine, IEO European Institute of Oncology, IRCCS, Milan, ITALY,* [2]*INFN National Institute of Nuclear Physics, Section of Rome, Rome, ITALY,* [3]*Division of Urology, IEO European Institute of Oncology, IRCCS, Milan, ITALY,* [4]*Division of Pathology, IEO European Institute of Oncology, IRCCS, Milan, ITALY,* [5]*INFN National Institute of Nuclear Physics, Section of Rome, Milan, ITALY.*

Aim/Introduction: The primary aim of this analysis was to evaluate the diagnostic accuracy of the combined approach with a DROP-IN positron detector (β-Probe) and 68Ga-PSMA-11 PET/CT (PSMA-PET) in the correct identification of lymph node metastases, in high-risk prostate cancer (PCa) patients undergoing robotic radical prostatectomy (RARP) and extended pelvic lymph-node dissection (ePLND). The standard of reference was the histopathological analysis. ***Materials and Methods:*** This is a prospective, single-arm, single-center, non-interventional, phase II trial (NCT05596851), aimed at enrolling fifteen (n=15) PCa patients. We present an interim analysis in the first eight consecutive (n=8) patients enrolled. Inclusion criteria were: a) biopsy proven, high-risk PCa; b) patients candidate to RARP + ePLND as primary therapy; c) PSMA-PET performed within 6 weeks prior to surgery; d) PSMA-positive nodes in PSMA-PET; e) age>18. The surgery procedure started with the intravenous injection of 1.1 MBq/Kg of 68Ga-PSMA-11 directly in the surgery theatre. After the injection the surgery procedure proceeded first with ePLND followed by RP. The in-vivo measurements of the surgery templates with β-Probe were performed with a DROP-IN system, inserting the probe into a trocar. All removed nodes were also measured ex-vivo. The tumor-to-background-ratio (TBR) was evaluated graphically in a display showing real-time counts per time. Furthermore, a dedicated, operator-independent, algorithm to reliably identify pathologic vs. non-pathologic nodes was developed. PSMA-staining was performed in all specimens. Data derived by the PSMA-PET, β-Probe and histopathological analysis were compared in a per-region analysis. ***Results:*** The live β-Probe-guided ePLND was a feasible procedure, without significant changes in the surgery practice. No side effects have been observed during ePLND. In total, 64 specimens were removed and analyzed. Pathology results were used to validate in vivo and ex-vivo β-Probe counts interpreted according to the operator-indipendent algorithm. Four (n=4) false positive and seven (n=7) false negative findings were detected. The intra-operative β-Probe sensitivity to detect PCa nodal metastasis was 76.7%, while specificity was 88.2%. ***Conclusion:*** These are the first ever published data derived from a live surgery experience using a β-Probe to identify PSMA-positive lymph nodes. This new approach proved to be feasible and safe. Visual TBR interpretation (operator-dependent) revealed to be more challenging than expected. After the implementation of a dedicated, operator-independent, algorithm for the identification of a cut-off in TBR analysis, the diagnostic accuracy improved. The completion of this phase II trial will provide more data about the efficacy of this new generation image-guided approach.

OP-039

[^{68}Ga]PSMA PET/CT vs. mpMRI in patients with suspicion of prostate cancer and previous negative biopsy: preliminary data from PROSPET-BX trial.

E. Lopci, *M. Lazzeri, L. Disconzi, P. Colombo, A. Saita, D. Maffei, V. Fasulo, R. Hurle, K. Marzo, L. Leonardi, R. Peschechera, A. Benetti, S. Zandegiacomo, L. Pasini, J. Jandric, R. Zanca, P. Casale, M. Rodari, L. Balzarini, G. Guazzoni, N. Buffi, G. Lughezzani;*
IRCCS - Humanitas Research Hospital, Rozzano MI, ITALY.

Aim/Introduction: Herein we present the preliminary data obtained from our prospective trial, designed to compare in parallel [^{68}Ga]PSMA PET/CT with mpMRI/TRUS fusion prostate biopsy in men with high suspicion of prostate cancer (PCa) after at least one negative biopsy. ***Materials and Methods:*** Patients enrolled from April 2022 until April 2023, have been considered for the analyses. Inclusion criteria: PSA level >4.0ng/ml; free-to-total PSA ratio <20%; progressive rise of PSA levels; serum blood tests suspicious for PCa; at least one previous negative biopsy; ASAP and/or high-grade PIN; negative DRE. All eligible patients have undergone [^{68}Ga]PSMA PET/CT and mpMRI scans, followed by biopsy session within one month distance. TRUS-fusion needle biopsy has been performed for all lesions detected with PET and mpMRI. ***Results:*** At present, 60 patients have been enrolled, of which 50 have already completed the diagnostic pathway and have undergone prostate biopsy. Median age is 64 years (range 51-83) and median PSA 10.5 ng/ml (range 4.49-25). The majority of the patients had undergone one previous biopsy, while 8 patients (16%) had more biopsy sets. Median SUVmax and SUVratio of targeted areas resulted 3.7 (range 1.7-41.99) and 1.5 (range 0.74-14), respectively. According to re-biopsy results, 7 patients presented with clinically significant PCa (csPCa), 3 with GS 6, while the majority had a negative biopsy (80%). mpMRI showed the following findings: 31 patients with PI-RADS 2 (62%), 2 with PI-RADS 3 (4%), 12 patients with PI-RADS 4 (24%), and 5 patients with PI-RADS 5 (10%). Median SUVmax and SUVratio resulted 3.6 and 1.3 for benign versus 8.9 and 3.2 for malignant lesions, respectively (P<0.001). While csPCa presented with a median SUVmax and SUVratio of 12.8 and 6.7, respectively. ROC analyses allowed to identify optimal cut-off points for malignancy and csPCA, which resulted for SUVmax >6 (AUC 0.746) and >7.48 (AUC 0,819), respectively, whereas for SUVratio the cut-off was >2.79 in both cases (AUC 0.808 versus 0.833, respectively). When combining [^{68}Ga]PSMA PET/CT with mpMRI data, all unnecessary prostate re-biopsies could be spared, i.e. 80% of the cohort , while granting a detection rate of 90% for PCa. ***Conclusion:*** In these

very preliminary results, the combination of [^{68}Ga]PSMA PET/CT with mpMRI in patients candidate to rebiopsy, can help increase the detection rate of prostate cancer lesions up to 90%, by spearing all unnecessary repeat biopsies. ***References:*** This study is financially supported by Ministero della Salute with the Grant GR-2018-12366240.

OP-040

Pre-surgical ^{68}Ga-PSMA-11 PET for biochemical recurrence risk assessment: a surrogate of Pelvic Lymph Node Dissection? Follow-up analysis of a Multicenter Prospective Phase 3 Imaging Trial.

L. Djaileb[1], *W. Armstrong*[2], *D. Thompson*[3], *A. Gafita*[2], *A. Farolfi*[2], *T. Grogan*[2], *M. Cooperberg*[4], *P. Carroll*[5], *S. Washington*[4], *R. Reiter*[6], *J. Czernin*[2], *H. Thomas*[3], *J. Calais*[2];
[1]*University Grenoble-Alpes, INSERM, CHU Grenoble Alpes, Nuclear Medicine Department, LRB, Grenoble, FRANCE,* [2]*UCLA, Los Angeles, CA, UNITED STATES OF AMERICA,* [3]*Department of Radiology and Biomedical Imaging, University of California, San Francisco, CA, UNITED STATES OF AMERICA,* [4]*Department of Urology, University of California, San Francisco, CA, UNITED STATES OF AMERICA,* [5]*Department of Urology, University of California, San Francisco, UCSF, CA, UNITED STATES OF AMERICA,* [6]*Institute of Urologic Oncology, University of California, Los Angeles, CA, UNITED STATES OF AMERICA.*

Aim/Introduction: To compare the prognostic value of presurgical PSMA-PET and pelvic lymph nodes invasion (pN1) for biochemical recurrence (BCR) free-survival (FS) in patients with intermediate-risk to high-risk prostate cancer (PCa) treated with radical prostatectomy (RP) and pelvic lymph node dissection. ***Materials and Methods:*** This is a follow-up study of the surgery cohort included in the multicenter prospective phase 3 imaging trial (n=277; NCT03368547, NCT02611882, NCT02919111). Each ^{68}Ga-PSMA-11-PET scan was read by three blinded independent readers. Local histopathology risk score (CAPRA-S (Cancer of the Prostate Risk Assessment) score without pN data), PSMA-PET extra-prostatic disease (N1/M1), and pN were used to assess risk of BCR. Patients were followed up after RP by the local investigators using electronic medical records. BCR was defined by a prostate-specific antigen (PSA) level ≥0.2 ng/ml after RP or an initiation of PCa specific secondary treatment (>6 months after surgery). Univariate, multivariate Cox model, and c-statistic index were performed to assess the prognostic value of PSMA-PET, LNI and its added value to Local histopathology risk score. ***Results:*** From December 2015 to December 2019, 277 patients underwent surgery after PSMA-PET. Clinical follow-up was obtained in 240/277(87%) patients. Median follow-up from surgery was 32.4 (IQR 23.3-42.9) months. Ninety-one/240 BCR events (38%) were observed. PSMA-PET N1/M1 and pN1 were found in 41/240 (17%) and 67/240 (28%) patients respectively. Local histopathology risk score, PSMA-PET and pN were significant univariate predictors of BCR. Only Local histopathology risk score and PSMA PET were significant in multivariate analysis (HR [95% CI] 1.4 (1.2-1.5) p<0.0001) and (1.7 (1-2.9) p=0.03). Prognostic value of model combining local histopathology and PSMA-PET was not significantly different than model combining local histopathology and pN (c-statistic 0.74 (0.69-0.79) vs 0.73 (0.68-0.78); p= 0.69). In patient group with low-risk Local histopathology score and PSMA-PET N0-M0 only 4/109 (5%) were pN1. In patients with high-risk local histopathology score, a PSMA-PET N1/M1 was associated with a significant lower BCR-FS than a PSMA-PET N0-M0 (median survival (95% CI) 32.7 (14.9-NR) vs 8 (3.2-15.5) p= 0.001). pN1 was found in respectively 25/34 (74%) and 34/90 (38%)**.** ***Conclusion:*** Combination of pre-surgical PSMA-PET and Local histopathology was not statistically different than the reference standard, i.e local histopathology and pN to predict BCR-FS. Interestingly rate of discrepancy with pN was low among patient with low histopathology risk and PSMA-PET (N0-M0) and patient with high histopathology risk and PSMA-PET (N1/M1).

OP-041

Updated Automated PROMISE assessment: Treatment response evaluation approach on metastatic prostate cancer patients based on PSMA PET/CT

S. Duriseti[1,2], *H. Sahlstedt*[3], *J. Brynolfsson*[3], *G. Berenji*[1,2], *S. Tsai*[2], *N. Kane*[1], *W. Fendler*[4], *M. Rettig*[1,2], *N. Nickols*[1,2];
[1]*University of California, Los Angeles, Los Angeles, CA, UNITED STATES OF AMERICA,* [2]*Greater Los Angeles VA Medical Center, Los Angeles, CA, UNITED STATES OF AMERICA,* [3]*Exini Diagnostics AB, Lund, SWEDEN,* [4]*University of Essen, Essen, GERMANY.*

Aim/Introduction: The response evaluation criteria in prostate-specific membrane antigen (PSMA) PET/CT (RECIP) were recently presented by Gafita et al. and has since been included in the second version of Prostate Cancer Molecular Imaging Standardized Evaluation (PROMISE v2). However, manual measurement of total tumour volumes (TTV) and lesion tracking between multiple time points are cumbersome. We evaluated software-aided longitudinal tracking of 18F-DCFPyL-avid lesions to generate a RECIP class for each evaluated patient. ***Materials and Methods:*** RECIP compares PSMA tracer-avid lesions from a baseline PET (bPET) and a follow-up PET image (fPET), and then classifies the response as either complete response (CR, no tracer avidity in the fPET), partial response (PR, TTV decrease of ≥30% without new lesions), progressive disease (PD, TTV increase ≥20% and new lesions), or stable disease (SD, defined as neither CR, PR, nor PD). Here, PSMA tracer-avid lesions were identified using an automated detection algorithm employing convolutional neural networks trained and validated on separate 18F-DCFPyL PET/CT image sets. The detected lesions were manually approved, and if needed, corrected by an experienced clinician. TTV was also calculated by the detection algorithm. The bPET and fPET were co-registered to automatically match individual lesions. Co-registered fPET and bPET lesions were considered a match if they were from the same anatomic disease compartment (prostate/prostate bed, lymph node, bone, or visceral) and had either overlap or a centre-of-masses distance <10 mm (for rib lesions, this distance was <50 mm to account for respiratory motion). The automated RECIP was evaluated on 33 patients, each with one bPET and one fPET acquired, both with 18F-DCFPyL. Of the 33 cases, 9 were manually categorized as CR, 8 as PR, 12 as SD, and 4 as PD.For each lesion annotated in the fPET, a match was sought in the corresponding bPET. If a match was not found, the lesion was denoted as a "new lesion". ***Results:*** The algorithm automatically assigned the correct RECIP classification in all cases. There were 217 total lesions identified in all bPET images, and 100 total lesions in the fPET images, respectively. The automated algorithm matched 61 bPET lesions to 53 lesions in the corresponding fPET. The remaining 47 fPET lesions were considered "new lesions." ***Conclusion:*** For response assessment using 18F-DCFPyL PET/CT and RECIP criteria, the automated algorithm and manual detection achieved the same clinical classifications. The precision and accuracy this automated process is being validated in prospective clinical studies.

OP-042

PSMA PET/CT for the Targeting of Prostate Biopsies: Additional Value over MRI?

C. J. W. M. Morré[1], *J. J. Boer*[1], *S. P. Rynja*[1], *M. J. Hagens*[2], *M. A. Noordzij*[1];
[1]*Spaarne Gasthuis, Hoofddorp, NETHERLANDS,* [2]*Antoni van Leeuwenhoek cancer institute, Amsterdam, NETHERLANDS.*

Aim/Introduction: Current guidelines recommend MRI-directed targeted prostate biopsies (TBx) and systematic prostate biopsies (SBx) for diagnosing prostate cancer (PCa), but performing only TBx has shown to miss approximately 15% of clinically significant PCa (csPCa) cases. While PSMA PET/CT is increasingly used for metastatic screening, recent literature has suggested its diagnostic value for detecting local disease and targeting prostate biopsies. This retrospective pilot study aimed to compare PSMA-directed biopsies to MRI-directed Tbx in detecting csPCa. ***Materials and Methods:*** The study identified men subjected to PSMA PET/CT between November 2020 and December 2022, within six months after prostate MRI and prostate biopsies from a comprehensive institutional database. Indications for PSMA PET/CT were: PSA > 20, stage T_{3-4} and aggressive histology (ISUP ≥ 3). Abnormalities found on prostate MRI (PI-RADS classification V2.1), PSMA PET/CT (classified as normal, inconclusive, or suspect), and biopsies (ISUP grade groups) were localized according to the Ginsburg protocol, a protocol dividing the prostate into twenty-four sectors along the transversal plane. The study used ^{18}F-JK-PSMA-7 as a PSMA tracer on a EARL accredited PET-CT scanner. The maximum standardized uptake value (SUV_{max}) was measured for each suspicious lesion on the PSMA PET/CT. The analysis was conducted on the level of the Ginsburg regions. ***Results:*** A total of 366 men were included in the analysis, with both TBx (PI-RADS 3-5 regions) as well as SBx (PI-RADS 1-2 regions) taken. PSMA PET/CT was concordant with MRI in 56.5% of regions (1237 of 2190). PSMA classification was strongly correlated with ISUP scores on prostate biopsies from the corresponding region (Chi2-test, p=<0.001). For normal MRI regions (PI-RADS 1-2), where SBx were taken, csPCa was found in 32% (194 of 611), of which PSMA PET/CT detected 88% (169), with specificity of 40%. The median SUV_{max} per ISUP grade group was 4.8 for Ginsburg regions with benign histology, 10.6 for ISUP 1-2 (clinically insignificant PCa), and 17.5 for ISUP 3-5 (csPCa). Measured in the normal MRI regions, the SUV_{max} was 5.0, 13.4, and 18.4, respectively. ***Conclusion:*** PSMA PET/CT identifies more csPCa cases compared to MRI while distinguishing high- from low-grade PCa. However, it results in more false-positive results. The SUV_{max} appears to be a promising indicator for (cs)PCa. The retrospective design of this study makes it uncertain whether regions with high uptake without biopsy data may yield more false-positive results. Further research is needed to determine whether similar results are observed in a broader population.

207

Sunday, September 10, 2023, 8:00 AM - 9:30 AM
Hall F1

Neuroimaging Committee - Featured Session: Methods in NeuroImaging: Spotlight on Brain Connectivity

OP-043

The Molecular Connectivity in Neurology

M. Perovnik
University Medical Centre Ljubljana, Ljubljana, SLOVENIA.

OP-044

Aging and changes in intrinsic connectivity networks of the brain

S. Ha, *I. Chung, W. Ryoo, J. Min, S. Kwon, J. O;*
The Catholic University of Korea, Seoul, KOREA, REPUBLIC OF.

Aim/Introduction: ^{18}F-FDG PET/CT scan evaluates glucose metabolism and can be used as a proxy for neural activity of brain. Local changes as well as the cooperative network characteristics of various regions of the brain are important in understanding how the human brain works. The purpose of this study is to observe changes in intrinsic brain networks during normal aging. ***Materials and Methods:*** A total of 827 PET/CT scans obtained from 357 healthy individuals (male/female=334/23, age=32-90) who underwent health checkups at a single institution from January 2009 to July 2022 were analyzed. The PET slices of the brain were separated and spatial and intensity normalized using Statistical Parametric Mapping (SPM) 8. Independent Component Analysis (ICA) with threshold Z >2 was used to generate masks of 21 intrinsic connectivity networks (ICN). The sum of SUVR in each ICN within each subject was defined as total glycolysis of ICN (ICN-TG). Spearman's test was performed on age and ICN-TG to test linear change during aging. Significant ICN-ICN interrelationship was identified with Spearman's test (rho) of ICN-TG for the entire age group. In order to find ICN-ICN combinations with age-related differences, Fisher's Z-test was used to examine the rho between the ICN-TGs of individuals in their 30s and 80s. The connectivity strength measured by Spearman's correlation, rho, of ICN-TG between the 30s and 80s was transformed as a Z-score for each age group (30's, 40's, 50's, 60's, 70's, and 80's) and analyzed using cubic regression according to age. Multiple testing correction was performed with the Benjamini-Hochberg procedure with adjusted p-value less than 0.05. ***Results:*** Among the 21 ICNs, negative correlations were found between age and ICN-TG in 20 ICNs. Twenty-seven ICN-ICN combinations showed significant connectivity across all ages, with differences in connection strength between individuals in their 30s and 80s. 26 ICN-ICN combinations showed significantly lower connection strength in individuals in their 80s compared to those in their 30s. The connectivity of 26 ICN-ICN combinations showed a good fit for cubic regression (R2, range 0.681-0.980; adjusted p <0.05) and demonstrated two decreasing slopes, one generally in ages 30s-40s and another for ages 60s and older. ***Conclusion:*** During normal aging, intrinsic brain networks may show a continuous

decline in neural activity, and the connectivity strength between functionally connected ICN-ICN may also gradually weaken. These aging-related weakening of connectivity accelerates during young adulthood, slows down in middle age, and accelerates again during old age.

OP-045

Dynamic reconfiguration of metabolic brain connectivity during progression from MCI to Alzheimer's disease dementia

S. Caminiti[1], *A. Galli*[2], *A. Sala*[3], *M. Inglese*[4], *L. Presotto*[5], *C. Tassorelli*[1], *D. Perani*[6], *the Alzheimer's Disease Neuroimaging Initiative;*
[1]Department of Brain and Behavioral Sciences, University of Pavia, Pavia, ITALY, [2]Neurology Unit, Department of Clinical and Experimental Sciences, University of Brescia, Brescia, ITALY, [3]GIGA Consciousness, University of Liege, Liege, BELGIUM, [4]Department of Biomedicine and Prevention, University of Rome Tor Vergata, Roma, ITALY, [5]Department of Physics, University of Milano-Bicocca, Milano, ITALY, [6]Vita-Salute San Raffaele University, Milano, ITALY.

Aim/Introduction: We investigate brain connectivity reconfigurations along the progression from mild cognitive impairment (MCI) to Alzheimer's disease (AD) dementia, using a longitudinal design based on brain metabolic information provided by FDG-positron emission tomography (FDG-PET) at three time points obtained from ADNI. ***Materials and Methods:*** We analyzed the FDG-PET images of patients with AD according to the ATN-classification in MCI (AD-MCI, N=31), mild dementia (mild-AD, N=31) and full-blown dementia (AD-D, N=20) stages. A group of age/sex-matched healthy controls (HC) was longitudinally evaluated for comparison. Grey-matter parcellation was applied for whole-brain network construction. Pearson correlations were calculated between each pair of regions across subjects to obtain adjacent matrices. Z-test was run between adjacent matrices of clinical group and matched HC group to extract metabolic connectivity alterations for each time point. Levels of connectivity alterations were quantified for each time point with summary indices. The obtained indices also served as input for k-means (KM) cluster analysis. In a first approach each time point was clustered individually to describe stage-specific connectivity alterations (KM1). A second approach clustered the three time points longitudinally, to describe patterns of connectivity reconfiguration along the AD course (KM2). ***Results:*** The AD-MCI showed less connectivity alterations than the mild-AD and AD-D, specifically characterized by relatively higher numbers of gained than lost connections. KM1 analysis identified two clusters: "altered cluster" and "spared cluster". In AD-MCI, altered cluster involved connections of subcortical and limbic regions, occipito-parietal cortices, and cerebellum. At mild-AD and AD-D stages, the altered cluster involved a large portion of connections within occipito-parietal cortices and cerebellum. The KM2 identified four different clusters: Cluster1 included nodes with low levels of lost and gained connections in frontal cortex, insula, and basal ganglia across the whole disease course; Cluster2 grouped nodes with high levels of gained connections in occipito-tempo-ro-parietal regions; Cluster3 grouped nodes with high levels of lost connections in subcortical and limbic regions; in Cluster4 only the precuneus showed the highest levels of connectivity alterations, both as loss and gain, which remained consistently present along the whole disease course. ***Conclusion:*** The connectivity alterations initially involve limbic and AD-prototypical cortical regions, with prevalent hyperconnectivity, which might represent an early phase response to the neurodegenerative processes. As disease progresses, the most altered connectivity is limited to the cortical associative regions and cerebellum only. Moreover, our results shed light on the critical role of precuneus in the dynamic connectivity reconfigurations of AD pathology.

OP-046

Is energy consumption linked to structural and functional connectivity in the healthy human brain?

Y. Mayr[1], *A. Lizarraga*[1], *A. Sala*[1,2,3], *I. Yakushev*[1];
[1]Department of Nuclear Medicine, Klinikum rechts der Isar, Technical University of Munich, Munich, GERMANY, [2]Coma Science Group, GIGA-Consciousness, University of Liege, Liege, BELGIUM, [3]Centre du Cerveau2, University Hospital of Liege, Liege, BELGIUM.

Aim/Introduction: Operation of any communication system requires energy input. Consumption of glucose, the main source of energy for the brain, was shown to correlate with functional connectivity, while its relationship to structural connectivity remains unexplored. Here, we studied the relationship between glucose metabolism and structural as well as functional connectivity in the healthy human brain. ***Materials and Methods:*** We analyzed diffusion weighted imaging (DWI), resting-state functional magnetic resonance imaging (fMRI), and fluorodeoxyglucose (FDG) positron emission tomography (PET) data of 56 healthy, middle-aged individuals. Brain volumes were spatially parcellated into 106 regions. Regional standard uptake value ratio (SUVr) was calculated by division with the mean uptake in the whole gray matter. Structural connectivity (SC) was estimated from the DWI data by probabilistic tractography. Functional connectivity (FC) was estimated from the fMRI data. FC weights were computed as Pearson correlation between blood-oxygen-level-dependent signals of each pair of regions. Using graph theory, we calculated Spearman correlation (r) between node strength and regional SUVr. The node strength of a region is defined as the sum of all its connectivity weights. To understand how each connection individually contributes to regional SUVr, we fitted multiple linear regression (MLR) models between connectivity weights and SUVr. Herewith, the complete dataset was split into training (80%) and test (20%) sets, stratified by region. Significance level=0.05 with Bonferroni correction; confidence interval was estimated from 10,000 bootstraps. ***Results:*** Across subjects, median SUVr mildly correlated with median SC ($r=0.29$, $p=0.002$) and FC ($r=0.35$, $p<0.001$) node strength. With MLR, SC explained around half of the variance in SUVr (training $R^2=0.48$, test $R^2=0.49$), and 42 of the 106 predictors were statistically significant. The corresponding MLR model with FC explains a moderate portion of variance (training $R^2=0.22$, test $R^2=0.19$), and is not sufficient to analyze predictor importance. ***Conclusion:*** We found a positive relationship between glucose metabolism and connectivity in the healthy human brain. Notably, SC explained a much larger proportion of variance in glucose metabolism than FC did, suggesting that brain energy consumption is more strongly linked to its white matter infrastructure. Apart from neurobiological implications, these findings serve a reference for studying energy-connectivity (de) coupling in neurodegenerative and demyelinating diseases.

OP-047

Cortical stimulation-induced ictal [^{99m}Tc]Tc-HMPAO SPECT for surgery planning in epilepsy patients

T. Pyka[1], *S. Barlatey*[2], *K. Krieger*[1], *C. Friedrichs-Maeder*[3], *K. Schindler*[3], *A. Rominger*[1], *M. Baud*[3];
[1]*Department of Nuclear Medicine, Inselspital Bern, Bern, SWITZERLAND,* [2]*Department of Neurosurgery, Inselspital Bern, Bern, SWITZERLAND,* [3]*Department of Neurology, Inselspital Bern, Bern, SWITZERLAND.*

Aim/Introduction: Ictal [^{99m}Tc]Tc-HMPAO SPECT is an informative tool to detect and confirm epileptic foci for surgery planning. However, its diagnostic value crucially relies on prompt tracer injection after seizure onset, which for spontaneous seizures is often unpredictable. Triggering seizures by epileptogenic medication has been described [1], but is relatively unreliable with unclear safety and has not lead to a generalized adaptation of the method. In contrast, invasive cortical stimulation with grey matter stereoelectroencephalography (sEEG) is a mainstay investigation before epileptic surgery [2]. Our study combines for the first time this technique with a triggered ictal SPECT. ***Materials and Methods:*** At the time of writing, five patients with suspected temporal lobe epilepsy had been investigated in an ongoing prospective study (20 planned in total). Grey matter surface electroencephalography (sEEG) contacts were implanted and screened for triggering patient-typical seizures. On the next day, triggering was repeated and 406-511 MBq [^{99m}Tc]Tc-HMPAO were administered immediately after seizure confirmation. Clusters of hyperperfused voxels were determined by statistical parametric mapping using a normal template and compared with the signal of the implanted electrodes. Therefore, we computed bipolar traces of adjacent contacts and estimated seizure-power per dipole in terms of z-values over baseline. Cortical reconstruction based on MRI data was computed using FreeSurfer and imported into Lead-DBS for co-visualization with the SPECT z-map and sEEG contacts. ***Results:*** In all patients, ictal SPECT was successfully obtained with injection within 12 seconds of triggered seizure onset without any adverse event. In 4 out of 5 cases, there was a good correlation between deep electrode and SPECT signal, confirming a regional origin. In one case no clear ictal signal could be derived in SPECT nor sEEG. In two cases SPECT revealed areas of hyperperfusion in eloquent cortex that were not sampled by sEEG but corroborated patient-typical peri-ictal aphasia. ***Conclusion:*** Cortical stimulation-triggered ictal SPECT constituted a safe and easy-to-use method for imaging early seizure propagation networks, with good correlation with and complementing electrophysiological exploration. The method could lead to a revival of ictal SPECT imaging, as it is readily implementable at any specialized epilepsy center where sEEG is available. ***References:*** 1. Enev M, McNally KA, Varghese G, et al. Imaging onset and propagation of ECT-induced seizures. Epilepsia. Feb 2007;48(2):238-442. 2. Cuello Oderiz C, von Ellenrieder N, Dubeau F, et al. Association of Cortical Stimulation-Induced Seizure With Surgical Outcome in Patients With Focal Drug-Resistant Epilepsy. JAMA Neurol. Sep 1 2019;76(9):1070-1078.

OP-048

The Value of ^{18}F-FDG PET/MRI in the Preoperative Localization of Epileptogenic Zone in Patients With Drug-resistant Epilepsy

C. Zeng[1], *H. Zhou*[2], *X. Ling*[1], *Y. Tang*[1], *Z. Tan*[1], *H. Wu*[1], *Y. Cheng*[1], *J. Shang*[1], *Q. Guo*[3], *H. Xu*[1];
[1]*Department of Nuclear Medicine, The First Affiliated Hospital of Jinan University, Guangzhou, CHINA,* [2]*Department of Radiology, Central People's Hospital of Zhanjiang, Zhanjiang, CHINA,* [3]*Epilepsy Center, Guangdong 999 Brain Hospital, Affiliated Brain Hospital of Jinan University, Guangzhou, CHINA.*

Aim/Introduction: Currently, there is a lack of large sample size clinical studies on the value of ^{18}F-FDG PET/MRI for preoperative localization in patients with epilepsy. This study aimed to compare the localization rates of the epileptogenic zone (EZ) between invasive and noninvasive preoperative assessments based on a large sample size of clinical data, to explore in which situation noninvasive assessments may replace stereotactic electroencephalography (SEEG), and to further reveal the value of ^{18}F-FDG PET/MRI for preoperative localization in patients with drug-resistant epilepsy. ***Materials and Methods:*** Patients with drug-resistant epilepsy who underwent surgery and preoperative ^{18}F-FDG PET/MRI were retrospectively included, and all patients were followed up for at least 12 months after surgery. Patients underwent video electroencephalography (VEEG) and SEEG according to clinical indications. The correct localization rates of EZ were calculated for SEEG and noninvasive modalities, using the surgical resection site and postoperative follow-up for at least 12 months as reference standard. Chi-square test or Fisher's exact test was used to compare the localization rates of SEEG with noninvasive modalities. ***Results:*** A total of 594 patients, including MRI-negative (n = 104) and MRI-positive (n = 490), were included in this study, 273 of whom underwent SEEG. The localization rate of EZ with SEEG (83.9%) was comparable to PET-VEEG concordance in MRI-negative patients (75.0%, P = 0.875) and PET-MRI-VEEG concordance in MRI-positive patients (75.0%, P = 0.115). In temporal lobe epilepsy (TLE), the localization rate with SEEG (100.0%) was comparable to PET/MRI+VEEG in MRI-negative patients (100.0%) and PET/MRI+VEEG in MRI-positive patients (92.9%, P = 0.169). In extratemporal epilepsy (ETLE), the localization rate of EZ with SEEG (97.1%) was higher than PET/MRI+VEEG in MRI-negative patients (65.0%, P = 0.005) and PET/MRI+VEEG in MRI-positive patients (69.6%, P = 0.002). In multilobar epilepsy, the localization rate of EZ with SEEG (70.3%) was higher than PET/MRI+VEEG in MRI-negative patients (0.0%, P < 0.001) and PET/MRI+VEEG in MRI-positive patients (8.3%, P < 0.001). When the resection included insula, the localization rate of EZ with SEEG was significantly higher than noninvasive modalities. ***Conclusion:*** When the preoperative noninvasive modalities are concordant with each other, or when TLE is considered, patients with drug-resistant epilepsy can undergo direct surgery without SEEG if EZ does not involve the eloquent area. It is necessary to accept SEEG preoperatively when ETLE or multilobar epilepsy is considered. When insula is included in the resection, accepting SEEG preoperatively is necessary for patients.

OP-049

Effects of Deep Learning-based Quantification for Amyloid PET on Visual Reading: A retrospective, multicenter, multireader study

H. Ryoo[1], *K. Cho*[2], *Y. Kim*[3], *S. Ha*[4], *S. Kwon*[4], *R. Lee*[5], *J. Seok*[6], *S. Kang*[7], *Y. Kang*[2], *B. Kim*[7], *J. Jeong*[8], *H. Yoon*[9], *M. Yoo*[10], *G. Kim*[11], *J. Choi*[12], *J. Park*[12], *E. Lee*[13], *J. Kim*[14], *H. Song*[14], *K. Park*[14], *J. Ha*[15], *A. Chong*[15], *S. Jang*[16], *J. Bang*[16], *I. Hong*[17], *S. Choi*[17], *S. Jeong*[18], *I. Jo*[18], *H. Choi*[2,19,20];
[1]*Department of Nuclear Medicine, Seoul National University Bundang Hospital, Seongnam, KOREA, REPUBLIC OF,* [2]*Department of Nuclear Medicine, Seoul National University Hospital, Seoul, KOREA, REPUBLIC OF,* [3]*Department of Nuclear Medicine, Seoul Metropolitan Government Seoul National University Boramae Medical Center, Seoul, KOREA, REPUBLIC OF,* [4]*Division of Nuclear Medicine, Department of Radiology, College of Medicine, The Catholic University of Korea, Seoul, KOREA, REPUBLIC OF,* [5]*Department of Nuclear Medicine, Chung-Ang University Gwangmyeong Hospital, Gwangmyeong, KOREA, REPUBLIC OF,* [6]*Department of Nuclear Medicine, Chung-Ang University Hospital, Seoul, KOREA, REPUBLIC OF,* [7]*Department of Nuclear Medicine, Ewha Womans University Seoul Hospital, Ewha Womans University College of Medicine, Seoul, KOREA, REPUBLIC OF,* [8]*Department of Neurology, Ewha Womans University Seoul Hospital, Ewha Womans University College of Medicine, Seoul, KOREA, REPUBLIC OF,* [9]*Department of Nuclear Medicine, Ewha Womans University Mokdong Hospital, Ewha Womans University College of Medicine, Seoul, KOREA, REPUBLIC OF,* [10]*Department of Nuclear Medicine, Inha University Hospital, Incheon, KOREA, REPUBLIC OF,* [11]*Department of Neurology, Ewha Womans University Mokdong Hospital, Ewha Womans University College of Medicine, Seoul, KOREA, REPUBLIC OF,* [12]*Department of Nuclear Medicine, Soonchunhyang University Bucheon Hospital, Bucheon, KOREA, REPUBLIC OF,* [13]*Department of Neurology, Soonchunhyang University Bucheon Hospital, Bucheon, KOREA, REPUBLIC OF,* [14]*Department of Nuclear Medicine, Chonnam National University Hospital, Gwangju, KOREA, REPUBLIC OF,* [15]*Department of Nuclear Medicine, Chosun University School of Medicine, Gwangju, KOREA, REPUBLIC OF,* [16]*Department of Nuclear Medicine, CHA Bundang Medical Center, CHA University, Seongnam, KOREA, REPUBLIC OF,* [17]*Department of Nuclear Medicine, Kyung Hee University Hospital, Kyung Hee University School of Medicine, Seoul, KOREA, REPUBLIC OF,* [18]*Department of Nuclear Medicine, Kyungpook National University Chilgok Hospital, Daegu, KOREA, REPUBLIC OF,* [19]*Institute of Radiation Medicine, Medical Research Center, Seoul National University College of Medicine, Seoul, KOREA, REPUBLIC OF,* [20]*Department of Nuclear Medicine, Seoul National University College of Medicine, Seoul, KOREA, REPUBLIC OF.*

Aim/Introduction: Amyloid PET imaging is a valuable tool for early Alzheimer's diagnosis and management. However, visual interpretation has limitations, including inter-observer variability. Although quantitative software exists, it is not routinely used in clinical practice due to complexity and the need for MRI co-registration. We conducted a retrospective, multicenter, and multireader study to assess the efficacy of a deep learning-based quantification system that only uses amyloid PET images. Our goal was to evaluate if this system could improve inter-reader agreement and confidence in visual interpretation. ***Materials and Methods:*** We retrospectively collected 435 amyloid PET scans from 7 centers with mild cognitive impairment and early Alzheimer's disease. All collected PET scans were analyzed for this study. Deep learning-based quantification software which provides AI-based PET quantitative analysis without MR images was used for the amyloid PET reading [1]. For the randomized-blind-reader study, more than two readers were assigned to each center and reading was composed of two sessions: visual session (PET reading without aid of deep-learning quantification software) and quantification session (PET reading with aid of deep-learning quantification software). The order of visual and quantification session was randomly assigned, and the order of images between two sessions was randomly shuffled. The qualitative assessment was based on binary point scale (positive or negative for amyloid deposit). The confidence score for each session was evaluated by a 2-point scale (0: equivocal, 1: definite to decide). Inter-reader reliability was calculated based on Cohen kappa score. ***Results:*** Our results showed that the deep learning-based software improved inter-reader agreement and confidence of amyloid PET reading. Inter-reader reliability was measured median 0.80 (range, 0.39-1.00) and 0.92 (range, 0.39-1.00) for visual and quantification sessions, respectively. The pooled confidence score was 0.85 ± 0.35 and 0.93 ± 0.24 (mean ± standard deviation) for visual and quantification sessions. Four readers showed a significant increase in confidence score in the quantification session. ***Conclusion:*** The deep learning-based amyloid PET quantification software without MRI can increase inter-reader agreement and confidence of amyloid PET reading. This has strong clinical implications for the objective and accurate diagnosis of Alzheimer's disease. ***References:*** [1] Kang SK, Kim D, Shin SA, Kim YK, Choi H, Lee JS. Fast and accurate amyloid brain PET quantification without MRI using deep neural networks. J Nucl Med. 2023;64:659-666.

OP-050

Brain metabolic correlates of Cytokine Release Syndrome and Immune effector cell-associated neurotoxicity in patients with Diffuse Large B-Cell Lymphoma (DLCBL) treated with CAR-T

T. Di Raimondo[1], *M. Gambella*[2], *A. Raiola*[2], *F. D'Amico*[1], *L. Sofia*[1], *F. Lanfranchi*[1], *C. Ghiggi*[2], *C. Lapucci*[3], *G. Sambuceti*[1], *M. Bauckneht*[1], *M. Inglese*[3], *E. Angelucci*[2], *S. Morbelli*[1];
[1]*Nuclear Medicine Unit, Department of Health Sciences (DISSAL), University of Genoa, Genova, ITALY,* [2]*Department of Hematology and Cellular Therapy, IRCCS Ospedale Policlinico San Martino, Genova, ITALY,* [3]*Department of Neuroscience, Rehabilitation, Ophthalmology, Genetics, Maternal and Child Health (DINOGMI), IRCCS Ospedale Policlinico San Martino, University of Genoa, Genova, ITALY.*

Aim/Introduction: Chimeric antigen receptor (CAR) T-cell therapy is potentially associated to treatment-related toxicities mainly consisting in cytokine release syndrome (CRS) and immune-effector cell-associated neurotoxicity syndrome (ICANS). We aimed to evaluate brain metabolic correlates of CRS with and without ICANS in DLBCL patients treated with CAR-T and to investigate the relationship between both baseline metabolic tumor volume (MTV) and total lesion glycolysis (TLG) and the occurrence of CRS and ICANS. ***Materials and Methods:*** Twenty-one patients with refractory DLCBL underwent whole-body and brain [18F]FDG PET just before and 30-days after treatment with CAR-T. Five patients did not develop inflammatory-related side effects, eleven patients developed CRS (CRS group), in further 5 patients CRS evolved in ICANS (ICANS group). Baseline and post-CAR-T brain FDG-PET were compared with a local controls dataset (SPM12) to identify hypometabolic patterns both at single-patient and group level ($p<0.05$ after correction for family-wise error (FWE) as significant). MTV and TLG were computed on baseline FDG-PET and compared between patients' subgroups (t-test). ***Results:*** After therapy with CAR-T, ICANS patients showed an extended and bilateral pattern of hypometabolism mainly involving orbito-frontal, frontal dorso-lateral cortex, anterior

cingulate (p FWE-corrected <0.003). Patients who experienced CRS without ICANS showed significant hypometabolism in less extended clusters mainly involving bilateral medial and lateral temporal lobes, posterior parietal lobes, anterior cingulate and cerebellum (FWE-corrected p<0.002). When ICANS and CRS subgroups were directly compared, patients with ICANS showed a more prominent hypometabolism in orbitofrontal and frontal dorso-lateral cortex in both hemispheres (FWE-corrected p<0.002). Mean baseline MTV and TLG were significantly higher in ICANS patients with respect to patients with CRS only (p<0.02). ***Conclusion:*** Patients with ICANS after treatment with CAR-T are characterized by a fronto-lateral hypometabolic signature in line with the hypothesis of ICANS as a predominant frontal syndrome and with the more prominent susceptibility of frontal lobes to cytokine-induced inflammation.

OP-051

A pilot study comparing myelin measurements from [18F]-Florbetaben PET and quantitative T1 map imaging in multiple sclerosis (MS)

L. Sofia[1], *M. Donegani*[1], *A. Donniaquio*[2], *A. Chincarini*[3], *L. Roccatagliata*[4], *M. Pardini*[2], *R. Gianeri*[3], *F. Sensi*[3], *F. D'Amico*[1], *T. Di Raimondo*[1], *C. Bagnara*[5], *M. Riondato*[1], *G. Novi*[6], *A. Laroni*[2], *A. Murialdo*[6], *G. Ribizzi*[6], *A. Uccelli*[2], *M. Inglese*[2], *S. Morbelli*[1]; [1]*Nuclear Medicine Unit, Department of Health Sciences, University of Genoa, Genoa, ITALY,* [2]*Department of Neuroscience, Rehabilitation, Ophthalmology, Genetics, Maternal and Child Health (DINOGMI), University of Genoa, Genoa, Genoa, ITALY,* [3]*National Institute of Nuclear Physics (INFN), Genoa section, Genoa., Genoa, ITALY,* [4]*Neuroradiology Unit, University of Genoa, Genoa, Genoa, ITALY,* [5]*Medical Physics, IRCCS Policlinico San Martino, Genoa, Genoa, ITALY,* [6]*Division of Neurology, IRCCS Policlinico San Martino, Genoa, Genoa, ITALY.*

Aim/Introduction: PET imaging with β-amyloid ligands (amy-PET) is emerging as a molecular imaging technique targeting quantitative measurement of myelin content changes in MS. T1 relaxation time maps have been recently proposed for the qualitative and quantitative classification of MS lesions according to myelin content and to track lesional myelination changes over time. However, this MRI metrics has not yet been validated, and no data are to-date available on the relationship between T1-map and AMY-PET-based myelin measurements. We aimed to explore the correlation between lesional white matter (WM) amy-PET uptake and quantitative (q) T1 map metrics. ***Materials and Methods:*** Patients with relapsing-remitting (RR) and primary progressive (PP) MS were recruited in a project funded by the Italian Ministry of Health. All patients underwent both 3T MRI with standard sequences and qT1 map and dual dynamic amy-PET imaging with [18F]Florbetaben (early dynamic of the first 30 minutes and late steady-state acquisitions 90-110 minutes p.i.). Lesions were segmented on 3T MRI and for every lesion T1/T2 ratio (considered a rough measure of myelination) and intensity and coefficient of variance (capturing lesions' heterogeneity) on qT1 map were measured. PET images were spatially and intensity normalized. SUVratio was measured on early dynamic and late static PET images in the individual lesions and in the contralateral normal appearing white matter (NAWM). Correlation between WM amy-PET on one side and T1/T2 ratio and T1 map on the other were assessed by means of Pearson's correlation coefficient. ***Results:*** 607 WM lesions were analyzed in nineteen MS patients (10 primary-progressive, 9 relapsing-remitting) and were included in the analysis. In the lesion based analysis, both early-dynamic and steady state SUVr was significantly correlated with both T1/T2 and qT1 map. This correlation was significant with both lesions' intensity and coefficient of variation and was not affected by lesions' volume and patient's clinical phenotypes (p<0.0001 in both cases). When looking at the NAWM, the voxel-to-voxel correlation coefficient was higher in the gray-white matter transition zone. ***Conclusion:*** Both early and late steady state metrics derived from amy-PET correlate with advanced qT1 map data. Amy-PET seems to be able to reflect both the degree of demyelination and lesions' heterogeneity; however the potential influence of the topography of the lesions on PET signal seems to affect SUVr measurement and should be considered in more clinically-oriented studies.

208

Sunday, September 10, 2023, 8:00 AM - 9:30 AM

Hall F2

Paediatrics Committee - TROP Session: Paediatric PET/CT & PET/MR

OP-052

Predictive value of FDG PET/CT parameters in pediatric Hodgkin Lymphoma: initial results of an Italian prospective study

E. Lopci[1], *C. Elia*[2], *V. De Re*[2], *L. Mussolin*[3], *A. Piccardo*[4], *A. Cistaro*[5], *P. Zucchetta*[6], *E. Borsatti*[2], *M. Bianchi*[7], *S. Buffardi*[8], *P. Farruggia*[9], *A. Garaventa*[10], *A. Sala*[11], *L. Vinti*[12], *C. Mauz-Koeholz*[13], *M. Mascarin*[2]; [1]*IRCCS - Humanitas Research Hospital, Rozzano MI, ITALY,* [2]*CRO, Aviano, ITALY,* [3]*Pediatric Hemato-Oncology Clinic, Padoa, ITALY,* [4]*Galliera Hospital, Genoa, ITALY,* [5]*Salus Alliance Medical, Genoa, ITALY,* [6]*Padova University Hospital, Padoa, ITALY,* [7]*Regina Margherita Hospital, Turin, ITALY,* [8]*Hospital Santobono-Pausilipon, Naples, ITALY,* [9]*A.R.N.A.S. Ospedali Civico, Palermo, ITALY,* [10]*IRCCS G.Gaslini Hospital, Genoa, ITALY,* [11]*Hospital San Gerardo, Monza, ITALY,* [12]*Ospedale Bambino Gesù, Rome, ITALY,* [13]*Zentrum für Kinderheilkunde der Justus-Liebig-Universität Gießen, Gießen, GERMANY.*

Aim/Introduction: FDG PET/CT represents an essential tool for pediatric Hodgkin lymphoma (HL). In this context, volumetric analyses might be a valuable tool to discriminate disease prognosis and response. To validate this assumption, the AIEOP Hodgkin Lymphoma Study Group has designed a parallel study of the cohort of patients enrolled in the EuroNet-PHL-C2 trial. Herein, we present the initial results obtained from this cohort. ***Materials and Methods:*** We analyzed data from the first 200 patients (94M, 106F; median age 15years) with HL enrolled in 24 Italian centers from January 2017 to December 2020 for the EuroNet-PHL-C2 protocol. The cohort was classified based on treatment level: TL1 (31 patients), TL2 (90 patients) and TL3 (79 patients), of whom 71 with bulky masses. Response was classified into adequate (AR) and inadequate response (IR) as per protocol. The primary objective of the study was to define the predictive role of volumetric and semiquantitative analyses, i.e., SUVmax, SUVmean, MTV and total lesion glycolysis (TLG), as well as lymphoma dissemination (Dmax), at FDG PET/CT at baseline and during therapy. In particular, treatment response was assessed at early (ERA) and late evaluation (LRA). Semi-automatically delineated contours of the lesions were performed by using a fixed SUV threshold of 2.5. All parameters and their variations (Δ) were analyzed with respect to response. ***Results:*** At baseline, our cohort presented a median SUVmax of 12.5 (95%CI: 12.1-13.1), median SUVmean

4.3 (95%CI: 4.2-4.5), median MTV 223 (95%CI: 183-264), median TLG 1009 (95%CI: 868-1213) and median Dmax of 18 (95%CI: 14.7-21.7). There was a statistically significant difference of median baseline SUVmax (P=0.002), MTV (P=0.022), TLG (P=0.005) and Dmax (P=0.003) and treatment evaluation at ERA PET. Median variations from baseline resulted respectively: 81% for SUVmax, 59% for SUVmean, 92% for MTV, 97% for TLG and 40% for Dmax, with ΔSUVmax and ΔSUVmean showing a significant correlation to LRA (P=0.027 and 0.020, respectively). There was a significant correlation of semi-quantitative and volumetric parameters at baseline also at logistic regression for SUVmax (P=0.0025), MTV (P=0.0272), TLG (P=0.0078) and Dmax (P=0.0045). While pooled together with other clinical data (i.e. stage, TL, and bulky masses), multiple regression defined as independent predictive factors TL and bulky masses (P=0.0071 and 0.0078, respectively). ***Conclusion:*** Semi-quantitative and volumetric FDG PET/CT parameters correlate to ERA results and their variations show a statistically significant correlation to LRA. Dmax seems to have a potential role as predictor of response in pediatric HL.

OP-053

Interim TLG and MTV vs Deauville Score as Predictors in Pediatric Non-Hodgkin Lymphoma Patients

G. KAYA[1], *B. Volkan Salancı*[1], *B. Aydın*[2], *P. Özgen Kıratlı*[1];
[1]*Hacettepe University Medical School Department of Nuclear Medicine, Ankara, TÜRKIYE,* [2]*Hacettepe University Medical School Department of Pediatric Oncology, Ankara, TÜRKIYE.*

Aim/Introduction: Evaluation of interim FDG PET/CT scans of pediatric Non-Hodgkin lymphoma (NHL) patients is still a challenge. Apart from Deauville Score (DS), total lesion glycolysis (TLG) and metabolic tumor volume (MTV) are semiquantitative parameters originated from PET/CT data. The aim of this study is to assess the role of interim DS, TLG, and MTV in pediatric NHL patients. ***Materials and Methods:*** Interim PET images of pediatric FDG avid NHL patients were evaluated retrospectively. $MTV_{2.5}$ and $TLG_{2.5}$ values were calculated according to "SUVmax cut-off: 2.5", as well as DS of interim scans. $MTV_{2.5}$ and $TLG_{2.5}$ values ">0" and DS "≥3" were accepted as residual disease. Survival analysis and diagnostic parameters of each parameter were analyzed. Death and disease progression were accepted as an event. ***Results:*** The study group included 119 PET scans of 119 children (F/M: 36/83, mean age: 9.6y (SD 4.6) diagnosed as NHL, between 2011-2022. High-grade B cell lymphoma (47.5%), lymphoblastic lymphoma (28.3%), and anaplastic large cell lymphoma (11. 7%) composed the majority of the study group. On interim PET scans, median $MTV_{2.5}$ was 0 cm^3 (range: 0-453), $TLG_{2.5}$ was 0 (range: 0-3163) and DS was 1 (range: 1-5). Twenty-four patients were accepted positive for the minimal residual disease on MTV and TLG analysis, while 39 were positive in the DS group. There were no patients evaluated as positive on DS but negative on $MTV_{2.5}$ and $TLG_{2.5}$. Patients evaluated as positive in these methods significantly differ from each other ($p<0.001$). Kaplan-Meier analysis showed mean time-to-event was significantly shorter (6.7 years; $p<0.001$) in patients who were positive in TLG&MTV. The estimated median survival was not reached for only-DS-positive patients and also patients evaluated as negative on both methods. Cox analysis showed that the proportional hazard ratio was 5.4 for TLG&MTV positivity (lower 2.2 and upper 13.1, CI 95%; $p<0.001$). The negative predictive value of interim PET/CT was 86.3%. ***Conclusion:*** The results of this ongoing study suggest that $MTV_{2.5}$ & $TLG_{2.5}$ and DS assessments significantly differ in pediatric NHL patients. $MTV_{2.5}$ & $TLG_{2.5}$ exceed DS in the estimation of disease progression significantly in this group of patients.

OP-054

Application value of 18F-FDG PET/MR whole body imaging in children's rhabdomyosarcoma staging

S. Yun;
Hangzhou Universal Imaging diagnostic center, Hangzhou, CHINA.

Aim/Introduction: To evaluate the value of a Hybrid ^{18}F-FDG PET/MR in staging of pediatric nephroblastoma. ***Materials and Methods:*** The clinical data of 77 patients who were diagnosed as nephroblastoma were retrospectively analyzed from April 2017 to July 2019.Patients were divided into the pre-treatment group (n=40) and post-treatment group (n=37).The PET/MR characteristics was analyzed, and the size,shape, signal characteristics, relationship with surrounding tissues, SUVmax value, metastasis and staging characteristics of the tumor were observed. Pathological and clinical diagnosis results are the gold standard. ***Results:*** Based on NWTS-V staging,the 40 cases pre-treatment group included 3 cases (7.5%) in stage I, 5 cases (12.5%) in stage II, 14 cases (35.0%) in stage III, 16 cases (40.0%) in stage IV and 2 cases (5.0%) in stage V.20 (50.0%) tumors occurred in the right kidney, 17 (42.5%) in the left kidney, 2 (5.0%) in both kidneys, and 1 (2.5%) outside the kidney (in the spinal canal). The average maximum diameter of the lesions was 10.25 ± 4.12 cm; The average value of SUVmax was 13.58 ± 6.74. 28 cases (70%) had smooth and clear boundary and pseudocapsule; There were 26 cases (65%) with uneven density, necrosis, hemorrhage and cystic transformation; "Residual kidney sign" was found in 28 cases (70%), and 8 cases (20%) were of whole kidney invasion type. Tumor thrombus in renal vein or inferior vena cava in 5 cases (12.5%); Lymph node metastasis occurred in 21 cases (52.5%); 17 cases (42.5%) had distant metastasis, including 9 cases of lung metastasis, 8 cases of bone metastasis, 2 cases of liver metastasis and 2 cases of brain metastasis. In the post-treatment group, 12 cases (32.4%) had lymph node metastasis and 10 cases (27.0%) had remote metastasis.Staging after PET/MR imaging: 15 patients (37.5%) in the pre-treatment group had stage changes, 11 of them increased from III to IV, 4 from II to IV. In the post-treatment group, 12 cases (32.4%) had stage changes, of which 7 cases increased from stage 0 to stage IV, 2 case increased from stage III to stage IV, 3 cases decreased from stage IV to stage 0 due to negative FDG uptake. ***Conclusion:*** ^{18}F-FDG PET/MRI is superior to clinical in staging of pediatric nephroblastoma.It has more advantages in detecting the invasion and distant metastasis around the tumor, and obviously improves the accuracy of the primary staging and re-staging of the nephroblastoma.

OP-055

Prognostic Value of 18FDG PET/CT Parameters for the Outcome in Pediatric Sarcoma Patients

B. Soydas Turan[1], *B. Volkan-Salancı*[2], *G. B. Aydın*[3], *P. Özgen Kıratlı*[2];
[1]*Etlik City Hospital, Department of Nuclear Medicine, Ankara, TÜRKIYE,* [2]*Hacettepe University Faculty of Medicine, Department of Nuclear Medicine, Ankara, TÜRKIYE,* [3]*Hacettepe University Faculty of Medicine, Department of Pediatric Oncology, Ankara, TÜRKIYE.*

Aim/Introduction: To explore which metabolic 18FDG PET/CT parameters acquired at staging are predictive of overall survival (OS) and progression-free survival (PFS) in children with bone or soft tissue sarcomas. ***Materials and Methods:*** Pediatric patients with histologically proven Ewing sarcoma (ES), Osteosarcoma (OST) and Rhabdomyosarcoma (RMS) who referred to 18FDG PET/CT for staging before any treatment between January 2010 and

December 2020 were retrospectively enrolled. SUVmax, metabolic tumor volume (MTV), total lesion glycolysis (TLG) of primary tumor were obtained. MTV was defined with a threshold of 40% of SUVmax. TLG was defined as the product of MTV and SUVmean. MTV and TLG of all FDG avid metastatic lesions were also noted. Summation of MTV and TLG of all pathological lesions yielded the wb-MTV and wb-TLG, respectively. Kaplan-Meier curves and log-rank test were used to compare survival experience between PET parameters on cut-off values (median/upper quantile). ***Results:*** PET/CT scan of 87 patients with ES (n: 46, mean age 10.22 ± 3.79 years, 17 females), OST (n: 26, mean age 11.35 ± 3.17 years, 11 females) and RMS (n: 15, mean age 8.27 ± 5.35 years, 7 females) were analyzed. 19 patients (41.3%) with ES, 8 (30.8%) with OST and 9 (56.3%) with RMS presented with metastases. Median follow-up was 55 months (range 7-125). 36 patients (41.3%; 19 ES, 11 OST, 6 RMS) had relapse/progression and 28 patients (32.2%; 11 ES, 12 OST, 5 RMS) deceased. In ES group, patients with SUVmax > 7.25 (70 vs 108 months, p: 0.013), wb-MTV > 129.36 (66 vs 109 months, p: 0.028) and wb-TLG > 719.10 (47 vs 109 months, p: 0.003) had lower OS. Also, wb-TLG > 719.10 was significantly associated with early progression (37 vs 83 months, p: 0.048). Patients with wb-MTV > 129.36 had shorter PFS but not reaching statistical significance (53 vs 85 months, p: 0.088). In OST group, SUVmax > 7.17 (48 vs 90 months, p: 0.026) and wb-MTV > 134.25 (40 vs 85 months, p: 0.017) were associated with increased mortality. No relationship was found in RMS group, possibly due to limited number of patients. ***Conclusion:*** Staging 18FDG PET parameters can be used as a prognostic indicator in ES and OST. High SUVmax and wb-MTV were associated with worse OS. Additionaly, high wb-TLG was associated with poor OS and PFS in ES.

OP-056

Bone marrow involvement detection by FDG PET-CT in newly diagnosed Ewing Sarcomas : comparison to bone marrow aspiration and biopsy, and assessment of visual interpretation criteria with junior doctors

V. Isnardi[1], *A. Guinot*[1], *H. Bahri*[1], *E. Paquet*[1], *M. Fazel*[1], *L. Besson*[2], *M. Brahmi*[1], *N. Corradini*[1], *P. Marec-Berard*[1];
[1]*Lumen Centre Léon Bérard, Lyon, FRANCE,*
[2]*University Hospital, Saint Etienne, FRANCE.*

Aim/Introduction: Ewing sarcoma (ES) is an aggressive tumour with an unfavourable prognosis when bone marrow metastasis are present at diagnosis. Cancer staging identifies 30% of patients as metastatic at diagnosis, among them 20 % presents bone marrow involvement or bone metastasis. The overall 5 years survival is approximately 70% without metastasis and drop to 25% in case of bone marrow involvement. Bone marrow aspiration and biopsy (BMAB) are the gold standard for bone marrow assessment. However recent studies suggest that these invasive and painful procedures could be replaced by FDG PET-CT (FDG PET). FDG PET is indeed a sensitive technique for the detection of ES metastasis and typical sinctigraphic patterns could easily distinguish bone marrow involvement and focal bone metastasis. ***Materials and Methods:*** We compared the FDG-PET results of 180 patients with newly diagnosed ES, recorded at the Centre Léon Bérard over the past 10 years, with BMAB results. Marrow metastatic status was determined by the nuclear physician's interpretation at diagnosis. A blinded centralized review of positive or suspicious FDG PET was performed by an experienced nuclear medicine physician. Scintigraphic pattern of bone marrow involvement was defined by a diffuse, and frankly heterogeneous hypermetabolism of the axial and proximal appendicular skeleton, and focal bone metastase was defined by intense focal uptake. Then 3 junior doctors performed a blind review of an extracted panel of 24 FDG PET of the 180, including discordant ones according to the previous centralized review. They had to classify images as bone marrow involvement, focal bone metastasis or negative. ***Results:*** Of the 180 FDG-PET, 12 were true positive, one false positive, 166 true negative, one false negative. The sensitivity of FDG PET was 92.3% and the specificity 99.4%. The three junior doctors (2 nuclear medicine physicians, one oncologist) correctly classify 22, 21 and 20 on the panel of 24 FDG-PET respectively. In addition to the false positive case and the false negative case previously described, they misclassified none, one patient, and 2 patients respectively. ***Conclusion:*** FDG PET demonstrated a high sensitivity and specificity as well as a good repeatability and reproducibility, even by junior doctor. These results suggest that, excepted in situation of clinical research protocol, BMAB should no longer be systematically performed for the staging at the diagnosis of ES in case of typical scintigraphic pattern of bone marrow involvement on FDG PET and in case of localised ES or pulmonary metastasis alone.

OP-057

Role of F18 FDG PET/CT inEwing's Sarcoma Family Of Tumours (ESFT)

A. Tiwary Vyas[1], *A. Vyas*[2];
[1]*Janakpuri Superspeciality Hospital, New Delhi, INDIA,* [2]*Max Superspeciality Hospital Vaishali, New Delhi, INDIA.*

Aim/Introduction: The role of F-18 FDG PET/CT in staging, restaging and response assessment of Ewing's Sarcoma Family of Tumors (ESFT) - an Indian experience ***Materials and Methods:*** 37 patients of ESFT were assessed by FDG PET/CT after histopathological diagnosis. The patients had mean age of 21 years (range 5-45 years); male :female - 4.2: 1. Response was assessed as per PERCIST 1.0 criteria by follow up PET/CT in 26 cases after completion of treatment (surgery for resectable tumors & chemotherapy / radiotherapy for advanced tumors). Data was interpreted using qualitative (liver & mediastinal blood pool) & semi-quantitative (Standardized Uptake Value- SUV max). Resolution of metabolic activity was marker of response to therapy. ***Results:*** Out of 37, 29 cases were of skeletal Ewing's sarcoma (ES) - 17spinal & 12 extra-spinal,04 Extraskeletal Ewing's (ESE), 02 Askin`s tumour of chest wall & 02 PNET (in brain and orbit). 16 (43.2%) cases of stage IIa, 01 (2%) IIb, 01 (2%) III, 08 (21%) IVa & 11 (29.7%) IVb. Spine was the most frequent primary involvement, followed by extremities. A mixed sclerotic- lytic lesion is seen with associated soft tissue component and variable heterogeneous FDG uptake was seen in most of the skeletal lesions. Mean SUVmax of primary lesion 6.1(range 2.5 to 19.3). Regional lymphnodes (57 % cases) were most common site of metastases, 37% distant metastases. Lung (21.6 %) followed by bone(18.9 %). there was CMR 09 /26(34.6%), PMR 07/26 (26.9%), SD 01/26 (3%) & PD 09/26 (34.6%) respectively. ***Conclusion:*** Molecular imaging with F-18 FDG PET/CT is a helpful tool for staging & restaging of ESFT as well as for localization of distant metastases. It is a valuable in response assessment of all the types of Ewing sarcoma family of tumors by using qualitative & semi-quantitative (SUVmax) methods.Further prospective studies are recommended. ***References:*** 1.Iwamoto Y (February 2007)."Diagnosis and treatment of Ewing sarcoma". Jpn. J. Clin. Oncol. 37 (2): 79 89. doi:10.1093/jjco/hyl142. PMID 17272319.2. Ludwig JA. Ewing sarcoma: historical perspectives, current state-of-the-art, and opportunities for targeted therapy in the future. Curr Opin Oncol 2008; 20(4):412-418.3.Gerth HU, Juergens KU, Dirksen U, Gerss J,Schober O, Franzius C. Significant benefit of multimodal imaging:PET/CT compared with PET alone

in staging and follow-up of patients with Ewing tumors. J Nucl Med 2007;48(12):1932-1939.4. Wahl RL, et al. (2009). From RECIST to PERCIST: Evolving considerations for PET response criteria in solid tumors .J Nucl Med, 50, 122S-150S.

OP-058

Pediatric tumor patients scanned with a long axial field of view scanner - a single center experience of reduced administered doses of [^{18}F]FDG

C. Bregenzer[1], *K. Krieger*[1], *H. Sari*[1,2], *K. Zeimpekis*[1], *N. Gözlügöl*[1], *Â. Cardoso*[1], *Â. Mendes*[1], *A. Rominger*[1], *A. Afshar-Oromieh*[1];
[1]*Department of Nuclear Medicine, Inselspital, University Hospital Bern, University of Bern, Bern, SWITZERLAND,*
[2]*Advanced Clinical Imaging Technology, Siemens Healthcare AG, Lausanne, SWITZERLAND.*

Aim/Introduction: The administered activity for [^{18}F]FDG-PET/CT in children has always been a subject of discussion. Current guidelines recommend a dose of 3.7-5.2 MBq/kg body weight (BW), although the consensus is to use lowest doses as reasonably possible. The advent of latest generation scanners offers the opportunity of reducing the administered dose. Here we report our first experiences with pediatric patients scanned with reduced doses using a long axial field of view (LAFOV) PET/CT scanner. ***Materials and Methods:*** Twenty-seven [^{18}F]FDG-PET/CT scans from 21 children and adolescences (age limit 18 y/o) with different tumors were included in this retrospective analysis. Amongst them, three groups were identified depending on the administered activity: 1 MBq/kg BW, 2 MBq/kg BW and 3 MBq/kg BW. Acquisition duration was 10 minutes beginning 1h post injection. A LAFOV-PET/CT scanner (field-of-view: 106cm) was used for all scans. In addition to the aforementioned groups, a fourth group was formed by simulating 0.5 MBq/kg BW by histogramming only the first 5 minutes of PET data obtained with 1 MBq/kg scans. The quality of all scans was assessed in a blinded manner by two readers using a 5-point Likert scale, with 5 being the best quality and 1 the worst. ***Results:*** The children's average age was 11.8 ± 5.6 years, the average body weight was 42.3 ± 22.1 kg. The average Likert scale of the different groups were as follows: 2.7 ± 0.7 for 0.5 MBq/kg (n=10 scans); 3.4 ± 0.8 for 1 MBq/kg (n=10); 4.4 ± 0.5 for 2 MBq/kg (n=9) and 5.0 ± 0 for 3 MBq/kg (n=8). There was a significant association between higher doses and higher Likert scales: p=0.004 for the comparison between group 1 MBq/kg vs. group 0.5 MBq/kg, p=0.002 for the comparison between group 2 MBq/kg vs. group 1 MBq/kg and p=0.013 for the comparison between group 3 MBq/kg vs. group 2 MBq/kg. ***Conclusion:*** The image quality obtained with 3 MBq/kg and the LAFOV-PET/CT scanner was outstanding, although this dose is lower than recommended by the guidelines. As expected, image quality decreased significantly with lower doses of [^{18}F]FDG. The results indicate that scans with 0.5 MBq/kg were lower quality and this dose might not be suitable with 10-min long pediatric scans. Currently we are pursuing further assessments including lesion detectability and a comparison with scans derived from a standard PET/CT-scanner, which shall help to find the best compromise between 1 and 3 MBq/kg.

OP-059

Sedation-free pediatric ^{18}F-FDG imaging on totalbody PET/CT with the assistance of artificial intelligence

X. Zhou[1], *S. Xue*[2], *Q. Xia*[1], *A. Rominger*[2], *J. Liu*[1], *K. Shi*[2];
[1]*Shanghai Jiaotong University, Shanghai, CHINA,* [2]*Inselspital, Bern University Hospital, University of Bern, Bern, SWITZERLAND.*

Aim/Introduction: Sedation is frequently used to ensure that PET examinations of infants and small children maintain their diagnostic quality, despite known side effects. However, there are two key challenges to achieving sedation-free pediatric PET imaging: fast imaging and CT-free attenuation and scatter correction (ASC). This study focuses on developing solutions to these challenges on a total-body PET scanner. ***Materials and Methods:*** First, we explored the solutions based on retrospective investigation of sedated total-body PET (uExplorer) imaging of 20 pediatric patients (<3 years old) to determine the shortest time of acceptable PET imaging and to check the feasibility of CT-free ASC. We assessed the image quality by a 5-point scale and quantitative metrics including signal to noise ratio (SNR), tumor-to-background ratio (TBR), root mean square error (RMSE), and peak-to-mean ratio (PMR) of liver, mediastinum, and lesions. The deep learning-based method was adapted for the pediatric CT-free ASC [1]. Then, we validated the proposed solutions on PET imaging of 5 young children without sedation. ***Results:*** Compared to standard imaging of 300 s, there was no significant difference in the diagnostic sensitivity, specificity and quantification of tumor lesions for fast imaging until the reduction to 15s ($p>0.05$). The image quality of MIP and lesion in 15s total-body PET scan is more than 2 score. Compared with 300s, there was no significant difference in PMR of liver, mediastinal and lesion for 15s imaging ($p>0.05$). The RMSE of 15s was 27.16±10.58. Only liver lesions smaller than 1 cm and SUVmax < 2.5 may be missed in 15s imaging. The deep learning-based CT-free ASC can accurately correct ultrafast PET images. NRMSE and PSNR are 0.52%+ 0.03%, 48.1+4.5. With the two solutions, we successfully anesthesia-free PET imaging in 5 children. ***Conclusion:*** The proposed solutions of 15s ultrafast total-body PET imaging and CT-free ASC has the potential to preserve the image quality and diagnostic requirements for sedation-free pediatric PET imaging. ***References:*** [1] Guo R, Xue S, Hu J, et al. Using domain knowledge for robust and generalizable deep learning-based CT-free PET attenuation and scatter correction. Nature communications. 2022;13:5882.

209

Sunday, September 10, 2023, 8:00 AM - 9:30 AM
Hall G2

e-Poster Presentations Session 1 - Oncology & Theranostics Committee: Neuroendocrine Tumours and Gynecological Malignancies

EPS-002

SPECT and SPECT/CT Somatostatin Receptor Scintigraphy in the Follow-Up of Neuroendocrine Neoplasms of Appendix

***V. Artiko**, J. Petrovic, D. Sobic Saranovic, N. Petrovic;*
Center for Nuclear Medicine, University Clinical Center of Serbia, Faculty of Medicine University of Belgrade, Belgrade, SERBIA.

Aim/Introduction: Neuroendocrine tumors of appendix (ANETs), are rare tumors, usually discovered during emergency surgical conditions. In spite of lot of data of somatostatin receptor scintigraphy (SRS) in gastrointestinal neuroendocrine tumors, there is no much data about ANETs particularly. Our aim was to establish the role of somatostatin receptor scintigraphy (SRS) in the follow-up of these patients. ***Materials and Methods:*** The total of 58 patients was investigated, 36 females and 22 males, average age (48.3 ± 17.8 years). All patients had histological diagnosis of ANET (55 carcinoids of appendix and 3 tubular carcinoid). Majority of tumors (38) have been found incidentally during surgery, while 20 patients had diagnosis of appendiceal tumor before the surgery. Twenty two patients had tumor grade (G) G1, 19G2 and 17G3. The right hemicolectomy was performed in 32, while the rest of the patients had appendectomy only. SRS was performed for restaging in all the patients after surgery early (2 h) and late (24 h) after i.v. application of 740 MBq Tc-99m-HYNIC TOC. In 45 patients only planar viewes and SPECT were performed, while SPECT/CT was performed in 13. ***Results:*** There were 23 true positive (TP), 29 true negative, 4 false positive and 2 false negative SRS results. Sensitivity of the method (including both SPECT and SPECT/CT) was 92%, specificity 87.9%, positive predictive value 85.2%, negative predictive value 93.6% and accuracy 89.7%. Receiver operating characteristics analysis showed that SRS scintigraphy is a good test for detection of TP cases (area under the curve of 0.850, 95% confidence interval (CI): 0.710-0.990, P < 001). SPECT contributed to diagnosis in 12 TP findings in comparison to planar images. SPECT/CT contributed in 7/15 patients, in 5 confirming the positive finding (Krenning score 2) and in 2 excluding it in comparison to SPECT. In 12 patients Krenning score was 4, in 6 patients 3 and in 5 patients 2. In 21 patients SRS significantly changed the management of the patients (in 8 surgery was repeated, in 10 somatostatin analogues included and in 3 peptide receptor radionuclide therapy performed). Median progression-free survival in SRS positive patients was 53 months (95%CI: 39.8-118.1 months) while in SRS negative patients it was 61 month (95%CI: 42.9-77.9 mo), without statistically significant difference between the two groups (P = 0.434). ***Conclusion:*** SRS proved the value in the follow-up of the patients with ANETs after surgery, with added value with SPECT and particularly with SPECT/CT.

EPS-003

Total tumour volume in a GEP-NET patient cohort treated with intraarterial Lu-177 DOTATATE PRRT

***H. Schmid**, S. Kunte, G. Sheikh, A. Holzgreve, P. Bartenstein, L. Unterrainer, M. Zacherl;*
Departement of Nuclear Medicine University Hospital, LMU Munich, Munich, GERMANY.

Aim/Introduction: Peptide radio-receptor therapy (PRRT) with Lu-177 DOTATATE has been approved for the treatment of patients with well-differentiated gastroenteropancreatic neuroendocrine tumours (GEP-NET). In the case of predominantly hepatic metastasis, attempts have been made to achieve an increased therapeutic effect on these metastases by local intraarterial PRRT. Different results have been published regarding a possible therapeutic benefit. Hence, to the best of our knowledge for the first time in our study we investigate a new approach, the influence of local intraarterial and intravenous tumour therapy on the total tumour volume (TTV) in an inter-individual comparison. ***Materials and Methods:*** 20 patients with GEP-NET undergoing Lu-177 DOTATATE therapy were retrospectively included in the study. Of these, 10 patients received PRRT intraarterially via port catheters placed in the hepatic arterial vessels. The comparison group of 10 patients was treated with intravenous infusion of PRRT. The matched comparison group was primarily selected according to visual hepatic tumour burden and primary location of the neuroendocrine tumours. The total tumour volume (TTV) in Ga-68 DOTA-TATE PET/CT was determined at fixed thresholds. Clinical and laboratory parameters as well as follow up imaging were evaluated before and after two cycles of Lu-177 DOTATATE therapy. ***Results:*** The mean baseline TTV was comparable with 764.0 ml vs 864.2 ml for the intraarterial and intravenous patients, respectively, with a reduction to 703.3 ml vs 753.1 ml after two cycles of therapy, a mean percentage reduction corresponding to -10.8% vs -21.0 % respectively. There were no significant differences in TTV after two cycles in either the intraarterial or intravenous groups (p=0.55 vs p=0.13). There was no significant difference in the change of laboratory parameters, such as the renal retention parameter creatinine (p>0.99 vs p=0.26) and the tumour marker chromogranin A (p=0.09 vs p=0.62) or the PET parameters SUVmax (p=0.19 vs p=0.22) and SUVmean (p=0.22 vs p=0.70). In contrast, serotonin showed a significant decrease in both patient groups (p=0.002 vs p=0.04). In a direct comparison of both patient groups, there was no significant difference in the percentage decrease of TTV (p=0.82), the renal retention parameters creatinine (p=0.58) and TER (MAG3) (p=0.73) or the PET parameters SUVmax (p=0.91) or SUVmean (p=0.32). ***Conclusion:*** Total tumour volume (TTV) did not show significant difference in reduction between patients receiving intraarterial and intravenous Lu-177-DOTATATE therapy in a comparable patient population. The percentage changes in TTV also did not show significant correlations with the clinical and imaging data.

EPS-004

Somatostatin receptor antagonist PET/CT imaging provides better staging of lymph node than contrast enhanced CT prior to lymph node dissection in patients with duodenum and pancreatic neuroendocrine tumors

W. Zhu, *B. Yin, X. Wang, M. Liu, Q. Xu, W. Wu, L. Huo;*
Peking Union Medical College Hospital, Beijing, CHINA.

Aim/Introduction: Somatostatin receptor (SSTR) antagonist PET/CT is an effective modality to evaluate well-differentiated neuroendocrine tumors (NETs). For patients with pancreatic NET (pNET), especially those with small tumors, lymph node dissection is not routinely planned and sometimes enucleation is performed. However, this would leave the patients at risk of recurrence if there is lymph node metastasis. There's, so far, few evidence regarding the value of presurgical SSTR-targeted imaging in the assessment of lymph node metastasis in these patients. In this study, we aim to assess the value of presurgical antagonist PET/CT imaging using pathological results as ground truth and compare it to presurgical contrast-enhanced CT (ceCT). ***Materials and Methods:*** We retrospectively reviewed patients who had presurgical SSTR antagonist PET/CT as well as ceCT and underwent surgical resection in our hospital. The surgical procedure, whether lymph node dissection was performed, the number of lymph node dissected, and the number, location, and size of metastatic lymph nodes were recorded. The PET/CT images and ceCT images were also reviewed. The number and location of positive lymph nodes were recorded, respectively. ***Results:*** A total of 28 patients were reviewed, of whom 9 patients did not have lymph node dissection (enucleation in 4 patients) and were ruled out in the further analysis. In the remaining 19 patients (12 pancreatic NETs, 7 duodenum NETs), a total of 230 lymph nodes were dissected. Of them, 19 metastatic lymph nodes were found in 9 patients. The patient-level sensitivity, specificity, and accuracy were 78% (7/9), 100% (10/10), and 89% (17/19) for antagonist PET/CT and 33% (3/9), 100% (10/10), and 68% (13/19) for ceCT, respectively. The lesion-level sensitivity, specificity, and accuracy were 47% (9/19), 98% (207/211), and 94% (216/230) for antagonist PET/CT and 26% (5/19), 100% (211/211), and 94% (216/230) for ceCT, respectively. The average size of detected and undetected metastatic lymph nodes was 0.71 cm (0.3 - 1.2cm) and 0.34 cm (0.2 - 0.5 cm), respectively. ***Conclusion:*** Antagonist PET/CT is better than ceCT for lymph node staging prior to lymph node dissection in patients with duodenum and pancreatic NET.

EPS-005

Normalization and 2-bit-quantization of PSMA-PET using the visual miPSMA Score for training an deep learning AI for prostate cancer detection

B. Schemmer*;*
Uniklinik Bonn, Bonn, GERMANY.

Aim/Introduction: Prostate cancer is a leading cause of death in men worldwide, early detection is crucial for effective treatment. Positron Emission Tomography (PET) is a widely used imaging modality for prostate cancer detection with the standard uptake value (SUV) commonly used as a measure of tumor activity. However, SUV has limitations, and new methods are being developed to improve the value of PET imaging. One such method is the miPSMA Score, which uses a visual qualitative scoring system for the interpretation of tumor uptake with blood-pool, liver and parotid gland as references for uptake. ***Materials and Methods:*** We included patients with histologically confirmed prostate cancer who underwent PSMA-PET/CT imaging for primary staging or biochemical recurrence with at least one PSMA-PET study and one PSA-value per patient, to train and validate our AI model. We included 50 patients, median age 71 years (range, 55-86 years). The majority had intermediate-risk or high-risk disease (78%), most had a PSA-level >5 ng/mL (61%). The AI was based on deep learning and provided with whole-body PET-images as well PSA-values. The AI was specifically not trained to find any subtle metastasis with uptake below blood-pool. The PET-images were preprocessed, uptake values below blood-pool were no longer present in the training images. Detection was evaluated as successful when there was a corresponding labeled metastasis in the data. To increase the amount of training data, the whole bodies were presented as single image slices (~50*400 images). ***Results:*** The results of the study showed that using the visual miPSMA Score as quantization/normalization method for AI training a reliable detection of suspicious lesions is possible with a small dataset. We achieved a good sensitivity of 74% (mainly due to low uptake lesions in the pelvis and lesions close to other higher uptake lesions). However specificity was only 62% due to misinterpretation of unspecific findings such as ureter, inflammation and vaccination, on the other hand only lesions that need human interpretation were detected. ***Conclusion:*** This study demonstrates the potential of normalization and 2-bit-quantization of PSMA-PET using the visual miPSMA Score for deep learning AIs as a method to eliminate irrelevant image findings from PET images, thus reducing the workload of the reader. The AI itself currently still has a lot to learn, especially in regard to unspecific findings and low uptake lesions.

EPS-006

Retrospective Analysis of 666 Gallium-68 Labeled Somatostatin Receptor Antagonist PET/CT Imaging in Over 500 Patients: Experience from a Single Center in China

W. Zhu[1], *M. Liu*[1], *Y. Cheng*[1], *R. Jia*[2], *C. Bai*[1], *L. Huo*[1];
[1]*Peking Union Medical College Hospital, Beijing, CHINA,* [2]*The Fifth Medical Center, General Hospital of PLA, Beijing, CHINA.*

Aim/Introduction: Somatostatin receptor (SSTR) antagonist is a type of somatostatin analogues characterized by low internalization rate and high tumor affinity. Promising results have been observed in preclinical and small-sample clinical studies using Gallium-68 labelled SSTR2 antagonist to characterize neuroendocrine tumors (NETs). We present here a large cohort of SSTR antagonist imaging studies in patients with confirmed/suspected NETs. ***Materials and Methods:*** We retrospectively reviewed all SSTR antagonist PET/CT imaging studies performed at our center from Nov 2018 to Mar 2023. The patient's demographic characteristics, indication, primary tumor, tumor grade, imaging probe, and imaging results (binary and quantitative) were recorded. A final clinical diagnosis was made for each patient based on all information available, including pathological results, clinical characteristics, complementary imaging modalities, and follow-up. It was recorded as positive/negative for NETs and served as ground truth to calculate the patient-level diagnostic efficacy of antagonist imaging. Comparative imaging was also performed in some patients using either ^{68}Ga-DOTATATE or another SSTR antagonist. The quantitative parameters and binary imaging results were compared. ***Results:*** A total of 666 antagonist studies were reviewed in 593 patients. In 25 patients, the final diagnosis could not be made based on current information and required further follow-up. In the other 568 patients, 641 antagonist studies were performed, 64% (411/641) of which

were performed with ^{68}Ga-NODAGA-LM3, 9% (58/641) with ^{68}Ga-NODAGA-JR11, 16% (105/641) with ^{68}Ga-DOTA-LM3, and 10% (67/641) with ^{68}Ga-DOTA-JR11. The indications included NET (98%, 555/568) and PPGL (2%, 13/568). The primary locations of NET were from pancreas (54%, 301/555), rectus (12%, 66/555), small intestine (11%, 61/555), stomach (5%, 29/555), lung (5%, 27/555), thymus (3%, 17/555), others (4%, 21/555), and unknown (6%, 33/555). The patient-level sensitivity, specificity, and accuracy of antagonist imaging (all tracers combined) were 88.9% (487/548), 94.6% (88/93), and 89.7%(575/641), respectively. In particular, the patient-level sensitivity, specificity, and accuracy of ^{68}Ga-NODAGA-LM3 was 89.1% (310/348), 93.7% (59/63), and 89.8% (369/411). Overall, the SUVmax of antagonist imaging is similar to agonist (39.6 vs. 39.5, n=133). However, remarkable differences were noted between different antagonists. While ^{68}Ga-NODAGA-LM3 demonstrated higher uptake than ^{68}Ga-DOTA-TATE (57.1 vs 40.0, n=30), ^{68}Ga-NODAGA-JR11 (39.7 vs. 34.3, n=23) and ^{68}Ga-DOTA-LM3 (38.0 vs. 37.8, n=40) showed similar uptake compared to ^{68}Ga-DOTA-TATE and ^{68}Ga-DOTA-JR11 showed the lowest uptake (28.1 vs. 43.8, n=40). ***Conclusion:*** Antagonist PET/CT is a powerful tool for NET imaging with high diagnostic efficacy. Of different antagonists, ^{68}Ga-NODAGA-LM3 seems to have the best imaging profile.

EPS-007

[^{18}F]F-Al-NOTA-Octreotide versus [111In]In-DTPA-Octreotide for neuroendocrine tumours imaging: results of first 10 patients

B. Arruda Matheos de Lima[1], *R. C. M. Felix*[1], *P. B. Pujatti*[1], *D. A. Bulzico*[1], *M. P. Carneiro*[1], *M. A. S. Cardoso*[1], *M. L. Gomes*[1], *T. T. Guimarães*[1], *J. W. E. Silva*[1], *E. R. Oliveira*[1], *C. H. F. Costa*[1], *R. G. Silva*[1], *A. C. Bispo*[2], *D. M. Zouain*[2];
[1]*Brazilian National Cancer Institute, Rio de Janeiro, BRAZIL,* [2]*R2IBF Radiopharmaceuticals, Rio de Janeiro, BRAZIL.*

Aim/Introduction: SPECT with [^{111}In]In-DTPA-octreotide is still an option in the context of public health systems of developing countries for neuroendocrine tumor (NET) imaging. However, it is well known this technique has several limitations that adversely affect its accuracy. Positron emission tomography (PET/CT) imaging using [^{18}F]F-AlF-NOTA-Octreotide would be a viable option, as it offers greater spatial resolution and better anatomical localization than SPECT/CT and the radiopharmaceutical is superior in technical aspects of its implementation and costs, being the choice for services that could not prepare [^{68}Ga] Ga-somatostatin analogues. ***Materials and Methods:*** This study was a prospective, non-randomised, controlled and blinded clinical trial, designed to compare, for the first time, the effectiveness of PET/CT with [^{18}F]F-AlF-NOTA-Octreotide and SPECT/CT with [^{111}In] In-DTPA-octreotide, in detecting lesions during staging, restaging and follow-up of neuroendocrine tumors. Patients referred to the nuclear medicine service of a public hospital for SPECT with [^{111}In]In-DTPA-octreotide were invited to also undergo the PET/CT with [^{18}F]F-AlF-NOTA-Octreotide; no later than three weeks after SPECT. ***Results:*** So far, 10 patients were included, seven female; mean age 57.7 ± 11.9 years; grade I (n = 2) and grade II (n = 8); gastrointestinal (n = 6), pancreatic (n = 2), lung (n = 1) or primary unknown NET (n = 1). [^{111}In]In-DTPA-octreotide identified hepatic metastasis in seven patients - one patient with one, one with 2-5 and five with >5 lesions (Kreening 3-4) - and [^{18}F]F-AlF-NOTA-Octreotide in eight patients - three with 2-5 and five patients with >5 lesions [SUVmax 19.07 ± 8.1 and tumour-to-background ratio (TBR) 4.16 ± 1.2]. Positive lymph nodes were found in three patients with [^{111}In]In-DTPA-octreotide - one in two patients and 2-5 in one patient (Kreening 3) - and five in PET/CT with [^{18}F] F-AlF-NOTA-Octreotide - one in one patient; 2-5 in two and >5 in five patients (SUVmax 8.94 ± 8.5; TBR 0.61 ± 0.3) in PET/CT (p = 0.345). In addition, [^{18}F]F-AlF-NOTA-Octreotide imaged lesions in pancreas in two patients (SUVmax 16.00 ± 8.7; TBR 3.10 ± 0.9) and in bone in three patients (SUVmax 3.05 ± 1.8; TBR 0.50 ± 0.0), which were not previously identified by [^{111}In]In-DTPA-octreotide. ***Conclusion:*** These preliminary results showed that PET/CT with [^{18}F]F-AlF-NOTA-Octreotide detected a greater number of lesions than SPECT/CT with [^{111}In]In-DTPA-octreotide in liver and lymph nodes and extra-hepatic disease, not identified in SPECT/CT with [^{111}In]In-DTPA-octreotide (upstaging) and a high liver TBR, which enables better lesion delineation.

EPS-008

Quantification of ^{177}Lu-DOTATATE uptake in neuroendocrine tumors using a fast whole-body 360° CZT-SPECT/CT camera for monitoring and prediction of treatment response

C. Boursier[1,2,3], *J. Grangeret*[1], *E. Chevalier*[1], *G. Karcher*[3], *L. Imbert*[1,2,3], *P. Marie*[1,2,3];
[1]*Université de Lorraine, Department of Nuclear Medicine, CHRU Nancy, Vandoeuvre-les-Nancy, FRANCE,* [2]*Université de Lorraine, IADI, INSERM U1254, Nancy, FRANCE,* [3]*Nancyclotep Imaging Platform, Nancy, FRANCE.*

Aim/Introduction: This study aimed to assess the results provided by whole-body SPECT images recorded after ^{177}Lu-DOTATATE injection using a high-speed whole-body 360° CZT-SPECT camera for monitoring and prediction of treatment response in patients with metastatic neuroendocrine tumors (NET), with a comparison to pre-therapeutic ^{68}Ga-DOTATOC PET. ***Materials and Methods:*** We included consecutive patients with metastatic NET treated by 2 to 4 injection-cycles of ^{177}Lu-DOTATATE and who underwent a pre-therapeutic ^{68}Ga-DOTATOC PET and subsequently, 18-minute whole-body ^{177}Lu 360° CZT-SPECT recording after each ^{177}Lu-DOTATATE injection. The tumor Standardized Uptake Values (SUV) were compared according to the presence or absence of a significant volume change (> 28%) between pre- and post-therapeutic MRI investigations. ***Results:*** A total of 39 tumors from 14 patients (67±11 years, 7 women) were considered and among these tumors, 8 from 4 patients had a decreased volume (V-), 24 from 11 patients had an unchanged volume (V±), and 7 from 5 patients had an increased volume (V+) during treatment. The V- NETs were strongly predicted by high tumor SUV measured on either: (i) the ^{177}Lu-DOTATATE SPECT recorded after the first injection (for SUV mean, V-: 17.9±8.4 vs. V±: 8.5±4.8 or V+: 4.7±5.0, both $p \leq 0.001$) or (ii) the pre-therapeutic ^{68}Ga-DOTATOC PET (V-: 42.9±21.9 vs. V±: 13.0±6.4 or V+: 10.8±7.2, both $p<0.001$). However, this initial higher uptake within V- NETs was not observed on the ^{177}Lu-DOTATATE SPECT recorded after the 2nd, 3rd, or 4th injections and there was no difference in all SUV comparisons made between V± and V-. The tumor uptake of ^{177}Lu-DOTATATE exhibited a decrease during treatment in V- (p=0.01 for both SUV max and SUV mean), whereas no significant changes with time were observed on SUV from the V± or V+ tumor groups. ***Conclusion:*** The shrinkage of NETs treated by ^{177}Lu-DOTATATE may be predicted by a particularly high tumor uptake on the whole-body ^{177}Lu-SPECT recorded after the first injection, and a similar prediction may be achieved on a pre-therapeutic ^{68}Ga-DOTATOC PET. By contrast, the ^{77}Lu-SPECT recorded after the 2nd, 3rd or 4th ^{177}Lu-DOTATATE injections are poorly predictive, presumably because of treatment-related remodeling factors.

EPS-009

Bone marrow absorbed doses during treatment with [177Lu]Lu-DOTATATE assuming a specific uptake in the red marrow

L. Hagmarker[1], *J. Svensson*[2], *T. Rydén*[1], *M. Van Essen*[3], *A. Sundlöv*[4], *P. Gjertsson*[3], *K. Sjögreen Gleisner*[5], *P. Bernhardt*[1]; [1]*Department of Radiation Physics, Gothenburg, SWEDEN,* [2]*Sahlgrenska Academy, Gothenburg, SWEDEN,* [3]*Department of Clinical Physiology, Gothenburg, SWEDEN,* [4]*Department of Oncology and Pathology, Clinical Sciences, Lund, SWEDEN,* [5]*Department of Radiation Physics, Lund, SWEDEN.*

Aim/Introduction: Treatment with [177Lu]Lu-DOTATATE irradiates the radiosensitive hematopoietic stem cells in red marrow causing grade ¾ hematological toxicities in up to 10% of patients. Expression of somatostatin receptors subtype 2 on CD34+ stem cells has been previously identified, potentially leading to retention in the bone marrow cavities. Accurate yet accessible dosimetry methods are crucial to understand and potentially prevent hematological toxicities in the future as peptide receptor radiotherapies are increasingly utilized. Considering the specific uptake in red marrow, our aim has been to investigate a new hybrid dosimetry method. ***Materials and Methods:*** The study includes the first two treatment fractions of 49 patients treated with [177Lu]Lu-DOTATATE. 4 planar images (2, 24, 48 and 168 h.p.i.) and a SPECT-CT (24 h.p.i.) were collected. In planar images, the body was divided into a high-uptake compartment (HC) consisting of liver, spleen, kidneys, and tumours, and a low-uptake compartment (LC) consisting of the rest of the body. The bone marrow absorbed dose (BM) was calculated as the sum of the cross-doses from the HC and LC and the self-dose, estimated using the kinetics from the planar images, adjusted by the activity concentration in the lumbar vertebrae in the SPECT images. Two methods were employed: utilizing the kinetics of the LC or the HC. ***Results:***The median BM where estimated to 0.32 Gy/7.4 GBq and 0.29 Gy/7.4 GBq using the kintics of LC for treatment fraction one and two, respectively. Using the kinetics of the HC, the median BMs were 0.39 and 0.40 Gy/7.4 GBq. The correlation between the BM and the level of platelet counts were significant for both methods after treatment fraction one and two with r-values at 0.43 and 0.72 using the kinetics of the LC and 0.45 and 0.65 using the kinetics of the HC. ***Conclusion:*** Due to the prolonged retention observed for [177Lu]Lu-DOTATATE in bone cavities, the kinetics of the bone marrow was equated to that of the high-uptake compartment. The correlation between BM and platelet count was expected to be stronger when utilizing the kinetics of the HC. However, this was only achieved after treatment fraction one. ***References:*** Hagmarker L, Svensson J, Rydén T, Gjertsson P, Bernhardt P. Segmentation of Whole-Body Images into Two Compartments in Model for Bone Marrow Dosimetry Increases the Correlation with Hematological Response in ^{177}Lu-DOTATATE Treatments. Cancer Biother Radiopharm. 2017 Nov;32(9):335-343. doi: 10.1089/cbr.2017.2317. Epub 2017 Nov 10. PMID: 29125780.

EPS-010

Inpatient admissions for hormone secretion management in patients with neuroendocrine neoplasms treated with [177Lu]Lu-DOTA-Octreotate therapy over a 3-year period at a single high volume treatment centre

L. Neeson[1], *E. Boehm*[1], *T. Akhurst*[2], *R. Alipour*[1], *A. Cardin*[1], *C. Chiang*[1], *M. Hofman*[1], *M. Lee*[1], *M. Michael*[2], *A. S. Ravi Kumar*[2], *N. Sachithanandan*[1], *J. Saghebi*[1], *H. Wong*[1], *G. Kong*[2]; [1]*Peter MacCallum Cancer Centre, Melbourne, AUSTRALIA,* [2]*Peter MacCallum Cancer Centre and Sir Peter MacCallum Department of Oncology, University of Melbourne, Melbourne, AUSTRALIA.*

Aim/Introduction: Peptide Receptor Radionuclide Therapy (PRRT) is an effective therapeutic option for patients with somatostatin receptor expressing neuroendocrine neoplasms. However, patients with functional tumours may develop an acute flare of symptoms during or after PRRT. The aim of this study was to review the incidence and outcomes of patients requiring hospital admission for hormone secretion within the 14 days following [177Lu]Lu-DOTA-Octreotate (LuTate) at one NET centre. Outcomes measured were elective versus unplanned admissions, length of stay and level of care required. ***Materials and Methods:*** A retrospective review of all patients who received LuTate between March 1 2020 and March 31 2023 was performed. Before treatment, all patients were reviewed by the Nuclear Medicine Team and identified as high risk if they had any of the following risk factors: a functional tumour with high tumour markers, previous hospital admissions for functional syndromes, high burden of disease or baseline uncontrolled symptoms on maximal medical therapy. Patients were discussed at a Multi Disciplinary Meeting to determine requirements for elective inpatient LuTate. Prior to elective admission the oncology, endocrinology, high-acuity management teams, and ward staff were formally notified, and patients' medical status optimised by specialist physicians. ***Results:*** 265 patients (150 males, age range 11 to 94 years, median 65 years) received a total of 716 cycles of LuTate. 20 patients (8%), 24 treatments, were admitted electively for hormone secretion management (12 phaeochromocytoma/paraganglioma, 7 carcinoid, 3 insulinoma, 2 Cushing's), of whom 7 patients (9 treatments total, 38% of admitted treatments) experienced a flare in hospital. Only one patient had an unplanned admission due to hormonal flare post LuTate (management of Cushing's syndrome). Median length of stay was 2 days (range 2-19) for the elective group vs the 14 day stay for the single unplanned admission. All patients received multidisciplinary inpatient care. None of the elective/unplanned admissions required escalation of care above ward level management. There were no deaths in this time period. ***Conclusion:*** This study suggests that hormone flare should be considered as a risk for patients with functional NET undergoing PRRT. With identification of high-risk patients, adequate pre-treatment patient preparation, and planned multidisciplinary involvement, the incidence of unplanned admission for hormone flare and requirement for intensive care utilisation is very low at our hospital after LuTate treatment.

EPS-011

Impact of volumetric parameters applied to ^{177}Lu-DOTATATE SPECT-CT in the survival of NET patients after PRRT

S. Menendez-Sanchez[1], *V. Betech-Antar*[1], *E. Guillen*[2], *J. Rosales*[1], *L. Garcia-Belaustegui*[2], *A. Bronte*[1], *J. Bastidas*[1], *T. Cuenca*[1], *P. Echegoyen*[1], *A. Chopitea*[1], *E. Prieto*[1], *J. Martí-Climent*[1], *J. Arbizu*[1]; [1]*Clínica Universidad de Navarra, Pamplona, Navarra, SPAIN,* [2]*Clínica Universidad de Navarra, Madrid, SPAIN.*

Aim/Introduction: To evaluate differences in volumetric parameters of 177Lu-DOTATATE SPECT/CT between PRRT cycles as a potential marker of survival prognosis. ***Materials and Methods:*** We studied 19 NET patients (5 foregut / 5 midgut / 5 hindgut /3 pheochromocytoma-paraganglioma / 1 lung), mean age 55yo [±14.2], 52.6% males, referred to PRRT using 177Lu-DOTATATE. Mean activity was 28.8 GBq [±2.05]). Volumetric parameters of SPECT-CT performed 24 hours after first (C1) and fourth (C4) cycles included Metabolic -Tumor- Volume (MTV) and

Total- Lesion -Activity (TLA) of selected regions. MTV and TLA were obtained using both three-dimensional volume-of-interest isocontouring and whole-body thresholding techniques combined with automated segmentation of liver, and skeleton on CT images, with lesions outside those organs separately assigned to abdomen as appropriate, using work in progress syngo.via MI General Anatomy Segmentation software (Siemens Healthineers, Knoxville, TN). Sign test and Cox regression statistical analyses of volumetric parameters between C1 and C4 PRRT cycles with respect to PFS and OS were conducted. ***Results:*** Changes in the calculated MTV and TLA values between C1 and C4 cycles in the selected regions of the whole population didn't reach statistical significance (table 1). On the other hand, TLA in the selected regions, when present, remained stable in 11 patients, decreased in 7 patients and increased in 1 patient, but didn't correlate with survival. PFS rates at one, two and three years after PRRT were 81.7% (95% CI: 0.53 - 0.93), 44.95% (95% CI: 0.19 - 0.68) and 33.7% (95% CI: 0.10 - 0.59), respectively. OS rates were 88.8% (95% CI: 0.62 - 0.97), 73.79% (95 CI: 0.43 - 0.89) and 59.03% (95 CI: 0.23 - 0.82)respectively.Patients with reductions in Liver MTV and TLA showed a longer OS (HR:0.99; p=0.03; and HR:0.99; p=0.06, respectively), but does not correlate with increase of PFS (p=0.36). However, neither Abdomen nor Skeleton MTV and TLA reductions showed a longer OS or PFS (table 2). ***Conclusion:*** Liver MTV and TLA reduction between PRRT cycles correlate with longer OS and might be used as an effective tool for PRRT response assessment. Validation of the results with a larger cohort is recommended.

EPS-012

Metabolic tumor volume response on FDG-PET after [^{131}I]MIBG radiotherapy in patients with metastatic pheochromocytomas and paragangliomas predicts their prognosis

J. Takenaka[1,2], *S. Watanabe*[1,2], *T. Abe*[3], *T. Tsuchikawa*[4], *S. Takeuchi*[5], *K. Hirata*[1,2,6], *R. Kimura*[1,7], *N. Wakabayashi*[1,2], *N. Shinohara*[3], *K. Kudo*[1,6,7];
[1]*Department of Diagnostic Imaging, Graduate School of Medicine, Hokkaido University, Sapporo, JAPAN,* [2]*Department of Nuclear Medicine, Hokkaido University Hospital, Sapporo, JAPAN,* [3]*Department of Renal and Genitourinary surgery, Hokkaido University Graduate School of Medicine, Sapporo, JAPAN,* [4]*Department of Gastroenterological Surgery II, Hokkaido University Graduate School of Medicine, Sapporo, JAPAN,* [5]*Department of Medical Oncology, Faculty of Medicine and Graduate School of Medicine, Hokkaido University, Sapporo, JAPAN,* [6]*Division of Medical AI Education and Research, Hokkaido University Graduate School of Medicine, Sapporo, JAPAN,* [7]*Department of Diagnostic and Interventional Radiology, Hokkaido University Hospital, Sapporo, JAPAN.*

Aim/Introduction: Pheochromocytomas and paragangliomas (PPGLs) are rare neuroendocrine tumors producing catecholamines. Radionuclide therapy with [^{131}I]metaiodobenzylguanidine(MIBG) is a first-line treatment for MIBG-avid unresectable or metastatic PPGLs. Previously, we reported high metabolic tumor volume (MTV) can be a poor prognosis factor. In this study, we evaluated metabolic response (i.e., MTV change) to first [^{131}I]MIBG therapy in unresectable or metastatic PPGLs patients in relation to other clinical factors. ***Materials and Methods:*** Between 2001 and 2020, 28 patients with unresectable or metastatic PPGL could be followed up for at least 1 month after the first [^{131}I]MIBG therapy at our institute. Excluding patients with unavailable prognosis data, clinical data insufficiency except FDG-PET, we analyzed 20 patients undergoing FDG-PET before and after first [^{131}I]MIBG therapy. We utilized a single dose of 5.5GBq of [^{131}I]MIBG three times basically, although for some cases the number of treatments were increased or decreased considering treatment efficacy and side effects. MTV was calculated using liver SUV (mean+3SD) as a threshold on the free software Metavol (Hirata K, et al. PLoS ONE. 2014). Partial remission (PR) was defined as a ≥30% decrease in MTV, progressive disease (PD) as a ≥30% increase, and stable disease (SD) as a change between -30% and +30%. We divided the patients into PD group and non-PD group and OS of each group was compared using log-rank test. Relationship between metabolic response and other factors (age, sex, tumor type (pheochromocytoma vs. paraganglioma), metastatic sites, history of chemotherapy or external radiation, and 24-hour urine catecholamine levels) were evaluated using logistic regression analysis. ***Results:*** Median follow-up time was 55.5 months (range: 2-136) and 9 (45%) patients died. The number of [^{131}I]MIBG therapy per patient ranged 1 to 8 (median 3[HK1]). Semi-quantitative analysis showed median pre- vs. post-treatment MTV 1. 63×10 (range: 0-2.02×10^2) mL vs. 2.12×10 (range: 0-8.60×10^2) mL. Two patients were classified as PR, 10 patients as SD, and 8 patients as PD There was a significant difference in prognosis between the PD and non-PD groups as assessed by MTV (p = 0.0141). Higher urinary dopamine was significantly associated with poor metabolic response ([OR] = 1.002, p = 0.029); however, the other clinical parameters were not significant. ***Conclusion:*** Poor metabolic response, measured with MTV, to first [^{131}I]MIBG therapy in unresectable or metastatic PPGLs was related to shorter OS. Poor metabolic response can be predicted using urinary dopamine level.

EPS-013

Late toxicity after peptide receptor radioligand therapy (PRRT) therapy in neuroendocrine neoplasm.

D. Handkiewicz-Junak*, A. Sygula, A. Ledwon, K. Hassse-Lazar, B. Jurecka-Lubieniecka, E. Paliczka-Cieślik, A. Kropinska, T. Olczyk, T. Gawlik;*
Maria Sklodowska-Curie National Research Institute of Oncology, Gliwice, POLAND.

Aim/Introduction: Radioligand therapy is an effective treatment of neuroendocrine tumors. Apart from efficacy toxicity is a important factor when establishing the best therapeutic approach. The aim of our study was to evaluate late toxicity of PRRT in patients with well differentiated neuroendocrine tumors. ***Materials and Methods:*** The study enrolled 115 NET patients treated with PRRT therapy from 08.2005 to 11.2012. Patients were treated either with 4 cycles of 90Y-DOTATATE (80 mCi per cycle) or 4 cycles of 90Y-DOTATATE (80 mCi per cycle) and 1 cycle of 177Lu-DOTATATE (200 mCi). After the completition of the theraoy patients were randomly assigned to somatostatin analouges therapy or observation. ***Results:*** The mean follow-up time from the first cycle of isotopic treatment to the last observation or death was 6.6 (3.18-10.22) years. During this time late and persistent creatinine elevation occurred in 46/115 patients (40%) and was of G1 grade in almost half of the patients 22 (19.1%). Eleven 11/115 (9.6%) developed G3/4 nephrotoxicity. In the univariate analysis, there was no statistically significant correlation between - chemotherapy, MIBG therapy, computed tomography with iodinated contrast, hypertension/diabetes, age or with somatostatin analogues after PRRT - and elevated creatinine.Acute bone marrow damage after isotope treatment was mostly mild and reversible, occurring in 33/115 (28.7%) patients, mainly in grade G1/G2 3(0/115 patients; 26%). In 3 patients (2,6%) thrombocytopenia G3 was

diagnosed. In 4/115 (3.5%) patients serious, late haematological complications were diagnosed. In 1 patient, acute myeloblastic leukemia was diagnosed approximately 10 years after completion of chemotherapy (platinum based) and 8 years after completion of isotope treatment. Three patients underwent only isotopic treatment. No other malignancies were diagnosed. ***Conclusion:*** PRRT treatment is well tolerated but serious, late toxicity is diagnosed in up to 10% of patients.

EPS-014

RadioLigand Therapy: is it time to move towards a different dosimetric approach?

A. Filice[1], *R. Durmo*[1], *F. Fioroni*[2], *E. Grassi*[2], *C. Coruzzi*[1], *G. Besutti*[3], *S. Fanello*[4], *A. Frasoldati*[5], *S. Cavuto*[6], *L. Savoldi*[6], *A. Versari*[1];
[1]*Nuclear Medicine Unit Azienda USL-IRCCS, Reggio Emilia, ITALY,* [2]*Medical Physics Unit Azienda USL-IRCCS, Reggio Emilia, ITALY,* [3]*Radiology Unit, Azienda USL-IRCCS, Reggio Emilia, ITALY,* [4]*Medical Oncology Unit Azienda USL-IRCCS, Reggio Emilia, ITALY,* [5]*Department of Endocrinology and Metabolism Unit Azienda USL-IRCCS, Reggio Emilia, ITALY,* [6]*Clinical Trials and Statitistics Unit Azienda USL-IRCCS, Reggio Emilia, ITALY.*

Aim/Introduction: The correlation between the tumour absorbed dose and radioligand therapy (RLT) response is very difficult to assess and so far, it has not been established. RLT has been shown to be very effective in patients with neuroendocrine tumours (NETs) but disease progression is reported in 20%-30% of patients. Treatment failure probably depends on many factors and our hypothesis is that it could also depend on the lower dose received by some lesions during treatment. Hence, we aim to evaluate a dose-response correlation for NET patients treated with RLT. ***Materials and Methods:*** The DOTATER-1 trial consisted in the administration of tandem Y90/177Lu-DOTATOC therapy in patients with advanced NET in a prospective, single-center, non-randomized phase II clinical study (EudraCT:2015-005546-63). 177Lu-DOTATOC was administered during the first course of therapy in order to obtain tumour absorbed dose, derived from the acquisition of 4 sequential SPECT/CT. An experienced nuclear medicine physician (AF) manually segmented lesions on 24-h SPECT/CT. Therapy response was assessed 3 months after RLT by CT using response assessment criteria in solid tumours (RECIST 1.1) or MRI, in particular for bone lesions. For statistical analysis, logistic regression for repeated measures was used. ***Results:*** Fifty-five patients 69.62%) with stable disease (SD) or partial response (PR) were classified as responders and 24 (30.38%) as non-responders. In total 258 lesions were analyzed: 209 (81%) with SD or PR classified as responders and 49 (19%) as non-responders. Hepatic lesions were 164 (63.6%), lymph node 40 (15.5%), bone 20 (7.7%), lung 4 (1.6%), pancreas 13 (5%), intestinal lesions 4 (1.6%) and other organs 13 (5%). Higher total lesion absorbed dose (TLAD) was related to PRRT response (OR 0.52, 95% CI 0.3-0.91; p=0.02). There was a statistically significant association between TLAD and response status for lymph node (OR = 1.20, p=0.0007; median dose 67 vs 6 Gy) and bone (OR = 1.13, p = 0.0147; median dose 88 vs 15 Gy) and a borderline result for liver (OR = 1.01, p=0.0595; median dose 105 vs 71 Gy). Finally, in terms of trend, the result obtained for other organs (OR = 1.02, p=0.0967; median dose 53 vs 35 Gy) was also interesting, considering the limited number of available lesions. ***Conclusion:*** Based on dosimetric evaluation significant results were obtained exploring the correlation between tumour absorbed dose and RLT response. These results suggest that dosimetric approach may be useful for predicting treatment response.

EPS-015

Value Of Early Metabolic Response For Predicting Axillary Pathological Complete Response During Neoadjuvant Systemic Therapy In Triple-negative And Her2-positive Breast Cancers: Impact Of Molecular Subtypes

L. Guichard*, P. Nunes, C. Jankowski, A. Bertaut, S. Ladoire, E. Michel, C. Coutant, A. Cochet, J. Alberini;*
Centre George Francois Leclerc, Dijon, FRANCE.

Aim/Introduction: In the era of therapeutic de-escalation, the opportunity to move from systematic axillary lymph node dissection (ALND) to sentinel lymph node (SLN) or target axillary dissection (TAD) in axillary node-positive breast cancer patients after neoadjuvant systemic therapy (NST) is currently considered. The purpose of this study was to identify FDG-PET parameters associated with axillary pathological complete response (pCRAx) in the most proliferative molecular subtypes, eg triple negative (TN) and Her2+. ***Materials and Methods:*** Patients with newly-diagnosed TN or Her2+ breast cancer, with histologically-proven axillary node metastasis, no distant metastasis and indication of NST were prospectively included. FDG PET/CT scans were performed at baseline and after one cycle of NST. Metabolic parameters at baseline (1) and their variations (Delta Δ) were assessed: Standard Uptake Values (SUVmax, ratio SUVmax/SUVmax hepatic, SUVpeak, SUVmean), Total Lesion Glycolysis (TLG), Metabolic Total Volume (MTV) for axillary node (Ax). All patients underwent ALND after NST. Logistic regressions with ROC curves were used to determine parameters associated with pCRAx. Optimal thresholds for quantitative parameters were determined using the Youden index method. ***Results:*** 61 patients (24 TN (a), 19 non-luminal Her2+ (b) and 18 luminal Her2+ (c)) were recruited. pCRAx was observed for 35 patients (54%, 79% and 39% in a, b and c groups). Median value of Axillary SUVmax at baseline (AxSUVmax1) were 7.9, 7.0 and 5.2 and of Axillary DeltaSUVmax (AxΔSUVmax) -62%,-60% and -47% in a, b and c groups, respectively. In univariate model, in the whole population, AxΔSUVmax showed the greatest AUC for prediction of pCRAx (0.72 [95%CI: 0.59-0.85]), whereas AxSUVmax1 AUC was not statistically significant (AUC=0.6 [95%CI: 0.46-0.74]). Specificity and sensitivity of AxΔSUVmax were 96% and 49% respectively for predicting pCRAx with an optimal threshold of -69%. Odd Ratio (OR) associated with AxΔSUVmax<-69% compared to ≥-69% was 24.0 [95%CI: 2.9-194]. In multivariate model, adjusted on molecular subtypes, AxΔSUVmax was still significantly associated with pCRAx (OR=20.7 [95%CI: 2.5-172]). AUCs adjusted on the molecular subtype were not significantly modified compared to univariate model (for AxΔSUVmax: AUC=0.72 [95%CI: 0.59-0.85]; p=0.45 compared to unadjusted AUC) suggesting that thresholds were not significantly different in each molecular subtype. ***Conclusion:*** Axillary DeltaSUVmax seems to be the most relevant metabolic parameter to predict an axillary pathological complete response and early metabolic response could be a valuable tool for selecting patients eligible for axillary surgical de-escalation after NST, regardless molecular subtypes.

EPS-016

Detection of HER2-low lesions using HER2-targeted PET imaging in patients with HER2-negative metastatic breast cancer

R. Yeh[1], *S. K. Lyashchenko*[1], *B. M. Zeglis*[1,2], *J. S. Lewis*[1], *G. A. Ulaner*[3,1];
[1]*Memorial Sloan Kettering Cancer Center, New York, NY, UNITED STATES OF AMERICA,* [2]*Hunter College - City University of New York, New York, NY, UNITED STATES OF AMERICA,* [3]*Hoag Family Cancer Institute, Irvine, CA, UNITED STATES OF AMERICA.*

Aim/Introduction: Trastuzumab deruxtecan (T-DXd), a HER2-targeted antibody-drug conjugate, has led to a major paradigm shift in the treatment of patients with HER2-low breast cancer and established HER2-low as a new targetable patient population, shifting away from the historical binary categorization of HER2 status as either HER2-positive or -negative. Our prior experience with HER2 PET imaging with radiolabeled anti-HER2 antibodies demonstrated a high number of false positives for HER2-positive malignancy when compared to biopsy, limiting clinical utility (1-3). We hypothesize that HER2 PET imaging may be detecting HER2-low lesions in addition to HER2-positive lesions, thus possibly explaining the high false positive rate. ***Materials and Methods:*** We retrospectively reviewed the pathology and imaging results from a prior prospective clinical trial (ClinicalTrials.gov NCT02286843) evaluating HER2 PET imaging with 89Zr-trastuzumab and 89Zr-pertuzumab PET/CT in women with HER2-negative breast cancer. In this study, patients with tracer avid lesions underwent biopsy. HER2 status was determined using HER2 immunohistochemistry (IHC) and in situ hybridization (ISH). HER2-positive was defined as IHC 3+ or 2+ with positive ISH, HER2-low as IHC 1+ or 2+ with negative ISH, and HER2-zero as IHC 0. ***Results:*** Forty-four patients underwent HER2 PET imaging, 20 patients with 89Zr-trastuzumab and 24 patients with 89Zr-pertuzumab. In the 89Zr-trastuzumab cohort, 9 out of 20 patients had suspicious tracer-avid lesions with subsequent biopsies demonstrating 6 HER2-low (66.7%) and 3 HER2-positive lesions (33.3%). In the 89Zr-pertuzumab cohort, 7 out of 24 patients had suspicious tracer-avid lesions with subsequent biopsies demonstrating 5 HER2-low (71.4%) and 2 HER2-positive lesions (28.6%). No lesions were classified as HER2-zero. ***Conclusion:*** We performed a re-analysis of our prior prospective clinical trial of HER2 PET imaging in the context of HER2-low breast cancer and found that most tracer-avid lesions previously classified as HER2-negative were in fact HER2-low. This finding most likely explains what we previously considered false positive HER2 PET scans and suggests that HER2 PET may be useful for detecting HER2-low lesions and allow patients to qualify for T-DXd therapy. ***References:*** 1.Ulaner,G, et al., Identification of HER2-Positive Metastases in Patients with HER2-Negative Primary Breast Cancer by Using HER2-targeted (89)Zr-Pertuzumab PET/CT. Radiology, 2020. 2.Ulaner,G., et al., 89Zr-Trastuzumab PET/CT for Detection of Human Epidermal Growth Factor Receptor 2-Positive Metastases in Patients With Human Epidermal Growth Factor Receptor 2-Negative Primary Breast Cancer. Clin Nucl Med, 2017. 3.Ulaner, G., et al., Detection of HER2-Positive Metastases in Patients with HER2-Negative Primary Breast Cancer Using 89Zr-Trastuzumab PET/CT. J Nucl Med, 2016.

EPS-017

Clinical utility of [18F]FDG PET/CT in triple-negative breast cancer patients treated with neoadjuvant chemotherapy with or without immunotherapy

R. Seban[1], *E. Arnaud*[2], *D. Loirat*[2], *L. Cabel*[2], *P. Cottu*[2], *L. Djerroudi*[3], *S. Hescot*[1], *P. Loap*[4], *C. Bonneau*[5], *F. Bidard*[6], *V. Huchet*[7], *N. Jehanno*[7], *A. Berenbaum*[1], *L. Champion*[1], *I. Buvat*[8];
[1]*Department of Nuclear Medicine and Endocrine Oncology, Institut Curie, Saint-Cloud, FRANCE,* [2]*Department of Medical Oncology, Institut Curie, Paris, FRANCE,* [3]*Department of Pathology, Institut Curie, Paris, FRANCE,* [4]*Department of Radiation Oncology, Institut Curie, Saint-Cloud, FRANCE,* [5]*Department of Surgery, Institut Curie, Saint-Cloud, FRANCE,* [6]*Department of Medical Oncology, Institut Curie, UVSQ/Paris-Saclay University, Saint-Cloud, FRANCE,* [7]*Department of Nuclear Medicine, Institut Curie, Paris, FRANCE,* [8]*Laboratoire d'Imagerie Translationnelle en Oncologie, Inserm U1288, PSL University, Institut Curie, Orsay, FRANCE.*

Aim/Introduction: Clinical trials demonstrated increased rates of pathologic complete response (pCR) at the time of surgery with the addition of pembrolizumab, an anti-PD1 immune checkpoint inhibitor (ICI), to neoadjuvant chemotherapy (NAC) for patients with early triple-negative breast cancer (eTNBC). However, ICI leads to immune-related adverse events (irAEs). We aimed to determine if pretreatment [18F]FDG PET/CT could contribute to predicting pCR after NAC +/- pembrolizumab (NAC vs NAC+p) and the risk of developing ICI-induced hypothyroidism. ***Materials and Methods:*** In this retrospective bicentric study, we included eTNBC patients who underwent [18F]FDG PET/CT before NAC +/- pembrolizumab between March 2017 and August 2022. Clinical, biological and pathological data were collected. Endpoints were the rate of pCR and the occurrence of ICI-induced hypothyroidism. Total metabolic tumor volume (TMTV: p [primary] +/- ln [lymph node(s)] using a 41%-SUVmax threshold), tumor (p or ln) and thyroid SUVmax were measured. Cut-off values were determined by maximizing the Younden index. A multivariable model was developed using logistic regression to predict pCR. ***Results:*** A total of 191 patients were included (n=91/NAC; n=100/NAC+p). pCR rates were 53% and 70% in patients treated with NAC and NAC+p, respectively ($p<0.01$). In univariable analysis, high Ki67, high tumor SUVmax (>12.3) and low TMTV (≤ 3.0 cm3) were predictors of pCR in the NAC cohort while tumor staging classification (<T3), BRCA1/2 germline mutation, high tumor SUVmax (>17.2) and low TMTV (≤ 7.3 cm3) correlated with pCR in the NAC+p cohort. In multivariable analysis, only high tumor SUVmax (NAC: OR 8.8, $p<0.01$; NAC+p: OR 3.7, $p=0.02$) and low TMTV (NAC: OR 6.6, $p<0.01$; NAC+p: OR 3.5, $p=0.03$) were independent factors for pCR in both NAC and NAC+p patients, albeit at different thresholds. ICI-induced hypothyroidism was diagnosed in 10 patients (10%) in the NAC+p cohort. Thyroid SUVmax before pembrolizumab exposure predicted ICI-induced hypothyroidism with an area under the ROC curve of 0.67. Thyroid SUVmax was higher in patients who developed ICI-induced hypothyroidism compared to patients who did not without reaching statistical significance. ***Conclusion:*** High tumor metabolism and low tumor burden on pretreatment [18F]FDG PET/CT could predict pCR after NAC regardless of the addition of pembrolizumab. Our data suggest that high thyroid uptake may help in the early detection of patients at higher risk of developing ICI-induced hypothyroidism. Further validation studies are needed to determine how these biomarkers could be used to develop more personalized and effective treatment strategies for TNBC patients.

EPS-018

Dynamic ^{18}F-FLT PET Radiomics: a Novel and Promising Approach for an Improved Breast Cancer Prognosis Prediction

M. Inglese[1,2], *M. Ferrante*[1], *T. Boccato*[1], *N. Toschi*[1,3];
[1]*University of Rome Tor Vergata, Rome, ITALY,*
[2]*Imperial College London, London, UNITED KINGDOM,*
[3]*Athinoula A. Martinos Center for Biomedical Imaging, Boston, MA, UNITED STATES OF AMERICA.*

Aim/Introduction: Breast cancer (BC) is the most prevalent malignancy among women[1]. Existing imaging techniques for BC categorization and prediction are limited in sensitivity and specificity due to clinical and technological factors[2]. In this context, positron emission tomography (PET) identifies abnormal metabolic activity, offering crucial qualitative and quantitative tumor-related metabolic data[3]. In particular, ^{18}F-Fluorothymidine (FLT), a labeled thymidine analogue, exhibits correlations with Ki-67 in breast, lung, and brain cancers, and generally demonstrates higher specificity and reproducibility[4,5] as compared to conventional tracers[6].While PET data is commonly processed through radiomics approaches in a static manner, in this study we posit that extending radiomics techniques to the time domain ("dynamic radiomics") has the potential to extract more clinically useful information from the dynamic PET signal. ***Materials and Methods:*** A public clinical dynamic 18F-FLT PET dataset (44 BC patients from The Cancer Imaging Archive-ACRIN 66888-10, comprising 19 partial (PR) and 12 complete responders (CR)) was employed[7,8,9]. An experienced radiologist manually contoured volumes of interest around tumor and healthy regions on static PET images. 107 radiomic features for each dynamic PET frame were extracted using the Pyradiomics module (Python), after which their median and median absolute deviation(MAD) across time were computed and reduced to 7 features using principal component analysis(on training sets only - the transformation matrix was then reapplied to test sets). We used the XGBoost model in 5-fold nested cross-validation fashion, including hyperparameter optimization(inner loop) and performance quantification(outer loop) to discriminate 1) tumor vs. reference tissue and 2) CR vs. PR with both conventional static and dynamic radiomic features. Dynamic radiomics (using median, MAD and median + MAD radiomic feature values) was also compared to raw PET data given as input to deep learning models used in[10]. ***Results:*** Tumor vs. reference tissue: radiomics (both static and dynamic) surpassed standard PET image use, achieving 94% accuracy (0.94 AUC) compared to 61% accuracy(0.59 AUC) and 75% accuracy(0.81 AUC) obtained with 3D and 4D PET data, respectively. CR/PR classification: dynamic radiomics attained the highest performance at 86% accuracy (0.83 AUC), outperforming both static radiomics (71% accuracy, 0.67 AUC) and standard PET data (both static(59% accuracy, 0.51 AUC) and dynamic(60% accuracy, 0.59 AUC)). ***Conclusion:*** This study marks the first application of a radiomic approach to dynamic FLT-PET data, demonstrating its superiority in assessing treatment response compared to the conventional static radiomic approach, which is only adequate for simpler tasks, such as lesion/reference tissue classification. ***References:*** 1. Sollini, doi: 10.1016/j.ymeth. 2020.01.007; 2. Conti, doi:10.1016/j.semcancer.2020.04.002; 3. Yang, doi: 10.3348/kjr.2007.8.5.429;4.Romine,doi:10.1186/s13058-021-01464-1;5. Sanghera,doi:10.4103/0972-3919.130274;6.Adejolu,doi:10.2214/AJR.11.7130;7.Kinahan,doi:10.7937/K9/TCIA.2017.ol20zmxg;8. Kostakoglu,doi:10.2967/jnumed.115.160663;9.Clark,doi:10.1007/s10278-013-9622-7;10.Inglese,doi: 10.1109/TRPMS.2023.3268361

EPS-019

The Influence of Histological Subtypes and Tumour Grade on the Performance of [^{18}F]FDG-PET/CT and [^{18}F] FES-PET/CT in Staging Patients with Estrogen Receptor Positive Breast Cancer

J. J. Knip[1,2], *R. Iqbal*[1,2], *A. van Zweeden*[3], *L. H. Mammatas*[4], *J. J. M. Teunissen*[4], *S. van der Velde*[1], *E. Barbé*[1], *K. M. Duvivier*[1], *D. E. Oprea-Lager*[1], *A. D. Windhorst*[1], *R. Boellaard*[1], *C. W. Menke-van der Houven van Oordt*[1,2];
[1]*Amsterdam UMC, Amsterdam, NETHERLANDS,* [2]*Cancer Center Amsterdam, Amsterdam, NETHERLANDS,*
[3]*Ziekenhuis Amstelland, Amstelveen, NETHERLANDS,*
[4]*Reinier de Graaf Gasthuis, Delft, NETHERLANDS.*

Aim/Introduction: Patients with clinical stage II/III or locoregional recurrent (LRR) estrogen receptor positive (ER+) breast cancer (BC) have a significant risk (10-25%) of metastatic disease at presentation. Correct identification of all tumour lesions (i.e., staging) is paramount for an optimal treatment plan. Current guidelines advise staging with positron emission tomography (PET) using 2-[^{18}F]fluoro-2-deoxy-D-glucose ([^{18}F]FDG), combined with diagnostic computed tomography (CT). However, [^{18}F] FDG-PET/CT can be false negative with lobular and low-grade ER+ BC. An alternative is 16α-[^{18}F]-fluoro-17β-estradiol ([^{18}F]FES), a PET tracer which accumulates in ER+ lesions regardless of metabolic activity. The aim of this study was to investigate the influence of histological subtypes and tumour-grade on the performance of [^{18}F]FDG-PET/CT and [^{18}F]FES-PET/CT in staging patients with ER+ BC. ***Materials and Methods:*** We analysed patients with stage II/III or LRR ER+ BC that were included in a prospective multicentre clinical trial (NCT03726931). All patients underwent an [^{18}F]FDG-PET/CT and [^{18}F]FES-PET/CT within a time-frame of 21 days with at least 24h between the scans. Both scans were independently assessed. Visually suspect lesions for malignancy were verified pathologically (by biopsy or fine needle aspiration) or by conventional imaging (mammography, ultrasound, magnetic resonance imaging, CT). The stage of disease was determined independently, based on conventional diagnostics (conventional imaging and pathology) and [^{18}F]FDG-PET/CT or [^{18}F]FES-PET/CT, respectively. ***Results:*** 40 patients were included, with 43 primary breast tumours. For invasive lobular carcinoma (ILC), [^{18}F]FDG-PET/CT correctly staged 9/15 (60%), whereas [^{18}F]FES-PET/CT correctly staged 14/15 (93%). All 6 patients incorrectly staged with [^{18}F] FDG-PET/CT were correctly staged with [^{18}F]FES-PET/CT, with up-staging in 5 patients and down-staging in one. For grade-1 ILC (n = 3), staging by [^{18}F]FDG-PET/CT was incorrect in all cases, while [^{18}F]FES-PET/CT was correct. For invasive ductal carcinoma (IDC), [^{18}F]FDG-PET/CT and [^{18}F]FES-PET/CT correctly staged 21/26 (81%) and 22/26 (85%), respectively. Of the 5 patients incorrectly staged with [^{18}F]FDG-PET/CT, 3 were correctly staged with [^{18}F]FES-PET/CT with up-staging in 2 and down-staging in one. For grade-1 IDC (n = 7), [^{18}F]FDG-PET/CT correctly staged 5/7 (71%), and [^{18}F] FES-PET/CT correctly staged 7/7 (100%). For all grade-1 tumours combined, [^{18}F]FDG-PET/CT and [^{18}F]FES-PET/CT correctly staged 6/12 (50%) and 11/12 (92%), respectively. ***Conclusion:*** Both histological subtype and tumour-grade influence staging based on [^{18}F]FDG-PET/CT and [^{18}F]FES-PET/CT. The largest benefit of additional staging with [^{18}F]FES-PET/CT is seen in ILC and grade-1 tumours. These data can help to further define the role of [^{18}F] FES-PET/CT in staging patients with stage II/III and LRR ER+ BC.

EPS-020

Utility of 18F-FDG PET-CT in the evaluation of para-aortic lymph nodes in the staging of locally advanced cervical cancer

G. Cuesta Domingo[1], *C. Rodríguez Rey*[1], *A. Ortega Candil*[1], *R. Cano Carrizal*[2], *P. Nespral*[1], *P. Bascuñana*[1], *P. Romero Fernández*[1], *A. Berardinelli Isea*[1], *M. Meneses Navas*[1], *M. Cabrera Martín*[1]; [1]*Department of Nuclear Medicine, Instituto de Investigación Sanitaria San Carlos (IdISSC). Hospital Clínico San Carlos, Universidad Complutense., Madrid, SPAIN,* [2]*Department of Cardiology, Hospital Infanta Sofia, Madrid, SPAIN.*

Aim/Introduction: In locally advanced cervical cancer (LACC), the status of para-aortic lymph nodes is crucial in planning radiotherapy treatment. There is controversy regarding the best method for para-aortic lymph node staging: para-aortic lymphadenectomy (PLND) versus imaging staging (PET-CT). The aim of our study is to analyze the negative predictive value (NPV) of PET-CT in detecting para-aortic lymph node involvement when there are positive pelvic lymph nodes. ***Materials and Methods:*** Retrospective study between 2010-2023 that includes 188 patients with LACC (stages IB3-IVA) who come to our center for staging. Those patients with pelvic lymph node involvement and without para-aortic involvement on PET-CT who underwent subsequent PLND were included in the analysis, resulting in a final sample of 42 patients. ***Results:*** The mean age of the patients was 48.54±11.10 years. 69.05% (29) were stage IIB, being squamous cell carcinoma (88.10%) the most frequent histological subtype. Of the 42 patients included, 19 (45.24%) had pathological uptake in unilateral pelvic lymph nodes (more frequently on the left side, 63.16%) and 23 (54.80%) in bilateral pelvic lymph nodes. Of the 42 patients, 5 (11.9%) had para-aortic lymph node involvement on PLND, resulting in a NPV of PET-CT of 88.10%. The proportion of patients with para-aortic involvement on PLND was similar in those with bilateral or unilateral pelvic lymph node involvement (8.70% vs 15.79%; p=0.48). ***Conclusion:*** PET-CT shows a high NPV in detecting retroperitoneal lymph node involvement in LACC when there is pelvic lymph node affectation. However, we cannot ignore the number of false negatives of the technique, so it would be necessary to appropriately select, based on risk, those patients who would benefit from PLND.

EPS-021

Surgical evidence-based comparison of ^{68}Ga-FAPI PET/MRI and DW-MRI for assisting debulking surgery decision in ovarian cancer

X. Li[1], *F. Kang*[1], *S. Liu*[2], *T. Han*[3], *J. Wang*[1]; [1]*Department of Nuclear Medicine, Xijing Hospital, Fourth Military Medical University, Xi'an, CHINA,* [2]*Department of Gynaecology and Obstetrics, Xijing Hospital, Fourth Military Medical University, Xi'an, CHINA,* [3]*Department of Nuclear Medicine, Xijing Hospital, Fourth Military Medical University, Xi'an, CHINA.*

Aim/Introduction: Imaging assessment of tumor burden is important for debulking surgery choice in ovarian cancer patients. This study aims to evaluate the diagnosticefficiency of fibroblast activation protein (FAP) targeted ^{68}Ga-FAPI PET/MRI and DWI-MRI for assessing abdominopelvic tumor burden of ovarian cancer and its impact to debulking surgery decision. ***Materials and Methods:*** Thirty-six patients were prospectively enrolled and underwent integrated ^{68}Ga-FAPI PET/MR-DWI scan before debulking surgery. The ^{68}Ga-FAPI PET/MRI and DWI-MRI results were independently analyzed by per-lesion comparison referenced with surgical proof. The accuracy, sensitivity, specificity, missing rate, consistency and inconsistency of the two modalities were analyzed in region/ patient-based manner. Relationship of FAP expression and implants size were also analyzed. ***Results:*** ^{68}Ga-FAPI PET/MRI outperformed DWI-MRI in 11/19 patients (57.9%), and most abdominal/pelvic regions (19/24). ^{68}Ga-FAPI PET/MRI displayed higher accuracy (84.9% vs. 80.7%), higher sensitivity (76.8% vs.59.9 %), and lower missing rate (23.2% vs. 40.1%) than DWI-MRI. Furthermore, the accuracy of ^{68}Ga-FAPI PET/MR is higher than DWI-MRI in PDS patients but lower in IDS patients who already received chemotherapy. About 15% lesions displayed inconsistency between the two modalities, of them, ^{68}Ga-FAPI PET/MRI correctly identified more lesions than DWI-MRI, particularly in PDS patients. In addition, FAP expression was independent of metastatic lesion size. ***Conclusion:*** ^{68}Ga-FAPI PET/MRI shows superior efficiency than DWI-MRI for assessing abdominopelvic tumor burden of OC. Integrated ^{68}Ga-FAPI PET/MR-DWI imaging may be a valuable method for debulking surgery decision in ovarian cancer patients. ***References:*** 1. Liu S, Feng Z, Xu X, Ge H, Ju X, Wu X, et al. Head-to-head comparison of [(18)F]-FDG and [(68) Ga]-DOTA-FAPI-04 PET/CT for radiological evaluation of platinum-sensitive recurrent ovarian cancer. Eur J Nucl Med Mol Imaging. 2023. doi:10.1007/s00259-022-06096-x.2. Zheng W, Liu L, Feng Y, Wang L, Chen Y. Comparison of 68 Ga-FAPI-04 and fluorine-18-fluorodeoxyglucose PET/computed tomography in the detection of ovarian malignancies. Nucl Med Commun. 2023;44:194-203. doi:10.1097/mnm.0000000000001653.3. Dendl K, Koerber SA, Finck R, Mokoala KMG, Staudinger F, Schillings L, et al. (68)Ga-FAPI-PET/CT in patients with various gynecological malignancies. Eur J Nucl Med Mol Imaging. 2021;48:4089-100. doi:10.1007/s00259-021-05378-0.

210

Sunday, September 10, 2023, 08:00 - 09:30
Hall K

CTE 1 - Technologists Committee / SNMMI: Technologists' Guide launch – Gastro Intestinal Molecular Imaging Studies Launch

OP-060

Introduction

A. Pietrzak;
Greater Poland Cancer Centre, Nuclear Medicine Department, Poznan, POLAND.

OP-061

Hepatobiliary and spleen studies

D. Gilmore;
Massachusetts College of Pharmacy and Health Sciences, Boston, UNITED STATES OF AMERICA.

OP-062

Scintigraphy of gastroesophageal reflux, pulmonary aspiration and gastric emptying in children

Z. Bar-Sever;
Schneider Children's Medical Center Israel, Department of Nuclear Medicine, Petah Tikva, ISRAEL.

OP-063

Oncological studies (SPECT & PET)

R. Massa;
The Christie NHS Foundation Trust, Nuclear Medicine Department, Manchester, UNITED KINGDOM.

301

Sunday, September 10, 2023, 09:45 - 11:15
Hall A

CME 2 - Translational Molecular Imaging & Therapy + Oncology & Theranostics + Radiopharmaceutical Sciences Committee: FAP - Moving Towards Therapy

OP-064
FAP Inhibitors and Substrates
J. Milul;
Postdoctoral Scientist at Universitätsspital Basel, University Hospital Basel, University of Basel, Basel, SWITZERLAND.

OP-065
Dosimetric Aspects in FAP Radioligand Therapies
W. Fendler;
Department of Nuclear Medicine, West German Cancer Center (WTZ), University Hospital Essen, University of Duisburg-Essen, Essen, GERMANY.

OP-066
RLT Using Cancer-Associated Fibroblasts as Target in Solid Tumors: First Clinical Experiences
C. Nanni;
NuclearMedicine, IRCCS Azienda Ospedaliero-Universitaria di Bologna, Bologna, ITALY.

OP-067
Theranostic FAP Inhibitors: From Monomers for Diagnosis to Dimers for Therapy?
F. Rösch;
Department of Chemistry-TRIGA, Institute of Nuclear Chemistry, Johannes Gutenberg University, Mainz, GERMANY.

302

Sunday, September 10, 2023, 09:45 - 11:15
Hall D (Arena)

Challenge the Expert 1 - Thyroid Committee: Integrated Diagnostics of Thyroid Disease

OP-068
Integrated Diagnostics of Thyroid Disease
D. Deandreis; Nuclear Medicine, Universita degli Studi di Torino, Turin, ITALY

303

Sunday, September 10, 2023, 09:45 - 11:15
Hall E1

LIPS Session 2 - Radiation Protection Committee / EFOMP: Careers in Radiation Protection

OP-072
The current status of the medical physicist profession in Europe
E. Amato;
Universityof Messina, Department of Biomedical Sciences, Messina, ITALY.

OP-073
Requirements for the medical physicist training in Europe.
D. Visvikis;
National Institute of Health and Medical Research (INSERM), Medical Imaging Processing Lab, Paris, FRANCE.

OP-074
Building and maintaining competence in radiation protection of nuclear medicine professionals
J. Vassileva ;
International Atomic Energy Agency, Radiation Protection of Patients Unit, Vienna, AUSTRIA.

304

Sunday, September 10, 2023, 9:45 AM - 11:15 AM
Hall E2

M2M Track - TROP Session: Validating Methodology: In Vitro and in Vivo Models

OP-076
Role and Impact of Anaesthetic Procedures for Preclinical Radiotracer Development Using Small Animal Positron Emission Tomography-Computed Tomography Imaging
T. Ebenhan[1,2], *C. H. S. Driver*[1,3], *C. Swanepoel*[1], *J. Visser*[1];
[1]*Preclinical Imaging Facility, Nuclear Medicine Reseach Infrastructure NPC, Pretoria, SOUTH AFRICA,* [2]*Nuclear Medicine, University of Pretoria, Pretoria, SOUTH AFRICA,* [3]*Radiochemistry, Necsa, Pelindaba, SOUTH AFRICA.*

Aim/Introduction: Non-invasive, functional imaging techniques such as Positron Emission Tomography-Computed Tomography (PET-CT) provide the means for studying physiological and pharmacological processes in real-time, both within the preclinical and clinical setting. PET-CT imaging has made a major footprint in preclinical research of pharmacology and medical sciences which has an impact on how we study neurological or oncological disease, detect inflammation/infection and conduct cardiovascular research. This investigation aims to systematically align different anaesthetics with common radiotracers for PET-CT imaging studies to provide information that can enhance the radiotracer representation according to their targeting mechanism in rodents to advance quality and translatability of microPET/CT-derived data. ***Materials and Methods:*** The following anaesthetics were mainly assessed for suitability towards imaging

with [18F]FDG-, but also for [68Ga]Ga-DOTA-TATE-, and [68Ga]Ga-PSMA-11-microPET-CT diagnostics: isoflurane, sevoflurane, pentobarbital, propofol, or combination of fentanylcitrate-fluanisone/diazepam, and ketamine/xylazine. These anaesthetic agents were compared based on animal physiology (respiration rate, body temperature, apparent glucose metabolism and expected radiotracer biodistribution). ***Results:*** The investigated anaesthetics caused altered respiration rate, body temperature, glucose metabolism and have effects on target organs which affected radiotracer biodistribution. Isoflurane inhalation is the most desired anesthetic procedure; however, both sevoflurane and isoflurane (also ketamine/xylazine administration) induced hypoglycemia. Sevoflurane can be suggested over isoflurane for cardiac imaging. Propofol is suitable for [18F]FDG imaging but should be avoided for neuroimaging causing decreased cerebral glucose metabolism. Pentobarbital does not alter the blood glucose metabolism but has a lower safety margin for rodent anesthesia. Fentanylcitrate-fluanisone/diazepam the preferred injectable anesthetic option for [18F]FDG being the least interfering with glucose metabolism. Tumor imaging quality using [68Ga]Ga-DOTA-TATE- or [68Ga]Ga-PSMA-11-microPET-CT was supported by isoflurane or sevoflurane; however, higher glucocorticoid levels and certain neuroendocrine abnormalities occurred (may originated by hypothermia). ***Conclusion:*** This investigation proves that anaesthetics used for preclinical research using microPET/CT-imaging need to be carefully aligned with the radiotracer half-life, and metabolism, to warrant an uninterrupted image acquisition of high quality. Better understanding of the interplay between radiotracers and available anesthesia agents can allow for the best choice of anesthesia that will improve the performance and outcome of imaging studies. Thus, radiotracers are supported to show their full research potential to become non-invasive in vivo biomarker or sensitive drug efficacy monitoring tools.

OP-077

Feasibility of in vivo small animal imaging using a clinical total-body PET/CT scanner

J. Mannheim[1,2], *W. Lan*[3], *M. A. Krueger*[1], *C. la Fougère*[2,3], *F. P. Schmidt*[1,3];
[1]*Werner Siemens Imaging Center, Department of Preclinical Imaging and Radiopharmacy, Eberhard-Karls University Tuebingen, Tuebingen, GERMANY,* [2]*Cluster of Excellence iFIT (EXC 2180) "Image Guided and Functionally Instructed Tumor Therapies", University of Tuebingen, Tuebingen, GERMANY,* [3]*Department of Nuclear Medicine and Clinical Molecular Imaging, University hospital Tuebingen, Tuebingen, GERMANY.*

Aim/Introduction: Utilizing clinical PET scanners for preclinical animal imaging has been of interest ever since preclinical in vivo research has gained its importance. Constraints in this regard were the limited spatial resolution and sensitivity of clinical scanners compared to dedicated preclinical scanners. With the availability of total-body PET scanners with axial FOVs longer than 1 m, the limitation of sensitivity has been overcome. The aim of this study was to evaluate the in vivo quantification accuracy for 9 mice scanned simultaneously on a total-body PET/CT scanner compared to individual scans on a dedicated preclinical PET scanner. ***Materials and Methods:*** 9 healthy mice were injected with n 13.4 ± 0.4 MBq [18F]FDG. After 1h uptake time, mice were sacrificed and flash-frozen in the same position. 90 min p.i., static scans were performed for each animal individually on a dedicated preclinical PET scanner. All mice were subsequently transferred to a clinical total-body PET/CT scanner and a static scan was performed for all 9 mice simultaneously in a back-to-back arrangement to cover the 106 cm axial FOV. Preclinical images were also Gauss filtered to match the voxel size of the clinical system. VOIs were placed in the liver, muscle, left and right striatum, cortex and cerebellum. SUV_{mean} was calculated; one-way ANOVA was performed to test for statistically significant differences between the PET scans. ***Results:*** Reproducible SUV_{mean} values between the clinical total-body and preclinical PET scanner (original and filtered data) were determined for the liver and muscle, as well as for the right striatum and cortex. Furthermore, liver and muscle uptake were reproducible for frame durations as short as 10 s for the clinical total-body PET/CT scanner. For the left striatum and cerebellum, significant differences were determined between the original and filtered preclinical data (p=0.0495 and p=0.0363, respectively), whereas reproducible uptake was determined between the preclinical and clinical scans for these regions. ***Conclusion:*** Although the spatial resolution is considerably different between a preclinical and clinical PET scanner (~1 mm vs. 3-4 mm), it was feasible to perform reproducible mice studies with a clinical total-body PET/CT system due to the high sensitivity. Our study demonstrated that - with optimized protocols - clinical total-body PET/CT scanners can be utilized for preclinical in vivo imaging with the unique advantage of scanning multiple animals (>10) simultaneously. Future work will focus on a voxel-wise comparison of the individual regions.

OP-078

Is multiple-mouse PET/MR imaging possible in preclinical oncology?

A. Courteau[1,2], *A. Oudot*[2], *R. Garipov*[3], *P. Doughty*[3], *J. McGrath*[3], *A. Cochet*[1,2,4], *F. Brunotte*[1], *J. M. Vrigneaud*[1,2];
[1]*ICMUB laboratory, UMR CNRS 6302, University of Burgundy, Dijon, FRANCE,* [2]*Georges-François Leclerc Cancer Centre, Unicancer, Dijon, FRANCE,* [3]*MR Solutions Ltd, Guildford, UNITED KINGDOM,* [4]*CHU François Mitterrand, Dijon, FRANCE.*

Aim/Introduction: Although integrated positron emission tomography (PET)/magnetic resonance (MR) imaging provides high tissue contrast facilitating organ segmentation, the low throughput of PET/MR limits its widespread use. We present here preliminary results obtained with a mouse multibed accessory to overcome this limitation. ***Materials and Methods:*** The accessory consisted of a triangular arrangement of mouse cradles fitting a birdcage radiofrequency (RF) coil specifically designed and fine-tuned for mouse multibed imaging on our integrated 7 T preclinical PET/MR system. Firstly, three mouse-sized homogeneous cylinders were injected with 10.2 ± 0.3 MBq of 18F-fluorodeoxyglucose prior to a 30-min PET acquisition. Data were reconstructed with ordered-subset expectation maximization algorithm applying 2 iterations, 32 subsets, corrections for scatter, random, decay, normalization, and dead-time. A volume of interest extending over 75% of the phantom length and diameter was drawn to measure standardized uptake value (SUV) and coefficient of variation (CoV) per phantom. Regarding MRI, multi-echo gradient echo (GRE), and double flip angle (FA) GRE sequences were used to produce respectively principal magnetic field (B0) distortion maps in part per million (ppm), and FA maps representing RF field variations. Complementary axial and coronal two-dimensional (2D) fast spin echo T1- and T2-weighted and three-dimensional (3D) fast-low angle shot acquisitions were tested to assess the homogeneity and absence of artifacts. These MR scans were repeated during an in vivo imaging session on subcutaneous tumor-bearing mice. Acquisition parameters were modulated to achieve an optimal trade-off between image quality, tissue contrast, and acquisition duration.

Results: SUV of 1.00, 1.00, and 0.99 and CoV of 4.2%, 3.9%, and 5.9% were measured respectively on left, right, and top positions. The MR image homogeneity and absence of artifacts was verified with 2D and 3D imaging. On the three phantoms the measured B0 distortion was lower than 0.3 ppm/cm in the coronal plane, and the average FA variation did not exceed 3 degrees from the expected value. PET quantification accuracy and MR fields homogeneity were consistent with single-phantom results obtained on the same system. In vivo, an optimal MR image quality was obtained applying four signal averages, leading to an acquisition duration of seven to eleven minutes per sequence. Tumour heterogeneity was clearly visible in T2-weighted imaging, and the contouring of abdominal and pelvic organs was possible on the three animals. ***Conclusion:*** Preliminary results from the on-going study suggest that this system provides high tissue discrimination and quantitative PET data in a multi-bed configuration.

OP-079

In situ tumour response PET imaging without radiopharmaceuticals in particle therapy: a feasibility study in rats

C. Toramatsu*, A. Mohammadi, N. Nitta, C. Seki, Y. Ikoma, I. Kanno, T. Yamaya;*
National Institutes for Quantum Science and Technology (QST), Chiba, JAPAN.

Aim/Introduction: Positron emission tomography (PET) has been used for treatment verification in charged particle therapy. Without using radiopharmaceuticals, positron emitters such as ^{15}O and ^{11}C, which are produced through fragmentation reactions in a patient, are imaged. For accurate dose verification, modelling and correction of the biological washout effect of the positron emitters, which is influenced by the tumour vasculature condition, has been an issue. Conversely, the biological washout effect may indicate changes of the tumour vasculature condition, which is known to influence radiation response. At present, blood circulatory changes in a tumour are measured clinically using dynamic contrast-enhanced magnetic resonance imaging (DCE-MRI) to evaluate tumour radiation response [1]. Here, measuring of the biological washout rate of the produced positron emitters may also function to evaluate tumour radiation response, in a similar manner to DCE-MRI. The aim of this study is the comparison of the washout rates in rats between in-beam PET during treatment beam (^{12}C ion) irradiation and DEC-MRI. ***Materials and Methods:*** Different vascular types of the tumour model were prepared using six nude rats. The tumour of each nude rat was irradiated by a ^{12}C ion beam and, at the same time, scanned by an in-house-made in-beam PET system on the first day. On the second day, the DCE-MRI experiment was performed for the same six nude rats. The main washout rate of the produced positron emitters ($k_{2,1st}$) and the MRI contrast agent (k_{2a}) were derived using the single tissue compartment model which is commonly used in nuclear medicine. ***Results:*** A linear correlation was observed between $k_{2,1st}$ and k_{2a}. A heterogeneous morphology, which corresponds to a low metabolic area such as necrosis and haemorrhage, was observed in the MRI images of each tumour. The values for the ratio of the volume of the necrotic area to the volume of the whole tumour (fractional necrotic volume) was inversely related to the biological washout rate ($k_{2,1st}$ and k_{2a}). ***Conclusion:*** This was the first study that reported the biological washout rate of the positron emitters produced via a nuclear fragmentation reaction correlates to the washout of the MRI contrast agent administrated intravenously, which reflects a tumour vascular condition. The rat study findings suggest that the washout rate in in-beam PET may function as a predictor of tumour response in particle therapy. ***References:*** 1) Zahra MA et al 2007 Lancet Oncol 8 63-74

OP-080

Demonstrating the Quantitative Potential of Terbium-161 SPECT/CT Imaging: An Anthropomorphic Phantom Study

F. Westerbergh*[1], N. P. van der Meulen[2,3], C. Müller[3], A. Grings[4], P. Ritt[4], P. Bernhardt[1,5];*
[1]Department of Medical Radiation Sciences, Institute of Clinical Sciences, University of Gothenburg, Gothenburg, SWEDEN, [2]Laboratory of Radiochemistry, Paul Scherrer Institute, Villigen-PSI, SWITZERLAND, [3]Center for Radiopharmaceutical Sciences, Paul Scherrer Institute, Villigen-PSI, SWITZERLAND, [4]Clinic of Nuclear Medicine, University Hospital Erlangen, Erlangen, GERMANY, [5]Department of Medical Physics and Biomedical Engineering (MFT), Sahlgrenska University Hospital, Gothenburg, SWEDEN.

Aim/Introduction: Due to the large proportion of Auger and conversion electrons emitted in its decay, ^{161}Tb has been proposed as a superior alternative to ^{177}Lu—especially in the treatment of single cancer cells and small metastases. Much like ^{177}Lu, ^{161}Tb emits photons imageable by the γ-camera, making SPECT-based ^{161}Tb dosimetry a topic of interest. The study aimed to evaluate the quantitative potential of ^{161}Tb SPECT imaging by assessing activity quantification errors for a patient-like source geometry. ***Materials and Methods:*** Imaging was performed on a Discovery NM/CT 670 Pro system with a 5/8" NaI(Tl) crystal, using three different collimators: low-energy high-resolution (LEHR), extended low-energy general-purpose (ELEGP), and medium-energy general-purpose (MEGP). A 74.6 keV±10% photopeak window with two adjacent ±5% scattering windows was employed. Projections were acquired with a 256×256 matrix and 3° angular sampling. Reconstruction was performed with a Monte Carlo-based OSEM algorithm with 6 iterations and 10 subsets. Uniformity maps were acquired separately for each collimator using a ^{161}Tb-filled flood source phantom. A cylindrical, homogeneously filled phantom (V = 6.89 L; C = 45.7 MBq/L) was used to establish SPECT calibration factors. Recovery coefficients (RCs) for partial volume correction were determined with a Jaszczak Phantom™ with six spherical inserts (V = 0.5-16 mL; C = 0.78 MBq/mL). To evaluate the quantitative accuracy, an anthropomorphic phantom study was carried out using an Elliptical Lung-Spine Phantom™, containing eight fillable spheres (V = 2, 4, 8, and 16 mL, two per volume; C = 1.35 MBq/mL) mounted in various positions. Different activity levels were explored: i) a "cold" background; ii) a sphere-to-background ratio (SBR) of 20:1; iii) a SBR of 10:1. Listmode data was retrieved to enable spectral analyses. ***Results:*** The highest RCs were obtained with LEHR (0.32-0.70), followed by ELEGP (0.26-0.67) and MEGP (0.27-0.63). The mean relative quantification error in the anthropomorphic measurements was -2.63±9.04% for LEHR, -0.18±6.44% for ELEGP, and 3.58±6.41% for MEGP, respectively. Generally, errors decreased with increasing sphere volume. With LEHR, an underestimation of activity was observed at higher activity levels (i.e., SBR = 10:1 and 20:1). Spectra acquired with LEHR and ELEGP revealed distinct peaks at 292 and 475 keV, with subsequent down-scatter. Peaks were removed with MEGP. ***Conclusion:*** Accurate SPECT-based ^{161}Tb activity quantification using a 74.6 keV±10% photopeak window appears feasible. Although LEHR produces the highest resolution, this collimator option may not be optimal for quantification purposes due to penetration from higher-energy emissions.

OP-081

RadioFACS reveals [^{18}F]FDG uptake in a KRAS induced lung cancer model is driven by immune cells but not tumor cell metabolism

C. Vraka[1], *M. Homolya*[2], *T. Patsch*[1], *A. Spittler*[3], *E. Casanova*[2], *S. Grünert*[1], *M. Hacker*[1], *C. Philippe*[1];
[1]*Department of Biomedical Imaging and Image-guided Therapy, Medical University of Vienna, Vienna, AUSTRIA,* [2]*Institute of Pharmacology, Center of Physiology and Pharmacology, Medical University of Vienna, Vienna, AUSTRIA,* [3]*Core Facility Flow Cytometry and Department of Surgery, Research Laboratories, Medical University of Vienna, Vienna, AUSTRIA.*

Aim/Introduction: Cellular heterogeneity within and across tissues has been a major obstacle in treating cancer, but bulk analysis of tissues masks their complex heterogeneity. 2-[^{18}F] fluoro-2-desoxy-D-glucose Positron Emission Tomography ([^{18}F] FDG-PET) enables non-invasive functional in vivo imaging and is successfully used for tumor diagnostics and metastases discovery in cancer patients. However, the relatively poor resolution of PET limits the appraisal of tumor heterogeneity and the contribution of the tumor microenvironment (TME). Consequently, little is known about the uptake of tracers by different cell types, which however may hold critical information on the course of a pathology. The aim of this work was to investigate the [^{18}F] FDG uptake on single-cell level in the TME of a KRAS induced lung cancer mouse model using the novel method radioFACS. ***Materials and Methods:*** A C57BL6/N KRAS (K-ras^{G12D}:p53$^{\Delta Lep/\Delta Lep}$) orthotopic transplantation mouse model [1] was injected with [^{18}F] FDG intravenously. After 60 min tracer distribution in conscious animals, a 10 min static µPET/CT was conducted under isoflurane anesthesia. Subsequently, animals were sacrificed and lungs were harvested for gamma counting, Fluorescence Activated Cell Sorting (FACS), autoradiography and immunofluorescence. For radioFACS, single cell suspensions were obtained with a tumor dissociation kit, labelled with fluorescent antibodies and sorted by a ARIAFusion cell sorter. The sorted cell fractions were immediately measured in a gamma-counter and normalized to 10^5 cells. ***Results:*** [^{18}F]FDG uptake in the total lung was 5.8±1.6%ID/cc and 3.5±0.3%ID/g. RadioFACS analysis of these lungs showed a robust cell type specific uptake pattern across experiments. We present that the PET signal predominantly derives from [^{18}F]FDG uptake in the immune cells (CD45+, F4/80-: 78.3±6.6% and macrophages: 13.9±4.3%), whereas tumor cells (dTom+) only contributed with 2.8±1.0%, which was in the same range as structural cells (CD45-, dTom-: 5.0±2.3%). Normalization depicted that macrophages have the highest glucose metabolism (61.5±3.8%CPM/10^5) followed by the remaining immune cells (27.2±0.7%CPM/10^5). Tumor cells had a significantly lower glucose metabolism rate (7.1±2.7%CPM/10^5). The results were confirmed by autoradiography overlayed with immunofluorescence of dTom-expressing tumor cells. Additionally, ex vivo cell sorting and subsequent in vitro cell uptake of [^{18}F]FDG showed 7.0±10.0%CPM/10^5 in sorted macrophages and 1.0±1.0%CPM/10^5 tumor cells. ***Conclusion:*** RadioFACS was able to uncover that the [^{18}F]FDG signal mainly results from infiltrated immune cells and not tumor cells. These results indicate that the impact of immune cell infiltration upon therapy should be considered when interpreting [^{18}F]FDG uptake in tumor lesions to assess therapy response. ***References:*** [1] Breitenecker et al., Sci Transl Med (2021);13(601):eabc3911.

OP-082

Impact of inoculation-driven immune response on TSPO and amino acid PET imaging in experimental orthotopic glioblastoma

L. Gold[1], *E. Barci*[2], *M. Brendel*[1], *M. Orth*[3], *J. Cheng*[2], *S. V. Kirchleitner*[4], *L. M. Bartos*[1], *L. M. Unterrainer*[1], *L. Kaiser*[1], *S. Ziegler*[1], *L. Weidner*[5], *M. J. Riemenschneider*[5], *M. Unterrainer*[1], *C. Belka*[3], *J. Tonn*[4], *P. Bartenstein*[1], *M. Niyazi*[3], *L. von Baumgarten*[4], *R. Kälin*[2], *R. Glass*[2], *N. L. Albert*[1], *A. Holzgreve*[1];
[1]*Department of Nuclear Medicine, University Hospital, LMU Munich, Munich, GERMANY,* [2]*Neurosurgical Research, Department of Neurosurgery, University Hospital, LMU Munich, Munich, GERMANY,* [3]*Department of Radiation Oncology, University Hospital, LMU Munich, Munich, GERMANY,* [4]*Department of Neurosurgery, University Hospital, LMU Munich, Munich, GERMANY,* [5]*Department of Neuropathology, Regensburg University Hospital, Regensburg, GERMANY.*

Aim/Introduction: The translocator protein (TSPO) has proven great potential as a target for PET-imaging of glioblastoma. However, there is an ongoing debate about the potential various sources of the PET-signal, since TSPO has been shown to be highly overexpressed both in glioblastoma cells and in inflammatory cells. This work investigates the impact of the inoculation-driven immune response on the PET-signal in experimental orthotopic glioblastoma. ***Materials and Methods:*** We conducted a longitudinal dual tracer TSPO and amino acid PET study in direct comparison to tissue-based analyses. Serial [^{18}F]GE-180 and [^{18}F] FET PET-scans were performed at day-7/8 and day-14/15 after inoculation of GL261 mouse glioblastoma cells (n=24) or saline (sham, n=6) into the right striatum of immunocompetent C57BL/6 mice. Additional n=25 sham mice underwent [^{18}F]GE-180 PET and autoradiography (ARG) at days 7, 14, 21, 28, 35, 50 and 90 in order to monitor potential reactive processes that were solely related to the inoculation procedure. In vivo imaging results were directly compared to tissue-based analyses including ARG and immunohistochemistry. ***Results:*** We found that the inoculation process represents an immunogenic event which significantly contributes to TSPO-radioligand uptake. [^{18}F]GE-180 uptake in GL261-bearing mice surpassed [^{18}F]FET uptake both in the extent and the intensity, e.g., mean target-to-background ratio (TBR_{mean}) in PET at day-7/8: 1.22 for [^{18}F]GE-180 vs. 1.04 for [^{18}F]FET, $p<0.001$. Sham mice showed increased [^{18}F]GE-180 uptake at the inoculation channel, which however continuously decreased over time (e.g., TBR_{mean} in PET: 1.20 at day-7 vs. 1.09 at day-35, $p=0.04$). At the inoculation channel, the percentage of TSPO/IBA1 co-staining decreased, whereas TSPO/GFAP co-staining increased over time ($p<0.001$). ***Conclusion:*** We found that the invasive inoculation process used for generating preclinical glioblastoma in vivo models represents a relevant immunogenic event which significantly contributes to TSPO-radioligand uptake in glioblastoma-bearing and sham-operated mice. The inoculation-driven immune response should therefore be considered for the planning of PET imaging studies in orthotopic glioblastoma models. Furthermore, we provide information about the longitudinal changes of TSPO PET findings and the underlying TSPO-positive cell populations after penetrating traumatic brain injury.

OP-083

From 2D to 3D: Developing an improved in vitro model for radiopharmaceutical evaluation

L. van den Brink, *M. J. Klomp, S. Erkens-Schulze, W. M. van Weerden, S. U. Dalm;*
Erasmus Medisch Centrum, Rotterdam, NETHERLANDS.

Aim/Introduction: In vitro cell assays are one of the first methods used for evaluating the potential of newly developed radiopharmaceuticals. Currently, two-dimensional (2D) cell cultures are commonly used to assess binding capability, specificity and efficacy of radiopharmaceuticals. However, with recent advances in three-dimensional (3D) cell culture techniques, we can now much better recapitulate true tissues with important aspects such as target heterogeneity, perfusion and, importantly for determining efficacy, the irradiation range of radionuclides. This information is normally only taken into account at later stages when in vivo animal studies are conducted. Moreover, such an approach would serve to reduce the animals use as much as possible as well as reduce costs. With the aim of creating a more relevant in vitro model, we studied 3D spheroids for radiopharmaceutical evaluation. ***Materials and Methods:*** Prostate-specific membrane antigen (PSMA)-expressing human prostate cancer LNCaP cells were cultured in 2D and 3D setting. To obtain 3D spheroids, single cells were plated in natural extracellular matrix-based matrigel or synthetic noviogel, and subsequently cultured for seven days to form multiple 3D spheroids per gel dome. Uptake and viability studies were performed in 2D and 3D. Uptake was determined by incubating cells for 4h or 22h with 1nM [^{111}In]In-PSMA-I&T (20MBq/nmol) +/- 1µM unlabeled tracer. Cell viability was determined using CellTiter Glo six days after 4h incubation with 0.1-4MBq/mL (60MBq/nmol) of [^{177}Lu]Lu-PSMA-I&T or [^{177}Lu]Lu-DTPA. ***Results:*** At both time points, specific uptake of [^{111}In]In-PSMA-I&T was significantly higher in 2D versus 3D (approximately 2-3-fold, $p<0.05$ for both 3D systems). No differences in uptake were measured between spheroid cultures in matrigel or noviogel. Cell viability was therefore only determined for 2D and 3D-matrigel cultured cells, showing a similar reduction in viability despite the difference observed in uptake between the two models. No significant effect of [^{177}Lu]Lu-DTPA on viability was observed. ***Conclusion:*** We successfully used a spheroid model to test selectivity, uptake and cytotoxicity studies of radiopharmaceuticals. Tracer uptake in cells was lower in de 3D versus 2D system, possibly because of radiopharmaceutical perfusion through the gel. Interestingly, cells cultured in spheroids needed less dose to achieve the same reduction in viability, which is most likely due to cross-fire radiation. These preliminary results demonstrate the feasibility and additional value of 3D models for radiopharmaceutical studies. We are further optimizing and evaluating the developed method e.g. using radionuclides with different linear energy transfer, such as 161-Tb and 225-Ac.

OP-084

Theranostic Digital Blueprint Predicts Higher Therapeutic Efficacy using Radiopharmaceuticals with Higher Albumin Affinity

A. Fele Paranj[1], *C. Uribe*[1], *F. Benard*[2], *A. Rahmim*[1], *B. Saboury*[3];
[1]*University of British Columbia, Vancouver, BC, CANADA,*
[2]*BC Cancer, Vancouver, BC, CANADA,* [3]*National Institutes of Health (NIH), Bethesda, MD, UNITED STATES OF AMERICA.*

Aim/Introduction: Radiopharmaceutical therapy (RPT) is a promising approach to cancer treatment, and efforts are ongoing to improve its efficacy. One such effort is the development of radiopharmaceuticals with varying albumin affinities. Albumin, the most abundant protein in the serum, has numerous important roles in the body and can potentially be utilized to enhance RPT. However, in vivo and in vitro studies to evaluate the use of albumin in RPT are costly and time-consuming. In this study, we developed a physiologically based pharmacokinetic (PBPK) model to study the kinetics of radiopharmaceuticals, taking into account varying albumin affinities and their potential role in increasing treatment efficacy. ***Materials and Methods:*** Our PBPK model incorporates subcompartments of organs and tumors, including vascular, interstitial, binding sites, and internalization into cells. We implemented the model in the SimBiology toolbox in Matlab using realistic population averaged values for the model parameters. In a virtual in-silico experiment, we injected 11.7GBq of 177Lu-PSMA with a specific activity of 104MBq/µg and varying albumin affinities (KD of albumin-binding ranging from 1-200nanomole/liter). The time-integrated-activity (TIA) in tumors and organs at risk (OARs) which include kidney and salivary glands was calculated to determine the absorbed dose to tissue. Therapeutic-efficacy (TE) was defined as the tumor-to-OAR-dose-ratio normalized to the same ratio if albumin binding was off. ***Results:*** We found that a lower dissociation constant for albumin-binding decreases the delivered dose to tumors and OARs, reducing the delivery yield (about a 3-fold decrease). However, a lower dissociation constant for albumin binding enhances RPT treatment by enhancing the differential dose delivery to the tumor with respect to OARs (up to a 2-fold increase). Albumin-bound radiopharmaceuticals do not enter the interstitial media of OARs, but due to the mechanical properties of the tumor vasculature structure, albumin leaks to the tumor interstitial medium, improving the tumor targeting index for the radiopharmaceuticals. Changes in different parameters and modeling components may alter these results, providing insight into subtle aspects of radiopharmaceutical deliveries and varied findings in experimental studies. ***Conclusion:*** Our PBPK model fine-tuned for radiopharmaceuticals with albumin affinity shows that a low dissociation constant for albumin binding can enhance the tumor-targeting efficacy of radiopharmaceuticals (up to 2-fold increase), despite potentially reducing the delivery yield (about 3-fold decrease). These findings have implications for the development and optimization of radiopharmaceutical therapies for cancer treatment. ***References:*** Paranj AF, et al. Non-linearities in the Transition from Imaging Radiotracers to Therapeutic Radiopharmaceuticals. JNM.2022;63:2821-2821.

305

Sunday, September 10, 2023, 9:45 AM - 11:15 AM
Hall B

Cutting Edge Science Track - Featured Session: Radiomics

OP-085
State of the Art and Perspectives
M. Hatt;
INSERM, Brest, FRANCE.

OP-086
Prognostic value of [^{18}F]FDG PET radiomics to detect peritoneal and distant metastases in locally advanced gastric cancer - a side-study of the prospective multicentre PLASTIC study
W. A. Noortman[1], *L. C. E. Pullen*[2], *L. Triemstra*[3], *C. de Jongh*[3], *F. J. Rademaker*[2], *R. Spijkerman*[2], *G. M. Kalisvaart*[1], *E. C. Gertsen*[3], *L. F. de Geus-Oei*[1], *N. Tolboom*[3], *W. O. de Steur*[1], *M. Dantuma*[2], *R. H. J. A. Slart*[4], *R. van Hillegersberg*[3], *P. D. Siersema*[5], *J. P. Ruurda*[3], *F. H. P. van Velden*[1], *E. Vegt*[6], *PLASTIC Study Group;*
[1]*Leiden University Medical Center, Leiden, NETHERLANDS,* [2]*University of Twente, Enschede, NETHERLANDS,* [3]*University Medical Center Utrecht, Utrecht, NETHERLANDS,* [4]*University Medical Center Groningen, Groningen, NETHERLANDS,* [5]*Radboud University Medical Center, Nijmegen, NETHERLANDS,* [6]*Erasmus University Medical Center, Rotterdam, NETHERLANDS.*

Aim/Introduction: Accurate staging of gastric cancer is crucial to prevent futile gastrectomies. Recently, a Dutch multicentre study investigated the role of visual assessment of [^{18}F]FDG-PET/CT in staging [1]. The aim of this side-study was to improve identification of peritoneal and distant metastases in locally advanced gastric cancer using [^{18}F]FDG-PET radiomics. ***Materials and Methods:*** [^{18}F]FDG-PET scans of 206 patients acquired in 16 different Dutch hospitals in the prospective multicentre PLASTIC-study were analysed. Tumours were delineated using an adaptive threshold of 50% SUV_{peak} and 105 radiomic features were extracted. Three classification models were developed to identify peritoneal and distant metastases (incidence: 21%): a model with clinical variables, a model with radiomic features, and a clinicoradiomic model, combining clinical variables and radiomic features. To exclude features with high mutual correlations, redundancy filtering of the Pearson correlation matrix was performed (r=0.9). A least absolute shrinkage and selection operator (LASSO) regression classifier was trained and evaluated in a 100-times repeated random split, stratified for the presence of peritoneal and distant metastases. Model performances were expressed by the area under the receiver operating characteristic curve (AUC). In addition, subgroup analyses based on Lauren classification were performed. ***Results:*** None of the models could identify metastases with low AUCs of 0.59, 0.51, and 0.56, for the clinical, radiomic, and clinicoradiomic model, respectively. Subgroup analysis of intestinal and mixed-type tumours resulted in low AUCs of 0.67 and 0.60 for the clinical and radiomic model, and a moderate AUC of 0.71 in the clinicoradiomic model. Subgroup analysis of diffuse-type tumours did not improve the classification performance. ***Conclusion:*** Similarly to qualitative assessment of [^{18}F]FDG PET, [^{18}F]FDG-PET-based radiomics did not contribute to the preoperative identification of peritoneal and distant metastases in patients with locally advanced gastric carcinoma. In intestinal and mixed-type tumours, the classification performance of the clinical model slightly improved with the addition of radiomic features, but this slight improvement does not outweigh the laborious radiomic analysis. ***References:*** 1. Gertsen et al. 18F-Fludeoxyglucose-Positron Emission Tomography/Computed Tomography and Laparoscopy for Staging of Locally Advanced Gastric Cancer: A Multicenter Prospective Dutch Cohort Study (PLASTIC). JAMA Surg 2021, 156, e215340.

OP-087
Feasibility and reproducibility of radiomic features in real world whole-body [^{18}F]FDG PET/CT oncology studies
C. S. Constantino, *M. Silva, F. P. M. Oliveira, D. C. Costa;*
Champalimaud Clinical Centre, Champalimaud Foundation, Lisbon, PORTUGAL.

Aim/Introduction: The use of radiomics has been increasing in clinical studies to characterize disease and/or predict treatment response. Our goal is to study the feasibility and reproducibility of radiomic features to characterize lesions in whole-body [^{18}F]FDG PET/CT images from oncology patients. ***Materials and Methods:*** Fifty-three oncologic patients with diverse primary tumors were studied twice in two distinct scanners after a single injection of [^{18}F]FDG (246±60 MBq). The second scan started immediately after the first. Approximately half of the patients performed the first scan in one equipment (Philips GEMINI TF16) and the other half in the other equipment (Philips Digital Vereos). Both acquisition and reconstruction protocols are in accordance with EARL1 standards. Voxels are isotropic (4×4×4 mm^3). Lesions were identified by an experienced nuclear medicine physician and were all visible in both scanner-based images. Then, they were segmented automatically and independently using a validated and robust Bayesian-based method [1]. 103 radiomic features compliant with the image biomarker standardisation initiative (IBSI) were extracted using LIFEx software [2]. They were subdivided into morphological (12), intensity-based (19), histogram intensity-based (17) and textural features (55). The intraclass correlation coefficient (ICC) for absolute agreement between the correspondent lesion features was assessed and used as a measure of reproducibility. ***Results:*** A total of 289 [^{18}F]FDG avid lesions were identified. Following IBSI guidelines, only 103 lesions had the minimum size (>64 voxels) for textural analysis. Thus, only these were included in the statistical analysis. All morphological features showed excellent agreement (ICC≥0.90) between the lesions extracted from the two scanner-based images. Intensity-based features showed good or excellent agreement (ICC≥0.75). The majority of histogram-based features showed moderate to poor agreement, although good agreement in a few cases (0.28≤ICC≤0.86). Textural features had a wide variety of agreement results (0.29≤ICC≤0.96), with more than 50% of the features with poor or moderate agreement. ***Conclusion:*** In the real world application, morphological and intensity-based features are more reproducible than textural and histogram-based features and can be computed in small lesions. Extraction of texture features is only feasible in large lesions; 36% of our dataset. In addition, poor or moderate reproducibility is frequent. Therefore, independently of their value, application in the real world is limited. ***References:*** [1] Constantino et al., Journal of Digital Imaging 2023; https://doi.org/10.1007/s10278-023-00823-y [2] Nioche C. et al., Cancer Research 2018; https://doi.org/10.1158/0008-5472.CAN-18-0125

OP-088

Explainable machine learning model to diagnose giant cell arteritis based on texture features in aortic [18F]FDG-PET images

H. Vries[1,2], *G. van Praagh*[1], *P. Nienhuis*[1], *L. Alic*[2], *R. Slart*[1,2];
[1]*University Medical Centre Groningen, Groningen, NETHERLANDS,* [2]*University of Twente, Enschede, NETHERLANDS.*

Aim/Introduction: Accurate diagnosis for giant cell arteritis (GCA) is important to prevent serious side effects involved in treatment by high-dose glucocorticoids. Current-standard-of-care to diagnose GCA involves 2-deoxy-2-[18F]fluoro-D-glucose([18F]FDG) positron emission tomography (PET) imaging. However, distinguishing between GCA and atherosclerosis can be visually challenging, as both conditions show similar elevated [18F]FDG uptake. Therefore, the primary aim of this study was to investigate the feasibility of an explainable machine learning (ML) model to differentiate between GCA and atherosclerosis in aortic [18F]FDG-PET images. The secondary aim was to compare the ML model with the clinical assessment of the nuclear medicine physician to detect active GCA in follow-up [18F]FDG-PET images. ***Materials and Methods:*** In total, 64 [18F]FDG-PET scans (i.e., 34 with GCA, and 34 with type 2 diabetes mellitus - as this group contains high incidence of atherosclerotic plaques) were retrospectively included. The aorta was delineated into four segments (ascending, arch, descending, and abdominal aorta). From each segment, 93 radiomic features, $SUL_{mean,}$ and SUL_{max} were extracted from each segment. All segments were randomly split into a training (n=190; 80%) and test set (n=48; 20%). A total of 441 ML models were trained using ten-fold cross-validation: i.e., a combination of seven feature selection methods, seven classifiers, and nine individual number of features. Performance of the model was assessed by area under the curve (AUC), accuracy, positive predictive value (PPV), and negative predictive value (NPV). The best performing ML model (based upon test set) was compared to the clinical assessment by a nuclear physician in 19 follow-up scans (7 active GCA, 12 inactive GCA). An occlusion sensitivity map of the follow-up scans was created to illustrate the regions of the aorta contributing to the ML model. ***Results:*** The fifteen-feature model with feature selection method ANOVA and classifier extra-tree-classifier, showed the highest performance (accuracy=0.84, PPV=0.87, NPV=0.81, and AUC=0.91) to distinguish GCA from atherosclerosis. Compared with the clinical report in the follow-up scans, this model showed a higher NPV (0.83 and 0.79), equal accuracy (0.79 and 0.79), and lower PPV (0.71 and 0.80, respectively) in the detection of active GCA. The occlusion map illustrated the descending aorta as important segments contributing to the prediction of the ML model. ***Conclusion:*** The ML model based upon textural features in [18F]FDG-PET scans was able to differentiate GCA from atherosclerosis. The performance of this model was comparable to the clinical report findings in the detection of active GCA in follow-up [18F]FDG-PET.

OP-089

PET-CT Radiomics of Lung Cancer with Local Nodes; Dissemination Features are Linked to Survival

K. Albattat, *C. Marshall, R. Smith, N. Morley;*
Cardiff University, Cardiff, UNITED KINGDOM.

Aim/Introduction: Lymph Node (LN) stage is strongly related to prognosis in Non-Small Cell Lung Cancer (NSCLC). Few studies have investigated PET radiomics with inclusion of metastatic LN. Complex morphology and controversy about integration of multiple sites make this more difficult than analysis of a primary mass, but also likely to be more important. Recent EANM/SNMMI radiomics guideline [1] discusses this issue. We utilize a dissemination feature and asses it's performance along with radiomic features (RF) from LNs in assessing NSCLC survival. ***Materials and Methods:*** 224 LNs from 208 patients with NSCLC, stage IIb-IIIB (N≥1) were included. Primary endpoint was overall survival in days (OS) over a 3-year follow-up. LNs segmented and analysed as a single structure. Several lesion RF selection/aggregation methods were explored e.g. the average RFs from the lesions (LNs) (model 1), RFs from LNs with highest SUV (model 2), RFs from LNs with largest MTV (model 3) and conventional metrics (SUVmax, MTV, TLG etc.) along with a dissemination feature (average distance of all nodes from primary) (model 4). 204 RFs (5 conventional PET, 23 morphological, 41 intensity, 135 texture) were extracted for an assessment of patient-level disease burden. Multivariate regression prognostic models assessed RF's correlation with OS. Univariate testing initialized variable selection, multicollinearity was assessed using the variance inflation factor. 8 RF with P values (<0.05) were included (stat-COV, GLCM-contrast, GLRLM-glnu, GLRLM-percentage, GLSZM-hgze, GLSZM-szhge, GLDZM-variance, NGTD-complexity). Regression coefficients, hazard ratios and confidence intervals were estimated for the models. ***Results:*** GLRLM-percentage and GLSZM-szhge from model 1 showed significantly higher prediction of OS (HR 7.172 P-value 0.007 and HR 4.752 p-value 0.029 respectively). None of the RFs from model 2 or model 3 showed significant prediction of OS. An interesting initial finding is that the dissemination features (node-tumor spread by measuring Euclidian distance) from dataset of patients with > 2 metastatic LNs showed significant prediction of survival rate (HR 5.729, p-value 0.017) as compared to the textural RFs extracted from this cohort, which displayed no significant predictive ability. Risk of death in NSCLC with more than 2 metastatic LNs demonstrates a ~6-fold increase. ***Conclusion:*** This early work investigating different approaches for assessing radiomics of metastatic lymph nodes. We demonstrate a dissemination feature is highly predictive of survival that could contribute to discussions of clinical prognosis. Embracing radiomics of multiple disease sites will be crucial to advance this work. ***References:*** [1] Joint EANM/SNMMI guideline on radiomics in nuclear medicine (2023)

OP-090

The Effect of Feature Selection Methods on Prognostic Analysis of 18F-FDG PET Radiomics in Lymphoma

L. Yong[1], *X. Wong*[1], *Y. Chen*[2,3], *S. Liu*[1,3], *H. Lin*[4,5], *K. Lue*[1];
[1]*Tzu Chi University of Science and Technology, Hualien, TAIWAN,* [2]*Tzu Chi University, Hualien, TAIWAN,* [3]*Hualien Tzu Chi Hospital, Hualien, TAIWAN,* [4]*Chang Gung University, Taoyuan, TAIWAN,* [5]*Keelung Chang Gung Memorial Hospital, Keelung, TAIWAN.*

Aim/Introduction: 18F-FDG PET radiomic features have prognostic value in patients with lymphoma. However, it is unclear whether different feature selection methods affect survival prediction outcomes. This study aimed to investigate the performance of various feature selection methods for 18F-FDG PET radiomics-based survival prediction in patients with lymphoma. ***Materials and Methods:*** One hundred and eleven patients with a pathological diagnosis of lymphoma who underwent baseline 18F-FDG PET were retrospectively enrolled in our study. The 18F-FDG-avid lesions were segmented using a standardised uptake value threshold above 4.0 to measure the total metabolic tumour volume (TMTV). The volumes of interest based on TMTV were used to compute 93 radiomic features. To ensure generalisability, we

preselected 22 radiomic features that were robust to the ^{18}F-FDG tracer uptake time, image acquisition/reconstruction parameters, and respiratory motion. Six feature-selection approaches were employed for the preselected features, encompassing filter, wrapper, and embedded types. After selecting the features, the Cox proportional hazard regression models were used to assess their correlation with progression-free survival (PFS) and overall survival (OS). The prognostic performances of the models were evaluated using the Harrell's C-index. The survival curve was plotted using the Kaplan-Meier method, and the survival difference between subgroups was estimated using a log-rank test. ***Results:*** The median follow-up period of the patients was 47.9 months (interquartile range, 18.7-86.9 months). The 5-year PFS and OS rates were 58.6% 67.8%, respectively. Our results indicated that different feature selection approaches (based on chi-square test, minimum redundancy, maximum relevance, Relief algorithm, support vector machine, random forest, and least absolute shrinkage selection operator) identified different potential radiomic features for survival prediction. The multivariate Cox analysis further identified features that maintained prognostic significance. Prognostic models were constructed by integrating the Ann Arbor stage and TMTV (widely suggested as a prognostic factor in the literature) with selected radiomics features using estimated Cox regression coefficients. Survival curves showed significant differences in PFS and OS among the distinct risk groups. The C-indices for evaluating the survival prediction performance (ranging from 0.630 to 0.673 for both PFS and OS) did not significantly differ among the feature selection approaches. ***Conclusion:*** Different feature selection approaches can be used to identify different radiomic features for survival prediction. The performance of the prognostic model based on the selected radiomic features was comparable. A standardised feature selection method should be considered for ^{18}F-FDG PET radiomics-based survival predictions for lymphomas.

OP-091

Exploring Correlations between PSA Levels and PSMA-PET Images in Recurrent Prostate Cancer using Machine Learning, Tensor Radiomics and Deep Features Analysis

A. Toosi[1], *S. Harsini*[2], *H. Abdollahi*[1], *F. Bénard*[2,3], *C. F. Uribe*[2,3], *A. Rahmim*[1,4,3];
[1]*Department of Integrative Oncology, BC Cancer Research Institute, Vancouver, BC, CANADA,* [2]*BC Cancer, Vancouver, BC, CANADA,* [3]*Department of Radiology, University of British Columbia, Vancouver, BC, CANADA,* [4]*Department of Physics and Astronomy, University of British Columbia, Vancouver, BC, CANADA.*

Aim/Introduction: While prostate-specific antigen (PSA) is a widely used biomarker for prostate cancer (PCa) diagnosis and treatment decisions, its correlation with prostate-specific membrane antigen (PSMA) positron-emission tomography/computed tomography (PET/CT) imaging findings is still being investigated. We aimed to study correlations between PSA level at PET/CT and characteristics of metastatic lesions on PSMA PET images. ***Materials and Methods:*** This is a post-hoc analysis of a prospective clinical trial. In 380 whole-body [^{18}F]DCFPyL PET/CT images of patients with biochemical recurrence following initial curative-intent treatment, all active lesions were delineated by a nuclear medicine physician. Each image had 1.92±1.21 lesions with average active volume of 4.03±7.02 ml. One hundred fifty radiomics features were calculated on the most active lesions. Nine different filters were utilized in radiomics features extraction. Six pre-trained CNNs were used for deep feature extractors. Random forest regression models were trained to predict the PSA levels at PET/CT. To better highlight the relation between metastatic tumors' features and the corresponding PSA levels, PSA levels were dichotomized in a range (2 - 20 ng/mL). Two classification methods were used to investigate the relation between the PSA range and the features of the most active metastatic lesions. Fifty-repetition-5-fold cross-validation was used for evaluations. ***Results:*** Pearson correlation analysis of 10 highest scoring features showed a range of correlations of 0.2 to 0.39 (negative and positive) between the most active lesion's features and the PSA levels. Highest correlated features are related to the entropy features of lesions (0.38-0.39). Besides, only one feature is extracted from CT images while others are from filtered PET images. Classification analysis on the range of PSA levels shows a consistent pattern indicating that with a cut-off between 14 to 16, there is a strong relation between the appearance of metastatic lesions and PSA levels. Comparing classification results of tensor radiomics [1] and deep features, there is a visible increase in area under the ROC curve using deep features to explain the appearance of the metastatic lesions (AUC 0.6-0.8). ***Conclusion:*** The correlation we observed between the extracted radiomics features of metastatic PCa lesions and the PSA level suggests that these features could be used as additional biomarkers to assess disease progression and guide treatment decisions. Further studies are warranted to validate these findings and optimize their clinical utility. ***References:*** [1] Rahmim, Arman, et al. "Tensor Radiomics: Paradigm for Systematic Incorporation of Multi-Flavoured Radiomics Features." arXiv preprint arXiv:2203.06314 (2022).

OP-092

Improving Outcome Prediction in Multicentric Data: Novel Harmonization Techniques and MCA-Based Imputation for Radiomic Feature Analysis

N. Abdallah[1], *J. Marion*[2], *C. Tauber*[1], *T. Carlier*[3], *P. Chauvet*[2], *M. Hatt*[4];
[1]*Imaging & Brain, INSERM, Tours, FRANCE,* [2]*LARIS, Angers, FRANCE,* [3]*CRCINA, INSERM, CNRS, Université d'Angers, Université de Nantes, Nantes, FRANCE,* [4]*LaTIM, INSERM, Brest, FRANCE.*

Aim/Introduction: This study aimed at developing an outcome prediction pipeline incorporating novel harmonization techniques to explicitly address the multicentric nature of the data and to evaluate the benefit of imputing missing clinical variables using Multiple Correspondence Analysis (MCA). ***Materials and Methods:*** We proposed two ComBat-alternative harmonization techniques, including rescaling data through mean and standard deviation, and rescaling based on the extent of variable distribution. Missing clinical variables were imputed using MCA, and its effectiveness was compared to other popular machine learning-based methods (Extra Trees and K-Nearest Neighbours). We conducted sensitivity analyses on the imputer and survival methods' hyperparameters. Our survival analysis methods included Random Survival Forest (RSF) and Gradient Boosting (GB). We used the HECKTOR 2021 dataset containing 325 head and neck cancer patients from six clinical centers for evaluation, which included FDG PET/CT images. Moreover, clinical variables such as age, gender, T, N, and M stages, treatment, and HPV status were available but with missing values, particularly for HPV status (e.g., ~65 patients provided HPV status, and 74 patients reported tobacco and alcohol status). All models were evaluated using the concordance index (C-index) on the test set (101 patients out of the 325). ***Results:*** The best model achieved a c-index of 0.73 (beating the

highest score of 0.72 in in HECKTOR), using radiomic features and MCA-based imputation. The harmonization approach increased the c-index from 0.655 to 0.715 using RSF and from 0.668 to a maximum of 0.721 using GB. The first harmonization approach achieved a maximum c-index of 0.712 using RSF and 0.717 using GB. ComBat also showed comparable performance with a maximum c-index of 0.713 using RSF and 0.719 using GB. Results obtained with the Extra Trees and K-Nearest Neighbours methods were poor (0.57 and 0.55, respectively). ***Conclusion:*** This study emphasizes the importance of imputation and harmonization in a multicentric context. The proposed harmonization techniques and MCA-based imputation significantly improved models performance. One advantage of these harmonization transformations is their applicability to novel datasets without the need to retrain the model, like for ComBat. Further research is needed to enhance imputation and harmonization techniques. Future work will focus on strengthening these results using the larger HECKTOR 2022 dataset.

OP-093

DEBI-NN: Distance-Encoding Biomorphic-Informational Neural Networks in PET Radiomics

B. Ecsedi, *D. Haberl, C. P. Spielvogel, T. Traub-Weidinger, M. Hacker, L. Papp;*
Medical University of Vienna, Vienna, AUSTRIA.

Aim/Introduction: Modern artificial neural networks (ANNs) are challenging to apply in fields operating with small, albeit representative healthcare data and are prone to overfitting due to their large trainable parameter counts. A novel distance-encoding biomorphic-informational neural network (DEBI-NN) [1] has been proposed to significantly minimise the number of trainable parameters compared to traditional ANNs. For a 3D animation of the DEBI-NN training example, see [2]. This analysis aims to investigate the predictive performance of DEBI-NN in comparison with a traditional neural network (NN) model in the selected PET radiomic datasets that are small, albeit clinically relevant and challenging to be leveraged by most ANNs. ***Materials and Methods:*** This study involved 86 ^{11}C-MET PET glioma cases to predict three-year survival [3], and 52 [^{68}Ga]Ga-PSMA-11 prostate cancer cases to predict low-vs-high risk [4]. A 100-fold Monte Carlo cross-validation scheme was performed with 90-10% train-test ratio in both cohorts. Data pre-processing including redundancy reduction, class imbalance correction, and feature ranking was performed in all training subsets. Confusion matrix analytics were utilised across all test subset cohorts. The analysis was conducted on the DEBI-NN in comparison with a fully-connected feedforward neural network with harmonised and comparable network configurations and hyperparameters. ***Results:*** The DEBI-NN yielded a balanced accuracy (arithmetic mean of sensitivity and specificity) of 65% and 74%, while the baseline NN produced 63% and 50%, resulting in a difference of +2% and +24% for the glioma and prostate datasets, respectively. In the prostate cancer cohort, in particular, the DEBI-NN resulted in a more balanced classifier with 72% sensitivity and 75% specificity compared to the baseline NN which yielded 100% sensitivity and 0% specificity. ***Conclusion:*** While small medical datasets remain a challenge for traditional ANNs to successfully utilise, our initial findings are encouraging for clinical applications. The DEBI-NN - operating with a fraction of the trainable parameters in conventional NNs - has shown a more balanced behaviour over the baseline NN, even on datasets with high imbalance. Our findings imply the DEBI-NNs have the potential to become widely applicable in future radiomic studies.

References: [1] Papp, L., et al. (2022). DOI: 10.21203/rs.3.rs-2384764/v1[2] https://youtu.be/S4Dj5qc7Rno[3] Papp, L., et al. (2018). DOI: 10.2967/jnumed.117.202267[4] Papp, L., et al. (2021). DOI: 10.1007/s00259-020-05140-y

306

Sunday, September 10, 2023, 9:45 AM - 11:15 AM
Hall C

Clinical Oncology Track - Featured Session: Haematological Disease

OP-094

Haematological Disease

OP-095

Significance of ^{11}C-acetate PET/CT for the prediction of complete remission post induction therapy in newly diagnosed multiple myeloma: a prospective study

S. Chen, *Y. Wong, K. Wu, J. C. Chim, C. Ho;*
Hong Kong Sanatorium & Hospital, Hong Kong, HONG KONG.

Aim/Introduction: The International Myeloma Working Group (IMWG) has recently accepted PET/CT as a new modality for assessment of Bone status in the "CRAB" criteria for evaluation of organ damage in active multiple myeloma (MM). Our previous studies showed that ^{11}C-acetate (ACT) was a better molecular biomarker than ^{18}F-FDG (FDG) for diagnosis and prognostic prediction of active MM. On the other hand, the advent of novel agents in induction therapy for MM improves the complete remission (CR) rate. In this prospective study, we aim to evaluate whether baseline ACT-PET/CT might predict CR post induction therapy in newly diagnosed MM. ***Materials and Methods:*** From Mar-2019 to Dec-2021, clinically suspected MM patients were referred for ACT and FDG (dual-tracer) PET/CT. Clinical criteria for active MM was ≥10% clonal plasma cells in bone marrow plus at least one CRAB criterion defined by IMWG. PET/CT criteria for active MM were: (1) focally hypermetabolic bone lesions (FBLs) avid for ACT or FDG, and/or (2) diffusely increased marrow metabolism with L3 vertebra ACT-SUV$_{max_}$L3>=3.8 or FDG-SUV$_{max_}$L3>=3.0 (from prior database). Induction therapy to active MM patients was initiated after baseline PET/CT. Post-induction MM patients achieving "serological CR" (by IMWG criteria) underwent post-treatment dual-tracer PET/CT for evaluation of "molecular CR": metabolic quiescence in all the FBLs with ACT-SUV$_{max_}$L3<3.8 and FDG-SUV$_{max_}$L3<3.0. The pretreatment factors for univariate prediction of CR were: (1)%clonal bone marrow plasma cells, (2) beta-2 microglobulin, (3)no. of ACT-avid FBLs, (4)ACT-SUV$_{max_}$L3; (5)no. of FDG-avid FBLs, (6)FDG-SUV$_{max_}$L3. ROC curve analysis was performed. ***Results:*** 62 patients (M:F=32:30; age range:44-87 years, mean=59.7±9.7 years) were finally confirmed as active MM by IMWG criteria. ACT-PET/CT identified 59/62 (95.2%) and FDG-PET/CT identified 34/62 (54.8%). After induction therapy, 39/62 (62.9%) patients achieved serological CR, and of these 39 serological CR patients, 35/39 (89.7%) achieved molecular CR, while 4/39 (10.3%) patients had minimal residual disease in FBLs or mild ACT activity in bone marrow seen on PET/CT, hence continued with consolidation therapy. Among all the 6 pretreatment factors, only ACT-SUV$_{max_}$L3 was the significant predictor for CR post induction therapy (SUV$_{max_}$L3=4.59+/-1.62 vs. 6.88+/-1.86 for CR vs. non-CR).

ROC curve analysis identified baseline "ACT-SUV_{max}_L3<5.45" as the cut-off for the prediction of CR (AUC=0.834, P<<0.05). ***Conclusion:*** ^{11}C-acetate is the preferred molecular PET biomarker for diagnosis and prediction of CR after induction therapy in MM. It is also a recommended PET tracer to monitor residual disease. MM patients achieving serological plus molecular CR need further follow-up to evaluate overall survival.

OP-096

A prospective comparison of ^{68}Ga-Pentixafor PET/CT and ^{18}F-FDG PET/CT for the detection of intramedullary and extramedullary lesions in multiple myeloma

S. Tang*, Y. Wang, Y. Tian, C. Li, Z. Xiao, J. Chen, Y. He;*
Department of nuclear medicine, Zhongnan Hospital of Wuhan University, Wuhan, Hubei, CHINA.

Aim/Introduction: Chemokine receptor 4 (CXCR4) is a key factor for tumor growth and metastasis in multiple myeloma (MM). Since ^{18}F-FDG PET/CT has some limitations in evaluating MM, we design the study to compare the ability of ^{68}Ga-Pentixafor PET/CT targeting CXCR4 and ^{18}F-FDG PET/CT for the detection of intramedullary and extramedullary lesions in MM. ***Materials and Methods:*** The study included 38 newly diagnosed MM patients who had undergone paired ^{68}Ga-Pentixafor PET/CT and ^{18}F-FDG PET/CT in a week. The diagnostic performance of the two tracers was calculated and compared for intramedullary and extramedullary lesions with the reference standards from histopathological findings, typical radiological appearances, and clinical imaging follow-up. Intramedullary lesions were divided into seven regions (skull, cervical spine, thoracic spine, lumbar spine, pelvis, long bones, ribs and the rest) and scored by a scoring system to compare. The characteristics of extramedullary lesions in each patient were recorded for two imaging methods separately. Furthermore, we assessed the maximum standardized uptake value (SUVmax), tumor-to-mediastinal blood pool ratio (TBR), and tumor-to-liver ratio (TLR) for paired positive patients in both intramedullary and extramedullary lesions. ***Results:*** ^{68}Ga-Pentixafor PET/CT had a higher positive rate than ^{18}F-FDG PET/CT in subjects (97.4% [37/38] vs. 73.7% [28/38], p< 0.05). In intramedullary lesions analysis, the scores of each region and the total of the whole bone marrow were all significantly higher in ^{68}Ga-Pentixafor PET/CT than in ^{18}F-FDG PET/CT (all p< 0.05). It also showed higher median SUVmax (11.95 vs. 4.90), TBR (3.81 vs. 1.80), and TLR (3.82 vs. 1.29) than those with ^{18}F-FDG PET/CT in the intramedullary lesions (all p< 0.05). As for extramedullary lesions, ^{68}Ga-Pentixafor PET/CT showed slightly more patients with positive extramedullary lesions (50% [19/38] vs. 47.4% [18/38]) and with mildly higher median SUVmax (10.00 vs. 7.10), TBR (3.27 vs. 2.61), although neither of them had statistical difference (all p> 0.05). However, the TLR of ^{68}Ga-Pentixafor PET/CT was approximately two times that of ^{18}F-FDG PET/CT in extramedullary lesions (3.85 vs. 2.16, p< 0.05). Especially for lymph nodes of extramedullary lesions, ^{68}Ga-Pentixafor PET/CT detected more positive lesions than ^{18}F-FDG PET/CT (43 vs. 26, p< 0.05). ***Conclusion:*** ^{68}Ga-Pentixafor PET/CT is significantly more sensitive than ^{18}F-FDG PET/CT in all regions of intramedullary lesions. As for detecting extramedullary lesions, ^{68}Ga-Pentixafor PET/CT has a slight advantage over ^{18}F-FDG PET/CT. Moreover, it has a better positive rate in hematogenous spread lymph nodes by lesion-based analysis, which shows the potential for prognostic stratification.

OP-097

Assessment of the Diagnostic and Staging Potential of ^{68}Ga-Pentixafor PET/CT in Multiple Myeloma - A Comparison With ^{18}F-FDG PET/CT

L. Aridhasan Meenakshi*, V. Rajaraman, B. Dubashi, D. Halanaik;*
Jawaharlal Institute of Postgraduate Medical Education and Research, Puducherry, INDIA.

Aim/Introduction: ^{68}Ga-Pentixafor Positron Emission Tomography/ Computed Tomography (PET/CT) localises the expression of Chemokine receptor-4 (CXCR4), a receptor which is overexpressed in Multiple Myeloma. We aim to assess and compare the diagnostic and staging potential of ^{68}Ga-Pentixafor with ^{18}F-Fluorodeoxyglucose (FDG) PET/CT. ***Materials and Methods:*** Twenty-one (10F; 11M; Median Age= 57.7 years) newly diagnosed treatment-naive Multiple Myeloma patients were enrolled prospectively from January 2021 to April 2023. All participants underwent ^{68}Ga-Pentixafor and ^{18}F-FDG PET/CT imaging within one week. ^{68}Ga-Pentixafor (130-174 MBq) was injected intravenously followed by PET/CT acquisition at 45 minutes. The positivity rate and pattern of disease involvement were evaluated for both tracers. Quantitative parameters including Standardised Uptake Value - Maximum (SUVmax) and Tumour-to-Background Ratio (TBRmax) were calculated and compared for both tracers. Durie Salmon Plus (DSP) Stage was assigned based on CT, ^{68}Ga-Pentixafor PET/CT and ^{18}F-FDG PET/CT separately. ***Results:*** 68Ga-Pentixafor PET/CT showed a higher positivity rate of 100% (21/21), as compared to 90.5% (19/21) with ^{18}F-FDG PET/CT. ^{68}Ga-Pentixafor PET/CT showed significantly (p=0.028) higher TBRmax values (5.5; IQR6.6) as compared to ^{18}F-FDG PET/CT (2.2; IQR1.61). However, no significant difference (p=0.053) in SUVmax values was observed between ^{68}Ga-Pentixafor PET/CT (3.3; IQR 2.97) and ^{18}F-FDG PET/CT (2.2; IQR1.61). ^{68}Ga-Pentixafor PET/CT and ^{18}F-FDG PET/CT detected paramedullary lesions in 11 and 9 patients, respectively. One extramedullary lesion in the renal cortex was picked up by both modalities. Three patients had extramedullary ^{68}Ga-Pentixafor uptake but no ^{18}F-FDG uptake, of which one was histopathologically evaluated, and found to be benign. SUVmax and TBRmax of both tracers did not show any significant correlation with plasma cell percentage and beta-2-microglobulin levels. Out of 21 patients, 14 patients fell under the same DSP stage in CT, ^{18}F-FDG and ^{68}Ga-Pentixafor PET/CT. 2 patients (10%) were upstaged by ^{18}F-FDG PET/CT and 6 patients (29%) were upstaged by ^{68}Ga-Pentixafor PET/CT. ***Conclusion:*** A significant proportion of patients undergo a change in staging and prognostication due to the higher disease burden estimation by ^{68}Ga-Pentixafor PET/CT as compared to ^{18}F-FDG PET/CT. Improved comprehension of tumour heterogeneity in Multiple Myeloma can be achieved through the use of dual tracer imaging. With the recent progress in CXCR4-based therapeutics, the expanding role of ^{68}Ga-Pentixafor imaging in Multiple Myeloma is inevitable. ***References:*** Pan Q et al. Chemokine receptor-4 targeted PET/CT with 68Ga-Pentixafor in assessment of newly diagnosed multiple myeloma: comparison to 18F-FDG PET/CT. Eur J Nucl Med Mol Imaging. 2020 Mar;47(3):537-46.

OP-098

Prognostic value of FDG PET/CT biomarkers in patients withrecurrent/refractary MM treated with CAR-T Cells

V. Betech-Antar, *F. Minguez, L. Tamariz, A. Bronte, M. Romera, J. Rosales, J. Bastidas, S. Menendez-Sanchez, M. Panizo, S. Huerga, J. San-Miguel, P. Rodriguez-Otero, M. García-Velloso;*
Clínica Universidad de Navarra, Pamplona, SPAIN.

Aim/Introduction: To analyse the prognostic value of FDG PET/CT biomarkers at diagnosis, 1-month and 3-months after treatment with CAR-T Cells in patients with recurrent/refractary MM ***Materials and Methods:*** Whole-body ^{18}F-FDG PET/CT scans were performed in patients with recurrent MM before and after Chimeric antigen receptor T-cell (CAR-T) therapy targeted against B-cell maturation antigen (BCMA). The five-point Deauville scale (DS) was applied to describe 18F-FDG uptake in bone marrow (BM) and focal lesions (FL). The number of FL, presence of paramedullary disease (PMD) and extramedullary disease (EMD) were recorded. ***Results:*** Fifty-nine patients (29 male, 30 female; median age 59 years) were included. One-month after CAR-T 14/59 (23.7%) patients had complete response by PET (PETCR), and 3-months after CAR-T 13 more patients (22%) achieved PETCR. Patients without PETCR 3-months after CAR-T had shorter PFS (median 5.3 months [95% CI 2.5- 10.8] versus 11.9 [95% CI 5.7 - 16] (p = 0.001) and shorter OS (median 7.8 months [95% CI 5.1 - 18.4] versus 16 [95% CI 8.9 - 25.9] (p = 0.004); than those with PETCR (n = 24 [44%]). ***Conclusion:*** These results indicate that PET-CR can predict durable remission after CAR-T Cells. Further analysis with larger population could inform early post-CAR-T management and response-adapted stratification in clinical trials.

OP-099

Multicenter development of a PET-based risk assessment tool for product-specific outcome prediction in large B-cell lymphoma patients undergoing CAR T-cell therapy

C. Voltin[1], *S. Flossdorf*[2], *A. Paccagnella*[3], *M. Winkelmann*[4], *J. Heger*[1], *B. Casadei*[3], *L. Beckmann*[1], *K. Herrmann*[2], *N. Kutsch*[1], *P. Borchmann*[1], *S. Fanti*[3], *W. G. Kunz*[4], *M. Subklewe*[4], *C. Kobe*[1], *P. L. Zinzani*[3], *M. Stelljes*[5], *K. S. Roth*[1], *A. Drzezga*[1], *R. Noppeney*[2], *H. C. Reinhardt*[2], *B. von Tresckow*[2], *R. Seifert*[2,5], *J. C. Albring*[5], *V. Blumenberg*[4], *A. Farolfi*[3], *P. Gödel*[1], *C. Hanoun*[2];
[1]*University of Cologne, Cologne, GERMANY,* [2]*University of Duisburg-Essen, Essen, GERMANY,* [3]*University of Bologna, Bologna, ITALY,* [4]*Ludwig Maximilian University of Munich, Munich, GERMANY,* [5]*University of Münster, Münster, GERMANY.*

Aim/Introduction: Chimeric antigen receptor (CAR) T-cell therapy fundamentally changed the management of individuals with relapsed and refractory large B-cell lymphoma. However, real-world data have shown divergent outcomes for the approved constructs. The present study therefore aimed to evaluate potential risk factors in a larger cohort. ***Materials and Methods:*** Our analysis set included 88 patients, from four German university hospitals and one Italian center, who underwent ^{18}F-fluorodeoxyglucose positron emission tomography (PET) before CAR T-cell therapy with tisagenlecleucel (n = 62) or axicabtagene ciloleucel (n = 26). We first determined the predictive value of conventional risk factors, treatment lines, and response to bridging therapy for progression-free survival (PFS) through forward selection based on Cox regression. In a second step, the additive potential of two common PET parameters was assessed. Their optimal dichotomizing thresholds were calculated individually for each CAR T-cell construct. ***Results:*** Extra-nodal involvement emerged as the most relevant of conventional tumor and patient characteristics. Moreover, we found that inclusion of metabolic tumor volume (MTV) further improves outcome prediction. The hazard ratio for a PFS event was 1.68 per unit increase of our proposed risk score (95% confidence interval [1.20, 2.35], p = 0.003) which comprised both lymphoma burden and extra-nodal disease. While the most suitable MTV cut-off among patients receiving tisagenlecleucel was 11 mL, a markedly higher threshold of 259 mL showed optimal predictive performance in those undergoing axicabtagene ciloleucel treatment. ***Conclusion:*** Our analysis demonstrates that the presence of more than one extra-nodal lesion and higher MTV in large B-cell lymphoma are associated with inferior outcome after CAR T-cell treatment. Based on an assessment tool including these two factors, patients can be assigned to one of three risk groups. Importantly, as shown by our study, metabolic tumor burden might reflect the extent of bridging therapy needed individually for each construct.

OP-100

Performance of PET/CT using [^{18}F]Fludarabine for initial staging and therapeutic evaluation of symptomatic multiple myeloma (MM) patients in first line treatment or first relapse : preliminary results of an exploratory multicenter phase 2 study

C. François[1], *M. Santiago-Ribeiro*[2,3], *B. Jamet*[4], *S. Guillouet*[5], *C. Perrio*[5], *A. Abbas*[6], *F. Gourand*[5], *S. Querellou*[7,8], *T. Chalopin*[9], *C. Dubegny*[4], *C. Touzeau*[10,11], *N. Blin*[10,11], *F. Kraeber-Bodéré*[4,11], *C. Bodet-Milin*[4,11];
[1]*Nuclear Medicine department, Lille University Hospital, Lille, FRANCE,* [2]*Nuclear Medicine department, Tours University Hospital, Tours, FRANCE,* [3]*UMR 1253, iBrain, Université de Tours, Inserm, Tours, FRANCE,* [4]*Nuclear Medicine department, Nantes University Hospital, Nantes, FRANCE,* [5]*Normandie Univ, UNICAEN, CEA, CNRS, UAR 3408 Cyceron, Bd Henri Becquerel, 14000, Caen, FRANCE,* [6]*Normandie univ, UNICAEN, PSL Université Paris, EPHE, INSERM, U1077, CHU de Caen, GIP Cyceron, Neuropsychologie et Imagerie de la Mémoire Humaine, 14000, Caen, FRANCE,* [7]*Nuclear Medicine department, Brest University Hospital, Brest, FRANCE,* [8]*GETBO UMR U_1304, Inserm, UBO, Brest, FRANCE,* [9]*Hematology department, Tours University Hospital, Tours, FRANCE,* [10]*Hematology department, Nantes University Hospital, Nantes, FRANCE,* [11]*Nantes Université, Angers Université, INSERM, CNRS, CRCI2NA, Nantes, FRANCE.*

Aim/Introduction: [^{18}F]Fludarabine showed promising results in human lymphoproliferative disease imaging and in a murine MM model. To investigate its potential usefulness in human MM, we propose a prospective phase II clinical study comparing ^{18}F-Fludarabine-PET/CT (FludaPET) with ^{18}F-FDG-PET/CT (FDG-PET) for initial staging and therapeutic evaluation of symptomatic MM patients. ***Materials and Methods:*** This study aims to include 35 symptomatic MM patients according to IMWG criteria. Whole-body PET/CT are acquired 60 minutes after injection of 4 MBq/kg of [^{18}F]Fludarabine and 3 MBq/kg of [^{18}F]FDG. PET/CT are interpreted by MM experts nuclear medicine physicians defining focal lesion (FL), paramedullary disease (PMD), extra-medullary disease (EMD), and diffuse bone marrow involvement (BMI). The maximal standardized uptake value (SUVmax) and the target to pool ratio (TBR), defined as SUVmax/SUVblood pool, are calculated for BMI, FL, PMD and EMD. ***Results:*** At the time of analysis, 9/35 patients were included, 7 underwent both FludaPET and FDG-PET (2 screen failures). Both FludaPET and FDG-PET were performed for initial staging. No adverse effects were reported. Per-patient analysis : PET/CT showed abnormalities in all 7 patients, with 1 normal FludaPET and 2 normal FDG-PET. FludaPET and FDG-PET were concordant for patient 2 with FL+PMD and discordant for the 6 other patients :

for patients 1 and 5, FL+BMI with FludaPET and FL with FDG, for patient 3 BMI with FludaPET but FL with FDG, for patient 4 FL with FDG but negative FludaPET and, for patients 6 and 7 BMI with FludaPET and negative FDG-PET. Per-lesion analysis : FludaPET detected 11 FL, 1 PMD and 5 BMI, while FDG-PET identified 25 FL, 1 PMD and no BMI. In total, both methods detected 27 FL, 1 PMD and 5 BMI. SUVmax and TBR of FL/PMD ranged from 2.6 to 5.05 and 1.63 to 3.78 with FludaPET, and from 3 to 13.20 and 1.3 to 3.88 with FDG, respectively. For BMI, SUVmax and TBR ranged from 3.77 to 5.43 with FDG and from 2.23 to 4.08 with FludaPET. Fluda-PET showed uptake in supra and infra-diaphragmatic lymph nodes in 4 patients, but its nature remains unclear at the time of analysis. In 3 patients, FDG-PET detected bone and vertebral fractures, without significant [^{18}F]Fludarabine uptake, consistent with weaker [^{18}F]Fludarabine uptake in inflammatory processes. High presumably physiological splenic uptake was also observed (SUVmax 3.85-7.48). ***Conclusion:*** These first images of ^{18}F-fludarabine-PET/CT in MM suggest potential complementarity with ^{18}F-FDG-PET/CT, particularly for the detection of BMI.

OP-101

Patterns of PET positive residual tissue at early interim staging and risk of treatment failure in advanced-stage Hodgkin's Lymphoma: an analysis of the randomized phase III HD18 trial by the German Hodgkin Study Group

J. Ferdinandus[1], *L. van Heek*[1], *K. S. Roth*[1], *M. Dietlein*[1], *H. Eich*[2], *C. Baues*[1], *P. Borchmann*[1], *C. Kobe*[1], *German Hodgkin Study Group;*
[1]*University Hospital Cologne, Cologne, GERMANY,*
[2]*University Hospital Münster, Münster, GERMANY.*

Aim/Introduction: The randomized phase III HD18 trial introduced PET-2 adapted chemotherapy with eBEACOPP and demonstrated that reduction of chemotherapy in PET-2 negative patients is possible without loss of efficacy. [1] The aim of this study is to describe the patterns of PET-2 positivity in HD18 and determine wether multifocal residual disease is associated with inferior progression-free survival (PFS) compared to uni- or oligofocal disease. ***Materials and Methods:*** We analyzed data from all PET-2 positive patients included in HD18 (NCT00515554). Residual tissue was visually compared with reference regions according to the Deauville score (DS). PET-2 positivity was defined as residual tissue with uptake above the liver (DS4). PFS was defined as the time from completion of staging until progression, relapse, or death from any cause, or to the day when information was last received on the patient's disease status and analyzed according to Kaplan-Meier, using Cox regression for comparisons. ***Results:*** Between May 2008 and July 2014, 2101 patients aged 18-60 years with newly diagnosed, advanced-stage cHL were recruited in HD18. Of these, 480 patients had a positive PET-2 (DS4) and were therefore eligible for this analysis. The upper and lower mediastinum was involved in almost half of all patients: 230 (47.9%) and 195 (40.6%), respectively. A majority of patients had few positive regions in PET-2; 210 (43.8%) had one positive region, and 1-2 or 1-3 involved regions were observed in 372 (77.5%) and 433 (90.2%) patients, respectively. 5y-PFS for patients with 1-2 regions was 91.2% (CI95: 88.2-94.2) vs. 81.2% (CI95: 73.6% vs 89.5%) for those with >2 regions with a corresponding hazard ratio of 2.1 (CI95: 1.2-3.8). ***Conclusion:*** PET-2 positive residuals of cHL are most often located in the mediastinum and a majority of patients have 1-2 affected regions. In comparison, risk of progression was twofold higher in patients with more than two positive regions in PET-2. ***References:*** [1] Borchmann P, Goergen H, Kobe C, et al. PET-guided treatment in patients with advanced-stage Hodgkin's lymphoma (HD18): final results of an open-label, international, randomised phase 3 trial by the German Hodgkin Study Group. Lancet. 2017 Dec 23;390(10114):2790-2802. doi: 10.1016/S0140-6736(17)32134-7. Epub 2017 Oct 20. PMID: 29061295.

OP-102

Combining Baseline and End of Treatment Quantitative PET Parameters to Improve Progression-Free Survival Prediction in DLBCL

G. Zwezerijnen[1], *A. L. Bes*[2], *M. W. Heymans*[3], *U. Dührsen*[4], *J. Eertink*[2], *S. Wiegers*[1], *P. Lugtenburg*[5], *A. Hüttmann*[4], *L. Kurch*[6], *C. Hanoun*[4], *N. Mikhaeel*[7], *L. Ceriani*[8], *E. Zucca*[9], *S. Czibor*[10], *T. Györke*[10], *M. Chamuleau*[2], *S. Fanti*[11], *S. Lee*[12], *J. Zijlstra*[2], *S. Barrington*[13], *R. Boellaard*[1];
[1]*Amsterdam UMC, Vrije Universiteit Amsterdam, department of Radiology and Nuclear Medicine, Cancer Center Amsterdam, Amsterdam, NETHERLANDS,* [2]*Amsterdam UMC, Vrije Universiteit Amsterdam, department of Hematology, Cancer Center Amsterdam, Amsterdam, NETHERLANDS,* [3]*Amsterdam UMC, Vrije Universiteit Amsterdam, department of Epidemiology and Data Science, Amsterdam Public Health research institute, Amsterdam, NETHERLANDS,* [4]*Department of Hematology, West German Cancer Center, University Hospital Essen, University of Duisburg-Essen, Essen, GERMANY,* [5]*Erasmus MC Cancer Institute, University Medical Center Rotterdam, department of Hematology, Rotterdam, Rotterdam, NETHERLANDS,* [6]*Klinik und Poliklinik für Nuklearmedizin, Universitätsklinikum Leipzig, Leipzig, GERMANY,* [7]*Department of Clinical Oncology, Guy's Cancer Centre and School of Cancer and Pharmaceutical Sciences, King's College London University, London, UNITED KINGDOM,* [8]*Department of Nuclear Medicine and PET/CT Centre, IIMSI - Imaging Institute of Southern Switzerland, Bellinzona, Università della Svizzera Italiana, Bellinzona Switzerland; SAKK - Swiss Group for Clinical Cancer Research, Bern, SWITZERLAND,* [9]*Department of Oncology, IOSI - Oncology Institute of Southern Switzerland, Bellinzona; Università della Svizzera Italiana, Bellinzona, Switzerland; SAKK - Swiss Group for Clinical Cancer Research, Bern, SWITZERLAND,* [10]*Department of Nuclear Medicine, Medical Imaging Centre, Semmelweis University, Budapest, HUNGARY,* [11]*Nuclear Medicine department, Sant'Orsola-Malpighi Hospital, Bologna, ITALY,* [12]*Department of Molecular Imaging and Therapy, Austin Health, Melbourne, AUSTRALIA,* [13]*King's College London and Guy's and St Thomas' PET Centre, School of Biomedical Engineering and Imaging Sciences, King's Health Partners, Kings College London, London, UNITED KINGDOM.*

Aim/Introduction: Diffuse large B-cell lymphoma (DLBCL) is the most common aggressive non-Hodgkin lymphoma, with 70% of patients achieving curative responses to first-line treatment. The 5-point visual Deauville score (DS) assesses therapy response at End-of-Treatment (EoT) FDG PET. Although the Negative Predictive Value (NPV) is 85%, the Positive Predictive Value (PPV) using traditional DS criteria at EoT PET is suboptimal, ranging between 38 and 80%. This ongoing study, aims to determine if PPV could be improved without affecting NPV by using quantitative PET characteristics both at baseline and at EoT assessment. ***Materials and Methods:*** DLBCL patients from the PETRA database (www.petralymphoma.org) with a baseline and a positive EoT PET (DS4-5) were included. Lymphoma lesions were segmented on EoT and baseline PET using an adaptive semi-automatic delineation approach that applies either the SUV4.0 or MV3 method depending on tumor uptake values (Zwezerijnen et al. J. Nucl. Med 2021). Total Metabolic Tumor Volume (TMTV), SUV_{peak}, Total Lesion Glycolysis (TLG), Tumor-to-Liver ratio SUV metrics, and the absolute and relative difference in SUV for both timepoints were obtained. The outcome measure was 2-year progression-free

survival (2-yr-PFS). Descriptive statistics and Wilcoxon-rank testing with Bonferroni correction were applied to evaluate differences in TMTV and SUV metrics between patients with and without 2-yr-PFS. The predictive ability of each quantitative PET feature for 2-yr-PFS was assessed using the Receiver Operating Characteristic curve, from which the optimal threshold and performance metrics, such as positive predictive value (PPV), negative predictive value (NPV), and accuracy, were determined. ***Results:*** 140 DLBCL patients were included. Significant differences were detected in TMTV (median 5.2 vs 29.5mL), SUV_{peak} (3.9 vs 9.6), TLG (19.4 vs 174.7), and $TumorSUV_{peak}$/$LiverSUV_{mean}$-ratio (1.7 vs 4.3) at EoT between patients with and without 2-yr-PFS. Furthermore, compared to baseline, the relative change in SUV_{peak} (77.4 vs 45.2%) at EoT showed significant differences in 2-yr-PFS. The $\%\Delta SUV_{peak}$ showed the highest accuracy (71%) in predicting 2-yr-PFS, followed by SUV_{peak} (56%), $TumorSUV_{peak}$/$LiverSUV_{mean}$-ratio (56%), TMTV (53%), and TLG (54%). The PPV values ranged from 45% (TMTV and TLG) to 60% ($\%\Delta SUV_{peak}$), while the NPV values ranged from 73% (TLG) to 88% ($TumorSUV_{peak}$/$LiverSUV_{mean}$-ratio) within this DS4-5 group. ***Conclusion:*** This ongoing study suggests that several quantitative PET parameters, such as TMTV and SUV_{peak}, can be used to improve prediction of 2-yr-PFS in DLBCL patients with DS4-5 at EoT. Moreover, relative changes in uptake at EoT compared to baseline PET may further add to improved 2-yr-PFS prediction.

307

Sunday, September 10, 2023, 9:45 AM - 11:15 AM
Hall F1

Neuroimaging Committee - TROP Session: Amyloid, Tau and More in Neurodegenerative Disorders Tau

OP-103

Quantification of baseline amyloid load in individuals with subjective cognitive decline can identify future risk of amyloid accumulation

G. Kolinger[1], *M. Marquié*[2,3], *O. Sotolongo-Grau*[2], *N. Roé-Vellvé*[1], *E. Pérez-Martínez*[1], *N. Koglin*[1], *A. Stephens*[1], *J. Tartari*[2], *Á. Sanabria*[2,3], *A. García-Sánchez*[2], *L. Tárraga*[2,3], *A. Ruiz*[2,3], *S. Bullich*[1], *M. Boada*[2,3];
[1]*Life Molecular Imaging GmbH, Berlin, GERMANY,* [2]*Ace Alzheimer Center Barcelona – Universitat Internacional de Catalunya, Barcelona, SPAIN,* [3]*Centro de Investigación Biomédica en Red de Enfermedades Neurodegenerativas (CIBERNED), Instituto de Salud Carlos III, Madrid, SPAIN.*

Aim/Introduction: Amyloid-beta (Aβ) positron emission tomography (PET) with [^{18}F]florbetaben is an established tool for detecting in-vivo Aβ deposition in the brain. The quantitative analysis of such brain PET images allows for a precise measurement of the Aβ deposition and can be a powerful tool for assessing longitudinal changes in Aβ load. This study aimed to determine whether Centiloid (CL) at baseline can identify groups with distinct Aβ load increase. ***Materials and Methods:*** 197 subjects with subjective cognitive decline (SCD) enrolled in the Fundació ACE Healthy Brain Initiative (FACEHBI) study underwent at least two [^{18}F]florbetaben PET/CT scans. The latest follow-up scans were performed two, three, or five years after baseline (n=51, 27, and 119, respectively). Scans were quantified and classified according to CL cut-offs: Aβ-negative (Aβ-, CL≤20), Grey Zone (GZ, 20<CL≤35), and Aβ-positive (Aβ+, CL>35). A CL-based progression was established given each subject's baseline and follow-up PET scan quantification. Statistical comparisons were carried using a Wilcoxon rank sum test. ***Results:*** Mean age of participants was 65.6±7.2 years at baseline, 63.5% were females, and had 15.2±4.5 years of education. At baseline, 169 subjects (85.8%) were Aβ-. In their latest follow-up (4.2±1.5 years after baseline), 153 remained negative, 9 progressed to the GZ and 7 to Aβ+. Within the 8 subjects in the GZ at baseline, 6 increased their CL above the Aβ+ threshold. All 20 Aβ+ subjects remained in the same group on follow-up. There was a statistically significant ($p<0.001$) group difference on baseline CL (CL_{bl}) between the stable Aβ- subjects (CL_{bl} = -2.15±6.24; CL accumulation (CL_{acc}) = 0.20±1.37/year) and the ones that progressed from Aβ- to GZ (CL_{bl} = 7.36±4.21; CL_{acc}=4.04±1.86/year) and from Aβ- to Aβ+ (CL_{bl} = 12.2±5.5; CL_{acc} = 6.37±1.22/year). There were not enough subjects in the baseline GZ group for a comparison between the stable GZ subjects and those that progressed to Aβ+. The Aβ- subjects with higher CL values at baseline ($10<CL_{bl}<20$) showed a significantly higher ($p<0.01$) CL yearly increase rate than those with lower CL values ($CL_{bl}\leq10$) (CL_{acc} = 3.22±3.53/year vs CL_{acc} = 0.43±1.66/year, respectively). ***Conclusion:*** Baseline CL value was able to differentiate SCD individuals who accumulated amyloid load over time from those who remained stable. Most subjects in the GZ at baseline continued to accumulate Aβ longitudinally and progressed to the Aβ+ group. Similarly, Aβ- subjects showed a higher Aβ accumulation rate when their CL at baseline was closer to the GZ threshold.

OP-104

Association of plasma glial fibrillary acidic protein with neurofibrillary tau tangles in the brain and cognitive decline independent of amyloid-B

D. Peretti[1], *F. Ribaldi*[1,2], *C. Boccalini*[1,3,4], *M. Marizzoni*[5], *N. Ashton*[6,7,8], *H. Zetterberg*[6,9,10], *K. Blennow*[6], *G. Frisoni*[1,2], *V. Garibotto*[1,2];
[1]*University of Geneva, Geneva, SWITZERLAND,* [2]*Geneva University Hospitals, Geneva, SWITZERLAND,* [3]*Vita-Salute San Raffaele University, Milan, ITALY,* [4]*IRCCS San Raffaele Scientific Institute, Milan, ITALY,* [5]*IRCCS Istituto Centro Sand Giovanni di Dio Fatebenefratelli, Brescia, ITALY,* [6]*The Sahlgrenska Academy at the University of Gothenburg, Molndal, SWEDEN,* [7]*Maurice Wohl Clinical Neuroscience Institute, London, UNITED KINGDOM,* [8]*NIHR Biomedical Research Centre for Mental Health & Biomedical Research Unit for Dementia at South London & Maudsley NHS Foundation, London, UNITED KINGDOM,* [9]*University College London, London, UNITED KINGDOM,* [10]*Hong Kong Center for Neurodegenerative Diseases, Hong Kong, CHINA.*

Aim/Introduction: Alzheimer's disease (AD) is pathologically defined by the accumulation of extracellular amyloid plaques and intracellular neurofibrillary tangles of hyperphosphorylated tau. Increasing evidence shows that neuroinflammation is a possible modulator of the effects of tau spread on cognitive impairment in AD. Circulating plasma markers of neuroinflammation have recently become available, and first observations suggest a robust association with AD pathology. Among these, one of the most promising is the glial acidic fibrillary protein (GFAP). The aim of this study was to assess the correlation between plasma GFAP and topographical tau pathology, and its interaction with cognitive decline. ***Materials and Methods:*** A cohort of 123 subjects from the Geneva Memory Centre underwent amyloid- and tau-PET, blood collection, and mini-mental state examination (MMSE). Amyloid uptake was calculated as centiloid values and tau was quantified as standardised uptake value ratio (SUVR). Voxel-based linear regression to assess the topographical correlation between

tau SUVR and plasma GFAP was performed, corrected for age, education, gender, and amyloid accumulation. A sub-sample of 95 subjects underwent a follow up MMSE at least 1 year after baseline. Linear regression was used to assess the effect of GFAP on the annual rate of change of MMSE (corrected for centiloid, global tau, age, gender, and education), and a Wilcoxon test was performed to assess significant differences in GFAP values between subjects that presented cognitive decline or not. ***Results:*** The mean (SD) age of the participants was 72.6 (7.6) years, and 50% of subjects were men. GFAP was associated with increased tau-PET uptake in the lateral temporal and inferior frontal lobes independently of amyloid, gender, age, education, and MMSE scores after multiple comparisons corrections (β=0.001, p<0.01). The annual rate of MMSE change was significantly correlated with GFAP (β=0.006, p<0.01), and a global measure of tau SUVR (β=3.9, p<0.01), but not with amyloid burden. A significant difference in GFAP values was found between stable subjects and decliners (W=1325, p<0.01). ***Conclusion:*** Elevated plasma GFAP levels are associated with increased tau deposition in lateral temporal and frontal regions and also associated with accelerated cognitive decline, independently from tau and amyloid load. These results support neuroinflammation and astrogliosis as a relevant contributor to AD pathology, which can be monitored in blood, and suggest neuroinflammation as a potential target for future disease-modifying therapeutic trials targeting tau pathology.

OP-105

The functional long-distance relationship of amyloid and tau pathology

M. Hoenig[1], *A. Weller*[2], *E. Doering*[3], *G. Bischof*[4], *A. Drzezga*[4], *T. van Eimeren*[4];
[1]*Research Center Juelich, Juelich, GERMANY,* [2]*University of Cologne, Cologne, GERMANY,* [3]*German Center for Neurodegenerative Diseases, Bonn, GERMANY,* [4]*University Clinic Cologne, Cologne, GERMANY.*

Aim/Introduction: We recently identified spatial patterns of baseline regional amyloid-burden that were associated with spatially diverging patterns of tau-pathology spread (e.g. frontal baseline amyloid pattern was linked to temporal and precuneal tau increase). Given the spatial divergence between these identified spatial patterns of baseline amyloid and subsequent tau-pathology increase, we assessed whether functional connectivity serves as a mediator bridging the observed spatial gap between these proteinopathies. ***Materials and Methods:*** The regional patterns of baseline amyloid (18F-AV45) and subsequent tau-pathology increase (longitudinal 18F-AV1451 time points) were derived using parallel independent component analysis (pICA) based on data of 98 amyloid-positive subjects from the ADNI cohort. The pICA yielded six component pairs linking spatial patterns of baseline amyloid (i.e. regional amyloid pattern) to longitudinal tau increase (i.e. regional tau increase pattern). The degree of spatial divergence of the corresponding component patterns of each pair was quantified using Dice Similarity Coefficient (DSC). To examine the potential role of functional connectivity as mediator bridging the spatial gap between regional amyloid and tau-pathology increase, we used the region of maximum coefficient per component (of the respective regional amyloid or the regional tau increase pattern of each component pair) as seeds for functional connectivity analyses in a dataset of younger healthy controls. This resulted in six pairs of amyloid- and tau-derived seed-based networks (SBN). Subsequently, the spatial overlap between these SBNs and the respective component patterns (regional baseline amyloid OR tau increase pattern of each pair) and the combined component pairs (regional amyloid And tau increase pattern) were quantified. ***Results:*** Using pICA, we identified six component pairs of regional amyloid and tau increase that partly spatially overlapped, but also spatially diverged. Amyloid-derived SBNs presented greater spatial overlap with their respective amyloid components (24%-54%) than the tau-derived SBNs with the respective tau increase components (16%-40%). Importantly, the spatial combination of the regional baseline amyloid and tau increase component pairs showed highest spatial overlap with the amyloid-derived SBNs (up to 62% vs. 39% for the tau-derived SBNs) suggesting that amyloid causes initial tau spread within the same network. ***Conclusion:*** Mechanistically, it appears that the regional associations of amyloid and tau-pathology are driven by underlying large-scale functional networks. Functional connections may thereby transmit soluble amyloid to remote brain regions within the same network. The transmission of soluble amyloid likely results in increased phosphorylation of tau, which eventually triggers insoluble tau-pathology aggregation and spread outside the initially affected network.

OP-106

Validation of a topographic visual assessment method for ^{18}F-Flortaucipir based on Subtype and Stage Inference Model (SuStaIn)

G. Mathoux[1,2], *C. Boccalini*[3,4], *A. Arnone*[3], *D. E. Peretti*[3], *M. Scheffler*[5], *G. B. Frisoni*[6,7], *V. Garibotto*[2,3,8];
[1]*Università degli Studi di Milano-Bicocca, Monza, ITALY,* [2]*Division of Nuclear Medicine and Molecular Imaging, Geneva University Hospitals, Geneva, SWITZERLAND,* [3]*Laboratory of Neuroimaging and Innovative Molecular Tracers (NIMTlab), Geneva University Neurocenter and Faculty of Medicine, University of Geneva, Geneva, SWITZERLAND,* [4]*Università Vita e Salute San Raffaele, Milano, ITALY,* [5]*Division of Radiology, Geneva University Hospitals, Geneva, SWITZERLAND,* [6]*Memory Clinic, Department of Rehabilitation and Geriatrics, Geneva University and University Hospitals, Geneva, SWITZERLAND,* [7]*Laboratory of Neuroimaging of Aging (LANVIE), University of Geneva, Geneva, SWITZERLAND,* [8]*CIBM Center for Biomedical Imaging, Geneva, SWITZERLAND.*

Aim/Introduction: Substantial variability in the spreading pattern of tau pathology in Alzheimer's disease (AD) population is widely accepted. The Subtype and Stage Inference algorithm (SuStaIn) has distinguished four distinct spatiotemporal trajectories of tau pathology [1]: the limbic (S1), medial temporal lobe-sparing (S2), posterior (S3), and lateral temporal (S4). However, the validation of a visual method to identify them has not yet been proposed and would be important for its clinical translation. Our study aims to provide evidence for tau accumulation subtypes in a clinical setting applying a topographic visual method for tau-PET based on SuStaIn staging. ***Materials and Methods:*** We included 245 participants from the Geneva Memory Clinic, who underwent ^{18}F-Flortaucipir-PET. Three blinded physicians visually evaluated all scans for tau (T) status and SuStain subtypes. In case of discordance, a consensus was reached. Standardized uptake value ratio (SUVr) values were obtained from a global meta-region of interest (ROI).To test the agreement between raters we used Cohen's kappa (k). Chi-squared and Kruskal-Wallis tests were used to test the differences in clinical features, tau, and amyloid (Aβ) loads between the subtypes. Differences in cognitive trajectories between subtypes were tested using linear mixed-effects models. ***Results:*** Our study showed good agreement between different raters in visually interpreting tau pattern subtypes (k>0.65, p<0.001). T+ individuals performed worse on the MMSE than T-

independently from the subtypes (p<0.001). Individuals with S2 subtype were younger than S1 and S3 individuals (p<0.001) and had worse MMSE scores (p<0.05) than S4 and S1. We observed a systematic increase in global tau SUVr in T+ individuals compared to T- individuals (p<0.001), with the higher accumulation in S2 subtype compared to S1, S3, and S4 (p<0.05). Similarly, Aβ burden was found to be systematically increased in T+ individuals compared to T- individuals (p<0.001).T+ individuals showed significantly faster cognitive decline than T- group (p<0.001), with the S2 subtype exhibiting the fastest decline, with a greater slope in comparison with other subtypes. ***Conclusion:*** Our results support the existence of different tau accumulation subtypes, based on SuStaIn staging, that can be visually assessed with a good inter-rater agreement. Visually identified tau subtypes differ in tau and amyloid loads, clinical profiles, and long-term prognoses. Thus, the visual detection of different patterns might be useful for personalized clinical care and, ultimately, individualized therapy. ***References:*** 1. Vogel,et al."Four distinct trajectories of tau deposition identified in Alzheimer's disease." Nature medicine vol.27,5(2021).

OP-107

A Biological Staging Scheme for Alzheimer's disease: Results from the Tau Propagation over Time (T-POT) Cohort

E. Doering[1], *M. Hönig*[2], *V. Dzialas*[1], *J. Lothmann*[1], *K. Giehl*[2], *H. Theis*[3], *E. Jäger*[1], *G. Andrassy*[1], *A. Bauer*[2], *D. Elmenhorst*[2], *T. Kroll*[2], *A. Matusch*[2], *P. Krapf*[4], *B. Neumaier*[4], *C. Lerche*[5], *L. Tellmann*[5], *S. Frensch*[2], *P. Zeyen*[6], *F. Sand*[6], *N. Richter*[6], *F. Jessen*[6], *Ö. Onur*[3], *A. Ramirez*[6], *T. van Eimeren*[3], *A. Drzezga*[1], *G. Bischof*[1];
[1]*University of Cologne, Faculty of Medicine and University Hospital Cologne, Department of Nuclear Medicine, Cologne, GERMANY,* [2]*Research Center Jülich, Institute of Neuroscience and Medicine - Molecular Organization of the Brain (INM-2), Juelich, GERMANY,* [3]*University of Cologne, Faculty of Medicine and University Hospital Cologne, Department of Neurology, Cologne, GERMANY,* [4]*Research Center Jülich, Institute of Neuroscience and Medicine - Nuclear Chemistry (INM-5), Juelich, GERMANY,* [5]*Research Center Jülich, Institute of Neuroscience and Medicine - Medical Imaging Physics (INM-4), Juelich, GERMANY,* [6]*University of Cologne, Faculty of Medicine and University Hospital Cologne, Department of Psychiatry, Cologne, GERMANY.*

Aim/Introduction: Alzheimer's disease (AD) is characterized by the cerebral accumulation of amyloid-beta (A), tau (T), and progressive neurodegeneration (N). The widely used ATN system, with regard to positron emission tomography (PET) biomarkers, categorizes AD based on the mean signal in specific regions of interest (ROI). However, this procedure disregards the spatial extent of pathology and neurodegeneration. Here, we propose an alternative quantification of the volume, i.e., fill states, of A, T, and N in (pre-)clinical AD. ***Materials and Methods:*** We analyzed data from the Tau Propagation over Time (T-POT) study, including cognitively unimpaired individuals (CU, n=58), and patients with mild cognitive impairment (MCI, n=20) or AD dementia (n=4). C11-PIB-PET (A), 18F-AV1451 (T) and perfusion-phase 18F-AV1451 scans (N) were spatially and intensity-normalized (reference: cerebellum). To quantify the volume of A, T and N, we z-standardized and subsequently binarized all scans within-modality using a z-score threshold. Fill states were then computed as the sum of abnormal voxels relative to a whole-brain mask. Finally, mean fill states were compared across groups of clinical status (CU, MCI, AD) and partial correlations of either fill states or mean PET signal in established, tracer-specific ROIs with cognitive performance (Mini-Mental State Examination; MMSE) were computed, adjusting for age, sex and education. ***Results:*** Mean fill states reflected clinical status, as they increased with disease progression (CU: A=4%, T=4%, N=3%; MCI: A=15%, T=11%, N=4%; AD dementia: A=20%, T=23%, N=5%). Moreover, A and T fill states were negatively associated with MMSE (rho_A = -.299, p < .001; rho_T = -.318, p < .01; rho_N = -.147, p = .20), while associations of mean PET signal and MMSE tended to be weaker ($rho_{A(global)}$ = -.255, p = .03; $rho_{T(temporalmetaROI)}$ = -.275, p = .01; $rho_{N(MetaROI)}$ = .179, p = .12). ***Conclusion:*** We present a competitive volume-based staging scheme for AD that is associated with both, clinical status and cognitive performance. These results, while currently validated in a larger sample, suggest that the spatiotemporal dynamics of pathology and neurodegeneration in the AD continuum are well captured by our multi-parametric approach, which is possibly superior compared to classification from mean PET signal intensity. The extended cross-sectional and longitudinal comparison of the two classification schemes is a matter of ongoing research.

OP-108

[^{18}F]PI-2620 PET Imaging of 3R Pick Tau in Frontotemporal Lobar Degeneration - A Multi-Centre Study

H. Barthel[1], *M. Brendel*[2], *V. Villemagne*[3], *K. Marek*[4], *T. van Eimeren*[5], *M. Rullmann*[1], *M. Schroeter*[1], *D. Saur*[1], *M. Patt*[1], *J. Classen*[1], *J. Seibyl*[4], *A. Drzezga*[5], *O. Sabri*[1], *German Imaging Initiative for Tauopathies;*
[1]*Leipzig University Medical Centre, Leipzig, Germany, GERMANY,* [2]*Ludwig Maximillian University Munich, Munich, GERMANY,* [3]*University of Pittsburgh, Pittsburgh, AL, UNITED STATES OF AMERICA,* [4]*InviCRO, Boston, MA, UNITED STATES OF AMERICA,* [5]*University of Cologne, Cologne, GERMANY.*

Aim/Introduction: Certain types of frontotemporal lobar degeneration (FTLD) are histopathologically characterized by 3R Pick tau aggregates. These aggregates cannot be imaged so far in vivo. This shortcoming provided motivation to investigate the respective potential of the second-generation tau PET tracer [^{18}F]PI-2620. ***Materials and Methods:*** In this observational study we included participants from five centres, 46 patients with FTLD according to established clinical criteria (50% females, age 65±10yrs, symptom duration 3.7±2.1yrs, MMSE scores 24±6, Neuropsychiatric Inventory scores 8±9) and 26 age- and gender-matched HCs. The FTLD group consisted of Aβ(PET or CSF sampling)-negative patients with behavioural-variant frontotemporal dementia (bvFTD, n=18), semantic-variant primary progressive aphasia (svPPA) (n=7), or non-fluent-variant (nfv)PPA (n=17), as well as of Aβ-positive patients with logopenic-variant (lv)PPA (n=4). [^{18}F]PI-2620 PET data were acquired dynamically 0-60min p.i. Parametric distribution volume ratio (DVR) images were obtained from kinetic modelling (MRTM2, reference region=lower cerebellum) and analysed globally (AAL template) as well as for four Pick tau stage VOIs which were created according to histopathology literature. ***Results:*** [^{18}F]PI-2620 DVRs were significantly higher in the FTLD patients as compared to the HCs in several frontal and temporal cortical regions as well as in cingulate gyrus, striatum, thalamus, cerebellar cortex, medulla/midbrain/pons, and cerebral/cerebellar white matter brain regions. This was also the case for the Pick tau stage 1_limbic (p=0.016), stage 1_neocortical (p=0.011), stage 2 (p<0.001), and all stages/meta (p<0.001) VOIs. On an individual level, 87% of the FTLD patients were positive (>mv+2sd of the HCs) in at least one of the Pick tau stage VOIs. These were 41%, 46%, 83%, 2%, and 13% for the Pick tau stage 1_limbic, 1_neocortical, 2, 3, and 4 VOIs. 67%

of the FTLD patients followed a hierarchical staging. With regard to the FTLD subtypes, 100% of the nfvPPAs, 100% of the lvPPAs, 78% of the bvFTDs, and 71% of the svPPAs were PET-positive. ***Conclusion:*** In conclusion, PET imaging of 3R Pick tau in FTLD seems to be possible by [^{18}F]PI-2620. To further understand the tracer behaviour in this dementia category, we will also focus on alternatives to the current hierarchical Pick tau staging system, on the question of how the diagnostic potential of our tracer relates to that of structural MRI/[^{18}F]FDG PET imaging, and on elucidating the potential impact of TDP-43 pathology on the PET readouts.

OP-109

Tau-PET signal in Alzheimer's disease is related to immune activation and synaptic signaling measured with CSF proteomics

E. Van de Giessen*, R. M. Rikken, E. Vromen, E. M. Coomans, D. Visser, F. Barkhof, L. E. Collij, R. Boellaard, S. V. S. Golla, B. N. M. van Berckel, R. Ossenkoppele, A. den Braber, J. Vijverberg, W. M. van der Flier, Y. A. L. Pijnenburg, C. E. Teunissen, P. J. Visser, B. Tijms; Amsterdam UMC, Amsterdam, NETHERLANDS.*

Aim/Introduction: Tau tangles are one of the pathological hallmarks of Alzheimer's disease (AD) and can be quantified using PET. It remains unclear which molecular processes are related to tau aggregation. Protein levels in CSF can be used to study such underlying processes. This study aims to identify biological processes related to tau-PET using unbiased CSF proteomics in participants along the AD continuum. ***Materials and Methods:*** We included 89 participants with CSF proteomic and [^{18}F]flortaucipir (tau)-PET data available from the Amsterdam Dementia Cohort and the EMIF-preclin AD study (N=68 with abnormal CSF Aβ42 [64.7% cognitively impaired, 67.6% tau-PET visual read positive] and N=21 controls [normal cognition and normal CSF AD biomarkers]). [^{18}F]flortaucipir BP_{ND} was quantified in the temporal meta-ROI (Braak I, Braak III, Braak IV). CSF proteomics was measured using untargeted LC-MS/MS based on TMT labelling. We included proteins available in the whole sample (n=1421 proteins). Protein concentrations were normalized to the control group. We determined the relationship between tau-PET BP_{ND} (outcome) with protein levels (determinant) using linear regressions with sex and age as covariates, stratified for group. GO database was used for biological pathway enrichment analyses within the AD group for proteins thresholded at $p<0.05$ for positive and negative associations separately. ***Results:*** Higher CSF tau levels were associated with higher tau-PET BP_{ND} ($\beta=0.092$, $p=0.002$). In total, 458 proteins were associated with tau-PET BP_{ND} in AD. A higher tau-PET BP_{ND} was related to higher levels of 140 proteins and lower levels of 318 proteins. Proteins that showed higher levels with increasing tau-PET BP_{ND} were mainly involved in immune system processes, while the proteins with lower levels were predominantly related to synaptic processes and cell signaling. No significant associations were found within controls. ***Conclusion:*** Using CSF proteomics, we identified 458 proteins associated with tau-PET in AD. Higher tau burden was associated with increased levels of proteins involved in immune activation suggesting a role of the immune system in tau accumulation. Furthermore, higher tau burden was associated with lower levels of proteins related to synaptic process hinting at a role for tau in synaptic degeneration.

OP-110

Regional Desynchronization of Microglial Activity is Associated with Cognitive Decline in Alzheimer's Disease

A. Zatcepin[1,2]*, J. Gnörich*[1,2]*, B. Rauchmann*[3]*, L. M. Bartos*[1]*, N. Franzmeier*[4,5,6]*, M. Malpetti*[7]*, X. Xiang*[8,9]*, Y. Shi*[2]*, S. Parhizkar*[10]*, M. Grosch*[11]*, K. Wind-Mark*[1,2]*, S. T. Kunte*[1]*, L. Beyer*[1]*, G. Biechele*[1]*, A. Finze*[1]*, F. Eckenweber*[1]*, P. Bartenstein*[1]*, S. Tahirovic*[2]*, M. Simons*[2,4,6]*, C. Haass*[2,8,6]*, R. Rupprecht*[12]*, N. L. Albert*[1,13,14]*, G. U. Höglinger*[2,15,16]*, S. I. Zielger*[1]*, M. Brendel*[1,2,6]*;*
[1]Department of Nuclear Medicine, University Hospital, LMU Munich, Munich, GERMANY, [2]German Center for Neurodegenerative Diseases (DZNE), Munich, GERMANY, [3]Department of Radiology, University Hospital, LMU Munich, Munich, GERMANY, [4]Institute for Stroke and Dementia Research, University Hospital, LMU Munich, Munich, GERMANY, [5]Department of Psychiatry and Neurochemistry, Institute of Neuroscience and Physiology, The Sahlgrenska Academy, University of Gothenburg, Gothenburg, SWEDEN, [6]Munich Cluster for Systems Neurology (SyNergy), Munich, GERMANY, [7]Department of Clinical Neurosciences, Cambridge University Hospitals NHS Trust, University of Cambridge, Cambridge, UNITED KINGDOM, [8]Biomedical Center (BMC), Division of Metabolic Biochemistry, Faculty of Medicine, LMU Munich, Munich, GERMANY, [9]CAS Key Laboratory of Brain Connectome and Manipulation, the Brain Cognition and Brain Disease Institute, Shenzhen Institutes of Advanced Technology, Chinese Academy of Sciences, Shenzhen-Hong Kong Institute of Brain Science-Shenzhen Fundam. Res. Inst., Shenzhen, CHINA, [10]Department of Neurology, Washington University in St. Louis, St. Louis, MO, UNITED STATES OF AMERICA, [11]German Center for Vertigo and Balance Disorders, University Hospital of Munich, LMU Munich, Munich, GERMANY, [12]Department of Psychiatry and Psychotherapy, Molecular Neurosciences, University of Regensburg, Regensburg, GERMANY, [13]German Cancer Consortium (DKTK), Partner Site Munich, German Cancer Research Center (DKFZ), Heidelberg, GERMANY, [14]Bavarian Cancer Research Center (BZKF), Erlangen, GERMANY, [15]Department of Neurology, University Hospital, LMU Munich, Munich, GERMANY, [16]Department of Neurology, Hannover Medical School, Hannover, GERMANY.

Aim/Introduction: Microglial activation is a hallmark of Alzheimer disease (AD) neuropathology, but the regional interaction of microglia cells in the brain is poorly understood. To address this, we explored the existence and accessibility of a microglia connectome in both mouse models and humans with AD and performed a translational assessment of microglial desynchronization as a potential AD biomarker. ***Materials and Methods:*** To validate the concept, we depleted the microglia using CSF1R inhibition in wild-type mice and examined whether interregional correlation coefficients (ICC) of 18kDa translocator protein (TSPO)-PET with [^{18}F]GE-180 were affected by the lack of microglia. We further investigated the effect of dysfunctional microglia ($TREM2^{-/-}$) and AD pathophysiology (β-amyloidosis, tauopathy) on TSPO-PET ICC in mouse brain, and then extended the methodology to analyze a human TSPO-PET dataset comprising of cognitively normal individuals and patients with prodromal and dementia stages of AD. We explored stage-dependent differences of microglia synchronicity and correlated personalized microglia desynchronization index (DI) in AD-specific subregions with cognitive performance measured by Mini-Mental State Examination (MMSE) score. ***Results:*** Microglia-depleted mice demonstrated a dramatic reduction of TSPO-PET ICCs among all compartments of the brain. Wild-type mice and APPPS1 mice with TREM2 deficiency indicated significant reductions of TSPO-PET ICC when compared to $TREM2^{+/+}$ groups. Our study revealed

substantial alterations in TSPO-PET ICC in all the investigated AD models when compared to the age-matched controls. Notably, we observed these changes not only in mice with moderate neuropathology (5.0-6.0 months of age), but also in mice at the neuropathology onset (2.0-2.5 months of age). Humans with AD indicated a stage-depended reduction of both the number of significant connections and microglia DI in six parietal and four temporal regions. Strong negative correlations were observed between the MMSE score and microglia DI in four parietal and two temporal regions. ***Conclusion:*** Using TSPO-PET imaging of mice with depleted microglia, we provide the first evidence that a microglia connectome can be assessed in the mouse brain. Microglia synchronicity is closely associated with cognitive decline in AD and could be utilized as an independent personalized biomarker for neuroinflammation-associated disease progression.

OP-111

PET-based synaptic density measure, its amyloid-independent association with APOE e4 in cognitively impaired individuals

K. He[1], *F. Xie*[1], *Y. Huang*[2], *K. Chen*[3], *Y. Guan*[1], *B. Li*[4], *J. Wang*[5], *Q. Huang*[5];
[1]*Department of Nuclear Medicine & PET Center, Huashan Hospital, Fudan University, Shanghai, CHINA,* [2]*PET Center, Department of Radiology and Biomedical Imaging, Yale University School of Medicine, New Haven, New Haven, CT, UNITED STATES OF AMERICA,* [3]*Banner Alzheimer Institute, Arizona State University, University of Arizona and Arizona Alzheimer's Consortium, Phoenix, AZ, UNITED STATES OF AMERICA,* [4]*Clinical Neuroscience Center, Ruijin Hospital,Shanghai Jiao Tong University School of Medicine, Shanghai, CHINA,* [5]*Department of Nuclear Medicine & PET Center, Huashan Hospital, Fudan University, Shanghai, CHINA.*

Aim/Introduction: Apolipoprotein &#9494 (APOE &#9494) is the strongest genetic risk factor for sporadic Alzheimer's disease (AD). However, the relationship of the APOE induced synaptic loss and the cognitive impairment is still not fully understood. Investigation of the effect of APOE on synaptic loss is significant for the development of genotype-specific therapy in AD. We aimed to investigate the effect of APOE &#9494 on synaptic density and the associations between synaptic density and AD biomarkers in cognitively impaired (CI) participants. ***Materials and Methods:*** Fifty-eight cognitive impaired(CI) participants and 27 cognitively normal (NC) participants who underwent amyloid positron emission tomography (PET) with florbetapir and synaptic density PET with ^{18}F-SynVesT-1 were included. Thirty-seven participants underwent tau PET scanning with ^{18}F-MK6240. Analyses were stratified by APOE genotype. ***Results:*** Among the CI participants, APOE &#9494 carriers displayed significant synaptic loss in the medial temporal and neocortices compared to APOE &#9494 noncarriers. Synaptic loss was mainly in the bilateral hippocampal bodies and tails. Similar results were found in the comparisons between APOE &#9493 homozygotes and APOE &#9494 heterozygotes. Female APOE &#9494 carriers displayed significantly decreased synaptic density in the medial temporal cortex compared with female APOE &#9494 noncarriers. Global amyloid deposition was only associated with hippocampal synaptic density in APOE &#9494 carriers, but it was associated with synaptic density in the hippocampus and parahippocampal gyrus in APOE &#9494 noncarriers. However, significant associations between synaptic density with tau pathology and hippocampal volume were observed in the APOE &#9494 carriers ***Conclusion:*** APOE plays a significant role in synaptic density loss. APOE &#9494 carriers showed a significantly decreased synaptic density in medial temporal and neocortices compared to noncarriers, and only one copy of the APOE &#9494 allele reduced the synaptic density in the hippocampus. Furthermore, the effects of the APOE &#9494 allele on synaptic density were observed only in females. APOE &#9494 also potentiated the associations of synaptic density with tau pathology and hippocampal volume. Our study supports the hypothesis that the APOE &#9494 allele affects synaptic density in individuals with cognitive impairments.

308

Sunday, September 10, 2023, 09:45 - 11:15
Hall F2

Joint Symposium 1 - Cardiovascular + Inflammation & Infection Committee / EACVI: PET in Valvular Diseases - All In!

OP-112

Endocarditis

P. Erba;
Department of Nuclear Medicine, Ospedale Papa Giovanni XXIII, Bergamo, ITALY.

OP-113

Calcification

J. Kwiecinski;
Department of interventional cardiology and angiology, Institute of Cardiology, Warsaw, POLAND.

OP-114

Myocardial Inflammation and Fibrosis

F. Bengel;
Department of Nuclear Medicine, Hannover Medical School, Hannover, GERMANY.

309

Sunday, September 10, 2023, 9:45 AM - 11:15 AM
Hall G2

e-Poster Presentations Session 2 - Paediatrics Committee: Paediatric Nuclear Medicine & Adults General Nuclear Medicine

EPS-022

Gravity-Assisted Diuresis Renography with method F+10(sp) for clinical management and post-operative assessment of primary megaureter.

G. Tartaglione[1], *F. P. Ieria*[1], *N. Foschi*[2];
[1]*Cristo Re Hospital, Nuclear Medicine, Rome, ITALY,* [2]*Urology, Fondazione Policlinico Universitario Agostino Gemelli IRCCS, Rome, ITALY.*

Aim/Introduction: Primary obstructive megaureter is an uncommon disease defined as intrinsic ureteral dilatation caused by congenital abnormality of the lower ureteral tract. It may be discovered earlier by ultrasound, or later in life by imaging studies for urinary tract infections. When obstruction is not present, conservative management is the best treatment choice; otherwise, ureteroneocistostomy (UCNS) is recommended. Reflux is usually diagnosed with no difficulty on voiding cystography, while the

major diagnostic challenge is to recognize obstruction. Imaging tests in supine position may be misleading, because due to the dilated collecting system, the drainage of the urine is delayed also in the absence of true obstruction. Currently, renal scintigraphy is the key test to opt for surgical or conservative treatment, but only the drop of split renal function (SRF) is often a criterion for surgical treatment. We propose gravity-assisted diuresis renography with F+10(sp) (seated position) method for clinical management of primary megaureter. ***Materials and Methods:*** Twenty-six patients (15 m, 11 f), median age 42 y (18-73 y), median serum creatinine level 1.0 mg/dL (0.75-1.69). Based on radiological findings, megaureter was bilateral in 2 pts, and unilateral in 24 pts. 11 patients underwent a UCNS, and 15 patients received conservative treatment. In total 41 Diuresis Renography (82 kidneys) were assessed. We studied patients in seated position, using F+10(sp) method. We injected IV a dose of 150-200 MBq, 99mTc-MAG3 at time 0', and a dynamic study started at once after tracer injection. The patient drank 400-500 mL of water at 5 min and received IV a dose of 0.25 mg/Kg (maximum 20 mg) of Furosemide at 10 min. SRF, Tmax, Ratio 20 min/peak, were measured. ***Results:*** SRF (NV = 0.45-0.55) was decreased in 27 (32.9%) kidneys (14 Left, 13 Right). Tmax (NV <6 min) was increased in 43 (52.4%) kidneys (24 Left, 19 Right). Ratio 20min/peak (NV <0.25) was abnormal in 30 (36.6%) kidneys (16 Left, 14 Right). Serum creatinine level was >1.2 mg/dL in 4 (9.5%) studies. In post operative assessment, we found a discordance between SRF and Ratio findings in 14 (17.1%) kidneys. No adverse events have been observed. ***Conclusion:*** The Ratio 20min/peak, measured in condition of favorable gravity with F+10(sp) method, improves accuracy in obstruction detection and in post operative assessment of obstructive megaureter, preventing renal impairment. A drop of SRF is a late index of obstruction, his diagnostic value is limited in post-operative assessment of obstructive megaureter.

EPS-023

Evaluation of the use of [^{99m}Tc]Tc-MAG3 in the quantification of effective renal plasmatic flow in patients with autosomal dominant renal polycystosis. Preliminary data

L. Baz-Sanz, *R. Maestre-Cutillas, G. Rubio-Fernández, M. Álvarez-Nadal, L. Cebollada-Cameo, R. Castro-Velasco, C. Juan-Piriz, J. Pérez-Iruela;*
Hospital Ramón y Cajal, Madrid, SPAIN.

Aim/Introduction: Autosomal dominant polycystic kidney disease (ADPKD) is the most common inherited kidney disease with a prevalence of 5-10 cases/10,000 people. Factors predicting the rate of disease progression are genetic, total kidney volume (TKV) and effective renal plasma flow (ERPF). Identification of rapid progressors is beneficial for initiating treatment with tolvaptan. Due to the correlation of renal clearance of [^{99m}Tc]Tc-MAG3 with ERPF, this can be used as a predictor. The aim of this work is to validate our technique by correlating our preliminary [^{99m}Tc]Tc-MAG3 clearance data with VKT. ***Materials and Methods:*** ERPF was quantified by the Russell method in 41 patients with ADPKD divided into four groups (1A, 1B, 1C and 1D) according to Mayo Clinic criteria. The technique was performed using the radiopharmaceutical [^{99m}Tc]Tc-MAG3, which was prepared according to the technical data sheet. Two doses of 1mCi/1ml were prepared, one for intravenous administration and the other for the preparation of the standar. Blood was withdrawn 43min post-injection and centrifuged 10min/3900rpm. 2ml of plasma and standard were pipetted in triplicate. Their activity was determined with a gamma counter. ***Results:*** The mean clearance of the radiopharmaceutical and VKT of each group was calculated:[^{99m}Tc]Tc-MAG3 clearance: 1A(n=4), 167±40.00ml/min; 1B(n=20), 136±43.53ml/min; 1C(n=16), 119±47.43ml/min; 1D(n=1), 98ml/min. VKT: 1A(n=4), 282.25±88.75ml; 1B(n=20), 708.44±189.43ml; 1C(n=16), 1189.25±327.66ml; 1D(n=1), 1796ml. Pearson's correlation between radiopharmaceutical clearance and VKT: r=-0.487 and p=0.001. ***Conclusion:*** We obtained a moderate correlation between [^{99m}Tc]Tc-MAG3 clearance results and VKT, which indicates that our preliminary data are encouraging for future validation of our technique, expanding the number of patients. It is a simple, fast and convenient test for the patient, the implementation of which would be a benefit compared to diagnostic tests with a longer waiting list and more expensive, such as MRI.

EPS-024

Comparison Between In Vivo Gates Method and In Vitro Plasma Sampling Technique for Glomerular Filtration Rate Measurement in Voluntary Kidney Donors

M. Radulovic, *M. Sisic, B. Miljuš, L. Radosavcev, B. Ajdinovic;*
Institute of Nuclear Medicine, Military Medical Academy, Belgrade, SERBIA.

Aim/Introduction: Glomerular Filtration Rate (GFR) is defined as the volume of plasma that is filtered by the glomeruli per unit of time. Experience from our country shows that potential donors have been frequently assessed as ineligible due to lower GFR measured by in vivo Gates method. Aim of this study was to compare GFR measured by the radionuclide plasma sampling technique with Gates camera based method. ***Materials and Methods:*** Patient preparation consisted of the placement of intravenous cannula and adequate hydration. Before the beginning of renography study, preinjection syringe containing 185MBq of Tc-99m diethylenetriaminepentaacetic acid (DTPA) was counted using dual head gamma camera. Then a bolus dose of the tracer was intravenously administrated and the time recorded. Radiorenography was performed in 44 patients, potential kidney donors, for 35 minutes (30 frames lasting 2 seconds followed by 136 frames lasting 15 seconds) in the posterior position. The post-injection syringe was counted at the end of the study. Sampling: venous blood was taken according to required schedule - 180 minutes after administration of radioactive tracer. The samples of 10ml were taken from the arm contralateral to the administration site. Vials containing blood samples were centrifuged without postponement for 10 minutes at 1000 RPM. Two plasma samples, 1ml each, were taken from vials. A standard solution was prepared with 185MBq of Tc-99m in 1000ml of demineralized water. Standard sample containing 1ml of solution was prepared and counted after aprox. 24 hours using gamma counter. At that point, plasma samples were also counted. The decay of radioactivity was corrected. GFR was calculated according to guidelines. Gates GFR was calculated using gamma camera's software. Region of interest (ROI) for each kidney was drawn manually, and background ROIs were placed around the lower outer renal margins. Each patient provided serum creatinine findings within 48 hours of the study. ***Results:*** Mean values of GFR estimated using plasma sampling and Gates method were 82.26±16.05 ml/min/1.73m^2 and 69.93±15.57 ml/min/1.73m^2, respectively. There was significant difference between these values. Additionally, GFR was calculated using creatinine based equations (MDRD, CKD-EPI). The results showed that there was also significant difference between GFR estimated by radionuclide plasma sampling and creatinine based equations. ***Conclusion:*** Gates method tended to underestimated GFR

compared to plasma sampling method. Thus, calculation of GFR using in vitro radionuclide plasma method is essential in donor's work up protocol for kidney transplantation.

EPS-025

Glomerular filtration rate quantification in patients on antiretroviral therapy. Preliminary data

L. Baz-Sanz, *R. Maestre-Cutillas, G. Rubio-Fernández, V. Lopes-Martin, L. Cebollada-Cameo, M. Vaquero-Palomo, S. Horcas-Villaverde, J. Pérez-Iruela;*
Hospital Ramón y Cajal, Madrid, SPAIN.

Aim/Introduction: Some antiretroviral drugs inhibit tubular secretion of creatinine (Cr) without causing renal toxicity. Thus, an increase in plasma Cr concentration has been observed, with a consequent decrease in its estimated clearance, without producing a decrease in the actual glomerular filtration rate (GFR). The aim of this work is to identify whether patients really suffer a decrease in their GFR or, on the contrary, they are patients with a decrease in their tubular Cr secretion who do not need a change in their therapeutic planning. For this purpose, GFR estimation using serum Cr-based estimation formulae, such as MDRD4, will be compared in patients on antiretroviral therapy with the radioisotopic technique using the radiopharmaceutical [^{99m}Tc]Tc-DTPA, where the increase in serum Cr does not affect its determination. ***Materials and Methods:*** GFR was determined in 17 patients on antiretroviral therapy whose GFR estimates using the MDRD4 formula were below reference ranges. For this purpose, the radiopharmaceutical [^{99m}Tc]Tc-DTPA will be used, which was labelled according to the technical data sheet. A standard dose and a patient dose of 500 µCi were prepared. After administration of the radiopharmaceutical, blood samples were drawn at 2, 3 and 4 hours. Plasma was quantified in a gamma counter and GFR was determined using the Christensen and Groth method.They were divided into 2 groups: group 1, whose GFR estimated by isotopic method was>75ml/min/1.73m^2 (normal GFR); group 2, patients with GFR<75ml/min/1.73m^2. ***Results:*** Within group 2, only one patient required treatment modification due to a decrease in GFR, while the rest of the patients underwent closer monitoring without modification of their therapeutic regimen. The Mann-Whitney U-test was performed comparing both techniques in the two groups and statistically significant differences were obtained (p<0.05), so the null hypothesis is rejected. ***Conclusion:*** The analysis of results reveals that there are statistically significant differences between GFR determined by the MDRD4 method and the radioisotopic technique in patients on antiretroviral therapy. This supports the idea that antiretrovirals may underestimate GFR when using plasma Cr methods. In these cases, it may be advisable to use the radioisotopic technique, where increases in plasma Cr are not affected.

EPS-026

Body surface area as a determining factor in assessing glomerular filtration rate

G. Rubio-Fernández, *R. Maestre-Cutillas, L. Baz-Sanz, L. Cebollada-Cameo, V. Lopes-Martín, M. Vaquero-Palomo, S. Horcas-Villaverde, J. Pérez-Iruela;*
Hospital Ramón y Cajal, Madrid, SPAIN.

Aim/Introduction: The objective is to assess how body surface area index (BSI) affects glomerular filtration rate (GFR) by comparing the radiopharmaceutical test performed with [^{99m}Tc]Tc-DTPA with the biochemical, MDRD4 equation, which does not take into account BSI. ***Materials and Methods:*** An observational and retrospective study of the GFR of 47 patients with different pathologies who had undergone a test to determine GFR between 2019-2023 with two techniques, one biochemical (MDRD4) and one with radioisotopes (radiopharmaceutical [^{99m}Tc]Tc-DTPA). The BSI according to Dubois and Dubois is considered high if it is >1.9m^2 in men and >1.6m^2 in women. The radiopharmaceutical was administered to patients and samples were collected at 2, 3 and 4 hours. Plasma was quantified in a gamma counter and GFR was determined using the Christensen and Groth method. A GFR >75ml/min/1.73m^2 is considered normal. ***Results:*** 35/47(74.46%) patients are male and 12/47(25.53%) are female. Of the males 22/35(62.85%) have high ISC(>1.9m^2) whose GFR with [^{99m}Tc]Tc-DTPA and MDRD4 respectively are: 68.62±20.79ml/min/1.73m^2 and 49.45±9.86 ml/min/1.73m^2.86ml/min/1.73m^2 and of the females 11/12(25.53%) have high BSI (>1.6m^2) whose GFR with [^{99m}Tc]Tc-DTPA and MDRD4 respectively is: 50.01±23.71ml/min/1.73m^2 and 43.26±16.04ml/min/1.73m^2. Of the men with high BSI 19/22(86.36%) had a higher GFR with [^{99m}Tc]Tc-DTPA than with the MDRD4 equation (73.42±17ml/min/1.73m^2 and 50.32±9.16ml/min/1.73m^2 respectively). 16 ml/min/1.73m^2 respectively) and in the case of women with high BSI 7/11(63.63%) had a higher GFR with [^{99m}Tc]Tc-DTPA than with MDRD4 (57.98±26.68ml/min/1.73m^2 and 43.14±20.48ml/min/1.73m^2 respectively). The results obtained on GFR revealed in the case of the [^{99m}Tc]Tc-DTPA test that 34/47(72.34%) had a value <75ml/min/1.73m^2 while according to MDRD4 it was 46/47(97.87%). 39/47(82.97%) patients have a higher GFR with the radiopharmaceutical test than with MDRD4 (61.94±22.74ml/min/1.73m^2 and 46.55±11.57ml/min/1.73m^2 respectively. Comparing patients with high ISC in the radiopharmaceutical test and the MDRD4 equation yields p>0.05. ***Conclusion:*** The values obtained with the MDRD4 method have a lower GFR than those obtained with [^{99m}Tc]Tc-DTPA. It is observed that a high percentage of both male and female patients tested have a high BSI. Those patients with a high BSI had a lower GFR with MDRD4. Despite a decrease in GFR with MDRD4 compared to [99mTc]Tc-DTPA, there is no statistically significant difference. Obesity increases the risk of chronic kidney disease, therefore we found that many of these patients have an elevated BSI. This is probably due to the fact that the MDRD4 equation does not take into account the BSI unlike the [^{99m}Tc]Tc-DTPA test, which does.

EPS-027

Estimation of GFR Using Camera Based Method- Is There Any Role of CT?

S. Garg[1], *S. G. Ravindra*[1], *A. Khurana*[1], *K. J. Das*[2], *A. Singhal*[2], *V. Jaiswal*[2], *C. S. Bal*[1];
[1]*All India Institute of Medical Sciences, New Delhi, INDIA,*
[2]*National Cancer Institute - AIIMS, Jhajjar, INDIA.*

Aim/Introduction: There are various methods available for estimation of Glomerular Filtration Rate(GFR) using the renal radiopharmaceutical Technetium-99m-diethylenetriaminepentaacetic acid. Amongst these, the camera based methods are convenient as they do not require blood sampling. ***Materials and Methods:*** This is a prospective study wherein patients underwent a renal dynamic scan and a low dose CT scan simultaneously using GE NM/CT 870 DR. The GFRs were calculated using the following methods: 'GE Renal Analysis' software without filling the renal depth; formulae (Tonnesen's, Itoh K's, and Taylor's) based estimation of renal depths; CT based estimation of renal depth. The renal depths measured by the above mentioned techniques were compared to the Modified estimated GFR (eGFR) calculated using CKD-EPI equation. Statistical analysis was performed using

MedCalc Software with a p-value < 0.05 considered statistically significant. ***Results:*** Twenty-six patients were enrolled. The mean age and gender distribution (male: female) of patients was 44.7 ± 17.0 years and 12:14. The mean modified eGFR was 120.5 ± 69.6 mL/min. The mean GFRs calculated by the system, three formulae and CT were 68.7 ± 26.9, 68.4 ± 25.3, 81.7 ± 29.3, 78.2 ± 25.3 and 80.5 ± 30.4 respectively. All of them correlated well with modified eGFR with p<0.01. A good consistency was seen between the calculated GFR by system's inherent calculation technique, Tonnesen's, Itoh K's, Taylor's formulae, CT guided renal depth estimation and the modified eGFR(p<0.01). The right renal depth was significantly smaller using Tonessen's formula than those measured using the other two formulae but was not significantly different when compared to CT scan depth. The left renal depth measurement was not significantly different using any of the above methods(p>0.01). The right renal depth (6.1 cm, CI-5.8-6.5) was always larger than the left (5.9 cm, CI-5.7-6.2) (p<0.01). On pairwise comparison, system calculated (68.9 ± 27.0) and Tonessen's formula (68.4 ± 25.3) GFR(ml/min) were significantly lower as compared to CT aided(80.5 ± 30.4), Itoh K's(81.7 ± 29.3), Taylor's method(78.2 ± 25.3) GFR(ml/min). ***Conclusion:*** GFR calculated with CT guided, Itoh K's and Taylor's method is consistently higher than that calculated using system's inherent calculation technique and Tonessen's method. The Itoh K's and Taylor's method calculated renal depth correlates nicely with the CT aided depth measurement. These findings prove valuable as incorporation of low dose CT scan causes additional radiation burden to the patient.

EPS-028

Predictive role of ^{18}F-FDG PET/CT in renal function in patients with kidney disease

H. Jiao, *Y. Qiu, Z. Chen, Y. Fan, L. Kang;*
Peking University First Hospital Beijing, CHINA.

Aim/Introduction: Kidney disease appears to be both a potential cause and consequence of cancer. For patients with kidney disease, timely detection of tumors is particularly important. The ^{18}F-FDG distribution in tissues can reflect the level of local glucose metabolism. However, it has not been demonstrated by any studies yet whether detecting ^{18}F-FDG uptake in the renal cortex can provide relevant clinical information. In this study, we aimed to evaluate the value of ^{18}F-FDG PET/CT in patients with kidney disease. ***Materials and Methods:*** We retrospectively reviewed 182 ^{18}F-FDG PET/CT subjects diagnosed with kidney diseases and 32 subjects without any kidney disease from January 2018 to May 2022 in our hospital. Patients with kidney disease were divided into three groups: AKD, A/C, and CKD. The CKD groups were divided into G1, G2, G3, G4+G5 upon CKD-EPI-based estimated glomerular filtration rate (eGFR). The regions of interest (ROIs) were drawn in the left renal cortex of both upper and lower poles, liver, aorta and lesions with abnormal uptake. The SUVmax and SUVmean were measured for each ROI. The ratios of renal cortex SUVmax to the liver SUVmean and to the blood pool SUVmean were obtained, respectively. Statistical analysis was performed using the Kruskal-Wallis test and Spearman relation analysis. ***Results:*** Among 182 patients, 154 patients were found with abnormal FDG uptake (84.6%), of which the SUVmax of malignant lesions was significantly higher than that of benign lesions. The three most common malignant lesions included multiple myeloma, lymphoma and lung cancer. The sensitivity and specificity of PET/CT in the diagnosis of malignant lesions were 89.5% and 100%, respectively. The renal cortex SUV values of AKD, A/C and CKD group were significantly different from the normal group, and the renal cortex SUV values of the AKD group were also significantly higher than those of the CKD group. There were significant differences in the renal cortex SUVmax and SUVmean between G1 and G4+G5. In addition, there were significant differences in the renal cortex SUV values between primary kidney disease and secondary kidney disease. In CKD group, increased renal cortex SUVmax and SUVmean were associated with decreased serum creatinine, blood urea nitrogen, and increased eGFR. ***Conclusion:*** For patients with kidney disease, ^{18}F-FDG PET/CT can be used to systematically screen tumors and other abnormal uptake lesions. The ^{18}F-FDG uptake of renal cortex may predict different types of kidney diseases and be associated with renal function.

EPS-029

Clinical Significance of SPECT/CT Imaging in Dynamic Renal Scintigraphy for Work-up of Patients with Different Nephro-urological Conditions

T. Sofiyanski[1], *S. Sergieva*[1], *M. Dimcheva*[1], *B. Robev*[2];
[1]*Sofia Cancer Center, Sofia, BULGARIA,* [2]*University Hospital St. Ivan Rilski, Sofia, BULGARIA.*

Aim/Introduction: Dynamic ^{99m}Technetium diethylenetriaminepetaacetic acid (^{99m}Tc-DTPA) renal scintigraphy is a generally used imaging technique for evaluating renal function of patients with various nephron-urological conditions. The additional value of subsequent SPECT/CT to the renal scintigraphy has rarely been discussed in the medical literature. The aim of the study was to evaluate the benefits of subsequent SPECT/CT to the dynamic renal scintigraphy in the management of patients with different nephron-urological conditions. ***Materials and Methods:*** Thirty two patients /21 females and 11 males, aged 17-83 years/ underwent dynamic nephroscintigraphy with subsequent SPECT/CT. A dose of 185MBq (5mCi) ^{99m}Tc-DTPA was administered i.v. to perform dynamic imaging followed by SPECT/CT. The CT scan was performed with a low dose protocol. ***Results:*** Our analysis demonstrated impaired relative renal function in various degrees of left kidney in 18 patients and of the right kidney in 14 patients. SPECT/CT imaging revealed the specific cause, responsible for the renal dysfunction in the cases. The hybrid imaging demonstrated calculosis in 11 patients, postoperative strictures of ureter in 5 patients, tumor formation of kidney, ureter of urinary bladder in 4 patients, external compression of ureter from ovarian cyst in 1 patient and compression of ureter due to nephroptosis in 1 patient as a possible obstructive cause. In 9 patients congenital renal anomalies were the identified causes of impaired renal function - hypoplastic kidney in 3 patients, duplex kidney in 2 patients, multiple cortical cysts in 2 patients, aberrant vessel obstructing the pyelo-ureteral segment in 1 patient and horseshoe kidney in 1 patient. ***Conclusion:*** The combination of conventional dynamic renal scintigraphy and SPECT/CT could provide not only functional and anatomical information of kidneys and ureters in the evaluation of obstructive uropathies and congenital renal abnormities, but may also show the cause of the disease in the right patient. Our study indicated the usefulness of hybrid imaging in renal scintigraphy that can change the clinical management.

EPS-030

Added value of SPECT/CT to Planar Lymphoscintigraphy in Patients with Secondary Extremity Lymphedema: A Retrospective Cohort Study

H. Yoon[1], *D. Kim*[2], *K. Woo*[3], *B. Kim*[1], *J. Kim*[4];
[1]*Department of Nuclear Medicine, Ewha Womans University School of Medicine, Seoul, KOREA, REPUBLIC OF,* [2]*Department of Emergency Medicine, Incheon St. Mary's Hospital, The Catholic University of Korea, Incheon, KOREA, REPUBLIC OF,* [3]*Department of Plastic Surgery, Ewha Womans University School of Medicine, Seoul, KOREA, REPUBLIC OF,* [4]*Department of Nuclear Medicine Ewha Womans University Mokdong Hospital, Seoul, KOREA, REPUBLIC OF.*

Aim/Introduction: Lymphoscintigraphy is a standard modality to examine the functional status of the lymphatic system. In this study, we investigated the added value of SPECT/CT over planar lymphoscintigraphy for initial staging in patients with secondary extremity lymphedema. Furthermore, we developed a hybrid SPECT/CT classification combining dermal backflow (DBF) of SPECT and honeycomb pattern (HP) of CT, correlated it with lymphoscintigraphic staging and clinical severity. ***Materials and Methods:*** We retrospectively evaluated 41 patients with secondary extremity lymphedema who underwent lymphoscintigraphy with SPECT/CT from April 2022 to December 2022. Lymphoscintigraphic staging was performed according to the Taiwan Lymphoscintigraphy Staging (TLS) staging system, and clinical severity was evaluated using CT volumetry. Both CT-based and SPECT-based quantitative analyses were conducted. We examined the changes in TLS staging when SPECT/CT was added to planar scintigraphy alone. We analyzed quantitative parameters of CT-based (HP volume ratio) and SPECT-based (DBF volume ratio), as well as the hybrid classification according to the presence of HP and DBF, based on clinical severity and TLS staging. ***Results:*** Adding SPECT/CT to planar scintigraphy showed a 19.5% modification rate in TLS staging. HP volume ratio significantly differed among clinical severity groups and increased with severity ($p<0.001$) and among TLS staging groups with an increase in stage ($p=0.001$). DBF volume ratio did not differ significantly among clinical severity groups ($p=0.256$). However, DBF volume ratio showed significant differences according to TLS staging with an expected increase and decrease pattern ($p=0.008$). Hybrid SPECT/CT lymphoscintigraphic classification showed strong positive correlation with clinical severity and TLS staging. ***Conclusion:*** Our results demonstrated substantial modification of lymphoscintigraphic staging by adding SPECT/CT to a conventional planar scintigraphy. In addition, a hybrid SPECT/CT is expected to provide new indicators reflecting lymphoscintigraphic staging and clinical severity by providing both of functional DBF and anatomical HP information. ***References:*** Rockson, Stanley G. "Lymphedema after breast cancer treatment." New England Journal of Medicine 379.20 (2018): 1937-1944.Bae, Jae Seok, et al. "Evaluation of lymphedema in upper extremities by MR lymphangiography: Comparison with lymphoscintigraphy." Magnetic Resonance Imaging 49 (2018): 63-70. Cheng, Ming-Huei, et al. "Validity of the novel Taiwan lymphoscintigraphy staging and correlation of Cheng lymphedema grading for unilateral extremity lymphedema." Annals of surgery 268.3 (2018): 513-525.

EPS-031

Analysis and clinical response to bile acid sequestrants of patients with diarrhoea and borderline ^{75}SeHCAT results

S. Bondia-Bescós*, P. Notta, M. Pudis, B. Hervás-Sanz, J. Díaz-Moreno, A. Rodriguez-Gasen, A. Palomar-Muñoz, J. Robles-Barba, M. Cortés-Romera;*
Nuclear Medicine-PET (IDI) Department, Bellvitge University Hospital, Barcelona, SPAIN.

Aim/Introduction: The aim of this study is to evaluate the prevalence of bile acid diarrhoea (BAD) in patients with an abdominal retention score (ARS) 10-15% in ^{75}SeHCAT tests and to assess the clinical response to bile acid sequestrants (BAS) in those patients. ***Materials and Methods:*** A retrospective evaluation of ^{75}SeHCAT test results performed between April 2010 and January 2020. The SeHCAT test was performed as a measurement of the 7-day ARS. Oral administration of 370KBq of tauroselcholic acid and a collimated gamma camera was used in all cases. We divided SeHCAT results into three groups: A = ARS<10% (positive result), B = ARS between 10-15% (borderline result) and C = ARS>15% (negative result). Clinical data regarding response to BAS was obtained from the medical records of group B patients. ***Results:*** A total of 2678 SeHCAT tests were evaluated. ARS results on 7-day was, group A = 1144p, group B = 413p (275 women) and group C = 1025p. A total of 122 patients of group B received treatment with BAS, but in 20p it was not possible to know the response to BAS. 13p without follow-up just after the test were excluded. A good response to treatment in group B was obtained in 61.8% (63/102), intolerance in 12.7% (13/102) and non-response in 25.5% (26/102). In table 1 we divided the response to treatment of group B patients according to the type of BAD. ***Conclusion:*** In our study, a high percentage of patients with borderline SeHCAT results (ARS 10-15%) had a suitable clinical response to BAS. BAD type II subgroup showed the best response to BAS followed by BAD type III, therefore patients with borderline ARS results should be considered candidates to BAS treatment for correct clinical management. ***References:*** Barkun AN, Love J, Gould M, Pluta H, Steinhart H. Bile acid malabsorption in chronic diarrhea: pathophysiology and treatment. Can J Gastroenterol. 2013;27(11):653-659. Wedlake L, A'Hern R, Russell D, Thomas K, Walters JR, Andreyev HJ. Systematic review: the prevalence of idiopathic bile acid malabsorption as diagnosed by SeHCAT scanning in patients with diarrhoea-predominant irritable bowel syndrome. Aliment Pharmacol Ther. 2009 Oct;30(7):707-17.

EPS-032

Ukrainian experience of interictal FDG PET/CT brain scan for pharmacoresistant epilepsy in children as a part of a presurgical assessment

O. Oliinichenko[1]*, M. Tkachenko*[2]*;*
[1]*Kyiv Center of Nuclear Medicine, Kyiv, UKRAINE,* [2]*Bogomolets National Medical University, Kyiv, UKRAINE.*

Aim/Introduction: The aim of this study is introduction in practice in Ukraine routine use of brain ^{18}F-FDG PET/CT scans before surgical treatment of pharmacoresistant epilepsy in children and to optimize interpretation using a streamlined, automated solution for analysis and quantification of PET FDG - Cortex ID Suite. Over the past 4 years despite the epidemic and the war in our country surgical treatment of drug-resistant epilepsy continues to develop. One of the factors contributing to this was the use of an ^{18}F-FDG PET/CT scan. ***Materials and Methods:*** Our study included 100 children (1-17 years old, 55 female, 45 male) with normal or doubtful MRI that underwent an interictal 18F-FDG PET

as a part of a presurgical assessment. 18F-FDG PET was performed according to EANM procedure guidelines for brain PET imaging. Every patient received a dose of tracer injection according to the EANM Pediatric Dose calculator. Report of PET brain scans performed in two ways: the first -using only visual assessment and the second - reporting brain scans in Cortex ID. Among them, eight patients were excluded from the study because of short-term seizures after administration of FDG or 1 or 2 hours before scans appeared. Unfortunately, the parents hid this information. Among them, in 30 patients, we already have the pathohistological results after surgical treatment that revealed in 17 patients FCD, eight patients - hippocampal sclerosis, 3 with FCD in the combination of hippocampal sclerosis, 1 - pyloric gliosis, and one cavernous angioma. ***Results:*** Application of Cortex ID for patient reports showed that 65% of it helps to evaluate the epileptogenic focus in more detail even though the control Z - score database for adults, the correlation of visual assessment with 3D SSP methods for uptake ratio and Z-score data allows more focused detection of signs of hypometabolism caused by an epileptogenic focus, rather than distant consequences. ***Conclusion:*** Using 18 F- FDG PET CT brain scan in pediatric practice in presurgical diagnostic of drug-resistant epilepsy with negative or doubtful MRI results helps to select candidates for neurosurgical treatment. A combination of a visual and quantitative assessment of PET brain, using 3D SSP methods for uptake ratio and Z-score images helps more carefully and in detail to assess the interictal glucose metabolism of the brain to find the source of epilepsy.

EPS-033

Age variations in the normal physiological distribution of 18F-FDG

J. Hagerman[1], *D. Minarik*[2], *E. Trädgårdh*[1], *J. Oddstig*[2];
[1]*Clinical Physiology and Nuclear Medicine, Skåne University Hospital, Lund/Malmö, SWEDEN,* [2]*Radiation Physics, Skåne University Hospital, Lund/Malmö, SWEDEN.*

Aim/Introduction: The biodistribution of fluorine-18-fluorodeoxyglucose (18F-FDG) mimics the rate of tissue glucose utilization and is distributed in healthy/diseased tissue to varying degrees. Knowledge of the physiological accumulation of the tracer is central when interpreting positron emission tomography (PET) images. Clinical observations recognize differences in the physiological accumulation of 18F-FDG between adults and children - potentially associated with changes in glucose metabolism and/or body composition during a child´s development. Weight is recognized to influence biodistribution in adults, as white adipose tissue contributes to weight but is usually metabolically inactive. We aimed to investigate age-related quantitative differences in the normal distribution of 18F-FDG in children and adults. ***Materials and Methods:*** 18F-FDG PET images from 208 clinical patients (164 children), 0-76 years, were retrospectively included. Only presumed healthy tissue (according to PET) from the aorta, liver, spleen, lung, gluteus maximus, and pelvis skeleton were segmented in the PET images (assistance of corresponding computer tomography (CT) images), using a convolutional neural network with manual correction, generating a diversity of volumes-of-interest. Biodistribution was measured as the mean standardized uptake value (SUVmean). Patients were stratified into children (<20 years), adults (>20 years), and 0-8, 9-15, 16-19, and >20 years and analyzed in relation to their body composition. ***Results:*** Children had lower SUVmean than adults in the aorta (1.32 ±0.30, 1.64 ±0.34, p<0.001) (mean ±standard deviation), liver (1.66 ±0.42, 2.10 ±0.44, p<0.001), and gluteus maximus (0.51 ±0.10, 0.61 ±0.12, p<0.001), higher in the pelvic skeleton (1.13 ±0.20, 0.93 ±0.14, p<0.001), but similar in the lung (0.59 ±0.13, 0.61 ±0.14, p=0.396) and spleen (1.51 ±0.39, 1.58 ±0.33, p=0.258). Body composition was equivalent to normal weight for all adults, while obesity (6%), pre-obesity (16%), and underweight (10%) were present among the children. With a variation in significance level, the SUVmean among children for the aorta, liver, and spleen increased with age. In contrast, an initial increase, followed by a plateau, was observed for the lung, gluteus maximus, and pelvic skeleton. Regression analysis exposed SUVmean differences between adults and each younger group that remained significantly lower after adjusting for body mass index for the aorta, liver, and gluteus maximus. ***Conclusion:*** Our study confirms that SUVmeans generally increase, or remain constant, with age. Significantly lower accumulation of 18F-FDG was observed in children´s aorta, liver, and gluteus maximus compared to adults, which remained after adjusting for body composition. The result is important to recognize when reviewing/interpreting children´s 18F-FDG PET images.

EPS-034

The impact of the COVID-19 pandemic on oncological disease extent in children at FDG PET/MR staging

Y. Xu;
Hangzhou Universal Medical Imaging Diagnostic Center, Hangzhou, CHINA.

Aim/Introduction: To evaluate the impact of coronavirus disease 2019 (COVID-19) pandemic on tumor staging and treatment of 18F-FDG PET/MR in children. ***Materials and Methods:*** Retrospective observational study including biopsy-proven, newly diagnosed Malignant tumor in children using whole-body FDG PET/MR staging in two selected intervals: May 1, 2017 to January 31, 2020 (Group A), and February 1, 2020 to June 30, 2022 (Group B). Data regarding primary tumour, regional lymph nodal (N) status and number of involved regional lymph nodal stations, and presence and number of distant metastases (M) were collected. ***Results:*** 1415 children(398 neuroblastomas, 104 blastomas, 73 hepatoblastomas, 394 lymphomas, 119 Langerhans histiocytosis, 98 rhabdomyosarcomas, 21 osteosarcomas, 24 malignant teratomas, 31 endodermal sinus tumors, 40 germ cell tumors, 19 Ewing's sarcoma, 15 hyaline cell sarcoma, and 79 other types of tumors) were included (672 in Group A vs 743 in Group B, respectively). The median intervals to PET/MR from the initial symptom in group A and group B were 7.3 (1.0-28.6) and 8.5(1.2-30.4) days, respectively (p<0.05). The median intervals to treatment from the initial symptom in group A and group B were 15.2 (5.6-30.5) and 16.4 (6.3-28.3) days, respectively (p>0.05). There was no statistically significant difference between the two groups in the staging of various types of tumors(p>0.05). ***Conclusion:*** For children with malignant tumors in Zhejiang Province, China, after the start of isolation restriction, although the median interval from initial symptoms to PET/MR was extended, there was no significant delay in PET/MR staging and treatment.

EPS-035

^{18}F-FDG PET/MR Imaging findings of pediatric neuroblastoma with different MYCN amplification status

J. Liang;
CHINA.

Aim/Introduction: To observe the ^{18}F-FDG PET/MR imaging features of pediatric neuroblastoma (NB) with different MYCN gene amplification status. ***Materials and Methods:*** 140 pediatric neuroblastoma patients were enrolled and divided into MYCN group (n=62) and

unamplified group (n=78) according to MYCN gene copy number. The lesion location, size, morphology, shape, calcification, cystic degeneration and necrosis of tumors were compared between the two groups. The SUVmax and mean ADC values of tumor parenchyma were both compared between groups. ***Results:*** There were significant differences in tumor size, calcification, cystic degeneration and necrosis among groups (P <0.05), but there were no significant differences in tumor location, morphology and growth across the median line (P>0.05). The relationship between tumor and blood vessels and the invasion of neighboring organs were statistically different among the groups (P <0.05). There were statistically significant differences in SUVmax and mean ADC values of tumor parenchyma between groups (P <0.05). The SUVmax value of tumor parenchyma in MYCN group was significantly higher than that in unamplified group (P <0.05), while the mean ADC value in MYCN group was significantly lower than that in unamplified group (P <0.05). ***Conclusion:*** ^{18}F-FDG PET/MR imaging features of pediatric neuroblastoma patients with different MYCN gene amplification status are different.

EPS-036

Value of qPET in Pediatric Patients With Hodgkin Lymphoma

M. Mehesen[1,2], *E. Moussa*[3,2], *M. S. Zaghloul*[1,2], *M. Elwakeel*[1,2], *W. Elsayed*[1,2], *N. Ali*[1,2];
[1]*National Cancer Institute., Cairo, EGYPT,*
[2]*Children's Cancer Hospital Egypt, Cairo, EGYPT,*
[3]*Menoufya University, Menoufya, EGYPT.*

Aim/Introduction: qPET is a semi-automatic quantitative measurement used to assess the FDG-PET response in lymphoma. 898 scans of children with Hodgkin lymphoma from the EuroNetPHL-C1 (C1) trial were used to develop qPET. The aim of this study was to compare qPET and the Deauville score, then find their concordance in childhood HL patients treated at an Egyptian children's cancer hospital. ***Materials and Methods:*** qPET is computed by dividing the peakSUV of the hottest residual uptake by the meanSUV of the liver. Interim PET (after two cycles of chemotherapy) will be evaluated in accordance with qPET and DS, and the degree of concordance between the two will be determined. ***Results:*** We retrospectively analyzed 424 pediatric patients with newly diagnosed Hodgkin lymphoma (122 females and 302 males, with a mean age of 10.1 (2-18) years). In terms of pathologic subtypes, lymphocyte depletion was observed in 9 patients, mixed cellularity in 143 patients, NLPHL in 2 patients, lymphocytic rich in 15 patients, and nodular sclerosis in 255 patients. In 51 patients, stage IA was identified, then stage IB in 12 patients, stage IIA in 104 patients, stage IIB in 40 patients, stage IIIA in 61 patients, stage IIIB in 59 patients, stage IV A in 35 patients, and stage IVB in 62 patients. Based on PETCT measurements, DS was identified as DS1 in 24 patients, DS2 in 106 patients, DS3 in 187 patients, DS4 in 77 patients, and DS5 in 30 patients. 317 patients were negative (DS 1-3) and had an adequate response, while 107 were positive (DS 4-5) and had an inadequate response. qPET revealed that 341 patients were negative (less than 1.3) and 83 were positive.We found that 25 patients had a DS 4 (positive) and a qPET 3 (negative), while one patient had a DS 3 (negative) and a qPET 4 (positive). Two patients out of twenty-five (2/25) who were positive by DS and negative by qPET experienced a relapse, while the remaining twenty-three patients were in complete remission. EFS was 90.4% for negative DS and 80.1% for positive DS at 2 years (P = 0.004).EFS at 2 years was 88.3% for negative qPET and 83.9% for positive qPET (P = 0.03). ***Conclusion:*** Our qPET results indicate that it is a suitable semi-automatic quantitative method for evaluating response in pediatric HL patients. qPET thresholds from childhood HL in CCHE gave 73 % concordance for vDS and qPET.

EPS-037

Role of semi-quantitative assessment of ^{123}I-MIBG uptake in pediatric neuroblastoma.Does semiquantitative evaluation of uptake improve the diagnostic accuracy of^{123}I-MIBG scintigraphy in pediatric neuroblastoma ?

C. Altini[1], *M. Villani*[1], *M. Pizzoferro*[1], *A. Castellano*[2], *A. Serra*[2], *M. De Ioris*[2], *D. Ciucci*[3], *C. Polito*[3], *E. Solfaroli Camillocci*[3], *V. Cannatà*[3], *E. Villanucci*[1], *V. Nicoloso*[1], *G. Marchetti*[1], *M. Garganese*[1];
[1]*IRCCS Bambino Gesù Children's Hospital, Nuclear Medicine Unit, Imaging Department, Rome, ITALY,*
[2]*IRCCS Bambino Gesù Children's Hospital, Department of Oncohematology, Rome, ITALY,* [3]*IRCCS Bambino Gesù Children's Hospital, Medical Physics Unit, Rome, ITALY.*

Aim/Introduction: ^{123}I-MIBG scintigraphy is indispensable in neuroblastoma staging and in the evaluation of response to treatment. Qualitative scoring systems are a known and reliable method of evaluation to assess response to therapy in bone and bone marrow metastatic sites but the determination of response in primary tumour is challenging, as qualitative evaluation of images is often not sufficient. Aim of our study is to evaluate the usefulness of semiquantitative assessment of tracer uptake in ^{123}I-MIBG scintigraphies in the estimation of response to treatment in pediatric patients affected by neuroblastoma. ***Materials and Methods:*** we retrospectively evaluated staging scintigraphy and after induction chemotherapy scintigraphy of 33 patients affected by neuroblastoma (age range: 4 months - 17 years), for a total of 66 scintigraphies. All the studies (planar images and xSPECT/TC acquisitions) were performed from April 2021 to April 2023 in Our Center with an hybrid gamma camera (Symbia Intevo BoldTM, Siemens Healthineer). Treatment response after every treatment was classified as progressive disease or stable disease (PD and SD), partial and complete response (PR and CR) based on a comprehensive evaluation (CT data, qualitative evaluation of ^{123}I-MIBG scan, trephines data) and correlated to the variation of the ratio of SUVmax lesion (SUVmaxLE)/SUVaverage liver (SUVavgLI). ***Results:*** we found in 29/33 cases (89,5%) a concordance between the overall classification of the response and the variation of the SUVmaxLe/SUVavgLI ratio; only in 4 cases we found a mismatch. Despite the classification of the response in stable disease, ^{123}I-MIBG scintigraphy showed an increase of the SUVmax LE/SUVavgLI ratio in primary tumor above 50%. Among these patients, 3/4 presented metastatic disease at diagnosis, while 1/4 had localized disease, but segmental chromosome aberrations. ***Conclusion:*** in our experience, semiquantitative assessment of tracer uptake in primary tumor can improve the diagnostic accuracy of 123I-MIBG scintigraphy in Patients affected by neuroblastoma. Further studies with long term follow up are required in order to understand how semi-quantification of metabolic activity in primary tumor affects clinical management and outcome of these patients.

EPS-038

Dynamic Renal Scintigraphy In Pediatric Hydronephrosis: Imapct In Therapeutic Decision

L. Zaabar[1,2], *M. ElOuni*[3], *T. Ben Ghachem*[1,2], *D. Ben Sellem*[1,2], *B. Letaief*[1,2], *A. Mhiri*[1,2];
[1]*Salah Azaeiz Institute, Tunis, TUNISIA,* [2]*Faculté de Médecine de Tunis, Tunis, TUNISIA,* [3]*Health Ministery, Tunis, TUNISIA.*

Aim/Introduction: Pyeloureteral junction syndrome is an urodynamic disorder responsible for ureteropelvic dilation upstream of an organic or functional obstruction. Its imaging modalities and therapeutic choices are controversial.The aim of this study was to evaluate the contribution of dynamic renal scintigraphy (DRS) using ^{99m}Tc-MAG3 in initial and postoperative management of pediatric hydronephrosis. ***Materials and Methods:*** It was a five-year retrospective and descriptive study, conducted in the Nuclear Medicine Department of Salah Azaiez Institute, involving 89 children referred for exploration of their non-congenital hydronephrosis. All patients performed DRS using ^{99m}Tc-MAG3 with hyperdiuresis provocation test, then they were defined as renal unit (RU), giving us a total number of 176 RU. ***Results:*** The average age was 6.47± 3.34 years. Sex ratio M/F was 1.17. Among the 107 RU with ureteropelvic dilation, 98 RU (91.6%) had non-obstructive isotopic nephrogram (IN). Only nine percent of the RU with ultrasound-documented UPD had obstructive type of IN. We noticed a non progression towards aggravation in 40 DRS (85%) among the 47 control DRS. We identified the change in Tmax between the initial and the 1st DRS control as the most significant parameter of the follow-up (p=0.026), and found statistically significant difference in the separate relative function between each two successive DRS throughout the follow-up (p=0.02). The comparison of postoperative status of IN did not show any adverse evolution in 12 of the 13 cases. We calculated NORA (NOrmalized Residuel Activity) for 39 RU on all performed DRS (initial, control and postoperative DRS), and we noticed 27 favorable results (69%) including 12 displacements all to a better result, and in particular the cancellation of five obstructive IN and therefore the eventual surgery. ***Conclusion:*** DRS with ^{99m}Tc-MAG3 allows to identify kidneys at risk of damage and, consequently, to guide the most appropriate therapeutic management. Based on our findings, we present recommendations involving DRS as a cornerstone for initial management and monitoring of non-congenital hydronephrosis in children.

EPS-039

Predicting the clinical outcome of antenatally detected unilateral pelvi-ureteric junction obstuction.

R. Belakroum;
Central Military Hospital, Algiers, ALGERIA.

Aim/Introduction: To determine, in children with antenatally detected pelviureteric junction (PUJ) stenosis, which factors may be predictive for deterioration of differential renal function (DRF) in case of initially conservative attitude. Initial level of hydronephrosis, quality of renal drainage and cortical transit were analyzed and compared to the late DRF outcome. ***Materials and Methods:*** We have followed the 80 consecutive children with antenatally diagnosed PUJ stenosis during a 5-year period (between 2016 and 2020). From this cohort, we retained 80 children with unilateral PUJ and strictly normal contralateral kidney with a median follow up of 42 months. Repeated ultrasounds, voiding cystourethrography, and Tc-99m-ethylene-dicysteine (EC) renograms were performed in all children. ***Results:*** Among the 80 patients of the study, 51 patients did not underwent a surgical intervention (64%), while surgical repair (Anderson-Hynes dismembered pyeloplasty) was performed in 29 (36 %). Early pyeloplasty was performed in 19 patients at a median age of 6 months and late pyeloplasty in 10 cases at a median age of 33 months. During conservative follow-up, DRF deterioration was observed in 11,5% of cases. When analyzing the DRF evolution in function of the initial antero-posterior renal pelvic diameter, the quality of renal drainage, and abnormal cortical transit, only renal pelvic APD≥40mm and abnormal cortical transit were predictive of DRF deterioration in case of conservative approach. ***Conclusion:*** Conservative management of children with unilateral PUJ stenosis is a safe procedure. Impaired cortical transit in renogram seems the best scnitigraphic criterion for identifying children for whom pyeloplasty is mandatory. ***References:*** [1]- Koff SA, Campbell KD. The nonoperative management of unilateral neonatal hydronephrosis : natural history of poorly functioning kidneys. J Urol 1994 Aug :593e5., 152(2 Pt.[2]- Koff SA, Campbell K. Nonoperative management of unilateral neonatal hydronephrosis. J Urol. 1992 et 148 :525-31.[3]- Schlotmann A, Clorius JH, Clorius SN. Diuretic renography in hydronephrosis : renal tissue tracer transit predicts functional course and thereby need for surgery. Eur J Nucl Med Mol Imaging. 2009 et 36 :1665-1673.[4]- S. Arena1 & R. Chimenz E. Antonelli F. M. Peri P. Romeo P. Impellizzeri C-A long-term follow-up in conservative management of unilateral ureteropelvic junction obstruction with poor drainage and good renal function-European Journal of Pediatrics. 2018 [5]- Piepsz A, Gordon I, Brock J 3rd, et al. Round table on the management of renal pelvic dilatation in children. J Pediatr Urol.2009 [6]- Hong Phuoc Duong, Amy Piepsz, Frank Collier, Karim Khelif-UROLOGY 82 : 691e696, 2013.

EPS-040

A Classic Never Goes Out of Style: Fusion Kidney Malformations, a 10 Years Retrospective Analysis

I. Grierosu[1,2], *R. Tibu*[2], *I. Starcea*[1,3], *A. Mocanu*[3], *R. Bogos*[3], *T. Lazaruc*[3], *R. Stamate*[2], *L. Rau*[2], *D. Raileanu*[2], *V. Cernov*[2], *A. Iacoban*[1], *W. Jalloul*[1], *T. Ionescu*[1], *C. Stolniceanu*[1], *A. Statescu*[2], *C. Stefanescu*[1,2];
[1]*UMF, Iasi, ROMANIA,* [2]*County Emergency Hospital „Sf. Spiridon", Iasi, ROMANIA,* [3]*Emergency Children Hospital „Sf. Maria", Iasi, ROMANIA.*

Aim/Introduction: The most notorious renal malformation is the horseshoe kidney (HK). HK is a congenital anomaly in which the kidneys are usually united, forming an U-shape, hence the name horseshoe kidney. The incidence of HK is estimated at 0.25 % of the general population and occurs twice as often in men comparing to women. Most of the time it is incidentally discovered during abdominal ultrasonography but nevertheless, there are also many other types of fused kidney malformations. ***Materials and Methods:*** In this retrospective analysis, we aim to share our 10 years of experience regarding fusion kidney malformations in pediatric nuclear medicine from the North-Eastern Region of Romania. The retrospective group of patients is represented by 540 patients with one of these ultrasonographical diagnoses: renal hypoplasia, renal dysplasia, renal ectopia, renal agenesia, renal malformation, renal malrotation, pyeloureteral duplication, vesicoureteral reflux and HK. All patients underwent a ^{99m}Tc-DMSA renal scan, static images and SPECT, using a Siemens DIACAM double headed Gamma camera. ***Results:*** From all the cases, 38 were diagnosed with a type of kidney malformation after a ^{99m}Tc-DMSA renal scan. They were aged between 1 and 17 years old. We noticed a higher incidence in males (65.78 %) and also

a higher incidence of parenchymal isthmus fusion malformation (28.94 %). The others types of malformations were: fibrous isthmus (15.78 %), L-shaped left ectopia (18.42 %), L-shaped right ectopia (10.52 %), supernumerary kidney (15.78 %), sigmoid kidney (2.6 %), lump kidney (2.6 %), infero-superior left fusion (2.6 %), infero-superior right fusion (2.6 %). ***Conclusion:*** ^{99m}Tc-DMSA has a major role in the diagnostic algorithm of renal malformations for the pediatric patients, with very low radiation exposure and essentially minimally invasive. It is certain that in the PET-CT and PET-MRI era, there is still an important place for classic scintigraphy.

EPS-041

Risk of renal damage in children with VUR grade III according to ^{99m}Tc-DMSA scan grading

D. Chroustova[1], *J. Trnka*[1], *J. Langer*[1], *I. Urbanova*[2], *L. Cerna*[1], *R. Kocvara*[1];
[1]*Charles University, 1st Faculty of Medicine and General University Hospital, Prague, CZECH REPUBLIC,* [2]*University Hospital Bulovka, Prague, CZECH REPUBLIC.*

Aim/Introduction: Renal changes can have long-term consequences, and their prevention is the main goal of vesicoureteral reflux (VUR) treatment. Renal scintigraphy using ^{99m}Tc-DMSA scan is considered as the gold standard to prove the presence and extent of renal parenchymal changes and to determine split renal function. The aim of this study was to determine the risk of renal damage in children diagnosed with VUR grade III, which is generally considered (along with VUR I and II) as a low-grade VUR, according to the occurrence of renal changes using the ^{99m}Tc-DMSA scan grading. ***Materials and Methods:*** A total of 132 patients were examined (56 boys, 76 girls aged 6 months -11 years) 6 months after acute pyelonephritis with a diagnosis of VUR. Planar static scintigraphy of the kidneys was performed using GE Infinia gamma camera 2 h after i.v. administration of 18-80 MBq ^{99m}Tc-DMSA according to EANM paediatric dosage card. Determination of the degree of kidney involvement according to the ^{99m}Tc-DMSA grading G0-G4 (Mattoo et al) with our modification of the G4 grade was based on the number of affected segments (0-12) as follows: Grade G0: no involvement G1: 1-2 segments, G2: 2-4 segments G3: more than 4 segments, G4 smaller kidney (A without focal changes, B with marginal changes). For purpose of statistical analysis, the number of pathological segments/scars was assessed in each involved kidney. For G0-G3, the numbers were counted exactly, whereas for G4 the numbers were estimated based on expected count in this group. Mean values within each VUR grade were calculated and evaluated using Student´s t-test. ***Results:*** A total of 201 kidneys were evaluated: VUR I in 19 kidneys, VUR II in 32 kidneys, VUR III in 63 kidneys, IV in 62 kidneys, VUR V in 25 kidneys regardless of unilateral or bilateral occurrence. VUR III demonstrated significantly higher value of expected scars (3.11 vs 1.67, p=0.001) than the remaining low-risk grades I and II. On the other hand, when compared with high-risk grade IV, the value was not significantly lower (3.11 vs 3.77, p = 0.08). ***Conclusion:*** VUR III is linked to a higher incidence of high-grade ^{99m}Tc-DMSA changes, especially grade G3, G4B which can be considered a risk factor leading to permanent renal damage. Therefore, we recommend excluding VUR III from the low-grade group and considering it as a standalone grade of moderate risk.

310

Sunday, September 10, 2023, 09:45 - 11:15
Hall K

CTE 2 - Technologists Committee: Head and Neck Updates

OP-116

Head and Neck molecular imaging – state of the art

W. Cholewiński;
Greater Poland Cancer Centre/Poznan University of Medical Sciences, Nuclear Medicine/Electroradiology Department, Poznan, POLAND.

OP-117

Head and Neck cancer patient management using the PET-MRI method

M. Kinggaard Federspiel;
Rigshospitalet, Copenhagen, DENMARK.

OP-118

New radiopharmaceuticals for Head and Neck tumours evaluation and therapy

G. Gorgoni;
IRCCS Sacro Cuore, Department of Radiopharmacy, Negrar di Valpolicella Verona, ITALY.

401

Sunday, September 10, 2023, 11:30 - 13:00
Hall A

Plenary 2 New Imaging Techniques - Jump Aboard or Watch and Wait

OP-119

Introduction by Chairpersons

OP-120

AI technology: living up to expectations?

F. Buffa;
Bocconi University, Department of Computing Sciences, Milan, ITALY.

OP-121

SPECT/CT CZT based systems: jump aboard

L. Imbert;
CHRU Nancy, Nancy, FRANCE.

OP-122

SPECT/CT CZT based systems: watch and wait?

J. Dickson;
UniversityCollege London Hospitals, Institute of Nuclear Medicine, London, UNITED KINGDOM.

OP-123

Total Body PET: watch and wait?

A. Dimitrakopoulou-Strauss;
German Cancer Research Center, Heidelberg, GERMANY.

OP-124
Total Body PET: jump aboard
A. Rominger;
Universityof Bern, Inselspital, Dept. of Nuclear Medicine, Bern, SWITZERLAND.

OP-125
PET/MR: is it still worth it?
S. Wan;
UniversityCollege London Hospitals, Institute of Nuclear Medicine, London, UNITED KINGDOM.

OP-126
Innovation and sustainability in Nuclear Medicine: the IAEA perspective
R. Grossi;
IAEA, Vienna, AUSTRIA

501

Sunday, September 10, 2023, 15:00 - 16:30
Hall A

CME 3 - Cardiovascular Committee: Nuclear Imaging in Cardiac Amyloidosis - What Else?

OP-127
Background and novel therapies
M. Papathanasiou;
UniversityHospital Essen, University Duisburg-Essen, West German Heart- and Vascular Center, Department of Cardiology and Vascular Medicine, Essen, GERMANY.

OP-128
Bone scan – all you need to know
O. Lairez;
Cardiology Department, Rangueil University Hospital, Toulouse, FRANCE.

OP-129
PET – do we really need it?
D. Genovesi;
Fondazione Toscana Gabriele Monasterio, Division of Nuclear Medicine, Pisa, ITALY.

OP-130
Nuclear imaging for therapy response
H. Tingen;
UniversityMedical Center G, Groningen, NETHERLANDS.

502

Sunday, September 10, 2023, 15:00 - 16:30
Hall D (Arena)

Challenge the Expert 2 - Oncology & Theranostics Committee: Risk in Diagnostic and Therapeutic Nuclear Medicine

OP-131
Radiation risks in Nuclear Medicine: informed consent and effective communication
S. Leide Svegborn;
Skåne University Hospital, Department of Radiation Physics, Malmö, SWEDEN.

OP-132
Challenger cases
R. Teixeira Ferreira;
Hospital Garcia de Orta, E.P.E., Department of Nuclear Medicine, Almada, PORTUGAL.

OP-133a
Challenger cases
J. Castro Ferro;
Department of Nuclear Medicine, Instituto Português de Oncologia do Porto Francisco Gentil, E.P.E, Porto, PORTUGAL.

OP-133b
Challenger cases
B. Ribeiro Pereira;
Department of Nuclear Medicine, Centro Hospitalar Universitário de São João, E.P.E, Porto, PORTUGAL.

OP-133c
Challenger cases
M. Monteiro;
Department of Nuclear Medicine, Centro Hospitalar e Universitário de Coimbra, E.P.E, Coimbra, PORTUGAL.

503

Sunday, September 10, 2023, 15:00 - 16:30
Hall E1

LIPS Session 3 - Thyroid Committee: Rational Use of PET/CT with 18F-FDG in DTC

OP-134
Adding FDG-PET to the diagnostic work-up of indeterminate thyroid nodules: expensive gadget or cost-effective?
L. de Geus-Oei;
Leiden University Medical Center (LUMC), Department of Radiology, Leiden, NETHERLANDS.

OP-135
18F-FDG in staging DTC: when and why
S. Kusacic Kuna;
Clinical Department of Nuclear Medicine and Radiation Protection, University Hospital Centre, Zagreb, CROATIA.

OP-136
Role of 18F-FDG in restaging DTC and as a tool for response evaluation
M. Tuncel;
Department of Nuclear Medicine, Hacettepe University, Ankara, TÜRKIYE.

504

Sunday, September 10, 2023, 3:00 PM - 4:30 PM
Hall E2

M2M Track - TROP Session: Radioligand Therapy - New and Old Targets

OP-137

Preclinical Characterization of a Novel EphA2-Targeted Peptide Radioligand for Treatment of Solid Tumors

G. Li[1], *R. Clift*[1], *S. Richardson*[1], *T. Ehara*[2], *H. Yanagida*[2], *I. Hung*[1], *Z. Amso*[1], *K. Salvador*[1], *M. Guest*[1], *G. Han*[1], *A. Bhat*[1], *D. Cole*[1], *E. Bischoff*[1];
[1]*RayzeBio, San Diego, CA, UNITED STATES OF AMERICA,* [2]*PeptiDream, Kawasaki-Shi, JAPAN.*

Aim/Introduction: Ephrin type-A receptor 2 (EphA2) is a type I transmembrane glycoprotein which belongs to the ephrin receptor subfamily. EphA2 is primarily expressed during embryonic development, and its expression levels are low or absent in normal adult tissues. EphA2 overexpression has been observed in multiple tumors such as bladder, cervical, ovarian, colorectal, lung and esophageal cancers. The broad overexpression in solid tumors and relatively low expression in normal adult tissues make EphA2 attractive for targeted radiopharmaceutical therapy (RPT). ***Materials and Methods:*** RAYZ-6114 is comprised of a macrocyclic peptide binder to EphA2, a linker, and DOTA chelator which can be complexed with different radiometals. RAYZ-6283 shares the same peptide binder and chelator with RAYZ-6114 but differs in the linker. The binding affinity, selectivity and cross-species reactivity to EphA2 and other Ephrin proteins were determined by surface plasma resonance (SPR). Target-mediated internalization was measured using flow cytometry. In vivo biodistribution and anti-tumor efficacy studies were performed in tumor-bearing athymic nude mice. A coagulopathy study was performed in Sprague Dawley rats. For tumor type identification, EphA2 immunohistochemistry (IHC) was performed on tumor microarrays (TMA) representing diverse tumor types. ***Results:*** IHC analyses of TMAs confirmed the expression of EphA2 in a multitude of solid tumors, with the highest positivity rates in cervical, pancreatic, bladder, colorectal, esophageal and non-small cell lung cancers. RAYZ-6114 showed high binding affinity to human EphA2 with a K_D of 0.03 nM. High-affinity binding was conserved across mouse, cynomolgus monkey and human EphA2. No binding to other Ephrin type-A or Ephrin type-B proteins was detected, nor to EphA2-knockout cells. The binder rapidly and efficiently internalized in EphA2-positive H1299 cells upon target engagement, with ~75% internalized by 1 hour. In PC3 xenograft mice, ^{177}Lu-RAYZ-6283 showed sustained tumor uptake (~25% ID/g) for up to 48 hours and tumor/kidney ratios of 2.7, 3.3 and 5.9 at 24h, 48h and day 7, respectively. Low uptake was seen in other normal tissues. Both ^{177}Lu- and ^{225}Ac- labelled RAYZ-6114 significantly inhibited tumor growth. Particularly, durable tumor regression and survival benefit were achieved by a single dose of ^{225}Ac-RAYZ-6114 (3 uCi), out-performing ^{177}Lu-RAYZ-6114 dosed at 3 mCi. No adverse clinical signs or changes in coagulation parameters were observed in Sprague Dawley rats. ***Conclusion:*** RAYZ-6114 and RAYZ-6283 are first-in-class, highly potent and selective macrocyclic peptide binders. Preclinical pharmacodynamic, pharmacokinetic, biodistribution and efficacy data demonstrated their potential for treatment of patients with EphA2-positive tumors.

OP-138

Preclinical Characterization of a Novel Peptide Binder to Glypican-3 for Targeted Radiopharmaceutical Therapy of Hepatocellular Carcinoma

G. Li[1], *F. Lin*[1], *R. Clift*[1], *T. Ehara*[2], *H. Yanagida*[2], *S. Horton*[1], *K. Salvador*[1], *S. Richardson*[1], *M. Guest*[1], *A. Noncovich*[1], *A. Bhat*[1], *G. Han*[1];
[1]*RayzeBio, San Diego, CA, UNITED STATES OF AMERICA,* [2]*PeptiDream, Kawasaki, JAPAN.*

Aim/Introduction: Glypican-3 (GPC3) is a membrane-associated heparan sulfate proteoglycan with no or minimal expression in normal adult tissues. Significant upregulation of GPC3 protein in hepatocellular carcinomas (HCC) has been observed in up to 75% cases, whereas no expression is seen in cirrhotic liver or intrahepatic cholangiocarcinoma. The differential expression of GPC3 between tumor and normal tissues provides an opportunity for GPC3-targeted radiopharmaceutical therapy (RPT) to treat HCC, a leading cause of cancer-related deaths worldwide. ***Materials and Methods:*** RAYZ-8009 is comprised of a novel macrocyclic peptide binder to GPC3, a linker, and chelator DOTA that can be complexed with different radioisotopes. The affinity of peptide binders to GPC3 was determined by surface plasma resonance (SPR), as well as a radioligand binding assay in human HCC cell line HepG2. The cross-species binding was assessed by radioligand binding using recombinant mouse, cynomolgus monkey, and human GPC3 proteins. Target-mediated internalization in HepG2 cells was measured using Microbeta at various time points. Circulating GPC3 levels were measured using plasma collected from athymic nude mice harboring HepG2 tumors of different sizes. In vivo biodistribution and anti-tumor efficacy studies were performed in GPC3+ tumor-bearing athymic nude mice. ***Results:*** RAYZ-8009 showed high binding affinity to human GPC3 with a K_D of 0.7 nM as determined by SPR. Binding affinity was maintained across mouse, cynomolgus monkey and human GPC3. Potent cellular binding was confirmed in GPC3+ HepG2 cells, and was independent of choice of isotope. ^{177}Lu-RAYZ-8009 showed fast and efficient internalization with 42% internalized by 20 minutes in HepG2 cells. In vivo biodistribution of ^{177}Lu-RAYZ-8009 showed tumor uptake of 19.8, 16.6, 16.4, and 8.8 %ID/g at 2, 24, 48, and 96 hours, respectively. Renal uptake was 16.1, 4.7, 1.6, and 0.7 %ID/g at the same timepoints, with tumor/kidney ratios of 1.3, 3.7, 11.3, and 15.0, respectively. Minimal uptake was observed in other normal tissues. Tumor-specific uptake and retention were also observed when tumors were implanted orthotopically with no uptake in non-malignant liver tissue. Circulating GPC3 was detectable in mouse plasma but had no impact on biodistribution or clearance. Furthermore, significant tumor growth inhibition and survival benefit were achieved with ^{225}Ac- or ^{177}Lu-labelled RAYZ-8009 in GPC3+ HCC xenografts. ***Conclusion:*** Preclinical pharmacodynamic, pharmacokinetic, biodistribution and efficacy data demonstrate the potential of RAYZ-8009 as a RPT agent for the treatment of patients with GPC3-positive HCC.

OP-139

A Novel Anti-L1CAM Antibody-Radionuclide-Conjugate (ARC) as New Treatment Option for Ovarian Cancer

C. Geraths[1], *M. Behe*[2], *D. Winkler*[1], *M. Hackebeil*[1], *A. Blanc*[2], *T. Chiorazzo*[2], *S. Imobersteg*[2], *R. van der Kant*[3,4], *J. Schymkowitz*[3,4], *F. Rousseau*[3,4];
[1]*CIS Pharma AG, Bubendorf, SWITZERLAND,* [2]*Paul-Scherrer-Institut, Villigen, SWITZERLAND,* [3]*Switch Laboratory - VIB KU Leuven Center for Brain and Disease Research, Leuven, BELGIUM,* [4]*KU Leuven - Department of Cellular and Molecular Medicine, Leuven, BELGIUM.*

Aim/Introduction: We present a novel ARC against the human cell adhesion molecule L1CAM which is upregulated in different cancers. Since it is related to a poor prognosis, L1CAM is a highly interesting target for an ARC. Our aim was to develop an improved humanised antibody targeting L1CAM, radiolabel it with Lu-177 and test it in vitro as well as in vivo. ***Materials and Methods:*** A humanisation of chimeric antibody chCE7[(1)] using latest in-silico modelling tools was performed thereby optimising physicochemical properties like affinity, stability, immunogenicity and aggregation behaviour. Further the antibody was a-glycosylated to be compatible with site specific coupling with transglutaminase. We generated DOTA and polymer-$(DOTA)_x$ (x = 2-5). We attached two DOTAs or two polymers to the functionalised antibody via click chemistry resulting in ARCs with drug (here chelator) to antibody ratios (DAR) 2-10. We tested the Lu-177 labelled ACR in vitro as well as in vivo. ***Results:*** The humanised huCE7 shows high binding affinity (K_D = 64 pM). In-silico modelling for identification of aggregation prone regions compensated the negative effect of a-glycosylation leading to a robust and stable antibody. Melting temperatures (Tm1 = 64.6 °C; Tm2 = 79.0 °C) characterised by dynamic scanning fluorometry showed higher stability compared to the chimeric de-glycosylated chCE7 (Tm1 = 60.3 °C; Tm2 = 73.6 °C). These DOTA-coupled constructs were labelled with Lu-177 with high radiochemical purity (>99 %) in less than 10 min (37 °C) and subsequently tested for tumour-cell interaction and in a mouse xenograft model (SKOViP3, ovarian cancer). The lead ARC (DOTA coupled to the humanised Ab) showed a favourable biodistribution with low uptake in healthy tissue (e.g., liver after 96 h 4.7 ± 0.7 % iA/g) and a constant accumulation in the tumour tissue (maximum after 96 h = 67.5 ± 15.1 % iA/g). The overall survival (OS) in the treatment group (4 MBq Lu-177-huCE7, day 13 after tumour implantation, 10 mice per group) was 64 days (control group = 35 days). ***Conclusion:*** Here we present the first results of a novel ARC against L1CAM positive tumours, which showed a good in vivo efficacy in an aggressive ovarian cancer model. In the next steps the linker as well as dosing regime will be optimised to generate a candidate for investigative new drug enabling. ***References:*** [(1)]Amstutz et al. - Production and characterization of a mousehuman chimeric antibody directed against human neuroblastomaInt. J. Cancer: 53,147-152 (1993)

OP-140

In vitro evaluation of [^{225}Ac]Ac-DOTA-C595 for pancreatic ductal adenocarcinoma

A. Hull[1], *W. Hsieh*[2], *W. Tieu*[3], *A. Borysenko*[4], *D. Bartholomeusz*[2], *E. Bezak*[1];
[1]*University of South Australia, Adelaide, AUSTRALIA,* [2]*SA Medical Imaging, Adelaide, AUSTRALIA,* [3]*The University of Adelaide, Adelaide, AUSTRALIA,* [4]*Environment Protection Authority, Adelaide, AUSTRALIA.*

Aim/Introduction: Pancreatic ductal adenocarcinoma (PDAC) continues to have a poor prognosis with limited curative treatments available. Targeted alpha therapy (TAT) using monoclonal antibodies (mAb) conjugated to alpha-emitting radionuclides such as Actinium-225 (Ac-225) may hold promise in treating PDAC. Cancer-specific mucin 1 (MUC1-CE) is a promising therapeutic target for PDAC TAT. MUC1-CE is overexpressed on over 90% of PDAC with minimal normal tissue expression. The C595 mAb effectively binds to MUC1-CE. The aim of this study was to develop a novel radioimmunoconjugate, [^{225}Ac]Ac-DOTA-C595, and characterise its in vitro ability to target PDAC cells via MUC1-CE. ***Materials and Methods:*** C595 was conjugated to p-SCN-Bn-DOTA chelator. The resulting conjugate was labelled to Ac-225. Cell binding with 0 - 500nM of [^{225}Ac]Ac-DOTA-C595 at 1 h was assessed in a series of four pancreatic cancer cell lines with varying MUC1-CE expression: PANC-1 (high expression), CAPAN-1 (moderate expression), BxPC-3 (low expression), AsPC-1 (low expression). An internalisation assay was performed in the cell lines to evaluate the rate of internalisation over 48h. The ability of [^{225}Ac]Ac-DOTA-C595 to induce double-strand DNA breaks (DSBs) was assessed in PANC-1 and AsPC-1 cells using γH2AX staining detected via flow cytometry. Clonogenic assays were performed in PANC-1 and AsPC-1 cells to establish the in vitro cytotoxicity of [^{225}Ac]Ac-DOTA-C595. ***Results:*** [^{225}Ac]Ac-DOTA-C595 had significantly greater binding to PANC-1 cells compared to CAPAN-1, BxPC-3 and AsPC-1 cells at concentrations of 50 nM and above. All cell lines showed rapid internalisation ranging from 15% of internalised activity within 1 h to 49% internalisation at 48 h. PANC-1 cells exhibited significantly more γH2AX foci than AsPC-1 cells within 1 h of [^{225}Ac]Ac-DOTA-C595 exposure ($p = 0.0069$). At 48 h post-[^{225}Ac]Ac-DOTA-C595 exposure, PANC-1 cells had significantly less γH2AX foci than that observed at 1 h ($p = 0.0083$), suggesting cell death or DSB resolution. The clonogenic survival of AsPC-1 and PANC-1 cells decreased as the concentration of [^{225}Ac]Ac-DOTA-C595 increased. The survival of PANC-1 cells was significantly lower than AsPC-1 cells at 1 and 5 nM of [^{225}Ac]Ac-DOTA-C595 ($p < 0.0001$), although cell survival was similar at higher concentrations. ***Conclusion:*** At an in vitro level, [^{225}Ac]Ac-DOTA-C595 efficiently binds to MUC1-CE positive PDAC cells and is rapidly internalised. The cytotoxic effects of [^{225}Ac]Ac-DOTA-C595 are heightened in cells with high MUC1-CE expression, although a therapeutic effect is evident in weakly expressing cells. Future work will include in vivo studies to further assess [^{225}Ac]Ac-DOTA-C595 as a therapeutic radioimmunoconjugate against PDAC.

OP-141

Preclinical Comparison of the GRPR Antagonists AMTG and RM2 Labelled With Terbium-161 and Lutetium-177 - A PRISMAP Project

T. Günther[1], *N. Holzleitner*[1], *T. Cwojdzinski*[1], *R. Beck*[1], *N. Urtz-Urban*[1], *C. C. Hillhouse*[2], *P. V. Grundler*[2], *N. P. van der Meulen*[2], *Z. Talip*[2], *S. Ramaekers*[3], *M. Van de Voorde*[3], *B. Ponsard*[3], *A. Casini*[1];
[1]*Technical University of Munich, Garching, GERMANY,*
[2]*Paul Scherrer Institute, Villingen, SWITZERLAND,*
[3]*Belgian Nuclear Research Centre, Mol, BELGIUM.*

Aim/Introduction: To improve the metabolic stability of gastrin-releasing peptide receptor (GRPR) ligands, we recently substituted Trp^8 by α-methyl tryptophan (α-Me-Trp^8) in RM2 (DOTA-Pip^5-D-Phe^6-Gln^7-Trp^8-Ala^9-Val^{10}-Gly^{11}-His^{12}-Sta^{13}-Leu^{14}-NH_2) to achieve AMTG (α-Me-Trp^8-RM2). Other than retaining the favourable pharmacokinetics of RM2 irrespective of the radiometal used (copper-64, gallium-68, lutetium-177), a distinctly higher in vivo stability was observed for [^{177}Lu]Lu-AMTG (as compared to [^{177}Lu]Lu-RM2), which led to a significantly enhanced activity retention in the tumour over time. In this study, we labelled AMTG and RM2 with terbium-161 and carried out a

preclinical comparison by state-of-the-art experiments including their ^{177}Lu-labelled analogues. ***Materials and Methods:*** ^{161}Tb- and ^{177}Lu-labelling was carried out at 90°C within 5 min (1.0 M NaOAc buffer, pH=5.5). GRPR affinity (IC_{50}, n=3) and internalisation (37 °C, 1 h, n=6) were evaluated on PC-3 cells. Metabolic stability was investigated in vivo at 30 min post-injection (p.i.) in CB17-SCID mice (n=3). Biodistribution studies were carried out at 1, 4, 24 and 72 h p.i. in PC-3 tumour-bearing CB17-SCID mice (n=4, 100 pmol each). ***Results:*** ^{161}Tb- and ^{177}Lu-labelling proceeded nearly quantitatively (>98%). The Tb-labelled compounds showed a slightly higher GRPR affinity than their Lu-labelled analogues (IC_{50} (nM) of Tb-RM2: 2.46±0.16, Tb-AMTG: 2.16±0.09, Lu-RM2: 3.45±0.18, Lu-AMTG: 3.04±0.08). Internalisation studies revealed that 75-84% of the cell-associated activity was receptor-bound for both [^{161}Tb]Tb-/[^{177}Lu]Lu-RM2 and [^{161}Tb]Tb-/[^{177}Lu]Lu-AMTG. Lipophilicity (expressed as n-octanol/PBS distribution coefficient, $logD_{7.4}$, n=8) of the ^{161}Tb-labelled analogues was slightly lower as compared to their ^{177}Lu-labelled derivatives ([^{161}Tb]Tb-/[^{177}Lu]Lu-RM2: −2.63±0.05/−2.51±0.02, [^{161}Tb]Tb-/[^{177}Lu]Lu-AMTG: −2.48±0.07/−2.28±0.06). In vivo, both [^{161}Tb]Tb- and [^{177}Lu]Lu-AMTG displayed a distinctly higher stability (91-93% intact in serum, 68-74% in urine) than [^{161}Tb]Tb- and [^{177}Lu]Lu-RM2 (11-23% intact in serum, 0-1% in urine) at 30 min p.i. In vivo, all four compounds revealed a similar biodistribution profile at all time points, showing a rapid activity clearance from the pancreas and further off-target tissues. [^{161}Tb]Tb-AMTG exhibited the highest activity levels in the tumour as compared to the other three derivatives at 4 (16.0 versus 10.4-12.2 %ID/g), 24 (12.0 versus 9.1-11.5 %ID/g) and 72 h p.i. (5.3 versus 3.0-4.3 %ID/g). ***Conclusion:*** [^{161}Tb]Tb-AMTG demonstrated attractive in vitro (GRPR affinity, lipophilicity, receptor-bound fraction) and in vivo (metabolic stability, pharmacokinetics, activity retention in the tumour) characteristics. Due to its high in vivo stability and the higher number of Auger electron emissions per decay of terbium-161 as compared to lutetium-177, an enhanced therapeutic efficacy is anticipated for [^{161}Tb]Tb-AMTG over [^{177}Lu]Lu-AMTG and [^{161}Tb]Tb-/[^{177}Lu]Lu-RM2, which will be further evaluated in future studies.

OP-142

Preclinical Evaluation of a ^{68}Ga/^{177}Lu-based CXCR4 Radioligand: A Theranostic Tool Against Advanced Prostate Cancer

I. Astiazaran-Rascon[1,2], *H. Kuo*[1], *H. Merkens*[1], *N. Colpo*[1], *P. Ng*[1], *C. Ong*[2,3], *Y. Wang*[1,2,3], *K. Lin*[1,2], *F. Bénard*[1,2];
[1]BC Cancer, Vancouver, BC, CANADA, [2]University of British Columbia, Vancouver, BC, CANADA, [3]Vancouver Prostate Center, Vancouver, BC, CANADA.

Aim/Introduction: Neuroendocrine prostate cancer (NEPC) is an aggressive subtype of advanced prostate cancer with poor prognosis and limited treatment options, necessitating the development of novel diagnostic and therapeutic approaches. CXCR4 radioligands have been evaluated against haematologic malignancies; however, their application in advanced prostate cancer has not been explored yet. Our group has developed a series of macrocyclic peptide-based radioligands with high affinity to CXCR4 for the targeted delivery of radionuclides. The theranostic pair [^{68}Ga]Ga/[^{177}Lu]Lu-BL34 was chosen as the lead candidate for preclinical evaluation as an imaging and therapeutic agent in NEPC patient-derived xenograft (NEPC PDX) models. ***Materials and Methods:*** The preclinical evaluation of [^{68}Ga]Ga/[^{177}Lu]Lu-BL34 was conducted in three different NEPC PDX models (LTL331R, LTL352 and LTL545). Protein expression of CXCR4 was confirmed ex vivo in tumour-bearing mice by molecular techniques. Also, expression levels of CXCR4 mRNA were analyzed from a publicly available dataset of advanced prostate cancer patients and PDX models. The in vivo tumour uptake of [^{68}Ga]Ga/[^{177}Lu]Lu-BL34 was evaluated by PET/SPECT imaging and biodistribution studies at 1h (n=6) or at 1, 4, 24 and 72h post-injection (n=5), respectively. ***Results:*** The relative CXCR4 protein expression levels are shown to be higher in LTL331R and LTL352 models in comparison to LTL545. This is in line with the documented mRNA levels for each model. Elevated expression of CXCR4 relative to SSTR2 mRNA was observed in a cohort of advanced prostate cancer clinical samples and PDX supporting its clinical relevance. We showed high and specific accumulation of [^{68}Ga]Ga-BL34 in LTL331R (13.48±3.48 %ID/g), LTL352 (12.37±3.95 %ID/g) and LTL545 (3.80±0.59 %ID/g) tumour-bearing mice 1h after injection. The LTL331R model was selected for further studies as it showed the highest tumour uptake of our radioligand. Time course biodistribution studies showed that [^{177}Lu]Lu-BL34 reaches maximum tumour uptake 1h after intravenous administration in LTL331R tumour-bearing mice (11.97±1.76 %ID/g), with a significant decrease observed after 4h (5.96±2.1 %ID/g). High tumour-to-blood (37:1), tumour-to-kidney (4:1) and tumour-to-liver ratio (16:1) were observed 1h after injection indicating its fast clearance from circulation. ***Conclusion:*** The results presented show that both [^{68}Ga]Ga-BL34 and [^{177}Lu]Lu-BL34 accumulate at high levels in the tumour site with minimal uptake in major organs. Currently, dose-escalation studies are being performed to evaluate the therapeutic response. The blood clearance of [^{68}Ga]Ga-BL34 is optimal for non-invasive imaging of NEPC and future work may increase the tumour retention time of [^{177}Lu]Lu-BL34 to improve the dose delivery for therapy.

OP-143

Albumin Binder-modified Radiolabeled Heterodimer Probe for Cancer Imaging and Therapy

B. Yang, *Y. Gai, X. Song, X. Lv, Y. Long, Y. Wang, Y. Feng, R. An, X. Lan;*
Dept of Nuclear Medicine and PET center,Union Hospital, Tongji Medical College,HUST, Wuhan, CHINA.

Aim/Introduction: Integrin $\alpha_v\beta_3$ and CD13 (aminopeptidase N, APN) are two important biomarkers involved in tumor angiogenesis, overexpressed by tumor neovascular endothelial cells and tumor cells, promoting angiogenesis, tumor growth and metastasis. RGD (Arg-Gly-Asp) and NGR (Asp-Gly-Arg) are two extensively investigated peptides targeting integrin $\alpha_v\beta_3$ and CD13, respectively. On the basis of heterodimer probe RGD-NGR, RGD-NGR-Ab-01, 02, 03 was synthesized by modifying the molecular structure and adding albumin binder. The study aimed to explore the feasibility of using ^{177}Lu-RGD-NGR-Ab for in vivo radioligand therapy by single-dose administration in a BxPC-3 tumor bearing nude mouse model. ***Materials and Methods:*** ^{177}Lu-RGD-NGR-Ab-01, 02, 03 were synthesized, and labelling efficiency and radiochemical purity were determined. The in vitro stability of the probes was investigated by measuring its radiochemical purity at different time points, and the protein binding rate and lipid water partition coefficient of the probes were measured separately. Preclinical pharmacokinetics were determined in BxPC-3 tumor bearing nude mouse model using SPECT/CT and biodistribution experiments. In the radioligand therapy study, mice were randomized into 4 groups: 37 MBq ^{177}Lu-NGR-RGD, 18.5 MBq ^{177}Lu-RGD-NGR-Ab-03, 37 MBq ^{177}Lu-RGD-NGR-Ab-03, and PBS (control). A single-dose administration was applied at

the beginning of therapy studies. Tumor volume, body weight were monitored every 2 days. After the end of therapy, mice were euthanized. Tumors were then weighed, and systemic toxicity was evaluated via blood testing and histological examination of healthy organs. ***Results:*** All probes were successfully prepared with high purity and stability. ^{177}Lu-RGD-NGR-Ab-01, 02, 03 were stable in PBS (pH 7.4) and saline for at least 72h. They exhibit excellent stability in vitro, with high protein binding rate and good water solubility. SPECT imaging and biodistribution studies of ^{177}Lu-RGD-NGR-Ab-01, 02, 03 have proved their prominently improved tumor accumulation and retention at 96 h post-injection, especially for ^{177}Lu-RGD-NGR-Ab-03, high tumor uptake and low background signal make it the optimal compound. In radioligand therapy studies, tumor growth was significantly suppressed in the 37 MBq ^{177}Lu-RGD-NGR-Ab-03 group compared to other groups. ***Conclusion:*** Radioligand therapy using ^{177}Lu-RGD-NGR-Ab-03 significantly suppressed tumor growth and prolonged survival time in BxPC-3 tumor bearing nude mice without obvious toxicity, indicating that ^{177}Lu-RGD-NGR-Ab-03 is promising for clinical application and transformation.

OP-144

Preclinical Evaluation of [^{212}Pb]VMT-α-NET Targeted Alpha Therapy for High-Risk Metastatic Neuroblastoma

D. Liu[1], *J. T. Ewald*[1], *Z. Dai*[2], *C. Robels-Plannels*[3], *B. S. Cagle*[1], *S. N. Rodman III*[1], *M. Li*[1], *R. Rastogi*[2], *E. Sagastume*[1], *F. L. Johnson*[1], *D. Zepeda-Orozco*[3], *M. K. Schultz*[1,2];
[1]*Perspective Therapeutics Inc, Coralville, IA, UNITED STATES OF AMERICA,* [2]*University of Iowa, Iowa City, IA, UNITED STATES OF AMERICA,* [3]*Nationwide Children's Hospital, Columbus, OH, UNITED STATES OF AMERICA.*

Aim/Introduction: High-risk neuroblastoma (NB) in pediatric patients is an aggressive disease often accompanied by liver and bone marrow metastases, which leads to treatment failure and relapse (4-year survival <10%). NB tumors almost universally express SSTR2, suggesting a potential for improvements using peptide-receptor radionuclide therapy (PRRT). Here, we evaluate preclinically the use of theranostic pair $^{203/212}$Pb for PRRT using SSTR2-targeted agonist PSC-PEG2-TOC (VMT-α-NET) for NB image-guided therapy. In this study, we established a robust metastatic mouse model of NB and evaluated the efficacy of [$^{203/212}$Pb]VMT-α-NET for image-guided treatment of metastatic disease. ***Materials and Methods:*** VMT-α-NET was radiolabeled with ^{203}Pb as SPECT imaging diagnostic radiotracer and ^{212}Pb as targeted alpha therapeutic radiopharmaceutical. Maximum tolerated dose (MTD) was determined by administrating escalating levels of [^{212}Pb]VMT-α-NET (0 - 4.44 MBq) via tail vein to tumor-free SCID mice for a 32-day observation window. Two million IMR32-luc cells were implanted systemically via intracardiac injection into immunocompromised NSG mice and bioluminescence imaging was used to monitor tumor progression. For the efficacy study, 3 weeks post-inoculation, tumor-bearing mice (n=6-7/group) were administered a total of 2.22 MBq [^{212}Pb]VMT-α-NET by single, 2 or 3 fractionated dosing regimens, with vehicle mice receiving 8 mg of DL-Lysine/saline only. Endpoints include total tumor burden (bioluminenscence > 1000 times of the initial level), body weight changes >20%, overt toxicity. Hematological and renal responses were evaluated by periodic complete blood counts , urine and kidney biomarkers, serum chemistry and pathological read out of major organs. ***Results:*** A robust metastatic NB mouse model was established by intracardiac injection of IMR32-luc cells. Within two weeks, lesions were found mostly in liver, bone marrow and lung - and occasionally in brain, heart, mesentery as observed via bioluminescence imaging. Sequential SPECT imaging and biodistribution analysis using [^{203}Pb]VMT-α-NET confirmed metastases as well as highly tumor-specific targeting to metastatic lesions. The MTD of [^{212}Pb]VMT-α-NET in SCID mice was determined as 2.22 MBq without acute toxicity. For the 90-day efficacy study, median survival days for vehicle control, single and 2 fractionated dose groups were 37, 66.5 and 84, respectively. Three fractionated doses of 740 kBq of [^{212}Pb]VMT-α-NET produced 100% overall survival, with partial response and stable disease, while a single high dose of 2.22 MBq produced less benefit. More evaluation data will be updated. ***Conclusion:*** Multiple fractionated doses of [^{212}Pb]VMT-α-NET demonstrated effective tumor control and were well tolerated. Future studies will include combination therapy and optimizing the fractionation dose regimen.

OP-145

Preclinical Evaluation of ^{225}Ac-rhPSMA-10.1, a Novel Radiohybrid PSMA Compound for Targeted Alpha Therapy of Prostate Cancer

V. Vassileva[1], *B. Waldron*[1], *A. Wurzer*[2], *C. D'Alessandria*[2], *R. Veggerby Grønlund*[3], *M. Wikke Hallund*[3], *D. Gauden*[1], *D. Stevens*[1], ***C. Foxton***[1];
[1]*Blue Earth Therapeutics, Oxford, UNITED KINGDOM,* [2]*Department of Nuclear Medicine, Technical University of Munich, Munich, GERMANY,* [3]*Minerva Imaging, Ølstykke, DENMARK.*

Aim/Introduction: Theranostic "radiohybrid" prostate-specific membrane antigen (rhPSMA) ligands can be radiolabelled with ^{18}F for diagnostic imaging or alpha or beta-emitting radiometals for therapeutic use in prostate cancer. Significant preclinical efficacy has been previously demonstrated with novel rhPSMA radiopharmaceutical, ^{177}Lu-rhPSMA-10.1, now under evaluation in a Phase 1/2 trial (NCT05413850). Here, we present data on the preclinical evaluation of ^{225}Ac-labelled rhPSMA-10.1, as a potential alpha-targeted therapy for prostate cancer, compared to ^{177}Lu-rhPSMA-10.1. ***Materials and Methods:*** Binding affinity and cellular internalization assays were conducted in LNCaP cells, using ^{177}Lu-PSMA-I&T as a reference compound. PSMA binding affinity (IC_{50}) was evaluated in a competitive binding assay using rhPSMA-10.1 complexed with natural Lanthanum (^{nat}La), serving as a cold surrogate for ^{225}Ac, or natural Lutetium (^{nat}Lu). Cellular internalization was assessed by measuring free, surface-bound, and internalized activity after 1-hour incubation with ^{225}Ac-rhPSMA-10.1 or ^{177}Lu-rhPSMA-10.1 using γ-counting, and normalized to ^{177}Lu-PSMA-I&T (% internalization). The lipophilicity of ^{225}Ac-rhPSMA-10.1 and ^{177}Lu-rhPSMA-10.1 was determined by the shake-flask method, measuring the distribution coefficient in n-octanol and PBS at pH 7.4 (log $D_{7.4}$). Therapeutic response to single-administration of ^{225}Ac-rhPSMA-10.1 (30 kBq) or ^{177}Lu-rhPSMA-10.1 (30 MBq) was evaluated in 22Rv1 tumour-bearing mice (n=8 per group). Efficacy was assessed based on relative tumour growth (change in tumour volume from treatment administration day/baseline) and survival of mice versus untreated controls ≤49 days post-treatment initiation. Body weights were monitored throughout for toxicity assessment. Two-way ANOVA and Tukey's multiple comparisons test (data analyzed until n=3 remained per group), and Kaplan-Meier, Log-rank survival analyses were performed ($p \leq 0.05$ considered significant). ***Results:*** Both ^{nat}La-rhPSMA-10.1 and ^{nat}Lu-rhPSMA-10.1 showed excellent PSMA binding affinity (IC_{50} = 3.6±0.6 nM and 1.6±0.1 nM, respectively). High cellular internalization and similar lipophilicity were observed for both ^{225}Ac-rhPSMA10.1 and

^{177}Lu-rhPSMA-10.1 (% internalization = 99±14 and 108±5; log$D_{7.4}$ = -3.4±0.2 and -3.8±0.1; respectively). ^{225}Ac-rhPSMA-10.1 treatment significantly reduced tumour growth in vivo versus controls (from day 14 to 31, p<0.05), and prolonged survival of mice (median survival: 27, 43.5, and 42 days for untreated, ^{225}Ac-rhPSMA-10.1, and ^{177}Lu-rhPSMA-10.1 groups, respectively). There were no significant differences in tumour growth suppression or survival between the ^{225}AcrhPSMA-10.1 and ^{177}Lu-rhPSMA-10.1 groups, and both treatments were well-tolerated. ***Conclusion:*** These preclinical analyses demonstrate a promising therapeutic profile for ^{225}Ac-rhPSMA10.1, using a 1000-fold lower activity than ^{177}Lu-rhPSMA-10.1. Similar in vitro characteristics and in vivo therapeutic efficacy were observed for both ^{225}Ac-rhPSMA-10.1 and ^{177}LurhPSMA-10.1. ^{225}Ac-rhPSMA-10.1 represents a novel alpha-targeted therapy with planned clinical trial application submission in 2023.

505

Sunday, September 10, 2023, 3:00 PM - 4:30 PM
Hall B

Cutting Edge Science Track - TROP Session: From Cells to Human via the Fish

OP-146

Radiosensitivity of neuroendocrine cancer cells to ^{177}Lu-DOTATATE and radiobiological implications for peptide radionuclide therapy

G. Tamborino[1,2], *P. Engbers*[2,1], *T. de Wolf*[2,1], *T. Reuvers*[2,1], *M. Konijnenberg*[1], *J. Nonnekens*[2,1];
[1]*Department of Radiology and Nuclear Medicine, Erasmus University Medical Center, Rotterdam, NETHERLANDS,*
[2]*Department of Molecular Genetics, Erasmus University Medical Center, Rotterdam, NETHERLANDS.*

Aim/Introduction: Despite the efficacy of peptide receptor radionuclide therapy (PRRT) for treatment of metastatic tumours, the radiobiology underlying the dose-response is poorly understood.This work aims to determine the relative biological effectiveness (RBE) of PRRT in comparison to external beam radiotherapy (EBRT) for cell death in a relevant neuroendocrine tumour cell-line (GOT1), while establishing a framework for realistic cellular dosimetry calculations in a cluster-forming scenario. ***Materials and Methods:*** ^{177}Lu-DOTATATE uptake (membrane-bound and internalized fractions) was measured over a 4-hour incubation period and excretion into the medium was subsequently measured. Time-integrated activities were calculated for source regions up to 14 days(d). Viability was assessed at 7d (CellTiterGlo assay) and cell-death (flow cytometry) at 4,7,11 and 14d of exposure for 0.1-2.5MBq/mL of ^{177}Lu-DOTATATE. For comparison, response to 0.5-2Gy x-ray irradiation was measured.Geant4/GATE was used to simulate the absorbed dose per decay (S-value) of lutetium-177 during in vitro cell irradiation.The absorbed dose calculations (MIRD-formalism) during the 4h-uptake (floating) and follow-up (plated) phase account for single cells and clusters of variable size, derived from microscopic image, assuming homogeneous or heterogeneous activity distribution (receptor: μ=log(1), σ=0.05 and/or cellular placement within cluster). Cross-absorbed dose is calculated either by weighting in-cluster S-values using a closed packing algorithm for cluster-size frequency, neglecting cross-cluster contribution, or by simulating the set-up from 8 microscopic images of plated cells. ***Results:*** Cross-cluster absorbed dose (from single cells and cluster) during 4h-uptake phase was negligible (<1%). The in-cluster S-value for 3D cellular clusters up to n=100 cells followed a saturation profile (cross S-value=B_{max}*n/(k_d+n), B_{max}=4.69E-03±2.11E-04 Gy/Bq s, 1.77E-03±7.87E-05 Gy/Bq s and k_d=30±3, 13±5 for centre- and edge-cell, respectively). Self-, in-cluster, and medium (10mL) absorbed doses contributed 8%, 8-10%, and 83% of the 4h-absorbed dose, respectively. During the plated phase, the cross-cluster absorbed dose formed a substantial contribution to the total cross-absorbed dose per decay. Hence, the perfect packing approach underestimated it substantially (66% for membrane and 90% for cytoplasm sources). Assuming homogenous uptake, the average absorbed dose (1 MBq/mL) after 7d ranged between 2.9±1.0 Gy and 3.8±1.2 Gy, depending on the intra- and inter- set-up variability. Assuming a gradually reducing uptake in the cluster centre can reduce the absorbed dose per set of 0.5-1.1 Gy. Preliminary calculations indicate RBE=0.34±0.12 using as biological end-point the loss of viability at 7d and homogeneous uptake. ***Conclusion:*** According to our results, PRRT requires an absorbed dose three times higher than EBRT to achieve an equivalent effect.

OP-147

Stochastic microscale dosimetry in breast cancer micrometastasis model for alpha-emitter radiopharmaceutical therapy

R. Bastiaannet, *M. Hasan, I. Liatsou, R. F. Hobbs, G. Sgouros; Johns Hopkins University School of Medicine, Baltimore, MD, UNITED STATES OF AMERICA.*

Aim/Introduction: The alpha particles in alpha-emitter radiopharmaceutical therapy (αRPT) are very cytotoxic. But αRPT uptake is typically non-uniform, which combined with the short range of alphas in tissue (<100μm), necessitates dosimetry on a near-cellular spatial scale. We have previously developed a framework to perform in vitro dosimetry on a single-cell level. Using high-resolution confocal microscopy, we performed Monte Carlo-based dosimetry for >550 measured -rather than modeled- individual live cells. This allowed for a statistical approach to cell survival modelling, which fit the measured data significantly better [1]. The purpose of this work was to build on these results and apply our empirical approach to a clinically more relevant model: micrometastases. ***Materials and Methods:*** Micrometastasis-like 3D spheroids were grown using the NT2.5 cell line, which is a HER2+ breast cancer cell line. After 5 days, the spheroids reached a diameter of ~400 μm and were harvested. The spheroids were incubated with an anti-HER2 antibody (7.16.4; fluorescently labelled AF488) for 1-72 hours. Nuclei were stained using DRAQ5. Spheroids were imaged in 3D on a high-resolution confocal microscope, using a water-emersion objective with a long working distance. Attenuation and photobleaching were corrected for. Antibody penetration was measured as a function of time and a diffusion-binding/internalization pharmacokinetic model was fit to the data. Cell nuclei were segmented. This data was imported into our GEANT4-based Monte Carlo framework and the microdosimetric absorbed dose distributions to cell nuclei were calculated for a total of 18 spheroids, collectively consisting of thousands of cells. ***Results:*** Antibody penetration remained limited(<~5-8cell diameters), even after 3 days of incubation (binding site barrier problem). This results in a large fraction of the spheroid not receiving significant amounts of absorbed dose. In our previous work on cell monolayers, we found that over 50%

of cells do not receive any dose in most experimental conditions. But that was due to the random nature of the direction of the particle emissions. We found that this number is approaching zero in the 3D case of spheroids. ***Conclusion:*** Careful assessment of antibody penetration and stochastic microscale dosimetry allows for a better understanding of radiobiology in micrometastases. Work on relating this dosimetry to growth after treatment is currently ongoing. ***References:*** 1. Bastiaannet R, Liatsou I, F Hobbs R, Sgouros G (2023) Large-scale in vitro microdosimetry via live cell microscopy imaging: implications for radiosensitivity and RBE evaluations in alpha-emitter radiopharmaceutical therapy. J Transl Med 21:1-14

OP-148

Nephron Morphology Influences the Dosimetry of Microscopic Renal Tissues of Non-Uniform Activity Distributions of Alpha Particle and Low Energy Electron Emitters

M. Andersson[1,2], *N. Goudin*[3], *M. Pontoglio*[4], *H. Levillain*[2], *N. Reynaert*[2], *C. Saldarriaga Vargas*[1];
[1]*Belgian Nuclear Research Centre (SCK CEN), Mol, BELGIUM,* [2]*Faculté de Médecine, Université Libre de Bruxelles (ULB), Brussels, BELGIUM,* [3]*Necker Bioimage Analysis platform SFR Necker US24/UAR 3633, Paris, FRANCE,* [4]*Institut National de la Santé et de la Recherche Médicale, Centre National de la Recherche Scientifique, Université de Paris, Paris, FRANCE.*

Aim/Introduction: Mouse renal dosimetry at the level of nephron substructures is of interest for preclinical investigations of nephrotoxicity in radiopharmaceutical therapy with alpha-particle and electron emitters. As the distribution of radiopharmaceutical can be heterogeneous across different nephron substructures of kidney tissues, and even between different nephron types [1]. This study investigated the influence of nephron morphology on mouse kidney dosimetry. ***Materials and Methods:*** A realistic computational model of murine nephrons was developed based on 3D multiphoton microscopy images of mouse kidney tissues [2]. Three nephrons with distinctive morphology were modelled: a superficial (glomerulus in the outermost renal cortex), a juxtamedullary (glomerulus near the renal medulla) and a mid-cortical (intermediate) nephron. The shape and size (length) of the different nephron sub-compartments (glomerulus, proximal tubule (PT), loop of Henle and distal tubule) differ between each nephron type. S-values and energy absorbed fractions (AF) were calculated (GATE v9.2) for the different nephron sub-compartments for various Auger-electron, beta- and alpha emitting radionuclides (^{177}Lu, ^{161}Tb, ^{211}At), assuming a uniform radionuclide source in each nephron PT (or glomerulus). ***Results:*** For a source in the PT, the AF for self-irradiation is significantly higher for the juxtamedullary nephron than for the superficial nephron for all radionuclides (40% and 20% higher, respectively for ^{177}Lu and ^{161}Tb Auger and internal conversion electrons). The PT self-irradiation AF of beta particles are similar ($0.03 \leq AF \leq 0.06$) for all nephrons. The difference in AF between the mid-cortical nephron was within 20% higher for all particles of both radionuclides. For ^{211}At, the AF for alpha particle PT self-irradiation is 70% and 20% higher for the juxtamedullary nephron than for the superficial and mid-cortical nephron, respectively. However, for all radionuclides, the S-values are substantially higher for the superficial nephron than for the mid-cortical (approximately 50% higher) and juxtamedullary (90% higher) nephron, as the PT mass of the superficial nephron is respectively 66% and 51% lower than the mass of the mid-cortical and juxtamedullary PTs. ***Conclusion:*** Differences in the morphology and substructure sizes of different nephrons significantly influences microscopic renal tissue dosimetry of low energy electron and alpha particle emitters with a heterogeneous activity distribution in murine kidneys. Therefore, consideration of nephron morphology and size characteristics in dosimetry calculations might be needed in cases of differential radioligand distributions across different nephron types to effectively support the preclinical investigation of nephrotoxicity in radiopharmaceutical therapy. ***References:*** [1] EJNMMI 2005;32(10):1136-43. https://doi.org/10.1007/s00259-005-1793-0 [2] Kidney International 2021;99(3):632-45. https://doi.org/10.1016/j.kint.2020.09.032

OP-149

Small-scale anatomical modeling of the salivary gland for alpha-particle and beta-article radiopharmaceutical therapy

R. Hobbs*, I. Marsh, R. Bastiaannet, I. Liatsou, C. Brayton, K. Gabrielson, T. Yusufaly;*
Johns Hopkins, Baltimore, MD, UNITED STATES OF AMERICA.

Aim/Introduction: Salivary gland toxicity is a serious quality of life issue from both beta-particle (^{131}I or ^{177}Lu-PSMA) and alpha-particle (^{211}At or ^{225}Ac-PSMA) radiopharmaceutical therapy (RPT). Clinical sequelae include xerostomia, sialedenitis and tooth decay. These clinical observations do not correlate well with whole organ dosimetry as the uptake of the radioisotope or radiopharmaceutical is confined to a small sub-set of cells within the salivary glands, resulting in a higher absorbed dose to a whole category of cells (ductal cells) as compared to the average whole organ absorbed dose. We present an anatomically representative model of ductal branching inside the salivary gland to model the relative absorbed dose to the different cell types. ***Materials and Methods:*** The salivary gland, which produces and secretes saliva, is modeled as a sphere containing acinar cells, with varying radius to represent SG size distributions. Embedded within the bulk is a branched network of intra- and interlobular ducts, with tunable branching angles, number of levels, and segment lengths. Occupancy of the ductal cells and spacing of the branches are derived from ex vivo murine histopathology. Monte Carlo simulations for the relevant isotopes were run and the S values for the model obtained. Dose coefficients were obtained for the different compartments assuming activity uptake in the ductal cells, and compared to the whole organ dose coefficient as a function of salivary gland size. ***Results:*** Dose coefficients to the ductal cells are markedly higher than the average salivary gland dose coefficient. For ^{131}I, this value is about 4 (depends on the organ size), while for most alpha-emitters it is closer to 14, with less variation as a function of size and with narrower distributions of absorbed dose per cell. ***Conclusion:*** A simple branching model with stylized parameters allows us to relate the average organ absorbed dose to cell-specific dosimetry, to which bio-kinetic modeling can then be applied (BED or EQD2). Experiments are ongoing to provide the measured apportionment factors (small scale activity distribution in the different ductal cell sub-types)and in vivo RBE determination, each specific to each SG type for model refinement. The human model will be supplemented with data from human cadaver studies. For RPT, the ductal cells are expected to be the dose-limiting sub-compartment of the salivary glands.

OP-150

Zebrafish embryos as experimental model to advance pre-clinical research in nuclear medicine

C. Morgat[1,2], *G. Siefried*[3,4], *S. Bodin*[1,2], *F. Cavelier*[5], *E. Hindié*[1,2,6], *M. Khatib*[3];
[1]*Nuclear Medicine Department - University Hospital of Bordeaux, Bordeaux, FRANCE,* [2]*INCIA, University of Bordeaux, CNRS, EPHE, UMR 5287, Bordeaux, FRANCE,* [3]*RyTME, Bordeaux Institute of Oncology (BRIC)-UMR1312 Inserm, Pessac, FRANCE,* [4]*Xenofish, Pessac, FRANCE,* [5]*Institut des Biomolécules Max Mousseron IBMM, UMR 5247 Pôle Chimie Balard, Montpellier, FRANCE,* [6]*Institut Universitaire de France, Paris, FRANCE.*

Aim/Introduction: The current xenografted mice model has limitations to evaluate the efficacy of novel therapeutic radionuclides emitting short-range particles due to difficulties in identifying and following tumor cell clusters and micrometastases. Zebrafish allows the implantation of human tumor cells that can next metastasize ***Materials and Methods:*** The triple negative breast cancer cell line MDA-MB-231, overexpressing neurotensin receptor-1 was stably transfected with the pIRES2-EGFP empty vector. Following incubation with the neurotensin analogue [^{111}In]In-JMV 6659 at 1 or 2MBq/mL, cells were microinjected in zebrafish embryo perivitelline space. Embryos were then imaged under fluorescence imaging and the relative primary tumor area and the number of metastases were determined at several time points ***Results:*** [^{111}In]In-JMV 6659 at 2MBq/mL was able to eliminate almost all metastases, whilst its effect on the primary tumors was limited. ***Conclusion:*** Zebrafish embryos stand as a novel model to better evaluate the efficacy of short-range emitters on tumor cell clusters and micrometastases.

OP-151

Biodistribution and dosimetry of lipiodol with various beta emitters: a preclinical study

A. Dieudonne[1], *R. Santus*[2], *P. Vera*[1], *S. Becker*[1], *X. Violas*[2];
[1]*LITIS-Quantif, Centre Henri Becquerel, Rouen, Rouen, FRANCE,* [2]*Research and Development Division, Laboratoire Guerbet, Aulnay-sous-Bois, FRANCE.*

Aim/Introduction: Radioembolization is one therapeutic options for the treatment of early-intermediate stage hepatocellular carcinoma. Lipiodol based agents were developed and used in research (1). The aim of this study was to compare lipiodol with several beta emitters. ***Materials and Methods:*** VX2 tumours were implanted on New Zealand rabbits, that further received an injection of lipiodol in the left hepatic artery. Tumours were explanted and imaged with X-ray micro computerized tomography (µCT) at 15 min, 1, 2, 6, 9 and 12 days. The voxel size was 141 µm or 172 µm depending on the field-of-view. Tumours were frozen and cut into 12 µm for histologic analysis. Absorbed dose distributions were simulated for ^{32}P, ^{90}Y, ^{131}I, ^{177}Lu and ^{188}Re from the µCT biodistributions of lipiodol and using a dose-point kernel approach in water. Average absorbed dose per administered activity in the tumour (S/λ) were reported. Equivalent uniform biological effective dose (EUBED) were calculated for an average absorbed dose of 100 Gy, using α and β values of respectively 0.037 Gy^{-1} and 0.0028 Gy^{-2} (2). ***Results:*** Over the 19 rabbits included, 14 had exploitable data. The histologic analysis showed that the lipiodol distributes homogeneously in the tumour up to 12 days after injection. Average tumour S/λ value was statistically higher for ^{32}P with 62.8 ± 94 Gy.MBq^{-1}, followed by ^{90}Y (14.9 ± 22 Gy.MBq^{-1}), ^{131}I (10.8 ± 16 Gy.MBq^{-1}), ^{177}Lu (6.9 ± 11 Gy.MBq^{-1}), ^{166}Ho (4.92 ± 7.4 Gy.MBq^{-1}) and ^{188}Re (3.43 ± 5.1 Gy.MBq^{-1}). EUBED values for a tumour absorbed dose of 100 Gy for ^{90}Y with 45.3 ± 20 Gy, followed by ^{188}Re (39.8 ± 18 Gy), ^{32}P (36.5 ± 16 Gy), ^{166}Ho (36.1 ± 16 Gy), were statistically higher than ^{131}I (17.5 ± 9 Gy) and ^{177}Lu (12.0 ± 7 Gy). ***Conclusion:*** This study showed the ability of lipiodol to penetrate into the tumour and to remain in the compartment. It showed also the better dosimetry efficacy of ^{90}Y and ^{188}Re, thus confirming that they are the best candidates for radioembolisation. ***References:*** 1. Bouvry C, Palard X, Edeline J, Ardisson V, Loyer P, Garin E, et al. Transarterial Radioembolization (TARE) Agents beyond 90 Y-Microspheres. BioMed Res Int. 2018;2018:114. 2. Leeuwen CM van, Oei AL, Crezee J, Bel A, Franken NAP, Stalpers LJA, et al. The alfa and beta of tumours: a review of parameters of the linear-quadratic model, derived from clinical radiotherapy studies. Radiat Oncol. 2018;13(1):96.

OP-152

DNA damage repair in PBMCs after internal ex vivo irradiation with ^{177}Lu

I. Strobel[1], *H. Scherthan*[2], *J. Hahn*[1], *J. Müller*[2], *S. Schumann*[1], *A. K. Buck*[1], *M. Port*[2], *M. Lassmann*[1], *U. Eberlein*[1];
[1]*Department of Nuclear Medicine, University Hospital Würzburg, Würzburg, GERMANY,* [2]*Bundeswehr Institute of Radiobiology affiliated to the University of Ulm, Munich, GERMANY.*

Aim/Introduction: The aim of this study was to investigate DNA damage induction and repair in peripheral blood mononuclear cells (PBMCs) after internal ex vivo irradiation of whole blood with the β-emitter ^{177}Lu. ***Materials and Methods:*** Blood samples of seven healthy volunteers were collected and divided in five aliquots each, of which one served as non-irradiated baseline. The remaining blood samples were incubated for 1h with varying ^{177}Lu activities to achieve total absorbed doses to the blood between 3mGy to 100mGy, followed by PBMCs isolation. The PBMCs were divided in three subsamples to study the time course of the DNA damage repair and either fixed directly with 70% ethanol or 4h and 24h after culture in RPMI. Immunostaining of DNA double-strand break (DSB) markers γ-H2AX and 53BP1 revealed co-localised DSB foci in the PBMCs' nuclei that were counted microscopically in 100 nuclei per sample. To quantify the repair rates, a monoexponential model was used. ***Results:*** Mean absorbed doses to the blood of (3.4±1.5)mGy, (23.0±1.4)mGy, (47.3±2.0)mGy and (89.7±4.6)mGy were achieved. Directly after 1h internal irradiation, the mean of the average number of radiation-induced foci (RIF) per cell were 0.13±0.09 (3mGy), 0.30±0.09 (25mGy), 0.65±0.25 (50mGy) and 1.23±0.09 (100mGy). The average number of RIF showed a linear correlation to the absorbed dose (r^2= 0.96). After 4h the RIF per cell decreased significantly ($p<0.05$) to 0.30±0.08 (50mGy) and 0.41±0.18 (100mGy). Repair was complete within uncertainties after 24h, with RIF values of -0.01±0.12 (50mGy) and 0.13±0.14 (100mGy). The decrease in RIF at 3mGy and 25mGy was not significant due to large scatter of RIF values in the low dose range. The repair rate of the RIF were (0.15±0.12)h^{-1} (25mGy; r^2=0.44), (0.21±0.03)h^{-1} (50mGy; r^2=0.89) and (0.36±0.06)h^{-1} (100mGy; r^2=0.90). The repair rate induced by 50mGy Lu-177 irradiation is in agreement with the value of (0.28±0.03)h^{-1} obtained for ^{131}I at an absorbed dose of 50mGy [1]. ***Conclusion:*** This study shows a linear increase of RIF for total absorbed doses between 3mGy and 100mGy directly after internal irradiation with ^{177}Lu. A significant reduction of RIF to baseline values after 50 and 100mGy β-irradiation over 24h of culture indicates successful DSB repair. In addition, our data suggest a repair rate of DNA DSBs after low-dose internal irradiation that increases with the absorbed dose. ***References:*** [1] Schumann et al, EJNMMI, 49, 2022, 1447-1455

OP-153

From bench to bedside: ^{64}Cu/^{177}Lu 1C1m-Fc anti TEM-1: mice-to-human dosimetry extrapolations for future theranostic applications

J. Delage[1], *N. Chouin*[2], *M. Cherel*[3], *S. M. Dunn*[4], *N. Schaefer*[5], *A. Faivre-Chauvet*[3], *J. O. Prior*[5], *S. Gnesin*[6];
[1]*Radiopharmacy Unit, Department of Pharmacy, Lausanne University Hospital and University of Lausanne, Lausanne, SWITZERLAND,* [2]*University of Nantes, Inserm, CNRS, University of Angers, Oniris, CRCI2NA, Nantes, FRANCE,* [3]*University of Nantes, CHU Nantes, CNRS, Inserm, CRCINA, Nantes, FRANCE,* [4]*LAbCore, Ludwig Institute for Cancer Research, Lausanne University Hospital and University of Lausanne, Epalinges, SWITZERLAND,* [5]*Department of Nuclear Medicine and Molecular Imaging, Lausanne University Hospital and University of Lausanne, Lausanne, SWITZERLAND,* [6]*Institute of Radiation Physics, Lausanne University Hospital and University of Lausanne, Lausanne, SWITZERLAND.*

Aim/Introduction: The development of diagnostic and therapeutic radiopharmaceuticals is a hot topic in nuclear medicine. Several radiolabeled antibodies are under development necessitating both biokinetic and dosimetry extrapolations for effective human translation. The validation of different animal-to-human dosimetry extrapolation methods still is an open issue. We previously developed and tested preclinically a fully human single-chain variable fragment (scFv) Fc fusion, 1C1m-Fc, cross-reacting with both murine and human TEM-1. This fusion protein antibody was conjugated with DOTA and radiolabeled with ^{64}Cu for PET imaging and with ^{177}Lu for therapeutic purposes. ***Materials and Methods:*** This study reports the mice-to-human dosimetry extrapolation of ^{64}Cu/^{177}Lu 1C1m-Fc anti-TEM-1 for theranostic application in soft-tissue sarcomas. We applied four different dosimetry methods; direct mice-to-human extrapolation (M1); extrapolation considering a relative organ-specific mass scaling factor (M2), application of a metabolic scaling factor (M3) and combination of M2 and M3 (M4). Furthermore, we evaluated the viability of using [^{177}Lu]Lu-1C1m-Fc as therapeutic agent in treating soft-tissue sarcomas (STS) investigating the administered activity that would results in reaching safety limits (in kidneys, red marrow, liver, spleen and gonads) and expected efficacy (in STS). ***Results:*** For the four dosimetry methods described above (M1-M4), we reported the average values of source organ TIACs extrapolated to the human from previously published mice data. Predicted in-human dosimetry for the [^{64}Cu]Cu-1C1m-Fc resulted in an effective dose of 0.05 mSv/MBq, favorable for diagnosis use. Absorbed dose (AD) extrapolation for the [^{177}Lu]Lu-1C1m-Fc indicated that the AD of 2 Gy and 4 Gy to the red-marrow and total-body can be reached with 5-10 GBq and 25-30 GBq of therapeutic activity administration respectively depending on applied dosimetry method. ***Conclusion:*** Dose estimation based on animal data is a mandatory requirement, providing important insights and guidance for predicting safety and efficacy of any radiolabeled compound prior to its diagnostic and/or therapeutic in-human translation. Different methods for animal-to-human dosimetry extrapolations have been reported in the literature but no consensus presently exists on the appropriate approach to apply for any specific radiolabeled compound. For our theranostic couple ^{64}Cu/^{177}Lu 1C1m-Fc anti TEM-1, dosimetry extrapolation methods provided significantly different absorbed doses in organs. Even if dosimetry properties for the [^{64}Cu]Cu-1C1m-Fc are suitable for a diagnostic in-human use, the therapeutic application of [^{177}Lu]Lu-1C1m-Fc presents challenges and would benefit from further assessments in animals' models such as dogs before moving into the clinic.

OP-154

Simulations of the relative effectiveness of tumor stroma and cancer cell targeting radiopharmaceuticals

Y. Song[1,2], *J. Brosch-Lenz*[1], *C. D'Alessandria*[1], *K. Shi*[3], *W. Weber*[1];
[1]*Department of Nuclear Medicine, Klinikum rechts der Isar, Technische Universität München, Munich, GERMANY,* [2]*Department of Nuclear Medicine, Union Hospital, Tongji Medical College, Huazhong University of Science and Technology, Wuhan, CHINA,* [3]*Department of Nuclear Medicine, Inselspital, University of Bern, Bern, SWITZERLAND.*

Aim/Introduction: Fibroblast activation protein (FAP) is a promising target for radiopharmaceutical therapy (RPT) because it is expressed in the stroma of many malignant tumors while its expression in normal tissues is highly restricted. However, there is a potentially higher heterogeneity of radiation dose to the cancer cells than for RPT directed against targets expressed by the cancer cells. The aim of this study was to explore the magnitude of this effect for Y-90 and Lu-177 labeled FAP ligands. ***Materials and Methods:*** The effects for RPT were modelled for spherical aggregates of cells (diameter: 20 µm) ranging from 400 µm to 2 mm in MIRDcell. The radioactivity was either distributed homogenously in all cells (scenario for RPT directed against targets expressed by cancer cells) or accumulated in only 50% or 25% of the cells, randomly distributed within the sphere (scenario for FAP ligands targeting fibroblasts in the tumor stroma). The biological half-life of the FAP radioligand was assumed to 10.1 h as previously published by Ferdinandus et al. (JNM 2022). Surviving tumor cell fractions were calculated using the alpha/beta parameters provided by MIRDcell. ***Results:*** When all the cells accumulated the same amount of radioactivity, the activity per cell required to kill 90% of the cells in spheres with diameters from 400 µm to 2 mm ranged between 0.98 Bq and 0.93 Bq for Lu-177, and between 1.5 Bq and 3.1 Bq for Y-90. When these amounts of radioactivity were accumulated by only 50% and 25% of the cells, the fractional cell kill of the unlabeled cells ranged between 30% and 60% for Lu-177 and 38% and 78% for Y-90. The loss of efficacy diminished for both isotopes with increasing lesion size. ***Conclusion:*** For the same total tumor uptake of radioactivity, radiopharmaceuticals targeting the tumor stroma deliver lower doses to the tumor cells than radiopharmaceuticals targeting the cancer cells. This effect is more pronounced for smaller lesions and only slightly improved by a high energy beta emitter such as Y-90. ***References:*** Ferdinandus J, Costa PF, Kessler L, et al. Initial Clinical Experience with 90Y-FAPI-46 Radioligand Therapy for Advanced-Stage Solid Tumors: A Case Series of 9 Patients. J Nucl Med. 2022;63(5):727-734. doi:10.2967/jnumed.121.262468.

506

Sunday, September 10, 2023, 3:00 PM - 4:30 PM
Hall C

Clinical Oncology Track - TROP Session: Gastrointestinal Malignancies

OP-155

Evaluation of [64Cu]Cu-ATSM PET-CT as a response predictor to neoadjuvant therapy in locally advanced rectal cancer: preliminary results

M. Le Thiec[1], *L. Ferrer*[1,2], *M. Colombié*[1], *M. Lacombe*[3], *A. Devillers*[4], *P. Salaün*[5,6], *S. Hiret*[1], *J. Raimbourg*[1], *L. Doucet*[1], *E. Rio*[1], *S. Lesourd*[4], *P. Tremolières*[3], *M. Heymann*[1,7], *N. Varmenot*[1,2], *A. Vidal*[8,9,10], *F. Haddad*[8,9,10], *N. Allam*[1], *M. Chérel*[1,2], *F. Kraeber-Bodéré*[11,2], *L. Campion*[1], *M. Bourgeois*[11,2,8], *C. Rousseau*[1,2];
[1]ICO Gauducheau, Saint Herblain, FRANCE, [2]Nantes Université, Univ Angers, INSERM, CNRS, CRCI2NA, Nantes, FRANCE, [3]ICO Papin, Angers, FRANCE, [4]Cancer Institute Eugène Marquis, Rennes, FRANCE, [5]University Hospital, Brest, FRANCE, [6]UMR Inserm 1304 GETBO, University Western Brittany, Brest, FRANCE, [7]Research pathology platform, Tumor Heterogeneity and Precision Medicine, Saint-Herblain, FRANCE, [8]Arronax, Saint-Herblain, FRANCE, [9]SUBATECH, IMT Atlantique, CNRS/IN2P3, Nantes, FRANCE, [10]Université de Nantes, Nantes, FRANCE, [11]CHU Nantes, Nantes, FRANCE.

Aim/Introduction: Neoadjuvant radiochemotherapy is the standard treatment for locally advanced rectal cancers with variable anatomopathological responses on the surgical specimen with known treatment resistance factors including tumor hypoxia. This study aims to evaluate interest of [64Cu] Cu-ATSM (Cu-ATSM) PET-CT to predict neoadjuvant treatment response for locally advanced rectal cancers. ***Materials and Methods:*** T3 or T4 rectal adenocarcinoma patients with or without regional lymph node involvement on conventional imaging were included in this multicenter pilot study (NCT03951337). Before any neoadjuvant treatment, all patients performed [18F] FDG PET-CT (FDG1) and Cu-ATSM PET-CT and most patients performed preoperative FDG2. Acquisitions were performed on the pelvic region, 1- and 24-hours post-injection of 3 MBq/kg Cu-ATSM. Semi-quantitative image analyses were conducted. Rectal tumor and gluteal VOIs were respectively delineated with a 70% threshold and a manual delineation on 64Cu-ATSM images whereas a varying threshold was used for rectal tumor delineation on FDG examinations. SUVmax, SUVmean, tumor-to-muscle-ratio, Hypoxic-Tumor-Volume (HTV), and Hypoxic-Burden (HB: HTV x SUVmean) were calculated on Cu-ATSM images. ΔMTV and ΔTLG (FDG1-FDG2/FDG1) were calculated with 30% decrease considered as response. Anatomopathological Rödel score defined on the surgical specimen was used to classify patients as responders (R score=3-4), and non-responders (NR score=0-2). Progression-free survival was followed for 2 years. ***Results:*** Of 24 patients included in this study, only 14 had surgical intervention (sex ratio1/1, median age 67 years [49-77], MRI median rectal tumor height 44mm [33-105], 12 and 2 patients classified respectively as T3 and T4): 10 had a positive histological response to neoadjuvant therapy. Progression-free survival at 12 months was 81.8%; IC 95% [44.7-95.1]. Cu-ATSM quantitative analysis revealed an uptake increase between 1h and 24h for any SUV features as well as the tumor-to-muscle ratio. Indeed, median SUVmax, SUVmean, and tumor-to-muscle ratio increased from 3.81 [2.74-6.65] to 6.34 [2.81-11.69], 3.07 [2.23-5.10] to 5.25 [2.29-9.05], and 4.38 [2.63-7.25] and 6.7 [1.75-21.03] respectively. Conversely, median HTV and HB decreased respectively from 4.67cm^3 [1-18.74] to 0.95 cm^3 [0.34-9.27] and 14.88 cm^3 [5.12-58.32] to 4.05 cm^3 [1.03-44.05]. Population analysis (R vs NR) was not significant (p: 0.32-1.00). Additionally, early and late Cu-ATSM uptake did not correlate with FDG1 (p: 0.26-0.91). FDG ΔTLG was correlated to HB at 24h on Cu-ATSM (r =-0.68; p=0.02). ***Conclusion:*** These preliminary results showed that a greater tumor hypoxic volume (HB) at 24 hours was correlated with a poorer metabolic response (ΔTLG). Supplementary data will be presented during the congress for this ongoing study.

OP-156

The effect of free thyroxine on glucose metabolic activity in primary hepatic neoplasm: A study of PET-CT scans

Z. Zhao[1], *X. Wang*[2], *J. Xiao*[1], *D. Wang*[1], *Z. Luo*[1];
[1]Affiliated Hospital of Guangdong Medical University, Zhanjiang, CHINA, [2]Children's Hospital Affiliated to Zhengzhou University, Zhengzhou, CHINA.

Aim/Introduction: The glucose metabolic activity was an important characteristic in many malignant tumors, including the primary hepatic neoplasm. The standard uptake value (SUV) was a useful indicator in the 18F-FDG positron emission tomography (PET) examination, which could reflect the glucose metabolic activity. Some early research showed that the thyroid hormones, including the free thyroxine (FT4), also had effects on the malignant tumors. While the relationship of the FT4 and the glucose metabolic activity of primary hepatic neoplasm is largely unknown. In this study, we tried to explore this relationship using 18F-FDG PET examination. ***Materials and Methods:*** 18 patients with primary hepatic neoplasm were enrolled in this study. All of them received the 18F-FDG PET scanning. Hand-painted measurement was used to get the SUV. In this study, the SUVmax was used only. All of the patients received the thyroid hormones level measurement, including the FT4 level. The average of the FT4 level was 15.7 pmol/L. The FT4 levels in 10 patients (group 1) were higher than 15.7 pmol/L. The FT4 levels in 8 patients (group 2) were lower than 15.7 pmol/L. Differences between groups were estimated using the students t test. Nominal P values of less than 0.05 were considered to demonstrate statistically significant differences. ***Results:*** The media SUVmax was 8.92±3.74 in group 1 and 4.55±4.05 in group 2. The highest SUVmax was 13.4 in group 1 and 11.0 in group 2. The lowest SUVmax was 0.8 in group 1 and 0.7 in group 2. The SUVmax were higher in the group 1 than that in group 2. The difference was significant (P = 0.033). ***Conclusion:*** This study demonstrated the significant difference of SUVmax between the primary hepatic neoplasm patients with the higher level of FT4 and the lower level of FT4. The SUVmax were higher in the patients with the higher level of FT4 than those with the lower level of FT4. The results showed that the FT4 may effect the glucose metabolic activity of primary hepatic neoplasm. This maybe one of the reason why the thyroid hormones affect tumor growth, as some of the early research had studied.

OP-157

Assesment of biological parameters of esophageal cancer in pre-, and post-treatment 18F-FDG-PET/CT in patient with early relapse.

A. Filipczuk[1], *A. Lewandowska*[1], *A. Pietrzak*[1], *W. Cholewiński*[2];
[1]*Greater Poland Cancer Center, Poznan, POLAND,*
[2]*Medical University of Poznan, Poznan, POLAND.*

Aim/Introduction: Esophageal cancer is one of the most agressive gastrointestinals tumor, and it is characterised with early relapse after radical treatment.PET/CT with the glukose analog 18F-FDG in esophageal cancer, is frequently used for staging, and evaluation of treatment response.After radical radiochemotherapy, heterogeneous and persistent FDG uptake in esophagus, may be cause by various reasons, including inflammation after treatment, or residual cancer process.The aim of the study, is to evaluate the link, between biological parameters of esophageal cancer before, or after radical treatment, and early relapse. ***Materials and Methods:*** Forty patients (64±9 years, 30M, 10F), with histologically confirmed esophageal cancer (35 with squamos cell carcinoma, and 5 with adenocarcinoma), underwent 18F-FDG-PET/CT scan 60min after tracer injection. All patients had first PET/CT scan before any treatment, and second scan 10 weeks after radiochemotherapy. According to pre treatment diagnosis - 32 patients were in stage II, 6 in III, and 2 in IV.Tumor's maximal and mean standarized uptake value (SUVmax, SUVmean), total lesion glycolysis (TLG), and metabolic tumor volume (MTV), before and after treatment were included in the analysis. ***Results:*** Average values of SUVmax, SUVmean, MTV and TLG before radiochemotherapy in patients with squamos cell carcinoma were: 14,0±5,5; 7,6±2,9; 25±26; 155±224, respectively. In patients with adenocarcinoma evaluated values were: 6,4±2,7; 3,3±1,0; 10,0±5,5; 43,1±31,7, respectively.In two patients, SUVmax after treatment was higher than before.In the remaining patients, SUVmax decreased after treatment to 5,7±3,6 (range 2,5-8,9).36 patients had relapse within 1 year, and 4pts in 2 years after radiochemotherapy.Average relative decrease of glucose metabolism after radiochemotherapy was 58% (±27%, range 2%-86%), and was associated in all patients, with an early relapse. ***Conclusion:*** Combination of biological parameters, delivered from pre-and post-treatment PET/CT, may be useful in the prediction of early relapse, in patients with esophageal cancer.

OP-158

Comparison of ^{18}F-FDG PET/CT and ^{18}F-FDG PET/MRI in Detection of Liver Lesions in Hepatocellular Carcinoma for Staging and Restaging

B. Demir[1], *C. Soydal*[1], *E. Dursun*[1], *M. Araz*[1], *D. Kuru Oz*[2], *N. O. Kucuk*[1];
[1]*Ankara University School of Medicine Department of Nuclear Medicine, Ankara, TÜRKIYE,* [2]*Ankara University School of Medicine Department of Radiology, Ankara, TÜRKIYE.*

Aim/Introduction: ^{18}F-FDG PET/CT is a widely accepted and useful imaging modality in staging and re-staging of various malignant solid tumours. However, in hepatocellular carcinoma(HCC) patients its ability to detect lesions is significantly affected due to the variable affinity and uptake patterns seen in HCC lesions. In this study we aimed to investigate additive value of liver-specific PET/MRI compared to routine whole-body PET/CT imaging. ***Materials and Methods:*** A total number of 77 patients and 99 pairs of PET/CT and dedicated respiratory gated contrast-enhanced PET/MRI acquired in same session that was performed between September 2018-December 2022, were included in this retrospective study. Total FDG-avid lesion numbers, affected liver segment numbers, SUVpeak, SUVmean, metabolic tumour volume(MTV), total lesion glycolysis(TLG) and tumour-background ratio(TBR) were assessed in each study. Lesion numbers were grouped as no lesion, 1 lesion, 2-4 lesions, 5-10 lesions and >10 lesions. Detected lesion and affected segment numbers compared between PET/CT and PET/MRI with Chi-Square test. ***Results:*** Indications of molecular imaging were for staging in 37 studies and for re-staging in 62 studies. Median AFP level of patients was 11.7ng/mL (min-max:1-33477). Whole-body PET/CT was positive for lymph node metastasis in 36 studies, lung metastasis in 15 studies, bone metastasis in 5 studies and adrenal metastasis in 5 patients. In PET/CT and PET/MRI studies median SUVpeak, SUVmean, MTV, TLG and TBR values were 6.9 vs. 7.9, 4.3 vs. 4.6, 168 vs. 160.98 cm^3, 1021.5 vs 1040 gr/mLxcm^3 and 2.1 vs. 2.1, respectively. Both PET/CT and PET/MR studies were negative for FDG-avid lesions in liver for 29 studies (29%). In 41 studies(41%) PET/CT and PET/MRI detected similar numbers of lesions. However, in the remaining 29 studies(29%) PET/MRI detected significantly higher numbers of lesions(p=0.001). Also, in 9 studies (9%) PET/MRI detected FDG-avid lesions in liver, while there was no pathological uptake in liver on PET/CT images. The number of affected segments was same in 43 studies(43%) on both modalities. But in 27 studies (27%) PET/MR detected higher number of affected segments than PET/CT (p=0.001). Average affected segment numbers on PET/CT and PET/MRI were 2.13 and 2.52 respectively. ***Conclusion:*** Certain variable biological features of HCC could complicate the detection of liver lesions. In order to overcome this setback imaging with a dedicated liver PET/MRI protocol can enhance diagnostic ability of PET imaging. In this study we have demonstrated superiority of PET/MRI against standard whole-body PET/CT imaging in the detection of HCC liver lesions.

OP-159

A proposed first-line treatment regime for Lenvitinib or Nivolumab based on dual-tracer PET/CT may improve progression free survival for advanced stage HCC patients

S. Chen, *S. Cheung, K. Cheng, Y. Yip, W. Leung, C. Ho;*
Hong Kong Sanatorium & Hospital, Hong Kong, HONG KONG.

Aim/Introduction: HCC is known to be a highly heterogeneous malignant tumor with poor prognosis. Lenvatinib (a multi-TKI) and Nivolumab (a PD-1 blocker) are both first-line anti-cancer drugs approved for advanced/inoperable HCC. In our preliminary study, we showed that Lenvatinib could have significant difference in treating ^{11}C-acetate (ACT)-avid HCC versus ^{18}F-FDG (FDG)-avid HCC. On the other hand, literature data reported on PD-1/PD-L1 blockade effects for advanced HCC were also highly heterogeneous. We aim to evaluate if advanced HCC patients randomized into 2 treatment arms, Lenvatinib or Nivolumab, could have different progression-free survival (PFS) outcomes using dual-tracer PET as metabolic differentiators. ***Materials and Methods:*** This is a prospective study between year 2017 and 2020. All patients with advanced stage HCC (BCLC stage C) underwent baseline ACT and FDG (dual-tracer) PET/CT. They were then randomized into systemic treatment by either Lenvatinib or Nivolumab. Follow-up dual-tracer PET/CT were performed every 2-3 months after initiation of Lenvatinib or Nivolumab treatment until disease progression, death or to a maximum of 36 months. Patients were classified into 4 groups: (1) ACT-avid HCC treated by Lenvatinib (ACT-LVN), (2) FDG-avid HCC by Lenvatinib (FDG-LVN), (3) ACT-avid HCC by Nivolumab (ACT-NVM), (4) FDG-avid HCC

by Nivolumab (FDG-NVM), with PFS as endpoint. PFS time was calculated using the KaplanMeier method and analyzed using a logrank test. ***Results:*** Study recruited 75 patients (male:66, female:9 ; HBV:70, HCV:2; mean age=54.5±12.0 years, range:33-82 years): 42 treated by Lenvatinib and 33 by Nivolumab, with no significant difference in patient age, sex, hepatitis status, AFP level, and presence of extrahepatic metastases between the 2 treatment arms. Lenvatinib arm (ACT-LVN+FDG-LVN) and Nivolumab arm (ACT-NVM+FDG-NVM) had similar median PFS (6.0 vs 7.0 months). However, within the Lenvatinib arm, ACT-LVN group had a significantly longer PFS than FDG-LVN (8.0 vs 4.0 months); while in the Nivolumab arm, FDG-NVM group had a significantly longer PFS than ACT-NVM group (9.0 vs 3.0 months). These results suggest that if patients with ACT-avid HCC were treated by Lenvatinib and FDG-avid HCC by Nivolumab, differential PFS could be significantly improved at 6-month (71.1 vs 47.6%), 9-month (35.6 vs 23.8%), 1-year (24.4 vs 11.9%), 2-year (8.9 vs 2.4%) and 3-year (8.9 vs 2.4%), when compared with all patients treated by Lenvatinib first-line. ***Conclusion:*** With dual-tracer PET as metabolic differentiators, our proposed treatment regime for advanced stage HCC was to treat ACT-avid HCC first-line with Lenvatinib, and FDG-avid HCC first-line with Nivolumab.

OP-160

18F-Fluorodeoxyglucose (FDG) and 18F-Fluorocholine (FCH) Positron Emission Tomography (PET) as Early Predictive Factorsof Overall Survival in Patients With Advanced Hepatocellular Carcinoma Treated WithSorafenib: a prospectivemulticentricstudy

V. BESSON[1], *C. Tabouret-Viaud*[1], *A. Fouquier*[2], *J. Bronowicki*[3], *E. Chevalier*[4], *A. Heurgue*[5], *D. Papathanassiou*[6], *J. Blanc*[7], *J. Pinaquy*[8], *L. Bengrine*[9], *X. Palard*[10], *H. Bourien*[11], *A. Bertaut*[2], *S. Manfredi*[12], *A. Cochet*[13];
[1]*Department of Nuclear Medicine, Centre Georges François Leclerc, Dijon, FRANCE,* [2]*Department of Statistics, Centre Georges-François Leclerc, Dijon, FRANCE,* [3]*Department of Gastro-Enterology and Hepatology, University Hospital of Nancy, Nancy, FRANCE,* [4]*Department of Nuclear Medicine, University Hospital of Nancy, Nancy, FRANCE,* [5]*Department of Hepato-Gastro-Enterology, University Hospital of Reims, Reims, FRANCE,* [6]*Department of Nuclear Medicine, Institut Jean Godinot, Reims, FRANCE,* [7]*Department of Hepato-Gastro-Enterology, University Hospital of Bordeaux, Bordeaux, FRANCE,* [8]*Department of Nuclear Medicine, University Hospital of Bordeaux, Bordeaux, FRANCE,* [9]*Department of Medical Oncology, Centre Georges-François Leclerc, Dijon, FRANCE,* [10]*Department of Nuclear Medicine, Centre Eugene-Marquis, Rennes, FRANCE,* [11]*Department of Medical Oncology, Centre Eugene-Marquis, Rennes, FRANCE,* [12]*Department of Hepato-Gastro-Enterology, Dijon, FRANCE,* [13]*ICMUB, UMR CNRS 6302, University of Burgundy, Dijon, FRANCE.*

Aim/Introduction: Hepatocellular Carcinoma (HCC) is the third cause of cancer-related death and is most often diagnosed at an advanced stage. Sorafenib remains one of the recommended treatments for advanced HCC; however, its efficacy remains inconstant and the incidence of treatment-related adverse events is high. Thus, our aim was to evaluate the clinical significance of dual radiotracers studies, ^{18}F-Fluorodesoxyglucose (FDG) and ^{18}F-Fluorocholine (FCH) performed before and after one month of Sorafenib therapy, in patients with advanced HCC for the prediction of one-year survival. ***Materials and Methods:*** Patients with advanced HCC and eligible for Sorafenib therapy were recruited in the prospective open-label non-randomized multicentric PREMETHEP trial (NCT02847468; 6 recruiting centres). Patients were assessed to perform FDG and FCH PET/CT before treatment initiation and one month after in order to evaluate baseline and residual tumor metabolism. The following parameters were extracted from each scan: SUV_{max} , SUV_{avg} and Tumor to Normal liver Ratio (TNR= SUV_{max} of the tumor/ SUV_{avg} of normal liver) for the most significant lesion, volumetric parameters of the intra-hepatic tumor burden: Metabolic Tumor Volume (MTV), Total Lesion Glycolysis (TLG) for FDG, Total Lesion Choline Kinase activity (TLCK) for FCH. The tumor metabolic response (ΔSUV_{max}, ΔSUV_{avg}, ΔSUV_{mean}, ΔTNR, ΔMTV, ΔTLG and ΔTLCK) was also calculated. Patients were followed during one year after treatment initiation. Logistic regressions with ROC curves were used to determine parameters associated with 1-year survival status (binary outcome). Optimal thresholds for quantitative parameters were determined using the Youden index method. Univariate and bivariate Cox analysis were performed to determine predictors of death. ***Results:*** Sixty-two patients (age 70±7 years) were included. All patients received Sorafenib therapy during at least one month. Median follow-up was 12 months. Twenty-two patients died during follow-up. In univariate analysis, only parameters reflecting high FDG tumor burden at baseline were significantly associated with death: TNR>1.5 (Hazard Ratio [HR]:7.1, 95% Confidence Interval [95%CI]:2.1-24.5, p=0.002), MTV>18 mL (HR:8.4, 95%CI:2.5-28.-, p<0.001; Sensitivity=86%, Specificity=71%), TLG>53g (HR:10.6, 95%CI:2.4-45.9, p=0.002) and presence of extra-hepatic lesions (HR:2.5, 95%CI:1.1-6.0, p=0.04). In contrast, neither follow-up FDG parameters, FCH parameters (baseline or follow-up), clinical and biological data had a prognostic significance. After adjustment on age, MTV>18 mL on baseline FDG PET/CT remained an independent predictor of death (HR:9.6, 95%CI:2.7-33.8, p<0.001). ***Conclusion:*** Baseline metabolic tumor burden determined with FDG PET/CT is a strong prognostic factor in patients with advanced HCC receiving Sorafenib therapy. FCH PET/CT does not seems to provide additional prognostic information.

OP-161

Assessing the performance of ^{68}Ga-Fibroblast activating protein inhibitor-04 (FAPI) PET/CT in the diagnosis of cholangiocarcinoma - A prospective pilot study.

D. Halanaik, *V. Rajaraman, L. Aridhasan Meenakshi, A. Jeba Selvaraj, B. Pottakkat;
Jawaharlal Institute of postgraduate medical education and Research, Puducherry, INDIA.*

Aim/Introduction: Initial studies have indicated favourable levels of FAPI expression in cholangiocarcinoma (CC). Even though F18-Fluorodeoxyglucose (FDG) positron emission tomography/ Computed tomography (PET/CT) is a frequently utilized method for assessing various malignancies, its application in cholangiocarcinoma was restricted. Therefore, our objective was to investigate the effectiveness of Ga-68 FAPI PET/CT in detecting cholangiocarcinoma and to evaluate its performance against that of F-18 FDG PET/CT. ***Materials and Methods:*** Patients suspected to have CC were recruited prospectively from January 2021 to March 2023. FDG and FAPI PET/CT studies were completed within 1 week. The final diagnosis of malignancy was achieved by tissue diagnosis (Either histopathological examination or fine needle aspiration cytology), radiological correlation from conventional modalities and serological correlation of Alpha-fetoprotein (AFP), Carcinoembryonic antigen (CEA) & Cancer antigen 19-9 (CA 19-9). Results were compared with the final diagnosis and expressed as sensitivity, specificity, positive predictive value (PPV), negative predictive value (NPV) and diagnostic accuracy (DA).

Results: 28 patients with suspected cholangiocarcinoma were included. Out of 28, 9 were metastatic and 17 were non-metastatic. For diagnosis of primary CC, FAPI PET/CT showed a sensitivity of 95.65% (CI:78-99.89%), specificity of 100% (CI:29.24-100%) & DA of 96.15% (CI:80.36-99.9%), whereas FDG PET/CT showed a sensitivity of 47.83% (CI:26.82-69.41%), specificity of 100% (CI:29.24-100%), and DA of 53.85% (CI:33.37-73.41%). Out of the 9 metastatic diseases, FDG and FAPI PET/CT detected 5 and 8 metastatic diseases, respectively. While the sensitivity of FAPI PET/CT was satisfactory, its effectiveness in identifying lesions was impeded by diffuse FAPI uptake in the liver (50%) and pancreas caused by pre-existing cirrhosis and periductal inflammation. ***Conclusion:*** In the diagnosis of primary and metastatic cholangiocarcinoma, FAPI PET/CT has demonstrated significant advantages over FDG PET/CT. Additional studies are necessary to assess the predictive value of FAPI PET/CT in the prognosis of cholangiocarcinoma.

References: Kratochwil C, Flechsig P, Lindner T, Abderrahim L, Altmann A, Mier W, et al. 68 Ga-FAPI PET/CT: Tracer Uptake in 28 Different Kinds of Cancer. J Nucl Med. 2019 Jun;60(6):801-5.

OP-162

Static and Dynamic^{68}Ga-FAPI PET/CT in Mass Forming Pancreatitis and Pancreatic Ductal Adenocarcinomas (PDAC)

M. Preussig[1], *M. Lang*[2], *C. Schroeter*[1], *E. Gutjahr*[3], *U. Haberkorn*[1], *M. Röhrich*[1];
[1]*Department of Nuclear Medicine, University Hospital Heidelberg, Heidelberg, GERMANY,* [2]*Department of General, Visceral, and Transplantation Surgery, University Hospital Heidelberg, Heidelberg, GERMANY,* [3]*Department of Pathology, University Hospital Heidelberg, Heidelberg, GERMANY.*

Aim/Introduction: The differentiation between mass forming pancreatitis and pancreatic ductal adenocarcinomas (PDAC) based on conventional imaging methods like ultrasound, CT and MRI is frequently not possible. Here, we applied static (60 minutes post injection) and dynamic PET/CT with ^{68}Gallium-labelled Fibroblast Activated Protein Inhibitors (^{68}Ga-FAPI-PET/CT) in 17 preoperative, treatment-naive patients with unclear pancreatic masses to evaluate the potential diagnostic value of this new imaging method for the differentiation between mass forming pancreatitis and PDAC. ***Materials and Methods:*** 17 Patient with unclear pancreatic masses underwent static and dynamic ^{68}Ga-FAPI-PET/CT before surgical resection or biopsy of the pancreas and subsequent histological diagnoses. Static parameters (SUVmax and SUVmean) were generated from VOIs of pancreatic masses. Time activity curves and dynamic parameters including kinetic modeling were extracted from dynamic PET data using PMOD software. ***Results:*** Histology revealed PDAC in 10 patients and inflammation in 7 patients. We observed a markedly higher ^{68}Ga-FAPI-uptake in PDACs than in inflammatory lesions (SUVmax: 17,93+/-4,95 versus 10,87+/-3,18 SUVmean: 10,76+/-2,96 versus 6,42+/-1,92). In dynamic PET-imaging, PDAC and inflammatory lesions showed distinctive and characteristic time activity curves: Whereas PDAC increased for 15+/-5 minutes followed by a plateau phase after the perfusion peak, the inflammatory lesions showed a steady and slow decrease after a perfusion peak. The average time to peak was markedly longer for PDAC (19 minutes) than for inflammatory lesions (4 minutes). PDAC showed higher K1and K2 values than the inflammations (K1:0,64+/-0,25 versus 0,33 +/-0,1, K2:0,77+/-0,63 versus 0,26+/-0,13). ***Conclusion:*** ^{68}Ga-FAPI-PET/CT should be considered for patients where other imaging methods are not able to distinguish between malignant and inflammatory pancreatic masses. Overall, PDAC show higher ^{68}Ga-FAPI-uptake than mass forming pancreatitis. However, an overlap of PDAC and pancreatitis-related uptake is possible. Dynamic time activity curves are distinctive for both PDAC and inflammation, which underlines the additional value of dynamic ^{68}Ga-FAPI-PET acquisition.

OP-163

The Role of [^{68}Ga]Ga-DOTA-FAPI-04 PET/CT on Detecting Lesions and Altering Stage in Patients With Digestive System Malignencies With Non-FDG-avid Lesions

G. Beydagi[1], *N. Alan-Selcuk*[1], *K. Akcay*[1], *E. Demirci*[1], *O. Sonmez*[2], *M. Ocak*[3], *T. Toklu*[1], *S. Celik*[4], *B. B. Oven*[4], *L. Kabasakal*[1,5];
[1]*Yeditepe University, Department of Nuclear Medicine, Istanbul, TÜRKIYE,* [2]*Yeditepe University, Faculty of Medicine, Istanbul, TÜRKIYE,* [3]*Istanbul University, Faculty of Pharmacy, Department of Pharmaceutical Technology, Istanbul, TÜRKIYE,* [4]*Yeditepe University, Department of Medical Oncology, Istanbul, TÜRKIYE,* [5]*Istanbul Unıversity-Cerrahpasa, Department of Nuclear Medicine, Istanbul, TÜRKIYE.*

Aim/Introduction: ^{68}Ga-labeled FAP ligands (^{68}Ga-FAPI) have emerged as a promising alternative for cancer patients presenting with FDG-negative lesions. The objective of this study is to assess the potential efficacy of ^{68}Ga-FAPI PET/CT in the detection, staging, and restaging of digestive system malignancies characterized by low FDG uptake or FDG-negativity. ***Materials and Methods:*** Obtaining approval from the Clinical Research Ethics Committee, we prospectively enrolled patients with pathologically confirmed primary tumors or metastases. All participants underwent ^{68}Ga-FAPI-04 and ^{18}F-FDG PET/CT within one week, either for initial assessment (detection, staging) or for recurrence detection (restaging). Two senior nuclear medicine physicians reviewed all studies by consensus. ***Results:*** ^{68}Ga-FAPI PET/CT imaging was conducted in 69 patients diagnosed with digestive system malignancies, who presented with suspicious lesions on FDG PET/CT. Among the 69 patients, 43 had gastric cancer, 13 had colorectal cancer, 7 had pancreatic cancer, 4 had hepatocellular carcinoma, and 2 had appendix cancer. Twenty cases with gastric cancer and two cases with colon cancer were diagnosed with signet ring cell carcinoma. In comparison to FDG PET/CT, the primary malignancy stage increased in 31 patients (45%) on FAPi PET/CT. Moreover, the primary malignancy stage increased in 64% of patients diagnosed with signet ring cell cancer. Peritoneal metastases were observed in 47 patients (68%). Although peritoneal metastases were FDG-negative in 27 patients, peritoneal metastases could not be demonstrated in just one case with a colon cancer diagnosis on FAPi PET/CT. Consequently, in the entire patient cohort, major changes were implemented in the treatment approach for 27 patients (39%), while minor changes were made for 4 patients (6%). ***Conclusion:*** ^{68}Ga-FAPI PET/CT demonstrates superiority in the detection, staging, and restaging of low FDG-avid tumors, particularly in gastro-entero-pancreatic cancers or in regions with an unfavorable tumor-to-background ratio on FDG-PET/CT. In accordance with our findings, 68Ga-FAPI PET/CT alters the disease stage in 45% of gastrointestinal malignancies.

507

Sunday, September 10, 2023, 3:00 PM - 4:30 PM
Hall F1

Paediatrics Committee - TROP Session: Adults General Nuclear Medicine

OP-164

The value of chemokine receptor type 4 targeted PET imaging in primary aldosteronism preoperative localization diagnosis compared with adrenal venous sampling

N. Lu[1], *C. Li*[1], *Y. Tian*[1], *Z. Xiao*[1], *D. Xing*[1], *J. Zhong*[1], *W. Li*[1], *D. Zeng*[1], *W. Luo*[1], *H. Guo*[1], *Z. Meng*[2], *Y. He*[1];
[1]*Department of Nuclear Medicine, Zhongnan Hospital of Wuhan University, Wuhan, CHINA,* [2]*Department of Urology, Zhongnan Hospital of Wuhan University, Wuhan, CHINA.*

Aim/Introduction: Primary aldosteronism (PA) is the most common cause for secondary hypertension, some of which are curable by resecting the dominant aldosterone-producing lesions. However, how to accurately recognize the functional adenoma or differentiate the dominant side in bilateral lesions by CT scans are still challenging. Chemokine receptor type 4 is found highly expressed in aldosterone-producing tissues. We aimed to evaluate the preoperative localization diagnostic efficiency of ^{68}Ga-PentixaFor PET imaging targeting CXCR4 in PA patients, compared with adrenal venous sampling (AVS), the current gold standard for PA differentiation. ***Materials and Methods:*** We prospectively recruited 19 PA patients (13 males and 6 females, 45±11 years old). All patients underwent PET/CT imaging of adrenal region 30 min (early scan) and 2 h (delayed scan) after injection of ^{68}Ga-PentixaFor, as well as AVS before surgery, with 2-5 months following-up. The SUVmax of adrenal lesions in both scans were measured. The correlations of above data with AVS and pathological results were then analyzed. The threshold of SUVmax to differentiate the dominant side in PA was determined by receiver operating characteristic (ROC) analysis. ***Results:*** 8(42%) patients with unilateral lesion and 7(37%) patients with bilateral lesions performing dominant avid ^{68}Ga-PentixaFor uptake, consistent with AVS results, turned out to be aldosterone-producing adenoma (APA), aldosterone-producing nodules (APNs), or aldosterone-producing micronodules (APMs) by pathological immunohistochemistry staining. 4(21%) patients with bilateral lesions showed weak ^{68}Ga-PentixaFor uptake but had dominant side by AVS. These lesions were APNs/APMs according to pathological results. All of these patients were cured of hypertension post adrenalectomy. A total of 36 adrenal lesions in 19 patients were analyzed. The mean SUVmax of 24.8±11.0 and 19.3 ±11.5 at early and delayed phases separately of APA, the most common type of aldosterone-producing tissues, was significantly elevated than that of APNs/APMs (7.5±5.4 and 5.3 ±3.9, separately), (P<0.005). To differentiate dominant side in PA patients, the optimal cut-off level of early SUVmax=7.9 and delayed SUVmax=7 was associated with sensitivity of 94%, specificity of 100%, and Youden's index of 94%. ***Conclusion:*** ^{68}Ga-PentixaFor PET imaging, as a non-invasive method compared with AVS, performed excellent ability in detecting APA and differentiating dominant lesions in PA patients. However, for some APNs or APMs patients with weak ^{68}Ga-PentixaFor uptake, AVS should be supplied to distinguish the lesions need surgery.

OP-165

Incidental Findings on ^{18}F-Fluorocholine PET for Parathyroid Imaging

A. Namazova[1], *A. NAZARI*[1], *B. Ince*[2], *S. Sağer*[1], *K. Sonmezoğlu*[1];
[1]*Istanbul University-Cerrahpaşa, Department of Nuclear Medicine, Istanbul, TÜRKIYE,* [2]*Istanbul University-Cerrahpaşa, Department of Nucleer Medicine, Istanbul, TÜRKIYE.*

Aim/Introduction: The aim of our study is to investigate the etiology of incidentally detected choline accumulation in non-parathyroid tissues in patients who underwent FCH-PET scan for the purpose of investigating parathyroid adenoma in our center ***Materials and Methods:*** We retrospectively analyzed 235 patients who underwent FCH-PET for the purpose of investigating parathyroid adenoma in our center between 2017 and2022. After the patients were injected with 0.1mci/kg intravenous 18F-fluorocholine, PET/MR images of the neck and upper mediastinum were taken at the 15th minute, and PET/CT images of the vertex-upper thigh were taken at the 45th minute. Images were interpreted by competent readers in the field, and areas showing abnormal choline uptake were recorded. SUVmax values of abnormal choline uptake were obtained. Each finding was correlated with follow-up data from the electronic medical records. ***Results:*** Incidental findings were observed in 23 (9.79%) of the 235 patients examined. The median age of the patients was 61 (29-84). Focal FCH accumulation was detected in the prostate gland of 8 male patients (80%), the median age of these patients was 69 (38-71) and the median serum PSA value was 1.05 (0.2-3.03). The patients were found to be clinically and radiologically compatible with BPH in the urological examinations. Focal FCH uptake in the breast was observed in 4 female (30.7%) patients. The mammography and clinical examinations of these patients were evaluated in benign processes. In 4 patients (3 M, 1 F), focal FCH uptake was observed in the thyroid nodules, and FNAB result of 1 female patient was reported as benign and 3 male patients as malignant. Total thyroidectomy operation was performed on patients whose FNAB results were interpreted as malignant, and the pathology result of the patients was papillary thyroid carcinoma. In addition, adrenal uptake (adenoma) in 1 patient, pituitary uptake in 1 patient (physiological), bone marrow uptake in 1 patient (aplastic anemia), focal liver uptake in 1 patient (FNH), uptake in the left nasopharynx in 1 patient (scc carcinoma in situ?), 1 patient meningioma and axillary lymph node uptake were observed in 1 patient, and it was thought to be secondary to the covid-19 vaccination. There was no significant correlation between the SUVmax values of benign and malignant lesions and the nature of the lesions. ***Conclusion:*** Although FCH-PET imaging is routinely used for imaging parathyroid adenoma and prostate cancer, FCH accumulation can be seen incidentally in some other malignant and benign conditions.

OP-166

Correlation between kidney ^{18}F-FDG uptake and renal function in patients with chronic kidney disease.

F. Dondi[1], *A. Talin*[2], *D. Albano*[2], *A. Calabrò*[2], *M. T. Volpe*[2], *P. Furtuna*[2], *F. Bertagna*[2];
[1]*Spedali Civili di Brescia, Brescia, ITALY,* [2]*Università degli Studi di Brescia, Brescia, ITALY.*

Aim/Introduction: The aim of the study was to underline a possible correlation between kidney uptake at ^{18}F-fluorodeoxyglucose (^{18}F-FDG) positron emission tomography/computed tomography (PET/CT) and creatinine (Cr) values in patients with chronic kidney disease (CKD). ***Materials and Methods:*** Patients

were retrospectively enrolled. Cr levels, estimated glomerular filtration rate (eGFR) and class of renal impairment at the time of the scan were collected. Kidney uptake (Ku), expressed as the average standardized uptake value (SUVmax) of 5 region of interest (ROIs) for each kidney, was sampled and ratios with liver (Ku-L) and blood-pool (Ku-BP) uptakes were calculated. T-test and Anova test were used to compare renal uptakes between the different classes of renal impairment. Pearson's correlation coefficient was used to evaluate the correlation between Cr levels, eGFR levels and PET/CT results. Moreover, in the case of patients with multiple scans, the temporal evolution of Cr levels (dCr) and eGFR (deGFR) were calculated and compared to the evolution of ^{18}F-FDG PET/CT parameters. ***Results:*** A total of 126 patients (81 male, mean age 71) who performed a total of 167 ^{18}F-FDG PET/CT scans were enrolled. Seventeen patients were functionally monokidney, 90 had two functioning kidneys and 19 subjects were transplanted: 17 had a functioning transplanted kidney while 2 had uptake on both native kidneys and transplanted one. In the total cohort of patients, significant negative correlations for Cr with Ku, Ku-L and Ku-BP were reported; positive correlations for eGFR were demonstrated with the same parameters. In evolutional terms, negative correlation for dCr with Ku and Ku-BP and for deGFR with Ku, Ku-L and Ku-BP were reported. In the group of patients with two functioning kidneys, negative correlations for Cr with Ku, Ku-L and Ku-BP and positive correlation for eGFR with the same parameters were confirmed. In the same group, dCr had a significant negative correlation with Ku and Ku-BP as also deGFR did. In the cohort of transplanted subjects, no significant correlations between the aforementioned parameters were reported. Significantly different Ku-L and Ku-BP dichotomizing the patients based on a value of Cr of 1.2 mg/dL were reported. Significantly different Ku, Ku-L and Ku-BP between the different classes of CKD were demonstrated. ***Conclusion:*** Correlation between kidney ^{18}F-FDG uptake with Cr and eGRF levels were reported, with the exception of transplanted patients. These insights were also confirmed between the temporal evolution of tracer uptake and renal functional parameters.

OP-167

Renal blood flow quantification for the evaluation of stress induced kidney imaging using Rubidium-82 PET/CT

A. van de Burgt[1,2], *F. H. P. van velden*[2], *F. Smit*[1,2], *L. F. de Geus-Oei*[2,3,4], *I. A. Dekkers*[2];
[1]*Alrijne hospital, Leiderdorp, NETHERLANDS,*
[2]*Leiden University Medical Center, Leiden, NETHERLANDS,*
[3]*University of Twente, Enschede, NETHERLANDS,*
[4]*Delft University of Technology, Delft, NETHERLANDS.*

Aim/Introduction: Chronic kidney disease (CKD) is a worldwide health problem. There is a need for novel quantifiable (image) biomarkers to define the underlying mechanisms of early-stage CDK. Renal blood flow (RBF) and renovascular reserve (RVR), defined as the ratio between RBF during stress and rest, might enable evaluation of disease activity and treatment response monitoring. The aim of this study is to develop a compartment model using dynamic Rubidium-82 (^{82}Rb) PET/CT imaging and to evaluate RVR by using stress induced kidney ^{82}Rb PET/CT imaging. ***Materials and Methods:*** Compartment models were developed based on the linkage and number of compartments and the delineation of the volume of interest (VOI). Image-derived input functions (IDIF) were derived from kidney, left-ventricular blood pool (LVBP), ascending thoracic aorta (ATA) and abdominal aorta (AA) VOIs. Subsequently, retrospective data were collected from 10 patients (5 impaired kidney function and 5 controls) undergoing dynamic myocardial ^{82}Rb PET/CT imaging. Finally, obtained K_1 values were converted to RBF in rest and pharmacological stress, and the RVR was composed to evaluate the potential of stress induced kidney ^{82}Rb PET/CT imaging. ***Results:*** A three-tissue compartment model was developed to distinct between cortex and medulla in three layers. No significant differences were found between the three layers ($p>0.05$). Subsequently, a one-tissue compartment model was developed based on myocardial blood flow models and showed a decrease in K_1 values in stress compared to rest for controls and patients with impaired kidney function of 20.6% and 7.9% (median in %) respectively when ISO-contouring and AA as IDIF were applied. The RVR for the controls were overall significantly lower compared to the impaired kidney function group, with the smallest median(IQR) of 0.40(0.28-0.66) and 0.96(0.62-1.15), respectively ($p<0.05$). ***Conclusion:*** In this proof-of-concept study, it was demonstrated that obtaining RBF in rest and stress using ^{82}Rb PET/CT is feasible for a one-tissue and a three-tissue compartment model. As the three-tissue compartment model cannot distinguish between the cortex and medulla, the one-tissue compartment model is preferred. In the impaired kidney function group, response to adenosine was absent and might be explained by the inability of the diseased kidney to respond with increased RBF after adenosine administration. However, further research is necessary to assess the use of adenosine for stress induced kidney imaging. To show sufficient evidence for the use of stress induced kidney ^{82}Rb PET/CT imaging in clinical practice, validation should take place in a future clinical study.

OP-168

Segmentation and Volumetric Analysis of Pulmonary Reperfusion after Pulmonary Thromboembolism using Lung Perfusion SPECT/CT

N. Alvarez Mena*, F. Sebastián Palacid, M. García Aragón, R. Zambrano Infantino, A. Hurtado Romero, R. Ruano Pérez;*
Hospital Clínico Universitario de Valladolid, Valladolid, SPAIN.

Aim/Introduction: To assess pulmonary reperfusion in patients under follow-up for pulmonary thromboembolism (PTE) by segmental and volumetric analysis in lung perfusion SPECT/CT. ***Materials and Methods:*** Prospective study from November 2020 to December 2022, in which we included 40 patients with PTE diagnosed by lung perfusion scintigraphy (planar images associated with SPECT/CT), who underwent a scintigraphic control 6 months later. Variables such as age, sex and degree of reperfusion were analysed. For reperfusion assessment, 3D visual and quantification analysis was performed using SPECT/CT segmentation (Q.Volumetrix software, GE). In volumetric analysis, the mean volumes and counts of the defect at baseline and at scintigraphic control were assessed to calculate the relative evolution (%). It was considered as no reperfusion ≤ 15%, minor partial reperfusion > 15-50%, major partial reperfusion > 50-80% and complete reperfusion > 80%. In addition, concordance between visual and quantitative analysis was assessed ($\chi 2$ test). ***Results:*** Mean age 71 years (36-89). 70% female. In scintigraphic control assessed by visual analysis was objectified 55% of patients no reperfusion, 20% partial reperfusion and 25% complete reperfusion. In quantitative analysis, 17% of patients no reperfusion, 33% minor partial reperfusion, 39% major partial reperfusion and 11% complete reperfusion were observed. In the 29 patients with partial reperfusion, 21 patients

had, on average, a relative decrease in defect volume (RDV) of 39% (16-79%), 4 patients with relative increase in mean defect counts (RImC) of 34% (17-64%) and 4 patients with RDV and RImC > 15%. When statistically comparing both methods, no significant concordance was noted between the scintigraphic results of the visual and quantitative analysis (p=0.05). Fifty-two per cent of patients with partial reperfusion on volumetric analysis (15/29) were considered non-reperfused by visual analysis. ***Conclusion:*** In the follow-up of pulmonary thromboembolic disease, volumetric analysis by lung perfusion SPECT/CT is superior to visual analysis. Furthermore, it is a tool that facilitates the assessment of reperfusion in patients in whom no significant improvement is observed in visual analysis as it may avoid unnecessary and prolonged treatment if reperfusion is noted by quantification.

OP-169

Could FAPI and MIBI scans help in diagnostic dilemmas in interstitial lung disease (ILD) for distinguishing fibroinflammatory process? Ongoing translational exploratory study

M. Assadi[1], *M. Bahtouee*[2], *E. Jafari*[1], *R. Mazarei*[2], *M. Khazaei*[3];
[1]*Department of Nuclear Medicine, Molecular Imaging, and Theranostics, Bushehr Medical University Hospital, School of Medicine, Bushehr University of Medical Sciences, Bushehr, IRAN, ISLAMIC REPUBLIC OF,* [2]*Department of Internal Medicine (Division of Pulmonary Medicine), Bushehr Medical Center Hospital, Bushehr University of Medical Sciences, Bushehr, IRAN, ISLAMIC REPUBLIC OF,* [3]*Department of Radiology, Bushehr Medical Center Hospital, Bushehr University of Medical Sciences, Bushehr, IRAN, ISLAMIC REPUBLIC OF.*

Aim/Introduction: The distinction of active fibroinflammatory process from an inactive form of the disease is of great value in the management of interstitial lung disease (ILD). There is no specific non-invasive method for this purpose, we aim to evaluate the diagnostic values of FAPI and MIBI scanning for fibrosis and inflammation in patients suspected to ILD. ***Materials and Methods:*** In this prospective exploratory study, 8 ILD patients suspected to ILD according to the high-resolution CT and their symptoms underwent FAPI and MIBI studies till now. The imaging assessed to determine where and to which degree the FAPI tracer and MIBI accumulate in lung tissues of patients with interstitial lung disease. Positive FAPI scan was considered as active fibrotic process and also positive MIBI scan considered as active inflammation. ***Results:*** Of eight patients, five patients showed positive FAPI scan but negative MIBI scan. One patient showed mild uptake of MIBI and also positive FAPI scan. Both scans were negative for two patients. ***Conclusion:*** FAPI scan might be considered as a promising procedure for diagnosis and monitoring of progression and therapeutic effect in ILD patients. Subsequent to the continuing evidence on the many-sided pathophysiology of ILD, there is a need for a precise approach for the management of ILD patients, especially in intractable patients using the existing treatment. ***References:*** 1. Bahtouee M , Saberifard J, Javadi H, Nabipour I, Raeisi A, Assadi M, Eftekhari M. 99mTc-MIBI Lung Scintigraphy in the Assessment of Pulmonary Involvement in Interstitial Lung Disease and Its Comparison With Pulmonary Function Tests and High-Resolution Computed Tomography: A Preliminary Study. Medicine (Baltimore). 2015;94(47):e2082.2. Bahtouee M, Saberifard J, Javadi H, Nabipour I, Malakizadeh H, Monavvarsadegh G, Ilkhani Pak H, Sadeghi A, Assadi M. 99mTc-IgG-Lung Scintigraphy in the Assessment of Pulmonary Involvement in Interstitial Lung Disease and Its Comparison With Pulmonary Function Tests and High-Resolution Computed Tomography: A Preliminary Study. Iran J Radiol. 2015;12(4):e14619

OP-170

The Role Of [^{99m}Tc] Sodium Pertechnetate Pulmonary Ventilation Single Photon Emission Computed Tomography/Computed Tomography (Spect/Ct) In The Early Location Of Prolonged Pulmonary Air Lack In Adults. Our Experience.

A. Peñaherrera Cepeda*, F. Gómez Caminero, J. Villanueva Curto, J. Badell Martínez, E. Campaña Díaz, P. García Talavera, E. Martín Gómez, S. Rama Alonso, M. Fuentes Gago., P. Tamayo Alonso;*
Complejo asistencial universitario de Salamanca, Salamanca, SPAIN.

Aim/Introduction: To evaluate the role of [99mtc] sodium pertechnetate pulmonary ventilation single photon emission computed tomography/computed tomography (SPECT/CT) in the early location of prolonged pulmonary air lack in adults to guide de surgical approach. ***Materials and Methods:*** Twenty two patients referred from the Thoracic Surgery Department (5 females; 17 males), mean age 64 +/- 13 years, with prolonged pulmonary air leak (greater than 5 days) were evaluated during February 2021 to March 2023. They were studied by pulmonary ventilation SPECT/CT for pre-surgical localisation of the air leak. All of them underwent a mixed morphofunctional tomographic study after a mean dose of 571.10 MBq with [^{99m}Tc] sodium pertechnetate, administered thanks to the Technegas® system. ***Results:*** Nineteen of the 22 SPECT/CT studies were positive and useful for the exact anatomical localisation of the peripheral air leak, 68% of which were in the upper lobes. Eighteen of these 19 patients underwent surgery, most of them with atypical segmentectomy of the lobe indicated by this technique, with immediate resolution of the pneumothorax in 100% of the operated patients. These patients were discharged 24 hours after surgery, compared to the patients who could not be operated (4 patients, 3 because the leakage point could not be located by this technique and 1 because it was not surgically accessible), who had prolonged hospital stays of up to 21 days in one of them. ***Conclusion:*** The [99mTc] sodium pertechnetate pulmonary ventilation SPECT/CT hybrid imaging, allows a very efficient localisation of pulmonary air leaks, thus allowing the correct surgical approach, minimising possible risks, guiding the surgeon to the exact location of the leak and reducing operating room time and hospital stay.

OP-171

Oropharyngoesophageal scintigraphy (OPES) in Systemic Sclerosis Patients: A Valuable Tool for Evaluating Dysphagia

A. Marciano[1], *M. Di Battista*[2], *M. Scarpuzza*[1], *A. Ambrogio*[1], *G. Nonne*[1], *A. Leo*[1], *E. Esposito*[1], *A. Valevich*[2], *M. Grosso*[1], *D. Volterrani*[1];
[1]*Nuclear Medicine, Department of Translational Research and New Technology in Medicine, University of Pisa, Pisa, ITALY,* [2]*Rheumatology Unit, University of Pisa, Pisa, ITALY.*

Aim/Introduction: Evaluate the performance of oropharyngoesophageal scintigraphy (OPES) in assessing oropharyngeal and esophageal motility in patients with systemic sclerosis (SSc), both with and without dysphagia. ***Materials and Methods:*** The study enrolled adult SSc patients (129 patients, 87.7% female, mean age 57±16 years, median time from diagnosis 4.65 years) who underwent OPES. OPES was performed with both liquid and semisolid boluses (6 boluses) labelled with of ^{99m}Tc nanocolloid and provided information on oropharyngeal transit time (OPTT), esophageal transit time (ETT), oropharyngeal retention index (OPRI), esophageal retention index (ERI), and site of bolus retention. ***Results:*** OPES identified at least one anomaly in 98%

of patients, and the results were generally worse for the semisolid bolus. Esophageal motility was widely impaired, with 78.9% of patients showing an increased ERI for the semisolid bolus, and the middle-lower esophagus was the most frequent site of bolus retention (57.3%). Although not statistically significant, there were increased retention indices in the male population. Oropharyngeal impairment was highlighted by widespread increased OPRI, especially for the semisolid bolus (96.1%). Considering only patients without a history of dysphagia at the examination (48 patients, 79.1% female, mean age 56±18 years, mean time from diagnosis 3 years), OPES identified at least one anomaly in 95.8% of patients, showing a similar distribution of anomalies to the whole population examined. Although dysphagic patients showed a higher median ERI (for the semisolid boluses) than those without a history of dysphagia, the difference is not statistically significant (p=0.061). ***Conclusion:*** In SSc patients OPES revealed similar alterations of the oropharingoesophageal motility in patients with and without history of dysphagia showing a marked SSc esophageal impairment, with slowed transit time and increased bolus retention. These findings suggest that OPES can provide valuable insights into dysphagia in systemic sclerosis patients and may aid in the early diagnosis and management of this pathology.

OP-172

Correlation Between Lymphoscintigraphy And Clinical Staging In Diagnosis Of Lymphedema

A. Kilicaslan, *B. Okudan Tekin;*
Ankara City Hospital, Ankara, TÜRKIYE.

Aim/Introduction: Appropriate diagnosis, staging, and selection of the best treatment of patients with extremity lymphedema are essential for patient management. Lymphoscintigraphy is still accepted as the gold standard imaging method for the diagnosis of lymphedema (1-3). In this study, we aimed to retrospectively evaluate the staging of Lymphedema with lymphoscintigraphy findings and their compatibility with clinical practice. ***Materials and Methods:*** 131 patients who underwent lymphoscintigraphy imaging in our clinic between 2021 and 2023 with a preliminary diagnosis of lymphedema were included. Lymphoscintigraphies were re-evaluated retrospectively by two different physicians without clinical knowledge. For lymphoscintigraphy staging, normal lymphatic flow, the number of multi and/or dilated channels, transition to proximal lymph nodes, presence of deep lymph nodes and dermal-backflow were evaluated. Lymphoscintigraphies were classified between normal and Grade I-IV according to the criteria of "An Atlas of Clinical Nuclear Medicine". Statistical analysis was performed using Chi-Square and Kendalls tau tests in the IBM SPSS 26 program. ***Results:*** 59 of the patients were male and 72 were female. The median age was 62 years. In the clinical staging, 41 (31.2%) of the patients were stage 1, 66 (50.4%) stage 2, and 24 (8.4%) stage 3. In the lymphoscintigraphy evaluation, 41 (31%) of the patients were found to be scintigraphically normal. In the clinical staging of the patients who were evaluated as normal scintigraphically, 36 (87.8%) were stage 1, 6 (14.6%) were stage 2 and 3 (7.3%) were stage 3. In lymphoscintigraphy staging, a positive correlation was found between both readers (correlation coefficient for right and left: 0.87; 0.89, respectively). A positive correlation was found between the staging of both readers and the clinical staging (P<0.05). Among the readers, a positive correlation was found between reduced transition to proximal lymph nodes, multichannel lymphatic flow, dermal-backflow and clinical staging (p<0.05). However, no positive correlation was found between deep lymph nodes and clinical staging (p>0.05). ***Conclusion:*** There is a clinical correlation with the presence of decreased passage to proximal lymph nodes, multichannel and/or dilated lymphatic duct, and dermal-backflow. According to the results of our study, we think that lymphoscintigraphy, which is accepted as the gold standard in the literature in the diagnosis and follow-up of lymphedema, is an important auxiliary technique in patient management, as a reproducible and objective evaluation criterion.

508

Sunday, September 10, 2023, 15:00 - 16:30
Hall F2

Joint Symposium 2 - Oncology & Theranostics Committtee / EORTC: Nuclear Medicine Imaging of the Immune System

OP-173

Molecular Imaging of the Immune System

W. Cai;
Universityof Wisconsin, Molecular Imaging and Nanotechnology Laboratory, Madison, UNITED STATES OF AMERICA.

OP-174

Radiolabeled Markers of Immune Response

S. Heskamp;
Radboud University Medical Center, Department of Medical Imaging (Nuclear Medicine), Nijmegen, NETHERLANDS.

OP-175

Imaging Tumor Metabolism and its Heterogeneity

E. Lopci;
IRCCS–Humanitas Research Hospital, Nuclear Medicine, Milan, ITALY.

OP-176

Translating Immuno-PET for immune-oncology treatments into the Clinic

E. G. E. de Vries;
UniversityMedical Centre Groningen, Department of Medical Oncology, Groningen, NETHERLANDS.

509

Sunday, September 10, 2023, 3:00 PM - 4:30 PM
Hall G2

e-Poster Presentations Session 3 - Inflammation & Infection Committee: More on Infection and Inflammation Imaging

EPS-042

Role of scintigraphy in the staging of necrotizing otitis externa in diabetics

T. Ben Ghachem, *R. Ghodhbane, L. Zaabar, I. Slim, A. Mhiri;*
Salah Azaiez Institute, Tunis, TUNISIA.

Aim/Introduction: Malignant external otitis (MEO) is a rare but serious infectious pathology which develops from the external auditory canal, and which occurs mainly in diabetic subjects. The aim of our study is to determine the interest of bone scintigraphy with 99mTc-MDP in the diagnosis and assessment of extension of MEO.

Materials and Methods: We report a retrospective study of 21 diabetic patients, collected over a 10-year period (2009-2019), referred for extension assessment of a confirmed MEO. The average age is 66.5 years with extremes ranging from 52 to 87 years. All subjects underwent a 99mTc-MDP bone scan with early and late skull-centered static image acquisition, a whole-body scan at 120 minutes, and a skull-centered tomoscintigraphy coupled with CT scan (SPECT/CT) scan. ***Results:*** Among the 21 diabetic subjects, 18 were insulin-requiring (71.4%). The diabetes was relatively unbalanced with an HbA1C between 8 and 10%. Bone scintigraphy with 99mTc-MDP was positive in 15 cases and negative in 6 cases. Extension to surrounding bony structures was found in 12 patients. This extension was present at the level of the temporomandibular joint in 1 case, of the petrous bone in 3 cases, of the mastoid in 3 cases and extended to the mastoid and the petrous bone in 5 cases. ***Conclusion:*** Bone scintigraphy with 99mTc-MDP is considered the examination of choice for the early diagnosis of MEO. It allows to make the initial assessment to know the degree of extension to the neighboring bone structures. SPECT/CT significantly improved its specificity.

EPS-043

A promising tool for excluding knee and hip prosthetic infection with a novel semiquantitative index in double-phase bone scintigraphy

R. Zambrano Infantino*, J. Piñerúa-Gonsálves, F. Sebastian Palacid, N. Álvarez Mena, M. Alonso Rodríguez, M. García Aragón, B. Pérez López, C. Gamazo Laherran, M. González Soto, R. Ruano Pérez;*
Hospital Clínico Universitario de Valladolid, Valladolid, SPAIN.

Aim/Introduction: Pain following hip and knee arthroplasty is a frequent issue, with aseptic loosening and prosthetic joint infection as the leading causes. Distinguishing between these conditions promptly is essential, as their treatment approaches differ significantly. This study aims to assess the accuracy of the Blood Pool Ratio-Delayed Ratio variation index in semiquantitative analysis of double-phase bone scintigraphy as a tool for the diagnosis of prosthetic joint infection in the hip and knee. ***Materials and Methods:*** A retrospective study was performed, including patients who underwent surgical intervention for suspected knee and hip prosthetic infection. A semiquantitative analysis was performed on planar images obtained from double-phase bone scintigraphy (blood pool and delayed phase) following the administration of 99mTc-hydroxymethylene-diphosphonate (99mTc-HMDP). In the blood pool phase, a region of interest (ROI) was placed on the affected area, and a corresponding position in the contralateral joint was selected as the control area. The Blood Pool ratio (BPr) was obtained by calculating the ratio between the two areas. Subsequently, the ROI was applied to the same areas in the delayed phase to determine the Delayed Ratio (Dr). The BPr-Dr variation index was calculated as [(Dr - BPr) / BPr] x 100. The results were compared with the culture and/or presence of intraoperative purulent joint fluid, and the accuracy of the semi-quantitative analysis was evaluated using ROC analysis. The Youden index was used to determine the optimal cut-off point of the BPr-Dr variation index for predicting infection. ***Results:*** Forty-seven patients with suspected prosthetic joint infection were included in the study. The semiquantitative analysis showed moderate model performance, with an area under the curve of 0.76 (95% CI 0.58-0.94). The optimal cut-off point for predicting prosthetic joint infection was an increase of 20.6% of the BPr-Dr index, with a sensitivity of 75.0%, specificity of 71.4%, negative predictive value of 89.9%, and positive predictive value of 47.3%. ***Conclusion:*** The proposed semiquantitative method appears to be a useful tool for excluding knee and hip prosthetic infection due to its high negative predictive value, which could potentially reduce the need for other tests such as scintigraphy with labeled autologous leukocytes. ***References:*** 1. Quartuccio N, Panareo S, Urso L, Sturiale L, et al. Initial results of the use of a novel semiquantitative parameter in three-phase bone scan to predict 99mTc-HMPAO-labeled leukocyte scintigraphy in patients with unilateral total knee replacement. Nucl Med Commun. 2021. 1;42(2):198-204.

EPS-044

Assessment of disease severity in Sjögren's syndrome using semi- quantitative parameters on salivary gland scintigraphy.

T. Singhal*, P. Singh, A. Rehman, K. Kandula, G. Parida, P. Kumar, K. Bishnoi, R. Emerson, S. Patro, K. Agrawal;*
AIIMS Bhubaneswar, Bhubaneswar, INDIA.

Aim/Introduction: Sjögren's syndrome(SS) is a chronic autoimmune disease characterized by lymphocytic infiltration and destruction of exocrine glands. SS characteristically involves salivary glands with presence of xerostomia in majority (>93%) of patients. Severity of xerostomia can vary from mild to severe and debilitating. Labial histopathology and ANA are commonly used in diagnosis of SS but do not corelate well with disease severity. Tests available for objective assessment of disease severity include sialometry and salivary gland scintigraphy (SGS) (1). This study aims to correlate severity of xerostomia with semi-quantitative parameters on SGS. ***Materials and Methods:*** Sixty-one patients with diagnosis of SS who underwent SGS were analyzed. Based on clinical symptoms, the severity of xerostomia was graded into mild, moderate and severe. Semi-quantitative parameters (maximum uptake and excretion fractions(EFs)) for all salivary glands were calculated on SGS. Pearson's correlation coefficients were calculated to assess correlation with clinical disease severity. Also, correlation between ANA and disease severity was evaluated, when available(n=38). ***Results:*** Sixty-one patients (47 females and 14 males) with median age of 41 years (Range: 4-85y) were included. Of these, 38 had mild, 17 had moderate, while only 6 had severe disease. Mean values of SGS parameters are described in Table1 which were highest in mild and lowest in severe disease group ($p<0.05$). Pearson's correlation coefficient for left and right parotids & left and right submandibular glands EFs with disease severity were -.304, -.331, -.360 and -.365, respectively ($p<0.05$). Correlation coefficient for maximum uptake with disease severity were -.361, -.385, -.258 and -.221, respectively. The EFs showed significant negative correlation with disease severity while maximum uptake showed significant negative correlation for bilateral parotid and left submandibular gland. No significant correlation of ANA with disease severity was noted. ***Conclusion:*** Semi-quantitative parameters on SGS show reduction with increase in severity of xerostomia. Additionally, maximum uptake and EFs correlated well with severity of xerostomia of SS, whereas ANA levels showed no significant correlation with disease severity. SGS can serve as an objective parameter of clinical severity of xerostomia, which is otherwise difficult to determine clinically. ***References:*** 1. Chen YC, Chen HY, Hsu CH. Recent Advances in Salivary Scintigraphic Evaluation of Salivary Gland Function. Diagnostics (Basel). 2021 Jun 28;11(7):1173.

EPS-045

Oral Gallium -67 citrate Scintigraphy as a new highlighter for guided biopsiescolonoscopy in Inflammatory bowel disease.

J. Calegaro[1], *J. Tajra*[1,2], *J. Tajra*[3];
[1]*Secretaria de Estado de Saúde, Brasília, BRAZIL,*
[2]*Hospital de Base do Distrito Federal, Brasilia, BRAZIL,*
[3]*Centro Universitário UNIEURO, Brasília, BRAZIL.*

Aim/Introduction: Histologic remission has been added prognostic information in Crohn´s disease, however colonoscopy randomized biopsies had a doubt results. AIM: this study analyzes the useful of oral gallium as a new highlighter for hot spot activity at guided biopsies by colonoscopy. ***Materials and Methods:*** This is a prospective study with 41 Crohn's disease treated patients in follow up treatment from 2016 to 2022. The patients underwent digestive transit studies with 67-Gallium Citrate (300uCi) after oral ingestion of 10 ml of water. The radionuclide protocols were performed at 1, 6, 12, 24, 48 and 72 h. A total of 20 patients were submitted to colonoscopy with randomized biopsies and 21 patients were underwent to colonoscopy guided biopsies with oral 67-gallium scintigraphy. The sample was evaluated by yearly SES-CD endoscopic score (mucosal healing for SES-CD<2). GHAS histologic score was used as referent test (remission for GHAS<4). Values of receiver operating characteristic (ROC) curve were obtained and compared. Significance test level was 0,05. ***Results:*** The population included 41 patients (13 men; 28 women); average age was 37,9; illness time was 4,48 years. In patients with mucosal healing (39%), there were 68% of histological activity identifiedwith sensitivity of 57% and specificity of 45% by oral ^{67}Ga scintigraphy group. In the randomized biopsies group, there were 27% with mucosal healing and 45% of histological activity. Biopsies guided by oral ^{67}Ga has a Mann-Whitney test with p =0,03. ***Conclusion:*** Oral ^{67}Ga scintigraphy may be a useful and inexpensive test for guided biopsies in Crohn´s disease patients particularly in colonoscopies with mucosal healing. ***References:***
1. Mazzuoli S, Guglielmi FW, Antonelli E, Salemme M, Bassotti G, Villanacci V. Defnition and evaluation of mucosal healing in clinical practice. Dig Liver Dis. 2013;45(12):969-77. 2. Maconi G, Armuzzi A. Beyond remission and mucosal healing in Crohn's disease. Exploring the deep with cross sectional imaging. Dig Liver Dis. 2017;49(5):457-8.3-Becker W, Meller J. The role of nuclear medicine in infection and inflammation. Lancet Infect Dis. 2001;1(5):326-33.

EPS-046

Evolving Nuclear Imaging of Infection - The South African Initiative for Novel Radiopharmaceuticals

T. Ebenhan[1,2], *A. H. Mdlophane*[3,4], *J. Duvenhage*[1], *C. A. Grouws*[5,1], *M. Kaths-Lundie*[6], *O. Gheysens*[7], *T. Govender*[8,3], *T. Naicker*[5,3], *H. G. Kruger*[5], *J. Zeevaart*[4,2,3], *M. M. Sathekge*[3,9];
[1]*Preclinical Imaging Facility, Nuclear Medicine Reseach Infrastructure NPC, Pretoria, SOUTH AFRICA,* [2]*Nuclear Medicine, University of Pretoria, Pretoria, SOUTH AFRICA,* [3]*Nuclear Medicine Reseach Infrastructure NPC, Pretoria, SOUTH AFRICA,* [4]*Radiochemistry, Necsa, Pelindaba, SOUTH AFRICA,* [5]*Catalysis and Peptide Research Unit, University of KwaZulu Natal, Durban, SOUTH AFRICA,* [6]*Radiochemistry, Sefako Makgatho Health Science University, Pretoria, SOUTH AFRICA,* [7]*Department of Nuclear Medicine, Cliniques Universitaires Saint- Luc, and Institute of Clinical and Experimental Research, Université Catholique de Louvain, Leuven, BELGIUM,* [8]*Department of Chemistry, University of Zululand, KwaDlangezwa, SOUTH AFRICA,* [9]*Nuclear Medicine and Steve Biko Academic Hospital, University of Pretoria, Pretoria, SOUTH AFRICA.*

Aim/Introduction: Positron emission tomography/computed tomography imaging has made remarkable inroads as a technique to advance diagnostics and monitoring of infectious diseases. Currently, the diagnostic toolbox of routine tracers includes metabolic imaging using [^{18}F]FDG or [$^{67/68}$Ga]citrate, imaging host response to infection using radiolabeled blood elements / radiolabeled antibodies. However, the initial diagnosis or specific therapy monitoring can be elaborate due to limited capabilities of available radiopharmaceuticals to decipher sterile inflammatory processes from active infection. With South Africa tracking an almost 20-year record of clinical research in utilizing [^{18}F]FDG-/[^{68}Ga]Ga-citrate-PET/CT imaging to battle various infection, a preclinical research program to develop more pathogen-specific PET-imaging agents has been in focus since 2014. This work will highlight the different strategies to advance novel radiopharmaceuticals for PET-imaging of infectious diseases. ***Materials and Methods:*** Better understanding of the more intricate infectious diseases, such as tuberculosis, MRSA, or malaria sparked an emergence of innovative, more-selective ligands with known targeting mechanism. Small molecules (A-EK, DnL, TB-Sid), antibiotics (DBI1-16, Purm) and peptide derivatives (UBI29-41, TBAI101, LL-37, CP1-3, Ph1, a-H8, PD-P1/-C1) were labelled with either copper-64 or gallium-68. The antibody (Ab) Pf-BII-6, the Ab-fragment Pf-McG45 and specific blood-derived elements (LE, PISC) were labelled with zirconium-89. Radiochemical synthesis and characterization as well as a preclinical assessment addresses tracer selectivity, accuracy and sensitivity to pursue with more disease-specific in vivo investigations. ***Results:*** A radiolabeling strategy developed for [^{68}Ga]Ga-UBI29-41 was further tailored for subsequent peptide-based molecules (or small molecules) thereby achieving >95% radiochemical purity and now undergoing full characterization during their preclinical assessment (except for LL-37). Promising results from radio-characterization suggesting [^{68}Ga]Ga-CDPx, -DnL, -Ph1, -a-H8 as candidates for more disease-specific in vivo imaging investigations. Facile radiolabeling, tracer inertness and favorable PET/CT imaging-guided pharmacokinetics motivates for [^{89}Zr] Pf-McG45 to become relevant for preclinical, malaria-specific applications. ***Conclusion:*** The stages of radiopharmaceutical research for various potential infection PET-imaging agents are presented. By meeting the requirement for infection imaging, Ga-68-labeled UBI29-41, -Purm and -CDPx are suited for potential translation to the clinical nuclear medicine setting whereas [^{89}Zr] Zr-Pf-McG45 based PET/CT imaging can become a preclinical biomarker tool to support antimalarial drug development. Using radiolabeled molecules with known predetermined functionalities, e.g., a bacteria-specific mechanism of action or targets may better facilitate diagnosis of infection or allow fast-tracking current antimicrobial drug development. However, based on this experience, future radiopharmaceutical development should give better attention to specific molecule design that meets the rather unique requirements of an infection imaging agent.

EPS-047

The Importance of FDG PET/CT in the Diagnosis of Left Ventricular Asist Device Infection

Y. Okar, *I. Sezgin, R. Horal, M. Urhan, B. Akkas;*
Sultan Abdulhamid Han Training and Research Hospital, Istanbul, TÜRKIYE.

Aim/Introduction: Pre-transplant LVAD (left ventricular assist device) is a very important treatment approach in patients with end-stage heart failure. However, infection of the LVAD device is a condition that can result in high morbidity and mortality. In the presence of suspected infection, laboratory tests, blood culture and thorax X-ray, thorax CT, USG can be performed. These methods are insufficient in imaging LVAD device infections. Gram staining and culture of the LVAD device are recommended for the definitive

diagnosis of the presence of infection. In this study, our aim is to evaluate the success of FDG PET/CT in imaging the presence and extent of infection in patients with suspected LVAD infection. ***Materials and Methods:*** Twelve male patients(age:30-60) who applied to our clinic with the suspicion of LVAD infection between 2019-2023 were evaluated retrospectively. The pump part of the LVAD located in the intrathoracic area and the circumference of the intrathoracic and abdominal parts of the drive line were evaluated visually and semiquantitatively on PET/CT images. Areas with increased FDG uptake were confirmed with NAC (non attenuation correction) images and recorded as positive uptake. The definitive diagnosis of LVAD infection was decided based on the results of microbiological analysis (Table 1). ***Results:*** In PET/CT, 9/12(75%) patients were true positive, 2/12(17%) patients were true negative, 1/12(8%) patients were false positive was detected (table 1).Staphylococcus aureus and Pseudomonas aeuroginosa pathogens were grown in the microbiological evaluation of drive line exit site. Clinical and laboratory results of patients (9/12) who were found to be true positive in PET/CT strongly suggested the presence of LVAD infection. In true negative patients (2/12) laboratory values were normal and there was no growth in the culture. Laboratory results of the patient(1/12), whose result was false positive, were normal and there was no growth in the culture. All components of the device were replaced in 2 patients with involvement in the pump parts of the LVAD. Seven patients who showed involvement in favor of drive line infection on PET/CT were considered responsive to treatment because their clinical and laboratory values returned to normal after antibiotic treatment and there was no growth in the control culture. Sensitivity:100%, specificity:66%, PPV:90%, NPV:100% were calculated. ***Conclusion:*** In the presence of high clinical and laboratory suspicion of infection in LVAD device infection, PET/CT has a high advantage in demonstrating the presence and extent of infection.

EPS-048

Clinical Value and Utility of the ^{18}F-FDG PET/CT in Detecting Prosthetic Infection After the Aortic Valve and Thoracic Aorta Reconstruction.

V. Carrero-Vásquez[1], *I. Sánchez-Rodríguez*[1], *F. Escrihuela-Vidal*[2], *L. Gracia-Sánchez*[1], *P. Notta*[1], *M. Pudis*[1], *S. Bondia-Bescós*[1], *A. Blasco*[3], *B. Hervas-Sanz*[1], *C. Martínez-Ramos*[1], *P. Perlaza-Jiménez*[1], *M. Cortés-Romera*[1];
[1]*Nuclear Medicine Department, Bellvitge University Hospital, Barcelona, SPAIN,* [2]*Infectious Diseases Department. Bellvitge University Hospital., Barcelona, SPAIN,* [3]*Cardiovascular Surgery Department, Bellvitge University Hospital, Barcelona, SPAIN.*

Aim/Introduction: To assess the utility of 18F-FDG PET/CT in detecting infection in aortic vascular prostheses. Identify the morphometabolic characteristics that allow discerning between post-surgical inflammatory changes and the infectious process. Correlate PET/CT findings with clinical data. ***Materials and Methods:*** A retrospective descriptive study in patients undergoing reconstruction of the aortic valve and thoracic aortic artery with prosthetic devices who presented clinical suspicion of prosthetic infection and underwent an examination with 18F-FDG PET/CT for diagnostic purposes. Twelve patients were reviewed from March 2016 to December 2021. Demographic data, vascular devices, symptoms, clinical analysis, and the characteristics of the PET/CT study were studied, contrasting with the final diagnosis. ***Results:*** 12 patients (8 men) with a mean of 71 years old (53-82) were analyzed. The 2 patients that PET/CT classified as positive were true positives; 3 were classified as doubtful: 1 was positive, and the other 2 were negative. Two of those positive for endocarditis presented heterogeneous uptake; the other showed a focal uptake on the PET image. The positive patients showed a higher semiquantitative uptake index (SUVmax) in the suspicious images and a slight elevation of leukocytes compared to the negative patients. The CT identified abscesses in 2 of the 3 positive patients. The 7 patients that PET/CT classified as negative were true negatives. ***Conclusion:*** ^{18}F-FDG PET/CT allowed us to reject all negative patients, avoiding unnecessary surgeries and prolonged courses of antibiotic therapy. It demonstrated excellent performance in the detection and localization of infectious processes. The focal uptake pattern and the abscess were the PET/CT image findings that were most associated with the diagnosis of infection.

EPS-049

Role of [18F]FDG PET/CT in patients with suspected ventricular assist device infection. Experience in a PET/CT dedicated cardio center.

B. Hervás Sanz[1], *L. M. Gràcia-Sánchez*[1], *I. E. Sánchez-Rodríguez*[1], *P. C. Notta*[1], *V. A. Carrero-Vásquez*[1], *C. Martínez-Ramos*[1], *A. Palomar-Muñoz*[1], *M. Pudis*[1], *S. Bondia-Bescós*[1], *J. L. Díaz-Moreno*[1], *C. Díez-López*[2], *J. González-Costello*[2], *L. Herrador-Galindo*[2], *F. Escrihuela-Vidal*[3], *N. Sabé-Fernández*[3], *D. Ortiz-Berbel*[4], *K. Osorio-Higa*[4], *M. Cortés-Romera*[1];
[1]*Nuclear Medicine-PET (IDI) Department, Bellvitge University Hospital-IDIBELL, L'Hospitalet de Llobregat, SPAIN,* [2]*Cardiology Department, Bellvitge University Hospital-IDIBELL, L'Hospitalet de Llobregat, SPAIN,* [3]*Infectious Disease Department, Bellvitge University Hospital-IDIBELL, L'Hospitalet de Llobregat, SPAIN,* [4]*Cardiovascular Surgery Department, Bellvitge University Hospital-IDIBELL, L'Hospitalet de Llobregat, SPAIN.*

Aim/Introduction: Ventricular assist devices (VAD) are used in patients with heart failure either as bridge therapy to cardiac transplantation or as destination therapy.The aim of this study is to evaluate the usefulness and diagnostic capability of [18F]FDG PET/CT in patients carrying VADs with suspected underlying infectious processes. ***Materials and Methods:*** Retrospective descriptive study of patients (p) carrying VAD, with performance of [18F]FDG PET/CT for suspected infection between July 2018 and January 2023. Demographic data, baseline pathology, VA purpose and PET/CT findings were studied. ***Results:*** 11p (5 female, 5 male, 1 transgender female) with a mean age of 55.4 years [31-76], affected by dilated cardiomyopathy (8 ischaemic, 2 toxic secondary to chemotherapeutic treatment, 1 idiopathic) were analysed. 7p were VAD carriers as bridging therapy and 4p as destination. The reasons for requesting PET/CT were in 10p clinical suspicion of device infection and in 1p suspicion of interstitial nephritis. 5p presented PET/CT suggestive of infection (4 on driveline entry and subcutaneous tract; 1 on ventricular device and mediastinal cannulae). Microbiological analysis was performed in all of them and was positive in only 3p. Despite this, all 5p received antibiotic treatment with beta-lactams (4p with resolution of the infectious condition and 1p requiring cardiac transplantation). 1p presented a discrete increase in metabolism at the level of the subcutaneous driveline tract attributable to an inflammatory process. 5p showed no findings suggestive of infection by PET/CT and the final diagnosis was unrelated to the VAD (2p without infection and 3p with infection in locations other than the VAD). The median SUVmax of patients with extrathoracic infection (driveline entry and subcutaneous tract) was 2.5 g/ml vs. 1.36 g/ml in relation to the rest of the patients without infection.The median SUVmax of patients with intrathoracic infection was 4.99 g/ml vs. 3.6 g/ml for

the rest of the patients without infection. ***Conclusion:*** 18F]FDG PET/CT has been able to detect in our sample, in a non-invasive way, infection related to ventricular assist devices, presenting higher diagnostic yield and a high negative predictive value with respect to microbiological analysis.

EPS-050

Asesessment Of Splenic And Bone Hypermetabolism As Indirect Signs Of Infection/Inflammation In Patients With Suspected Infective Endocarditis Or Implantable Cardiac Device Infection.

A. Padilla Bermejo[1], *F. J. Pena Pardo*[1], *M. Amo Salas*[2], *M. N. Sicilia Pozo*[1], *C. Lucas Lucas*[1], *M. Contreras Ameduri*[1], *L. García Zoghby*[3], *M. Cruz Montijano*[3], *E. Noriega Álvarez*[1], *A. M. García Vicente*[3], *Á. Soriano Castrejón*[3], *M. P. Talavera Rubio*[1], *V. M. Poblete García*[1]; [1]*Nuclear Medicine Department, University General Hospital of Ciudad Real, Ciudad Real, SPAIN,* [2]*Mathematics Department, Castilla la Mancha University of Ciudad Real, Ciudad Real, SPAIN,* [3]*Nuclear Medicine Department, University General Hospital of Toledo, Toledo, SPAIN.*

Aim/Introduction: To determine the association of indirect signs of infection/inflammation on 18F-FDG PET/CT, such as spleen and bone marrow (BM) hypermetabolism with the diagnosis of infective endocarditis (IE), when assessed in patients with suspected IE in native valves (NV), prosthetic valves (PV) or implantable cardiac electronic device endocarditis/infection (ICEDI). ***Materials and Methods:*** Patients with suspected IE undergoing 18F-FDG PET/CT from April/2019 to January/2022 (60 min of FDG incorporation, all patients under myocardial suppression) were retrospectively included. SUVmax was determined in spleen and vertebral body of L2 for BM assessment, classifying as positive those values higher than hepatic SUVmax. The diagnosis of IE was established by a multidisciplinary team. The association of BM and/or splenic positivity with the final diagnosis of endocarditis and myocardial uptake was assessed on the overall patient group and the analysis by subgroups using Pearson's Chi-square test and exact two-tailed and asymptotic, respectively. ***Results:*** 85 patients were analysed, 34 with suspected IE in NV, 33 with IE in PV and 18 with ICEDI. IE was finally considered definite in 27 patients and 9 patients were diagnosed with device infection. In the overall patient group, the prevalence of BM hypermetabolism was 25.5% (30/85), 22.1% (26/85) in case of splenic hypermetabolism, 12.5% (15/85) of both simultaneously and 48.2% (41/85) in case of splenic and/or BM hypermetabolism. There was a statistically significant relationship between the final diagnosis of IE and increased splenic (P=0.004), BM (P=0.015) and splenic and/or BM (P=0.020) metabolism. There was no statistically significant relationship between myocardial uptake and splenic and/or BM hypermetabolism. In the subgroup analysis, the prevalence of splenic hypermetabolism was 43.75% (7/16) in definite IE and 15% (7/44) in probable IE. The prevalence of splenic hypermetabolism and BM hypermetabolism in definite IE was 37.5% (6/16). A statistically significant association was found between definite IE and splenic hypermetabolism (P=0.034) and between definite IE and BM and splenic hypermetabolism (P=0.037). ***Conclusion:*** In this cohort the presence of splenic, with or without bone marrow hypermetabolism, was related to the diagnosis of IE and may be useful as an additional indirect sign to support the suspicion of IE.

EPS-051

Assessment in clinical practice of the valvular uptake index with [18F]FDG-PET/CT in patients with prosthetic valve endocarditis

S. Guzmán Ortiz*, B. Rodriguez Alfonso, K. Velásquez Díaz, I. Obedkova, M. Grajeda Gallardo;*
Puerta de Hierro University Hospital, Madrid, SPAIN.

Aim/Introduction: The uptake pattern of infective prosthetic endocarditis (PVE) with [18F]FDG-PET/CT can be visually complex and subjective. The valvular uptake index (VUI) has been proposed to improve the diagnostic performance of qualitative analysis. Our aim was to assess the outcome of its application in clinical practice. ***Materials and Methods:*** Retrospective analysis of patients with suspected PVE with [18F]FDG-PET/cardiac CT and optimal myocardial suppression from 05/2017 to 12/2018. Quantification was performed on a VOI manually adjusted over the entire 10 mm thick valvular area, and drawn on morphometabolic fusion images in a cross-sectional projection. The VUI was calculated with the formula (SUVmax-SUVmean)/SUVmax. Cut point VUI ≥ 0.45 was suggestive of PVE. Sensitivity, specificity, PPV, NPV, accuracy, precision of visual analysis and SUV was calculated. The clinical decision of the multidisciplinary endocarditis team was considered as the reference standard. ***Results:*** Sixteen patients with suspected PVE were included. In 9 patients a definitive diagnosis of PVE was made and in 7 it was ruled out. Visual PET/CT analysis showed a sensitivity of 89%, specificity 71%, PPV 80%, NPV 83%, accuracy 81% and precision 80%. Visual PET/CT analysis in the aortic valve showed sensitivity 75%, specificity 100%, PPV 100%, NPV 71%, accuracy 85% and precision 100%. In mitral valve, sensitivity 100%, specificity 75%, PPV 80%, NPV 100%, accuracy 88% and accuracy 80%.In relation to the VUI, it presented sensitivity 100%, specificity 57%, PPV 75%, NPV 100%, accuracy 81% and precision 75%. The VUI analysis in the aortic valve showed sensitivity 88%, specificity 100%, PPV 100%, NPV 83%, accuracy 92% and precision 100%. In the mitral valve sensitivity 100%, specificity 25%, PPV 60%, NPV 100%, accurancy 63% and precision 60%.Of the 9 patients with PVE, 4 had positive PET/CT (positive VUI); 1 negative PET/CT (positive VUI) and 4 doubtful PET/CT (3 had positive VUI and 1 negative VUI). Of the 7 patients without PVE, 3 had negative PET/CT (negative VUI) and 1 doubtful PET/CT (negative VUI); 2 negative PET/CT (positive VUI) and 1 positive PET/CT (positive VUI). ***Conclusion:*** The VUI showed good performance and diagnostic accuracy, especially in the aortic prosthetic valve, and clarified the doubtful cases of visual analysis. ***References:*** 1. Roque A, Pizzi MN, Fernández-Hidalgo N, et al. The valve uptake index: improving assessment of prosthetic valve endocarditis and updating [18F]FDG PET/CT(A) imaging criteria. Eur Heart J Cardiovasc Imaging. 2022;23(9):1260-1271. doi:10.1093/ehjci/jeab279.

EPS-052

Utility of PET/CT with ^{18}F-FDG for the localization of malignant and pre-malignant colorectal disease and its correlation with different microorganisms in patients studied for suspected prosthetic infective endocarditis and/or intracardiac devices.

J. Badell*, F. Gómez-Caminero López, P. García-Talavera San Miguel, J. C. Cañadas Salazar, E. Campaña Díaz, S. López Puche, S. Rama Alonso, E. Casillas Sagrado, P. Tamayo Alonso;*
Hospital Clinico Universitario de Salamanca, Salamanca, SPAIN.

Aim/Introduction: To establish the relationship between pathological ^{18}F-FDG uptake in colon and malignant/pre-malignant colorectal disease and its association with microorganisms (enteropathogenic/non-enteropathogenic) in patients studied for suspected prosthetic infective endocarditis (IE) and/or intracardiac devices (ICD). ***Materials and Methods:*** We included 122 patients with suspected IE/DIC who were referred to our service. A PET/CT study was performed with ^{18}F-FDG from the base of the skull to the thighs 60 minutes after intravenous administration of

^{18}F-FDG after myocardial suppression (diet 48-72 hours + fasting 12-18 hours + fractionated heparin at 50IU/kg). Pathological valvular foci, possible colorectal deposits and their correlation with morphological images were identified. PET/CT findings were evaluated with anatomopathological and microbiological results. ***Results:*** 84 men and 38 women (67.6 years ± 14.05 years). PET/CT detected 11 pathological deposits of ^{18}F-FDG in colorectal location. Thirty-nine underwent colonoscopy for other indications. Of these, 8 had a normal study, 14 had benign macroscopic lesions and 17 had suspicious lesions histologically studied as benign lesions (3), pre-malignant lesions (13) and malignant lesions (1). Of the 14 pre-malignant/malignant lesions, microorganisms were detected in 8, predominantly streptococci: viridans (1), gallolyticus (1), gordonii (1), staphylococci: aureus (2), haemolyticus (1) and enterobacteria: E. coli (2). Of the 11 patients with colonic deposition on PET/CT, 6 corresponded to malignant/premalignant lesions, associated with the enterococci subgroup. ***Conclusion:*** PET/CT with ^{18}F-FDG for IE/ICD study can identify, incidentally, colorectal uptake that correlates with malignant/premalignant lesions, especially in patients with streptococcal and enterobacterial bacteremia, so any hypermetabolic focus seen on PET/CT should be studied with colonoscopy and histologically.

EPS-053

The Role of [18F]FDG-PET/MRI in Patients with Large-Vessel Vasculitis

G. Argalia[1], *M. Fogante*[2], *G. Biscontini*[1], *F. M. Fringuelli*[1], *A. Palucci*[1], *C. Romagnolo*[1], *C. Cottignoli*[1], *N. Schicchi*[2], *P. Esposto Pirani*[2], *P. Fraticelli*[3], *L. Burroni*[1];
[1]*Nuclear Medicine, Department of Radiological Sciences, University Hospital of Marche, Ancona, ITALY,* [2]*Radiology, Department of Radiological Sciences, University Hospital of Marche, Ancona, ITALY,* [3]*Internal Medicine, Department of Radiological Sciences, University Hospital of Marche, Ancona, ITALY.*

Aim/Introduction: Investigate the role of [18F]FDG-PET/MRI in the management of patients with large vessel vasculitis (LVV), at different stages of the disease. ***Materials and Methods:*** We retrospectively enrolled all consecutive patients with LVV who underwent [18F]FDG-PET/MRI at our department from July 2022 to February 2023. Inclusion criteria were: 1) clinical diagnosis of LVV: Takayasu's arteritis, giant cell arteritis, aortitis and periaortitis and IgG4-related vasculitis; 2) [18F]FDG-PET/MRI performed at any time during the disease course (pre-therapy, during therapy and follow-up). [18F]FDG-PET/MRI scans were performed with a hybrid PET/MRI tomograph enabling simultaneous acquisition of PET and 3Tesla-MRI images. Contrast-agent was injected intravenously. Four PET/MRI patterns were defined: 1) Positive [18F]FDG-PET/MRI (vessel wall uptake equal-to or greater-than hepatic uptake) and positive contrast-agent-MRI (stenosis/wall thickening): active inflammation; 2) Negative [18F]FDG-PET/MRI and negative contrast-agent-MRI: normal; 3) Negative [18F]FDG-PET/MRI and positive contrast-agent-MRI: fibrous; 4) Positive [18F]FDG-PET/MRI and negative contrast-agent-MRI: metabolic. ***Results:*** Overall, 23 patients were included; 7 females and 16 males with a median age of 69 yrs. The sample was divided and analysed into three groups: 1) Pre-therapy (7 patients); 2) During therapy (15 patients); 3) Follow-up (1 patient). The four PET/MRI patterns are distributed as follows: pre-therapy: 3/7 active inflammation, 1/7 normal, 3/7 metabolic; during therapy: 8/15 active inflammation, 1/15 normal, 4/15 fibrous, 2/15 metabolic; follow-up: 1/1 fibrous. PET/MRI was able to evaluate the anatomical alterations of the vessel wall and the metabolic ones allowing, pre-therapy, an early assessment (often the metabolic alteration precedes the anatomical one); during therapy an accurate evaluation of its effectiveness (and its possible modification) distinguishing between active inflammation and fibrosis and in follow-up a possible relapse of the disease in patients with vessel walls' alterations. ***Conclusion:*** [18F]FDG-PET/MRI with contrast-agent can be useful in different phases of the clinical history of LVV. The two most important purposes of the examination were the metabolic evaluation of the disease and the exact localization of the anatomical vascular damage. The multidisciplinary approach and the fact that the two most important exams for LVV assessment are performed synchronously makes the [18F]FDG-PET/MRI with contrast-agent a very accurate exam. According to our preliminary results the [18F]FDG-PET/MRI could play a role in the management of patients with LVV.

EPS-054

Role of 18F-FDG PET/CT in patients with Hemophagocytic lymphohistiocytosis (HLH)

R. Goel, *K. Chandekar, N. A. Damle, Y. Dharmashaktu, C. Bal, R. Kumar, M. Tripathi, P. Kumar;*
All India Institute of Medical Sciences (AIIMS), New Delhi, INDIA.

Aim/Introduction: Hemophagocytic lymphohistiocytosis (HLH) is a rare, life-threatening, multi-organ disorder caused by immune system dysregulation and characterized by fever, hepatosplenomegaly, cytopenias, and progressive multiple-organ failure. HLH is often secondary to autoimmune diseases, cancers (most commonly lymphoid cancers and leukemias), or infections in contrast to familial HLH[1]. This study aims to evaluate the role of 18F-FDG PET/CT in patients with a clinical suspicion of HLH ***Materials and Methods:*** We retrospectively reviewed data of 12 patients(2 female, 10 males; age 4-52 years) with a clinical suspicion of HLH by HLH-2004 criteria[2] referred from the medicine department of our tertiary care hospital between January 2018 to April 2023. All patients underwent 18F-FDG PET/CT to identify the possible trigger for HLH and were correlated with histopathology. ***Results:*** 10/12 (83.4%) patients were found to have anemia, 11/12(91.6%) had thrombocytopenia, 6/12(54.5%) had hypertriglyceridemia. Elevated levels of ferritin were found in 10/12 (83.4%) patients. On PET/CT images, splenomegaly was found in 6 (50%) patients, out of which 5 (83.4%) had diffusely increased FDG uptake and 1(16.6 %) showed focal splenic lesions. Hepatomegaly was observed in 4/12(33.4%) patients. Diffuse bone marrow uptake in the visualized skeleton was seen in 5/12(41.6 %) patients and 2/12 (16.6%) patients showed focal increased FDG uptake in marrow. Lymphadenopathy with increased FDG uptake was seen in 7(58.3 %) patients and all had involvement of two or more nodal groups. Based on scan findings suspicious for lymphoma/leukemia, histopathological correlation was advised for 8/12 (66.7 %) patients. Of these, histopathological reports of 5/8 (62.5%) patients were positive for malignancy [HL:3 (60%), Leukemia:1 (20%), B cell lymphoma:1 (20%)] whereas histopathological reports of 3/8 (37.5%) patients did not reveal any malignancy. PET/CT images of 4/12 (33.3%) patients did not reveal any findings suggestive of underlying malignancy. ***Conclusion:*** 18F FDG PET/CT was able to correctly detect haematolymphoid malignancy in 5/12 (41.6%) patients and accurately rule it out in 4/12 (33.3%) patients, thereby benefitting 9/12 (75%) patients with clinical suspicion of HLH. Thus, it is helpful for identifying the possible trigger (particularly malignant disease), extent of disease in secondary HLH and aids in guiding site for biopsy. However, more studies on a larger patient population are required to

validate the same. ***References:*** 1.Fisman DN. Hemophagocytic syndromes and infection. Emerg Infect Dis. 2000;6(6):601-8. 2.Henter J-I, Horne A, Aricó M, Egeler RM, Filipovich AH, Imashuku S, et al. HLH-2004: Diagnostic and therapeutic guidelines for hemophagocytic lymphohistiocytosis. Pediatr Blood Cancer. 2007;48(2):124-31.

EPS-055

Establishing The Ideal Time Point In Imaging Patients With ^{99m}Tc-Ethambutol Scintigraphy In Extrapulmonary Tuberculosis

D. Khan, *N. A. Damle, S. Sagar, A. Ghazal, V. Tiwari, C. Bal, M. Tripathi, S. Sikdar, P. Ranjan, V. Manhas, P. Kumar;*
AIIMS Delhi, Delhi, INDIA.

Aim/Introduction: Tc99m labelled ethambutol (EMB) is a non-invasive modality to image tuberculosis, however there is scarce literature to suggest optimal scan time, resulting in few serial images till 6-24 hours. We aimed to identify ideal time point for imaging of tubercular lesions in Tc99m ethambutolscintigraphy in order to reduce number of scans acquired to single time point. ***Materials and Methods:*** We prospectively studied 24 tuberculosis (20 confirmed, 4 suspected) over 1 year in our center. Patients were injected with 10mCi of radiolabelled 99mTc-ethambutol and serial whole-body scans were acquired on SPECT/CT gamma camera. Scans were acquired as 5 min dynamic and static images over 15, 30 and 45 min and 1,2,4 ,6,12 and 24 hrs. We attempted to acquire atleast 4 sets ofimages. SPECT/CT scan was acquired at time of peak uptake in known pathologic lesion. Any abnormal focus of uptake outside known normal biodistribution of the drug was considered positive. ***Results:*** Mean age of patients was 39.7±13.2 with 11 male and 13 female patients. Ethambutol (EMB) was successfully labelled with 99mTc with a mean labelling efficiency of 95±1.5%(n=24) with optimal QC. In 20 clinically diagnosed patients, 16 had bone (80%), 2 lymph nodal(10%) and 2 had abdominal TB(10%) .Out of 16 patients with bone TB, 6 patients had spinal TB, 1 had sternal TB, 5 had Knee TB, 1 had elbow, 2 had hip TB and 1 had femoral TB. Ideal time points for imaging of tubercular lesions using EMB scan were assessed visually and quantitively. On visual analysis, 9 out of 20 (45%) patients showed ideal time point at 45 min post injection of 99mTc-EMB. Rest of the patients showed optimal uptake with adequate background clearance at 1 hr(5/20,25%), 2hr (4/20,20%) and 4 hr (2/20, 10%) post injection. Quantitative analysis was done by calculating lesion to background ratios (LBR) over serial time point images. Region of interests (ROI) were drawn over lesion and liver (background). We found that in 20 positive cases, highest mean LBR ratios was 3.3±2.8 obtained at 1 hr image post injection with significant p value of 0.008($p<0.05$) using Kruskal Wallis Test. ***Conclusion:*** Ideal time point for 99mTc-EMB scintigraphy evaluated through qualitative and quantitative analysis for visualization of bone lesions in tuberculosis is 45-60 minutes after injection of 99mTc-Ethambutol and a single whole body image acquired at this time point appears sufficient for evaluation of tubercular lesions.

EPS-056

^{18}F-FDG PET/CT metabolic parameters as predictors of immune status and disease severity in the patients with non-tuberculous mycobacteria

D. Chen[1], *Y. Chen*[2], *S. Yang*[1], *T. Li*[1], *K. Liu*[1], *Z. Wang*[1], *T. Zhang*[1], *G. Wang*[1], *K. Zhao*[1], *X. Su*[1];
[1]*Department of Nuclear Medicine, The First Affiliated Hospital, Zhejiang University School of Medicine, Hangzhou, CHINA,* [2]*State Key Laboratory for Diagnosis and Treatment of Infectious Diseases, Hangzhou, CHINA.*

Aim/Introduction: Non-tuberculous mycobacteria (NTM) infection is an increasing health problem due to delaying an effective treatment. The decision of therapy strategy relies strongly on the immune status, extent of lesion involvement, and disease severity in NTM patients. However, there is very little data on the use of imaging methods including ^{18}F-FDG PET/CT for predicting these risk factors of NTM treatment. Herein, the aim of the present study was to investigate predictive value of ^{18}F-FDG PET/CT for evaluating immune status, extent of lesion involvement and disease severity in NTM patients. ***Materials and Methods:*** A total of 23 patients with confirmed diagnosis of NTM infection who underwent ^{18}F-FDG PET/CT imaging were analyzed retrospectively. The clinical data, including the patients' immune status, lesion distribution, severity of NTM pulmonary disease (NTM-PD), clinical manifestation, and laboratory examination, and ^{18}F-FDG PET/CT imaging characteristics were reviewed. ^{18}F-FDG PET/CT images were analyzed visually and semi-quantitatively by measuring maximum standardized uptake value (SUV_{max}), SUV_{max} of the most FDG-avid lesion (SUV_{Top}), the most FDG-avid lesion-to-liver SUV_{max} ratio (SUR_{Liver}) , the most FDG-avid lesion-to-blood pool SUV_{max} ratio (SUR_{Blood}), metabolic lesion volume (MLV) and total lesion glycolysis (TLG).The optimal cut-off of ^{18}F-FDG was determined using receiver operating characteristic curve (ROC). ***Results:*** Of the 23 patients with NTM infection, there were 6 patients (26.09%) with localized pulmonary diseases and 17 patients (73.91%) with disseminated diseases. Moreover, among these patients, there were a total of 22 cases with lung involvement, 17 cases with extra-pulmonary involvement. These involved lesions had high or moderate ^{18}F-FDG uptake (median SUV_{Top}: 8.2±5.7). For the patients' immune status, the median SUV_{Top} in immunocompromised and immunocompetent patients was 10.0 and 5.2, and the difference was significant (P=0.038). As for the distribution of NTM lesions, SUR_{Liver} and SUR_{Blood} in localized pulmonary and disseminated diseases were 1.9 vs.3.8, and 2.7 vs. 5.5, respectively, with significant difference (P=0.016 and 0.026). Moreover, For the severity of NTM-PD, SUV_{max} of lung lesion ($SUV_{l\text{-}lung}$), SUV_{max} of marrow (SUV_{Marrow}), platelet count in the severe group were 7.7, 4.4, and 314.0±119.3×10^9/L, respectively, and significantly higher than those in the non-severe group (4.3, 2.4 and 194.3±73.1×10^9/L) (P= 0.027, 0.036 and 0.003). ***Conclusion:*** ^{18}F-FDG PET/CT is a unique and powerful tool in the diagnosis, evaluation of lesion activity, immune status and extent of lesion involvement in the NTM patients and can contribute to planning the appropriate treatment of NTM.

EPS-057

Correlation of Total Lesion Glycolysis with Inflammatory and Immune Biomarkers in Talaromyces Marneffei Infection Patients: A Cross-sectional and Longitudinal FDG PET/CT Study

W. Bao[1], *X. Zhang*[1], *Q. Huang*[1], *S. Ren*[1], *F. Hua*[2], *C. Zuo*[1], *F. Xie*[1], *Y. Guan*[1];
[1]*Huashan Hospital, Shanghai, CHINA,*
[2]*Longhua Hospital, Shanghai, CHINA.*

Aim/Introduction: Talaromyces marneffei (T. marneffei) is an emerging opportunistic fungal infection, particularly affecting immunocompromised patients. Accurate evaluation of disease activity and response to treatment is essential for optimal patient management. This study aims to investigate the correlation between total lesion glycolysis (TLG) derived from FDG PET/CT and inflammatory and immune biomarkers in patients with T. marneffei infection. Additionally, the study provides a longitudinal assessment of these parameters, including three post-treatment follow-ups, to evaluate the potential of TLG as a non-invasive imaging biomarker for disease monitoring and treatment response evaluation. ***Materials and Methods:*** Eighteen patients diagnosed with T. marneffei infection underwent a baseline FDG PET/CT scan, out of which three had follow-up scans after the initiation of treatment. Quantitative PET parameters, including TLG, were obtained from each lesion group. Inflammatory and immune biomarkers, such as CRP, ESR, and IgG level, were collected concurrently with imaging. Pearson correlation coefficients were calculated to assess the relationship between TLG and biomarkers at baseline and follow-up time points. Paired t-tests were performed to evaluate the changes in TLG and biomarkers between the baseline and follow-up scans for the three patients with follow-up data. ***Results:*** At baseline, significant correlations were observed between TLG and inflammatory and immune biomarkers (CRP, ESR, and CD4+ T-cell counts) in the 18 patients (CRP: r=0.66, p=0.001; ESR: r=0.83, p<0.001; IgG level: r=0.80, p<0.001). In the three patients with follow-up data, paired t-tests demonstrated significant changes in TLG ($t(2) = 4.92$, p<0.001) and biomarker levels between the baseline and post-treatment scans (CRP: $t(2) = 5.41$, p<0.001; ESR: $t(2) = 6.23$, p<0.001; IgG level: $t(2) = 4.87$, p<0.001). These changes suggest a strong association between TLG and the patients' response to treatment, as evidenced by the alterations in inflammatory and immune biomarker levels. ***Conclusion:*** This study demonstrates a significant correlation between TLG derived from FDG PET/CT and inflammatory and immune biomarkers in patients with Talaromyces marneffei infection. The results also suggest that TLG may serve as a potential non-invasive imaging biomarker for disease monitoring and treatment response evaluation in these patients. The findings, however, are limited by the small number of patients with follow-up data. Further studies with larger cohorts and multiple follow-up time points are needed to confirm the utility of TLG in evaluating disease progression and response to therapy in Talaromyces marneffei infection.

EPS-058

Head-to-head comparison of ^{18}F-FDG PET and labelled leucocyte scintigraphy for the monitoring of treatment response in malignant external otitis

S. Melki[1], *M. Hurstel*[1], *A. Vasseur*[2], *D. Nguyen*[2], *C. Rumeau*[2], *A. Verger*[1,3];
[1]*Department of Nuclear Medicine and Nancyclotep, University Hospital of Nancy, Nancy, FRANCE,* [2]*Department of ENT, University Hospital of Nancy, Nancy, FRANCE,* [3]*IADI, INSERM, UMR 1254, Université de Lorraine, 54000, Nancy, FRANCE.*

Aim/Introduction: Malignant external otitis (MEO) is a rare disease associated with high morbidity-mortality, with no currently available consensus concerning the imaging modality to apply to assess the treatment response. The aim of this study is to directly compare the diagnostic performances of ^{18}F-FDG PET and labelled leucocyte scintigraphy (LS) for the monitoring of treatment response in MEO ***Materials and Methods:*** Consecutive patients with MEO performed a ^{18}F-FDG PET scan, at least one week after the end of antibiotic therapy, as well as planar and SPECT labelled leucocyte scintigraphy within one month of delay. Semi-quantitative analyses were performed with calculation of ratios of affected/non-affected sides for PET, 4h and 24h LS time acquisitions as well as kinetic of ratios in PET (at diagnosis and after treatment) and LS (4h-24h). The final treatment response was assessed by two experimented ENT physicians gathering clinical, otoscopic and biological information. ***Results:*** Seventeen patients (74.0 ±10.6 years old, 5 women) were included in this longitudinal study. The best diagnostic performances were obtained with SUV_{max}-lesion-to-background ratio in PET and lesion-to-background ratio in 4h time acquisitions in LS (respective thresholds of 4.1, 1.05 in planar and 1.11 in SPECT with 94%, 94% and 88% of accuracies). In multivariate analysis, SUV_{max}-lesion-to-background ratio in PET was the only predictive factor of non-treatment response when associated to all clinical parameters (p=0.003). ***Conclusion:*** ^{18}F-FDG PET is a widely accessible imaging modality for evaluating the treatment response in MEO, with high diagnostic performances, equivalent to those of LS. 4h time acquisitions with LS seem to be sufficient to evaluate the treatment response in MEO.

EPS-059

Dynamic [^{18}F]FDG PET/CT imaging with a LAFOV PET/CT camera system to differentiate between infection and inflammation.

N. D. van Rijsewijk, *J. H. van Snick, F. F. A. Ijpma, M. Wouthuyzen-Bakker, J. van Sluis, A. W. J. M. Glaudemans;*
University Medical Center Groningen, Groningen, NETHERLANDS.

Aim/Introduction: [^{18}F]FDG PET/CT is commonly used for imaging infection and inflammation in nuclear medicine. However, distinguishing infection from inflammation on static images after 1 hour post injection can be challenging. In this study, we aim to differentiate between infection and inflammation by leveraging dynamic imaging. ***Materials and Methods:*** Patients referred to the nuclear medicine department with suspected infection or inflammatory disease were dynamically scanned on a long axial field of view (106 cm) PET/CT system for 65 minutes immediately following [^{18}F]FDG injection. PET data were reconstructed using 31 frames as follows: 6x10 sec, 3x20 sec, 6x30 sec, 5x1 min, 11x5 min. Additionally, static images were reconstructed from the last 3 min. All images were reconstructed using both clinically optimized settings (CLIN) and European Association of Nuclear Medicine Research Ltd. (EARL) standard 2 settings (EARL2). Volumes of interest were drawn at various locations: infection and inflammation sites, spleen, liver, aorta, bone marrow in L5 and/or iliac crest, femoral artery, gluteus muscle and caput femoris. Time activity curves (TACs) were generated based on the dynamic reconstruction, and standardized uptake values (SUVs) were calculated at CLIN and EARL2 reconstructions after correction for blood glucose, following EANM guidelines. ***Results:*** To date, a total of three infection sites (2 fracture related infections and 1 lead infection of a left ventricular assist device) and four inflammation sites were identified in four patients. For EARL2 reconstructed images, SUV_{peak} for infection sites was 2.94, 6.50 and 6.89, and 3.19, 7.01 and 8.22 for CLIN reconstructed images. For inflammation sites, SUV_{peak} ranged between 1.56 - 4.02 (EARL2) and 1.73 - 3.45 (CLIN). The increase in SUV_{peak} from 30 - 65 minutes post-injection was at least 10% (10%, 26%, and 31%, absolute:

0.41, 2.05, and 1.96 SUV, respectively) for EARL2 reconstructed images and at least 18% (18%, 28%, and 37%, absolute: 0.81, 2.30, and 2.65 SUV, respectively) for CLIN reconstructed images for infection sites, both with a clear increasing slope. In contrast, for inflammation sites, the percentual increase or decrease in SUV_{peak} during the same time frame showed a more stagnating curve and a more erratic pattern: from -1% to 5% (absolute: -0.04 - 0.17 SUV) on EARL2 images and from -5% to 3% (absolute: -0.10 - 0.11 SUV) on CLIN images. ***Conclusion:*** Preliminary results show that TACs might be helpful to differentiate infection from inflammation using the increase of [^{18}F]FDG uptake in time.

EPS-060

Exploring the clinical ambit of ^{68}Ga-NOTA-UBI PET/CT as an infection imaging technique

N. Damle, *Y. Dharmashaktu, A. Singhal, S. Ballal, R. Goel, S. D. Maurya, V. Tiwari, A. Gawande, S. Sagar, J. Jaleel, C. Bal, M. Ansari, V. Kumar;*
All India Institute of Medical Sciences, New Delhi, INDIA.

Aim/Introduction: Ubiquicidin (UBI) is a cationic antimicrobial peptide with tremendous potential for imaging of infectious diseases as it helps in differentiating between sterile inflammation and various infections. Here we have labelled UBI with chelator NOTA complexed with Ga-68 and used the radiolabelled compound to look for infective etiology in clinically challenging scenarios. ***Materials and Methods:*** Labelling of UBI conjugated with NOTA and Ga-68 was optimized at 95°C, pH of 4-5 with the radiochemical purity of at least 95% and higher. We retrospectively reviewed the ^{68}Ga-NOTA-UBI scans of 22 patients (5 female, 17 male; age range 23-65 years) between January 2022 to March 2023 done at our institution. Patients were injected with 3-5 mCi of ^{68}Ga-NOTA-UBI intravenously and early whole body and delayed regional PET/CT images were acquired at 45-60 mins and 90 mins post injection respectively. Lesions were graded as positive, suspicious and negative for infection by three independent Nuclear Medicine physicians. ***Results:*** Normal tracer biodistribution was visualized in cardiac blood pool, liver, kidneys, bladder and occasionally in spleen & rarely in marrow. Out of 22 patients, 9/22 were referred with a suspicion of orthopedic implant associated infection, 6/22 to differentiate between malignancy & infection, 1/22 for pyrexia of unknown origin (PUO), 1/22 for suspected aspergilloma and 5/22 for miscellaneous infections. 7/9 (77.7%) patients with implant associated infection suspicion showed significant increased soft tissue tracer uptake around the implant and were interpreted as positive for infection while 2/9 were reported suspicious. Of the 6 scans done for differentiating infection from malignancy, 2/6 were reported as positive for infection, 3/6 as negative and 1 patient was reported equivocal. 1 patient who was referred for PUO evaluation had multiple focal marrow lesions with increased tracer uptake suggestive of infection. 1 patient with clinical suspicion of aspergillosis was reported positive for infection involving right orbit and right lung. Out of 5 scans done for miscellaneous infections 3/5 were positive while 2/5 were suspicious and negative for infection respectively. ***Conclusion:*** ^{68}Ga-NOTA-UBI is a promising PET/CT imaging agent for detecting orthopedic implant associated infection with a strong evolving role in distinguishing infective and non-infective pathology. However, studies on a larger patient cohort are required to validate the same and establish its definitive role.

EPS-061

Correlation Between Emotional and Psychological Symptoms and Brain Glucose Metabolism on PET/CT in Patients with Long Covid

L. Wichert-Ana, *D. L. Ferreira, L. E. Lopes-Santos, A. C. Trevisan, G. D. Angelis, J. S. Sakamoto, B. G. Coretti, L. Alexandre-Santos, M. P. Foss, O. Y. Fukumori, M. Kato, F. A. Pitella, V. Tumas, F. B. Rodrigues;*
Ribeirão Preto Medical School - University of São Paulo, Ribeirao Preto, BRAZIL.

Aim/Introduction: The SARS-CoV-2 pandemic is a global health problem characterized by multiple variants, different levels of severity and high morbidity. Persistent symptoms after the acute phase of COVID-19 have been reported, including post-traumatic stress disorder, mood and anxiety disorders, fibromyalgia, and chronic fatigue syndrome. Most of these symptoms may be related to the infection itself, the way of coping with the disease or the stress generated by the pandemic. However, the topography and pathophysiology of post-COVID brain involvement, whether due to the neuro-infection or clinical and therapeutic factors, are still not entirely known. This study correlated psychological and emotional symptoms with brain glucose metabolism changes in PET/CT in long COVID patients. ***Materials and Methods:*** Twenty-two patients with persistent cognitive complaints after mild COVID and 20 healthy controls underwent psychological assessment and [18F]FDG brain PET/CT. The psychological evaluation measured levels of executive dysfunction, anxiety and depression symptoms, and physical and mental fatigue. PET/CT data were modelled by CortexID software. ***Results:*** Mann-Whitney U test revealed significant differences between groups in all psychological variables, with greater severity of self-reported symptoms in the mild COVID group compared to healthy controls. We observed negative correlations between left anterior cingulate cortex (ACC) metabolism and symptoms of anxiety (ρ = -0.305, p = 0.049), physical fatigue (ρ = -0.351, p = 0.023), and executive dysfunction (ρ = -0.304, p = 0.050). Our results support the hypothesis of different patterns of ACC activation in response to threat and anticipatory anxiety, in which hypervigilance to external stimuli was associated with ventral ACC deactivation. ***Conclusion:*** The anatomoclinical correlations evidenced by brain PET/CT may help understand the pathophysiology of neuropsychiatric disorders and contribute to therapeutic strategies for the psychological symptoms associated with Long COVID. ***References:*** Straube, T., Schmidt, S., Weiss, T., Mentzel, H. J., & Miltner, W. H. (2009). Dynamic activation of the anterior cingulate cortex during anticipatory anxiety. Neuroimage, 44(3), 975-981.

EPS-062

Brain Perfusion SPECT, DAT SPECT, and [18F]FDG PET/CT and PET/MRI Findings in Patients with Long COVID

L. Wichert-Ana[1], *L. S. C. Wellingta*[1], *L. E. Lopes-Santos*[1], *K. J. C. C. Lacerda*[1], *V. R. Sá*[2], *F. E. Padovan-Neto*[2];
[1]*Ribeirão Preto Medical School - University of São Paulo, Ribeirao Preto, BRAZIL,* [2]*Department of Psychology, Faculty of Philosophy, Sciences and Letters of Ribeirão Preto, University of São Paulo, Ribeirao Preto, BRAZIL.*

Aim/Introduction: Prolonged COVID-19 affects patients after the acute phase of infection, beyond 12 weeks, with persistent symptoms such as fatigue, cognitive dysfunction, and respiratory difficulties. In addition, the virus demonstrates neurotropism, causing neurological and psychiatric disorders. This study aims to review the main findings of perfusion

SPECT, DAT SPECT, and [18F]FDG PET/CT brain in patients with neuropsychiatric manifestations of long COVID. ***Materials and Methods:*** A systematic literature review was conducted in the PUBMED, SCOPUS, and EMBASE databases, searching for articles published on brain findings post-COVID-19 and up to 02/12/2022. The keywords "COVID-19 And PET/CT And BRAIN" and "COVID-19 And SPECT And BRAIN" were entered in the search fields. After excluding publications relating to non-brain studies, the search resulted in 05 articles on cerebral SPECT and 15 articles on cerebral PET/CT in Long COVID. ***Results:*** Perfusion SPECT findings in patients with Long COVID showed hyperperfusion in the cerebellum and diffuse hypoperfusion, especially in the frontal lobes, which recovered after a few months. Studies with tracers for dopaminergic transporters demonstrated reduced DAT density in the striatum, worse in the putamen and on the left side. In addition, the [18F]FDG PET/CT and PET/MRI findings demonstrated areas of glycolytic hypometabolism in various brain regions (frontal lobes, temporal lobes, left insula, and diffuse areas in the parietal and occipital lobes). Moreover, brain regions with glycolytic hypermetabolism were also observed, mainly in the cerebellum, subthalamic nucleus, and right thalamus. ***Conclusion:*** Perfusion SPECT, DAT SPECT, and cerebral PET/CT contribute to the evaluation of brain changes associated with prolonged COVID-19, allowing quantification of regional cerebral blood flow and regional cerebral glucose metabolic rate. Changes in cerebral SPECT are milder than those described in PET/CT and PET/MRI, possibly due to the lower spatial resolution of the technique. These findings help understand the pathophysiology of neuropsychiatric manifestations of Long COVID and guide future therapeutic strategies.

510

Sunday, September 10, 2023, 3:00 PM - 4:30 PM
Hall K

Technologists Oral Presentations 1: SPECT-CT in Diagnosis and Therapy

OP-177

Deep learning-based abnormality classification in ^{123}I-ioflupane SPECT imaging

T. Yamao, *R. Yamakuni, N. Takahashi, K. Miwa, Y. Kaneko, N. Miyaji, H. Ito;*
Fukushima Medical University, Fukushima, JAPAN.

Aim/Introduction: Diagnosis of dopamine transporter (DAT) single-photon emission computed tomography (SPECT) imaging is based on visual interpretation combined with quantitative analysis. Quantitative analysis evaluates the specific binding to DAT in the striatum. However, quantitative assessment of the spatial distribution of striatal accumulation remains to be established. The present study aimed to develop a deep learning system to discriminate abnormalities in striatal accumulation on DAT SPECT. ***Materials and Methods:*** The subjects were 60 DAT SPECT images (normal; 23, abnormal; 37). All images were anatomically standardized by ^{123}I-ioflupane template [1]. The area surrounding of the striatum was cropped from the whole brain. Seven continuous images were used as input to a convolutional neural network. The network was based on pre-trained VGG19 model, and fine-tuning was performed on 840 images from 60 subjects with data augmentation by horizontal flipping. An ensemble of seven axial slices of VGG19 was used to determine normal and abnormal. Classification performance was evaluated using five-fold cross-validation. Receiver operating characteristic (ROC) analysis was performed to compare the area under the curve (AUC), VGG19, specific binding ratio (SBR) and asymmetry index (AI). A heat map based on the gradient-class activation map (Grad-CAM) was generated to demonstrate how the VGG19 model classified the DAT SPECT image. ***Results:*** The proposed method exhibited an accuracy of 91.9%, sensitivity of 91.1%, and specificity of 94.1%, as determined by the five-fold cross-validation method. The AUC values for VGG19, SBR, and AI were 0.898, 0.919, and 0.872, respectively. In the normal subject, the heat map displayed activation in only a narrow region of the striatum, whereas in the abnormal subject, activation was observed in a broader region around the striatum. ***Conclusion:*** The proposed method allowed to discriminate normal and abnormal images in DAT SPECT images with high accuracy. Our current system might provide reliable support for diagnosing patients with parkinsonism. ***References:***
García-Gómez FJ, García-Solís D, Luis-Simón FJ, et al. Elaboration of the SPM template for the standardization of SPECT images with 123I-Ioflupane. Rev Esp Med Nucl Imagen Mol. 2013;32(6):350-356.

OP-178

Quantitative evaluation of SPECT/CT performance for therapeutic Lu177 radionuclide with NEMA standards

P. Dwivedi[1], *V. Sawant*[1], *A. Jha*[2], *V. Rangarajan*[2];
[1]*Advanced Centre for Treatment Research and Education In Cancer, Mumbai, INDIA,* [2]*Tata Memorial Hospital, Mumbai, INDIA.*

Aim/Introduction: The use of quantitative SPECT/CT imaging for targeted radionuclide therapy with 177Lu holds excellent potential for developing imaging based personalized dose assessment. The study aims to evaluate the quantitative performance of SPECT/CT and its effect on image quality parameters for 177Lu by utilising standard NEMA image quality phantom and PET/CT quality assurance methodology. ***Materials and Methods:*** The study was performed on a dedicated SPECT/CT system using a NEMA standard image quality phantom having 6 sphere inserts (inner diameter 10, 13, 17, 22, 28, and 37 mm) and a lung insert. Except for the largest 37 mm sphere (filled with water), all other spheres were filled with an activity 177Lu concentration of 440 kBq/mLmL.At minimum three degree angle and for minimum of 30 seconds per projection, the phantom images were collected with a four spheres to background activity concentration ratio (no background,1:4, 1:8, 1:16). Also, the accuracy of attenuation correction was determined using lung insert. The attenuation corrected images reconstructed with OSEM iterative reconstruction method were analysed. The region of interest (ROI) was drawn in a transverse image slice containing the sphere's center and adjacent slices, calculating average counts in the sphere. Percent contrast recovery was calculated for each sphere to background ratio. A total of 12 ROI for each sphere diameter were drawn in central and adjacent slices for background variability assessment for each hot sphere to background ratio. ***Results:*** The highest percent contrast recovery in hot sphere was observed in the 28 mm sphere for a 16:1 hot sphere to background ratio, whereas the 10 mm sphere shows the least per cent recovery ranges in all sphere to background ratios. The background variability was maximum for the 10 mm sphere diameter and the least was noted for the 28 mm sphere. The 37 mm cold spheres show highest contrast recovery in all sphere volumes. The highest lung error was seen in no background concentration ratio images. The

maximum lung error was seen in the 16:1 sphere to background concentration ratio. ***Conclusion:*** The study results show that percent contrast increases with an increase in the sphere size where there is significant effect of background concentration on percent contrast recovery and background variability.The results indicates overall good quantitative performance of SPECT CT for therapeutic radionuclide 177Lu when experimented with NEMA standards. This also concludes that NEMA methodology for PET/CT can be applied to SPECT/CT for quality assurance tests.

OP-179

Broad quantification calibration of various isotopes for quantitative analysis and the assessment of their SUVs in a SPECT/CT scanner

H. Ko, *J. Choi, S. Park;*
Asan Medical Center, Seoul, KOREA, REPUBLIC OF.

Aim/Introduction: Broad Quantification Calibration(B.Q.C) is used for the quantitative analysis of the Standard Uptake Value(SUV) in a SPECT/CT scanner. B.Q.C was performed for Tc-99m, I-123, I-131 and Lu-177, then we acquired the phantom images to ascertain whether the SUVs were measured accurately. Because there is no standard method for assessing SUV in SPECT, we used the ACR Esser PET phantom alternatively. The purpose of this study was to lay the groundwork for the quantitative analysis with various isotopes in a SPECT/CT scanner. ***Materials and Methods:*** Symbia Intevo 16 and Intevo Bold SPECT/CT scanners were used for this study. The B.Q.C procedure has two steps: the first is point source sensitivity cal. and the second is volume sensitivity cal. to calculate the volume sensitivity factor(VSF) using a cylinder phantom. To verify the SUVs, we acquired the images using the ACR Esser PET phantom, then we measured the SUV_{mean} on background and SUV_{max} on hot vials(25, 16, 12 and 8 mm). The SPSS software was used to perform Mann-Whitney test to analyze the difference in the SUVs obtained using the Intevo 16 and Intevo Bold. ***Results:*** The results of sensitivity(CPS/MBq) for Detector 1, 2 and VSF were as follows(Intevo 16 D1 sensitivity/D2 sensitivity/VSF and Intevo Bold); 87.7/88.6/1.08 and 91.9/91.2/1.07 for Tc-99m, 79.9/81.9/0.98 and 89.4/89.4/0.98 for I-123, 124.8/128.9/0.69 and 130.9/126.8/0.71 for I-131, 8.7/8.9/1.02 and 9.1/8.9/1.00 for Lu-177, respectively. The results of the SUV assessment using the ACR PET phantom were as follows(Intevo 16 BKG SUV_{mean}/25mm SUV_{max} /16mm/12mm/8mm and Intevo Bold); 1.03/2.95/2.41/1.96/1.84 and 1.03/2.91/2.38/1.87/1.82 for Tc-99m, 0.97/2.91/2.33/1.68/1.45 and 1.00/2.80/2.23/1.57/1.32 for I-123, 0.96/1.61/1.13/1.02/0.69 and 0.94/1.54/1.08/0.98/0.66 for I-131, 1.00/6.34/4.67/2.96/2.28 and 1.01/6.21/4.49/2.86/2.21 for Lu-177, respectively. The SUVs obtained using the Intevo 16 and Intevo Bold showed no statistically significant difference($p>0.05$). ***Conclusion:*** In the past, only qualitative analysis was possible using a gamma camera. On the other hand, it is possible to not only acquire anatomic localization, 3D tomography, but also achieve the quantitative analysis of the SUVs in SPECT/CT scanners. We could lay the groundwork for quantitative analysis of various isotopes, such as Tc-99m, I-123, I-131 and Lu-177 by B.Q.C and verify the accuracy of SUV measurements using the ACR phantom. Moreover, periodic calibration is necessary to maintain the precision of the quantitative evaluation. Thus, we can perform the quantitative analysis of isotopes in follow-up scans obtained using the SPECT/CT examinations and evaluate therapeutic responses in theranostics.

OP-180

Differential Diagnosis of Lewy Body Dementia andAlzheimer's Disease in ECD SPECT Images Using 2D and 3D CNN Methods

Y. Ni[1], *Z. Lin*[1], *S. Tsen*[1], *M. Pai*[2], *P. Chiu*[3], *G. Hung*[4], *K. Lin*[5], *I. Hsiao*[6], *C. Chang*[7], *Y. Chang*[8];
[1]*Health Physics Division, Institute of Nuclear Energy Research, Atomic Energy Council, Taoyuan, TAIWAN,* [2]*Alzheimer's Disease Research Center, National Cheng Kung University Hospital, Taiwan, TAIWAN,* [3]*Department of Neurology, Show Chwan Memorial Hospital, Changhua, TAIWAN,* [4]*Department of Nuclear Medicine, Chang Bing Show Chwan Memorial Hospital, Changhua, TAIWAN,* [5]*Department of Nuclear Medicine and Molecular Imaging Center, Linkou Chang Gung Memorial Hospi-tal, Taoyuan, TAIWAN,* [6]*Department of Medical Imaging and Radiological Sciences & Healthy Aging Center, Chang Gung University, Taoyuan, TAIWAN,* [7]*Department of Neurology, Kaohsiung Chang Gung Memorial Hospital, Kaohsiung, TAIWAN,* [8]*Department of Neurology, Institute of translational research in biomedicine, Kaohsiung Chang Gung Memorial Hospital, Chang Gung University College of Medicine, Kaohsiung, TAIWAN.*

Aim/Introduction: The purpose of this study was to evaluate the differential diagnostic performance of 2D and 3D CNN deep learning models on Tc-99m ECD SPECT images of Alzheimer's disease (AD) and Lewy Body Dementia (LBD). ***Materials and Methods:*** Since Taiwan's insurance pays Tc-99m ECD SPECT for the diagnosis of dementia, in order to facilitate future clinical application scenarios, this study was conducted using the brain nuclear medicine imaging database established in Taiwan, which includes 4 hospitals. In order to balance the amount of training data, Tc-99m ECD SPECT images of 112 AD patients and 127 LBD patients were selected. The method of image standardization was to perform spatial normalization through SPM5 software and use the whole cerebellum as a reference region for intensity normalization. We used 2D and 3D convolutional neural networks for the AD/DLB classification task, where the 2D model used the InceptionV3 pre-trained model for transfer learning, and the 3D model used composed of 4 layers of 3D convolutional layer architecture. 90% of all the data was used as a training set, and the other 10% was used as an independent test set. And used 5-fold cross-validation to reduce the issues of overfitting and selection bias. During the training process, the t-SNE method was used to visualize the data distribution of the classification. The performances of the models were analyzed by indicators such as sensitivity, specificity, precision, accuracy, and F1 score. ***Results:*** As shown in Table 1, the performances of the AD/LBD classification task on the independent test set using the 2D and 3D CNN models. In the 2D CNN model, the sensitivity for detecting LBD was 1.0, the specificity was 0.77, the precision was 0.79, the accuracy was 0.88, and the F1 score was 0.88; in the 3D CNN model, the above indicators were 1.0, 0.85, 0.85, 0.92, and 0.92, respectively. ***Conclusion:*** In this study, using Tc-99m ECD SPECT images, both 2D and 3D CNN deep learning models can distinguish the two most common neurodegenerative diseases AD and LBD. The research results show that the performance of the 3D CNN model is better than that of the 2D CNN model, which might due to the relatively complete preservation of the spatial relationship of the 3D image.

OP-181

Validation of dramatic CT topogram dose reduction with use of tin filter

K. Christensen[1], *P. C. Holdgaard*[1], *L. L. Østergård*[1], *N. A. Bebbington*[2];
[1]*Lillebaelt University Hospital, Vejle, Vejle, DENMARK,*
[2]*Siemens Healthcare A/S, Aarhus, DENMARK.*

Aim/Introduction: The CT tin (Sn) filter reduces unnecessary dose compared with conventional filtration. Saltybaeva et al. (1) found optimal Sn-topogram settings of Sn100kV/75mA in abdominal phantoms, providing large dose savings compared to non-Sn topograms. However, scan ranges outside the abdomen are often performed in PET-CT and SPECT-CT. The aim was to find the optimal Sn-topogram settings for ranges outside the abdomen. ***Materials and Methods:*** The Kyoto Kagaku adult whole-body phantom was scanned on a PET-CT system with standard and obese habitus, with several Sn-topogram (Sn140kV/Sn100kV and 75mA/20mA) and non-Sn topogram settings (20mA with 100kV/120kV (conventional reference)/140kV). Dose Length Product (DLP) was recorded for each topogram. To evaluate effect on tube current modulation, CT scans were made after each topogram, and mAs-profiles plotted (Z-direction). To determine effect on visual identification of anatomical landmarks for planning scan ranges, 16 landmarks were scored for visibility on a scale of 1-3. 4 metal objects were placed on the phantom (1 abdominal, 2 thoracic, 1 mandibular), to determine visibility for applying Metal Artefact Reduction. Landmarks and metal artifacts were evaluated by one trained observer. All findings were compared to the conventional reference. ***Results:*** DLP (mGy.cm) for the conventional reference (120kV/20mA) was 4.8. DLP was reduced with settings of 100kV/20mA (2.6mGy.cm), Sn140kV/20mA (1.6mGy.cm), Sn100kV/75mA (1.1mGy.cm) and Sn100kV/20mA (0.3mGy.cm), representing dose savings of 46%, 67%, 77% and 94% respectively. For standard and obese patients, all mAs profiles were comparable to the conventional reference, apart from in the abdominal scan range at Sn100kV/20mA for the obese patient, showing mAs reduction of up to 10%. Similarly, Sn100kV/20mA did not allow visualization of the abdominal metal object in standard and obese modifications. All other ranges and settings showed all metal objects. At Sn100kV/20mA for the standard patient, visibility of 14/16 landmarks were comparable with the conventional reference, whilst visibility of the scapulae and the bottom of the liver were reduced, and for the obese patient, visibility of the lumbar spine and iliac crests were reduced in addition. ***Conclusion:*** Sn100kV/75mA should be used for scan ranges which include the abdomen, providing 77% topogram dose saving compared with the conventional reference. However, if the scan range does not include the abdomen, Sn100kV/20mA appears to be adequate, and saves an additional 73% topogram dose compared with Sn100kV/75mA. ***References:*** 1.Saltybaeva N,Krauss A,Alkadhi H. Technical note: radiation dose reduction from computed tomography localizer radiographs using a tin spectral shaping filter. Med Phys. 2019;46(2):544-549.

OP-182

Clinical Application of SPECT Phantoms Created Using Paper Phantoms

T. Nagahara[1], *T. Katafuchi*[2], *T. Inagaki*[1], *R. Isobe*[1], *K. Kato*[1];
[1]*Nagoya University Graduate School of Medicine, Nagoya, JAPAN,* [2]*Gifu University, Gifu, JAPAN.*

Aim/Introduction: In recent years, single-photon emission computed tomography (SPECT) research has become mainstream in nuclear medicine, with increasing use of three-dimensional phantoms. In contrast, two-dimensional paper phantoms are restricted for evaluating planar images because they lack thickness and cannot be easily applied to three-dimensional SPECT images. However, previous studies have shown that paper phantoms can be applied in SPECT evaluation and that 3D images can be delineated from 2D images. This study examined the optimal conditions for evaluating SPECT images using a SPECT phantom created from paper phantoms and discussed the possibility of its clinical application. ***Materials and Methods:*** Paper phantoms were designed using PowerPoint based on Burger's phantom and were created by mixing $^{99m}TcO_4$-prepartation and black ink, loading it into an ink cartridge, and printing it using an inkjet printer. Subsequently, a SPECT phantom was fabricated by alternately overlapping the paper phantoms with polystyrene foams or acrylic plates to determine its thickness. This was used for the SPECT collection with a gamma camera, and the differences in the images obtained were compared. To determine the optimal conditions, the pixel size was divided into two classes: one in which the pixel size was smaller than the distance between the paper phantoms, and the other in which the pixel size was approximately the same as the distance between the paper phantoms. In addition, another SPECT phantom was created using clinical images as the design for the paper phantoms, and the images of SPECT and static acquisition were compared. ***Results:*** Under clinical conditions, a pixel size smaller than the phantom spacing was appropriate for evaluating SPECT images using a SPECT phantom created from paper phantoms. The counts obtained using acrylic plates decreased by >50% compared to those obtained using polystyrene foams, resulting in a smaller visible area. Furthermore, the SPECT images had indistinct edges, whereas the static images showed an overall clearer image. ***Conclusion:*** A study with a view to clinical applications, such as creating a SPECT phantom using acrylic plates and clinical images and evaluating the images, suggests that this phantom can be applied in clinical practice.

OP-183

SPECT/CT-ONLY Imaging for Sentinel Lymph Node Biopsy in Breast Cancer: Efficient and Effective

B. Bosveld[1], *R. A. Valdés Olmos*[2], *W. van der Bruggen*[1], *C. D. Bavelaar-Croon*[3], *B. F. Bulten*[1];
[1]*Slingeland Hospital, Doetinchem, NETHERLANDS,*
[2]*Leiden University Medical Center, Leiden, NETHERLANDS,*
[3]*Alexander Monro Hospital, Bilthoven, NETHERLANDS.*

Aim/Introduction: For nuclear imaging prior to sentinel lymph node biopsy in breast cancer (SLNB), current international guidelines propose flexible directives. A previous survey of 57 nuclear medicine departments in the Netherlands showed wide variation in interpretation of those directives. Nearly all scanning protocols (98%) were based on planar scintigraphy, with Single Photon Emission Computed Tomography combined with Computed Tomography (SPECT/CT) used exclusively in cases of inadequate sentinel lymph node (SLN) visualisation. One hospital skipped planar imaging and directly applied SPECT/CT to identify SLNs, which is an efficient protocol in terms of capacity planning for staff and gamma cameras. We therefore investigated whether SPECT/CT-ONLY could safely replace our standard planar scintigraphy protocol. ***Materials and Methods:*** We conducted a randomised non-inferiority trial comparing SLNB operation time after SPECT/CT versus planar scintigraphy. Enrolled patients were assigned 1:1 to a control group (planar protocol, i.e. multidirectional static images plus skin marking) and an intervention group (SPECT/CT protocol, i.e. SPECT/CT-ONLY without skin marking).

Informed consent was obtained. Participants received two periareolar intracutaneous injections into the affected breast. Two hours later they underwent the scanning protocol they were assigned to. Surgery was performed three to four hours post injection. To answer our primary research question, we calculated the 95% confidence interval for difference in SLNB operation time between the two groups. A 95% confidence interval entirely below 5 minutes additional operation time after SPECT/CT would demonstrate significant non-inferiority. Secondary outcomes were SLNs identified by nuclear medicine physicians and SLNs removed by surgeons. ***Results:*** Between April 1 and December 31, 2022, 79 adult women were enrolled. For 65 of these 79 participants (82%) SLNB operation time could be analysed. Mean difference in operation time between SPECT/CT and planar group was -1.83 minutes, i.e. shorter operation time in the SPECT/CT group. The 95% confidence interval (-4.73;+1.08min) was entirely below +5 minutes. In all 79 participants one (85%), two (13%) or three (2%) SLNs were preoperatively identified. In 8 participants (10%) not all preoperatively identified SLNs were removed. This occurred 7 times in the planar group and 1 time in the SPECT/CT group. ***Conclusion:*** SPECT/CT-ONLY seems to be not only an efficient, but also an effective preoperative nuclear medicine imaging protocol for SLNB in breast cancer. Operation time was significantly non-inferior after SPECT/CT compared to planar scintigraphy, and we reported lower incidence of non-removed SLNs in the SPECT/CT group.

OP-184

Contamination of the Isolation Room After Iodine-131 Ablation Treatment

K. Levänen*, N. Miettinen, H. Leskinen, J. Heikkinen;*
Department of Radiology and Nuclear Medicine, The wellbeing services county of South Savo, Mikkeli, FINLAND.

Aim/Introduction: Orally ingested iodine-131 is used for the treatment thyroid grand cancers. Due to the radiation hazard that the high energy radiation (max. energy 364 keV) of I-131 induces, isolation of the treated patients is a necessary procedure. The Finnish Radiation and Nuclear Safety Authority requires that the residual activity inside the patient is under 800 MBq (a measured dose rate of <40 µSv/h) before ending the isolation. During the isolation, patients contaminates the room with their excretion. Therefore, conducting a thorough decontamination as part of the room cleaning is a vital part of the radiation safety procedures in the hospital. A dose rate exceeding 5 µSv/h measured from an item is considered a radiation hazard and the item in question needs to be stored in a decay-in-storage before wash or disposal. This study aims to determine the frequency of contamination in different locations in the isolation room. ***Materials and Methods:*** The contamination level of ten selected locations of the isolation room was measured after 30 patients treated with 1110, 1850 or 3700 MBq of iodine-131. The measurements were conducted using handheld dose rate meter after the patient left the isolation room. The measured locations were: both sides of the pillow, bed linen, patient clothing, patient slippers, toilet seat, toilet bowl, floor drain and waste containers in bathroom and patient room. ***Results:*** The isolation room was found contamined (dose rate >5 µSv/h) frequently at least in one location. However, the contamined locations were mostly the patient room and bathroom waste containers (50% and 33% of the times respectively). Patient clothing was found contamined two times (max 147µSv/h), pillow and bed linen both a single time. The dose rates of the toilet bowl and the floor drain did not exeed the threshold of contamination. The contamination of these locations was found to be caused by saliva, sweat or urine. ***Conclusion:*** The results indicate that the contamination in the isolation room after iodine-131 treatment is minimal. Since the contamination was mostly found from the waste containers where contamination can be expected, we can conclude that the patients have been well-informed of the radiation hazards of the treatment. The results of this study helps to keep the personell, who clean the room after isolation, better informed of the radiation safety of their work furhermore preventing the contamination spread from the isolation room. ***References:*** Finnish Radiation and Nuclear Safety Regulation stuklex (2013)

OP-185

Dose rate evaluation of patients performing diagnostic Nuclear Medicine procedures

A. Santos*, P. Colarinha;*
Hospital Cuf Descobertas, Lisbon, PORTUGAL.

Aim/Introduction: Patients submitted to Nuclear Medicine (NM) procedures are non-sealed sources of radiation. Diagnostic NM is considered to involve small amounts of radiation to both the patient and the public. The aim of this study is to answer three of the most common questions asked by patients, regarding public exposure, with the use of a quantitative method and relate the results with legal dose limits and international recommendations. ***Materials and Methods:*** Dose-rate (microsievert/hour) was measured at 1m distance, at the end of three diagnostic procedures (Geiger-muller counter): 1) Bone Scintigraphy (BS) with ^{99m}Tc-HDP (N=48), 2) Myocardial Perfusion Scintigraphy (MPI) with ^{99m}Tc-Tetrofosmine (N=31) and 3) PET with ^{18}F-FDG (FDG) (N=50). The average dose was used to calculate the cumulative dose on 3 hypothetical scenarios, corresponding to three of the most common questions asked, in regard to public irradiation: A) I will travel for 2h in a private car, is the dose to my driver within legal limits? B) Will we be within public dose limits if I sleep tonight with my spouse? C) Can I go to work tomorrow? ***Results:*** Dose-rate was measured and its average determined (table 1). The cumulative dose for each scenario was calculated (table 1). ***Conclusion:*** Public legal annual limit of 1mSv was not reached in any of the studied scenarios. Only in Scenario B) for MPI group was reached the cumulative dose of 0,3mSv. This study allowed our group to communicate with patients about the public exposure in an informed and evidence-based manner. ***References:*** • Radiation Protection Nº 180 - Medical Radiation Exposure of the European Population. European Commission (2014). Available at: https://ec.europa.eu/energy/sites/ener/files/documents/RP180.pdf • Bartlett ML. Estimated dose from diagnostic nuclear medicine patients to people outsider the nuclear medicine department. Radiation Protection Dosimetry. 2013; 157(1):44-52. • European Council Directive 2013/59/Euratom on basic safety standards for protection against the dangers arising from exposure to ionising radiation and repealing Directives 89/618/Euratom, 90/641/Euratom, 96/29/Euratom, 97/43/Euratom and 2003/122/ Euratom. Official Journal of the European Union 2014;L13:1-17. • Harding LK, et al. Dose rates from patients having nuclear medicine investigations. Nuclear Medicine Communications. 1985; 6:191-194. • Mountford PJ, et al. Radiation dose rates from adult patients undergoing nuclear medicine investigations. Nuclear Medicine Communications. 1991; 12: 767-777. • Harding LK, et al. Radiation doses to those accompanying nuclear medicine department patients: a waiting room survey. 1994; 21(11):1223-1226.

511

Sunday, September 10, 2023, 3:00 PM - 4:30 PM
Hall G1

Theranostics Track - Oncology & Theranostics Committee / EARL - Featured Session: Old but Novel Techniques

OP-186

K. Herrmann;
University Hospital Essen, Department of Nuclear Medicine, Essen, GERMANY.

OP-187

Predictive value of [18F]F-Choline and PSMA-based quantitative parameters for response to [177Lu] Lu-PSMA-617 therapy in mCRPC: The added value of dynamic FDG acquisition using Patlak method

S. Miet[1], *B. Maucherat*[1], *P. Baumgartner*[1], *E. Picot-Dilly*[1], *P. Lalire*[1], *A. Morel-Thierry*[1], *D. Rusu*[1], *M. Le Thiec*[1], *V. Nicolas*[2], *F. Rolland*[1], *C. Rousseau*[2], *L. Ferrer*[2];
[1]*ICO René Gauducheau, F-44800 Saint-Herblain, Nantes, FRANCE,* [2]*ICO René Gauducheau, F-44800 Saint-Herblain, Nantes Université, Univ Angers, INSERM, CNRS, CRCI2NA, F-44000, Nantes, FRANCE.*

Aim/Introduction: [177Lu]Lu-PSMA-617 (Lu-PSMA) is a promising therapy for metastatic castration-resistant prostate cancer (mCRPC), but there is still a need for reliable predictive tools to balance risk and benefit. Recent studies suggest that FDG PET/CT (FDG) may have added value in predicting response to therapy compared to [68Ga]Ga-PSMA-11 PET/CT (PSMA)[1]. This study compared the predictive value of [18F]F-Choline (FCH), PSMA and FDG-based quantitative parameters and assesses the added value of dynamic FDG acquisition using the Patlak method[2]. ***Materials and Methods:*** We retrospectively enrolled 26 patients with mCRPC, of which 10 had complete pre-therapeutic data (FCH, PSMA, and FDG and FDG dynamic PET/CT) and sufficient clinical follow-up (2023-059). Tumour volumes were delineated using semi-automatic segmentation (3DSLICER), and PSA changes were recorded according to the Prostate Cancer Working Group Criteria (PCWGC3) after three cycles of Lu-PSMA. PET/CT quantitative parameters were compared with PSA early change response. For all acquisition types, patient global scores were defined as the maximum and median of SUVmax, SUVmean, SUVmedian, and TLG. ***Results:*** In total, 1099, 625, 681 and 993 segmentations were respectively delineated on FCH, FDG,FDG dynamic PET/CT and PSMA images. Lesion volumes defined on FCH and PSMA examinations were not different (p-value=0.06) as opposed to those compared on FDG/FCH and FDG/PSMA examinations (p-value<0.005). Lesion volumes defined on Patlak's Ki images were not different to volumes defined on the other modalities (p-values>0.10) except for FDG (p-value=0.005). Regarding PSA change, 7 patients had a positive response defined as a drop-off superior to 30%. The three non-responders exhibited the lowest maximum SUVmax values on PSMA examinations (p-value=0.01). ***Conclusion:*** This study aimed to provide insights into the predictive value of FDG, FCH and PSMA-based quantitative parameters for response to Lu-PSMA therapy in mCRPC. Preliminary results showed that patients with the highest PSMA SUVmax better respond to 177Lu-PSMA therapy. The dynamic FDG acquisition benefit using Patlak method still needs to be addressed. These findings may help improve patient selection for Lu-PSMA therapy. ***References:*** 1. Jadvar H. The VISION Forward: Recognition and Implication of PSMA-/18F-FDG+ mCRPC.J Nucl Med. 2022;63:812-815. 2. Dias AH, Pedersen MF, Danielsen H, Munk OL, Gormsen LC. Clinical feasibility and impact of fully automated multiparametric PET imaging using direct Patlak reconstruction: evaluation of 103 dynamic whole-body 18F-FDG PET/CT scans. Eur J Nucl Med Mol Imaging. 2021;48:837-850.

OP-188

FAP-Targeted Radiopeptide Therapy using ^{177}Lu-, ^{225}Ac- and90Y-labeled 3BP-3940 in Diverse Advanced Solid Tumors: First-in-Humans Results

J. Zhang[1], *V. Jakobsson*[1], *A. Mishra*[2], *A. Eismant*[2], *L. Greifenstein*[2], *C. Kramer*[2], *A. Klega*[2], *C. Landvogt*[2], *C. Mueller*[2], *R. P. Baum*[2];
[1]*National University of Singapore, Singapore, SINGAPORE,* [2]*Curanosticum Wiesbaden-Frankfurt, Center for Advanced Radiomolecular Precision Oncology, Wiesbaden, GERMANY.*

Aim/Introduction: The purpose of this study was to determine the feasibility of using a novel FAP-targeted cyclic peptide 3BP-3940 for peptide targeted radionuclide therapy (PTRT) and present first-in-humans results using ^{177}Lu, ^{90}Y and ^{225}Ac labeled 3BP-3940 in end-stage cancer patients. ***Materials and Methods:*** 40 patients (23 men and 17 women; mean age 60.8±10.2 years) with advanced metastatic cancers of the pancreas, breast, lung, esophagus, hepatocellular, appendix, ovary, prostate and bowel presented with disease progression after previous treatments and were treated with ^{177}Lu-, ^{225}Ac- and ^{90}Y- PTRT between March 2021 and October 2022. Pre-treatment PET/CT imaging was done with ^{68}Ga-3BP-3940 to determine tumor uptake. Treatment response was evaluated according to RECIST and EORTC. Kaplan-Meier survival analysis was performed to calculate overall survival (OS), defined from the start of PTRT. ***Results:*** Cumulative activity was for ^{177}Lu 7.0 ± 2.0 GBq; range 2 - 12 GBq (n, patients=33, 82.5%), ^{90}Y 5.3 ± 2.0 GBq; range 1.9- 7.6 GBq (n, patients = 10, 25%) and ^{225}Ac 8.9 ± 3.4 MBq; range 5.0 - 18 MBq (n, patients = 28, 70 %). Visual analysis of posttherapy whole-body scans and SPET/CT scans demonstrated significant uptake and retention of 3BP-3940 in tumor lesions on delayed imaging in all patients, with very high tumor-to-background ratio. Dosimetry was calculated for one pancreas cancer patient who received 9.73 GBq 177Lu, uptake was for the brain 37 mGy, for the lungs 161 mGy, for healthy liver tissue 86 mGy, for the pancreas 142 mGy, for the kidneys 265 mGy, and for the primary pancreas lesion 2200 mGy. 6-8 weeks after the first cycle, responses were progressive disease (n=7, 27 %), partial remission (n=13, 50 %), mixed pattern (n=2, 8 %), and stable disease (n=4, 15 %). Patient 17 is after two cycles 3BP-3940 PTRT in complete remission. For the entire cohort from the start of PTRT (n = 40), the median OS was 10.0 months. In the subgroup of patients with advanced pancreatic adenocarcinoma (n = 10), the median OS was 7.5 months. ***Conclusion:*** 3BP-3940 PTRT is feasible with ^{177}Lu/^{90}Y/^{225}Ac either alone or as TAndEM treatment of end-stage cancer patients. Treatments were well-tolerated without significant adverse effects. 3BP-3940 PTRT demonstrated a favorable biodistribution, significant uptake and retention in tumor lesions with very high tumor-to-background ratio, and should objective responses in advanced metastatic adenocarcinomas and sarcomas. The survival benefit for pancreatic adenocarcinoma patients seems to be very promising.

OP-189

Static and dynamic 68Ga-FAPI-46 PET in 18F-FDG-negative pulmonary lesions - target validation and imaging properties

M. Roehrich, *J. Daum, J. Hoppner, F. Eichhorn, K. Schlamp, E. Gutjahr, H. Winter, U. Haberkorn;*
University Hospital Heidelberg, Heidelberg, GERMANY.

Aim/Introduction: Fibroblast activation protein (FAP) expressing Cancer associated fibroblasts (CAFs) are crucial for the progression of malignant tumors, among them lung cancer (LC). In particular, CAFs are present in lepidic LCs. This subtype of LC is frequently 18F-FDG-negative, but also other LC subtypes can exhibit variable glucose metabolism. Given the strong expression of FAP in the stroma of LC, 68Ga-FAPI-PET is a promising imaging modality for LC in general and particularly for primary FDG-negative pulmonary lesions as 18F-FDG-negativity cannot exclude malignancy in these cases. Here, we have confirmed FAP-expression of CAFs in lepidic LCs and evalauted the diagnostic potential of 68Ga-FAPI-PET for 18F-FDG-negative pulmonary lesions. ***Materials and Methods:*** HE staining and FAP-immunohistochmistry of paraffin embedded sections of 24 lepidic LC was performed. Static (60 minutes p.i.) and dynamic 68Ga-FAPI-46 PET was applied in 20 patients with 18F-FDG negative pulmonary lesions. After PET imaging, all patients underwent lung biopsy and histological diagnosis. Pulmonary lesions and healthy appearing lung tissue were contured manually and SUVmax, SUVmean and corrresponding target to background ratios of 68Ga-GAPI-46-PET and 18F-FDG imaging were calculated. Dynamic 68Ga-FAPI-46 PET data was analzyed qualitatively and quantitatively (time to peak and kinetic modeling). ***Results:*** Immonohistochemistry showed strong FAP-expression in lepidic LC. Histology revealed LC in 6/15 patients and benign results in 9/15. LCs showed markedly higher 68Ga-FAPI-46 uptake than 18F-FDG uptake (average SUVmax 3,93 +/- 0,89 versus 1,54 +/- 0,52, average SUVmean 2,47 +/- 0,54 versus 1,08 +/- 0,38). In particular, a lepidic LC was well decernable in 68GA-FAPI-46-PET (SUVmax 3,80, SUVmean 1,75 versus 0,60), but not in 18F-FDG (SUVmax 0,94). Benign lesions also showed higher 68Ga-GAPI-46-uptake than 18F-FDG-uptake (SUVmax 3,12 +/- 1,95 versus 2,16 +/- 1,24, SUVmean 1,89 +/- 1,34 versus 1,26 +/- 0,81), but the average 68Ga-FAPI-46/18-FDG average ratio was higher in LC than in benign lesions (3,64 +/- 1,59 versus 1,89 +/- 0,32). In dynamic imaging, LC and benign lesions showed different time activity curves with increasing uptake for 15-20 minutes followed by slow washout for LC and constant washout for benign lesions, which was reflected by prolonged time to peak of (815 +/- 330 seconds versus 410 +/- 440 seconds). ***Conclusion:*** Static and dynamic 68Ga-FAPI-46 PET is a promising approach for the characterization of 18F-FDG-negative pulmonary lesions. As 68Ga-FAPI-46 PET reflects the presence of CAFs in LC, it provides tumor biology-based imaging information and may impact future clinical decision making in this challenging setting.

OP-190

^{68}Ga-FAPI-46 vs ^{18}F-FDG PET/CT and contrast-enhanced CT in patients with advanced gastrointestinal stroma tumors (GIST)

T. Bartel[1], *K. M. Pabst*[1], *A. Milosevic*[2], *S. Bauer*[3], *J. Falkenhorst*[3], *H. Lanzafame*[1], *I. A. Mavroeidi*[3], *M. Nader*[1], *J. T. Siveke*[3,4,5], *K. Herrmann*[1], *R. Hamacher*[3], *W. P. Fendler*[1];
[1]*Department of Nuclear Medicine, West German Cancer Center, University Hospital Essen, Essen, GERMANY,* [2]*Department of Diagnostic and Interventional Radiology and Neuroradiology, University Hospital Essen, Essen, GERMANY,* [3]*Department of Medical Oncology, West German Cancer Center, University Hospital Essen, Essen, Germany, Essen, GERMANY,* [4]*Bridge Institute of Experimental Tumor Therapy, West German Cancer Center, University Hospital Essen, Essen, GERMANY,* [5]*Division of Solid Tumor Translational Oncology, German Cancer Consortium (DKTK, Partner Site Essen) and German Cancer Research Center, DKFZ, Heidelberg, GERMANY.*

Aim/Introduction: GISTs are the most common mesenchymal tumors of the gastrointestinal tract. Contrast-enhanced CT is current clinical standard diagnostic, however lacks detection of small lesions and peritoneal deposits. ^{68}Ga-FAPI-46 PET images tumor-associated fibroblast in a wide range of tumor entities with high accuracy. Our aim was to investigate tracer uptake and detection efficacy of ^{68}Ga-FAPI-46 PET compared to ^{18}F-FDG PET/CT and contrast-enhanced CT in patients with GIST. In addition, we aimed to assess the impact on treatment management. ***Materials and Methods:*** All patients with GIST in our prospective database of 899 patients who underwent ^{68}Ga-FAPI-46 PET/CT between June 2020 and March 2023 were retrospectively reviewed. Clinical data, histo- and molecular pathology including mutation status (c-KIT, PDGFRA) were collected. Lesion- and region-based detection efficacy was assessed compared to ^{18}F-FDG PET/CT and contrast-enhanced CT, subdivided into true-/false-positive and true-/false-negative findings. Histopathology/follow-up were standard of reference. SUV_{max}/SUV_{mean}/SUV_{peak} and Tumor-to-Background Ratios (TBR) of both tracers were compared using Wilcoxon test. Impact on management was assessed by pre- and post-imaging questionnaire sent to the treating physicians. ***Results:*** A total of n=10 patients with a median age of 61 years (range: 55-84 years) and advanced GIST were analyzed. C-KIT/PDGFRA mutation was present in n=7/1 patients. Overall, n=56 tumor lesions were detected (local: n=35 (62%), lymph node: n=1 (2%), distant (soft tissue/organ): n=20 (36%)). Detection rates for contrast-enhanced CT/^{18}F-FDG PET/^{68}Ga-FAPI-46 PET were n=34/32/11 (local tumor), n=1/1/1 (lymph node), n=20/13/13 (distant)). N=14 lesions (19.7%; lymph nodes in one patient (histopathology available: n=4)) were false-positive on contrast-enhanced CT/^{18}F-FDG PET and true-negative on ^{68}Ga-FAPI-46 PET. N=1 lesion (1.4%; distant metastasis) was false-positive on ^{68}Ga-FAPI-46 PET and true-negative on both other imaging modalities. In a patient-based analysis, interpatient heterogeneity was observed for both tracers with average SUV_{peak} values ranging from 1.0 to 12.7 for ^{68}Ga-FAPI-46 PET and from 1.6 to 6.3 for ^{18}F-FDG PET. SUV_{max}/SUV_{mean} showed no significant difference between both tracers (^{18}F-FDG vs. ^{68}Ga-FAPI-46: 5.0 (±2.1) vs. 4.9 (±4.3); p=0.23/3.1 (±1.3) vs. 3.0 (±2.6); p=0.28). TBR_{muscle} (p=0.028) was significantly higher for ^{18}F-FDG PET and $TBR_{bloodpool/liver}$ showed no difference (p=0.75/p=0.48). Biopsy was prevented (n=1)/performed additionally (n=2) due to ^{68}Ga-FAPI-46 PET. ***Conclusion:*** Tracer uptake was heterogeneous for ^{18}F-FDG and ^{68}Ga-FAPI-46 PET resulting in highest detection rate for contrast-enhanced CT alone. Due to additional detection

of distant metastases on ^{68}Ga-FAPI-46 PET, management changed in one third of patients. Accuracy will be further evaluated in an ongoing prospective trial (NCT05160051).

OP-191

Radiolabeled Somatostatin Receptor Antagonist versus Agonist for Peptide Receptor Radionuclide Therapy in Patients with Therapy-resistant Meningiomas - Phase 0 Part of the Promenade Study

C. Eigler[1], *L. McDougall*[1], *A. Bauman*[1], *P. Bernhardt*[2], *M. Hentschel*[1], *K. A. Blackham*[1], *G. Nicolas*[1], *M. Fani*[1], *D. Cordier*[1], *D. Wild*[1];
[1]*University Hospital Basel, Basel, SWITZERLAND,*
[2]*University of Gothenburg, Gothenburg, SWEDEN.*

Aim/Introduction: Our aim was to compare the meningioma and organ absorbed doses of the new radiolabeled somatostatin receptor antagonist [^{177}Lu]Lu-DOTA-JR11 with the established radiolabeled somatostatin receptor agonist [^{177}Lu]Lu-DOTATOC in the same patients with progressive meningiomas that are refractory to standard treatment. ***Materials and Methods:*** In this prospective, single-center, open label phase 0 study (NCT04997317), 6 patients were included: 3 men and 3 women (mean age 63.5 years, age range from 39 to 83 years). Patients received 6.9-7.3 GBq (standard activity) [^{177}Lu]Lu-DOTATOC followed by 3.3-4.9 GBq (2 GBq/m^2 x body surface area) [^{177}Lu]Lu-DOTA-JR11 in an interval of 10±1 weeks. In total one [^{177}Lu]Lu-DOTATOC and 2-3 [^{177}Lu]Lu-DOTA-JR11 treatment cycles were performed. Quantitative SPECT/CT was done at ~24, ~48 and ~168 h after injection of both radiopharmaceuticals in order to calculate meningioma and organ doses (3D segmentation approach). Disease control rate (DCR) was calculated. ***Results:*** The median (range) of the mean meningioma absorbed dose of one treatment cycle was 11.5 (4.7-22.7) Gy for [^{177}Lu]Lu-DOTA-JR11 and 3.4 (0.8-10.2) Gy for [^{177}Lu]Lu-DOTATOC, (P=0.03). The mean bone marrow and kidney absorbed doses after one treatment cycle were 0.28 (0.16-0.39) and 3.6 (1.6-5.9) Gy for [^{177}Lu]Lu-DOTA-JR11 as well as 0.11 (0.05-0.17) and 3.0 (1.3-5.3) Gy for [^{177}Lu]Lu-DOTATOC, respectively. According to the CTCAE v5.0 two patients developed reversible grade 2 lymphopenia after one cycle [^{177}Lu]Lu-DOTATOC. Afterwards, two patients developed reversible grade 3 lymphopenia and one patient developed reversible grade 3 lymphopenia and neutropenia after 2-3 cycles [^{177}Lu]Lu-DOTA-JR11. No grade 4 or 5 adverse events were observed ≥15 months after therapy start. DCR (all stable disease) was 83% (95% CI, 53-100%) at ≥12 months after inclusion. ***Conclusion:*** [^{177}Lu]Lu-DOTA-JR11 shows 2.2-5.7 times higher meningioma and 1.7-3.1 times higher bone marrow absorbed doses compared to [^{177}Lu]Lu-DOTATOC despite 1.4-2.1 times lower injected activities. First efficacy results indicate a high DCR with an acceptable safety profile in this conventional treatment-resistant meningioma patients. Therefore, larger studies with [^{177}Lu]Lu-DOTA-JR11 are warranted.

OP-192

Inter-institutional differences and common ground in ^{177}Lu-PSMA radionuclide therapy: International survey in 95 theranostic centers

A. Farolfi[1,2], *W. Armstrong*[2], *L. Djaileb*[3], *A. Gafita*[4], *M. Hotta*[2], *M. Auerbach*[2], *L. Unterrainer*[2], *W. P. Fendler*[5], *M. Rettig*[6], *M. Eiber*[7], *M. Hofman*[8], *B. Hadaschik*[9], *K. Herrmann*[5], *J. Czernin*[2], *J. Calais*[2], *M. Benz*[2];
[1]*Division of Nuclear Medicine, IRCCS Azienda Ospedaliero-Universitaria di Bologna, Bologna, ITALY,* [2]*Ahmanson Translational Theranostics Division, Department of Molecular and Medical Pharmacology, University of California Los Angeles, Los Angeles, CA, UNITED STATES OF AMERICA,* [3]*Nuclear Medicine Department, Univ. Grenoble Alpes, INSERM, CHU Grenoble Alpes, Grenoble, FRANCE,* [4]*The Russell H. Morgan Department of Radiology and Radiological Science, Johns Hopkins University School of Medicine, Baltimore, MD, UNITED STATES OF AMERICA,* [5]*Department of Nuclear Medicine and German Cancer Consortium (DKTK), University Hospital Essen, University of Duisburg-Essen, Essen, GERMANY,* [6]*Department of Urology, University of California Los Angeles, Los Angeles, CA, UNITED STATES OF AMERICA,* [7]*Department of Nuclear Medicine, Klinikum Rechts Der Isar, Technical University of Munich, Munich, GERMANY,* [8]*Prostate Cancer Theranostics and Imaging Centre of Excellence, Molecular Imaging and Therapeutic Nuclear Medicine, Peter MacCallum Cancer Centre, Melbourne, AUSTRALIA,* [9]*Department of Urology, University of Duisburg-Essen and German Cancer Consortium-University Hospital Essen, Essen, GERMANY.*

Aim/Introduction: ^{177}Lutetium-labeled prostate-specific membrane antigen (Lu-PSMA) radionuclide therapy has proven its effectiveness in prospective randomized clinical trials and received FDA and EMA approval in 2022. Patient numbers and number of theranostic centers are expected to significantly increase, requiring standardization/harmonization of patient selection, therapy protocols, therapy response assessment and treatment discontinuation criteria. The aim of this international questionnaire study was to assess operational differences and similarities between Lu-PSMA treatment centers. ***Materials and Methods:*** The web-based questionnaire comprised 62 questions. The survey was designed by a core team of 5 physicians and externally reviewed by international experts before an e-mail invitation for study participation was sent in June 2022. E-mail recipients included 1) all centers involved in patient recruitment for the TheraP and VISION trials 2) PubMed search for corresponding authors on clinical Lu-PSMA publications, and 3) international key contacts. Duplicates were removed. The survey was closed in late September 2022. ***Results:*** 95 out of 211 (45%) contacted centers completed the questionnaire. Most participating centers were located in Europe (51%), followed by north- and south-America (22%), Asia (22%), Oceania (3%), and Africa (2%). During the 12 months prior to this study, a total of 5906 patients received Lu-PSMA therapy in the 95 participating centers. Most patients in these last 12 months were treated in Europe (2840/5906; 48%), followed by Asia (1313/5906; 22%) and Oceania (1225/5906; 21%). To assess patient eligibility, PSMA-ligand PET or SPECT was performed in all centers and ^{68}Ga-PSMA-11 was the most frequently injected radiotracer (77%). Mean standard injected activity per cycle was 7.3 GBq (range 5.5-11.1 GBq). Additional pre-therapy imaging included FDG-PET/CT, contrast enhanced CT, renal and bone scintigraphy in 49%, 32%, 30%, and 15% of centers for clinical standard of care/compassionate care/local research protocols, and 26%, 60%, 21%, and 67% respectively for industry sponsored trials. PSMA-PET eligibility criteria included subjective qualitative assessment of PSMA positivity in 33%, VISION criteria in 23%, and TheraP criteria in 13% of centers. 33/95 (35%) centers did not apply standardized response assessment criteria. Of the remaining centers, PSMA PET Progression Criteria (PPP) for treatment response were applied by 37%, RECIST by 24%, PCWG3 by 22%, RECIP by 11%, and PERCIST by 7%. ***Conclusion:*** Results revealed inter-institutional differences in Lu-PSMA radionuclide therapy. Standardization/harmonization of protocols and criteria is desirable in anticipation of increasing number of patients and theranostic centers.

OP-193

Safety and dosimetry evaluation of personalized dose I131-apamistamab prior to HCT in the phase 3 SIERRA trial for patients with relapsed/refractory acute myeloid leukemia (R/R AML)

N. Pandit-Taskar[1], *M. Natwa*[2], *M. Chen*[3], *W. Yap*[4], *G. Wiseman*[5], *E. Leung*[6], *A. Desai*[7], *P. Brodin*[7], *E. Haeuber*[7], *A. Nahar*[7], *R. L. Wahl*[8];
[1]Molecular Imaging and Therapy, Memorial Sloan Kettering Cancer Center, New York, NY, UNITED STATES OF AMERICA, [2]Ohio State University, Columbus, OH, UNITED STATES OF AMERICA, [3]Yale New Haven Hospital, New Haven, CT, UNITED STATES OF AMERICA, [4]University of Kansas Medical Center, Kansas City, KS, UNITED STATES OF AMERICA, [5]Mayo Clinic Rochester, Rochester, MN, UNITED STATES OF AMERICA, [6]The Ottawa Hospital, Ottawa, ON, CANADA, [7]Actinium Pharmaceuticals, Inc., New York, NY, UNITED STATES OF AMERICA, [8]Washington University St. Louis, St. Louis, MO, UNITED STATES OF AMERICA.

Aim/Introduction: I131-apamistamab is a radioimmunoconjugate to CD45 that delivers high-dose targeted radiation to hematopoietic cells, allowing for myeloablation prior to allogeneic hematopoietic cell transplant (aHCT) in patients with active R/R AML. Here we present a safety and dose-response evaluation of targeted high-dose I131-apamistamab from the SIERRA randomized controlled Phase 3 trial, compared to physician's choice of conventional care (CC). ***Materials and Methods:*** Patients with active R/R AML were randomized to I131-apamistamab vs. CC. Patients on the I131-apamistamab arm received study drug with fludarabine and total body irradiation (2 Gy) followed by aHCT. Pts on CC arm received physician's choice of salvage therapy. Organ-specific uptake and dosimetry estimates based on gamma camera imaging following tracer dose administration was used to individually tailor the prescribed activity of the therapeutic dose of I131-apamistamab. Estimated total integrated activity coefficients (TIACs) and organ-specific absorbed dose estimates were calculated for each patient. The estimated absorbed doses to organs-at-risk were tabulated along with the rates of relevant non-hematological grade ≥3 adverse events in this heavily pre-treated patient population. ***Results:*** Out of the 153 patients enrolled in the SIERRA trial, 76 were in the I131-apamistamab arm and 77 in the CC arm. All 66 patients that received the therapeutic dose of I131-apamistamab went on to receive an aHCT vs. only 14 patients (18.2%) on the CC arm using standard conditioning regimens, and the 66 patients treated with I131-apamistamab form the subset for this analysis. I131-apamistamab prior to aHCT was well tolerated with low rates of non-hematological grade≥3 adverse events in the form of sepsis (4/66, 6.1%), mucositis (10/66, 15.2%), pneumonitis (2/66, 3.0%), acute kidney injury (3/66, 4.5%), acute GVHD (4/66, 6.1%) and acute liver injury (2/66, 3.0%). Median estimated absorbed dose to bone marrow was 16 Gy (range: 5 to 45 Gy), with median dose to relevant organs-at-risk being generally low at 2.5 Gy to lungs, 2.4 Gy to small intestine, 4.1 Gy to kidneys and 3.6 Gy to stomach. Liver was considered the dose limiting organ-at-risk in this trial with maximum tolerated dose of 24 Gy, and median received dose of 21.6 Gy, with very few grade ≥3 liver toxicities observed. ***Conclusion:*** I131-apamistamab conditioning followed by aHCT proved safe and tolerable in this population of heavily pre-treated patients with active R/R AML. This treatment delivered high-dose targeted radiation to leukemic cells, while doses to organs-at-risk were well below safety limits established from external beam radiation.

OP-194

^{89}Zr-DFO-girentuximab PET/CT imaging for clear cell renal cell carcinoma - ZIRCON study results of diagnostic performance, including in very small lesions

S. Martina[1], *P. Mulders*[2], *B. M. Shuch*[3], *A. J. Pantuck*[3], *M. A. Morris*[4], *V. Master*[5], *A. Scott*[6,7,8], *C. van Praet*[9], *C. Bailly*[10], *B. Önal*[11,12], *T. Aksoy*[13], *R. Merkx*[2], *D. M. Schuster*[5], *S. Lee*[14], *N. Pandit-Taskar*[15,16], *A. C. Fan*[17], *L. Tauchmanova*[1], *K. Schmidt*[18], *P. Allman*[19], *K. Vadali*[1], *C. Hayward*[1], *J. Bernhard*[20];
[1]Telix Pharmaceuticals, Melbourne, AUSTRALIA, [2]Radboud University Medical Center, Nijmegen, NETHERLANDS, [3]UCLA, Los Angeles, CA, UNITED STATES OF AMERICA, [4]Advanced Molecular Imaging and Therapy, Glen Burnie, MD, UNITED STATES OF AMERICA, [5]Emory University School of Medicine, Atlanta, GA, UNITED STATES OF AMERICA, [6]Austin Health, Melbourne, AUSTRALIA, [7]University of Melbourne, Melbourne, AUSTRALIA, [8]Olivia Newton-John Cancer Research Institute, Melbourne, AUSTRALIA, [9]Universitair Ziekenhuis Gent, Gent, BELGIUM, [10]Nantes University Hospital, Nantes, FRANCE, [11]Istanbul University, Istanbul, TÜRKIYE, [12]Cerrahpasa Medical, Istanbul, TÜRKIYE, [13]Istanbul Training and Research Hospital, Istanbul, TÜRKIYE, [14]Austin Health, Heidelberg, AUSTRALIA, [15]Memorial Sloan Kettering Cancer Center, New York, NY, UNITED STATES OF AMERICA, [16]Weil Cornell Medical Center, New York, NY, UNITED STATES OF AMERICA, [17]Stanford University School of Medicine, Stanford, CA, UNITED STATES OF AMERICA, [18]ABX-CRO advanced pharmaceutical services Forschungsgesellschaft mbH, Dresden, GERMANY, [19]Premier Research, Morrisville, NC, UNITED STATES OF AMERICA, [20]CHU de Bordeaux, Bordeaux, FRANCE.

Aim/Introduction: Accurate noninvasive techniques to risk stratify patients with renal mass remains an unmet need. Girentuximab is a chimeric monoclonal antibody with high affinity for carbonic anhydrase IX (CAIX), which is highly expressed in clear cell renal carcinoma (ccRCC); thus, ^{89}Zr-DFO-girentuximab may aid diagnosis, characterization, and differentiation of ccRCC and other renal lesions. ZIRCON was an open label, multicenter clinical trial evaluating the performance of ^{89}Zr-DFO-girentuximab PET/CT for detection of ccRCC. We present data on diagnostic performance of in very small renal lesions, and inter-/intrareader consistency. ***Materials and Methods:*** 300 patients with an IDRM (≤7 cm; cT1) scheduled for partial or radical nephrectomy within 90 days from planned ^{89}Zr-DFO-girentuximab administration received a single dose of ^{89}Zr-DFO-girentuximab IV (37 MBq±10%; 10mg girentuximab) on Day 0 and underwent abdominal PET/CT imaging on Day 5 (±2days). Blinded central histology review determined ccRCC status. PET positivity was assessed by 3 independent blinded central readers. The coprimary objectives were to evaluate both the sensitivity and specificity of ^{89}Zr-DFO-girentuximab PET/CT imaging in detecting ccRCC, using histology as the standard of truth. Key secondary objectives included both sensitivity and specificity in the subgroup of patients with IDRM ≤4cm (cT1a). Other secondary objectives included safety and tolerability. Fleiss' kappa statistics determined agreement between qualitative visual assessment of ^{89}Zr-DFO-girentuximab tumour targeting (tracer uptake in target lesion: yes/no); an intra-class kappa of ≥0.70 was considered acceptable. Cohen's kappa statistics determined intra-reader reproducibility. ***Results:*** 300 patients received ^{89}Zr-DFO-girentuximab (mean age 62±12 y; 71% Male). The primary analysis included 284 evaluable patients (central histology and readable PET). Across all 3 readers, the average [95% CI] sensitivity and specificity was 86% [80%, 90%] and 87% [79%, 92%] respectively for coprimary endpoints, and 85% [77%, 91%] and 90% [79%, 95%] resp. for key secondary. Sensitivity and specificity in lesions ≤2cm ranged from 90-100% . Inter- and

Intra-reader consistency was 91% and 100%, respectively. Of 263 adverse events (AEs) in 124 patients, 2 AEs of mild intensity were treatment related. ***Conclusion:*** ^{89}Zr-DFO-girentuximab PET/CT is a well-tolerated, accurate, noninvasive modality for imaging of renal masses for detection and characterization of ccRCC, supporting patient treatment/management decision making. ***References***: ClinicalTrials.gov Identifier: NCT03849118. Disclosures: Telix Pharmaceuticals sponsored this study.

601

Sunday, September 10, 2023, 16:45 - 18:15
Hall A

CME 4 - Oncology & Theranostics Committee: Update in Multiple Myeloma

OP-195
Genomic vs FDG Patterns
C. Nanni;
IRCCS Azienda Ospedaliero-Universitaria di Bologna, Nuclear Medicine, Bologna, ITALY.

OP-196
Radioligand Therapy
A. Buck;
UniversityHospital Würzburg, Dept. Of Nuclear Medicine, Wurzburg, GERMANY.

OP-197
FDG PET/CT, DWI or Both?
C. Mesguich;
NuclearMedicine Department, Centre Hospitalier Universitaire de Bordeaux, Pessac, FRANCE.

OP-198
ImmunoPET
F. Krabere-Bodere;
NuclearMedicine department, CHU Nantes, ICO, CRCINA, Nantes University, Nantes, FRANCE.

602

Sunday, September 10, 2023, 16:45 - 18:15
Hall D (Arena)

Challenge the Expert 3 - Dosimetry Committee: Dosimetry Live

OP-199
Dosimetry Calculation Live on Stage
M. Konijnenberg;
Eurasmus MC, Radiology & Nuclear Medicine, Rotterdam, NETHERLANDS.

OP-200
Dosimetry Calculation Live on Stage
J. Gear;
Royal Marsden NHSFT, Sutton , UNITED KINGDOM.

OP-201
Dosimetry Calculation Live on Stage
C. Stokke;
Division of Radiology and Nuclear Medicine, Oslo University Hospital, Oslo, NORWAY, Department of Physics, University of Oslo, Oslo, NORWAY.

603

Sunday, September 10, 2023, 16:45 - 18:15
Hall E1

LIPS Session 4 - Oncology & Theranostics Committee: Residents for Residents

OP-206
PET/CT cases in thoracic oncological disorders
R. Metz;
CHU Nantes, Service de Médecine Nucléaire, Nantes, FRANCE.

OP-207
PET/CT cases in abdominal/pelvic oncological disorders
S. Himmen;
UniversityHospital Essen, Nuclear Medicine, Essen, GERMANY.

OP-208
PET/CT cases in neurology
S. Sperti;
Universityof Padova, Nuclear Medicine, Padova, ITALY.

OP-209
PET/CT cases in infectious diseases
S. Erdkamp;
Amsterdam UMC, Department of Radiology and Nuclear Medicine, Amsterdam, NETHERLANDS.

604

Sunday, September 10, 2023, 4:45 PM - 6:15 PM
Hall E2

M2M Track - TROP Session: Novel Imaging Targets in Oncology

OP-212
Computer-Aided Development of Trop-2-Targeted Peptides for Radiotheranostic Applications for Pancreatic Cancer
H. Hong[1], *J. Hu*[1], *Y. Cong*[1], *X. Li*[1], *Y. Wang*[2];
[1]*Nanjing University, Nanjing, CHINA,* [2]*China Pharmaceutical University, Nanjing, CHINA.*

Aim/Introduction: Trophoblast cell-surface antigen 2 (Trop-2) is involved in the proliferation and progression of various solid tumors. Trop-2 targeted antibody drug conjugates have showed good efficacy and safety profile in patients with many cancer types. Thus, a noninvasive method for fast delineation of Trop-2 can significantly benefit cancer diagnosis and therapy monitoring. The goal of this study is to develop peptide ligands with strong affinity to Trop-2 was and labeled them with different radiometals for positron emission tomography (PET) imaging and targeted radiotherapy of pancreatic cancer. ***Materials and Methods:*** With the analysis of crystal structure from human Trop-2, molecular docking strategies (e.g. SiteMap and FT Map) was used to find

five potential binding pockets inside Trop-2, and determined the critical amino acids inside. We identified five peptide sequences with strong binding affinity against Trop-2. One candidate (named TP1) was conjugated with p-SCN-Bn-NOTA and subsequently radiolabeled with gallium-68. Flow cytometry, microscopy studies, cell internalization assay, and competitive binding assay were conducted to investigate the cellular interaction behavior of TP1 peptide in Trop-2 positive BxPC-3 pancreatic cancer cells. PET imaging with ^{68}Ga-NOTA-TP1 was carried out in pancreatic tumors with different Trop-2 expression levels. Western blot of tumor lysate was conducted to correlate the uptake of ^{68}Ga-NOTA-TP1 with Trop-2 expression level. Finally, lutetium-177 was also labeled with NOTA-TP1 to treat BxPC-3 tumors. ***Results:*** Both TP1 (Kd = 0.62 nM) and NOTA-TP1 (Kd = 15.1 nM) showed good binding affinity and specificity against uPA, confirmed by abovementioned assays. ^{68}Ga-NOTA-TP1 had a fast internalization into Trop-2^{+} BxPC-3 cells, significantly higher than that in AsPC-1 cells (Trop-2 low). Serial PET imaging revealed that ^{68}Ga-NOTA-TP1 had a fast and strong accumulation in BxPC-3 tumors (6.8 ± 1.4 %ID/g at 1 h p.i., n = 4), significantly higher than those in AsPC-1 tumors at all time points examined. In vivo Trop-2 specificity was confirmed and the tumor uptakes obtained from PET correlated with Trop-2 expression in tumor measured by Western Blotting. ^{177}Lu labeling of NOTA-TP1 was also achieved with a radiochemical yield of 34.2 ± 6.4% (n = 4) and good radiochemical purity, while ^{177}Lu-NOTA-NP1 showed significant tumor growth inhibition for BxPC-3 in vivo, with no noticeable toxicity incurred. ***Conclusion:*** Quantitative PET imaging with ^{68}Ga-labeled TP1 peptides can facilitate oncologists to adopt more relevant treatment planning, and ^{177}Lu-labeled TP1 can kill pancreatic cancer selectively. Those radiolabeled peptides can serve as good radiotheranostic agents for pancreatic cancer.

OP-213

Glioblastoma and Pancreatic Adenocarcinoma - Versatile radiolabeled probe targeting Low Density Lipoprotein Receptors (LDLR)

I. Tworowska[1], *L. Flores*[1], *X. Qu*[1], *C. Malicet*[2], *R. Zielinski*[3], *P. Lecorche*[1], *E. Delpassand*[4], *J. Temsamani*[5];
[1]*RadioMedix Inc., Houston, TX, UNITED STATES OF AMERICA,* [2]*Vect-Horus, Marseille, FRANCE,* [3]*MDAnderson, Houston, TX, UNITED STATES OF AMERICA,* [4]*RadioMedix, Houston, TX, UNITED STATES OF AMERICA,* [5]*Vect-Horus, Marseille Cedex 15, FRANCE.*

Aim/Introduction: RMX-VH is a proprietary chelator modified-peptide developed for radiotheranostic targeting the Low-Density Lipoprotein Receptors (LDLR)-overexpressing in solid tumors. The overexpression of LDLR has been reported in multiple solid tumors and correlated with disease prognosis. In addition, LDLRs are known to facilitate the transport of endogenous ligands through the blood-brain barrier (BBB). RMX-VH can serve as a delivery vector to pass the BBB and target LDLR-overexpressed GBM. Our goal was to synthesize and characterize ^{212}Pb-RMX-VH, develop a protocol of SPECT ^{212}Pb-imaging, and perform to complete in vitro/in vivo pre-clinical studies in relevant glioblastoma (GBM) and pancreatic-ductal adenocarcinoma (PDAC) models. In parallel, we evaluated the distribution and safety of ^{68}Ga-RM-VH in eIND studies. ***Materials and Methods:*** The labeling of RMX-VH (25ug) with ^{212}Pb chloride was done using a manual approach in acetate buffer pH=6.0 in the presence of 40mg/ml ascorbate used as a scavenger. The radio/chemical purity was analyzed using iTLC chromatography, radio/UV HPLC, and gamma counter normalized for ^{212}Pb and ^{212}Bi energy windows. The uptake studies were completed in multiple GBM cancer cell lines (U87MG, A172, U373) and PDAC (HPAF-II, BxPC-3, and MiaPaCa2) showing various levels of LDLR expression. The SPECT images were acquired using a gamma-eye camera at 2h, 4h, and 24h post-injection with follow-up biodistribution studies. The organs and tumor were collected, weighed, and the tissue radioactivity was measured with a gamma counter. The percentage of injected dose-per-gram of tissue (%ID/g) was calculated and decay-corrected. ***Results:*** Our results showed that the radiopharmaceutical had a radiochemical purity of over 98% and no indication of radiolysis at 4 hours post-synthesis. The cellular uptake studies confirmed time-dependent accumulation of the agent reaching the highest uptake at 24h for HPAFII (13.7 %ID/g), BXPC3 (10.9 %ID/g) and lower for MiaPaca2 (3.6 %ID/g), and Colo357 (2.99 ID/g). The SPECT imaging studies showed selective accumulation of the agent in the orthotopic models of PDAC50 as early as 2h post-injection. The uptake correlated with bioluminescent data and PET/CT imaging studies using diagnostics analog, ^{68}Ga-RMX-VH. The bioD studies have shown (7.05 %ID/g) retention of the agent in the orthotopic PDAC at 2h post-injection, slightly reduced at 4h (4.56 %ID/g) and 24h (5.44 %ID/g) with renal excretion from the bloodstream as the main route of elimination. ***Conclusion:*** Our findings suggest that RMX-VH has favorable LDLR-tumor targeting properties. Ongoing studies include the evaluation of the companion diagnostic ^{68}Ga-RMX-VH in eIND clinical studies in the USA.

OP-214

Preparation and preclinical evaluation of ACE1 targeting molecular probe ^{68}Ga-DOTA-BPP

Q. Zhang, *Z. Yang, Z. Hua;*
Peking University Cancer Hospital, Beijing, CHINA.

Aim/Introduction: Triple negative breast cancer (TNBC), is estrogen receptor (ER), progesterone receptor (PR) and human epidermal growth factor receptor 2 (HER2) are all negative breast cancer by pathological examination, and the prognosis of this type of breast cancer is extremely poor. Angiotensin-converting enzyme 1 (ACE) is an important part of human renin-angiotensin-aldosterone system. Relevant literature has shown that ACE1 is highly expressed in the TNBC cell line MDA-MB-231. Therefore, ACE1 is expected to become a new target of TNBC. In this study, ^{68}Ga-DOTA-BPP, a novel peptide nuclide molecular imaging probe targeting ACE1 was constructed. The tumor-specific molecular imaging ability of the probe was evaluated by MDA-MB-231 and MCF-7 tumor models using Micro-PET/CT equipment. ***Materials and Methods:*** The peptide DOTA-BPP was radiolabeled with positron nuclide 68Ga. The labeling rate and radiochemical purity of the peptide were determined by Radio-HPLC. The in vitro stability of the peptide in normal saline and 5% human serum albumin (5% HSA) was analyzed. Pharmacokinetics were used to investigate the metabolism of the probe in the blood of normal mice. Immunohistochemical methods were used to analyze the expression of ACE1 in clinical TNBC specimens, and then two breast cancer models of MDA-MB-231 and MCF-7 were constructed to verify the specificity of the probe. The mouse model was injected with 3.7 MBq ^{68}Ga-DOTA-BPP in the tail vein, and Micro-PET/CT imaging was performed on the mouse model with tumor. To investigate the tumor imaging ability of ^{68}Ga-DOTA-BPP ***Results:*** The radiochemical purity of the product was greater than 99% after purification by C18 column. The radiochemical purity of the product was greater than 95% after the probe was placed in normal saline and 5% HSA for 2 hours. The mean expression rate of ACE in 143 clinical TNBC specimens was about 27%. The half-life of ^{68}Ga-DOTA-BPP in the blood of normal mice was 1.41 min and 14.18 min, respectively, indicating that the probe could be rapidly metabolized in the blood. Imaging results showed that

the probe was concentrated at the tumor site of MDA-MB-231 in ACE positive breast cancer model, but no significant uptake was observed at the tumor site of MCF-7 in ACE negative breast cancer model. ***Conclusion:*** Molecular probe ^{68}Ga-DOTA-BPP has good stability in vitro, and preliminary studies have shown that this probe has good targeting to TNBC tumors. Therefore, this study is expected to provide a new strategy for the diagnosis and treatment of TNBC.

OP-215

Construction of a novel PET probe of Iodine-124 labeled ADC for Trop-2 targeting and Micro-PET imaging

Z. Zeng[1], *D. Li*[1], *X. Yan*[2], *L. Li*[1], *J. Ding*[1], *X. Sheng*[2], *H. Zhu*[1], *Z. Yang*[1];
[1]*Department of Nuclear Medicine, Peking University Cancer Hospital & Institute, Beijing, CHINA,* [2]*Department of Genitourinary Oncology, Peking University Cancer Hospital & Institute, Beijing, CHINA.*

Aim/Introduction: Trop-2 is closely associated with the development and progression of various tumors, and its high expression is indicative of poor prognosis. Non-invasive imaging of Trop-2 in vivo can be achieved with an iodine-124 (^{124}I) labeled antibody drug conjugates (ADC, IMMU-132) positron emission tomography (PET) probe, which offers an essential approach for diagnosing and monitoring tumors with anti-Trop-2 clinical practice. ***Materials and Methods:*** In this study, we stained Trop-2 in pancreatic cancer tissue samples from patients with varying survival rates and developed a novel Trop-2 targeting molecular probe, ^{124}I-IMMU-132. We investigated the targeting and binding abilities of the probe to Trop-2 positive tumors in Capan-1/MDA-MB-468/Mcf-7 cells and their animal models. ***Results:*** Immunofluorescent staining revealed that Trop-2 is highly expressed in human pancreatic cancer and can predict the prognosis. The constructed ^{124}I-IMMU-132 probe had reliable radio-chemical characteristics and maintained binding affinity (Kd = 2.200 nmol/L). The probe uptake by Trop-2 positive Capan-1/MDA-MB-468 cells increased in a time-dependent manner. The probe specifically bound to Capan-1/MDA-MB-468 tumors in vivo, and the T/muscle ratio of SUVmax gradually increased with time from 4.30 ± 0.55 to 10.78 ± 1.80 ($p<0.01$) in the Capan-1 model and from 8.84 ± 0.95 to 32.20 ± 2.9 ($p<0.001$) in the MDA-MB-468 model. The biodistribution and pharmacokinetics of ^{124}I-IMMU-132 in the mouse model were consistent with the imaging, and the estimated dosimetry for humans was acceptable (the effective radiation dose was less than 4.2 mSv when 70 MBq probe was injected). ***Conclusion:*** ^{124}I-IMMU-132 PET is a promising imaging technique for delineating Trop-2 positive tumors, with great potential in early diagnosis and targeted population selection of patients.

OP-216

Immuno-PET Imaging of Tumor Mesothelin Expression with Gallium-68 Radiolabeled Nanobody

X. Lv[1,2], *Z. Xu*[3], *X. Song*[1,2], *Y. Gai*[1,2], *D. Jiang*[1,2], *P. Lei*[3], *W. Wei*[4], *Y. Zhang*[1,2], *R. An*[1,2], *X. Lan*[1,2];
[1]*Department of Nuclear Medicine, Union Hospital, Tongji Medical College, Huazhong University of Science and Technology, Wuhan, CHINA,* [2]*Hubei Province Key Laboratory of Molecular Imaging, Wuhan, CHINA,* [3]*Department of Immunology, School of Basic Medicine, Tongji Medical College, Huazhong University of Science and Technology, Wuhan, CHINA,* [4]*Department of Nuclear Medicine, Institute of Clinical Nuclear Medicine, Renji Hospital, School of Medicine, Shanghai Jiao Tong University, Shanghai, CHINA.*

Aim/Introduction: Mesothelin (MSLN) overexpresses in various solid tumors especially in pancreatic cancer and ovarian cancer while limited in normal tissues, making it a promising candidate for molecular imaging and targeted therapy. Nanobodies, the smallest antibody derived fragment, are facile to modify for functional agent conjugation, together with ideal characteristics appropriate to aforementioned application. Then immuno-positron emission tomography (Immuno-PET) could provide valuable whole-body information for analysis of related target properties and potential lacks. The objective of this work was to evaluate the in vivo distribution property of the nanobody (MS3) as MSLN-overexpressing tumor-directing agent via immuno-PET study. ***Materials and Methods:*** By labeling a MSLN-specific nanobody with Gallium-68, we developed a MSLN-targeted immune-PET imaging probe [^{68}Ga]Ga-NOTA-MS3. The in vivo characteristics and specificity of the probe was estimated in preclinical tumor models bearing different level of MSLN. Then we strived to reduce renal uptake with premedication of sodium maleate, thereby improving visualization of intraperitoneal tumor lesions and protecting from radiation-induced nephrotoxicity. The mean percentage of injected dose per gram (%ID/g) for various tissues were obtained by drawing regions of interest. Human cancer cells lines BxPC-3 and HuH-7 were identified as respectively high and low MSLN-expressing, and the BxPC-3 MSLN knockout (BxPC-3 KO) cell line was successfully constructed for comparative study. ***Results:*** The non-decay corrected yield of ^{68}Ga-NOTA-MS3 was around 47%, and the radiochemical purity exceeded 98% according to radio-high-performance liquid chromatography. Consistent with the results from western blot and immunohistochemistry, the tumor uptake of ^{68}Ga-NOTA-MS3 was ranked from highest to lowest in BxPC-3, BxPC-3 KO and HuH-7. Apart from the half-hour point imaging greatly affected by blood-pool signal, the tumor uptakes, tumor-to-muscle (T/M) and tumor-to-blood (T/B) ratios of BxPC-3 on each time point were significantly higher than those in the other two groups. The highest tumor uptake, T/M and T/B of BxPC-3 come to 1.28%ID/g at 30 minutes post-injection, 22.2 and 8.18 at 4 h post-injection, respectively. Furthermore, the pre-administration of sodium maleate significantly reduced renal uptake of ^{68}Ga-NOTA-MS3, from 32.2 to 7.52%ID/g at 30 minutes post-injection, without compromising tumor uptake, hence ameliorate the delineation of tumor in situ. ***Conclusion:*** We successfully validated one specific MSLN nanobody, MS3, and the derived immune-PET probe ^{68}Ga-NOTA-MS3 showed precise visualization for accurate diagnosis of MSLN-expressing lesions.

OP-217

CD70-targeted immunoPET imaging of renal carcinomas

X. Zhou, *Q. Xia, J. Liu, W. Wei;*
shanghai jiaotong university, Shanghai, CHINA.

Aim/Introduction: The diagnosis of primary and metastatic lesions in renal cell carcinoma (RCC) remains a clinical challenge. The cluster of differentiation (CD70) is specifically expressed in RCC making it a potential diagnostic and therapeutic target for RCC. This work aims to develop an immuno-positron emission tomography (immunoPET) imaging strategy targeting CD70 and to assess the diagnostic value of new molecular probes in preclinical RCC models. ***Materials and Methods:*** CD70 expression was detected in various types of RCCs and normal kidney tissues using immunohistochemical staining. Two novel CD70-specific single-domain antibodies (sdAbs) and their albumin-binding domain (ABD) variants were produced and labeled with gallium-68 (^{68}Ga, $T_{1/2}$ = 1.1 h) and zirconium-89 (^{89}Zr, $T_{1/2}$ = 78.4

h) to develop radiolabelled agents with different half-lives. The diagnostic properties of the developed tracers targeting CD70 ([^{68}Ga]Ga-NOTA-B3, [^{68}Ga]Ga-NOTA-B6, and [^{89}Zr]Zr-DFO-ABDB6) were evaluated in subcutaneous RCC patient-derived xenograft (PDX) models. For clinical study, PET/CT images were acquired at 1 h after injection of [^{68}Ga]Ga-NOTA-B6 (1.85-3.7 MBq/kg) in 3 RCC patients with metastases. ***Results:*** Expression of CD70 was associated with gender, tumor differentiation, tumor thrombus, necrosis, distant metastasis, and overall survival. SdAbs targeting CD70 and ABD fusion proteins had high affinity for recombinant human CD70. ImmunoPET imaging with [^{68}Ga]Ga-NOTA-B3 and [^{68}Ga]Ga-NOTA-B6 visualized subcutaneous RCC with clarity. Tumor uptake of [^{68}Ga]Ga-NOTA-B6 was significantly reduced after the blockade of CD70. [^{68}Ga]Ga-NOTA-ABDB6 had significantly prolonged in vivo circulation time. Multi-time point immunoPET imaging with [^{89}Zr]Zr-DFO-ABDB6 showed that tumors were visible within 144 h after injection, with the best tumor-to-background ratio achieved at 72 h after injection. In 3 RCC cancer patients, there was no adverse reaction during study. The uptake of [^{68}Ga]Ga-NOTA-B6 had signifcantly high tumor uptake in CD70-positive metastatic lesions at 1h post-injection. ***Conclusion:*** CD70 is expressed in primary and metastatic lesions of most ccRCCs and is strongly associated with patient survival. We have successfully developed sdAb-derived CD70-targeted immunoPET tracers and characterized their superior diagnostic accuracies in preclinical RCC models.

OP-218

Screening, development and preliminary evaluation of CLDN18.2 specific peptide PET probes

Z. Wang[1], *C. Zhao*[2], *J. Ding*[1], *H. Zhu*[1];
[1]*Key Laboratory of Carcinogenesis and Translational Research (Ministry of Education/Beijing), Key Laboratory for Research Evaluation of Radiopharmaceuticals (National Medical Products Administration), Department of Nuclear Medicine, Peking University Cance, Beijing, CHINA,*
[2]*Key Laboratory of Carcinogenesis and Translational Research (Ministry of Education/Beijing), Department of Biochemistry and Molecular Biology, Peking University Cancer Hospital and Institute, Beijing, Beijing, CHINA.*

Aim/Introduction: Gastric cancer (GC) remains prevalent worldwide, especially in Asian countries. Recent global clinical trials have shown that CLDN18.2 is an ideal target for the treatment of gastric cancer and patients with high CLDN18.2 expression can benefit from targeted therapy. Therefore, accurate and comprehensive detection of CLDN18.2 expression is important to the effective use of this target. The objectives of this study are to screen and obtain CLDN18.2 specific targeted peptides, and construct ^{68}Ga labeled molecular probes to achieve real-time and comprehensive evaluation of CLDN18.2 in vivo. ***Materials and Methods:*** Phage display technology was used to screen CLDN18.2 specific peptides from 100 billion libraries. 293T$^{CLDN18.1}$ cells were used to exclude non-specific binding and CLDN18.1 binding sequences while 293T$^{CLDN18.2}$ cells were used to screen CLDN18.2 specific binding peptides. The monoclonal clones obtained from phage screening were sequenced and peptides were synthesized based on the sequencing results. Binding specificity and affinity were assessed with FITC conjugated peptide using ELISA, flow cytometry and immunofluorescence experiments. DOTA conjugated peptide was also synthesized for ^{68}Ga radio labeling. The in vitro stability, in vivo molecular imaging and biodistribution were also characterized. ***Results:*** Overall, 54 monoclonal clones were selected after phage display screening. Subsequently, based on cell ELISA results, CLDN18.2 preference monoclonal clones were selected for DNA sequencing, and four 7-peptide sequences were obtained after sequence comparison. Among them, a peptide named T37 was further validated in vitro and in vivo. The T37 peptide specifically recognized CLDN18.2 but not CLDN18.1 and bound strongly and specifically to CLDN18.2-positive cell membranes. The ^{68}Ga-DOTA-T37 probe has good properties and high stability in vitro. It has high biological safety and PET/CT studies have shown that it can specifically target CLDN18.2 protein and CLDN18.2-positive tumors in mice. ***Conclusion:*** A CLDN18.2-specific peptide T37 was obtained. ^{68}Ga-DOTA-T37 demonstrated the superiority and feasibility of being a CLDN18.2 specific probe in PCT/CT imaging that deserves further development and exploitation.

OP-219

Immuno-PET of Colorectal Cancer with A CEA-Targeted ^{68}Ga-Nanobody: From Bench to Bedside

L. Li[1], *X. Lin*[1], *X. Ma*[1], *F. Liu*[1], *B. Jia*[2], *Z. Yang*[1];
[1]*Peking University Cancer Hospital & Institute, Beijing, CHINA,* [2]*Peking University, Beijing, CHINA.*

Aim/Introduction: The accurate diagnosis of colorectal carcinoma (CRC) can assist physicians in developing reasonable therapeutic regimens, thereby significantly improving patient's prognosis. Carcinoembryonic antigen (CEA)-targeted PET imaging shows great potential for this purpose. Despite showing remarkable abilities to detect CRC, previously reported CEA-specific antibody radiotracers or pretargeted imaging are not suitable for clinical use due to poor pharmacokinetics and complicated imaging procedures. In contrast, nanobodies exhibit ideal characteristics for PET imaging, for instance, rapid clearance rates and excellent distribution profiles, allowing same-day imaging with sufficient contrast. In this study, we developed a novel CEA-targeted nanobody radiotracer, ^{68}Ga-HNI01, and assessed its tumor imaging ability and biodistribution profile in preclinical xenografts and patients with primary and metastatic CRC. ***Materials and Methods:*** HNI01 was generated by immunizing lama with CEA proteins and site-specifically with ^{68}Ga using the THP as chelator. Micro PET imaging and biodistribution studies were performed in CEA-positive LS174T and CEA-negative HT-29 xenografts. Following successful preclinical assessment, a phase I study was conducted in 9 patients with primary and metastatic CRC. Participants received 151.21 ± 25.25 MBq of intravenous ^{68}Ga-HNI01 and underwent PET/CT scan at 1 h and 2 h post injection. Patients 01-03 also underwent whole-body dynamic PET imaging within 0-40 minutes p.i. All patients underwent ^{18}F-FDG PET/CT imaging within 1 week after ^{68}Ga-HNI01 imaging. Tracer distribution, pharmacokinetics and radiation dosimetry were calculated. ***Results:*** ^{68}Ga-HNI01 was successfully synthesized within 10 minutes under mild conditions with radiochemical purity > 98% without purification. Miro PET imaging revealed clear visualization of LS174T tumors, while signals from HT-29 tumors were significantly lower. Biodistribution studies indicated that uptake of ^{68}Ga-HNI01 in LS174T and HT-29 was 8.83 ± 3.02 %ID/g and 1.81 ± 0.87 %ID/g, respectively, at 2 h p.i. No adverse events occurred in all clinical participants after injection of ^{68}Ga-HNI01. A fast blood clearance and low background uptake were observed, and CRC lesions could be visualized with high contrast as early as 30 minutes after injection. ^{68}Ga-HNI01 PET could clearly detect metastatic lesions in the liver, lung and pancreas, and showed superior ability than ^{18}F-FDG PET/CT in detecting small metastases. ***Conclusion:*** ^{68}Ga-HNI01 is a novel CEA-targeted

PET imaging radiotracer with excellent pharmacokinetics and favorable dosimetry profiles. ^{68}Ga-HNI01 PET is an effective and convenient imaging tool for detecting CRC lesions, particularly for identifying small metastases.

OP-220

Increasing the Tumor-to-Blood Ratio by Click-Cleavable Radioimmunoimaging with [^{89}Zr]Zr-DFO-Trans-Cyclooctene-Trastuzumab in Mice

K. E. de Roode[1,2], *M. Vlastara*[1], *R. Rossin*[1], *F. J. M. Hoeben*[3], *M. Boswinkel*[2], *L. H. J. Kleijn*[1], *J. Nagarajah*[2], *S. Heskamp*[2], *M. Rijpkema*[2], *M. S. Robillard*[1];
[1]*Tagworks Pharmaceuticals, Nijmegen, NETHERLANDS,* [2]*Department of Medical Imaging, Radboud University Medical Centre, Nijmegen, NETHERLANDS,* [3]*SyMO-Chem, Eindhoven, NETHERLANDS.*

Aim/Introduction: Positron-emission tomography (PET) imaging using ^{89}Zr-labeled monoclonal antibodies is limited by the long blood circulation time of these antibodies, resulting in low tumor-to-background ratios. To overcome this drawback, we developed a ^{89}Zr-labeled Trastuzumab (Tmab) construct, [^{89}Zr]Zr-TCO-Tmab comprising a chemically cleavable trans-cyclooctene (TCO) linker [1, 2] between antibody and radiometal-chelate. Upon in vivo reaction with tetrazine (trigger) in blood, but not inside tumor cells, a bioorthogonal click-to-release reaction leads to liberation of rapidly clearing [^{89}Zr]Zr-DFO from the antibody construct. ***Materials and Methods:*** Several [^{89}Zr]Zr-TCO-Tmab construct variants were synthesised and their [^{89}Zr]Zr-DFO release upon reaction with trigger was evaluated in vitro. The best performing candidate was studied in vitro on BT-474 cancer cells to determine the rate of internalisation, and subsequently in healthy and BT-474 tumor-bearing mice to determine the biodistribution with and without trigger. In addition, PET imaging of tumour-bearing mice administered with [^{89}Zr]Zr-TCO-Tmab was performed before and after trigger administration. ***Results:*** The best performing [^{89}Zr]Zr-TCO-Tmab and trigger pair demonstrated 83% release of [^{89}Zr]Zr-DFO fragment in mouse plasma, and in line with predicted HER2 internalization over time, successful internalisation of [^{89}Zr]Zr-TCO-Tmab into BT-474 cells was observed in vitro. In tumor-bearing mice we observed a striking increase of the tumour-to-blood ratio from 1.0 ± 0.4 to 2.3 ± 0.6 (p=0.0057) and from 2.5 ± 0.7 to 6.6 ± 0.9 (p<0.0001) when the trigger was administered at 6 h and 24 h post-mAb, respectively. Same-day PET imaging confirmed a clear increase in tumor-to-background ratio after administration of trigger. ***Conclusion:*** We demonstrated successful enhancement of tumor-to-background ratios in mice using a click-cleavable [^{89}Zr]Zr-TCO-Tmab construct. The results presented here demonstrate the potential of click-cleavable strategies to reduce radiation doses and overcome inconvenient lengthy intervals in PET imaging with full-size antibodies. ***References:*** 1. Versteegen, R.M., et al., Click to release: instantaneous doxorubicin elimination upon tetrazine ligation. Angew Chem Int Ed Engl, 2013. 52(52): p. 14112 6. 2. Rossin, R., et al., Chemically triggered drug release from an antibody-drug conjugate leads to potent antitumour activity in mice. Nat Commun, 2018. 9(1): p. 1484.

605

Sunday, September 10, 2023, 4:45 PM - 6:15 PM
Hall B

Cutting Edge Science Track - TROP Session: Segmentation and Denoising

OP-221

Deep learning is a promising tool for fully automatic malignant lesions identification and segmentation in whole-body bone scans

F. Oliveira, *Â. Silva, J. Castanheira, M. Silva, C. Constantino, D. C. Costa;*
Champalimaud Foundation, Lisboa, PORTUGAL.

Aim/Introduction: Automated identification of malignant lesions in whole-body bone scans (BS) as well as the delineation of those lesions for the computation of the bone scan index are important tasks for disease quantification. We aim to assess the feasibility of fully automatic malignant lesion detection and segmentation in BS using deep learning based on a U-Net architecture. ***Materials and Methods:*** We randomly selected, from our archives, 434 whole-body BS obtained with ^{99m}Tc-HDP (^{99m}Tc-hydroxydiphosphonate), in anterior and posterior projections. Two nuclear medicine physicians reviewed the BS and all information contained in the patients' clinical records. Thereafter, they labeled all bone lesions suspected of malignancy. A self-adaptative Bayesian classifier was used for semiautomatic lesion segmentation [1]. For each malignant lesion, the segmentation was done in the projection displaying higher contrast to the background. In cases where two segmentations were obtained (one per projection), they were fused afterward. For fully automatic lesion detection and segmentation, we trained a two-channel 2D U-Net using the nnU-Net framework [2]. The dataset was randomly split into 384 BS for training and the remainder 50 for the test. The posterior projection of each BS was mirrored to match the anterior projection pixel-by-pixel and then used as a second channel in the 2D U-Net. The Dice coefficient was used to measure the pixelwise agreement between the semiautomatic and fully automatic segmentations. ***Results:*** In total, 155 BS were identified by the physicians as having at least one malignant lesion, 137 were included in the training, and 18 were in the test set. Most of the "non-malignant" BS were from oncological patients with only degenerative bone and joint disease. After applying the 2D U-Net model obtained in the training process to the test set, 16 out of 18 BS were correctly identified as having malignant lesions (sensitivity 89%), and 31 out of 32 without malignant lesions (specificity 97%). The BS classification predictive positive value (PPV) was 94%. Regarding the quality of the segmentation on the 18 BS of the test set with malignant lesions, the median Dice coefficient was 0.68 (interquartile range 0.48-0.77), with sensitivity of 54%, and PPV of 90%. ***Conclusion:*** The solution here implemented using deep learning is a promising tool for the automatic identification of BS with malignant lesions and their segmentation. Financial support: Project LISBOA/NORTE-01-0247-FEDER-017685, from PORTUGAL2020. ***References:*** [1] Constantino et al. J Digit Imaging. 2023. doi:10.1007/s10278-023-00823-y. [2] Isensee et al. Nature Methods. 2021 doi:10.1038/s41592-020-01008-z.

OP-222

Using a 3-D UNet artificial intelligence model to segment PSMA-avid lesions in ^{68}Ga-PSMA-11 PET/CT images

E. Greenblatt[1], *M. Maker*[1], *A. Kadumberi*[1], *S. Wail*[2], *P. Kuo*[1];
[1]*Invicro, Needham, MA, UNITED STATES OF AMERICA,*
[2]*Telix Pharmaceuticals, North Melbourne, AUSTRALIA.*

Aim/Introduction: ^{68}Ga-PSMA-11, a PET imaging radiopharmaceutical, is utilized for staging and detection of biochemical recurrence of prostate cancer. PSMA-avid lesion segmentation enables assessment of quantitative volumetric and SUV metrics. Segmentation is resource demanding - particularly with extensive multi-system disease. The aim was to develop artificial intelligence segmentation of lesions trained with ^{68}Ga-PSMA-11 image datasets. ***Materials and Methods:*** 660 PET/CT images were gathered from three sites. Images from two sites were divided into training (n=585) and benchmark (n=30) datasets; the third site's images (n=45) were test data. A standard was developed for disease below 3g/ml that may be clinically relevant in low disease burden patients. Semi-automated tools were utilized to label bone, lymph node, liver, prostate/prostate bed, peritoneal, pleura, and adrenal lesions. UNet models were trained to predict lesion classes at both high and low resolution; several included a physiological uptake segmentation class. Models were tested in cross-validated predictions of training data, and lead models were evaluated with benchmark and validation datasets. For each lesion class the average, median, and volume-weighted average dice ($Dice_{vw}$) scores described model performance. R^2 between predicted versus ground truth volume, SUV mean, SUV maximum, PSMA load, and the fraction of cases that were purely false-positive or false-negative characterized the model's stratification of disease burden across patients. ***Results:*** Bone segmentations matched experts in all datasets and models ($0.79<Dice_{vw}<0.92$). Lymph node performance was more varied ($0.44<Dice_{vw}<0.76$), as was the prostate class where cases were available ($0.06<Dice_{vw}<0.68$). R^2 across patients followed a similar pattern among classes with bone showing the strongest relationships ($0.83<R^2<1.00$), while these measures were highly varied for lymph node and prostate ($0<R^2<1.00$). Low disease, liver and other class performed poorly. One high-resolution model with the physiological uptake class was highest performing across datasets, although the high-resolution model without such segmentation had superior lymph node segmentation in the benchmark and test datasets. Clinical review of the segmentations found bone and lymph node segmentations to be valuable and beneficial in volumetric analysis of ^{68}Ga-PSMA-11 images. ***Conclusion:*** High-resolution models trained on this population are advantageous for segmenting large bone lesions at resolutions twice the PET image. Lymph node and prostate segmentations also performed well but require review in the pelvic region. Segmentation of prostatic lesions are difficult to distinguish from the bladder. The models segment low disease, liver and other lesion classes poorly. The addition of more training data, including no lesion images, may improve future models.

OP-223

A Feature-Based Ensemble of 3D U-Nets for Computed Tomography (CT) Lung Lobe Segmentation

E. Amini[1,2], *R. Klein*[1,3,4];
[1]*Ottawa Hospital Research Institute, Ottawa, ON, CANADA,* [2]*Carleton University, Ottawa, ON, CANADA,* [3]*The Ottawa Hospital Department of Nuclear Medicine, Ottawa, ON, CANADA,* [4]*University of Ottawa Department of Medicine, Ottawa, ON, CANADA.*

Aim/Introduction: Lung lobe segmentation is a critical step in the diagnosis, treatment, and monitoring of lung diseases. Recent advances in deep learning-based approaches have shown promising results for accurate and efficient lung lobe segmentation. However, the clinical applicability of these algorithms is challenging due to a wide variation in fissure anatomy, disease and imaging methods. We propose a novel segmentation method explicitly trained on a unique, heterogenous image set. ***Materials and Methods:*** The study used a dataset of 120 CT scans with annotations for lung lobes and trachea. Images were stratified by difficulty of lung lobe segmentation by visual score on a 3-level scale based on factors such as fissure perceptibility, completeness, and presence of disease patterns. Data were then split randomly into 80% for training and 20% for testing preserving stratification. To prepare the training data, eigenvalue analysis of the Hessian matrix at three different scales was performed on each scan to generate tubular structures (e.g., blood vessels and airways) in the image, at three levels of detail (coarse to fine). Consequently, each lobe presents as its own network of airways and blood vessels; revealing the fissures as gaps between these networks. Each CT scan was then masked with the filtered image and its associated trachea label, and a 3D U-Net architecture was separately trained for each detail level. A fourth model was trained on the unprocessed CT scans. As a final step, a random forest classifier was trained to combine the outputs from these models to segment each lobe. The performance of the proposed method is evaluated using the dice similarity coefficient (DSC) and the mean surface distance (MSD). ***Results:*** The proposed method DSC correlated with difficulty class (DSC = 0.93±0.01, 0.91±0.09 and 0.71±026 for easy, moderate, and hard, respectively). However, MSD (0.46±0.15, 0.44±0.09, and 0.48±0.14 mm) was consistent between difficulty classes. These results are consistent with visual impression of segmentation results in which erroneous segments tended to crisscross the fissures. ***Conclusion:*** In this study, we performed a lung lobe segmentation using a feature-based ensemble of 3D U-Net models using CT scans and tubular structure-filtered images. The segmentation performance correlates with visual impression of the task difficulty, achieving clinically useful results with good image quality and good fissure visibility. Future efforts must address difficult cases by improving automation and/or enabling manual tweaking of automatic segmentation results.

OP-224

Improving Automated Lesion Detection and Segmentation in PET/CT Scans: A Comparative Study of 3D UNet-Based Configurations

M. Namías, *Y. V. Rotstein Habarnau;*
Fundación Centro Diagnóstico Nuclear, Buenos Aires, ARGENTINA.

Aim/Introduction: Fluorodeoxyglucose (FDG) positron emission tomography / computed tomography (PET/CT) scans are routinely used for oncologic staging and response assessment. In this context, automatic lesion detection and segmentation is still a challenging task, since lesions are not the only FDG-avid regions, with physiological uptake also present on healthy tissues. Moreover, lesions of different shapes, sizes and FDG uptake may be found in diverse body regions. In this work, we explore different deep learning strategies to improve the rate of both false positive and false negative results in automated lesion detection and segmentation. ***Materials and Methods:*** We compared the performance of different 3D UNet-based configurations that automatically segment the lesions in PET/CT images. We trained

a 3D UNet using different input channels: PET image, a denoised PET image, the fusion of PET and CT images, and the fusion of PET, CT and organ segmentations obtained from the CT images. We also trained a mirror-UNet: one path segments the organs from a CT image and the other one segments the lesions from the PET image, with both paths sharing the bottleneck and thus obtaining a multimodal representation of image features. We trained and validated our networks on the AutoPET MICCAI 2022 Challenge dataset [1], considering only the studies with lesions. We used the Dice score, false positive (FPV) and false negative (FNV) volumes as performance metrics, averaged over the studied test cases. ***Results:*** We found that combining the PET and CT reduces the FPV compared to the unimodal PET model (12.13 ml vs 25.27 ml), but slightly increases the FNV (8.67 ml vs 5.70 ml). They both have similar Dice coefficients (0.65 for PET/CT vs 0.64 for PET). Adding a tissue segmentation channel as an input reduces the FPV compared to unimodal PET (13.02 ml), at the expense of FNV and Dice performance (14.70 ml and 0.57 respectively). The denoised version of the PET model had a very similar performance to that of the original PET (Dice=0.64, FPV=26.51 ml, FNV=5.04 ml). The mirror-UNet configuration gave the best Dice and FNV and a better FPV than de unimodal PET: Dice=0.67, FPV=18.93 ml and FNV=4.13 ml. ***Conclusion:*** We successfully compared the performance of different 3D UNet-based configurations for automatic lesion detection and segmentation in PET/CT, of which the mirror-UNet variant is the best-performing one. ***References:*** [1] https://autopet.grand-challenge.org/

OP-225

A Hybrid Neural Network Architecture to improve low-dose PET Image Reconstruction

S. Kaviani[1], *A. Sanaat*[2], *M. Mokri*[1], *C. Cohalan*[3], *J. Carrier*[1,4]; *[1]Université de Montréal, Montréal, QC, CANADA, [2]University of Geneva, Geneva, SWITZERLAND, [3]CHUM - Centre hospitalier de l'Université de Montréal, Montréal, QC, CANADA, [4]CHUM - Centre hospitalier de l'Université de Montréal, Montreal, QC, CANADA.*

Aim/Introduction: Positron emission tomography (PET) images are prone to noise, resulting in low contrast and reduced spatial resolution, particularly in low-count settings typical for dynamic acquisitions. The challenge of low-count PET data is a major concern in clinical practice, as it leads to difficulties in image interpretation and may compromise the accuracy of diagnosis. Therefore, developing an accurate and efficient image reconstruction method for low-count PET data is essential. In this work, we propose a novel deep-learning approach for low-dose PET image reconstruction. ***Materials and Methods:*** The novel deep learning approach for low-dose PET image reconstruction by combining two neural network architectures, the Transformer and UNet, and incorporating them into the unrolled maximum a posteriori estimation (MAPEM) algorithm. Our proposed approach was evaluated using both simulated and real patient data. The simulated dataset was generated using NiftyPET to simulate forward projection operators and noise models to generate ground truth images and simulated projection data, while the real patient dataset was acquired using a Siemens Biograph mMR PET scanner. We also implemented state-of-the-art methods for comparison purposes: OSEM, MAPEM, and unsupervised denoising. The reconstructed images are compared to ground truth images using metrics such as peak signal-to-noise ratio (PSNR), structural similarity index (SSIM), and relative root mean square error (rRMSE) to quantitatively evaluate the accuracy of the reconstructed images. ***Results:*** For the simulated data, our approach achieved an average PSNR of 38.91, an average SSIM of 0.976, and an average rRMSE of 0.077. These results outperformed 3 state-of-the-art methods, which had average PSNRs of 36.54, 37.15, and 37.88, average SSIMs of 0.969, 0.972, and 0.974, and average rRMSEs of 0.105, 0.093, and 0.089. For the real patient data, our approach achieved an average PSNR of 33.72, an average SSIM of 0.955, and an average rRMSE of 0.129. These results also outperformed other methods which had average PSNRs of 31.89, 32.12, and 32.87, average SSIMs of 0.944, 0.947, and 0.950, and average rRMSEs of 0.159, 0.149, and 0.145. ***Conclusion:*** These results demonstrate that our proposed approach can effectively reconstruct low-dose PET images with reduced noise levels and better edge preservation compared to other reconstruction and post-processing algorithms. Our method shows potential for clinical use as it can reconstruct smooth images while preserving edges.

OP-226

A deep learning method for the recovery of standard-dose imaging quality from ultra-low-dose PET on wavelet domain

S. Xue[1], *F. Liu*[1], *H. Wang*[2], *M. Viscione*[1], *R. Guo*[2], *A. Rominger*[1], *B. Li*[2], *K. Shi*[1]; *[1]University of Bern, Bern, SWITZERLAND, [2]Shanghai Jiao Tong University School of Medicine, Shanghai, CHINA.*

Aim/Introduction: Recent development in positron emission tomography (PET) dramatically increased the effective sensitivity by increasing the geometric coverage leading to total-body PET imaging. This encouraging breakthrough brings the hope of ultra-low dose PET imaging equivalent to transatlantic flight with the assistance of deep learning (DL)-based methods. A critical bottleneck for conventional DL-based methods is their limited capability in the application in the heterogeneous domain of PET imaging. We aim to develop a wavelet-based DL method that can recover high-quality imaging from ultra-low-dose PET. ***Materials and Methods:*** In contrast to traditional DL techniques that perform denoising on the image domain, we propose to feed the network with the wavelet-decomposed high frequency component of PET imaging, where the noise is mainly concentrated. The effectiveness and robustness of our proposed approach was verified in tests of different imaging tracers on different scanners. Total-body PET images of 550 patients using ^{18}F-FDG, ^{18}F-PSMA, ^{68}Ga-DOTA-TOC, ^{68}Ga-DOTA-TATE, acquired using total-body PET scanners, including Biograph Vision Quadra (Siemens Healthineers), uEXPLORER (United Imaging) in Shanghai and Bern, were included for the development and testing of the proposed method [1]. The generated image quality was evaluated with customized scoring system, using weighted global physical metrics and local clinical-relevant features. ***Results:*** Although the method was developed using data from one scanner, it achieved score of 2.16 on both Quadra and Explorer, which improved over conventional deep learning methods (2.09) and non-AI enhanced images (1.66). Our deep learning methodology showed advantages on all DRF ($p < 0.05$). ***Conclusion:*** The proposed wavelet-based DL method leads to fast computation and despeckling with well-preserved image details, which can improve the performance and robustness of image quality recovery on ultra-low-dose PET imaging. It may improve the trustworthiness and clinical acceptability of DL-based dose reduction. ***References:*** Xue, Song, et al. "A cross-scanner and cross-tracer deep learning method for the recovery of standard-dose imaging quality from low-dose PET." European journal of nuclear medicine and molecular imaging (2021): 1-14.

OP-227

Sequential Deep Learning Image Enhancement Models Improve Diagnostic Confidence, Lesion Detectability and Image Reconstruction Time in PET

M. Dedja[1], *A. Mehranian*[2], *K. M. Bradley*[3], *M. D. Walker*[1], *S. D. Wollenweber*[4], *R. Johnsen*[4], *D. R. McGowan*[1,5];
[1]*Oxford University Hospitals, Oxford, UNITED KINGDOM,* [2]*GE Healthcare, Oxford, UNITED KINGDOM,* [3]*Cardiff University, Cardiff, UNITED KINGDOM,* [4]*GE Healthcare, Waukesha, WI, UNITED STATES OF AMERICA,* [5]*University of Oxford, Oxford, UNITED KINGDOM.*

Aim/Introduction: Investigate the potential benefits of sequential deployment of two deep learning (DL) algorithms namely DL Enhancement (DLE) and DL-based time-of-flight (ToF) (DLT). DLE aims to enhance the rapidly reconstructed ordered subset expectation maximisation algorithm (OSEM) images towards block-sequential-regularised-expectation-maximisation (BRSEM) images [1], whereas DLT aims to improve the quality of BRSEM images reconstructed without ToF [2]. As the algorithms differ in their purpose, the sequential application may allow the benefits from each to be combined. ***Materials and Methods:*** 20 FDG PET-CT scans were performed on a GE Healthcare PET-CT D710 scanner. List-mode data was reconstructed with four combinations of algorithms: 1.BRSEMToF, 2.BRSEMnonToF+DLT, 3.OSEMToF+DLE and 4.OSEMToF+DLE+DLT. To assess image noise, 30mm-diameter spheres were drawn in both lung and liver to measure standard deviation of voxels within the volume. In a blind clinical reading, an experienced reader rated the images in a five-point Likert scale (5 best) based on diagnostic confidence and lesion detectability. The reader also ranked the images based on the same metrics (1 best). Statistical differences were corrected for multiple comparisons using Bonferroni correction. ***Results:*** For reconstructions 1-4 noise in the liver was 0.24±0.04,0.23±0.06,0.19±0.04,0.19±0.04. There was a significant decrease in image noise for 3&4 compared to the reference reconstruction (1) (Bonferroni corrected p<0.02), demonstrating that reconstructions with DLE have lower liver noise. Conversely, for the lung 0.07±0.02,0.08±0.02,0.07±0.02,0.07±0.02 with no statistical difference across reconstructions (p>0.05). Clinical image reading scores showed a significant preference for OSEMToF+DLE+DLT over other reconstructions in both lesion detectability(p<0.05) and diagnostic confidence(p<0.05). The score for lesion detectability in reconstructions 1-4 was 3.85±0.48,3.75±0.54,3.6±0.66,4.8±0.40 and the ranking was 2.40±0.80,2.65±1.01,2.55±1.02,1.00±0.00. For diagnostic confidence the score was: 3.50±0.59,3.35±0.65,3.65±0.57,4.8±0.40, the ranking was: 2.65±0.91,2.85±1.01,2.30±0.84,1.00±0.00. ***Conclusion:*** The combination of DLE and DLT increases diagnostic confidence and lesion detectability compared to BRSEM images, and to each DL algorithm in isolation. As DLE+DLT uses input OSEM images, and because DL inferencing is fast, there is a significant decrease in overall reconstruction time. This could have applications to total body PET as reconstruction time increases with the axial field of view. Future work will include multiple blinded readers and additional test cases. ***References:*** [1]Mehranian, A. et al.(2021) "Image enhancement of whole-body oncology [18F]-FDG PET scans using deep neural networks to reduce noise,"European Journal of Nuclear Medicine and Molecular Imaging, 49(2), pp. 539-549. [2]Mehranian, A. et al.(2022) "Deep learning-based time-of-flight image enhancement of non-ToF PET scans," European Journal of Nuclear Medicine and Molecular Imaging, 49(11), pp. 3740-3749.

OP-228

The Effect of Multimodal Anatomical Images in Deep Learning-enhanced Low-dose Amyloid PET Imaging

S. Kuo[1], *M. Lee*[1], *C. Ko*[2], *K. T. Chen*[1];
[1]*National Taiwan University, Taipei, TAIWAN,* [2]*National Taiwan University Hospital, Taipei, TAIWAN.*

Aim/Introduction: Amyloid PET has been commonly used in Alzheimer's disease diagnoses [1]. As the potential risk of radiation exposure remains a concern, deep learning methods have been proposed to generate full-dose PET images from simulated low-dose PET images [2, 3]. This study aims to investigate the contribution of multimodal anatomical images (CT and MRI) by leveraging all available imaging information. ***Materials and Methods:*** The images used in this study were obtained from 52 (mean±standard deviation [SD]: 65.4±12.2 years) participants and acquired separately on PET/CT and MR scanners; 410±102 MBq of the amyloid radiotracer 11C-Pittsburgh Compound-B were administered to the participant. The dynamic PET scan time was 70 minutes. In each PET dataset the last 3 frames (40-70 minutes post-injection) were averaged to create the full-dose ground truth image. The third last frame (40-50 minutes post-injection) was chosen as the simulated low-dose PET image (about 1/3 dose). U-nets [4] were trained in this work with the inputs being combinations of multimodal images (Case 1: low-dose PET image only, Case 2: low-dose PET and CT images, Case 3: low-dose PET and T2-weighted MR images, and Case 4: low-dose PET, CT, and T2-weighted MR images). 10-fold cross-validation was used to prevent testing on the same datasets. The metrics PSNR and SSIM were used to evaluate image quality. ***Results:*** The results generated from these networks all demonstrated significant improvements (p-value < 0.001) in terms of metrics when compared to the low-dose PET images and resembled the full-dose ground truth images. The incorporation of additional modalities into network training all yielded relatively higher SSIM and PSNR scores. Comparing SSIM in models incorporating other modalities, namely Case 2 (mean±SD: 0.9825±0.0099), Case 3 (0.9844±0.0087), and Case 4 (0.9837±0.0095), to Case 1 (0.9720±0.0349), statistically significant improvements in all 3 comparisons were observed (p-value < 0.05). The addition of MR images (Case 3 and Case 4) also showed significant improvement (p-value < 0.05) in PSNR compared to Case 1. ***Conclusion:*** This study demonstrated that incorporating CT and MR information into a deep learning network for predicting full-dose PET images from low-dose PET images significantly improved image quality. These findings also highlighted the value of utilizing anatomical imaging information for PET-related deep learning tasks. ***References:*** [1] GD Femminella et al. Int J Mol Sci. 2018.[2] KT Chen et al. Radiology. 2019.[3] KT Chen et al. Eur J Nucl Med Mol Imaging. 2020.[4] O Ronneberger et al. MICCAI. 2015.

OP-229

Iterative Deep-Learning Denoising in Bone SPECT-CT Reconstruction Based on Simulations from Clinical Data

O. Ziv, *B. Yuzefovich, J. Sachs, G. Kovalski;*
GE Healthcare, Haifa, ISRAEL.

Aim/Introduction: In Single-Photon Emission Computed Tomography (SPECT) imaging, achieving adequate signal-to-noise ratio is often limited by high statistical photonic noise. A fundamental problem in applying noise reduction techniques, is that small findings are typically similar to the image noise characteristics. Therefore, suppressing noise without impairing clinical image features is challenging with conventional algorithms.

Deep-Learning (DL) techniques have shown great potential in improving image quality in medical imaging applications. However, for SPECT it can be impractical to acquire high quality clinical images for the model learning targets. This study proposes a simulation-based DL approach to improve image quality of bone SPECT scans. ***Materials and Methods:*** Data generation: total of 2184 simulations were generated for the model training directly from clinical data including SPECT projections and CT images from 55 whole-body Tc99m bone exams. Realizations generation contains 4 steps: (1)Noise-free objects generation using dedicated algorithms, (2)Insertion of lesions with known location and contrast, (3)Noise insertion to depict a given scan time, (4)Final image reconstruction for training. DL model: a supervised 3D residual U-Net model was trained with input noisy image data and the ideal target data, using mean squared error loss function. During inferencing, the DL model is applied iteratively within the reconstruction iterations for incremental denoising process towards convergence. Both attenuation-corrected (AC) and non-corrected (NC) exams were processed. ***Results:*** The DL model was evaluated using digital phantom (XCAT with inserted lesions, 100 realizations) and clinical data (80 SPECT-CT exams, 6 expert readers). Both image characteristics (Structural Similarity Index (SSIM), Peak Signal-to-Noise Ratio (PSNR)) and lesion characteristics (Contrast-to-Noise Ratio (CNR), Contrast Recovery Coefficient (CRC)) were calculated on the digital phantom images. The clinical images were evaluated using a 5-points Likert score for Image Quality (IQ), Image Resolution (IR) and Noise Level (NL). The results (including 3 systems, 5 contrast ratios) represent an average improvement as compared to a standard reconstruction protocol (AC, NC respectively). Image characteristics improvement in SSIM (+4.8%, +3.8%) and PSNR (+12.1%, +2.9%) and lesion characteristics improvement in CNR (+29.6%, +42.4%) and CRC (+9.1%, +1.8%) were obtained. The clinical review demonstrated an improvement in IQ (+17.9%, +16.5%), IR (+27.2%, +25.7%) and NL (+12.2%, +17.0%). ***Conclusion:*** This study demonstrates a simulation-based DL approach integrated within the image reconstruction process to improve SPECT image quality. This approach effectively reduces noise, enhances image resolution and contrast, which led to improved image quality and potentially enhanced diagnostic accuracy.

606

Sunday, September 10, 2023, 4:45 PM - 6:15 PM
Hall C

Clinical Oncology Track - TROP Session: Neuroendocrine Tumors Treatment

OP-230

A phase I theranostic study evaluating the safety and tolerability of ^{177}Lu-satoreotide tetraxetan with ^{68}Ga-satoreotide trizoxetan companion imaging in participants with extensive-stage small-cell lung cancer (ES-SCLC) on atezolizumab maintenance therapy

L. Emmett[1], *J. Cardaci*[2], *K. O'Byrne*[3], *S. Arulananda*[4], *A. Prawira*[5], *B. Pais*[6,7], *M. Crumbaker*[1], *N. Lenzo*[8];
[1]*St Vincent's Hospital, Sydney, AUSTRALIA,* [2]*Hollywood Private Hospital, Nedlands, AUSTRALIA,* [3]*Princess Alexandra Hospital, Brisbane, AUSTRALIA,* [4]*Monash Health, Clayton, AUSTRALIA,* [5]*Obatica, Zetland, AUSTRALIA,* [6]*Ariceum Therapeutics, Berlin, GERMANY,* [7]*SRT-Biomedical, Soest, NETHERLANDS,* [8]*GenesisCare, Murdoch, AUSTRALIA.*

Aim/Introduction: ES-SCLC is a neuroendocrine carcinoma with a dismal prognosis. Etoposide/platinum-based chemotherapy (E/P-CT) has been the standard of care for patients with ES-SCLC for decades. Recently, immune checkpoint inhibition (ICI) with atezolizumab or durvalumab added to E/P-CT, followed by ICI maintenance therapy, has resulted in survival benefit. However, the need for improved treatment options remains as the median progression free (mPFS) and overall survival (mOS) is still not more than 5-7 and 13-14 months, respectively. Somatostatin receptor 2 (SST2) is expressed in the majority of SCLC lesions and SST2 targeted radioligand therapy has proven safe and effective in other neuroendocrine tumors. We therefore hypothesise that adding the SST2-antagonist ^{177}Lu-satoreotide tetraxetan (^{177}Lu-SSO110) to maintenance treatment with atezolizumab is safe and will result in efficacy benefits for patients with ES-SCLC eligible for maintenance treatment. ***Materials and Methods:*** The main objective of this study is to assess the safety and tolerability of ^{177}Lu-SSO110 and the recommended phase 2 dose in combination with atezolizumab. The secondary objective is to assess the preliminary anti-tumour activity. The exploratory objectives include the assessment of the level of concordance of lesions visible on ^{68}Ga-satoreotide trizoxetan (^{68}Ga-SSO120) PET/CT versus lesions visible on contrast-enhanced CT and/or FDG PET. Inclusion criteria include histologically or cytologically confirmed ES-SCLC, adequate organ and bone marrow function, a life expectancy >18 weeks, and ≥1 positive lesion on ^{68}Ga-SSO120 PET/CT. The first dose of ^{177}Lu-SSO110 will be administered after the 1st or 2nd cycle of atezolizumab maintenance therapy. Each patient will be treated with 4 doses of ^{177}Lu-SSO110 6-9 weeks apart, which may be extended up to 7 in case of clinical benefit. The study will follow a BOIN design to determine the recommended phase 2 dose with a target dose-limiting toxicity (DLT) rate of 0.30. The ^{177}LuSSO110 starting dose is 3.7 GBq which can be (de)escalated to 2.3, 3.0, 4.5, and 5.2 GBq, as required. ***Results:*** Preliminary results of this ongoing, open label study will be presented at the meeting. ***Conclusion:*** This study will support the selection of a recommended phase 2 dose and assess preliminary safety and efficacy of ^{177}Lu-SSO110 in patients with ES-SCLC on atezolizumab maintenance therapy.

OP-231

Evaluation of Progression-Free Survival (PFS) in Patients with Advanced, Non-resectable, Progressive GEP-NET Treated Using Combine Radioligand and CAPTEM therapy.

J. Cwikla[1], *A. Zrajkowska*[2], *G. Nowicka*[3], *J. Pałucki*[4], *N. Seklecka*[2], *A. Kolasińska-Ćwikła*[4];
[1]*University of Warmia and Mazury, Olsztyn, POLAND,* [2]*Diagnostic and Therapy Center – "Gammed" Warsaw, Poland, Warsaw, POLAND,* [3]*Warsaw Medical University, Warsaw, POLAND,* [4]*Maria Skłodowska-Curie National Research Institute of Oncology, Warsaw, POLAND.*

Aim/Introduction: Prospective, single-arm, open-label, case series study with assessment efficacy and safety of combined radioligand therapy (RLT) and CAPTEM in, advanced, unresectable progressive GEP-NET (NCT04194125). Primary endpoint: locally assessed RECIST 1.1 progression-free survival (PFS). Secondary goals: objective response rate (ORR), disease control rate (DCR), clinical response based on performance status (PS), additional safety (AEs). ***Materials and Methods:*** Twenty-one patients in group of 23 screened subjects between 18 February 2019 to 01 May 2023 included into analysis. All patients with confirmation of GEP-NETs at advanced, progressive, non-resectable stage.

Combine RLT (^{177}Lu DOTATOC) and CAPTEM used in all subjects. Clinical follow-up at least 48 months. Mean age 58.6 +12.6, male to female ratio 8/13. Tumour characteristics: NETG1=9, G2=10, G3=2. Disease status and treatment efficiency were evaluated by clinical assessment including PS, ORR, also biochemical response and safety profile of combine therapy. ***Results:*** Pancreatic (panNET) n=14, midgut n=7. Cumulative activity ^{177}Lu (GBq) of whole therapy; median=25.1GBq (20.4-27.0), per therapy median=6.5 GBq (5.8-6.8). Median PFS for all subjects (IQR) 31.5 months (16.0-n.r.), panNET PFS 28.0 m (14.0-n.r.), midgut PFS=31.5 months (24.5-n.r). After 6 weeks of follow-up 9 pts (42%) had partial response (PR) and 11 (52%) had stable disease (SD), after 3 m 9 had PR, 8 had SD, single had disease progression (DP). After 6 m 9 PR, 9 SD and 2 DP, after 12 m single 1 complete response, 10 PR, 5 SD and 2 DP. DCR after 6 weeks all patients, after 3 months 17 subjects (90%), 6 months 18 patients (85%) and after 12 months 16 subjects (89%). Clinical evaluation including PS=1 in 12 subjects improved at 6 to PS=0 in 2 cases PS=2 improve to PS=1, no change in 7 subjects. Treatment-emergent adverse events (TEAEs) were reported in most of them. The most common AEs was a transient lymphopenia G2 (44%) and G3 (8%); others AEs and their significant intensity (at least G3) were observed sporadically, no G4, during and after therapy. Persistent lymphopenia in treated subjects noted in 16% of cases. ***Conclusion:*** Combine therapy (RLT&CAPTEM) is effective in GEP-NET in terms of improvement of PFS in those who had documented DP. Clinical response, DCR of combine therapy seen in most of subjects during follow-up. Significant benefit in terms of ORR reported in panNET but not in midgut. In panNET who had PR four of them had primary tumor removal, single with CR for 4 years.

OP-232

Safety and organs-at-risk dosimetry in patients with gastroenteropancreatic neuroendocrine tumours (GEP-NETs) treated with ^{177}Lu-DOTATATE peptide receptor radionuclide therapy (PRRT): data from prospective phase II clinical trial

M. Mileva[1], *C. Van Bogaert*[2], *G. Marin*[3], *H. Levillain*[3], *C. Artigas*[1], *C. Marin*[3], *R. Danieli*[3], *A. Deleporte*[4], *C. Jungels*[4], *B. Vanderlinden*[3], *Z. Wimana*[1,5], *A. Hendlisz*[4], *P. Flamen*[1], *I. Karfis*[1];
[1]*Nuclear Medicine Department, Institut Jules Bordet, H.U.B, Brussels, BELGIUM,* [2]*Nuclear Medicine Department, Hôpital Erasme, H.U.B, Brussels, BELGIUM,* [3]*Medical Physics Department, Institut Jules Bordet, H.U.B, Brussels, BELGIUM,* [4]*Medical Oncology Department, Institut Jules Bordet, H.U.B, Brussels, BELGIUM,* [5]*Radiopharmacy Department, Institut Jules Bordet, H.U.B, Brussels, BELGIUM.*

Aim/Introduction: Safety of PRRT through evaluation of adverse events (AEs) and glomerular filtration rate (GFR) changes in patients with GEP-NETs, and their association with organs-at-risk (OARs) dosimetry and patient progression-free-survival (PFS). ***Materials and Methods:*** Patients with progressive GEP-NETs were prospectively included and treated with four cycles of ^{177}Lu-DOTATATE every 12 weeks, afterwards followed every 6mo until disease progression. AEs (CTCAEv4.03) occurring from the day of first treatment injection until 12 weeks after the last PRRT injection were collected and followed up until resolution (or patient end-of-study). GFR was calculated using plasma clearance of ^{51}Cr-EDTA or ^{99m}Tc-DTPA, at baseline, end-of-treatment and every 6mo during follow-up. Dosimetry of kidneys, bone marrow (BM) and spleen, was performed after each PRRT cycle, as previously published [1]. The %change of GFR at last available follow-up from baseline was correlated with the radiation dose received by the kidneys using Spearman correlation coefficient. Differences of BM and spleen dose between patients with high (2-4) and low grade (0-1) of haematological toxicity were assessed using Mann-Whitney U-Test. Kaplan-Meier method and log-rank test was used to estimate the PFS. ***Results:*** In 37pts included, median PFS was 28mo. Most patients (28/37) received four PRRT cycles. Most common AEs of any grade were anaemia and lymphopenia (65%), followed by thrombocytopenia and fatigue (51%), alopecia (46%) and nausea (41%). Most common grade ≥3 AEs were lymphopenia and increase in gamma-glutamyl transferase, in 43% and 14% of patients, respectively. After median of 23.4mo from the first cycle, median GFR decrease was 11% (95%CI:6%-18%). Median cumulative biological effective dose (BED) received by the kidneys and BM was 27.8Gy and 0.8Gy respectively. Median cumulative absorbed dose (AD) to the spleen was 40.9Gy. No correlation was found between GFR %decrease and kidneys' cumulative BED (Spearman ρ=-0.09; p=ns). BED of the BM was higher for patients developing high grade (n=6, median: 0.8Gy) versus low grade thrombocytopenia (n=31, median: 0.55Gy) (p=0.04). No association between BM BED and grades of lymphopenia and anaemia was demonstrated, as well as between the spleen AD and haematological toxicities. No statistical evidence was found for association between GFR decrease or the development of haematological toxicity and PFS. ***Conclusion:*** We confirm the global safety of PRRT. Apart from association between BM BED and thrombocytopenia, no other haematological toxicities were associated with dose to BM and spleen or with PFS, similarly to GFR decrease and dose to kidneys. ***References:*** 1.Marin G et al: Phys Med.2018;56:41-9.

OP-233

Efficacy and Safety of 177Lu-DOTATATE in Lung Neuroendocrine Tumors: A multicenter study

M. Mitjavila Casanovas[1], *V. Pubul*[2], *P. Belló*[3], *B. Miguel*[4], *J. Cano*[5], *D. Balaguer*[6], *A. García-Burillo*[7], *A. Mariño Méndez*[8], *E. Rodeño*[9], *A. Custodio*[10], *A. Piñeiro*[11], *L. García-Cañamaque*[12], *M. Castellon*[13], *M. Orduña*[14], *A. Carmona-Bayonas*[15], *P. Jimenez-Fonseca*[16];
[1]*Hospital Universitario Puerta de Hierro Majadahonda, Madrid, SPAIN,* [2]*Hospital Complejo Universitario Santiago, Santiago de Compostela, SPAIN,* [3]*Hospital Universitario La Fe, Valencia, SPAIN,* [4]*Hospital Universitario de Burgos, Burgos, SPAIN,* [5]*Hospital General Universitario de Ciudad Real, Ciudad Real, SPAIN,* [6]*Hospital Universitario Doctor Peset, Valencia, SPAIN,* [7]*Hospital Universitario Vall d'Hebron, Barcelona, SPAIN,* [8]*Hospital Universitario Central Asturias, Oviedo, SPAIN,* [9]*Hospital Universitario Cruces, Bilbao, SPAIN,* [10]*Hospital Universitario La Paz, Madrid, SPAIN,* [11]*Hospital Universitario Virgen de las Nieves, Granada, SPAIN,*
[12]*HM Hospitales Madrid, Madrid, SPAIN,* [13]*Hospital Universitario Virgen de la Arrixaca, Murcia, SPAIN,* [14]*Hospital Ramón y Cajal, Madrid, SPAIN,* [15]*Hospital Universitario Morales Meseguer, Murcia, SPAIN,* [16]*Hospital Universitario Central de Asturias, Oviedo, SPAIN.*

Aim/Introduction: Clinical trial evidence supporting the effectiveness of 177Lu-DOTATATE therapy (PRRT) is primarily focused on gastroenteropancreatic neuroendocrine neoplasms (NENs). Nevertheless, it is reasonable to consider that this therapy may also be effective in other NENs that express somatostatin receptors. This study aims to evaluate the efficacy and safety of PRRT in patients with advanced, non-resectable bronchopulmonary NENs. ***Materials and Methods:*** SEPTRALU represents a national, multicenter (23 hospitals) registry encompassing patients with advanced neuroendocrine neoplasms (NEN) who have undergone treatment with 177Lu-DOTATATE in clinical practice. This analysis includes patients with advanced bronchopulmonary

NENs treated between 2014 and 2022. The Kaplan-Meier method was utilized to analyze survival, the RECIST 1.1 criteria determined response rate, and the Common Terminology Criteria for Adverse Events (CTCAE) version 3.0 served as the basis for classifying toxicity. ***Results:*** Of the 706 patients registered with NEN, 9.35% (n=66) had bronchopulmonary NENs, with a median age of 62 years (range, 21-83) among these patients. 78% were male (n=51), and 84% had an ECOG performance status of 0-1 at diagnosis (n=55). The most common histological subtype was atypical carcinoid (53%, n=35), with neuroendocrine carcinomas accounting for 16% (n=11). The most frequent metastasis location was the liver (80%, n=53), followed by lymph nodes (53%, n=35), and bone (48%, n=32). Lutetium was administered as a second-line treatment in 31% of cases (n=20), as a third-line treatment in 58% (n=38), and in subsequent lines for the remaining patients (n=8). Prior to lutetium treatment, 54% of patients (n=36) had undergone primary cancer resection, 92% (n=61) had received somatostatin analogs, and 43% (n=28) had been treated with everolimus. The duration from diagnosis to the initiation of PRRT was 35 months (95% CI, 3-52). The response rate was 34% (n=22), with 52% (n=34) achieving stabilization. With 41/66 progression events and 26/66 deaths, progression-free survival was 18.4 (95% confidence interval (CI), 15.8-33.4) months, and overall survival was 47.9 (95% CI, 20-NA) months. The most common toxicity was neutropenia (44%, n=29), with 7% (n=5) of cases presenting as grade 3-4. ***Conclusion:*** 177Lu-DOTATATE is safe and active in patients with advanced bronchopulmonary NEN treatment in clinical practice. This study supports the development of phase III clinical trials to definitively determine the role of 177Lu-DOTATATE in bronchopulmonary NEN and the optimal treatment sequence. .

OP-234

Cylindrical TGR as Early Radiological Predictor of RLT Progression in GEPNETs. A Proof of Concept

F. Scalorbi[1], *E. Garanzini*[1], *G. Calareso*[1], *C. Marzi*[2], *S. Mazzaglia*[3], *G. Di Rocco*[1,4], *G. Argiroffi*[1], *L. Mascitti*[1,4], *M. Cuomo*[1,4], *S. Pusceddu*[1], *M. Milione*[1], *M. Baccini*[2], *E. Seregni*[1], *A. Marchianò*[1], *M. Maccauro*[1];
[1]*Istituto Nazionale Tumori Milano, Milan, ITALY,* [2]*Department of Statistics, Computer Science, Applications (DiSIA), University of Florence, Firenze, ITALY,* [3]*ASST Santi Paolo e Carlo, San Paolo University Hospital, Milan, ITALY,* [4]*University of Milan, Milan, ITALY.*

Aim/Introduction: Tumor Growth Rate (TGR) allows for early and quantitative assessment of SSAs (somatostatin analogues) and systemic treatments in GEPNETs (gastro-entero-pancreatic neuroendocrine tumors). Recently, TGR application has been proposed in the prediction of radio ligand therapy (RLT) response too. The aim is to evaluate the accuracy of cylindrical TGR (cTGR, obtained modifying the TGR formula) in the prediction of early progression after RLT, compared with the conventional TGR. ***Materials and Methods:*** Progressive metastatic G1-G2 GEPNETs treated with RLT (177Lu-DOTATATE, 4 administrations, 7.4 GBq) from April 2019 to October 2022 were considered. Inclusion criteria were three contrast enhancement CT scans per patient: one within three months of RLT start (i.e. baseline CT), one after two RLT administrations (i.e. interim CT) and one within three months after RLT (i.e. follow-up CT). RLT response was assessed at follow-up, according to RECIST1.1, as percentage variation of lesion diameters over time (a continuous value), and as four different classes: complete response (CR), partial response (PR), stable disease (SD) or progressive disease (PD). TGR was computed by comparing baseline and interim CT, in two ways: by approximating lesion volume to (i) a sphere (i.e., conventional TGR) or (ii) an elliptical cylinder (cTGR). Multivariate linear regression was performed to model the relationship between the change in TGR (conventional or cylindrical) and the continuous response to RLT, including the following covariates: age, gender, primary tumor, grading, ECOGPS, lines of therapy, and WHO grading. Moreover, ROC curves and optimal TGR cut-off values were computed to predict the PD class. STATA v16 software was used. ***Results:*** 58 patients (34 females, mean age 62.8) were included, resulting in 58.6% midgut, 41.4% foregut, 55.2% G2. In accordance with RECIST, 8.6% had early progression (PD) after RLT. In the PD prediction task, cTGR showed the best AUROC (0.82), compared with TGR(0.78). The optimal cut-off points were 6.57%/month (80% sensitivity, 94.34% specificity) and 5.96%/month (80% sensitivity, 92.45% specificity) for cTGR and TGR, respectively. Results were confirmed by multivariate analysis where both the TGRs were independent predictors of PD, with a higher coefficient for cTGR (1.16) compared to the conventional one (1.11). ***Conclusion:*** Both the TGRs are good predictors of RLT response with a better performance of cTGR. This study is a proof of concept that paves the way for clinical trials on the purpose of introducing cTGR in clinical practice. ***References:*** Dromain C. BMC Cancer 19,66(2019) - Pettersson OJ, Endocr Connect. 2021 Apr 22;10(4):422-431

OP-235

Safety and Efficacy of Lu-177-DOTATATE in Metastatic or Inoperable Pheochromocytoma/Paraganglioma: An Interim Analysis

F. Lin[1], *J. Carrasquillo*[1], *J. del Rivero*[1], *I. Shami*[1], *Z. Joy*[1], *B. Turkbey*[1], *J. Klubo*[1], *Y. Teng*[2], *A. Jha*[1], *E. Mena*[1], *M. L. Lindenberg*[1], *C. Chen*[1], *P. Herscovitch*[1], *C. Millo*[1], *K. Pacak*[1];
[1]*National Institutes of Health, Bethesda, MD, UNITED STATES OF AMERICA,* [2]*Henry M Jackson Foundation for the Advancement of Military Medicine, Bethesda, MD, UNITED STATES OF AMERICA.*

Aim/Introduction: Pheochromocytoma/Paraganglioma (PPGL) are rare neuroendocrine tumors that express somatostatin receptors (SSTR) and can be treated with radiolabeled somatostatin analogues. We report on the safety and efficacy of Lu-177-DOTATATE in the treatment of metastatic or inoperable PPGL in a prospective phase 2 clinical trial. ***Materials and Methods:*** This is an open-label, single-arm phase 2 study to evaluate the efficacy and safety of Lu-177-DOTATATE in patients with PPGL (NCT03206060). Patients are divided into apparent sporadic and SDHx cohorts. The primary endpoint is progression free survival (PFS) at 6 months post initiation of treatment. Eligibility criteria include: SSTR+ tumor and progression by RECIST 1.1 within 12 months. Anatomic scans as well as F-18-FDG and Ga-68-DOTATATE PET scans are acquired at baseline, 4 weeks after the second cycle, and 8 weeks after the fourth cycle,. Lu-177-DOTATATE is administered at 200 mCi (7.4 GBq) every 8 weeks x 4 cycles with amino acid renal blocking. An interim analysis is built-in for both the sporadic and SDHx cohorts when each has reaches 18 participants. ***Results:*** 36 patients (18 per cohort) were evaluated. For the sporadic cohort, 16 (89%) patients achieved stable disease (SD) while 2 (11%) had partial response (PR). In the SDHx (SDHA=2, SDHB=15, SDHD=1) cohort, 10 (55%) patients had SD, 3 (17%) patients had PR, and 5 (28%) patients had progression. 31/36 (86%) met the primary study end point, and the mean PFS is 19.1 months. Patients in the sporadic cohort had longer average PFS of 22.7 months vs 15.4 months in the SDHx cohort. Adverse events unique to the PPGL population include increased catecholamine-related symptom starting as early as

during the Lu-177-DOTATATE infusion and persisting for days to weeks after treatment. Serum catecholamine levels often surged quickly, which likely accounts for the increase in symptoms, and on average peaked at 24 hours post-administration (median increase = 60%, maxincrease 10x baseline). Despite these acute increases and associated symptoms, catecholamine levels inmost patients returned approximately to baseline by Day 28. ***Conclusion:*** Lu-177-DOTATATE has high efficacy and a good safety profile for metastatic PPGL in both the sporadic and SDHx cohorts, although the PFS in the spordic group (24.6 months) is longer than in the SDHx (13.2 months) group. While catecholamine crisis related to surging serum catecholamine levels occurs, levels usually return to near baseline and patients can be safety treated, though ICU care is sometimes needed.

OP-236

Efficacy and safety of dosimetry-based, personalized ^{177}Lu-DOTATATE PRRT of neuroendocrine tumours: an update from the P-PRRT trial

M. Morin, *F. A. Buteau, A. Beaulieu, F. Arsenault, G. Bouvet, A. Desy, N. Lafrenière, G. April, J. M. Beauregard; Department of Radiology and Nuclear Medicine, and Cancer Research Center, Université Laval, Quebec City, Canada; Department of Medical Imaging, and Research Center (Oncology Axis), CHU de Québec – Université Laval, Quebec City, QC, CANADA.*

Aim/Introduction: Peptide receptor radionuclide therapy (PRRT) is widely administered using a fixed activity per cycle, despite the consequent high interpatient variability in healthy tissues dosimetry, and the growing evidence that such a one-size-fits-all approach may leave most patients undertreated. The P-PRRT clinical trial is a phase 2 study of a personalized PRRT regime in which the ^{177}Lu-DOTATATE activity is tailored to deliver a prescribed renal absorbed dose (NCT02754297). The updated efficacy and safety results are presented. ***Materials and Methods:*** Patients with inoperable progressive and/or symptomatic neuroendocrine tumours (NETs) showing sufficient SSTR expression on scintigraphy or PET were eligible. They received up to four induction cycles of ^{177}Lu-DOTATATE every two months, with a personalized activity to achieve a target cumulative renal absorbed dose of 26.5 Gy, assessed using quantitative SPECT/CT. RECIST v1.1 criteria were used to assess the best radiological response and the progression-free survival (PFS). Overall survival (OS) was recorded. PFS and OS were also assessed in the subgroup of participants with midgut NETs whose characteristics matched the eligibility criteria of the NETTER-1 trial. Blood counts and creatinine-based estimated glomerular filtration rate results were compiled to determine the frequency of grade 3 and 4 haematological and renal toxicities according to CTCAE v5.0. The incidence of secondary haematological malignancies was assessed. ***Results:*** 226 participants with NETs of various origins, functional statuses and grades were enrolled and treated with 813 induction cycles averaging 9.54 GBq (0.67-33.68 GBq) of ^{177}Lu-DOTATATE. The overall response rate was 30.4% and the disease control rate was 95.9% (1.8% complete response, 28.6% partial response, 19.8% minor response, 45.6% stable disease and 4.1% progressive disease). Overall, the median PFS and OS were 26.0 and 44.0 months, respectively. In the NETTER-1 subgroup (n=53), the median PFS and OS were 36.0 and 42.3 months, respectively. 61 participants (27%) experienced at least one grade 3-4 non-lymphopenia haematological toxicity: thrombocytopenia in 14.6%, leucopoenia in 11.5%, anaemia in 11.1%, and neutropenia in 9.3%. In the vast majority of cases, the haematological toxicity was reversible and did not significantly interfere with patient care. Two participants (0.9%) developed a myelodysplastic syndrome. One patient developed grade 3 renal toxicity that could be attributable to PRRT. ***Conclusion:*** Personalized ^{177}Lu-DOTATATE PRRT based on renal dosimetry is feasible and shows an acceptable toxicity profile. It allows to escalate the injected activity in most patients suffering from a wide range of SSTR-expressing NETs, with encouraging efficacy results. ***References:*** NEJM 2017;376:125-135. EJNMMI 2019;46:728-742.

OP-237

Extended Peptide Receptor Radionuclide Therapy: Evaluation of Nephrotoxicity and Therapeutic Effectiveness in Neuroendocrine Tumor Patients Receiving More Than Four Treatment Cycles

X. Fan[1], *T. Zhao*[2], *V. Jakobsson*[2], *X. Chen*[2], *R. P. Baum*[3], *J. Zhang*[2]; [1]*Department of Nuclear Medicine, Shanghai Tenth People's Hospital, Tongji University School of Medici, Shanghai, CHINA,* [2]*Department of Diagnostic Radiology Yong Loo Lin School of Medicine, National University of Singapore, Singapore, SINGAPORE,* [3]*CURANOSTICUM Wiesbaden-Frankfurt, Center for Advanced Radiomolecular Precision Oncology, Wiesbaden, GERMANY.*

Aim/Introduction: To evaluate the nephrotoxicity and therapeutic effectiveness of peptide receptor radionuclide therapy (PRRT) with more than four treatment cycles. ***Materials and Methods:*** This retrospective study included 751 patients who underwent multiple PRRT treatments, with complete follow-up information available for 637 patients after four treatment cycles. The overall renal function indicators before and after multiple treatments were analyzed. Nephrotoxicity was compared between patients receiving four cycles and those receiving more than four cycles, considering creatinine levels and CTCAE creatinine grades. Treatment effectiveness was evaluated using survival analysis, focusing on overall survival and disease-specific survival (DSS). ***Results:*** The study included 281 patients in the four-cycle treatment group and 356 in the more-than-four-cycle treatment group. No significant differences in baseline characteristics and renal function were observed between the groups before treatment. Mean post-treatment creatinine levels were 89.30 ± 51.19 μmol/L in the four-cycle group and 93.20 ± 55.98 μmol/L in the >4-cycle group, with no significant differences between the groups ($P = 0.364$). CTCAE creatinine grading of renal function was not statistically significant between the groups ($P = 0.448$). Adverse renal events occurred in 1/281 (0.4%) patients in the four-cycle group and 4/356 (1.1%) in the >4-cycle group. The median follow-up time was 88.3 months (95% CI: 79.3-97.3). Median overall survival was 66.1 months (95% CI: 61.2-71.0) for the entire cohort, 52.8 months (95% CI: 45.5-60.2) for the four-cycle group, and 72.8 months (95% CI: 66.2-79.5) for the >4-cycle group. Cox regression analysis indicated a better prognosis for the >4-cycle group in terms of overall survival (HR: 0.580, $P < 0.001$) and DSS (HR: 0.599, $P < 0.001$). ***Conclusion:*** For neuroendocrine tumor patients undergoing PRRT, multiple treatments are feasible, effective, and safe. Patients experiencing disease recurrence or progression after the standard four-cycle treatment may benefit from additional treatment cycles.

OP-238

Outcome prediction in patients with gastroenteropancreatic neuroendocrine tumours (GEP-NETs) treated with ^{177}Lu-DOTATATE peptide receptor radionuclide therapy (PRRT): results from a prospective phase II clinical trial

M. Mileva[1], *G. Marin*[2], *H. Levillain*[2], *C. Artigas*[1], *C. Van Bogaert*[3], *C. Marin*[2], *R. Danieli*[2], *A. Deleporte*[4], *C. Jungels*[4], *B. Vanderlinden*[2], *Z. Wimana*[1,5], *A. Hendlisz*[4], *P. Flamen*[1], *I. Karfis*[1];
[1]*Nuclear Medicine Department, Institut Jules Bordet, H.U.B, Brussels, BELGIUM,* [2]*Medical Physics Department, Institut Jules Bordet, H.U.B, Brussels, BELGIUM,* [3]*Nuclear Medicine Department, Hôpital Erasme, H.U.B, Brussels, BELGIUM,* [4]*Medical Oncology Department, Institut Jules Bordet, H.U.B, Brussels, BELGIUM,* [5]*Radiopharmacy Department, Institut Jules Bordet, H.U.B, Brussels, BELGIUM.*

Aim/Introduction: To predict outcome of patients with gastroenteropancreatic neuroendocrine tumours (GEP-NETs) early during the course of treatment with ^{177}Lu-DOTATATE peptide receptor radionuclide therapy (PRRT) using ^{68}Ga-DOTATATE-PET/CT and tumour absorbed dose (AD). ***Materials and Methods:*** Patients with progressive GEP-NETs were prospectively included and treated with four cycles of 7.4GBq of ^{177}Lu-DOTATATE (NCT01842165). ^{68}Ga-DOTATATE-PET/CT was performed at baseline and ten to twelve weeks after the first injection. Specific uptake parameters ($SUV_{max/mean}$, tumour-to-blood, tumour-to-spleen ratio) and volumetric parameters (SSTR-tumour volume (TV), total-lesion SSTR expression) were measured in maximum five target lesions per patient. Dosimetry was performed using three timepoint SPECT/CTs after the ^{177}Lu-DOTATATE injections to calculate tumour AD at cycle 1 (C1). Average values of the ^{68}Ga-DOTATATE-PET/CT parameters (baseline and relative changes after the first PRRT cycle from baseline) and minimal, maximal and mean C1 tumour AD in each patient, were tested for association with progression-free survival (PFS). Kaplan-Meier method and log-rank test was used to estimate the PFS. Optimal cut-offs of continuous variables were determined with the Contal and O'Quigley method. ***Results:*** 37 patients were included, mean age at inclusion of 66y (±8.1). Most common primary NET was small-intestinal (23/37), followed by pancreatic (10/37) and colorectal (4/37). Most NETs were of grade 2 (22/37). All patients received at least one prior line of treatment (median: 2). Most patients (28/37) received four cycles of ^{177}Lu-DOTATATE. Median PFS was 28mo. 11/37 (30%) patients achieved partial response (RECIST1.1). SSTR-TV decrease of more than 10% after the first PRRT cycle from baseline, discriminated patients with significantly longer median PFS of 51.3mo, compared to mPFS of 22.8mo in patients in which SSTR-TV increased or decreased less than 10% after one PRRT cycle from baseline (p=0.003; HR:0.35, 95% CI:0.16-0.75). Similarly, total-lesion SSTR expression decrease of more than 10% from baseline after the first PRRT cycle discriminated patients with a mPFS of 32.2mo compared to 26.2mo (p=0.05; HR:0.42,95%CI:0.17-1.0). Patients receiving minimal C1 AD of 35Gy in all target lesions exhibited significantly longer PFS (48.1mo vs 26.2mo, HR:0.37,95%CI:0.17-0.82; p=0.02). There was no statistical evidence of an association between the uptake ^{68}Ga-DOTATATE-PET/CT parameters or the maximal and mean C1 AD and PFS. ***Conclusion:*** Changes of volumetric parameters on ^{68}Ga-DOTATATE-PET/CT after the first treatment cycle could be used for early therapy response assessment in patients with GEP-NETs treated with ^{177}Lu-DOTATATE. The association of the minimal tumour AD at C1 with the patient outcome, provides basis for personalised dosimetry-guided treatment strategies.

607

Sunday, September 10, 2023, 4:45 PM - 6:15 PM
Hall F1

Cardiovascular Committee - TROP Session: Functional Imaging, Plaque and Total-Body PET

OP-239

Comparing left ventricular function derived from CMR and gated ^{13}N-ammonia PET-MPI - An evaluation of reproducibility using hybrid PET/MR

D. F. Sager[1], *N. Manz*[2], *S. Manser*[2], *L. Laubscher*[3], *A. W. Stark*[4], *J. Schuetze*[4], *P. A. Kaufmann*[1], *C. Gräni*[4], *R. R. Buechel*[1];
[1]*Department of Nuclear Medicine, University Hospital Zurich, Zurich, SWITZERLAND,* [2]*Faculty of Medicine, University of Bern, Bern, SWITZERLAND,* [3]*Department of Health Science and Technology, ETH Zurich, Zurich, SWITZERLAND,* [4]*Department of Cardiology, University Hospital Bern, Bern, SWITZERLAND.*

Aim/Introduction: Cardiac magnetic resonance (CMR) and electrocardiogram gated ^{13}N-ammonia positron emission tomography myocardial perfusion imaging (PET-MPI) provide accurate and highly comparable global left ventricular ejection fraction (LVEF) measurements. Beyond accuracy, however, reproducibility becomes vital when serial LVEF assessments are required. Avoiding variations caused by intra- or inter-reader variability is essential, as they could potentially negatively impact treatment decisions. The aim of this study was to compare reproducibility of LVEF measurements derived from simultaneously acquired CMR and PET-MPI. ***Materials and Methods:*** Ninety-three patients undergoing hybrid PET/MR imaging for evaluation of suspected or known coronary artery disease, or with history of myocarditis were retrospectively included. LVEF was derived from CMR and PET-MPI in a blinded fashion at two separate core labs with two expert readers each, using two state-of-the-art software packages for CMR (cvi42 version 5.13.8 and Medis Suite MR version 3.2.48.8) and PET-MPI (QPET version 2017.7 and CardIQ Physio version 2.06-3), respectively. Intra- and inter-reader reproducibility were assessed using correlation and Bland-Altman (BA) analyses. ***Results:*** BA analyses showed smaller biases for LVEF derived from PET-MPI (intra-reader bias -0.1% for QPET and 0.9% for CardIQ, inter-reader bias -0.4% for QPET and -0.8% for CardIQ) than those derived from CMR (intra-reader bias 0.7% for cvi42 and 2.8% for Medis, inter-reader bias -0.9% for cvi42 and -2.2% for Medis) with comparable results for limits of agreement. Intra- and inter-reader correlations of LVEF were high among both modalities and all four software packages ($r \geq 0.87$ and ICC ≥ 0.91, all correlations significant at $p < 0.0001$). Notably, LVEF derived from PET-MPI and analyzed with QPET outperformed all other analyses, yielding near-perfect correlations ($r = 0.99$ and $r = 0.98$ for intra- and inter-reader reproducibility, respectively, QPET correlations significantly higher than other software packages at $p \leq 0.0001$). ***Conclusion:*** Electrocardiogram gated ^{13}N-ammonia PET-MPI provides equivalent, if not better intra- and inter-reader reproducibility of LVEF than CMR. Hence, it may serve as a valid alternative to CMR for patients requiring serial LV functional assessments.

OP-240

Use of First-Pass Non-Gated ^{15}O-water PET for Evaluation of Left Heart Remodelling and Cardiac Function in Severe Mitral Regurgitation

J. Sigfridsson, *H. J. Harms, J. Bergsten, M. Lubberink, T. Kero, T. Baron, F. A. Flachskampf, J. Sörensen;*
Uppsala University, Uppsala, SWEDEN.

Aim/Introduction: Patients with severe primary mitral valve regurgitation (MiR) are serially evaluated for signs of progression, and decisions on surgical intervention are based on symptoms and quantification of regurgitation severity, left ventricular and left atrial dilatation with echocardiography or gold standard cardiac magnetic resonance (CMR). PET has currently no role in MiR evaluation and regurgitant volume measurements require ECG-gated images, which are generally of insufficient quality on non-digital PET. However, the ratio of forward stroke volume (FSV) and LV end-diastolic volume (LVEDV) obtained from CMR corresponds to both mitral regurgitant fraction (RegFraction) and LV dilatation, and predicts future need of valvular surgery. This ratio, as well as left atrial volume (LAV), can be measured with ^{15}O-water PET first-pass images analysed with indicator dilution techniques. Our aim was to study if ^{15}O-water-PET with first-pass imaging can be used for assessing MiR severity. ***Materials and Methods:*** We included 45 asymptomatic patients with moderate-severe/severe MiR and 9 healthy volunteers (HV). LVEF was >60% in all MiR by CMR. Patients underwent same-day scanning with ^{15}O-water-PET, echocardiography and CMR, and HV only PET. PET-scans were performed on an older BGO-based PET/CT (DST, n=28) or modern digital PET/CT (DMI, n=26). First-pass PET-analysis was conducted using in-house developed software, enabling fully automated quantitation of LAV, FSV and LVEDV, using previously validated methods. For comparison, echo-based LAV and CMR-based FSV, LVEDV, FSV/LVEDV and regurgitant fraction (RegFraction) were derived. PET-based prediction of time to surgery was evaluated using Cox regressions. ***Results:*** PET-based LAVi, LVEDVi in MiR were elevated, and FSV/LVEDV reduced, compared to HV (LAV: 58±21 vs 26±3ml/m^2; LVEDV: 108±25 vs 65±11 ml/m^2; FSV/LVEDV: 42±10 vs 71±11 %, all p<0.0001), but FSVi was preserved (43±6 vs 45±4 ml/m^2, p=0.32). PET-LAV correlated with echocardiographic LAV (r=0.73, p<0.0001) and PET-based FSV, LVEDV and FSV/LVEDV correlated with CMR (FSV: r=0.82; LVEDV: r=0.87; FSV/LVEDV: r=0.82, P<0.0001 for all). Both PET-based LAV and FSV/LVEDV correlated with CMR-based RegFraction (LAV: r=0.67; FSV/LVEDV: r=-0.81, both p<0.0001). Twenty-two patients progressed to surgery during follow-up (median 2.7y). PET-based LAV and FSV/LVEDV predicted time to surgery (p<0.02 for both). PET results were not significantly affected by PET/CT device (ST or DMI). ***Conclusion:*** Automated measurements of left heart morphology and function in MiR are feasible using non-gated ^{15}O-water-PET even on older PET/CT devices. PET-based LAV and FSV/LVEDV correlated with gold standard regurgitation severity and were predictive of progression requiring surgery.

OP-241

Added value of automatic coronary artery calcium scoring from low dose CT ^{15}O-water PET scans in MACE prediction in comparison to the reference, calcium scoring CT scans.

M. Dobrolinska[1], *R. Jukema*[2], *S. van Velzen*[3], *P. van Diemen*[3], *M. Greuter*[1], *N. Prakken*[1], *N. van der Werf*[4], *P. Raijmakers*[3], *R. Slart*[1], *P. Knaapen*[3], *I. Isgum*[3], *I. Danad*[4];
[1]*UMCG, Groningen, NETHERLANDS,* [2]*UMC Amsterdam, Amsterdam, NETHERLANDS,* [3]*Amsterdam UMC, Amsterdam, NETHERLANDS,* [4]*UMC Utrecht, Utrecht, NETHERLANDS.*

Aim/Introduction: We sought to assess the value of coronary artery calcium (CAC) scored automatically from LDCT scans acquired during MPI ^{15}O-water-PET scanning and CAC scored from a reference, CSCT scans, in predicting long-term major adverse cardiac events (MACE). ***Materials and Methods:*** Between 2008 and 2014, 505 consecutive patients, with suspected CAD, who underwent myocardial perfusion ^{15}O-water - PET with LDCT and dedicated CSCT scan, regardless of CSCT and CT angiography results, were included in this single centre study. For CAC scoring from CSCT scans, the reference Agatston method was applied. For automatic scoring in LDCT, a previously described method was applied. Briefly, to enable calcium quantification in LDCT scans with large slice thickness, low image resolution and cardiac motion artifacts, the automatic scoring does not apply the standardly used 130 HU threshold for calcium detection. Instead, it mimics visual scoring to quantify calcium on LDCT scans using a generative adversarial deep learning approach. Subsequently, each patient was assigned to one out of five point scale equivalent to Agatston risk groups (0; 1-100; 101-400; 401-1000; >1000 Agatston score). MACE was defined as a composite of all-cause death, myocardial infarction, late and urgent revascularization (PCI and CABG), and unstable angina. ***Results:*** During the median follow up of 6.8 (interquartile range 4.8-7.8) years, 16.8% of patients experienced an end-point event. The agreement in risk classification between reference CSCT manual scoring and automatic scoring from LDCT was 0.58 (95%CI: 0.53-0.62). Based on multivariable Cox regression analysis of associations with MACE between CAC scored from CSCT scans and myocardial perfusion defects, increasing CAC was associated with an increased risk of MACE, which was significant for patients with CAC 1-100 (hazard ratio (HR) 3.84, 95%CI 1.64-9.00, P=0.002), CAC 101-400 (HR 4.27, 95%CI 1.76-10.36, P=0.001), CAC 401-1000 (HR 8.87, 95%CI 3.50-22.47, P<0.001), CAC>1000 (HR 9.59, 95%CI 3.80-24.21, P<0.001) compared with patients with CAC 0. Based on automatic analysis, the risk of MACE was significantly higher only in patients with CAC>400 (CAC 401-1000: HR 2.30, 95%CI 1.23-4.29 P=0.009, CAC>1000: HR 3.77, 95%CI 1.81-7.84, P<0.001). ***Conclusion:*** Both, automatic CAC scoring from LDCT scans and CAC scoring from a reference CSCT scans, improved identification of patients at higher risk of long-term MACE, independently from the MPI ^{15}O-water-PET results. Nevertheless, due to decreased detectability of CAC from LDCT scans, adding a CSCT scans to myocardial perfusion scans should be considered.

OP-242

Impact of data driven motion correction on accuracy of summed stress and rest scores measured with NH3 cardiac PET.

S. Lazarenko[1], *L. van Wunnik*[1], *F. M. van der Zant*[1], *T. S. Martinez-Lucio*[2], *O. I. Mendoza-Ibañez*[2], *C. Hayden*[3], *B. Spottiswoode*[3], *R. J. J. Knol*[1];
[1]*Noordwest Ziekenhuisgroep, Alkmaar, NETHERLANDS,* [2]*University Medical Centre Groningen, Groningen, NETHERLANDS,* [3]*Siemens Medical Solutions United States Of America, Inc., Knoxville, TN, UNITED STATES OF AMERICA.*

Aim/Introduction: The summed stress score (SSS) is a powerful independent predictor of all ischemic cardiac events [1,2]. Abnormal SSS (>3) is associated with a significantly higher cardiac event rate in patients with an intermediate to high pretest probability of CAD. Normal SSS (≦3) is associated with a low event rate in patients with any pretest probability of CAD [1,2]. High respiratory motion during PET acquisition typically degrades image quality as this produces blurry images and possible underestimation of perfusion in some myocardial areas.

This may subsequently lead to an incorrect, overestimated SSS. The aim of this study was to investigate the impact of data driven motion correction (DDMC) software prototype on the accuracy of SSS and summed rest scores (SRS) measured with NH3 cardiac PET. ***Materials and Methods:*** 26 patients who underwent a PET/CT (Biograph Vision 600) examination from July 2020 to February 2021 in the Noordwest Ziekenhuisgroep Alkmaar (Netherlands) were retrospectively included. Inclusion criteria: no prior history of CAD, high MBF, normal LV-function, ongoing follow-up since the scan without major adverse cardiac events (MACEs) or recurrent chest pain. Datasets without motion correction and with DDMC were analyzed with Corridor 4DM, which was used to determine the SSS and SRS. Differences were analyzed using paired sample t-tests in SPSS. ***Results:*** For the selected group of patients SSS and SRS <4 were expected. SSS and SRS measured from DDMC datasets were significantly lower in compared to uncorrected, original datasets, 2.1±2.0 vs 5.5±5.0 p=0,001 for SSS and 1.4±2.1 vs 3.4±3.6 p=0,002 for SRS, respectively. Only 4 patients had SSS >3 following DDMC, whereas 16 patients had SSS >3 in the data without motion correction. ***Conclusion:*** Data driven motion correction improves image quality and the accuracy of summed stress and rest scores measured with NH3 cardiac PET ***References:*** [1] Brophey MD, Farukhi IM, Castanon R, DeLaPena R, Bradshaw L, Banerjee S. Accuracy of 82Rb PET/CT myocardial perfusion imaging with regadenoson stress, including 3-year clinical outcomes. J Nucl Med Technol. 2017;45:75-81.[2] Imamura Y, Fukuyama T, Nishimura S, Nishimura T; Japanese Assessment of Cardiac Events and Survival Study (J-ACCESS). Normal myocardial perfusion scan portends a benign prognosis independent from the pretest probability of coronary artery disease. Sub-analysis of the J-ACCESS study. J Cardiol. 2009 Aug;54(1):93-100.

OP-243

The role of motion correction tools in left ventricular function parameters as measured by gated ^{13}N-NH$_3$ PET/CT

T. Martinez-Lucio[1], *R. J. J. Knol*[2], *O. I. Mendoza-Ibanez*[1], *L. van Wunnik*[2], *F. M. van der Zant*[2], *C. Tsoumpas*[1], *R. H. J. A. Slart*[1], *S. V. Lazarenko*[2];
[1]*University Medical Center Groningen, Groningen, NETHERLANDS,* [2]*Northwest Clinics Alkmaar, Alkmaar, NETHERLANDS.*

Aim/Introduction: Gated cardiac positron emission tomography (PET) is an imaging technique that synchronizes acquired PET data to the heart cycle based on electrocardiogram (ECG) signal. Gated series provide quantitative functional parameters of the left ventricle (LV), namely LV ejection fraction, end-systolic volume (ESV) and end-diastolic volume (EDV), typically used for risk stratification and prognosis in coronary artery disease (CAD). However, cardiac PET often comprises artifacts related with cardiac, respiratory and/or patient motion, which can lead to misinterpretation of the results. Previous studies have suggested that LV function parameters, particularly ESV and EF could be under- and overestimated respectively, due to presence of motion artifacts. Motion correction (MC) tools have been developed to overcome this drawback, such as CardioFreeze with dual-gating technology and data driven motion correction (DDMC). This study aims to elucidate the effect of these tools in LV function assessment. ***Materials and Methods:*** Twenty-four patients with suspected CAD that underwent gated ^{13}N-NH$_3$ PET/CT in the Northwest Clinics Alkmaar (Netherlands) from 28-07-2020 to 15-12-2020 were retrospectively included. Inclusion criteria: no history of CAD, normal perfusion and LV-function, follow-up since the time of study without major adverse cardiac events or recurrent symptomatology. Four reconstructions were performed: no motion correction (NMC), CardioFreeze, DDMC and DDMC & CardioFreeze. Analysis was done with Cedars-Sinai QPET software. Clinical data, LVEF and LV volumes in rest and stress were acquired for the final analysis. For statistical analysis paired T-tests were performed to compare the LV parameters with and without the MC tools. ***Results:*** Study population consisted of 24 patients (62.5% women), all patients older than 42 years old, and 22 (91.6%) vasodilated with adenosine. With regard to EDV rest and stress, significant differences were found only between the NMC and DDMC groups (p<0.01). Regarding ESV and EF in both rest and stress significant differences were found between NMC with CardioFreeze, DDMC and CardioFreeze & DDMC (p<0.001). Larger mean differences with NMC are measured after applying CardioFreeze & DDMC (ESV rest: -5.42, ESV stress: -6.54, LVEF rest: 5.13% and LVEF stress: 6.08%) Interestingly, of both individual MC tools, CardioFreeze demonstrated larger mean differences. ***Conclusion:*** The use of motion correction tools increase significantly ESV values and decrease significantly EF values, with larger differences after applying two combined tools of motion correction, CardioFreeze & DDMC. ***References:*** Tang et. al. Enhancing ejection fraction measurement through 4D respiratory motion compensation in cardiac PET imaging. Phys Med Biol. 2017 Jun 7;62(11):4496-4513

OP-244

The prognostic value of non-perfusion parameters on CZT SPECT in patients with normal myocardial perfusion imaging: a large scale single-center retrospective cohort study.

K. Ko[1], *C. Lin*[2], *L. Tang*[2], *C. Liu*[2], *D. Wang*[3];
[1]*National Taiwan University Cancer Center, Taipei, TAIWAN,* [2]*National Taiwan University Hospital, Taipei, TAIWAN,* [3]*Tri-Service General Hospital, Taipei, TAIWAN.*

Aim/Introduction: The purpose of this study is to evaluate the clinical significance of non-perfusion variables derived from thallium-201 CZT SPECT in patients with normal myocardial perfusion. ***Materials and Methods:*** Data for 2017-2019 from an integrated health care information system of a single hospital were analyzed. A total of 1635 patients with normal myocardial perfusion (summed stress score of 3 or less) using vasodilator stress were identified. We collected non-perfusion variables from gated thallium-201 CZT SPECT imaging. Patients were followed up at least 2 years for major adverse cardiovascular events (MACEs), including cardiovascular death, nonfatal myocardial infarction, hospitalization due to stroke, heart failure, unstable angina or revascularization. ***Results:*** Out of 1634 patients, MACEs occurred in 96 (5.9%) patients and the mean follow-up period was 20.7±11.5 months. In these patients, 64 of them were diagnosed as significant coronary artery stenosis. After adjusted for potential clinical prognostic factors, multivariable Cox regression analysis revealed post-stress increased lung-to-heart (L/H) ratio (HR: 4.625; 95% CI: 2.022 to 10.578; p = 0.008), post-stress increased RV uptake (HR: 2.378; 95% CI: 1.152 to 4.907; p = 0.021) and post-stress ejection fraction (EF) worsening (HR: 2.196; 95% CI: 1.392 to 3.464; p = 0.003) as independent predictors of MACEs. Kaplan-Meier survival curve analysis for MACEs according the number of non-perfusion imaging predictors showed that patients with 2 or more factors as above mentioned had the higher incidence of MACEs.

Conclusion: Normal myocardial perfusion might confer low risk of obstructive coronary artery disease. However, care must be taken for post-stress lung uptake, RV uptake and post-stress EF worsening, which were associated with higher adverse cardiac events.

OP-245

A machine-learning-based prediction model of lethal arrhythmic events by using the ^{123}I-meta-iodobenzylguanidine derived late heart-to-mediastinum ratio: Application into separate Japanese and European cohorts

K. Nakajima[1], *T. Doi*[2], *T. Nakata*[3], *H. Tada*[1], *D. O. Verschure*[4], *V. Frantellizzi*[5], *H. J. Verberne*[6];
[1]*Kanazawa University, Kanazawa, JAPAN,* [2]*Teine Keijinkai Hospital, Sapporo, JAPAN,* [3]*Hokodate-Goryoukaku Hospital, Hokodate, JAPAN,* [4]*Zaans Medical Center, Zaans, NETHERLANDS,* [5]*Sapienza University of Rome, Rome, ITALY,* [6]*University of Amsterdam, Amsterdam, NETHERLANDS.*

Aim/Introduction: A machine-learning (ML)-based prediction model for differentiating events in heart failure (HF) patients was created by using the ^{123}I-meta-iodobenzylguanidine (mIBG) derived late heart-to-mediastinum (H/M) ratio in combination with clinical variables. This study focused on lethal arrhythmic events (ArE) using two retrospective cohorts; a Japanese cohort (Cohort-J) of non-specific chronic HF patients and a European cohort (Cohort-E) of HF patients mainly referred for cardiac device implantation (ICD/CRTD). ***Materials and Methods:*** The ML model was based on 13 variables (age, sex, left ventricular ejection fraction (LVEF), NYHA functional class, comorbidities, etc.) from 526 Japanese patients with chronic HF. The primary outcome parameters for this study were ArE (arrhythmic death, sudden cardiac death and appropriate ICD therapy) and HF death (HFD) after 2 years. The test group (Cohort-J) consisted of 581 Japanese patients with chronic HF who underwent mIBG scintigraphy (mean age 68±12y, LVEF 31±11%, mean follow-up 29 months, and 86% in NYHA I-II). The European test group (Cohort-E) included 246 patients (mean age 64±11y, LVEF 29±9 %, mean follow-up 31 months, and 91% in NYHA II-III). ICD/CRTD was implanted in 18% and 66% in Cohorts-J and E, respectively. ArE probability was calculated for each patient. The indication for ICD/CRTD therapy was predicted and actual outcomes were compared. ***Results:*** Based on the ML-based model, baseline risk for ArE+HFD was calculated as 19±20% and 35±25% in Cohort-J and E, respectively, and actual event rate was 22% and 34%, respectively (p=0.0006). When ArE risk of <3%, 3-9%, and >9% was respectively defined as low, intermediate and high ArE risk, ICD/CRTD was implanted in 7%/18%/25% for low/intermediate/high risk groups in Cohort-J (p<0.0001), and 56%/66%/78% for Cohort E (p=0.01) during 2-year follow-up. In the Cohort-J ArE was observed in 3%/8%/12% for low/intermediate/high risk groups (p=0.009). However, in the Cohort E ArE occurred in 36%/35%/30% in the three risk groups, respectively (p=ns). There was a "bell-shaped" relationship between ArE rate and H/M in the Cohort-E. ***Conclusion:*** Patients with higher ArE risk were more often indicated for ICD/CRTD in both cohorts. The subsequent ArE outcome was adequately predicted in the Japanese population, but not in the Cohort-E. This failure in prediction could be explained by differences in baseline characteristics between the Japanese and European cohorts; amongst others potentially high-risk ArE patients were more prominently included in the latter. ***References:*** (ML model) Nakajima K, et al. J Nucl Cardiol 2022;29:190-201

OP-246

Long-axial field-of-view PET/CT scanners improve the detection of inflamed coronary artery plaques with [^{68}Ga] Ga-DOTA-TOC imaging

C. Mingels, C. Bregenzer, N. Gözlügöl, L. Knappe, I. Alberts, A. Rominger, ***F. Caobelli****;*
Department of Nuclear Medicine, Inselspital, Bern University Hospital, University of Bern, Bern, SWITZERLAND.

Aim/Introduction: Inflamed coronary artery plaques are major determinants of myocardial infarction and sudden cardiac death. Hence, it is crucial that prone-to-rupture coronary lesions are identified, to risk-stratify patients with coronary artery disease (CAD). While positron emission tomography (PET) with somatostatin receptor 2 ligands (SST_2) like [^{68}Ga]Ga-DOTA-TOC may reveal inflammation due to activated monocyte-derived macrophages, many reports in literature, featuring standard PET scanners, showed limited sensitivity and spatial resolution. Recently, a new generation of PET/CT scanners with a long-axial field of view (LAFOV) has been introduced, characterized by increased sensitivity over standard scanners. We therefore aimed to investigate, whether this gain in sensitivity also pertains to [^{68}Ga]Ga-DOTA-TOC LAFOV PET/CT. ***Materials and Methods:*** We retrospectively evaluated 113 patients with neuroendocrine tumors and without history nor symptoms of CAD, who underwent a [^{68}Ga]Ga-DOTA-TOC LAFOV PET/CT during their oncological workup. Images were acquired on a LAFOV Biograph Vision Quadra (Siemens Healthineers) PET scanner (FOV 106cm) 60 minutes after intravenous administration of 154±19.77 MBq [^{68}Ga]Ga-DOTA-TOC. If a high ^{68}Ga-DOTA-TOC uptake of the coronary plaque was visually detected, standardized uptake values ($SUV_{max/mean/peak}$) and Hounsfield Units (HU) were measured by placing an isocontour VOI with 40% threshold. Lesion-to-background (LBR) ratios and lesion to mediastinal blood pool (LMR) ratios were calculated. Patients with coronary artery calcifications were divided into 3 Group according to the number of affected vessels (1= one-vessel disease, 2=two-vessel disease, 3=three-vessel disease). A linear regression model was used to correlate the semi-quantitative values with the degree of calcification (HU). ANOVA testing was performed to reveal differences in the [^{68}Ga]Ga-DOTA-TOC uptake according to the Likert scale of calcification. ***Results:*** 68.8% of our patients showed calcifications of any degree in the coronary arteries (Likert-score median: 1, IQR: 2.25). In 56.3% at least one calcified plaque was identified as [^{68}Ga]Ga-DOTA-TOC-avid (SUV_{max}: 1.26±0.42; HU: 75±49.05, LMB >1.0). [^{68}Ga]Ga-DOTA-TOC uptake within coronary plaques was significantly higher in Patients with 3-vessel disease compared to other groups (p= 0.02, Figure 1). There was only a weak correlation between plaque calcification density and $SUV_{maxc/mean/peak}$ (R^2: 0.159/0.139/0.185, p=0.23/0.26/0.21). ***Conclusion:*** [^{68}Ga]Ga-DOTA-TOC LAFOV PET/CT yields a high detection rate of inflamed coronary plaques, which is superior to what reported in literature for standard PET scanners. Patients with higher burden of calcified plaques showed significantly higher [^{68}Ga]Ga-DOTA-TOC uptake, indicating that the detected uptake is probably expression of prone-to-rupture lesions.

OP-247

Adequacy of whole-body parametric imaging of regional tissue perfusion using the recent total-body PET system and i.v. ^{15}O-water

H. Iida[1], *H. Merisaari*[2], *N. Ono*[3], *N. Kudomi*[4], *T. Tolvanen*[5], *V. Saunavaara*[5], *H. Sari*[6], *J. Knuuti*[1], *L. Nummenmaa*[1], *P. Nuutila*[1]; [1]*Turku PET Centre, University of Turku and Turku University Hospital, Turku, FINLAND,* [2]*Department of Radiology, University of Turku, Turku, FINLAND,* [3]*Nara Institute of Science and Technology, Ikoma, JAPAN,* [4]*Kagawa University School of Medicine, Kagawa, JAPAN,* [5]*Department of Medical Physics, Turku University Hospital, Turku, FINLAND,* [6]*Advanced Clinical Imaging Technology, Siemens Healthcare AG, Lausanne, SWITZERLAND.*

Aim/Introduction: Total-Body PET (TBPET) is attractive for whole-body imaging with much higher sensitivity but could be restricted due to limited counting rate performance. We aim to evaluate the adequacy of simultaneous parametric imaging of whole-body tissue perfusion. ***Materials and Methods:*** Seven volunteers (3 males and 4 females with ages: 21-50 and 31-60 yo, body weight: 74-108 and 61-124 kg, BMI: 23.4-31.2 and 22.7-42.9, respectively) participated in the PET experiments involving 8 scans at 4 different i.v. bolus ^{15}O-water doses ranging from 20 to 700 MBq. The administration was to the brachial vein with the arms on the side. True, random, and total prompt rates were obtained and the noise-equivalent count rates (NECR) (1) were calculated during all PET scan periods. Dynamic images were reconstructed for Maximum-Ring-Distance of 85 to which 40 volumes-of-interest (VOI) were selected to calculate quantitative tissue perfusion (TP) and distribution volume (DV) assuming a single tissue compartment model with a vascular component (1TCM). The arterial input function (AIF) was obtained from the aorta time-activity curve. Administration dose dependency in TP and DV was then evaluated. The pixel-by-pixel calculation of TP and DV was also evaluated in selected scans to identify potential sources of errors. ***Results:*** NECR and prompt rates decreased monotonically after the completion of ^{15}O-water administration to the vein, suggesting that the coincidence slew rate was not saturated even at the maximum administration dose of 700MBq, though the breakdown was seen for a 20 cmφ cylinder phantom already at 400MBq, due to smaller attenuation. VOI analysis did not demonstrate a significant reduction or difference in TP or DV at 700MBq compared with other administration doses for VOIs of TP>0.3 ml/min/g. Significant intra-subject variation was seen if not corrected for inconsistent positioning of VOIs both for AIF and tissues due to movement, and inappropriate delay particularly in peripheral regions, e.g., the branchial/thigh muscle and intra-organ delay in the liver and also in the brain in some extent. The parametric images for TP and DV were visually superior with a larger administration dose, particularly in small TP regions. ***Conclusion:*** Despite the wide range of TP from 0.01 to 5 ml/min/g, ^{15}O-water PET is feasible for providing whole-body TP and DV, and even parametric images. Further technical advances are required for organ-specific adaptation of the model including adequate corrections for intra-and inter-organ delay in AIF and the partial volume effect. ***References:*** (1) J Nucl Med 2005; 46:1825-1834

608

Sunday, September 10, 2023, 4:45 PM - 6:15 PM
Hall F2

Inflammation & Infection Committee - TROP Session: Infection and Inflammation Imaging: New Frontiers

OP-248

^{99m}Tc-Ethambutol Single Photon Emission Computed Tomography/Computed Tomography (SPECT/CT) Scan in Pulmonary Tuberculosis: Correlation of ^{99m}Tc-Ethambutol Avidity with CT Manifestations

F. Aghahosseini[1,2], *Y. Salehi*[1,2], *S. Farzanefar*[1,2], *M. Abbasi*[1,2], *F. Saboktakin*[1,2], *N. Vahidfar*[1,2], *P. Sheikhzadeh*[1]; [1]*Tehran University of Medical Science, Tehran, IRAN, ISLAMIC REPUBLIC OF,* [2]*Nuclear Medicine Department, Valiasr Hospital, Imam Khomeini Complex Hospital, Tehran, IRAN, ISLAMIC REPUBLIC OF.*

Aim/Introduction: Technetium - 99m - ethambutol (99mTc-ethambutol) scintigraphy, as a molecular imaging modality, can be potentially used to identify the biological process of anatomical changes at cellular and subcellular levels. The present study aimed to investigate the correlation between 99mTc-ethambutol avidity and computed tomography (CT) manifestations of pulmonary TB. ***Materials and Methods:*** This study was conducted on 10 previously untreated patients with a culture-proven diagnosis of pulmonary TB, who underwent chest CT scan and 99mTc-ethambutol single photon emission computed tomography (SPECT)/CT scan within seven days. Each individual pulmonary lesion in the chest CT scans was investigated for 99mTc-ethambutol uptake on SPECT/CT images and further categorized as positive (if 99mTc-ethambutol uptake exceeded the background activity) and negative vice versa. For the purpose of semiquantitative analysis, a scoring system was developed on a per-subsegment basis, in which each segment was divided into three subsegments, based on the maximum number of lesion types counted in a single segment. The summation of scores for each individual lesion type was compared between the two 99mTc-ethambutol positive and negative groups. Moreover, CT manifestations were classified dichotomously as destructive (i.e., cavities, bronchiectasis, and fibro-destructive changes) and non-destructive (i.e., non-cavitary nodules, consolidation, centrilobular nodular infiltration, and miliary pattern) lesions and further assessed for any significant differences regarding 99mTc-ethambutol uptake. ***Results:*** Out of the 359 involved sub-segments, 57 were predominantly occupied by cavities (score=67, 18.7%), followed by bronchiectasis (score=56, 15.6%) and fibro-destructive changes (score=54, 15%). The 99mTc-ethambutol uptake occurred in 52/54 sub-segments with predominant feature of bronchiectasis (92.9%), 50/54 with fibro-destructive changes (92.6%), and 54/67 with cavities (80.6%), while no significant 99mTc-ethambutol uptake was found in 11/11 sub-segments with non-destructive fibrosis (100%), 37/41 with consolidation (90.2%), 44/49 with non-cavitary nodules (89.8%), 48/54 with miliary pattern (88.9%), and 21/25 with centrilobular nodular infiltration (84%) (P=0.000). Comparison of 99mTc-ethambutol uptake between the two groups of destructive and non-destructive lesions revealed a significantly higher rate of 99mTc-ethambutol positivity in the first group (156/177, 88.1% vs. 19/180, 10.6%; P=0.000). ***Conclusion:*** The current study

revealed that 99mTc-ethambutol uptake occurs significantly more frequent in destructive lesions such as bronchiectasis, fibro-destructive changes, and cavities, all of which contribute to the lung remodeling process, compared to non-destructive CT manifestation. It may be presumed that 99mTc-ethambutol scintigraphy may have the potential to provide prognostic information on the development of pulmonary impairment after tuberculosis (PIAT).

OP-249

Head to head comparison of ultrasound and Tc - 99m glucosamine SPECT/CT imaging of patients with rheumatoid arthritis of the knee.

O. Evbuomwan, *G. Engelbrecht;*
University Of The Free State, Bloemfontein, SOUTH AFRICA.

Aim/Introduction: The evaluation of disease activity in rheumatoid arthritis (RA) is challenging and requires very sensitive, feasible and reliable investigations. Ultrasound (US) and MRI have been the forefront imaging modalities in the management of patients with RA. If properly used, US has been shown to offer a very high diagnostic accuracy, because of its ability to accurately measure blood flow to inflamed joints and detect early synovial changes. However, it is an operator dependent technique and could be cumbersome in imaging multiple joints in a single patient. These disadvantages are not associated with nuclear medicine functional imaging. In this prospective study we aimed at assessing RA synovitis of the knee, with SPECT/CT imaging using the SPECT glucose analogue ^{99m}Tc glucosamine in comparison of US imaging. ***Materials and Methods:*** This was a prospective study, in which 10 patients with proven rheumatoid arthritis and active disease of the knee were recruited. Each participant was injected with 20-25mCi of ^{99m}Tc labelled glucosamine. SPECT/CT (2 hours post injection) imaging of the knees were performed. Joints were qualitatively assessed for abnormal increased uptake of the radiotracer in the suprapatellar, lateral, medial, and popliteal regions. Ultrasound of the knees were performed on the same day during the waiting period between the blood pool and SPECT/CT imaging. An experienced radiologist assessed each US scan for suprapatellar, lateral, and medial synovitis and popliteal bursitis. ***Results:*** Eight sites in both knees of each participant were assessed for disease activity, making a total of 80 sites assessed. The median (interquartile range) age was 65 (53-68) years, and the majority (n = 7; 87.5%) were females. The overall calculated sensitivity and specificity of 99mTc glucosamine was 96% and 44% respectively. However, taking each knee as a single site, the specificity increased to 90%. ***Conclusion:*** This study revealed that 99mTc glucosamine imaging had a very high sensitivity in the imaging of patients with RA of the knee, and it compares very well with US. The overall low specificity might be as a result of associated osteoarthritis in these patients, the detection of subclinical disease not picked up by US imaging or a combination of both. Further studies are however warranted to establish its role in the management of patients with RA.

OP-250

SUV-Based Assessment of Known or Suspected Polyarthritis on Double-Phase Whole-Body Bone Tomoscintigraphies Provided by a High-Speed CZT Camera

F. Rajadhas[1], *C. Morizot*[2], *D. Loeuille*[2], *I. Chary-Valckenaere*[2], *V. Roch*[1], *P. Marie*[1,3], *L. Imbert*[1,3], *A. Bahloul*[1,3];
[1]*CHRU-Nancy, Department of Nuclear Medicine and Nancyclotep Imaging Platform, Nancy, FRANCE,* [2]*CHRU-Nancy, Department of Rheumatology, Nancy, FRANCE,* [3]*Université de Lorraine, INSERM U1254, IADI, Nancy, FRANCE.*

Aim/Introduction: New whole-body high-speed CZT-cameras provide high-quality images with absolute quantification that is useful for monitoring 177Lu-based therapy. However, the usefulness of such quantification remains to be demonstrated for double-phase bone scintigraphy. This study, conducted in patients referred to bone scintigraphy for known or suspected poly-arthritis, aimed to determine whether the SUV maximal (SUVmax), observed within articular regions during the blood-pool (BP) and delayed (DP) phases, may predict the results achieved from a conventional visual analysis by experienced observers. ***Materials and Methods:*** We included 56 patients (48±15 years-old, 37 women), who had been referred to bone scintigraphy for a suspected or known polyarthritis. High-speed whole-body 3D recordings were started 5 min after the intravenous injection of 482 to 641 MBq of 99mTc-HMDP (BP phase with 9 minutes SPECT recording) and almost 3 hours later (DP phase with 18 minutes SPECT recording). Results of visual analysis of the SPECT and CT images, achieved by a consensus of two experienced observers, were regrouped into 26 different articular regions and further correlated with the SUVmax from the same regions. ***Results:*** Among the 1456 joint regions considered, 201 were visually judged abnormal at DP, of which 88 were additionally judged abnormal at BP. The SUVmax of the remaining 1255 normal articular regions were independently influenced by the joint locations and body mass index (both $p<0.001$), but not by age and sex, and they could be regrouped into 4 different joint groups with equivalent SUVmax levels: G1, ankles, feet and hands joints (95% confidence intervals: 1.28-1.37 at BP and 1.82-1.99 at DP); G2, wrists, knees and elbows (1.71-1.85 at BP and 2.68-2.98 at DP); G3, shoulders, hips and sterno-clavicular joints (2.21-2.33 at BP and 4.86-5.14 at DP); and G4, sacroiliac joints and thoracic and lumbar spine (3.03-3.24 at BP and 6.01-6.39 at DP). The criterion of a SUVmax setting above the upper limit of the 95% confidence interval, which had been determined for the corresponding normal articular group and scintigraphy phase, provided high specificities for the prediction of visually abnormal regions at BP (96% (1304/1360)) and DP 96% (1204/1250)). Whereas the corresponding sensitivities were lower (78% (69/88)) and (66% (132/201)), respectively). ***Conclusion:*** In patients referred to double-phase whole-body bone tomoscintigraphies using a high-speed 360° CZT-camera for a known or suspected polyarthritis, the BP and DP joint SUVmax are highly predictive of the results provided by a conventional visual analysis from experienced observers.

OP-251

Assessing the augmentive value of 18F-FDG PET/CT over 99mTc-MDP bone scan in distinguishing infection from aseptic loosening of prostheses.

S. Shamim, *H. Khairwa, S. Sagar, D. Khan, K. Sivashankar, N. Kundu, N. Kumar, G. Arora, R. Kumar;*
AIIMS New Delhi, Delhi, INDIA.

Aim/Introduction: Methylene diphosphonate (MDP) bone scan is a valuable tool for distinguishing between infection and aseptic loosening of prostheses, but in cases where patients have already received antibiotics, the MDP uptake can persist for a prolonged period, making it challenging to differentiate between the two conditions. Our study aimed to assess the additional benefit of using Flurodeoxyglucose (18F-FDG)-PET/CT in conjunction with 99mTc-MDP bone scan to distinguish between infection and aseptic loosening in patients who are experiencing symptoms related to their prostheses. ***Materials and Methods:*** At a tertiary care centre in India, we conducted a prospective study that included all patients referred to our department with suspected infection or aseptic loosening of prostheses between January 2019 and March 2023 having doubtful finding on MDP scan. Patient underwent 99mTc-MDP planar imaging and SPECT/CT according to our department protocol. Patient having clear diagnosis on bone scan were excluded from the study. 18F-FDG PET/CT was performed if the MDP scan findings were inconclusive. Clinical follow-up and post operative findings were considered gold standard. Two experienced nuclear medicine physicians reviewed both types of scans, and their results were compared. ***Results:*** There were 16 patients fulfiling inclusive criteria and having inconclusive bone scan were included in the study, 11 were male and 5 were female, with an average age of 48.63±18.63 years. Out these 16 patients FDG-PET/CT showed increased metabolic activity in 11 patients (68.75%) and FDG-PET/CT showed negative results in 05 patients (31.25%). As a result, 18F-FDG PET/CT was able to exclude infection in 5 out of 16 (31.25%) patients and confirmed infection in 11 out of 16 (68.75%) patients. On clinical follow up, the 11 patients diagnosed as positive based on the scans responded to antibiotics while 5 patients who were negative on FDG PET/CT scan were operated for loosening with good post operative outcome and there was no evidence of infection found during surgery and post surgery culture. ***Conclusion:*** We concluded that patients with negative or clearly positive bone scan results, there is no need to undergo additional 18F-FDG PET/CT scans. However, in patient having inconclusive bone scan, 18F-FDG PET/CT may have a promising role for confirming or excluding infection.

OP-252

[^{18}F]FDG PET/CT identified infections and inflammation in persistent critical illness

B. van Leer, *K. M. Demenaga, M. W. N. Nijsten, J. H. van Snick, R. H. J. A. Slart, A. W. J. M. Glaudemans, J. Pillay;*
UMCG, Groningen, NETHERLANDS.

Aim/Introduction: In patients with persistent critical illness (PerCI), prognosis after day 10 is no longer determined by the initial admission diagnosis, but by a cascade of events resulting in new and persistent organ failure.[1] Acquired immune paralysis, resulting in occult infections or persistent inflammation both play a role in PerCI.[2] [^{18}F]FDG PET/CT can be used as a method to image (low-grade) infection and inflammation.[3] Our aim is to investigate the value of [^{18}F]FDG PET/CT in patients with PerCI. ***Materials and Methods:*** Patients (≥18 years) admitted to the ICU of the University Medical Center Groningen between 2010 and 2023 by whom a [^{18}F]FDG PET/CT was performed ten days or more after ICU admission were retrospectively included. [^{18}F]FDG PET/CT report was evaluated for infection foci and in combination with clinical records therapy change was scored. Therapy change was defined as any therapeutic decision (e.g. starting, stopping, continuing or restricting) reported to be made directly after the [^{18}F]FDG PET/CT. In addition, we assessed whether presence of infection on the [^{18}F]FDG PET/CT was associated with length of ICU stay and all-cause mortality using Kaplan-Meier with Log-Rank test. ***Results:*** 18 patients were included. Clinical signs of Inflammation or infection was the main reason to perform a [^{18}F]FDG PET/CT scan. In 13 (72%) patients an infectious focus was found. [^{18}F]FDG PET/CT was followed by therapy change in 11 patients (61%). In 9 patients a decision was made regarding antibiotic therapy. Corticosteroids were started in 2. Furthermore, in 2 patients drainage of infected collections was performed and in one patient supportive therapy was limited. Two patients died. Mean ICU admission time was 47 days. No association between presence of infection on [^{18}F]FDG PET/CT and ICU stay and all-cause mortality was observed. ***Conclusion:*** In patients with PerCI and clinical suspicion of inflammation, [^{18}F]FDG PET-CT contributes to identification of an infectious or inflammatory focus and results in therapy change. Larger prospective studies are needed to determine the impact of [^{18}F]FDG PET/CT on length of stay and mortality in this patient category. ***References:*** 1. Iwashyna TJ, et al. Timing of onset and burden of persistent critical illness in Australia and New Zealand: a retrospective, population-based, observational study. LancetRespirMed.2016;4(7):566-573. doi:10.1016/S2213-2600(16)30098-42. Zhang B, et al. Association of Monocyte-to-Lym hocyte and Neutrophil-to-Lymhocyte Ratios With Persistent Critical Illness in Patients With Severe Trauma. JTraumaNurs.2022;29(5):240-251.doi:10.1097/JTN.0000000000000672 3. Pijl JP, et al. FDG-PET/CT in intensive care patients with bloodstream infection. CritCare.2021;25(1). doi:10.1186/S13054-021-03557-X 4.

OP-253

Comparison of [^{18}F]FDG and [^{18}F]DPA714 for the visualization of the pathogenesis of pulmonary tuberculosis in rhesus monkeys (Macaca mulatta)

M. Stammes[1], *M. Vierboom*[1], *C. Sombroek*[1], *J. Bakker*[1], *R. Vervenne*[1], *S. Hofman*[1], *A. Windhorst*[2], *J. Langermans*[1,3], *F. Verreck*[1];
[1]*BPRC, Rijswijk, NETHERLANDS,* [2]*Amsterdam UMC, Amsterdam, NETHERLANDS,* [3]*Utrecht University, Utrecht, NETHERLANDS.*

Aim/Introduction: Tuberculosis (TB) remains a global threat with a mortality rate of 1.5 million people in 2020. To fight tuberculosis a better understanding of pathogenesis and the complex host-pathogen interactions at different disease stages is essential. Dedicated tracers to follow spatiotemporal changes by molecular imaging like PET would help providing such insight. The most extensively studied tracer in TB, used both in the clinic and in research, is [^{18}F]FDG which is highly sensitive but not specific. A more specific tracer that has been developed targets the mitochondrial translocator protein (TSPO), which is upregulated in activated microglia and mononuclear phagocytes. Since macrophages are the target cells of Mycobacterium tuberculosis (Mtb) infection playing a critical role in host immunity including the formation of TB granulomas, such tracers are interesting candidates to study in the context of TB. In this study we set out to pioneer the use of the TSPO tracer [^{18}F]DPA714 in the primate host, along with [^{18}F]FDG as

a control, to visualize the pathogenesis of pulmonary tuberculosis upon experimental infection of rhesus monkeys (Macaca mulatta). ***Materials and Methods:*** Three adult healthy male rhesus monkeys were challenged 8 times at one-week intervals by repeated limiting dose exposure to Mtb. Next to baseline scans, PET-CTs were recorded 4, 5, 6 and 7 weeks after the primary challenge, alternating the use of[^{18}F]DPA714 or [^{18}F] FDG, respectively. Eleven weeks after the primary challenge the animals were euthanized, and a full necropsy was performed. ***Results:*** While experimental infection was verified postmortem by pathological examination and by increasing immune diagnostic signals from the blood along the infection phase, also both tracers demonstrated spatiotemporal alterations in lungs and mediastinal lymph nodes from 4 weeks after the primary challenge onwards. Remarkably, as the [^{18}F]FDG tracer showed an elevating trend, the initial [^{18}F]DPA714 signals at week 4 appeared decreasing 2 weeks later. Histological assessment of TSPO showed a staining pattern that was in concordance with the expression of CD68, a marker of innate macrophages, more than CD3, which is specific to adaptive T lymphocytes. ***Conclusion:*** The results of this pilot study indicate that the TSPO tracer [^{18}F]DPA714 has the potential to detect experimental Mtb infection at early stages in the primate host through measurement of inflammatory responses. The disparate dynamics of [^{18}F] DPA714 versus [^{18}F]FDG signals warrant further investigation and suggest that, during the development of TB disease, increasing inflammatory metabolism is not correlated with macrophage recruitment and/or activation.

OP-254

68Ga-triacetylfusarinine C (TAFC) Siderophore PET/CT for Detection of Invasive Aspergillus Infection: the SPECIFIC Clinical Trial Protocol

S. M. Levy[1,2,3], *B. Z. Sim*[4,2], *M. Haskali*[1,2], *C. Decristoforo*[5], *H. Haas*[6], *M. Slavin*[4,2], *M. Hofman*[1,2], *A. Douglas*[4,2];
[1]*Molecular Imaging and Therapeutic Nuclear Medicine, Cancer Imaging, Peter MacCallum Cancer Centre, Melbourne, AUSTRALIA,* [2]*Sir Peter MacCallum Department of Oncology, The University of Melbourne, Melbourne, AUSTRALIA,* [3]*Department of Nuclear Medicine, The Royal Melbourne Hospital, Melbourne, AUSTRALIA,* [4]*Department of Infectious Diseases, Peter MacCallum Cancer Centre, Melbourne, AUSTRALIA,* [5]*Department of Nuclear Medicine, Medical University of Innsbruck, Innsbruck, AUSTRIA,* [6]*Institute of Molecular Biology, Biocenter, Medical University of Innsbruck, Innsbruck, AUSTRIA.*

Aim/Introduction: Invasive Aspergillus infection (IAI) is a common infection in immunocompromised patients undergoing cancer therapies. Prompt diagnosis is paramount given high morbidity and mortality. Whilst 18F-fluorodeoxyglucose (FDG) PET/CT is useful in diagnosis, it remains non-specific. Siderophore-radiolabelled PET/CT may facilitate rapid and non-invasive diagnosis of IAI. Siderophores are natural scavengers of iron produced by pathogens, essential for pathogen function, and quite specific for certain pathogens. Aspergillus fumigatus secretes two siderophores - fusarinine C and TAFC. TAFC is relatively specific for acute IAI and not taken up by human cellular systems. 68Ga is an attractive radionuclide for TAFC radiolabelling, due to equal charge and comparable radius to ferric iron, allowing iron displacement by 68Ga. Preclinical studies demonstrate diagnostic potential of 68Ga-TAFC PET/CT with specific visualisation of Aspergillus fumigatus infection [1]. This study aims to evaluate whether these pre-clinical findings can be confirmed in humans with proven or probable IAI. ***Materials and Methods:*** This is a first-in-human pilot observational cohort imaging study of patients with probable or proven IAI. 10 patients satisfying inclusion and exclusion criteria will be recruited to undergo 68Ga-TAFC-PET/CT within two weeks of IAI diagnosis, in addition to standard of care (SOC) imaging. 68Ga-TAFC will be compounded on-site. Baseline and post-imaging clinical data, haematologic, renal and liver function will be collected. Whole body PET/CT will be performed at 15, 60 and optionally 180 minutes following intravenous injection of 1.8-2.2 MBq/kg 68Ga-TAFC. Findings pertinent to IAI and physiologic uptake will be qualitatively and quantitatively analysed, including scan classification as positive or negative, measurement of SUVmax, SUVmean and MTV, and safety. Findings will be compared to existing SOC imaging (18F-FDG-PET/CT or CT). ***Results:*** 68Ga labelling was optimised to yield 68Ga-TAFC quantitatively at 50 C (pH 4.0) in 7 minutes. Production was then automated on a radiochemistry module and validated to produce high purity and pyrogenic free formulation for clinical administration. Clinical trial is anticipated to commence mid-2023. ***Conclusion:*** This proof-of-concept clinical trial aims to evaluate suitability of 68Ga-TAFC PET/CT for imaging IAI. ***References:*** [1] Journal of Fungi 2021; doi: 10.3390/jof7070558

OP-255

FAPI PET/CT Imaging of Pulmonary Hypertension Caused by Fibrosing Mediastinitis and FAPI Radiotargeted Therapy

L. Song, *Z. Wu, C. Zan;*
First Hospital of Shanxi Medical University, Taiyuan, CHINA.

Aim/Introduction: To propose an innovative strategy for the integration of diagnosis and treatment of fibrous mediastinitis (FM) through targeting fibroblast activation protein inhibitor (FAPI) for fibrosis rats, and provide a theoretical basis for patients with pulmonary hypertension caused by fibrosing mediastinitis (PH-FM) based on PET/CT imaging. ***Materials and Methods:*** By performing ^{18}F-FAPI PET/CT scan on patients with PH-FM, we determined the presence of FAPI-avid in FM lesions. We then injected ^{177}Lu-FAPI-46 into a fibrosis rat model for SPECT/CT scan, evaluated the therapeutic effect, and estimated the absorbed dose and effective dose for this agent in the treatment of patients with FM. ***Results:*** PET/CT imaging of patients with 349.13±46.39 MBq of ^{18}F-FAPI showed high-level uptake (SUVmax=7.94±0.26) in FM lesions. ^{18}F-FAPI PET/CT imaging of fibrosis rats (8.28±0.91 MBq) suggested significant uptake of ^{18}F-FAPI in the fibrotic lesions (SUVmax=2.11±0.23). SPECT/CT imaging of fibrosis rats injected with 17.87±1.99 MBq of ^{177}Lu-FAPI-46 showed that the fibrotic lesions displayed FAPI-avid up to 60 h. These fibrosis rats were set as the control group (n=6), not treated by ^{177}Lu-FAPI-46, and other three treatment groups were the 30 MBq group (n=6, 33.32±1.28 MBq), the 100 MBq group (n=6, 112.07±11.64 MBq), and the 300 MBq group (n=4, 299.00±10.06 MBq). No spontaneous healing of lesions was observed during the treatment period in the control group, and there was complete healing on day 9, day 11 and day 14 in the 30 MBq, 100 MBq and 300 MBq groups, respectively. With a significant difference in the free of event rate in the Kaplan-Meier curve among these four groups (log-rank chi-squared value=25.593, P-value < 0.001), the dose of 300 MBq displayed the best therapeutic effect, and no damage was observed in the kidney. We further presumed organ-absorbed doses and an effective dose (ED=0.4320 mSv/MBq) of ^{177}Lu-FAPI-46 for patients. ***Conclusion:*** ^{18}F-FAPI PET/CT can be a potentially valuable tool for the clinical diagnosis of PH-FM. Using ^{177}Lu-FAPI-46 may be a novel and safe strategy for the integration of diagnosis and treatment of FM.

OP-256

Increased Colonic TSPO Expression in Inflammatory Bowel Diseases by the Translocator Protein 18kDa Radioligand [18F]DPA-714

Q. He[1], *D. Jiang*[2], *Y. Guan*[2], *A. Fei*[1], *F. Xie*[2];
[1]*Department of General Medicine, Xinhua Hospital Affiliated to Shanghai Jiaotong University School of Medicine., Shanghai, CHINA,* [2]*Department of Nuclear Medicine & PET center, Huashan Hospital, Fudan University, Shanghai, CHINA.*

Aim/Introduction: Currently specific means of non-invasive imaging examination for inflammatory bowel disease is still lacking. Considering that the Translocator Protein (TSPO) is widely expressed in intestine and participates in intestinal immune response, [18F]DPA-714 is used to explore the colitis degree of DSS-induced chronic colitis mice, so as to provide a new non-invasive examination method. ***Materials and Methods:*** Colon biopsies were obtained from IBD patients and HC, including patients with active CD (A-CD, n = 24), patients with CD in remission (R-CD, n = 10), patients with active UC (A-UC, n = 25), patients with UC in remission (R-UC, n = 7) and healthy controls (HC, n = 16). TSPO was determined by qRT-PCR. CD-SES/UCEIS was recorded at the same time. Correlation between TSPO and CD-SES/UCEIS was performed by Spearman rank correlation. Male C57BL/6 mice were administrated with 2% DSS in drinking water for 7 consecutive days, followed by 14 days for recovery. The cycle was repeated for 3 times before all mice were sacrificed. [18F]DPA-714 scans were performed in the end. Ten mins static PET imaging at 40 min post-injection of [18F]DPA-714 was involved in this study. ***Results:*** TSPO was significantly increased in the inflamed mucosa of active IBD patients compared with that in HC or IBD patients in remission. However, no difference was found between HC and patients with CD or UC in remission. Correlation between TSPO expression in colon mucosa and CD simple endoscopic score (CD-SES) of CD patients and UCEIS of UC patients, respectively. As a result, a positive association was observed between TSPO and CD-SES or UCEIS. Successful establishment of chronic colitis mice model was verified by intestinal immunohistochemical staining. [18F]DPA-714 scan was performed to evaluate the colitis degree. A remarkably higher uptake in intestinal was observed in colitis mice compared to controls. ***Conclusion:*** TSPO is significantly increased in active IBD patients and positively correlated with disease activity. The Translocator Protein 18kDa Radioligand [18F] DPA-714 could be used as a non-invasive evaluation examine method for IBD patients.

609

Sunday, September 10, 2023, 4:45 PM - 6:15 PM
Hall G2

e-Poster Presentations Session 4 - Thyroid Committee: Thyroid and Parathyroid Disease

EPS-063

Implementing a Clinical Pathway for Treatment with I 131 for Differentiated Thyroid Cancer: Evaluation of Quality Objectives

J. Cruz Vasquez*, A. Alonso Echarte, I. Blanco Saiz, E. Anda Apiñaniz, A. Alomar Casanovas, I. Saura Lopez, A. Barrera Cerpa, N. Rudic Chipe, M. Ribelles Segura, E. Goñi Gironés, A. Camarero Salazar;*
Hospital Universitario de Navarra, Pamplona, SPAIN.

Aim/Introduction: A clinical pathway (CPW) is a healthcare plan applied to a clinical process with a predictable course, detailing a sequence of interventions carried out by healthcare professionals through a multidisciplinary perspective, with the objective of reducing the variability in care and aiding in decision-making. This clinical management tool allows for periodic evaluation of quality of care, improvement of the transmission of information to patients, patients' assessment of the process and safety, the optimization of resources, and maintaining updated training for professionals. After the planning, development, and implementation of a CPW for the metabolic therapy with I-131 in our hospital, the objective was to meet the quality objetives in ≥ 80% of patients and to identify areas for improvement. ***Materials and Methods:*** During the implementation (2019-2022), data from the CPW and satisfaction surveys from all patients with DTC and an indication for post-surgical therapy with I-131 was analyzed. We evaluated the following time interval objectives: surgery to I-131 administration < 4 months (T1); surgery to Endocrinology appointment <2 months (T2); NuclearMedicine appointment to I-131 administration <2 months (T3). Other objetives were median hospital stay 1-3 days and a global patient satisfaction index >8 (scale 1 to 10). ***Results:*** From 131 patients, 84 women (64.1%) had a median age of 51 years (IQR: 11-85). 118 (90.1%) had papillary carcinoma and 13 (9.9%) had follicular carcinoma. 96 patients (73.3%) had stage 1, 27 (20.6%) had stage 2, 5 (3.8%) had stage 3, and 2 (1.5%) had stage 4. The dose administered of the radiopharmaceutical was between 1.11-7.4 Gbq. The median T1 was 102.55 days (47-268), meeting the objective in 96 patients (77%). The median T2 was 58.58 days (24-206), meeting the objective in 71 patients (56.8%). The median T3 was 28.67 days (13-121), meeting the objective in 127 patients (96.9%). The median hospital stay was 2.03 days (1-5). There was a significant positive correlation between the hospital stay and the activity of administered I-131 (r=0.556, p=0.00). Satisfaction surveys were collected from a total of 51 patients. Overall, 90% of patients assessed their care with 8-10 points. ***Conclusion:*** The quality objectives met were time between Nuclear Medicine appointment and treatment, hospital stay, and patient satisfaction. There is room for improvement in time between surgery and treatment and time between Endocrinology appointment and treatment. There is a possibility these objectives were not met due to patient and/or hospital clinical variations.

EPS-064

FNA-Tg in Metastatic Lymph Node Predictions Local Recurrence Following Lateral Neck Dissection in Papillary Thyroid Carcinoma

Y. Yang[1], *X. Jia*[1], *J. Hui*[2], *A. Yang*[1], *R. Gao*[1];
[1]*the First Affiliated Hospital of Xi 'an Jiaotong University, Xi 'an, Shaanxi, CHINA,* [2]*Shaanxi Cancer Hospital, Xi 'an, Shaanxi, CHINA.*

Aim/Introduction: Lateral lymph node metastasis (LLNM) is associated with distant metastasis and locoregional recurrence in papillary thyroid carcinoma (PTC). Still, the prognostic significance of LLNM, as well as that of concurrent predictors, remains unclear. Thyroglobulin through fine-needle aspiration (FNA-Tg) is frequently practiced in the preoperative diagnosis of LNM, and LNM with a high FNA-Tg level was related with a higher tumor load. The goal of this study was to evaluate the FNA-Tg as a risk factor to prediction of local recurrence following therapeutic lateral neck dissection (LND) for PTC. ***Materials and Methods:*** This cohort study reviewed medical records of patients with PTC suspected of having LLNM and underwent cytology through FNA+FNA-Tg

as well as therapeutic LND in our institution, between January 1, 2019, and January 1, 2021. The relationships between clinical outcomes and FNA-Tg in LLNM were analyzed using logistics regression analysis. Receiver operating characteristic (ROC) curve analysis was used to obtain the cut-off value for FNA-Tg. ***Results:*** The study cohort included 65 patients (34 male, 31 female; median age, 41.7 years) with a median follow-up of 31.5 months after surgery. Local recurrence (including persistent disease) and distant metastasis were revealed in 22 (33.85%) and 3 (13.64%) cases, respectively. The median FNA-Tg levels of metastatic LNs respectively were 500.00 ng/mL and 335.90 ng/mL in patients with and without recurrence. Comparing recurrence patients who required further attention or treatment with those who did not recur, no significant difference was found concerning sex, age, BRAF, tumor size, capsular invasion, histology and pT stage. In univariate analysis, FNA-Tg value, FNA-Tg beyond the measurement limit, number of primary lesions, multifocal, extraglandular invasion, lateral lymph nodes ratio (LLNR), and number of iodine treatments were risk factors for local recurrence/persistence in LLND ($P < 0.05$). Multivariate analysis revealed that above factors were independent risk factors ($P < 0.05$),except for number of primary lesions. Noteworthy, FNA-Tg greater than 460.00 ng/mL was predictive of recurrence, which combined LLNR had higher predictive value with 89.50% sensitivity and area under ROC curve of 0.814 (95%CI: 0.689-0.938). Combined with FNA-Tg exceeding the measurable upper limit (>500 ng/mL), FNA-Tg showed an advantage in predicting local recurrence/persistence. ***Conclusion:*** FNA-Tg is an independent risk factor to predict local recurrence/persistent disease before therapeutic LND. And FNA-Tg combined LLNR can potentially assist in guiding the extent of LLND and identifying at-risk patients who need aggressive treatment and intensive surveillance for postoperative recurrence.

EPS-065

Role of ^{18}F-NaF PET/CT on bone evaluation in patients with differentiated thyroid cancer undergoing radioactive iodine therapy and ^{18}F-FDG PET/CT: preliminary results

F. Volpe[1], *C. Nappi*[1], *E. Zampella*[1], *E. Nicolai*[2], *L. Piscopo*[1], *D. Bianco*[3], *C. Vallone*[1], *F. Volpicelli*[1], *M. Falzarano*[1], *L. Pace*[4], *A. Cuocolo*[1], *M. Klain*[1];
[1]*Department of Advanced Biomedical Sciences, University Federico II, Naples, Italy, Napoli, ITALY,* [2]*IRCCS SDN, Diagnostic Imaging, Naples, Napoli, ITALY,* [3]*CIRA - Italian Aerospace Research Centre, Capua, ITALY, Capua, ITALY,* [4]*Dipartimento di Medicina, Chirurgia e Odontoiatria "Scuola Medica Salernitana" /DIPMED, Salerno, ITALY.*

Aim/Introduction: Differentiated thyroid cancer (DTC) is the most frequent endocrine malignancy. After surgery, DTC patients are referred to ^{131}I radioactive (RAI) therapy and a post-therapeutic total-body scintigraphy (PT-WBS) to identify local and/or remote metastases. In presence of high levels of thyroglobulin and suspicion of no-iodine avid metastasis, PET/CT with ^{18}F-FDG is also indicated. ^{18}F-NaF PET/CT has been recently introduced for evaluation of bone metastases in oncological patients. However, no data are available regarding the comparison between ^{18}F-FDG and ^{18}F-NaF PET/CT in DTC patients with suspicion of bone metastasis at ^{131}I-PT-WBS.We compared the role of ^{18}F-NaF PET/CT with ^{131}I-PT-WBS and ^{18}FDG-PET/CT on bone evaluation in DTC patients. ***Materials and Methods:*** We enrolled consecutive DTC patients undergoing RAI therapy avid bone uptake on PT-WBS, referred to ^{18}F-NaF PET/CT and ^{18}F-FDG PET/CT from June 2020 to November 2022. Findings on the 3 scans were compared for detection rates and imaging concordance. ***Results:*** A total of 10 patients (3 men, 66±13 years) were included. Thyroglobulin levels at time of RAI therapy were 2441±4048 ng/dL (mean thyroid stimulating hormone: 66±36 mUI/mL). The administered ^{131}I dose was 4748±1455 MBq. At ^{131}I-PT WBS 2 patients showed residual thyroid bed uptake and latero-cervical avid nodes, 6 also demonstrated lung avid foci and all 10 patients had skeletal involvement with a total of 22 bone iodine avid lesions. At ^{18}F-FDG PET/TC, 20 bone lesions (in 9 patients) demonstrated 18F-FDG uptake and densitometric alterations, and 2 lesions (in 1 patient) did not show any pathological finding. Five more pathological foci were observed on thyroid bed (2/2), latero-cervical nodes (2) and lung (1/6) taking into consideration that the other 5 lung lesions were <5 mm size on CT evaluation and hence not metabolically evaluable. Similarly, at ^{18}F-NaF PET/CT the same 20 bone lesions also demonstrated abnormal uptake and the other 2 did not. Additionally, other 13 focal bone sites with benign densitometric pattern at CT were observed in 7 subjects. ***Conclusion:*** ^{18}F-NaF PET/CT did not add information on metastatic skeletal involvement in DTC patients over ^{131}I-PT-WBS and ^{18}F-FDG PET/CT, with comparable specificity for bone evaluation but with a not negligible rate of nonspecific findings. Moreover, both ^{131}I-PT-WBS and ^{18}F-FDG PET/CT also allowed to evaluate other potential disease compartments such as thyroid bed, nodes and lungs confirming the highest disease detection rate for ^{131}I-PT-WBS over other imaging modalities.

EPS-066

Correlation of thyroglobulin reduction index after ^{131}I therapy with RECIST1.1 assessment results in DTC with microscopic pulmonary metastases

T. Tian, *R. Huang;*
West China Hospital, Sichuan University, Chengdu, CHINA.

Aim/Introduction: This study analyzed the relationship between the stimulated thyroglobulin reduction index (TRI) and RECIST1.1 assessment results in DTC patients with microscopic pulmonary metastases (< 1 cm), aiming to provide a reliable evidence for the clinical decision of ^{131}I therapy in such patients. ***Materials and Methods:*** The clinical data of patients with pulmonary metastatic DTC underwent ^{131}I therapy in our department from 2009 to 2022 were retrospectively analyzed, and all pulmonary metastases in each patient were < 1 cm in diameter. Stimulated thyroglobulin (sTg) was measured before ^{131}I treatment (interval > 6 months), TRI=100×(sTg1-sTg2)/sTg1. Response evaluation was performed 6-12 months after each ^{131}I therapy according to RECIST criteria. ***Results:*** A total of 78 patients with DTC with lung metastases < 1 cm in diameter were included in the study. The median follow-up time was 5.8 years (range: 2-33 years), during which TRI was measured and response was evaluated 236 times, and the median number of ^{131}I treatments was 4 (range: 2-11). The median s-Tg was 116.10 ng/mL (range: 2.8-5000 ng/mL) and the median TRI value was 35.2% (range: - 403.2% - 95.4%). According to RECIST version 1.1, no patients in the study cohort achieved CR, 13 patients with PD (5.5%), and 222 patients (94.5%) with non-CR non-PD. The ROC curve yielded an optimal cut-off value of -28% for TRI for predicting PD, and patients in the TRI < -28% group were more likely to have PD than those with higher TRI levels (23.8% vs. 3.7%. $P < 0.001$). In the non-CR non-PD group, 17.1% (38/222) showed a reduction in the number of pulmonary metastatic lesions after ^{131}I therapy. ROC curve analysis showed that the best cut-off value for TRI to predict lesion reduction was 15.2 %, with

a sensitivity of 92.1%. There were far more patients with reduced lesions in the TRI > 15.2% group than in those with TRI ≤ 15.2% (21.9% vs. 4.8%, P=0.002). Multifactorial analysis showed that TRI was associated with reduced pulmonary metastatic lesions after ^{131}I therapy (HR: 5.196, 95% CI: 1.159-17.774, P=0.009), whereas type of pathology, interval of ^{131}I treatment, cumulative dose of ^{131}I therapy were not associated with reduced pulmonary metastatic lesions. ***Conclusion:*** TRI can objectively indicate the efficacy of ^{131}I therapy. In DTC patients with non-CR non-PD pulmonary metastases assessed by RECIST 1.1 criteria, TRI >15% can predict a better response and can be used to guide subsequent ^{131}I therapy.

EPS-067

Towards clinical translation of a novel antibody-based ^{177}Lu-labeled radiopharmaceutical for treatment of anaplastic thyroid cancer

A. Mortensen[1,2], *H. Berglund*[2], *T. Mohajer Shojai*[2], *H. Lotsholm Persson*[3], *A. Stenman*[1], *P. Jha*[2], *C. Juhlin*[1], *P. Bernhardt*[4], *J. Zedenius*[1], *F. Frejd*[2], *M. Nestor*[2,3,3];
[1]*Karolinska Institutet, Stockholm, SWEDEN,* [2]*Uppsala University, Uppsala, SWEDEN,* [3]*Science for Life Laboratory, Stockholm, SWEDEN,* [4]*University of Gothenburg, Gothenburg, SWEDEN.*

Aim/Introduction: Anaplastic thyroid cancer (ATC) is a rare but dire disease with few therapeutic options that offer more than simply palliative care. The cancer-associated cell-surface antigen CD44v6 is overexpressed in approximately 50% of all ATC and can be utilized for molecular radiotherapy. In collaboration with the Science for Life Laboratory, Drug Discovery and Development platform (SciLifeLab, DDD), we have developed a novel, antibody-based radiopharmaceutical targeting CD44v6. ***Materials and Methods:*** Phage selection and affinity screening was performed in an IP-free library created by DDD. Antibody candidates were assessed in vitro for specificity, affinity and off-target binding. The primary candidates were evaluated in vivo in mice bearing ATC xenografts using ^{125}I and a final candidate was selected. A dual-nuclide study (^{125}I/^{177}Lu) provided dosimetry data and a pilot therapy study using ^{177}Lu-labeled antibody was evaluated in an ATC xenograft model. Affinity maturation was performed and candidates were evaluated in vitro and in vivo in several xenograft models with varying CD44v6-expression levels. The lead drug candidate was evaluated for therapy in two ATC xenograft models and imaged using small-animal SPECT. A biodistribution study in rabbits was performed as a secondary toxicology species using ^{111}In-labeled antibody. Further, ^{68}Ga-PET/CT in cynomolgus was performed to confirm lack of unspecific binding. ***Results:*** Affinity, off-target binding and in vivo distribution studies resulted in the selection of Akir-1par as the primary lead candidate antibody. The dosimetry study indicated that ^{177}Lu would significantly increase the tumor dose compared to ^{131}I and the pilot therapy study resulted in 100% survival in the therapy group compared to controls in a high CD44v6-expressing xenograft model. Affinity-matured candidates demonstrated superior binding compared to the parental antibody and a final candidate was chosen, Akir-1. A dose-dependent therapeutic response to ^{177}Lu-Akir-1 was demonstrated using a high CD44v6-expressing xenograft model. Surprisingly, even a moderate dose of ^{177}Lu-Akir-1 resulted in complete remission of all treated animals in a low/moderate CD44v6-expressing xenograft model, cementing the superiority of Akir-1 compared to Akir-1par. The biodistribution of ^{111}In-Akir-1 in rabbits confirmed the previous pattern of low or non-existent uptake in normal tissues and no active binding to bone marrow. PET/CT in cynomolgus using ^{68}Ga confirmed low uptake in healthy tissues. ***Conclusion:*** The accumulated results from all animal studies cement the validity of ^{177}Lu-Akir-1 as a promising, novel antibody-based radiopharmaceutical targeting CD44v6 in ATC and a clinical phase 1 study is planned for 2024.

EPS-068

Differentiating subcentometer pulmonary metastases in differentiated thyroid cancer patients by integration of machine learning and deep learning: a retrospective, multicenter study

X. Gao*;*
Department of Radiology, Zhejiang Cancer Hospital, Hangzhou, CHINA.

Aim/Introduction: Diagnosing subcentimeter pulmonary metastases in indeterminate pulmonary nodules is crucial for patients with differentiated thyroid cancer.We aim to develop and validate novel integration models combing machine learning and deep learning for diagnosing subcentimeter pulmonary metastases in differentiated thyroid cancer patients. ***Materials and Methods:*** Models were developed in a primary center included 1244 subcentimeter pulmonary metastases on CT. Lesions were randomly assigned (7:3) to training or internal validation. Integration models based on machine learning were built with selected radiomics features and deep learning features and compared with classic machine learning models or deep learning models to classify the indeterminate subcentimeter lung nodules as pulmonary metastases or benign nodules. External validation contained 161 subcentimeter differentiated thyroid cancer pulmonary metastases in two independent centers. Stepwise validation was further performed according to the nodule's largest diameter in order to test models' generalization ability for subcentimeter nodules of different sizes. ***Results:*** Among all the machine learning models, the support vector machine showed the best discrimination in external validation, with a 0.910 AUC and a 0.935 AUC in internal validation. The deep learning model also showed good discrimination, with a 0.952 AUC in internal validation and a 0.893 AUC in external validation. All the integration models were significantly better than machine learning or deep learning alone, with the best AUC of 0.969 and 0.967 in internal validation and external validation, respectively. Stepwise validation demonstrated that with the PM diameter decreasing from 9mm to 2mm, the AUC initially remained stable and gradually decreased in all models and the integration models were the most stable. ***Conclusion:*** The novel integration models combining traditional radiomics and deep learning features provided noninvasive discrimination of subcentimeter pulmonary metastases from benign pulmonary nodules, even with minimal sizes, and was more effective than machine learning or deep learning alone.

EPS-069

Modeling Clinical Radioiodine Uptake by Using Organoids Derived from Differentiated Thyroid Cancer

X. Zhang[1], *J. Liu*[2], *Z. Li*[2], *R. Huang*[1];
[1]*Department of Nuclear Medicine, West China Hospital, Sichuan University, Chengdu, CHINA,* [2]*Department of Thyroid Surgery, West China Hospital Sichuan University, Chengdu, CHINA.*

Aim/Introduction: The majority of differentiated thyroid cancers (DTC) exhibit excellent prognosis under comprehensive treatments. However, about 2/3 of DTC with distant metastasis tend to de-differentiate and lose their capacity to uptake iodine, known as RAI-refractory DTC (RAIR-DTC), which may not benefit

from RAI therapy. Therefore, we intend to establish a primary tumor derived organoid model to predict ^{131}I uptake of tumor residue and investigate potential mechanism of sodium iodine symporter (NIS) regulation. ***Materials and Methods:*** Organoids were cultured from fresh tumor tissues origined from either treatment-naive DTC patients with distant metastasis or post-RAI therapy DTC patients with tumor recurrence. The corresponding clinicopathologic data was gathered, and the consistency of the morphological and histological features between organoid and parental tissue were analyzed. RAI uptake ability of organoid was assessed by ^{131}I uptake assay and its predictive sensitivity was checked by comparing with ^{131}I whole-body scan of corresponding patient. Transcriptome sequencing of RAI-avid and RAIR tissues was performed to search differentially expressed genes. ***Results:*** Eight DTC patients' organoids were created. One patient had bone metastasis alone, three had lung metastasis alone, and two patients had both. One patient presented residual lymph nodes metastasis, while another had recurrence in thyroid bed. Morphological and histological analysis showed that organoids faithfully recapitulated main features of origin tumor tissue, displaying similar expression pattern of thyroid-specific markers (PAX8, TTF-1, TSHR and TG), transporter necessary for iodine uptake (NIS), and proliferation marker (Ki-67). All patients received RAI therapy after surgery, and according to their post-therapy whole-body scintigraphy, patients were designated as either RAI-avid or RAIR DTC. RAIR DTC organoids showed comparable ^{131}I uptake level to an anaplastic thyroid cancer organoid control (53.0±45.8 vs 41.5±0.7 cpm/10^5 cells, p=0.087), while RAI-avid group presented significant higher ^{131}I uptake (1335.8±2047.4 cpm/10^5 cells, P=0.027). Predictive sensitivity was 87.5% when a cut-off value less than 300 cpm/10^5 cell was used to distinguish RAIR from RAI-avid organoids. Transcriptome analysis revealed that 668 mRNAs were up-regulated in RAIR DTC and 743 were down-regulated. The differentially expressed genes mainly enriched in ECM-receptor interaction, PPAR signaling pathway and cGMP-PKG signaling pathway. Moreover, SLC5A5, which encoding NIS, showed substantial discrepancy (p<0.001). ***Conclusion:*** Patient derived organoids from DTC recapitulated main characteristics of their parental tissue and preserved ability to uptake radioiodine, showing potential in predicting clinical ^{131}I-uptake status. Differentially expressed markers between RAI-avid and RAIR tissue may be latent targets in future attempt of re-differentiation therapy.

EPS-070

Cytoreductive efficacy of radioiodine treatment in hyperfunctioning thyroid nodules.

A. Alomar, *I. Blanco, F. Lozada, A. Irigaray, J. Pineda, M. Ollero, I. Saura, J. Cruz, A. Barrera, N. Rudic, M. Ribelles, A. Camarero, E. Anda, E. Goñi;*
Hospital Universitario de Navarra (HUN), Pamplona, SPAIN.

Aim/Introduction: The treatment of choice for patients with autonomous thyroid nodule without compressive symptoms and/or suspicion of malignancy is radioactive 131-I (RAI). Although the efficacy in normalizing thyroid function is widely demonstrated, there are currently few studies that determine the effectiveness of RAI in reducing the size of the autonomous thyroid nodule. The main objective of this study is to investigate the cytoreductive effect of RAI in the treatment of hyperthyroidism in autonomous thyroid nodule, as well as the clinical, radiological, scintigraphic, and dosimetric variables that influence this effect. ***Materials and Methods:*** Two senior nuclear medicine physicians, blinded to all clinical-radiological data, reviewed treatments with radioiodine (empirical dose) for hyperthyroidism indication between 2017 and 2020. Only those cases with a clearly dominant high uptake nodule in the thyroid scintigraphy with initial and follow-up ultrasound where selected. An analysis of scintigraphic images was performed (planar acquisition 20min. post iv injection of 185MBq of 99mTc-Pertechnetate) collecting data from ROIs (total, mean, and maximum counts) in thyroid nodules/s, thyroid parenchyma, and background. Additionally, maximum diameter and volumes of the nodule/s were collected using ultrasound, both before and after treatment, as well as clinical and biochemical data to evaluate thyroid function. Follow-up was performed between 12-18 months post-treatment. ***Results:*** A total of 39 nodules (20 multinodular goiters and 19 autonomous nodules) in 38 patients were included with a mean age of 54.6±2.1 years being women 34(87.2%). After radioiodine treatment (mean dose of 13.5±0.32mCi ranging from 10 to 15mCi), a significant decrease in nodule volume was observed (p=0.000) with a volume reduction ratio (VRR) of 64.9% [IQR: 47.3-92.7] (min: 5.2%, max: 96.7%), being significantly higher in nodules <3cm (74.1%±3.0 vs 52.5%±6.1; p=0.002). The VRR was not associated with any scintigraphic characteristic studied (total, mean, or maximum counts) neither the administered dose (rho=0.285; p=0.08). Two patients (5.2%) remained hyperthyroid while 7 (18.4%) became hypothyroid at one year follow-up. No relationship was found between scintigraphic uptake in remaining thyroid parenchyma and the rate of subsequent hypothyroidism. ***Conclusion:*** This study demonstrates that the administration of a single dose of 131-I presents a significant cytoreductive effect (measured as volume decrease) at 12-18 months post-treatment for autonomous thyroid nodule, which is especially significant in nodules <3cm. There was no significant association between VRR and any of the pre-treatment scintigraphic features neither the administered dose.

EPS-071

The effect of radioiodine therapy I-131 in patients with non-toxic nodular goitre

S. Abdelrazek, *J. Mysliwiec, P. Szumowski, W. Madra, L. Zukowski;*
Department of Nuclear Medicine, Medical University of Bialystok, Bialystok, POLAND.

Aim/Introduction: Simple goitre is defined as the enlargement of the thyroid gland, in the absence of autoimmune thyroid disease, malignancy, or inflammation, still constitutes a major diagnostic and therapeutic challenge. Radioiodine therapy (RAIT) is non-invasive, safe and cost effective method of therapy for reduction of goitre. There is no consensus regarding the optimum treatment of benign non-toxic goitre. Randomised studies have shown that levothyroxine has poor evidence of efficacy and is inferior to radioiodine therapy regarding goitre reduction. The aim of our study was to evaluate the short term efficacy of radioiodine therapy to reduce thyroid volume with minimal risk of hypothyroidism in patients with non-toxic nodular goitre. ***Materials and Methods:*** We treated 2200 patients, aged 20-90 years; (72%) of the studied groups were female and (24%) male; the mean radioiodine uptake (RAIU) was 42% and thyroid volume ranged between 42-190ml. Qualification of these patients were based on normal levels of serum fT3, fT4, TSH and characteristic appearance on thyroid scans and ultrasound. Malignant changes were excluded in all suspected nodules by fine needle aspiration biopsy. The activity dose was calculated by the use of Marinelli's formula and ranged between 200 -800 MBq (465 ± 191 MBq). The mean absorbed dose was 204 ± 25 Gy, and was proportional to

thyroid volume. Thyroid ultrasonography, and thyroid scan with RAIU at 24hours was done before and after 12 months of RAIT. Follow up control for the evaluation of fT4, TSH was done every 6 weeks. ***Results:*** After 12 months of radioiodine therapy a mean thyroid volume reduction of 51% was achieved. Approximately half of the effect is obtained within the first 3 months. Euthyroidism persist in 91% of patients, and hypothyroidism develop in 9% of patients. All patients were highly satisfied; with improvement in obstructive symptoms and exercise tolerance in the majority of patients. ***Conclusion:*** Radioiodine is non-invasive, safe and cost effective method of therapy for reduction of the goiter volume and should not be restricted to elderly patients, or to patients with high operative risk, but should be used as first choice in every patient with non toxic nodular goitre with thyroid volume > 40 ml. Surgery should be reserved as first choice if malignancy is suspected. The reduction of thyroid volume with low percent of hypothyroidism, were due to well accurate measurement of administered activity, relatively high effective half-life, & well-organised follow up.

EPS-072

Variables Associated With Positive [^{18}F]F-Choline Pet/Ct Uptake In Primary Hyperparathyroidism With Negative [^{99m}Tc]Tc-Mibi Scintigraphy

M. Guerra Gómez, *J. Cuenca Cuenca, N. Valerdiz Menéndez, A. Rodríguez Pajuelo, J. Tirado Hospital, J. Jiménez-Hoyuela García; University Hospital Virgen del Rocío, Seville, SPAIN.*

Aim/Introduction: The aim of this study was to identify the variables associated with positive uptake on [^{18}F]F-Choline PET/CT in cases of primary hyperparathyroidism (PHP) with negative preoperative [^{99m}Tc]Tc-MIBI scintigraphy. ***Materials and Methods:*** An observational case-control study was performed. Patients with histopathologically confirmed PHP with negative [^{99m}Tc]Tc-MIBI scintigraphy and positive [^{18}F]F-Choline PET/CT were included as cases. Patients with histopathologically confirmed PHP with positive [^{99m}Tc]Tc-MIBI scintigraphy were included as controls. Baseline clinical, biochemical and ultrasound variables before surgical treatment were analysed. Additionally, the incidence of post-surgical hypoparathyroidism was studied in both cohorts, as well as the histological variables (predominant cell type, growth pattern, location and size of adenoma). Logistic regression analysis was used to analyze the factors that influence the uptake of [^{18}F]F-Choline. ***Results:*** 79 patients were included. 26 cases (mean age 56.6 years, 76.9% female) and 53 controls (mean age 60.2 years, 76.4% female). Pre-surgical ultrasound study showed a higher frequency of cystic adenomas with calcifications and lobulated borders in cases compared to controls ($p < 0.05$). Multiglandular disease was also more frequent in PHP cases with positive [^{18}F]F-Choline uptake compared to controls (30.8% vs. 13.2%, p=0.061), as was the incidence of post-surgical hypocalcemia (19.2% vs. 7.5%, p=0.125) and lower post-surgical PTH level (16.1 vs. 47 pg/ml, p=0.052). Histological analysis showed a lower glandular volume in cases compared to controls (1.5 vs. 2.02 cc, $p < 0.001$). No significant differences were found in predominant cell type. A higher frequency of follicular growth pattern was observed in cases compared to controls (31.6% vs. 10.6%, p=0.03). In multivariate analysis, [^{18}F]F-Choline uptake in patients with negative [^{99m}Tc]Tc-MIBI scintigraphy was associated with lower glandular volume (adjusted Odds Ratio (AOR) 0.371, 95% CI [0.15, 0.94], p=0.037), follicular growth pattern (AOR 0.1, 95% CI [0.01, 0.87], p=0.037) and the presence of atypical ultrasound features (AOR 6.18, 95% CI [1.43, 26.69], p=0.015). ***Conclusion:*** Our findings suggest that lower glandular volume, multiglandular disease, presence of atypical ultrasound features and follicular growth pattern are associated with negative [^{99m}Tc]Tc-MIBI scintigraphy uptake and positive [^{18}F]F-Choline PET/CT in primary hyperparathyroidism. These results support the use of [^{18}F]F-Choline PET/CT in cases of PHP with a negative preoperative localization study.

EPS-073

Incremental value of Tc-99m-sestamibi SPECT/CT in patients with positive planar scintigraphy in the detection of additional lesions in patients with Primary hyperparathyroidism

R. Goel, *N. Damle, Y. Dharmashaktu, C. Bal, P. Kumar, A. Goyal, R. Gupta, Y. Gupta, R. Aphale, G. Puri, S. Chumber; All India Institute of Medical Sciences (AIIMS), New Delhi, INDIA.*

Aim/Introduction: Tc-99m-sestamibi scintigraphy is of value in non-invasively localizing abnormal parathyroid glands before surgical exploration as well as for ruling out ectopic glands in patients with primary hyperparathyroidism. However, most centres in India restrict to planar scintigraphy rather than SPECT/CT. In this retrospective analysis, we aim to demonstrate the incremental value of Tc-99m-sestamibi SPECT/CT over planar scintigraphy in detecting additional culprit lesions in patients with primary hyperparathyroidism. ***Materials and Methods:*** We retrospectively reviewed data of 313 patients(205 female, 108 male; age 2.5-80 years) with biochemical evidence of hyperparathyroidism referred from Endocrinologists(mainly from our institute) between January 2021 to December 2022. All patients were injected with 20mCi of Tc-99m-sestamibi intravenously. Planar images were acquired at 15-minute, 50-minute, and 2-hour intervals. SPECT/CT images were acquired at 50 minutes. The imaging findings were correlated with histopathology. ***Results:*** Out of the total 313 patients, 219(144-female, 75-male; age 14-80 years) patients had primary hyperparathyroidism with a mean iPTH of 360.3 pg/mL. In patients with primary hyperparathyroidism, planar scintigraphy was positive for presence of hyperfunctioning parathyroid in 146/219 patients(66.67%), while SPECT/CT detected lesions over and above planar imaging in 31/146 patients(21.2%). Of these 31 patients, planar imaging detected a total of 34 lesions, of which 4 were in right superior location, 12 in right inferior, 5 in left superior and 13 in left inferior. SPECT/CT of these 31 patients revealed 41 additional lesions out of which 14 lesions were in right superior location, 9 in right inferior, 9 in left superior and 7 in left inferior location and 2 in ectopic location(prevertebral and left upper paratracheal location respectively). Out of the 41 additional lesions on SPECT/CT, 6 were considered positive, 21 suspicious and 14 indeterminate for a parathyroid adenoma.17/31 patients underwent surgery and a total of 36 supposed lesions were excised. On a per patient analysis, SPECT/CT correctly identified lesions over and above planar imaging in 9/17 patients. On lesion-based analysis, 29/36 lesions were positive on histopathology for adenoma/hyperplasia. Of these 29 lesions, 16 were described in planar and SPECT/CT imaging. 12 were described only in SPECT/CT images. 3/12 lesions were given as positive, 6/12 as suspicious, and 3/12 as indeterminate on SPECT/CT for a parathyroid adenoma. One lesion was not described in planar or SPECT/CT images. ***Conclusion:*** Tc-99m-sestamibi SPECT/CT provides incremental value over planar scintigraphy in the detection of additional lesions thus reducing the possibility of failed parathyroidectomy in patients with primary hyperparathyroidism.

EPS-074

18F-Choline PET/MR for the Localization of Hyperplastic Parathyroid: Preliminary Analysis from a Monocentric Study

C. Gagliani, *P. Bartoletti, V. Camozzi, S. Sperti, F. Torresan, M. Iacobone, L. Evangelista;*
Azienda Ospedaliera Universitaria di Padova, Padova, ITALY.

Aim/Introduction: To evaluate the role of PET/MR with 18F-Choline in identifying hyperfunctioning parathyroids in patients with a history of primary or recurrent hyperparathyroidism but a negative or doubtful conventional imaging (i.e., neck ultrasonography and/or 99mTc-sestamibi scintigraphy). ***Materials and Methods:*** Between January 2020 and April 2023, 105 patients underwent PET/MR investigation with 18F-Choline. All images were reviewed by at least 2 nuclear physicians and 1 radiologist. For the interpretation of the images, both visual and semiquantitative assessment were used for PET, while MR images were only visually analyzed. For the semiquantitative PET analysis, the maximum standardized uptake value (SUVmax) was obtained. Data about surgical approach were considered, when available. ***Results:*** The detection rates of PET and MR for the localization of hyperplastic parathyroids were 82% and 56%, respectively. PET/MR was able to identify 100% of hyperplastic parathyroids in 11 patients who previously had a parathyroidectomy. The median value of SUVmax at the level of the hyperfunctioning parathyroid was 11.31 (range 2.1 - 39.7). PET/MR was positive mainly in patients with high serum calcium (median values: 14.09 vs. 2.69 mg/dL, respectively in positive and negative PET/MR), while a poor correlation with serum parathormone (PTH) was observed (median values: 105 vs. 108 pg/mL, respectively in positive and negative PET/MR). Data about surgery was available in 21/105 (20%) patients. In all 21 patients PET/MR was positive (100% true positive rate) with a final histological analysis compatible with parathyroid adenomas. ***Conclusion:*** The present study demonstrates that 18F-Choline PET/MR shows greater identification of parathyroids than MR alone. In addition, the value of serum calcium seems to play an important role in guiding patient selection, whereas serum PTH seems to play a limited role.

EPS-075

CXCR4-directed [^{68}Ga]Ga-PentixaFor PET/CT as a novel diagnostic modality in primary aldosteronism

A. Chaman Baz[1], *M. Gotthardt*[1], *W. Spiering*[2], *B. de Keizer*[2], *J. Deinum*[1], *J. F. Langenhuijsen*[1];
[1]*Radboudumc, Nijmegen, NETHERLANDS,*
[2]*UMC Utrecht, Utrecht, NETHERLANDS.*

Aim/Introduction: PA is a growing recognized form of secondary hypertension, affecting an estimated 2.6% of the hypertensive population (1). Primary aldosteronism (PA) is caused by autonomous overproduction of aldosterone by either a unilateral aldosterone-producing adenoma (APA) or by bilateral adrenal hyperplasia (BAH). Distinction ('subtyping') is crucial, PA is cured by adrenalectomy in unilateral PA and is treated by medication in bilateral PA. The reference standard in subtyping PA is currently adrenal vein sampling (AVS). However, it is invasive, costly, has limited availability and is accompanied by risk of serious complications. We propose a new diagnostic imaging modality employing the PET-tracer [^{68}Ga]Ga-PentixaFor, which has high accuracy in detecting APAs in PA (2). The goal of this study is to determine concordance of [^{68}Ga]Ga-PentixaFor PET/CT and AVS. Secondary outcomes are optimal timepoint for scanning and quantitative criteria for lateralization at the optimal timepoint. ***Materials and Methods:*** This study is part of a two-step diagnostic trial. We included patients with PA from Radboudumc Nijmegen and UMC Utrecht, confirmed by an intravenous salt-loading test. Patients underwent AVS and [^{68}Ga]Ga-PentixaFor PET/CT. A dynamic scan was performed to determine the optimal timepoint for scanning in the first 6 patients. The main outcome was the concordance of AVS and [^{68}Ga]Ga-PentixaFor PET/CT. The SUV_{max} was used to determine lateralization in [^{68}Ga]Ga-PentixaFor PET/CT. ***Results:*** Twenty-four patients underwent adrenal vein sampling and a [^{68}Ga]Ga-PentixaFor PET/CT. Two patients had inconclusive AVS results and were excluded from analysis. The optimal timepoint of scanning was 1h post-injection. Using a cut-off of SUV-max-ratio of 1.4 we reached a concordance of 68%, sensitivity of 64% and specificity of 75%. Using a Bayesian prediction model, the predicted-concordance was: 67% (CI80%=54-78). ***Conclusion:*** [^{68}Ga]Ga-PentixaFor PET/CT is an imaging modality with high concordance with AVS. With these results we have sufficient evidence to proceed to step-2: A randomized controlled diagnostic trial, where patients will be randomized in [^{68}Ga]Ga-PentixaFor PET/CT or AVS. ***References:***

1. Kayser SC, Deinum J, de Grauw WJ, Schalk BW, Bor HJ, Lenders JW, et al. Prevalence of primary aldosteronism in primary care: a cross-sectional study. Br J Gen Pract. 2018;68(667):e114-e22.
2. Hu J, Xu T, Shen H, Song Y, Yang J, Zhang A, et al. Accuracy of Gallium-68 Pentixafor Positron Emission Tomography-Computed Tomography for Subtyping Diagnosis of Primary Aldosteronism. JAMA Network Open. 2023;6(2):e2255609-e.

EPS-076

Role of 68Ga-DOTANOC, 18F-FDOPA and 68 Ga- Exendin PET/CT imaging in adult patients with Hyperinsulinemic Hypoglycemia(HI)

S. Sagar, *N. A. Damle, D. Khan, P. Kumar, C. Bal, M. Tripathi, N. Tandon, Y. Gupta;*
AIIMS, Delhi, INDIA.

Aim/Introduction: Hyperinsulinemic hypoglycemia (HI) is a rare but potentially fatal condition. At our institution, we aimed to evaluate three tracers- 18F-FDOPA,68Ga-DOTANOC and 68Ga-EXENDIN-4 PET/CT in identifying focal pancreatic lesions in patients with HI. These imaging techniques have been shown to be useful for this purpose. ***Materials and Methods:*** 68Ga-DOTANOC and 68 Ga- ExendinPET/CT scans and clinical details of 23 adults with biochemical and clinical diagnosis of HI were reviewed. The adult patients were administered 2-3mCi 68Ga-DOTANOC, 18F-FDOPA and 68Ga-Exendin and the scan was acquired on dedicated PET/CT scanners (Biograph mCT, Siemens Inc and Discovery PET/CT, GE). Abdominal spot images over 1-2 bed positions were acquired with 18F-FDOPA and 68 Ga- Exendin while whole body images were acquired with 68Ga-DOTANOC. ***Results:*** Out of 23 adults (14 female and 9 male), 10 adults underwent 18F-DOPA PET/CT,19 adults underwent 68Ga-DOTANOC PET/CT between 2017 to 2023 at our institution.Our results showed diffuse uptake in all 10 patients whereas 5 patients had both FDOPA PET/CT and 68-Ga DOTANOC PET/CT and DOTANOC was able to detect focal lesion in 4 patients (2 had focal uptake at head and the other 2 had uptake in the tail of pancreas).Out of these 10 patients, 5 patients also had both FDOPA PET/CT and 68-Ga EXENDIN PET/CT and EXENDIN was able to detect focal lesions in 5 patients. Out of these 5 patients 4 patients had both EXENDIN And DOTANOC PET/CT with focal localisation to same site. ***Conclusion:*** In adult patients with hyperinsulinemic hypoglycemia (HI), both 68Ga-DOTANOC and 68Ga-Exendin PET/CT are effective methods

for identifying focal pancreatic lesions. Compared to 18F-DOPA PET/CT without Carbidopa premedication, the detection rate is significantly higher for both of these imaging techniques.

EPS-077

Association between BAT detection (and activity) with FDG PET/CT and cancer prognostic: an Artificial Intelligence (AI) enhanced systematic review.

P. Jané[1], *E. Jané*[2], *E. Pirazzo Teixeira*[1], *V. Garibotto*[1], *K. Gariani*[3];
[1]*Service of Nuclear Medicine and Molecular Imaging, Hôpitaux Universitaires de Genève, Genève, SWITZERLAND,* [2]*Universidad Politécnica de Madrid, Madrid, SPAIN,* [3]*Service of Endocrinology, Diabetes, Nutrition and Therapeutic education, Hôpitaux Universitaires de Genève, Genève, SWITZERLAND.*

Aim/Introduction: Brown adipose tissue (BAT) represents the main source of adaptive thermogenesis in humans providing an attractive pharmacological target to counteract obesity, insulin resistance and cardio-vascular disorders. BAT usually displays an increased uptake of 18F-FDG in positron emission tomography/computed tomography (PET/CT), making this modality the most established approach for the detection and quantification of BAT in the clinic. Some associations between BAT activity and cancer evolution have been described, however the role of BAT on cancer prognostic and development remains uncertain, thus motivating this AI-enhanced systematic review. ***Materials and Methods:*** We used the Entrez API and a local copy of the 2022 Medline dataset (courtesy of the National Library of Medicine, U.S.A) to search and retrieve all articles involving BAT and PET. We then built an automated systematic review pipeline with the help of different python tools for Natural Language Processing like Spacy, Scispacy and the Scibert model to perform text classification, entity recognition and entity linking to the Unified Medical Language System (UMLS) Metathesaurus. We defined 35 variables for the meta-analysis including study characteristics, patients' demography, clinical data, and imaging findings and created ad-hoc algorithms for the automated extraction of the necessary data from the full texts. ***Results:*** Our (semi)-automated systematic review identified an initial number of 847 articles with finally eight articles with a total of 6290 patients that fulfilled the quality criteria for inclusion after screening of titles, abstracts and full texts. The cancers studied were breast cancers, lung cancer, lymphoma, gastrointestinal cancer, thyroid cancer, melanoma, genitourinary cancer and sarcoma/carcinoma of unknown origin. The results collected from the included studies suggested that BAT activity is greater in patients with active cancer compared to age-, sex-, and BMI-matched BAT-positive patients without active cancer. In particular, patients with breast cancers have a BAT activity that appears greater than in patients with other solid tumor malignancies. Furthermore, the presence of atypical FDG uptake in neck and/or supraclavicular lesion, which may represent active BAT, was associated with HER2 and PgR expressions, and was an independent prognostic factor for patients with breast cancers. ***Conclusion:*** This (semi)-automated systematic review suggests that BAT activity detected with PET/CT is greater in patients with malignancies, especially breast cancers and may represent eventually a prognostic factor. The implementation of AI in the systematic review process significantly increases its sensitivity and efficiency, and reduces the time and resources needed.

EPS-078

^{68}Ga-DOTATATE PET/CT versus ^{18}F- FDG PET/CT in TENIS syndrome - Impact in management and theranostics strategies - Pilot study

L. Almeida[1], *A. Santos*[1], *T. O. Costa*[2], *M. Araújo*[1], *L. Assumpção*[1], *M. Lima*[1], *T. Souza*[1], *D. Wittmann*[1], *E. Etchebehere*[1];
[1]*Campinas University, Campinas, BRAZIL,* [2]*Ebserh, Bahia, BRAZIL.*

Aim/Introduction: TENIS syndrome (Thyroglobulin-Elevated Negative Iodine Scintigraphy) is characterized by reduced expression of sodium-iodine symporter, rising serum thyroglobulin levels (Tg), and negative whole-body I-131 scans. In such patients, somatostatin receptor imaging with ^{68}Ga-DOTATATE PET/CT (SSR PET/CT) and ^{18}F-FDG PET/CT (FDG PET/CT) can identify metastases. To compare the uptake pattern of SSR PET/CT and FDG PET/CT with patients with TENIS Syndrome under two conditions: elevated (eTSH) and suppressed (sTSH) TSH serum levels. Based on imaging findings in these patients, we intend to identify potential candidates for peptide receptor radionuclide therapy (PRRNT). ***Materials and Methods:*** Fifteen patients with TENIS Syndrome were prospectively enrolled. All patients underwent both SSR PET/CT and FDG PET/CT with sTSH and eTSH. All images were blindly evaluated for differences in SUVmax values and lesion detectability (local recurrence and lymph node (LN), lung, and bone metastases). The reference standard consisted of neck ultrasound, CT, MRI, PET/CT, biopsy, and follow-up. Five patients were selected for PRRNT due to lesion uptake similar to or higher than the liver. ***Results:*** On a per-patient and on a per-lesion based analysis, sTSH SSR PET/CT detected a greater number of cervical and distant LNs (both p = 0.0253 on per-patient and p=0.0176 and p=0.0391 on per-lesion, respectively) when compared to sTSH ^{18}F-FDG PET/CT**.** Likewise, eTSH SSR PET/CT detected a greater number of patients with local recurrences (p=0.0455) and distant LN metastases (p=0.0143) and in a per-lesion based analysis greater number of cervical and distant LNs (p=0.0337 and p=0.0039, respectively) when compared to eTSH ^{18}F-FDG PET/CT**.** No differences were found in lesion detectability for lung and bone metastases. One of three patients submitted to 3 cycles of PRRNTpresented with a visual partial response, a 20% reduction in quantitative analyses and stable disease regarding Tg and ATgAb levels. ***Conclusion:*** In patients with TENIS Syndrome, SSR PET/CT detected a greater number of loco-regional and distant LN metastases than FDG PET/CT with both sTSH and eTSH. One patient submitted to PRRNT presented a partial response to treatment. Our findings may impact in patient restaging, management and theranostics strategies with radiolabeled somatostatin analogs.

EPS-079

Role of Integrated ^{18}F-Fluorocholine PET/4DCT in the localization of culprit lesions in patients with primary hyperparathyroidism

Y. Dharmashaktu, *N. A. Damle, C. Bal, M. Tripathi, P. Kumar, R. N. Wakankar, S. Chumber, Y. Gupta, D. K, S. Agarwal, C. Kumar, R. Goel;*
All India Institute of Medical Sciences, Delhi, INDIA.

Aim/Introduction: 4D-CT and FCH PET/CT are excellent modalities that have evolved in the last decade to substitute the deficiencies of MIBI scan and Ultrasound in primary hyperparathyroidism. However literature is scarce on the role of integrated FCH PET/4D-CT. In the present study we assessed the lesion detection rate of integrated FCH PET/CT and 4D-CT imaging in comparison to both modalities individually. ***Materials and Methods:*** 45 patients with PHPT were evaluated from October 2020 to May 2022. All

patients underwent integrated FCH PET/4D-CT from angle of mandible to diaphragm. Scans were interpreted by a Nuclear Medicine physician and a radiologist independently with blinding and lesions were graded as positive, suspicious and negative. ***Results:*** There were 45 patients (14 males, 31 females) with mean age of 41.8 years. Mean iPTH was 163 pg/mL. 27/45 patients underwent surgery and a total of 43 lesions were excised.Overall, FCH PET/CT was able to detect lesions in 36/45 (80%) patients, 4D-CT in 32/45 (71.1%) patients and integrated FCH PET/4DCT in 39/45 (86.6%) patients.In the 27 operated patients, 4D-CT was able to detect a culprit lesion in 23/27 (85.1 %) patients and FCH PET/CT in 26/27 patients (96.2%).On a per patient analysis based on histopathology, FCH PET/CT was able to correctly detect the culprit lesion(s) in 25/27 patients (92.5%), 4D-CT in 21/27 (77.7%) patients and integrated in 25/27 patients (92.5%), i.e. true positive cases.Hence, on per patient based analysis, both the sensitivity and lesion detection rates of FCH PET/CT, 4D-CT and integrated FCH PET/4D-CT were same i.e., 92.5%, 77.7% and 92.5% respectively. On per lesion based analysis, sensitivity, specificity and detection rate for FCH PET/CT, 4D-CT and integrated FCH PET/4D-CT was 91.8%, 50%, 94.4%; 72.9%, 66.6%, 72.9% and 91.8%, 50%, 94.4% respectively. ***Conclusion:*** FCH PET/CT performed equally well on a per patient and per lesion basis in the operated group of patients. Integrated imaging however increased surgeon confidence in going ahead with the surgeryIntegrated FCH PET/4D-CT imaging also ensures patient comfort (single sitting procedure) along with lesser radiation by avoiding one extra NCCT compared to separate procedures Integrated imaging may be preferred if both investigations are planned anyway.

EPS-080

18F-Fluorocholine PET/CT and scintigraphy detection rate stratified by PTH levels in parathyroid imaging

N. Jacquet-Francillon, *I. Morelec, M. Dietz, A. Clotagatide, J. Tordo, L. Al-Mansour, S. Isal, A. Flaus;*
Hospices Civils de Lyon, Lyon, FRANCE.

Aim/Introduction: [^{18}F]-Choline PET/CT is used more and more in addition to [^{99m}Tc]-SestaMIBI scintigraphy and ultrasonography, sometimes even as a first-line imaging modality for parathyroid imaging. The aim of our study is to evaluate the detection rate (DR) of [^{18}F]-Choline PET/CT and [^{99m}Tc]-SestaMIBI scintigraphy according to the PTH level. ***Materials and Methods:*** In one academic center, we retrospectively included 253 patients with hyperprathyroidism. The detection rate of hyperfunctioning parathyroid glands was calculated in 7 subgroups of serum PTH level for [^{18}F]-Fluorocholine PET/CT and [^{99m}Tc]-SestaMIBI scintigraphy. Linear and exponential regression curves have been calculated. ***Results:*** DR of [^{18}F]-Fluorocholine PET/CT varied from 45.5% for serum PTH < 50 ng/mL to 89.2% for serum PTH > 150 ng/mL. DR of [^{99m}Tc]-SestaMIBI scintigraphy varied from 40.0% for serum PTH < 50 ng/mL to 90.5% for serum PTH > 150 ng/mL. Linear and exponential regression curves confirmed a relationship between DR and PTH level. Detection rate of [^{18}F]-Fluorocholine PET/CT is slightly superior to that of scintigraphy for the lowest PTH levels. ***Conclusion:*** Our study establishes a pre-test probability of identifying a parathyroid lesion before [^{18}F]-Choline PET/CT or [^{99m}Tc]-SestaMIBI scintigraphy . ***References:*** [1] Araz M, Soydal Ç, Özkan E, Kır MK, İbiş E, Güllü S, et al. The efficacy of fluorine-18-choline PET/CT in comparison with 99mTc-MIBI SPECT/CT in the localization of a hyperfunctioning parathyroid gland in primary hyperparathyroidism. Nucl Med Commun. Lippincott Williams and Wilkins; 2018;39:989-94. [2] Parikshak M, Castillo ED, Conrad MF, Talpos GB. Impact of hypercalcemia and parathyroid hormone level on the sensitivity of preoperative sestamibi scanning for primary hyperparathyroidism. Am Surg [Internet]. 2003;69:393-8. [3] Jacquet-Francillon N, Morelec I, Germain N, Prades JM, Habouzit V, Mariat C, Bonnefoy PB, Prevot N. Performance of quantitative measurements in [18F]fluorocholine positron emission tomography/computed tomography for parathyroid imaging (P2TH study). Front Med (Lausanne). 2022 Aug 2;9:956580.[4] Rutledge R, Stiegel M, Thomas CG, Wild RE. The relation of serum calcium and immunoparathormone levels to parathyroid size and weight in primary hyperparathyroidism. Surgery. 1985;98:1107-12. [5] Moretz WH, Watts TL, Virgin FW, Chin E, Gourin CG, Terris DJ. Correlation of intraoperative parathyroid hormone levels with parathyroid gland size. Laryngoscope. 2007;117:1957-60. [6] Bossert I, Chytiris S, Hodolic M, Croce L, Mansi L, Chiovato L, et al. PETC/CT with 18 F-Choline localizes hyperfunctioning parathyroid adenomas equally well in normocalcemic hyperparathyroidism as in overt hyperparathyroidism. J Endocrinol Invest. 2019;42:419-26.

EPS-081

Concordance between 18F-Fluorocholine PET-CT and surgery in the localization of parathyroid adenomas in patients with primary hyperparathyroidism

P. Daudén Oñate[1], *A. Ortega Candil*[1], *C. Rodríguez Rey*[1], *G. Cuesta Domingo*[1], *S. Ochagavía Cámara*[1], *R. Cano Carrizal*[2], *I. Domínguez Serrano*[1], *S. Mera Carreiro*[1], *M. Meneses Navas*[1], *P. Nespral Torres*[1], *P. Romero Fernández*[1], *A. Berardinelli*[1], *M. Cabrera Martín*[1], *P. Bascuñana Almarcha*[1];
[1]*Hospital Clínico San Carlos, Madrid, SPAIN,*
[2]*Hospital Infanta Sofía, Madrid, SPAIN.*

Aim/Introduction: Parathyroid adenomas are the most common cause of primary hyperparathyroidism, being solitary in 90% of the cases. Definitive treatment consists of surgical resection of the hyperfunctioning gland, being essential its pre-surgical localization using imaging tests. Our aim is to determine the concordance between 18F-fluorocholine positron emission tomography / computed tomography (choline PET/CT) and surgical findings in the localization of parathyroid adenoma in patients with primary hyperparathyroidism. We also intend to test whether the acquisition on digital equipment increases the reliability of the technique. ***Materials and Methods:*** Retrospective study of 154 patients with primary hyperparathyroidism and negative/discordant conventional imaging tests (neck ultrasound and technetium-99m sestamibi (MIBI) scintigraphy), who underwent choline PET/CT between 2019-2023. We included those patients who underwent resection up to the date of analysis, constituting a final sample of 48 patients. We defined four quadrants of parathyroid adenoma localization: right superior, right inferior, left superior and left inferior. Twenty-seven studies were acquired in analog equipment (AE) and 21 in digital equipment (DE). ***Results:*** The mean age was 63.9±10.6 years, being more frequent in women (81,25%). The interval between PET-CT and surgery was 340±234 days, being the right lower pole the most frequent location (39,62%). The mean PET-CT lesion size was 7.22±3.63mm with mean Standardized Uptake Value (SUVmax) 6.22±4.14. PTH values 10 minutes after resection decreased significantly (-66.88pg/mL, p<0.001). The observed agreement between surgical localization and PET-CT localization was 81,1%, with a Kappa index 0.74 (95% CI 0.60-0.87, p<0.001). The agreement observed with DE was significantly higher than that observed with AE (p=0.025): 95,5% vs 71%. The Kappa index in the ED was 0.94 (95% CI 0.82-1.00, p<0.001), compared to 0.61 (95% CI 0.41-0.81,

p<0.001) in the AE. ***Conclusion:*** Choline PET-CT is a reliable tool in the localization of parathyroid adenoma in patients with primary hyperparathyroidism and inconclusive/discordant conventional imaging tests, especially with the new DE. This allows a minimally invasive surgical approach, reducing surgical morbidity.

EPS-082

Impact of Radioactive Iodine on Survival outcomes for Differentiated Thyroid Carcinoma - Understanding the Factors at Play

A. Al ibraheem, *U. Al-Rasheed, A. S. Abdlkadir, N. Mashhadani, S. Ruzzeh, D. A. Al-Adhami, I. Mohamad, B. Hamdan, R. Kheetan, M. E. Juweid, A. Mansour, F. Istatieh;*
King Hussein Cancer Center, Amman, JORDAN.

Aim/Introduction: Differentiated thyroid cancer (DTC) is the most common type of endocrine cancer, and its incidence is increasing worldwide. Treatment of DTC is multi-factorial, involving a combination of surgical, hormonal, and nuclear medicine (NM) therapies. NM therapies typically involve the administration of radioactive iodine (RAI). RAI is administered following thyroid surgery in order to thyroid remnant ablation, deliver adjuvant therapy, or treat identifiable disease. There is a scarcity of reports on the long-term outcome of DTC in developing countries at centers of excellence. The purpose of this study was to evaluate the effect of radioactive iodine therapy (RAI) and other patient-related factors on the five-year survival of 555 patients with primary thyroid cancer who were diagnosed and treated at KHCC from 1998 to 2021. ***Materials and Methods:*** Data from a tertiary referral cancer center were collected and analyzed retrospectively. A cohort of 555 patients who were diagnosed with biopsy-proven thyroid cancer was investigated. Baseline statistics were reported using measures of central tendency and dispersion for continuous variables and proportions for categorical variables. Descriptive data were compared across groups using Student's t-test for continuous variables and Chi-square or Fisher's exact tests for categorical variables. A univariate and multivariate analysis was performed using a Cox regression model. The Kaplan-Meier method was used for survival analysis. A log-rank test was used to compare the survival curves. All tests were two-sided, and a p value of less than 0.05 was considered statistically significant. ***Results:*** A total of 26 patients died from thyroid cancer during the median follow-up period of 73 months. It's noteworthy that 18 other patients died from non-disease specific reasons (breast cancer, Sepsis, Ischemic heart disease, and renal failure due to diabetes) were censored in the present study. The 5-year survival for patients with DTC was found to be high (91%), with a mean estimated survival time of 168.3 months. Age and distant metastasis were identified as the main negative prognostic factors, while RAI treatment was found to be a significant factor in improving prognosis. ***Conclusion:*** The large majority of patients with thyroid cancer (93.33%) in our study cohort had an excellent prognosis, comparable to published data from other studies. Radioiodine therapy was found to be protective against poor prognosis. These findings suggest that appropriate treatment and adherence to clinical guidelines can improve outcomes for patients with DTC.

EPS-083

Differential serum miRNA profile in well differentiated thyroid cancer and benign thyroid disease. Prognosis of patients with this miRNA profile five years after radioiodine treatment

O. Bourogianni[1], *N. Kapsoritakis*[1], *E. Tsitoura*[2], *A. Tsaroucha*[1], *G. Lamprakopoulos*[1], *M. Stathaki*[1], *E. Papadaki*[1], *S. Koukouraki*[3];
[1]*Department of Nuclear Medicine, University Hospital of Crete, Heraklion, GREECE,* [2]*Laboratory of Molecular and Cellular Pneumonology, Medical School, University of Crete, HERAKLION, GREECE,* [3]*Department of Nuclear Medicine, Medical School, University of Crete, Heraklion, GREECE.*

Aim/Introduction: The increased incidence of papillary thyroid cancer (PTC) in Crete, led us to study the expression of a panel of 84 mature miRNAs in patients of the island of Crete. MiRNAs are small non-coding RNAs of approximately 19-25 nucleotides in length that are responsible for the posttranscriptional regulation of gene expression. The objective of the current study was to identify circulating miRNAs that might be used as clinical biomarkers in patients with PTC. We set out to identify (1) circulating miRNAs in preoperative serum samples from patients with PTC (2) different expression of miRNAs in patients with PTC and patients with benign thyroid nodules (3) the efficacy of radioiodine treatment (4) the prognosis of patients with this miRNAs profile five years after total thyroidectomy and radioiodine treatment(RAIT). ***Materials and Methods:*** Blood samples of peripheral venous blood were obtained one day before surgery. Centrifugation at 2500 g for 10 minutes was performed to separate serum from other blood components. The supernatant was separated from the cellular layer and immediately stored at -80°C A biobank of 45 samples was generated. All pathological findings were confirmed after surgery. The enrolled patients were divided into two groups: benign nodules (BN) and PTC. RNA was isolated. For the analysis of microRNA expression levels, total RNA were used in reverse transcriptase and quantitative PCR reactions. The efficacy of RAIT and clinical outcome 5 years later was evaluated according to the biochemical or structural evidence of disease. ***Results:*** By analyzing data using special data analysis tools we identified 2 miRNAs significantly deregulated in PTC compared to BN. These included 1 upregulated and 1 downregulated miRNAs. Especially miR23a-3p and miR- 574-3p were the most accurate in discriminating between PTC patients and patients with benign thyroid nodules. None of the rest of 84 miRNAs was significantly different between the two groups, although the mean preoperative serum level of miR-150-5p, miR-21-5p in the PTC group was more than 2 fold than that found in samples from patients with BN. The clinical outcome five years following RAIT ablation in all patients with PTC was excellent, ***Conclusion:*** Identification of miRNA signatures in serum for PTC diagnosis could probably serve as a stable, sensitive, and non-invasive biomarker for discrimination between PTC and benign thyroid disease. Prognosis of patients with this miRNA profile seems to be excellent five years after thyroidectomy and radioiodine treatment.

610

Sunday, September 10, 2023, 16:45 - 18:15
Hall K

CTE 3 - Technologists Committee: Patient Care in Nuclear Medicine

OP-257
Improving understanding of patients' experience
A. Grilo;
Escola Superior de Tecnologia da Saúde, Instituto Politécnico, Lisbon, PORTUGAL.

OP-258
Looking beyond the images: practical examples in paediatrics
I. Baeta;
Kings College Hospital NHS Foundation Trust, Nuclear Medicine and PET/CT Department, London, UNITED KINGDOM.

OP-259
Shaping patient experience in PET-CT, PET-MRI, and Clinical Trials
P. Turco;
Department of Medicine DIMED, University-Hospital of Padova, Padova, ITALY.

611

Sunday, September 10, 2023, 16:45 - 18:15
Hall G1

Special Symposium 1 - EANM/EARL: Harmonisation and Accreditation Accelerate Research and Clinical Translation

OP-260
To EARL" or "Not To EARL" in Clinical Practice?
S. Stroobants;
Antwerp University Hospital, Antwerp, BELGIUM.

OP-261
EARL 1 and EARL 2. Where are we now?
I. Hristova;
EARL, Vienna, AUSTRIA.

OP-262
Accreditation for Brain PET studies
R. Boellaard;
Amsterdam UMC, Amsterdam, NETHERLANDS.

OP-263
Harmonisation in quantitative SPECT and its challenges
J. Tran-Gia;
Universitätsklinikum Würzburg, Würzburg, GERMANY.

701

Monday, September 11, 2023, 08:00 - 09:30
Hall A

CME 5 - Oncology & Theranostics Committee: Will the Microenvironment Become Even More Important in Nuclear Medicine?

OP-269
The future of the oldest Megaimportant Nuclear Medicine marker of the menvironment
S. Carrilho Vaz;
Champalimaud Centre for the Unknown, Champalimaud Foundation, Department of Nuclear Medicine - Radiopharmacology, Lisbon, PORTUGAL.

OP-270
Hypoxia - The importance of spotting such a hostile menvironment
W. Weber;
Technical University of Munich, Department of Nuclear Medicine, Munich, GERMANY.

OP-271
Immune system – Immunotherapy enthusiasm will fuel new techniques in Nuclear Medicine?
N. Schäfer;
Lausanne University Hospital, Nuclear Medicine and Molecular Imaging Department, Lausanne, SWITZERLAND.

OP-272
Cancer-associated fibroblasts - Highlighting no-malignant cells that are in the dark, serving malignant cells
S. Dalm;
Erasmus MC, Radiology & Nuclear Medicine Department, Rotterdam, NETHERLANDS.

702

Monday, September 11, 2023, 08:00 - 09:30
Hall D (Arena)

Debate 2 - Neuroimaging Committee: What is the Best Tracer for Molecular Brain Tumour Imaging?

OP-273
Conventional tracers: Is it all about amino acid tracers or is there still a role for FDG?
F. Cicone;
Dipartimento di Medicina Sperimentale e Clinica (DMSC) Università degli Studi "Magna Graecia" di Catanzaro (ITALY) Università degli Studi "Magna Graecia" di Catanzaro, Catanzaro, ITALY.

OP-274
Novel radiotracers: why do we need more than amino acid tracers?
N. Albert;
Klinikum der Ludwig-Maximilians-Universität, Munich, GERMANY.

703

Monday, September 11, 2023, 08:00 - 09:30
Hall E1

LIPS Session 5 - Cardiovascular + Physics Committee: Challenges in MBF Quantification

OP-279
Patient motion and data-driven motion correction
I. Armstrong;
Manchester University NHS Foundation Trust, Nuclear Medicine, Manchester, UNITED KINGDOM.

OP-280
SPECT: is there anybody out there?
L. Imbert;
CHRU Nancy Brabois, Nuclear Medicine Department, Nancy, FRANCE.

OP-281
Accuracy of MBF estimates and cut-off values
M. Lubberink;
Uppsala University, Nuclear Medicine & PET, Uppsala, SWEDEN.

OP-282
Challenges of using quantification in clinical practise
I. Danad;
Utrecht University Medical Centre / Amsterdam University Medical Centre, Cardiology, Utrecht, NETHERLANDS.

704

Monday, September 11, 2023, 8:00 AM - 9:30 AM
Hall E2

M2M Track - TROP Session: Imaging Inflammatory Processes in Cardiovascular Diseases

OP-284
Dynamic Expression of Myocardial Sigma-1 Receptor in Doxorubicin-Induced Cardiomyopathy using Radioiodine Labeled 2-[4-(2-iodophenyl)piperidino]cyclopentanol (OI5V) Imaging
Z. Chen[1], *H. Wakabayashi*[1], *H. Mori*[1], *T. Hiromasa*[1], *X. Zhang*[1], *T. Kozaka*[2], *K. Ogawa*[3], *S. Kinuya*[1], *J. Taki*[4,1];
[1]*Department of Nuclear Medicine, Kanazawa University Hospital, Kanazawa, JAPAN,* [2]*Division of Probe Chemistry for Disease Analysis, Research Center for Experimental Modeling of Human Disease, Kanazawa University, Kanazawa, JAPAN,* [3]*Institute for Frontier Science Initiative, Kanazawa University, Kanazawa, JAPAN,* [4]*PET Center, Kanazawa Advanced Medical Center, Kanazawa, JAPAN.*

Aim/Introduction: In doxorubicin-induced cardiomyopathy (DIC), drug-induced cardiomyocyte damage or death occurs via various molecular mechanisms, including endoplasmic reticulum stress, oxidative stress, iron metabolism, Ca^{2+} homeostasis dysregulation, sarcomeric structure alterations, gene expression modulation, and apoptosis. However, it is still unclear how sigma 1 receptors (σ1R) are related to DIC. In this study, we aimed to evaluate the expression of the σ1R using radiolabeled 2-[4-(2-iodophenyl) piperidino]cyclopentanol (OI5V) in the DIC rat model. ***Materials and Methods:*** Wistar rats were injected with doxorubicin (2 mg/kg/week, intraperitoneal), while the control group was injected with saline (2 mL/kg/week, intraperitoneal) (n=4-6 for each group). Gated ^{99m}Tc-MIBI SPECT was performed on the rats to evaluate cardiac function before and at 3, 5, 7, and 8 weeks after injection. We measured organ uptake (heart, blood, kidney, lung, pancreas, liver, and muscle) of ^{125}I-OI5V, and heart uptake of ^{99m}Tc-MIBI was measured before and at 3, 5, 7, and 8 weeks after injection. ***Results:*** The rats did not die during the observation period and showed increased body weight. In cardiac function, end-diastolic and end-systolic volume significantly increased 5 weeks after doxorubicin injection and ejection fraction started to decrease 7 weeks after injection. Post-mortem tissue counting showed that ^{125}I-OI5V uptake started to decrease 5 weeks after injection in the heart and kidney, and started to increase 5 weeks after injection in the blood. The uptake in the lung, pancreas, liver, and muscle was not changed in the observation period. ^{99m}Tc-MIBI uptake of the heart correlated well with ^{125}I-OI5V uptake ($R^2 = 0.8$, $P < 0.0001$). ***Conclusion:*** Our study confirmed the dynamic expression pattern of σ1R after doxorubicin injection, with a decrease of σ1R expression in the heart demonstrated by post-mortem tissue counting. σ1R may be a feasible target for monitoring DIC by confirming the decline in expression.

OP-285
Early evaluation of organ fibrosis in Angiotensin II-induced hypertensive mouse model using ^{68}Ga-FAPi46 PET
J. Byun[1,2,3], *Y. Kim*[1,3], *Y. Lee*[1], *J. Paeng*[1], *K. Kang*[1], *G. Cheon*[1];
[1]*Department of Nuclear Medicine, Seoul National University Hospital, Seoul, KOREA, REPUBLIC OF,* [2]*Department of Biomedical Sciences, Seoul National University, Seoul, KOREA, REPUBLIC OF,* [3]*Cancer Research Institute, Seoul National University, Seoul, KOREA, REPUBLIC OF.*

Aim/Introduction: In chronic hypertension (HT), injury and fibrosis occurs in major organs. This study aims to evaluate the feasibility of ^{68}Ga-FAPi46 PET in the early assessment of cardiac and renal fibrosis in a HT animal model. ***Materials and Methods:*** To induce HT in mice, Angiotensin II was infused to Balb/c male (8 weeks old) mice via subcutaneously implanted osmotic minipumps for 4 weeks. As a treatment group, losartan was treated to a subgroup of the model. Biodistribution study and ^{68}Ga-FAPi46 PET/MRI were performed 1, 2 and 4 weeks after HT induction. Target-to-background ratio (TBR) and percent of injected dose per gram (%ID/g) were measured in PET images and biodistribution, respectively. ***Results:*** At the first week, the heart and kidney uptake of ^{68}Ga-FAPi46 was significantly increased in HT model (2.18±0.38 vs. 1.36±0.28, $P < 0.001$, TBR; 2.91±0.92 vs. 1.11±0.29, $P < 0.001$, %ID/g). ^{68}Ga-FAPi46 uptake was also increased at the second week (2.60±0.24, $P < 0.001$ TBR; 2.99±1.52, $P < 0.05$, %ID/g), the uptake was normalized by losartan treatment (1.49±0.3, $P < 0.001$ TBR; 2.11±0.6, %ID/g). However, there was no pathological fibrosis at the first and second weeks. There was also no renal function change shown on serum blood urea nitrogen (31.44±5.72 vs. 31.28±4.02mg/dL) and creatinine levels (0.36±0.01 vs. 0.30±0.01mg/dL). ***Conclusion:*** In the HT mouse model, ^{68}Ga-FAPi46 uptake is increased early after HT before pathological or functional change occurs. This study implies that ^{68}Ga-FAPi46 PET can be used for early evaluation and diagnosis of cardiac and renal fibrosis progression in hypertensive organ injury.

OP-286

The evolution and prognostic value of ^{68}Ga-Pentixafor uptake in the myocardium after acute infarction

P. Wu[1,2], *S. He*[3], *M. Yan*[1], *H. Wang*[1,2], *X. Liu*[4], *Z. Xiang*[1], *L. Xu*[1,5], *Y. Zhao*[1,5], *X. Li*[6], *M. Hacker*[6], *Z. Wu*[1,2], *S. Li*[1,2];
[1]*Department of Nuclear Medicine, First Hospital of Shanxi Medical University, Taiyuan, CHINA,* [2]*Shanxi Key Laboratory of Molecular Imaging, Shanxi Medical University, Taiyuan, CHINA,* [3]*Department of Radiology, First Hospital of Shanxi Medical University, Taiyuan, CHINA,* [4]*Department of Radiology, Shanxi Bethune Hospital(Shanxi Academy of Medical Sciences, Tongji Shanxi Hospital, Third Hospital of Shanxi Medical University), Taiyuan, CHINA,* [5]*Collaborative Innovation Center for Molecular Imaging of Precision Medicine, Shanxi Medical University, Taiyuan, CHINA,* [6]*Division of Nuclear Medicine, Department of Biomedical Imaging and ImageGuided Therapy, Medical University of Vienna, Vienna, AUSTRIA.*

Aim/Introduction: Dynamic visualization of inflammation is crucial to the anti-inflammation strategy for patients with acute myocardial infarction (AMI). The evolution and prognostic value of ^{68}Ga-Pentixafor uptake targeting chemokine receptor 4 (CXCR4) in the myocardium of pigs has not been reported before. ***Materials and Methods:*** Six AMI and four Sham pigs serially underwent ^{68}Ga-Pentixafor imaging early (Day 2 and Day 7) and late (Day 28 or Day 46) post-operation. The SUV of infarcted myocardium (SUVmax_MI) and remote myocardium (SUVmax_RE, SUVmean_RE) were measured, and the TBR_MI was calculated to indicate the uptake intensity. The early inflammation area by ^{68}Ga-Pentixafor was assessed. Gated ^{18}F-Flurpiridaz stress MPI was performed to obtain the sum stress score (SSS), and CMRI was performed to obtain cardiac function and the area of late gadolinium enhancement (LGE). To observe the inflammation ripple effect, correlation analysis of SUV_RE with SUVmax_MI at different time points and with the late cardiac function was conducted. ***Results:*** The TBR_MI of ^{68}Ga-Pentixafor peaked before Day 2 after AMI, significantly dropped to half on Day 7, and sustained a slightly reduced level in the late phase. The late LVEF in the AMI group was significantly reduced compared to that in the Sham group (48.76±8.76% vs 65.27±2.18%, $P = 0.017$). The SUVmax_MI on Day 2 and TBR_MI on Day 7 were strongly correlated with the late LVEF and ESV ($P < 0.05$). The TBR_MI on Day 2 was strongly correlated with the late SSS ($r = 0.891$, $P = 0.017$). No significant difference was found among SUV_RE at different time points ($P > 0.05$). However, on Day 2 early after AMI, SUVmax_RE ($r = 0.854$, $P = 0.031$) and SUVmean ($r = 0.861$, $P = 0.028$) were significantly correlated with SUVmax_MI. A strong correlation was found between SUV_RE on Day 2 and the late ESV ($r = 0.886$, $P = 0.019$). The early inflammatory area assessed by ^{68}Ga-Pentixafor was strongly correlated with the LGE area assessed by CMRI ($r = 0.989$, $P = 0.001$). ***Conclusion:*** The inflammation in the infarcted myocardium surged 2 days early after AMI and dropped dramatically in the first week. The higher the early ^{68}Ga-Pentixafor uptake in the infarcted myocardium, the worse the following perfusion or cardiac function. The inflammation response at peak spread to the remote myocardium, which may involve the contemporary or following cardiac function. Further studies are warranted to clarify the prognostic value and the relative mechanism of the remote myocardium.

OP-287

Translocator protein 18kDa positron emission tomography imaging of ^{18}F-FDPA in rabbits with vulnerable atherosclerosis plaques

W. Dong*, J. Jiao, T. Mou, Y. Zhang, H. Mi;*
Beijing Anzhen Hospital, Beijing, CHINA.

Aim/Introduction: The aim of this study was to investigate the potential of N, N-diethyl-2-(2-(4-^{18}F-fluorophenyl)-5,7-dimethylpyrazolo[1,5-a] pyrimidin-3-yl) acetamide (^{18}F-FDPA), a translocator protein 18kDa (TSPO) targeted radiotracer, for vulnerable atherosclerotic plaques (VAP) imaging. ***Materials and Methods:*** Eighteen New Zealand rabbits were randomly divided into group A (abdominal aortic strain and high-fat diet, n=6), group B (abdominal aortic strain, high-fat diet and subcutaneous injection of Evolocumab 7 mg/kg/2 weeks, n=6), and group C (sham surgery and normal diet, n=6). Optical coherence tomography (OCT) was performed at 8, 12 and 20 weeks after the operation. On the day after OCT, 18F-FDPA PET/CTA was performed. Standardized uptake value (SUVmax) of 18F-FDPA was measured on abdominal aorta. Standardized uptake value (SUVmean) of 18F-FDPA in left ventricular SUVblood pool served as background reference. The target-to-background ratio (TBRmax) was calculated as follows: TBRmax = SUVmax/SUVblood pool. At the 8th and 12th weeks, one rabbit was killed in each group after PET/CTA. Others were killed 20 weeks after PET/CTA. The abdominal aorta was obtained and performed micro-PET/CT imaging immediately. Pathological HE staining, TSPO and CD68 immunofluorescence staining and TSPO western blot analysis were performed on arterial sections. ***Results:*** There was no statistically significant difference in TBRmax between group A and group B at 8 weeks and 12 weeks after operation. At 20 weeks after operation, TBRmax in group A was significantly higher than that in the group B (4.78 ± 1.04 vs. 2.21 ± 0.16, $P = 0.048$) and group C (4.78 ± 1.04 vs. 0.78 ± 0.20, $P < 0.001$). In OCT images, more large lipid core, thin fibrous caps and macrophages were observed in group A than in group B, especially in the area with high TBRmax of 18F-FDPA. In the PET/CTA study, the radioactivity of low density lipid plaques was higher than that of normal aorta. The micro-PET/CT images in vitro showed that the radioactivity in the white protruding plaque area increased. The HE staining study showed that there were more vulnerable plaques of AHA type in these areas, indicating the relation between TBRmax and VAP. TSPO and CD68 staining and western blot analysis confirmed the increased expression of TSPO and macrophages in these areas. In addition, more VAP was observed in group A than that in group B, which was consistent with the results of PET/CTA. ***Conclusion:*** 18F-FDPA PET imaging can visualize VAP and evaluate the vulnerability of arterial plaque after the intervention of Evolocumab.

OP-288

^{99m}Tc-AFN: A Nanobody-Based SPECT Radiotracer with Clinical Potential for Noninvasive Monitoring of Fibroblast Activity After Myocardial Infarction

X. Zhang[1], *Z. Ai*[1], *C. Li*[2], *B. Jia*[2], *M. Yang*[1];
[1]*Department of Nuclear Medicine, Beijing Chaoyang Hospital, Beijing, CHINA,* [2]*Medical Isotopes Research Center and Department of Radiation Medicine, School of Basic Medical Sciences, Peking University, Beijing, CHINA.*

Aim/Introduction: Myocardial infarction (MI) is the most prevalent cause of morbidity and mortality among all cardiovascular diseases[1]. The temporospatial presence of activated fibroblasts in the injured myocardium predicts the quality of cardiac

remodeling after MI. Therefore, noninvasive monitoring of activated fibroblasts after MI is of great significance. Fibroblast activation protein (FAP) expression is upregulated in activated fibroblasts. PET imaging with radiolabeled FAP inhibitors (FAPIs) has been developed and characterized for post-MI fibroblast activation in previous studies. However, challenges remain for FAPIs based imaging probes due to slow clearance from the blood stream and relative low specificity. It is an urgent clinical need for an improved noninvasive tool to evaluate the FAP expression levels to guide the treatment and the prognosis in MI patients. Nanobodies, also known as single-domain antibodies, are the smallest antibody fragment with antigen-binding capability. Nanobodies have been developed rapidly as targeted probes for molecular imaging owing to their high affinity, improved stability and rapid blood clearance. Therefore, FAP targeted nanobody can be a promising molecular probe for noninvasive imaging of activated fibroblasts with high signal to noise ratios and fast blood elimination in preclinical studies. ***Materials and Methods:*** The FAP-targeting nanobody (AFN) was produced after immunization of healthy alpacas with recombinant FAP protein. ^{99m}Tc-AFN was prepared by site-specific labeling. MI mice were scanned with ^{99m}Tc-AFN or ^{99m}Tc-FAPI SPECT/CT (3, 7, 14, 28 d after MI). Dynamic ^{99m}Tc-AFN SPECT and blocking studies were performed on MI mice 7 d after coronary ischemia reperfusion. Autoradiography, HE staining and immunofluorescence staining were carried out for ex vivo validation, aiming to evaluate the correlation of fibrosis degree and SPECT serial imaging. ***Results:*** ^{99m}Tc-AFN uptake in the injured myocardium peaked on day 7 after coronary ischemia reperfusion. The tracer accumulated intensely in the MI territory, with much higher signal to noise ratios compared with ^{99m}Tc-FAPI. ***Conclusion:*** ^{99m}Tc-AFN represents a promising radiotracer for in vivo SPECT imaging of post-MI fibroblast activation. ***References:*** 1. Yap, J.; Irei, J.; Lozano-Gerona, J.; Vanapruks, S.; Bishop, T.; Boisvert, W. A., Macrophages in cardiac remodelling after myocardial infarction. Nat Rev Cardiol 2023 Jan 10. doi: 10.1038/s41569-022-00823-5.

OP-289

Temporal characterisation of inflammation and active collagen biosynthesis in the rat heart post myocardial infarction, using novel Positron Emission Tomography (PET) radiotracers.

V. Reid[1,2], *M. G. MacAskill*[1,2], *K. Pandya*[1], *A. Arcidiacono*[1], *C. Alcaide Corral*[1,2], *T. E. F. Morgan*[1,2], *V. Balogh*[1], *L. M. Riley*[3], *T. Fujisawa*[1], *N. L. Mills*[1,4], *R. J. Lennen*[1,2], *M. A. Jansen*[1,2], *G. A. Gray*[1], *A. H. Baker*[1,5], *D. E. Newby*[1], *A. Sutherland*[3], *A. A. S. Tavares*[1,2];
[1]Centre for Cardiovascular Sciences, University of Edinburgh, Edinburgh, UNITED KINGDOM, [2]Edinburgh Imaging, University of Edinburgh, Edinburgh, UNITED KINGDOM, [3]School of Chemistry, University of Glasgow, Glasgow, UNITED KINGDOM, [4]The Usher Institute, University of Edinburgh, Edinburgh, UNITED KINGDOM, [5]CARIM, School for Cardiovascular Diseases, Maastricht University, Maastricht, NETHERLANDS.

Aim/Introduction: Myocardial infarction (MI) is a common precursor of Heart Failure (HF) and remains a leading cause of death worldwide. Following an MI, inflammation and active collagen biosynthesis are fundamental for myocardial repair and are key contributors to aberrant ventricular remodelling. The mechanisms underlying this close interaction between inflammation and collagen synthesis remain unknown and can be difficult to investigate due to lack of selective, in vivo biomarkers for active collagen synthesis. This study aims to characterise the temporal profile of cardiac inflammation and active collagen biosynthesis in a rat coronary artery permanent ligation model using novel Positron Emission Tomography (PET) radiotracers, [^{18}F]LW223 [1], cis-4-[^{18}F]fluoro-L-proline, and trans-4-[^{18}F]fluoro-L-proline [2]. ***Materials and Methods:*** Adult male Sprague-Dawley rats underwent permanent coronary artery ligation (CAL) to induce MI. At 1-, 2-, 4-, and 12-weeks post-MI, in vivo PET/CT imaging was performed with cis-4-[^{18}F]fluoro-L-proline and trans-4-[^{18}F]fluoro-L-proline which measure fibrillary collagen and triple-helical collagen respectively. Cardiac MRI and T1 mapping were completed to assess extracellular volume (ECV), infarct size and functional outcome. In vitro autoradiography with [^{18}F]LW223, a ligand for the inflammatory biomarker translocator protein (TSPO), was completed on MI heart sections post-scanning to assess the temporal profile of inflammation in this model. ***Results:*** Significant upregulation of both cis- and trans-4-[^{18}F]fluoro-L-proline occurred within the infarct region of the anterior left ventricle (LAV) following MI. Relative Standard Uptake Value (SUVr) for trans-4-[^{18}F]fluoro-L-proline increased at 2, 4 and 12-weeks post-MI ($p<0.05$), relative to naïve controls, while cis-4-[^{18}F]fluoro-L-proline uptake peaked at 4weeks post-MI ($p<0.01$). Peak signal for both tracers in the remote, non-infarcted region of the posterior left ventricle (LPV) occurred at 12-weeks post-MI, indicative of detrimental ventricular remodelling. Cardiac MRI imaging showed significant increases in ECV in the LAV from 1-week post-MI onwards ($p<0.0001$), relative to naive, but was not able to detect changes in the LPV. Binding of [^{18}F]LW223, measured as ratio of Total to Non-Specific binding (T:NS), peaked at 2-days and 4-weeks post-MI in the LPV ($p<0.01$) and remains elevated across all time-points in the LAV post-MI. ***Conclusion:*** [^{18}F]LW223, cis-4-[^{18}F]fluoro-L-proline and trans-4-[^{18}F]fluoro-L-proline can be used to assess temporal changes in inflammation and collagen biosynthesis at a regional level in the heart post-MI. Time-course dynamics indicate potential interplay between these two responses and identify critical intervention time-points for modulation of post-infarct cardiac inflammation and collagen biosynthesis. ***References:*** [1] MacAskill et al. J. Nuc. Med. 2021; 62:536-544 [2] Morgan et al. J. Org. Chem. 2021; doi: 10.1021/acs.joc.1c00755

OP-290

Positive Protective Effects of Sigma-1 Receptor Stimulation with Fluvoxamine after Myocardial Ischemia and Reperfusion in Rat

X. Zhang[1], *H. Wakabayashi*[1], *H. Mori*[1], *T. Hiromasa*[1], *Z. Chen*[1], *T. Kozaka*[2], *K. Ogawa*[3], *S. Kinuya*[1], *J. Taki*[1,4];
[1]Department of Nuclear Medicine, Kanazawa University Hospital, Kanazawa, Ishikawa, JAPAN, [2]Division of Probe Chemistry for Disease Analysis, Research Center for Experimental Modeling of Human Disease, Kanazawa University, Kanazawa, Ishikawa, JAPAN, [3]Institute for Frontier Science Initiative, Kanazawa University, Kanazawa, Ishikawa, JAPAN, [4]PET Center, Kanazawa Advanced Medical Center, Kanazawa, Ishikawa, JAPAN.

Aim/Introduction: Sigma-1 receptor (Sig-1R) is considered a pluripotent modulator with multiple functional manifestations in the living system. Sig-1R is expressed in cardiomyocytes as a chaperon, regulates the response to ER stress, modulates calcium handling, and affects the function of voltage-gated ion channels in abnormal statutes, including myocardial ischemia. However, the role of Sig-1R in postischemic myocardium is still unclear. This study investigated the impact of protective effect with stimulation of Sig-1R by fluvoxamine, an agonist of the Sig-1R, after myocardial ischemia and reperfusion in a rat. ***Materials and Methods:*** The left coronary artery occlusion was performed for 20 min on Wistar rats (n=24), followed by reperfusion. Rats were randomly divided

into two groups for two weeks of intraperitoneal therapy with saline (control group) or fluvoxamine (10 µg/kg each, F group). Electrocardiography (ECG)-gated SPECT with ^{99m}Tc-MIBI was performed on the 1, 14, and 28 days after reperfusion, respectively, to evaluate the function of the left ventricle. Triple-tracer autoradiography with ^{125}I-OI5V (a vesamicol analog allows the noninvasive imaging of Sig-1R expression), ^{99m}Tc-MIBI, and ^{201}TlCl was performed 29 days after reperfusion to assess the salvaged and nonsalvaged areas. Paired t-test was used to evaluate the efficacy after dosing. ***Results:*** The left ventricular ejection fraction (LVEF) of the F group demonstrated an improvement after 2-week dosing (D14-D1: 6±7, p=0.03), while it didn't occur in rats of the control group (D14-D1: -1±11, n.s.), and this tendency remained 2 weeks after medication (D28-D1, F group: 8±5, p<0.01 vs. D28-D1, control group: 1±10, n.s.). End diastolic volume (EDV) and end-systolic volume (ESV) increased in both groups after ischemia and reperfusion. However, the rise tended to be smaller in the F group (D14-D1 ESV: 36±42, p=0.03) than in the control group (D14-D1 ESV: 80±111, p=0.03). The increase showed a slight fallback once the medication was stopped in the F group (D28-D14 EDV: -7±69, n.s.; D28-D14 ESV: -12±61, n.s.), while it tended to continue in the control group (D28-D14 EDV: 23±54, n.s.; D28-D14 ESV: 3±42, n.s.). The autoradiography confirmed no differences between the groups in the salvaged and non-salvaged areas. Though with no significant difference, a lower OI5V uptake was observed in the F group than in the control group. ***Conclusion:*** Stimulating Sig-1R with fluvoxamine contributed to LV remodeling suppression and LVEF recovery after ischemia-reperfusion injury. We confirmed that this pathway is cardioprotective, and targeting the Sig-1R can potentially be effective as a new cardioprotective therapeutic strategy.

OP-291

C-X-C Motif Chemokine Receptor 4-Directed PET Signal in the Arterial Tree is not Consistently Linked to Calcified Plaque Burden and Cardiovascular Risk

N. Hasenauer[1], *A. Kosmala*[1], *S. E. Serfling*[1], *K. Michalski*[1], *M. Fröhlich*[2], *N. Dreher*[1], *P. E. Hartrampf*[1], *T. Higuchi*[1,3], *A. K. Buck*[1], *A. Weich*[2,4], *T. Reiter*[5], *R. A. Werner*[1,4,6];
[1]*Department of Nuclear Medicine, University Hospital Würzburg, Würzburg, GERMANY,* [2]*Internal Medicine II, University Hospital Würzburg, Würzburg, GERMANY,* [3]*Faculty of Medicine, Dentistry and Pharmaceutical Sciences, Okayama University, Okayama, JAPAN,* [4]*NET-Zentrum Würzburg, European Neuroendocrine Tumor Society Center of Excellence (ENETS CoE), University Hospital Würzburg, Würzburg, GERMANY,* [5]*Internal Medicine I, University Hospital Würzburg, Würzburg, GERMANY,* [6]*Johns Hopkins School of Medicine, The Russel H Morgan Department of Radiology and Radiological Sciences, Baltimore, MD, UNITED STATES OF AMERICA.*

Aim/Introduction: C-X-C motif chemokine receptor 4 (CXCR4) is overexpressed on a multitude of cells involved in inflammatory processes and has been shown to play an important mediating role during the evolution of atherosclerotic plaques. Therefore, we analyzed focal tracer uptake in the arterial tree in patients imaged with CXCR4-directed PET/CT and aimed to determine relevant associations between vessel wall calcification (derived from CT as a known non-invasive imaging biomarker of cardiovascular risk) and cardiovascular risk factors (CVRF). ***Materials and Methods:*** 55 oncologic patients who underwent CXCR4-directed [^{68}Ga] Ga-PentixaFor PET/CT were examined. Arterial wall CXCR4 uptake in 7 large arterial vessel segments was assessed visually (providing the number of CXCR4(+) sites) and quantitatively (to determine target-to-background ratios [TBR]). PET-based findings were then correlated with CVRF, calcified plaque burden (including number of calcified plaques, plaque thickness and calcification circumference), and image noise by using coefficient of variation (CoV; derived from unaffected hepatic parenchyma). We also investigated interactions between CXCR4-avid tumor volume (TV) and in-vivo arterial uptake. ***Results:*** In 55/55 (100%), CXCR4(+) arterial sites were recorded in 996 instances, with concomitant calcification in 360/996 (36.1%). CXCR4(+) sites correlated significantly with number of calcified plaques (r=0.28, P=0.04). A comparable trend was also observed for calcified plaque thickness and calcification circumference (r=0.26 and P=0.06, respectively). PET-derived TBR, however, showed no relevant correlations with calcified plaque burden (r≤0.03; P≥0.80). In univariate analysis, the following clinical parameters were associated with the number of CXCR4(+) sites in the arterial tree: sex (female; Odds Ratio [OR], 0.59), age (OR, 1.03), BMI (OR, 1.07), and image noise-related CoV (OR, 1.08, P≤0.03). On multivariate analysis, however, only sex (OR [female], 0.81), age (OR, 1.02), and CoV (OR, 1.05) remained significant (P≤0.01). For TBR, we recorded relevant associations with CoV (OR, 1.02) and BMI (OR, 1.03; P≤0.01, respectively) on univariate analysis. Multivariate testing, however, showed significance only for CoV (OR, 1.02; P<0.05). Last, there was no relevant association between CXCR4-avid TV and arterial wall-derived TBR (r=0.11; P=0.42). ***Conclusion:*** CXCR4-directed molecular imaging provides high focal arterial wall uptake and is moderately associated with calcified plaque burden. This phenomenon, however, was not persistently linked to CVRF, but rather driven by image noise.

OP-292

Molecular Imaging in Cardio-Oncology: Detecting Cardiotoxicity of Breast Cancer Treatments Through Radionuclide Ventriculography and Novel Cardiac Biomarkers Assessment

A. Lazar[1], *M. Mutuleanu*[1,2], *I. Irimescu*[1,3], *R. Maaz*[1], *C. Petroiu*[1], *M. Gherghe*[1,2];
[1]*Institute of Oncology "Professor Doctor Alexandru Trestioreanu", Bucharest, ROMANIA,* [2]*University of Medicine and Pharmacy "Carol Davila", Bucharest, ROMANIA,* [3]*Applied Sciences Doctoral School, Politehnica University, Bucharest, ROMANIA.*

Aim/Introduction: Human epidermal growth factor receptor 2 (HER2) is overexpressed in roughly 20% of the breast cancers diagnosed nowadays, paving the path for treatment with HER2-inhibitors. The monoclonal antibodies trastuzumab and pertuzumab represent the main HER2 inhibitors used for the treatment of HER2-positive breast cancer, associated or not with chemotherapy. The clinical benefits of HER2-inhibitors are well documented, however the possible cardiac adverse reactions need to be considered. The aim of our study was to determine whether monitoring cardiac function through radionuclide ventriculography (RNV) and cardiac biomarkers could detect the cardiac involvement in breast cancer patients following combination therapy with trastuzumab, pertuzumab and docetaxel. ***Materials and Methods:*** Our prospective study included 22 patients suffering from HER2-positive breast cancer, who had their left ventricular ejection fractions (LVEF) and cardiac biomarkers assessed both at the beginning (T0) and after 6 months (T1) of treatment with trastuzumab, pertuzumab and docetaxel. Among all of the enrolled patients, two blood specimens were collected to assess circulating cardiac biomarkers: cardiac troponin I (cTnI), amino-terminal fragment of the prohormone brain-type natriuretic peptide (NT-proBNP), amino-terminal fragment of

the prohormone atrial-type natriuretic peptide (NT-proANP), suppression of tumorigenicity 2 protein/interleukin-33R (ST2/IL33), growth differentiation factor 15 (GDF-15). After "in vivo" radiolabeling of the erythrocytes with ^{99m}Tc-pyrophospate, planar RNV and bloodpool single photon emission computed tomography (BP-SPECT) were performed in each patient on a for both timepoints. Obtained results were statistically correlated. ***Results:*** The average LVEF decrease between the two timepoints was approximately 4%. Five patients (22.72%) fulfilled the criteria for cardiotoxicity, presenting a decrease in LVEF of over 10%, to below 50%, between T0 and T1. LVEF obtained on BP-SPECT were slightly higher than those obtained on gated planar images: mean LVEF of 57.77±6.21% on planar RNV versus 57.95±5.89% on BP-SPECT for T0, respectively of 53.36±7.30% on planar RNV versus 54.95±6.89% on BP-SPECT for T1. NT-proBNP negatively correlated with the LVEF values obtained both at T0 and T1 ($r=-0.615$ for T0 and $r=-0.751$ for T1, $p<0.05$ for both). The ST2/IL-33R proved statistically significant correlations at T1 ($r=-0.547$, $p<0.05$). The values of the other cardiac biomarkers evaluated in our study changed between the two examinations, but with no statistical significance. ***Conclusion:*** Our results confirmed the good cardiac safety profile of this therapeutic scheme, while suggesting that a combination of radionuclide ventriculography and dosing of NT-proBNP and ST2-IL33R could help in early detecting the cardiac impairment.

705

Monday, September 11, 2023, 8:00 AM - 9:30 AM
Hall B

Cutting Edge Science Track - Featured Session: Imaging Guided Surgery

OP-293

Surgical Radioguidance with Beta emitting Radionuclides

P. Fragoso Costa;
Department of Nuclear Medicine at University Hospital Essen, Essen, GERMANY.

OP-294

Translation of a drop-in beta probe for robotic radio guided surgery

F. Collamati[1], *R. Mirabelli*[1], *R. Faccini*[2], *F. Ceci*[3], *E. Bertani*[4], *G. Musi*[5], *M. N. van Oosterom*[6], *F. van Leeuwen*[7], *S. Morganti*[1]; [1]*INFN Rome, Roma, ITALY,* [2]*Università Roma Sapienza, Roma, ITALY,* [3]*1.IEO European Institute of Oncology, Nuclear Medicine, Milano, ITALY,* [4]*2.IEO European Institute of Oncology, Division of Digestive Surgery, Milano, ITALY,* [5]*IEO European Institute of Oncology, Division of Urology, Milano, ITALY,* [6]*Leiden University Medical Center | Interventional Molecular Imaging Laboratory, Department of Radiology, Leiden, NETHERLANDS,* [7]*Leiden University Medical Center | Interventional Molecular Imaging Laboratory, Department of Radiology, Leiden, ITALY.*

Aim/Introduction: Recently, an innovative approach to radio guided surgery has been proposed, exploiting the intraoperative localization of beta-particle-emitting tracers (e.g., 18F-FDG, 68Ga-PSMA or 90Y-DOTATOC). After laboratory and Monte Carlo tests, this technique, based on the detection of short-penetration beta particles, has been recently validated in vivo with encouraging results. The surgical trend to move towards (robotic) minimal-invasive surgery has created a need for compatible tethered modalities [1]. In this paper, we present the design and clinical translation of a drop-in beta probe. ***Materials and Methods:*** The drop-in beta probe is based on a scintillating crystal of p-terphenyl read by a silicon photomultiplier. Designs were driven by practical requirements to in vivo use with the robotic surgical platform, including: the small form factor (needing to enter via the 12 mm trocar), biocompatible materials, adaption to the common robotic instruments and compatibility with sterilization protocols. To optimize the detection sensitivity, tailored Monte Carlo simulations were used. Specifically, CT data were used to reconstruct in Geant4 the geometry of the patients, and PET images to generate primary particles, with the aim of estimating the far-background counting (i.e. the one from annihilation photons in the whole patient), tissue-background counting and tissue-target counting. Following ex vivo tissue validation [2], the technique was evaluated during 68Ga-PSMA/68Ga-DOTATOC radioguided surgery. ***Results:*** A tethered drop-in beta probe was created that is fully compliant with the requirements of robotic surgery, proving to withstand several sterilization cycles, while remaining sensitive to beta particles. Its overall efficiency was found to be comparable to the open surgery version (~% to gammas and >90% to >100keV betas). After insertion in the surgical field, the surgeon was able to autonomously manipulate the probe using the robotic ProGrasp Forceps instrument. As compared to real tissue/in vivo data, the Monte Carlo simulations proved to have an accuracy of the order of 20% in the estimation of the "far tissue background" to probe countings. Sensitivity/Specificity of the order of 70%-90% were found in first in vivo tests on 68Ga-PSMA prostate cancer robotic RGS[3]. ***Conclusion:*** We present our translational efforts regarding a tethered drop-in beta probe for robotic guided surgery. Our findings underscore the validity of this form of RGS, thereby providing a basis for the more widespread implementation of PET-tracers during radioguided robotic surgery. ***References:*** [1] Dell'Oglio et al., Eur Urol, 2021 [2] Collamati et al., EJNMMI Res, 2020 [3] Ceci, talk at EAU 2023

OP-295

Live Nuclear/X-ray Imaging during Radioembolization Interventions using a Novel Hybrid C-arm Scanner

M. Dietze*, M. B. M. Meddens, R. van Rooij, A. J. A. T. Braat, B. de Keizer, R. C. G. Bruijnen, M. G. E. H. Lam, M. L. J. Smits, H. W. A. M. de Jong;*
University Medical Center Utrecht, Utrecht, NETHERLANDS.

Aim/Introduction: The current hepatic radioembolization workflow consists of a pre-treatment procedure using Tc-99m-MAA particles for safety and planning purposes after which the treatment with Y-90 ionizing microspheres is performed. Ideally, the pre-treatment procedure and the treatment would be merged in a single session since this reduces the number of interventions from two to one and potentially improves the prognostic power of the Tc-99m-MAA distribution. Such a single-session procedure requires the distribution of the Tc-99m-MAA particles to be evaluated during the intervention, which is currently not feasible. ***Materials and Methods:*** In the UMC Utrecht, we have developed a compact and mobile hybrid c-arm scanner (named IXSI) dedicated to the intervention room which can perform simultaneous fluoroscopic x-ray, planar scintigraphic and SPECT/CBCT imaging using a novel dual layer detector [1]. We have tested the safety and feasibility of using IXSI in radioembolization in a clinical study with 12 patients. For all 12 patients, images were acquired during the injection of Tc-99m-MAA to study dynamic

processes in the particle distributions. For nine patients, a SPECT/CBCT scan was acquired in the intervention room directly after the injection of Tc-99m-MAA. And for six patients, the lung-shunt fraction was measured in the intervention room using planar imaging. ***Results:*** Based on questionnaires and tracking of adverse events, it was determined that IXSI can be safely introduced in the intervention room during radioembolization interventions. The planar hybrid images had adequate angiographic and nuclear image quality and live imaging demonstrated that the Tc-99m-MAA particle distribution can change as more particles are injected. The SPECT images from IXSI were compared with the SPECT images from a conventional clinical scanner and found to have a similar dosimetric quality. The lung-shunting fraction as measured by IXSI was compared with the measurement by a clinical scanner and found to be lower owing to the shorter time between injection and imaging. ***Conclusion:*** A new hybrid c-arm scanner can safely be incorporated into the radioembolization workflow for real-time x-ray/nuclear guidance and dosimetry during the intervention. New insights into the dynamics of radioembolization interventions were obtained. The next stage of this project is to move towards a single-session radioembolization treatment. ***References:*** [1] Dietze, Martijn MA, et al. "A compact and mobile hybrid C-arm scanner for simultaneous nuclear and fluoroscopic image guidance." European Radiology 32.1 (2022): 517-523

OP-296

Investigation of a CZT-based hand-held gamma-camera for pre-clinical imaging of alpha-emitter ^{225}Ac

D. Roth[1], *Z. Ells*[2], *M. Dahlbom*[2], *J. Strand*[3,4], *C. Mona*[2,5], *P. Jean Jean*[2,5], *M. Ljungberg*[1], *S. Strand*[1];
[1]*Medical Radiation Physics, Lund, Lund University, Lund, SWEDEN,* [2]*Ahmanson Translational Theranostics Division, Department of Molecular and Medical Pharmacology, David Geffen School of Medicine, University of California – Los Angeles, Los Angeles, CA, UNITED STATES OF AMERICA,* [3]*Department of Clinical Sciences Lund, Oncology, Lund University, Lund, SWEDEN,* [4]*Department of Hematology, Oncology, Radiation Physics, Skåne University Hospital, Lund University, Lund, SWEDEN,* [5]*Jonsson Comprehensive Cancer Center, University of California – Los Angeles, Los Angeles, CA, UNITED STATES OF AMERICA.*

Aim/Introduction: ^{225}Ac is an alpha-emitting radionuclide with promising applications for radiopharmaceutical therapy. Its decay-chain releases alpha and beta particles, as well as two gamma-photons with energies and yields suitable for imaging: 218 keV (11 %) from ^{221}Fr and 440 keV (26 %) from ^{213}Bi. Activity-quantification and dosimetry is important for assessing or predicting treatment outcome. The aim of this project is to investigate the capabilities of a small gamma-camera for imaging and activity-quantification of ^{225}Ac in a pre-clinical setting. ***Materials and Methods:*** A CdZnTe-based hand-held gamma-camera was used with a medium-energy high-resolution parallel-hole collimator, providing imaging with a 4x4 cm^2 field-of-view and a 16x16 image-matrix (1). The camera was operated using in-house written software, allowing energy spectra to be saved for each individual image-pixel after each measurement. In subsequent analyses, images were created for energy-windows placed over the 218 keV and 440 keV peaks. Calibration and characterisation and measurements were performed to assess the camera's image-uniformity, sensitivity, and spatial resolution for ^{225}Ac. Image-quality was additionally evaluated using a 3D-printed mouse phantom with a fillable tumour and liver cavity, for which ventral planar images were acquired. SPECT projections were also acquired of the mouse phantom using a motorised rig. In-vivo measurements were performed on NCG mice with PC3-PIP tumours implanted on the upper flank. Imaging was performed at different time points up to 25 h after injection of [^{225}Ac]Ac-PSMA-617. ***Results:*** Imaging of ^{225}Ac was feasible, although septal penetration of 440 keV photons was notable. Due to the energy-response of the CdZnTe-detector, the 218 keV window was also affected. At a source-collimator distance of 10 mm, the sensitivity was 81 cps/MBq and 68 cps/MBq, for the 218 keV and 440 keV windows, respectively. At 100 mm, the corresponding values were 25 cps/MBq and 15 cps/MBq. Measurements on the mouse phantom demonstrated that the liver and tumour could be distinguished. Septal-penetration-related background was present in images for both energy-windows, but lower in the 218 keV window. The bio-distribution of [^{225}Ac]Ac-PSMA-617 could be measured in the mice. Further analysis will be carried out and presented. ***Conclusion:*** Pre-clinical imaging of ^{225}Ac can be performed with the hand-held camera. ***References:*** 1. Roth D, Larsson E, Sundlöv A, Sjögreen Gleisner K. Characterisation of a hand-held CZT-based gamma camera for ^{177}Lu imaging. EJNMMI Physics. 2020;7(1).

OP-297

CT-guided percutaneous marking of small pulmonary nodules with [^{99m}Tc]Tc-Macrosalb is very accurate and allows minimally invasive lung-sparing resection: a single-centre quality control

N. Doncic*, C. J. Zech, D. Wild, H. Bachmann, M. Mallaev, N. Tsvetkov, A. Hojski, M. T. L. Takes, D. Lardinois;*
Basel University Hospital, Basel, SWITZERLAND.

Aim/Introduction: The detection of small lung nodules in thoracoscopic procedure is difficult when the lesions are not localized within the outer border of the lung. In the case of ground-glass opacities, it is often impossible to palpate the lesion. The marking of lung nodules with radiotracer is a known technique. We analysed the accuracy and safety of the technique and the potential benefits of operating in a hybrid operating room. ***Materials and Methods:*** 57 patients, including 33 (58%) females with a mean age of 63.3 years (range 21-82) were included. In 27 patients, we marked and resected the lesion in a hybrid room. In 30 patients, the lesion was marked at the department of radiology the day before resection. [99mTc]Tc- Macrosalb was used at an activity of 1 MBq in the hybrid room and at an activity of 3 MBq the day before to get technical feasible results. Radioactivity was detected using the gamma detection system with endoscopic probe. ***Results:*** Precise detection and resection of the nodules was possible in 95% of the lesions and in 93% of the patients. Complete thoracoscopic resection was possible in 90% of the patients. Total conversion rate was 10%, but conversion due to failure of the marking of the nodule was observed in only 5% of the patients. Histology revealed 28 (37%) primary lung cancers, 24 (32%) metastases and 21 (28%) benign lesions. In 13 (23%) of the patients, minor complications were observed. None of them required additional interventions ***Conclusion:*** The radio-guided detection of small pulmonary nodules is very accurate and safe after CT guided injection of [99mTc]Tc-Macrosalb. Performing the operation in a hybrid room has several logistic advantages and allows using lower technetium-99m activities. The technique allows minimally invasive lung sparing resection and prevents overtreatment of benign and metastatic lesions. ***References:*** 1. Ambrogi MC, Melfi F, Zirafa C, Lucchi M, De Liperi A, Mariani G, et al. Radio-guided thoracoscopic surgery (RGTS) of small pulmonary

nodules. Surg Endosc. 2012;26:914-9. 2. Grogan EL, Jones DR, Kozower BD, Simmons WD, Daniel TM. Identification of small lung nodules: technique of radiotracer-guided thoracoscopic biopsy. Ann Thorac Surg. 2008;85:S772-7. 3. Galetta D, Rampinelli C, Funicelli L, Casiraghi M, Grana C, Bellomi M, et al. Computed Tomography-Guided Percutaneous Radiotracer Localization and Resection of Indistinct/Small Pulmonary Lesions. Ann Thorac Surg. 2019;108:852-8.

OP-298

A truncated 14-amino acid myelin protein zero targeting peptide for fluorescence-guided nerve preserving surgery

N. Berehova, *M. P. van Meerbeek, S. Azargoshasb, L. J. Slof, S. Navaei Lavasani, M. N. van Oosterom, F. W. B. van Leeuwen, T. Buckle;*
Leiden University Medical Center, Leiden, NETHERLANDS.

Aim/Introduction: The growing implementation of image-guided head-and-neck surgery have exposed the need to exploit molecular targeted nerve-sparing interventions, an application that relies on the availability of nerve specific tracers. In this paper we describe the development of a truncated peptide that has an optimized affinity for protein zero (P0), the most abundant protein on myelin. ***Materials and Methods:*** Further C- and N-terminal truncation was performed on the lead peptide Cy5-$P0_{101-125}$. The resulting nine Cy5 labelled peptides were characterized based on their (photo)physical properties, P0 affinity and in vitro staining. These characterizations were combined with P0 crystal structure evaluations to select the optimized tracer Cy5-$P0_{112-125}$. A near-infrared Cy7-functionalized derivative (Cy7-$P0_{112-125}$) was used to perform initial fluorescence-guided surgery evaluations in a porcine model. ***Results:*** The 26 amino acid lead compound Cy5-$P0_{101-125}$ could be reduced to the 14 amino acid Cy5-$P0_{112-125}$, while inducing a 1.5-fold affinity gain. The peptide design could be corroborated by interactions observed in the crystal structure of the extracellular portion of P0. The near-infrared analogue Cy7-$P0_{112-125}$ supported nerve illumination during nerve surgery in a porcine head-and-neck model. ***Conclusion:*** Methodological truncation yielded a second generation P0-specific peptide. Initial surgical evaluations suggest the peptide can support molecular targeted nerve imaging. ***References:*** Buckle, T.; Hensbergen, A.W.; van Willigen, D.M.; Bosse, F.; Bauwens, K.; Pelger, R.C.M.; van Leeuwen, F.W.B. Intraoperative visualization of nerves using a myelin protein-zero specific fluorescent tracer. EJNMMI Res 2021, 11, 50, doi:10.1186/s13550-021-00792-9. Shapiro, L.; Doyle, J.P.; Hensley, P.; Colman, D.R.; Hendrickson, W.A. Crystal structure of the extracellular domain from P0, the major structural protein of peripheral nerve myelin. Neuron 1996, 17, 435-449, doi:10.1016/s0896-6273(00)80176-2

OP-299

Metabolic 18F FDG PET/CT Guided Intrathoracic Tumor Biopsies: An Analysis of Initial Experience from Central India.

M. Ravina, *R. Ganga, A. Behera, T. Lukose, S. Krishna, S. Dasgupta, R. Kote, A. Rath;*
All India Institute of Medical Sciences, Raipur, Raipur, INDIA.

Aim/Introduction: The purpose of this study is to investigate the feasibility and diagnostic efficacy of the robotic navigation system assisted 18F FDG PET/CT guided biopsy of intrathoracic tumors. ***Materials and Methods:*** 30 Patient with FDG avid intrathoracic tumors were included in the study. These patients underwent robotic navigation system assisted 18F FDG PET/CT guided biopsies. Patients were immobilized using a vacuum assisted patient arrestor bed during the entire procedure. Regional single bed preprocedural PET/CT imaging was acquired and transferred into the automated robotic navigation system (ARNS). A target lesion and safe trajectory from entry point were chosen using the images on the planning console. Biopsy trajectory and site was decided based on the safety of the needle path, tumor location, its relation to the vital structures, accessibility, avidity and presence of necrosis. The trajectory was then confirmed and the data was fed to the robotic arm system. Planned trajectory was executed using the robotic arm. Proposed entry site was highlighted with laser markers on the patient's chest. Multiple biopsies were taken using Semiautomatic Core Biopsy Gun. Low dose check CT was done to look for any complications. ***Results:*** 30 patients were included in the study. Mean age of patients was 56.13 years (95% CI: 51.78-60.49yrs) and 73.3% (n:22) of patients were male. Left lung mass was seen in 60% (LUL:03, LLL:10, LLL:07), 40% had right lung mass (RUL:01, RML:08, RLL:01). Mean size of the tumor was 5.74cm x5.13cm x7.14cm (min: 1 patient had diffuse FDG uptake with no tumour localization). 100% patents had heterogenous uptake in 18F FDG PET/CT. Mean SUV max was 17.63 (95% CI: 14.11-21.19). Mean target distance was 40.8mm (95%CI: 35.6-45.9; min:17mm max:80mm). 56.7% (n:17) and 43.3% (n:13) underwent biopsy in supine and prone positions respectively. Mean of number of cores taken was 4.47 (min:03 max:06). Sample adequacy and positive diagnosis was achieved in 100% of the patients. 70%(n:21) had non-small cell lung cancer, 16.7% (n:5) had tuberculosis, 2 patients had metastasis from carcinoma rectum; small cell lung cancer, lymphoma and neuroendocrine tumor was diagnosed in 1 patient each. 83.3% (n:25) had no complications. 3 patients had minimal pneumothorax and 1 patient had minor bleeding from biopsy site. Mean VAS score for pain was 1.63 (95% CI:1.26-2.01). ***Conclusion:*** The study confirms that PET/CT guided intrathoracic lung mass biopsy has a good diagnostic yield to establish a pathological diagnosis.

OP-300

Gamma-Flex, a novel flexible gamma probe for minimal invasive laparoscopic interventions

M. van Oosterom[1], *L. J. Slof*[1], *S. Navaeilavasani*[1], *S. Azargoshasb*[1], *K. Schwenkenbecher*[2], *J. Scheltes*[3], *F. W. B. van Leeuwen*[1];
[1]*Leiden University Medical Center, Leiden, NETHERLANDS,* [2]*Crystal Photonics, Berlin, GERMANY,* [3]*DEAM, Amsterdam, NETHERLANDS.*

Aim/Introduction: Radioguided surgery is commonly used as a means to intraoperatively localize lesions e.g., sentinel lymph nodes or PSMA expressing metastases [1]. Thereby the technique allows surgeons to identify the exact lesions intraoperatively as found during preoperative imaging at the Nuclear Medicine department. To this end, the handheld gamma detection probe has been the staple modality. Unfortunately, moving to minimal-invasive laparoscopic applications, working through key-holes (i.e., trocars) has drastically limited its utility. Especially the restriction in movements limits the intraoperative target-identification process [2]. To enable laparoscopic radio guidance with a greater degree-of-freedom, we have devised a steerable laparoscopic gamma probe. ***Materials and Methods:*** A laparoscopic steerable gamma probe was designed using 3D CAD software and produced using computerize-numerical-control turning machines. Collimation designs were fabricated out of tungsten, the detector was based on GAGG(Ce) scintillation

crystals, the probe shaft was created out of medical grade stainless steel (SS 316L) and medical grade plastics (i.e., POM). To allow for monitoring of probe movements during its use and evaluate the benefit with respect to rigid laparoscopic gamma probes, a miniaturized electromagnetic sensor was incorporated in the probe detection head. In a laparoscopic phantom model (simulating typical pelvic lymph node applications), the effect of the enhanced flexibility on the dexterity was directly compared to a traditional rigid laparoscopic probe based on similar detector configurations. ***Results:*** The Gamma-Flex prototype supports radio-guidance with 6 degrees-of-freedom, where the traditional rigid instrument only supports 4. Bending angle of the steerable shaft supported a movement range from -45 to +45° over two angles around the instrument's shaft, facilitated by the bending flexure joint. Multi-parametric kinematic tracking of the detector demonstrated superior dexterity compared to the rigid instrument during radioactive lymph node guidance in the laparoscopic phantom, a feature that directly related to the probe's utility during localization. Moreover, the anatomical reach of the gamma-flex prototype was superior to that of the rigid probe. ***Conclusion:*** With the creation of the Gamma-Flex prototype, a second-generation laparoscopic gamma probe has been introduced. Initial preclinical evaluation demonstrates improvements in maneuverability. Further in vivo follow-up is needed to see how this will help improve the surgical performance. ***References:*** [1] van Oosterom et al., Expert Review Medical Devices, 2019 [2] Dell'Oglio et al., European Urology, 2021

OP-301

Performance Evaluation of ^{18}F-PSMA and ^{68}Ga-PSMA in a Novel MicroPET/CT System Dedicated to Radioguided Surgery

A. Moraitis[1], *C. Darr*[2], *T. Kahl*[2], *L. Püllen*[2], *W. Jentzen*[1], *D. Kersting*[1], *B. Hadaschik*[2], *K. Herrmann*[1], *W. P. Fendler*[1], *P. Fragoso Costa*[1];
[1]*Department of Nuclear Medicine at University Hospital Essen, Essen, GERMANY,* [2]*Department of Urology at University Hospital Essen, Essen, GERMANY.*

Aim/Introduction: ^{18}F-PSMA and ^{68}Ga-PSMA are highly relevant radiotracers for prostate cancer and have demonstrated feasibility for intraoperative margin assessment in the context of radical prostatectomy. In this phantom study, we report the imaging properties of both tracers in a novel silicon photomultiplier based microPET/CT system dedicated to radioguided surgery. ***Materials and Methods:*** Spatial resolution (FWHM), linearity, and detectability (given as contrast-to-noise ratio, CNR) were determined for ^{18}F and ^{68}Ga using a line-source phantom and a sphere-phantom consisting of a cylindrical background region and a 1-ml spherical insert. The line-source phantom was filled with 15 MBq/ml (≈ 1 µl effective volume) to provide good count statistics. The sphere-phantom was filled with around 20 kBq/ml (sphere) at a sphere-to-background ratio of eight, based on observations in prostate specimens. The sphere-phantom was scanned over several half-lives (until activity concentration < 0.3 kBq/ml). All scans were performed on the Aura 10 microPET/CT system (XEOS, Ghent, Belgium). Emission times were default 10 minutes and attenuation and scatter corrected images were reconstructed into a 252×252 transverse matrix with a cubical voxel size of $(0.4\ mm)^3$ using a 3D-MLEM algorithm with 20 iterations. ***Results:*** Axial and transaxial spatial resolution (FWHM) were 1.77 mm and 1.87 mm for ^{18}F, and 3.19 mm and 3.24 mm for ^{68}Ga, based on gauss-fitting over line profiles in consecutive image slices. The lower volume limit was therefore estimated to be 0.003 ml and 0.017 ml for ^{18}F and ^{68}Ga, respectively. Linearity of the imaged signal was given for a wide activity concentration range with each ^{18}F and ^{68}Ga (r^2 = 0.98 down to 1 kBq/ml). Initial CNR was 14 for ^{18}F at 18 kBq/ml, and 16 for ^{68}Ga at 27 kBq/ml, and decreased gradually to 3.9 for ^{18}F at 0.22 kBq/ml and 3.7 for ^{68}Ga at 0.24 kBq/ml. Minimum detectable activity concentration was 0.4 - 0.5 kBq/ml for both radionuclides. Segmentation of the sphere based on visual assessment and thresholding was impaired for activity concentrations below 1 kBq. ***Conclusion:*** Given the default acquisition and reconstruction parameters, the Aura 10 performs well with ^{18}F and ^{68}Ga for intraoperative specimen imaging. The spatial resolution is compatible with clinical requirements, and the high detectability allows for implementation of several intraoperative imaging workflows. Further optimisation is required to attain accurate and reliable segmentation at low activity concentrations.

706

Monday, September 11, 2023, 8:00 AM - 9:30 AM
Hall C

Clinical Oncology Track - TROP Session: Neuroendocrine Tumors - Diagnosis

OP-302

First-in-human Study of an Optimized, potential Kit-type, SSTR Antagonist ^{68}Ga-DATA^{5m}-LM4 in Neuroendocrine Tumors

J. Zhang[1], *L. Greifenstein*[2], *V. Jakobsson*[1], *C. Kramer*[2], *C. Landvogt*[2], *C. Mueller*[2], *R. P. Baum*[2];
[1]*National University of Singapore, Singapore, SINGAPORE,* [2]*Curanosticum Wiesbaden-Frankfurt, Center for Advanced Radiomolecular Precision Oncology, Wiesbaden, GERMANY.*

Aim/Introduction: The aim of this study was to assess the feasibility of using a novel kit-type SSTR antagonist ^{68}Ga-DATA^{5m}-LM4 for PET imaging and evaluate the safety, biodistribution, and preliminary diagnostic efficacy of ^{68}Ga-DATA^{5m}-LM4 in patients with metastatic neuroendocrine tumors. ***Materials and Methods:*** Twenty-seven patients (19 male and 8 female; mean age, 61.0 ± 12.1y) with histopathologically confirmed well-differentiated NETs underwent ^{68}Ga-DATA^{5m}-LM4 PET/CT for the staging and restaging or patient selection for PRRT. All the patients underwent PET/CT scans 60 min after intravenous injection of 1.85 MBq (0.05 mCi) per kilogram of body weight (151 ± 54 MBq mean ± SD) of ^{68}Ga-DATA^{5m}-LM4. ***Results:*** ^{68}Ga -DATA^{5m}-LM4 was well tolerated in all patients, with no adverse symptoms being noticed or reported. The normal organ uptake of ^{68}Ga-DATA^{5m}-LM4 in the thyroid gland, pancreas, and spleen was significantly lower ($P < 0.05$), particularly in the liver as compared to ^{68}Ga-DOTA-TATE (3.90 ± 0.88 vs 9.12 ± 3.64, $P < 0.000001$). ^{68}Ga-DATA^{5m}-LM4 uptake in the liver and spleen was significantly lower than the ^{68}Ga-DOTA-TOC uptake ($P = 0.0166$ and $P = 0.0098$, respectively). In NETs patients, tumors lesions showed high uptake intensity on ^{68}Ga-DATA^{5m}-LM4 PET/CT, with the highest SUVmax up to 167.93 (mean ± SD, 44.47 ± 36.22). With SUVmean of healthy liver parenchyma, the kidney, and blood pool as background, tumor-to-background ratios were 20.32 ± 19.97, 4.30 ± 3.03, and 38.63 ± 35.97, respectively. ***Conclusion:*** The new SSTR antagonist ^{68}Ga-DATA^{5m}-LM4 can be conveniently labeled with high radiochemical yields and purities. Our first clinical data demonstrate excellent imaging performance of the new antagonistic SSTR ligand ^{68}Ga-DATA^{5m}-LM4. Application of the tracer in patients with disseminated metastases NETs showed a superior biodistribution with very high tumor contrast and low uptake in thyroid glands and spleen, and especially in the liver as compared to the agonistic SSTR ligands, which facilitates favorable lesion detection of ^{68}Ga-DATA^{5m}-LM4. The advantageous imaging

characteristics, along with the very convenient, potential „kit-type" production, makes ^{68}Ga-DATA^{5m}-LM4 an overall extraordinary promising radiopharmaceutical for the staging and restaging of NET patients and especially for the detection of very small hepatic metastases.

OP-303

A Prospective Evaluation of [^{18}F]AlF-NOTA-LM3 in Patients with Well-differentiated Neuroendocrine Tumors: Head-to-head Comparison with^{68}GaDOTATATE

***M. Liu**, W. Zhu, Y. Zhang, C. Ren, H. Zhang, Z. Huang, L. Huo;*
Peking Union Medical College Hospital, Beijing, CHINA.

Aim/Introduction: SSTR antagonists have shown better performance than analogs for somatostatin receptor imaging. The aim of this study was to evaluate safety, biodistribution and diagnostic efficacy of [^{18}F]AlF-NOTA-LM3 PET/CT in patients with well-differentiated neuroendocrine tumors. And compare with ^{68}Ga-DOTATATE PET/CT. ***Materials and Methods:*** Patients aged 18 to 80, with histologically confirmed well-differentiated neuroendocrine tumors (G1 and G2) were prospectively recruited to the study. All patients performed [^{18}F]AlF-NOTA-LM3 PET/CT and ^{68}Ga-DOTATATE PET/CT within a week and the interval between the two scans were at least 24 hours. Safety of [^{18}F]AlF-NOTA-LM3 were assessed. Physiologic normal-organ uptake, lesion numbers, standardized uptake values (SUVmax) of tumor, and tumor-to-background ratio (TBR) were compared head-to-head. ***Results:*** A total of 15 patients were enrolled in this study. No adverse events related to the radiopharmaceuticals were reported. The physiological uptake of [^{18}F]AlF-NOTA-LM3 was significantly lower than ^{68}Ga-DOTATATE in abdominal organs (including liver, spleen, pancreas, stomach, small intestine, renal cortex) and bone marrow. On per-patient basis, [^{18}F]AlF-NOTA-LM3 had a higher detection rate for liver lesions and lymph node lesions. In 9 patients with liver metastases, 78% (7/9) showed more liver lesions on [^{18}F]AlF-NOTA-LM3 than on ^{68}Ga-DOTATATE, 11% (1/9) showed the opposite, and the remaining 11% (1/9) showed identical results. In 8 patients with lymph node metastases, 75% (6/8) detected more lymph node lesions on [^{18}F]AlF-NOTA-LM3, whereas 25% (2/8) showed comparable results with both tracers. On per-lesion basis, [^{18}F]AlF-NOTA-LM3 detected significantly more liver metastases (275 vs. 219, P=0.028) and lymph node metastases (21 vs. 14, P=0.020) than ^{68}Ga-DOTATATE. Both tracers were comparable in detection of pancreatic lesions (21 vs. 20, P = 0.317), duodenum lesions (5 vs. 5, P = 1.000), and bone metastases (5 vs. 6, P = 0.317). No significant difference of tumor SUVmax were observed between [^{18}F]AlF-NOTA-LM3 and ^{68}Ga-DOTATATE PET/CT. However, [^{18}F]AlF-NOTA-LM3 showed higher TBR of liver lesions, pancreatic lesions, and bone lesions. ***Conclusion:*** [^{18}F]AlF-NOTA-LM3 performed better in detection of liver metastases and lymph node metastases than ^{68}Ga-DOTATATE, with a better tumor-to-background ratio.

OP-304

Superiority of ^{68}Ga-DOTATATE PET/CT compared to ^{18}F-FDG PET/CT, MRI of the spine, and whole-body diagnostic CT and MRI in the detection ofspinal bone metastases associated with pheochromocytoma and paraganglioma

***A. Jha**[1], M. Patel[1], A. Ling[1], R. Shah[1], C. C. Chen[1], C. Millo[1], M. A. Nazari[1], N. Sinaii[1], K. Charles[1], M. J. Kuo[1], T. Prodanov[1], B. Saboury[1], S. Talvacchio[1], A. Derkyi[1], J. del Rivero[1], G. O'Sullivan Coyne[1], A. P. Chen[1], N. Nilubol[1], P. Herscovitch[1], F. I. Lin[1], D. Taïeb[1], A. C. Civelek[2], J. A. Carrasquillo[1], K. Pacak[1];*
[1]National Institutes of Health, Bethesda, MD, UNITED STATES OF AMERICA, [2]Johns Hopkins Medicine, Baltimore, MD, UNITED STATES OF AMERICA.

Aim/Introduction: Pheochromocytomas and paragangliomas (PPGLs) are rare catecholamines-producing neuroendocrine tumors that cause life-threatening complications. Bone-metastases are observed in upto 71% of metastatic PPGL patients. Furthermore, 20% of metastatic PPGL patients have metastasis exclusively to bone with spine being the most common location (81%). Bone-metastases weaken and destroy skeletal tissue and predispose patients to skeletal-related-events. Data regarding head-to-head comparison between functional and anatomic imaging modalities to detect spinal bone metastases in PPGL are limited. The aim of this study is to compare the diagnostic performance of ^{68}Ga-DOTATATE PET/CT, ^{18}F-FDG PET/CT, MRI of the spine (MRI_{spine}), and contrast-enhanced whole-body CT (CT_{WB}) and MRI (MRI_{WB}) for the detection of PPGL-related spinal bone-metastases. ***Materials and Methods:*** Between 2014 and 2020, PPGL participants with spinal bone-metastases underwent ^{68}Ga-DOTATATE PET/CT, ^{18}F-FDG PET/CT, MRI_{spine} (sagittal T1w, sagittal STIR, axial T1w, and axial T2w), MRI_{WB}, and CT_{WB}. Per-patient and per-lesion detection rates were calculated. Counting of spinal bone-metastases was limited to a maximum of one lesion per vertebrae. A composite of all scans served as an imaging comparator. McNemar test was used to compare detection rates between the scans. Two-sided p values <0.05 were considered statistically significant. ***Results:*** Forty-three consecutive participants [females, 22; median age, 22 years, harboring mutations in SDHx (N=30), NF1 (N=1), HIF2A (N=1), and negative for mutations (N=11)] with MRI_{spine} were included in this prospective study. They also underwent ^{68}Ga-DOTATATE PET/CT (N=43), ^{18}F-FDG PET/CT (N=43), MRI_{WB} (N=24), and CT_{WB} (N=33). Forty-one of 43 participants were positive for spinal bone-metastases, with 382 lesions on the imaging comparator. ^{68}Ga-DOTATATE demonstrated a per-lesion detection rate of 377/382 (98.7%) which was significantly superior compared to ^{18}F-FDG (72.0%, 275/382, p<0.001), MRI_{spine} (80.6%, 308/382, p<0.001), MRI_{WB} (55.3%, 136/246, p<0.001) and CT_{WB} (44.8%, 132/295, p<0.001). The per-patient detection rate of ^{68}Ga-DOTATATE was 41/41 (100%) which was higher compared to ^{18}F-FDG (90.2%, 37/41), MRI_{spine} (97.6%, 40/41), MRI_{WB} 22/23 (95.7%,), and CT_{WB} 27/33 (81.8%), statistical significance reached only with CT_{WB} (p=0.041). Furthermore, ^{68}Ga-DOTATATE was found to detect greater or equal true-positive lesions compared to ^{18}F-FDG in 40/41 (97.6%), MRI_{spine} (41/41, 100.0%), MRI_{WB} (23/23, 100.0%), and CT_{WB} (33/33, 100.0%). ***Conclusion:*** ^{68}Ga-DOTATATE showed a significantly superior per-lesion detection rate of spinal bone-metastases compared to ^{18}F-FDG, MRI_{spine}, MRI_{WB}, and CT_{WB}. Besides providing a whole-body analysis, it maybe the imaging modality-of-choice to evaluate metastatic spine disease especially in the treatment planning and response assessment of the targeted-radionuclide-therapy ($^{223}RaCl_2$, ^{177}Lu/^{90}Y DOTA-analogs) in patients with bone-only metastatic PPGL.

OP-305

Prognostic Value of C-X-C motif Chemokine Receptor 4-directed Molecular Imaging in Patients with Advanced Adrenocortical Carcinoma

***W. Schlötelburg**[1], P. E. Hartrampf[1], A. Kosmala[1], S. E. Serfling[1], A. Schirbel[1], A. K. Buck[1], M. Fassnacht[2], S. Hahner[2], R. A. Werner[1,3];*
[1]Department of Nuclear Medicine, University Hospital of Würzburg, GERMANY, [2]Division of Endocrinology and Diabetes, Department of Medicine I, University Hospital of Würzburg, GERMANY, [3]The Russel H. Morgan Department of Radiology and Radiological Science, Johns Hopkins Unversity School of Medicie, MD, UNITED STATES OF AMERICA.

Aim/Introduction: In an ex-vivo setting, C-X-C motif chemokine receptor 4 (CXCR4) is highly expressed in sites of disease in patients affected with adrenocortical carcinoma (ACC)(1). We aimed to determine the predictive value of CXCR4-targeting [^{68}Ga]

Ga-PentixaFor PET/CT for outcome relative to clinical parameters. ***Materials and Methods:*** We identified 41 advanced, metastasized ACC patients imaged with [^{68}Ga]Ga-PentixaFor PET/CT. Scans were assessed visually and on a quantitative level by manually segmenting the tumor burden (providing tumor volume, peak/mean/maximum standardized uptake values [SUV] and fractional tumor activity [FTA], defined as mean SUV multiplied by TV). Clinical parameters included sex, previous therapies, age, Weiss-Score, and Ki67 index. Following imaging, overall survival (OS) was recorded. ***Results:*** After [^{68}Ga]Ga-PentixaFor PET/CT, median OS was 257 days (range, 27 - 2913 days). On univariable analysis, only presence of CXCR4-positive peritoneal metastases (PM, HR 2.04, 95%CI 1.02 - 4.07) was significantly linked to shorter OS (P=0.04). FTA revealed a trend towards significance (P=0.07), while all other PET-based parameters were not associated with survival (P≥0.14). Moreover, none of the clinical parameters (Sex, age, Weiss-Score, Ki67 index) showed relevant associations with OS (P≥0.66). On Kaplan-Meier analysis, presence of CXCR4-positive PM was linked to decreased survival (no PM, median OS, 11.41 months vs presence of PM, 6.41 months, P<0.04), which was also observed for increased FTA (above median [434], 13.3 months vs below median, 6.41 months, P<0.02). ***Conclusion:*** In advanced ACC patients, presence of CXCR4-expressing peritoneal lesions and increasing FTA on [^{68}Ga]Ga-PentixaFor PET/CT may be linked to less favorable outcome, while clinical parameters failed to provide outcome benefits. Funding: IZKF Z-2/91 ***References:*** (1) Bluemel C et al. Investigating the Chemokine Receptor 4 as Potential Theranostic Target in Adrenocortical Cancer Patients. Clin Nucl Med . 2017 Jan;42(1):e29-e34.

OP-306

"Novel ^{99m}Tc-labelled somatostatin antagonists in the diagnostic algorithm of neuroendocrine neoplasms" - results of a multicenter phase I clinical trial - TECANT

M. Opalinska[1], *I. Virgolini*[2], *L. Lezaic*[3], *G. di Santo*[2], *C. Decristoforo*[2], *P. Kolenc*[3], *R. Mikolajczak*[4], *A. Studen*[5], *P. Garnuszek*[4], *U. Simoncic*[5], *M. Trofimiuk-Muldner*[1], *C. Rangger*[2], *B. Glowa*[6], *K. Skorkiewicz*[6], *M. Fani*[7], *A. Sowa-Staszczak*[1], *B. Janota*[4], *M. Kroselj*[3], *S. Rep*[3], *A. Hoermann*[2], *A. Hubalewska-Dydejczyk*[1];
[1]*Chair and Department of Endocrinology, Jagiellonian Medical College, Krakow, POLAND,* [2]*Department of Nuclear Medicine, Medical University Innsbruck, Innsbruck, AUSTRIA,* [3]*Department of Nuclear Medicine , University Medical Centre Ljubljana, Ljubljana, SLOVENIA,* [4]*National Centre for Nuclear Research Radioisotope Centre POLATOM, Otwock, POLAND,* [5]*Faculty of Mathematics and Physics, University of Ljubljana, Ljubljana, SLOVENIA,* [6]*Nuclear Medicine Unit, University Hospital in Krakow, Krakow, POLAND,* [7]*Universitätsspital Basel, Basel, SWITZERLAND.*

Aim/Introduction: The management of patients with neuroendocrine neoplasms (NEN) has improved substantially since the introduction of radiolabelled somatostatin analogues targeting overexpressed somatostatin receptors (SSTR). Accurate assessment of SSTR status of primary focus/metastases is crucial to determine the personalized approach to the treatment. Recently it has been shown that novel molecular probes, SSTR2-antagonists, recognize more binding sites in comparison to the widely used SSTR2-agonists and hence they improve diagnostic efficacy, especially when the density of SSTR is low. The aim of the project is to initiate a clinical feasibility study with a novel ^{99}mTc-labelled SSTR2-antagonist as a sensitive probe to assess the SSTR status in NEN patients, and to develop a robust, reproducible quantitative imaging method. ***Materials and Methods:*** On the basis of extensive preclinical studies the most promising SSTR2 antagonist N4-LM3 (p-Cl-Phe-cyclo(D-Cys-Tyr-DAph(Cbm)-Lys-Thr-Cys)-D-Tyr-NH2 (TECANT1) was selected for clinical translation.Ten patients with advanced NEN and SSTR positivity confirmed by routinely used SSTR imaging based on a radiolabelled agonist were enrolled in this phase I multicentre clinical study(EudraCT no: 2019-003379-20). Safety, tolerability, human pharmacokinetics, dosimetry and NEN targeting properties of the compound tested were assessed. Comparability of clinical and imaging data collected at all clinical centres were provided by centralized secured database for standardization of image analysis and integration of statistical tools. ***Results:*** By now SPECT/CT imaging with the [^{99m}Tc]Tc-TECANT1 as Investigational Medicinal Product (IMP) was performed in 7 out of 10 patients. No IMP related side effects were observed. Rapid distribution with predominant renal excretion with typical pattern of SST analogues was observed, [^{99m}Tc]Tc-TECANT1 tumour uptake was visible as early as 5minutes after its administration and was retained 24 hours p.i. NEN lesions were very well visible in all examined patients. In certain patients lesion contrast was superior to images obtained with 68Ga-SSTR agonists. In all cases high tumour to background ratio was obtained, with the highest values at 4 hours after IMP injection. ***Conclusion:*** Images obtained with the ^{99m}Tc-labelled SSTR2-antagonist TECANT1 appear to be of great clinical value. Favourable toxicological and pharmacological profile was observed. Detailed quantitative analysis will be reported to support the initial highly comparable diagnostic performance to SSTR-PET.TECANT1 holds great promise to enable a reliable and widely available method for quantitative assessment of SSTR status and to improve the decision-making diagnostic and therapeutic algorithm as one of the key elements in a personalised approach to the management of NEN patients. Funding: ERAPerMed, FWF Austria, NCBiR Poland, MIZS Slovenia

OP-307

Comparison of [^{68}Ga]Ga-DOTANOC and [^{68}Ga]Ga-DATA^{5m}-LM4 PET/CT in the same patient group with neuroendocrine tumors.

R. V[1], *S. Ballal*[1], *M. Yadav*[1], *F. Roesch*[2], *P. Sheokand*[1], *M. Martin*[2], *M. Tripathi*[1], *R. Sahoo*[1], *C. Bal*[1];
[1]*AIIMS, Delhi, INDIA,* [2]*Johannes Gutenberg university of Mainz, Mainz, GERMANY.*

Aim/Introduction: Neuroendocrine tumors (NETs) are slow-growing tumors that express high levels of somatostatin receptors (SSTRs). SSTR imaging uses radio-labeled somatostatin analogs which bind to the somatostatin receptors (SSTR1-5), commonly over-expressed in NETs. NETs have shown a rising trend in incidence over the past four decades due to increasing awareness and better diagnostic tools. Recent studies have shown radiolabeled SSTR antagonists are superior for cancer theranostics compared with agonists (1-3). In this retrospective study, we aim to compare the diagnostic efficacy between [^{68}Ga]Ga-DOTANOC with [^{68}Ga]Ga-DATA^{5m}-LM4 in the detection of primary and metastatic lesions in NET patients. ***Materials and Methods:*** Histologically proven NET patients who underwent [^{68}Ga]Ga-DOTANOC and [^{68}Ga]Ga-DATA^{5m}-LM4 PET/CT scans were retrospectively analysed. Both imaging modalities were compared according to patient-based and lesion-based analysis. The qualitative analysis involved visual judgment of radiotracer uptake that was validated by the morphological findings on CT which was considered as the reference standard.Quantitative comparisons between the radiotracers were presented as standardised uptake value (SUV) corrected for lean body mass:

SULpeak, and SULavg. ***Results:*** 29 patients with a mean age of 49 years (range: 25 - 67 years; 14 women and 15 men) with confirmed NET were evaluated. Histology revealed low-grade NETs (G1) in 13 patients, intermediate grade (G2) in 7, and high grade (G3) in 9. 51.7% of patients (15/29) had distant metastases, and 48.2% (14/29) of patients demonstrated locally advanced disease. In total, 390 lesions were confirmed by cross-sectional diagnostic CT. The lesion-based sensitivity of [^{68}Ga]Ga-DATA^{5m}-LM4 PET was 84% (328/390), compared with 66.6% (260/390) for [^{68}Ga]Ga-DOTANOC PET (P<0.0001). According to lesion-based analysis, on diagnostic CT, 29 patients had 25 primary tumors, 69 lymph nodes, 7 lung metastases, 261 liver metastases, and 28 bone metastases. [^{68}Ga]Ga-DATA^{5m}-LM4 scan identified more abnormal lesions than [^{68}Ga]Ga-DOTANOC in all the primary and metastatic sites with a maximum marked difference in the liver [87.3% vs 67% ; P <0.0001 (228 vs. 175 compared to 261 lesions on CT) and bone metastases [100% vs 32%; P<0.0001 (28 vs. 9 compared to 28 lesions on CT)]. Quantitatively, the tracer uptake [SULpeak, and SULavg] was significantly higher in [^{68}Ga]Ga-DATA^{5m}-LM4 than with [^{68}Ga]Ga-DOTANOC PET for primary tumor (P<0.05). ***Conclusion:*** The SSTR ligand antagonist tracer [^{68}Ga]Ga-DATA^{5m}-LM4 detected significantly more lesions than the [^{68}Ga]Ga-DOTANOC in patients with NETs. [^{68}Ga]Ga-DATA^{5m}-LM4 is a promising radiopharmaceutical for the staging and restaging of NETs. However, the clinical significance has to be proven in a larger sample size.

OP-308

Prognostic value of the post-treatment ^{177}Lu-DOTATOC scintigraphy in NET patients undergoing PRRT.

S. Leyser[1,2], *H. Lanzafame*[1,2], *D. Kersting*[1,2], *R. Seifert*[1,2], *F. Zarrad*[1], *H. Lahner*[3], *N. Unger*[3], *W. P. Fendler*[1,2], *K. Herrmann*[1,2], *M. M. Weber*[1,4];
[1]*Department of Nuclear Medicine, West German Cancer Center, University Hospital Essen, Essen, GERMANY,* [2]*German Cancer Consortium (DKTK), Partner site University Hospital Essen, Essen, GERMANY,* [3]*Department of Endocrinology West German Cancer Center, University Hospital Essen, Essen, GERMANY,* [4]*German Cancer Consortium (DKTK), Partner site University Hospital Essen, Essen, Germany, Essen, GERMANY.*

Aim/Introduction: With the 2018 FDA approval of [^{177}Lu]-DOTATATE following the successful NETTER-1 trial peptide radioreceptor therapy (PRRT) has been established as a 2nd line treatment option for grade 1-2 neuroendocrine tumors (NETs) of gastroenteropancreatic origin. However, assessment of sufficient target expression was performed in this trial with somatostatin receptor (SSR) scintigraphy, a modality largely replaced by SR-PET due to superior sensitivity creating a need for alternative imaging parameters. We therefore aimed to evaluate the prognostic value of other imaging, such as semiquantitative analysis of the PET/CT as well as the Krenning-Score evaluated on the planar 1st cycle post-treatment [^{177}Lu]-DOTATOC-scintigraphy (PTS1), acquired 24h p.i. with regards to progression-free (PFS) and overall survival (OS). ***Materials and Methods:*** We included patients with histopathological diagnosis of NET, who underwent at least 2 PRRT cycles between January 2009 and July 2019, with available PTS1. Target SR expression was graded using the established, SRS-based Krenning criteria and mean SUVmax/-mean on baseline [^{68}Ga]-DOTATOC PET/CT for up to 9 lesions per patient. Progression free survival was defined as the interval from the first PRRT cycle to radiological progression (RECIST 1.1), clinical progression (ruled by a board-certified endocrinologist) or death. Time-to-event data (PFS and OS) were described using Kaplan-Meier curves and compared by use of log-rank test. ***Results:*** 115 patients were deemed eligible; of these 33 (28.7 %) had grade 1, 73 (63.5%) grade 2, and 9 (7.8%) grade 3 NETs. Median PFS was 22.3 months (range 2.8-148.9) and median OS was 48 months (range 4.3-157.1). 55 (47.8%) and 60 (52.2%) patients were classified as Krenning 3 and 4 on the post-treatment scintigraphy, respectively. In the Kaplan-Meier-analysis, Krenning score 4 vs. 3 was associated with a significantly longer PFS (35.9 vs. 16.2 months; p<0.001), as well as a significantly longer OS (75.3 vs. 41.8 months; p=0.001). Baseline [^{68}Ga]-DOTATOC PET/CT SUV was not significantly associated with PFS (p=0.36) and OS (p=0.53), underlining the independent value of the [^{177}Lu]-DOTATOC based Krenning score. ***Conclusion:*** Krenning score evaluated on PTS1 was a strong prognosticator for PFS and OS, whereas SUV was not. Patients with a Krenning score 3 demonstrated shorter survival and might thus benefit from a intensified treatment and folllow-up.

OP-309

Optimized segmentation of neuroendocrine tumor lesions on somatostatin receptor PET/CT imaging for therapy response assessment

A. Chaban[1], *J. Brosch-Lenz*[1], *Y. Song*[1], *V. Dinkel*[1], *L. Bodei*[2], *W. Weber*[1];
[1]*Klinikum rechts der Isar, der Technischen Universität München, Munich, GERMANY,* [2]*Memorial Sloan Kettering Cancer Center, New York, NY, UNITED STATES OF AMERICA.*

Aim/Introduction: There is increasing interest in using somatostatin receptor PET/CT (SSTR-PET/CT) for monitoring neuroendocrine tumor (NET) response to therapy. However, the conventional approach of using index lesions for response assessment is inherently limited because NETs frequently present with many metastases. We therefore investigated different approaches to capture tumor burden in patients with NETs. ***Materials and Methods:*** In this dual center study, we explored several approaches to delineate NET lesions in 156 SSTR PET/CT studies, including a global minimum SUV, a global SUV threshold based on liver or spleen SUVs, and separate thresholds for lesions in different sites of the body (liver, abdomen outside the liver, and lung/skeleton). Promising approaches were further evaluated in a group of 30 patients with a total 295 of well-defined lesions. In this group sensitivity, specificity, and area under the curve (AUC) were calculated for correct localization of metastases. The total tumor volume (TTV) of the best automated approach was compared with the sum of tumor volumes determined by segmenting lesions with a 42% threshold of their respective SUVmax which served as the reference standard. Finally, the inter-observer variability of the automated method was assessed. ***Results:*** Global thresholds for lesion delineation did not result in a reliable delineation of metastases and were not further investigated. In contrast, site-specific thresholds allowed for accurate lesion delineation. The best threshold for segmentation of liver metastases was normal liver SUVmax+2.2 g/ml, which resulted in a sensitivity, specificity, and AUC of 0.95, 0.97, and 0.96, respectively. The best threshold for bone and intrapulmonary metastases was a SUV of 2.0 g/ml with a sensitivity, specificity, and AUC of 1.00, 0.97, and 0.98, respectively. For extrahepatic lesions the best threshold was the liver SUVmax with a sensitivity, specificity, and AUC of 0.94, 0.83, and 0.89, respectively. Median TTVs measured with the automated approach was systematically larger (mean: 62 ml, range: 3 ml-588 ml) than TTV measured by individual segmentation of lesions (mean: 53 ml, range: 2 ml358ml,

p<0.01) but both parameters were closely correlated (r=0.88). The automated approach showed excellent reproducibility of TTV measurements between the two observers (r=0.99). ***Conclusion:*** SUV-based thresholding of SSTR PET images with site-specific thresholds is a promising approach for automated segmentation of NET lesions that can be easily implemented clinically. TTVs derived from this approach may be used as a new measure of tumor burden and to assess tumor response to therapy.

OP-310

Diagnostic performance of functional imaging with ^{68}Ga-DOTATATE PET/CT, ^{18}F-FDG PET/CT, and ^{18}F-FDG PET/CT, and anatomic imaging with whole-body CT and/or MRI in the detection ofSDHD-related pheochromocytoma and paraganglioma - A comparative prospective study

A. Jha, *M. Patel, A. Ling, C. C. Chen, C. Millo, K. Charles, M. Kuo, T. Prodanov, M. A. Nazari, S. Talvacchio, A. Derkyi, J. del Rivero, A. P. Chen, N. Nilubol, P. Herscovitch, F. I. Lin, D. Taïeb, J. A. Carrasquillo, A. C. Civelek, K. Pacak;*
National Institutes of Health, Bethesda, MD, UNITED STATES OF AMERICA.

Aim/Introduction: Patients with germline SDHD pathogenic variants (encoding succinate dehydrogenase subunit D) predominantly develop head and neck paragangliomas (HNPGLs), and might coexist with paragangliomas arising from other locations. The risk of metastatic disease is approximately 5%, however, multifocality of paragangliomas is observed in about 75% of patients. The performance of ^{68}Ga-DOTATATE PET/CT in SDHD-related pheochromocytomas/paragangliomas (PPGLs) is currently unknown. The purpose of this prospective study was to evaluate and compare the diagnostic performance of ^{68}Ga-DOTATATE PET/CT to ^{18}F-FDG PET/CT, ^{18}F-L-dihydroxy-phenylalanine (^{18}F-FDOPA) PET/CT, and whole-body CT and/or MRI (CT/MRI) in detection of SDHD-related PPGLs. ***Materials and Methods:*** ^{68}Ga-DOTATATE PET/CT was prospectively performed in 38 patients (females:males, 24:14; mean age, 44±13 years) with SDHD-related PPGLs. All patients also underwent ^{18}F-FDG PET/CT and CT/MRI, with 35/38 patients also undergoing ^{18}F-FDOPA PET/CT. Per-patient and per-lesion detection rates were compared for all imaging modalities. The median duration between ^{68}Ga-DOTATATE and ^{18}F-FDG, ^{18}F-FDOPA, and CT/MRI were 2, 1, and 2.5 days, respectively. A composite of all functional and anatomical imaging studies served as an imaging comparator. McNemar test was used to compare detection rates between ^{68}Ga-DOTATATE PET/CT and the other imaging modalities. Two-sided p values <0.05 were considered significant. ***Results:*** All patients were positive for PPGLs demonstrating 249 lesions on the imaging comparator. Thirty-five patients presented with HNPGLs whereas 13 presented with additional primaries located outside the head and neck region (adrenal, n=4; mediastinum, n=8, and abdomen, n=6), and 2 presented with metastases alone. Twenty-six (17 in head and neck and 14 outside the head and neck) patients also demonstrated metastases. ^{68}Ga-DOTATATE PET/CT demonstrated a per-lesion detection rate of 243/249 [97.6%, 95% confidence interval (CI): 94.8-99.1%]. ^{18}F-FDG PET/CT, ^{18}F-FDOPA PET/CT, and CT/MRI showed significantly lower per-lesion detection rates of 130/249 (52.2%, 95% CI: 45.8-58.6%; p<0.001), 203/244 (83.2%, 95% CI: 77.9-87.7%; p<0.001), and 211/249 (84.7%, 95% CI: 79.7-89.0%; p<0.001), respectively. The per-patient detection rates of ^{68}Ga-DOTATATE PET/CT, ^{18}F-FDG PET/CT, ^{18}F-FDOPA PET/CT, and CT/MRI were 38/38 (100%, 95% CI: 90.8-100%), 35/38 (92.1%, 95% CI: 78.6-98.3%), 34/35 (97.1%, 95% CI: 85.1-99.9%), and 38/38 (100%, 95% CI: 90.8-100%), respectively. ***Conclusion:*** ^{68}Ga-DOTATATE PET/CT showed a significantly superior per-lesion detection rate compared to all other functional and anatomical imaging modalities and may be the preferred functional imaging modality to evaluate SDHD-related PPGLs. Furthermore, owing to the ^{68}Ga-DOTATATE avidity of PPGLs in these patients, cold somatostatin analog and/or peptide receptor radionuclide therapy can be considered as one of the therapeutic options.

707

Monday, September 11, 2023, 8:00 AM - 9:30 AM
Hall F1

Paediatrics Committee - TROP Session: Neuroblastoma & Non-PET Paediatric Studies

OP-311

Prognostic and predictive value of imaging features in neuroblastoma using pre-treatment 123I-MIBG SPECT/CT: is there a place for radiomics?

M. Luporsi[1], *H. Brisse*[2], *C. Nioche*[3], *N. Jehanno*[1], *H. Fokem-Fosso*[3], *I. Buvat*[3], *G. Schleiermacher*[4], *F. Orlhac*[3];
[1]*Department of nuclear medicine, Institut Curie, PSL Research University, Institut Curie, Inserm , LITO-U1288, Paris, FRANCE,* [2]*Institut Curie, Inserm , LITO-U1288, Department of radiology, Institut Curie, PSL Research University, Paris, FRANCE,* [3]*Institut Curie, Inserm , LITO-U1288, Orsay, FRANCE,* [4]*SiREDO Integrated Pediatric, adolescents and young adults Oncology Center, Laboratory of translational research in pediatric oncology INSERM-U830, Institut Curie, Paris, FRANCE.*

Aim/Introduction: Recent studies based on 123I-MIBG SPECT/CT have suggested that some radiomic features - mainly reflecting the primary tumor's volume and its shape - could be promising prognostic tools in neuroblastoma (NB). Yet, available data remain sparse and have only involved small series. The aim of this study is to assess the prognostic significance of NB's primary tumor radiomic features calculated from pre-therapeutic 123I-MIBG SPECT/CT (MIBG) images and to explore their ability to predict NMYC status. ***Materials and Methods:*** Patients (<18 yo) with a newly diagnosed NB and a pre-therapeutic 123I-MIBG scan performed on a SPECT/CT (Discovery GE 670) between 2012 and 2020 in our institution were retrospectively included. Genomic, histological, biological and CT data at diagnosis as well as survival (> 2 years of follow-up) were collected from medical records. The segmentation of the primary tumor and extraction of 18 radiomic features were performed using LIFEx software (version 7.3.25) [1]. The ability of radiomic features to identify NMYC status was assessed using the Youden Index (=Se+Sp-1) and the Wilcoxon test. Kaplan-Meier analysis was performed and the estimated OS probabilities for two different groups of patients were obtained for the cut-off that leads to the lowest p-value in log-rank tests. ***Results:*** 92 patients were enrolled (32 female) with a mean age of 27±32 months at diagnosis (range [1-178], < 18 months: 52%). 52/92 patients had a metastatic disease (42 stage M, 10 Ms) and 36/92 patients were considered with a high-risk NB . 9 features were independently associated with the NMYC amplification (Wilcoxon test: p<0.05). NMYC amplified tumors (18/92) exhibited higher Metabolic Volume values (volume normalized by the body surface area, p=0.005), higher Asphericity values (p<0.001) and higher Kurtosis values (p=0.017) than non-NMYC amplified lesions. Asphericity was the most discriminant feature with a Youden index of 0.48 (Se=78%;Sp=70%). Established prognostic features

at diagnosis (age, INRGSS stage, LDH, MKI, INPC, genomic profiles and baseline SIOPEN score) were all predictive of survival ($p<0.05$). Metabolic Volume, Asphericity and Kurtosis of the primary tumors were additionally predictive of survival (log-rank test: $p\leq0.05$). ***Conclusion:*** In this largest series to date, radiomic features extracted from pre-therapeutic MIBG are strongly associated with the NMYC status and overall survival, and could be used for as new biomarkers for prognostic stratification. ***References:*** [1] Nioche et al. Cancer Res 2018.

OP-312

Comprehensive Analysis of 18F-MFBG Biodistribution and Variability in Pediatric Neuroblastoma Patients

P. Wang[1,2], *H. Zhang*[1], *Y. Zhang*[1], *T. Li*[1], *H. Jing*[1], *F. Li*[1], *J. Zhang*[2];
[1]*Department of Nuclear Medicine, Peking Union Medical College Hospital, Beijing, CHINA,* [2]*Department of Diagnostic Radiology, National University of Singapore, Singapore, SINGAPORE.*

Aim/Introduction: ^{18}F-MFBG is a promising PET tracer for diagnosing neural crest tumors, particularly neuroblastoma. This study aims to provide a comprehensive analysis of 18F-MFBG biodistribution in pediatric neuroblastoma patients, focusing on the uptake in normal organs and the variability observed in the liver, pancreas, and brown adipose tissue. ***Materials and Methods:*** We retrospectively analyzed consecutive ^{18}F-MFBG PET/CT scans of patients with neuroblastoma. Two experienced nuclear medicine physicians interpreted the PET/CT studies using MIM software, and quantitative analysis was performed on normal tissues, reporting the SUVmax. ***Results:*** Quantitative analysis of ^{18}F-MFBG biodistribution was performed on 10 patients with negative PET findings, confirmed by follow-up. ^{18}F-MFBG exhibited stable and reproducible biodistribution in normal organs, with the highest SUVmax observed in the salivary glands (9.0 ± 0.8; range, 3.8-16.2), myocardium (6.9 ± 0.4; range, 3.0-10.3), and adrenal glands (4.5 ± 0.2; range, 3.1-6.0). Lower SUVmax was observed in the small intestine, renal parenchyma(1.6 ± 0.1; range, 0.9-2.9), and spleen, and stomach, while the lowest SUVmax was found in muscle, bone (0.6 ± 0.05; range, 0.3-1.0), and lungs. The head of the pancreas displayed higher uptake (3.0 ± 0.2 vs. 2.6 ± 0.2; P=0.007) compared to the body and tail. In an extended analysis of 121 neuroblastoma patients, we observed three patterns of 18F-MFBG uptake in normal liver tissue: (1) uniform uptake with LRR of 1.2 ± 0.1 (range, 1.0-1.4); (2) higher uptake in the left lobe with uniform uptake in both lobes (LRR, 1.8 ± 0.3, range, 1.5-2.8); and (3) increased uptake in the hepatic margin with IRR of 2.0 ± 0.5 (range, 1.5-3.4). Uniform uptake in the whole liver was observed in similar proportions of 38.5% and 36.4% in adults and children, respectively. High gallbladder uptake was observed in one patient. Brown adipose tissue was detected in 11 patients (9.1%), with five located around the neck and supraclavicular region, and six along the T1-2 spine. These findings are particularly important as they provide insights into the variability of ^{18}F-MFBG uptake that may impact image interpretation. ***Conclusion:*** Understanding the biodistribution of ^{18}F-MFBG and its variability is essential for accurate image interpretation and clinical management of pediatric neuroblastoma patients. This study presents a comprehensive analysis of ^{18}F-MFBG biodistribution, which will aid physicians in better interpreting PET images and making more informed clinical decisions.

OP-313

The ^{18}F-FDG PET/MRI radiomics nomogram for differentiating high-risk and non-high-risk patients of the International Neuroblastoma Risk Group Staging System

J. Liang;
杭州通用医学影像诊断中心，杭州，*CHINA.*

Aim/Introduction: To develop and validate an ^{18}F-FDG PET/MRI radiomics nomogram to distinguish high-risk and non high-risk patients in the International Neuroblastoma Risk Group staging system (INRGSS). ***Materials and Methods:*** The ^{18}F-FDG PET/MRI imaging data of 124 patients with neuroblastoma were analyzed retrospectively, which were divided into training set (n=93) and verification set (n=31). The radiomics features were extracted from PET images and T2WI images, and a radiomics score (Rad score) was calculated. Then single factor and multivariate logistic regression analysis were used to screen out independent clinical factors and build a clinical model. Based on Rad score and independent clinical factors, a radiomics nomogram was developed. The performance of the clinical model, Rad score and nomogram was evaluated by receiver operating characteristic (ROC) curve, calibration curve and decision curve analysis (DCA). ***Results:*** Eight radiomics features were selected to construct the radiomics model. There were significant differences between high-risk and non high-risk patients in patient age, INRG stage, MTV(metabolic tumor volume), TLG (total lesion glycolysis) and Rad scores. The radiomics nomogram combining Rad scores with the clinical factors described above showed favorable predictive value for distinguishing high and non-high risk, with AUC values of 0.973 and 0.969 in the training and validation sets, respectively. The calibration curve showed that the nomogram of radiomics had goodness of fit, and DCA proved that the nomogram of radiomics was useful in clinical practice. ***Conclusion:*** The radiomics nomogram combining Rad score and clinical factors can well predict high-risk and non high-risk patients of INRGSS. It may be helpful for disease follow-up and management in clinical practice, and assist in individualized and precise treatment of neuroblastoma.

OP-314

First clinical experience with [^{64}Cu]Cu-NOTA-ch14.18/CHO to visualize GD2 by PET in several pediatric tumor entities - Biodistribution and preliminary dosimetry

N. Trautwein[1,2], *J. Schwenck*[1,2,3], *C. Seitz*[4,5], *S. von Beschwitz*[1], *G. Reischl*[2], *S. Scheuermann*[4,5], *P. Lang*[4], *J. Schaefer*[6], *B. Pichler*[2,3], *C. la Fougère*[1,3], *H. Dittmann*[1];
[1]*1Department of Nuclear Medicine and Clinical Molecular Imaging, Tuebingen, GERMANY,* [2]*2Werner Siemens Imaging Center, Department of Preclinical Imaging and Radiopharmacy, Tuebingen, GERMANY,* [3]*3Cluster of Excellence iFIT (EXC 2180) "Image-Guided and Functionally Instructed Tumor Therapies", Tuebingen, GERMANY,* [4]*4Department of General Pediatrics, Hematology and Oncology, University Children's Hospital Tuebingen, Tuebingen, GERMANY,* [5]*5Cluster of Excellence iFIT (EXC 2180) "Image-Guided and Functionally Instructed Tumor Therapies", Tuebingen, GERMANY,* [6]*6Department of Diagnostic and Interventional Radiology, Tuebingen, GERMANY.*

Aim/Introduction: The disialoganglioside GD2 is overexpressed in several malignant tumor entities. Since EMA approval in 2017, dinutuximab beta, a GD2 targeting antibody, has been established to treat neuroblastoma (1). Currently clinical trials for the treatment of osteosarcoma (NCT02484443) and initial trials in Ewing sarcoma are ongoing. Due to the variable GD2

expression of tumors and severe side effects of dinutuximab beta therapy, non-invasive evaluation of GD2 expression is highly desirable. To address this issue, a GD2-targeting PET-tracer, [^{64}Cu]Cu-NOTA-ch14.18/CHO (^{64}Cu-GD2) was developed (2). Here, we evaluated the biodistribution and estimated the dosimetry of the ^{64}Cu-GD2 PET-Tracer. ***Materials and Methods:*** A total of 11 patients (7 male, 4 male, mean age: 13.9 ± 5.0). Patients had a histology confirmed neuroblastoma (6), osteosarcoma (3) or Ewing sarcoma (2). ^{64}Cu-GD2 PET/MRI was performed in approximately 21 hours (range: 17-25 hours) after i.v. injection of 2-5 MBq/kg of ^{64}Cu-GD2. In 6 patients, a second scan was executed 43 hours p.i. (range: 41-44 hours) tumor and organ doses were estimated in the subgroup of patients who had two scans using OLINDA® software. Tissue uptake in organs was quantified by SUV_{max} and SUV_{mean} of a defined spherical volume of interest (VOI), while SUV_{mean} of tumor lesions was evaluated by a 41% isocontour of the SUV_{max}. In two patients tumorlesion were resected and stained. ***Results:*** No high-grade side effects were observed; one patient reported minor dizziness. In 9 of 11 patients (81%), suspicious tumor lesions were detected by PET/ MRI. In 8 of these 9 patients (89%) at least one metastasis with an increased ^{64}Cu-GD2 uptake was detected. A high tumor uptake (SUV_{max} >10) was measured in 4 of 8 patients (50%). In the case of GD2-positive lesions, an excellent tumor to background ratio with at least 6-fold higher uptake was observed in bones, muscles or lungs. The highest organ dose was measured in the liver (mean: 0.15 mGy/MBq; range: 0.04-0.21) while whole body dose was 0.03 mGy/MBq (0.02-0.04). ***Conclusion:*** ^{64}Cu-GD2 PET is a promising tool to visualize GD2 expression in various cancers. By using the universal NOTA chelator, labeling with ^{177}Lu seems feasible. Due to uptake values up to SUVmax 30, future considerations of radioimmunotherapy will be possible. Since dinutuximab beta is already an approved therapy for neuroblastoma, ^{64}Cu-GD2 may be used for therapy stratification. ***References:*** (1) EMA. European public assessment report for Qarziba (2) Schmitt J, Translational immunoPET imaging using a radiolabeled GD2 Theranostics

OP-315

Reaching the target dose with one single [^{131}I]-mIBG treatment in high-risk neuroblastoma. The determinant impact of the primary tumour

F. Fiz[1], *A. Cirone*[1], *S. Righi*[1], *M. Massollo*[1], *L. Amoroso*[2], *G. Bottoni*[1], *M. Conte*[2], *M. Gambaro*[1], *F. Massone*[1], *G. Semino Bruzzone*[1], *S. Orengo*[1], *S. Sorrentino*[2], *A. Garaventa*[2], *A. Piccardo*[1];
[1]*Ospedale Galliera, Genova, ITALY,* [2]*IRCCS Istituto Giannina Gaslini, Genova, ITALY.*

Aim/Introduction: [^{131}I]I-MIBG is an efficacious treatment for children with metastasized neuroblastoma (NBL). However, treatment effectiveness is linked to the effective dose absorbed by the target; to achieve a sufficient effect, a 4 Gy whole-body dose threshold has been proposed. Achieving this goal often requires administering [^{131}I]I-MIBG twice back-to-back (tandem therapy), which may cause high-grade haematological toxicity. In this study, we tried to assess the factor predicting the achievement of 4 Gy whole-body dose with a single radiopharmaceutical administration. ***Materials and Methods:*** Children affected by metastatic NBL and treated with a high [131I]I-MIBG activity (>450 MBq/Kg) were evaluated retrospectively. Kinetics measurements were carried out at multiple time points to estimate the whole-body dose. The resulting whole-body dose was compared with clinical and activity-related parameters. ***Results:*** Seventeen children (12 girls, median age 3 years, age range 1,5-6,9 years) were included. Eleven of them still bore the primary tumour. They received an average activity of 563±80 MBq of [^{131}I]I-MIBG per Kg of body weight. The resulting median whole-body dose was 2,88 Gy (range 1,63-4,22 Gy). There was a direct correlation between the tracer biological half-life and the whole-body dose (R: 0,878, p<0,001); in turn, the volume of the primary tumour was correlated with the [^{131}I]I-MIBG half-life. As a result, children who had a "bulky" primary (>30 ml) received a higher whole-body dose than those with smaller or surgically removed primaries (3,42±0,74 Gy vs 2,48±0,65 Gy, respectively p=0,016). Conversely, the correlation between activity/Kg and whole-body dose was moderate (R: 0,42 p=0,093). ***Conclusion:*** These data suggest that the presence of a bulky primary tumour can significantly prolong the [^{131}I]I-MIBG biological half-life, effectively increasing the absorbed whole-body dose. This information could be used to model the administered activity, allowing to attain the target dose without the need of a two-step radiopharmaceutical administration.

OP-316

Utility and Optimal Scan Time of Diagnostic and Post-therapeutic Whole-Body Scan in Children and Young Adult Patients Administered with Iodine-131

P. Kumar*, C. Bal, N. A. Damle;*
All India Institute of Medical Sciences, New Delhi, INDIA.

Aim/Introduction: The utility of Dx-WBS (diagnostic whole-body scan) in patients with differentiated thyroid cancer (DTC) is controversial. The optimal time of acquisition of WBS has not yet been established even extensive routine use of the same in clinical practice. Moreover, the optimal time of WBS acquisition is important in children as it has potential to alter the patient management. The aim of this study was to find out the optimal time of acquisition of WBS of both the diagnostic and post-therapy scan (PTS) in children and young adults with DTC. ***Materials and Methods:*** Children and young adults (≤21 y) with DTC had undergone serial WBS at 24h, 48h and/or ≥72h after diagnostic as well as therapeutic dosage administration. All the serial WBSs were blinded and reviewed by nuclear medicine physicians for detection of lesions. The utility of Dx-WBS and PTS was determined based on the additional lesion(s) that could alter the administered therapy activity of ^{131}I. The optimal time of acquisition for Dx-WBS/PTS was evaluated based on the first appearance of lesion in ^{131}I WBS. ***Results:*** Ninety-five children and young adults (M=27; F=68) with mean age of 17.9±3 y were evaluated. Ten patients (10.5%) had no evidence of disease on Dx-WBS and were considered surgically ablated, and hence were excluded from the study. Eighty-five included patients received 74 MBq (2 mCi) of ^{131}I administered for Dx-WBS followed by the therapeutic activity ranging from 1.11-5.55 GBq (30-150 mCi) ^{131}I depending on the extent of disease. There were no additional lesions seen on serial Dx-WBS or PTS in patients with intact thyroid lobe and thyroid remnant. In patients with nodal metastases, additional nodes were seen in 2/32 patients in ≥48h Dx-WBS and 1/32 patients in PTS at 72h but was clinically not relevant as it did not alter the Rx dosage of ^{131}I. The serial Dx-WBS missed pulmonary metastases in 3/17 (17.6%) patients that was visualized in PTSs. The optimal time of acquisition of Dx-WBS and PTS was found to be at 48 h and 72 h, respectively in children and young adult patients with pulmonary metastases. ***Conclusion:*** The Dx-WBS and PTS both appear useful in children and young patients with DTC and should be done at 48h and 72h, respectively.

OP-317

SPECT/CT in the diagnosis of Ectopic Gastric Mucosa-Meckel's Diverticulum

Z. Koç[1], *P. Özcan*[1], *F. Tuncel*[2], *C. İsbir*[3], *Y. Usta*[4];
[1]Mersin University Hospital Nuclear Medicine Dpt., Mersin, TÜRKIYE, [2]Mersin University Hospital Pathology Dpt., Mersin, TÜRKIYE, [3]Mersin University Hospital Pediatric Surgery Dpt., Mersin, TÜRKIYE, [4]Mersin University Hospital Pediatric Gastroenterology Dpt., Mersin, TÜRKIYE.

Aim/Introduction: The imaging of Meckel's Diverticulum (MD) is based of accumulation of Tc-99m pertechnetate in the Ectopic Gastric Mucosa (EGM) content. Although the diagnostic accuracy of this imaging modality is high there are some overlap patients with coexisting gastrointestinal bleeding and false positive causes hampering diagnostic power. Althogh there are several case reports about the diagnostic facility of SPECT/CT in ectopic gastric mucosa determination there are no large studies in the literature (1-3). The aim of this study was to evaluate the possible contribution of SPECT/CT in EGM-MD diagnosis and to determine the indication of this additional imaging modality. ***Materials and Methods:*** 52 pediatric patients (24 girls, 28 boys; mean: 8,06±5,22 years old) who have suspicion of MD and referred for scintigraphy were evaluated retrospectively. Additional SPECT/CT were performed to selected five cases among the group. The results of the scintigraphy as well as SPECT/CT were compared with endoscopy, pathology and/or follow up results. ***Results:*** There were nine patients with equivocal study results, twelve positive results and the others were considered negative MD scintigraphy. One patient was out of follow up and ten patients underwent surgery. Only one single patient was negative during surgery but scintigraphy was also negative. The diagnostic sensitivity, specificity and accuracy were 100%, 95% and 96% respectively. Among 5 patients with SPECT/CT results one patient was only diagnosed by only SPECT/CT who had EGM in duplication cyst, one equivocal patient was diagnosed as descending colon bleeding and one patient's lesion was clearly delineated by SPECT/CT. ***Conclusion:*** SPECT/CT has clear advantages over standard planar scintigraphy imaging in EGM-MD determination. This modality might decrease equivocal and false positive results but this issue has to be addressed with further studies.

References: Yang J, Tian D, Wu L, Dong M, Zhong J.Meckel's diverticulum with polypoid hyperplasia of ectopic gastric mucosa diagnosed by double-balloon enteroscopy and single-photon emissioncomputed tomography/computed tomography.J Int Med Res. 2020 Sep;48(9):300060520955055. Mittl GS, Servaes SE, Zhuang H.An Atypical Case of Meckels Diverticulum Assessed by SPECT/CT Imaging.Clin Nucl Med. 2022 Apr 1;47(4):372-374. Zhu Y, Dong M, Weng W, Yang J.Spontaneous perforation and intraabdominal abscess due to Meckels diverticulum revealed on SPECT/CT with 99m-technetium pertechnetate: A case report. Medicine (Baltimore). 2018 Oct;97(43):e13004.

OP-318

Re-evaluating the milk scan protocol, perplexing or potentially prognostic?

K. Hlongwa[1], *A. Brink*[1], *S. M. Peters*[2], *S. More*[1];
[1]Red Cross War Memorial Children's Hospital and University of Cape Town, Cape Town, SOUTH AFRICA, [2]Groote Schuur Hospital and School of Public Health and Family Medicine, University of Cape Town, Cape Town, SOUTH AFRICA.

Aim/Introduction: Gastro-oesophageal reflux (GER) and pulmonary aspiration occur in children of all ages. Milk scans have been used for the detection of GER for decades. There are various documented protocols for milk scans in search of GER with no universally accepted protocol. We recently amended our protocol from imaging patients for 30 minutes and assessing gastric emptying at 2 hours to imaging patients for 60 minutes and assessing gastric emptying at 3 hours due to the potential of missing episodes of reflux and overclassifying delayed emptying when normal. This study aims to assess the value of the change in protocol in being able to detect significant number of refluxes. ***Materials and Methods:*** We retrospectively reviewed the scans of all patients who presented for milk scans at the Red Cross War Memorial Children's Hospital from 1 November 2021 to 30 November 2022. The number of reflux episodes detected in patients imaged with the 30-minute protocol in comparison to the number detected with the 60-minute protocol was reviewed. The episodes of reflux were classified with an in-house severity scale and gastric emptying was evaluated at different time intervals. Delayed gastric emptying at 2 hours was quantified as residual activity in the stomach >37% and at 3 hours as >80% emptying into the bowel. ***Results:*** A total of 205 studies were reviewed over the 13-month period. In the 30-minute studies, 400 reflux episodes were observed in 70 patients, 7 were classified as normal, 9 mild reflux, 19 moderate reflux, 35 severe reflux, with 21 patients demonstrating delayed gastric emptying at the 2-hour images. 11/21 patients with delayed gastric emptying had no reflux and 10/21 patients had reflux of varying classifications.In the 60-minute studies, 537 reflux episodes were observed in 65 patients, 16 were classified as normal, 8 mild reflux, 15 moderate reflux, 26 severe reflux with 12 patients demonstrating delayed gastric emptying at the 3-hour images. 8/12 patients with delayed emptying had no reflux and 4/12 had reflux of varying classifications.No statistically significant difference was seen between the detection of refluxes in 30-minute vs 60-minute studies. Chi-Square statistic = 5.201, p-value = 1.57659. ***Conclusion:*** Our findings did not demonstrate an additional benefit of changing the milk scan protocol imaging time. A standardized study comparing similar patient populations with the question of reflux may be valuable in order to establish a common practice.

OP-319

Predictive Value of Diuretic Renogram for Progressive Hydronephrosis in Perinatally Detected Unilateral Hydronephrosis

C. Lin[1], *P. Chuang*[2], *I. Tsai*[3], *M. Cheng*[4];
[1]National Taiwan University Hospital, Taipei City, TAIWAN, [2]Department of Nuclear Medicine, National Taiwan University Hospital Yunlin Branch, Douliu City, TAIWAN, [3]PEDIATRICS National Taiwan University Children Hospital and National Taiwan University College of Medicine, Taipei City, TAIWAN, [4]Nuclear Medicine National Taiwan University Hospital and National Taiwan University College of Medicine, Taipei City, TAIWAN.

Aim/Introduction: The aim of our study was to review the long-term outcome of perinatally detected hydronephrosis and try to find the predictors by first diuretic renogram. ***Materials and Methods:*** We retrospectively analyzed patients who received diuretic renogram with furosemide in a tertiary medical center. Predictive values derived from diuretic renogram included: differentiated renal function (DRF), furosemide half-clearance time ($T_{1/2}$), cortical transit time (CTT) and response to furosemide stimulation (RFS). Decreased DRF was defined as DRF below 45% at the hydronephrotic side. The diuretic $T_{1/2}$ was the time at which the time-activity curve decreases to half its maximal activity. Prolonged isotope washout rate was defined if $T_{1/2} > 15$

minutes. Delayed CTT was defined as the absence activity in the subcortical structures within 3 minutes of tracer injection. Patients were followed at least 2 years to monitor for disease deterioration. The primary endpoint is the time of first occurrence of one of the signs of disease deterioration, defined as urinary tract infection, flank pain, upgraded hydronephrosis defined by Society of Fetal Urology (SFU) grade in serial renal ultrasound (US), or intervention to relieve hydronephrosis. Cox proportional hazard model and Kaplan-Meier Method were applied to identify predictors. ***Results:*** From January 2013 to March 2021, a total of 31 infants (24 boys and 7 girls) received diuretic renogram at mean age of 9.01 ± 9.68 months. Out of 31 patients, disease deterioration occurred in 16 (51.6%) patients and the mean follow-up period was 24.9 months (IQR: 3.4 to 44.9). By Cox regression analysis, decreased DRF was the only factor significantly associated with disease deterioration (HR: 3.501; 95% CI: 1.240 - 9.885; p = 0.018). Patients with decreased DRF (<45%) had shorter time to deterioration of 3.19 ± 2.11 months. In contrast, the median time to deterioration period in patients with preserved DRF (>45%) at the hydronephrotic kidney was not reached at the time of analysis (p = 0.012). ***Conclusion:*** Decreased DRF (<45%) in initial diuretic renogram is a prognostic factor for disease deterioration in children with perinatally detected unilateral hydronephrosis. In addition, lower DRF indicate rapid deterioration, and may need earlier intervention.

708

Monday, September 11, 2023, 08:00 - 09:30
Hall F2

Special Symposium 2 - Inflammation & Infection Committee: Usefulness of PET in the Evaluation of Inflammatory Rheumatisms

OP-320
Clinical spectrum and imaging of inflammatory rheumatisms: a clinician's perspective
K. van der Geest;
UniversityMedical Center Groningen, Department of Rheumatology and Clinical Immunology, Groningen, NETHERLANDS.

OP-321
[18F]FDG PET/CT in inflammatory rheumatic disorders in elderly (PMR vs EORA vs SpA)
F. Besson;
Hôpitaux Universitaires Paris-Saclay, AP-HP, CHU Bicêtre, Department of Nuclear Medicine and Molecular Imaging, Paris, FRANCE.

OP-322a
[18F]FDG PET/CT in rheumatoid arthritis and other rheumatic disorders
P. Guglielmo;
Instituto Oncologico Veneto, Castelfranco Veneto, ITALY.

OP-322b
Beyond [18F]FDG in inflammatory rheumatisms
C. van der Laken;
Amsterdam UMC, Department of Rheumatology, Amsterdam, NETHERLANDS.

709

Monday, September 11, 2023, 8:00 AM - 9:30 AM
Hall G2

e-Poster Presentations Session 5 - Physics Committee: SPECT/CT, PET/CT, PET/MR Quantitative Imaging

EPS-084
ThyroPIX - Mobile Compton camera based on Timepix3 technology for monitoring of thyroid gland cancer treatment
E. Trojanova[1], *D. Doubravova*[1], *R. Kaderabek*[2], *V. Poriz*[3], *T. Kracmerova*[4];
[1]*ADVACAM s.r.o, Prague, CZECH REPUBLIC,* [2]*Radalytica as.s, Prague, CZECH REPUBLIC,* [3]*Radalytica a.s., Prague, CZECH REPUBLIC,* [4]*Fakultní nemocnice v Motole, Prague, CZECH REPUBLIC.*

Aim/Introduction: Thyroid tumors are relatively rare, but their incidence is steadily increasing in recent times. The goal of preclinical and clinical studies is therefore to find a way to detect and successfully treat this type of cancer early. The main problem is that the current imaging methods don't provide sufficient spatial resolution to reveal the remnants after the chirurgical removal of the gland. Due to their presence the disease relapses. ThyroPIX is a new-generation multimodal device for imaging the thyroid gland and thyroid cancer treatment monitoring. ***Materials and Methods:*** . ThyroPIX is a new-generation multimodal device for imaging the thyroid gland and thyroid cancer treatment monitoring. The ThyroPIX device is equipped with a fully spectral single-photon counting detector of a new generation based on Timepix3 technology which exploits the ability to measure the position, energy, and time of every detected particle. Thanks to this information related to very precise time detection of every incoming gamma photon is possible to determine the position of the interaction of primary and Compton scattered photons in sensitive layers of detector materials. Together with the energy information direction of a primary photon is then calculated and based on the backward reconstruction the source is localized in space.This new imaging method concept called the Compton camera brings possibilities of emission imaging for various types of radioisotopes of a broad range of energies. This approach leads to the development of a unique system without using any other usually necessary equipment (e.g. heavy collimators). Besides the absence of collimators, the main benefits of the novel system include better spatial resolution, low weight, and significantly higher sensitivity. Thanks to the implementation of the detector on a mobile collaborative robotic arm and the execution of either a planar or tomographic image, it will be possible to perform a quick, basic examination of the patient in any part of the hospital. ***Results:*** This contribution presents the imaging system and shows the measured data and its results in the framework of preclinical tests on phantoms. ***Conclusion:*** Thanks to the implementation of the detector on a mobile collaborative robotic arm and the execution of either a planar or tomographic image, it will be possible to perform a quick, basic examination of the patient in any part of the hospital. ***References:*** [1] TURECEK, D., J. JAKUBEK, E. TROJANOVA a L. SEFC. Compton camera based on Timepix3 technology. Journal of Instrumentation [online]. 2018, 13(11)

EPS-085

Quantification of amyloid load from [18F]florbetaben PET scans agrees with histopathology, visual read, and clinical progression

G. Kolinger[1], *L. Tiraboschi*[1], *F. Padovano*[2], *D. Braca*[2], *M. Spitilli*[2], *G. Lucidi Pressanti*[3], *S. Bullich*[1], *R. Mazza*[2];
[1]*Life Molecular Imaging GmbH, Berlin, GERMANY,* [2]*Nuclear Medicine Unit, "G. Mazzini" Hospital, Teramo, ITALY,* [3]*Services Department, "G. Mazzini" Hospital, Teramo, ITALY.*

Aim/Introduction: Positron emission tomography (PET) with [18F]florbetaben allows the detection of amyloid-beta (Aβ) plaques in the brain. While quantification of amyloid PET is already commonly done in research studies and clinical trials, quantification can also assist clinicians in interpreting [18F]florbetaben images. However, quantification can be software-dependent, therefore it is important to test available software before clinical use. To this end, this work compared quantitative results from CortexID (v1.6 ext.6, GE Healthcare) with histopathology confirmation of Aβ in the brain, visual read (VR) from five independent readers, and longitudinal progression of clinical status and Aβ load. ***Materials and Methods:*** In total, 338 scans were quantified using the whole cerebellum as reference region and the Composite as target region for the calculation of Standardized Uptake Value Ratio (SUVR). 87 scans of subjects with histopathology confirmation of presence/absence of Aβ plaques in the brain (using a combination of Bielschowsky silver staining and immunohistochemistry as standard of truth) were used to define a Aβ positivity quantitative cut-off using receiver operator characteristic curve analysis. Meanwhile, the scans of 100 healthy control subjects with a consensus negative VR were used to define an early pathology cut-off by the 95% quantile. To assess the concordance between the positivity cut-off and VR, an independent set of 174 images was quantified and evaluated by five independent readers. Finally, 40 subjects with mild-cognitive impairment (MCI) had at least one follow-up scan 1 and/or 2 years after baseline and clinical assessment 2 and/or 4 years after baseline. This cohort was quantified to evaluate longitudinal changes in Aβ load and clinical progression. ***Results:*** Quantitative results agreed with histopathology (sensitivity of 0.94[0.84-0.99] and specificity of 0.94[0.81-0.99]), leading to an optimal positivity cut-off of SUVR=1.24 and an agreement of 95%[92%-99%] with VR. Furthermore, an early pathology cut-off based on healthy controls was found to be SUVR=1.15, therefore quantification below that on the Composite region indicates absence or sparse presence of Aβ plaques in the brain. None of the MCI subjects with Composite SUVR<1.24 at baseline (n=19) progress to Alzheimer's disease (AD) at clinical follow-up. Meanwhile 19 of 21 MCI subjects above the cut-off at baseline progressed to AD. However, the accumulation rate between those groups was not significantly different. ***Conclusion:*** Quantification of [18F]florbetaben amyloid PET scans using CortexID can be a valuable tool as adjunct to VR in cross-sectional settings.

EPS-086

2-layer Hemispheric PET featuring different materials on each layer

K. Scheiff*, A. Pashazadeh, C. Hoeschen;
Otto-von-Guericke-University Magdeburg, Magdeburg, GERMANY.*

Aim/Introduction: Positron Emission Tomography (PET) is used for the diagnostic and research purposes of a wide range of brain diseases, requiring high resolution of about 1mm. To achieve such resolution, brain-dedicated geometries have been proposed and prototyped in recent years. [1] Many of these PET-systems use (hemi-)spherical geometries to minimize the scanner's radius and reach a desired resolution. [2] Like most PET-systems, brain-dedicated geometries commonly utilize detectors with pixelated crystals. However, over the last decade, detectors using monolithic crystals have achieved intrinsic resolutions comparable to pixelated ones. [3] Since the intrinsic resolution of monolithic crystals is related to their thickness, a second layer of detectors can be added to achieve the same total crystal depth as that used in pixelated detectors and to close gaps in the positioning of the first layer. By having pixelated crystals on the inner layer and monolithic detectors on the outer layer, time-of-flight resolution and depth of interaction resolution can be achieved, respectively. Use of two layers also allows the combination of different materials on each layer. In the simulation study, we compared the sensitivity performance of three 2-layer geometries, with different material combinations. ***Materials and Methods:*** The simulation study was conducted using the GEANT4 toolkit GATE. We simulated several 2-layer hemispheric PET-geometries with detectors, employing pixelated crystals in the inner layer and monolithic crystals in the outer layer. To assess the performance of the three crystal combinations, we used LSO-LSO as the benchmark for LSO-BGO, and LYSO-LYSO for LYSO-BGO, and LYSO-LSO as the proposed inner-outer layer crystals. ***Results:*** Depending on the material combination, sensitivity modification differs 6,6% for one of the simulated LSO-BGO geometries and up to 167% for one LYSO-BGO geometries, depending on the activity. ***Conclusion:*** The usage of different materials on each layer shows high enhancement of sensitivity for the two investigated LYSO combinations. Further investigation on the coincidence distribution and impact on measurement precision are highly interesting for improving the sensitivity of 2-layer geometries. ***References:*** [1] Ciprian Catana, Development of Dedicated Brain PET Imaging Devices: Recent Advances and Future Perspectives, J. Nucl. Med. 2019 Aug.; 60(8):1044-1052. [2] Hideaki Tashima et al 2019, First prototyping of a dedicated PET system with the hemisphere detector arrangement, 2019 Phys. Med. Biol. 64 065004 [3] Andrea Gonzalez-Montoro et al, Evolution of PET Detectors and Event Positioning Algorithms Using Monolithic Scintillation Crystals, IEEE Transactiom on radiation and plasma medical sciences, Vol. 5, No. 3, May 2021

EPS-087

Survey of Patient Journeys throughout Nuclear Medicine Services

A. Brink[1], *K. Pathmaraj*[2], *M. Marengo*[3], *B. Arends*[4], *Z. Jawa*[5], *R. Jaimovich*[6], *T. Pascual*[7], *S. Rubow*[8], *L. Torres*[9], *S. Vinjamuri*[10], *E. Woodrow*[11], *M. Dondi*[1], *D. Paez*[1];
[1]*International Atomic Energy Agency, Vienna, AUSTRIA,* [2]*Austin Health, Melbourne, AUSTRALIA,* [3]*University of Bologna, Bologna, ITALY,* [4]*Catharina Ziekenhuis, Eindovhen, NETHERLANDS,* [5]*SQUH, Muscat, OMAN,* [6]*Universidada Catolica de Chile, Santiago, CHILE,* [7]*PNRI, Manila, PHILIPPINES,* [8]*University of Stellenbosch, Stellenbosch, SOUTH AFRICA,* [9]*CENTIS, Havana, CUBA,* [10]*Liverpool University Hospital, Liverpool, UNITED KINGDOM,* [11]*Singapore General Hospital, Singapore, SINGAPORE.*

Aim/Introduction: Quality standards in health care are increasing, knowledge and experience in the use of tools for quality management (QM) has to grow accordingly. The International Atomic Energy Agency (IAEA) developed and supported the implementation of the QUality Audits in Nuclear Medicine (QUANUM). The QUANUM portfolio includes the QUANUM

self-assessment and audit-tool, staffing calculator and "the Basics of Quality Management for NM Practices" book, it will be expanded by introducing quality indicators aimed at surveying the overall journey of a patient in a NM Department, integrating the use of patient and referring physician surveys. ***Materials and Methods:*** A QUANUM advisory committee, composed of NM professionals with experience in QM and auditing prepared a Patient Journey Audit Tool (PJAT) based on an audit tool developed and applied at the Department of Molecular Imaging and Therapy, Austin Health, Australia. The IAEA-PJAT, is constructed to monitor all the phases of the process including; referral; procedure justification; booking the appointment; patient and appointment instructions; clinical history assessment; patient consent and preparation; the procedure itself; adverse or unexpected events; deviations from standard practice; post procedure instructions; patient release/discharge; report generation and dissemination. The instrument is suited to monitor diagnostic and therapeutic procedures. "Customer" satisfaction surveys were developed. The patient satisfaction survey comprises 13 questions, with checkboxes to rate an answer and a field for free text comments or suggestions. The referrers survey includes 19 questions, assessing the level of satisfaction of clinical practictioners who refer patients to NM. ***Results:*** The example initiative at Austin Health evaluated over 60 patient journey experiences and resulted in a significant improvement on aspects of medication safety, reducing risk of extravasation and misadministration, helping to keep administered radiopharmaceutical doses under relevant Diagnostic Reference Levels (DRL), and improving timing of NM and PET/CT scans, amongst others. This showed that patient journey audits are essential to prove compliance with regulatory standards, international or national guidelines as well as IAEA recommendations. It is expected that the application of the IAEA-PJAT tool, developed to monitor all the phases of the NM services under the QUANUM umbrella, will contribute significantly to the same goals at a global scale. ***Conclusion:*** The IAEA-PJAT tool will shortly be available at the IAEA's Human Health Campus as a spreadsheet that can be used "as it is" or adapted according to local needs. It is envisaged that this will help improve quality and safety central to patient care.

EPS-088

Development of phantom analysis software package for Japanese Society of Nuclear Medicine PET imaging site qualification program

K. Matsumoto[1], *H. Daisaki*[2], *S. Yoshida*[3], *K. Nishida*[3], *N. Tamaki*[1]; [1]*Kyoto College Of Medical Science, Kyoto, JAPAN,* [2]*Gunma Prefectural College of Health Sciences, Maebashi, JAPAN,* [3]*Nihon Medi-Physics Co.,Ltd., Tokyo, JAPAN.*

Aim/Introduction: The Japanese Society of Nuclear Medicine (JSNM) certifies PET imaging site for the purpose of standardization of imaging methods and improvement of data reliability in PET imaging [1,2]. It is important to confirm phantom test of procedures and meet the criteria prior a PET imaging site certification before. The purpose of this study was to develop an analysis software "PETquactIE (PET quality control tool of image of image evaluate)" for the brain amyloid [3] and the whole-body FDG imaging [4]. ***Materials and Methods:*** The developed analysis software is capable of semi-automatically analyzing the geophysical evaluations in the phantom test procedure, absolute quantitation, resolution, recovery coefficient, contrast, uniformity, image noise etc., and the analysis results can be displayed and saved. A PETquactIE also has a ROI template to calculate contrast in NEMA Body phantom and Hoffman phantom. The method was evaluated on a diverse set of 10 NEMA and 10 Hoffman phantom PET/CT scans. NEMA phantoms were filled with radioactive tracer solution at 4:1 activity ratio over background, and Hoffman phantoms were filled with 20 MBq of ^{18}F solution [2]. This analysis software method was compared to the manual analysis of PET phantom images by JSNM experts. ***Results:*** Results of all analyses were comparable to the JSNM evaluations. ***Conclusion:*** A PETquactIE, which allows easy phantom analysis, was considered a useful tool prior to the PET imaging site certification, and could be also used to set conditions for the PET camera. ***References:*** [1] Senda M. Standardization of PET imaging and site qualification program by JSNM: collaboration with EANM/EARL. Ann Nucl Med. 2020;34(11):873-874. [2] Japanese Society of Nuclear Medicine. Standard PET imaging protocols and phantom test procedures and criteria: executive summary. http://jsnm.org/archives/3561/ Feb 2017. Accessed 24 April 2023 [3] Fukukita H, Suzuki K, Matsumoto K, et al. Japanese guideline for the oncology FDG-PET/CT data acquisition protocol: synopsis of Version 2.0. Ann Nucl Med. 2014;28(7):693-705. [4] Ikari Y, Akamatsu G, Nishio T, et al. Phantom criteria for qualification of brain FDG and amyloid PET across different cameras. EJNMMI Phys. 2016;3(1):23.

EPS-089

Insertion of Synthetic Lesions for the Clinical Assessment of AI-based reconstruction algorithms

Q. Maronnier[1], *A. Latgé*[1], *K. Su*[2], *F. Courbon*[1], *O. Caselles*[1]; [1]*Oncopole Claudius Regaud, Toulouse, FRANCE,* [2]*GE Healthcare, Waukesha, WI, UNITED STATES OF AMERICA.*

Aim/Introduction: Over the past decade, Artificial Intelligence (AI) solutions spread widely in healthcare especially for clinical application. A deep learning software called Precision Deep Learning (PDL) is available in our nuclear medicine department, but not currently used in clinical practice. This solution simulates Time-Of-Flight effect on PET images for the improvement of small lesion detectability. In this study, we assess the first results of its quantitative impact on clinical data using the Insertion of Synthetic Lesions (ISL) method. ***Materials and Methods:*** The study was performed on the Omni Legend (General Electric Healthcare, Waukesha, WI USA). We selected two 18F-FDG cases of different Body Mass Index (BMI) (20 and 32) and used each one as a baseline for the insertion of 8 synthetic lesions distributed in relevant anatomical locations. For each insertion site, we simulated spherical lesions with varying diameters (6, 8 and 10 mm) and contrasts (4:1, 6:1, 8:1 and 10:1). All resulting datasets were reconstructed using Bayesian penalized likelihood (BPL) reconstruction algorithm without and with PDL. We used the three PDL settings: High (H), Medium (M) and Low (L). These parameters correspond to different levels of contrast-enhancement-to-noise trade off [1]. For each clinical case, we calculated the Signal-to-Noise Ratio (SNR) measured from the liver. We also assessed lesions quantitation by measuring SUVmean with spherical VOIs of the same volume as the corresponding synthetic lesions. Finally, we calculated Recovery Coefficient (RC) from theoretical and measured SUV (RC-SUV) and then compared the results obtained according to the reconstruction algorithm. ***Results:*** PDL application showed enhanced SNR calculated from the liver of each patient. The magnitude of this improvement stems from the PDL parameter used (SNR-Native < SNR-PDL-H < SNR-PDL-M < SNR-PDL-L). Regarding SUV metrics of synthetic lesions, we highlighted an average increase of 20% in RC-SUV using PDL-H, 5% with PDL-M and an average decrease of 7% with PDL-L.

Comparing the results obtained for each patient, we observed a significant improvement for the case presenting the highest BMI. ***Conclusion:*** The ISL method is an efficient tool for assessing the impact of new AI-based software solutions through ground truth. ***References:*** [1] Mehranian A, Wollenweber SD, Walker MD, Bradley KM, Fielding PA, Huellner M, et al. Deep learning-based time-of-flight (ToF) image enhancement of non-ToF PET scans. Eur J Nucl Med Mol Imaging. 2022 Sep 1;49(11):3740-9.

EPS-090

Anatomy-based correction of kidney PVE on ^{177}Lu SPECT images

J. Salvadori[1], *O. Allegrini*[1], *I. Namer*[1,2];
[1]*Institut de cancérologie Strasbourg Europe (ICANS), Strasbourg, FRANCE,* [2]*ICUBE UMR 7357, Strasbourg, FRANCE.*

Aim/Introduction: In peptide-receptor-radionuclide-therapy (PRRT), accurate quantification of kidney activity on post-treatment SPECT images paves the way for patient-specific treatment. Due to the poor spatial resolution of SPECT images, partial volume effect (PVE) is one of the most important quantitative biases. Thanks to PET research in this area, effective anatomy-based PVE correction techniques are freely available. In this study, we aimed to evaluate the possibility to use these methods for SPECT modality and their performances to recover the accurate activity concentration of realistic kidney geometries on ^{177}Lu SPECT images recorded in clinical condition. ***Materials and Methods:*** Based on the patients' CT scan data, three pairs of fillable kidneys with surface area-to volume ratio ranging from 1.5 to 2.8 cm^{-1}, were 3D printed. A modular fixation system dedicated to the IEC phantom was also modeled and printed. Fully quantitative ^{177}Lu SPECT/CT recordings were performed for the three modified IEC phantoms and for 6 different kidney-to-background ratios (KBRs: 2, 4, 6, 8, 10, 12) using our optimized clinical protocol for ^{177}Lu-DOTATATE. Two VOI-based [Geometric Transfert Matrix (GTM) and Labbé (LAB)] and three voxel-based [iterative Yang (IY), multi-target correction (MTC) and region-based voxel-wise correction (RBV)] methods were evaluated on this data set. The kidney recovery coefficients (RCs) were determined from anatomical CT-based segmentations. Additionally, background RC was determined for voxel-based method by using the background ROIs defined in the image quality test of the NEMA NU-2 2018 protocol. ***Results:*** For all recordings, accurate background quantification was achieved with RCs ranged 0.99 to 1.06 (mean 1.04). Without PVE correction, the kidney RCs ranged from 0.62 to 0.84 (mean 0.75). For a KBR of 12, all anatomy-based method were able to recover the kidneys activity concentration with an error < 7%. All methods had a similar degradation of performances with decreasing KBR. Compared with a KBR of 12, the average loss of recovery was 3, 8, 13, 26, and 56% for KBRs of 10, 8, 6, 4, and 2, respectively. The LAB method was the less sensitive to PSF mismatch (mean positive bias of 10% for an overestimation of 4 mm). All others methods had the same behavior (mean positive bias of 14% for an overestimation of 4 mm). Among the voxel-based methods, IY and RBV performed better than MTC in the vicinity of high-gradient areas. ***Conclusion:*** Anatomy-based PVE correction enable accurate SPECT quantification of the ^{177}Lu activity concentration inside realistic kidney geometries.

EPS-091

The optimum earliest total-body 68Ga-FAPI-04 PET scan timing: An evidence-based single-centre study

Z. Zheng*, H. Gao, Y. Lin, H. Yu, W. Mao, R. Yang, Y. He, X. Chen, H. Wu, P. Hu, H. Shi;*
Zhongshan Hospital, Fudan University, Shanghai, CHINA.

Aim/Introduction: We aimed to investigate the optimum earliest positron emission tomography (PET) scan timing after ^{68}Ga-fibroblast activation protein inhibitor-04 (^{68}Ga-FAPI-04) injection to shorten patients' waiting time, reduce patient discomfort, and improve the diagnostic workflow. ***Materials and Methods:*** In this prospective study, we enrolled 30 patients with suspected malignant tumours who underwent 60-min dynamic ^{68}Ga-FAPI-04 total-body PET/CT scans with reconstruction at 10-min intervals (G0-10, G10-20, G20-30, G30-40, G40-50, and G50-60) and evaluated the ^{68}Ga-FAPI-04 uptake patterns. The standardised uptake value (SUV), the liver signal-to-noise ratio (SNR), and the lesion-background ratios (LBRs) for the different time windows were calculated to evaluate image quality and lesion detectability. The 30-40 min period was then split into 5-min intervals starting from every minute for further evaluation of image quality. The G50-60 values were considered as the reference. ***Results:*** The SUVmean of normal organs decreased with time. In the images reconstructed at 10-min intervals, the liver SNR decreased with time. Longer acquisition times were associated with lower background uptake and better image quality. Some lesions could not be detected until G30-40. The lesion detection rate, uptake, and LBRs of all lesions did not differ significantly among the G30-40, G40-50, and G50-60 scans (all $P > 0.05$). The SUVmean and LBRs of primary tumours in the reconstructed images obtained at 5-min intervals between 30 to 40 min did not differ significantly; however, for metastatic and other positive lesions, the G34-39 and G35-40 images showed significantly better SUVmean and LBRs than the other images. The G34-39 and G50-60 scans showed no significant differences in lesion uptake, LBRs, and lesion detection rate (all $P > 0.05$). ***Conclusion:*** The optimum earliest time point to start acquisition was 34-min after injection of ^{68}Ga-FAPI-04. With a reasonable acquisition time, the image quality could still meet diagnostic requirements.

EPS-092

Comparison of a 3D printed wall-less phantom with a conventional NEMA phantom for establishing threshold-based segmentation methods

A. Zounek[1], *A. Zatcepin*[1,2], *A. Delker*[1], *F. Gildehaus*[1], *A. Bollenbacher*[1], *G. Böning*[1], *P. Bartenstein*[1,2], *N. L. Albert*[1,3,4], *S. Ziegler*[1], *L. Kaiser*[1];
[1]*Department of Nuclear Medicine, University Hospital, LMU Munich, Munich, GERMANY,* [2]*German Center for Neurodegenerative Diseases (DZNE), Munich, GERMANY,* [3]*German Cancer Consortium (DKTK), Partner Site Munich, German Cancer Research Center (DKFZ), Munich, GERMANY,* [4]*Bavarian Cancer Research Center (BZKF), Erlangen, GERMANY.*

Aim/Introduction: Phantoms are an important tool for quality control and calibration of PET systems. Performance measurements are routinely performed according to NEMA standards using phantom designs with fillable inserts. However, previous studies have shown that inactive walls may lead to quantification errors for non-zero background signal [1]. The aim of this work was to confirm whether the NEMA phantom can be reliably applied to establish or validate threshold-based segmentation methods. This was achieved by comparing phantom measurements using the

NEMA NU-2001 PET body phantom with measurements using 3D printed and thus wall-less radioactive spheres [2]. ***Materials and Methods:*** The 3D printed phantom was designed in CAD software to resemble NEMA specifications and manufactured using a stereolithography printer. Radioactive spheres were obtained by mixing [^{18}F]FDG with the resin before printing. Images were acquired on a Siemens Biograph mCT PET/CT system with two different background fractions (BF_{3D}) of 0.12 and 0.6. To ensure comparability, PET images of the NEMA phantom were acquired according to the EARL accreditation protocol with BF_{EARL}=0.1. The conventional NEMA and the 3D printed phantoms were compared using background-corrected volume reproducing thresholds (VRT). ***Results:*** The VRT values were similar for both phantoms in the high contrast images (BF_{EARL}=0.1 and BF_{3D}=0.12), ranging from 45% to 50% for all six sphere diameters with a mean percentage difference of 3%. VRT values were also similar for both measurements of the 3D printed phantom (BF_{3D}=0.12 and 0.6), ranging from 37% to 50% with a mean percentage difference of 7%. ***Conclusion:*** The feasibility of 3D printing as a method for producing radioactive wall-less objects as demonstrated in previous studies [2] was confirmed successfully. The high-contrast NEMA phantom measurement using fillable spheres yielded almost identical VRTs as the measurement with the wall-less spheres phantom and is therefore equally suitable for the validation of threshold-based segmentation methods. Moreover, the measured phantom data confirm the theoretical findings of Hofheinz et al. [1], indicating a low influence of cold walls for high contrast images and predicting that VRT is independent of BF in wall-less phantoms. Objects of higher geometrical complexity and lower contrast, which are potentially stronger affected by wall-related effects, can easily be produced in the future using 3D printing. ***References:*** 1.Hofheinz et al. Effects of cold sphere walls in PET phantom measurements on the volume reproducing threshold. Physics in Medicine and Biology. 2010;55(4):1099-113.2.Gillett et al. 3D printing 18F radioactive phantoms for PET imaging. EJNMMI Physics. 2021;8(1).

EPS-093

Discrepancies in commercial Y-90 vial's activity assessments: Monte Carlo simulations provide a possible explanation

L. Auditore[1,2], *D. Pistone*[1,2], *A. Italiano*[3,4], *E. Amato*[1,2], *S. Gnesin*[5]; *[1]Department of Biomedical and Dental Sciences and of Morphofunctional Imaging (BIOMORF), University of Messina, Italy, Messina, ITALY, [2]INFN, National Institute for Nuclear Physics, Section of Catania, Italy, Catania, ITALY, [3]Istituto Nazionale di Fisica Nucleare (INFN) - Sezione di Catania, Catania, ITALY, [4]Department of Mathematical and Computer Science, Physical Sciences and Earth Sciences (MIFT), University of Messina, Italy, Messina, ITALY, [5]Institute of Radiation Physics, Lausanne University Hospital and University of Lausanne, Lausanne, SWITZERLAND.*

Aim/Introduction: Selective Internal RadioTherapy (SIRT), also known as Trans-Arterial RadioEmbolization (TARE), performed with resin/glass ^{90}Y-labeled microspheres, is currently employed worldwide and an accurate determination of the therapeutic administered activity is key in dose/response studies aiming at the optimization of the treatment safety and efficacy. In a recent multicentre study [1] discrepancies between PET/CT measured activity and vendor-calibrated activity for ^{90}Y glass and resin microspheres were found. This study investigated the possible origin of these discrepancies using Monte Carlo (MC) simulations. ***Materials and Methods:*** We used the GAMOS MC software to model three vial configurations: ^{90}Y-chloride, ^{90}Y-labeled glass and resin microspheres, hosted in a commercial activity-meter. For the three considered configurations, we estimated the electric signal per unit of activity (I) generated in the active volume of the activity-meter.We additionally considered the production of Internal Bremsstrahlung (IB) photons, accompanying the beta decay. IB was demonstrated [2,3] playing a relevant role in determining the response of an activity-meter. The electric currents obtained for ^{90}Y glass (I_{glass}) and resin (I_{resin}) microspheres were compared in terms of relative percent difference respect to that of ^{90}Y-chloride (ε_{glass} and ε_{resin}), and each other (δ). The findings of this work were then compared with the experimental results from the PET multicentre study. ***Results:*** The relative percent differences, ε_{glass} and ε_{resin}, resulted to be (30.7±5.2)% and (-17.2±2.5)% respectively, while δ was (57.8±2.4)%. By including IB in the source term the estimates of ε_{glass}, ε_{resin}, and δ become (24.6±3.9)%, (-15.0±2.2)% and (46.5±1.9)%, respectively. The relative percent difference between glass and resin microsphere activity calibrations, δ^*, obtained by Gnesin et al. [1] is (46.00±0.15)% in a remarkable good agreement with the MC estimates including IB contribution. ***Conclusion:*** Our results corroborate and potentially explain the results reported in a recent multicentre study [1]. The MC simulation estimates indicate that the different geometry of the specific commercial vials and the metrological approach adopted for activity-meter calibration with ^{90}Y chloride liquid source can explain the reported PET-based experimental discrepancies. Furthermore, IB photons confirmed to play a relevant role in accurately determining the response of the activity-meter. ***References:*** [1] Gnesin S et al. J Nucl Med. 2022;jnumed.122.264458.[2] Italiano A et al. Phys Med. - EJMP 2020;76:159-165.[3] Auditore L et al. Phys Med. - EJMP 2021;90:158-63.

EPS-094

Characterization of an innovative small animal PET scanner based on a proprietary acquisition method

F. M. Ribeiro[1], *P. M. C. C. Encarnação*[1], *P. M. M. Correia*[1], *A. L. M. Silva*[1], *A. X. Pinto*[1], *R. G. Oliveira*[1], *A. C. M. Magalhães*[1], *J. Sereno*[2], *A. Abrunhosa*[2], *I. F. Castro*[3], *J. F. C. A. Veloso*[1]; *[1]Institute for Nanostructures, Nanomodelling and Nanofabrication (i3N), Department of Physics, University of Aveiro, Aveiro, PORTUGAL, [2]Institute for Nuclear Sciences Applied to Health (ICNAS), University of Coimbra, Coimbra, PORTUGAL, [3]Radiation Imaging Technologies Lda. (RI-TE), University of Aveiro Incubator, PCI - Creative Science Park, Ílhavo, PORTUGAL.*

Aim/Introduction: The easyPET.3D [1] is a benchtop Positron Emission Tomography (PET) scanner dedicated to high-resolution imaging of mice, with an exclusive scanning method based on a U-shape board with two axes of motion and two modules of detectors always face-to-face. We present the scanner's performance evaluation following the National Electrical Manufacturers Association (NEMA) NU 4-2008 standard [2]. ***Materials and Methods:*** Each detector module of the scanner consists of a 32 × 2 pixelated LYSO scintillator array with individual crystals measuring 2.0 × 2.0 × 30 mm^3. The crystal arrays are coupled to 1.3 × 1.3 mm^2 silicon photomultipliers via one-to-one coupling. The transaxial field-of-view (FOV) is adjustable up to 50 mm diameter and the axial length of 72 mm is suitable for imaging whole-body mice. The performance characterization includes the spatial resolution, sensitivity, counting rate performance, scatter fraction, and image quality characteristics. Furthermore, mice were scanned to evaluate the in vivo imaging capability of the easyPET.3D scanner. ***Results:*** The measured spatial resolution at the center of the axial FOV in radial, tangential, and axial directions using full width at half-maximum was 0.94, 0.99 and 0.81 mm

(0.77 mm^3), respectively. A peak absolute sensitivity of 0.20% was measured for 100-700 keV energy window. The peak noise equivalent counting rate for the mouse-like phantom was 177 cps at 7 MBq (350-650 keV). The recovery coefficients for 5, 4, 3, 2, and 1 mm diameter rods in the image quality phantom were: 0.64, 0.62, 0.45, 0.23, and 0.15, respectively. The uniformity was 14% and the spill-over ratios in the images of air and water filled chambers were 0.08 and 0.02, respectively. In the additional in vivo experiments, small structures such as striatum in brain imaging and vertebras in bone imaging were resolved proving the scanner's suitability for mice high-resolution molecular imaging. ***Conclusion:*** The easyPET.3D scanner provides a significant improved spatial resolution (0.87 mm^3 at a radial offset of 5 mm) over current commercially available preclinical PET scanners (<1-14.2 mm^3 at a radial offset of 5 mm). The system is suitable for the low range of activities used for small animal imaging. The overall performance showed that the easyPET.3D can produce high-quality images for preclinical applications. ***References:*** [1] https://www.ri-te.pt/[2] NEMA Standards Publication NU 4-2008, "Performance Measurements of Small Animal Positron Emission Tomographs," National Electrical Manufacturers Association, Rosslyn, 2011.

EPS-095

Triple and dual PET quantification of a Small-Animal Multi-Pinhole PET/SPECT/CT System

P. Echegoyen*, T. Cuenca Bandín, M. Ecay, E. Prieto, M. Collantes, F. Pareja, J. Simón Martínez, I. Peñuelas, J. Martí-Climent;*
Clínica Universidad de Navarra, Pamplona, SPAIN.

Aim/Introduction: Small animal devices offer the possibility to image multiple isotopes simultaneously. However, quantitative accuracy might be affected by physical interferences. The aim was to evaluate quantitative accuracy of dual- and triple-isotope simultaneous acquisitions, combining gamma and positron emitters in a small animal PET/SPECT/CT scanner. ***Materials and Methods:*** Initially, system performance for each of the three isotope under investigation (^{111}In, ^{99m}Tc and ^{18}F) was characterized in terms of sensitivity, energy resolution and spatial resolution using standard procedures. Then, micro test tubes (~0.17 mL) were filled 4 to 6 MBq of ^{111}In, ^{99m}Tc and ^{18}F. A custom methacrylate phantom was built to place the different sources in adjacent positions and to facilitate the positron annihilation. These sources were acquired individually, and then all possible dual and triple combinations were scanned. Triple acquisition was repeated switching relative positions of the sources. All data were acquired in list-mode with 1 min/bed position. Images were reconstructed with 20% window width for all photopeaks except for the 171 keV ^{111}In photopeak for which window width was reduced to 15% to avoid overlapping with the 140 KeV photopeak. Images were reconstructed using SROSEM algorithm with filter and voxel size adapted to each radionuclide including decay, scatter and attenuation corrections. Calibration factors, previously obtained from individual sources following manufacturer protocol, were used to convert counts into activity. Images were analyzed with PMOD 4.2. Then, total activity observed in the image for each isotope was calculated and compared to the expected activity. Deviations less than 10 % were considered for acceptance. ***Results:*** Energy resolutions were 10.1% for 140 keV, 10.2% for 171 keV, 10.0% for 245 keV and 8.5% for the 511 keV peak. Measured sensitivities are 0.6 % for ^{99m}Tc, 0.8 for ^{111}In and 0.4 % for ^{18}F. Spatial resolution of gamma emitters was better (0.8 mm for ^{99m}Tc and 0.9 mm for ^{111}In) than for ^{18}F (1.1 mm). Quantification errors obtained for the single acquisitions were [-0.8, 4.8] %. For dual acquisitions, error increased slightly to [-6.8, 7.1] % being higher for ^{99m}Tc and ^{111}In affected by Compton scattering of higher energy photons. The same tendency was observed for the triple-isotope scan, where quantification error increased to [1.1, 8.8] %. ***Conclusion:*** Quantitative accuracy was preserved in simultaneous dual- and triple-isotope PET/SPECT acquisitions despite physical interferences between isotopes.

EPS-096

ComBat harmonization in different PET imaging scenarios

M. Gandia-Ferrero*[1], I. Torres-Espallardo[2,1], S. Prado-Wohlwend[2], B. Martínez-Sanchis[2], E. Muñoz[3], C. Morera[3], P. Bello-Arques[2], M. Vázquez-Martínez[2], S. Ginés-Cárdenas[1], Á. Almendros-Riaza[1], L. Martí-Bonmatí[2,1];*
[1]Health Research Institute La Fe, Valencia, SPAIN,
[2]La Fe University and Polytechnic Hospital, Valencia, SPAIN, [3]Oncovision, Valencia, SPAIN.

Aim/Introduction: The extraction of quantitative information from PET images is fundamental and aids in the establishment of objective threshold values. Nowadays, different PET systems provide varying quantitative values based on many scanner parameters. Due to the increasing number of PET procedures, many hospitals have different PET devices in the same center, so there is a need to harmonize these images to get reproducible results regardless of the device. The main aim of this study is to evaluate the potential effects of harmonizing key features extracted from PET images on the diagnosis outcomes. ***Materials and Methods:*** Harmonization was performed in 2 different scenarios: for an oncology and a neurology application. In the former, 25 [68Ga]Ga-DOTA-TOC PET images form patients with uncommon neuroendocrine tumours were acquired in the same day both on a PET/CT and a PET/MR device. Since tumour uptake must be greater than the liver uptake for [177Lu] Lu-DOTA-TATE Peptide Receptor Radionuclide Therapy to be considered, SUVmax measurements from the liver and 125 lesions were harmonized between both scanners. The kappa coefficient was calculated to compare the devices agreement. In the latter, 80 [18F]FDG PET brain images were acquired in the same day both on a PET/CT and a brain-dedicated PET scanner. Since for the diagnosis of neurology diseases the SUVr values are used, those of 27 brain ROIs were harmonized between both devices. Bland-Altman analysis for each ROI was performed before and after harmonization. All data was collected from the Nuclear Medicine service of our hospital. The harmonizing technique used for the analysis was ComBat. Three different reference systems have been used for harmonization, including using each device and an arbitrary reference. ***Results:*** The kappa coefficient (k) assessed on the [177Lu]Lu-DOTA-TATE therapy consideration before harmonization was k = 0.54 (moderate agreement), and after harmonization, selecting the PET/CT, the PET/MR, and an arbitrary reference system, k was equal to 0.68 (substantial agreement), 0.04, and 0.19 (insignificant agreement), respectively. In contrast, on the harmonization of the 28 ROI SUVr values between PET/CT and brain-dedicated PET, while the Bland-Altman analysis revealed differences when comparing between both devices (e.g. Basal_Ganglia_Right: 15%; average difference: 6%) excellent results were provided after harmonization (average differences: 0%) whatever reference system was selected. ***Conclusion:*** Harmonization is a powerful tool that should be used when comparing results from different scanners to obtain information that can provide a reproducible analysis. However, choosing the appropriate variables to harmonize is crucial.

EPS-097

Elimination of not yet Reported Artifacts in Myocardial Perfusion Imaging Studies on Semiconductor Cardiac Gamma Camera by Covering Radiopharmaceutical Injection Site with a Shield

A. Owczarek[1], *P. Cichocki*[1], *Z. Adamczewski*[1], *A. Plachcinska*[2]; *[1]Nuclear Medicine Department, Medical University of Lodz, Lodz, POLAND, [2]Department of Quality Control and Radiological Protection, Medical University of Lodz, Lodz, POLAND.*

Aim/Introduction: Myocardial perfusion imaging (MPI) is one of the most common studies in nuclear medicine used in diagnosis of coronary artery disease (CAD). Dedicated cardiac gamma cameras with semiconductor detectors perform MPI faster and acquire higher quality images than traditional cameras. However, while working on the device for a long time, a previously unreported artifact, caused by residual activity of the radiopharmaceutical in injection site (RAiIS) in cubital fossa caught in the camera field of view (FOV) was observed. ***Materials and Methods:*** Study included 39 patients, referred for MPI using Discovery NM 530c cardiac gamma camera in last quarter of 2022, in whom RAiIS was observed in stress or rest study. In such cases image acquisition was immediately repeated, without moving the patient or changing camera settings, with injection site covered by a thyroid shield with extra layers of lead (4,5mm in total). All 39 patients were male, aged 40 to 83, and examined in routine, two day stress-rest protocol in prone position, with head and arms placed on a dedicated support. Acquired images were assessed by two experienced nuclear medicine physicians (separately for studies with and without the shield) and evaluated using a 0-4 point scale in each segment (where 0 - normal perfusion and 4 - total absence of perfusion). Summed stress, rest and difference scores (SSS, SRS and SDS, respectively) were calculated for the whole myocardium and 3 main vascular territories. ***Results:*** SSS, SRS and SDS were assessed as abnormal most often in RCA territory, least often in LCx territory. Activity in injection site was observed more often in stress studies (31/39 cases). Elimination of this artifact changed the assessment of SSS, SRS or SDS from normal to abnormal or vice versa in almost 20% of studies. LAD and RCA vascular territories were affected the most often. For stress-induced perfusion defects, in 8% of assessed vascular territories initially found defects were no longer present after applying the shield, while in 5% using the shield revealed previously invisible defects. ***Conclusion:*** Artifacts caused by RAiIS reduce the image quality and can potentially generate or obscure perfusion defects. They can be observed in patients examined in prone position, with radiopharmaceutical injected in the area of cubital fossa. Lead shield used in this study effectively mitigated them. Using such shielding or avoiding cubital fossa as injection site should be considered in patients examined in prone position.

EPS-098

Match/mismatch between aortic Na[^{18}F]F uptake on PET and macrocalcifications on CT

G. van Praagh[1], *M. Davidse*[2], *J. M. Wolterink*[2], *R. H. J. A. Slart*[1]; *[1]University Medical Center Groningen, Groningen, NETHERLANDS, [2]University of Twente, Enschede, NETHERLANDS.*

Aim/Introduction: Sodium[^{18}F]fluoride (Na[^{18}F]F) has been shown to bind to active atherosclerotic processes. The evidence on the presentation of vascular Na[^{18}F]F in clinical PET/CT is limited. Therefore, the aim of this study is to establish a match/mismatch score between calcified plaque content on CT and Na[^{18}F]F-uptake on PET in the aorta. ***Materials and Methods:*** In total, 186 Na[^{18}F]F-PET/CT scans were retrospectively collected. The aorta was manually segmented on low-dose CT from the aortic valve to the iliac bifurcation. A publicly available deep learning algorithm was used to segment the vertebrae in each CT image.[1] The vertebral mask was dilated by 10 mm and subtracted from the aortic mask to avoid skeletal spill-over of Na[^{18}F]F. For each patient, calcium HU values were retrieved using a 130 HU threshold on CT and Na[^{18}F]F-hotspot values using an adaptive 50% SUV_{peak} threshold on PET. To get a population image of the distribution of these values, all aortic masks were registered onto one patient using SimpleElastix.[2] Heatmaps for Na[^{18}F]F-uptake and calcium were made by obtaining a surface mesh and projecting the masks from the centerline onto the surface. For every surface point, a Spearman's correlation with Bonferroni correction was done between calcium values and Na[^{18}F]F values of that point and its 500 closest points. Besides, in every slice in every patient, target-to-bloodpool ratios (TBR) were calculated within the calcium masks and in the aortic wall except the calcium masks. ***Results:*** A strong positive correlation (r=0.77, P<0.0001) was found between the calcium values and Na[^{18}F]F values on the population image. Of all locations, 79% had a correlation above zero (63% P<0.05), of which 25% above 0.6 (all P<0.05), whereas 21% was below zero (9% P<0.05) and 0% below -0.6. Calcifications were most clearly present in the inferior abdominal aorta and the inferior aortic arch. For most Na[^{18}F]F-uptake this was similar (match), but also in the superior abdominal aorta. Significantly higher TBR values were found outside the calcium masks than inside the calcium masks (P<0.0001) (mismatch). ***Conclusion:*** This in-depth analysis of clinical Na[^{18}F]F-PET/CT images demonstrated a high match in location of macrocalcifications detectable on CT and Na[^{18}F]F-uptake on PET. Contrarily, a mismatch was found of uptake inside and outside the macrocalcifications. This might suggest that Na[^{18}F]F is taken up in noncalcified plaques, but not in late-phase calcified plaques. The population image provides additional insight in the uptake pattern of Na[^{18}F]F in the population. ***References:*** 1. doi:10.1016/j.media.2019.02.005; 2. doi:10.1109/CVPRW.2016.78

EPS-099

Metabolic connectivity changes of patients with post-COVID-19 condition: a reorganization of the olfactory cognitive pathway?

M. Doyen[1,2], *T. Horowitz*[3], *A. Bruyere*[4], *F. Goehringer*[4], *A. Verger*[1,2], *E. Guedj*[3]; *[1]Department of Nuclear Medicine and Nancyclotep Imaging Platform, CHRU Nancy, F-54000 Nancy, FRANCE, [2]Université de Lorraine, IADI, INSERM U1254, F-54000 Nancy, FRANCE, [3]Nuclear Medicine Department, Aix-Marseille University, APHM, CNRS, Centrale Marseille, Institut Fresnel, Timone Hospital, CERIMED, Marseille, France, Marseille, FRANCE, [4]Department of Infectious Diseases, CHRU Nancy, 54000, Nancy, FRANCE.*

Aim/Introduction: Post-COVID-19 condition could be associated with a brain network impairment from olfactory pathway. The aim of this study was to evaluate the metabolic changes of connectivity in post-COVID-19 conditions patients. ***Materials and Methods:*** One hundred and eighty patients (48.5±11.8 years old, 112 women) with post-COVID-19 condition having performed a brain 18F-FDG PET in two French centers (113 in Marseille, 67 in Nancy) were included. Brain 18F-FDG PET scans of patients were compared with age and sex-matched healthy controls (respectively 56 and 64 in Marseille and Nancy) using voxel-to-voxel groups comparisons. Metabolic connectivity of post-COVID-19 condition patients, as compared to those of

healthy controls, was studied through seed correlations of the maximal cluster extracted from the group's comparisons and sparse inverse covariance estimations (SICE). ***Results:*** Patients with post-COVID-19 condition showed hypometabolisms in the bilateral temporal lobes with a right predominance, the right thalamus, the right fronto-orbital cortex, the brainstem and the cerebellum (p-voxel<0.005, corrected for the cluster volume). Seed correlations from the maximal hypometabolic cluster involving the right temporal lobe and the cerebellum showed increased connectivity with the cerebellum and the left thalamus and decreased connectivity with bilateral temporal lobes and the prefrontal cortex especially in the olfactory gyri. SICE confirmed these findings with an increase connectivity between the prefrontal cortex, the cerebellum, the thalamus and the brainstem, observed in both the whole population and in each center respectively, and a decreased of connectivity of temporal lobes, especially the right one, with the right fronto-orbital cortex. ***Conclusion:*** The study of metabolic connectivity in post-COVID-19 conditions patients shows a switch of connectivity within the hypometabolic post-COVID-19 network with a decrease of connectivity from the temporal lobes, preferentially the right one and with the olfactory cortex and an increase of connectivity within the cerebellum, the thalamus and the brainstem. These findings suggest a reorganization of the cognitive olfactory pathway.

EPS-100

Impact of ^{68}Ga-specific PET Reconstruction on Image Quality of Patient Data

P. Gavriilidis[1,2,3], *A. Marinus*[4,1], *M. Koole*[3], *T. W. Deller*[5], *F. P. Jansen*[5], *F. M. Mottaghy*[6,1,2], *R. Wierts*[1,2];
[1]*Maastricht University Medical Center, Maastricht, NETHERLANDS,* [2]*Maastricht University, Maastricht, NETHERLANDS,* [3]*Katholieke Universiteit Leuven, Leuven, BELGIUM,* [4]*Eindhoven University of Technology, Eindhoven, NETHERLANDS,* [5]*GE HealthCare, Waukesha, WI, UNITED STATES OF AMERICA,* [6]*RWTH University Hospital, Aachen, GERMANY.*

Aim/Introduction: In recent years, the utilization of ^{68}Ga in clinical positron emission tomography (PET) imaging has increased. However, in comparison to the commonly used ^{18}F, ^{68}Ga features higher positron range (PR) affecting image quality. We present a positron range correction (PRC) method to enhance ^{68}Ga PET image quality and quantification. ***Materials and Methods:*** The PR distribution profile of ^{68}Ga in water was determined using Monte Carlo simulations and modeled as a spatially invariant Gaussian function. Of this function, the FWHM was calculated. PRC was performed by adding this to the Gaussian filter applied in the image space of the Hybrid-Space PET Point Spread Function (Hybrid PSF) [1] after subtracting the FWHM of ^{18}F. ^{68}Ga-specific Hybrid PSF (^{68}Ga-specific PSF) reconstructions were introduced as corrections to OSEM+PSF (2 iterations, 34 subsets) and Q.Clear (β=700) and were compared to the clinical used non-corrected corresponding reconstructions. The SUVmean (50% threshold of SUVmax) and SUVpeak (1 mL sphere with highest uptake) were calculated for 38 lesions from 10 patients administered with ^{68}Ga-PSMA or ^{68}Ga-DOTATOC. For each lesion, the contrast-to-noise ratio (CNR) was defined as the difference between the mean lesion activity concentration and mean background activity concentration scaled by the background noise. Wilcoxon signed rank test (α=0.05) was performed. ***Results:*** Analysis on all lesion showed that for both OSEM and Q.Clear reconstructions ^{68}Ga-specific PSF significantly increased the CNR (16%; 11%) and SUVpeak (3%, 7%). For OSEM, ^{68}Ga-specific PSF reconstructions showed similar increase in CNR (15-17%) and SUVpeak (3%) for ^{68}Ga-DOTATOC and ^{68}Ga-PSMA (both 19 lesions). For Q.Clear, ^{68}Ga-specific PSF showed higher increase for ^{68}Ga-DOTATOC compared to ^{68}Ga-PSMA the CNR (13% vs 9%) and similar increase for SUVpeak (6-8%). SUVmean values only showed significant increase for Q.Clear (9% ^{68}Ga-DOTATOC, 3% ^{68}Ga-PSMA), but not for OSEM which can be explained by a slower rate of convergence of the ^{68}Ga-specific PSF reconstruction. For both OSEM and Q.Clear, lung lesions (4 lesions) showed smaller, non-significant, changes in CNR (6% OSEM, 6% Q.Clear) and SUVpeak (-1% OSEM, 5% Q.Clear) compared to the significant changes observed in soft-tissue (26 lesions; CNR:17% OSEM, 10% Q.Clear; SUVpeak:3% OSEM, 6% Q.Clear) and bone lesions (8 lesions; CNR:16% OSEM, 17% Q.Clear; SUVpeak: 6% OSEM, 10% Q.Clear). ***Conclusion:*** PRC of ^{68}Ga improves the quality and quantification of ^{68}Ga PET patient data. ***References:*** [1] T. W. Deller et al., IEEE Nucl Sci Symp Conf Rec, 2021, pp. 1-5.

EPS-101

Clinical evaluation of a deep learning-based CT-free attenuation and scatter correction

S. Xue[1], *H. Zhou*[1], *R. Guo*[2], *M. Viscione*[1], *A. Rominger*[1], *B. Li*[2], *K. Shi*[1];
[1]*University of Bern, Bern, SWITZERLAND,* [2]*Shanghai Jiao Tong University School of Medicine, Shanghai, CHINA.*

Aim/Introduction: The burden of ionizing radiation is a significant concern in the practice of positron emission tomography/computed tomography (PET/CT) imaging, which limits its application in many situations. Deep learning (DL)-based methods have been proposed as a substitute for CT-based PET attenuation and scatter correction for CT-free PET imaging [1]. However, evaluation based on physical metrics alone is inadequate. The purpose of this study is to systematically evaluate the clinical potential of the developed CT-based PET attenuation and scatter correction method. ***Materials and Methods:*** Whole body PET images of 359 patients using ^{18}F-FDG, ^{18}F-PSMA, ^{68}Ga-DOTA-TOC, ^{68}Ga-DOTA-TATE, ^{68}Ga-FAPI, acquired with clinical PET scanners, including Biograph Vision (Siemens Healthineers), United Imaging uMI 780 (United Imaging), Discovery MI (General Electric Healthcare) in Shanghai and Bern, were included for the clinical evaluation. DL-corrected PET images were compared to reference locations of clinically or pathologically proven metastases to determine the normalization score for each lesion and the normalization score for each case. ***Results:*** Among all tested methods, the Decomposition-based DL method achieved the highest mean score (98.9), outperforming both the conventional 2D DL (90.9) and 3D DL (77.8). From the CT-based corrected PET scans, a total of 1018 lesions were detected, with the highest number of true positive markings observed for the Decomposition-based DL method (965), followed by 2D (820) and 3D (765) DL. False positives were also detected for some cases (117 for 2D, 125 for 3D, and 65 for Decomposition-based DL). Case studies of uptake lesions revealed the superior lesion detection sensitivity of the Decomposition-based DL method, particularly in internal organs such as the liver, lungs, and spine. ***Conclusion:*** The clinical evaluation of various external imaging tracers on different scanners confirms the effectiveness and robustness of the Decomposition-based DL method, although the observed missing lesions in some cases require further development. ***References:*** [1] Guo, R. et al., Nat Communications 13, 5882 (2022).

EPS-102

Influence of coils and attenuation correction methods on the performance and image quality of a preclinical PET/MR insert

C. Kuntner[1], *J. Friske*[1], *A. Stessl*[2], *M. Haas*[3], *L. Breyer*[1], *T. Wanek*[1], *M. Hacker*[1], *T. Helbich*[1], *I. Rausch*[1];
[1]Medical University of Vienna, Vienna, AUSTRIA, [2]University of Applied Science, Wiener Neustadt, AUSTRIA, [3]Bruker BioSpin Preclinical Imaging Division, Ettlingen, GERMANY.

Aim/Introduction: Quantitative PET/MR imaging relies on applying different corrections to the PET data to obtain reliable and reproducible results. These corrections typically include normalization, decay correction, randoms correction, scatter- and attenuation correction whereby the last two rely on the knowledge of the material distribution within the scanner. In simultaneous PET/MR scanners, attenuation correction (AC) can be deduced from the MR images and predefined attenuation templates of hardware parts. However, MR-based AC is still not optimized for any imaging, and the RF coils within the PET field-of-view (FoV) may influence the scanner's performance. Therefore, the aim was to test the influence of coils and AC on the performance of a preclinical PET/MR insert. ***Materials and Methods:*** Scanner performance was evaluated using the NEMA NU-4-2008 [1] standard for assessing sensitivity, spatial resolution, noise-equivalent count (NEC) rate, and image quality. All measurements were done with three different RF coils within the PET FoV: mouse-dedicated, rat-dedicated (not PET-optimized), and big-rat-dedicated coil. In addition, the accuracy of the AC was quantitatively tested using homogeneously filled phantoms of different sizes and activity. ***Results:*** Peak absolute sensitivity depended on the presence of the different coils, whereas the spatial resolution measurements did not depend on the coils' presence. The mouse phantom NEC curve (peak 441.2 kcps at 29.3 MBq) was highest when the mouse-dedicated coil was in place. The rat phantom-based NEC curve was tested using only the rat-dedicated coils and exhibited the NEC peak of 203.1 kcps at 27.5 MBq (big-rat-dedicated coil). Activity concentrations in the NEMA IQ phantom were underestimated when using standard MR-AC, which was attributed to the absence of the phantom walls in the generated μ-maps. For the uniformly filled phantoms with wall thicknesses <1 mm, AC works fine. ***Conclusion:*** We conclude that the presence of the RF coils only slightly influences the performance of the PET/MR insert, with the most prominent variation seen for the not PET-optimized coil. AC based on generated μ-maps performed well for the uniformly filled phantoms with negligible wall size. ***References:*** [1] National Electrical Manufacturers Association. NEMA Standard Publication NU 4-2008: Performance Measurements of Small Animal Positron Emission Tomographs. Rosslyn, VA: National Electrical Manufacturers Association; 2008.

EPS-103

Impact of patient size on image quality of OSEM3D and BSREM reconstruction in [^{68}Ga]Ga-DOTA-TATE PET/MR

C. P. W. Cox*, T. Brabander, F. A. Verburg, M. Segbers;
Erasmus MC, Rotterdam, NETHERLANDS.*

Aim/Introduction: Previous [^{18}F]FDG and [^{68}Ga]Ga-DOTA-TATE PET/CT studies using ordered subset expectation maximization (OSEM3D) based reconstruction algorithms, demonstrated non-linear relations between body weight and image quality [1-3]. Block Sequential Regularized Expectation Maximization (BSREM) algorithm reduces noise amplification during reconstruction. The impact of the reconstruction algorithm on the relation between image quality and patient size in digital [^{68}Ga]Ga-DOTA-TATE PET may differ from OSEM3D. The amount of activity administered to the patient is usually adjusted based on this relationship with patient size. Therefore, the aim of this study is to investigate the relation between patient size and image quality in OSEM3D and BSREM [^{68}Ga]Ga-DOTA-TATE PET/MR reconstructions. ***Materials and Methods:*** This study included prospective 20 and respective 28 patients who underwent a diagnostic [^{68}Ga]Ga-DOTA-TATE PET/MR (1.5MBq/kg and 3 (≤70kg) or 4 (≥71kg) minutes per bedposition), which was reconstructed with both OSEM3D (VUE Point FX, SharpIR, 28 iterations, 4 subsets and a 7mm Gaussian filter) and BSREM (factor β=450). PET image quality was determined by the signal-to-noise ratio (SNR) in the right liver lobe. This ratio was normalized for injected activity and acquisition time (SNRnorm). Curve fitting between SNRnorm was used with body weight, body length, body mass index, body weight/body length and lean body mass using two power fits, a nonlinear two-parameter model αp^{-d} and a linear single-parameter model $\alpha p^{-0.5}$. Akaike's corrected information criterion (AICc) model selection was applied to select the preferred model. ***Results:*** OSEM3D image SNR (mean=9.8±1.8, range=8.2)was significantly (t(47)=3.7, p<0.001) lower than BSREM SNR (mean=11±2.0, range=8.2). Body mass, the best predictor for both algorithms, clarified 58% (nonlinear with α=39 and d=1.0) and 43% (linear with α=4.4) of the variance in image SNR for OSEM3D. Whereas, body mass clarified only 24% of the variance for BSREM (both nonlinear with α=3.5 and d=0.44 and linear with α=4.6). AICc preferred the nonlinear (probability of correct=99.7%) model for OSEM3D. ***Conclusion:*** Body mass is the best predictor of digital PET/MR [^{68}Ga]Ga-DOTA-TATE image quality for both BSREM and OSEM3D. Although, this prediction is weaker for BSREM. Minimizing the effect of patient size on PET/MR [^{68}Ga]Ga-DOTA-TATE image quality for BSREM and OSEM3D might require different body mass adjusted dose regimens. ***References:*** 1.deGrootEH, PostN, BoellaardR, WagenaarNR, WillemsenAT, van DalenJA. Optimized dose regimen for whole-body FDG-PET imaging. EJNMMI Res. 2013;3(1):63.2.CoxCPW, vanAssemaDME, VerburgFA, BrabanderT, KonijnenbergM, SegbersM. A dedicated paediatric [^{18}F]FDG PET/CT dosage regimen. EJNMMI Research. 2021;11(1):65.3.CoxCPW, SegbersM, GravenLH, BrabanderT, van AssemaDME. Standardized image quality for [^{68}Ga]Ga-DOTA-TATE PET/CT. EJNMMI Res. 2020;10:27.

EPS-104

Impact of 2.5-dimensional Deep Learning for Zero-TE MR-based Attenuation Correction on Chest FDG PET/MRI: Comparison with Conventional and 2-dimensional Deep Learning Approach

M. Tachibana[1], *M. Nogami*[2,3], *H. Matsuo*[1], *M. Nishio*[1], *J. Inukai-Inoue*[1], *F. Zeng*[1], *T. Kurimoto*[4], *K. Kubo*[2], *T. Murakami*[1,2];
[1]Kobe University Graduate School of Medicine, Kobe, JAPAN, [2]Department of Radiology, Kobe University Hospital, Kobe, JAPAN, [3]Division of Medical Imaging, Biomedical Imaging Research Center, University of Fukui, Fukui, JAPAN, [4]GE Healthcare, Hino, JAPAN.

Aim/Introduction: Conventional magnetic resonance-based attenuation correction by 2-point Dixon MR images in the chest may underestimate the standardized uptake value (SUV) compared with positron emission tomography/ computed tomography due to the lack of bone components. In our previous study, pseudo-CT (pCT) with bone components from 360 ZTE-MRI training data set using the 2-dimensional (2D) deep learning (DL) method including unsupervised generative adversarial networks (GAN) yielded

μmaps with bone components ($\mu map_{bone\text{-}2D}$) in combination with conventional bone-lacking μmaps ($\mu map_{no\text{-}bone}$) in the chest. This study aimed to assess the feasibility of pCT and μmap ($\mu map_{bone\text{-}2.5D}$) from ZTE using 2.5-dimensional (2.5D) DL method and compare the quantitative values of the normal tissues and lesions between $\mu map_{no\text{-}bone}$-, $\mu map_{bone\text{-}2D}$-, and $\mu map_{bone\text{-}2.5D}$-besed reconstruction. ***Materials and Methods:*** Thirty-six cases with paired fluorine-18 fluorodeoxyglucose ZTE PET/MRI and PET/CT were retrospectively evaluated to compare the mean SUV (SUVmean) of the normal bone and liver in the chest region. Twenty-seven cases with lesions on chest FDG PET/MRI were also retrospectively assessed to compare the maximum SUV (SUVmax) of lesions in four regions: the lungs, mediastinum, extra-thorax, and bone. For the 2.5D method, the value of a loss function in the GAN was calculated for each of the three consecutive 2D slices, and the weighted sum of those was defined as the 2.5D loss function. Each μmap was applied to PET reconstruction on the offline workstation. The Wilcoxon signed-rank test was used to assess the SUVmean and the SUVmax. The similarity of the histogram by $\mu map_{no\text{-}bone}$, $\mu map_{bone\text{-}2D}$ and $\mu map_{bone\text{-}2.5D}$ to CTAC was estimated by the correlation coefficients. The image-quality of $pCT_{bone\text{-}2D}$ and $pCT_{bone\text{-}2.5D}$ was evaluated by two radiologists using a three-point scoring system regarding bone delineation and bone continuity. ***Results:*** The SUVmean by $\mu map_{bone\text{-}2.5D}$ was significantly larger than $\mu map_{bone\text{-}2D}$ in the normal bone and the liver ($p=0.0009$, $p< 0.0001$). The SUVmax by $\mu map_{bone\text{-}2.5D}$ was significantly larger than $\mu map_{bone\text{-}2D}$ in all regions ($p= 0.0176$). The correlation coefficients of the histogram for $\mu map_{bone\text{-}2.5D}$ and $\mu map_{bone\text{-}2D}$ were significantly higher than $\mu map_{no\text{-}bone}$ in the bone ($p<0.0001$). The image-quality scores of $pCT_{bone\text{-}2.5D}$ for bone delineation and bone continuity were significantly higher than $pCT_{bone\text{-}2D}$ in both readers ($p= 0.0106$, $p< 0.0001$). ***Conclusion:*** $\mu map_{bone\text{-}2.5D}$ are assumed to yield smaller differences in SUV with μmap_{CT} than $\mu map_{no\text{-}bone}$ and $\mu map_{bone\text{-}2D}$ in normal tissues and lesions. The result supports the feasibility of using the 2.5D method for the generation of bone components from ZTE with DL.

710

Monday, September 11, 2023, 8:00 AM - 9:30 AM

Hall K

Technologists Oral Presentations 1: All about PET-CT!

OP-323

Double acquisition protocol for the study of washout in PET/CT parathyroids examination with 18F-Choline

M. Anelli[1], *M. Nicoletto*[2], *A. Zambelli*[3], *A. Di Nicola*[1];
[1]*Azienda Sanitaria Locale di Pescara, Pescara, ITALY,*
[2]*Policlinico di Abano Terme, Abano Terme (PD), ITALY,* [3]*Azienda Ospedaliera Universitaria di Padova, Padova, ITALY.*

Aim/Introduction: PET/CT studies with 18F-Choline are mainly performed to localize parathyroid glands adenomas. Scintigraphy with 99mTc-sestamibi is the elective examination to study neoformations and identify abnormal and ectopic parathyroid tissue in the neck area. Occasionally, further investigations with high-resolution methods, such as PET/CT with 18F-Choline, might be necessary. This paper aims to provide our centre's radiographers with a practical guidance on double PET/CT acquisition examinations for parathyroid adenomas after findings with conventional imaging (parathyroid scintigraphy or ultrasonography). ***Materials and Methods:*** In our nuclear medicine unit, PET/CT acquisition protocol for studying parathyroids with Choline-F18 is performed through two different scans executed at standard time intervals in order to assess and evaluate SUV changes.Patients were included in the study based on the following procedure1. Blood glucose level examination showing values below 180 mg/dl;2. Injection of Choline-F18, 3.4 mBq/Kg3.Patients had to wait in a comfortable area before the examination;4.First acquisition, 5 minutes after injection;5.Second acquisition, with the same parameters, 60 minutes after the injection.Both acquisitions started from the vertex to the liver domes; acquisition time was 4' for each bed. ***Results:*** After examining a sample of 30 patients (18M, 12F, age 28-73), a new protocol to optimize parathyroids 18F-Choline PET/CT examination was developed in 2022. This allowed us to best evaluate and compare 18F-Choline absorption in the scanned area with specific and standard time intervals. The results concerning the 2021 study allowed us to standardize two acquisitions performed after 5 and 60 minutes to evaluate the choline washout times at the level of the parathyroid glands. ***Conclusion:*** Our findings show that double acquisition leads to an optimal radiopharmaceutical kinetics evaluation, and the highest Choline-F18 uptake occurs at 60 min after injection. In particular, these acquisition parameters allow us to carry out an accurate qualitative assessment of SUVmax and average over the area of interest. After the completion of this study, an internal acquisition protocol was also drafted. The double acquisition allows us to understand a real data on the parathyroid washout after first acquisition. In order to optimize the procedure, patients that have to undergo this examination are generally scheduled at the end of the F18-choline daily session, so that double scans can be performed without interruption.

OP-324

Reduction of scan time in ^{18}F-FMM PET/CT-scans in the diagnosis of Alzheimer's disease

J. Terzic[1,2], *J. K. Fuglsang*[2], *R. Ismail*[3];
[1]*Vejle Hospital, Vejle, DENMARK,* [2]*Aalborg University, Aalborg, DENMARK,* [3]*Odense University Hospital, Odense, DENMARK.*

Aim/Introduction: Alzheimer's disease (AD) is the most common form of dementia. The protein β-amyloid is a diagnostic biomarker for AD. Patients with AD have an increased accumulation of β-amyloid in cerebrum. ^{18}F-Flutemetamol (^{18}F-FMM) PET/CT scans are used to provide information about the accumulation of β-amyloid in cerebrum. This information is strongly correlated with post mortem findings. The relatively long scan time of 20 minutes may result in cooperation difficulties which can cause movement artifacts. This can affect image quality and the diagnostic accuracy. For this patient group it may be beneficial to reduce the scan time. The aim of this study was to investigate, via visual and quantitative evaluation, whether reduced scan times for ^{18}F-FMM PET/CT scans affected the diagnostic accuracy in the diagnosis of AD. ***Materials and Methods:*** The ^{18}F-FMM PET/CT scans were performed at the Department of Nuclear Medicine, Vejle Hospital. 25 patients were included in this study. 185±2.4 MBq ^{18}F-FMM was injected intravenously 88.9±3.3 minutes prior to the PET scan. PET data was acquired in list mode and CT was used for attenuation correction. The acquisition time for the PET scan was 20 minutes in accordance to international guidelines. The images were reconstructed into periods of 10, 15 and 20 minutes which resulted in three sets of data per patient. A blinded, experienced nuclear medicine physician visually evaluated the

scans as positive, negative or borderline. Standard uptake value ratios for 13 auto segmented regions in cerebrum were used for quantitative evaluation of the scans. Pons was used as the reference region. Friedman's test was used for statistical analysis, to test whether there was a significant difference between the three scan times. For the post hoc analysis a Wilcoxon test with Bonferroni correction was applied. The concordance between visual and quantitative evaluation was furthermore evaluated. ***Results:*** There was no significant difference in the diagnosis between 10, 15 and 20 minutes scan times in the visual evaluations, nor in the quantitative evaluations (p>0.05 in all 13 regions). The concordance between the visual and quantitative evaluations was 80-84%. ***Conclusion:*** Visual and quantitative evaluation showed no significant difference in the diagnosis of AD between 10 or 15 minutes scan times compared to 20 minutes scan time. Based on these findings a reduced scan time may have potential for use in clinical practice. This may reduce cooperation difficulties for patients with AD.

OP-325

Optimization of TOF-BPL reconstruction using clinical images in [18F]flutemetamol amyloid PET

S. Fukuda[1], *K. Miwa*[2], *K. Wagatsuma*[1,3], *Y. Yakushiji*[1], *T. Yamao*[2], *Y. Kamitaka*[3], *T. Hasegawa*[1];
[1]*Kitasato University Graduate School of Medical Sciences, Kanagawa, JAPAN,* [2]*Fukushima Medical University, Fukushima, JAPAN,* [3]*Tokyo Metropolitan Institution of Gerontology, Tokyo, JAPAN.*

Aim/Introduction: Bayesian penalized likelihood reconstruction with Q.Clear and time-of-flight (TOF-BPL) are useful for oncological, but not brain images acquired using positron emission tomography (PET). The β value controls the global strength of noise suppression, whereas the γ factor in the relative difference penalty (RDP) controls the degree of edge preservation in Q.Clear. Block sequential regularized expectation maximization (BSREM) is applied in Q.Clear as an optimizer. Here, we optimized the γ factor and iteration number in BSREM to acquire amyloid PET images using a phantom. This study aimed to confirm quantitative values in [18F]flutemetamol images and further optimize TOF-BPL reconstruction for amyloid PET. ***Materials and Methods:*** We analyzed imaging data from 30 patients who were positive (n = 13) or negative (n = 17) for amyloid and assessed by [18F]flutemetamolPET. All data were reconstructed using Duetto toolbox (GE HealthCare) running on MATLAB All data were reconstructed under the following algorithms and conditions: the γ factor 2 (β value, 300; iteration, 8; with PSF), γ factor 5 (β value, 500; iteration, 1; without PSF), and γ factor 10 (β value, 800; iteration, 1; without PSF). The β values and iterations of γ factors 5 and 10 were optimized in a previous phantom study. We calculated composite standardized uptake value ratios (SUVr) using the pons as a reference region, then the Centiloid scale (CL). Correlation coefficients were calculated between the composite SUVr and the CL in three γ factors, and areas under receiver operating characteristic (ROC) curves (AUC) were calculated for SUVr and CL. ***Results:*** The SUVr was increased slightly more by γ factor 5, than 2 and 10. The CL of γ factors 5 and 10 were slightly lower than that of γ factor 2. The coefficient correlations were higher for γ factors 5 and 10 than 2. The AUCs for SUVr and CL were almost identical under γ factors 5 and 2, and lower under γ factor 10. ***Conclusion:*** A γ factor > 2 in TOF-BPL was appropriate, and TOF-BPL reconstruction without PSF, γ factor = 5, β = 500, iterations, 1, and PSF OFF were the optimal conditions for [18F] flutemetamol.

OP-326

Influence of the number of iterations on image quality and semiquantitative accuracy in [18F]FDG PET imaging using a Long Axial Field-of-View PET/CT system

M. van der Vegt, *R. A. J. O. Dierckx, A. W. J. M. Glaudemans, J. van Sluis;*
University Medical Centrum Groningen, Groningen, NETHERLANDS.

Aim/Introduction: Long Axial Field-of-View (LAFOV) PET/CT systems are characterised by increased sensitivity, resulting in improved image quality. Improved performance characteristics of LAFOV PET have been shown to allow reduction in activity administration and/or shorter scan duration while maintaining image quality in terms of signal-to-noise ratio and semiquantitative accuracy [1, 2]. However, to date, the influence of the number of iterations on image quality using a LAFOV PET/CT has not been evaluated yet. Therefore, the aim of the current study was to explore the influence of the number of iterations on image quality and semiquantitative accuracy in [18F]FDG PET imaging using a LAFOV PET/CT system. ***Materials and Methods:*** So far, six oncological patients underwent a 3-min listmode [18F]FDG PET/CT acquisition and received a weight-based activity injection of 2 MBq/kg. PET data were reconstructed using European Association of Nuclear Medicine Research Ltd. (EARL) 2 compliant settings with various iterations: 2, 4, 6, 8, and 10. Six tumour lesions and liver tissues were segmented [AWJM1] using in-house developed software to obtain Standardized Uptake Values (SUV), Coefficient of Variation (COV) in the liver and Tumour to Background Ratio (TBR). Also the maximum intensity projection (MIP) images were visually assessed on image quality. ***Results:*** Median SUV_{max} of the tumour lesions increased from 9.42 to 9.93 from 2-10 iterations, respectively, with almost no difference between 6-10 iterations. The median SUV_{peak} increased even less. From 2-10 iterations the median COV increased from 4.2% to 8.7%, respectively, with the largest increase between 4 to 6 iterations. The highest TBR was seen in the images reconstructed using 8 and 10 iterations, however there is merely a 5% increase in TBR between from 2-10 iterations. Also, image quality MIPs in all cases are sufficient for diagnostic purposes, but the noise was considered higher when having more iterations. ***Conclusion:*** The number of iterations influence noise levels in the obtained images resulting in the highest COV in the images reconstructed using 10 iterations, whereas TBR improved slightly with the number of iterations. Because of the largest increase in COV between 4-6 iterations, we recommend to use 4 iterations or less to obtain optimal image quality with minimal interference of noise. Future research will determine the influence of the number of iterations on convergence rate. ***References:*** [1] van Sluis J et al. Eur J Nucl Med Mol Imaging. 2022 Nov;49:4652-4660. [2] Alberts I et al. Eur J Nucl Med Mol Imaging. 2021 Jul;48:2395-2404.

OP-327

Comparison of the quadratic scheme suggested by EANM guidelines and manufacturer-recommended dose factor for Fluorine-18 FDG imaging on PET-CT system with SiPM detectors: evaluation on image quality

A. Hurtado de Mendoza, *M. Yaryes, C. Soza-Ried, H. Amaral;*
Positronmed, Santiago, CHILE.

Aim/Introduction: The aim of this study is to compare the Fluorine-18 FDG activity determined by the quadratic scheme suggested by the European Association of Nuclear Medicine (EANM) guidelines with the manufacturer-recommended dose factor for PET-CT imaging. Additionally, we aim to evaluate the impact of these dose factors on image quality, measured by

signal-to-noise ratio (SNR) tumor-to-background ratio (TBR), Coefficient of Variation (COV), and Exposure Internal Dose (EID) in mSv to assess radiation protection. ***Materials and Methods:*** We included 60 oncology patients, divided into two groups of 30 each. The first group underwent FDG PET imaging with the manufacturer-recommended dose factor of 0.06 mCi/kg/body weight, while the second group received activity of 0.08 mCi/kg/body weight, determined using the quadratic linear method following the technical note provided by the EANM. Image acquisition parameters, including 4 iterations, 5 subsets, 4-mm Gaussian filter, OSEM PSF + TOF reconstruction method, and 1 minute per bed, were kept constant for both groups. We measured SNR and COV in the liver and TBR. Lesions were evaluated by nuclear medicine physicians with over 10 years of experience, using VOI isocontour with a threshold of 41% for SUVmax. SNR and TBR were compared between the two groups using Wilcoxon Test. For COV, we used descriptive statistics and considered values under 15% as acceptable for both groups. EID was compared using Student's t-test. ***Results:*** SNR values were significantly higher in the group receiving 0.08 mCi/kg/body weight compared to the group receiving 0.06 mCi/kg/body weight ($p < 0.01$). In contrast,TBR values did not show significant differences between groups ($p = 0.74$). The internal exposure dose was significantly higher in the group receiving 0.08 mCi/kg/body weight compared to the group receiving 0.06 mCi/kg/body weight ($p < 0.05$). The COV values remained below 15% in both groups. ***Conclusion:*** Our study shows that digital PET-CT technology allows the use of the manufacturer-recommended dose factor of 0.06 mCi/kg/body weight for FDG imaging without compromising image quality. Our findings demonstrate that there is no significant impact in TBR between the two dose factors, which is crucial for accurate lesion evaluation. Furthermore, COV values are acceptable for both methods. From a radiation protection perspective, the 0.06 mCi/kg/body weight dose factor may result in lower internal exposure dose (mSv) to patients. Therefore, we recommend using the manufacturer-recommended dose factor for FDG PET imaging to achieve optimal image quality while minimizing radiation exposure to patients. ***References:*** 1. https://doi.org/10.1186/s40658-016-0135-5.

OP-328

The Impact of a New Breathing Movement Correction Method On FDG Uptake and Volume Determination of Body Lesions

M. Schiavini[1], *F. Buffoni*[1], *M. Bardo*[1], *M. Giavarini*[2], *D. Capolongo*[1], *R. Leo*[1], *M. Rognoni*[1], *C. Sdraiati*[1], *L. Sembele*[3], *M. Castellani*[1];
[1]*IRCCS Fondazione "Cà Granda" Osp. Maggiore Policlinico di MILANO, Milan, ITALY,* [2]*UNIMI, Milan, ITALY,* [3]*Latvian Maritime Medical Center, Riga, LATVIA.*

Aim/Introduction: Patient's respiratory movement is a common problem occurring during whole body PET/CT (WB-PET/CT) images acquisition. Due to overestimation of lesion volume and underestimation of radiotracer concentration, this kind of artefact generates not only an important loss of the image quality but also leads to a change of PET and CT quantitative parameters. ***Materials and Methods:*** [^{18} F] FDG PET/CT (Biograph Vision 450 Siemens) images of sixty-four patients with one or more hyper-enhancing lesions (chest and/or abdomen) were retrospectively analysed over the last four months. Two sets of reconstructed WB images with and without OF respiratory gating were processed. After a visual comparison of the PET/CT fused images quality of two image sets, a manually delineation of an iso-contour volume of interest (VOI) was obtained. Standardized uptake values (SUVs) of the lesions along with their metabolic volumes were calculated. ***Results:*** A more precise correspondence between focal FDG uptake area and CT profile of the lesions was found at WB-OF reconstructed images. An increase of the percent mean variations of SUVmax and SUVmean (13.74% ± 11.44%) and a decrease of volumes (-39.21% ± 45.20%) were respectively calculated at WB-OF images in comparison to standard WB image group. ***Conclusion:*** Our data indicated that the DDG methods and particularly OF-AI may reduce the effects of respiratory artefacts, leading to a better quality of images and to a different FDG uptake values and lesion volumes, in comparison to WB images obtained without OF reconstruction.

OP-330

Occupational Radiation exposure from PET/CT during patient positioning

R. Siyanbola*, M. Coelho, P. Fragoso Costa, A. Moraitis, K. Herrmann, H. Hautzel;*
Department of Nuclear Medicine, University Hospital Essen, University Duisburg - Essen, Essen, GERMANY.

Aim/Introduction: Due to increasing PET/CT throughput rates occupational radiation exposure (ORE) to technicians is of major interest. Previously, both tracer injection and patient positioning contributed almost equally to the radiation exposure and accounted for more than 90% of the total dose [1]. Nowadays injection-related exposure is negligible due to automated i.v.-application systems. Therefore, patient handling is now the main ORE source. Aim of this ongoing project is to identify factors leading to increased dose exposure in the course of PET/CT patient positioning. ***Materials and Methods:*** Dose rates using a FH 40 G-L 10 Survey Meter (Thermo Fisher Scientific, USA) and the time being with the patients were collected during (1) accompanying the patient into the scanner room and positioning her/him in the PET/CT (inPET-procedure) and (2) taking the patient out of the scanner/scanner room (outPET-procedure). From these variables total dose per procedure were calculated. Further data collected were: type of disease, injected activity, time point of injection, time point into the scanner, time point out of the scanner. After testing for normality two-sided t-tests and Spearman's Rho correlational analyses were calculated whenever appropriate. ***Results:*** Up to now 44 consecutive patients were included, predominately suffering from lung or prostate cancer. Patients were positioned in the PET/CT 61±17 min after injection of 240±45 MBq [^{18}F]-labelled tracers. After 88±17 min patients were removed from the scanner. Measures for inPET-procedure were: time consumption 2.9±1.9 min, dose rate 26.8±11.2 µSv/h, ORE 1384±1623 nSv per procedure. Results for outPET-procedure were: time consumption 1.4±0.8 min, dose rate 14.2±8.0 µSv/h, ORE 413±622 nSv per procedure. outPET-procedure was significantly faster than inPET-procedure. Consequently, ORE was correlated with the type of procedure but not with the injected activity or type of disease. Decay correction of the inPET-procedure dose rate to the time point of the outPET-procedure resulted in 23.2±9.5 µSv/h. Of note, that was still significantly higher than the dose rate of the outPET-procedure. ***Conclusion:*** From our preliminary data one might infer that the inPET-procedure is about twofold more time-consuming than the outPET-procedure. However, its contribution to the total ORE is threefold indicating that not only timing matters but potentially also the distance between the technician and the patient during positioning within the scanner. This assumption is supported by the fact that even the decay corrected dose rate of the inPET-procedure is significantly higher than the corresponding outPET-procedure dose rate. ***References:*** [1] Costa P.F. et al.; Radiat Prot Dosimetry. 2018;179(3):291-298

OP-331

Eye lens exposure of nuclear medicine technologists during PET/CT procedures: compliance with dose limits and eye lens vs whole-body dosimetry

M. Ryser, *S. Figueiredo, S. Medici, J. O. Prior, N. Cherbuin; CHUV, Lausanne, SWITZERLAND.*

Aim/Introduction: Following the recommendations of the International Commission of Radiological Protection, the Swiss Radiological Protection Regulation drastically decreased the annual equivalent dose limit for the eye lens from 150 to 20 mSv for workers professionally exposed to ionizing radiation. Eye lens exposure can be either measured by dedicated dosimeters worn close to the eye or extrapolated from whole-body dosimeters worn on the chest. The aim of this work was to quantify the annual eye lens dose of nuclear medicine technologists performing different PET/CT-related activities in our department and determine whether the dose extrapolation from the chest-worn dosimeter provides a conservative approximation of the eye lens exposure. ***Materials and Methods:*** This study was performed on a monthly basis using optically-stimulated luminescent (OSL) passive dosimeters: one whole-body worn on the left side of the chest allowing to retrieve $H_p(10)$, $H_p(0.07)$ and $H_p(3)$ and two eye lens (left and right) calibrated in $H_p(3)$. A total of 17 technologists wore two sets of dosimeters during their work routine on a digital PET/CT: one set for the technologist at the console acquisition (T1) and the other for the technologist in charge of patient care, including radiopharmaceutical injection (T2). ***Results:*** According to our preliminary results obtained over a 3-month surveillance period, approximately 85% of the monitored procedures involved F-18 while the remaining were performed with Ga-68. The radionuclides were bond to different vectors and 42% of the injections were performed manually, while 58% were performed using an automatic injector (administered activity 2 MBq/kg). The monthly normalized $H_p(3)$ for T1 were 4.0 µSv/GBq and 4.2 µSv/GBq for the left and right eye respectively, and 5.3 µSv/GBq and 6.5 µSv/GBq for T2. Thus, the predicted annual eye lens doses are significantly below the legal dose limits, with a maximum estimated $H_p(3)$ for T2 of 2.52 mSv for the right eye. For T1, the ratio between $H_p(3)$ provided by the eye lens (left and right) and whole-body dosimeters was 0.67 and 0.70, respectively. For T2, these values were 0.78 and 0.95. ***Conclusion:*** The annual eye lens legal dose limit is unlikely to be exceeded by the technologists for the PET/CT procedures and workload considered during this study. Given the predicted eye lens dose, a dosimetric surveillance based on the whole-body dosimeter is sufficient. The whole-body dosimeter generally provides a conservative estimator of the eye lens dose.

711

Monday, September 11, 2023, 8:00 AM - 9:30 AM

Hall G1

Theranostics Track - TROP Session: What's New in Prostate Cancer?

OP-332

Radioligand Therapy with [^{177}Lu]Lu-PSMA I&T in the Elderly - Safety, Efficacy and Prognosticators of Survival

S. Weber[1], *A. Seitz*[2], *H. Kübler*[2], *A. K. Buck*[1], *R. A. Werner*[1,3], *P. E. Hartrampf*[1];
[1]*University Hospital Wuerzburg, Department of Nuclear Medicine, Wuerzburg, GERMANY,* [2]*University Hospital Wuerzburg, Department of Urology and Paediatric Urology, Wuerzburg, GERMANY,* [3]*Johns Hopkins University School of Medicine, Baltimore, MD, UNITED STATES OF AMERICA.*

Aim/Introduction: Peak rate of prostate cancer (PC) is above 75 years of age, rendering elder patients as the main target population for novel treatment options. We aimed to evaluate safety and efficacy of prostate-specific membrane antigen (PSMA)-targeted radioligand therapy (RLT) using [^{177}Lu]Lu-PSMA I&T in individuals of minimum 75 years of age, including predictors of overall survival (OS). ***Materials and Methods:*** We identified 56 men (≥75 years) affected with metastatic castration resistant PC (mCRPC), which were treated with PSMA RLT using [^{177}Lu]Lu-PSMA I&T. Adverse events were classified according to the Common Terminology Criteria for Adverse Events (CTCAE) v5.0, by investigating haematological (platelets, leukocytes, haemoglobin) and renal (eGFR, creatinine) parameters. In addition, baseline liver enzymes (aspartate aminotransferase [AST], alkaline phosphatase [AP]), lactate dehydrogenase (LDH), C-reactive protein (CRP), and Gleason-Score were also recorded. PSA response was evaluated by comparing PSA levels from baseline and last available follow-up (n=43). We performed univariable cox regression, followed by multivariable analyses to determine an association with OS. ***Results:*** Median age at 1st cycle was 78 years (range, 75-95 y) with an initial Gleason Score of 8 (5-10). Median 3 (range, 1-9) cycles of RLT were administered using a median cumulative activity of 18.2 GBq (range, 4.9-54.8 GBq) [^{177}Lu]Lu-PSMA I&T. Median decrease for platelet counts, leucocytes and haemoglobin was 11.4%, 7.4% and 6.2%, respectively. After RLT, the following grade I/II haematologic CTCAE were recorded: anaemia in 21%, followed by leukocytopenia in 17%, and thrombocytopenia in 7%. eGFR decreased by 2.5%, with respective grade I/II CTCAE in 19% (creatinine increase by 5%; creatinine CTCAE grade I/II, 14%). No CTC grade ≥III occurred. 33/43 (76.7%) exhibited a PSA decrease of median 57% (range, 0.6 - 99%), with the vast majority (22/33 [66.7%]) achieving a decline by more than 50%. Median OS was 11 months, while 32/56 (57.1%) patients died. Univariable analysis provided the following significant parameters: PSA, CRP, LDH, AST, AP, haemoglobin (p<0.05, each). In multivariable cox regression, baseline CRP (per mg/dl, Hazard Ratio [HR], 1.233 [95%CI 1.098-1.373]; P<0.001), PSA (per ng/ml, HR, 1.001 [95%CI, 1.000-1.002]; P<0.01), and LDH (per U/l, HR, 1.001 [95%CI 1.000-1.002]; P<0.02) remained significant, indicative for an independent prognostic value for OS. ***Conclusion:*** RLT with [^{177}Lu]Lu-PSMA I&T is safe in elderly patients (above 75 years of age) and showed comparable outcome to previously published data. Initial lower PSA, lower CRP and lower LDH were associated with longer OS in those patients.

OP-333

Evaluation of Nephrotoxicity of Extended Lu^{177}-PSMA in Patients with Metastatic Castration-Resistant Prostate Cancer

E. Topal[1], *B. Kovan*[1], *D. Has Simsek*[1], *C. Civan*[1], *M. Sanli*[2], *M. Basaran*[3], *Y. Sanli*[1];
[1]*Istanbul University, Istanbul Medical Faculty, Department of Nuclear Medicine, Istanbul, TÜRKIYE,* [2]*Istanbul University, Istanbul Medical Faculty, Department of Urology, Istanbul, TÜRKIYE,* [3]*Istanbul University, Oncology Institute, Department of Medical Oncology, Istanbul, TÜRKIYE.*

Aim/Introduction: We aimed to investigate the effect of extended Lu^{177}-PSMA radioligand treatment (PSMA-RLT) on renal function in patients with metastatic castration-resistant prostate cancer. ***Materials and Methods:*** The cohort included 54 patients who received ≥4 cycles of PSMA-RLT. All patients underwent post-treatment whole body and SPECT/CT images at 4th, 24th and 96th hours after each cycles. Renal dosimetry for

each cycles were calculated using the OLINDA/EXM 1.1 program. Pre and post-treatment blood creatinine values were measured and nephrotoxicity was graded according to CTCAE v4.0. Risk factors for nephrotoxicity included pre-existing renal disease, comorbidities and history of chemotherapy and radiotherapy were recorded. ***Results:*** Median of PSMA-RLT cycles was 6 and the number of cycles of PSMA-RLT were 4 in 13 patients, 5-8 in 38 patients and 9-10 in 3 patients. The median age was 71 (range, 54-89) years and the median baseline creatinine value was 0.83 mg/dL (range,0.5-2,19). Median of cumulative renal dose (cRD) of 4 cycles in 54 patients was 12.71 Gy (IQR: 4,83). After 4 cycles, maximum cRD was 20,64 Gy. In 38 patients who received 5-8 cycles, median of cRD was 21.8 Gy (IQR:7,15) and maximum cRD was 35,1 Gy. In 3 patients who received 9-10 cycles, median of cRD was 39.1 Gy (IQR:7,5) and maximum cRD was 44,27 Gy. According to CTCAE v4.0, none of the 54 patients received grade 2 or more than 2 nephrotoxicity. After PSMA-RLT, 13 patients (24%) had grade 1 nephropathy. Of those, 5 patients had grade 1 nephropathy at baseline. In 8 patients, who developed grade 1 nephropathy, median and maximum cRD were 23,25 and 44,27 Gy, respectively. 7 patients (13%) received cRD more than 28 Gy without any severe nephrotoxicity. ***Conclusion:*** Our results showed that extended PSMA-RLT is safe for renal function. PSMA-RLT could be continued in patients who responded treatment with personalized dosimetric evaluation without any severe nephrotoxicity. Maximum cumulative renal doses of PSMA-RLT should be determined in prospective, multi-centric studies.

OP-334

Safety and Efficacy of Extended ^{177}Lu-PSMA Therapy: Multi-Center Retrospective Analysis

T. Telli[1,2,3], *R. Seifert*[1,2,3], *C. Lapa*[4], *T. Hekimsoy*[5], *W. Weber*[5], *C. Pfob*[4], *K. Herrmann*[1,2,3], *K. Rahbar*[6], *M. Eiber*[5], *W. Fendler*[1,2,3];
[1]*Department of Nuclear Medicine, University Hospital Essen, Essen, GERMANY,* [2]*German Cancer Consortium (DKTK), University Hospital Essen, Essen, GERMANY,* [3]*West German Cancer Center, University Hospital Essen, Essen, GERMANY,* [4]*Department of Nuclear Medicine, University Hospital Augsburg, Augsburg, GERMANY,* [5]*Department of Nuclear Medicine, University Hospital of Munich Technical University, Munich, GERMANY,* [6]*Department of Nuclear Medicine, University Hospital Münster, Münster, GERMANY.*

Aim/Introduction: Therapy continuation or re-challenge with ^{177}Lu-PSMA is a viable option for patients with favorable response to ^{177}Lu-PSMA therapy. This study aims to determine the feasibility, efficacy, and safety of continuous or re-challenge ^{177}Lu-PSMA extended therapy. ***Materials and Methods:*** In this multicenter study, we retrospectively analyzed 111 patients who were treated with more than six cycles of either continuous (n=43) or re-challenge (n=68) ^{177}Lu-PSMA therapy at the Nuclear Medicine Departments of Munich Technical University, University Hospitals Essen, Münster, and Augsburg. The primary endpoints of the study were to analyze efficacy with overall survival(OS)and therapy response, as well as the safety of extended therapy options of ^{177}Lu-PSMA. PSA response was assessed after 8-12 weeks after first therapy cyle. Biochemical partial response(PR) was defined as at least 50% decrease of PSA value, while progression(PD)was defined as any increase from baseline. Any other differences were considered as biochemical stable disease(SD). The severity of adverse events was graded according to Common Terminology Criteria for Adverse Events (CTCAE) v5.0 criteria. ***Results:*** Median cumulative doses for continuous and re-challenge therapy patients were 57.4(IQR: 51.6-59.5) and 60.8(IQR: 54.9-73.1) GBq. The estimated median OS from the beginning of initial therapy of the total cohort was 31.3 months (95% CI: 26.3-36.3) and the projected two-year OS rate was estimated 69%. For the continuous therapy group estimated median OS from the beginning of the first ^{177}Lu-PSMA administration was 23.2 months(95% CI: 20.4-25.9). For the rechallenge therapy group estimated median OS from the beginning of the first ^{177}Lu-PSMA administration and from the beginning of rechallenge therapy were 40.2(95% CI: 31.8-48.7) and 20(95% CI: 11.8-28.3) months, respectively. Biochemical PR, SD, and PD 8-12 weeks after the first ^{177}Lu-PSMA cycle were seen in 10/42(23.8%), 21/42(50%), 11/42(26.2%) in the continuous therapy group, and 37/65(56.9%), 24/65(36.9%), 4/65(6.2%) in re-challenge therapy patient group, respectively. 8-12 weeks after the first re-challenge ^{177}Lu-PSMA cycle biochemical PR, SD, and PD were seen in 22/63(34.9%), 22/63(34.9%), 19/63(30.2%), respectively. Grade 3 anemia, thrombocytopenia, leukocytopenia, neutropenia, and decrease in GFR occurred in 7/43(16.3%), 3/43(7%), 1/43(2.3%), 1/39(2.6%) 2/43(4.7%) for continuous therapy group and 12/68(17.6%), 2/68(2.9%), 2/67(3%), 0(0%), 5/68(7.4%) for rechallenge group. One patient(1.5%) in the re-challenge group had grade 4 thrombocytopenia. ***Conclusion:*** Patients who received more than 6 cycles of ^{177}Lu-PSMA therapy presented a median OS of 31.3 months with favourable toxicity . In selected patients with favorable initial response and better response biomarkers, ^{177}Lu-PSMA treatment continuation or re-challenge is feasible.

OP-335

AcTION: A phase 1 study of [^{225}Ac]Ac-PSMA-617 in men with PSMA-positive prostate cancer with or without prior [^{177}Lu]Lu-PSMA-617 radioligand therapy

M. Sathekge[1], *M. Crumbaker*[2], *A. M. Joshua*[2], *F. Bruchertseifer*[3], *T. Kreisl*[4], *S. Emeneni*[5], *J. Wehbe*[6], *M. Korn*[4], *A. Morgenstern**[3,7], *L. Emmett**[2,7];
[1]*University of Pretoria and Steve Biko Academic Hospital, Pretoria, SOUTH AFRICA,* [2]*St Vincent's Hospital, Sydney, AUSTRALIA,* [3]*European Commission, Joint Research Centre, Karlsruhe, GERMANY,* [4]*Novartis Pharmaceuticals Corporation, East Hanover, NJ, UNITED STATES OF AMERICA,* [5]*Novartis India, Hyderbad, Telangana, INDIA,* [6]*Novartis Institutes for BioMedical Research, Basel, SWITZERLAND,* [7]**Co-senior author, GERMANY, AUSTRALIA.*

Aim/Introduction: Lutetium (^{177}Lu) vipivotide tetraxetan ([^{177}Lu]Lu-PSMA-617; ^{177}Lu-PSMA-617) plus standard of care (SoC) significantly prolongs radiographic progression-free survival (rPFS) and overall survival relative to best SoC alone in patients with prostate-specific membrane antigen (PSMA)-positive metastatic castration-resistant prostate cancer (mCRPC). The AcTION study will assess the novel PSMA-targeted radioligand [^{225}Ac]Ac-PSMA-617 (^{225}Ac-PSMA-617), which delivers PSMA-guided ^{225}Ac, a high-energy α-emitter able to create DNA double-strand breaks. ***Materials and Methods:*** AcTION (NCT04597411) is an international, open-label, dose-escalation, phase 1 study. The primary endpoint is to determine the recommended phase 2 dose and schedule of administration of ^{225}Ac-PSMA-617 in men with progressive PSMA-positive mCRPC with or without prior exposure to ^{177}Lu-PSMA-617. Approximately 60 patients with PSMA-positive disease (determined by [^{68}Ga]Ga-PSMA-11 positron emission tomography/computed tomography) will be assigned to one of three groups (20 patients per group): (A) prior chemotherapy/androgen receptor pathway inhibitors (ARPI) received, no prior ^{177}Lu-PSMA-617; (B) naïve to chemotherapy and novel ARPI; (C) prior ^{177}Lu-PSMA-617. Enrolled patients will receive intravenous

^{225}Ac-PSMA-617 once every 8 weeks (±1 week) for a maximum of 6 cycles. Dose escalation will proceed using a Bayesian logistic regression model with a starting dose of 4 MBq. Subsequent dose levels will increase by 2 MBq increments to a maximum of 10 MBq. The lowest dose tested will be reduced to 2 MBq if required. In each group, at least three patients will be treated at each dose and evaluated for ≥ 6 weeks before consideration of patient enrolment into the next dose. The maximum tolerated dose will be that at which the posterior probability of targeted toxicity exceeds 50% (≥ 6 patients treated at this dose and observed for 6 weeks) or at which a minimum of 15 participants have already been treated in the trial. Patients may also receive supportive care, including palliative radiation therapy, but cannot receive concurrent anti-cancer therapies. Secondary endpoints are overall safety and tolerability, response according to RECIST v1.1 (overall response rate, duration of response, disease control rate), progression-free survival (radiographic disease progression, clinical progression and prostate specific antigen progression), biochemical response, and health-related quality of life (HRQoL). Safety follow-up will be performed approximately 60 days following the final dose of ^{225}Ac-PSMA-617, or before any subsequent anti-cancer treatment. Long-term follow-up will include HRQoL, survival and treatment update every 3 months (± 1 month) for 12 months.

OP-336

Prediction of resistance to PSMA-617 Lu-177 by assessment of circulating tumor DNA biomarkers

O. Sartor[1], *E. Ledet*[2], *M. Huang*[1], *J. Schwartz*[2], *A. Lieberman*[2], *B. Lewis*[2], *J. Layton*[2], *A. Jang*[2], *O. Pocha*[2], *S. Lanka*[2], *M. Hawkins*[2], *K. Harris*[2];
[1]*Mayo Clinic, Rochester, MN, UNITED STATES OF AMERICA,*
[2]*Tulane University, New Orleans, LA, UNITED STATES OF AMERICA.*

Aim/Introduction: Response to radiopharmaceuticals remains incompletely understood despite pre-treatment imaging being a well established biomarker. Herein we explore the possibility of using circulating tumor DNA (ctDNA) as a prognostic biomarker for metastatic castrate resistant prostate cancer (mCRPC) treated with PSMA-617 Lu-177 (PSMA Lu-177) + standard of care (SOC). ***Materials and Methods:*** Blood for ctDNA (Guardant360 assays) was obtained <50 days before treatment with PSMA Lu-177 + SOC. This assay uses deep sequencing to assess mutations in 83 genes, deletions in 7 genes, and amplification in 17 genes. All assessed genes are implicated in cancer growth, progression, and/or metastases. PSMA Lu-177 responses were assessed by PSA declines (>50% decline or not). Patients selection for treatment used VISION criteria for inclusion/exclusion. ***Results:*** Fourty-four patients had baseline ctDNA. Of these 28/44 (63.6%) had a PSA response., whereas 16/44 (36.3%) did not. Unresponsive patients were more likely to have amplifications detected in their ctDNA assays; 75% vs 39.2% (P=0.03). When examining alterations on a gene by gene basis, three genes were distinct. Amplification in CCNE1 and FGFR1 and pathogenic mutations in CDK12 were more frequently detected in patients without a PSA response. A total of 0% of responders had CCNE1 amplification vs 31.2% of non-responders (P=0.004). Responders had 0% FGFR1 amplifications vs 25% of non-responders (P=0.01). For CDK12, 3.6% of responders were pathologically mutated compared to 25% of non-responders (P=0.05). ***Conclusion:*** CCNE1 and FGFR1 amplifications and CDK12 pathogenic mutations are associated with resistance to PSMA Lu-177 therapy in mCRPC patients. Alterations in each of these genes are implicated in other studies of drug resistance, including resistance to DNA damaging agents such as platinum. Limitations include a small sample sizes and a single institution study. In addition, Guardant assays are known to incompletely assess ctDNA alterations in prostate cancer. More and larger studies with more complete ctDNA assessments are needed to confirm these initial findings.

OP-337

Implementation of PSMA-PET/CT improves treatment outcomes after salvage radiotherapy for recurrent or persistent prostate cancer after surgery

C. Zamboglou[1,2], *P. Staus*[3], *M. Wolkewitz*[3], *N. S. Schmidt Hegemann*[4], *T. Wiegel*[5], *L. Emmett*[6], *S. Fanti*[7], *A. L. Grosu*[2], *S. Koerber*[8], *S. G. C. Kroeze*[9], *F. Ceci*[10], *J. C. Peeken*[11], *S. Hayoz*[12], *D. M. Aebersold*[13], *A. Vrachimis*[1], *P. Ghadjar*[14];
[1]*German Oncology Center, Limassol, CYPRUS,* [2]*Department of Radiation Oncology, University of Freiburg - Medical Center, Freiburg, GERMANY,* [3]*Institute of Medical Biometry and Statistics, Division Methods in Clinical Epidemiology, Faculty of Medicine and Medical Center, University of Freiburg, Freiburg, Germany, Freiburg, GERMANY,* [4]*Department of Radiation Oncology, University of Munich, Munich, GERMANY,* [5]*Department of Radiation Oncology, University of Ulm, Ulm, GERMANY,* [6]*St VIncent's Public Hospital Sydney, University of New South Wales, Sydney, AUSTRALIA,* [7]*Department of Nuclear Medicine, University of Bologna, Bologna, ITALY,* [8]*Department of Radiation Oncology, University of Heidelberg, Heidelberg, GERMANY,* [9]*Department of Radiation Oncology, University of Zuerich, Zuerich, SWITZERLAND,* [10]*European Institute of Oncology, Milano, ITALY,* [11]*Department of Radiation Oncology, Technical University of Munich, Munich, GERMANY,* [12]*Swiss Group for Clinical Cancer Research (SAKK), Bern, SWITZERLAND,* [13]*Department of Radiation Oncology, University of Bern, Bern, SWITZERLAND,* [14]*Department of Radiation Oncology, Charite Berlin, Berlin, GERMANY.*

Aim/Introduction: Due to its high diagnostic accuracy and impact on the treatment decision making, prostate-specific membrane antigen positron emission tomography (PSMA-PET) is increasingly used to guide salvage radiotherapy (sRT) for prostate cancer patients with prostate specific antigen (PSA) persistence or relapse after prostatectomy. Whether the implementation of PSMA-PET is leading to improved outcomes in these patients is not answered yet. ***Materials and Methods:*** Patients who underwent sRT from two separate patient cohorts were included. Cohort 1 consists of 344 patients from the phase III SAKK 09/10 trial (no PSMA-guided sRT). Cohort 2 consists of 1201 patients from a retrospective multicentre cohort (12 hospitals, 5 countries, PSMA-guided sRT). Patients with positive lymph nodes in primary surgery, initial cM1 status, cM1 status on PET imaging, PSA>0.5 ng/ml and with missing stratification variables were excluded. Subsequently, the cohorts were balanced (inverse probability of treatment weighting) based on ISUP score, PSA before sRT, PSA recurrence vs. persistence and pT/R status in surgery. Finally, biochemical recurrence-free survival (BRFS) and recurrence patterns were compared. Biochemical recurrence was defined as PSA nadir after sRT +0.2 ng/ml. ***Results:*** In total, 654 patients (cohort 1 and 2: 256 and 398) with median follow-up of 75 and 36 months (cohort 1 and 2) were included. The cohorts were well balanced (standardized mean differences <0.1). The delivered sRT dose to the fossa/local relapse in PET was <66 Gy in 188 (49%) and 41 (10%), 66-70 Gy in 194 (51%) and 201 (51%) and 70 Gy in 0 and 150 (38%) patients of cohort 1 and 2, respectively. In cohort 1 no patient had androgen deprivation therapy (ADT) and no sRT to elective pelvic lymph nodes (PLN) was performed. In cohort 2, 70 (82.2%) patients had PET-positive pelvic LNs, two (0.5%) patients received ADT and in 86 (21.6%) patients PLNs were irradiated.

Three years BRFS rates were 70% (95%CI 64-77%) and 78% (95%CI 73-83%) for cohort 1 and 2 (p=0.012, weighted log-rank test). Recurrence patterns showed that within the first 3 years, 33 (83%) and 14 (58%) of the patients in cohort 1 and 2, respectively, had relapse in regional or distant lymphatics. ***Conclusion:*** Our data suggests a significant improvement in BRFS with the inclusion of PSMA-PET for sRT guidance. One possible reason is the individualized coverage of local and regional disease in the sRT field based on PET . Currently, prospective studies are ongoing to validate this finding.

OP-338

LuTectomy: phase 1/2 study evaluating dosimetry, safety and potential benefit of pre-surgery [^{177}Lu]Lu-PSMA-617 radioligand therapy in patients with high-risk localised prostate cancer

M. Hofman[1], *R. Eapen*[1], *J. P. Buteau*[1], *P. Jackson*[1], *C. Mitchell*[1], *S. Oon*[1], *O. Alghazo*[2], *L. McIntosh*[1], *N. Dhiantravan*[3], *J. O'Brien*[1], *A. McVey*[1], *S. Sandhu*[1], *A. A. Azad*[1], *S. G. Williams*[1], *G. Sharma*[1], *B. Emmerson*[1], *M. B. Haskali*[1], *M. Bressel*[1], *D. Moon*[1], *N. Lawrentschuk*[1], *P. Neeson*[1], *D. G. Murphy*[1];
[1]*Peter MacCallum Cancer Centre, Melbourne, AUSTRALIA,* [2]*Flinders University, Adelaide, AUSTRALIA,* [3]*Royal Brisbane & Women's Hospital, Brisbane, AUSTRALIA.*

Aim/Introduction: High-risk localised prostate cancer (HRCaP) is associated with high chances of local and systemic recurrence. ^{177}Lu-PSMA-617 (LuPSMA) is effective for patients with metastatic castration-resistant prostate cancer. LuTectomy is a phase I/II study evaluating LuPSMA in men with HRCaP before undergoing radical prostatectomy (RP). The primary objective was to measure tumour radiation absorbed dose. ***Materials and Methods:*** Patients with HRCaP (PSA >20 ng/mL, ISUP grade group (GG) 3-5, ≥cT2c or N1), high tumour uptake (SUVmax≥20) on ^{68}Ga-PSMA-11 PET/CT and scheduled for RP were eligible. Cohort A (n=10) received 1 cycle of 5GBq LuPSMA and Cohort B (n=10) received 2 cycles of 5GBq LuPSMA followed by RP scheduled 6 weeks after treatment completion. Radiation dose was estimated using post-therapy SPECT/CT at 4, 24 and 96 hours utilising voxel-based 3-phase exponential clearance model with partial-volume correction. Adverse events (AE) [CTCAE v5], surgical safety [Clavien-Dindo], PSA decline≥50% (PSA50-RR) at 6 weeks post-LuPSMA were evaluated. ***Results:*** 20 patients with a median age of 66 and median PSA (IQR) of 18 (11-35) ng/mL were enrolled 5/2020-4/2022. 6/20 (30%) had N1 disease. The median (IQR) baseline SUVmax was 31 (26-36).The median (IQR) highest tumour absorbed dose after cycle 1 for all lesions was 36Gy (20-50) with a median of 20Gy (11-48) for the prostate and 38Gy (33-50) for lymph nodes.PSA50-RR occurred in 9/20 (45%). AE were mainly G1 including fatigue (8), dry mouth (7), nausea (6) and lymphopenia (5). One patient in cohort B developed Grade 1 thrombocytopenia that precluded a 2nd dose of LuPSMA as per protocol. No grade 3/4 toxicities.All patients underwent robotic RP, with PLND in 18/20. Surgical difficulty levels were similar to expected for 15/20 (75%) of men, with minor increase in surgical difficulty in 5 pts. Length of hospitalisation was 1 night in 19/20 (95%) and urinary catheters were removed by day 17 in all patients. No Clavien 3-5 complications were recorded. 16/20 (80%) had evidence of treatment effect on histopathology and one patient had minimal residual disease in the prostate. No complete pathologic responses were seen. ***Conclusion:*** LuPSMA before RP in men with HRCaP delivered high radiation doses with few toxicities and without compromising surgical safety. Significant PSA reductions were achieved. LuPSMA in this setting warrants further evaluation ***References:*** [1] Clinical Trial Protocol: doi: 10.1016/j.euf.2020.09.021

OP-339

Lutetium-177-PSMA-617 in oligo-metastatic hormone sensitive prostate cancer (Bullseye)

B. Privé[1], *C. H. J. Muselaers*[1], *D. Meijer*[2], *W. A. Van Gemert*[1], *B. Timmermans*[1], *M. J. R. Janssen*[1], *M. A. Jonker*[1], *M. de Groot*[1], *I. M. van Oort*[1], *N. Mehra*[1], *W. R. Gerritsen*[1], *E. Alevroudis*[3], *A. Vrachimis*[3], *J. A. Gietema*[4], *M. Gotthardt*[1], *A. N. Vis*[2], *I. J. de Jong*[4], *A. J. Witjes*[1], *W. Noordzij*[4], *D. E. Oprea-Lager*[2], *J. Nagarajah*[1];
[1]*Radboudumc, Nijmegen, NETHERLANDS,* [2]*Amsterdam University Medical Centers, Amsterdam, NETHERLANDS,* [3]*German Oncology Center, Limassol, CYPRUS,* [4]*University Medical Center Groningen, Groningen, NETHERLANDS.*

Aim/Introduction: [^{177}Lu]Lu-PSMA-617 radioligand therapy (RLT) is a novel treatment for patients with metastatic castration resistant prostate cancer. Previously, we showed that [^{177}Lu]Lu-PSMA-617 could be offered to patients with PSMA-expressing oligometastatic hormone-sensitive prostate cancer (HSPC), with encouraging results and minimal toxicity (CCR, 2021). Due to [^{177}Lu]Lu-PSMA-617 RLT, androgen deprivation therapy (ADT) could be postponed and thus delaying the time to ADT-related toxicity. We hereby report interim results of a randomized trial analyzing the time without ADT using [^{177}Lu]Lu-PSMA-617 RLT versus deferred ADT (current standard of care; SoC). ***Materials and Methods:*** This is an ongoing international, multicenter, open-label, randomized phase 2 trial (NCT04443062). Fifty-eight patients will be randomized in a 1:1 ratio. Eligibility consists of fast-progressing HSPC (PSA doubling time <6 months) following local treatment, with a maximum of 5 metastases on [^{18}F]PSMA-PET/CT. Patients can receive 2+2 cycles of 7.4 GBq [^{177}Lu]Lu-PSMA-617. The primary outcome is progression-free survival (i.e., ADT free time). Progressive disease (PD) is defined as the initiation of ADT, a 100% increase in PSA since randomization, and radiographic or clinical progression. Secondary outcomes are PSA response and toxicity, following CTCAE v5.0. ***Results:*** To date (April 3rd, 2023), 42 patients were included. Their median PSA at inclusion was 4.5 ng/mL (range: 1.3 - 38). During a median follow-up of 6 months (range 1-20 months), 77% (17/22) and 10% (2/20) of the SoC and [^{177}Lu]Lu-PSMA-617 arm, respectively, reached the definition for PD. The median progression-free survival was 4 months in the SoC arm vs. not reached in the [^{177}Lu]Lu-PSMA-617 arm (HR 0.03; 95% CI 0.004 to 0.227; p < 0.001). The most common treatment-related adverse events were grade 1 xerostomia (70%), grade 1 fatigue (61%), grade 1 nausea (35%), grade 1 bone marrow toxicity (30%). Grade ≥2 adverse events were observed in less than 10% of patients. One patient developed grade 3 xeropthalmia and grade 2 xerostomia. The median percentage PSA change was +114% vs. -91% in the SoC vs. [^{177}Lu]Lu-PSMA-617 arm, respectively. At present, 55% (11/20) of the patients that underwent treatment had a PSA drop exceeding 90%, with five patients having a complete biochemical response. ***Conclusion:*** [^{177}Lu]Lu-PSMA-617 RLT shows promising efficacy in oligometastatic HSPC patients to defer from ADT, with minimal and mostly transient side effects. After surgery and external beam radiotherapy, [^{177}Lu]Lu-PSMA-617 could become a third metastases-directed therapeutic option for oligometastatic hormone-sensitive prostate cancer patients, to prolong the ADT-free interval.

OP-340

Association of baseline quantitative [68Ga]Ga-PSMA-11 PET imaging parameters with clinical outcomes in patients with mCRPC receiving [177Lu]Lu-PSMA-617: a VISION sub-study

P. H. Kuo[1], *M. Morris*[2], *A. T. Kendi*[3], *K. Rahbar*[4], *X. X. Wei*[5], *B. Fang*[6], *A. J. Armstrong*[7], *J. Hesterman*[8], *K. Chi*[9], *J. de Bono*[10], *K. Fizazi*[11], *B. Krause*[12], *O. Sartor*[3], *S. T. Tagawa*[13], *S. Ghebremariam*[14], *M. Brackman*[15], *C. Wong*[16], *A. M. Catafau*[17], *T. Benson*[18], *K. Herrmann*[19];
[1]*University of Arizona, Tucson, AZ, UNITED STATES OF AMERICA,* [2]*Memorial Sloan Kettering Centter, New York City, NY, UNITED STATES OF AMERICA,* [3]*Mayo Clinic, Rochester, MN, UNITED STATES OF AMERICA,* [4]*University Hospital Münster, Münster, GERMANY,* [5]*Dana-Farber Cancer Institute, Boston, MA, UNITED STATES OF AMERICA,* [6]*Astera Cancer Care, East Brunswick, NJ, UNITED STATES OF AMERICA,* [7]*Duke Cancer Institute Center for Prostate and Urologic Cancers, Durham, NC, UNITED STATES OF AMERICA,* [8]*Invicro, Needham, MA, UNITED STATES OF AMERICA,* [9]*British Columbia Cancer Agency, Vancouver Centre, Vancouver, BC, UNITED STATES OF AMERICA,* [10]*The Institute of Cancer Research and Royal Marsden Hospital, London, UNITED KINGDOM,* [11]*Gustave Roussy Institute, University of Paris Saclay, Villejuif, FRANCE,* [12]*Rostock University Medical Center, Rostock, GERMANY,* [13]*Weill Cornell Medicine, New York City, NY, UNITED STATES OF AMERICA,* [14]*Novartis Pharmaceuticals Corporation, East Hanover, NJ, UNITED STATES OF AMERICA,* [15]*Novartis Pharmaceuticals Corporation, Indianapolis, IN, UNITED STATES OF AMERICA,* [16]*Novartis Pharmaceuticals Corporation, Cambridge, MA, UNITED STATES OF AMERICA,* [17]*Novartis Pharmaceuticals Corporation, Geneva, SWITZERLAND,* [18]*Novartis Pharmaceuticals Corporation, St George, UT, UNITED STATES OF AMERICA,* [19]*University Hospital Essen, Essen, GERMANY.*

Aim/Introduction: In the phase 3 VISION study, patients with PSMA-positive metastatic castration-resistant prostate cancer (mCRPC) benefited from addition of lutetium (^{177}Lu) vipivotide tetraxetan ([^{177}Lu]Lu-PSMA-617, ^{177}Lu-PSMA-617) to standard of care (SoC). This sub-study aimed to correlate the pattern and level of PSMA expression at baseline with response to ^{177}Lu-PSMA-617 targeted radioligand therapy. ***Materials and Methods:*** In VISION, lesion PSMA positivity was visually assessed as greater than liver uptake on ^{68}Ga-PSMA-11 PET. In this exploratory post hoc analysis, quantitative ^{68}Ga-PSMA-11 PET parameters were based on standardized uptake values (SUVs) in bone, lymph node, liver, soft tissue and whole body. SUV_{mean}, SUV_{max}, PSMA-positive tumour volume, tumour load and presence of PSMA-positive lesions by disease site were assessed for associations with efficacy outcomes. All patients randomized were eligible for quantitative analysis, 551 in the ^{177}Lu-PSMA-617 plus SoC arm and 280 in the SoC alone arm. The study was not powered for post hoc analyses. ***Results:*** Analysable ^{68}Ga-PSMA-11 PET scans from 826 patients were included. Baseline quantitative ^{68}Ga-PSMA-11 PET parameters were well balanced between the study arms. rPFS and OS were prolonged with ^{177}Lu-PSMA-617 plus SoC versus SoC alone in all whole-body SUV_{mean} quartiles. In the highest quartile (rPFS, ≥10.1; OS, ≥9.9), hazard ratio (HR) was 0.34 (95% CI: 0.20-0.56) for rPFS (median: 13.8 vs 3.9 months) and 0.47 (0.32-0.68) for OS (median: 21.4 vs 15.0 months). In the lowest quartile (rPFS, <6.0; OS, <6.0), HR was 0.75 (0.45-1.26) for rPFS (median: 5.8 vs 4.0 months) and 0.87 (0.60-1.27) for OS (median: 14.5 vs 11.3 months). rPFS and OS differed significantly between the treatment and control arms at all SUV_{mean} cut-points and no optimal cut-point was identifiable. Whole-body tumour load and presence of lesions in bone or liver (as compared with node only) on ^{68}Ga-PSMA-11 PET were associated with increased rPFS and OS event risk in both arms of the study. ***Conclusion:*** Baseline ^{68}Ga-PSMA-11 SUV_{mean} was predictive of ^{177}Lu-PSMA-617 efficacy in patients with PSMA-positive mCRPC in the VISION study. Among patients with higher SUV_{mean}, addition of ^{177}Lu-PSMA-617 to SoC resulted in greater improvements in rPFS and OS. Nevertheless, ^{177}Lu-PSMA-617 improved outcomes across all SUV_{mean} quartiles and at all SUV_{mean} cut-points. Higher SUV_{mean} values indicate higher PSMA expression, which may increase ^{177}Lu-PSMA-617 tumour dose and enhance anti-tumour activity. These results indicate that the VISION ^{68}Ga-PSMA-11 PET eligibility criteria identify patients with widely ranging tumour PSMA expression, but who are suitable candidates for ^{177}Lu-PSMA-617 treatment.

801

Monday, September 11, 2023, 09:45 - 11:15

Hall A

CME 6 - Dosimetry Committee: Understanding Radiobiology for Dosimetry-Guided Molecular Radiotherapy

OP-341

General Aspects of Radiobiology Applied to Molecular Radiotherapy

J. Pouget;
Cancer Research Institute/INSERM, Montpellier, FRANCE.

OP-342

Radiobiological Aspects Applied to Different Molecular Radiotherapies

D. Taieb;
La Timone University Hospital, Department of Nuclear Medicine, Marseille, FRANCE.

OP-343

Relevance of the Absorbed Dose, Fractionation, and Time Interval Between Cycles

L. Strigari;
Universityof Bologna, Department of Medical and Surgical Sciences, Bologna, ITALY.

OP-344

Particular Aspects of the Radiobiology of Alpha and Beta Emitters

J. Nonnekens;
Erasmus Medical Center, Department of Radiology and Nuclear Medicine, Rotterdam, NETHERLANDS.

802

Monday, September 11, 2023, 09:45 - 11:15

Hall D (Arena)

Round Table 1 - Translational Molecular Imaging & Therapy + Oncology & Theranostics + Radiopharmaceutical Sciences Committee: Dialogue with the Treating Physician

OP-345

Dialogue with the Treating Physician - Immunoocologist

A. Digklia;
Centre hospitalier universitaire Vaudois, Department of Oncology, Lausanne, SWITZERLAND.

OP-346
Dialogue with the Treating Physician - Cardiologist
C. Kamani;
Leeds Teaching Hospitals NHS Trust, Cardiorespiratory Department, Leeds, UNITED KINGDOM.

OP-347
Dialogue with the Treating Physician - Urologist
T. Maurer;
Universitätsklinikum Hamburg-Eppendorf, Martini-Klinik, Department of Urology, Hamburg, GERMANY.

OP-348
Dialogue with the Treating Physician - Dermatologist
E. Guenova-Hoetzenecker;
CHUV, Department of Dermatology, Lausanne, SWITZERLAND.

OP-349
Dialogue with the Treating Physician - Nuclear Medicine Physician
E. Lopci;
RCCS – Humanitas Research Hospital, Nuclear Medicine, Department of diagnostic imaging, Rozzano, ITALY.

OP-350
Dialogue with the Treating Physician - Radiopharmacist
P. Laverman;
Radboud University Medical Center, Department of Radiology and Nuclear Medicine, Nijmegen, NETHERLANDS.

803

Monday, September 11, 2023, 09:45 - 11:15
Hall E1

LIPS Session 6 - Neuroimaging + Cardiovascular + Inflammation & Infection Committee: Molecular Imaging to Solve the Problem of Long COVID

OP-351
The lung impairment in long COVID
D. Albano;
NuclearMedicine, University of Brescia and Spedali Civili Brescia, Brescia, ITALY.

OP-352
The vascular impairment in long COVID
M. Sollini;
Department of Biomedical Sciences, Humanitas University, Milan, ITALY.

OP-353
The brain impairment in long COVID
E. Guedj;
Aix Marseille Universite, APHM, CNRS, Centrale Marseille, Institut Fresnel, Timone Hospital, CERIMED, Nuclear Medicine Department, Marseille, FRANCE.

804

Monday, September 11, 2023, 9:45 AM - 11:15 AM
Hall E2

M2M Track - TROP Session: TME and Therapy: Direct Targeting and Secondary Effects

OP-355
Optimisation of FAP-targeted radionuclide therapy through molecular evolution of OncoFAP derivatives and combination with immunocytokines
A. Galbiati[1], *M. Bocci*[1], *E. Gilardoni*[1], *J. Mock*[1], *D. Neri*[2], *S. Cazzamalli*[1];
[1]*Philochem AG, Otelfingen, SWITZERLAND,* [2]*Philogen, Siena, ITALY.*

Aim/Introduction: Fibroblast Activation Protein (FAP) is abundantly expressed on the surface of stromal cells of the majority of solid human cancers. High-affinity small molecule FAP ligands labelled with ^{18}F or ^{68}Ga, are excellent diagnostic tools for the detection of lesions in many different types of cancer. [1,2] For therapeutic applications, more stringent requirements on affinity are needed, as ligands need to remain at the tumor site for several days, with negligible uptake in normal organs. We have recently identified OncoFAP, an ultra-high affinity small molecule ligand of FAP whose targeting performance has been validated in patients with a wide variety of solid malignancies.[3,4] Here, we describe the development of novel OncoFAP-based RLTs with enhanced tumor uptake and residence time. Combination therapy with a targeted cytokine (L19-IL2, a clinical-stage tumor-targeted interleukin2) strongly potentiates the anticancer efficacy of OncoFAP-based RLTs. ***Materials and Methods:*** We exploited DNA-encoded chemical libraries and conventional medicinal chemistry approaches to mature OncoFAP affinity. The novel derivatives were coupled to DOTAGA chelator, suitable for radiolabelling with ^{177}Lu. In vitro characterization was performed using recombinant human FAP and transfected FAP-expressing cell lines. Tumor-targeting properties and therapeutic efficacy of the novel derivatives were investigated in comparative biodistribution and therapy studies, alone and in combination with L19-IL2. ***Results:*** BiOncoFAP, OncoFAP-11 and OncoFAP-23 were identified as promising candidates from chemical engineering activities. ^{177}Lu-OncoFAP-23 emerged for its superior uptake and residence time in tumors (i.e., ~20% ID/g at 24 h and ~16% ID/g at 96 h) and for its favorable tumor-to-kidney ratio (i.e., ~17-to-1 at 24 h and ~22-to-1 at 96 h). Moreover, when administered at very low doses (e.g., 250 MBq/kg), ^{177}Lu-OncoFAP-23 exhibited an enhanced anticancer activity compared to other ^{177}Lu-labeled OncoFAP derivatives. ^{177}Lu-OncoFAP-23 showed a dose-dependent therapeutic activity and strong synergism with L19-IL2. Mechanistic studies revealed a potent activation of NK cells, with a significant enhancement of the expression of biocidal granzymes and perforin-1 after combination treatment. ***Conclusion:*** Our findings demonstrate the superior tumor uptake and residence time of OncoFAP-23 compared to other FAP-targeted ligands. The combination with L19-IL2 represents an avenue to achieve promising anti-tumor activity at low activities, thus further reducing the radioactive burden. ***References:*** 1.Calais J et al. J Nucl Med. 2020;61(2):163.

doi: 10.2967/jnumed.119.241232. 2.Kratochwil C et al. J Nucl Med. 2019;60:801-805. doi: 10.2967/jnumed.119.227967. 3.Millul J et al. Proc National Acad Sci. 2021;118:e2101852118. doi: 10.1073/pnas.2101852118. 4.Backhaus P et al. Eur J Nucl Med Mol Imaging. 2022 May;49(6):1822-1832. doi: 10.1007/s00259-021-05653-0.

OP-356

Tumor-targeted Interleukin-2 Boosts the Anti-cancer Activity of FAP-directed Radioligand Therapeutics

P. Backhaus[1,2], *P. Dorten*[2], *A. Galbiati*[3], *E. Gilardoni*[3], *F. Gierse*[2], *M. Bocci*[3], *A. Zana*[3], *J. Mock*[3], *M. Claesener*[1], *J. Cufe*[1], *F. Büther*[1], *K. Schäfers*[2], *S. Hermann*[2], *D. Neri*[4,5], *M. Schäfers*[1], *S. Cazzamalli*[3];
[1]*University Hospital Münster, Münster, GERMANY,* [2]*European Institute for Molecular Imaging, University of Münster, Münster, GERMANY,* [3]*Philochem AG, R&D department, Otelfingen, SWITZERLAND,* [4]*Swiss Federal Institute of Technology, Department of Chemistry and Applied Biosciences, Zurich, SWITZERLAND,* [5]*Philogen S.p.A, Siena, ITALY.*

Aim/Introduction: We studied the anti-tumor efficacy of a combination of Lutetium-177-labelled Radio Ligand Therapeutics (RLTs) targeting the Fibroblast Activation Protein (OncoFAP and BiOncoFAP) with the antibody-cytokine fusion protein L19-IL2 providing targeted delivery of Interleukin-2 to tumors. ***Materials and Methods:*** The biodistribution of ^{177}Lu-OncoFAP and ^{177}Lu-BiOncoFAP was studied in mice bearing subcutaneous HT-1080.hFAP tumors via SPECT/CT at different molar amounts (3 nmol/kg vs 250 nmol/kg) of injected ligand and self-absorbed tumor and organ doses were calculated. In vivo anti-cancer effect of 5 MBq of the radiolabelled preparations was evaluated as monotherapy or in combination with L19-IL2 in subcutaneously implanted HT-1080.hFAP and SK-RC-52.hFAP tumors. Tumor samples from animals treated with ^{177}Lu-BiOncoFAP and/or with L19-IL2 were analyzed by mass spectrometry-based proteomics to identify therapeutic signatures on cellular and stromal markers of cancer, and on immunomodulatory targets. ***Results:*** ^{177}Lu-BiOncoFAP led to significantly higher self-absorbed dose in FAP-positive tumors (0.293 ± 0.123 Gy/MBq) compared to ^{177}Lu-OncoFAP (0.157 ± 0.047 Gy/MBq, p=0.01), and demonstrated favorable tumor-to-organ ratios at high molar amounts of injected ligand. Administration of L19-IL2 or ^{177}Lu-BiOncoFAP as single agents led to cancer cures only in a limited number of treated animals. In ^{177}Lu-BiOncoFAP + L19-IL2 combination therapy, complete remissions were observed in all injected mice (7/7 C.R. for the HT-1080.hFAP model, and 4/4 C.R. for the SK-RC-52.hFAP model), suggesting therapeutic synergy. Proteomic studies revealed a mechanism of action based on the activation of NK cells, with a significant enhancement of the expression of granzymes and perforin-1 in the tumor microenvironment after combination treatment. ***Conclusion:*** The combination of OncoFAP-based RLTs with concurrent targeting of interleukin-2 shows synergistic anti-cancer effects in the treatment of FAP-positive tumors. This experimental finding should be corroborated by future clinical studies.

OP-357

FAP directed target modules for UniCAR T cell therapy and radionuclide-based tumour theranostics

C. Neuber*, L. Loureiro, L. Hoffmann, M. Kubeil, C. Arndt, A. Feldmann, M. Bachmann;*
Helmholtz-Zentrum Dresden-Rossendorf, Dresden, GERMANY.

Aim/Introduction: Expression of fibroblast activation protein (FAP) is restricted to activated fibroblasts. In line with this, there is very limited FAP expression on healthy adult tissue. As FAP is mainly found on cancer-associated fibroblasts (CAFs) in the tumour stroma, it is a widespread tumour target and a variety of attempts have been made to address FAP using radiotracers. Our aim is to use FAP not only as a target for radionuclide-based tumour theranostics but also to address this protein via UniCAR T cell therapy. The modular universal chimeric antigen receptor (UniCAR) platform is a promising immunotherapeutic approach that reduces the risk for on-target/off-tumour toxicities and cytokine release syndrome since the UniCAR T cells are exclusively activated in the presence of a target module (TM) that specifically establishes the crosslinking between target cells and UniCAR T cells. ***Materials and Methods:*** We established TMs by fusing the single-chain variable fragment (scFv) of an anti-human FAP mAb to the peptide epitope E5B9 that is recognized by UniCAR T cells. In addition to this low molecular weight TM (αFAP scFv) that is rapidly eliminated, a TM based on the human IgG4 Fc-domain with an extended half-life was developed (αFAP IgG4). TMs were charcterized for their potetial in UniCAR T cell therapy and as FAP-directed radiotracers. ***Results:*** Both αFAP TMs bind to FAP-expressing cells with a K_d in the low nanomolar range and enabled specific killing of FAP-positive tumour cells by UniCAR T cells both in vitro and in vivo. In addition, αFAP TMs were conjugated to different chelators, e.g. Bispidines, NODAGA, and CHX-A-DTPA to allow for radiolabelling with either Copper-64 or Lutetium-177 for PET and SPECT imaging, respectively. PET and SPECT imaging in NMRI nude mice bearing both FAP-negative and FAP-overexpressing HT1080 tumours revealed an excellent FAP-specific tracer enrichment at the FAP-positive tumour site, especially for αFAP IgG4, resulting in SUV_{mean} up to 25 with almost no background. Considering the results found with ^{177}Lu-radiolabelled αFAP IgG4, also regarding tumour growth, this TM is a promising candidate for not only diagnostic imaging but also targeted radionuclide therapy. ***Conclusion:*** We demonstrated suitability of novel FAP specific TMs with different molecular weights not only for immunotherapeutic approaches using UniCAR T cells but also for diagnostic PET and SPECT imaging as well as targeted radionuclide therapy. Given their immunotherapeutic as well as radionuclide-based theranostic potential these TMs might be able to improve individualized cancer therapy.

OP-358

Evaluation of Therapeutic and Immunological Action of CAIX-Targeted Lutetium-177 Radionuclide Therapy Combined with Immune Checkpoint Inhibition

S. Kleinendorst[1], *M. Konijnenberg*[1], *G. Franssen*[1], *J. Molkenboer-Kuenen*[1], *S. Wenker*[1], *D. Boreel*[1], *D. Kroon*[1], *M. Gloudemans*[1], *K. Twumasi-Boateng*[2], *M. Wheatcroft*[2], *E. Oosterwijk*[3], *S. Heskamp*[1];
[1]*Department of Medical Imaging, Radboud University Medical Center, Nijmegen, NETHERLANDS,* [2]*Telix Pharmaceuticals Ltd., Melbourne, AUSTRALIA,* [3]*Department of Urology, Radboud University Medical Center, Nijmegen, NETHERLANDS.*

Aim/Introduction: Treatment response to immunotherapy differs widely among tumours, which is often reliant on their immunogenicity. Shifting this immunogenic phenotype towards a more responsive one is an attractive approach to enhance tumour sensitivity to immune checkpoint inhibition (ICI). This is exemplified by the in situ vaccination effect that can result from ionizing radiation, releasing neo-antigens and triggering inflammatory signalling. We aim to evaluate therapeutic action of combined targeted radionuclide therapy (TRT) and ICI in mouse tumour models of distinct immunogenicity. ***Materials and Methods:*** Renca-hCAIX or CT26-hCAIX tumour cells were injected subcutaneously in the flank of Balb/c mice. Tumour PD-L1 and

CD3 expression was characterized by immunohistochemistry. For therapeutic experiments, treatment was initiated when tumours reached 50-100mm^3. Subsequently, tumour-bearing mice were randomized as follows: (1) control, (2) ICI, (3) TRT ([^{177}Lu]Lu-DOTA-hG250, recognizing hCAIX), (4) TRT+ICI combination. Each tumour growth curve was quantified as mean tumour volume (MTV) and reported as median with interquartile range. Mice with complete tumour regressions were re-challenged with hCAIX-positive and hCAIX-negative tumour cells. In a follow-up experiment, Renca-hCAIX tumour-bearing mice will be sacrificed at 0, 5, or 8 days after treatment and immunological TME changes will be characterized by flow cytometry, immunohistochemistry, and transcriptional profiling. ***Results:*** Renca-hCAIX tumours were classified as poorly immunogenic with homogeneous PD-L1 expression and poor T cell infiltration, whereas CT26-hCAIX tumours showed heterogeneous PD-L1 expression and extensive T cell infiltration, thus were classified as highly immunogenic. The pharmacokinetic and pharmacodynamic behaviour of [^{177}Lu]Lu-DOTA-hG250 was comparable for both tumour models. Therapy studies demonstrated significantly reduced tumour growth after combined treatment regimens (11 or 32 Gy TRT with aPD1+aCTLA4 for Renca-hCAIX and 11 Gy TRT with aPD1 for CT26-hCAIX) compared with control groups ($MTV_{11Gy+ICI}$="58(70)"mm^3 and $MTV_{32Gy+ICI}$="55(61)"mm^3 vs $MTV_{control}$="270(320)"mm^3, $p<0.01$ for Renca-hCAIX, and $MTV_{11Gy+ICI}$="23(42)"mm^3 vs $MTV_{control}$="344(161)"mm^3, $p<0.05$ for CT26-hCAIX). Only for Renca-hCAIX, tumour control was significantly better after combination therapy compared with TRT alone (MTV_{11Gy}="414(280)"mm^3, $p<0.05$ and MTV_{32Gy}="166(179)"mm^3, $p<0.05$). Furthermore, complete tumour regression was most frequent after combination treatments (80% for Renca-hCAIX and 78% for CT26-hCAIX) and re-challenge of these mice resulted in 100% rejection of hCAIX-positive cells and 94% and 17% rejection of parental Renca and CT26 cells, respectively. Preliminary immunohistochemistry experiments suggest increased DNA damage and neutrophil infiltration after TRT compared to control, and further TME characterization is ongoing. ***Conclusion:*** Combined TRT and ICI resulted in significant tumour control in both Renca-hCAIX and CT26-hCAIX models and complete tumour responses were abundantly observed.

OP-359

RAYZ-15170, a novel small-molecule binder to carbonic anhydrase IX (CA9) for targeted radiopharmaceutical therapy of clear cell renal cell carcinoma and other CA9 expressing tumors

N. Smith*, J. Tran, A. Lai, Y. Bravo, A. Cieniewicz, P. Mondala, R. Clift, T. Lo, G. Chen, G. Li, K. Lidberg, L. Nyiranshuti, S. Richardson, A. Hudson;*
RayzeBio, Inc., San Diego, CA, UNITED STATES OF AMERICA.

Aim/Introduction: Carbonic anhydrase IX (CA9) is a cell surface enzyme that plays a key role in microenvironmental pH regulation, cell growth, survival and migration, with limited expression in normal tissues. In up to 95% of clear cell renal cell carcinoma (ccRCC), loss of Von Hippel Lindau function results in overexpression of CA9 and is associated with worse prognosis. Compared to the long circulating half-life of antibodies, a small-molecule, CA9-targeting radiopharmaceutical therapy (RPT) with selectivity over related CA isozymes such as CA12 that are more widely expressed in normal tissues, would provide a valuable way to treat ccRCC and other CA9 expressing tumors. ***Materials and Methods:*** RAYZ-15170 is comprised of a small-molecule CA9 binder attached to a DOTA chelator that is used to complex different radioisotopes. The affinity of RAYZ-15170 to mouse, monkey and human CA9 and CA12 was determined by surface plasma resonance (SPR), and cell-based potency was determined in a HT-29 cell-line in which CA12 had been knocked out. In vivo biodistribution of RAYZ-15170 was examined using both SPECT imaging and ex-vivo cut/count techniques in SK-RC-52 tumor bearing mice (ccRCC tumor line). Anti-tumor efficacy studies were also performed in SK-RC-52 tumor-bearing mice with both ^{225}Ac and ^{177}Lu constructs. ***Results:*** ^{175}Lu-RAYZ-15170 showed potent binding affinity to human CA9 with a K_D of 0.094 nM and high selectivity over human CA12 of >1,500x. Binding affinity was maintained across mouse, monkey and human CA9. Potent cell-binding of ^{175}Lu-RAYZ-15170 was confirmed in a HT29 cell line (IC_{50} = 1.6 nM). In vivo biodistribution of ^{177}Lu-RAYZ-15170 in SK-RC-52 tumor bearing mice using SPECT imaging showed sustained tumor uptake of 10, 8.1, 8.0 and 5.4 %ID/g at 2, 24, 48, and 96 hours, respectively. Uptake was low in kidney, stomach and intestines from the 24 hour time-point onward (%ID/g < 3%). Biodistribution measured by ex-vivo cut/count gave a similar result with tumor uptake of 19, 5.7 and 5.7 %ID/g at the 2, 24 and 48 hr time-points, and kidney, stomach and intestines wall <3% ID/g from 24 hours onward. Minimal uptake was observed in other normal tissues. Efficacy studies with ^{225}Ac and ^{177}Lu constructs showed significant tumor-growth regression and survival benefit in SK-RC-52 tumor-bearing mice. ***Conclusion:*** Preclinical in-vitro potency and selectivity together with biodistribution and efficacy data demonstrate the potential of RAYZ-15170 as a RPT agent for the treatment of patients with clear cell renal cell carcinoma (ccRCC) and other CA9 expressing tumors.

OP-360

[^{225}Ac]Ac-DPI-4452, a new peptide radioligand targeting Carbonic Anhydrase IX, displays strong anti-tumoral activity in colorectal cancer and clear cell renal cell carcinoma mouse models

N. Wiedemann*, A. Attinger, E. Da Costa Branquinho, U. Andersson;*
Debiopharm International SA, Lausanne, SWITZERLAND.

Aim/Introduction: The transmembrane metalloenzyme Carbonic Anhydrase IX (CAIX) is an attractive diagnostic and therapeutic target with expression in hypoxic tumor types such as colorectal cancer (CRC) and clear cell renal cell carcinoma (ccRCC) and a limited number of healthy organs. The cyclic peptide DPI-4452 selectively binds CAIX and its DOTA cage allows labelling with different radionuclides for diagnostic and therapeutic purposes. Previously, promising theranostic potential of [^{68}Ga]Ga-DPI-4452 and [^{177}Lu]Lu-DPI-4452 has been demonstrated in CRC and ccRCC xenograft mouse models. Here we characterized the ex vivo biodistribution and the in vivo efficacy of [^{225}Ac]Ac-DPI-4452 in CRC and ccRCC xenograft mouse models. ***Materials and Methods:*** CAIX-positive human cancer cell lines HT-29 (CRC) or SK-RC-52 (ccRCC) were subcutaneously implanted in immunodeficient mice. Treatments were initiated at a mean group tumor volume of 140-180 mm^3, and tumor volume and tolerability monitored. Groups of 7-10 mice received a single intravenous administration of either 15 kBq, 45 kBq or 135 kBq of [^{225}Ac]Ac-DPI-4452. Efficacy was assessed at 14 days post-treatment by one-way ANOVA and p-values below 0.05 deemed significant. Radioactivity uptake (as % of injected dose/gram tissue; %ID/g) in tumors, kidney, stomach, small and large intestine at secular equilibrium was assessed in separate groups of 4-5 mice 4h upon a single administration of 15 kBq of [^{225}Ac]Ac-DPI-4452 using an automated gamma counter.

Results: Mice displayed high radioactivity uptake in tumors 4h after administration of 15 kBq of [^{225}Ac]Ac-DPI-4452 as analyzed by ex vivo gamma counting, with SK-RC-52 tumors (39.1 %ID/g) showing more than 3-fold higher uptake than HT-29 tumors (11.3 %ID/g). Kidneys showed the highest non-target organ uptake with tumor-to-kidney ratios remaining above 1 in both models, whereas tumor-to-organ ratios were above 10 for the other organs. All [^{225}Ac]Ac-DPI-4452 treatments were well tolerated in both models as indicated by stable or increasing body weights. Significant dose-dependent tumor growth inhibition (TGI) was observed 14 days post-treatment in the 45 kBq (56% TGI) and 135 kBq (78% TGI) groups in the HT29 model, and for all 3 dose levels in the SK-RC-52 model (TGI of 57%, 64% and 67% for 15 kBq, 45 kBq and 135 kBq groups, respectively). ***Conclusion:*** [^{225}Ac]Ac-DPI-4452 displays promising therapeutic potential in CAIX-expressing CRC and ccRCC xenograft mouse models demonstrating that DPI-4452 is a versatile peptide radioligand suitable for use with the alpha-emitting radionuclide Ac-225 for efficacious treatment of CAIX-expressing tumors.

OP-361

Extracellular Matrix-Targeted Radionuclide Therapy Remodels Tumor Microenvironment Landscape and Enhances Immunotherapy in Triple-Negative Breast Cancer

L. Li, *Z. Zeng, F. Liu, X. Ma, B. Jia, Z. Yang;*
Peking University Cancer Hospital & Institute, Beijing, CHINA.

Aim/Introduction: Although immunotherapy has significantly impacted triple-negative breast cancer (TNBC) treatment, its benefits remain confined to a small patient subset, emphasizing the urgent need for immunomodulatory approaches that overcome resistance. In this study, we examined the potential of a targeted radionuclide therapy (TRT) method employing a novel nanobody-based therapeutic tracer (^{177}Lu-HMI02-ABD035) targeting the fibronectin, a key component of tumor extracellular matrix, as an immunomodulator to reshape the TNBC microenvironment and enhance immunotherapy effectiveness. ***Materials and Methods:*** We analyzed TCGA data to compare fibronectin expression in TNBC tumors and normal breast tissues. A novel nanobody (HMI02) was acquired by immunizing llama with fibronectin protein and fused with albumin binder ABD030 (HMI02-ABD035) to extend its blood half-life. ^{177}Lu radiolabeling was achieved via the chelator DOTA that was site-specifically attached to the C terminus of HMI02-ABD035. Micro SPECT imaging, biodistribution studies and TRT monotherapy were conducted in mice bearing syngeneic EMT-6 TNBC tumors. Combination therapy with ^{177} Lu-HMI02-ABD035 and anti PD-1 was assessed in EMT-6 and 4T1 xenografts that were resistant to immunotherapy. Post-treatment immune cells infiltration was analyzed using multiplex immunohistochemistry. ***Results:*** The TCGA analysis of TNBC data revealed significantly higher fibronectin expression in tumor regions compared to normal tissues. Fibronectin overexpression occurred frequently (67.3%) in TNBC patients. SDS-PAGE and MALDI-TOF analysis confirmed the high purity and accurate fusion of HMI02-ABD035, respectively. Excellent uptake and retention of ^{177}Lu-HMI02-ABD035 were observed in EMT-6 tumors (28.24 ± 1.65%ID/g at 48 h p.i. and 11.20 ± 2.23%ID/g at 120 h p.i.). The normal tissues showed low uptakes of tracer, and the tumor to muscle ratios were as high as 31 ± 3.24 at 48 h p.i. Low-dose ^{177}Lu-HMI02-ABD035 (9.3 MBq per mouse) significantly inhibited tumor growth and extended overall survival in EMT-6 xenografts. ^{177}Lu-HMI02-ABD035 monotherapy reduced the cancer-associated fibroblast population in tumor and enhanced dendritic cell infiltration. Combining TRT with anti PD-1 improved antitumor efficacy compared to either monotherapy in both tested tumor models, resulting in complete tumor regression in most EMT-6 tumor-bearing mice (4/7). Combination therapy also induced tumor-specific memory, as demonstrated by protection against tumor rechallenge and induction of effector and memory T cells. ***Conclusion:*** Our results suggest that fibronectin-targeted ^{177}Lu-HMI02-ABD035 TRT holds potential for treating TNBC and sensitizing treatment-resistant tumors to immunotherapy. This indicates that combining ^{177}Lu-HMI02-ABD035 with anti-PD-1 therapy may be a promising approach to treating TNBC patients in the clinic.

OP-362

Profiling the influencing factors of radiopharmaceutical therapy: spatial transcriptomics and computational modeling in microenvironment

J. Hong[1], *S. Bae*[2], *L. Cavinato*[3], *M. Ryhiner*[1], *A. Rominger*[1], *H. Choi*[2], *K. Shi*[1];
[1]*University of Bern/Inselspital, Bern, SWITZERLAND,*
[2]*Seoul National University Hospital, Seoul, KOREA, REPUBLIC OF,* [3]*Politecnico di Milano, Milan, ITALY.*

Aim/Introduction: Computational modeling of radiopharmaceuticals in microenvironment has contributed to the investigation of dosimetry in radiopharmaceutical therapy (RPT). Recently, a novel technique, Spatial Transcriptomics (ST), has been introduced which counts the number of transcripts of a gene at distinct spatial locations in a tissue. We used a novel approach that combines computational modeling with ST which profiles the distribution of the influencing factor of RPT. In particular, we incorporated ST of hypoxia M10508 (Harris hypoxia) and Folate Hydrolase 1 (FOLH1) expression, which are associated with hypoxia and prostate tumor, respectively, to modeling spatiotemporal distribution as well as dosimetry of both ^{177}Lu-PSMA and ^{225}Ac-PSMA. ***Materials and Methods:*** We employed a prostate cancer single-cell transcriptomic dataset to fingerprint Harris hypoxia and FOLH1 expression in each spot composing the ST data. We then calculated the proportion of cell types that included endothelial cells in the same spatial ST domain, which was used to contour the vessel. To generate an arterial input function (AIF) of each ^{177}Lu-PSMA and ^{225}Ac-PSMA within those vessels, we used a well-established physiological-based-pharmacokinetic-modeling (PBPK) model where the injected amount was determined to deposit 10Gy in the prostate tumor 20 days post-injection. We established convection-reaction-diffusion (CRD) model to simulate spatiotemporal distribution, assuming that once radiopharmaceutical enters the tumour interstitium from the vessels, it is transported through the interstitial volume by diffusion down concentration gradients and convection from regions of high to low interstitial fluid pressure, finally exiting the compartment via a cellular uptake and backflow into the vasculature. ST of FOLH1 was integrated into the simulation to serve as parameter associated with receptor density, and all other parameters were taken from the previous literature. Dose-voxel kernel (DVK) method was utilized to derive the dosimetry using MIRD cell. Cell survival rate was derived in each ST locations using hypoxia information from Harris hypoxia ST and linear quadratic model. ***Results:*** The average simulated dose in PSMA abundant area was 15.02 Gy and 10 Gy for ^{177}Lu-PSMA and ^{225}Ac-PSMA, respectively. On the other hand, in PSMA depleted area, the absorbed dose was 0.48 Gy and 0.06 Gy for ^{177}Lu-PSMA and ^{225}Ac-PSMA, respectively. However, cell survival rate was largely

decreased in the PSMA depleted area in ^{225}Ac-PSMA compared to ^{177}Lu-PSMA, indicating that ^{225}Ac-PSMA therapy outcome is more sensitive to hypoxia than ^{177}Lu-PSMA. ***Conclusion:*** This pilot study confirmed the feasibility of ST to enhance the computational modelling in the investigation of RPT dosimetry.

805

Monday, September 11, 2023, 9:45 AM - 11:15 AM
Hall B

Cutting Edge Science Track - TROP Session: Image Reconstruction and Data Corrections

OP-363

Fast Penalized Maximum Likelihood Method for Positron Lifetime Image Reconstruction Using Adaptive Time Framing

J. Qi, *B. Huang;*
UC Davis, Davis, CA, UNITED STATES OF AMERICA.

Aim/Introduction: Positronium lifetime imaging (PLI) has attracted growing interest due to its potential for examining tissue microenvironment and identifying hypoxia regions. However, it has been commonly believed that the spatial resolution of PLI is limited by the time-of-flight (TOF) resolution of a PET scanner. A previous study has shown a spatial resolution of 3 cm with 460 ps TOF resolution and that achieving 5 mm spatial resolution would require 50 ps TOF resolution [1], which is far beyond the capability of current state-of-the-art scanners. Previously we developed a list-mode based penalized maximum likelihood method for reconstructing high-resolution positronium lifetime images using an existing TOF PET [2], but the method was computationally intensive for practical use. Here we present a new fast penalized maximum likelihood method for positronium lifetime image reconstruction using adaptive time framing. ***Materials and Methods:*** List-mode coincidence events are adaptively divided into frames based on their measured delay times between positron annihilation and prompt gamma. In each frame, the coincidence data follow a Poisson distribution with the expectation of events in each LOR related to the lifetime of each voxel through a positron decay model and the system matrix of the PET scanner. Using the optimization transfer method, we decoupled the reconstruction of positron decay curve in each voxel and lifetime estimation. The proposed method allows for the use any positron lifetime model in the fitting procedure. For the mono-exponential decay model, a closed form update equation is obtained. ***Results:*** Simulation studies demonstrate that the proposed method can reconstruct positronium lifetime images at much better spatial resolution than the limit set by the TOF resolution of the PET scanner. The new method substantially reduced the computation time by more than a factor of 10 compared to the list-mode maximum likelihood method without sacrificing the accuracy of lifetime estimation. Additionally, the proposed penalized maximum likelihood method achieves lower variance than methods that perform reconstruction and lifetime estimate in two separate steps. ***Conclusion:*** The proposed fast and efficient method for positronium lifetime image reconstruction enables high-resolution PLI using existing PET scanners. This method opens opportunities of using PLI for studying tissue microenvironment in various diseases in human and animal models. ***References:*** [1] Moskal et al., "Performance assessment of the 2γ positronium imaging with the total-body PET scanners," EJNMMI Physics, 7(1):44, 2020. [2] Qi and Huang, "Positronium Lifetime Image Reconstruction for TOF PET," IEEE Transactions on Medical Imaging, 41(10):2848-2855, 2022.

OP-364

Direct versus indirect parametric whole body [^{18}F]FDG Patlak imaging using a LAFOV PET/CT system

J. van Sluis[1], *L. Providência*[1], *J. H. van Snick*[1], *A. W. J. M. Glaudemans*[1], *R. H. J. A. Slart*[1], *R. A. J. O. Dierckx*[1], *C. Tsoumpas*[1], *R. Boellaard*[1,2];
[1]*University Medical Center Groningen, Groningen, NETHERLANDS,* [2]*Amsterdam University Medical Centers, Amsterdam, NETHERLANDS.*

Aim/Introduction: Whole body axial coverage and high sensitivity of long axial field-of-view (LAFOV) PET systems allow whole body dynamic acquisition and precise measurements of image-derived input functions (IDIF). Commonly, estimation of kinetic parameters derived from dynamic PET data is done indirectly following individual frame reconstruction. However, because of the use of an approximated noise model and high noise levels, especially in shorter time frames, indirect parametric images may be noisy. Alternatively, parametric images can be estimated directly from raw dynamic PET data, hereby taking into account all acquired dynamic data instead of per frame. This allows more precise modelling of the noise distribution resulting in improved image quality. Here, we aimed to compare the quality of parametric images obtained with indirect and direct [^{18}F]FDG Patlak reconstruction using a LAFOV PET/CT system. Dynamic PET data were acquired using a maximum ring difference (MRD) of 85 (high sensitivity mode) which equals a photon acceptance angle of 18 degrees, and using an MRD of 322 (ultra-high sensitivity mode) equivalent to a photon acceptance angle of 52 degrees. ***Materials and Methods:*** Eleven oncological patients received a weight-based injection of [^{18}F]FDG and underwent a 65-min dynamic PET acquisition. First, dynamic PET data frames were reconstructed individually. From these dynamic frames, an IDIF from the ascending aorta was extracted and used for Patlak parametric image generation (indirectly); this IDIF also served as input for the direct Patlak reconstructions. For both Patlak methods (t* = 30 min) [^{18}F]FDG influx rate constant (K_i) images were obtained. Herein, tumour lesions as well as liver tissues were segmented to derive K_i and information regarding image noise levels. All reconstructions were performed offline using prototype research software (Siemens Healthineers). Indirect parametric image conversion and all image segmentations were performed using in-house developed software. ***Results:*** Lesion K_i differed minimally (~3%) between indirectly and directly reconstructed parametric images and applied MRDs. However, large differences between the liver coefficient of variation (COV) between the indirect and direct reconstruction methods were found: indirect MRD85 and MRD322 mean COV were 37.1% and 32.3%, direct MRD85 and MRD322 mean COV were 10.5% and 9.1%. ***Conclusion:*** Direct reconstruction of parametric Patlak images results in similar K_i but a substantial decrease in noise levels compared with indirect Patlak analysis. Improved signal-to-noise ratio and increased image quality is obtained with direct Patlak reconstruction which may enable future reduction of dynamic imaging duration for a more feasible clinical implementation.

OP-365

O-15 water in acceptance angle comparison high sensitivity vs ultra-high sensitivity

H. Merisaari[1], *N. Ono*[2], *T. Tolvanen*[3,4], *V. Saunavaara*[3,4], *J. Knuuti*[3], *L. Nummenmaa*[3], *P. Nuutila*[3], *H. Iida*[3];
[1]*Department of Radiology, University of Turku, Turku, FINLAND,* [2]*Department of Information Science, Nara Institute of Science and Technology, Turku, FINLAND,* [3]*Turku PET Centre, University of Turku and Turku University Hospital, Turku, FINLAND,* [4]*Department of Medical Physics, Turku University Hospital, Turku, FINLAND.*

Aim/Introduction: The acceptance angle during PET reconstruction determines the spatial resolution and sensitivity of the PET scanner. A larger acceptance angle means that more gamma ray pairs are detected. This can improve the sensitivity of the scanner, allowing use of lower injected activity in PET acquisition, and shorter acquisition times [1]. However, a larger acceptance angle can also lead to a lower spatial resolution, as the position of the annihilation event along the LOR may be less accurately determined. The purpose of this study was to evaluate potential benefits of higher acceptance angle in full body water O-15 PET acquisition with large FOV PET scanner. ***Materials and Methods:*** One patient underwent full body water O-15 PET scan with Biograph Vision Quadra (Siemens Healthineers), with four injected activity amounts (50, 100, 300, and 700 MBq activities), with one subject. To evaluate the effect of injected activity to image quality, we applied bootstrapping approach taking 50% of activations 10 times for each acquisition. We evaluated high sensitivity mode with maximum ring difference (MRD) of 85 and ultra high sensitivity mode with MRD 322 in the image reconstruction, with PSF-TOF as reconstruction method. The image quality was evaluated with Coefficient of Variation (CoV=SD/mean) across the 10 bootstrap permutations for each frame of dynamic series. We used 38 Volumes of Interest including brain, heart, lungs, artery, pancreas, kidney, and bone marrow. We evaluated time activity curves and modelled K1 and k2 parameters. ***Results:*** The CoV across bootstraps in ROI mean values were significantly lower for the higher acceptance angle, giving up to 20% average reduction. In K1 and k2 parameters, the K1 and k2 parameter CoVs were generally improved in the heart left ventricle, pancreas, kidney and bone marrow, with CoV improvements being dependent on the ROI in question. As expected, biggest improvements were observed with lowest dose acquisitions (50 and 100 MBq). ***Conclusion:*** Increased acceptance angle provided promising image data quality, and may allow to reduce injected dose in clinical acquisitions in the future. ***References:*** [1] Mingels, C., Weidner, S., Sari, H., Buesser, D., Zeimpekis, K., Shi, K., Alberts, I. and Rominger, A., 2023. Impact of the new ultra-high sensitivity mode in a long axial field-of-view PET/CT. Annals of nuclear medicine, pp.1-6.

OP-366

Impact of different collimator response models on quantitative ^{177}Lu-SPECT reconstructions

W. Claeys[1], *W. Deckers*[2], *V. Nuttens*[3], *C. Deroose*[1,2], *K. Goffin*[1,2], *K. Baete*[1,2], *M. Koole*[1];
[1]*KU Leuven, Leuven, BELGIUM,* [2]*UZ Leuven, Leuven, BELGIUM,* [3]*OLV Aalst, Aalst, BELGIUM.*

Aim/Introduction: ^{177}Lu-DOTATATE and ^{177}Lu-PSMA are increasingly used for radiopharmaceutical therapy. For these therapies, post-therapy SPECT-CT is important to estimate the absorbed dose to tumor and organs at risk. However, quantitative ^{177}Lu-SPECT-CT reconstruction protocols are not standard yet. Therefore, our aim was to investigate the impact of different collimator response models on the quantitative properties of ^{177}Lu-SPECT imaging. ***Materials and Methods:*** Quantitative SPECT acquisitions were performed on a Siemens Intevo Bold SPECT-CT system with medium energy collimators. The NEMA IEC PET body phantom comprising hot spheres (2MBq/ml) on a cold background was used. The standard 10mm diameter sphere was replaced by a 60mm sphere, resulting in diameters between 13 and 60mm. Reconstructions were performed using the vendor neutral reconstruction software MIM Encore (MIM Inc., Cleveland, OH, USA) with and without a simple geometric resolution model, and with Siemens Flash3D and xSPECT Quant software, including a Gaussian model and measured collimator response respectively. Number of subsets was set to 2 while the number of iterations was varied between 5 and 80. Reconstructed data were smoothed with a Gaussian kernel and varying Full Width Half Maximum (FWHM) from 0 to 25mm. Quantitative accuracy was evaluated based on the recovery coefficients (RC) for different sphere sizes while Gibbs artefacts (GA) were quantified as the relative difference between the central minimum and sphere maximum of the activity concentration. ***Results:*** Reconstruction without collimator modeling gives poor quantitative accuracy (RC_{max} = 64% for the 60mm sphere). With collimator model, increasing the number of updates increases the RC for all spheres up to approximate convergence at 80 updates. Using a more advanced model further increases quantitative accuracy, but only moderately at convergence (RC_{max} of the 60mm sphere is 88%, 91% and 94% for MIM, Flash3D and xSPECT respectively). In the largest sphere, Gibbs artefacts are present, which increase with number of updates and are amplified with the inclusion of a more advanced collimator model (GA_{max} = 28%, 38% and 50% for MIM, Flash3D and xSPECT). In the smaller spheres, visual heterogeneities were observed for MIM and Flash3D, but not for xSPECT. Increasing the smoothing level decreases Gibbs artefacts and hotspots, at the cost of lower RC. Varying the number of subsets while maintaining the number of updates does not affect RC nor Gibbs artefacts. ***Conclusion:*** Quantitative ^{177}Lu-SPECT-reconstructions with a more advanced collimator response model provide better quantitative accuracy at the expense of larger Gibbs artefacts.

OP-367

Towards the clinical implementation of quantitative^{177}Lu SPECT/CT with a ring-shaped CZT-based camera: comparison of OSEM and Q.Clear reconstruction algorithms

R. Danieli[1], *M. Stella*[2], *J. Leube*[3], *J. Tran Gia*[3], *H. Levillain*[1], *C. Marin*[1], *B. Vanderlinden*[1], *N. Reynaert*[1], *P. Flamen*[1];
[1]*Institut Jules Bordet, Brussels, BELGIUM,* [2]*GE HealthCare, Diegem, BELGIUM,* [3]*University Hospital Würzburg, Würzburg, GERMANY.*

Aim/Introduction: Dosimetry after radiopharmaceutical therapy with ^{177}Lu (^{177}Lu-RPT) relies on quantitative SPECT/CT, for which suitable reconstruction algorithms are required. Q.Clear is a reconstruction algorithm that has recently been made available for a CZT ring-shaped SPECT/CT camera (StarGuide, GE HealthCare), as alternative to the well-established OSEM. This study represents a first step towards the definition of an optimal reconstruction protocol for dosimetry after ^{177}Lu-RPT and compares the performance of three different algorithms (OSEM and Q.Clear with and without RDP regularization). ***Materials and Methods:*** The six spherical inserts of a NEMA phantom (diameter range: 10-37mm) and a cylindrical phantom (filling volume: 5.4L) were filled with

1.6MBq/ml and 700MBq of ^{177}Lu, respectively. Each phantom was scanned on a StarGuide for 15 minutes, with emission and scatter windows centred at 208keV (±6%) and 185keV (±5%), respectively. Acquired projections were reconstructed with OSEM and Q.Clear, both including resolution recovery, attenuation and scatter correction, with 1 subset and a number of iterations varying from 12 to 576. In addition, Q.Clear reconstructions including RDP regularization were performed (Q.ClearRDP). The noise was quantified as the coefficient of variation of the counts in a volume of interest drawn inside the cylindrical phantom. The spatial resolution was calculated by a matched-filter analysis based on the NEMA phantom [1]. ***Results:*** Visually, OSEM reconstructions presented more evident Gibbs-like artefacts compared to Q.Clear and Q.ClearRDP. After 12 iterations, all algorithms provided similar noise (~10%) and spatial resolution (~20 mm). Increasing the number of iterations, however, OSEM exhibited a faster noise build-up than Q.Clear and Q.ClearRDP (63%, 22% and 14%, respectively, after 576 iterations). After 72 iterations, a resolution of 9 mm, 11 mm and 12 mm was determined for OSEM, Q.Clear and Q.ClearRDP, respectively. From 72 to 576 iterations, minor improvements down to 7 mm, 8 mm and 10 mm were observed. Similar trade-offs between noise build-up and resolution improvement were found after 48, 96 and 192 iterations for OSEM, Q.Clear and Q.ClearRDP, respectively. ***Conclusion:*** When imaging ^{177}Lu on a StarGuide system, Q.ClearRDP succeeds considerably better than OSEM in reducing the accumulation of noise for a growing number of iterations, while also reducing Gibbs-like artefacts. However, when the reconstruction parameters are chosen with care, similar quality, noise and spatial resolution can be obtained with all considered algorithms (OSEM, Q.Clear and Q.ClearRDP). ***References:*** [1] Tran-Gia, Lassmann. Characterization of Noise and Resolution for Quantitative ^{177}Lu SPECT/CT with xSPECT Quant. J Nucl Med. 2019;60(1):50-59. doi:10.2967/jnumed.118.211094

OP-368

Positron-Range Correction for an On-Chip PET Scanner using Deep Learning

C. Clement[1], *G. Birindelli*[1], *F. Pagano*[2,3], *M. Pizzichemi*[2,3], *M. Kruithof-De Julio*[1], *S. Ziegler*[4], *A. Rominger*[1], *E. Auffray*[2], *K. Shi*[1];
[1]*Inselspital Bern, Bern, SWITZERLAND,* [2]*CERN, Geneva, SWITZERLAND,* [3]*University of Milano-Bicocca, Milan, ITALY,* [4]*University Hospital Munich, Munich, GERMANY.*

Aim/Introduction: Organs-on-Chips (OOCs) are an innovative technology designed to replicate human organ functions in vitro. OOCs provide a promising alternative to traditional in vitro and animal models for drug development, disease modeling, and toxicity testing [1]. As OOCs emerge as a potent tool for studying human physiology and drug responses, there is an increasing demand for dedicated PET scanners that can precisely and effectively image these microfabricated devices. However, the spatial resolution of existing small-scale PET systems is inadequate for OOC imaging. One key factor limiting PET scanner spatial resolution is the positron range, which refers to the distance a positron travels before colliding with an electron. In prior work, we introduced a dedicated On-Chip PET scanner capable of imaging OOCs [2]. In this study, we present enhanced performance results of the scanner by implementing a deep learning-based positron-range correction algorithm. ***Materials and Methods:*** We generated a dataset comprising pairs of non-corrected and corrected images using a Monte-Carlo simulation of a realistic OOC phantom and a fully three-dimensional Maximum-Likelihood Expectation-Maximization (MLEM) iterative reconstruction algorithm. We then developed and trained an image-to-image deep learning (DL) model that accepts a non-positron-range corrected reconstructed image as input and outputs a positron-range corrected image. ***Results:*** The mean full-width at half-maximum (FWHM) values of the non-positron-range corrected, ground truth, and DL-corrected reconstructed images of the test set are 0.260 mm, 0.169 mm, and 0.177 mm, respectively. These values were calculated using line profiles in the x-, y-, and z-directions drawn through the four sources in each compartment of the OOC phantom. Moreover, we compared the quality of the predicted images and ground truth images using the Peak Signal-to-Noise Ratio (PSNR) and Structural Similarity Index Measure (SSIM) metrics. The reconstructed test images achieved a PSNR of 48.9 dB and an SSIM of 0.994. ***Conclusion:*** Our findings demonstrate the effectiveness of the DL-based positron-range correction algorithm in enhancing the overall quality of the reconstructed images. This approach has the potential to serve as a valuable tool for advancing the study of 3D models in radiopharmaceutical research. Overall, this study highlights the potential of using a deep learning-based positron-range correction algorithm to improve the performance of a dedicated PET scanner for imaging OOCs. ***References:*** [1] L. A. Low et al., Nature Reviews Drug Discovery 20.5 (2021). [2] C. Clement et al., EJNMMI Physics 9.1 (2022).

OP-369

Implementation and performance evaluation of artificial intelligence based SPECT attenuation correction on clinical SPECT images

M. Szolikova[1], *A. Kovacs*[1], *B. Husztik*[1], *N. Meszaros*[1], *F. Nagy*[2], *I. Garai*[2], *S. Barna*[2];
[1]*Mediso Ltd., Budapest, HUNGARY,* [2]*ScanoMed Nuclear Medicine Centers, Debrecen, HUNGARY.*

Aim/Introduction: Accurate attenuation correction (AC) is essential for precise quantification and improved image quality in single-photon emission computed tomography (SPECT) imaging. While non-uniform AC through computed tomography (CT) is the standard method in clinical practice, it may produce artifacts due to patient movement, misalignment between SPECT and CT images, presence of metal implants and contrast agents in the body. Additionally, CT scans expose patients to higher levels of radiation. SPECT-only systems are still widely used, which do not allow transmission imaging, therefore CT-based AC is not available. We aimed to develop an artificial intelligence (AI) assisted method that generates synthetic CT images from bone SPECT measurements. This novel technique enables SPECT imaging comparable to CT-based correction, without requiring an actual CT scan. ***Materials and Methods:*** Our team developed a convolutional neural network solution that employs supervised and unsupervised techniques. The objective was to produce a synthetic CT-like image from SPECT data and a corresponding attenuation map. Retrospective study involved 1300 clinical subjects injected with ^{99m}Tc-MDP, images were acquired using 3-headed SPECT/CT system. The clinical sample was heterogeneous in terms of sex, age, BMI, disease, and regions examined. We randomly selected 900 images for network training, 200 for testing, 200 for evaluation. SPECT projection data was reconstructed three ways: AC using the original CT volume (CT-AC), AC using the synthetic CT volume (SCT-AC), non-attenuation-corrected (Non-AC). Both the attenuation maps and the reconstructed SPECT images were compared by considering the original CT-based method as reference. Image-derived metrics

such as mean absolute error, structural similarity index (SSI), peak signal-to-noise ratio (SNR), Dice coefficient, and region-based clinically relevant values such as activity concentrations were evaluated. ***Results:*** Evaluation of 200 independent samples (noninvolved in neural network learning and hyperparameter optimization) indicated that the synthetic attenuation maps were both qualitatively and quantitatively consistent with the CT-based attenuation maps. There were no significant differences in terms of SNR and activity concentration between the SPECT volumes reconstructed using CT-AC and SCT-AC methods. Both CT-AC and SCT-AC methods outperformed the Non-AC method in terms of SNR. Furthermore, when using SCT-AC, misregistration error is excluded due to the main principle of our method. ***Conclusion:*** Our study has shown that accurate attenuation maps can be generated exclusively from the emission data for bone SPECT imaging. Our proposed method offers several clinical benefits, including reduced radiation exposure to the patient and elimination of CT and motion artifacts from SPECT images.

OP-370

Deep-Learning-based Partial Volume Correction in SPECT

T. Kaprélian*, A. Extebeste, D. Sarrut;*
Université de Lyon, CREATIS; CNRS UMR5220; Inserm U1044; INSA-Lyon; Université Lyon 1; Centre Léon Bérard, France., Lyon, FRANCE.

Aim/Introduction: Image resolution and quantification on SPECT is limited by Partial Volume Effects (PVE) [1]. PVE are dominated by collimator response and depend on source-to-detector distance and source size, making lesions smaller than the system's resolution volume hard to detect. A widely used Partial Volume Correction (PVC) method is the Resolution Modeling (RM) during reconstruction, which improves spatial resolution but generates Gibbs artifacts. We propose a deep learning framework (PVCNet) to compensate for the collimator's PSF on projections, before reconstruction. ***Materials and Methods:*** We generated an analytical database counting 5000 sources containing a cylindrical background and 1 to 8 ellipsoidal lesions with background-to-source activity ratios between 10^{-3} and 1/8. Each source was then projected twice for each angle on a 256^2 pixels detector with ray-tracing using RTK [2]: once without RM (P_{noPVE} projection) and once with RM corresponding to a realistic SPECT system followed by Poisson noise ($P_{PVE,noise}$ projection). We then trained a UNet taking $P_{PVE,noise}$ projections as input and corresponding projections from P_{noPVE} as targets. The UNet takes six projections as input: the projection to correct, the two adjacent angles, the two orthogonal and the opposite ones. It contains a convolutional layer followed by 4 encoding/decoding blocks. We used L1 loss, Adam optimizer, and learning rate starting from $4x10^{-4}$. PVCNet method was tested on a simulated IEC phantom containing 6 spheres of 10, 13, 17, 22, 28 and 37mm radius, with source-to-background activity ratio of 40. Recovery Coefficients (RC) were compared on three reconstructed images: the image reconstructed with P_{noPVE} without PVC (Rec_noPVE_noPVC), with $P_{PVE,noise}$ and RM (Rec_PVE_RM) and with PVCNet-corrected projections (Rec_PVE_PVCNet). All reconstructions were made with RTK's OSEM algorithm (5 iterations, 10 subsets), except for Rec_PVE_RM (20 iterations). ***Results:*** Training PVCNet took 20 hours, on 4 GPUs. RCs on Rec_noPVE_noPVC image were close to 1 while RCs on Rec_PVE_PVCNet were always at least 12% higher than Rec_PVE_RM (on the 17mm radius sphere 0.649 (PVCNet) / 0.531 (PVC-RM)) although the smallest sphere was more affected by artifacts. RMSE was divided by a factor of 1.46 and CNR by 1.36. ***Conclusion:*** PVCNet shows encouraging results reducing PVE on synthetic data compared to standard PVC-RM method. Increased realism of the training dataset and further testing of the PVCNet on real data are necessary. ***References:*** [1] Erlandsson et. al 2012 Phys. Med. Biol. vol. 57, no. 21, pp. R119-R159, 2012[2] Rit et al. 2014 Phys: Conf. Ser., vol. 489, p. 012079

OP-371

Deep-learning based partial volume correction for ^{177}Lu SPECT/CT imaging based on a large Monte Carlo simulated dataset

J. Leube*[1], J. Gustafsson[2], M. Lassmann[1], M. Salas Ramirez[1], J. Tran-Gia[1];*
[1]University Hospital Würzburg, Würzburg, GERMANY,
[2]Lund University, Lund, SWEDEN.

Aim/Introduction: The partial volume effect is a major obstacle in quantitative SPECT/CT imaging and image-based dosimetry. In this work, a deep-learning based method for partial volume correction (PVC) of ^{177}Lu SPECT/CT imaging is presented. The method was developed and tested based on a large dataset of randomly shaped SPECT images generated by Monte Carlo (MC) simulations. ***Materials and Methods:*** A dataset of 10,000 activity distributions was generated by randomly placing random voxelized shapes [1] inside artificially generated XCAT body phantoms. Using the SIMIND MC program [2] low-noise ("noisefree") SPECT projection sets (120 projections, 128x128 matrices, 0.48x0.48 cm2 pixels, 20% energy window at 208 keV) were simulated for a Siemens Intevo bold SPECT/CT system (MELP collimator, 3/8" crystal). SPECT reconstructions were performed based on noisefree and noisy (created by adding Poisson noise) projections using standard OSEM without (CASToR [3], 2 iterations, 10 subsets, AC, SC) and with PSF modeling (STIR [4], 6 iterations, 6 subsets, AC, SC). Based on these four different sets of SPECT reconstructions, four different u-shaped convolutional neural networks (u-nets) were trained (input: SPECT reconstructions, output: original activity distributions, 60 epochs, L1 loss function). The dataset was divided in 9000/500/500 for training/validation/testing. For quantitative analysis, SSIM, NRMSE and volume activity accuracy (VAA, a new metric describing the percentage of voxels with activity in which the determined activity concentration deviates from the true activity concentration by less than 5%) between original activity distributions and SPECT reconstructions without / after PVC were calculated for all test data. ***Results:*** For CASToR, the PVC resulted in significant improvements (paired Wilcoxon test, $p<0.01$) in the quality parameters for noisefree (no PVC: 0.852/1.15%/10.7%, PVC: 0.960/0.66%/38.4% [SSIM/NRMSE/VAA]) and noisy reconstructions (no PVC: 0.816/1.29%/7.8%, PVC: 0.942/0.81%/30.7%). For STIR, the same behavior was found for noisefree (no PVC: 0.903/0.99%/11.7%, PVC: 0.965/0.64%/41.4%) and noisy reconstructions (no PVC: 0.893/1.04%/11.5%, PVC: 0.944/0.80%/32.9%). PVC based on STIR performed significantly better ($p<0.01$) than based on CASToR. ***Conclusion:*** In this work, the great potential of deep-learning based PVC is presented. A simulated data set was used to demonstrate the functionality of the presented method for different standard reconstructions (OSEM with and without PSF modeling). Overall, the method could help to alleviate the major problem of poor spatial resolution in SPECT. ***References:*** [1] Leube et al., EJNMMI Phys, 2022(9) [2] Ljungberg et al., Comput Meth Prog Bio, 1989(29) [3] Merlin et al., Phys Med Biol, 2018(63) [4] Thielemans et al., Phys Med Biol, 2012(57)

806

Monday, September 11, 2023, 9:45 AM - 11:15 AM
Hall C

Clinical Oncology Track - Featured Session: FAP Imaging

OP-372
FAP Imaging
J. Calais;
UCLA, Los Angeles, UNITED STATES OF AMERICA

OP-373
Dual-phase ^{68}Ga-FAPI-04 PET/CT: the pancreatic FAPI uptake characteristics and differentiation of pancreatic diseases
H. Wu*, C. Li, Y. Tian, Z. Xiao, Y. Jiang, Y. He;*
Zhongnan Hospital of Wuhan University, Wuhan, Hubei Province, CHINA.

Aim/Introduction: This study aims to evaluate the diagnostic performance of dual-phase ^{68}Ga-FAPI-04 PET/CT in differentiation of pancreatic disease and explore the factors affecting pancreatic ^{68}Ga-FAPI-04 uptake. ***Materials and Methods:*** We retrospectively analyzed patients who received dual-phase point ^{68}Ga-FAPI-04 PET/CT scan from May 2022 to October 2022. PET/CT scans were performed in at 30~60 minutes (rang from the base of the skull to mid-thigh). and at 2 hours (from the lower chest to mid abdomen for full coverage of pancreas). Multiple clinical data were collected to analyze its relationship with pancreatic ^{68}Ga-FAPI-04 uptake. Quantitative parameters including the maximum standardized uptake (SUVmax), tumor to mediastinal blood pool ratio (TBR) at both time points for the pancreas were measured or calculated to evaluate the diagnostic performance for pancreatic diseases. The threshold of SUVmax to differentiate between malignant and non-malignant pancreas was determined by receiver operating characteristic (ROC) analysis. The reference standard was based on histopathological findings, clinical data typical imaging data (CT, MRI, ultrasound and ^{18}F-FDG PET/CT) and imaging follow-up. ***Results:*** A total of 98 patients (63/98 males; median age, 56 years) were evaluated. The pancreatic FAPI uptake was significantly correlated with age ($P = 0.032$). There was no significant correlation between pancreatic FAPI uptake and body mass index (BMI), blood glucose, bilirubin, serum amylase, lipase, tumor markers, abdominal surgery ($P > 0.05$). Meanwhile, the SUVmax and TBR of malignant pancreas at dual-phases were significantly elevated than those of benign or normal pancreas ($P < 0.05$). The SUVmax and TBR of dual-phase ^{68}Ga-FAPI-04 PET/CT scans performed excellent diagnostic performance in differentiating malignant and non-malignant condition of the pancreas. The optimal cut-off level of early SUVmax= 13.6 and delayed SUVmax=9.8 were associated with sensitivity of 91.7% and 66.7%, specificity of both was 90.7%. And the cut-off level of early TBR= 9.8 and delayed TBR=7.1 were associated with sensitivity of 100% and 66.7%, specificity of 88.4% and 84.9 respectively. ***Conclusion:*** The pancreatic ^{68}Ga-FAPI-04 uptake was age-dependent, with older individuals more likely to experience pancreatic FAPI uptake. More importantly, the dual-phase ^{68}Ga-FAPI-04 PET/CT scan can be used to distinguish between malignant, benign disease and normal pancreas.

OP-374
^{68}Ga-labeled Fibroblast Activation Protein Inhibitor PET/CT in the clinical diagnosis and management of breast cancer: Comparison with [^{18}F]FDG PET/CT
W. Guo[1]*, W. Xu*[1]*, H. Fu*[1]*, Y. Pang*[1]*, L. Zhao*[1]*, L. Sun*[1]*, H. Chen*[2]*;*
[1]*The first affiliated hospital of Xiamen University, Xiamen, CHINA,* [2]*The first affiliated hospital of Xiamen University, Xiamen city, CHINA.*

Aim/Introduction: Quinoline-based fibroblast activation protein inhibitors (FAPIs) have shown promising results in the diagnosis of cancer. PET imaging using ^{68}Ga-FAPI shows a greater tumour-to-background ratio (TBR) than [^{18}F]FDG in various types of cancer, particularly in breast cancer. However, the further clinic role of [^{68}Ga]Ga-FAPI in the detection, staging/re-staging, and cancer management of breast cancer have not been systematically investigated. In this study, we investigated the diagnostic accuracy and clinical impact of [^{68}Ga]Ga-FAPI PET/CT in primary and metastatic breast cancer and compare the results with those of standard-of-care imaging (SCI) and [^{18}F]FDG PET/CT. ***Materials and Methods:*** This was a single-centre post-hoc retrospective study of a sub-cohort of patients from a previously acquired database. Patients with diagnosed or suspected breast cancer who underwent concomitant [^{68}Ga]Ga-FAPI (FAPI-46) and [^{18}F]FDG PET/CT scans from October 2019 to March 2022 were retrospectively analysed. Breast ultrasound (US) imaging was performed in all treatment-naïve patients as SCI. The maximum standard uptake value (SUVmax),TBR, lesion detection rate, and tumour-node-metastasis (TNM) classifications between [^{68}Ga]Ga-FAPI and [^{18}F]FDG PET/CT were evaluated and compared. ***Results:*** Thirty female patients (median age, 52 y; range, 28-80 y) were included. Among them, 5 patients underwent evaluation for a definitive diagnosis of suspected breast lesions, 9 underwent initial staging, and 16 were evaluated for the detection of recurrence. The sensitivities of breast US, [^{18}F]FDG, and [^{68}Ga]Ga-FAPI PET/CT for detecting primary breast tumours were 80%, 70%, and 100%, respectively. Regarding the diagnosis of recurrent/metastatic lesions, the per-lesion detection rate of [^{68}Ga]Ga- FAPI PET/CT was significantly higher than that of [^{18}F]FDG, which including local and regional recurrence (129 vs. 88), neck lymph node(LN) metastases (33 vs. 15), abdomen LN metastases (28 vs. 3), bone metastases (146 vs. 59), and liver metastases (28 vs. 11). Compared with [^{18}F]FDG, [^{68}Ga]Ga-FAPI PET/CT upstaged eight patients' TNM staging/re-staging (8/29, 28%) and changed six patients' clinical management (6/29, 21%). Compared to SCI, [^{68}Ga]Ga-FAPI changed eleven patients' TNM staging/re-staging (11/29, 33%) and eight patients' therapeutic regimens(8/29, 28%). There was no significant association between FAPI-derived SUVmax and receptor status/histologic type in both primary and metastatic lesions. ***Conclusion:*** [^{68}Ga]Ga-FAPI PET/CT was superior to [^{18}F]FDG in diagnosing primary and metastatic breast cancer, with higher radiotracer uptake and TBR, especially in the detection of primary/recurrent tumour, abdominal LN metastases, liver, and bone metastases. [^{68}Ga]Ga-FAPI PET/CT is superior to [^{18}F]FDG and SCI in TNM staging and may improve tumour staging, recurrence detection, and implementation of necessary treatment modifications.

OP-375

Role of PET/CT using [68Ga]Ga-DOTA-FAPI-04 in the Detection of Lesions and Staging of Various Malignancies, Excluding Gastrointestinal Tract Malignancies with Non-FDG Avid Lesions.

G. Beydagi[1], *N. Alan-Selcuk*[1], *K. Akcay*[1], *E. Demirci*[1], *O. Sonmez*[1], *M. Ocak*[2], *T. Toklu*[1], *S. Celik*[3], *B. Oven*[3], *L. Kabasakal*[4,1];
[1]*Yeditepe University, Department of Nuclear Medicine, Istanbul, TÜRKIYE,* [2]*Istanbul University, Faculty of Pharmacy, Department of Pharmaceutical Technology, Istanbul, TÜRKIYE,* [3]*Yeditepe University, Department of Medical Oncology, Istanbul, TÜRKIYE,* [4]*Istanbul Unıversity-Cerrahpasa, Department of Nuclear Medicine, Istanbul, TÜRKIYE.*

Aim/Introduction: The emergence of 68Ga-labeled FAP ligands, also known as 68Ga-FAPI, has provided a promising alternative for cancer patients with FDG-negative lesions. Various studies have demonstrated the effectiveness of FAPi PET/CT in detecting digestive system malignancies. This study aims to evaluate the potential effectiveness of 68Ga-FAPI PET/CT in detecting, staging, and restaging different malignancies, excluding digestive system malignancies, which are characterized by low FDG uptake or FDG-negativity. ***Materials and Methods:*** After obtaining approval from the Clinical Research Ethics Committee, we prospectively enrolled patients with primary tumors or metastases confirmed by pathology. All participants underwent 68Ga-FAPI and 18F-FDG PET/CT scans within one week for either initial assessment (detection and staging) or recurrence detection (restaging). Two senior nuclear medicine physicians reviewed all studies by consensus. ***Results:*** A total of 52 patients with suspicious lesions on FDG PET/CT underwent 68Ga-FAPI PET/CT imaging. Of these, 15 had ovarian cancer, 11 had breast cancer, 7 had pancreatic cancer, 4 had hepatocellular carcinoma, 4 had renal cell carcinoma, 2 had lung cancer, 2 had leiomyosarcoma, 1 had thyroid papillary carcinoma, 1 had gastrointestinal stromal tumor, 1 had endometrium cancer, 1 had squamous cell carcinoma, and 2 had unknown primary. Compared to FDG PET/CT, FAPi PET/CT showed an increase in the primary malignancy stage in 16 patients (31%). Specifically, 75% of patients (n=3/4) diagnosed with lobular carcinoma of the breast had an increase in primary malignancy stage. Peritoneal metastases were detected in 28 patients (68%). Although 10 patients had FDG-negative peritoneal metastases, FAPi PET/CT could detect them in all but one patient with a gastrointestinal stromal tumor diagnosis. As a result, major treatment changes were made for 11 patients (21%) and minor changes for 5 patients (10%) in the entire patient cohort. ***Conclusion:*** 68Ga-FAPI PET/CT has demonstrated superiority in the detection, staging, and restaging of low FDG-avid tumors, not only in gastrointestinal malignancies but also in other malignancies where the tumor background ratio in FDG-PET/CT is unfavorable.

OP-376

Impact of ^{68}Ga-FAPI PET/CTimaging in the diagnosis and management of primary and recurrent epithelial ovarian cancer

K. Xu, *J. Chen, C. Li, Y. Tian, L. Li, Y. Jiang, Z. Xiao, D. Xing, B. Wen, Y. He;*
Zhongnan Hospital of Wuhan University, Wuhan, China, CHINA.

Aim/Introduction: Gallium-68-labeled fibroblast activation protein inhibitor (^{68}Ga-FAPI) has showed promising application prospects in many malignant tumors. This study aims to evaluate the diagnostic performance and impact on the clinical management of ^{68}Ga-FAPI PET/CT in epithelial ovarian cancer (EOC) compared with conventional imaging (CI). ***Materials and Methods:*** Forty-one patients with EOC were retrospectively recorded between October 2021 and January 2023. All participants underwent both CI and [^{68}Ga]Ga-FAPI-04 PET/CT. PET images were analyzed for judging complete resectability according to SUIDAN scoring system(PET scores). The associations between the PET score, peritoneal cancer index (PCI) score, and Esienkop score of preoperative [^{68}Ga]Ga-FAPI-04 PET/CT imaging were also evaluated. A receiver operating characteristic (ROC) curve analysis was performed to assess the accuracy of the PET score in predicting complete postoperative resection and guide therapeutic management. The recommended treatment was determined by imaging according to the NCCN guidelines. The final diagnosis and treatment were determined by pathological criteria and a dedicated multidisciplinary team. The diagnostic performance according to [^{68}Ga]Ga-FAPI-04 PET/CT was compared with CI and changes in oncologic management were recorded. ***Results:*** [^{68}Ga]Ga-FAPI-04 PET/CT significantly outperformed CI in diagnostic accuracy (86.5% vs. 51.2%, respectively, p< 0.001), especially in the stage III to IV. The PET score had a significant positive correlation with tumor burden (Eisenkop: r=0.768, P< 0.001; PCI: r=0.777, P< 0.001). The ROC showed that preoperative PET score ≥ 6 and score≥ 3 predicted a high risk of incomplete resection for primary and secondary debulking surgeries, respectively. Based on the final treatment, the coincidence rate of PET score guided treatment was significantly higher than that of CI (90.2% vs. 62.5%, p<0.001). Compared with CI, [^{68}Ga]Ga-FAPI-04 PET/CT modified the diagnosis in 34.6% of patients. [^{68}Ga]Ga-FAPI-04 PET/CT led to an upgrade in 45.0% and 33.3% of treatment-naive and relapse participants, resulting in management changes in 30.0% and 28.6% of patients compared with CI. ***Conclusion:*** [^{68}Ga]Ga-FAPI-04 PET/CT is a promising imaging modality for the diagnosis performance and therapeutic management. The preoperative PET score can noninvasively reflect tumor burden and helps predict complete resection after surgery in EOC patients.

OP-377

Fibroblast activation protein and glycolysis in lymphoma diagnosis: comparison of^{68}Ga-FAPI PET/CT and ^{18}F-FDG PET/CT

X. Chen, *S. Wang, Y. Lai, G. Wang, M. Wei, X. Jin, J. Ding, Y. Zhang, Y. Shi, F. Wang, H. Zhu, Z. Yang, X. Wang;*
Peking University Cancer Hospital & Institute, Beijing, CHINA.

Aim/Introduction: o compare the diagnostic performances of gallium 68 (^{68}Ga)-labeled fibroblast activation protein inhibitor (FAPI) and fluorine 18 (^{18}F)-labeled fluorodeoxyglucose (FDG) PET/CT in diagnosing lymphomas and to characterize the influences of fibroblast activation protein (FAP) and glycolytic markers on tracer uptake by involved lesions. ***Materials and Methods:*** Participants with different lymphoma subtypes, who were prospectively recruited from May 2020 to December 2021, underwent ^{68}Ga-FAPI and ^{18}F-FDG PET/CT. Immunohistochemistry was performed to evaluate FAP, hexokinase 2 (HK2), and glucose transporter 1 (GLUT1) expression, and paired samples t-test and Wilcoxon signed-rank test were used to compare parameters. Correlation between the immunochemistry results and tracer uptake was determined by Spearman's rank correlation coefficient. ***Results:*** In total, 186 participants (median age: 52 years [interquartile range: 41-64 years]; 95 women) were included. Dual-tracer imaging produced three types of imaging profiles. ^{18}F-FDG PET possessed a higher staging accuracy (98.4%) than ^{68}Ga-FAPI PET (86.0%). In 5980 lymphoma lesions, ^{18}F-FDG PET/

CT detected more nodal (4624 vs. 2196) and extranodal lesions (1304 vs. 845) than ^{68}Ga-FAPI PET/CT. Additionally, 52 FAPI+/FDG− lesions and 2939 FAPI−/FDG+ lesions were observed. In many lymphoma subtypes, semiquantitative evaluation revealed no significant differences in maximum standardized uptake values (SUV_{max}) and target-to-liver ratios between ^{68}Ga-FAPI and ^{18}F-FDG PET/CT (P > .05). Interestingly, GLUT1 and HK2 were overexpressed in both lymphoma cells and the tumor microenvironment, while FAP was only expressed in stromal cells. FAP and GLUT1 expression were positively correlated with $SUV_{max\text{-}FAPI}$ (r = 0.622, P = .001) and $SUV_{max\text{-}FDG}$ (r = 0.835, P < .001), respectively. ***Conclusion:*** ^{68}Ga-FAPI PET/CT was inferior to ^{18}F-FDG PET/CT in diagnosing lymphomas with low FAP expression. However, the former may supplement the latter and help reveal the molecular profile of lymphomas.

OP-378

[68Ga]GaFAPI-RGD PET/CT in the evaluation of renal carcinoma: comparison with [18F]FDG/[68Ga]Ga-PSMA PET/CT

R. Lin[1], *J. Zang*[1], *C. Wang*[1], *S. Chen*[1], *J. Zhang*[1], *Y. Yang*[1], *F. Xu*[1], *J. Zhang*[2], *X. Chen*[2], *W. Miao*[1];
[1]*Department of Nuclear Medicine, the First Affiliated Hospital, Fujian Medical University, Fuzhou, Fujian Province, CHINA,*
[2]*National University of Singapore, Singapore, SINGAPORE.*

Aim/Introduction: To compare the potential efficiency of [^{68}Ga]Ga-FAPI-RGD with that of [^{18}F]FDG/[^{68}Ga]Ga-PSMA PET/CT for detecting renal cell carcinoma (RCC) and to explore parameters derived from [^{68}Ga]Ga-FAPI-RGD PET/CT for discriminating pathological characteristics in RCC. ***Materials and Methods:*** Twenty-five RCC patients confirmed by pathology with a total of 28 lesions were enrolled in this prospective study. 16 patients underwent paired [^{68}Ga]Ga-FAPI-RGD and [^{18}F]FDG PET/CT, and the other 9 patients underwent paired [^{68}Ga]Ga-FAPI-RGD and [^{68}Ga]Ga-PSMA PET/CT. The activity of tracer accumulation in lesions was assessed by maximum standardized uptake value (SUVmax) and tumor-to-background (TBR). Pathological characteristics included WHO/ISUP grade and adverse pathology (tumor necrosis or sarcomatoid or rhabdoid feature). Values of radiological parameters were compared within subgroups of pathological characteristics. ***Results:*** [^{68}Ga]Ga-FAPI-RGD PET/CT showed a higher detection rate for primary lesions than those of [^{18}F]FDG and [^{68}Ga]Ga-PSMA (FAPI-RGD vs. FDG: 76.5% [13/17] vs. 23.5% [4/17], P < 0.001; FAPI-RGD vs. PSMA: 81.8% [9/11] vs. 54.5% [6/11], P = 0.361). [^{68}Ga]Ga-FAPI-RGD showed higher SUVmax (6.6 vs. 3.7, P = 0.005) and TBR (2.6 vs. 1.7, P = 0.011) in RCC compared with [^{18}F]FDG, and it also showed higher TBR (2.9 vs. 0.5, P = 0.003) and TBR-delay (2.8 vs. 0.3, P = 0.003) compared with [^{68}Ga]Ga-PSMA PET/CT. The SUVmax, TBR and TBR-delay significantly differed by WHO/ISUP grade and adverse pathology (all P < 0.05), the TBR significantly differed by clinical grade and M stage (P = 0.018, P = 0.002), and the SUVmax-delay significantly differed by pT stage (P = 0.019). SUVmax and TBR could effectively differentiate WHO/ISUP grade (3-4 vs. 1-2) and adverse pathology (positive vs. negative) (SUVmax: AUC 0.81, P = 0.04, cutoff 9.1, sensitivity 80%, and specificity 93% for WHO/ISUP grade; AUC 0.80, P = 0.033, cutoff 10.5, sensitivity 67%, and specificity 100% for adverse pathology; TBR: AUC 0.84, P = 0.026, cutoff 4.0, sensitivity 80%, and specificity 87% for WHO/ISUP grade; AUC 0.85, P = 0.014, cutoff 3.8, sensitivity 67%, and specificity 94% for adverse pathology). ***Conclusion:*** [^{68}Ga]Ga-FAPI-RGD is a promising new diagnostic PET tracer for RCC imaging and can effectively identify aggressive pathological features of RCC.

OP-379

Diagnostic Accuracy of ^{68}Ga-FAPI and ^{18}F-FDG PET/CT for Localizing Primary Tumor in the Head and Neck Cancer of Unknown Primary

B. Gu, *X. Du, Z. Yang, S. Song, Z. Yang;*
Fudan University Shanghai Cancer Center, Shanghai, CHINA.

Aim/Introduction: To investigate the diagnostic accuracy of gallium 68 (^{68}Ga)-labeled FAP inhibitor (FAPI) PET/CT for the detection of primary tumor of head and neck cancer of unknown primary (HNCUP), compared with fluorine 18 (^{18}F)-labeled fluorodeoxyglucose (FDG). ***Materials and Methods:*** A total of 91 patients (18 females, 73 males; median age: 60 years, range: 24-76 years) with negative or equivocal findings of primary tumor by comprehensive clinical examination comprehensive clinical examination and conventional imaging were prospectively enrolled from June 2020 to September 2022. Images from paired ^{18}F-FDG and ^{68}Ga-FAPI PET/CT underwent within 1 week were analyzed. Suspected primary sites were further verified by biopsy or histopathologic examination. Paired t test and Wilcoxon signed-rank test were used to compare the differences of maximum of standardized uptake value (SUV_{max}) and tumor-to-liver blood pool ratio (TLR) between ^{18}F-FDG and ^{68}Ga-FAPI in primary tumor and metastatic lesions. The survival analyses were performed using Kaplan-Meier method. ***Results:*** Of the 91 patients, primary tumor was detected in 46 patients (50.55%) after a thorough diagnostic workup. Compared to ^{18}F-FDG, ^{68}Ga-FAPI PET/CT detected more primary lesions (17 vs. 46, P < 0.001) and outperformed in sensitivity, positive predictive value and accuracy for the locating the primary tumor (25% vs. 51.11%, 42.50% vs. 97.87%, and 18.68% vs. 50.55%, respectively). Furthermore, ^{68}Ga-FAPI PET/CT led to T upstaging in 22 of 91 (24.18%) patients compared with ^{18}F-FDG. Moreover, in terms of SUV_{max} and TLR, primary tumors demonstrated significantly higher semiquantitative uptake values of ^{68}Ga-FAPI than ^{18}F-FDG (SUV_{max}: 6.11 ± 4.30 and 3.16 ± 5.11, P < 0.001; TLR: 10.85 ± 6.81 and 1.45 ± 2.31, P < 0.001). Kaplan-Meier curve illustrated that patient with unidentified primary tumor had a significant worse prognosis than patient with identified primary tumor (Hazard rate (HR) = 5.77, 95% confidence interval (CI): 1.86-17.94, P = 0.0097). ***Conclusion:*** ^{68}Ga-FAPI PET/CT outperforms ^{18}F-FDG in detecting primary lesions, and could serve as a sensitive, reliable and reproducible imaging modality for HNCUP patients.

OP-380

Head-to-head comparison of^{68}Ga-FAPI46 PET/CT,^{18}F-FDG PET/CT, and contrast-enhanced CT in patient with various solid tumors

M. Watanabe, *H. Grafe, N. Hirmas, R. Hamacher, H. Lanzafame, K. M. Pabst, M. Nader, J. T. Siveke, W. P. Fendler, K. Herrmann, M. Weber;*
Essen University Hospital, Essen, GERMANY.

Aim/Introduction: FAPI-PET/CT is characterized by visualization of high tumor specific uptake and low background accumulation, enabling the detection of tumor lesions with high sensitivity. We aimed to compare the diagnostic performance of ^{68}Ga-FAPI46 PET/CT vs. ^{18}F-FDG PET/CT vs. contrast-enhanced CT (CE-CT) in patients with solid tumors. ***Materials and Methods:*** 241 patients underwent ^{68}Ga-FAPI46 PET/CT,^{18}F-FDG PET/CT, and CE-CT within 4 weeks from October 2018 to September 2022. Detection rates were assessed by a blinded reader, with at least 2 weeks between scans of the same patient to avoid recall bias, per-lesion, per-region and per-patient. In addition, the highest SUVmax in each region

was measured. A separate sub-analysis was carried out for 629 histopathologically validated lesions to calculate sensitivity, specificity, positive predictive values (PPV), negative predictive values (NPV) and accuracy. Detection rates among different modalities were compared using McNemar's test. ***Results:*** The total lesion-based detection rates in ^{68}Ga-FAPI46 PET/CT, ^{18}F-FDG PET/CT, and CE-CT were 91.5% (1635/1787), 82.7% (1477/1787) and 60.2% (1075/1787). Separate for regions, the lesion-based analyses were 95.4% (185/194), 88.7% (172/194) and 78.9% (153/194) for primary lesions, 82.7% (335/405), 88.4% (358/405), 51.6% (209/405) in cervicothoracic nodal metastases, 93.1% (338/363), 72.7% (264/363) and 47.7% (173/363) in abdominopelvic nodal metastases, 96.2% (178/185), 93.0% (172/185) and 93.0% (172/185) in lung metastases, 95.6% (215/225), 73.3% (165/225) and 58.7% (132/225) in liver metastases, 92.1% (176/191), 76.4% (146/191) and 43.5% (83/191) in other visceral metastases, 92.9% (208/224), 89.3% (200/224) and 68.3% (153/224) in bone metastases, respectively. Per-region detection rates were 95.7% (441/461), 84.8% (391/461) and 70.3% (324/461), and per-patient analysis was 99.5% (210/211), 92.9% (196/211) and 90.5% (191/211), respectively. As well as the per-region and per-patient analyses, per-lesion detection rates were significantly higher in ^{68}Ga-FAPI46 PET/CT than ^{18}F-FDG PET/CT for total, primary, abdominopelvic nodal, liver, and other visceral lesions ($p<0.05$). There were no significant differences of SUVmax between ^{68}Ga-FAPI46 PET/CT and ^{18}F-FDG PET/CT.In the sub-analysis, sensitivity, specificity, PPV, NPV and accuracy were 75.7%, 94.9%, 85.4%, 90.9% and 89.5% in^{68}Ga-FAPI46 PET/CT, 71.2%, 94.0%, 82.4%, 89.3% and 87.6% in ^{18}F-FDG PET/CT, and 65.5%, 96.2%, 87.2%, 87.7% and 87.6% in CECT, respectively. ***Conclusion:*** ^{68}Ga-FAPI46 PET/CT outperforms ^{18}F-FDG PET/CT and CE-CT in a variety of solid tumors with regards to the detection rate, while also lowering the risk of false-positive findings, especially for primary, abdominopelvic nodal, liver, and other visceral lesions. Further studies on which entities draw particular benefit from ^{68}Ga-FAPI46 PET/CT are warranted to aid appropriate diagnostic workup.

807

Monday, September 11, 2023, 9:45 AM - 11:15 AM
Hall F1

Cardiovascular Committee - TROP Session: Clinical Perfusion Imaging with PET

OP-381

Cardiac one stop shop: Performance of a Rapid Diagnostic Outpatient Clinic using Rubidium-82 PET-CT Imaging.

J. Boer, *M. Ros, P. Bot;*
Spaarne Gasthuis, Haarlem, NETHERLANDS.

Aim/Introduction: Atherosclerotic vascular disease is a major cause of death worldwide, and in the Netherlands, coronary heart disease affects a large number of people.To speed up the diagnosis of myocardial ischemia due to severe atherosclerotic narrowing of coronary arteries, a one-stop-shop (OSS) was introduced that utilizes rubidium-82 myocardial perfusion PET-CT imaging (Rb-82 PET-CT). The aim of this clinic is to analyze patients within a week and all appointments on the department of cardiology and nuclear medicine take place on the same day. The study aims to determine whether the use of the OSS results in shorter throughput times, thus decreasing the risk for patients with severe coronary artery disease without compromising efficiency and healthcare costs. ***Materials and Methods:*** The study was conducted by retrospectively comparing the throughput times between the OSS and the traditional outpatient clinic. The date of referral and the date of the follow-up appointment after the examination for all patients referred for examination at the OSS were recorded, as well as the number of patients who actually underwent an examination. The Duke score was calculated, and a pre-test likelihood of >15% indicated the need for additional testing according to the guideline of the European Society of Cardiology (ESC). The study's main outcome was the potential reduction in days of the diagnostic process through the use of the OSS compared to the control group. ***Results:*** In total, 152 patients were analyzed, and the results showed that the throughput times in the OSS were on average 9 days compared to 68 days in the control group. Ischemia was found in 25% of patients in the OSS and 10% of controls. Six percent of patients dropped out of the OSS because the indication was rejected by the cardiologist, and 8% of patients in the OSS had a pretest likelihood of below 15%. Examinations with a Duke score below 15% or with non-specific complaints were considered not useful and deemed as over diagnosis. ***Conclusion:*** The implementation of a OSS utilizing Rb-82 PET-CT imaging has the potential to dramatically expedite the diagnosis of myocardial ischemia in patients with suspected coronary artery disease with an average reduction of 59 days. The OSS was more effective in selecting patients with ischemia, where 25% of patients had ischemia compared to 10% in the control group. Dropout rates and overdiagnosis occurred in 14% of cases.

OP-382

Prognostic value of coronary flow capacity by rubidium-82 PET/CT in patients with suspected CAD and normal myocardial perfusion imaging

A. D'Antonio[1], *E. Zampella*[1], *R. Assante*[1], *T. Mannarino*[1], *V. Gaudieri*[1], *P. Buongiorno*[1], *M. Falzarano*[1], *R. Lepre*[1], *F. Reina*[1], *M. Panico*[2], *P. Arumugam*[3], *A. Cuocolo*[1], *W. Acampa*[1];
[1]*Department of Advanced Biomedical Sciences, University of Naples "Federico II", Naples, ITALY,* [2]*Institute of Biostructure and Bioimaging, CNR, Naples, ITALY,* [3]*Department of Nuclear Medicine, Central Manchester Foundation Trust, Manchester, UNITED KINGDOM.*

Aim/Introduction: Vasodilator capacity of coronary circulation is an important diagnostic and prognostic tool in patients with suspected and known coronary artery disease (CAD). Non-invasive assessment of myocardial blood flow (MBF) and myocardial perfusion reserve (MPR) is able to evaluate both epicardial disease and microvascular dysfunction. Coronary flow capacity (CFC) has been evaluated as comprehensive of the coronary circulation, integrating both MBF and MPR measurements. We aimed to assess the prognostic value of impaired CFC, evaluated by Rubidium-82 positron emission tomography/computed tomography (PET/CT), in patients with suspected CAD and normal myocardial perfusion imaging (MPI) ***Materials and Methods:*** We evaluated 2454 patients with suspected CAD who underwent stress/rest Rubidium-82 cardiac PET/CT. Patients with normal MPI (n=2005), defined as a total perfusion defect <5%, were included. Hyperemic MBF and MPR were calculated and considered abnormal when < 1.8 ml/min/g and <2, respectively. In order to evaluate CFC, four patient groups were identified based on the concordant or discordant impairment of MBF or MPR. CFC was considered impaired in the presence of both abnormal MBF and MPR. End- points were defined as major adverse cardiovascular

events (MACEs), such as cardiovascular death, nonfatal myocardial infarction, unplanned hospitalization for any cardiac reasons, and unplanned coronary revascularization. Annualized event rates (AER) were calculated. A parametric survival model was also used to identify how the variables influenced time to event and to estimate risk-adjusted event rates during the follow-up ***Results:*** Follow-up was available in 1896 (95%) patients (median age 59±13 years). During a median time of 44 months (range 3-111), 72 events occurred (cumulative rate 4%, AER 0.8%). Both MBF and MPR were concordant abnormal in 141 (7%) subjects with impaired CFC, concordant normal in 1402 (74%), discordant with impaired MBF in 112 (6%) and discordant with impaired MPR in 241 (13%). According to MBF and MPR categories, AER was higher in patients with impaired CFC (AER 3.2%) as compared to concordant normal (AER 0.4%), discordant patients with impaired MBF (1.3%) and those discordant with impaired MPR (AER 0.9%) (p for trend <0.001). At Weibull parametric survival analysis, the highest probability of cardiac events and the major risk acceleration were observed in patients with both impaired MBF and MPR ***Conclusion:*** In patients with suspected CAD and normal MPI, impaired CFC was associated with a higher risk of MACEs. The CFC evaluation can help identify patients candidates to additional therapies in order to prevent future events

OP-383

Quantitative relationship between coronary artery calcium and myocardial blood flow by hybrid rubidium-82 PET/CT imaging in heart transplanted patients

T. Mannarino[1], *R. Assante*[1], *E. Zampella*[1], *A. D'Antonio*[1], *F. Cacciatore*[2], *C. Amarelli*[3], *M. Falzarano*[1], *F. Reina*[1], *R. Lepre*[1], *I. Mattucci*[3], *R. Chiappetti*[2], *V. Gaudieri*[1], *P. Buongiorno*[1], *M. Panico*[1], *C. Maiello*[3], *A. Cuocolo*[1], *W. Acampa*[1];
[1]*Department of Advanced Biomedical Sciences, University of Naples Federico II, Naples, ITALY,* [2]*Department of Translational Medical Sciences, University of Naples "Federico II", Naples, ITALY,* [3]*Department of Cardiac Surgery and Transplantation, Monaldi, Azienda Ospedaliera dei Colli, Naples, Naples, ITALY.*

Aim/Introduction: Cardiac myocardial perfusion imaging (MPI) by positron emission tomography (PET)/ computed tomography (CT) represents a noninvasive method used for an integrated measurement of myocardial blood flow (MBF), myocardial flow reserve (MFR) and coronary calcium content. No study has investigated the relationship between coronary atherosclerotic burden and vascular function in heart transplanted patients. Thus, we assessed the relationship between CAC score, MBF and MFR in heart transplant patients undergoing hybrid ^{82}Rb positron emission tomography (PET)/computed tomography (CT) imaging. ***Materials and Methods:*** We enrolled a total of 100 (mean age 60±13 years) consecutive patients referred to hybrid ^{82}Rb PET/CT myocardial perfusion imaging for evaluation of myocardial ischemia. CAC score was measured according to the Agatston method and patients were categorized into 4 groups (0, 0.01-99.9, 100-399.9, and ≥400). Baseline and hyperemic MBF were automatically quantified. MFR was calculated as the ratio of hyperemic to baseline MBF and it was considered reduced when <2. The Spearman correlation coefficient was assessed between continuous CAC score and MBF or MFR values. Univariable and multivariable logistic regression analyses were used to determine the variables associated with reduced MFR. ***Results:*** Global CAC score showed a significant inverse correlation with hyperemic MBF (r=-0.28, P < .05) and MFR (r=-0.40, P < .001), while no correlation between CAC score and baseline MBF was found (P = 0.9). CAC score was zero in 71 (71%) patients, 0.1-99.9 in 8 (8%), 100-399.9 in 12 (12%), and ≥400 in 9 (9%). Global baseline MBF was comparable among the four groups of patients at different levels of CAC score (F = 0.040, P = 0.989). Whereas hyperemic MBF (F = 2.897) and CFR (F = 4.344) progressively decreased with increasing CAC levels (P for trend <0.05). Univariable analysis demonstrated that age, diabetes, and CAC score (all P < .05) were associated with reduced MFR. At multivariable logistic regression analysis only age and CAC score (both P < .05) were independently associated with reduced MFR. The addition of CAC score to clinical data, increased the global chi-square value for predicting reduced MFR from 18.79 to 25.66 (P < .01). ***Conclusion:*** In heart transplanted patients there was an inverse relationship between CAC score and MFR. The evaluation of calcium content might be helpful for identifying patients with a reduced MFR, at high risk to develop cardiac allograft vasculopathy.

OP-384

MPI - from Rb to [^{15}O]water with a dedicated cyclotron

M. Lonsdale*, S. Fuglsang, M. Krakauer, A. Larsen, I. Rasmussen, U. Talleruphuus, P. Hovind;*
Bispebjerg Hospital, Copenhagen, DENMARK.

Aim/Introduction: [^{15}O]water PET is considered the reference for non-invasive in vivo measurement of myocardial blood flow[1]. Advantages over ^{82}Rb include metabolical inertness and a linear relationship between tracer uptake and myocardial blood flow. The main disadvantages are the need for an on-site cyclotron due to the half-life of ^{15}O and software to calculate parametric images as no static uptake images can be acquired. We present our experiences transitioning perfusion studies from ^{82}Rb to [^{15}O]water with a dedicated mini-cyclotron at a hospital with no previous cyclotron installation. ***Materials and Methods:*** Supply chain disruptions, economic uncertainties, and the ambition to provide state-of-the-art myocardial perfusion imaging (MPI) services initiated the transition from ^{82}Rb to [^{15}O]water. A self-shielded cyclotron dedicated to the production of ^{15}O was installed in a technical building without radiation shielding features. Production of ^{15}O, synthesis to [^{15}O]water and i.v. administration is performed using standard procedures which are exclusively performed by the departments' technologists - without other cyclotron staff. Initial training included physicists (cyclotron troubleshooting), technologists (production of ^{15}O and [^{15}O]water, QC - all according to GMP) and medical doctors (software, reading of images). All patient handling and scanning procedures could be easily translated 1:1 from ^{82}Rb. ***Results:*** Economics: The return-of-investment is less than 5 years, with the extra advantage of greater flexibility. For ^{82}Rb generators, the cost is driven by the number of ^{82}Rb-generators, regardless of utilization. In contrast, cyclotron running costs are dominated by its actual use. No extra staff was necessary apart from a part-time consulting radiochemist acting as QP for GMP. Clinical: After 12 months of exclusive use of [^{15}O]water for MPI, the impact on the referral pattern was the most notable change. Patient referrals decreased from 125 per months to around 100. During implementation of [^{15}O]water, the interprofessional collaboration with cardiology was improved significantly (teaching sessions, more frequent multidisciplinary conferences and continuous case-oriented dialogue) leading to increased awareness and knowledge in pearls and pitfalls in MPI studies in general - all in all leading to more clinically appropriate and relevant referrals. "Stress-only" studies for selected populations offer extra patient comfort. As a minor positive side-effect

radiation dose to patients and exposed staff was reduced to about 50%. ***Conclusion:*** We have demonstrated the possibility to offer high-volume, state-of-the-art MPI studies at a hospital with no prior cyclotron installation. Clinical experience is positive. ***References:*** [1] R Sciagrà et al: EANM procedural guidelines for PET/CT quantitative MPI, EJNMMI. 2021;48:1040-69.

OP-385

^{82}Rb and [^{15}O]H_2O Myocardial perfusion PET imaging - a prospective head to head comparison

L. Marner[1], *M. Krakauer*[1], *A. Ismail*[1], *U. Talleruphuus*[1], *A. C. Henriksen*[1], *M. N. Lonsdale*[1], *I. L. Rasmussen*[1], *S. Fuglsang*[1], *E. Prescott*[2], *P. Hovind*[1], *L. Marner*[1];
[1]*Copenhagen University Hospital Bispebjerg, Department of Clinical Physiology and Nuclear Medicine, Copenhagen NV, DENMARK,* [2]*Copenhagen University Hospital Bispebjerg, Department of Cardiology, Copenhagen NV, DENMARK.*

Aim/Introduction: ^{82}Rb PET and [^{15}O]H_2O PET are both validated tracers for myocardical perfusion imaging but have not previously been compared in a prospective cohort of patients in diagnosing possible myocardial ischemia. During our site's clinical transition from ^{82}Rb PET to [^{15}O]H_2O PET, we performed a head-to-head comparison measuring myocardial perfusion in a mixed population with suspected ischemic heart disease. ***Materials and Methods:*** A total of 37 patients were examined with both ^{82}Rb and [^{15}O]H_2O PET on the same day in rest and during adenosine-induced stress. Significant regional perfusion defects were suspected in ^{82}Rb PET if a relative defect was >10% and in [^{15}O]H_2O PET if two segments had perfusion ≤ 2.3 mL/(g·min). Significant global reduction was suspected in ^{82}Rb PET if the perfusion reserve (relative increase) was ≤ 1.8 and in [^{15}O]H_2O PET if all segments were ≤ 2.3 mL/(g·min). Further, a less sensitive assessment of total perfusion defects of 10% (TPD) was evaluated for [^{15}O]H_2O PET. Results were rated by two blinded readers to assess agreement between methods and interrater agreement. ***Results:*** Agreement between methods was 59% as [^{15}O]H_2O PET identified more patients compared to ^{82}Rb PET with regional perfusion defects during pharmacological stress. Using the less sensitive TPD, the agreement increased to 84% corresponding to a Cohen's kappa of 0.57 [95% C.I.: 0.25 - 0.87]. Interrater agreement was 95% corresponding to a kappa of 0.89 [95% C.I.: 0.74 - 1.00]. ***Conclusion:*** In conclusion, [^{15}O]H_2O myocardial perfusion PET is a sensitive imaging modality with a high interrater agreement. However, we found a moderate agreement between methods as [^{15}O]H_2O PET identifies more patients with signs of ischemia than ^{82}Rb PET especially in patients with previous heart disease. When performing a clinical transition from ^{82}Rb PET to [^{15}O]H_2O PET, the higher sensitivity for perfusion defects should be taken into account.

OP-386

Splenic switch-off as marker of adenosine response in myocardial perfusion imaging with O-15-H2O PET

M. Jochumsen[1,2], *L. C. Gormsen*[1,2], *L. P. Tolbod*[1,2], *J. Brorson*[1,2];
[1]*Dept of Nuclear Medicine and PET-Centre, Aarhus University Hospital, Aarhus, DENMARK,* [2]*Department of Clinical Medicine, Aarhus University, Aarhus, DENMARK.*

Aim/Introduction: Surrogate markers of sufficient adenosine response during positron emission tomography (PET) myocardial perfusion imaging (MPI) are important for discriminating between adenosine non-responders and patients with severe balanced ischemia. These results is part of a larger study to validate splenic switch-off as a marker of sufficient adenosine response on ^{15}O-H_2O-PET MPI using both qualitative and quantitative analysis and examines the splenic switch-off in a cohort with verified sufficient adenosine response. ***Materials and Methods:*** A cohort of patients with sufficient adenosine response was identified (n=90), including patients with normal MPI (n=30), regional ischemia (n=30), and global/balanced ischemia (n=30). To determine whether the adenosine response was sufficient, two criteria were used: (1) a 1.5-fold increase in myocardial blood flow in at least two adjacent segments following adenosine administration, and (2) at least two of the following: hemodynamic response, side effects, and ECG changes. All patients were scanned according to facility standards and international guidelines on a GE Discovery MI Digital Ready PET/CT (GE Healthcare, Waukesha, Wisconsin, USA). Since ^{15}O-H_2O is not a retention tracer, images of summed activity and parametric blood flow images are used for visual assessment of splenic switch-off. Furthermore, spherical VOIs of the spleen, liver, and blood were drawn on both summed activity and parametric blood flow images for quantitative analysis. ***Results:*** Summed activity images: Visual splenic switch-off: positive (71%), inconclusive (16%), negative (13%). Spleen signal: >10% decrease (84%), 0-10% decrease (6%), increase (10%). Hepatic signal: >10% increase (30%), 0-10% increase (27%), decrease (43%). Spleen-liver-ratio: >10% decrease (81%), 0-10% decrease (11%), increase (8%). Parametric blood flow images: Visual splenic switch-off: positive (86%), inconclusive (6%), negative (8%). Spleen signal: >10% decrease (92%), 0-10% decrease (5%), increase (3%). Hepatic signal: >10% increase (66%), 0-10% increase (15%), decrease (19%). Spleen-liver-ratio: >10% decrease (91%), 0-10% decrease (4.5%), increase (4.5%). When comparing stress-rest-ratios for splenic switch-off, hepatic switch-on and decrease in spleen-liver-ratio, parametric images highly significantly outperformed summed images on all parameters (p<0.0001). ***Conclusion:*** The presence of splenic switch-off, and decrease in spleen-liver-ratio are reliable markers of sufficient adenosine response on ^{15}O-H_2O-PET MPI, whereas the absence of these does not necessarily indicate a lack of adenosine response. For both visual and quantitative assessment, parametric blood flow images should be preferred; however, summed images can serve as a convenient alternative in clinical routine.

OP-387

RV to LV Myocardial Blood Flow Ratio With ^{15}O-water PET as a Risk Marker for Cardiac Events in Patients With Left Ventricular Hypertrophy

P. Svanström, *J. Sigfridsson, H. J. Harms, T. Kero, K. Eggers, N. Regula, M. Lubberink, J. Sörensen;
Uppsala University, Uppsala, SWEDEN.*

Aim/Introduction: Left ventricular hypertrophy (LVH) is a well-established cardiac risk factor. Increased risk in LVH is associated with microvascular dysfunction, but LVH might also increase poor outcome by diastolic dysfunction and subsequent pulmonary hypertension (PH), which is less well studied. LVH is diagnosed as increased septal wall thickness (WT) or left ventricular mass (LVM), which can be measured with ^{15}O-water PET [1]. Using ^{15}O-water PET, a ratio of right ventricle (RV) and LV resting myocardial blood flow ($MBF_{RV/LV}$) larger than 67% diagnosed PH and predicted poor outcome with high accuracy in cardiac amyloidosis patients [2]. This study aimed to determine the prognostic value of $MBF_{RV/LV}$ in a clinical cohort of patients with LVH. ***Materials and Methods:*** We retrospectively identified LVH from a single-centre cohort of 500 consecutive patients with suspected coronary artery disease

referred for routine rest/adenosine-stress ^{15}O-water PET. LVH was determined from resting PET according to standard criteria (LVM >85g/m^2 or WT >12 mm). Cardiac events were defined as cardiac death, acute heart failure or acute myocardial infarction. The prognostic value of $MBF_{RV/LV}$ was compared to LV stress-MBF, coronary flow reserve (CFR), WT and LVM using Cox hazards ratio (HR[95% confidence interval]). ***Results:*** LVH was diagnosed in 105 patients (21%), in which 24 cardiac events were registered (median follow-up 4.1 years). Significant prognostic value in univariate analysis was found for $MBF_{RV/LV}$ (HR 1.61[1.20-2.12] per 10%), stress-MBF (HR 0.93[0.87-0.98] per 0.1 ml/min/g) and CFR (HR 0.43[0.25-0.71]), but not WT (HR 1.00[0.84-1.19] per mm) or LVM (HR 1.01[0.99-1.03] per g/m^2). In multivariate analysis $MBF_{RV/LV}$ and CFR remained independently significant. Using receiver-operating characteristic analysis $MBF_{RV/LV}$ > 67.7% was the best cut-off (HR 5.2[2.2-12], P < 0.001). ***Conclusion:*** A $MBF_{RV/LV}$-ratio from ^{15}O-water PET was independently prognostic in patients with LVH. Surprisingly, the best predictive cut-off for $MBF_{RV/LV}$ in generic LVH equalled the best cut-off previously shown in cardiac amyloidosis patients. Prospective trials to establish $MBF_{RV/LV}$ as a clinical risk marker are warranted. ***References:*** 1. Sörensen, J., et al., Diagnosis of left ventricular hypertrophy using non-ECG-gated (15)O-water PET. J Nucl Cardiol, 2022. 29(5): p. 2361-2373. 2. Harms, H.J., et al., Association of Right Ventricular Myocardial Blood Flow With Pulmonary Pressures and Outcome in Cardiac Amyloidosis. JACC Cardiovasc Imaging, 2023. doi: 10.1016/j.jcmg.2023.01.024

OP-388

Evaluation of DOTA as a marker of myocardial blood flow by comparison of ^{68}Ga-DOTA to^{15}O-water-PET

M. Lubberink[1], *S. Kvernby*[1], *C. Rischpler*[2], *K. Azarbar*[1], *J. Sörensen*[1], *I. Velikyan*[1], *T. Kero*[1];
[1]*Uppsala University, Uppsala, SWEDEN,*
[2]*Klinikum Stuttgart, Stuttgart, GERMANY.*

Aim/Introduction: Gd-DOTA (DOTAREM) and similar MRI contrast agents are often suggested as non-invasive markers for myocardial blood flow (MBF). Accurate quantification of MBF with MR contrast agents requires (1) correct conversion of the MR signal to Gd concentration which is challenging; (2) analysis with an appropriate kinetic model; and (3) correction for the limited extraction of Gd-DOTA using the relationship between the uptake rate of the contrast agent and true MBF. Contrary to MRI, the PET signal is directly proportional to radioactivity concentrations and hence a PET analogue of DOTAREM, ^{68}Ga-DOTA, could be used to assess the kinetics of DOTA without the challenge of converting MR signal to Gd concentration. The aim of the present work was to assess the kinetics of DOTA by comparing ^{68}Ga-DOTA to the gold standard for non-invasive measurement of MBF, ^{15}O-water PET. ***Materials and Methods:*** Twenty-five patients referred for assessment of ischemia using ^{15}O-water-PET underwent 4 min dynamic ^{15}O-water-PET scans during rest and adenosine stress followed by 10 min dynamic ^{68}Ga-DOTA-PET scans during rest and adenosine stress on a Signa PET/MR scanner. ^{15}O-water PET was analysed automatically using aQuant software, and volumes of interest were transferred to the co-registered ^{68}Ga-DOTA-PET images. ^{68}Ga-DOTA-PET was analysed using single- and two-tissue irreversible compartment models and the uptake rate constant K_1 of ^{68}Ga-DOTA was compared to that of ^{15}O-water. Permeability-surface area product for ^{68}Ga-DOTA was estimated using the Renkin-Crone equation. ***Results:*** Kinetics of ^{68}Ga-DOTA were well described by a single-tissue compartment model. Correlation between ^{68}Ga-DOTA and ^{15}O-water K_1 values was moderate (Spearman rho 0.82 at the global and 0.71 at the regional level, P < 0.005). Extraction of ^{68}Ga-DOTA was low with average whole myocardium ^{68}Ga-DOTA K_1 values ranging from 0.22 to 0.80 mL/cm^3/min compared to 0.72 and 4.2 mL/cm^3/min for ^{15}O-water. The permeability surface area product of ^{68}Ga-DOTA was 0.41 (CI 0.30-0.53) mL/cm^3/min. ***Conclusion:*** Extraction of DOTA is low, and lower than for ^{82}Rb or even ^{99m}Tc-sestamibi, resulting in a high uncertainty in hyperemic MBF and coronary flow reserve values. Based on these results, DOTA cannot be considered a suitable agent for accurate measurement of MBF.

OP-389

The Second Phase-3 Multi-Center Trial of^{18}F-Flurpiridaz PET Myocardial Perfusion Imaging for Coronary Artery Disease Evaluation

J. Knuuti[1], *D. Agostini*[2], *T. Bateman*[3], *J. J. Bax*[4], *R. Beanlands*[5], *D. Berman*[6], *S. Dorbala*[7], *E. V. Garcia*[8], *J. Feldman*[9], *G. V. Heller*[10], *P. Martinez-Clark*[11], *M. Pelletier-Galarneau*[12], *B. Shepple*[13], *N. Tamaki*[14], *F. Tranquart*[15], *J. E. Udelson*[16], *J. Maddahi*[17];
[1]*Turku University Hospital, Turku, FINLAND,* [2]*University Hospital Caen, Caen, FRANCE,* [3]*Mid-America Heart, Kansas City, KS, UNITED STATES OF AMERICA,* [4]*Leiden University Medical Center, Leiden, NETHERLANDS,* [5]*Ottawa Heart Institute, Ottawa, ON, CANADA,* [6]*Cedars Sinai Medical Center, Los Angeles, CA, UNITED STATES OF AMERICA,* [7]*Brigham and Women's Hospital, Boston, MA, UNITED STATES OF AMERICA,* [8]*Emory University, Atlanta, GA, UNITED STATES OF AMERICA,* [9]*Memorial City and Katy Cardiology, Katy, TX, UNITED STATES OF AMERICA,* [10]*Morristown Medical Center, Morristown, NJ, UNITED STATES OF AMERICA,* [11]*North Miami Beach, Miami, FL, UNITED STATES OF AMERICA,* [12]*Montreal Heart Institute, Montreal, QC, CANADA,* [13]*University of Tennessee Medical Center, Tennessee, TN, UNITED STATES OF AMERICA,* [14]*Kyoto Prefectural University of Medicine, Kyoto, JAPAN,* [15]*GE Healthcare, Chalfont St Giles, UNITED KINGDOM,* [16]*Tufts Medical Center, Boston, MA, UNITED STATES OF AMERICA,* [17]*David Geffen School of Medicine at University of California, Los Angeles, CA, UNITED STATES OF AMERICA.*

Aim/Introduction: ^{18}F-flurpiridaz (flurpiridaz) is a novel PET myocardial perfusion imaging tracer. The aim of this study was to further assess the diagnostic efficacy and safety of flurpiridaz PET for the detection and evaluation of coronary artery disease (CAD) defined as >50% stenosis by quantitative invasive coronary angiography (ICA) in a multi-center prospective international clinical trial. The primary end point was to assess the diagnostic sensitivity and specificity of flurpiridaz for the detection of significant CAD. The secondary end points were to compare the diagnostic performance of flurpiridaz vs. Tc-99m SPECT MPI in the detection of CAD in all patients and in the clinically important subgroups of women, patients with BMI≥30 kg/m^2, and those with diabetes. The safety of flurpiridaz was also evaluated. ***Materials and Methods:*** 730 patients with suspected CAD from 48 clinical sites in US, Canada and Europe were enrolled. Patients underwent 1-day rest/stress (pharmacological or exercise) flurpiridaz PET and rest-stress Tc-99m labeled SPECT before ICA. PET and SPECT images were read by 3 experts blinded to clinical and ICA data. ICA was quantified by a core laboratory expert blinded to clinical and image data. ***Results:*** 578 patients (age, 63.7+9.5 years) were evaluable. Flurpiridaz met the prespecified primary endpoint of the study; sensitivity and specificity were significantly higher than the prespecified threshold value of 60% by two of the three readers. Analysis of the secondary endpoints showed that flurpiridaz sensitivity and specificity met the predefined criterion of being significantly higher than SPECT by two of three readers in the overall population as well as in women, in patients with

BMI≥30 kg/m^2, and in diabetic patients. Sensitivity and specificity of flurpiridaz were 80.3% and 63.8% that were significantly higher (p<0.0004) than those of SPECT 63.8% and 61.7%. Furthermore, ROC area under the curves were significantly higher than SPECT in the overall population (0.80 vs 0.68, p<0.0001), in women and in patients with BMI≥30 kg/m^2. Flurpiridaz was also superior to SPECT for assessment of defect extent/severity (p<0.0001). Image quality (% excellent or good) was significantly better than SPECT for rest images, pharmacological stress images and treadmill exercise images. Radiation exposure was less for flurpiridaz than SPECT. ***Conclusion:*** This second flurpiridaz MPI multicenter trial demonstrates that flurpiridaz has promise as a new tracer for detection and evaluation of CAD. This is particularly so in women and patients with BMI≥30 kg/m^2.

808

Monday, September 11, 2023, 9:45 AM - 11:15 AM
Hall F2

Thyroid Committee- Featured Session: Iodine-131 Therapy and Beyond in Differentiated Thyroid Cancer

OP-390

An Overview on Nuclear Medicine Therapy of Differentiated Thyroid Cancer

M Kreissl;
UniversityHospital Magdeburg, Division of Nuclear Medicine, Department of Radiology and Nuclear Medicine, Magdeburg, GERMANY.

OP-391

Radioactive Iodine Therapy for Low-risk Papillary Thyroid Cancer: Long-term Recurrence Risk Reduction in a Matched Cohort Study

S. Bilgic[1], *R. C. Meral*[2], *M. S. Sağer*[3], *K. Sönmezoğlu*[3];
[1]Sirnak State Hospital, Sirnak, TÜRKIYE, [2]University of Michigan, Ann Arbor, MI, UNITED STATES OF AMERICA, [3]Istanbul University-Cerrahpasa, Cerrahpasa Medical Faculty, Department of Nuclear Medicine, Istanbul, TÜRKIYE.

Aim/Introduction: The aim of this study was to investigate the factors associated with the recurrence of low-risk papillary thyroid cancer patients as defined by the American Thyroid Association (ATA) guidelines and the effect of radioactive iodine (RAI) therapy on long-term treatment success(1). ***Materials and Methods:*** Patients with papillary thyroid carcinoma or papillary microcarcinoma who were classified as low risk and underwent total or near-total thyroidectomy, treated at Nuclear Medicine Department of Cerrahpaşa Medical Faculty between 2004 and 2016 were included in the study. Risk groups were determined according to the 2015 ATA guidelines. Patients who did not have a complete set of postoperative data, interim evaluation results, and follow-up data for more than 40 months were excluded. Age at diagnosis, gender, pathology reports, and scintigraphic findings were analyzed. ***Results:*** Our patient cohort predominantly comprises women (85.0%; n=495), with a median follow-up duration of 76.5 (40-189) months. Low-risk patients who received RAI therapy (n=396) and those who did not (n=196) were matched using 1:1 Mahalanobis distance matching. In order to make the distribution of low-risk patients more homogeneous, women with no high anti-tg levels (<135 IU/ml) and tumor diameter less than 16 mm were matched in the analysis. After matching, 173 patients were obtained from both groups. Static results for up to 6 months, dynamic results for up to 24 months, and long-term outcomes were evaluated. RAI therapy reduced the risk of late recurrence by 13-fold in patients with low-risk papillary thyroid carcinoma and papillary microcarcinoma (p=0.0014). Unsuccessful initial RAI ablation, and high postoperative thyroglobulin levels were predictors of disease recurrence in this cohort. ***Conclusion:*** Due to the latent nature of low-risk papillary thyroid cancer, observing the effectiveness of RAI treatment is only possible through long-term follow-ups. Factors associated with recurrence in papillary thyroid cancer patients differ considerably depending on whether they receive RAI therapy. ***References:*** 1. Haugen BR, Alexander EK, Bible KC, et al. 2015 American Thyroid Association Management Guidelines for Adult Patients with Thyroid Nodules and Differentiated Thyroid Cancer: The American Thyroid Association Guidelines Task Force on Thyroid Nodules and Differentiated Thyroid Cancer. Thyroid : official journal of the American Thyroid Association 2016; 26:1-133

OP-392

Comparison of 1.1 gbq and 2.2 gbq^{131}I activities in patients with low-risk differentiated thyroid cancer requiring postoperative iodine-131 therapy.

A. Campenni'[1], *R. Ruggeri*[1], *M. Garo*[2], *A. Raffa*[1], *M. Siracusa*[1], *G. Restuccia*[1], *A. Rappazzo*[1], *H. Rosarno*[1], *A. Nicocia*[1], *D. Cardile*[1], *P. Petranović Ovčariček*[3], *S. Baldari*[1], *L. Giovanella*[4];
[1]Ospedale Gaetano Martino, Messina, ITALY, [2]Mathsly Research, Roma, ITALY, [3]University Hospital Center Sestre Milosrdnice, 10 000 Zagreb, CROATIA, [4]Clinic for Nuclear Medicine and Competence Centre for Thyroid Diseases, Imaging Institute of Southern Switzerland, Ente Ospedaliero Cantonale, 6500 Bellinzona, SWITZERLAND.

Aim/Introduction: Thyroid surgery followed by risk-adapted postoperative ^{131}I therapy (RIT) is considered the current standard of care for many DTC patients, leading to an excellent response in >80% of them. This study was aimed to compare the efficacy of low and moderate ^{131}I activities in low-risk DTC patients requiring postoperative RIT in a real-world clinical setting. ***Materials and Methods:*** We reviewed the records of 299 (F=225, M=74; female-to-male ratio=3:1; median age=52, range=18-81) low-risk DTC patients [pT1-T2, Nx(0),Mx]. Papillary thyroid cancer was carried in 246/296 (82%) patients while 47 (16%) had a follicular thyroid carcinoma and 6 (2%) had a Hurthle cell carcinoma. All patients had undergone (near)-total thyroidectomy followed by RIT, using either low (1.1 GBq) or moderate (2.2 GBq) radioiodine activities. A post-therapy whole body scintigraphy coupled with SPECT-CT (pT-imaging) was obtained 2-5 days after RIT. Finally, the response to initial treatments was evaluated 8-12 months after RIT using basal and rhTSH-stimulated Tg measurements, neck-ultrasound and ^{123}I-Diagnostic whole body scintigraphy associated to SPECT/CT imaging. Then, patients were classified according to 2015 American Thyroid Association guidelines (2015 ATA). ***Results:*** At the time of pT-imaging, 246 (82.3%) patients showed thyroid remnants alone, while 53 (17.7%) patients showed thyroid remnants and metastases (i.e., loco-regional lymph-node metastases, n=51; lung metastases, n=1; lymph-node and lung metastases, n=1). Among patients carrying metastases, 22 (41.5%) received low ^{131}I activity (Group A), while 31 (58.5%) moderate one (Group B) (p= not significant).An excellent response (ER) to initial treatments was observed in 274/299 (91.6%) patients, specifically, in 119/139 (85.6%) and 155/160 (96.9%) patients treated with low and moderate ^{131}I activities, respectively (p=0.029). The

biochemical indeterminate or incomplete response was observed in 17 (22.2%) patients treated with low ^{131}I activities and 3 (1.8%) patients treated with moderate ^{131}I activities (p=0.001). Five patients showed a structural incomplete response, among them 3 and 2 received low and moderate ^{131}I activities, respectively (p=0.654). Notably, 25/53 (47.2%) patients carrying metastatic disease at pT-imaging showed less than ER at follow-up [20/22 Group A (91%) and 5/31 Group B (16%), p<0.0001]. No differences were found between these patients before RIT. ***Conclusion:*** The incidence of metastatic disease may be unexpectedly high in low-risk DTC patients in real life settings. When ^{131}I therapy is indicated, we encourage the use of moderate instead of low activities, in order to reach an ER in a significantly larger patients' proportion, including patients with unexpected persistence of disease.

OP-393

Integrating ^{131}I SPECT-based RPT dosimetry into stereotactic external beam treatment planning for patients with metastatic radioiodine-refractory thyroid cancer, preliminary clinical trial results

I. Marsh[1], *H. Quon*[1], *P. Santhanam*[1], *P. Ladenson*[1], *B. He*[2], *D. Kaplin*[1], *K. Lowe*[1], *H. Wang*[1], *G. Sgouros*[1], *R. F. Hobbs*[1];
[1]*Johns Hopkins University, Baltimore, MD, UNITED STATES OF AMERICA,* [2]*RAPID LLC, Baltimore, MD, UNITED STATES OF AMERICA.*

Aim/Introduction: Treatment of well differentiated thyroid cancer with radioiodine (^{131}I) has a long and successful history. However, tumor uptake of ^{131}I can be diminished in patients with recurrent metastatic disease resulting in sub-therapeutic absorbed doses (AD) to the tumors. Here we present results from an ongoing clinical trial combining ^{131}I with stereotactic radiotherapy (SRT), using personalized dosimetry. ***Materials and Methods:*** Four patients have been enrolled in the trial to date. Patients are simulated for external beam treatment planning and then administered a tracer amount of ^{131}I, with multiple time point whole body probe and blood activity measurements aquired. These measurements are used in a two source compartment S-value dosimetry model to determine the patient-specific maximum tolerated therapeutic activity based on bone marrow constraints. Following administration of the therapeutic ^{131}I, three SPECT/CT images are acquired using the patient-specific immobilization devices from the SRT simulation, which improves the registration of images across time and reduces the uncertainty in ^{131}I AD calculations. SPECT images undergo quantitative reconstruction and are registered to the simulation CT where target lesion(s) are delineated. S-value dosimetry is used to determine mean lesion AD, which is then converted to EQDX, where X is the dose per fraction of the SRT treatment, determined as the amount needed to deliver a cumulative 80 Gy EQD2 to the target lesion(s). ***Results:*** In the case of the first patient, two lesions were identified and treated, the ^{131}I portion was calculated to have delivered ADs of 16.6 and 12.5 Gy (14.7 and 11.0 Gy EQDX), respectively, to lesion PTVs. The lesions were then treated with five fractions of SRT of 9.0 Gy and 9.5 Gy (66.0 Gy and 71.3 Gy EQD2), respectively. Following treatment, the patient experienced tumor volume reduction and pain relief. Thyroglobulin levels fell from 89,000 to 55,000 ng/ml three months post-treatment and TSH increased to 9.0 mU/L, indicating reduction in overactive thyroid tissue. The other patients have received similar treatments with follow-up data to come. ***Conclusion:*** Personalized dosimetry-based combination radiopharmaceutical therapy (RPT)-SRT is feasible, allows for effective AD delivery to target lesions that is unachievable through either modality alone, and may benefit from reduced toxicity. The low level of AD from ^{131}I observed in this work may indicate a need for a more quantitative triage approach and a wider application of this methodology. This work sets the groundwork for more generalized routine clinical RPT-external beam combinations.

OP-394

Is radio iodine therapy really as bad as it is made out to be? A look at secondary neoplasms using the SEER database.

B. Schemmer*;*
Uniklinik Bonn, Bonn, GERMANY.

Aim/Introduction: It is frequently noted that radio iodine therapy (RIT) is associated and causal for secondary primary neoplasms. Our goal was to find evidence in support of the induction of secondary neoplasms due to RIT. ***Materials and Methods:*** We searched the SEER Research Plus Data 12 Registries (excl AK), Nov 2021 Sub (1992-2019) database for cases of papillary thyroid carcinoma (only ICD-O-3 8260/3) using the MP-SIR tool. We used the Radioisotopes(1988+) variable and the system supplied Summary Stage 2000 to analyze both cumulative observed to expected ratios (O/E) as well as latency. p<0.05 was considered statistically significant(#). ***Results:*** For localized, regional and distant papillary carcinomas the O/E was 1.22#, 1.24# and 1.1 for non-iodine and 1.14#, 1.41# and 1.71# for RIT. In total 23461/21335 (non iodine/RIT) patients were considered, 381/439 died and 23080/20896 were lost to follow-up @ 360 months post diagnosis. The total number of observed/expected events was 1018/834, 205/165 and 18/16 for non-iodine and 590/518, 704/501 and 83/48 events for RIT. Confidence intervals of non-iodine and RIT patients overlaped for localized (1.15-1.30 vs 1.05-1.23), regional (1.08-1.42 vs 1.30-1.51) and distant stages (0.65-1.73 vs 1.37-2.13). The latency from exposure to event (secondary primary tumor) was 14 years (mean age at exposure 48.9 years, mean age at event 62.9), 16.6 (45.3,61.9) and 10 (60.2,70.4) years for localized, regional and distant for non-iodine and 15.6 (46.3,61.9), 16.5 (44.2,60.7) and 14.7 (51.4,66.1) years for RIT. The most common cancers out of 6030 neoplasms for 2785 patients in the case files treated with radio iodine (non-iodine) were 348(356) breast, 145(98) prostate, 121(150) lung and bronchus, 113(95) melanomas, 81(81) kidney, 75(67) corpus uteri, 45(36) urinary bladder, 33(19) ovary, 30(48) pancreatic, 79(63) NHL, 60(39) leucemias (acute and chronic), 17(20) myelomas, 6(3) hodgkin. ***Conclusion:*** Using the SEER Research Data Plus database we did not find evidence that RIT causes any one specific cancer. We did not find a significant difference between patients treated with radio iodine and non-iodine patients regarding type and onset of secondary primary neoplasms, the most common types of cancers do correspond to those also most common in the general population. Due to the rarity of thyroid carcinomas, even if the relative risk may appear large, the absolute risk of leukemia potentially induced by RIT appears to be minuscule (on the order of 0.1%).

OP-395

Radioguided Occult Lesion Localization (ROLL) in patients with persistence/recurrence of differentiated thyroid cancer: a 10-years single-centre experience

C. Manni[1], *G. Follacchio*[1], *G. Gesuelli*[2], *R. Scibè*[2], *G. Ferrara*[3], *M. Capponi*[4], *G. Ciccioli*[4], *F. Capoccetti*[1];
[1]*Nuclear Medicine Unit, Macerata Hospital, Italy, Macerata, ITALY,* [2]*Surgery Unit, Macerata Hospital, Italy, Macerata, ITALY,* [3]*Anatomic Pathology and Cytopathology Unit, Istituto Nazionale Tumori di Napoli, IRCCS "G. Pascale", Naples, ITALY,* [4]*Radiology Unit, Macerata Hospital, Italy, Macerata, ITALY.*

Aim/Introduction: Surgery is the elective treatment in cervical recurrence from differentiated thyroid cancer (DTC), but it is burdened by risk of failure and morbidity. We report results of 10-years single-center experience with Radioguided Occult Lesion Localization (ROLL) in this setting. ***Materials and Methods:*** Patients with DTC persistence/recurrence who underwent ROLL procedure in our Institution between 2012 and 2022 were considered. All patients were previously treated with thyroidectomy and at least one radiometabolic therapy with 131-Iodine. DTC persistence/recurrence was diagnosed by neck ultrasonography (US), PET/CT and Fine-Needle Aspiration Citology (FNAC) on suspect lesions associated to Thyroglobulin Wash Test (Thy-WT). On the day before surgery, target lesions were marked by intralesional injection of 99mTc-radiolabelled human albumin macroaggregates (99mTc-MAA - mean activity 11.1 MBq) under US guidance. During tracer injection, Thy-WT was repeated. SPECT/CT neck scan was then performed. For locoregional recurrence, a mini-invasive ROLL-guided excision was performed; for nodal metastases, ROLL-guided lymph-node excision was associated to a modified neck dissection. A hand-held gamma-probe was employed for intraoperative lesion detection. Thy-WT was performed on all radioactive surgical specimens. First follow-up evaluation was performed 3 months after surgery with serum Thyroglobulin measurement and neck US, then repeated every 6 months. ***Results:*** 23 patients were included in the study. DTC persistence/recurrence was localized in thyroid bed in 4 patients and in loco-regional lymph-nodes in 19 patients. A total of 26 lesions was identified and marked with 99mTc-MAA. SPECT/CT scan confirmed in every case a correct lesion localization. Intraoperatively all radioactive areas were correctly localized and resected without surgical complications.Final histology showed DTC persistence/recurrence in 22/26 lesions, in accordance with Thy-WT on surgical specimens. In 4/26 lesions, characterized by highly suspect cytology and a slight increase in Thy-WT, malignancy was not confirmed. At 3-months follow-up, patients were classified in complete response (n=16/23), partial response due to biochemical disease persistence (n=5/23) and no evidence of structural disease (n=2/23). During complete follow-up (mean 52 months, range 3-115), 11/23 patients remained in complete response, 5/23 patients with biochemical disease persistence underwent radiometabolic treatment, 7/23 developed disease progression: in 3 patients ROLL was repeated and 4 patients underwent external-beam radiotherapy. ***Conclusion:*** Radioguided surgery in DTC persistence/recurrence can be a useful tool to optimize radical surgical treatment minimizing local morbidity due to repeated neck surgery.

OP-396

High Ki-67 LI is an Important Factor for Good Early Outcomes After Radioiodine Therapy in Patients with Intermediate to High-Risk Papillary Thyroid Cancer

X. Luo, *W. Ouyang;*
Department of Nuclear Medicine, Zhujiang Hospital of Southern Medical University, Guangzhou, Guangdong Province, CHINA.

Aim/Introduction: This study aims to correlate Ki-67 expression with outcomes after radioiodine (RAI) therapy in papillary thyroid cancer (PTC) with different risk stratifications. ***Materials and Methods:*** Samples from 221 patients with PTC were studied for expression of Ki-67 labelling index (LI) between January 2015 and December 2019. Ki-67 LI was determined immunohistochemically. Samples were divided into low (≤4) and high (>4) groups according to mean value. Then correlations of Ki-67 LI with clinicopathological variables were analyzed by Chi-square test, and survival curves were evaluated by Kaplan-Meier methods. Furthermore, univariate and multivariate analysis were performed to assess the diagnostic values of Ki-67 LI by the Cox regression model. ***Results:*** Ki-67 LI was considered low in 54.3% and high in 45.7%. High Ki-67 LI was associated with vascular invasion (OR=3.684,95%CI:1.463-9.276,P=0.006), distant metastases (OR=8.089, 95%CI: 1.690-38.706, P=0.009), and central lymph node ratio (LNR) >0.28 (OR=0.427, 95%CI: 0.230-0.794, P=0.007), and was an independent prognosticator of disease-free survival (DFS) in multivariate analysis (HR=0.523, 95%CI: 0.319-0.858, P=0.010). Moreover, intermediate and high-risk patients with high Ki-67 LI had decreased risk for DFS (P=0.018, P=0.396). On contrary, low-risk patients with high Ki-67 LI had increased risk for DFS (P=0.067). ***Conclusion:*** In summary, our data show that high Ki-67 LI in intermediate to high-risk PTC is associated with good early outcomes after RAI therapy compared with patients with low Ki-67 LI, so the high radioiodine activities may change the initial poor outcomes caused by high Ki-67 LI to some extent. ***References:*** 1. Haugen BR, Alexander EK, Bible KC, et al. 2015 American Thyroid Association Management Guidelines for Adult Patients with Thyroid Nodules and Differentiated Thyroid Cancer: The American Thyroid Association Guidelines Task Force on Thyroid Nodules and Differentiated Thyroid Cancer. Thyroid Off J Am Thyroid Assoc 2016;26(1):1-133; doi: 10.1089/thy.2015.0020. 2. Lindfors H, Ihre Lundgren C, Zedenius J, et al. The Clinical Significance of Lymph Node Ratio and Ki-67 Expression in Papillary Thyroid Cancer. World J Surg 2021;45(7):2155-2164; doi: 10.1007/s00268-021-06070-y. 3. Melling N, Kowitz CM, Simon R, et al. High Ki67 expression is an independent good prognostic marker in colorectal cancer. J Clin Pathol 2016;69(3):209-214; doi: 10.1136/jclinpath-2015-202985.

OP-397

Redifferentiation Therapy for RAI-Refractory Differentiated Thyroid Cancers Based on Tumor Genomic Assay

D. Shen[1,2], *H. Chan*[1], *F. Tsai*[1], *Y. Chiu*[1], *T. Liang*[1], *Y. She*[1], *S. Li*[1];
[1]*Kaohsiung Veterans General Hospital, Kaohsiung, TAIWAN,* [2]*Tri-Service General Hospital, Taipei, TAIWAN.*

Aim/Introduction: Radioiodine (RAI)-refractory thyroid cancers (RR-DTCs) are usually treated with tyrosine kinase inhibitors (TKIs) and certain TKIs might offer advantage of re-differentiation effect, i.e. restoration of tumor RAI avidity, allowing for further RAI therapy. Such strategy is based on the salvage of cancer-related aberrant mechanism to re-induce Na^+/I^- sympoter (NIS) by targeting oncogene-involved signaling pathways. We intend to investigate whether the use of TKIs specific to cancer-related

genes for RR-DTC patients based on the oncogene identified can lead to effective redifferentiation effects. ***Materials and Methods:*** RR-DTC patients without RAI-avid lesion were recruited and their tumor tissues were subjected for next generation sequencing to identify driver-genes; then they were treated with different TKIs to inhibit mutated bRAF, RET fusion, NTRK fusion, or ROS-1 fusion, according to genomic assay results. Since the start of TKI treatment, serum markers, i.e. thyroglobulin (Tg) and anti-Tg antibody (ATA) were monitored monthly. FDG PET/CT was used to assess tumor response and RAI therapy (120~150 mCi) was administered in week 16~22 after TKIs treatment. Post-RAI whole body scans were checked to see any lesion RAI avidity. ***Results:*** Totally 57 patients with RR-DTCs in progression were included for tumor genomic assay. 23 (10 females; age: 56.3+/- 15.5, 23~79) of them received > 16 weeks of TKIs specifically to target their tumor-related gene alterations, i.e. bRAFV600E (n=18), RET fusion (n=3), NTRK fusion (n=1), and ROS-1 fusion (n=1). In week 16~22 post TKIs treatment, decreased tumor lesion FDG avidity was noticed (16~99% decrease of SUVmax). With PET-based therapeutic response criteria, there were 8(35%), 12(52%) and 3(13%) patients classified as complete, partial and stable metabolic response, respectively. Post-RAI whole body scans demonstrated significant tumor I-131 uptake in 20 (87.0%) patients; among them, four of 20 cases showed unexpected extra-cervical lesion I-131 uptake, i.e. pulmonary metastases. Tumor marker assay after TKI treatment showed a decrease of ATA level in 3/3 of RR-DTC patients with positive ATA while significant increment (up to >200%) of serum Tg level in 19/20 of ATA-negative patients during the TKI therapy. ***Conclusion:*** In our study, we demonstrated the potential of using oncogene-specific TKIs to restore RAI uptake for RR-DTCs and 16 weeks of TKI therapy might be sufficient to induce redifferentiation effect. The findings of unexpected pulmonary metastases shown on post-RAI scans and opposite-direction change of serum marker between ATA and Tg post TKI treatment warrant for further study.

OP-398

Radioligand Therapy with ^{177}Lu-EB-FAPI for the Treatment of Metastatic Radioiodine Refractory Thyroid Cancer: First-in-Human Dose-Escalation Clinical Trial

H. Fu, *J. Huang, W. Guo, L. Sun, H. Wu, H. Chen;*
The First Affiliated Hospital of Xiamen University, Xiamen, CHINA.

Aim/Introduction: This study is designed to explore the safety, tolerability, dosimetry, recommended dose, and preliminary effects of administration of ^{177}Lu-EB-FAPI with 3+3 escalating doses in metastatic radioiodine refractory thyroid cancer (mRAIR-TC) patients suffer from disease progression after tyrosine kinase inhibitors (TKIs) treatment. ***Materials and Methods:*** 12 mRAIR-TC patients were recruited, divided into 3 groups, and treated with escalating doses. Group A received 1.85-2.22GBq/cycle; Group B, 3.33-3.7GBq/cycle, and Group C, 4.44-4.81GBq/cycle. The treatment was planned for up to 2 cycles. All the patients underwent serial whole-body planar scans at 1, 4, 24, 48, 72, 96, and 168 h and SPECT/CT at 72h after the first treatment. Treatment-related adverse events were graded according to the National Cancer Institute Common Terminology Criteria for Adverse Events (CTCAE), version 5.0. The dosimetry was calculated using the Hermes system and OLINDA/EXM 1.1 software. ***Results:*** Administration of ^{177}Lu-EB-FAPI was well tolerated, without life-threatening adverse events. None of 3 patients experience dose-limiting toxicity (DLT) in Group A. CTCAE grade 4 thrombocytopenia was recorded in one patient in Group B, hence, another 3 patients enrolled in Group B, and none of these patients experienced DLT. CTCAE grade 3 hematotoxicity (thrombocytopenia) was recorded in 2 patients in Group C. No hepatotoxicity and nephrotoxicity were observed. All the patients recovered within a short period after drug intervention. The whole-body effective dose (mean±SD) was 0.16±0.02 mSv/MBq. The mean absorbed organ doses for kidney and red marrow were 1.32±0.69 mSv/MBq and 0.11±0.03 mSv/MBq, respectively. Intense uptake and prolonged tumor retention of ^{177}Lu-EB-FAPI resulted in high absorbed tumor doses (7.55±6.68 Gy/GBq). The effective half-lives (mean±SD) for whole body and tumor were 90.20±7.68 h and 96.91±8.54 h, respectively. Up to now evaluation results were obtained in 10 of the 12 patients, three patients showed partial response, one patient showed progressive disease and the other 6 patients showed stable disease. ***Conclusion:*** ^{177}Lu-EB-FAPI was well tolerated in all patients, and demonstrated increased uptake and prolonged tumor retention. At the dose of 3.33-3.7GBq/cycle, ^{177}Lu-EB-FAPI displayed acceptable side effects. Prospective clinical studies are warranted.

809

Monday, September 11, 2023, 9:45 AM - 11:15 AM
Hall G2

e-Poster Presentations Session 6 - Oncology & Theranostics Committee: Prostate Cancer

EPS-105

The Probability of Prostate Cancer Metastases within different Prostate-Specific Antigen ranges using Primary Staging Prostate-Specific Membrane Antigen PET/CT in Patients with Newly Diagnosed Prostate Cancer

W. Luining[1], *M. J. Hagens*[2], *D. Meijer*[1], *S. Srbljin*[3], *J. C. C. Koppes*[1], *R. J. J. Knol*[4], *P. J. van Leeuwen*[2], *A. N. Vis*[1], *D. E. Oprea-Lager*[1];
[1]*Amsterdam UMC, Amsterdam, NETHERLANDS,* [2]*Netherlands Cancer Institute - Antoni van Leeuwenhoek Hospital (NCI-AVL), Amsterdam, NETHERLANDS,* [3]*Zaans Medisch Centrum, Zaandam, NETHERLANDS,* [4]*Northwest Clinics, Alkmaar, NETHERLANDS.*

Aim/Introduction: Prior research on prostate-specific membrane antigen (PSMA) positron emission tomography/computed tomography (PET/CT) has predominantly focused on patients with biochemical recurrence following curative treatment for prostate cancer (PCa), whereas data on outcomes of primary staging at the time of initial diagnosis is limited (1-3). This is the first study to investigate, in a large patient cohort, the association between the serum prostate specific antigen (PSA) levels and the findings on PSMA PET/CT for primary staging, regarding the proportion and site of prostate cancer metastases. ***Materials and Methods:*** Patients with newly diagnosed PCa, in whom a PSMA PET/CT was performed for primary staging between January 2017 and April 2022, were retrospectively studied. The primary objective of this study was to evaluate the risk of metastatic disease on PSMA PET/CT, based on stratification by PSA levels. Additionally, the study aimed to investigate the proportion of PSMA-positive lesions in different anatomical locations (miN1, miM1a-c). A logistic regression analysis was performed to investigate the association between iPSA levels and the findings on PSMA PET. ***Results:*** Overall, 1306 patients were included with a median PSA of 16.5 ng/mL (IQR 8.4-40.4). Of these, 42% (548/1306) were found to have metastatic disease (miN1, and/or miM1a-c) on PSMA PET/CT. The proportion of patients with metastatic disease increased with

rising PSA levels, with PSMA PET/CT detecting metastases in 19%, 30%, 39%, 41%, 60%, 73%, and 89% of patients with PSA levels <10, 10-15, 15-20, 20-35, 35-50, 50-100, and >100 ng/mL, respectively. On PSMA PET/CT, 37% (477/1306) of patients had miN1, 16% (208/1306) miM1a, 22% (283/1306) miM1b, and 2.5% (33/1306) had miM1c PCa. The PSA level was a significant predictor for the presence of metastases on PSMA PET/CT (p<0.05). ***Conclusion:*** Metastatic disease was found in 42% of patients at primary staging using modern PSMA PET/CT imaging. The initial PSA level was a significant predictor of the presence of metastases on PSMA PET/CT. These findings support the use of PSMA PET/CT in the initial staging of PCa. The current results might have important implications for the counseling and treatment of patients with PCa. ***References:*** 1. HofmanMS,LawrentschukN,Fran isRJ, Tang-C,Velal,ThomasP,et al. Prostate-specific_membrane_ ntigen_ PET-CT-_in_patients_with_high-risk_prostate_cancer_before_ curative-intent_surgery_or_radiotherapy(proPS A): a_prospective, randomised, multicentre_study. Lancet. 2020;395(10231):1208-16. 2. MottetN,vandenBerghRCN,BriersE,VandenBroeckT, Cum erbatchMG,DeSantisM,et al. EAU-EANM-ESTRO-ESUR-SIOG Guidelines_on_Prostate_Cancer-2020_Update.Part 1: Screening, Diagnosis, and Local Treatment with Curative Intent. EurUrol.2020. 3. PereraM,PapaN,RobertsM,WilliamsM,UdovicichC,Velal,et al. Gallium-68 Prostate-specific Membrane Antigen Positron Emission Tomography in Advanced Prostate Cancer-Updated Diagnostic Utility, Sensitivity, Specificity, and Distribution of Prostate-specific Membrane Antigen-avid Lesions: A Systematic Review and Meta-analysis. EurUrol.2020;77(4):403-17.

EPS-106

A systematic review and meta-analysis of the diagnostic test accuracy of PSMA PET for tumor staging in newly diagnosed prostate cancer patients, compared to histopathology

F. Gossili[1,2], *A. W. Mogensen*[1,2], *T. C. Konnerup*[3], *K. Bouchelouche*[4], *I. L. Alberts*[5], *A. Afshar-Oromieh*[5], *H. D. Zacho*[1,2];
[1]*Department of Nuclear Medicine and Clinical Cancer Research Center, Aalborg University Hospital, Aalborg, DENMARK,* [2]*Department of Clinical Medicine, Aalborg University, Aalborg, DENMARK,* [3]*Unit of Clinical Biostatistics, Aalborg University Hospital, Aalborg, DENMARK,* [4]*Department of Nuclear Medicine & PET-Centre, Aarhus University Hospital, Aarhus, DENMARK,* [5]*Department of Nuclear Medicine. Inselspital, Bern University Hospital, University of Bern, Bern, SWITZERLAND.*

Aim/Introduction: The current clinical guidelines suggest the utilization of PSMA-PET tracers for identifying metastatic prostate cancer in the primary staging. However, their efficacy in localizing the index tumor and tumor stage is not well-defined. This study aims to determine the diagnostic accuracy of PSMA-PET tracers for tumor-staging in newly diagnosed prostate cancer patients using histological confirmation as the reference standard. ***Materials and Methods:*** We conducted a systematic literature search of the PubMed, Embase, Web of Science, and Cochrane Library databases using a set of specific search terms, which included 'PSMA PET', 'primary staging', and 'prostate cancer'. Two reviewers independently evaluated all the studies based on predetermined inclusion criteria; one of the main inclusion criteria was the use of histopathology as reference standard. The reviewers extracted relevant data, and assessed the quality of evidence, with the aid of a third reviewer to resolve any discrepancies. The random-effects Sidik-Jonkman model was utilized to perform a meta-analysis and estimate the diagnostic accuracy on a per-patient basis, along with 95% confidence intervals. Furthermore, an assessment of potential publication bias and small-study effect was conducted through both Egger's test and visual analysis of the funnel plot. ***Results:*** The analysis encompassed a total of twenty-three papers, consisting of 969 patients, which were examined using both qualitative and quantitative approaches. The findings revealed that the estimated diagnostic accuracy of PSMA PET/CT and PSMA PET/MRI, regardless of PSMA-tracer type, for intraprostatic tumor detection was 86% (95% CI: 76-96%) and 97% (95% CI: 94-100%), for extraprostatic extension detection was 73% (95% CI: 64-82%) and 77% (95% CI: 69-85%), and for seminal vesicle involvement detection was 87% (95% CI: 80-93) and 90% (95% CI: 82-99%), respectively. ***Conclusion:*** The present analysis has demonstrated that PSMA PET/MRI exhibits greater diagnostic accuracy than the currently recommended mpMRI, while PSMA PET/CT displays comparable diagnostic accuracy in the detection of intra-prostatic tumors, when compared to mpMRI. Nonetheless, the analysis uncovered potential limitations, such as small study effects, and a risk of publication bias, which may influence the overall conclusions drawn from the study.

EPS-107

A multi-center European study to explore the detection of oligometastatic disease by PSMA-PET/CT in intermediate to high-risk Prostate Cancer

G. Zuccotti[1], *F. Mattana*[1], *A. Barone*[1], *L. Muraglia*[1], *R. Mei*[2], *A. Farolfi*[2], *P. Rajwa*[3], *M. Miszczyk*[4], *V. Kasivisvanathan*[5], *F. Zattoni*[6], *G. Gandaglia*[7], *A. Briganti*[7], *S. Shariat*[3], *P. Castellucci*[2], *S. Fanti*[2], *F. Ceci*[1];
[1]*Division of Nuclear Medicine, IEO European Institute of Oncology IRCCS, Milano, ITALY,* [2]*Service of Nuclear Medicine, Sant'Orsola-Malpighi University Hospital IRCCS, Bologna, ITALY,* [3]*Department of Urology, University of Vienna, Vienna, AUSTRIA,* [4]*Department of Nuclear Medicine, Narodowy Instytute Onkologii, Gliwice, POLAND,* [5]*Department of Urology, Imperial College of London, London, UNITED KINGDOM,* [6]*Department of Urology, University of Padova, Padova, ITALY,* [7]*Department of Urology, San Raffaele Hospital, Milano, ITALY.*

Aim/Introduction: The accurate staging of prostate cancer (PCa) prior to primary therapy is crucial, as metastatic disease is related to less favorable outcome compared to locally confined ones. Recently, the addition of metastasis-directed therapy to conventional radical therapy (surgery or radiotherapy) has been proposed. Nevertheless, evidences about the incidence of oligo-metastatic disease (OMD) detected by PSMA-PET are still limited.The primary objective was to compare the positivity rate of PSMA-PET vs. conventional imaging (CI) (CT and bone scan) to identify OMD. Secondary objectives were: a) to assess the overall detection of OMD in intermediate vs high-risk PCa; b) to assess the overall detection of OMD in M1a/M1b vs. M1c; c) the intention-to-treat analysis to evaluate potential changes in clinical management. ***Materials and Methods:*** This is a retrospective, multicenter, head-to-head comparative analysis involving seven high-volume centers in Europe. All patients were affected by a biopsy proven intermediate to high-risk PCa, and performed PSMA-PET and CI (CT and/or bone scan) prior radical therapy within four months each other. According to literature, the proportion of OMD detected with CI was in the 5-10% range. We hypothesized that PSMA-PET was able to identify a higher proportion of OMD compared to CI. The Mc-Nemar test for paired proportions was used. ***Results:*** Overall, 359 patients met the inclusion criteria (high-risk=260/359; intermediate-risk=99/359). PSMA-PET identified metastatic disease in 88/359 (24,5%) and disease confined to the pelvis in 47/359 (13%), while CI identified

metastatic disease in 39/359 (10,8%) and disease confined to the pelvis in 33/359 (9,2%).The primary end-point analysis was performed in 256 patients who performed both CT and bone scan. PSMA-PET detected OMD in 29/256 patients (11,3%), while CI in 17/256 patients (6,6%). In 6/256 (2,3%) patients PSMA-PET and CI were concordant in the identification of OMD, 6/256 patients (2,3%) were considered OMD by CI and upstaged as multi-metastatic by PSMA-PET, 23/256 patients (9%) showed OMD in PSMA-PET while were negative on CI.In the overall population (n=359), PSMA-PET detected OMD in 41/359 patients (11,4%) all M1a/M1b. In the intermediate-risk sub-cohort, PSMA-PET detected OMD in 9/99 patients (9%), while CI in 3/99 patients (3%). In the high-risk sub-cohort, PSMA-PET detected OMD in 32/260 patients (12,3%), while CI in 22/260 (8,4%). ***Conclusion:*** PSMA-PET identified a higher proportion of metastatic disease compared to CI, as expected. Accordingly, the proportion of patients presenting with OMD at PSMA-PET was approximately the double compared to CI.

EPS-108

Role of AL^{18}F-labeled prostate specific membrane antigen (PSMA-BCH) PET/CT in detecting extracapsular extension of localized prostate cancer.

Z. Jie[1], *Y. Zhi*[2], *L. Chen*[2];
[1]*Shanxi Cancer Hospital, Taiyuan, CHINA,* [2]*Peking University Cancer Hospital and Institute, Bejing, CHINA.*

Aim/Introduction: In this study, we evaluated the usefulness of AL^{18}F-PSMA-BCH PET/CT in detecting extracapsular extension before radical prostatectomy for localized prostate cancer. ***Materials and Methods:*** The study consisted of thirty patients with localized prostate cancer who underwent AL^{18}F-PSMA-BCH PET/CT befor either open or laparoscopic radical prostatectomy between January 2018 and August 2022. Intraprostatic tumor extent, maximum diameter of the index tumor, SUVmean, SUVmax were evaluated on the PET/CT scans in the thirty patients and compared with postoperative histopathology to analyze the detectability of AL^{18}F-PSMA-BCH in localized prostate cancer using one sample t-test and ROC curve by SPSS 25.0. ***Results:*** In the thirty patients with localized prostate cancer were diagnosed age at 55-81 years and the median age was 69 years; Gleason score in preoperative biopsy was 6-10, median Gleason score was 7; Gleason score was 6-9 in postoperative pathology, median Gleason score was 7; the range of tumor volume was 1227.5-36891.6 mm3, the median volume was 9289.25 mm3;maximum diameter of the index tumor was 20.4-62.3mm, the maximum diameter was 38.5mm; the range of SUVmean was 2.19-4.95, the median SUVmean was 3.585; the range of SUVmax was 3.41-29.33, and the median SUVmax was 9.04. In AL18F-PSMA-BCH PET/CT images, there were significant differences in tumor volume, the maximum diameter , SUVmean and SUVmax between prostate cancer patients with and without extracapsular invasion ($P < 0.05$). When the cutoff value of tumor volume is 12805.9mm3, tumor extracapsular invasion AL18F-PSMA-BCH has better diagnostic value in tumor extracapsular invasion. The AUC value was 0.638 and the Youden index was 0.286. The sensitivity and specificity of detecting tumor extracapsular invasion were 50% and 78.6% respectively. ***Conclusion:*** The tumor volume in AL^{18}F-PSMA-BCH PET/CT can detective tumor extracapsular invasion in localized prostate cancer effectively, which can guide the treatment plan for patients with localized prostate cancer helpfully .

EPS-109

Exploring the Correlation between Multiparameters Detected in Primary Prostate Cancer using 18F-PSMA-1007 PET/MRI and thier Potential for Predicting Lymph Node and Bone Metastatses

S. Cheewadhanaraks[1], *K. Sereeborwornthanasak*[2], *C. Chotipanich*[1], *D. Siripongsatian*[1], *C. Promteangtrong*[1], *A. Kunawudhi*[1], *P. Kiatkittikul*[1], *A. Jantarato*[1], *N. Boonsingma*[1], *N. Boonkawin*[1];
[1]*National Cyclotron and PET Centre, Chulabhorn Hospital, Bangkok, THAILAND,* [2]*Bhumibol Adulyadej Hospital, Bangkok, THAILAND.*

Aim/Introduction: Prostate cancer is the second most common cancer in men. A novel tool so called PSMA PET/MRI has emerged as having a better diagnostic performance than mpMRI alone. To further enhance the value of PET/MRI, there have been studies of quantitative parameters, including ADC value, SUVmax, PSMA-TLU, and PSMA-TV of the primary cancer. This is the first study evaluating the correlation of those parameters using 18F-PSMA-1007 PET/MRI and their potential for predicting lymph node and bone metastases. ***Materials and Methods:*** This retrospective study was performed in 51 patients with primary prostate cancer who underwent initial staging at National Cyclotron and PET Centre (NCPC), Chulabhorn Hospital, Thailand between September 2020 and September 2022. The SUVmax, PSMA-TLU, and PSMA-TV were automatically calculated in primary prostate tumors. The ADC value was then measured in the darkest area of the primary tumor. The metastases were recorded by locations. Bone metastases were further divided into two groups based on the exclusion of the non-specific bone lesion (NSBL). ***Results:*** There was a significant inverse correlation between ADC value and other quantitative parameters. ADC value was significantly lower in patients with lymph node metastasis ($p = 0.0342$). Whereas, PSMA-TLU, PSMA-TV, SUVmax/ADC, PSMA-TLU/ADC, and PSMA-TV/ADC ratios were significantly higher ($p = 0.0479$, 0.0006, 0.0044, 0.0252, 0.006, and 0.0026, respectively). From ROC analysis, PSMA-TLU ratio was the best predictor of lymph node metastasis with sensitivity and specificity of 76.47% and 79.41%, respectively. No significant correlation was noted between the presence of bone metastases with NSBL and those parameters. After excluding NSBL, ADC value was significantly lower in patients with bone metastasis ($p = 0.0053$). While, SUVmax, PSMA-TLU, PSMA-TV, SUVmax/ADC, PSMA-TLU/ADC, and PSMA-TV/ADC ratios were significantly higher ($p = 0.0137$, 0.0129, 0.0111, 0.0089, 0.0108, and 0.0089, respectively). From ROC analysis, PSMA-TLU/ADC and PSMA-TV/ADC ratios could be the best predictors of bone metastasis with sensitivity of 76.92% and 61.54%, as well as specificity of 60.53% and 97.37%, respectively. ***Conclusion:*** There is a significant inverse correlation between ADC values and other quantitative parameters in primary prostate cancer using 18F-PSMA-1007 PET/MRI. Moreover, a strong correlation is noted between such parameters and the presence of metastases in lymph nodes and bones without NSBL. PSMA-TLU/ADC ratio can be the best predictor of lymph node metastasis. Meanwhile, both PSMA-TLU/ADC and PSMA-TV/ADC ratios are the best predictors of bone metastasis.

EPS-110

The Updated Prostate Cancer Molecular Imaging Standardized Evaluation (PROMISE V2.0) Framework for Standardized Reporting of PSMA-PET

R. Seifert[1], *L. Emmett*[2], *K. Herrmann*[1], *B. Hadaschik*[1], *J. Calais*[3], *S. Fanti*[4], *T. A. Hope*[5], *M. S. Hofman*[6], *M. Eiber*[7], *W. P. Fendler*[1];
[1]*University Hospital Essen, Essen, GERMANY,* [2]*St Vincent's Hospital, Sydney, AUSTRALIA,* [3]*David Geffen School of Medicine at UCLA, Los Angeles, CA, UNITED STATES OF AMERICA,* [4]*IRCCS AOU di Bologna, Bologna, ITALY,* [5]*University of California, San Francisco, San Francisco, CA, UNITED STATES OF AMERICA,* [6]*University of Melbourne, Melbourne, AUSTRALIA,* [7]*Technical University of Munich, Munich, GERMANY.*

Aim/Introduction: Prostate-specific membrane antigen (PSMA) targeting PET imaging is becoming the reference standard examination for patients with prostate cancer. It is widely used for early stages with localized treatment options, for staging advanced disease undergoing systemic treatment, and to assess eligibility for PSMA-targeting radioligand therapy. Therefore, the PROMSIE framework has been introduced to standardize the reporting of PSMA-PET derived findings. However, new applications for PSMA-PET have emerged, such as prostate imaging in biopsy-naïve patients as well as to response monitoring to systemic anti-cancer therapy. Therefore, a comprehensive and updated version of the PROMISE framework is needed. ***Materials and Methods:*** To address this need, the updated and expanded PROMISE V2.0 framework is introduced. It now comprises three layers of assessment: certainty of the diagnosis (expressed by the PRIMARY score for local tumors or by the harmonized PSMA-expression score), extent of the tumors or metastases (expressed by a revised miTNM score), and tumor volume as exploratory endpoint for clinical trials. ***Results:*** A literature review of the currently used PROMISE framework confirmed the association of PSMA-PET derived parameters with clinically relevant outcomes, such as overall survival or progression-free survival. In addition, there is growing evidence that PSMA-PET has an important role in measuring response. Especially total tumor volume changes may be associated with the outcome in advanced stages (response evaluation criteria in PSMA PET, RECIP framework). However, a lesion-based reporting approach might be more suited for earlier stages of the disease (PSMA PET Progression Criteria, PPP criteria). To facilitate the assessment with already proposed response frameworks like PPP or RECIP, but also enable new response frameworks, a standardized reporting template is proposed by PROMISE 2.0. In this way, all PSMA-PET derived characteristics that are of relevance for response assessment or outcome prognostication are clearly defined. ***Conclusion:*** The updated and extended PROMISE V2.0 framework provides a comprehensive basis for standardized PSMA-PET reporting. In addition, novel parameters are proposed to facilitate the use of PSMA-PET for response monitoring in clinical trials. ***References:*** Gafita, Andrei, et al. "Novel Framework for Treatment Response Evaluation Using PSMA PET/CT in Patients with Metastatic Castration-Resistant Prostate Cancer (RECIP 1.0): An International Multicenter Study." Journal of Nuclear Medicine63.11 (2022): 1651-1658. Fanti, Stefano, Boris Hadaschik, and Ken Herrmann. "Proposal for systemic-therapy response-assessment criteria at the time of PSMA PET/CT imaging: the PSMA PET progression criteria." Journal of Nuclear Medicine 61.5 (2020): 678-682.

EPS-111

PRIMARY scores on PSMA PET/CT and MpMRI: Role in initial evaluation of prostate cancer.

S. Kumar*, Y. Mathur, H. Singh, B. Mittal, R. Kumar;*
PGIMER, Chandigarh, INDIA.

Aim/Introduction: Multiparametric MR (MpMR) with the PIRADS (Prostate Imaging Reporting and Data Systems) forms the cornerstone of non-invasive modalities used in the initial evaluation of prostate cancer. PSMA PET/CT is a well-established modality for extent assessment, but its ability for initial evaluation of patients is less explored. The PRIMARY score provides a hierarchical approach to prostatic PSMA uptake pattern determination. The study aims to evaluate the ability of PIRADS and primary scores to identify patients with cs PC (clinically significant prostate cancer). ***Materials and Methods:*** 101 patients who underwent diagnostic MpMR and presented to PGIMER, for initial staging and/or patients suspected to have Ca prostate referred for initial evaluation were retrospectively reviewed. PRIMARY scoring of the PSMA PET/CT was done by two independent nuclear medicine physicians and compared with the PIRADS score on MpMRI. The patients were followed up for confirmation of diagnosis (Malignant vs Benign) based on TRUS/PET guided biopsy findings and/or follow-up serum PSA levels. ***Results:*** Of the 101 men with a mean age of 66.5 years included in the study, 15 %(15/101) were lost to follow up and 50% (51/101) patients had csPC. PRIMARY score 1-5 was seen in 22% (22), 12% (12), 10% (10), 11% (11), and 45% (46) of the patients. PIRADS SCORE 1-5 were seen in 0%(0), 13%(13), 15%(15), 32%(32) and 40%(41) of the patients. SUV max values respectively among the PRIMARY score 1-5 were score 1 (4.7), score 2 (6.5), score 3 (6.9), score 4 (9.6), and score 5 (24.6). Sensitivity, specificity, PPV, and NPV for PRIMARY score 1,2 (low-risk patterns) vs PRIMARY score 3-5 (high-risk patterns) were 92, 73, 84, and 86 %. Sensitivity, specificity, PPV, and NPV for PIRADS score 1,2,3 (low-risk patterns) vs score 4-5 (high-risk patterns) was 90, 63, 78 and 81% respectively. PIRADS and PRIMARY score were discordant in 6 (PIRADS - and PSMA +) and 18(PIRADS - and PSMA +) patients. ***Conclusion:*** PRIMARY Score was able to accurately identify patients who were seen to have csPC. MpMRI and PSMA PET/CT at the time of initial evaluation may act as complementary tools in the initial assessment for csPC. ***References:*** Emmett LM, Papa N, Buteau J, Ho B, Liu V, Roberts M, et al. The PRIMARY Score: Using intra-prostatic PSMA PET/CT patterns to optimise prostate cancer diagnosis. Journal of Nuclear Medicine [Internet]. 2022 Mar 1 [cited 2022 Oct 16]; Available from: https://jnm.snmjournals.org/content/early/2022/03/17/jnumed.121.263448

EPS-112

European Association of Urology Biochemical Recurrence (EAU BCR) Risk Groups after radical prostatectomy in the era of PSMA PET/CT

C. Artigas*, C. Leplat, Q. Shagera, T. Jabbour, R. Diamand, P. Flamen;*
Institut Jules Bordet, Université Libre de Bruxelles, Brussels, BELGIUM.

Aim/Introduction: After radical prostatectomy about a third of patients present with biochemical recurrence (BCR). The European Association of Urology (EAU) BCR risk grouping relies on data from historical cohorts that used conventional imaging techniques. Assessing the pattern of recurrence is essential to distinguish local relapse, oligometastatic disease or extended metastatic disease, as treatments and prognosis differ. The aim of this study was to compare the rate and patterns of positivity of ^{68}Ga-PSMA-11 PET/

CT across EAU-BCR risk groups and to provide insight on positivity predictors. ***Materials and Methods:*** From a local database of 1185 ^{68}Ga-PSMA-11 PET/CT performed for BCR, we analyzed a homogenous population of 435 patients. All patients were treated by radical prostatectomy, with or without adjuvant or salvage radiotherapy and presenting BCR as defined by the EAU. Patients that were in biochemical persistence or under androgen deprivation therapy (ADT) were excluded. PSA and PSA kinetics were measured at the time of PSMA-PET/CT. Oligometastasis was defined as ≤ 5 lesions according to ESTRO-ASTRO consensus. The Mann-Whitney U-test was used to compare continuous variables, and chi-squared test for categorical variables. Univariate and multivariable logistic regressions were performed searching for predictive factors of positivity. Cut-offs were defined using ROC curves. ***Results:*** ^{68}Ga-PSMA-11 PET/CT detected at least one lesion suspicious for prostate cancer recurrence in 236 (54%) patients. In 51% of cases with a positive PET/CT, lesions were limited to the pelvis. 43 (18,2%) patients were cM1a, 59 (25%) cM1b and 14 (5,9%) cM1c respectively. In the EAU-BCR Low-risk group, the positivity rate was 36% (n=35), compared to 59% (n=201) in the High-risk group (p<0,001). Among the BCR Low-risk patients with a positive PSMA-PET/CT, 100% had oligometastatic disease, compared to 89% in the High-risk group (p<0.001). In addition, EAU-BCR High risk patients had an increased risk for PSMA-PET/CT positive extra-pelvic lymph node (p=0,008) and bone (p=0,007) lesions. Multivariable logistic regression analysis showed that EAU-BCR risk groups (OR 2,2; CI 95% 1,3-3,8; p=0,004) and PSA at PET/CT (OR 2,7; CI 95% 1,7-4,4; p<0,001) were independent predictive factors of PSMA-PET/CT positivity. ***Conclusion:*** This study confirms that the EAU-BCR risk groups have different rates of PSMA-PET/CT positivity. We highlight the high rate of oligometastatic disease in EAU-BCR Low risk patients with a positive PSMA-PET/CT. Such patients may benefit from metastasis directed therapy, delaying ADT and its toxicities. Future prospective studies are still needed to validate the above findings and assumptions.

EPS-113

Multispectral fluorescence imaging as a means to separate healthy from diseased lymphatics during radioguided robotic surgery

F. van Leeuwen[1], *A. Berrens*[2], *M. van Oosterom*[1], *P. van Leeuwen*[2], *I. Slof*[1], *t. buckle*[1], *h. van der Poel*[2];
[1]*Leiden University Medical Center, Leiden, NETHERLANDS,*
[2]*NETHERLANDS cancer institute, Amsterdam, NETHERLANDS.*

Aim/Introduction: Within the management of prostate cancer with a 5% chance of lymph node invasion, it is common practice to perform an (extended) pelvic lymph node (LN) dissection (ePLND) during (robot-assisted) radical prostatectomy (RARP). This, however, often comes at the cost lymph edematous complications. A previous preclinical proof-of-concept studies in porcine surgery [1], suggests that not all LNs within the ePLND template are related to the prostate. In this clinical study we aimed to categorize LNs within the ePLND template by employing multispectral fluorescence imaging to intraoperatively differentiate the lymphatic drainage pathway from the prostate (and tumor) to that of non-disease related anatomies such as the leg and the abdominal wall. ***Materials and Methods:*** Thirteen patients with elevated risk of LN involvement were prospectively included and underwent RARP + ePLND. All men underwent a sentinel node (SN) procedure by intraprostatic administration of indocyanine green (ICG)-99mTc-nanoscan and preoperative SPECT/CT imaging. Prior to RARP, Fluorescein was injected intradermally with two deposits into the upper leg (group 1; n=8) or the abdominal wall (group 2; n=5). Multicolor fluorescence imaging was performed in and ex vivo using a Firefly (da Vinci Xi; ICG only) camera and Image 1 HUB HD + D-light P (Karl Storz; ICG and Fluorescein) fluorescence laparoscope. Imaging data was correlated to histopathological findings. ***Results:*** A median of 4 SNs (interquartile range [IQR] 3-6, n=13) were identified per patient on both SPECT/CT and intraoperative ICG imaging. The additional Fluorescein did not result in discomfort at the site of injection or abnormal postoperative recovery. In group 1, in 5/8 patients (63%) fluorescein was clearly visible within the ePLND template. In group 2, this increased to 5/5 patients (100%). There was a discordance in nodal staining for Fluorescein and ICG, suggesting separate drainage routes of the prostate (and cancer) vs. the lower limbs or the abdominal wall. Of the 11 tumor positive LNs, 91% (10) were ICG-positive SNs and 0% was fluorescein positive. Damage to fluorescein positive lymphatic ducts revealed leakage and fluorescein containing urine was shown to contaminate the surgical field during prostatectomy. ***Conclusion:*** For the first time, discordance of lymph drainage patterns of the leg and prostate, or the abdominal wall and prostate, was presented in humans. Thereby providing a first step towards lymph node sparing ePLND strategies. ***References:*** [1] Meershoek et al., J Nucl Med, 2018

EPS-114

Significance of interim ^{18}F-PSMA-1007 PET/CT for early prediction of ^{177}Lu-PSMA-I&T treatment effect in metastatic castration-resistant prostate cancer patients

S. Cheung*, S. Chen, Y. Wong, Y. Yip, C. Ho;*
Hong Kong Sanatorium & Hospital, Hong Kong, HONG KONG.

Aim/Introduction: A common approach for monitoring the efficacy of ^{177}Lu-PSMA radionuclide therapy is by serial evaluation of serum PSA (PSA Response) and a PSMA-targeted PET/CT (Imaging Response) after completion of 4 treatment cycles. However, serum PSA dynamics are known to be affected by a number of inherent factors such as cytological heterogeneity, tumor grade and differentiation, free-to-protein-bound ratios and treatment flare effects. We aimed to investigate whether an interim ^{18}F-PSMA-1007 PET/CT after 2 cycles of ^{177}Lu-PSMA-I&T treatment in mCRPC patients could provide early prediction of response to guide further treatment decisions. ***Materials and Methods:*** Between Aug-2020 and Dec-2022, we recruited mCRPC patients who completed 4 cycles of ^{177}Lu-PSMA-I&T therapy (~7.4 GBq at six-week intervals). They all had serum PSA bioassay and ^{18}F-PSMA-1007 PET/CT: (1) baseline (bPET), (2) after 2 cycles of treatment (interim PET, iPET), (3) 3 months after 4 cycles (fPET). We used a "PSA Response" criterion proposed by PCWG3 with "PSA decline≥50%" from baseline as positive response. Whereas, we followed the RECIP-1.0 proposal to calculate Total PSMA-avid tumor volume (PSMA-VOL, automatically by MIMContouring) as a tumor burden parameter for gauging "Imaging Response" on 3 sets of PET/CT. "Imaging Response" was defined as complete (CR), partial (PR) or nonresponse (NR) based on iPET and fPET changes compared with bPET. CR: all PSMA-1007-avid lesions normalized; PR: decline≥30% in PSMA-VOL with no emergence of new lesions; NR: progressive or decline<30% in PSMA-VOL or emergence of new lesions. Final therapeutic outcome was judged by the combined "PSA+imaging responses" 3 months after 4 cycles. ***Results:*** This study recruited 24 patients (mean age=73.5±11.1 years, range:54-92 years). After the 2nd cycle of treatment, interim "PSA Response" rate was 79% (19/24); while interim "Imaging Response" rate was significantly lower, only 46% (11/24: 1 CR+10 PR). After

the 4th cycle, "PSA Response" rate was 46% (11/24); while "Imaging Response" rate was 42% (10/24: 10 PR). The primary outcome based on combined "PSA+imaging responses" identified 11/24 patients (46%) as responders. Interim "Imaging Response" was consistent with the primary outcome for all patients classified as Response/Nonresponse, while interim "PSA Response" misclassified 8/19 (42%) patients as positive response, who were found to have new tumors on iPET and confirmed on fPET, with rebounded PSA after 4 cycles of treatment. ***Conclusion:*** Interim ^{18}F-PSMA-1007 PET/CT after the 2nd cycle of ^{177}Lu-PSMA-I&T treatment in mCRPC patients has prognostic value as a surrogate biomarker for monitoring treatment and predicting final therapeutic outcome.

EPS-115

Absorbed dose prediction for subsequent therapy cycles from 1st cycle of ^{177}Lu-PSMA-617 therapy of mCRPC patients

J. Brosch-Lenz[1], *N. Colpo*[2], *I. Bloise*[1], *X. Hou*[1], *W. R. Parulekar*[3], *C. Dellar*[3], *F. Saad*[4], *K. Chi*[2], *D. Wilson*[2], *F. Bénard*[2], *A. Rahmim*[1], *C. Uribe*[2];
[1]*BC Cancer Research Institute, Vancouver, BC, CANADA,* [2]*BC Cancer, Vancouver, BC, CANADA,* [3]*Canadian Cancer Trials Group, Queen's University Kingston, Kingston, ON, CANADA,* [4]*Prostate cancer research, Montreal Cancer Institute / CRCHUM, Montreal, QC, CANADA.*

Aim/Introduction: ^{177}Lu-PSMA-617 was approved as a radiopharmaceutical for patients suffering for metastatic, castration-resistant prostate cancer (mCRPC) that is administered using fixed activities. However, mCRPC patients may present with very different tumor burden and extent of disease besides natural differences such as age, weight, height, and pre-therapy history. Consequently, a personalized activity prescription approach based on dosimetry is advisable to maximize the therapeutic effect, while minimizing the radiation exposure to healthy tissues. The aim of this study was to estimate the accuracy of dose predicted for subsequent therapy cycles based on the first therapeutic administration. This work is based on early experience from the Canadian Cancer Trials Group PR21 trial (NCT 04663997). ***Materials and Methods:*** Four patients with six therapy cycles each were included in this study. Healthy organs (kidneys, liver, spleen) were segmented on the CT images using an AI-model and salivary glands were segmented using a threshold-based approach on the quantitative ^{177}Lu-SPECT. Organ-specific time-activity-curves were fitted to a mono-exponential function for the first therapy cycle, while a single time point dosimetry approach was used for the subsequent therapy cycles. Monte Carlo simulations were used for 3D dosimetry in GATE using the patients' organ time-integrated activity images and CT per cycle. The organ absorbed doses (ADs) per injected activity from first cycle were extrapolated to subsequent therapy cycles and compared with the actual calculated ADs per cycle. ***Results:*** Median injected activity was 7718±205MBq across patients and cycles. Kidney ADs increase by +37%, liver ADs by +21%, spleen ADs by +20%, while salivary gland ADs decreased by -9% from cycle 1 to 6. Percentage differences between predicted AD and actual AD per cycle was -9%, -12%, -22%, -26%, and -19% for kidneys (cycle 2 to 6); 0%, -13%, -19%, -28%, and -16% for liver (cycle 2 to 6); -8%, -16%, -23%, -31%, and -26% for spleen (cycle 2 to 6); and 0%, -3%, -8%, -1%, and -6% for salivary glands (cycle 2 to 6). ***Conclusion:*** The results of this preliminary analysis indicate that a simple extrapolation of healthy organ ADs from the cycle 1 to 2 to 6 is not advisable. We observed large AD underestimation up to -31% compared to individual dosimetry per cycle. The differences increased towards higher cycles, which may be related to the tumor sink effect. It is planned to expand this analysis to a larger patient cohort of the PR21 trial.

EPS-116

Pre-treatment ^{68}Ga-PSMA PET/CT Parameters Could Predict Response to ^{177}Lu-PSMA Treatment and Overall Survival in Metastatic Castration Resistant Prostate Carcinoma Patients Treated with ^{177}Lu-PSMA

E. Özkan[1], ***B. Demir***[1], *M. Ozturk*[1], *M. Araz*[1], *C. Soydal*[1], *B. Dursun*[2], *Y. Urun*[2], *N. O. Kucuk*[1];
[1]*Ankara University School of Medicine Department of Nuclear Medicine, Ankara, TÜRKIYE,* [2]*Ankara University School of Medicine Department of Medical Oncology, Ankara, TÜRKIYE.*

Aim/Introduction: Response to ^{177}Lu-PSMA treatment is highly variable and the factors that can be useful in predicting response to ^{177}Lu-PSMA treatment and their correlation to overall survival of the patients have not been clearly established yet. In this study we aimed to determine parameters that are contributing to predict therapy response and overall survival, derived from pre-treatment ^{68}Ga PSMA PET/CT. ***Materials and Methods:*** We analysed a total number of 55 patients treated with ^{177}Lu-PSMA therapy in this retrospective study. Baseline PET/CT of all patients were segmented and total tumour metabolic volume (TT-MV), SUVmax, SUVmean, SUVpeak and total tumour PSMA uptake (TT-PSMA) values were noted. Also, overall survival time after PET/CT imaging and PSA response based on a decline of at least 50% for responders were determined for available patients. ROC analysis for PET/CT parameters was performed in predicting PSA response. For overall survival, Kaplan-Meier survival analysis between PSA responders/non-responders and the groups generated from PET/CT parameters based on median values was performed. ***Results:*** PSA responder and non-responder groups median SUVmax, SUVmean, SUVpeak, TT-MV and TT-PSMA values were 47.78 vs. 26.80, 13.62 vs. 8.47, 32.25 vs. 16.96, 162.12 vs. 168.61 and 839.68 vs 1627 respectively. Between two groups SUVmax (p=0.002), SUVmean (p=0.038) and SUVpeak (p=0.007) values were significantly higher in responder group. In ROC analysis AUC for SUVmax, SUVmean and SUVpeak were 0.772, 0.681 and 0.736 respectively. A high specificity cut-off were determined for SUVmax value to predict PSA response was 50.70 (sensitivity: 47.1%, specificity: 87.9%). In survival analysis overall median survival time after PET/CT for PSA responder group (513 days) was significantly (p=0.003) longer than non-responder group (305 days). Also, the patients with TT-MV smaller than 162.12 cm3 had longer median overall survival time (567 days) than TT-MV>162.12cm3 (279 days) group (p<0.001). ***Conclusion:*** SUVmax, SUVmean and SUVpeak values in pre-treatment ^{68}Ga-PSMA PET/CT were significantly higher in PSA responder group. Also, PSA responder patients to ^{177}Lu-177 PSMA treatment and the patients with lower TT-MV values had significantly longer overall survival. Understanding of contributing factors to predict response in ^{177}Lu-PSMA treatment may help better selection of suitable patients to ^{177}Lu-PSMA treatment.

EPS-117

Changes in PSA levels after two cycles of radioligand therapy appear superior to changes in PSMA PET for outcome prediction

P. Hartrampf[1], *T. Hüttmann*[1], *A. K. Seitz*[2], *H. Kübler*[2], *T. Higuchi*[1], *S. E. Serfling*[1], *W. Schlötelburg*[1], *K. Michalski*[1], *A. K. Buck*[1], *R. A. Werner*[1];
[1]*Klinik und Poliklinik für Nuklearmedizin, Würzburg, GERMANY,* [2]*Klinik und Poliklinik für Urologie, Würzburg, GERMANY.*

Aim/Introduction: In patients with prostate carcinoma (PC) undergoing PSMA-directed radioligand therapy (RLT), current guidelines recommend restaging using PSMA-directed PET/CT after two cycles of treatment along with monitoring of PSA levels. We aimed to determine whether changes of quantitative parameters on molecular imaging are superior for prediction of overall survival (OS) when compared to alterations of PSA levels. ***Materials and Methods:*** In this retrospective study, 73 PC patients were imaged with [^{18}F]-PSMA-1007 PET prior to and after two cycles of RLT using [^{177}Lu]Lu-PSMA I&T. By analyzing the whole tumor burden on both scans, we recorded changes (provided as delta [Δ]) of quantitative PET-based parameters (including mean/maximum SUV, PSMA-avid tumor volume [PSMA-TV], and total lesion PSMA [TL-PSMA, defined as PSMA-TV * mean SUV). We also determined PSA levels at baseline and after the second cycle. Moreover, subjects were stratified according to biochemical PCWG3 criteria (with progressive disease [PD] defined as PSA increase ≥ 25%) and PET-based RECIP 1.0 (PD defined as increase ≥ 20% in PSMA-TV and appearance of new lesions). We performed univariable cox regression analysis, followed by multivariable and Kaplan Meier analyses for survival prediction. ***Results:*** Median OS was 17 months [mo], while 28 patients died. On univariable analysis, ΔPSMA-TV, ΔTL-PSMA and ΔPSA were associated with OS (P<0.01, each). Multivariable cox regression revealed only ΔPSA (per unit, HR, 1.003, 95% CI 1.001-1.005; P<0.001) as prognosticator for OS, while ΔPSMA-TV (P=0.06) narrowly failed to reach significance. On Kaplan Meier analysis, we observed significant segregation between individuals with (21 mo) vs. without any PSA response (13 mo, HR 0.4, 95% CI 0.2-1.0; P=0.02). Using PD classification according to RECIP (no PD, 21 mo vs. PD, 11 mo [HR 2.5, 95% CI 1.0-6.3; P=0.008]) or PCWG3 criteria (no PD, 21 mo vs. PD, 11 mo [HR 3.0, 95% CI 1.2-7.2; P=0.001]) showed shorter OS for patients with PD. Combination of RECIP 1.0 and PCWG3 criteria provided improved segregation (no PD, 21 mo vs. PD, 11 mo [HR 3.6, 95% CI 1.6-8.3; P<0.001]). ***Conclusion:*** After two cycles of RLT, changes in PSA levels may better identify patients prone to shorter survival when compared to alterations on PSMA-PET. Standardized frameworks combining biochemical (PCWG3 criteria) and PET-based changes (RECIP 1.0) may further refine response evaluation.

EPS-118

Analysing the Tumour Transcriptome of Prostate Cancer to Predict Efficacy of Lu-PSMA Therapy

A. Handke[1], *C. Kesch*[1], *W. Fendler*[1], *T. Telli*[1], *Y. Liu*[2], *A. Hakansson*[2], *E. Davicioni*[2], *J. Hughes*[2], *H. Song*[3], *K. Lückerath*[1], *K. Herrmann*[1], *B. Hadaschik*[1], *R. Seifert*[1];
[1]*Universitätsklinikum Essen, Essen, GERMANY,* [2]*Decipher Bioscience, Vancouver, BC, CANADA,* [3]*Stanford University, Stanford, CA, UNITED STATES OF AMERICA.*

Aim/Introduction: Radioligand therapy with ^{177}Lu-PSMA is a promising treatment option for patients with PSMA-positive mCRPC. However, treatment failure is seen frequently and the interplay of immune-related features and efficacy of177Lu-PSMA therapy is poorly understood. Therefore, the analysis of the immune tumour microenvironment could help identifying patients who are best candidates for ^{177}Lu-PSMA radioligand therapy. ***Materials and Methods:*** Between March 2018 and December 2021, we screened a total of 168 patients who were referred to ^{177}Lu-PSMA therapy in our department and received a mean dose of 21.9 GBq (3 cycles in mean). All patients underwent a baseline PSMA PET. Of this group of patients, primary pathology was requested from the primary pathology institutes; a total of 34 samples were successfully retrieved. Sufficient RNA passing quality for subsequent analysis was available in n = 23 patients. In this subset, tumour RNA transcriptomic analyses measured 74 immune-related features. From these features, n=24 signatures were not co-correlated and therefore investigated further for outcome prognostication. Univariable and multivariable Cox proportional hazards models were used for the OS analysis; Bonferroni correction was used to minimize the risk of alpha error accumulation. Kaplan Meier plots were used to visualize survival difference between patients; for that, signature scores were dichotomized by their median value and log-rank tests were used to investigate the statistical significance of differences in OS. ***Results:*** PD-L1 was not significantly associated with OS (hazard ratio (HR) per standard deviation (SD) change [95% confidence interval (CI)] 0.74 [0.42-1.30]; p=0.29) in patients who received ^{177}Lu-PSMA therapy. However, PD-L2 was positively associated with longer OS (HR per SD change 0.46 [0.29-0.74]; p=0.001; median OS 17.2 vs. 5.7 months in higher vs. lower PD-L2 patients). Furthermore, PD-L2 levels correlated with PSA-response (ϱ = -0.46; p=0.04). The ability of PD-L2 for OS prognostication was significantly associated with LDH levels (Cox model interaction p=0.01). ***Conclusion:*** The presented preliminary evidence suggests a crosstalk between the tumor immune microenvironment and the outcome of patients treated with Lu-PSMA therapy. Higher PD-L2 expression seems to be associated with improved outcome of patients treated with ^{177}Lu-PSMA therapy by a currently unknown relationship of radiation efficiency and immune environment.

EPS-119

Initial clinical study results of ^{68}Ga/^{177}Lu-NYM032, a new generation of PSMA-targeting theranostic radiopharmaceuticals, in patients with metastatic prostate cancer

H. He[1], *Y. Wang*[1], *Y. Mi*[1], *C. Yan*[2], *P. Fang*[2], *W. Eng*[2], *H. Fu*[1], *C. Yu*[1];
[1]*Affiliated Hospital of Jiangnan University, Wuxi, CHINA,* [2]*Norroy bioscience Co. Ltd., Wuxi, CHINA.*

Aim/Introduction: The current study was aimed at developing a new generation of prostate specific membrane antigen (PSMA)-targeting radiopharmaceuticals that have the characteristics of longer tumor uptakes and faster circulatory elimination. ^{68}Ga/^{177}Lu-NYM032 is a novel small-molecule theranostic radiopharmaceutical targeting PSMA. This study adopted a clinical design of a head-to-head comparison with the well-known radiopharmaceutical, PSMA617, to mainly investigate and analyze the diagnostic imaging capability and biodistribution of ^{68}Ga/^{177}Lu-NYM032 in patients with metastatic prostate cancer. ***Materials and Methods:*** Through several iterations of structural optimization and preclinical studies, the small-molecule lead derivative with an optimized structure, NYM032, was obtained. In the current head-to-head comparative study, the radiation doses of ^{68}Ga-NYM032 and ^{68}Ga-PSMA617 for each patient, were maintained the same, i.e., with an intravenous injection dose of about 2-4 mCi of both radiopharmaceuticalsto each patient, and the repeated PET scanning time points were at 1 and 2 h after injection. In the imaging studies of ^{177}Lu-NYM032 (with SPECT) and ^{68}Ga-NYM032 (with PET) in each patient, the injected radioactive dose of ^{177}Lu-NYM032 was about 15-30 mCi, and multiple (tomographic SPECT) scanning time points between 0.5 h and 504 h were selected; while the radioactive dose of ^{68}Ga-NYM032 at injection, which was about 24-96 h prior to the administration

of ^{177}Lu-NYM032, was about 3-5 mCi, with a PET scanning time point at 1 h after ^{68}Ga-NYM032 injection. ***Results:*** Among the 10 patients with metastatic prostate cancer who have completed the entire research study, the results of ^{68}Ga-NYM032, as compared to ^{68}Ga-PSMA617, showed higher tumor radiation uptakes and a lower uptake in the heart blood pool, thus demonstrating a high tumor target-to-background ratio. The SPECT scanning results of in three patients who have received ^{177}Lu-NYM032 showed a prolonged residence time of radioactivity in tumors (persisted more than 504 h, with an average $t_{1/2\ eff}$ >150 h in most tumor lesions) and a low uptake in the circulation, thus supporting the notion that ^{177}Lu-NYM032 has stronger therapeutic and higher safety potential. ***Conclusion:*** ^{68}Ga/^{177}Lu-labeled versions of the small-molecule radiopharmaceutical, NYM032, with an optimized structure exert a high specificity for PSMA-positive tumor lesions, leading to higher lesion uptakes, and a prolonged and persistent residence time of radioactivity in the target tissues. Therefore, ^{68}Ga/^{177}Lu-NYM032 have a great potential as a novel and powerful theranostic for prostate cancer.

EPS-120

Detection Rate of ^{64}Cu-SAR-Bombesin-PET/CT in Men with Biochemically Recurrent Prostate Cancer and Negative or Equivocal ^{68}Ga-PSMA-11-PET/CT

S. Li[1], *A. Nguyen*[1,2], *W. Counter*[1], *N. John*[1], *J. De Leon*[3], *G. Hruby*[4,3,5], *A. M. Joshua*[6,7,8], *P. Stricker*[9,5,10], *K. Wong*[1], *V. Liu*[1], *E. Lengyelova*[11], *S. Agrawal*[1,6,7], *L. Emmett*[1,7,2];
[1]Department of Theranostics and Nuclear Medicine, St Vincent's Hospital, Sydney, AUSTRALIA, [2]St Vincent's Clinical School, University of New South Wales, Sydney, AUSTRALIA, [3]Genesis Cancer Care, Sydney, AUSTRALIA, [4]Department of Radiation Oncology, Royal North Shore Hospital, Sydney, AUSTRALIA, [5]Faculty of Medicine, University of Sydney, Sydney, AUSTRALIA, [6]The Kinghorn Cancer Care Centre, St Vincent's Hospital, Sydney, AUSTRALIA, [7]Garvan Institute of Medical Research, Sydney, AUSTRALIA, [8]St. Vincent's Clinical School, University of New South Wales, Sydney, AUSTRALIA, [9]Department of Urology, St Vincent's Hospital, Sydney, AUSTRALIA, [10]Faculty of Medicine, University of New South Wales, Sydney, AUSTRALIA, [11]Clarity Pharmaceuticals, Sydney, AUSTRALIA.

Aim/Introduction: Despite a high detection rate of ^{68}Ga Prostate-specific Membrane Antigen (PSMA) PET/CT in biochemical recurrence (BCR) of prostate cancer (PCa), a significant proportion of men have negative ^{68}Ga-PSMA-11 PET/CT. Identifying sites of disease recurrence is critical in better targeting salvage treatment (sRT) post radical prostatectomy (RP). Gastrin-releasing peptide receptor, targeted by ^{64}Cu-SAR-BBN PET/CT is also overexpressed in PCa. In this Phase IIa, prospective, single-site study, we investigate the added diagnostic value of PET/CT imaging with the copper-chelated analogue ^{64}Cu-labelled-Bombesin (^{64}Cu-SAR-BBN) in patients with ^{68}Ga-PSMA-11 PET/CT that is negative or equivocal in BCR (NCT 0561384) ***Materials and Methods:*** 20 men with BCR (defined as PSA >0.2ng/mL) with negative or equivocal ^{68}Ga-PSMA-11 PET/CT underwent ^{64}Cu-SAR-BBN PET/CT within 3 months (median 1.0). ^{64}Cu-SAR-BBN median dose was 211MBq (IQR 186-225) with scans acquired at 1 and 3 hours. Delayed 24-hour imaging was undertaken in 13/20. All images were reviewed, with site, intensity of tracer uptake and certainty of disease involvement recorded. PET results were released to referring clinicians, and any further treatments or investigations undertaken to confirm imaging findings were obtained. ***Results:*** Median age 71 (range 58-81). Prior RP in 19/20, RP and sRT in 12/20. Median PSA at imaging 0.73 (IQR 0.50-2.28). Median PSA doubling time of 4.6 months (IQR 2.5-7.3). 15/20 had negative ^{68}Ga-PSMA-11 PET studies and 5/10 reported as equivocal probably negative. ^{64}Cu-SAR-BBN PET avid disease was identified in 6/20 (30% detection rate). These comprised 2/20 with local recurrence, 2/20 with nodal disease (pelvic) and 2/20 with distant disease (lung). 40% (8/20) of all patients underwent subsequent treatment, 7/8 targeted and 1/8 systemic. On follow-up, 2/8 had targeted treatment response (pelvic node) or biopsy confirmation (lung biopsy), considered true positive disease on^{64}Cu-SAR-BBN PET/CT. Physiological uptake was noted in mediastinal lymph nodes in 7 patients. No adverse events from ^{64}Cu-SAR-BBN administration were reported. ***Conclusion:*** ^{64}Cu-SAR-BBN PET/CT demonstrates sites of disease recurrence in 30% of BCR cases with negative or equivocal ^{68}Ga-PSMA-11 PET/CT. Further evaluation to confirm diagnostic benefit is warranted.

EPS-121

Impact of ^{68}Ga-PSMA-11 PET/CT on salvage radiation treatment concept in males with early biochemical relapse of prostate cancer after radical prostatectomy

M. Dyankova[1,2], *T. Stoeva*[1], *Z. Dancheva*[1], *S. Chausheva*[1], *T. Yordanova*[1], *B. Chaushev*[1], *A. Klisarova*[1];
[1]Medical University Varna "Prof. Dr. Paraskev Stoyanov", Department of Imaging Diagnostics, Interventional Radiology and Radiotherapy, Varna, BULGARIA, [2]St. Marina University Hospital, Department of Nuclear Medicine, Varna, BULGARIA.

Aim/Introduction: Salvage radiation treatment (SRT) is well settled in males with biochemical recurrence (BCR) after radical prostatectomy (RP) in the absence of distant metastases. The aim of this study was to assess the impact of 68Ga-PSMA-11-PET/CT on SRT concept in males with early biochemical relapse in the low-range values up to prostate-specific antigen (PSA) ≤ 0.5 ng/ml after RP. ***Materials and Methods:*** We performed a retrospective analysis in 85 consecutive patients with BCR (up to PSA ≤ 0.5 ng/ml) after RP. The patients were planned for SRT after PSMA PET/CT scan. An experienced radiation therapists defined the concept of upcoming SRT by two different approaches: first based on the clinical and pathological characteristics hypothetically, where after based on the obtained PET/CT scans. ***Results:*** The mean age of the patients was 69.3 years. The mean ISUP grade group was 3 and the mean PSA level was 0.354 ng/mL (0.2-0.5). Without taking into account the results of the PSMA PET/CT, all 85 patients would have been referred for RT: 65 (76.5%) to the prostate bed and seminal vesicles fossa only, and 20 (23.5%) furthermore to the regional pelvic lymph nodes due to high-risk histopathologic features. A total of 44 patients (51.8%) showed at least one positive lesion. ^{68}Ga-PSMA PET/CT detection rate varied according involved regions as follows: local recurrence- 21.2% (18) : in the prostate bed- 11.8% (10) in the seminal vesicle fossa- 9.4% (8), lymph node metastases: regional- 12.9% (11), distant- 9.4% (8); bone metastases- 20.0% (17), distant metastases as a whole- 23.5% (20). Additional data from 68Ga-PSMA-11-PET/CT guide to alter of RT planning in 28 (32.9%) males. There were modification with mild adaptation of RT, included the supplementary inclusion in the irradiated area of seminal vesicle fossa in 8 patients (9.4%). The significant differences in the target volume included the supplementary RT of lymph nodes or the added or particular RT of bone metastatic lesions in 20 patients (23.5%). PSA response was achieved in 47 (92%) patients from the available PSA levels in 65 patients 6 months after accomplishment of SRT. ***Conclusion:*** ^{68}Ga-PSMA-11-PET/CT showed a high impact on SRT concept in

males with early biochemical relapse of PC after RP. A change in the treatment planning was indicated in 32.9% of patients with BCR at PSA levels ≤ 0.5 ng/ml. Thus, PSMA PET/CT can significantly contribute to a personalized approach in RT planning, which may improve progression-free survival.

EPS-122

Effects of novel androgen receptor signaling inhibitors on PSMA PET signal intensity in patients with castrate-resistant prostate cancer: a prospective exploratory serial imaging study

I. Sonni[1,2], *A. Gafita*[1,3], *R. M. Alano*[1], *S. Lira*[1], *L. Unterrainer*[1,4], *J. Shen*[1], *A. Drakaki*[1], *T. Grogan*[1], *M. B. Rettig*[1], *J. Czernin*[1], *J. Calais*[1];
[1]*University of California, Los Angeles, Los Angeles, CA, UNITED STATES OF AMERICA,* [2]*Università Magna Graecia, Catanzaro, ITALY,* [3]*Johns Hopkins University, Baltimore, MD, UNITED STATES OF AMERICA,* [4]*Ludwig-Maximilians-University, Munich, GERMANY.*

Aim/Introduction: PSMA expression on prostate cancer (PCa) cells is influenced by hormonal status. Studies investigating the effects of androgen-receptor (AR) targeting treatments on PSMA expression produced unclear results. Aim of this study was to evaluate changes on serial whole-body (WB) PSMA PET parameters and PSA levels in patients with metastatic castrate-resistant prostate cancer (mCRPC) in response to AR-signaling inhibitor (ARSI). ***Materials and Methods:*** This was a single-center, exploratory, prospective study designed to enroll 30 patients. Inclusion criteria were known mCRPC and planned initiation of treatment with a new ARSI. Patients underwent serial serum PSA measurements and 68Ga-PSMA-11 PET/CT (PSMA PET) at baseline (pre-ARSI - visit #1), 1-week (visit #2) and 3-months (visit #3) post-ARSI. Follow-up with PSA was conducted every 3 months after visit #3 (at 6, 9, and 12-months post-ARSI). The imaging analysis was conducted using qPSMA by a board-certified nuclear medicine physician who contoured all PSMA-avid lesions to extract WB quantitative parameters (SUVmean, SUVmax and tumor volume). We assessed changes in PSA and WB-PSMA PET parameters at all time-points. Changes ≤10% were considered stable and >10% as clinically significant. We correlated PSA and WB-PSMA PET changes to outcome at 1-year post-ARSI. PSA levels and WB-PSMA PET changes were considered concordant with outcome in case of an increase with unfavorable outcome or in case of a decrease, or stable with favorable outcome. ***Results:*** Nine patients/30 were prospectively enrolled between 02/2020 and 11/2021. All patients underwent PSA and PSMA PET at visit #1 and #2, 6/9 patients had PSA and PSMA PET at visit #3. Changes in PSA, PSMA-VOL, SUVmean and SUVmax were -12%, +5%, +3%, and +10% at 1-week in 9/9 patients, -42%, -16%, -15% and -17% at 3-months in 5/9 patients, respectively. Six/9 patients had unfavorable outcome, 2/9 died and 4/6 experienced biochemical recurrence during the 1-year follow-up. 1-week PSA changes were discordant with 1-year outcome in 4/6 patients. Three/9 patients had favorable outcome with stable or decreasing PSA at 1-year, and none had increase in any of the PSMA PET metrics at 1-week or 3-months post-ARSi initiation. ***Conclusion:*** In this prospective study we found a heterogeneous response to the AR pathway modulation, and in most cases discordance between PSA kinetics and whole-body PSMA PET measurements. The modulation induced by ARSI to the PSMA expression of the whole tumor burden of mCRPC patients was not observed at 1- week.

EPS-123

Comparison of SUV and tumour net uptake rate values using dynamic whole-body ^{68}Ga-PSMA-11 PET/CT in patients with metastatic castrate-resistant prostate cancer

N. Payan[1], *J. M. Vrigneaud*[1,2], *A. Cochet*[1,2];
[1]*George François Leclerc Centre, Department of Nuclear Medicine, Dijon, FRANCE,* [2]*ICMUB Laboratory, UMR CNRS 6302, University of Burgundy, Dijon, FRANCE.*

Aim/Introduction: ^{68}Ga-PSMA-11 PET ligand targeting the prostate specific antigen (PSMA) is widely used in patients with prostate cancer. This radiopharmaceutical has also recently gained popularity in assessing patients' eligibility for ^{177}Lu-PSMA therapy. However, there is a paucity of data focused on the complementarity of ^{68}Ga-PSMA-11 PET SUV and parametric images-based values. The aim of this study was to assess whether SUV-based values in tumour lesions do correlate with the net influx rate Ki as a representation of the PSMA receptor expression in patients with metastatic castrate-resistant prostate cancer (mCRPC). ***Materials and Methods:*** Ten patients with mCRPC who underwent diagnostic ^{68}Ga-PSMA-11 PET scans were prospectively included. Immediately after ^{68}Ga-PSMA-11 injection, a 6-min chest-centered static acquisition was used to generate the bolus part of the image-derived input function (IDIF) extracted from descending aorta. Then, six dynamic whole-body PET/CT acquisitions were performed in continuous bed motion, for one hour. Parametric Ki images were computed with the graphical Patlak method, using a fully-automated IDIF extracted from the static and dynamic acquisitions. Five lesions per patient were delineated using isocontours of 40% of the SUV_max and were transferred on the Ki parametric images. Correlation analyses were carried out between SUV, Tumour-to-Blood Ratio (TBR) and Ki (mL/min/mL) mean values. Correlations of Tumour-to-Liver (TLR) and Tumour-to-Spleen (TSR) ratios were analysed between both, SUV and Ki parameters (TLR_SUV, TLR_Ki, TSR_SUV and TSR_Ki respectively). Linear and non-linear regressions were tested. R squared were calculated for linear regressions and the goodness of the fits was evaluated using residual standard error. ***Results:*** A total of 50 malignant lesions were included. Strong correlations between SUV-based and Ki-based parameters' values were noted using linear relationships, with the highest correlations observed between TBR and Ki values (adjusted R^2=0.92, 0.95, 0.97 and 0.97 with p-values <0.001, for SUV/Ki, TLR_SUV/TLR_Ki, TSR_SUV/TSR_Ki and TBR/Ki respectively). Slightly lower residual standard errors were noted using non-linear regressions except for TBR/Ki (7.6 vs 8.2, 0.95 vs 1.01, 0.96 vs 0.97 and 2.54 vs 2.39 using non-linear and linear regressions, between SUV/Ki, TLR_SUV/TLR_Ki, TSR_SUV/TSR_Ki and TBR/Ki respectively). ***Conclusion:*** Strong correlations between Ki and SUV-based values were observed, including when SUV and Ki parameters were corrected by liver or spleen mean values, reflecting a good agreement between the SUV extracted from ^{68}Ga-PSMA-11 PET scans and the lesions' PSMA receptor density. A stronger correlation between TBR and Ki would suggest that TBR reflects lesions' PSMA receptor density slightly better than SUV_mean.

EPS-124

Predictive ^{18}F-rhPSMA 7.3 PET parameters for outcome assesssment of ^{177}Lu-PSMA RLT

K. Hansen, *C. Fütterer, T. Langbein, M. Heck, W. A. Weber, M. Eiber, I. Rauscher;*
Klinikum rechts der Isar, Munich, GERMANY.

Aim/Introduction: Several clinical/laboratory parameters as well as 68Ga-PSMA-11 PET-based imaging parameters have been proposed as predictors for outcome of PSMA-radioligand therapy (RLT) in patients with metastatic castration-resistant prostate

cancer (mCRPC). Increasingly, 18F-labelled PSMA-targeting agents are used in preference to 68Ga-PSMA-11. The aim of this retrospective analysis was to evaluate the use of a 18F-rhPSMA-7.3 in conjunction with clinical/laboratory parameters as prognostic marker of outcome in patients receiving 177Lu-PSMA RLT. ***Materials and Methods:*** A total of 188 mCRPC patients were included. Prognostic factors included clinical parameters, routine laboratory parameters and findings on baseline 18F-rhPSMA-7.3 PET. For each patient, all tumor lesions were semi-automatically delineated using aPROMISE software and different quantitative parameters were calculated (e.g., SUV mean/max/peak, total lesion number, total tumor volume (TTV)). Overall survival (OS) was calculated and uni- and multivariable Cox regression analyses were performed to determine the association with OS. Further, the Kaplan-Meier method was used for estimation of event time distributions and log rank tests were used for group comparisons. ***Results:*** Overall, OS was 11.8 months (95% CI, 10.0 to 13.0). Univariable Cox regression analysis revealed total lesion number, TTV, rising levels of AP, LDH, PSA, decreasing hemoglobin, prior chemotherapy, and the presence of visceral metastases at baseline as negative prognostic factors for OS. In multivariable analysis, total lesion number on 18F-rhPSMA-7.3 PET, rising levels of LDH and the presence of visceral metastases were identified as significant prognosticators. Further, patients presenting with a higher TTV (≥ median of 394 ml) and a higher number of metastatic lesions (≥ median of 127 lesions) on 18F-rhPSMA-7.3 PET presented with a significant reduced OS (10.1 vs. 15.9 months for TTV and 9.7 vs. 16.3 months for lesion number; p<0.001 each, respectively). ***Conclusion:*** Our results indicate that 18F-rhPSMA-7.3 PET increasingly replacing 68Ga-PSMA-11 yields prognostic value in patients undergoing 177Lu-PSMA RLT. In addition to clinical and laboratory parameters, the total number of metastatic lesions on baseline 18F-rhPSMA-7.3 PET prior to 177Lu-PSMA RLT is an independent prognosticator of OS.

EPS-125

Associations between antihormonal-treatment status and ^{68}Ga-PSMA-HBED-CC PET biodistribution

K. Kluge[1], *D. Haberl*[1], *H. Einspieler*[1], *D. Muin*[1], *L. Shiyam Sundar*[2], *S. Gutschmayer*[2], *L. Kenner*[3], *A. Haug*[1], *M. Hacker*[1];
[1]*Medical University of Vienna - Dept. of Nuclear Medicine, Vienna, AUSTRIA,* [2]*Medical University of Vienna - Dept. of Medical Physics, Vienna, AUSTRIA,* [3]*Medical University of Vienna - Dept. of Pathology, Vienna, AUSTRIA.*

Aim/Introduction: Androgen deprivation therapies (ADT) are known to influence the prostate-specific membrane antigen (PSMA) expression of prostate cancers, potentially complicating the interpretation of PSMA ligand positron-emission tomography (PET) findings and affecting PSMA radioligand therapy (RLT). However, the impact of ADT on the PSMA ligand biodistribution in non-tumorous organs is not well understood. ***Materials and Methods:*** Fifty men with histological-proven prostate cancer who underwent ^{68}Ga-PSMA-HBED-CC PET/computed tomography (CT) between March 2019 and July 2021 at the Medical University Vienna with known ADT status were retrospectively recruited. 25 patients were on ADT at the time of imaging (treatment group), while 25 patients with no history of ADT served as a control group. Patients on androgen-receptor, 5α-reductase or CYP17A1 (1) inhibitors were excluded.Physiologically PSMA-expressing organs (salivary glands, kidneys, liver, spleen) were delineated (2,3) and their uptake values were compared according to their data distributions. Multivariate regression analysis was performed to assess the relationship between renal as well as salivary gland SUVmean values and the explanatory variables metabolic tumour volume (MTV), glomerular filtration rate (GFR) and ADT status. ***Results:*** ADT was associated with lower levels of PSMA uptake in the kidneys (SUVmean Δ[ADT - Control]=-6.46; CI=[-10.26;-2.66]; p=0.002) and salivary glands (SUVmean - Δ[ADT - Control]=-2.45; CI=[-4.03;-0.86]; p=0.004), but no significant differences were observed in hepatic or splenic PSMA uptake between the control and treatment groups. In a multivariate analysis, ADT was found to be associated with lower renal SUVmean values (β=-7.84, CI=[-11.32; -4.36], p= <0.0001), while GFR was associated with higher levels of renal SUVmean values (β=0.279, CI=[0.152; 0.405], p <0.0001). Salivary glandular SUVmean levels were only associated with ADT (β=-2.83, CI=[-4.67; -0.991], p= 0.0034), but not with GFR or MTV. ***Conclusion:*** These findings suggest that long-term ADT modulates PSMA expression in a systemic fashion, which may have implications for treatment-optimizing and side-effect minimizing strategies of PSMA radioligand therapies, particularly those using more potent but toxic ^{225}Actinium labelled PSMA-conjugates.

References: 1) Crawford ED, Schellhammer PF, McLeod DG, et al. Androgen Receptor Targeted Treatments of Prostate Cancer: 35 Years of Progress with Antiandrogens. J Urol. 2018;200:956-966.; 2) Shiyam Sundar LK, Yu J, Muzik O, et al. Fully-automated, semantic segmentation of whole-body 18F-FDG PET/CT images based on data-centric artificial intelligence. J Nucl Med. June 2022.; 3) Beichel RR, Van Tol M, Ulrich EJ, et al. Semiautomated segmentation of head and neck cancers in 18F-FDG PET scans: A just-enough-interaction approach. Med Phys. 2016;43:2948-2964.

810

Monday, September 11, 2023, 09:45 - 11:15
Hall K

CTE 4 - Technologists Committee: Prostate Cancer Theranostics

OP-399

Prostate Cancer Theranostics – What's its Role and Why we Need it?

P. Sandach*;*
Universitätsklinikum, Nuclear Medicine Department, Essen, GERMANY.

OP-400

The utility of Theranostics in Various Stages of Prostate Cancer

R. Madru*;*
Skånes Universitetssjukhus, Lund, SWEDEN.

OP-401a

The role of Nuclear Medicine Technologist in Theranostics

A. Santos*;*
NuclearMedicine Department, CUF Descobertas Hospital, Lisbon, PORTUGAL.

OP-401b

The role of Nuclear Medicine Technologist in Theranostics in the USA

D. Beyder;
Barnes-Jewish Hospital, Mallinckrodt Institute of Radiology, Missouri, UNITED STATES OF AMERICA.

811

Monday, September 11, 2023, 09:45 - 11:15

Hall G1

Special Symposium 3 - EANM / EJNMMI: You, the EANM and the EJNMMI

OP-402

Setting a world stage for the EANM Journal: a voyage through 50 volumes

A. Chiti;
Professor in Diagnostic Imaging and Radiotherapy Faculty of Medicine and Surgery, Vita-Salute San Raffaele University
Director, Department of Nuclear Medicine, IRCCS Ospedale San Raffaele
Editor in Chief, European Journal of Nuclear Medicine and Molecular Imaging, Milan, ITALY.

OP-403

Ethics and metrics of scientific publication: what you should know

I. Carriò;
Autonomous University of Barcelona, Barcelona, SPAIN.

901

Monday, September 11, 2023, 11:30 - 13:00

Hall A

Plenary 3: Radiotheranostics: What's New?

OP-406

PRRT in Neuroendocrine Tumours as a Paradigm for Progress in Radiopharmaceuticals: Where are we and where will we be?

J. Strosberg;
Moffitt Cancer Center Tampa, Florida, UNITED STATES OF AMERICA.

OP-407

2023: PSMA State of the Art

M. Hofman;
Peter MacCallum Cancer Centre, University of Melbourne, Melbourne, AUSTRALIA

OP-408

PSMA 2.0

S. Heskamp;
Radboud University Nijmegen Medical Centre, Nijmegen, NETHERLANDS.

OP-409

CXCR4: Ready for Prime Time!

A. Buck;
Universitätsklinikum Würzburg, Würzburg, GERMANY.

OP-410

Targeting the Tumour Microenvironment: Next Breakthrough?!

K. Lückerath;
UniversityHospital Essen, Essen, GERMANY.

OP-411

Dark Horses of Theranostics

L. Unterrainer;
Department of Nuclear Medicine, LMU Munich, Munich , GERMANY, Department of Nuclear Medicine, UCLA, UNITED STATES OF AMERICA.

1001

Monday, September 11, 2023, 15:00 - 16:30

Hall A

CME 7 - Thyroid + Dosimetry Committee: New NM Guidelines of Benign Thyroid Disease

OP-414

Radioiodine Therapy of Hyperthyroidism: An Overview on the New EANM GL

A. Campennì;
UniversityHospital "Gaetano Martino", Messina. Department of Biomedical and Dental Sciences and Morpho-Functional Imaging, Nuclear Medicine Unit, Messina, ITALY.

OP-415

Radioiodine Therapy in Hyperthyroid Pediatric Patients

F. Verburg ;
Department of Radiology and Nuclear Medicine, Erasmus Medical Center, Dr. Molewaterplein 40, 3015 CE, Rotterdam, NETHERLANDS.

OP-416

Radioiodine Therapy in Non-Toxic Benign Thyroid Disorders: Who, When, How

B. Katica;
Department of Nuclear Medicine, University Medical Centre Ljubljana and Faculty of Medicine, University of Ljubljana, Ljubljana, SLOVENIA.

OP-417

Adverse Effects of Radioiodine Therapy: A Real Point of View

P. Petranović Ovčariček;
UniversityHospital Center Sestre Milosrdnice, Department of Oncology and Nuclear Medicine Hospital/Institute; School of Medicine, University of Zagreb, Zagreb, CROATIA.

1002

Monday, September 11, 2023, 15:00 - 16:30

Hall D (Arena)

Award Session: EANM Sanjiv Sam Gambhir Award - Compete and Win!

1003

Monday, September 11, 2023, 15:00 - 16:30
Hall E1

LIPS Session 7 - Inflammation & Infection Committee: Tips and Tricks in the Study of Prosthesis Infection

OP-424
Tips and Tricks in Orthopedic Prosthesis
E. Noriega-Álvarez *;*
General University Hospital of Ciudad Real, Department of Nuclear Medicine, Ciudad Real, SPAIN.

OP-425
Tips and Tricks in Heart Valve Prosthesis
L. Leccisotti*;*
Fondazione Policlinico Universitario Agostino Gemelli IRCCS, Nuclear Medicine Unit, Rome, ITALY.

OP-426
Tips and Tricks in Vascular Prosthesis
A. Glaudemans*;*
UniversityMedical Center Groningen, Department of Nuclear Medicine and Molecular Imaging, Groningen, NETHERLANDS.

1004

Monday, September 11, 2023, 3:00 PM - 4:30 PM
Hall E2

M2M Track - TROP Session: New Roads Towards FAP-directed Theranostics

OP-427
Clinical Evaluation of ^{68}Ga-FAPI-RGD for Imaging of Fibroblast Activation Protein and Integrin $\alpha_v\beta_3$ in Various Cancer Types
Y. Pang*, l. zhao, w. xu, j. cai, l. sun, h. chen;*
Department of Nuclear Medicine & Minnan PET Center, Xiamen Cancer Center, The First Affiliated Hospital of Xiamen University, School of Medicine, Xiamen University, Xiamen, China, xiamen, CHINA.

Aim/Introduction: Radiolabeled fibroblast activation protein (FAP) inhibitors (FAPIs) and Arg-Gly-Asp (RGD) peptides have been extensively investigated for imaging of FAP- and integrin $\alpha_v\beta_3$-positive tumors. In this study, a FAPI-RGD heterodimer was radiolabeled with ^{68}Ga and evaluated in patients with cancer. We hypothesized that the heterodimer, recognizing both FAP and integrin $\alpha_v\beta_3$, would be advantageous because of its dual-receptor-targeting property. ***Materials and Methods:*** The effective dose of ^{68}Ga-FAPI-RGD was evaluated in 3 healthy volunteers. The clinical feasibility of ^{68}Ga-FAPI-RGD PET/CT was evaluated in 22 patients with various types of cancer, and the results were compared with those of ^{18}F-FDG and ^{68}Ga-FAPI-46. ***Results:*** ^{68}Ga-FAPI-RGD was tolerated well, with no adverse events in any of the healthy volunteers or patients. The effective dose from ^{68}Ga-FAPI-RGD PET/CT was 1.01 x 10^{-2} mSv/MBq. In clinical investigations with different types of cancer, the radiotracer uptake and tumor-to-background ratio (TBR) of primary and metastatic lesions in ^{68}Ga-FAPI-RGD PET/CT were significantly higher than those in ^{18}F-FDG PET/CT (primary tumors: SUVmax, 18.0 vs. 9.1 [P<0.001], and TBR, 15.2 vs. 5.5 [P<0.001]; lymph node metastases: SUVmax, 12.1 vs. 6.1 [P<0.001], and TBR, 13.3 vs. 4.1 [P<0.001]), resulting in an improved lesion detection rate and tumor delineation, particularly for the diagnosis of lymph node (99% vs. 91%) and bone (100% vs. 80%) metastases. ^{68}Ga-FAPI-RGD PET/CT also yielded a higher radiotracer uptake and TBR than ^{68}Ga-FAPI-46 PET/CT did. ***Conclusion:*** ^{68}Ga-FAPI-RGD exhibited improved tumor uptake and TBR compared with ^{18}F-FDG and ^{68}Ga-FAPI PET/CT. This study demonstrated the safety and clinical feasibility of ^{68}Ga-FAPI-RGD PET/CT for imaging of various types of cancer.

OP-428
Quantitative SPECT/CT Imaging of the Radiation Dosimetry of ^{99m}Tc-Labeled FAPI Tracer in Healthy Subjects, and Compared with ^{68}Ga-PET/CT in Gastrointestinal Tumor
C. ZHOU*, G. Li, F. Kang, J. Wang;*
Department of Nuclear Medicine, Xijing Hospital, Fourth Military Medical University, Xi'an, China, CHINA.

Aim/Introduction: Fibroblast activation protein (FAP) is a potential target for tumor diagnosis and treatment because it is selectively expressed on the cell membrane of Cancer-associated fibroblasts (CAFs) in most solid tumor stroma. Professor Zhang's team from Beijing Normal University previously reported a new ^{99m}Tc-labeled FAPI imaging agent([^{99mTc}]Tc-DP-FAPI), and they have verified the effect and stability of this agent in cell and animal experiments. The research reported the dosimetric profile of [^{99mTc}]Tc-DP-FAPI in healthy volunteers, and gastrointestinal solid tumors, to assess its diagnostic accuracy for gastrointestinal tumor imaging, and to evaluate the prognosis. ***Materials and Methods:*** Five healthy individuals were included for dosimetric studies based on their physical examination. Ten patients with different types of cancer (pancreatic cancer (n=5), gastric cancer (n=3), liver cancer(n=1), cholangiocarcinoma (n=1)) were included. The patients underwent quantitative SPECT/CT 2 h after the intravenous application of [^{99mTc}]Tc-DP-FAPI (740MBq). ^{68}Ga-FAPI PET/CT image acquisition was performed on the second day after the completion of [^{99mTc}]Tc-DP-FAPI quantitative SPECT/CT image acquisition. Tumor/background ratios (T/B) were calculated by delineating volumetric regions of interest (VOIs) (3D) around tumor areas (T) and healthy tissue as background (B), including: liver (T/Bl).In the [^{99mTc}]Tc-DP-FAPI and ^{68}Ga-FAPI images, the maximum standardized uptake value (SUV max) was quantified. ***Results:*** The equivalent dose received by the five healthy subjects was 3.8 mSv. The calculated effective dose for [99mTc]Tc-DP-FAPI is safety. Visual comparison between [^{99mTc}]Tc-DP-FAPI quantitative SPECT/CT and ^{68}Ga-FAPI PET/CT molecular imaging techniques revealed that both radiotracers accumulated in the same primary tumor lesions, with an excellent image quality. And that is [^{99mTc}]Tc-DP-FAPI quantitative SPECT/CT detected primary tumor (100%) and the SUVmax was 3.22-11.33 and the T/Bl (tumor/background liver) was range from 1.58 to 3.58, which reflect significant contrast. ***Conclusion:*** In conclusion, [^{99mTc}]Tc-DP-FAPI for the tumor imaging of FAP showed high tumor uptake and target to non-target ratios. The calculated effective dose and biodistribution for [^{99mTc}]Tc-DP-FAPI is safe, and there are no obvious toxic and side effects were observed, and it had the high sensitivity for the identification of several primary tumors. ***References:*** 1. Qi, N.; Meng, Q.; You, Z.; Chen, H.; Shou, Y.; Zhao, J., Standardized uptake values of 99mTc-MDP in normal vertebrae assessed using quantitative SPECT/CT for differentiation diagnosis of benign and malignant

bone lesions. BMC Medical Imaging 2021, 21 (1).2. Armstrong, I. S.; Hoffmann, S. A., Activity concentration measurements using a conjugate gradient (Siemens xSPECT) reconstruction algorithm in SPECT/CT. Nucl Med Commun 2016, 37 (11), 1212-7.

OP-429

Preclinical evaluation of a novel ^{18}F-labeled probe for fibroblast activation protein-targeted imaging and side by side comparison with FAPI-04

F. Elvas, *N. Filippi, Y. Van Rymenant, S. Grintsevich, L. Cianni, I. De Meester, P. Van der Veken;*
University of Antwerp, Wilrijk, BELGIUM.

Aim/Introduction: Fibroblast activation protein (FAP) is an abundant, practically universal biomarker of cancer that is expressed on the surface of cancer-associated fibroblasts in >90% of carcinomas. Currently, great attention goes to the use of FAP as a tumoral anchor point for cancer diagnostics and therapeutics. ^{68}Ga-labeled FAPI-04 is one of the most clinically investigated FAP-radioligands, showing excellent lesion visualization in a variety of cancers(1). Soon after, ^{18}F-labeled derivatives were developed to benefit from the larger batch size, longer half-life and better image quality. However, there are only a few suboptimal examples available. With the aim of improving pharmacokinetics and tumor targeting, we have developed and evaluated a novel ^{18}F-labeled FAP radioligand for PET imaging in cancer. ***Materials and Methods:*** A lead compound structurally derived from our FAP inhibitor - UAMC1110 - and having a polar linker between the pharmacophore and the radiolabel, was synthesized and characterized in vitro, comprising affinity and selectivity determination(2). The precursor was synthesized and radiolabeled with fluorine-18 using a fluoroalkylation strategy yielding [^{18}F]UAMC-4522. The reference radioligand, FAPI-04, was radiolabeled with gallium-68 as described before(3). A series of in vitro assays were performed to characterize radioligands' lipophilicity and stability. The pharmacokinetic profile of [^{18}F]UAMC-4522 was evaluated by micro-PET imaging and ex vivo biodistribution in nude mice. In addition, PET imaging and biodistribution studies were conducted in U87MG xenografts to evaluate in vivo FAP targeting. Ex vivo validation of radiotracer uptake in the tumors was performed by autoradiography and histological analysis of FAP expression. ***Results:*** UAMC-4522 showed excellent affinity for FAP (0.32±0.02 nM) and excellent selectivity with respect to PREP (> 10 μM), when compared to the reference compounds UAMC1110 and FAPI-04. [^{18}F]UAMC-4522 was radiolabeled with a 2.6±1.2% isolated radiochemical yield (decay-corrected) and a high radiochemical purity of >99%. The ^{18}F-labeled FAP ligand showed a less polar profile when compared to [^{68}Ga]Ga-DOTA-FAPI-04 (logD=-1.77 vs -3.46, respectively), which led to mixed renal-hepatobiliary excretion of [^{18}F]UAMC-4522. Compared to the reference radiotracer, [^{68}Ga]Ga-DOTA-FAPI-04, [^{18}F]UAMC-4522 showed high in vivo stability. Micro-PET imaging of U87MG xenografts revealed higher specific tumor uptake of [^{18}F]UAMC-4522 compared to [^{68}Ga]Ga-DOTA-FAPI-04 (10.98±1.73%ID/g vs 3.67±0.73%ID/g), in accordance with FAP expression in the tumors. ***Conclusion:*** [^{18}F]UAMC-4522 showed excellent FAP affinity and selectivity, favourable in vivo pharmacokinetics, and high and specific tumor uptake. These results suggest that [^{18}F]UAMC-4522 has potential clinical usefulness in oncology. ***References:*** 1.Giesel FL, et al. JNM.2019;60(3):386-92. 2.Jansen K, et al. JMC.2014;57(7):3053-74. 3.Lindner T, et al. JNM.2018;59(9):1415-22.

OP-430

Enhancing the tumor-to-background ratio of FAP-positive PET/CT scans with the novel ^{61}Cu-Kalios derivatives: synthesis, in vitro and in vivo characterization

J. Millul[1], *T. Basaco Bernabeu*[1], *R. H. Gaonkar*[1], *F. De Rose*[2], *L. Jaafar-Thiel*[2], *R. Mansi*[1], *M. Fani*[1];
[1]*University Hospital Basel, Basel, SWITZERLAND,*
[2]*Nuclidium AG, Basel, SWITZERLAND.*

Aim/Introduction: Fibroblast Activation Protein (FAP)-targeting ligands labeled with the positron-emitters Ga-68 and F-18 have gained increased attention for imaging of solid tumors and fibrotic diseases. Nevertheless, due to the relatively short half-life and the logistic of the clinically-used radionuclides, delayed time-points PET/CT scans are rarely doable. We propose the use of Kalios, a class of novel FAP-targeting ligands bearing the NODAGA chelator and radiolabeled with the cyclotron-produced Copper-61 ($t_{1/2}$ = 3.33 h), as an alternative to ^{68}Ga- and ^{18}F-based FAP PET/CT imaging. ***Materials and Methods:*** Four new ligands, Kalios-01, Kalios-02, Kalios-01M and Kalios-02M were synthesized, conjugated with NODAGA, and radiolabeled with Cu-61 in high yield and radiochemical purity. In vitro affinity against the isolated protein, log D, and cellular distribution on human fibrosarcoma cell line HT-1080 transduced with hFAP were evaluated for all four radioligands. In vivo PET/CT imaging and ex vivo biodistribution were assessed at different time points in mice bearing FAP-positive and FAP-negative tumors after the intravenous administration of ^{61}Cu-labeled ligands. ***Results:*** All Kalios derivatives were radiolabeled with Cu-61 at room temperature in quantitative yields and >95% radiochemical purity at apparent molar activity of 24 MBq/nmol. All four ^{61}Cu-Kalios showed high hydrophilicity (log D range from -3.32 to -3.09) and high affinity (KD from 1.50 nM to 3.44 nM and IC50 from 26.2 pM to 232 pM) against FAP. The radioligands were mainly internalized after incubation with FAP-positive cells. PET/CT images performed at 0-1h (dynamic scans) and 4h p.i. (static scans) illustrated the ability of all radioligands to visualize the tumors. Quantitative biodistribution studies confirmed the feasibility and advantage of delayed time-point imaging, with tumor-to-background ratios increasing at 4h, especially for two out of 4 radioligands, ^{61}Cu-NODAGA-Kalios-02 and ^{61}Cu-NODAGA-Kalios-01M. ***Conclusion:*** ^{61}Cu-Kalios ligands are a new class of FAP-targeting PET tracers. Kalios ligands can be easily labeled with ^{61}Cu and allow delayed time-point imaging due to the physical half-life of Cu-61 and the improved signal-to-noise ratio. The selection of the best candidate for clinical translation is planned after direct comparison with ^{68}Ga-FAPI-46.

OP-431

Effects of Linker and Attachment Position on Binding Affinity, Tumor Uptake and Tumor-to-background Contrast of ^{68}Ga-labeled Pyridine-based Fibroblast Activation Protein Inhibitors

A. Verena, *H. Kuo, H. Merkens, N. Colpo, P. Ng, F. Bénard, K. Lin;*
BC Cancer Research Centre, Vancouver, BC, CANADA.

Aim/Introduction: Most of the emerging fibroblast activation protein (FAP)-targeted tracers incorporate a quinoline-based pharmacophore. Recently, we reported two FAP-targeted tracers containing a pyridine-3-carbonyl- ([^{68}Ga]Ga-AV02053) or pyridine-4-carbonyl-based pharmacophore ([^{68}Ga]Ga-AV02070), and a 1,2-dimethylethylenediamine linker attached to the pyridine ring at the ortho position to the pyridine nitrogen. Both tracers showed significantly better tumor-to-background image contrast than the

clinically validated [^{68}Ga]Ga-FAPI-04 (Verena A, et al. Pharmaceuticals 2023;16:449), making the pyridine-based pharmacophore a promising candidate for the design of FAP-targeted tracers. Here, we aim to investigate the effects of linker and the position to attach the linker to the pyridine ring on FAP binding affinity, tumor uptake and tumor-to-background uptake ratios. ***Materials and Methods:*** AV02093, a DOTA-conjugated ligand containing a 3-(piperazin-1-yl)propan-1-ol linker (the same one in [^{68}Ga]Ga-FAPI-04) attached to the meta position (to the pyridine nitrogen) of the pyridine-4-carbonyl-based pharmacophore, was synthesized in 5 steps: coupling methyl 3-hydroxyisonicotinate with Boc-protected 3-(piperazin-1-yl)propan-1-ol via Mitsunobu reaction, hydrolysis of the methyl ester, coupling with (S)-1-(2-aminoacetyl)-4,4-difluoropyrrolidine-2-carbonitrile, Boc-deprotection with trifluoroacetic acid, and the final coupling with the DOTA chelator. Gallium (^{nat}Ga and ^{68}Ga) complexation was conducted in acetate (0.1 M, pH 4.5) and HEPES (2 M, pH 5.0) buffers, respectively. FAP binding affinity was determined by enzyme-based competition binding assay. PET imaging and biodistribution studies were conducted in HEK293T:hFAP tumor-bearing mice at 1h post-injection. ***Results:*** AV02093 was obtained in 5.4% overall yield over 5 steps. Ga-AV02093 was obtained in 38% yield. The decay-corrected radiochemical yields of [^{68}Ga]Ga-AV02093 were 46-50% with >57 GBq/µmole molar activity and >99% radiochemical purity. The binding affinity of Ga-AV02093 (IC_{50}=72.9±4.16 nM) was lower than Ga-AV02070 (IC_{50}=17.1±4.60 nM), but higher than Ga-AV02053 (IC_{50}=187±52.0 nM). The HEK293T:hFAP tumor xenografts were clearly visualized with good contrast on PET images acquired at 1h post-injection. The tumor uptake of [^{68}Ga]Ga-AV02093 (5.33±0.87 %ID/g) was comparable to [^{68}Ga]Ga-AV02070 (7.93±1.88 %ID/g) and [^{68}Ga]Ga-AV02053 (5.60±1.12 %ID/g). The tumor-to-background (blood, muscle and bone) uptake ratios of [^{68}Ga]Ga-AV02093 (7.00±1.35, 16.9±5.84 and 4.66±1.35, respectively) were significantly lower than [^{68}Ga]Ga-AV02070 (22.9±10.1, 45.7±9.88 and 34.3±7.35, respectively) and [^{68}Ga]Ga-AV02053 (25.2±1.97, 51.2± 19.8 and 38.1±5.03, respectively). ***Conclusion:*** Replacing the 1,2-dimethylethylenediamine linker with a 3-(piperazin-1-yl)propan-1-ol linker and changing its attachment position (ortho to meta of the pyridine nitrogen) on the pyridine-4-carbonyl-based pharmacophore generated [^{68}Ga]Ga-AV02093 with retained tumor uptake, but significantly decreased tumor-to-background contrast ratio. Our data suggest that attaching the linker to the ortho position to the pyridine nitrogen is more preferable for the design of pyridine-4-carbonyl-based FAP-targeted tracers.

OP-432

Preclinical side by side comparison of two [^{177}Lu]Lu-labeled FAP-based inhibitors: A promising therapeutic approach for targeted radionuclide therapy of stromal tumors

T. Läppchen[1], *A. Bilinska*[1], *E. Pilatis*[1], *E. Menéndez*[1], *S. Imlimthan*[1], *E. S. Moon*[2], *F. Rösch*[2], *A. Rominger*[1], *E. Gourni*[1];
[1]*Department of Nuclear Medicine, Inselspital, Bern University Hospital, University of Bern, 3010 Bern, SWITZERLAND,*
[2]*Department of Chemistry – TRIGA site, Johannes Gutenberg - University Mainz, 55128 Mainz, GERMANY.*

Aim/Introduction: Cancer-Associated Fibroblasts (CAFs) account for approximately 80% of all fibroblasts in tumor microenvironment and are identified by several biomarkers with Fibroblast Activation Protein (FAP) being one of them. FAP is highly expressed on the surface of CAFs and promotes tumor growth invasion, metastasis and immunosuppression and its inhibition may increase the antitumor biological response. It also appears to be an appealing target in the nuclear medicine field, since it has the potential to be used for non-invasive radionuclide-based in vivo tumor imaging and therapy. Herewith, we report a side-by-side comparison of the in vitro and in vivo performance of two FAP-based inhibitors, the monomer DOTA.SA.FAPi and the dimer DOTAGA.(SA.FAPi)2, labeled with lutetium-177 for SPECT imaging and potential therapeutic applications. ***Materials and Methods:*** DOTA.SA.FAPi and DOTAGA.$(SA.FAPi)_2$ were labeled with lutetium-177. Their lipophilicity and tendency to bind to human plasma proteins was investigated. The human hTERT PF179T CAF cells which overexpress FAP as proven by western blot and immunofluorescence staining, was used for their further in vitro (saturation, internalization and efflux studies studies) evaluation. In addition, biodistribution and SPECT imaging studies were performed in PC3 xenografts. ***Results:*** [^{177}Lu]Lu-DOTA.SA.FAPi and [^{177}Lu]Lu-DOTAGA.$(SA.FAPi)_2$ were prepared in >95% radiochemical purity and apparent molar activities between 8 and 12 GBq/µmol exhibiting a $logD_{octanol/PBS}$ of -2.86, and -1.71, respectively. The % of the radioactivity bound to human serum proteins was 9 for [^{177}Lu]Lu-DOTA.SA.FAPi and 25 for [^{177}Lu]Lu-DOTAGA.$(SA.FAPi)_2$ after 30 min of incubation. $^{177/nat}$Lu-DOTA.SA.FAPi and $^{177/nat}$Lu- DOTAGA.$(SA.FAPi)_2$ exhibited high affinity for the CAF cells, with K_d values of 0.82±0.22, and 1.35±0.68 nM, respectively. After 60 min of incubation with the stromal cells, approximately 20% of the total added activity was internalized for [^{177}Lu]Lu-DOTA.SA.FAPi and about 15% for [^{177}Lu]Lu-DOTAGA.$(SA.FAPi)_2$. The efflux studies revealed the superiority of [^{177}Lu]Lu-DOTAGA.$(SA.FAPi)_2$ compared to [^{177}Lu]Lu-DOTA.SA.FAPi with regard to their residency in CAFs. After 24 h, 51% of the internalized [^{177}Lu]Lu-DOTAGA.$(SA.FAPi)_2$ activity was released from CAFs, versus 87% in case of [^{177}Lu]Lu-DOTA.SA.FAPi. Biodistribution studies revealed specific tumor uptake of 8.9±0.3 %IA/g for [^{177}Lu]Lu-DOTA.SA.FAPi and 8.6±0.7 %IA/g for [^{177}Lu]Lu-DOTAGA.$(SA.FAPi)_2$ at 1h p.i. Over time, the accumulated activity in the tumor was faster washed out for [^{177}Lu]Lu-DOTA.SA.FAPi compared to [^{177}Lu]Lu-DOTAGA.$(SA.FAPi)_2$, with values of 1.1±0.3 %IA/g and 3.9±0.5 %IA/g, respectively, at 72h p.i. These findings were also illustrated by SPECT imaging. ***Conclusion:*** The superior in vitro and in vivo behaviour of [^{177}Lu]Lu-DOTAGA.$(SA.FAPi)_2$ compared to [^{177}Lu]Lu-DOTA.SA.FAPi paves the way towards improved FAP-directed therapy of stromal tumors.

OP-433

Novel Co-culture Model of Pancreatic Cancer to Accurately Predict the Efficacy of Fibroblast Activation Protein Targeted Radionuclide Therapy using [^{161}Tb]Tb-FAP-2286 and [^{177}Lu]Lu-FAP-2286

C. D. van der Heide[1], *A. Lak*[1], *R. McMorrow*[1,2,3], *L. Mezzanotte*[1,2], *S. U. Dalm*[1];
[1]*Department of Radiology & Nuclear Medicine, Erasmus MC, Rotterdam, NETHERLANDS,* [2]*Department of Molecular Genetics, Erasmus MC, Rotterdam, NETHERLANDS,* [3]*Percuros B.V, Leiden, NETHERLANDS.*

Aim/Introduction: Fibroblast activation protein (FAP) is almost exclusively expressed by cancer-associated fibroblasts (CAFs). When targeting FAP on CAFs for targeted radionuclide therapies (TRT), the neighboring cancer cells will be irradiated via cross-radiation, unlike conventional TRT in which the radiation is being delivered to the cancer cells themselves. Improved in vitro models that accurately mimic this indirect irradiation are necessary for a more accurate evaluation of FAP-directed TRT. Therefore, we aim to develop a co-culture system that mimics the stromal disposition of pancreatic tumors and that can be used to correctly

evaluate the efficacy of FAP-TRT. Moreover, we are evaluating the binding and cytotoxicity of both [^{161}Tb]Tb-FAP-2286 and [^{177}Lu]Lu-FAP-2286 using this novel system. ***Materials and Methods:*** The human pancreatic cancer cell line PANC-1, transduced to express GFP and near-infrared click beetle luciferase (λ=740 nm) (PANC-1-CBR2), and the pancreatic stellate cell line PS-1 were used. Co-cultures were optimized by seeding different ratios of PANC-1-CBR2 and PS-1 cells. Images of the co-cultures were obtained with fluorescence microscopy and compared to three pancreatic cancer patient samples on which FAP immunohistochemistry staining was performed. The correlation between the bioluminescent signal and the number of PANC-1-CBR2 cells was evaluated by seeding the cells in increasing numbers in monoculture or co-culture. Uptake studies on PS-1 cells were performed by incubating cells with 1 nM [^{161}Tb]Tb-FAP-2286 or [^{177}Lu]Lu-FAP-2286 for 45 minutes, with and without 1 µM of UAMC-1110 for blocking. ***Results:*** Fluorescent microscopy images demonstrated that in a ratio of 1:1 and 1:2 PS-1 cells densely collect and surround clusters of the PANC-1-CBR2 cell, which resembles the FAP-positive fibroblast density observed in patient samples. The bioluminescent signal of PANC-1-CBR2 correlated with the number of cells for both monoculture and co-culture (R^2 of 0.91 and 0.97 respectively). A FAP-specific uptake of 2.5% and 3.0% added dose/200,000 cells was measured for [^{161}Tb]Tb-FAP-2286 and [^{177}Lu]Lu-FAP-2286, respectively, with 75% of the radionuclide being membrane-bound. ***Conclusion:*** The developed co-culture system presents a relatively simple method to combine fibroblasts and cancer cells to resemble the patient's situation more closely. The bioluminescent signal of PANC-1-CBR2 allows for cell death quantification of cancer cells and fibroblasts separately which is relevant for cytotoxicity studies. The first uptake studies demonstrate no big difference in uptake between [^{161}Tb]Tb-FAP-2286 and [^{177}Lu]Lu-FAP-2286 on PS-1 cells. How this affects cytotoxicity in the co-culture system is currently still being determined.

OP-434

Radioligand Therapy in GBM: Fibroblast Activation Protein (FAP) Promises

P. Jeanjean[1,2], *S. Kwock*[1,2], *T. Cloughesy*[1], *J. Calais*[1,2], *J. Czernin*[1,2], *G. Carlucci*[1,2], *D. Nathanson*[1,2], *C. Mona*[1,2], *E. Besserer-Offroy*[1,2];
[1]*Department of Molecular and Medical Pharmacology, David Geffen School of Medicine, University of California - Los Angeles, Los Angeles, CA, UNITED STATES OF AMERICA,* [2]*Ahmanson Translational Theranostics Division, David Geffen School of Medicine, University of California - Los Angeles, Los Angeles, CA, UNITED STATES OF AMERICA.*

Aim/Introduction: Glioblastomas (GBM) are grade IV gliomas, and, with a dismal 5-year survival rate of 4%, are the most aggressive and fatal type of brain cancer. Despite intensive research efforts leading to various pharmacological approaches, cure has remained elusive. Recently, Fibroblast Activation Protein (FAP) has emerged as a new therapeutic target. Expressed both by Cancer-Associated Fibroblasts (CAFs) and GBM cells[1], FAP has been targeted by radiolabeled small molecules used as pan-cancer theranostics agents[2]. This study aims to evaluate the relevance of FAP inhibitor-46 (FAPi-46) as a molecular probe for Positron Emission Tomography (PET) imaging and Radioligand Therapy (RLT) in GBM models. ***Materials and Methods:*** U87MG and U138MG, human glioblastoma-derived cell lines reported to express FAP, were used as xenograft models. NSG mice were inoculated with U87MG or U138MG cells subcutaneously. FAP expression was assessed by ^{68}Ga-FAPi-46 PET imaging. Mice were subsequently randomized into four groups: vehicle, 5mg/kg temozolomide (TMZ), 60kBq ^{225}Ac-FAPi-46, and 5mg/kg TMZ + 60kBq ^{225}Ac-FAPi-46. Tumor growth and overall survival were evaluated. Additionally, DNA-damage and FAP expression were assessed by immunohistochemistry (IHC) on resected tumors, respectively, 24h after ^{225}Ac-FAPi-46 treatment or at sacrifice endpoints. ***Results:*** FAP-targeted RLT was first performed on U87MG model. Following confirmation of FAP expression by ^{68}Ga-FAPi-46 PET imaging (SUVmax=6.1±1.2), mice treated with a single ^{225}Ac-FAPi-46 injection showed tumor growth delay compared to vehicle-treated animals (median survival of 30 and 23 days, respectively). Treatment with TMZ induced a significant delay in tumor growth of 23 days. Finally, the combination of ^{225}Ac-FAPi-46 and TMZ significantly improve the survival rate compared to TMZ alone (median survival of 67 and 46 days, respectively). IHC confirmed FAP expression and DNA-damage after ^{225}Ac-FAPi-46 treatment. FAP-targeted RLT on U138MG tumors is ongoing and preliminary results are promising. ***Conclusion:*** Since FAP is expressed by both tumor cells and microenvironment in GBM, FAP-targeted RLT can act on these two tumor compartments. Our results suggest that ^{225}Ac-FAPi-46 has a real theranostics potential on subcutaneous GBM tumors combined with TMZ. As observed with many GBM therapeutic agents, FAPi-46 is not able to cross the blood brain barrier to reach orthotopic tumors at a therapeutic concentration. Subsequent conjugation of FAPi-46 with a cell penetrating peptide moiety[3] will be required to improve brain uptake and recapitulate therapeutic effects observed on subcutaneous models. ***References:*** 1.Fitzerald, A. et al. Cancer Metastasis Rev.(2020) 2.Mona, C. et al. J. Nucl. Med. (2022) 3.Demeule, M. et al. J. Pharmacol. Exp. Ther.(2008)

OP-435

Targeted Covalent Radiopharmaceutical (TCR) Could be a Promising Modality for Delivering Radionuclides to Tumour

X. Cui[1], *Z. Liu*[2,1];
[1]*Changping Lab, Beijing, CHINA,* [2]*Peking University, Beijing, CHINA.*

Aim/Introduction: The success of therapeutic radiopharmaceutical requires perfect tumour targeting, rapid blood clearance, and sufficiently long tumour retention. Yet, balancing blood clearance and tumour retention of a drug is often a dilemma. A general technology platform that irreversibly fixes radiopharmaceuticals to cancer targets in a tumour-selective manner, if successfully developed, would ideally solve the above dilemma but has not been established. Herein, we aimed to develop a Targeted Covalent Radiopharmaceutical (TCR), installing radiopharmaceutical molecule with a suitable covalent warhead rationally, to gain the function of irreversible ligation but avoid loss of affinity. ***Materials and Methods:*** The rational engineering was started with an unprecedentedly accurate docking of metal-chelated FAPI, which is targeting fibroblast activated protein (FAP). A covalent-engineered FAPI derivative (TCR-FAPI) was designed and synthesized. TCR-FAPI with DOTA is compatible for ^{68}Ga or ^{177}Lu-radiolabelling and quality control was performed by radio-HPLC. The stability of ^{177}Lu-TCR-FAPI was assessed both in vitro and in vivo. An SDS-PAGE-autoradioluminography tandem assay was developed to detect the irreversible covalent binding of TCR-FAPI with FAP protein. The PET-CT imaging studies of ^{68}Ga-TCR-FAPI were performed in mice bearing HT-1080-FAP xenografts on shoulder. ***Results:*** The molecule docking provided a solid basis for computer-assisted design. ^{68}Ga-TCR-FAPI and ^{177}Lu-TCR-FAPI

can be labelled with high radio-yield and radio-purity. The autoradioluminography shows ^{177}Lu-TCR-FAPI presented efficient (over 90% ligation yields) and robust (at least 144 h) covalent binding with FAP in an irreversible manner. In HT-1080-FAP tumour-bearing mice, the maximum standard uptake value in the tumour of ^{68}Ga-TCR-FAPI is increased to 10.5±1.3 ID%/g at 1-hour post-injection, which is doubled that of ^{68}Ga-labelled original FAPI. ***Conclusion:*** A covalent-engineered TCR-FAPI was developed and evaluated for delivering radionuclides to FAP-expressed tumour. The administration of ^{68}Ga-TCR-FAPI allowed for higher uptake of tumor xenografts in mice, with only slightly higher uptake in the normal tissues. The irreversible covalent interaction of TCR-FAPI and FAP was validated at molecule level, which should be the root cause for the improved pharmacokinetics. The chemical modification of this hit to leading molecule is underway. ***References:*** 1. Verdonk, M.L., et al . Improved protein-ligand docking using GOLD. Proteins: Structure, Function, and Bioinformatics 52, 609-623 (2003). 2. Jansen, K. et al. Extended Structure-Activity Relationship and Pharmacokinetic Investigation of (4-Quinolinoyl)glycyl-2-cyanopyrrolidine Inhibitors of Fibroblast Activation Protein (FAP). Journal of Medicinal Chemistry 57, 3053-3074 (2014). 3. De Cesco, S., et al. , N. Covalent inhibitors design and discovery. European Journal of Medicinal Chemistry 138, 96-114 (2017).

1005

Monday, September 11, 2023, 3:00 PM - 4:30 PM
Hall B

Cutting Edge Science Track - TROP Session: Clinical Dosimetry I - ^{177}Lu / ^{225}Ac and ^{161}Tb RLT

OP-436

Bone Marrow Dosimetry in Radioligand Therapy using AI-Enabled Whole Body Spongiosa Segmentation and Complementary Marrow/Lesion Maps from ^{99m}Tc-Sulfur Colloid SPECT/CT and [^{68}Ga]Ga-PSMA-11 PET/CT

A. Peterson[1,2], *S. J. Wilderman*[1], *J. Blakkisrud*[1,3], *K. Wong*[1], *K. A. Frey*[1], *Y. K. Dewaraja*[1];
[1]*University of Michigan, Ann Arbor, MI, UNITED STATES OF AMERICA,* [2]*Wayne State University, Detroit, MI, UNITED STATES OF AMERICA,* [3]*Oslo University Hospital, Oslo, NORWAY.*

Aim/Introduction: In metastatic castrate resistant prostate cancer (mCRPC) patients treated with [^{177}Lu]Lu-PSMA-617 radioligand therapy, lesion infiltration of bone causes heterogeneous distributions of hematopoietically active (red) bone marrow making dosimetry challenging. We present a methodology for patient-specific Monte Carlo (MC)-based bone marrow dosimetry which uses [^{177}Lu]Lu-PSMA-617 SPECT/CT in combination with complementary information from ^{99m}Tc-sulfur colloid (SC) SPECT/CT and [^{68}Ga]Ga-PSMA-11 PET/CT for red marrow and lesion localization. ***Materials and Methods:*** [^{68}Ga]Ga-PSMA-11 PET/CT, ^{99m}Tc-SC SPECT/CT, and sequential cycle 1 [^{177}Lu]Lu-PSMA-617 2-bed-SPECT/CT were rigidly coregistered for seven mCRPC patients. Using open-source AI-based segmentation tools[1], the skeletal anatomy in the field-of-view (FOV) was delineated on CT and processed to extract spongiosa ("FOV spongiosa"). A "reference spongiosa" region was defined as a vertebra with little ^{68}Ga-PET uptake but strong, uniform ^{99m}Tc-SPECT uptake and assigned an age-based cellularity according to [2]. This allowed for patient-specific conversions from ^{99m}Tc-SPECT images to red marrow mass maps. ^{177}Lu time-integrated activity (TIA) maps were generated by voxel-level time-activity fitting. Lesion voxels were determined by a 3 SUV threshold on the ^{68}Ga-PET map that was transferred to the ^{177}Lu-TIA map with partial volume correction. Voxels with active marrow were determined by applying a threshold to the red marrow mass map. Where lesion and marrow thresholds overlapped, voxels were randomly assigned to lesion or marrow and red marrow mass was displaced from lesion voxels while TIA was displaced from marrow voxels. Dose to red marrow in the FOV spongiosa was computed using an in-house MC code with routines for marrow voxels that apportion energy while accounting for material composition (bone fraction/cellularity/lesion fraction) of each voxel given TIA, CT-derived density, and red marrow mass maps. ***Results:*** Cycle 1 absorbed dose to red marrow in the FOV spongiosa ranged from 0.14-4.24 Gy (0.02-0.59 Gy/GBq) and was significantly correlated with percent change at 6 weeks post-cycle 1 relative to baseline for platelets (Spearman r=-0.79,P=0.036) and neutrophils (r=-0.93,0.003) indicating a potential dose-toxicity trend. Correlation with other toxicity measures was not significant (white blood cells: r=-0.75,P=0.052; hemoglobin: r=-0.61,P=0.148; lymphocytes: r=0.00,P=1.000). ***Conclusion:*** Absorbed dose to red marrow was calculated with MC using ^{99m}Tc-SC and [^{68}Ga]Ga-PSMA-11 imaging for marrow and lesion localization/quantification. Dosimetry correlates with toxicity markers motivating studies with larger cohorts to establish robust dose-toxicity relationships. ***References:*** [1] Wasserthal J, et al. TotalSegmentator: robust segmentation of 104 anatomical structures in CT images. 2022. [2] Dunnill MS, et al. Quantitative histological studies on age changes in bone. J Pathol Bacteriol. 1967;94(2):275-291.

OP-437

Radiation absorbed dose in patients with metastatic castration-resistant prostate cancer treated with [^{161}Tb]Tb-PSMA-I&T: first results of the VIOLET phase I/II study

B. Emmerson[1], *L. McIntosh*[1], *J. P. Buteau*[1,2], *P. Jackson*[1,2], *L. Kostos*[2,3], *T. Akhurst*[1,2], *R. Alipour*[1,2], *A. Cardin*[1,2], *A. S. Ravi Kumar*[1,2], *R. Kashyap*[1], *R. Ravi*[1], *G. Kong*[1,2], *J. Saghebi*[1], *S. Sandhu*[2,3], *B. Tran*[2,3], *M. B. Haskali*[2,4], *C. Martin*[5], *P. Opar*[6], *E. Medhurst*[1,2], *A. Azad*[2,3], *M. S. Hofman*[1,2];
[1]*Prostate Cancer Theranostics and Imaging Centre of Excellence; Molecular Imaging and Therapeutic Nuclear Medicine, Cancer Imaging, Peter MacCallum Cancer Centre, Melbourne, AUSTRALIA,* [2]*Sir Peter MacCallum Department of Oncology, University of Melbourne, Melbourne, AUSTRALIA,* [3]*Department of Medical Oncology, Peter MacCallum Cancer Centre, Melbourne, AUSTRALIA,* [4]*Radiopharmaceutical Production and Research Laboratory, Peter MacCallum Cancer Centre, Melbourne, AUSTRALIA,* [5]*Parkville Cancer Clinical Trials Unit, Peter MacCallum Cancer Centre, Melbourne, AUSTRALIA,* [6]*Centre of Biostatistics and Clinical Trials, Peter MacCallum Cancer Centre, Melbourne, AUSTRALIA.*

Aim/Introduction: [^{177}Lu]Lu-PSMA is an effective therapy for men with metastatic castration-resistant prostate cancer (mCRPC). Terbium-161 (^{161}Tb) offers comparable beta emission to ^{177}Lu with the addition of Auger electrons which have high linear energy transfer and very short range. [^{161}Tb]Tb-PSMA has shown superior in-vitro and in-vivo results in comparison with [^{177}Lu]Lu-PSMA. We calculated radiation absorbed dose to normal organs in patients with mCRPC who were treated with [^{161}Tb]Tb-PSMA-I&T. ***Materials and Methods:*** VIOLET (NCT05521412) is a single-center, single-arm, phase I/II trial recruiting 30 to 36 men with progressive mCRPC. The phase I dose-escalation is designed with a 3+3 design to establish the maximum tolerated dose of [^{161}Tb]

Tb-PSMA-I&T using initial administered radioactivities of 4.4, 5.5 and 7.4 GBq. Dose calibration was performed for local vial and syringe geometry using supplier activity as reference and verified using high-purity germanium gamma spectroscopy. [^{161}Tb]Tb-PSMA-I&T was produced using an automated radiochemistry module with extensive process validation. Quantitative SPECT/CT sensitivity was derived from serial phantom imaging with activity ranging from 50-5400 MBq. Three time-point SPECT/CT from vertex to mid-thigh were acquired at 2-6h, 18-24h and 72-120h. Acquisitions were obtained on low energy high resolution collimators, using a triple energy window peaked at 74keV with upper and lower scatter limits. Retention of [^{161}Tb]Tb-PSMA-I&T was estimated from voxel-based time-activity curves based on a multi-phase exponential clearance model and convolved using a GATE-derived voxel dose kernel based on decay of ^{161}Tb in ICRP soft tissue to yield three-dimensional absorbed dose maps. ***Results:*** Nine patients received their first cycle of [^{161}Tb]Tb-PSMA-I&T; three patients each receiving 4.4, 5.5 and 7.4 GBq. The mean absorbed dose per GBq (standard deviation) for parotid glands, submandibular glands, kidneys, liver and spleen was 0.14 (± 0.03), 0.14 (±0.06), 0.35 (± 0.10), 0.07 (±0.03), 0.07 (± 0.03) Gy/GBq, respectively. The highest dose cohort potentially receiving 40 GBq cumulative activity over 6 cycles are estimated to receive 5.60 (± 1.20), 5.60 (±2.40), 14 (±4.00), 2.8 (±1.2), 2.8 (±1.2) Gy/GBq for the same organs in above order. The dosimetry owing to beta emission are inline with known dose estimates for [^{177}Lu]Lu-PSMA. However, we did not apply additional radiation weighting factor for Auger electrons as subcellular distribution knowledge is required to determine Auger biological effects. ***Conclusion:*** Radiation absorbed doses following [^{161}Tb]Tb-PSMA-I&T are within a safe and expected range for normal organs with physiological uptake.

OP-438

Evaluation of a Phantom-Independent Dual-Energy Quantitative Computed Tomography (PI-DEQCT) Method for Selecting Bone-Site Specific S-Values in Bone Marrow Dosimetry in Molecular Radiotherapy

J. Pereira-Cubillo[1], *E. Mora-Ramirez*[2], *M. Salas-Ramirez*[3];
[1]*University of Costa Rica, Escuela de Física, San José, COSTA RICA,* [2]*University of Costa Rica, Escuela de Física, CICANUM, San José, COSTA RICA,* [3]*University Hospital of Würzburg, Department of Nuclear Medicine, Würzburg, GERMANY.*

Aim/Introduction: Accurately quantifying the volume fraction of cortical bone, fat, and water is crucial for applying bone site-specific S-Values for active bone marrow absorbed dose quantification. This study aims to evaluate a DEQCT method [1] for quantifying the volume fraction of cortical bone, fat, and water by investigating the impact of kVp, quality reference mAs (QRM), pitch, and beam hardening on the acquired images. ***Materials and Methods:*** Several CT scans of the Advanced Electron Density Phantom (Sun Nuclear) were obtained using various combinations of kilovoltage (70 kVp, 80 kVp, 100 kVp, 120 kVp, and 140 kVp), QRM (35 mAs, 45 mAs, and 55 mAs), and pitch values (1.2 and 1.4) in a PET/CT (Biograph Vision, Siemens Healthineers). The scans were performed with and without the phantom head and external shell (attenuation medium). For each combination, the attenuation coefficients were parameterized relative to water using a method described in [2], and lookup tables (F(Z)) were generated to parametrize the effective atomic number (Zeff) and effective mass density (ρeff) of the material mixture. Finally, a three-material decomposition using a phantom-dependent DEQCT [3] (PD-DEQCT) and a phantom-independent DEQCT (PI-DEQCT) [1] method was performed in a section of a bone sample of a pig inside a NEMA IEC PET body phantom, with and without water filling (attenuation). The volume fractions of cortical bone, fat, and water were quantified using low-dose (80 kVp, 55 mAs; 120 kVp, 35 mAs) and high-dose (100 kVp, 45 mAs; 140 kVp, 35 mAs) kVp-combinations. ***Results:*** The steepness of the F(Z) curves depends on the selected kVp-combination and attenuation conditions. Moreover, the kVp-combinations with the 70 keV data were found to be inapplicable for clinical purposes. The relative error quantifying the volume fraction of cortical bone, fat, and water between the PD-DEQCT (reference) and PI-DEQCT methods were 30.9%, 14.3%, and 36.2% for 80/120 kVp and 12.5%, 8.1%, and 51.8% for 100/140 kVp combinations without attenuation, and 2%, 20%, and 4.1% for 100/140 kVp with attenuation. The quantification using 80/120 kVp with attenuation was not feasible. ***Conclusion:*** The PI-DEQCT method shows promise for accurate quantification of the volume fraction of cortical bone, fat, and water using a commercial hybrid (PET/)CT system, but its accuracy is affected by the kVp-combination and beam hardening. ***References:*** [1] Salas-Ramirez M. et al. ZMedPhys. 2022. [2] Martines L. et al. PhysMed. 2012.[3] Goodsitt M. et al. MedPhys. 2014

OP-439

Hematological Toxicity Correlates with Monte Carlo-derived Absorbed Dose to the Red Marrow in Patients Treated with [^{177}Lu]Lu-DOTA-TATE

J. Blakkisrud[1,2], *G. Kingkiner*[1], *A. B. Peterson*[1,3], *S. J. Wilderman*[1], *K. Wong*[1], *K. A. Frey*[1], *Y. K. Dewaraja*[1];
[1]*University of Michigan, Ann Arbor, MI, UNITED STATES OF AMERICA,* [2]*Oslo University Hospital, Oslo, NORWAY,* [3]*Wayne State University, Detroit, MI, UNITED STATES OF AMERICA.*

Aim/Introduction: Observed toxicities in peptide receptor radionuclide therapy (PRRT) of neuroendocrine tumours (NET) have been primarily hematological. In this work we investigate the relationship between absorbed dose to the red marrow and hematological toxicity in patients treated with PRRT. ***Materials and Methods:*** Nineteen patients with somatostatin-positive NETs who were treated with four cycles of [^{177}Lu]Lu-DOTA-TATE and underwent multi-timepoint post cycle 1 SPECT/CT-imaging were included in this study. Vertebrae in the field of view (FOV) were segmented on CT by an AI-segmentation tool [1] with manual fine-tuning when necessary. Vertebrae time-integrated activity (TIA) maps were generated following exponential and trapezoidal fitting of time-activity. Absorbed dose to the red marrow was calculated coupling TIA-maps with an in-house developed Monte Carlo (MC) code. The code allows for specification of the fraction of red marrow cells, the location of the activity within each skeletal site (i.e. red and yellow marrow and trabecular bone) and a CT-based density correction for the trabecular bone fraction. The patient level absorbed dose to red marrow was calculated as the median of the red marrow dose in all vertebrae in the FOV, excluding those with focal uptake in metastatic disease. Hematological toxicity was monitored with neutrophil (ANC), thrombocyte (Plt), white blood cell (WCC) and lymphocyte (ALC) count. The change in values compared to baseline before cycle two as well as three and six months after the last treatment cycle were used for dose-toxicity correlation and tested with the Spearman rank test. The absolute values at the sampling times were also investigated. ***Results:*** The vertebrae-median absorbed dose (absorbed dose per administered activity in parenthesis) of cycle 1 ranged from 0.16 (0.02 Gy/GBq) to 0.79 (0.11 Gy/GBq) with an average of 0.38 Gy (0.053 Gy/GBq). Of the evaluated toxicity markers, a significant dose-toxicity correlation was identified

for relative platelet counts before the second cycle (r = -0.51, p = 0.026) and after six months (r = -0.57, p = 0.041). ***Conclusion:*** A correlation between the absorbed dose to red marrow and toxicity markers was found, suggesting that dosimetry can be used to manage and potentially predict treatment-related toxicities for dosimetry-guided treatment in the future. ***References:*** 1) Wasserthal et. al. TotalSegmentator: robust segmentation of 104 anatomical structures in CT images, 2022. arXiv: 2208.05868

OP-440

Dosimetry estimates of ^{177}Lu-PNT2002 in oligorecurrent prostate cancer: preliminary dosimetry results from a randomized phase 2 trial (LUNAR)

Z. Ells[1], *L. Unterrainer*[1,2], *D. Sennung*[1], *R. Alano*[1], *K. Booker*[1], *C. Felix*[1], *A. Daley*[1], *A. Farolfi*[1,3], *J. Czernin*[1], *M. Dahlbom*[1], *A. Kishan*[1], *J. Calais*[1];
[1]*University of California - Los Angeles, Los Angeles, CA, UNITED STATES OF AMERICA,* [2]*Ludwig Maximilian University of Munich, Munich, GERMANY,* [3]*Universita di Bologna, Bologna, ITALY.*

Aim/Introduction: The phase II trial LUNAR (NCT05496959) randomizes oligo-recurrent prostate cancer patients with 1-5 lesions visible by PSMA-PET to neo-adjuvant ^{177}Lu-PSMA-I&T (PNT2002) and stereotactic body radiotherapy (SBRT) versus SBRT alone (no ADT). Here we report preliminary dosimetry data of PNT2002 in these patients. ***Materials and Methods:*** Patients randomized to the intervention group received 2 cycles (6.8GBq/cycle) of neo-adjuvant PNT2002. Quantitative SPECT images were obtained with Siemens Intevo 6 at 4, 24, and 72-96 hours after the injection of the first cycle (3 bed positions, 120 views, 10s per view, 256x256 pixels (2.4 mm)^2). Siemens quantitative image reconstruction (xSPECT) was completed using 48 iterations, 1 subset, and 0mm Gaussian filter. The CT from the second and third timepoint was deformably registered to the first, creating a voxel wise dose map in which SPECT voxels at each timepoint represent the same volumes using HERMES (2.15.0). Tumor lesions and organs of interest (kidneys, parotids, submandibular glands, liver) were manually delineated with HERMES Affinity Viewer. Time integrated activity curves were created for each segmentation. The absorbed dose calculations were done on a voxel-level basis (electrons considered absorbed locally, photons modeled using semi-monte-carlo modeling). ***Results:*** By March 2023, 14 patients were randomized to the PNT2002 group and were included in the analysis. Patients received an average of 6.97 GBq ± 0.31 (SD) of PNT2002 for their first cycle. The average dose to the right and left, kidneys, parotid and submandibular glands, and liver were 3.51 ± 1.33; 3.51 ± 1.35; 0.96 ± 0.34; 1.09 ± 0.53; 1.04 ± 0.28; and 0.97 ± 0.15, 0.29 ± 0.20 Gy/cycle, respectively. The average dose to and volume of the 9 bony and 22 lymph node lesions were 0.51 ± 0.61 Gy/cycle, 1.20 ± 0.87 mL and 1.90 ± 1.51 Gy/cycle, 0.63 ± 0.63mL respectively. ***Conclusion:*** For organs at risk the absorbed dose estimates remained within the same range as in a higher burden of disease setting. There was significant interpatient absorbed dose variation. Due to the small size of the tumor lesions partial volume corrections will need strong consideration. ***References:*** Support: Point Biopharma

OP-441

Modelling the effect of daughter migration on dosimetry estimates for actinium-225 in targeted alpha therapy

S. Tronchin[1], *J. C. Forster*[1,2], *K. Hickson*[2,3], *E. Bezak*[1,4];
[1]*Department of Physics, The University of Adelaide, Adelaide, AUSTRALIA,* [2]*Medical Physics & Radiation Safety, South Australia Medical Imaging, Adelaide, AUSTRALIA,* [3]*Allied Health & Human Performance, University of South Australia, Adelaide, AUSTRALIA,* [4]*Cancer Research Institute, University of South Australia, Adelaide, AUSTRALIA.*

Aim/Introduction: Actinium-225 (^{225}Ac) has demonstrated promising results in Targeted Alpha Therapy. A concern with ^{225}Ac is that the decay energy can break the bond to the targeting vehicle, releasing free daughter radionuclides in the body. Daughter migration is generally not considered in clinical dosimetry. The effect of daughter migration needs to be studied to assess the reliability of dose estimates which do not account for daughter migration. The aim of this work is to develop a compartment model that includes individual biokinetics for the daughter isotopes of ^{225}Ac. ***Materials and Methods:*** A multilevel compartment model for ^{225}Ac and its daughters was developed, where the daughter isotopes of ^{225}Ac are assigned their own unique transfer coefficients between compartments. The developed compartment model was used to build a program in Python. Computer simulations were performed for ^{225}Ac-DOTATATE. The initial distribution of ^{225}Ac-DOTATATE was obtained from the literature for patients with meningioma and neuroendocrine tumours. Each decay of ^{225}Ac was assumed to release the daughter isotope from the DOTATATE peptide. Simulations were performed for scenarios where: 1) the daughters have unique biokinetics, and 2) the daughters decay at the site of ^{225}Ac-DOTATATE. Absorbed doses to the tumour and normal organs were determined in each case. The impact of tumour cell internalisation was also studied in the following way: If ^{225}Ac-DOTATATE was internalised, then the daughters remained internalised. For non-internalised ^{225}Ac-DOTATATE in the tumour, the decay released the daughter into the plasma. ***Results:*** When the daughter isotopes had unique biokinetics and no ^{225}Ac-DOTATATE was internalised in tumour cells, the kidneys and tumour received doses of 0.79 Gy/MBq and 7.11 Gy/MBq, respectively. This is a change in dose of +12% for the kidneys and decrease in tumour dose by a factor of almost 5 compared to when the daughter isotopes decayed at the site of ^{225}Ac-DOTATATE. When 100% of ^{225}Ac-DOTATATE was internalised in tumour cells, the kidneys and tumour received doses of 0.75 Gy/MBq and 33.76 Gy/MBq, respectively. This is a change in dose of +6% for the kidneys and 0% for the tumour compared to when the daughter isotopes decayed at the site of ^{225}Ac-DOTATATE. ***Conclusion:*** When the daughter isotopes have unique biokinetics, there is a 6-12% increase in kidney dose compared to when the daughters decayed at the site of ^{225}Ac-DOTATATE. Tumour cell internalisation had a minor effect on normal organ dose but a substantial effect on tumour dose.

OP-442

Image Quantification and Quality Assessment of Dual-Isotope^{99m}Tc and^{177}Lu SPECT for Bone Marrow Dosimetry: a Simulation Study

C. Miller, *X. Hou, J. Brosch-Lenz, A. Rahmim, C. Uribe;*
BC Cancer Research Institute, Vancouver, BC, CANADA.

Aim/Introduction: Bone marrow (BM) is the organ-at-risk in metastatic castration-resistant prostate cancer (mCRPC) treatment with ^{177}Lu-PSMA. Although ^{177}Lu-SPECT imaging enables dosimetry, the active BM distribution is not necessarily known as BM is considered a non-imageable organ and bone metastases might change the BM distribution. The aim of this work is to test the feasibility for localization and quantification of active BM activity distributions by performing a ^{99m}Tc-sulphur colloids (SC) scan simultaneously with one of the ^{177}Lu dosimetry scans. This can lead to improved image-based BM dosimetry in radiopharmaceutical therapies. ***Materials and Methods:*** We tested two phantom configurations: i) a cylindrical phantom containing three spheres filled with ^{99m}Tc, ^{177}Lu, or both, with hot

background and varying ratios of ^{177}Lu:^{99m}Tc up to 50:1 and ii) the XCAT anthropomorphic phantom, with four ^{177}Lu-PSMA and two ^{99m}Tc-SC biodistributions. ^{177}Lu biodistributions were based on 14 SPECT images of 8 mCRPC patients treated at our institution and scanned at 4, 24, and 48 hours post-injection of ^{177}Lu-PSMA. The ^{99m}Tc-SC cases represented patients with high/low BM uptakes (5% and 25% of administered activity, respectively) based on ^{99m}Tc-SC biodistribution data. All the phantoms were imaged with a medium energy collimator using the Simind Monte-Carlo code. The projections of each radionuclide were combined to replicate dual-isotope scans. Seven energy windows were used to estimate the counts for the photopeaks and scatter of ^{99m}Tc and ^{177}Lu and remove the ^{177}Lu scatter from the ^{99m}Tc photopeak. Images were reconstructed using our PyTomography software with 10 subsets, 6 iterations, attenuation and scatter correction (using our 7-energy windows). Spherical ROIs were placed in the spheres or pelvic bones to assess quantitative accuracy of ^{99m}Tc. Images were assessed qualitatively to determine if BM localization could be determined. ***Results:*** For the spheres in the water cylinder, quantification of ^{99m}Tc was acceptable (within 12% of baseline (^{99m}Tc alone)) up to a 10:1 ratio of ^{177}Lu:^{99m}Tc. For the XCAT phantom, when BM uptake was high, quantitative accuracy was always within 10% of baseline. When uptake was low, accuracy was within 17% of baseline 4-24 hours post-injection and within 3% at 48 hours. Qualitatively, dual-isotope ^{99m}Tc images appeared identical to images of ^{99m}Tc alone and BM could be identified. ***Conclusion:*** Active BM localization in mCRPC patients could be possible with a ^{99m}Tc-SC scan in the presence of ^{177}Lu. Best quantification for ^{99m}Tc-SC was achieved when the scan was performed 48 hours post-injection of ^{177}Lu.

OP-443

Uncertainty analysis for Lu-177-PSMA in clinical routine

V. Nuttens[1], *M. Koole*[2], *O. De Winter*[1], *P. De Bondt*[1];
[1]*OLVZ, Aalst, BELGIUM,* [2]*KU Leuven, Leuven, BELGIUM.*

Aim/Introduction: There is a large interest in performing personalized post-therapy dosimetry for patients treated with Lu-177-PSMA as this allows to determine dose-response relationships and adapt dosing schemes for each patient individually. But is Lu-177-PSMA dosimetry feasible with acceptable uncertainties using current state-of-the-art SPECT/CT systems? How will a new generation 360° CZT SPECT/CT camera impact these uncertainties? Current clinical routine uses the validated protocol for a DH (dual-head) Anger-type SPECT/CT. [1] ***Materials and Methods:*** Uncertainty analysis was performed according to EANM recommendations [2] with a model implemented in Python. The mean absorbed dose D= Ã*S (with Ã the cumulated activity) as defined in the MIRD model, gives the following: $[u(D)/D]^2 = [u(Ã)/Ã]^2+[u(S)/S]^2+2u(Ã,S)/(ÃS)$ The last term considers the covariance as specified by the law of propagation of uncertainty (LPU). The uncertainty of Ã consists of its different subcomponents; A0 administered activity (as the uncertainty of the dose calibrator), λ effective decay constant, Q calibration factor, R recovery coefficient ($=C_{observed}/C_{true}$), C count rate, φ error function and c_2 a fitting constant of the S-factor. This analysis was done for a kidney volume of 176 mL, a tumour volume of 13 mL, with measured values for DH and datasheet values for the 360° CZT SPECT/CT. ***Results:*** The volume has the largest fractional uncertainty in DH with 51.1% and 21.4% for tumour and kidney volumes respectively. For the 360° CZT these are lower and correspond to 33.1% and 13.9%. The large volume error propagates through the total chain as R, C and the S-factor are all directly influenced by it. This leads for the DH to dose uncertainties of 36.4% and 14.1% for tumour and kidney volumes. For the 360° CZT the corresponding uncertainties are 22.9% and 10.7% respectively. Additionally, a 25% uncertainty corresponds to an 11 mL lesion for the 360° CZT while this is 30 mL for the DH. ***Conclusion:*** Volume is a dominating factor in the total uncertainty chain. Findings demonstrated that a SPECT/CT system with smaller pixel size and better spatial resolution such as these newly 360° CZT SPECT/CT's drastically decreases the dose uncertainty, especially for smaller lesions. ***References:*** [1] Marin G et al. Accuracy and precision assessment for activity quantification in individualized dosimetry of 177Lu-DOTATATE therapy. EJNMMIPhys. 2017Dec;4(1):7. doi:10.1186/s40658-017-0174-7. [2] Gear JI et al. EANM practical guidance on uncertainty analysis for molecular radiotherapy absorbed dose calculations. Eur J Nucl Med Mol Imaging. 2018Dec;45(13):2456-2474. doi:10.1007/s00259-018-4136-7.

OP-444

Tumour dosimetry after ^{177}Lu-RPT with a ring-shaped CZT-based camera requires inclusion criteria based on volume and activity concentration

R. Danieli[1], *C. Marin*[1], *M. Stella*[2], *B. Vanderlinden*[1], *H. Levillain*[1], *N. Reynaert*[1], *P. Flamen*[1];
[1]*Institut Jules Bordet, Brussels, BELGIUM,* [2]*GE HealthCare, Diegem, BELGIUM.*

Aim/Introduction: Partial volume effect (PVE) corrections based on recovery coefficients (RC) are widely adopted to enhance the accuracy of tumour dosimetry after radiopharmaceutical therapy (RPT) with ^{177}Lu. This study aims to maximise the confidence in our RC-based PVE correction by assessing the RC accuracy and repeatability at different levels of activity concentration. ***Materials and Methods:*** The six spherical inserts of a NEMA phantom (volume range: 1.2-113.1ml) were filled with 1.8MBq/ml of ^{177}Lu. Nine acquisitions of 60 minutes each were performed over one month (activity concentration range: 0.1-1.8MBq/ml) on a ring-shaped CZT-based camera (StarGuide, GE HealthCare), with emission and scatter windows centred at 208keV(±6%) and 185keV(±5%), respectively. Acquired projections were reframed with the Lister tool to obtain 5 independent sets of projections of 12 minutes each (total: 45 sets). These resulting projections, as well as the 60-minutes projections corresponding to the highest activity level, were reconstructed with the protocol suggested by the manufacturer. For each sphere and reconstructed image, volumes of interest (VOI) were obtained by a region-growing tool based on the nominal volume. RC were determined by dividing the measured activity concentration inside each VOI by the nominal activity concentration. RC obtained with the first 60-minutes acquisition were taken as reference (RC_ref). All the other RC were normalized by the corresponding RC_ref (RC_norm). For each sphere, the median and range (maximum-minimum) of RC_norm on all the reconstructed images were computed to assess the RC accuracy and repeatability, respectively. To investigate the dependency of the RC accuracy and repeatability on the activity concentration, the same analysis was repeated including only the 30 reconstructed images corresponding to activity concentrations arbitrarily >0.3MBq/ml. ***Results:*** RC_ref ranged from 19% (1.2ml sphere) to 73% (113.1ml sphere). Median(range) RC_norm were 1.07(1.96), 0.99(0.62), 1.03(0.34), 1.04(0.16), 1.05(0.15), 1.05(0.16) for the 1.2, 2.6, 5.6, 11.5, 26.5 and 113.1ml sphere, respectively. When considering activity concentrations higher than 0.3MBq/ml, RC_norm were 1.04(1.13), 1.00(0.22), 1.02(0.21), 1.03(0.12),

1.03(0.13), 1.03(0.10). ***Conclusion:*** For all spheres and activity concentrations, high RC accuracy was measured with respect to the chosen reference (median RC_norm < 1.07). Low repeatability was found in the RC of the three smallest spheres (RC_norm range between 0.34 and 1.96). Limiting the analysis to activity concentrations >0.3MBq/ml and to volumes >11.5mL improved both accuracy and repeatability (<1.04 and <0.13, respectively). Our results suggested that inclusion criteria based on volume and activity concentration should be considered for accurate tumour dosimetry after ^{177}Lu-RPT with StarGuide.

1006

Monday, September 11, 2023, 3:00 PM - 4:30 PM
Hall C

Clinical Oncology Track - Featured Session: Melanoma

OP-445
Pitfalls in Melanoma Imaging

OP-446
Predictive value of baseline quantitative parameters of 2-[^{18}F]FDG-PET/CT for brain metastases in melanoma patients

F. Kalantari[1,2], *L. Hehenwarter*[1], *G. Rendl*[1], *G. Schweighofer-Zwink*[1], *W. Hitzl*[3], *P. Koelblinger*[4], *C. Pirich*[1], *M. Beheshti*[1];
[1]*Division of Molecular Imaging & Theranostics, Department of Nuclear Medicine, University Hospital, Paracelsus Medical University Salzburg, Salzburg, AUSTRIA,* [2]*Iran University of Medical Sciences, Tehran, IRAN, ISLAMIC REPUBLIC OF,* [3]*Biostatistics and Publication of Clinical Trial Studies, Research and Innovation Management (RIM), Paracelsus Medical University Salzburg, Salzburg, AUSTRIA,* [4]*Department of Dermatology, University Hospital, Paracelsus Medical University Salzburg, Salzburg, AUSTRIA.*

Aim/Introduction: Malignant melanoma represents a public health challenge due to its increasing incidence over the last decades, its aggressive nature, and its high tendency for brain metastases. Therefore, accurate identification of patients at higher risk of developing brain metastases (BM) is crucial for effective surveillance and optimal treatment management. In this study, we assessed the predictive value of baseline organ-specific metabolic parameters of 2-[^{18}F]FDG-PET/CT for brain metastases free survival (BMFS) in malignant melanoma. ***Materials and Methods:*** 159 patients with malignant melanoma (45.3% female, 54.7% male; mean age: 71 ± 14 years) who underwent primary staging by 2-[^{18}F]FDG-PET/CT and brain MRI and had available clinical and imaging follow-up data. Semi-quantitative 2-[^{18}F]FDG-PET parameters as well as clinical and histopathological variables were collected for survival analysis. Exclusion criteria were undefined disease stage, infection, atypical histopathological findings, brain metastases at initial diagnosis, and second primary malignancies. Predictive value of organ-specific semi-quantitative 2-[^{18}F]FDG-PET parameters (i.e. SUVmax, SULpeak, MTV, TLG) of the primary tumor, lymph nodes-, bone-, liver-, and lung-metastases were analyzed. ***Results:*** Median patient follow-up time was 6.3 years, and BM were found in 59 patients (37%) with a median time to brain metastasis-free survival (BMFS) of 60.58 months (range: 2-221 months). A negative 2-[^{18}F]FDG-PET/CT scan at the initial staging was significantly associated with BMFS, irrespective of the initial stage, gender, and BRAF mutation. The significant clinical predictors of BMFS were tumor thickness and the primary stage of the disease. No significant correlation was observed between the metabolic tumor burden on 2-[^{18}F]FDG-PET/CT and BMFS. There was significant correlation between SULpeak and SULmax of the prominent lymph node metastasis (P value 0.02), and SULpeak of the primary tumor with BMFS (P value 0.009). Patients were classified into low-risk (<20% probability of BM in mean-time of 10 years), intermediate-risk (>50% probability of BM in mean-time of 5 years) and high-risk (>75% probability of BM in mean-time of 1 year) based on a survival curve derived by SULpeak of <2, between ≥2 and 14.6, and > 14.6, respectively. ***Conclusion:*** Baseline organ-specific metabolic parameters of 2-[^{18}F]FDG-PET/CT showed promising markers for independent prediction of brain metastases in patients with melanoma. Furthermore, such quantitative metabolic imaging parameters could potentially be incorporated into existing clinical survival prediction models for accurate stratification of high-risk melanoma patients, who may benefit from further imaging surveillance and prophylactic treatment approaches.

OP-447
Lymphoid organs' glucose metabolism and its role in predicting the outcomes of patients with malignant melanoma treated with immunotherapy

L. Evangelista[1], *A. Bianchi*[2], *A. Annovazzi*[3], *R. Sciuto*[3], *S. Di Treglia*[3], *A. G. Nappi*[4], *C. Ferrari*[4], *G. Rubini*[4], *S. Panareo*[5], *L. Urso*[6], *M. Bartolomei*[6], *D. Arico*[7], *M. Bombaci*[7], *D. Caponnetto*[7], *S. Gusella*[8], *A. Spimpolo*[8], *C. Carriere*[9], *M. Balma*[2], *A. Buschiazzo*[2], *R. Gallicchio*[10], *G. Storto*[10], *M. L. De Rimini*[11];
[1]*Nuclear Medicine Unit, University of Padua, Padova, ITALY,* [2]*Nuclear Medicine Unit, SC Medicina Nucleare ASO S.Croce e Carle Cuneo, Cuneo, ITALY,* [3]*Nuclear Medicine Unit, IRCCS Regina Elena National Cancer Institute, Rome, Italy, Rome, ITALY,* [4]*Section of Nuclear Medicine, Interdisciplinary Department of Medicine, University of Bari "Aldo Moro", Bari, Italy, Bari, ITALY,* [5]*Nuclear Medicine Unit, Oncology and Haematology Department, University Hospital of Modena, Italy, Modena, ITALY,* [6]*Nuclear Medicine Unit, Oncology and Specialistic Department, University Hospital of Ferrara, Italy, Ferrara, ITALY,* [7]*Servizio di Medicina Nucleare, Humanitas Istituto Clinico Catanese, Misterbianco (CT), Italia., Catania, ITALY,* [8]*Nuclear Medicine Department,Central Hospital Bolzano (SABES-ASDAA), Bolzano-Bozen, Italy, Bolzano, ITALY,* [9]*Dermatology Department, Central Hospital Bolzano (SABES-ASDAA), Bolzano-Bozen, Italy., Bolzano, ITALY,* [10]*Nuclear Medicine Unit, IRCCS CROB Referral Cancer Center of Basilicata, Rionero in Vulture (PZ), Italia, Rionero in Vulture, ITALY,* [11]*Nuclear Medicine Unit - Department of Health Service- AORN Ospedali dei Colli, Naples, Italy, Naples, ITALY.*

Aim/Introduction: The aims of the present study were to assess if the changes of mean SLR, bone marrow uptake and the site of new metabolic lesions at 2-[18F]-FDG PET/CT can predict patients' outcomes. ***Materials and Methods:*** From August 2013 to December 2020, data about [18F]FDG PET/CT obtained for 92 consecutive patients with malignant melanoma were collected. The following inclusion criteria were adopted: 1) a confirmed diagnosis of malignant melanoma; 2) age >18 years; and 3) a follow-up of at least 12 months after the first PET/CT scan. The scans were named as following: baseline PET when performed before starting immuno-therapy (within 3 months), PET1, PET2 and PET, respectively made after 6, 18 and 36 months from starting immunotherapy. Mean standardized uptake value (SUVmean) of the liver (SUVmean_L) and the spleen (SUVmean_spleen) were

measured. The Spleen Liver Ratio (SLR) was calculated as the ratio between SUVmean_spleen and the SUVmean_L. Bone marrow uptake was visually quantified by using a scale system from 1 to 5. ***Results:*** Data for both baseline PET and PET1 was available in all 92 patients, while 70 (76%) and 34 (37%) patients underwent PET2 and PET3 scans, respectively. Median values of SLR across the scans were similar, there was a slight increase in the bone marrow uptake between the baseline PET and PET1 (the score 4/5 moved from 2.2% to 6.5%, respectively in the baseline and PET1 scan), while it was substantially stable in PET2 an PET3. After a median follow-up period of 41 (4-312 months), 41 (44.6%) patients had a progressive disease. Moreover, 32 (34.8%) died after 61 (range 5-342) months. At baseline PET and PET3, median values of SLR were slightly higher in patients with a good prognosis (0.83 vs. 0.70 and 0.78 vs. 0.72, respectively in alive vs. dead patients), while they were substantially similar in PET1 and PET2 (0.79 vs. 0.76 and 0.75 vs. 0.74, respectively in alive vs. dead patient). Bone marrow uptake tended to be higher (score > 2) in PET1, PET2 and PET3 in patients with a worse prognosis, although not statistically significant. ***Conclusion:*** FDG uptake in lymphoid organs would be useful as a prognostic parameter in patients with malignant melanoma undergoing immunotherapy. Larger study population is mandatory to accertain this evidence. ***References:*** Cancers (Basel). 2023 Jan 31;15(3):878.Cancer Biother Radiopharm. 2023 Apr 25. doi: 10.1089/cbr.2022.0092.

OP-448

First-in-human PET imaging and evaluation of melanin-targeted ^{18}F-DMPY2 in malignant melanoma patients.

Y. Yang[1], *M. Zhou*[1], *N. Chen*[1], *J. Su*[2], *X. Chen*[2], *S. Hu*[1];
[1]*Department of Nuclear medicine, Xiangya Hospital, Central South University, Changsha City, Hunan Province, CHINA,* [2]*Department of Dermatology, Xiangya Hospital, Central South University, Changsha City, Hunan Province, CHINA.*

Aim/Introduction: Early diagnosis and accurate staging of malignant melanoma (MM) have significant and decisive value in clinical practice. ^{18}F-DMPY2 is a promising PET tracer in vivo with high affinity and selectivity for melanin. The study aims to investigate biodistribution and radiation dosimetry in healthy volunteers and the potential clinical application of ^{18}F-DMPY2 in MM patients. ***Materials and Methods:*** ^{18}F-DMPY2 was synthesized via a one-pot reaction. The biodistribution, radiation dosimetry, and safety of the new probe were estimated in 3 healthy volunteers. 31 MM patients underwent ^{18}F-DMPY2 and/or ^{18}F-FDG PET/CT scans to explore the clinical use in the early detection of melanoma metastasis. Besides, we studied its diagnostic performance in 51 lymph node basins of 27 MM patients after node dissection by comparing PET uptake with the postoperative pathological results. ***Results:*** ^{18}F-DMPY2 was well tolerated by healthy volunteers and MM patients. The calculated effective dose of ^{18}F-DMPY2 was 0.0122 mSv/MBq. In MM patients, we observed prominent ^{18}F-DMPY2 tumor uptake and high tumor-to-background ratios in primary tumors. Diagnostic Performance of ^{18}F-DMPY2 in Lymph Node Metastases is significantly better than ^{18}F-FDG. The sensitivity, specificity, accuracy, and positive and negative predictive values of ^{18}F-DMPY2 were 66.7%, 100%, 88.9%, 100%, and 85.7% respectively. Nevertheless, those of ^{18}F-FDG were 50%, 42.8%, 46.6%, 50%, and 42.8%. Some distant metastases were detected in ^{18}F-DMPY2, but not in ^{18}F-FDG PET, such as brain and bone. Additionally, ^{18}F-DMPY2 PET imaging had a unique advantage in distinguishing ^{18}F-FDG false-positive lesions. ***Conclusion:*** ^{18}F-DMPY2 is a safe and well-tolerated melanin PET tracer. ^{18}F-DMPY2 PET/CT is a powerful imaging tool in the early detection and clinical staging of MM patients. ***References:*** Pyo A, Kim DY, Kim H, Lim D, Kwon SY, Kang SR, Kim HS, Bom HS, Min JJ. Ultrasensitive detection of malignant melanoma using PET molecular imaging probes. Proc Natl Acad Sci U S A. 2020 Jun 9;117(23):12991-12999. doi: 10.1073/pnas.1922313117.

OP-449

The prognostic value of [^{18}F]FDG PET/CT based response monitoring in metastatic melanoma patients undergoing immunotherapy: comparison of different metabolic criteria

C. Sachpekidis[1], *V. Weru*[1], *A. Kopp-Schneider*[1], *J. C. Hassel*[2], *A. Dimitrakopoulou-Strauss*[1];
[1]*German Cancer Research Center (DKFZ), Heidelberg, GERMANY,* [2]*National Center for Tumor Diseases (NCT), University Hospital Heidelberg, Heidelberg, GERMANY.*

Aim/Introduction: To investigate the prognostic value of [^{18}F]FDG PET/CT as part of response monitoring in metastatic melanoma patients treated with immune checkpoint inhibitors (ICIs). ***Materials and Methods:*** Sixty-seven patients underwent [^{18}F]FDG PET/CT before start of treatment (baseline PET/CT), after two cycles (interim PET/CT) and after four cycles of ICIs administration (late PET/CT). Metabolic response evaluation was based on the conventional EORTC and PERCIST criteria, as well as the newly introduced, immunotherapy-modified PERCIMT, imPERCIST5 and iPERCIST criteria. Metabolic response to immunotherapy was classified according to four response groups (complete metabolic response [CMR], partial metabolic response [PMR], stable metabolic disease [SMD], progressive metabolic disease [PMD]), and further dichotomized by response rate (responders= [CMR] + [PMR] vs. non-responders= [PMD] + [SMD]), and disease control rate (disease control= [CMR] + [PMR] + [SMD] vs. [PMD]). The spleen-to-liver SUV ratios (SLR_{mean}, SLR_{max}) and bone marrow-to-liver SUV ratios (BLR_{mean}, BLR_{max}) were also calculated. The results of PET/CT were correlated with patients' overall survival (OS). ***Results:*** Median patient follow up [95% CI] was 61.5 months [45.3 - 66.7 months]. On interim PET/CT, the application of the novel PERCIMT demonstrated significantly longer survival for metabolic responders, while the rest criteria revealed no significant survival differences between the different response groups. Respectively on late PET/CT, both a trend for longer OS and significantly longer OS were observed in patients responding to ICIs with metabolic response and disease control after application of various criteria, both conventional and immunotherapy-modified. Moreover, patients with lower SLR_{mean} values demonstrated significantly longer OS. ***Conclusion:*** In patients with metastatic melanoma PET/CT-based response assessment after four ICIs cycles is significantly associated with OS after application of different metabolic criteria. The prognostic performance of the modality is also high after the first two ICIs cycles, especially with employment of novel criteria. In addition, investigation of spleen glucose metabolism may provide further prognostic information.

OP-450

Early monitoring of immunotherapy using ^{18}F-FDG-PET-CT in patients with stage IV melanoma treated with PD-1 inhibitors

D. Hochmuth[1], *C. Sachpekidis*[1], *J. Hassel*[2], *L. Pan*[1], *A. Dimitrakopoulou-Strauss*[1];
[1]*German Cancer Research Center, CCU Nuclear Medicine, Heidelberg, GERMANY,* [2]*Department of Dermatology, University Hospital Heidelberg and NCT Heidelberg, Heidelberg, GERMANY.*

Aim/Introduction: The aim of the present study is to evaluate the value of ^{18}F-FDG-PET-CT in patients with metastatic melanoma treated with PD-1 inhibitors and to find out at what point in therapy an initial follow-up examination provides a predictive value in terms of survival. Furthermore, the intention is to find out what additional information can be gained from dynamic PET-CT, which has been used until now primarily within research purposes. ***Materials and Methods:*** The study group included twenty-three patients with unresectable, metastatic melanoma treated with PD-1 inhibitors. PD-1 inhibitors were administered either as monotherapy or as combination treatment with a CTLA-4 inhibitor. Therapy monitoring was performed before the start of treatment (baseline), after two treatment cycles (interim) and after four treatment cycles (late) and consisted of dynamic PET-CT of the thorax and upper abdomen as well as static whole-body PET-CT. Patterns of physiological ^{18}F-FDG uptake and irAEs were documented and distinguished from actual tumor lesions. Treatment response was assessed based on the application of the EORTC criteria and the PERCIMT. Patients' response to treatment was classified as either MB (metabolic benefit), including CMR, PMR and SMD, or no-MB (no metabolic benefit) in case of PMD. The actual clinical response was determined individually by the patients' PFS (progression-free survival) which was measured from the start of treatment until disease progression or death from any cause. ***Results:*** Tumor lesions and irAEs could be assessed in all planes and clearly differentiated from normal tissue due to the high ^{18}F-FDG uptake. Survival analysis showed that both late and interim PET-CT were able to provide predictive value regarding PFS. Based on both follow-ups, patients with predicted MB showed significantly longer PFS compared to patients with predicted PMD. This significant survival benefit was seen when both criteria were used, with lower p-values and higher hazard ratios expressing superiority of the EORTC criteria (interim: $p = 0.021$, hazard ratio = 3.36; late: $p = 0.022$, hazard ratio = 5.25) over the PERCIMT (interim: $p = 0.048$, hazard ratio = 2.82; late: $p = 0.049$, hazard ratio = 4.23). ***Conclusion:*** The results show that ^{18}F-FDG-PET-CT has predictive value in the early course of treatment with ICIs and is suitable for identifying early on which patients will benefit from therapy. The additional use of dynamic PET-CT enables a better understanding of the pathophysiology of malignant and inflammatory processes as well as the mechanism of action of ICIs.

OP-451

FDG PET/CT Biomarker Dissemination Features In Metastatic Melanoma Patients Treated With Immunotherapy: Association With Survival

H. Saadani[1,2], *E. A. Aalbersberg*[1], *M. T. Kayembe*[1], *J. B. A. G. Haanen*[1], *O. S. Hoekstra*[2], *R. Boellaard*[2], *M. P. M. Stokkel*[1];
[1]*NETHERLANDS Cancer Institute, Amsterdam, NETHERLANDS,* [2]*Amsterdam UMC, Vrije Universiteit Amsterdam, Cancer Center Amsterdam, Amsterdam, NETHERLANDS.*

Aim/Introduction: In metastatic melanoma treated with immunotherapy, patient risk stratification to determine treatment benefit remains an unsolved clinical problem. FDG Positron Emission Tomography/Computed Tomography ([^{18}F]FDG PET/CT) is an established technique for staging malignant melanoma. Melanoma shows heterogeneous metastatic patterns, with certain distributions associated with worse prognosis. Advanced PET dissemination features can quantify malignant spread in a simplified manner. However, the additional value of advanced image analysis and quantification is unknown yet. The aim of this study was to evaluate the association of [^{18}F]FDG PET/CT uptake metrics and dissemination features with overall survival (OS) in metastatic melanoma patients treated with immunotherapy. ***Materials and Methods:*** Consecutive metastatic melanoma patients who received first-line immunotherapy from 2016 to April 2021 were eligible. Inclusion criteria were histopathological confirmed metastatic/unresectable melanoma, a baseline [^{18}F]FDG PET/CT scan and initiation of immunotherapy within a maximum 12 weeks of baseline scan. Exclusion criteria included aggressive concurrent malignancies within 5 years prior to the baseline scan, brain metastasis and less than two lesions. On a patient level, 18 dissemination features and 5 conventional PET metrics (SUVmax, SUVpeak, SUVmean, TLG, TMTV) were extracted. From the 18 dissemination features, 5 provide quantitative measures for spatial distribution over the body, 10 for the variability in SUV across lesions and 3 for the variability in tumor volume across all lesions. Clinical baseline characteristics were collected including: age, sex, stage, tumour type, immunotherapy type, mutations, LDH, performance status and metastasized organ sites. Univariate and multivariate Cox regression analyses were used to assess association between PET features and OS. The Spearman's rank correlation (rho) between predictor variables was used to test for potential multicollinearity. ***Results:*** Eighty five patients were included, and their mortality rate was 60%. At current follow-up, the median OS time was 33 months. Patients were mostly treated with pembrolizumab, nivolumab and ipilimumab/nivolumab. Two spatial dissemination features and one volume dissemination feature, were significantly associated with OS in the univariate analysis. Conventional PET metrics were not associated with OS. In the multivariate analysis, one spatial dissemination feature remained significantly associated with OS. ***Conclusion:*** Spatial dissemination measuring the distance between the largest and any other lesion within metastatic melanoma patients was associated with worse OS, whereas the conventional PET metrics were not. We showed a first exploratory independent association between spatial dissemination and OS, however we're working on further in-depth examination and validation necessary before clinical implementation can be considered.

OP-452

Correlation of thyroid FDG uptake on 18F-FDG PET/CT with response to immunotherapy in metastatic melanoma patients

K. Zevnik[1,2], *N. Hribernik*[1,2], *K. Strašek*[3], *A. Studen*[3,4], *A. Doma*[1,2], *K. Škalič*[1], *M. Reberšek*[1,2];
[1]*Oncology Institute Ljubljana, Ljubljana, SLOVENIA,* [2]*Faculty of Medicine, University of Ljubljana, Ljubljana, SLOVENIA,* [3]*Faculty of Mathematics and Physics University of Ljubljana, Ljubljana, SLOVENIA,* [4]*Experimental Particle Physics Department, Jožef Stefan Institute, Ljubljana, SLOVENIA.*

Aim/Introduction: Previous studies showed conflicting results about the occurrence of immune-related (IR) thyroiditis in cancer patients on immunotherapy (ICI) and clinical benefit. Positive correlation between higher thyroid metabolic activity on PET/CT and IR thyroiditis has been shown in previous studies. Our aim was to analyse whether the increase of thyroid metabolic activity on 18F-FDG PET/CT in metastatic melanoma (MM) patients on ICI correlates with clinical outcome ***Materials and Methods:*** In this prospective single-arm, one-centre clinical study, 67 MM patients on ICI were included. Patients were monitored with 18F-FDG PET/CT at the baseline, 1, 4 and 8 months (M1, M4, M8) after ICI treatment initiation. Thyroid gland was segmented on PET/CT scans using a convolutional neural network (CNN). To quantify 18F-FDG thyroid uptake a novel quantitative biomarker was

used - 75th percentile of SUV distribution (SUV75%), which was proven to be optimal for detection of IR-thyroiditis in one of our previous studies. We determined clinical best overall response (BOR) status of patients up to 8 months. We divided the patients into two groups based on their BOR, with progressive patients (PD) being in the non-clinical response group (non-CB) and all the other patients (CR, PR, SD) being in the clinical benefit group (CB). We analysed the correlation of SUV75% on M1 and M4 PET/CT scans with clinical BOR of the patients subdivided into the before mentioned CB and non-CB groups using the Pearson correlation method. Secondarily we analysed the correlation of grade 2 (G2) thyroiditis and any grade thyroiditis (AG), diagnosed in the follow-up period of 8 months, with SUV75% and with BOR. ***Results:*** Clinical BOR status of 67 patients was defined as CR (16 patients), PR (18 patients), SD (7 patients) and PD (26 patients). 41 patients were categorized in the CB group and 26 in the non-CB group. There was no correlation of SUV75% from either M1 or M4 PET/CT with BOR. No threshold was found to distinguish between the two groups (CB and non-CB). G2 thyroiditis was present in 11 pts. and AG thyroiditis in 13 pts. There was no correlation of G2 thyroiditis and AG thyroiditis with BOR. M4 SUV75% had high correlation with G2 thyroiditis and AG thyroiditis. ***Conclusion:*** Our prospective study showed no statistical correlation between higher 18F- FDG PET/CT thyroid uptake and clinical response to immunotherapy. PET/CT seems to be a good diagnostic tool for detection of IR -thyroiditis.

OP-453

Prediction of Additional Regional Lymph Node Metastases in Cutaneous Melanoma Patients With Positive Sentinel Lymph Node Biopsy

L. Radosavcev[1], *M. Rajovic*[2], *M. Radulovic*[1], *N. Petrov*[3], *L. Kandolf Sekulovic*[4];
[1]*Institute of Nuclear Medicine, Military Medical Academy, Belgrade, SERBIA,* [2]*Clinic for Plastic and Reconstructive Surgery , Military Medical Academy, Belgrade, SERBIA,* [3]*Institute of Pathology and Forensic Medicine , Military Medical Academy, Belgrade, SERBIA,* [4]*Department of Dermatology and Venerology, Military Medical Academy, Belgrade, SERBIA.*

Aim/Introduction: Sentinel lymph node (SLN) biopsy is the standard of care for nodal staging in clinically node-negative melanoma patients. The impact of complete lymph node dissection (CLND), after a positive SLN biopsy is still debatable. Examining the factors associated with increased risk of metastases in non-sentinel lymph node (NSLN) is important to identify patients who could still benefit from CLND. ***Materials and Methods:*** We retrospectively analyzed clinicopathologic and lymphoscintigraphic characteristics in 420 cutaneous melanoma patients who underwent lymphoscintigraphy and SLN biopsy. Univariate and multivariate logistic regression analysis was performed using (non) SLN metastasis (yes/no binary outcome), with odds ratios representing effect size. ***Results:*** The overall detection rate of SLNs was 97.6. Metastatic SLNs were found in 81 patients (19.7%) and CLND was recommended. Among patients who underwent CLND at our institution, additional metastatic nodes (positive CLND) were shown in 26 (32.1 %) patients, while negative CLND was found in 55 (67.9%) patients. Positive NSLN was no associated with a gender, age, localization, presence of ulceration, regression, hystopathological type and mitotic rate of primary melanoma. Breslow thickness in patients with positive NSLN tended to be higher (median 4.8mm) versus 4.4 mm in NSLN negative group, but without reaching statistical significance. In addition, characteristics on lymphoscintigraphy like the time to procedure, number of draining basins, number of SLN visualized on scintigraphy and excised for patients were no associated with NSLN positivity. ***Conclusion:*** Patients and primary tumor characteristics as well as the lymphoscintigraphy imaging characteristics were not significant predictors of metastatic involvement of additional lymph node(s) in regional basins.

1007

Monday, September 11, 2023, 3:00 PM - 4:30 PM
Hall F1

Neuroimaging Committee - TROP Session: Imaging Neurotransmission in Movement Disorders

OP-454

Effects Of Medications On Dopamine Transporter Imaging Using ^{123}I-FP-CIT SPECT In Routine Practice

Y. Piatkova[1], *M. Doyen*[1], *S. Frismand*[2], *L. Hopes*[2], *L. Imbert*[1], *A. Verger*[1];
[1]*Université de Lorraine, Department of Nuclear Medicine and Nancyclotep Imaging Platform, CHRU Nancy, Nancy, FRANCE,* [2]*Université de Lorraine, Department of Neurology, CHRU Nancy, Nancy, FRANCE.*

Aim/Introduction: Dopamine transporter (DAT) imaging is used as a diagnostic tool to support the diagnosis of neurodegenerative parkinsonian disorders. Medications have been described as potentially influencing the interpretation of ^{123}I-FP-CIT SPECT scan, but with limited data. The aim of the current study was to evaluate in routine practice the potential effects of medications on interpretation of ^{123}I-FP-CIT SPECT scan. ***Materials and Methods:*** Consecutive patients undergoing a ^{123}I-FP-CIT SPECT/CT scan on a 360° CZT camera between September 2019 and December 2022 were included. An exhaustive interrogation of medications (antidepressants,antipsychotics,anti-epileptics,anti-parkinsonians, benzodiazepines, lithium, opioids and stimulants) taken by each patient was performed. Two experienced nuclear physicians, blinded to the report of medications, interpreted the ^{123}I-FP-CIT SPECT scans visually as well as semi-quantitatively through striatal and occipital masks obtained after a Montreal National Institute spatial normalization of each CT scan registered to the SPECT. ***Results:*** Three hundred and five patients (71.0 ± 10.4, 135 women) were included with 145 (47.5%) of visually interpretated normal scans. In normal scans, the striatum/occiput ratio was decreased by noradrenergic and specific serotonergic antidepressant (n=15, average decrease of 15%) and opioid (tramadol, n=6, average decrease of 12%) medications in association with a lower age in a multivariate analysis. In the overall population, the striatum/occiput ratio was not influenced by these medications since only consensual visual analysis associated with age, sex, and anti-parkinsonian medications, were significant predictors. ***Conclusion:*** This study confirms the potential impact of antidepressant (noradrenergic and specific serotonergic) and opioid (tramadol) medications on semi-quantitative analysis of ^{123}I-FP-CIT SPECT scans. However, the impact of these medications did not influence the interpretation of ^{123}I-FP-CIT SPECT scans, based on visual analysis associated with the already known factors of age, sex and parkinsonian disease status.

OP-455

Disease-tailored z-score cut-offs for striatal binding ratio of DaT SPECT for the diagnosis of Dementia with Lewy Bodies (DLB): a multicenter study

F. Lanfranchi[1,2], *D. Arnaldi*[2,3], *V. Garibotto*[4], *C. Boccalini*[4], *L. Bonanni*[5], *M. V. Mattoli*[6], *V. Costa*[2,3], *S. Raffa*[1,2], *S. Chiola*[1,2], *F. Massa*[2,3], *M. Losa*[2,3], *M. Pardini*[2,3], *G. Frisoni*[7], *N. Nicastro*[8], *G. Sambuceti*[1,2], *M. Bauckneht*[1,2], *S. Morbelli*[1,2];
[1]*Nuclear Medicine Unit, Department of Health Sciences (DISSAL), University of Genoa, Genoa, ITALY,* [2]*IRCCS Ospedale Policlinico San Martino, Genoa, ITALY,* [3]*Department of Neuroscience, Rehabilitation, Ophthalmology, Genetics, Maternal and Child Health (DINOGMI), University of Genoa, Genoa, ITALY,* [4]*Division of Nuclear Medicine and Molecular Imaging, University Hospitals and NIMTLab, Geneva University, Geneva, SWITZERLAND,* [5]*Department of Neuroscience, Imaging and Clinical Sciences, University G. d'Annunzio, Chieti-Pescara, ITALY,* [6]*Nuclear Medicine Unit, Presidio Ospedaliero Santo Spirito, Pescara, ITALY,* [7]*Laboratory of Neuroimaging of Aging (LANVIE), University of Geneva, Geneva, SWITZERLAND,* [8]*Division of Neurorehabilitation, Department of Clinical Neurosciences, Geneva University Hospitals, Geneva, SWITZERLAND.*

Aim/Introduction: There's an emerging evidence about the need to identify disease-specific Z-score (ZS) cut-off for striatal binding ration (SBR) for DLB diagnosis. In a cohort of DLB patients from Genoa, a ZS of -1 for the putamen was identified as the most accurate cut-off to support the differential diagnosis with Alzheimer's Disease (AD). We aimed to assess the accuracy of -1 ZS to support the diagnosis of DLB in an independent sample and in a multicenter setting. ***Materials and Methods:*** Two-hundred patients (150 DLB and 50 AD; age 74.8±8.3 vs. 76.9±6.1; females 48 vs. 27) underwent DaT SPECT in three different European centers. Patients' final clinical diagnosis served as gold-standard (regardless of DaT SPECT results). Age-adjusted ZS of striatum and substriatal regions for both hemispheres were computed with Datquant®, a commercially available software. ROC curve was used to test the accuracy of the previously identified cut-off (-1 ZS) in an independent sample of patients (Chieti and Geneva, 100 DLB and 30 AD) and then in the whole population. Sensitivity (Se), specificity (Sp), positive and negative predictive values (PPV and NPV, respectively), and Youden's index (YI) were calculated and compared to the widely used cut-off of -2 ZS. ***Results:*** In the independent population, the whole putamen of both hemispheres was confirmed as the most accurate parameter for the discrimination between DLB and AD (AUC=0.95 and AUC=0.94 for left and right hemisphere, respectively; p<0.0001 for both), and -1 ZS showed a higher accuracy (Se=0.84, Sp=0.90, PPV=0.97, NPV= 0.63, YI=0.74) with respect to -2 ZS (Se=0.65, Sp=0.93, PPV=0.97, NPV=0.44, YI=0.58). Similarly, the bilateral putamen remained the most accurate parameter to discriminate between DLB and AD (AUC=0.95 and AUC=0.94 for left and right hemisphere, respectively; p<0.0001 for both) in the whole group. Again, a cut-off very close to -1 ZS (-0.96 ZS) resulted more accurate (Se=0.87, Sp=0.92, PPV=0.97, NPV= 0.70, YI=0.79) than -2 ZS (Se=0.69, Sp=0.94, PPV=0.97, NPV=0.51, YI=0.63). ***Conclusion:*** In an independent multi-centric sample, -1 ZS for SBR of both putamen was confirmed as an accurate cut-off to tell apart DLB from AD patients. The experimental exploration of the whole multicenter cohort showed -0.96 ZS for bilateral putamen SBR as the most accurate cut-off for the differential diagnosis between DLB and AD. The use of this less conservative cut-offs provided higher sensitivity than -2 ZS without a measurable loss in specificity.

OP-456

Dopamine dysregulation in depression: a 123I-FP-CIT SPET study

D. Pizzuto[1], *E. Perrone*[1,2], *F. Cocciolillo*[1], *F. Pesaresi*[3,4], *L. Di Benedetto*[3,4], *A. D'Onofrio*[3,4], *G. Camardese*[3,4], *D. Di Giuda*[1,2];
[1]*Nuclear Medicine Unit, Diagnostic Imaging, Radiation Oncology and Hematology Department, Fondazione Policlinico Universitario Agostino Gemelli IRCCS, Rome, ITALY,* [2]*Nuclear Medicine Institute, University Department of Radiological and Hematological Sciences, Università Cattolica del Sacro Cuore, Rome, ITALY,* [3]*Institute of Psychiatry and Psychology, Department of Geriatrics, Neuroscience and Orthopedics, Fondazione Policlinico Universitario Agostino Gemelli IRCCS, Rome, ITALY,* [4]*Department of Psychiatry, Università Cattolica del Sacro Cuore, Rome, ITALY.*

Aim/Introduction: A decrease in dopamine (DA) transmission has long been thought to be involved in the pathophysiology of depression. Preclinical data suggest plastic changes in Dopamine Transporter (DAT) availability depending on striatal DA levels. However, in-vivo evidence from neuroimaging studies in Major Depressive Disorder (MDD) is inconclusive. The aim of this study was to investigate the relationships between striatal DAT availability and psychopathological dimensions of MDD in a large cohort of patients using 123I-FP-CIT SPET. ***Materials and Methods:*** A retrospective study was conducted on 120 drug-free patients (M: 66; mean age: 66±12 years) with a current Major Depressive Episode (MDE) in MDD (DSM-5 criteria) and 62 healthy subjects (M: 29; mean age: 64±14 years) from a previous 123I-FP-CIT SPET database. All depressed patients showed no DAT-SPET alterations and no neurological diseases were diagnosed in the subsequent three-year clinical follow-up. On the same day as SPET, patients underwent a psychiatric interview and psychometric evaluation: the severity of depression symptoms, levels of anxiety, anhedonia and psychomotor retardation were assessed by the Hamilton Depression Rating Scale (HAMD), Hamilton Anxiety Rating Scale (HAMA), Snaith Hamilton Pleasure Scale (SHAPS) and Depression Retardation Rating Scale (DRRS), respectively. SPECT was carried out 3 hours after 148 MBq 123I-FP-CIT intravenous injection. A semiquantitative assessment was performed using SPM and VOI analysis. Specific to non-specific 123I-FP-CIT binding ratios (SBRs) were calculated. ***Results:*** There were no differences in age and gender between patients and healthy subjects. Depressed patients showed decreased DAT availability in the left caudate (p=0.006), right putamen (p=0.001) and left putamen (p=0.008) in comparison with healthy subjects. Inverse correlations were found between the severity of depression symptoms (HAMD total scores) and DAT availability in the right putamen (p=0.042) and left putamen (p=0.003). Anxiety levels (HAMA total scores) inversely correlated with DAT availability in the right putamen (p = 0.042) and left putamen (p = 0.023). Similarly, psychomotor impairment (DRRS total scores) was associated with lower DAT availability in the right putamen (p = 0.032) and left putamen (p = 0.006), whereas levels of anhedonia (SHAPS total scores) inversely correlated with DAT availability in the left putamen (p=0.015). ***Conclusion:*** This study provided evidence for decreased striatal DAT availability in a large cohort of depressed patients, hypothesising a compensatory down-regulation of DAT in response to blunted DA transmission. Our findings are consistent with prior reports of negative associations between striatal DAT availability and psychopathological dimensions of MDD.

OP-457

Comparison of ^{123}I-FP-CIT SPECT and ^{18}F-FE-PE2I PET in patients with parkinsonism and persistent diagnostic uncertainty

M. Dhadamus[1,2], *A. Delva*[3], *W. Vandenberghe*[3], *K. Van Laere*[1,2];
[1]*Division of Nuclear Medicine, University Hospitals Leuven, Leuven, BELGIUM,* [2]*Nuclear Medicine and Molecular Imaging, KU Leuven, Leuven, BELGIUM,* [3]*Neurology, University Hospitals Leuven, Leuven, BELGIUM.*

Aim/Introduction: Imaging of dopamine transporters (DAT) in the brain has shown to be a highly performant tool in the diagnostic work-up of clinically uncertain parkinsonism. DAT SPECT radioligands such as ^{123}I-FP-CIT are widely used in daily clinical practice. Recently, ^{18}FFE-PE2I was introduced as a highly specific alternative for PET. In several patients, despite ^{123}I-FP-CIT imaging, diagnostic uncertainty remains. In this study, we have compared follow-up ^{18}FFE-PE2I PET to previous ^{123}I-FP-CIT SPECT in patients with parkinsonism and persistent diagnostic uncertainty. ***Materials and Methods:*** All subjects who had a ^{18}F-FE-PE2I PET scan between 02/2017 and 03/2023 because of persistent diagnostic difficulties and had already previously undergone ^{123}I-FP-CIT SPECT imaging at our tertiary referral centre were included in this retrospective study. All images were visually assessed by experienced nuclear medicine physicians and classified as normal or abnormal striatal binding. Concordances and discrepancies between both imaging modalities were analysed. ***Results:*** In our database, 46 subjects (26F/20M, 69.1 ± 10.4 years) underwent ^{123}I-FP-CIT SPECT and subsequent ^{18}F-FE-PE2I PET. ^{123}I-FP-CIT SPECT was performed between 2008 and 2022. The average time between ^{123}I-FP-CIT SPECT and ^{18}F-FE-PE2I PET imaging (ΔT) was 2.3 ± 2.3 years (range 0.1 - 11.4 years). Thirty-three subjects (72%) had a concordant result for ^{18}F-FE-PE2I PET and ^{123}I-FP-CIT SPECT, i.e., both modalities classified 24 and 9 participants as abnormal and normal, respectively. By contrast, the results were discrepant in 13 subjects (28%). In 6 subjects (13%), ^{123}I-FP-CIT SPECT was judged to be abnormal, but subsequent ^{18}F-FE-PE2I PET was normal (ΔT= 0.4-7.2 years). In 7 subjects (15%) ^{123}I-FP-CIT SPECT was normal, but ^{18}F-FE-PE2I PET abnormal, which may reflect conversion over the time course (ΔT= 0.5-4.7 years). Visual ^{18}F-FE-PE2I PET assessments agreed with a semiquantitative age-adjusted comparison to an in-house normal dataset in 93% of cases. ***Conclusion:*** In our sample of parkinsonism patients with persistent uncertain clinical diagnosis, 6 out of 30 cases with an abnormal ^{123}I-FP-CIT SPECT scan had qualitatively and quantitatively normal ^{18}F-FE-PE2I PET at follow-up. A semiquantitative correlation analysis of both DAT imaging modalities is underway, but this visual analysis already suggests additional clinical value of ^{18}F-FE-PE2I PET. ***References:*** 1. Delva, A. et al. Quantification and discriminative power of 18F-FE-PE2I PET in patients with Parkinson's disease. EJNMMI 47, 1913-1926 (2020) 2. Marner, L et al. [18F]FE-PE2I PET is a feasible alternative to [123I]FP-CIT SPECT for dopamine transporter imaging in clinically uncertain parkinsonism. EJNMMI Res 12, 56 (2022).

OP-458

Within-subject comparison of ^{11}C-PE2I and ^{18}F-FE-PE2I PET for dopamine transporter availability and relative blood flow measures

M. Jonasson*, L. Appel, S. Roslin, G. Antoni, D. Nyholm, T. Danfors, M. Lubberink;*
Uppsala University, Uppsala, SWEDEN.

Aim/Introduction: PE2I is a PET ligand with high affinity and sensitivity to the dopamine transporter (DAT). It can be labelled with either carbon-11 (^{11}C-PE2I) or fluorine-18 (^{18}F-FE-PE2I) to measure DAT availability in vivo. Relative tracer delivery, as a measure of relative cerebral blood flow (rCBF), can be estimated as well based on a dynamic scan with either of these tracers. At Uppsala University Hospital, ^{11}C-PE2I is used as clinical routine investigation using both DAT-availability and rCBF for differential diagnosis of patients with parkinsonism [1], and so far, more than 1200 patients has been investigated. However, the short half-life of carbon-11 can be a disadvantage making fluorine-18 a more clinically feasible alternative. The aim of this study is to compare ^{11}C-PE2I and ^{18}F-FE-PE2I, regarding DAT-availability and rCBF measures, in the same individuals. ***Materials and Methods:*** Ten healthy controls have been included so far in this ongoing study. They each received an 80 min dynamic ^{11}C-PE2I PET scan and a 60 min dynamic ^{18}F-FE-PE2I scan within one week. Parametric images were generated using a basis function implementation of the simplified reference tissue model, showing binding potential (BP_{ND}) as a measure of DAT-availability, and rCBF. In addition, DAT availability was estimated as the standardized uptake value ratio (SUVR) at a 30-40 min interval. Grey matter cerebellum was used as the reference region. Average regional voxel values were extracted from the parametric images in striatal VOIs (caudate and putamen) and in cortical VOIs (frontal, temporal, parietal and occipital). ***Results:*** High corelation was found for DAT availability between ^{11}C-PE2I and ^{18}F-FE-PE2I in striatum; r=0.85 and 0.79 for BP_{ND} and SUVR-1 respectively. Both BP_{ND} and SUVR-1 values were significantly lower for ^{18}F-FE-PE2I than for ^{11}C-PE2I ($p<0.0001$). Mean BP_{ND} values were 3.16 ± 0.90 for ^{18}F-FE-PE2I and 6.56 ± 1.39 for ^{11}C-PE2I, and mean SUVR-1 values were 3.73 ± 1.05 and 4.84 ± 1.20, respectively. Correlation and agreement were high for rCBF in both striatal VOIs (r=0.95, slope=1.09) and cortical VOIs (r=0.98, slope=1.10). ***Conclusion:*** A strong correlation was seen between the two tracers regarding both DAT availability and rCBF. However, both BP_{ND} and SUVR-1 were significantly lower for ^{18}F-FE-PE2I than ^{11}C-PE2I, which may reduce discrimination between patients with parkinsonism and healthy subjects. More data (controls and Parkinson's disease patients) will be included in the near future. ***References:*** [1] Appel et al. Use of ^{11}C-PE2I PET in differential diagnosis of parkinsonian disorders. J Nucl Med. 2015;56(2), 234-242

OP-459

Relationship between cerebral blood flow and dopamine transporter availability in healthy individuals

M. Jonasson*, L. Appel, S. Roslin, D. Nyholm, T. Danfors, M. Lubberink;*
Uppsala University, Uppsala, SWEDEN.

Aim/Introduction: A dual-biomarker approach with PET, where both blood flow and receptor or transporter availability is assessed from the same scan, can be used for differential diagnosis of patients with neurodegenerative disorders. PE2I is a PET ligand that binds to the dopamine transporters (DAT) and can be label with either carbon-11 or fluorine-18. In a recent study we found a significant correlation between dopamine transporter (DAT) availability and relative tracer delivery (R_1) as a measure of relative cerebral blood flow (rCBF) in striatum with both ^{11}C-PE2I and ^{18}F-FE-PE2I PET [1]. This suggests that a more active dopamine system requires a higher striatal perfusion, or that the activity of the dopamine system is flow limited. However, to date, the relation between DAT availability and absolute blood flow has not been investigated. The aim of this study is to investigate the relation between cerebral blood flow (CBF) and both DAT availability and tracer delivery using ^{15}O-water and ^{18}F-FE-PE2I PET. ***Materials and Methods:*** Ten healthy controls have been included so far in this ongoing study. Each subject underwent a 6-minute dynamic

^{15}O-water PET scan and a 60-minute dynamic ^{18}F-FE-PE2I PET scan. Parametric images showing ^{15}O-water CBF were generated using a single tissue compartment model and rCBF was calculated relative to cerebellar grey matter. ^{18}F-FE-PE2I BP_{ND} and R_1 were generated using a basis function implementation of the simplified reference tissue model using cerebellar grey matter as reference tissue. Average regional voxel values were extracted from striatal VOIs (caudate and putamen) as well as cortical VOIs (frontal, temporal, parietal and occipital). ***Results:*** A significant positive relationship was found between ^{15}O-water CBF and ^{18}F-FE-PE2I BP_{ND} in striatum (r=0.68, p<0.0001). A strong correlation was also seen between ^{15}O-water rCBF and BP_{ND} (r=0.78, p<0.0001). When comparing the relative measures ^{15}O-water rCBF and ^{18}F-FE-PE2I R_1, the correlation in the striatal region was high (r=0.87, p<0.0001) but only moderate in the cortical regions (r=0.65, p<0.0001) due to the narrow range of the cortical R_1 values. ***Conclusion:*** These results indicate an association between DAT availability and absolute blood flow in striatum and confirms that relative tracer delivery correlates to relative blood flow. More data (controls and Parkinson's disease patients) will be included in the near future. ***References:*** [1] Jonasson et al. Striatal dopamine transporter and receptor availability correlate with relative cerebral blood flow measured with [^{11}C]PE2I, [^{18}F]FE-PE2I and [^{11}C]raclopride PET in healthy individuals. J Cereb Blood Flow Metab. 2023, in press

OP-460

FDG-PET related pattern expression and survival in Parkinson's disease

G. Martí-Andrés[1], *V. Betech*[2], *E. Prieto*[2], *C. Espinoza-Vinces*[2], *M. Riverol*[2], *M. Luquin*[2], *J. Arbizu*[2];
[1]*Hospital Universitario de Navarra, Pamplona, SPAIN,*
[2]*Clínica Universidad de Navarra, Pamplona, SPAIN.*

Aim/Introduction: Aim: To assess FDG-PET metabolic findings as a possible risk factor of mortality in a cohort of patients with a clinical diagnosis of Parkinson's disease (PD). Background: Many studies have revealed clinical factors associated with a higher risk of mortality in PD patients however, it is less known about the impact of FDG-PET findings on survival. ***Materials and Methods:*** We performed a retrospective cohort study and included a total of 114 patients with a final clinical diagnosis of PD according to the MDS-PD criteria, who were referred for an FDG-PET scan throughout the disease course. We performed a systematic review of medical charts and obtained clinical and FDG-PET variables, including the date of death or last follow-up visit date in subjects who were alive in December 2022. We included the individual expression of a predefined PD-related pattern (PDRP)[1] obtained using a multivariate Scaled Subprofile Model/Principal Component Analysis (SSM/PCA) into FDG-PET scans. A Kaplan-Meier test was performed to calculate the median of survival. The risk of death in PD patients was calculated using a Cox proportional hazard model in univariate analysis. Moreover, we analyzed the impact on the risk of death at the time of onset of preselected clinical milestones. ***Results:*** PD patients were followed up for a median of 13 years when a total of 30 PD patients died. The median survival was 26.9 years. Higher PET-FDG PDRP expression, increased age at disease onset, presence of dysphagia in the first 5 years, and lower disease duration at PET were independent risk factors of mortality [Table 1]. ***Conclusion:*** A more severe FDG-PET PDRP, older age at onset, and early appearance of dysphagia have a negative impact on survival in PD patients. ***References:*** [1] Martí-Andrés, G., et al. Clinical correlates of Parkinson's disease metabolic pattern: not only a diagnostic tool. 25th international congress of Parkinson´s disease and movement disorders. MDS virtual congress 2020.

OP-461

Identification of Synaptic Alterations in Idiopathic REM Sleep Behavior Disorder: A Preliminary Study using ^{18}F-SynVesT-1 PET/CT Imaging

J. Li[1], *J. Huang*[2], *J. Guo*[2], *S. Hu*[1];
[1]*1.Department of Nuclear Medicine (PET Center), Xiangya Hospital Central South University, Changsha, CHINA,* [2]*1.Department of Neurology, Xiangya Hospital Central South University, Changsha, CHINA.*

Aim/Introduction: Idiopathic Rapid Eye Movement (REM) Sleep Behavior Disorder (RBD) is a parasomnia characterized by abnormal motor movements during REM sleep, which has been linked to neurodegenerative diseases such as Parkinson's Disease (PD), Dementia with Lewy bodies (DLB), and Multiple System Atrophy (MSA). Previous research shows that individuals with idiopathic RBD demonstrate disruptions in brain regions associated with sleep-wake regulation and motor control. Synaptic loss is an early indication of many neurodegenerative conditions, and Positron Emission Tomography (PET) imaging of synaptic vesicle glycoprotein 2A (SV2A) could serve as a promising biomarker of synaptic density. This study aims to use ^{18}F-Synaptic Vesicles Transporter-1 (^{18}F-SynVesT-1) PET/CT imaging to determine whether synaptic loss occurs in patients with idiopathic RBD. ***Materials and Methods:*** In this study, we recruited 7 participants diagnosed with idiopathic RBD (mean age 57 years, range 41-68 years; 6 males, 1 female) and 10 healthy controls (mean age 57 years, range 47-69 years; 5 males, 5 females). All subjects underwent ^{18}F-SynVesT-1 PET imaging and 3D-T1-weighted structural magnetic resonance imaging (MRI). The T1-weighted images were used for accurate PET spatial normalization, and regions of interest (ROIs) were defined using the Anatomical Automatic Labeling (AAL) 3 template in Montreal Neurological Institute (MNI) standard space. The standardized uptake value ratio (SUVR) relative to centrum semiovale was computed and used to compare the SUVRs of the RBD and healthy control groups using a two-sample t-test. ***Results:*** Compared with healthy individuals, RBD patients demonstrated significant decreases in ^{18}F-SynVesT-1 uptake in regions of the brain involved in sleep regulation, such as the locus coeruleus (mean SUVR 1.66 versus 1.80, p=0.049), ventral tegmental area (mean SUVR 1.44 versus 1.66, p=0.008), and pons (mean SUVR 1.15 versus 1.25, p=0.039). The nigrostriatal pathway, which is associated with the motor symptoms of Parkinson's disease, also exhibited reduced 18F-SynVesT-1 uptake in RBD patients, including the substantia nigra (mean SUVR 1.53 versus 1.69, p=0.03) and Putamen (mean SUVR 4.40 versus 4.78, p=0.036). ***Conclusion:*** This study provides the first evidence of synaptic loss in brain regions that regulate sleep and motor control in living patients with idiopathic RBD. Our findings suggest that ^{18}F-SynVesT-1 PET imaging could serve as a new biomarker for early detection and monitoring of neurodegeneration in this population. However, larger sample size studies

OP-462

Neurobiological dysfunctional substrates for the self-medication hypothesis in adult individuals with ADHD and cocaine use disorder: an18F-FDG PET study

A. Martini[1], *G. Carli*[2], *M. Bruscoli*[3], *L. Presotto*[4], *C. Mazzeo*[1], *S. Sestini*[1], *D. Perani*[5];
[1]*Unit of Nuclear Medicine, Department of Diagnostic Imaging, N.O.P. - S. Stefano, U.S.L. Toscana Centro, Prato, ITALY,* [2]*Department of Nuclear Medicine and Molecular Imaging, University Medical Center Groningen, Groningen, NETHERLANDS,* [3]*UFC Farmacotossicodipendenze, Department of Drug Addiction, N.O.P. - S. Stefano, U.S.L. Toscana Centro, Prato, ITALY,* [4]*Department of Physics G. Occhialini, Università degli Studi di Milano Bicocca, Milano, ITALY,* [5]*In vivo human molecular and structural neuroimaging Unit, Division of Neuroscience, IRCCS San Raffaele Scientific Institute;*
NuclearMedicine Unit, San Raffaele Hospital, Milano, ITALY.

Aim/Introduction: Attention-deficit hyperactivity disorder (ADHD) in adulthood shows high co-occurrence rates with cocaine use disorder (CoUD). The self-medication hypothesis (SMH) provides a theoretical explanation for this comorbidity. This study investigates the neurobiological mechanisms that could support SMH in adult patients with ADHD-CoUD. ***Materials and Methods:*** We included 19 ADHD-CoUD (84.2% male; age: 32.11 [7.18]) and 16 CoUD (68.7% male; age: 36.63 [8.12]). All subjects underwent an ^{18}F-FDG-PET brain scan. We tested brain metabolism differences between ADHD-CoUD and CoUD patients using voxel-based and regions of interest (ROIs)-based analyses. The correlation between dependence/abstinence duration and regional brain metabolism was also assessed in the two groups. Lastly, we investigated the integrity of brain metabolic connectivity of mesocorticolimbic and nigrostriatal dopaminergic systems, and large-scale brain networks involved in ADHD and addictions. ***Results:*** The voxel-wise and ROIs-based approaches showed that ADHD-CoUD patients had a lower metabolism in the thalamus and increased metabolism in the amygdala and parahippocampus, bilaterally, compared to CoUD subjects and HC. Metabolism in the thalamus negatively correlated with years of dependence in ADHD-CoUD patients. Moreover, connectivity analyses revealed that ADHD-CoUD had a more preserved metabolic connectivity than CoUD in the dopaminergic networks and large-scale networks involved in self-regulation mechanisms of attention and behaviours (i.e., ADMN, ECN, SAN). ***Conclusion:*** We demonstrated distinct neuropathological substrates underlying substance-use behaviours in ADHD-CoUD and CoUD. Furthermore, we provided neurobiological evidence in support of SMH, demonstrating that ADHD-CoUD might experience short-term advantages of cocaine assumption (i.e., compensation of dopaminergic deficiency and related cognitive-behavioural deficits).

1008

Monday, September 11, 2023, 15:00 - 16:30
Hall F2

Joint Symposium 3 - Translational Molecular Imaging & Therapy Committee + Oncology & Theranostics + Physics / EAU: Metastases Directed Prostate Cancer Surgery - Translational Challenges and Possibilities

OP-463
Surgical removal of nodal metastases in prostate cancer, what is the clinical value?
E. Mazzone;
Dept. of Urology, San Raffaele Scientific Institute, URI - Urological Research Institute, Milan, ITALY.

OP-464
Translation and implementation of (radio)tracers for nodal management of prostate cancer
T. Buckle;
Leiden University Medical center, Radiology, Leiden, NETHERLANDS.

OP-465
An engineers overview of radioguided surgery modalities that support targeted nodal dissections in the pelvis
T. Wendler;
Technical University Munich, CAMP, Munich, GERMANY.

OP-466
State of the art in PSMA-guided surgery
S. Knipper;
Vivantes Klinikum am Urban, Urology, Berlin, GERMANY.

1009

Monday, September 11, 2023, 3:00 PM - 4:30 PM
Hall G2

e-Poster Presentations Session 7 - Cardiovascular Committee: Cardiovascular Imaging e-Posters

EPS-126
Positron Range Correction for ^{82}Rb myocardial PET: Validation in a healthy cohort
M. Lassen[1,2], *H. Kertesz*[3], *I. Rausch*[4], *A. Kjaer*[1,2], *V. Panin*[5], *D. Bharkhada*[5], *R. DeKemp*[6], *T. Beyer*[4], *P. Hasbak*[1];
[1]Department of Clinical Physiology and Nuclear Medicine, University Hospital Copenhagen – Rigshospitalet, Copenhagen, DENMARK, [2]Cluster for Molecular Imaging, Department of Biomedical Sciences, Faculty of Health and Medical Sciences, University of Copenhagen, Copenhagen, DENMARK, [3]Image X Institute, Faculty of Medicine and Health, The University of Sydney, Sydney, AUSTRALIA, [4]QIMP Team, Center for Medical Physics and Biomedical Engineering, Medical University of Vienna, Vienna, AUSTRIA, [5]Siemens Medical Solutions UNITED STATES OF AMERICA, Inc, Knoxville, TN, UNITED STATES OF AMERICA, [6]National Cardiac PET Centre, University of Ottawa Heart Institute, Ottawa, ON, CANADA.

Aim/Introduction: To assess the feasibility of applying a positron-range (PR) correction (PRC) method for routinely acquired myocardial perfusion imaging (MPI) employing ^{82}Rb PET. ***Materials and Methods:*** The PRC was implemented into the vendor-based image reconstruction algorithm as a blurring kernel applied to the image estimate during iterative reconstruction. A spatially variant and tissue-dependent PR-kernel was generated for every voxel. The PR-kernels were composed of simulated uniform PR distributions (within lung, water, and bone densities) based on the underlying tissue compositions derived from the attenuation correction map. The PRC method was evaluated in 25 healthy volunteers (11F/14M, mean age 23-y) who underwent serial rest/stress ^{82}Rb MPI sessions on the Siemens Biograph mCT system. Static and 8-ECG gated reconstructions (employing a 400x400x109 matrix, PSF+TOF + 5mm post-filter), with and without PRC (PRC (3iterations, 21 subsets) and Standard (2iterations, 21 subsets), respectively; of note, PRC was optimized to compare the results), were evaluated in this study. We report changes in the signal-to-noise ratio (SNR) and contrast-to-noise ratio (CNR) for the static images. Further, for the ECG-gated reconstructions, we evaluated the changes introduced in end-diastolic and systolic volumes (EDV and ESV, respectively), the stroke volume (SV), the left ventricular ejection fraction (LVEF), and the LVEF reserve (stress-rest LVEF) in QPET (Cedars-Sinai). Finally, we evaluate the test-retest repeatability coefficients (Bland-Altman method) for the volumetric assessments. ***Results:*** Image quality of static

reconstructions improved for both rest and stress MPI following PRC (%-change (Rest/Stress): (25±22)%/(34±30)% (SNR) and (35±27)%/(41±34)% (CNR), all p<0.05. When correcting for the PR, EDV and ESV increased (EDV change (Rest/Stress) [mL]: (9±5) / (4±3), (PRC volumes = (110±32) / (131±37)); ESV change (Rest/Stress) [mL]: (9±7) / (9±3), (PRC volumes = (53±24) / (47±22)), all p<0.0001). However, PRC did not change SV during resting conditions (SV change (Rest/Stress) [mL]: (-1±5) / (-5±9), (PRC volumes = (57±10) / (84±17)), p=0.61 and 0.015, respectively). PRC significantly reduced the LVEF without affecting the LVEF reserve (LVEF [%] (Rest/Stress): Standard = (58±7) / (72±7), PRC = (54±9) / (66±7), both p< 0.001, LVEF Reserve: Standard = (13±3), PRC = (12±4), p=0.05). Excellent repeatability coefficients are reported for all volumetric assessments with test-retest variations <7% for both the standard and PRC reconstructions. ***Conclusion:*** In a cohort of healthy volunteers, PRC significantly improves SNR and CNR and changes the majority of the volumetric assessments without affecting the repeatability measures. Follow-up studies in patient cohorts are planned.

EPS-127

Metabolic pretest calculator to improve cardiac FDG PET/CT imaging

S. Hartikainen[1], *T. Tompuri*[1], *T. M. Laitinen*[1], *T. Laitinen*[1,2];
[1]*Kuopio University Hospital, Kuopio, FINLAND,*
[2]*University of Eastern Finland, Kuopio, FINLAND.*

Aim/Introduction: Poor myocardial glucose metabolism suppression (MGS) may hamper differentiation between cardiac inflammatory manifestations and physiological 18F-FDG uptake. Even a strict one or two-day ketogenic diet (KD) and prolongated fasting with or without heparin premedication doesn't always induce adequate MGS. This may lead to additional imaging or myocardial biopsies. The aim of our study was to develop a pretest probability calculator of adequate MGS based on medical history, body composition and β-hydroxybutyrate (BHB) level. ***Materials and Methods:*** We recruited 193 adults (95 female), median age 66 years (19-87), with any clinical indication for whole body 18F-FDG-PET/CT. 62 patients followed KD 1-2 days before scan and had fasted for at least 12 hours. Blood glucose and β-hydroxybutyrate (BHB) level were measured with a point-of-care device. Electronic health record was searched for the presence of previously diagnosed diseases, including diabetes and hypertension, and use of sodium-glucose transport 2 inhibitor (SGLT2i) medication. Liver and spleen attenuation in a low-dose CT were measured to assess the presence of fatty liver. Adequate MGS was defined as myocardial uptake below left ventricular blood pool. Correlations between MGS and metabolic factors were calculated. Logistic regression analysis was performed using the variables that showed statistically significant correlation. The ability of BHB test and pretest calculator to predict MGS was evaluated with ROC analysis. ***Results:*** Median BMI was 26.9 (range 17.0-55.2), median SUV 1.75 (0.72-19.10) and BHB 0.2 (0.0-5.1) mmol/l. Youden index suggested a cut-off of 0.35 mmol/l for BHB. For patients with low BHB, adequate MGS was seen more often in patients with diabetes (p = 0.003), obesity (p = 0.002) or fatty liver (p = 0.002). Using information attainable before imaging and logistic regression analysis, the most prominent variables to predict MGS were BHB (B = -2.463, p < 0.001) and KD (B = -1.484, p = 0.001), followed by diabetes (B = -1.744, p = 0.003) and obesity (B = -1.237, p = 0.018). We found a tendency towards SGLT2i usage to predict MGS (B = -0.979, p = 0.238). We thereby created a pretest calculator of inadequate MGS. AUC for pretest calculator is 0.857 and for BHB alone 0.802. ***Conclusion:*** BHB measured with a point-of-care device is useful in predicting MGS. Using information attainable before imaging, a pretest calculator may further increase patient-to-patient customization of preparation protocol to ensure proper diagnostics or exclusion of an inflammatory cardiac disease.

EPS-128

Diagnostic accuracy of global parameters obtained during dynamic PET/CT with 13N-Ammonia and vasodilator stress in patients with triple-vessel stenotic lesion of coronary arteries and stable form of CAD

A. Shakhova*, E. Golukova, I. Aslanidis, I. Shurupova, N. Surkova, M. Rumyantseva, I. Ekaeva;*
A.N. Bakulev Scientific Center for Cardiovascular Surgery of the Ministry of Health of the Russian Federation, Moscow, RUSSIAN FEDERATION., Moscow, RUSSIAN FEDERATION.

Aim/Introduction: Balanced ischemia with triple vessel (3v) coronary artery disease (CAD) is difficult to diagnose with semiquantitative myocardial perfusion imaging (MPI).The aim was to find out the features of 3v CAD by means of global parameters derived from dynamic PET combined with computer tomography (PET/CT) in patients with a stable form of CAD ***Materials and Methods:*** 135 patients with known CAD and angiographic narrowing >70% in at least of one (of the major) coronary artery were enrolled: 13 - with 3V CAD, 122 - one or two-vessel CAD; 54 had chronic total occlusions (CTO). PET/CT with 13N-ammonia at rest and after adenosine stress test was performed in dynamic mode. The global summed stress and difference score (SSS and SDS respectively) were calculated. Myocardial blood flow (MBF) at rest and stress, myocardial flow reserve (MFR) were quantified. ***Results:*** Patients with 3v CAD had significantly increased SRS, SSS, and SDS compared to patients without it: 4.0 (2.0; 6.0) versus 1.0 (0.0; 3.0), 22.0 (17.0; 27.0) versus 9.0 (4.3; 16.0) and 19.0 (15.0; 21.0) versus 7.0 (3.0;13.0),respectively (p<0.001). There was similar resting MBF between patients with and without 3v CAD: 0.92 (0.87; 0.98) versus 0.83 (0.79; 0.92) ml/g/min (p=0.198), but significantly lower stress MBF of 1.29 (1.19; 1.51) versus 1.89 (1.64; 2.31) ml/g/min, and simillary lower MFR of 1.6 (1.5; 2.1) versus 2.6 (2.1; 3.0), (p<0.001). The prevalence of CTOs was highter in 3v group: 77% (n=10) versus 35% (n=43), p=0,003. The discriminant function to expect 3-vessel CAD was: for SSS AUC 0,858 (p<0,001) with cutoff >13 (sensitivity (Se), specificity (Sp), positive predictive value (PPV), negative predictive value (NPV) and diagnostic accuracy (DA) of 92%, 60%, 20%, 99% и 63%, respectively; for SDS AUC = 0.834 (p<0.001) with cutoff >15 (77%, 83%, 32%, 97% и 82% respectively). For absolute values AUCs with optimal cutoff were: MBF < 1.51 ml/g/min and AUC 0.787 (p<0.001) (Se, Sp, PPV, NPV and DA were 77%, 86%, 37%, 97% and 85%, respectively); MFR < 1,8 and AUC 0,843 (p<0.001) (69%, 93%, 53%, 97% и 91% %, respectively). ***Conclusion:*** MFR showed the highest accuracy in identifying 3V CAD due to a high specificity of 93% and allowable sensitivity of 69%. The high sensitivity of the SSS in is associated with the widespread of CTOs which leads to a more pronounced "heterogeneity" of perfusion severity, practically excluding the presence of "balanced" ischemia.

EPS-129

Does global value of myocardial flow reserve using 13N-ammonia positron emission tomography independently predict identification of multivessel coronary artery disease

A. Shakhova*, E. Golukhova, I. Aslanidis, I. Shurupova, N. Surkova, M. Rumyantseva, I. Ekaeva;*
A.N. Bakulev Scientific Center for Cardiovascular Surgery of the Ministry of Health of the Russian Federation, Moscow, RUSSIAN FEDERATION.

Aim/Introduction: Standard relative myocardial perfusion imaging (MPI) is widely used for the assessment of obstructive coronary artery disease (CAD), but when multivessel (MV) CAD is present,

total perfusion defect (PD) scoring can lead to underestimation of degree of obstructive atherosclerotic burden. The aim of this study was to assess whether assessment of global myocardial flow reserve (MFR) measured with 13N-ammonia PET is an independent predictor of severe MV CAD. ***Materials and Methods:*** In this study 135 consecutive patients with available 13N-ammonia PET within 3 months of invasive coronary angiography (ICA) and no cardiac events between them were included. 87 patients had significant single-vessel, 48 had two- or three-vessel lesion, (64.1 ± 10.3 years, 75% men), those with myocardial scar, history of coronary artery bypass graft (CABG), severe valvular disease and ejection fraction < 40% were exclude. PET/CT with 13N-ammonia at rest and after adenosine stress test was performed in dynamic mode. The global summed stress score (SSS) was derived, quantitative values of myocardial blood flow (MBF) at rest and stress, with subsequent calculation of myocardial flow reserve (MFR) was made. The presence or absence of transient ischemic dilatation (TID) on visual analysis was also noted. ECG was monitored continuously during adenosine stress for ST-depression. Crude odds ratio (COR) and adjusted odds ratio (AOR) were calculated from regression coefficients. ***Results:*** On univariable analysis MFR (COR: 0.15 (95% CI: 0.07-0.32, p<0.001) and SSS (COR: 1.12 (95% CI: 1.07-0.19, p<0.001), as well as ST-depression during stress test (COR: 5.46 (95% CI: 1.61-18.52, p=0.006) were associated with MV CAD, while TID was not (p=0,678). The multivariable analysis suggests that MFR and SSS independently predicts MV CAD after considering significant confounders mentioned above: AOR: 0.23 (95% CI: 0.10-0.54, p<0.001) and 1.09 (95% CI: 1.02-1.16, p=0.007) respectively. ***Conclusion:*** The global MFR is a strong predictor of MV CAD and further facilitates the identification detection of "hight risk" CAD. A 1.0 unit reduction in MFR, increases the likelihood MV CAD by 6.8 times. The traditional non-parametric predictors of MV CAD didn't demonstrate diagnostic capability in the presence of parametric PET/CT indices.

EPS-130

Defining a Significant Change with serial assessment of myocardial perfusion metrics, obtained during dynamic Positron Emission Tomography with 13 N-Ammonia in patients with CAD

A. Shakhova*, E. Golukhova, I. Aslanidis, I. Shurupova, M. Rumyantseva, N. Surkova, I. Ekaeva;*
A.N. Bakulev Scientific Center for Cardiovascular Surgery of the Ministry of Health of the Russian Federation, Moscow, RUSSIAN FEDERATION.

Aim/Introduction: Serial perfusion assessment is attractive for clinical status evaluation in patients with stable coronary artery disease (CAD). The aim was to determine the direction and magnitude of change of global parameters obtained during dynamic positron emission tomography (PET/CT) in patients receiving optimal medical therapy (OMT) of CAD alone. ***Materials and Methods:*** In total 26 patients with known or suspected CAD were retrospectively enrolled (59.1 ± 12.8 years, 66% men) who did not underwent coronary revascularization between routine serial dynamic PET/CT scans. The median interval between baseline and follow-up PET scans was 18 (12.0; 36.8) months with no cardiac events between them. PET/CT with 13N-ammonia at rest and after adenosine stress test was performed in dynamic mode. The global summed stress score (SSS), summed rest score (SRS), and summed difference score (SDS) were calculated. Based on the obtained global quantitative values of myocardial blood flow (MBF) at rest and stress, myocardial flow reserve (MFR) was quantified. The rate pressure product was calculated by multiplication of systolic pressure with heart rate. ***Results:*** There was not significant difference between serial PET MPI measurement: for SRS 2.0 (1.0; 4.0) at baseline versus (vs) 2.0 (0,0; 5.0) at follow-up (p=0.612), for SSS 7.0 (3.0; 12.3) at baseline vs 6.5 (3.0; 11.3) at follow-up (p=0.809) and for SDS 4.5 (0.0; 7.3) at baseline vs 4.0 (2.0; 6.5) at follow-up (p=0.617). Within absolute MBF values there was not significant difference for MBF at rest and stress: 0.81 (0.63; 1.04) vs 0.80 (0.63; 0.92) mg/l/min (p=0.328) and 2.08 (1.80; 2.38) vs 2.17 (1.95; 2.37) mg/l/min respectively. Significant improvement of global MFR, however, was observed in 19 (73%) cases, with increasing from 2.5 (2.2; 3.0) to 3.1 (2.4; 3.5) (p=0.017). The rate pressure product (RPP) at follow-up was lower than at the baseline: 9878 (8231; 11765) vs 11024 (7551; 14023). Mean difference in MFR was 0.27+/-0.67 (25%+/-17). ***Conclusion:*** Observed improvement of global MFR is probably due to individual variability in RPP and, as a consequence, MBF at rest between two PET/CT examinations, and is not suitable by oneself for the assessment in MBF changes in patients on OMT alone. We should be more careful when drawing the conclusion about the improvement of MBF based only on global MFR metrics with expected variability about 25%, if evaluation of serial studies is necessary.

EPS-131

Relationship between myocardial flow reserve measured by a dynamic cadmium-zinc-telluride camera and increase rate in myocardial uptake of radionuclide during exercise

T. Niimi[1]*, K. Hirayama*[1]*, S. Yoshida*[2]*;*
[1]*Japanese Red Cross Aichi Medical Center Nagoya Daini Hospital, Nagoya, JAPAN,* [2]*Nagoya University, Nagoya, JAPAN.*

Aim/Introduction: A cadmium-zinc-tellurium (CZT) camera can simultaneously evaluate myocardial flow reserve (MFR) and perform myocardial perfusion imaging. Therefore, unlike conventional single-photon emission computed tomography (SPECT) cameras, it can detect the presence of multi-vessel coronary artery disease (CAD) without underestimating it. However, obtaining MFR measurements by routine SPECT examination is difficult. To determine if the increase rate could be an alternative in the absence of MFR measurements, we examined the relationship between MFR measured simultaneously with a dynamic CZT camera and the increase rate in myocardial radionuclide uptake during exercise. ***Materials and Methods:*** We evaluated 40 patients with suspected or known CAD who underwent dynamic CZT SPECT after injection of 250 MBq and 820 MBq of 99mTc-sestamibi for rest and stress imaging, respectively. Radionuclide was injected at 1 ml^3/s using an automatic injector and flushed with 30 ml of saline. Dynamic CZT SPECT imaging data for calculating MFR was net-retention analyzed using commercially available software. An increase of radionuclide uptake in myocardial during exercise was defined as an increase rate, and CAD detection was tested from myocardial perfusion imaging. An increase rate was calculated as an exercise image/rest image normalized by dose. ***Results:*** Comparing the global CAD diagnostic performance of MFR and increase rate, the area under the receiver operating characteristic curve was 77% for MFR and 58% for increase rate (p=0.114, cutoff value of MFR was 2.68 and increase rate was 1.31). However, in cases of three-vessel lesions (2 of 40 cases), which were difficult to evaluate with relative distribution images, both showed lower than the cutoff value (MFR: 1.23 ± 0.37, increase rate: 0.82 ± 0. 28) and assisted diagnosis. ***Conclusion:*** The relationship between MFR measured by a dynamic CZT camera and the increase rate

in myocardial uptake of radionuclide during exercise was verified. Although the global CAD diagnostic performance of the increase rate was lower than that of the MFR, the detection accuracy was similar to that of MFR in cases of three-vessel lesions that were difficult to assess on relative distribution images. The increased rate of myocardial uptake of radionuclide during exercise may provide additional information to myocardial perfusion imaging, such as the diagnosis of multi-vessel lesions, even when MFR measurements are not possible.

EPS-132

Stress-only versus rest-stress SPECT MPI in the detection and diagnosis of myocardial ischemia and infarction by machine learning

F. Wang[1], *H. Yuan*[1], *L. Jiang*[1,2];
[1]*PET Center, Department of Nuclear Medicine, Guangdong Provincial People's Hospital (Guangdong Academy of Medical Sciences), Southern Medical University, Guangzhou, CHINA,*
[2]*Guangdong Provincial Key Laboratory of Artificial Intelligence in Medical Image Analysis and Application, Guangzhou, CHINA.*

Aim/Introduction: To investigate the performance of stress-only versus rest-stress SPECT myocardial perfusion imaging (MPI) in detecting and diagnosing myocardial ischemia and infarction by machine learning (ML). ***Materials and Methods:*** 276 patients with suspected coronary artery disease (CAD) were randomly divided into training (184 patients) and test (92 patients) cohorts. Variables extracted from clinical, physiological, and rest-stress SPECT MPI were screened. Stress-only and rest-stress MPI using ML were established and compared using the training cohort. Then the diagnostic performance of two models in diagnosing myocardial ischemia and infarction was evaluated in the test cohort. ***Results:*** Using 6 ML algorithms, stress-only MPI models were constructed entering summed stress score (SSS), summed wall thickness score of stress% (sSTS%), and end-diastolic volume of stress (sEDV). Stress-only MPI performed equally good as rest-stress MPI in detecting myocardial ischemia and infarction (area under the curve [AUC] using logistic regression [LR] model: 0.863 vs. 0.877, P=0.519). Furthermore, using ML models, stress-only MPI showed a reasonable prediction of reversible deficit as shown by rest-stress MPI (AUC using LR model: 0.861). Subsequently, predictive nomograms for myocardial ischemia and reversible perfusion deficit using the above-identified variables in the stress-only MPI were constructed, which showed good discrimination in the training and test cohorts. ***Conclusion:*** Stress-only MPI demonstrated similar diagnostic performance compared with rest-stress MPI using 6 ML algorithms. ML models based on stress-only MPI might replace rest-stress MPI to differentiate the reversibility of perfusion deficit, and hence ischemia from scar.

EPS-133

A Meta-Analysis of Bone Tracer Scintigraphy in the Diagnosis of Cardiac Amyloid ATTR and Al, Comparing HMDP with DPD and PYP Sensitivity and Specificity in Biopsy Proven Cases

A. ALDEHLAUI[1,2], *C. Fowler*[2];
[1]*King Abdullah Medical City, Makkah, SAUDI ARABIA,*
[2]*King's College London, London, UNITED KINGDOM.*

Aim/Introduction: Cardiac amyloidosis (CA) is an underdiagnosed cause of heart failure with preserved ejection fraction. Two types of cardiac amyloidosis, transthyretin (ATTR) and light-chain (AL), are treated differently. Both ^{99m}Tc-DPD and ^{99m}Tc-PYP scintigraphy already have well-established roles in diagnosing ATTR and differentiating it from AL CA. ^{99m}Tc-HMDP is another radiopharmaceutical that has been studied for the same purpose and acknowledged by the ASNC and EANM guidelines but has no clear established role in this clinical context yet. To the best of our knowledge, there is no published review comparing HMDP to DPD or PYP in the same cohort. The study aims to systematically assess and validate the diagnostic sensitivity and specificity of^{99m}Tc-HMDP whole-body planar scintigraphy in biopsy-proven ATTR CA studies of patients compared to DPD and PYP as a meta-analysis. ***Materials and Methods:*** AA comprehensive online literature search using PubMed, Embase, and Medline databases of studies on HMDP, DPD, and PYP imaging diagnostic values in cardiac amyloidosis was conducted in 2021 to identify high-quality studies on cardiac amyloidosis in single-photon imaging and diagnosis based on HMDP, DPD, and PYP radiopharmaceuticals. The relevant identified studies were filtered based on biopsy-proven patients who had undergone bone scintigraphy, including 20 subjects or more, patients' medical history must be free of other myocardiopathies, and tracer related specificities and sensitivities to distinguish ATTR CA from AL. Then the quality of the studies was assessed using NIH Quality Assessment Tool for Before-After (Pre-Post) Studies With No Control Group. Finally, the mean sensitivity and specificity of nuclear bone scintigraphy in the differentiation of ATTR from AL amyloidosis were calculated from the selected studies for the three tracers. ***Results:*** Eight selected studies were identified on HMDP, DPD, and PYP bone scintigraphy in cardiac amyloidosis, including 868 biopsy-proven patients that were included in the meta-analysis, provided the following ***results:*** the pooled and calculated sensitivity for ATTR of HMDP, DPD, and PYP is 98.3%, 99.6% and 97.4%; and specificity 98.6%, 87.6% and 93.8% respectively. The sensitivity of the tracers in diagnosing AL was 5.0%, 41.3%, and 35.0%, and specificity was 2.0%, 12.8%, and 8.3%, respectively. ***Conclusion:*** A meta-analysis of the literature shows HMDP has equivalent sensitivity and higher specificity in comparison with DPD and PYP for diagnosing ATTR cardiac amyloidosis.

EPS-134

CT-free attenuation correction for cardiac-dedicated CZT SPECT: preliminary results of the CASCTEC study

M. Hesse, *B. El Jari, F. Dupont, O. Gheysens, R. Lhommel, V. Roelants;*
Cliniques Universitaires Saint-Luc, Brussels, BELGIUM.

Aim/Introduction: It is known that attenuation-correction (AC) improves the diagnostic accuracy of myocardial perfusion scintigraphy (MPS) for detecting coronary artery diseases (CAD). However, most clinical cardiac-dedicated CZT cameras are not equipped with a CT to reduce costs and footprint. Therefore, the CASCTEC clinical study aims at developing an approach to generate AC images from emission scans only on a pinhole CZT camera, without the need for CT. ***Materials and Methods:*** CASCTEC is a single-center prospective study enrolling patients referred for MPS. Two-day stress/rest myocardial SPECT imaging was performed on a pinhole CZT camera. A standard of care (SOC) 5-10 minute acquisition was immediately followed by an additional 5-minute acquisition after retracting the detectors without moving the patient. Subsequently all patients underwent SPECT/CT imaging serving as reference. The acquisition with retracted detectors allowed to delineate the patient body contour, and together with the SOC acquisition, enabled the segmentation of soft and lung tissues to generate an attenuation map. Non-corrected (NC) and AC pinhole CZT images were compared among themselves and

against the SPECT/CT images using the AHA 17-segment model and visual evaluation of stress and rest summed scores. ***Results:*** 12 patients have been included until March 2023. CASCTEC-AC stress and rest perfusion images showed a more homogeneous tracer distribution, especially in the inferior wall, similar to the reference. All perfusion defects observed on the SPECT/CT-AC images were also visible on CASCTEC-AC images. The mean visual summed score for AC images was 17.7±3.8 for CASCTEC and 19.9±4.5 for SPECT/CT (p=0.002). The CASCTEC mean relative uptake increased by up to 30% in the inferior segments compared to the NC image. Changes by less than 10% were observed for all other segments, except for the apical segment that decreased by up to 30%. The differences of the changes in summed scores from NC to AC between CASCTEC and SPECT/CT images were -0.5±5.2 (p=0.37) and 0.5±3.6 (p=0.35), respectively for stress and rest scans. ***Conclusion:*** These preliminary results show that the CT-free patient-specific attenuation map enhances NC perfusion in the inferior wall similarly to CT-based AC images from a SPECT/CT acquisition. This method might enhance the diagnostic accuracy of current cardiac pinhole CZT systems for detecting obstructive CAD but further studies are warranted.

EPS-135

The effect of Ursodeoxycholic Acid on early hepatic clearance of 99mTc-sestamibi in patients undergoing myocardial perfusion scintigraphy

E. Hosseinzadeh*, M. Ghodsirad, H. Garavand;*
Nuclear medicine department, shohadaye tajrish hospital, Shahidbeheshti university, Tehran, IRAN, ISLAMIC REPUBLIC OF.

Aim/Introduction: The aim of this study is to investigate the effect of Ursodeoxycholic Acid (UDCA) on hepatic clearance of 99mTc-sestamibi in patients undergoing myocardial perfusion scintigraphy (MPS). 99mTc-sestamibi is a commonly used radiopharmaceutical that is used in MPS to assess myocardial blood flow. However, the clearance of 99mTc-sestamibi from the liver is important for accurate diagnosis and reducing artifacts.UDCA has a choleretic effect and facilitates the excretion of bile acid from hepatocytes, and in addition it has cell protection, membrane stabilization, and immune modulator effects. ***Materials and Methods:*** This study involved 174 patients who underwent MPS and were divided into two groups: the UDCA group (n=90) and the control group (n=84). The UDCA group received a single dose of UDCA (300 mg) and underwent MPS after one and four hours, while the control group received a placebo. The hepatic clearance of 99mTc-sestamibi was measured in both groups using a gamma camera, and the results were compared. ***Results:*** The results showed that after four hours, the mean hepatic clearance of 99mTc-sestamibi was significantly higher in the UDCA group compared to the control group ($p<0.05$). Additionally, the mean hepatic uptake of 99mTc-sestamibi and hepatic to cardiac ratio were significantly lower in the UDCA group compared to the control group ($p<0.05$). However, there was no significant difference between the UDCA and control groups in after one-hour MPS. ***Conclusion:*** In conclusion, this study suggests that administering UDCA four hours prior to MPS can significantly improve hepatic clearance of 99mTc-sestamibi and reduce hepatic uptake in patients undergoing MPS. Therefore, UDCA may be considered as a potential treatment option to improve the accuracy of MPS in patients. However, further studies are needed to confirm these findings and determine the optimal dosage and duration of UDCA treatment.

EPS-136

The Role Of Myocardial Perfusion Scintigraphy In Asymptomatic Patients With 50-70% Coronary Artery Stenosis In Coronary Ct

A. Doumas[1]*, D. Boundas*[2]*, E. Giannoula*[1]*, P. Exadaktylou*[1]*, A. Tsangaridi*[1]*, N. Papadopoulos*[1]*, G. Gerasimou*[1]*, E. Papanastasiou*[1]*, I. Iakovou*[1]*;*
[1]Aristotle University, Thessaloniki, GREECE, [2]Private Nuclear Medicine Centre, Ippokratis, Thessaloniki, GREECE.

Aim/Introduction: Angiography of the coronary vessels using 64 or 128-slice CT (CTA) has become a widely used method for the exclusion of possible coronary artery disease, especially in young people with low probability of coronary artery stenosis as recommended by the new guidelines of the American Heart Association. The aim of the study was to define the role of myocardial perfusion scintigraphy in asymptomatic patients with 50-70% coronary artery stenosis in CTA. ***Materials and Methods:*** 136 subjects, 87 men and 49 women with an average age of 67 years (43-79 years) underwent heart scintigraphy after stress (94 subjects), or drug-related stress (42 subjects). All of them had abnormal CTA with stenoses in the range of 50-70%. A dual-head gamma camera (General Electric Millennium MG) was used for heart scintigraphy following an exercise-rest protocol after administration of 8 mCi SESTAMIBI at stress and 25 mCi at rest. The results were analyzed quantitatively (Emory Toolbox). If the image after stress was normal, the study was terminated (stress only), otherwise imaging was repeated at least two hours later. ***Results:*** The presence of ischemia was detected in only 11 subjects (8%), quantitative analysis showed that of these 11 subjects only 4 had ischemia exceeding 10% of the total myocardial mass. ***Conclusion:*** A very small percentage of the 50-70% of stenoses discovered on CTA are hemodynamically significant and of these, a very small percentage require revascularization surgery. It may be necessary for the cardiology community to reconsider the "critical" percentage of stenosis, as CTA tends to overestimate the extent of lesions compared to conventional coronary angiography.

EPS-137

Artefacts and False Positive Results of Myocardial Perfusion SPECT with CZT D-SPECT Camera

M. Esnault[1]*, D. Legallois*[2]*, D. Agostini*[2]*, P. Richard*[3]*, M. Alain*[2]*;*
[1]Caen University, Caen, FRANCE, [2]Caen University Hospital, Caen, FRANCE, [3]Hospital Privé Saint Martin, Caen, FRANCE.

Aim/Introduction: The artifacts occurring during myocardial perfusion SPECT acquisition with a CZT camera potentially reduce the specificity of the results and are poorly documented. The aim of our study was to analyze the relationship between these artefacts and the occurrence of false-positive myocardial SPECT examinations. ***Materials and Methods:*** Quality control of myocardial SPECT images from 60 consecutive patients with a True Positive (TP) (n=30) or False Positive (FP) (n=30) perfusion SPECT was retrospectively analyzed. All examinations were performed with a D-SPECT camera (Spectrum dynamics, Caesarea, Il), using a 99mTc-labeled radiopharmaceutical and a 1-day stress/rest protocol. All patients had coronary angiography within 3 months after myocardial perfusion SPECT. Artefacts were considered and classified as follows: (1) inadequate positioning of the heart within the cardio-focal area (0%, 30%, 60%, or 100% outside), (2) nonidentical patient positioning during stress and rest acquisition, (3) number of patient movements during stress and rest acquisition (graded as 0 [no movement], 1 [single movement], to 2 [more than 1 movement]), (4) quality of ECG-gating (good or poor), and (5) stress and rest myocardial count statistics (<500 kcts or ≥500 kcts). ***Results:*** Our study revealed that there was a majority

of men in both groups (n=21, 70% for TP and n=22, 73% for FP). In the FP group, the main indication for SPECT was diagnostic SPECT for suspected coronary artery disease (n=25, 83%), whereas in the TP group, the main indication was risk assessment in patients with documented coronary artery disease (n=16, 53%). Patients considered FP were younger (mean age = 64±11 vs. 69±10 y/o in VP, p< 0.05) with an increased BMI (32±8.6 vs. 27±5.3 kg/m^2 in VP, p=0.02). Among the quality control characteristics, the occurrence of a false-positive SPECT examination was significantly associated with the inadequate position of the heart in the cardio-focal area (p < 0.05), non-identical patient positioning during stress and rest imaging (p < 0.05), number of patient movements (p < 0.05), and low count statistics at rest (p < 0.05). The number of artefacts was strongly associated with the occurrence of false-positive examinations, with an 80% false-positive rate in patients with at least 2 artefacts (p = 0.0003). ***Conclusion:*** In this retrospective study, the false-positive rate dramatically increased with the number of artefacts, which shows the importance of having a robust quality control.

EPS-138

Impact of Initial Myocardial Perfusion Imaging versus Coronary Angiography on Costs and Outcomes in Patients with Coronary Artery Disease in China

L. Yang, *Y. Hu, S. Li;*
First Hospital of Shanxi Medical University, Taiyuan, CHINA.

Aim/Introduction: In patients with stable coronary artery disease (CAD), there are two main options for guiding treatment: initial coronary angiography (CAG) or selective CAG after the risk stratification of myocardial perfusion imaging (MPI). Debate continues regarding whether patients with suspected or stable coronary artery disease might benefit from initial myocardial perfusion imaging or coronary angiography. This study compares and analyses costs and clinical outcomes in our hospital regarding the two strategies. ***Materials and Methods:*** This study included 664 patients who presented to the hospital between January 2018 and end of December 2019 with suspected or known stable CAD, excluding patients with acute coronary syndrome, previous myocardial infarction (MI) or coronary revascularization. Patients were divided into two groups based on initial use of CAG or MPI, and each group was followed up to the end of 2022 for costs due to suspected or known stable CAD, and rates of myocardial revascularization, myocardial infarction and all-cause mortality. Univariate and multivariate COX proportional risk models were used to estimate the risk of events. ***Results:*** There were 332 patients in the MPI and CAG groups respectively, with a similar Charlson comorbidity index (CCI). In terms of cost, initial MPI strategy was on average 61% cheaper than CAG strategy (P<0.0001). In terms of clinical outcomes, the MPI group had a significantly and dramatically lower incidence of cardiac events (27 vs. 92, P<0.0001) than the CAG group. Further, the incidence of revascularization (19 vs. 60, P<0.0001), MI (6 vs. 27, P<0.001), and all-cause mortality (2 vs. 5, P>0.05) were also lower in the MPI group than in the CAG group. Multivariable analysis adjusting for age, gender, CCI, and comorbidities showed that in the MPI group fewer patients had revascularization (HR 0.20, 95% CI 0.11-0.34) and MI (HR 0.18, 95% CI 0.07-0.45) than CAG group, and the rate of all-cause mortality was lower (HR 0.80, 95% CI 0.12-5.58). ***Conclusion:*** In patients with suspected or stable CAD, this study showed that a diagnostic strategy guided by MPI could reduce costs and the incidence of cardiac events, resulting in savings in healthcare resources and health insurance funds.

EPS-139

The value of gated blood pool SPECT in assessment of stress-induced changes of the right ventricular contractile function.

V. Shipulin, *S. Andreev, V. M. Shipulin, S. Polikarpov, K. Zavadovsky;*
Cardiology Research Institute, branch of the Federal State Budgetary Scientific Institution «Tomsk National Research Medical Center of the Russian Academy of Sciences», Tomsk, RUSSIAN FEDERATION.

Aim/Introduction: There is increasing attention for the investigation of the role of right ventricle (RV) contractile function in ischemic heart failure (IHF). However, the precise assessment of RV function, particularly its stress-induced changes, is a quite challenging task. The wide use of gamma cameras equipped with solid-state CZT detectors makes possible to reduce GBPS acquisition time up to 5 min and perform examinations on pharmacological stress tests, in particular, with dobutamine. The purpose of current study was to assess the feasibility of CZT GBPS in evaluation of stress-induced changes of RV contractile function. ***Materials and Methods:*** A total of 63 patients with IHF were included in this study. All patients underwent GBPS at rest and on the stepwise increased doses of dobutamine (10/15μg/kg/min) on CZT gamma camera (GE Discovery NM/CT 570c). The following parameters were estimated: end-diastolic and end-systolic (ESV) volumes, ejection fraction (EF), stroke volume (SV), peak ejection (PER) and filling (PFR) rates, as well as mechanical dyssynchrony (MD) indices (phase standard deviation, phase bandwidth (HBW) and phase entropy) of RV and interventricular dyssynchrony. ***Results:*** Significant changes in EF were observed at a dobutamine dose of 10 μg/kg/min (p<.001), while to detect stress-induced changes in SV (p<.001), ESV (p<.001), PER (p<.001) and PFR (p=.005) the dobutamine dose of 15 μg/kg/min was required. Neither interventricular nor intraventricular MD indices showed significant changes during stress test, despite a decreasing trend. Among all patients, 18 (29%) have shown drop of EF at the dobutamine dose of 15 μg/kg/min, which was accompanied by a significant increase of HBW (p<.001). ***Conclusion:*** CZT GBPS is feasible to assess RV volume and contractility on dobutamine stress test in patients with IHF. Dobutamine dose of 10 μg/kg/min is sufficient to achieve diagnostically significant stress-induced changes of RV EF, while to detect changes in SV, ESV, PER and PFR higher doses are required. Moreover, the association between RV EF drop on 15 μg/kg/min dobutamine dosage and increase of HBW was found.

EPS-140

Simultaneous PET/MRI myocardial perfusion measurements using Gd-DOTA CMR and 68Ga-DOTA-PET

S. Kvernby[1], *T. Kero*[1], *K. Azarbar*[1], *C. Rischpler*[2], *J. Sörensen*[1], *I. Velikyan*[1], *M. Lubberink*[1];
[1]*Uppsala University, Uppsala, SWEDEN,*
[2]*Klinikum Stuttgart, Stuttgart, GERMANY.*

Aim/Introduction: Myocardial perfusion imaging using magnetic resonance imaging (MRI) often includes the use of a gadolinium-based contrast agent bound to the DOTA-molecule (DOTAREM). Quantification of myocardial blood flow (MBF) using MRI aims to measure the shortening of the T1 relaxation time that occurs in the myocardium when the Gd-DOTA molecules pass through the myocardium. For accurate MBF quantification, the MRI signal needs to be converted to Gd-concentration, which is challenging. The extraction rate of the DOTA-molecule is also

limited and has to be established when converting Gd-uptake rate to MBF. In contrast to MRI, the signal in a PET image is direct proportional to the radioactivity concentration in tissue. The aim of this study is to use a ^{68}Ga PET-analog of DOTAREM to evaluate the kinetics of the DOTA-molecule and compare it with that of Gd-DOTA in a simultaneous PET/MRI scanner. ***Materials and Methods:*** Eight patients referred for assessment of ischemia underwent 10 min dynamic ^{68}Ga-DOTA-PET scans during rest and during adenosine stress on a PET/MRI scanner. Simultaneously with the PET scan, an MRI-perfusion scan was performed by injection of Gd-DOTAREM (0.05 mmol Gd/kg body weight) using an ultrafast gradient echo sequence (FGRE) together with myocardial T1-mapping for individual estimation of the native T1-relaxation time. Both the ^{68}Ga-DOTA-PET and the Gd-DOTA MRI scan were analyzed using single-tissue reversible compartment model. For the MRI perfusion data, a conversion was first made from signal-curve to T1-curve and then to Gd-concentration curve. The uptake rate constant K_1 was compared between the two DOTA-perfusion methods. ***Results:*** The myocardial uptake rate constant K_1 had a moderate correlation between ^{68}Ga-DOTA-PET and the MRI Gd-DOTA (Pearson correlation coefficient, r=0.75 for whole myocardium and r=0.46 for the 16 segment model). Extraction was low for both methods with average whole myocardium ^{68}Ga-DOTA K_1 ranging from 0.22-1.66 mL/cm^3/min and Gd-DOTA K_1 ranging from 0.37-1.82 mL/cm^3/min. Average K_1 was significantly higher for Gd-DOTA than for ^{68}Ga-DOTA (paired t-test, p<0.05). ***Conclusion:*** Quantitative myocardial perfusion using ^{68}Ga-DOTA-PET in a simultaneous PET/MRI demonstrated moderate correlation with the Gd-DOTA-MRI myocardial uptake rate constant K_1. Extraction rate was low for both methods but was significantly higher for Gd-DOTA compared with ^{68}Ga-DOTA.

EPS-141

Detection of mental stress induced myocardial ischemia with myocardial perfusion imaging in patients with anxiety and/or depression after coronary revascularization

W. Dong*, J. Jiao, N. Nan, T. Mou, H. Mi, X. Song;*
Beijing Anzhen Hospital, Beijing, CHINA.

Aim/Introduction: The aim of this study was to detect mental stress induced myocardial ischemia (MSIMI) and long-term changes of MSIMI in CAD patients with anxiety and/or depression after coronary revascularization using baseline and follow-up myocardial perfusion imaging (MPI). ***Materials and Methods:*** Patients with anxiety and/or depression(GAD-7≥5 and/or PHQ-9≥5)who underwent coronary revascularization from Dec 2018 to Dec 2019 were prospectively recruited. Mental stress was induced by the Stroop Color and Word Test (SCWT). All participants underwent baseline mental stress/rest MPI at least 4 weeks after coronary revascularization, and were followed-up 12 months with mental stress/rest MPI. At baseline and during follow-up, all participants received secondary prevention of CAD, but did not receive intervention in psychotropic drugs. MSIMI was defined as the presence of at least one of four abnormal MPI phenomena: reversible perfusion defect (RPD), transient ischemic dilation (TID), reverse redistribution (RR), and stress ejection fraction (EF) decreased by ≥5%. Kendall's tau-b correlation coefficient was used to test the consistency of the two MPI results. ***Results:*** 93 patients with anxiety and/or depression after coronary revascularization completed the baseline MPI and follow-up MPI for 14.25 ±4.42 months. Among them, 51 patients (54.8%, 51/93) detected MSIMI at baseline and 42 patients (45.2%, 42/93) detected MSIMI at follow-up. The agreement rate was 58.1%, which was not statistically significant (Kendall's tau-b 0.172, P = 0.098). The incidence of abnormal components of MSIMI from high to low was RPD (25.8%, 24/93) >stress EF decreased by ≥5% (14.0%, 13/93) >TID (10.8%, 30/93) >RR (6.5%, 6/93) at baseline MPI and RPD (24.7%, 23/93) >RR (9.7%, 9/93) >stress EF decreased by ≥5% (7.5%, 7/93) =TID (7.5%, 7/93) at follow-up MPI. Among the four MSIMI abnormal components, RPD accounted for the highest proportion of MSIMI. Of the 24 patients with RPD at baseline, 17 patients (17/24, 70.8%) still had RPD at follow-up. Only the two MPI results of RPD were highly consistent (Kendall's tau-b 0.630, P < 0.001). ***Conclusion:*** MSIMI can be well identified by MPI in patients with anxiety and/or depression after coronary revascularization. In addition, RPD has always existed in patients at baseline and during long-term follow-up MPI. As for these high-risk patients with MSIMI, more attention should be paid to emotional control and early intervention.

EPS-142

Radionuclide Assessment of Myocardial Mitochondrial Dysfunction in Patients with Multivessel Coronary Artery Disease

K. Zavadovsky*[1], A. Kalinovsky[2], M. Gulya[1], K. Kopyeva[1], N. Kamenshikov[1];*
[1]Cardiology Research Institute, branch of the Federal State Budgetary Scientific Institution "Tomsk National Research Medical Center of the Russian Academy of Sciences", Tomsk, RUSSIAN FEDERATION, [2]Siberian State Medical University, Tomsk, RUSSIAN FEDERATION.

Aim/Introduction: Myocardial perfusion single-photon emission computed tomography of the myocardium (SPECT) with ^{99m}Tc-sestamibi (MIBI) is widely used in CAD patients for diagnostic and prognostic purposes. MIBI accumulates in cardiomyocytes by passive diffusion, predominantly (up to 90%) in mitochondria, thus allows to assess mitochondrial dysfunction. Although, there's data regarding diagnostic value of MIBI washout rate in severe heart failure patients, there is lack of knowledge about mitochondrial dysfunction in multivessel CAD (MVCAD) patients. MIBI washout rate could be potentially used as a marker for the detection of MVCAD, even when perfusion images show a mild or moderate decrease in myocardial perfusion. The aim of this study is to evaluate the MIBI washout rate in patients with MVCAD as compared to those without obstructive lesion. ***Materials and Methods:*** A total of 38 patients were enrolled in the study. Multivessel group (MVCAD) consists of 18 patients (male=12, age=65±7 years; CHF NYHA I-III). 10 (56%) patients have a history of acute myocardial infarction. Risk factors are diabetes mellitus (17%), smoking (39%). 20 patients (male=12, age=62.0±6 years; without obstructive CAD were recruited as a comparison group (NOCAD)). Risk factors are hypertension (75%), diabetes mellitus (8%), smoking (7%). All patients underwent stress/rest SPECT. As a part of a research protocol rest study was acquired twice - 1h and 4h after ^{99m}Tc-MIBI injection. The washout rate (WR) was quantified using the percentage difference in ^{99m}Tc-MIBI accumulation adjusted for the half-life of ^{99m}Tc (6.04 h). For MVCAD group, the number of significant stenoses was estimated. Statistical processing was performed in Statistica 12.0. The differences were considered statistically significant at the level of p<0.05. ***Results:*** Obstructive multivessel coronary artery lesion was diagnosed in all MVCAD patients: LMA - 4 patients (22%), LAD - 13 (72%), LCX - 7 (39%), RCA - 7 (39%). A statistically significant increase in the WR was revealed in the MVCAD group 8,26 (IQR 6.88; 16.65) compared with the group without obstructive lesions (3.72 (IQR 1.03; 5.42))

(p<0.001). The median value of LVEF was comparable (p=0.8) in MVCAD and NOCAD patients: 65% (IQR 56; 69) and 64.25% (IQR 62.40; 65.60), respectively. ***Conclusion:*** An increase in the ^{99m}Tc-MIBI WR in patients with MVCAD occurs despite the preserved ejection fraction what may be due to the presence of mitochondrial dysfunction resulting from chronic myocardial ischemia. Thus, the assessment of the ^{99m}Tc-MIBI WR by serial SPECT is valuable for the assessment of chronic ischemia in MVCAD.

EPS-143

Multidisciplinary approach for the early detection of amyloid in patients who undergo carpal tunnel syndrome or lumbar stenosis surgery. Results of an ongoing study.

N. Orta[1,2], *T. Ripoll*[3,2,4], *S. Rubí*[1,2,4], *J. Pons*[1,2], *E. Fortuny*[1,2], *M. Bosch*[1,2,4], *C. Nadal*[1], *I. Torralba*[1], *G. Salvà*[1,4], *N. Mora*[1,4], *S. Lirola*[1], *R. Marí*[5], *J. Femenias*[1], *M. Llabrés*[1], *A. Álvarez*[1], *B. Barceló*[1,2,4], *V. Daza-Cajigal*[1,2], *A. Pérez*[1,2], *D. Heine*[1,2], *A. Sharma*[1], *A. Piñar*[1], *M. Villar*[1], *C. Peña*[1,2];
[1]*Hospital Universitari Son Espases, Palma, SPAIN,* [2]*IdISBa, Palma, SPAIN,* [3]*Hospital Universitari Son Llàtzer, Palma, SPAIN,* [4]*Department of Medicine, University of the Balearic Islands, Palma, SPAIN,* [5]*Hospital Sant Joan de Déu, Palma-Inca, SPAIN.*

Aim/Introduction: Symptomatic carpal tunnel syndrome(CTS) and lumbar stenosis(LS) seem to precede the cardiac manifestations of cardiac amyloidosis(CA) due to transthyretin amyloidosis(ATTR), so they could represent early markers of CA. CTS is more commonly present in CA due to wild-type ATTR(ATTRwt), although it can also be present in its hereditary variant(ATTRv) and in primary amyloidosis caused by immunoglobulin light chain deposition(AL). Therefore,in this ongoing study, our aim is to evaluate the prevalence of amyloidosis in patients undergoing CTS or LS surgery, in an endemic area of the TTR mutation Val50Met(ATTRv). ***Materials and Methods:*** To date,234 operated patients have been included(180 CTS,54 LS) in whom an intraoperative biopsy was obtained(ligamentum flavum in LS; synovial tissue or flexor retinaculum in CTS) for histopathological analysis using Congo Red staining for amyloid detection and immunohistochemistry(IHC) or mass spectrometry(MS) for subtyping in amyloid A(AA), kappa,lambda and ATTR. Blood and urine test to rule out a monoclonal component and a cardiac scintigraphy(CS) with ^{99m}Tc-DPD to detect myocardial uptake were performed, which analysis was visual by Perugini scale. A cardiac SPECT/CT was performed in cases with a positive planar imaging,according to the ASNC/EANM Cardiac Amyloidosis Practice Points. ***Results:*** Total of 192 biopsies were obtained(144 CTS,48 LS), 14 of them were amyloid positive(6 CTS,8 LS).All IHC were negative for AA, kappa and lambda. IHC for ATTR and MS analysis are still pending. 33 operated patients without biopsy(29 CTS,4 LS). Nine biopsies are pending for histopathological result. 194 laboratory tests and CS have been performed: 4/194 CS were positive(grade 3) and underwent CTS surgery with 3/4 positive biopsies for amyloid(1/4 without biopsy). 190/194 CS were negative(grade 0). In 14/194 laboratory tests, a monoclonal component was detected. 119/145 completed cases have completed the study (all tests negative). To date, positivity for amyloid has been obtained in 17/234 cases(7.3%): 13 positive biopsies (one of them with a positive blood test for monoclonal gammopathy of undetermined significance, 2 with positive CS and 10 with negative blood/urine test and CS), 2 positive biopsies with CS and blood/urine test still pending and 2 CS positive without biopsy and normal blood/urine test. In the follow-up(1.75 years) of patients with positivity, 23.5%(4/17) manifests cardiomyopathy, 3 of them with positive CS, and 88.2%(15/17) has previously other orthopedic manifestations. ***Conclusion:*** The estimated prevalence of amyloidosis in our series of surgically treated patients with CTS or LS is 7.3% to date. These are preliminary data from an ongoing study.

EPS-144

A 3-month of physical exercise reduces stress-related neurobiological activity in obese women: a prospective 18F-FDG PET/CT study

K. Pahk, *H. Kwon, S. Kim;*
Korea University College of Medicine, Seoul, KOREA, REPUBLIC OF.

Aim/Introduction: Psychological stress is considered as a major risk factor for cardiovascular disease (CVD). Chronic exercise is known to reduce CVD risk partly through attenuating psychological stress. Obesity has been linked with increased levels of psychological stress. We aimed to prospectively evaluate whether physical exercise could alleviate stress-associated amygdala metabolic activity, assessed by ^{18}F-fluorodeoxyglucose (FDG) positron emission tomography/computed tomography (PET/CT) in women with obesity. ***Materials and Methods:*** A total of 43 participants were enrolled in this study. Twenty-three obese women were participated in a physical exercise program 5 days per week for 3 months. The exercise program consisted of aerobic exercise and resistance training. Serial ^{18}F-FDG PET/CT was taken before the start of physical exercise program (baseline) and after finishing the program (post-exercise). A total of 20 participants who underwent ^{18}F-FDG PET/CT for general health check-up were enrolled as non-obese control group. Brain amygdala activity (AmygA) was calculated as maximum standardized uptake value (SUVmax) of amygdala normalized to mean SUV of temporal lobe. ***Results:*** Chronic physical exercise significantly reduced AmygA and improved body adiposity and systemic inflammation. AmygA was highest in baseline, intermediate in post-exercise, and lowest in non-obese control group (0.76 ± 0.17, 0.61 ± 0.1, 0.52 ± 0.09, $p < 0.001$). Furthermore, physical exercise also abrogated the association of AmygA with systemic inflammation. ***Conclusion:*** Chronic physical exercise reduced stress-associated amygdala metabolic activity and broke its association with systemic inflammation in obese women. This study could explain the putative mechanism underlying the health beneficial effect of exercise on CVD via attenuation of stress neurobiology.

EPS-145

Prognostic Value of 18F-FDG PET/CT Brain metabolism and Brain Network in Patients with Heart Failure

Y. Bai, *M. Yun, X. Zhang;*
Beijing Anzhen Hospital, Capital Medical University, Beijing, CHINA.

Aim/Introduction: To investigate the cerebral neurometabolic ventricular dyssynchrony interactome in patients with heart failure with reduced ejection fraction (HFrEF), and the association with prgnosis. ***Materials and Methods:*** Patients with HFrEF who underwent gated single-photon emission computed tomography/computed tomography (CT), myocardial perfusion imaging and the brain ^{18}F-fluorodeoxyglucose positron emission tomography/CT were prospectively enrolled. Relationships between the regional brain metabolism and major arrhythmic events were assessed using Cox models and mediation analyses. ***Results:*** A total of 392 patients [age: 59.0 (51.0, 65.0) years, 88.5% male] were included in the current study, and 60 (15.3%) patients experienced MAEs during a median follow-up time of 3.9 years. Compared with patients without MAEs (n = 332), patients

with MAEs (n = 60) showed decreased glucose metabolism in some brain regions, mainly located in the insula, hippocampus, amygdala, cingulate gyrus, caudate nucleus and thalamus, which are related to the autonomic nervous system (all P value< 0.001). The decreased cerebral glucose metabolism activity in the autonomic nervous system related brain regions such as the insula, hippocampus, amygdala, cingulate gyrus, caudate nucleus and thalamus were independent predictors of MAEs in patients HF (all P value < 0.05). The glucose metabolism activity in the insula, hippocampus, amygdala, cingulate cortex, and caudate nucleus was correlated with the ventricular dyssynchrony (r = -0.10- 0.24, P value < 0.05). Mediation analysis showed that the metabolic activity of autonomic nervous system related brain regions such as the insula, hippocampus, amygdala, cingulate gyrus, and caudate nucleus was reduced, which affected ventricular mechanical dyssynchrony and electrical dyssynchrony, and mediated the occurrence of MAEs in patients with HF. In patients with HF, compared with non-MAEs patients, the central autonomic neural networks were damaged in patients with MAEs (P value < 0.05). Compared with the sympathetic neural network, the parasympathetic neural network was more severely disturbed, that is, the central autonomic neural network is imbalanced. ***Conclusion:*** The decreased glucose metabolism related to the autonomic nervous system is associated with MAEs in patients with HF. Neuronal metabolism affects ventricular mechanical dyssynchrony and ventricular electrical dyssynchrony, and mediates the occurrence of MAEs. In addition, central autonomic neural network imbalance can predict MAEs in patients with HF.

EPS-146

Characterization of brain structure and metabolism in heart failure patients with reduced or preserved ejection fraction: a simultaneous PET/MR study

C. Zheng[1], *Y. Cui*[1], *Q. Ge*[2], *Y. Yang*[3], *X. Li*[4], *J. Lu*[1];
[1]*Department of Radiology and Nuclear Medicine, Xuanwu Hospital, Capital Medical University, Beijing, CHINA,* [2]*Central Research Institute, United Imaging Healthcare, Shanghai, CHINA,* [3]*Beijing United Imaging Research Institute of Intelligent Imaging, Beijing, CHINA,* [4]*Division of Nuclear Medicine Department of Biomedical Imaging and Image-guided Therapy. Vienna General Hospital Medical University of Vienna, Vienna, AUSTRIA.*

Aim/Introduction: It is controversial whether the cognitive impairment associated with heart failure (HF) is due to left ventricular ejection fraction (LVEF). The purpose of this study was to determine whether HF patients with reduced ejection fraction (HFrEF) or ejection fraction preserved heart failure (HFpEF) exhibits evidence of cognitive impairment and brain alterations compared to healthy controls (HC). ***Materials and Methods:*** A total of 78 subjects were included in this study, including 26 patients with HFrEF, 20 patients with HFpEF, and 32 age- and sex-matched individuals with HC. All HF patients suffer from left ventricular myocardial infarction. Basic clinical information and clinical cognitive scale assessments were collected, including the Mini-Mental State Examination (MMSE) and Montreal Cognitive Assessment (MoCA). All subjects underwent an integrated 18F-fluorodeoxyglucose (^{18}F-FDG) PET/MR scan. High-resolution T1-weigthted imaging structural images and ^{18}F-FDG PET images were acquired for all subjects. The normalized gray matter volume (GMV) images and normalized PET standardized uptake value ratio (SUVR) with pons as the reference region images were obtained using the CAT12 and SPM12 toolboxes. Voxel-wise analysis was used to evaluate abnormalities in brain metabolism and structure in the HF patients. Age and gender were used as covariates of no interest in PET image comparison, and age, gender, and total intracranial volume were used for GMV images. ***Results:*** There were no significant differences in education, hyperlipidemia, or other vascular risk factors among the three groups. Both HFrEF and HFpEF patients showed reduced MOCA and MMSE scores compared to HC subjects (all P<0.05). However, there was no significant difference in MMSE and MoCA scores between the two HF groups. Compared to HC, HFrEF patients showed hypometabolism in the bilateral inferior temporal gyrus, insula, and superior frontal gyrus, as well as the right inferior temporal gyrus and right hippocampal GMV loss. HFpEF patients showed hypometabolism in the bilateral thalamus, bilateral hippocampus, bilateral caudate nucleus, bilateral superior temporal gyrus, and GMV loss in the medial superior frontal gyrus, compared to HC. Nevertheless, no differences were found in glucose metabolism and GMV between the two groups of HF patients. ***Conclusion:*** Our findings demonstrate that patients with HF with reduced or preserved LVEF have impairments in brain metabolism and gray matter structures in cognitively relevant areas of the brain. These results may provide imaging evidence for clinical patient management.

1010

Monday, September 11, 2023, 3:00 PM - 4:30 PM
Hall K

Technologists' e-Poster Presentations Session - Technologists Committee: Techs' e-Posters

TEPS-001

Description of an imaging protocol in patients with glioblastoma treated with [^{177}Lu]Lu-DOTA-TATE.

E. Córdoba Cañete[1], *M. Caballero Vivancos*[1], *N. González Corredera*[1], *E. Triviño Ibañez*[1], *R. Sánchez Sánchez*[2];
[1]*Hospital Universitario Virgen de las Nieves, Granada, SPAIN,*
[2]*Hospital Universitario Virgen de las Nieves, Maracena, SPAIN.*

Aim/Introduction: Glioblastoma is the most commonly occurring malignant central nervous system tumor accounting for 14.6% of all tumors. It is an aggressive primary brain tumor, with a high mortality rate despite extensive efforts to develop new treatments. "[177Lu]Lu-DOTA-TATE" is a targeted radioligand therapy binding with high-affinity to somatostatin receptors (SSTR), with highest affinity for subtype 2 receptors (SSTR2). Pathologic conditions, including brain tumors (i.e. GB) and chemical or physical stimuli such as surgery, RT, some chemotherapy agents, could increase the blood brain barrier (BBB) permeability disrupting its integrity. [68Ga]Ga-DOTA-TATE PET/CT (or PET/MRI) will be performed during screening to select patients presenting uptake in the tumoral region before the administration of the first dose of [177Lu]Lu-DOTA-TATE.The aim of our job is to present our imaging protocol in gliobalstoma patients treated with [177Lu]Lu-DOTA-TATE ***Materials and Methods:*** Whole body planar image will be acquired on the day of [177Lu]Lu-DOTA-TATE administration 1 to 3 hours after end of [177Lu]Lu-DOTA-TATE infusion. Matrix 256 x1024 Zoom 1. Both detectors. supine position. Exploration extension from 200 cm to 10 cm/min scanning speed. Automatic contours. Photopeak centered at 208 Kev with a window of +-15%. Two more attached windows are enabled both above and below the main 4% picking up the top and bottom dispersion. SPECT/CT scan will be acquired in 24 hours after the end of [177Lu]Lu-DOTA-TATE infusion. Matrix 128 x 128 60 images at 20sec/image on two beds including head-thorax-abdomen. 360 degrees of rotation. 180 degree detector configuration. Orbits not circular in advance and take. Energy window of 208 Kev. CT parameters Using the CareDose 4D method of dose modulation, a CT scan is performed with 3-slices. mm with window reconstructions of the abdomen (B31s medium homog) and bone (B70sdefined) and mediastinal window with expanded Fov for attenuation correction. ***Conclusion:*** The introduction of therapy with new radioligands makes it necessary to optimize the acquisition protocols for the correct evaluation of the images.

TEPS-002

[^{18}F]AlF-complexation of pamidronic acid, a NOTA-conjugated bisphosphonate, as a potential tracer for PET bone imaging

H. Hassan[1], *M. Othman*[2], *H. Abdul Razak*[3], *Z. Zakaria*[4], *F. Ahmad Saad*[1];
[1]*Universiti Putra Malaysia, Serdang, MALAYSIA,* [2]*Universiti Teknologi MARA, Bandar Puncak Alam, MALAYSIA,*
[3]*University of Exeter, Devon EX1 2LU, UNITED KINGDOM,*
[4]*Universiti Malaysia Sabah, Kota Kinabalu, MALAYSIA.*

Aim/Introduction: The use of radiopharmaceuticals in nuclear imaging offers greater advantages than conventional diagnostic imaging. Although [^{18}F]sodium fluoride ([^{18}F]NaF) is recognised to be superior to [^{99m}Tc]-Tc-methyl diphosphate ([^{99m}Tc]Tc-MDP) and 2-deoxy-2-[^{18}F]fluoro-D-glucose (2-[^{18}F]FDG) in bone diagnostics, there is a concern that [^{18}F]NaF uptake is not cancer-specific, leading to a higher number of false-positive interpretations. Therefore, in this study, a bisphosphonate drug, pamidronic acid, was conjugated to a NOTA for [^{18}F]AlF complexation of pamidronic acid using the aluminium fluoride (Al-F) technique and evaluated for its in vitro uptake. ***Materials and Methods:*** The conjugation of NOTA-pamidronic acid was prepared using the N-hydroxysuccinimide (NHS) ester strategy and validated by liquid chromatography-mass spectrometry analysis (LC-MS) before being isolated in pure form. The conditions for the [^{18}F]AlF complexation of pamidronic acid were optimised to achieve an acceptable radiochemical yield (RCY) between 40 and 60% and radiochemical purity (RCP) above 90%. It was ensured that [^{18}F]AlF-NOTA-pamidronic acid met all quality control requirements for radiopharmaceuticals prior to in vitro bone binding assay with hydroxyapatite and in vitro cell uptake studies with normal human osteoblast cell lines (hFOB 1.19) and human osteosarcoma cell lines (Saos-2) were performed. ***Results:*** Conjugation of NOTA-pamidronic acid in a molar ratio of 5:1 of pamidronic acid to NOTA-NHS at room temperature for 4 hours with pH adjusted to 8 successfully yielded 24.13% of NOTA-pamidronic acid. The purity of the NOTA-pamidronic acid fractions was 92%, with no free NOTA impurities detected. [^{18}F]AlF-NOTA-pamidronic acid prepared in a 1:1 molar ratio of aluminium chloride ($AlCl_3$) to NOTA-pamidronic acid and heated at 100 °C for 15 minutes in the presence of 50% ethanol (v/v) proved to be optimal. [^{18}F]AlF-NOTA-pamidronic acid also successfully met all radiopharmaceutical quality control requirements and was also stable in the final formulation and in human plasma (n = 6). The in vitro bone-binding study showed that [^{18}F]AlF-NOTA-pamidronic acid was as sensitive as [^{18}F]NaF in binding hydroxyapatite. Although [^{18}F]NaF was more strongly taken up by both cell lines, the results nevertheless demonstrated that [^{18}F]AlF-NOTA-pamidronic acid was specific, as a higher cellular uptake of [^{18}F]AlF-NOTA-pamidronic acid was observed in the Saos-2 cell lines. ***Conclusion:*** The novel radioconjugate [^{18}F]AlF-NOTA-pamidronic acid prepared by the Al-F technique appears to be a potential PET tracer for bone imaging. The preliminary in vitro results indicate that further preclinical studies with [^{18}F]AlF-NOTA-pamidronic acid are needed before it can be translated to clinical research.

TEPS-003

Evaluation of Variation method to Improve the Sensitivity of Immunoradiometric Assay

W. Kwon, *J. Kim;*
Seoul National University Bundang Hospital, Seongnam-si, Gyeonggi-do, KOREA, REPUBLIC OF.

Aim/Introduction: The concentration of PSA (Prostate Specific Antigen) after radical prostatectomy in prostate cancer patients is a predictor of biochemical recurrence, and the AUA (American Urological Association) is defined as biochemical recurrence when the concentration of PSA is measured at 0.2 ng/ml or more, and when the concentration is measured at 0.2 ng/ml or more at the retest. This standard is also applied our hospital. In this laboratory, the PSA reagent using IRMA (Immunoradiometric Assay) is used, and the sensitivity at a very low value was not as good as the reagent used in the department of laboratory medicine. This study aims to increase the reliability of the results by improving the precision and sensitivity of very low values. ***Materials and Methods:*** As a reagent for the study, PSA reagent using IRMA was used. As a method to improve the precision and sensitivity of very low values, a variation method on the serum volume(25ul, 50ul, 100ul, 200ul) was studied, and variation usefulness evaluation was conducted. The evaluation items were compared the results of precision, analytical sensitivity, recovery rate, dilution test, high-dose hook test, parallel test and very low concentration values(n = 20). ***Results:*** The validation results were displayed in the order of 25ul, 50ul, 100ul, 200ul. As the serum volume increased, it was confirmed that CV (Coefficient of Variation)(%) improved. Analytical sensitivity(ng/ml) was 0.038, 0.041, 0.017, 0.015 and recovery rate(%) was 101±3, 101±3, 99±2, 97±4. very low concentration values(ng/ml) between each volume(n=20) were 0.135±0.068, 0.076±0.050, 0.048±0.034, 0.046±0.034. and high dose hook effect appeared as the serum volume increased. ***Conclusion:*** Through the variation usefulness evaluation, it was confirmed that as the serum volume increased, the precision and sensitivity improved at very low concentration values. However, it is necessary to pay special attention to the occurrence of high-dose hook effect as the serum volume increases. In the case of tests that requires very low concentration values, it is thought that the reliability of the result will be increased if the variation method is properly used after the variation usefulness evaluation.

TEPS-004

Comprehensive management of paediatrics in nuclear medicine: sharing the experience of technologists in a leading cancer center

M. GOLVET, *M. Luporsi, N. Jehanno, S. Lasalle, N. Sanchez Bertomeu;*
Department of nuclear medicine, Institut Curie, Paris, FRANCE.

Aim/Introduction: In our nuclear medicine department, located in one of the leading cancer centers in Europe, we are used to taking care of patients of all ages. However, management of paediatrics is one of the most challenging part of our daily activities. Therefore we had to develop several technical and communication skills in order to perform the best image quality while offering the least invasive procedure as possible. In this poster, we would like to share our experience enriched by decades of daily practice. ***Materials and Methods:*** Paediatrics management is based on a collaborative approach between all members of imagery department, relying as much on secretaries, as the physicists, the radiopharmacist, the physician and finally the technologist. The versatility of the technologists on other modalities such as MRI and CT helps to ensure effective pediatric care. We mainly focus here on the involvement of the technologists for the well running of nuclear medicine imaging involving paediatric patients. ***Results:*** In 2022 we performed respectively 83 MIBG scan (range [1 months-17 yo], <6yo : 46/83) and 123 PET/CT (range [3months-17yo] ; < 6 yo : 17/123) on paediatrics, without requiring any general anesthesia and with only a very rare use of premedication for anxiolysis. Many soft strategies help us to welcome the child and his/her family in a pleasant and secure environment (attractive stickers on walls and equipements, toys in waiting rooms, colourful light diffusers, DVD and music players). Then a communication adapted to the child's language and his comprehension appeases everyone and helps to install a relionship of trust between the caregiver, the child and the parents, actively involving them into the procedure. Some of our technologists are also specifically trained in pain management (inhalation of nitrous oxide for injection, anaesthetic cream) and in conversational hypnosis to facilitate injection and/or installation. Optimal installation and immobilization with age-adapted devices is finally on of the key point of the procedure (cushions, paediatric cradle⋯) ***Conclusion:*** Thanks to a multidisciplinary approach and the development of technical and communication skills over the years, we take care of children and teenagers every day, for PET/CT and scintigraphies, trying to perform the best image quality while remaining as less invasive as possible.

TEPS-005

Ultra-fast Gallium-68 is it possible in the era of digital PET/CT imaging

Z. Alqallaf[1], *L. Ghadhanfer*[2], *A. Sadeq*[1], *H. Alfake*[1], *F. Marafi*[1];
[1]*Jaber Al Ahmed Center For Nuclear Medicine & Molecular Imaging, Sabah Medical area, KUWAIT,* [2]*Faculty of Allied Health Kuwait university, Jabriya, KUWAIT.*

Aim/Introduction: Digital PET/CT scanners system has higher sensitivity when compared to analog PET/CT scanners. New digital PET/CT has enhanced specifications with higher count statistic, time-to-flight ratio, and camera resolution contributing to better sensitivity. Gallium68 is an isotope labeled with a wide range of radiotracers used in oncology and inflammatory diseases due to the availability of Germanium-68/Gallium-68 generator. However, it has less favorable properties that lower image quality mainly due to lower positron yield (89.14%) and higher positron energy (1,899 keV) with higher kinetic energy resulting in further distance between positron emission and annihilation. This reflect on the image resolution and contrast as it increases the scatter and therefore image noise. The aim of this study is to determine the possibility of ultra-fast imaging time with optimal OSEM and Q. Clear filter for better image resolution in digital PET/CT imaging. ***Materials and Methods:*** Flangeless PET phantom was used which has solid cylindrical shaped attached to the lid with diameter of 8, 12, 16mm, and three with diameter of 25mm. Gallium-68 was added to the phantom with ratio of 8:1 concentration of cylindrical shape to background, starting from 25 followed by 8, 12,16mm sequentially. The other 25mm cylindrical shape one filled with water and the other is filled with air for attenuation purposes. In the other end of the phantom there are cold rods diameters: 4.8, 6.4, 7.9, 9.5, 11.1 and 12.7 mm* Height of rods: 8.8 cm. The images were acquired by digital PET/CT camera at different time points per bed starting with 5min, 4min, 3min, 2:30min, 2min, 1:30min, 1min, and 0:30sec. The images were reconstructed using OSEM and Q.Clear filters, and it was analyzed by two nuclear medicine physicians. ***Results:*** In both the iterative reconstruction and Q.Clear all the hot lesions were identified clearly by the two

readers, up to 4mm at 30sec per bed. However, the cold lesions in 4.8 and 6.4mm were blurred in iterative reconstruction, while the resolution were enhanced and identified in the Q.Clear. ***Conclusion:*** In the era of the digital PET system, this preclinical study demonstrates the ability of obtaining high quality images with optimal contrast to background ratio and better image resolution. This study could establish a new opportunity for ultra-fast digital PET scanning providing potentials for clinical trials in which patients can be imaged in shorter time. Q.Clear filter showed superiority over iterative reconstruction especially with cold lesions of smaller diameter.

TEPS-006

The Effect of Using Radiopharmaceutical Multidose Injector for 18F FDG on the Received Effective Doses of Radiographers

D. Sercic*, J. Peric, U. Cotar;*
Institute of Oncology Ljubljana, Ljubljana, SLOVENIA.

Aim/Introduction: To determine the possible impact of using radiopharmaceutical multidose injector for ^{18}F Fluorodeoxyglucose (FDG) on the received effective dose of employed radiographers. ***Materials and Methods:*** The retrospective study included data on the received effective doses of 10 radiographers over a period of 12 months (a total of 120 received effective doses). During that period, radiographers were 6 months applicated ^{18}F FDG manually and 6 months using radiopharmaceutical multidose injector. Thermoluminescent dosimeters (TLDs) were used to measure and calculate received effective doses monthly. Depending on the data normality, Mann-Whitney U test were used to determine potential impact of using radiopharmaceutical multidose injector for ^{18}F FDG on the received effective dose. ***Results:*** Data analysis showed that the received effective dose of radiographers is significant different between manual application of ^{18}F FDG and using radiopharmaceutical multidose injector for application ^{18}F FDG (p=0.046). Mean ± STD of measured effective dose during manual application of radiopharmaceutical ^{18}F FDG was 0.137 ± 0.143 mSv per month and effective dose measured during use radiopharmaceutical injector was 0.083 ± 0.044 mSv per month. ***Conclusion:*** The difference of effective dose between two methods of radiopharmaceuticals application was statistically significant. Results showed that mean of measured effective dose during manual application of ^{18}F FDG was 39.4% higher in comparison with measured effective dose during use radiopharmaceutical multidose injector.

TEPS-007

Decontamination of Lu-177-PSMA and Tc-99m-Pertechnetate Spills from Laboratory Floor: Comparing Four Cleansing Agents

S. Rajala[1]*, I. Rantala*[1]*, L. Elg*[2]*, A. Honkanen*[2]*, J. Lehto*[2]*, E. Hippeläinen*[2]*, V. Ahtiainen*[1,3]*, M. Ladev*[1]*, M. Eskola*[1]*, S. Keskimäki*[4]*, K. Kiviluoto*[4]*, J. Tervonen*[4]*, M. Salomaa*[1]*, V. Reijonen*[1]*;*
[1]HUS Comprehensive Cancer Center, Helsinki, FINLAND, [2]HUS Diagnostic Center, Helsinki, FINLAND, [3]University of Helsinki, Helsinki, FINLAND, [4]HUS Pharmacy, Helsinki, FINLAND.

Aim/Introduction: Accidental spills may occur when one works with unsealed radioactive sources. Nuclear medicine staff are trained to prevent, monitor and handle radioactive contamination that may result from the use of radiopharmaceuticals. The selection of diagnostic and therapeutical radiopharmaceuticals is versatile, and new agents are developed and coming to clinical use. The optimal choice of decontamination solvent for each radiopharmaceutical and surface material is different, which is why ready-made cleansing mixtures can be a practical solution for daily routine. ***Materials and Methods:*** Small pieces of plastic laboratory floor material (polyurethane-coated polyvinyl chloride) were contaminated with a low activity of either Lutetium-177-PSMA (prostate-specific membrane antigen, peptide) or Technetium-99m-pertechnetate: 10 µl droplet was pipetted and spread with glass rod on a 2 cm x 2 cm area. The contaminated pieces were left to dry in a laminar flow hood for 1 hour or 24 hours. The pieces were then decontaminated with wipes moistened with a cleansing agent: water, 80% ethanol, commercial solution 1, or commercial solution 2. In order to equalise the decontamination process, we constructed an apparatus: Two plastic tiles were covered with disposable tape, and the wipe was placed between these two. Each contaminated piece was then pushed through the gap between the plastic tiles, with a 966 g lead block placed above to apply constant pressure. The contaminated pieces were measured just before the decontamination (that is, after drying), and after decontamination. ***Results:*** For Lu-177-PSMA, the decontamination efficiency (reported as an average of two measurements for each cleansing agent) after 1 hour/24 hour drying time was 99%/99% with water, 95%/91% with ethanol, 99%/99% with commercial solution 1, and 99%/99% with commercial solution 2. For Tc-99m-pertechnetate, 72%/48%, 87%/36%, 87%/52%, and 81%/65%, respectively. For Lu-177-PSMA, all four decontaminating agents were efficient for both 1 and 24 hour spills. However, decontamination efficiency with ethanol was slightly lower than for the other agents. For Tc-99m-pertechnetate, the average decontamination efficiency was higher after 1 hour drying time compared to 24 hours drying time, indicating the longer the spill had time to dry, the harder it was to decontaminate. ***Conclusion:*** The differences in cleansing efficiency between all four tested decontamination solutions were minor. Decontamination of Tc-99m-pertechnetate was more difficult after 24 hours than 1 hour of drying time, whereas Lu-177-PSMA was easy to clean in both cases.

TEPS-008

Development of a specialized image reconstruction technique for dedicated breast positron emission tomography

K. Hanaoka[1]*, S. Watanabe*[1]*, D. Ishikawa-Morimoto*[1]*, Y. Yamakawa*[2]*, T. Kobayashi*[2]*, A. Ohtani*[2]*, S. Kumakawa*[2]*, T. Ito*[3]*, Y. Komoike*[3]*, H. Kaida*[1]*, K. Ishii*[1]*;*
[1]Institute of Advanced Clinical Medicine, KINDAI University, Osaka-sayama, JAPAN, [2]Shimadzu Corporation, Kyoto, JAPAN, [3]Division of Breast and Endocrine Surgery, KINDAI University, Osaka-sayama, JAPAN.

Aim/Introduction: FDG dedicated breast PET (db-PET) has been employed for clinical presentation and diagnosis. However, the quality of images has been compromised at the periphery of the patient's field of view(FOV), i.e., near the chest wall, due to out-of-field scattered radiation from the brain and heart, as well as decreased sensitivity of detection at the edges during db-PET acquisition. To address this issue, the present study endeavors to develop a db-PET reconstruction technique and evaluate its effectiveness. ***Materials and Methods:*** In an effort to balance noise reduction and preservation of resolution, we have developed a novel reconstruction methodology that combines a 3x3x3 Median filter and a Non-Local Means filter(I:0.5, S:3, P:6). This method was evaluated using data acquired from the BresTome, manufactured by Shimadzu Corporation. The performance of this new method was contrasted against that of the conventional reconstruction

approach utilizing a 2.2 mm Gaussian filter, by utilizing both phantom and clinical data. This assessment began with a 5-minute acquisition of a 20 cm diameter cylindrical phantom containing 10 MBq, where the coefficient of variation(CV values) within the central homogeneous region in each slice after reconstruction was measured along the depth direction from the edge of the FOV and compared between the different reconstructions. Furthermore, the maximum standard uptake value(SUVmax) in 53 lesions and SUVavg on mammary grand and fat were compared between reconstructions in a cohort of 30 breast cancer cases. ***Results:*** The new method was found to be effective in reducing CV values by a mean of 27% when compared to the conventional method. This effect was observed to be independent of the depth from the periphery of the FOV. In clinical cases, the mean SUVmax of 53 lesions(mean size 11.6±7.9 mm) and mean SUVavg of normal mammary tissue were not significantly difference in new method compared to conventional method(9.11±5.83 vs 8.92±5.62, p=0.332 and 0.93±0.29 vs 0.90±0.30, p=0.984). On the other hand, the mean SUVavg on fat tissue tended to be lower in new method compared to conventional method(0.24±0.10 vs 0.31±0.14, p<0.001). The image quality was found to be improved in all cases with the use of the new technique. ***Conclusion:*** The reconstruction method developed, which incorporates a Non-Local Means filter, has the ability to effectively reduce background noise encountered in db-PET. ***References:*** 1) Ishii K, Hanaoka K, et al. J Nucl Med 2023;64, 2) Morimoto-Ishikawa D, Hanaoka K, et al. EJNMMI Phys. 2022;9:88.

TEPS-009

Impact of Image Space PSF Correction on Quantitative Values and SNR of Clinical PET Images in SiPM-based PET/CT with List-Mode Acquisition

Y. Shirakawa*, K. Ebine, M. Kawada, J. Suyama;*
Kyorin University Hospital, Tokyo, JAPAN.

Aim/Introduction: The Cartesion Prime (Canon) SiPM-based PET/CT scanner employs list-mode acquisition and reconstruction, along with image space PSF (iPSF) correction for spatial resolution improvement. This study aimed to evaluate the impact of iPSF on the quantitative values and signal-to-noise ratio (SNR) of clinical images in a high spatial resolution SiPM-based PET/CT scanner. ***Materials and Methods:*** Lung cancer cases (83 nodules) classified as T1a (≤ 1 cm), T1b (1 cm < ≤ 2 cm), or T1c (2 cm < ≤ 3 cm) in the Tumor-Node-Metastasis (TNM) classification (UICC 8th edition) were analyzed in 78 patients undergoing ^{18}F-FDG PET/CT examination. All patients fasted for at least 4 hours before PET/CT and received an intravenous infusion of 215.7±40 MBq of ^{18}F-FDG followed by a 60-minute resting period. The injection dose per body weight was 3.6±0.4 MBq/kg, and acquisition began 60 minutes after administration. Collection was performed at 3 minutes/bed. Image reconstruction was performed by 3D-OSEM with subset 12, iteration 3, time-of-flight (+), iPSF correction (-/+), Gaussian filter FWHM 4 mm. SUV_{max} and liver SNR (n=78) of lung nodules were measured with and without iPSF, and cases of lung nodules were divided into sizes based on T1a-c classification, and statistical analysis was performed using Wilcoxon signed rank test. P values less than 0.05 were considered statistically significant in all analyses. ***Results:*** SUV_{max} was 5.0±1.9 for nodule diameter ≤1 cm without iPSF, 8.2±2.7 for 1 cm < nodule diameter ≤2 cm, 12.0±2.9 for 2 cm < nodule diameter ≤3 cm, and 5.9±2.4, 9.5±3.3 and 13.4±3.5 with iPSF, respectively. The liver SNR was 10.5±1.6 without iPSF and 12.5±2.2 with iPSF. ***Conclusion:*** Although the application of iPSF resulted in a higher liver SNR, the effect was small, and the guideline recommendations were met without any problem without iPSF, thus limiting the effect of the iPSF. ***References:*** 1) Tong S, Alessio AM, Kinahan PE. Noise and signal properties in PSF-based fully 3D PET image reconstruction: an experimental evaluation. Phys Med Biol. 2010 Mar 7;55(5):1453-73.2) D. Bharkhada, V. Panin, M. Conti, M. E. et al. Listmode Reconstruction for Biograph Vision PET/CT Scanner. 2019 IEEE Nuclear Science Symposium and Medical Imaging Conference (NSS/MIC), Manchester, UK, 2019, pp. 1-6.

TEPS-010

Comparison between MIRD-based and Monte Carlo simulation-based patient-specific dosimetry in177Lu-DOTATATE

N. Miyaji*[1], K. Miwa[1], K. Yamashita[2], T. Yamao[1], K. Hasegawa[1], N. Oriuchi[3], T. Terauchi[2];*
[1]Fukushima Medical University, Fukushima, JAPAN, [2]Cancer Institute Hospital of Japanese Foundation for Cancer Research, Tokyo, JAPAN, [3]Advanced Clinical Research Center, Fukushima Medical University, Fukushima, JAPAN.

Aim/Introduction: Patient-specific image-based dosimetry for PRRT is beneficial for assessing adequate lesion response while minimizing normal tissue toxicity. The present study aimed to compare the absorbed dose derived from voxel-level dosimetry using Medical Internal Radiation Dosimetry (MIRD) and Monte Carlo simulation (MC). ***Materials and Methods:*** We retrospectively investigated four patients treated with 7.4 GBq ^{177}Lu-DOTATATE. Each patient underwent an abdominal SPECT/CT scan using the Symbia Intevo 16 (Siemens Healthcare) at 24 and 168 hours after injection. The SPECT images were acquired in a step-and-shoot mode with 60 views using a 128×128 matrix and low-medium energy general purpose collimators. The energy window was set to a photopeak of 113, 208 keV with a 15% width. Liver, spleen, kidneys and lesion absorbed dose distributions were calculated from the projection data using a MIRD-based and MC-based dosimetry software (Hermes Medical Solutions)[1)]. The absorbed dose with MC was calculated at single or two time-points of estimation (24, 168 and 24/168 hours). ***Results:*** The MC-based absorbed doses at each time point showed higher values in the order of 24-hour point, 24/168-hour point, 168-hour point. The MC-based mean absorbed doses at two time points were higher, ranging from 1.6 to 6.3 Gy, than the MIRD-based doses (with average relative differences ranging between 27.4% and 127.2%) in the kidneys. However, no patient had received greater than the accepted threshold for renal toxicity of 23 Gy. In the lesions, the MC-based mean absorbed doses at the 24-hour time point were lower, ranging from -0.4 to -7.3 Gy, than the doses at two time points. In contrast, the absorbed dose at the 168-hour time point was higher, ranging from 1.3 to 10.2 Gy, than the doses at two time points. ***Conclusion:*** The MC-based dosimetry at single time point of the early or late phase caused variation in the absorbed dose. Multipoint MC-based dosimetry can be expected to provide a reliable assessment compared with uncertain MIRD-based dosimetry. ***References:*** 1) Hippeläinen ET, Tenhunen MJ, Mäenpää HO, Heikkonen JJ, Sohlberg AO. Dosimetry software Hermes Internal Radiation Dosimetry: from quantitative image reconstruction to voxel-level absorbed dose distribution. Nucl Med Commun. 2017;38(5):357-365.

TEPS-011

[18F]fluorocholine PET is more resource-effective than conventional [99mTc]sestamibi scintigraphy in patients with primary hyperparathyroidism

S. Rep[1,2], *I. Slodnjak*[1], *K. Sirca*[3], *K. Zaletel*[1,4], *M. Hocevar*[3], *L. Lezaic*[1,4];
[1]*Department for Nuclear Medicine, University Medical Centre Ljubljana, Ljubljana, SLOVENIA,* [2]*University of Ljubljana, Faculty of Health Sciences, Medical Imaging and Radiotherapy Department, Ljubljana, SLOVENIA,* [3]*Department of Oncological Surgery, Institute of Oncology Ljubljana, Ljubljana, SLOVENIA,* [4]*University of Ljubljana, Faculty of Medicine, Ljubljana, SLOVENIA.*

Aim/Introduction: Minimally invasive parathyroidectomy is the treatment of choice in patients with primary hyperparathyroidism, but it needs a reliable preoperative localization method to detect hyperfunctioning parathyroid tissue. Higher sensitivity and lower radiation exposure were demonstrated for [18F]fluorocholine PET/CT (FCh-PET) in comparison to [99mTc]sestamibi (MIBI) scintigraphy. However, data of its cost-effectiveness is lacking. The aim of our study was to determine the cost-effectiveness of FCh-PET in comparison to conventional MIBI scintigraphy. ***Materials and Methods:*** A group of 234 patients who underwent surgery after MIBI scintigraphy was compared to a group of 163 patients who underwent surgery after FCh-PET.The whole working process from the implementation of imaging to the completion of surgical treatment was analysed. The economic costs were expressed in the time needed for the required procedures. ***Results:*** The time needed to perform imaging was reduced by 80 % after FCh-PET in comparison to MIBI scintigraphy. The time needed to perform surgery was reduced by 41 % when intraoperative parathyroid hormone monitoring was not used. There was no significant difference in the time of surgery between FCh-PET and MIBI scintigraphy. Postoperative complications occurred in 16.6 % of patients after SS and SPECT/CT and 6.1% of patients after FCh-PET (p= < 0.001). ***Conclusion:*** FCh-PET reduces the time of imaging and the time of surgery and potentially reduces the number of reoperations for persistent disease. ***References:*** 1. Hocevar M, Lezaic L, Rep S, Zaletel K, Kocjan T, Sever MJ, Zgajnar J, Peric B. Focused parathyroidectomy without intraoperative parathormone testing is safe after pre-operative localization with 18F-Fluorocholine PET/CT. Eur J Surg Oncol. 2017 Jan;43(1):133-137. DOI: 10.1016/j.ejso.2016.09.016. Epub 2016 Oct 21. PMID: 27776943. 2. Lezaic L, Rep S, Sever MJ, Kocjan T, Hocevar M, Fettich J. ^{18}F-Fluorocholine PET/CT for localization of hyperfunctioning parathyroid tissue in primary hyperparathyroidism: a pilot study. Eur J Nucl Med Mol Imaging. 2014 Nov;41(11):2083-9. DOI: 10.1007/s00259-014-2837-0. Epub 2014 Jul 26. PMID: 25063039. 3. Rep S, Hocevar M, Vaupotic J, Zdesar U, Zaletel K, Lezaic L. 18F-choline PET/CT for parathyroid scintigraphy: significantly lower radiation exposure of patients in comparison to conventional nuclear medicine imaging approaches. J Radiol Prot. 2018 Mar;38(1):343-356. DOI: 10.1088/1361-6498/aaa86f. Epub 2018 Jan 17. PMID: 29339573.

TEPS-012

Does ^{18}F-FDG-PET require withdrawal of Glucagon-like peptide 1 (GLP-1) analogs in diabetic patients?

B. Olsson[1], *U. Bitzén*[1], *S. Garpered*[1], *S. Leide-Svegborn*[2], *A. Stenvall*[2];
[1]*Clinical Physiology and Nuclear Medicine, Malmö/Lund, SWEDEN,* [2]*Radiation Physics, Malmö/Lund, SWEDEN.*

Aim/Introduction: Many patients undergoing ^{18}F-FDG-PET examinations have diabetes mellitus and their medication can potentially alter the physiological ^{18}F-FDG distribution. Glucagon-like peptide 1 (GLP-1) analogues, a group of diabetes type 2 pharmaceuticals introduced some years ago, stimulate the release of insulin from pancreas. To date, no literature was found about possible effects of these pharmaceuticals in ^{18}F-FDG-PET. The aim was to study if GLP-1 analogues affect the physiological ^{18}F-FDG distribution. ***Materials and Methods:*** Twenty-two diabetic patients (46 ^{18}F-FDG PET/CT scans) with BMI range 22-41 and medicated with GLP-1 analogues, either once daily with liraglutide (5 patients, 14 scans) or once weekly with semiglutide (17 patients, 32 scans) referred for 18F-FDG-PET were retrospectively included. As a control group 30 non-diabetic patients with BMI range 22-40 were included. They were all injected with 4 MBq/kg and scanned after 60 minutes on a PET/CT with SiPM detectors. In each scan three volumes-of-interest (VOIs) were drawn, one in each of the reference organs mediastinal blood pool, liver and thigh muscle. SUVmean were determined for each VOI. SUVmean were related to BMI and blood glucose level at time of ^{18}F-FDG injection. ***Results:*** No obvious difference in SUVmean in any of the reference organs; mediastinal blood pool, liver or muscle was found for GLP-1 medicated diabetics compared to a control population. This result was regardless of BMI, blood glucose level or GLP-1 analogue regimen investigated. ***Conclusion:*** The physiological ^{18}F-FDG distribution, reflected by SUVmean in reference organs, was similar in patients with GLP-1 analogues compared to the control group. Hence, ^{18}F-FDG-PET does not require withdrawal of GLP-1 analogues in diabetic patients.

TEPS-013

^{99m}Tc-Colloid residuals dependency on the syringe and needles

D. Teixeira Macarico[1], *C. Laurins*[1], *L. Hogg*[2], *R. Williamson*[1], *J. Dennis*[1], *A. Nicol*[1];
[1]*Nuclear Medicine Department, Queen Elizabeth University Hospital, Department of Clinical Physics and Bioengineering, NHS Greater Glasgow and Clyde, Glasgow, UNITED KINGDOM,* [2]*Medical Physics, Royal Alexandra Hospital, Department of Clinical Physics and Bioengineering, NHS Greater Glasgow and Clyde, Glasgow, UNITED KINGDOM.*

Aim/Introduction: Lymphoscintigraphy is a common nuclear medicine procedure essential for the prognosis and treatment of breast cancer, allowing identification of sentinel lymph nodes during theatre using gamma probes and subsequent biopsy. The administration technique performed in our department was by subdermal injection of ^{99m}Tc-Nanocoll (10MBq or 40MBq for same-day or following day surgery) with a 25G (0.5mm) needle and 1mL syringe, peri-areolar at the same quadrant as the tumour. Following feedback from the surgical team of some patients with lower counts, a review was performed including the syringe & needle and an audit of syringe residual activity. Peer review at other centres identified the use of a different needle gauge (insulin needle and syringe system 29G 0.33mm) and this was adopted. The aim of this study is to compare radiopharmaceutical retention (RR) with both needle gauges. ***Materials and Methods:*** Experiments were performed by dispensing 10MBq/40MBq of ^{99m}Tc-Nanocoll and measuring RR, similar to a patient administration. A total of 16 experiments were performed by two operators using the 25G needle and 1mL syringe and 8 experiments using the 29G insulin syringe system. Additionally, retrospective analysis of administrations using the 25G needle (54 patients) and prospective analysis with the 29G needle (4 patients to date - data collation is ongoing) were performed to determine RR after administration. ***Results:*** The experiments showed a RR of 20% (SD=8.2%) for the 25G needles and RR of 7.9% (SD=2%) for 29G needles (t-test shows differences statistically significant for p<0.01). The analysis of the patient administrations with the 25G needle showed an average of RR of 21% (SD =

8%). For the 29G syringe the average of RR was 5% (SD = 2%). These differences were statistically significant (t-test, p<0.01). ***Conclusion:*** A significantly lower RR of the radiopharmaceutical was observed for the insulin syringe and needle (29G) system in both experiments and patients administrations, which can help explain some lower counts in the lymph nodes reported by the surgical team. Following these results, the standard operator protocols were changed and positive feedback is reported by the surgical team. Acknowledgements: thanks to Nuclear Medicine teams in all Glasgow sites.

TEPS-014

Usefulness of ^{99m}Tc-MIBI Myocardial SPECT/CT Subtraction Protocol with CZT Gamma Camera

K. Nam, *H. Cho, J. Lee, W. Lee;*
Seoul National University Bundang Hospital, Seoul, KOREA, REPUBLIC OF.

Aim/Introduction: This study introduces ^{99m}Tc-MIBI gated myocardial SPECT/CT subtraction protocol with CZT gamma camera (NMCT 870 CZT) which can reduce examination time and provide a comfortable examination for patients. ***Materials and Methods:*** Medical staff performed a pharmacologically induced stress test on the patient. The heart rate and blood pressure were monitored during this phase. 296 MBq of ^{99m}Tc-MIBI was injected in the middle of the test. After the test, the patient ingested fatty meals to reduce uptake of liver. After at least 30 min, myocardial SPECT stress scan was started with 6 degree angle, 30 projections and 40 sec of each acquisition. Also, helical CT scan was performed with 120 kVp, 20 mA and 18.75 mm/rot for attenuation correction. Immediately after the stress scan, 925 MBq of ^{99m}Tc-MIBI has been injected and myocardial SPECT rest scan was started with 6 degree angle, 30 projections and 30 sec of each acquisition. Afterwards, technician subtracted myocardial stress images from rest images with arithmetic software installed as standard and reconstructed true rest images. ***Results:*** Pharmacologically induced stress test took 6 min. After 30 min, myocardial SPECT stress scan was performed for 10 min. CT scan was performed for 2 min. Myocardial SPECT rest scan took 8 min. Overall ^{99m}Tc-MIBI myocardial perfusion SPECT/CT subtraction protocol was completed within 56 min. ***Conclusion:*** ^{99m}Tc-MIBI myocardial perfusion SPECT/CT single isotope subtraction protocol with CZT gamma camera is expected to reduce overall examination time within an hour, which will increase the patient's satisfaction, be more useful for patients who have difficulty in examination for a long time, and improve the efficiency of equipment usage. ***References:*** Heiba Sherif I ,Hayat Nasser J ,Salman Hani S ,Higazy Ezzat,Sayed Mohammed E ,Saleh Zuhair,Khalaf Ali I ,Naeem Mohammed,Bourosly Suhair. "Technetium-99m-MIBI myocardial SPECT" The Journal of nuclear medicine : 1510-1514."Acquisition method study on ^9^9^mTc-MIBI myocardial SPECT" NUCLEAR TECHNIQUES : 285-288.Robinson V J B,Chernick R J,Corley J H,Litaker M S,Raibon S A,Reece S J,Yoder J H,Burke G J. "Improvement of Spect TL-201 Myocardial Perfusion Image Quality with Exercise Prior to Adenosine Infusion" Journal of investigative medicine : p30A.

TEPS-015

Validation of Diagnostic Accuracy for Primary Aldosteronism with Quantitative Adrenal SPECT: Comparison with Adrenal Venous Sampling

T. Sato[1], *N. Matsutomo*[2], *T. Yamamoto*[2], *M. Fukami*[2], *T. Kono*[3];
[1]*Chiba Aoba Municipal Hospital, Chiba, JAPAN,* [2]*Kyorin University, Tokyo, JAPAN,* [3]*Chiba University, Chiba, JAPAN.*

Aim/Introduction: The type of disease that cause primary aldosteronism (PA) is characterized by lateralization of adrenal hormone secretion. Adrenal venous sampling (AVS) is the gold standard test for differentiating them and determining the course of treatment, meanwhile it is invasive and can fail at times. This study aimed to evaluate the diagnostic accuracy for PA with the maximum and mean standardized uptake values (SUVmax and SUVmean) on ^{131}I-6B-iodomethyl-19-norcholesterol (NP-59) single-photon emission computed tomography (SPECT) and compared with AVS in clinical study to verify whether it can be established alternatively. ***Materials and Methods:*** Adrenal NP-59 SPECT was acquired under the optimized image parameters determined by preliminary phantom experiment using Symbia Intevo in 14 patients with suspected PA. In addition, AVS was also performed in 7 of them. SPECT images using two-way reconstruction method were analyzed with region of interest to measure the adrenal lesion SUVmax and SUVmean and their ratios to the values on the contralateral side (SUVRmax and SUVRmean). ***Results:*** SUVmax and SUVmean on NP-59 SPECT images using the ordered-subset conjugate gradient minimization (OSCGM), a high-resolution reconstruction algorithm, were significantly higher for aldosterone-producing adenoma (APA) than for bilateral adrenal hyperplasia (BAH) or nonfunctioning adenoma (P=0.0475 and P=0.0447). The areas under the receiver-operating characteristic curve for SUVmax and SUVmean were the same 0.933 with OSCGM and 0.844 with the three-dimensional ordered-subset expectation maximization (3D-OSEM), while SUVRmax and SUVRmean were the same 0.725 with OSCGM and 0.750 with 3D-OSEM. Quantitative SPECT improved PA diagnostic accuracy over visual inspection. The lesion SUVmax and SUVmean were higher than on the contralateral side, and SUVRmax and SUVRmean were higher than 1.0 in 5 of the 6 cases (except one patient with bilateral APA) in which the aldosterone concentration on the lesion side or the lateralized ratio exceeded the cutoff value on AVS. Additionally, both SUV and aldosterone concentration of AVS on the side with the lesion were higher for APA than for BAH. ***Conclusion:*** SUV and SUVR of NP-59 SPECT with OSCGM algorithm appear to hold promise as indices for PA diagnosis. Furthermore, SUV and SUVR were associated with the diagnostic features on AVS and consistent with lateralization of adrenal hormone secretion by AVS in most patients. Quantitative adrenal SPECT can be an alternative to AVS. ***References:*** Yen RF, Wu VC, Liu KL, et al. 131I-6beta-iodomethyl-19-norcholesterol SPECT/CT for primary aldosteronism patients with inconclusive adrenal venous sampling and CT results. J Nucl Med. 2009;50(10):1631-7.

TEPS-016

Image characteristics of ^{99m}Tc myocardial perfusion SPECT/CT using a new multi-focal collimator: comparison with conventional SPECT with LEHR collimator

K. Takami[1], *M. Onoguchi*[1], *T. Shibutani*[1], *A. H. Vija*[2], *F. Massanes*[2], *T. Shimizu*[2], *H. Yoneyama*[3], *T. Konishi*[3], *K. Nakajima*[4];
[1]*Department of Quantum Medical Technology, Graduate School of Medical Sciences, Kanazawa University, Kanazawa Japan, Kanazawa, JAPAN,* [2]*Siemens Medical Solutions UNITED STATES OF AMERICA, Inc., Hoffman Estates, IL, UNITED STATES OF AMERICA,* [3]*Department of Radiological Technology, Kanazawa University Hospital, Kanazawa Japan, Kanazawa, JAPAN,* [4]*Department of Functional imaging and Artificial Intelligence, Kanazawa University, Kanazawa Japan, Kanazawa, JAPAN.*

Aim/Introduction: A multi-focal collimator for SPECT imaging with a suitable high resolution and extended magnification volume (SZHRX) was used in cardiac, neurologic, and orthopedic applications. We evaluated the characteristics of myocardial perfusion imaging with the SZHRX collimator to compare with low-energy high-resolution (LEHR) collimator. ***Materials and Methods:*** A Symbia Intevo 16 (Siemens Healthineers) SPECT/CT system was used and equipped with LEHR and SZHRX collimators. An anthropomorphic phantom was filled with 99mTc. The radioactive concentration ratio between myocardium, liver and background was set to 14:8:1. Normal myocardium and inferior defect myocardium were used as myocardial models. Traditional SPECT data with LEHR collimator was acquired with 64×64 matrixes, 1.45 zoom, 6.6mm pixel size, with a circular body centered orbit radius of 24cm, and angular step of 6 deg. Subsequently. SPECT data with SZHRX collimator was acquired with 256×256 matrixes, 2.4mm pixel size, with a circular body centered orbit radius of 26 and 28cm, and continuous mode. Image reconstruction of the SPECT data with LEHR collimator was used Flash3D and SZHRX collimator was used a prototype quantitative xSPECT using the ordered subset conjugate gradient minimizer (OSCGM) including attenuation, scatter, and resolution corrections. A Gaussian filter with a full width at half-maximum of 10 mm was used as a post filter. For physical analysis, %CV and %uptake used 17 segments of polar map, and contrast was calculated for normal myocardium. The %uptake for defect myocardium used circumferential profile curve. ***Results:*** The %CV for LEHR and SZHRX collimator with the radius of 26 cm and 28 cm was 5.6%, 8.7% and 8.8% respectively. The %CV for xSPECT with SZHRX collimator was equivalent to traditional SPECT with LEHR collimator. The contrast for LEHR and SZHRX collimator with the radius of 26 cm and 28 cm was 53.2%, 78.1% and 77.5%. The contrast for SZHRX collimator was higher values than that of the LEHR collimator. The defect %uptake for LEHR and SZHRX collimator in the radius of 26 cm and 28 cm was 39.1%, 26.8%, and 32.3% respectively. ***Conclusion:*** The %CV for SPECT image using the new multi-focal SZHRX collimator was equivalented to the traditional LEHR collimator, and the contrast for SZHRX collimator was higher than that for LEHR. Then, the defect detectability for the SZHRX collimator was superior to that for LEHR.

TEPS-017

The effect of data-driven respiratory gating on myocardial SPECT

T. Shibutani[1], *M. Onoguchi*[1], *A. H. Vija*[2], *F. Massanes*[2], *T. Shimizu*[2], *H. Yoneyama*[3], *T. Konishi*[3], *K. Nakajima*[4];
[1]*Department of Quantum Medical Technology, Institute of Medical, Pharmaceutical and Health Sciences, Kanazawa University, Kanazawa, Ishikawa, JAPAN,* [2]*Siemens Medical Solutions UNITED STATES OF AMERICA, Inc., Hoffman Estates, IL, UNITED STATES OF AMERICA,* [3]*Department of Radiological Technology, Kanazawa University Hospital, Kanazawa, Ishikawa, JAPAN,* [4]*Department of Functional Imaging and Artificial Intelligence, Kanazawa University, Kanazawa, Ishikawa, JAPAN.*

Aim/Introduction: A cardiac study often exhibits motion, which affects the image quality and quantitation of myocardial single-photon emission computed tomography (SPECT). While data-driven respiratory gating (DDG) correction is clinically established in positron emission tomography, data-driven methods for SPECT scans have not yet been clinically adopted. We demonstrated the effect of DDG on myocardial SPECT. ***Materials and Methods:*** A SPECT/CT scanner (Symbia Intevo 16, Siemens Healthneers) with a low-energy high-resolution collimator was used. Two myocardial models of normal myocardium and anterior wall infarction were created using an anthropomorphic myocardial phantom. The myocardial, liver, and background areas were filled with ^{99m}Tc solutions of 93, 53 and 6.6 kBq/mL. The SPECT data was acquired with 256 matrices, 2.4 mm pixel size, with non-circular orbit and 3 deg sampling angular step using list-mode. The anthropomorphic myocardial phantom was moved in a cycle at a steady speed to simulate respiratory motion, with a respiratory rate of 18 breaths/min and movement distances of ±0.5, ±1, and ±1.5 cm, respectively. A stationary myocardial phantom was acquired as a reference. The projection data was reconstructed by the ordered subset conjugate gradient method with attenuation and scatter corrections using a prototype reconstruction engine. Subset and iteration were set at 1 and 48, and a Gaussian filter of the full width at half maximum (FWHM) was applied as a post-filter. We created two images with and without DDG correction. Cavity contrast, percent coefficients of variance (%CV), %uptake and wall thickness with FWHM of normal myocardial model and the %uptake of anterior wall defect model were used to compare with and without DDG correction. ***Results:*** The %uptake of normal myocardium was decreased by 4-8% in the anterior wall and 10~20% in the inferior wall more than ± 1 cm compared with the reference. Cavity contrast and %CV of movement distance ±1.5 cm was approximately 40% decreasing and 5% increasing compared with the reference. The %uptake, cavity contrast and %CV were improved by DDG correction. The FWHM of anterior and inferior walls was higher with increasing movement distances without DDG correction. While the FWHM of DDG correction showed constant values independent of movement distance. ***Conclusion:*** The influence of respiratory motion on myocardial SPECT was particularly severe for motion exceeding ±1 cm, which improved the image quality and physical indices by DDG correction.

TEPS-018

High dose adenosine overcomes the effect of caffeine intake in Rubidium PET perfusion

B. Ribeiro, *S. Townrow, C. Pacheco, C. Lopez Martinez, E. Reyes, L. Menezes;*
Barts Health NHS Trust, London, UNITED KINGDOM.

Aim/Introduction: Caffeine reduces the vasodilatation effect of adenosine stress in myocardial perfusion imaging (MPI). Almost 10% of patients may be under-stressed (Manisty et al. Radiology 2015). High dose adenosine overcomes caffeine antagonism (Reyes et al. JACC 2008). This study sought to confirm its effectiveness in practice in Rubidium PET perfusion. ***Materials and Methods:*** A retrospective review of the department database to identify patients who received 210 mcg/kg/min adenosine, over 4 years, due to recent caffeine ingestion. Tolerability, conduction abnormalities, the haemodynamic effects, any reduction of splenic counts during stress, normalcy rates, and global myocardial flow reserve, were recorded. ***Results:*** 142 out of 4972 patients were identified on the 210 mcg/kg/min adenosine protocol. 111 were male, 31 female, with mean age 66.3 ± 11.7. Only one patient was

unable to tolerate the 6 minute of adenosine infusion due to side effects, while minor and well tolerated side effects were reported in all the other patients. There were no sustained episodes of AV block. Heart rate increased by 19.2 ± 14.8 bpm. Systolic BP decreased by 9.0 ± 21.5 mmHg and diastolic BP decreased by 4.9 ± 16.6 mmHg. The spleen was included in the FoV in 100% of patients. There was a reduction in splenic uptake in 96.5% of studies. The global myocardial flow reserve was 2.22 ± 0.86, 59.9% patients had a global MFR of >2. ***Conclusion:*** High dose adenosine is safe and well tolerated and overcomes the antagonist effects of caffeine as evidenced by a reduction in splenic uptake, and an average global MFR>2. The haemodynamic effects are modest. It can be reliably used in PET MPI and by extension in SPECT MPI, rather than cancelling or rebooking a patient who has ingested caffeine.

TEPS-019

Dose reduction for nuclear medicine technicians through implementation of automated dispensing and infusion devices: a retrospective study

E. Hendrikse, *W. Huisman, J. Medema, P. H. Elsinga, A. T. M. Willemsen;*
University Medical Center Groningen, Groningen, NETHERLANDS.

Aim/Introduction: Over the last years the number of Positron Emission Tomography (PET) procedures in the department of Nuclear Medicine and Molecular Imaging (NGMB) of the University Medical Center Groningen (UMCG) has risen. The dose report of Mirion Dosimetry Services reported an increasing whole-body and extremity dose of personnel as a possible result of the increasing number of procedures. Shielded automated dispensing and infusion devices have recently been introduced. Unlike manual preparation and injection, these automatic devices offer the technicians more protection against radiation exposure and allow them to keep more distance during the procedures. The aim of the study was to evaluate the effect of an automatic syringe dispensing and injection system on the whole-body and extremity dose of technicians compared to manual dispensing and injection. ***Materials and Methods:*** The whole-body and extremity dose per four weeks (one period) for all personnel working at the PET were measured with ring and badge dosimeters and compared between four periods of manual (12-08-2019 to 08-12-2019) and four periods of automatic (16-08-2021 to 5-12-2021) dispensing and injection. ***Results:*** The mean whole-body dose rate was not significant different between the periods of automatic and manual dispensing and injection (p=0,236). However the extremity dose rate reduced from 35,72 ± 39,84 µSv/h to 9,97 ± 8,97 µSv/h (p<0,001). ***Conclusion:*** The use of an automatic syringe dispensing and injection system resulted in a 72,1 ± 40,8% reduction of the extremity dose. At the same time the whole-body dose did not change. Additional investments are needed to further reduce the whole-body dose for technicians.

TEPS-020

A comparative study regarding deep inhalation breath-hold and free-breathing total-body PET/CT with half-dose [18F]-FDG

J. Jia, *K. Yuan, M. Liu, Y. Cui, S. Tang, C. Zhou, W. Zhang;*
Sun Yat-Sen University Cancer Center, Department of Nuclear Medicine, Guangzhou, Guangdong, China., Guangzhou, CHINA.

Aim/Introduction: To compare the image quality and diagnostic efficacy between 30-seconds deep inspiration breath-hold (DIBH) PET/CT 8 min and free-breathing (FB) using a total-body PET-CT (uEXPLORER) with half-dose [18]F-FDG. ***Materials and Methods:*** From July 2022 to February 2023, 19 patients with suspected or confirmed upper abdominal malignancies who underwent half-dose (0.05mCi/kg) [18]F-FDG PET/CT in Sun Yat-sen University Cancer Center were enrolled. They underwent a 30-seconds DIBH PET/CT quick scan after a FB 8 min total-body PET-CT scanning. PET images of FB-8min, FB-30s, and DIBH-30s were reconstructed, and the SUVmax of the liver, spleen, bone marrow, mediastinal blood pool, upper lung, and lower lung were measured as background reference. Distances of the hepatic dome of PET and CT were used as quantitative measurements for image registration of FB-8min, FB-30s, and DIBH-30s, respectively. We measured the lesion center offset, SUVmax, SUVmean, SUVpeak, MTV, and TBR in a free-breathing scan and DIBH quick scan. ***Results:*** DIBH scanning was successfully performed in 16 of 19 cases, a total of 43 lesions were detected in 19 patients. 37 (86%) lesions' PET and CT were well aligned. There was no significant difference in SUVmax of the liver, spleen, bone marrow, and mediastinal blood pool of PET between the FB-30s group and DIBH-30s group, and both were higher than that of FB-8min. For upper abdominal lesions: the focal center deviation (mm) of DIBH-30s vs. FB-30s vs. FB-8min was 1.67±2.35 vs. 4.66±3.43 vs. 4.43±3.27. DIBH-30s showed a significantly lower focal center deviation compared with the other groups (p<0.001). The SUVmax of DIBH-30s vs. FB-30s vs. FB-8min was 11.05±3.36vs. 8.99±3.14vs. 8.39±2.93, DIBH-30s was significantly higher than other groups (p<0.001). The MTV value of DIBH-30s vs. FB-30s vs. FB-8min was 0.69±0.90 vs. 0.80±0.99 vs. 0.84±1.05, where the DIBH-30s was significantly lower than other groups (p<0.05). The TBR of DIBH-30s vs. FB-30s vs. FB-8min was 4.15±1.26 vs. 3.40±1.20 vs. 3.47±1.28, DIBH-30s was significantly higher than other groups (p<0.001). ***Conclusion:*** Compared to routine free-breathing PET-CT, DIBH PET/CT can effectively improve PET-CT registration of the lesion, and improve the semi-quantitative measurements. Half-dose 18F-FDG breath-hold PET/CT is feasible in clinical practice and may increase diagnostic confidence for abdominal lesions.

TEPS-021

Developments in Radiochemical Processing of Solid Targets for Radiopharmaceuticals Production

G. Sciacca[1], P. Martini[2], S. Cisternino[1], L. Mou[1], G. Balajan[1], J. Amico[3], J. Esposito[1], G. Gorgoni[3], ***E. Cazzola[3];***
[1]INFN-LNL, Legnaro, ITALY, [2]University of Ferrara, Ferrara, ITALY, [3]Sacro Cuore Don Calabria Hospital, Negrar di Valpolicella, ITALY.

Aim/Introduction: Accelerator-produced radiometals are growing in importance in nuclear medicine applications. In this regard, for their efficient production solid precursor materials are usually preferred. However, this implies the need to properly manage the target dissolution process for radioisotope recovery. For this purpose, various systems based on a patent by INFN (Italian National Institute for Nuclear Physics) have been developed by our research group to perform this operation with automated synthesis modules. This was done in the framework of a collaboration between the LARAMED (LAboratory of RAdionuclides for MEDicine) project of INFN, the radiopharmacy department of the Sacro Cuore Don Calabria Hospital (Negrar, VR), and the radiochemistry laboratories of the Ferrara University. ***Materials and Methods:*** The developed reactors consist of an open-bottom vial, installed on one of the module's motors for syringe plungers via a frame connection system, and a target holder designed to be plugged into the module's reactor heater. For target processing, once the irradiated target is placed on

its holder, the vial is pressed over it by the module's motor to confine the chemical attack by means of an interposed O-ring. To guarantee adequate sealing, the connecting system is engineered to automatically correct any misalignment between the vial and the target. ***Results:*** This reactor configuration allows to remotely perform all the synthesis operations in a single hot cell and to selectively dissolve only the precursor material if a composite target with an inert interlayer is used. It has been successfully tested with various modules by different brands in radioisotope recovery and radiopharmaceutical synthesis operations. The simplicity of this system has paved the way for the ongoing STarDiS (Solid Target Dissolution System) project, funded by the INFN National Committee for Technology Transfer (CNTT) to develop a prototype for production routine in good manufacturing practice environments. ***Conclusion:*** A new concept of solid target dissolution reactor is here proposed. It allows the use of automatic modules for rapid, cheap, and easy integration in radiopharmaceutical facilities already equipped for radioisotope recovery from solid targets. ***References:*** 1) G.Sciacca et al., Molecules. 2021 26. 6255. 2) V.Palmieri et al., WO/2019/053570, 7 September 2018. 3) J.Esposito et al., Molecules. 2018 Dec 21; 24(1):20.

1011

Monday, September 11, 2023, 3:00 PM - 4:30 PM
Hall G1

Case Report Session 1 - TROP Session: Learning from Single Cases in Theranostics

OP-467

Feasibility of ^{177}Lu-PSMA-617 radioligand therapy in a patient with recurrent high-grade glioma

A. Holzgreve[1], *A. Delker*[1], *V. Wenter*[1], *M. J. Zacherl*[1], *N. Thon*[2], *P. Harter*[3], *M. Brendel*[1], *L. M. Unterrainer*[1], *M. Niyazi*[4], *P. Bartenstein*[1], *L. von Baumgarten*[2], *N. L. Albert*[1];
[1]*Department of Nuclear Medicine, University Hospital, LMU Munich, Munich, GERMANY,* [2]*Department of Neurosurgery, University Hospital, LMU Munich, Munich, GERMANY,* [3]*Center for Neuropathology and Prion Research, LMU Munich, Munich, GERMANY,* [4]*Department of Radiation Oncology, University Hospital, LMU Munich, Munich, GERMANY.*

Aim/Introduction: ^{177}Lu-based radioligand therapy (RLT) targeting the prostate-specific membrane antigen (PSMA) is a well-established treatment for advanced prostate cancer (PCa) and has been approved in 2022 by both the FDA and EMA. Although other tumour entities also overexpress PSMA and an application of PSMA-RLT has been continuously propagated for those entities, it has scarcely been performed beyond PCa. Here, we present preliminary data on PSMA-RLT in a glioma patient. ***Materials and Methods:*** A 31-year old patient with anaplastic oligodendroglioma, IDH-mutant, 1p/19q-codeleted, CNS WHO grade 3 presented for a re-recurrence. The initial diagnosis had been made 13 years earlier, and the patient had undergone multiple prior treatments including repeated resections, chemoradiotherapy with concomitant temozolomide, interstitial brachytherapy, a combination of lomustine and olaparib, and others. In view of the repeated recurrences and a lack of established further therapy lines, the interdisciplinary tumour conference made a decision to evaluate and perform PSMA-RLT under compassionate use in compliance with §13.2b of the German Medicinal Products Act (AMG). Pre-therapeutic PET imaging showed increased tumoral PSMA-radioligand uptake. There were no contraindications including sufficient kidney function and bone marrow reserve. ***Results:*** 7912 MBq of ^{177}Lu-PSMA-617 were intravenously injected. The patient received concomitant prophylactic dexamethasone. There were no immediate adverse events of PSMA-RLT, the treatment was well tolerated. Post-therapeutic 2-bed position SPECT and low-dose CT scans of the head, neck, thorax, and upper abdomen were performed at 3h, 24h, 48h, 5d, and 7d p.i., and used for dosimetry analyses, values were not recovery-corrected. The tumor volume was 1.9 ml, mean tumor dose was 1.34 Gy. A focally increased tumoral uptake was found until 7 days p.i. Mean dose in the kidneys was 1.87 Gy, in the parotid glands 0.85 Gy and in the submandibular glands 0.80 Gy. Continuous follow-up over 5 weeks showed no adverse events, a second cycle was planned. ***Conclusion:*** As shown by this preliminary data, the dose of ^{177}Lu-PSMA-617 in organs-at-risk in a patient with high-grade glioma was not superior to those known for patients with advanced PCa, despite the significantly lower total tumour volume compared to advanced PCa. ^{177}Lu-PSMA-617 showed a prolonged retention in the tumor. The tumor dose was low compared to PCa and a previously reported glioblastoma case, however the association between dose and efficacy in glioma deserves further consideration, and may encompass immunological mechanisms of action. More data are warranted to evaluate safety and efficacy of ^{177}Lu-PSMA-RLT in glioma.

OP-468

First-In-Human CXCR4 & FAP Instillation Theranostics in Muscle invasive bladder cancer patients predicted not to respond to Neoadjuvant chemotherapy within the Bladder BRIDGister.

R. Wirtz[1,2,3], *L. Kastner*[4], *P. C. Voß*[5], *F. Friedersdorff*[6], *D. Barski*[7], *T. Otto*[8], *M. Waldner*[9], *E. Veltrup*[1], *F. Linden*[1], *M. Schwandt*[1], *R. Hake*[3], *S. Eidt*[1], *J. Roggisch*[10], *C. Rieger*[4], *S. Koch*[11,12], *T. H. Ecke*[13], *A. Heidenreich*[14], *L. Greifenstein*[15], *R. P. Baum*[2,15];
[1]*STRATIFYER Molecular Pathology GmbH, Cologne, GERMANY,* [2]*ICPO Foundation, Ravensburg, GERMANY,* [3]*Institute of Pathology at the St. Elisabeth Hospital, Cologne, GERMANY,* [4]*Dpt. of Urology, University Clinic Cologne, Cologne, GERMANY,* [5]*Dpt. of Urology, Charité - Universitätsmedizin Berlin, Berlin, GERMANY,* [6]*Dpt. of Urology, Evangelisches Krankenhaus Königin Elisabeth Herzberge, Berlin, GERMANY,* [7]*Dpt. of Urology, Rheinlandklinikum, Neuss, GERMANY,* [8]*Dpt. of Urology, Rheinlandklinikum, Cologne, GERMANY,* [9]*Dpt. of Urology St. Elisabeth Hospital, Cologne, GERMANY,* [10]*Institute of Pathology, HELIOS Hospital, Cologne, GERMANY,* [11]*Brandenburg Medical School, DE-14770 Brandenburg, Berlin, GERMANY,* [12]*Institute of Pathology, HELIOS Hospital, Bad Saarow, GERMANY,* [13]*Department of Urology, HELIOS Hospital, Berlin, GERMANY,* [14]*Dpt. of Urology, University Clinic Cologne, Cologne, GERMANY,* [15]*CURANOSTICUM Wiesbaden-Frankfurt, Wiesbaden, GERMANY.*

Aim/Introduction: Patients with muscle invasive urothelial carcinoma (MIBC) achieving pathological complete response (pCR) upon neoadjuvant chemotherapy (NACT) have improved prognosis. CXCR4 and FAP is found in chemoresistant, stroma-associated MIBC. This study aimed to prospectively validate the predictive value of molecular target typing and to assess CXCR4 & FAP radioligand instillation imaging and therapy in selected patients of the „Bladder BRIDGister". ***Materials and Methods:*** Formalin fixed paraffin embedded (FFPE) tissues from transurethral resections (TUR) before chemotherapy and cystectomy samples after NACT of 36 patients were retrospectively

collected and 650 TURB samples were prospectively collected as part of the Bladder BRIDGister. RNA from FFPE tissues were extracted by commercial kits, relative gene expression of subtyping markers (KRT5, KRT20, FGFR1) and radioligand target genes (CXCR4, FAP) were analyzed by standardized RT-qPCR systems (STRATIFYER Molecular Pathology GmbH, Cologne). PET/CT Imaging by ^{68}Ga-CXCR4 instillation was performed after completion of cisplatinum based NACT. ^{177}Lu-FAP treatment was performed subsequently by instillation +/- systemic application. ***Results:*** The retrospective NACT cohort consisted of 36 patient (median age: 69, male: 83%). Hierarchical clustering revealed that CXCR4 and FAP are elevated in stromal rich, KRT5 & KRT20 negative tumors not responding to NACT. Elevated FAP above mdian mRNA expression was significantly associated with resistance to NACT (chi^2 4.314 p=0,0378). Combining elevated FAP and CXCR4 mRNA expression did identify 28% of the patients to be at high risk of NACT resistance (90%). TUR biopsies from MIBC patients undergoing NACT were molecularly analyzed for subtype and radioligand expression. Exemplarily one pT2 G3 MIBC patient was selected for PET/CT imaging after two cycles that was predicted to be unresponsive to NACT. As CXCR4 radioligand imaging is associated with hematologic toxicity we instilled ^{68}Ga CXCR4 and did see tumor specific uptake into the chemotherapy-resistant MIBC invading the adjacent soft tissue. Subsequent instillation and systemic therapy cycles with ^{177}Lu-FAP also revealed strong uptake into the invading MIBC and a newly developed cancer site within the bladder. ***Conclusion:*** We show that the mRNA expression of the radioligand targets CXCR4 and FAP in TURB tissue of MIBC patients is associated with aggressive, stromal-like tumors not responding to neoadjuvant chemotherapy. This could be validated by selecting patients for FAP & CXCR4 PET/CT and imaging of resistant tumor residues invading surrounding soft tissue. Instillation of radioligands into the bladder revealed to be safe and effective for imaging and therapy of patients being unresponsive to standard therapies.

OP-469

Dual-tracer PET/CT imaging in response assessment to peptide receptor radionuclide therapy - a case report

I. Próspero, *G. Ferreira, J. C. Ferro, D. Barbosa, D. G. Silva, S. Fontão de Castro, J. P. Teixeira, H. Duarte, I. Lucena Sampaio; Instituto Português de Oncologia do Porto, Porto, PORTUGAL.*

Aim/Introduction: Dual-tracer positron emission tomography/computed tomography (PET/CT) using 2-[^{18}F]FDG PET/CT combined with somatostatin receptor (SSTR) PET/CT identifies tumor heterogeneity in neuroendocrine neoplasms (NENs), providing prognostic information and allowing optimal therapeutic decision. Nevertheless, standardized criteria for its selective use in NENs assessment before and after peptide receptor radionuclide therapy (PRRT) are not yet established. ***Materials and Methods:*** We report a case of a 63-year-old man with an asymptomatic Grade 2 (G2) Pancreatic Neuroendocrine Tumour (Pan-NET) with hepatic metastasis, diagnosed in 2011. He underwent a distal pancreatectomy and splenectomy in 2012, three procedures of embolization with polyvinyl alcohol (PVA) between 2011 and 2014, three cycles of PRRT with [^{177}Lu]Lu-DOTATATE in 2016, and has been under long-acting somatostatin analogue therapy since 2013. The disease was considered stable for almost 4 years after PRRT. Due to new hepatic lesions detected in [^{68}Ga]Ga-DOTANOC PET/CT in 2020 and 2021, the patient was referred for a PRRT retreatment (consisting of 2 cycles of 7400 MBq each), which he completed in December 2021. ***Results:*** The evaluation of treatment response in a [^{68}Ga]Ga-DOTANOC PET/CT performed two months later showed a decrease in the number of hepatic lesions expressing SSTR relatively to the imaging acquired before PRRT retreatment. A 2-[^{18}F]FDG PET/CT carried out two weeks afterwards demonstrated two lesions DOTANOC-negative/FDG-positive and one lesion DOTANOC-positive/FDG-positive, with the remaining hepatic metastasis classified as DOTANOC-positive/FDG-negative. An abdominal MRI (Magnetic Resonance Imaging) acquired nine months after the last PRRT cycle confirmed disease progression. The patient remained asymptomatic. It was then decided to treat the liver metastasis with transarterial embolization, which was performed in January 2023. ***Conclusion:*** The results suggest that functional imaging response assessment to PRRT by SSTR PET/CT alone may not be sufficient in some metastatic NENs. Furthermore, disease characterization before PRRT retreatment could have been performed with 2-[^{18}F]FDG PET/CT, additionally to SSTR PET/CT, since histological grade may have evolved over time from the first biopsy, developing a more aggressive disease pattern, which could eventually change treatment choice. Therefore, this case highlights the role of dual-tracer PET/CT imaging in NENs, particularly in the context of PRRT retreatment, with the potential for a better optimization of treatment decision and response evaluation.

OP-470

Bone-Marrow dosimetry with 177Lu-DOTATATE treatment in a hemodialysis patient.

S. CHAIB[1,2], *P. Tylski*[1], *C. Lachachi*[1], *T. Keniza*[1], *E. Levigoureux*[1,2]; [1]*Hospices Civils de Lyon, Lyon, FRANCE,* [2]*Claude Bernard Lyon 1 University, Lyon Neuroscience Research Center, CNRS, INSERM, Lyon, FRANCE.*

Aim/Introduction: The main excretion for the 177Lu-DOTATATE targeted therapy is renal. Consequently doses to organs at risk for hemodialysis patients may be higher, but there is no recommendation to adapt the prescribed activity. In absence of nephrotoxicity, the bone marrow is the primary organ at risk. This case study details a hemodialysis-dependant patient with a metastatic neuroendocrine tumor treated with 177Lu-DOTATATE. ***Materials and Methods:*** A 63-year-old female patient with stage V chronic renal failure was hospitalized for 3 days to receive an injection of 3700 MBq of 177Lu-DOTATATE. Two hemodialysis sessions were performed at day +1 and day +3 post-injection. Seven whole blood samples were collected during the stay and counted in duplicate. During this period, five whole-body images were acquired and a SPECT/CT scan was acquired 3 hours after the start of injection. The 177Lu-DOTATATE elimination and the dose to the bone marrow were estimated using two methods, one based on blood counts and another based on planar imaging (1) , distinguishing between low- and high-uptake compartments. Additionally, measurements for radiation protection were taken for medical staff and the environment. ***Results:*** During the first dialysis, 177Lu removed was 76% and 41% in blood for the 2nd dialysis session. The estimated number of disintegrations in the bone marrow compartment was 0.71 MBq.h/MBq using the image-based method and 0.97 MBq.h/MBq using the blood based method. The corresponding absorbed dose to the bone marrow was 0.66 Gy and 0.74 Gy using the two methods respectively, corresponding to doses per injected activity of 185 and 207 mGy/MBq. The dose rate measurements taken from the patient during the period between injection and discharge ranged from 400 to 266 µSv/h at contact and 14.1 to 6.5 µSv/h at 1 meter away. The operational dosimeters worn by the dialysis

nurses recorded doses of 19 µSv and 16 µSv during the first and second hemodialysis sessions, respectively. ***Conclusion:*** The mean doses estimated are below the toxicity threshold of 2 Gy for the bone marrow suggesting a safe administration for hemodialysis patients although the estimated doses are higher than those typically reported for patients without renal failure (between 2 and 150 mGy/MBq). ***References:*** 1. Svensson, J. et al. A novel planar image-based method for bone marrow dosimetry in 177Lu-DOTATATE treatment correlates with haematological toxicity. EJNMMI physics 3, 1-12 (2016).

OP-471

Evaluation of the potential use of [^{18}F]F-Al-NOTA-Octreotide as a theranostic probe for PRRT with [^{177}Lu]Lu-DOTA-TATE compared to [^{111}In]In-DTPA-Pentetreotide

B. A. M. Lima*, R. C. M. Felix, D. A. Bulzico, P. B. Pujatti;*
Brazilian National Cancer Institute, Rio de Janeiro, BRAZIL.

Aim/Introduction: To evaluate uptake sites in [^{18}F]F-Al-NOTA-Octreotide PET/CT and [^{111}In]In-DTPA-Octreotide SPECT/CT of a 49 years old female patient submitted to [^{177}Lu]Lu-DOTA-TATE. Initially submitted to enterectomy after intestinal obstruction in 2017 with intraoperative mesenteric mass and liver nodules. Pathology study revealed a G2 neuroendocrine tumour (Ki67 of 10%). Liver disease progression was observed in conventional imaging methods two years later and the patient was submitted to liver metastasectomy and retroperitoneal lymphadenectomy. After this second surgery [^{111}In]In-DTPA-Octreotide scan showed one focal liver uptake (Krenning 3). Asymptomatic, she lost follow-up, returning in July 2022 referring flushing and dhiarrhoea. New [^{111}In]In-DTPA-Octreotide scan abnormal focal uptakes were noticed in the liver and in a supraclavicular lymph node (Krenning 3) and long acting somatostatin analogue therapy was introduced. Imaging control exams were performed in December 2022 including a new [^{111}In]In-DTPA-Octreotide that revealed two new mesenteric foci. After tumour board discussion, the patient was referred to peptide receptor radionuclide therapy (PRRT) with [^{177}Lu]Lu-DOTA-TATE. ***Materials and Methods:*** As our Institution is conducting a clinical trial comparing [^{18}F]F-Al-NOTA-Octreotide PET-CT with [^{111}In]In-DTPA-Octreotide SPECT-CT in the context of cost-effectiveness of somatostatin-receptor imaging in a Public Health System of a developing country, she was invited to participate, conceived formal consent and prior to PRRT was submitted to PET-CT scan 90 minutes after i.v. injection of 4.4 MBq/kg of [^{18}F]F-Al-NOTA-Octreotide. ***Results:*** PET/CT showed uptake in three hepatic lesions (SUVmax 25,1), the supraclavicular lymph node (SUVmax 17,2) and others lymph nodes in paraesophageal, retroperitoneal, paraortic and mesenteric regions (SUVmax of 8,4, 7,2 and 4,4, respectively), and two pancreatic foci (SUVmax 14,4). So far, she has been submitted to two cycles of 7.4 GBq of [^{177}Lu]Lu-DOTA-TATE and the post-PRRT scans shows uptake in one hepatic lesion, the supraclavicular and two mesenteric lymph nodes and one discrete uptake in the mid paraesophageal lymph node observed in PET-CT. ***Conclusion:*** This case report shows that not only the same lesions with somatostatin receptor expression in [^{111}In]In-DTPA-Octreotide SPECT/CT were observed in the post-PRRT scans but also in [^{18}F]F-Al-NOTA-Octreotide PET-CT, a new probe with suitable pharmacokinetics and high somatostatin receptor affinity[1] suggested to be able to outperform current gold standard [^{68}Ga]Ga-DOTA-TATE[2], indicating its adequate use for theranostics purpose. ***References:*** 1.Laverman P, et al. A novel facile method of labeling octreotide with (18)F-fluorine. J Nucl Med. 2010 Mar;51(3):454-61. 2.Pauwels E, et al. ^{18}F-AlF-NOTA-Octreotide Outperforms ^{68}Ga-DOTATATE/NOC PET in Neuroendocrine Tumor Patients: Results from a Prospective, Multicenter Study. J Nucl Med. 2023 Apr;64(4):632-638.

OP-472

Peptide receptor radionuclide therapy (PRRT) with [177Lu]Lu-DOTA-TATE in the treatment of malignant insulinoma: a case report of remarkable clinical and imaging response

D. Barbosa*, H. Duarte, A. Paula Santos, J. Ferro, I. Próspero, D. Silva, S. Gil-Santos, R. Calheiros, S. Fontão de Castro, G. Ferreira, J. P. Teixeira, I. Lucena Sampaio;*
Portuguese Institute of Oncology, Oporto, PORTUGAL.

Aim/Introduction: Malignant insulinomas are a rare type of functional pancreatic neuroendocrine tumors (panNETs), often associated with high morbidity and mortality, mainly due to life-threatening hypoglycemic episodes. Since studies on its therapeutic algorithm are scarce, we present the case of a patient with malignant insulinoma treated with PRRT just 4 months after diagnosis. ***Materials and Methods:*** A 78 year-old woman with apparently non-functional metastatic panNET G2 performed a [68Ga]68Ga-DOTA-Somatostatin Analog Positron Emission Tomography/Computed-Tomography ([68Ga]68Ga-DOTA-SSA-PET/CT) revealing high somatostatin receptors (SSTRs) expression in pancreatic body/tail, in a celiac lymph node and in several hepatic lesions. 2-[18F]fluoro-2-desoxi-D-glucose PET/CT (2-[18F]FDG-PET/CT) was also performed and didn´t reveal discordant lesions (FDG+;SSTR-). Careful review of symptoms at our Institute revealed episodes of nocturnal sweating and dizziness. Symptomatic hypoglycemia and endogenous hyperinsulinism due to malignant insulinoma was confirmed (elevated insulinemia, proinsulin and C-peptide). Therapy with sub-cutaneous 100mcg octreotide was introduced. Due to worsening of hypoglycemic episodes, lanreotide was added every 28 days and octreotide frequency was increased. Given the high expression of SSTRs in most lesions and the rapid onset of symptoms, the patient underwent 4 cycles of PRRT with [177Lu]Lu-DOTA-TATE with an interval of 8-10 weeks (cumulative activity: 29,6GBq). ***Results:*** Just 10 days after the first cycle of PRRT, the patient showed significant clinical improvement with only 2 episodes of hypoglycemia; in 1 month, octreotide was discontinued and C-peptide and insulin values reverted to normal. After the second cycle, the patient normalized the number of daily meals (4-5) and revealed a great improvement in symptoms. Ten weeks after fourth PRRT cycle, the patient remained without hypoglycemic crises with grade 1 hematological toxicity. Abdominal reassessment CT (3 months after fourth PRRT cycle) revealed a decrease in number and lesion size. [68Ga]68Ga-DOTA-SSA-PET/CT performed 6 months after the end of treatment (13 months after the first cycle and 17 months after diagnosis) revealed a decrease in the extent of radiopharmaceutical uptake in the pancreas and the disappearance of uptake in most liver lesions and in the celiac lymph node. Currently, 20 months after diagnosis, the patient remains under follow-up, asymptomatic, with a clear improvement in her quality of life and a persistent tumor burden reduction in imaging studies. ***Conclusion:*** The optimal time to initiate PRRT in malignant insulinomas is still up for debate. This case supports that PRRT is safe and can be considered as a second-line treatment for progressive malignant insulinomas. More studies, with larger samples, are required.

OP-473

Peptide receptor radionuclide therapy as neoadjuvant treatment in pancreatic neuroendocrine tumours

I. Próspero, *G. Ferreira, J. C. Ferro, D. Barbosa, D. G. Silva, S. Fontão de Castro, J. P. Teixeira, H. Duarte, I. Lucena Sampaio; Instituto Português de Oncologia do Porto, Porto, PORTUGAL.*

Aim/Introduction: In pancreatic neuroendocrine tumours (Pan-NETs), peptide receptor radionuclide therapy (PRRT) is traditionally recommended in unresectable or metastatic, progressive disease, after failure of other systemic therapies. Therefore, its role as a neoadjuvant treatment is not yet established in current treatment guidelines. ***Materials and Methods:*** A 52-year-old man, presenting with weight loss, was diagnosed in 2017 with a Grade 2 (G2) Pan-NET through radiological studies and a biopsy. The lesion, measuring 60 x 58 mm in the axial plane, was located in the pancreatic head, causing dilation of the main pancreatic duct, and had extensive contact with the superior mesenteric vein and the inferior vena cava; hence, invasion of these structures could not be excluded. Staging through [^{68}Ga] Ga-DOTANOC PET/CT and 2-[^{18}F]FDG PET/CT revealed intense uptake of [^{68}Ga]Ga-DOTANOC [maximum standardized uptake value (SUVmax)= 76,9] and moderate glycolytic metabolism (SUVmax= 4,0), with no evidence of metastasis. The tumour was considered potentially unresectable, and the patient was referred for PRRT, with the objective of reducing the tumour volume and subsequent reevaluation of the feasibility of a surgical approach. ***Results:*** The patient underwent three cycles of PRRT with [^{177}Lu] Lu-DOTATATE (7400 MBq per cycle; 12 weeks between cycles) from March to September 2018, with no clinically significant toxicity. He started long-acting somatostatin analogue therapy in the following month. Restaging through morphologic imaging (three months after completing PRRT) revealed a reduction in the tumour size to 48 x 44 mm (-20% in the longest axial diameter), and absence of invasion of the (aforementioned) vascular structures. The patient was submitted to a pancreaticoduodenectomy with curative intent in February 2019. Subsequent treatment assessments through morphologic and functional imaging have revealed no signs of residual disease or recurrence to date, for a follow-up period of approximately 49 months. ***Conclusion:*** PRRT exhibits potential as an effective neoadjuvant therapy in unresectable localized Pan-NETs, contributing to tumour downsizing and subsequent resectability, namely in the context of suspected vascular invasion and large tumour size, with promising disease free survival results. ***References:*** 1. Pavel M, Öberg K, Falconi M, Krenning EP, Sundin A, Perren A, et al. Gastroenteropancreatic neuroendocrine neoplasms: ESMO Clinical Practice Guidelines for diagnosis, treatment and follow-up [Internet]. Vol. 31, Annals of Oncology. Elsevier BV; 2020. p. 844-60. Available from: http://dx.doi.org/10.1016/j.annonc.2020.03.304

OP-474

Safety and Efficacy in a Recurrent Squamous Cell Carcinoma of the Foot treated with Sequential Applications of 188Re-resin

L. Vetrone[1], *P. Castellucci*[2], *C. Baraldi*[3], *S. Vichi*[4], *F. Zagni*[5], *B. Piraccini*[3], *L. Strigari*[5], *S. Fanti*[1,6];
[1]*Nuclear medicine, Alma Mater Studiorum University of Bologna, BOLOGNA, ITALY,* [2]*Nuclear Medicine, IRCCS, Azienda Ospedaliero-Universitaria di Bologna, BOLOGNA, ITALY,* [3]*Dermatology Unit, IRCCS Azienda Ospedaliero-Universitaria di Bologna, BOLOGNA, ITALY,* [4]*Clinical Engineering Department, IRCCS, Azienda Ospedaliero-Universitaria di Bologna, BOLOGNA, ITALY,* [5]*Medical Physics Department, IRCCS Azienda Ospedaliero-Universitaria di Bologna, BOLOGNA, ITALY,* [6]*Nuclear Medicine, IRCCS, Azienda Ospedaliero-Universitaria di Bologna, Bologna, ITALY.*

Aim/Introduction: Brachytherapy using ^{188}Re-resin is an emerging and promising technique to treat Non-Melanoma Skin Cancers. However, most of the (scarse) literature is based on single treatments since the response rate ranges between 90-95%. Aim of this report is to assess feasibility, efficacy and safety of multiple sequential treatments using ^{188}Re-resin in a 69 years old female with recurrent squamous cell carcinoma (SCC). ***Materials and Methods:*** The patient was enrolled according to the following inclusion criteria: histologically proven SCC; lesion's thickness lower than 3 mm; difficult to treat with surgery, evaluation with biopsy and dermoscopy after 6 months. Toxicity was evaluated according to Common Terminology Criteria for Adverse Events (CTCAE-5.0) scale, while cosmetic results were assessed according to the Radiation Therapy Oncology Group (RTOG) scale. The patient had a biopsy proven SCC on the left foot with a surface area of 14.5cm^2 and 1mm of neoplastic invasion. We treated the lesion using 400MBq ^{188}Re-resin for 61minutes of application time; absorbed dose at 0.5 mm depth was 27Gy, absorbed dose at 1mm was 15Gy, superficial absorbed dose was 78Gy. Seven months after therapy, the patient showed an 8cm^2 recurrence of SCC 1mm thick. Two months later a retreatment was performed using 126 MBq ^{188}Re-resin for 146 minutes; absorbed dose at 0.5mm was 32Gy, absorbed dose at 1mm was 20Gy and superficial dose was 106Gy. Eight months later a second smaller recurrence has been observed showing a surface area of 2cm^2 and 1.5mm neoplastic invasion. A third ^{188}Re-resin treatment was performed using 150MBq for 50minutes; absorbed doses were: 40Gy at 0.5mm, 25Gy at 1.5mm and 130Gy at the surface. ***Results:*** Five weeks after each treatment toxicity was G1 according to the CTCAE scale; the first two treatments showed excellent cosmetic results according to the RTOG scale. Not significant adverse events nor pain during and after treatments were reported, however we cannot report the efficacy of the third treatment since the patient is still under follow up. ***Conclusion:*** In this case the early recurrences were probably due to an underestimation of the real thickness of the lesion since, especially in large lesions, it is possible that neoplastic invasion is deeper than the one assessed by biopsy. For this reason, it should be always recommended to perform multiple biopsies before 188Re-resin therapy. Finally, re-treatment with ^{188}Re-resin in case of recurrence is safe even after several applications in the same area.

1101

Monday, September 11, 2023, 16:45 - 18:15
Hall A

CME 8 - Oncology & Theranostics Committee: Assessing Response to Peptide Receptor Radionuclide Therapy in Patients with Neuroendocrine Tumors

OP-475

PRRT Combinations in On-Going Trials

I. Virgolini *;
Department of Nuclear Medicine, Medical University Innsbruck, Innsbruck, AUSTRIA.*

OP-476
RECIST and Beyond: How Can Radiological Assessment Be Improved?
L. Solnes;
The Russell H Morgan Department of Radiology and Radiological Science, Johns Hopkins School of Medicine, Baltimore, UNITED STATES OF AMERICA.

OP-477
Functional Nuclear Medicine Parameters (Predictive and/or Prognostic)
V. Ambrosini;
NuclearMedicine, Alma Mater Studiorum, University of Bologna, IRCCS Azienda Ospedaliero-Universitaria di Bologna, Bologna, ITALY.

OP-478
How to Structure Pts' Follow-Up After PRRT: Guidelines and Beyond
J. Strosberg;
Moffitt Cancer Center Tampa, Tampa, UNITED STATES OF AMERICA.

1102

Monday, September 11, 2023, 17:15 - 18:15
Hall D (Arena)

Debate 3 - Physics Committee: AI in Nuclear Medicine: Fear or Embrace?

OP-479
Embrace Artificial Intelligence
M. Sollini;
Department of Nuclear Medicine, IRCCS Humanitas Research Hospital, Milan, ITALY.

OP-480
Beware of Artificial Intelligence
G. Gaglio;
Professor of Sociology, Research Group in Law, Economics and Management (GREDEG), Côte d Azur University, Nice, FRANCE.

1103

Monday, September 11, 2023, 16:45 - 18:15
Hall E1

LIPS Session 8 - Cardiovascular Committee: Stiff to Sweet - Infiltration and Inflammation

OP-481
Infiltrative cardiac disease: Harder muscle, softer interpretation
S. Ben Haim;
UniversityHospital Hadassah, Jerusalem, Department of Nuclear Medicine, Jerusalem, ISRAEL.

OP-482
Inflammatory cardiac diseases. The sweeter it gets, the hottest it is.
F. Caobelli;
Universitätsklinik für Nuklearmedizin Inselspital Bern, Bern, SWITZERLAND.

OP-483
Quantification: The cherry on top?
M. Burniston;
Head of Nuclear Medicine Physics Barts Health NHS Trust, London, UNITED KINGDOM.

1104

Monday, September 11, 2023, 4:45 PM - 6:15 PM
Hall E2

M2M Track - TROP Session: Efficient Radiolabelling: Key for Clinical Translation

OP-487
Functionalized rigidified pentadentate chelators useful for the [Al^{18}f]$^{2+}$labeling of biomolecules
L. Tei[1], *J. Martinelli*[1], *L. Russelli*[2], *G. Multhoff*[3], *C. D'Alessandria*[2]; [1]*Department of Science and Technological Innovation, University of Piemonte Orientale, Alessandria, ITALY,* [2]*Department of Nuclear Medicine, Technical University Munich, Munich, GERMANY,* [3]*Department of Radiation Oncology, TranslaTUM, Technical University Munich, Munich, GERMANY.*

Aim/Introduction: Al(III) complexes have been recently investigated for their use in PET imaging by formation of ternary complexes with the radioisotope fluorine-18 (^{18}F). The gold standard chelator for such methodology is NOTA (1,4,7-triazacyclononane-1,4,7-triacetic acid), although it requires high temperature to obtain reasonable radiochemical yields.[1,2] Thus, non-macrocyclic, semi-rigid pentadentate chelators having two N- and three O-donor atoms such as RESCA1 and AMPDA-HB have been recently proposed with the aim to allow room temperature [Al^{18}F]$^{2+}$ labelling of temperature sensitive biomolecules.[3,4] ***Materials and Methods:*** The 2-aminomethylpiperidine (AMP)-based chelators 2-AMPTA, 2-AMPDA-HB and NHB-2-AMPDA were synthesized and labelled with [Al^{18}F]$^{2+}$ at different temperatures (25-90°C) and in the pH range 4-6.5.[3] Once found the most effective chelator for [Al^{18}F]$^{2+}$ labelling, bifunctional derivatives bearing NHS-activated ester (2-AMPDA-HB-NHS) and maleimide (2-AMPDA-HB-mal) groups were synthesized and conjugated to an antibody fragment anti-Galectin-3 (antiGal3-F(ab')) and to a tumor cell-penetration peptide probe (TPP), recognizing the tumor-specific membrane heat shock protein 70 (Hsp70) expression. After purification, the purity of the tracers was confirmed via radio-HPLC and radio-TLC, whereas their stabilities were measured in vitro (up to 4h in PBS, Serum and EDTA) and in vivo in a syngeneic subcutaneous breast cancer (4T1) mouse model. ***Results:*** The chelator AMPDA-HB showed the best [Al^{18}F]$^{2+}$ labelling performance at 37°C and pH 5.5-6 (70-80%). In vivo experiments in in tumor-free mice highlighted high rapid hepatobiliary and renal excretion of the labelled complex and low accumulation in the bones. The labelling with AlF-18 of the bioconjugates 2-AMPDA-HB-antiGal3-F(ab') and 2-AMPDA-HB-mal-TPP resulted in a radiochemical yield respectively of 28 and 22% (radio-TLC), and a radiochemical purity of >94% after purification. Once the in vitro stability was confirmed in human serum, the AlF-18 labelled 2-AMPDA-HB-mal-TPP was injected i.v. in 7 mice with subcutaneous breast cancer (4T1). PET scans were acquired 1h after injection of the tracer for 15 min after which the tracer accumulated in the tumor as determined in biodistribution assays. The in vivo study on 2-AMPDA-HB-antiGal3-F(ab') is ongoing. ***Conclusion:*** The development of the

AMP-based pentadentate chelators and their conjugation to selected biomolecules brings important innovation in the field of AlF-18 radiolabelling providing a new tool for the application of Al-F18 approach to oncological or ImmunoPET imaging. ***References:*** [1] Schmitt, S.; Moreau, E. Coord. Chem. Rev. 2023, 480, 215028. [2] Archibald, S.J.; Allott, L. EJNMMI 2021, 6, 30. [3] Russelli, L. et al. ChemMedChem, 2020, 15, 284-292. [4] Cleeren, F. et al. Nat. Prot. 2018, 13, 2330-2347.

OP-488

Development of a kit formulation of Technetium-99m labeled holmium microspheres as scout dose for radioembolization treatment planning.

M. Boswinkel[1], *P. Laverman*[1], *T. Weisheit*[2], *R. Drescher*[2], *J. F. W. Nijsen*[1];
[1]*Department of Medical Imaging, Radboud University Medical Center, Nijmegen, NETHERLANDS,* [2]*Clinic of Nuclear Medicine, University Hospital Jena, Jena, GERMANY.*

Aim/Introduction: Treatment planning of radioembolization with holmium-166 microspheres (^{166}Ho-MS) is currently performed using technetium-99m macroaggregated albumin particles (^{99m}Tc-MAA) or a scout dose of ^{166}Ho-MS. While the distribution ^{166}Ho-MS better corresponds to the therapeutic dose of ^{166}Ho-MS, it must be pre-ordered, ^{99m}Tc-MAA provides better imaging quality. Therefore we developed a kit formulation to label non-radioactive Holmium-165 microspheres (Ho-MS) with Tc-99m, to obtain a product with reliable distribution, optimal availability, and good imaging quality. ***Materials and Methods:*** Sterilized GMP-grade Ho-MS (60 mg) were labeled with 300 MBq [^{99m}Tc]pertechnetate in the presence of various amounts of stannous chloride, and incubated for various temperatures and durations. Parameters investigated included stannous chloride concentration, incubation temperature and duration, and the use of a glass vial or an Eppendorf tube. Quality control was performed using ITLC and centrifugation (supernatant and radiolabeled microspheres were separated, and radioactivity measured in each sample). Radiochemical purity (RCP) and maximal specific activity were determined. Stability tests were performed in 0.1% pluronic at room temperature (RT), and in plasma at 37 °C for 2 h. Microsphere integrity was investigated using multisizer analysis, microscopy, and free acetylacetonate (AcAc) concentration. ***Results:*** Optimization of the ^{99m}Tc labeling was performed in several steps. A stannous chloride concentration of 100 µg was found optimal, and a temperature of 37 °C more efficient than RT. Using a glass vial the RCP increased from 72% to 94%. In addition, the incubation time could be decreased from 2 h to 15 min. Specific activity was increased from 2.5 MBq/mg to 5 MBq/mg Ho-MS, by using a higher starting activity, resulting in a final product containing of 300 MBq/60 mg Ho-MS (single patient dose). Preliminary tests showed that the integrity of the microspheres was not affected by ^{99m}Tc labeling. Microscopy images showed intact structure of the microspheres, multisizer analysis showed that the microspheres had a mean diameter of 27 µm (range 15-60 µm), and free AcAc concentration was less than 0.4 wt%, indicating good integrity. Radiolabeled product was stable in 0.1% pluronic and plasma, with a RCP of 95% and 83%, respectively, after 2 h. ***Conclusion:*** ^{99m}Tc-labeled Ho-MS can be labeled in 15 min and are a therefore promising for scout dosing of radioembolization patients. Using these ^{99m}Tc-Ho-MS as a scout dose may lead to optimized and flexible treatment planning with high similarity to the therapeutic ^{166}Ho-MS dose and with better imaging quality.

OP-489

Large-scale, GMP-compliant production and quality control of Al[^{18}F]F-NOTA-Octreotide

V. Kramer[1,2], *A. Bispo*[3], *C. Gomez*[3], *D. Zouain*[3], *L. Cantuarias*[1], *C. Soza-Ried*[1,2], *N. Emmanuel*[4], *G. Decoux*[4], *C. Goncalves Gameiro*[4];
[1]*Positronpharma, Santiago de Chile, CHILE,* [2]*Nuclear Medicine & PET/CT Center Positronmed, Santiago de Chile, CHILE,* [3]*R2IBF, Rio de Janeiro, BRAZIL,* [4]*Ion Beam Applications, Louvain-la-Neuve, BELGIUM.*

Aim/Introduction: [^{68}Ga]Ga-DOTATATE is well established for PET/CT imaging of neuroendocrine tumors (NET). Al[^{18}F]F-NOTA-Octreotide is an emerging radiotracer for the same indication, allowing for large-scale, centralized production improving patient access to precision imaging for the same indication[1]. In this work, our objective was to evaluate the production capacity and the influence of starting activities on critical parameters such as radiochemical yields (RCY), purity (RCP), reliability and stability. ***Materials and Methods:*** A GMP-compliant production process for Al[^{18}F]F-NOTA-Octreotide was developed, optimized, and validated at two independent radiopharmacies. Briefly, [^{18}F]fluoride was trapped on a QMA cartridge, rinsed with water, and eluted with EtOH/NaCl 0.9%. Subsequently, the precursor solution was added and heated to 100 **°C** for 10 minutes before standard workup and reformulation. Quality control was performed including appearance, pH, radionuclidic, radiochemical, and chemical purity, residual solvents, endotoxins, and sterility, compliant with the European pharmacopeia. We collected and analyzed 60 production records from executed between August 2022 and March 2023, applying the same methods for production and quality control. ***Results:*** From starting activities of 157,8 ± 47,5 GBq we obtained an overall average of 51,0 ± 23,5 GBq (31,8 ± 9,8 % RCY n.d.c., n=57) Al[^{18}F]F-NOTA-Octreotide with 96,5 ± 2,9 % RCP. The implemented process can provide up to 100 GBq of Al[^{18}F]F-NOTA-Octreotide with high RCPs and stability was confirmed of up to 10h EOS. Of a total of n=61 analyzed production batches, n=3 (5%) were out of specification, n=1 (1.6%) resulted in no product and from n=57 batches, 550 doses have been supplied to >10 PET imaging sites with excellent clinical results as previously published[3] ***Conclusion:*** Al[^{18}F]F-NOTA-Octreotide can be obtained in large amounts, with excellent and reliable radiochemical yields and purity, and improves patient access to precision diagnostic imaging of NETs. ***References:*** 1. Pauwels, E.; Cleeren, F.; Tshibangu, T.; Koole, M.; Serdons, K.; Boeckxstaens, L.; et al. (18)F-AlF-NOTA-octreotide outperforms (68)Ga-DOTA-TATE/-NOC PET in neuroendocrine tumor patients: results from a prospective, mul-ticenter study. J Nucl Med. 2022. Epub 2022/10/21. doi: 10.2967/jnumed.122.264563. PubMed PMID: 36265911. 2. Tshibangu, T.; Cawthorne, C.; Serdons, K.; Pauwels, E.; Gsell, W.; Bormans, G.; et al. Automated GMP compliant production of [(18)F]AlF-NOTA-octreotide. EJNMMI Radiopharm Chem. 2020;5(1):4. Epub 2020/01/31. doi: 10.1186/s41181-019-0084-1. PubMed PMID: 31997090; PubMed Central PMCID: PMCPMC6989705. 3. Haeger A.; Soza-Ried C.; Kramer V. et al.; Al[18F]F-NOTA-Octreotide Is Comparable to [68Ga] Ga-DOTA-TATE for PET/CT Imaging of Neuroendocrine Tumours in the Latin-American Population. Cancers 15 (2), 439

OP-490

Fully Automated Radiosynthesis of [^{89}Zr]Zr-Crefmirlimab Berdoxam for Clinical Multi-Centre PET Imaging of CD8$^+$ T-Cell Trafficking

C. Wichmann[1], *Z. Cao*[1], *A. McDonald*[1], *N. Guo*[1], *S. Poniger*[2], *F. Scott*[1], *F. Jia*[3], *K. Brady*[3], *W. Le*[3], *A. Scott*[1];
[1]*Olivia Newton John Cancer Research Institute, Heidelberg, AUSTRALIA,* [2]*iPhase Technologies Pty Ltd, Rowville, AUSTRALIA,* [3]*ImaginAb Inc., Inglewood, CA, UNITED STATES OF AMERICA.*

Aim/Introduction: Presence of CD8$^+$ tumour infiltrating lymphocytes in the tumour microenvironment is critical for the immune-oncology therapy response in solid tumours and lymphoma. [^{89}Zr]Zr-crefmirlimab berdoxam (formerly [^{89}Zr]Zr-Df-IAB22M2C) is a promising novel radiotracer that can reveal whole body CD8$^+$ T-cell distribution using positron emission tomography [1]. [^{89}Zr]Zr-crefmirlimab berdoxam is currently being investigated in clinical trials (e.g. iPREDICT study, NCT05013099). In order to support Australian trials, we have developed a fully automated protocol for the clinical radiosynthesis of [^{89}Zr]Zr-crefmirlimab berdoxam. ***Materials and Methods:*** Based on our prior work, automated radiolabelling of Df-Crefmirlimab with ^{89}Zr, formulation, and sterile filtration was established using a disposable cassette-based synthesis module. Starting activity and protein amount were optimized to satisfy patient dose requirements avoiding further manual intervention. Quality control was performed on the formulated product to satisfy clinical release and stability criteria over 6 days. ***Results:*** Df-Crefmirlimab with an approximate chelator-to-minibody ratio of 2 was used for radiolabelling experiments. Radiolabelling reactions were performed in sodium succinate pH 6 with 0.02% Tween 80 which gave >95% conversion after 15 minutes at ambient temperature. Overall process yield of formulated sterile [^{89}Zr]Zr-crefmirlimab berdoxam was 76% ± 7% (n=15) at end-of-synthesis (EOS) with a process time of 45 minutes. Product was formulated in a volume of 10.2 mL ± 0.6 mL (n=15) with maximum total and apparent specific activities at EOS of 205 MBq and 105 MBq/mg, respectively. Calibrated patient dose activity was 40.5 MBq ± 2.9 MBq (n=15) and patient protein dose was 1.53 mg ± 0.17 mg (n=15). Radiochemical purity and immunoreactive fraction at EOS were 99.4% ± 0.5% (n=15) and 95.6% ± 1.8% (n=15), respectively, and dropped to 98.6% ± 0.6% (n=4) and 88.4% ± 1.7% (n=4), respectively, after storage at 4-8°C for 6 days. Size-exclusion HPLC analysis of formulated [^{89}Zr]Zr-crefmirlimab berdoxam demonstrated antibody integrity of 92.7% ± 2.1% (n=15) with 5.5% ± 2.1% (n=15) aggregation. pH of formulated [^{89}Zr]Zr-crefmirlimab berdoxam was 6.47 ± 0.05 (n=15) and sterility and endotoxin levels passed clinical release criteria. ***Conclusion:*** Fully automated production of [^{89}Zr]Zr-crefmirlimab berdoxam for clinical use was achieved with minimal exposure to the operator and excellent stability over 6 days allowing for centralised production. This demonstrates feasibility of automated production of ^{89}Zr-radiopharmaceuticals in a clinical setting. ***References:*** [1] Pandit-Taskar N, Postow MA, et al. First-in-Humans Imaging with ^{89}Zr-Df-IAB22M2C Anti-CD8 Minibody in Patients with Solid Malignancies: Preliminary Pharmacokinetics, Biodistribution, and Lesion Targeting. J Nucl Med. 2020 Apr;61(4):512-519.

OP-491

Radiopharmaceutical production of [^{61}Cu]Cu-NODAGA-LM3 injection solution

M. Alejandre Lafont[1], *T. Basaco Bernabeu*[1], *M. Blagoev*[2], *A. Johayem*[2], *F. De Rose*[3], *C. Porcelli*[3], *L. Jaafar-Thiel*[3], *M. Fani*[1];
[1]*Division of Radiopharmaceutical Chemistry, University Hospital Basel, Basel, SWITZERLAND,* [2]*Department of Nuclear Medicine, University Hospital of Zürich, Zürich, SWITZERLAND,* [3]*Nuclidium AG, Basel, SWITZERLAND.*

Aim/Introduction: Copper based radiotracers are promising compounds in Nuclear Medicine with a broad application field in diagnosis and therapy.[1] Based on pre-clinical results in our group, we present the radiopharmaceutical production of [^{61}Cu]Cu-NODAGA-LM3 (where NODAGA is 1,4,7-triazacyclononane,1-glutaric acid, 4,7-acetic acid and LM3 is p-Cl-Phe-cyclo(D-Cys-Tyr-D-Aph(Cbm)-Lys-Thr-Cys)D-Tyr-NH_2)), including an automatic labeling process and a full set of quality control procedures. This work serves as a preparation for a phase I clinical study on [^{61}Cu]Cu-NODAGA-LM3, which will be launched at University Hospital Basel. Additionally, we present a new and efficient validation procedure for radio-HPLC. ***Materials and Methods:*** [^{61}Cu]$CuCl_2$ was produced using a Nickel solid target irradiated at 40 µA for 2 h at the University Hospital Zurich cyclotron followed by cassette-based automated separation. NODAGA-LM3 was labeled on a clinical scale with [^{61}Cu]$CuCl_2$ in sodium acetate solution with our own labeling procedure, using a modified commercially available cassette mounted on a Modular-Lab PharmTracer synthesizer (EZAG). Chemical and radiochemical purity were determined by radio-HPLC and by radio-iTLC. Sterile filter integrity was proven with a self-designed semi-automatic device and other tests such as ethanol content, pH, ascorbate content and endotoxin testing were performed. ***Results:*** [^{61}Cu]$CuCl_2$ purified solution was obtained in 0.05 M HCl at activity levels of 1.5-2.0 GBq. We successfully developed a fast and reliable automated labeling method to produce [^{61}Cu]Cu-NODAGA-LM3 injection solution with radiochemical yield of around 95 % within 12 min. The achieved radiochemical purity and radio labelling yield were > 90 %. The new radio-HPLC method was successfully validated with proven linearity for chemical (R^2 = 0,9996) and for radiochemical (R^2 = 0.9994) purity, specificity, precision, recovery rate, trueness and sensitivity. The ethanol, and ascorbate content as well as the pH values were all within narrow ranges and met the required specifications. The process was validated for activity amounts on clinical scale. ***Conclusion:*** A production process of high-quality [^{61}Cu]$CuCl_2$ as an active pharmaceutical ingredient (API) was established on a routine basis. Following this, a new [^{61}Cu]Cu-NODAGA-LM3 production process was successfully established and can be carried out completely using a commercially available reagent kit and labeling cassette. It is supported by a new and validated radio-HPLC method and established additional QC-methods with suitable product specifications. A clinical phase I study based on these processes is pending. ***References:*** [1] M. Fani et al., J Nucl Med 2011; 52:1110-1118.

OP-492

Development of an ACE2-Targeting Radiotracer for PET Imaging of the SARS-CoV-2 Entry Receptor

C. Müller[1], *D. Beyer*[1], *J. Wang*[2], *C. Vaccarin*[1], *Y. He*[2], *L. Mu*[2], *J. W. Bode*[2], *R. Schibli*[1];
[1]*Paul Scherrer Institute, Villigen-PSI, SWITZERLAND,*
[2]*ETH Zurich, Zurich, SWITZERLAND.*

Aim/Introduction: The expression level and dynamics of the angiotensin-converting enzyme-2 (ACE2) may be decisive for the susceptibility for SARS-CoV-2 infection and COVID-19 progression and outcome. In previous studies, we and others reported on the development of DX600-based radiopeptides for non-invasive imaging of ACE2, potentially enabling the identification of patients at risk for severe disease progression [1-3]. The aim of this study was to develop an ^{18}F-based PET radiotracer based on the ACE2-binding inhibitor MLN-4760 [4]. ***Materials and Methods:*** ($SnMe_3$)-MLN4760 was synthesized as a precursor for the preparation of [^{18}F]F-MLN-4760, while F-MLN-4760 was synthesized as the reference compound [^{18}F]F-MLN-4760 was obtained in high yields (>1GBq). The radiotracer was investigated on ACE2- and ACE-expressing HEK cells to determine ACE2-specific uptake. The ACE2-binding affinity was determined in displacement experiments using F-MLN-4760 and [^{3}H]MLN-4760. Biodistribution and PET/CT imaging studies were performed at 15 min, 1 h and 3 h after injection of [^{18}F]F-MLN-4760 in nude mice bearing HEK-ACE2 and HEK-ACE xenografts. ***Results:*** ACE2-binding affinity of F-MLN-4760 (IC_{50}: 21.5 ± 2.3 nM) was similar to the original compound MLN-4760 (IC_{50}: 13.5 ± 2.5 nM). [^{18}F]F-MLN-4760 showed specific uptake in HEK-ACE2 cells (45 ± 4% and 63 ± 3% after 1 h and 3 h, respectively), whereas the co-incubation with excess MLN-4760 to block ACE2 prevented it (<1.5%). Binding of [^{18}F]F-MLN-4760 to HEK-ACE cells was negligible (<0.3%). The tissue distribution of [^{18}F]F-MLN-4760 (5 MBq/mouse) showed specific accumulation in HEK-ACE2 xenografts (13 ± 2% IA/g, 1 h p.i.), which declined over time (5.8 ± 0.9% IA/g at 3 h p.i.). No activity accumulation was observed in the HEK-ACE xenograft (<0.3% IA/g). Renal clearance of [^{18}F]F-MLN-4760 was relatively fast (5.1 ± 1.5% IA/g; 1 h p.i.), while substantial activity retention in the intestines was observed (28.2 ± 4.6% IA/g and 5.0 ± 4.8% IA/g after 1 h and 3 h, respectively). No radiodefluorination was observed. ***Conclusion:*** The study data confirmed ACE2-specific binding of [^{18}F]F-MLN-4760 in vitro and in vivo. Structural optimization of the radiotracer will be necessary to improve retention at the target and reduce hepatobiliary excretion. This will be particularly important to enable the imaging of (patho)physiological expression levels of ACE2 in COVID-19 patients. ***References:*** [1] Parker et al. Nucl Med 2021 62:1631. [2] Zhu et al. Adv. Sci. 2021, 8: 2100965. [3] Beyer & Vaccarin et al. EJNMMI Research 2023, 13:32. [4] Towler et al. J Biol Chem 2004, 279, 17996.

OP-493

One-pot combinatorial 18F fluorination: Innovative high-throughput radiolabelling for acceleration of tracer development

S. Xiao[1], *M. Kominia*[1], *A. Domling*[2], *B. Cornelissen*[1], *P. Elsinga*[1];
[1]*University Medical Center Groningen, Groningen, NETHERLANDS,* [2]*Palacky University, Department of Innovative Chemistry, Olomouc-Holice, CZECH REPUBLIC.*

Aim/Introduction: Positron emission tomography (PET) heavily relies on the employment of radiolabeled molecules. These obtained radiopharmaceuticals are rationally designed or screened from a library of radiolabelled compounds. Selection of suitable lead candidates can be a drawn-out process which is often slow as a construction of the library of radiolabelled compounds is required with high affinity and high specificity. Thus, high-throughput screening and structure-activity relationship studies would be very helpful to accelerate the development of tracers. Currently, molecules can already be synthesized in high-throughput by the multicomponent reaction (MCR). Therefore, rapid, simple and high-throughput radiolabelling methods would be highly advantageous. We investigated whether high-throughput radiolabelling methods were feasible and chose tetrazole compounds as the test system. Some derivatives of tetrazoles could be used to treat neurodegenerative disorders such as Alzheimer's and Parkinson's disease. Several tetrazoles with different lipophilicities were designed for investigating brain penetration. Fluorine-18 has extensive clinical and research applications in PET due to its compatible half-life and chemistry, matching a wide variety of radiolabelled small molecules. This work aims to achieve fast and multiplexed fluorine-18 radiolabelling of a panel of tetrazoles for screening tracer uptake in brain. ***Materials and Methods:*** A panel of tetrazoles containing aryl boronic pinacol esters (Bpins) and the corresponding fluorine-19 versions are synthesized using MCR. Then, the multiple Bpins are converted to radioactive ^{18}F-fluoro compounds in one pot using $Cu(OTf)_2(Py)_4$ as a catalyst. The conditions of the labeling experiment are optimized to improve radiochemical conversion (RCC) with respect to base, solvent, the amounts of reagent and catalyst. ***Results:*** Several Bpins with different lipophilicities and their fluorine-19 versions were synthesized. Five different Bpins were simultaneously and successfully converted into fluorine-18 compounds at small-scale in a one-pot reaction. Relatively high RCC was obtained with potassium oxalate, dimethylacetamide, 25 µmol of precursors and 7.5 µmol of catalysts. Under optimized conditions, the cumulative RCC for all ^{18}F-compounds was 66% ±10% (n=3). ***Conclusion:*** A fast and multiplexed fluorine-18 radiolabelling method was constructed. Next, we will expand the types and quantities of precursors and explore the interaction between precursors. In short, MCR and bulk radiolabelling may offer a fast and simple method to compile and screen larger numbers of radiolabelled compounds for PET.

OP-494

To Have and To Hold: The exceptional attraction of ^{225}Ac and Macropa

A. Amor Coarasa[1,2], *M. Friebe*[1], *S. Ponnala*[1], *P. K. Singh*[1], *S. DiMagno*[1], *J. W. Babich*[1];
[1]*Ratio Therapeutics Inc, Boston, MA, UNITED STATES OF AMERICA,* [2]*Albert Einstein College of Medicine, Bronx, NY, UNITED STATES OF AMERICA.*

Aim/Introduction: Actinium-225 radiopharmaceutical development displays significant tumor cell-killing effect in vivo, but is fraught with challenges. To date, there are two macrocyclic chelators proven to form stable complexes with ^{225}Ac: DOTA and Macropa. DOTA is a versatile chelator, but not selective for ^{225}Ac. Moreover, labeling requires elevated temperatures, a condition not compatible with labile targeting ligands. This work characterizes the radiolabeling and stability of [^{225}Ac]Macropa and [^{225}Ac]DOTA constructs. ***Materials and Methods:*** We evaluated four different Macropa containing PSMA targeting ligands, a bifunctional version of Macropa ($M\text{-}NH_2$), and an equivalent DOTA containing PSMA targeting ligand for comparison. Labeling was performed in 1 M NH_4OAc to produce a clinically-relevant radioconcentration [25-35 µCi/ml injectable solution] of ^{225}Ac-labeled formulated

drug product. We evaluated labeling conditions, impact of metal impurities, and long-term stability in the absence of anti-oxidants or radical scavengers using various QC methods. ***Results:*** [^{225}Ac]Macropa labeling experiments uniformly showed ≥99% yields (25ºC, 30 minutes). A 7-day stability study showed no change in RCP (>99%) of the ^{225}Ac-Macropa complexes. This study also showed that while ^{221}Fr is released from the chelator, its longer half-life daughter (^{213}Bi) is readily complexed by Macropa (92.5±1.2%), thereby ensuring high drug product purity at any given time prior to injection. Macropa demonstrated remarkable selectivity; deliberate contamination (50 ppm) with common metal ions (Zn, Al, Cu, Co, Ni, Mn, Cr, and Fe) did not interfere with the formation of the [^{225}Ac]Macropa at 25ºC (RCP>99%). In comparison, DOTA chelation at 95ºC did not produce pure (54.4%<RCP<78.7%) drug products in the presence of such metal ion contaminants, even when challenged at a significantly lower concentration (5 ppm). In addition, Macropa complexes (confirmed by MS) of isotopically stable Ce, Bi, Sm, and Lu ions underwent quantitative displacement by ^{225}Ac (25ºC, 30 minutes). Finally, a sequential dilution experiment showed that Macropa will quantitatively label actinium in concentrations as low as 1-10 µM, or a molar ratio of approximately 50:1. ***Conclusion:*** Macropa possesses remarkable advantages as an actinium chelator: it labels quantitatively at room temperature, even in the presence of high levels of metal ion impurities, the 225Ac complex remains stable for at least 7 days, and it complexes 213Bi released via alpha decay from 221Fr at dose levels present in the formulated drug product solution kept at room temperature. The rapid labeling kinetics, solution stability, ease of use, and daughter recapture supports Macropa as the actinium chelator of choice for medicinal products.

1105

Monday, September 11, 2023, 4:45 PM - 6:15 PM
Hall B

Cutting Edge Science Track - TROP Session: Current Issues of Radiation Protection

OP-495

Radiation Protection of Undertakers (Transport/ Embalming of the Body) and Crematorium Staff in Case of a Patient Death Shortly After Radionuclide Therapy

C. Michel, *H. Caplin, D. Célier, E. Blanchardon, A. Mathieu, A. Isambert;*
Institute for Radiation Protection and Nuclear Safety (IRSN), Fontenay-aux-Roses, FRANCE.

Aim/Introduction: A patient death shortly after a radionuclide therapy is rare. Nevertheless, this situation can be complicated to manage by healthcare professionals, undertakers, and crematorium staff as there are few radiation protection guidelines, and especially for the new therapeutic radionuclides. That is why, at the request of the French nuclear safety authority (ASN), the French Institute for radiation protection and nuclear safety (IRSN) performed a study (1) about occupational radiation protection issues in the case where a patient dies shortly after radionuclide therapy with new radiopharmaceuticals. The objectives of this piece of work were to perform a synthesis of the recommendations about death and cremation of nuclear medicine patients, and to assess the doses which could be received by undertakers (performing transport and embalming of the body) and crematorium staff. ***Materials and Methods:*** IRSN reviewed European recommendations about death and cremation. These European data were completed with some recommendations from countries outside Europe (USA, Canada) and data from international organisations (i.e. International Commission on Radiological Protection, and International Atomic Energy Agency). For 4 most promising new therapeutic radionuclides identified in a previous IRSN study (2) - Lutetium-177, Radium-223, Holmium-166, and Actinium-225 - the doses which could be received by undertakers and crematorium staff were assessed using realistic scenarios and conservative hypotheses. For instance, for transport and embalming, the times of presence near the body, namely at 50 cm, were 1 and 2 hours, respectively. ***Results:*** For Radium-223 and Actinium-225, the immediate transport and embalming of the body is possible as the assessed doses for undertakers are negligible. For Lutetium-177 and Holmium-166, a few days period after the death is necessary before the transport and the embalming to comply with regulatory dose constraints, without exceeding the French legal time frame for funeral operations.For cremation, the assessed doses are usually under 0.3 mSv per cremation (excepted for Actinium-225). ***Conclusion:*** Considering the assessed occupational doses, practical radiation protection proposals were established in case of a patient death shortly after radionuclide therapy, which may be useful for radiation protection authorities, undertakers, and crematorium staff. ***References:*** (1) French Institute for Radiation Protection and Nuclear Safety (IRSN), Avis 2023-00004, January 2023, https://www.irsn.fr/sites/default/files/2023-02/Avis-IRSN-2023-00004.pdf (2) French Institute for Radiation Protection and Nuclear Safety (IRSN), Nouveaux radionucléides en médecine nucléaire - Première partie : étude bibliographique des nouveaux radionucléides et perspectives d'utilisation clinique en France - Rapport IRSN 2021-00083, February 2021, https://www.irsn.fr/FR/expertise/rapports_expertise/Documents/radioprotection/IRSN_Rapport-2021-00083-nouveaux-radionucleides-medecine.pdf

OP-496

Justification of the radiation dose to a pregnant carer and comforter

E. Morris[1,2], *F. Sansum*[2], *M. Easty*[2], *L. Biassoni*[2], *M. Burniston*[1];
[1]*Barts Health NHS Trust, London, UNITED KINGDOM,* [2]*Great Ormond Street Hospital for Children, London, UNITED KINGDOM.*

Aim/Introduction: Generally, individuals who are pregnant would not be accepted as a carer and comforter within Nuclear Medicine. However, in a busy children's hospital, preventing a pregnant individual from supporting their child may prohibit that child from having a medically necessary scan. In UK legislation, the Ionising Radiation Regulations 2017 states the annual radiation dose limit for a member of the public (including foetuses) to be 1 mSv [1] and the Ionising Radiation (Medical Exposures) Regulations 2017 specifies no dose limit for carers and comforters, requiring locally set dose constraints and justifiaction of the exposure by a practitioner [2]. The aim of this project is to provide evidence to allow the Nuclear Medicine Practitioner to justify the exposure to a pregnant carer and comforter whilst having confidence that the radiation dose received by the foetus will remain under 1 mSv. Additionally, to give pregnant individuals appropriate information to allow them to knowingly and willingly agree to act as a carer and comforter. ***Materials and Methods:*** Non-pregnant individuals attending with their child wore a calibrated electronic personal dosemeter on their waistband which recorded total radiation dose received by the abdomen for the duration of their time in the

department. The radiation dose received after the individual had left the department was estimated from a dose rate measured at the end of the exam and calculated assuming normal close contact patterns. These results were summed to estimate of the total radiation dose received by the abdomen due to that appointment. Activity remaining in the patient at the end of the appointment which could be excreted or vomited was calculated to allow estimations of the potential risk to the carer and comforter from contamination. ***Results:*** Abdominal radiation doses received by studied carers and comforters were routinely low for most investigations, with little risk of breaching the 1mSv dose limit. ***Conclusion:*** In situations where the carer and comforter is pregnant, the additional information acquired in this study provides greater confidence for the practitioner justifying the exposure and has contributed to the development of improved information leaflets for pregnant carers and comforters. If a child were to undergo multiple studies within the pregnancy, a personalised dose estimate for the carer and comforter should be completed. ***References:*** [1] The Ionising Radiations Regulations. 2017. Accessed: Apr. 14, 2023. [Online]. Available: https://www.legislation.gov.uk/uksi/2017/1075/contents/made [2] The Ionising Radiation (Medical Exposure) Regulations. 2017. Accessed: Apr. 14, 2023. [Online]. Available: https://www.legislation.gov.uk/uksi/2017/1322/made?view=plain

OP-497

Investigating the contamination risk during ^{177}Lu-PSMA and ^{225}Ac-PSMA therapies of advanced prostate cancer patients

J. Brosch-Lenz*, S. Nekolla, L. Tischendorf, J. Allmann, W. Weber, M. Eiber;*
Klinikum rechts der Isar, der Technischen Universität München, Munich, GERMANY.

Aim/Introduction: ^{177}Lu-PSMA radiopharmaceutical therapy (RPT) is an approved treatment option for metastatic castration-resistant prostate cancer (mCRPC) using beta-radiation. In cases of beta-resistance, alpha-emitting ^{225}Ac-PSMA RPT has also shown promising results. mCRPC patients typically present with many comorbidities including urinary incontinence. The aim of this work was to investigate the contamination risk in patient rooms during ^{177}Lu- and ^{225}Ac-PSMA RPT to avoid unintended dispersion of radioactivity. ***Materials and Methods:*** Wipe samples were collected to detect a possible contamination of high-touch areas (door handles, faucet, toilet seat, chairs) in patient rooms at 24h and 48h after RPT. After patient discharge, floors were screened with a hand-held contamination monitor and further wipe samples were collected when local contaminations were detected. All samples were measured in a gamma counter that was calibrated for ^{177}Lu and ^{225}Ac and the activities were decay corrected to the time point of sample collection. ***Results:*** Samples were taken from a total of 19 ^{177}Lu- and 5 ^{225}Ac-PSMA RPT patients with median injected activities of 7.39 GBq and 7.84 MBq, respectively. A total of 251 samples was measured and maximum detected activities were 46.70 kBq and 5.62 kBq, respectively. The surfaces with highest contaminations were the toilet seats followed by faucets and door handles. Mean activities were 0.56 kBq and 0.01 kBq (faucet), 6.64 kBq and 1.13 kBq (toilet seats), 0.28 kBq and 0.03 kBq (door handles), and 0.18 kBq and 0.05 kBq (chairs) for ^{177}Lu and ^{225}Ac, respectively. Floor contaminations were found in 88 % (21 out of 24) of therapies with a maximum of 5163.60 kBq/m^2 and 4.70 kBq/m^2, respectively. These floor contaminations were detected in patients' bathrooms and decontamination measures were taken. ***Conclusion:*** Our investigation indicates an increased contamination risk in patient bathrooms and on door handles. As a first step, cautious instructions to avoid any contamination during bathroom cleaning and when sharing bathrooms should be introduced. This especially applies when using alpha emitters which are more harmful in case of incorporation. In addition, our results may yield further specifications for radiation protection actions in hospital and patient households for out-patient treatment.

OP-498

Assessment of Occupational Radiation Exposure During Administration of [^{177}Lu]Lu-DOTA-TATE Using Active and Passive Dosimetry

M. Riveira-Martin*[1], L. Struelens[2], J. Muñoz Iglesias[3], W. Schoonjans[2], J. M. Nogueiras Alonso[4], O. Tabuenca[3], F. J. Salvador Gomez[5], A. Lopez Medina[5];*
[1]Galicia Sur Health Research Institute, Vigo, SPAIN, [2]Belgian Nuclear Research Centre (SCK CEN), Mol, BELGIUM, [3]Meixoeiro Hospital, University Hospital of Vigo, Nuclear Medicine Department (SERGAS), Vigo, SPAIN, [4]Meixoeiro Hospital, University Hospital of Vigo, Nuclear Medicine Department (GALARIA), Vigo, SPAIN, [5]Meixoeiro Hospital, University Hospital of Vigo, Medical Physics and RP Department (GALARIA), Vigo, SPAIN.

Aim/Introduction: [^{177}Lu]Lu-DOTA-TATE has become popular for treating neuroendocrine tumours, but its high demand, novelty, and inconsistencies in procedures, can increase exposure of the staff. However, there is a shortage of data on the resulting occupational radiation exposure. This study aims to investigate radiation doses received by the staff during the administration of [^{177}Lu]Lu-DOTA-TATE. ***Materials and Methods:*** At our institution, [^{177}Lu]Lu-DOTA-TATE is administered by a physician and a nurse (7.4 GBq/session). Four nurses and two physicians were monitored throughout 32 sessions. Five thermoluminescent dosimeters (TLDs) in different positions on both dominant (D) and non-dominant (ND) hand provided doses in terms of Hp(0.07). Eye lens dosimeters measured Hp(3) values. Effective doses in terms of Hp(10) were obtained with Optically Stimulated Luminescence (OSL) dosimeters placed at chest level, under the lead apron. These detectors were provided and analysed by the Belgian Nuclear Research Centre (SCK CEN). Additionally, dose rates and effective dose in terms of Hp(10) were recorded with personal electronic dosimeters (PEDs). Staff wore lead aprons (0.5 mm lead equivalent), although three sessions were performed without aprons to evaluate the effect on Hp(10) using the PEDs. Dose values were normalized to the total administered activity (A). A P-value<0.05 was considered significant. ***Results:*** Lead aprons reduced dose rates/effective doses by 71%/69% for the physician, and by 56%/68% for the nurse. On average, Hp(10)/A showed lower values with electronic (0.65 ± 0.18 µSv/GBq) than with OSL (11.6 ± 2.9 µSv/GBq) dosimeters, so further measurements are needed. Median [range] of maximum Hp(0.07)/A values for all workers involved were (µSv/GBq): 41.5[33.8 - 49.2] for ND and 28.8[20 - 37.6] for D hand for physicians; 15.4[8.5 - 33.1] for ND and 13.9[9.5 - 14.8] for D hand for nurses. Doses are significantly higher for physicians as they manipulate the vial closer, but not significantly different between D and ND hands. The thumb and index fingertip receive the highest doses more frequently. Physicians should correct their middle/ring finger doses by at least a factor of 5/6 to account for maximum doses (on ND hand) and nurses by 3/4 (irrespective of the hand). Maximum Hp(3)/A ranged from (µSv/GBq) 1.4 - 2.2 (physicians) and 0.5 - 1.3 (nurses).

Conclusion: Under appropriate safety measures, administration of [^{177}Lu]Lu-DOTA-TATE is a safe procedure. However, regular monitoring is recommended to ensure that the annual dose limits are not exceeded. Acknowledgments: Funded by Euratom 2019 - 2020 under GA 945196 (SINFONIA)

OP-499

Tracer validation for non [^{18}F]FDG PET pharmaceuticals in automatic injector

M. Hammar[1], *R. Solem*[2], *F. Mörnsjö Centofanti*[2], *E. Evetovic*[2], *A. Akbari*[1], *K. Benner*[2], *B. Olsson*[1], *E. Höljer*[2], *J. Oddstig*[2];
[1]*Skane University Hospital, Malmö, SWEDEN,*
[2]*Skane University Hospital, Lund, SWEDEN.*

Aim/Introduction: Automatic injectors have been shown to reduce personal dose, especially to fingers, compared to manual administration for PET radiopharmaceuticals [1]. As our clinic's use of ^{18}F-PET tracers increases we wanted to validate our Iris automatic injectors for other tracers, namely ^{18}F-labelled PSMA, Roche, FET and Flutemetamol. ***Materials and Methods:*** For each radiopharmaceutical the following injector characteristics were validated 1. The trueness, as average percentage deviation, of the injector administered activity compared to a stand-alone dose calibrator (geometry calibrated against secondary standard Fidelis dose calibrator) for three injections. 2. An appropriate rinsing volume with respect to residual activity in the patient line. 3. Radiopharmaceutical quality control of the third injection and, if radiopharmaceutical was diluted by injector, on the radiopharmaceutical vial after finished run. This quality control is identical to the one routinely performed post-production. Data points for rinsing volumes were collected by performing two consecutive 4 ml rinsing's into separate vials after an administration (which include a variable initial rinsing). The activity in the vials was measured in a dose calibrator and the initial rinsing was set to 10, 15 and 20 ml for the three test injections. Quality control measuring presence of solvent (ethanol/acetonitrile) and radiochemical purity (TLC/HPLC) was performed on third injection. For [^{18}F]FET and [^{18}F]PSMA-1007 QC was also performed on radiopharmaceutical vial after the run. ***Conclusion:*** All four radiopharmaceuticals were successfully validated. Injections of [^{18}F]PSMA-1007 and [^{18}F]FET have since been performed using automatic injection in clinical routine. However, for [^{18}F]Flutemetamol and [^{18}F]Roche, errors in estimated vial activity concentration ("Measure bulk") was observed and the errors lead to the injector not being able to withdraw and inject the prescribed activity unless being repeatedly recalibrated. Lipophile substances, like Roche and Flutemetamol, are known to adsorb on surfaces. Individual tubing parts were measured separately in a dose calibrator post injection and a significant amount of activity was adsorbed in the initial tube connecting the radiopharmaceutical vial to the 4 way manifold for both radiopharmaceuticals. The same measurement for [^{18}F]PSMA shows little residual activity in tubing. Therefore, [^{18}F]Flutemetamol and [^{18}F]Roche has not been implemented despite being validated. ***References:*** [1] Cunha L, Dabin J, Leide-Svegborn S, Zorz A, Kollaard R, Covens P. Extremity exposure of nuclear medicine workers: results from an EANM and EURADOS survey. Q J Nucl Med Mol Imaging. 2023 Jan 11.

OP-500

Implementation of CT tin filter in PET-CT: dose savings and image quality evaluation for tissues and dose levels relevant to PET-CT

P. Holdgaard[1], *N. A. Bebbington*[2], *K. B. Christensen*[1], *L. L. Østergård*[1];
[1]*Lillebælt University Hospital, Vejle, DENMARK,*
[2]*Siemens Healthcare A/S, Aarhus, DENMARK.*

Aim/Introduction: CT dose optimisation is particularly important in PET-CT since most examinations cover the whole-body. The tin filter has demonstrated dramatic dose savings for a range of clinical indications in standalone (diagnostic-level) CT. The aim was to evaluate tin filter dose and image quality in high- and in low contrast tissues at dose-levels relevant to PET-CT. ***Materials and Methods:*** The Kyoto-Kagaku adult CT-body-phantom underwent 39 whole-body (WB, vertex-to-knee) scans in standard and obese patient configurations, with standard CT settings used in clinical practice for localisation/characterisation of FDG (120kV/40mAs-eff-ref) and NaF (120kV/20mAs-eff-ref) examinations, and with a range of tin filter settings utilising Sn100kV and Sn140kV spectra with 25-500mAs-ref. Dose length product (DLP) was recorded, and effective dose (ED) calculated from DLP. Two expert observers scored image quality (IQ) in three low-contrast areas (aqueduct in pons cerebri, liver veins, renal pelvis) and two high-contrast areas (bronchial branching, bone/facet joint). Scores were made on a 5-point scale: 1=not detectable, 2=barely visible (AC only), 3=acceptable (localisation), 4=good (characterisation), 5=excellent (diagnostic). Exposure settings and doses with tin filter used to provide a given level of IQ in the respective tissue was determined, and dose savings for comparable IQ to non-tin CT were calculated. ***Results:*** Reference scan: The 120kV/40mAs-eff-ref clinical FDG scan settings gave a WB-ED of 1.21mSv in the standard phantom configuration. Observer 1 gave IQ scores of 3 to the aqueduct, liver and renal pelvis, and scores of 4 to the bronchi and bone/facets. IQ was matched using the tin filter with relative dose reductions of 39% (aqueduct), 57% (liver), 48% (kidney pelvis), 89% (bronchi) and 57% (bone). Observer 2 gave IQ scores of 3 to the aqueduct and renal pelvis, 4 to the liver, and 5 to the bronchi and bone/facets. IQ was matched using the tin filter with relative dose reductions of 39% (aqueduct), 39% (liver), 57% (bronchi) and 48% (bone). Sn100kV provided greater dose reduction than Sn140kV in all tissues. Both observers deemed WB-ED as low as 0.14mSv (89% lower than FDG clinical reference) sufficient for localisation in bone/facets and characterisation in bronchi. Although absolute doses were greater with the obese phantom configuration, similar dose-savings for comparable IQ to the obese reference scan were observed. ***Conclusion:*** The tin filter allows localisation and characterisation CT IQ for PET-CT at ultra-low WB doses, providing large dose reductions compared with standard (non-tin) settings, with the greatest benefits noted in high-contrast structures.

OP-501

Ultra-low Dose CT With and Without Tin Filter for PET Attenuation Correction: Dose Savings and Quantification

N. Bebbington[1], *K. B. Christensen*[2], *L. L. Østergård*[2], *P. C. Holdgaard*[2];
[1]*Siemens Healthcare A/S, Aarhus, DENMARK,* [2]*Department of Nuclear Medicine, Lillebælt University Hospital, Vejle, DENMARK.*

Aim/Introduction: A tin (Sn) filter can be used to reduce CT radiation dose to patients by filtering out a greater proportion of lower energy x-rays from the beam, compared with standard aluminium filtration. The aim was to determine by how much

dose can be reduced with ultra-low-dose (ULD) Sn- and non-Sn CT protocols, without significantly impacting PET quantification. ***Materials and Methods:*** The NEMA image quality phantom was imaged under three conditions: (1) water-filled (0HU representing soft tissue) with ^{18}F-FDG; (2) cylindrical insert containing homogenous mix of sand, flour, water (SFW, approximately 400HU representing trabecular bone) and ^{18}F-FDG, with water background; (3) cylindrical insert containing sand (approximately 1200HU representing cortical bone) and ^{18}F-FDG, with water background. Each phantom condition underwent a 1 bed position PET-CT scan (26.3cm axial field-of-view) comprising 1 PET and 13 CT acquisitions. CT acquisitions used tube current modulation and were performed at 120kV/50mAs-ref (reference standard), 100kV/7mAs-ref (current ULDCT for attenuation correction (AC) standard), Sn140kV (mAs range 7-50-ref) and Sn100kV (mAs range 12-400-ref). PET data were reconstructed with μ-maps provided by each CT dataset, and volumes of interest assigned to measure PET activity concentration. Differences in CT dose length product (DLP) and PET quantification were determined relative to the 120kV/50mAs-ref reference standard. ***Results:*** At all tube voltages, differences in PET quantification were greater with increasing material density and reducing mAs. Compared with reference standard CT, differences in PET quantification for the 100kV/7mAs scans for the three phantom conditions were ≤1.7%, and DLP was reduced by 85.0% (DLP in water phantom =7.0 mGy.cm). For Sn100kV scans, differences in PET quantification were negligible (≤1.2%) for all three phantom conditions down to 50mAs-ref (DLP in water phantom=2.8mGy.cm, effective dose=0.04mSv), giving 94.2% DLP reduction compared with the reference, and 60% DLP reduction compared with the non-Sn ULDCT protocol. Below this level, differences in PET quantification were >2% for at least one of the three phantom conditions (2.3% at 25mAs-ref in SFW and 6.4% at 12mAs-ref in sand). At Sn140kV, quantification differences were ≤0.6% for all scans in the water phantom, increasing to 1.7-2.1% in SFW, and 2.9-3.7% in sand. DLP reductions at Sn140kV ranged from 65.2% (50mAs-ref) to 92.7% (7mAs-ref). ***Conclusion:*** CT protocols for PET AC with and without Sn filter (Sn100kV/50mAs-ref and 100kV/7mAs-ref) provide ultra-low doses with negligible impact on PET quantification. This Sn protocol provides 60% lower dose than the non-Sn ULDCT protocol for PET AC.

OP-502

How Low Can You Go With Ultra-low-dose Tin Filter CT in PET-CT? Evaluation of Dose and Artifacts in a Whole-body Patient Phantom

N. Bebbington[1], *K. B. Christensen*[2], *P. C. Holdgaard*[2], *L. L. Østergård*[2];
[1]*Siemens Healthcare A/S, Aarhus, DENMARK,* [2]*Department of Nuclear Medicine, Lillebælt University Hospital, Vejle, DENMARK.*

Aim/Introduction: A CT tin filter can be used to reduce patient dose, and previous work demonstrated accurate PET quantification in the NEMA PET image quality phantom at such ultra-low dose CT (ULDCT). However, in patient CT scans, artifacts can sometimes be seen in images between structures providing very high attenuation, such as the shoulders and femoral heads, and could in turn affect PET attenuation correction (AC). The aims were to measure artifacts in standard low-dose (SLD) scans and ULD tin filter scans, to help determine appropriate exposure settings for ULDCT for AC in whole-body PET imaging, and to measure whole-body CT effective dose (ED). ***Materials and Methods:*** An adult whole-body CT phantom underwent repeated CT scans in standard and obese configurations, with tube current modulation at 120kV/20mAs-ref (SLD reference for PET bone imaging with localisation/characterisation CT), 100kV/7mAs-ref (non-tin ULDCT for AC protocol), Sn140kV (mAs range 7-50-ref) and Sn100kV (mAs range 12-400-ref). A semi-quantitative artifact score was calculated for each dataset, by identifying the most severe artifact in each group of 20 axial slices, and measuring the difference in HU (through placement of ROIs) for the most affected area and a corresponding unaffected area. Differences of 0-20HU, 20-30-HU, 30-50HU, 50-70HU and >70HU gave artifact scores of 0-4, respectively, for each group of slices. Whole-body artifact scores were calculated as the sum of all slice groups. Dose-length-product (DLP) was converted to whole-body (vertex-to-knee) ED for each scan using a DLP to ED whole-body conversion factor. ***Results:*** With SLD settings, whole-body artifact scores were 17 and 31, and EDs 1.4mSv and 2.3mSv, for standard and obese phantoms, respectively. At Sn100kV/50mAs-ref, artifact scores were considered matched to those with SLD settings, at 15 and 28, for standard and obese phantoms, with EDs at 0.2mSv and 0.4mSv. At Sn100kV/25mAs-ref, artifact scores increased to 37 and 98, albeit at lower doses of 0.1mSv and 0.2mSv. At Sn140kV, its highest artifact scores of 7 and 18 were provided at 7mAs-ref, with EDs of 0.2mSv and 0.3mSv, for standard and obese phantoms. At 100kV/7mAs-ref, artifact scores were 45 and 75, with EDs at 0.6mSv. ***Conclusion:*** ULDCT scans for PET AC with tin filter give a whole-body ED of 0.2mSv in a standard patient, whilst providing comparable or lower artifact scores to the SLD CT scan, with 85% lower dose. Artifact scores and EDs are also considerably lower than those for the current non-tin ULDCT protocol.

OP-503

Ultra-low-dose CT for Long Axial Field of View PET/CT: A Phantom Study

S. Mostafapour[1], *M. Greuter*[2], *P. van Snick*[1], *J. van Sluis*[1], *A. A. Lammertsma*[1], *C. Tsoumpas*[1];
[1]*Department of Nuclear Medicine and Molecular Imaging, University Medical Center Groningen, Groningen, NETHERLANDS,* [2]*Department of Radiology, University Medical Center Groningen, Groningen, NETHERLANDS.*

Aim/Introduction: Attenuation correction (AC) CT contributes to the overall radiation exposure associated with (repetitive) whole-body PET/CT scans. Several approaches have been investigated to reduce CT radiation dose in whole-body PET/CT examinations (1). In some new CT scanners, a tin (Sn) filter can potentially reduce radiation dose without degrading PET image quality. The purpose of this phantom study was to evaluate ultra-low dose attenuation correction CT using various dose reduction options, such as a tin (Sn) filter, reducing the tube current, increasing the pitch factor, and applying tube current modulation. ***Materials and Methods:*** The ultra-low dose CT protocol was evaluated using five phantoms that mimic a wide range of tissue densities: 1) Tissue Characterization Phantom, 2) NEMA IQ phantom, 3) CT Whole Body Phantom, 4) Head Phantom, and 5) Anthropomorphic Torso Phantom. All phantoms were scanned on a LAFOV PET/CT scanner, applying the various CT dose reduction parameters. Two metrics (CT dose index volume available from the scanner and dose length product) were used to determine the dose resulting from the CT scans in the whole body. Several volumes of interest (VOIs) and voxel-based evaluations were performed to assess the effects of CT protocol changes. These assessments were performed by analysing the ultra-low dose CT images in some phantoms or the PET-AC scans in other phantoms against corresponding scans acquired and

reconstructed using a reference CT. CT images of the Whole-Body Phantom were compared in terms of contrast-to-noise ratio (CNR) and signal-to-noise ratio (SNR) as well. ***Results:*** Using the tin filter and applying other dose reduction parameters resulted in a reduction of the effective radiation dose by almost 97%. At the same time, the reduction in SNR and CNR within the CT images was less than 65%. VOI and voxel-based comparisons of PET images showed a relative difference of less than 5% for all parts of the Torso phantom. ***Conclusion:*** Using a tin filter during CT scanning substantially reduces the overall radiation dose of whole-body PET/CT without a large impact on image quality. Nevertheless, future studies are needed to assess the effect of this method of dose reduction on PET quantification in human PET/CT studies therefore, the patient part of this study is scheduled. ***References:*** 1. Prieto, E., et al., 2021. Ultra-low dose whole-body CT for attenuation correction in a dual tracer PET/CT protocol for multiple myeloma. Phys Med, 84, 1-9.

1106

Monday, September 11, 2023, 4:45 PM - 6:15 PM
Hall C

Clinical Oncology Track - TROP Session: Prostate Cancer Biochemical Recurrence

OP-504

Final Analysis of a Prospective, Single-center, Phase II/III Imaging Trial of ^{68}Ga-RM2 PET/MRI in Patients with Biochemical Recurrence of Prostate Cancer

H. Duan, *F. Moradi, G. A. Davidzon, T. Liang, H. Song, A. Loening, S. Vasanawala, S. Srinivas, J. D. Brooks, S. L. Hancock, A. Iagaru; Stanford University, Stanford, CA, UNITED STATES OF AMERICA.*

Aim/Introduction: The recent NCCN guideline has included prostate-specific membrane antigen (PSMA)-targeted PET for the detection of biochemical recurrent (BCR) prostate cancer (PC). However, up to 10% of PC do not express PSMA, and given the high intratumor heterogeneity, targeting a single tumor characteristic might not be sufficient to reflect full extent of disease. Gastrin releasing peptide receptors (GRPR) have shown to be overexpressed in PC and can be targeted with ^{68}Ga-RM2. In this study, we evaluated the diagnostic performance of ^{68}Ga-RM2 PET/MRI in BCR PC. ***Materials and Methods:*** This prospective, single-center, open-label, single-arm, phase II/III trial was performed at Stanford University. Patients ≥18 years with Karnofsky performance ≥50, rising PSA ≥0.2 ng/mL after prostatectomy, or ≥2 ng/mL above nadir after radiotherapy, and non-contributory conventional imaging (negative CT and/or bone scan) were eligible. The primary outcome was to assess diagnostic performance of ^{68}Ga-RM2 PET/MRI vs MRI alone. Each PET scan was interpreted by three independent masked readers using a standardized evaluation criteria. This study is registered with ClinicalTrials.gov NCT02624518 and is complete. ***Results:*** Between December 12, 2015 and July 27, 2021, 209 patients were screened for eligibility, of whom 100 were included. The primary endpoint was met; ^{68}Ga-RM2 PET/MRI showed significantly higher detection rates than MRI alone (143 vs 96 lesions, respectively; P<0.001) and sensitivity (85.2%; 95% CI 75.6, 92.1 vs 49.4%; 95% CI 38.1, 60.7, respectively; P<0.001) while specificity was comparably high (100.0%; 95% CI 82.4, 100.0 vs 94.7%; 95% CI 74.0, 99.9, respectively; P=0.303). ***Conclusion:*** ^{68}Ga-RM2 PET/MRI showed better diagnostic performance than MRI alone in BCR PC with significantly higher detection rates, sensitivity, and accuracy. Therefore, ^{68}Ga-RM2 PET should be considered in BCR PC patients in aiding disease detection and management decision. Further prospective comparative studies with PSMA-targeted PET are needed to gain a better understanding of GRPR and PSMA expression patterns in BCR PC.

OP-505

Prospective Single-Centre Phase II Clinical Trial On The Diagnostic Accuracy of Fully Hybrid [68Ga]Ga-PSMA-11 PET/MRI and [68Ga]Ga-RM2 PET/MRI in Patients with Biochemically Recurrent Prostate Cancer

S. Ghezzo[1,2], *P. Mapelli*[1,2], *A. Samanes Gajate*[2], *A. Palmisano*[3], *V. Cucchiara*[4,5], *G. Brembilla*[1,3], *C. Bezzi*[1,2], *N. Suardi*[6], *P. Scifo*[2], *A. Briganti*[1,4,5], *F. De Cobelli*[1,3], *A. Chiti*[1,2], *A. Esposito*[1,3], *M. Picchio*[1,2]; [1]*Vita-Salute San Raffaele University, Milan, ITALY,* [2]*Department of Nuclear Medicine, IRCCS San Raffaele Scientific Institute, Milan, ITALY,* [3]*Department of Radiology, IRCCS San Raffaele Scientific Institute, Milan, ITALY,* [4]*Department of Urology, IRCCS San Raffaele Scientific Institute, Milan, ITALY,* [5]*Division of Experimental Oncology, URI, Urological Research Institute, Milan, ITALY,* [6]*IRCCS Ospedale San Martino, Genova, ITALY.*

Aim/Introduction: This study aims to evaluate the diagnostic accuracy of [68Ga]Ga-PSMA-11 PET/MRI and [68Ga]Ga-RM2 PET/MRI in patients with biochemically recurrent prostate cancer (PCa). The secondary aim is to compare the patient and region-based detection rates of these imaging modalities. Furthermore, the association between imaging findings and clinical data is explored. ***Materials and Methods:*** Forty-four patients with biochemically recurrent PCa underwent [68Ga]Ga-PSMA-11 PET/MRI and [68Ga]Ga-RM2PET/MRI within 16 days (median:2,range:2-16 days). Two Radiologists interpreted MRI and two Nuclear Medicine physicians analysed PET images. Images were then re-examined to produce an integrated PET/MRI report for both [68Ga]Ga-PSMA-11 and [68Ga]Ga-RM2. In the integrated report, imaging was considered positive for malignancy if at least one imaging modality was clearly positive for PCa recurrence or if both modalities were concordant in the suspect of recurrence. Clinical and instrumental follow-up (median follow-up:22.8,range:6-31.5 months) was used to validate imaging findings at the patient-level. Diagnostic performance was assessed with accuracy, sensitivity, specificity, positive and negative predictive value. McNemar's test was used to compare sensitivity and specificity on a per-patient base and detection rate on a per-region base. Prostate bed, locoregional lymph nodes, non-skeletal distant metastases, and bone metastases were considered. Univariable logistic regression was used to identify the role of age, ISUP grade, time to biochemical recurrence, PSA at time of scans, initial PSA, PSA doubling time and PSA velocity for the prediction of positive imaging. P-value significance was defined below the 0.05 level after correction for multiple testing. ***Results:*** Patients' median age was 69.8 years (IQR=61.8-75.1) and median PSA level at time of imaging was 0.53 ng/mL (IQR=0.33-2.04). Evidence of PCa recurrence was observed in 31/44 patients at follow-up. [68Ga]Ga-RM2 PET showed lower sensitivity compared to [68Ga]Ga-PSMA-11 PET and MRI (0.613 vs 0.839 and 0.871,p=0.046 and 0.043, respectively), while specificity was comparable among the imaging modalities (1 vs 0.846 and 0.692,p=0.479 and 0.134; respectively). Combining MRI with[68Ga]Ga-PSMA-11 PET and [68Ga]Ga-RM2 PET resulted in sensitivity =1 and 0.935 and specificity of 0.692 and 0.692; respectively. The integrated assessment of PET (both with [68Ga]Ga-PSMA-11 and [68Ga]Ga-RM2) and MRI improved the detection rate of locally

recurrent PCa. No significant associations were found between the investigated clinical data and imaging findings. ***Conclusion:*** PET/MRI is useful to characterize patients with biochemically recurrent PCa. Furthermore, it was reported high sensitivity for [68Ga]Ga-PSMA-11 PET and MRI, while the utility of [68Ga]Ga-RM2 PET in absence of a simultaneous whole-body/multiparametric MRI remains to be determined.

OP-506

Higher Preoperative Maximum Standardised Uptake Values (SUV_{max}) are Associated with Higher Biochemical Recurrence Rates After Robot-Assisted Radical Prostatectomy for ^{68}Ga-PSMA-11 and ^{18}F-DCFPyL PET/CT

K. De Bie[1], *H. Veerman*[1], *Y. J. L. Bodar*[1], *D. Meijer*[1], *P. J. van Leeuwen*[2], *H. G. van der Poel*[2], *M. Donswijk*[2], *A. N. Vis*[1]; [1]*Amderdam UMC, Amsterdam, NETHERLANDS,* [2]*Nederlands Kanker Instituut, Amsterdam, NETHERLANDS.*

Aim/Introduction: In patients with primary prostate cancer (PCa), the visual and semi-quantitative measuring of PSMA tracer uptake in the prostate lesions by the maximum standardized uptake value (SUV_{max}) are essential. We evaluated whether in patients with primary PCa, the SUV_{max} on preoperative PSMA PET/CT was associated with the development of biochemical recurrence (BCR) after robot-assisted radical prostatectomy (RARP). ***Materials and Methods:*** We retrospectively analysed 446 PCa patients who underwent a ^{68}Ga-PSMA or ^{18}F-DCFPyL PSMA PET/CT scan prior to RARP. PET/CT scan images were visually and semi-quantitatively analysed by measuring SUV_{max} in the clinically suspicious prostate cancer lesions. BCR was defined as two consecutive PSA values ≥0.2 ng/mL after RARP. The predictive value of SUV_{max} for BCR was evaluated using uni- and multivariable Cox regression analyses, adjusting for preoperative variables: radiologic tumor stage (mT), biopsy International Society of Urological Pathology grade group (bISUP), and positive lymph nodes on PSMA PET/CT (miN1), or postoperative variables: pathologic ISUP group (pISUP), pathologic T-stage (pT), and positive surgical margins (R1). Based on the SUV_{max} distribution among the patients, SUV_{max} was classified into two groups (high: SUV_{max} >10 and low: SUV_{max} ≤10). ***Results:*** SUV_{max} >10 was a significant predictor for BCR (p<0.001). This was also true for the subgroups bISUP3-5, mT3, and EAU classification: high risk for BCR (p<0.001, p=0.002, and p=0.004, respectively). Negative lymph node status (miN0) was associated with developing BCR (p=0.01), as opposed to miN1 (p=0.11). In multivariable analysis, adjusting for mT, bISUP, and miN1, SUV_{max} was an independent preoperative predictor for the development of BCR (p=0.03). ***Conclusion:*** PSMA tracer expression of the dominant prostate cancer lesion on PSMA PET/CT, defined as SUV_{max}, was an independent predictor for BCR after RARP in patients with primary PCa. SUV_{max} >10 might be used as a prognostic factor for an unfavourable outcome after RARP.

OP-507

Staging with [68Ga]Ga-PSMA-11 PET/CT in patients with intermediate and high-risk prostate cancer prior surgery. Is there any association between semiquantitative parameters and biochemical recurrence?

J. Rosales[1], *J. Bastidas*[1], *A. Bronte*[1], *V. Betech-Antar*[1], *F. Minguez*[1], *M. Romera*[1], *F. Pareja*[1], *E. Guillen*[2], *S. Menendez-Sanchez*[1], *C. Beorlegui*[3], *J. Arbizu*[1], *J. Peréz Gracia*[4], *M. Rodriguez-Fraile*[1]; [1]*Nuclear Medicine Department, University Clinic Of Navarra, Pamplona, SPAIN,* [2]*Nuclear Medicine Department, University Clinic Of Navarra, Madrid, SPAIN,* [3]*Planning Evaluation and Knowledge Management Health Department, Government of Navarra, Pamplona, SPAIN,* [4]*Oncology Department, University Clinic Of Navarra, Pamplona, SPAIN.*

Aim/Introduction: We aimed to describe semiquantitative parameters of PSMA-PET in intermediate and high-risk prostate cancer (PCa) patients prior to surgery and their prognostic value for biochemical recurrence (BR). ***Materials and Methods:*** Fifty PCa patients referred for PSMA-PET/CT for initial staging and scheduled for radical prostatectomy (RP) were included. PET-parameters including tumor SUVmax, Prostate Molecular Tumor Volume (pMTV), Prostate Volume (pV), Prostate Total Lesion Activity (pTLA) and Prostate Disease Burden % (pDB) were recorded. pV was obtained by automated segmentation of prostate gland on CT images using work in progress syngo.via MI General Anatomy Segmentation software (Siemens Healthineers, Knoxville, TN). pDB was calculated using the formula (pMTV x 100 / pV). Moreover, other clinical and tumor-specific characteristics were also analyzed. Receiver-operating-characteristic (ROC) curve analysis was used to determine optimal cut-off values for the PET parameters to identify BR. Univariate and multivariate logistic regression analysis were used to determine the association between clinicopathologic variables, PET-parameters before RP and the occurrence of BR. ***Results:*** Twenty-two intermediate-risk (IR) and twenty-eight high-risk (HR) PCa patients were included. The median SUVmax was 10.85 (9.96-12.90) in the IR group and 13.49 (7.08-17.76) in the HR group. The median pMTV and pTLA in the HR group were 3.85 cm3 (2.43-7.97) and 28.10 (14.99-60.19) respectively and 2.86 cm3 (1.87-5.65) and 19.05 (11.44-25.57) in the IR group. After a median follow-up of 24 months (± 8.8), 42% of patients experienced BR within 2 years of RP. pMTV, pTLA, pDB were statistically higher in patients with BR than in patients who remained with undetectable PSA levels (p<0.05 each, Table 1). The ROC curves showed that a pDB cut-off value of 8.10% had a sensitivity of 77% and a specificity of 75% (AUC=0.716 [95%CI: 0.55-0.87; p=0.014]), for discriminating those patients who experienced BR during follow-up. On multivariate regression analysis, both Gleason Score ≥8 (OR=5.5 [95%CI: 1.2-25.8, p=0.030]) and pDB >8.10% (OR=6.8 [95%CI:1.6-29, p=0.010)], significantly predicted BR at the last follow-up, whereas other clinical, tumor-specific and semiquantitative parameters did not. ***Conclusion:*** Preoperative PSMA-PET semiquantitative parameters (pMTV, pTLA and pDB) were significantly higher in patients with BR than in patients who remained with undetectable PSA levels. Both Gleason Score ≥8 and pDB >8.10% were significant predictors for the risk of postoperative BR. Further studies with a larger number of patients and longer follow-up periods are necessary.

OP-508

From CHAARTED low- and high-volume disease to PSMA PET imaging volume in mHSPC patients: an international multicenter retrospective study

L. Unterrainer[1,2], *T. A. Hope*[3], *H. Ndlovu*[4], *F. Barbato*[5], *W. P. Fendler*[5,6], *K. Herrmann*[5,6], *M. Sathekge*[4], *J. Czernin*[1], *J. Calais*[1]; [1]*UCLA, Los Angeles, CA, UNITED STATES OF AMERICA,* [2]*LMU Munich, Munich, GERMANY,* [3]*UCSF, San Francisco, CA, UNITED STATES OF AMERICA,* [4]*University of Pretoria, Pretoria, SOUTH AFRICA,* [5]*University Hospital Essen, Essen, GERMANY,* [6]*German Cancer Consortium (DKTK)-University Hospital Essen, Essen, GERMANY.*

Aim/Introduction: In patients with mHSPC, the volume of disease (high-volume disease (HVD) / low-volume disease (LVD)) as defined by the CHAARTED criteria based on conventional imaging (CT + bone scan (BS)), is associated with overall survival and used for treatment decisions. PSMA-PET has a higher sensitivity and specificity than conventional imaging. It remains unknown how the definition of HVD and LVD can be

transferred to PSMA-PET-based criteria. ***Materials and Methods:*** In this retrospective study, mHSPC patients who underwent a ^{68}Ga-PSMA-11 PET/CT or PET/MRI and a BS (CI) (within a maximum time interval of 100 days) at 4 international sites were included. Patients with treatment in between both scans were excluded. HVD and LVD was retrospectively determined on the BS and the CT/MRI component acquired with PET. Additionally, CHAARTED stratification into HVD and LVD was applied to PSMA-PET. HVD was defined by the presence of visceral metastases and / or ≥ 4 bone metastases (with ≥ 1 beyond spine and pelvis). EXINIbone™ 3.4 (EXINI Diagnostics) was used to obtain the number / localization of bone metastases on BS and the quantitative bone scan index. The whole-body (WB) PSMA-PET positive tumor volume (PSMA-TV) was obtained using a semi-automatic thresholding method on Affinity 3.0.2 (Hermes Medical Solutions). ***Results:*** 40 mHSPC patients with paired PSMA-PET+BS were included. Median PSA was 42.2 (0.2 - 5675.0) ng/ml. 12/40 patients had disease detected in the prostate fossa, 23/40 in lymph nodes, 25/40 in bones and 2/40 in visceral organs by CI and 24/40, 24/40, 20/40 and 2/40 by PSMA-PET, respectively. 12/40 patients had CI_{HVD} (30%) and 28/40 CI_{LVD} (70%) based on CI, and 16/40 patients had PSMA-PET_{HVD} (40%) and 18/40 PSMA-PET_{LVD} (45%) by PSMA-PET. 6/40 (15%) patients had no PSMA-positive lesion or only in the prostate fossa while CI was at least CI_{LVD}. Overall, mean WB-PSMA-TV was 394.9 ml (0 - 3734.0 ml). In CI_{HVD}, mean WB PSMA-TV was 961.1 (0.3 - 3734.0) ml, in CI_{LVD}, 111.9 (0-1201.0) ml and in PSMA-PET_{HVD} 870.8 (0 - 1427.0) ml and in PSMA-PET_{LVD} 59.7 (0 - 117.0) ml, respectively. Upstaging (LVD to HVD) from CI to PSMA-PET occurred in 5/40 patients (12.5%), and downstaging in 6/40 patients (15.0%). ***Conclusion:*** Stage migration between LVD/HVD from conventional imaging to PSMA-PET occurs both by upstaging and downstaging. Correlation with outcome of the new definitions of HVD/LVD based on PSMA-PET/CT is warranted.

OP-509

Head-to-head comparison of ^{68}Ga-PSMA-11 PET with ^{99}mTc-MDP bone scan for detection of bone disease in prostate cancer patients with biochemical progression during ADT: a single center prospective study

A. Gafita*, R. Alano, M. Rettig, J. Shen, W. Armstrong, T. R. Grogan, S. Liu, M. R. Benz, J. Czernin, J. Calais;*
University of California, Los Angeles, Los Angeles, CA, UNITED STATES OF AMERICA.

Aim/Introduction: ^{68}Ga-PSMA-11 PET/CT (PSMA-PET) was approved in patients with prostate cancer (PCa) at primary staging or biochemical recurrence. However, it is unclear if bone scan (BS) remains indicated in men with PCa and with biochemical progression under ADT. This study aimed to compare the detection rate of bone disease for PSMA-PET vs BS in men with PCa and with biochemical progression during ADT. ***Materials and Methods:*** This was a prospective single-center, open-label, single-arm, head-to-head comparison, prospective phase 2 study (NCT04928820). Men with i) biopsy-proved PCa, ii) who had rising PSA levels on 2 successive occasions ≥1 week apart, iii) were receiving treatment with hormonal therapy, iii) and had an absolute PSA value ≥1 ng/ml were eligible. Men who were enrolled received PSMA-PET and bone scan within 30 days. The primary endpoint was detection rate of bone disease for PSMA-PET vs BS. Secondary endpoint was the number of bone lesions detected by PSMA-PET vs BS. Number of lesions was categorized into: 0 vs 1 vs 2 vs 3 vs 4 vs 5 vs >5. A p <0.05 was considered statistically significant. ***Results:*** 22 men were enrolled between July 8, 2021 and June 9, 2022. The median patients age was 71 years (range: 56-94). The median time between scans was 12 days (range: 1-29). The median PSA value was 9.5 ng/ml (range: 1.2 - 1717). 11/22 (11%) patients had hormone-sensitive PCa, while 11/22 (50%) had castration-resistant PCa prior to receiving the scans. The positivity rate for bone disease was equal for PSMA-PET and BS in all cases: 7/22 (32%) patients had negative scans on both imaging modalities and 15 (68%) had ≥1 bone lesion detected on both imaging modalities (p=1.00). In 15/22 (68%) men, both imaging modalities showed equal number of bone lesions: 0 lesions in 7/22 (32%) men and >5 lesions in 8/22 (36%) men. In 3/22 (14%) men BS showed higher number of lesions, while in 4/22 (18%) men PSMA-PET showed higher number of lesions (Table 1). No statistical difference was noticed between PSMA-PET and BS in number of bone lesions detected (p>0.05). PSMA PET scan detected non-bony disease in 13/22 (59%) men: TrN0M0 in 10/22 (45%), TxN1-M1a in 7/22 (32%), and TxNxM1c in 4/22 (18%) men. ***Conclusion:*** In this prospective study of patients with prostate cancer with rising PSA levels under hormonal therapy, ^{68}Ga-PSMA-11 PET and ^{99}mTc-MDP bone scan had similar detection rate for bone disease.

OP-510

Factors Affecting Diagnostic Performance of Ga-68 PSMA PET/MRI in Biochemical Recurrent Prostate Cancer and Nomogram Model

S. Küçükali*, U. Aydos, E. Balcı, Ü. Akdemir, L. Atay;*
Gazi University, Faculty of medicine, Ankara, TÜRKIYE.

Aim/Introduction: This study aimed to evaluate the diagnostic performance of imaging and to examine the factors affecting the detection rate in prostate cancer (PC) patients who underwent Ga-68 PSMA PET/MR imaging for biochemical recurrence (BCR) after radical prostatectomy (RP). ***Materials and Methods:*** This study included 104 PC patients who underwent PET/MRI between 2016 and 2022 due to post-RP BCR. In the visual evaluation, the presence, localization and number of pathological lesions were assessed. Total PSA(ng/ml), ISUP Gleason grades(GG), presence of androgen deprivation therapy (ADT), and PSA doubling time (PSAdt) were recorded. Logistic regression analysis was performed to determine the factors predicting PET/MRI positivity. Additionally, a nomogram was created to determine the probability of PET/MRI positivity in the early BCR group (PSA<1.0 ng/ml) by using the lrm() and nom() functions in the R software rms package. ***Results:*** In 73 (70.2%) patients, positive findings consistent with recurrence were detected on imaging. Of the patients, 11 had local recurrence, 50 had pelvic lymph node involvement, 17 had distant lymph node metastasis, 13 had bone metastasis, and 8 had visceral organ metastasis. In multivariate logistic regression analysis, total PSA and PSAdt were found as independent predictive factors for imaging positivity (Table 1). According to total PSA values, imaging positivity rates were 38% in patients with a PSA level of <0.2, 41.2% in patients with a PSA level between 0.2-<0.5, 75% in patients with a PSA level between 0.5-<1.0, 94.1% in patients with a PSA level between 1.0-<2.0, and 100% in patients with a PSA level of ≥2.0. The imaging positivity rate was 97.6% in the patient group with total PSA value of ≥1.0 ng/ml. In patients with early BCR (n=62), the detection rate was 80% in patients with a PSAdt ≤3 months, 68.2% in patients with a PSAdt between 3 months and 6 months, and 20% in patients with a PSAdt >6 months. Figure 1 shows the nomogram that predicted imaging positivity in patients with PSA<1.0 ng/ml. In the nomogram, the variables are scored on a 0-100 scale, and the probability of PSMA PET/MR positivity can be calculated

according to the total score. ***Conclusion:*** If PSA level is ≥1.0 ng/ml in PC patients with BCR after RP, Ga-68 PSMA PET/MRI has a very high lesion detection rates. In patients with PSA<1.0 ng/ml, the PSAdt is very effective in the diagnostic performance of the imaging method and should be considered in patient selection.

OP-511

The diagnostic performance of ^{68}Ga-PSMA-11 PET/CT versus multiparametric MRI for detecting intra-prostatic radiorecurrent prostate cancer

A. Light[1], *S. Lazic*[2], *M. Bayne*[3], *M. J. Connor*[1], *H. Tam*[2], *H. U. Ahmed*[1], *T. T. Shah*[1], *T. D. Barwick*[2];
[1]*Imperial Prostate, Imperial College London, London, UNITED KINGDOM,* [2]*Department of Radiology, Charing Cross Hospital, Imperial College Healthcare NHS Trust, London, UNITED KINGDOM,* [3]*Imperial Urology, Charing Cross Hospital, Imperial College Healthcare NHS Trust, London, UNITED KINGDOM.*

Aim/Introduction: For patients with biochemical recurrence after radiotherapy for prostate cancer, PSMA PET/CT is increasingly used to detect extra-prostatic disease. However, its ability to localise intra-prostatic lesions is unclear, with previous studies omitting histological verification of imaging findings. This is important for planning any local salvage treatment. Using a histopathological reference standard, we evaluated the diagnostic accuracy of ^{68}Ga-PSMA-11 PET/CT for this purpose and compared this to mpMRI. ***Materials and Methods:*** In this single-centre retrospective series (2017-2022), men with a rising PSA post-radiotherapy underwent mpMRI, ^{68}Ga-PSMA-11 PET/CT and systematic and/or targeted biopsy. PET/CT was performed with both standard knees-to-vertex acquisitions (mean 61 minutes post-injection) and delayed post-micturition pelvic acquisitions (mean 91 minutes post-injection). Each PET/CT was reported in sextants by a single expert blinded to previous imaging and clinical data. Suspicion of intra-prostatic radiorecurrence was denoted by a 5-point Likert score, with scores 3-5 indicating a suspicious scan. Diagnostic accuracy metrics were calculated comparing PET/CT versus MRI, and comparing PET/CT with MRI used together versus MRI alone. Analyses were performed at the hemi-gland level using cluster bootstrapping with 1,000 resamples. ***Results:*** 35 men (70 hemi-glands) were included. 45/70 (64%) hemi-glands had a suspicious PET/CT, and 41/70 (59%) had a suspicious MRI. When using both modalities in conjunction, 55/70 (79%) hemi-glands were deemed suspicious. 43/70 hemi-glands (61%) had cancer on biopsy. PET/CT missed 6/43 (14%; 95%CI 6-28%). MRI missed 12/43 cancers (28%; 95%CI 17-43%), with 10/12 of these cancers detected by PET/CT. PET/CT sensitivity and specificity were 0.86 (95%CI 0.76-0.95) and 0.71 (95%CI 0.54-0.87), respectively, which were not significantly different to MRI sensitivity and specificity (sensitivity: 0.72, 95%CI 0.61-0.83, p=0.2; specificity: 0.64, 95%CI 0.44-0.83, p=0.8). PET/CT PPV was 0.83 (95%CI 0.70-0.93), and NPV was 0.76 (95%CI 0.58-0.92), both also not significantly different to MRI (PPV: 0.76, 95%CI 0.62-0.90, p=0.3; NPV: 0.59, 95%CI 0.41-0.75, p=0.09). When both PET/CT and MRI were used together, sensitivity was 0.95 (95%CI 0.89-1.00), significantly higher than MRI alone (p=0.004). NPV was 0.88 (95%CI 0.67-1.00), also significantly higher than MRI alone (p=0.004). Specificity was 0.50 (95%CI 0.30-0.68), and PPV 0.75 (95%CI 0.62-0.87), both not significantly different versus MRI alone (p=0.1 and 0.8, respectively). ***Conclusion:*** ^{68}Ga-PSMA-11 PET/CT has high sensitivity, though the use of both ^{68}Ga-PSMA-11 PET/CT and mpMRI together, provides a significantly greater sensitivity and NPV than mpMRI alone. Negative imaging with both modalities could therefore be a useful rule-out tool in this population.

OP-512

The imaging characteristics of theranostic ^{99m}Tc/^{188}Re-PSMA-GCK01 is equivalent to dedicated diagnostic ^{99m}Tc-HYNIC-iPSMA in prostate cancer

E. Mamlins[1], *J. Cardinale*[1,2], *M. Krotov*[1], *E. Winter*[2], *H. Rathke*[2,3], *U. Haberkorn*[2], *C. Kratochwil*[2], *F. Giesel*[1];
[1]*Department of Nuclear Medicine, Medical Faculty and University Hospital Duesseldorf, Heinrich-Heine-University Duesseldorf, Duesseldorf, GERMANY,* [2]*Department of Nuclear Medicine, University Hospital Heidelberg, Heidelberg, GERMANY,* [3]*Department of Nuclear Medicine, Inselspital Bern, Bern, SWITZERLAND.*

Aim/Introduction: Radiolabelled PSMA-ligands play a major role in today's nuclear medicine. Since approval of ^{177}Lu-PSMA-617 for therapy of metastatic prostate cancer, both the capacity of PSMA-PET and the availability of ^{177}Lu became bottleneck of supply due to the high demand. Recently a theranostic PSMA-ligand, PSMA-GCK01, was developed which can be labelled either diagnostically or therapeutically based on de-centralized available ^{99}Mo/^{99m}Tc and ^{188}W/^{188}Re generator nuclides. This novel tracer might solve supply limitations. In this investigation, the diagnostic imaging characteristics of ^{99m}Tc-PSMA-GCK01 were compared with the purely diagnostic reference compound ^{99m}Tc-HYNIC-iPSMA in patients with advanced stage prostate cancer. ***Materials and Methods:*** Between 01/2021 and 02/2022 two cohorts (n=21 vs. n=22) of patients with metastatic castration-resistant prostate cancer matched for age, tumor stage and total Gleason score underwent a planar gamma camera imaging with ^{99m}Tc-HYNIC-iPSMA and ^{99m}Tc-PSMA-GCK01 prior to PSMA-ligand therapy for PSMA-phenotyping. The imaging data were retrospective analysed for salivary gland, kidney, liver, soft-tissue and tumor-uptake on a semi-automated ROI-analysis using Hermes Medical Solution (HMS, Sweden). ***Results:*** Out of the cohort of ^{99m}Tc-HYNIC-iPSMA, two patients has been excluded due to incomplete records. All other data set were semi-automated quantified on a ROI-based analysis. The tumor-to-background presented equal results of ^{99m}Tc-PSMA-GCK01 compared to ^{99m}Tc-HYNIC-iPSMA. The physiological PSMA-positive organs like salivary gland presented also equal uptake in counts/MBq (salivary gland median 9,48 ^{99m}Tc-PSMA-GCK01 vs. median 9,11 ^{99m}Tc-HYNIC-iPSMA), while liver-to-kidney ratio presented a slide shift to the liver parenchyma using ^{99m}Tc-PSMA-GCK01 (0,83) compared to ^{99m}Tc-HYNIC-iPSMA (0,55) with no statistical significance. ***Conclusion:*** The novel theranostic tracer ^{99m}Tc/^{188}Re-PSMA-GCK01 demonstrates comparable diagnostic imaging characteristic compared with diagnostic reference compound ^{99m}Tc-HYNIC-iPSMA. These results pave the way for the PSMA-targeting imaging and theranostic agents for a broader, rather low-cost, generator applied radio-ligand therapy utilisation.

References: Cardinale et. al., JNM 2023

1107

Monday, September 11, 2023, 4:45 PM - 6:15 PM
Hall F1

Inflammation & Infection Committee - TROP Session: Vasculitis and Endocarditis: Current and New Evidence

OP-513

99mTc-white blood cell scintigraphy performance in thoracic aortic vascular graft infection: be careful in early post-operative period

B. Mahida[1,2], *M. Para*[2,3], *C. Regis*[1,4], *L. Deconinck*[5], *K. Ben Ali*[1,2], *X. Duval*[3,6], *B. IUNG*[3,7], *F. Rouzet*[1,2];
[1]*Nuclear medicine department, Bichat Hospital, AP-HP, Paris, FRANCE,* [2]*Université Paris Cité, Paris, FRANCE,* [3]*Department of Cardiovascular Surgery and Transplantation, Bichat Hospital, AP-HP, Paris, FRANCE,* [4]*Department of Medical Imaging, Institut de cardiologie de Montréal, Université de Montréal, Montréal, QC, CANADA,* [5]*Infectious Disease Department, Bichat Hospital, AP-HP, Paris, FRANCE,* [6]*Clinical Investigation Center, Bichat Hospital, AP-HP, Paris, FRANCE,* [7]*Cardiology Department, Bichat Hospital, AP-HP, Paris, FRANCE.*

Aim/Introduction: Thoracic aortic vascular graft infection (TAVGI) is rare, yet it is associated with a high morbidity and mortality. TAVGI diagnosis in early postoperative stages is challenging particularly with conventional anatomic imaging tools. The aim of this study was to assess the value and performance of 99mTc-hexamethypropylene amine oxime labeled autologous white blood cell (WBC scintigraphy) in the diagnosis of TAVGI during early postoperative period following TAVG surgery. ***Materials and Methods:*** From January 2011 to February 2022, 46 patients with suspected TAVGI who underwent WBC scintigraphy were retrospectively included. The final diagnosis was established by local multidisciplinary team considering clinical, bacteriological and imaging findings after a >6-month follow-up. Since 2 patients were lost to follow-up, the final analysis was performed on 44 patients. The median age was 63 years (range 22-85). A majority of patients underwent Bentall procedure (72%). Twenty-seven patients were finally diagnosed with TAVGI. They were all treated with antibiotics alone (n=22) or in combination with redo surgery (n=5). The rest of the study population underwent medical observation. The mean delay between initial vascular graft surgery and WBC scintigraphy was 734±1226 days. ***Results:*** In the overall study population, the diagnostic sensitivity, specificity, positive predictive value, and negative predictive value were 81.5%, 64.7%, 78.6%, and 68.8% respectively. Out of 29 patients with positive WBC scintigraphy, 6 were false positive because no relapse occurred during the follow-up without antibiotic treatment. The delay between vascular graft procedure and WBC scintigraphy was <35 days in 4 of them. One of the 2 other false positive patients underwent iterative embolization procedures, 2 months prior to scintigraphy and showed intense uptake on the vascular plugs sites, while the other patient had progressing pseudoaneurysm at the site of positive scintigraphy. When WBC scintigraphy was performed in the early postoperative period (<35 days), all scans were positive (n=13) with 100% sensitivity and 4 false positive conversely to the 33 scans performed ≥ 35 days after surgery with a 72% sensitivity and a 84.6% specificity. ***Conclusion:*** WBC scintigraphy is reliable to rule out thoracic aortic vascular graft infection. However its specificity decreases in the early post-operative period following surgery (<35 days).

OP-514

Fast-Track Pathway for Early Diagnosis and Management of Giant Cell Arteritis At University College London Hospital: Positive Impact of FDG PET-CT for Detection of Active Vasculitis

A. Alduraibi[1,2], *D. Ludwiga*[3], *S. Vöö*[4], *V. Morrisa*[3];
[1]*Department of Radiology, College of Medicine, Qassim University, qassim, SAUDI ARABIA,* [2]*University College London Hospitals Nhs Foundation Trust, London, UNITED KINGDOM,* [3]*Department of Rheumatology, University College London Hospital, University College London Hospitals NHS Foundation Trust (UCLH) and bInstitute of Nuclear Medicine, UCLH, London, UNITED KINGDOM,* [4]*Institute of Nuclear Medicine, University College London Hospital, London, UNITED KINGDOM.*

Aim/Introduction: Giant cell arteritis (GCA) is the most common type of vasculitis characterized by systemic inflammation, arteritis, and critical ischemia. Immediate, accurate diagnosis and access to appropriate treatment are key factors in preventing morbidity associated with this disease. Recent developments in vascular imaging prompted a review of our management of GCA patients. Here, we present the newly implemented Fast-track pathway (FTP) in GCA at the University College London Hospital, using combined temporal artery ultrasound (TAUS) and [18F]-fluorodeoxyglucose PET- computed tomography (FDG PET-CT). ***Materials and Methods:*** All patients with clinical suspicion of GCA were prospectively included in the study and evaluated following the existent GCA FTP. Patient underwent temporal artery ultrasound (TAUS) and temporal artery biopsy (TAB) within 24 h of presentation and FDG PET-CT within 72 h. Imaging protocol and interpretation were based on current clinical guidelines. FDG PET-CT images were considered positive if FDG uptake in vascular regions (thoracic aorta, abdominal aorta, subclavian arteries, axillary, carotid, vertebral, iliac, and femoral arteries) was higher or equal to the background FDG uptake in the liver. Imaging results were correlated with TAB outcomes and gold-standard clinical follow up. ***Results:*** Of 21 patients assessed by FTP (from June to December 2019), 13 patients (61.9%) had a positive diagnosis of GCA. TAB was positive in less than half of the GCA-positive cases (5/13). Of the TAB-positive cases, there was a strong correlation observed between TAB and imaging (TAUS + FDG PET-CT) findings. Most GCA-positive cases on TAB demonstrated GCA-positive features on imaging (4/5), indicating an excellent positive predictive value for our FTP in GCA. Eight patients (8/13) were negative on TAB, with high clinical suspicion of GCA demonstrated and typical GCA features on imaging (TAUS and FDG PET-CT). Two of these positive patients (2/13) had positive PET-CT, whereas both TAB and TAUS were negative for temporal artery involvement. Two GCA-mimics were detected on FDG PET-CT (2/21): one case of malignancy and one skull base infection. ***Conclusion:*** The use of FDG PET-CT increases the diagnostic yield of FTP for early detection of GCA. The combination of TAUS and FDG PET-CT shows a higher diagnostic accuracy compared to TAB. In addition, FDG PET-CT is valuable in identifying GCA-mimics, preventing inappropriate steroid therapy, and prompts for further secondary referrals in GCA-mimic cases.

OP-515

[18F]FDG-PET/CT as a Prognostic Inflammatory Imaging Marker in Giant Cell Arteritis

P. Nienhuis, *Y. Van Sleen, E. Brouwer, R. H. J. A. Slart;*
University Medical Center Groningen, Groningen, NETHERLANDS.

Aim/Introduction: Giant cell arteritis (GCA) is a large vessel vasculitis affecting the aorta, its major branches, and the arteries of the head and neck. Predicting its disease course is difficult because clinical presentation and inflammatory biomarkers are not disease specific. Hence, adequate management of the disease may be challenging. [18F]-fluoro-deoxyglucose (FDG) positron emission tomography-computed tomography (PET/CT) is an established diagnostic tool in GCA, but its prognostic value remains unclear. This study aimed to investigate [18F]FDG-PET/CT as a prognostic tool for GCA. ***Materials and Methods:*** This study involved patients with newly diagnosed GCA enrolled a prospective cohort study who underwent [18F]FDG-PET/CT prior to glucocorticoid therapy. The aorta, its major branches, and the cranial arteries were visually scored on a scale of 0-3, after which the scores were summed for a total vascular score (TVS). The same arteries were also manually segmented for volumetric semiquantitative analysis using total lesion glycolysis (TLG), which is a multiplication of the mean standardized uptake value and the volume of inflamed arterial wall. The relationship between [18F]FDG-PET/CT data and clinical outcomes was examined, with treatment-free remission as the primary endpoint. ***Results:*** In total, 29 patients were included in the study. The a median follow-up time was 4.4 years (range 1.0-9.8 years). Using receiver operating characteristics (ROC) analysis, TLG was able to distinguish patients who achieved treatment-free remission at 3 years (AUC 0.82, p=0.0076). Those having high TLG scores were more likely to have achieved treatment-free remission. Using the optimal ROC-based cut-off, Kaplan-Meier analysis showed that patients with high TLG achieved treatment-free remission faster (p=0.0442). No significant differences were observed when using TVS. ***Conclusion:*** High TLG was linked to a better response to treatment in GCA patients, while TVS did not show any association with disease course. These findings contrast with previous studies that reported a high TVS to be associated with a more complicated disease course or to have no relationship with disease course [1,2]. TLG provides a more comprehensive measure of the degree of inflammation in the vessel wall compared to visual scoring, which may explain the contrasting findings of this study. Moreover, high volumetric FDG uptake reflects heightened metabolic and inflammatory activity and therefore may indicate a greater responsiveness to anti-inflammatory medication. ***References:*** [1] Grayson et al. Arthritis Rheumatol 70.3 (2018): 439. doi: 10.1002/art.404032 [2] Sammel et al. Int J Rheum Dis 23.4 (2020): 582-588. doi: 10.1111/1756-185X.13724

OP-516

18F-FDG-PET/CT imaging on the LAFOV-PET/CT in patients with suspected large vessel vasculitis: reference values and diagnostic performance.

L. Knappe, *C. Bregenzer, N. Gözlügöl, C. Mingels, A. Rominger, F. Caobelli;*
Department of Nuclear Medicine, Inselspital Bern, Bern, SWITZERLAND.

Aim/Introduction: 18F-FDG PET/CT is an important diagnostic tool in suspected large vessel vasculitis (LVV). However, reference values and diagnostic performances are still unknown for PET-scanner with long-axial field-of-view (LAFOV). ***Materials and Methods:*** Images of 110 patients with suspected LVV were retrospectively evaluated. All underwent 18F-FDG PET/CT on a LAFOV-PET/CT-Scanner 60 minutes after injection of 3.0 MBq/Kg FDG. Semiquantitative parameters were calculated for supra-aortal vessels (temporal, carotid and subclavian arteries) and aortic/infra-aortal vessels (thoracic and abdominal aorta, external iliac and femoral arteries). To liver and bloodpool (BP) normalized values were also calculated in all vessels. The final diagnosis was obtained by consensus in a multidisciplinary meeting. ***Results:*** 50 of 110 patients (45.5%) had a final diagnosis of LVV. Both for supra-aortic and infra-aortic vessels, all semi-quantitative parameters were significantly different between patients with and without LVV (p<0.01 for all). At ROC-Curves analysis the following parameters yielded highest diagnostic accuracy for supra-aortal LVV: to-liver-SUV_{max} (AUC 0.90, threshold 0.65 with sensitivity 86% and specificity 77%), to-BP-SUV_{max} (AUC 0.92, threshold 1.00 with sensitivity 90% and specificity 79%), to-liver-SUV_{peak} (AUC 0.87, threshold 0.61 with sensitivity 80% and specificity 72%), to-BP-SUV_{peak} (AUC 0.90, threshold 0.94 with sensitivity 88% and specificity 80%) and for infra-aortal LVV: to-liver-SUV_{max} (AUC 0.98, threshold 0.83 with sensitivity 96% and specificity 90%), to-BP-SUV_{max} (AUC 0.97, threshold 1.27 with sensitivity 92% and specificity 92%), to-liver-SUV_{peak} (AUC 0.96, threshold 0.76 with sensitivity 94% and specificity 87%), to-BP-SUV_{peak} (AUC 0.95, threshold 0.94 with sensitivity 90% and specificity 95%). ***Conclusion:*** Our results confirm the usefulness of 18F-FDG-PET/CT in the diagnostic workup of LVV. In this regard LAVOF-PET/CT may yield increased diagnostic accuracy thanks to improved spatial and temporal resolution. Similarly, to what already reported normalized semi-quantitative values appear to be more robust in the diagnostic workup. However, thresholds for LAFOV-PET/CT may differ from those reported in literature for different scanners. Hence, prospective studies are warranted to implement new reference values in clinical practice when using high sensitivity scanners.

OP-517

C-X-C Motif Chemokine Receptor 4-directed PET/CT in Newly Diagnosed Giant Cell Arteritis - Initial Results from a Phase II Trial

M. Fröhlich[1], *S. E. Serfling*[2], *K. V. Guggenberger*[3], *T. Higuchi*[2], *M. Gernert*[1], *S. Samnick*[2], *M. Schmalzing*[1], *A. K. Buck*[2], *T. A. Bley*[3], *R. A. Werner*[2];
[1]*Medical Department II, Rheumatology, University Hospital Würzburg, Würzburg, GERMANY,* [2]*Department of Nuclear Medicine, University Hospital Würzburg, Würzburg, Germany, Würzburg, GERMANY,* [3]*Institute of Diagnostic and Interventional Radiology, University Hospital Würzburg, Würzburg, GERMANY.*

Aim/Introduction: We aimed to report on initial results of inflammatory-targeting, C-X-C motif chemokine receptor 4 (CXCR4)-directed imaging in newly diagnosed patients with giant cell arteritis (GCA). ***Materials and Methods:*** In a phase II trial NCT05604482, seven treatment-naïve patients with confirmed GCA received dual-tracer imaging without therapy between PET/CT using [18F]FDG (FDG) and [68Ga]PentixaFor (PEN). A total of 13 arterial segments were analyzed per patient. In addition, eight joints were analyzed for concurrent polymyalgia rheumatica. We compared both scans on a visual (using PETVAS) and quantitative level (by calculating target-to-background ratios (TBR) with blood pool serving as reference). CXCR4 is expressed by lymphocytes; therefore, quantitative PET results were also correlated with peripheral blood white blood cell counts (WBC) at the time of imaging. ***Results:*** On a visual level, PETVAS on FDG (24.29 ± 5.5) was higher relative to PEN (20.14 ± 3.18, P=0.19). TBR from FDG (2.38 ± 1.11) was not significantly different when compared to PEN

(1.55 ± 0.44, P=0.78). Of note, interquartile ranges (IQR) were lower for PEN (IQR, 0.46) when compared to FDG (IQR, 1.81), indicative for less scatter and higher accuracy on CXCR4-directed PET-based quantification. This phenomenon was also observed for joints (PEN: IQR, 0.25; FDG: IQR, 0.49). We observed higher correlative indices between TBR and WBC in patients imaged with PEN (PEN, R=0.45, P=0.45) when compared to FDG (R=0.27, P=0.65). ***Conclusion:*** In newly diagnosed patients with GCA, quantitative assessment of PEN was not inferior to FDG for vessel wall and joint read-outs. The quantified PEN signal may emerge as an image biomarker for active inflammation, provide guidance towards novel anti-inflammatory treatment or be useful in the context of artificial intelligence applications.

OP-518

[^{68}Ga]Ga-FAPI-46 PET/CT in patients with Large Vessel Vasculitis and comparison with age gender-matched controls.

J. Rosales[1], *J. Hoppner*[2], *U. Haberkorn*[2], *W. Merkt*[2], *P. Kvacskay*[2], *M. Röhrich*[2];
[1]*University Clinic Of Navarra, Pamplona, SPAIN,* [2]*University Hospital of Heidelberg, Heidelberg, GERMANY.*

Aim/Introduction: Giant Cell Arteritis and Takayasu Arteritis are the main forms of Large Vessel Vasculitis (LVV). Evaluation of disease activity is often difficult and different imaging modalities have been used in the assesment of structural and inflammatory changes. Fibroblast Activation Protein-PET (FAPI-PET) has shown promising results as a new imaging method not only in cancer patients but also in nonmalignant-inflammatory diseases. We aim to describe FAPI-PET semiquantitative parameters in patients with active and clinically inactive LVV and compare them with control subjects. ***Materials and Methods:*** We present a retrospective analysis of [^{68}Ga]Ga-FAPI-46 PET/CT semiquantitative parameters in eight patients with LVV performed at University Hospital Heidelberg. Three males with active disease (median-age: 58) and five females with clinically inactive disease (median-age: 59) were included. Eight age-gender-matched patients with no previous history of vascular inflammation served as controls [median-age: 58]. SUVmax, SUVmean and TBR were obtained placing a small ROI over the highest uptake in seven vascular segments: subclavian artery, ascending aorta, aortic arch, thoracic descending aorta, abdominal aorta, iliac and femoral arteries in all three groups. Patient-based and segment-based analysis were performed and compared with clinical data and MRI findings as a standard of reference. ***Results:*** On a patient-based analysis, SUVmax was significantly higher in patients with active disease than in clinically inactive cases and age-gender-matched controls (active, median-value, 3.35, inactive: 2.71 and controls: 1.76; p<0.005 each). SUVmean and TBR were also higher in active cases than inactive and control cases (p<0.05). On a segment-based analysis, average SUVmax and average SUVmean were significantly higher in the active group when compared with age-gender-matched controls in four vascular segments: ascending aorta, aortic arch, thoracic descending aorta and abdominal aorta (p<0.05 each). TBR was also significantly higher in active LVV group but only in the ascending aorta, descending aorta and abdominal aorta (p<0.05 each). Interestingly, average SUVmax and average SUVmean in the ascending aorta, aortic arch, thoracic descending aorta and abdominal aorta were significantly higher in the inactive group than in controls (p<0.05 each). Active and inactive cases did not differ significantly in terms of either SUVmax, SUVmean or TBR in patient-based or segment-based analysis. ***Conclusion:*** [^{68}Ga]Ga-FAPI-46 PET/CT is a promising new imaging modality and could potentially play a role in the evaluation of patients with LVV, not only to determine the extension of the disease in newly diagnosed cases, but also for the assesment and follow-up of clinically inactive cases.

OP-519

Improved [^{18}F] FDG PET/CT diagnostic accuracy for infective endocarditis: cardiac motion correction using different gating strategies

D. ten Hove[1,2], *B. Sinha*[1,2], *P. J. H. Van Snick*[1,2], *R. H. J. A. Slart*[1,2], *A. W. J. M. Glaudemans*[1,2];
[1]*Rijksuniversiteit Groningen, Groningen, NETHERLANDS,* [2]*University Medical Center Groningen, Groningen, NETHERLANDS.*

Aim/Introduction: Infective endocarditis is a serious and diagnostically challenging condition. The most recently published European Society of Cardiology's guidelines includes [18F] FDG-PET/CT as a major diagnostic criterion for the diagnosis due to its high sensitivity and specificity, particularly in patients with prosthetic heart valves. However, [18F]FDG-PET/CT is susceptible to motion related artefacts, which are not routinely corrected for in clinical practice. This study investigated the potential benefits of incorporating cardiac motion correction into [18F]FDG-PET/CT to enhance its diagnostic accuracy and clinical interpretability. ***Materials and Methods:*** In this prospective case series, patients receiving [18F] FDG-PET/CT for suspected IE underwent one or two additional motion corrected sequences using a conventional and/or a novel, list-mode data derived cardiac gating sequence. PET/CT scan preparation, acquisition and evaluation were performed in accordance with EANM recommendations. Scans were assessed for signs of IE by two experienced nuclear medicine physicians who were blinded to patients' clinical context. Clinical diagnosis of IE was established based on surgical findings or multidisciplinary consensus after a minimum of 4 months follow-up. ***Results:*** A total of 7 patients participated in the study, undergoing both an ungated [18F] FDG-PET/CT and a scan with cardiac gating. Cardiac gating improved interpretability of suspected intracardiac infection in 3 out of 4 patients with valvular lesions, regardless of the method of motion correction used. Importantly, in one of these 3 patients IE was confirmed, while the diagnosis was missed on ungated PET/CT. In another of the 3 patients, motion corrected PET demonstrated fluttering of a vegetation at the aortic valve. ***Conclusion:*** Motion correction of [18F] FDG PET/CT improved the diagnostic interpretability of [18F]FDG PET/CT. This is may improve the sensitivity of PET/CT while patient burden is negligible beside limited extra time in the scanner. Further larger comparative studies are necessary to confirm the additive value of the motion correction methods. ***References:*** Habib G et al. EHJ. 2015. Baddour LM et al. Circulation. 2015. Scholtens AM et al. JACC Cardiovasc Imaging. 2016. Gould FK et al. J. Antimicrob. Chemother. 2012.

OP-520

Impact and diagnostic performance of dedicated cardiac [^{18}F]-FDG digital PET/CT in infective endocarditis

S. Notohamiprodjo[1], *K. Scheidhauer*[1], *M. Eiber*[1], *I. Yakushev*[1], *S. Kleiner*[1], *J. Kraus-Deuringer*[1], *H. W. A. Krebs-Fleischmann*[1], *A. G. Villagran Asiares*[1], *S. G. Nekolla*[1], *R. Eggerstedt*[2], *B. Eglseder*[3], *W. A. Weber*[1];
[1]*Technical University of Munich, Munich, GERMANY,* [2]*German Heart Centre Munich, Munich, GERMANY,* [3]*Krankenhaus GmbH Landkreis Weilheim-Schongau, Weilheim, GERMANY.*

Aim/Introduction: For modified Duke criteria (mDC) for the diagnosis and management of patients with suspected infective endocarditis (IE), FDG-PET/CT was recently introduced as a new criterion, but not routinely recommended due to low sensitivity and lack of clinical impact. But recently a new generation of digital PET/CT-systems are commercially available with improved spatial resolution and equipped with integrated ECG

and respiratory-gating. As data regarding such a sophisticated acquisition approach in diagnosis of endocarditis are currently lacking, this study aimed to assess the impact and diagnostic performance of a dedicated cardiac protocol for [18F]-FDG-PET/CT, that includes state-of-the-art digital PET and a dual-ECG-respiratory-gating technique (dedicated-cardiac-PET), compared to conventional whole-body-PET in diagnosis of IE determined by the consultant and nuclear medicine physician in training (trainee). ***Materials and Methods:*** 44 patients suspected for IE underwent conventional whole-body- and dedicated-cardiac-PET on a digital PET/CT-system after overnight fasting. Visual and semiquantitative analyses were performed and the diagnostic performances were determined. The readers were instructed to describe findings and to confirm/reject the diagnosis of IE, blinded to the protocols used for the examination and other criteria for mDC. Consensus of multidisciplinary IE task force served as gold standard. ***Results:*** The median of maximum-Standardized-Uptake-Value (SUVmax) for confirmed IE was 5.2, respectively, for rejected IE 2.5. In ROC-analysis a cutoff value of SUVmax > 3.8 identified positive cases with sensitivity and specificity of 92% and 77%. High resolution dedicated-cardiac-PET revealed higher interobserver reliability of valvular uptake characteristics for IE-focus detectability than conventional-PET, indicating higher diagnostic confidence. Consultant-group determined pooled sensitivity, specificity and accuracy of >91% in dedicated-cardiac-PET and of >77% in conventional-PET. Trainee-group established values of >69% in dedicated-cardiac-PET and >48% in conventional-PET. Compared to conventional-PET, substantial improvement of the diagnostic performance in diagnosis of native valve endocarditis using dedicated-cardiac-PET in consultant and trainee group was evident. Substantial improvement in diagnosis prosthetic valve endocarditis was found in trainee-group, but only minimal in consultant-group at initial high performance in conventional-PET. In consultant-group, dedicated-cardiac-PET revealed remarkable higher interobserver reliability in scoring of FDG-uptake characteristic and of confidence of scoring than in conventional-PET, indicating higher diagnostic confidence. The interobserver reliability in trainee-group was poor. The high intraobserver reliability in consultant and trainee-group demonstrated robust reproducibility. ***Conclusion:*** Dedicated-cardiac-PET has the potential as an adequate adjunctive diagnostic modality in challenging possible IE-cases and may have a significant impact on IE-related morbidity, mortality and patient's management, provided the investigators have the desired expertise.

OP-521

New semiquantitative parameters to improve diagnostic accuracy of FDG-PET/CT in suspected endocarditis

C. Bregenzer, *L. Knappe, C. Mingels, N. Gözlügöl, A. Rominger, F. Caobelli;*
Department of Nuclear Medicine, Inselspital, University Hospital Bern, University of Bern, Bern, SWITZERLAND.

Aim/Introduction: Infective endocarditis (IE) is an infection of the endocardium involving native and prosthetic valves. In the diagnostic workup, FDG-PET is now recommended in uncertain cases. However, the image-derived diagnosis relies mostly on a visual interpretation and is often challenging, especially in patients with prosthetic valves. We aimed to evaluate semiquantitative parameters able to yield an accurate diagnosis of IE. ***Materials and Methods:*** In our center, patients with suspected IE in native and prosthetic valves who underwent a [18F]FDG-PET/CT scan after 72-hours of low-carb diet were included. If a focal increased uptake was present, it was evaluated semiquantitatively. Standardized uptake value (SUV) max/mean/peak and normalized values (to-liver, to-mediastinum, to-surrounding uptake) were calculated with a volume of interest (VOI) and a 40% isocontour around detectable hypermetabolic foci. Sorrounding activity was defined as the presence of homogeneous and circumferential uptake at the valve/prosthesis level. Final diagnosis of confirmed or rejected IE was obtained by consensus in a multidisciplinary board, by evaluating clinical, laboratory and imaging data. ***Results:*** Fifty patients (44 males), aged 57.99 ± 18.86y were evaluated. Forty-five (90%) had a prosthetic valve, in the remaining IE was suspected on native valves. IE was confirmed in 25/50 patients and rejected in 25. Visually detectable hypermetabolic foci (n=44) were seen in 28 patients (56%). Of these, 20 were finally diagnosed with IE. Several semiquantitative measures on the foci of increased uptake as well as normalized values differed between patients with and without IE (values expressed as median [IQR]): SUV_{peak} (5.45 [2.32] vs. 3.37 [2.04], p=0.02), to-liver SUV_{max} (2.31 [1.34] vs. 2.13 [2.1], p=0.001), to-liver SUV_{mean} (1.31 [0.39] vs. 1.2 [1.2], p=0.001), to-liver SUV_{peak} (1.97 [1.18] vs. 1.49 [1.23], p<0.001), to-mediastinum SUV_{max} (3.13 [1.14] vs. 2.64 [3.53], p =0.001), to-mediastinum SUV_{mean} (1.66 [0.62] vs. 1.44 [1.47], p=0.001), to-mediastinum SUV_{peak} (2.37 [1.3] vs.1.66 [1.53], p<0.001), to-surrounding-activity SUV_{max} (1.75 [0.8] vs. 1.25 [1.62], p<0.001), to-surrounding-activity SUV_{mean} (1.29 [0.38] vs. 1.15 [0.45], p<0.001) and to-surrounding-activity SUV_{peak} (1.6 [0.92] vs. 1.04 [0.97], p<0.001). Highest accuracy was yielded by ROC-Curves analysis for SUV_{peak} (AUC 0.79, p=0.02, threshold 3.93 with sensitivity 85% and specificity 75%), and to-surrounding activity SUV_{peak} (AUC 0.79, p=0.02, threshold 1.23 with sensitivity 85% and specificity 75%). ***Conclusion:*** Semiquantitative parameters in our cohort proved to be accurate and should be recommended in clinical practice to assist in the interpretation of [18F]FDG-PET/CT in patients with suspected IE.

1108

Monday, September 11, 2023, 4:45 PM - 6:15 PM
Hall F2

Thyroid Committee - TROP Session: Iodine-131 Therapy in Differentiated Thyroid Cancer: Present and Future Perspective

OP-522

Efficacy of ^{131}I therapy and its influencing factors in children and adolescents with differentiated thyroid cancer lung metastases: comparative analysis with youth using propensity score matching

X. Zhang[1], *H. Feng*[2];
[1]*Department of Nuclear Medicine, Zhujiang Hospital Southern Medical University, Guangzhou,Guangdong Province, CHINA,* [2]*Department of Nuclear Medicine, Zhujiang Hospital Southern Medical University, 广州市, CHINA.*

Aim/Introduction: The aim of this study was to analyse the factors influencing lung metastases in pediatric patients with differentiated thyroid cancer(DTC) and to evaluate the efficacy of ^{131}I therapy. To compare its efficacy with that of young differentiated thyroid cancer patients by propensity score matching. ***Materials and Methods:*** We performed a retrospective analysis of DTC pediatric patients who were hospitalized in our institution between 2010 and 2018. All patients had undergone

total thyroidectomy and ^{131}I treatment. According to the cut-off point of age 14 years old, The group was divided into children (≤14 years old) and adolescents (15-21 years old). Efficacy evaluation was divided into PD and non-PD (non-PD, including CR, PR, SD). Factors affecting lung metastasis were identified and evaluated for ^{131}I treatment efficacy by univariate and multifactorial COX regression analysis. In order to compare the prognosis of pediatric patients with lung metastases with youth patients, Patients with DTC in pediatric patients from 2014 to 2018 were matched in a ratio of 1:6 through propensity score matching. ***Results:*** A total of 1095 patients were included in our study, including 168 paediatric patients and 927 youth patients. The median follow-up time of was 70.2 months, and the incidence of lung metastases was 25.9%. Age, gender, underlying disease (i.e. no underlying disease versus Hashimoto's thyroiditis-containing disease), number of lesions, involvement of glands, and lateral cervical lymph nodes metastasis were found to be significant predictors of the presence of lung metastases in pediatric patients in a univariate analysis ($p > 0.05$); In Cox regression analysis of pediatric patients, no statistically significant difference was found between the treatment outcome of ^{131}I in patients with lung metastases and that of patients with non-lung metastases. After propensity score matching, no statistically significant difference in ^{131}I treatment outcome was obtained between pediatric patients with lung metastases and youth patients. ***Conclusion:*** The incidence of lung metastases was higher in pediatric patients with DTC. The treatment effect of ^{131}I in children with lung metastases was the same as that in children without lung metastases. The treatment effect of ^{131}I in patients with pediatric patients lung metastases was similar to that in youth patients with lung metastases, and both had good treatment effect.

OP-523

Prognostic factors in children with differentiated thyroid cancer

S. Zakavi[1], *F. Nesari Javan*[1], *E. Askari*[1], *S. Shafiee*[1], *V. Roshanravan*[1], *A. Aghaei*[1], *N. Ayati*[2];
[1]*Nuclear Medicine Research Center, Mashhad University of Medical Sciences, Mashhad, IRAN, ISLAMIC REPUBLIC OF,* [2]*Cancer Imaging, Peter MacCallum Cancer Centre, Melbourne, AUSTRALIA.*

Aim/Introduction: Prognostic factors of follicular cell derived differentiated thyroid carcinoma (DTC) are not studied extensively. In this study, we analyzed prognostic factors in children with DTC who have been treated in a single center in the last 27 years. ***Materials and Methods:*** We studied 126 children with an age range of 5 to 18 years. The patients have been treated by near-total thyroidectomy followed by radio-iodine therapy and thyroid hormone administration for the purpose of TSH suppression. Follow-up of the patients was done more frequently in the first year after treatment (2, 6, and 12 months) and then by yearly evaluation. Response to treatment was defined according to the American Thyroid Association (ATA) guideline ***Results:*** Majority of the patients (93.7%) had papillary thyroid cancer and 52.4% had lymph node metastasis at presentation, which was extensive (>5) in 30% of the patients. All patients with extranodal extension had extensive lymph node invasion. Distant metastasis was seen in 8.8%, and the majority of them (90.9%) were in the lung. The mean initial dose of I-131 was 3.7±1.9 GBq in total or 74±42.2 MBq/kg of body weight. The median follow-up was 82 months and the median time to achieve an excellent response was 29 months. One year after therapy, 18% of the patient achieved excellent response, and the figure increased to 46.4% in the last follow up. The pre-ablation stimulated thyroglobulin (psTg) level was 153.0±245.7 ng/ml in patients with incomplete response compared to 11.2±17.5 ng/ml in others (P<0.001). Furthermore, using logistic regression, the psTg level was the only significant predictor of distant metastasis. Additionally, distant metastasis was more common in boys (14.7%) than girls (6.5%), and it took longer time for boys to achieve an excellent response. Younger children tended to have more advanced diseases. ***Conclusion:*** The pre-ablation sTg level was the only significant predictor of incomplete response and distant metastases in children with DTC. Boys had more advanced diseases and worse prognosis than girls.

OP-524

Impact of micro-extrathyroidal extension and bilateral topography of malignancy on clinical initial stating and early outcome of differentiated thyroid cancer (<4cm) patients.

A. Campenni'[1], *R. Ruggeri*[1], *M. Siracusa*[1], *D. Cardile*[1], *S. Russo*[1], *A. Nicocia*[1], *A. Rappazzo*[1], *V. Davi*[1], *A. Alibrandi*[1], *S. Baldari*[1], *L. Giovanella*[2];
[1]*Ospedale Gaetano Martino, Messina, ITALY,* [2]*Ente Ospedaliero Cantonale, 6500 Bellinzona, SWITZERLAND.*

Aim/Introduction: The latest 2017 American Joint Committee on Cancer downstaged the impact of micro-extrathyroidal extension (mETE) on both clinical tumor staging and outcome of differentiated thyroid cancer (DTC) (<4 cm) patients. However, literature data showed conflicting evidence. This study was aimed to assess mETE impact on initial tumor staging and outcome of DTC patients in a real clinical scenario. ***Materials and Methods:*** We reviewed the records of 360 (F=295, M=82) low or intermediate-risk DTC patients [pT1-T3,Nx(0,1),Mx(0)]. Papillary thyroid cancer was carried out in 324/360 (90%) patients while 24 (6.6%) had a follicular thyroid carcinoma and 12 (3.4%) had a Hurthle cell carcinoma. In 75, 109, 122 and 54 DTC patients, malignant lesion(s) was localized in bilateral, left, right and multi-focal-unilateral lobes, respectively. mETE was diagnosed in 73/360 (20.3%) DTC patients.All patients had undergone (near)-total thyroidectomy followed by iodine-131 therapy (RIT) with ablative or adjuvant purpose. A post-therapy whole body scintigraphy coupled with SPECT-CT (pT-imaging) was obtained 2-5 days after RIT. The response to initial treatments was evaluated 8-12 months after RIT and patients were classified according to 2015 American Thyroid Association guidelines (2015 ATA). ***Results:*** At initial diagnosis/treatments, metastatic disease was noted in 36/73 (49.3%) and 75/287 (26.1%) patients with or without mETE, respectively (p= <0.001). In DTC patients with or without mETE, an excellent response (ER) or less than excellent response to initial treatments (i.e. bio-chemical or structural persistent disease) was noted in 62/73 (84.9%), 269/287 (93.7%), 11/73 (15.1%) and 18/287 (6.3%) cases, respectively (p=0.014). mETE emerged as an independent risk factor for having both metastatic disease at initial diagnosis/treatments and persistent disease at early follow-up (p=0.01).Interestingly, DTC had a bilateral topography in 6/11 (54.5%) patients with mETE and less than ER (p= 0.005). In such patients, the risk of having metastatic disease at initial diagnosis/treatments or persistent disease at early follow-up was higher than other patients (Odds Ratio=1.869 and 3.007, respectively; p=0.008 and p=0.005, respectively).Noteworthy, the association between mETE and bilaterality emerged at multivariate analysis as an independent risk factor for having persistent disease at early follow-up (p=0.008). ***Conclusion:*** The prevalence of metastatic disease at initial diagnosis/treatment

such as persistent disease at early follow-up is significantly higher in DTC patient with mETE than others. The association between mETE and bilateral DTC topography is an independent risk factor for significantly increasing the risk of metastatic disease at initial diagnosis/treatment and persistent disease at early follow-up.

OP-525

Postoperative Thyroglobulin as a Yard-stick for Radioiodine Therapy: Decision Tree Analysis in a European Multicenter Series of 1317 Patients with Differentiated Thyroid Cancer

L. Giovanella[1], *L. Milan*[1], *W. Roll*[2], *M. Weber*[3], *S. Schenke*[4], *M. Kreissl*[4], *A. Vrachimis*[5], *K. Pabst*[6], *T. Murat*[7], *P. Petranović Ovčariček*[8], *B. Riemann*[9], *L. Ceriani*[1], *A. Campenni'*[10], *R. Goerges*[6];
[1]*Imaging Institute of Southern Switzerland, Bellinzona, SWITZERLAND,* [2]*University Hospital Muenster, Muenster, GERMANY,* [3]*University Hospital of Essen, Essen, GERMANY,* [4]*University Hospital Magdeburg, Magdeburg, GERMANY,* [5]*German Oncology Center, Limassol, CYPRUS,* [6]*University Hospital Essen, Essen, GERMANY,* [7]*Hacettepe University, Ankara, TÜRKIYE,* [8]*University Hospital Center "Sestre milosrdnice", Zagreb, CROATIA,* [9]*University Hospital Münster, Münster, GERMANY,* [10]*Ospedale Universitario di Messina, Messina, ITALY.*

Aim/Introduction: An accurate postoperative assessment is pivotal to inform postoperative ^{131}I treatment in patients with differentiated thyroid cancer (DTC). Our study developed a predictive model for post treatment-whole body scintigraphy (PT-WBS) results (as a proxy for persistent disease) by adopting a decision tree model. ***Materials and Methods:*** Age, sex, histology, T stage, N stage, risk classes, remnant estimation, TSH, and Tg were identified as potential predictors and were put into regression algorithm (conditional inference tree, ctree) to develop a risk stratification model for predicting the presence of metastasis in PT-WBS. ***Results:*** The lymph node (N) stage identified a partition of the population into two subgroups (N positive vs negative). In N positive patients a Tg value >23.3 ng/mL conferred a 83% probability to have metastatic disease compared to those with lower Tg values. Additionally, N negative patients were substratified in three subgroups with different risk rates according to their Tg values. The model remained stable and reproducible in the iterative process of cross validation. ***Conclusion:*** We developed a simple and robust decision tree model able to provide reliable informations on the probability of persistent/metastatic DTC after surgery. Provided informations may guide post-surgery ^{131}I administration by selecting patients requiring curative rather than adjuvant ^{131}I therapy schedules.

OP-526

Diffuse Sclerosing Variant of Papillary Thyroid Carcinoma is Related to A Poor Outcome: A Comparison Study Using Propensity Score Matching

L. Yang*, M. Zhao, L. Xiao, L. Li, P. Dong;*
Department of Nuclear Medicine, West China Hospital, Sichuan University, Chengdu, CHINA.

Aim/Introduction: Clinical outcome of diffuse sclerosing variant of papillary thyroid carcinoma (DSV-PTC) remains still controversial. We aimed to determine whether DSV-PTC is associated with increased risk of persistent/recurrent disease. ***Materials and Methods:*** We performed a retrospective cohort study of DSV-PTC and classic variant of papillary thyroid carcinoma (CV-PTC) after post-surgical radioactive iodine therapy. We used the propensity score matching (1:3 matching ratio) to account for differences between recipients of DSV-PTC vs CV-PTC. Univariable and multivariable analysis were performed to assess the independent factors for persistent/recurrent disease. Kaplan-Meier curve analyses were used to compare disease-free survival (DFS). ***Results:*** In total, 35 (12.7%) patients with DSV-PTC and 240 (87.3%) patients with CV-PTC were included. After propensity score matching, 35 pairs of patients were selected (DSV-PTC, n = 35; CV-PTC, n = 105). In the matched analysis, higher proportions of DSV-PTC experienced persistent/recurrent disease compared with CV-PTC (25.7% vs 5.7%; p = 0.003). In multivariate analyses of clinical and tumor characteristics, only the histologic type of DSV-PTC (odds ratio, 6.288; 95% confidence interval, 1.900-20.811; p = 0.003) was associated with increased risk of persistent/recurrent disease. The five-year DFS rates for the DSV-PTC and CV-PTC groups were 69.2% and 93.6%, respectively. The Kaplan-Meier analysis indicated that the DSV-PTC group (p = 0.001) had shorter DFS. ***Conclusion:*** This propensity-matched analysis found that the histologic type of DSV-PTC may increase the risk of persistent/recurrent disease.

OP-527

Radiomics approaches for predicting non-iodine-avid status of lung metastases in patients with differentiated thyroid cancer based on CT: a prospective observational study

X. Gao*;*
Department of Radiology, Zhejiang Cancer Hospital, Hangzhou, CHINA.

Aim/Introduction: Identifying non-iodine-avid status of lung metastases (LMs) in time is crucial to avoid radioactive I^{131} for patients with differentiated thyroid cancer (DTC) who will not benefit from it. In this study, we speculated that vivid radiomics features and deep learning features of routine chest CT scans may reflect different tumor heterogeneity between noniodine-avid and iodine-avid LMs. To evaluate this hypothesis, different radiomics models were built with machine learning, deep learning and novel integration of radiomics features and deep learning features to discriminate non-iodine-avid LMs from iodine-avid LMs in patients with DTC. ***Materials and Methods:*** Models were built in 1445 pretreated LMs of 270 consecutive DTC patients with pretreated initially diagnosed LMs who underwent both chest CT and radioiodine whole-body scanning between January 2010 and December 2019 in Zhejiang Cancer Hospital. Integration models based on machine learning were built with selected radiomics features and deep learning features and compared with classic machine learning models (Random Forest, K-Nearest Neighbor, Logistic Regression, and Support Vector Machine), or deep learning models to predict non-iodine-avid status of lung metastases**.** To validate these radiomics approaches prospectively, we recruited 244 consecutive patients with 876 LMs between January 2020 to October 2022. ***Results:*** Among all the machine learning models, the Support Vector Machine showed the best discrimination, with a 0.815 area under the curve (AUC), a 0.754 sensitivity and a 0.730 specificity. The deep learning model reached a 0.869 AUC, a 0.794 sensitivity and a 0.798 specificity. All the integration models were significantly better than classic machine learning or deep learning alone, with the best AUC of 0.904, sensitivity of 0.812, specificity of 0.823. ***Conclusion:*** Radiomics features and deep learning features of routine chest CT scans can reflect different tumor heterogeneity between noniodine-avid and iodine-avid LMs. Our study highlights a possible role of radiomics approaches from routine chest CT as a noninvasive, less radioactive and cost-effective way to evaluate iodine-avid status of LMs in DTC.

OP-528

Could Coprococcus catus be used as a biomarker for the treatment response of I-131 in thyroid cancer patients?

A. Fernandes[1], *R. Soares*[2], *P. Barata Coelho*[3];
[1]*Centro Hospitalar e Universitário São João, Porto, PORTUGAL,* [2]*Faculdade de Medicina da Universidade do Porto, Porto, PORTUGAL,* [3]*Universidade Fernando Pessoa, Porto, PORTUGAL.*

Aim/Introduction: Given the growing evidence that highlights the connection between the gut microbiota and response to certain therapeutics and that the gut microbiota may act as a regulator of immunity and, therefore, may indirectly play a role in tumorigenesis, we conducted a prospective observational study to assess whether there were microbial signatures that correlated with therapeutic response to RAIT. To do this, we profiled baseline samples of responders and non-responders of differentiated thyroid cancer patients to find potential biomarkers for predicting response after RAIT. ***Materials and Methods:*** Faecal samples of 37 thyroid cancer patients with the indication for RAIT were collected 2 to 3 days before therapeutics. After DNA extraction, the overall composition of the gut microbiota was studied by shotgun metagenomics. Patients were separated into responders if they had negative TgAb and Thyroglobulin (suppressed Tg<0.2ng/mL or stimulated Tg<1 ng/mL) and non-responders if they did not achieve these parameters. Those without follow-up or with an indeterminate response were excluded (n=11). Finally, 13 patients were considered responders and 13 non-responders. To explore key phylotypes that may contribute to the observed differences in microbial communities between cohorts, linear discriminant analysis (LDA) effect size (LEfSe) was performed to estimate differentially abundant features with biological consistency and statistical significance, with an LDA threshold value of > 3.0. $\rho < 0.05$ values were considered statistically significant. ***Results:*** LEfSe analysis showed that the specie Coprococcus catus was enriched in patients with thyroid cancer that responded to therapeutics, with an LDA score of 3.069, p=0.01. ***Conclusion:*** Our results suggest that the pre-existing changes in the gut microbial ecology may serve as a potential predictive marker to identify patients more likely to respond to treatment. Coprococcus catus is a short-chain fatty acid (SCFA) producer bacteria. SCFAs improve gut health through several local effects, including maintaining and improving intestinal barrier integrity, increased absorption of some nutrients and mineral elements, mucus production, and protection against inflammation. In addition, SCFAs can inhibit histone deacetylase and activate NIS re-expression in thyroid cancer cells, thereby inducing re-differentiation and iodine uptake. The relationship between thyroid cancer and SCFA-producing bacteria has also been investigated, and investigations have deduced that the loss of these bacteria might promote the development of thyroid cancer. This study provides a conceptual basis for further investigations that may increase our comprehension of response to therapeutics. ***References:*** doi: 10.1016/j.jare.2021.04.001; 10.3389/fendo.2022.943408.

OP-529

Determination of whole-body effective half-life of I-131 on differentiated thyroid cancer patients with a cloud-based remote dose meter

L. Kääriä[1,2], *M. Lapela*[3,2], *M. Seppänen*[4,2], *J. Ruohola*[3,2], *A. Ålgars*[5,2], *T. Noponen*[6,2];
[1]*Department of Nuclear Medicine, Turku University Hospital and Wellbeing services county of Southwest Finland, Turku, FINLAND,* [2]*University of Turku, Turku, FINLAND,* [3]*Department of Oncology, Turku University Hospital and Wellbeing services county of Southwest Finland, Turku, FINLAND,* [4]*Department of Clinical Physiology, Nuclear Medicine and Turku PET Centre, Turku University Hospital and Wellbeing services county of Southwest Finland, Turku, FINLAND,* [5]*Deparment of Oncology, Turku University Hospital and Wellbeing services county of Southwest Finland, Turku, FINLAND,* [6]*Department of Clinical Physiology, Nuclear Medicine, Turku PET Centre and Medical Physics, Turku University Hospital and Wellbeing services county of Southwest Finland, Turku, FINLAND.*

Aim/Introduction: We analysed continuously monitored external dose rate signals from remote dose rate meters to determine the effective half-life of I-131 in differentiated thyroid cancer (DTC) patients. The aim is to gain novel understanding of the retention of radioiodine in DTC patients and to demonstrate that remote cloud-based dose rate meter solutions can be reliably used in the real-time monitoring of external dose rate and discharging radionuclide therapy patients. ***Materials and Methods:*** 135 DTC patients who received postoperative radioiodine therapy between September 2018 and February 2022 in Turku University Hospital were studied retrospectively. The activity administered in 29 low-risk patients ranged from 1.055 to 1.223 GBq and in 106 higher-risk patients from 3.149 to 4.048 GBq. The external dose rates of the patients were continuously monitored during their hospitalization with a remote dose rate meter fixed on the ceiling of the radiation isolation room. Patients' normal movements in the isolation room affect to the measured dose rate signals. Therefore, location correction factors were determined from the calibration measurements of the meter using a radioiodine capsule in the isolation room. The dose rate signals were adjusted by using the location correction factors that transferred the location of the patient moving around the room into a standardized location on the hospital bed. The dose rate signal of each patient was location corrected and resampled whereafter monoexponential function was fitted in the signal. Finally, the effective half-life was calculated from the fitted equation. The group differences of effective half-lives were statistically analysed with Mann-Whitney U test. A possibility to use the remote dose-rate measurements to discharge the radioactive therapy patients was also evaluated. ***Results:*** The mean effective half-life was 13.47 ± 5.43 h for all patients. For low-risk patients the mean effective half-life was 13.78 ± 5.51 h and for higher-risk patients 13.38 ± 5.43 h. There were no statistically significant difference (p=0.718) in half-lives observed between the groups administered the activities of 1.1 and 3.7 GBq. The remotely measured dose rate signals could reliably be used to discharge the patients. ***Conclusion:*** The administered activity has no effect on whole-body effective half-life of the patient. With the continuously measured dose rate signals, it may be possible to obtain more accurate information on the removal of radioiodine than before. This information can be used to optimize the length of radiation isolation period, discharge instructions and be utilized for dosimetry purposes.

OP-530

Preliminary results from a clinical trial combining ^{131}I and external beam radiotherapy for treatment of metastatic radioiodine-refractory thyroid cancer

R. Hobbs, *I. Marsh, H. Quon, P. Santhanam, P. Ladenson, B. He, D. Kaplin, K. Lowe, H. Wang, G. Sgouros;*
Johns Hopkins, Baltimore, MD, UNITED STATES OF AMERICA.

Aim/Introduction: Treatment of well differentiated thyroid cancer with radioiodine (^{131}I) has a long and successful history. However, tumor uptake of ^{131}I can be diminished in patients with recurrent metastatic disease resulting in sub-therapeutic absorbed doses (AD) to the tumors. Here we present results from an ongoing clinical trial combining ^{131}I with stereotactic radiotherapy (SRT), using personalized dosimetry. ***Materials and Methods:*** Four

patients have been enrolled in the trial to date. Patients are simulated for the external beam portion of the therapy and then administered a tracer amount of ^{131}I, with multiple time point whole body probe and blood activity measurements. These measurements are used in a two source compartment S value dosimetry model to determine the patient-specific maximum tolerated therapeutic activity based on bone marrow constraints. Following administration of the therapeutic ^{131}I, three SPECT/CT images are acquired using the patient-specific fixation device(s) from the SRT simulation, which improves the registration of images across time and reduces the uncertainty in the ^{131}I AD calculations. The images are reconstructed, registered, and the target lesion(s) delineated. S value dosimetry is used to determine mean lesion AD, which is then converted to EQDX, where the X is the dose per fraction of the SRT treatment, determined as the amount needed to deliver a combined total of 80 Gy of EQD2 to the target lesion(s). ***Results:*** In the case of the first patient, two lesions were identified and treated, the ^{131}I portion was calculated to have delivered ADs of 16.6 and 12.5 Gy (14.7 and 11.0 Gy EQDX), respectively, to lesion PTVs. The lesions were then treated with 5 fractions of SRT of 9.0 Gy and 9.5 Gy (66.0 Gy and 71.3 Gy EQD2), respectively. Following treatment, the patient experienced tumor volume reduction and pain relief. Thyroglobulin levels fell from 89,000 to 55,000 ng/ml three months post-treatment and TSH increased to 9.0 mU/L, indicating reduction in overactive thyroid tissue. The other patients have received similar treatments with follow-up data to come. ***Conclusion:*** Personalized dosimetry-based combination radiopharmaceutical therapy (RPT)-SRT is feasible and allows for AD delivery to target lesions that would not be achievable by either single modality alone and may benefit from reduced toxicity. The low level of AD from ^{131}I seen here may indicate a need for a more quantitative triage approach and a wider application of this methodology. This work sets the groundwork for more generalized routine clinical RPT-external beam combinations.

1109

Monday, September 11, 2023, 4:45 PM - 6:15 PM
Hall G2

e-Poster Presentations Session 8 - Neuroimaging Committee: E-Poster Neurology: It's in the Brain!

EPS-147

Improving the quantification of tau pathology in Alzheimer's Disease: A data-driven analysis using 18F-PI2620 PET.

G. Bischof[1,2], *M. Kanekiyo*[3], *M. Irrizari*[3], *A. Stephens*[4], *T. van Eimeren*[1], *A. Drzezga*[1,2,5];
[1]*University Hospital Cologne, Cologne, GERMANY,* [2]*Molecular Organization of the Brain, Institute for Neuroscience and Medicine (INM2), Juelich, GERMANY,* [3]*Eisai Inc., Nutley, NJ, UNITED STATES OF AMERICA,* [4]*Life Molecular Imaging, Berlin, GERMANY,* [5]*German Center for Dementia Research (DZNE), Bonn, GERMANY.*

Aim/Introduction: The second-generation tau tracer 18F-PI2620 has been developed with high on-target affinity to tau pathology in Alzheimer's Disease (AD), paralleled by reduced off-target binding. However, due to the lack of autopsy studies, optimal reference regions to quantify standard uptake value ratios (SUVRs) are missing. The identification of suitable reference regions is however imperative to optimize quantification of on-target binding patterns of tau deposition for disease staging. ***Materials and Methods:*** We analyzed static images of 18F-PI2620 PET of AD patients (N=88) and healthy controls (HC; N=9) to assess regions as candidates for reference regions. In the discovery sample we evaluated differences in off-target binding between HC vs. AD patients (N=28) using a data-driven non-parametric statistical mapping technique. Results were applied to the testing sample (N=60) and SUVRs were computed for a global measure and for a temporal meta- region of interest (ROI). Two-sample t-tests and effect sizes (Hedges g') were computed for each potential region that could serve as a suitable reference region. ***Results:*** We identified several sub-regions of the cerebellum as reference regions Computed SUVRs showed significant differences between AD vs. HC for most of the examined regions and effect sizes were in the range of 0.8-1.7. AAL2- cerebellum 6 and a data-driven cerebellar cluster yielded the highest effect sizes. ***Conclusion:*** Here we improve the quantification of in vivo tau PET imaging in a non-parametric data-driven fashion. This novel reference region can lead to improved SUVR estimates and allows better staging of disease severity.

EPS-148

Single Tracer ATN Assessment With Dynamic 18F-PI-2620 Recordings

J. Gnörich[1], *M. Zaganjori*[1], *M. Groß*[1], *M. Scheifele*[1], *A. Bronte*[2], *R. Perneczky*[3], *K. Bürger*[4], *J. Levin*[5], *O. Sabri*[6], *P. Bartenstein*[1], *H. Barthel*[6], *N. Franzmeier*[4], *M. Brendel*[1];
[1]*LMU Munich, Department of Nuclear Medicine, Munich, GERMANY,* [2]*Universidad de Navarra, Pamplona, SPAIN,* [3]*LMU Munich, Department of Psychiatry and Psychotherapy, Munich, GERMANY,* [4]*Institute for Stroke and Dementia Research, LMU Munich, Munich, GERMANY,* [5]*LMU Munich, Department of Neurology, Munich, GERMANY,* [6]*Department of Nuclear Medicine, Leipzig, GERMANY.*

Aim/Introduction: Patients with neurodegenerative diseases are now molecular categorized by the A/T/N classification system, which can use characteristic features derived from amyloid-PET (A), tau-PET (T), and FDG-PET (N). Recent studies showed that the early perfusion phase of tau-PET recordings can serve as a surrogate of neuronal injury comparable to FDG-PET (i.e. "N"). We evaluated if dynamic tau-PET with [^{18}F]PI-2620 can also serve to predict the amyloid status (i.e. "A") via tissue clearance (k2) in tau-positive regions, with the goal of testing PET based assessment of A/T/N in individual patients during a single imaging session. ***Materials and Methods:*** We obtained dynamic PET recordings with [^{18}F] PI-2620 from 19 participants with a clinical diagnosis of probable AD (3/4-repeat(R)-tauopathy; amyloid-PET positive) and from 30 suspected amyloid-negative controls with corticobasal syndrome (CBS) and progressive supranuclear palsy (PSP) (4R-tauopathies). [^{18}F]PI-2620-PET scans were acquired 0-60 min p.i. and z-scores, the delivery (R1), efflux (k2) and distribution volume ratio (DVR) were calculated via simplified reference tissue modeling 2 (SRTM2), all values being compared between 3/4R- and 4R-tauopathies. [^{18}F] PI-2620-positive cortical regions were defined as a DVR z-score ≥ 2 and patients exceeding 5 tau-positive regions of interest (ROIs) extracted from the Brainnatome atlas were considered tau-positive. Neurodegeneration was examined by assessment of cortical R1, whereas patients exceeding R1 z-score < -1,5 in more than 5 regions were assigned as neuronal impaired. ***Results:*** [^{18}F] PI-2620 indicated significant elevation of cortical tracer binding in 11/19 patients of the AD cohort and 10/30 patients of the 4RT cohort. After exclusion of tau-negative participants, multiple logistic regression considering k2 as a surrogate for amyloid status revealed a negative predictive value of 90% and positive predictive value of 91%. Receiver operating characteristic showed

an area under the curve of 0.98 for prediction of amyloid-PET by k2 (p=0.0003). 8/19 AD patients showed impaired [18F]PI-2620 delivery compared to 9/30 patients in the 4R-tauopathy cohort confirming previous findings for R1 as a surrogate marker of neuronal injury. ***Conclusion:*** [18F]PI-2620 imaging may facilitates assessment of PET based A/T/N in a single dynamic PET session.

EPS-149

Early-phase [18F]FBB PET vs [18F]FDG PET in atypical dementia: preliminary data from a multicentric study (AMY-ITA).

D. Cecchin[1], *A. Chincarini*[2], *S. Mozzetta*[3], *C. Gagliani*[3], *A. Osele*[3], *S. Morbelli*[4], *S. Sestini*[5], *F. Dore*[6], *M. Dottorini*[7], *L. Ruffini*[8], *G. Trifirò*[9], *M. Farsad*[10], *L. Turk*[3], *A. Cagnin*[3];
[1]*Nuclear Medicine University Hospital Padova, Padova, ITALY,* [2]*Istituto Nazionale di Fisica Nucleare (INFN), Genova, ITALY,* [3]*University of Padova, Padova, ITALY,* [4]*University of Genoa, Genoa, ITALY,* [5]*Hospital of Prato, Prato, ITALY,* [6]*Azienda sanitaria universitaria Giuliano Isontina, Trieste, ITALY,* [7]*Azienda Ospedaliera di Perugia, Perugia, ITALY,* [8]*Azienda Ospedaliero Universitaria di Parma, Parma, ITALY,* [9]*ICS Maugeri, Pavia, ITALY,* [10]*Ospedale di Bolzano, Bolzano, ITALY.*

Aim/Introduction: Amyloid PET and [18F]FDG PET scans are commonly used in patients with uncertain diagnosis of AD. Different studies showed that early frames of amyloid PET correlate well with FDG PET images, providing perfusion-like information, thus being a potential surrogate for FDG PET. However, there is still limited evidence in certain classes of patients. We investigated whether the early frames of the FBB PET scan are comparable to the FDG PET images in terms of regional uptake deficits, in patients with a clinical suspicion of an atypical form of Alzheimer's disease. ***Materials and Methods:*** AMY-ITA is a still ongoing prospective multicenter study conducted in 9 Italian centres. Until now, 81 patients have been enrolled, collecting data from brain magnetic resonance imaging, FBB and FDG PET scan. Each patient underwent dual time-point FBB PET, acquiring images 0 - 15 min and 90 - 110 min after injection of the tracer. The brain was divided into 8 different regions in both FDG and early-frames FBB PET scans. Then each region for each tracer was visually and blindly analysed, defining the tracer uptake abnormality, using a scale of 0 to 3. A statistical analysis was then performed using Spearman and Wilcoxon tests. ***Results:*** Visual analysis of the brain was performed on available data and revealed similar patterns between early-frame FBB PET and FDG PET images in atypical forms of Alzheimer's disease; however, the scores of abnormal uptake were globally higher in FDG PET. The Spearman test showed a statistically significant correlation in all brain regions (ρ from 0.798 to 0.927, P< 0.0001), however Wilcoxon's test, showed a statistically significant difference in the temporal and parietal regions (from 0.001 to 0.041, P< 0.05). ***Conclusion:*** Early-phase FBB PET acquisitions correlated well with FDG PET scans in atypical forms of dementia, showinga metabolic-like image, suggesting the use of the amyloid tracer as a surrogate marker of synaptic dysfunction. A consequence of this would be the possibility to eliminate the FDG PET scan, reducing patient radiation exposure and health costs.

EPS-150

Clinical outcomes up to 9 years after [18F]flutemetamol amyloid-PET in a symptomatic memory clinic population

L. Collij[1,2], *G. Farrar*[3], *M. Zwan*[1], *E. M. van de Giessen*[1], *R. Ossenkoppele*[1,2], *F. Barkhof*[1,4], *A. Rozemuller*[1], *Y. Pijnenburg*[1], *W. M. Van der Flier*[1], *F. Bouwman*[1];
[1]*Amsterdam UMC, location VUmc, Amsterdam, NETHERLANDS,* [2]*Lund University, Lund, SWEDEN,* [3]*GE Healthcare, Amersham, UNITED KINGDOM,* [4]*University College London, London, UNITED KINGDOM.*

Aim/Introduction: Previous studies demonstrated increases in diagnostic confidence and change in patient management after amyloid-PET. However, studies investigating longitudinal outcomes over an extended period of time are limited. We therefore aimed to investigate clinical outcomes up to 9 years after amyloid-PET to support the clinical validity of the imaging technique. ***Materials and Methods:*** We analyzed longitudinal data from 200 patients (M_{age}=61.8, 45.5% female, M_{MMSE}=23.3) suspected of early-onset dementia that underwent [18F]flutemetamol-PET. Baseline amyloid status was determined through visual read (VR). Information on mortality was available with a mean follow-up of 6.7 years (range=1.1-9.3). In a subset of 108 patients, longitudinal cognitive scores and clinical etiological diagnosis (eDx) at least 1 year after amyloid-PET acquisition was available (M=3.06 years, range=1.00-7.02). VR- and VR+ patients were compared on mortality rates with Cox Hazard's model, prevalence of stable eDx using chi-square test, and longitudinal cognition with linear mixed models. Neuropathological data was available for 4 patients (mean delay=3.59±1.82 years, range = 1.2-6.3). ***Results:*** At baseline, 184 (92.0%) patients were considered to have dementia. Majority of VR+ patients had an etiological diagnosis of AD (122/128, 95.3%), while the VR- group consisted mostly of non-AD etiologies, mainly frontotemporal lobar degeneration (29/72, 39.7%). Overall mortality rate was 48.5% and did not differ between VR- and VR+ patients. eDx at follow-up was consistent with baseline diagnosis for 92/108 (85.2%) patients, with most changes observed in VR- cases (VR-=14/35, 40% vs VR+=2/73, 2.7%, χ^2=26.03, p<0.001), who at no time received an AD diagnosis. Within the VR- group, 7/35 still had a primary etiological diagnosis of AD at baseline after disclosure of the amyloid-PET status. Etiological diagnosis changed at follow-up for 5/7 of these cases, with 2 cases receiving a 'dementia other' diagnosis, 1 primary psychiatric disorder, 1 FTLD, and 1 primary vascular etiology. VR+ patients declined faster than VR- patients based on MMSE (β=-1.17, p=0.004), episodic memory (β=-0.78, p=0.003), fluency (β=-1.44, p<0.001), and attention scores (β=16.76, p=0.03). Amyloid-PET assessment was in line with post-mortem confirmation in all cases; two cases were VR+ and showed widespread AD pathology, while the other two cases were VR- and showed limited amyloid pathology. ***Conclusion:*** In a symptomatic population, we observed that amyloid-status did not impact mortality rates, but is predictive of cognitive functioning over time across several domains. Also, we show particular validity for a negative amyloid-PET assessment, as these patients did not receive an AD diagnosis at follow-up.

EPS-151

Gender influences the expression of metabotropic glutamate receptor 5 in the brain of cognitively impaired individuals: a PET/MR study

W. Jie[1], *Y. Guan*[2], *F. Xie*[2];
[1]*Fudan University, shanghai, CHINA,* [2]*Department of Nuclear Medicine & PET Center, Huashan Hospital, Fudan University, Shanghai, CHINA.*

Aim/Introduction: To investigate the differences in the expression of metabotropic glutamate receptor 5 (mGluR5) as seen on PET imaging between normal controls and cognitively impaired individuals, as well as the impact of gender on its expression. ***Materials and Methods:*** The study included 31 individuals with cognitive impairment and 25 normal controls who underwent [18F]Florbetapir PET/CT and [18F]PSS232 PET/MR scans, as well as neuropsychological testing. Based on the region of interest analysis, we compared the expression of mGluR5 between the two groups using a two-sample t-test and explored the impact of gender using a one-way variance.To investigate the differences in the expression of metabotropic glutamate receptor 5 (mGluR5) as seen on PET imaging between normal controls and cognitively impaired individuals, as well as the impact of gender on its expression. ***Results:*** In the whole cohort, individuals with cognitive impairment had decreased mGluR5 expression compared to normal controls in the medial temporal lobe (P = 0.046). Males had more mGluR5 expression than females in the occipital cortex (P = 0.044), precuneus (P = 0.022), frontal lobe (P = 0.042), medial temporal lobe (P = 0.014), and posterior cingulate cortex (P = 0.007). In stratified analyses, there was no significant difference in mGluR5 expression between male and female individuals with cognitive impairment, while in the normal controls, males had more mGluR5 expression than females in the lateral parietal lobe (P = 0.040), precuneus (P = 0.013), frontal lobe (P = 0.042), and posterior cingulate gyrus (P = 0.024). In the female subgroup, individuals with cognitive impairment had decreased mGluR5 expression compared to normal controls in the lateral parietal lobe (P = 0.017), precuneus (P = 0.011), frontal lobe (P = 0.035), and medial temporal lobe (P = 0.036). No such differences were observed in the male subgroup. ***Conclusion:*** Our findings indicate reduced mGluR5 expression in the brains of individuals with cognitive impairment compared to normal controls on 18F-PSS232 PET/CT imaging, This expression was influenced by gender and was more pronounced in the female group.

EPS-152

Prevalence of Limbic-predominant Age-related TDP-43 Encephalopathy (LATE) in Tertiary Care Cognitive Disorder Clinics

E. Park*, C. J. Cliatt-Brown, Y. Anzai, S. Minoshima;*
University of Utah, Salt Lake City, UT, UNITED STATES OF AMERICA.

Aim/Introduction: The prevalence of a recently recognized form of neurodegenerative dementia, limbic-predominant age-related TDP-43 encephalopathy (LATE), was investigated among patients referred for imaging evaluation by cognitive disorder clinics. ***Materials and Methods:*** This retrospective study involved 404 consecutive patients who were referred for imaging evaluation of dementia by cognitive disorder clinics at a tertiary healthcare center. Each patient underwent standard clinical assessments, brain FDG PET, and MRI with or without regional volumetric analysis. PET images were analyzed voxel-by-voxel compared to those of age-similar healthy subjects. Since there is currently no specific biomarker for TDP-43, the diagnosis of probable LATE was established by identifying unique patterns of reported imaging findings: 1) accentuated glucose hypometabolism (Z-score > 3) involving medial temporal lobes and orbitofrontal cortices and 2) accentuated atrophy in the medial temporal lobe. In addition, the concomitant presence of the established pattern of Alzheimer's disease (AD) was independently assessed on PET within the probable LATE group. ***Results:*** Fifty-four of 404 patients (13%) were diagnosed as probable LATE based on the findings of FDG PET and MRI. Additional 35 patients (9%) showed the findings consistent with probable LATE and concomitant AD, totaling 22% of LATE among the dementia patients referred for imaging evaluation. Age of patients with probable LATE only was significantly older than that of non-LATE group (77.1±5.6 years, mean±SD, vs. 69.0±8.6 years, respectively, p<0.00001). Age of patients with probable LATE with or without concomitant AD was also significantly older (74.5±7.8 years, p<0.00001). The gender distribution was similar between the probable LATE (Men:Women = 59%:41%) and non-LATE (54%:46%) groups. ***Conclusion:*** A notable fraction of the patients who are referred for imaging evaluation by the cognitive disorder clinics at a tertiary healthcare center demonstrates imaging findings consistent with probable LATE with or without a concomitant AD pattern. These patients are significantly older than the patients with non-LATE dementia. The recognition of the LATE patterns on the brain FDG PET and MRI is critical in the evaluation of dementia patients. ***References:*** Nelson PT, Dickson DW, Trojanowski JQ, et al. Limbic-predominant age-related TDP-43 encephalopathy: consensus working group report. Brain. 2019;142:1503-1527. Minoshima S, Frey Ka, Koeppe RA, et al. A diagnostic approach in Alzheimer's disease using three-dimensional stereotactic surface projections of fluorine-18-FDG PET. J Nucl Med.1995;36:1238-1248. Grothe MK, Moscoso A, Silva-Rodriguez J, et al. Differential diagnosis of amnestic dementia patients based on an FDG-PET signature of autopsy-confirmed LATE-NC. Alzheimer's Dement. 2023;19:1234-1244.

EPS-153

Application of principal component analysis on amyloid-PET and clinical data to predict conversion from mild cognitive impairment to Alzheimer's disease

E. Perrone[1,2], *F. Cocciolillo*[2], *S. Taralli*[2], *D. Quaranta*[3], *D. Santoni*[4], *M. Mazzei*[4], *C. Marra*[5], *M. L. Calcagni*[1,2];
[1]*Nuclear Medicine Institute, University Department of Radiological and Hematological Sciences, Università Cattolica del Sacro Cuore, Rome, ITALY,* [2]*Nuclear Medicine Unit, Diagnostic Imaging, Radiation Oncology and Hematology Department, Fondazione Policlinico Universitario Agostino Gemelli IRCCS, Rome, ITALY,* [3]*Neurology Unit, Fondazione Policlinico Universitario Agostino Gemelli IRCCS, Rome, ITALY,* [4]*Institute for System Analysis and Computer Science "Antonio Ruberti", National Research Council of Italy, Rome, ITALY,* [5]*Memory Clinic, Fondazione Policlinico Universitario Agostino Gemelli IRCCS, Rome, ITALY.*

Aim/Introduction: Principal component analysis (PCA) is a multivariate analysis used to manage large multidimensional dataset eliminating redundant features, looking for relevant uncorrelated variables. Amyloid-PET is used for non-invasive assessment of cortical amyloid burden in patients with mild cognitive impairment (MCI). This study aimed to evaluate whether PCA, applied to clinical-neuropsychological data and semi-quantitative PET parameters, can predict conversion from MCI to Alzheimer's disease (AD). ***Materials and Methods:*** Clinical-neuropsychological assessment and amyloid-PET were performed in 61 patients: 37 with amnestic-MCI single-domain

(aMCI-sd), 14 with amnestic-MCI multi-domain (aMCI-md), 10 with subjective cognitive impairment (SCI). 18F-Flutemetamol (180.9±7.9 MBq) PET/CT was acquired in dynamic list-mode (20min). Images were considered positive when amyloid uptake in grey matter was equal or higher than that in white matter. SUVr was calculated in ten cortical VOIs and in whole grey matter, considering the cerebellum as reference. PCA was applied to clinical (age, education, neurological scores) and SUVr data. PCA was carried out through ad-hoc designed software and the statistical pipeline was implemented through R Package R version 4.1.3. The principal components (PCs) were listed in decreasing order of importance in terms of variance. ***Results:*** After mean follow-up of 3.4 years, 36/61 (59%) patients converted to AD (22 aMCI-sd, 10 aMCI-md; 4 SCI). Among converters, 31/36 were amyloid-PET positive with mean time to conversion of 2.1 years (vs. 2.4 years in 5/36 amyloid-PET negative patients). Among 25 non-converters patients, 14/25 were amyloid-PET positive, 11/25 were amyloid-PET negative. PCA resulted in two main components explaining the 63% of the total variance: PC1 was represented by SUVr data, accounting for 45%; PC2 included two cognitive scores, semantic verbal fluency and delayed recall, accounting for 18%. PCA did not extract any differences in amyloid uptake among cortical regions. ***Conclusion:*** Global amyloid cortical burden is the strongest component able to predict conversion from MCI to AD, independently of neurological data, regional or lateralised amyloid uptake, followed by episodic memory and executive function impairment. Non-converters AD patients with amyloid-positive PET could represent a subpopulation in which amyloid does not exert pathologic action for some factors, including individual cognitive reserve and resilience. Longer follow-up should be considered also. Converters-AD patients with amyloid-negative PET could represent a subpopulation of different AD phenotypes including primary age related tauopathy, or TDP-43 pathology, characterized by the absence of amyloid plaques.

EPS-154

Clinical utility of Amyloid Brain PET in patients with Mild Cognitive Impairment

M. Pudis[1], *L. Rodríguez-Bel*[1], *M. Suarez-Piñera*[1], *C. Martínez-Ramos*[1], *J. Gascón-Bayarri*[2], *J. Campdelacreu-Fumado*[2], *S. Bondia-Bescós*[1], *B. Hervás-Sanz*[1], *J. Diaz-Moreno*[1], *M. Cortés-Romera*[1];
[1]*Nuclear Medicine - PET (IDI), Bellvitge University Hospital, L'Hospitalet de Llobregat, Barcelona, SPAIN,* [2]*Neurology Department, Bellvitge University Hospital, L'Hospitalet de Llobregat, Barcelona, SPAIN.*

Aim/Introduction: Several studies have demonstrated that a negative Amyloid Brain PET scan is associated with a low risk of progression to Alzheimer's disease (AD) in patients with mild cognitive impairment (MCI). The aim of this study was to assess, through statistical parameters, the diagnostic accuracy of amyloid brain PET in patients with MCI. ***Materials and Methods:*** A retrospective study of 153 patients with clinical criteria for MCI who underwent an Amyloid Brain PET was performed between the years 2014 and the end of 2021. The patients were subclassified, according to the PET result, into two subgroups: positive (+) and negative (-). In both subgroups, PET results were correlated with follow-up for a mean of 5 years [15-101 months] and possible conversion to AD by clinical criteria. We calculated the sensitivity (Se), specificity (Sp), positive predictive value (PPV) and negative predictive value (NPV) of this diagnostic technique. ***Results:*** Out of 85 patients with (+) amyloid PET, 70 patients during the follow-up were diagnosed with AD with a mean conversion time of 26 months [5-68 months] and 15p did not show AD conversion during a mean follow-up time of 4,5 years [19-101 months]. Of the 68p with amyloid PET (-), 6 patients were diagnosed with AD with a mean conversion time of 24.33 months [8-50]. The calculated sensitivity was 92%, specificity 81%, PPV 82% and NPV 91%. ***Conclusion:*** Amyloid brain PET in the workup of patients with MCI has a high diagnostic value beyond what can be obtained through a comprehensive clinical evaluation. The negative result helped to rule out conversion to AD with a high negative predictive value. The positive result helped to confirm the presence of amyloid plaques with high sensitivity, confirming the conversion to AD with a mean time of 2 years.

EPS-155

Unilateral Nasal Septal Deviation Mediates Contralateral Loss of Striatal Dopamine Transporter Uptake in Patients with Parkinson's Disease

J. Wang[1,2], *J. Ge*[1], *F. Liu*[3], *M. Tian*[2], *J. Wang*[3], *C. Zuo*[1];
[1]*Department of Nuclear Medicine/PET center, Huashan Hospital, Fudan University, Shanghai, CHINA,* [2]*Human Phenome Institute, Fudan University, Shanghai, CHINA,* [3]*Department of Neurology, Huashan Hospital, Fudan University, Shanghai, CHINA.*

Aim/Introduction: Laterality is a key feature of Parkinson's disease (PD), usually manifesting in the early stages, but the underlying mechanism remains unclear. In our previous study, we found that injecting lipopolysaccharide (PM2.5 component) unilaterally into the nasal cavity of mice resulted in reduced striatal dopamine transporter (DaT) uptake and α-synuclein aggregation in the substantia nigra, causing apparent asymmetric motor features[1]. Since the nasal cavity is a gateway for environmental neurotoxins to enter the brain, our study aimed to investigate the correlation between asymmetric loss in striatal subregions and unilateral nasal septal deviation (NSD). ***Materials and Methods:*** We retrospectively reviewed 453 PD patients who underwent ^{11}C-CFT or ^{18}F-FP DTBZ PET/CT at Huashan Hospital between March 2011 and February 2020, all of whom met the diagnostic criteria of the United Kingdom Parkinson Disease Society (UKPDS). Quantitative analyses were calculated based on six volume-of-interest templates of bilateral striatal subregions, including the caudate, anterior putamen (AP), and posterior putamen (PP). These measures included the ratio of specific to nonspecific binding, the intersubregional gradient from PP to AP (PP/AP), and the caudate to putamen (C/P) ratio. We also defined the NSD index (NSDI) as the degree of NSD and the asymmetry index (AI) as the degree of DaT laterality between the two hemispheres. ***Results:*** 82.1% of PD patients with left-NSD had greater deficit on the right side of the putamen, while 73.3% of patients with right-NSD had greater deficit on the left side (χ^2=17.9, P<0.001). The Cohen's kappa test demonstrated a significant negative agreement between the direction of NSD and the side with more affected DaT (kappa=-0.6, P<0.001). Patients with right-NSD had a significantly higher AI than those with left-NSD (P<0.001 for AP, PP, and caudate). The PP/AP was significantly higher in patients with right-NSD than in those with left-NSD (P<0.01), while the C/P was significantly lower in patients with right-NSD compared to those with left-NSD (P<0.05). For early PD, the Spearman test showed a significant negative correlation between NSDI and PP AI (r=-0.51, P<0.001). ***Conclusion:*** Our findings suggest that PD patients with unilateral NSD exhibit contralateral DaT loss. Moreover, the degree of NSD deviation is positively correlated with the extent of contralateral dopamine loss. These results provide a basis for further investigation of the underlying mechanisms of PD laterality.

References: He Q, et al. Intranasal LPS-mediated Parkinson's model challenges the pathogenesis of nasal cavity and environmental toxins. PLoS One. 2013;8(11).

EPS-156

Dopamine D_1 receptor availability in Gilles de la Tourette syndrome measured by [11C]SCH23390 PET

M. Rullmann[1], *D. Gkotsoulias*[2], *S. Schmitt*[3], *C. Fremer*[3], *C. Klages*[3], *K. Hartung*[3], *A. Bujanow*[2], *F. Zientek*[1], *K. Messerschmidt*[1], *M. Patt*[1], *O. Sabri*[1], *K. Müller-Vahl*[3], *H. Möller*[2], *H. Barthel*[1];
[1]*Department of Nuclear Medicine, University of Leipzig, Leipzig, GERMANY,* [2]*Max Planck Institute for Human Cognitive and Brain Sciences, Leipzig, GERMANY,* [3]*Clinic of Psychiatry, Social Psychiatry and Psychotherapy, Hannover Medical School, Hannover, GERMANY.*

Aim/Introduction: Clinically, Gilles de la Tourette syndrome (GTS) is characterized mainly by motor and vocal tics. Current treatment strategies are often unsatisfactory. Therefore, it is necessary to further elucidate the underlying pathophysiology. The literature suggests a dysregulated dopaminergic system, with the selective dopamine D_1 receptor (D_1R) antagonist ecopipam showing promising treatment results in children and adults. To date, D_1Rs have not been studied in vivo in GTS. We hypothesize that patients with GTS have reduced D_1R availability that correlates with clinical disease severity. ***Materials and Methods:*** We performed a D_1R PET scan with [11C]SCH23390 on a Siemens hybrid PET/3T-MRI system in patients with GTS and age- and sex-matched healthy control participants (HCs). After a 90 bolus injection of 474 ± 30 MBq, participants underwent a 90-minute dynamic PET scan. Dynamic data were motion corrected and coregistered with individual T1-MP2RAGE MRI data. We performed kinetic modeling to generate parametric maps of binding potential (BP_{ND}) and relative delivery (R_1) using MRTM2 with cerebellar cortex as the reference region. Parametric data were analyzed voxel-wise in SPM12 ($p < 0.001$ unc., $k > 10$ voxels). Clinical severity was assessed using the Yale Global Tic Severity Scale (YGTSS). ***Results:*** Our preliminary analysis of 20 GTS patients and 20 HCs suggests reduced $BP_{ND}s$ in patients with GTS in caudate, insula and putamen. R_1 levels were reduced in patients with GTS in occipital cortex. $BP_{ND}s$ were negatively correlated with YGTSS scores and subscores in precentral, striatal and parietal areas. ***Conclusion:*** These preliminary results suggest an altered D1R system in patients with GTS in relation to clinical severity. The analysis of additional data is still ongoing. As such, our first results will help to provide a more comprehensive picture of neurochemical abnormalities in GTS, especially when combined with MRI measures such as 1H-MRS and quantitative susceptibility mapping.

EPS-157

Multiparametric ^{11}C-MET PET/MR for predicting survival of postsurgical glioma patients

Y. Xu, *C. Li, F. Liu, F. Hu, W. Ruan, X. Lan;*
Department of Nuclear Medicine, Union Hospital, Tongji Medical College, Huazhong University of Science and Technology, Wuhan, CHINA.

Aim/Introduction: The study is aimed to evaluate the value of multiparametric ^{11}C-MET PET/MRI for predicting survival for glioma patients after surgery. ***Materials and Methods:*** Newly diagnosed glioma patients with histologically confirmation were consecutively enrolled and evaluated by postsurgical ^{11}C-MET PET/MR. A 10-min PET scan was started 20 minutes after injection, together with anatomical MR sequences, diffusion-weighted imaging (DWI), 3D Arterial Spin Labeling (3D ASL) perfusion imaging and magnetic resonance spectroscopy (MRS). Images were analyzed with visual evaluation and quantitative parameters such as SUV_{max}, SUV_{mean}, TBR_{max} and TBR_{mean} (lesion/contralateral normal frontal lobe), ADC, ADC ratio (lesion/normal thalamus), CBF, CBF ratio (lesion/contralateral brain), Cho/Cr and Cho/NAA for residual tumor lesions. Residual tumor lesions were then segmented with the thresholds of TBR above 1.3, 1.6 and 40%SUV_{max} to get the metabolic tumor volume (MTV) and total lesion methionine metabolism (TLMM), avoiding physiological uptake or postsurgical alterations. Patient went through standard radiochemotherapy. Overall survival (OS) and progression-free survival (PFS) were determined by long-term follow-up. Log-rank test and COX regression model were used to analyze the association between image parameters, clinical features, and patient survival. Least absolute shrinkage and selection operator (LASSO) regression model was used to screen the parameters to establish a nomogram prediction model for internal validation. ***Results:*** Seventy-three patients were enrolled. During follow-up, 35 patients developed disease progression, 38 patients did not develop disease progression, 8 patients developed disease progression but still survive, and 28 patients died (including a patient who died before disease progression). Multivariate COX regression analysis showed that SUV_{max}, SUV_{mean}, TBR_{max}, TBR_{mean}, MTV (1.3TBR), MTV (1.6TBR), TLMM (1.3TBR), TLMM (1.6TBR), Cho/Cr and Cho/NAA were significantly associated with PFS. Only MTV (1.3TBR) was significantly associated with OS. A nomogram prediction model for overall survival was established including patient age, WHO grade, IDH mutation status and MTV(1.3TBR), whose concordance index could reach 0.900. ***Conclusion:*** Postsurgical ^{11}C-MET PET/MR imaging had prognostic value for glioma patients. SUV_{max}, SUV_{mean}, TBR_{max}, TBR_{mean}, MTV, TLMM, Cho/Cr, and Cho/NAA were significantly associated with PFS. Only MTV with the threshold of TBR above 1.3 was significantly associated with OS.

EPS-158

A Feasibility Study of Ga68-PSMA PET/CT in Differentiating Brain Metastases from Radiation Necrosis

F. Lattuada[1], *S. Wagemaker*[2], *L. de Wit-van der Veen*[2], *D. Brandsma*[2], *M. Stokkel*[2];
[1]*Post Graduate School of Nuclear Medicine, University of Milano-Bicocca, Milano, ITALY,* [2]*NKI-AVL, Amsterdam, NETHERLANDS.*

Aim/Introduction: Prostatic-specific membrane antigen (PSMA) targeted radionuclide imaging has shown excellent results for the assessment and management of prostate cancer. Nevertheless, heterogeneous degrees of PSMA expression have been proven in other malignancies, including primary non-small cell lung cancer (NSCLC) and its metastases. Using conventional imaging methods, recurrent disease and treatment-related changes, including radiation necrosis (RN), in the brain are often indistinguishable on MRI. As RN represents a primary complication of stereotactic radiation therapy (SRT), this study aims to assess the diagnostic role of 68Ga-PSMA PET/CT in differentiating NSCLC brain metastasis and radiation necrosis in irradiated NSCLC brain metastasis. ***Materials and Methods:*** Two different cohorts of patients were selected: the first group (n=11) comprises patients with newly diagnosed NSCLC brain metastases, and the second group (n=13) patients with defined RN after irradiation of NSCLC brain metastases. All patients received 100 MBq of 68Ga-PSMA intravenously followed by a PET/CT scan 45 minutes post-injection. We selected 37 lesions with a diameter ≥ 1.0 cm based on

contrast-enhanced MRI in order to obtain a reliable quantification. All the lesions has been evaluated using semi-quantitative (SUVmax and SUVpeak) and visual assessment. ***Results:*** Of 37 lesions, 15 were brain metastases and 22 were RN. Mean SUVmax values for the brain metastasis group and the RN group were 7.62 (95% CI 5.10 - 10.15) and 4.05 (95% CI 2.98 - 5.12), respectively (p= 0.013). Mean SUVpeak values for the brain metastasis group and the RN group were 3.71 (95% CI 2.40 - 5.01) and 2.09 (95% CI 1.57 - 2.61), respectively (p=0.013). We also calculated semi-quantitative values normalized to background uptake identified as ΔSUVmax and ΔSUVpeak. Mean ΔSUVmax values for the brain metastasis group and the RN group were 7.38 (95% CI 4.86 - 9.89) and 3.72 (95% CI 2.65 - 4.78), respectively (p=0.009). Mean ΔSUVpeak values for the brain metastasis group and the RN group were 3.62 (95% CI 2.32 - 4.92) and 1.96 (95% CI 1.43 - 4.92), respectively (p=0.010). Visual assessment did not reveal additional value. ***Conclusion:*** This feasibility study showed a significant difference between brain metastases and RN uptake values on 68Ga-PSMA PET/CT imaging. A subsequent study will be initiated including a larger cohort of patients to be able to find a cut-off value that enables differentiation of the two entities in clinical practice.

EPS-159

Feasibility and initial experience of chemokine receptor-4 receptor-4 (CXCR4) expression using 68Ga-Pentixafor and O-2-18F-fluoroethyl-l-tyrosine (18F-FET) PET-MR image fusion in low- and high-grade gliomas

H. Dadgar[1,2], *N. Norouzbeigi*[1], *M. Assadi*[3], *B. Al-balooshi*[4], *A. Al-Ibraheem*[5], *Y. Omar*[6], *H. Muhsin Al-Alawi*[7], *S. Usmani*[8], *M. Ricci*[9], *A. Cimini*[10], *H. Arabi*[11], *H. Zaidi*[11,12,13];
[1]*Nuclear Medicine and Molecular imaging research center, Mashad, IRAN, ISLAMIC REPUBLIC OF,* [2]*Cancer Research Center, RAZAVI Hospital, Imam Reza International University, Mashhad, Iran, Mashhad, IRAN, ISLAMIC REPUBLIC OF,* [3]*The Persian Gulf Nuclear Medicine Research Center, Department of Molecular imagingand Radionuclide Therapy, Bushehr Medical University Hospital,Bushehr University of Medical Sciences, IRAN, Bushehr, IRAN, ISLAMIC REPUBLIC OF,* [4]*Dubai Nuclear Medicine & amp; Molecular imaging center-Dubai Academic Health corporation-DAHC, UAE, Dubai, UNITED ARAB EMIRATES,* [5]*Department of Nuclear Medicine, King Hussein Cancer Center, Amman, Jordan-Devision of Nuclear Medicine/Department of Radiology and Nuclear Medicine, University of Jordan, Amman, Jordan, Amman, JORDAN,* [6]*PET-CT department at Misr Radiology Center, Heliopolis, Egypt, Heliopolis, EGYPT,* [7]*Nuclear Medicine department, Amir Al-momineen Specialty Hospital, Al-Najaf Governorate, Iraq Middle Euphrates Cancer Hospital, Al-Najaf Governorate, Iraq, Mashad, IRAQ,* [8]*Department of Nuclear Medicine Sultan Qaboos Comprehensive Cancer Care and Research Center (SQCCCRC), Seeb, Oman, Seeb, OMAN,* [9]*Nuclear Medicine Unit, Cardarelli Hospital, Campobasso, Italy, Campobasso, ITALY,* [10]*Nuclear Medicine Unit, St. Salvatore Hospital, 67100 L'Aquila, Italy, L'Aquila, ITALY,* [11]*Division of Nuclear Medicine and Molecular Imaging, Department of Medical Imaging, Geneva University Hospital, CH-1211 Geneva 4, Switzerland, Geneva, SWITZERLAND,* [12]*Geneva Neuroscience Center, Geneva University, CH-1205 Geneva, Switzerland, Geneva, SWITZERLAND,* [13]*Department of Nuclear Medicine and Molecular Imaging, University of Groningen, University Medical Center Groningen, 9700 RB Groningen, NETHERLANDS, Groningen, NETHERLANDS.*

Aim/Introduction: Amino acid agents and CXCR4 have been reported to be overexpressed in glioma cells, particularly in glioblastoma multiform. The current study aimed to evaluate the feasibility of MRI, 18F-FET, and 68Ga-Pentixafor PET to increase diagnostic accuracy and to improve the discrimination of treatment-emergent changes in low- and high-grade gliomas. ***Materials and Methods:*** We analyzed two separate databases; in the first subgroup, 29 patients with recurrent glioblastoma underwent 68Ga-Pentixafor PET/CT to examine CXCR4 expression before/after tumor mass resection. The second subgroup included 11 patients with histopathologically proven brain tumor suspected of having recurrent changes 3-4 months after surgery who were referred for an 18F-FET PET/CT scan. In addition, PET/MR image fusion for both 68Ga-Pentixafor and 18F-FET was performed. For both PET probes, visual and semi-quantitative calculation of image-derived metrics, SUVmax and tumor-to-background ratios (TBR), were performed. ***Results:*** Among eleven patients (age: 27-73 years; mean age of 47 ± 13 years) referred to 18F-FET PET/CT/MR imaging, nine cases (82%) had a positive MRI, six cases (55%) had a positive PET/CT and PET/MRI, and tumor recurrence was observed in 6 patients (55%). Sample follow-up indicated that accuracy, sensitivity, specificity, positive predictive value (PPV), and negative predictive value (NPV) were 64%, 85%, 25%, 67%, 50% for MRI alone and 91%, 85%, 100%, 100% and 80% for PET/CT/MRI, respectively. The results of 29 patients who underwent 68Ga-Pentixafor PET/CT were also evaluated visually and semi-quantitatively. Visual assessment of 68Ga-Pentixafor PET revealed that 27/29 cases were positive with a mean SUVmax of 3.92 (13 patients were female (13/29) and 16 patients were male (16/29); the mean age of the patients was 57.36 years). 17.24% (5/29) of patients had WHO grade III pathologies (anaplastic oligodendroglioma/anaplastic astrocytoma). 3 out of 29 participants had a stereotactic biopsy. The interval time between biopsy and imaging was 14-38 days (mean 21.71 days). The mean SUVmax of WHO grade IV lesions was significantly higher than grade III (3.131 ± 3.01 vs. 1.99 ± 0.45) and the mean SUVmax of blood pool activity was reported as 1.277 at the superior sagittal sinus area. While the mean target-to-background ratio of grade IV patients was 29.45, all grade III gliomas showed lower lesion uptake than background activity considered at the contralateral cortex. ***Conclusion:*** This study concluded that 68Ga-Pentixafor had a higher TBR (lower background in the cortex) than 18F-FET PET, with the ability to bond with 177Lu-Pentixather. 68Ga-Pentixafor imaging could improve recurrence detection.

EPS-160

Histopathological validation of 18F-FACBC uptake in high- and low-grade glioma

B. Vindstad[1], *L. K. Pedersen*[2], *E. M. Berntsen*[1,3], *O. Solheim*[3,1], *I. Reinertsen*[4,1], *H. Johansen*[3], *A. J. Skjulsvik*[1,3], *L. Eikenes*[1], *A. Karlberg*[1,3];
[1]*Norwegian University of Science and Technology, Trondheim, NORWAY,* [2]*University Hospital of North Norway, Tromsø, NORWAY,* [3]*St. Olavs Hospital, Trondheim, NORWAY,* [4]*SINTEF Digital, Trondheim, NORWAY.*

Aim/Introduction: Accurate diagnosis, grading and tumor delineation of gliomas is essential for treatment planning and prognosis estimation. PET can provide quantitative information of cellular activity and metabolism, and amino acid PET is recommended as a complement to MRI for patients with suspected glioma. 18F-FACBC is an amino acid tracer with a very low uptake in normal brain parenchyma compared to the currently recommended tracers for glioma imaging, which could be beneficial in diagnostic applications for patients with gliomas.The aim of the study was to investigate the relationship between 18F-FACBC uptake and histopathology in patients with gliomas. The tracer was evaluated as a predictor for high-grade

and low-grade glioma, as well as individual molecular parameters associated with glioma. ***Materials and Methods:*** Patients with suspicion of primary or recurrent gliomas (n=27) were scanned with hybrid PET/MRI systems (Siemens Biograph mMR) prior to surgery. PET and MR images were used in the neuronavigation during sampling of a total of 61 image localized biopsies from eligible patients (n = 18, up to 4 biopsies per patient). 44 biopsies were analysed for increased cell density and IDH1 and ATRX mutation status, and an estimation of glioma grade in each biopsy (HGG, LGG or normal tissue) was made based on the histopathological results. Tumor-to-background ratio (TBR) of 18F-FACBC uptake was calculated for each biopsy location. The TBR value was evaluated as predictor for both the individual molecular parameters (cell density, IDH1 and ATRX) and the estimated diagnosis using ROC analysis. ***Results:*** 18F-FACBC uptake predicted classification of increased cell density, IDH1 and ATRX mutation status (high cell density: threshold = 3.69, AUC = 0.9; moderate or high cell density: threshold = 1.77, AUC = 0.73; IDH1 mutation: threshold = 2.44, AUC = 0.8; ATRX mutation: threshold = 2.44, AUC = 0.86). Preliminary results based on the estimates of diagnosis suggest that 18F-FACBC may predict HGG vs LGG/normal tissues (threshold = 3.41, AUC = 0.88), but has lower sensitivity for HGG/LGG vs normal tissues prediction (threshold = 1.68, AUC = 0.53). ***Conclusion:*** 18F-FACBC TBR is a good predictor of various molecular parameters associated with glioma. Increased cell density as well as IDH1 and ATRX mutation was predicted with high sensitivity. Preliminary results also suggest 18F-FACBC as a good predictor for HGG, but less so for LGG.

EPS-161

Prognostic Role of Preoperative [^{11}C]Methionine PET in IDH-Wildtype Astrocytomas

G. Ninatti[1], *M. Sollini*[2,3], *B. Bono*[2], *L. Antunovic*[4], *F. Gelardi*[2], *C. Landoni*[1,5], *F. Pessina*[2,3], *M. Rodari*[3], *A. Chiti*[6,4];
[1]*University of Milano Bicocca, Monza, ITALY,* [2]*Humanitas University, Pieve Emanuele, ITALY,* [3]*IRCCS Humanitas Research Hospital, Rozzano, ITALY,* [4]*IRCCS San Raffaele Scientific Institute, Milan, ITALY,* [5]*IRCCS-San Gerardo, Monza, ITALY,* [6]*Vita-Salute San Raffaele University, Milan, ITALY.*

Aim/Introduction: IDH-wildtype astrocytomas are the most common and aggressive type of primary brain tumors. [^{11}C]Methionine (MET) positron emission tomography (PET) is commonly used for the preoperative evaluation of patients with glial neoplasms. This study aimed to investigate the prognostic role of [^{11}C]MET PET in newly-diagnosed IDH-wildtype astrocytic gliomas who underwent surgical treatment. ***Materials and Methods:*** Patients with a histomolecular diagnosis of IDH-wildtype astrocytoma who underwent surgery and preoperative (<100 days) [^{11}C]MET PET/CT were retrospectively included. Qualitative and semi-quantitative analyses of [^{11}C]MET PET images were performed. For qualitative analysis, lesions were classified as positive in case of increased radiopharmaceutical uptake compared to the normal brain and negative in all other cases. The mean and maximum tumor-to-background ratio (TBR), calculated as ratios between SUV_{max} and SUV_{mean} of the metabolic tumor volume, respectively, and uptake values of contralateral normal brain, were used for the semi-quantitative analysis. Progression-free survival (PFS) rates were analyzed by Kaplan-Meier curves and compared using the log-rank test. Cox proportional-hazards regression was used to test the association of imaging and clinical data to PFS. A p-value < 0.05 was considered statistically significant. ***Results:*** A total of 48 patients (M/F: 25/23; median age 55) were included in the study. At visual analysis 39 lesions (81%) were defined as positive at [^{11}C]MET PET, while 9 (19%) as negative. All IDH-wildtype astrocytomas with a known TERT promoter mutation were positive at [^{11}C]MET PET (9/9, 100%). Patients with positive [^{11}C]MET PET at diagnosis had a shorter median PFS compared to patients with a negative scan (15.9 months vs. undefined, p = 0.0427). Considering only the 29 patients (60%) who underwent complete surgical resection of the lesion, positive preoperative [^{11}C]MET PET scan was still significantly associated with shorter median PFS (16.8 vs. undefined, p = 0.0304). Extent of surgical resection (EOR), lesion contrast enhancement on MRI, TBR_{max} and TBR_{mean} at [^{11}C]MET PET were significantly associated with PFS on univariate analysis. EOR was an independent predictor of PFS on multivariate analysis. ***Conclusion:*** Preoperative [^{11}C]MET PET is able to identify the most aggressive IDH-wildtype glial neoplasms and to predict patient prognosis. [^{11}C]MET PET results may reflect the presence of genetic parameters typical of IDH-wildtype astrocytomas with a negative prognostic impact. Our findings highlight the usefulness of [^{11}C]MET PET for the preoperative assessment of this glioma type.

EPS-162

^{99m}Tc-ECD SPECT Predicts Neurological Recovery in Cardiac Arrest Survivors

P. Chuang[1], *Y. Chen*[2], *Y. Huang*[2], *C. Wang*[3], *W. Chang*[4], *Y. Wu*[5], *M. Cheng*[2];
[1]*Department of Nuclear Medicine, National Taiwan University Hospital Yunlin Branch, Douliu City, TAIWAN,* [2]*Department of Nuclear Medicine, National Taiwan University Hospital, Taipei City, TAIWAN,* [3]*Department of Emergency Medicine, National Taiwan University Hospital Yunlin Branch, Douliu City, TAIWAN,* [4]*Department of Emergency Medicine and Cardiology, National Taiwan University Hospital, Taipei City, TAIWAN,* [5]*Department of Nuclear Medicine and Cardiology, Far Eastern Memorial Hospital, New Taipei City, TAIWAN.*

Aim/Introduction: Neuroprognostication plays a pivotal role in managing patients who have been successfully resuscitated from cardiac arrest, particularly when facing the decision to withdraw or continue life-sustaining treatment. We aim to investigate whether ^{99m}Tc-ECD SPECT helps to predict neurological outcome among cardiac arrest survivors. ***Materials and Methods:*** We conducted a retrospective analysis of a prospectively established cohort from January 2010 to February 2022 in a tertiary referral centre in Northern Taiwan. Patients successfully resuscitated from cardiac arrest were consecutively enrolled. Brain ^{99m}Tc-ECD SPECT was performed 5 to 10 days after the index event. Individuals with traumatic cardiac arrest causes or major intracranial insults revealed by non-enhanced CT were excluded. The standard of reference was the neurological outcome assessed using the cerebral performance category (CPC) score at hospital discharge or 30 days after the index event, with scores of 3 to 5 denoting poor outcomes. ^{99m}Tc-ECD SPECT/CT images were analysed by two experienced nuclear medicine specialists independently. Each image was segmented into 8 cortical brain areas (including bilateral frontal, parietal, occipital, and temporal lobes) and 5 areas of the ascending reticular activating system (including upper brainstem, bilateral thalami, and basal ganglia). Hypoperfusion severity in each brain area was graded on a scale of 0 (preserved perfusion) to 4 (no perfusion). A brain area graded >2 was considered hypoperfused. Semi-quantitative analysis was computed using PMOD software, with uptake ratios representing the mean count activity of each segmented brain area normalized to that of the bilateral temporalis muscles. The Youden's method

was used to determined cut-off values for uptake ratios, and a brain area with an uptake ratio below its cut-off value was also considered hypoperfused. Logistic regression analysis was used to identify predictors for poor neurological outcomes. ***Results:*** We analyzed 224 patients (138 men, 86 women; mean age, 66.8 ± 16.2 years), of which 176 patients (78.6%) had poor neurological outcome. The whole brain area showed no evidence of perfusion in ^{99m}Tc-ECD SPECT significantly associated with poor outcome (OR, 18.99, 95% CI, 1.13-318.60; p=0.006). The number of hypoperfused brain areas in the ascending reticular activating system independently predicted neurological outcome with adjusted OR of 1.70 (95% CI, 1.10-2.63; p=0.017) using visual assessment, and 1.84 (95% CI, 1.32-2.56; p<0.001) using uptake ratios. ***Conclusion:*** Brain hypoperfusion evaluated with ^{99m}Tc-ECD SPECT is helpful in predicting neurological recovery in cardiac arrest survivors, which might assist in informed decision-making for post-resuscitation care.

EPS-163

Cerebral perfusion imaging with [^{15}O]H_2O and an image derived input function from an additional scan of the heart

L. Marner[1], *M. E. Larsen*[1,2], *A. O. Kellberg*[1], *A. C. Henriksen*[1], *S. Fuglsang*[1], *M. N. Lonsdale*[1], *L. Marner*[3];
[1]*Copenhagen University Hospital Bispebjerg, Department of Clinical Physiology and Nuclear Medicine, Copenhagen NV, DENMARK,* [2]*Copenhagen University Hospital Rigshospitalet, Department of Anestesiology, Copenhagen, DENMARK,* [3]*Copenhagen University Hospital Bispebjerg, Department of Clinical Physiology and Nuclear Medicine, Copenhagen, DENMARK.*

Aim/Introduction: Quantitative cerebral perfusion imaging with [^{15}O]H_2O PET is used for assessment of high risk stroke patients but has been limited by the need for invasive arterial cannulation. We aimed to validate a new method with an additional scan of the heart to achieve a non-invasive image derived input function (IDIF) compared to the reference standard with an arterial input function (AIF). ***Materials and Methods:*** Six patients suspected for cerebral hemodynamic insufficiency undergoing cerebral perfusion imaging with [^{15}O]H_2O PET during clinical routine and two healthy elderly subjects were included. Participants had a total of four [^{15}O]H_2O PET scans: a heart and a brain scan at rest followed by infusion of approx. 1 g of acetazolamide to induce vasodilation. After 20 min, the heart and brain scans were repeated. During all four scans, continuous arterial sampling was performed to achieve an AIF. The IDIF was extracted from a manual delineated volume-of-interest (VOI) in the left ventricle of the heart. After correction for injected dose and time-shifting, the IDIF's and AIF's were compared by means of area under curve (AUC) and sums-of-squares (SOS) from an averaged AIF. Using an univariate general linear model, two subsequent AIF's were compared, IDIF's were compared to AIF's, and the regional cerebral perfusion (rCBF) estimated from the AIF and IDIF, respectively, were compared. ***Results:*** Of the 32 scans, 26 had successful arterial sampling. Two subsequent injections of [^{15}O]H_2O resulted in AIF's that were significantly dependent only on subject (p<0.001), and AUC and SOS were highly correlated between measurements (p<0.001 and p<0.000001, n=11 repeated measurements in 6 subjects). Further, AIF and IDIF were highly correlated and dependent on subjects (p<0.007 and p<0.001) but AUC were also significantly lower for IDIF (p<0.02). The lower AUC resulted in higher rCBF (p<0.001) for IDIF compared to AIF. rCBF were still highly dependent on subject (p<0.001, n=15 in 8 subjects). Bland Altman plot showed a positive bias of 3% [-7%, + 14%] using IDIF compared to AIF. ***Conclusion:*** Replacing the invasive arterial cannulation by an additional scan of the heart to achieve an IDIF results in an acceptable bias of 3% higher rCBF estimations. The method is applicable to all scanner systems and is independent of advanced partial volume correction methods.

EPS-164

Hypermetabolism in the Cerebellum is Related to M1 Microglial Activation in Temporal Lobe Epilepsy

Y. Tang*, L. Xiao, J. Yang, J. Hou, B. Chen, S. Hu;*
Xiangya Hospital Central South University, Changsha, CHINA.

Aim/Introduction: The cerebellum is a crucial subcortical structure involved in epileptic networks. Our previous study found hypermetabolism in the bilateral cerebellum among patients with temporal lobe epilepsy (TLE). However, the underlying pathophysiological mechanism remains unclear. This study aimed to explore the potential mechanism of abnormal cerebellar metabolism in TLE, providing deeper insights into the pathophysiology and furthering the search for new drug targets for better management of TLE. ***Materials and Methods:*** Twenty-one patients with TLE and 21 sex- and age-matched healthy controls who underwent [^{18}F]F-FDG PET/CT were enrolled in our study. Regional cerebral metabolic patterns were analyzed using statistical parametric mapping. Then, a rat model of TLE induced by lithium chloride-pilocarpine was subjected to [^{18}F]F-FDG micro-PET/CT imaging and dynamic metabolism changes in the cerebellum were analyzed. [^{18}F]F-DPA-714 micro-PET/CT imaging was implemented to confirm cerebellar neuroinflammation. Immunohistochemistry and western blotting were conducted to investigate the quantities of neurons, Purkinje cells, glial cells and glucose transporters. Flow cytometry and a Luminex assay were applied to verify cerebellar microglial activation and an immune inflammatory reaction. ***Results:*** Compared to healthy controls, patients with TLE showed hypermetabolism in the bilateral cerebellum in addition to hypometabolism in the temporal lobe. In the rat model of TLE, increased [^{18}F]F-FDG and [^{18}F]F-DPA-714 uptake in the cerebellum was confirmed in the chronic phase. We observed the loss of Purkinje cell without a significant decrease of Neun-expressing neurons, and the expression of glucose transporter-1 (Expressed in microglia) increased while there was no change of the glucose transporter-3 (Expressed in neurons) in the cerebellum, indicating that hypermetabolism in the cerebellum is not associated with increased glucose uptake of neurons. Compare to control animals, the immunofluorescence and Western blotting results showed that not only the number of microglia increased, but also the cell body of microglia increased and dendrites decreased in morphology in the chronic stage, there was no significant changes for astrocytes in cerebellum. Furthermore, we found an increase in M1-phenotype microglia, a decrease in M2-phenotype microglia, and an increase in inflammatory factors in the cerebellum. ***Conclusion:*** Patients with TLE exhibited hypermetabolism in the cerebellum, which was confirmed in the chronic phase in TLE rat model. Hypermetabolism of cerebellum may be associated with activation of M1 microglia and immune-driven neuroinflammation, which supports the network theory of epilepsy pathogenesis and may aid the selection of appropriate drug and network regulation targets for TLE interventions designed to address cerebellar inflammation.

EPS-165

Brain Networks Involved in Cancer Treatment Response:Insights from 18F-FDG PET Scans

M. Namías[1], *M. Perovnik*[2], *D. T. Huff*[3], *C. Tinetti*[1,4], *M. Azar*[4], *R. Jeraj*[5,6];
[1]*Fundación Centro Diagnóstico Nuclear, Buenos Aires, ARGENTINA,* [2]*University Medical Center Ljubljana, Ljubljana, SLOVENIA,* [3]*University of Wisconsin-Madison, Madison, WI, UNITED STATES OF AMERICA,* [4]*Instituto de Oncología "Ángel H. Roffo", Buenos Aires, ARGENTINA,* [5]*University of Wisconsin School of Medicine and Public Health, Madison, WI, UNITED STATES OF AMERICA,* [6]*Faculty of Mathematics and Physics, University of Ljubljana, Ljubljana, SLOVENIA.*

Aim/Introduction: Neuroimmunology studies of the interaction between the nervous and immune systems. This field has shed light on how the brain coordinates behavior, metabolism, and immune response, and how psychological and physiological factors can affect the functioning of the immune system, including its ability to fight cancer. In this study, we aimed to investigate whether pre-treatment brain 18F-FDG PET metabolic patterns could predict treatment outcomes in oncology. Our research questions were: 1) Can we identify an 18F-FDG metabolic pattern of the brain that correlates with treatment outcome in oncology? 2) Is this pattern stable across cancer types and treatment modalities? We also sought to explore the cognitive implications of the identified patterns by evaluating differences in the expression of different brain networks. ***Materials and Methods:*** We retrospectively analyzed two 18F-FDG PET datasets from different cancer types and treatment modalities, including advanced metastatic melanoma patients treated with anti-PD1 immunotherapies and stage III breast cancer patients undergoing neoadjuvant chemotherapy. We extracted the brain region from whole-body PET scans and developed uptake patterns as group-level differences between patients who responded to treatment vs. non-responders. Individual pattern expression scores were obtained by multiplying brain scans with the t-score pattern. Scores between groups were compared by performing the Mann-Whitney U test and receiver operating characteristic curves. Classification performance was evaluated by performing both intra- and across-group crossvalidation. We also evaluated the expression of 10 brain networks obtained from the analysis of the BrainMap activation database. ***Results:*** The metabolic pattern was distributed across different brain regions, with regions of relative hypermetabolism in non-responders including the precuneus, Brodmann areas 7, 31 and 40, the cingulate gyrus, left angular gyrus and the middle temporal gyrus, and the cerebellum being the main region with relative hypometabolism. The metabolic pattern was stable across these two cancer types and treatment modalities, and can classify responders vs. non-responders to cancer treatment with areas under the curve of 0.68 and 0.86 for melanoma and breast cancer respectively. Finally, significant differences were found in the expression of the default mode and cognition-language networks between groups. ***Conclusion:*** Our results demonstrate that metabolic patterns of the brain correlate with treatment outcome in cancer patients. We anticipate our work to contribute to the understanding of the interrelation of the central nervous system and treatment response in the context of cancer therapies.

EPS-166

Correlation between neovascularization and macrophage inflammation in carotid atherosclerotic plaques evaluated by hybrid ^{18}F-FDG PET/MR:a fused image-based histological validation study

Y. Zhang[1,2], *B. Cui*[1,2], *H. Yang*[1,2], *Y. Ma*[3], *J. Lu*[1,2];
[1]*Department of Radiology and Nuclear Medicine, Xuanwu Hospital Capital Medical University, Beijing, CHINA,* [2]*Beijing Key Laboratory of Magnetic Resonance Imaging and Brain Informatics, Beijing, CHINA,* [3]*Department of Neurosurgery, Xuanwu Hospital Capital Medical University, Beijing, CHINA.*

Aim/Introduction: Rupture of carotid atherosclerotic plaque is the primary cause of cerebral infarction. Inflammation may cause the occurrence, development and rupture of atherosclerotic plaque, but its physiological mechanism and relationship with the outcome of atherosclerotic plaque are unclear. Neovascularization and macrophage inflammation are the important components of inflammation and their interaction leads to plaque progression. MRI and PET are the non-invasive imaging technology and increasingly used to evaluate atherosclerotic plaque. As dynamic enhanced MRI is used for imaging neovascularization with high spatial resolution, ^{18}F-FDG-PET can be used for quantitative imaging macrophages metabolism of response to inflammation with high sensitivity and specificity. This study determines to investigate the correlation between neovascularization and macrophage inflammation in atherosclerotic carotid plaques with hybrid ^{18}F-FDG PET/MR, further to verify accuracy by histological examination, and to evaluate the clinical potential of hybrid ^{18}F-FDG PET/MR. ***Materials and Methods:*** Twenty-five patients with transient ischemic attack or minor stroke in carotid territory and ipsilateral carotid artery stenosis of 50% to 90% were included. All patients underwent hybrid PET/MR a median of 130 min after injection of ^{18}F-FDG. ^{18}F-FDG standard uptake values with target-to-background ratio (TBR) were determined on corresponding PET sections. Neovascularization was quantified by transfer constant (K^{trans}) on corresponding DCE-MRI sections. A cohort of symptomatic patients (n=12) with carotid stenosis scheduled for carotid endarterectomy (CEA) was separately imaged with hybrid ^{18}F-FDG PET/MR and findings were correlated with histochemical assessment of intact carotid plaques. Spearman rank correlation coefficients between TBR and K^{trans} were calculated. ***Results:*** The correlation between TBR and K^{trans} was only marginal in the whole study sample (r=0.25, p=0.043). The two variables correlated with each other in the symptomatic plaques (r=0.71, p=0.013), but were independent in the asymptomatic plaques (r=0.03, p=0.473). Neither TBR nor K^{trans} was significantly higher in the symptomatic plaques, but both showed inverse relationships with time since last cerebrovascular ischemic event (r=-0.92 and -0.74 for TBR and K^{trans}, respectively). Histological findings from CEA confirmed that inflammation and neovascularization expression was localized within carotid vulnerable plaques. Co-localization of cellular CD31 and CD68 expression in the plaque was observed by immunofluorescence staining. ***Conclusion:*** The correlation between neovascularization and macrophage inflammation in carotid atherosclerotic plaques with hybrid ^{18}F-FDG PET/MR varied with clinical conditions, pointing to a complex interplay between macrophages and neovessels under different pathophysiological conditions. Hybrid ^{18}F-FDG PET/MR systems might help to evaluate the correlation between neovascularization and macrophage inflammation in carotid atherosclerotic plaques.

EPS-167

Brain-dedicated PET system shows non-inferiority compared to conventional PET-CT

P. Nespral[1], *P. Bascuñana*[1], *G. Cuesta Domingo*[1], *A. Canora*[1], *A. Delgado-Cano*[1], *J. Matías-Guiu*[2], *J. Carreras-Delgado*[1], *M. Cabrera-Martín*[1];
[1]*Department of Nuclear Medicine, Instituto de Investigación Sanitaria San Carlos (IdISSC). Hospital Clínico San Carlos, Universidad Complutense, Madrid, SPAIN,*
[2]*Department of Neurology. Instituto de Investigación Sanitaria San Carlos (IdISSC). Hospital Clínico San Carlos, Universidad Complutense, Madrid, SPAIN.*

Aim/Introduction: Conventional PET-CT equipment is often saturated due to the high demand for preferential oncological studies. The development of a dedicated brain PET would allow greater accessibility for PET studies in patients with neurodegenerative disease. This would allow for a broadening of clinical indications in addition to enabling improvements in sensitivity and spatial and temporal resolution, better quantification of small areas and nuclei, and the performance of dynamic studies, among other advantages. ***Materials and Methods:*** A total of 422 studies were performed in 211 patients (mean age 70.78±9.57(27-89)), 57.3% of whom were women. They were referred from the Neurology Department of the Hospital Clínico San Carlos for 18F-FDG PET-CT. The patients underwent a brain imaging study in the conventional PET-CT scanner and subsequently in the dedicated PET scanner after signing the informed consent form. Two nuclear physicians with more than 15 years of experience in neuroimaging evaluated the images without clinical information from the patients, establishing the degree of hypometabolism of the main brain regions and an image-based diagnose. The percentage of agreement between the PET diagnosis and the clinical diagnosis was estimated for both scans. The percentage of agreement and Cohen's Kappa between both scans were also evaluated. ***Results:*** The diagnostic ability of PET vs. clinical diagnosis (degenerative vs. non-degenerative cause) was 82.35% in the dedicated PET and 75.55% using the conventional PET-CT. Similarly, the agreement with the broad diagnosis of neurodegenerative diseases was 80.3% for the dedicated PET vs 75.23% for the conventional PET-CT. The inter-evaluator concordance percentage for degenerative vs. non-neurodegenerative was 83.8% in dedicated PET and 76.7% in conventional PET-CT. ***Conclusion:*** We found good concordance of the dedicated tomograph with conventional PET-CT equipment, having even slightly superior diagnostic capacity. These findings validate the clinical use of this new dedicated brain PET for the diagnosis of neurodegenerative diseases. .

1110

Monday, September 11, 2023, 16:45 - 18:15
Hall K

CTE 5 - Technologists Committee: Cardiac Inflammatory Disease

OP-531

Nuclear Medicine's input in Cardiac Inflammation – clinical overview

P. Erba;
Università di Pisa, Department of Translational Research on New Technologies in Medicine and Surgery, Bergamo, ITALY.

OP-532

The importance of patient preparation

V. Mautone;
Instituto Romagnolo per lo Studio dei Tumori "Dino Amadori" - IRST IRCCS, Meldola, ITALY.

OP-533a

Nuclear Medicine's input in Cardiac Amyloidosis

O. Gheysens;
UCLouvain Louvain-la-Neuve Belgium, Nuclear Medicine Department, Brussels, BELGIUM.

OP-533b

Multimodality in cardiac Imaging: who are the imagers?

S. Pereira;
King's College London and Guy's and St Thomas' Hospital NHS Foundation Trust, Clinical PET Centre, London, UNITED KINGDOM.

1111

Monday, September 11, 2023, 4:45 PM - 6:15 PM
Hall G1

Case Report Session 2 - TROP Session: Successful Molecular Targeting in Oncology

OP-534

Triple Imaging in a Patient with Symptomatic Multiple Myeloma at Staging: Which Is More Informative?

M. Di Franco[1], *D. Bezzi*[1], *A. Cattabriga*[2], *S. Brocchi*[2], *C. Mosconi*[2,3], *E. Zamagni*[4], *M. Talarico*[4], *C. Gaudiano*[2], *L. Vetrone*[1], *R. Mei*[5], *S. Fanti*[1,5], *C. Nanni*[5];
[1]*Nuclear medicine, Alma Mater Studiorum University of Bologna, Bologna, ITALY,* [2]*Department of Radiology, IRCCS Azienda Ospedaliero Universitaria Di Bologna, Bologna, ITALY,* [3]*DIMEC, IRCCS, Azienda Ospedaliero-Universitaria di Bologna, Bologna, ITALY,* [4]*Istituto di Ematologia "Seràgnoli", IRCCS Azienda Ospedaliero-Universitaria di Bologna, Bologna, ITALY,* [5]*Nuclear Medicine, IRCCS, Azienda Ospedaliero-Universitaria di Bologna, Bologna, ITALY.*

Aim/Introduction: This is a case report of a patient diagnosed with symptomatic multiple myeloma (MM) who was staged with [18F]F-FDG PET/CT (FDG-PET/CT), [68Ga]Ga-PSMA PET/CT (PSMA-PET/CT) and Whole-Body Magnetic Resonance with Diffusion Weighted Imaging (DWI-WB-MRI). ***Materials and Methods:*** A 56-year-old woman with recent diagnosis of MM underwent double-tracer PET/CT with [18F]F-FDG and [68Ga]Ga-PSMA in December 2022 (within a clinical protocol approved by local IRB, n° 538/2021/Oss/AOUBo) and DWI-WB-MRI in January 2023, 4 weeks apart from the first to the last imaging procedure. All the scans were carried out with standard procedure and before therapy onset. Upon imaging completion, the patient started pre-transplantation induction therapy, still ongoing. ***Results:*** FDG-PET/CT showed a low focal uptake corresponding to osteorarefaction and bulge of the tenth costovertebral joint and the lateral part of the eighth left rib ("cold" lesions, DS3). On the contrary, PSMA-PET/CT showed multiple areas of focal uptake in the skull (three lytic lesions with a SUVmax=5.3 in the left frontoparietal region), ribs (lytic lesion of the eighth left rib, with para-medullary extension, SUVmax=5.1; paravertebral part of the tenth rib, SUVmax=5.2) and the right sacral wing (SUVmax=4.8) with no corresponding morphological abnormalities. The subsequent DWI-WB-MRI, reported according to the MY-RADS criteria, showed signal alterations corresponding exactly to PSMA-PET/CT findings.

No bone marrow involvement nor extramedullary sites of myeloma were found by any of the imaging procedures. ***Conclusion:*** In this particular case, PSMA-PET/CT result was superimposable to DWI-WB-MRI and both of them turned out to detect more focal findings as compared to FDG-PET/CT at staging. However, no prognostic impact of PSMA-DWI positive / FDG negative lesions has ever been investigated so far. Despite that, this case suggests a possible role of PSMA-PET/CT to estimate the disease extension in newly diagnosed MM in the light of a subsequent theranostic approach. A larger patient population is needed to finally assess the potential of theranostics in this field.

OP-535

Anthracosis: a potential pitfall in 18F-FCH PET/CT and 18F-PSMA-1007 PET/CT interpretation

A. Cimini[1], *M. Ricci*[2], *A. Marzullo*[1], *M. Menichini*[1], *F. Di Stasio*[1], *M. Di Pietro*[1], *H. Arabi*[3], *H. Dadgar*[4], *G. L. Gravina*[5]; *[1]Nuclear Medicine Unit, St. Salvatore Hospital, L'Aquila, ITALY, [2]Nuclear Medicine Unit, Cardarelli Hospital, Campobasso, ITALY, [3]Division of Nuclear Medicine and Molecular Imaging, Department of Medical Imaging, Geneva University Hospital, Geneva, SWITZERLAND, [4]Cancer Research Center, RAZAVI Hospital, Imam Reza International University, Mashhad, IRAN, ISLAMIC REPUBLIC OF, [5]Department of Applied Clinical Sciences and Biotechnologies Division of Radiotherapy, University of L'Aquila, L'Aquila, ITALY.*

Aim/Introduction: 18F-Fluorocholine (18F-FCH) and 18F-Prostate Specific Membrane Antigen (18F-PSMA)-1007 are two PET radiopharmaceuticals commonly used in the evaluation of prostate cancer: nonetheless, other conditions such as inflammations may present high uptake of these two radiopharmaceuticals. In this case report, we describe the findings of both 18F-FCH PET/CT and 18F-PSMA-1007 PET/CT in a patient with anthracosis, a type of pneumoconiosis caused by repeated inhalation of coal dust. ***Materials and Methods:*** A 66-year-old man with history of prostate cancer (previously treated with radical prostatectomy) underwent 18F-FCH PET/CT scan due to biochemical recurrence (PSA 1.34 ng/ml): images showed significant uptake of the radiopharmaceutical in lymph nodes of the mediastinum and right pulmonary hilar region, and no uptake of 18F-FCH in subdiaphragmatic lymph nodes. Due to the rarity of spread to supradiaphragmatic lymph nodes, a subsequent 18F-PSMA-1007 PET/CT scan was performed, revealing high uptake of the radiopharmaceutical in lymph-nodes of the mediastinal and right pulmonary hilar region; subdiaphragmatic lymph nodes did not show significant uptake of the radiopharmaceutical also in this case. Therefore, a biopsy of mediastinal and hilar lymph nodes was performed. ***Results:*** 18F-FCH PET/CT scan showed uptake of the radiopharmaceutical in one lymph node located in the mediastinum (SUVmax 2.7) and in one lymph node of the right pulmonary hilum (SUVmax 4.9). Interestingly, 18F-PSMA-1007 PET/CT scan revealed high uptake of the radiotracer in two mediastinal lymph nodes (respectively with SUVmax 23.4 and SUVmax 8.3) and in two lymph nodes of the right pulmonary hilar region (respectively with SUVmax 6.3 and SUVmax 5.9). The biopsy revealed anthracosis and no malignant cells. Subsequently, the patient communicated previous exposures to coal dust due to his job. ***Conclusion:*** To our knowledge, this is the first report describing a patient with anthracosis evaluated both with 18F-FCH PET/CT and 18F-PSMA-1007 PET/CT: nuclear medicine physicians should be aware of potential pitfalls due to inflammatory conditions. Interestingly, 18F-PSMA-1007 PET/CT scan revealed a greater number of inflammatory lymph nodes, suggesting a possible higher sensitivity of this radiotracer for the detection of anthracosis.

OP-536

Epididymal metastasis of prostate adenocarcinoma in [^{68}Ga]Ga-PSMA-11

B. Martins*, T. Timóteo, C. Loewenthal; Hospital da Luz, Lisboa, PORTUGAL.*

Aim/Introduction: Reporting the clinical case of a 76-year-old man, with a personal history of dyslipidemia and high blood pressure, diagnosed with high-risk prostate adenocarcinoma in January 2015 - PSAi 48.34 ng/mL, Gleason score 9 (4+5), without perineural invasion, staged as cT3bN0M0. He was treated with neoadjuvant hormone therapy, followed by 70Gy (28 fractions) of external radiotherapy with fields on the prostate, seminal vesicles and lymphatic chains until October 2015, having been medicated with adjuvant hormone therapy from May 2015 until June 2018 (nadir PSA of 0,04ng/mL). The patient was clinical reassessed with the usual periodicity, maintaining excellent general condition (ECOG 0) and monitored with PSA, referred for PET-CT with [^{68}Ga]Ga-PSMA-11 with PSA of 1.82ng/mL in July 2022. ***Materials and Methods:*** A dynamic study of the pelvis was carried out immediately after intravenous administration of [^{68}Ga]Ga-PSMA-11 and a whole body image approximately one hour later, complemented with delayed images of the pelvis. Low-dose CT was obtained for attenuation correction and anatomical referencing. ***Results:*** Normal biodistribution of the radiopharmaceutical was observed, with no evidence of disease recurrence in the prostate gland. However, two foci of increased radiopharmaceutical uptake were observed - one on the left testicle (about 1x1.3cm - ApxLL) with SUVmax of 25.72 (which rose to 37.34 in the late images) and a second in a left paraaortic lymph node, with approximately 7x5mm and SUVmax of 6.18. No adenopathies were documented in the remaining lymphatic territories, nor images suggestive of visceral or bone involvement. In the subsequent clinical evaluation, the testicular nodule was palpated on physical examination and a scrotal ultrasound was performed, the result of which favored an inflammatory process of the left epididymis. ***Conclusion:*** The patient was subsequently submitted to bilateral orchidectomy. The pathological result confirmed prostatic metastasis in the left epididymis. The left para-aortic adenopathy was irradiated with SBRT. In subsequent evaluations, a progressive reduction in PSA was documented, which stabilized at 0.02ng/mL in January 2023. In general, the secondary involvement of prostate adenocarcinoma in the epididymis is rare and may result from direct invasion by the vas deferens or by venous or lymphatic retrograde dissemination[1]. In this case [^{68}Ga]Ga-PSMA-11 identified a true positive (image-histology match) uncommon site of prostate cancer secondary involvement, in a context in which the ultrasound suggested an inflammatory etiology. ***References:*** Zhang J. et al: Prostatic adenocarcinoma presenting with metastases to the testis and epididymis: A case report. Oncol Lett 11: 792-794, 2016

OP-537

PET/CT with ^{18}F-FDG and ^{68}Ga-DOTATOC: a case of negative findings in a Solitary Fibrous Tumor.

L. Jonghi-Lavarini[1], *F. Bono*[2], *A. Tuoro*[3], *C. Crivellaro*[4], *L. Guerra*[4,1], *C. Landoni*[4,5,6]; *[1]University Milano-Bicocca, Milan, ITALY, [2]Department of Pathology, IRCCS San Gerardo dei Tintori Hospital, Monza, ITALY, [3]Thoracic Surgery Department, IRCCS San Gerardo dei Tintori Hospital, Monza, ITALY, [4]Department of Nuclear Medicine, IRCCS San Gerardo dei Tintori Hospital, Monza, ITALY, [5]University of Milano–Bicocca, Milan, ITALY, [6]Tecnomed Foundation, Monza, ITALY.*

Aim/Introduction: A 63-year-old woman affected by IBD and asthma during an Rx chest found a nodule in the right lung. A CT chest study confirmed a parenchymal pedicled nodule connected to the visceral pleura in the right upper lobe, with contrast enhancement uptake suggestive of a neuroendocrine tumour. ***Materials and Methods:*** The patient underwent PET imaging with [18F]-FDG and [68Ga]-DOTATOC radiotracers at the Nuclear Medicine Department of San Gerardo Hospital on a GE Discovery MI scanner with 3D acquisition mode according to the EANM guidelines. PET acquisition was performed after at least 6 hours of fasting, with glycemia < 160 mg/dL. About 250 MBq of [18F]-FDG and 150 MBq of [68Ga]-DOTATOC were administered and both acquisitions were performed 60 min after radiotracer injection. ***Results:*** The [18F]-FDG PET/CT study was performed the nodule showed a mild tracer uptake (SUVmax 1.37) consistent with low metabolic activity. Since such behaviour could be compatible with carcinoid, hamartoma, or bronchogenic carcinoma, a [68Ga]-DOTATOC PET/CT was performed without significant uptake at the lesion (SUVmax 1.46); no other uptake abnormalities of radiolabelled somatostatin analogues have been detected in the rest of the body. The bronchoscopic cytologic smear (without the chance to perform any special stain) of the lesion supported the suspicion of a carcinoid tumour due to uniform plasmacytoid bland nuclei and a scant amount of cytoplasm; thus, she underwent surgical resection of the involved lung lobe and some mediastinal lymph nodes. The final diagnosis was Solitary Fibrous Tumour (SFT), and immunostains confirm it through STAT6+, CKpool-, synaptophysin-, TTF1-, p63-, smooth muscle actin-. Ki67 index was 1-2% and mitotic count was low. ***Conclusion:*** SFT is a rare mesenchymal tissue-originating spindle cell tumour that can develop in all parts of the body, most frequently the pleura, with an annual incidence of 0.2/100,000 per year. In this case the location of the growth was the lung parenchyma, with its characteristic "adenofibromatous appearance". Due to its slow rate of growth, [18F]-FDG PET uptake is usually similar to the mediastinal blood pool. Some authors showed that SFTs may overexpress somatostatin receptors (SSTR), mimicking neuroendocrine tumours at [68Ga]-DOTATOC PET scan; on the other hand, in our case, SFT showed no significant uptake on either FDG or DOTA-peptide scan, and this is the first case, to the best of our knowledge. This is additional information for the characterization of lung lesions by using a combination of FDG and DOTA-PET scans.

OP-538

Flip-flop phenomenon on dual SSTR PET and amino acid PET in a case of pre-treated atypical meningioma CNS WHO grade 2

A. Holzgreve[1], *S. Quach*[2], *P. Harter*[3], *R. Forbrig*[4], *C. Schichor*[2], *J. Tonn*[2], *M. Niyazi*[5], *P. Bartenstein*[1], *L. von Baumgarten*[2], *N. L. Albert*[1]; [1]*Department of Nuclear Medicine, University Hospital, LMU Munich, Munich, GERMANY,* [2]*Department of Neurosurgery, University Hospital, LMU Munich, Munich, GERMANY,* [3]*Center for Neuropathology and Prion Research, LMU Munich, Munich, GERMANY,* [4]*Institute of Neuroradiology, University Hospital, LMU Munich, Munich, GERMANY,* [5]*Department of Radiation Oncology, University Hospital, LMU Munich, Munich, GERMANY.*

Aim/Introduction: Meningiomas overexpress somatostatin receptors (SSTRs) and, therefore, are susceptible to SSTR-targeted PET imaging. Amino acid PET, e.g. using the tyrosine analogue fluoroethyl-l-tyrosine (FET), is recommended for the imaging of glioma but has no established role in meningioma imaging. We here illustrate the potential value of dual SSTR and amino acid PET in a challenging case of pre-treated meningioma with heterogeneous imaging findings. ***Materials and Methods:*** A 65-year old patient in continuous clinical follow-up presented with a new unclear lesion on MRI near the left sphenoid bone, 5 years after stereotactic radiotherapy with 54 Gy and 1 year after craniotomy and tumor resection for a left temporal atypical meningioma CNS WHO grade 2. The patient received ongoing treatment with everolimus and octreotid for dural tumor remnants. At the current presentation, MRI showed new-onset edema and an increasing contrast-enhancing lesion in the left brainstem extending into the left cerebellar peduncle in direct vicinity to and/or continuation of the previously known meningioma remnant. MRI findings were rather suggestive of reactive changes but could not exclude vital tumor tissue. A decision was made to perform PET imaging. ***Results:*** SSTR-targeted PET/CT with 187 MBq [^{18}F]SiTATE showed a marked increase in SSTR-expression at the known meningioma residue, whereas the adjacent new lesion only showed low tracer uptake. SSTR PET therefore substantiated the suspicion of a radiation necrosis. Due to the uncommon late-onset 5 years after radiotherapy, however, additional amino acid PET imaging with 173 MBq [^{18}F]FET was performed. In contrast to SSTR PET, FET PET displayed only a minor uptake in the previously known meningioma residue, whereas the new lesion showed a markedly increased uptake typical for malignant tumor tissue. Taken together, the findings were suggestive for meningioma recurrence with signs of dedifferentiation or a radiation-induced secondary tumor. Subsequently, a stereotactic biopsy was performed and revealed malignant tumor tissue (classification of the tumor type currently ongoing); a radiation necrosis on the contrary could not be confirmed. Based on the imaging and consecutive biopsy results, the patient was scheduled for a surgical tumor resection ***Conclusion:*** Additional amino acid PET imaging in meningioma may be helpful in case of equivocal MRI and SSTR PET findings. Here, in a case of pre-treated atypical meningioma CNS WHO grade 2, a "flip-flop" constellation on dual SSTR and amino acid PET enabled to detect malignant tumor tissue, which might have been missed using MRI and SSTR PET alone.

OP-539

"Not always a zebra" - Clear Cell Renal Cell Carcinoma Metastasis detected in [^{68}Ga]Ga-DOTA-NOC PET/CT

J. C. Ferro*, J. P. Teixeira, I. Próspero, D. Barbosa, D. G. Silva, S. Fontão de Castro, G. Ferreira, L. Violante, F. Lopes, H. Duarte, I. Lucena e Sampaio;*
Instituto Português de Oncologia do Porto Francisco Gentil, Oporto, PORTUGAL.

Aim/Introduction: Renal cell carcinoma (RCC) constitutes approximately 3% of all malignant neoplasms diagnosed in adults, with clear cell RCC (ccRCC) being the most common histological type. Up to 30% of patients experience recurrence after surgery with curative intent, with distant metastases commonly occurring in the lung, bone, liver, and occasionally in the pancreas. The high recurrence rate underscores the importance of diligent follow-up, with computed tomography (CT) being considered the standard imaging modality for detecting disease recurrence after surgery. Positron emission tomography (PET) and CT with 2-[^{18}F]FDG (FDG-PET/CT) for restaging is not recommended due to limited sensitivity. However, the usefulness of ^{68}Ga-labelled somatostatin analogues (DOTA-SST-PET/CT) for restaging RCC patients remains uncertain, despite high expression of somatostatin receptors in ccRCC, particularly subtype SST receptor 2. ***Materials and Methods:*** A 64-year-old female patient with a clinical picture of

abdominal pain, anorexia, and weight loss, underwent abdominal CT that revealed a mass in the body of the pancreas, suspicious for primary malignant pancreatic neoplasm. Relevant medical history includes ccRCC in remission, for which she underwent left radical nephrectomy 13 years ago. ***Results:*** In the context of staging, FDG-PET/CT was performed, which revealed a mass in the body of the pancreas and two lung nodules with mild 2-[^{18}F]FDG uptake. In contrast, DOTA-NOC-PET/CT showed intense and moderate uptake, respectively; incidentally, an expansive brain lesion centred in the right lateral ventricle was identified. Carcinoembryonic antigen (1.14ng/mL) and carbohydrate antigen 19-9 (11.2U/mL) were normal, and chromogranin A was high (1342.05ng/mL). Percutaneous biopsy of the pancreatic mass and one of the lung nodules was performed, and the histology was consistent with metastases from ccRCC, suggestive of metachronous metastasis. Later, the lesion in the right ventricle was characterized as meningioma. The patient initiated a tyrosine kinase inhibitor (pazopanib), resulting in stable disease on serial CT scans and normalization of chromogranin A levels. ***Conclusion:*** This clinical case serves as a reminder that [^{68}Ga]Ga-DOTA-SST uptake is not pathognomonic for neuroendocrine tumours and the possibility of ccRCC metastases should be considered in the differential diagnosis in an appropriate clinical scenario. Accurate restaging of RCC patients can impact therapeutic decisions and influence disease outcomes. Although FDG-PET/CT can effectively be used for restaging of RCC, the overall sensitivity for detecting distant metastases is limited, suggesting that DOTA-SST-PET/CT may be a useful imaging tool for detecting ccRCC metastases.

OP-540

Brain [^{18}F]FET PET/CT in acute myeloid leukemia

G. Crosta[1], *A. Castello*[2], *S. Pacella*[2], *V. Longari*[2], *L. Florimonte*[2], *M. Castellani*[2];
[1]*University of Milan, Milan, ITALY,* [2]*Fondazione IRCCS Ca' Granda Ospedale Maggiore Policlinico, Milan, ITALY.*

Aim/Introduction: Involvement of central nervous system (CNS) in patients with acute leukemia is relatively rare, accounting for 4-7% of patients with acute lymphoblastic leukemia and for 1-3% with Acute Myeloid Leukemia (AML) [1,2]. However, the presence of CNS lesions at diagnosis or relapse is associated with a worse prognosis. MRI is the first imaging technique used for the diagnosis of either primary or secondary brain tumours, although it is not free from drawbacks [3]. Morevoer, due to high uptake of healthy brain parenchima, [^{18}F]FDG PET/CT shows limited accuracy for characterization of brain lesions. ***Materials and Methods:*** [^{18}F]FET, analogue of the L-tyrosine, is an artificial amino acidic radiotracer that presents no uptake in normal cerebral cortex, with a higher tumor-to-background signal and low uptake in inflammatory cells. Therefore, it is used to characterize brain lesions, to differentiate between tumor progression and treatment related changes, for planning biopsy and radiotherapy, as well as for monitoring treatment. ***Results:*** A 58-year-old woman, with a history of AML in complete response, was referred to the Emergency department of our hospital for loss of consciousness. A brain MRI showed an intracranial mass suggestive for either primary brain tumor or brain metastasis. [^{18}F]FET PET/CT, performed for guiding stereotactic biopsy, revealed increased uptake of the lesion localized at the genu of the corpus callosum. Metastasis from AML was diagnosed after brain biopsy. To complete staging before starting chemotherapy, patient underwent [^{18}F]FDG PET/CT, including brain acquisition, that showed an uptake slightly below the adjacent healthy brain and physiological distribution of glucose without sites of abnormal extra-cranial accumulation. ***Conclusion:*** according RANO guidelines, brain [^{18}F]FET PET/CT is recommended for both glial tumors and suspected secondary localizations. Our case confirms the higher sensitivity of ^{18}F-FET than ^{18}F-FDG in the assessment of this rare case of brain metastasis from AML. ***References:*** 1 Ganzel C, Lee JW, Fernandez HF, et al. CNS involvement in AML at diagnosis is rare and does not affect response or survival: data from 11 ECOG-ACRIN trials. Blood Adv. 2021;5:4560-4568. 2 Cheng CL, Li CC, Hou HA, et al. Risk factors and clinical outcomes of acute myeloid leukaemia with central nervous system involvement in adults. BMC Cancer. 2015;15:344. 3 Langen KJ, Galldiks N, Hattingen E, Shah NJ. Advances in neuro-oncology imaging. Nat Rev Neurol. 2017;13:279-289.

OP-541

Two Cases of Diffuse Mild-Moderate 18F-Fluoroestradiol Lung Uptake in Women with Metastatic Estrogen Receptor Positive Breast Cancer

E. Phillips*, P. Karak;*
Hartford Hospital, Hartford, CT, UNITED STATES OF AMERICA.

Aim/Introduction: 18F-Fluoroestradiol (FES) is a radiotracer that binds to estrogen receptors (ER) and is utilized for suspected disease recurrence or metastatic disease in patients with ER positive breast cancer. However, FES will also bind to wherever estrogen receptors are located within the body. Although estrogen receptors are located within the lungs, FES does not routinely demonstrate uptake within them. To date, FES has only been shown to demonstrate uptake within a focal region of the lung status post radiation therapy, but no cases have demonstrated diffuse uptake within the lungs which we do here. ***Materials and Methods:*** We reviewed the images from all patients at our institution, Hartford Hospital, who had 18F-Fluoroestradiol PET/CT scans performed. Data analysis and extensive literature search were performed. We present two patients with stage IV ER positive breast cancer who underwent FES PET/CT imaging to evaluate for metastatic disease. Both of the scans demonstrated mild-moderate diffuse uptake within the bilateral lungs. ***Results:*** We found that 2 of the 11 total patients who had 18F-Fluoroestradiol PET/CT scans done demonstrated diffuse mild-moderate bilateral lung uptake for a total of 0.18%. The first patient had a severe lung injury, acute respiratory distress syndrome and acute interstitial pneumonia, which was improving but still present at the time of her imaging. The second patient had a remote history of right breast radiation therapy for a prior breast cancer as well as emphysema. ***Conclusion:*** As breast cancer is the most commonly diagnosed cancer in women, FES PET/CT imaging will likely become more commonly performed. Therefore, it's important to understand where the radiotracer might demonstrate uptake and why. To date, only focal FES uptake has been demonstrated within the lungs which was secondary to fibrotic changes from prior radiation therapy. As diffuse bilateral mild-moderate lung uptake has not yet been reported we highlighted two unique cases that demonstrated such findings to provide further information about FES. Overall, we conclude that diffuse bilateral mild-moderate FES uptake within the lungs is likely secondary to inflammation, interstitial disease, or a combination thereof.

OP-542

The ultimate indication for surgical probe use: a case of an ectopic intraesophageal parathyroid adenoma.

A. Doumas[1], *I. Pliakos*[2], *T. Papavramidis*[2], *P. Exadaktylou*[1], *D. Boundas*[3], *E. Giannoula*[1], *A. Tsangaridi*[1], *G. Gerasimou*[1], *E. Papanastasiou*[1], *N. Papadopoulos*[1], *I. Iakovou*[1];
[1]*Aristotle University, Thessaloniki, GREECE,* [2]*1st Surgery Clinic of Aristotle University of Thessaloniki, University Hospital AXEPA, Thessaloniki, GREECE,* [3]*Private Nuclear Medicine Centre, Ippokratis, Thessaloniki, GREECE.*

Aim/Introduction: The scintigraphic demonstration of parathyroid adenomas in patients with known hyperparathyroidism is currently the main preoperative strategy. The combination of ultrasound and scintigraphic study by experienced imaging specialists increases the probability of accurate detection of adenoma to about 90%. In addition, the intraoperative use of the surgical probe after administration of a small amount of isonitrile (SESTAMIBI) contributes to the successful excision of the adenoma, reduces the operating time, and increases the surgeon's confidence. Our target is to present the validity of the intraoperative use of probe in patients with particularly challenging surgical localization of parathyroid adenoma. ***Materials and Methods:*** We present the case of a 53-year-old woman, with a clear suspicion of overactive parathyroid tissue evidenced by a history of nephrolithiasis for several years, very high PTH values and serum Ca consistently above 10 mg/dl for the past three years. In 2022, the patient underwent parathyroid scintigraphy, which revealed a parathyroid adenoma located at the lower left lobe of the thyroid and towards the midline. The imaging suggested that the adenoma was mobile, providing further evidence of its presence. Thyroid ultrasound also detected the adenoma. The patient was operated on by an experienced endocrine gland surgeon; however, despite a thorough exploration of the neck, the adenoma could not be located. Parathyroid hormone levels remained high both perioperatively and in the following months. Finally, 4 months later, the scintigraphy was repeated, with the same picture as an outcome. A few months after the last scintigraphy, the patient was administered 6mCi SESTAMIBI, and two hours later, using the surgical probe, the parathyroid gland was located intraesophageally and successfully excised. The intraoperative finding of successful adenoma excision by means of the probe was positive in the excised adenoma compared to the surrounding tissues. Furthermore, the intraoperative PTH value dropped by 70% in the next hour ***Conclusion:*** The intraoperative use of a surgical probe is the most reliable, fast, cheap, and absolutely necessary solution for the endocrine gland surgeon for the successful removal of parathyroid adenomas, especially when there is a suspicion of their ectopic location.

1201

Tuesday, September 12, 2023, 08:00 - 09:30

Hall A

CME 9 - Bone & Joint + Physics Committee: Current Bone SPECT/CT (including 360 CZT)

OP-543

360 CZT Bone SPECT/CT How to report it and Case Examples

D. Little*;*
Royal United Hospital, Radiology Department, Bath, UNITED KINGDOM.

OP-544

CT findings in SPECT/CT – Bone and Incidental

I. Bruno*;*
Regional General Hospital "F. Miulli", Bari, ITALY.

OP-545

Extent of scan in SPECT/CT Whole Body vs Single and Multiple Fields of View

S. Redman*;*
Royal United Hospital, Radiology Department, Bath, UNITED KINGDOM.

OP-546

SUV in Bone SPECT/CT

B. Geist*;*
Medical University of Vienna, Department of Biomedical Imaging and Image-guided Therapy, Vienna, AUSTRIA.

1202

Tuesday, September 12, 2023, 08:00 - 09:30

Hall D (Arena)

Round Table 2 - Radiation Protection Committee: Establishing and Running a Theranostics Center in a Clinical Setting

OP-547

Why theranostics and future challenges, the clinical perspective

K. Herrmann*;*
UniversityHospital Essen, Department of Nuclear Medicine, Essen, GERMANY.

OP-548

Staff, infrastructure and instrumentation, and related regulatory issues

A. Sundlöv*;*
Swedish Medical Products Agency, Uppsala, SWEDEN.

OP-549

Patient management and radiation protection considerations of staff, patients, carers, and the public

N. Cherbuin*;*
Centre Hospitalier Universitaire Vaudois, Institut de Radiophysique, Lausanne, SWITZERLAND.

OP-550

New theranostic agents and future challenges

S. Heskamp;
Department of Medical Imaging, Nuclear Medicine, Radboud University Medical Center Nijmegen, Nijmegen, NETHERLANDS.

1203

Tuesday, September 12, 2023, 08:00 - 09:30

Hall E1

LIPS Session 9 - Paediatrics Committee: Paediatric Nephro-Urology - Beyond Hydro-Nephrosis

OP-551

Renal scintigraphy in kidney abnormalities other than hydronephrosis

A. Santos;
Hospital Garcia de Orta, Nuclear Medicine Department, E.P.E. , Almada, PORTUGAL.

OP-552

MAG3 or DMSA in congenital renal malformation

J. Rogasch;
Charité-Universitätsmedizin Berlin, Department of Nuclear Medicine, Berlin, GERMANY.

OP-553

DMSA, MAG3, sonography and functional MRI: contribution in complex ectopic, duplex and horseshoe kidneys

P. Zucchetta;
Padova University Hospital, Department of Medicine, Nuclear Medicine Unit, Padova, ITALY.

1204

Tuesday, September 12, 2023, 8:00 AM - 9:30 AM

Hall E2

M2M Track - TROP Session: Imaging the Brain from all Angles

OP-555

First imaging of PARP1 in the living human brain - a translational PET study with [^{11}C]AZ3391

M. Schou[1,2], *A. Pike*[3], *A. Jucaite*[1,2], *P. Johnström*[1,2], *M. Cortes Gonzalez*[2], *A. Högnäsbacka*[2], *K. Dahl*[1,2], *A. Ghosh*[4], *J. Johannes*[4], *A. Staniszewska*[3], *E. Leo*[3], *P. Hamerlik*[3], *B. Davies*[3], *S. Cosulich*[3], *J. Swales*[3], *R. Lawrence*[3], *M. Squatrito*[3], *N. Mueller*[5], *V. Sousa*[2], *J. Bartek*[2], *G. Stragliotto*[2], *P. Stenkrona*[2], *L. Farde*[2], *C. Halldin*[2], *Z. Cselényi*[1,2];
[1]*AstraZeneca, Stockholm, SWEDEN,* [2]*Karolinska Institutet, Stockholm, SWEDEN,* [3]*AstraZeneca, Cambridge, UNITED KINGDOM,* [4]*AstraZeneca, Waltham, MA, UNITED STATES OF AMERICA,* [5]*AstraZeneca, Gaithersburg, MD, UNITED STATES OF AMERICA.*

Aim/Introduction: PARP1 is a key enzyme in DNA damage repair implicated in the pathophysiology of cancer and neurodegenerative disorders. We herein report the discovery and development of a blood-brain barrier (BBB) penetrant, subtype-selective high affinity PARP1 inhibitor, [^{11}C]AZ3391, as a novel PET radioligand for PARP1. ***Materials and Methods:*** The preclinical evaluation of [^{11}C]AZ3391 was conducted using in vitro autoradiography and PET in non-human primates (NHPs) (n=7, 23 PET in total). After giving informed consent, nine healthy volunteers and one patient were enrolled in the human study, which included 19 PET measurements. Total binding was estimated using semiquantitative (standardized uptake value, SUV) and quantitative (volume of distribution, V_T) analyses, the latter obtained using a two-tissue compartment model. ***Results:*** AZ3391 was labelled using ^{11}C-methylation at high molar activity (162 GBq/μmol) and high radiochemical purity (>99%). In vitro autoradiography demonstrated dense binding of [^{11}C]AZ3391 to A549 tumour xenograft tissue as well as rat, mouse, NHP and human cerebellum. The binding could be obliterated (>99% inhibition) by co-incubation with two structurally distinct PARP inhibitors, namely olaparib (that targets PARP1 and other members of the PARP family) and AZD5305 (PARP1-selective), thus confirming specific binding to PARP1 in vitro**.** NHP PET demonstrated binding of [^{11}C]AZ3391 to PARP1 in bone marrow, pituitary, spleen and brain with highest regional binding in cerebellum. The binding was blocked in a dose-dependent manner after pre-treatment with two structurally distinct PARP-inhibitors (up to 99% inhibition), namely AZD9574 (PARP1-selective) and pamiparib (that targets PARP1 and other members of the PARP family), thus confirming specific [^{11}C]AZ3391 binding to PARP1 in vivo. PET measurements in healthy volunteers confirmed that [^{11}C]AZ3391 crossed the human BBB. Consistent with that observed in NHP PET, high binding was observed in the pituitary, bone marrow and cerebellum. Absolute test-retest variability (TRV) of the regional SUV estimates ranged from 5% to 10%. The TRV for V_T ranged from 10% to 22%. A case study in a patient with glioblastoma multiforme (GBM) demonstrated several-fold higher total [^{11}C] AZ3391 binding in the tumor region compared to normal brain tissue. Interestingly, there was considerable heterogeneity in radioligand binding across the tumor. ***Conclusion:*** [^{11}C]AZ3391 is the first BBB penetrant and subtype-selective PET radioligand for PARP1. Its development opens up new opportunities for clinical research in cancer and neurodegenerative disorders as well as for dose-setting in clinical drug development.

OP-557

Development of a PET imaging agent for the detection of amyotrophic lateral sclerosis

B. Guérin[1], *S. Ait-Mohand*[1], *V. Dumulon-Perreault*[2], *J. Rousseau*[1], *O. Sarrhini*[2], *S. Tremblay*[1], *M. Maier*[3], *M. Salzmann*[3];
[1]*Universite de Sherbrooke, Sherbrooke, QC, CANADA,* [2]*CRCHUS/CIUSSSE CHUS, Sherbrooke, QC, CANADA,* [3]*Neurimmune AD, Zurich, SWITZERLAND.*

Aim/Introduction: Amyotrophic lateral sclerosis (ALS) is a rare neurodegenerative disease resulting from the loss of motor neurons in the motor cortex, brainstem, and spinal cord. It currently affects 2.1 to 3.8 per 100 000 person-years in Europe. Of all ALS cases ~10% are inherited (FALS) and the rest arise sporadically (SALS). Mutations in the superoxide dismutase 1 (SOD1) gene, leading to the misfolding of its protein product, are the second most common genetic cause of ALS. SALS patients had increased levels of misfolded SOD1 (mSOD1).[1] Currently, there is no approved diagnostic tool for ALS. We developed a recombinant human monoclonal antibody (AP-101) conjugated to ^{89}Zr-desferoxamine (^{89}Zr-DFO), which selectively targets mSOD1. The purpose of this study was to validate ^{89}Zr-DFO-AP-101 radiotracer for PET imaging of mSOD1. ***Materials and Methods:*** DFO-AP-101 was prepared

by conjugating AP-101 antibody with p-SCN-Bn-DFO and labelled with ^{89}Zr ($t_{½}$=78.41h). A longitudinal imaging study was performed to identify the optimal mice age and time post administration of ^{89}Zr-DFO-AP-101 (20-30 MBq) for the detection mSOD1 aggregation in transgenic (Tg, [B6.Cg-Tg(SOD1*G93A)1Gur/J)]) mice expressing mSOD1 and in wild type (Wt) mice. As control, a subset of mice were co-injected with AP-101 (100 mg/kg) to assess target specificity. PET/CT data were expressed as percent injected dose per gram of tissue (%ID/g). ***Results:*** ^{89}Zr-DFO-AP-101 was able to engage mSOD1 aggregates in the spinal cord of Tg mice and imaging was optimal in 126-day-old Tg mice and at day 10 post administration. The number of detected aggregates was more important at day 10 (18) as compared to day-7 (6). All the spots found between the T11 and L2 vertebra. The concentration of ^{89}Zr-DFO-AP-101 in the spinal cord and vertebra of the Tg mice significantly exceeded that of the Wt mice ($p = 0.01$). Co-injection with AP-101 considerably reduced the amount of mSOD1 aggregates detected from 67% (6/9) to 15% (2/13). The intensity of the aggregates was also decreased from 8.05 ± 1.30 %ID/g to 5.73 ± 0.28 with ^{89}Zr-DFO-AP-101 alone or in presence of AP-101 in excess. Blocking with AP-101, significantly reduced the spinal cord ($p < 0.001$) and vertebra ($p < 0.0001$) uptake of ^{89}Zr-DFO-AP-101. ***Conclusion:*** Our lead ^{89}Zr-DFO-AP-101 can exhibited unprecedented detection of mSOD1 aggregate in transgenic mice. Such a PET tracer would find application in the early diagnostic of ALS and in the monitoring of therapeutic interventions. ***References:*** 1. Maier M, et al. Sci Transl Med. 2018;10(470).

OP-558

In vivo performance of different ^{18}F-labelled cannabinoid receptor 2 radioligands

D. Guendel[1], *W. Deuther-Conrad*[1], *L. Ueberham*[2], *R. Teodoro*[1,3], *G. Bormans*[4], *M. Toussaint*[1], *E. Hey-Hawkins*[2], *K. Kopka*[5,6], *P. Brust*[1,7], *R. Moldovan*[1];
[1]*Helmholtz-Zentrum Dresden-Rossendorf, Institute of Radiopharmaceutical Cancer Research, Department Neuroradiopharmaceuticals, Leipzig, GERMANY,* [2]*Leipzig University, Faculty of Chemistry and Mineralogy, Institute of Inorganic Chemistry, Leipzig, GERMANY,* [3]*Life Molecular Imaging GmbH, Berlin, GERMANY,* [4]*Laboratory for Radiopharmacy, KU Leuven, Leuven, BELGIUM,* [5]*Helmholtz-Zentrum Dresden-Rossendorf, Institute of Radiopharmaceutical Cancer Reserach, Dresden, GERMANY,* [6]*Faculty of Chemistry and Food Chemistry, School of Science, Technische Universität Dresden, Dresden, GERMANY,* [7]*University Medical Center Schleswig-Holstein, The Lübeck Institute of Experimental Dermatology, Lübeck, GERMANY.*

Aim/Introduction: Cannabinoid receptor 2 (CB2) expression in healthy brain is very low and the upregulation is associated with inflammation, traumatic brain injury, neurodegeneration and cancer[1]. In view of the increasing interest in CB2-targeted therapies, PET offers an attractive strategy to quantify the availability of CB2 in the diseased brain. To achieve this goal, we developed a number of ^{18}F-labelled CB2 ligands and biologically evaluated them in rodents. Here we present a comparative overview of the obtained results. ***Materials and Methods:*** Structure-activity-relationships-driven target compound identification, organic synthesis and radiofluorination was performed for compounds of the thiazole ([^{18}F]JHU94620[2] and [^{18}F]LUZ5[3]), naphthyridin-2-one ([^{18}F]LU14[4] and [^{18}F]LU13[5]) and indole ([^{18}F]RM365) families. The new radioligands were assessed in vitro by binding experiments using CHO(hCB2) cell membranes and rat spleen homogenates and by autoradiography on cryosections of rodent spleen. Furthermore, the radioligands were examined for their metabolic stability and biodistribution by PET. Furthermore, for selected radioligands the binding to highly expressed hCB2 in a rat model overexpressing hCB2(D80N) in the right striatum (AAV-hCB2)[6] was investigated. ***Results:*** The low- to subnanomolar hCB2 affinities of the presented radioligands were demonstrated in vitro by K_d values ranging from 0.4 to 2.9 nM with a hCB2 selectivity against hCB1 of >1000-fold. The highest metabolic stability was observed for [^{18}F]RM365 with 55% and 90% and the lowest for [^{18}F]JHU94620 with 7% and 36% of the initial fraction in plasma and brain 30 min p.i., respectively. The in vivo experiments confirmed the in vitro autoradiographic results, and showed high uptake for [^{18}F]JHU94620, but low or non-displaceable uptake for [^{18}F]LU14, [^{18}F]LUZ5 and [^{18}F]RM365 in spleen. Contrary to the low uptake of [^{18}F]LUZ5 in the brain of naïve Wistar rats, target-specific and displaceable uptake for [^{18}F]LU14 and [^{18}F]RM365 was demonstrated in the AAV-hCB2 rat model, with the highest signal-to-noise ratio determined for [^{18}F]RM365 expressed as SUVR of 20 and lowest for [^{18}F]LU14 expressed as SUVR of 6. ***Conclusion:*** A novel series of CB2 receptor radioligands has been developed and preliminarily evaluated in rodents. Binding affinity to the CB2 varies between species, however PET scans with an AAV-hCB2 rat model revealed a high brain uptake and target specificity for hCB2 with excellent signal-to-noise ratios and displaceable binding. ***References:*** [1]Stasiulewicz et al. IJMS, 2020, 21,2778; [2]Moldovan et al. JMC, 2016, 59,17; [3]Ueberham et al. JMC, 2023; [4]Teodoro et al. IJMS, 2021, 22,15; [5]Gündel et al., JMC 2022, 65,13; [6]Attili et al. BJP, 2019, 176,1481

OP-559

^{18}F-FDS PET imaging as a quantitative marker to investigate the magnitude and dynamics of enhanced of blood-brain barrier permeability induced by regadenoson

B. Hosten*, S. Goutal, S. Leterrier, A. Winkeler, L. Breuil, M. Goislard, C. Truillet, N. Tournier;*
Université Paris-Saclay, INSERM, CNRS, CEA, Biomaps, Orsay, FRANCE.

Aim/Introduction: The development of strategies to overcome the blood brain barrier (BBB) and enable drug delivery to the brain is tightly linked to the availability of translational biomarkers of BBB permeability to evaluate their efficacy in the living brain. Among translational imaging techniques, PET imaging benefits from absolute quantitative performances, which enables kinetic modeling. ^{18}F-2-deoxy-2-fluoro-D-sorbitol (^{18}F-FDS, MW: 183 Da) is a non-metabolized hydrophilic small molecule repurposed as a PET marker of BBB permeability. ^{18}F-FDS PET was optimized to capture the dynamics of transient BBB disruption induced by regadenoson a selective adenosine A2 receptor (A_2R) agonist. ***Materials and Methods:*** ^{18}F-FDS was easily obtained by chemical reduction of commercial ^{18}F-FDG. In anesthetized rats, regadenoson (0.05 mg/kg) or saline (control) was administered i.v., immediately before ^{18}F-FDS microPET injection (bolus, 34 ± 5 MBq) followed by dynamic microPET acquisition. Six rats underwent arterial canulation for the determination of the arterial input function (AIF) of ^{18}F-FDS during PET acquisition in both the control and regadenoson (n=3) to validate an image derived input function (IDIF). Other rats (6 control, 5 regadenoson) underwent bolus ^{18}F-FDS PET without AIF. Kinetic modeling was performed from time-activity curves obtained in the brain and the left ventricle (IDIF) to estimate the total volume of distribution (V_T, Logan plot analysis) of ^{18}F-FDS in brain regions. Then dynamic

^{18}F-FDS PET acquisition (90 min) using a bolus-infusion strategy (48 MBq bolus followed by 26 MBq/90 min infusion, i.v.) was tested to capture the dynamics of BBB disruption induced by regadenoson, injected 20 min after the start of infusion. ***Results:*** A significant correlation was observed between the AIF and IDIF (R = 0.88, p<0.001). In the whole-brain, regadenoson increased brain V_T of ^{18}F-FDS (+93.9+/-6.2% p <0.001). The effect was significantly different across brain regions (p<0.001) and was maximal in the striatum (+176.0+/-26.3% p<0.001) and minimal in the cerebellum (+76.0+/-5.9% p<0.001), consistent with the regional expression of A_2R. In the bolus-infusion experiments, an increase in ^{18}F-FDS brain uptake relative to control rats was observed immediately after regadenoson injection and stopped after 24 min. ***Conclusion:*** The readily available ^{18}F-FDS PET provides a convenient, quantitative and translational imaging techniques to evaluate and compare strategies of BBB permeabilization in vivo. Regadenoson offers a simple and efficient way for transient BBB permeabilization with perspectives for drug delivery to the brain.

OP-560

The 5-HT1A receptor modulates motor/exploratory activity, object recognition and DAT binding in the dorsal and ventral striatum of the rat

S. Nikolaus[1], *M. Beu*[1], *J. Henke*[1], *C. Antke*[1], *B. Fazari*[2], *E. Mamlins*[1], *F. L. Giesel*[1];
[1]*University Hospital Düsseldorf, Düsseldorf, GERMANY,*
[2]*Heinrich-Heine University, Düsseldorf, GERMANY.*

Aim/Introduction: Both dopamine (DA) and serotonin (5-HT) are relevant for motor control as well as learning. In the present study, we assessed the effect of the 5-HT1A receptor (R) agonist 8-OH-DPAT on motor/exploratory behavior, memory for object and place and dopamine (DAT) and serotonin transporter binding (SERT) in the rat brain. ***Materials and Methods:*** Rats (n=41) underwent a 5-min exploration trial in an open field with two identical objects. A 5-min test trial with one of the objects replaced by a novel one and the other object transferred to a novel place was conducted 30 min after intraperitoneal injection of either 8-OH-DPAT (0.1 and 3 mg/kg) or vehicle (0.9% NaCl). Subsequently, 123I-FP-CIT; 11±4 MBq was injected into the tail vene. Specific binding of 123I-FP-CIT to DAT and SERT was determined by subtracting unspecific binding in the cerebellar reference region from radioligand concentrations obtained in the individual regions of interest (DAT: cingulate, caudateputamen, nucleus accumbens; SERT: thalamus, dorsal and ventral hippocampus, brainstem). Duration and frequency of object exploration, ambulation, sitting, rearing, head-shoulder-motility and grooming were evaluated with Ethovision XT. ***Results:*** 8-OH-DPAT (3 mg/kg) increased DAT binding in the caudateputamen relative to both vehicle (p=0.001) and 0.1 mg/kg 8-OH-DPAT (p=0.015). In the nucleus accumbens, DAT binding was decreased after 3 mg/kg 8-OH-DPAT relative to vehicle (p=0.006). In the test trial, 8-OH-DPAT dose-dependently increased ambulation and exploratory head-shoulder motility, whereas rearing was dose-dependently decreased (0.001≤p≤0.05). 3 mg/kg 8-OH-DPAT induced a memory deficiency for object relative to vehicle (p<0.05). Moreover, memory for place was impaired relative to both 0.1 mg/kg 8-OH-DPAT (p=0.003) and vehicle (p<0.001). ***Conclusion:*** Findings indicate that the 5-HT1AR modulates motor/exploratory behaviors, memory for object and place and regional DA function in the rat. It may be hypothesized that 8-OH-DPAT initially augmented neostriatal DA (possibly via a disinhibition of GABAergic microcircuits), resulting in the compensatory downregulation reflected by the increase of radioligand binding to the DAT. Conversely, in the NAC, 8-OH-DPAT may have reduced excitatory input from neocortex and hippocampus, resulting in the increase of available DA reflected by the decrease of radioligand binding to the DAT.

OP-561

Brain mitochondrial function and cerebral glucose utilization in non-human primate of Parkinson disease model with α-synuclein propagation via the olfactory system: a^{18}F-BCPP-EF and^{18}F-FDG PET imaging study

H. Onoe[1], *M. Sawamura*[2], *T. Hirato*[2], *H. Tsukada*[3], *T. Nakako*[4], *T. Nakayama*[4], *K. Ikeda*[4], *C. Chen*[5], *K. Isa*[5], *M. Nakamura*[5], *T. Isa*[5], *R. Takahashi*[2];
[1]*Human Brain Research Center, Kyoto University Graduate School of Medicine, Kyoto, JAPAN,* [2]*Department of Neurology, Kyoto University Graduate School of Medicine, Kyoto, JAPAN,* [3]*Central Research Laboratory, Hamamatsu Photonics K.K., Hamakita, JAPAN,* [4]*Sumitomo Pharma Co., Ltd., Osaka, JAPAN,* [5]*Department of Physiology and Neurobiology, Kyoto University Graduate School of Medicine, Kyoto, JAPAN.*

Aim/Introduction: Parkinson's disease (PD) is a neurodegenerative disorder characterized by degeneration of dopaminergic neurons in the substantia nigra and the formation of alpha-synuclein (α-Syn) inclusion called Lewy bodies in neurons. PD is thought to progress through the amplification and propagation of α-Syn aggregates in the brain in a prion-like manner. Patients with Lewy body diseases exhibit variable degrees of cortical and subcortical hypometabolism. However, the underlying causes behind this progressive hypometabolism remain unresolved. Mitochondrial dysfunction, especially the impairment of complex I (MC-I), has been implicated in PD. Previously, we have developed a marmoset PD model with inoculation of α-Syn fibrils into the olfactory bulb, which induced α-Syn propagation through the olfactory system, and subsequent decreases in regional cerebral glucose utilization (rCGU) measured by ^{18}F-FDG-PET. The aim of this study was to investigate whether mitochondrial dysfunction is proportionally linked to the magnitude of hypometabolism and α-Syn pathology by performing ^{18}F-BCPP-EF-PET, which can measure MC-I activity, as well as ^{18}F-FDG-PET using this model. ***Materials and Methods:*** We inoculated 3.2 μg α-Syn fibrils into the two sites of the bilateral olfactory bulbs. ^{18}F-BCPP-EF-PET and ^{18}F-FDG-PET were performed on four adult marmosets 1, 3, 6, 9 and 12 months after as well as before α-Syn inoculation. Immunohistochemical analysis for phosphorylated α-Syn has been performed after the last imaging, and a regression analysis of PET images has been performed for temporal changes from pre-inoculation to 12 months post-inoculation. Correlation between α-Syn pathology and result of PET at 12 months (Spearman's rank correlation coefficient analysis) was performed using region of interests (ROIs) in the marmoset standard brain MRI atlas. ***Results:*** We observed phosphorylated α-Syn aggregates, mainly in the olfactory pathway in accordance with our previous study. PET image analysis showed that MC-I activity decreased in the olfactory bulb, prefrontal area, piriform cortex, and amygdala while rCGU decreased particularly in the occipital lobe. Statistical analysis revealed that α-Syn pathology was significantly negatively correlated with MC-I activity (r_s=-0.33, p=0.0001) but had no correlation with rCGU, indicating that α-Syn aggregation was associated with mitochondrial dysfunction. ***Conclusion:*** Mitochondrial dysfunction is proportionally linked to the magnitude of α-Syn pathology but not directly associated with hypometabolism in non-human primate PD model. ^{18}F-BCPP-EF-PET is expected as a biomarker of prodromal

synucleinopathies for PD, especially disease-associated α-Syn aggregates. ***References:*** Sawamura M. et al, Lewy body disease primate model with α-synuclein propagation from the olfactory bulb, Mov Disord, 37(10):2033-2044, 2022.

OP-562

Discovery of Novel PET tracer [^{18}F]F-diarylbisthiazoles for α-Synucleinopathies Imaging

B. Hooshyar Yousefi[1], *B. Uzuegbunam*[2], *S. Bagheri*[3], *G. B. Kotipalli*[3], *W. Paslawski*[4], *J. Li*[5], *E. Nasisi*[6], *F. Geibl*[6], *M. Henrich*[6], *P. Svenningsson*[4], *H. Ågren*[5], *M. Luster*[7], *W. Weber*[8], *T. Arzberger*[9], *D. Librizzi*[10];
[1]*Nuclear Medicine Department, Radiopharmacy section, Philipps University Marburg, Marburg, GERMANY,* [2]*Nuclear Medicine Department, Radiopharmacy section, Philipps University, Munich, GERMANY,* [3]*Nuclear Medicine Department, Radiopharmacy section, Philipps University, Marburg, GERMANY,* [4]*Department of Clinical Neuroscience, Karolinska Institutet, Stockholm, SWEDEN,* [5]*Department of Physics and Astronomy, Uppsala University, Uppsala, SWEDEN,* [6]*Department of Neurology, Philipps University Marburg, Marburg, GERMANY,* [7]*Nuclear Medicine Department, Philipps University, Marburg, GERMANY,* [8]*Department of Nuclear Medicine, Technical University of Munich, Munich, GERMANY,* [9]*Neurobiobank Munich, Ludwig-Maximilians-University of Munich, Munich, GERMANY,* [10]*Nuclear Medicine Department, Philipps University Marburg, Marburg, GERMANY.*

Aim/Introduction: Development of a specific ^{18}F-labeled PET tracer for α-synucleinopathies imaging, based on diarylbisthiazole (DABTA), with high binding affinity to α-synuclein fibrils (α-syn), excellent selectivity over β-amyloid and tau fibrils and a suitable brain uptake kinetic. As an α-synuclein PET tracer, can specially monitor disease progression and evalute potetial disease modifying therapies for PD and DLB. ***Materials and Methods:*** We apply in silico, molecular dynamics and quantum/molecular mechanics approaches to design DABTAs with excellent binding properties and a favorable pharmacokinetics (PK). The precursors and ^{18}F-labeled lead DABTAs, with high affinity to α-syn with excellent selectivity and PK, are synthesized and used for brain uptake kinetic and PET/CT in a group of 12 weeks post intrastriatal injection of preparation of human aSYN preformed fibrils (PFF) mice study. The leads with appropriate PK and in vivo stability were further studied within our translational research, screened via experimental lipophilicity and assays, plasma stability, biodistribution, in vivo metabolite analyses and postmortem autoradiography of human brain slices with α-Synucleinopathies. ***Results:*** Autoradiography of three promising DABTAs (with K_i <3 nM and >>100 folds selectivity) show high density binding to α-Synucleinopathies in regions of PD, DLB and MSA postmortem brains then confirmed by IHC. The most promising tracer [^{18}F]F5 with excellent binding properties (K_i ≤1 nM), logD 2.6, based on the biodistribution results in healthy mice showed initial brain uptakes of up to 7 %ID/g and with fast washout from brain at 120 mins p.i. down to 0.6 %ID/g. It shows an excellent plasma and brain stability. The PET/CT and kinetic modelling results of the PFF mice show elevated tracer retention where α-synuclein aggregates are in left brain hemisphere including striatum and amygdala but not in WT mice which fit to to the immunohistochemical results showing abundant α-Synucleinopathies. ***Conclusion:*** The in silico modeling helps rational design of the tracers with desired properties. The promising in vitro and in vivo results encourage us to further study the tracer by in vivo imaging nonhuman primate and translation to first in human investigation. [^{18}F]F5 is a groundbreaking tool to the highly desirable, but as yet unmet, medical need to detect and quantify the presence, severity, and regional distribution of α-syn and its clinical manifestations in individuals with α-synucleinopathies in vivo. ***References:*** This project was supported by ParkinsonFonds Deutschland.

OP-563

In vivo quantification of [^{11}C]BIO-1819578, a novel radioligand for O-GlcNAcase, in non-human primates using Positron Emission Tomography

M. Bolin[1], *S. Nag*[1], *P. Datta*[1], *R. Arakawa*[1], *Y. Khani Meynaq*[1], *E. Lin*[2], *N. Genung*[2], *H. Hering*[2], *K. Guckian*[2], *L. Martarello*[2], *M. Kaliszczak*[2], *L. Farde*[1], *P. Stenkrona*[1], *C. Halldin*[1], *A. Forsberg Morén*[1];
[1]*Centre for Psychiatry Research, Department of Clinical Neuroscience, Karolinska Institutet, & Stockholm Health Care Services, Region Stockholm, Stockholm, SWEDEN,* [2]*BIOGEN MA Inc., 225 Binney St., Cambridge, MA, UNITED STATES OF AMERICA.*

Aim/Introduction: The novel radioligand [^{11}C]BIO-1819578 has been labelled from [^{11}C]CO and developed to study how drugs targeting O-GlcNAcase (OGA) interact with the enzyme in the CNS. The aim of the present study was to further validate [^{11}C]BIO-1819578 binding to OGA in the non-human primate brain. For that purpose, kinetic compartment analyses (1TCM and 2TCM) and a graphical analysis (MA1Logan) were evaluated using a radio-metabolite corrected arterial input function. The total volume of distribution (V_T) was the outcome estimate and used for comparisons between the models. ***Materials and Methods:*** Three cynomolgus monkeys were examined a total of seven times using a HRRT PET system (Siemens Medical Solutions). PET data were collected for 93 minutes immediately after injection of [^{11}C]BIO-1819578 (83.6±5.3 MBq, MA: 18.1±6.3 GBq/μmol); One pre-treatment scan was perform with a mass dose of the selective OGA inhibitor Thiamet-G. Arterial blood was measured continuously for the first 3 minutes followed with discrete samples at several time points. The fraction of unchanged radioligand in plasma was determined from HPLC analysis and used to produce the metabolite corrected input function. The outcome measure of the kinetic and graphical analyses was V_T in hippocampus, frontal cortex, putamen, occipital cortex, and cerebellum. To guide method selection in future studies with [^{11}C]BIO-1819578, the second-order corrected Akaike Information Criterium (AICc) was calculated for all quantitative approaches. ***Results:*** The regional time activity curves were overall better described by the two-tissue compartment model (2TCM) in comparison with the one-tissue compartment model (1TCM), (mean AICc for 2TCM ~ 47.6±29.3 and 1TCM ~ 52.3±34.2). V_Ts of OGA binding at baseline conditions obtained by 2TCM were (Hippocampus V_T ~ 34 mL/cm^3, Frontal Cortex V_T ~ 30 mL/cm^3, Putamen V_T ~ 28 mL/cm^3, Occipital Cortex V_T ~ 18 mL/cm^3 and Cerebellum V_T ~ 16 mL/cm^3). The V_T values obtained by the graphical method were a few percent lower in comparison with the estimates from 2TCM. Pre-treatment with Thiamet-G indicated a uniform reduction of uptake across the brain and a mean V_T decrease of 89 %. ***Conclusion:*** The regional TACs could be described by the 2TCM which performed better than the 1TCM. The V_Ts were similar for the kinetic and graphical approaches. Pre-treatment data indicates ~ 90 % specific binding of [^{11}C]BIO-1819578 to OGA. Furthermore, no region appeared to be devoid of specific binding and hence future studies with [^{11}C]BIO-1819578 will require an arterial plasma input function for quantification.

1205

Tuesday, September 12, 2023, 8:00 AM - 9:30 AM
Hall B

Cutting Edge Science Track - TROP Session: Total Body PET Methods

OP-564

Application of the long axial field-of-view PET/CT with direct and indirect Patlak parametric imaging

L. Pan, *C. Sachpekidis, A. Dimitrakopoulou-Strauss;*
German Cancer Research Center, Heidelberg, GERMANY.

Aim/Introduction: Patlak imaging by ^{18}F-FDG PET/CT is an important parametric imaging tool of disease diagnostics. The recent introduction and clinical application of long axial field-of-view (LAFOV) PET/CT scanners has yielded very promising results regarding image quality and sensitivity in oncological patients. We, herein, aim to evaluate whether Patlak imaging is feasible in a new LAFOV Biograph Vision 600 PET/CT (Siemens Healthcare) system and whether it improves lesion detectability as compared with the 55-60-min SUV images. ***Materials and Methods:*** 37 oncological patients (n= 23 melanoma, n= 7 lung cancer, n= 5 sarcoma, n= 1 lymphoma, n= 1 urothelial carcinoma) were enrolled in the study. All patients underwent PET/CT from the skull vertex to the upper leg in one bed position (each 60-min acquisition in list mode, field-of-view 106 cm) after i.v. injection of 2.0 MBq/kg ^{18}F-FDG. Three sets of images were compared: direct Patlak k_i images from Siemens e7-tools, indirect Patlak k_i images from PMod software, as wells as static 55-60-min SUV images. Three sets of images were reviewed visually (qualitatively) by the reading physicians, and 260 individual tumor lesions were quantitatively analyzed using the target-to-background (TBR) metrics. ***Results:*** Concerning visual analysis, no significant differences were observed between the three applied imaging approaches (direct Patlak k_i, indirect Patlak k_i, static SUV images) regarding both number of pathologic scans and number of lesions. Quantitatively, direct Patlak k_i TBR was significantly higher than SUV TBR in 255/260 lesions, and indirect Patlak k_i TBR was significantly higher than SUV TBR in 259/260 lesions. Besides, indirect Patlak k_i TBR was significantly higher than direct Patlak k_i TBR in 179/260 lesions. All three set TBR are significantly different to each other according to Wilcoxon signed-rank test. ***Conclusion:*** Dynamic FDG PET/CT is feasible with the new LAFOV PET/CT scanner and produces Patlak k_i images of good visual quality and better lesion contrast than SUV images regardless of the applied Patlak method (direct or indirect). In addition, indirect Patlak k_i images are relatively better than direct Patlak k_i image in terms of lesion contrast.

OP-565

Kinetic modeling and parametric imaging of 18F-PSMA-11: an evaluation based on total-body dynamic PET scan

H. Yuan, *L. Jiang;*
Guangdong Provincial People's Hospital, Guangzhou, CHINA.

Aim/Introduction: Despite the increasing clinical utilization of 18F-PSMA-11, the in vivo visualization of its kinetic feature in humans remains lacking, and hence the normal in vivo distribution of 18F-PSMA-11 remains unclear. With the recent advancement of long axial FOV total-body PET equipment, the whole-body dynamic scan enabled the visualization and quantification of radiotracer kinetics . Hence, this study aimed to evaluate the in vivo kinetic features of 18F-PSMA-11 in healthy volunteers and visualize these features using parametric imaging based on the total-body dynamic PET scan. ***Materials and Methods:*** A total of 8 healthy volunteers (7 males; 1 female) underwent total-bodyPET/CT imaging at 1 h and 2 h post-injection (p.i.) of 18F-PSMA-11, of which 7subjects underwent total-body dynamic PET scans lasting 30 min. Two-tissuecompartments (2TC) and Patlak models were fitted based on the voxel-based time activity curves (TACs), with the parametric images generated subsequently.Additionally, semi-automated segmentation of multiple organs was performed in the dynamic images to measure the SUVmean at different time points and in theparametric images to estimate the mean value of the kinetic parameters of theseorgans. ***Results:*** 18F-PSMA-11 was rapidly cleared from blood circulation and predominantly-excreted through the urinary system. High and rapid radiotracer accumulation was observed in the liver, spleen, lacrimal glands, and salivary glands, whereas gradual accumulation was observed in the skeleton. Net influx (Ki) values generated using Patlak models showed a good correlation with Ki values of 2TC models ($r=0.858$, $P<0.05$). However, the 2TC parametric images might suffer from estimation errors from moving artifacts (e.g., lungs) and variations of blood supply (e.g., liver). A scanning time point of 30-35 min p.i. was then suggested for decreased abdominal organ uptake and controlled skeletal background of the radiotracer. ***Conclusion:*** Patlak model-based Ki measurement showed good consistency with, thusis recommended over 2TC model-based Ki calculation on dynamic 18F-PSMA cans for substantially quicker calculation and less susceptibility to errors. Based on the dynamic imaging analysis, a shorter uptake time (30-35min) might be preferred for a better balance of background radioactive accumulation within the visceral organs vs. the bones.

OP-566

Multi-tracer image-derived input function validation using a long axial field of view PET scanner

X. Palard-Novello[1,2], *D. Visser*[2], *N. Tolboom*[3], *C. Smith*[2], *G. Zwezerijnen*[2], *E. van der Giessen*[2], *M. den Hollander*[2], *F. Barkhof*[2], *B. Windhorst*[2], *B. N. M. van Berckel*[2], *R. Boellaard*[2], *M. Yacub*[2];
[1]*Centre Eugène Marquis, Rennes, FRANCE,* [2]*Amsterdam Universitair Medische Centra, Amsterdam, NETHERLANDS,*
[3]*Universitair Medisch Centrum Utrecht, Utrecht, NETHERLANDS.*

Aim/Introduction: Highly sensitive large axial field of view (LAFOV) PET scanners could avoid the need of an arterially measured input function by using an image-derived input function (IDIF) for kinetic modelling of dynamic PET studies. The aim of this study is to validate the use of IDIF for two different tracers. ***Materials and Methods:*** Four dynamic 70 minutes 18F-FDG scans and 10 dynamic 60 minutes [18F]DPA-714 scans were acquired on the Quadra PET/CT scanner. For [18F] DPA-714, continuous online arterial and manual arterial blood samples were acquired. Venous blood samples were available for the [18F]FDG study. PET images were reconstructed using a large variability of different reconstruction settings (number of iterations, matrix size, maximum ring difference, gaussian filter and scatter correction) with EARL2 as reference. IDIFs were taken from ascending aorta (AA), descending aorta (DA), and left ventricular cavity (LV) locations and calibrated using blood samples. Patlak linearization was performed to extract K_i for [18F] FDG in striatum and Logan linearization was performed to extract V_T for [18F]DPA714 in frontal region. To assess only the effects

of various IDIFs, frontal and striatum time-activity-curves were extracted from EARL2 reconstruction. ***Results:*** For [18F]FDG, the results showed a low variability of the calibration factors (CF) for the different IDIFs (AA_EARL2_IDIF: mean CF = 0.86 with standard deviation (SD) = 0.04). Compared to striatum K_i extracted using AA_EARL 2 IDIF as reference, striatum K_i mean differences were <10% using other locations or reconstruction settings to derive IDIFs. For [18F]DPA714, the results showed high variability of the CF for the different IDIFs (AA_EARL2_IDIF: mean CF = 0.87 with SD = 0.13). The CF improved to 1.0 using more iterations but the variability also increased (AA_10iterations_5subsets_nofilter_IDIF: mean CF = 0.99 with SD = 0.21). Compared to frontal V_T extracted using continuous sampler input as reference, frontal V_T mean differences were <10% for the other IDIFs, except for DA_EARL2_IDIF (frontal V_T mean relative difference = +11% with SD = 6%) and LV_EARL2_IDIF (frontal V_T mean relative difference = +16% with SD = 11%). ***Conclusion:*** EARL2-based IDIF from LAFOV PET scanner can replace venous samples for [18F]FDG. For [18F]DPA714, it can replace the use of continuous arterial sampling but may only be used in combination with recalibration using several manual arterial blood samples. So the accuracy and precision of IDIFs obtained with the LAFOV PET/CT system are tracer dependent and depend also on reconstruction settings and locations.

OP-567

The ENHANCE-PET Framework: An initiative to engage the imaging community in Advancements in Total-Body PET Analysis

L. Shiyam Sundar[1], *B. A. Spencer*[2], *J. Callahan*[3], *S. R. Cherry*[2], *R. D. Badawi*[2], *I. Buvat*[4], *D. Lewis*[5], *D. Ferrara*[1], *S. Gutschmayer*[1], *R. Hicks*[3], *M. Lassen*[6], *J. Mannheim*[7], *O. Muzik*[8], *M. Pires*[1], *J. Yu*[1], *T. Beyer*[1];
[1]*Medical University of Vienna, Vienna, AUSTRIA,* [2]*University of California-Davis, Davis, CA, UNITED STATES OF AMERICA,* [3]*Melbourne Theranostics Innovation Center, Melbourne, AUSTRALIA,* [4]*Institut Curie, Paris, FRANCE,* [5]*CRUK Glasgow, Glasgow, UNITED KINGDOM,* [6]*Rigshospitalet Copenhagen, Copenhagen, DENMARK,* [7]*Uniklinikum Tuebingen, Tuebingen, GERMANY,* [8]*Wayne State University, Detroit, MI, UNITED STATES OF AMERICA.*

Aim/Introduction: With its wide field-of-view coverage and simultaneous tracking of physiological activities, total-Body PET (TB-PET) is revolutionising nuclear medicine and offers potential for novel insights into human physiology and disease processes. To effectively analyze large TB-PET datasets and foster collaboration among TB-PET stakeholders, we introduce the ENHANCE-PET framework. This approach supports the open sharing of tools, datasets, and experiences through the user-friendly, centralized enhance.pet web platform. The bespoke tools though aimed at TB-PET, works seamlessly for regular whole-body (WB) PET images as well. ***Materials and Methods:*** In a previous iteration of this framework, presented at EANM 2022, the platform featured open-access tools for automated image segmentation (MOOSE), motion correction (FALCON), and inter-organ connectivity assessment (PIGEON). Ongoing efforts and community collaboration have since resulted in four additional tools: voxelwise metabolic aberration mapping (OCELOT), a PET-CT image alignment tool for dual-modality, static and dynamic PET/CT scans (ORCA), a tool to generate non-kinetic modeling-based multi-parametric images from short-duration dynamic PET scans (STING-RAY), and a tool for evaluating voxel-/organ-wise metabolic changes during health-to-disease transitions (WOLF). To evaluate these tools, we analyzed several datasets from different vendors: For ORCA, we used 19 WB FDG PET/CT datasets; for STING-RAY, we analyzed 10 TB PSMA PET/CT datasets; for OCELOT, we examined 15 WB FDG PET/CT datasets; and for WOLF, we assessed 10 longitudinal WB FDG PET/CT datasets. The integration of these diverse datasets demonstrates the versatility and practicality of the ENHANCE-PET framework across various contexts. ***Results:*** We showcased the feasibility of these newly developed tools by applying them to various TB/WB-PET datasets from a range of clinical situations as proof-of-concept. OCELOT effectively identified voxelwise intensity and morphometric changes in a lung cancer patient with cachexia. ORCA improved the accuracy of image registration, while STING-RAY successfully produced informative non-kinetic modeling-based multi-parametric images from short-duration dynamic scans. WOLF proved to be useful in monitoring metabolic changes over time, thereby enhancing our understanding of disease progression and treatment response. ***Conclusion:*** The ENHANCE-PET framework, strengthened by contributions from a global community, offers an extensive set of tools for thorough TB/WB-PET analysis. The enhance.pet platform encourages collaboration and promotes open sharing, ultimately contributing to a better understanding of human physiology and disease mechanisms. We are excited to announce the launch of the enhance.pet community website at the EANM conference, fostering continued innovation and cooperation within the nuclear medicine community.

OP-568

Walk-Through Flat-Panel Total Body PET: System Design and Comparison of Body Motion with a standard PET-CT

F. Muller[1], *J. Maebe*[1], *N. Withofs*[2], *S. Vandenberghe*[1];
[1]*Medical Image and Signal Processing, Faculty of Engineering and Architecture, Ghent University, Ghent, BELGIUM,* [2]*Division of Nuclear Medicine and Oncological Imaging, Department of Medical Physics, CHU of Liege, Quartier Hôpital, Liège, BELGIUM.*

Aim/Introduction: Current Total Body PET (TB-PET) scanners come at high costs which limits their acquisition in standard nuclear medicine departments. TB-PET systems have become so sensitive that 30-second torso acquisitions seem feasible, practical patient throughput is however limited by patient positioning. We describe the design of a new dual flat-panel Walk-Through (WT) TB-PET scanner for patient imaging in upright position; enabling fast and efficient patient throughput at lower component cost. The extent of motion, potentially larger for standing patients, was tested in a mock-up of the WT-TB-PET and compared to motion of patients lying on a conventional PET-CT scanner bed. ***Materials and Methods:*** To define the dimensions of the WT-TB-PET, patients size (vertex-ischium length, shoulder width, patient depth) were measured from 40 PET-CT scans. For the motion tests, healthy volunteers (n=9) and patients (n=13) were asked to step into the WT-TB-PET mock-up and stand still between the two flat-panels for 30s (feasible acquisition time). A Microsoft Kinect camera tracked motion of infrared markers placed on subjects' shoulders, head, chest and abdomen. After 30s normal breathing test, we investigated whether breath-hold or leaning back against the flat-panel can feasibly be associated with reduced patient movement. Motion results were compared with those of patients lying on a conventional Biograph Vision PET-CT (CHU Liège). ***Results:*** The WT-TB-PET system consists of two flat-panel detectors that are 70x106cm^2 in size and spaced 50cm apart, leading to a WT-TB-PET footprint (2-4m^2) much smaller than current PET-CTs (±35m^2). Motion of patients standing in the WT-TB-PET was larger (factor 1.5-3) compared with patients lying in the conventional PET-CT. When patients stood upright

in the WT-TB-PET for 30s, most movement was observed along the y-axis (front-back) which was ~2x the motion ranges seen along the x-axis (right-left); with head motion the largest (y-axis: 5.7mm). Motion was reduced by factor 1.7±0.2mm when patients held their breath; breath-hold was not possible for 1 out of 4 patients. When subjects were leaning back against a flat-panel while standing inside the WT-TB-PET, body motion was reduced to motion ranges comparable to those recorded on conventional PET-CT (in mm: $head_{WT\text{-}TB\text{-}PET(y)}$=0.52, $head_{PET\text{-}CT(y)}$=0.49, $head_{WT\text{-}TB\text{-}PET(x)}$=1.07, $head_{PET\text{-}CT(x)}$=0.52, $chest_{WT\text{-}TB\text{-}PET(y)}$=0.63, $chest_{PET\text{-}CT(y)}$=0.85, $chest_{WT\text{-}TB\text{-}PET(x)}$=0.36, $chest_{PET\text{-}CT(x)}$=0.43). ***Conclusion:*** A new TB-PET scanner was proposed with patients standing upright between two flat-panels. Motion tracking studies with the WT-TB-PET mock-up showed that body motion is limited (i.e., close to the expected spatial resolution of 2 mm) for a design configuration with leaning backwards.

OP-569

TOF Data Compression Strategies for 3D Fourier-Based Analytical Reconstruction of Long Axial Field of View (LAFOV) scanners data

V. Panin;
Siemens Medical Solutions United States Of America, Knoxville, TN, UNITED STATES OF AMERICA.

Aim/Introduction: The Direct Inversion Fourier Transform Time-of-Flight (3D DIFTOF) algorithm is a tool for resolution and unbiased image assessment. However, analytical reconstruction on LAFOV scanners faces challenges due to suboptimal signal-to-noise ratio (SNR) resulting from poor quality oblique data, which are susceptible to noise amplification during attenuation correction. This is in contrast to iterative methods, which can statistically weight these data to improve SNR. This study aims to investigate different TOF data compression methods for LAFOV scanner data to improve the SNR while maintaining axial resolution in 3D DIFTOF reconstructed images. ***Materials and Methods:*** A long 20 cm diameter cylinder phantom that completely covered the axial scanner FOV (1 m) and was filled with F-18 was scanned on a Biograph Vision Quadra scanner (Siemens Healthineers) using two different TOF data compression schemes. The first, standard, method used uniform TOF axial line-of-responses (LORs) spanning, while the second added an additional axial compression on the most oblique tilts (47^0-52^0), combining them into one tilt. The reconstructed images were also evaluated using the NEMA resolution assessment data, which included a Na-22 point source located at various positions. ***Results:*** The standard data compression method led to a 20% decrease in SNR in the axial central part of the image using all data, compared to an "optimal" Maximum Ring Difference (MRD) of about 40^0. However, the modified compression method reversed this trend, with the axial central part of the image showing a marginal increase in SNR. The axial resolution was not practically affected by additional compression of the most oblique tilts. ***Conclusion:*** A more extensive axial TOF compression scheme should be used to accurately reflect better SNR when more oblique data are being used. This is consistent with the idea of TOF down sampling, where worse axial resolution data should be compressed more to improve computational efficiency.

OP-570

Comparison of the standard and ultra-high sensitivity modes on a long axial FOV PET/CT system

M. Roya, *J. van Sluis, J. H. van Snick, A. W. J. M. Glaudemans, C. Tsoumpas;*
University Medical Center Groningen, Groningen, NETHERLANDS.

Aim/Introduction: Recently, long axial field of view (LAFOV) PET/CT systems have been introduced. Compared to short axial field of view systems, the image quality is superior due to the increased sensitivity in photon detection. This increase may allow very short scan duration in order to minimise motion artifacts[1]. This work aims to study the feasibility of ultra-fast protocols compared to routine scans. ***Materials and Methods:*** 6 patients referred for routine PET/CT were asked to participate in this study. The formal need for a METc approval was waived. The acquisition protocol was completed on a 106-cm long LAFOV in listmode. The data was used to reconstruct 15 and 30-second images with the full maximum ring distance (MRD322) and the routine 2-minute protocols with the standard setting (MRD85) using the e7tools. The vendor-recommended reconstruction settings were used, which are optimised for clinical diagnosis. The noise levels in healthy tissue were compared between the ultra-fast and routine protocols using the coefficient of variation (COV). The liver, spleen, abdominal aorta (blood pool) and bone marrow (spinal segment L4) were chosen as healthy tissue due to their proximity to the centre of the axial field of view, where the sensitivity profile is the highest[2]. ***Results:*** The mean COV for the 2-minute scan was .17. The mean COV for 30s (MRD322) scan was .25. The mean COV for 15s (MRD322) was .34. The COV was found to be significantly different for all healthy tissue between the three reconstruction durations ($p < 0.008$). ***Conclusion:*** This study suggests that with full maximum ring distance (MRD322) 15 and 30 seconds scans do not match the noise level of routine 2-minute acquisitions. However, the effect of ultra-short scan durations with full MRD on the standardised uptake in healthy tissue and lesions remains to be further explored in ongoing research. ***References:*** 1. Slart R, Tsoumpas C, Glaudemans A, Noordzij W, Willemsen ATM, Borra RJH, et al. Long axial field of view PET scanners: a road map to implementation and new possibilities. Eur J Nucl Med Mol Imaging. 2021;48:4236-45. doi:10.1007/s00259-021-05461-6. 2. Prenosil GA, Sari H, Furstner M, Afshar-Oromieh A, Shi K, Rominger A, et al. Performance Characteristics of the Biograph Vision Quadra PET/CT System with a Long Axial Field of View Using the NEMA NU 2-2018 Standard. J Nucl Med. 2022;63:476-84. doi:10.2967/jnumed.121.261972.

OP-571

Sub-minute acquisition with deep-learning reconstruction in the diagnosis of colorectal cancers using total-body 18F-FDG PET/CT

E. Liu, *Z. Lyu, L. Jiang;*
Guangdong Provincial People's Hospital, Guangdong Academy of Medical Sciences, Guangzhou, CHINA.

Aim/Introduction: This study aimed to retrospectively evaluate the feasibility of total-body ^{18}F-FDG PET/CT ultrafast acquisition combined with deep-learning reconstruction (DLR) in the diagnosis of colorectal cancers (CRCs). ***Materials and Methods:*** The clinical and preoperative imaging data of patients with CRCs were collected. All patients underwent a 300-second list-mode total-body ^{18}F-FDG PET/CT. The entire dataset was divided into groups of durations of 10, 20, 30, 60, and 120-second. PET images were reconstructed using ordered subset expectation

maximisation (OSEM) and deep-learning reconstruction (DLR). Considering the 300-second OSEM reconstruction image as a standard, a 5-point Likert scale and semi-quantitative analysis were used to compare the effects of OSEM and DLR on image quality, detection rate, and uptake value of primary and liver metastases of CRCs at different acquisition durations. ***Results:*** All 34 recruited patients with CRCs had single colorectal lesions, and the diagnosis was verified pathologically. Of total patients, 11 had liver metastases, and 113 liver metastases were detected. The 10-second dataset cannot be evaluated because of high noise, whether it is reconstructed by OSEM or HYPER DLR. The signal-to-noise ratio (SNR) of the liver and mediastinal blood pool of 10, 20, 30, and 60-second acquisition duration images reconstructed with the same reconstruction parameters was lower than that of the 300-second OSEM reconstruction images ($P<0.01$). DLR significantly improved the SNR and visual image quality score compared to OSEM reconstruction ($P<0.01$). No significant difference was observed in the SNR of the liver and mediastinal blood pool, SUVmax and TBR of CRCs and liver metastases, and the number of detectable liver metastases between the 20 and 30-second DLR and 300-second OSEM reconstruction images ($P>0.05$). ***Conclusion:*** DLR can significantly improve the image quality of total-body ^{18}F-FDG PET/CT ultrafast acquisition. Notably, without affecting the diagnosis of CRCs and liver metastases, DLR allowed decreasing the acquisition time of total-body PET images to 20-second. Compared with the standard acquisition, the 20-second and 30-second DLR images have the same accuracy in identifying and quantitatively evaluating CRCs and liver metastases.

OP-572

Diagnostic image quality and quantitative PET parameters of low-dose ^{18}F-FDG-PET/CT in a total-body PET/CT scanner: How low can we go?

E. Calderón[1], *F. P. Schmidt*[1,2], *W. Lan*[1], *H. Dittmann*[1], *C. la Fougère*[1,3], *L. S. Kiefer*[1];
[1]*Department of Nuclear Medicine and Clinical Molecular Imaging, University Hospital Tübingen, Tübingen, GERMANY,* [2]*Werner Siemens Imaging Center, Department of Preclinical Imaging and Radiopharmacy, Eberhard-Karls University Tübingen, Tübingen, GERMANY,* [3]*Cluster of Excellence iFIT (EXC 2180) "Image Guided and Functionally Instructed Tumor Therapies", University of Tübingen, Tübingen, GERMANY.*

Aim/Introduction: Total-body PET/CTs with a long axial field-of-view have a higher sensitivity and allow for a reduction of the injected activity while maintaining diagnostic image quality and quantitative PET parameters. Lower doses of injected activity reduce radiation exposure, which is especially beneficial for oncological patients routinely exposed during their radiological follow-up. This study aims to evaluate the lowest activity limits of ^{18}F-FDG for standard clinical use in a total-body PET/CT. ***Materials and Methods:*** Twenty-two randomly selected oncological patients who underwent a clinically indicated ^{18}F-FDG-PET/CT in a total-body PET/CT scanner were included in this study. Standard 5 min scans were acquired with an injected dose of 3 MBq/kg and subsequently rebinned for lower frame durations to simulate doses of 0.5 MBq/kg, 0.25 MBq/kg, and 0.125 MBq/kg for acquisition times of 5 and 10 min, respectively. The impact of limited and maximum acceptance angle modes was assessed by performing reconstructions with the manufacturer's proprietary software. Whole-body images were analyzed by two nuclear medicine physicians in consensus read using a 5-Point Likert scale, evaluating overall image quality, lesion conspicuity, and image noise. Afterwards, eighty-two tumor lesions were randomly selected for further analysis. Thereby, standard uptake PET parameters SUV_{mean}, SUV_{max}, SUV_{peak}, total-lesion-glycolysis (TLG), and tumor-to-background ratio (TBR) were measured for each lesion and normalized for analysis. TBR was determined as the ratio of SUV_{max} to SUV_{mean} of the background (a 14 cm^3 spherical VOI in the right liver lobe). ***Results:*** Subjective image rating showed degradation of diagnostic image quality and increased noise starting at 0.25 MBq/kg (5 min). A lesion detection rate of 95% was recorded for 0.5 MBq/kg (5 min), corresponding to 0.25 MBq/kg (10 min), which considerably decreased with the further reduction of simulated injected activity. Lesion conspicuity was significantly influenced by the size of tumor lesions and their contrast to background. SUV_{max} and TBR increased by 24% and 29% for the lowest simulated injected activity compared to the original scan data at 3 MBq/kg. The maximum decrease of SUV_{mean}, SUV_{peak}, and TLG was recorded at 8%, 3%, and 8%, respectively (0.125 MBq/kg). ***Conclusion:*** This study indicates that the lowest activity dose for acquiring clinically diagnostic images in a total-body PET/CT is 1/12th of the standard injected activity using the maximum acceptance angle mode and an acquisition time of 10 minutes. Thereby, lesion detection was assured, and diagnostic image quality was maintained without any relevant deterioration of quantitative PET parameters.

1206

Tuesday, September 12, 2023, 8:00 AM - 9:30 AM
Hall C

Clinical Oncology Track - TROP Session: Gynaecological Malignancies

OP-573

Molecular imaging predicts response absence to T-DM1 in advanced HER2-positive breast cancer: final results from a prospective phase II ZEPHIR trial

M. Mileva[1], *E. G. de Vries*[2], *T. Guiot*[3], *Z. Wimana*[4], *A. Deleu*[1], *C. Schröder*[5,6], *Y. Lefebvre*[1], *M. Paesmans*[7], *S. Stroobants*[8], *M. Huizing*[9], *P. Aftimos*[10], *J. Tol*[11], *W. Van der Graaf*[12], *W. Oyen*[13,14,15], *D. Vugts*[16], *C. Menke-van der Houven van Oordt*[12], *A. Brouwers*[17], *M. Piccart-Gebhart*[10], *P. Flamen*[1], *G. Gebhart*[1];
[1]*Department of Nuclear Medicine, Institut Jules Bordet, Hôpital Universitaire de Bruxelles (H.U.B), Université Libre de Bruxelles (ULB), Brussels, BELGIUM,* [2]*Department of Medical Oncology, University of Groningen, University Medical Center Groningen, Groningen, NETHERLANDS,* [3]*Department of Medical Physics, Institut Jules Bordet, Hôpital Universitaire de Bruxelles (H.U.B), Université Libre de Bruxelles (ULB), Brussels, BELGIUM,* [4]*Department of Radiopharmacy, Institut Jules Bordet, Hôpital Universitaire de Bruxelles (H.U.B), Université Libre de Bruxelles (ULB), Brussels, BELGIUM,* [5]*Department of Medical Oncology, University of Groningen, University Medical Center Groningen, Groningen, NETHERLANDS,* [6]*Department of Medical Oncology, Antoni van Leeuwenhoek-NETHERLANDS Cancer Institute, Amsterdam, NETHERLANDS,* [7]*Data center, Institut Jules Bordet, Hôpital Universitaire de Bruxelles (H.U.B), Université Libre de Bruxelles (ULB), Brussels, BELGIUM,* [8]*Department of Nuclear Medicine, Antwerp University Hospital, Edegem, Antwerp, BELGIUM,* [9]*Department of Medical Oncology, Antwerp University Hospital, Edegem, Antwerp, BELGIUM,* [10]*Department of Medical Oncology, Institut Jules Bordet, Hôpital Universitaire de Bruxelles (H.U.B), Université Libre de Bruxelles (ULB), Brussels, BELGIUM,* [11]*Department of Internal Medicine, Jeroen Bosch Ziekenhuis,*

Den Bosch, NETHERLANDS, Den Bosch, NETHERLANDS, [12]Department of Medical Oncology, Amsterdam UMC location VUMC, Cancer Centre Amsterdam, Amsterdam, NETHERLANDS, [13]Humanitas Clinical and Research Center, Humanitas University, Milan, ITALY, [14]Department of Radiology and Nuclear Medicine, Rijnstate Hospital, Arnhem, NETHERLANDS, [15]Department of Radiology and Nuclear Medicine, Radboud University Medical Center, Nijmegen, NETHERLANDS, [16]Department of Radiology and Nuclear Medicine, Amsterdam UMC, Vrije Universiteit, Cancer Center Amsterdam, Amsterdam, NETHERLANDS, [17]Department of Nuclear Medicine and Molecular Imaging, University of Groningen, University Medical Center Groningen, Groningen, NETHERLANDS.

Aim/Introduction: Efficacy of the human epidermal growth factor receptor (HER)2-targeting trastuzumab emtansine (T-DM1) in breast cancer (BC) relies on HER2 status obtained on tissue samples. Heterogeneity in HER2 expression, however, generates interest in whole-body assessment using molecular imaging. Previously published interim results of a patient-based analysis demonstrated high negative predictive value (NPV) of zirconium-89 (^{89}Zr) trastuzumab (HER2)-PET/CT in identifying patients with metastatic BC who will not benefit from T-DM1 [1]. Here we present the final results of the study's primary objective, namely a lesion-based analysis to evaluate the role of HER2-PET/CT, early FDG-PET/CT response, and their combination in detecting lesions unlikely to respond to T-DM1. ***Materials and Methods:*** The ZEPHIR trial is an international, single-arm phase II trial, including patients with locally advanced or metastatic HER2-positive BC. Patients underwent HER2-PET/CT, FDG-PET/CT and diagnostic CT before T-DM1 initiation. Maximum 10 (5 per organ) unequivocally neoplastic lesions were selected as target lesions on baseline FDG-PET/CT. Based on ^{89}Zr-trastuzumab uptake, target lesions were visually classified as HER2-positive (visible/high uptake) or HER2-negative (background/close to background activity). A week before the second treatment cycle, early metabolic lesion response was assessed on FDG-PET/CT (≥15% SUVmax decrease from baseline). After three T-DM1 cycles, lesion response was assessed anatomically on CT (size decrease ≥30% from baseline) and metabolically on late FDG-PET/CT (≥30% SUVmax decrease from baseline). NPVs of HER2-PET/CT, early FDG-PET/CT response, and combination of both, were evaluated for their prediction of the lesion anatomic and late metabolic non-responses post three T-DM1 cycles. ***Results:*** Ninety patients were included, median prior treatment lines of 3. 83/90p received median of 12 T-DM1cycles (1-114). In 383 target lesions, 148 (39%) were HER2-negative. In the anatomically evaluable lesions (265/383), 93 (35%) were classified as HER2-negative. HER2-PET/CT correctly identified 75/93 HER2-negative lesions as anatomically non-responding with NPV of 81%. NPV of HER2-PET/CT for the lesion late metabolic response was 63%. Early FDG-PET/CT predicted lesion anatomic and late metabolic response with NPV of 81% and 69%, respectively. Combination of both imaging modalities predicted lesion anatomic and late metabolic response with NPV of 91% and 84%, respectively. ***Conclusion:*** Molecular imaging can assess HER2 heterogeneity in HER2-positive BC and can predict very early on lesions not responding to T-DM1, further improved by adding an early metabolic response assessment. Similar efforts should be displayed for improved tailoring of the highly active but also toxic new generations of antibody-drug conjugates. ***References:***

1. Gebhart G et al.Annals of Oncology27:619-624,2016

OP-574

First Clinical experience with^{68}Ga-Nitroimidazole imaging in cancer of the cervixuteri

K. Mokoala[1,2], *I. O. Lawal*[3,1], *L. C. Maserumule*[1,2], *K. N. Hlongwa*[4], *H. Ndlovu*[1], *J. D. Reed*[1], *J. Jeong*[5], *J. Mahapane*[1], *C. Davis*[1,2], *C. van de Wiele*[6], *A. Maes*[7], *M. Vorster*[8], *M. M. Sathekge*[1,2];
[1]*University of Pretoria, Pretoria, SOUTH AFRICA,* [2]*Nuclear Medicine Research Infrastructure (NuMeRI), Pretoria, SOUTH AFRICA,* [3]*Emory University, Atlanta, GA, UNITED STATES OF AMERICA,* [4]*University of Cape Town, Cape Town, SOUTH AFRICA,* [5]*Seoul National University College of Medicine, Seoul, KOREA, REPUBLIC OF,* [6]*Katholieke University Leuven, Leuven, BELGIUM,* [7]*University of Ghent, Ghent, BELGIUM,* [8]*University of Kwazulu Natal, Durban, SOUTH AFRICA.*

Aim/Introduction: Hypoxia in solid tumours is associated with increased tumour aggressiveness and resistance to chemoradiotherapy. Hypoxia in cervical cancer has been associated with a poor prognosis. Molecular markers and PET imaging methods have been investigated for assessing and mapping hypoxic lesions. Several ^{18}F-labelled and $^{60/64}$Cu tracers have been studied for imaging hypoxia in cervical cancer with variable yet encouraging results. Over the years ^{68}Ga labelled nitroimidazoles have been studied and have shown improved kinetics with improved tumour to background ratios. We present the first translational imaging of hypoxia PET in cervical cancer with ^{68}Ga-Nitroimidazole derivative and ^{18}F-FDG PET/CT. ***Materials and Methods:*** We prospectively recruited twenty women with histologically proven cervical cancer who underwent both ^{18}F-FDG and ^{68}Ga-Nitroimidazole PET/CT imaging. The ^{68}Ga-Nitroimidazole PET was performed at 30 and 60-minutes post tracer injection. Qualitative and semi-quantitative analyses were performed on both scans, with ^{68}Ga-Nitroimidazole scans being scored qualitatively from 0 - 3 and a score above 2 considered as positive. We also documented SUVmax and SUVmean of the primary lesions as well as tumour to muscle ratio (TMR), tumour to blood (TBR), metabolic tumour volume (MTV) and hypoxic tumour volume (HTV). ***Results:*** The mean age of the population was 44.65±11.43years. Twelve patients had uptake considered positive on ^{68}Ga-Nitroimidazole PET. The median SUVmax, SUVmean, MTV, TMR, TBR of the primary tumour on ^{18}F-FDG were 17.41, 6.78, 150.51cm^3, 28.50 and 9, respectively. The median SUVmax, SUVmean, HTV, TMR, TBR on ^{68}Ga-Nitromimidazole PET were 3.63, 1.49, 60.85cm^3, 10.50 and 3.27, respectively. The areas of ^{68}Ga-Nitroimidazole uptake in the primary lesion were smaller than the metabolic area on ^{18}F-FDG PET, with the hypoxic subvolume as a percentage of the MTV ranging from 2% - 98% (median 37%). ***Conclusion:*** Two-thirds of the patients demonstrated hypoxia on ^{68}Ga-Nitroimidazole PET imaging. ^{68}Ga-Nitroimidazole PET may play a complementary role in patients with a high index of suspicion for hypoxia.

OP-575

2-[^{18}F]FDG-PET/CT in the early prediction of histopathological response in breast carcinoma: results of the German multi-center Gepar-PET study

B. Krause[1], *W. Mohnike*[2], *S. Dresel*[3], *H. Rudolf*[4], *F. H. H. Müller*[5], *J. Farahati*[6], *H. Palmedo*[7], *S. M. Schwarzenböck*[1], *M. Untch*[8], *J. Kurth*[1], *K. Mohnike*[2];
[1]*Department of Nuclear Medicine, University Medical Center Rostock, Rostock, GERMANY,* [2]*Center for Nuclear Medicine, DTZ Berlin, Berlin, GERMANY,* [3]*Department of Nuclear Medicine, Helios Clinics Berlin-Buch, Berlin, GERMANY,* [4]*Institute for Biostatistics and Informatics in Medicine and Ageing Research, University Medical Center Rostock, Rostock, GERMANY,* [5]*Radiologie und Nuklearmedizin Ludwigshafen, Ludwigshafen, GERMANY,* [6]*Department of Nuclear Medicine, Ev. Krankenhaus BETHESDA zu Duisburg, Duisburg, GERMANY,* [7]*Institute of Nuclear Medicine and Radiology, Kaiserpassage, PET/CT Center Johanniter Hospital, Bonn, GERMANY,* [8]*Department of Gynecology and Obstetrics, Helios Clinics Berlin-Buch, Berlin, GERMANY.*

Aim/Introduction: To demonstrate the preoperative predictive value of 2-[F]FDG -PET/CT in reducing the rate of mastectomy in high-risk breast cancer patients undergoing neoadjuvant chemotherapy (CTx), in addition to conventional staging methods, as a primary endpoint. Sensitivity and specificity of a partial/complete PET/CT early response for predicting pathological complete response (pCR) at the end of CTx, among others, were analyzed as a secondary endpoint. ***Materials and Methods:*** 94 patients (median age 48.5; with triple neg., HER2-pos. or high-risk HR+/HER2) from the prospective GeparOcto (NCT02125344) study were recruited for the Gepar-PET substudy. Within the main study protocol, randomization and subsequent adaptation of the treatment protocol within the study arms took place depending on the receptor status. The patients included in the sub-study underwent FDG-PET/CT before neoadjuvant CTx (PET1) and 2 weeks after the start of therapy (PET2) to assess the early response to therapy. Following a further randomization, a sub group of patients received a 3rd PET/CT (PET3) after the completion of neoadjuvant CTx. ΔSUV_{max} and ΔSUV_{peak} were assessed to evaluate treatment response according to the primary endpoint using histopathology as the reference. The statistical evaluation included the determination of cut-off values by means of ROC analysis (max. Youden's Index) and subsequently the corresponding sensitivities and specificities. ***Results:*** 53 of 94 (56%) patients were histopathological responder and 41 (44%) were histopathologic non-responder. A threshold of 70% decrease in SUV_{peak} evaluation (PET2 - PET1) identified 25 of 53 responders. Histopathological responders were identified with a positive predictive value of 81%. ***Conclusion:*** The Gepar PET-study demonstrates that in patients with advanced breast cancer FDG PET/CT differentiates histopathologic responders from non-responders early in the course of neoadjuvant treatment. Thus, FDG-PET/CT may be helpful for improved patient management by reducing the rate of mastectomy in high-risk breast cancer patients.

OP-576

Evaluation of a Dual Integrin αvβ3 and Gastrin-Releasing Peptide Receptor Targeting PET tracer [^{68}Ga]Ga-RM26-RGD in Breast Cancer Patients

R. Wang[1,2,3], *X. Wen*[4], *P. Xu*[5], *X. Zhang*[4], *Z. Guo*[4], *Z. Zhu*[1,2,3], *X. Chen*[6,7,8], *J. Zhang*[6,7,8];
[1]*Peking Union Medical College Hospital, Chinese Academy of Medical Sciences, Peking Union Medical College, Beijing, CHINA,* [2]*State Key Laboratory of Complex Severe and Rare Diseases, Beijing, CHINA,* [3]*Beijing Key Laboratory of Molecular Targeted Diagnosis and Therapy in Nuclear Medicine, Beijing, CHINA,* [4]*State Key Laboratory of Molecular Vaccinology and Molecular Diagnostics & Center for Molecular Imaging and Translational Medicine, School of Public Health, Xiamen University, Xiamen, CHINA,* [5]*Institute of Clinical Pharmacy & Pharmacology, Jining First People's Hospital, Jining Medical University, Jining, CHINA,* [6]*Departments of Diagnostic Radiology, Yong Loo Lin School of Medicine, National University of Singapore, Singapore, SINGAPORE,* [7]*Nanomedicine Translational Research Program, NUS Center for Nanomedicine, Yong Loo Lin School of Medicine, National University of Singapore, Singapore, SINGAPORE,* [8]*Clinical Imaging Research Centre, Centre for Translational Medicine, Yong Loo Lin School of Medicine, National University of Singapore, Singapore, SINGAPORE.*

Aim/Introduction: Radiolabeled RM26 and RGD peptide analogs have been investigated for imaging gastrin releasing peptide receptor (GRPR) and integrin αvβ3 receptor expression in multiple types of tumors. In this study, we synthesized a novel RM26-RGD heterodimer, radiolabeled with [^{68}Ga]Ga and applied it for the first time in breast cancer patients to assess its clinical performance. ***Materials and Methods:*** RM26-RGD heterodimer was synthesized from GRPR antagonist RM26 and integrin αvβ3 antagonist RGD through conjugating with 1,4,7-triazacyclononanetriacetic acid (NOTA) and labeled with [^{68}Ga]Ga. The dual receptor binding affinity of [^{68}Ga]Ga-RM26-RGD was determined using cell uptake and competition binding assay. PET/CT imaging of [^{68}Ga]Ga-RM26-RGD was performed to identify the tumor targeting effect and pharmacokinetic properties. With institutional review board approval and informed consent, a total of 32 patients with breast cancer (24 patients with primary tumor confirmed by puncture pathology and 8 patients with suspected recurrence or metastasis) were recruited. 6 patients underwent 2-h dynamic acquisition of [^{68}Ga]Ga-RM26-RGD PET/CT for dosimetry estimation, and the other patients underwent [^{68}Ga]Ga-RM26-RGD PET/CT scan at 45 min after intravenous injection. ***Results:*** [^{68}Ga]Ga-RM26-RGD had GRPR and integrin αvβ3 dual receptor binding affinity in vitro and in vivo, which showed higher tumor uptake values and tumor/muscle ratios than [^{68}Ga]Ga-RM26 and [^{68}Ga]Ga-RGD in PC3 tumor model. In clinical applications, all patients tolerated the examination well and no significant adverse event was reported in correlation with the study in any of the patients. The total body absorbed dose and the effective dose of [^{68}Ga]Ga-RM26-RGD were 1.00E-02 ± 1.20E-03 and 3.25E-02 ± 7.94E-03 mSv/MBq, respectively. [^{68}Ga]Ga-RM26-RGD detected a total of 23 primary lesions in all 25 lesions of 24 patients (92%). The mean SUVmax of primary tumor lesions on [^{68}Ga]Ga-RM26-RGD PET/CT was 4.6 ± 2.1. In a recurrent breast cancer patient with brain metastases who also underwent [^{18}F]-FDG PET/CT, [^{68}Ga]Ga-RM26-RGD showed a superior tumor/background ratio (15.5 vs. 1.1) than [^{18}F]-FDG PET/CT. ***Conclusion:*** [^{68}Ga]Ga-RM26-RGD was synthesized and radiolabeled with high radiochemical purity and stability. This pilot study indicates the safety and the first clinical application of [^{68}Ga]Ga-RM26-RGD in breast cancer. Further investigation of the detection performance of [^{68}Ga]Ga-RM26-RGD in metastatic lymph nodes and the differences between dual- and single- target tracers in larger scale clinical studies are warranted

OP-577

Tumor and metastatic lymph nodes metabolic activity on ^{18}F-FDG PET/CT to predict progression-free survival in locally advanced cervical cancer

J. Song*;*
Zhejiang Cancer Hospital, Hangzhou, CHINA.

Aim/Introduction: The present study investigated the predictive diseases progression value of preoperative fluorodeoxyglucose (FDG) positron emission tomography/computed tomography (PET/CT) in patients with local advanced cervical cancer (LACC). ***Materials and Methods:*** In total, 267 patients [median age 58 (range: 27-85) years old] with LACC underwent ^{18}F-FDG PET/CT prior to any treatment. The maximum standardized uptake values (SUV_{max}), metabolic tumor volume (MTV) and total lesion glycolysis (TLG) of the primary lesion and metastatic lymph nodes were measured on PET/CT and correlated with clinicopathological features and progression-free survival (PFS). ***Results:*** The median follow-up was 36.52 (range: 3.09-61.29) months. During the observation period, 80 (30.0%) patients exhibited disease progression. Univariate analysis showed that FIGO stage, concurrent chemoradiotherapy (CRT), serum level of carcinoembryonic antigen (CEA) and squamous cell carcinoma antigen (SCC-Ag), primary tumor MTV (pMTV) and TLG (pTLG), lymph nodes SUV_{max} (nSUV_{max}) and TLG (nTLG), and total

metabolic activity (sMTV, sTLG) were associated with PFS. $nSUV_{max}$ ≥5.29, CEA≥7.11ng/ml and deficiency of concurrent CRT were independent risk factor for PFS (P = 0.006, P=0.008, P=0.014). The 3-year PFS for patients with high $nSUV_{max}$ were 42.2% compared to 56.3% for low $nSUV_{max}$ values. ***Conclusion:*** Pretreatment cervical and lymph nodes metabolic parameters were associated with PFS in patients with LACC.

OP-578

HER2-specific Affibody Molecule [^{99m}Tc]Tc-ZHER2:41071: phase I clinical trial

V. Tolmachev[1], *O. Bragina*[2], *M. Larkina*[3], *A. Rybina*[2], *R. Zelchan*[2], *M. Oroujeni*[1], *A. Loftenius*[4], *A. Orlova*[5], *J. Sörensen*[6], *F. Frejd*[1], *V. Chernov*[2];
[1]*Department of Immunology, Genetics and Pathology (IGP), Uppsala University, Uppsala, SWEDEN,* [2]*Cancer Research Institute, Tomsk National Research Medical Center, Tomsk, RUSSIAN FEDERATION,* [3]*Research Centrum for Oncotheranostics, Research School of Chemistry and Applied Biomedical Sciences, Tomsk Polytechnic University, Tomsk, RUSSIAN FEDERATION,* [4]*Affibody AB, Solna, SWEDEN,* [5]*Department of Medicinal Chemistry, Uppsala University, Uppsala, SWEDEN,* [6]*Radiology and Nuclear Medicine, Department of Surgical Sciences, Uppsala University, Uppsala, SWEDEN.*

Aim/Introduction: Imaging of human epidermal growth factor receptor type 2 (HER2) expression in breast and gastric cancers may be instrumental for selection of patients responding to HER2-targeting therapy. Affibody molecules are small (58 amino acids) targeting proteins based on non-immunoglobulin scaffold, which provide highly sensitive molecular imaging at the day of injection. Contemporary SPECT/CT scanners provide good sensitivity and sufficient accuracy for quantitative measurements of activity in vivo. Implementation of a ^{99m}Tc-labelled Affibody molecule would increase availability of HER2 imaging for clinical community. Affibody molecule [^{99m}Tc]Tc-ZHER2:41071 (affinity 68 pM) was developed for SPECT/CT imaging of HER2 expression. The aim of this Phase I trial was an evaluation of safety, biodistribution and dosimetry of [^{99m}Tc]Tc-ZHER2:41071. ***Materials and Methods:*** A prospective, open-label, non-randomized Phase I diagnostic study was performed in patients with untreated primary breast cancer (ClinicalTrials.gov Identifier: NCT05203497). Thirty one patients were divided in three cohorts. Each cohort included at least five patients with high HER2 expression (immunohistochemistry (IHC) score 3+ or FISH-positive and IHC score 2+) and five patients with low HER2 expression in tumors (FISH negative and IHC score 2+ or lower). The injected protein mass was either 500, 1000, or 1500 µg ZHER2:41071 for cohort 1, 2 and 3, respectively. The injected activity was 451±71 MBq [^{99m}Tc]Tc-ZHER2:41071. Planar scintigraphy followed by SPECT/CT was performed after 2, 4, 6 and 24 h. Vital signs were monitored before, during and after the imaging. The imaging data were used for calculation of dosimetry using OLINDA/EXM 1.1 (female phantom). The uptake values were analyzed using one-way ANOVA (for comparison of different groups) or Mann-Whitney U test (comparison of tumor uptake). ***Results:*** Injections of [^{99m}Tc]Tc-ZHER2:41071 were not associated with any adverse events. The effective dose was 0.019±0.004 mSv/MBq. Injection of with 1000 µg enabled the best discrimination between HER2-positive and HER2-negative tumors. The uptake in tumors with high expression (SUVmax 16.9±7.6) was significantly (p<0.005, Mann-Whitney U test) higher than in tumors with low expression (SUVmax 3.6±1.4) in this case already 2 h post injection. The uptake of [^{99m}Tc]Tc-ZHER2:41071 in HER2-positive lymph node metastases was also significantly (p < 0.05) higher than in HER2-negative 2 h after injection of 1000 µg. ***Conclusion:*** Injections of [^{99m}Tc]Tc-ZHER2:41071 are safe. Dosimetry data permit multiple injections of [^{99m}Tc]Tc-ZHER2:41071. Injection of 1000 µg is ensures the best discrimination between tumors with high and low expression of HER2.

OP-579

HER2-targeting [^{68}Ga]Ga-ABY-025 PET Predicts Early Metabolic Response in Metastatic Breast Cancer

A. Alhuseinalkhudhur[1,2], *H. Lindman*[2], *P. Liss*[3], *T. Sundin*[4], *F. Y. Frejd*[2,5], *J. Hartman*[6,7], *V. Iyer*[1], *J. Feldwisch*[5], *M. Lubberink*[1,8], *C. Rönnlund*[6,7], *V. Tolmachev*[2], *I. Velikyan*[1], ***J. Sörensen***[1];
[1]*Nuclear Medicine and PET, Department of Surgical Sciences, Uppsala University, Uppsala, SWEDEN,* [2]*Department of Immunology, Genetics and Pathology, Uppsala University, Uppsala, SWEDEN,* [3]*Radiology, Department of Surgical Sciences, Uppsala University, Uppsala, SWEDEN,* [4]*Clinical Research and Development Unit, Uppsala University Hospital, Uppsala, SWEDEN,* [5]*Affibody AB, Solna, SWEDEN,* [6]*Department of Oncology-Pathology, Karolinska Institute, Stockholm, SWEDEN,* [7]*Department of Clinical Pathology and Cancer Diagnostics, Karolinska University Hospital, Stockholm, SWEDEN,* [8]*Medical Physics, Uppsala University Hospital, Uppsala, SWEDEN.*

Aim/Introduction: Imaging using human epidermal growth factor receptor 2 (HER2) binding tracer [^{68}Ga]Ga-ABY-025 was shown to reflect HER2 status determined by immunohistochemistry and in situ hybridization (ISH) in metastatic breast cancer (MBC). This single-center open-label Phase II study aimed to investigate how [^{68}Ga]Ga-ABY-025 uptake corresponds to biopsy results and early treatment response in both primary breast cancer (PBC) planned for neoadjuvant chemotherapy and MBC. ***Materials and Methods:*** Forty patients with known positive HER2 status were included, 19 PBC and 21 MBC (median three previous treatments). [^{68}Ga]Ga-ABY-025 PET/CT, [^{18}F]F-FDG PET/CT, and core needle biopsies from targeted lesions were performed at baseline. [^{18}F]F-FDG PET/CT was repeated after two cycles of therapy to calculate the directional change in tumor lesion glycolysis (delta-TLG). Largest lesions (up to five) were evaluated in all three scans per patient. Standardized uptake values (SUV) from [^{68}Ga]Ga-ABY-025 PET/CT were compared to biopsied HER2 status and delta-TLG by receiver operating characteristics (ROC) analyses. ***Results:*** Trial biopsies were HER2-positive in 31, negative in six, and borderline-positive in three patients. [^{68}Ga]Ga-ABY-025 PET SUVmax 6.0 cut-off predicted delta-TLG lower than -25% with 86% sensitivity and 67% specificity in soft tissue lesions (AUC 0.74 [95% CI, 0.67-0.82] [P = 0.01]). Compared to HER2 status, this cut-off resulted in clinically relevant discordant findings in 12 of 40 patients. Metabolic response (delta-TLG) was more pronounced in PBC (-71% [95% CI, -58% to -83%]) than MBC (-27% [95% CI, -16% to -38%]) (P < 0.0001), but [^{68}Ga]Ga-ABY025 SUVmax values were similar in both with a mean SUVmax of 9.8 (95% CI, 6.3-13.3) and 13.9 (95% CI, 10.5-17.2), respectively (P = 0.10). In multivariate analysis, global delta-TLG was positively associated with the number of previous treatments (P = 0.0004) and negatively with [^{68}Ga]Ga-ABY025 SUVmax (P = 0.018), but not with HER2 status (P = 0.09). ***Conclusion:*** [^{68}Ga]Ga-ABY025 PET predicted early metabolic response to HER2-targeted therapy in HER2-positive BC. Metabolic response was attenuated in recurrent disease. [^{68}Ga]Ga-ABY025 PET appears to provide an estimate of the HER2-receptor expression required to induce tumor metabolic remission by targeted therapies and might be useful as an adjunct diagnostic tool.

OP-580

^{68}Ga-NeoB PET for Glioma and Breast Cancer: First Results from a Prospective Observational Trial

D. Kersting[1], *L. Lazaridis*[2], *F. Barbato*[1], *S. Kebir*[2], *S. Kümmel*[3], *A. Welt*[4], *L. Umutlu*[5], *A. Milosevic*[5], *M. Nader*[1], *P. Fragoso Costa*[1], *T. Schmidt*[2], *C. Oster*[2], *C. Deuschl*[5], *U. Sure*[1], *M. Stuschke*[6], *C. Kleinschnitz*[2], *B. Scheffler*[7], *H. Hautzel*[1], *M. Schuler*[4], *M. Glas*[2], *W. P. Fendler*[1], *K. Herrmann*[1];
[1]*Department of Nuclear Medicine, University Hospital Essen, University of Duisburg-Essen, Essen, GERMANY,* [2]*Department of Neurology and Center for Translational Neuro- and Behavorial Sciences (C-TNBS), Division of Clinical Neurooncology, University Medicine Essen, University of Duisburg-Essen, Essen, GERMANY,* [3]*Breast Unit Kliniken Essen-Mitte, Essen, GERMANY,* [4]*Department of Medical Oncology, University Hospital Essen, University of Duisburg-Essen, Essen, GERMANY,* [5]*Institute of Diagnostic, Interventional Radiology and Neuroradiology, University Hospital Essen, University of Duisburg-Essen, Essen, GERMANY,* [6]*Department of Radiotherapy, University Hospital Essen, University of Duisburg-Essen, Essen, GERMANY,* [7]*DKFZ-Division Translational Neurooncology at the West German Cancer Center (WTZ), DKTK Partner Site, University Medicine Essen, University Duisburg-Essen, Essen, GERMANY.*

Aim/Introduction: The ^{68}Ga-labelled gastrin-releasing peptide receptor (GRPR) antagonist NeoB is a novel PET tracer for imaging tumors with high target expression. Here we aim to assess ^{68}Ga-NeoB-uptake in glioma and breast cancer patients. ***Materials and Methods:*** Eligible patients with glioma or breast cancer were offered clinical PET and subsequently enrolled in a prospective observational trial. PET data were acquired 81 min (mean) after injection of 95 MBq (mean) of ^{68}Ga-NeoB. In glioma, lesion SUV_{max} values were determined and compared among distinct entities according to the recently revised WHO Classification. In breast cancer, NeoB-uptake (NeoB-positivity defined as visually markedly higher uptake than local background) was reported in five regions ("breast", "lymph nodes", "liver", "bone", "other"). Only patients/regions with at least one clinically verified tumor lesion (by either histopathology, CT/MRI/PET, or tumor board) were included in a patient-/region-based analysis. Mean SUV_{max} values from all NeoB-positive regions were calculated per breast cancer patient for global assessment of NeoB-uptake. ***Results:*** We investigated n=24 glioma patients (n=16 diagnosed with glioblastoma, n=6 with IDH-mutant astrocytoma, n=2 with IDH-mutant oligodendroglioma). Mean SUV_{max} was 1.1 (range: 0.3-2.4) among all, 0.7 (0.3-1.9) among non-glioblastoma, and 1.3 (0.4-2.4) among glioblastoma patients. Highest SUV_{max} values were measured in glioblastoma patients with histopathological relapse confirmation. In n=11 glioblastoma patients with relapse-suspicious MRI at NeoB PET examination, mean SUV_{max} was 1.4 (0.6-2.4); n=7/11 (63.6%) of these patients underwent FET PET examination within two weeks with FET showing higher uptake (mean SUV_{max}: 2.2 versus 1.6; range: 1.2-3.5 versus 0.7-2.4). We investigated n=20 breast cancer patients with clinically verified tumor in at least one region (n=8 at initial staging, n=12 with advanced disease), n=14/20 (70%) were NeoB-positive. In a patient-based analysis regarding hormone receptor status, n=12/14 patients (85.7%) with estrogen receptor-positive/HER2-negative breast cancer (ER+/HER2-) and n=2/6 patients (33.3%) with other hormone receptor status were NeoB-positive. In NeoB-positive ER+/HER2- patients, mean SUV_{max} was 12.3 (4.1-25.9) and n=7/12 (58.3%) patients showed high (mean $SUV_{max} \geq 10$), n=4/12 (33.3%) intermediate ($10 >$ mean $SUV_{max} \geq 5$), and n=1/12 (8.3%) low ($SUV_{max} < 5$) global NeoB-uptake. In the region-based analysis, n=20/26 (76.9%) of regions in ER+/HER2- patients were NeoB-positive (mean SUV_{max}: 14.3; range: 3.5-44.0). ***Conclusion:*** NeoB-uptake and lesion detection were low for glioma and heterogeneous for breast cancer. Glioblastoma showed higher uptake than other glioma. ER+/HER2- breast cancer demonstrated higher uptake than other hormone receptor status; more than 50% of those patients showed intense global uptake and could be candidates for GRPR-directed radioligand therapy.

OP-581

Prognostic Value Of [^{18}F]-FDG PET/CT In Patients With Metastatic Breast Cancer Treated With Cyclin-Dependent Inhibitors

D. Maccora[1], *A. Annovazzi*[1], *S. Rea*[1], *L. Pizzuti*[2], *G. Ferretti*[3], *P. Vici*[4], *F. Cappuzzo*[2], *R. Sciuto*[1];
[1]*Nuclear Medicine Unit, IRCCS Regina Elena National Cancer Institute, Rome, ITALY,* [2]*Division of Medical Oncology 2, IRCCS Regina Elena National Cancer Institute, Rome, ITALY,* [3]*Division of Medical Oncology 1, IRCCS Regina Elena National Cancer Institute, Rome, ITALY,* [4]*Phase IV Clinical Trial Unit, IRCCS Regina Elena National Cancer Institute, Rome, ITALY.*

Aim/Introduction: The addition of cyclin-dependent kinase 4/6 inhibitors (CDK4/6i) (i.e. palbociclib, ribociclib, abemaciclib) to endocrine therapy impressively improved the outcome of patients with hormone receptor-positive metastatic breast cancer. Despite their great efficacy, not all patients respond to treatment and many of them develop acquired resistance. We aimed to assess the role of [^{18}F]-FDG PET/CT in evaluating treatment response and in predicting progression-free survival (PFS) and overall survival (OS) in breast cancer patients treated with CDK4/6i. ***Materials and Methods:*** One hundred fourteen patients who performed an [^{18}F]-FDG PET/CT scan before (PET1) and 2-6 months after (PET2) starting treatment were retrospectively enrolled. Metabolic response was evaluated by EORTC criteria, PERCIST and Deauville score and correlated to PFS and OS. Four response groups were considered: complete metabolic response (CMR), partial metabolic response (PMR), stable metabolic disease (SMD), and progressive metabolic disease (PMD). The 5-point Deauville score was evaluated considering the hottest lesion at PET2 using the well-known scores according to background and liver uptake (1 to 5). In addition, pre-treatment Total Metabolic Tumour Volume (TMTV), a surrogate for tumour burden, as well as clinic-pathologic tumour variables were analysed and correlated to PFS or OS. ***Results:*** Disease progression occurred in 69 patients (median follow-up time 35.8 months). In patients who did not progress at PET2 (n = 90), PFS rates were not significantly different between classes of response by EORTC criteria and PERCIST. Conversely, patients showing a Deauville score ≤3 had a longer PFS (median PFS 42 vs 21 months; p = 0.008). A higher TMTV at PET1 (TMTV1) was associated with a shorter PFS (median PFS 18 vs 42 months; p = 0.0026). PMD at PET2 was associated with a shorter OS (36-month survival rate 29.8 vs 84.9%, median OS 24 months vs not reached; p<0.0001), as well as some baseline clinical features, such as ECOG status, administration of CDK4/6i therapy in second- or later line and liver metastases. Deauville score and TMTV1 were the only independent prognostic factors for PFS at multivariate analysis and their combination stratified the population in four definite classes of relapse risk. ***Conclusion:*** Metabolic response by Deauville score and TMTV were significant prognostic factors for PFS in patients with breast cancer treated with CDK4/6i, PMD and the presence of liver metastases for OS. Their determination could help physicians to select patients who may need a closer follow-up.

1207

Tuesday, September 12, 2023, 8:00 AM - 9:30 AM
Hall F1

Neuroimaging Committee - Featured Session: Breadth of Tracers and Approaches in Neuro-Oncology

OP-582

Breadth of Tracers and Approaches in Neuro-Oncology

***I. Law*;**
University of Copenhagen, Faculty of Health and Medical Sciences Consultant Department of Clinical Physiology and Nuclear Medicine Rigshospitalet, Copenhagen, DENMARK

OP-583

Fibroblast activation protein staining in tissue samples of high-grade gliomas

***N. Tolboom**, S. Sabunchi, A. Muhlebner, P. A. J. T. Robe, T. J. Snijders;*
University Medical Centre Utrecht, Utrecht, NETHERLANDS.

Aim/Introduction: Fibroblast activation protein (FAP) shows low expression in normal tissue and high expression in certain types of cancer and is therefore a promising potential target for non-invasive imaging and treatment of patients. Limited information is available on expression in gliomas. The aim of this study was to examine the staining pattern of a FAP-specific antibody in high-grade glioma tissue samples, to determine the potential of FAP and [68Ga]FAPI-PET for glioma imaging and theranostics.
Materials and Methods: Tissue samples from patients with high-grade gliomas (WHO grade 3-4) were primed on tissue microarrays (TMA) and immunohistochemically stained with a FAP-specific antibody. Samples were assessed consecutively and systematically on extent of staining by two readers and classified in a binary fashion as low/focal or high/diffuse. Furthermore, pattern of staining (perivascular and/or diffuse intraparenchymal) and heterogeneity of FAP expression across gliomas was examined. The association between isocitrate dehydrogenase (IDH) mutation status and extent of staining and expression pattern was tested with Chi-square tests or Fisher's exact test and regression models. ***Results:*** 418 samples from 191 patients (107 male, 84 female, mean age of 59 years) were available for analysis. The samples consisted of tissue, mostly from grade 4 gliomas (n=406), 9 grade 3 astrocytomas and 3 grade 3 oligodendrogliomas. IDH mutation status was available for 332 samples. In the total sample studied, negative FAPI staining was more common than positive staining (68% versus 32%). Of these positive cases, most tumour samples stained only perivascular but about a fifth of the samples did show diffuse intraparenchymal or a combination of diffuse intraparenchymal and perivascular staining. High/diffuse staining was seen in 27 out of 315 IDH wildtype glioma (mostly glioblastoma according to WHO2021) samples and 5 out of 17 IDH mutant glioma samples. Heterogeneity of staining was found within patients. FAP expression was not related to survival. ***Conclusion:*** In a large cohort of patients with high-grade gliomas, the majority of the samples did not stain with FAP. However, of the samples that did stain, a subset showed a high and diffuse intraparenchymal FAP expression pattern, suggesting a potential for [68Ga]FAPI-PET in a select set of patients. However, heterogeneity in staining pattern within patients was observed which needs to be further investigated. These findings give useful insights, in light of the recent interest in [68Ga]FAPI-PET based imaging and potential theranostic therapies in gliomas.

OP-584

Postoperative ^{68}Ga-DOTATATE-/PET-CT imaging is prognostic for progression-free survival survival in meningioma WHO grade 1:A prospective single center study

***N. Teske**, A. Biczok, S. Quach, F. J. Dekorsy, R. Forbrig, R. Bodensohn, M. Niyazi, J. Tonn, N. L. Albert, C. Schichor, M. Ueberschaer;*
Munich University Hospital, LMU Munich, Munich, GERMANY.

Aim/Introduction: Microsurgical tumor resection represents the first-line treatment for symptomatic meningiomas, and extent of resection has been shown to be of prognostic importance. Assessment of tumor remnants with somatostatin receptor PET proves to be superior to intraoperative estimation with Simpson grading or MRI. However, prognostic relevance of postoperative PET for progression-free survival in meningiomas remains unclear.
Materials and Methods: We conducted a prospective study including patients with surgically removed meningioma WHO grade 1 and collected clinical and imaging data. All patients received postoperative MRI and ^{68}Gallium-DOTATATE/PET, and were followed regularly with MRI surveillance scans for detection of tumor recurrence/progression. ***Results:*** We included 46 patients with 49 tumors. Mean age at diagnosis was 57.8 ± 1.7 years with a male-to-female ratio of 1:1.7. Local tumor progression occurred in 7/49 patients (14%) after a median follow-up of 52 months. Positive PET was associated with an increased risk for progression (*p = 0.015) and a lower progression-free survival (*p = 0.029) whereas MRI was not. 20/20 patients (100%) with negative PET findings remained recurrence-free. Location of recurrence/progression on MRI was adjacent to regions where postoperative PET indicated tumor remnants in all cases. Gross tumor volumes were higher on PET compared to MRI (*p = 0.032). ***Conclusion:*** Our data show that ^{68}Ga-DOTATATE/PET is highly sensitive in revealing tumor remnants in patients with meningioma WHO grade 1. Negative PET findings were associated with a higher progression-free survival, thus improving surveillance. In patients with tumor remnants, additional PET can optimize adjuvant radiotherapy target planning of surgically resected meningiomas.

OP-585

^{18}F-DOPA PET imaging in re-irradiation with proton therapy of recurrent glioblastoma.

***D. Donner**[1], D. Amelio[2], D. Scartoni[2], L. Picori[1], S. Agostini[1], F. Magnani[1], A. Palermo[1], M. Cianchetti[2], F. Chierichetti[1];*
[1]Nuclear Medicine Unit, Azienda Provinciale per i Servizi Sanitari, Trento, ITALY, [2]Centro di Protonterapia, Azienda Provinciale per i Servizi Sanitari, Trento, ITALY.

Aim/Introduction: After Photon Therapy, recurrent glioblastoma (rGBM) may be treated again with re-irradiation by Proton Therapy (PT). We evaluated the impact of adding 18FDOPA PET data, with respect to MRI planned treatment, in defining the target volumes for PT. ***Materials and Methods:*** 54 patients (pts) with rGBM underwent morphological MRI with Gadolinium-based contrast agent and 18F-DOPA PET imaging at baseline. 18F-DOPA tumor uptake, using a tumor-to-normal brain ratio > 2, identified the so-called Biological Tumor Volume (BTV). We investigated the differences in volume and relationship of MRI vs. 18F-DOPA PET-derived gross tumor volumes (GTVs). MRI T1 positive for contrast enhancement was used for MRI-based GTV (MRGTV). Definitive GTV included MRGTV plus BTV. Finally, clinical target volume was generated by adding to GTV a 3mm uniform margin in the proximity of anatomical barriers. All pts received 36 GyRBE

in 18 fractions. We also evaluated the median PFS at 4th and 6th month after PT and where the recurrence occurred. ***Results:*** MRGTV (mean 17.8 ± 16.07 cc) was smaller than BTV (mean 23.41 ± 21.28 cc) although this difference was not statistically significant (p = 0.11). The PT irradiation of PET-integrated target volumes provided a median progression-free survival (PFS) of 4 months; 6-month PFS rate was 28%; median survival after PT was 8.5 months. After re-irradiation with protons, the recurrence occurs in the re-irradiated field in 70% of cases and 30% of cases in the marginal outfield regions. ***Conclusion:*** 18F-DOPA PET helped detect the rGBM intratumoral heterogeneity, more accurately defining the tumor burden and catching non-enhancing pathological areas in rGBM, outside the conventional MRGTV. This provided larger volumes in treatment planning. The possible effect on outcome and survival needs further evaluation. ***References:*** 1) Heikki Minn, Saila Kauhanen, Marko Seppänen, Pirjo Nuutila. 18F-FDOPA: A Multiple&#8211Target Molecule. Journal of Nuclear Medicine Dec 2009, 50 (12) 1915-1918; DOI: 10.2967/jnumed 109.065664 2) Pafundi DH, Laack NN, Youland RS, Parney IF, Lowe VJ, Giannini C, Kemp BJ, Grams MP, Morris JM, Hoover JM, Hu LS, Sarkaria JN, Brinkmann DH. Biopsy validation of 18F&#8211DOPA PET and biodistribution in gliomas for neurosurgical planning and radiotherapy target delineation: results of a prospective pilot study. Neuro Oncol. 2013 Aug;15(8):1058-67. doi: 10.1093/neuonc/not002. Epub 2013 Mar 3. PMID: 23460322; PMCID: PMC3714146. 3) Scartoni, D., Amelio, D., Palumbo, P. et al. Proton therapy re-irradiation preserves health-related quality of life in large recurrent glioblastoma. J Cancer Res Clin Oncol 146, 1615-1622 (2020). https://doi.org/10.1007/s00432-020-03187-w

OP-586

Amino-acid PET for monitoring temozolomide adjuvant therapy after a Stupp protocol in gliomas

T. Zaragori[1,2], *S. Ahrari*[1,2], *A. Zinsz*[2], *A. Mortada*[2], *L. Taillandier*[3,4], *M. Blonski*[3,4], *F. Rech*[5,4], *L. Imbert*[1,2], *A. Verger*[1,2];
[1]*Université de Lorraine, IADI, INSERM, UMR 1254, Vandoeuvre-lès-Nancy, FRANCE,* [2]*Department of Nuclear Medicine & Nancyclotep Imaging Platform, CHRU-Nancy, Université de Lorraine, Vandoeuvre-lès-Nancy, FRANCE,* [3]*Department of Neuro-Oncology, CHRU-Nancy, Université de Lorraine, Nancy, France, Vandoeuvre-lès-Nancy, FRANCE,* [4]*Centre de Recherche en Automatique de Nancy CRAN UMR 7039, CNRS, Université de Lorraine, Vandoeuvre-lès-Nancy, FRANCE,* [5]*Department of Neurosurgery, CHRU-Nancy, Université de Lorraine, Vandoeuvre-lès-Nancy, FRANCE.*

Aim/Introduction: Studies investigating the value of amino-acid PET for monitoring temozolomide adjuvant therapy (TMZ) in literature are scarce with limited and heterogeneous populations. The aim of this study was to evaluate the performances of amino-acid PET to monitor adjuvant therapy in gliomas within a homogeneous population of patients having beneficiated from TMZ after a Stupp protocol. ***Materials and Methods:*** Consecutive patients with grades II-IV gliomas who performed a dynamic ^{18}F-FDOPA PET imaging within 3 months of the end of a TMZ after a Stupp protocol were included. Clinical and histo-molecular factors, responses to RANO criteria for MRI and static and dynamic PET parameters were correlated to progression-free and overall survivals (PFS and OS). The biological tumor volumes (BTV) were defined semi-automatically with a 1.6 threshold from the healthy brain. ***Results:*** Sixty-seven patients (57.1±14.4 years old, 27 women) from whom 59 (88%) with IDH-wildtype glioblastomas, having beneficiated from 3 to 24 cures of TMZ, were included. In a subgroup of 19 patients with multiples PET during TMZ cures, decrease in tumor-to-background ratios were associated to PFS at 1 year with an accuracy of 84% (p=0.03). In the overall population, the presence of a BTV was associated to significant lower PFS and OS (respectively 9.0 vs. 22.4 months, p<0.001 and 21.7 vs. 50.0 months, p=0.01). In multivariate analysis, the combination of the presence of a BTV, RANO criteria, the grade of the tumor and the slope were associated to PFS. ***Conclusion:*** Amino-acid PET is an efficient tool to monitor TMZ therapy in patients with gliomas. In a homogeneous population of patients having beneficiated from TMZ after a Stupp protocol, the presence of a BTV is an independent predictor of survivals.

OP-587

Predictive values of preoperative [^{68}Ga]Ga-PSMA-11 PET/CT in patients with suspected brain tumours of glial origin.

K. Pelka[1,2], *K. Koczyk*[3], *L. Koperski*[4], *T. Dziedzic*[3], *A. Nowak*[3], *L. Królicki*[1], *P. Kunert*[3], *J. Kunikowska*[1];
[1]*Nuclear Medicine Department, Medical University of Warsaw, Warsaw, POLAND,* [2]*Laboratory of Centre for Preclinical Research, Department of Research Methodology, Medical University of Warsaw, Warsaw, POLAND,* [3]*Department of Neurosurgery, Medical University of Warsaw, Warsaw, POLAND,* [4]*Department of Pathology, Medical University of Warsaw, Warsaw, POLAND.*

Aim/Introduction: PET/CT targeting the prostate-specific membrane antigen (PSMA) is commonly used in patients with prostate cancer, however its expression has been found in other solid tumors like renal cell carcinoma, hepatocellular carcinoma, and primary brain tumors like glioblastoma (GB). It has been found in the recurrence of GB. The aim of this study to evaluate usefulness of preoperative [^{68}Ga]Ga-PSMA-11 PET/CT of patients with suspected brain tumours of glial origin. ***Materials and Methods:*** In this prospective study we screened patients as a consecutive series, which were referred to the hospital for surgery with suspicion of a tumor of glial origin in previously performed imaging examinations. The PET/CT image acquisition was performed from the skull to the mid-thigh with a CT scan for anatomic correlation and attenuation correction 60 min post injection of [^{68}Ga]Ga-PSMA-11 (2 MBq per kg body weight). Additional acquisition of 5 min was used for brain imaging. The PET/CT qualitative and quantitative results were compared to the histological examination. The collected results were compared to GB diagnostics or differentiation between high-grade (HGG) and low-grade gliomas (LGG). Additional histopathological staining for PSMA has been performed to gain more data. ***Results:*** 44 patients met the inclusion criteria. 20 of them had positive and 24 negative PET/CT scan. The sensitivity, specificity, positive predictive value and negative predictive value for HGG diagnosis 71.4 (95% confidence interval - 51.3-86.8), 100.0 (79.4-100.0), 100.0 (83.1-100.0), 66.7 (44.7-84.4) respectively. Due to tracer uptake in all lesions finally diagnosed as HGG, for the quantitative analysis the area under the receiver operating characteristic curve was used for differentiation GB vs non-GB, with the best results for tumor-to-backgound ratio parameter: 0.81 (0.66-0.96; 42.2) (95% CI; cut-off). The comparison with immunohistochemical examination showed a correlation in qualitative and quantitative analysis. ***Conclusion:*** The PSMA PET/CT showed a great potential in detection of HGG. More prospective trials are still needed for a differentiation between GB and non-GB. the proposed interpretation of the study allows to distinguish a high-risk group from patients with suspected tumor of glial origin, which may allow better treatment planning.

OP-588

Tumoral TSPO-radioligand uptake on PET prior to radiotherapy is associated with overall survival in glioblastoma patients

A. Holzgreve[1], *D. V. Nelwan*[1], *D. F. Fleischmann*[2], *S. Quach*[3], *K. von Rohr*[1], *L. Kaiser*[1], *N. Teske*[3], *L. M. Unterrainer*[1], *L. M. Bartos*[1], *V. C. Ruf*[4], *M. Brendel*[1], *M. J. Riemenschneider*[5], *C. Wetzel*[6], *J. Herms*[4], *R. Rupprecht*[6], *N. Thon*[3], *J. Tonn*[3], *C. Belka*[2], *P. Bartenstein*[1], *L. von Baumgarten*[3], *M. Niyazi*[2], *M. Unterrainer*[1], *N. L. Albert*[1];
[1]*Department of Nuclear Medicine, University Hospital, LMU Munich, Munich, GERMANY,* [2]*Department of Radiation Oncology, University Hospital, LMU Munich, Munich, GERMANY,* [3]*Department of Neurosurgery, University Hospital, LMU Munich, Munich, GERMANY,* [4]*Center for Neuropathology and Prion Research, LMU Munich, Munich, GERMANY,* [5]*Department of Neuropathology, Regensburg University Hospital, Regensburg, GERMANY,* [6]*Department of Psychiatry and Psychotherapy, University of Regensburg, Regensburg, GERMANY.*

Aim/Introduction: PET imaging targeting the 18-kDa translocator protein (TSPO) is increasingly applied in glioblastoma patients. Data correlating TSPO-PET imaging results with survival in glioblastoma patients, however, are lacking. Therefore, we here investigated the prognostic value of TSPO-PET imaging in patients with proven glioblastoma prior to radiotherapy. ***Materials and Methods:*** 45 patients (median age 63.3 years, range 30.6-84.2) with newly-diagnosed glioblastoma (CNS WHO Grade 4) prior to radiotherapy were included. 23/45 (51.1%) patients received conventional chemoradiotherapy (60 Gy dose and temozolomide), and 22/45 (48.9%) patients received hypofractionated radiotherapy (40.05 Gy dose, either with or without temozolomide). Pre-therapeutic image analysis included assessment of tumoral uptake intensity on TSPO-PET (SUV_{max}) and delineation of tumor volumes on MRI (ceT1 and T2/FLAIR). Additionally, the TSPO binding affinity status of each patient was assessed using polymorphism genotyping. Further clinical parameters included MGMT status and TERT status. Univariate survival analysis was performed using Kaplan-Meier estimation and Log-rank test regarding progression-free survival (PFS) and overall survival (OS) for all imaging-based and further clinical data. Parameters found to be prognostic in the univariate analysis were subsequently included in a multivariate survival analysis using Cox proportional hazards model. A two-tailed p-value < 0.05 was considered as statistically significant. ***Results:*** On TSPO-PET, the median tumoral SUV_{max} was 2.2 (range, 1.0-4.7). SUV_{max} was associated with clinical outcome: Patients with a high tumoral uptake intensity on TSPO-PET prior to radiotherapy (i.e., median split $SUV_{max} > 2.2$) had a significantly shorter survival than patients with a lower SUV_{max} (8.3 vs. 17.8 months, p=0.037). No such correlation was found regarding PFS. Other parameters with a significant association to overall survival in the univariate analysis included the T2w-tumor volume on MRI (p=0.031), age (p=0.046), and MGMT status (p=0.032). Contrast-enhancement on MRI was present at a higher proportion in patients with $SUV_{max} \geq 2.2$ (p=0.022), otherwise there were no group differences between patients with low vs. high tumoral uptake on TSPO-PET (for each other imaging-based or clinical parameter, p>0.05). Tumoral SUV_{max} on TSPO-PET was still significantly associated with overall survival when performing multivariate survival analysis (p=0.023). The hazard ratio for death in cases with a $SUV_{max} > 2.2$ was 2.212 (95% CI, 1.115-4.386). ***Conclusion:*** In patients with newly-diagnosed glioblastoma, a high tumoral TSPO-radioligand uptake on PET prior to radiotherapy is associated with significantly shorter survival. TSPO-PET seems to add prognostic insights in glioblastoma beyond established clinical parameters.

OP-589

Imaging PD-L1 in the brain - journey from the lab to the clinic

G. Kramer-Marek[1,2], *D. Dar*[1], *M. Rodak*[2], *C. Da Pieve*[1], *M. Niedbala*[3], *G. Sharma*[1], *I. Gorczewska*[2], *P. Bzowski*[2], *A. d'Amico*[2], *E. Chmielik*[2], *B. Bobek-Bilewicz*[2], *E. Nowicka*[2], *R. Tarnawski*[2], *W. Kaspera*[3];
[1]*The Institute of Cancer Research, London, UNITED KINGDOM,* [2]*Maria Sklodowska-Curie National Research Institute of Oncology, Gliwice, POLAND,* [3]*Medical University of Silesia, Katowice, POLAND.*

Aim/Introduction: Patients with glioblastoma (GBM) eventually relapse, mainly due to a relatively immune-depleted ("cold") tumour microenvironment. High levels of programmed death ligand-1 (PD-L1) have been associated with GBM invasiveness and immuno-resistance. Presently, there is no standardised assessment of PD-L1 expression level that would help in predicting the response to immune checkpoint inhibitors. To fulfil this exigency, we investigated the suitability of ^{89}Zr-radiolabelled Atezolizumab (anti-PD-L1 mAb) to measure the expression of PD-L1 in xenograft and syngeneic mouse models and patients with GBM. ***Materials and Methods:*** The immunoreactivity, binding affinity, and specificity of ^{89}Zr-DFO-Atezolizumab were assessed in vitro using GBM cell lines with different PD-L1 expression levels. Mice with human and murine orthotopic GBM tumours were injected with ~2 MBq (110 µg) of the radioconjugate and PET/CT images were acquired 24, 48 and 72 h post-injection. Biodistribution studies, IHC staining of brain sections and immunophenotyping of tumour samples using flow cytometry (FC) were performed. GBM patients (n=6) enrolled in the clinical trial (NCT05235737), with and w/o neoadjuvant pembrolizumab treatment, received ~37 MBq of ^{89}Zr-DFO-Atezolizumab (1 mg) together with unlabelled antibody (10 mg) and underwent PET/CT scans 48 and 72 h post-injection. Following the surgery, the tumour samples were collected for IHC and FC analysis. ^{89}Zr-DFO-Atezolizumab uptake was measured in the VOIs placed in the tumour mass and normal tissues. The data, expressed as the standardised uptake value (SUV_{max}/SUV_{mean}/SUV_{peak}) were correlated with PD-L1 IHC staining and tumour lymphocytes infiltration. ***Results:*** Atezolizumab was radiolabelled with high radiochemical yield (RCY=88-92%) and purity (RCP>98%). The cell-associated radioactivity in vitro corroborated PD-L1 expression levels assessed by FC. ^{89}Zr-DFO-Atezolizumab specifically recognised PD-L1 expressing brain tumours in vivo providing high contrast images at 24 and 48 h post-injection. Patients experienced no ^{89}Zr-DFO-Atezolizumab-related side effects. High radioconjugate accumulation was observed in the vital part of the tumours 48 h post-administration. However, the radioconjugate uptake varied between the patient's with and w/o neoadjuvant pembrolizumab (SUV_{max}: 3.4 vs 6.9). In normal tissues, uptake was seen in the spleen, liver, and intestines. The radioconjugate tumour targeting was associated with PD-L1 expression assessed by IHC and was consistent with an increased T-cell infiltration. ***Conclusion:*** ^{89}Zr-DFO-Atezolizumab detects with high specificity different expression levels of PD-L1 in the preclinical GBM models and patients with newly diagnosed GBM. It also provides complementary tumour-specific and/or immune-specific information to ex vivo methods.

OP-590

Profiling Functional Clusters of Short Chain Fatty Acids Metabolism in Primary Brain Gliomas for Phenotype Prediction

M. Inglese[1,2], *T. Boccato*[1], *M. Ferrante*[1], *S. Islam*[2], *M. Williams*[2], *A. D. Waldman*[3], *K. O'Neill*[4], *E. O. Aboagye*[2], *N. Toschi*[1,5];
[1]*University of Rome "Tor Vergata", Rome, ITALY,* [2]*Imperial College London, London, UNITED KINGDOM,* [3]*University of Edinburgh, Edinburgh, UNITED KINGDOM,* [4]*Imperial College Healthcare NHS Trust, London, UNITED KINGDOM,* [5]*Athinoula A. Martinos Center for Biomedical Imaging, Boston, MA, UNITED STATES OF AMERICA.*

Aim/Introduction: Glioblastoma multiforme (GBM) genetic profiling significantly influences diagnosis, therapy, and patient survival. The primary GBM biomarker is isocitrate dehydrogenase (IDH), with IDH mutations(mu) associated with markedly improved survival compared to the wild-type(wt)[1]. Pathological sampling, the gold standard for GBM diagnosis, poses risks due to spatial heterogeneity and variable genetic expression. Additionally, technical limitations hinder IDH mutation pathological testing, necessitating non-invasive diagnostic techniques to supplement pathologic data[2]. However, IDH mutation currently lacks a distinct radiologic signature[3]. This study aims to classify GBMs' genetic profiles using 18F-fluoropivalate(FPIA) PET tracer kinetics, targeting brain gliomas' specific mechanism involving short-chain fatty acid(SCFA) oxidation for energy production and proliferation4,5. ***Materials and Methods:*** Ten primary brain glioma patients(5 IDH1mu, 5 IDHwt) were recruited. ^{18}F-FPIA PET/MR images were obtained using a Signa PET/MR scanner. For each patient, an average of 25202(±14337) time activity curves(TACs) were extracted voxelwise from dynamic PET data using a lesion mask generated manually by an expert radiologist. A K-means clustering approach for time series grouped standardized TACs into k=4 clusters (k defined by optimizing distortion score using the elbow method), generating four lesion subregions (DynamicFPIA_clustering). For each patient and subregion, the percentage of voxels and average MRI-derived diffusion/perfusion parameters were assessed for classification. A support vector machine(SVM) model was trained on in a 5-fold nested cross validation fashion, which comprised hyperparameter optimization(inner loop) and perforamnce quantification (outer loop). This approach was compared to two others: one using parameters evaluated in subregions defined by clustering SUV voxels (StaticFPIA_clustering), and another assessing average MRI parameter values across the entire lesion(standard approach). ***Results:*** The DynamicFPIA_clustering approach classified GBM phenotypes with 80%(±20) accuracy (AUC=0.8±0.2), with the 3rd subregion's percentage dimension and the 2nd subregion's CBF as the most significant features. Accuracy decreased to 70%(±24) (AUC=0.7±0.2) using StaticFPIA_clustering and 60%(±37) (AUC=0.6±0.4) with the standard approach without subregions. Average and standard deviation evaluated across outer folds. ***Conclusion:*** This study leverages the inherent spatial heterogeneity of GBMs, which significantly affects biopsy, diagnosis, and survival outcomes, to non-invasively identify four distinct profiles of SCFA kinetics. By combining these profiles with MRI-derived parameters, our approach classifies GBM phenotypes with 80% accuracy. The findings demonstrate the potential of integrating dynamic FPIA PET/MR imaging with machine learning techniques as a valuable, non-invasive diagnostic tool. Moreover, this innovative method could contribute to more accurate and personalized treatment strategies for GBM patients, minimizing the risks associated with invasive biopsies. ***References:*** 1.Wang,doi: 10.1016/j.gde.2014.12.002.2.Pasquini,doi: 10.3390/jpm11040290.3.Johnson,doi: 10.1148/rg.2017170037.4.Kant,doi: 10.1038/s41419-020-2449-5.5.Mashimo,doi: 10.1016/j.cell.2014.11.025

1208

Tuesday, September 12, 2023, 08:00 - 09:30
Hall F2

Joint Symposium 4 - Dosimetry Committee / ESTRO: Dosimetry in Different Modalities - Where We Are and Where We Want To Be

OP-591

Dosimetry for EBRT and Brachytherapy

E. Gershkevitsh;
North Estonia Medical Centre, Tallinn, ESTONIA.

OP-592

Dosimetry for Selective Internal Radiotherapy

C. Hindorf;
Karolinska University Hospital, Solna, SWEDEN.

OP-593

Dosimetry for Molecular Radiotherapy

J. Gear;
Royal Marsden NHSFT and Institute of Cancer Research, Joint Department of Physics, Sutton, UNITED KINGDOM.

OP-594

Comparisons and future perspectives

M. Cremonesi;
Istituto Europeo Di Oncologia, Department of Medical Imaging and Radiation Sciences, Milan, ITALY.

1209

Tuesday, September 12, 2023, 8:00 AM - 9:30 AM
Hall G2

e-Poster Presentations Session 9 - Physics Committee: Artificial Intelligence and Radiomics

EPS-168

Development of deep learning model for generalized utilization to restore short-scanning PET images using three radiopharmaceuticals

Y. Jeong[1], *S. Cheon*[1], *H. Park*[2], *K. Jeon*[2];
[1]*Dong-A University Hospital, Busan, KOREA, REPUBLIC OF,* [2]*National Institute for Mathematical Science, Daejeon, KOREA, REPUBLIC OF.*

Aim/Introduction: We proposed a deep learning (DL) model that restores 2-minute amyloid positron emission tomography (PET) images as 20-minute standard images and recently developed this model to be commonly applicable to amyloid PET images using three radiopharmaceuticals. The performance of the DL model commonly applicable to three radiopharmaceuticals for amyloid PET was evaluated. ***Materials and Methods:*** We enrolled a total of 873 F-18 florbetaben (FBB), 415 F-18 flutemetamol (FMM), and 208 F-18 florapronol (FPN) PET images of our hospital. These PET images were divided into training, internal validation, and temporal validation sets as follows: 734,119, and 20 for FBB-PET, 365, 30, and 20 for FMT-PET, and 173, 15, and 20 for FPN-PET, respectively. For all PET images, 20-minute images were used as ground truth images, and the first 2-minute images among 20-minute data were used

as short-scanning images. Using our DL network, we generated a 20-minute PET-like image from a 2-minute PET image. We verified our model by measuring peak signal-to-noise ratio (PSNR), structural similarity (SSIM), and root-mean-square error (RMSE). We also compared these quantified results with other DL models. ***Results:*** In internal and temporal validation datasets, our DL model showed better performance than the existing models in restoring short-scanning PET images. (Table 1, 2). In addition, it was confirmed that the performance of our DL model was commonly stable for various types of amyloid PET images obtained with three radiopharmaceuticals. ***Conclusion:*** It was confirmed that our image restoration DL model could be applied to all amyloid PET images using three different radiopharmaceuticals and that the image quality is well maintained. The proposed method using domain labels for short-scanning amyloid PET image restoration can be a promising approach to overcoming the challenges of multi-domain learning in PET imaging. ***References:*** Jeong YJ, Park HS, Jeong JE, Yoon HJ, Jeon K, Cho K, Kang DY. Restoration of amyloid PET images obtained with short-time data using a generative adversarial networks framework. Sci Rep. 2021 Mar 1;11(1):4825.

EPS-169

Deep-learning based classification of dual-phase 18F-FP-CIT PET images for the diagnosis of Parkinsonism

D. Kim[1], *K. Choo*[1], *D. Kim*[2], *H. Lim*[2], *M. Yun*[2];
[1]*Yonsei University, Seoul, KOREA, REPUBLIC OF,* [2]*Yonsei University College of Medicine, Seoul, KOREA, REPUBLIC OF.*

Aim/Introduction: With new cases of Parkinsonism being reported at an accelerating rate, physicians are under pressure to study tens of PET images a day. To alleviate this burden, this study aims to develop a deep-learning based framework that helps with the analysis of dual-phase 18F-FP-CIT PET images to detect persons with normal condition (NC), idiopathic Parkinson's disease (IPD), progressive supranuclear palsy (PSP), and multiple system atrophy (MSA). ***Materials and Methods:*** This retrospective study involved 388 cases collected internally from 2015 to 2022. Labels were assigned on the consensus of two experts, one nuclear medicine physician and one clinician. The data were split into train, validation, and test set by the ratio 8:1:1 to assess the effects of model architecture, regularization, and dual-phase imaging. Candidate models were then selected based on F1 score and accuracy, upon which 5-fold cross validation was performed. Finally, the performance of each of the five models was compared with their ensemble. The best-performing ensemble model has been prospectively examined for one month on 76 cases. ***Results:*** DenseNet, EfficientNet, and a custom convolutional neural network are chosen as candidate architectures, among which the custom CNN showed best performance (F1 score, accuracy: 0.90, 0.90) in single model. Regularization on the custom CNN improved its accuracy to 0.92. However, when trained only on each of delay-phase and early-phase images, the custom CNN's F1 score and accuracy dropped to 0.62, 0.77 and 0.83, 0.82 respectively. Among the candidates, DenseNet showed best performance in 5-fold cross-validation, with an average F1 score of 0.90 (std 0.05) and an average accuracy of 0.92 (std 0.04). In ensemble, the F1 score and the accuracy improved to 0.94 and 0.95. This ensemble model yielded a F1 score of 0.71 and an accuracy of 0.92 during the prospective study. ***Conclusion:*** Convolutional neural network has shown to be capable of classifying 18F-FP-CIT PET images at the level of a skilled nuclear medicine physician. Further research may explore the possibility of performing classification on data from different PET devices.

EPS-170

Feasibility of transfer learning in decoding hibernating myocardium from rest myocardial perfusion images

B. Khangembam*, J. Jaleel, A. Roy, P. Gupta, C. Patel;*
All India Institute of Medical Sciences, New Delhi, INDIA.

Aim/Introduction: To assess the feasibility of a transfer learning approach to automatically predict hibernating myocardium from rest myocardial perfusion imaging (MPI). ***Materials and Methods:*** Data of patients who underwent 99mTc-sestamibi MPI and 18F-FDG cardiac PET/CT for myocardial viability assessment from January 2017 to September 2022 were assessed. Replicable and stratified data sampling allocated 70% (146) of the dataset to the training set and the remaining 30% (62) to the testing set. The gold standard for defining hibernating myocardium was the presence of mismatched perfusion-metabolism defect with impaired myocardial contractility at rest. Rest MPI data were processed on ECToolbox and polar maps were saved using NFile PMap tool. Image embedding was implemented on the polar map images using VGG-16, a 16-layer deep neural network model trained on the ImageNet dataset. Image features in the vector space were ranked by Gini Index scoring method. The 17 best-ranked features were selected for training the machine learning (ML) algorithms. 13 supervised ML algorithms were trained with 10-fold stratified cross-validation on the training set with hyperparameter optimization to yield optimal performance. The trained ML algorithms with a LogLoss of <0.693 were then tested on the testing set. Various performance matrices of the algorithms were assessed including area under the curve (AUC), classification accuracy (CA), F1 score, precision, recall, and specificity. ***Results:*** A total of 208 patients (186 males; mean age 56 ± 11 years) were enrolled in the study. Among the 13 ML algorithms, Naive Bayes and Decision Tree had a LogLoss of >0.693 in the cross-validation step while 9 ML algorithms had AUC >0.800. These were Gradient Boosting (scikit-learn), Stochastic Gradient Descent (SGD), Support Vector Machine (SVM), Gradient Boosting (xgboost), Logistic Regression (LR), Neural Network (NN), Random Forest (RF), Gradient Boosting (catboost), and Gradient Boosting Random Forest (xgboost). On testing, 8 ML algorithms had AUC >0.750 which included k-Nearest Neighbours (kNN) and all the above algorithms with the exception of SGD and LR. Gradient Boosting (xgboost) and Gradient Boosting (catboost) were the most optimal models (AUC 0.813 and 0.803 respectively) with similar F1 Score (0.762), precision (0.750), specificity (0.742) and could decode hibernating myocardium in 24/31 (77.4%) patients with an overall CA of 75.8% (47/62). ***Conclusion:*** Machine learning using a transfer learning approach can decode the presence of hibernating myocardium from rest myocardial perfusion images. Gradient Boosting (xgboost) and Gradient Boosting (catboost) were the most consistent and optimal models for the purpose.

EPS-171

Synthetic Attenuation Correction Maps for SPECT Imaging using Deep Learning: A Study on Myocardial Perfusion Imaging

M. Namías[1], *M. A. Prieto Canalejo*[2], *A. Palau San Pedro*[1], *R. Geronazzo*[1], *D. M. Minsky*[3], *L. E. Juarez Orozco*[4];
[1]*Fundación Centro Diagnóstico Nuclear, Buenos Aires, ARGENTINA,* [2]*Universidad Tecnológica Nacional, Facultad Regional Buenos Aires, Buenos Aires, ARGENTINA,* [3]*Comisión Nacional de Energía Atómica, San Martín, ARGENTINA,* [4]*University Medical Center Utrecht, Utrecht, NETHERLANDS.*

Aim/Introduction: CT-based attenuation correction of SPECT images is essential for obtaining quantitative images of the activity concentration inside the human body. However, there are many SPECT systems that do not have an associated CT scanner. Performing additional CT scans also implies larger radiation doses for patients. The objective of this work is to estimate linear attenuation coefficient maps from SPECT emission images reconstructed without attenuation correction, using deep learning methods. ***Materials and Methods:*** 398 myocardial perfusion studies with ^{99m}Tc-sestamibi SPECT were included. A deep convolutional neural network (DCNN) based on a 2D U-Net architecture was trained using information from 312 patients. The quality of the synthetic attenuation correction maps (ACM) and reconstructed emission values was evaluated using three metrics and compared to standard of care data using Bland-Altman plots. Finally, a quantitative evaluation of myocardial uptake was performed, followed by semi-quantitative evaluation of myocardial perfusion (summed stress score) using the Emory Cardiac Toolbox. ***Results:*** For 66 test patients, the ACM quality metrics were: MSSIM = 0.97 ± 0.001 and NMAE = 3.08 ± 1.26 (%), and the reconstructed emission quality metrics were MSSIM = 0.99 ± 0.003 and NMAE = 0.23 ± 0.13 (%). The 95% limits of agreement (LoA) at the voxel level for reconstructed SPECT images were: [-9.04; 9.00] %, and for the segment level were [-11; 10] %. The 95% LoA for the Summed Stress Score values between images reconstructed were [-2.8, 3.0]. When the global perfusion scores were assessed, it was observed that 2 out of 66 patients showed changes in categories. The 95% LoA for percent myocardium abnormal were [-4.2, 4.4]%. ***Conclusion:*** We implemented a generative deep learning model to estimate attenuation correction maps from non-attenuation corrected SPECT images. This method can produce high-quality attenuation maps suitable for attenuation correction in myocardial perfusion SPECT imaging.

EPS-172

Human vs Machine: Comparison of manual and deep learning semantic segmentation algorithm generated tumour volumes on [177Lu]Lu-PSMA-617 post therapy SPECT/CT images

R. Karri, *P. Jackson, L. McInstosh, J. P. Buteau, G. Kong, T. Akhurst, A. S. Ravi Kumar, D. G. Murphy, S. Sandhu, M. S. Hofman;*
Peter MacCallum Cancer Centre, Melbourne, AUSTRALIA.

Aim/Introduction: [177Lu]Lu-PSMA-617 is a new life-prolonging treatment in patients with metastatic castrate-resistant prostate cancer following at least one line of chemotherapy and androgen receptor pathway inhibitors. Post therapy imaging can provide information on biodistribution and tumour response to treatment. Tumour volume and intensity of PSMA uptake on the post therapy SPECT/CT images (potential prognostic biomarkers) can be estimated with advanced image processing. This is a time consuming manual process and not all centres have software to facilitate. We compared the accuracy and agreement of manually contoured and AI generated tumour volumes on the post therapy SPECT/CT images ***Materials and Methods:*** Post-therapy quantitative SPECT CT images 24 hrs post administration of cycle 1 of [177Lu]Lu-PSMA-617 in a 50 patient single-centre phase II study were analysed[1,2]. Manual contouring of tumour excluding any physiologic uptake was performed using a standardised uptake value (SUV) threshold of 3. Molecular Tumour Volume (MTV), SUVmax and SUVmean were recorded. Contours were also generated using a novel semantic deep learning segmentation workflow called Global Threshold Regional Consensus Network (GTRC-Net). The similarity of the parameters using the two techniques was estimated using dice scores and Pearson's correlation. Bland Altman analysis were also performed. ***Results:*** The mean dice coefficient for the MTV was 0.965. The Pearson correlation was 0.99 for TTB, SUVmax and SUVmean. Bland Altman analysis demonstrated bias between the two techniques of 35.61 ± 338.8 for MTV, 0.07±0.64 for SUVmax and 0.04±0.64 for SUVmean. The plot shows excellent agreement between both techniques with few outliers. A difference in contours of more than 100ml was noted in 9 scans. These were due to incorrect contouring by expert in 2 and false positive or false negative contours by AI in 7 scans. False positive contours by AI were predominantly in the bowel loops, lacrimal / salivary glands while false negatives were in proximity to kidney and in the liver. Processing time of the tumour contour by the AI workflow is about a minute per scan. ***Conclusion:*** The novel deep-learning enabled algorithm has excellent agreement in delineating tumour burden on post therapy SPECT/CT images; potentially permitting large-scale clinical use. Further work is required to define the role of SPECT-based quantitative parameters as predictive or prognostic biomarkers. ***References:*** Lancet Oncology. Jun;19(60) 2018:825-833. J Nucl Med. 2020 Jun;61(6):857-865.

EPS-173

Primary tumour type impacts 3D U-Net for [^{18}F]FDG PET lesion segmentation performance in cases of lung cancer, melanoma, and lymphoma

M. Sobral[1,2], *M. Oliveira*[1,3], *C. Constantino*[1], *F. Oliveira*[1], *N. Matela*[4], *D. C Costa*[1];
[1]*Champalimaud Foundation, Lisboa, PORTUGAL,*
[2]*Departamento de Física, Faculdade de Ciências, Universidade de Lisboa, Lisboa, PORTUGAL,* [3]*Escola Superior de Biotecnologia, Universidade Católica Portuguesa, Porto, PORTUGAL,*
[4]*Instituto de Biofísica e Engenharia Biomédica, Faculdade de Ciências, Universidade de Lisboa, Lisboa, PORTUGAL.*

Aim/Introduction: We aim to evaluate the importance of the type of primary tumour used to train a deep learning network to segment different types of tumours. ***Materials and Methods:*** This study includes 432 whole-body [^{18}F]FDG PET images and corresponding manual tumour segmentations, from the MICCAI AutoPET Challenge [1-3]. There are three cohorts: 144 images of lung cancer, 144 of melanoma, and 144 of lymphoma. Each cohort was divided into 114 images for training, 15 for internal validation, and 15 for testing. All images and segmentations were resampled to isotropic voxels of 4×4×4 mm^3. A 3D U-Net with a depth of 4 convolutional blocks, and a patch size of 128×128×128 voxels was chosen for the deep learning-based segmentation. The optimal weights were obtained by minimising the generalised Dice loss while using the Adam optimiser, over 600 epochs. Therefore, 3 networks were trained, one for each cohort. Each network was applied to the three test sets and the Dice similarity coefficient (DSC) was calculated, using the manual segmentations as gold standard. The Wilcoxon signed-rank test was used for statistical inference. P-values were adjusted for multiple comparisons using the Bonferroni method. ***Results:*** The segmentations of the test set from lymphoma patients achieved median DSC of 0.43, 0.57, and 0.68 when using the networks trained with the lung, melanoma, and lymphoma patients, respectively. The network trained with the lymphoma patients had significantly higher DSC values when compared to the others (p_{adj}<0.05). The median DSC regarding the segmentation of the lung cancer patients' test set were 0.79, 0.64, and 0.54 using the networks trained with lung cancer, melanoma, and lymphoma patients, respectively. When comparing the DSC

values, the network trained with lung cancer patients originated statistically higher values than the others (p_{adj}<0.01). The median DSC obtained from the melanoma test dataset were 0.45, 0.64, and 0.41, for the networks trained with lung cancer, melanoma, and lymphoma patients, respectively, without statistically significant difference between them (p_{adj}>0.05). ***Conclusion:*** Tumour segmentation of [^{18}F]FDG PET images using the 3D U-Net should be trained with images from patients with the same tumour type as per case under evaluation. This seems to be more important in the cases of lung cancer and lymphoma than melanoma. ***References:*** [1] Gatidis et al. (2022), The Cancer Imaging Archive. DOI: 10.7937/gkr0-xv29 [2] Gatidis et al. (2022), Scientific Data. DOI: 10.1038/s41597-022-01718-3 [3] Clark et al. (2013) Journal of Digital Imaging. DOI: 10.1007/s10278-013-9622-7

EPS-174

A systemic analysis of [18F]FDG PET/CT data for early detection of cachexia in lung cancer patients

D. Ferrara[1], *A. Frille*[2], *E. Abenavoli*[3], *T. Beyer*[1], *S. Duke*[4], *S. Gruenert*[5], *M. Hacker*[5], *S. Hesse*[2], *L. Hofmann*[2], *S. Holm*[4], *M. Rullmann*[2], *R. Sciagrà*[3], *L. Shiyam Sundar*[1], *A. Tönjes*[2], *H. Wirtz*[2], *J. Yu*[1,5], *O. Sabri*[2];
[1]*QIMP Team, Medical University of Vienna, Vienna, AUSTRIA,* [2]*University Hospital of Leipzig, Leipzig, GERMANY,* [3]*Division of Nuclear Medicine, Azienda Ospedaliero Universitaria Careggi, Florence, ITALY,* [4]*University of Copenhagen, Copenhagen, DENMARK,* [5]*Division of Nuclear Medicine, Medical University of Vienna, Vienna, AUSTRIA.*

Aim/Introduction: Cancer-associated-cachexia (CAC) substantially decreases quality of life and survival of cancer patients, especially those with lung cancer. Early detection of CAC can aid in identifying lung cancer patients (LCP) requiring increased multi-professional clinical support at the time of LC diagnosis and treatment planning. Using a multi-organ analysis, we sought to extract distinct "metabolic fingerprints" from [18F] FDG-PET images of LCP who subsequently developed CAC. ***Materials and Methods:*** A retrospective cohort included LCP (N=209, 59F/150M) who underwent [18F]FDG-PET/CT imaging for initial clinical staging. The body mass index (BMI)-adjusted weight loss (WL) grading system (WLGS) helped stratify LCP into two metabolic phenotypes: a non-cachectic (WLGS-0: N=121, 32F/89M, 68±9 years) and a cachectic (WLGS-3-4: N=88, 27F/61M, 62±12 years). Abdominal organs, muscles, subcutaneous and visceral adipose tissue were segmented automatically from PET/CT data [1]. Standardized-uptake-values normalized to lean body mass (SUV_{lbm}) and organ volumes were extracted from each segmented organ and their averages reported across both cohorts. A multi-organ network analysis was conducted to study inter-organ connectivities using Spearman correlations. Significant (p<0.05) correlations were visualized in a chord plot for both WLGS-0 and WLGS-3-4 groups. The individual organ degree of centrality (i.e., the number of inter-organ connections) was investigated. A machine-learning model was trained to classify the LCP in WLGS-0 or WLGS-3-4 respectively. Techniques of explainable artificial-intelligence (AI: feature importance plots and SHAP analysis) were employed to identify the parameters that primarily contributed to disease development for each patient. ***Results:*** SUV_{lbm} of visceral and subcutaneous adipose tissue were higher in patients with WLGS-3-4 than in WLGS-0. Corresponding volumes were smaller in the WLGS-3-4 cohort than in the WLGS-0 cohort. The multi-parametric correlation analysis revealed a lower degree of centrality for gluteus muscle SUV_{lbm} and fat volumes in WLGS-3-4. Machine-learning based classification into cachectic and non-cachectic phenotypes was 88% accurate. Feature importance plots and SHAP analysis identified volumes of fat segmentations and SUV_{lbm} of gluteus regions as the parameters that mainly influenced the prediction. ***Conclusion:*** The multi-organ networks in LCP were distinct for patients without (WLGS-0) and with (WLGS-3-4) cachexia phenotype. The inter-organ analysis highlighted differences in adipose tissue and gluteus connectivity profiles between the two clinical phenotypes. Explainable AI helps extract a "metabolic fingerprint" for LCP at risk of developing CAC. ***References:*** [1] L. K. Shiyam Sundar et al. "Fully-automated, semantic segmentation of whole-body [18F]FDG PET/CT images based on data-centric artificial intelligence". In: Journal of Nuclear Medicine (2022).

EPS-175

Comparison of a deep learning model to denoise low dose 18F-FDG PET images trained using synthetic image versus acquired low dose images

L. Sibille*, R. Chamberlain;*
Subtle Medical, Menlo Park, CA, UNITED STATES OF AMERICA.

Aim/Introduction: Recently, deep learning techniques have emerged as a promising solution for enhancing low photon count image quality, thus facilitating faster acquisitions. State of the art methods to denoise low dose 18F-FDG PET images rely on a large number of paired images (low dose, full dose) which are difficult and expensive to collect. This study investigated the capabilities of a diffusion model to capture the degradation process to generate realistic synthetic low dose PET from a full dose image applied to low dose image denoising. ***Materials and Methods:*** A 2.5D Convolutional Neural Network was trained to denoise synthetic low dose images (sCNN) and compared against an identically trained network using the acquired low dose images (rCNN). Synthetic low dose images were generated from a full dose image using a conditional diffusion probabilistic model (cDDPM) trained from pairs of low dose (50%, 25%, 10%, 5% and 1% of dose) and full dose images. Additionally, the cDDPM used an extra embedding based on scanner manufacturer and dose level to control the generative process. Evaluation was performed using acquired low dose image. Regions suspicious for cancer were manually delineated using 41% of SUVmax and manually adjusted if necessary. SUVmax and SUVmean quantification was performed on these regions. ***Results:*** 192 patients were retrospectively used to train (N=160) the the cDDPM, sCNN and rCNN and evaluated (N=32) on an independent dataset. The mean difference of SUVmax quantification between synthetic and acquired images was not significant (P>0.93) and similarly for SUVmean (P>0.12). L1 (sCNN=0.140, rCNN=0.120) and SSIM (sCNN=0.985, rCNN=0.987) were comparable. SUVmax error (sCNN=0.149, rCNN=0.176) and SUVmean error (sCNN=0.130, rCNN=0.151) were lower for the CNN trained using synthetic images. ***Conclusion:*** cDDPM was found to be a promising approach to generate realistic synthetic images to be used for low count image denoising. Our results indicate training a PET denoising model using synthesize low dose data could improve the quantitative accuracy the denoised images.

EPS-176

Multi-tracer Deep Learning-based Time-of-Flight (DL-ToF) Image Enhancement of non-TOF PET Scans

A. Mehranian[1], *S. Wollenweber*[2], *K. Bradley*[3], *M. Walker*[4], *K. Su*[2], *R. Johnsen*[2], *F. Jansen*[2], *D. McGowan*[4,5];
[1]*GE HealthCare, Oxford, UNITED KINGDOM,* [2]*GE HealthCare, Waukesha, WI, UNITED STATES OF AMERICA,* [3]*Wales Research and Diagnostic PET Imaging Centre, University Hospital of Wales, Cardiff, UNITED KINGDOM,* [4]*Oxford University Hospitals NHS FT, Oxford, UNITED KINGDOM,* [5]*Department of Oncology, University of Oxford, Oxford, UNITED KINGDOM.*

Aim/Introduction: To evaluate the generalizability of a deep learning time-of-flight (DL-ToF) model trained using fluorodeoxyglucose (FDG) and non-FDG PET images in order to provide ToF like image quality for multi-tracer non-ToF PET scans ***Materials and Methods:*** A multi-tracer DL-ToF model was trained using 315 (289 training, 26 validation) whole-body PET exams scanned on GE Discovery MI (DMI) ToF (3-5 ring) scanners from eleven different sites (US, Europe and Asia). The training and validation pairs consisted of ToF (target) and non-ToF (input) Q-Clear reconstructions using site-preferred regularisation parameters (beta values). The tracer distribution of training and validation pairs was 74% FDG and 26% with four different non-FDG tracers (68Ga-PSMA, 68Ga-Dotatate, 18F-Fluciclovine and 18F-Fluorine). A total of 25 FDG and 7 non-FDG whole-body DMI exams were selected for quantitative analysis based on standardised uptake value (SUV) in selected regions of interest (ROI). A subset of 15 exams (8 FDG and 7 non-FDG) were further selected for blinded clinical readings based on diagnostic confidence, lesion detectability and image noise/quality on a 5-point Likert score ***Results:*** Quantitative analysis of 67 lesions identified on 25 FDG test exams showed that the non-ToF and DL-ToF images resulted in -36±17% and -10±24% difference in SUVmax, respectively, compared to target ToF images. The SUVmean percent difference, averaged over 5 ROIs per organ per exam, were 7±13% and 1±11% for lungs and 5±5% and 0±4% for liver, respectively. For 7 non-FDG test exams (4 different tracers), results for non-TOF and DL-ToF were as follows: SUVmax percent difference for 12 identified lesions of -27±19% and -1±20%, lung SUVmean percent difference of -1±23% and -5±19%, and liver SUVmean percent difference of -5±5% and -0±5%, respectively. Clinical readings of all 15 selected exams were as follows: ToF, non-ToF and DL-ToF scored 4.6±0.6, 3.3±0.6 and 4.9±0.3 for diagnostic confidence, 4.9±0.5, 3.3±0.6 and 4.9±0.4 for lesion detectability and 3.8±0.7, 4.4±0.8 and 4.4±0.6 for image noise/quality metrics, respectively. Additionally, DL-ToF showed the reduction of photopenic areas caused by attenuation mismatch artefacts similar to ToF reconstruction method ***Conclusion:*** This study demonstrated that the DL-ToF model developed is generalizable to both FDG and non-FDG tracers and could be utilized for BGO-based PET scanners to provide ToF like image quality. This work will be extended by including multi-tracer exams from GE Discovery IQ and OMNI Legend PET/CT scanners and more readers

EPS-177

Deep learning based missing data retrieval of small animal PET using a conditional GAN (Pix2Pix)

Z. Karimi[1], *A. Ghafari*[2], *M. Farahani*[2], *P. Sheikhzadeh*[3], *M. Ay*[2]; [1]*Faculty of Physics, University of Isfahan, Isfahan, IRAN, ISLAMIC REPUBLIC OF,* [2]*Research Center for Molecular and Cellular Imaging (RCMCI), Advanced Medical Technologies and Equipment Institute (AMTEI), Tehran University of Medical Sciences (TUMS), Tehran, IRAN, ISLAMIC REPUBLIC OF,* [3]*Department of Nuclear Medicine, Imam Khomeini Hospital Complex, Tehran, IRAN, ISLAMIC REPUBLIC OF.*

Aim/Introduction: The Pix2Pix conditional generative adversarial network (Pix2Pix cGAN) is used to retrieve and fill missing data in preclinical PET sinograms caused by inter-block gap. Missing areas in sinogram domains can cause distortions in the resulting reconstructed image and can lead to errors in quantitative data analysis. ***Materials and Methods:*** The Pix2Pix cGAN model was trained on a total of 4700 2D PET sinograms with gaps from the real moused scanned by animal PET scanner. The sinograms filled with interpolation method were modified as target. The artificial gaps were applied on the target sinograms with different width (3 - 4 - 5 pixels) similar to original gaps pattern. These artificial gaps were also located at different places except the interpolation areas as input of the network and tested on a separate set of 300 original sinograms. The quality of the generated sinograms was quantitatively assessed using normalized mean square error (NMSE) and structural similarity index (SSIM) metrics. ***Results:*** The SSIM and NMSE of the generated sinograms from the model trained was 0.99 ± 0.000024 and 0.0026 ± 0.000082 considering the corresponding interpolated sinograms as target, respectively. So, the predicted sinograms demonstrated improvements quantitatively compared to input sinograms. This approach can recover missing data in sinograms prior to reconstruction which indicates more accuracy and consistency than the conventional interpolation method. ***Conclusion:*** This proposed approach can retrieve the missing data present in the sinograms by learning a mapping derived from the whole sinogram compared to the adjacent pixels used in the conventional interpolation method used. ***References:*** Shiri, I., Sheikhzadeh, P., & Ay, M. R. (2019). Deep-fill: Deep learning based sinogram domain gap filling in positron emission tomography. arXiv preprint arXiv:1906.07168.

EPS-178

Enhanced characterization of functionally significant coronary lesions using machine learning techniques with radiomics-based analysis

G. Kalykakis[1,2], *F. V. Driest*[3], *A. Broersen*[4], *D. Terentes-Printzios*[5], *A. Antonopoulos*[5], *N. Anousakis Vlachichristou*[1], *R. Liga*[6], *D. Visvikis*[7], *A. Scholte*[8], *J. Knuuti*[9], *D. Neglia*[10], *C. D. Anagnostopoulos*[1]; [1]*Biomedical Research Foundation Academy of Athens, Athens, GREECE,* [2]*Ionio University, Corfu, GREECE,* [3]*Leiden University Medical Center, Department of Cardiology, Leiden, NETHERLANDS,* [4]*University Medical Center, Division of Image Processing, Leiden, NETHERLANDS,* [5]*Hippocration General Hospital of Athens, Athens, GREECE,* [6]*University of Pisa, Pisa, ITALY,* [7]*University of Bretagne Occidentale, Brest, FRANCE,* [8]*Leiden University Medical Center, Leiden, NETHERLANDS,* [9]*Turku University Hospital, Turku, FINLAND,* [10]*Institute of Clinical Physiology, Pisa, ITALY.*

Aim/Introduction: Computed Tomography Coronary Angiography (CTCA) is an effective non-invasive imaging modality for anatomo-functional assessment of coronary artery disease (CAD). Radiomics features have been used for diagnosis or outcome prediction, however, their potential value for characterizing flow limiting coronary lesions has not been explored. The aim of the study is to assess whether application of novel radiomics and machine learning (ML) techniques on CTCA derived datasets improves characterization of functionally significant coronary lesions. ***Materials and Methods:*** Consecutive patients with stable chest pain and intermediate pre-test likelihood for CAD, who underwent CTCA and PET-or SPECT-Myocardial Perfusion Imaging (MPI) respectively, were prospectively evaluated and included in the analysis. PET-MPI was considered abnormal when >1 contiguous segments showed both stress Myocardial Blood Flow ≤ 2.3mL/g/min and Myocardial Flow Reserve (MFR) ≤ 2.5 for 15O-water or < 1.79 mL/g/min and ≤ 2.0 for 13N-ammonia respectively. Defect reversibility (DR) was defined as a summed difference score (SDS) between stress and rest images ≥ 2. CTCA and functional images were fused to assign each myocardial segment to the pertinent coronary territory. Stenosis severity, plaque characteristics and radiomic

plaque features were assessed in the total length of the 3 main coronary vessels. In total, 1765 features were extracted from each vessel and a feature reduction and model creation pipeline was constructed. Two separate datasets: a) coronary stenosis (≥ 50%) + plaque characteristics and b) coronary stenosis (≥ 50%) + plaque characteristics + radiomics were formulated and compared in terms of AUCs accordingly. ***Results:*** The study analyzed 140 vessels having corresponding PET-MPI data and 152 vessels having SPECT MPI data. For PET-MPI, plaque burden and stenosis severity were identified as the only independent predictors of impaired myocardial perfusion, with an area under the curve (AUC) of 0.749 (95% CI: 0.658-0.826). However, when additional radiomics features were combined with stenosis severity, the prediction performance improved significantly, with an AUC of 0.854 (95% CI: 0.775-0.914, p-diff: 0.02, 95% CI: 0.0165-0.194). For SPECT-MPI, stenosis severity was the only predictor of a reversible perfusion defect, with an AUC of 0.624 (95% CI: 0.542-0.702). However, combining additional radiomics features with stenosis severity significantly improved the prediction performance, with an AUC of 0.816 (95% CI: 0.745-0.875, p-diff: 0.006, 95% CI: 0.152-0.329). ***Conclusion:*** Radiomic futures can be combined with anatomical and morphological characteristics of coronary lesions in CTCA imaging and provide valuable complementary information for characterizing functionally significant coronary lesions.

EPS-179

Volume dependence and repeatability of ^{99m}Tc SPECT radiomic parameters

A. Gemmell[1,2,3], *C. Brown*[1,2], *S. Ray*[3], *S. Small*[1,2];
[1]*Nuclear Medicine, Gartnavel General Hospital, Glasgow, UNITED KINGDOM,* [2]*Department of Clinical Physics & Bioengineering, Glasgow, UNITED KINGDOM,* [3]*School of Mathematics & Statistics, University of Glasgow, Glasgow, UNITED KINGDOM.*

Aim/Introduction: Guidelines on radiomics in Nuclear Medicine [1] have recommended that users test for volume dependence and repeatability of radiomic parameters, including proposing the use of a "revolver" phantom, originally applied to PET imaging by Forgacs et al [2]. This study applies a modified version of the suggested methodology to identify reproducible SPECT radiomics parameters using ^{99m}Tc. ***Materials and Methods:*** A uniform phantom containing 297 MBq of ^{99m}Tc was imaged and 15 Volumes of Interest (VoI) of increasing size ranging from 0.9 ml to 1021 ml were placed in the reconstructed image. 67 radiomics parameters (IBSI compliant) were calculated and correlated against the VoI size. Due to the poorer resolution of SPECT relative to PET, three "revolver" inserts were tested, each using 7 syringes of 2.5 ml, 5 ml and 10 ml syringes respectively. Each were filled with ^{99m}Tc in syringe:background concentrations of: 4:1, 8:1 and 16:1. The inserts were placed into a phantom and SPECT imaging performed four consecutive times. VoIs were drawn around the inserts using a SUV_{max} threshold of 2.5 times background. The mean and standard deviation for the 67 parameters was recorded and Coefficient of Variation (CoV) was calculated for comparison to the recommended criteria of CoV <10%. ***Results:*** For volume dependence, 32 features showed convergence above a minimum VoI size of 50 ml. 35 features showed increasing, decreasing or a random distribution with increasing VOI size. 4 parameters exceeded 10% CoV for the "revolver" insert constructed of 2.5 ml syringes, 6 parameters for the 5ml insert and 1 parameter for the 10 ml insert. Parameters in common across the three insert sizes that would be excluded from any future studies are Excess Kurtosis and multiple Grey Level Zone Length Matrix parameters. ***Conclusion:*** The guideline recommendation for phantom studies to assess volume dependence and repeatability of radiomics parameters can be applied to ^{99m}Tc SPECT imaging and can help to exclude features that will not prove reliable in radiomics patient studies. ***References:*** 1. Hatt M, Krizsan AK, Rahmim A, Bradshaw TJ, Costa PF, Forgacs A, et al. Joint EANM/SNMMI guideline on radiomics in nuclear medicine. Eur J Nucl Med Mol Imaging [Internet]. Springer Berlin Heidelberg; 2022; Available from: https://doi.org/10.1007/s00259-022-06001-6 2. Forgacs A, Pall Jonsson H, Dahlbom M, Daver F, Difranco MD, Opposits G, et al. A study on the basic criteria for selecting heterogeneity parameters of F18-FDG PET images. PLoS One. 2016;11:1-14.

EPS-180

The biological counterpart of radiomics in pancreatic cancer: a preliminary simulation study

L. Cavinato[1], *J. Hong*[2], *S. Reinhard*[2], *M. Wartenberg*[2], *F. Ieva*[1,3], *K. Shi*[2];
[1]*Politecnico di Milano, Milano, ITALY,* [2]*University of Bern, Bern, SWITZERLAND,* [3]*Human Technopole, Milan, ITALY.*

Aim/Introduction: Radiomics extracts quantitative features from medical images and use them to predict clinical outcomes. However, to fully realize the potential of radiomics, these features need to be associated with a biological meaning. Linking radiomics features to underlying biological processes is still an open matter, yet crucial to achieve a deeper understanding of disease mechanisms and identify potential biomarkers. In this work, we employ a multidisciplinary approach that integrates radiomics and other fields, to correlate radiomics features with biological characteristics of different tissues affected by pancreatic cancer at different stages. ***Materials and Methods:*** We analysed the histopathological samples (Whole Slide Imaging - WSI) of four patients affected by different stages of pancreatic cancer. Three different markers were used to stain patients' specimens to highlight different biological structures: CD31 antigen (Cluster of Differentiation 31) to marks (micro)vessels; the FAP (Fibroblast Activation Protein) that is usually expressed by stromal cells; the Ki67 antigen that is a marker of active cell proliferation in both normal and tumoral cell populations. We developed and implemented a simulation framework for estimating the spatiotemporal uptake throughout the tissues of the 18F-fluorothymidine tracer ([18F] FLT).The framework consisted of several steps including the creation of the computational domain from CD31 WSI and the implementation of a spatiotemporal model to describe the [18F]FLT uptake via Partial Differential Equations (PDE). From time-varying uptake maps of the tissues, we simulated the dynamic PET imaging and extracted 43 radiomic feature maps describing the tissue texture. Each of these feature maps was correlated with tissue biological characteristics (spatial location of vessel, stroma, and cell density), cell proliferation index and overall tracer uptake, and the overall tracer uptake with carcinoma grade describing tumour aggressiveness. We used Pearson correlation to quantify the relationship between the variables. ***Results:*** The overall uptake was higher in carcinomas with higher grades and lower in slides with no or reduced cancer. GLCM_features_Entropy (0.27), NGTDM_features_Complexity (0.26) and GLCM_features_Homogeneity (0.25) correlated the most with stromal tissue; GLCM_features_AutoCorrelation (0.15), GLSZM_features_LZHGE (0.13) and NGTDM_features_Complexity (0.12) correlated with cell density; GLCM_features_Entropy (0.54) , GLCM_features_Homogeneity (0.53) and GLRLM_features_LRE (0.51) with cells proliferation index. ***Conclusion:*** The proposed framework

represents a sound pipeline for evaluating the biological meaning of radiomics. With a properly extended sample size, this work can provide valuable insights into the biological counterpart of the texture analysis.

EPS-181

A machine learning approach based on rest myocardial perfusion image radiomics to detect the presence of hibernating myocardium: a single institutional experience on 239 patients with 371 perfusion defects

C. Patel, *B. Khangembam, J. Jaleel, A. Roy, P. Gupta;*
All India Institute of Medical Sciences, New Delhi, INDIA.

Aim/Introduction: To assess the feasibility of a machine learning (ML) approach using radiomics features of perfusion defects on rest myocardial perfusion imaging (MPI) to detect the presence of hibernating myocardium. ***Materials and Methods:*** Data of patients who underwent 99mTc-sestamibi MPI and 18F-FDG cardiac PET/CT for myocardial viability assessment were retrieved. Rest MPI data were processed on ECToolbox and polar maps were saved using NFile PMap tool. The gold standard for defining hibernating myocardium was the presence of mismatched perfusion-metabolism defect with impaired myocardial contractility at rest. Radiomics analysis was performed on LIFEx-7.3.21. Perfusion defects on the polar maps were delineated with regions of interest (ROIs) after spatial resampling and intensity discretization. Replicable random sampling allocated 80% (257) of the perfusion defects of the patients from January 2017 to September 2022 to the training set and the remaining 20% (64) to the validation set. An independent dataset of perfusion defects from 29 consecutive patients from October 2022 to January 2023 was used as the testing set for model evaluation. A total of 110 first and second-order texture features were extracted for each ROI. After feature normalization and imputation, 26 best-ranked features using Information Gain scoring were selected to train the ML algorithms. 13 ML algorithms were trained with 10-fold stratified cross-validation on the training set and validated on the validation set. The ML algorithms with a Log Loss of <0.688 and <0.672 in the cross-validation and validation steps respectively were evaluated on the testing set. Performance matrices of the algorithms assessed included area under the curve (AUC), classification accuracy (CA), F1 score, precision, recall, and specificity. ***Results:*** In total, 239 patients (214 males; mean age 56 ± 11 years) were enrolled in the study. On cross-validation, 6 ML algorithms had AUC >0.800. These were Support Vector Machine, Gradient Boosting (xgboost), Neural Network (NN), Random Forest (RF), Gradient Boosting (catboost) and Gradient Boosting Random Forest (xgboost). On validation, 5 ML algorithms had AUC >0.800 with RF achieving the highest AUC of 0.842. On model evaluation on the testing set, 7 ML models had AUC >0.800 with NN achieving the highest AUC of 0.877 and could decode hibernating myocardium in 21/29 (72.4%) perfusion defects with a precision of 87.5% (21/24), specificity 85.7% (18/21), CA 78.0% (39/50) and F1 Score 0.792. ***Conclusion:*** Machine learning using radiomics features of perfusion defects on rest myocardial perfusion images can decode the presence of hibernating myocardium.

EPS-182

Clinical Evaluation of ^{18}F-FDG PET Radiomics Stability to Respiratory Motion Using a Data-Driven Respiratory Gating Algorithm

K. Lue[1], *K. Kan*[2,3], *Y. Chen*[2,4], *S. Liu*[1,2], *I. Shih*[5], *H. Lin*[6,7];
[1]*Tzu Chi University of Science and Technology, Hualien, TAIWAN,* [2]*Hualien Tzu Chi Hospital, Hualien, TAIWAN,* [3]*Fu Jen Catholic University Hospital, New Taipei City, TAIWAN,* [4]*Tzu Chi University, Hualien, TAIWAN,* [5]*GE HealthCare, Taipei, TAIWAN,* [6]*Chang Gung University, Taoyuan, TAIWAN,* [7]*Keelung Chang Gung Memorial Hospital, Keelung, TAIWAN.*

Aim/Introduction: ^{18}F-FDG PET-based quantitative features are susceptible to respiratory motion. However, few studies have explored the impact of respiratory motion on ^{18}F-FDG PET radiomic features using clinical patient data. In this study, we investigated the stability of radiomics features in clinical ^{18}F-FDG PET images using a data-driven respiratory motion correction technique. ***Materials and Methods:*** Oncological pathologies of 65 patients who underwent whole-body ^{18}F-FDG PET scans using a digital PET/computed tomography system (Discovery MI, GE Healthcare, Milwaukee, USA) were retrospectively included in this study. A commercially available data-driven gating algorithm combined with a motion-correction technique (MotionFree, GE HealthCare, Milwaukee, USA) was used to extract the PET images with respiratory motion correction. ^{18}F-FDG-avid lesions from the lower lung to the upper abdomen were analysed using motion-corrected and non-motion-corrected images. The lesions were segmented with a 40% threshold of the maximum standardised uptake value to define the metabolic tumour volume (MTV). A total of 725 radiomic features were computed from the segmented images, including first-order, shape, texture, and wavelet features. The intraclass correlation coefficient (ICC) and coefficient of variation (COV) were calculated to evaluate feature reproducibility and variability. An ICC above 0.9 and a COV below 5% were considered high stability. All images were analysed using the PMOD image processing software version 4.2 (PMOD Technologies Ltd., Zurich, Switzerland). The Pyradiomics software package version 3.0.1 (Harvard Medical School, Boston, USA) was used to compute the radiomic features. Statistical analyses were performed using MedCalc 20.218 (MedCalc Software, Ostend, Belgium). ***Results:*** In total, 133 lesions with and without respiratory motion correction were analysed. The median MTV was 2.60 mL (interquartile range: 1.69-6.28 mL). Our results indicated that ^{18}F-FDG PET radiomics features are sensitive to respiratory motion. For lesions with MTV larger than 3 mL, 13 radiomic features were very stable, including first-order_entropy, shape_sphericity, grey-level cooccurrence matrix (GLCM) sum entropy, three grey-level run length matrix (GLRLM) features (run_entropy, run_percentage, and short_run_emphasis), and seven wavelet features (first-order_entropy, GLCM_joint_entropy, GLCM_sum_entropy, GLRLM_run_entropy, GLRLM_run_length_nonuniformity_normalized, GLRLM_run_percentage, GLRLM_short_run_emphasis) in the three axes of PET images in low-pass filtering (wavelet-LLL). For all lesions, only six features (GLRLM_run_entropy, shape_sphericity, wavelet-LLL_first-order_entropy, wavelet-LLL_GLCM_joint_entropy, wavelet-LLL_GLCM_sum_entropy, and wavelet-LLL_GLRLM_run_entropy) were highly stable for respiratory motion. ***Conclusion:*** Respiratory motion has a significant impact on ^{18}F-FDG PET radiomic stability. Several highly stable features were identified that may be potential candidates for machine-learning modelling.

EPS-183

Does fdg pet-based radiomics have an added value for prediction of overall survival in non-small cell lung cancer?

G. Giovacchini[1], *E. Giovannini*[1], *F. Tutino*[1], *A. Milano*[1], *L. Florimonte*[2], *E. Bonatto*[3], *C. Bareggi*[2], *L. Dellavedova*[4], *A. Castello*[5], *C. Aschele*[1], *M. Castellani*[2], *A. Ciarmiello*[1];
[1]*S. Andrea Hospital, La Spezia, ITALY,* [2]*Fondazione IRCCS Ca' Granda, Milano, ITALY,* [3]*University of Milan, Milano, ITALY,* [4]*ASST Ovest Milanese, Legnano, ITALY,* [5]*IRCCS Ca' Granda, Milano, ITALY.*

Aim/Introduction: Machine-learning and radiomics are promising approaches to improve the clinical management of NSCLC. However, the additive value compared to clinical and standard imaging variables is less investigated. We aimed to assess the prognostic role of combined use of machine-learning and radiomics in NSCLC patients. ***Materials and Methods:*** 320 NSCLC patients underwent PET/CT with FDG. A total of 49 predictors, including 43 textural features extracted from PET studies, and SUVmax, MTV, TLG, TNM stage, age and gender. A least absolute shrinkage and selection operator (LASSO) regression was used to select features with highest predictive value. Overall survival were calculated with Kaplan-Meier curves. ***Results:*** Five variables including one textural feature (NGTDM coarseness), SUVmax and TNM stage (stage II, stage III, stage IV) showed highest predictive value at LASSO regression analysis. These variables were used to create a test model (TNM, SUVmax and NGTDM Coarseness) and a reference model (TNM, SUVmax). The test model did not significantly better predict survival in NSCLC patients than the reference model. ***Conclusion:*** These data indicate that radiomics, as selected and assessed by our study design, should not be used as an additional tool in clinical practice to predict prognosis when tumor stage and SUVmax, as derived by FDG PET, are available

EPS-184

Improving Outcome Prediction in Multicentric Data: Novel harmonization and clustering Techniques for Radiomic Feature Analysis

N. Abdallah[1], *J. Marion*[2], *C. Tauber*[1], *T. Carlier*[3], *P. Chauvet*[2], *M. Hatt*[4];
[1]*Imaging & Brain, INSERM, Tours, FRANCE,* [2]*LARIS, Angers, FRANCE,* [3]*CRCINA, INSERM, CNRS, Université d'Angers, Université de Nantes, Nantes, FRANCE,* [4]*LaTIM, INSERM, Brest, FRANCE.*

Aim/Introduction: This study aimed at developing a survival analysis pipeline incorporating innovative clustering and harmonization techniques, explicitly addressing the multicentre nature of the data to maximize outcome prediction. ***Materials and Methods:*** We introduced a linear regression (RL) harmonization approach and compared it to ComBat. We also developed two novel methods for training separate models for two sub-populations of the cohort: one based on a latent feature generated from a Partial Least Squares (PLS) Regression model, the other based on clustering according to the feature most correlated with progression-free. IBSI-compliant features were extracted with PyRadiomics, followed by feature selection. Survival analysis employed Random Survival Forest (RSF) and Gradient Boosting (GB), with performance evaluated using the concordance index (C-index). We evaluated our pipeline using the HECKTOR 2021 dataset containing 325 head and neck cancer patients from six clinical centers. FDG PET/CT images with expert-defined GTV masks were provided for Pyradiomics feature extraction. Clinical variables with missing values were imputed using a Logistic Regression Model trained for each variable. ***Results:*** The base model (without clustering) achieved a c-index of 0.64 using the RSF method and our RL harmonization approach on CT features. The c-index increased to 0.69 when combining CT features, PET features, and clinical variables with imputed values. Using PLSRegression clustering, a maximum weighted c-index of 0.70 was reached with ComBat harmonization and the RSF method on concatenated CT and PET features with imputed clinical variables. For the first cluster, the highest c-index of 0.82 was achieved using our RL harmonization approach on PET images concatenated with imputed clinical variables. For the second cluster, the highest c-index was 0.69, utilizing concatenated CT and PET features with imputed clinical variables and ComBat harmonization. We also investigated clustering using features most correlated with time, achieving a maximum weighted c-index of 0.682 based on the c-index of 0.642 (RSF) in cluster 1 and 0.728 in cluster 2. ***Conclusion:*** Relying on models trained specifically on sub-populations of the cohorts automatically determined through clustering improved the overall model, as demonstrated in this study. The base model had a c-index of 0.68, while our novel clustering approaches combined with harmonization achieved a maximum c-index of 0.70. Additionally, we emphasized the importance of using imputed clinical variables for survival analysis, as shown by the increase in c-index from 0.64 to 0.69.

EPS-185

[18F]FDG-PET/CT Tumor Spread and Dissemination Measured from the Spleen in Lymphoma: How Predictive of the Outcome?

K. Girum[1], *A. Cottereau*[2], *J. Clerc*[2], *L. Vercellino*[3], *O. Casasnovas*[4], *F. Morschhauser*[5], *C. Thieblemont*[6], *I. Buvat*[1];
[1]*LITO laboratory, U1288 Inserm, Institut Curie, University Paris-Saclay, Orsay, FRANCE,* [2]*Department of Nuclear Medicine, Cochin Hospital, AP-HP, Paris Descartes University, Paris, FRANCE,* [3]*Department of Nuclear Medicine, Saint-Louis Hospital, AP-HP, Paris, FRANCE,* [4]*Department of Hematology, University Hospital of Dijon, Dijon, FRANCE,* [5]*Department of Hematology, Claude Huriez hospital, University Lille, EA 7365, Research Group on Injectable Forms and Associated Technologies, Lille, FRANCE,* [6]*Department of Hematology, Saint Louis Hospital, AP-HP, Paris, FRANCE.*

Aim/Introduction: To investigate the predictive value of new baseline [18F]-FDG PET/CT features that characterize how tumor spreads and disseminates in Diffuse Large B-Cell Lymphoma (DLBCL) patients. Assuming the spleen plays a particular role in DLBCL, we assessed whether spleen-based features improved the prediction of progression-free survival (PFS) and overall survival (OS) when combining them with the total metabolic tumor volume (TMTV). ***Materials and Methods:*** This is a retrospective analysis of DLBCL patients from the REMARC (NCT01122472) cohort. Experts delineated lymphoma lesions on the [18F]-FDG PET/CT images, from which the TMTV and recently introduced tumor dissemination features (Dmax (distance between two farthest lesions) and Dbulk (the maximum distance between the largest lesion and another lesion)) were calculated. Artificial intelligence method was used to segment the spleen from the CT images [1]. An image-processing pipeline was developed to check the quality of the spleen segmentation and correct it. The distance between the centroid of the spleen and all other lesions was measured. The standard deviation (SD) of the measured distances was defined as the lesion spread (LS). The maximum distance of a lesion from the spleen for each patient (DLS) was computed. Univariate and multivariate survival analyses were evaluated using Kaplan-Meier estimates and time-dependent receiver-operating-characteristic curves (tdAUC).

Results: 282 patients (mean age ± SD, 68.33 ± 5.42, y; 164 men) were evaluated. LS and DLS were uncorrelated with TMTV (Pearson r<0.23) and moderately correlated with Dmax and Dbulk (r≤0.78). The median values, used as a cut-off value in the Kaplan-Meier survival analysis, were 6.67 and 32.43 cm, respectively. LS and DLS classified patients into two-risk groups significantly for PFS and OS (P<0.001). The hazard ratios (95% confidence interval) for OS were DLS: 19.4 (2.9-90.7), LS: 10.3 (1.6-46.1), TMTV: 17.6 (2.1-82.5), Dmax: 6.4 (1.0-18.7), Dbulk: 7.9 (1.2-28.6), and IPI: 5.9 (1.3-16.3). The tdAUC (95% confidence interval) for OS were DLS: 0.6 (0.6-0.7), LS: 0.6 (0.6-0.7), TMTV: 0.7 (0.6-0.7), Dmax: 0.6 (0.5-0.7), Dbulk: 0.6 (0.5-0.7), and IPI: 0.6 (0.5-0.7). Combining TMTV with LS or DLS can classify the patients into three-risk groups for both OS and PFS significantly (P<0.001). ***Conclusion:*** The two introduced simple LS and DLS PET/CT features characterizing the lesion locations with respect to the spleen are predictive of PFS and OS in DLBCL. Both biomarkers complement TMTV to characterize the disease. Further evaluation on an external cohort and other lymphatic diseases is underway. ***References:*** [1] Wasserthal et al., arxiv, 2022

EPS-187

Quantitative Analysis of Dual Time Point in FDG PET/CT images

N. Reshtebar[1], *S. Hosseini*[1], *A. Rahmim*[2], *p. Sheikhzadeh*[3]; *[1]Sharif University of Technology, Tehran, IRAN, ISLAMIC REPUBLIC OF, [2]University of British Columbia, Vancouver, BC, CANADA, [3]Tehran University of Medical Sciences, Tehran, IRAN, ISLAMIC REPUBLIC OF.*

Aim/Introduction: In single-time-frame whole-body PET/CT, the SUV parameter is commonly utilized for assessment of disease. By contrast, dynamic imaging can provide significant information via extraction of kinetic features and quantitative analysis based on temporal information. We aimed to assess textural features in parametric Patlak K_i images as generated from dual time point images in comparison with K_i from entire data (Standard Patlak) and SUV images. ***Materials and Methods:*** The XCAT human torso phantom was used to simulate dynamic whole-body FDG PET imaging. Thirty-nine realistic tumors were modeled in lung tissue with various irregularly shaped heterogeneities and varying levels of uptake. Finally, the texture features in parametric K_i (Patlak-DTP) images (at 60-min post injection for early and 90-min post injection for the late scan) in comparison with K_i (Patlak-full) ^{18}F-FDG WB PET and SUV images were assessed. ***Results:*** Using the 40% threshold segmentation, The average value of MTV in K_i (Standard Patlak) and K_i (Pat-DTP) images was smaller than (28%) average value of this parameter in SUV images. It was also observed that most mean radiomics features did not significantly differ between K_i (Standard Patlak) and K_i (Pat-DTP) images, and there was high correlation (>80%) between the evaluated texture features in K_i (Standard Patlak) and K_i (Pat-DTP) images. ***Conclusion:*** A simulation study was used to assess performance of heterogeneity metrics in parametric K_i (Pat-DTP) images (at 60-min post injection for early and 90-min post injection for the late scan). Quantitative analysis indicated that parametric K_i (Pat-DTP) images may have larger heterogeneity than SUV images. We concluded that parametric K_i (Pat-DTP) images from dual-time-point imaging can be an alternative to more common parametric K_i (Standard Patlak) images, and can provide complementary images with respect to conventional SUV. ***References:*** Kotasidis FA, Tsoumpas C, Rahmim A. Advanced kinetic modelling strategies: Towards adoption in clinical PET imaging. Clin Transl Imaging . Rahmim A, Lodge MA, Karakatsanis NA, Panin VY, Zhou Y, McMillan A, et al. Dynamic whole-body PET imaging: principles, potentials and applications. Eur J Nucl Med Mol Imaging 2019;. Zhuang M, Karakatsanis NA, Dierckx RAJO, Zaidi H. Quantitative Analysis of Heterogeneous [18F]FDG Static (SUV) vs. Patlak (Ki) Whole-body PET Imaging Using Different Segmentation Methods: a Simulation Study. Mol Imaging Biol 2019;. Zaker N, Kotasidis F, Garibotto V, Zaidi H. Assessment of Lesion Detectability in Dynamic Whole-Body PET Imaging Using Compartmental and Patlak Parametric Mapping. Clin Nucl Med 2020;45:.

EPS-188

Predicting overall survival in non-Hodgkin lymphoma patients using baseline ^{18}F-FDG PET radiomic features

T. Husevåg, *A. M. Løndalen, J. Blakkisrud, C. Stokke; Oslo University Hospital, Oslo, NORWAY.*

Aim/Introduction: [^{177}Lu]Lu-lilotomab satetraxetan was developed as an anti CD37 radioimmunotherapy and investigated in a phase 1/2a study for relapsed / refractory indolent non-Hodgkin B-cell lymphoma. This study aims to investigate the relationship between radiomic features extracted from tumour volumes in positron emission tomography (PET) images at baseline and the patient outcome, to identify potential imaging biomarkers with prognostic potential. ***Materials and Methods:*** The LYMRIT37-01 activity escalation study included administration of 10-20 MBq per kg of body weight of [^{177}Lu]Lu-lilotomab satetraxetan to non-Hodgkin lymphoma patients, with varying pre-treatment and pre-dosing of rituximab and lilotomab, across five study arms. Using 2-[^{18}F]FDG PET-images at baseline from 28 patients, 107 radiomic features (RFs) were extracted following the imaging biomarker standardization initiative [1]. The tumour volumes of interest (VOIs) were segmented by thresholding in the SUV3.0 to SUV4.0 range, with manual corrections for physiological uptake in collaboration with a nuclear medicine physician. First-order, shape-based and texture-features were extracted from a single VOI for each patient. The patients were followed up until 10.4 years post-treatment to assess overall survival (OS). Clinical factors such as age, bodyweight, and gender were also assessed as covariates. An elastic-net regularized cox proportional hazard model was used for predicting overall survival. Using leave-one-out cross-validation with nested 3-fold cross-validation for hyperparameter tuning, the RFs having stable non-zero coefficients were identified and used for prediction. ***Results:*** The median survival for all patients was 6.09 years. Using clinical factors, only age obtained a non-zero model weight with a hazard ratio of 1.043. The model scored a concordance-index (c-index) of 0.578, an integrated brier score (IBS) of 0.207, and a cumulative dynamic area under the receiver operating characteristic (CDAUC) of 0.506. Age and three texture-features were selected, scoring a c-index of 0.736, IBS of 0.170, and CDAUC 0.709. Stratifying the survival data by median predicted risk yielded significantly different survival probabilities under the log-rank test (p=0.039). NGTDM-busyness had the highest hazard rate at 1.370, while GLCM-IMC had the lowest at 0.629. ***Conclusion:*** Radiomic features from 2-[^{18}F]FDG PET images at baseline demonstrated the potential to predict overall survival, with three texture-features identified as stable predictors having complementary information to the baseline age. As the patient cohort is small, there are treatment variations across study arms and subsequent treatments, validation is needed to assess the reproducibility of the results. ***References:*** [1] Zwanenburg et al., "Image biomarker standardisation initiative - feature definitions", Dec. 2016.

1210

Tuesday, September 12, 2023, 08:00 - 09:30
Hall K

CTE 6 - Technologists Committee: Extravasation Incidents Management

OP-595
Extravasation incidents – theoretical principles and examples in Conventional Nuclear Medicine
M. Cruz;
Centro Hospitalar de Lisboa Ocidental, EPE - Hospital de Santa Cruz, Nuclear Medicine, Carnaxide, PORTUGAL.

OP-596
Extravasation incidents with PET agents and contrast media
J. Elliott;
Canterbury Christ Church University, School of Allied and Public Health Professions (Diagnostic Radiography), Canterbury, UNITED KINGDOM.

OP-597
Extravasation in radionuclide therapy – a step by step guide
N. Ahmadi Bidakhvidi;
UZ Leuven, Nuclear Medicine and Molecular Imaging, Leuven, BELGIUM.

1211

Tuesday, September 12, 2023, 08:00 - 09:30
Hall G1

Special Symposium 4 - Lung scintigraphy for pulmonary embolism diagnosis and long term management

OP-598
Clinical challenge of acute pulmonary embolism diagnosis
H. Robert-Ebadi;
Division of angiology and hemostasis, Geneva, SWITZERLAND.

OP-599
Clinical challenge of long-term management after an acute pulmonary embolism
G. Le Gal;
Universityof Ottawa, Department of Medicine, Ottawa, CANADA.

OP-600
Role and interpretation of lung scintigraphy for the diagnosis and follow up of pulmonary embolism
P. Le Roux;
UniversityHospital of Brest, Department of Nuclear Medicine - UMR U1304 -GETBO, Brest, FRANCE.

1301

Tuesday, September 12, 2023, 09:45 - 11:15
Hall A

CME 10 - Radiation Protection + Paediatrics Committee + Women´s Empowerment Task Force: Radiation Protection in Motherhood and Childhood - What is so Special?

OP-602
Radiobiological aspects to consider during pregnancy, neonates and small children
U. Eberlein;
Universityof Würzburg, Department of Nuclear Medicine, Würzburg, GERMANY.

OP-603
Dilemmas of the pregnant or breastfeeding radiation worker, patient and carer
S. Leide-Svegborn;
Department of Radiation Physic, Skåne University Hospital Malmö, Lund University, Lund, SWEDEN.

OP-604a
Common diseases during childhood and the role of Nuclear Medicine
P. Zucchetta;
Universityof Padua, Nuclear Medicine Unit, Padua, ITALY.

OP-604b
Family management in therapeutics and diagnostics of children
L. Cunha;
IsoPor-Azores, Department of Nuclear Medicine and Molecular Imaging, Azores, PORTUGAL.

1302

Tuesday, September 12, 2023, 09:45 - 11:15
Hall D (Arena)

Debate 4 - Physics + Oncology & Theranostics Committee: Whole Body Parametric Imaging

OP-605
Whole-body parametric imaging is ready for clinic
A. Tavares;
University/BHF Centre for Cardiovascular Science, University of Edinburgh, The Queen's Medical Research Institute, Edinburgh, UNITED KINGDOM.

OP-606
Whole-body parametric imaging is not ready for clinic
D. Visvikis;
National Institute of Health and Medical Research (INSERM), Medical Image Processing Lab, Brest, FRANCE.

1303

Tuesday, September 12, 2023, 09:45 - 11:15
Hall E1

LIPS Session 10 - Neuroimaging Committee: The Sunrise of Alpha-Synuclein in vivo Brain Imaging

OP-611
The Need of an Alpha-Synuclein Biomarker
R. Smith;
Lund University, Memory Clinic at Skåne University Hospital, Lund, SWEDEN.

OP-612
Alpha-Synuclein in Parkinson's Disease
D. Van Weehaeghe;
KU Leuven UZ Gasthuisberg, Division of Nuclear Medicine, Leuven, BELGIUM.

OP-613a
Alpha-Synuclein in Lewy Body Dementia
N. Tolboom;
UniversityMedical Centre Utrecht, Department of Radiology, Utrecht, NETHERLANDS.

OP-613b
Alpha-Synuclein in Multi System Atrophy
H. Barthel;
Leipzig University Medical Centre, Department of Nuclear Medicine, Leipzig, GERMANY.

1304

Tuesday, September 12, 2023, 9:45 AM - 11:15 AM
Hall E2

M2M Track - TROP Session: Emerging Theranostic Concepts

OP-614
Radio-theragnostics targeting CXCR4 based on the endogenous ligand EPI-X4 for oncological applications
R. Gaonkar[1], *J. Millul*[1], *R. Mansi*[1], *M. Harms*[2], *J. Münch*[2], *M. Fani*[1];
[1]University Hospital Basel, Basel, SWITZERLAND, [2]Institute of Molecular Virology, Ulm University Medical Center, Ulm, GERMANY.

Aim/Introduction: The C-X-C chemokine receptor 4 (CXCR4) is highly expressed in various cancers and plays an important role in proliferation and metastasis, while its level of expression is correlated with poor prognosis. Previously we had reported on radiolabeled derivatives (work presented in EANM 2022) from Endogenous Peptide Inhibitor of CXCR4 (EPI-X4), a human serum albumin fragment (1). The derivative ^{68}Ga-/^{177}Lu-JMF-04 (dILRWSRKK(^{68}Ga-/^{177}Lu-DOTA)-NH_2) was able to visualize CXCR4 expressing tumors in xenografted mice. However, it had undesirably high kidney uptake and therefore in a follow-up structure optimization study, we developed two optimized derivatives, JMF-10 and JMF-11, reported herein. ***Materials and Methods:*** JMF-10 and JMF-11 were labeled with Lu-177 and compared against the lead ^{177}Lu-JMF-04. Their hydrophilic nature was assessed via log D values, and the shelf-life was determined at room temperature at 1 up to 24h. SPECT/CT images (200 pmol, 15MBq) and biodistribution studies (200 pmol, 1MBq) were performed in CXCR4-expressing Jurkat T cell xenografts at 1 h post injection (p.i.) followed by performing blocking studies using AMD3100 in high excess. Additionally, in vivo the metabolic stability of ^{177}Lu-JMF-10 was evaluated in blood, while PET/CT imaging and biodistribution studies were performed with ^{68}Ga-JMF-10, in a theragnostic approach. ***Results:*** Radiochemical yield of the radioligands was >95% and remained >90% after 4h. At 24h, ^{177}Lu-JMF-10 showed higher stability than ^{177}Lu-JMF-11 and ^{177}Lu-JMF-04 (79±1% vs. 72±2% vs. 66±0%, respectively). ^{177}Lu-JMF-10 and ^{177}Lu-JMF-11 displayed similar lipophilicity (log D = -2.99±0.1 and -2.88±0.3, respectively), being higher than that of ^{177}Lu-JMF-04 (-3.45±0.1). Both, ^{177}Lu-JMF-10 and ^{177}Lu-JMF-11 were able to visualize CXCR4-expressing tumors and showed significant reduced accumulation in the kidneys as compared to ^{177}Lu-JMF-04 in SPECT/CT imaging studies. Biodistribution studies at 1h, revealed a 15-fold reduction in the kidneys for ^{177}Lu-JMF-10 and ^{177}Lu-JMF-11 (~5% %IA/g), as compared to ^{177}Lu-JMF-04 (83±25 %IA/g), without hampering the tumor uptake (1.5-2 %IA/g). ^{177}Lu-JMF-10 displayed the best tumor-to-background ratios and remained ~50% intact in the blood 30 min p.i. Its ^{68}Ga-counterpart, ^{68}Ga-JMF-10, behaved identically to ^{177}Lu-JMF-10 in the PET/CT imaging and biodistribution studies. ***Conclusion:*** Structural optimization of the endogenous CXCR4 antagonist EPI-X4 led to the identification of new radioligands with significantly improved biodistribution profile and lower unspecific accumulation in non-targeted organs without compromising the tumor uptake. Among the developed derivatives, ^{177}Lu/^{68}Ga-JMF-10 was identified as the best theragnostic pair for CXCR4-expressing malignancies. ***References:*** 1.Zirafi O et al., Cell Reports 11, 737-747, 2015.

OP-615
Next Generation Theranostics Based on the Tetrazine Ligation
U. Battisti[1,2], *V. Shalgunov*[1], *C. B. M. Poulie*[1], *L. Hvass*[3], *M. Muller*[2], *A. S. Clausen*[3], *E. Hansson*[4], *E. H. K. Aneheim*[5], *M. El Fakiri*[6], *M. Eder*[6], *S. Lindegren*[5], *A. Kjaer*[3], *H. J. Jensen*[7], *A. T. I. Jensen*[1], *M. M. Herth*[1,2];
[1]Tetrakit Technologies, Copenhagen, DENMARK, [2]Department of Drug Design and Pharmacology, Faculty of Health and Medical Sciences, University of Copenhagen, Copenhagen, DENMARK, [3]Department of Clinical Physiology and Nuclear Medicine & Cluster for Molecular Imaging, Copenhagen University Hospital – Rigshospitalet & Department of Biomedical Sciences, University of Copenhagen, Copenhagen, DENMARK, [4]Atley solution, Gothenburg, SWEDEN, [5]Sahlgrenska Academy, University of Gothenburg, Gothenburg, SWEDEN, [6]Faculty of Medicine, Albert-Ludwigs-Universität Freiburg, Freiburg, GERMANY, [7]PET and Cyclotron Unit, Copenhagen University Hospital, Copenhagen, DENMARK.

Aim/Introduction: Radiolabeling with ^{18}F/^{211}At employs complex radiosynthesis with multi-step purifications. Procedures are typically not quantitative and not compatible with aqueous media. In particular, no easily implementable method exists for employing ^{18}F/^{211}At as a theranostic pair. Last year´s Nobel Prize in chemistry highlighted the promise of click chemistry in addressing such challenges. Unfortunately, conventional click chemistry is too slow to reach completion for micromolar scale reactions. Reaction times of month would be needed. Recently, the tetrazine ligation has been explored as next generation click chemistry with rate constants suitable for quantitative radiolabeling within 5-10 minutes. [1, 2] However, this reaction results in a complex

mixture of isomers which can be an unsurmountable challenge for regulatory approval. [3] Here, we present a new radiolabeling technology, which provides just a single isomeric product from the tetrazine ligation within 20 minutes, without the need for any purification. This methodology holds the promise of labeling any targeting vector with ^{18}F/^{211}At. ***Materials and Methods:*** In order to avoid the formation of multiple isomers, a new trans-cyclooctene (T4CO) was developed. T4CO was synthesized and conjugated to two established vectors; PSMA and octreotate. ^{18}F/^{211}At-tetrazines were synthesized[4, 5] and clicked to the vectors. The procedure was performed at room temperature using micromolar starting amount of the vectors. All ^{18}F-structures were µPET scanned in naïve and tumor bearing mice. Different linkers were employed to optimize the excretion profile. The lead PSMA analogue was labeled with ^{211}At and evaluated in ex vivo biodistribution studies. ***Results:*** Radiolabeled tetrazines were clicked quantitively to the T4CO-vectors resulting in ready-to-inject radiopharmaceuticals within 20 minutes. All products were isomerically pure with a RCP ≥ 95%, thus avoiding the need of HPLC purification. ^{18}F-derivatives demonstrated tumor uptake in vivo. Careful design of the linkers with respect to polarity and overall net charge allowed to steer the excretion profile of these radiopharmaceuticals. Our best ^{18}F-PSMA targeting ligand showed a comparable tumor and excretion pattern as ^{68}Ga-PSMA-11/^{18}F-PSMA-1007. The ^{211}At version of our lead showed promising results in ex vivo biodistribution studies in tumor bearing mice indicating that it can be used as a therapeutic. ***Conclusion:*** We have demonstrated that the tetrazine ligation can be used to ^{18}F/^{211}At-labelel any targeting vector. Our platform can produce ready-to-inject radiopharmaceuticals within minutes without the need of purification. ***References:*** 1. BioconjugateChem. 2022, 1393. 2. Bioorg.Med. Chem.Lett. 2011, 5011. 3. J.A.C.S. 2018, 3603. 4. Chemical Science, 2021, 11668. 5. J.Med.Chem. 2021, 15297.

OP-616

CD83 as a Theranostic Target for Acute Myeloid Leukemia

K. Ott[1], *A. J. Robertson*[1], *J. P. Gallant*[1], *K. K. Walton*[2], *B. C. Betts*[2], *A. M. LeBeau*[1];
[1]*The University of Wisconsin-Madison, Madison, WI, UNITED STATES OF AMERICA,* [2]*The University of Minnesota, Minneapolis, MN, UNITED STATES OF AMERICA.*

Aim/Introduction: Acute Myeloid Leukemia (AML) is the most common form of acute leukemia among adults, accounting annually for the majority of leukemia related deaths in the US. Patients with AML are additionally at an increased risk of developing myeloid sarcomas (MS). MS is reported in 2-8% of AML patients as a single or multifactorial tumor and has been increasingly seen as an initial manifestation of relapse in previously treated AML patients in remission. Patients presenting with MS concurrent with AML is traditionally considered a marker for poor clinical outcome and shorter survival (5-year survival: 28%). Management and treatment of the disease is often hindered by dose limiting toxicity and drug resistance. In an effort to overcome these issues, we have identified the target antigen, CD83, which is uniquely overexpressed across AML subtypes. Using phage display we identified an anti-CD83 camelid antibody (C10) and engineered into a number of constructs. Here, we aim to use these novel camelid constructs as a platform theranostic technology for the imaging of AML associated MS as well for the development of a novel CD83 drug conjugate treatment. ***Materials and Methods:*** Biolayer interferometry (BLI) and Flow Cytometry were used to assess binding ability of the camelid antibody constructs for CD83. For imaging studies, mice bearing subcutaneous U937 xenografts were injected with ^{89}Zr-labeled C10-Fc and imaged for up to 144H post-injection. Injected dose per gram quantities were determined for non-specific and tumor-specific tissues. Cell viability assays using the AML cell line, U937, were used to determine the specificity, efficacy, and potency of the developed C10-Fc anthracycline based drug conjugate. ***Results:*** Engineering the C10 camelid antibody into a human Fc scaffold (C10-Fc) increases affinity for CD83 by 16-fold (K_D = 39.8 nM:2.60 nM) as determined by BLI. C10-Fc binds cellularly expressed CD83 with even greater affinity (K_D = 44.98 pM) making the construct suitable for in vivo experimentation. As an nuclear imaging agent, [^{89}Zr]Zr-C10-Fc rapidly localizes to the tumor site at 4h and largely remains up to 48h with little background from non-specific tissues. The C10-Fc drug conjugate is highly potent against the U937 AML cell line with an IC_{50} of 0.308 nM. ***Conclusion:*** We conclude that our anti-CD83 camelid antibody construct, C10-Fc, is an effective theranostic tools for PET imaging of AML as well as for the delivery of highly potent drugs.

OP-617

Development of [^{18}F]F-[^{nat}Lu]Lu-/[^{19}F]F-[^{177}Lu]Lu-DOTA-rhCCK-84, a Radiohybrid-Based Minigastrin Analogue With High Tumour and low Kidney Accumulation: A Viable Clinical Option for Imaging and Radioligand Therapy of Medullary Thyroid Carcinoma?

T. Günther[1], *N. Holzleitner*[1], *I. Maniyankerikalam*[1], *L. Greifenstein*[2], *R. Beck*[1], *D. Di Carlo*[1], *R. P. Baum*[2], *H. Wester*[1];
[1]*Technical University of Munich, Garching, GERMANY,* [2]*CURANOSTICUM Wiesbaden-Frankfurt, Wiesbaden, GERMANY.*

Aim/Introduction: To address kidney retention issues of previous radiohybrid-based minigastrin analogues, such as [^{18}F]F-[^{nat}Lu]Lu-/[^{19}F]F-[^{177}Lu]Lu-DOTA-rhCCK-18 ([^{18}F]F-[^{nat}Lu]Lu-/[^{19}F]F-[^{177}Lu]Lu-DOTA-dap(SiFA)-(γ-glu)$_8$-Ala-Tyr-Gly-Trp-Asp-Nle-Phe-NH$_2$), we substituted negatively charged D-γ-glutamate by hydroxyproline (Hyp) moieties and introduced a polyethylene glycol moiety, which yielded DOTA-rhCCK-84 (DOTA-dap(SiFA)-γ-glu-(Hyp)$_6$-γ-glu-(PEG)$_3$-Trp-(N-Me)Nle-Asp-1-Nal-NH$_2$). In vitro and in vivo properties of [^{18}F]F-[^{nat}Lu]Lu-/[^{19}F]F-[^{177}Lu]Lu-DOTA-rhCCK-84 were investigated via state-of-the-art experiments and compared to internal ([^{18}F]F-[^{nat}Lu]Lu-/[^{19}F]F-[^{177}Lu]Lu-DOTA-rhCCK-18) and external references ([^{68}Ga]Ga-/[^{177}Lu]Lu-DOTA-MGS5) to pave the way for a first-in-man application. ***Materials and Methods:*** ^{177}Lu-labelling was performed at 90°C within 15 min (1.0 M NaOAc buffer, pH=5.5). ^{18}F-labelling was conducted via isotopic exchange reaction at 60°C within 5 min (ammonium formate in anhydrous DMSO) using previously dried [^{18}F]fluoride (~400 MBq) with subsequent purification by cartridge. CCK-2R affinity (IC_{50}, n=3) was evaluated on AR42J cells. In vivo stability was investigated at 30 min post-injection (p.i.) in CB17-SCID mice (n=3). Biodistribution studies were carried out at 1 and 24 h p.i. in AR42J tumour-bearing CB17-SCID mice (n=4, 100 pmol each). ***Results:*** ^{177}Lu-labelling resulted in radiochemical yields (RCY) and purities (RCP) of >99% and molar activities of 30-40 GBq/µmol. ^{18}F-labelling resulted in RCYs and RCPs of 15-45% and >95%, respectively, and molar activities of up to 85 GBq/µmol. [^{19}F]F-[^{nat}Lu]Lu-DOTA-rhCCK-84 showed a slightly lower CCK-2R affinity than [^{19}F]F-[^{nat}Lu]Lu-DOTA-rhCCK-18 and [^{nat}Lu]Lu-DOTA-MGS5 (IC_{50} (nM): 7.9±0.3 versus 4.7±0.6 and 5.2±0.8, respectively). Lipophilicity (expressed as n-octanol/PBS distribution coefficient, $logD_{7.4}$, n ≥5) of [^{19}F]F-[^{177}Lu]Lu-DOTA-rhCCK-84 was comparable or slightly higher than those

of [19F]F-[177Lu]Lu-DOTA-rhCCK-18 and [177Lu]Lu-DOTA-MGS5 (−2.14±0.06 versus −2.69±0.06 and −2.21±0.08, respectively). In vivo, [18/19F]F-[nat/177Lu]Lu-DOTA-rhCCK-84 revealed high stability at 30 min p.i. (94±2% intact in serum, 55±9% in urine) and a noticeably higher tumour accumulation than [18/19F]F-[nat/177Lu]Lu-DOTA-rhCCK-18 at 1 h p.i. (36.3±3.7 versus 24.1±4.2 %ID/g, respectively), while kidney uptake was distinctly lower (16.8±1.1 versus 97.2±14.0 %ID/g, respectively). At 24 h p.i., [19F]F-[177Lu]Lu-DOTA-rhCCK-84 exhibited slightly lower activity levels in the tumour than [19F]F-[177Lu]Lu-DOTA-rhCCK-18 and higher levels than [177Lu]Lu-DOTA-MGS5 (18.8±1.4 versus 25.4±4.7 and 10.9±1.2 %ID/g, respectively), while activity levels in the kidneys were distinctly lower than those of [19F]F-[177Lu]Lu-DOTA-rhCCK-18 and only slightly higher than those of [177Lu]Lu-DOTA-MGS5 (9.5±1.7 versus 134±18 and 1.3±0.4 %ID/g, respectively). Based on these encouraging results, clinical translation of [18F]F-[natLu]Lu-/[19F]F-[177Lu]Lu-DOTA-rhCCK-84 has already been initiated. ***Conclusion:*** In contrast to previous radiohybrid-based minigastrin analogues, [18F]F-[natLu]Lu-/[19F]F-[177Lu]Lu-DOTA-rhCCK-84 displayed distinctly lower activity levels in the kidneys, while high tumour accumulation and retention was retained. A first-in-man application of [18/19F]F-[nat/177Lu]Lu-DOTA-rhCCK-84 will elucidate whether this compound could be a viable option for imaging and radioligand therapy of medullary thyroid cancer.

OP-618

Construction and preclinical evaluation of a 124/125Ilabeled specific antibody targeting CD147 in pan-cancer

X. Ma, *T. Liu, H. Zhu, Z. Yang;*
Peking University Cancer Hospital, Beijing, CHINA.

Aim/Introduction: Objectives:Tumor microenvironment (TME) is a multifaceted and dynamic environment that surrounds tumors, consisting of immune cells, signaling molecules, blood vessels, and extracellular matrix (ECM). Recent studies have demonstrated that extracellular matrix metalloproteinase inducer (CD147) contributes to pan-cancer immunity and progression. The purpose of this study is to provide guidance for the noninvasive detection of CD147 in pan-cancer. ***Materials and Methods:*** Flow cytometry (FCM), Western blot (WB), and Immunofluorescence (IF) were used to verify the expression of CD147 on the surface of human colon cancer cells LS174T, human pharyngeal squamous cell carcinoma cells FADU, human prostate cancer cells 22RV1, human pancreatic cancer cells ASPC1 and human gastric cancer cells BGC823. 124/125I-anti-CD147 was prepared using N-bromine succinimide (NBS) as oxidant and purified by PD-10 column. The physicochemical properties, affinity, metabolic characteristics, biodistribution and immunoPET imaging of 124/125I-anti-CD147 were performed. 124I-IgG and 18F-FDG were used as controls. Finally, the correlation analysis between tumor uptake and CD147 expression level was established. ***Results:*** LS174T, FADU and 22RV1 cells showed high CD147 expression, while ASPC1 and BGC823 showed low expression of CD147. The radiochemical purity was over 99% and maintained over 85% in saline or 5% Human Serum Albumin (HSA) for more than 7 d. The K_d value of 125I-anti-CD147 to CD147 protein was 6.344 nM, while that of 125I-IgG was over 100 nM. 125I-anti-CD147 showed significantly higher uptake in CD147 high-expression cells than that in CD147 low-expression cells (P<0.001). The biological half-life of distribution and clearance phases were 0.63 h and 19.60 h, respectively. 125I-anti-CD147 showed high initial uptake in blood pool and liver, and the uptake was decreased with time. The effective dose of 124I-anti-CD147 estimated from the biodistribution data was 0.104 mSv/MBq. In vivo immunoPET imaging showed that the tumor-to-muscle ratio of 124I-anti-CD147 were higher than that of 124I-IgG and 18F-FDG (P<0.01) in CD147 (+) tumors. The expression levels of CD147 in cells and tumors had positive correlation with SUV_{max} values (P<0.01). ***Conclusion:*** 124/125I-anti-CD147 showed high targeting and affinity to CD147, which represents a tremendous potential for the imaging of CD147 positive tumors. The development of 124I-anti-CD147 may provide new insights for the regulation of TME and the formulation of precision diagnosis and treatment programs for tumors.

OP-619

CD47-targeted nanobody theranostics

W. Wei;
Shanghai Jiao Tong University, Shanghai, CHINA.

Aim/Introduction: Overexpression of CD47 is frequently found in various types of human malignancies. By mapping biomarker expression, immuno-positron emission tomography has been increasingly used for patient screening and response monitoring in clinical settings. However, molecular imaging tracers targeting human CD47 remain to be developed. Moreover, CD47-targeting radionuclide therapy may provide alternative treatment options for CD47-expressing malignancies. ***Materials and Methods:*** By immunization alpacas with recombinant human CD47, we prepared a CD47-targeting nanobody C2 and further engineered a nanobody deriative termed as ABDC2, which simutaneously targeting human CD47 and human/murine serum albumin. Following this, we carried labeling with C2/ABDC2 with 68Ga, 89Zr, and 177Lu and theranostic studies in CD47-humanized mice models. ***Results:*** Both C2 and ABDC2 specifically reacted with human CD47 with a high K D value of 23.50 and 84.57 pM, respectively. [68Ga]Ga-NOTA-C2 was developed with high radiochemical purity (99 >%, n = 4) and visualized CD47 expression in the nude mice and CD47-humanized NCG models. In comparison to the rapid renal clearance and short half-life of [68Ga]Ga-NOTA-C2, both [68Ga]Ga-NOTA-ABDC2 and [89Zr]Zr-DFO-ABDC2 showed prolonged circulation and increased tumor uptake, with the highest uptake of [89Zr]Zr-DFO-ABDC2 occurring at 72 h post-injection. Moreover, [177Lu]Lu-DOTA-ABDC2 radioimmunotherapy suppressed the tumor growth but was associated with toxicity, warranting further optimization of the treatment schedules. ***Conclusion:*** Taken together, we reported a series of nanobody-derived CD47-targeted agents, of which [68Ga]Ga-NOTA-C2 and [89Zr]Zr-DFO-ABDC2 are readily translatable. Optimization and translation of CD47-targeted theranostic pair may provide new prospects for CD47-targeted management of solid tumors. ***References:*** 1. Wei et al. Med. 2023 Feb 10;4(2):69-74.2. Wei et al. J Nucl Med. 2022 Oct;63(10):1475-1479.3. Wei et al. Eur J Nucl Med Mol Imaging. 2021 Aug;48(9):2749-2760.4. Wei et al. Chem Rev. 2020 Apr 22;120(8):3787-3851.

OP-620

Preclinical Evaluation of [18F]F-[natLu]Lu-/[19F]F-[177Lu]Lu DOTA-rhCCK-18, a Radiohybrid-Based Minigastrin Analog With High Target Affinity and Tumor Accumulation: First Steps Towards Clinical Translation

N. Holzleitner[1], *T. Günther*[1], *L. Greifenstein*[2], *N. Urtz-Urban*[1], *D. Di Carlo*[1], *C. Lapa*[3], *R. Baum*[2], *H. Wester*[1];
[1]*Technical University Munich, Munich, GERMANY,* [2]*Center for Advanced Radiomolecular Precision Oncology, Wiesbaden, GERMANY,* [3]*University of Augsburg, Augsburg, GERMANY.*

Aim/Introduction: In comparison to a recently introduced radiohybrid-based minigastrin analogue, [177Lu]Lu-(R)-DOTAGA-rhCCK-16 ([177Lu]Lu-(R)-DOTAGA-dap(SiFA)-(D-γ-Glu)$_6$-Ala-Tyr-Gly-

Trp-Asp-Nle-Phe-NH_2), the novel [^{177}Lu]Lu-DOTA-rhCCK-18 ([^{177}Lu]Lu-DOTA-dap(SiFA)-(D-γ-Glu)$_8$-Ala-Tyr-Gly-Trp-Asp-Nle-Phe-NH_2) revealed a significantly increased CCK-2R affinity (~4-fold improved IC_{50}) by a simple DOTA-for-(R)-DOTAGA substitution. In this study, we investigated the human serum albumin (HSA) and plasma protein binding and in vivo properties of [$^{18/19}$F]F-[$^{nat/177}$Lu]Lu-DOTA-rhCCK-18 to pave the way for a first evaluation in humans. ***Materials and Methods:*** All compounds were synthesised via automated Fmoc-based solid phase peptide synthesis (SPPS). ^{177}Lu-labelling was performed at 90°C within 15 min (1.0 M NaOAc buffer, pH = 5.5). ^{18}F-labelling was conducted at 60°C within 5 min (ammonium formate in DMSO) using previously dried [^{18}F] fluoride with subsequent purification by cartridge. Human serum albumin (HSA) and plasma protein binding was determined via an ultrafiltration method (3200 rpm, 40 min). Biodistribution studies were carried out at 1 and 24 h post-injection (p.i.) in AR42J tumor-bearing CB17-SCID mice. ***Results:*** Automated SPPS with concomitant purification via RP-HPLC yielded 5-20% peptide precursor. ^{177}Lu-labelling resulted in high radiochemical purity (RCP, >95%) and molar activity of A_m = 40 GBq/μmol. ^{18}F-labelling proceeded in radiochemical yields of 10-30%, RCP >95% and molar activities of A_m ~85 GBq/μmol. High HSA (62±3%) and plasma protein (95±1%) binding in vitro was determined for [^{19}F]F-[^{177}Lu]Lu-DOTA-rhCCK-18. In vivo at 1 h p.i., [^{18}F]F-[^{nat}Lu]Lu-DOTA-rhCCK-18 revealed high activity levels in the tumour and the kidneys (31.2 and 146 %ID/g, respectively) but a low bone uptake (<1.7 %ID/g), underlining the high stability of the Si-^{18}F bond in vivo. Apart from high activity accumulation in the kidneys overall background was low in non-target tissues. At 24 h p.i., [^{19}F]F-[^{177}Lu]Lu-DOTA-rhCCK-18 exhibited high activity retention in both the AR42J tumour xenograft and the kidneys (25.4±4.7 and 134±18 %ID/g, respectively), while further off-target retention was low, leading to superior tumour-to-background ratios for [^{19}F]F-[^{177}Lu]Lu-DOTA-rhCCK-18 compared to the reference compound [^{177}Lu]Lu-DOTA-PP-F11N ([^{177}Lu]Lu-DOTA-(D-Glu)$_6$-Ala-Tyr-Gly-Trp-Asp-Nle-Phe-NH_2). Based on these encouraging results, clinical translation of [^{18}F]F-[^{nat}Lu]Lu-DOTA-rhCCK-18 has already been initiated. Apart from the general pharmacokinetics it will be investigated whether the unfavourable high kidney uptake is obtained in humans as well. ***Conclusion:*** [$^{18/19}$F]F-[$^{nat/177}$Lu]Lu-DOTA-rhCCK-18 demonstrated favourable in vitro and in vivo properties, particularly high tumor accumulation and retention. A first-in-human application using either [^{18}F]F-[^{nat}Lu]Lu-DOTA-rhCCK-18 or [^{19}F]F-[^{68}Ga]Ga-DOTA-rhCCK-18 will elucidate if elevated kidney uptake observed in animals is reflected in humans. If not, the radiohybrid-based DOTA-rhCCK-18 could be a viable theranostic agent for positron emission tomography imaging and radioligand therapy of medullary thyroid cancer.

OP-621

In vitro and in vivo evaluation of BCY18469, a novel EphA2-targeting Bicycle® for radiotheranostic applications

M. El Fakiri[1,2,3], *G. E. Mudd*[4], *J. Mitschke*[5,1], *P. Huxley*[4], *K. McDonnell*[4], *A. R. Regupathy*[4], *N. Klemm*[5], *L. Domogalla*[2,1], *A. C. Eder*[1,2], *T. Reinheckel*[5,1], *M. Eder*[1,2];
[1]*German Cancer Consortium (DKTK), Partner Site Freiburg, and German Cancer Research Center (DKFZ), Freiburg, GERMANY,* [2]*Department of Nuclear Medicine, University Medical Center Freiburg, Faculty of Medicine, University of Freiburg, Freiburg, GERMANY,* [3]*Faculty of Biology, University of Freiburg, Freiburg, GERMANY,* [4]*BicycleTx Limited, Cambridge, UNITED KINGDOM,* [5]*Institute of Molecular Medicine and Cell Research, University of Freiburg, Freiburg, GERMANY.*

Aim/Introduction: Targeting specific and selective binding sites with radioisotope bearing molecules offers immense value in the personalized management of cancer patients, enabling imaging and treatment of a wide range of tumours. EphA2, a tyrosine kinase involved in cell-cell interactions, is overexpressed in various tumours and has been linked to poor prognosis. To target cancer-overexpressed receptors, bicyclic peptides have gained attention due to their constrained nature, high tissue penetration, and improved stability compared to their linear counterparts. This work presents an in vitro and in vivo preclinical evaluation of BCY18469, a novel bicyclic peptide-based radiotheranostic that targets EphA2. ***Materials and Methods:*** To evaluate the preclinical efficacy of BCY18469, the bicyclic peptide was radiolabelled with gallium-68 and lutetium-177, and its stability assessed in mouse and human plasma. In vitro properties such as binding affinity and internalization were evaluated using the EphA2-overexpressing cell line HT1080. The peptide demonstrated a favourable in vitro profile, and was subsequently evaluated in vivo. Firstly, through μPET/MR imaging and biodistribution studies in an HT1080 mouse xenograft (BALB/c nu/nu), and secondly, in a μPET/MR longitudinal study on a transgenic immunocompetent breast cancer mouse model (MMTV-PyMT). ***Results:*** The EphA2-targeting bicyclic peptide BCY18469 was labelled with gallium-68 and lutetium-177 (RCY's ≥ 98%). Following 24 hours of incubation, ~90% of BCY18469 remained intact in human plasma, while 30% degradation was observed in mouse plasma. In vitro assays demonstrated specific binding of BCY18469 to EphA2-expressing cells, with nanomolar binding affinity. In vivo μPET/MR imaging of [^{68}Ga]Ga-BCY18469 on HT1080 xenograft mice showed high tumour enrichments at early time-points, with an SUV value of 1.18 g/mL 2 hours post-injection. Biodistribution studies with [^{177}Lu]Lu-BCY18469 in the HT1080 xenograft were consistent with μPET/MR imaging results, demonstrating high tumour accumulation at early time-points (19.50 ± 3.50 %ID/g 1 hour post-injection, n = 3). Additionally, [^{68}Ga]Ga-BCY18469 was able to stage and image disease progression from the formation of the first palpable tumours until end-point in MMTV-PyMT breast cancer mice. ***Conclusion:*** Targeting the EphA2 receptor has the potential to enable imaging and treatment of various cancerous diseases that overexpress it. The high tumour accumulation observed for BCY18469 at early time-points makes it a promising candidate for molecular imaging using short-lived radionuclides. Furthermore, the capacity of BCY18469 to detect cancerous lesions over time in an immunocompetent mouse model strengthens the hypothesis that bicyclic peptides are an effective tool for PET imaging of solid tumours during all the disease stages.

OP-622

Theranostic role of^{89}Zr/^{177}Lu-labeled aflibercept in triple-negative breast cancer

L. Kang*, Q. Yang, Z. Chen, Y. Qiu, W. Huang, L. Song;*
Peking University First Hospital, Beijing, CHINA.

Aim/Introduction: Breast cancer is the most common cancer among women around the world. Although systemic therapy has improved outcomes for patients, the development of new molecularly targeted drugs and treatment regimens is imperative. Vascular endothelial growth factor (VEGF) represents a growth factor with important pro-angiogenic activity. Targeting and blocking angiogenesis could help the diagnosis and treatment of breast cancer. Aflibercept (Abe), a chimeric recombinant protein, contains the ligand-binding domains of both VEGFR-1 and VEGFR-2 and can sequester all isoforms of VEGF-A, PlGF, and VEGF-B, therefore affecting pathological and physiological

angiogenesis. In this study, the theranostic role of ^{89}Zr- and ^{177}Lu-labeled aflibercept was investigated for PET imaging and treatment in breast cancer murine models. ***Materials and Methods:*** Aflibercept was conjugated with desferrioxamine (Df) and 1,4,7,10-Tetraazacyclododecane-1,4,7,10-tetraacetic acid (DOTA) for radiolabeling with ^{89}Zr ($t_{1/2}$ = 78.4 h) and ^{177}Lu ($t_{1/2}$ = 6.65 d). After the breast cancer 4T1 tumor-bearing mice model was established, PET imaging and biodistribution studies were performed for 7 days after injection of ^{89}Zr-Df-aflibercept. Further, six groups were employed for the treatment study, including PBS, aflibercept, ^{177}Lu-only, ^{177}Lu-DOTA-IgG (human non-specific), ^{177}Lu-DOTA-aflibercept-low, and ^{177}Lu-DOTA-aflibercept-high. Tumor sizes and body weight were measured within 16 days post-injection (n = 5-8). Mice injected with Cy5.5-aflibercept (n=4) and Cy5.5-IgG (n=4) were imaged for optical imaging. Finally, histological analysis was performed to examine VEGF expression in tumors. ***Results:*** PET imaging of ^{89}Zr-Df-aflibercept showed an increased tumor uptake with the maximum SUVmax of 5.61±0.92 at 120 h post-injection for 4T1 tumors (n = 3). After being labeled with Cy5.5 in optical imaging, the uptake of tumors in the experimental group was higher obviously than control IgG. The tumor-to-blood and tumor-to-muscle ratios increased over time. The above results suggest the high uptake of tumors from radiolabeled aflibercept. We further labeled ^{177}Lu with aflibercept. The results showed that for the treatment group of ^{177}Lu-DOTA-aflibercept-high, significant inhibition of tumor growth was observed. Within 16 d, the standard tumor volume of ^{177}Lu-DOTA-aflibercept-high was significantly less than other groups. Therefore, the effectiveness of the treatment was demonstrated in our study. Besides, the body weight of ^{177}Lu-DOTA-aflibercept-high did not change significantly, indicating the safety of radiolabeled aflibercept in vivo. ***Conclusion:*** ^{89}Zr- and ^{177}Lu-labeled aflibercept displayed a significant VEGF positive tumor affinity and effective tumor therapy without significant toxicity. Therefore, radiolabeled aflibercept could be further investigated in the theranostic field of breast cancer.

1305

Tuesday, September 12, 2023, 9:45 AM - 11:15 AM

Hall B

Cutting Edge Science Track - TROP Session: Quantitative SPECT/CT Imaging

OP-623

Comparison of lesion detectability in Whole-Body Bone Scan images: A Monte Carlo study of CdZnTe- and NaI(Tl)-based Gamma Cameras

R. Madru[1], *N. Karindotter-Borgendahl*[2], *M. Dahlbeck*[2], *M. Ljungberg*[3];
[1]*Skane University Hospital, Lund, SWEDEN,* [2]*Skane Sjukhus Nordost, Kristianstad, SWEDEN,* [3]*Lund University, Lund, SWEDEN.*

Aim/Introduction: Whole-body-bone-scintigraphy (WBBS) is a high-sensitive imaging method to detect metabolic changes at the early stages of the disease. Here, we study the detectability of the lesions by simulating the modern Cadmium-Zinc-Telluride (CZT) gamma camera (high energy resolution) and compare it to the conventional NaI(Tl) camera (high sensitivity) by using SIMIND Monte Carlo simulations with XCAT virtual patients. The aims were to a) create patient-like WBBS images with realistic activity distribution, including "tumors" of different sizes and intensities in the skeleton and b) simulate a WB scanning situation for CZT- and NaI(Tl)-gamma camera and compare detectability of tumors from these images to ground truth. ***Materials and Methods:*** Whole-body images of ten virtual patients with increased metabolic activity situated at 7-10 different locations in the skeleton (volume range 0.5-8 cm^3) were simulated. The intensity of the metabolic activity was randomly altered between five different values in the different locations, based on clinical experience, to mimic bone-scintigraphy images of prostate cancer patients. The bone-to-kidney activity concentration ratio was set to 3:1 and bone-to-background to 30:1. Virtual patient images were simulated for CZT- and NaI(Tl) gamma camera with specific parameters regarding the different collimators (WEHR/LEHR), energy resolution (5.9%/9.2% FWHM), intrinsic spatial resolution (2.46/3.8 mm), measured sensitivity (83/90 cps/MBq), pixel size (2.46/2.39 mm). To obtain a realistic noise level as obtained in clinical images, Poisson noise was added to the simulated images (assuming 570 MBq injected activity and scanning speed 15 cm/min). Two experienced physicians visually evaluated the images using third-party software and graded metabolic changes as 1) possibly-, 2) probably-, and 3) certainly positive. The results were compared with the expected findings. The inter-rater reliability was determined and a p-value<0.05 was considered statistically significant. ***Results:*** A lower percentage true positive lesions was detected in CZT-images compared to conventional NaI(Tl) gamma camera (39% vs 50%). The lesions in the spine and sacrum regions were found more difficult to detect for both types of cameras. The inter-rater reliability showed no significant differences between the two readers (p-value=0.003; K=0.185). ***Conclusion:*** According to preliminary results, WBBS images simulated for CZT-camera show a slightly lower sensitivity compared to conventional NaI(Tl). In a clinical setting, the CZT-camera may include contrast enhancement and advanced noise filtering, which was not considered in this study. Further studies regarding the noise and its impact on lesion detectability is ongoing.

OP-624

CZT swiveling-detectors ring SPECT enables 3D dynamic acquisitions

M. Hesse*, F. Dupont, R. Lhommel;*
Cliniques Universitaires Saint-Luc, Brussels, BELGIUM.

Aim/Introduction: CZT detector ring cameras (CZTR) with their PET-like design including a dozen of swiveling detectors set around the patient enable fast SPECT acquisitions. In pure swiveling motion, sampling resolution down to 5 seconds is achievable, allowing fast dynamic SPECT scans, which is still out of reach with conventional rotating-heads SPECT. However, more developments and validations are required before a potential clinical implementation. This study aims at validating 4D scans on CZTR with the help of a dedicated phantom setup. ***Materials and Methods:*** The phantom consisted in a hermetic bottle filled with 100ml of water to which two entries and one output lines were connected through the rubber stopper. One entry was connected to a 50ml perfusion bag filled with about 3mCi of ^{99m}Tc and the other one to a water tank. The later allowed a continuous infusion to maintain the water volume in the phantom leading to an exponential total activity decrease. This setup typically simulates a ^{99m}Tc-MAG3 dynamic kidney study. Fifteen minutes dynamic acquisitions were performed first as a 3D SPECT on a CZTR in pure swiveling mode, then in 2D on a conventional gamma camera with 5-15 seconds frames. The CZTR SPECT list file was sorted to produce different SPECT bin durations that

were then reconstructed to a dynamic SPECT image. Total and partial bottle counts kinetic curves were generated. ***Results:*** As expected the corresponding reconstructed SPECT images become noisier the smaller the frame duration. However, total counts in the bottle could still be extracted and used to create low noise kinetic curves down to 5 seconds sampling resolution. The dynamic SPECT curve displayed the usual uptake phase and slower exponential decrease associated to the ^{99m}Tc release. When normalized, the dynamic SPECT curve nicely fit the 2D dynamic curve with a mean square deviation lower than 2.5%. Very similar values were found for the time to reach the curve maximum and the release half-life between the planar (178 s and 92 s) and SPECT (165 s and 94 s) dynamic images. From 4D-SPECT, release half-life for the six 8mm-thick coronal slices of the bottle was 94.6 ± 6.2 seconds. ***Conclusion:*** Dynamic SPECT imaging is feasible on CZT swiveling-detectors ring cameras and provides dynamic curves in good agreement with planar dynamic images on conventional gamma camera. 4D-SPECT also enables kinetic modeling of specific organ region. Further in vivo testing is required to confirm these promising results.

OP-625

SPECT image reconstruction from sparse projection data using deep learning model trained by randomly generated training phantom

R. Yano[1], *Y. Okura*[2], *M. Yamamoto*[2];
[1]*Graduate School of Medical Technology and Health Welfare Sciences, Hiroshima International University, Higashihiroshima, JAPAN,* [2]*Department of Clinical Radiology Faculty of Health Sciences, Hiroshima International University, Higashihiroshima, JAPAN.*

Aim/Introduction: In general, the acquisition time of whole-body single photon emission computed tomography (SPECT) is long. One of the methods to shorten acquisition time is to reduce the number of projection data at SPECT acquisition. However, a small number of projection data affect the quality of resultant SPECT images. On the other hand, deep learning technology made remarkable progress in recent years. In general, deep learning techniques require a large number of images for training the model. However, the number of available SPECT images is limited. This study aims to develop a method to obtain sufficient quality SPECT images from sparse projection data and image data other than SPECT images by deep learning and to evaluate the quality of the resultant SPECT images. ***Materials and Methods:*** We constructed a deep learning model by modifying 3D U-Net model so that the number of output frames is twice the number of input frames. To train the model, we used two types of data sets. One was a projection image obtained by Radon transforming CT images available as open data. The other data set was a projection image created from a random point image. Using the trained model, by inputting sparse projection data, we obtained the output image consisting of twice the frame as interpolated projection images. SPECT images were reconstructed by OSEM using the obtained projection images. To evaluate the SPECT images, we used three numerical phantom data from viewpoints of spatial resolutions, image noise, and Image quality. SPECT images by developed methods were compared with reference SPECT images using %CV, FWHM, and PSNR/SSIM. ***Results:*** SPECT image noise by the developed method was approximately 10% lower than that of the reference SPECT image. However, spatial resolutions were not improved so clearly. PSNR and SSIM were comparable between the CT image trained model and the random point trained model. ***Conclusion:*** We constructed the method to reconstruct SPECT images from sparse projection data using deep learning trained other than the projection images. We found that the deep learning model trained by random point data is available for improvement SPECT images. It was suggested that projection images of sufficient quality could be obtained without using SPECT images. ***References:*** Ryden T, Van Essen M, Marin I, Svensson J, Bernhardt P. Deep-Learning Generation of Synthetic Intermediate Projections Improves 177Lu SPECT Images Reconstructed with Sparsely Acquired Projections. J Nucl Med. 2021;62(4):528-35.

OP-626

Assessing the Efficacy of the Relative Difference Prior for SPECT Dosimetry

L. Polson;
University of British Columbia, Vancouver, BC, CANADA.

Aim/Introduction: Radiopharmaceutical therapies (RPTs) are gaining interest due to the promising results in prostate cancer and neuroendocrine tumor treatment. However, current approaches follow a "one size fits all" paradigm that does not account for physiological differences between patients. An alternative to this approach requires quantitative images and standardization of SPECT imaging and reconstruction protocols. The aim of this work was to test if the Bayesian BSREM algorithm with relative difference prior (RDP) could improve accuracy and reduce the variability in image quantification. ***Materials and Methods:*** The XCAT phantom was used to generate 8 different realistic activity uptake scenarios of ^{177}Lu. Lesions of different size (2-16mm diameter) and locations were included. SPECT scans were simulated using the SIMIND Monte Carlo code with a medium energy collimator, 120 projections, and a 0.3x0.3cm^2 pixel size. The OSEM and the BSREM algorithms were used with 8 subsets and a varying number of iterations (1 to 120). Recovery coefficients (RC) vs. noise curves were created, where image noise was computed from the variance in the liver, and RCs were estimated as the ratio of the measured and true activity for both organs and lesions. While organs were segmented using the true mask from XCAT, a 40% threshold was used for lesions to account for some of the spill out due to their small size. Statistical significance between different algorithms was determined using the paired t-test. ***Results:*** Qualitatively, images reconstructed using the BSREM algorithm were smoother (i.e., less noise) compared to OSEM generated ones after 120 iterations. For both algorithms, the bias is reduced with increasing iteration number, but OSEM resulted in increased image noise. In the kidneys, for example, 120 iterations of OSEM and BSREM led to RCs of -4.4±0.8% and -10.4±0.7% respectively (significant difference, $p<10^{-7}$), while the difference in image noise was 35.7±4.6% and 19.6±4.1% respectively (significant difference, $p<10^{-5}$). Lesion quantification was less dependent on iteration numbers for BSREM than OSEM. For example, in 16mm lesions, OSEM yielded RCs of 55.4±10.4% (40 iterations) and 76.2±9.6% (120 iterations) while BSREM yielded RCs of 35.4±7.7% (40 iterations) and 36.8±7.6% (120 iterations). ***Conclusion:*** Usage of BSREM tended to decrease image noise but resulted in worse RCs for all organs and lesions. The invariance of BSREM with respect to iteration number when measuring lesion RCs, however, could be used to reduce the variability in image quantification. Future work should explore alternative parameter configurations for BSREM.

OP-627

Head-to-head comparison of SPECT and MRI based holmium-166 dosimetry

L. E. L. Westlund Gotby[1], *Y. X. Mak*[2], *N. J. M. Klaassen*[1], *J. Roosen*[1], *M. W. M. van Wijk*[1], *M. W. Konijnenberg*[1,3], *M. Abayazid*[2], *J. F. W. Nijsen*[1];
[1]*Department of Medical Imaging, Radboud University Medical Center, Nijmegen, NETHERLANDS,* [2]*Robotics and Mechatronics, University of Twente, Enschede, NETHERLANDS,* [3]*Department of Radiology and Nuclear Medicine, Erasmus Medical Center, Rotterdam, NETHERLANDS.*

Aim/Introduction: Both SPECT/CT, acquired during free-breathing, and MRI, acquired during breath-hold, can be utilized for quantifying the dose distribution in the liver after transarterial radioembolization (TARE) with holmium-166 (^{166}Ho) microspheres (MS). In the clinic, the true ^{166}Ho-MS biodistribution in a patient is unknown, which makes it difficult to assess the accuracy of the estimated dose distribution, the discrepancies between the two imaging modalities, and the impact that respiratory motion has on the quantification. We aim bridge this knowledge gap by modelling a known dose distribution in a liver after TARE and perform a head-to-head comparison of the image based dose information acquired using SPECT/CT and MRI. ***Materials and Methods:*** A mock-up for the liver phantom was created by adding (non-radioactive) ^{165}Ho-MS to agarose gel that was put in a plastic container (1500 mL). Tumors were modelled by three agarose gel spheres (14, 35, and 112 mL) also placed in the container. A ^{165}Ho-MS sphere-to-background concentration ratio ($S:BG_{ratio}$) of 4:1 was used. The mock-up phantom was imaged using MRI and the integrity of this model was evaluated based on the $S:BG_{ratio}$ and the homogeneity of the distribution. A pneumatically driven, MRI compatible, robotic phantom [1] will be used to simulate the respiratory induced liver motion. This robotic phantom moves in the superior-inferior, as well as in the anterior-posterior directions and is programmable to match the patient population characteristics. Both phantoms (^{166}Ho-MS liver and robotic) will be positioned in the SPECT/CT and MRI scanner, respectively, and imaged for optimal conditions (no motion, both scanners), for free-breathing (SPECT/CT only), and various breath-hold disturbances (MRI only). Dose distributions are evaluated using Q-suite and MATLAB. ***Results:*** MRI based results for the ^{165}Ho-MS phantom showed $S:BG_{ratio}$ of 4.29, 4.41, and 4.44 for each sphere, respectively. The ^{165}Ho-MS distribution in the background region is deemed to be sufficiently homogenous based on a mean±SD of 0.252±0.038 mg/ml. Experiments with the ^{166}Ho-MS liver and robotic phantoms are ongoing. ***Conclusion:*** With this phantom setup we will be able to simulate a known activity distribution after TARE, and quantify the measured dose based on SPECT/CT and MR imaging. This experiment will indicate which image modality should be considered the state-of-the-art for evaluating ^{166}Ho-MS TARE, and whether any of these two imaging modalities yields dose information that is accurate enough to pursue voxel-based dosimetry. ***References:*** [1] Naghibi, H. et al. Proc. IEEE RAS EMBS Int. Conf. Biomed. Robot. Biomechatronics 2018-Augus, 577-582 (2018)

OP-628

Holmium-166 SPECT/CT imaging for dosimetry: a multi-center optimization study in the Netherlands

L. E. L. Westlund Gotby[1], *M. Stella*[2], *C. D. E. van Speybroeck*[1], *D. Lobeek*[1], *D. M. V. de Vries-Huizing*[3], *B. J. de Wit-van de Veen*[3], *E. J. Rijkhorst*[4], *R. Wierts*[5], *M. K. Stam*[6], *F. H. P. van Velden*[6], *P. Dibbets-Schneider*[6], *R. van Rooij*[2];
[1]*Department of Medical Imaging, Radboud University Medical Center, Nijmegen, NETHERLANDS,* [2]*Department of Radiology and Nuclear Medicine, University Medical Center Utrecht, Utrecht, NETHERLANDS,* [3]*Department of Nuclear Medicine, NETHERLANDS Cancer Institute, Amsterdam, NETHERLANDS,* [4]*Department of Medical Physics and Technology, NETHERLANDS Cancer Institute, Amsterdam, NETHERLANDS,* [5]*Department of Radiology and Nuclear Medicine, Maastricht University Medical Center, Maastricht, NETHERLANDS,* [6]*Department of Radiology, Leiden University Medical Center, Leiden, NETHERLANDS.*

Aim/Introduction: Reliable dosimetry based on SPECT/CT imaging is essential to achieve personalized ^{166}Ho radioembolization planning and post-treatment evaluation. This study quantitatively evaluates image quality of ^{166}Ho SPECT/CT reconstructions performed at five Dutch centers with the purpose of optimizing acquisition and reconstruction parameters for ^{166}Ho SPECT/CT dosimetry. ***Materials and Methods:*** At each center, a cylindrical (~6.7 or 9 L) and a NEMA IEC phantom were filled with ~250 MBq of ^{166}Ho-chloride. An 8:1 sphere-to-background activity concentration ratio and a cold lung insert were used for the NEMA phantom. The phantoms were imaged using SPECT/CT scanners from two vendors; one Discovery NM/CT 670 Pro and one Discovery NM/CT 870 DR (GE HealthCare), two Symbia Intevo Bold and three Symbia T (Siemens Healthineers). Data were acquired for 20 minutes with a photopeak window at 81 keV (15% width). Two adjacent scatter windows (8% width), and an upper scatter window at 118 keV (12% width) were used for triple energy window (TEW) and dual energy window (DEW) scatter correction, respectively. The TEW and DEW reconstructions were performed with vendor specific software. A vendor neutral software (Hermes Medical Solutions) was used to reconstruct the data with Monte Carlo (MC) based scatter correction. All images were reconstructed using 10 iterations and 8 subsets without post-reconstruction filtering. The image quality was evaluated by quantifying the coefficient of variation (COV; noise) in the cylindrical phantom, and contrast recovery coefficients (CRCs) and contrast-to-noise ratios (CNRs) measured in the NEMA phantom. ***Results:*** The COV increased for TEW compared to DEW but was reduced for MC reconstruction (GE DEW range: 38-44%, Siemens DEW range: 17-20%, GE TEW range: 48-50%, Siemens TEW range: 20-24%, MC range: 16-35%). The CRCs for the largest sphere were higher for TEW compared to DEW reconstruction for all scanners (GE DEW range: 0.36-0.42, Siemens DEW range: 0.43-0.47, GE TEW range: 0.40-0.48, Siemens TEW range: 0.54-0.58). Additionally, MC reconstructions consistently yielded the highest CRCs for the largest sphere of all datasets (range: 0.50-0.68). The CNRs for the largest sphere were similar for DEW and TEW, while on average 43% higher for MC. ***Conclusion:*** TEW and MC reconstructions improved image quality compared to DEW for all scanners, which enables more accurate ^{166}Ho SPECT/CT based dosimetry. Additionally, implementing the TEW protocol is more straightforward than DEW and this, in combination with the better image quality, facilitates comparison of SPECT/CT based ^{166}Ho dosimetry after radioembolization in multi-center, multi-scanner studies.

OP-629

Quantitative ^{177}Lu SPECT/CT imaging with a ring-shaped CZT-based camera: 208 vs 113 keV photopeak

R. Danieli[1], *M. Stella*[2], *C. Marin*[1], *J. Tran Gia*[3], *J. Leube*[3], *C. Uribe-Munoz*[4], *M. Hesse*[5], *H. Levillain*[1], *B. Vanderlinden*[1], *N. Reynaert*[1], *P. Flamen*[1];
[1]*Institut Jules Bordet, Bruxelles, BELGIUM,* [2]*GE HealthCare, Diegem, BELGIUM,* [3]*University Hospital Würzburg, Würzburg, GERMANY,* [4]*University of British Columbia, Vancouver, BC, CANADA,* [5]*Cliniques Universitaires Saint-Luc, Bruxelles, BELGIUM.*

Aim/Introduction: Quantitative ^{177}Lu SPECT/CT with NaI-based gamma cameras is commonly performed using the 208 keV photopeak, as it contains less scatter than the 113 keV. However, when using CZT-based systems, the use of the 113 keV photopeak might be reconsidered. This study aims to find the most suitable photopeak for quantitative ^{177}Lu SPECT/CT imaging with a ring-shaped CZT-based camera by assessing the stability of the calibration at multiple activity concentrations. ***Materials and Methods:*** A cylindrical phantom (filling volume: 5.4L) filled with 640MBq of ^{177}Lu was used to calibrate the camera. For verification, a similar phantom (5.8L) was prepared and acquired for nine times over two months (activity concentrations from 920 to 2kBq/ml). All acquisitions were performed on a StarGuide (GE HealthCare), with energy windows centred at 208 keV(±6%) and 113 keV(±10%), and scatter windows centred at 185 keV(±5%), 129 keV(±3.5%) and 97 keV(±4.5%). Acquisition duration was set at 15 minutes. Each photopeak was reconstructed separately using the vendor protocol, including attenuation correction, scatter correction (SC) and resolution recovery (SmartConsole V.1.0.10). SC for the 113 keV photopeak was performed with a standard triple-energy window method. For the 208 keV photopeak, a dedicated dual-energy window SC taking into account the "tailing effect" typical for CZT detectors was used. A large volume of interest (VOI) encompassing the whole phantom was drawn on each SPECT reconstruction. For the two reconstructions of the 5.4-L phantom (113 and 208 keV), a calibration factor (CF) was computed by dividing the total counts inside the VOI by the acquisition duration and by the nominal activity. For all eighteen reconstructions of the 5.8-L phantom, the error in the activity quantification was computed as percentage difference between measured and nominal activity. Measured activities were obtained by dividing the total counts inside the VOI by the acquisition duration and by the CF corresponding to the same photopeak. ***Results:*** CFs for the 208 and 113 keV photopeaks were 94.6 and 86.3cps/MBq, respectively. For the 208 keV photopeak, acceptable errors of less than 4% were measured. For the 113 keV photopeak, similar errors were measured for activity concentrations higher than 40kBq/ml. As the activity concentration in the phantom decreased, errors in the activity quantification increased, reaching the maximum value of 70% at 2kBq/ml. ***Conclusion:*** Our results suggest that quantitative ^{177}Lu SPECT/CT imaging with StarGuide for a clinically realistic range of activity concentrations is currently best performed using the 208 keV photopeak.

OP-630

Hyperthyroidism Etiological Diagnosis: a Multilabel Classification using Convolutional Neural Networks on Thyroid Scans

M. Abdi[1], *Q. Naili*[1], *M. Habbeche*[1], *M. Bourouba*[2], *S. Berrani*[3];
[1]*Centre d'imagerie scintigraphique Blida, Blida, ALGERIA,* [2]*Clinique Fatema Al Azhar, Alger, ALGERIA,* [3]*National Polytechnic School of Algiers (Ecole Nationale Polytechnique), Algiers, ALGERIA.*

Aim/Introduction: Primary hyperthyroidism has diverse causes and treatments, but it is difficult to diagnose the specific etiology due to overlapping imaging features[1]. A new approach is proposed to identify the main etiologies from thyroid scans, even when more than one disease is present in the same scan. This approach is based on a multilabel classification using convolutional neural networks (CNN). Previous work used a multiclass approach[2]. ***Materials and Methods:*** 1482 thyroid scans have been collected between 2016 and 2023 (patients with hyperthyroidism). The scans were labeled with three classes: Graves' disease, thyroiditis, and hot nodules, based on the interpretation of two experienced nuclear medicine physicians (taking into account clinical, ultrasound, and biological findings [1]). To evaluate the performance of this approach, Two test sets have been collected. The first test set (test 1) consisted of 132 scans from the same department (with documented Thyrotropin Receptor Antibodies). The second test set included 185 scans from another department. Using a transfer learning approach, different CNN architectures have been compared. A 5-level cross-validation was used, and the results are displayed as mean values, with standard deviation (95% confidence level). Each model acted as a multi-label classifier, predicting each etiology independently. We evaluated the precision of the models based on their ability to classify the scans into their respective etiologies. ***Results:*** Multiple CNNs have been trained, and evaluated on two test sets (internal and external). The Xception architecture outperformed the other CNNs in terms of training speed, and precision. On test 1, the CNN achieved a loss value of 0.3911±0.0061 and precision scores of 83.58%±3.57%, 72.64%±1.75%, and 94.57%±6.83% for Graves' disease, thyroiditis, and hot nodules, respectively. The CNN was particularly effective in recognizing the features associated with hot nodules, achieving a precision of 93.43%±3.22% on the test 2 set (external). The CNN also performed well for thyroiditis and Graves' disease, with precision scores of 87.64±2.52% and 70.6%±4.71%, respectively. ***Conclusion:*** This study demonstrated that a multilabel approach based on Xception architecture is effective in identifying the main etiologies of hyperthyroidism from thyroid scans. The use of a multilabel classifier can improve the precision of the diagnosis of hyperthyroidism. This can provide better targeted treatment options. ***References:*** 1: Intenzo, Charles M., et al. "Scintigraphic features of autoimmune thyroiditis." Radiographics 21.4 (2001): 957-964. 2: Ma, Liyong, et al. "Thyroid diagnosis from SPECT images using convolutional neural network with optimization." Computational intelligence and neuroscience 2019 (2019).

OP-631

Fundamental study on brain SPECT denoising using deep image prior

T. Zeniya[1], *A. Yabe*[1], *Y. Aita*[1], *K. Matsubara*[2], *K. Koshino*[3], *H. Watabe*[4], *T. Yuasa*[5];
[1]*Hirosaki University, Hirosaki, JAPAN,* [2]*Akita Prefectural University, Yurihonjo, JAPAN,* [3]*Hokkaido Information University, Ebetsu, JAPAN,* [4]*Tohoku University, Sendai, JAPAN,* [5]*Yamagata University, Yonezawa, JAPAN.*

Aim/Introduction: We are developing a high spatial resolutiion SPECT system, but the image becomes noisy when sufficient counts are not obtained. Recently, it has been reported that deep image prior (DIP), a deep learning method that does not require prior learning, is effective for PET image denoising. The aim of this study was to evaluate the effects of DIP, and the combination of DIP and total variation (TV) regularization on noise reduction

in SPECT images. Futhermore, the possibility of shortening the imaging time is investigated. ***Materials and Methods:*** A brain phantoms filled with Tc-99m solution were scanned by high-resolution SPECT under development, and similar simulations were performed. After DIP processing the projection data, the images were reconstructed with MLEM (DIP+MLEM) and EMTV (DIP+EMTV). Image quality was evaluated by PSNR and SSIM in addition to visual evaluation.Quantitative accuracy of images was also evaluated by ROI value. In addition, we investigated the possibility of short-time imaging by reducing amount of data. ***Results:*** The images reconstructed with non-DIP+MLEM, with DIP+MLEM and with DIP+EMTV had PSNRs (dB) of 32.09, 41.68 and 41.98, respectively, and SSIMs of 0.856, 0.948 and 0.951, respectively. DIP greatly the image quality of SPECT, and the combination of DIP and EMTV further improved the image. The error between the reconstructed image using DIP and the original image was 2.7 %, demonstrating high quantitative accuracy. The evaluation results of the images reconstructed from the reduced amount of data suggested the possibility of short-time imaging by the proposed method. ***Conclusion:*** This study suggested that DIP was effective in reducing noise and improving the image quality for brain SPECT.

1306

Tuesday, September 12, 2023, 9:45 AM - 11:15 AM
Hall C

Clinical Oncology Track - TROP Session: Lung

OP-632

Residual total metabolic tumor volume, assessed on post-therapeutic 18F-FDG PET/CT, is a game-changer in the early monitoring of patients with metastatic non-small cell lung cancer treated with immunotherapy.

P. Tricarico*;*
Centre Antoine Lacassagne, Nice, FRANCE.

Aim/Introduction: Because of atypical progressive imaging patterns in patients with metastatic non-small cell lung cancer (NSCLC) treated with immune checkpoint inhibitors (ICPIs), new biomarkers are needed for a better monitoring of treatment efficacy. The aim of this prospective study was to evaluate the prognostic value of volume-derived PET parameters on baseline and follow-up 18FDG-PET exams, and to compare their performance to conventional PERCIST criteria. ***Materials and Methods:*** Patients with metastatic NSCLC were included in two different single-center prospective trials. 18FDG-PET exams were performed before the start of immunotherapy (PETbaseline), after 6-8 weeks (PETinterim1) and after 12-16 weeks (PETinterim2) of treatment, using PERCIST criteria for tumor response assessment. Different metabolic parameters were evaluated : absolute values of SUVmax of the most intense lesion, total metabolic tumor volume (TMTV), total lesion glycolysis (TLG), but also their percentage changes between PET studies (ΔSUVmax, ΔTMTV and ΔTLG). For tumor segmentation, a fixed threshold of SUV4.0 was applied. The median follow-up of patients was 19.3 [7.6-32.2] months. Prognostic values and optimal thresholds of PET parameters were estimated by ROC curve analysis of 12-month overall survival (12M-OS) and 6-month progression-free survival (6M-PFS). Tumor progression needed to be confirmed by a multi-disciplinary tumor board. ***Results:*** 119 patients were prospectively included. On PETbaseline, TMTV and TLG were predictive of 12M-OS (AUC=0.65; 95%CI=0.55-0.75 and AUC=0.63; 95%CI=0.52-0.73, respectively); whereas SUVmax was not (AUC=0.52). On PETinterim1 and PETinterim2, all metabolic parameters, excepted ΔTLG on PETinterim2, were predictive for 12M-OS and 6M-PFS, the residual TMTV on PETinterim1 (termed TMTV1) being the strongest prognostic biomarker (AUC=0.82; CI=0.74-0.90, for both 12M-OS and 6M- PFS). Using the optimal threshold by ROC Curve to classify patients into three TMTV1 subgroups (0cm3; 0-57cm3; >57cm3), TMTV1 prognostic stratification outperformed PERCIST criteria. Subgroup analysis demonstrated that TMTV1 remained a strong prognostic biomarker of 12M-OS for both responding (p<0,0001) and non-responding patients (p=0.0003) according to PERCIST criteria. In the specific group of patients with PERCIST progression on PETinterim1, low residual tumor volume (<57cm3) was associated with a still very favorable patients' outcome (6M-PFS=69%; 24M-OS=54%). ***Conclusion:*** Residual metabolic tumor volume, assessed 6-8 weeks after the start of ICPI, is a strong prognostic biomarker in patients with metastatic NSCLC, surpassing and complementing the conventional PERCIST criteria. Its clinical value is to identify, among patients with a first PERCIST progression on PETinterim1, those who maintain a very favorable outcome. ICPI should be maintained beyond the first PERCIST progression for these patients.

OP-633

Predictive value of primary tumor metabolic heterogeneity of ^{18}F-FDG PET/CT for lung cancer progression

X. Li[1,2]*, M. Hou*[3]*, X. Wang*[1,2]*, C. Cui*[1,2]*, Z. Wu*[1,2]*;*
[1]Department of Nuclear Medicine, First Hospital of Shanxi Medical University, Taiyuan, Shanxi, CHINA, [2]Collaborative Innovation Center for Molecular Imaging of Precision Medicine Shanxi Medical University, Taiyuan, Shanxi, CHINA, [3]Department of Respiratory, First Hospital of Shanxi Medical University, Taiyuan, Shanxi, CHINA.

Aim/Introduction: To compare the metabolic heterogeneity of primary lung cancer foci of different histological types based on ^{18}F-FDG PET/CT and analyze its correlation with Ki67, staging and disease progression. ***Materials and Methods:*** A retrospective analysis of consecutive cases with pre-treatment ^{18}F-FDG PET/CT whole-body examination and pathologically confirmed primary lung cancer was performed. The primary tumors with SUVmax 40%-90% percent threshold were outlined and different MTVs were obtained. A correlation straight line of MTV-threshold (40%-90%) function was fitted and the absolute value of the slope of the straight line was defined as the Heterogeneity Factor (HF). Differences in HF between histological types were compared and correlations with Ki67, staging and disease progression were analyzed. ***Results:*** A total of 116 lung cancer cases were included, including 98 NSCLC and 18 SCLC. 73 cases in the disease progression group and 32 in the non-progression group. Mann-Whitney U-test analysis yielded a difference between NSCLC and SCLC of HF (U=462.00, P<0.001). At each percentile, HF was higher in SCLC than in NSCLC. The best cut-off value for HF to discriminate NSCLC or SCLC was 0.700 [95% CI=0.624, 0.874]. However, HF did not differ between squamous carcinoma (SQCC) and Adenocarcinoma (ADC) (U=1011, P=0.670). HF was positively correlated with Ki67 ($r_{Spearman}$=0.267, P=0.008) only in NSCLC. Further analysis of the histological subtypes of NSCLC revealed a positive correlation between HF and Ki67 only in ADC ($r_{Spearman}$=0.482, P=0.008). Multivariate ordered logistic regression analysis was performed by dividing all cases of HF

into four grades according to quartiles, with lung cancer T-stage and overall stage as dependent variables, respectively, and HF quartiles were independent risk factors for both stages (χ^2=84.039, P<0.001; χ^2=10.790, P=0.029). The highest quartile of HF (Q4) was associated with ORs for T-stage and overall staging risk compared with the lowest quartile (Q1) were 5.225 [95% CI=3.834, 6.616] and 1.507 [95% CI=0.426, 2.588], respectively. When the proportion of tumors in T-stage versus overall stage was stratified by quartiles of HF, trend analysis showed a positive correlation between HF and both T-stage and overall stage (P=0.011; P=0.009).Spearman correlation analysis showed a positive correlation between HF and disease progression (r=0.295, P=0.001). The best cut-off value for HF in primary tumors of lung cancer to predict disease progression was 0.7634 [95% CI=0.586, 0.786]. ***Conclusion:*** HF was positively correlated with disease progression, suggesting that metabolic heterogeneity of primary lung cancer tumors assessed by pre-treatment ^{18}F-FDG PET/CT could predict disease progression.

OP-634

Prognostic role of pre-operative 18F-FDG PET/CT in surgically treated patients with early-stage non-small-cell lung cancer

S. Taralli[1], *F. Vocaturo*[1,2], *E. Perrone*[1,2], *P. C. Pafundi*[3], *S. Ricciardi*[4], *G. Cardillo*[4], *M. L. Calcagni*[1,2];
[1]*Nuclear Medicine Unit, Diagnostic Imaging, Radiation Oncology and Hematology Department, Fondazione Policlinico Universitario Agostino Gemelli IRCCS, Rome, ITALY,* [2]*Nuclear Medicine Institute, University Department of Radiological and Hematological Sciences, Università Cattolica del Sacro Cuore, Rome, ITALY,* [3]*Epidemiology and Biostatistics Research Core Facility, GEMELLI GENERATOR, Fondazione Policlinico Universitario Agostino Gemelli IRCCS, Rome, ITALY,* [4]*Thoracic Surgery Unit, San Camillo Forlanini Hospital, Rome, ITALY.*

Aim/Introduction: Even after curative surgery, patients with early-stage (I-II) non-small-cell lung cancer (NSCLC) still present unsatisfactory prognosis, with >50% developing disease-recurrence. Early prognostic stratification is essential to improve outcome, as high recurrence-risk patients might benefit from more aggressive treatments. In this setting, literature on the prognostic role of pre-operative 18F-FDG PET/CT reported heterogeneous and no definitive results. We thus aimed to investigate, among pre-operative 18F-FDG PET/CT parameters, potential predictors of disease-recurrence in a highly-selected early-stage NSCLC population. ***Materials and Methods:*** We retrospectively analysed 320 consecutive patients (68.2±8.6 years;59.7% males) with surgically-treated early-stage NSCLC (IA-IB=291/320, IIA-IIB=29/320; all pN0 with negative surgical-margins) undergone pre-operative 18F-FDG PET/CT for staging between 2005-2017. The following PET, anatomical, histopathological and clinical parameters were evaluated: 1) tumour activity (SUVmax, SUVmean, SUVpeak, MTV, TLG); 2) tumour size, lung-side, lobe-site, peripheral/central-location, T-stage; 3) histotype, grading, lymphatic and vessel angioinvasion, pleural infiltration, necrosis; 4) patients' age, gender, adjuvant therapy. Potential predictors of recurrence-free survival (RFS) were assessed by Cox regression models and plotted into a nomogram scoring-system. After dichotomization, PET parameters were analysed by Kaplan-Meier survival analysis. A subgroup-analysis was performed in adenocarcinoma-subtype patients (246/320). Statistical analyses were performed with R-software v4.2.2 (statistical significance: p<0.05). ***Results:*** At diagnosis: 246/320 tumours showed peripheral-location, 129/320 high-grade, 110/320 lymphatic-angioinvasion, 140/320 vessel-angioinvasion, 85/320 pleural-infiltration, 107/320 necrosis; 24/320 patients received adjuvant therapy (AT). Disease-recurrence occurred in 71/320 patients (22.2%; median RFS=49.0months from surgery). At univariable analysis, in overall and adenocarcinoma patients: higher SUVmax, SUVmean, SUVpeak and TLG values were significantly associated with disease-recurrence (HR>>1;p<<0.05), alongside AT and histopathological aggressive-features; female-gender and peripheral-location were positive prognostic predictors. At multivariable analysis: AT was independent negative predictor of RFS in overall (HR=1.98;95%CI=1.02-3.84;p=0.043) and adenocarcinoma patients (HR=2.38;95%CI=1.03-5.52;p=0.043); SUVpeak was independent and stronger negative predictor of RFS in adenocarcinoma-subgroup (HR=1.50;95%CI=1.07-2.11;p=0.018). At predictive-model represented by nomogram: SUVpeak showed the highest impact on individual RFS-probability at 1, 3 and 5-years from surgery. At Kaplan-Meier analysis: patients with SUV-parameters and TLG above cut-offs showed a significantly lower RFS, with major RFS-differences in adenocarcinoma-subgroup for SUVpeak (34.7months if >2.84 vs 61.0months if ≤2.84) and SUVmean (23.1months if >6.06 vs 54.7months if ≤6.06). ***Conclusion:*** Tumour metabolic parameters at pre-operative 18F-FDG PET/CT are valuable prognostic predictors in selected early-stage NSCLC population candidate to surgery, able to identify higher recurrence-risk patients. Pre-operative unfavourable metabolic parameters could be considered as additional prognostic risk-factors to practically tailor/guide the planned surgical strategy and decide for adjuvant therapy need.

OP-635

The variability and diagnostic value of respiratory-gated 4D PET/CT based radiomics features in lung lesions compared to ungated PET/CT

S. Huang[1], *C. Cao*[2], *L. Guo*[1], *C. Li*[1], *W. Mu*[2,3], *Y. Liang*[1,4];
[1]*National Cancer Center/National Clinical Research Center for Cancer/Cancer Hospital & Shenzhen Hospital, Chinese Academy of Medical Sciences and Peking Union Medical College, Shenzhen, CHINA,* [2]*School of Engineering Medicine, Beihang University, Beijing, CHINA,* [3]*Key Laboratory of Big Data-Based Precision Medicine, Ministry of Industry and Information Technology of the People's Republic of China, Beijing, CHINA,* [4]*National Cancer Center/National Clinical Research Center for Cancer/Cancer Hospital, Chinese Academy of Medical Sciences and Peking Union Medical College, Beijing, CHINA.*

Aim/Introduction: To assess the impact of respiratory motion artifact on tumor heterogeneity using radiomics features in PET/CT is essential for quantitative characterize and diagnosis of lung lesions. The purpose of this study was to investigate the variability of respiratory-gated (RG) 4D PET/CT based radiomics features compared to ungated (UG) PET/CT, as well as their diagnostic value in the differentiation between non-small cell lung cancer (NSCLC) and benign lung lesions. ***Materials and Methods:*** 117 patients with suspected lung lesions underwent ungated PET/CT and chest respiratory-gated 4D PET/CT were prospectively included. 6 patients failed RG PET/CT. A total of 209 lung lesions in 111 cases were segmented manually using ITK-SNAP by two nuclear medicine physicians. For each lesion, 377 Image Biomarker Standardization Initiative (IBSI) radiomics features were extracted from PET images of each scan, including 71 histogram-related features, 89 shape-related features, 62 textural features and 155 wavelet features. We firstly perform variability comparison via t-test. The subgroup of 126 non-metastasis lesions in 91 patients without treatment before PET/CT were included for diagnosis

analysis and were randomly distributed in training and validation sets. We compared the diagnostic efficiencies in feature-level by ROC curves. Then we selected and developed two radiomics models with UG features (i.e. UGModel) and RG features (i.e. RGModel). And the model-level comparison was performed by comparing the diagnostic value of logistic regression models developed with different scans using five-fold cross-validation. ***Results:*** For the variability analysis, 101/377 (26.8%) RG features showed significant difference compared to UG features ($p < 0.05$). As for the diagnosis analysis, 55 benign lesions of 27 cases and 71 malignant lesions of 64 cases were analyzed. For the feature-level comparison, 61/377(16.2%) RG features showed better discriminant ability in malignant recognition ($p < 0.05$). As for the model-level comparison, the average AUC, accuracy, sensitivity, specificity, PPV and NPV of the two radiomics-based models were 0.80, 79.4%, 73.2%, 87.3%, 88.1%, 71.6% for RGModel, and 0.75, 65.9%, 57.7%, 76.4%, 75.9%, 58.3% for UGModel, respectively. ***Conclusion:*** Respiratory-gated PET/CT improves image quality and quantitative characterization of lung lesions by reducing respiratory motion-related artifacts. Compared to ungated PET/CT, respiratory-gated 4D PET/CT based radiomics features showed incremental diagnostic value in both feature-level and model-level for differentiation of NSCLC and benign lung lesions.

OP-636

Improved imaging of small lung nodules using LAFOV [^{18}F]FDG-PET and data-driven motion compensation method

C. Bregenzer[1], *C. Mingels*[1], *M. Viscione*[1], *H. Sari*[1,2], *K. Shi*[1], *A. Rominger*[1], *T. Pyka*[1];
[1]*Department of Nuclear Medicine, Inselspital, University Hospital Bern, University of Bern, Bern, SWITZERLAND,* [2]*Advanced Clinical Imaging Technology, Siemens Healthcare AG, Lausanne, SWITZERLAND.*

Aim/Introduction: Detection and characterization of lung nodules with PET has traditionally been imposed a size limit (e.g. ≥8mm) due to decreasing sensitivity of former analogue PET scanners in smaller lesions. The newly introduced long axial field of view (LAFOV) PET scanners have been shown to be superior to traditional standard axial field of view (SAFOV) scanners in term of system sensitivity. In order to improve imaging of lung lesions, data driven gating-based motion correction algorithm (DDG-MC) is available to compensate for respiratory movement. Herein, we present the first data evaluating LAFOV PET for lung lesions compared to simulated SAFOV (sSAFOV) acquisitions with and without motion correction. ***Materials and Methods:*** At the time of writing, 24 consecutive patients with a total of 40 lung lesions which had undergone [^{18}F]FDG-PET/CT on a LAFOV PET/CT scanner (106 cm FOV) were included. Data for both ultra-high sensitivity mode (UHS, maximum ring difference (MRD) 322) and sSAFOV acquisition (120 s per bed position, high sensitivity (HS) mode, MRD 85) with and without data driven gating-based motion correction were reconstructed. Lesions were measured in three dimensions (diagnostic inspiratory CT if available, else low-dose CT). Standard uptake values $(SUV)_{mean/max/peak}$ of liver, blood pool and lung background, likewise tumor volume and lesion uptake were calculated with a volume of interest using a 40% isocontour approach. SNR and CNR with lung background were calculated. ***Results:*** Median largest lesion size was 7 mm (Q25: 5mm, Q75: 10 mm). Lesion signal intensity above liver was found in 8/22 small lesions (<8 mm, SUV_{max} 2.15±1.84; ≥8 mm in 15/18, SUV_{max} 7.01±5.25) and above blood pool in 12/22 (≥8 mm in 15/18). SNR and CNR were significantly increased in LAFOV compared to sSAFOV mode ($p \leq 0.01$; HS 2 min 53.43±73.75/50.0±73.43, HS 2 min+DDG-MC 63.21±82.19/59.8±81.9, UHS 6 min 62.45±87.03/58.11±86.67, UHS 6 min+DDG-MC 73.68±98.0/69.35±97.58). sSAVOF 2min with DDG-MC was comparable to UHS 6 minutes without motion correction (SNR: p=0.41, CNR: p=0.30). ***Conclusion:*** UHS acquisition on LAFOV PET/CT with DDG-MC motion correction showed significantly higher SNR and CNR in small lung lesions. Higher detection rates compared to SAFOV PET/CT for lung lesions in PET/CT even <8 mm can be achieved. Further correlation with the final diagnosis is planned. LAFOV PET/CT might be of clinical advantage in the assessment of small lung lesions, possibly pushing the lower size limits for reliable characterization.

OP-637

Predicting survival of metastatic non-small cell lung cancer (NSCLC) patients treated by anti-PD-1 by combining clinical and radiomic features

J. Auriac[1], *N. Captier*[1], *E. Woff*[1,2], *M. Luporsi*[1,3], *C. Nioche*[1], *N. Girard*[4], *I. Buvat*[1], *F. Orlhac*[1];
[1]*Institut Curie, Inserm, Université Paris-Saclay, U1288-LITO, Orsay, FRANCE,* [2]*Université libre de Bruxelles, Jules Bordet Institut, Department of Nuclear Medicine, Bruxelles, BELGIUM,* [3]*Institut Curie, Department of Nuclear Medicine, Paris, FRANCE,* [4]*Institut du Thorax Curie-Montsouris, Paris, FRANCE.*

Aim/Introduction: To determine whether the combination of clinical and radiomic features could predict overall survival (OS) in metastatic patients with non-small cell lung cancer (NSCLC) treated by anti-PD-1 immunotherapy. ***Materials and Methods:*** Baseline FDG-PET/CT images and clinical data were retrospectively collected for 74 metastatic NSCLC patients treated by pembrolizumab. All lesions were segmented with a threshold set to 4 SUV. The Total Metabolic Tumor Volume (TMTV) and the distance between the 2 most distant lesions (Dmax) were extracted using LIFEx [1]. Advanced lung cancer inflammation index (ALI) [2-3] was calculated based on body mass index, serum albumin and neutrophil-to-lymphocyte ratio. For each feature, the optimal cut-off (i.e. giving the lowest p-value in log-rank tests) to distinguish two different groups of patients based on OS was determined. Risk categories were defined based on the presence of risk factors: low ALI, high age, high TMTV and/or high Dmax. Then, different combinations of these 4 binarized features were tested. To compare these combinations, survival analyses were performed for each using the Kaplan Meier method with the log-rank test and Cox proportional hazard regression model, including calculation of adjusted hazard ratios (HRs) with 95% confidence intervals (CI) and Harrell's C-index. ***Results:*** Four univariate models (ALI; age; TMTV; Dmax) and 11 multivariate models (M1 to M11) were tested. High ALI values (>42.4) were significantly associated with longer OS (C-index=0.575, log-rank: p=0.0270). Similarly, young age (<60 yo, C-index=0.600, p=0.0052), low TMTV values (<90 mL, C-index=0.589, p=0.0170) or low Dmax values (<28.4 cm, C-index=0.624, p=0.0008) were associated with longer OS. Comparing the C-index of multivariate models, M4 (ALI+Dmax+Age) outperformed other models to predict OS (C-index=0.708, log-rank: p<0.0001) using 3 risk categories: low (0 or 1 risk factor, n=20), intermediate (2 risk factors, n=33) and high (3 risk factors, n=21). M4 was significantly better than ALI (Z-test [4]: p=0.0001), Dmax (p=0.0009), TMTV (p=0.0042) or age (p=0.0007), and better than 3 multivariate models: M3 (ALI+Dmax, p=0.0106), M5 (ALI+TMTV, p=0.0199) and M6 (ALI+age, p=0.0235). ***Conclusion:*** The performance of ALI can be improved by combining it with simple radiomic features and age. The

combination of ALI, Dmax and age yielded the best performance on predicting OS for metastatic NSCLC patients treated with immunotherapy, and warrants further evaluation. ***References:*** [1] Nioche et al. Cancer Res 2018. [2] Jafri et al. BMC Cancer 2013. [3] Mountzios et al. ESMO Open 2021. [4] Kang et al. Stat Med 2015.

OP-638

Variables Derived From 18F-FDG PET/CT In Predicting Patterns Of Recurrence In Patients With Non-Small Cell Lung Cancer (Stage I-III)

G. Jimenez Londoño[1], *A. M. Garcia Vicente*[2], *J. J. Bosque*[3], *J. Perez-Beteta*[3], *M. Amo-Salas*[4], *A. F. Honguero-Martinez*[5], *E. Noriega Alvarez*[1], *C. Lucas Lucas*[1], *V. M. Perez-Garcia*[3], *A. M. Soriano Castrejon*[2];
[1]*Department of Nuclear Medicine, Hospital General Universitario de Ciudad Real, Ciudad Real, SPAIN,* [2]*Department of Nuclear Medicine, Complejo Hospitalario Universitario de Toledo, Toledo, SPAIN,* [3]*Department of Mathematics, Mathematical Oncology Laboratory (MOLAB), Universidad de Castilla-La Mancha, Ciudad Real, SPAIN,* [4]*Department of Mathematics, Universidad de Castilla-La Mancha, Ciudad Real, SPAIN,* [5]*Department of Surgery, Hospital General Universitario de Albacete, Albacete, SPAIN.*

Aim/Introduction: This study aimed to analyse the metabolic parameters derived from 18F FDG PET/CT staging that can predict recurrence patterns in non-small cell lung cancer (NSCLC) ***Materials and Methods:*** Retrospective study including NSCLC patients who had a baseline 18F-FDG PET/CT scan. Inclusion criteria required stage I-III, complete surgical resection, absence of neoadjuvant treatment, lung lesions with significant 18FDG avidity, diameter ≥10 mm and clinical/radiological follow-up ≥24 months. Relapse patterns were analysed based on location (Distant vs. local recurrence), lesion number (poly vs. oligometastasic disease) and organ-specific recurrence. Polymetastases involved >3 lesions in one organ, recurrence in ≥2 organs or widespread pleural/pericardial involvement, with mediastinal lymph nodes counted as one organ.Clinical variables such as age, tumour location, stage, histology, lymph nodal infiltration and lymphovascular and pleural invasion were recorded. After semi-automatic lung tumour segmentation, SUV and volume-based metrics, global texture, geometrical variables and textural parameters based on run-length matrices and co-occurrence matrices were obtained. Uni-Multivariate logistic regression were performed ***Results:*** Out of 173 patients, 104 experienced recurrence, with 39 having local recurrence, 42 exhibiting distant recurrence, and 23 presenting both. The mean time between surgery and the appearance of local and distant recurrence was not significantly different (18.80±16.5 months and 18.07±17.82 months, respectively). Furthermore, 43.3% of patients were classified as oligometastatic and 56.7% as polymetastatic, with the lung, regional lymph nodes, brain and bone being the most commonly affected sites of metastasis. In multivariate analysis, adenocarcinoma tumours, LRLGE (Long run low gray-level emphasis) and SRHGE (Short run high gray-level emphasis) were identified as independent variables for distant recurrence. The analysis also found that patient age, number of affected lymph nodes, Sphericity, nSCD (normalized SUVpeak to centroid distance), Entropy, LGRE (Low gray-level run emphasis), and HGRE (High gray-level run emphasis) were independent variables for polymetastatic disease. Regional lymph node recurrence was related to number of affected lymph nodes and Dissimilarity, while lung recurrence was associated with upper lobe tumour, SUVmax, Sphericity, and nSPD (normalized SUVmax perimeter distance). Brain recurrence was related with adenocarcinoma tumours and lymph node invasion at diagnosis, and bone recurrence was related to the number of affected lymph nodes and GLNU (Gray-level non-uniformity). ***Conclusion:*** Metabolic variables obtained from 18F-FDG PET/CT were found to be predictive of recurrence patterns that are closely linked to the overall survival of NSCLC patients. These findings could help in the development of personalized treatment strategies based on an individual's recurrence pattern

OP-639

18F-FDG PET/CT and Coefficient of Variation of Primary Tumors and Metastatic Lymph Nodes To Assess the Heterogeneity of Glycolytic Phenotype in Patients With Advanced NSCLC

S. Pellegrino[1], *R. Fonti*[1], *C. Vallone*[1], *A. Catapano*[1], *R. Morra*[2], *S. De Placido*[2], *S. Del Vecchio*[1];
[1]*Department of Advanced Biomedical Sciences, University Federico II, Naples, ITALY,* [2]*Department of Clinical Medicine and Surgery, University Federico II, Naples, ITALY.*

Aim/Introduction: The aim of the present study was to test whether the Coefficient of Variation (CoV) of 18F-FDG PET/CT images of primary tumors and metastatic lymph nodes may predict clinical outcome in patients with advanced non-small cell lung cancer (NSCLC). ***Materials and Methods:*** Ninety-two patients with advanced NSCLC who had undergone 18F-FDG PET/CT scan at diagnosis were studied. Imaging parameters including SUVmax, SUVmean, CoV (SD divided by SUVmean), MTV, TLG were determined in primary tumors and target lymph nodes along with Total MTV (MTV_{TOT}) and Whole-Body TLG (TLG_{WB}) of all malignant lesions. Univariate analysis of clinical and imaging variables was performed using Cox proportional hazards regression whereas survival analysis was performed using Kaplan-Meier method and log-rank tests. ***Results:*** A total of 150 lesions were analyzed including 92 primary lung tumors and 58 metastatic lymph nodes showing the highest SUVmax value in each patient. Mean SUVmax, SUVmean, CoV, MTV and TLG values were 12.00±5.77, 5.44±2.11, 0.36±0.13, 71.14±117.08 ml and 401.56±618.48 g in primary tumors while they were 11.89±8.54, 4.85±1.90, 0.37±0.16, 46.16±99.59 ml and 256.84±548.27 g in involved lymph nodes. At univariate analysis, overall survival (OS) was predicted by CoV of primary tumors (p=0.0141), SUVmax (p=0.0363), SUVmean (p=0.0200) and CoV (p=0.0139) of target lymph nodes, MTV_{TOT} (p=0.0165) and stage (p=0.0105). Then we performed Kaplan-Meier analysis by using the cutoff values of CoV of primary tumors (0.35) and CoV of target lymph nodes (0.29). OS was significantly better in patients with CoV of primary tumors>0.35 than those with CoV≤0.35 (χ^2=6.6933, p=0.0097), while patients with CoV of target lymph nodes≤0.29 showed significantly better OS as compared to patients having CoV>0.29 (χ^2=5.9570, p=0.0147). Finally, we combined CoV values of primary tumors and target lymph nodes in all possible arrangements for Kaplan-Meier analysis. Patients with CoV of primary tumors≤0.35 and CoV of target lymph nodes>0.29 had the worst prognosis, while the best OS was observed in patients with CoV of primary tumors>0.35 and CoV of target lymph nodes≤0.29 (χ^2=14.3992, p=0.0024). ***Conclusion:*** CoV of primary tumors and CoV of target lymph nodes can predict clinical outcome of NSCLC patients in opposite direction. In fact, heterogeneity of primary tumors derives mainly from the lower percentage of tumor cells having a glycolytic phenotype inside the malignant lesion whereas in metastatic lymph nodes, heterogeneity is due to a higher percentage of tumor cells having a glycolytic phenotype inside the target lesion.

OP-640

Use of 18F-FDG PET Imaging after Curative Treatment of Non-Small Cell Lung Cancer Patients: A Nationwide Cohort Study

K. Guldbrandsen[1], *L. Sopina*[2], *T. R. Rasmussen*[3], *B. M. Fischer*[1]; *[1]Dept. of Clinical Physiology, Nuclear Medicine & PET, Copenhagen University Hospital, Rigshospitalet, Copenhagen, DENMARK, [2]Danish Centre for Health Economics, DaCHE, Dept. of Public Health, University of Southern Denmark, Odense, DENMARK, [3]Department of Respiratory Diseases and Allergy, Aarhus University Hospital, Aarhus, DENMARK.*

Aim/Introduction: Surveillance imaging is essential for managing non-small cell lung cancer (NSCLC), as it enables early detection of disease recurrence, which remains a significant risk after curative-intent treatment. In recent years, [^{18}F]Fluorodeoxyglucose positron emission tomography-computed tomography (18F-FDG PET/CT) has become an essential imaging modality in lung cancer due to its high sensitivity and specificity for detecting malignant lesions and assessing tumour staging. However, little is known about how 18F-FDG PET imaging is utilized during surveillance. This study aimed to investigate changes over time and factors associated with the use of 18F-FDG PET imaging in patients after curative treatment of NSCLC. ***Materials and Methods:*** We analyzed data from 13,746 NSCLC patients diagnosed between 2007 and 2020 in the Danish Lung Cancer Registry who underwent curative-intent treatment. Multivariable regression was used to analyze trends in the use of 18F-FDG PET imaging over time and to identify factors associated with the use of 18F-FDG PET imaging during the first two years of surveillance after curative therapy. ***Results:*** The utilization rate of 18F-FDG PET scans per 100 patients increased from 9.9 per year in 2007 [95% confidence interval (CI), 4.7 to 15.1] to 40.0 per year in 2013 [95% CI, 36.7 to 43.3], followed by a period of stability. The proportion of patients who received at least one 18F-FDG PET scan during the first two years after treatment increased from 23% for patients diagnosed in 2007-08 to 38% in 2019-20. The utilization rate increased with increasing stage (percentage points, +19.0 [95% CI, 11.3 to 26.7] and +30.3 [95% CI, 22.2 to 38.4] for stages II and III, respectively). Additionally, the utilization rate was higher in patients who received definitive chemoradiation or stereotactic body radiotherapy (SBRT) when compared to surgery (pp, +25.5 [95% CI, 18.3 to 32.6]). ***Conclusion:*** There has been a substantial increase in 18F-FDG PET imaging after curative therapy for NSCLC. Notably, the use is increased in patients with advanced stage and after definitive chemoradiation or SBRT. These findings suggest that 18F-FDG PET imaging is increasingly important in managing these patients. Further research is needed to determine how this will impact patient outcomes and healthcare system efficiency.

1307

Tuesday, September 12, 2023, 9:45 AM - 11:15 AM
Hall F1

Cardiovascular Committee - TROP Session: Plaque, Fibrosis and Cardio-Oncology

OP-641

Value of Na[18F]F and 2-[18F]FDG PET/CT imaging in early stages of aortic valve degeneration assessment after transcatheter aortic valve (TAVI) implantation

M. Opalinska[1], *D. Sorysz*[2], *A. Sowa-Staszczak*[1], *A. Grochowska*[3], *A. Dziewierz*[2], *K. Malinowski*[4], *N. Maruszak*[2], *M. Bagieński*[5], *S. Bartuś*[2], *D. Dudek*[6];
[1]Department of Endocrinology, Jagiellonian University Medical College, Krakow, POLAND, [2]2nd Department of Cardiology, Institute of Cardiology, Jagiellonian University Medical College, Krakow, POLAND, [3]Department of Radiology, University Hospital, Krakow, POLAND, [4]Department of Bioinformatics and Telemedicine, Jagiellonian University Medical College, Krakow, POLAND, [5]Intensive Cardiac Care Unit, University Hospital, Krakow, POLAND, [6]Center for Digital Medicine and Robotics, Jagiellonian University Medical College, Krakow, POLAND.

Aim/Introduction: Severe symptomatic aortic stenosis is often in the elderly, caused by the degenerative process of valve leaflets associated with aging. Nowadays transcatheter aortic valve implantation (TAVI) is a standard, minimally invasive treatment in such cases. Unfortunately, in some of them we observe their fast degeneration, causing limited durability of TAVI. We aimed to investigate the utility of Na[18F]F and 2-[18F]FDG PET/CT in assessment of an early TAVI valve degeneration and the influence of microcalcification and inflammatory processes on TAVI durability. ***Materials and Methods:*** Seventy-one TAVI patients underwent baseline transthoracic echocardiography (TTE), transesophageal echocardiography, and PET/CT using Na[18F]F and 2-[18F]FDG. Of these, 30 patients had follow-up examinations, while the remainder were lost to mortality and the COVID pandemic. TAVI valve morphology and function were assessed using TTE and TEE. SUVmax, SUVmean and tissue-to-background (TBR) of Na[18F]F and 2-[18F]FDG uptake in the projection of the aortic valve were measured. Both Na[18F]F and 2-[18F]FDG uptakes were compared between baseline and follow-up PET/CT scans, performed 18.2 (±11.3) and 19.8 (±12.7) months after baseline, respectively. ***Results:*** Na[18F]F and 2-[18F]FDG PET/CT as well as echocardiography data were analyzed for 30 TAVI patients, all who underwent follow-up PET/CT scans. Median age of patients was 84.0 (IQR 80.0-87.0) years. After TAVI implantation, significant improvement in valve function was observed in all patients. During follow-up, valve function, assessed by TTE, remained stable, however PET/CT imaging has demonstrated an increase in TBR value of 2-[18F]FDG uptake in the inner (1.2 (IQR 1.0-1.7) to 1.7 (IQR 1.5-2.1), p = 0.009) and outer (IQR 1.3 (1.1-1.7) to 1.7 (IQR 1.5-2.1), p= 0.012) sites of the TAVI valve stent, while there were no difference in Na[18F]F uptakes in any site of TAVI (inner: baseline 1.4 (IQR 1.1-1.7), follow-up 1.5 (IQR 1.1-2.0), p = 0.17, outer: baseline 1.1 (IQR 0.9-1.2), follow-up 1.2 (IQR 0.9-1.4), p = 0.57). ***Conclusion:*** In average, 2 years after TAVI implementation, an increase of an inflammation marker (2-[18F]FDG) uptake was seen in PET/CT, while the uptake of the calcification marker (Na[18F]F) remained stable. That inflammation process, as evidenced by increased 2-[18F]FDG uptake, may play a pivotal role in the early stages

of TAVI valve degeneration, preceding the onset of calcification detected by Na[18F]F uptake. The possible use of PET/CT imaging for prediction of degenerative process on TAVI, as well as understanding of the pathomechanism of their destruction needs further investigation.

OP-642

The relationship between arterial calcification and hypoxia of the arterial wall detected by [18F] F-Fluoromisonidazole Positron Emission Tomography

J. Bellinge[1,2], *I. Barry*[3], *R. Francis*[1,2], *F. Picazo-Pineda*[3], *N. Altaf*[3], *C. Schultz*[1,3];
[1]*University of Western Australia, Perth, AUSTRALIA,*
[2]*Sir Charles Gairdner Hospital, Perth, AUSTRALIA,*
[3]*Royal Perth Hospital, Perth, AUSTRALIA.*

Aim/Introduction: Arterial calcification burden is a strong predictor of cardiovascular disease events. Hypoxia within the arterial wall may contribute to the development of arterial calcification. [18F]F-Fluoromisonidazole ([18F]F-FMISO) Positron Emission Tomography (PET) is a novel method for non-invasive detection of hypoxia of the arterial wall(1). We aimed to investigate the relationship between hypoxia of the arterial wall measured on [18F]F-FMISO PET and arterial calcification burden. ***Materials and Methods:*** This is a post-hoc analysis of 3 prospective observational studies investigating [18F]F-FMISO PET for tumoral hypoxia in patients with mesothelioma or pancreatic cancer (2,3). Arterial [18F]F-FMISO activity was quantified by drawing regions of interest around the adventitia of the thoracic aorta on consecutive axial slices. The SUVmax was measured for each slice and the most disease segment (MDS SUV), defined as the average of three consecutive slices centered on the highest SUVmax, was calculated for each territory of the thoracic aorta (ascending, arch and descending thoracic aorta). The MDS SUV was divided by blood pool SUVmean, measured from the right atrium, to result the tissue-to-background ratio (MDS TBR)(4). Arterial calcification was quantified from attenuation correction CT scans using the Agatston score. Imaging modalities were analysed by blinded observers. Spearmans' Rho (r) and independent t-tests were used appropriately, depending on the distribution of the variables tested. ***Results:*** Forty-one individuals underwent [18F]F-FMISO PET between 2009 and 2017 and were included in this analysis. The mean age was 64.3±9.1 and 85.4% were male. The MDS SUV correlated positively with the calcium score in the ascending (r=0.45, p=0.003) and descending aorta (r=0.37, p=0.019) but not the arch of aorta (r=0.29, p=0.06). The MDS TBR did not correlate with the calcium score in the ascending (r=-0.13, p=0.93), arch (r=0.00, p=0.99) or descending aorta (r=0.25, p=0.12). The maximum MDS SUV of the three thoracic aortic territories was higher in patients prescribed antihypertensive therapy (N=13) compared to those who were not (2.40±0.25 v 2.08±4.9, p=0.033). There were no other associations between thoracic arterial [18F]F-FMISO activity and traditional cardiovascular risk factors. ***Conclusion:*** Thoracic aortic [18F]F-FMISO activity is associated with arterial calcification burden, but the relationship is dependent on the method of quantification. Further studies are required to validate [18F]F-FMISO as a measure of hypoxia of the arterial wall. ***References:*** 1. Mateo et al. Circ Cardiovasc Imaging. 2014;7:312-20. 2. Segard et al. Clin Nucl Med. 2013;38:1-6. 3. Francis et al. Lung Cancer. 2015;90:55-60. 4. Bellinge et al. J Nucl Cardiol. 2022;29:1855-66

OP-643

Morphological and component features of advanced carotid plaque on MRI in correlation with inflammation on PET: a hybrid ^{18}F-FDG PET/MRI study

F. Yu, *Y. Zhang, J. Lu;*
Xuanwu Hospital, Capital Medical University, Beijing, CHINA.

Aim/Introduction: The aim of this study was to exploit the methodological opportunity of hybrid PET/MRI to simultaneously evaluate the morphological, component, and metabolic features of advanced atherosclerotic plaques, observe the relationship among features and explore the incremental value of PET over MRI. ***Materials and Methods:*** The study group comprised 280 patients with advanced plaque in the carotid bifurcation who underwent ^{18}F-FDG PET/MRI scan. Plaque morphological and component features were determined on MRI. Maximum standardized uptake values (SUV_{max}) and tissue to background ratio (TBR) on corresponding PET sections were calculated. Further, all patients were divided into high and low ^{18}F-FDG uptake group for subgroup analysis. ***Results:*** The degree of luminal stenosis (77.0% vs 59.0%, $p < 0.001$), the prevalence of complicated lesion-MR AHA type VI (50.6% vs 21.9%, $p < 0.001$), and the intensity of ^{18}F-FDG uptake (SUV_{max}=2.30[1.68-2.92] vs 1.93[1.52-2.49], p=0.007; TBR= 2.96[2.35-3.80] vs 2.32[1.81-3.00], $p < 0.001$) were significantly higher in the symptomatic plaques than the asymptomatic plaques. The degree of luminal stenosis and the MR AHA type was corelated with ^{18}F-FDG uptake separately (r=0.14, p=0.013 and r=-0.25, p=0.018). Subgroup analysis found higher prevalence of complicated plaque for the symptomatic plaques in both ^{18}F-FDG high uptake group and low uptake group (56.9% vs 27.5% and 41.7% vs 17.3%, p<0.001 and p=0.001 each). However, lower prevalence of MR AHA type IV-V lesion was identified for symptomatic plaques as compared with asymptomatic plaques only in low uptake group (25.0% vs 45.1%, p=0.026). In contrast, lower prevalence of MR AHA type VII lesion was identified for symptomatic plaques only in high uptake group (2.0% vs 6.9%, p=0.006). No significant difference for the prevalence of MR AHA type VIII lesion was found between the symptomatic and the asymptomatic plaques in both high and low uptake groups. ***Conclusion:*** Morphological and component features were associated with metabolic status in advanced atherosclerotic plaques. Moreover, the prevalence of lipid core (MR AHA type IV-V lesion) and calcification (MR AHA type VII lesion) in symptomatic plaques varied under different inflammatory uptake status. Hybrid ^{18}F-FDG PET/MRI can provide supplementary optimization information for the traditional MR AHA classification to identify vulnerable plaques in atherosclerosis subjects.

OP-644

Comparison between Cardiac ^{18}F-FAPI PET/CT and MRI for Assessment of Myocardial Fibrosis in Hypertrophic Cardiomyopathy

L. Wang[1], *Y. Wang*[2], *Y. Zhang*[1], *Z. Dong*[3], *J. Wang*[3], *X. Xi*[1], *B. Chen*[1], *S. Zhao*[3], *M. Yang*[1];
[1]*Beijing Chaoyang Hospital, Beijing, CHINA,*
[2]*Beijing Tsinghua Changgung Hospital, Beijing, CHINA,* [3]*Fuwai Hospital, Beijing, CHINA.*

Aim/Introduction: Myocardial fibrosis could be evaluated by cardiac MRI and fibroblast activation protein inhibitor (FAPI) PET/CT imaging. We aimed to explore the relationship between FAPI imaging and late gadolinium enhancement (LGE) and T1 mapping for assessment of myocardial fibrosis in hypertrophic cardiomyopathy (HCM). ***Materials and Methods:*** In this

prospective study from July 2021 to October 2022, participants with HCM underwent cardiac FAPI PET/CT imaging and MRI, which was performed within a median time of 2 days before or after FAPI imaging. Myocardial FAPI activity was quantified as intensity (target-to-background uptake ratio, TBR), extent (the percent of FAPI-avid myocardium of left ventricle, FAPI%), and amount (FAPI% × TBR). A segment with TBR of 2.3 or greater than was defined as FAPI-avid. LGE and extracellular volume fraction (ECV) by T1 mapping on MRI were employed to quantify focal and diffuse fibrosis, respectively. The extent of LGE was expressed as the percentage of left ventricular mass (LGE%). Segment with the presence of LGE or ECV≥29.6% was defined as abnormal. Univariable and multivariable linear regression analyses were used to identify factors related to the difference (ΔExtent%) in the extent of myocardial fibrosis detected by FAPI imaging and ECV mapping on MRI. ***Results:*** Fifty-three HCM participants (mean age: 46.0 ± 13.3 years, 30 men) with 848 segments were analyzed. Intense but inhomogeneous FAPI uptake was observed in all participants, most of whom were identified as having LGE (90.6%) and ECV expansion (77.4%). FAPI% varied to a greater scale (12.1%-92.2%) and was larger than ECV [49.7 (37.9, 64.5) vs. 32.0 (30.0, 36.9), P<0.0001)] and LGE% [6.6 (1.9, 15.2), P<0.0001]. Log-transformed ΔExtent% had a positive relationship with the log-transformed N-terminal pro-brain natriuretic peptide (NT-proBNP) [0.88 (95% confidential interval (CI): 0.35, 1.40)] and left ventricular mass [1.82 (95%CI: 0.40, 3.24)]. Notably, in segments without the presence of LGE and ECV expansion, there were still 127 segments (15.0%) showing FAPI activity. ***Conclusion:*** Cardiac FAPI PET/CT imaging was capable of detecting more injured myocardium than MRI. NT-proBNP and left ventricular mass were associated with the difference in the extent of myocardial fibrosis detected by FAPI imaging and ECV.

OP-645

Coronary microvascular dysfunction: main characteristics and prognostic value

K. Kopeva*, E. Grakova, A. Maltseva, A. Mochula, A. Gusakova, A. Smorgon, K. Zavadovsky;*
Cardiology Research Institute, branch of the Federal State Budgetary Scientific Institution «Tomsk National Research Medical Center of the Russian Academy of Sciences», Tomsk, RUSSIAN FEDERATION.

Aim/Introduction: The objective of this study was to evaluate the main clinical and instrumental features of coronary microvascular dysfunction (CMD) and to assess its prognostic value during 12 months of follow-up period. ***Materials and Methods:*** A total of 118 patients with non-obstructive CAD and preserved LVEF (62 [59; 64]%) were enrolled. Serum levels of biomarkers were analyzed by ELISA. CMD was defined as the presence of MFR ≤2 evaluated by dynamic CZT-SPECT. Two-dimensional transthoracic echocardiography with evaluation of left ventricle diastolic dysfunction was performed baseline. ***Results:*** Patients were divided into groups depending on the presence of CMD: group 1 included patients with CMD (n=45), and group 2 included patients without CMD (n=73). The lateral e' values were lower by 35% in group 1 (p=0.009) than in group 2. The peak rate of tricuspid regurgitation was higher by 12% (p=0.011), the E/e' ratio was higher by 21.4% (p =0.041) and indexed left atrial volume by 51.2% (p=0.038) in group 1 than group 2. In patients with CMD, the value of global longitudinal starin was lower by 29.7% (p=0.005) than in those without it. In patients with CMD, MFR values were lower by 48.3% (p<0.001) than in patients without it. In group 1, rest-MBF was higher by 30.1% (p<0.001) and stress-MBF was lower by 30.1% (p<0.001) compared to group 2. CRP concentrations were higher by 1.8 times (p=0.011), interleukin-10 concentrations were lower by 21.7% (p=0.048) and interleukin-1β was higher by 2.7 times (p=0.046) in group 1 compared to group 2. The levels of NT-proBNP were higher by 2.6 times (p=0.004), soluble ST2 by 18.1% (p<0.001), tissue inhibitor of metalloproteinase-1 by 2.3 times (p=0.011), matrix metalloproteinase-9 by 1.9 times (p=0.012) in group 1 compared to group 2. GDF-23 and tetranectin did not differ between groups. Multivariate regression analysis showed the presence of diastolic dysfunction (OR 3.27; 95% CI 2.26-5.64; p<0.001), the hyperexpression of NT-proBNP ≥ 760.5 pg/mL (OR 1.67; 95% CI 1.12-4.15; p=0.021), and soluble ST2 ≥ 31.4 ng/mL (OR 1.37; 95% 1.08-2.98; p=0.015) were independent factors associated with CMD. Kaplan-Meier analysis showed that the frequency of adverse outcomes were significantly (p<0.001) higher in patients with CMD (45.2%, n=19) than in patients without it (8.6%, n=6). ***Conclusion:*** The presence of CMD was associated with the severe diastolic dysfunction, hyperexpression of the biomarkers of fibrosis and inflammation. Patients with CMD had higher rate of adverse outcomes than those without it. ***Funding:*** MK-4257.2022.3.

OP-646

Comparative analysis of multi-modality cardiac imaging for prediction of cardiovascular outcomes in patients undergoing coronary artery bypass grafting

M. Gao[1]*, W. Wen*[2]*, J. Meng*[2]*, M. Yun*[2]*, H. Li*[1]*, Y. Yu*[1]*, X. Zhang*[2]*;*
[1]*Department of Cardiac Surgery, Beijing Anzhen Hospital, Capital Medical University, Beijing, CHINA,* [2]*Department of Nuclear Medicine, Molecular Imaging Lab, Beijing Anzhen Hospital, Capital Medical University, Beijing, CHINA.*

Aim/Introduction: Multidisciplinary quantitative analysis has not been well established in outcome studies in patients with ischemic cardiomyopathy post coronary artery bypass grafting (CABG). This comparative study aimed to evaluate coronary stenosis, micro & macro-calcification in predicting short and long-term cardiovascular outcomes in patients after CABG. ***Materials and Methods:*** Patients with three-vessel disease or left main disease underwent cardiac ^{18}F-NaF PET/CT, coronary angiography (SYNTAX score), and coronary artery calcium (CAC) scoring prior to the CABG procedure. Maximum coronary microcalcification activity (TBR_{max}) and global coronary microcalcification activity (TBR_{global}), represented the highest and average coronary ^{18}F-NaF uptake, were calculated. Radiomic features were extracted from PET, CT, and PET+CT fusion images to develop a multiparametric radiomics signature for cardiac events prediction. Perioperative myocardial infarction (PMI) after 7 days of CABG was defined as the primary endpoint. The major adverse cardiac and cerebrovascular events (MACCEs) and recurrent angina as the secondary endpoint. ***Results:*** 101 patients with coronary artery disease (CAD) were enrolled and followed up to 40.0 months. TBR_{max} (odds ratio, 1.445; P=0.011) and TBR_{global} (odds ratio, 1.797; P=0.018) significantly predicted the occurrence of PMI, outperforming SYNTAX score, CAC score, and blood biomarkers. Patients with threshold value of TBR_{max} > 3.0 had a >4-fold increase in PMI independent of age, sex and risk factors, respectively. Interestingly, the occurrence of PMI in the anterior wall ($PMI_{anterior}$) and the inferior wall ($PMI_{inferior}$) was related to the corresponding coronary ^{18}F-NaF uptake as TBR in the left anterior descending ($TBR_{LAD-max}$) (odds ratio, 2.154, P=0.036) and TBR in the right coronary artery ($TBR_{RCA-max}$) (odds ratio, 2.686; P=0.031). Furthermore, TBR_{max} was a predictor of MACCEs and threshold value of TBR_{max} >3.6 had a >6-fold

increase in the incidence of MACCEs. The Kaplan-Meier estimate of the survival rate for MACCEs decreased with the increase of TBR_{max}. TBR_{max} (HR = 1.261; p = 0.016) and TBR_{global} (HR = 1.327; p = 0.016) were significantly associated with the occurrence of recurrent angina in long term after CABG. ***Conclusion:*** Coronary microcalcification activity quantified by ^{18}F-NaF PET has superior potential in predicting cardiovascular outcomes after CABG compared to conventional coronary macrocalcification burden and stenosis severity.

OP-647

Coronary artery calcium score and epicardial adipose tissue from unenhanced whole-body PET-CT imaging in oncological patients with and without standard modifiable cardiovascular risk factors

C. Vallone[1], *C. Nappi*[1], *R. Lepre*[1], *L. Basile*[1], *A. Ponsiglione*[1], *C. Ferraioli*[1], *R. Green*[1], *V. Cantoni*[1], *C. Mainolfi*[1], *M. Imbriaco*[1], *M. Petretta*[2], *A. Cuocolo*[1];
[1]*Department of Advanced Biomedical Sciences, University of Naples Federico II, Naples, ITALY,* [2]*IRCCS Synlab SDN, Naples, ITALY.*

Aim/Introduction: Earlier diagnoses and more effective therapies lead to an improvement in the survival of patients with cancer. Hence, in cancer patients with high probability of long-term survival it is important to consider cardiovascular risk. Whole-body unenhanced PET-CT imaging performed for oncological reasons may provide additional parameters such as coronary artery calcification (CAC) and epicardial adipose tissue volume (EAT) with cost-effective predictive value in asymptomatic people, beyond traditional cardiovascular risk factors. The aim of the study was to investigate the characteristics of cardiac CT parameters (CAC and EAT) obtained from unenhanced whole-body PET-CT imaging in oncological patients with standard modifiable cardiovascular risk factors (SMuRFs) as compared to patients without (SMURF-less). ***Materials and Methods:*** We studied 109 consecutive patients without known CAD undergoing PET-TC with administration of ^{18}F-FDG in 92 and ^{18}F-Choline in 17 patients. For each patient, the exposure variable was defined as having at least one of the following SMuRFs: current smoker status, hypercholesterolemia, diabetes mellitus, or hypertension. Unenhanced CT images were retrospectively reviewed for CAC, EAT on a dedicated platform. CAC score was calculated according to the Agatston method with a threshold of ≥130 HU and EAT volume was quantified setting the range of attenuation for EAT segmentation between -30 and -190 HU. The ln(CAC+1) score transformation was used to adjust for the rightward skew of the data and to reduce heteroscedasticity. ***Results:*** From overall population (53 men, 49%), 44 subjects (40%) were SMuRF-less and 65 (60%) had ≥1 SMuRFs. SMURFs patients were older than SMuRF-less (51±17 vs. 62±12 years, p<0.001). ln(CAC+1) (1.8±2.5 vs. 3.3±2.6, p<0.004) and EAT volume (84±45 vs. 109±49 cm^3, p=0.006) were higher in SMURFs patients compared to SMuRF-less. EAT volume was also higher in patients with BMI ≥30 kg/m2 compared to those with BMI <30 kg/m2 (122±33 vs. 95±45 cm^3, p=0.04). At regression analysis, a significant relationship was detectable between ln(CAC+1) and EAT volume (p<0.001) in the entire population. At logistic regression analysis, ln(CAC+1) (p<0.005) and EAT volume (p<0.008) were significantly associated with the presence of SMuRFs. ***Conclusion:*** This study first demonstrates a strong association between SMURFs, CAC score and EAT in cancer patients, suggesting evaluating in a cost-effectiveness manner these parameters in all patients undergoing whole-body PET/CT imaging. This approach may imply substantial benefits allowing to evaluate cancer disease and atherosclerotic burden in a single test already included in the diagnostic program of oncological patients with radiation dose optimization.

OP-648

Immune checkpoint inhibitor treatment may induce abated reactive arterial inflammation in lung cancer patients with history of sysmatic therapy: trained immunity before immunotherapy?

R. Calabretta, *L. Beer, H. Prosch, D. Kifjak, P. Binder, S. Grünert, W. Langsteger, M. Mitterhauser, X. Li, M. Hacker;
Medical University of Vienna, Vienna, AUSTRIA.*

Aim/Introduction: Immunotherapy with immune checkpoint inhibitors (ICI), one of the most effective therapies in oncology today, is related to different immune-related adverse events (IRAEs) affecting also cardiovascular (CV) system, including accelerated progression of atherosclerosis. Positron emission tomography (PET) with 2-[^{18}F]fluoro-d-glucose (2-[^{18}F]FDG) is a validated imaging modality to study and to quantify inflammation in atherosclerosis, also in oncological patients. ***Materials and Methods:*** 2-[^{18}F]FDG PET/CT imaging pre/post ICI therapy of 47 patients with lung cancer were retrospectively analyzed. Maximum 2-[^{18}F]FDG standardized uptake values (SUV_{max}) and target-to-background ratios (TBRs) were calculated along six arterial segments. We classified the arterial PET lesions by pre-existing active inflammation (cut-off: TBR_{pre}≥1.6). 2-[^{18}F] FDG metabolic activity pre/post was also quantified in bone marrow, spleen, and liver. Circulating blood biomarkers like high sensitivity C-reactive protein (hsCRP) and neutrophil-lymphocyte ratio (NLR) were additionally collected at baseline and after ICI treatment. ***Results:*** ICI therapy resulted in a significantly increased arterial inflammatory activity, detected by increased TBRs, in all arterial PET lesions analyzed (n= 761; lesional-TBR_{pre}=1.73±0.42 vs. lesional-TBR_{post}=1.90±0.44; p<0.001). In particular, a significant elevation of arterial 2-[^{18}F]FDG uptake was recorded in PET lesions without pre-activating inflammation (n=305; $TBR_{inf(-)_pre}$=1.35±0.18 vs. $TBR_{inf(-)_post}$=1.79±0.39; p<0.001), in calcified (n=73; $TBR_{cal(+)_pre}$=1.75±0.42 vs. $TBR_{cal(+)_post}$=1.91±0.45; p<0.001) and in non-calcified lesions ($TBR_{cal(-)_pre}$=1.64±0.43 vs. $TBR_{cal(-)_post}$=1.99±0.38; p<0.001). Furthermore, a significant increase of arterial 2-[^{18}F]FDG meatbolic activity was observed in patients not previously treated with chemotherapy (n=19; $TBR_{CHT(-)_pre}$=1.64±0.26 vs. $TBR_{CHT(-)_post}$=1.91±0.36; p<0.001) or radiotherapy (n=25; $TBR_{RT(-)_pre}$=1.68±0.25 vs. $TBR_{RT(-)_post}$=1.93±0.38; p<0.001) as well as in those without CV risk factors (n= 29, $TBR_{RF(-)_pre}$= 1.72±0.28 vs. $TBR_{RF(-)_no_post}$= 1.89±0.34,p<0.01). No significant changes were recorded in 2-[^{18}F]FDG uptake of bone marrow ($SUV_{mean_BM_pre}$=1.17±0.20 vs. $SUV_{mean_BM_post}$=1.12±0.27; p=0.34), spleen ($SUV_{mean_spleen_pre}$=1.77±0.47 vs. $SUV_{mean_spleen_post}$=1.78±0.37; p=0.92), and liver ($SUV_{mean_liver_pre}$=1.99±0.33 vs. $SUV_{mean_liver_post}$=2.02±0.41; p=0.61) after ICI treatment. No significant modifications were seen in the blood biomarkers. ***Conclusion:*** Cancer immunotherapy with ICI might increase vascular inflammation in lung cancer patients absenting pre-exisiting arterial inflammation, while subjects priorly exposed to anti-ancer treatments or already presenting CV risk factors could have a lower immuno-response and, subsequently, a lower arterial activation after ICI, probably due to trained immunity.

OP-649

Leg-muscle perfusion preserve on 99mTc-MIBI stress-rest scintigraphy : the novel use of radionuclide imaging in peripheral arterial disease

G. Parida, *T. Singhal, P. Singh, P. Kumar, R. Emerson, K. Bishnoi, A. Rehaman, S. Patro, K. Agrawal;
All India Institute Of Medical Sciences, Bhubaneswar, INDIA.*

Aim/Introduction: Peripheral arterial disease (PAD) is typically believed to be associated with obstructive arteriopathy. However, real-time clinical studies showed a surprisingly weak correlation between the limb hemodynamics and walking capacity. This depicts other factors at play apart from the macrovascular

obstructive disease as initially believed. Thereby necessitating a need for non-invasive imaging that could detect the functional disturbances apart from hemodynamic disturbance and could predict their functional capacity. This study evaluated the utility of lower extremity 99mTc-MIBI imaging as a non-invasive correlate to lower extremity functional capacity (1, 2). ***Materials and Methods:*** Thirty-three patients including eight diabetics with no known history of PAD were included in the study. 99mTc-MIBI perfusion scintigraphy was performed for calf muscles at stress and rest. Counts are assessed on anterior and posterior images and a geometric mean of both was taken. Perfusion reserve (PR) for bilateral calves was calculated as: (average stress counts-average rest counts)/ average rest counts x 100. Correlation of PR of bilateral calves was assessed with respect to functional / exercise capacity (METs and exercise duration). ***Results:*** Thirty-three patients (26 male and 7 female) with median age of 46 (range 28-66) years were included in the study. Mean PR for left and right calf muscles was 75.35±49.1% and 70.57±44.4% respectively. There was significant correlation between functional capacity of the patients (METs achieved and exercise duration) and PR of bilateral calf muscles (Table 1). Besides, among the diabetics, there was mild negative correlation between duration of diabetes with perfusion reserve with a correlation coefficient of -0.3 and p value of 0.09. ***Conclusion:*** Radionuclide imaging with 99m-Tc MIBI may serve as an ideal non-invasive imaging to detect the macrovascular and microvascular perfusion disturbances in patients with PAD and diabetes much before appearance of clinical symptoms and to assess skeletal muscle adaptation in response to exercise therapy or other novel therapies. ***References:***
1. Manevska N, Stojanoski S, Pop Gjorceva D, Todorovska L, Vavlukis M, Majstorov V. Tissue-muscle perfusion assessed by one day 99mTc-MIBI rest-dipyridamol scintigraphy in non-diabetic and diabetic patients. Rev Esp Med Nucl Imagen Mol (Engl Ed). 2018 May-Jun;37(3):141-145. 2. Chou TH, Alvelo JL, Janse S, Papademetris X, Sumpio BE, Mena-Hurtado C, Sinusas AJ, Stacy MR. Prognostic Value of Radiotracer-Based Perfusion Imaging in Critical Limb Ischemia Patients Undergoing Lower Extremity Revascularization. JACC Cardiovasc Imaging. 2021 Aug;14(8):1614-1624.

1308

Tuesday, September 12, 2023, 9:45 AM - 11:15 AM
Hall F2

Thyroid Committee - TROP Session: ^{18}F-FDG and Novel Tracers in the Diagnostic Management of Patients with Thyroid Cancers

OP-650

Investigating the role of F18-FDG PET/CT and Ga68 DOTATOC PET/CT in the evaluation of differentiated thyroid cancer patients with increased serum thyroglobulin and negative I-131 whole body scan

A. Aghaee, *K. Aryana, M. Esmatinia, V. Roshan Ravan;*
Nuclear Medicine Research Center,Mashhad University Of Medical Sciences, Mashhad, IRAN, ISLAMIC REPUBLIC OF.

Aim/Introduction: Regarding increasing prevalence and incidence of thyroid cancer, defining a useful diagnostic protocol for choosing the proper treatment is inevitable. in the differentiation of thyroid cancers, the thyroid cancer population may express different receptors, including somatostatin. The aim of this study was to investigate the role of F18-FDG PET / CT and Ga68-DOTATOC PET / CT in these patients. ***Materials and Methods:*** In this retrospective study, 20 patients with differentiated thyroid carcinoma and Tg values above 10 with TSH stimulation by levothyroxine withdrawal or Tg values above 5 on TSH suppression) following surgery, thyroid ablation or iodine therapy along with recent negative whole body scans with I-131 were evaluated in this study. All patients underwent F18-FDG PET / CT scan first and underwent Ga68-DOTATOC PET / CT scan for a maximum period of one week. ***Results:*** 20 patients with TENIS syndrome were examined, The primary pathology of thyroid cancer was PTC in 19 patients and FTC in one case. The total number of positive findings based on the location of the lesions in both scans was 23/27 and based on the patient in Ga-DOTATOC and FDG were 65% (13/20) and 70% (14/20), respectively. Stage of the disease in most patients according to the seventh edition was stage IV (12 patients) and based on the eighth edition (10 patients) was in stage I of the disease. The overall results of both modalities based on discontinuation of the pill or TSH suppression were not significantly different (p-value < 0.999). The statistical relationship between the number of positive and negative findings of patients in the two PET tracers was not significant (p = 1). While there was a significant relationship between Tg levels and FDG findings (p-value = 0.015) there was no significant relationship between Tg levels and FDG positive findings in TSH stimulation state (p = 0.262). Also, there was no significant relationship between Tg levels and pathological subtypes (p-value = 0.602). ***Conclusion:*** Expression of somatostatin receptors by Ga68-DOTATOC PET / CT uptake is observed in significant percentage of TENIS patients . The positive findings of the two modalities are not significantly different and it seems that Ga-DOTATOC is effective in the treatment plan of patients who have a positive FDG PET / CT finding with no change in the management of the disease.

OP-651

Exploring the role of new angiogenic tracer, ^{68}Ga DOTAGA- IAC and comparison of its diagnostic performance with ^{18}F-FDG PET/CT in patients with radioiodine refractory differentiated thyroid carcinoma

S. Ananth Kumar, *A. Sood, J. Shukla, R. Kumar, P. Aggarwal, B. Rai Mittal;*
Postgraduate Institute Of Medical Education and Research, Chandigarh, Chandigarh, INDIA.

Aim/Introduction: ^{18}F-FDG PET/CT has proven to be an advantageous tool to predict the occurrence of recurrent/ residual disease in patients with radioiodine refractory differentiated thyroid carcinoma (RAIR-DTC). However its non-specificity and lack of a suitable theranostic pair has led to search of new molecular agents targeting various processes involved in the metastases. Integrin antagonist carbamate (IAC), a newer αvβ3 integrin antagonist peptidomimetic molecule in the pipeline, makes molecular imaging of tumour angiogenesis amenable. The study aims to investigate the clinical efficacy of ^{68}Ga DOTAGA-IAC PET/CT in the detection of RAIR-DTC and compare its diagnostic performance with ^{18}F-FDG PET/CT. ***Materials and Methods:*** This prospective pilot study included RAIR-DTC patients (previously histopathologically proven DTC patients) as defined by ATA guidelines who underwent whole body ^{18}F-FDG-PET/CT followed by ^{68}Ga DOTAGA-IAC PET/CT between Jan 2021 and April 2023 in a tertiary care centre. The imaging findings of both PET/CT were interpreted and quantitative parameters like SUVmax, SUVpeak, MTV and TLG were obtained and statistically analysed using SPSS version 26.0. A p value of <0.05 was considered statistically significant. ***Results:*** 27 patients (14 women) with a median age of 48.3 years (interquartile range-25) were included in the study, most of them being papillary carcinoma thyroid (92.6%). Majority

of the patients were risk stratified as intermediate (55.6%) and high (40.7%) initially respectively. Overall, most patients were stage I (51.9%), followed by stage II (40.7%), III (3.7%) and IV (3.7%) according to AJCC 8th edition. Median TSH and thyroglobulin levels of patients were 75µIU/ml and 154ng/ml respectively. The commonest sites of involvement on both PET/CT were locoregional lymph nodes (77.8%), followed by pulmonary nodules (59.3%), thyroid bed (22.2%), with least common site being liver and paracolic deposit (0.04% each). FDG uptake was significantly higher than IAC with median SUVmax and SUVpeak being 7.9 vs 2.5(p value <0.001) and 4.6 vs 1.7(p value <0.001). ^{18}F-FDG PET/CT performed better than ^{68}Ga DOTAGA-IAC PET/CT, predominantly in detecting locoregional lymph nodes (median SUVmax 8.9 vs 3.0, p value <0.001) and pulmonary nodules (median SUVmax 6.2 vs 1.5, p value <0.001). Volumetric parameters like median MTV and TLG of FDG outperformed IAC, with values being 6 vs 0.8(p value 0.007) and 24.9 vs 2.3(p value 0.006) respectively. ***Conclusion:*** Angiogenesis imaging with ^{68}Ga DOTAGA-IAC PET/CT appears to be inferior compared to ^{18}F-FDG PET/CT in the detection of lesions in patients with RAIR-DTC, retaining the domination of ^{18}F-FDG PET/CT imaging in clinical practice.

OP-652

Lactate dehydrogenase A is associated with glucose metabolism, radioiodine avidity and prognosis in differentiated thyroid cancer

T. Tian, *H. Dai, R. Huang;*
West China Hospital, Sichuan University, Chengdu, CHINA.

Aim/Introduction: ^{18}F-FDG PET/CT reflects the Warburg effect of tumours. Lactate dehydrogenase A (LDHA) is an enzyme responsible for the conversion of pyruvate to lactate and plays an important role in aerobic glycolysis. The aim of this study was to i) analyse the relationships among LDHA, glycolysis, and radioactive iodine (RAI) avidity and ii) explore the value of these parameters in the prognosis of differentiated thyroid cancer (DTC). ***Materials and Methods:*** DTC patients who underwent ^{18}F-FDG PET/CT and subsequent total thyroidectomy or metastasectomy at our centre from 2007-2021 were enrolled. The expression levels of LDHA, glucose transporter 1 (Glut1), glucose transporter 3 (Glut3) and Ki67 proteins in tumour tissue were measured using immunohistochemistry (IHC). The maximum standardized uptake value for the whole body (SUVmax), the maximum standardized uptake value for the lesion corresponding to the IHC specimen (lesion SUVmax), metabolic tumour volume (MTV) and total lesion glycolysis (TLG) were measured. A radioiodine whole body scan was used to determine lesion radioiodine avidity. Quantitative PCR and Western blotting were used to study the expression of Glut1 and Glut3 in thyroid cancer cell line (TPC-1) transfected with lentivirus overexpressing LDHA. ***Results:*** A total of 69 DTC patients were included in the study, and LDHA expression levels were correlated with Glut3 expression levels (P=0.003) and lesion SUVmax (P=0.002). 39 patients undergoing RAI therapy for structural disease. The median LDHA and lesion SUVmax of the RAI avidity group were lower than those of the non-RAI avidity group (200 vs. 285, P= 0.036; 3.06 vs. 8.38, P=0.038, respectively). After a median follow-up of 43 months (3-360 months), 53 patients were finally included in the assessment of clinical outcomes. Of these 53 patients, 18 (34.0%) had disease progression, and 5 (11.1%) died. Elevated SUVmax (log rank P=0.004), MTV (log rank P=0.014), TLG (log rank P=0.001) and LDHA expression (Breslow P=0.048) led to shorter time to progression (TTP). Cox regression analysis revealed that TLG (HR: 4.773, P=0.047) was an independent prognostic factor of TTP.In cellular experiments, overexpression of LDHA significantly increased TPC-1 proliferation, migration, and Glut1 and Glut3 expression. ***Conclusion:*** LDHA expression was highly correlated with the non-avidity of RAI and increased glycolysis. High LDHA expression levels are associated with worse progression. Cellular experiments confirmed that LDHA could regulate the expression of glut1 and Glut3, but immunohistochemical staining showed that LDHA was more closely related to Glut3 expression.

OP-653

The Complementary Role of PSMA Expression and [^{18}F] FDG PET/CT in Predicting Thyroid Cancer Outcome — from Black and White to Shades of Grey, in the Era of Precision Oncology

C. Pini[1], *M. Sollini*[2,3], *M. Kirienko*[4], *L. Di Tommaso*[2,5], *F. Gelardi*[2,3], *S. Ariano*[2,6], *C. Landoni*[1,7], *A. G. Lania*[2,6], *G. Mazziotti*[2,6], *G. Mercante*[2,8], *A. Chiti*[2,3];
[1]*School of Medicine and Surgery, University of Milano-Bicocca, Monza, ITALY,* [2]*Department of Biomedical Sciences - Humanitas University, Pieve Emanuele, ITALY,* [3]*Nuclear Medicine – IRCCS Humanitas Research Hospital, Rozzano, ITALY,* [4]*Fondazione IRCCS Istituto Nazionale dei Tumori, Milano, ITALY,* [5]*Pathology - IRCCS Humanitas Research Hospital, Rozzano, ITALY,* [6]*Endocrinology - IRCCS Humanitas Research Hospital, Rozzano, ITALY,* [7]*Nuclear Medicine Department, IRCCS Monza, San Gerardo Hospital, Monza, ITALY,* [8]*Otorhinolaryngology, IRCCS Humanitas Research Hospital, Rozzano, ITALY.*

Aim/Introduction: The diagnostic and prognostic value of Prostate-Specific Membrane Antigen (PSMA) in thyroid carcinoma (TC) is still largely unknown. We aimed to test the potential complementary role of PSMA and 2-[^{18}F]fluoro-2-deoxy-D-glucose ([^{18}F]FDG) as biomarkers for TC outcome prediction. ***Materials and Methods:*** From a retrospective cohort of TC patients we selected those fulfilling the following inclusion/exclusion criteria: thyroidectomy in our Institution, available primary tumor tissue PSMA immunostaining, [^{18}F]FDG PET/CT and follow-up data. We included 23 subjects. PSMA staining was visually assessed. PET/CT was considered positive in case of [^{18}F]FDG uptake higher than the background at the site of TC confirmed by cyto-/histology, and/or follow-up. Disease recurrence, radioiodine refractoriness (RAI-R) and status at last follow-up (LFU) were used as outcome endpoints. ***Results:*** Disease recurrence occurred in 18/23 patients (median time 11 months, range 1-40); among these 12/18 developed RAI-R (median time 28 months, range 2-221), and 13/18 cases had evidence of disease at LFU. Only one out of 11 patients classified at high risk of structural disease recurrence according to ATA Guidelines did not experience recurrence. PSMA expression was negative in 6/23 cases. PET/CT was negative in 11/23 patients (7/11 experienced recurrence). Nine out of 12 RAI-R patients had a positive PET/CT, while 10/13 cases with evidence of disease at LFU had a positive PET/CT. All patients who had a positive PET/CT had a positive PSMA immunostaining. Six out of 11 patients with negative PET/CT were positive at immunostaining. Patients with negative PET/CT exhibited lower PSMA expression (median score of 30%, range 0-80%) than patients with positive PET/CT. The TC samples without PSMA expression belonged to patients who resulted negative also at PET/CT (3 experienced recurrence, 2 were RAI-R, and 1 had disease at LFU). Four out of 11 patients who resulted negative at PET/CT exhibited very high PSMA expression (≥ 70%) and although 3 of them experienced recurrence, none resulted RAI-R, and only 1 had persistent disease at LFU. ***Conclusion:*** Primary tumour PSMA expression and [^{18}F]FDG seem to play a complementary role in TC. The majority of patients who expressed PSMA recurred. Patients with intermediate risk and negative PSMA

immunostaining recurred less than patients who belong to the same class risk and expressed PSMA. Notably, although patients with a negative [18F]FDG PET/CT had a favourable long-term outcome, PSMA assessment might be useful to timely identify subjects at higher risk of recurrence.

OP-654

Prospective study on the usefulness of 18FDOPA PET-CT in the management of medullary thyroid cancer patients with higt residual calcitonin rate after surgery

M. Terroir Cassou Mounat[1], *A. Lusque*[1], *E. Hindié*[2], *D. Taieb*[3], *L. Vija*[1], *J. Sarini*[1], *F. Courbon*[1], *A. Decotte*[4], *S. Grunenwald*[5], *S. Zerdoud*[1];
[1]*IUCT Oncopole, toulouse, FRANCE,* [2]*University Hospital of Bordeaux, Bordeaux, FRANCE,* [3]*La Timone University Hospital, Marseille, FRANCE,* [4]*University Hospital Rangueil-Larrey, toulouse, FRANCE,* [5]*Centre Hospitalier Universitaire de Toulouse, toulouse, FRANCE.*

Aim/Introduction: The reference treatment of medullary thyroid cancer (MTC) is surgery but calcitonin (ctn) remains often detectable postoperatively. In case of ctn level above 150 pg/ml, international recommendations suggest adding 18 fluoro-dopa positron emission tomography (18FDOPA PET) to conventional imaging (CI) workup. The aim of this study was to measure the impact of the 18FDOPA in the management of MTC patients with elevated ctn by determining its ability to identify residual lymph node and distant metastases compared to CI. ***Materials and Methods:*** This prospective, multicenter, open-label study (NCT02856347) evaluated the benefit of 18FDOPA imaging in the detection of metastatic lymph nodes and metastases, compared to CI in operated MTC patients with ctn above 150 pg/ml. The primary endpoint was the relative true-positive rate of metastatic lymph nodes on 18FDOPA compared with the CI in a per lymph node analysis. Secondary endpoints are discordance rate between 18FDOPA and CI in a per metastasis site analysis, changes in patient management after 18FDOPA determined by a multidisciplinary tumor board of experts (SZ, SG, AD and MT) and concordance between the reading of the 18FDOPA PET in the investigating center and a centralized review (MT). ***Results:*** The study prospectively included 24 patients from five French centers between 2017 and 2020. The median ctn was 824 pg/mL (range 176-16418). A total of 60 lymph nodes were detected by 18FDOPA or CI, fifty-three (35 FDOPA+CI, 18 FDOPA) were defined involved and 7 non-involved (2 FDOPA+CI, 4 FDOPA, 1 CI) after clinical examination (Gold Standard). 18FDOPA detected 1.5 (95%CI: 1.25-1.84) times more lymph nodes metastases compared to CI. For metastases, the discordance rate was 46.4% (95%CI 27.5-66.1), 13/28. After a multidisciplinary tumor board of experts, 14 patients (58.3%, 95%CI: 36.6-77.9) had a change in patient management after 18FDOPA results. Six patients would be monitored, seven patients would have had surgery or modified surgery, four patients a fine needle aspiration, two patients local treatment and three patients systemic treatment. The discordance rate for 18FDOPA between expert and local readers was 20.8% (95%CI: 7.1-42.2, 5/24 pts) for metastases. The expert review allowed catching up two metastatic sites. ***Conclusion:*** In this multicenter prospective study, 18FDOPA imaging changed MTC patient management in 58% of cases. These data confirm that 18FDOPA PET is particularly helpful for MTC workup and patient management. The results on the 18FDOPA expert reading suggest the importance of further improving the assessment of MTC with 18FDOPA.

OP-655

CCK_2-receptor targeted PET/CT in patients with medullary thyroid cancer using [68Ga]Ga-DOTA-CCK-66 - First clinical experience

O. Viering[1], *T. Günther*[2], *N. Holzleitner*[2], *H. Wester*[2], *A. Dierks*[1], *M. Kircher*[1], *G. Wienand*[1], *C. H. Pfob*[1], *R. A. Bundschuh*[1], *C. Lapa*[1];
[1]*Nuclear Medicine, faculty of medicine, University of Augsburg, Augsburg, GERMANY,* [2]*Chair of Pharmaceutical Radiochemistry, Technische Universität München, Munich, GERMANY.*

Aim/Introduction: Medullary thyroid cancer (MTC) is a neuroendocrine tumour arising from the parafollicular cells of the thyroid gland and accounts for approximately 5 % of all thyroid cancers. Since patients with MTC can only be cured by complete resection of the primary tumour and any locoregional or distant metastases, accurate imaging techniques for disease staging are required. Recently, cholecystokinin-2 (CCK_2)-receptor has been demonstrated as a suitable target for positron emission tomography/computed tomography (PET/CT) imaging of MTC (1). Here, we report on the first clinical experience with [68Ga]Ga-DOTA-CCK-66, a novel CCK_2R ligand. ***Materials and Methods:*** Eight patients (4 male, mean age 59±13 years) with a history of MTC and elevated tumour marker levels (calcitonin: 125 (13-720) pg/ml, CEA: 2.2 (0.8-6.9) ng/ml) underwent PET/CT imaging with 168±17 MBq [68Ga]Ga-DOTA-CCK-66 for re-staging purposes. In 3 patients additional imaging with [18F]FDG- (n=1) and [18F]F-DOPA-PET/CT (n=2) was available. Tumour detection rates were assessed and compared to tumour marker levels as well as doubling times. ***Results:*** PET imaging was well tolerated by all patients with no adverse effects. CCK_2-positive lesions were detected in 3/8 patients (37.5 %) with local recurrence in one patient, lymph node metastases in three subjects and bone and liver metastases in one patient. The median calcitonin level was higher in the PET-positive group (380 pg/ml vs. 120 pg/ml) and the PET-positive patients had a shorter median calcitonin doubling time before PET/CT imaging (10 months vs. 37 months). In comparison to [18F]FDG, additional lymph node, liver and bone metastases could be detected with [68Ga]Ga-DOTA-CCK-66. In comparison to [18F]F-DOPA the same number of lesions was documented. Apart from tumour lesions, [68Ga]Ga-DOTA-CCK-66 was only found in the CCK_2R-positive stomach as well as in the ureter and the bladder due to excretion. ***Conclusion:*** CCK_2-receptor-directed PET imaging with [68Ga]Ga-DOTA-CCK-66 is feasible, as the compound revealed a favourable biodistribution profile and good detection of tumour lesions. PET positivity is correlated with higher tumor marker levels and shorter doubling times. Further research to investigate a potential diagnostic superiority over already established imaging modalities and to assess the therapeutic option by means of 90Y- or 177Lu-labelled DOTA-CCK-66 are warranted.

References: (1) Refardt J, Hofland J, Kwadwo A, Nicolas GP, Rottenburger C, Fani M, Wild D, Christ E. Theranostics in neuroendocrine tumors: an overview of current approaches and future challenges. Rev Endocr Metab Disord. 2021 Sep;22(3):581-594.

OP-656

PET/CT imaging of differentiated and medullary thyroid carcinoma using the novel SSTR-targeting peptide [18F] SiTATE - first clinical experiences

S. Kunte[1], *V. Wenter*[1], *G. T. Sheikh*[1], *M. Unterrainer*[1], *S. Lindner*[1], *J. Toms*[1], *K. Jurkschat*[2], *C. Wängler*[3], *B. Wängler*[3], *R. Schirrmacher*[4], *J. Rübenthaler*[1], *C. J. Auernhammer*[1], *C. Spitzweg*[1], *P. Bartenstein*[1], *A. Holzgreve*[1], *L. M. Unterrainer*[1];
[1]LMU, Munich, GERMANY, [2]Technische Universität Dortmund, Dortmund, GERMANY, [3]Medizinische Fakultät Mannheim der Universität Heidelberg, Mannheim, GERMANY, [4]University of Alberta, Edmonton, Edmonton, AL, CANADA.

Aim/Introduction: The novel ^{18}F-labeled somatostatin-receptor (SSTR)-directed radiotracer [^{18}F]SiTATE demonstrated promising results in the imaging of various SSTR-expressing tumor entities and provides also a theranostic perspective. As thyroid carcinomas (TC) express SSTR, the use of SSTR-PET/CT might be useful with regard to therapeutic decisions beyond standard imaging. Data on [^{18}F]SiTATE PET/CT imaging in TC, however, are lacking. This study provides first [^{18}F]SiTATE PET/CT data in a patient cohort with histologically proven TC. ***Materials and Methods:*** Patients with either differentiated or medullary TC who underwent at least one [^{18}F]SiTATE PET/CT were included as part of a non-interventional, observational study. Mean SUV_{max} and SUV_{mean} of the tumoral lesions and mean total tumor volume (TTV) with their standard deviations (SDs) were determined using a 50%-isocontour-VOI. ***Results:*** Overall, 21 patients (mean age 62.24 ±13.9 years; 13 female / 8 male) with TC (10x medullary, 8x follicular, 2x papillary, 1x oncocytic) were included. 16/21 showed metastatic sites in the ^{18}F-SiTATE PET/CT scan. Altogether, 89 lesions were included. Three patients with medullary and one patient with follicular and papillary TC respectively showed no SiTATE uptake, which was aligned with no target lesions in CT. Analysis of osseous (31 lesions; SUV_{max} 8.3, SD 7.84; SUV_{mean} 5.6, SD 5.29) and nodal (37 lesions; SUV_{max} 8.7, SD 7.73; SUV_{mean} 5.7, SD 5.28) metastases showed the highest uptakes. Metastases were also localized in the lung (17 lesions; SUV_{max} 4.52, SD 1.82; SUV_{mean} 3.49, SD 1.67) and in the soft tissue (1 lesion; SUV_{max} 4.14; SUV_{mean} 2.35). One patient had not undergone thyroidectomy and in two patients, a local recurrence was present; the local tumoral uptake was markedly increased in all three cases (SUV_{max} 11.97, SD 9.66; SUV_{mean} 7.51, SD 5.61). Mean TTV in patients with differentiated TC was 539.21 ml (SD 1059.90), SUV_{max} 14.63 (SD 14.67) and SUV_{mean} 5.33 (SD 3.02). In patients with medullary TC analysis showed a mean TTV of 76.97 ml (SD 173.05), SUV_{max} 5.48 (SD 4.15) and SUV_{mean} 3.55 (SD 2.41). ***Conclusion:*** Our preliminary data demonstrate that [^{18}F]SiTATE PET/CT is highly feasible in patients with differentiated and medullary TC. These results suggest [^{18}F]SiTATE as a useful, novel SSTR-radioligand for TC beyond established Ga-labeled radioligands. Additionally, [^{18}F]SiTATE PET/CT might be helpful to select patients that could benefit from a SSTR-directed therapy. Further analyses comparing [^{18}F]SiTATE PET and standard imaging in correlation to clinical follow up are underway.

OP-657

Clinical Impact of Ga68-DOTATATE PET/CT Imaging in Medullary Thyroid Carcinoma, a retrospective single center study

A. Abdelrahman, *R. Akinlusi, S. Gavane;*
Icahn School of Medicine at Mount Sinai, New York, NY, UNITED STATES OF AMERICA.

Aim/Introduction: Medullary thyroid carcinoma (MTC) is a rare form of cancer that arises from neuroendocrine calcitonin-secreting cells accounting for 1-2% of all thyroid cancers, however, the mortality burden is up to 15%. As with other neuroendocrine tumors, MTCs overexpress L-type amino acid transporters as well as somatostatin receptors. Hence, they can be imaged by both by 18F-FDOPA and 68Ga-DOTATATE. FDOPA is not readily available in the US. In this study, we aim to investigate the impact of 68Ga-DOTATATE imaging on the management of patients with MTC and to compare its performance to FDG. ***Materials and Methods:*** From 1/1/2018 to 1/1/2023, all patients who had a biopsy proven diagnosis of medullary thyroid carcinoma and underwent 68Ga-DOTATATE PET/CT imaging were retrospectively reviewed. Imaging studies including 68Ga-DOTATATE and FDG PET/CTs have been independently reviewed by two nuclear medicine physicians. The association between qualitative imaging findings for both DOTATATE and FDG PET/CT and serum calcitonin levels was measured using Fischer's exact test. SUV max values were plotted against calcitonin levels in a linear regression model to measure correlation. ***Results:*** 16 patients have met the inclusion criteria. 14 patients (80%) had their DOTATATE imaging for restaging after surgical resection of the thyroid gland due to rising tumor markers and one patient was imaged for initial staging, and one patient was incidentally found to have increased uptake in the thyroid while undergoing DOTATATE PET/CT for NET. Mean calcitonin levels at the time of scan was 1704 (± 4467 SD, IQR: 15567). DOTATATE was positive in 11/16 patients (70%). It had 78% sensitivity and 100% specificity. 7/16 patients had FDG PET/CT along with DOTATATE PET/CT. In this subgroup, the comparison between the performance of DOTATATE and FDG is shown in table 1. The impact of DOTATATE PET/CT imaging on the management is shown in table 2. There was no significant correlation between calcitonin levels and DOTATATE SUV max values (R2 = 0.06, P value = 0.3). ***Conclusion:*** Our initial results demonstrate that DOTATATE PET/CT imaging had a positive impact on management as well as a clinical benefit particularly in detection of recurrent disease with elevated tumor markers. It detected local disease in 8 patients (50%), resulted in surgical intervention in 4 (25%), and upstaged 3/16 patients (19%). DOTATATE PET/CT was superior to FDG PET/CT in detecting recurrent disease. Additional data is being evaluated to assess lesion and per patient sensitivity and specificity for both tracers.

OP-658

18f tetrafluoroborate-pet in evaluation of thyroid cancer patients: preliminary results

K. Saglam, *O. Sahin, E. Karayel, H. Pehlivanoglu, R. Uslu Besli, A. Aygun, S. Asa, K. Sonmezoglu;*
Istanbul Univercity-Cerrahpasa Cerrahpasa Medical Faculty, Istanbul, TÜRKIYE.

Aim/Introduction: Sodium-iodide symporter (NIS) receptors mediate iodine transport into the thyrocytes. NIS receptors can be monitored by SPECT using radioactive iodine and PET imaging using I-124 PET and also the [18F]tetrafluoroborate ([18F] TFB-PET). PET imaging is known for better resolution comparing SPECT and gamma camera imaging methods. I-124 PET can also be used for diagnostic purposes, but its use is limited due to its expensiveness and higher radiation doses.We aimed to compare [18F]TFB-PET with SPECT for imaging the residual tissue, local recurrences, and distant metastases in thyroid cancer. ***Materials and Methods:*** For that ongoing study, we select patients prospectively, who underwent bilateral total thyroidectomy and have indications for RAI treatment. These patients were on a low-iodine diet and not taking any levothyroxine replacement therapy.TSH levels of patients were >50mIU/L. 3-6 mCi [18F]TFB injected and imaging performed with a 40 minutes delay from the injection. Seven patients were included in the study. Patients

treated with various RAI doses. Post-radioiodine therapy SPECT imaging was also performed. A total ten different lesions were identified from SPECT and PET. ROIs were drawn with a standard threshold of 42% and formulated as lesion/background activity count per volume for SPECT and lesion/background SUVMean for [18F]TFB-PET. ***Results:*** Two of the lesions were seen only in [18F] TFB-PET and one of them was evaluated in favor of temporal bone metastases, while the other one was evaluated as residual tissue. Another lesion, a local recurrence, was only seen in SPECT. 7 of 10 lesions were detected on both methods. While comparing with average of lesion/background activity count per volume in lesions detected by SPECT was 112,35, lesion/background SUVMean lesions detected by [18F]TFB-PET was 1005,64. Volumes of two lesions were also obtained by MRI. The results, which were found 0.258 and 0.212 cm^3 in MRI, were found to be 0.358, 0.355 cm^3 when measured with [18F]TFB-PET, and 5.26, 3.36 cm^3 when measured with SPECT, respectively. ***Conclusion:*** One lesion was not detected in [18F]TFB-PET, while two in SPECT. A markedly higher lesion-to-background ratio detected in [18F]TFB-PET; therefore, it is considered to have a better resolution in the [18F] TFB-PET. In addition, when the volume obtained from the [18F] TFB-PET is compared with the MRI, which has a better resolution than the other methods, it is more accurate than SPECT.

1309

Tuesday, September 12, 2023, 9:45 AM - 11:15 AM
Hall G2

e-Poster Presentations Session 10 - Oncology & Theranostics Committee: Haematological and Abdominal Malignancies / localised Treatments

EPS-189

Role of 68Ga-DOTATATE PET/CT Quantitative Parameters in the Differential Diagnosis of Adrenal Lesions

D. Denizmen[1], *D. Has Simsek*[1], *E. G. Isık*[1], *H. Hacısahinogulları*[2], *S. Kuyumcu*[1];
[1]*Istanbul University Istanbul Faculty of Medicine Nuclear Medicine Department, Istanbul, TÜRKIYE,* [2]*Istanbul University Istanbul Faculty of Medicine Endocrinology and Metabolic Diseases Department, Istanbul, TÜRKIYE.*

Aim/Introduction: Although most of the adrenal lesions consist of benign,non-functional lesions; adrenal tumors have metastatic potential and show aggressive course in advanced stages such as pheochromocytoma(FEO), paraganglioma(PGL), adrenal cortex carcinoma(ACC) [1] .In addition to clinical and laboratory findings,molecular-correlative imaging plays an important role in final diagnosis.[2]This study investigated the contribution of quantitative parameters defined by 68Ga-DOTATATE PET/CT(DOTAPET) in the differential diagnosis of adrenal gland lesions. ***Materials and Methods:*** Patients who referred for characterization of adrenal lesions or had adrenal insidentaloma in DOTAPET included to the study.Additionally, a control group was identified for comparison of normal adrenals by including normal DOTAPET scans verified by correlative CT/MRI.Final diagnosis of adrenal lesions was confirmed with histopathology results,initial or follow up CT/MRI findings.SUVmax values of liver,normal adrenal gland and adrenal lesions in addition to quantitative parameters such as SSTR-TV and SSTR-TL which demonstrates total tumor volume and SSTR expression of the lesions were documented.Diagnostic role of quantitative parameters examined by Mann-Whitney U and Kruskall Wallis tests, and the threshold was determined by ROC curve if parameters were significant. ***Results:*** A total of 85 patients were included to study.41 patients(46 lesions) had adrenal lesions, while 44 patients were in normal control group.25 lesions (n:3 bilateral) were evaluated for adrenal lesion characterization and 21 lesions(n:2 bilateral)were incidentalomas.The final diagnosis was confirmed by histopathology in 22 patients while remaining lesions were determined by MRI(n:18) or follow-up CT(n:6). Of the 46 lesions, 24 lesions were adenoma,14 lesions were FEO,two lesions were ACC and remaining lesions were other pathologies(Table 1).Only FEO and adenoma cases were included to the statistical analysis due to the limited number of other pathologies.Median SUVmax of normal adrenal,FEO and adenoma were calculated as 14.95, 22.27 and 11.45 respectively(p:0.003). SSTR-TV and SSTR-TL of FEO were 18.64 cc and 264.77 while 1.65 cc and 13.35 for adenoma which were significantly higher in FEO(p=0.003).ROC curves showed that SSTR-TV had the highest diagnostic power among all parameters in differentiation of FEO and adenoma(Table 2).The sensitivity and specificity of DOTAPET were found to be 93% and 96% respectively when threshold was 4cc for SSTR-TV(p:<0.001,AUC:0.927-1)(Table 3). ***Conclusion:*** This study indicates that volumetric parameters of DOTAPET had promosing results in differential diagnosis of FEO/adenoma with high diagnostic performance.Further research is required for inclusion in routine clinical practice. ***References:*** 1. Sherlock,et al."Adrenal incidentaloma."Endocrine Reviews41.6(2020):775-8202. 2.Mody,et al."ACR Appropriateness Criteria Adrenal Mass Evaluation:2021 Update."Journal of the American College of Radiology18.11(2021):S251-S267

EPS-190

Role of ^{68}Ga-PSMA-11 PET/CT in staging metastatic renal cell cancer: A pilot study

P. Aggarwal, *H. Singh, C. K. Das, R. S. Mavuduru, A. Lal, N. Kakkar, R. Kumar, U. Gorsi, B. R. Mittal;*
Post Graduate Institute of Medical Education and Research, Chandigarh, INDIA.

Aim/Introduction: The role of Prostate-specific membrane antigen (PSMA) based positron emission tomography (PET) tracers is well known in the management of prostate cancer. However, it is also an angiogenic imaging marker with a potential role in the imaging of hypervascular tumours like Renal cell cancer (RCC). Our study aims to assess the potential role of ^{68}Ga-PSMA-11 PET/CT in the staging workup of metastatic RCC and compare it with the current imaging standard (CECT) and ^{18}F-FDG PET/CT. ***Materials and Methods:*** Biopsy-proven RCC patients with known or suspected distant metastases underwent ^{68}Ga-PSMA-11 PET/CT for staging/restaging. Those patients who had undergone ^{18}F-FDG PET/CT within six weeks of ^{68}Ga-PSMA-11 PET/CT were also included. A patient-based and lesion-based analysis was done to compare the lesion detection rates of CECT, ^{18}F-FDG and ^{68}Ga-PSMA-11 PET. Additionally, PET-based quantitative parameters were compared between both the PET modalities. The degree of agreement between different imaging modalities was evaluated using Kohen's kappa and disagreement using the McNemar test. Statistical analysis was done using SPSS v26.0 (IBM Corp, Armank, NY). A p-value of <0.05 was considered significant. ***Results:*** Thirty-seven patients with median age 60 years ± 13 years (range = 26-76 years) were included in the final analysis. Twenty-seven patients had clear cell (cc) RCC, six had papillary RCC (pRCC), and one each had an eosinophilic variant

of ccRCC, collecting duct RCC, translocation RCC and poorly differentiated RCC. Fifteen patients also underwent ^{18}F-FDG PET. Overall, ^{68}Ga-PSMA-11 PET/CT identified more lesions than CECT in 27% of patients with lesion-based analysis showing higher lesion detection (568 vs 527, p = 0.215), especially for bone lesions (18.8% vs 9.1%, p <0.001). In ccRCC, there were 51 discordant PSMA+ CT- lesions (tumor thrombi and marrow-based lesions) and 11 discordant PSMA- CT+ liver lesions. ^{68}Ga-PSMA-11 PET was also superior to CECT in differentiating tumor thrombus from bland thrombus. It was also superior to ^{18}F-FDG PET/CT in lesion detection (312 vs 202, p < 0.001) with a significantly higher SUVmax (6.9 vs 5.2, p<0.001), SUVpeak (4.4 vs 3.8, p = 0.004) and TBR (5.7 vs 3.8, p <0.001), especially in ccRCC. ***Conclusion:*** ^{68}Ga-PSMA-11 PET/CT was superior to CECT and ^{18}F-FDG PET in metastatic clear cell RCC for lesion detection and baseline tumor burden assessment. Its potential role as an angiogenic imaging agent in managing RCC needs to be explored further.

EPS-191

Incremental value of ^{68}Ga-FAPI-04 to dual-tracer PET/CT for the evaluation of hepatobiliary masses with indeterminate CT/MR findings

I. Ho[1,2], *S. Chen*[2], *K. Cheng*[2], *K. Wu*[2], *C. Ho*[2];
[1]*The Chinese University of Hong Kong, Hong Kong, HONG KONG,* [2]*Hong Kong Sanatorium & Hospital, Hong Kong, HONG KONG.*

Aim/Introduction: Dual-tracer (DT) PET/CT with ^{11}C-acetate (ACT) and ^{18}F-FDG (FDG) has been widely used for the evaluation of hepatobiliary masses in localities with high liver cancer prevalence. In the past 2 decades, we have confirmed DT-PET/CT highly valuable in most primary liver tumors but may still encounter difficulties in some rare or complicated hepatobiliary pathologies such as hilar tumors (Klatskin tumors) that are non-avid for FDG. ^{68}Ga-FAPI-04 (FAPI-04) is a rapidly evolving PET tracer recently found useful in a number of tumors; we therefore aimed to evaluate the incremental value of FAPI-04 over DT-PET/CT for the evaluation of hepatobiliary masses with indeterminate CT/MR findings. ***Materials and Methods:*** During Jan-2022 to Feb-2023, 20 patients (M:14, F:6; age range:34-77 years, mean=58.7±14.0 years) underwent FAPI-04 PET/CT for evaluation of suspicious hepatobiliary lesions with indeterminate CT/MR And negative/atypical DT-PET/CT findings. Whole-body FAPI-04 PET/CT was performed within one week after DT-PET/CT. Imaging started at ~60 minutes post FAPI-04 injection (dosage:117±20 MBq, range:76-151 MBq). The SUV_{max} was measured for a maximum of 3 lesions per patient using MIM software. The gold standard for diagnosis was histopathology. One-way ANOVA analysis was performed to evaluate the semiquantitative FAPI-04 uptake among various types of malignancies and benign diseases. ***Results:*** 16/20 patients (M:13, F:3; age range:37-77 years, mean=59.1±12.9 years) with pathological confirmation were finally included for analysis. 12/16 patients were confirmed hepatobiliary malignancies: 5 intrahepatic cholangiocarcinoma (ICC: small-duct and Klatskin), 1 gallbladder adenocarcinoma (GBC), 3 well-differentiated hepatocellular carcinoma (HCC), 1 scirrhous HCC with fibrous features of bile ducts, 1 hepatic-angiosarcoma and 1 hemangioendothelioma. FAPI-04 PET/CT was strongly-avid in 9/12 (75%) hepatobiliary malignancies having negative ACT-PET/CT with/without mild FDG uptake, but completely non-avid in 3 well-differentiated HCC purely-avid for ACT. All "5 ICC+1 GBC" (6 patients: SUV_{max}=10.13±3.96, range:6.3-16.3) showed significantly greater intensities than the remaining 3 rare hepatobiliary malignancies (3 patients: SUV_{max}=4.40±1.40, range:3.3-6.3). 4/16 patients were confirmed benign but with little to mild uptake on FAPI-04 PET/CT (SUV_{max}=2.08±0.74, range 1.2-3.0): 1 FNH, 1 carvernous hemangioma, 1 dysplastic nodule and 1 steatosis. One-way ANOVA analysis showed significant differences among ICC+GBC, rare liver primary, well-differentiate HCC and benign diseases. ***Conclusion:*** FAPI-04 PET/CT has incremental value over FDG PET/CT in evaluation of hilar or small-duct ICC that are non-avid or minimally-avid for FDG, but cannot exclude well-differentiated HCC with pure avidity for ACT. False positive FAPI-04 for the above benign hepatobiliary entities have low uptake but need more cases for ROC differentiation.

EPS-192

Utility of CT-free attenuation and scatter correction in dual-tracer PET/CT for Evaluation of Gastric Cancer

S. Xue[1], *Y. Miao*[2], *M. Viscione*[1], *H. Wang*[2], *A. Rominger*[1], *R. Guo*[2], *B. Li*[2], *K. Shi*[1];
[1]*University of Bern, Bern, SWITZERLAND,* [2]*Shanghai Jiao Tong University School of Medicine, Shanghai, CHINA.*

Aim/Introduction: Ionizing radiation exposure is a major concern in PET/CT imaging, particularly for dual-tracer PET/CT studies where redundant anatomic imaging may add to the radiation burden. This study aims to explore the utility of CT-free deep learning (DL)-based methods for attenuation and scatter correction in the practice of gastric cancer diagnosis using dual-tracer PET/CT. ***Materials and Methods:*** Thirty-three patients with histopathologically confirmed gastric cancer underwent whole-body dual-tracer PET imaging (^{18}F-FDG and ^{68}Ga-FAPI, with an interval of less than 3 days) for pre-treatment evaluation [1]. We trained our previously developed CT-free Decomposition-based DL method [2] using 18F-FDG PET images from 1532 patients and applied it to 33 68Ga-FAPI PET images for attenuation and scatter correction. CT-corrected PET was used as a control. Two nuclear medicine physicians evaluated image quality using a 5-point Likert scale: 1-poor, 2-reasonable, 3-good, 4-very good, and 5-excellent quality. Clinically or pathologically confirmed lesion sites were counted to assess lesion detection sensitivity. ***Results:*** DL-corrected PET imaging achieved higher clinical utility scores (4.85) than CT-corrected PET imaging (4.30). DL-corrected PET imaging had less noise, better contrast, and sharper patterns, resulting in higher scores. Moreover, the number of detected lesions was identical in both datasets. ***Conclusion:*** The CT-free DL-based attenuation and scatter correction may enhance the potential of clinical translation in the dual-tracer PET/CT, which may largely ease the radiation burden for patients.

References: [1] Miao, Y. , Feng, R. , Guo, R. , Huang, X. , Hai, W. , & Li, J. , et al. Utility of [68ga]fapi-04 and [18f]fdg dual-tracer pet/ct in the initial evaluation of gastric cancer. European Radiology, 1-12. [2] Guo, R., Xue, S., Hu, J. et al. Using domain knowledge for robust and generalizable deep learning-based CT-free PET attenuation and scatter correction. Nat Commun 13, 5882 (2022).

EPS-193

^{68}Ga-NY104 PET/CT in patients with recurrent/metastatic clear cell renal cell carcinoma suspicion: a comparative study with ^{18}F-FDG

W. Zhu, *X. Li, Y. Zhang, L. Huo;*
Peking Union Medical College Hospital, Beijing, CHINA.

Aim/Introduction: ^{68}Ga-NY104 is a novel small molecule tracer targeting carbonic anhydrase IX (CAIX), which is overexpressed in clear cell renal cell carcinoma (ccRCC). The purpose of this study was to compare ^{68}Ga-NY104 PET/CT with ^{18}F-FDG in patients

with recurrent/metastatic ccRCC suspicion. ***Materials and Methods:*** The study was approved by the institutional review board of Peking Union Medical College Hospital (approval NO. ZS-3089). Patients with recurrent/metastatic ccRCC suspicion were prospectively recruited in the study. All patients received an intravenous injection of ^{68}Ga-NY104 (200Mbq ± 20%) and underwent whole body PET/CT scan at 45-75 min after injection. Comparative ^{18}F-FDG PET/CT was performed within a week. The efficacy of ^{68}Ga-NY104 and ^{18}F-FDG PET/CT scan was calculated at patient level and lesion level using a final diagnosis as ground truth, which was based on pathological results or comprehensive clinical evaluation. The SUVmax and tumor-to-background ratio (TBR) was also calculated using blood pool as background. ***Results:*** Fifteen patients were recruited in the study. Ten of them were later confirmed as recurrent/metastatic ccRCC while the other 5 patients were confirmed as non-ccRCC (2 inflammation, 2 adenocarcinoma, 1 papillary RCC). The final diagnosis in 12 patients (7 with ccRcc and 5 with non-ccRCC) were confirmed by pathological results and through comprehensive clinical evaluation in other 3 ccRCC patients. The patient-level sensitivity, specificity, and accuracy were 90% (9/10), 100% (5/5), and 93% (14/15) for ^{68}Ga-NY104 PET and 70% (7/10), 0 (0/5), and 46% (7/15) for ^{18}F-FDG, respectively. The lesion-level sensitivity, specificity, and accuracy were 88% (66/75), 100% (19/19), and 90% (85/94) for ^{68}Ga-sNY104 PET and 61% (46/75), 0 (0/19), and 49% (46/94) for ^{18}F-FDG, respectively. The SUVmax and TBR of matched lesions were significantly higher with ^{68}Ga-NY104 compared to ^{18}F-FDG (SUVmax, 17.5 ± 11.4 vs. 8.3 ± 5.3, TBR, 13.5 ± 11.1 vs. 3.7 ± 2.3 P<0.05). ***Conclusion:*** ^{68}Ga-NY104 PET/CT has better efficacy than ^{18}F-FDG in patients with recurrent/metastatic ccRCC suspicion.

EPS-194

First-in-human validation of enzymolysis clearance strategy for decreasing renal radioactivity using modified 68Ga-HER2 Affibody

M. Zhang*, T. Xing, J. Wang, T. Ma, G. Li, Z. Quan, W. Yang, F. Kang, J. Wang;*
Department of Nuclear Medicine, Xijing Hospital, Fourth Military Medical University, Xi'an, CHINA.

Aim/Introduction: Enzymolysis clearance strategy is verified a safe and effective way to reduce the renal radioactive accumulation in mice. However, the effectiveness of this strategy in humans remained unknow. Human epidermal growth factor receptor 2 (HER2) is overexpressed in various types of tumors, and radiolabeled HER2 Affibody is believed to be an attractive tool for HER2-targeted theranostics. However, its wide application is limited by the high and persistent radioactivity accumulation in kidney. In this study, we intend to validate the effectiveness of enzymolysis clearance strategy in reducing the renal accumulation by using modified HER2 Affibody. ***Materials and Methods:*** A new HER2 Affibody ligand, NOTA-MVK-$Z_{HER2:2891}$, containing with a cleavable Met-Val-Lys (MVK) linker was synthesized and labeled with ^{68}Ga. The microPET imaging study was performed in SKOV-3 tumor mice to assess the uptake in tumor and kidney both for the control ligand and the MVK one. Seven healthy volunteers were included for biodistribution and dosimetric studies with both the control and MVK ligands performed one week apart. Urine and blood samples from healthy volunteers were collected for in vivo metabolism study of the two ligands. Four HER2-positive and two HER2-negative patients were recruited for ^{68}Ga-NOTA -MVK-$Z_{HER2:2891}$ PET/CT imaging at 2 and 4 h post-injection (p.i.). ***Results:*** MicroPET images showed that the tumor uptake of ^{68}Ga-NOTA-MVK-$Z_{HER2:2891}$ was comparable to that of the control at all the time points, while the kidney uptake was significantly reduced after 40 min p.i. (p = 0.01). The biodistribution study in health volunteers showed that the kidney uptake of MVK ligand was extremely significantly lower than that of the control ligand after 1 h p.i. (p = 0.005), while the uptake of the two ligands in other organs showed no significant difference. The effective dose of the MVK ligand and the control one was 26.1 and 27.7 μSv/MBq, respectively. The enzymolysis fragment of ^{68}Ga-NOTA-Met-OH was observed in the urine samples of healthy volunteers injected with the MVK ligand, indicating that the enzymolysis clearance strategy worked in humans. The PET/CT study of patients showed that the range of SUV_{max} of HER2-positive lesions were 9.4-21, while that of HER2-negative lesions were 2.7-6.2. ***Conclusion:*** We for the first time demonstrated that enzymolysis clearance strategy can effectively reduce renal radioactivity accumulation in humans. This strategy is expected to decrease renal radiation dose of peptide and small protein-based radiotracers, especially in the field of radionuclide therapy.

EPS-195

Biodistribution of Monoclonal Antibodies: Defining New Baselines for ^{89}Zr-Immuno-PET-Derived Target Engagement In Vivo.

H. J. Sebus*[1,2], J. E. Wijngaarden[3,2], I. H. C. Miedema[1,2], J. J. Eertink[1,2], I. Bahce[4], A. J. De Langen[4,5], E. F. Smit[6], M. Cleveland[7], D. J. Vugts[3], G. J. C. Zwezerijnen[3,2], M. C. Huisman[3,2], C. W. Menke - van der Houven van Oordt[1,2];*
[1]Amsterdam UMC location Vrije Universiteit Amsterdam, Medical Oncology, De Boelelaan 1117, Amsterdam, NETHERLANDS, [2]Cancer Center Amsterdam, Imaging & Biomarkers, Amsterdam, NETHERLANDS, [3]Amsterdam UMC location Vrije Universiteit Amsterdam, Department of Radiology and Nuclear Medicine, Boelelaan 1117, Amsterdam, NETHERLANDS, [4]Department of Pulmonary Diseases, Cancer Center Amsterdam, Amsterdam University Medical Centers, Amsterdam, NETHERLANDS, [5]Department of Thoracic Oncology, NKI-AvL, Amsterdam, NETHERLANDS, [6]Department of Pulmonology, Leiden University Medical Center, Leiden, NETHERLANDS, [7]Bioimaging, Platform Technology and Science, GlaxoSmithKline, Stevenage, UNITED KINGDOM.

Aim/Introduction: Using ^{89}Zr-immuno-PET, the biodistribution of monoclonal antibodies (mAb) can be studied in vivo to assess target engagement. However, quantification with standard uptake values cannot separate reversible from irreversible uptake (K_i), which can be done using Patlak linearization. Additionally, K_i comprises non-target and target-specific uptake. To discriminate these, a baseline-K_i must be defined. We assume baseline-K_i equals the K_i of mAbs without target expression in the tissue (mAb_{neg}), and can also be derived through saturating all targets with unlabelled mAb (high mass dose) alongside ^{89}Zr-mAb (saturation effect). This study aims to determine baseline-K_i for tissues of interest in immune oncology treatments (e.g., the adrenal glands, bone marrow, inguinal lymph nodes, pituitary gland, spleen, thyroid and, tonsils) to identify target-specific uptake of (new) mAbs. ***Materials and Methods:*** This retrospective study analysed PET-scan series acquired in clinical trials with ^{89}Zr-anti-HER3 (N=5, NCT02345174), ^{89}Zr-cetuximab (N=5, NCT01691391), ^{89}Zr-durvalumab (N=4, EudraCT2019-004284-51), ^{89}Zr-ipilimumab (N=5, NCT03313323), ^{89}Zr-nivolumab (N=3, EudraCT2015-004760-11) and ^{89}Zr-pembrolizumab (N=3, NCT03065764), with multiple scans 24 hours (e.g. 48 and 144) after injection. Following manual volume of interest delineation, K_i were calculated using

Patlak linearization. Using the Human Protein Atlas, organ target expression was determined (mAb_{neg} and mAb_{pos}). When given an increased mass dose, e.g., 2 mg in cycle 1 versus 200 mg with the second tracer administration (N=15/25 series), saturation effects were evaluated to confirm target engagement. Baseline-K_i (reported as medians with interquartile ranges (IQR)) were reported per organ, using K_i of mAb_{neg} from both cycles, and mAb_{pos} in the second cycle. ***Results:*** Baseline-K_i (µL/g/h) in the inguinal lymph nodes (0.27 (IQR 0.18-0.34)), palatine tonsils (0.78 (IQR 0.58-0.98)), spleen (0.51 (IQR 0.42-0.58)), and thyroid (0.46 (IQR 0.39-0.58)) were identified. Baseline-K_i of the other tissues were heterogeneous (IQR > 0.5). Of all K_i (N=302), 79 were unreliable and excluded from analysis, due to small size and activity spill from neighbouring tissue, most frequently the case for the pituitary gland (N=32). The anti-PD-1 mAbs (2-4 mg in cycle 1) showed target engagement in the bone marrow, inguinal lymph nodes (0.56 (IQR 0.22-0.92)), palatine tonsils (1.05 (IQR 0.78-1.24)), spleen (3.12 (IQR 2.59-3.32)) and thyroid (0.90 (IQR 0.65-0.90)). Ipilimumab exhibited no saturation effect, possibly due to cycle 1's relatively high mass dose (10 mg). ***Conclusion:*** This study reports baseline-K_i for the inguinal lymph nodes, palatine tonsils, spleen and thyroid, to help identify target engagement of mAb in vivo using ^{89}Zr-immuno-PET.

EPS-196

Smouldering multiple myeloma: progression to symptomatic disease predicted by 18F-FDG PET-CT

C. Caldarella[1], *S. Taralli*[1], *F. Cocciolillo*[1], *T. Za*[2], *V. De Stefano*[2,3], *M. L. Calcagni*[1,4];
[1]*Dipartimento di Diagnostica per Immagini, Radioterapia Oncologica ed Ematologia, UOC di Medicina Nucleare, Fondazione Policlinico Universitario A. Gemelli IRCCS, Rome, ITALY,* [2]*Dipartimento di Diagnostica per Immagini, Radioterapia Oncologica ed Ematologia, UOC Servizio e Day Hospital di Ematologia, Fondazione Policlinico Universitario A. Gemelli IRCCS, Rome, ITALY,* [3]*Dipartimento di Scienze Radiologiche ed Ematologiche, Istituto di Ematologia, Università Cattolica del Sacro Cuore, Rome, ITALY,* [4]*Dipartimento di Scienze Radiologiche ed Ematologiche, Istituto di Medicina Nucleare, Università Cattolica del Sacro Cuore, Rome, ITALY.*

Aim/Introduction: Smouldering multiple myeloma (MM) is characterized by 10-60% bone marrow (BM) plasma cell infiltration in absence of MM-related symptomatology or MM-defining events. Despite its indolent course, the 2-year risk of progression to symptomatic MM may be as high as 73% in patients with unfavourable cytogenetics. In patients with smouldering MM, diffuse 18F-FDG uptake in BM may occur without focal active disease and/or lytic lesions on CT. Aim of this study is to determine whether diffuse 18F-FDG uptake in BM predicts progression to symptomatic MM. ***Materials and Methods:*** Thirty-eight patients (16M/22F), median age 64.98 y (range 43-87), with recently diagnosed smouldering MM and diffuse 18F-FDG uptake in BM on PET-CT, without focal active disease or lytic lesions on CT, were selected retrospectively from a 4-years interval (February 2017 - February 2021). Volumes of interest were placed on dorsal-lumbar spine (D10-L3), iliac crests and femoral diaphyses to obtain SUVmax and SUVmean. A second cohort of 22 patients (13M/9F) with smouldering MM and no significant 18F-FDG uptake was selected from the same time interval. Plasma cell % BM infiltration and M-component at the time of PET-CT were determined. Progression to symptomatic MM was based on IMWG criteria, and minimum 2-year follow-up. Possible differences in progression according to SUVmax or SUVmean (Mann-Whitney), and correlation between SUVmax or SUVmean and laboratory tests (Spearman) were assessed. Youden's Index extrapolated from Receiver Operating Characteristic (ROC) Curve allowed to discover a SUVmax or SUVmean cut-off for progression vs non-progression. ***Results:*** Progression to symptomatic MM was observed in 10/38 (26%) patients with BM diffuse 18F-FDG uptake, 22 months (median) after PET-CT, and in 2/22 (9%) patients with no significant 18F-FDG uptake in BM, 35 and 41 months after PET-CT, respectively. A trend to higher plasma cell % infiltration (median 19% vs 15%; P=0.067) was observed in patients with diffuse than in patients with no significant 18F-FDG uptake. SUVmax cut-off 3.79 for D10-L3 predicted progression to symptomatic MM which occurred in 50% patients with SUVmax > 3.79 (vs 12.5% patients with SUVmax < 3.79; P=0.032), with sensitivity 70% and negative predictive value 87.5%. No robust correlations were evident between SUVmax or SUVmean of selected BM districts and laboratory tests (Spearman's rho < 0.6). ***Conclusion:*** Degree of diffuse 18F-FDG uptake on PET-CT in dorsal-lumbar spine may identify patients with smouldering MM at higher risk of progression to symptomatic MM, with an expected impact on surveillance and treatment.

EPS-197

A novel prognostic index for diffuse large B-cell lymphoma combined baseline metabolic tumour volume with clinical and pathological risk factors

T. Yuan*, X. Chen, Y. Zhang, M. Wei, H. Zhu, Z. Yang, X. Wang;*
Peking University Cancer Hospital & Institute, Beijing, CHINA.

Aim/Introduction: This study aimed to develop a novel prognostic index integrating baseline metabolic tumour volume (MTV) along with clinical and pathological parameters for diffuse large B-cell lymphoma (DLBCL). ***Materials and Methods:*** The prospective trial enrolled 289 patients with newly diagnosed DLBCL (clinicaltrials.gov identifier: NCT02928861). The predictive value of novel prognostic index was compared with Ann Arbor staging and National Comprehensive Cancer Network International Prognostic Index (NCCN-IPI). We used the concordance index (C-index) and a calibration curve to determine its predictive capacity. ***Results:*** Multivariate analysis revealed high MTV (>191 cm^3), Ann Arbor stage (III-IV) and MYC/BCL2 double expression lymphoma (DEL) to be independently associated with inferior progression-free (PFS) and overall survival (OS). Ann Arbor stage and DEL could be stratified by MTV. Our index, combining MTV with Ann Arbor stage and DEL status, identified four prognostic groups: group 1 (no risk factors,), group 2 (one risk factor), group 3 (two risk factors), and group 4 (three risk factors). The 2-year PFS rates were 85.5%, 73.9%, 53.6%, and 13.9%; 2-year OS rates were 94.6%, 87.0%, 67.5%, and 24.2%, respectively. The C-index values of the novel index were 0.697 and 0.753 for PFS and OS prediction, which was superior to Ann Arbor stage and NCCN-IPI. ***Conclusion:*** The novel index including tumour burden and clinicopathological features may help predict outcome of DLBCL.

EPS-198

Lung dose prediction in radioembolization: ^{166}Ho-microspheres scout for ^{166}Ho-microspheres treatment vs. ^{99m}Tc-MAA scout for ^{90}Y-microspheres treatment

M. Wagemans*, R. van Rooij, A. J. A. T. Braat, M. L. J. Smits, R. C. G. Bruijnen, H. W. A. M. de Jong, M. G. E. H. Lam;*
Department of Radiology and Nuclear Medicine, UMC Utrecht, Utrecht, NETHERLANDS.

Aim/Introduction: Radiation pneumonitis is a rare, but serious complication of radioembolization, mostly described in patients with hepatocellular carcinoma (HCC). Treatment with

^{166}Ho-microspheres can be preceded by a lower scout dose consisting of the same microspheres. As individualized treatment planning improves overall patient selection and outcomes, a strong agreement between the scout and therapeutic dose distribution becomes increasingly important. It remains unclear how the predictive value of ^{166}Ho-microspheres scout compares to that of ^{99m}Tc-MAA for ^{90}Y-microspheres. The accuracy of lung mean dose (LMD) prediction was compared for ^{166}Ho-microspheres scout and treatment versus ^{99m}Tc-MAA and glass yttrium-90 (^{90}Y)-microspheres, in HCC patients. ***Materials and Methods:*** The ^{166}Ho-microspheres cohort was derived from the prospective HEPAR PRIMARY study.[1] Patients were retrospectively selected for the ^{90}Y-microspheres cohort (February 2012 to September 2020).[2] LMD for ^{166}Ho-microspheres scout, ^{166}Ho-microspheres treatment and ^{99m}Tc-MAA scout were assessed by SPECT/CT imaging, while ^{90}Y-microspheres treatment was assessed by PET/CT imaging. The Mann-Whitney U test was used to compare both groups, while Wilcoxon signed rank test was applied to analyse paired data. ***Results:*** In total, 78 HCC patients were included (^{166}Ho-microspheres cohort; 21, ^{90}Y-glass cohort; 57). The median absolute difference between ^{99m}Tc-MAA predicted LMD and ^{90}Y-microspheres LMD was 1.84 Gy (range: 0.09-79.38) and was found to be significant (p<0.01). No significant difference was found between the ^{166}Ho-microspheres scout predicted LMD and ^{166}Ho-microspheres treatment LMD; median absolute difference 0.16 Gy (range: 0.03-1.26). The Mann-Whitney U test revealed a significant difference in the median absolute differences between the cohorts (U = 140, p<0.01). ***Conclusion:*** Prediction of LMD by ^{166}Ho-microspheres scout for ^{166}Ho-microspheres treatment was significantly better than ^{99m}Tc-MAA LMD prediction for ^{90}Y-microspheres treatment. Despite inherent limitations in the comparison, these results support the use of ^{166}Ho-microspheres scout for treatment planning in HCC patients. ***References:*** 1. Reinders MTM, van Erpecum KJ, Smits MLJ et al. Safety and Efficacy of ^{166}Ho Radioembolization in Hepatocellular Carcinoma: The HEPAR Primary Study. J Nucl Med. 2022;63(12):1891-8. 2. Stella M, Rooij R van, Lam M. et al. Lung dose measured on post-radioembolization ^{90}Y-PET/CT and incidence of radiation pneumonitis. J Nucl Med 2022; 63:1075-1080.

EPS-199

Comparison of response evaluation criteria in diffuse large B-cell lymphoma: Lugano versus RECIL, and PERCIST

P. Tang, *R. Tian, M. Su;*
Department of Nuclear Medicine, West China Hospital, Sichuan University, Chengdu, CHINA.

Aim/Introduction: The objectives of this study were (1) to compare the interobserver agreement of the Lugano criteria, RECIL criteria, and PERCIST criteria in the response evaluation of DLBCL; and (2) to compare their performance in predicting patients' prognosis. ***Materials and Methods:*** 335 patients diagnosed with diffuse large B-cell lymphoma (DLBCL) were retrospectively analyzed. All patients underwent baseline 18F-FDG PET/CT and interim PET/CT (I-PET/CT) or end-of-treatment PET/CT (EoT-PET/CT). Scans were interpreted by two nuclear medicine physicians using Lugano, RECIL and PERCIST, and the agreement of two observers was compared. Those with inconsistent evaluations reached an agreement by discussion. Then, the RECIL and PERCIST were compared with Lugano for predicting progression-free survival (PFS) and overall survival (OS). Survival curves were estimated with Kaplan-Meier analysis and compared using the log-rank test. The discrimination of different response evaluation criteria was evaluated with C-index and compared using compare C. P < 0.05 was considered statistically significant. ***Results:*** The median follow-up was 47 months. 18F-FDG PET/CT-based response evaluation according to Lugano, RECIL, and PERCIST was determined at interim or end-of-treatment restaging. In the interobserver agreement comparison, the weighted kappa for Lugano, RECIL, and PERCIST were respectively 0.887, 0.798, and 0.740 in I-PET/CT and respectively 0.831, 0.781, and 0.807 in EoT-PET/CT. All three response criteria were significantly associated with PFS (P<0.001) and OS (P<0.001). In I-PET/CT, the C-index of Lugano criteria in predicting PFS and OS was higher than RECIL criteria (both P=0.043) and PERCIST criteria (P=0.008 and P=0.034). In EoT-PET/CT, the C-index for predicting PFS and OS according to Lugano was equal to RECIL, but not significantly different from PERCIST (P = 0.597 and P = 0.231). ***Conclusion:*** With Lugano, RECIL, and PERCIST interpretation, I-PET/CT and EoT-PET/CT were predictive of PFS and OS. But Lugano criteria showed greater interobserver agreement and better prediction of PFS and OS, highlighting the importance of Lugano in DLBCL response evaluation in I-PET/CT and EoT-PET/CT.

EPS-200

Voxel-Based Dosimetry with Integrated Y-90 PET/MRI Following TARE with Glass Microspheres and Dose-Response Relationships - Preliminary Results

B. Demir[1], *E. C. Celebioglu*[2], *C. Soydal*[1], *N. O. Kucuk*[1], *D. Kuru Oz*[2], *M. S. Bilgic*[2], *K. M. Kir*[1];
[1]*Ankara University School of Medicine Department of Nuclear Medicine, Ankara, TÜRKIYE,* [2]*Ankara University School of Medicine Department of Radiology, Ankara, TÜRKIYE.*

Aim/Introduction: During transarterial radioembolization (TARE) planning, multi-compartmental dosimetry is now recommended by multiple studies and guidelines, but the value of dose-volume histograms and dosimetry with Y-90 PET/MRI has yet to be determined. In this study we aimed to show feasibility of using integrated PET/MRI for an accurate voxel-based dosimetry. ***Materials and Methods:*** Patients who were treated with Y-90 glass microspheres and imaged with Y-90 PET/MRI between February 2021-May 2022 were retrospectively included in the study. Also, the patients who were treated after May 2022 included prospectively to this ambispective study. A total of 55 treatments of 46 patients were included in the study. For dosimetry, acquisition with respiratory gating enabled for most patients with 256 matrix, 1 iteration/16 subsets was employed. In a total of 245 perfused lesions, 165 lesions which could be delineated on pre-treatment PET were included in analysis. Individual average tumour doses(Davg) and dose-volume histograms were calculated. Response to treatment was evaluated with FDG or Ga-68-DOTATATE PET depending on histopathology. Response types were categorized as complete(CR), partial(PR), stable(SD) and progressive(PD). ***Results:*** Of the treatments 27 were for colorectal carcinoma, 12 for hepatocellular carcinoma and the remainder tumours were neuroendocrine, breast, cholangiocellular, pancreatic, thyroid carcinomas and uveal melanoma. Mean Davg values(in Gy) were calculated as 402.57, 201.29, 150.06 and 79.08 for CR, PR, SD and PD. Davg values for responder(CR+PR) lesions(mean:331.44/median:195.7) were significantly higher than non-responding(SD+PD) lesions(mean:96.82/median:79.90). Furthermore, for colorectal carcinoma Davg for responder lesions(mean:183.51/median:161.00) were significantly higher than non-responding(SD+PD) lesions(mean:88.12/median:69.50).

Additionally, CR lesions had significantly higher Davg compared to PR lesions. Also, for colorectal carcinoma lesions D70, D80, D90 and D99 were all significantly higher for responder lesions than non-responder lesions. Between CR and PR lesions D70 and D80 did not differ significantly but D90 and D99 were significantly higher in CR lesions compared to PR lesions. ROC analysis was performed for Davg, D70, D80, D90 and D99 values in colorectal responder and non-responder lesions. AUC for Davg, D70, D80, D90 and D99 were 0.814, 0.862, 0.867, 0.875 and 0.829. High specificity cut-offs were determined as 160.75, 96.50, 71.50, 42 and 29.50; for Davg, D70, D80, D90 and D99 respectively. ***Conclusion:*** In addition to average absorbed dose, D values from dose-volume histograms are also successful in predicting tumour response to TARE treatment. High resolution from PET/MRI with high soft tissue contrast of MRI may yield better registration and segmentation of tumours for Y-90 dosimetry.

EPS-201

Dose Distribution Pattern of Fractionally Administered Transarterial Radioembolization Holmium Microspheres in Non-Tumorous Human Liver Tissue

A. van den Brekel[1], *T. J. Snoeijink*[1], *J. Roosen*[1], *S. J. S. Ruiter*[2], *V. E. de Meijer*[2], *J. F. W. Nijsen*[1];
[1]*Department of Medical Imaging, Radboud University Medical Center, Nijmegen, NETHERLANDS,* [2]*Department of HPB Surgery and Liver Transplantation, University of Groningen, University Medical Center Groningen, Groningen, NETHERLANDS.*

Aim/Introduction: Transarterial radioembolization (TARE) is a local treatment modality for patients with hepatocellular carcinoma or liver metastases who are not eligible for curative-intent treatment. During TARE, radioactive microspheres containing a high energy beta emitter are injected into the hepatic artery via a microcatheter. High mean absorbed doses in the non-tumorous liver tissue are relatively well tolerated in TARE, which is hypothesized to be a result of a heterogeneous dose distribution in the non-tumorous liver tissue. This study investigated the dose distribution pattern in non-tumorous liver tissue after fractional administration of TARE microspheres using an experimental setup of ex situ perfused human livers, and compared this with patient data. ***Materials and Methods:*** TARE using non-neutron-activated holmium-165 loaded microspheres (^{165}Ho-MS) was performed during MRI in three discarded human donor livers under continuous dual hypothermic machine perfusion. Four fractions of 250 mg ^{165}Ho-MS with different fluorescent dyes were administered centrally in the hepatic artery using a microcatheter. Holmium-sensitive MRI scans were obtained after each fraction, enabling MRI-based dosimetry using a fictional specific activity. Tissue samples were obtained for histopathological analyses with both conventional and fluorescence microscopy. These data were compared to MRI dose distribution patterns of three patients who underwent TARE with holmium microspheres administered in four fractions. ***Results:*** The MRI-based dose maps of the three TARE-treated perfused human livers and the three TARE-treated patients were comparable upon visual inspection, and revealed a heterogeneous dose distribution pattern of several hotspots throughout the non-tumorous liver tissue, where each new fraction of ^{165}Ho-MS resulted in an increase of the already present hotspots. Histopathological analyses of the machine perfused human livers revealed accumulation of ^{165}Ho-MS of one or more fractions in the larger arterioles and arteries. ***Conclusion:*** TARE holmium microspheres distribute heterogeneously in non-tumorous liver tissue, where the injection of multiple fractions of microspheres from the same catheter position generally does not result in a more homogenous dose distribution. This implies that part of the non-tumorous liver tissue remains unexposed to lethal doses of ionising radiation during TARE, even when increasing the amount of administered microspheres. Together with the regenerating ability of the liver, this may explain why a relatively high mean absorbed dose can be given to the liver during TARE without inducing liver failure. Future (dose-escalation) studies are needed to investigate the safety of increasing the mean absorbed dose in the non-tumorous liver tissue during TARE.

EPS-202

Can Circulating Angiogenic Factors Predict ^{90}Y Microsphere Treatment Outcomes ?

M. Mavi[1], *B. Volkan Salancı*[2], *I. Lay*[3], *F. G. Eldem*[4], *B. Peynircioğlu*[4], *S. Yalçın*[5], *Ö. Uğur*[2], *M. F. Bozkurt*[2];
[1]*Karaman Training and Research Hopital Nuclear Medicine Department, Karaman, TÜRKIYE,* [2]*Hacettepe University Nuclear Medicine Department, Ankara, TÜRKIYE,* [3]*Hacettepe University Medical Biochemistry Department, Ankara, TÜRKIYE,* [4]*Hacettepe University Interventional Radiology Department, Ankara, TÜRKIYE,* [5]*Hacettepe University Medical Oncology Department, Ankara, TÜRKIYE.*

Aim/Introduction: Tumor angiogenesis plays a crucial role in cancer growth, invasion, and metastasis. Despite extensive research on the prognostic value of circulating angiogenic factors in transarterial chemoembolization, limited data are available on their relationship with ^{90}Y microsphere treatment response. This study aimed to investigate whether circulating angiogenic factors could have an impact to predict Y-90 microsphere treatment outcomes. ***Materials and Methods:*** A total of 22 patients with primary or metastatic liver cancer were included in this study. Blood samples were collected at different time points (on the day before the treatment and days 1,7 and 30 after treatment), and the levels of various angiogenic factors were measured. The patients underwent anatomic (CT and/or MRI) and molecular ([^{18}F]FDG PET-CT) imaging to assess early treatment response and overall survival. Response in treated liver region, non-target and extrahepatic progression status were assessed with mRECIST and PERCIST criteria, along with clinical follow-up. ***Results:*** The patients with non-target progression had significantly lower levels of Ang-2 on Day 1 (p=0,019) and Day 7 (p=0,02), while patients with extrahepatic progression had significantly higher levels of osteopontin on Day 30 (p=0,041) . The change in Ang-2 levels from the day before treatment to Day 1 (p=0,029) and from Day 1 to Day 30 (p=0,041), as well as the change in PDGF-BB levels from the day before treatment to Day 1 (p=0,017), were significantly different between patients with and without non-target progression. Patients with target (13,05±1,05 vs 8,15±0,94 months, p=0,028), non-target (14,38±0,66 vs 7,15±1,02 months, p<0,001), and extrahepatic (14,12±0,90 vs 8,49±1,01 months, p=0,012) progression had significantly shorter overall survival. ***Conclusion:*** This study suggests that serum Ang-2, PDGF-BB, and osteopontin levels, as well as the amount and trend of the change in levels after 90Y microsphere treatment, may have a predictive role in prognosis. Furthermore, early target, non-target, and extrahepatic progression after ^{90}Y microsphere treatment strongly predict shorter survival for patients. This information may be useful in patient management by enabling closer follow-up and/or combining ^{90}Y microsphere treatment with other possible treatments, such as antiangiogenic treatments, for these patients.

EPS-203

Improvement of minimally invasive parathyroidectomy through the introduction of radioguided surgical approach.

A. Alomar, *I. Blanco, I. Saura, J. Cruz, A. Barrera, P. Salvador, E. Anda, N. Rudic, F. Lozada, M. Ribelles, A. Camarero, E. Goñi;*
Hospital Universitario de Navarra (HUN), Pamplona, SPAIN.

Aim/Introduction: To demonstrate if the implementation of radioguided surgical procedure improves the conventional minimally invasive parathyroidectomy technique. ***Materials and Methods:*** A prospective study was carried out consecutively including 129 minimally invasive radioguided parathyroidectomy (MIRP) procedures between February 2020 and December 2022. This group was compared with 129 selective parathyroidectomy procedures prior to the introduction of radioguided surgery between March 2017 and January 2020. All the surgeries (258) were conducted at the same tertiary center on 254 patients with surgical indication of primary hyperparathyroidism. All of them underwent preoperative morphofunctional confirmation with US and Scintigraphy ± PET-CT. The MIRP group included 112(86.8%) MIBI procedures (i.v. injection of 185MBq of 99mTc-Sestamibi) 60min before surgery and 17(13.2%) MAA procedures (US-guided lesion injection of 18,5MBq of 99mTc-Macroaggregates) 6h before surgery. The intraoperative localization was accomplished with a portable gamma camera and gamma probe. Surgical success was evaluated through intraoperative biopsy. Criterion for cure was based on normal calcemia at 6 months. ***Results:*** The mean age was 61.5±11.7 with 101(78.2%) women in the MIRP group and 60.4±14.1y/o with 103(79.8%) women in the non-radioguided group. No significant differences (p>0.05) were found between the two groups in terms of preoperative calcemia, sex, age, BMI, excised gland weight, preoperative location of the pathological gland on MIBI and US or neck surgical history. The success rate in the surgical localization of the parathyroid glands was identical in both groups; 126(97.7%). Cure rate was slightly higher in the MIRP group [125(97.7%) vs. 120(93.7%), p=0.108 - one patient was lost to follow-up]. However, MIRP provides a significant reduction in surgical time (45min vs. 55min, p=0.005) with lower requirement for initial incision enlargement [4(3.2%) vs. 15(11.6%), p=0.008] and lower percentage of post-surgical complications [8(6.2%) vs. 20(15.5%), p=0.013]. In addition, a greater number of ectopic glands were removed in MIRP [30(23.2%) vs. 14(10.8%), p=0.008]. ***Conclusion:*** Radioguided surgery significantly reduced surgical time as well as the rate of initial incision enlargement with fewer surgical complications and a higher efficacy in the excision of ectopic glands. These benefits without compromising the high success and cure rate of the conventional minimally invasive parathyroidectomy. Moreover, the high percentage of localization and the ex vivo confirmation of radiotracer uptake in the excised gland may obviate the need for intraoperative pathological confirmation, leading to shorter surgical times.

EPS-204

^{188}Re-N-DEDC lipiodol trans-arterial radionuclide therapy (TART) in HCC patients: Modification in lung Shunt fraction (LSF) criteria and clinical implication on therapeutic dose estimation using scout dose of ^{188}Re-N DEDC lipiodol

N. Kumar, *P. Gupta, S. A. Shamim, S. Gamanagatti, S. Shalimar, C. Bal;*
All India Institute of Medical Sciences, New Delhi, INDIA.

Aim/Introduction: Accurate hepatopulmonary shunt assessment, typically performed by planar scintigraphy, is critical in dose planning and delivery of ^{188}Re-N-DEDC lipiodol TART. High lung shunt fractions (LSFs) may alter treatment and may induce pulmonary toxicity if radiation absorbed dose to lungs >30Gy. Thus, this study is aimed to modify the LSFs calculation criteria and to describe the potential clinical implications on therapeutic dose estimation based on partition model using transarterial injection of scout dose of ^{188}Re-N-DEDC lipiodol. ***Materials and Methods:*** The study included 20 patients (18 male; 2 female; mean age, 54 ±11 years) who underwent 5mCi scout ^{188}Re-N-DEDC lipiodol injected in each tumor artery. The planar and SPECT/CT scintigraphy was performed for artery mapping, LSF calculation and therapy dose planning. LSF using planar imaging (PLSF) was compared with LSF using SPECT/CT (SLSF) via automatically generated volumetric ROIs on Interview fusion imaging software around the lungs and liver with subsequent manual adjustments. The partition model was used to calculate the therapeutic activity to be injected transarterially in super selective artery of tumor. The LSFs values derived from planar and SPECT/CT data were compared using paired-t test. ***Results:*** Of 20 patients, 7 patients had Barcelona Clinic Liver Cancer-stage B (BCLC-B), while 13 had BCLC-C staging. Thirteen out of 20 patients had Child Pugh score A, while 7 had Child Pugh score B. Mean PLSF, 23.2±5.28%, was greater than mean SLSF, 7.4±4.06% ($p < 0.001$). In BCLC-C HCC patients, SLSF is significantly lower compared to PLSF, with a greater discrepancy among patients with a PLSF ≥ 10%, tumor size ≥ 8 cm, and child Pugh score B.None of patient had PLSF <10%, 5/20 patients had %PLSF between 10-20% and remained had >20% PLSF. All except 3 of 20 patients had SPECT/CT LSF was >15% and remained have qualified for standard radionuclide therapy as the estimated absorbed dose to lung was <20Gy in all patients when desired dose to tumor was kept >200Gy on calculated with partition model. ***Conclusion:*** LSF calculation is a subjective criteria, thus appropriate method must be used. The estimated absorbed dose to lung, liver and tumor also varies with LSF calculation and dosimetry method used. SPECT/CT should now be considered for clinical LSF calculations prior TART in HCC patients.

EPS-205

A controlled administration device for MRI-guided holmium-166 transarterial radioembolisation: MR-safe and fractional microsphere administration

M. W. M. van Wijk[1], *G. van Wolfswinkel*[2], *J. Roosen*[1], *M. J. Arntz*[1], *M. J. R. Janssen*[1], *J. F. W. Nijsen*[1];
[1]*Department of Medical Imaging, Radboud university medical center, Nijmegen, NETHERLANDS,* [2]*R&D TIO, Quirem Medical B.V. - a Terumo company, Deventer, NETHERLANDS.*

Aim/Introduction: Transarterial radioembolisation (TARE) is a treatment modality for palliative treatment of liver tumours. Current results from clinical trials show no added overall survival of TARE compared to or combined with systemic therapies, but clinical studies demonstrated the added value of reaching a high tumour dose to the overall and progression free survival of patients [1,2]. Dosimetry is therefore often stated as an important element of optimizing TARE, however, current clinical implementation is limited. Holmium-166 (^{166}Ho) microspheres facilitate quick, high resolution MRI-based dosimetry. This is currently used as an evaluation measure, however, it could also be used for intraprocedural dosimetry to optimize tumour and healthy liver dose to improve treatment outcome. MRI-guided

TARE requires accurate, controlled microsphere administration, which is not possible with the current administration systems used for TARE. Therefore, a controlled administration device (CAD) was developed and the safety and feasibility of using this device for fractional administration during MRI-guided TARE was investigated. ***Materials and Methods:*** The CAD system is an MR-safe device containing a rotating syringe to keep the microspheres in a homogeneous suspension, a control unit to set rotational speed and a battery pack for the power supply. The CAD was firstly tested ex-vivo, to determine the optimal settings for microsphere suspension homogenization, MR-safety and administration accuracy. After ex-vivo testing a clinical study (CONTROL) was performed to validate the use of the device in-vivo in an MRI-guided setting. Included patients got a holmium-scout procedure as normally performed to determine administration positions and lung shunt. During the treatment procedure, fluoroscopy was used to place the catheter, after which the patients were transferred to an adjacent 3T MRI system. Patients were positioned in the MRI and ^{166}Ho microspheres were administered in five fractions. After each fraction a multigradient echo was acquired for MRI-based dosimetry. MRI-based activity maps were used to validate the activity administration in-vivo. ***Results:*** Ex vivo validation of the CAD resulted in accurate, equally concentrated administration fractions of a total dose divided in 10 fractions. Preliminary results of three CONTROL study patients show no device or procedure related (S)AE's. The total activity on the MRI-based activity maps increases consistently with every fraction administered by the CAD. ***Conclusion:*** Preliminary results of in-vivo validation show a good usability of the new controlled administration device which enables MRI-guided TARE with personalized dose administration in a future clinical study (expected to start in June 2023). ***References:*** 1. 10.1148/radiol.2020191606 2. 10.1016/S2468-1253(20)30290-9

EPS-206

NOBLE (Nobody Left Behind) Registry: Initial Experience of [^{99m}Tc]Tc-HYNICiPSMA Imaging in the Detection of Prostate Cancer

S. Martina[1], *P. Tually*[2], *V. Garcia Quinto*[3], *Y. Omar*[4], *R. Yudistiro*[5], *M. Sathekge*[6], *G. Currie*[7], *P. Galette*[1], *N. Patel*[1], *T. Brown*[1], *G. Bolland*[8], *R. Lo bue*[8], *C. Hayward*[1];
[1]*Telix Pharmaceuticals, Melbourne, AUSTRALIA,* [2]*TeleMed Nuclear Imaging, Kalgoorlee, AUSTRALIA,* [3]*Hospital Galenia, Cancun, MEXICO,* [4]*Misr Rediology Center, Cairo, EGYPT,* [5]*Siloam International Hospitals, Tangerang, INDONESIA,* [6]*University of Pretoria, Pretoria, SOUTH AFRICA,* [7]*Charles Sturt Univeristy, Wagga Wagga, AUSTRALIA,* [8]*Oncidium Foundation, Brussels, BELGIUM.*

Aim/Introduction: [^{68}Ga]Ga-PSMA-11 PET/CT has emerged as the standard of care for prostate cancer (PC) imaging; however, accessibility to PET/CT can be limited by socioeconomic status, geographic factors, or health care structure and funding models. A PSMA-targeted tracer labelled with ^{99m}technetium (^{99m}Tc) that has a long half-life, is more abundant than PET/CT tracers, and could be used with SPECT may have substantial global health benefits. We present preliminary results from a global registry that aims to collect [^{99m}Tc]TcHYNIC-iPSMA SPECT images and patient-associated relevant clinical data. The primary and secondary objectives, respectively, are to assess the safety and tolerability of [^{99m}Tc]Tc-HYNIC-iPSMA administration and determine the clinical relevance of [^{99m}Tc]Tc-HYNIC-iPSMA SPECT in detecting disease at different stages of PC. ***Materials and Methods:*** This is a prospective, observational, multicenter registry; 100 patients with prostate cancer between 18 and 80 years old will be enrolled. Patients receive [^{99m}Tc]Tc-HYNIC-iPSMA intravenously prior to imaging (suggested dose for 70-kg patient is 555-740 MBq (1520 mCi) and 50 µg of HYNIC-iPSMA). Patient data are to be analyzed descriptively. An interim analysis is planned when data from 40 patients is collected. ***Results:*** As of abstract submission date, 40 patients have been enrolled in 6 countries (Australia, Azerbaijan, Egypt, Indonesia, South Africa, Mexico) and have received [^{99m}Tc]TcHYNICiPSMA tracer administration followed by planar and SPECT imaging. Preliminary data on patients are reported here. Demographics and disease information were collected prior to enrollment: age (mean 69 y), race (27 Caucasian, 4 Latino, 6 Asian, 2 Black/African American, 1 American Indian), rationale for [^{99m}Tc]Tc-HYNIC-iPSMA imaging (involving several indications including initial clinical staging, restaging of disease, therapy response assessment, biochemical recurrence) and PSA (average per indication at enrollment; initial clinical staging 67 ng/mL, restaging of disease 54 ng/mL, BCR 256 ng/mL, therapy response assessment 23 ng/mL). In 40% of subjects, a change in treatment due to the [^{99m}Tc]Tc-HYNIC-iPSMA imaging was reported . No adverse events have been reported. This study is still enrolling, and an interim analysis is underway. ***Conclusion:*** [^{99m}Tc]Tc-HYNIC-iPSMA is promising to identify PSMA-positive PC on SPECT and could enable improved patient access to PSMA imaging worldwide.Disclosure: The sites are sponsoring the registry, through the Principal Investigator/s, who are responsible for the initiation and conduct of the Registry. Telix is providing IP and, with Oncidium Foundation, providing clinical and operational support. Virginie Kinet and Carolina Mena (Telix Pharmaceuticals) provided operational/project management and editorial support.

EPS-207

BPH-related False Positive of [^{68}Ga]Ga-PSMA PET/CT in the Diagnosis of Prostate Cancer: the Achilles' Heel of Biopsy-free Radical Prostatectomy?

Y. Tang, *L. Xiao, J. Yang, J. Hou, B. Chen, S. Hu;*
Xiangya Hospital Central South University, Changsha, CHINA.

Aim/Introduction: Radical prostatectomy (RP) is the primary treatment for localized clinically significant prostate cancer. Generally, its application is based on prior biopsy and pathological diagnosis. [^{68}Ga]Ga-PSMA PET/CT has been considered in recent years to be effective in biopsy-free RP. However, the expression of PSMA in benign prostatic hyperplasia (BPH) and its related positive reaction are crucial concerns for no biopsy strategy. Currently, no large-scale study has explored the BPH-related false positive of [^{68}Ga]Ga-PSMA PET/CT in the detection of prostate cancer. Furthermore, the influence of SUVmax and PI-RADS on biopsy-free RP is also poorly characterized. ***Materials and Methods:*** Patients who received mpMRI and [^{68}Ga]Ga-PSMA PET/CT because of clinical suspicion of prostate cancer based on elevated prostate-specific antigen or abnormal digital rectal examination, subsequently were confirmed to be BPH or prostate cancer by pathological examination after systematic/targeted biopsy or/and RP. The mpMRI images were evaluated in accordance with the PI-RADS v2.1 and score ≥ 3 was considered positive. The PET/CT images were interpreted using a five-point Likert scale and those with a score of 3-5 were categorized as positive. The SUVmax value and PI-RADS score of the dominant lesion was recorded. The highest SUVmax in the prostate gland was also collected for negative cases with low-level radiotracer uptake. The Spearman rank correlation analysis was performed to estimate the correlation between the SUVmax and ISUP grade

group. The receiver operating characteristic curve was generated for SUVmax values, from which the area under the curve (AUC) and the Youden index was calculated. Sensitivity and specificity were calculated based on the cutoffs. ***Results:*** 89 BPH and 94 prostate cancer patients were included. 27 of the 89 BPH cases were considered PET/CT-positive, and were regarded as BPH-related false positive (30.3%). SUVmax could effectively distinguish BPH and grade group 1 patients with an AUC of 0.8562, the optimal SUVmax cutoff value was 9.750 with a sensitivity of 64.71% and a specificity of 97.22%. Considering the importance of specificity in biopsy-free RP, the optimal SUVmax cutoff value with 100% specificity was 14.60, with a sensitivity of 41.18%. Notably, using stringent PET and PI-RADS scores criteria (both ≥ 4) could exclude all positive BPH patients. ***Conclusion:*** In summary, our results revealed, for the first time, the BPH-related false positive rate of [^{68}Ga]Ga-PSMA PET/CT in the primary diagnosis of prostate cancer. Using SUVmax values or stringent PET and PI-RADS scores in biopsy-free RP can effectively exclude positive BPH patients.

EPS-208

FDG-PET/CT for lymph node staging prior to radical cystectomy

M. Markus[1], *V. Pihl*[2], *F. Liedberg*[2], *E. Trägårdh*[1];
[1]*Clinical Physiology and Nuclear Medicine, Malmö, SWEDEN,* [2]*Department of Urology, Malmö, SWEDEN.*

Aim/Introduction: ^{18}F-Fluorodeoxyglucose positron emission combined with computed tomography (FDG-PET/CT) has been proposed to improve preoperative staging in patients with bladder cancer subjected to radical cystectomy (RC). Our aim was to assess the accuracy of FDG-PET/CT for lymph node staging ascertained at the multidisciplinary tumor board (MDT) compared to lymph node status in the surgical lymphadenectomy specimen obtained at RC, and to explore potential factors associated with false positive FDG-PET/CT results. ***Materials and Methods:*** Consecutive patients with bladder cancer undergoing RC with extended lymph node dissection between 2011 and 2019 without preoperative chemotherapy in a tertial referral cystectomy unit were included in the study. Sensitivity, specificity, positive and negative predictive values, and likelihood ratios were calculated. Potential factors investigated for association with false positive FDG-PET/CT were; bacteriuria within four weeks prior to FDG-PET/CT, Bacillus Calmette-Guerin (BCG) treatment within 12 months prior to FDG-PET/CT and transurethral resection of bladder tumor (TURB) within four weeks prior to FDG-PET/CT. ***Results:*** Among 159 patients included for analysis, 46 (29%) were clinically node positive according to FDG-PET/CT. The sensitivity and specificity for detection of lymph node metastasis were 50% and 82%, respectively, and the corresponding positive predictive and negative predictive values were 59% and 76%. Positive and negative likelihood ratios were 2.8 and 0.6, respectively. No association were found between bacteriuria, previous BCG treatment or TURB within 28 days and false positive FDG-PET/CT results. ***Conclusion:*** Preoperative FDG-PET/CT prior to RC had a clinically meaningful high specificity (82%) but lower sensitivity (50%) for detection of lymph node metastases compared to lymph node status in an extended pelvic lymphadenectomy template. We could not identify any factors associated with false positive FDG-PET/CT outcomes.

EPS-209

One-day dual-tracer PET/CT protocol with [68Ga]-DOTA-FAPI-04 for negative orequivocal [18F]FDG

H. Li*, Z. Xiao, C. Li, Y. Tian, N. Lu, J. Chen, D. Xing, Y. He;*
Zhongnan Hospital of Wuhan University, Wuhan, CHINA.

Aim/Introduction: [68Ga]-FAPI is a tumor-stromal imaging agent that has shown complementary values to [18F]FDG in cancer imaging. We aimed to investigate the feasibility of a One-day dual-tracer PET/CT protocol with [68Ga]-DOTA-FAPI-04 following [18F]-FDG-PET/CT in patients presenting with negative or equivocal [18F]FDG. ***Materials and Methods:*** [68Ga]-DOTA-FAPI-04 was injected following the [18F]-FDG-PET/CT in patients presenting with negative or equivocal [18F]FDG on the same day (The interval between injection of the two tracers was 4-8 hours). The maximum tracer concentration (TCmax) of lesions (Bq/mL) was measured. The tumor-to-blood ratio (TBR), tumor-to-liver ratio (TLR), and tumor-to-cerebellum (TCR) were recorded and compared between the two imaging modalities. The standard for the final diagnosis was histopathologic findings and/or follow-up imaging (at least 3 months). ***Results:*** We prospectively recruited 15 patients (11 males and 4 females, mean age 55.7 ± 13.8). Of them, 5 (33.3%) for detection of the unknown primary site in biopsy-proven or conventional imaging highly suspected of metastatic malignancy with negative [18F]-FDG-PET/CT, 3 (20.0%) for the initial staging, and the other 7 (46.7%) for postoperative recurrence and metastasis detection. The TBR, TLR, and TCR of dual-tracer were significantly higher than those of [18F]FDG for detecting primary lesions and postoperative recurrence (TBR:10.0 vs. 2.8, P=0.006; TLR: 11.8 vs. 2.3, P=0.027; TCR: 8.4 vs.0.89, P=0.013), lymph node (TBR:12.2 vs. 6.9, P=0.042; TLR: 9.7 vs. 5.2, P=0.025; TCR: 4.9 vs. 1.9, P=0.008), and peritoneal metastases (TBR:6.2 vs. 2.0, P=0.012; TLR: 6.0 vs. 1.7, P=0.026; TCR: 4.8 vs. 0.7, P=0.005) in dual-tracer PET/CT than did [18F]FDG. In addition, dual-tracer PET/CT detected the primary site in 2/5 patients (40%) with unknown malignancy. Two patients (2/5) were eventually diagnosed with multiple myeloma or primary peritoneal carcinoma, respectively. Besides, dual-tracer PET/CT upgraded tumor staging in 1/3 of patients (33.3%) and detected more disease recurrence and metastatic lesions in 4/7 patients (57.1%). ***Conclusion:*** Dual-tracer PET/CT showed great potential for detecting primary tumors, postoperative recurrence and metastasis in patients with negative or equivocal for [18F]FDG findings. We will recruit a larger number of participants to further confirms our conclusion in the future.

1310

Tuesday, September 12, 2023, 9:45 AM - 11:15 AM
Hall K

Technologists Oral Presentations 3: NM Technologists: Competencies and Training

OP-659

Technologists´ interests and barriers toward healthcare research.

C. H. Led[1], *C. Baun*[1,2], *M. G. Hildebrandt*[1,2];
[1]*Department of Nuclear Medicine, Odense C, DENMARK,* [2]*Department of Clinical Research, University of Southern Denmark, Odense, DENMARK.*

Aim/Introduction: Clinical and preclinical research is a growing field in healthcare organizations. In the field of nuclear medicine, clinical research is often performed by nuclear medicine physicians or academia. Although technologists often have the primary contact to patients participating in clinical studies, their

role and voice is less defined. This study aims to gather knowledge of the technologists' interests and attitudes toward clinical and preclinical research. Furthermore, to identify incentives and barriers for technicians to participate in research projects. ***Materials and Methods:*** An electronic survey (SurveyXact, Rambøll) was carried out, in October 2022, at the Department of Nuclear Medicine, Odense University Hospital. The questionnaire was developed iteratively by a collaborative team comprising two nuclear medicine technologists and one senior nuclear medicine physician. The questionnaire underwent several pilot tests before the primary survey. The final digital questionnaire included 21 questions (19 forced multiple choice and two open-ended questions) and took approximately 10 minutes to complete. The survey was divided into five main sections; 1) Descriptive background, 2) General interest and visibility of research projects, 3) Interest in a collaborative role in research, and 4) interest in performing own projects. 5) Barriers and suggestions for improvements. The survey was shared by email, with a 14-day response time. After seven days, a reminder email was sent. ***Results:*** 1) Forty-one (76%) technologists completed the survey, of whom 24 (53%) had been employed at the department for >10 years. 2) All responders (100%) found clinical research interesting in general, but 38 (90%) reported that the information level about the ongoing and new projects in the department was insufficient. 3) Twenty-two (52%) of the respondents would like to take a collaborative role in a clinical research project, whereas only 10 (24%) were interested in preclinical projects. 4) Seventeen responders (41%) would like to perform their own research and quality assurance projects. 5) Twenty-six (62%) believe that a dedicated contact person for the technologist group would be beneficial. Finally, twenty-nine (71%) responders listed uncertainty about time, payment, and the priority of clinical tasks were potential barriers. ***Conclusion:*** Based on the results, we conclude that the technologist group in our department has a considerable interest in healthcare research in general. Furthermore, a dedicated subgroup of technicians would like to participate in collaborative- and own research projects. Improvements in visibility, information, and clear, practical framework are needed to ensure that research for technologists becomes more easily accessible.

OP-660

Framework for Online Radiographer Clinical Education (FORCE): results of students' evaluation of the Nuclear Medicine strand

P. Costa[1], *J. Lemos*[1], *R. Strudwick*[2], *P. Bezzina*[3], *N. Dalen*[4], *J. T. Huhtanen*[5], *M. Jaronen*[6], *T. Saila*[6], *C. Kamp*[7], *L. Rainford*[8], *K. Matthews*[8];
[1]*Nuclear Medicine Department, School of Health - Polytechnic Institute of Porto (ESS|P.Porto), Porto, PORTUGAL,* [2]*School of Health and Sports Sciences - University of Suffolk, Suffolk, UNITED KINGDOM,* [3]*Faculty of Health Sciences - University of Malt, Msida, MALTA,* [4]*Department of Health and Functioning - Western Norway University of Applied Sciences, Bergen, NORWAY,* [5]*Health and Well-being, Rehabilitation, Oral Health Care and Diagnostic Services - Turku University of Applied Sciences, Turku, FINLAND,* [6]*Social Services and Health Care - Tampere University of Applied Sciences, Tampere, FINLAND,* [7]*University of Applied Sciences FH Campus Wien, Wien, AUSTRIA,* [8]*School of Medicine - University College Dublin, Dublin, IRELAND.*

Aim/Introduction: The FORCE project is focused on the use of simulation in education and in such context it is being developed a set of virtual web-based learning resources where Radiography undergraduates can engage in interactive, problem-based development of knowledge, ability and professional awareness within the fields of Nuclear Medicine, Radiology and Radiotherapy. The project was already presented and disseminated in scientific events as well as with academic partners and professional associations and societies. The aim of this novel presentation is to present the current development of the project and to share feedback from students that already tested the first complete case of the specific strand of Nuclear Medicine. ***Materials and Methods:*** An original online questionnaire, based on SurveyMonkey, was developed and face-validity together with pilot tests were implemented to validate such data collection tool. A total of 36 students of the third year of a Medical Imaging and Radiotherapy degree course answered the questionnaire. ***Results:*** The complete simulation case is focused on a patient with an high-risk Prostate Carcinoma that was sent to the Nuclear Medicine Department with a referral for Bone Scintigraphy. Students revealed that time spent to explore the whole case was between 30 minutes and 2 hours (86%, n=31), and the majority of students considered the case as clear in terms of learning objectives and content (94%, n=34 and 92%, n=33, respectively). Global results showed that majority of students (86%, n=31) agree or strongly agree with the idea that studying these cases will improve their clinical learning. Other specific results related with the case structure and content, questions and interactivity, technical e-learning and navigation, multimedia, overall experience, and strengths/weaknesses analysis will be shared. ***Conclusion:*** The presentation will summarise the development process to date and provide a complete presentation of the case here evaluated together with global feedback from students already obtained. These results allowed the validation of the evaluation questionnaire, the collection of data related with students' feedback about the case and revealed very good acceptance of the learning resources that are being developed along this project.

OP-661

The evolution of our PSMA PET imaging service

L. Thomas;
St Vincent's Hospital Melbourne, Melbourne, AUSTRALIA.

Aim/Introduction: Over the past 7 years of our Prostate PET/CT service we have evolved the scanning procedure to be what it is today. ***Materials and Methods:*** We are a single PET/CT scanner department in a tertiary public hospital in Melbourne, Australia. The small size of our hotlab and having no radiopharmacist onsite does not allow us to have a Gallium generator, so we had to source our own supply externally. We were only able to source Gallium once a week and then we had to pick either PSMA or DOTATATE for that run (only 1-3 patient doses). In 2017 we jumped at the opportunity to utilise 18F-DCFPyL as our Prostate PET/CT imaging agent of choice. After starting to scan with 18F-DCFPyL we made quite a few protocol variations with our physicians and referrers. To start with, we performed dual time point half body scans at 1 and 2 hours. Then we moved to a half body scan at 1 hour and Modified CT IVP with 2 PET pelvis beds at 2 hours - logistically this was very hard to schedule. Finally we have settled on a protocol where we hand inject 50 mls of CT contrast and then get the patient walking around for 20 minutes. ***Results:*** Our current protocol has saved patients the extra CT dose along with significant scanner time, resulting in the ability to increase patient numbers. This protocol not only helps us to differentiate between ureters and lymph nodes but also bladder and recurrence in the prostate bed. ***Conclusion:*** Our current Prostate PET/CT protocol with ureteric contrast enhancement produces excellent

diagnostic PET/CT images along with efficient use of our limited scanner time. ***References:*** • Szabó, Z. et al. "Initial Evaluation of [18F] DCFPyL for Prostate-Specific Membrane Antigen (PSMA)-Targeted PET Imaging of Prostate Cancer." Molecular Imaging and Biology 17 (2015): 565-574. • Jansen BHE, Yaqub M, Voortman J, et al. Simplified methods for quantification of 18F-DCFPyL uptake in patients with prostate cancer. J Nucl Med. April 18, 2019 • Wondergem M, van der Zant FM, Knol RJJ, Lazarenko SV, Pruim J, de Jong IJ. 18F-DCFPyL PET/CT in the detection of prostate cancer at 60 and 120 minutes: detection rate, image quality, activity kinetics, and biodistribution. J Nucl Med. 2017;58:1797-1804.

OP-662

Comparison of calculated Left Ventricular Ejection Fraction (LVEF) from F-18 FDG dual-gated PET/CT, single-gated PET/MRI, and cardiac MRI

P. Toompong, *A. Jantarato, D. Siripongsatian, P. Panperee, C. Promteangtrong, A. Kunawudh, P. Kiatkittikul, P. Lerdsirisuk, S. Sombon, C. Chotipsnich;*
National Cyclotron and PET Centre, Bangkok, THAILAND.

Aim/Introduction: Left Ventricular Ejection Fraction (LVEF) is a critical parameter in evaluating cardiac function and guiding treatment decisions in breast cancer patients undergoing chemotherapy. Positron Emission Tomography (PET) with F-18-FDG uptake has emerged as a promising alternative to Multi-Gated Acquisition (MUGA) scan. This study aims to compare LVEF assessment using PET/CT, PET/MRI, and Cardiac Magnetic Resonance Imaging (MRI) as the gold standard. ***Materials and Methods:*** Ten breast cancer patients meeting inclusion criteria fasted for 12 hours before undergoing a glucose load of 60 mg and an injection of 18F-FDG. The uptake time was 60 minutes, after which patients underwent PET/CT using three different reconstruction techniques: Dual gating with Electro Cardiac Gated (ECG) and Respiratory gated (Dual Gated), Dual gated with AI-assisted list mode respiratory compensated PET/CT (List mode Dual gating PET/CT), and Single-gated (ECG) PET/CT. Additionally, the single-gated PET/MRI and cardiac MRI were performed for data collection on end-diastolic volume (ED), end-systolic volume (ES), and ejection fraction (EF). Statistical analysis was conducted using Stata, with $p < 0.05$ as statistically significant. ***Results:*** Statistical analysis revealed no significant difference in EF among cardiac MRI, dual-gated PET/CT, list mode PET/CT, single-gated PET/CT, and single-gated PET/MRI (F-ratio = 1.4273, $p = 0.240436$, $p < 0.05$). Dual-gated PET/CT showed the lowest average percentage difference when compared to cardiac MRI (6.45%). ED and ES showed no significant difference among PET-based methods ($p < 0.05$). However, MRI-based methods had significant differences in ED and ES when compared to all PET-based methods, with consistent percentage differences ranging from -37.64% to -39.38% for ED and -43.68% to -45.32% for ES. Intraclass correlation showed moderate to good reliability, and Pearson correlation coefficients indicated good to strong correlations between cardiac MRI and PET MRI-based methods, as well as among PET-based methods. ***Conclusion:*** PET-based methods may offer comparable results to MRI cardiac-based methods for the evaluation of LVEF in breast cancer patients undergoing chemotherapy. Utilizing PET-based methods may offer advantages in terms of convenience, accessibility, and cost-effectiveness, as a promising alternative for assessing LVEF in this population. ***References:*** Li Y, Wang L, Zhao S-H, et al. Gated F-18 FDG PET for Assessment of Left Ventricular Volumes and Ejection Fraction Using QGS and 4D-MSPECT in Patients with Heart Failure: A Comparison with Cardiac MRI. Lipinski M, ed. PLoS ONE. 2014;9(1):e80227. doi:10.1371/journal.pone.0080227

OP-663

A. Resende Geao, *A. Santos, P. Colarinha;*
Hospital Cuf Descobertas, Lisboa, PORTUGAL.

Aim/Introduction: 68Ga -PSMA (Prostate-Specific Membrane Antigen) is currently a tool with high clinical application in prostate cancer. In 2023, EANM provided updated guidance and standards of 68Ga-PSMA for prostate cancer imaging. In addition to the guideline recommendations in the available literature can be seen the clinical impact of acquiring an initial dynamic study. The aim of this project is to present the evolution of the technique of acquisition of the dynamic study in a nuclear medicine department. ***Materials and Methods:*** The NM department started to perform 68Ga-PSMA studies since 2018 and many changes have been implemented in the procedure. The timing of the injection and the applied technique has been changing throughout the years. Table 1 summarizes the major modifications implemented in technologists practice.The implementation of the dynamic study in these studies has several challenges, including defining the best technique for injection and determining the optimal image acquisition timing. One challenge is the timing of the injection of the radiopharmaceutical. Injection too early may result in incomplete uptake of the radiopharmaceutical in the tumor and surrounding tissues, while injection too late may result in excessive urinary excretion of the radiopharmaceutical, leading to reduced tumor-to-background contrast. Therefore, it is important to find the optimal time for injection. ***Results:*** The impact of protocol customization on the clinic can be significant, leading to improved imaging results, patient experience, and clinical efficiency. The dynamic study offers several advantages in the visualization of prostate cancer. The early images acquired during the dynamic study can provide information about the initial uptake and clearance of the radiopharmaceutical, allowing for improved visualization of the pelvic area and accurate staging of the disease. It is important for the multidisciplinary team to continually review and adapt protocols to meet the specific needs of patients and equipment, ensuring that the best possible outcomes are achieved for each individual case. ***Conclusion:*** The implementation in routine of the acquisition of a dynamic study in 68Ga-PSMA studies lead to the challenge of defining the best technique for injection of the radiopharmaceutical and image acquisition timing. Advantages and disadvantages can be found however, the advantages of early imaging and improved visualization of the pelvic area make it a valuable tool for diagnosis and management of prostate cancer. ***References:*** Fendler WP, Eiber M, Beheshti M, et al. PSMA PET/CT: joint EANM procedure guideline/SNMMI procedure standard for prostate cancer imaging 2.0. Eur J Nucl Med Mol Imaging. 2023;50(5):1466-1486.

OP-664

Short and long-term outcomes prediction using baseline FDG PET imaging in mCRPC patients treated with ^{177}Lu-PSMA radioligand therapy

Q. Shagera, *C. Broeckaert, T. Guiot, E. Barraco, S. Albeaini, L. Taraji, I. Karfis, P. Flamen, C. Artigas;*
Jules Bordet Institute, Université Libre de Bruxelles (ULB), Brussels, BELGIUM.

Aim/Introduction: Optimal selection of patients for radionuclide therapy is essential to obtain the expected results. Regarding ^{177}Lu-PSMA radioligand therapy (PSMA-RLT), it has been proposed to use the so-called dual tracer imaging approach, combining both the analysis of the target expression (PSMA-PET) together with the metabolic activity (FDG-PET). Those patients with mismatching lesions (FDG+/PSMA-) are not to be selected for

PSMA-RLT due to its poor outcome. On the other hand, patients without mismatch but with metabolically active metastatic lesions (FDG+/PSMA+) are still accepted for PSMA-RLT. Therefore, we aimed to evaluate the relationship between baseline FDG-PET imaging characteristics with short-term (PSA response and progression-free survival) and long-term outcomes (OS) in metastatic castration-resistant prostate cancer (mCRPC) patients treated with ^{177}Lu-PSMA-RLT. ***Materials and Methods:*** For this retrospective analysis, patients with dual tracer imaging (FDG-PET and PSMA-PET) performed within 8 weeks before ^{177}Lu-PSMA-RLT initiation were included. For each scan, all lesions were contoured using SUV=3 threshold for PSMA and liver SUVmean+2SD for FDG-PET. Quantitative parameters were measured, including the highest SUV (SUVmax), the total tumor volume (Vol), and the ratio FDG/PSMA-TV. Patient outcomes were calculated, including PSA response (decline of 50%) after 2 cycles, PSA-PFS (PCWG3 criteria), and overall survival (OS). The Mann-Whitney test was used to assess the association between baseline parameters and PSA response. The Cox regression model and Kaplan-Meier method were used for survival analysis. ***Results:*** A total of 87 patients were analyzed. 30 patients (34%) died, and 58 (67%) presented disease progression. The FDG-SUVmax, FDG-Vol, and FDG/PSMA-Vol ratio were significantly associated with PSA response (p=0.037, p=0.019, and p=0.001, respectively). PSA response was significantly associated with OS (HR 5.2, p=0.003). Regarding PFS, FDG-SUVmax and FDG/PSMA-Vol ratio presented significant associations (HR 1.06, p=0.006; and HR 2.6, p=0.001, respectively). For OS, FDG-SUVmax, FDG-Vol, and FDG/PSMA-Vol ratio (HR 1.09, p=0.004; HR 1.001, p=0.027 and HR 2.9, p=0.011, respectively). ***Conclusion:*** Our study findings show that baseline FDG-PET quantitative parameters may be used as factors predicting short- and long-term outcomes of patients with mCRPC treated with ^{177}Lu-PSMA-RLT. Those patients presenting with high glycolytic activity and high metabolic tumor volume compared to PSMA tumor volume are associated with lower response rates and shorter PFS and OS.

OP-665

Comparison of non-specific bone uptake of [^{18}F]AIF-PSMA-11 in prostate cancer patients acquired at different time intervals.

I. Cordero[1,2], *K. Suanes*[1,2], *P. Duarte*[1], *O. Alonso*[1,2];
[1]Centro Uruguayo de Imagenología Molecular, Montevideo, URUGUAY, [2]Unidad Académica de Medicina Nuclear e Imagenología Molecular, Facultad de Medicina, Universidad de la República, Montevideo, URUGUAY.

Aim/Introduction: Among many ^{18}F-labeled prostate-specific-membrane-antigen (PSMA) targeted PET/CT tracers, the novel [^{18}F]AIF-PSMA-11 produced in our center has demonstrated to be a good alternative for the diagnostic evaluation of prostate cancer (PCa). However, the limited time-dependent in vitro stability and consequently non-specific bone tracer uptake might hamper the visualization of small PCa bone metastases.To compare bone uptake of [^{18}F]AIF-PSMA-11 in different regions of interest at 30 minutes and 60 minutes post-administration of the radiotracer. ***Materials and Methods:*** From March 2018 to July 2021, 233 patients (median age: 68 years, range 49-89; median PSA: 24.2 ng/mL, range 0.11-834) at initial staging (21%) or with biochemical recurrence (79%) underwent ^{18}F-ALF-PSMA-11 PET/CT after the i.v. administration of 4.0 MBq/kg.Studies were performed with a 64-slice PET/CT scan with TOF correction and acquired at 60 minutes or at 30 minutes after injection (Group A and B, respectively).We measured the maximum SUV (SUVmax) and the SUVmax ratio (SR), defined as SUVmax bone/SUVmax background) in the following sites: shoulders, sternoclavicular joints, L5 and sacroiliac joints, in both groups. We selected femoral diaphysis as background. T-test for independent samples was performed using a significance level of 5%. ***Results:*** Abnormal foci were seen in the following sites: prostate gland (n=130), lymph nodes (n=68) and bone (n=74). We found a significantly higher SUVmax for group A (60 min) compared to Group B (30 min), in all studied regions as follows: SR Shoulders 60 vs 30 min: 1.77 (0.5 - 5.8) and 0.98 (0.38 - 2.5), median (range), for each group, respectively (P=0.000042).SR Sternoclavicular joints: 1.7 (0.7 - 3.5) and 1,28 (0, 56-2,8), for each group, respectively (P=0.000716). SR L5: 2.16 (0.4 - 4.0) and 1.72 (0.75 - 4.4), P=0.00002; SR Sacroiliac joints: 1.8 (0.8-3.3) and 1.48 (0.48 - 3.48), for each group, respectively (P< .00001). ***Conclusion:*** [^{18}F]AIF-PSMA-11 is a promising imaging technique for the evaluation of PC patients.However, it has demonstrated a time-dependent increase of radiotracer uptake in bone that may influence the accuracy of lesion detection in the skeleton and difficult image interpretation.

OP-666

The relentless pursuit for the best compromise between image quality and dose reduction - a single center experience with pediatric patients undergoing 18F-FDG PET/CT with long axial field of view scanner

A. Cardoso*, A. Mendes, C. Bregenzer, K. Krieger, H. Sari, K. Zeimpekis, N. Gözlügöl, A. Rominger, A. Afshar-Oromieh; Department of Nuclear Medicine, Inselspital, University Hospital Bern, University of Bern, Bern, SWITZERLAND.*

Aim/Introduction: Children are particularly sensitive to radiation exposure. Besides a cautious indication for nuclear medicine diagnostics, efforts should be made to reduce the radiation dose. Currently, guidelines recommend a dose of 3.7-5.2 MBq ^{18}F-FDG per kg body weight (BW). Recently, PET/CT-scanners with long axial field of view (LAFOV, also called "whole-body" scanners) have entered the market. They demonstrate a significantly improved performance compared to standard PET/CT-scanners. The aim of this evaluation was to assess the image quality of scans conducted with a whole-body PET/CT-scanner after injection of reduced doses of ^{18}F-FDG in pediatric tumor patients. ***Materials and Methods:*** From October 2020 until March 2023 a total of 27 ^{18}F-FDG-PET/CT scans were conducted in 21 children and adolescents (age limit 18 y/o) at our institute with a LAFOV-PET/CT-scanner (FOV: 105cm). Amongst them, three groups were identified depending on the injected activity: 1 MBq/kg, 2 MBq/kg and 3 MBq/kg. Acquisition started at 1h post injection and lasted for 10 minutes in all patients. In addition to the before-mentioned three groups, a fourth group was created simulating 0.5 MBq/kg BW by artificially reconstructing the images obtained with 1 with MBq/kg. The quality of all scans was assessed in a blinded read by the first and the last author using a 5-point Likert scale, with 5 being the best and 1 the worst quality. ***Results:*** Average age was 11.8 ± 5.6 years and average body weight 42.3 ± 22.1 kg. The Likert scales of the four groups were as follows: 2.7 **±** 0.6 for 0.5 MBq/kg (n=10 scans); 3.4 **±** 0.8 for 1 MBq/kg (n=10); 4.5 ± 0.4 for 2 MBq/kg (n=9) and 4.9 ± 0.2 for 3 MBq/kg (n=8). There was a significant association between higher doses and higher Likert scales: p=0.005 for the comparison between group 0.5 MBq/kg vs. group 1 MBq/kg, p=0.002 for the comparison between group 1 MBq/kg vs. group 2 MBq/kg and p=0.018 for the comparison between group 2 MBq/kg vs. group 3 MBq/kg. ***Conclusion:***

Although acquired with a lower dose than recommended by the guidelines, the image quality of scans conducted with 3 MBq/kg ^{18}F-FDG and the whole-body PET/CT-scanner was outstanding. As expected, the image quality decreased significantly with lower doses. Our results indicate that scans with 0.5 MBq/kg might not be suitable with a 10-min acquisition duration since the quality was lower compared to the other doses.

OP-667

Measuring GFR Using ^{51}Cr-EDTA: a Clinical Case Requiring Gamma Ray Spectra Analysis

P. Geleijnse, *S. Jentjens, K. Goffin, W. Deckers, K. Baete; Nuclear Medicine, University Hospitals Leuven, Leuven, BELGIUM.*

Aim/Introduction: Glomerular filtration rate (GFR) can be estimated from serum parameters, but in specific populations, such as children, or persons with obesity or cachexia, results are less accurate. For these populations, ^{51}Cr-EDTA clearance from blood plasma can provide a more accurate GFR measurement. The clearance can be assessed using 4 blood samples, taken one hour apart after ^{51}Cr-EDTA administration. The radioactivity in plasma samples, and reference samples derived from the administered activity concentration, can then be measured using a gamma counter (GC). The count rate measurements allow for a bi-exponential regression analysis of the data, estimation of the distribution volume and GFR computation using the Bröchner-Mortensen correction method. ***Materials and Methods:*** A 9-year-old girl was referred for GFR determination using ^{51}Cr-EDTA after ^{131}I-mIBG treatment for a stage 4 neuroblastoma. The paediatric oncologists requested an accurate GFR determination before starting chemotherapy 8 weeks after 2 cycles of ^{131}I-mIBG therapy, and 4 weeks after the last treatment cycle. Naturally, a considerable amount of ^{131}I radioactivity in plasma was suspected. In fact, the GC measurement procedure initially did not pursue inspection of the sample gamma ray spectra, besides the determination of the count rate. However, the low yield (9.9%) gamma rays of ^{51}Cr (320 keV) are near the high (81.2%) and low (6.1%) yield gamma rays of ^{131}I (364 and 284 keV, respectively). Moreover, factory GC energy window settings for ^{51}Cr (198 - 360 keV) are influenced by ^{131}I. Therefore, long-term GC measurements were performed, storing the gamma ray spectra for each sample. The spectra were corrected for background and a gaussian function was fitted to the 320 keV peak to determine its height and derive the ^{51}Cr activity concentration. The 284 keV peak of ^{131}I was ignored. ***Results:*** Initial sample count rate results showed very low plasma clearance and determined an unreliable GFR (28 ml/min/1.73m^2) due to significant influence of the ^{131}I activity concentration in blood. Using physical decay and long-term GC measurements, a more accurate ^{51}Cr activity concentration could be determined, leading to a more reliable GFR determination (65 ml/min/1.73m^2). Finally, a measurement of 18 hours per sample was performed 40 days after administration. ***Conclusion:*** This clinical case shows that it is possible to estimate the ^{51}Cr activity concentration in blood samples, containing other radionuclides, using advanced gamma ray spectra analysis. It also revealed potential pitfalls when using count rate results without thorough inspection of the sample energy spectra.

1311

Tuesday, September 12, 2023, 9:45 AM - 11:15 AM
Hall G1

Theranostics Track - TROP Session: What's New in Neuroendocrine Tumors?

OP-668

Primary tumor resection followed by PRRT in the treatment of patients with metastatic neuroendocrine ileal cancer: preliminary data from a retrospective single center study.

F. Mattana[1], *G. A. Zuccotti*[1], *A. Barone*[1], *E. Pisa*[2], *N. Fazio*[3], *U. Fumagalli Romario*[4], *C. M. Grana*[1], *F. Ceci*[1,5], *E. Bertani*[4]; [1]*IEO European Institute of Oncology, Nuclear Medicine, Milano, ITALY,* [2]*IEO European Institute of Oncology, Pathology, Milano, ITALY,* [3]*IEO European Institute of Oncology, Division of Gastrointestinal Medical Oncology, Milano, ITALY,* [4]*IEO European Institute of Oncology, Division of Digestive Surgery, Milano, ITALY,* [5]*Department of Oncology and Hemato-Oncology, University of Milan, ITALY.*

Aim/Introduction: A low volume disease is an independent positive prognostic factor for the evaluation of response to peptides-radiolabelled-receptor-therapy (PRRT). Data from a previous study[1] in patients with pancreatic-neuroendocrine-cancer (P-NET) showed that resection of the primary tumor before PRRT improves response to therapy and increases progression-free survival (PFS), namely in liver metastatic patients. Primary aim was to evaluate the PFS in two cohorts of patients (surgery + PRRT vs. PRRT alone) affected by ileal neuroendocrine neoplasm (ileum-NEN). Secondary aim was to evaluate the safety of this approach in clinical setting. ***Materials and Methods:*** this is a retrospective single-center study. Inclusion criteria were: 1) patients with histopathological diagnosis of G1-G2 ileum-NEN with synchronous liver metastasis; 2) not eligible for radical surgery; 3) eligible for PRRT. Exclusion criteria were: 1) not eligible for PRRT; 2)<18yo. Two match-comparison cohorts with a comparable total volume disease were identified: patients underwent resection of primary cancer followed by PRRT (group A) and patients underwent PRRT alone (group B). Progressive Disease (PD), Stable disease (SD) and Partial Response (PR) have been defined according clinical and radiological criteria (RECIST 1.1). PFS was evaluated in the two cohorts. ***Results:*** From 2000 to 2016 a total of 25 patients have been evaluated with an over-all median follow-up of 60 months (range 6-132 months). 13 patients were included in group A and 12 in group B. For group A, an average PFS of 52 was found vs. 44.33 months for group B. For group A 7 (54%) patients had PD, 4 (31%) SD, and 2 (15%) PR; in group B, the number of patients with PD, SD, and PR respectively was 9 (75%), 3 (25%) and 0 (0%). No adverse events have been reported in the two groups. ***Conclusion:*** Primary tumor resection prior to PRRT can be safely proposed in patients with G1-G2 metastatic ileum-NEN, as it seems to significantly improve PFS. However, more data deriving from a larger cohort of patients are needed to confirm these preliminary results. ***References:*** Bertani E, Fazio N, Radice D, Zardini C, Grana C, Bodei L, Funicelli L, Ferrari C, Spada F, Partelli S, Falconi M. Resection of the Primary Tumor Followed by Peptide Receptor Radionuclide Therapy as Upfront Strategy for the Treatment of G1-G2 Pancreatic Neuroendocrine Tumors with Unresectable Liver Metastases. Ann Surg Oncol. 2016 Dec;23(Suppl 5):981-989. doi: 10.1245/s10434-016-5550-3. Epub 2016 Sep 9. PMID: 27613553.

OP-669

First results from IEO 676 clinical study of PRRT in neuroendocrine tumors: is there still space for Y-90-DOTATOC?

C. Grana, *A. Barone, S. Papi, P. Rocca, S. Fracassi, M. Ferrari, F. Botta, F. Mattana, F. Ceci, C. Fodor, F. Spada, I. Clerici, N. Fazio, M. Rubino;*
European Institute of Oncology, IRCCS, Milano, ITALY.

Aim/Introduction: IEO 676 is a prospective phase II study of Peptide Receptor Radionuclide Therapy (PRRT) with Y-90-DOTATOC in progressive G1, G2, G3, neuroendocrine patients. PRRT has been in use since the late 1990s, with the introduction of 90Y-DOTATOC, which allowed objective responses in 10-30% of treated patients. There have been numerous studies that have led to the approval of Lu-177-oxodotreotide in G1-G2 GEP NETS. The aim of this phase II study is to evaluate the antitumor activity of 90Y-DOTATOC therapy in patients affected by sst2 positive neuroendocrine tumors, stratified for positive or negative FDG PET/CT. Although the comparison between the two patient populations is not an objective of the study, an analysis of these two groups can be carried out at a later stage, in order to evaluate the therapeutic efficacy based on the different activity administered for stratification obtained following positive-negative disease on 18F-FDG PET/CT. ***Materials and Methods:*** The protocol includes two level of administered activity: 5 cycles of 50 mCi of Y-90-DOTATOC in FDG-PET positive pts and 4 cycles in FDG negative pts. ***Results:*** From February 2020 to April 2023 we enrolled 25 out 29 pts: 13 bronchial NET, 2 unknow primary, 7 pNET G3, 1 G2 GEP NET, 1 ovarian NET, 1 paraganglioma. We have observed 1 CR, 1 PR, 11 SD, 5 PD; 7 patients are still in treatment. Therapy was well tolerated in all pts; no hematological toxicity was observed; 2 sindromic pts presented an increase of the syndrome after PRRT that was resolved with medical therapy. The pt obtaining a complete response was FDG negative. ***Conclusion:*** These first results are in line with literature results of PRRT tolerability, and the answer to the question in the title could be yes: PRRT with Y-90-DOTATOC in clinical trials is a treatment that can be proposed in NET, in particular in those patients that can not receive approved radiopharmaceuticals, but can have a benefit from PRRT

OP-670

Intra-arterial PRRT, a Prospective Clinical Study in NET Patients with Hepatic Metastases

S. Ebbers[1], *M. W. Barentsz*[1], *D. M. V. de Vries-Huizing*[2], *M. W. J. Versleijen*[2], *L. G. Klompenhouwer*[2], *M. E. T. Tesselaar*[2], *M. P. M. Stokkel*[2], *T. Brabander*[3], *H. Hofland*[3], *A. Moelker*[3], *A. J. A. T. Braat*[1], *M. G. E. H. Lam*[1];
[1]*University Medical Center Utrecht, Utrecht, NETHERLANDS,*
[2]*Netherlands Cancer Institute, Amsterdam, NETHERLANDS,*
[3]*Erasmus Medical Center, Rotterdam, NETHERLANDS.*

Aim/Introduction: The aim was to investigate whether tumor uptake in liver metastases can be enhanced by intra-arterial (IA) administration of ^{177}Lu-DOTATATE (Lutathera®, Novartis) via the hepatic artery, in order to improve tumor response without increasing toxicity. ***Materials and Methods:*** In this prospective RCT, a total of 27 patients with grade 1-2 NET, and bi-lobar liver metastases were randomized to receive IA PRRT in either the left or right hepatic artery for four consecutive cycles. The other liver lobe was treated via a 'second-pass' effect and was used as a control lobe. Up to 3 tumors per liver lobe were identified as target lesions at baseline (>3 cm). Tumor-to-normal (T/N) uptake ratios on 24h post-treatment SPECT/CT were calculated for each target lesion using the mean uptake and peak uptake (mean uptake in 1cm diameter sphere around maximum uptake voxel), and compared between IA-treated lobe (IAL) and control lobe (CL) using paired-samples t-test. Furthermore, response was recorded according to RECIST 1.1 at 3 and 6 months post-treatment. ***Results:*** A non-significant increase in both T/N_{mean} and T/N_{peak} uptake ratio was observed in the IAL: T/N_{mean}: CL = 16.2 vs. IAL = 17.9 (p = 0.299); T/N_{peak}: CL = 32.5 vs. IAL = 38.0 (p = 0.091). The mean relative increase in T/N_{mean} = 1.17 (95% CI [1.00; 1.37]), T/N_{peak} = 1.23 (95% CI [1.06; 1.42]). Overall, 67% of patients showed an increase in T/N_{mean} ratio. Tumor response rates were identical (25% PR and 75% SD at 3 mo; 35% PR, 61% SD and 4% PD at 6 mo in both IAL and CL). ***Conclusion:*** No clinically significant increase in hepatic tumor uptake on SPECT/CT after 24h, and no difference in response at 3 or 6 months follow-up could be identified after intra-arterial administration of ^{177}Lu-DOTATATE.

OP-671

Diagnostic Performance of [^{18}F]F-meta-fluorobenzylguanidine ([^{18}F]MFBG) PET/CT in Patients with Pheochromocytoma and Paraganglioma

P. Wang[1], *F. Li*[1], *J. Zhang*[2], *H. Jing*[1], *Y. Zhang*[1];
[1]*Peking Union Medical College Hospital, Beijing, CHINA,*
[2]*National University of Singapore, Singapore, SINGAPORE.*

Aim/Introduction: 123I-metaiodobenzylguanidine scintigraphy has demonstrated high specificity but low sensitivity for imaging pheochromocytoma and paraganglioma (PPGL) due to limited spatial resolution. 18F-meta-fluorobenzylguanidine ([^{18}F]MFBG) is a novel norepinephrine transporter (NET) -targeting PET tracer may address this limitation and enhance PPGL staging and restaging. ***Materials and Methods:*** We assessed the sensitivity, and specificity of 18F-MFBG PET in 17 patients with suspected PPGL using histopathology (n=10) and clinical validation (n=7) as reference standards. Additionally, we compared the detection rate of [^{18}F]MFBG PET/CT with [^{68}Ga]Ga-DOTATATE PET/CT on a per-patient and per-lesion basis in 31 patients with metastatic PPGL. Tumor uptake measured as tumor-to-background ratio (TBR) were compared between [^{18}F]MFBG PET/CT and [^{68}Ga]Ga-DOTATATE PET/CT. ***Results:*** [^{18}F]MFBG PET/CT was positive in 11 of 17 patients with suspected PPGL, with PPGL confirmed in 11 of 17. Sensitivity and specificity of 18F-MFBG PET/CT were 100% each. In 31 patients with metastatic PPGL, [^{18}F]MFBG PET was positive in 29 (93.5%). Two MFBG-negative patients exhibited multiple high-uptake foci on 68Ga-DOTATATE; both were on medications affecting NET during the exam. Combined [^{18}F]MFBG PET/CT and [^{68}Ga]Ga-DOTATATE PET/CT detected 691 lesions, with 676 (98%) and 658 (95%) visible on [^{18}F]MFBG PET/CT and [^{68}Ga]Ga-DOTATATE PET/CT, respectively. For matched lesions, [^{18}F]MFBG had a higher TBR for liver lesions (5.0 ± 1.8 vs. 3.8 ± 2.0; P=0.133). ***Conclusion:*** [^{18}F]MFBG PET/CT exhibits high accuracy for initial PPGL staging and high detection rate for restaging, indicating its potential as a first-line functional imaging modality in this clinical setting.

OP-672

^{225}Ac-DOTATATE Dosimetry Results from Part 1 of the ACTION-1 Trial

M. Morris[1], *G. Ulaner*[2], *T. Delie*[1], *S. Kotiah*[3], *D. Ferreira*[4], *K. Ma*[1], *J. Rearden*[4], *J. Li*[4], *S. Moran*[4], *E. Sneeden*[4], *B. He*[5], *M. Ghaly*[5], *E. Frey*[6], *A. Scott*[1], *C. Huffman*[1], *G. Sgouros*[6];
[1]*Advanced Molecular Imaging and Therapy, Glen Burnie, MD, UNITED STATES OF AMERICA,* [2]*Hoag Family Cancer Institute, Newport Beach, CA, UNITED STATES OF AMERICA,* [3]*Mercy Medical Center, Baltimore, MD, UNITED STATES OF AMERICA,* [4]*RayzeBio, San Diego, CA, UNITED STATES OF AMERICA,* [5]*5Radiopharmaceutical Imaging and Dosimetry, LLC (Rapid), Baltimore, MD, UNITED STATES OF AMERICA,* [6]*The Russell H. Morgan Department of Radiology and Radiological Science, School of Medicine, Johns Hopkins University, Baltimore, MD, UNITED STATES OF AMERICA.*

Aim/Introduction: RYZ101 (^{225}Ac-DOTATATE) is an alpha-emitting radiopharmaceutical being developed for somatostatin receptor 2-expressing (SSTR2+) solid tumors. ACTION-1 (NCT05477576) is a Phase 1b/3 trial comparing RYZ101 with standard-of-care therapy in SSTR2+, well-differentiated gastro-enteropancreatic neuroendocrine tumors (GEP-NETs) progressing following ^{177}Lu-labelled somatostatin analogue therapy. A dosimetry substudy was conducted during phase 1b to determine the feasibility of obtaining imaging data with ^{225}Ac to estimate RYZ101 absorbed doses to critical organs and tumors. ***Materials and Methods:*** Phase 1b primary objective: determine the recommended Phase 3 dose of RYZ101. Seventeen patients were assigned to the highest RYZ101 dose level (120kBq/kg) and observed for dose-limiting toxicities (DLTs) during cycle 1 (8w). Patients receive up to 4 cycles. Nine patients were enrolled in the dosimetry substudy. Dosimetry calculations are performed using SPECT/CT images acquired for Cycles 1 and 4 at 4±1h, 24±2h and 168±24h post-infusion. All SPECT/CT acquisitions utilizing ^{225}Ac are performed with a High Energy Collimator. Dual-radionuclide quantitative SPECT reconstruction was used to obtain ^{221}Fr and ^{213}Bi activity images, including compensation for crosstalk and other physical image-degrading effects. Activity in the liver, kidneys, spleen, red marrow and selected tumors is quantified. Absorbed doses to target organs and lesions are calculated using Medical Internal Radiation Dose (MIRD) Committee S-value methodology (Rapid software package, 3D-RD-S). ***Results:*** As of February 17, 2023, dosimetry results were available for 9 patients (Cycle 1) and 3 patients (Cycle 4). No DLTs were observed. Mean total activity administered in Cycle 1 was 8.9MBq (range 7.3-10.6MBq); mean total activity administered in Cycle 4 was 8.5MBq (range 5.4-11.0MBq). Mean weighted RBE (=5) absorbed dose coefficients for spleen, kidneys, liver, and red marrow in Cycle 1 were 0.88, 0.52, 0.45, and 0.029Gy/MBq and in Cycle 4 were 0.86, 0.42, 0.26, and 0.029Gy/MBq, respectively. Dose coefficients for selected tumors were in the range of 1.0-8.8Gy/MBq during Cycle 1 and 0.95-3.1Gy/MBq during Cycle 4. In general, there is comparable/higher tumor uptake of ^{221}Fr and ^{213}Bi in Cycles 1 and 4 compared with that observed in the kidneys and other organs. Imaging and dosimetry are ongoing. ***Conclusion:*** Imaging and obtaining quantitative information for dosimetry of ^{225}Ac are feasible, where ^{221}Fr and ^{213}Bi are imaged directly and simultaneously. This shows, for the first time, that ^{213}Bi stays mostly with the delivery agent (DOTATATE), with a minor fraction going to kidneys. Overall, initial data from ACTION-1 dosimetry suggest a favorable tumor-to-background profile for RYZ101 in SSTR+ GEP-NETs.

OP-673

Early results of^{212}Pb-VMT-α-NET Targeted Alpha Therapy in Metastatic Gastro-entero-pancreatic Neuroendocrine Tumors: First in Human Clinical Experience on Safety and Efficacy

D. Malik[1], *I. Sen*[1], *P. Thakral*[1], *S. Das*[1], *M. Schultz*[2];
[1]*Fortis Memorial research institute (FMRI), Gurugram, INDIA,* [2]*University of Iowa, Iowa, IA, UNITED STATES OF AMERICA.*

Aim/Introduction: There has been an increasing interest in targeted alpha therapy using ^{212}Pb. ^{212}Pb-VMT-α-NET, a proprietary molecule from Perspective has shown significantly improved performance in preclinical studies. ^{212}Pb-VMT-α-NET therapy was effective and well-tolerated in mice, achieving 100% complete response rate in tumor bearing mice. The objective of this study was to investigate the early results on the safety and efficacy of ^{212}Pb-VMT-alpha NET therapy (TAT) in patients with advanced, progressive, 177Lu-DOTATATE refractory, somatostatin receptor (SSTR) positive, metastatic gastro-entero-pancreatic neuroendocrine tumors (GEP-NETs). ***Materials and Methods:*** This exploratory first in human study was approved by the Institute Ethics Committee (IEC No:2023-002-EMP-40). We recruited 10-patients with well differentiated neuroendocrine tumours. Patients underwent a screening ^{68}Ga-DOTANOC PET/CT scan to assure high SSTR expression and progressive disease to prior therapies. ^{212}Pb-VMT-α-NET was administered (25MBq/Kg body weight) at an interval of 8 weeks up to 3 cycles. Hematologic, kidney, and liver function tests were repeated after every cycle of ^{212}Pb-VMT-α NET therapy at 2, 4 and 8-week intervals. Treatment-related side-effects were assessed every 2 weeks on the basis of physical examination, vital signs, laboratory results and adverse events graded according to the CTCAE v5.0. Efficacy assessment included assessment of clinical response, assessment of objective radiological response measured on the diagnostic contrast-enhanced CT and the receptor expression seen on ^{68}Ga-DOTANOC PET/CT scans. RECIST 1.1 criteria for changes in size and the changes in uptake of ^{68}Ga- DOTANOC were used to track response. ***Results:*** The most common adverse effects (AEs) were nausea, alopecia, fatigue and appetite loss. These adverse effects excluding alopecia usually resolved about 7 - 10 days post infusion. None of the patients experienced grade 3 or 4 hemato-toxicity, renal insufficiencies or hepatotoxicity. Morphological response assessment was assessed in all patients which revealed partial response in 9 and stable disease in 1 patient. All patients demonstrated good clinical response with an improvement in their quality of life. There was no treatment related death. ***Conclusion:*** Our initial results indicate ^{212}Pb-VMT-α-NET therapy as safe with low and transient side-effects. While all patients showed a good clinical response, most showed an objective radiological response to therapy even after a single dose of ^{212}Pb-VMT-Alpha NET therapy. None of the patients demonstrated a clinically significant grade 3 adverse event. This study is an ongoing trial and we have presented only the preliminary results. Long-term survival data will be derived after a longer duration of follow-up.

OP-674

The increase of LutaThera Therapy posology due to dosimetry could be give a better progression free survival (PFS) in GEPNets patients?

M. Cuomo[1,2], *G. Argiroffi*[2], *A. Lorenzoni*[2], *G. Aliberti*[2], *M. Bagnalasta*[2], *F. Scalorbi*[2], *M. Kirienko*[2], *C. Chiesa*[2], *E. Seregni*[2], *M. Maccauro*[2];
[1]*University of the study of Milan, Milan, ITALY,* [2]*Istituto Nazionale Tumori Milano, Milan, ITALY.*

Aim/Introduction: The NETTER-1 study demonstrated noticeably increased PFS in GEP-NET treated with 177Lu-DOTATATE respect to cold somatostatine analogs. Aim of our work was to check if

the registered LUTATHERA posology could be increased thanks to dosimetry. ***Materials and Methods:*** Toxicity, radiological responses, dosimetric evaluations and follow-up were collected respectively on 95, 58, 52, 61 patients who completed the 4 injections schedule. Renal toxicity was assessed through creatinine level and eGFR. RECIST responses were measured 3 months after the last administration. Dosimetry was performed after the first and last treatment, with two SPECT/CT scans 1 and 7 days after administration. Red marrow absorbed dose was evaluated encompassing the vertebral body in L2-L3-L4, correcting for the individual volume. The concept of global tumor dose (GTD) was the sum of lesion doses weighted by lesion mass. Cumulative-GTD (CGTD) was calculated as the mean between cycle 1 and 4 multiplied by 4. Patients were followed-up for at least one year, up to a maximum of three, through blood tests and ceCT. ***Results:*** Creatinine toxicity G1 was observed in 19/95 patients, while eGFR G1 in 42/80, and G2 in 18/80. Throbocytopenia G1 occured in 45/95 patients, and 1 G2, 2 G3, 2 G4 occurrences were observed. Anemia was reported as G1: 52/95; G2: 8/95; G3: 1/95. Leucopenia was observed with G1 in 11/95 and G2 in 18/95. No haematological stochastic effect was observed. . Dosimetry agreed with this mild toxicity scenario, with red marrow dose distribution after the first administration spanning from 0.01 to 0.62 Gy, median 0.1 Gy, 25th and 75th percentile at 0.0625 and 0.15 Gy. Cumulative kidney Biologically Effective Dose (BED) ranged from 5 to 32 Gy, median 16 Gy, with 75th percentile at 20 Gy. CGTD ranged from 23 to 650 Gy, median 74 Gy and 75th percentile at 160 Gy,which is the threshold for RECIST response according to Ilan et al 2005. So 75% of our patient got a tumour dose below the efficacy threshold, in perfect agreement with the observed responses. During the follow-up no complete response obtained, only 7/61 partial responses, 44/61 stabilization and 10/61 progression disease were observed. The median PFS of patients was 27.4months. ***Conclusion:*** Clinical outcome and dosimetry demonstrate that 75% of patients got a tumor dose below the efficacy threshold. Probably, increasing number of treatments would increase the rate of PFS, stable disease or tumor regression.

OP-675

Personalized, dosimetry-based PRRT therapy in patients with neuroendocrine tumors using [177Lu]Lu-DOTA-TATE or [177Lu]Lu/[90Y]Y-DOTA-TATE mixture - the initial results of DUONEN multicenter study

M. Opalinska[1], *G. Kaminski*[2], *M. Dedecjus*[3], *A. Kowalska*[4], *M. Kolodziej*[2], *M. Saracyn*[2], *D. Gasior-Perczak*[4], *W. Lenda-Tracz*[5], *A. Sowa-Staszczak*[1], *A. Borkowska*[6], *A. Budzynska*[7], *A. Kubik*[7], *W. Chalewska*[3], *K. Kacperski*[7], *P. Szubstarska*[7], *P. Garnuszek*[8], *R. Mikolajczak*[8], *A. Hubalewska-Dydejczyk*[1];
[1]*Chair and Department of Endocrinology, Jagiellonian University Medical College, Krakow, POLAND,* [2]*Department of Endocrinology and Isotope Therapy, Military Institute of Medicine - National Research Institute, Warsaw, POLAND,* [3]*Department of Endocrine Oncology and Nuclear Medicine, National Institute of Oncology, Warsaw, POLAND,* [4]*Collegium Medicum, Jan Kochanowski University in Kielce, Kielce, POLAND,* [5]*Department of Endocrinology, Oncological Endocrinology and Nuclear Medicine, University Hospital, Krakow, POLAND,* [6]*Faculty of Health Sciences, Jagiellonian University Medical College, Krakow, POLAND,* [7]*Department of Nuclear Medicine, Military Institute of Medicine - National Research Institute, Warsaw, POLAND,* [8]*Radioisotope Center POLATOM, National Centre for Nuclear Research, Otwock, POLAND.*

Aim/Introduction: Peptide Receptor Radionuclide Therapy (PRRT) is an effective treatment for disseminated neuroendocrine tumors (NETs) with good somatostatin receptors expression. Despite many published studies, the consensus on the optimal PRRT treatment algorithm has not been reached yet.The main objective of the DUONEN multicenter, randomized, phase III study (EUDRACT No: 2020-006068-99) is a development of a dosimetry-based personalized PRRT algorithm. The second goal include the assessment of the efficacy of dosimetry-based personalized therapy with mixture of [177Lu]Lu- and [90Y]Y-DOTA-TATE in comparison with use of [177Lu]Lu-DOTA-TATE in standard doses (7400MBq). The personalized dosimetry is design to deliver the maximal activity to the tumor tissue maintaining the safety of critical organs. ***Materials and Methods:*** Adult patients with advanced, unresectable well-differentiated (G1 and G2) NETs, progressing on long-acting somatostatin analogues are randomized into four arms: A -treated with [177Lu]Lu -DOTA-TATE with constant radioactivity of 7400MBq per cycle B -treated with mixture of [177Lu]Lu-DOTA-TATE and [90Y]Y-DOTA-TATE, initially at a ratio of 3700:1850MBq/MBq. The [177Lu]Lu-DOTATATE activity will be constant in all cycles, the [90Y]Y-DOTA-TATE activity will be adjusted in the second, the third and the fourth cycle, based on bone marrow and kidney dosimetry to obtain the highest radiation dose in tumor tissue.C -analogous to arm B, except that here the activity of [90Y]Y-DOTA-TATE will be constant and the activity of [177Lu]Lu-DOTA-TATE will depend on the results of dosimetry D -initially analogous to arm A and then with an individualized doses based on dosimetry results. The treatment efficacy is evaluated on morphological imaging (TK or MR) according to RECIST 1.1 criteria. The safety of PRRT is assessed by the kidney and bone marrow biochemical function. ***Results:*** 20 patients have been enrolled to the study (arm A-5, arm B-6, arm C-4, arm D-5). 39 cycles of PRTT were given, including 23 fixed doses (firsts doses or arm A). In case of 16 cycles provided for adjustment, the dose of radiopharmaceutical estimated on the basis of personalized dosimetry was increased in 11 and decreased in 5 cases. Four patients were withdrawn due to disease progression or its side effects. Two patients underwent the first post-PRRT evaluation assessed according to RECIST 1.1 criteria achieving 1 partial (arm A) and 1 complete (arm B) response. ***Conclusion:*** Personalized dosimetry allows for the PRRT dose adjustments (more frequently increase) in subsequent treatment cycles maintaining the safety of therapy.Acknowledgements: The study is funded by the Medical Research Agency (Project number 2019/ABM/01/00077-00).

OP-676

Quantitative somatostatin receptor image assessment for survival prediction: a full-body, longitudinal, individual lesion analysis of neuroendocrine tumors in patients treated with peptide receptor radiation therapy

V. Santoro-Fernandes[1], *B. Schott*[1], *A. Deatsch*[1], *Q. Keigley*[2], *T. Francken*[1], *R. Meeker*[1], *R. Lyer*[3], *F. Christos*[3], *S. Perlman*[2,4], *R. Jeraj*[1,4];
[1]*Department of Medical Physics, School of Medicine and Public Health, University of Wisconsin, Madison, WI, UNITED STATES OF AMERICA,* [2]*Section of Nuclear Medicine and Molecular Imaging, Department of Radiology, School of Medicine and Public Health, University of Wisconsin, Madison, WI, UNITED STATES OF AMERICA,* [3]*Division of GI Medicine, Department of Medicine, Roswell Park Comprehensive Cancer Center, Buffalo, NY, UNITED STATES OF AMERICA,* [4]*Carbone Cancer Centre, University of Wisconsin, Madison, WI, UNITED STATES OF AMERICA.*

Aim/Introduction: Baseline somatostatin-receptor image features (SRIF) are correlated with peptide receptor radionuclide therapy (PRRT) outcomes in metastatic neuroendocrine tumor (mNET) patients[1]. The predictive power of longitudinal SRIF derived from every individual lesion is unexplored. Here, we conducted such an investigation and evaluated how much longitudinal assessment improves the predictive power of SRIF to predict progression-free-survival (PFS) of mNET patients receiving PRRT. ***Materials and Methods:*** We retrospectively collected ^{68}Ga-DOTATATE PET/CT scans of mNET patients imaged before (baseline) and after ^{177}Lu-DOTATATE PRRT. PFS was determined based on chart review (median follow-up of 54 months) and used to stratify patients into poor and good responders. All lesions were contoured, and the quantitative features were extracted for every lesion. Lesions were matched between imaging time-points and feature variation was calculated. The lesion-level features were aggregated into patient-level features and separated into baseline and longitudinal sets. Using leave-one-out cross-validation, optimal features in each set were selected by maximum relevance and minimum redundancy. For each set, a multivariate linear regression (MLR) model was fitted for PFS regression and three machine-learning methods (LightGBM, XGBoost, and Random-Forest) were compared to it. Prediction performance was evaluated using RMSE, ROC, Kaplan-Meier, and Proportional-Hazards analyses. ***Results:*** Longitudinal images from 34 mNET patients were acquired. The median PFS was 20 months (min=4, max=54). Eighteen patients were classified as poor responders (PFS<31 months). Altogether, 2521 lesions were identified with median of 38.5 per patient (min=5, max=381). The MLR model using longitudinal SRIFs yielded a better fit than single time-point baseline SRIFs (RMSE=13.5 vs. 14.1). Classification accuracy was also better (AUROC=0.81 vs 0.74). Patient stratification was significant for longitudinal SRIFs and not-significant for baseline SRIFs (p=0.003 vs. 0.06, log-rank test). The hazard ratios showed superiority of longitudinal SRIFs: 0.92 (95% C.I. [0.88, 0.96]; P<0.001) vs. 0.96 (95% C.I. [0.92, 1.00]; P=0.04). Furthermore, the MLR model resulted in better PFS prediction than all machine-learning models. The best-performing machine-learning model (Random-Forest with longitudinal SIRFs) had RMSE of 14.1 vs. 13.5 for longitudinal MLR, and AUROC of 0.71 vs. 0.81 for longitudinal MLR. ***Conclusion:*** This work is the first to investigate the utility of full-body, longitudinal, lesion-wise SRI for clinical outcome prediction. Our results suggest that longitudinal SRIF adds value to PFS prediction when compared to baseline SRIF in mNET patients receiving PRRT. Interestingly, MLR outperformed machine learning models, possibly due to the limited training sample. ***References:*** 1. Haug AR et al. J Nucl Med. 2010;51(9):1349-1356.

1401

Tuesday, September 12, 2023, 11:30 - 13:00

Hall A

Plenary 4: Diagnostic Imaging: Proven Beyond Doubt?

OP-677

AI technology: FDG PET imaging and lymphomas: a proven certainty

J. Zijlstra;
Amsterdam UMC, Amsterdam, NETHERLANDS.

OP-678

PET imaging in every oncological guideline: what is still missing?

S. Carrilho Vaz;
Champalimaud Foundation, Lisbon, PORTUGAL.

OP-679

Impact without a cure: prospective evidence for diagnostic neuroimaging

A. Drzezga;
UniversityHospital of Cologne, Cologne, GERMANY.

OP-680

Cardiac imaging: prospective studies and the EURECA registry

D. Neglia;
Fondazione CNR/Regione Toscana G. Monasterio, Pisa, ITALY.

OP-681

Cost effectiveness molecular imaging studies

M. Gauthé;
SCINTEP, Grenoble, FRANCE.

OP-682

Real world data: an answer to all questions?

J. Kleesiek;
Institute for AI in Medicine (IKIM), Essen, GERMANY.

1501

Tuesday, September 12, 2023, 15:00 - 16:30

Hall A

CME 11 - Paediatrics Committee: Pediatric Lymphoma and Update on FDG

OP-685

Clinical background on pediatric lymphoma and what do clinicians expect from nuclear medicine

A. Attarbaschi;
St Anna's Kinderspital, Department of Hematology, Vienna, AUSTRIA.

OP-686

Role of Molecular Imaging (FDG PET-CT) in the evaluation pediatric lymphoma patients

P. Ozgen Kiratli;
Hacettepe University Hospital Department of Nuclear Medicine, Ankara, TÜRKIYE.

OP-687

Response to therapy assessment via FDG PET-CT

L. Kurch;
Universityof Leipzig Hospital, Department of Nuclear Medicine, Leipzig, GERMANY.

1502

Tuesday, September 12, 2023, 15:00 - 16:30
Hall D (Arena)

Challenge the Expert 4 - Neuroimaging Committee: Amyloid vs. Tau PET: Which is First in suspected Alzheimer Patients? Germany versus Italy

OP-688
Tau PET first in the AD flow-chart - Germany
H. Barthel;
Department of Nuclear Medicine, University of Leipzig, Leipzig, GERMANY.

OP-689
Challengers case - Germany
K. Messerschmidt;
Department of Nuclear Medicine, Leipzig University Hospital Centre, Leipzig, GERMANY.

OP-690
Challengers case - Germany
J. Gnörich;
Department of Nuclear Medicine, Ludwig Maximillian University Munich, Munich, GERMANY.

OP-691a
Amyloid PET first in the AD flow-chart - Italy
S. Morbelli;
Department of Nuclear Medicine, University of Genoa, Genoa, ITALY.

OP-691b
Challengers case - Italy
G. Polverari;
PET/CT Center, AFFIDEA-IRMET S.P.A., Turin, ITALY.

OP-691c
Challengers case - Italy
A. Martini;
NuclearMedicine Unit, Department of Diagnostic Imaging, N.O.P. - S. Stefano, U.S.L. Toscana Centro, Prato, ITALY.

1503

Tuesday, September 12, 2023, 15:00 - 16:30
Hall E1

LIPS Session 11 - Bone & Joint Committee: Pitfalls and Common Bony Findings in PET-CT/MRI using Novel Tracers

OP-692
PSMA PET/CT - atypical bony patterns using different radioligands - tips on assessment of bone metastases
A. Maurer;
UniversityHospital Zurich, Nuclear Medicine, Zurich, SWITZERLAND.

OP-693
FAPI PET/CT - what should be considered in interpretation of bony lesion?
K. Pabst;
UniversityHospital Essen, Nuclear Medicine, Essen, GERMANY.

OP-694
PET/MRI - Pitfalls and normal variations in assessment of bone metastases
S. Wan;
Institute of Nuclear Medicine, University College London, London, UNITED KINGDOM.

1504

Tuesday, September 12, 2023, 3:00 PM - 4:30 PM
Hall E2

M2M Track - TROP Session: Imaging the Components of the TME

OP-697
STING-targeted PET Tracer for Early Assessment of CRC Tumor Immunogenicity after Chemotherapy
D. Xu[1,2,3], *X. Lu*[1,3], *F. Yang*[2,3], *D. Li*[3,2];
[1]*Center for Interventional Medicine, the Fifth Affiliated Hospital, Sun Yat-sen University, Zhuhai, CHINA,* [2]*Department of Nuclear Medicine, the Fifth Affiliated Hospital, Sun Yat-sen University, Zhuhai, CHINA,* [3]*Guangdong Provincial Engineering Research Center of Molecular Imaging, the Fifth Affiliated Hospital, Sun Yat-sen University, Zhuhai, CHINA.*

Aim/Introduction: The objective clinical efficiency of immunotherapy for colorectal cancer (CRC) is less than 20%. The combination of chemotherapy and immunotherapy can effectively improve the therapeutic effect, mainly because chemotherapy can promote tumor elimination by activating interferon gene stimulating protein (STING) in immune cells at an early stage and converting CRC to an immunogenic state. However, there is a lack of reliable methods to monitor early tumor immunogenicity changes under the influence of chemotherapy. To standardize the rational use of immune checkpoint inhibitors and to screen the optimal strategy for combination immunotherapy, we used the STING targeted probe to monitor the changes in tumor immunogenicity during chemotherapy in CRC mice. ***Materials and Methods:*** The toluene sulfonate precursor was labeled with ^{18}F and then reacted with TFA to produce the STING targeted probe—[^{18}F]FBTA. [^{18}F]FBTA-PET imaging and biodistribution experiments were performed in CRC mice after oxaliplatin (OXA) and cisplatin (CDDP) treatment. CRC mice were also treated with low (CDDP-LD: 1 mg/kg) and medium (CDDP-MD: 2.5 mg/kg) doses of CDDP, PET imaging and biodistribution experiments were performed on the treated mice. The effects of different chemotherapeutic agents (OXA and CDDP) and different doses of CDDP on tumor innate immunity were verified by immunohistochemistry and flow cytometric sorting. ***Results:*** PET imaging of CRC mice showed significantly higher uptake in tumors treated with OXA (3.09 ± 0.25 %ID/g, ***P < 0.001) and CDDP (4.01 ± 0.18 %ID/g, ***P < 0.001), especially in CDDP treated tumors (**P < 0.01). Immunohistochemistry confirmed high levels of STING expression in tumors with high uptake in PET imaging. Flow cytometry results showed that both chemotherapeutic agents led to DC and macrophage infiltration in the tumor and were responsible for the increased level of STING expression. Both CDDP-LD and

CDDP-MD treatment elevated uptake in CRC tumors (***P < 0.001 and ***P < 0.001), especially in CDDP-MD-treated tumors (***P < 0.001). Histocytological experiments also confirmed significantly elevated levels of STING expression in DCs and macrophages after CDDP-LD and CDDP-MD treatment. ***Conclusion:*** In this study, the STING-targeted probe—[^{18}F]FBTA was demonstrated to monitor early changes in tumor immunogenicity in CRC mice after OXA or CDDP treatment. And there were differences in tracer uptake in CRC tumors treated with different doses of cisplatin. These studies provide key insights into innate immune activation after chemotherapy and suggest that [^{18}F]FBTA will be useful in the screening of chemotherapeutic agents and doses in combination with immunotherapy.

OP-698

Targeting PD-1 on Chronically Activated T cells with Radioimmunotherapy as a Novel Therapeutic Strategy for Multiple Sclerosis.

C. Frank[1], *H. E. Salapa*[2,3,4], *K. J. H. Allen*[1], *M. C. Levin*[2,3,4], *W. Dawicki*[5], *E. Dadachova*[1];
[1]*College of Pharmacy and Nutrition, University of Saskatchewan, Saskatoon, SK, CANADA,* [2]*Office of Saskatchewan Multiple Sclerosis Clinical Research Chair, CMSNRC (Cameco MS Neuroscience Research Center), College of Medicine, University of Saskatchewan, Saskatoon, SK, CANADA,* [3]*Department of Medicine, Neurology Division, University of Saskatchewan, Saskatoon, SK, CANADA,* [4]*Department of Anatomy, Physiology and Pharmacology, College of Medicine, University of Saskatchewan, Saskatoon, SK, CANADA,* [5]*Department of Biochemistry, Microbiology and Immunology, College of Medicine, University of Saskatchewan, Saskatoon, SK, CANADA.*

Aim/Introduction: Multiple sclerosis is a chronic neurodegenerative autoimmune disease partially characterized by inappropriate immune activation towards myelin proteins[1]. T lymphocytes drive early stages of multiple sclerosis immunopathology. Pathogenic T lymphocytes chronically stimulated by self-antigens develop characteristic "fatigued" receptors such as the programmed cell death protein 1 (PD-1)[1]. Specifically depleting chronically stimulated T lymphocytes by targeting PD-1 may reduce the ability of the immune system to promote the destruction of neurons. Here we report the effectiveness and tolerability of an anti-PD-1 radiolabeled monoclonal antibody in treating mice induced with experimental autoimmune encephalomyelitis (EAE). ***Materials and Methods:*** Female C57Bl/6 mice were induced with EAE and at days 0, 3, 6, 9 and 12 post paralysis development. Animals were euthanized, and spinal cords were stained for CD45, CD3, CD11b, Ly6C and PD-1 to investigate PD-1 expression on infiltrating immune cells. Female C57BL/6 mice were induced with EAE and treated at symptom onset intravenously with 2.22 MBq of [^{177}Lu]Lu-DOTA-RMP1-14 (Anti-PD-1), 2.22 MBq of [^{177}Lu]Lu-DOTA-Irrelevant Isotype control antibody, "cold" RMP1-14, 2.22 MBq of [^{177}Lu]Lu-DOTA-RMP1-14 in combination with 3 mg/kg of fingolimod (FTY720) or saline. Safety and tolerability of the [^{177}Lu]Lu-DOTA-RMP1-14 antibody was assessed using total blood counts and blood chemistry to assess liver and kidney toxicity. PET/CT imaging of EAE mice was performed using 3.7 MBq of [^{89}Zr]Zr-DFO-RMP1-14 at 0, 24, 48 and 96 hours. Biodistribution of EAE induced mice with 1.85 MBq of [^{203}Pb]Pb-DOTA-RMP1-14 on lymph nodes, brain, spinal cord, spleen and kidneys was performed. ***Results:*** PD-1 was expressed and sustained on spinal cord infiltrating T lymphocytes at symptom onset and guided [^{177}Lu]Lu-DOTA-RMP1-14 treatment at symptom onset. Administration of [^{177}Lu]Lu-DOTA-RMP1-14 significantly reduced the overall disease burden and clinical score in EAE induced animals compared to controls, demonstrated a favorable toxicity profile with no effect on liver and kidney function as well as on bone marrow. PET/CT imaging and biodistribution demonstrates uptake in the lymph nodes and spinal cords of active disease animals. ***Conclusion:*** Here we demonstrate a novel approach using radioimmunotherapy to specifically target and deplete pathogenic lymphocytes in an autoimmune disease animal model. This approach has the potential to be applied to other autoimmune disease to target and deliver cytocidal radiation to pathogenic immune cells. ***References:*** 1) Li, H., Zheng, C., Han, J., Zhu, J., Liu, S., & Jin, T. (2021). PD-1/PD-L1 Axis as a Potential Therapeutic Target for Multiple Sclerosis: A T Cell Perspective. Frontiers in cellular neuroscience, 15, 716747. doi: 10.3389/fncel.2021.716747

OP-699

The synthesis of a novel molecular imaging probe^{68}Ga-DOTA-PDL1P and applicationin malignant melanoma

Z. Yang;
Fudan University Shanghai Cancer Center, Shanghai, CHINA.

Aim/Introduction: Based on programmed cell death-ligand 1 targeted peptide (PD-L1P), to synthesize a programmed cell death-ligand 1 (PD-L1) agent on positron emission tomography (PET/CT) imaging and explore the clinical application. ***Materials and Methods:*** DOTA-PDL1P was labeled with gallium 68 (68Ga), and its radiochemical purity and stability were evaluated. Mouse B16-F10 cells were used for cell uptake and blocking in vitro to evaluate its specific targeting performance. Biological distribution and PET/CT tumor imaging were performed in B16-F10 tumor-bearing mice, and the uptake of 68Ga-DOTA-PDL1P in tumors was further evaluated by autoradiography of tumor samples. Finally, the expression of PDL1 in tumor tissues was evaluated by immunohistochemistry. ***Results:*** The labeling rate and radiochemical purity of 68Ga-DOTA-PDL1P were higher than 99% and maintained good stability. Cell uptake results showed that 68Ga-DOTA-PDL1P could be specifically taken up by B16-F10 cells, and this specific uptake could be blocked by PD-L1 antibody. The results of biological distribution indicated that 68Ga-DOTA-PDL1P was excreted mainly through the urinary system. PET imaging results of tumor in tumor bearing mice showed high uptake of 68Ga-DOTA-PDL1P in tumor tissues. The autoradiographic and immunohistochemical results of tumor tissue confirmed that the high uptake sites of 68Ga-DOTA-PDL1P were consistent with the positive areas of PD-L1 expression, which proved that 68Ga-DOTA-PDL1P could specifically screen malignant tumors with positive PD-L1 expression. ***Conclusion:*** The new PET imaging agent ^{68}Ga-DOTA-PDL1P synthesized in this study has good stability and high tumor targeting specificity, which is a promising new immune PET imaging agent targeting PD-L1 protein.

OP-700

A Novel PET Tracer ^{68}Ga-NOTA-XH05 Targeting LAG-3 for Evaluating the Efficacy of Immunotherapy in Tumors

P. Yuan[1,2], *Y. Long*[1,2], *N. Wei*[1,2], *Y. Gai*[1,2], *Y. Zhang*[1,2], *R. An*[1,2], *X. Lan*[1,2];
[1]*Department of Nuclear Medicine, Union Hospital, Tongji Medical College, Huazhong University of Science and Technology, Wuhan, CHINA,* [2]*Hubei Key Laboratory of Molecular Imaging, Wuhan, CHINA.*

Aim/Introduction: Lymphocyte activation gene 3 (LAG-3), which is a novel target for immune checkpoints blocking, is upregulated on activated T cells. Several clinical reports suggested that patients had a better prognosis when LAG-3 expression is observed on

tumor infiltrating lymphocytes, in which LAG-3 can be considered as a biomarker of T cell activation. In this study, a novel peptide PET tracer ^{68}Ga-NOTA-XH05 targeting LAG-3 was constructed to noninvasively detect LAG-3 expression in tumors after CpG-ODN treatment, in order to evaluate the efficacy of immunotherapy. ***Materials and Methods:*** The tracer ^{68}Ga-NOTA-XH05 was identified by high performance liquid chromatography (HPLC) after prepared and purified. The expression of LAG-3 in the B16-F10 subcutaneous tumors was monitored by flow cytometry, and its correlation with the uptake of the tracer was analyzed to evaluate the specificity of the tracer. PET imaging and biodistribution were conducted after TLR9 agonist, CpG-ODN, used for the treatment of unilateral or bilateral B16-F10 subcutaneous tumor models, to evaluate the ability of ^{68}Ga-NOTA-XH05 monitoring the efficacy of immunotherapy and the abscopal effect of CpG-ODN. ***Results:*** After purification, the radiochemical purity of ^{68}Ga-NOTA-XH05 was over 99%. The mean fluorescence intensity of LAG-3 in tumor cells was detected by flow cytometry and it was positively correlated with the uptake of ^{68}Ga-NOTA-XH05 (R^2=0.5213, P=0.0184), which suggested that the uptake of ^{68}Ga-NOTA-XH05 could reflect the expression level of LAG-3 in tumor. ^{68}Ga-NOTA-XH05 PET imaging of the mice with B16-F10 subcutaneous tumors was performed after intratumoral injection of CpG-ODN. The tumor blood ratio (TBR) was 2.234±0.386, which was significantly higher than that of the control (TBR=1.348±0.301, P=0.0001). The result of biodistribution was similar to the imaging result, indicating that ^{68}Ga-NOTA-XH05 could distinguish therapeutic efficacy. In bilateral subcutaneous tumors model, only the right tumors were treated with intratumoral injection of CpG-ODN. On day 2 after first treatment, ^{68}Ga-NOTA-XH05 PET imaging showed increased TBR of the right tumors, but no significant difference displayed between the left tumors and the control. On day 8, uptake of the left tumors was also significantly higher than that of the control, and even higher than that of the right tumors, indicating that ^{68}Ga-NOTA-XH05 can effectively monitor the abscopal effect of CpG-ODN. ***Conclusion:*** ^{68}Ga-NOTA-XH05 had a good correlation with the expression of LAG-3 in vivo. ^{68}Ga-NOTA-XH05 could be used to evaluate the immunotherapy response and monitor the abscopal effect of the therapy, which suggests potential clinical translational prospects.

OP-701

Preclinical evaluation of a small-molecule carbonic anhydrase IX targeting PET tracer in clear cell renal cell carcinoma

W. Zhu, *X. Li, Y. Zhang, L. Huo;*
Peking Union Medical College Hospital, Beijing, CHINA.

Aim/Introduction: Carbonic anhydrase IX (CAIX) is an isoform of carbonic anhydrases (CAs), which are a family of zinc metalloenzymes that catalyze the reversible hydration of carbon dioxide to bicarbonate and a proton. While CAIX is highly expressed in clear cell renal cell carcinoma (ccRCC), its expression in normal human tissue is limited, making it an ideal target for molecular imaging and precision drug delivery. The purpose of this study was to evaluate 68Ga-NY104, a small molecule CAIX-targeting PET agent, in ccRCC tumor models. ***Materials and Methods:*** 68Ga-NY104 was manually synthesized. The binding affinity (Kd) of ^{68}Ga-NY104 was measured using surface plasmon resonance. The blood pharmacokinetics were measured in ICR mice. The in vivo and ex vivo biodistribution and blocking study of ^{68}Ga-NY104 were investigated in CAIX-positive OS-RC-2 xenograft-bearing models. CAIX expression was further confirmed using immunohistochemistry. The binding of the tracer was further validated using autoradiography for human ccRCC samples. ***Results:*** NY104 can be labeled with high radiochemical yield (about 65% for a 30-min radiolabeling process) and purity (>95%). The tracer was stable for at least 3 hours. The binding affinity (Kd) of NY104 to CAIX is 5.75nM. ^{68}Ga-NY104 quickly cleared through kidney with a biexponential blood clearance: α-half-life, 0.15 h and β-half-life, 6.04 h. Approximately 75% of the administered activity was cleared in the α phase.High tumor accumulation of ^{68}Ga-NY104 was noted in OS-RC-2 tumors as early as 5 min after injection, which gradually increased until 3 h after injection with ID%/g of 29.29 ± 6.82. Besides, nonnegligible uptake was observed in the heart, lung, liver, stomach, and kidney. After blocking with unlabeled NY104, the tumor showed negligible uptake, confirming the specific binding of ^{68}Ga-NY104. In PC-3 models, barely any uptake of ^{68}Ga-NY104 was noted in the tumor. High CAIX expression was observed in OS-RC-2 xenograft tumors. Meanwhile, the PC-3 xenograft tumors were negative for CAIX immunohistochemical staining. Significant binding was detected using autoradiography on sections of human ccRCC tumor, while no significant binding was noted in the pancreatic cancer sample. ***Conclusion:*** ^{68}Ga-NY104 can efficiently and specifically bind to CAIX and may serve as a biomarker for ccRCC characterization.

OP-702

A Radiohapten Capture System for In Vivo CAR T Cell Tracking in Ovarian Cancer

L. Gajecki, *L. Eibler, K. Kurtz, S. Lovibond, D. Veach, S. Larson, D. Scheinberg, S. Krebs;*
Memorial Sloan Kettering, New York, NY, UNITED STATES OF AMERICA.

Aim/Introduction: CAR-T cell trials have shown remarkable response rates in hematologic malignancies, however, success has been limited in solid tumors. There remains an unmet need to understand why CAR T cell therapy fails, which would be aided through the creation of tools to track the engineered cells' biodistribution, persistence, expansion and functionality in vivo. Here we show that a humanized single-chain variable fragment (scFv) huC825, which specifically binds M-DOTA-haptens (ABD, "Proteus" (Pr)), can be expressed on CAR-T cells directed against the retained portion of MUC16 (MUC16^{ecto}) on human ovarian cancer cells. We demonstrate proof-of-principle for huC825 reporter gene function and MUC16 CAR-T tracking in vivo. ***Materials and Methods:*** Transduction of a SFG retroviral vector encoding the huC825 scFv and a second generation MUC16^{ecto}-directed CAR (4H1128ζ) into CD3-activated human T cells was confirmed by flow cytometry. In vitro function of the CAR was assessed by bioluminescence cytotoxicity assays on MUC16^{ecto}+ human ovarian cancer cells (SKOV3-MUC16^{ecto}) expressing firefly luciferase and in vivo functionality was assessed in xenograft mouse models. Flow cytometry using a biotinylated DOTA-probe (Biotin-Pr) in combination with streptavidin–fluorophore anti-biotin verified expression and in vitro functionality of huC825 in huC825-CAR-T cells. The feasibility of in vivo tracking of intravenously administered huC825-CAR-T cells was studied in immuno-deficient mice bearing subcutaneous SKOV3-MUC16^{ecto} xenografts with [^{86}Y] Y-ABD PET/CT performed at 16 h post-radiotracer injection. Image-based biodistribution was assessed for tumor ([%ID/g]max) and normal tissue ([%ID/g]mean) to determine tumor-to-normal tissue ratios. ***Results:*** We generated a panel of T cells expressing huC825 and/or CAR (huC825-CAR, CAR). We confirmed cell surface expression of the CAR and huC825 by flow cytometry. The

cytotoxic effector function of huC825 CAR-T was preserved with respect to control CAR-T cells. Using microPET/CT, tumoral uptake of the reporter probe [^{86}Y]Y-ABD (3.7 MBq) in mice given 5.0 x10^5 huC825-CAR-Ts was observed at day 14 post T cell administration indicating their accumulation (9.8 ± 6.5 [%ID/g]max, n=4). Excellent image contrast with tumor-to-kidney, tumor-to-blood and tumor-to-muscle ratios of 19.2, 127.6 and 205.2 were noted. In contrast, minimal tumoral uptake was observed in control mice (0.2 ± 0.03 [%ID/g]max, n = 4). ***Conclusion:*** CAR-T cell imaging in a solid tumor model was demonstrated in vitro and in vivo through selective DOTA-hapten capture by MUC16 CAR-T cells equipped with huC825 reporter scFv. These cells were tracked in vivo using PET/CT and CAR-T infiltration in SKOV3-MUC16^{ecto} cells was visualized with high contrast. Serial tracking studies are ongoing.

OP-703

Discovery and development of high-affinity macrocyclic peptide for PET imaging of human Granzyme-B

T. Nayak[1], *J. Schubert*[1], *Z. Zhou*[1], *I. Bennacef*[1], *X. Meng*[1], *M. Stenslik*[1], *K. Getty*[1], *J. Patteson*[1], *H. Zokian*[2], *J. Lee*[2], *E. DiNunzio*[2], *H. Wan*[2], *F. Orvieto*[3], *V. Piacenti*[3], *A. Saldanha*[2], *A. Walji*[1], *E. Hostetler*[1];
[1]*MSD, West Point, PA, UNITED STATES OF AMERICA,*
[2]*MSD, Kenilworth, NJ, UNITED STATES OF AMERICA,*
[3]*IRBM S.p.A, Rome, ITALY.*

Aim/Introduction: Granzyme B (GzmB) is a serine protease secreted by cytotoxic T lymphocytes. GzmB-induced cell death has been traditionally viewed as a primary mechanism used by immune cells to eliminate harmful target cells such as allogeneic, virally infected, and tumor cells. Linear tetrapeptides with moderate affinity have been used for PET imaging of GzmB. However, improvement in affinity and in vivo stability may be required for clinical success.In this study, we report macrocyclic peptides derived from mRNA display screening and selection of a high-affinity lead peptide for clinical translation. ***Materials and Methods:*** An mRNA-display screen against human GzmB yielded 66 macrocyclic peptides hits. Based on binding characteristics and physicochemical properties, two series were identified and peptides from each modified to incorporate a linker and NOTA-based chelator for [18F]AlF chemistry. In vivo PET imaging was performed in healthy mice and rhesus monkeys to assess biodistribution and clearance properties. To assess in vivo binding to human GzmB, xenogeneic Graft-Versus-Host-Disease (GvHD) was generated by engrafting human PBMC cells in NOG mice. Immunohistochemistry was performed on tissues collected after PET scans to confirm GzmB expression. ***Results:*** Despite single-digit nM binding affinity, some peptides were deprioritized due to undesirable off-target biodistribution and clearance properties for clinical translation.A 13 nM binding affinity peptide, and corresponding scrambled peptide (no GzmB binding) were tested in GvHD model. Lung uptake (SUVmean) was significantly greater in GvHD mice than NOG mice (0.23 ± 0.08 vs 0.04 ± 0.08, p = 0.0006). No significant difference in lung uptake was observed between GvHD and NOG mice injected with scrambled peptide, suggesting differences in the GvHD mice are GzmB specific. Similar observations were made in other affected tissues such as liver. GzmB expression measured by immunohistochemistry correlated with observations from PET scans. Based on the encouraging in vivo results, positional scanning mutagenesis and targeted SAR exploration was performed to identify lead peptide with 0.7 nM binding affinity. In vivo PET imaging in GvHD and radiation dosimetry studies were conducted in rhesus monkeys with this 0.7 nM and additional IND-enabling studies are on-going. ***Conclusion:*** High-affinity macrocyclic peptides for PET imaging of human GzmB were discovered and developed though mRNA-display screening and subsequent modifications. In vivo proof-of-concept was achieved in a GvHD model. Clinical studies with the current lead peptide are planned for early 2024.

OP-704

Evaluation of Affinity Matured Affibody Molecules for Imaging of Immune Check-Point Protein B7-H3

M. Oroujeni[1], *E. Bezverkhniaia*[2], *T. Xu*[1], *Y. Liu*[1], *E. Plotnikov*[2], *E. Ryer*[3], *I. Karlberg*[3], *A. Orlova*[1], *F. Frejd*[1], *V. Tolmachev*[1];
[1]*Uppsala University, Uppsala, SWEDEN,* [2]*Tomsk Polytechnic University, Tomsk, RUSSIAN FEDERATION,*
[3]*Affibody AB, Stockholm, SWEDEN.*

Aim/Introduction: B7-H3 is an immune checkpoint protein, which is a promising molecular target for immune therapy of malignant tumours. Sufficient B7-H3 expression level is a precondition for a successful therapy. Radionuclide molecular imaging is a promising technique for visualizing expression levels of molecular targets in vivo. The use of small radiolabelled targeting proteins would enable high-contrast radionuclide imaging of molecular targets if adequate binding affinity and specificity of an imaging probe could be provided. Affibody molecules, small engineered affinity proteins based on a non-immunoglobulin scaffold, have demonstrated an appreciable potential for the use as radionuclide imaging probes. Proof-of principle of radionuclide visualization of B7-H3 in vivo was demonstrated using the [^{99m}Tc]Tc-AC12-GGGC Affibody molecule. The aim of this study was to test the hypothesis that the affinity maturation of B7-H3-binding Affibody molecules could improve their targeting properties for imaging of B7-H3-expressing tumours. ***Materials and Methods:*** An affinity maturation of AC12 Affibody molecule enabling selection of clones with higher affinity was performed. The most promising clones were expressed with a -GGGC chelating sequence at the C-terminus and labelled with technetium-99m. In vitro characterization was performed using B7-H3-expressing cell lines. A head-to-head biodistribution of the affinity maturated Affibody binders and the parental variant AC12 (both labelled with ^{99m}Tc) was studied in mice bearing B7-H3-expressing SKOV-3 xenografts. Uptake in B7-H3-negative Ramos xenografts was used as a specificity control. ***Results:*** Radiolabelling with ^{99m}Tc resulted in radiochemical yield over 95 % and no further purification was performed. Binding to B7-H3-expressing cell lines was B7-H3-mediated. SYNT-179 showed a 3-8-fold improvement in affinity compared to the parental AC12 Affibody molecule. Biodistribution data 4 h after injection demonstrated that [^{99m}Tc]Tc-SYNT-179 showed the lowest blood concentration and uptake in almost all organs and tissues. Tumour uptake was 2.15 ± 1.01 %ID/g. Significantly ($p<0.05$) higher tumour-to-blood ratio for [^{99m}Tc]Tc-SYNT-179 (25.7±2.5) compared to [^{99m}Tc]Tc-AC12-GGGC (11.0±0.5) was observed. Tumour-to-bone ratio was significantly ($p<0.05$) higher for [^{99m}Tc]Tc-SYNT-179 (280.5 ± 50.8) than for [^{99m}Tc]Tc-AC12-GGGC (43.6 ± 5.7). ***Conclusion:*** The affinity maturation resulted in an increased affinity and lower hepatic uptake through an affinity maturation step. SYNT-179 could be a promising B7-H3 targeted candidate aiming at clinical application in the future.

OP-705

A ^{68}Ga labelled CD25 targeted cyclopeptide probe for activated T cell imaging

F. Liu[1], *S. Wang*[2], *P. Wang*[1], *Z. Yang*[1];
[1]*Peking University Cancer Hospital & Institute, Beijing, CHINA,*
[2]*Peking University Health Science Cente, Beijing, CHINA.*

Aim/Introduction: Immunotherapy and adoptive T cell therapy was developing rapidly in recent years and achieved promising outcomes in the treatment of various cancer. Tumor T cell activation is critical for treatment, and noninvasive imaging of T cell activation can provide early prediction of efficacy. CD25 is the-chain of IL-2 receptor, which shows negligible expression on naive T cells, while upregulated on activated T cells. To track the status of activated T cells in vivo, a cyclopeptide MCDQWERCKW containing DOTA chelating agent targeting CD25 was constructed and named DOTA-TCP. ***Materials and Methods:*** DOTA-TCP was synthesized by solid phase and purified by Pre-HPLC.^{68}Ga-DOTA-TCP was radiolabeled with ^{68}Ga eluted from a ^{68}Ge-^{68}Ga generator. The in vitro and in vivo stability of ^{68}Ga-DOTA-TCP was determined by Radio-HPLC in saline solution or 5% human serum albumin(HSA) and normal mice. Karpas299 tumor-bearing CB17-SCID mice with high CD25 expression were selected and were intravenously injected with 200 μL of ^{68}Ga-DOTA-TCP (7.4 MBq), and static Micro-PET/CT imaging was acquired at 1 h post-injection observe the uptake and metabolism of tumor, muscle and other areas of interest. ***Results:*** The purity of DOTA-TCP was > 95% and its structure was identified by ESI-MS. The radiochemical purity of ^{68}Ga-DOTA-TCP was >95% after purification by C18 cartridge. ^{68}Ga-DOTA-TCP had good stability in vitro and in vivo, the radiochemical purity can maintain >95% within 30min,The Micro-PET/CT Imaging results of ^{68}Ga-DOTA-TCP in karpas299 tumor-bearing mice showed that the probe had uptake at the tumor site, the relatively lower background uptake rendered higher tumor-to-background ratio and better PET/CT imaging quality. The tumor ratio of ^{68}Ga-DOTA-TCP was 3.29. ***Conclusion:*** ^{68}Ga-DOTA-TCP showed good in vitro and in vivo stability and rapid clearance by the kidney. It also showed sufficient specificity and tumor-background ratio when applied to the imaging of CD25-positive Karpas299 tumor bearing mouse model. Therefore ^{68}Ga-DOTA-TCP has a certain application prospect in noninvasive evaluation of T cell activation status in vivo.

1505

Tuesday, September 12, 2023, 3:00 PM - 4:30 PM
Hall B

Cutting Edge Science Track - TROP Session: AI Methods and Applications

OP-706

Primary prostate characterization in PSMA-11 PET on real quantum computers

L. Papp, *C. P. Spielvogel, M. Hacker, W. Drexler, S. Moradi;*
Medical University of Vienna, Vienna, AUSTRIA.

Aim/Introduction: Prostate cancer is one of the most common cancers in men. The routine diagnosis is based on inaccurate biopsy sampling. Radiomics combined with machine learning has shown feasible results regarding primary prostate cancer characterization in vivo. Nevertheless, conventional ML (CML) tends to be architecturally complex which complicates their generalization abilities, especially on small medical data. In contrast, quantum machine learning (QML) has the ability to build robust, algorithmically simple and potentially superior prediction models compared to CML. Nevertheless, existing so-called noisy intermediate scale quantum computers (NISQs) are still challenging to be utilized due to their high noise and error rates. Hence, this study aimed to investigate the feasibility of utilizing error mitigation techniques combined with QML in predicting prostate lesion risk in real NISQ devices. ***Materials and Methods:*** This study involved 121 [^{68}Ga]Ga-PSMA-11 (PSMA-11) primary prostate lesions having radiomic features with 60 low (≤ Gleason 3) and 61 high (≥ Gleason 4) Gleason risk as endpoint to predict. Ten-fold cross-validation was utilized with 90:10 train:test ratios to estimate predictive ML performance. Spearman rank reduncandy reduction combined with R-squared feature ranking and selection of 8 radiomic features per-train subset was performed. Multiple QML models were built per-fold in a quantum simulator environment: A simplified quantum support vector machine (qsSVM), a quantum kernel Gaussian process (qGP), and a quantum distance classifier (qDC). For comparison, respective CML models were built: support vector machine (cSVM), Gaussian process (cGP) and k-nearest neighbor (ckNN). Furthermore, quantum error mitigation was employed, followed by evaluating the QML approaches on the real IonQ device in a hold-out validation setting. ***Results:*** Predictive performance evaluation over 10-fold test subsets revealed an average 76% accuracy (ACC) for QML and 72% ACC for CML models in simulator environment, thus, demosntrating quantum advantage. The average test ACC in noiseless simulator environment was 75-83% for qDC, qGP and qsSVM approaches in the held-out validation setting. In contrast, the test ACC on the IonQ device without error mitigation was in the range of 42-75%. Utilizing error mitigation on IonQ yielded identical results to the noiseless simulator test performances in the qDC (77% ACC) and qsSVM (76% ACC) algorithms. ***Conclusion:*** We demonstrated that with error mitigation, quantum advantage can be achieved in real existing quantum computers when predicting low-vs-high risk in clinically-relevant primary prostate PSMA-11 cancer cohort.

OP-707

Image-based PSMA PET/MRI deep learning model for automatic prostate cancer grading

E. Solari[1], *S. Schachoff*[1], *I. Rauscher*[1], *M. Eiber*[1], *W. Weber*[1], *N. Navab*[2], *S. G. Nekolla*[1];
[1]*Klinikum rechts der Isar, Technical University Munich, München, GERMANY,* [2]*School of Informatics, Technical University Munich, München, GERMANY.*

Aim/Introduction: Gleason score (GS) is fundamental in the decision making process of prostate cancer (PCa) management. Post-surgical GS (psGS) originates from a radical prostatectomy, but patients who are not subjected to this treatment option rely on a biopsy GS (bGS), which is less accurate and only agrees with psGS in around 60% of the cases. Previously, we showed that it is possible to improve this agreement applying PSMA PET/MRI radiomics in a small cohort. In this work, we propose a novel tool to automate and improve psGS predictions from an initial PSMA PET/MRI study, based on a multi-step deep learning pipeline. ***Materials and Methods:*** 185 biopsy planning and primary staging 68Ga-PSMA PET/MR PCa studies from a single scanner were included. An automatic deep learning pipeline was implemented to predict psGS from only images (PET, T2w, ADC). A whole-prostate segmentation tool was trained on 90 T2w

images manually segmented by an expert. The segmentations were later transposed into the other modalities. Three separate convolutional neural networks (CNN) were trained to classify two psGS groups (GS<8, GS≥8) from each image modality (60/20/20 train/validation/test split), with weighted average voting for the final classification. Balanced accuracy (bAcc) was used as the main metric to compare our model vs bGS predictions. ***Results:*** The patient distribution among the two groups was balanced (G<8: 56%, n=103; GS≥8: 44%, n=82). The segmentation showed signs of overfitting, suggesting the necessity of more annotated images (Dice coeff. 75%). The three CNN were trained over 20 epochs to classify psGS. The final model outperformed bGS in the prediction of psGS overall (bAcc, CNN: 90%; bGS: 74%) and in sensitivity and specificity towards the higher GS groups (CNN vs bGS, GS≥8: sens. 92% vs 79%; spec. 87% vs 69% respectively). This explained the reduction in under- and overestimation of psGS groups with respect to bGS (CNN vs bGS, underestimates: 8 vs 20 cases; overestimates: 15 vs 28 cases). ***Conclusion:*** Our work shows that it is possible to automate the prediction of psGS by groups based on PSMA PET/MRI studies, outperforming bGS. Possible clinical implications are the reduction of unnecessary biopsies and the improvement of initial patient management.

OP-708

Increased sensitivity for AI-based detection of lymph node metastases on [18F]-PSMA-1007 PET-CT when adding synthetic data to the training data

E. Tragardh[1,2], *J. Ulén*[3], *O. Enqvist*[3,4], *L. Edenbrandt*[5], *M. Larsson*[3];
[1]*Skåne University Hospital, Malmö, SWEDEN,* [2]*Lund University, Malmö, SWEDEN,* [3]*Eigenvision AB, Malmö, SWEDEN,* [4]*Chalmers University of Technology, Gothenburg, SWEDEN,* [5]*Sahlgrenska Academy, Gothenburg, SWEDEN.*

Aim/Introduction: Obtaining manually annotated positron emission tomography-computed tomography (PET-CT) images for training artificial intelligence (AI) is laborious. Here we investigated if it is possible to develop a fully automated AI-based method for detecting suspected lymph node metastases in prostate-specific membrane antigen (PSMA) PET-CT images of patients with prostate cancer, by adding synthetic lymph node metastases to the images to expand the training set. ***Materials and Methods:*** Patients referred for clinically indicated [18F]-PSMA PET-CT due to staging of high-risk prostate cancer or recurrence were included. The synthetic data were derived from original training images to which new, synthetic, lymph node metastases were added. Lymph node metastasis templates were gathered from all training images and carefully placed in new images using an aligned lymph node positioning map. In this way, the original training set from a previously published study (ref 1) (n=420), was expanded by one synthetic image for every original image. The resulting training set, with double the size (n=840), was used to train the AI tool. The performance of the AI-method was compared to nuclear medicine physicians and to a previously developed AI in a test set of 120 patients. The human readers were alternately used as a reference and compared to either another reading or AI. ***Results:*** The AI had an average sensitivity of 84% for detecting lymph node metastases, compared with 78% for human readings. Our previously developed AI-method, without synthetic data, had an average sensitivity of 79%. The number of true positive lesions was slightly higher for the new AI compared to human readings and the previous AI, while the number of false negative lesions was lower. The number of false positive lesions increased from 3.3 per patient for the new AI compared to 2.8 for the previous AI. ***Conclusion:*** It was possible to use synthetic data to increase the performance of a fully automated AI to detect suspected lymph node metastases in PSMA PET-CT images. However, the number of false positive lesions increased somewhat. ***References:*** 1. Trägårdh E et al. Freely available, fully automated AI-based analysis of primary tumour and metastases of prostate cancer in whole-body [18F]-PSMA-1007 PET-CT. Diagnostics(Basel) 2022;12:2101.

OP-709

Deep learning-based PET Image harmonization improves robustness and discriminative power of quantitative imaging markers in multi-institutional studies

D. Haberl[1], *C. P. Spielvogel*[1], *D. Iommi*[1], *I. Buvat*[2], *A. R. Haug*[1], *L. Papp*[3];
[1]*Department of Biomedical Imaging and Image-Guided Therapy, Division of Nuclear Medicine, Medical University of Vienna, Vienna, AUSTRIA,* [2]*LITO laboratory, U1288 Inserm, Institut Curie, University Paris-Saclay, Orsay, FRANCE,* [3]*Center for Medical Physics and Biomedical Engineering, Medical University of Vienna, Vienna, AUSTRIA.*

Aim/Introduction: Quantitative PET/CT imaging has become a promising method providing information regarding diagnosis, prognosis, and treatment response monitoring. However, the sensitivity of quantitative imaging biomarkers (QIB) to different scanners and imaging protocols is a limiting factor in large-scale multi-institutional studies and hampers clinical translation. In response, we developed a deep learning harmonization method that aims to improve the reproducibility and discriminative power of QIB in multicentric studies. ***Materials and Methods:*** A cycle-consistent generative adversarial network (CycleGAN) was used to perform image style and texture translation among different centers and scanners. The capability of processing volumetric images was added to better deal with the 3D nature of tomographic biomedical images and to enable the application to whole-body PET scans. The method was evaluated by applying it on two different datasets and tasks. First, harmonization was performed on a dual-center whole-body lung cancer (LC) cohort where the SUV coefficient of variation (CV) in healthy liver tissue was evaluated. Second, the method was applied to a head and neck (HN) cancer cohort acquired from three centers. Here, the clinical impact of the method was analyzed by predicting the patient outcome (development of distant metastases) using a multivariate logistic regression model incorporating first-order statistics (n=18) and texture features (n=75) from baseline ^{18}F-FDG PET before and after harmonization. ***Results:*** The high structural similarity (SSIM) of 0.991±0.006 (mean±1sd) and low mean squared error of 0.012±0.015 in the LC cohort indicated successful style and texture transfer without altering global anatomical structures. Site-specific differences (p=0.0003) were observed for the liver CV which became insignificant (p=0.1207) after harmonization. Inter-site reproducibility of QIB in healthy liver tissue increased by 41±12% (GLCM), 38±10% (GLRLM), 37±10% (GLDM), 29±18% (GLSZM), 22±15% (NGTDM), and 16±15% (first-order statistics) on average through the proposed method. In the HN cancer cohort, the clinical outcome prediction improved from AUC=0.68 (95% CI 0.66-0.71) to AUC=0.73 (0.71-0.75) through the GAN-harmonization (p<0.0001). ***Conclusion:*** The proposed method has the potential to improve QIB reproducibility of quantitative PET/CT imaging between centers while retaining the clinically relevant biological information. The approach is - in contrast to existing feature-based PET harmonization methods - operating at the image level, allowing physicians and researchers to have access to the images after harmonization. The clinical relevance of the method was demonstrated by directly linking it to an improved outcome prediction for HN cancer patients.

OP-710

[^{11}C] CFT PET to [^{123}I] FP-CIT SPECT Domain Adaptation:A CycleGAN harmonization approach

L. Lopes[1,2], *S. Xu*[1], *J. Lu*[3], *T. Pyka*[1], *K. Krieger*[1], *R. Fahmi*[4], *B. Spottiswoode*[4], *A. Soliman*[4], *R. Buchert*[5], *M. Brendel*[6], *J. Hong*[1,2], *C. Clement*[1,2], *C. Bassetti*[7], *A. Rominger*[1], *P. Wu*[3], *K. Shi*[1];
[1]Department of Nuclear Medicine, Inselspital, University of Bern, Bern, SWITZERLAND, [2]Graduate School for Cellular and Biomedical Sciences, University of Bern, Bern, SWITZERLAND, [3]Department of Nuclear Medicine & PET Center, Huashan Hospital, Fudan University, Shanghai, CHINA, [4]Siemens Medical Solutions United States Of America, Inc., Knoxville, TN, UNITED STATES OF AMERICA, [5]Department of Diagnostic and Interventional Radiology and Nuclear Medicine, University Medical Center Hamburg-Eppendorf, Hamburg, GERMANY, [6]Department of Nuclear Medicine, University Hospital, LMU Munich, Munich, GERMANY, [7]Department of Neurology, University of Bern, Bern, SWITZERLAND.

Aim/Introduction: Dopamine transporter (DAT) imaging is routinely used in the diagnosis of Parkinson's Disease (PD) and atypical parkinsonian syndromes(APS). While CFT PET is widely accessible in East Asia with a substantial APS database to support AI advancements, DAT SPECT is widely used in Europe with only limited APS data. Cross-modality harmonization is still challenging, which is particularly relevant in longitudinal or multicenter studies. This study aims to develop a deep learning-based cross-modality synthesis to improve interoperability between CFT PET and DAT SPECT. ***Materials and Methods:*** A 3D CycleGAN was trained using unpaired CFT PET (n=705; 66% PD) and DAT SPECT (n=1033; 85% PD) brain images from PD and non-parkinsonian (NP) subjects. The network was used to generate synthetic SPECT from a real PET test set (n=116; 63% PD). A blind visual scoring analysis was performed by two nuclear medicine specialists in a mixed selection of 10 real and 10 synthetic SPECT images. Specialists scored the level of noise, presence of artifacts, confidence in diagnosis, and synthetic/real interpretation on a 3-point Likert scale. Quantitatively, striatal-specific binding ratios (SBR) were calculated in the real PET and real and synthetic SPECT test sets and compared. A convolutional neural network (CNN) for NP vs PD classification was trained with the synthetic SPECT dataset and tested on the real SPECT test set. ***Results:*** Visual assessment showed no significant differences in the mean synthetic/real score between real and synthetic datasets. The synthetic SPECT dataset has a slightly insignificant higher mean noise and artifacts score, and a significantly lower mean confidence in diagnosis score($P<0.05$) compared to real SPECT. The mean diagnostic accuracy of visual interpretation in the synthetic SPECT images was 75%, compared to 90% in real SPECT images. The SBR values of synthetic SPECT were not significantly different from those of real SPECT. Differences were significant between NP and PD in the synthetic SPECT($P<0.05$). The CNN trained with synthetic SPECT achieved a diagnostic accuracy of 97% in the real SPECT test set. ***Conclusion:*** Our CycleGAN successfully generated synthetic SPECT images visually indistinguishable from real SPECT images and preserved disease classification information. The developed PET-to-SPECT translation has the potential to improve the reproducibility of quantitative metrics and classification accuracy across the two modalities, which might facilitate multicenter studies and aid in the challenging differential diagnosis of PD and APS. Further studies with a higher number of visual assessments are needed to validate the approach.

OP-711

Estimating the Tumor Localization Performance via Class-Activation Map Explanations of a Slice Classification Neural Network Without Pixel-Level Supervision

S. Ahamed[1,2], *C. F. Uribe*[1,3], *A. Rahmim*[1,2];
[1]University of British Columbia, Vancouver, BC, CANADA, [2]BC Cancer Research Institute, Vancouver, BC, CANADA, [3]BC Cancer, Vancouver, BC, CANADA.

Aim/Introduction: Explainability of AI models in medical image analysis is important for building trust, ensuring regulatory compliance, facilitating clinical decision support, and beyond. They allow physicians to understand AI-generated results and make informed clinical decisions. We utilized class-activation maps (CAMs)-based explanation methods on our previously trained slice classification network[1]. The network was trained on a multi-centric dataset(n=466) of lymphoma PET axial slices using slice-level annotation (positive vs. negative for tumors). We explored the extent of (pixel-level) tumor localization using explanations on slices and performed localization receiver operating characteristic (LROC) analysis, without explicitly training on pixel-level supervision. ***Materials and Methods:*** The test set performance of our previously trained network was: sensitivity=73%, specificity=96%, precision=79%, F1-score=76%[1]. In this work, CAM-based methods (GradCAM, GradCAM++, EigenCAM, LayerCAM) were utilized for interpreting classification decisions. These methods computed gradients of target class with respect to feature maps of the last convolutional layer, resulting in heatmaps highlighting important regions influencing the model's prediction. An acceptance circle with varying radii R (between 3.12mm and 390mm) centered at the centroid of the explanation heatmap was constructed, and the fraction of tumors (ground-truth) encompassed by the circle was measured. The fraction of tumors localized (averaged over the whole set) was plotted as a function of the circle radius to generate LROC curves for each CAM method. ***Results:*** At a chosen R=6.2 cm on the empirical-LROC curves, the mean fraction of tumor localized on the slices via GradCAM, GradCAM++, EigenCAM, and LayerCAM was 0.537±0.401, 0.502±0.402, 0.560±0.398, and 0.531±0.402, respectively. Area under the LROC curves (AUC LROC) used as surrogates to represent the localization power of these methods were calculated to be 0.529, 0.487, 0.552, and 0.522, respectively. A simulated random localizer on the same set had a mean localization fraction=0.025±0.026 and AUC LROC=0. ***Conclusion:*** Utilizing the explanations of classification models could be an effective way for not just interpreting model predictions, but also localizing tumors without explicit pixel-level training/supervision. In our analysis, the EigenCAM method outperformed all other methods in the task of finding a tumor localization window via explanation. Future work will focus on improving localization performance for smaller window sizes. ***References:*** [1]S. Ahamed, el al, Proc. SPIE 12464, Medical Imaging 2023.

OP-712

Early experiences with the use of triplet networks for histological subtype classification in Non-Small Cell Lung Cancer

F. Gelardi[1,2], *F. Aksu*[1], *A. Chiti*[1,2], *P. Soda*[3,4];
[1]Department of Biomedical Sciences, Humanitas University, Pieve Emanuele (MI), ITALY, [2]Department of Nuclear Medicine, IRCCS Humanitas Research Hospital, Rozzano (MI), ITALY, [3]Research Unit of Computer Systems and Bioinformatics, Campus Bio-Medico University of Rome, Rome, ITALY, [4]Department of Radiation Sciences, Radiation Physics, Biomedical Engineering, Umea University, Umea, SWEDEN.

Aim/Introduction: Non-Small Cells Lung Cancer (NSCLC) is one of the leading neoplasms and causes of morbidity and mortality worldwide. Accurate histopathological assessment and disease extent staging by invasive and imaging techniques are essential for individualised patient management and outcome prediction, resulting in delayed treatment and costly procedures. Virtual biopsy through the development of deep learning (DL) methods exploiting routinely collected image scans is a promising strategy to address these issues. However, most well-known DL techniques require a large amount of data, while the available datasets are small, limiting the training of the model. We aimed to test whether triplet networks were able to classify the histological subtype of NSCLC on a small dataset and to compare their performance with plain Convolutional Neural Networks (CNNs). ***Materials and Methods:*** We retrospectively and randomly selected patients with new diagnosis of NSCLC, baseline [18F]FDG PET/CT and surgical intervention performed in the IRCCS Humanitas Research Hospital. We collected demographic data, tumour information and clinical outcome. We segmented semi-automatically primary tumour lesions on PET images using a commercial software (PET VCAR, GE Healthcare, Waukesha, WI, USA) and manually adjusted the volume of interest (VOI) on CT images in case of mismatch between CT and PET images. We performed different experiments using different pretrained CNNs and triplet selection methods on the CT image dataset extracted from PET/CT. We statistically compared performance scores, measured in terms of area under the receiver operating characteristics curve (AUROC) averaged over 25 runs. We considered a p-value ≤0.1 for statistical significance. ***Results:*** We included 87 patients with NSCLC (age 69±8, male-to-female ratio 3:1). The histological diagnosis was adenocarcinoma in 60 patients and squamous cell carcinoma in 27 patients. The triplet network approach was more robust to data scarcity compared to plain CNNs. ResNet-50 and GoogleNet were the best performing networks ($p \leq 0.01$), with an AUROC of 0.651 ± 0.136 in GoogleNet. ***Conclusion:*** Triplet networks outperformed plain CNNs in the classification of the histological subtype of NSCLC in almost all experiments. Triplet networks are a viable option to overcome the limitations of small datasets when applying deep learning techniques in medical imaging.

OP-713

Development and Multicenter Validation of an Artificial Intelligence System for the Detection of Cardiac Amyloidosis in ^{99m}Tc Scintigraphy

C. Spielvogel[1], *D. Haberl*[1], *J. Ning*[2], *R. Calabretta*[1], *T. Traub-Weidinger*[1], *R. H. Davies*[3], *I. Pierce*[4], *K. Patel*[4], *K. Kluge*[1], *T. Nakuz*[1], *A. Goellner*[1], *D. Amareller*[1], *M. Weber*[1], *M. Zhao*[5], *X. Ma*[6], *X. Li*[1], *A. R. Haug*[1], *L. Menezes*[4], *T. A. Treibel*[3], *M. Hacker*[1], *C. Nitsche*[7], *CS and DH are first authors with equal contribution;*
[1]*Department of Biomedical Imaging and Image-Guided Therapy, Division of Nuclear Medicine, Medical University of Vienna, Vienna, AUSTRIA,* [2]*Christian Doppler Laboratory for Applied Metabolomics, Medical University of Vienna, AUSTRIA,* [3]*Institute of Cardiovascular Science, University College London, London, UNITED KINGDOM,* [4]*Department of Cardiology, Bart's Heart Centre, St Bartholomew's Hospital, West Smithfield, London, UNITED KINGDOM,* [5]*Department of Nuclear Medicine, First Xiangya Hospital, Central South University, Changsha, CHINA,* [6]*Department of Nuclear Medicine, Second Xiangya Hospital, Central South University, Changsha, CHINA,* [7]*Department of Medicine II, Division of Cardiology, Medical University of Vienna, Vienna, AUSTRIA.*

Aim/Introduction: In Cardiac amyloidosis (CA), misfolded proteins aggregate to amyloid fibrils and accumulate in the myocardium, eventually leading to heart failure and death. The current diagnostic approach relies on difficult-to-standardize, visual interpretation of ^{99m}Tc-scintigraphy[1]. In addition to the resulting variability in image ratings, CA is sometimes an incidental finding in ^{99m}Tc-scintigraphy and not always correctly recognized or reported to the referring physician[2]. We developed an artificial intelligence (AI) system to detect CA on ^{99m}Tc-scintigraphy scans in a standardized and accurate way. Robustness, prognostic value, safety, and clinical applicability of the AI system were assessed by multicenter validation, outcome assessment with two clinical endpoints, a medical algorithmic audit[3], and a multi-case multi-reader (MCMR) study. ***Materials and Methods:*** Overall, 19201 scans from 16059 patients originating from eight centers in Austria, the United Kingdom, and China were included in the study. The AI system was developed using data from a single center and validated on the remaining seven centers. The AI system was trained to detect the presence of a CA-associated pattern (Perugini grade[4] ≥ 2). The system's performance was further compared to the diagnostic performance of five experienced physicians through a MCMR study. Outcome assessment was performed using multivariate Cox regression corrected for relevant confounders (median follow-up time 4.1 years, IQR 1.5-6.5). ***Results:*** The AI system achieved a 10-fold cross-validation performance of AUC 1.000 (95% CI: 1.000-1.000) for the Austrian cohort and independent external validation AUCs of 0.997 (95% CI: 0.993-0.999) and 0.925 (95% CI: 0.871-0.971) for the United Kingdom and China cohorts respectively. The AI system's predictions were prognostic for survival (HR 1.40; 95% CI: 1.04-1.90; p=0.029) and heart failure (HR 1.85; 95% CI: 1.15-3.00 ; p=0.012). Median follow-up was 3.1 years (IQR 1.4-6.5) after which 28% of patients were either affected by heart failure or death. In the MCMR study, disagreement among the physicians occurred in 10.2% of cases (Fleiss kappa 0.88) and with a mean performance of AUC 0.945 (range 0.911-0.970), while the AI system had an AUC of 0.997. The medical algorithmic audit suggested robustness across tracers, scanners, demographic factors and centers. ***Conclusion:*** The developed AI system reaches diagnostic performances comparable with nuclear medicine physicians and provides a standardized and fast approach for reliably detecting CA patients using ^{99m}Tc-scintigraphy scans. The AI system may be employed for CA screening among patients referred for 99mTc-scintigraphy. ***References:*** 1.Kittleson,-M.-et-al.-2023-ACC-Expert-Con ensus-Decision-Pathway-on-Compre ensive-Multidisciplinary-Care-for-the-Patient-With-Cardiac-Am loidosis.-J.-Am.-Coll.-Cardiol.-81,-1076-1126-(2023).2.Stan,-C.,-Mititelu,-R.,-Adam,-R.-D.-&-Jurcuț,-R.-Awareness-of-Nucler-Medicine-Physicians-in-Romania-Regarding-the-Diagnostic-of-Cardiac-Amyloidosis-A-Survey-Based-Study.-Diagnosics-(Basel)-12,-(2022).3.Liu,-X.-et-al.-The-medical-algorithmic-audit.-The-Lancet-Digial-Health-4,-e384-e397-(2022).4.Hutt,-D.-F.-et-al.-Prognostic-utility-of-the-Perugini-grading-of-99mTc-DPD-scintigraphy-in-transthyretin-(ATTR)-amyloidosis-and-its-relationship-with-skeletal-muscle-and-soft-tissue-amyloid.-Eur.-Heart-J.-Cardiovasc.-Imaging-18,-1344-1350-(2017).

OP-714

Deep learning-based image classification in differentiating lymphoma pulmonary involvement and other hypermetabolic pulmonary diseases on ^{18}F-FDG PET/CT

R. Cheng[1], *Y. Peng*[1], *M. Quan*[2], *B. Li*[1], *N. Wen*[2], *J. Hu*[1];
[1]*Department of Nuclear Medicine, Ruijin Hospital, Shanghai Jiao Tong University School of Medicine, Shanghai, CHINA,* [2]*Department of Radiology, Ruijin Hospital Shanghai Jiao Tong University School of Medicine, Shanghai, CHINA.*

Aim/Introduction: Lymphoma pulmonary involvement, lung cancer, and hypermetabolic benign pulmonary lesions share similar patterns on ^{18}F-FDG PET/CT frequently. To address this issue, we developed a deep learning model by utilizing multi-center PET/CT data to realize the auto-segmentation and classification of hypermetabolic pulmonary lesions on images of ^{18}F-FDG PET/

CT. ***Materials and Methods:*** This study employed two datasets. Dataset I included 1014 FDG PET/CT studies with malignant lymphoma, melanoma, lung cancer and negative controls from the AutoPET competition [1]. All the lesions were manually annotated. The dataset was divided into training and validation sets in a 4:1 ratio for initial model training. Dataset II consisted of 161 cases of PET/CT images (40 lyphoma, 60 lung cancer, 60 benign) acquired from our own institute. Lesion in the thoracic regions in Dataset II was segmented manually by two nuclear medicine physicians and extracted based on a 41% SUVmax threshold, resulting in 620 lesions. Then, it was partitioned into training, verification, and test sets using a 3:1:1 ratio. The images from both datasets underwent thoracic region cropping for model inputs. To train the lesion segmentation model, we employed a 3D UNet network model with ResNet-18 as the backbone [3D UNet (ResNet-18)], which was pre-trained using Dataset I and finetuned on Dataset II. Next, the 3D ResNet-18 was trained to classify the lesions based on the lesion. Subsequently, the lesion classification model was trained on Dataset II using the same 3D ResNet-18 model. ***Results:*** In the segmentation task, the model achieved a Dice coefficient of 0.699, with precision and recall scores of 0.869 and 0.614 respectively in the testing cohort. Meanwhile, in the classification task, the model achieved an area under the curve (AUC) of 0.975, with an accuracy rate of 87.9% (48/48 for lymphoma, 50/54 for benign, and 20/22 for lung cancer). ***Conclusion:*** The proposed deep learning model provides a practical approach for identifying hypermetabolic lung lesions to aid physicians in clinical decision making. Future studies should assess the model's diagnostic performance by comparing it with double-blind diagnoses made by physicians. ***References:*** [1] Gatidis S, Kuestner T. A whole-body FDG-PET/CT dataset with manually annotated tumor lesions (FDG-PET-CT-Lesions) [Dataset]. The Cancer Imaging Archive, 2022. DOI:10.7937/gkr0-xv29

1506

Tuesday, September 12, 2023, 3:00 PM - 4:30 PM
Hall C

Clinical Oncology Track - TROP Session: Prostate Cancer Treatment

OP-715

Can pre-therapy ^{68}Ga-PSMA-11 PET SUVs predict absorbed doses across multiple cycles of ^{177}Lu-PSMA-617 therapy of mCRPC patients?

J. Brosch-Lenz[1], *N. Colpo*[2], *I. Bloise*[1], *X. Hou*[1], *W. R. Parulekar*[3], *C. Dellar*[3], *F. Saad*[4], *K. Chi*[2], *D. Wilson*[2], *F. Bénard*[2], *A. Rahmim*[1], *C. Uribe*[2];
[1]*BC Cancer Research Institute, Vancouver, BC, CANADA,* [2]*BC Cancer, Vancouver, BC, CANADA,* [3]*Canadian Cancer Trials Group, Queen's University Kingston, Kingston, ON, CANADA,* [4]*Prostate cancer research, Montreal Cancer Institute / CRCHUM, Montreal, QC, CANADA.*

Aim/Introduction: ^{177}Lu-PSMA-617 is an approved radiopharmaceutical for the treatment of metastatic, castration-resistant prostate cancer. However, patient-individual therapy response is not yet understood. Therefore, we aimed at investigating how parameters from the pre-therapeutic ^{68}Ga-PSMA-11 PET/CT imaging may predict the absorbed dose in the total tumor burden (TTB) and kidneys across multiple cycles of ^{177}Lu-PSMA-617 therapy. This work is based on early experience from the Canadian Cancer Trials Group PR21 trial (NCT 04663997). ***Materials and Methods:*** Pre-therapy ^{68}Ga-PSMA-11 PET/CT and post-therapy ^{177}Lu-PSMA-617 SPECT/CT data from four patients with a total of 24 therapy cycles were analyzed. Healthy organs were segmented on the CT images using an AI-model, while tumors were segmented on the SPECT images using the qPSMA approach [1]. Tissue-specific time-activity-curves were fitted to a mono-exponential function for the first therapy cycle, while a single time point dosimetry approach [2] was used for the subsequent therapy cycles. S-value based dosimetry was performed in IDAC-Dose v2.1 using organ/lesion time-integrated activity and mass. A correlation analysis was performed between the TTB and kidneys on PET and TTB absorbed dose (AD) across therapy cycles and between TTB SUV_{max} and SUV_{mean} on PET and the TTB and kidney ADs. ***Results:*** PET-based TTB was 563±726 ml averaged across all patients. SUV_{max} and SUV_{mean} were 66.3±31.8 and 13.5±3.3 for TTB, averaged across all patients. Left and right kidney ADs increased on average by +38% and +36% from cycle 1 to 6. In contrast, ADs for TTB decreased on average by -39% from cycle 1 to 6. Intermediate correlation was found between PET-TTB and kidney AD (R^2 from 0.21-0.70) across cycles, while no correlation was found between PET-TTB and TTB AD. For tumors, small (R^2=0.20) to intermediate (R^2=0.45) correlation was found between SUV_{max} and TTB AD and SUV_{mean} and TTB AD for the 1st cycle. Varying correlation (R^2 from 0.00 to 0.98) was found between TTB $SUV_{max/mean}$ and kidney AD across cycles. ***Conclusion:*** Despite the small number of investigated patients, we believe that the TTB SUV_{mean} may be used as a predictor for tumor AD. However, contrary to the global approach in this work, a separate analysis between lesions in soft tissue and bone is advisable and might lead to better correlation. It is planned to expand this analysis to a larger patient cohort of the PR21 trial. ***References:*** [1] DOI: 10.2967/jnumed.118.224055; [2] DOI: https://doi.org/10.2967/jnumed.122.264594

OP-716

Safety and efficacy of PSMA-targeted radionuclide therapy with ^{177}Lu-ITG-PSMA-1 in metastatic castration resistant prostate cancer patients: Update on the prospective, multicentre, Swiss registry study

A. Chirindel[1], *A. Bauman*[1], *M. Fani*[1], *F. Forrer*[2], *A. Afshar-Oromieh*[3], *M. del Sol Pérez Lago*[4], *J. Blautzik*[5], *N. Schaefer*[6], *E. Nitzsche*[7], *D. Wild*[1], *G. Nicolas*[1];
[1]*University Hospital Basel, Basel, SWITZERLAND,* [2]*Kantonsspital St. Gallen, St Gallen, SWITZERLAND,* [3]*Inselspital, Berne, SWITZERLAND,* [4]*Luzerner Kantonsspital, Lucerne, SWITZERLAND,* [5]*Hirslanden Klinik St. Anna, Lucerne, SWITZERLAND,* [6]*University Hospital Lausanne, CHUV, Lausanne, SWITZERLAND,* [7]*Kantonsspital Aarau, Aarau, SWITZERLAND.*

Aim/Introduction: To assess safety and efficacy of ^{177}Lu-ITG-PSMA-1 (^{177}Lu-PSMA I&T) in progressive metastatic castration resistant prostate cancer (mCRPC) patients, implemented in day-to-day clinical practice in Switzerland. ***Materials and Methods:*** Prospective, multicenter national register study (EKNZ 2021-01271) of progressive mCRPC patients treated with ^{177}Lu-ITG-PSMA-1. The primary endpoint is safety, assessed by biweekly laboratory parameters, adverse events (as per CTCAE v5.0) and xerostomia questionnaire (XQ). Efficacy outcome measures comprise best biochemical (PSA_{50}: PSA decrease >50% from baseline) and imaging response (clinical evaluation based on all available imaging modalities: CT, MRI, quantitative PSMA SPECT- or PET-CT), time to progression, overall survival and quality-of-life (EORTC PR25, EORTC QLQ-C30 and Brief Pain

Inventory Questionnaires). Descriptive and comparative statistics will be used to evaluate therapy safety and response. Multivariate analysis and Kaplan-Meier statistics will be used to evaluate time-to-outcome events and prognostic factors. ***Results:*** So far 140 patients (age: 74±8 years, mean±SD)) treated since May 2020 until March 2023 with at least 1 cycle (number of cycles, median [IQR]: 3 [2-5],) and 1 follow-up. The activity per cycle (median [IQR]) was 7.1 [6.5-7.5] GBq. Treatment related ≥G3 anemia, leucopenia and thrombocytopenia were found in 20 (14.7%), 5 (4%) and 4 (3%) patients, respectively. Analysis of the XQ-score (0-80) in the first 75 patients showed an increase from 7±10 to 10±11 (mean±SD) between the first and the last cycle (p=0.009, paired t-test), while an increase ≥10 was observed in 16 patients (21%). PSA_{50} was achieved in 55/135 (41%), whereas any PSA decrease occurred in 89/135 (66%) patients. Partial imaging response (PR) was found in 47/89 patients (53%). PR occurred at cycle 2 in 68% (32/47), while only 6/47 (12%) responded after the 3rd cycle. The median time to progression and OS will be presented. ***Conclusion:*** Our preliminary analysis shows that ^{177}Lu-ITG-PSMA-1 therapy is safe and efficacious in most progressive mCRPC patients. Anemia appears to be the most frequent and clinically relevant subacute myelotoxicity; while during treatment, a marked XQ-score increase is reported only in a small minority of patients. Biochemical or imaging-based tumor response, was recorded in approximately half of the patients.

OP-717

Systematic evaluation of response and adverse events in mCRPC patients treated with different combinations of ^{225}Ac/^{177}Lu-PSMA-therapy

G. Sheikh[1], *M. J. Zacherl*[1], *A. Holzgreve*[1], *S. C. Kunte*[1], *V. Wenter*[1], *M. Unterrainer*[2], *W. Kunz*[3], *J. Casuscelli*[4], *C. Stief*[4], *P. Bartenstein*[1], *L. M. Unterrainer*[1];
[1]*Department of Nuclear Medicine, LMU Klinikum, Munich, GERMANY,* [2]*Die Radiologie, Munich, GERMANY,* [3]*Department of Radiology, LMU Klinikum, Munich, GERMANY,* [4]*Department of Urology, LMU Klinikum, Munich, GERMANY.*

Aim/Introduction: ^{225}Ac-Targeted alpha therapy is a potent and promising option for patients with metastatic castration-resistant prostate cancer (mCRPC) and failure of guideline-based therapies and ^{177}Lu-PSMA-radioligand therapy. Unfortunately, side effects associated with TAT can significantly affect quality of life. A combination treatment regimen adding ^{177}Lu and reducing ^{225}Ac activities may limit side effects while maintaining sufficient anti-tumour effect. We therefore evaluated different combinations ^{225}Ac-/^{177}Lu-PSMA-I&T (ALCT) with regard to response and adverse events. ***Materials and Methods:*** A total of 22 consecutive patients treated with ALCT on compassionate use basis at our department were evaluated. Patients were grouped into three different subgroups, depending on the ^{225}Ac/^{177}Lu-activity administered: group 1 (Gr1) received 4MBq and 4000MBq, group 2 (Gr2) 6MB and 1000 or 2000MBq and group 3 (Gr3) 8 MBq and 1000MBq per therapy cycle, respectively. Laboratory (PSA, ALP, LDH, Hb, Lc, Tc, Crea) and imaging parameters on ^{18}F-PSMA-PET/CTs (TTV, SUVmax/mean) at baseline and after 2 cycles of therapy were evaluated for the total patient population as well as each therapy subgroup and statistically compared. Adverse events (xerostomia, anemia, leukopenia, thrombocytopenia, weight loss) were recorded. Response evaluation criteria in PSMA-PET/CT (RECIP 1.0) was used for response evaluation. ***Results:*** Gr1 showed RECIP 1.0 response in 4/10 patients and progression in 3/10 patients, Group 2 showed response in 2/3 patients and progression in 1/3 patients and group 3 showed response in 4/8 patients and progression in 2/8 patients. There was no significant difference between the three subgroups in respect to absolute values after therapy or pre- and post-therapy difference in any of the laboratory or imaging parameters evaluated. A positive correlation could be found between ^{177}Lu-activity and bone marrow events and ^{225}Ac-activity and xerostomia. After 2 cycles of ALCT the following adverse events developed newly or worsened by at least one grade: anemia in 2/10 patients from Gr1 and 3/9 patients from Gr3; thrombocytopenia in 1/10 patients from Gr1; leukopenia in 4/10 from Gr1, 1/3 from Gr2 and 2/9 from Gr3; weight loss in 1/10 from Gr1 and 2/9 from Gr3 and xerostomia in 3/10 from Gr1, 1/3 from Gr2 and 5/9 from Gr3. ***Conclusion:*** Since there was no significant differences in efficacy between the three therapy groups, ALCT with lower ^{225}Ac-activity may be a good choice in cases in which conservation of salivary gland function is the main concern, but more careful monitoring of blood values is warranted in those patients.

OP-718

ProstACT GLOBAL: A Phase 3 Study of 177Lu-DOTA-rosopatamab (TLX591) With and Without the Best Standard of Care for Patients With PSMA Expressing Metastatic Castration-resistant Prostate Cancer Progressing Despite Prior Treatment with a Novel Androgen Axis Drug

S. Martina[1], *C. Hawkins*[1], *N. Patel*[1], *J. Gibson*[1], *T. Brown*[1], *N. Lenzo*[2], *C. Hayward*[1];
[1]*Telix Pharmaceuticals, Melbourne, AUSTRALIA,*
[2]*Genesis Care, Alexandria NSW 2015, AUSTRALIA.*

Aim/Introduction: The treatment of advanced prostate cancer (PC) is challenging, with undesirable side effects that impact patient quality of life. Radioimmunotherapy (RIT) can localize therapy to specific tumor cells in multiple organs to reduce or eliminate damage to normal tissue. The cell surface glycoprotein prostate-specific membrane antigen (PSMA) is an ideal therapeutic target as it is highly expressed by malignant prostate cells. There is a strong rationale for further investigation of the ^{177}Lu-labeled, chelator-conjugated antibody, ^{177}Lu-DOTA-rosopatamab, as a potential RIT candidate for the treatment of PC. ***Materials and Methods:*** In this multinational, multicenter, prospective, randomized, open label phase 3 study, 387 patients with PSMA-expressing metastatic castration-resistant PC (mCRPC) that have progressed despite prior treatment with a novel androgen axis drug will be enrolled in a 2:1 ratio to receive either the best standard of care (SoC) or 2 single intravenous (IV) injections of 76 milicuries (mCi) each (equivalent to a 45 mCi/m2 dose in a standard 1.7m2 individual) of ^{177}Lu-DOTA-rosopatamab, given 14 days apart, plus best SoC. Eligible patients must have received prior therapy with either enzalutamide or abiraterone plus prednisone, and 1 line of prior taxane therapy or have refused or are ineligible for taxanes. Patients must have adequate organ function including at least $150x10^9$ /L platelets, hemoglobin 10 g/dL, and have PSMA-positive disease on ^{68}Ga-PSMA-11 PET/CT imaging as confirmed by a central reader. Key exclusion criteria include small cell histology, increased risk of hemorrhage or bleeding, known brain or hepatic metastases, or history of stroke, seizure, or treatment with radioisotopes within 6 months prior to randomization. The primary endpoint is radiographic progression-free survival (PFS). Secondary endpoints include 5-year overall survival, tumor objective response rate, time to symptomatic skeletal event, PFS, and participant number with treatment-related adverse events. Effective treatment options for mCRPC with favorable safety and tolerability profiles continue

to be an unmet need. Combining the advantages of targeted radiotherapy and immunotherapy, along with proven patient selection capabilities of ^{68}Ga-PSMA-11 PET, provides reasonable justification for further evaluation of ^{177}Lu-DOTA-rosopatamab in a large-scale trial. ***Results:*** This study is ongoing; no results are available at the time of abstract submission. ***Conclusion:*** Effective treatment options for mCRPC with favorable safety and tolerability profiles continue to be an unmet need. Combining the advantages of targeted radiotherapy and immunotherapy, along with proven patient selection capabilities of ^{68}Ga-PSMA-11 PET, provides reasonable justification for further evaluation of ^{177}Lu-DOTA-rosopatamab in a large-scale trial.

OP-719

[^{225}Ac]Ac-PSMA-617 mutational landscape in circulating tumor DNA (ctDNA): early clinical outcome prediction in metastatic castration-resistant prostate cancer

M. Amghar[1], *T. Rausch*[2], *T. Hielscher*[1], *H. Ozgur*[2], *M. Roscher*[1], *U. Bauder-Wüst*[1], *M. Schick*[1], *Y. Remde*[1], *G. Bakos*[1], *M. Schäfer*[1], *F. Bruchertseifer*[3], *A. Morgenstern*[3], *V. Benеš*[2], *C. Kratochwil*[4], *M. Benešová-Schäfer*[1];
[1]*DKFZ, Heidelberg, GERMANY,* [2]*EMBL, Heidelberg, GERMANY,* [3]*European Commission, Joint Research Centre (JRC), Karlsruhe, GERMANY,* [4]*Department of Nuclear Medicine, University Hospital, Heidelberg, GERMANY.*

Aim/Introduction: First clinical experiences employing prostate-specific-membrane-antigen (PSMA)-addressing PSMA-617 with the alpha-particle-emitting radionuclide actinium-225 (^{225}Ac) exhibited astonishing responses in heavily pre-treated-metastatic castration- and chemo-resistant-prostate-cancer (PCa) patients. Thus, our efforts have been directed toward the investigation of functional predispositions of PCa-related radiation resistance and sensitivity to PSMA-directed targeted alpha therapy (TαT) with [^{225}Ac]Ac-PSMA-617. Preclinical and clinical studies reported that DNA-damage repair (DDR)-associated gene mutations can interfere with radiosensitivity of PCa. Therefore, non-invasive liquid biopsies, detecting early clinical outcome, represent an unmet clinical need. Whole-genome circulating tumor DNA (ctDNA) and its matching germline DNA (gDNA) sequencing will address the molecular alpha emitter-based radiation resistance mechanisms. ***Materials and Methods:*** Blood samples from PCa patients undergoing repeated cycles of TαT were collected within an ethical approval (S-882/2020). Digital-droplet-PCR (dd-PCR) was performed using androgen receptor (AR) copy number variation (CNV) assay, including NSUN3 as a reference gene, and ZXDB as a control. CNV analysis was performed using a linear mixed model accounting for repeated measurements and applying log-transformed CNV levels. gDNA and ctDNA whole genome sequencing (WGS) was performed to the requested depths. Targeted sequencing panel of ctDNA comprehended hotspot coverage: AKT1, EGFR (ERBB1), ERBB3, ESR1 (ERα), FBXW7, KRAS, PIK3CA (p110-alpha), SF3B1, and whole coding coverage: BRCA1, BRCA2, ERBB2 (HER-2, NEU), TP53 (p53). ***Results:*** The cohort consisted of 43 metastatic castration- and chemo-resistant PCa patients with a median age of 74 (57-84). Patients were divided into three groups: responders, non-responders and unknowns based on the prostate-specific antigen (PSA) value measured in blood. No significant correlation was observed between CNV estimates and PSA levels (p=0.07). No significant difference in cfDNA CNV levels (p=0.4) was observed between non-responders and responders. WGS data from 15 patients has been performed. Upon radiation resistance filter gene set, 23 genetic alterations were reported in 15 patients, comprising three frame shift, 18 missense mutations and one stop gained as well as three rearrangements. Overall, SIRT1 (100%), BARD1 (67%), and SFRP2 (53%) showed the highest mutation frequency. SIRT1 (100%), FANCD2 (93%), MUS81 (93%), IP6K3 (97%), and BARD1 (87%) were the genes showing the highest mutation frequency rate upon DDR filter gene set. ***Conclusion:*** The unique set of longitudinal patient probes undergoing PSMA-TαT harbors the potential to shed light on mechanisms of congenital and acquired resistances correlating genomic, molecular and clinical data on (progression-free) survival and might enable risk stratification, prognosis and therapy prediction for heavily pre-treated metastatic castration- and chemo-resistant PCa patients.

OP-720

Evaluation of labelingparameters of PSMA-617 with ^{213}Bi for targeted alpha-radionuclide therapy of metastatic castration-resistant prostate cancer

H. khoshhosn*, M. Davarpanah, H. Khoshhosn*, A. Gravand, Y. Tavakoli, N. Soltani, M. Harati, B. Kalantari, F.Johri;
Pars Isotope company, Tehran, IRAN, ISLAMIC REPUBLIC OF.

Aim/Introduction: Targeted alpha therapy (TAT) has a great potential for the treatment of metastatic castration resistant prostate cancer. Recent studies have shown that prostate-specific membrane antigen (PSMA) is an important target for radionuclide imaging and therapy of PCa. PSMA is selectively overexpressed in 90-100% of primary and metastatic PCa lesions.[(i),(ii)] The alpha emitter ^{213}Bi is a generator-based radionuclide and has a half-life of 46 minutes which can be obtained by an ^{225}Ac/ ^{213}Bi generator. The objective of this study was to validate a radiolabeling and quality control procedure of ^{213}Bi labeled PSMA-617 in routine clinical production. Effective parameters on labeling of ^{213}Bi-PSMA-617 were evaluated. Radionuclide purity was over 99.9%. Labeling yield and radiochemical purity were >99%. The production and labeling process of the ^{213}Bi-PSMA-617 was reproducible and stable. ***Materials and Methods:*** ^{213}Bi^{3+} obtained from an ^{225}Ac/ ^{213}Bi-generator was provided by ITG Co. without adding any carrier, PSMA-617 peptide was from Arian pazho Co., which was used in preparation of the radiopharmaceutical. The generator was eluted with 0.6 mL 0.1 M NaI in 0.1 M HCl. The generator eluate was transferred into the reaction vial which contains 0.6 mL of 1M sodium acetate buffer, 5 mg ascorbic acid and 20 µg PSMA-617 (19 nmol). The pH of the reaction mixture was determined to be 5.0. The labeling was accomplished after heating the solution for 12 minutes at 95°C. ***Results:*** Using this procedure the incorporation of ^{213}Bi was 99% with 50 MBq of ^{213}Bi. The pH of the reaction mixture and the final product was 5.0. After QC, the final product could be used directly without the need for a final purification step. The final reaction volume was about 1.2 mL and can be diluted further for dose administration to any desired volume. ITLC analysis of the final product revealed no evidence of free Bi after 3 hours. ***Conclusion:*** A routinely useful synthesis procedure for the radiopharmaceutical production of ^{213}Bi-PSMA-617 was validated. This protocol allows a routine production for the treatment of patients with metastatic castration-resistant prostate cancer. ***References:*** [1] Minner S, Wittmer C, Graefen M, et al. High level PSMA expression is associated with early PSA recurrence in surgically treated prostate cancer. Prostate 2011;71:281. [1] Silver DA, Pellicer I, Fair WR, et al. Prostate-specific membrane antigen expression in normal and malignant human tissues. Clin Cancer Res 1997;3:81.

OP-721

Safety, Dosimetry and Response of ^{177}Lu-LNC1003 in Patients with Metastatic Castration Resistant Prostate Cancer

J. Zang[1], *G. Wang*[2], *T. Zhao*[3], *Y. Yang*[1], *W. Miao*[1], *Z. Zhu*[2], *J. Zhang*[3], *X. Chen*[3];
[1]*Department of Nuclear Medicine, the First Affiliated Hospital, Fujian Medical University, Fuzhou, CHINA,* [2]*Department of Nuclear Medicine, Peking Union Medical College (PUMC) Hospital, Chinese Academy of Medical Science and PUMC, Beijing, CHINA,* [3]*Departments of Diagnostic Radiology, Yong Loo Lin School of Medicine, National University of Singapore, Singapore, SINGAPORE.*

Aim/Introduction: In our previous studies, to increase tumor accumulation and retention for radioligand therapy, we conjugated a truncated Evans blue (EB) molecule onto PSMA-617, and obtained the first-generation drug ^{177}Lu-EB-PSMA. To further optimize its pharmacokinetics, we designed and synthesized the second generation of drug ^{177}Lu-PSMA-EB-01 (or ^{177}Lu-LNC1003). This translational study is designed to assess the safety, dosimetry and therapeutic response to ^{177}Lu-LNC1003 in patients with metastatic castration-resistant prostate cancer (mCRPC). ***Materials and Methods:*** Following institutional review board approval and informed consent, ten patients with mCRPC were recruited. Patients were divided into 3 groups: group A (n = 4) was treated with about a 1.11 GBq (30 mCi) dose of ^{177}Lu-LNC1003. Group B (n = 3) was treated with about a 1.85 GBq (50 mCi) dose of ^{177}Lu-LNC1003. Group C (n = 3) was treated with around a 2.59 GBq (70 mCi) dose of ^{177}Lu-LNC1003. ***Results:*** ^{177}Lu-LNC1003 at different doses was well tolerated by all patients. No significant adverse effects were observed up to 2 months after the first cycle of treatment. Two patients in Group B experienced Grade 1 thrombocytopenia, but recovered within 8 weeks. Kidney function and liver function were not significantly changed within 2 months period of observation. The total body effective dose for ^{177}Lu-LNC1003 was 0.384 ± 0.050 mSv/MBq. The highest estimated radiation dose was calculated for lacrimal glands at 2.65 ± 1.98 mSv/MBq. For the kidneys and red bone marrow, the calculated absorbed doses were 2.09 ± 0.51 mSv/MBq and 0.195 ± 0.0329 mSv/MBq, respectively. The mean absorbed dose for bone metastases and lymph node metastases was 8.74 mSv/MBq and 9.51 mSv/MBq, respectively. After the first cycle of treatment, a decline in the PSA level was observed in 1 (25.0%), and 2 (66.7%) patients in groups A and B, respectively. A decline in the PSA level of greater than 50% (PR) occurred in 0 (0%), and 1 (33.3%) of patients in groups A and B, respectively. After the first treatment cycle, according to the adapted PERCIST 1.0, 0 (0%), 1 (25.0%) patient in group A and 2 (66.7%) patients in group B had PR. Patients in the group C had not yet reached the time for recheck. ***Conclusion:*** This first-in-human study demonstrated that ^{177}Lu-LNC1003 had higher accumulation than ^{177}Lu-EB-PSMA and ^{177}Lu-PSMA-617 in mCRPC and was well tolerated at the administered low dose. Further investigations with increased dose and frequency of administration are warranted.

OP-722

Extension of a ^{68}Ga-PSMA PET-based nomogram for outcome prediction of ^{177}Lu-PSMA radioligand therapy for the use of ^{18}F-rhPSMA-7.3

I. Rauscher[1], *K. Hansen*[1], *A. Gafita*[1], *W. A. Weber*[1], *M. Eiber*[2];
[1]*Department of Nuclear Medicine, Technical University of Munich, Klinikum rechts der Isar, Munich, GERMANY,* [2]*Technical University of Munich, Klinikum rechts der Isar, Munich, GERMANY.*

Aim/Introduction: Recently, ^{177}Lu-PSMA radioligand therapy (RLT) has been approved by the FDA and EMA for patients with metastatic-castration resistant prostate cancer (mCRPC). As response to ^{177}Lu-PSMA RLT is not achieved by all patients, nomograms, including pre-therapeutic ^{68}Ga-PSMA-PET, were established to predict outcomes. The increasing use of ^{18}F-labelled PSMA-ligands requires adaptation of these methods. Thus, the aim of this retrospective analysis was the extension of a recently published nomogram for use with ^{18}F-rhPSMA- 7.3 in a large cohort of patients with mCRPC. ***Materials and Methods:*** A total number of 180 patients were retrospectively included. First, pre-therapeutic outcome probabilities (PSA-progression-free survival (PFS) and overall survival (OS)) for each patient were estimated according to recently published ^{68}Ga-PSMA PET-based prediction models. (1). Parameters included the same clinical variables and imaging data now derived from ^{18}F-rhPSMA-7.3 PET (tumor SUVmean, number of lesions, presence of pelvic lymph node, bone and/or liver metastases). The observed and estimated outcome of each patient C-indexes were calculated for OS and PFS. OS and PFS were compared, stratifying patients in high- and low-risk groups based on the cut-off values determined by Gafita et al (1). ***Results:*** The estimated median PFS and OS were 3.7 months and 14.9 months, while the observed PFS and OS were 3.1 months and 12.1 months, respectively. For the OS survival model our data reached a C-index of 0.70 (95%CI 0.66-0.75), which is comparable to the development cohort and the validation cohort of Gafita et al. (C-index of 0.71 and 0.72, respectively). The C-index for PSA-PFS was 0.64 (95%CI 0.60-0.70) and substantially lower compared to a C-index of 0.71 (95%CI 0.65-0.78) in the validation cohort of Gafita et al. Low-risk patients presented with a significantly longer OS than high-risk patients (16.5 months (95%CI 15.1-17.8) vs. 8.8 months (95%CI 7.7-9.9), respectively; p-value < 0.0001). ***Conclusion:*** The use of data from ^{18}F-rhPSMA 7.3-PET substituting ^{68}Ga-PSMA in a recently proposed PET-based prediction nomogram performs well for assessing outcome of ^{177}Lu-PSMA RLT. Its high concordance of the C-indexes confirming the prediction models' ability to determine reliable outcome parameters. As prediction models might be beneficial in patient selection further improvement of the model is warranted. ***References:*** (1) Gafita A, Calais J, Grogan TR, et al., Nomograms to predict outcomes after (177)Lu-PSMA therapy in men with metastatic castration-resistant prostate cancer: an international, multicentre, retrospective study, Lancet Oncol, 2021;22:1115-1125.

OP-723

^{177}Lu-PSMA-617 therapy in advanced mCRPC patients: preliminary results of the phase 2 prospective trial IRST-185.03

I. Marini, *M. Sansovini, G. Paganelli, I. Grassi, F. Matteucci, S. Nicolini, U. De Giorgi, E. F. Giunta, F. Foca, M. Monti, M. Celli, P. Caroli, V. Di Iorio, A. Sarnelli, C. Lolli, G. Schepisi, N. Brighi, S. Severi; IRCCS Istituto Romagnolo per lo Studio dei Tumori (IRST) "Dino Amadori", Meldola, ITALY.*

Aim/Introduction: IRST-185.03 is an open-label, single-centre, phase 2 prospective study. We report the efficacy and toxicity of ^{177}Lu-PSMA-617 low dosages therapy, scheduled to identify the optimal cumulative activity to treat advanced mCRPC patients. The study is still ongoing. ***Materials and Methods:*** Progressive mCRPC patients, with positive 68Ga-PSMA PET-CT, were assigned to two distinct treatment groups based on age, prior therapies and risk factors for toxicity: a low-dosage group (LD - range 3.7-4.4 GBq per cycle) and a high-dosage group (HD - 5.5 GBq per cycle), both to

receive 4 (up to 6) cycles of ^{177}Lu-PSMA-617. The primary objective of this analysis was the assessment of best biochemical response (BR) defined as ≥50% PSA reduction from baseline. Secondary objectives were safety, median progression-free survival (mPFS) and median overall survival (mOS). ***Results:*** From April 2017 to October 2022 we prospectively enrolled 145 patients. We had 3 screening failure and 142 patients who received at least one ^{177}Lu-PSMA-617 cycle. 43 patients were assigned to the LD-group and 99 to the HD-group. All 142 patients were evaluated for BR, safety, OS and PFS. The median number of cycles was 4 and the median follow-up was 28.8 months. A PSA reduction ≥50% was achieved in 57 patients (40.1%), a reduction ≥30% in 69 patients (48.6%). 73 patients (51.4%) had a PSA increase or a PSA reduction <30%. ^{177}Lu-PSMA-617 therapy proved to be safe and well tolerated in both groups. Overall only 7 patients had a G3 toxicity, 5 haematological, 2 renal. No G4 toxicity was observed. The most common side effect was G1 anaemia (13.4% of patients). No significant salivary gland toxicity was registered. The mPFS was 6.8 months in the LD-group and 7.0 months in the HD-group (non-significant difference). The overall mPFS was 7.0 months. Overall, the 6-month mPFS rate was 53.9% and the 12-month mPFS rate was 18.9%. The mOS was 13.5 months in the LD-group, 16.4 months in the HD-group and 16.8 months overall. The total 12-month mOS rate was 51.1% for the LD-group and 64.9% for the HD-group. The total 12-month mOS was 60.4%. ***Conclusion:*** Our results, obtained with reduced dosages, are in line with previous literature data and demonstrated an improved tolerance profile. The search for a minimum effective and non-toxic dosage deserves to be pursued with a view to using 177Lu-PSMA-617 in combination with other treatments, within de-escalation protocols and at earlier stages of the disease.

1507

Tuesday, September 12, 2023, 3:00 PM - 4:30 PM
Hall F1

Cardiovascular Committee - TROP Session: Perfusion

OP-724

Prognostic role of coronary microvascular dysfunction in non-obstructive coronary artery disease

K. Kopeva*, A. Maltseva, E. Grakova, A. Mochula, K. Zavadovsky;*
Cardiology Research Institute, branch of the Federal State Budgetary Scientific Institution «Tomsk National Research Medical Center of the Russian Academy of Sciences», Tomsk, RUSSIAN FEDERATION.

Aim/Introduction: The objective of the study was to evaluate of the prognostic role of coronary microvascular dysfunction (CMD), obtained by dynamic SPECT, in the development and progression of HFpEF in patients with non-obstructive coronary artery disease (CAD) during a 12-month follow-up period. ***Materials and Methods:*** A total of 112 patients (70 men, median age of 62.0 (58.0; 69.0) years) with preserved LV EF and non-obstructive coronary artery disease were enrolled in the study. Dynamic CZT SPECT and coronary computed tomography angiography studies were performed baseline. Impaired Myocardial flow reserve (MFR) was defined as MFR ≤2. Coronary microvascular dysfunction (CMD) was therefore defined as the presence of impaired MFR in the absence of flow-limiting CAD. Serum levels of NT-proBNP were analyzed by ELISA. ***Results:*** All patients were divided into groups depending on the presence of CMD: group 1 included patients with CMD (CFR ≤2; n=42), and group 2 included patients without it (CFR >2; n=70). MFR levels and rest-MBF correlated with the level of NT-proBNP (r=-0.368; p=0.007 and r=0.354; p=0.042, respectively). The values of MFR also correlated with LAVI (r=-0.464; p=0.001) and septal e' (r=0.314, p=0.012), and rest-MBF correlated with E/e' (r=0.512; p=0.002). During 12 months of follow-up, 25 patients had adverse events. The Kaplan-Meier test showed that the frequency of adverse outcomes significantly (p<0.001) differed between groups. Patients with CMD had higher rates of adverse outcomes (8.6%, n=6) than those without it (45.2%, n=19). Based on ROC-analysis, only the levels of MFR ≤ 1.62 (sensitivity 85.7%, specificity 84.7%; AUC=0.884; p<0.001) and stress-MBF ≤ 1.35 ml/min/g (sensitivity 87.5%, specificity 62.5%; AUC=0.750; p<0.001) were identified as cut-off values predicting the adverse outcomes. Based on ROC-curve comparison analysis, MFR values were more significant predictor (p=0.034) of HFpEF development and progression. ***Conclusion:*** The presence of CMD, obtained by dynamic SPECT, helped to identify patients at high risk of developing and progressing HFpEF during the 12-month follow-up period. The values of MFR and stress-MBF can be used as a non-invasive predictor for risk evaluation of HFpEF development and progression in patients with non-obstructive CAD. ***References:*** Funding: MK-4257.2022.3

OP-725

Impact of coronary flow reserve on the mortality and major adverse cardiac and cerebrovascular event in hemodialysis patients, regardless of diabetes

S. Ohshima*;*
Nagoya Kyoritsu Hospital, Nagoya, JAPAN.

Aim/Introduction: Ischemic heart disease (IHD) is still a major problem not only in general patients but also in regular hemodialysis (HD) patients. We have reported about prognostic value of coronary flow reserve (CFR) derived from N13-ammonia PET in HD population for all-cause mortality and major adverse cardiac event (MACE) in prior studies. We investigated the impact of diabetes and low CFR on the mortality in HD population. ***Materials and Methods:*** A total 1,020 HD patients who undergone 13N-ammonia PET for suspected IHD were enrolled. We divided them into four groups according to CFR (cut off value = 2.0) and whether DM or not. We collected and evaluated their all-cause mortality, cardiovascular (CV) mortality and MACE, and analyzed using Kaplan-Meier methods and uni/multivariate cox regression model. ***Results:*** There were inter group differences in all-cause mortality, CV death, non-CV death and MACCE. Whether DM or not, CFR predicted HD patients' prognosis precisely. And HD patients with DM and low CFR had worst prognosis in all prognostic evaluation. Furthermore, multivariate Cox regression model showed CFR (continuous value) was an independent predictor for all-cause mortality (hazard ratio (HR); 0.7744, 95% confidential interval (CI) 0.6056-0.9790, p value=0.0368) and MACCE (HR0.7691, 95%CI0.6295-0.9320, p=0.0087) in DM HD population. Similarly, CFR predicted all-cause mortality (HR0.7313, 95%CI 0.5689-0.9401, p=0.0146) and non-CV death (HR0.6361, 95%CI0.4514-0.8963, p=0.0097) in non-DM HD population. ***Conclusion:*** Low CFR would predict the HD patients' unfavorable prognosis regardless of DM. Moreover, HD patients with DM and low CFR had worst prognosis in all-cause mortality, CV death, non-CV death and MACCE.

OP-726

Relationship between monocyte to high density lipoprotein cholesterol ratio and myocardial perfusion imaging findings

M. Sadic;
Division of Nuclear Medicine, Department of Radiology, University of Washington, Seattle, WA, UNITED STATES OF AMERICA.

Aim/Introduction: Monocyte to high density lipoprotein ratio (MHR) has been proposed as a novel prognostic indicator of CAD. Myocardial perfusion imaging is a useful non-invasive imaging test to evaluate the suspected or known CAD and to predict the prognosis as well. To the best of our knowledge, relationship between MHR and MPI findings such as TID in patients with suspected CAD has not stated clearly and this is the first study to evaluate the relationship between MHR and MPI parameters. In the light of relation between MHR and CAD, the goal of our study is to investigate the correlation between MHR and MPI findings. ***Materials and Methods:*** A total of 134 patients were included in our study. Patients were divided into groups according to the MPI findings and coronary angiography (CAG) results. They were evaluated due to possible cardiac events by gated single-photon emission computed tomography (GSPECT) MPI and coronary angiography (CA). Evaluations include the assessment of myocardial perfusion, wall motion and wall thickening and the measurement of LVEDV, LVESV, LVEF, SSS, SDS, SRS and TID parameters. We examined on these data to determine the value of TID. Their hematologic and biochemical data were obtained. The monocyte-to-high density lipoprotein ratio was calculated, and the relationship between the groups and the MHR was statistically analyzed. ***Results:*** The MHR was statistically higher in the patients with ischemia detected with MPI, than in patients who had normal MPI values (2.63 ± 1.71 and 2.04 ± 1.05, respectively). Therefore, the MHR was similar between patients who were both CAG positive and had ischemic MPI according to MPI findings. In addition, the MHR was similar for patients who had both normal MPS and CAG negative. MHR was detected as an independent predictor for coronary artery disease on logistic regression analysis (p = 0.005, OR = 1.29, 95% CI: 1.082 - 1.539). ***Conclusion:*** The MHR is an independent predictor for coronary artery disease. a high TID value was found to be well-correlated with the high of MHR in patient with CAD. This novel index is a beneficial identifier to interpret the results of MPI in terms of increasing diagnostic accuracy. This may provide valuable information to select the high-risk patients.

OP-727

Analysis of related factors of persistent or recurrent chest pain in patients with coronary artery disease after PCI based on gated myocardial perfusion imaging

Z. Yang[1,2], *J. Wang*[1,2], *Y. Wang*[1,2];
[1]*Department of Nuclear Medicine, The Third Affiliated Hospital of Soochow University, Changzhou, Jiangsu Province, CHINA,* [2]*Institute of Clinical Translation of Nuclear Medicine and Molecular Imaging, Soochow University, Changzhou, Jiangsu Province, CHINA.*

Aim/Introduction: We aimed to evaluate the influencing factors of persistent or recurrent chest pain in patients with coronary artery disease after percutaneous coronary intervention (PCI) using gated myocardial perfusion imaging (GMPI). ***Materials and Methods:*** This study prospectively enrolled 201 patients with coronary artery disease who underwent PCI. All subjects underwent GMPI within 1-2 months after PCI, and were followed up by telephone or medical record system at 1 year after PCI for persistent or recurrent chest pain. The clinical characteristics, cardiac Doppler ultrasound, electrocardiogram, GMPI, coronary angiography findings and PCI procedural factors were collected. PCI treatment methods are divided into complete revascularization and incomplete revascularization (incomplete revascularization due to technical reasons such as small coronary artery or preoperative non-culprit vascular functional evaluation). Multivariate logistic regression analysis was performed to define the independent risk factors of persistent or recurrent chest pain after PCI in patients with coronary artery disease. ***Results:*** Persistent or recurrent chest pain after PCI occurred in 59 (29.4%) out of 201 patients. The symptomatic group was significantly older than the asymptomatic group (63.0±9.6 years vs. 59.7±10.4 years, t=2.074, P=0.039). Compared with patients in the asymptomatic group, patients in the symptomatic group had a higher proportion of patients with residual myocardial ischemia and incomplete revascularization (66.1% vs. 49.3%, χ^2=4.743, P=0.029 and 54.2% vs. 35.2%, χ^2=6.247, P=0.012). However, there were no statistically significant differences between the symptomatic group and the asymptomatic group in terms of coronary artery disease type, highest troponin, left ventricular ejection fraction (LVEF), arrhythmia, Gensini score, and coronary collateral circulation (all P>0.05). Multivariate logistic regression analysis showed that residual myocardial ischemia (OR=2.237, 95%CI: 1.140-4.389, P=0.019) and incomplete revascularization (OR=2.117, 95%CI: 1.112-4.031, P=0.022) were independent risk factors for persistent or recurrent chest pain after PCI. ***Conclusion:*** Residual myocardial ischemia and incomplete revascularization are independent risk factors for persistent or recurrent chest pain after PCI. GMPI assessment of residual myocardial ischemia and the therapeutic strategy of complete revascularization have important clinical significance in predicting persistent or recurrent chest pain after PCI.

OP-728

Association between myocardial perfusion and peripheral endothelial function in patients with coronary artery disease

N. Vartiainen, *J. E. K. Hartikainen, T. M. Laitinen, H. Mussalo, P. Kuikka, T. P. Laitinen;*
Kuopio University Hospital, Kuopio, FINLAND.

Aim/Introduction: Hyperemic myocardial perfusion can be assessed quantitatively with ^{15}O-H_2O PET/CT by infusing intravenous adenosine to induce maximal vasodilation. It has been speculated that adenosine-induced vasodilation is a least partly mediated by coronary endothelial function, but this is still unclear. Impaired adenosine-mediated vasodilatation in coronary arteries has been frequently, but not always seen among patients with coronary endothelial dysfunction. Flow-mediated dilation (FMD) of brachial artery is a marker of peripheral endothelial function and a risk factor for adverse cardiovascular events. Our aim was to assess if there is a relationship between quantitative myocardial perfusion determined with ^{15}O-H_2O PET/CT and brachial artery FMD. ***Materials and Methods:*** We prospectively studied 56 patients (22 men, 34 women, aged 41-77 years), who had findings consistent with coronary artery disease in coronary CT angiography. Quantitative myocardial perfusion PET/CT was imaged at rest and during adenosine-induced maximal vasodilation by using ^{15}O-H_2O as a tracer. FMD was measured with ultrasound from the left brachial artery. FMD was determined by the increase in vessel diameter after reactive hyperemia relative to

the baseline diameter. ***Results:*** There was a statistically significant correlation between FMD and global stress perfusion (r=0.311, p=0.020). A statistically significant difference was observed in FMD between the patients grouped to the lowest and the highest tertile by global stress perfusion (3.9% vs. 7.0%, p=0.029). There was no statistically significant difference in FMD between patients with normal (n=40) and patients with impaired (n=16) stress perfusion (5.0% vs. 6.4%, p=0.414). ***Conclusion:*** Our study showed a statistically significant correlation between FMD of brachial artery and global myocardial stress perfusion in PET/CT. This strengthens the idea, that adenosine-induced hyperemic myocardial perfusion can be viewed as a marker of coronary endothelial function. FMD of brachial artery, however, doesn't function as surrogate marker for myocardial ischemia in patients with coronary artery disease.

OP-729

Relative stress perfusion deficit is an independent predictor of significant stenosis in a heterogenous population of patients examined with [^{15}O]H_2O PET

P. Mark[1], *E. Prescott*[2], *L. Marner*[1], *P. Hovind*[1], *M. Krakauer*[1];
[1]Department of Clinical Physiology and Nuclear Medicine, Copenhagen University Hospital - Bispebjerg Frederiksberg Hospital, Bispebjerg Bakke 23, 2400 Copenhagen, DENMARK, [2]Department of Cardiology, Copenhagen University Hospital - Bispebjerg Frederiksberg Hospital, Bispebjerg Bakke 23, 2400 Copenhagen, DENMARK.

Aim/Introduction: Myocardial perfusion imaging with [^{15}O]H_2O PET can detect coronary artery stenosis with high accuracy in patients with no history of ischemic heart disease. However, recent evidence suggests reduced accuracy in patients with previous ischemic heart disease[1]. We aimed to examine absolute and relative stress perfusion deficits as predictors of significant coronary artery stenosis in subsequent coronary angiography (CAG) in a heterogenous population. ***Materials and Methods:*** From May to December 2022 we retrospectively and consecutively included patients referred to CAG after [^{15}O]H_2O PET. The patients were divided into groups with significant vs. no significant stenosis (fractional flow reserve (FFR) ≤0.8 or a coronary artery narrowing of ≥70% when FFR was not available). Total perfusion deficit (TPD) was calculated as a combined continuous measure of the extent and severity of reduced stress perfusion as a percentage of the total left ventricle myocardium. The thresholds for decreased perfusion was <2.4 mL/min/g for absolute TPD (aTPD) and <0.7 relative to the individual highest perfusion for relative TPD (rTPD). Values of aTPD and rTPD are given as median (IQR). A multivariate logistic regression analysis was performed to test the adjusted associations (odds ratio (OR) with 95% CI) with subsequent detection of significant stenosis. ***Results:*** In a total of 144 patients, 78 patients had at least one significant stenosis and 66 patients had no significant stenosis. In groups of no stenosis vs. stenosis, aTPD was 22% (12-46) vs. 37% (16-66) (P=0.007) and rTPD was 9% (4-15) vs. 19% (9-29) (P<0.001). In an adjusted analysis rTPD ($OR_{10\%\ increase}$ = 1.92 (1.34-2.76), P<0.001), previous CABG (OR = 0.13 (0.04-0.41), P=0.001) and reduced LVEF (OR = 0.28 (0.09-0.88), P=0.03) were independently associated with coronary stenosis, whereas the association with aTPD ($OR_{10\%\ increase}$ = 1.15 (1.00-1.32) P=0.06) was borderline. ***Conclusion:*** In the presence of an absolute perfusion deficit, rTPD independently improves the detection of significant stenosis in a heterogenous population of patients examined with [^{15}O]H_2O PET. Furthermore, previous CABG and reduced LVEF are associated with non-stenotic perfusion deficiencies suggesting caution when interpreting myocardial perfusion measurements in patients with such confounders. ***References:*** 1. Driessen et al. Functional stress imaging to predict abnormal coronary fractional flow reserve: the PACIFIC 2 study. Eur Heart J 2022 Sep 1;43(33):3118-3128.

OP-730

Cardiac ^{15}O-water PET/CT predicts progression of Cardiac Dysfunction in Patients with Type 2 Diabetes and Diabetic Foot Ulcers

N. Christensen[1,2,3], *L. P. Tolbod*[1,2], *K. Bouchelouche*[1,2], *M. A. Madsen*[1], *C. S. Buhl*[3], *J. Sørensen*[1];
[1]Department of Nuclear Medicine & PET, Aarhus University Hospital, Aarhus N, DENMARK, [2]Aarhus University, Aarhus C, DENMARK, [3]Steno Diabetes Center Aarhus, Aarhus University Hospital, Aarhus N, DENMARK.

Aim/Introduction: Patients with type 2 diabetes (T2DM) and diabetic foot ulcers (DFU) are at an increased risk for developing cardiovascular disease. Cardiac ^{15}O-water PET/CT is a non-invasive method for evaluating myocardial blood flow (MBF) in detecting early signs of ischemic heart disease (IHD). Additionally, measurements of ankle-brachial index (ABI) and toe-brachial index (TBI) can provide information on the severity of peripheral artery disease (PAD). This study aimed to investigate the association between MBF and the occurrence of cardiac events in patients with T2DM and DFU. ***Materials and Methods:*** Cardiac ^{15}O-water PET/CT was performed at rest and during adenosine stress in 21 patients with T2DM and DFU. Peripheral hemodynamic measurements (ABI/TBI) were performed within four weeks prior to PET/CT. The PET scan was considered positive if maximal MBF in one or more vascular territories or globally was <2.3 mL/min/g. Cardiac events were recorded. ***Results:*** Ten (48%) patients had positive PET. Seven (33%) of these had known stable IHD. Five of the PET-positive patients developed chest pain or dyspnoea during follow-up (median 8 months). Cardiac symptoms were associated with lower maximal MBF (p=0.004). TBI correlated with maximal MBF (r=0.56, p=0.009) and coronary flow reserve (CFR) (r=0.68, p=0.0006), and ABI correlated with CFR (r=0.72, p=0.0008). Nine of 10 PET-positive patients had TBI below the reference level for PAD (p=0.0006). ABI measurements were obtained from eight PET-positive patients, of whom six had ABI values below the reference level for PAD (p=0.07). None of the PET-negative patients reported cardiac symptoms. ***Conclusion:*** Our study shows that PAD and significant IHD often coexist in T2DM patients with DFU. We found a significant association between maximal MBF and imminent worsening of cardiac symptoms, as well as a significant correlation between reduced coronary flow reserve and PAD severity, as measured by TBI and ABI. Our results suggest that cardiac PET/CT might be valuable in T2DM patients with DFU.

OP-731

Prevalence, characteristics and effect of cardiac motion in ^{13}N-ammonia PET/CT dynamic acquisitions

O. Mendoza-Ibanez[1], *T. S. Martinez Lucio*[1], *F. van der Zant*[2], *C. Hayden*[3], *R. J. J. Knol*[2], *R. H. J. A. Slart*[1], *S. V. Lazarenko*[2];
[1]University Medical Center Groningen, Groningen, NETHERLANDS, [2]Northwest Clinics Alkmaar, Alkmaar, NETHERLANDS, [3]Siemens Medical Solutions, Inc. United States Of America, TN, UNITED STATES OF AMERICA.

Aim/Introduction: Heart-wall motion negatively impacts PET/CT results. For dynamic acquisitions, motion can induce estimation errors up to 500% in myocardial blood flow (MBF) and myocardial flow reserve (MFR) values. Motion can present as inter-frame

motion (interMo) or as intra-frame motion (intraMo), and can differ between different axes and/or phase. A prototype data driven motion correction (DDMC) algorithm allows heart-wall motion tracking for each second of acquisition time in the 3D space what could allow better description of motion. This project aims to depict the prevalence, characteristics, and effect of cardiac motion in 13N-ammonia PET/CT dynamic acquisitions with the use of DDMC. ***Materials and Methods:*** 25 patients who underwent a cardiac PET/CT examination were retrospectively included. Inclusion criteria: no prior CAD, normal PET/CT results, and follow-up without major adverse cardiac events. DDMC was used to retrieve motion information in the later frames, as accuracy for the early frames was suboptimal. Data was retrieved in the left-right tranxial (x), anterior-posterior transaxial (y) and axial (z) directions. IntraMo was defined as the ratio between the sum of absolute differences in heart position and the frame-length for each frame. InterMo was defined as the difference in average heart position from one frame to the previous. Patients were classified with "significant motion" (sigMo) when InterMo >3mm was found. Absolute mean values of IntraMo and InterMo were used for final comparison between patients. Image processing was performed with Cedars Sinai QPET to retrieve values of MBF and CFR and compare them between the lower and upper tertile of motion. Differences were analyzed using Mann-Whitney U and McNemar tests. ***Results:*** Twenty-one patients (84%) had sigMo either in rest or stress. The prevalence of sigMo was significantly higher in z-axis both for rest [48% vs 12%(x) vs 12%(y)] and stress phase [68% vs 4%(x) vs 4%(y)]. InterMo in z-axis was higher in stress than rest, while intraMo was higher for all the axis in stress than rest ($p<0.05$). When comparing between axes, interMo and intraMo in z-axis were significantly higher than for the other axes both in rest and stress. Values of MBF in stress, Cx MFR and RCA MFR were significantly lower for the group with highest interMo in z-axis. ***Conclusion:*** A substantial percentage of patients present significant cardiac motion in PET/CT examinations. InterMo in the z-axis during stress appears highly relevant, as it leads to significantly lower values in stress MBF and CFR parameters.

OP-732

Role of motion correction tools in the estimation of microvascular coronary function by ^{13}N-ammonia hybrid-positron emission tomography

O. Mendoza-Ibanez[1], *R. J. J. Knol*[2], *R. H. J. A. Slart*[1], *C. Hayden*[3], *T. S. Martinez Lucio*[1], *S. V. Lazarenko*[2];
[1]University Medical Center Groningen, Groningen, NETHERLANDS, [2]Northwest Hospital Group Alkmaar, Alkmaar, NETHERLANDS, [3]Siemens Medical Solutions United States Of America, Tenesse, TN, UNITED STATES OF AMERICA.

Aim/Introduction: PET/CT is considered the gold-standard for the non-invasive determination of microvascular coronary function, by software-based estimations of regional and global values of myocardial blood flow (MBF) in rest and stress, and coronary flow reserve (CFR). The presence of motion artifacts can impact the quantification, leading to estimation errors up to 500% in MBF/CFR parameters. Some motion-corrections (MC) tools are now available, with their specific role yet to be proven. In-software MC tools (ISMC) are available within some commercial packages for PET processing, and, more recently, an innovative data driven motion correction (DDMC) has been developed to correct for motion prior the image reconstruction process. This work aims to elucidate the role of ISMC and DDMC in the determination of MBF and CFR values. ***Materials and Methods:*** Twenty-eight patients that underwent a ^{13}NH3-PET/CT examinations were retrospectively included. Inclusion criteria: no prior CAD/MI, normal LV-function, normal CFR, and no MACEs during follow-up. Image processing was made in three different software packages, namely Corridor.4DM (4DM), Cedars-Sinai QPET (QPET), and SyngoMBF (Syngo). Values of regional and global MBF in rest and stress and CFR without MC (NMC), with the use of ISMC and after processing with DDMC were acquired for the final analysis. Paired T-Tests, Bland-Altman plots and intraclass correlation coefficients were used for statistical analysis. ***Results:*** Population consisted of 17(65%) woman, all patients >42 yo, and 23(88%) of adenosine stress (12% regadenoson). QPET proved to be more sensitive to MC, as significantly higher values in all regional and global stress-MBF and CFR were obtained after the use of any MC technique ($p<0.001$). For 4DM, the impact of ISMC was higher than DDMC, with significant changes in seven parameters of rest-MBF and stress-MBF compared to only 3 with DDMC. For Syngo, no significant effect was observed by the use of any MC tool (all p-values >0.05). Bland-Altman and ICC plots showed that the use of any MC tool improves the agreement between software. DDMC demonstrated the higher improvements, achieving excellent agreement (ICC >0.9) in the RCA CFR. ***Conclusion:*** The effect of MC tools is related to the software used for image processing. QPET appear to underestimate values of regional and global stress-MBF and CFR when NMC is used, whereas the other packages does not appear that sensitive to motion. In general, the use of a MC technique seems valuable, particularly for DDMC, to improve reliability and agreement between software.

1508

Tuesday, September 12, 2023, 15:00 - 16:30
Hall F2

Joint Symposium 5 - Oncology & Theranostics Committee / ESMO: Prostate Cancer Theranostics: Where Do We Go?

OP-733

Biology and Treatment Landscape in advanced Prostate Cancer and unmet Medical Needs

E. Castro;
12 de Octubre University Hospital, Department of Medical Oncology, Madrid, SPAIN.

OP-734

Potential combination partners for PSMA radioligand therapy

B. Krause;
UniversityMedical Center, University of Rostock, Department of Nuclear Medicine, Rostock, GERMANY.

OP-735

Moving PSMA RLT to earlier lines

B. Privé;
Erasmus Medical Center, Department of Radiation oncology, Rotterdam, NETHERLANDS.

OP-736

The future role of radiotherapy of prostate cancer

1509

Tuesday, September 12, 2023, 3:00 PM - 4:30 PM
Hall G2

e-Poster Presentations Session 11 - Translational Molecular Imaging & Therapy Committee + Radiopharmaceutical Sciences Committee: Novel Therapeutic Approaches

EPS-210

In Vitro Evaluation of Radiation-induced DNA Damage and Repair within Targeted Radionuclide Therapies in Comparison to External Radiation

R. Winter, *U. Bauder-Wüst, M. Schäfer, M. Roscher, R. Lopez Perez, M. Benešová-Schäfer;*
German Cancer Research Center, Heidelberg, GERMANY.

Aim/Introduction: For late-stage cancer patients who do not respond to conventional therapies, Targeted Radionuclide Therapy (TRNT) and Targeted Alpha Therapy (TαT) have lately been aroused as highly potent treatment options. Despite the promising outlook, radioresistance development associated with mutations in DNA repair genes has been found in prostate cancer (PCa) patients. However, knowledge and understanding about the mechanism of DNA damage induction and repair after TRNT and TαT is still incomplete. Therefore, this study aims to investigate these mechanisms with the β-emitter ^{177}Lu as well as the α-emitters ^{227}Th and ^{223}Ra. External radiation with photons, as an established therapy, will serve as an alternative for further comparison and calibration. ***Materials and Methods:*** LNCaP was selected as PCa cell line. Cells were incubated with non-complexed radionuclides for 4 h with 100, 500, 1000 and 5000 kBq of [^{177}Lu]$LuCl_3$ or with 1, 5, 10 and 100 kBq of [^{227}Th]$ThCl_4$ or [^{223}Ra]$Ra(NO_3)_2$. After incubation, cells were fixated. The DNA damaging effects were compared to treatment with external radiation using doses ranging from 0.5 to 2.5 Gy in 0.5 Gy increments and fixated 30 min after irradiation. Systematic evaluation of nuclide- and dose-dependence of DNA damage was performed by visualization of DNA double-strand breaks via immunofluorescent staining of γH2AX. ***Results:*** Literature research showed a ratio of 1:700 for activities of α-emitters: β-emitter leading to comparable DNA damage. This observation was in line with our experiments. Calibration with external radiation showed 5000 kBq of ^{177}Lu equals 1.1 Gy external radiation dose whereas 5 kBq of ^{223}Ra equals 0.6 Gy. Since the same activity of ^{227}Th corresponds only to 0.2 Gy, ^{223}Ra showed higher damaging potential than ^{227}Th. For all treatments, signal intensity of foci was increasing linearly with dose, while foci area showed a broader size range for α-emitters than gamma and β-emitters. ***Conclusion:*** The results provide a deeper understanding of the DNA damage induction after TRNT and TαT, and highlight differences in β- and α-emitter-based therapies like higher damaging potential of ^{223}Ra. Hereby the short-lived daughter radionuclides of ^{223}Ra, namely the α-emitters ^{219}Rn and ^{215}Po with a half-life of 4.0 s and 1.9 ms, are increasing the frequency of emitted α-particles. Likewise, the study is setting a baseline for therapeutic dose estimation of different radionuclides. Subsequent experiments with PSMA-617 labelled radionuclides as well as other targets like neurokinin receptor 1 (NK-1) will provide further amelioration of TRNT and TαT.

EPS-211

Three-dimensional spheroids as in vitro preclinical model for radiobiology studies: the example of radium-223 in prostate cancer spheroids

A. Pires Lourenço[1,2,3], *I. A. Marques*[4,2,5], *D. Cancelinha*[4,6], *G. Costa*[7], *A. M. Abrantes*[4,2,3], *M. F. Botelho*[4,2,3];
[1]*Institute of Biophysics, Coimbra Institute for Clinical and Biomedical Research (iCBR) area of CIMAGO, Faculty of Medicine, University of Coimbra, Coimbra, PORTUGAL,* [2]*Center for Innovative Biomedicine and Biotechnology (CIBB), University of Coimbra, Coimbra, PORTUGAL,* [3]*Clinical Academic Center of Coimbra (CACC), Coimbra, PORTUGAL,* [4]*Univ Coimbra, Coimbra Institute for Clinical and Biomedical Research (iCBR) area of Environment Genetics and Oncobiology (CIMAGO), Institute of Biophysics, Faculty of Medicine, Coimbra, PORTUGAL,* [5]*Faculty of Pharmacy, University of Coimbra, Coimbra, PORTUGAL,* [6]*Faculty of Science and Technology, University of Coimbra, Coimbra, PORTUGAL,* [7]*Department of Nuclear Medicine, Centro Hospitalar e Universitário de Coimbra (CHUC), Coimbra, PORTUGAL.*

Aim/Introduction: Several radiopharmaceuticals have emerged for diagnostic, therapeutic or theragnostics. Conducting radiobiological studies during radiopharmaceuticals preclinical testing could provide relevant insights to improve the clinical outcomes. Usually, they are not included into this phase neither are done in 3D cell cultures, which better mimics the human tumor microenvironment. The aim of this study is to use and validate 3D spheroids as in vitro preclinical models for radiobiology research. Specifically, we propose prostate cancer spheroids to evaluate the radiobiology of the alpha-emitter radium-223. ***Materials and Methods:*** Prostate cancer (PCa) spheroids were developed using PC3 cells, a human metastatic PCa cell line derived from a bone metastasis. Three techniques for generating 3D spheroids were tested: magnetic levitation, hanging drop and liquid overlay technique (in ultra-low attachment plates). Spheroids with 5000 cells were generated, incubated with increasing volumic activities of radium-233 dichloride (Ra-223, 55-7040Bq/mL) for 24h, and then monitored for 7 days by optical microscopy. Radiobiology studies were done 7 days post-irradiation, namely spheroids' viability (ATP levels) and cell death profile (apoptosis or necrosis). Immunohistochemistry , invasion and migration assays were also performed, as well as dosimetry to correlate the biological effects with doses. ***Results:*** Spheroids generated by liquid overlay technique showed to be faster (48h) to develop and easier to irradiate, with high reproducibility among experiments. Generally, a decrease in spheroid size and integrity was observed with increasing activities of Ra-223 over time. Spheroids' area and viability, 7d post-irradiation with 5280Bq/mL, decreased to 1.27±0.04mm2($p<0.0001$) and 32.2±1.7% ($p<0.0001$), respectively, comparatively to control. These effects were associated with increased cell death, showed by an increasing in morphological features of apoptosis and higher levels of annexin-V staining. Compared to our previous results obtained in conventional 2D PC3 cell cultures, fewer biological effects are obtained in 3D spheroids, when exposed to the same volumic activity of Ra-223. ***Conclusion:*** Our results demonstrate that 3D spheroids may be used as an in vitro preclinical model for radiobiology studies. The advantages include a better mimic of the human microenvironment and, consequently, the radiopharmaceutical's biological effects and, in terms of radiological protection, allows carrying out analyzes easily and safely. Apart from the need to optimize the spheroid model for each cell line, it showed to be easily reproduced for similar assays with other cell lines, as well as, for other radiopharmaceuticals. Acknowledges: FCT PhD Scholarship to I.A.M.(SFRH/BD/136973/2018). Institutional funding from FCT strategic projects (UIDB/04539/2020,UIDP/04539/2020) and by COMPETE-FEDER (POCI-01-0145-FEDER-007440).

EPS-212

Comparison of biological effects produced by radioactively labeled antibodies in human cancer cells and fungal cells

J. Bonet, *M. E. Malo, K. J. Allen, C. Frank, R. Jiao, E. Dadachova; University of Saskatchewan, Saskatoon, SK, CANADA.*

Aim/Introduction: Radioimmunotherapy (RIT) has been used as an effective cancer therapy for decades. Current work includes the translation of this treatment modality into the field of opportunistic fungal infections. The aim of this project is to conduct mechanistic studies to compare the effects of RIT on both cancer and fungal cells. ***Materials and Methods:*** Human pathogenic yeast Cryptococcus neoformans and the human acute myeloid leukemia cell line OCI-AML3 were used as a model in vitro systems. C.neoformans was treated with 3.7 KBq and 2.59 KBq [^{225}Ac]Ac-DOTA-400-2 or 3.7 Mbq and 1.85 MBq [^{177}Lu]Lu-DOTA-400-2 monoclonal antibodies raised against the 1,3-β-glucan antigen. Cells were incubated with radiolabeled antibodies for 1 hour, washed, and cultured in a minimal medium. OCI-AML3 was comparatively treated with 3.7 KBq and 2.59 KBq of [^{225}Ac]Ac-DOTA-HuM195 (lintuzumab) or 3.7 Mbq and 1.85 MBq of [^{177}Lu]Lu-DOTA-HuM195 anti-CD33 antibody. Cells were incubated with radiolabeled antibodies for 1 hour, washed, and cultured in a complete medium. Mechanistic studies on the effect of RIT on eukaryotic cells were performed by visualizing DNA double-strand breaks (DSBs) via Gamma-Histone 2Ax (γ-H2Ax) immunofluorescence, cell viability via clonogenic and trypan blue survival assays, antibody internalization assays, and micronuclei formation assays. ***Results:*** Clonogenic survival assay demonstrated that both ^{177}Lu and ^{225}Ac-labeled antibodies were effective in killing leukemic and fungal cells, at 24, 48, and 72 hrs post-treatment. ^{225}Ac-labeled antibodies demonstrated greater potency in vitro and were more cytotoxic towards both fungal and leukemic cells compared to ^{177}Lu-labeled antibodies. Gamma-H2AX immunofluorescence demonstrated increased DSBs in ^{225}Ac-labeled antibody-treated fungal and leukemic cells 1 hr post-treatment compared to ^{177}Lu-labeled antibodies. ***Conclusion:*** Current comparative evaluation of the effect of RIT on fungal and human cells supports the predicted cytotoxic response of both fungal and cancer cell lines towards RIT. The eukaryotic nature of both fungal and human cells makes them respond in similar ways to the effects of antibody-delivered targeted radiation.

EPS-213

HDACi Treatment Increases SSTR2 mRNA and Protein Expression in Tumor-Bearing Animals: What is the Effect on Radiolabeled DOTATATE uptake?

M. J. Klomp, *L. van den Brink, P. M. van Koetsveld, C. M. A. de Ridder, D. C. Stuurman, L. J. Hofland, S. U. Dalm; Erasmus MC, Rotterdam, NETHERLANDS.*

Aim/Introduction: Somatostatin type-2 receptors (SSTR2) form a pivotal target for the treatment of neuroendocrine tumors (NET) using [^{177}Lu]Lu-DOTATATE. However, treatment responses are suboptimal and improvement is thus required. We aim to increase SSTR2 expression using epigenetic drugs, i.e. histone deacetylase (HDAC) inhibitors (HDACis), to increase the tumoral [^{177}Lu]Lu-DOTATATE dose for improved treatment responses. Promising results are described after HDACi treatment in vitro, but encouraging in vivo studies are lacking. Therefore, the objective of this study was to assess the effect of several HDACis on SSTR2 expression and [^{111}In]In/[^{177}Lu]Lu-DOTATATE uptake in tumor-bearing animals. Our second objective was to gain more insight into the association between HDAC and SSTR2 expression. ***Materials and Methods:*** Human NCI-H69 small-cell lung carcinoma cells and human BON-1 pancreatic NET cells were treated with an HDACi (i.e entinostat, mocetinostat (MOC), LMK235, CI994 or panobinostat (PAN)), and evaluated for SSTR2 mRNA expression levels and [^{111}In]In-DOTATATE uptake. Additionally, NCI-H69 and BON-1 tumor-bearing animals were treated with the HDACis, followed by [^{111}In]In/[^{177}Lu]Lu-DOTATATE injection and biodistribution studies. Tumors were collected to analyze SSTR2 expression. Additionally, HDAC and SSTR2 mRNA expression levels were measured in NCI-H69, BON-1, NCI-H727 (human pulmonary carcinoid) and GOT1 (human midgut NET) xenografts and/or cells. ***Results:*** All HDACis significantly enhanced SSTR2 mRNA expression levels and uptake of [^{111}In]In-DOTATATE in vitro. However, no significant increase in tumoral [^{177}Lu]Lu-DOTATATE uptake was observed after HDACi treatment in NCI-H69 xenografts, whereas tumoral SSTR2 mRNA expression levels were significantly upregulated after MOC, CI994 and PAN treatment (≤2.1-fold, $p<0.0001$) and SSTR2 protein expression levels after CI994 (1.3-fold, $p=0.0012$). In line with what is observed in PAN-treated NCI-H69 tumor-bearing animals, PAN-treated BON-1 xenografts only demonstrated significantly increased SSTR2 mRNA expression levels (2.0-fold, $p=0.003$). Moreover, BON-1 xenografts showed a significantly higher expression for six out of the eleven examined HDACs in comparison to NCI-H69 tumors. Focusing on these elevated HDACs in cell lines, an inverse correlation was found between HDAC3 and SSTR2 expression (Pearson $r=-0.92$, $p<0.0001$). ***Conclusion:*** Depending on the inhibitor, increased SSTR2 expression levels were observed after HDACi treatment in vitro and in vivo. Despite this, tumoral radiolabeled DOTATATE uptake levels were not significantly enhanced in vivo; not in NCI-H69, nor in BON-1 tumor-bearing animals regardless of higher HDAC expression levels. The discrepancy between the increased SSTR2 expression and unchanged radiolabeled DOTATATE uptake after HDACi treatment indicates the need for further investigations, including a better understanding of the association between HDACs and SSTR2.

EPS-214

Preclinical efficacy of novel anti-oxMIF/HSG bispecific antibody for pretargeted radioimmunotherapy

A. Puchol Tarazona, *I. Mirkina, M. Thiele, A. Schinagl; OncoOne Research & Development GmbH, Vienna, AUSTRIA.*

Aim/Introduction: This study aimed to evaluate a two-step pretargeting radioimmunotherapy based on an anti-oxMIF x anti-HSG (histamine-succinyl-glycyl) bispecific antibody and a ^{177}Lu-labelled di-HSG peptide hapten in murine models of colorectal and pancreatic cancer. The antibody targets oxMIF - the "oxidised", disease-related structural isoform of the pleiotropic cytokine MIF (macrophage migration inhibitory factor)[1]. ***Materials and Methods:*** An anti-oxMIF x anti-HSG bispecific antibody (cON-05) in the format Fab-scFv-Fc was designed, recombinantly expressed and purified. Infrared dye-labelled cON-05 was administered to Balb/c mice bearing subcutaneous CT26 cancer syngrafts to assess tumour uptake and retention by infrared imaging and to determine its half-life in circulation. Balb/c mice bearing subcutaneous CT26 tumours or Balb/c nude mice bearing subcutaneous CFPAC-1 tumours were given a single intravenous injection of the antibody (doses 1.0, 2.5 or 5.0 mg/kg). 3-5 days later, the mice received one tenth molar equivalents of a ^{177}Lu-labeled, di-HSG hapten peptide (3.7, 9.3 or 18.5 MBq). At least one control group given only the radiolabelled hapten

at the highest dose was included. Tumour volume and body weight were monitored for three weeks. ***Results:*** Rapidly growing subcutaneous CT26 tumours almost completely regressed when mice were given the highest treatment dose (5 mg/kg and 18.5 MBq) with a pretargeting delay of three days. Administered with a 5-day pretargeting interval, the highest dose arrested tumour growth in both CT26 and CFPAC-1-derived cancer models, while the lower doses reduced the tumour growth rate. In all cases, the highest treatment dose was well tolerated and resulted in 100% survival at the study endpoint, in contrast to 0% or 50% survival for the control groups in the CT26 and CFPAC-1 models, respectively. ***Conclusion:*** Our pretargeting therapy making use of an anti-oxMIF x anti-HSG bispecific antibody and a ^{177}Lu-loaded peptide hapten resulted in nearly complete tumour regression or stopped tumour growth in murine models of colorectal and pancreatic adenocarcinoma. The treatment led to 100% survival and was well tolerated. This intervention could prove effective at delivering high radioactive doses safely to tumours in oxMIF-positive patients. ***References:*** 1. Schinagl A, Thiele M, Douillard P, et al. Oxidized macrophage migration inhibitory factor is a potential new tissue marker and drug target in cancer. Oncotarget. 2016;7(45):73486-73496.

EPS-215

Combined Treatment with ^{177}Lu-DOTATOC and Histone Deacetylase Inhibitor s on SSTR2 Expression and Uptake in in vivo

H. Bakr[1,2], *A. Al-Awar*[1], *E. Forssell-Aronsson*[1,2];
[1]*Department of Medical Radiation Sciences, Institute of Clinical Sciences, Sahlgrenska Center for Cancer Research, Sahlgrenska Academy, University of Gothenburg, Gothenburg, SWEDEN,* [2]*Department of Medical Physics and Biomedical Engineering, Sahlgrenska University Hospital, Gothenburg, SWEDEN.*

Aim/Introduction: Patients with metastatic disease from neuroendocrine tumours are often successfully treated with ^{177}Lu-octreotate, but few are cured. Histone deacetylase inhibitors (HDACis) have been used for a long time in psychiatry and neurology, and have lately been proposed for treatment of cancer, They influence the regulation of gene expression, cell growth pathways, and cell cycle arrest in cancer cells, and have shown cytostatic effect. The aim of this study was to investigate the potentially increased therapeutic effect of combining radiation therapy with the HDACi valproic acid (VPA) in mice bearing the human small-intestine neuroendocrine GOT1 tumours. ***Materials and Methods:*** BALB/c mice bearing GOT1 tumours were divided into five groups of 5-6 animals/group. The mice received either 1) a single i.v injection with 30 MBq ^{177}Lu-octreotide alone, 2) VPA administered orally once daily for 5 days per week alone, 3) combined treatment 1 and 2, or 4) 2x15 MBq ^{177}Lu-octreotide 48h apart combined with treatment 2. One group was mock-treated and used as control. The body weight and tumour volume were measured three times per week. Animals were killed when the tumour weight was 10% of the body weight. ***Results:*** The animals in the combination therapy groups with 2x15 MBq ^{177}Lu-octreotide showed a reduction in relative tumor size during the first week, while there was no reduction in tumour size in the other groups. Furthermore, the animals in that group also had the longest median overall survival of 39 days (max 70 days), while corresponding values for the other groups were 18-32 days and maximal values of 25-44 days. ***Conclusion:*** The results showed that an increased therapeutic effect could be achieved with a combination of ^{177}Lu-octrotide and the HDACi VPA, both regarding tumour volume reduction and overall survival. Best results were obtained after fractionation of the ^{177}Lu-.octreotide. Future studies should aim for finding the most optimal treatment schedule including fractionation of both ^{177}Lu-octreotide/octreotate and the HDACi.

EPS-216

Effective treatment of SSTR2 positive small cell lung cancer using^{211}At-containing targeted α-particle therapy agent which promotes endogenous anti-tumor immune response.

F. Yu, *S. Qin, J. Zhang, M. Yang;*
Department of Nuclear Medicine, Shanghai Tenth People's Hospital, Tongji University School of Medicine, Shanghai, CHINA.

Aim/Introduction: Small cell lung cancer (SCLC) is a neuroendocrine tumor with a high degree of malignancy. Due to limited treatment options, patients with SCLC have a poor prognosis. ***Materials and Methods:*** We developed and evaluated biological effects of [^{211}At]SAB-Oct for targeted alpha therapy. Concurrently, we explored immunogenicity triggered by alpha-emitter ^{211}At and excavated its potential mechanisms. ***Results:*** We have found, however, that intravenously administered octreotide (Oct) armed with astatine-211 ([^{211}At]SAB-Oct) is effective against somatostatin receptor 2 (SSTR2)-positive SCLC tumor in SCLC tumor-bearing BALB/c nude mice. In biodistribution analysis, [^{211}At]SAB-Oct achieved a highest concentration in the SCLC tumors up to 3 hours after injection as time proceeded. A single intravenous injection of [^{211}At]SAB-Oct (370 kBq) was sufficient to suppress SSTR2-positive SCLC tumor growth in treated mice by inducing DNA double strand breaks. Additionally, a multi-treatment course (370 kBq followed by twice doses of 370 kBq for a total of 1110 kBq) inhibited the growth of the tumor compared to the untreated control group without significant off-target toxicity. Surprisingly, we found that [^{211}At]SAB-Oct could up-regulate the expressions of calcreticulin and major histocompatibility complex I (MHC-I) on the tumor cell membrane surface, suggesting that α-particle internal irradiation may activate endogenous anti-tumor immune response through the regulation of immune cells in the tumor microenvironment, which could synergically enhance the efficacy of immunotherapy. ***Conclusion:*** We conclude that [^{211}At]SAB-Oct is a potential new therapeutic option for SSTR2-positive SCLC.

EPS-217

DOTAGA-modified DB15 mimics for theranostic use in prostate cancer

P. Kanellopoulos[1], *A. Mattsson*[1], *A. Abouzayed*[1], *K. Obeid*[1], *B. A. Nock*[2], *V. Tolmachev*[1], *T. Maina*[3], *A. Orlova*[1];
[1]*Uppsala University, Uppsala, SWEDEN,* [2]*INRASTES, NCSR "Demokritos", Athens, GREECE,* [3]*INRASTES, NSCR "Demokritos", Athens, GREECE.*

Aim/Introduction: The gastrin-releasing peptide receptor (GRPR) is frequently overexpressed in primary and metastatic prostate cancer. We herein report on three mimics of the neprilysin (NEP)-resistant SPECT radiotracer [^{99m}Tc]Tc-DB15 (N_4-Ama-Dig-DPhe-Gln-Trp-Ala-Val-Sar-His-Leu-NHEt, N_4: 6-carboxy-1,4,8,11-tetraazaundecane, Ama: 4-aminomethylaniline, Dig: diglycolic acid) (1). These analogs carry the DOTAGA instead of the N_4 chelator, thus allowing for coordination of trivalent-radiometals, including the theranostic In-111/Lu-177 pair. To compensate for charge changes at the N-terminus, a Arg/DArg was introduced next to DOTAGA, yielding: AU-SAR-M1 (DOTAGA-Ama-Dig-DPhe-Gln-Trp-Ala-Val-Sar-His-Leu-NHEt), AU-SAR-M2 ([DOTAGA-Arg]

AU-SAR-M1) and AU-SAR-M3 ([DOTAGA-DArg]AU-SAR-M1). After labeling with In-111, the respective [111In]In-radiopeptides were compared in GRPR-expressing cell and animal models. ***Materials and Methods:*** After [^{111}In]In-labeling (30 min, 85°C), the metal-chelate stability was assessed under 1000x molar excess of EDTA (1 h). GRPR-specificity and cell-uptake over time were tested in PC-3 cells. Metabolic stability was determined in peripheral blood of healthy Swiss albino mice 5 min post-injection (pi), while biodistribution was performed in Balb/c nu/nu mice bearing PC-3 xenografts at 4 h pi. ***Results:*** Radiochemical yields and complex stability were high for all radiopeptides (>97% and >91%, respectively). All radiotracers displayed a sub-nanomolar receptor affinity and a highly GRPR-specific cell binding. Cell associated activity was: 39±2% of added activity for [^{111}In]In-AU-SAR-M1, 33±1% for [^{111}In]In-AU-SAR-M2 and 48±3% for [^{111}In]In-AU-SAR-M3. All radiopeptides displayed metabolic stabilities comparable or higher than [^{99m}Tc]Tc-DB15. During biodistribution, [^{111}In]In-AU-SAR-M1 (11±1 %IA/g) and [^{111}In]In-AU-SAR-M2 (12.7±0.8 %IA/g) displayed almost twice as high tumor uptake vs. [^{111}In]In-AU-SAR-M3 (6.7±0.3 %IA/g; $p<0.001$). On the other hand, [^{111}In]In-AU-SAR-M3 demonstrated the lowest pancreatic uptake (0.5±0.1 %IA/g), followed by [^{111}In]In-AU-SAR-M1 (2±1.2 %IA/g; $p<0.0001$) and [^{111}In]In-AU-SAR-M2 (9±2 %IA/g; $p<0.0001$). Renal uptake was lower for the first two radiopeptides (3.1±0.3 %IA/g and 3.4±0.4 %IA/g respectively; $p<0.001$ & $p<0.01$), whereas [^{111}In]In-AU-SAR-M2 had higher intestinal uptake than the other two analogs. Interestingly, [^{111}In]In-AU-SAR-M1 displayed the highest tumor-to-background ratios, although second in rank in terms of tumor uptake ***Conclusion:*** Three novel DB-15 mimics, coupled to DOTAGA for [^{111}In]In-labeling, were successfully prepared, showing higher resistance to NEP than the parent [^{99m}Tc]Tc-DB15. The introduction of basic Arg/DArg next to DOTAGA had no considerable impact on their biological performance. [^{111}In]In-AU-SAR-M1, lacking a basic Arg/DArg residue next to DOTAGA, displayed the best tumor-to-background ratios in PC-3 tumor-bearing mice. ***References:*** (1) Nock et al. Cancers. 2021; 13: 5093

EPS-218

Development and preclinical evaluation of biodistribution and dosimetry of ^{177}Lu-labelled PSMA targeting therapeutic with optimized linker for treatment of disseminated prostate cancer

A. Orlova[1], *A. Abouzayed*[1], *K. Seitova*[2], *F. Lundmark*[1], *V. Bodenko*[2], *M. Oroujeni*[1], *V. Tolmachev*[1], *U. Rosenström*[1];
[1]*Uppsala University, Uppsala, SWEDEN,* [2]*Tomsk Polytechnic University, Tomsk, RUSSIAN FEDERATION.*

Aim/Introduction: Prostate specific membrane antigen (PSMA) is highly expressed in metastatic castration-resistant prostate cancer (mCRPC) and is a promising therapeutic target. PSMA-targeting agents for diagnostic and therapy of PC are widely used in patient management and has shown an improved outcomes for patients with mCRPC. Using a computer modelling, we have performed an optimization of a urea-based probe for radionuclide visualization of PSMA expression in vivo[1]. With the purpose to develop a targeting agent equally suitable for radionuclide imaging and therapy, the agent containing DOTA chelator was designed (designated BQ7876). The aim of the study was to test the hypothesis that ^{177}Lu-labelled BQ7876 possesses target binding and biodistribution properties potentially enabling its use for radionuclide therapy. ***Materials and Methods:*** BQ7876 was synthesized using Fmoc solid-phase peptide synthesis and labelled with Lu-177. Specificity and affinity of [^{177}Lu]Lu-BQ7876 to PSMA-expressing PC3-pip cells was evaluated and its processing after binding to these cells was studied. Animal studies in mice were performed to assess its biodistribution in vivo, specificity of its accumulation in PSMA-expressing tumour xenografts and dosimetry. In a number of experiments, [^{177}Lu]Lu-PSMA-617 was simultaneously evaluated for comparison. ***Results:*** Peptide was labelled with Lu-177 with radiochemical yield >99%. Its binding to PSMA was specific in vitro and in vivo when tested in antigen saturation conditions and in PSMA-negative tumours, respectively. The binding of [^{177}Lu]Lu-BQ7876 to living PC3-pip cells was characterized by rapid association, while the dissociation included a rapid and a slow phase with affinities K_{D1}= 3.8 nM and K_{D2}= 25 nM. The half-inhibitory concentration for ^{nat}Lu-BQ7876 was 59 nM that is equal to 61 nM for ^{nat}Lu-PSMA-617. Cellular processing of [^{177}Lu]Lu-BQ7876 was accompanied by slow internalization. [^{177}Lu]Lu-BQ7876 was cleared from blood and normal tissues rapidly. Initial elevated uptake in kidneys decreased rapidly, and by 3 h pi, the renal uptake (13±3%ID/g) did not differ significantly from tumour uptake (9±3%ID/g). Tumour uptake was stable between 1 and 3 h followed by a slow decline. The calculated effective dose (0.00423 Sv/GBq) was somewhat lower than the clinical values for [^{177}Lu]Lu-PSMA-617 (~0.08 Sv/GBq). The highest absorbed dose was in kidneys, followed by organs and tissues in abdomen. ***Conclusion:*** Biodistribution studies in mice demonstrated that targeting properties of [^{177}Lu]Lu-BQ7876 are not inferior to properties of [^{177}Lu]Lu-PSMA-617. Phase I clinical study is required to evaluate if [^{177}Lu]Lu-BQ7876 offers any advantage in clinics. ***References:*** [1]Lundmark et al. Pharmaceutics. 2022;14:1098.

EPS-219

Theranostic approach in CD30 positive cancers with a radiolabeled antibody conjugated to the radiosensitizing antitubulin monomethyl auristatin E payload

C. Petitot[1], *J. Frenay*[2], *A. M. M. Dias*[1], *A. Oudot*[1], *A. Helbling*[1], *M. Moreau*[3], *M. Monterrat*[1], *M. Guillemin*[1], *N. Ranjit*[1], *A. Cochet*[4], *P. S. Bellaye*[5], *B. Collin*[6];
[1]*Pirp - Service de Médecine Nucléaire, Centre Georges-François Leclerc, Dijon, FRANCE,* [2]*Icb - Umr Cnrs 6303 / Pirp - Service de Médecine Nucléaire, Centre Georges-François Leclerc, Dijon, FRANCE,* [3]*Icmub - Umr Cnrs 6302, Dijon, FRANCE,* [4]*Icmub - Umr Cnrs 6302 / Pirp - Service de Médecine Nucléaire, Centre Georges-François Leclerc / Chu François Mitterrand, Dijon, FRANCE,* [5]*Pirp - Service de Médecine Nucléaire, Centre Georges-François Leclerc / Lnc - Umr Inserm 1231, Dijon, FRANCE,* [6]*Icmub - Umr Cnrs 6302 / Pirp - Service de Médecine Nucléaire, Centre Georges-François Leclerc, Dijon, FRANCE.*

Aim/Introduction: CD30 is a 120 kDa transmembrane glycoprotein that is the eighth member of the tumour necrosis factor receptor superfamily (TNFRSF8). It interacts with TRAF2 or TRAF5 proteins to activate nuclear factor kappa B (NF-κB), which leads to cellular proliferation and differentiation. CD30 represents an attractive theranostic target since it is overexpressed in many cancers such as lymphomas, melanoma, nasopharyngeal carcinoma or lung cancers. In this context, a theranostic probe based on brentuximab vedotin (BV, antibody drug conjugate approved in CD30 positive lymphomas) might be of great interest, especially for further combination with radiotherapy due to the radiosentization properties of its payload (monomethyl auristatin E, MMAE). Thus, this preclinical study aimed to develop a radiolabeled BV for theranostic PET imaging purposes. ***Materials and Methods:*** KARPAS 299 cell line (anaplastic large cell lymphoma) were used as CD30 positive tumour models. BV was randomly conjugated

to deferoxamine (DFO) to be radiolabeled with zirconium-89 (^{89}Zr). The radiochemical purity (RCP) was assessed by instant thin layer chromatography. In vitro binding assays were performed to ensure that bioconjugation and radiolabeling did not alter the affinity and immunoreactivity of the BV radioconjugate. For the in vivo experiments, a total of 10.10^6 cells were subcutaneously implanted in the right flank of irradiated NOD-SCID mice (n = 6). Finally, ^{89}Zr-DFO-BV (25 µg, 5 MBq per mouse in 100 µL, n = 3) was injected i.v. in tumor-bearing mice (target volume: 300-500 mm^3). In parallel, a blocking group was also performed with the same design plus a 50x excess of « cold » BV. Then, mice underwent PET/CT imaging at 24h, 48h and 72h post-injection and ex vivo gamma counting was performed after the last imaging timepoint. ***Results:*** After radiolabeling, we obtained an RCP systematically > 95% (specific activity of 100MBq/mg). In vitro assays demonstrated good affinity (Kd = 0.15 ± 0.026 nM) and immunoreactivity (about 60%). PET imaging of ^{89}Zr-DFO-BV showed the highest tumour uptake at 72h post-injection (30.4 ± 1.5 %ID/g) with a good specificity as demonstrated by the blocking group (uptake significantly decreased about 5 times, 6.2 ± 2.0 %ID/g) and confirmed by ex vivo gamma counting. ***Conclusion:*** Our study demonstrated that BV could be a suitable PET companion diagnostic in the frame of targeted therapy of CD30 positive cancers. It could also be of great interest for further association with external and/or molecular radiotherapy since the BV's payload (MMAE) is a well-known radiosensitizer

EPS-220

Testing the potential therapeutic use of [^{188}Re]Re-maSSS/maSES-PEG2-RM26 as part of a theranostic pair with their [^{99m}Tc]Tc-labeled counterparts

P. Kanellopoulos, *Q. Yu, A. Abouzayed, E. Bezverkhniaia, V. Tolmachev, A. Orlova;*
Uppsala University, Uppsala, SWEDEN.

Aim/Introduction: Despite the introduction of new radionuclides in use in nuclear medicine, tracers based on Tc-99m are still on high demand, due to its availability and the paired equipment worldwide. Recently two novel [99mTc]Tc-labeled radioantagonist based on the RM26 motif were reported. These two radiotracers ([^{99m}Tc]Tc-maSSS-PEG2-RM26 and [^{99m}Tc]Tc-maSES-PEG2-RM26) (1) displayed promising preclinical results, to the degree that the first one became subject in clinical trials (2). Based on the positive results and the lack of a potent GRPR-targeting theranostic pair for clinical use, we aimed to investigate the performance of these two agents after labeling with generator acquired Re-188. ***Materials and Methods:*** Both maSSS-PEG2-RM26 and maSES-PEG2-RM26 were labeled with Re-188, radiochemical yields were determined using iTLC with PBS or pyridine/CH_3COOH/water 5:3:1.5 as mobile phases and radiochemichal purity was accessed with reverse-phase radio-HPLC. The complex stability was tested with 1000x molar excess of L-Cystein at room temperature. Cell association and GRPR-specificity were tested in PC-3 (37°C, Cf=0.25nM peptide concentration), while for GRPR-blocking 100x molar excess of DOTAGA-PEG2-RM26 was used. The biodistribution profile of the two resulting radiotracers was accessed in Balb/c nu/nu mice bearing PC-3 xenografts. ***Results:*** Radiochemichal yields were 88±9% and 89±9% for maSSS-PEG2-RM26 and maSES-PEG2-RM26, respectively. The HPLC chromatogram showed excellent radiochemical purity for both compounds. Cysteine challenge show a robust metal-chelate with little to none Re-188 released within 1 h. Both radiotracers had a cell-uptake highly GRPR-specific with values reaching 8.5±0.1% of added activity and 5±0.3% respectively, after blocking these values dropped to 1.14±0.01% ($p<10^{-7}$) and 1.0±0.2% ($p<10^{-4}$). Both radiotracers displayed a typical for antagonist cell uptake pattern, with the bulk of the activity remaining on the membrane and a slow internalization over 24 h continues incubation. Both radiotracers displayed similar biodsitribution pattern with their previously reposted [^{99m}Tc]Tc-labeled counterpart (1). Biodistribution results for organ of interest such as liver, kidneys, pancreas and tumors are summarized in the following table. ***Conclusion:*** Despite their rapid washout from other tissues, both [^{188}Re]Re-labeled compounds displayed a descent tumor uptake and retention. Unfortunately, both had high hepatobiliary excretion with very high gastrointestinal activity uptake, hindering their potential therapeutic use due to radiotoxicity. ***References:*** (1) Abouzayed A et al Pharmaceutics. 2021;13(2):182. doi:10.3390/pharmaceutics13020182 (2) Chernov V et al. Cancers (Basel). 2023;15(6):1631 doi:10.3390/cancers15061631

EPS-221

Alpha-emitter radium-223 mediates tumor eradication via STING-dependent pyroptosis

F. Yu, *M. Yang, S. Qin, J. Zhang;*
Department of Nuclear Medicine, Shanghai Tenth People's Hospital, Tongji University School of Medicine, Shanghai, CHINA.

Aim/Introduction: Radium-223 (^{223}Ra) is the first-in-class alpha-emitter to mediate tumor eradication. Radiation emitted from alpha-emitter is usually regarded to reduce tumor burden by directly cleaving double-strand DNA and killing tumor cells. However, the immunogenic characteristics and various cell death modalities triggered by alpha-emitter ^{223}Ra remain unclear. ***Materials and Methods:*** We evaluated biological effects of ^{223}Ra in cancer cell lines and mice models by biological endpoints. Concurrently, we explored immunogenicity and cell death modalities triggered by ^{223}Ra and excavated its mechanisms of pyroptosis induction. Besides, synergistic effect with checkpoint blockade was also assessed. ***Results:*** ^{223}Ra exhibited efficient therapeutic antitumor effects, which examined by cell viability study and tumor regression. More importantly, the irradiated cells increased the pro-inflammatory damage-associated molecular patterns, including surface-exposed calreticulin, released HMGB1, and secreted HSP70, which actively shaped tumor immunogenicity. Pyroptosis, an immunogenic cell death, was also found to play significant roles in the modulation of cancer progression under the therapeutic ^{223}Ra. Mechanically, this synergistic effect relied on ^{223}Ra-induced DNA damage, which activated the STING-mediated DNA sensing pathway, leading to significant increase in the degree of the T cells activation and DCs maturation as well as NLRP3 inflammasome-dependent pyroptosis. Besides, it showed potent therapeutic efficacy in ^{223}Ra combining with checkpoint blockade anti-CD47 mAb. ***Conclusion:*** These findings reveal that alpha-emitter ^{223}Ra with high relative biological effectiveness values induces broad antitumor effects and triggers robust tumor immunogenicity mainly through STING-dependent pyroptosis, which may shed light on promising targets for tumor therapeutic interventions.

EPS-222

Fractionated therapy of the PSMA-targeted radioligand^{212}Pb-AB001 significantly delays tumor growth

A. Kjoel Tornes[1,2], *V. Y. Stenberg*[1,2], *A. Repetto-Llamazares*[1], *R. H. Larsen*[3,1], *A. Juzeniene*[2];
[1]*ArtBio AS, Oslo, NORWAY,* [2]*Department of Radiation Biology, Oslo University Hospital, Oslo, NORWAY,* [3]*Sciencons AS, Oslo, NORWAY.*

Aim/Introduction: Treatment with beta-emitting ^{177}Lu-PSMA-617 is approved for metastatic castration-resistant prostate cancer expressing prostate-specific membrane antigen (PSMA). Targeted

alpha therapy has resulted in favorable outcomes in patients both naïve or refractory to ^{177}Lu-PSMA-617. However, ^{225}Ac ($t_{1/2}$=9.9 days) is not available in high quantities for clinical use and has a long physical half-life compared to the circulatory half-life of anti-PSMA small molecules. Pb-212 ($t_{1/2}$=10.6h) is an in vivo generator of alpha particle emitters whose half-life matches that of small molecules, thereby potentially increasing the therapeutic efficacy of radioligand therapy. Previous studies with the novel PSMA-targeting radioligand ^{212}Pb-AB001 have shown preclinical efficacy in vitro and in vivo [1]. The current preclinical study aims to optimize treatment effectiveness and safety by investigating the treatment regimen of ^{212}Pb-AB001. ***Materials and Methods:*** Athymic nude mice with subcutaneous PC-3 PIP-luc xenografts were treated with ^{212}Pb-AB001 7-10 days post cell inoculation. All groups received a cumulative dose of 0.8 MBq ^{212}Pb-AB001 injected in 1 to 8 fractions in weekly or biweekly intervals. Tumor size and body weights were measured 2-3 times per week. Blood sampling for hematological and clinical chemistry analysis was performed at euthanasia and organs were collected for histology. Flow cytometry was performed to study cell cycle phase distribution and DNA damage in vitro. ***Results:*** Prolonged median survival and tumor growth delay were observed in all treatment groups receiving a cumulative dose of 0.8 MBq ^{212}Pb-AB001 compared to the control. Treatments administered as two injections of 0.4 MBq with a two-week interval or four injections of 0.2 MBq delivered weekly, resulted in significant tumor growth delay and improved overall survival compared to the single dose of 0.8 MBq. Weekly injections of 0.4 MBq or 0.1 MBq, or biweekly injections of 0.2 MBq resulted in similar median survival as the group receiving one dose of 0.8 MBq. No significant differences were observed in body weight, hematology or biochemistry parameters in the treatment groups at day 60. ^{212}Pb-AB001 demonstrated activity-dependent DNA damage (γH2AX), cell-cycle arrest in G2-M phase and apoptosis in vitro. ***Conclusion:*** The current results show that fractionated therapy with ^{212}Pb-AB001 represents a promising strategy to enhance therapeutic efficacy compared to single-dose treatment. The number of fractions, interval duration between fractions, and administered dose per fraction were identified as crucial factors influencing the treatment outcome. This study emphasizes the importance of determining optimal dosing regimen through further preclinical and clinical investigations of ^{212}Pb-AB001. ***References:*** [1]doi:10.3390/cancers14112784

EPS-223

Biodistribution Study and Pre-clinical Radiopharmaceutical Therapy with a CXCR4-targetted Compound on a Human CXCR4 Positive Multiple Myeloma Orthotopic Model

I. Bloise*, H. Kuo, N. Colpo, H. Merkens, P. Ng, D. Kwon, L. Escano, F. Kuchenbauer, K. Lin, F. Benard;*
BC Cancer, Vancouver, BC, CANADA.

Aim/Introduction: Despite recent treatment advances, Multiple Myeloma (MM) represents 10% of hematological malignancies and remains incurable. The chemokine receptor 4 (CXCR4), overexpressed in MM and other solid tumors and hematological malignancies, is an attractive target for radiopharmaceutical therapy (RPT). We developed an orthotopic model of MM applicable to pre-clinical studies involving CXCR4-targeted radiopharmaceuticals. In this study, we investigate the applicability of such model in RPT, including treatment efficacy, possible side effects and potential toxicity. ***Materials and Methods:*** SPECT/CT images and biodistribution studies were performed on luciferase-transfected AMO1 MM xenograft-bearing NRG male mice with [^{177}Lu]Lu-BL34. For RPT, NRG mice were intravenously injected with 10^6 luciferase-transfected AMO1 cells. Animals were clinically monitored once a week for the following 5 weeks, then divided into groups and injected with saline, 15MBq, 35MBq and 50MBq of [^{177}Lu]Lu-BL34 (control n=4/ RPT n=8). Disease engraftment and spread was also monitored weekly by in vivo bioluminescence imaging in a Perkin Elmer's IVIS Lumina 5, starting 3 weeks post-injection until RPT, and once 2 weeks after therapy due to radiation safety protocols. Animals were monitored daily following therapy until reaching humane endpoint criteria and their weights measured and recorded once a week. ***Results:*** Biodistribution study and SPECT/CT images showed high persistent uptake in xenografts and low uptake with quick washout in healthy organs. Limited mobility and hind limb paralysis were the most common symptoms leading to euthanasia in the different groups. No significant weight loss (>10% of body weight) was observed in any of the treatment groups. Extra-marrow tumor growth was observed in 3 mice in the 15MBq group and 1 mouse in the 35MBq, tumors involved the mandible, thorax, hips and lumbar spine. The median survival endpoint was reached by control, 15MBq, 35MBq and 60MBq in 20, 18, 20 and 24 days respectively. Statistical significance was achieved only in the highest activity treatment group (p=0.0158). ***Conclusion:*** Many clinical trials use CXCR4-targeted RPT for marrow ablation, in this pre-clinical study we were able to show potential treatment benefits using a non-myeloablative approach. Treatment was well tolerated, no acute side effects from therapy were evident regardless of the injected activity, and humane endpoint was reached due to disease progression. Further work is needed as many CXCR4-targeted radiopharmaceuticals are highly selective for human CXCR4, which may mask some undesirable effects of RPT in mouse models due to CXCR4 expression in normal hematopoietic stem cells and bone marrow stromal cells.

EPS-224

Design and evaluation of a new generation of long-acting SSTR2 antagonists for enhanced radionuclide therapy of NETs

M. Handula[1]*, S. Beekman*[1]*, Y. Seimbille*[1,2]*;*
[1]*Erasmus MC, Rotterdam, NETHERLANDS,*
[2]*TRIUMF, Vancouver, BC, CANADA.*

Aim/Introduction: The high expression of the somatostatin receptor subtype 2 (SSTR2) by the neuroendocrine tumors (NETs) makes it an ultimate target for the diagnosis and treatment of the malignancies. Various biovectors were developed to target NETs and among them, DOTA-JR11 a SSTR2-antagonist. Preclinical studies showed that high tumor uptake and favorable biodistribution were observed using the antagonist. However, rapid blood clearance was reported upon injection of the radioligand. Hence, there is a need to improve the bioavailability of the radioligand to achieve higher tumor uptake, and consequently enhance therapeutic efficacy. We report herein the development and evaluation of SSTR2-antagonists bearing palmitic fatty acid to improve the pharmacokinetic properties of DOTA-JR11. ***Materials and Methods:*** DOTA-JR11-Lys(N_3)-NH_2 (1) was synthesized by solid-phase peptide synthesis. Palmitic acid was conjugated either to bicyclononyne (BCN) or aza-dibenzocyclooctyne (DBCO) and coupled to 1 via the strain-promoted azide-alkyne cycloaddition to obtain compounds 2 and 3, respectively. Both peptides were radiolabeled with [^{177}Lu]$LuCl_3$ in optimized conditions. Stability studies in PBS and mouse serum, as well as hydrophilicity ($LogD_{7.4}$)

were determined for both compounds. Competitive binding assay as well as cell uptake and internalization were carried out in U2OS.SSTR2 cells. ***Results:*** Compounds 1, 2 and 3 were successfully synthesized and obtained in 15, 55 and 65% chemical yield, respectively. 2 and 3 were radiolabeled with lutetium-177 and obtained in excellent radiochemical yields (> 98%) and radiochemical purities (> 98%). [^{177}Lu]Lu-2 and [^{177}Lu]Lu-3 exhibited a $logD_{7.4}$ value of 0.63 and 0.56, respectively, and high stability in PBS (> 91%) at 24 h post incubation at 37 °C. However, [^{177}Lu]Lu-2 showed higher sensitivity towards peptidase digestion in mouse serum compared to [^{177}Lu]Lu-3 (24.2 and 98.7% intact radioligand at 24 h post incubation at 37 °C, respectively). The binding affinity of 2 and 3 was 1.1 and 9.7-fold lower than the binding affinity of the parent peptide DOTA-JR11 (4.1 nM and 37.0 nM vs. 3.8 nM). [^{177}Lu]Lu-2 and [^{177}Lu]Lu-3 had lower cell uptake compared to [^{177}Lu]Lu-DOTA-JR11 (26.3% AD and 16.1% AD, respectively, compared to 54.7% AD). However, uptake could be blocked, confirming the specificity of the binding to SSTR2. ***Conclusion:*** Our new DOTA-JR11 analogs were successfully synthesized and radiolabeled with lutetium-177. They exhibited good binding affinity to SSTR2 and showed acceptable cell uptake. Further optimization of the molecular structure to enhance the hydrophilicity and the pharmacokinetics is underway, as well as in vivo evaluation in tumor bearing mice.

EPS-225

DOTA-MGS5, a novel cholecystokinin-2 receptor-targeting peptide analogue for use in targeted therapy, preclinical evaluation for clinical translation

T. Zavvar[1], *A. A. Hoermann*[1], *M. Klingler*[1], *J. Hagenbuchner*[2], *L. Joosten*[3], *G. Franssen*[3], *P. Laverman*[3], *M. W. Konijnenberg*[4], *I. Skvortsova*[5], *L. Gruber*[6], *E. von Guggenberg*[1];
[1]*Department of Nuclear Medicine, Medical University of Innsbruck, Innsbruck, AUSTRIA,* [2]*Department of Pediatrics II, Medical University of Innsbruck, Innsbruck, AUSTRIA,* [3]*Department of Medical Imaging, Radboud University Medical Center, Nijmegen, NETHERLANDS,* [4]*Department of Radiology and Nuclear Medicine, Erasmus Medical Center, Rotterdam, NETHERLANDS,* [5]*Department of Therapeutic Radiology and Oncology, Medical University of Innsbruck, Innsbruck, AUSTRIA,* [6]*Department of Radiology, Medical University Innsbruck, Innsbruck, AUSTRIA.*

Aim/Introduction: Cholecystokinin-2 receptors (CCK2R) are overexpressed in medullary thyroid carcinoma (MTC) and some other malignancies. We recently reported on the development of DOTA-DGlu-Ala-Tyr-Gly-Trp-(N-Me)Nle-Asp-1-Nal-NH_2 (DOTA-MGS5), a novel minigastrin analogue that exhibits improved stability and enhanced tumour targeting properties. As a result, targeting CCK2R with DOTA-MGS5 provides a potential new theranostic strategy for patients with CCK2R expressing neoplasms. We conducted preclinical studies with the aim of clinical translation of [^{177}Lu]Lu-DOTA-MGS5 for peptide receptor radionuclide therapy (PRRT). ***Materials and Methods:*** A431 and AR42J cells expressing CCK2R were used to examine the receptor-specific cellular uptake of [^{177}Lu]Lu-DOTA-MGS5 up to 4h after incubation. In addition, confocal microscopy studies were performed using MGS5 conjugated with the fluorescent dye ATTO-488. Biodistribution studies were conducted in A431-CCK2R xenografted female BALB/c nude mice for up to seven days after injection. To investigate the therapeutic effect, cell viability studies were performed on A431-CCK2R cells. The radiation dose response after incubation with ~60 or ~240 kBq (~0.5-2 nM) [^{177}Lu]Lu-DOTA-MGS5 was compared to different doses of external beam radiation (2, 4, 8 Gy). ***Results:*** [^{177}Lu]Lu-DOTA-MGS5 exhibited a high and specific cell uptake of 68.0±2.3% in A431-cells and 48.6±2.2% in AR42J-cells after 4h incubation. Fluorescence microscopy confirmed a rapid receptor-specific translocation of ATTO-488-MGS5 from the cell membrane to the intracellular compartment in both cell lines. The radiolabelled peptide exhibited a favourable biodistribution profile in animals, with low non-specific radioactivity accumulation in the majority of tissues. The tumour uptake in A431-CCK2R xenografts was remarkably increased (28.9±7.2% and 12.6±3.3% IA/g at 1 and 3 days after injection) combined with a very favourable tumour-to-kidney ratio (13-15). In stomach, with physiological CCK2R expression, a somewhat prolonged retention of radioactivity was observed with a tumour-to-stomach ratio of 4-6. On the basis of the pharmacokinetic data acquired in mice, human dosimetry estimates were calculated. In the cell viability studies a reduction of total viable cells comparable to 4 Gy external beam radiation was achieved. ***Conclusion:*** A high receptor specific cell uptake and favourable tumour targeting properties was confirmed for [^{177}Lu]Lu-DOTA-MGS5. Improved tumour uptake and retention was determined in A431-CCK2R xenografted mice. The therapeutic effect observed in vitro and the dosimetry extrapolations from mice to human support the therapeutic use of [^{177}Lu]Lu-DOTA-MGS5 in patients with advanced MTC and other CCK2R-expressing tumours.

References: von Guggenberg, Elisabeth, et al. "Preliminary clinical experience of cholecystokinin-2 receptor PET/CT imaging using the 68Ga-labeled minigastrin analog DOTA-MGS5 in patients with medullary thyroid cancer." JNM (2023).

EPS-227

Preclinical evaluation of a radiotheranostic single-domain antibody against Fibroblast Activation Protein alpha

Y. Dekempeneer[1], *S. Massa*[1], *F. Santens*[1], *L. Navarro*[1], *M. Berdal*[1], *M. M. Lucero*[1], *A. Pombo Antunes*[1], *J. A. Van Ginderachter*[2,3], *T. Lahoutte*[1,4,3], *N. Devoogdt*[1,3], *M. D'Huyvetter*[1,3];
[1]*PRECIRIX NV/SA, Brussels, BELGIUM,* [2]*VIB Center for Inflammation Research, Brussels, BELGIUM,* [3]*Vrije Universiteit Brussel, Brussels, BELGIUM,* [4]*UZ Brussel, Brussels, BELGIUM.*

Aim/Introduction: Fibroblast activation protein alpha (FAP) is highly expressed on cancer associated fibroblasts of epithelial-derived cancers. Breast, colon and pancreatic tumors often show strong desmoplastic reactions which results in a dominant presence of stromal cells. FAP gains interest as a target for molecular imaging and targeted therapies. Single-domain antibodies (sdAbs) are the smallest antibody-derived fragments with beneficial pharmacokinetic properties for molecular imaging and targeted therapy. ***Materials and Methods:*** We describe the generation, selection and characterization of a sdAb against FAP. We assessed in mice its imaging and therapeutic potential after radiolabeling with biomarker dose Iodine-131 (^{131}I) and Gallium-68 (^{68}Ga) for respectively SPECT and PET imaging, and with Iodine-131 and Actinium-225 (^{225}Ac) for targeted radionuclide therapy. ***Results:*** The lead anti-FAP sdAb (=sdAb) was identified with picomolar affinity for a FAP conserved epitope that is away from the catalytic site, and recognized both purified and membrane-anchored FAP protein. The radiolabeled variants [^{68}Ga]Ga-DOTA-sdAb, [^{225}Ac]Ac-DOTA-sdAb and [^{131}I]I-GMIB-sdAb had radiochemical purities >95% and were functional on recombinant human FAP protein and FAP$^+$ GM05389 human fibroblasts. [^{68}Ga]Ga-DOTA-sdAb, [^{225}Ac]Ac-DOTA-sdAb and [^{131}I]I-GMIB-sdAb accumulated fast and specific in FAP$^+$human U87MG glioblastoma tumors upon intravenous

administration. Low but specific uptake (about 2-3 %IA/g) was observed in lymph nodes, uterus, bone and skin. Unbound [^{131}I]I-GMIB-sdAb was rapidly cleared from kidneys (<1%IA/g after 24h), while for [^{225}Ac]Ac-DOTA-sdAb it is slower (8.07+/-1.39%IA/g after 24h and 2.47+/-0.18%IA/g after 96h). Mice treated with [^{225}Ac]Ac-DOTA-sdAb and [^{131}I]I-GMIB-sdAb lived longer compared to mice treated with radioactive controls or vehicle solution, and this in a dose-dependent manner. ***Conclusion:*** [^{68}Ga]Ga-DOTA-sdAb and biomarker dose [^{131}I]I-GMIB-sdAb allow for specific detection of FAP^{+}tumors in mice. Therapeutic [^{225}Ac]Ac-DOTA-sdAb and [^{131}I]I-GMIB-sdAb revealed high and sustained tumor targeting, which translated into dose-dependent therapeutic effect in FAP^{+}tumor xenografted mice. This study confirms the potential of radiolabeled anti-FAP sdAb as radiotheranostic for FAP^{+}cancers and warrants clinical testing.

EPS-228

Auger electron therapy of prostate cancer: a preclinical evaluation of ^{58m}Co-DOTA-PSMA-617

C. Baun[1,2,3], *J. H. Dam*[1], *J. D. Ewald*[4,2], *B. W. Kristensen*[4], *V. S. Laursen*[1,2], *M. G. Hildebrandt*[1,2,3], *B. B. Olsen*[1], *H. Thisgaard*[1,2]; [1]*Department of Nuclear Medicine, Odense University Hospital, Odense C, DENMARK,* [2]*Department of Clinical Research, University of Southern Denmark, Odense, DENMARK,* [3]*Center for Personalized Response Monitoring in Oncology (PREMIO), Odense University Hospital, Odense, DENMARK,* [4]*Department of Pathology, Odense University Hospital, Odense C, DENMARK.*

Aim/Introduction: We have previously evaluated the novel theranostic pair [$^{55/58m}$Co]Co-DOTA-PSMA-617 in vitro and in vivo in prostate cancer. These preliminary studies demonstrated promising antiproliferative effects in vitro, while specific tumor targeting was achieved in xenograft mice (1). The current study aimed to evaluate the therapeutic efficacy and adverse effects of [^{58m}Co]Co-DOTA-PSMA-617 in vitro and in vivo in prostate cancer xenograft mice. ***Materials and Methods:*** The therapeutic effect of [^{58m}Co]Co-DOTA-PSMA-617 in vitro was evaluated by clonogenic assay of PSMA-positive (PC3-PIP) and PSMA-negative (PC3-flu) prostate cancer cells. Increasing activity concentrations (0-60 MBq/ml) of [^{58m}Co]Co-DOTA-PSMA-617 diluted in the incubation medium was added to cells followed by 24 h incubation. The therapeutic effect in vivo was investigated in male BALB/c mice (n=12) inoculated subcutaneously with 1x10^{6} PC3-PIP cells. Seven days after tumor inoculation, the mice were divided into two groups with equal visual tumor sizes. One group (n=6) was injected iv with [^{58m}Co]Co-DOTA-PSMA-617 (144.0±9.0 MBq, 2.3±0.1 nmol) and the other group (n=6) with saline. One week later, the treatment was repeated. The mice were monitored by body weight and tumor size measurements until the end of the observation period (90 days) or when they reached one of the humane endpoints, after which they were euthanized, and the kidneys and liver were collected for histopathological analysis**.** Two mice from the treated group had to be censored due to hostility between cage rivals, which resulted in terminal lesions. Survival was analyzed by Kaplan-Meyer analysis and log-rank (Mantel-Cox) test. ***Results:*** The clonogenic survival of PC3-PIP cells in vitro was significantly reduced by [^{58m}Co]Co-DOTA-PSMA-617 in an activity-dependent manner (2.5 MBq/mL: p<0.001; 5-60 MBq/mL: p<0.0001). In vivo, the treated mice had a significantly improved median survival time of 23 days compared to untreated mice, which only had a median survival time of 11 days (p=0.0014). Hence, a 110% increase in median survival was obtained. Further, 25% of the treated mice had a complete response and long-term survival. The histopathological assessment of liver and kidney tissue showed no signs of inflammation, fibrosis, or necrosis, and no visible differences were observed between the groups. ***Conclusion:*** Auger electron therapy with [^{58m}Co]Co-DOTA-PSMA-617 showed promising therapeutic effects in vitro and in vivo and resulted in significant survival benefits for tumor-bearing mice with no toxicities observed. ***References:***
[^{58m}Co]Co-DOTA-PSMA-617: A novel radioligand for Auger electron therapy of prostate cancer Thisgaard, H. et al. 2017. J. Label. Compd. Radiopharm. 60, Suppl. 1, S327, P 167.

EPS-229

Polymeric Micelles as Drug Delivery System for PARP Inhibitor-Based Chemo-Radiotherapy Combination Against Triple-Negative Breast Cancer

L. Schäfer[1], *A. Wang*[2], *Q. Peña*[2], *E. Henrard*[1], *T. Lammers*[2], *E. M. Buhl*[3], *M. Frings*[4], *C. Bolm*[4], *A. Morgenroth*[1], *F. M. Mottaghy*[1,5]; [1]*Department of Nuclear Medicine, RWTH Aachen University Hospital, 52074 Aachen, GERMANY,* [2]*Institute for Experimental Molecular Imaging, RWTH Aachen University Hospital, 52074 Aachen, GERMANY,* [3]*Electron Microscopy Facility, Institute of Pathology, RWTH Aachen University Hospital, 52074 Aachen, GERMANY,* [4]*Institute of Organic Chemistry, RWTH Aachen University, 52074 Aachen, GERMANY,* [5]*Department of Radiology and Nuclear Medicine, Maastricht University Medical Center, 6229 ER Maastricht, NETHERLANDS.*

Aim/Introduction: Poly (ADP-ribose) polymerase inhibitors (PARPi) are commonly used in the treatment against BRCA-mutated (BRCA^{mut}) tumors, such as triple negative breast cancer (TNBC). However, PARPi-based monotherapies have some inherent limitations, including the development of resistance. To overcome some of these drawbacks, combinations of PARPi with different chemotherapeutics or other cancer treatments (e.g., radiotherapy) have shown significant promise. We have previously established a therapeutic approach against BRCA^{mut} TNBC, based on combining the DNA damage response inhibition of PARPi with the radiotherapeutic effect of the Auger electron emitter 125-iodine (^{125}I). Yet, preliminary preclinical evaluation showed poor biodistribution and chemical instability of the developed ^{125}I-PARPi tracer. Hence, we here set out to develop a polymeric micelle-based formulation efficiently co-encapsulating non-radioactive and radioactive I-PARPi with the overall aim of improving tracer stability, biodistribution and target-site accumulation for more efficient chemo-internal radiotherapy combination. ***Materials and Methods:*** Radiolabeling was performed using a tributyltin-precursor with chloramine-T as catalyst. Radioactive and non-radioactive I-PARPi co-loaded polymeric micelles were prepared via nanoprecipitation method. Physicochemical and pharmaceutical properties were analyzed by high-performance liquid chromatography (HPLC), dynamic light scattering and transmission electron microscopy (TEM). Drug encapsulation efficiency (EE) and retention inside the micelles were analysed by HPLC. Cell uptake of the tracer was assessed in different TNBC BRCA^{mut} and BRCA wildtype cell lines, and analysed by Gamma-counter measurements. In vitro tracer stability was examined via HPLC. ***Results:*** TEM images of the co-loaded micelles showed a homogenous distribution of spherical particles, with sizes around 70 nm and polydispersity index (PDI) below 0.1, as confirmed by DLS. Radioactive and non-radioactive I-PARPi were efficiently co-encapsulated into the micelles (EE > 80 %), and these were stable over 14 days at 4 °C. Co-loaded micelles showed a similar release profile for both compounds (i.e., 50 % retained after 72 hours). Furthermore, formulation in micelles improved tracer stability about 10-fold by minimizing its deiodination in vitro,

as well as it enhanced tracer uptake in BRCA^{mut} TNBC cell lines. ***Conclusion:*** We have successfully developed a stable radioactive and non-radioactive I-PARPi co-loaded polymeric micelle formulation that holds potential for efficient chemo-radiotracer therapy combination in TNBC. Ongoing work involves in vivo investigation of the nanoformulation in terms of tracer stability in blood, its pharmacokinetics and therapeutic efficacy.

EPS-230

Successful treatment of human high-risk neuroblastoma using ^{177}Lu-octreotide combined with Lorlatinib in a mouse model

E. Forssell-Aronsson[1,2], *A. Romiani*[1], *D. Pettersson*[1], *K. Simonsson*[1], *H. Bakr*[1,2], *D. Lind*[1], *A. Kovacs*[1,2], *R. Palmer*[1], *B. Hallberg*[1], *K. Helou*[1], *J. Spetz*[1];
[1]*University of Gothenburg, Gothenburg, SWEDEN,*
[2]*Sahlgrenska University Hospital, Gothenburg, SWEDEN.*

Aim/Introduction: Children with high-risk neuroblastoma (HR-NB) has poor prognosis with less than 40% survival, and new treatment options should be developed. Many human HR-NBs overexpress somatostatin (SS) receptors (SSTRs) to a very high extent, and should be possible to successfully treat with, e.g., ^{177}Lu-labelled SS analogues. Recent clinical and preclinical studies show, however, unexpectedly low therapeutic effects of such treatment. HR.NBs often have gain-of-function mutations in anaplastic lymphoma kinase (ALK). The aim of this study was to investigate if treatment with ^{177}Lu-octreotide in combination with the ALK inhibitor lorlatinib would give enhanced effect in a human HR-NB mouse model. ***Materials and Methods:*** Balb/C mice were xenografted with human CLB-BAR HR-NB. Biodistribution of ^{177}Lu-octreotate and ^{177}Lu-octreotide were determined, and the absorbed dose was estimated to tumour and selected normal tissues. Initial therapeutic effects were studied in mice administered with different amounts of ^{177}Lu-octreotate or ^{177}Lu-octreotide. In the final therapy study, mice were treated with 30 MBq ^{177}Lu-octreotide, lorlatinib, or a combination of both treatments, and controls received saline. Tumour volume was followed and compared with controls. Tumour samples were analysed by qPCR and immunohistochemical (IHC) analyses for apoptosis. ***Results:*** Biodistribution data showed very high uptake and absorbed dose to tumour tissue for both radiopharmaceuticals. Tumour/Blood ^{177}Lu activity concentration ratios were 420 and 270 for ^{177}Lu-octreotide and ^{177}Lu-octreotate, respectively. Treatment with ^{177}Lu-octreotide gave somewhat better effects than ^{177}Lu-octreotate, but still a very low effect on tumour volume. No dose-response effects of ^{177}Lu-octreotate were obtained. Combination therapy with ^{177}Lu-octreotide and lorlatinib resulted in clear and synergistic tumour volume reduction, with a relative tumour volume of 0.39 compared with 4.6 and 1.2 for ^{177}Lu-octreotide and lorlatinib as monotherapy, respectively. Furthermore, more apoptosis-related genes were affected by combination than single-treatment. ***Conclusion:*** The gene regulation suggest apoptosis activation through the extrinsic pathway for both treatments. ALK mutations seems to results in radioresistance. ALK inhibitors may restore radiosensitivity and lead to successful therapeutic effects of ^{177}Lu-octreotide.

1510

Tuesday, September 12, 2023, 15:00 - 16:30
Hall K

CTE 7 - Technologists & Thyroid Committee: Molecular Thyroid Imaging - Qualitative and Quantitative Approaches

OP-737

Best practice on thyroid imaging: What's to know?!

M. Punda *;*
UniversityClinical Hospital Center "Sestre Milosrdnice", Department of Oncology and Nuclear Medicine, Zagreb, CROATIA.

OP-738

MIBI-Imaging of the thyroid and parathyroid: How to get most out of it.

M. Jessop*;*
Brighton and Sussex University Hospitals, Department of Nuclear Medicine, Brighton, UNITED KINGDOM.

OP-739

Imaging of thyroid cancer: From I-131 to FAPi.

J. Nagarajah*;*
Radboud UMC, Department of Nuclear Medicine, Nijmegen, NETHERLANDS.

OP-740

Update on new developments in thyroid ultrasound

T. Wendler*;*
Technical University of Munich, TUM School of Computation, Information and Technology, Munich, GERMANY.

1511

Tuesday, September 12, 2023, 15:00 - 16:30
Hall G1

EU Policy Symposium 1 - Policy & Regulatory Affairs Committee: Supply & Shortages of Radiopharmaceuticals

OP-742

Supply & Shortages of Radiopharmaceuticals

1601

Tuesday, September 12, 2023, 16:45 - 18:15
Hall A

CME 12 - Physics + Oncology & Theranostics + Translational Molecular Imaging & Therapy + Technologists Committee: Long Axial Field-of-View PET Scanners - A Copernical Revolution

OP-749

Hybrid Total Body PET scanners

I. Tsoumpas*;*
UMCG, Nuclear Medicine, Groningen, NETHERLANDS.

OP-750
Clinical Perspectives of Total Body PET/CT
A. Dimitrakopoulou-Strauss;
DKFZ, Nuclear Medicine, Heidelberg, GERMANY.

OP-751
Parametric Imaging with dynamic PET for oncological applications
J. van Sluis;
UMCG, Nuclear Medicine, Groningen, NETHERLANDS.

OP-752
Non Oncological applications
R. Boellaard;
Amsterdam UMC, Radiology and nuclear medicine, Amsterdam, NETHERLANDS.

1602

Tuesday, September 12, 2023, 16:45 - 18:15
Hall D (Arena)

Debate 5 - Bone & Joint + Cardiovascular Committee: NaF PET in cardiology and MSK: pro or cons?

OP-753
NaF PET in cardiology: pro
P. Hølund-Carlsen;
Odense University Hospital, Clinical Physiology and Nuclear Medicine Department, Odense, DENMARK.

OP-754
NaF PET in cardiology: cons
F. Hyafil;
Hopital européen Georges Pompidou, Nuclear medicine Department, Paris, FRANCE.

OP-755
NaF PET in musculoskeletal imaging: pro
H. Zacho;
Kræftforsknings-Center, Aalborg Universitetshospital og, Aalborg, DENMARK.

OP-756
NaF PET in musculoskeletal imaging: cons
D. Mak; *Guys and St Thomas' NHS, Nuclear medicine Department, London, UNITED KINGDOM.*

1603

Tuesday, September 12, 2023, 16:45 - 18:15
Hall E1

LIPS Session 12 - Neuroimaging + Inflammation & Infection Committee: The Role of FDG PET in the Diagnosis of Auto-Immune Encephalitis

OP-760
Interpretation of auto-immune encephalitis with brain FDG PET
A. Verger;
CHRU Nancy, Nuclear Medicine, Nancy, FRANCE.

OP-761
The role of the whole-body FDG PET in autoimmune encephalitis
I. Apostolova;
Department of Diagnostic and Interventional Radiology and Nuclear Medicine, University Medical Center Hamburg-Eppendorf, Hamburg, GERMANY.

OP-762
The complementary PET/MRI modalities in autoimmune encephalitis
D. Cecchin;
Department of Medicine, Nuclear Medicine Unit, University-Hospital of Padova, Padova, ITALY.

1604

Tuesday, September 12, 2023, 4:45 PM - 6:15 PM
Hall E2

M2M Track - TROP Session: Understanding and Improving RLT

OP-764
Novel DNA polymerase theta inhibitors induce efficient X-ray and proton therapy sensitisation in vitro and in vivo
J. Barlow[1], *A. Cicconi*[1], *M. Ranzani*[1], *G. Rodriguez-Berriguete*[2], *R. Prevo*[2], *M. Boursier*[1], *A. Galbiati*[1], *L. Geo*[1], *D. Grande*[1], *R. A. Heald*[1], *J. Majithiya*[1], *D. Piscitello*[1], *E. Rajendra*[1], *M. Stockley*[1], *P. Mariniello*[3], *G. Sawakuchi*[3], *G. Smith*[1], *G. S. Higgins*[2], *H. Robinson*[1];
[1]*Artios Pharma, Cambridge, UNITED KINGDOM,*
[2]*University of Oxford, Oxford, UNITED KINGDOM,*
[3]*University of Texas MD anderson Cancer Center, Houston, TX, UNITED STATES OF AMERICA.*

Aim/Introduction: DNA polymerase theta (Pol theta) is essential for DNA double strand break repair through microhomology-mediated end-joining (MMEJ). Pol theta has very restricted expression in normal tissues but is frequently overexpressed in cancer cells and its loss has been shown to sensitise cancer cells but not normal cells to ionising radiation (IR). This highlights Pol theta as a promising drug target for the potentiation of radiotherapy. Artios recently developed potent and highly selective Pol theta inhibitors showing in vitro and in vivo efficacy in cancer models[1]. The aim of this study was to explore the possible therapeutic applications of these inhibitors in combination with radiation. ***Materials and Methods:*** For this purpose a panel of cell lines (n=56) enriched for head & neck, colorectal and lung cancers was treated with either Pol theta inhibitor, X-rays or a combination of Pol theta inhibitor and X-rays then assessed for in vitro viability by colony formation assay and induction of DNA damage response markers by immunofluorescence. ***Results:*** It was observed that Pol theta inhibition sensitised a wide range of cancer cell lines but not normal cells to X-rays. This effect was enhanced with increasing number of X-ray fractions, a modality that closely reflects clinical treatment regimens. Additionally, it was shown that Pol theta inhibition combined with X-rays leads to increased DNA damage foci compared to the X-ray or Pol theta inhibitor treatment alone[2]. The combination of Pol theta inhibitor with X-rays was well tolerated in vivo during xenograft efficacy studies and induced a significant reduction in tumor growth compared to single agent treatment[2]. In studies to identify potential patient selection biomarkers, it was found that loss of the Shieldin

complex component SHLD2, sensitised cells to the combination treatment in vitro, which may have relevance for the treatment of tumors that have mutations in the 53BP1/Shieldin complex. In addition, it was confirmed that Pol theta inhibition potentiates the efficacy of fractionated protons both in vitro and in vivo in mouse xenotransplants, suggesting that Pol theta inhibition has the potential to increase the efficiency of different radiotherapies. ***Conclusion:*** Collectively, our results show that Artios' potent and selective Pol theta inhibitors are effective radiosensitisers in a wide range of cancer models, paving the way for testing Pol theta inhibitors with radiotherapy in clinical trials. ***References:*** 1. Zatreanu et al. Nature communications 2021. 2. Rodriguez-Berriguete, Ranzani, Prevo et al. Clinical Cancer Research 2023.

OP-765

Dissecting signaling network response to radiolabeled minigastrin analog reveals radiosensitizing targets in CCKBR-positive cancers

M. Grzmil[1], *Y. Qin*[1], *A. Blanc*[1], *T. Chiorazzo*[1], *P. Berger*[2], *S. Frank*[3], *R. Schibli*[1,4], *M. Behe*[1];
[1]*Center for Radiopharmaceutical Sciences, Paul Scherrer Institute, Villigen PSI, SWITZERLAND,* [2]*Laboratory of Nanoscale Biology, Paul Scherrer Institute, Villigen PSI, SWITZERLAND,* [3]*Division of Neuropathology, Institute of Pathology, University of Basel, Basel, SWITZERLAND,* [4]*Department of Chemistry and Applied Biosciences, ETH Zürich, Zürich, SWITZERLAND.*

Aim/Introduction: Identification of radiation-activated survival mechanisms in cancer cells provides opportunities to develop new therapeutic strategies based on the targeting signaling pathways, which are triggered during radiotherapy. Our recent study explored cancer responses to targeted beta radiation therapy and identified radiosensitizing targets including integrin or epidermal growth factor receptors [1]. In comparison to β-emitters, targeted alpha-particle therapy (TAT) with a relatively short range and high linear energy transfer shows higher toxicity to cancer cells. Nevertheless, the toxicity to healthy organs or cancer radioresistance can limit the efficacy. In the present study, we analyzed signaling network responses to TAT with actinium-225 labeled minigastrin analog [^{225}Ac]Ac-PP-F11N to improve the effectiveness of TAT by combinatory treatments. ***Materials and Methods:*** Quantitative phosphoproteomics and proteomics followed by the bioinformatics analysis identified alterations in the signaling networks in response to [^{225}Ac]Ac-PP-F11N in A431 cells, which overexpress cholecystokinin B receptor (CCKBR). Western blot (WB) analysis and confocal microscopy verified the activation of the induced pathways. Small-molecule inhibitors were used to validate the radiosensitizing strategies both in vitro and in A431/CCKBR tumor-bearing nude mice. ***Results:*** TAT-induced DNA damage response (DDR), cell cycle regulation, signal transduction, RNA transcription and processing as well as cell morphology and transport. WB analysis and microscopy confirmed increased phosphorylations of p53, p53BP1, histone deacetylases (HDACs), and H2AX. Inhibition of HDAC, ATM, and p38 kinases by TMP269, AZD1390, and SB202190, respectively, sensitized A431/CCKBR cells to TAT. Combination of [^{225}Ac]Ac-PP-F11N with HDAC inhibitor vorinostat (SAHA) showed significantly reduced viability and increased DNA damage of A431/CCKBR cells as well as the most pronounced tumor growth inhibition and the extended mean survival of treated tumor-bearing mice. ***Conclusion:*** The present study revealed alterations in cancer signaling networks in response to TAT and verified the radiosensitizing potential of HDAC inhibitors to [^{225}Ac]Ac-PP-F11N [2]. This research further recommends the development of radiosensitizing strategies by targeting radiation-activated and survival-promoting signaling pathways. ***References:*** 1. Grzmil M, Boersema P, Sharma A, Blanc A, Imobersteg S, Pruschy M, Picotti P, Schibli R, Behe M. Comparative analysis of cancer cell responses to targeted radionuclide therapy (TRT) and external beam radiotherapy (EBRT). J Hematol Oncol. 2022;15:123. 2. Qin Y, Imobersteg S, Frank S, Blanc A, Chiorazzo T, Berger P, Schibli R, Béhé MP, Grzmil M. Signaling Network Response to Alpha-Particle Targeted Therapy with Actinium-225 Labeled Minigastrin Analogue ^{225}Ac-PP-F11N Reveals Radiosensitizing Potential of HDAC Inhibitors. J Nucl Med. 2023; jnumed.122.264597

OP-766

p53 Stabilisation Potentiates ^{177}Lu-DOTATATE Treatment in Neuroblastoma

H. Berglund[1], *S. Lundsten Salomonsson*[2], *T. Mohajershojai*[1], *D. P. Lane*[1,3,4], *M. Nestor*[1];
[1]*Department of Immunology, Genetics and Pathology, Uppsala University, Uppsala, SWEDEN,* [2]*Ridgeview Instruments AB, Uppsala, SWEDEN,* [3]*Department of Microbiology, Tumour and Cell Biology, Karolinska Institute, Stockholm, SWEDEN,* [4]*p53Lab, Agency for Science Technology and Research (A*STAR), Singapore, SINGAPORE.*

Aim/Introduction: Targeted radionuclide therapy against somatostatin receptors using ^{177}Lu-DOTATATE is currently being explored as a treatment option for neuroblastoma. Combining molecular radiotherapy with radiosensitising drugs have been proposed as a viable strategy for enhancing the therapeutic efficacy while minimising adverse effects. p53 has been identified as a potential target for radiosensitisation due to its involvement in DNA damage response. The aim of this study was to investigate the novel wild-type p53-stabilising peptide VIP116 in neuroblastoma, both as monotherapy and together with ^{177}Lu-DOTATATE in neuroblastoma models in vitro and in vivo. ***Materials and Methods:*** Three neuroblastoma cell lines were characterised in vitro for specific uptake of ^{177}Lu-DOTATATE and sensitivity towards VIP116. Multicellular tumour spheroids using the IMR-32 cell line were established and subjected to mono- and combination treatment of varying concentrations of VIP116 and ^{177}Lu-DOTATATE. Biodistribution of ^{177}Lu-DOTATATE was performed in mice bearing IMR-32 or Neuro 2a tumour xenografts. A monotherapy study using VIP116 was done in mice with IMR-32 or Neuro 2a tumour xenografts. A combination therapy study was conducted in mice bearing IMR-32 tumour xenografts. This study included four treatment groups: control, VIP116 monotherapy, ^{177}Lu-DOTATATE monotherapy and a combination group. ***Results:*** Two out of three cell lines had a specific uptake of ^{177}Lu-DOTATATE in vitro. The sensitivity towards VIP116 was correlated with p53 mutational status, with cell lines harbouring mutant p53 displaying a higher IC_{50} value. Treatment with ^{177}Lu-DOTATATE and/or VIP116 showed growth inhibition of multicellular tumour spheroids, with the combination treatment displaying synergistic effects. Both IMR-32 and Neuro 2a had a specific uptake of ^{177}Lu-DOTATATE in vivo, with IMR-32 having a higher uptake in the tumour than Neuro 2a. Monotherapy with VIP116 resulted in growth inhibition of IMR-32 tumour xenografts, but not Neuro 2a tumour xenografts. The combination therapy study resulted in a doubled media survival for both monotherapies in comparison to the control (90 and 96.5 days vs. 50 days), with the combination treatment showing a median survival of >120 days. ***Conclusion:*** Both VIP116 and ^{177}Lu-DOTATATE inhibited neuroblastoma cell growth in vitro and prolonged the median survival in tumour bearing mice. The use of these two therapies, especially in combination, may therefore be a feasible future treatment option for neuroblastoma.

OP-767

Substantial Reduction of the Activity Retention in the Kidneys of Radiohybrid-Based Minigastrin Analogues by Modifying the Charge Distribution Within the Linker Section

N. Holzleitner[1], *T. Günther*[1], *S. Fischer*[1], *R. Beck*[1], *C. Lapa*[2], *H. Wester*[1];
[1]*Technical University Munich, Munich, GERMANY,*
[2]*University of Augsburg, Augsburg, GERMANY.*

Aim/Introduction: In order to reduce elevated activity retention in the kidneys of previous radiohybrid-based minigastrin analogues, such as [^{177}Lu]Lu-DOTA-rhCCK-18 ([^{177}Lu]Lu-DOTA-D-Dap(SiFA)-(D-γ-Glu)$_8$-Ala-Tyr-Gly-Trp-Asp-Nle-Phe-NH$_2$), we substituted the negatively charged poly-D-γ-glutamate chain by polyethylene glycol moieties of various length ((PEG)$_{4\text{-}11}$). We further evaluated the influence of a different charge distribution in proximity to the silicon-based fluoride acceptor (SiFA) moiety on CCK-2R affinity, lipophilicity and biodistribution properties by insertion of different SiFA building blocks (SiFA and SiFAlin) as well as a D-γ-glutamate moiety next to the D-Dap(SiFA/SiFAlin) unit. ***Materials and Methods:*** ^{177}Lu-labelling was performed at 90°C within 15 min (1.0 M NaOAc buffer, pH=5.5, 0.1 M sodium ascorbate). CCK-2R affinity (IC$_{50}$, n=3) was evaluated on AR42J cells. Lipophilicity (expressed as n-octanol/PBS distribution coefficient; logD$_{7.4}$) was determined. Biodistribution studies (n=4) were carried out at 24 h post-injection in AR42J tumour-bearing CB17-SCID mice. ***Results:*** Synthesis via solid-phase peptide synthesis yielded 4-8% RP-HPLC-purified labelling precursor. 177Lu-labelling proceeded in high radiochemical yields and purities of >95% and molar activities of 30-40 GBq/μmol. CCK-2R affinities of most compounds evaluated were found to be in a range of 8-20 nM, which resulted in slightly increased or comparable IC$_{50}$ values to [^{nat}Lu]Lu-DOTA-rhCCK-18 and [^{nat}Lu]Lu-DOTA-PP-F11N (IC$_{50}$: 4.7±0.6 and 12.8±2.8 nM), respectively. Lipophilicity was noticeably decreased for compounds containing a D-γ-glutamate moiety next to the D-Dap(SiFA) unit as compared to their counterparts lacking the additional negative charge. Combining the highest CCK-2R affinity and lipophilicity of all compounds investigated, [$^{177/nat}$Lu]Lu-DOTA-rhCCK-70 (DOTA-D-Dap(SiFA)-D-γ-Glu-(PEG)$_7$-D-γ-Glu-(PEG)$_3$-Trp-(N-Me)Nle-Asp-1-Nal-NH$_2$; IC$_{50}$: 12.6±2.0 nM; logD$_{7.4}$: −1.67±0.08) and [$^{177/nat}$Lu]Lu-DOTA-rhCCK-91 (DOTA-D-Dap(SiFAlin)-D-γ-Glu-(PEG)$_4$-D-γ-Glu-(PEG)$_3$-Trp-(N-Me)Nle-Asp-1-Nal-NH$_2$; IC$_{50}$: 8.6±0.7 nM; logD$_{7.4}$: −1.66±0.07) were further evaluated in vivo. Biodistribution data at 24 h post-injection for both [^{177}Lu]Lu-DOTA-rhCCK-70 and [^{177}Lu]Lu-DOTA-rhCCK-91 showed substantially decreased activity levels in the kidneys (8.4±0.8 and 6.6±0.5 %ID/g, respectively), when compared to [$^{177/nat}$Lu]Lu-DOTA-rhCCK-18 (134±18 %ID/g). However, activity levels in the tumour were found to be decreased as well (12.0±0.8 and 7.5±1.0 versus 25.4±4.7 %ID/g, respectively). In comparison to [^{177}Lu]Lu-DOTA-PP-F11N (tumour: 1.9±0.8 %ID/g, kidney: 3.0±0.5 %ID/g) activity levels in the tumour at 24 h post-injection were observed to be much higher for both compounds investigated, resulting in favourable tumour to kidney ratios (1.45±0.12 and 1.13±0.12 versus 0.62±0.30). ***Conclusion:*** In this study we could successfully demonstrate a reduction of activity accumulation in the kidneys by a reduction of negative charges in the linker section of radiohybrid-based minigastrin analogues, while maintaining a good tumour uptake, which led to more favourable tumour/kidney ratios in vivo compared to the references [^{177}Lu]Lu-DOTA-PP-F11N and [^{177}Lu]Lu-DOTA-rhCCK-18.

OP-768

Internalising radioimmunoconjugates to target KRAS in pancreatic cancer cells for simultaneous radionuclide therapy and radiosensitisation

K. Vallis[1], *J. Lourenco*[1], *N. Sereesongsaeng*[2], *O. Tietz*[3], *T. Rabbitts*[2];
[1]*University of Oxford, Oxford, UNITED KINGDOM,*
[2]*Institute of Cancer Research, London, UNITED KINGDOM,*
[3]*Macquarie University, Sydney, AUSTRALIA.*

Aim/Introduction: Mutant KRAS is a major oncogenic driver of pancreatic ductal adenocarcinoma (PDAC), a cancer of unmet need with 5-year survival of <10%. The goal of this study was to internalise radiolabelled anti-KRAS DARPin and anti-pan-RAS scFv into PDAC cells using a cell-penetrating peptide (CPP), Tri-cTatB, consisting of three copies of cyclised TAT peptide. Internalised KRAS binders were predicted to result in inhibition of downstream signalling, radiosensitisation and cytotoxicity. ***Materials and Methods:*** Recombinant immunomolecules were expressed in E. coli. PDAC cell lines (PSN1 [KRAS^{G12R}], PANC-1 [KRAS^{G12D}], BxPC3 [KRAS^{WT}]) were used. The intracellular uptake of fluorphore-DARPin/scFv, co-delivered with Tri-cTatB, was assessed using live cell immunofluorescence microscopy, and cell viability was assessed using CellTiter-Glo®. As KRAS interacts with the plasma membrane, the effect of farnesylation (DARPin-cFarn, scFv-cFarn) on intracellular distribution was investigated. The chloramine-T method was used to label DARPins/scFvs with 123-Iodine and the intracellular distribution of iodinated constructs was assessed in fractionation assays. Western blot analysis (WBA) was used to evaluate expression of proteins downstream of activated KRAS. Clonogenic assays were done to investigate the effect of internalised anti-KRAS molecules on sensitisation of PANC-1 cells to external beam radiation (EBR; caesium-137 gamma radiation, 0.81 Gy min^{-1}). ***Results:*** mCherry-labelled DARPin and scFv were efficiently uptaken by PDAC cells in the presence of Tri-cTatB (1-2 μM). The radiolabelling yield for [^{123}I]I-DARPin/scFv was ≥95%. The percentage of internalised [^{123}I]I-anti-KRAS DARPin accumulating in the membrane, cytoplasm and nuclei of PANC-1 cells was 29, 9 and 62% respectively. The addition of a farnesylation moiety, [^{123}I]I-DARPin-cFarn, resulted in redistribution of the internalised radioactivity with 62, 14 and 24% in the membrane, cytoplasm and nuclei. WBA showed downregulation of pERK in the PANC-1 cell line incubated with anti-KRAS DARPins/scFvs plus Tri-cTatB. DARPin-cFarn and scFv-cFarn (550 nM) plus Tri-cTatB (2 μM) reduced PANC-1 cell viability to <10% by 48 h, but had minimal effect on BxPC3 cells. In clonogenic assays the surviving fraction of PANC-1 cells incubated with or without scFv-cFarn plus Tri-cTatB after exposure to 2 Gy EBR was 37 and 60%, respectively. ***Conclusion:*** Internalising radiolabelled RAS targeting constructs result in KRAS inhibition with simultaneous radiosensitisation, and are cytotoxic and so hold promise as a new approach to radionuclide therapy for cancer.

OP-769

Human hematopoietic stem cells show SSTR2 expression and specific binding of radioligands providing a potential explanation for the hematotoxicity of ^{177}Lu-DOTA-JR11

S. Kossatz[1], *Y. Min*[1], *N. T. Nguyen*[1], *J. Rivière*[1], *M. van der Garde*[1], *S. Ghosh*[2], *L. Bartos*[3], *M. Brendel*[3], *F. Bassermann*[1], *K. Götze*[1], *A. Azhdarinia*[4], *W. A. Weber*[1];
[1]*Klinikum rechts der Isar at Technical University Munich, Munich, GERMANY,* [2]*University of Texas Health Science Center at Houston, Houston, VT, UNITED STATES OF AMERICA,* [3]*University Hospital of Munich, LMU Munich, Munich, GERMANY,* [4]*University of Texas Health Science Center at Houston, Munich, GERMANY.*

Aim/Introduction: Peptide Receptor Radionuclide Therapy (PRRT) with the somatostatin receptor subtype 2 (SSTR2) antagonist ^{177}Lu-DOTA-JR11 has shown promising results for treatment of neuroendocrine tumors (NET). However, hematologic toxicity occurred when patients received a macroscopic bone marrow dose of ≥ 1.44 Gy - <2 Gy, which was considered a well-tolerated dose for the agonist ^{177}Lu-DOTA-TATE[2]. We hypothesize that ^{177}Lu-DOTA-JR11 binds to SSTR2-positive subpopulations of hematopoietic stem cells, exerting increased hematotoxicity compared to agonist-PRRT. Here, we synthesized fluorescent analogs with comparable binding characteristics to DOTA-JR11 and DOTA-TOC and investigated their binding to human bone marrow stem cell subpopulations. ***Materials and Methods:*** We synthesized multimodal DOTA-JR11/TOC analogs by replacing DOTA with a multimodality chelator (MMC), and conjugating DBCO-functionalized dyes using copper-free click chemistry. We produced 5 MMC(Dye)-JR11/TOC variants and compared their cellular uptake, K_D and IC_{50} to ^{177}Lu-DOTA-JR11/TOC. Fluorescence characterization was done using microscopy and flow cytometry. To assess binding to bone marrow stem cell populations, isolated peripheral blood mononuclear cells (PBMCs) were stained for CD34, CD38, CD45RA and CD90, before incubation with MMC(Dye)-JR11/TOC. SSTR1-5 expression of bone marrow stem cell populations was assessed via qRT-PCR. ***Results:*** The Sulfo2Cy5 conjugates MMC(S2Cy5)-JR11/TOC were identified as lead compounds with comparable binding characteristics to ^{177}Lu-DOTA-JR11/TOC. In flow cytometry, the antagonist MMC(S2Cy5)-JR11 showed up to 10-fold higher binding than the agonists across cell lines, consistent with the binding properties of their radioligand counterparts. Analysis of binding to human bone marrow cells revealed specific, blockable binding to CD34+ PBMCs, but not CD34- PBMCs. Within the CD34+ population, specific binding was further observed to long-term (LT-HSC) and short-term (ST-HSC) multipotent stem cells and progenitors, but not to lineage-committed progenitors. In all cases, the antagonist showed 2-5 fold higher binding than the agonist. LT-HSCs showed the highest binding levels, which were almost comparable (10-20% lower) to the well-known SSTR2-overexpressing cell line AR42J. qRT-PCR to determine SSTR1-5 expression of stem cells and in vitro treatment of stem cells to determine cell viability and proliferation after ^{177}Lu-DOTA-TOC or -JR11 treatment are currently ongoing. ***Conclusion:*** We have successfully synthesized multimodal variants of clinically used PRRT agents and established protocols to investigate their binding to human bone marrow stem cell subpopulations. Our results indicate SSTR2-mediated binding to multipotent stem cells and progenitors. LT-HSC make up only 0.05-0.1% of the PBMCs, but if ablated, will lead to pancytopenia, as observed after multiple cycles of ^{177}Lu-DOTA-JR11 despite a tolerable total red marrow dose.

OP-770

Reducing the Effective Specific Activity of [^{225}Ac]-PSMA-617 to Minimize Salivary Gland and Renal Toxicity

T. Esposito*, T. Kalidindi, R. Payne, Z. Faudemer, K. Jones, N. Pillarsetty;*
Memorial Sloan Kettering Cancer Center, New York City, NY, UNITED STATES OF AMERICA.

Aim/Introduction: Peptide-based targeted radioligand therapy (TRT) against prostate-specific membrane antigen (PSMA) is a promising last-line treatment option for patients with metastatic castration-resistant prostate cancer (mCRPC). [^{177}Lu]-PSMA-617 (Pluvicto, Novartis) has recently received market authorization and clinical trials are underway with alpha-emitting TRTs, such as [^{225}Ac]-PSMA-617. However, dose-limiting xerostomia and renal toxicity limits the potential of PSMA-TRT. We have previously shown with a tracer dose of [^{177}Lu]-PSMA-617 (5 uCi, 1.5 pmol) that reducing its effective specific activity (ESA) can minimize salivary gland and kidney uptake without compromising radioligand uptake into PSMA-positive tumors in mice. In this work we explored how this approach works using a therapeutic dose of [^{225}Ac]-PSMA-617 in mice bearing xenografts of low- and high-PSMA expression. ***Materials and Methods:*** [^{225}Ac]-PSMA-617 was prepared at a clinically-relevant specific activity (~20 mCi/mmol) and injected intravenously into cohorts of mice bearing PC3-PIP (PSMA high) and CWR22RV1 (PSMA low) xenografts. The dose provided (1.58 ± 0.15 µCi, 83.2 ± 6.4 pmol) is equivalent when scaled to the 100 kBq/kg dose commonly used in clinical trials of [225Ac]-PSMA-617. [225Ac]-PSMA-617 was co-injected with between 0-2000 pmol of PSMA-11 to adjust the ESA. Biodistributions were performed at 1.5 h post-injection and tumor growth kinetics were monitored over a 2-month period. ***Results:*** The tumor uptake for the 22RV1 cohort ranged between 2-4 % ID/g. Though there was trend toward lowering of uptake in tumor with reduced ESA, particularly with the 2000 pmol PSMA-11 block, the change was not statistically significant. However, there was a remarkable reduction in the uptake of [^{225}Ac]-PSMA-617 in both the kidneys and salivary glands. For example, with the addition of 500 pmol PSMA-11 block, the activity concentration decreased from 12.9 ± 6.9 % ID/g to 2.5 ± 1.8 % ID/g in the kidney and from 0.12 ± 0.04 % ID/g to 0.047 ± 0.02 % ID/g in the salivary glands. For the PC3-PIP xenograft bearing mice, there was no reduction in uptake in the tumors (18-22 % ID/g) but a markedly reduced activity concentration in the kidneys and salivary glands. PC3-PIP xenografts regressed at a similar rate in mice treated with [^{225}Ac]-PSMA-617 regardless of the level of PSMA-11 block. ***Conclusion:*** Reducing the ESA of [^{225}Ac]-PSMA-617 appears to be an effective way at reducing salivary and kidney uptake without compromising its therapeutic effect. ***References:*** Kalidindi TM et al., Eur J Nucl Med Mol Imaging, PMID: 33495926. ***Funding:*** NIH RO1-1R01CA262675

OP-771

Improvement of the pharmacokinetic properties of PSMA-617 by introducing sarcosine moieties

N. M. Geis*[1,2,3], N. Steinacker[1,2], L. Domogalla[1,2], P. T. Meyer[1,2], M. Eder[1,2], A. Eder[1,2];*
[1]Department of Nuclear Medicine, University Medical Center Freiburg, Freiburg im Breisgau, GERMANY, [2]Division of Radiopharmaceutical Development, German Cancer Consortium, Freiburg im Breisgau, GERMANY, [3]Faculty of Biology, University of Freiburg, Freiburg im Breisgau, GERMANY.

Aim/Introduction: PSMA-specific radiopharmaceuticals that employ urea containing inhibitors like [^{177}Lu]Lu-Glu-urea-Lys-2Nal-ChX-DOTA ([^{177}Lu]Lu-PSMA-617) were shown to have significant clinical benefits for targeted radionuclide therapy of metastatic castration-resistant prostate cancer (mCRPC). Recently, the FDA and EMA approved the use of [^{177}Lu]Lu-PSMA-617 therapy under the name Pluvicto™. However, the potential efficacy of the treatment with beta- emitting [^{177}Lu]Lu-PSMA-617 and with the potentially more effective alpha-emitting [^{225}Ac]Ac-PSMA-617 is limited by side-effects like xerostomia. Earlier research showed major effects on biological activity by modifications of the linker region in PSMA-targeting inhibitors. Uncharged linker modifications have been identified as the key method

for developing the best pharmacokinetic profile for PSMA-617. To further improve the pharmacokinetic properties, repeated sarcosine moieties (3-15) were introduced into the linker region of PSMA-617 resulting in a series of modified structures with improved in vitro and in vivo properties. ***Materials and Methods:*** The linker-modified PSMA-targeting inhibitors were synthesized through the introduction of sarcosine moieties adjacent to the chelator of PSMA-617. The inhibitors were radiolabeled with gallium-68 and lutethium-177 to investigate their chemical and stability properties. The biological activity of the compounds was evaluated in competitive cell and internalization assays using PSMA-expressing LNCaP cells. To assess the pharmacokinetic profiles, small-animal PET/MRI imaging studies with ^{68}Ga-labeled compounds were conducted in BALB/c nu/nu mice bearing LNCaP xenografts. Organ distribution studies were performed at different time points using the ^{177}Lu-labeled variants with the most promising characteristics. ***Results:*** The novel PSMA-targeting inhibitors exhibited high radiolytic stability. Both reactions of the precursors with either ^{68}Ga or ^{177}Lu, respectively, resulted in high yields greater than 95%. The investigated compounds demonstrated a high affinity to PSMA (Ki down to 19.75 ± 9.42 nmol) and PSMA-specific internalization and surface binding in vitro. Small-animal PET imaging revealed high tumor uptake and rapid clearance from kidneys and circulation for the ^{68}Ga-labeled variants with three or fifteen sarcosine moieties, respectively, resulting in improved tumor-to-kidney ratios as compared to the reference PSMA-617 at 1 h p.i. (PSMA-617 (tumor-to-kidney ratio 0.33), sarcosine-3-moiety (0.96), and sarcosine-15-moiety (0.93)). The organ-distribution studies confirmed these findings of an improved pharmacokinetic profile. ***Conclusion:*** It can be concluded, that the introduction of sarcosine moieties into the linker region of PSMA-617 significantly affects the pharmacokinetic profile with strong improvements of the tumor-to-kidney ratio accompanied by enhanced excretion. Resulting dose reductions in crucial organs indicate potential advantages of the novel variants, highlighting their great potential as an improved treatment option of mCRPC.

OP-772

Preclinical toxicity study of [^{211}At]PSMA5 in mice and for the FIH clinical trial of targeted alpha therapy against refractory prostate cancer

T. Watabe[1], *K. Kaneda-Nakashima*[1], *Y. Kadonaga*[1], *K. Ooe*[1], *T. Sampunta*[1], *X. Yin*[2], *H. Haba*[2], *Y. Kon*[1], *A. Toyoshima*[1], *J. Cardinale*[3], *F. L. Giesel*[3], *K. Fukase*[1], *N. Tomiyama*[1], *Y. Shirakami*[1];
[1]*Osaka University, Suita, JAPAN,* [2]*RIKEN, Wako, JAPAN,*
[3]*University Hospital Duesseldorf, Duesseldorf, GERMANY.*

Aim/Introduction: Astatine (^{211}At) is an alpha emitter (half-life=7.2 h) that can be produced by a 30-MeV cyclotron using natural bismuth target. Targeted alpha therapy (TAT) using ^{211}At-labeled PSMA compound ([^{211}At]PSMA5) showed excellent tumor growth suppression using tumor xenograft model. In this study, we performed preclinical toxicity studies for the first-in-human (FIH) clinical trial which is scheduled to start in 2024. ***Materials and Methods:*** [^{211}At]PSMA5 solution was injected into the normal ICR mice (male (n = 60), body weight: 28.2 ± 1.4g) and Cynomolgus monkey (n=2, body weight: 2.1 kg). Mice were divided into four groups: 5 MBq/kg (n=15), 12 MBq/kg (n=15), 35 MBq/kg (n=15), and vehicle control (n=15). Mice were followed up for 1 day (main evaluation point for acute toxicity: n=40 (n=10 for each group)) or 14 days (evaluation point for recovery: n=20 (n=5 for each group)) to monitor general condition and body weight change. Monkeys were followed up for 24 hrs post administration of [^{211}At]PSMA5 (9MBq/kg). At the end of the observation period, autopsy, blood test, organ weight measurement, and histopathological examination were performed. ***Results:*** In 12 MBq/kg group (day5) and 35MBq/kg group (day10) of mice, significant decrease in body weight was observed compared to control. In the blood test of mice, no significant myelosuppression or renal dysfunction was observed either on the day1 or day14 after administration. In Cynomolgus monkey, mild leukopenia, mainly lymphopenia, was observed 24 hrs after administration. In the organ weight measurement of mice, there was a significant decrease in testis weight in the 12MBq/kg group (organ weight: 0.18 ± 0.02 g) and 35MBq/kg group (organ weight: 0.17 ± 0.003 g) compared to control group (0.24 ± 0.02 g) on day14. Irreversible toxicity was not observed in the histology of risk organs, such as thyroid, salivary gland, and kidneys in mice. ***Conclusion:*** In this toxicity study of [^{211}At]PSMA5 which was performed under reliability standard, no severe toxicity was observed. After confirming all pathological results, we will proceed to determine the starting dose in the FIH clinical trial. [^{211}At]PSMA5 is expected to be a next-generation TAT against prostate cancer with the domestic production of alpha emitter using cyclotron. ***References:*** Watabe T, Kaneda-Nakashima K, Shirakami Y, et al. Targeted α-therapy using astatine (211At)-labeled PSMA1, 5, and 6: a preclinical evaluation as a novel compound. Eur J Nucl Med Mol Imaging. 2023 Feb;50(3):849-858.

1605

Tuesday, September 12, 2023, 4:45 PM - 6:15 PM
Hall B

Cutting Edge Science Track - TROP Session: Data Analysis

OP-773

Using timestamps in fast time-of-flight positron emission tomography detectors to encode the depth of interaction of 511 keV gamma-photons in scintillators

V. Nadig[1], *K. Herweg*[1], *K. Weindel*[1], *D. Schug*[1,2], *H. Radermacher*[1], *F. Mueller*[1], *B. Weissler*[1,2], *V. Schulz*[1,2], *S. Gundacker*[1];
[1]*RWTH Aachen University, Aachen, GERMANY,* [2]*Hyperion Hybrid Imaging Systems GmbH, Aachen, GERMANY.*

Aim/Introduction: For positron emission tomography (PET), both precise depth-of-interaction (DOI) encoding, often realized via light-sharing concepts and determined via the energy deposit, and fast time-of-flight (TOF) resolution are key technological features to obtain a tomographic image with a high signal-to-noise ratio (SNR). While a TOF resolution of 100 ps (FWHM) would improve the SNR by a factor of 3.7 compared to a non-TOF scanner, resolving DOI allows to correct for a superposing effect, so-called parallax errors, which further improves the SNR. ***Materials and Methods:*** Since fast TOF-PET electronics require individual timing channels in addition to standard energy channels, resulting in a considerably higher form factor, we propose to omit the energy channel and encode the DOI via the mean time delay between adjacent detector pixels. We employ scalable detector units consisting of two LYSO:Ce,Ca scintillators (Taiwan Applied Crystal, evaluated in [1]) of 3x3x20mm^3 size separated by a triangular enhanced specular reflector sheet. These were coupled to two FBK NUV-MT silicon-photomultipliers (SiPMs) using

Cargille Meltmount (n=1.582) and read out by custom ultra-fast high-frequency (HF) electronics, which have been adapted from previous versions to read multiple detector channels [2,3]. ***Results:*** The mean time delay between two adjacent channels clearly increases towards DOIs close to the SiPMs. In contrast to double-sided readout techniques, the time delay measured here does not correspond to the actual optical photon travel time. Still, a mean DOI resolution of about 4 mm to 5 mm (RMSE) is obtained using the information of the timing channel, while a sub-150 ps (FWHM) TOF resolution is achieved. ***Conclusion:*** The DOI resolution obtained would allow to separate the scintillator into at least two DOI bins, which could be fed into reconstruction algorithms to correct for parallax. Together with a high TOF resolution, this would result in an improved SNR in the reconstructed image. ***References:*** This research project "ProtoTOF" is supported by the START-Program of the Faculty of Medicine of the RWTH Aachen University. This work did not involve human subjects or animals in its research. [1] Nadig et al 2023 Phys. Med. Biol. 68 075002. doi: 10.1088/1361-6560/acbde4 [2] Gundacker et al 2019 Phys. Med. Biol. 64 055012 doi: 10.1088/1361-6560/aafd52 [3] Krake et al 2022 NIMA. 1039. 167032. doi: 10.1016/j.nima.2022.167032

OP-774

Brain PET Quantitative and Qualitative Interpretation Using Sparse Detector Ring Configuration PET System

R. Fahmi[1], *J. Cabello*[1], *G. Platsch*[2], *B. Spottiswoode*[1];
[1]*Siemens Healthineers, Knoxville, TN, UNITED STATES OF AMERICA,* [2]*Siemens Healthineers, Erlangen, GERMANY.*

Aim/Introduction: Brain-PET imaging plays an important role in the diagnosis and prognosis of various neurodegenerative diseases and is being used both as an enrichment tool and an endpoint in various Alzheimer's disease-modifying drug trials. The aim of this work is to assess quantitative and qualitative brain-PET image interpretation using a simulated affordable PET system with a sparse-detector configuration. ***Materials and Methods:*** Using brain PET listmode data (N=7 ^{18}F-FDG, N=2 ^{18}F-FDOPA, and N=2 ^{11}C-PiB) acquired on a Vision scanner, we simulated detectors' decimation by removing 1-out-of-each-X coincidences to achieve decimation levels ranging from 5%-50%. Scanner normalization was kept the same throughout this study. We used commercial Database Comparison, Cortical Analysis, and Striatal Analysis quantification workflows to process reconstructed FDG, PiB, and FDOPA images, respectively. FDG images were also visually read by a clinical expert. ***Results:*** Decimated FDG images were each compared to the same normal database (nDB) and corresponding mean z-scores within 116 Automated-Anatomical-Labelling regions were all in good agreement (R^2>0.98) with those from original images compared to the same nDB. Lower agreements were found for 50%-decimation (R^2<0.77). About 87% of brain voxels, in both 5%-and-10% decimated images, had z-scores below 10 percent-error relative to z-scores from corresponding original images. Greater percent-errors were found at higher decimation levels. The fraction of z-scores below -2.5 (abnormal-looking) was relatively stable up to 30%-decimation. Visually, 5%-to-20% decimated images and corresponding z-score stereotactic-surface-projections were of acceptable quality for a clinical read. Increased artifacts and noise levels were seen at higher decimation levels rendering visual interpretation more challenging for clinical conditions such-as epilepsy where focal abnormalities may be present. For ^{11}C-PiB, mean composite SUV-ratio was relatively stable across decimation levels 5%-to-30% compared to original images, with a mean percent-error below 0.8%. For ^{18}F-FDOPA, striatal-binding-ratios within different striatal regions were all relatively stable up to 30% decimation. However, greater percent-errors were found for 20%-and-25% decimation compared to 30%-decimation level, indicating that the arrangement of removed detectors had greater impact on the quantification results. ***Conclusion:*** We assessed the effect of sparse detector configurations on brain-PET image interpretation. Results comparable to full detector coverage were obtained up to 30%-decimation level. We also observed that the spatial distribution can be more impactful than the number of removed detectors. Other decimation geometries will be evaluated to potentially achieve acceptable results even with fewer detectors. This could offer a cost-effective solution for dedicated brain PET imaging without compromising clinical interpretability.

OP-775

PUMA: PET Unification for Multi-Tracer Applications in Multiplexed PET Imaging

S. Gutschmayer[1], *B. A. Spencer*[2], *Y. G. Abdelhafez*[2], *R. D. Badawi*[2], *S. R. Cherry*[2], *T. Beyer*[1], *L. Shiyam Sundar*[1];
[1]*Quantitative Imaging and Medical Physics (QIMP) Team, Medical University of Vienna, Vienna, AUSTRIA,* [2]*Department of Biomedical Engineering and Radiology, University of California-Davis, Davis, CA, UNITED STATES OF AMERICA.*

Aim/Introduction: PET imaging provides functional information on tracer distribution, which can be extracted simultaneously across the entire human body with total-body PET imaging. Dual-tracer protocols have been introduced to complement readouts on diseases that may not be present on either tracer-PET, such as for lesion differentiation with [^{18}F]-FDG and [^{68}Ga]-DOTATATE or [^{68}Ga]-PSMA, as well as for assessing myocardial function using [^{82}Rb] and [^{18}F]-FDG. However, 2-tracer protocols are complex and not clinically viable. We present an automatic tool called PUMA (PET Unification for Multi-Tracer Applications) as part of the ENHANCE-PET framework for multiplexing different tracer information from the same patient undergoing sequential scans to improve clinical reading value. ***Materials and Methods:*** Eight subjects (4M, 4M) were enrolled in this IRB-approved study and underwent serial whole-body PET/CT imaging using [^{18}F]-FDG and [^{68}Ga]-DOTATATE (6 subjects, 2M/4F) or [^{18}F]-Fluciclovine (2 subjects, 2M). The PET images of each subject were aligned using a co-registration method that utilized both the PET and the structural information of the CT images. First, the CT images were resliced according to the corresponding PET image's dimension and spacing. The [^{18}F]-FDG PET/CT image of each patient was used as a reference in a multiscale co-registration procedure. The CT of the patient's other tracer ([^{68}Ga]-DOTATATE or [^{18}F]-Fluciclovine) PET/CT image was aligned to the CT of the [^{18}F]-FDG PET/CT image, and the resulting deformation field was applied to the corresponding PET image. For validation, an automated segmentation tool [1] delineated four target organs: lung, liver, brain and spleen. As with the PET information, extracted deformation fields were also applied to the resulting masks. The dice score was used as a metric to quantify the alignment. The mean intensity distribution within the masks was used to quantify the change in tracer information caused by interpolation after alignment. ***Results:*** After alignment, the dice scores between the first reference and the subsequent multiplexed scans improved on average by 47% (brain), 45% (liver), 64% (spleen) and 46% (lung). The mean intensity change within these reference organs remained below 2.5% on average. ***Conclusion:*** Based on PET/CT data, the proposed tool successfully aligned complementary

PET tracer information of the same patient. As a caveat, care must be taken regarding the PET-CT alignment in each PET/CT study, calling to action standardized imaging protocols and adequate patient positioning and instructions. ***References:*** [1] Sundar LKS, Yu J, Muzik O, et al. J Nucl Med. 2022; doi:10.2967/jnumed.122.264063. Online ahead of print.

OP-776

Comparison of Standardized Uptake Values of [18F]FDG-PET/CT imaging of healthy volunteers: a multi-country PET/CT study

D. Ferrara[1], *R. Badawi*[2], *T. Beyer*[1], *Z. Chen*[3], *S. Cherry*[4], *B. Geist*[5], *S. Gutschmayer*[1], *M. Hacker*[5], *S. Kinuya*[3], *L. Shiyam Sundar*[1], *B. Spencer*[4], *S. Takeda*[6], *J. Taki*[6], *H. Wakabayashi*[3];
[1]*QIMP Team, Medical University of Vienna, Vienna, AUSTRIA,* [2]*Department of Radiology, UC Davis, Sacramento, CA, UNITED STATES OF AMERICA,* [3]*Department of Nuclear Medicine, Kanazawa University Hospital, Kanazawa, Ishikawa, JAPAN,* [4]*Department of Biomedical Engineering, UC Davis, Davis, CA, UNITED STATES OF AMERICA,* [5]*Division of Nuclear Medicine, Medical University of Vienna, Vienna, AUSTRIA,* [6]*PET Center, Kanazawa Advanced Medical Center, Kanazawa, Ishikawa, JAPAN.*

Aim/Introduction: Whole-body [18F]FDG-PET/CT imaging is a clinically-viable means of oncology patient management. Standardized-uptake-values (SUVs) are used to assess disease and treatment response. Lately, the concept of inter-organ mapping of metabolic activities using whole-/total-body PET is gaining traction. To employ PET for studying inter-organ aberrations of metabolic profiles, a SUV normative database is required. This study aimed to investigate potential variations in SUVs among healthy volunteers with distinct geographic backgrounds. ***Materials and Methods:*** 15 Japanese (13M/2F, 71±11 kg), 19 European (10M/9F, 76±17 kg), and 15 American (6M/9F, 82±17 kg) healthy volunteers underwent whole-body [18F]FDG-PET/CT imaging at 60-min post-injection (test). A second scan (retest) was performed for European cohort 90 min after the first scan and for the Japanese cohort 1-y after the initial scan, each using the same protocol. Ten volumes-of-interest (VOI: aorta, brain, pancreas, spleen, thyroid, inferior-vena-cava, lung, skeletal-muscle, subcutaneous-fat, visceral-fat) were segmented automatically from the PET/CT images [1]. Mean SUVs normalized to body weight were extracted for each VOI. To limit confounders from different acquisition/reconstruction protocols, SUVs were normalized for each volunteer to their own liver uptake. The resulting SUV_{liver} across cohorts and test-retest were compared with relative %-differences (%D) and t-tests. To avoid potential sex-related differences, the analysis was subsequently repeated solely on male participants. ***Results:*** Across three cohorts, SUV_{liver} were comparable (%D<=15%) in all VOI, except for thyroid (%D=18%, p=0.01), brain (%D=32%, p<0.01), and visceral-fat (%D=90%, p<0.01). Further, SUV_{liver} was highest and most variable in brain. Japanese subjects had the lowest SUV_{liver}, ranging from 0.28 (lungs) to 2.42 (brain). Mean %D in SUV_{liver} were minimal between American and European cohorts, ranging from 1% (lung) to 23% (visceral-fat). Corresponding variations were higher between American and Japanese cohorts, ranging from 4% (skeletal-muscle) to 90% (visceral-fat). Notably, intra-group differences (test-retest) were not significant, with the highest %D of 5% (brain). Similar findings were observed when analysing only male participants for an imbalanced sex-distribution across the 3 cohorts. ***Conclusion:*** The overall differences in SUV_{liver} across American, European, and Japanese cohorts were relatively small, suggesting that it may be possible to establish a normative database across individuals with different geographic upbringings. Limitations of this study, such as differences in PET system calibration, demographics, and small sample size, will be addressed by expanding the sample sizes (ongoing) across the sites. ***References:*** [1] L.K. Shiyam Sundar et al. "Fully-automated, semantic segmentation of whole-body [18F] FDG-PET/CT images based on data-centric artificial-intelligence". In: J Nuc Med (2022).

OP-777

Non-rigid anatomical standardization of whole-body PET/CT identifies variation of FDG distribution with age and sex: an AI-assisted study

K. Hirata[1,2,3], *S. Watanabe*[1,2], *J. Takenaka*[1,2], *N. Wakabayashi*[1,2], *R. Kimura*[1,4], *T. Nagai*[5], *T. Ogawa*[6], *K. Kudo*[1,3,4];
[1]*Department of Diagnostic Imaging, Graduate School of Medicine, Hokkaido University, Sapporo, JAPAN,* [2]*Department of Nuclear Medicine, Hokkaido University Hospital, Sapporo, JAPAN,* [3]*Global Center for Biomedical Science and Engineering, Faculty of Medicine, Sapporo, JAPAN,* [4]*Department of Diagnostic and Interventional Radiology, Hokkaido University Hospital, Sapporo, JAPAN,* [5]*Department of Cardiovascular Medicine, Faculty of Medicine and Graduate School of Medicine, Hokkaido University, Sapporo, JAPAN,* [6]*Faculty of Information Science and Technology, Hokkaido University, Sapporo, JAPAN.*

Aim/Introduction: Anomaly detection algorithms are expected to play important roles in the development of AI diagnosis for whole-body FDG-PET/CT. While there have been reports on anomaly detection performed using deep learning without anatomical standardization (AS), methods using AS have not been extensively studied. AS for the brain PET has been well established, however, not for the whole-body PET. We aimed to investigate possibility of applying non-rigid transformation to thousands of whole-body FDG-PET/CT scans using a single template and to validate the adequacy of AS by comparing SUV by age and sex. ***Materials and Methods:*** We reviewed all the FDG-PET/CT studies performed at Hokkaido University Hospital from 2015 to 2019, including patients with various diseases. Three different PET/CT scanners were employed. While the field-of-view was either head-to-thigh or head-to-toe, we selected head-to-thigh images taken with arms raised. For this selection, we trained a deep neural network, VGG19, with one-year manually labeled dataset, and used to classify the rest of 4-year images. We then arbitrarily selected one female patient with no abnormal accumulation as a template and overlaid all other patient images using non-rigid deformation implemented with affine transformation. After anatomical standardization, a nuclear medicine physician placed ROIs to evaluate correlations with age and sex differences. ***Results:*** After excluding same-patient studies, 3835 (1723 females) were analyzed. The average image was blurrier compared to an individual image, however, the distribution did not change significantly, indicating the non-rigid deformation was reasonably performed. Regarding correlation analysis with age, no strong correlation was found in any area. However, a weak negative correlation (r=-0.18) was found in the frontal lobe, and weak positive correlations (r=0.20-0.22) were found in the neck subcutaneous tissue and gluteal muscles. Regarding sex differences, the values in parentheses represent the difference in SUV, with a plus indicating that females had higher values. Females had higher SUV in the frontal lobe (1.3), cerebellum (0.9), tongue (0.2), ascending aorta (0.2), liver (0.2), kidney (0.5), lumbar subcutaneous tissue (0.2), and lower part of bladder (1.7), while males had higher SUV in the neck subcutaneous tissue (-0.4),

left ventricular myocardium (-0.3), abdominal wall subcutaneous tissue (-0.2), upper part of bladder (-1.7), and external genitalia (-0.7). ***Conclusion:*** Although the analysis was limited to the particular field-of-view and posture, reasonable results were obtained in terms of correlations with sex and age differences, and this non-rigid transformation was considered applicable for constructing a normal database for anomaly detection.

OP-778

Noise and Sharpness estimation in Positron Emission Tomography (PET) images using radiomics and deep learning

P. Gurunath Bharathi*, F. Moradi, M. Khalighi;*
Stanford Medicine, Palo Alto, CA, UNITED STATES OF AMERICA.

Aim/Introduction: Noise and sharpness are important quality metrics in medical imaging. Here we examine if radiomics and deep learning approaches can be used to reliably measure these and compare them. ***Materials and Methods:*** This study utilized FDG PET from 52 patients, (40 patients for training, 6 patients each for testing and validation). The PET scans were reconstructed using Time-Of-Flight Block-Sequential Regularized Expectation Maximization (TOFBSREM) with beta values from 400 to 1200 or ordered subset expectation maximization (OSEM), for time/bed between 60 to 120 seconds. An expert radiologist annotated the liver to calculate the coefficient of variation (CV) as the ground truth noise values. The beta was used as a proxy of sharpness levels. To improve computational efficiency, the input axial scans were cropped into a 64 * 64 matrix to remove excess background. 160 slices above and below the liver position were extracted from each reconstructed volume. Radiomics features such as textural, wavelet, gabor features were extracted from these slices and fed into supervised classifier or regressor for estimating the sharpness and noise levels respectively. Similarly, the extracted slices were also given as input to deep learning model for estimating the sharpness and noise levels. ***Results:*** A total of 10,274 radiomics features were fed into the trained random forest classifier and regressor with 200 trees for sharpness and noise estimation respectively. The accuracy of sharpness and noise estimation through radiomics was 63.1% and coefficient of determination (r^2) was 0.583, respectively. On the other hand, deep learning approach showed 77.2% accuracy in sharpness estimation and $r^2 = 0.57$ for noise estimation. Table 1 provides a comprehensive comparison between the two methods. ***Conclusion:*** This study proposed a radiomics and deep learning approach to assess the sharpness and noise levels in PET scans. Our deep learning method achieved good performance in terms of accuracy and r^2, and efforts are ongoing to create an integrated approach that combines radiomics and deep learning for improving accuracy. This approach can be used to quantify how changing scan acquisition and reconstruction parameters affects image quality.

OP-779

Evaluation of potential dose reduction in O-15 water PET by simulation of low count data and sinogram denoising

M. Voskamp[1,2]*, F. Büther*[3]*, M. Mamach*[4,2]*, J. Lücke*[5,6]*, S. Salwig*[5]*, H. Mousavi*[5]*, F. M. Bengel*[1]*, T. Lenarz*[2,2]*, G. Berding*[1,2]*;*
[1]Department of Nuclear Medicine, Hannover Medical School, Hannover, GERMANY, [2]Cluster of Excellence "Hearing4all", Hannover, GERMANY, [3]Department of Nuclear Medicine, University Hospital, Münster, GERMANY, [4]Department of Medical Physics and Radiation Protection, Hannover Medical School, Hannover, GERMANY, [5]Department of Medical Physics and Acoustics, Carl von Ossietzky University Oldenburg, Oldenburg, GERMANY, [6]Cluster of Excellence "Hearing4all", Oldenburg, GERMANY, [7]Department of Otolaryngology, Hannover Medical School, Hannover, GERMANY.

Aim/Introduction: Positron Emission Tomography (PET) is capable to assess neuronal activity in brain regions using radioactive markers indicating higher regional blood flow. We simulated a reduction in used radioactivity and applied sinogram denoising to examine the feasibility of a lower radiation exposure. ***Materials and Methods:*** O-15 water PET studies of 5 patients with auditory implants in the cochlea (CI, n=1), brainstem (ABI, n=2) or midbrain (AMI, n=2), scanned during quiet and speech stimulation (3-6 per condition) using a Siemens Biography LSO-Duo PET/CT were included [1]. We simulated the application of lower radioactivity doses by randomly reducing the number of coincident events by a factor of 8 (this factor would have left the radiation exposure even below the limit of 1 mSv for the public according to the Euratom directive 2013/59). Those reduced datasets were then denoised by applying the BM4D (Block matching 4D) algorithm to the normalized, attenuation-, random-, and scatter-corrected sinograms. We used statistical parametric mapping (SPM) to compare the number of activated voxels in the auditory cortices ($p<0.001$, uncorrected, Brodmann areas (BA) 21, 22, 41, and 42) in the original, the reduced, and the reduced+denoised datasets. ***Results:*** In comparison to the mean number of activated voxels mapped inside the auditory cortices across patients based on the unreduced data (1130 +- 630 voxel, Zmax 4.96 +- 0.35) we saw significantly ($p<0.01$) less voxels in those areas in the reduced data (383 +- 400 voxel, Zmax 4.36 +- 0.41). When denoised with BM4D (655 +-775 voxel in the auditory cortices, Zmax 4.22 +- 0.45) the difference in comparison to the original data was no longer significant ($p>0.05$). Nevertheless, we did not find a significant difference between reduced and reduced+denoised data ($p>0.1$), and Zmax was significantly lower for both compared to unreduced data ($p<0.05$). ***Conclusion:*** Reducing the applied radioactivity in PET scans of auditory system function may improve the usability for diagnostic measurements by, for example, increasing the number of follow-up studies during auditory rehabilitation after implantation to better detect neuronal plasticity. Our results indicate that even with two-decade-old PET technology, which has lower sensitivity than current scanners, a reduction in the radioactivity by a factor 8 would have been possible if used in combination with advanced denoising algorithms. ***References:***
[1] Berding G et al. (2015) Positron Emission Tomography Imaging Reveals Auditory and Frontal Cortical Regions Involved with Speech Perception and Loudness Adaptation. PLoS ONE 10(6): e0128743. doi:10.1371/journal.pone.0128743

OP-780

Intra-arterial super-selective delivery of Yttrium-90 for the treatment of recurrent Glioblastoma: feasibility and safety results in virtual patients' cohort

G. Paolani[1]*, S. Strolin*[1]*, S. Minosse*[2]*, M. Santoro*[1]*, N. Pucci*[2]*, L. Oddo*[3]*, Y. Toumia*[3]*, E. Guida*[4]*, F. Di Giuliano*[4]*, R. Floris*[4]*, F. Garaci*[4]*, S. Dolci*[4]*, G. Paradossi*[3]*, F. Domenici*[3]*, V. Da Ros*[4]*, L. Strigari*[1]*;*
[1]Department of Medical Physics, IRCCS Azienda Ospedaliero-Universitaria di Bologna, Bologna, ITALY, [2]UOC Diagnostica per Immagini, University Hospital of Rome "Tor Vergata", Rome, ITALY, [3]Department of Chemical Science and Technologies, University of Rome "Tor Vergata", Rome, ITALY, [4]Department of Biomedicine and Prevention, University Hospital of Rome "Tor Vergata", Rome, ITALY.

Aim/Introduction: Glioblastoma (GBM) is the most common malignant neoplasia in the central nervous system. Surgical resection followed by external beam radiation therapy (EBRT) and adjuvant chemotherapy is the standard of care, but median life expectancy remains poor. In this study, the feasibility and safety

of IA injection of Poly(vinyl alcohol) Microbubble (^{90}Y-PVA MBs) in GBM recurrent patients are investigated using an ad-hoc tool to calculate the absorbed dose distribution from contrast-enhanced MRI images used as a surrogate of ^{90}Y-MBs distribution. A comparison between the EBRT approach and the ^{90}Y absorbed dose per injected activity is reported. ***Materials and Methods:*** Nine GBM patients (7 men and 2 women) were investigated. MRI examinations were performed using a 3T superconductive system to delineate the tumor volumes. CT scans co-registered with MRI images were used to delineate organs at risk, automatically segmented using Deep Learning-based software, and approved by an expert neuroradiologist. Volumetric Modulated Arc Therapy treatment plans with two coplanar arcs were generated using a clinical treatment planning system (TPS). We assumed that the relative intensity at the voxel levels from the MRI post-contrast T1-weighted images was a valid surrogate of ^{90}Y-MBs distribution post-AI.A specific ^{90}Y dose voxel kernel (DVK) obtained with a Monte Carlo simulation using DOSExyz was convolved with the MRI images using MATLAB, to obtain the ^{90}Y-MBs-based dose distribution. The ^{90}Y-MBs and EBRT-based plans were compared in terms of absorbed dose distribution using a clinical TPS for radioembolization. ***Results:*** The physical dose distribution obtained from the simulation of a total activity of 1GBq of ^{90}Y-MBs was rescaled to consider the prescribed ^{90}Y-MBs activities calculated in order to guarantee that the 95% of the prescribed dose is delivered to the 95% or the 99%, (i.e., $A_{95\%}$ and $A_{99\%}$). The calculated activities median [range] were $A_{95\%}$=269.2 MBq[63.6-2334.1] and $A_{99\%}$=370.6 MBq[93.8-3315.2], while the median [range] of mean doses to PTV were 58.21Gy [42.34;61.33] for the VMAT plan, and 133.62Gy[6.02;589.35], 161.33Gy[11.25;856.97] considering $A_{95\%}$ and $A_{99\%}$ respectively. In addition, the brain tissue was spared in the ^{90}Y simulations compared to the VMAT one with median [range] of mean doses of 13.89Gy [0;61.33] for the VMAT plan, and 6.24Gy [0;589.35] 8.12Gy [0;856.97] considering $A_{95\%}$ and $A_{99\%}$ respectively. ***Conclusion:*** Our results suggest that higher doses to tumor volumes and lower mean doses to the brain might be reached using ^{90}Y-MBs, compared with EBRT leading to a less toxic and higher treatment.

OP-781

Variational autoencoder for detecting coronary artery disease in myocardial perfusion SPECT

K. Okuda[1], *K. Nakajima*[2], *T. Hara*[3], *H. Yoneyama*[2], *S. Kinuya*[2];
[1]*Hirosaki University, Hirosaki, JAPAN,* [2]*Kanazawa University, Kanazawa, JAPAN,* [3]*Gifu University, Gifu, JAPAN.*

Aim/Introduction: The variational autoencoder (VAE) (1-2) has been used for unsupervised anomaly detection in medical images. This study evaluated the automatic anomaly detection from myocardial perfusion SPECT (MPS) images using convolutional VAE approach. ***Materials and Methods:*** All patients underwent ^{99m}Tc-sestamibi or tetrofosmin MPS, and stress polar maps were generated and used as two datasets. A total of 3,432 polar map images (49% male) without known coronary artery disease (CAD) were used as a training dataset, and 111 polar map images (59% male, 43% obstructive CAD) were also used as a validation dataset. By training the convolutional VAE on normal polar map images, we constructed an image generator that could reproduce normal myocardial perfusion distribution from any state of myocardial perfusion. Abnormal myocardial perfusion was automatically detected by performing image operations between the VAE-generated normal polar map images and original images using mean square error (MSE), structural similarity index (SSIM), and peak signal-to-noise ratio (PSNR). A summed stress score (SSS) was also calculated using sex-segregated normal databases. ***Results:*** VAE-based image generator successfully generated all normal polar maps irrespective of difference in male/female and normal/defect patterns. Moreover, MSE, SSIM, and PSNR were calculated automatically by the VAE-based image generator trained from sex-combined polar map images. The area under the receiver-operating characteristic curve for CAD detection was 0.873 (95% confidence interval: 0.792-0.931) for MSE, 0.860 (0.777-0.921) for SSIM, and 0.877 (0.797 to 0.934) for PSNR compared to 0.814 for SSS (p = n.s. for all comparisons). ***Conclusion:*** The convolutional VAE has the potential to improve the detection of CAD in MPS images. Although conventional quantitative analysis is based on sex-segregated normal databases, this new approach using VAE-based analysis does not need to consider the characteristics of myocardial perfusion in males and females. ***References:*** (1) Higaki A, Kawaguchi N, Kurokawa T, Okabe H, Kazatani T, Kido S et al. Content-based image retrieval for the diagnosis of myocardial perfusion imaging using a deep convolutional autoencoder. J Nucl Cardiol 2023; 30 :540-549.(2) He Z, Zhang X, Zhao C, Ling X, Malhotra S, Qian Z, et al. A method using deep learning to discover new predictors from left-ventricular mechanical dyssynchrony for CRT response. J Nucl Cardiol. 2023; 30:201-213.

1606

Tuesday, September 12, 2023, 4:45 PM - 6:15 PM
Hall C

Clinical Oncology Track - TROP Session: Head and Neck Imaging

OP-782

Dual time-point imaging of FAPI-04 in head and neck squamous cell carcinoma

J. Yaqun, *L. Chongjiao, H. Yong;*
Department of Nuclear Medicine, Zhongnan Hospital of Wuhan University, Wuhan, CHINA.

Aim/Introduction: ^{68}Ga-FAPI-04 has been most extensively studied clinically as imaging probe and shown favorable imaging properties, especially for HNSCC. However, the optimal acquisition time remains poorly understood. Therefore, we aimed to evaluate the diagnostic value of the dual time-point ^{68}Ga-FAPI-04 PET/CT in the staging of HNSCC, especially in lymph node metastasis. ***Materials and Methods:*** A total of 43 patients with diagnosed or suspected HNSCC were enrolled for final analysis, including 40 treatment-naïve and 3 relapsing patients. Each patient underwent a whole-body ^{68}Ga-FAPI-04 PET/CT at 30~60 min and a delayed scan in the head and neck region at 2 h post injection. The tracer uptake of primary and metastatic lesions was semiquantitatively determined using SUVmax and tumor-to-background ratio (TBR). The SUVmean was measured for contralateral normal tissues or organs (palatine tonsils, submandibular glands, sternocleidomastoid muscle, and internal jugular vein). Radiotracer uptake, TBR, retention index (RI), diagnostic performance, and T/N staging was explored. Findings were referred to histopathology or radiographic follow-up. ***Results:*** We evaluated 43 participants (38/43 men; median age, 61 years), including 2 maxillary sinus, 11 oral, 10 oropharyngeal, 13 laryngeal, and 7 hypopharyngeal cancer. As for primary tumors, the mean SUVmax was similar between early (16.91) and delayed scan (16.11, p = 0.315). However, the mean TBR of delayed imaging was significantly

higher than that of early scan (all $p < 0.05$). For the analysis of neck lymph nodes, 30 patients were visually quantified positive and 17 patients underwent neck dissection. Notably, metastatic lymph nodes showed higher mean SUVmax in delayed scan than early imaging (12.13 vs 10.63, $p = 0.000$), while non-metastatic lymph nodes showed the opposite results (delayed 2.53 vs early 3.42, $p = 0.028$). The mean RIs of metastatic and non-metastatic lymph nodes were 15.65% and -19.43%, respectively. N staging had been altered in 3 (3/30) patients based on delayed images. The mean SUVmean of submandibular glands and palatine tonsils was markedly decreased in delayed imaging (both $p = 0.000$). What's more, a second primary tumor which was masked at the early scan appeared on the delayed imaging in the submandibular gland, and the lesion was identified as secretory carcinoma by subsequent surgical pathology. ***Conclusion:*** For ^{68}Ga-FAPI-04 PET/CT imaging of HNSCC, delayed imaging can effectively acquire high-contrast images, especially adding diagnostic value for the discrimination of metastatic from non-metastatic lymph nodes and detecting hidden lesions near or within the tissues influenced by physiological uptake.

OP-783

Effectiveness of HAN-MI-RADS (Head and Neck Molecular Imaging-Reporting and Data System) criterion in head and neck squamous cell carcinoma post concurrent chemoradiotherapy

M. Gupta[1], *A. Jajodia*[2], *P. Ahlawat*[3], *M. Gairola*[3], *M. Agarwal*[4], *S. Goyal*[5], *P. Choudhury*[1];
[1]*Department of Nuclear Medicine, Rajiv Gandhi Cancer Institute and Research Centre, Delhi, INDIA,* [2]*Department of Radiology, Juravinski Hospital, McMaster University, ON, CANADA,* [3]*Department of Radiotherapy, Rajiv Gandhi Cancer Institute and Research Centre, Delhi, INDIA,* [4]*Department of Surgical Oncology, Rajiv Gandhi Cancer Institute and Research Centre, Delhi, INDIA,* [5]*Department of Medical Oncology, Rajiv Gandhi Cancer Institute and Research Centre, Delhi, INDIA.*

Aim/Introduction: Post-concurrent chemo-radiotherapy (CRT) response assessment have been challenging in locally advanced head and neck squamous cell carcinoma (LA-HNSCC) due to prevailing post-radiation changes. Molecular response methods have been encouraging, though further clarifications and validations were needed. We tested the effectiveness of a proposed semi-quantitative molecular response criterion in these patients. ***Materials and Methods:*** Two subspecialty-trained physicians evaluated FDG PET/CT of LA-HNSCC patients (n-83) post three months CRT using a five points HAN-MI-RADS (Head and Neck Molecular Imaging-Reporting and Data System) criterion. Where available, histopathology examination with clinical and imaging interpretation was taken as a reference for the disease. A diagnostic accuracy comparison was made with the existing Hopkins score. Further effectiveness was analyzed with disease-free survival (DFI) and overall survival (OS). ***Results:*** Metastasis was developed in 11/83 patients at 3 months of evaluation. Of 72 patients, 39, 2, and 31 patients had a complete response, equivocal response, and partial response as per HAN-MI-RADS. Per patient sensitivity, specificity, PPV, NPV, and accuracy for predicting loco-regional disease up to one year and two years was 93.3%, 92.5%, 90.3%, 94.9%, 92.9% and 84.9%, 91.9%, 90.3%, 87.2%, 88.6% respectively. One year and two years DFI for each HAN-MI-RADS score showed a statistically significant difference while it was not for OS. The ROC curve analysis showed significantly better outcome predictability of HAN-MI-RADS (AUC 0.884) than Hopkins (AUC 0.699). ***Conclusion:*** A five points HAN-MI-RADS criterion was found promising for response assessment with less equivocal results and statistically significant higher AUC than Hopkins for loco-regional recurrence prediction. ***References:*** 1. Mehanna H, Wong WL, McConkey CC, Rahman JK, Robinson M, Hartley AG, et al. PET-CT Surveillance versus Neck Dissection in Advanced Head and Neck Cancer. N Engl J Med. 2016;374:1444-54. 2. Werner RA, Bundschuh RA, Bundschuh L, Javadi MS, Higuchi T, Weich A, Sheikhbahaei S, Pienta KJ, Buck AK, Pomper MG, Gorin MA, Lapa C, Rowe SP. Molecular imaging reporting and data systems (MI-RADS): a generalizable framework for targeted radiotracers with theranostic implications. Ann Nucl Med.2018;32:512-22. 3. Marcus C, Ciarallo A, Tahari AK, Mena E, Koch W, Wahl RL, et al. Head and neck PET/CT: therapy response interpretation criteria (Hopkins Criteria)-interreader reliability, accuracy, and survival outcomes. J Nucl Med. 2014;55:1411-6.4.

OP-784

[^{18}F]FDG PET/CT in the Therapy Response Evaluation of Head and Neck Carcinoma. How to approach it?

V. Carrero-Vásquez[1], *B. Hervas-Sanz*[1], *L. Rodríguez-Bel*[1], *G. Reynes-Llompart*[2], *R. Martin-Vaello*[2], *A. Lozano-Borbalas*[3], *O. Bermejo-Segu*[4], *P. Perlaza-Jiménez*[1], *C. Martínez-Ramos*[1], *M. Cortés-Romera*[1];
[1]*Nuclear Medicine Department, Bellvitge University Hospital, Barcelona, SPAIN,* [2]*Radiophysics Department, Bellvitge University Hospital, Barcelona, SPAIN,* [3]*Radiation Oncology Department, Bellvitge University Hospital, Barcelona, SPAIN,* [4]*Plastic Surgery Department, Bellvitge University Hospital, Barcelona, SPAIN.*

Aim/Introduction: Despite advances in therapy, recurrence-rates in patients with head and neck squamous cell carcinoma (HNSCC), especially locoregional, are still high. Therefore, its early identification is of utmost importance; hence, it will change clinical management completely. [^{18}F]FDG-PET/CT-scan has shown effectiveness in the evaluation of therapeutic response(ETR), although there is no consensus on how to assess and report it using quantitatively with the standardized uptake value (SUVmax) and/or qualitatively with Likert scales like Hopkins(HS) and Deauville(DS) scores. Primary aims: assess the performance method in the evaluation of locoregional control(RC) and whether any technique is superior in predicting RC, progression-free survival(PFS) and overall survival(OS). Secondary aims: determine the relationship between HPV and p16 presence. ***Materials and Methods:*** 149 consecutive patients with HNSCC between 2010 and 2021 were selected; 73: 51 men, mean age 58(42-82) met the inclusion criteria: PET/CT-scan 3-6 months post-radiotherapy (postRT). The studies were scored using a qualitative 5-point-scale: HS and DS, grouped as positives(scores 4 and 5), negatives(scores 1,2,3) for primary tumour, right neck and left neck. The SUVmax was determined for each.All patients were followed until 2023. ***Results:*** 21 patients(p) had recurrence: 15p locoregional, 3p locoregional+metastatic, 3p metastatic. 52p did not show recurrence. The assessment of these positive PET/CT-postRT using the HS was positive in 15p, with a sensitivity, specificity, PPV, NPV, and accuracy of 71%, 100%, 100%, 90% and 91%, respectively, and a significant statistical correlation between HS-positive and recurrence (p=0.0083), HPV and p16-positive (p=0,05 and p=0,09). Using the DS, we observed 36p had positive PET/CT-postRT studies with sensitivity, specificity, PPV, NPV, and accuracy of 100%, 71%. 58%. 100% and 79%, respectively. DS-positive and recurrence also showed a high significance (p=0.028), and a good concordance index between the two scales HS-DS for the ETR was observed. Also, patients with higher SUVmax at the pre-treatment-PET/CT and lower decreased at the post-RT-PET/CT showed a significant

p-value with the recurrence rate (p=0.00972). The PFS (mean 10,3 months, range 2-30) and OS (mean 18,9 months, range 6-44) were lower in patients with HS-positive and DS-positive studies. ***Conclusion:*** Our study found that all assessment methods predicted RC, OS and PFS with high significance and almost equally well, according to the current published data. Regarding the Likert scales, our results showed a good performance in discriminating responders from nonresponders.Also, there was a high significance with the HPV and p16-positive association and a good concordance between the Likert scales.

OP-785

C-X-C motif chemokine receptor 4-directed PET/CT in newly diagnosed Head and Neck Squamous Cell Carcinoma - Initial Experience

S. Serfling, *R. Werner, S. Andreas, H. Takahiro, A. K. Buck, A. Kosmala, R. Hagen, S. Hackenberg, A. Scherzag, E. Gerhard-Hartmann, Y. Zhi;*
University Hospital Würzburg, Würzburg, GERMANY.

Aim/Introduction: In patients affected with head and neck cancer, [^{18}F]FDG is used as reference, but its diagnostic accuracy can be hampered by inflammatory processes. We aimed to determine the read-out capabilities of the novel C-X-C motif chemokine receptor 4 (CXCR4)-targeting radiotracer relative to [^{18}F]FDG in treatment-naïve individuals. ***Materials and Methods:*** Twelve patients with histologically confirmed head and neck squamous cell carcinoma (HNSCC) were scheduled for dual-tracer imaging without therapy between scans using [^{18}F]FDG (FDG) and [^{68}Ga]PentixaFor (PEN). We applied target-to-background ratios (TBR) with liver (TBR_L) and vena cava superior (TBR_{VCS}) serving as reference. 6/12 (50%) were scheduled for LN removal, thereby allowing to compare PEN-PET findings with surgical specimen. ***Results:*** On a visual assessment, [^{18}F]FDG identified more sites of disease, with increased detection rates for both the primary (FDG, 12/12 [100%], PEN, 9/12 [75%], P=0.08) and LN (FDG, 10/12 [83%], PEN, 9/12 [75%], P=0.4). Quantification provided slightly higher TBR for FDG relative to PEN for all lesions (TBR_L: FDG, 7.54 ± 3.5 vs PEN, 5.61 ± 1.82, P=0.17; TBR_{VCS}: FDG, 11.65 ± 8.49 vs PEN, 4.33 ± 1.32, P=0.03), primary (TBR_L: FDG, 9.2 ± 4.3 vs PEN, 5.57 ± 2.2, P=0.02; TBR_{VCS}: FDG, 13.6 ± 8.7 vs PEN, 4.16 ± 1.58; P<0.01), and LN (TBR_L: FDG, 5.43± 4.2 vs PEN, 5.61 ± 1.92; TBR_{VCS}: FDG, 9.3 ± 10.64 vs PEN, 4.4 ± 1.6; P≥0.24). Of note, in patients with available LN derived from surgical removal, PEN was true positive in 4/18 (22.2%) and false positive in 14/18 (77.8%), with the latter classified as reactive LNs by histological work-up. Respective sensitivity and specificity for FDG was 100% and 96%, which was higher relative to PEN (80% and 90.7%, respectively). ***Conclusion:*** In treatment-naïve HNSCC, FDG was superior for assessing the primary when compared to PEN. For LN, PEN achieved lower rates of sensitivity and specificity, with false-positive findings in reactive/inflammatory conditions probably due to the physiological expression of CXCR4 in germinal centers.

OP-786

Targeted imaging of αvβ6-integrin in patients of Head and Neck Squamous Cell Carcinoma and Pancreatic Ductal Adenocarcinoma with ^{68}Ga-Trivehexin PET/CT scan and correlation with immunohistochemistry- a pilot study

S. Das, *I. B. Sen, D. Malik, P. Thakral;*
Fortis Memorial Research Institute, Gurugram, INDIA.

Aim/Introduction: αvβ6-integrin is exclusively expressed in epithelial cells and is upregulated in many carcinomas, such as Pancreatic Ductal Adenocarcinoma (PDAC) and head and neck squamous cell carcinoma (H&N-SCC). Expression of αvβ6 integrin is almost always tumour specific. αvβ6 modulates invasion and inhibit apoptosis. Trivehexin is a trimerized αvβ6-integrin selective nanopeptide which can be used as a diagnostic agent after labelling with a positron emitter like ^{68}Gallium. This is a pilot study to assess the correlation between ^{68}Ga-Trivehexin positron emission tomography/computed tomography (PET/CT) tumour uptake and αvβ6-integrin expression by the tumour tissue on immunohistochemistry (IHC). ***Materials and Methods:*** 33 patients (19-76 years; 24 males) with suspected H&N-SCC (n=20), or PDAC (n=13) underwent 68Ga-Trivehexin PET/CT scans and 18F-FDG PET/CT scans on two-separate days. 29 patients underwent tissue biopsy from the suspected primary/ metastatic tumor site. An experienced pathologist categorized αvβ6-integrin expression on IHC using the immune-reactive score (IRS) and modified 4-point IRS classification. ***Results:*** ^{68}Ga-Trivehexin PET/CT images demonstrated good tracer uptake in 24/29 patients. 18F-FDG PET/CT images demonstrated good tracer uptake in 27/29 patients. Subsequent biopsy results from 29 lesions revealed 09 PDACs, 01 pancreatic neuroendocrine tumour, 01 adenocarcinoma colon, 15 H&N-SCCs, while benign inflammatory changes was observed in two patient and in one patient biopsy was inconclusive. All the 24 patients with PDACs and H&N-SCC showed good tracer uptake in the primary as well as the metastatic lesions on ^{68}Ga-Trivehexin PET/CT scan (mean SUVmax 6.04 ± 3.8) with a better tumor to background ratio in comparison to 18F-FDG PET/CT scan. The SUVmax of biopsied lesions calculated on ^{68}Ga-Trivehexin PET/CT scan demonstrates a strong correlation with the IRS scores with significant p-value (r=0.61; P=0.002), while there was no such correlation observed on the FDG PET/CT scan (r= 0.38; P=0.066). The αvβ6-integrins expression was higher along the tumor margins, than in the center, which was consistent with the pattern of ^{68}Ga-Trivehexin uptake. ***Conclusion:*** To our knowledge, this is the first in human study evaluating αvβ6 expression in various carcinomas by both in-vivo and in-vitro methods. Our study shows ^{68}Ga-Trivehexin as a promising molecular imaging agent for tumors expressing αvβ6 integrins with a good correlation with αvβ6 expression seen on IHC.

OP-787

Role of pet biomarkers (suvmax, tlg and mtv) in the response to treatment in patients with nasopharyngeal carcinoma and its evolution.

S. Lopez Puche, *F. Gómez-Caminero López, P. García-Talavera San Miguel, L. Diaz Gonzalez, E. Casillas Sagrado, J. Badell Martinez, S. Rama Alonso, E. Campaña Diaz, P. Tamayo Alonso;*
Hospital Universitario de Salamanca, Salamanca, SPAIN.

Aim/Introduction: To evaluate by means of PET biomarkers the response to QT/RT treatment in patients with nasopharyngeal carcinoma. ***Materials and Methods:*** Retrospective study including patients diagnosed with nasopharyngeal carcinoma between 2014-2022 treated with concomitant QT+RT (70Gy in main lesion [PTV1] and 56-63Gy in nodes [PTV2]). All underwent staging/planning PET/CT with [18F]-fluorodeoxyglucose (FDG) and response assessment PET/CT at 3 months post-treatment. Some patients received neoadjuvant QT (QTNA-scheme TPF with docetaxel, cisplatin and fluorouracil), with an early PET/CT study performed 3 weeks post-treatment. Pre/post-treatment biomarkers were measured by quantitative analysis (Syngovia® software). They were divided into two groups according to response to treatment and evolution: relapsed/non-relapsed. Statistical analysis by subgroups was performed with Jamovi® to evaluate the difference in the percentage

of pre/post-treatment biomarker decline in both groups and between those who received each treatment regimen. ***Results:*** 52 patients, excluding 8 as baseline PET was not available; final sample size: 44 patients (33 males and 11 females; mean age 56 years +/- 11.4 years). 13 with squamous cell carcinoma, 24 undifferentiated, 6 lymphoepithelioma and 1 low-grade papillary adenocarcinoma. Non recurrent (36): stage I (4), II (8), III (15) and IV (10). 24 received QT/RT; 13 QTNA+QT/RT. Pre/post-treatment decline was observed in PTV1 SUVmax 79% MTV 56% and TLG: 90% and in PTV2 SUVmax 88%; MTV 67% and TLG 96%. Currently, all remain under follow-up. Relapsed (8): stage III (3), IV (4). 5 received QT-RT and 2 QTNA+QT/RT, the decrease in PTV1 was (SUVmax 74%; MTV 54% and TLG: 86%) and in PTV2 (SUVmax 83%; MTV 74% and TLG 93%). Of these, 4 have died (57%). Mean values of all biomarkers in PTV1 and PTV2 were higher in patients who progressed, with a mean decrease in patients who did not relapse of (SUVmax 11.9%; MTV 35.9% and TLG 24.1) in PTV1 and of (SUVmax 16.8%; MTV 40.6% and TLG 53.1) in PTV2. Student's t-test showed statistical significance in the decrease of SUVmax PTV1 pre/post-treatment (p=0.032) and in TLG PTV2 (p=0.04) with no significance in the rest of parameters (p>0.05). ***Conclusion:*** PET/CT biomarkers were able to determine the metabolic response in most cases. Furthermore, the results obtained showed a statistically significant percentage decrease of SUVmax values in PTV1 and TLG in PTV2 pre- and post-treatment, as well as higher mean values of all biomarkers in patients who progressed, so they could be useful as prognostic markers of patient outcome.

OP-788

Evaluation of relationship between Total Tumor Metabolic Volume and tumour tissue modified viral Human papilloma virus DNA levels at initial staging in HPV driven oropharyngeal squamous cell carcinoma.

R. Kulkarni, *M. Posner, S. Roof, N. Ghesani;*
Mount Sinai Hospital, New York, NY, UNITED STATES OF AMERICA.

Aim/Introduction: The biology of Human papilloma virus (HPV) driven oropharyngeal squamous cell carcinoma (OPSCC) varies from non-HPV driven OPSCC. The NCCN guidelines therefore advise a separate management strategy for HPV driven OPSCC. Total metabolic tumor volume (TMTV) a volumetric parameter, derived from 18F-FDG PET/CT, is proven to be a more complete representation of disease burden than conventional response assessment criteria such as two-dimensional measurements and highest standardised uptake value (SUVmax) and recently has been validated in numerous malignancies. Tumor Tissue Modified Viral (TTMV) HPV DNA is a recently introduced highly sensitive serum marker for HPV driven OPSCC. TTMV-HPV DNA is produced during the break-down of integrated and/or episomal HPV DNA of malignant epithelial cells during the degradation of tumours. In this retrospective review, we studied correlation between TTMV-HPV DNA value and TMTV from 18F-FDG PET/CT scan at initial staging in patients with HPV driven OPSCC to understand tumor biology and disease burden and to explore complementary role between the two tests. ***Materials and Methods:*** TTMV from 18F-FDG PET/CT scans performed for initial staging in patients with biopsy proven HPV genotype positive OPSCC were obtained using a proprietary software. Voxels of interest (VOIs) were manually drawn around the lesions and the software analysed these VOIs to derive a TTMV. The TTMV-HPV DNA values were obtained from patient charts. Pearson's correlation co-efficient was used to derive the correlation between TTV at initial staging and TTMV-HPV DNA. The statistical significance of this correlation was assessed. Statistical significance was considered when the p value was <0.05. ***Results:*** 30 patients, 24 males and 6 females, average age of 64.4 were examined. The primary sites of malignancies were base of the tongue in 9/30 patients, palatine tonsils in 16/30, tonsils/base of tongue combined in 2/30, and pyriform sinus, nasal cavity, and watershed area of the nasopharynx/tonsil in remaining 3. 27/30 patients had biopsy proven nodal metastases and one with distal metastasis. 18F-FDG PET CT had 75% specificity and 100% sensitivity in detecting nodal metastases. The mean tumor volume was 43.9 mL and mean TTMV-HPV DNA value was 2354.2 fragment/mL. The Pearson's correlation co-efficient between TTMV-HPV DNA values and the TTV was 0.41 with a p value of 0.03 (p <0.05). ***Conclusion:*** TTV is well established as an imaging parameter of disease burden and on preliminary investigation, has a significant correlation with TTMV-HPV DNA values. This likely denotes a complementary relationship between the two parameters.

OP-789

A prospective Comparison of ^{68}Ga-FAPI and ^{18}F-FDG PET/MR in the Diagnosis of Residual Tumor Tissue for Head and Neck Squamous Cell Carcinoma Patients after Neoadjuvant Treatment

X. Zhong[1], *Y. Luo*[2], *M. Su*[3], *X. Peng*[2], *W. Zhang*[4];
[1]*Nuclear Medicine Department and Biomedical Big Data Center, West China Hospital of Sichuan University, Chengdu, CHINA,* [2]*Cancer Center, West China Hospital of Sichuan University, Chengdu, CHINA,* [3]*Nuclear Medicine Department, West China Hospital of Sichuan University, Chengdu, CHINA,* [4]*Biomedical Big Data Center, West China Hospital of Sichuan University, Chengdu, CHINA.*

Aim/Introduction: To perform a head-to-head comparison of ^{68}Ga-FAPI and ^{18}F-FDG PET/MR of their diagnostic capabilities for detecting residual tumor tissue in patients with head and neck squamous cell carcinoma (HNSCC) following neoadjuvant therapy. ***Materials and Methods:*** Our study included patients with HNSCC who underwent ^{68}Ga-FAPI and ^{18}F-FDG PET/MR examinations before and after neoadjuvant treatment starting from June 2022. Patients with primary malignant tumors other than HNSCC were excluded. Tracer uptake of primary tumor were compared by SUVmax and visual evaluation. A diagnosis of positive residual tumor tissue was made if a lesion or lymph node showed a higher uptake of ^{68}Ga-FAPI and ^{18}F-FDG than the surrounding normal soft tissues. Differences in SUVmax between groups were determined by paired t test. The diagnostic abilities of ^{68}Ga-FAPI and ^{18}F-FDG PET/MR were compared by chi-square test. Two-tailed p values of less than 0.05 were considered statistically significant. ***Results:*** Currently, a total of 8 patients with primary tumors located in the oropharynx (n=1), hypopharynx (n=6), and tonsil (n=1) were included. All included patients underwent radical surgery after treatment. The comparison of SUVmax of ^{68}Ga-FAPI versus ^{18}F-FDG PET/MR showed no significant difference before neoadjuvant therapy with values of 16.77±5.01 vs. 16.40±3.91 (P=0.803) but significantly different after therapy with values of 9.00±3.28 vs. 5.62±3.18 (P=0.011). ΔSUVmax before and after neoadjuvant therapy of the two imaging methods were significantly different with values of 7.77±4.62 vs. 10.78±5.69 (P=0.016). In total, 32 cervical lymph node regions were dissected. The sensitivity, specificity and accuracy of ^{68}Ga-FAPI vs. ^{18}F-FDG PET/MR for diagnosing residual malignant lymph node regions were 57.14% vs. 57.14% (P>0.05), 60.00% vs. 88.00% (P<0.05), and 59.38% vs. 81.25% (P<0.05), respectively. Postoperative pathology revealed

that one patient had no residual malignant tumor in the primary tumor area after neoadjuvant therapy. Although the diagnosis of ^{18}F-FDG PET/MR was negative, ^{68}Ga-FAPI PET/MR was positive for this patient. For the other seven patients, pathological results showed different quantities of residual malignant tumor tissues in the primary tumor area, of which 4 cases were diagnosed correctly by ^{18}F-FDG PET/MR, while all cases were correctly diagnosed by ^{68}Ga-FAPI PET/MR. ***Conclusion:*** ^{68}Ga-FAPI PET/MR is superior to ^{18}F-FDG PET/MR in the diagnosis of residual malignant tumor of HNSCC patients in the primary focus.

OP-790

Preclinical and clinical evaluation of^{68}Ga-FAPI-LM3 for PET imaging in nasopharyngeal carcinoma

L. Zhao, *H. Chen, Q. Lin;*
the First Affiliated Hospital of Xiamen University, Xiamen, CHINA.

Aim/Introduction: Radiolabeled fibroblast activation protein inhibitors (FAPIs) and LM3 peptides have been extensively widely explored for imaging of FAP- and SSTR2 positive tumors. A FAPI-LM3 heterodimer that was radiolabeled with ^{68}Ga and evaluated in tumor xenografts and NPC patients with cancer. ***Materials and Methods:*** FAPI-LM3 was synthesized based on FAPI-46 and LM3, and then radiolabeling with ^{68}Ga to creat^{68}Ga-FAPI-LM3. Its dual-receptor-binding affinity was evaluated in vitro and in vivo. Preclinical studies, including micro-PET and biodistribution studies, were performed using HT-1080-FAP+ HT-1080-SSTR2 xenografts. The effective dosimetry of ^{68}Ga-FAPI-LM3 was evaluated in three healthy volunteers. The clinical feasibility of ^{68}Ga-FAPI-LM3 PET/CT was evaluated in 6 NPC patients (5 for primary staging and 1 for restaging). ***Results:*** ^{68}Ga-FAPI-LM3 was stable in phosphate buffered saline and fetal bovine serum for 2 h. ^{68}Ga-FAPI-LM3 yielded FAP- and SSTR2-binding affinities comparable to those of monomeric FAPI (IC_{50}, 4.4nM vs. 11.7nM) and DOTA-LM3 (IC_{50}, 13.2nM vs. 1.3nM), respectively. The tumor uptake of ^{68}Ga-FAPI-LM3 was significantly higher than that of ^{68}Ga-FAPI-46 (14.78 ± 0.76 %ID/g vs. 8.08 ± 1.51 %ID/g at 1h, P<0.001; 17.68 ± 2.46 %ID/g vs. 7.11 ± 0.99 %ID/g at 4h, P<0.001) and ^{68}Ga-DOTA-LM3 (14.78 ± 0.76 %ID/g vs. 7.88 ± 1.10 %ID/g at 1h, P<0.001; 17.68 ± 2.46 %ID/g vs. 5.46 ± 0.41 %ID/g at 4h, P<0.001) in HT-1080-FAP+ HT-1080-SSTR2 double-target-positive xenografts, while the normal organs showed low tracer uptake. The tumor uptake of ^{68}Ga-FAPI-LM3 at 1 h p.i. (14.78 ± 0.76 %ID/g) was mostly suppressed by FAPI46+DOTA-LM3 (0.86% ± 0.06%, 94% blockade), partially inhibited by FAPI46 (6.51 ± 0.89 %ID/g, 56% blockade) and DOTA-LM3 (6.34 ± 0.77 %ID/g, 57% blockade) in HT-1080-FAP+ HT-1080-SSTR2 double-target-positive xenografts. ^{68}Ga-FAPI-LM3 was tolerated well, with no adverse events in any of the healthy volunteers or patients. The effective dose from ^{68}Ga-FAPI-LM3 PET/CT was 1.96×10^{-2} mSv/MBq. In clinical investigations with NPC, the radiotracer uptake of primary and metastatic lesions in ^{68}Ga-FAPI-LM3 PET/CT was significantly higher than those in ^{18}F-FDG PET/CT (median SUVmax: primary tumors, 13.8 vs. 9.0, P=0.043; regional lymph nodes, 10.7 vs. 9.2, P=0.039; distant metastases, 12.9 vs. 5.2, P<0.001). Moreover, 3 bone metastases and 1 liver metastasis were found to be negative in 18F-FDG PET/CT but positive in 68Ga-FAPI-LM3 PET/CT. ***Conclusion:*** ^{68}Ga-FAPI-LM3 exhibited promising FAP and SSTR2 dual-receptor-targeting properties, leading to favorable tumor imaging in NPC patients. This study demonstrated the safety and clinical feasibility of ^{68}Ga-FAPI-LM3 PET/CT for imaging of NPC patients.

1607

Tuesday, September 12, 2023, 4:45 PM - 6:15 PM
Hall F1

Neuroimaging Committee - TROP Session: New PET Tracers for Brain Imaging

OP-791

Potentially incremental role of ^{18}F-DPA714 PET to conventional MRI in the detection and therapeutic monitoring of autoimmune encephalomyelitis

M. Zhang[1], *H. Meng*[2], *S. Chen*[2], *B. Li*[1];
[1]*Department of Nuclear Medicine, Ruijin Hospital, Shanghai Jiao Tong University School of Medicine, Shanghai, CHINA,*
[2]*Department of Neurology, Ruijin Hospital, Shanghai Jiao Tong University School of Medicine, Shanghai, CHINA.*

Aim/Introduction: Our previous case reports have shown the potential value of translocator protein (TSPO) radioligand 18F-DPA714 positron emission tomography (PET) in the detection of autoimmune encephalomyelitis (AE) [1]. Therefore, we aim to further assess the role of 18F-DPA714 PET in the detection and therapeutic monitoring of AE compared to conventional MRI in our clinical trial (Trial registration number ClinicalTrials.gov: NCT05293405). ***Materials and Methods:*** Forty-one patients with a definite diagnosis of AE underwent hybrid 18F-DPA714 PET and conventional MRI sequences, modified Rankin scale (mRS) scores assessment and antibody titer testing at baseline. The intensity and extent of 18F-DPA714 uptake in involved brain regions were evaluated. Ten healthy volunteers (HVs) were recruited in the study as normal controls on 18F-DPA714 PET. Fourteen of 41 patients further underwent follow-up PET/MRI at an average of 7 months after receiving immunosuppressive therapy. ***Results:*** Higher physiological uptake of 18F-DPA714 in the thalamus and brainstem than that in other brain cortical regions was observed in HVs (P < 0.05). The overall detection positive rate of AE on 18F-DPA714 PET was significantly higher than that on conventional MRI (53.66% vs. 36.58%, P = 0.027). For sixteen seronegative AE patients, abnormal 18F-DPA714 uptakes were observed in four patients whereas only one patient had positive MRI findings. For the patents with positive findings on 18F-DPA714 PET, the extent and intensity of 18F-DPA714 uptake at baseline showed no significant correlation with mRS score or antibody titer. However, significant decrease in the uptake extent and intensity of 18F-DPA714 in involved brain regions after receiving immunosuppressive therapy was clearly observed. ***Conclusion:*** 18F-DPA714 PET might have potentially incremental role to conventional MRI for detection and therapeutic monitoring of AE. ***References:*** 1. Shen R, Shen D, Zhou Q, Zhang M, Chen S. Antibody-mediated autoimmune encephalitis evaluated by (18) F-DPA714 PET/MRI. Brain Behav Immun Health 2022;26:100535. doi: 10.1016/j.bbih.2022.100535

OP-792

Activated Microglia Detected by TSPO PET in Anti-N-Methyl-D-Aspartate Receptor (NMDAR) Encephalitis: Distinct Pattern of Disease

J. Ge, *J. Wang, P. Wu, Y. Guan, C. Zuo;*
Huashan Hospital, Shanghai, CHINA.

Aim/Introduction: Autoimmune encephalitis (AIE) constitutes a group of inflammatory brain disorders that are characterized by prominent neuropsychiatric symptoms and are associated

with antibodies against neuronal cell-surface proteins, ion channels, or receptors. The disorders most frequently recognized on clinical grounds are anti-N-methyl-D-aspartate receptor (NMDAR) encephalitis and autoimmune limbic encephalitis (ALE) such as anti-leucine-rich glioma-inactivated 1 (LGI1) protein encephalitis and anti-γ-aminobutyric acid receptor-B (GABAB) encephalitis. We have previously reported that patients with ALE exhibited abnormal microglial activation, primarily in the bilateral hippocampus, as detected by 18-kDa translocator-protein (TSPO) PET imaging [1]. While brain MRI in anti-NMDAR encephalitis is often normal, this study aimed to investigate the activated microglia pattern of anti-NMDAR encephalitis and to evaluate its correlation with clinical phenotype. ***Materials and Methods:*** Twenty patients with anti-NMDAR encephalitis from the AIE cohort in Huashan hospital and ten controls with ALE or non-inflammatory diseases were included in the current study. All patients with anti-NMDAR encephalitis were diagnosed based on clinical manifestations and positive anti-NMDAR antibodies both in serum and in CSF samples. Cerebral TSPO PET imaging with 18F-DPA714 was performed in individual subjects. The abnormal microglial activation of anti-NMDAR encephalitis was evaluated by comparing TSPO PET images between individual patients with anti-NMDAR AIE and those of the ten controls using visual reading, voxel-wise statistical parametric mapping analysis, and semi-quantitative analysis with standardized uptake value ratios normalized to the cerebellum (SUVRc), respectively. ***Results:*** Remarkable and extensive microglial activation in the frontal-parieto-temporal lobes was demonstrated in anti-NMDAR AIE. Notably, the changes of abnormally activated microglia in individual patients commonly involved unilateral cerebral hemisphere or exhibited an apparently asymmetric pattern of two hemispheres. The semi-quantification of the affected frontal-parieto-temporal regions showed significant difference between anti-NMDAR AIE and controls with ALE or non-inflammatory diseases ($P<0.05$). Longitudinal analysis of two cases showed normalization of the pattern of cerebral microglial activation with recovery. ***Conclusion:*** This study revealed that anti-NMDAR encephalitis has a distinctive pattern presented by TSPO PET imaging, which indicated underlying mechanisms of microglia in pathogenesis and clinical phenotype. We propose that this pattern may offer valuable information for the diagnosis, treatment decision and prognosis prediction of this elusive but treatable disease. ***References:*** 1Wang J, Ge J, Jin L, et al: Characterization of neuroinflammation pattern in anti-LGI1 encephalitis based on TSPO PET and symptom clustering analysis. Eur J Nucl Med Mol Imaging 2023.

OP-793

Safety, biodistribution, and dosimetry of [18F]OP-801, a novel neuroinflammation PET biomarker, in healthy individuals

F. Moradi[1], *M. Jovin*[1], *N. Malik*[1], *J. H. Park*[1], *V. Ferri*[1], *M. L. James*[1], *J. L. Cleland*[2], *S. Maricich*[2];
[1]*Stanford University, Stanford, CA, UNITED STATES OF AMERICA,* [2]*Ashvattha Therapeutics, Redwood City, CA, UNITED STATES OF AMERICA.*

Aim/Introduction: [18F]OP-801, a fluorine labeled hydroxyl dendrimer, is a novel PET radiopharmaceutical for neuroinflammation. Pre-clinical studies showed that [18F]OP-801 crossed blood-brain barrier in areas of neuroinflammation and was selectively taken up by activated microglia and macrophages, predominantly via fluid phase endocytosis[1]. The degree of uptake correlated linearly with severity of neuroinflammation, and in contrast to TSPO PET which is complicated by TSPO expression across many cell types, nonspecific uptake was minimal. We are now conducting a first in human, phase 1/2 clinical trial in healthy controls and patients with amyotrophic lateral sclerosis (NCT05395624), and hereby reporting the results of the first cohort (healthy volunteers). ***Materials and Methods:*** Healthy individuals without personal or family history of neurodegenerative disorders were recruited for the study. Exclusion criteria include recent acute illness or use of anti-inflammatory medications. [18F]OP-801 (RCY_{EOS-dc} 10%; Radiochemical purity ~100%; SA>55 GBq/mg) was produced using automated radiosynthesis[2]. Following intravenous administration of 400 MBq [18F]OP-801, PET/MR images of vertex to lower legs were acquired using a 3 Tesla GE SIGNA scanner at 0, 1, 2, and 3 hours post injection. Blood and urine samples were collected and measured for activity up to 6 hours. Clinical, laboratory and ECG data were acquired at baseline and after administration, and participants were followed up for 15 days. Image-based dosimetry was performed using MIRDCalc version 1.1 (MIRDsoft.org). ***Results:*** Three male and two female healthy volunteers completed the study without experiencing any adverse events related to the radiopharmaceutical. PET images demonstrated blood pool activity followed by renal excretion. No significant uptake was observed in the brain, spine, or any other organs. A very small amount of biliary excretion was present in the gallbladder after first hour, with visualization of low-level activity in small bowel in subsequent time points. The overall biodistribution and dosimetry were similar to the mouse model in preclinical studies, with kidney and bladder wall receiving the highest dose. ***Conclusion:*** As expected from pre-clinical studies, [18F]OP-801 is safe and has favorable biodistribution with no or little background uptake in normal central nervous system, and non-uptaken circulating radiopharmaceutical is eliminated via urinary excretion, resulting in low effective radiation dose. ***References:*** 1. Henningfield et al. Alzheimers Dement. 2020, 16 (S2), e040661. 2. Jackson et al. Clinical Radiosynthesis and Translation of [18F] OP-801: A Novel Radiotracer for Imaging Reactive Microglia and Macrophages. Submitted

OP-794

Dopaminergic Damage Pattern Predicts Phenoconversion Time in Isolated Rapid Eye Movement Sleep Behaviour Disorder

J. Ge, *Q. Xu, H. Lin, Y. Guan, C. Zuo, P. Wu, H. Yu; Huashan Hospital, Shanghai, CHINA.*

Aim/Introduction: The exact phenoconversion time from isolated rapid eye movement sleep behaviour disorder (iRBD) to synucleinopathies remains unpredictable. This study investigated whole-brain dopaminergic damage pattern (DDP) with disease progression and predicted phenoconversion time in individual patients. ***Materials and Methods:*** Age-matched 33 iRBD patients and 20 healthy controls with ^{11}C-CFT-PET scans were enrolled. The patients were followed up 2-10 (6.7 ± 2.0) years. The phenoconversion year was defined as the base year, and every two years before conversion was defined as a stage. Support vector machine with leave-one-out cross-validation strategy was used to perform prediction. ***Results:*** We found dopaminergic degeneration of iRBD occurred about 6 years before conversion and then abnormal brain regions gradually expanded. Using DDP, area under curve (AUC) was 0.879 (90% sensitivity and 88.3% specificity) for predicting conversion in 0-2 years, 0.807 (72.7% sensitivity and 83.3% specificity) in 2-4 years, 0.940 (100%

sensitivity and 84.6% specificity) in 4-6 years and 0.879 (100% sensitivity and 80.7% specificity) over 6 years. In individual patients, predicted stage correlated with whole-brain dopaminergic level (r = -0.740, p < 0.001). ***Conclusion:*** Our findings suggest that DDP could accurately predict phenoconversion time of individual iRBD patients, which may help to screen patients for early intervention.

OP-795

[^{18}F]F-SynVesT-1 and [^{18}F]F-FDG PET imaging in the pre-surgical evaluation of MRI-negative children with focal cortical dysplasia

L. Xiao, *Y. Tang, J. Yang, S. Hu;*
Department of Nuclear Medicine, Xiangya Hospital, Central South University, Changsha, CHINA.

Aim/Introduction: Focal cortical dysplasia (FCD) is the most common cause of drug-resistant epilepsy in children undergoing epilepsy surgery. In children with epilepsy caused by FCD, MRI-negative focal epilepsy is one of the most challenging cases in surgical epilepsy treatment, which represent approximately one-third of the total cohort. It is difficult to identify the epileptogenic zone (EZ) in MRI-negative cases, and these cases have poor surgical outcomes, with postoperative seizure-free rates as low as 50%. Our study aims at utilizing quantitative positron emission tomography (QPET) analysis to complement [^{18}F]F-SynVesT-1 and [^{18}F]F-FDG positron emission tomography (PET) imaging to facilitate the identification of EZ in MRI-negative children with FCD. ***Materials and Methods:*** We prospectively enrolled 17 MRI-negative patients with FCD who underwent [^{18}F]F-SynVesT-1 and [^{18}F]F-FDG PET before undergoing surgical resection. QPET was analyzed using statistical parametric mapping (SPM) with comparison to age- and gender-matched normal controls. The sensitivity, specificity, and area under the curve (AUC) of [^{18}F]SynVesT-1 PET, [^{18}F]FDG PET, [^{18}F]SynVesT-1 QPET, and [^{18}F]FDG PET QPET in EZ localization were assessed. Additionally, logistic regression analyses were performed based on electroencephalography (EEG), [^{18}F]F-SynVesT-1 and [^{18}F]F-FDG PET. ***Results:*** The AUC values of EEG, [^{18}F]F-FDG PET, and [^{18}F]F-SynVesT-1 PET were 0.849 (sensitivity = 100.0%, specificity = 69.7%), 0.924 (sensitivity = 94.1%, specificity = 90.8%), and 0.908 (sensitivity = 82.4%, specificity = 99.2%), respectively. [^{18}F]F-FDG QPET showed reduced sensitivity (64.7%) but increased specificity (95.8%) when compared to visual assessment, whereas [^{18}F]F-SynVesT-1 QPET exhibited increased sensitivity (94.1%) but reduced specificity (97.5%). Notably, the hybrid model that relied on EEG, [^{18}F]F-FDG PET, and [^{18}F]F-SynVesT-1 PET demonstrated the highest AUC value (AUC = 0.996, sensitivity = 100.0%, specificity = 96.6%) among all models. ***Conclusion:*** The study outcomes exhibit a favorable utilization of a multivariate prediction model that incorporates EEG, [^{18}F]SynVesT-1 PET, and [^{18}F]FDG PET as a tool for enhancing the precision of diagnostic tests designed to identify the location of EZ. Also, the research indicates that QPET analysis holds great potential for refining the precision of diagnostic tests utilized for EZ localization, specifically in situations where only [^{18}F]FDG PET or [^{18}F]SynVesT-1 PET data are attainable. These research results suggest that QPET analysis could potentially lead to better surgical outcomes for MRI-negative children with FCD.

OP-796

Mapping Sudden sensorineural hearing loss-related brain activation: a preliminary study by Using [18 F] SynVesT-1 and PET Imaging.

J. Zhong[1], *S. Hu*[1], *E. Zhou*[2];
[1]*Department of Nuclear Medicine, XiangYa Hospital, Central South University, Changsha, CHINA,* [2]*2Department of Otolaryngology Head and Neck Surgery, Hunan Provincial People's Hospital (First Affiliated Hospital of Hunan Normal University), Changsha, CHINA.*

Aim/Introduction: Sudden sensorineural hearing loss (SSNHL) is commonly encountered in audiologic and otolaryngologic practice. SSNHL is most commonly defined as sensorineural hearing loss of 30 dB or greater over at least three contiguous audiometric frequencies occurring within a 72-hr period. Although the differential for SSNHL is vast, for the majority of patients an etiologic factor is not identified. In recent years, some studies suggested that the essence of SSNHL is hearing loss caused by nerve injury.As an consequence, the neurologic cause arise our interest. Synaptic vesicle protein 2A(SV2A) can reflect neuronal abnormality. The abnormalities of synaptic density in SSNHL has not yet been tested directly by SV2A. In this positron emission tomography (PET) study with the new tracer ^{18}F-SynVesT-1, we evaluated SV2A abnormalities in patients with SSNHL. ***Materials and Methods:*** Twenty patients with SSNHL and twenty-five healthy controls were recruited. All SSNHL patients and healthy controls underwent magnetic resonance imaging (MRI) and static PET imaging with 18F-SynVesT-1.Visual assessment of PET images and ROI analysis by whole brain analyses were undertaken. Standardized uptake value (SUV) of ^{18}F-SynVesT-1 and ratio (SUVr) were computed between regions of interest. ***Results:*** Lesions in the brain of tinnitus patients had increased ^{18}F-SynVesT-1 uptake compared with controls. The patients revealed increased metabolism of the unilateral hemisphere, including 11 brain areas prior to the bilateral Accumbens Area , bilateral Caudate,Putamen and posterior cingulate,left angular gyrus ,right frontal pole ,right lingual gyrus.^{18}F-SynVesT-1 PET indicated high lesion uptake in 17 cases (85%). Further SPM assessment indicated that the degree and frequency of SSNHL are related to high ^{18}F-SynVesT-1 uptake (P<0.05). ***Conclusion:*** SV2A PET with ^{18}F-SynVesT-1 is the first in vivo evidence linking higher synaptic density to network alterations and confirming to the hypothesis of increased neuronal activity in SSNHL. Our findings provide further incentive to evaluate interventions that restore synaptic connections to treat SSNHL.

OP-797

Lower synaptic density and its association with cognitive dysfunction in patients with obsessive-compulsive disorder

J. Hou, *Q. Xiao, L. Xiao, S. Hu;*
Xiangya Hospital, Central South University, Changsha, CHINA.

Aim/Introduction: The exploration of synaptic alteration of obsessive-compulsive disorder (OCD) is helpful for detecting pathological mechanism, but there is still a lack of in vivo research. The aim of this study is to investigate the synaptic density indicators of OCD, and to explore the relationship between cognitive dysfunction of OCD and synaptic density changes. ***Materials and Methods:*** This research enrolled 28 drug-naïve adults with OCD aged 18-40 years and 16 healthy controls (HCs). A 3D-T1 weighted structural Magnetic resonance imaging (MRI) and ^{18}F-SynVesT-1 Positron Emission Computed Tomography

(PET) was collected. In this study, the Wisconsin cart sorting test (WCST) was used to test cognitive function in patients with OCD and HCs. Correlative analysis of synaptic density reduction with cognitive dysfunction was also calculated. ***Results:*** Compared with HCs, patients with OCD showed reduced synaptic density in regions of the cortico-striato-thalamo-cortical (CSTC) circuit such as bilateral putamen, left caudate, left parahippocampal gyrus, left insula, and left parahippocampal gyrus as well as in the left middle occipital lobe (voxel P <0.001, with cluster level above 50 contiguous voxels). The Percent Conceptual Level Responses of WCST were positively associated with the synaptic density reduction in the left middle occipital gyrus (R^2=0.1690, P=0.0298), the left parahippocampal gyrus (R^2=0.1464, P=0.0445), and left putamen (R^2=0.1967, P=0.0181) in OCD patients. ***Conclusion:*** There was lower 18F-SynVesT-1 uptake in adults with OCD relative to HCs, potentially reflecting lower synaptic density. This study is the first attempt to explore the synaptic density of vivo OCD patients, and is helpful to find biological targets for cognitive dysfunction in OCD. ***References:*** 1. Hazari N, Narayanaswamy JC, Venkatasubramanian G. Neuroimaging findings in obsessive-compulsive disorder: A narrative review to elucidate neurobiological underpinnings. Indian J Psychiatry 2019; 61(Suppl 1): S9-S29. 2. Holmes SE, Scheinost D, Finnema SJ, Naganawa M, Davis MT, DellaGioia N et al. Lower synaptic density is associated with depression severity and network alterations. Nat Commun 2019; 10(1): 1529. 3. Piantadosi SC, Chamberlain BL, Glausier JR, Lewis DA, Ahmari SE. Lower excitatory synaptic gene expression in orbitofrontal cortex and striatum in an initial study of subjects with obsessive compulsive disorder. Mol Psychiatry 2021; 26(3): 986-998. 4. Millet B, Dondaine T, Reymann JM, Bourguignon A, Naudet F, Jaafari N et al. Obsessive compulsive disorder networks: positron emission tomography and neuropsychology provide new insights. PLoS One 2013; 8(1): e53241.

OP-798

A1 adenosine receptor availability and perfusion in the human brain during acute normobaric hypoxia measured with [F-18]CPFPX PET/MRI

H. Weis[1,2], *M. Michno*[3], *J. Schmitz*[4], *A. Foerges*[3], *S. Beer*[3], *B. Neumaier*[5], *A. Drzezga*[1], *D. Aeschbach*[4], *A. Bauer*[3], *J. Tank*[4], *E. Elmenhorst*[6], *D. Elmenhorst*[3];
[1]*Department of Nuclear Medicine, University Cologne, Germany, Cologne, GERMANY,* [2]*Institute of Aerospace Medicine, German Aerospace Center, Cologne, Germany, GERMANY,* [3]*Institute of Neuroscience and Medicine (INM-2), Forschungszentrum Jülich, Jülich, GERMANY,* [4]*Institute of Aerospace Medicine, German Aerospace Center, Cologne, GERMANY,* [5]*Institute of Neuroscience and Medicine (INM-5), Forschungszentrum Jülich, Jülich, GERMANY,* [6]*Institute of Aerospace Medicine, German Aerospace Center, Cologne, Cologne, GERMANY.*

Aim/Introduction: Hypoxia alters cerebral metabolism, perfusion, and electric activity. The neuromodulator adenosine is produced/and or released into the interstitial space during hypoxia and may mediate some of these effects. A1 adenosine receptor (A_1AR) antagonism or knock-out attenuates this neuronal inhibition in mice. Here we tested the hypothesis that exposure to short term hypoxia compared to normoxia reduces the availability of A1AR in the human brain, providing evidence for a hypoxia-induced increase in endogenous adenosine. As exploratory objectives, we tested the hypotheses that psychomotor vigilance is affected during hypoxia and that perfusion is altered. ***Materials and Methods:*** Ten healthy volunteers (32 ± 13 years, 3f) completed a 110-min bolus plus constant infusion [F-18]CPFPX PET-MRI hybrid experiment: Subjects spent 60 minutes in normoxia followed by 30 minutes of normobaric hypoxia with peripheral oxygen saturation of 70 - 75 %, followed by 20 minutes of normoxia. Blood samples were used to calculate metabolite-corrected steady-state distribution volumes (V_T) of A1AR (i. e., 40 - 100 min after start of [F-18]CPFPX administration). Brain perfusion was measured using arterial spin labeling. A 3-minute psychomotor vigilance test (PVT) was conducted every 10 minutes. Heart rate and peripheral blood oxygen saturation were measured continuously. ***Results:*** Compared to normoxia, acute hypoxia reduces A_1AR availability in the cerebral cortex by 11 % ($p = 0.033$). Cortical gray matter brain perfusion on the other hand increased by 25 % ($p < 0.001$). Heart rate increased by 22 % ($p < 0.001$). PVT mean reaction time was longer by 7 ms ($p = 0.027$). ***Conclusion:*** Acute normobaric hypoxia reduces cerebral A_1AR availability, indicating increased adenosine concentration and receptor occupancy. Simultaneously cognitive performance is impaired and brain perfusion increases.

OP-799

mGluR5 and glutamate involvement in Autism spectrum disorder (ASD) adult patients : a multimodal imaging study

A. Dupont[1,2], *N. Arlicot*[1,2,3], *L. Barantin*[4], *J. Vercouillie*[4], *C. Tauber*[5], *V. Gissot*[6], *F. Bonnet-Brilhault*[7,2], *M. Santiago-Ribeiro*[8,2,3];
[1]*Radiopharmacie, CHRU Tours, Tours, FRANCE,* [2]*Inserm U 1253, Tours, FRANCE,* [3]*Inserm CIC 1415, Tours, FRANCE,* [4]*Inserm U 1253, Tours, FRANCE,* [5]*Inserm U1253, Tours, FRANCE,* [6]*CIC1415, Chru Tours, Tours, FRANCE,* [7]*Centre Universitaire de Pédopsychiatrie, Chru Tours, Tours, FRANCE,* [8]*Médecine nucléaire, Chru Tours, Tours, FRANCE.*

Aim/Introduction: Autism Spectrum Disorder (ASD) is a neurodevelopmental disorder whose pathophysiological mechanisms are still unclear. Hypotheses suggest a role for glutamate dysfunctions in ASD development and more precisely the mGlu5 receptor. To further understand the role of the glutamatergic transmission and the mGluR5 in the pathophysiology of ASD, we conducted a multimodal clinical study combining proton magnetic resonance spectroscopy (^{1}H-MRS) and Positron Emission Tomography (PET) to explore the cerebral glutamate levels along with the brain mGluR5 density in adults with ASD and controls. ***Materials and Methods:*** Two groups consisting in 12 adult males with ASD and 14 healthy adult males were recruited and matched on age. Before PET scan, each subject underwent a MRI study for brain anatomical imaging to define Regions Of Interest. Glutamate (Glu) and glutamine (Gln) levels were assessed from ^{1}H-MRS data collected from the anterior-cingulate cortex (ACC). After a CT acquisition for attenuation correction, healthy volunteers were intravenously injected with [^{18}F]FPEB as a bolus, and underwent a 90 min brain dynamic acquisition. To shorten the acquisition duration for the ASD group, PET data were collected between 30 and 50 minutes post [18F]FPEB injection. Thus, the same time window of 20-minute images from 30 to 50 minutes post [^{18}F]FPEB injection was used for comparison between the two groups. ***Results:*** No modifications in cingulate Glu levels were observed between individuals with ASD and control subjects. Our imaging results showed an overall increased density in mGluR5 in adults with ASD. The z-score maps comparing the SUVr obtained in ASD individuals and controls revealed significant differences in binding in almost all the studied brain areas at the exception of the pallidum and hippocampus. In the cortex, higher values in SUVr were detected in the frontal, parietal, temporal, occipital and insular lobes. Lower values in SUVr in the ASD group vs controls were only observed in parts of the medial precentral and inferior

temporal cortices. ***Conclusion:*** No modifications in Glu levels were observed supporting the difficulty to evaluate modifications in excitatory transmission using spectroscopy in this population, and the complexity of its glutamate-related changes. Only two other studies suggested higher densities in adult subjects with ASD in the cerebellum and postcentral gyrus using PET but were either post-mortem or limited by a small number of participants. We showed that adult individuals with ASD exhibit higher mGluR5 densities in almost all the cortex and subcortical areas.

1608

Tuesday, September 12, 2023, 4:45 PM - 6:15 PM
Hall F2

Thyroid Committee - TROP Session: Nuclear Medicine Imaging in Thyroid and Parathyroid Disorders

OP-800

The Risk of Malignancy of Thyroid PET-Avidomas on ^{18}F-FDG PET/CT using the Bethesda System for Reporting Thyroid Cytopathology

H. Coerts[1], *F. J. van Kemenade*[1], *F. A. Verburg*[1], *B. de Keizer*[2], *J. L. F. Raithel*[1], *T. M. van Ginhoven*[1];
[1]*Erasmus Medical Center, Rotterdam, NETHERLANDS,*
[2]*University Medical Center Utrecht, Utrecht, NETHERLANDS.*

Aim/Introduction: Incidental PET-positive thyroid lesions are detected on PET scans performed for non-thyroid indications. This study aims to investigate the risk of malignancy, as classified according to the Bethesda System for Reporting Thyroid Cytopathology, in patients with PET-avidomas and non-PET patients. ***Materials and Methods:*** The national pathology database (PALGA) was used to identify all patients who underwent fine needle biopsy of one or more thyroid nodules between 2012 and 2022 in the Netherlands. Bethesda classifications and indications for performing fine needle aspiration cytology were extracted from the record. ***Results:*** A total of 50,782 PALGA reports were evaluated, and the incidence of Bethesda classes in the Netherlands was as follows: 27.0% Bethesda 1 (n=13703), 55.0% Bethesda 2 (n=27951), 7.4% Bethesda 3 (n=3771), 5.1% Bethesda 4 (n=2588), 2.8% Bethesda 5 (n=1440) and 2.6% Bethesda 6 (n=1329). Among patients with a PET-avidoma who underwent surgery, the risk of malignancy by Bethesda classification was as follows: 30.3% (44/145) for Bethesda 1, 31.4% (22/70) for Bethesda 2, 29.4% (37/126) for Bethesda 3, 35.8% (100/279) for Bethesda 4, 86.1% (155/180) for Bethesda 5 and 99.4% (172/173) for Bethesda 6. Among patients who did not undergo PET and had surgery, the risk of malignancy by Bethesda classification was as follows: 14.8% (362/2446) for Bethesda 1, 9.8% (366/3740) for Bethesda 2, 26.4% (424/1607) for Bethesda 3, 39.8% (790/1983) for Bethesda 4, 83.0% (901/1086) for Bethesda 5 and 98.6% (872/884) for Bethesda 6. ***Conclusion:*** In conclusion, our findings suggest that thyroid PET-avidomas have a higher a priori risk of malignancy compared to non-PET patients.

OP-801

Iodine-123 diagnostic imaging in the early follow-up of differentiated thyroid cancer patients: wich is the best acquisition timing ?

A. Campenni'[1], *R. Ruggeri*[1], *M. Siracusa*[1], *A. Rappazzo*[1], *V. Davì*[1], *A. Nicocia*[1], *D. Cardile*[1], *S. Baldari*[1], *L. Giovanella*[2];
[1]*Ospedale Gaetano Martino, Messina, ITALY,* [2]*Ente Ospedaliero Cantonale, 6500, Bellinzona, SWITZERLAND.*

Aim/Introduction: In differentiated thyroid cancer (DTC) patients, the response to initial treatments is evaluated 6-12 months after radioiodine therapy (RIT) according to 2015 American Thyroid Association (2015 ATA) criteria. In selected patients, diagnostic $^{131/123}$I whole body scintigraphy (Dx-WBS) is recommended. ^{123}Iodine offers physical advantages compared to iodine-131 but up to date no data have been reported on the best timing to perform imaging study. We evaluated the diagnostic-performance of ^{123}I-Dx-WBS-SPECT/CT (^{123}I-Dx-imaging) in the early follow-up of DTC patients and compared early (+3 hours) and late (+20 hours) imaging results for identifying the best acquisition timing. ***Materials and Methods:*** We reviewed the records of 61 (F=43, M=18; female-to-male ratio=2.38:1; mean age=45.4±13.8, median=45, range=18-78) low (n=21) or intermediate-risk DTC patients [pT1-T3,Nx(0,1),Mx]. Papillary thyroid cancer was carried out in 58/61 (95.1%) patients while 3 had a follicular thyroid carcinoma. All patients had undergone (near)-total thyroidectomy followed by RIT, using low (1.1 GBq) or moderate (2.2 GBq) radioiodine activities. A post-therapy whole body scintigraphy coupled with SPECT-CT (pT-imaging) was obtained 2-5 days after RIT. The response to initial treatments was evaluated 8-12 months after RIT using basal and rhTSH-stimulated Tg measurements, neck-ultrasound (nUS) and ^{123}I-Dx-imaging. The latter was obtained 3 and 20 hours after tracer administration. Then patients were classified according to 2015 ATA. ***Results:*** According to 2015 ATA criteria, 31, 13 and, 17 DTC patients were classified to have excellent response (ER), indeterminate (n=9) or incomplete bio-chemical response (BIndR/BIR) or structural incomplete response (SIR), respectively. In all patients with SIR, metastatic disease was detected by ^{123}I-Dx-imaging while nUS was positive in 4 (16%) patients only (regional lymph-node metastases, n=3; local lymph-node metastasis, n=1). ^{123}I-Dx-imaging was positive at early, late or both acquisition in 2, 5, 10 patients, respectively. Acconrdingly, late ^{123}I-Dx-imaging was able to detect structural disease in 15/17 (88.2%) patients. Early, late or both planar imaging was positive in 1, 1, 4 patients, respectively. Accordingly, planar imaging was able to detect structural disease in 6/17(35.3%) patients only. ***Conclusion:*** Our data confirms the role of ^{123}I-Dx-imaging in assessing the response to initial treatments in DTC patients being able to change response assessment (from biochemical to SIR) in 13/31 (41.9%) patients with persistent disease after initial treatments. SPECT/CT imaging sensitivity is significantly superior than planar imaging. According to our preliminary results, late acquisition should be considered as the best timing for ^{123}I-Dx-imaging being able to increase diagnostic performance and reduce patients' discomfort.

OP-802

Prospective comparison of F-18-TFB and I-124 PET/CT in metastatic thyroid cancer

P. Backhaus[1,2], *K. Pentlow*[2], *A. L. Ho*[2,3], *A. Mauguen*[2], *J. A. Fagin*[2], *N. V. K. Pillarsetty*[2], *S. K. Lyashchenko*[2], *E. Burnazi*[3], *R. A. Ghossein*[2], *S. Chhabra*[2], *M. Abusamra*[2], *S. M. Larson*[2], *H. Schöder*[2], *J. O'Donoghue*[2], *W. Weber*[4], *R. K. Grewal*[2];
[1]*University Hospital Münster, Münster, GERMANY,* [2]*Memorial Sloan Kettering Cancer Center, New York City, NY, UNITED STATES OF AMERICA,* [3]*Weill Cornell Medical College, New York City, NY, UNITED STATES OF AMERICA,* [4]*Technical University Munich, München, GERMANY.*

Aim/Introduction: Fluorine 18 labelled tetrafluoroborate (F-18-TFB) is a substrate for the sodium/iodide symporter. In thyroid cancer, F-18-TFB-PET/CT may be an alternative to iodine imaging to evaluate the extent of disease and eligibility to radioiodine treatment. We report the results of the pilot study "Study of PET Imaging With 18-F-TFB in Patients With Thyroid Cancer" (NCT03196518) to determine tumor uptake of F-18-TFB and to compare properties to I-124 PET/CT in thyroid cancer. ***Materials and Methods:*** 5 patients were included in a prospective study. Following application of 0.9 mg thyrotropin alfa (Thyrogen, Sanofi Genzyme, Paris, France) on two consecutive days, patients received PET/CT 1 h after injection of 356 ± 12 MBq F-18-TFB. On the same day, patients were given 230 ± 9 MBq I-124 orally followed by PET/CT after 48 h. PET/CTs were analyzed by two board certified specialists. Detection rates and Spearman correlation for F-18-TFB and I-124 was calculated. ***Results:*** Two patients had metastatic papillary and three patients had poorly differentiated thyroid cancer. Patients with poorly differentiated cancer were treated on a redifferentiation trial preceding near-simultaneous I-124 and F-18-TFB PET/CT and had additional I-124 PET/CT at baseline. Overall 81 metastatic lesions were detected. Of these 19 (23 %) were F-18-TFB positive, whereas 78 lesions (96 %) were I-124 positive. Lesions' F-18-TFB and near-simultaneous I-124 SUV_{max} did not show a good correlation (R = 0.06, P = 0.61). In patients undergoing redifferentiation therapy, 48 lesions were newly seen in I-124-PET/CT compared to baseline with SUV_{max} up to 285. All these lesions were F-18-TFB negative. ***Conclusion:*** F-18-TFB can strongly underestimate radioactive iodine uptake. Future studies may resolve whether such relevant underestimation is a unique feature of certain redifferentiation therapies in poorly differentiated thyroid cancer or can appear also in redifferentiation naïve differentiated thyroid cancer.

OP-803

Diagnostic value of [99mTc] Tc-HYNIC-TOC scintigraphy in the management of differentiated thyroid cancer with elevated thyroglobulin and negative radioiodine whole-body scan

A. Aghaee, *E. Askari, S. Shafiei, K. Aryana;*
Nuclear Medicine Research Center,Mashhad University Of Medical Sciences, Mashhad, IRAN, ISLAMIC REPUBLIC OF.

Aim/Introduction: Negative radioiodine (131I) whole-body scan with elevated serum thyroglobulin (Tg) level are found in 20% of patients with differentiated thyroid cancer (DTC), which can be a diagnostic challenge. We evaluated the efficacy of Technetium-99m-Hydrazinonicotinyl-Tyr3-Octreotide ([99mTc] Tc-HYNIC-TOC) somatostatin receptor scintigraphy (SRS) for detection of non-iodine-avid metastases and its impact on staging and management of these patients. ***Materials and Methods:*** The study population consisted of 35 DTC patients (25 females; PTC = 88.2%, FTC = 11.8%) who had elevated serum Tg levels despite negative post-ablation radioiodine whole-body scan. All patients underwent whole body SRS 3-4 hours after intravenous injection of 20mCi (740 MBq) of [99mTc]Tc-HYNIC-TOC. Sites of suspected radiotracer accumulation were confirmed with anatomic imaging. Ultimately, corresponding changes in the staging and management were recorded. ***Results:*** SRS was positive in 27 (77.1%) cases. Patients with positive scan had significantly higher Tg levels at the time of scan, compared to those with negative scans (154.5±188.6 vs. 28.2±32.7 ng/mL, p-value = 0.005). Interestingly, previous history of neck external beam radiation therapy (EBRT) was significantly correlated with [99mTc] Tc-HYNIC-TOC avidity (Likelihood ratio = 11.2, p = 0.005). Addition of SSTR scintigraphy changed overall staging and management in 11% and 32.4% of the patients, respectively. ***Conclusion:*** SRS can be a useful diagnostic adjunct in DTC patients with highly elevated Tg and negative radioiodine whole-body scan. The likelihood of positive findings on [99mTc]TcHYNICTOC was higher in cases with previous history of EBRT or high Tg levels (i.e. suppressed-Tg >80 ng/mL) at the time of scan.

OP-804

Dual time ^{18}F-Fluorocholine PET/CT in patients with primary hyperparathyroidism

L. Vija[1], *A. Latgé*[1], *M. Sinigaglia*[1], *C. Renaud*[2], *S. Grunenwald*[2], *P. Pascal*[1], *S. Kanoun*[1], *S. Zerdoud*[1], *S. Brillouet*[1], *M. Terroir Cassou-Mounat*[1], *T. Cassou Mounat*[1], *L. O. Dierickx*[1], *F. Courbon*[1];
[1]*Institut Claudius Regaud-Oncopole, Toulouse Cedex 9, FRANCE,* [2]*CHU Toulouse, Toulouse Cedex 9, FRANCE.*

Aim/Introduction: ^{18}F-Fluorocholine (^{18}F-FCH) PET/CT is becoming the reference imaging method to locate hyperfunctioning parathyroid glands in patients with primary hyperparathyroidism (pHPT), due to its increasing availability and better performances compared to ^{99m}Tc- MIBI scan and neck ultrasound. Despite a growing body of evidence, the acquisition protocol still remains unstandardized and can vary significantly (single vs dual time, early vs late acquisition). With this study, we aimed to assess the value of dual-time acquisition and discuss possible ways for optimization. ***Materials and Methods:*** Patients who were referred to our center from March 2016 to April 2022 for 18F-FCH PET/CT in the context of pHPT were included in the analysis. History of neck surgery, biology and genetic results were considered. Dual time PET/CT was performed at 10 minutes (early phase) and 60 minutes (late phase) after 18F-FCH injection. For patients who benefited from neck surgery after PET/CT exploration, histology analysis of parathyroids was used as gold standard. Both phases were evaluated by two nuclear medicine physicians (consensual reading). Presence, location, SUVmax, SUVpeak and parathyroid-to-thyroid ratio of presumed hyperfunctioning glands were reported. ***Results:*** 145 patients and 165 glands were evaluated. Mean corrected calcemia was 2.58 ± 0.48 mmol/l ; mean PTH was 89.92 ± 42.88 pg/ml. Mean SUVmax of hyperfunctioning lesions was superior at 60 min p.i compared to 10 min p.i (5.77 ± 3.33 vs 5.16 ± 2.97, p < 0.01), with no significant variation of SUVpeak (2.83 ± 1.64 vs 2.92 ± 1.73, p = 0.10). Parathyroid-to-thyroid ratio was higher at 60 min p.i compared to 10 min p.i (1.78 ± 0.98 vs 1.46 ± 0.77, p < 0.01). 99 patients benefited from neck surgery after PET/CT and 119 glands were removed: 91 adenomas, 18 hyperplasias, 9 unspecified or normal glands. Lesion-based performances of PET/CT versus surgery were 87.88% for sensitivity and 86.14% for predictive positive value. We observed higher SUVmax for operated hyperplasia compared to adenoma at 10 min p.i (6.47 ± 1.98 vs 4.94 ± 2.96 ; p = 0.03) no difference at 60 min p.i. All

hyperfunctioning glands were seen on both acquisition times; only 27/119 (23%) operated glands (78% adenomas) presented higher uptake on early FCH PET. ***Conclusion:*** All hyperfunctioning glands were detected on both acquisition times, with higher SUVmax and lesion/background ratio on ^{18}F-FCH PET-CT late acquisition. Compared to pathology results, in our cohort, SUVmax was more intense for hyperplastic glands on early PET acquisition.

OP-805

^{18}F-fluorocholine (FCH) PET/CT performance to detect hyperfunctioning parathyroid glands in patients with no definite kidney disease and whose PTH serum level and/or calcemia are within the normal range. 786 PET/CTs in one centre.

J. Talbot[1], *C. Aveline*[2], *J. Zhang-Ying*[2], *O. Belissant-Benesty*[2], *J. Ohnona*[2], *S. Périé*[3], *S. Gaujoux*[4], *I. Wagner*[2], *M. Bennis*[5], *F. Ménégaux*[4], *S. Christin-Maître*[5], *J. Haymann*[1], *B. Baujat*[6], *S. Balogova*[7], *F. Montravers*[2];
[1]*APRAMEN, Hopital Tenon, Paris, FRANCE,* [2]*Hopital Tenon, Paris, FRANCE,* [3]*CH privé Ambroise Paré Hartmann, Neuilly sur seine, FRANCE,* [4]*GH Pitié-Salpétrière, Paris, FRANCE,* [5]*Hôpital St Antoine, Paris, FRANCE,* [6]*Hôpital Tenon, Paris, FRANCE,* [7]*Comenius University, Bratislava, SLOVAKIA.*

Aim/Introduction: In the current EANM Guidelines for parathyroid imaging, primary hyperparathyroidism (pHPT) is characterised by high serum PTH levels due to the presence of enlarged hyperfunctioning parathyroid gland(s) (PT); calcemia in some cases may be normal; rarely, PTH levels are normal with concomitant hypercalcemia. We aimed to check the performance of FCH PET/CT to detect abnormal PTs according to whether those two serum markers were in the normal range or not. ***Materials and Methods:*** From our database, we gathered 786 FCH-PET/CTs performed in patients with pHPT, excluding secondary HPT, in particular CKD grade>3 or hemodialysis or renal graft, or genetically-proven familial HPT. Four groups were considered: G0 (n=389): hypercalcemia with high PTH level, the reference for indication of HPT imaging, G1 (n=245): high PTH level but normocalcemia (<=2.6 mmol/L), G2 (n=84): hypercalcemia (>2.6 mmol/L) with inappropriate PTH level but still within the normal range, G3 (n=68) normocalcemia and normal PTH level. We determined in each group the FCH-PET/CT positivity rate, and in operated (PTX) patients, patient-based sensitivity (Se), multiglandular disease (MGD) detection, gland based sensitivity and specificity, with histology of the removed PTs as standard of truth. FCH foci interpreted as equivocal were considered negative. G0 results were compared with those of the other groups with the chi-2 test, * notes significant difference p<0.05 if the 4x2 overall test is significant ***Results:*** FCH positivity rate. G0: 330/389=85%, G1: 147/245=60%*, G2: 65/84=77%, G3: 36/68=33%* No follow-up was obtained in 98 patients whose data were excluded from further analysis. PTX rate. G0: 272/353=77%, G1: 123/207=59%*, G2: 54/74=73%, G3: 31/54=57%* FCH Se patient-based. G0: 230/256=90%, G1: 88/115=77%*, G2: 46/50=92%, G3: 22/27=81% MGD at PTX. G0: 31/272=11%, G1: 24/123=20%*, G2: 6/52=12%, G3: 8/27= 33%* FCH MGD detection. G0: 14/31=45%, G1: 8/24=33%, G2: 3/6=50%, G3: 2/8=25% FCH Se gland-based. G0: 238/283=84%, G1: 90/158=57%*, G2: 49/58=84%, G3: 26/40=65%* Adenomas / abnormal PTs. G0: 228/283=81%, G1: 71/158=45%*, G2: 39/58=67%*, G3: 17/40=43%* FCH gland-based specificity. G0: 27/36=75%, G1: 12/14=86%, G2+G3: 2/2(=100%) ***Conclusion:*** In case of pHPT, high serum levels of both PTH and calcium are not mandatory for a successful detection of hyperfunctioning PTs with FCH PET/CT. Group G2 shared several patterns with the reference group G0. The results in groups G1 and G3 with normal calcemia were rather different, with a higher frequency of MGD and a minority of adenomas vs. hyperplastic PTs, with a trend to a lower FCH sensitivity compared with hypercalcemic pHPT.

OP-806

First-line FCH PET/CT versus MIBI SPECT/CT in the surgical management of primary hyperparathyroidism: the multicentre APACH2 phase III trial

E. Quak[1], *A. Lasne-Cardon*[1], *M. Cavarec*[2], *B. Lireux*[1], *V. Bastit*[1], *N. Roudaut*[2], *P. Salaun*[2], *N. Keromnes*[2], *G. Potard*[2], *P. Vaduva*[3], *A. Esvant*[3], *F. Jegoux*[3], *O. Crouy-Chanel*[3], *A. Devillers*[4], *C. Guery*[4], *C. Lasnon*[1], *R. Ciappuccini*[1], *M. Sali-Dauda*[1], *B. Legrand*[1], *A. Estienne*[1], *J. Grellard*[1], *S. Bardet*[1], *B. Clarisse*[1];
[1]*Francois Baclesse Cancer Centre, Caen, FRANCE,* [2]*University Hospital of Brest, Brest, FRANCE,* [3]*University Hospital of Rennes, Rennes, FRANCE,* [4]*Eugene Marquis Cancer Institute, Rennes, FRANCE.*

Aim/Introduction: Whether F18-choline PET/CT (FCH PET/CT) should replace Tc99m-sestaMIBI SPECT/CT (MIBI SPECT/CT) as a first-line imaging technique for preoperative localisation of parathyroid adenomas in primary hyperparathyroidism (pHPT) is unclear. ***Materials and Methods:*** We conducted a multicentre randomized open diagnostic intervention phase III trial in adults with primary hyperparathyroidism and indication for surgical treatment (NCT04040946). Patients were assigned in a 1:1 ratio to receive first-line FCH PET/CT (FCH1) or MIBI SPECT/CT (MIBI1). In case of negative or inconclusive first-line imaging, patients received second-line FCH PET/CT (FCH2) after MIBI1 or MIBI SPECT/CT (MIBI2) after FCH1. The main aim of the trial was to compare the proportions of patients in whom the first-line imaging method resulted in successful mini-invasive parathyroidectomy (MIP) and cure, defined as the normalisation of serum calcium and parathyroid hormone levels at 1 month. We hypothesized a 30% superiority of FCH1 over MIBI1 for sample size determination (Quak_2021). ***Results:*** From 11/2019 to 05/2022, 58 patients were assigned to receive FCH1 (n=30) or MIBI1 (n=28). Baseline patient characteristics were similar between groups. FCH1 was positive in 23/29 patients and led to successful MIP and cure in 22/23 patients. MIBI1 was positive in 18/28 and led to MIP in 16/17 operated patients, and video-assisted thoracoscopy (VATS) in 1/17 patient. Cure was obtained in 15/17 patients. The proportion of patients in whom the first-line imaging exam led to successful MIP and cure was 22 (76%) for FCH1 and 13 (50%) for MIBI1 (p=0.047). Diagnostic performances were superior for FCH1 than for MIBI1: sensitivity (92% vs 68%), specificity (100% vs 75%), positive predictive value (100% vs 94%), negative predictive value (67% vs 30%), and area under the ROC curve (96% vs 71%, p=0.022), respectively. Ten patients received FCH2 and 6 patients received MIBI2. FCH2 was positive in 8/10 patients, leading to 7/9 MIP and 2/9 bilateral cervical explorations (surgery recused in 1 patient), and cure in 9/9 patients. MIBI2 was positive in 2/6 patients, leading to 1 MIP and 1 VATS; all 6 patients were cured. No adverse events related to imaging and 4 adverse events related to surgery were reported. ***Conclusion:*** The proportion of patients who underwent correct imaging-guided MIP leading to cure was higher for FCH1 than for MIBI1, 76% vs 50% respectively. Diagnostic performances were better for FCH1 than for MIBI1. Cost-benefit analyses should elucidate whether first-line FCH PET/CT in pHPT management is justified. ***References:*** Quak et al, PMID: 33413316

OP-807

PET/CT with [11C]-methionine in the diagnosis of tertiary hyperparathyroidism

M. Kolodziej[1], *M. Saracyn*[1], *A. Lubas*[2], *M. Dziuk*[3], *A. Mazurek*[3], *J. Smoszna*[2], *O. Kaminska*[3], *S. Niemczyk*[2], *G. Kaminski*[1];
[1]*Department of Endocrinology and Isotope Therapy, Military Institute of Medicine - National Research Institute, Warszawa, POLAND,* [2]*Department of Internal Medicine, Nephrology and Dialysis, Military Institute of Medicine - National Research Institute, Warszawa, POLAND,* [3]*Department of Nuclear Medicine, Military Institute of Medicine - National Research Institute, Warszawa, POLAND.*

Aim/Introduction: Tertiary hyperparathyroidism (tHP) may develop in patients treated with hemodialysis or peritoneal dialysis. Parathyroidectomy may be a chance for a significant reduction in the severity of symptoms. For the effective surgical treatment of hyperparathyroidism proper localization of the parathyroid glands prior to surgery is essential. The sensitivity of scintigraphy in the diagnosis of tHP is lower than in the diagnosis of primary hyperparathyroidism. In recent years, positron emission tomography (PET/CT) has been gaining importance, usually as a complementary technique. The aim of the study was to determine the usefulness of PET/CT with [11C]MET in the preoperative localization diagnosis of patients with tertiary hyperparathyroidism caused by chronic kidney disease, in whom first-line diagnostic methods did not allow the localization of pathologically parathyroid glands. ***Materials and Methods:*** The study was conducted in a group of 19 adult patients with severe tHP, resistant or intolerant for non-invasive treatment with negative results of scintigraphy and ultrasound of the neck. The study protocol included measurement the concentration of calcium, phosphorus and PTH in the blood serum and performing PET/CT with [11C]MET. ***Results:*** A positive result of PET/CT was obtained in 89.5% of patients (17/19). Among patients with positive PET/CT with [11C]MET results, parathyroidectomy was performed in 52.9% of them (9/17) with full consistency of the histopathological examinations with a positive results of PET/CT with [11C]MET. On this basis, the sensitivity of PET/CT with [11C]MET in the preoperative localization diagnosis of patients with tHP was assessed at 100%. Multiple lesions were visualized in 57.9% of patients (11/19). Ectopic lesions were visualized in 21.1% of patients (4/19). ***Conclusion:*** PET/CT with [11C]MET is a sensitive technique of the second-line pre-operative imaging of parathyroid glands in patients with tertiary hyperparathyroidism, in whom first-line examinations such as ultrasound and scintigraphy failed.

OP-808

Performance of multiphase iodine contrast enhanced CZT SPECT-CT in the detection of parathyroid adenomas

M. Ochoa Figueroa, *F. Askling, T. Lööw, P. Norberg, M. Ressner, J. Dahl, V. Sanchez-Rodriguez;
Universitetssjukhuset i Linköping, Linköping, SWEDEN.*

Aim/Introduction: The aim of this study was to evaluate the performance of a CZT SPECT-CT camera using 99mTc-MIBI, imaging in three different time-points and using a three phase contrast-enhanced CT protocol for preoperative localization of parathyroid adenomas. ***Materials and Methods:*** Thirty patients with suspected parathyroid adenoma (22 females and 8 males, mean age 65 y.o.) were prospectively evaluated with a CZT SPECT-CT camera using a three time-point SPECT protocol (10, 90 and 160 minutes after the intravenous administration of 500 MBq of 99mTc-MIBI), nonenhanced CT and contrast enhanced CT in the arterial and venous phase from December 2020 to October 2022. In 11 patients, the imaging results could be correlated with histopathology after surgery. The rest of the patients have a follow-up time of at least 5 months. All focal 99mTc-MIBI uptake suspicious of adenoma was quantified using a VOI sphere. ***Results:*** The overall results of the multimodality study was a sensitivity of 96%, specificity of 80%, positive predictive value of 96%, negative predictive value of 80% and an accuracy of 93%. The median maximum concentration for the adenoma suspicious uptake at 10 minutes was 27,6 kBq/ml, at 90 minutes 18,1 kBq/ml and at 160 minutes 12,1 kBq/ml. The combination of a focal 99mTc-MIBI lesion at 90 minutes in CZT SPECT and a pathological contrast enhanced soft tissue lesion in CT provided the most useful imaging information to reach diagnosis. ***Conclusion:*** Our CZT SPECT-CT iodine contrast enhanced CT protocol has provided satisfactory performance for parathyroid adenoma detection, allowing quantification of the suspicious adenoma uptake providing better characterization of the lesion and could be of help to avoid potential pitfalls like thyroid tissue, cysts and lymph nodes. Further research is required to confirm our results.

1609

Tuesday, September 12, 2023, 4:45 PM - 6:15 PM
Hall G2

e-Poster Presentations Session 12 - Dosimetry
Committee: Dosimetry Simphony

EPS-231

Estimation of absorbed tumour doses in patients treated with Yttrium-90 radioembolization in the prospective TRACE trial

B. Lambert[1], *Y. D'Asseler*[2], *E. Dhondt*[2], *L. Hermie*[2], *L. Huyck*[2], *H. Van Vlierberghe*[3], *L. Defreyne*[3];
[1]*AZ Maria Middelares en AZ Jan Palfijn Gent, Gent, BELGIUM,* [2]*Ghent University Hospital, Gent, BELGIUM,* [3]*Ghent University, Gent, BELGIUM.*

Aim/Introduction: In the prospective TRACE-trial Yttrium-90 radioembolization compared favorable to chemo-embolization in unresectable HCC. The trial was designed with activity prescription according to the TheraSphere package insert at that time. It was planned to deliver ≥120Gy in the perfused liver volume, unless risk factors such as high exposed volumes, liver dysfunction or low tumour-to-background ratio favored a reduction to 80-100Gy. In this subanalysis we estimate the absorbed tumour dose and confront the absorbed doses with outcome. ***Materials and Methods:*** We retrospectively calculated the absorbed tumour dose in the subset of patients treated with TheraSphere in the TRACE-trial[1]. Tumour dose was estimated with Simplicity® based on Tc99mMAA-SPECT/CT and the actual net 90-Yttrium activity given. We compared the absorbed tumour dose of the target lesions with the mRECIST response at 6months. We dichotomized the group in patients with a minimum tumour dose of 205Gy. ***Results:*** We investigated 27 patients. The median perfused volume was 694ml (min82-max2200). The median net administered activity 90Y was 1,28GBq (min0,22-max3,94). Based on monocompartimental dosimetry we obtained a median perfused liver dose of 87Gy (min67-max159) whereas median tumour doses were estimated 259Gy (min64-max1100). Sixteen patients had tumour doses ≥205Gy: 15 showed a good response at 6months; 1 patient suffered from new lesions outside the treated area. 11 patients had an estimated tumour dose <205Gy: 3 without response vs 8

with reponse. ***Conclusion:*** We retrospectively assessed absorbed tumour doses in 27 HCC-patients treated with TheraSphere in the prospective TRACE trial. The median absorbed tumour dose was 259Gy. 23/27 patients in this dosimetric subanalysis showed complete or partial response in the whole liver at 6 months on imaging, of whom respectively 8 and 15 presented with a tumour dose <205Gy and ≥205 Gy. 1/16 patients with a tumour dose ≥205Gy did not achieve a response. ***References:*** 1.Dhondt E, 90Y Radioembolization versus Drug-eluting Bead Chemoembolization for Unresectable Hepatocellular Carcinoma: Results from the TRACE Phase II Randomized Controlled Trial. Radiology. 2022

EPS-232

A Dosimetric Study of Liver and Tumors for Patients Undergoing HO-166 Microspheres Radioembolization

L. Miseo[1], *G. Iaccarino*[1], *M. D'Andrea*[1], *S. Ungania*[1], *A. Soriani*[1], *F. Murtas*[1], *M. Pacilio*[2], *D. Maccora*[3], *R. Sciuto*[3], *G. E. Vallati*[4], *B. Cassano*[1];
[1]*Laboratory of Medical Physics and Expert Systems, IRCCS Regina Elena National Cancer Institute, Rome, ITALY,* [2]*Medical Physics Division, Azienda Ospedaliera-Universitaria Policlinico Umberto I, Rome, ITALY,* [3]*Nuclear Medicine Unit, IRCCS Regina Elena National Cancer Institute, Rome, ITALY,* [4]*Interventional Radiology Unit, IRCCS Regina Elena National Cancer Institute, Rome, ITALY.*

Aim/Introduction: Holmium-166 labeled microspheres (Ho-166-ms) have been successfully introduced, in the last few years, in transarterial radioembolization treatments. Ho-166-ms have two main advantages, compared to Y-90 microspheres: the former is an 81 keV photopeak, that permits the acquisition of SPECT/CT quantitative images, and the latter is that can be used in both Pre-Treatment administrations (PTa) and In-Treatment ones (ITa). The reporting of the therapeutic administered activities was the goal of this study, aiming to not exceed a mean absorbed dose (mAD) to the whole liver of 60 Gy, and to study the PTa predictive power on the ITa. ***Materials and Methods:*** A cohort of fifteen patients was enrolled, diagnosed with a cumulative count of 25 hepatic metastases. Every patient underwent the PTa (that ranged into 180-250 MBq of Ho-166-ms) and, after two weeks, the ITa. Contours of liver and metastases were delineated on the PTa SPECT/CT scan, and transferred, with a rigid registration (based on liver contour), to the images acquired after the treatment. The co-registration quality was assessed with the Pearson Corelation Coefficient. For both PTa and ITa a Local Deposition Method-based dosimetric evaluation was performed: the former had the aim to determine the therapeutic activity to keep the liver mAD under or equal to 60 Gy, and the latter to calculate the in-treatment mAD of the liver and the metastases. In order to study the reproducibility of the dose spatial distribution, a local gamma function analysis was performed, with 10% dose difference and 10 mm Distance to Agreement (DTA). ***Results:*** The ITa activities varied in a (median[min;max]) 6.9[4.6;11.2] GBq range, with a tumor mAD of 115[60;315] Gy. A simulation of a 1 GBq administration was performed, resulting in a linear correlation of the liver mAD in PTa and ITa, with an R^2 equal to 0.95 (their respective differences ranged between -0.76[-2.54;0.23] Gy). The local gamma function analysis gave a minimum pass rate of 80%. None of the patients had reported toxicity symptoms within the first month. ***Conclusion:*** Considering the limit of maintaining the liver mAD within 60 Gy, the Ho-166-ms treatment is a safe choice, even with activity administration that are greater than 10 GBq. The advantage of using the same radionuclide in both of the administrations leads to having liver mAD differences that confirm a high predictive power.

EPS-233

Quantification accuracy evaluation of Yttrium-90 PET for post-therapeutic voxelised dosimetry on three generations PET/CT scanners: a phantom study

G. Croes*, J. van Sluis, A. Willemsen, W. Noordzij, O. Ivashchenko; UMCG, Groningen, NETHERLANDS.*

Aim/Introduction: Post-therapeutic dosimetry plays an important role in predicting response in patients undergoing liver radioembolization with ^{90}Y-microspheres. Although accurate quantification of ^{90}Y distribution is challenging regardless of the imaging modality, multiple studies have shown that PET/CT imaging of low incidence positrons emitted by ^{90}Y (0.003% branching) has better accuracy compared to Bremsstrahlung SPECT/CT. Nevertheless, associated effects on dosimetric accuracy have not yet been investigated. We evaluate the quantification accuracy of post-therapeutic dosimetry calculation using voxelised local energy deposition models (LDM) of ^{90}Y for three generation PET/CT systems: analogue, digital and long axial field of view (LAFOV) using phantom scans. ***Materials and Methods:*** PET/CT systems used were analogue, digital and digital-LAFOV scanners. To evaluate quantitative accuracy, two types of phantoms were utilized: uniform (6.2 L) and a NEMA-IQ phantom. Each was filled with 0.24 and 0.22/2.92 MBq/ml (13.3 sphere-to-background ratio) of $^{90}YCl_3$, respectively. Citric acid solution (0.05M) was used to prevent material interaction. Next, a 30-minute list mode acquisition was performed for each phantom-scanner combination. They were reconstructed using 15- and 30-minute frames with 4 iterations and 5 subsets (digital, digital-LAFOV) and 3 iterations 21 subsets (analogue), 3D-OSEM with PSF modelling, to mimic clinical protocols. Effects of all-pass, 7- and 9-mm Gaussian filtering were evaluated. Quantitative accuracy was assessed by means of Coefficient of Variation (COV) in the uniform and mean Recovery Coefficient (RC-mean) in the NEMA-IQ phantom. Theoretical LDM dosimetry within NEMA-IQ spheres was compared to CE-marked software calculations, with and without partial volume effect (PVE) correction. ***Results:*** In the uniform phantom, COV, activity concentration and total activity accuracies were [127%/9.7%/12%; 36%/1.7%/11%; 28%/6.8%/-6%] (analogue), [58%/-3%/11.1%; 20%/-2.5%/11.2%; 13%/-0.1%/3.5%] (digital) and [76%/-0.3%/-0.3%; 24%/-2.0%/3.0%; 17%/-0.2%/3.2%] (digital-LAFOV), for all-pass, 7- and 9-mm filtered reconstruction, respectively. The RC-mean for 22-mm sphere (clinically relevant tumour size) was [1.37/0.92/0.79] (analogue), [1.16/0.84/0.74] (digital) and [1.04/0.74/0.67] (digital-LAFOV), for all-pass, 7- and 9-mm filtered reconstruction. Absorbed dose error varied from 13%-75% for NEMA-IQ spheres, without differences in the mean, yet significant uncertainty variations between the scanners. On average, PVE correction resulted in dosimetry error reduction from 27% to 13% (sphere of 22 mm). ***Conclusion:*** Despite variations in noise levels for ^{90}Y scans between tested PET/CT scanners, the average activity concentration remained comparable. Our results suggest that to exploit the full potential of digital-LAFOV PET/CT for ^{90}Y, improved scatter correction techniques are needed. Additionally, accurate quantification of ^{90}Y PET/CT dosimetry with clinically relevant tumour size range requires PVE-correction.

EPS-234

Overestimation in 90Y-PET/CT based mean lung doses following 90Y-radioembolization

S. Kappadath*, B. P. Lopez, E. C. Henry, B. M. Kelley, A. Mahvash; UT MD Anderson Cancer Center, Houston, TX, UNITED STATES OF AMERICA.*

Aim/Introduction: Accurate and practical clinical estimates of delivered lung doses after ^{90}Y-radioembolization are sparsely reported in publications but are essential to address radiation dose concerns as ^{90}Y-activity prescriptions are increased in pursuit of curative radioembolization treatments. We investigate the effects of image noise and respiratory motion in post-treatment ^{90}Y-PET/CT for lung dose estimation. ***Materials and Methods:*** Thirty-four ^{90}Y-microsphere radioembolization patients underwent pre-therapy ^{99m}Tc-MAA planar (Siemens SymbiaT16) and post-therapy ^{90}Y-PET/CT (GE DMI 5-Ring, 25-minute single bed) imaging as part of a prospective clinical trial (NCT03896646). Left and right lung dose-volume histograms (DVH) were calculated using local deposition dosimetry with patient-specific CT-based lung densities (g/mL) and PET-based ^{90}Y-activity concentrations (Bq/mL). For each patient, we defined left lung median dose (D50L) as the reference dose and report the right lung median dose (D50R), the left and right lung average (DavgL, DavgR), and the predicted lung dose using pre-therapy ^{99m}Tc-MAA planar lung and liver ROI counts, 1 kg mass, and administered ^{90}Y activity (Dplanar). Respiratory motion mismatch in PET was assessed visually. To assess impact of image noise, the ^{90}Y-PET images were denoised by removing "hot" lung voxels with activity concentrations exceeding the median value by >10x the interquartile range (IQR). ***Results:*** PET and CT data required manual registration in 21/34 (62%) patients to minimize breathing motion misalignment. The median (25^{th}-75^{th}) reference ^{90}Y-PET left lung doses D50L of 0.6 (0.4-1.1) Gy were substantially lower than Dplanar values of 3.5 (2.1-8.0) Gy. While PET right lung doses D50R were modestly higher (factor of 2) than reference doses, the median absolute difference was <1 Gy. In contrast, the PET lung average doses (DavgL & DavgR) were respectively 8 to 10 times higher than the reference doses (i.e., 4 to 8 Gy median differences). The denoising algorithm removed a median 2.9% (2.1%-3.8% IQR) of the hottest lung voxels. D50L and D50R estimates were minimally affected by de-noising (<1 Gy change) while DavgL and DavgR values decreased by about 50%, corresponding to 2 to 4 Gy changes. Mean DVH values approximated median DVH values after de-noising. ***Conclusion:*** Post-treatment ^{90}Y-PET/CT mean lung doses can be considerably over-estimated by the presence of a small number of hot noisy voxels in the reconstructed images. This dose bias can be easily mitigated by extracting median, instead of mean, dose values from ^{90}Y-PET lung contour data or by applying simple data-driven thresholds to remove unrealistic hot voxels.

EPS-235

A Model to Describe the DNA Damage Response in Blood Cells During Radioiodine Therapy

S. Schumann[1], *H. Scherthan*[2], *S. Schoof*[2], *P. Hartrampf*[1], *A. K. Buck*[1], *M. Port*[2], *M. Lassmann*[1], *U. Eberlein*[1];
[1]*Department of Nuclear Medicine, University Hospital Würzburg, Würzburg, GERMANY,* [2]*Bundeswehr Institute of Radiobiology affiliated to the University of Ulm, Munich, GERMANY.*

Aim/Introduction: The aim of the study was to develop a model describing patient-specifically the absorbed-dose-dependent DNA damage response in blood cells during radionuclide therapy. For this purpose we used data sets collected as part of the MEDIRAD project which analysed blood samples from patients with differentiated thyroid carcinoma. ***Materials and Methods:*** Blood samples of 18 patients receiving their first radioiodine therapy were collected at up to nine different time points up to 168 h after therapy start and analysed for radiation-induced gamma-H2AX+53BP1 foci (RIF) as markers of DNA double-strand breaks (DSBs) in peripheral blood mononuclear cells (PBMCs). Blood-based dosimetry was performed as described by Eberlein et al. [1]. To describe the time course of the number of RIF, a linear two-compartment model was developed, which assumes that the change in RIF is proportional to the dose rate. The induction is described by a proportionality constant c and the repair by a time-constant rate k. Since potentially not all DSB damage repair is described by a single constant repair rate, time-dependent induction and repair are characterized by a fast (k_1) and a slow (k_2) repair rate. Fits were performed for all patients separately taking into account patient-specific blood dosimetry data. ***Results:*** 4 of 18 patients had to be excluded due to insufficient data points (< 8) or large errors of the fit parameters. In all other patients, the data were described well by the model ($r^2 > 0.83$). Fit parameters differed substantially between patients. The median value of c is 0.026 mGy^{-1} (min: 0.012; max: 0.109) and, in average, 96% of the damage is repaired with k_1 varying between 0.19 h^{-1} and 3.03 h^{-1} while k_2 ranged from 0 to 0.04 h^{-1}. Our analysis revealed that patients can be divided into two groups based on their k_1-values: Patients with faster repair rates (n=6, $k_1 > 1.1$ h^{-1}) and patients with slower repair rates (n=8, $k_1 < 0.6$ h^{-1}). ***Conclusion:*** Our model is well suited to describe patient-specific DNA damage induction and repair in PBMCs in vivo during radioiodine therapy. It indicates that repair rates vary strongly between individual patients and that different patient groups need to be considered separately. In a next step, correlations with clinical parameters will be tested. ***References:*** [1] Eberlein et al., JNM 2016 (10.2967/jnumed.115.164814)

EPS-236

Validation of a Monte Carlo Simulation Model for Quantification of DNA Double-Strand Breaks in Lymphocyte Nuclei by Ex Vivo Internal Irradiation with Radionuclides

M. Salas Ramirez[1], *L. Maigne*[2], *G. Fois*[2], *H. Scherthan*[3], *M. Lassmann*[1], *U. Eberlein*[1];
[1]*University Hospital Würzburg, Department of Nuclear Medicine, Würzburg, GERMANY,* [2]*Physics Laboratory of Clermont, University of Clermont Auvergne, Clermont, FRANCE,* [3]*Bundeswehr Institute of Radiobiology affiliated to the University of Ulm, Munich, GERMANY.*

Aim/Introduction: The aim of this study was to validate a radiation transport model that quantifies the number of DNA double-strand breaks (DSBs) produced in lymphocyte nuclei by internal ex vivo irradiation of whole blood with radionuclides at low absorbed doses (<100 mGy). The Monte Carlo simulation was performed using the GATE/Geant4 code at the macroscopic level and the Geant4-DNA code at the cellular level. ***Materials and Methods:*** The simulation in GATE reproduced an 8 ml cylindrical water-equivalent medium contained in a vial mimicking the geometry of ex vivo blood irradiation. Lymphocytes were simulated as randomly distributed spheres with a radius of 3.75 µm and a concentration of 125 spheres/ml. At the cellular level, the clustering example based on a density-based spatial clustering of applications with a noise algorithm was used for each of the simulated radionuclides (^{90}Y, ^{99m}Tc, ^{123}I, ^{131}I, ^{177}Lu, ^{223}Ra, and ^{225}Ac). The absorbed dose coefficients for lymphocyte nuclei (d_{Lymph}) were calculated and compared with reference absorbed dose coefficients for whole blood (d_{Blood}) [1]. For gamma/beta-emitting radionuclides, the number of DSBs·$cell^{-1}$·mGy^{-1} was quantified by modeling and compared with the number of radiation-induced foci per cell and absorbed doses (RIF·$cell^{-1}$·mGy^{-1}) obtained from experimental data [2]. For alpha emitters, the number of αtracks·$cell^{-1}$·mGy^{-1}, DSBs·$µm^{-1}$ and the number of DSBs·$cell^{-1}$·Gy^{-1} were calculated using thresholds

derived from experiments for the αtrack lengths and DBSs·track^{-1} values. The results were compared with an ex vivo study with ^{223}Ra [3, 4]. ***Results:*** The d_{Lymph} values differed from the d_{Blood} values by -1.0% (^{90}Y), -5.2% (^{99m}Tc), -22.3% (^{123}I), 0.35% (^{131}I), 2.4% (^{177}Lu), -5.6% (^{223}Ra) and -6.1% (^{225}Ac). The number of DSB·cell^{-1}·mGy^{-1} for each beta/gamma emitting radionuclide was 0.015 DSB·cell^{-1}·mGy^{-1} (^{90}Y), 0.012 DSB·cell^{-1}·mGy^{-1} (^{99m}Tc), 0.014 DSB·cell^{-1}·mGy^{-1} (^{123}I), 0.012 DSB·cell^{-1}·mGy^{-1} (^{131}I), and 0.016 DSB·cell^{-1}·mGy^{-1} (^{177}Lu). For ^{223}Ra and ^{225}Ac, the number of α-tracks·cells^{-1}·mGy^{-1}, the linear density of DSBs·µm^{-1} of α-track length, and the number of DSBs cell^{-1}·Gy^{-1} were 0.00144 αtracks·cell^{1}·mGy^{1} and 0.00151 α-tracks·cell^{-1}·mGy^{-1}, 11.13 DSBs·µm^{-1} and 10.86 DSBs·µm^{-1}, and 67.9 DSBs·cell^{-1}·Gy^{-1} and 69.1 DSBs·cell^{-1}·Gy^{-1}, respectively. These results are in agreement with experimental data [2, 3, 4]. ***Conclusion:*** In conclusion, this study presents and validates a radiation transport model that simulates the α-tracks and DNA damage in lymphocyte nuclei induced by internal ex vivo irradiation with alpha emitters radionuclides. ***References:*** [1] Salas-Ramirez, M. et al. ZMedPhys. 2023 [2] Eberlein, U. et al. PLoSOne. 2015 [3] Göring, L. et al. EJNMMI. 2022 [4] Scherthan, H. et al. Cancers. 2019

EPS-237

Dose-dependent relative biological effectiveness of ^{225}Ac compared to ^{177}Lu during [^{225}Ac]Ac-PSMA and [^{177}Lu]Lu-PSMA radionuclide therapy

M. Rumiantcev[1], *W. Li*[2], *S. Lindner*[1], *G. Liubchenko*[1], *S. Resch*[1], *P. Bartenstein*[1], *S. Ziegler*[1], *G. Böning*[1], *A. Delker*[1];
[1]*Department of Nuclear Medicine, LMU Hospital, Munich, GERMANY,* [2]*Federal Office for Radiation Protection, Oberschleißheim, GERMANY.*

Aim/Introduction: [^{225}Ac]Ac-PSMA radionuclide therapy, which utilizes α-emitting ^{225}Ac, has evolved as a promising treatment option for patients with advanced metastatic castration-resistant prostate cancer (mCRPC) who became resistant to [^{177}Lu]Lu-PSMA therapy. For α-particle emitter treatments, improved knowledge on the relative biological effectiveness (RBE) is required. Therefore, this simulation study aimed to determine the RBE of ^{225}Ac compared to ^{177}Lu during [^{225}Ac]Ac-PSMA and [^{177}Lu]Lu-PSMA in a wide range of absorbed doses to the cell nucleus . ***Materials and Methods:*** This study employed the TOol for PArtcile Simulation (TOPAS) [1,2] based on the Geant4 simulation toolkit. Simulation of the nuclear DNA and the damage scoring were performed using the TOPAS-nBio [3] extension of TOPAS. DNA repair was modeled utilizing the Python-based program MEDRAS [4,5]. The number of double-strand breaks was considered as the biological endpoint. Five different cell geometries of equal volume and two radionuclide internalization assumptions, as well as two cell arrangement scenarios (2D and 3D) were considered. The radionuclide activity (number of source points) was adopted on the basis of SPECT images of patients undergoing [^{177}Lu]Lu-PSMA-617 or [^{177}Lu]Lu-PSMA-I&T therapy. ***Results:*** ^{225}Ac emitting high-LET α-particles revealed a linear dose-effect relationship, whereas ^{177}Lu showed a linear-quadratic dose-effect relationship. Based on the simulated dose-effect curves, the RBE of ^{225}Ac compared to ^{177}Lu as a function of ^{225}Ac nucleus absorbed dose was derived in a wide range of doses. ***Conclusion:*** Considering DNA damage repair, a dependence of the RBE of ^{225}Ac on the nucleus absorbed dose was observed. The dose-dependent RBE values can improve clinical dosimetry for radionuclide therapy with ^{225}Ac. ***References:*** [1]. Perl J et al. TOPAS: An innovative proton Monte Carlo platform for research and clinical applications. Med Phys. 2012;39(11):6818-37. [2]. Faddegon B et al. The TOPAS tool for particle simulation, a Monte Carlo simulation tool for physics, biology and clinical research. Phys Medica. 2020 Apr 1;72:114-21. [3]. Schuemann J et al. TOPAS-nBio: An Extension to the TOPAS Simulation Toolkit for Cellular and Sub-cellular Radiobiology. Radiat Res. 2019;191(2):125-38. [4]. Mcmahon SJ et al. Mechanistic Modelling of DNA Repair and Cellular Survival Following Radiation-Induced DNA Damage. Sci Rep. 2016;6(April):1-14. [5]. McMahon SJ et al. A general mechanistic model enables predictions of the biological effectiveness of different qualities of radiation. Sci Rep. 2017;7(1):1-14.

EPS-238

PET Quantification Performance of the Oversize-Volume-of-Interest Approach in the Context of Tumour Dosimetry in Radionuclide Therapy Planning

N. Hammersen*, W. Jentzen, F. Stawitzki, K. Herrmann, D. Kersting, P. Fragoso Costa, A. Moraitis;*
Department of Nuclear Medicine at University Hospital Essen, Essen, GERMANY.

Aim/Introduction: In PET imaging, the partial-volume effect (PVE) is an important factor impairing quantification of tumour uptake - a key quantity for predicting tumour absorbed dose in radionuclide therapy planning. Applying an effective and easy PVE correction in clinical routine is of great interest. Aims of this study were to provide a procedure for the application of the oversize-volume-of-interest (VOI) approach and to compare its performance to the commonly used contour-VOI approach that utilizes phantom-based recovery coefficients. ***Materials and Methods:*** A mathematical sphere model was applied to determine the oversize volume (in units of the PET spatial resolution) that contained 98% of the total activity. Experimental investigations involving phantom and clinical data were conducted to study the performance of the applied PVE correction approaches. All phantom measurements were performed in a novel PET/CT scanner using 12 spherical tumour-inserts (diameters of 3.7 to 37.4 mm) containing solution with ^{18}F. Both PVE correction approaches were compared for various imaged signal-to-background ratios (20 to 3). Performance was evaluated based on percentage deviation between the PVE-corrected and the actual activity concentrations. In clinical application, both approaches were applied to images acquired with ^{18}F-PSMA in patients with prostate cancer. ***Results:*** To reduce the contribution of background correction while containing at least 98 % of the total activity, we used an oversize-VOI diameter of two PET spatial resolutions larger than the physical sphere diameter. In comparison, the oversize-VOI approach showed a favorable performance for tumours below 10 mm in diameter, whereas the contour-VOI approach is more suitable for sizes above 10 mm. Both approaches were robust against varying phantom and clinical imaging conditions. ***Conclusion:*** The oversize-VOI approach is an accurate and easy to implement PVE correction approach, especially for small tumours, that may be used for pre-therapeutic tumour dosimetry. A systematic analysis of the influence of PET quantification approaches on tumour dose predictions is further warranted.

EPS-239

Investigating various parameters on the labeling efficiency of ^{67}Ga-phytate and its absorbed dose estimation in humans based on mouse data

z. bayat[1], *N. Vahidfar*[2], *E. Saeedzadeh*[1], *M. Sadeghi*[3], *S. Farzanefar*[2];
[1]*Radiation Medical Engineering, Science and Research branch, Islamic Azad University, Tehran, Iran, ISLAMIC REPUBLIC OF,* [2]*Department of Nuclear Medicine, Vali-Asr Hospital, Tehran University of Medical Sciences, Tehran, Iran, ISLAMIC REPUBLIC OF,* [3]*Medical Physics Department, School of Medicine, Iran University of Medical Sciences, Tehran, Iran, ISLAMIC REPUBLIC OF.*

Aim/Introduction: lymphoscintigraphy is one of the most considerable and common methods for early detection of breast cancer in the world.Among the routine radiopharmaceuticals for this purpose, [^{99m}Tc]Tc-phytate have been demonstrated remarkable results in pre-surgery detection of metastatic axillary

lymph nodes in clinical trials. According the longer half-life of ^{67}Ga compared to ^{99m}Tc (78.25 h versus 6 h), introducing and development of an appropriate alternative radiopharmaceutical including ^{67}Ga for lymphoscintigraphy in order to extension of evaluation and surgery procedure time will be an important deal in the clinic.In this study radiolabeling of phytic acid with ^{67}Ga was accomplished. Based on radioactive thin layer chromatography (RTLC), radiochemical purity (RCP) was estimated >99%.The final product represented satisfactory stability in human serum circumstances which was calculated >89% during 3 days of study. Pre-clinical studies confirmed urinary system as the main excretion way for the radiopharmaceutical.Finally human estimation dosimetry study based on preclinical data was reported. ***Materials and Methods:*** The radiochemical purity of the labeled compound was investigated at 100 degrees Celsius and at times of 1, 5, 10, 15, 20 and 30 minutes.All the experiments were done in a laboratory scale and repeated three times (n=3).Since the pH of the final product was acidic, NaHCO3 (0.1 M) was used to adjust pH=6-7. The radiochemical purity of the final compound was determined using thin layer radiochromatography (RTLC). ***Results:*** The results of the stability study of the labeled compound showed that this compound will still have a radiochemical purity higher than 89% even after 48 hours at room temperature and in human blood serum.(100 °C, 30 min, 10 mg phytic acid).The absorbed dose of different human organs after the injection of ^{67}Ga-phytate labeled compound was estimated using the RADAR formulation based on the rat biodistribution data.The results of the dose evaluation show that most of the organs did not receive a relatively high dose, and the equivalent and effective dose in humans after the injection of the labeled compound ^{67}Ga-phytate was estimated as 1.949 mGy/MBq and 0.015 mSv/MBq, respectively. ***Conclusion:*** In this study, after producing the labeled compound ^{67}Ga-phytate with a radiochemical purity of more than 99% under optimal conditions, the biodistribution of the compound was investigated in healthy mice. The results showed that the marked compound has high accumulation in lymph nodes and kidneys.

EPS-240

Head-to-head comparison of ^{177}Lu-DOTATATE dosimetry between high-speed 360° CZT-SPECT/CT and conventional SPECT/CT systems

L. Imbert, *C. Boursier, V. Roch, E. Chevalier, P. Marie;*
CHU Nancy Hopital Brabois Adultes,
Vandoeuvre Les Nancy, FRANCE.

Aim/Introduction: ^{177}Lu-DOTATATE is an efficient therapy for neuroendocrine tumors expressing somatostatin receptors. A drawback is a possible deleterious effect due to excessive absorbed dose (AD) by several critical organs, especially kidneys and bone marrow. These ADs may be determined through serial conventional SPECT (Conv-SPECT) recorded after ^{177}Lu-DOTATATE injection, however recording times are too long for clinical routine. The aim of this study was to determine whether the ADs determined by a high-speed whole-body 360° CZT-SPECT camera are equivalent to those provided by Conv-SPECT in the same patients. ***Materials and Methods:*** Thirteen patients referred for ^{177}Lu-DOTATATE treatment were enrolled and underwent, during a single treatment cycle and at 3 time-points (i.e., 24 hours, 96 hours and 7 days after ^{177}Lu-DOTATATE injection), (i) a thoraco-abdominopelvic Conv-SPECT recording of 32 min, immediately followed by (ii) a whole-body CZT-SPECT recording of 18 minutes (1). Right and left kidneys, bone marrow and spleen were automatically segmented by an artificial intelligence-based tool on the CT acquisitions from each system recorded at 24 hours. Time-integrated activity curves, convolved by the voxel S value kernel, were computed with a well-validated dosimetry software to determine the AD from kidneys, bone marrow and spleen. Partial volume effect was corrected by fitting recovery coefficients with the volume's spheres from an IEC body phantom and with a 10/1 tumor-to-background ratio. The ADs from Conv-SPECT and CZT-SPECT were compared using paired Student's t-tests. ***Results:*** Mean ADs, determined in the 13 patients (6 women, 63±12 years-old, 25±4 kg.m^{-2} body mass index) and expressed per MBq of injected ^{177}Lu-DOTATATE, were not significantly different between Conv-SPECT and CZT-SPECT for kidneys (0.42±0.13 vs. 0.44±0.15 mGy/MBq, p=0.11), bone marrow (0.05±0.04 vs. 0.06±0.04 mGy/MBq, p=0.09), and spleen (0.53±0.29 vs. 0.55±0.28 mGy/MBq, p=0.57). ***Conclusion:*** This head-to-head comparison shows that the ADs determined after ^{177}Lu-DOTATATE injection for kidneys, bone marrow and spleen with this 360° whole-body CZT-SPECT/CT system, are concordant with those obtained with a conventional SPECT/CT, but with the advantages of much shorter recording times and the added ability to determine AD on a whole-body scale. ***References:*** (1) Chevalier E, Boursier C, Claudin M, Marie PY, Imbert L. Feasibility of ^{177}Lu Therapy Monitoring Using Fast Whole-Body SPECT Recordings Provided by a High-Speed 360° CZT Camera. Clin Nucl Med. 2020 Nov;45(11):e493-e494.

EPS-241

Validation of Lu-177 PSMA dosimetry from 113keV energy peak using digital 3D SPECT/CT imaging system

H. Gröhn, *M. Hakulinen, K. T. Tapani, T. M. Laitinen;*
Kuopio University Hospital, Kuopio, FINLAND.

Aim/Introduction: Our clinical dosimetry protocol consists of two imaging sessions, 4h and 24h post Lu-PSMA treatment, and is based on Lu-177 208keV energy peak with analog SPECT/CT. Current imaging sessions are challenging for patients due to long acquisition time. Our new digital 3D SPECT/CT system allows markedly shorter (<50%) imaging time for the same anatomical coverage. However, the 3D SPECT/CT system utilizes 113keV energy peak instead of 208keV peak for Lu-177 imaging. The aim of this study was to validate the use of lower energy peak of Lu-177 for our clinical PSMA dosimetry protocol. ***Materials and Methods:*** Ten patients were scanned using both analog SPECT/CT utilizing 208keV energy peak and 3D digital SPECT/CT utilizing 113keV peak, 4h and 24h after Lu-PSMA treatment. Absorbed doses were calculated for kidneys and salivary glands based on MIRD dosimetry. Four raters drew VOIs based on experience from current protocol for both data sets. Then criteria for drawing VOIs were optimized for new dataset and VOIs were redrawn. Interrater variability was estimated using intraclass correlation coefficient (ICC) with two-way random effects, absolute agreement, multiple raters. Difference between means was evaluated using paired t-test. ***Results:*** Preliminary results from the first five patients are presented here. After optimizing VOI drawing criteria, interrater reliability increased both for kidneys (from ICC=0.96 [0.83-1.00, 95% confident interval] to ICC=0.99 [0.97-1.00]) and salivary glands (from ICC=0.84 [0.43-0.98] to ICC=0.99 [0.96-1.00]). At group level, there was no difference in absorbed doses between approaches utilizing different energy peaks (p=0.39 and p=0.66, kidneys and salivary glands, respectively). However, in some of the individual patients there were marked differences in absorbed doses up to 26% and 27% for kidney and salivary glands, respectively. ***Conclusion:*** Lu-PSMA dosimetry from 113keV energy peak gave promising results after optimizing VOI drawing criteria.

There was no significant difference between absorbed doses calculated from different peaks, nor trend towards consistently higher values with one of the approaches. The relatively large differences between approaches in some patients could be due to lack of experience in evaluating images from the new system with different reconstruction parameters and resolution. To validate in more detail the difference between approaches, we are currently measuring IQ phantom and analyzing already scanned patients. We are confident that after optimization and validation is completed, dosimetry with 3D digital SPECT/CT utilizing 113keV peak will become preferred method for clinical workflow saving scan time and increasing patient comfort.

EPS-242

Semiautomatic Segmentation for Tumour Dosimetry in PSMA Radiopharmaceutical Therapy using a Novel Digital Twins Framework

R. Fedrigo[1,2], *L. Polson*[1,2], *C. Li*[1,2], *S. Harsini*[1], *I. Bloise*[1], *J. Brosch-Lenz*[1], *B. Saboury*[3], *F. Bénard*[1,2,4], *A. Rahmim*[1,2,4], *C. Uribe*[1,2,4];
[1]*BC Cancer Research Institute, Vancouver, BC, CANADA,*
[2]*University of British Columbia, Vancouver, BC, CANADA,*
[3]*National Institutes of Health (NIH), Bethesda, MD, UNITED STATES OF AMERICA,* [4]*BC Cancer, Vancouver, BC, CANADA.*

Aim/Introduction: Prostate-specific membrane antigen radiopharmaceutical therapy (PSMA-RPT) has shown promising results for treating metastatic prostate cancer (mPCa). Conventionally, PET images are obtained for initial diagnosis and staging, while SPECT is used to quantify radiopharmaceutical uptake and monitor the effects of treatment in real-time. To gain understanding of dose-response relationships, a method that can aid in tumor segmentation is required. The aim of this study was to test qPSMA [1], a semiautomatic liver-based thresholding method for lesion segmentation, that is based on ^{68}Ga-PSMA scans, and to determine new thresholds that can extend it to ^{18}F-DCFPyL PET and ^{177}Lu-PSMA-617 SPECT. ***Materials and Methods:*** Sixteen digital twins (i.e., very realistic digital versions of a patient) were created for two imaging paradigms: (i) ^{18}F-DCFPyL, and (ii) ^{177}Lu-PSMA-617, with 64 metastases positioned in the pelvis and abdomen. Data was simulated for a GE Discovery RX PET/CT with Ashrafinia 2017 code and Siemens Symbia SPECT/CT using Simind Monte Carlo. Images were processed using clinical parameters (8subsets,4iterations) and compared to 20-40 iterative updates. Lesions were segmented with qPSMA using population-based liver parameter; SUV_{pop}=4.3. We determined new SUV_{pop}=6.2 and 1.18 by analyzing images of 10 patients imaged with ^{18}F-DCFPyL and ^{177}Lu-PSMA-617, respectively. Lesion detection sensitivity was measured for each SUV_{pop}. We used Fisher's exact test to determine if differences observed with each SUV_{pop} were statistically significant. We performed 8 noise realizations for each phantom and verified recovery coefficients (RCs) for total tumour activity. ***Results:*** Lesion detection sensitivity was 87.5% for the ^{18}F-DCFPyL scans, which did not significantly differ for the modified threshold (p=0.80). In ^{177}Lu-PSMA-617, detection sensitivity significantly increased from 12.5% to 65.6% (p<0.0001). Lesion quantification was most accurate for ^{18}F-DCFPyL using clinical reconstruction parameters, with RCs of 16.3%, 56.9%, 84.9%, 79.6%, for the 4,8,12,16mm spheres, respectively. For ^{177}Lu-PSMA-617 with the adjusted population threshold, RCs were 23.4%, 43.8%, 52.1%, 53.1% using 4 iterations, which increased to 8.3%, 57.8%, 89.2%, 87.5% using 20 iterations, for the 4,8,12,16mm spheres, respectively. ***Conclusion:*** The qPSMA method showed that adequate detection sensitivity and quantification can be obtained in 2-16mm PCa metastases. Performing additional iterative updates (20-40) in combination with an updated liver threshold, can greatly improve tumour quantification accuracy in ^{177}Lu-SPECT. Overall, our results suggest that qPSMA tumour detection for dosimetry can be reliably performed with ^{18}F-PET and ^{177}Lu-SPECT imaging. This tool can help in closing the knowledge gap between absorbed dose and tumor response in RPTs. ***References:*** 1. Gafita, JNM, 60(9):1277-1283, 2019.

EPS-243

Does urinary excretion rate change over the courses of 177Lu-PSMA therapies ?

L. Ferrer[1,2], *M. CHABIRON*[3], *C. Rousseau*[1,2], *N. Varmenot*[1,2];
[1]*ICO René Gauducheau, St Herblain cedex, FRANCE,*
[2]*Nantes Université, Univ Angers, INSERM, CNRS, CRCI2NA, Nantes, FRANCE,* [3]*Nantes Université, Nantes, FRANCE.*

Aim/Introduction: Patients with refractory metastatic prostate cancer (mCRPC) are referred to 177Lu-PSMA therapies. Some studies [1,2] have shown that patient's renal excreted mean activities can be as high as 80% of the initial injected activity in the first hours of this treatment. This study aims at assessing a patient's urine activity as a renal excreted activity surrogate and at evaluating its changes according to the therapy cycles'number. ***Materials and Methods:*** Patients with mCRPC were treated with one to six injections of 7.4 GBq 177Lu-PSMA between March-2022 and April-2023. The patient's normal renal function was assessed prior to any given treatment. Their urines were collected in 2L containers until they performed their first SPECT/CT examination 3 to 5 hours later. Each container was weighted without and with the urines on a scale (±5g) and 20ml samples were withdrawn and measured with a 177Lu-calibrated well counter. Urine's activity per unit of injected activity (%I.A) as well as its concentration per minute (rate_%I.A) were derived at the injection time. Statistical tests were conducted with Scipy's statistics module (v1.10.1). ***Results:*** Twenty-one patients benefited from 79 treatments (N = [21, 20, 15, 12, 7, 4] treated with 1 to 6 cycles). All urines were collected between the injection and the first imaging time with a delay of 280.6 min [±34.5 min]. The urine volume was 461.5 ml [±320 ml]. Two patients urinated more than 1000 ml (2 times). Neither the median %I.A [nor rate_%I.A] for all patients were different among the cycles: 18%, 21%, 20%, 17%, 25%, and 28% [0.09, 0.13, 0.11, 0.12, 0.13, 0.15 %/(L.min) resp.] for the cycle 1 to 6 respectively (Kruskal-Wallis p-value: 0.4 [0.49 resp.]). But some patients' treatment exhibited extreme values as low as 4% or as up to 43%. ***Conclusion:*** This study's findings are not completely in line with previously published data suggesting an incomplete vesical voiding. Nonetheless, we showed that the urine excretion did not change much from cycle to cycle regardless of tumor response to treatment. Further investigations are undergoing to extract urine activity from SPECT images and look after correlations with renal function indices. ***References:*** [1]: Kurth, J., Krause, B.J., Schwarzenböck, S.M. et al. External radiation exposure, excretion, and effective half-life in 177Lu-PSMA-targeted therapies. EJNMMI Res 8, 32 (2018). [2]: Demir M, Abuqbeitah M, Uslu-Beşli L, et al. Evaluation of radiation safety in (177)Lu-PSMA therapy and development of outpatient treatment protocol. J Radiol Prot. 2016 Jun;36(2):269-78

EPS-244

Outcome-Driven Assessment of Single-Time-Point Dosimetry for PSMA-Directed Radiopharmaceutical Therapy

J. Hu, *S. Xue, C. Vinicius Gomes Ferreira, L. Mercolli, A. Afshar-Oromieh, A. Rominger, K. Shi;*
University of Bern, Department of Nuclear Medicine, 3008 Bern, SWITZERLAND.

Aim/Introduction: Single time point (STP) dosimetry is preferred in the practice of monitoring radiation dosimetry in radiopharmaceutical therapy. However, the current development of STP methodology is often guided by the assumed ground-truth of multiple-time-point (MTP) dosimetry. Unfortunately, MTP dosimetry is typically based on limited measurements and modeling, with no established common sense and limited accuracy. Considering the ultimate goal of dosimetry monitoring, we propose an alternative perspective to assess and develop STP dosimetry methodologies using treatment outcomes. ***Materials and Methods:*** 20 mCRPC patients with multiple ^{177}Lu-PSMA-617 treatment cycles with SPECT/CT dosimetry measurements (2-4 h, and at least 2 time-point (TPs) of 24 h/48 h/72 h/4-9 days p.i.) were retrospectively included. STP dose-map generated with the measurements at different time points were generated using voxel dosimetry module (Version 1.1) from Hermes Medical Solution. Mean absorbed doses were estimated for organs at risk (OARs) and whole-body tumor, and corresponding individual cumulated dose (MTP/STPDose) for each therapy cycle were calculated. Therapy outcomes were evaluated by overall survival (OS), PSA response rate and toxicity assessment. The predictive accuracy of MTP/STPDoses for treatment outcomes and toxicity were analyzed. ***Results:*** Patients with greater OS than 18 months (9/20) had significantly higher tumor MTPDose ($p<0.05$), higher STPDose of 24h ($p<0.05$) and 4-9D ($p<0.02$). Patients with PSA reduction of ≥ 50% (17/20) had a significantly higher tumor MTPDose ($p<0.05$) and STPDose of 4-9D ($p<0.05$). For patients with hematotoxicity ≥ grade 3 (3/20), only bone marrow STPDose of 24h (Spearman's $r=.22$, $p<0.05$) was identified as independent indicators. ***Conclusion:*** Our study provides an alternative perspective for the investigation of STP dosimetry and our preliminary results suggested that late scan (>72h) is preferred for STP dosimetry while early scan (24h) is preferred for STP dosimetry for toxicity assessment. The current study was limited by the number of patients, which shall be improved in the follow-up study.

EPS-245

Comparison of the Images Taken at the 1st and 4th Hours After ^{99m}TC-MAA Injection in ^{90}Y TARE Treatment Planning

B. Kovan[1], *E. Işık*[1], *Y. Şanlı*[1], *S. Kuyumcu*[1], *B. Demir*[2];
[1]*Istanbul Faculty of Medicine, Nuclear Medicine Department, Istanbul, TÜRKIYE,* [2]*Istanbul University, Faculty of Science, Istanbul, TÜRKIYE.*

Aim/Introduction: In the treatment of ^{90}Y Radioembolization, ^{99m}Tc-MAA imaging is an important step in treatment planning and dose calculation. There may be changes in the activity distribution depending on time due to reasons such as the physical shape of MAA, its fragility, and due to free pertechnetate released from ^{99m}Tc-MAA. In this study, the distribution of MAA in early and late imaging after ^{99m}Tc-MAA application were evaluated. ***Materials and Methods:*** A total of 51 patients (22 F, 29 M, (60.86 years ±12.65)) diagnosed with HCC (n:22), mCRC (n:11), and liver metastases secondary to other malignancies (n:18) who were applied ^{99m}Tc-MAA simulation application before ^{90}Y microsphere treatment are included to the study. SPECT/CT imaging of the whole body and liver were performed within 1 hour after ^{99m}Tc-MAA application. Whole body and SPECT imaging of the patients were repeated 3 hours after the first imaging. SPECT/CT images were analysed using a software. Perfused volume (PV) was detected in both images using the threshold values of 5% and 10%. In addition, lung shunt ratios (LSF) were determined from SPECT/CT images. Obtained values were compared with Student's T test. ***Results:*** Averages of LSF in the whole patient group were 4.59 (±4.19) and 6.00 (±4.67) in early and late imaging, respectively ($p:<0.01$). By using 10% threshold values, the mean PV was calculated as 559 cm^3 (±412) and 565 cm^3 (±421) in early and late imaging. Mean PV values by using 5% threshold values were calculated as 825 cm^3 (± 573) and 836 cm^3 (± 573) in early and late imaging ($p:<0.01$). ***Conclusion:*** In our study, it was determined that there were changes in the activity distribution in case of late imaging after ^{99m}Tc-MAA application. When a comparison are made between In the early and late images, LSF values showed an average increase of 30.71%, and the highest increase was found to be 162% in late imaging. PV values by using 10% threshold increased by an average of 1% in late imaging, maximum increase was 40.77% and the maximum decrease was 16.66%. PV values increased by an average of 1.4% with a threshold of 5%, maximum increase was 33.02% and the maximum decrease was 14.42% in the late image. Since the differences in the late imaging of LSF and PV values change the dose calculations to be applied to the patient, imaging within the 1st hour after ^{99m}Tc-MAA application provides a more accurate dose calculation.

EPS-246

Evaluation of a portable high-resolution gamma camera for personalized dosimetry during radioiodine treatment ofthyroid diseases

T. Bossis[1,2], *M. Verdier*[1,2], *L. Pinot*[1], *F. Bouvet*[1], *T. Beaumont*[3], *D. Broggio*[3], *S. Lamart*[3], *O. Caselles*[4], *S. Zerdoud*[4], *L. Ménard*[1,2];
[1]*IJCLab - CNRS/IN2P3, Université Paris-Saclay, Orsay, FRANCE,* [2]*IJCLab - CNRS/IN2P3, Université Paris Cité, Orsay, FRANCE,* [3]*Internal Dose Assessment Laboratory, IRSN, Fontenay-aux-Roses, FRANCE,* [4]*Institut Claudius Regaud, IUCTO, Toulouse, FRANCE.*

Aim/Introduction: In the recent years, molecular radiotherapy has been in great expansion thanks to new radiopharmaceuticals for more targeted therapies or theranostic approaches. As for external radiotherapy, a patient specific planning and post-treatment control are strongly recommended. However, in clinical practice, personalized dosimetry is the exception rather than the rule. This is mainly due to a lack of dedicated imaging devices and standardized dosimetry protocols. In that context, we propose to develop a portable gamma-camera dedicated to reinforce dosimetry during radioiodine treatment of thyroid diseases. ***Materials and Methods:*** The performance of the gamma-camera was optimized for quantitative imaging with ^{131}I. Its field of view is 10x10cm^2 and the detection of gamma-rays is done by a monolithic $CeBr_3$ scintillator coupled to a 16x16 SiPMs array. This detection module reaches an intrinsic energy resolution of 8% at 356keV and an intrinsic spatial resolution of 1.15mm, thanks to a convolutional neural network. Two high-energy parallel-holes tungsten collimators made with 3D printing were developed for treatment planning (high-sensitivity, HS) and post-treatment control (high-resolution, HR). The camera is shielded from background radiations to optimize signal-to-noise ratio for early imaging after treatment administration. The counting capability reaches 160kcps with negligible deadtime.

The camera is mounted on a mobile structure to adjust its position to the patient neck. An accurate sensitivity calibration was performed with cylindrical ^{131}I sources of varying radius depending on the source distance and the attenuation media. The quantification performance was assessed with various 3D thyroid phantoms (from 3 to 30ml) by implementing different quantification protocols, optimized correction (scattering and attenuation) and delineation methods. ***Results:*** The sensitivity of the camera at a 5cm distance is 45 and 268cps/MBq and its spatial resolution is 5.2 and 10mm for the HR and HS collimator, respectively. The recovery coefficient measured with the thyroid phantoms ranges between 100 and 101% and between 98% and 104% with the HR and HS collimator, respectively. Optimal quantification was achieved when using an anterior view to measure the activity biodistribution combined with a lateral view for estimation of anatomical dimensions. ***Conclusion:*** We developed a high-resolution portable gamma-camera dedicated to thyroid quantitative imaging with ^{131}I. Its optimized imaging features enable near 100% activity recovery coefficients to be achieved, even for small sources. The quantification performance on heterogeneous thyroid phantoms, mimicking toxic nodules or tumor remnants, will be also presented at the conference. ***References:*** Trigila et al. Phys. Med. Biol. 67 (2022) 035011

EPS-247

3D Whole-Body SPECT images for dosimetry of ^{177}Lu-PSMA treatment using a 360° CZT gamma camera

L. Vergnaud[1], *A. Giraudet*[2], *E. Paquet*[2], *T. Baudier*[1], *J. Badel*[1], *D. Sarrut*[1];
[1]*Centre Léon Bérard / CREATIS, Lyon, FRANCE,*
[2]*Centre Léon Bérard, Lyon, FRANCE.*

Aim/Introduction: Monitoring and dosimetry of patients treated with ^{177}Lu-PSMA require wide field of view SPECT/CT acquisitions (4-5 beds instead of 2) and therefore, a longer total acquisition time. This time can be reduced with 360° CZT gamma cameras which are more sensitive than conventional cameras. However, some detectors have a SPECT energy range of less than 200 keV while the 208 keV photopeak is recommended. For this type of detector, we tested the feasibility of dosimetry for patients treated with ^{177}Lu-PSMA based on 3D whole-body SPECT images. ***Materials and Methods:*** Thirteen patients with castration-resistant metastatic prostate cancer were treated with ^{177}Lu-PSMA at the Léon Bérard centre. They received between 1 and 6 injections of 6601±437 MBq of ^{177}Lu at six week intervals. Three 3D whole-body SPECT/CT acquisitions were performed with a 360° CZT gamma camera after the first treatment at 4h, 24h and between 96h and 144h and then a single acquisition after each other treatment at 24h. Attenuation and scatter corrections were applied during the reconstruction process which includes 12 iterations and 8 subsets. For each time-point, a dose-rate map was calculated using low-statistic Monte Carlo simulations and CT-based contours of the organs at risk (kidneys, liver and spleen) were made to compute mean organ dose-rates. A tri-exponential function was used to model the time dose-rate curve and to estimate the absorbed doses by time integration. For cases with a single acquisition, the procedure used was described in article [1]. ***Results:*** Absorbed doses by left and right kidneys, liver and spleen for all cycles and all patients were 0.56 ± 0.19 Gy/GBq (mean ± std), 0.61 ± 0.18 Gy/GBq, 0.12 ± 0.10 Gy/GBq and 0.11 ± 0.07 Gy/GBq. The acquisition time is about 25 minutes for a 3D whole-body SPECT acquisition, three times less than with a conventional gamma camera (4-5 beds of 15 minutes). ***Conclusion:*** Dosimetry of patients treated with ^{177}Lu-PSMA is feasible using 3D whole-body SPECT acquisition and gives results comparable to those in the literature although the acquisition time is reduced compared to conventional gamma cameras. ***References:*** [1] Vergnaud et al. EJNMMI Physics, 2022

EPS-248

Comparison of Model Implementations in SAAM II and MATLAB/SimBiology: a PBPK model for PRRT with [^{177}Lu]Lu-DOTATATE

V. Vasic[1,2], *J. Gustafsson*[3], *E. Yousefzadeh-Nowshahr*[1,2], *A. Beer*[1], *K. Sjögreen Gleisner*[3], *G. Glatting*[1,2];
[1]*Department of Nuclear Medicine, Ulm University Medical Centre, Ulm, GERMANY,* [2]*Medical Radiation Physics, Department of Nuclear Medicine, Ulm University, Ulm, Germany, Ulm, GERMANY,* [3]*Medical Radiation Physics, Lund University, Lund, Sweden, Lund, SWEDEN.*

Aim/Introduction: Physiologically-based pharmacokinetic (PBPK) models allow simulation and prediction of the biodistribution of radiopharmaceuticals and have the potential to accomplish individualised treatment planning in molecular radiotherapy. In this work, the same model for peptide receptor radionuclide therapy (PRRT) with [^{177}Lu]Lu-DOTATATE is implemented and analysed in SAAM II (version 2.3, The Epsilon Group, Charlottesville, Virginia 22901, USA) and Simbiology (MATLAB version 2021a, The MathWorks Inc., Natick, Massachusetts 01760, USA). The concordance of the results is investigated to establish the performance of the model implemented in MATLAB. ***Materials and Methods:*** A PBPK model for a combined evaluation of [^{68}Ga]Ga-DOTATATE and [^{177}Lu]Lu-DOTATATE was developed and implemented in SAAM II and SimBiology. The data from 12 patients (8 males, 4 females, aged (65±12 years)) with low-grade metastatic neuroendocrine tumours were analysed retrospectively (1). Patients received (1.7 ± 0.4) pmol and (197 ± 48) MBq [^{68}Ga]Ga-DOTATATE and (10.26 ± 0.09) nmol and (7.46 ± 0.07) GBq [^{177}Lu]Lu-DOTATATE. Accurate dosimetry has been done previously (2), and the biokinetic data were used to fit the model parameters. Time-activity curves were calculated using both software and compared for (a) identical pharmacokinetic parameter values and (b) fitted parameter values. The absorbed dose (AD) for kidney, spleen, liver and lesions were calculated according to the MIRD guidelines (3). ***Results:*** Simulations with the same parameters gave maximum differences in ADs for kidneys, spleen, liver, and tumours of -14 mGy (0.25%), 23 mGy (0.17%), 5 mGy (0.12%), and 74 mGy (0.17%), respectively. The fitted parameters in both software were equal within the 95% confidence level. The Akaike Information Criterion (AIC) of the Simbiology/MATLAB fit was lower than that of the SAAM II fit. After fitting, the maximum differences in AD in kidneys, spleen, liver, and tumours were -0.17 Gy (3.4%), -0.29 Gy (4.0%), -0.07 Gy (1.9%), -1.84 Gy (17%), respectively. ***Conclusion:*** A model implemented in Simbiology/MATLAB is now available, which has been tested against SAAMII. The Simbiology/MATLAB model provides easy access to the calculation system and is, therefore, more flexible to changes in the primary functions and for future improvements. The differences reported after the fit is due to the different minimisation algorithms. Based on the AIC, the fit with the sbiofit function of MATLAB is better than the Rosenbrock fit of SAAM II. ***References:*** 1) Sundlöv et. al, Eur J Nucl Med Mol Imag. 2022;49:3830-3840 2) Stenvall et. al, EJNMMI Res 2022;12:75 3) Bolch et.al, J Nucl Med. 2009;50:477-84

EPS-249

Current Practice in Reporting Internal Dosimetry for [177Lu]Lu-DOTA-TATE Therapy: Literature Review

O. Ivashchenko[1], *J. O'Doherty*[2], *T. Perez*[3], *J. Tran-Gia*[4], *E. Hippeläinen*[5], *M. Sandström*[6], *C. Stokke*[7], *G. Glatting*[8], *M. Cremonesi*[9];
[1]*University Medical Center Groningen, Groningen, NETHERLANDS,* [2]*Siemens Medical Solutions, Malvern, PA, UNITED STATES OF AMERICA,* [3]*University Hospital of Gran Canaria Dr. Negrín, Las Palmas de Gran Canaria, SPAIN,* [4]*University Hospital Würzburg, Würzburg, GERMANY,* [5]*University of Helsinki and Helsinki University Hospital, Helsinki, FINLAND,* [6]*Uppsala University, Uppsala, SWEDEN,* [7]*Oslo University Hospital, Oslo, NORWAY,* [8]*Ulm University Hospital, Ulm, GERMANY,* [9]*European Institute of Oncology IRCCS, Milan, ITALY.*

Aim/Introduction: Radionuclide therapy (RNT) has experienced rapid growth in recent years. Given the wide variety of mathematical techniques that can be used to calculate image-derived radiation absorbed dose, initiatives have been taken to standardise the reporting of dosimetry results, such as the EANM Dosimetry Committee guidance 2010. Clear guidelines are given about the minimum detail necessary to guarantee the reproducibility of published work and to make research comparable. EFOMP's SIGFRID workgroup on time-activity data fitting decided to review a selection of published papers on [177Lu]Lu-DOTA-TATE therapy (as showcase example) to evaluate the quality of reported parameters according to EANM guidance and to note whether sufficient data are provided to reproduce the methodologies presented. ***Materials and Methods:*** A retrospective meta-analysis was conducted. Articles in PubMed published up to December 17, 2022 focused on [177Lu]Lu-DOTA-TATE RNT, including tumour, renal dosimetry, used SPECT imaging, were searched. Subsequently, the results were screened for duplicates and refined using the following criteria: a clinical study with >=5 patients (no case reports) and the presence of dosimetric results. Each article meeting these criteria was reviewed and compared to the EANM Dosimetry Reporting Guidance. ***Results:*** A total of 110 articles were extracted, 46 of which met the search criteria. Of these, 93% fully complied with reporting guidelines for imaging equipment used, 85% image acquisition, 89% image processing, 85% corrections applied, 56% phantom and calibration measurements, 100% sequential imaging scheme, 82% time-activity fit type, 74% fit integration and extrapolation procedure, 63% reference dosimetry phantom used, 70% reported S-values used, 87% described tumour dosimetry calculation, 76% mentioned dosimetry software name, 100% reported absorbed doses, and 14% provided statistical error calculations. Only 21% of papers fully complied with the EANM guidance. ***Conclusion:*** Although EANM guidelines for clinical dosimetry reporting have been in place for more than 13 years, these recommendations are insufficiently implemented in articles on RNT dosimetry. While data collection information is well documented, details on actual dosimetric calculations are scarce. To establish reproducible and comparable RNT dosimetry studies, quality criteria for RNT dosimetry reporting must be adopted and enforced by major nuclear medicine and medical physics journals, as has been done, for example, in radiomics, AI, and radiochemical nomenclature.

References: 1. Lassmann et al. EANM Dosimetry Committee guidance document: good practice of clinical dosimetry reporting. Eur J Nucl Med Mol Imaging. 2011 Jan;38(1):192-200.

EPS-250

Clinical dosimetry in [177Lu]Lu-PSMA therapy: kidney mean absorbed dose difference between subsequent cycles

E. Owers, *E. Rijkhorst, M. Dotinga, L. J. de Wit-van der Veen, D. M. V. de Vries - Huizing;*
Antoni van Leeuwenhoek, Amsterdam, NETHERLANDS.

Aim/Introduction: Peptide radioligand therapy (PRLT) is an established treatment for stage IV metastatic castration resistant prostate cancer (mCRPC). Most studies to date have implemented a standard therapeutic activity of 7.4 GBq [177Lu]Lu-PSMA per cycle without any personalised dosimetric considerations. By introducing dosimetry, the maximum dose to normal tissue can be determined, thereby allowing a personalised approach. However, post-therapy scans required for individual dosimetry are resource consuming and taxing on the patient. Therefore, an optimal clinical regimen must be determined to overcome these aspects. This study aims to determine differences in the kidney mean absorbed dose (MAD) between the first and second therapy cycle in patients with mCRPC. ***Materials and Methods:*** In this retrospective analysis, a total of 37 patients with mCRPC were included. All patients had progressive disease with an indication for PRLT and were treated with 7.4 GBq [177Lu]Lu-PSMA-I&T under our standard protocol with 2 administrations injected 2 weeks apart. Post-treatment SPECT/CT imaging was performed after 24 hours and 5-7 days. Segmentation of the kidney cortex on low-dose CT and calculation of the dose-rate (convolution kernel) was performed in PLANET Onco and Dose (DOSIsoft), after which a mono-exponential fit was used to determine the MAD. The MAD averaged over both kidneys was used for analysis to exclude intra-patient bias. The difference ΔMAD in Gy/GBq between the subsequent treatment cycles was evaluated using Bland-Altman analysis and the reliability using the intraclass correlation coefficient (ICC, two-way random effects, absolute agreement). ***Results:*** The median kidney MAD was 0.44 Gy/GBq [interquartile range (IQR) 0.35-0.68] and 0.46 Gy/GBq [IQR 0.38-0.63] for cycle 1 and cycle 2, respectively. The median of the ΔMAD between cycles was -0.03 Gy/GBq [IQR -0.10-0.08]. With respect to the dose in Gy/GBq, the bias was -0.009 ± 0.097 Gy/GBq [95% limits of agreement -0.200-0.181] with an ICC of 0.856 [95% CI 0.738-0.923]. ***Conclusion:*** The difference in kidney MAD between the first two cycles was limited and showed a good reliability. This suggests that the kidney MAD of the first treatment cycle can be used as an estimate of the kidney MAD of the second cycle. This could allow the omission of post-therapy imaging after the second therapy cycle in this patient population and treatment protocol. However, in case of any clinical changes that could lead to differences in kidney kinetics and uptake, post-therapy imaging should be repeated after the second therapy cycle.

EPS-251

Implementation of an 18F PET / 177Lu SPECT Phantom Study for Personalized Theranostics in PSMA Radiopharmaceutical Therapies

R. Fedrigo[1,2], *J. Tran-Gia*[3], *J. Brosch-Lenz*[1], *P. Petric*[4], *L. Fougner*[1], *K. Sabo*[4], *R. Ralea*[5], *S. Harsini*[1], *I. Bloise*[1], *J. Beauregard*[6], *F. Bénard*[1,2,4], *A. Rahmim*[1,2,4], *C. Uribe*[1,2,4];
[1]*BC Cancer Research Institute, Vancouver, BC, CANADA,* [2]*University of British Columbia, Vancouver, BC, CANADA,* [3]*University of Würzburg, Würzburg, GERMANY,* [4]*BC Cancer, Vancouver, BC, CANADA,* [5]*Vancouver General Hospital, Vancouver, BC, CANADA,* [6]*Laval University, Laval, QC, CANADA.*

Aim/Introduction: The development of prostate-specific membrane antigen (PSMA)-targeting radiopharmaceuticals has shown the promising capabilities of theranostics in diagnosing and treating metastatic prostate cancer (mPCa). PET imaging is used to verify that the target is present (diagnosis), while SPECT is used to monitor radiopharmaceutical uptake and perform dosimetry calculations during therapy. The aim of this work was to develop a first-of-its-kind theranostics phantom for ^{18}F-PET and ^{177}Lu-SPECT imaging, such that the information from the higher quality PET images can be used towards improving image-based dosimetry with SPECT. ***Materials and Methods:*** Our ^{18}F/^{177}Lu theranostics phantom consisted of re-purposed shells from the Probe-IQ [1] and Q3P [2] phantoms to model the thorax and head, respectively. A fillable liver and two-compartment kidney were 3D-printed based on ICRP templates (Tran-Gia 2021). To ensure reproducible comparison between ^{18}F-PET and ^{177}Lu-SPECT, a negative-cast modeling technique was used to create small target regions (24 metastases, 4 salivary glands) that were simultaneously prepared with ^{18}F and ^{177}Lu. Due to the short half-life of ^{18}F relative to ^{177}Lu, the ^{18}F activity was imaged with a GE Discovery MI PET/CT (2.5min/bed), followed by ^{177}Lu acquisitions with a Siemens Symbia SPECT/CT (15s/projection). Images were reconstructed using OSEM (8subsets, 1-12iterations, 6.4mm) with attenuation and scatter correction. Regions-of-interest were segmented using 20-60% of SUV_{max} fixed thresholding and recovery coefficients (RCs) were computed for total activity. Recovery factors will be determined for converting RCs between ^{18}F-PET and ^{177}Lu-SPECT acquisitions, and to improve detection of low-contrast lesions for ^{177}Lu-SPECT. ***Results:*** We report initial results for our ^{18}F-PET images, though analysis and comparison of ^{177}Lu-SPECT scans will be released shortly. Applying our diagnostic ^{18}F-PSMA PET/CT protocol, we found that accurate kidney and liver quantification can be achieved using 5% and 15% fixed thresholds, with RCs 96.1±0.2% and 99.4±0.6%, respectively. Threshold-based activity quantification was reasonably accurate for salivary glands (73.0±0.1% to 122.4±0.7%) and mid-sized tumours (107.1±0.9% and 98.5±3.5% for 14,16mm), but consistently overestimated metastases <10mm. ***Conclusion:*** Our initial results show that threshold-based activity measurements may be used for ^{18}F-PET quantification of larger organs (i.e., kidneys, liver), although more robust segmentation methods may be needed for smaller glands and metastases. Our next steps include correlating recovery factors between ^{18}F-PET and ^{177}Lu-SPECT for better mass estimation needed for dosimetry, and incorporating lesions that can be detected by PET but missed in SPECT scans for improved dosimetry calculations. ***References:*** 1. Fedrigo, EJNMMI Physics, 9(2), 2022. 2. Fedrigo, EJNMMI, 48(Suppl.1),S255-S256, 2021.

1610

Tuesday, September 12, 2023, 16:45 - 18:15

Hall K

CTE 8 - Technologists Committee: Gynaecological Studies

OP-809

Gynaecological studies: where NM is and its importance

K. Dendl;
Heidelberg University Hospital, Department of Nuclear Medicine, Heidelberg, GERMANY.

OP-810

Radiotracers used in gynaecological studies

N. Hartman;
Swansea University, Head of nuclear medicine, Singleton Hospital, Swansea, UNITED KINGDOM.

OP-811

The role of the Technologists in Gynaecological studies: protocols and patient care

G. Paixão;
Hospital Garcia de Orta, Departamento de Medicina Nuclear Hospital Garcia de Orta, Almada, PORTUGAL.

1611

Tuesday, September 12, 2023, 16:45 - 18:15

Hall G1

EU Policy Symposium 2 - Policy & Regulatory Affairs Committee: Regulatory Challenges of Radiopharmaceuticals

OP-813

Regulatory Challenges of Radiopharmaceuticals

1701

Wednesday, September 13, 2023, 08:00 - 09:30

Hall A

CME 13 - Translational Molecular Imaging & Therapy + Oncology & Theranostics + Radiopharmaceutical Sciences Committee: Diagnostic Imaging and Theranostics in Breast Cancer - Old Targets, New Tracers

OP-819

Targeting HER2 from Preclinical to the Clinics

M. Keyaerts;
Department of Nuclear Medicine, Faculty of Medicine and Pharmacy, University Hospital Brussels, Free University Brussels, Jessa Hospital, Hasselt, BELGIUM.

OP-820

Estrogen Receptor-Targeted Imaging: Appropriate Use Criteria (AUC) and Interpretation

G. Ulaner;
Hoag Family Cancer Institute, New Port Beach, UNITED STATES OF AMERICA.

OP-821

Clinical Targets Beyond the Classical Approaches

P. Backhaus;
Department of Nuclear Medicine, University Hospital Munster, Münster, GERMANY.

1702

Wednesday, September 13, 2023, 08:00 - 09:30
Hall D (Arena)

Debate 6 - Oncology & Theranostics Committee / EHA: Staging Lymphoma - Ann Arbour Outdated and Replaced by MTV?

OP-822
Staging Lymphoma: Ann Arbour outdated and replaced by Metabolic Tumor Volume? - Pro
A. Cottereau;
Department of Nuclear Medicine, Cochin Hospital, Assitance Publique Hôpitaux de Paris, Université de Paris, Paris, FRANCE.

OP-823
Staging Lymphoma: Ann Arbour outdated and replaced by Metabolic Tumor Volume? - Contra
B. von Tresckow;
Department of Hematology and Stem Cell Transplantation, University of Duisburg-Essen and German Cancer Consortium (DKTK)-University Hospital Essen, Essen, GERMANY.

1703

Wednesday, September 13, 2023, 08:00 - 09:30
Hall E1

LIPS Session 13 - Dosimetry Committee: Case Reading - Dosimetry in SIRT

OP-827
Dosimetry in whole liver and whole lobe targeting
E. Garin;
Cancer Centre Eugene Marquis, Department of Nuclear Medicine, Rennes, FRANCE.

OP-828
Dosimetry in specific tumour and oligosegmental targeting
A. Harteveld;
Erasmus Medical Center, Department of Radiology and Nuclear Medicine, Rotterdam, NETHERLANDS.

OP-829
Dosimetry of off-target accumulation
C. Chiesa;
Department of Nuclear Medicine, Foundation IRCCS Istituto Nazionale Tumori, Milan, ITALY.

1704

Wednesday, September 13, 2023, 8:00 AM - 9:30 AM
Hall E2

Dosimetry Committee - TROP Session: Clinical Disimetry II - Tutti Frutti

OP-831
An Update on Normal Tissue Absorbed Doses for Patients Treated with [^{177}Lu]Lu-lilotomab satetraxetan; Results From Two Studies
J. Blakkisrud[1,2], *A. Løndalen*[1], *R. Midthun*[1], *C. Stokke*[1,3];
[1]*Oslo University Hospital, Oslo, NORWAY,* [2]*University of Michigan, Ann Arbor, MI, UNITED STATES OF AMERICA,* [3]*University of Oslo, Oslo, NORWAY.*

Aim/Introduction: [^{177}Lu]Lu-lilotomab satetraxetan is an anti-CD37 antibody radionuclide conjugate developed to treat B-cell non-Hodgkin lymphoma. Liver, spleen, kidney and red bone marrow (RM) are known source organs for this treatment, and RM is the primary organ at risk. Previously we have reported absorbed dose for patients in the LYMRIT 37-01 phase I/IIa-trial [1]. The current work presents absorbed dose to normal tissues in the two studies LYMRIT 37-01 phase IIb, and the activity escalation trial LYMRIT 37-07. The latter included [^{177}Lu]Lu-lilotomab satetraxetan in combination with rituximab. ***Materials and Methods:*** Ten patients from the LYMRIT 37-01 phase IIb (n = 4) and the LYMRIT 37-07 (n = 6) were included for dosimetry. In both trials pre-dosing with unlabelled lilotomab was given. In the LYMRIT 37-01 phase IIb trial patients were randomized into receiving either 100 mg/m^2 body surface area of lilotomab and 20 MBq/kg body mass of [^{177}Lu]Lu-lilotomab satetraxetan or a fixed amount of 40 mg lilotomab and 15 MBq/kg body mass of [^{177}Lu]Lu-lilotomab satetraxetan. In LYMRIT 37-07, patients were either given 10, 15 or 20 MBq/kg body mass of [^{177}Lu]Lu-lilotomab satetraxetan. Organ level absorbed dose calculations were performed based on four SPECT/CT-scans nominally conducted 4, 24, 96 and 168 hours post administration. Absorbed dose to RM was calculated using the lumbar vertebrae L2-L4. Two patients, one in each trial, were excluded from RM-dosimetry due to previous external beam radiation therapy to the lumbar area. ***Results:*** Median absorbed doses for liver, spleen and kidneys in the two arms of the LYMRIT 37-01 IIb trial were 0.97, 1.40 and 0.58 mGy/MBq (100 mg/m^2 lilotomab), and 0.72, 2.67 and 0.47 (40 mg lilotomab). Median absorbed doses per administered activity for liver, spleen and kidneys in the LYMRIT 37-07 trial were 1.01, 2.38 and 0.58 mGy/MBq, respectively. Across both studies, liver, spleen, and kidneys received absorbed doses below 2.0, 3.7 and 1.2 Gy, respectively. In the LYMRIT 37-01 phase IIb trial, the median absorbed doses to RM were 0.73 mGy/MBq (100 mg/m^2 lilotomab) and 0.91 mGy/MBq (40 mg lilotomab). For RM, absorbed dose per administered activity was 0.84 mGy/MBq in the LYMRIT 37-07 trial. ***Conclusion:*** The absorbed doses to normal tissues for LYMRIT 37-01 phase IIb patients treated with [^{177}Lu]Lu-lilotomab satetraxetan were in agreement with phase I/IIa results. The addition of rituximab in the LYMRIT 37-07 study did not significantly change the biodistribution. ***References:*** 1) Stokke et. al EJNMMI 2018(45)

OP-832

Absorbed Doses to Kidneys and Tumours for Alpha-Emitter Peptide Receptor Radionuclide Therapies Estimated with [^{177}Lu]Lu-DOTATATE SPECT Images and Biokinetic Models

M. Kvassheim[1,2], *J. Blakkisrud*[1,3], *M. E. Revheim*[4,2,5], *A. J. Tulipan*[4,6], *C. Stokke*[1,7];
[1]*Department of Physics and Computational Radiology, Division of Radiology and Nuclear Medicine, Oslo University Hospital, Oslo, NORWAY,* [2]*Faculty of Medicine, University of Oslo, Oslo, NORWAY,* [3]*University of Michigan, Ann Arbor, MI, UNITED STATES OF AMERICA,* [4]*Department of Nuclear Medicine, Division of Radiology and Nuclear Medicine, Oslo University Hospital, Oslo, NORWAY,* [5]*The Intervention Centre, Oslo University Hospital, Oslo, NORWAY,* [6]*Nuclear Medicine/PET center, Department of Radiology, Haukeland University Hospital, Bergen, NORWAY,* [7]*Department of Physics, University of Oslo, Oslo, NORWAY.*

Aim/Introduction: Alpha-emitter therapies are proposed for patients with tumours requiring higher and more localised absorbed doses than practical and feasible with beta-emitters. Insight into expected absorbed doses to organs at risk and tumours from different alpha-emitters for a carrier might guide the choice of radionuclide. To estimate absorbed doses to kidneys and tumours for potential alpha-emitter somatostatin receptor therapies, we utilised [^{177}Lu]Lu-DOTATATE as a surrogate for alpha-emitters ^{212}Pb, ^{212}Bi, ^{213}Bi, ^{211}At, ^{225}Ac, ^{227}Th, and ^{149}Tb, and modelled redistribution of released radioactive daughters. ***Materials and Methods:*** Post-therapy SPECT/CT (day 0, 1, 4, and 7) images from six patients receiving their first fraction of [^{177}Lu]Lu-DOTATATE were analysed to estimate time-activity-curves for kidneys, livers, spleens, and tumours. The corresponding kinetics were simulated for alpha emitters assuming biological behaviour was unaffected by the radionuclide substitution. Redistribution of daughters was modelled with IDACAlpha (ABX-CRO) using patient specific uptake data, allowing dose estimations for a range of daughter retention values. The uptake values of the specified organs were subtracted from whole body retention constructed from probe measurements. This remaining activity was assumed to reside in the 'other' compartment in the biokinetic model, with instant uptake and two retention coefficients. To estimate the ratio of daughters to parents at injection, a parent half-life was assumed to pass from production to injection. Absorbed doses from alpha and beta radiations were calculated, with the CT-defined mass and assuming local energy deposition (1). ***Results:*** Setting z as the fraction of daughters released from the carrier and leaving the tumour before decaying, and y as the fraction released from the carrier in normal tissues, the tumour-to-kidney absorbed dose ratio is: tumour-to-kindey absorbed dose ratio = (A+(1-z)×B) / [(C+(1-y)×D)+y×E+z×F], with A and B as the parent and daughter contributions to dose in the tumours, respectively, and C and D as the parent and daughter contributions to dose in the kidneys, respectively. E and F are the modelled dose contributions from free daughters, from normal tissues and tumours respectively, to the kidney. F was mostly negligible (<7% of E). ***Conclusion:*** The physical half-life of the radionuclide and redistributing daughters released from their carriers are the main factors influencing the tumour-to-kidney absorbed dose ratio. For some alpha-emitters, daughters may contribute strongly to the kidney dose, while for others it will have a smaller effect. ***References:*** (1) ICRP. Nuclear Decay Data for Dosimetric Calculations. ICRP Publication 107 Annals of the ICRP. 2008; 38 (3).

OP-833

Comparison of Commercial Software Solutions for ^{177}Lu Labelled Radiopharmaceutical Therapies

S. Beykan, *M. Lassmann, S. Schlögl;*
University Hospital Würzburg, Würzburg, GERMANY.

Aim/Introduction: Dosimetry is an important tool for determining safety and efficacy of radiopharmaceutical therapies and requires robust and reliable software solutions. The main aim of this project was to create a measured phantom data set for testing the dosimetry calculation process and suggesting improvements or additional features. ***Materials and Methods:*** A NEMA phantom with 6 spheres (^{177}Lu activity concentration per sphere: 2.14 MBq/ml) was used for analysis of three commercial software solutions. SPECT/CT scans were acquired at 1,8,12 and 19 d post-injection with two Siemens SPECT/CTs with different crystal thicknesses. The phantom positioning was identical except at 8 d post-injection for one camera (test 1) (phantom rotation: 180°). To simulate kidney time-activity curves of a patient, the phantom was scanned five times at day 1 post-injection by using different acquisition durations (test 2). Test 1 aimed to check the ability of the software to convert count-based images to activity-based images with variable scan-dependent image calibration factors (ICFs) (use case: different cameras are used for same patient). Test 2 tested the user-freedom to manipulate e.g. acquisition times and the ability to integrate time-activity values that increase and decrease. All scans were reconstructed with FLASH-3D and xSPECTquant with attenuation and scatter correction without post-filtering. The alignment, segmentation and fitting were checked for both reconstructed data sets. The resulting activities, fitting parameters, time-integrated activity coefficients (TIACs) and absorbed doses (ADs) were compared to the reference. ***Results:*** All programs were able to work with count-based images and apply variable ICFs. For high differences in positioning, either manual scan or manual segment alignment was required instead of automatic alignment. Editing the drawn segment for each SPECT and CT scan individually and using 2 different segments for the same organ to quantify the activity and the volume was possible for all programs. 2/3 programs allowed manipulation of acquisition times for test 2. For test 1 and all programs, the relative differences in the activities, TIACs and ADs were <±4.7%, similar to the activity calculations for test 2. Nevertheless, a large heterogeneity in the fitting process was observed in test 2. Relative differences in TIACs of 10% and <120% were obtained for 2/3 programs. ***Conclusion:*** Independent of the dosimetry-software, imaging protocols, segmentation, alignment and fitting impact the dosimetry results considerably. Performing similar workflows result in differences in the same order of magnitude. Improvements especially with respect to fitting would be desirable for all software solutions.

OP-834

Determination of the treatment coverage of theragnostic ^{124}I-8H9 antibody to treat diffuse pontine glioma by convective enhance delivery

A. França Velo[1], *A. Giantini Larsen*[2,3], *J. Humm*[1], *P. Zanzonico*[1], *M. Souweidane*[3], *N. Pandit-Taskar*[4];
[1]*Department of Medical Physics, Memorial Sloan Kettering Cancer Center, New York, NY, UNITED STATES OF AMERICA,* [2]*Department of Neurosurgery, Memorial Sloan Kettering Cancer Center, New York, NY, UNITED STATES OF AMERICA,* [3]*Department of Neurological Surgery, Weill Medical College of Cornell University, New York, NY, UNITED STATES OF AMERICA,* [4]*Department of Radiology, Memorial Sloan Kettering Cancer Center, New York, NY, UNITED STATES OF AMERICA.*

Aim/Introduction: The aim of this study was to evaluate intra-lesional distribution and dosimetry of an ^{124}I-labeled antibody administered by convection-enhanced delivery (CED) in diffuse intrinsic pontine glioma following treatment. ***Materials and Methods:*** Patients from a phase 1-2 trial underwent MRI scans and serial PET-CT scans at multiple times; on average 3 (immediately after, 24 and 48 hr) following infusion by CED. In this study, ^{124}I was used both as the diagnostic PET isotope and the therapeutic isotope. The brain stem lesions were delineated on the MRI scans using MIM Sureplan MRT by a neurosurgeon and nuclear medicine physician and saved as RT structures. Similarly, the distribution volume of the injected radiotracer from the PET scan was segmented using a 42% threshold. The volumetric intersection between the PET and MRI delineations were calculated and represent the percentage coverage of the target volume. Worth to mention that all calculations are based on a single injection using a single catheter. Using a MIM workflow, the PET/CT images were co-registered and used to generate voxelwise absorbed dose distributions. Dose volume histograms were calculated from the activity distribution to the target volume. ***Results:*** The dosimetry was performed for 38 patients with diffuse intrinsic pontine glioma. The range of administered activity was from 8.8 to 369 MBq. The overlap of the MRI target volume by the PET volume ranged from 22 to 95% with a median of 83%. The median and maximum absorbed doses to the overlap volume ranged from 5.06 to 55.6 Gy and 15.2 to 165 Gy respectively, depending upon the treatment activity and therefore the infuscate volume and the target volume. In 21 of 38 patients, the coverage volume was greater than 80%. ***Conclusion:*** Our study showed that CED allows for distribution and radiation delivery to large parts of the tumor of a therapeutic absorbed doses objective. These are the first data to quantitively assess the accuracy of coverage of intra-lesional CED of a targeted radioimmunotherapy. ***References:*** Souweidane MM, Kramer K, Pandit-Taskar N, Zhou Z, Haque S, Zanzonico P, Carrasquillo JA, Lyashchenko SK, Thakur SB, Donzelli M, Turner RS, Lewis JS, Cheung NV, Larson SM, Dunkel IJ. Convection-enhanced delivery for diffuse intrinsic pontine glioma: a single-centre, dose-escalation, phase 1 trial. Lancet Oncol. 2018 Aug;19(8):1040-1050. doi: 10.1016/S1470-2045(18)30322-X. Epub 2018 Jun 18. Erratum in: Lancet Oncol. 2018 Aug;19(8): e382. PMID: 29914796; PMCID: PMC6692905.

OP-835

Accuracy of single-time-point dosimetry using a population-based model selection and Bayesian fitting method

B. Patrianesha[1], *A. Jundi*[1], *M. Naqiyyun*[2], *D. Hardiansyah*[1];
[1]*Medical Physics and Biophysics Research Group, Physics Department, Faculty of Mathematics and Natura, Depok, INDONESIA,* [2]*Nuclear Medicine Department, MRCCC Siloam Hospital, Jakarta, INDONESIA.*

Aim/Introduction: Population-based model selection with shared parameters (SP-PBMS) performed better in calculating the time-integrated activity (TIAs) compared to the individual model selection (IBMS) [1]. The aim of this study was to investigate the accuracy of single-time-point (STP) dosimetry using SP-PBMS and Bayesian fitting (BF) method. ***Materials and Methods:*** Biokinetic data of ^{177}Lu-DOTATATE in kidneys were obtained from the literature [2]. In brief, the biokinetics in the kidneys were collected using SPECT/CT after injection of (6.9±1.1) GBq of ^{177}Lu-DOTATATE at either two (N=4) or four (N=8) time points. The sum of exponentials (SOE) function $A_1/\{((1-\alpha)/(\lambda1+\lambda phys))-(\alpha/(\lambda2+\lambda phys))-((1-2\alpha)/(\lambda bc+\lambda phys))\}$ $e^{-\lambda phys(t)}$ $\{(1-\alpha)e^{-\lambda1(t)}-\alpha e^{-\lambda2(t)}-(1-2\alpha)e^{-\lambda bc(t)}\}$ which was selected as the best model for the kidney data of ^{111}In-DOTATATE in the literature [3] was used as the basic structure of the mathematical model in our study. The function parameters were fitted to all-time-point data with different combinations of parameter settings, i.e. as shared-fitting, individual-fitting and fixed parameter as reported in the literature [3]. The best combination of parameter settings was selected using the SP-PBMS method based on the Goodness-of-fit, i.e. visual inspection of the fitted curves and the coefficient of variations of the fitted curves <0.5, and the Akaike weight. The SOE function with the best parameter setting from SP-PBMS (SOE-SP-PBMS) was used to derive reference time-integrated activities (rTIAs). The STP with BF Method and the SOE-SP-PBMS was done with Jackknife at time point that has been shown as the best time point for STP dosimetry, i.e. (99.8 ± 1.5) p.i. [2], to determine the predicted time-integrated activity (pTIAs). The accuracy of STP dosimetry was assessed by calculating the relative deviation (RD) and root-mean-square error (RMSE) between rTIAs and pTIAs. ***Results:*** Parameter setting with shared-fitting of λ2, individual-fitting of A1 and λ1, and fixed value of α to the literature value for ^{111}In-DOTATATE was selected as the SOE-SP-PBMS. The RD and RMSE of the SOE-SP-PBMS at (99.8 ± 1.5) p.i. between pTIAs and rTIAs was (1.4±16.9) % and 16.9%, respectively. ***Conclusion:*** In this study, we showed the accuracy of STP dosimetry in PRRT using the SP-PBMS and BF methods. This approach could be a beneficial recommendation for clinicians to improve patient care while lowering costs and improving overall treatment efficiency. ***References:*** [1]D. Hardiansyah, et al., Z. Med. Phys., pp. 1-9, 2023, doi: 10.1016/j.zemedi.2023.01.007.[2]T. P. Devasia, et al., J. Nucl. Med., vol. 62, no. 8, pp. 1118-1125, 2021, doi: 10.2967/jnumed.120.256255.[3]D. Hardiansyah, et al., EJNMMI Phys., pp. 1-12, 2023, doi: 10.1186/s40658-023-00530-1.

OP-836

AI-Generated Synthetic Intermediate Projections could enable SPECT-based bone marrow dosimetry with reduced acquisition time

K. Smits[1], *F. Westerbergh*[1], *J. Hemmingsson*[1], *J. Svensson*[2], *T. Rydén*[3], *P. Bernhardt*[1,3];
[1]*Department of Medical Radiation Sciences, Institute of Clinical Sciences, Sahlgrenska Academy at University of Gothenburg, Gothenburg, SWEDEN,* [2]*Department of Oncology, Institution of Clinical Sciences, Sahlgrenska Academy at University of Gothenburg, Gothenburg, SWEDEN,* [3]*Department of Medical Physics and Biomedical Engineering (MFT), Sahlgrenska University Hospital, Gothenburg, SWEDEN.*

Aim/Introduction: Over the last few years, the number of patients treated with [^{177}Lu]Lu-DOTATATE has rapidly increased. However, clinical resources are limited, making shorter acquisition times desirable. Short acquisitions are problematic in vertebral bone marrow dosimetry, as the low signal results in significant degradation from noise. The aim of this study was to determine if synthetic intermediate projections (SIPs) could be used to compensate for the loss of image quality caused by a decreased acquisition time, by examining different clinically realistic noise levels. ***Materials and Methods:*** A Jaszczak phantom with spherical inserts was filled with a sphere-to-background activity concentration ratio of 5:1 (0.937:0.191 MBq/mL of 177Lu). The phantom was imaged with a GE Discovery NM/CT 670 Pro system (120 projections, 66 s per projection). The four largest spheres (2-16 mL) were analysed based on their size being roughly the same as the volumes-of-interest used for vertebral delineation. Poisson-distributed noise was added to the SPECT

projection data (10%, 5%, 1%, 0.5%, and 0.1% relative to the true acquisition time) to mimic noise levels observed in the vertebral (T8-L5) bone marrow in 177Lu-DOTATATE patients examined 24 h p.i. (n = 16). Thus, five noise levels were obtained, ranging from the maximum concentration observed in patients to 60% of the minimum. Thirty realizations were generated for each noise level. The images were reconstructed using a Monte Carlo-based OSEM algorithm (6i10s), with either 120 projections, 30 projections, or 30 projections + 90 SIPs. Recovery coefficient (RCs) and uncertainties (coefficient of variation) of the RCs were determined for each reconstruction method. ***Results:*** The uncertainties for SIPs, 120 projections and 30 projections for the 2 mL-sphere were 50%, 98%, and 267%, respectively. The corresponding values for the 16 mL-sphere were 26%, 22%, and 53%, respectively. When including SIPs, RCs tended to decrease with increasing noise, indicating a greater loss of resolution at high noise levels. ***Conclusion:*** When using conventional projections and small spheres, high variations were observed between realizations, risking large quantitative errors when calculating the absorbed dose. With larger spheres, the uncertainties decreased substantially, indicating that the smallest bone marrow cavities are less appropriate for bone marrow dosimetry. The loss of resolution obtained at higher noise levels might decrease the quantitative accuracy for SIPs reconstructions. Nevertheless, for larger volumes, uncertainties were similar for SIPs and 120 projections, highlighting SIPs potential to improve bone marrow dosimetry for SPECT protocols with sparsely acquired projections.
.

OP-837

RPT-TEC assessment of normal organ toxicity avoidance thresholds for alpha-emitter radiopharmaceutical therapy - an appeal for data.

J. Hesterman[1], *R. Hobbs*[2], *G. Sgouros*[2], *Radiopharmaceutical Therapy Normal Tissue Effectsin the Clinic (RPT-TEC);*
[1]Ratio Therapeutics, Boston, MA, UNITED STATES OF AMERICA, [2]Johns Hopkins University, Baltimore, MD, UNITED STATES OF AMERICA.

Aim/Introduction: To determine the normal organ toxicity avoidance (NOTA) dose thresholds for alpha-emitter radiopharmaceutical therapy (αRPT). ***Materials and Methods:*** The inaugural Radiopharmaceutical Therapy Normal Tissue Effects in the Clinic (RPT-TEC) meeting was held in September 2022 to establish NOTA dose thresholds in approved radiopharmaceutical therapy (RPT), consistent with previous projects for external beam NOTA thresholds, QUANTEC and HyTEC. A committee, consisting of physicists and clinicians from industry and academia, was formed to pursue the determination of thresholds specifically for αRPT. A three-phase approach was identified. First, characterization of available clinical data to increase understanding of the relationships between administered activity (AA), absorbed dose (AD), and toxicity. Second, application of robust, existing methods to compute consistent whole organ dosimetry values, particularly for cases with observed toxicity. These data are used to determine an interim set of NOTA dose thresholds, based on whole organ EQD2 and BED. Third, extending existing dosimetry methodology specific to the concerns of αRPT, including RBE, daughter radionuclides, and small-scale modeling with standardized apportionment factors. ***Results:*** An assessment of existing clinical αRPT evidence revealed a lack of data. While studies assessing long-term safety and/or administered activity escalation of ^{223}Ra-dichloride exist[1-3], inter- and intra-patient data spanning AA, AD estimates, and toxicity are unavailable. These limitations extend to other αRPTs. Only 11 publications were identified that include dosimetry values estimated directly from administered alpha therapy in people. Generally, minimal toxicity is reported. Related biomarkers, important to extending understanding of individual radio-sensitivity, are lacking. New clinical trials should bring new data. A clinicaltrials.gov search of the "Hopeful Eight" αRPT radionuclides[4] identified 176 alpha therapy trials, of which 45 have a "Start Date" within the last three years and only 26 with results reported. Additionally, 115 trials are funded by industry with 19 unique industry sponsors represented. Early phase trials must include dosimetry, making them essential to generating AA, AD, and toxicity data capable of supporting NOTA dosimetry. A reporting template has been developed and disseminated to industry and academic groups to facilitate the collection of these data. ***Conclusion:*** There is an urgent need to improve collection and standardization of intra- and inter-patient administered activity, absorbed dose, and toxicity data in αTRT. Clinical workflows and early phase clinical trials must acquire and report these data consistently to improve our understanding of αRPT dose-response relationships, thus enabling a NOTA dose threshold paradigm. ***References:*** 1. 10.1016/j.eururo.2017.06.021, 2. 10.1056/NEJMoa1213755, 3. 10.3389/fmed.2022.1070392, 4. 10.3390/pharmaceutics13060906

OP-838

Impact Of Small Patient Motion During SPECT/CT Scans Onto Activity Quantification Of ^{177}Lu-PSMA Based on A Phantom Simulation

S. Resch[1], *X. Shen*[1], *M. Reymann*[2], *F. Basi Massanes*[3], *P. Bartenstein*[1], *G. Platsch*[2], *A. Vija*[3], *G. Böning*[1], *A. Delker*[1];
[1]LMU Klinikum Großhadern, München, GERMANY, [2]Siemens Healthcare GmbH, Molecular Imaging, Forchheim, GERMANY, [3]Siemens Medical Solutions UNITED STATES OF AMERICA Inc., Molecular Imaging, Hoffman Estates, IL, UNITED STATES OF AMERICA.

Aim/Introduction: ^{177}Lu-PSMA patients commonly suffer from progressing bone metastases causing severe pain. Thus, lying still during long SPECT scans (>20min.) can be difficult and uncomfortable. To alleviate pain, they may perform sudden movements, which distort the activity distribution, the quantification and ultimately the dosimetry. The aim of this preliminary study was to investigate the impact of this sudden motion onto the recovery coefficients (RCs) of a simulated NEMA body phantom. ***Materials and Methods:*** The NEMA body phantom (sphere-to-background ratio 8:1, 781MBq ^{177}Lu-solution) was used as input for the SIMIND Monte Carlo program (128 projections, 5 and 15s acquisition times, 256x256 pixels, Symbia Intevo T16 (Siemens Healthineers) SPECT/CT, MELP collimator, emission peak at 208keV, width 15% plus lower and upper scatter windows). In addition to a baseline tomography (BL), different positions of the phantom were simulated (shifted 5, 10, 20mm in lateral and anterior direction). These simulations were stacked together randomly, creating different motion-affected tomographic data sets. It is assumed that the phantom moves instantaneously to a shifted position, remains there for a motion duration (MD) of either 5 or 15s, and moves back instantaneously. The mean motion frequency (MMF) was randomly sampled from a normal distribution with a mean of 1/60 or 1/120s^{-1} (σ = 10%), allowing for a motion at any time during the scan. Motion magnitudes and directions were randomly chosen from the simulated parameter sets. Ten different scans per parameter combination were generated leading to 240 reconstructions in total. The RCs of the three largest spheres (37, 28, 22 mm diameter) and their

deviation from the BL data were calculated. ***Results:*** The RCs of the BL are 0.84, 0.80, 0.69 and 1.00, 0.88, 0.64 for decreasing sphere size and 5 and 15s acquisition times, respectively. Assuming a MMF of 1/60s^{-1} and a MD of 15s, the RCs deviated from the BL by -4, -18, -27% and -9, -11, -9% for acquisition times of 5 and 15s, respectively. The latter changed to -4, -6, -3% for half the MMF (1/120s^{-1}). Reducing the MD to a third (5s) with a MMF of 1/60s^{-1} and an acquisition time of 15s resulted in deviations of -5, -7, -6%. ***Conclusion:*** This preliminary study shows that small, even visually non-detectable motions, can lead to strong distortions of the activity quantification during ^{177}Lu-PSMA SPECT/CT scans. These results motivate further simulations, evaluations of the motion parameters and their impact on quantification and dosimetry.

OP-839

Comparison of transmission-dependent and energy-window based scatter correction methods for quantitative SPECT imaging for ^{225}Ac

G. Liubchenko, *M. Rumiantcev, S. Resch, M. Zacherl, F. Gildehaus, P. Bartenstein, S. Ziegler, G. Böning, A. Delker;*
LMU Klinikum Munich, Munich, GERMANY.

Aim/Introduction: In single photon emission computed tomography (SPECT), photon scatter leads to a reduction of image quality and impairs image quantification. The aim of this study was to compare a transmission-dependent (TD[1]) and an energy-window-based scatter corrections embedded in a MAP-EM algorithm for ^{225}Ac SPECT imaging. ***Materials and Methods:*** Quantitative SPECT reconstructions for both, the 440keV and 218keV peak, were carried out via in-house MAP-EM, including attenuation correction, resolution modelling and TD or energy-window-based scatter correction. To generate the scatter kernels for TD method, SIMIND[2] Monte Carlo program was used to simulate line profiles behind water slabs of varying thicknesses (2-20 cm). For all slab thicknesses, the tails of the scatter signal were fitted using mono-exponential function, and scatter-to-primary fractions were obtained from SIMIND. The scatter kernels were convolved with the current image estimate to generate a scatter image. For every iteration and projection angle, the scatter image was forwardprojected and added to the current projection estimate. To compare the scatter correction methods, a self-made phantom (3 volumes-of-interest (VOIs) with 20, 45, 200ml) filled with ^{225}Ac (64 projections; 128x128 matrix; foreground-to-background ratio of 6; three measurements with 2s and 6s (imitating the patient cases), and 60s (high count case) per projection) was imaged. In addition, 24h post injection (p.i.) SPECT/CT scans of three patients treated with 8 MBq [^{225}Ac]Ac-PSMA-I&T were evaluated using both scatter correction methods. ***Results:*** For the self-made ^{225}Ac phantom study, comparable recovery coefficients were observed for energy-window-based and TD methods for both 440 and 218keV peaks (440kev, TD: 15.02%-47.7%; DEW: 15.92%-47.51%; 218kev, TD: 17.29%-35.98%, TEW: 18.13%-36.72%). TD method, however, resulted in higher SNRs (12-34%) for all VOIs and step times, for both, the 440 and 218keV peak. For the patient cases and the 440keV peak, the absorbed dose and the SUV at 24h p.i. in the kidneys were found to be 3-7% and 5-9% higher for the TD method, respectively. The lesion evaluation showed comparable absorbed doses and SUV at 24h p.i. For the 218keV peak, the absorbed dose and the SUV at 24h p.i. in the kidneys were found to be 14-36% and 21-36% higher for the TD method, respectively. The lesion absorbed dose and the lesion SUV at 24h p.i. were found to be 6-21% and 20-38% higher for the TD method, respectively. ***Conclusion:*** TD method showed improved SNR for the phantom and higher recovered activities for the patient studies. ***References:*** 1. https://doi.org/10.1007/s12149-008-0170-z. 2. https://doi.org/10.1201/b13073-8.

1705

Wednesday, September 13, 2023, 8:00 AM - 9:30 AM
Hall B

Cutting Edge Science Track - Featured Session: Dynamic Imaging

OP-840

State of the Art in Quantitative Dynamic Imaging

G. Wang;
Department of Radiology, University of California Davis Health, Scacramento, UNITED STATES OF AMERICA

OP-841

Prediction of bone turnover in chronic kidney disease with hemodialysis patients using K_i-Patlak dynamic ^{18}F-NaF PET/CT imaging

K. Khamwan[1], *V. Sanoesan*[1], *J. Phannajit*[1], *T. Sawatnatee*[2], *B. Phromphao*[2], *C. Sukprakhun*[1], *P. Susantitaphong*[1], *K. Kingpetch*[1];
[1]*Chulalongkorn University, Bangkok, THAILAND,* [2]*King Chulalongkorn Memorial Hospital, Bangkok, THAILAND.*

Aim/Introduction: The diagnosis of renal osteodystrophy (ROD) is based on the bone turnover, mineralization, and volume (TMV system), which can be assessed through bone histomorphometry from bone biopsy. While bone biopsy is considered the gold standard for ROD classification, it is an invasive and painful procedure that is limited to a single bone site and requires considerable expertise to interpret specimens. This study aimed to evaluate the use of ^{18}F-NaF PET/CT kinetic parameters of bone metabolic flux in chronic kidney disease (CKD) patients on hemodialysis to predict bone turnover rate as a non-invasive biomarker. ***Materials and Methods:*** Thirty-five CKD patients (16 males and 19 females) with an average age of 55.6 ± 9.6 years and biochemical abnormalities indicative of mineral and bone disorder were enrolled in the study. Following injection with 111-185 MBq of 18F-NaF, dynamic PET/CT scans were acquired for 60 minutes covering the T12 to anterior iliac crest to determine the Patlak-derived influx rate constant (Ki). The images were reconstructed into 37 frames of 12 × 5 s, 6 × 10 s, 8 × 30 s, and 11 × 300 s. 3D volumes of interest (VOIs) were drawn at L1-L4 and both anterior iliac crests to generate time-activity curves (TACs) for kinetic modeling using PMOD software. Kinetic parameters for the Ki Patlak model were derived using an image-derived input function (IDIF) drawn at the abdominal aorta. The Ki-Patlak values calculated from dynamic ^{18}F-NaF were compared with biochemical markers to evaluate bone turnover rate. ***Results:*** We found a strong correlation of K_i-Patlak between the average influx rate of L1-L4 and each lumbar region, as well as between the average L1-L4 and both iliac crests. Using a cut-off value of 0.040 mL/min/mL in the lumbar region or at the anterior iliac crest, low bone turnover was detected in 7 patients (20%) while high bone turnover was detected in 28 patients (80%) based on the biochemical markers. ***Conclusion:*** This study indicated a potential of dynamic ^{18}F-NaF PET/CT scans as a noninvasive diagnostic tool for determining bone turnover rate in CKD hemodialysis patients.

OP-842

Automated and reproducible processing and kinetic modelling of whole-body [15O]H2O PET/CT data

S. Palonen[1], *J. Tuisku*[2], *H. Kärpijoki*[2], *S. Nesterov*[2], *V. Oikonen*[2], *R. Klén*[2], *L. Nummenmaa*[2], *J. Knuuti*[1];
[1]*Turku PET centre, Turku University, Turku, FINLAND,*
[2]*Turku PET centre, Turku, FINLAND.*

Aim/Introduction: Manual pre-processing of PET-data is time-consuming and less reproducible than automated methods, particularly when multiple target tissues need to be analysed. Several tools exist for automated brain-PET data processing, but similar pipelines are not yet widely available for whole-body PET data. Here we present a novel method for automated and reproducible processing and kinetic modelling for whole-body PET dynamic [^{15}O]H_2O data. ***Materials and Methods:*** Automated analysis was developed and tested using whole-body [^{15}O]H_2O PET/CT data from 36 subjects with suspected coronary artery disease. In the proposed approach, CT-based segmentation (TotalSegmentator1) is used for extracting the regional PET tissue time-activity curves for all major organs (including brain, myocardium, lungs, liver, kidney, pancreas, spleen, gut, gluteal muscle). Manually defined image-based input (abdominal aorta) is corrected for radiotracer delay separately for each organ before 1-tissue compartment model fitting process, providing blood flow estimates for each organ. Voxel-level parametric maps are calculated for each organ separately by using the delay-corrected input curves, after which they are combined in parametric 3D flow-maps. As a separate analysis branch, the brain is extracted from the PET images, followed by motion correction, template-based normalization, automated ROI-delineation, and regional and voxel-level kinetic modelling by using an in-house magia-toolbox[2] for brain PET data processing. ***Results:*** Based on visual inspection, the 1-tissue compartment model fits had good quality, and the automated process produced consistent regional and voxel level blood flow estimates with minimal user input. ***Conclusion:*** The present study describes an example framework for the automated processing of whole-body [^{15}O]H_2O PET data from multiple organs with minimal manual labour. This framework will provide means to study characteristics of the inter-organ blood flow such as brain-body interactions. A detailed comparison against the results of manual workflow is warranted. ***References:*** 1. J. Wasserthal et al., TotalSegmentator: robust segmentation of 104 anatomical structures in CT images. arXiv preprint arXiv:2208.05868, (2022).2. T. Karjalainen et al., Magia: Robust automated modeling and image processing toolbox for PET neuroinformatics. Frontiers in Neuroinformatics, 604835 (2020).

OP-843

Shortening Dynamic [^{11}C]PK11195 PET Protocol for Parametric Imaging Using Supervised Clustering to Improve Clinical Feasibility

D. B. A. Mantovani[1], *M. S. Pitombeira*[1], *P. N. Schuck*[2], *C. Buchpiguel*[1], *D. de Paula Faria*[1], *A. Marques da Silva*[1];
[1]*University of Sao Paulo, Sao Paulo, BRAZIL,* [2]*Weill Cornell Medical College, New York, NY, UNITED STATES OF AMERICA.*

Aim/Introduction: Positron emission tomography (PET) quantification using parametric imaging is superior to semi-quantitative parameters extracted from static images. However, there are many obstacles to incorporating parametric imaging into clinical practice, such as the time-consuming of dynamic PET acquisitions. While input functions from reference regions provide a good approach for PET quantification, some tracers, such as the 18kDa Translocator Protein (TSPO) ligand [^{11}C]PK11195, are spread in the central nervous system, with no reference region available. In this case, pseudo-reference regions are identified by a supervised clustering algorithm (SVCA). This work investigates the shortening of the dynamic [^{11}C]PK11195 PET acquisition protocol while obtaining reliable distribution volume ratio (DVR). ***Materials and Methods:*** Pseudo-reference regions were extracted using the SVCA approach (1) with a full-time scan (60 min) and a reduced-time scan (40 min) from dynamic [^{11}C]PK11195 PET-MR images of 24 relapsing-remitting multiple sclerosis (RRMS) patients and 16 healthy volunteers (HV). Gray matter, white matter, and blood pool classes were extracted from the HV group, while the specific-binding class was extracted from the patients' thalamus (2). Using the reference-tissue-based Logan analysis, DVR values were determined in the gray matter, white matter, caudate nucleus, putamen, pallidum, thalamus, brainstem, and nucleus accumbens. In addition, the DVR correlation between the full-time (SVCA60) and reduced-time (SVCA40) were tested. ***Results:*** Pseudo-reference regions extraction was not affected significantly by shortened scan, showing that the SVCA approach applies to reduced [^{11}C]PK11195 PET acquisitions. The reduced-time PET scan produced DVR values comparable to the full-time scan, with a Pearson correlation coefficient in all brain regions between 0.77-0.95 ($p<0.0001$) for HV group and 0.61-0.95 (<0.0001) for RRMS group. SVCA40 showed good correlations with SVCA60 ($r2 = 0.9118$ for HV and $r2 = 0.8986$ for RRMS) and the arterial input function approach ($r2 = 0.9170$ for HV and $r2 = 0.8998$ for RRMS). ***Conclusion:*** A 40-minute [^{11}C]PK11195 PET acquisition produces reliable SVCA pseudo-reference regions and DVR values. This may improve the clinical feasibility of kinetic modeling and dynamic PET imaging for MS patients. ***References:*** (1)-Yaqub M, van Berckel BN, Schuitemaker A, Hinz R, Turkheimer FE, Tomasi G, et al. Optimization of Supervised Cluster Analysis for Extracting Reference Tissue Input Curves in (R)-[11 C]PK11195 Brain PET Studies. J Cereb Blood Flow Metab. 2012 Aug;32(8):1600-8. (2)-Turkheimer FE, Edison P, Pavese N, Roncaroli F, Anderson AN, Hammers A, et al. Reference and target region modeling of [11C]-(R)-PK11195 brain studies. J Nucl Med. 2007 Jan;48(1):158-67.

OP-844

Feasibility of Dynamic Total-Body Pre-therapy PET for Predicting Radiopharmaceutical Therapy (RPT) Dosimetry: a simulation study

J. Hong[1], *M. Kassar*[2], *A. Rominger*[1], *K. Shi*[1];
[1]*University of Bern/Inselspital, Bern, SWITZERLAND,*
[2]*Technical University Munich, Munich, GERMANY.*

Aim/Introduction: The dosimetry of radiopharmaceutical therapy (RPT) is determined by whole-body pharmacokinetics. The dynamic total-body PET enables us to characterize the multi-organ pharmacokinetics of radiopharmaceuticals. This study aimed to predict the dosimetry of RPT from pre-therapy imaging in voxel level using deep learning method. For proof-of-concept, the realistic computational simulation PET images were utilized for this work. ***Materials and Methods:*** We aimed to predict ^{177}Lu-PSMA-617 dosimetry from dynamic ^{68}Ga-PSMA-11 total-body PET in voxel-level using seq2seq model. We simulated 200 pairs of dynamic ^{68}Ga-PSMA-11 pre-therapeutic PET images and ^{177}Lu-PSMA-617 dosimetry images using 4D XCAT phantom, of which we divided 150 and 50 for training and test, respectively. 2 ellipsoidal tumor lesions were placed in the regions frequently reported: liver, lung, bone, or lymph node. We then

performed physiologically based pharmacokinetic (PBPK) model to simulate the dynamic time-activity curve (TAC) of each organ in the phantom for each ^{177}Lu-PSMA-617 and ^{68}Ga-PSMA-11. The kinetic parameters were taken from literatures and noise was added to generate more individual variations. The parameters such as kidney volume, kidney receptor density, and flow rate to the kidney, as well as those of tumor, were randomly sampled from Gaussian distribution; Height and weight were sampled from multivariate Gaussian distribution. For dynamic ^{68}Ga-PSMA-11 total-body PET, the time frames were set as [1(min)*2; 3(min)*1; 5(min)*1; 20(min)*3; 30(min)*1]. The dynamic pre-therapeutic images were then reconstructed by ordered subset expectation maximization (OSEM) algorithm. Similarly, the paired dosimetry images were simulated by applying the dose voxel kernel (DVK) to the integral of TAC over 20 days that is generated by PBPK model for ^{177}Lu-PSMA-617. The reduction of lesion volume was considered in simulation by using the linear-quadratic model and exponential tumor growth. The seq2seq model was established to predict the dosimetry images from the dynamic pre-therapeutic images. ***Results:*** The dynamic ^{68}Ga-PSMA-11 total-body PET simulation agreed well with the previous literatures except for lung and liver. The activity of lung was overestimated and that of liver was underestimated across full frame. On average, the prediction underestimated 0.016 Gy/GBq in tumor, and the bias and variance were 0.888 and 0.145. However, MAE, variance and bias showed a positive relationship with the ground truth absorbed dose in organs($p<0.05$); the higher the absorbed dose was, the prediction error was higher in organs. ***Conclusion:*** Dosimetry of RPT may be predicted by dynamic pre-therapy PET scans using deep learning model.

OP-845

Voxel-wise parametric imaging of 4D PET data :evaluation of new software solution for [^{18}F]-FDG PET kinetic modeling at the whole FOV level.

F. Besson[1,2], *E. Marchal*[1], *S. Faure*[3];
[1]*CEA / Inserm / CNRS / Université Paris Saclay, BioMaps, Orsay, FRANCE,* [2]*Department of Nuclear Medicine-Molecular Imaging, Hôpitaux Universitaires Paris Saclay, AP-HP, Le Kremlin-Bicêtre, FRANCE,* [3]*Laboratoire de Mathématique d'Orsay, CNRS, Université Paris Saclay, Orsay, FRANCE.*

Aim/Introduction: voxel-wise PET kinetic modeling constitutes a high computational challenge at the whole FOV level. Here we assessed the performance of a new dedicated software solution we developed to perform parametric imaging from 4D PET data in a very fast and efficient way. ***Materials and Methods:*** the one-hour dynamic thoracic PET data from 12 patients with NSCLC who had prospectively undergone [^{18}F]-FDG PET/MR for oncology purpose were processed with our software solution to generate, at the whole FOV level (5 million voxels, whole blood image-derived input function defined in the aorta), the parametric maps of the net influx constant Ki, both using Patlak (Ki_{Patlak}) and the irreversible 2 tissue compartment model (Ki_{2TCM}). We compared the computation times, robustness and Ki values with those estimated by PMOD kinetic tool (PKIN, PMOD Technologies LLC 1996-2022, Zurich, Switzerland) within 3 small volumes of interest (VOI < 300 voxels) - tumor, tissue and bone targets respectively - due to the inability of PMOD to compute whole FOV parametric images. Quantitative data are expressed as median [interquartile ranges]. ***Results:*** per patient, our solution took around 1 minute to read, compute and write the whole FOV parametric maps (Ki_{Patlak} and Ki_{2TCM}, 5 millions voxels) from the 4D PET data, whereas PKIN took 10 seconds to compute Ki_{Patlak} and 7 minutes [4.2; 10.6] to compute Ki_{2TCM} within the VOIs (< 300 voxels). The voxel fitting failure rate (i.e. 0 or negative values) per target was for Ki_{Patlak}: 0% [0; 0], 0% [0; 0], 0% [0; 0] with our soft and 44% [35; 68], 76.1% [73.7; 78.6], and 70.4% [64.5; 77.4] with PKIN. And for Ki_{2TCM}: 11% [6; 16.8], 10.3% [3.8; 16.7], 0% [0; 0.9] with our soft and 13.1% [9.2; 14.7], 14.6% [11.9; 15.9], 12.4% [0; 15.3] with PKIN. On average, the differences between our soft and PKIN were 33% [28; 65], 131% [86; 164], 109% [47; 200] for Ki_{Patlak} and -6% [-13; 8], 9% [0; 18], 13% [7; 20] for Ki_{2TCM}. ***Conclusion:*** our solution overpassed PKIN for Ki_{Patlak} and provided less than 20% median differences for Ki_{2TCM} within the VOIs. Our soft appears promising for fast and robust IDIF-based voxel-wise PET kinetic modeling at the whole FOV level.

OP-846

Incorporating prior knowledge with physics-informed neural networks to predict arterial input functions from dynamic PET images

M. Ferrante[1], *M. Inglese*[1], *L. Brusaferri*[2], *A. C. Whitehead*[3], *M. L. Loggia*[4], *N. Toschi*[1];
[1]*University of Rome Tor Vergata, Roma, ITALY,* [2]*Department of Radiology, Athinoula A. Martinos Center for Biomedical Imaging, Boston, MA, UNITED STATES OF AMERICA,* [3]*Institute of Nuclear Medicine, University College London, (UNITED KINGDOM), London, UNITED KINGDOM,* [4]*2)Department of Radiology, Athinoula A. Martinos Center for Biomedical Imaging, Boston, MA, UNITED STATES OF AMERICA.*

Aim/Introduction: Translocator protein 18kDa (TSPO) is a critical target for [^{11}C]PBR28 PET-based in-vivo imaging of neuroinflammation [1,2,5] as it is upregulated by activated microglia and macrophages. Quantitative PET imaging requires sampling of the arterial input function (AIF) through invasive arterial cannulation, which poses several challenges, including higher clinical staff demands and additional patient burden. In this study, we aimed to estimate the AIF from a dynamic PET acquisition while employing a parameter-efficient, physics-informed convolutional neural network (PINN) [3,4] that combines the advantages of model-based and data-driven methods. ***Materials and Methods:*** We performed [^{11}C]PBR28 PET/MRI brain scans on 50 individuals and collected arterial blood samples for each subject. Our architecture consisted of six depthwise separable 3D strided convolution layers, which repeatedly downsampled the dynamic 4D PET image by a factor of two. The interaction between channels was split through the implementation of depthwise and pointwise convolutions, resulting in both a considerable reduction of parameter count and computation of spatiotemporal features. The multilayer perceptron of depth 3 with hyperbolic tangent activation functions mapped the features onto the ten parameters of the Parker's model. ***Results:*** After training, the estimated AIF in the test set was used to model [^{11}C]PBR28 kinetics with the 2TCM-1k, leading to an estimation of the distribution volume VT. No statistical difference in VT values was found when comparing estimates from the estimated and real AIF in various regions of interest, including the hippocampus, thalamus, and frontal cortex. Furthermore, the intraclass correlation coefficient (ICC) indicated strong agreement between the estimated and real AIF-derived VT values. The PINN model demonstrated robustness across different brain regions and maintained high accuracy in the presence of varying noise levels, providing more confidence in the use of the estimated AIF for quantitative PET. ***Conclusion:*** Our results demonstrate the potential of incorporating prior knowledge into neural networks and employing depthwise

separable convolutions to handle high-dimensional time series data, achieving comparable performance to real-world measured plasma components even with limited data availability. This work has the potential to reduce the invasiveness of quantitative PET and promote the use of this technique, which has greater diagnostic and prognostic power than static PET imaging. Further advancements in this field could lead to practical applications in clinical settings, enabling quantitative PET without the need for invasive measurements. ***References:*** 1. SandströmA, KimM, WeerasekeraA, Castro-BlancoK, LinY, AlshelhZ, Torrado-CarvajalA, MukerjiSS, GandhiRT, ChuJ, PollakL, NapadowV, EdwardsRR, RataiEM, LoggiaML. 1H-MRSBrain Metabolites and Quantitative Sensory Testingin People Living With HIV and HIV-Related Neuropathic Pain. USASP (2023).Durham, UC, US. 2. Dimitrakopoulou-Strauss, Antonia, Leyun Pan, and Christos Sachpekidis. "Kinetic Modeling and ParametricImaging with Dynamic PET for Oncological Ap

OP-847

Impact of AI-based Image Denoising on Quantitative Kinetic Analysis in Dynamic PET imaging

B. Liu[1], *G. Hu*[2], *X. Wang*[2], *L. Huo*[2], *H. Ding*[1], *H. Zhang*[1]; [1]*Tsinghua University, Beijing, CHINA,* [2]*Peking Union Medical College Hospital, Beijing, CHINA.*

Aim/Introduction: AI^{18}F-PSMA-617 has excellent detectability of tumors and favorable pharmacokinetic profiles, while dynamic PET imaging provides valuable parameters for quantitative description of the physiological state. This study aims to investigate whether AI-based denoising process affects the quantitative accuracy in kinetic analysis of AI^{18}F-PSMA-617 PET imaging compared to the traditional method. ***Materials and Methods:*** 12 PCa patients recruited in this study underwent a 60-min dynamic AI^{18}F-PSMA-617 PET scan. The list mode data were reconstructed with and without Gauss filtering, images without Gauss filter processing were sent to the AI-based denoising algorithm named a novel segmentation guided style based generative adversarial network (SGSGAN). Physicians' perceptions of image quality were determined by scoring image preference and anatomical clarity on a 5-point Likert scale, while objective evaluation was conducted by calculating signal-to-noise (SNR). The reversible two-tissue compartment model was used and validated based on R^2 values. Statistical analysis was performed with P values, AUCs, and ICCs. ***Results:*** The two physicians showed good consistency in ratings with coefficients of agreement (COA) > 60%, agreed that AI denoising improved image quality compared to traditional method, which was also revealed by significantly increased SNR. R^2 was 0.838±0.132 and 0.805±0.085 for lesions and normal tissues in the Gauss group, while in the AI group there was a significant improvement to 0.940±0.056 and 0.885±0.062. Kinetic parameter Ki were 0.103±0.095 and 0.030±0.013 / 0.111±0.106 and 0.027±0.013 for lesions and normal tissues in Gauss / AI group, Vd were 9.361±7.004 and 1.166±0.347 / 8.677±6.715 and 1.234±0.396, all exhibited significant differences (P<0.0005) between tumors and normal tissues. Ki AUCs in the Gauss and AI group were 0.927 (P=0.0004) and 0.948 (P=0.0002), Vd AUCs were both 1 (P<0.0001) in two groups, indicating that diagnostic efficiency was improved after AI noise reduction for Ki, while Vd had even higher differentiation ability that was barely affected by noise reduction. ICC values for Ki were 0.989 (P<0.0001) and 0.973 (P<0.0001) for lesions and normal tissues, and for Vd were 0.962 (P<0.0001) and 0.951 (P<0.0001), revealing excellent consistency between two groups. ***Conclusion:*** AI-based denoising techniques are effective in enhancing image quality without compromising the quantitative accuracy and diagnostic efficiency of kinetic analysis for dynamic PET imaging. Future research should explore other factors affecting kinetic analysis stability to enhance clinical parameter utilization.

OP-848

Myocardial Dynamic Positron Emission Tomography Later Time Frames Prediction Using Deep Learning

M. Mokri[1], *M. Safari*[2], *L. Archambault*[2], *S. Kaviani*[1], *D. Juneau*[3], *C. Cohalan*[3], *J. Carrier*[1,3]; [1]*Université de Montréal, Montreal, QC, CANADA,* [2]*Université Laval, Quebec City, QC, CANADA,* [3]*Centre hospitalier de l'Université de Montréal, Montreal, QC, CANADA.*

Aim/Introduction: Dynamic Myocardial Positron Emission Tomography (PET) imaging is a technique for assessing myocardial uptake. The long acquisition time of dynamic PET might hinder its applications due to the patient's discomfort and movement. Deep learning (DL) techniques have been utilized for medical image synthesis. Our goal is to utilize deep learning techniques to predict the late time frames of myocardial PET images using the initial time frames, which will reduce the acquisition time. ***Materials and Methods:*** This study used dataset of 350 patients to train two DL models. The patients underwent ^{13}N-ammonia myocardial PET/CT scans constituting 21 time frames. We introduced a temporal normalization in the preprocessing step to keep the correlation between different time points. The networks were Unet and Attention Unet with self-attention layers that capture dependencies between feature maps, which focus on more relevant regions of the image. We used L1 regressor to train the networks. The networks were used for two independent prediction scenarios: to predict the last 10 and 14 late time frames, respectively, using the initial 11 and 7 time frames. ***Results:*** For both models, the predicted frames showed a close resemblance in appearance and texture compared to the reference frames. Qualitative examinations illustrate a comparable pattern of radiotracer uptake biodistribution in predicted images and reference images. Quantitative metrics including Peak Signal-to-Noise Ratio (PSNR), Mean squared Error (MSE) and (Structural Similarity Index Measure) SSIM, were used to assess performance in terms of image distortion and structural similarity. For the prediction of 10 time frames, Attention Unet outperformed Unet with average PSNR of 39.14, and MSE of 0.003 compared to Unet's PSNR of 35.56, and MSE of 0.0051. Attention Unet demonstrated higher average SSIM value of 0.96 compared to Unet with SSIM value 0.91. For the prediction of the last 14 time frames, Attention Unet performed Unet with average PSNR of 38.88, SSIM of 0.95, and MSE of 0.0035 compared to Unet's PSNR of 31.35, SSIM of 0.89, and MSE of 0.0056. Attention-Unet outperformed Unet in terms of PSNR and SSIM, as determined by a pairwise t-test (p-value < 0.05). ***Conclusion:*** We developed and evaluated deep learning models to predict the late time frames of dynamic myocardial images from initial data points. The quantitative metrics indicate that Attention Unet outperformed Unet for two different prediction scenarios. The results demonstrate the potential of deep learning models for predicting late frames for dynamic PET.

1706

Wednesday, September 13, 2023, 8:00 AM - 9:30 AM
Hall C

Clinical Oncology Track - TROP Session: Localised Treatments

OP-849

Is there any factor that influences the quality of the I125 placement in non palpable breast lesions?

O. Ajuria Illarramendi, *A. Martinez Lorca, U. Vera Schmulling, P. Azpeitia Hernandez, M. Gutierrez Guerrero, P. Paredes Rodriguez, T. Navarro Martinez, M. Orduña Diez;*
Hospital universitario ramon y cajal, Madrid, SPAIN.

Aim/Introduction: Radioguided Seed Localization(RSL) has become the elected technique to perform the surgery of non palpable breast lesion at our institution. The success of the technique is related to the correct placement of the seed in the lesion. The aim of this study is to find out if the histology of the lesion, the size of the lesion or the imaging technique used to deploy the seed influence the result of the placement. ***Materials and Methods:*** We review 533 consecutive patients who underwent RSL technique at our institution. The histology (invasive ductal carcinoma(CDI), invasive lobulilllar carcinoma(CLI), in situ(IS) or non tumoral(NT)); the size and the imaging technique (US, stereotactic or MRI) used to deploy the seed were recorded. Correct placement was considered when the seed was deployed inside or within 5mm the lesion, marginal placement was considered when the seed was released above 5mm the lesion and failure of the placement was considered when another marking technique was necessary to accomplish the excision of the lesion. All the sizes of the lesions were recorded in cm. ***Results:*** In 456/533 the seed was released guided by US: 435/456(95,4%) had correct placement, 17/456(3,7%) marginal and 4/456(0,9%) failed. 76/533 were guided by stereotactic: 55/76 (72,4%) had correct placement, 13/76 (17,1%) marginal and 8/76(10, 5%) failed. 1/533 was deployed guided by MRI and failed. Statistical significance was achieved with p<0,001. According to the histology: 91,8% CDI, 97,5% CLI, 87,5% IS and 93,2% NT had correct placement, while 5,8% CDI, 2,5% CLI, 8,9% IS and 3,4% NT had marginal placement and in 2,4% CDI, 0% CLI, 3,6% IS and 3,4% NT the placement failed. There was no statistical significance with p:0,665. When the influence of the size was analyzed there was no statistical significance neither (p:0,266). ***Conclusion:*** The success on the seed placement is related to the imaging technique that is used to guide the deployment, earning better results when using the US. On the other hand, there is no relation between the histology or the size of lesion with the result of the seed placement.

OP-850

Investigation on Dose-Toxicity and Dose-Response Relationship in Neuroendocrine Liver Metastases treated with Holmium-166 Radioembolization

K. Ramdhani, *J. J. Verduin, S. C. Ebbers, M. L. J. Smits, R. C. G. Bruijnen, M. G. E. H. Lam, A. J. A. T. Braat;*
University Medical Center Utrecht, Utrecht, NETHERLANDS.

Aim/Introduction: Aim of this study was to investigate a lesion-based dose-response relationship and patient-based dose-toxicity relationship in neuroendocrine liver metastases (NELM) treated with holmium-166-radioembolization. ***Materials and Methods:*** Single center, retrospective study including patients with NELM that received holmium-166-radioembolization with post-treatment SPECT/CT and evaluation imaging. SPECT was scaled based on total net administered activity to calculate tumor and whole liver healthy tissue (Dh) absorbed dose. Clinical and laboratory toxicity was graded by Common Terminology Criteria for Adverse Events (CTCAE), version 5 at baseline and three months follow-up. Response was determined according to RECIST 1.1. ***Results:*** Twenty-seven treatments in 25 patients were included, with a total of 114 tumors. Sixteen patients had grade 1-2 clinical toxicity and only one patient with grade 3. No new grade 4-5 toxicity was encountered. No clear dose-toxicity relationship was found. None of the treatments with Dh <30 Gy experienced any clinical toxicity. There was minimal change in laboratory parameters (57%, grade 1-2). Of the treatments with Dh >30 Gy, 66% experienced clinical toxicities (max grade 2) and 71% laboratory toxicities (max grade 3). Six tumors had CR, 36 tumors had PR, 69 tumors had SD and only three tumors had PD, resulting in a disease control rate of 97% of target lesions. The mean dose in non-responders (PD+SD) was 68 Gy versus 118 Gy in responders (CR+PR), p=0.01. On patient level, there was no significant difference between responders and non responders with a mean tumor absorbed dose of 76 Gy in the non responders and 81 Gy in the responders group, p=0.7 ***Conclusion:*** This study confirms the safety of holmium-166-radioembolization in NELM in a real-world setting, with a clear dose-response relationship, high disease control rates (97%) and limited toxicities.

OP-851

Radioembolization of HCC Patients for Curative Intent with Personalized Yttrium-90 Dosimetry (RAPY90D)

S. Kappadath, *E. C. Henry, B. P. Lopez, A. Mahvash;*
UT MD Anderson Cancer Center, Houston, TX, UNITED STATES OF AMERICA.

Aim/Introduction: To report on a single-arm single-institution prospective clinical trial (NCT03896646) on ^{90}Y-glass radioembolization for hepatocellular carcinoma (HCC) patients (n=40) using patient-specific voxel-dosimetry treatment planning. The primary endpoint was localized mRECIST objective response rate (ORR) at 6-month follow-up. Secondary analysis evaluated concordance between planned and delivered absorbed doses based on pre- and post-therapy quantitative SPECT/CT and PET/CT. ***Materials and Methods:*** Eligibility criteria included all adult HCC patients eligible for ^{90}Y-glass radioembolization with non-infiltrative tumors of maximum single dimension ≥3 cm (index tumors). All patients underwent hepatic angiography with fan-beam CT (AngioCT), received ^{99m}Tc-MAA injections at all planned treatment sites, and imaged with SPECT/CT. AngioCT and ^{99m}Tc-MAA SPECT/CT were used to determine the volume of perfused territories and to calculate the ^{90}Y-microsphere activities needed to achieve tumor mean dose (D_{mean}) ≥200 Gy and normal liver D_{mean} ≤100 Gy with voxel dosimetry. Localized mRECIST tumor responses and overall toxicities (CTCAE v5.0) were determined at 6-month follow-up. Post-treatment imaging for dose verification was performed within 24 hours using both ^{90}Y-SPECT/CT and ^{90}Y-PET/CT. Inter-modality concordance of D_{mean} for tumors and normal livers were assessed. The delivered D_{mean} was defined as the average of bias-corrected ^{90}Y-SPECT and ^{90}Y-PET estimates. ***Results:*** Forty patients received ^{90}Y-radioembolization, and 37 patients (58 tumors and 48 index tumors) completed 6-month follow-up. The median (range) index lesion effective-diameter

was 4.7 (2.8-13.0) cm. Bland-Altman analyses between ^{90}Y-PET and ^{90}Y-SPECT yielded, on average (95% limits-of-agreement), higher ^{90}Y-PET tumor D_{mean} by 16% (±28%) and lower ^{90}Y-PET normal liver D_{mean} by 11% (±27%). The median (range) planned and delivered tumor D_{mean} were 350 (224-574) Gy and 357 (206-981) Gy, respectively. Pre- and post-therapy doses were strongly correlated (R^2=0.92) and clinically comparable (within ±20%) in 83% of cases. Similarly, post-therapy bias-corrected ^{90}Y-SPECT and ^{90}Y-PET doses were strongly correlated (R^2=0.95) and clinically comparable (within ±20%) in 85% of cases. The ORR at 6-month follow-up was 97% (56/58), with CR=72% (42/58), PR=24% (14/58), and SD=3% (2/58). Two patients experienced one nontreatment-related grade 3 toxicity, and one patient developed duodenal ulcer with grade 5 toxicity. ***Conclusion:*** RAPY90D trial has demonstrated the feasibility and clinical benefits of prospective, ^{99m}Tc-MAA-SPECT-based, patient-specific voxel dosimetry treatment planning for ^{90}Y-radioembolization of HCC patients. A 97% tumor response rate was achieved by targeting high tumor doses (≥200 Gy) while minimizing normal liver doses. Excellent concordance between planned and delivered doses were achieved through careful image-guided treatment planning, delivery, and verification.

OP-852

166Holmium-SIRT after PRRT (HEPAR PLuS) versus PRRT-only in Patients with Metastatic Neuroendocrine Tumors: a Propensity-score Matched Analysis

A. Braat[1], *T. Walter*[2], *D. de Vries-Huizing*[3], *J. Theysohn*[4], *S. Barton*[5], *E. Ekkelenkamp*[6], *B. Lachachi*[2], *R. de Jong*[6], *L. van Golen*[3], *H. Lanzafame*[4], *L. Milot*[2], *H. Lahner*[4], *W. Veldhuis*[1], *M. Tesselaar*[3], *M. Lam*[1];
[1]*University Medical Center Utrecht, Utrecht, NETHERLANDS,* [2]*Hospices Civils de Lyon, Lyon, FRANCE,* [3]*NKI-AVL, Amsterdam, NETHERLANDS,* [4]*University Hospital Essen, Essen, GERMANY,* [5]*Barton Biostatistics Ltd, London, UNITED KINGDOM,* [6]*Medical Affairs Interventional Oncology Terumo Europe NV, Leuven, BELGIUM.*

Aim/Introduction: Patients with bulky neuroendocrine liver metastases undergoing peptide receptor radionuclide therapy (PRRT) with [^{177}Lu]Lu-DOTATATE have a worse survival than patients with limited liver metastases.[1] Previously, safety and efficacy of additional selective internal radiotherapy (SIRT), using ^{166}Holmium microspheres, directly following PRRT in patients with liver metastatic neuroendocrine tumors (mNET) was confirmed in the prospective HEPAR PLuS study.[2] Aim of the current study is to provide insight into efficacy and progression-free survival (PFS) benefit of ^{166}Ho SIRT+PRRT over PRRT-only by means of a propensity score matched historical cohort ***Materials and Methods:*** A multicenter retrospective data collection of patients treated with PRRT-only was initiated to match with prospectively collected HEPAR PLuS study patients. Demographic, clinical, laboratory and imaging data were collected. All imaging data was centrally re-assessed: RECIST 1.1 response and liver tumor load segmentation. Matching criteria included liver tumor burden, RECIST 1.1 response after PRRT, primary tumor location and resection, Ki-67 score, days from liver metastases diagnosis to PRRT initiation, previous treatments, extrahepatic disease, albumin, gender and age. Primary endpoint is proportion of patients with PFS (defined as surviving, not requiring subsequent treatment and radiological PFS) at 2 years after start of PRRT. Secondary endpoints include proportion of patients with 2-years hepatic PFS (hPFS), general PFS and hPFS, objective response rates (ORR), and overall survival. ***Results:*** 24 SIRT+PRRT-treated patients and 24 PRRT-only patients were included in the analysis set. All key matching criteria were balanced between cohorts. The proportion of patients with PFS and hPFS at 2 years was 68% and 82% with SIRT+PRRT versus 55% and 50% with PRRT-only. Time to median PFS (i.e. 50% probability of PFS) was comparable (31 versus 30 months). However, notable in mNET patients with primary intestinal tumors (i.e. small intestine+colon+rectal) a delay in PFS was observed in SIRT+PRRT patients (75% probability of PFS at 26 versus 20 months). A delay in hPFS was also observed in SIRT+PRRT mNET patients (75% probability of PFS 27 versus 22 months) and most notably in intestinal tumors (75% probability of PFS at 26 versus 15 months). Best ORR was 71% with SIRT+PRRT versus 25% with PRRT-only. ***Conclusion:*** SIRT+PRRT results in a higher PFS-rate at 2 years and best objective response compared to PRRT-only. A delay in hPFS was observed in the patients treated with PRRT+SIRT compared to PRRT-only. ***References:*** [1]Strosberg J et al EJNMMI 2020;47(10). [2]Braat AJAT et al. Lancet Oncology 2020;21(4):561-570.

OP-853

Intratumoral Holmium-166 Microsphere Brachytherapy in Patients with Pancreatic Ductal Adenocarcinoma: The Sloth Project

C. Y. Willink, *S. F. M. Jenniskens, M. W. J. Stommel, M. J. R. Janssen, J. J. Fütterer, K. J. H. M. van Laarhoven, J. F. W. Nijsen; Radboudumc, Nijmegen, NETHERLANDS.*

Aim/Introduction: To evaluate the safety and feasibility of intratumoral holmium-166 microsphere brachytherapy in patients suffering from pancreatic ductal adenocarcinoma (PDAC). ***Materials and Methods:*** The multi-disciplinary research project comprises a pre-clinical study (SLOTH ex-vivo) and clinical pilot studies (SLOTH-1 and SLOTH-2). In the SLOTH ex vivo: phantoms and ex vivo PDAC tumors are used to establish basic injection parameters. With both MRI and CT for holmium-165 (stable isotope) visualization and quantification, microsphere distribution within the target-area and off-target tracking are evaluated. The SLOTH-1 study is the first pilot study in which 3 patients, in whom PDAC resection is not possible during explorative surgery, are directly treated with ultrasound guided intratumoral holmium-166 microsphere brachytherapy. Safety (CTCAE v4.0) and feasibility (SPECT) are primary outcomes after a follow-up of 12 weeks. SLOTH-2 is a second pilot study in which 6 patients with terminal PDAC will receive CT-guided percutaneous holmium-166 microsphere brachytherapy. Primary outcomes are safety (CTCAE v5.0) and feasibility (SPECT) with a follow-up of 16 weeks and Quality of Life as exploratory outcome. ***Results:*** Feasibility of intratumoral injection of holmium microspheres was established in ex vivo PDAC with sufficient control of needle placement and injections. Basic injection and imaging parameters were established and applied in the SLOTH-1 clinical trial. In the SLOTH-1 trail, two patients are currently treated, one was identified with metastasis and the other with irresectable disease. Preliminary dosimetry by SPECT showed a mean tumor dose of 8.9 Gy and 71.5 Gy with off-target irradiation up to 0.3 Gy in the lungs, liver and colon. Treatment was well tolerated with two procedure-related AEs grade 1-2 and non-related 23 grade 1-2, five grade 3 and zero grade 4-5 AEs. Screening and inclusion for the SLOTH-2 trial will commence in Q2 2023. Approval by the Medical Research Ethics Committee and Radiation Safety has already been granted. ***Conclusion:*** Intratumoral holmium-166 microsphere brachytherapy is a potential treatment option for patients suffering from pancreatic ductal adenocarcinoma. Preliminary feasibility is demonstrated and short toxicity seems acceptable. Additional research will be conducted during the SLOTH-project.

OP-854

A phase II trial to evaluate the accuracy of an intra-operative radio-guided approach with a beta probe for 68Ga-DOTATOC in patients affected by GEP-NET of the ileum.

F. Mattana[1], *E. Bertani*[2], *F. Collamati*[3], *R. Mirabelli*[3], *A. M. Bonomi*[2], *A. Barone*[1], *L. L. Travaini*[1], *M. Ferrari*[4], *E. Pisa*[5], *N. Fusco*[5], *U. Fumagalli Romario*[2], *F. Ceci*[1,6];
[1]*IEO European Institute of Oncology, Nuclear Medicine, Milano, ITALY,* [2]*IEO European Institute of Oncology, Division of Digestive Surgery, Milano, ITALY,* [3]*INFN National Institute of Nuclear Physics, Nuclear Physics, Rome, ITALY,* [4]*IEO European Institute of Oncology, Medical Physics, Milano, ITALY,* [5]*IEO European Institute of Oncology, Pathology, Milano, ITALY,* [6]*Department of Oncology and Hemato-Oncology, University of Milan, ITALY.*

Aim/Introduction: The primary aim was to evaluate the diagnostic accuracy of intra-operative positron detector (beta-Probe) to detect Gastro-Entero-Pancreatic-Neuroendocrine-Tumor (GEP-NET) lesions, using histopathology of the surgical specimens as reference standard. The secondary aim was to evaluate feasibility and safety of the intra-operative beta-probe RGS approach. ***Materials and Methods:*** This is a prospective, single-arm, single-center, non-interventional, phase II trial (NCT05448157) performed at our institution between May2022 and April2023. Inclusion criteria were:1)proven ileum GEP-NET;2)baseline 68Ga-DOTATOC-PET/CT(SSR-PET) performed within 4weeks from surgery;3)SSR-PET performed for initial staging or disease recurrence;4)age≥18 years-old;5)willing to sign informed consent form. Exclusion criteria were:1)patients not fit for surgery;2)negative SSR-PET. 1.1 MBq/Kg of 68Ga-DOTATOC was intravenously administered in the surgery theatre 10 minutes before surgery. The in-vivo measurements were performed by the surgeon using hand-held (open-surgery procedures) or DROP-IN (laparotomic procedures) systems. The tumor-to-background-ratio(TBR) was evaluated using real-time counts per second(CPS). Data derived from the SSR-PET, beta-Probe and histopathological analysis were compared. The primary endpoint was explored with a per-lesion analysis. ROC curve analysis was used to calculate the CPS cut-off with the highest accuracy. The absorbed dose for the surgery staff was measured using an electronic personal dosimeter (EPD). The sample size calculation consisted in 20 patients. ***Results:*** The intra-operative RGS approach was feasible in all cases, without significant changes in surgery timing and no side effects. A total of 132 specimens (26 ileum specimens, 31 lymph nodes, 75 omental or mesenteric fat specimens; mean of 6.6 specimens per-patient) have been surgically removed and considered for primary end-point analysis. The per-lesion specificity, sensibility, PPV and NPN were 86%, 89%, 89%, 86% respectively. The CPS cut-off with the higher performance was 1.3. The mean absorbed dose from the surgery staff was 30μSv (range 12-41μSv). ***Conclusion:*** These first ever published data derived from a live-surgery-experience using a beta-probe, showed optimal accuracy in detecting lesions of GEP-NET of the ileum. A favorable TBR has been observed also in the latest phases of the surgical procedures suggesting the possibility to use a lower activity while maintaining good performance. The procedure was safe, feasible, easily reproducible in the daily clinical practice with a limited absorbed dose from the surgeon. ***References:*** El Lakis M, Gianakou A, Nockel P, Wiseman D, Tirosh A, Quezado MA, Patel D, Nilubol N, Pacak K, Sadowski SM, Kebebew E. Radioguided Surgery With Gallium 68 Dotatate for Patients With Neuroendocrine Tumors. JAMA Surg. 2019 Jan 1;154(1):40-45. doi: 10.1001/jamasurg.2018.3475. PMID: 30267071; PMCID: PMC6439858.

OP-855

Prediction of acute radiation-induced lung toxicity after SBRT using dose-volume parameters from functional mapping on Gallium-68 lung perfusion PET/CT

P. Le Roux, *D. Bourhis, F. Pinot, M. Hamya, G. Goasduff, F. Blanc, S. Hennebicq, M. Mauguen, K. Kerleguer, U. Schick, M. Consigny, O. Pradier, G. Le Gal, P. Salaun, V. Bourbonne, F. Lucia;
Brest University Hospital, Brest, FRANCE.*

Aim/Introduction: Stereotactic body radiotherapy (SBRT) has an increasing role in the treatment of both primary and secondary lung tumors. However, while local tumor control rate is higher than 90%, lung SBRT remains associated with significant radiation-induced lung toxicity (RILT). The aim of this study was to evaluate the performance of anatomical and functional dosimetric parameters based on Gallium-68 lung perfusion PET/CT imaging to predict the risk of symptomatic acute RILT in patients with lung tumors treated with SBRT. ***Materials and Methods:*** 59 patients were prospectively included and underwent, before lung SBRT, lung perfusion PET/CT after administration of [68Ga] Ga-MacroAggregatted Albumin (MAA). Mean lung dose (MLD) and volumes receiving xGy (VxGy, 5 to 30 Gy) were calculated in five lung volumes: the conventional anatomical volume (AV) delineated on CT images, three lung functional volumes defined on lung perfusion PET imaging (FV50%, FV70%, FV90%, i.e. the minimal volume containing 50%, 70% and 90% of the total activity within the AV), and a low functional volume (LFV = AV-FV90%).The primary endpoint of this analysis was grade ≥2 acute RILT at 3 months as assessed with NCI CTCAE v.5. Dose volume parameters in patients with and without acute RILT were compared. ROC curved to assess the ability of dose-volume parameters to discriminate between patients with and without acute RILT were generated and area under the curves (AUC) were calculated. ***Results:*** Out of the 59 patients, 10 (17%) had grade ≥2 acute RILT. The MLD and the VxGy (5 to 30 Gy) in the AV and LFV were not statistically different in patients with and without acute RILT. In contrast, all dose volume parameters were significantly higher in the FV50%, FV70% and FV90% volumes in patients with acute RILT ($p<0.05$). AUCs of MLD FV70% and FV90% were significantly higher than AUC of MLD AV ($p<0.05$). AUCs of V20 FV50%, FV70% and FV90% were significantly higher than AUC of V20 AV ($p<0.05$). ***Conclusion:*** In our study, the predictive value of PET perfusion-based functional parameters outperformed the standard CT-based dose-volume parameters for the risk of grade ≥2 acute RILT in patients treated with lung SBRT. Functional parameters could be useful to guide radiotherapy planning to reduce the risk of acute RILT.

OP-856

Intra-arterial Administration of PRRT in Patients with Advanced Meningioma

A. Amerein[1], *A. Rinscheid*[2], *A. Gäble*[1], *A. Krebold*[1], *O. Viering*[1], *A. Berlis*[3], *C. Maurer*[3], *C. Lapa*[1], *C. Pfob*[1], *R. Bundschuh*[1];
[1]*Nuclear Medicine, faculty of medicine, University of Augsburg, Augsburg, GERMANY,* [2]*Medical Physics, University Hospital Augsburg, Augsburg, GERMANY,* [3]*Neuroradiology, faculty of medicine, University of Augsburg, Augsburg, GERMANY.*

Aim/Introduction: Peptide Receptor Radionuclide Therapy (PRRT) is a treatment option in advanced WHO CNS grade 1 and 2 meningioma. Recently, intra-arterial application of the radiolabelled somatostatin receptor agonist has been introduced as an alternative to standard intravenous procedures. In this study, we evaluated the safety, achievable tumor doses as well as efficacy of intra-arterial PRRT in patients with progressive

meningioma. ***Materials and Methods:*** Eight patients (5 female, mean age, 70±13 years) with advanced progressive meningioma underwent intra-arterial PRRT (median, 3 cycles; range, 1-4) using [^{177}Lu]Lu-DOTA-TATE (mean activity per cycle, 7436±77 MBq). Safety of PRRT was assessed according to Common Terminology Criteria for Adverse Events (CTCAE) v5.0. During the first treatment cycle, dosimetry including whole-body scans (0.5, 4, 24, 46-48 and 90-120 h p.i.) and single photon emission computed tomography/computed tomography (SPECT/CT; 4 and 46-48 h p.i.) was performed to estimate achieved tumor doses. Four to twelve weeks after the second treatment cycle, early treatment response was evaluated using somatostatin receptor-directed positron emission tomography/CT and magnetic resonance imaging. ***Results:*** Treatment was well tolerated by all individuals with no acute adverse events. One patient died of treatment-unrelated complications four weeks after the first treatment cycle before follow-up imaging. In the remaining seven patients, no grade 3 or higher toxicity according to CTCAE v5.0 was observed. Mean achievable meningioma doses were 2.05 (range, 0.25-12.6) Gy/GBq administered activity, resulting in a maximum per cycle tumor dose of 91.2 Gy. At first follow-up, all subjects presented with disease stabilization. ***Conclusion:*** Intra-arterial PRRT of meningioma is feasible and safe. It might result in favorable tumor doses as compared to standard intravenous therapy. Further research to corroborate these initial findings as well as to investigate long-term treatment outcome is highly warranted.

OP-857

Preliminary Clinical data in the Phase 1/2a Dose Escalation Trial of 186RNL (Rhenium-186 nanoliposome) (186Re) Obisbemeda in Leptomeningeal Metastases (LM): the ReSPECT-LM Trial

W. Phillips[1], *A. Bao*[2], *N. LaFrance*[3], *M. Hedrick*[3], *M. Moore*[3], *T. Patel*[4], *J. Floyd*[1], *M. Youssef*[4], *J. Michalek*[1], *A. Brenner*[1];
[1]*The University of Texas Health Science Center at San Antonio, San Antonio, TX, UNITED STATES OF AMERICA,* [2]*Case Western Reserve University, San Antonio, TX, UNITED STATES OF AMERICA,* [3]*Plus Therapeutics, Inc, Austin, TX, UNITED STATES OF AMERICA,* [4]*UT Southwestern Medical Center, Dallas, TX, UNITED STATES OF AMERICA.*

Aim/Introduction: Leptomeningeal metastases (LM) are a devastating clinical complication where the primary cancer spreads to the leptomeninges. Treatment options for LM are limited, and survival is dismal. Rhenium (^{186}Re) obisbemeda (^{186}RNL) is a BMEDA-chelated ^{186}Re encapsulated in nanoliposomes β-emitter with a ~2 mm path length, allowing directly targeted radiation therapy delivery with limited exposure to surrounding tissue. We present preliminary clinical data for the first 9 patients from our ReSPECT-LM trial (NCT05034497). ***Materials and Methods:*** ReSPECT-LM is a multi-center, sequential cohort, open-label, dose-escalation, phase 1/2a clinical trial evaluating the safety, tolerability, and activity of a single dose of ^{186}RNL given by a direct CNS intraventricular [Ommaya Reservoir] route in LM adult patients. Primary objectives are: maximum tolerated dose/maximum feasible dose in up to 21 LM patients in 7 cohorts using a modified 3x3 Fibonacci design, 3 cohorts have been enrolled beginning at 6.6 mCi with administered dose doubling at each successive cohort to 26.4mCi administered in 5 mL through a Ommaya reservoir. Whole body planar and SPECT/CT imaging were obtained up to 7 days following treatment for dosimetry, distribution and CSF tumor cells/ml using microfluidic chamber assay were assessed up to 56 days. Patients were followed for safety, progression, and survival. ***Results:*** A total of 9 LM patients [3 each in Cohorts 1-3} have been treated. Patients had primary diagnoses of small cell carcinoma, metastatic breast cancer (both triple negative), and lung adenocarcinoma. ^{186}RNL showed prompt, complete distribution throughout the CSF with durable retention in the subarachnoid space and leptomeninges through protocol defined observation on Day 7 and achieved absorbed doses ranging from 18.7 to ~200 Gray (Gy) to the ventricles and cranial subarachnoid spaces. All patients experienced a decreased CSF cell count ranging from 46% to 92%. Patient treatment started in March of 2022, eight patients remain alive [1 patient has died due to primary tumor progression. No patients had treatment related adverse events (AEs) greater than Grade 1, and the most common AE was headache. ***Conclusion:*** Preliminary, interim results of this ongoing phase 1 trial showed that a single treatment with ^{186}RNL delivered by an intraventricular catheter (Ommaya reservoir) in 9 adult patients is well tolerated, without dose limiting toxicity and with decreased CSF tumor cell counts durable through at least 30 days. Enrollment and dose escalation is continuing, and repeated dosing will be explored.:

1707

Wednesday, September 13, 2023, 8:00 AM - 9:30 AM
Hall F1

Cardiovascular Committee - TROP Session: Heart Failure, Sarcoidosis and Amyloidosis

OP-858

Current practices and access to cardiac bone scans for the detection of transthyretin cardiac amyloidosis based on the results of a large national electronic survey

F. Hyafil[1,2], *W. Amara*[3], *T. Bardin*[4], *B. Bouquillon*[5], *G. Canali*[6], *M. Dubois*[6], *P. Fournier*[7], *S. Guignard*[8], *C. Labeyrie*[9], *D. Legallois*[10], *S. Oghina*[11], *N. Piriou*[12], *P. Sabouret*[13], *C. Sauvage*[5], *O. Toulza*[14], *R. Tresorier*[15], *M. Walle*[16], *T. Damy*[17];
[1]*AP-HP, Paris, FRANCE,* [2]*APHP, European Hospital Georges-Pompidou, Department of Nuclear Medicine, Paris, FRANCE,* [3]*GHI Le Raincy-Montfermeil, Department of Cardiology, Montfermeil, FRANCE,* [4]*University Hospital Strasbourg, Department of Internal Medicine, Strasbourg, FRANCE,* [5]*Carely, Lille, FRANCE,* [6]*Pfizer, Paris, FRANCE,* [7]*University Hospital Toulouse, Department of Cardiology, Toulouse, FRANCE,* [8]*University Hospital Henri Mondor, UPEC, Department of Rheumatology, Créteil, FRANCE,* [9]*University Hospital Bicêtre, Referral Center for Familial Amyloid Neuropathy and other Rare Peripheral Neuropathies, Department of Neurology, Paris, FRANCE,* [10]*University Hospital of Caen-Normandy, Department of Cardiology, Caen, FRANCE,* [11]*APHP (Assistance Publique-Hôpitaux de Paris), Department of Cardiology, French Referral Centre for Cardiac Amyloidosis, Cardiogen Network, Henri Mondor University Hospital, Paris, FRANCE,* [12]*University Hospital of Nantes, Department of Cardiology, Thorax Institute, Nantes, FRANCE,* [13]*Cardiovascular Prevention Institute, Paris, FRANCE,* [14]*University Hospital of Toulouse, Department of Geriatrics, Toulouse, France, Toulouse, FRANCE,* [15]*University Hospital of Clermont Ferrand, Department of Cardiology, Clermond Ferrand, FRANCE,* [16]*Edouard Herriot Hospital, HCL, Department of Upper Limb Orthopedic Surgery, Lyon, FRANCE,* [17]*APHP (Assistance Publique-Hôpitaux de Paris), Department of Cardiology, French Referral Centre for Cardiac Amyloidosis, Cardiogen Network, Henri Mondor University Hospital, Créteil, FRANCE.*

Aim/Introduction: The diagnosis of transthyretin cardiac amyloidosis (ATTR-CM) requires a good collaboration between physicians to confirm the diagnosis. This study aimed to assess current practices of nuclear medicine (NM) physicians for cardiac scintigraphy with bone radiotracers and to evaluate access to cardiac bone scintigraphy in the healthcare circuit for the diagnosis of ATTR-CM. ***Materials and Methods:*** A nationwide electronic survey was sent to 13 830 French physicians including 775 nuclear medicine (NM) physicians to assess their knowledge of 1. clinical signs of amyloidosis and 2. the recommended diagnostic algorithm to identify TTR cardiac amyloidosis. In addition, accessibility, appointment delays and results interpretation difficulties for each of the explorations required to confirm the diagnosis of ATTR-CM were evaluated among different medical specialists. A part of the questionnaire was exclusively dedicated to NM to understand their current practice regarding acquisitions protocols and reporting of cardiac bone scans. ***Results:*** 1264 physicians including 148 NM physicians (19 % of all NM physicians contacted) completed the survey. NM physicians who answered to the survey worked in academic hospitals (35 %), general hospitals (31 %), or private practices (26 %). Cardiac bone scans using early acquisitions were performed by 20 % of NM and SPECT acquisitions by 72 %. Grading of cardiac uptake of bone tracers using the Perugini score was carried out by 93 % of the NM but only 31% and 5% of NM systematically performed heart/whole body or heart/mediastinum signal quantification, respectively. Median (Q1; Q3) delay to obtain results for a cardiac bone scan was estimated at 2 (2; 4) weeks compared to 4 (3; 8) weeks for cardiac MRI, and 2 (2; 4) weeks for a biopsy. Among physicians, 68% rarely or never faced difficulties for cardiac scintigraphy. The main difficulties encountered were: appointment delay (60%), geographical distance (17%), interpretation (12%). ***Conclusion:*** In this large French national survey, access to cardiac bone scintigraphy for patients with a suspicion of ATTR cardiac amyloidosis and quality of reports appear excellent thanks to good adherence of NM physicians to the recommended acquisition protocols for cardiac bone scans and the widespread use of the Perugini grading scale in reports. However, quantitative measurements of cardiac uptake of bone tracers were performed only in one third of bone scans underscoring room for improvement in the next procedural guidelines for cardiac bone scans.

OP-859

SPECT/CT SUV based metrics: a promising diagnostic tool in patients with suspected transthyretin cardiac amyloidosis.

S. Koukouraki[1,2], *N. Kapsoritakis*[1,2], *O. Bourogianni*[1,2], *M. Stathaki*[1,2], *I. Zaganas*[3,4], *A. Patrianakos*[3,5], *A. Plevritaki*[1,5], *D. Corela*[6], *M. Marketou*[7], *E. Foukarakis*[6];
[1]*Medical School, University of Crete, Heraklion-Crete, GREECE,* [2]*Nuclear Medicine department, Medical School, University of Crete, Heraklion, crete, GREECE,* [3]*Medical School, University of Crete, HERAKLION, CRETE, GREECE,* [4]*Neurology Department, Medical School, University of Crete, Heraklion, crete, GREECE,* [5]*Cardiology Department , Medical School University of Crete, Heraklion, crete, GREECE,* [6]*Cardiology Department Venizeleion Hospital, Heraklion-Crete, GREECE,* [7]*Cardiology Department, Medical School, University of Crete, Heraklion-Crete, GREECE.*

Aim/Introduction: The purpose of this study was to investigate the additional contribution of SPECT/CT SUV-based metrics to diagnostic confidence in patients suspected of ATTR-CA. ***Materials and Methods:*** One hundred four pts suspected of ATTR-CA underwent planar scintigraphy (PS), and a subset of 48 pts received additional SPECT/CT. Pts were classified according to the Perugini grading scale, the H/CL, H/Bone and H/Bkg ratios. SPECT/CT SUV measurements of the heart, myocardium, lungs, liver, soft tissues and bone, together with the ratios SUVmaxmyo, SUVmax,lungs, SUVmaxliver, SUVmaxbone and SUVmaxst, were evaluated in order to investigate potential critical metrics that would differentiate pts with different Perugini grades. ***Results:*** 33.7% of pts were considered grade 0, 34.6% grade 1 and 31.7% grade 2 or 3. The most reliable marker for differentiating grade 0 or 1 versus grades 2 or 3 was the H/CL ratio. A combination of H/CL>1.33 and H/Bone>0.85 showed sensitivity 100%. SUV-based metrics clearly differentiated grade 0 or 1 versus grades 2 or 3 with statistical significance, whereas no significant difference was found between grades 0 and 1, or between grades 1 and 2.The combined cut-off values H/CL 1.33 and SUVmaxmyo 2.88 yielded 100% sensitivity and 84.6% specificity in differentiating ATTR-CA positives versus negatives. The metric SUVmaxmyo/SUVmaxliver was able to differentiate pts with grade 1 as negative (grade 0) or positive (grade 2 or 3). ***Conclusion:*** Among SPECT/CT SUV metrics, the ratio SUVmaxmyo/SUVmaxliver was the only parameter able to classify pts with grade 1 as negative (grade 0) or positive (grade 2 or 3) for ATTR-CA

OP-860

99mTc-hydroxydiphosphonate Uptake in Soft Tissue Reflects Amyloid Load in Subcutaneous Abdominal Fat Tissue and Harbors Prognostic Value in Wild Type Transthyretin Amyloidosis Patients

H. Tingen[1], *D. Groothof*[1], *A. Tubben*[1], *E. J. Houwerzijl*[1], *F. L. H. Muntinghe*[1], *P. van der Meer*[1], *B. P. C. Hazenberg*[1], *H. L. A. Nienhuis*[1], *R. H. J. A. Slart*[1,2];
[1]*University Medical Center Groningen, Groningen, NETHERLANDS,* [2]*University Twente, Enschede, NETHERLANDS.*

Aim/Introduction: Wild type transthyretin (ATTRwt) amyloidosis is a progressive protein misfolding disease mainly characterized by cardiomyopathy. Cardiac tracer uptake on bone scintigraphy is the cornerstone of non-invasive diagnosis of ATTRwt amyloidosis. Extracardiac tracer uptake on bone scintigraphy might reflect amyloid deposition and its presence has been associated with worse prognosis in patients with cardiac tracer uptake. We investigated whether intensity of soft tissue tracer uptake reflects amyloid load in subcutaneous abdominal fat tissue and whether it has added prognostic value compared to current staging systems. ***Materials and Methods:*** In this retrospective study, 89 ATTRwt amyloidosis patients who underwent whole-body 99mTc-hydroxydiphosphonate scintigraphy at the University Medical Center Groningen in The Netherlands between 2012 and 2021 were included. Twenty-six amyloid-negative heart failure patients were included as controls. Regions of interest were drawn in the skull, shoulders, heart, sixth left rib, elbows, wrists, abdominal soft tissue and thigh soft tissue on anterior planar images. Region-to-rib ratios were calculated. Differences between ATTRwt amyloidosis patients and controls were assessed with a Mann-Whitney U test. A trend between soft-tissue-to-rib (ST/rib) ratio and amyloid load as measured by Congo Red score in abdominal fat tissue aspirates was assessed with a Jonckheere-Terpstra test. Cox proportional hazards regression was used to evaluate whether ST/rib ratio was prognostically relevant. Bonferroni correction for multiple testing was applied. ***Results:*** Differences in ST/rib ratio, heart/rib ratio and skull/rib ratio were found between ATTRwt amyloidosis patients and controls (respectively 0.30 [0.24-0.38] vs 0.26 [0.22-0.29], p=.004; 1.92 [1.60-2.34] vs 0.86 [0.71-0.96], p<.001; 0.33 [0.27-0.40]

vs 0.67 [0.47-0.89], p<.001; median [interquartile range]). The Jonckheere-Terpstra test showed a statistically significant trend of higher median ST/rib ratio's with higher Congo Red scores in ATTRwt amyloidosis patients (T_{JT} = 1669.0, z=3.022, p=.003). Cox regression revealed that ST/rib ratio has prognostic value on top of currently used staging systems when corrected for age, with a hazard ratio of 1.476 (1.025-2.127) (p=.036) for the Grogan staging system and 1.570 (1.017-2.424) (p=.042) for the Gillmore staging system and an improvement in -2 Log Likelihood from 161.921 to 157.836 (p=.043) and 165.316 to 161.160 (p=.041) respectively. ***Conclusion:*** ST/rib ratio on bone scintigraphy reflects amyloid load in subcutaneous abdominal fat tissue in ATTRwt amyloidosis patients and harbors prognostic value on top of currently used staging systems. As bone scintigraphy is performed in nearly every ATTRwt amyloidosis patient, measurement of soft tissue uptake could easily be applied in clinical practice.

OP-861

Agreement of 68Ga-DOTANOC PET/CT with 18F-FDG PET/CT and Cardiac MR in sarcoid patients with suspected cardiac involvement: A tertiary care center experience

R. Solanki, *A. Sood, S. Kumar, B. R. Mittal;*
Post Graduate Institute of Medical Education and Research (PGIMER), Chandigarh, INDIA.

Aim/Introduction: Sarcoidosis is an inflammatory disease, characterized by non-caseous granulomas predominantly involving the lung and lymph nodes. Cardiac sarcoidosis (CS) is a rare presentation with poor prognosis. Imaging modalities like cardiac magnetic resonance imaging (CMR), positron emission tomography (PET) and radionuclide scans are helpful in early diagnosis and treatment of CS. ^{18}F-FDG PET/CT in CS provides inflammatory disease activity information and helps in early detection and therapy monitoring, but requires prior preparation in order to suppress the variable physiological uptake. ^{68}Ga-DOTANOC has high affinity for somatostatin receptors (SSTR) 2, 3 and 5 expressed in inflammatory cells in sarcoid granulomas without physiological uptake. Therefore ^{68}Ga-DOTANOC can be an alternative to ^{18}F-FDG without the need for suppression of physiological FDG uptake. ***Materials and Methods:*** Twenty-three patients recruited from the pulmonary out- patient department (OPD) with biopsy proven pulmonary sarcoidosis with suspected cardiac involvement and patients from cardiology OPD with a primary cardiac abnormality, in whom systemic sarcoidosis was diagnosed on the basis of clinical/histopathological features were prospectively included in this study. Patients underwent cardiac specific imaging like CMR, ^{13}N-NH_3 PET/CT for myocardial perfusion, ^{18}F-FDG PET/CT for glucose metabolism and ^{68}Ga-DOTANOC PET/CT for abnormal SSTR expression in the myocardium. Intermodality agreement between CMR, ^{18}F-FDG PET/CT and ^{68}Ga-DOTANOC PET/CT was evaluated. ***Results:*** CMR could be done in only 19 out of 23 patients. CMR and ^{18}F-FDG PET/CT were concordant in 17/19 (89.4%) patients and discordant in 2/19 (10.5%) with a substantial intermodality agreement with Cohen's kappa=0.774 and p value of 0.001 (statistically significant). CMR and ^{68}Ga-DOTANOC PET/CT were concordant in 16/19 (84.2%) patients and discordant in 3/19 (15.7%) with substantial intermodality agreement with Cohen's kappa=0.671 with p value of 0.003 (statistically significant) and ^{18}F-FDG and ^{68}GaDOTANOC were concordant in 18/23 (78.2%) patients and discordant in 5/23 (21.7%) with moderate intermodality agreement with Cohen's kappa =0.563 and p value of 0.007 (statistically significant). ***Conclusion:*** The physiological cardiac suppression with ^{18}F-FDG PET/CT is a tedious process and may not be achieved in many patients, whereas SSTR imaging with ^{68}GaDOTANOC PET/CT has this advantage. In our study, although both ^{18}F-FDG and ^{68}GaDOTANOC PET/CT had strong inter-modality agreement with CMR, the role of these imaging techniques is more complementary. Though there is paucity of data to validate its role, but with more sample size and evidence, SSTR imaging has the potential to replace ^{18}F-FDG PET/CT in the diagnosis, prognostication and response assessment in the upcoming future.

OP-862

Cardiac Viability Imaging With 15O-H2O/18F-FDG Positron Emission Tomography Does Not Predict Left Ventricular Ejection Fraction Improvement After Revascularization in Patients With Chronic Ischemic Heart Failure

M. Gram Kjærulff[1], *K. Pryds*[2], *R. Nielsen*[2], *S. Madsen*[1], *T. V. Luong*[1], *L. P. Tolbod*[1], *L. C. Gormsen*[1];
[1]*Department of Nuclear Medicine & PET Centre, Aarhus University Hospital, Aarhus, DENMARK,* [2]*Department of Cardiology, Aarhus University Hospital, Aarhus, DENMARK.*

Aim/Introduction: Different imaging methods can assess cardiac viability, including positron emission tomography (PET) which differentiates hibernating myocardium from scar tissue by assessing myocardial perfusion and metabolism simultaneously. Previous observational studies have demonstrated that imaging-guided revascularization improved patient outcomes. However, the usefulness of viability imaging in revascularization decision-making is debated due to newer randomized studies showing the opposite. To our knowledge, there have been no PET studies conducted on this issue using ^{15}O-H_2O combined with ^{18}F-FDG. The aim of this study was therefore to assess the predictive value of ^{15}O-H_2O/^{18}F-FDG PET metrics on improving left ventricular ejection fraction (LVEF) following revascularization in patients with chronic ischemic heart failure (iHF). ***Materials and Methods:*** In this prospective study, 78 chronic iHF patients with reduced LVEF (mean baseline LVEF 33.7±10.7) underwent viability imaging using ^{15}O-H_2O and ^{18}F-FDG prior to potential revascularization. The primary outcome measure was an absolute increase of at least 5% in LVEF from baseline to follow-up, as assessed by echocardiography. The significance of PET metrics in predicting LVEF improvement was assessed by receiver operating curves (ROC) and their respective area under curve (AUC) values analysing PET metrics, including scar percent, hibernation score, and myocardial flow reserve (MFR). ***Results:*** Of the 78 patients undergoing viability imaging by PET, 32 (41%) underwent revascularization. The proportion of patients with an LVEF improvement of ≥5% was not significantly different between revascularized and non-revascularized patients (47% vs. 53%; p = 0.36). In revascularized patients, the ROC analysis of the predictive value of PET metrics resulted in AUC values of 0.46 for scar (95% confidence interval (CI): 0.25-0.67), 0.45 for hibernation (95% CI: 0.24-0.65), and 0.58 for MFR (95% CI: 0.34-0.83). The predictive value of PET metrics was equally poor in the non-revascularized group. ***Conclusion:*** No significant difference in LVEF improvement between revascularized and non-revascularized patients with chronic ischemic herat failure was observed. No PET metrics obtained from ^{15}O-H_2O/^{18}F-FDG PET viability imaging could predict LVEF improvement following revascularization. The clinical use of viability PET imaging should therefore be questioned.

OP-863

Epicardial adipose tissue is differently associated with myocardial remodeling and perfusion in heart failure with reduced and preserved ejection fraction

Y. Cui, *C. Zheng, S. Gu, J. Lu;*
Department of Radiology and Nuclear Medicine, Xuanwu Hospital, Capital Medical University, Beijing, CHINA.

Aim/Introduction: Epicardial adipose tissue (EAT) has been investigated in patients with heart failure (HF) and suggested to play a pathogenic role[1]. However, different association of EAT with cardiac haemodynamic and metabolic profile has been presented in HF patients with reduced (HFrEF) and preserved (HFpEF) ejection fraction [2]. We aimed to evaluate the relationship of EAT with myocardial remodeling and perfusion by using integrated PET/MR in patients with HFrEF and HFpEF. ***Materials and Methods:*** Fifty-two consecutive HF patients (HFrEF n=24, HFpEF n=28) who underwent resting cardiac ^{13}N-NH_3 PET/MR were retrospectively included. EAT volume, left ventricular volume and function parameters, myocardial native T1 value, and scar volume were analyzed from cardiac MR images, and global absolute myocardial blood flow (MBF) was calculated from dynamic PET data. The difference of EAT volume between HFrEF and HFpEF was assessed with the independent sample t-test. Pearson correlation coefficient and multiple linear regression analysis was used to estimate the relationship between PET/MR parameters and EAT. ***Results:*** Patients with HFrEF and HFpEF showed similar EAT volume (83.89 ± 35.54 mL vs. 80.90 ± 23.00 mL, P = 0.716). For all HF patients, EAT volume was positively correlated with age (r = 0.28, P = 0.043) and MBF (r = 0.37, P = 0.023), and negatively correlated with myocardial native T1 value (r = 0.30, P = 0.033). Increased EAT volume was associated with higher left ventricular ejection fraction (r = 0.42, P = 0.041), and lower end-systolic volume (r=0.44, P=0.032) and myocardial native T1 value (r = 0.51, P = 0.013) in patients with HFrEF. However, EAT volume was not significantly associated with other PET/MR parameters in patients with HFpEF. Multiple linear regression analysis showed native T1 value was independently associated with EAT in patients with HFrEF (P = 0.013). ***Conclusion:*** Increased EAT volume is associated better myocardial remodeling and perfusion in HFrEF, but not in HFpEF, indicating different roles of EAT in the two HF phenotypes. ***References:*** 1. Packer M. Epicardial Adipose Tissue May Mediate Deleterious Effects of Obesity and Inflammation on the Myocardium. J Am Coll Cardiol. 2018;71(20):2360-2372.2. Pugliese NR, Paneni F, Mazzola M, et al. Impact of epicardial adipose tissue on cardiovascular haemodynamics, metabolic profile, and prognosis in heart failure. Eur J Heart Fail. 2021;23(11):1858-1871.

OP-864

Relationship between left ventricular mechanical dyssynchrony with cardiac resynchronization therapy response in chronic heart failure patients with CRT-D

T. Atabekov, *A. Mishkina, R. Batalov, S. Sazonova, S. Krivolapov, V. Saushkin, M. Khlynin, Y. Varlamova, K. Zavadovsky, S. Popov;*
Cardiology Research Institute, branch of the Federal State Budgetary Scientific Institution "Tomsk National Research Medical Center of the Russian Academy of Sciences", Tomsk, RUSSIAN FEDERATION.

Aim/Introduction: Cardiac resynchronization therapy (CRT) improves outcomes in only two-thirds of patients (pts) with chronic heart failure (CHF) and implanted CRT devices with cardioverter-defibrillator function (CRT-D). These pts qualified as responders to CRT. Unfortunately, in the remaining one-third of pts, there is no improvement of the left ventricular (LV) contraction and clinical status. We aimed to investigate the relationship between LV mechanical dyssynchrony with CRT response in CHF pts with CRT-D. ***Materials and Methods:*** Forty nine pts (male - 34 [69.4%], average age 58.3 ± 11.4 years) with sinus rhythm, permanent left bundle branch block (LBBB) with QRS duration ≥ 150 ms and New York Heart Association (NYHA) II-III functional class (FC) of CHF were included to the study. In addition to full examination, myocardial perfusion scintigraphy (MPS) and gated blood pool single-photon emission computed tomography (gBPS) were performed before and 6 month after CRT-D implantation. Pts were considered as responders to CRT if they fulfilled after 6 month follow-up the following combined criteria: NYHA FC improvement ≥ 1 class + LV end systolic volume (LVESV) decrease > 15% or NYHA FC improvement ≥ 1 class + LV ejection fraction (LVEF) improvement > 5%. ***Results:*** The 1st and 2nd groups included 35 (71.4%) and 14 (28.6%) pts with and without the response to CRT respectively. Groups were comparable in terms of pre CRT-D implantation clinical and instrumental parameters, with the exception of MPS and gBPS parameters. The multivariate logistic regression with the inclusion factors such as baseline QRS duration, ΔQRS, female gender, non-ischemic CHF, LV lead lateral position, quadripolar LV lead, biventricular pacing percentage, MPS and gBPS indicators had shown that only ΔSkewness (adjusted odds ratio [OR] 0.1293; 95% confidence interval [CI] 0.0226-0.7396; p=0.02), LV septal phase standard deviation (PSD) (OR 1.0669; 95% CI 1.0118-1.1251; p=0.01) and interventricular dyssynchrony (IVD) (OR 1.0625; 95% CI 1.0202-1.1067; p=0.003) were the independent predictors to CRT response. The univariate ROC-analysis showed that ΔSkewness decrease ≤ -0.06 (AUC=0.809; p<0.0001), LV septal PSD increase > 23° (AUC=0.708; p=0.01) and IVD increase > 67.2 ms (AUC=0.851; p<0.0001) were predictors to CRT response. ***Conclusion:*** The mechanical dyssynchrony assessed by MPS and gBPS may be useful in identifying responders to CRT. ΔSkewness decrease ≤ -0.06, LV septal PSD increase > 23° and IVD increase > 67.2 ms are predictors to CRT response. Further investigations of their predictive significance are warranted.

OP-865

The prognostic value of mechanical and electrical dyssynchrony and hibernating myocardium in patients with ischemic heart failure: a comparative study of medical and revascularization therapy

L. Shan[1], *X. Zhang*[2];
[1]*Department of Cardiology, Beijing Anzhen Hospital, Beijing, CHINA,* [2]*Department of Nuclear Medicine, Molecular Imaging Lab, Beijing Anzhen Hospital, Beijing, CHINA.*

Aim/Introduction: We aimed to assess the prognostic value of QRS duration, LV mechanical dyssynchronization (LVMD) and hibernating myocardium (HM) in patients with ischemic heart failure (IHF), and to guide for therapeutic strategy decision-making. ***Materials and Methods:*** Two hundred and forty-seven (age, 59 (31, 82) y, 213 men) consecutive IHF patients with gated SPECT-LVEF≤35%, who underwent gated ^{99m}Tc-sestamibi SPECT myocardial perfusion imaging (MPI) and gated ^{18}F-FDG PET imaging, were followed-up for a median of 3.4 y (range, 0.1-5.7 y). LVMD was defined as standard deviation (SD)> 30 or histogram bandwidth (BW)>120 by gated MPI and ROC analysis. HM+ was defined as >10% LV of HM (perfusion defect mismatche score of 1.0 or greater). Electrical dyssynchrony was defined as QRS duration ≥130 ms. Patients were classified into 4 subgroups according to LVMD, combined with QRS or HM. All-cause death

served as the only endpoint. The estimated survival curve was analyzed and compared with the log-rank test. Cox proportional hazards regression analysis identified the independent predictors for all-cause death. ***Results:*** A total of 59 patients (23.8%) suffered all-cause death. The correlation between the QRS duration and BW (r = 0.223; p = 0.001) or SD (r = 0.213; p = 0.002) was weak, even in subgroup of patients with QRS<130ms. Among 4 subgroups, the cardiac survival in patients with QRS<130ms and LVMD- (BW≤120 or SD≤30) was the highest, which was significantly higher than that in patients with QRS<130ms and LVMD+ (BW>120, P = 0.016; SD>30, P = 0.008, respectively). Additionally, in subgroup of patients with QRS<130ms, the lowest survival was observed in patients with HM+ and LVMD+ (BW>120, P = 0.048; SD>30, P = 0.024, respectively). Revascularization could significantly improve the survival in comparison with medical therapy in these patients (HM+ and BW>120: χ 2 = 10.439, P = 0.001; HM+ and SD>30: χ 2 = 13.528, P < 0.001). Multivariate Cox analysis identified that age, QRS duration ≥ 130 ms, gated PET LVEF>25%, and BW >120 were independent predictors of all-cause death in patients with IHF (all P<0.05). By combining the four independent determinants, the prognostic power significantly (P < 0.0001) increased maximally to 28.86. ***Conclusion:*** Mechanical dyssynchrony by gated MPI provided an incremental prognostic value in patients with electrical dyssynchrony. Compared with medical therapy, coronary revascularization was significantly associated with improved long-term survival in patients with HM accompanied with mechanical dyssynchrony.

OP-866

C-X-C Motif Chemokine Receptor 4-directed Molecular Imaging of the Cardiac Lymphatic System after Acute Myocardial Infarction - Initial Results from the Phase II LOMI Trial

A. Kosmala[1], *A. Dörrler*[1], *N. Hasenauer*[1], *N. Kraus*[2], *S. E. Serfling*[1], *P. E. Hartrampf*[1], *A. K. Buck*[1,3], *T. Higuchi*[1,3,4], *T. Reiter*[2], *R. A. Werner*[1,3,5]; [1]*Department of Nuclear Medicine, University Hospital Würzburg, Würzburg, GERMANY,* [2]*Department of Internal Medicine I, Cardiology, University Hospital Würzburg, Würzburg, GERMANY,* [3]*Comprehensive Heart Failure Center, University Hospital Würzburg, Würzburg, GERMANY,* [4]*Faculty of Medicine, Dentistry and Pharmaceutical Sciences, Okayama University, Okayama, JAPAN,* [5]*The Russell H Morgan Department of Radiology and Radiological Sciences, Johns Hopkins School of Medicine, Baltimore, MD, UNITED STATES OF AMERICA.*

Aim/Introduction: After acute myocardial infarction (MI), the cardiac lymphatic system mediates resolution of the local inflammatory response in the infarct territory by immune cell trafficking to heart-draining mediastinal lymph nodes (MLN). Image biomarkers providing a quantitative read-out of the lymphatic-immune cell axis may identify subjects at increased risk for cardiac functional decline. ***Materials and Methods:*** We report on initial results of a Phase II Trial (NCT05519735), which enrolls patients with acute ST-elevation MI followed by reperfusion and imaged with C-X-C motif chemokine receptor 4 (CXCR4)-directed PET/CT using [^{68}Ga]Ga-PentixaFor. At baseline, patients are scheduled for molecular imaging and cardiac magnetic resonance (CMR). To determine functional decline, CMR will be repeated six months after the acute event. [^{68}Ga]Ga-PentixaFor uptake (SUV_{peak}) in the myocardium and MLN is determined, providing infarct/remote myocardial (IRR) and MLN/Remote LN Ratios (LNR). Association of uptake with adverse outcome is also tested. ***Results:*** At day of abstract submission, 20 patients were imaged median 4.5 days after STEMI (available follow-up after 6 months, 14/20 [70.0%]). SUV_{peak} from infarcted myocardium (3.35±0.55) and LN (4.00±0.67) were elevated when compared to blood-pool (2.30±0.32, P≤0.05). Respective IRR (2.23±0.59) and LNR (2.25±0.70) were consistently >1, with variance among patients (IRR, 1.34-2.99; LNR, 1.16-3.45). Upon first follow-up, CMR-derived left ventricular ejection fraction (LVEF) was improved when compared to baseline (48.4±7.88 vs 53.6±4.99, P<0.05), while late gadolinium enhancement (LGE, in g) declined (32.55±17.18 vs 18.06±13.99, P<0.05). Derived changes of cardiac outcome parameters correlated with LNR (%LVEF, R=0.59; LGE, R=0.62; P<0.05, each), but not with IRR (%LVEF, R=0.01; LGE, R=-0.06, P≥0.85). Comparing cohorts with declining vs. improved LVEF, LNR was increased in subjects with deteriorating LVEF (2.87±0.60 vs. improved LVEF, 1.99±0.48, P<0.05). In regression analysis, increased LNR was associated with declining LVEF (Odds Ratio, 20.04, P<0.05), while conventional parameters were not significantly associated with LVEF changes (including baseline-LGE/-LVEF, IRR, high sensitivity-Troponin T, B-type natriuretic peptide, creatine kinase, C-reactive protein, white blood cell count, P≥0.08). ***Conclusion:*** CXCR4-directed imaging of inflammatory leukocytes provides information on the extent of local and systemic tissue inflammation in patients after first acute MI. Chemokine receptor imaging of MLN involved in the adaptive immune response also identifies subjects at risk for cardiac functional decline. This novel image biomarker may guide reparative interventions for selective stimulation of cardiac lymphangiogenesis, which may prevent inflammatory-driven on-set of heart failure in coronary artery disease. ***Funding***: German Research Foundation (453989101, 507803309).

1708

Wednesday, September 13, 2023, 08:00 - 09:30

Hall F2

Joint Symposium 6 - Neuroimaging Committee / EAN: Progress in Multimodal Imaging of Parkinson's Disease

OP-867

Novel MR Techniques to Image Parkinson's Disease

E. van de Giessen;
Amsterdam UMC, Radiology and Nuclear Medicine, Amsterdam, NETHERLANDS.

OP-868

Transcranial Sonography to Image Parkinson's Disease

R. Yilmaz;
Ankara University Faculty of Medicine, Ibni Sina Hospital, Ankara, TÜRKIYE.

OP-869

Novel PET Tracers to Image Parkinson's Disease

S. Jakobsen Mo;
Umeå University, Department of Radiation Sciences, Umeå, SWEDEN.

1709

Wednesday, September 13, 2023, 8:00 AM - 9:30 AM
Hall G2

e-Poster Presentations Session 13 - Oncology & Theranostics Committee: Head and Neck Tumours, Lung, Melanoma and Others

EPS-252

Predictors for Disease Free and Progression Free Survival in Metabolic Responders and Non-responders on follow-up FDG PET/CT after Chemoradiation in Nasopharyngeal Cancers

M. Zaman[1], *N. Fatima*[2], *R. Tahseen*[3], *A. Ahmed*[1], *A. Zaman*[4], *S. Zaman*[5], *U. Zaman*[6];
[1]*Dept of Radiology, Aga Khan University Hospital, Karachi, PAKISTAN,* [2]*Dept of Radiology, Aga Khan University Hospital, KARACHI, PAKISTAN,* [3]*Dept of Radiation Oncology, Aga Khan University Hospital, Karachi, PAKISTAN,* [4]*Dept of Medicine, Sunny Downstate Medical Centre, NY, New York, NY, UNITED STATES OF AMERICA,* [5]*Dept of Medicine, Dr Ruth Pfau Hospital, Karachi, PAKISTAN,* [6]*Dept ogf Hem Oncology, Oklahoma University, Okla, Oklahoma, OK, UNITED STATES OF AMERICA.*

Aim/Introduction: Aim/Introduction: To determine disease free survival (DFS) and progression free survival (PFS) in patients with nasopharyngeal cancer (NPC) having achieved complete (CMR) and partial metabolic response (PMR) on post-chemoradiation (CRT) FDG PET/CT. ***Materials and Methods:*** Retro-prospective study conducted at PET/CT Section of JCIA accredited healthcare facility of Pakistan. Total 68 patients of NPC patients who had baseline and post-CRT FDG PET/CT were included and prospectively followed till predefined study end points of recurrence or disease progression or death from April-2016 till October 2022. Based on CMR on post-CRT FDG PET/CT, 40 patients labelled as responders and 18 as non-responder based on PMR respectively. By using ROC analysis, the predictors of PMR and recurrence were analyzed. Kaplan Meier's survival plots were analyzed to measure DFS in responders and PFS in non-responders respectively. ***Results:*** On follow-up, mean DFS in responders was 49.6 ± 6.3 month, 78% survival and recurrence was found in 09 (22%) patients. Baseline SUVmax >8.3 of primary tumor, stage IV, body mass index >24.609 and male gender were found significant predictors of recurrence in responder group using ROC ($p < 0.05$). In non-responders group, the mean PFS was 6.8 ± 1.8 months. Higher SUVmax >9.5 and more stage IV disease on baseline FDG PET/CT were found significant predictors of shorter PFS in non-responders on ROC ($p < 0.05$). ***Conclusion:*** Male gender, higher BMI and primary tumor SUVmax (>8.3) on baseline FDG PET/CT predict shorter DFS in patients who achieved complete metabolic response after CRT. In patients with partial metabolic response on post-CRT, higher primary tumor SUVmax >9.5 and stage IV disease on baseline FDG PET/CT were found significant predictors of shorter PFS.

EPS-253

Performance of hybrid [^{18}F]FDG PET-MRI for staging of head and neck cancer

E. Droogers, *I. J. Pruis, A. W. A. van der Eerden, A. A. Harteveld, R. Valkema, S. E. M. Veldhuijzen van Zanten;*
Erasmus Medical Center, Rotterdam, NETHERLANDS.

Aim/Introduction: This is the first retrospective study in the Netherlands to evaluate the diagnostic yield of hybrid 2-[18F] fluoro-2-deoxy-d-glucose ([18F]FDG) PET-MRI for staging of head and neck squamous cell carcinoma (HNSCC). ***Materials and Methods:*** Patients suspected of HNSCC underwent hybrid [18F] FDG PET-MRI following dedicated head and neck and whole-body protocol, either at time of initial diagnosis or suspected tumor recurrence. Images were analyzed in the setting of regular clinical care by both a nuclear medicine physician as well as a dedicated neuro/H&N radiologist. Data on the interpretation of multiple variables related to the primary tumor (T), lymph nodes (N), distant metastases (M) and second primary tumors (SPT) were extracted from the radiology reports retrospectively. Based on the combined interpretation of both PET and MRI, all lesions (T/N/M/SPT) were denominated as malignant, suspicious or not malignant/ absent and compared to reference values, including pathology and/or follow-up (clinical and/or imaging), to enable lesion-wise and patient-wise analyses on the diagnostic accuracy. ***Results:*** Ninety-five patients (68.4% male, mean age of 64.7) with histologically proven HNSCC were included. The true positive rate for T was 97.5% (79/81 correct diagnosis), the true negative rate was 100% (14/14). The latter group included nine patients with carcinoma of unknown primary (CUP) and five patients with unmeasurable T due to previous treatment. A true positive and true negative rate of 100% was shown for lymph nodes denominated as malignant (both in lesion-wise and patient-wise analyses) or benign (only patient-wise analysis possible). The lesion-wise analysis of suspicious lymph nodes demonstrated a true positive rate of 22.1% (15/68), i.e., a correct diagnosis in 1/5 patients, and overcall in 4/5 patients. Ten suspicious sites for M and sixteen suspicious sites for SPT were detected in eight and thirteen patients, respectively. ***Conclusion:*** Hybrid [18F]FDG PET-MRI in patients with HNSCC has a high diagnostic yield with particular high true positive/negative rates for primary tumors and pronounced malignant or benign lymph nodes. Further research is needed, however, to develop and validate optimal criteria for reading [18F]FDG PET-MRI, particularly for accurate interpretation of suspicious lymph nodes, and to compare its performance with [18F]FDG PET-CT. Additionally, novel radiotracers beyond [18F] FDG for diagnosis of head and neck cancer may be promising and must therefore be further analyzed.

EPS-254

The Validity of F-18-FDG PET/CT in the Management of the Patients with Laryngeal Carcinoma After Therapy

J. Petrovic, *J. Milovanovic, A. Jotic, D. Sobic Saranovic;*
Center for Nuclear Medicine, University Clinical Center of Serbia, Faculty of Medicine, University of Belgrade, Belgrade, SERBIA.

Aim/Introduction: The aim of this investigation is to estimate the diagnostic performance of positron emission tomography/ computed tomography using fluorine-18 fluoro-deoxyglucose (FDG PET/CT) in the follow up of the post-treatment laryngeal squamocellular squamous cell cancer carcinoma (SCC), as well as survival rate. ***Materials and Methods:*** Total of 68 patients (57 males and 11 females), mean age (69.1±6.8), with post-treatment laryngeal SCC were investigated. Indications for FDG PET/CT

were: staging after surgery, restaging after therapy with positive/uncertain CT, follow-up, suspected recurrence on CT. FDG PET/CT findings were compared to clinical follow-up of up to 12 years after imaging. Degree of metabolic activity was analyzed visually and semi-quantitatively using maximal standardized uptake value (SUVmax). ***Results:*** High accumulation of radiopharmaceutical was found in 48 (70.6%) patients (42 males and 6 females) who were considered true positive, physiological in 17 patients (25%) (13 males and 4 females) and only 3 (3.5%) (2 males and one female) were false positive. Overall sensitivity of FDG PET/CT was 100%, specificity 85.0%, positive predictive value 94.0%, negative predictive value 100% and accuracy 95.6%. In 25 cases (36.8%) PET/CT findings significantly influenced further management of the patients. Progression free survival (PFS) in the FDG positive group was 41.8 ± 12.9 months, median 40, range 21-70, while in FDG negative group it was 47.6 ± 19.7 months, median 44, range 17-97, without significant differences between the groups (p= 0.30). Statistically significant correlation between SUVmax and PFS was not observed (p>0.05). ***Conclusion:*** FDG PET/CT is a valuable tool for follow-up of laryngeal SCC due to its high sensitivity, specificity, PPV, NPV and accuracy. It can influence the patients' management in significant number of cases. Patients with negative FDG PET/CT findings had longer PFS than those with positive ones, but without statistical significance. SUVmax was not proven to be a strong predictor of the disease-free survival of the patients.

EPS-255

PET/CT-guided GTV delineation during radiotherapy planning and prognosis evaluation in recurrent oral cavity squamous cell carcinoma

Y. Tian, *Y. Zhang, C. Li, Y. He;*
Zhongnan Hospital of Wuhan University, Wuhan, CHINA.

Aim/Introduction: To evaluate the usefulness of PET/CT in gross tumor volume (GTV) delineation during radiotherapy planning and the prognostic value in recurrent oral cavity squamous cell carcinoma (OSCC). ***Materials and Methods:*** 20 patients with recurrent OSCC underwent PET/CT and MRI. The GTV for primary tumor and lymph nodes (nGTV) were defined on CT (GTV-CT) and compared to GTVs obtained from PET (GTV-PET) and MRI (GTV-MRI) images. Two methods of GTV determination were used: visual interpretation of CT, PET (GTV-PETvis) and MRI images and quantitative automatic method based on a chosen threshold value (20%, 30%, 40%, 50% 60%) of standardized uptake values (SUVmax) from PET examination (GTV-PET20%, GTV-PET30%, etc.). Statistical analysis of differences in GTV values obtained from CT, PET and MRI studies was performed. GTV-CT was used as a reference. SUVmax, whole-body metabolic tumor volume (WBMTV), and whole-body total lesion glycolysis (WBTLG) derived from PET/CT were measured. Using receiver operator characteristic (ROC) curves, Kaplan-Meier analysis, and log-rank tests, we identified the optimal cutoff values for SUVmax, WBMTV, and WBTLG to determine independent predictors of survival. ***Results:*** In all, 70% of GTV-MRI and 40% of GTV-PETvis were larger than GTV-CT. GTV-PET 30% were the most closely related volumes to GTV-CT from all threshold methods in 50% of patients. GTV-PETvis generated the most similar volumes to GTV-CT from all PET measurements. Compared to nGTV-CT, 70% of nGTV-MRI and 20% of nGTV-PETvis were larger. The remaining nGTV-MRI and nGTV-PETvis measurements were smaller than nGTV-CT. nGTV-PET20% were the most closely related volumes to nGTV-CT in 40% of the cases. GTV-PET20%, nGTV-PETvis, and nGTV-PET50% ($p < 0.05$) diverge significantly from nGTV-CT results. ROC's optimal cutoff values of the primary focus SUVmax, WBMTV, and WBTLG, were 10.36, 9.52cm^{3}and 52.12, respectively. Patients with WBMTV < 9.52 cm^3 had significantly better 3-year overall survival (OS) ($P = 0.003$) and disease-free survival (DFS) ($P < 0.001$) than patients with a WBMTV ≥ 9.52 cm^3. Patients with WBTLG < 52.12 had significantly better 3-year OS (90.9% vs. 76.9%, $P = 0.002$) and DFS (90.0% vs. 66.3%, $P < 0.001$) than patients with a WBTLG ≥ 52.12. Multivariate Cox regression modeling showed WBMTV (HR, 0.425) and WBTLG (HR, 0.317) could be predictive of OS and DFS. ***Conclusion:*** PET/CT provides more information during target tumor mass delineation in radiotherapy planning in recurrent OSCC. PET/CT measurements of WBMTV and WBTLG could predict survival.

EPS-256

Detection of Perineural Tumour Spread in Head and Neck Cancers by 18F-FDG PET/CT

A. Ormanci, *M. Tuncel;*
Hacettepe University Faculty of Medicine, Department of Nuclear Medicine, Ankara, TÜRKIYE.

Aim/Introduction: Perineural spread(PNS) refers to tumour growth along large nerves. It most commonly occurs in head and neck cancers(HNC). Accurate detection of PNS is crucial since it changes treatment plans and prognosis. However accuracy of PET/CT in detection of PNS is not extensively studied. Therefore, our study aimed to retrospectively analyse the PNS detection rate of 18F-FDG-PET/CT in patients with HNC. ***Materials and Methods:*** We have retrospectively analysed the 18F-FDG-PET/CT images of 478 patients with HNC.Among these patients,26 were diagnosed as having PNS by MRI and/or clinical findings. These patients had whole-body PET/CT scans within one-month of MRI.Seven of the 26 patients also had dedicated head and neck PET images. PET/CT images were re-evaluated by two nuclear medicine physicians(rePET). SUVmax and SUVmean values of the primary tumour region and PNS were measured. PNS pattern (focal/linear/focal+lineer),agreement with the MRI findings and original PET/CT reports were evaluated. ***Results:*** Our retrospective study enrolled 26 patients (F/M:7/19, median age:56 range:11-81) with FDG-avid HNC. Of these patients, 19/26(73%) had SCC,6/26(23%) had adenoid cystic carcinoma and 1/26(4%) had salivary ductus carcinoma. The primary tumor localisation was nasopharynx in 13/26(50%), oral cavity in 9/26(34%),nasal cavity in 1/26(4%),sphenoid sinus in 1/26(4%),maxillary sinus in 1/26(4%) and parotid gland in 1/26(4%) patients. While 14/26(54%) patients were newly diagnosed,12/26(46%) were evaluated after surgery and/or chemoradiotherapy. In 20/26(77%) patients, primary tumour was detected in PET/CT images, whereas in 6/26(23%) patients primary tumour was not detected because of previous treatments.The number of patients in which rePET and MRI were fully compatible was 19/26(73%).In 5/26(19%) patients MRI showed more extensive disease than rePET, and in 2/26(8%)patients MRI showed PNS, whereas rePET was negative. The median PET SUVmax values of the primary tumours were 12(range:3,27-41) and PNS was 8,6(range:2-41). Out of 24 patients that rePET detected PNS; 15/24(63%)had focal, 1/24(4%)had linear and 8/24(33%) had both focal & linear PNS.V2 nerve involvement was observed in 7/24(29%),V3 in 12/24(50%) and both V2 & V3 nerve involvement was observed in 5/24(21%) of patients. In 10/26(38%) of patients, rePET and original PET/CT reports described PNS consistently. However, in 16/26(62%) of patients, rePET detected PNS which was not reported at the original PET/CT report. ***Conclusion:*** 18F-FDG-PET/CT had lower sensitivity in the detection of PNS when compared to MRI. However, careful and dedicated interpretation of PET/CT images could detect more lesions compatible with PNS and can assist MRI findings.

EPS-257

18F-FDG PET CT andTumour Tissue Modified Viral (TTMV) -Human papilloma virus DNA : Role in Recurrent HPV driven oropharyngeal squamous cell carcinoma.

R. Kulkarni, *M. Posner, S. Roof, M. Ghesani, N. Ghesani;*
Mount SInai Hospital, New York, NY, UNITED STATES OF AMERICA.

Aim/Introduction: Human papilloma virus (HPV) driven oropharyngeal squamous cell carcinoma (OPSCC) has better outcomes than HPV negative ones. While around 1/5 of the patients develop locoregional failure, treatment with curative intent is still an option. Surveillance is therefore important for early detection of recurrence. Image-guided surveillance with ^{18}F Fluorodeoxyglucose (FDG)-positron emission tomography/computerized tomography (PET/CT) has demonstrated excellent survival rates and quality of life benefits. Liquid biomarkers such as Tumour Tissue Modified Viral (TTMV) -HPV DNA offer potential for early detection of recurrence. In this presumably first study of its kind, retrospective study, we present the preliminary data comparing the TTMV HPV DNA levels and tumour burden, represented by tumour lesion glycolysis (TLG). This is a volumetric parameter, more representative of disease burden than traditional criteria such as highest standardised uptake value (SUVmax), derived from ^{18}F-FDG PET CT studies. The utility of this parameter has been validated in large volume diseases. We are attempting to understand the role in oligometastases and locoregional recurrence. We are also studying the relationship between tumor burden and the TTMV HPV DNA to understand tumor biology and a possible complementary role between imaging and liquid biopsies. ***Materials and Methods:*** Patients with OPSCC positive for HPV 16 genotype at initial diagnosis and recurrence were included. Surveillance ^{18}F-FDG PET/CTs at recurrence, and for restaging prior to definitive treatment of recurrence were studied. Voxels of interest were drawn around the lesions and a proprietary software derived the TLG, SUVmax and SUVmean. Correlation between the TLG and the TTMV HPV DNA levels for each disease site was assessed using Pearson's correlation coefficient. ***Results:*** 25 patients, 22 males and 3 females, mean age 69.1 years, with biopsy proven, recurrent HPV positive OPSCC were included. Primary tumor sites were base of tongue cancer in 9/25 pts, palatine tonsil in 13/25, left nasal cavity, pyriform sinus SCC and unknown in rest. 5/25 had local, 8/25 had regional nodal, 5/25 had loco-regional recurrences and 7/25 had distant metastases. At recurrence, 25/25 patients had positive PET CT studies and 17/25 patients had a positive TTMV HPV DNA. Comparing the average site-specific tumour burden and the TTMV HPV DNA values when considering (Table 1), we see a strong positive correlation with a Pearson's correlation co-efficient of 0.99. ***Conclusion:*** In small volume disease, site-specific tumour burden correlates to the average TTMV HPV DNA. More sophisticated methods are needed to study overall tumor volumes and burden.

EPS-258

Convolutional Neural Network for Prediction of Early Disease Progression in Patients with Advanced Epidermal Growth Factor Receptor-Mutated Lung Adenocarcinoma Receiving Tyrosine Kinase Inhibitor Therapy Based on 18F-FDG PET Images

K. Lue[1], *Y. Chen*[2,3], *L. Yong*[1], *X. Wong*[1], *S. Liu*[1,2], *H. Lin*[4,5];
[1]*Tzu Chi University of Science and Technology, Hualien, TAIWAN,* [2]*Hualien Tzu Chi Hospital, Hualien, TAIWAN,* [3]*Tzu Chi University, Hualien, TAIWAN,* [4]*Chang Gung University, Taoyuan, TAIWAN,* [5]*Keelung Chang Gung Memorial Hospital, Keelung, TAIWAN.*

Aim/Introduction: Patients with advanced epidermal growth factor receptor (EGFR)-mutated lung adenocarcinoma are known to respond to first-line tyrosine kinase inhibitor (TKI) treatment. However, approximately half of the patients who initially respond to TKI experience drug resistance within 12 months. In this study, we used a convolutional neural network (CNN) based on ^{18}F-FDG PET images to predict disease progression in patients with advanced EGFR-mutated lung adenocarcinoma treated with TKI. ***Materials and Methods:*** In total, 112 patients diagnosed with EGFR-mutated lung adenocarcinoma were retrospectively enrolled. ^{18}F-FDG PET images were acquired before the TKI treatment. A standardised uptake value threshold > 2.5 was used for primary tumour segmentation. The segmented images were augmented via the intersection of the three-dimensional domain with triples of orthogonal planes, which were used as input images for the CNN model. The augmented images were randomly divided into training (80%), validation (10%), and testing (10%) datasets. The ResNet-50 architecture was adopted to construct a deep-learning CNN and predict the disease progression within 12 months. Random rotation, reflection, and scaling were applied to the images during the training to avoid overfitting. Predictive power was assessed using the area under the receiver operating characteristic curve (AUC). A confusion matrix was generated to estimate the performance, including sensitivity, specificity, positive predictive value (PPV), negative predictive value (NPV), and accuracy. An occlusion sensitivity map was used to visualise the important areas of a PET image for prediction. MATLAB with the Deep Learning Toolbox Release 2022a (MathWorks, Natick, USA) was used in this study. ***Results:*** In the study population, 19 and 93 patients were diagnosed with stage IIIB and IV disease, respectively. Fifty-one patients experienced disease progression within 12 months of receiving TKI treatment. The CNN ResNet-50 model was trained, fine-tuned, and utilised to predict early disease progression in the testing dataset. The AUC estimation was 0.93, accuracy was 93.3%, sensitivity and specificity were 88.4% and 97.4%, respectively, and PPV and NPV were 96.5% and 91.0%, respectively. The occlusion method for trained model interpretability highlighted important areas in regional parts of the primary lung tumour. ***Conclusion:*** The CNN ResNet-50 model based on ^{18}F-FDG PET images can predict disease progression within 12 months in patients with advanced EGFR-mutated lung adenocarcinoma treated with TKI. This model may be clinically helpful for facilitating the management of patients with advanced EGFR-mutated lung adenocarcinomas.

EPS-259

Role Of Novel Geometric Variables Derived From 18F-FDG PET/CT As Predictive Factors In Patients With Non-Small Cell Lung Cancer

G. Jimenez Londoño[1], *A. M. Garcia Vicente*[2], *J. J. Bosque*[3], *J. Perez-Beteta*[3], *M. Amo-Salas*[4], *A. F. Honguero-Martinez*[5], *E. Noriega Alvarez*[1], *C. Lucas Lucas*[1], *V. M. Perez-Garcia*[3], *A. M. Soriano Castrejon*[2];
[1]*Department of Nuclear Medicine, Hospital General Universitario de Ciudad Real, Ciudad Real, SPAIN,* [2]*Department of Nuclear Medicine, Complejo Hospitalario Universitario de Toledo, Toledo, SPAIN,* [3]*Department of Mathematics, Mathematical Oncology Laboratory (MOLAB), Universidad de Castilla-La Mancha, Ciudad Real, SPAIN,* [4]*Department of Mathematics, Universidad de Castilla-La Mancha, Ciudad Real, SPAIN,* [5]*Department of Surgery, Hospital General Universitario de Albacete, Albacete, SPAIN.*

Aim/Introduction: This retrospective study aimed to compare the prognostic significance of traditional and novel geometric parameters obtained from pretreatment 18F-FDG PET/CT scans in patients diagnosed with non-small cell lung cancer (NSCLC). ***Materials and Methods:*** The study included NSCLC patients who had a baseline 18F-FDG PET/CT scan. Inclusion criteria required

stage I-III, complete surgical resection, absence of neoadjuvant treatment, lung lesions with significant 18FDG avidity, diameter ≥10 mm and clinical/radiological follow-up ≥24 months. Clinical variables such as age, Charlson Comorbidity Index, Haemoglobin, tumour location, TNM stage, histology, differentiation degree, lymph nodal infiltration and lymphovascular and pleural invasion were recorded. Lung lesions were segmented in 3D using a semi-automatic algorithm, and parameters were obtained including SUV and volume-based metrics, global texture, sphericity, and two novel metrics, SUVpeak to centroid distance (SCD) and SUVmax to perimeter distance (SPD). SCD measured the distance between the SUVpeak voxel centre and tumor centre on PET images, while SPD represented the shortest distance from the SUVmax voxel to the tumor border in the same axial slice. Size dependence was eliminated by normalizing these metrics with the mean spherical radius of tumour, resulting in nSCD and nSPD. In the statistical analysis, early recurrence (ER) and short-term mortality (STM) were the outcome variables, defined as disease-free survival under 12 months and overall survival under 36 months, respectively. Univariate and multivariate logistic regression analyses were conducted for ER and STM. ***Results:*** A total of 173 patients were included in the study. After semi-automatic segmentation, 15 cases needed manual adjustment. Forty-nine of 104 patients developed ER and 100 patients died, 53 of whom had STM. Age, pathological lymphovascular invasion, lymph nodal infiltration, TNM stage, nSCD, and nSPD were all linked to ER. However, only age (OR=1.06, p=0.002), pathological lymphovascular invasion (OR=3.40, p=0.022), and nSPD (OR=0.02, p=0.018) were significant independent predictors of ER in multivariate analysis. Age, lymph nodal infiltration, TNM stage, nSCD, and nSPD were predictors of STM. Nonetheless, age (OR=1.05, p=0.006), lymph nodal infiltration (OR=2.72, p=0.005), and nSPD (OR=0.03, p=0.022) were significantly associated with STM in multivariate analysis. SUV and volumetric metabolic variables, as well as coefficient of variation (COV) and SUVmean/SUVmax ratio, were not significant predictors of ER or STM. ***Conclusion:*** The novel geometric variables nSCD and nSPD are reliable biomarkers for predicting unfavourable outcomes in NSCLC patients when compared to traditional PET variables. The use of these novel parameters could assist in treatment planning and patient management.

EPS-260

Correlation between 18F-FDG-PET parameters and outcome od Durvalumab treatment in unresectable locally advanced Non Small Cell Lung Cancer (NSCLC, stage IIIa-b-c)

K. Beshiri[1], *F. G. Dall'Olio*[1], *M. Aldea*[1], *C. Genova*[2], *F. Barlesi*[1], *A. Botticella*[1], *A. Levy*[1], *C. Le Pechoux*[1], *P. Lavaud*[1], *M. Frelaut*[1], *P. Abdayem*[1], *J. Remon Masip*[1], *D. Planchard*[1], *B. Besse*[1], *S. Ponce-Aix*[1], *F. Selhane*[1], *D. Deandreis*[1], *M. Bauckneht*[2], *C. Garcia*[1];
[1]*Institute Gustave Roussy, Villejuif, FRANCE,* [2]*IRCCS Ospedale Policlinico San Martino, Genova, ITALY.*

Aim/Introduction: Unresectable locally advanced NSCLC is commonly treated with curative-intent chemo-radiotherapy followed by Durvalumab consolidation. However, around 70% of patients progress at 5 years despite PDL-1 expression, highlighting the need for new prognostic biomarkers. The potential role of 18F-FDG-PET-derived parameters as biomarkers in patients receiving immune checkpoint inhibitors (ICIs) has been investigated, especially in advanced NSCLC. This study aims to evaluate whether 18F-FDG-PET-derived parameters could serve as prognostic biomarkers for unresectable locally advanced NSCLC and predictive biomarkers for those undergoing consolidation immunotherapy with Durvalumab. ***Materials and Methods:*** This is a retrospective study enrolling patients with unresectable locally advanced NSCLC. Patients were divided into two arms one receiving, after chemo-radiotherapy, consolidation treatment with Durvalumab (arm A) and the other without consolidation (arm B). 18F-FDG-PET images were obtained 40 days before treatment initiation. SULmax, SULpeak were recorded for primary lesions and for the whole examination, Total Lesion Glycolysis (TLG), and Metabolic Tumoral Volume (MTV) was calculated for all lesion >1cm3, using for segmentation 42% SULmax thresholding in a dedicated commercial software (PETVcar; GE-Healthcare). Per patient, Total body (TB)MTV and TBTLG was obtained by summing all segmented lesion's. Cox models had been used for the statistical analysis in order to correlate the variables to PFS/OS calculated from C1D1. ***Results:*** 112 patients were included, 66% were male, median age was 64 years, 65% were smokers, and 93% had an ECOG PS of 0-1. Concomitant chemo-radiotherapy was performed in 75% and 67.3% of patients of arm A and B, respectively. The ORR were 67% and 52%. The median PFS was not reached in arm A and 24 months in arm B. The survival at 50 months was 48% in Durvaluamb arm vs 27% in no-Durvalumab arm. ORR was respectively 67% vs 52%. Patients' PFS in the Durvalumab arm was not significantly predicted by TBTLG and TBMTV (p≥0.6, 0.7). In this cohort a positive correlation with PFS was observed between SULmax, SULpeak and Durvalumab cohort (HR 0.3, 0.37; p 0.035), which was not confirmed by multivariate analysis. No 18F-FDG-PET parameters correlation was found for OS in both arms. ***Conclusion:*** Our restrospective study showed in a univariate analysis a predictive role of SULmax and SULpeak in unresectable locally advanced stage III NSCLC receiving curative chemo-radiotherapy and Durvalumab consolidation. This result was not confirmed in a multivariate analysis. Further studies with a larger cohort and eventually a prospective trial design are needed to confirm the results.

EPS-262

Usefulness of imaging parameters by FDG-PET/CT and conventional CT in early T-stage lung adenocarcinoma patients who underwent surgery

S. Tsukamoto*, S. Koyasu, M. Hamaji, H. Date, Y. Nakamoto; Kyoto University, Kyoto, JAPAN.*

Aim/Introduction: Recently, evidence for the effectiveness of wedge resection in early-stage lung cancer has been accumulated [1]. Prior stratification by imaging is desired to improve outcomes, but its usefulness is not well established. The aim of this study was to evaluate the relationship between preoperative imaging parameters and histopathological findings or gene mutation status in surgically resected early T-stage lung cancer patients. ***Materials and Methods:*** We retrospectively enrolled pTis or pT1 lung adenocarcinoma which underwent preoperative FDG-PET/CT and conventional CT examination and surgically resected during 2020. The following imaging parameters were obtained using three-dimensional semiautomatic segmentation system: tumor volume of the entire lesion (TV) and percentage of the solid component (SC) by conventional CT, maximum standardized uptake value (SUVmax), metabolic tumor volume (MTV) and total lesion glycolysis (TLG) by FDG-PET/CT delineated with a threshold of SUV value 1.0 [2]. The relationship between these radiological parameters and histopathological high-risk findings such as international association for the study of lung cancer (IASLC) grade and spread through air space (STAS) as well as gene mutation status (EGFR, KRAS) was evaluated.

Results: A total of 72 lesions was included and the TNM classification was: pStage 0, I, II, III = 6, 62, 3, 1, respectively. The part solid (n=39), solid (n=20) and pure GGO type (n=13) were classified by conventional CT. In the tumors with IASLC grade 3 (n=8), SC, SUVmax, MTV and TLG were significantly higher (p=0.0007, 0.0008, 0.0329, and 0.0013, respectively) than those in tumors with IASLC grade 1-2 (n=57). In terms of STAS, SC, SUVmax and TLG of the STAS-positive tumors (n=14) were significantly higher (p= less than 0.0001, 0.0002, and 0.0002, respectively) than that of negative tumors (n=53), which was not observed in MTV (p=0.0625). TV with EGFR mutation (n=32) was significantly higher (p=0.0377) than that without EGFR mutation (n=34), and SC with KRAS mutation (n=10) was significantly higher (p=0.0175) than that without KRAS mutation (n=51). The significant differences of FDG-PET/CT parameters were not observed depending on the status of these gene mutations. ***Conclusion:*** In early T-stage lung cancer, the parameters obtained by FDG-PET/CT were significantly higher in tumors with STAS or higher IASLC grade. FDG-PET/CT parameters may be useful to stratify early T-stage lung adenocarcinoma with higher histopathological risk factors. ***References:*** [1] Aokage et al. Lancet Respir Med. 2023 (ahead of print) [2] Iwano et al. Clin Nucl Med. 44:560 2019.

EPS-263

Prognostic Value of Total Body Metabolic Tumour Volume in Patients with Advanced SCLC Treated by Chemotherapy and Immunotherapy.

A. CABARET[1], *C. GARCIA*[1], *F. DALL-OLIO*[1], *E. AUCLIN*[2], *B. BESSE*[1], *P. LAVAUD*[1];
[1]*Institut Gustave Roussy, Villejuif, FRANCE,*
[2]*Hopital George Pompidou, Paris, FRANCE.*

Aim/Introduction: ICI in association with a platine-based chemotherapy are the first agents in the last decades to determine a statistical improvement in OS and PFS in patients with advanced SCLC. Only a small fraction of patients experiences a long-term benefit. Reliable predictive and prognostic markers are lacking to identify these patients. We aim to investigate the prognostic and predictive values of different baseline metabolic parameters, from ^{18F}FDG PET-CT imaging in patients receiving first line treatment for a metastatic SCLC. ***Materials and Methods:*** In this retrospective monocentric cohort study, we selected all patients between October 2013 and December 2021 with advanced SCLC who underwent baseline ^{18F}FDG PET-CT within 4 weeks before treatment initiation : chemotherapy (CT-group) or chemotherapy + immunotherapy (CT-IO group). Metabolically active tumour regions were segmented on pretreatment PET using a commercial software with a 42% SULmax threshold. Total body Metabolic tumor volume (TBMTV, defined as the addition of the tumor volume segmented with ≥ 42% of the SULmax for all lesions >1cm^3), Total body Total Lesions Glycolysis (TBTLG, defined as the addition of MTV x SULmean), SULmax and SULPeak of the biggest lesion, were calculated in both groups. Association between these parameters and OS or PFS was evaluated. ***Results:*** 67 patients were enrolled, 29 treated with CT-IO and 38 treated with CT. Median follow up was 48,3 months for the CT group and 18,4 months for the CT-IO group. A high TBMTV and a high TBTLG were significantly associated with a poorer OS in the CT group.Median OS was 6,3 months in patients with high TBTLG versus 15,4 months in patients with low TBTLG (p=0.001). In the CT-IO group, the same trend was found but not statistically significant, probably due to the small number of patients in this cohort (p=0.3). In patients with high tumour volume (high TBTLG or TBMTV) there was a statistically significant difference between patients treated with CT alone and patients treated with CT-IO in terms of overall survival (p=0.04). SULmax and SULpeak of the biggest lesion were both associated with OS (HR 3.657 (p=0.009) and HR 1.104 (p=0.019) respectively). ***Conclusion:*** Our results indicate that TBMTV and TBTLG as well SULmax and SULpeak of the predominant lesion, are strong prognostics factors for OS in patients with metastatic SCLC and suggest that the addition of immunotherapy to chemotherapy appears to provide a greater benefit for patients with a high tumour volume.

EPS-264

Lymph Node Ultrasound Prior to Sentinel Lymph Node Biopsy in 414 Patients with Melanoma: Usefulness in the Era of Adjuvant Systemic Therapy

G. Horvatic Herceg[1], *S. Kusacic-Kuna*[2], *M. Ciglar-Hlasc*[2], *D. Herceg*[3], *L. Simetic*[3], *D. Mijatovic*[4];
[1]*University Hospital Zagreb, Zagreb, CROATIA,* [2]*Department of nuclear medicine and radiation protection, University Hospital Zagreb, Zagreb, CROATIA,* [3]*Clinic of oncology, University Hospital Zagreb, Zagreb, CROATIA,* [4]*Clinic of surgery, University Hospital Zagreb, Zagreb, CROATIA.*

Aim/Introduction: Sentinel lymph node biopsy (SLNB) in melanoma has still been the subject of discussions. Namely, it is a staging procedure for melanoma which is thicker than 0.8mm or thinner in the presence of ulceration. Following with the complete lymph node dissection (CLND), in case of positive sentinel node, it provides better locoregional disease control, however it does not prevent distant metastases. Furthermore, SLNB provides crucial information for both prognostic and treatment purposes. The aim of this study is to evaluate contribution of preoperative ultrasound (US), power Doppler, and US-guided FNAC in the diagnosing non-palpable, metastatic lymph nodes in melanoma patients. ***Materials and Methods:*** We performed a prospective study of 414 patients (194 females and 220 males; mean age 54 years, range: 19-82 years) with clinical stage I-II primary melanoma who underwent locoregional lymph node ultrasound prior to SLNB between 2010 and 2022. Median tumor depth was 2.38 mm (range 0.5- 15.0). The rate of ulceration was 39,13%. All patients were examined by US before preoperative lymphoscintigraphy and FNAC was performed in suspicious lymph nodes (round shaped, eccentric cortical hypertrophy and the presence of peripheral vascularization). In cases of malignant results, patients were submitted to CLND. The US-guided FNAC was considered positive, if US and FNAC were positive. If US was suspicious of malignancy, but FNAC was negative, the US-guided FNAC was considered negative. The findings were correlated with histopathology results after CLND. ***Results:*** US and US-guided FNAC were true positive in 59 cases, with no false positive results. All FNAC findings were confirmed by histopathology. There were 37 false negative results out of 355 patients with negative echographic findings. In those patients histopathology revealed metastases in form of tumor cells' foci, which were less than 1 mm in 16 patients, 1-5 mm in 4 patients and individual tumor cells were found in 17 patients. The sensitivity, specificity, positive predictive value, and negative predictive value of US combined with FNAC were 61.46%, 100%, 100% and 89.58%. ***Conclusion:*** Unnecessary surgical sentinel node staging can be avoided by ultrasound detection of regional melanoma metastases, combined with power Doppler and FNAC. In case of a negative US examination of the lymph nodes SLNB is required for adequate staging, furthermore it is of crucial importance for therapy planning. Due to the vast growing usage of novel adjuvant systemic treatment strategies for stage III melanoma, SLNB has been established as even more important.

EPS-265

Could lymphadenectomy be avoided in a selection of patients diagnosed with cutaneous melanoma with metastatic sentinel lymph node biopsy?

B. Hervás-Sanz[1], *M. T. Bajén-Lázaro*[1], *J. G. Reyes-Junca*[1], *A. M. Benítez-Segura*[1], *I. E. Sánchez-Rodríguez*[1], *S. Maymó-Garrido*[2], *J. L. Díaz-Moreno*[1], *M. A. Crespí-Busquets*[2], *M. Pudis*[1], *S. Bondia-Bescós*[1], *R. M. Penín-Mosquera*[3], *J. Marcoval-Caus*[4], *J. O. Bermejo-Segú*[5], *J. J. Martín-Liberal*[6], *I. Linares-Galiana*[7], *M. Cortés-Romera*[1]; [1]*Nuclear Medicine-PET (IDI) Department, Bellvitge University Hospital-IDIBELL, L'Hospitalet de Llobregat, SPAIN,* [2]*Radiopharmaceutical Department, Bellvitge University Hospital-IDIBELL, L'Hospitalet de Llobregat, SPAIN,* [3]*Anatomical Pathology Department, Bellvitge University Hospital-IDIBELL, L'Hospitalet de Llobregat, SPAIN,* [4]*Dermatology Department, Bellvitge University Hospital-IDIBELL, L'Hospitalet de Llobregat, SPAIN,* [5]*Plastic Surgery Department, Bellvitge University Hospital-IDIBELL, L'Hospitalet de Llobregat, SPAIN,* [6]*Medical Oncology Department, Institut Català d'Oncologia, L'Hospitalet de Llobregat, SPAIN,* [7]*Radiation Oncology Department, Institut Català d'Oncologia, L'Hospitalet de Llobregat, SPAIN.*

Aim/Introduction: Current protocols for cutaneous melanoma recommend primary tumor excision with safety margins and sentinel lymph node biopsy (SLNB) depending on Breslow thickness after confirmation by anatomopathological study. When metastasis is identified in the sentinel lymph node (SLN), the standard procedure to date has been full lymph node dissection (LND) in the region of the SLN metastasis. The aim of this study is to determine whether lymphadenectomy can be avoided in a group of patients (p), depending on Breslow's depth and SLNB metastases size. ***Materials and Methods:*** We retrospectively studied 393p diagnosed with cutaneous melanoma between January 2011 and December 2020. 10p were excluded from the study: 3 for non-detection of the SLN and 7 for loss to follow-up. The remaining 383p underwent SLNB and in all these patients, a lymphoscintigraphy was performed the day before the surgery, after the perilesional injection of 185 MBq of 99mTc-nanocolloid. In those patients with metastatic SLNB, a LND of the corresponding lymphatic station was performed. The following parameters were analyzed: Breslow's depth, number of lymphatic stations with metastatic SLNB, metastases size (<1mm or >1mm), number of LND and number of LND with additional lymph nodes (LN) metastasis. ***Results:*** Among the 383p analyzed, we found 106 lymphatic stations with metastatic SLNB. LND was performed in 100 out of the 106 (it did not take place in three cases because of patient's rejection, in two cases because of pulmonary metastasis diagnosis and in one case because of patient's exitus). Patients were classified as follows:<1mm Breslow's depth: 68p → 4 lymphatic stations with metastatic SLNB: 2 >1mm and 2 <1mm → 0/4 LND with additional LN metastasis (0%).1-2 mm Breslow's depth: 130p → 14 lymphatic stations with metastatic SLNB: 8 >1mm, 6 <1mm → 0/12 LND with additional LN metastasis (0%).2,01-4 mm Breslow's depth: 95p → 36 lymphatic stations with metastatic SLNB: 26 >1mm, 10 <1mm → 8 (all with SLNB metastases >1mm) out of 35 LND with additional LN metastasis (22,9%).>4 mm Breslow's depth: 90p → 52 lymphatic stations with metastatic SLNB: 42 >1mm, 10 <1mm → 13 (12 with SLNB >1mm and 1 <1mm) out of 49 LND with additional LN metastasis (26,5%). ***Conclusion:*** According to our results, LND could be avoided in patients with Breslow equal or lower than 2 mm and in patients with Breslow between 2,01-4 mm with SLNB metastases <1mm. However, more prospective studies should be performed.

EPS-266

Can physiologic colonic [18F]FDG uptake in PET/CT imaging predict response to immunotherapy in metastatic melanoma?

C. Sachpekidis[1], *C. K. Stein-Thoeringer*[2], *A. Kopp-Schneider*[1], *V. Weru*[1], *A. Dimitrakopoulou-Strauss*[1], *J. C. Hassel*[3]; [1]*German Cancer Research Center (DKFZ), Heidelberg, GERMANY,* [2]*Laboratory of Translational Microbiome Science, Internal Medicine I, University Clinic Tuebingen, Tuebingen, GERMANY,* [3]*Department of Dermatology and National Center for Tumor Diseases (NCT), University Hospital Heidelberg, Heidelberg, GERMANY.*

Aim/Introduction: To investigate if physiologic colonic [^{18}F]FDG uptake in PET/CT before start of immune checkpoint inhibitors (ICIs) correlates with clinical outcome of metastatic melanoma patients. The relation between [^{18}F]FDG uptake in lymphoid cell-rich organs and long-term patient outcome is also assessed. ***Materials and Methods:*** 119 patients scheduled for immunotherapy with ipilimumab underwent baseline [^{18}F]FDG PET/CT. PET/CT data analysis consisted of standardised uptake value (SUV), metabolic tumor volume (MTV) and total lesion glycolysis (TLG) calculations in the colon as well as measurements of the colon-to-liver SUV ratios (CLR_{mean}, CLR_{max}). Visual grading of colon uptake based on a four-point scale was also performed. Moreover, the spleen-to-liver SUV ratios (SLR_{mean}, SLR_{max}) and the bone marrow-to-liver SUV ratios (BLR_{mean}, BLR_{max}) were calculated. We also measured serum lipopolysaccharide (LPS) levels as a marker for bacterial translocation and surrogate for mucosal defense homeostasis. The results were correlated with patients' best clinical response, progression-free survival (PFS), and overall survival (OS) as well as clinical signs of colitis. ***Results:*** Median follow-up [95%CI] from the beginning of immunotherapy was 64.6 months [61.0 - 68.6 months]. Best response to treatment was progressive disease (PD) for 60 patients, stable disease (SD) for 37 patients, partial response (PR) for 18 patients and complete response (CR) for 4 patients. Kaplan-Meier curves demonstrated a trend for longer PFS and OS in patients with lower colonic SUV and CLR values, however no statistical significance was demonstrated. On the other hand, patients showing disease control as best response to treatment (SD, PR, CR) had significantly lower colonic MTV and TLG than those showing PD. Moreover, in multivariate analysis, colonic MTV and TLG correlated significantly with patient survival, with higher values of these parameters having an adverse effect on PFS. With regard to lymphoid cell-rich organs, significantly lower baseline SLR_{max} and BLR_{max} were observed in patients responding with disease control than progression to treatment, Furthermore, patients with lower SLR_{max} and BLR_{max} values had a significantly longer OS when dichotomized at their median. ***Conclusion:*** Physiologic colonic [^{18}F]FDG uptake, as assessed by means of SUV, before start of ipilimumab does not seem to independently predict patient survival of metastatic melanoma . On the other hand, colonic volumetric PET parameters, such as MTV and TLG, may identify patients showing disease control to immunotherapy, and significantly correlate with PFS. Finally, the investigation of glucose metabolism in the spleen and the bone marrow, may offer prognostic information.

EPS-267

The role of 18F-FDG PET/CT in changing the therapeutic plan in cutaneous melanoma patients at different clinical stages and time points of the disease.

Z. Dancheva, *T. Stoeva, M. Dyankova, S. Chausheva, T. Yordanova, B. Chaushev, A. Klisarova;*
Medical University, "Prf. Dr. Paraskev Stoyanov", Varna, BULGARIA.

Aim/Introduction: A definite survival benefit has been found in patients with cutaneous melanoma (CM) after radical metastasectomy, with 2-year survival as high as 50%. Therefore, it is important to identify the group of metastatic patients who would have a chance for radical surgery. In most cases 18F-FDG PET/CT upstages the patient, which leads to the redirection to targeted and immunotherapy that could improve significantly the one-year survival rates from 25% to over 70%. Our aim was to investigate the role of 18F-FDG PET/CT in changing the therapeutic plan in CM patients at different clinical stages and time points. ***Materials and Methods:*** We retrospectively analyzed 347 patients, 117 (33.7%) females and 230 (66.3%) males, aged between 10 and 87 years (mean 59.6 years). We divided the patients, according to the initial stage and by the clinical indication (staging, suspicion recurrence, restaging after first and second recurrence, and systemic therapy assessment). We investigated the relationship between the increase in stage and current clinical setting and the change in the therapeutic plan determined by 18F-FDG PET/CT. ***Results:*** 18F-FDG-PET/CT lead to change in treatment plan in 302 (87.8%) patients. The results demonstrated that the change correlates with the advanced initial stage of the patient. Notably, in patients with stage IIC and higher, 18F-FDG PET/CT significantly influenced the therapeutic decisions in over 83.0 % (p=0.035). We had data on the type of treatment changed in 280 of the patients. Stage II diagnosis was predominated by an earlier finding of operable lesions (56.09%- 65.3%). In patients diagnosed in stage III, 18F-FDG PET/CT was associated with a more frequent conversion to systemic treatment (59.3%.-85.7%). At staging a substantial amount of patients required additional surgical treatment (43.3%) or systemic treatment- 23.3%. In patients referred for suspected progression, we identified a similar number of cases suitable for surgery (36.4%) and systemic treatment in 40.3%. Among the patients after the first and second relapse, those suitable for systemic treatment or for changing the latter significantly were respectively 53.4% and 66.7%. ***Conclusion:*** 18F-FDG PET/CT is a whole body scanning and very sensitive procedure for CM because of their high glucose metabolism, which permit visualization the whole body, including the limbs, and allow the detection of small subclinical metastases. This study elicits the substantial role of 18F-FDG PET/CT in CM therapy management and precise redirection of patients to the most appropriate therapy for extending of their life expectancy.

EPS-268

Prognostic Value of Restaging FDG-PET/CT for Detecting Recurrence in Patients with Malignant Cutaneous Melanoma

M. Contreras Ameduri[1], *E. Noriega-Álvarez*[1], *M. Sicilia Pozo*[1], *C. Lucas Lucas*[1], *A. Padilla Bermejo*[1], *M. Cruz Montijano*[2], *L. García Zoghby*[2], *F. Pena Pardo*[1], *M. Talavera Rubio*[1], *A. García Vicente*[2], *Á. Soriano Castrejón*[2], *V. García Poblete*[1];
[1]*Servicio de Medicina Nuclear, Hospital General Universitario de Ciudad Real, Ciudad Real, SPAIN,* [2]*Servicio de Medicina Nuclear, Hospital Universitario de Toledo, Toledo, SPAIN.*

Aim/Introduction: To analyse the diagnostic capacity of FDG-PET/CT for the detection of tumoral recurrence in patients with malignant cutaneous melanoma (MM). ***Materials and Methods:*** Retrospective observational study of consecutive patients with confirmed MM referred for restaging FDG-PET/CT due to suspected recurrence between 2011 and 2022. Final diagnosis of recurrence was established by histopathological analysis or clinical follow-up of at least 6 months. Sensitivity, specificity, positive predictive value (PPV), negative predictive value (NPV) and diagnostic accuracy values were calculated. Statistical analysis was performed with SPSS v25 program (p<0.05 was considered significant). Univariant correlations between qualitative (sex, recurrence, localization of recurrence) and quantitative variables (age, initial MM stage) were measured with Chi-Square, Kendall's Tau_b and Pearson correlation indexes. Cox multivariate regression analysis between qualitative-quantitative variables was performed, including overall survival (OS) and progression-free survival (PFS). PFS and OS were assessed using Kaplan-Meier curves. ***Results:*** We evaluated 234 patients (101 women) with a mean age of 59.5 years (range: 22-88 years). Tumoral recurrence was detected in a total of 117 patients with pathologic FDG-PET/CT results in 111. Remaining 117 patients showed no recurrence, with negative FDG-PET/CT in 113. FDG-PET/CT sensitivity, specificity, PPV, NPV and accuracy values were 94.9%, 96.6%, 96.5%, 95% and 95.7%, respectively (χ^2:195.8; p<0.01). In univariate analysis with Pearson and Kendall's Tau_b correlation indexes, FDG-PET/CT results showed significant correlation with recurrence, location and initial stage of MM (p<0.01), and sex of the patients (p<0.05). Cox regression analysis showed that cutaneous lesions had greater risk of death, and increased risk of recurrence/death in bone lesions (p<0.01 and p=0.001). Tumour stage II showed higher risk of recurrence (p=0.009), while tumour stages II-IV showed higher risk of death (p=0.02). Male patients also had greater risk of recurrence (p=0.03) or death (p=0.04). Analyzing Kaplan-Meier curves, both OS and PFS were significantly higher in patients with negative restaging FDG-PET/CT scans than positive ones, showing a mean OS of 329.1 months (95%CI: 312.5-345.8) vs. 72.8 months (95%CI: 65.8-82.8), and mean PFS of 315.9 months (95%CI: 300.6-331.3) vs. 38.6 months (95%CI: 32.2-44.9), respectively. Comparing OS by sex in FDG-PET/CT positive patients, a shorter survival was found in men, with median OS of 119 (95%CI: 96.2-141.8) vs. 172.9 months (95%CI: 132.5- 209.3) in women. ***Conclusion:*** In concordance with the existing literature, we verified that restaging FDG-PET/CT has excellent diagnostic performance for detection of recurrences in patients with malignant cutaneous melanoma, and also seems to have prognostic value.

EPS-269

Survival and risk factors analysis for locoregional and distant metastases in patients with sentinel lymph node-negative cutaneous melanoma

A. Leiva Montejo, *A. Blesa Jimenez, A. De Agrela Serrao, C. Ruiz Corbalán, D. Cáceres Silva, J. Contreras Gutierrez, J. Navarro Fernández, A. Hernandez Martinez, T. Rodriguez Lorcano, L. Frutos Esteban, L. Mohamed Salem, M. Castellon Sánchez;*
Hospital Virgen de la Arrixaca, Murcia, SPAIN.

Aim/Introduction: Sentinel lymph node biopsy(SLNB) is a staging surgical procedure for patients with melanoma who are at risk of having occult nodal metastases which are the most important prognostic factor in early-stage melanoma. However, the rate of metastasic melanoma following negative SLNB long-term is from 6 to 24%. The aim of this study was to analyze the overall

survival and risk factors for regional and systemic metastases in patients with SLNB-negative melanoma during the clinical follow-up. ***Materials and Methods:*** Designed as a retrospective study, a multivariate analysis was done using the SPSS version 28 program. Data from 294 patients with negative and positive SLNB were collected since 2013 until 2023. A total of 211 SLNB-negative patients were analyzed. Variables studied were sex, age, tumor characteristics (melanoma subtype, tumor thickness, ulceration), location (head and neck, trunk and extremities), positive, negative and false negative SLNB. Metastases were classified as regional lymph node/locoregional cutaneous metastases and distant metastases. p<0.05 was considered statistically significant. Overall survival(OS) and Progression Free Survival(PFS) was calculated since the diagnosis date until death date and until progression date, respectively. Both were studied with Kaplan-Meier. ***Results:*** 294 patients were included, SLNB were positive in 83(28.24%) and negative in 211(71.76%). A total of 24(11.37%) SLNB-negative developed metastases, including 10(41.66%) distant and 14(58.33%) locoregional. SLNB-negative patients who progressed were older[(68.17+/-2.82years)(p<0.044)]. SLNB-negative patients that didn't progress had mostly the superficial spreading melanoma(SSM) subtype[155(82.9%)(p<0.05)]. Tumor ulceration was present in 9(37.5%)SLNB-negative patients with metastases and in 23(12.29%)SLNB-negative patients without metastases. (p<0.05). SLNB-false negative patients were 10(4.73%) and they were compared to SLNB-positive patients. SLNB-false negative patients were mostly men[6(60%)(p=0.04)], with the SSM subtype[7(70%)(p=0.033)]. A higher tumor thickness[(3.33cm+/-0.29)(p<0.001)] was related to a SLNB-positive.Mean follow-up was 61 months. SLNB-negative patients: 20(9.47%) died from melanoma and 180(85.30%) remained alive and stable. Median OS for SLNB-negative patients was 125.18 months (IC95% 120.33-130.03) and for SLNB-positive patients was 86.86 months (IC95% 76.56-97,16)(p=0.00). Mean PFS for SLNB-negative was 122.50 months (IC95% 117-127.9) ***Conclusion:*** Our patients who underwent SLNB in early stages were mostly negative. Only 24 SLNB-negative patients progressed during the clinical follow-up. Age and tumor ulceration are significant risk factors for developing melanoma metastases in this kind of patients. OS and PFS were almost the same in SLNB-negative patients.

EPS-270

A steerable modality for simultaneous radio- and fluorescence-guidance during robotic surgery

M. van Oosterom[1,2], *L. J. Slof*[1], *S. I. van Leeuwen*[1], *S. Azargoshasb*[1], *A. Berrens*[2], *K. Houwing*[1], *H. G. van der Poel*[2], *F. W. B. van Leeuwen*[1];
[1]*Leiden University Medical Center, Leiden, NETHERLANDS,* [2]*NETHERLANDS Cancer Institute - Antoni van Leeuwenhoek Hospital, Amsterdam, NETHERLANDS.*

Aim/Introduction: Intraoperative image guidance is needed to facilitate surgeons in the quest to resect diseased tissues with a high precision. Hybrid tracers have demonstrated to be more than the sum of their parts by fully integrating the complementary image-guidance provided via radioactive emissions (in-depth target localization) and fluorescent emissions (high resolution superficial target delineation) [1]. In parallel the engineering of steerable DROP-IN gamma probes has helped open up the way for robotic radioguided surgery [2]. Building on these findings, and new concepts such as the Click-On gamma probe [3] and handheld Optonuclear probe [4], we generated a miniaturized hybrid Click-On detector and evaluated it on clinical specimens. ***Materials and Methods:*** The hybrid Click-On detector was designed for a ProGrasp robotic forceps, and to facilitate both radio-tracing (^{99m}Tc) and near-infrared fluorescence detection (indocyanine green; ICG). Following the mechanical engineering, the system was produced using 3D printing and multi-axis precision milling. The technical aspects of the prototype modality were characterized and its compatibility with the robotic platform was evaluated on freshly excised tissue specimens of seven prostate cancer patients that underwent a sentinel lymph node procedure guided by the hybrid tracer ICG-^{99m}Tc-nanoscan [5]. A computer-vision algorithm was built to register the probe movements during the evaluations [3], and to visualize the recorded counts with respect to the anatomic areas visible in the endoscopic view. ***Results:*** When 'clicked on' the daVinci ProGrasp instrument, the Click-On Optonuclear provided the surgeon with autonomous and fully 6 degrees of freedom maneuverable molecular detection at the tips of the laparoscopic instrument. The modalities sensitivity for ^{99m}Tc was found to be $>10^{-4}$ MBq and sensitivity for ICG $>10^{-6}$ mg/mL. During the analysis of 17 specimens, the system was able to correctly identify both tracer signatures. The tracking algorithm, allowed us to augment the endoscopic view with a heat-map based display of the radioactive and fluorescent count rates. ***Conclusion:*** With the steerable hybrid Click-On modality, a first step towards 'fingertip' radio- and fluorescence-sensing by surgical instruments has been realized. At the same time the sensing capabilities help support robotic molecular imaging. A potentially new approach to image guided surgery. ***References:*** 1. Wit et al., Eur J Nucl Med Mol Imaging, 20232. Dell'Oglio et al., Eur Urol, 20213. Azargoshasb et al., Eur J Nucl Med Mol Imaging, 20214. Vidal-Sicart et al., IJCARS, 20195. Vreeburg et al., Eur J Nucl Med Mol Imaging, 2023

EPS-271

Feasibility of [99mTc] Tc-FAPI-SPECT Imaging for Detection of Primary Tumors, Lymph Node, and Distant Metastasis in Various Cancers

S. Rezaei*, E. Gharepapagh, S. Dabiri Oskue;*
Department of Nuclear Medicine, Medical School, Tabriz University of Medical Sciences, Tabriz, IRAN, ISLAMIC REPUBLIC OF.

Aim/Introduction: Cancer-associated fibroblasts (CAFs) express high levels of fibroblast activation protein (FAP). A variety of cancers with desmoplastic reactions, such as breast cancer, can be imaged with SPECT imaging with FAP inhibitors (FAPIs) since FAP is almost absent from healthy tissue. This study evaluated ^{99m}Tc-labeled FAP inhibitor radioligand ([^{99m}Tc] Tc-FAPI) for tumor stroma imaging in patients with various cancers and analyzed results from the perspective of stromal heterogeneity. ***Materials and Methods:*** Twenty patients with confirmed breast, lung, and colorectal cancers were included in this study. The patients had previously undergone other scans to evaluate the disease. SPECT imaging was performed one hour after [^{99m}Tc] Tc-FAPI injection. Lesions were categorized into three types: primary tumors, lymph node metastases, and distant metastases (Dm). Tumor-to-background ratios (T/B) were used to calculate semi-quantitative lesion uptake analysis. In all cases, histopathology corroborated the oncological diagnosis. ***Results:*** [^{99m}Tc] Tc-FAPI detected primary tumors, with 100% and 94% sensitivity and specificity, respectively. Moreover, Tc-FAPI demonstrated lymph nodes and distant metastases with high accuracy due to lower background activity and higher uptake in sub-centimetric lesions. Compared to lymph nodes and distant metastases, [^{99m}Tc] Tc-FAPI uptake was greater in primary tumors in the T/B data. Interestingly, [^{99m}Tc] Tc-FAPI was well absorbed in

peritoneal carcinomatosis lesions in recurrent colorectal cancer. ***Conclusion:*** [^{99m}Tc] Tc-FAPI SPECT imaging can provid valuable information about the microenvironment surrounding tumors and is considered a promising tool in the prognostic assessment of tumors, particularly breast cancer and recurrent colorectal cancers.

EPS-272

The Role of [18F]FDG PET/CT for predicting histology and prognosis in patients with thymic lesions

A. Castello[1], *P. Mendogni*[2], *M. Cattaneo*[2], *L. Rosso*[2], *G. A. Croci*[3], *S. Pacella*[1], *L. Florimonte*[1], *F. Lococo*[4], *S. Margaritora*[4], *S. Ferrero*[3], *M. Nosotti*[2], *M. Castellani*[1];
[1]*Department of Nuclear Medicine, Fondazione IRCCS Ca' Granda, Ospedale Maggiore Policlinico, Milan, ITALY,* [2]*Thoracic Surgery, Fondazione IRCCS Ca' Granda, Ospedale Maggiore Policlnico, Milan, ITALY,* [3]*Division of Pathology, Fondazione IRCCS Ca' Granda, Ospedale Maggiore Policlinico, Milan, ITALY,* [4]*Department of Thoracic Surgery, Fondazione Policlinico Universitario A. Gemelli, IRCCS, Rome, ITALY.*

Aim/Introduction: We aimed to investigated whether metabolic parameters by [^{18}F]FDG PET/CT were associated with histology and their potential prognostic role in patients with resected thymic lesions. ***Materials and Methods:*** A total of 84 patients (36 male, 48 female; mean age 56.9 y) who underwent thymectomy and preoperative [^{18}F]FDG PET/CT from 2012 to 2022 were retrospectively analyzed. Associations between histology and metabolic parameters (i.e. SUVmax, SUVmean, SUVpeak, TLG, and MTV), as well as the tumor-to-mediastinum (T/M) and SUVmax/Tcm ratios were examined. Progression-free-survival (PFS) was determined and compared using the Kaplan-Meier and the log-rank test. The median follow-up was 46 months (range 3-121 months). ***Results:*** The anterior mediastinal masses included 22 thymic hyperplasia, 32 low-risk thymomas (LRT, types A, AB, B1), and 30 high-risk thymomas (HRT, types B2, B3, and carcinoma). We observed a statistically significant difference between LRT and HRT among metabolic parameters, expressed by SUVmax (mean 3.89 ± 2.56 vs 6.10 ± 3.37, p=0.001), SUVmean (mean 2.36 ± 1.43 vs 3.10 ± 1.99, p=0.003), SUVpeak (mean 3.28 ± 2.20 vs 5.12 ± 2.70, p=0.001), TLG (mean 398 ± 1290 vs 258 ± 387, p=0.021), and T/M (mean 2.22 ± 1.47 vs 3.70 ± 2.75, p=0.001). Moreover, patients with median SUVmax lower than 4.3, as well as those with median SUVmean and median SUVpeak lower than 2.87 and 4.03, respectively, showed a longer PFS (p = 0.009, p= 0.05, and p=0.05), whereas volumetric parameters (i.e. MTV, and TLG) and metabolic ratios (i.e. T/M, and SUVmax/Tcm) were not associated with PFS. ***Conclusion:*** In our study metabolic parameters, derived from preoperative [^{18}F]FDG PET/CT, seem to provide useful information to differentiate thymic histotypes. Furthermore, SUVs-based parameters appear promising prognostic factors in terms of recurrence. ***References:*** Chiappetta M, Mendogni P, Cattaneo M, et al. Is PET/CT Able to Predict Histology in Thymic Epithelial Tumours? A Narrative Review. Diagnostics (Basel). 2022;13(1):98. Han S., Jungsu K., Seung S.O., Seo Y., Jae M., Geun P., Lee D., Choi S., Ryul H., Yong K., et al. Diagnostic and Prognostic Values of 2 [18 F] FDG PET/CT in Resectable Thymic Epithelial Tumour. Eur. Radiol. 2021;32:1173-1183.

1710a

Wednesday, September 13, 2023, 08:00 - 09:00
Hall K

Mini Course 1 - Technologists Committee: Radiotherapy Planning Using PET/CT and PET/MR

OP-871

Hybrid imaging in radiotherapy and the role of technologists

B. Bak;
Radiotherapy Department II, Greater Poland Cancer Centre, Poznan, POLAND.

OP-872

PET/CT based radiotherapy planning

V. Mautone;
Instituto Romagnolo per lo Studio dei Tumori "Dino Amadori" - IRST IRCCS U.o.s Medicina Nucleare Diagnostica, Meldola (FC), ITALY.

OP-873

PET/MRI based radiotherapy planning

D. Sipos;
Somogy County Kaposi Mór Teaching Hospital, Dr. József Baka Center, Department of Radiation Oncology, Kaposvár, HUNGARY.

1710b

Wednesday, September 13, 2023, 09:05 - 10:05
Hall K

Mini Course 2 - Technologists Committee: AI in the Technologists Practice

OP-875

Improving PET imaging based on artificial intelligence

M. De Summa;
Medipass S.p.a. c/o Fondazione Policlinico Universitario A. Gemelli IRCCS, PET-CT, Radiopharmacy and AI Research Laboratory, Rome, ITALY.

OP-876

AI in the Technologists Practice.

C. Votta;
Fondazione Policlinico Universitario A. Gemelli IRCCS, Deparmtnet of Diagnostic Imaging, Oncological, Radiotherapy and Hematology, Rome, ITALY.

1710c

Wednesday, September 13, 2023, 10:15 - 11:15
Hall K

Mini Course 3 - Technologists Committee: Phantoms Management

OP-940

The use of phantoms in QC & QA

K. Matuszewski;
Greater Poland Cancer Centre, Medical Physics Dep, Poznan, POLAND.

OP-941

Gamma Camera & PET-CT vs PET-MRI phantoms management

***D. Sørensen**;*
Department of Nuclear Medicine, Odense University Hospital, Odense, DENMARK.

OP-942

Phantoms in practice & Computer-based phantom models

***C. Abreu**;*
Royal Marsden NHS Foundation Trust, London , UNITED KINGDOM.

1711

Wednesday, September 13, 2023, 8:00 AM - 9:30 AM

Hall G1

Case Report Session 3 - TROP Session: Every Day a Discovery with FAP and Novel Targets

OP-878

FAPi imaging identified occurrence of fibrosis may indicate rapid progression of liver failure induced by immune checkpoint inhibitor

***X. Jia**[1], R. Tao[1], Y. Yang[1], Y. Wang[1], X. Li[1], B. Jia[2], R. Gao[1];*
[1]The first hospital of Xi'an jiaotong university, Xi'an, CHINA, [2]Medical Isotopes Research Center and Department of Radiation Medicine, School of Basic Medical Sciences, Peking University, Beijing, CHINA.

Aim/Introduction: The emergence of immune checkpoint inhibitors (ICIs) offers hope for the treatment of malignant tumors; however, they may lead to immune-related adverse reactions (irAE). ICI-related liver injury is a poorly understood irAE with varied clinical presentations and histopathological correlates, and there is still lack of non-invasive predictor to differentiate patients who will soon escalate to acute liver failure (ALF). ***Materials and Methods:*** A 34-year-old male patient with extensive-stage small cell lung cancer was treated with durvalumab (an anti-PD-L 1 antibody) and developed Grade 1 liver irAE during the eighth treatment. Slightly elevated liver enzyme was observed and abdomen US and CT revealed fatty liver. With exclusion of other potential liver disease, including liver metastasis, alcoholic hepatitis, and viral hepatitis, a diagnose of liver irAE was made. The ICIs induced liver injury slowly progressed to Grade 2 though prednisone (80mg/d for 1 week) was applied. In the mean time, Fapi imaging was prescribed to evaluate the tumor burden. ***Results:*** Except for tumor uptake in left lung, strong and diffuse fibroblast activation protein expression in hepatic tissue was imaged by radiolabled FAP inhibitor . The patient presented with abdominal distention and nausea, and abrupt rise of liver enzymes and bilirubin in the following week after FAPI imaging. Despite prompt administration of high dose intravenous methylprednisolone (240 mg/d) and plasmapheresis (2000 mL/d), the patient's liver enzymes rise rapidly. Hepatic encephalopathy, characterized by confusion and disturbed conscious occurred and the patient died within the following 24 hrs. Liver tissue from patients with ALF showed hepatic stellate cells (HSCs) activation and collagen deposition, which is thought to serve as a scaffolding that maintains hepatic integrity in the rapid progression of liver failure. The HSCs activation caused short-term occurrence of fibrosis, which identified by FAPI imaging in this ICIs induced ALF, is reported to be an important step in this process. The other 9 cases with mild ICIs-induced liver injury underwent FAPI imaging provided further support: except for focal concentration in liver metastasis, no diffuse uptake of the FAPI was revealed in their hepatic tissue. All 9 patients responded well to routine therapy and their liver dysfunction was promptly improved. ***Conclusion:*** Our data suggest that FAPI imaging has the potential to serve as a new diagnostic basis for early ICI-induced ALF.

OP-879

Is This a Real [68Ga]Ga-FAPI Scan? The Strange Case of [68Ga]Ga-FAPI-avid Liver

***E. Fortunati**[1], G. Cuzzani[1], S. Telo[2], C. Nanni[3], P. Castellucci[3], A. Farolfi[3], L. Zanoni[3], T. Galasso[4], M. Ferrari[4], F. Natali[4], G. Bandelli[4], P. Candoli[4], S. Fanti[1,3];*
[1]Nuclear Medicine, Alma Mater Studiorum University of Bologna, Bologna, ITALY, [2]Nuclear Medicine Unit, AUSL Romagna, Cesena, ITALY, [3]Nuclear Medicine, IRCCS, Azienda Ospedaliero-Universitaria di Bologna, Bologna, ITALY, [4]Interventional Pulmunology Unit, IRCCS, Azienda Ospedaliero-Universitaria di Bologna, Bologna, ITALY.

Aim/Introduction: A 68y.o. patient with history of smoking, heavy-drinking, hepatic cirrhosis(Child-Pugh Score:B7)with ascites, severe portal hypertension and previous HBV-infection, underwent both[18F]F-FDG-PET/CT and [68Ga]Ga-FAPI-PET/CT to stage lung neoplasia in the right lower lobe. As it is well known,[68Ga]Ga-FAPI presents low uptake and high Tumour-to-Background-Ratio(TBR) in healthy liver parenchyma, thus offering the opportunity to better study liver metastases. Fibroblast activation protein(FAP) expression is associated with the activation of hepatic stellate cells in fibrotic conditions involving the liver leading to cirrhosis and derived from different chronic causes. ***Materials and Methods:*** The patient was enrolled to perform a staging [18F]F-FDG-PET/CT for lung cancer within a prospective interventional study conducted in our Nuclear Medicine Department. He later underwent[68Ga]Ga-FAPI-46-PET/CT and images were acquired both at 10'and at60'. The two PET/CTs were performed 13days apart. ***Results:*** Blood tests have confirmed the presence of cirrhosis by showing altered bilirubin values, both total(2.76mg/dL) and fractionated (direct 0.8mg/dL;indirect 1.96mg/dL), elevated transaminases(AST:52U/L) and gamma glutamyl transferase values(215U/L). Both [18F]F-FDG and [68Ga]Ga-FAPI-PET/CT showed radiotracer uptake of the known pulmonary lesion and of a focality at the 10th left rib, described as a metastasis. Early(10') and late(60') [68Ga]Ga-FAPI-scans confirmed the uptake in correspondence of the primary lesion and of the bone localization. Intense and diffuse uptake was detected in the liver parenchyma (SUVmax10'=9.9;SUVmax60'=7.2;SUVmean10'=7.1;SUVmean60'=4.7). In a sample of 10 patients who underwent [68Ga]Ga-FAPI-PET/CT without any liver disease or liver parenchyma alterations at conventional imaging, the average SUVmax of liver parenchyma is1.3[median:1.3;range:0.8-1.9] at10'scan and 1.2[median:1.2;range:0.9-1.4] at 60'scan. The average SUVmean of liver parenchyma is 0.8[median:0.8;range:0.5-1] at10'scan and 0.6[median:0.6;range:0.4-0.7] at60'scan. ***Conclusion:*** This case-report is an extremely brilliant example of what already reported in literature[1-3] on how the presence of cirrhosis leads to an increased [68Ga]Ga-FAPI uptake in liver parenchyma. This is a relevant finding because it leads to a reduced TBR with a consecutive lower detection of possible liver metastasis. The collection of an accurate anamnesis before PET/CT is also of primary importance, in order to avoid mistakes in interpretation of similar findings. This case pointed out how [68Ga]Ga-FAPI-PET/CT could be an important tool to precociously recognize fibrosis in non-oncological disease, also before the execution of conventional imaging.

OP-880

Role of 68Ga FAPI-04 PET/CT in detecting cardiac sarcoidosis in a patient mimicking malignancy and its comparison with 18F-FDG PET/CT

S. Patel, *P. Sundaram, P. Sundaram, F. Saju;*
Amrita Institute of Medical Sciences & Research Center, Kochi, INDIA.

Aim/Introduction: 1. To characterize specific imaging findings of cardiac sarcoidosis using ^{68}Ga FAPI-04 PET/CT.2. To compare the study findings obtained from ^{68}Ga FAPI-04 PET CT and ^{18}F-FDG PET/CT in a patient with cardiac sarcoidosis.3. To evaluate the diagnostic role of ^{68}Ga FAPI-04 PET CT in differentiating cardiac and systemic sarcoidosis from lymphoma, tuberculosis, and other systemic inflammatory diseases. ***Materials and Methods:*** A patient suspected of having lymphoma and recently diagnosed with non-infective endocarditis was enrolled for the study. 4 millicuries (mCi) of Gallium-68 (^{68}Ga)-conjugated FAP inhibitor-04 (FAPI) were injected intravenously. A diagnostic whole-body imaging CECT was acquired, followed by PET images in 3D mode from the head to the upper thigh. Following appropriate dietary preparation a second PET/CT scan was scheduled after 3 days with ^{18}F-FDG (0.1 mCi/Kg). ***Results:*** The images obtained from the left ventricular myocardium showed significant heterogeneous ^{68}Ga-FAPI uptake throughout the myocardium with a maximum standardized uptake value (SUVmax) of 20.4, compared to FDG which showed uptake in the apico-anterior region with SUVmax of 16.6. Additionally, the images obtained from ^{68}Ga-FAPI PET CT showed a mediastinal lymph node uptake pattern more characteristic of sarcoidosis. Non-specific FDG uptake in the brain, inflammatory cervical lymph nodes, and degenerative bone changes, seen using ^{18}F-FDG, were not seen in ^{68}Ga-FAPI PET CT, further aiding in a more accurate disease diagnosis. ***Conclusion:*** The life-threatening complications associated with cardiac sarcoidosis underscore the importance of early diagnosis and management. Increasing role FDG PET/CT in patients with systemic and cardiac sarcoidosis has proven to be a valuable diagnostic tool[1]. Advent of novel radiopharmaceuticals such as ^{68}Ga-FAPI has significantly enhanced the potential of PET imaging. By selectively targeting cardiac fibroblast cells with high FAP expression [2], ^{68}Ga-FAPI exhibits increased specificity in detecting myocardial involvement in sarcoidosis. In this case study ^{68}Ga-FAPI PET CT was helpful in accurately diagnosing cardiac sarcoidosis with higher specificity compared to ^{18}F-FDG PET CT, with higher target-to-background ratio, and independence from euglycemic state maintenance being observed as additional benefits. Further investigations are warranted to fully explore its clinical utility. ***References:*** [1]. Keijsers RGM, Grutters JC. In Which Patients with Sarcoidosis Is FDG PET/CT Indicated. J Clin Med. 2020 Mar 24;9(3):890. [2]. Siebermair J, Kessler L, Kupusovic J, Rassaf T, Rischpler C. Cardiac fibroblast activation detected by 68Gallium-FAPI-46 positron emission tomography-magnetic resonance imaging as a sign of chronic activity in cardiac sarcoidosis. Eur Heart J Case Rep. 2022 Jan;6(1):ytac005.

OP-881

An Example of How [68Ga]Ga-FAPI PET/CT can Potentially Help Changing The Therapeutic Process of Patients with Sarcoma

G. Cuzzani[1], *E. Fortunati*[1], *M. Focaccia*[2], *S. Telo*[3], *A. Farolfi*[4], *C. Nanni*[4], *P. Castellucci*[4], *T. Frisoni*[2], *B. Spazzoli*[2], *C. Plenteda*[5], *D. M. Donati*[2], *S. Fanti*[1,4];
[1]*Nuclear medicine, Alma Mater Studiorum University of Bologna, Bologna, ITALY,* [2]*Orthopaedic Oncology Unit, IRCCS Istituto Ortopedico Rizzoli, Bologna, ITALY,* [3]*Nuclear Medicine Department, AUSL Romagna, Romagna, ITALY,* [4]*Nuclear Medicine IRCCS, Azienda Ospedaliero-Universitaria di Bologna, Bologna, ITALY,* [5]*Hematology and Bone Marrow Transplant Center Unit, Parma University Hospital, Parma, ITALY.*

Aim/Introduction: A 63-year-old man with a history of hematologic disorder, idiopathic Multicentric Castleman Disease(iMCD) who has been treated with Siltuximab for 3years encountered a growing mass in his right shoulder.A contrast ultrasound-guided biopsy was performed and the histological diagnosis was sclerosing epithelioid fibrosarcoma,a rare soft tissue sarcoma. Conventional imaging(CT and MRI)reported a solid lesion and multiple adenopathies of the right shoulder's region,but could not distinguish whether they were of sarcomatoid origin or from Castleman Disease.A high expression of fibroblast activation protein(FAP) was observed in multiple sarcomas,indicating an enormous potential for PET/CT using 68Ga-radiolabeled inhibitors of FAP (FAPI)[1]. ***Materials and Methods:*** Therefore,the patient was addressed to our Nuclear Medicine Department to be enrolled in a prospective interventional study and perform both a [18F]F-FDG and a [68Ga]Ga-FAPI-46 PET/CT. The patient underwent a [18F]F-FDG PET/CT at 60minutes from the radiotracer injection with a Field of View extended from the vertex to the toes; a [68Ga]Ga-FAPI-46 PET/CT was performed the following day and images were acquired both at 10and 60minutes. ***Results:*** The [18F]F-FDG PET/CT showed intense uptake of a solid lesion involving the right pectoralis region, part of the right scapula,axilla,clavicle and the overlying skin,along with multiple right axillary lymph nodes and of the shoulder's region. In addition,it detected small nodules at both lungs reported as metastases and not previously detected at conventional imaging.The [68Ga]Ga-FAPI-46 PET/CT was concordant, presenting a higher SUVmax of the shoulder's lesion(8.8 for [18F]F-FDG and 20.2 for [68Ga]Ga-FAPI); furthermore,it also displayed a liver focality located at segment V-VI with SUVmax=4.7,unknown at previous imaging and suspicious for metastasis. ***Conclusion:*** Determine patients' management is often challenging; the standard of care of fibrosarcoma is surgical excision with adequate margins in association with radiotherapy. In this particular case,due to the size and location of the neoplasm, the radical surgical treatment would have been a forequarter amputation of the dominant upper limb, with huge affection of quality of life. [18F]F-FDG and [68Ga]Ga-FAPI PET/CTs had reported systemic disease: for this reason and for clinical condition,the patient was addressed to palliative radiotherapy after multidisciplinary evaluation and patient's consult. Overall, an accurate detection rate for new metastases or suspicious lesions to examine and a high tumour-to-background ratio are fundamental to address patients to the correct therapeutic process; hence, [68Ga]Ga-FAPI-46 PET/CT is considered a promising tracer for sarcomatoid malignancies. ***References:*** [1]Koerber,S.A.,Finck,R.,Dendl,K.et al.Novel FAP ligands enable improved imaging contrast in sarcoma patients due toFAPI-PET/CT.Eur J Nucl Med Mol Imaging48,3918-3924(2021). https://doi.org/10.1007/s00259-021-05374-4

OP-882

[68Ga]Ga-FAPI PET/CT: a Valid Aid in Breast Cancer Not Only for Malignancies Reporting

G. Cuzzani[1], *E. Fortunati*[1], *S. Telo*[2], *C. Nanni*[3], *P. Castellucci*[3], *A. Farolfi*[3], *S. Zanotti*[4], *S. Grendele*[5], *D. Rosini*[4], *M. Taffurelli*[4], *S. Fanti*[1,3];
[1]*Nuclear medicine, Alma Mater Studiorum University of Bologna, Bologna, ITALY,* [2]*Nuclear Medicine Department, AUSL Romagna, Romagna, ITALY,* [3]*Nuclear Medicine, IRCCS, Azienda Ospedaliero-Universitaria di Bologna, Bologna, ITALY,* [4]*Breast Surgery, Department of Oncology and Hematological Diseases, IRCCS Azienda Ospedaliero-Universitaria di Bologna, Bologna, ITALY,* [5]*Breast Surgery, Department of Functional Oncology, AULSS 7 Pedemontana, Santorso Hospital, Vicenza, ITALY.*

Aim/Introduction: [68Ga]Ga-FAPI is known to be a promising PET/CT imaging tracer,showing an advantage when compared to[18F]F-FDG in those tissues which present a natural diffuse FDG uptake,such as liver and brain; furthermore,it shows high performance in the detection of breast cancer malignancies[1]. This is a case of a 66-year-old woman who was diagnosed with invasive ductal carcinoma of the left breast and presented a homolateral axillary lymph node suspicious for malignancy at traditional imaging(ultrasound and mammography).At a physical examination the left nipple showed a small ulcer and bloody discharge,so a cytologic evaluation was performed.The patient was offered neoadjuvant chemotherapy subject to a staging [18F] F-FDG PET/CT. ***Materials and Methods:*** The patient was enrolled in a prospective interventional study ongoing in our Nuclear Medicine Department and underwent both a [18F]F-FDG and a [68Ga]Ga-FAPI-46 PET/CT. The two scans were performed seven days apart;images were acquired 60 minutes after the [18F]F-FDG injection, while for [68Ga]Ga-FAPI-46 image acquisition occurred at 10 minutes("early scan")and at 60 minutes("standard scan")from the radiotracer injection. ***Results:*** The [18F]F-FDG PET/CT showed intense uptake in the upper outer quadrant of the left breast(SUVmax=17.6),agreeing with traditional imaging on the localization of the primary tumour,and focal uptake of a left axillary lymph node(SUVmax=18.6)reported as nodal metastasis. The subsequent [68Ga]Ga-FAPI-46 PET/CT confirmed the known mammary and axillary findings(which presented increasing SUVs from the early to standard scan)but also reported focal uptake of the left nipple(early SUVmax=8.3,standard SUVmax=7.7).In addition,[68Ga]Ga-FAPI-46 revealed mild uptake of the lateral-posterior arch of the sixth right rib(early SUVmax=5.5,standard SUVmax=5.7)which was reported to be more likely a benign formation according to the bone remodeling appearance at CT images,such as an enchondroma or fibrous dysplasia.The cytologic evaluation of the nipple's bloody discharge later resulted in "absence of malignancy" and it was reported as adenoma(which needed surgery despite being a benign condition),while the rib finding was confirmed stable at a CT scan performed seven months later. ***Conclusion:*** It is important to keep in mind that oncologic and collateral findings are equally common,therefore expertise and pathology are essential for the right diagnosis;knowing the causes of FAPI uptake is fundamental for an accurate image interpretation and to avoid false positives.This case is an example of how [68Ga] Ga-FAPI-46 PET/CT identified two additional findings which were negative at a prior [18F]F-FDG PET/CT and could have easily been mistaken for breast cancer metastases. ***References:*** [1]Kömek,-Can,Güzel,Oruç,Gündoğan,Yildirim,Kaplan,Erdur,Yıldırım,Çakabay.68Ga-FAPI-04 PET/CT,a new step in breast cancer imaging:a comparative pilot study with the18F-FDG PET/CT.Ann Nucl Med.2021Jun;35(6):744-752.doi:10.1007/s12149-021-01616-5. Epub2021May 2.PMID:33934311.

OP-883

Comparative PET/CT imaging in a patient with metastatic clear cell renal cell carcinoma: 68Ga-NY104 versus 68Ga-PSMA versus 18F-FDG

W. Zhu, *X. Li, Y. Zhang, Y. Li, L. Huo;*
Peking Union Medical College Hospital, Beijing, CHINA.

Aim/Introduction: ^{68}Ga-NY104 is a novel small molecule tracer targeting carbonic anhydrase IX (CAIX), which is overexpressed in clear cell renal cell carcinoma (ccRCC). ^{68}Ga-PSMA PET/CT has also been proven effective in RCC imaging due to neovascularization. However, no comparative study has been done to compare the two imaging modalities. ***Materials and Methods:*** A 53-year-old male had radical nephrectomy due to ccRCC of left kidney in 2008. In 2022, an avidly-enhancing right kidney mass was found on ceCT during follow-up, as well as multiple other lesions in the liver, abdominal wall, pancreas, and seminal vesical. ^{68}Ga-NY104 and ^{68}Ga-PSMA PET/CT was performed for restaging given the suspicion of metastatic ccRCC. A comparative ^{18}F-FDG PET/CT was also performed. The study was approved by the institutional review board of Peking Union Medical College Hospital (approval NO. ZS-3089 and ZS-2532). Metastatic ccRCC was later confirmed by biopsy of the abdominal wall lesion. ***Results:*** A total of 10 PET-positive lesions were identified on either of the three PET scans, including 1 right kidney lesion, 1 hepatic lesion, 1 pancreatic lesion, 2 abdominal wall lesions, 1 seminal vesicle lesion, 2 pulmonary lesions (0.6cm), 1 abdominal lymph node, and 1 left thigh lesion. On ^{68}Ga-NY104 PET/CT, all lesions were PET positive, demonstrating intensive uptake (SUVmax 27.5). On ^{68}Ga-PSMA PET/CT, only 6 lesions (1 hepatic, 1 pancreatic, 2 abdominal wall, 1 seminal vesicle, and 1 left thigh lesion) showed substantial uptake (SUVmax 12.9). On ^{18}F-FDG PET/CT, only mild uptake was noted in 4 lesions (1 right kidney, 1 pancreatic, 1 abdominal wall, and 1 seminal vesicle lesion) with SUVmax of 4.5. For all lesions, ^{68}Ga-NY104 demonstrated much higher tumor uptake and tumor-to-background ratio than ^{68}Ga-PSMA and ^{18}F-FDG. ***Conclusion:*** ^{68}Ga-NY104 PET/CT is a powerful tool to evaluate metastatic ccRCC and has the potential to surpass ^{68}Ga-PSMA and ^{18}F-FDG.

OP-884

[99mTc]Tc-HYNIC-TOC as an alternative to [123I]mIBG for Neuroblastoma Staging, a Comparative Case Series

K. Hlongwa, *A. Brink, O. Kolade, A. Alnabulsi, S. More;*
Red Cross War Memorial Children's Hospital and
University of Cape Town, Cape Town, SOUTH AFRICA.

Aim/Introduction: Neuroblastoma is the most common solid extracranial malignant paediatric tumour and is of neuroectodermal origin. Molecular imaging plays a key role in staging, evaluation of response to therapy, and follow-up. [^{123}I] mIBG has played an essential role in evaluating neuroblastoma patients with prognostic significance. Neuroblastomas have demonstrated expression of somatostatin receptors and successfully imaged with somatostatin analogue (SSA), [^{68}Ga] Ga-DOTA-TATE. During the COVID-19 pandemic, the supply of [^{123}I]mIBG was challenging, and in our hospital, access to PET/CT for paediatric patients is limited and not on-site. Therefore, our multi-disciplinary team opted to image patients with [^{99m}Tc] Tc-HYNIC-TOC and [^{123}I]mIBG once it became available to see the feasibility of using SSA in times of the unavailability of [^{123}I]mIBG. ***Materials and Methods:*** Paediatric patients referred for initial staging of neuroblastoma during 2021 and 2022 COVID pandemic were scanned with [^{99m}Tc]Tc-HYNIC-TOC and [^{123}I]mIBG within a 2-week interval of each other prior to chemotherapy. Consent was obtained from the parents prior to imaging. Images were reviewed by 2 Nuclear Physicians and a nuclear medicine registrar. Information regarding the N-myc amplification was also recorded for each patient. ***Results:*** Six patients were imaged with [^{99m}Tc] Tc-HYNIC-TOC and 3 were excluded due to incomplete imaging or chemotherapy prior to [^{123}I]mIBG imaging. Three patients were included in the review with respective ages of 4, 1 year 7 months, and 2 years 4 months. There was 100 % concordance in the imaging findings of [^{99m}Tc]Tc-HYNIC-TOC and [^{123}I]ImIBG in the 3 patients. Two patients with well-differentiated disease and N-myc

gain had positive [^{99m}Tc]Tc-HYNIC-TOC and [^{123}I]mIBG scans, one demonstrated localised disease and the other had metastases. One patient with differentiating disease and N-myc gain had negative [^{99m}Tc]Tc-HYNIC-TOC and [^{123}I]mIBG scans. ***Conclusion:*** Our limited case series demonstrates the potential for easily accessible and affordable [^{99m}Tc]Tc-HYNIC-TOC as an alternative to [^{123}I]mIBG for staging neuroblastoma in a resource-limited setting. Prospective large-scale studies will be necessary in order to validate these findings.

OP-885

[18F]F-SynVesT-1 PET In a Rare Case of Paraneoplastic Neurological Syndrome Associated With Isolated Anti-amphiphysin Antibodies

Y. Tang, *L. Xiao, J. Yang, S. Hu;*
Xiangya Hospital Central South University, Changsha, CHINA.

Aim/Introduction: Paraneoplastic neurological syndrome (PNS) is a rare immune-mediated neurological disorder that can be challenging to diagnose and treat. PNS related to anti-amphiphysin autoantibody, a 128 KD nerve terminal protein located on the synaptic vesicles, usually presented as stiff person syndrome. [^{18}F]F-SynvesT-1 is a novel radioligand for PET imaging targeting synaptic vesicle glycoprotein 2A (SV2A), which could observe the effect of anti-amphiphysin antibodies directly on the nervous system in patients with PNS. ***Materials and Methods:*** A 48-year-old man has suffered from progressive unresponsiveness and slurred speech for 10 months. Neuropsychological examination revealed inadequate numeracy, memory, and disorientation with dysarthria. The patients got 13/30 on Montreal Cognitive Assessment (MoCA). Routine laboratory, cerebrospinal fluid (CSF) analyses, and brain magnetic resonance imaging (MRI) were normal. Serological workup with paraneoplastic encephalitis panel showed positive evidence of anti-amphiphysin. ***Results:*** [^{18}F]F-FDG PET and [^{18}F]F-FDG PET/MRI images showed hypometabolism throughout the bilateral frontal and temporal lobes asymmetrically, while [^{18}F]F-SynvesT-1 PET and [^{18}F]F-SynVesT-1 PET/MRI showed a more restricted area of low uptake in these two lobes. Ambulatory EEG recording showed slow waves in the bilateral frontotemporal regions. Meanwhile, systemic [^{18}F]F-FDG PET did not identify any occult neoplasm. After being diagnosed with PNS, the patient's symptoms improved significantly with lymphatic plasma exchange and glucocorticoid therapy. ***Conclusion:*** Both [^{18}F]F-FDG and synaptic vesicle protein PET imaging can provide a diagnostic basis for localization for PNS. [^{18}F]F-SynVesT-1 PET is more specific than [^{18}F]F-FDG PET which plays an important role in the evaluation of PNS, not only an insight into disease characteristics and treatment directions.

1801

Wednesday, September 13, 2023, 09:45 - 11:15
Hall A

CME 14 - Neuroimaging + Paediatric Committee: Modern Imaging of Paediatric Epilepsy

OP-886

Clinical Point of View on Paediatric Epilepsy with a Focus on [18F]FDG PET/MR

L De Palma;
Ospedale Pediatrico Bambino Gesù, Dipartimento di Neuroscienze e Neuroriabilitazione, Rome, ITALY.

OP-887

Cortical Morphology and MR Post Processing in Paediatric Epilepsy

A. Hammers;
Kings College, London, UNITED KINGDOM.

OP-888

How Imaging Helps the Surgeon in Paediatric Epilepsy

K. Goffin;
UZ Leuven, Leuven, BELGIUM.

OP-889

Are We Really Ready to Go with New PET Tracers in Paediatric Epilepsy?

D. Van Weehaeghe;
KU Leuven UZ Gasthuisberg, Gent, BELGIUM.

1802

Wednesday, September 13, 2023, 09:45 - 11:15
Hall D (Arena)

Round Table 3 - Women´s Empowerment Task Force: Women in Science - Special Focus on Nuclear Medicine

OP-890

Women in Nuclear Medicine: the past and the present

O. Israel;
Nuclear Medicine, Rambam Health Care Campus, Haifa, ISRAEL.

OP-891a

The challenges of Women Technologists in Nuclear Medicine

A. Santos;
Department of Nuclear Medicine, Hospital Cuf Descobertas, Lisbon, PORTUGAL.

OP-891b

Women in Nuclear Medicine: the present and the future

L. de Geus-Oei;
Department of Radiology, Leiden University Medical Center (LUMC), Leiden, NETHERLANDS.

OP-891c

Radiochemist and to be a woman: what are the main challenges?

E. Eppard;
Institute of Nuclear Chemistry, Johannes Gutenberg-University, Mainz, GERMANY.

OP-891d

Physicist, Woman, Nuclear Medicine: how to conjugate them?

C. Stokke;
Department of Physics and Computational Radiology, Division of Radiology and Nuclear Medicine, Oslo, NORWAY.

1803

Wednesday, September 13, 2023, 09:45 - 11:15
Hall E1

LIPS Session 14 - Translational Molecular Imaging & Therapy + Physics + Radiation Protection + Oncology & Theranostics + Ethics Committee: Beta Emitters for Radioguided Surgery - Challenges and Opportunities

OP-892
Developments in instrumentation and probes
K. Shi;
Department of Nuclear Medicine, Inselspital, Bern University Hospital, University of Bern, Bern, SWITZERLAND.

OP-893
Radiation protection in beta RGS nuts and bolts
E. Ciarrocchi;
Department of Physics "E. Fermi", University of Pisa, Pisa, ITALY.

OP-894
Protocols and clinical relevance of beta RGS
C. Darr;
Department of Urology, University Hospital Essen, Essen, GERMANY.

1804

Wednesday, September 13, 2023, 9:45 AM - 11:15 AM
Hall E2

M2M Track - TROP Session: New Therapeutic Radiopharmaceuticals

OP-895
Radiometal modification of JMV6659 for theranostic approach of NTS1 targeting
S. Bodin[1,2], *S. Previti*[3], *S. Fernandez*[4], *D. Vimont*[2], *F. Masmejean*[2], *E. Rémond*[3], *A. Khatib*[5], *P. Garrigue*[4,6], *B. Guillet*[4,6], *E. Hindié*[7,2], *F. Cavelier*[3], *C. Morgat*[1,2];
[1]*Radiopharmacy, Nuclear Medicine, Bordeaux Hospital University Center, Bordeaux, FRANCE,* [2]*IMT, INCIA UMR-5287 CNRS, University of Bordeaux, Bordeaux, FRANCE,* [3]*Univ. Montpellier, CNRS, Institut des Biomolécules Max Mousseron, IBMM, UMR-5247, Montpellier, FRANCE,* [4]*Aix Marseille Univ, CNRS, CERIMED, Marseille, FRANCE,* [5]*RyTME, Bordeaux Institute of Oncology (BRIC), UMR 1312 Inserm, University of Bordeaux, Bordeaux, FRANCE,* [6]*Radiopharmacy, La Timone University Hospital, CERIMED, Aix-Marseille University, Marseille, FRANCE,* [7]*Nuclear Medicine, Bordeaux Hospital University Center, Bordeaux, FRANCE.*

Aim/Introduction: Neurotensin receptor-1 (NTS_1) is a G-protein coupled receptor overexpressed in several cancer types including pancreatic adenocarcinoma, triple negative breast cancer and others. We have previously reported that [^{68}Ga]Ga-JMV6659 (DOTA-APAc-Lys-Lys-Pro-Tyr-Ile-TMSAla-OH) as a promising peptide-based radiopharmaceutical for NTS1 imaging. In this work, we evaluated the impact of N-terminal radiometal modification of JMV6659 for theranostic purpose. As [^{68}Ga]Ga-JMV6659 showed also blood uptake, this finding was also deeply evaluated. ***Materials and Methods:*** JMV6659 was radiolabeled with ^{111}In and ^{161}Tb (^{89}Zr and ^{177}Lu ongoing). The resulting radiopharmaceuticals were investigated regarding their affinity, internalization, membrane bound fraction and efflux using colon cancer HT-29 cells. Cultured as 2D and 3D (organoids), HT-29 were also used to quantify the uptake of the radiopharmaceuticals. Finally, biodistribution of [^{111}In]In-JMV6659 was investigated in nude mice 24h after subcutaneous injection of HT-29 cells. ***Results:*** Saturation binding curves showed a preserved high affinity (nanomolar range) of [^{111}In]In-JMV6659 towards NTS1 with a K_d value of 3.91±2.70nM. [^{161}Tb]Tb-JMV6659 displayed a somewhat lower affinity with a K_d of 21.06±6.61 nM. [^{111}In]In-JMV6659 and [^{161}Tb]-JMV6659 exhibited high and specific NTS_1-mediated internalization which was maximum at 1h (68.17±5.97 and 82.97±3.12%, respectively) and slightly decreased to 54.48±9.59% and 60.74±12.00 at 4h. Contrarily, the membrane-bound fraction was 12.87±2.57 and 3.94±3.86%, respectively, at 1h and increased up to 25.43±7.38 and 23.00±5.43% at 4h. Human lymphocytes showed weak nonspecific binding of [^{111}In]In-JMV6659, whereas a higher specific binding was observed on human neutrophils up to 2h. Human plasma proteins bound [^{111}In]In-JMV6659 at about 2%IA/mg.On the monolayer HT-29 cells, uptake of [^{111}In]In-JMV6659 was up to 6051.6±634.2 Bq vs 2093.5±182.7 Bq for [^{161}Tb]Tb-JMV6659 when 800 kBq (8MBq/mL) were applied. On spheroids, the uptakes were respectively 460.4±46.9 Bq and 473.5±132.4 Bq at the same concentration.On biodistribution, uptake of [^{111}In]In-JMV6659 in HT-29 tumors was still 0.41±0.07 %ID/g at 24h. All other organs, except kidneys (8.92±5.55 %ID/g), were cleaned from radioactivity at 24h. To verify the receptor-mediated specificity, blocking experiments were performed using excess of neurotensin. Only uptake in HT-29 tumor was significantly displaced (0.41±0.07 %ID/g vs 0.19±0.09 %ID/g). Blood sampling was also performed at 2h, 4h and 24h to elucidate the underlying kinetics. At 2h, uptake in blood was 1.04±0.36 %ID/mL and decreased to 0.24±0.13 %ID/mL at 4h. At 24h, no significant signal was detected in blood. ***Conclusion:*** Radiolabeled JMV6659 stands as promising radiotherapeutic analogue suitable for targeted radionuclide therapy of NTS1-positive tumors.

OP-896
Prostate Specific Membrane Antigen in Human and Mouse Tissue
T. Kalidindi, *T. Esposito, D. Adilbay, P. Demetrio De Souza Franca, R. payne, N. Pillarsetty;*
Memorial Sloan Kettering Cancer Center, New York, NY, UNITED STATES OF AMERICA.

Aim/Introduction: PSMA targeted alpha therapy (TAT) agents such as [^{225}Ac]Ac-PSMA-617 have shown great efficacy in treating mCRPC patients. However, dose limiting adverse effects such as renal toxicity and xerostomia have limited their potential. We have demonstrated that reducing the effective specific activity (ESA) of the PSMA-TRT agent [^{177}Lu]Lu-PSMA-617 via co-injection of PSMA-11 can significantly reduce salivary gland and renal uptake while maintaining PSMA+ tumor uptake in mice. To determine if [^{225}Ac]Ac-PSMA-617 uptake in these off-target organs is due to passive accumulation or PSMA expression in these sites, we made a comparative analysis of PSMA expression in human and mouse tissue to see if ESA reduction could limit salivary gland and renal uptake in humans undergoing PSMA-TAT, aligning with our findings in mice. ***Materials and Methods:*** Analyzed PSMA using immuno-histochemistry (IHC), quantitative autoradiography (QAR) and western blot (WB) in samples collected from the kidneys, salivary glands (SG), and lacrimal glands (LG) of both

mouse and human cadavers. IHC was performed on paraffin embedded 5 µm slides using anti-PSMA antibody (Proteintech, 13163-1-AP). QAR was performed on 10µm fresh frozen tissue sections incubated with 0.5µCi of [^{177}Lu]Lu-PSMA-617 for 1h and quantified using autoradiography film. Tissues were homogenized and analyzed for PSMA and actin by WB using anti-PSMA (Cell Signaling, 12702) and anti-actin (Cell Signaling, 5152) antibodies. ***Results:*** QAR analysis revealed, [^{177}Lu]Lu-PSMA-617 mean uptake (pCi/mm^3) of 23.28 ± 0.51 in LNCaP , 5.29 ± 0.02 in LG, 6.23 ± 1.42 in parotid, 3.67 ± 0.20 in submandibular, 3.40 ± 1.56 in kidney (cortex), 1.08 in muscle of human tissue and 0.95 ± 0.05 in SG, 16.4 ± 2.61 in Kidney of mouse tissue. IHC analysis revealed percentage PSMA positive cells of 89.92 ± 4.03 in LNCaP xenograft, 61.71 ± 7.02 in LG, 65.96 ± 0.63 in parotid, 68.48 ± 4.53 in submandibular, 41.80 ± 3.12 in kidney (cortex), 19.11 ± 7.05 in muscle of human tissue and 36.12 ± 9.39 in SG, 53.58 ± 2.04 in kidney (cortex) of mouse tissue. WB analysis revealed significantly higher PSMA expression in LNCaP xenografts compared to SG, LG and kidney of human tissue. ***Conclusion:*** Our preliminary data demonstrated PSMA is prominently expressed in SG, LG and kidneys in human tissue and actively binds to PSMA-TRT agents. Therefore developing methods to limit off-target toxicity of PSMA-TRT agents becomes crucial. ***References:*** Kalidindi TM et al., Eur J Nucl Med Mol Imaging, PMID: 33495926. Funding: DOD- W81XWH-19-1-0536, NIH RO1-1R01CA262675-01A1.

OP-897

DARPin platform for the development of powerful targeting agents for radioligand therapy

C. Lizak[1], *A. Bosshart*[1], *S. Wullschleger*[1], *M. Behe*[2], *A. Blanc*[2], *S. Imobersteg*[2], *A. Constantinescu*[1], *J. Blunschi*[1], *L. Abduli*[1], *S. Schütz*[1], *J. Wolter*[1], *Z. Ziauddin Siddiqui*[1], *M. Matzner*[1], *A. Auge*[1], *N. Fic*[1], *W. Ali Abobaker Hassan*[1], *T. Chiorazzo*[2], *C. Reichen*[1], *A. Croset*[1], *A. Villa*[1], *P. Legenne*[1], *A. Goubier*[1], *R. Schibli*[2], *D. Steiner*[1];
[1]*Molecular Partners AG, Schlieren, SWITZERLAND,*
[2]*Paul Scherrer Institute, Villigen, SWITZERLAND.*

Aim/Introduction: DARPins (Designed Ankyrin Repeat Proteins) are small binding proteins that combine short systemic half-life, ideal binding properties and high stability. DARPin molecules with very high affinity and specificity can be generated against a broad range of tumor targets. We have previously shown that increased DARPin affinity correlates with elevated tumor uptake and extended tumor retention in mouse models suggesting that radiolabelled binders with picomolar affinity will lead to tumor uptake levels meaningful for therapeutic applications. The robust architecture of DARPins provides high thermal stability, which is beneficial for labelling with radionuclides that require harsh conditions, and which enables engineering approaches that are not compatible with other protein scaffolds. The limitation of small-sized, protein-based targeting agents originates from their renal clearance pathway, which leads to a strong kidney accumulation of coupled residualizing radionuclides resulting in kidney toxicities. To overcome this problem, we have undertaken an extensive engineering campaign to optimize the surface of the DARPin scaffold for reduced kidney reabsorption. ***Materials and Methods:*** Several surface-optimized DARPin variants were engineered against different tumor targets and were analysed for their biophysical properties. Building on the absence of cysteines in the DARPin scaffold, we generated single-cysteine versions for site-specific conjugation to different linker/chelators using maleimide chemistry. Molecules radiolabelled with different radionuclides (e.g., Indium-111, Lutetium-177) were analysed for their in vivo biodistribution properties in different xenografted tumor models. Furthermore, tumor penetration of candidates was analysed by immunohistochemistry on tumor sections. ***Results:*** In vitro characterization showed that engineered DARPin molecules maintained good biophysical properties and high affinities to the target antigen. In vivo biodistribution studies with surface-engineered DARPins showed strongly improved profiles as compared to parental binders. Kidney accumulation was reduced by up to 90% at four hours post injection, while tumor uptake was not affected. This effect was confirmed with different DARPin candidates suggesting a general applicability of the approach. Additionally, orthogonal kidney protecting strategies have been identified that showed superior effects than commonly used nephro-protectants. Combining the different strategies on Her2 binding candidates resulted in an additive effect and an improvement of the tumor-to-kidney ratio from 1:34 to 1:3 in preclinical mouse models. Refinement of the applied strategies to further optimize the tumor-to-kidney ratio are currently ongoing. ***Conclusion:*** The presented results show that our proprietary "Radio DARPin Therapy" platform represents an attractive solution for the development of next-generation RLTs. Several programs in indications with high unmet medical need are currently underway.

OP-898

[198Au]Au Labeled Gold Nanoparticle Depot ([198Au]Au-NPD) Inhibits the Growth of a 4T1 Murine Mammary Carcinoma Tumor on Immunocompetent BALB/c Mice without Normal Tissue Toxicity and Causes an Abscopal Effect on a Distant Non-irradiated Tumor

Z. Cai[1], *C. J. Georgiou*[1], *M. Kondo*[1], *C. Chan*[1], *R. Liu*[1], *M. Moran*[2], *A. Armstrong*[2], *R. M. Reilly*[1,3,4];
[1]*Department of Pharmaceutical Sciences, Leslie Dan Faculty of Pharmacy, University of Toronto, Toronto, ON, CANADA,*
[2]*McMaster Nuclear Reactor, McMaster University, Hamilton, ON, CANADA,* [3]*Department of Medical Imaging, Temerty Faculty of Medicine, University of Toronto, Toronto, ON, CANADA,* [4]*Joint Department of Medical Imaging and Princess Margaret Cancer Centre, University Health Network, Totonto, ON, CANADA.*

Aim/Introduction: To study the effectiveness and normal tissue toxicity of a nanoparticle depot (NPD) embedded with [^{198}Au]Au-gold nanoparticles ([^{198}Au]Au-NPD) for intratumoral β-particle radiotherapy of a 4T1 murine mammary carcinoma tumour in immunocompetent BALB/c mice and for causing an abscopal effect on a distant non-irradiated tumor. ***Materials and Methods:*** [^{198}Au]AuNP were synthesized by sodium citrate reduction of H[^{198}Au]AuCl$_4$ and stabilized with lipoic acid-polyethylene glycol, then characterized by UV/Vis spectroscopy, Transmission Electron Microscope (TEM) and Dynamic Light Scattering (DLS). 4 × 10^{11} [^{198}Au]AuNP were embedded in a calcium alginate seed (ϕ 0.8×4mm). Subcutaneous 4T1 tumors were initiated in BALB/c mice in the right shoulder (T1) at 7 days (d) before treatment and in the left flank (T2) outside the β-particle range at 1 d prior to treatment. Mice (n=5) received no treatment or intratumoral implantation in T1 of two non-radioactive Au-NPD, one (3.0 ± 0.5 MBq) or two (4.5 ± 0.6 MBq) [^{198}Au]Au-NPD. Tumor size (T1 and T2) and body weight were monitored 3 times/week. At 14 d post treatment, mice were sacrificed. Blood biochemistry and hematology were analysed. T2 was immunostained for CD4$^+$ and CD8$^+$ cells and flow cytometry was performed for CD45$^+$, CD3$^+$, CD4$^+$, CD8$^+$ and PD-1$^+$ Tumour Infiltrated Lymphocytes (TILs). ***Results:*** Spherical 23 nm [^{198}Au]AuNP were synthesized (>99% yield) and embedded into a NPD. Intratumoral implantation of one

or two [^{198}Au]Au-NPD increased T1 doubling-time (DT) by 1.8-fold (7.6±0.6 d) and 3.4-fold (14.9±3.7 d), respectively vs. no treatment (4.3±0.3 d, p<0.0001). DT of T2 was increased by treatment of T1 with one or two [^{198}Au]Au-NPD (3.9±1.0 or 4.1±1.1 d) vs. no treatment (3.0±0.5 d, p<0.0001). Treatment of T1 with two Au-NPD did not inhibit T1 or T2 growth (DT=4.7±0.6, 3.1±0.6 d, respectively). Body weight, blood biochemistry and hematology showed no normal tissue toxicity. Treatment of T1 with two Au-NPD, one or two [^{198}Au]Au-NPD decreased CD45$^+$, CD45$^+$CD3$^+$, CD45$^+$CD3$^+$CD8$^+$, CD45$^+$CD3$^+$CD4$^+$ TILs in T2 by 45-86 %. T1 treatment with two Au-NPD or one [^{198}Au]Au-NPD decreased PD-1 mean fluorescence intensity (MFI) on CD45$^+$CD3$^+$CD8$^+$ TILs by 33% or 43%, and on CD45$^+$CD3$^+$CD4$^+$ TILs by 34% or 42%, respectively. T1 treatment with two [^{198}Au]Au-NPD decreased PD-1 MFI on CD45$^+$CD3$^+$CD8$^+$ TILs by 33%, but increased on CD45$^+$CD3$^+$CD4$^+$ TILs by 23%. ***Conclusion:*** Intratumorally implanted [^{198}Au]Au-NPD inhibited 4T1 growth, and caused an abscopal effect on a distant tumor, possibly mediated by PD-1 expression on CD45$^+$CD3$^+$CD8$^+$ and CD45$^+$CD3$^+$CD4$^+$TILs.

OP-899

Radioactive immuno-imaging and radioimmunotherapy of 131I-labeled human single-chain variable fragment antibodies against anaplastic thyroid cancer in tumor-bearing nude mice

Q. Liu[1], *H. Pang*[2];
[1]*the Second Affiliated Hospital of Chengdu Medical College, China National Nuclear Corporation 416 Ho, Chengdu, Sichuan, CHINA,* [2]*The First Affiliated Hospital of Chongqing Medical University, Chongqing, P.R. China, Chongqing, Sichuan, CHINA.*

Aim/Introduction: Anaplastic thyroid carcinoma has a high degree of malignancy and lacks effective treatment, as the tumor tissue does not respond to radioactive iodine therapy. With the continuous development of immunotherapy, we investigated the use of 131 iodine-labeled antibodies, to explore a new treatment method. ***Materials and Methods:*** Total RNA was extracted from the lymphatic tissue near the anaplastic thyroid carcinoma which was used to amplified VH and VL fragments with RT-PCR, and joined with their linkers. VH and VL were used to produce the scFv fragments by the way of splicing-overlap-extension PCR. The scFv gene was cloned in pCANTAB-5E plasmid, and the recombinant phagemids were transformed to susceptible E. coli TG1. Enzyme-linked immunosorbent assay (ELISA) was used to detect the expression of scFv. The expression and relative molecular mass of soluble scFv were tested by sodium dodecyl sulfate polyacrylamide gel electrophoresis (SDS-PAGE) and western blotting, respectively. The chloramine T method was used to label scFv with ^{131}I. ^{131}I-scFv was injected via the tail vein into nude mice to analyze the distribution of ^{131}I-scFv in body tissues and organs. Static single photon emission-computed tomography (SPECT) imaging was performed at 12, 24, 48, and 72 h after injection to observe the intratumoral accumulation of radioactivity. The treatment group is divided into 4 groups. The tumor volume change was observed the tumor inhibition rate was calculated. The survival time of each mouse was also recorded. The tumor tissue was removed from each mouse within 1 h after death, and made pathological sections and observe under electron microscopy. ***Results:*** The human anaplastic thyroid carcinoma phage antibody library was constructed successfully. Phage ELISA results showed specific binding to ARO cells. SDS-PAGE and western blotting showed that the relative molecular mass of soluble scFv was approximately 29 kD. The labeling rate was 91.66% and the radiochemical purity was 93.1 ± 0.32%. SPECT imaging showed that 131I-scFv selectively accumulated in tumor tissue. The target/non-target (T/NT) value was highest and clearest at 48 h, and SPECT/CT image fusion results were in agreement with the biodistribution results. The survival times of the four groups of tumor-bearing nude mice were 39.5, 43.0, 54.5, and 55.0 d. ***Conclusion:*** Human single chain variable fragment antibodies against ATC were successfully generated. We found that 131I-scFv provided a more effective diagnosis and treatment method for the clinical treatment of anaplastic thyroid carcinoma.

OP-900

Preparation of 47SC-labeled DOTA-RGD4 tetramer and preliminary preclinical study on its application in iodine-refractory differentiated thyroid carcinoma

X. Jiang;
Second Affiliated Hospital of Chengdu Medical College (China National Nuclear Corporation 416 Hospital), chengdu, CHINA.

Aim/Introduction: Thyroid cancer is the most common malignant endocrine tumour and its incidence has been increasing in recent years. The 10-year survival rate of radioactive iodine-refractory differentiated thyroid cancer (RAIR-DTC) is only 10%, which is a key challenge in the clinical management of thyroid cancer. The αvβ3 is highly expressed in thyroid cancer, suggesting that radiolabeling can target αvβ3. Arg-Gly-Asp (RGD) may be a new strategy for the integration of RAIR-DTC treatment. In this study, ^{47}Sc-labelled 1,4,7,10-tetraazacyclododecane-1,4,7,10-tetraacetate (DOTA)-RGD tetramer (RGD_4) was used for the first time to explore its efficacy in the treatment of RAIR-DTC. ***Materials and Methods:*** In this study, ^{47}Sc labelling of DOTA-RGD_4 was efficiently performed. LogP values, in vivo and in vitro metabolic stability, cellular uptake and specific binding of the labelled product were determined. The tumour targeting ability and therapeutic potential of the radiotracer was investigated in CAL-62 mice, while imaging studies were performed at different time intervals (2 4 24 48 72h) by SPECT/CT. ***Results:*** The radiochemical yield of ^{47}Sc-labelled DOTA- RGD_4 was >90% and the radiochemical purity was >99%. the LogP value was -2.376. the radiotracer showed good in vivo, in vitro and metabolic stability, with a specific binding rate of >95%. the SPECT/CT and biodistribution studies showed that the radiopeptide accumulated heavily in the tumour, with maximum tumour uptake at 4 hours post-injection and a tumour background ratio of 8.13±3.67. The drug was excreted mainly by the urinary route. The treatment results suggested that not only was tumour growth inhibited but also significant tumour shrinkage was observed following administration of this radiopharmaceutical to mice. ***Conclusion:*** Preclinical data indicate that ^{47}Sc-DOTA-RGD_4 is highly efficient and stable in vitro and vivo, and that SPECT imaging and biodistribution data demonstrate significant tumor uptake and specificity, allowing for effective treatment of RAIR-DTC and other cancers overexpressing αvβ3 integrin receptors, as well as for staging and follow-up imaging.

OP-901

PSMA-Targeted Single Domain Antibody Fragment NB7: Preliminary Evaluation as a Scaffold for Targeted α-particle Therapy of Prostate Cancer

T. Huynh[1], *Y. Feng*[1], *R. Meshaw*[1], *X. Zhao*[1], *L. Rosenfeld*[2], *N. Papo*[2], *M. Zalutsky*[1];
[1]*Duke University, Durham, NC, UNITED STATES OF AMERICA,* [2]*Ben-Gurion University of the Negev, Beer-Sheva, ISRAEL.*

Aim/Introduction: Single domain antibody fragments (sdAbs) are an attractive platform for targeted α-particle therapy (TAT) because of their ~15 kDa size, high stability, fast normal tissue clearance and excellent tumor targeting and penetration. We developed a PSMA-targeted sdAb, NB7, with high affinity and a different

binding site on PSMA than the small molecule PSMA-targeted agents. Herein, we report the in vitro and in vivo evaluations of radiohalogenated NB7 conjugates using residualizing prosthetic agents designed for use with radioiodine and ^{211}At. ***Materials and Methods:*** NB7 sdAb was labeled using both the 1,3,5 and 1,3,4 isomers of N-succinimidyl guanidinomethyl [*I]iodobenzoate ([^{125,131}I]SGMIB), and their astatinated analogues [^{211}At]SAGMB s. Binding affinity, cell uptake and internalization were evaluated using PSMA+ PC3 PIP and PSMA- PC3 flu prostate cancer cells. A paired-label biodistribution study was performed to compare 1,3,4-[^{131}I]SGMIB-NB7 and 1,3,5-[^{125}I]SGMIB-NB7 conjugates (both without His6-tag) in athymic mice with subcutaneous PSMA+ PC3 PIP xenografts. A single-label study was performed with 1,3,5-[^{125}I] SGMIB-NB7His (with a His6-tag at the C-terminus) in the same animal model. ***Results:*** [^{131}I]SGMIB-NB7 showed high binding affinity (6.4 ± 2.0 nM), PSMA-specific cell uptake (51.6 ± 0.6 % at 2 h), and high internalization (30-70% internalization at 2 h). Good tumor uptake (7.2 ± 1.5 %ID/g at 1 h) and fast kidney clearance (3.2% ID/g at 4 h) was seen in PSMA+ PC3 PIP xenografts. Notably, less than 3% ID/g uptake was seen in salivary gland and lacrimal gland at 1h, which cleared quickly (< 1% ID/g at 4 h). Paired-label biodistribution found no distinctions between SGMIB isomers. No discernible differences were observed for radioiodinated NB7 conjugates with/without a His6 tag at the C-terminus. Similar to the radioiodinated conjugates, [^{211}At]SGMAB-NB7 demonstrated high PSMA-specific uptake in PSMA+ PC3 PIP cells (41.5 ± 1.5 % at 2 h). ***Conclusion:*** ^{125,131}I-labeled and ^{211}At-labeled NB7 conjugates via these guanidino bearing prosthetic agents demonstrated excellent PSMA-specific binding, cell uptake and internalization in PSMA+ PC3 PIP cells. Radioiodinated NB7 showed good tumor uptake, rapid kidney clearance and low retention in salivary glands and lacrimal glands. Our results suggest that NB7 offers a potentially valuable alternative scaffold for PSMA-targeted therapy with a size and pharmacokinetic profile intermediate between small molecule PSMA inhibitors and intact antibodies. Further evaluation of ^{211}At-labeled for TAT is underway.

OP-902

177Lu-labeled aflibercept for theranostic application in renalcancer models

L. Kang, *Z. Chen, Q. Yang, Y. Qiu, W. Huang, L. Song, X. Sun;*
Peking University First Hospital, Beijing, CHINA.

Aim/Introduction: Aflibercept, a chimeric recombinant protein, can sequester all isoforms of VEGF-A, PlGF, and VEGF-B, therefore affecting pathological and physiological angiogenesis. In this study, the role of ^{177}Lu-labeled aflibercept was investigated for SPECT imaging and treatment in renal cancer models. ***Materials and Methods:*** Aflibercept was conjugated with 1,4,7,10-Tetraazacyclododecane-1,4,7,10-tetraacetic acid (DOTA) for radiolabeling with ^{177}Lu ($t_{1/2}$ = 6.65 d). After the renal cancer Renca tumor-bearing mice model was established, SPECT imaging and biodistribution studies were performed after the injection of ^{177}Lu-DOTA-aflibercept. Further, five experimental groups of five mice each were formed and then treated as follows by tail vein injection: ^{177}Lu-DOTA-aflibercept, ^{177}Lu-DOTA-IgG (human non-specific), ^{177}Lu, aflibercept, and PBS. Measurements of tumor size were conducted every other day. Tumor sizes and body weight were measured within 14 days post-injection. Mice injected with CY5.5-aflibercept (n=4), CY5.5-IgG (n=4), and CY5.5-aflibercept-block (n=4) were imaged for optical imaging. Finally, histological analysis was performed to examine VEGF expression in tumors and hematological analysis was for evaluating the toxicity of therapy. ***Results:*** The labeling yields were more than 90% for ^{177}Lu (n=5). The SPECT imaging of ^{177}Lu-aflibecept showed that the tumor uptake of Renca tumor reached the highest on the fifth day. Ex vivo biodistribution results validated and quantified the planer imaging results. According to the results of fluorescence imaging, Cy5.5-aflibercept group mice showed significant accumulation in tumors, which was significantly higher than the control group and blocking group. The results showed that for the treatment group of ^{177}Lu-aflibercept, significant inhibition of tumor growth was observed. The standardized tumor volume of ^{177}Lu-aflibercept is only 180.4 ± 107.8% at 14 days, much smaller than PBS group (PBS=1064.3 ± 706.0%; P=0.002) and other treatment groups (^{177}Lu=461.9 ± 36.4%, ^{177}Lu-IgG=370.9 ± 176.4%, aflibercept=331.6 ± 101.1%). Immunofluorescence images showed positive signals of VEGF and CD31 expression in cells of different groups after treatment. The ^{177}Lu-aflibercept group had the least VEGF expression positive signals. However, there was no significant difference in CD31 expression signals between different groups. Therefore, the effectiveness of the treatment was demonstrated in our study. Besides, the bodyweight of ^{177}Lu-aflibercept did not change significantly and there was no significant long-term blood toxicity, indicating the safety of radiolabeled aflibercept in vivo. ***Conclusion:*** ^{177}Lu-labeled aflibercept displayed a significant VEGF-positive tumor affinity and effective tumor therapy without significant toxicity. Therefore, ^{177}Lu-labeled aflibercept could be further investigated in the theranostic field of renal cancer in the clinic.

OP-903

Development of cobalt-55 labelled neurotensin antagonist NOTA-SR142948 for cobalt-58m NTSR1 targeted radionuclide therapy

W. Lin[1], *G. O. Fonseca Cabrera*[2], *E. Aluicio Sarduy*[1], *T. E. Barnhart*[1], *Z. Li*[2], *Z. Wu*[2], *J. W. Engle*[1];
[1]*University of Wisconsin Madison, Madison, WI, UNITED STATES OF AMERICA,* [2]*University of North Carolina at Chapel Hill, Chapel Hill, NC, UNITED STATES OF AMERICA.*

Aim/Introduction: Neurotensin receptors (NTSR) are known for stimulating tumor proliferation through neurotensin (NTS) activation and are expressed in a variety of cancers including breast, pancreatic, prostate, colon and non-small cell lung cancers. NTS antagonists have achieved greater in vivo tumor uptake than NTS agonist-based ligands due to their improved metabolic stability, leading to phase I/II clinical trials in humans. We investigated the therapeutic potential of SR142948 conjugated with NOTA chelator for cobalt-58m targeted radionuclide therapy (TRT) via its diagnostic congener, cobalt-55, using NTSR1-positive HT29 human colorectal adenocarcinoma cells as the cancer model. ***Materials and Methods:*** Cobalt-55 (^{55}Co) was produced via deuteron irradiation of iron-54 targets and purified with ion exchange/extraction chromatography. Trace metals were quantified with microwave plasma - atomic emission spectroscopy (MP-AES). NOTA-SR142948 ("SR") was labelled with ^{55}Co (pH 4.5, 1 h, 55°C, 2 mg/mL sodium gentisate). Labelled compounds were purified using HLB solid-phase extraction columns following HPLC purification and subsequently dried under argon flow before reconstitution in PBS to <10% ethanol. Radioanalytical-HPLC was used to determine the radiochemical purity of the labelled compounds. [^{55}Co]Co-SR binding saturation and internalization assays were evaluated using HT29 cells in triplicate, and surface bound activity was removed with stripping buffer (0.1 M citrate pH 2). Female nude mice (N=4) were

xenografted with a 1:1 mixture of 10^6 HT-29 cells and Matrigel, and then PET imaged after 7 days. NTSR1-negative CaCo2 tumors were xenografted contralaterally. Each mouse received 2.1 MBq [^{55}Co]Co-SR. Pharmacokinetic profiles were acquired by PET imaging at 1, 4, 9 and 24 h post injection. Major organs and tissues were quantified at 24 h post injection to confirm image-derived uptake values. ***Results:*** Apparent molar activity of [^{55}Co]Co-NOTA was 146±18 MBq/nmol (N=2) end of the bombardment and verified by MP-AES. HPLC verified quantitative [^{55}Co]Co-SR radiolabelling at 74 MBq/nmol (37 MBq/nmol at time of injection) and sodium gentisate effectively mitigated radiolysis. >35% of bound [^{55}Co]Co-SR activity was internalized by HT29 cells after 3 h of incubation and measured NTSR1 K_D = 3±2 nM. PET imaging with [^{55}Co]Co-SR showed predominantly renal clearance with high, persistent tumor uptake (14±1 %ID/g at 24 h) and high tumor-to-organ ratios (>6 for kidney). ***Conclusion:*** In vitro and in vivo data from [^{55}Co]Co-SR show promising results for [^{58m}Co]Co-SR NTSR1 TRT. Future work will assess the subcellular compartmentalization of the internalized activity and evaluate the cytotoxicity of [^{58m}Co]Co-SR for HT29 cells before translation to in vivo therapy studies.

1805

Wednesday, September 13, 2023, 9:45 AM - 11:15 AM
Hall B

Cutting Edge Science Track - TROP Session: Clinical Dosimetry III - Time & Co.

OP-904

Single-time-point [68Ga]Ga-DOTATATE-PET/CT for model-based prediction of the time-integrated activity of [177Lu]Lu-DOTATATE during therapy

V. Vasic[1,2], *J. Gustafsson*[3], *E. Yousefzadeh-Nowshahr*[1,2], *A. Beer*[1], *K. Sjögreen Gleisner*[3], *G. Glatting*[1,2];
[1]*Department of Nuclear Medicine, Ulm University Medical Centre, Ulm, GERMANY,* [2]*Medical Radiation Physics, Department of Nuclear Medicine, Ulm University, Ulm, Germany, Ulm, GERMANY,* [3]*Medical Radiation Physics, Lund University, Lund, Sweden, Lund, SWEDEN.*

Aim/Introduction: Prediction of the time-integrated activity (TIA) based on single-time-point (STP) pre-treatment PET/CT could simplify patient-specific [^{177}Lu]Lu-DOTATATE therapy. The knowledge integrated into a physiologically based pharmacokinetic (PBPK) model, together with a [^{68}Ga]Ga-DOTATATE measurement and Bayesian information of the corresponding patient population, could suffice for a prediction of the TIA for [^{177}Lu]Lu-DOTATATE biokinetics during therapy. The objective is to evaluate the accuracy of the TIA calculation using STP and Bayesian information. ***Materials and Methods:*** Data from 12 patients (8 males, 4 females; (65±12) years) with well-differentiated metastatic neuroendocrine tumours (NETs) from the Iluminet trial (1,2) were eligible for the study. Patients received (1.7±0.4) pmol and (197±48) MBq of [^{68}Ga]Ga-DOTATATE and (10.26±0.09) nmol and (7.46±0.07) GBq of [^{177}Lu]Lu-DOTATATE. Accurate dosimetry as presented previously (1) was performed on four total-body planar gamma-camera images acquired at 1 h, 24 h, 96 h, and 168 h p.i. and one SPECT/CT at (22±1) h p.i. For the study, one PET/CT image (63±5) min p.i. was used, and a whole-body PBPK model was developed and implemented in SimBiology/MATLAB. First, Bayesian values were estimated from an initial fit with all measured data (diagnostic+therapy). Second, reference parameters were obtained using PET/CT, scintigraphic measurements and Bayesian information. Finally, two fits of STP pre-treatment PET/CT using Bayesian information were performed: a) using the reference parameters as start values and b) using the Bayes values as start values. The deviation from the reference TIA value was evaluated for the most relevant organs and lesions in percent. ***Results:*** In case a), median [min, max] of the deviation of the TIA from reference TIA in kidney, spleen, liver, tumour and total body without bladder activity are 0.2[0, 0.4]%, 0.2[0, 0.4]%, 1.2[0.7, 4.6]%, 0.4[0, 1.1]%, 0.8[0.4, 1.3]%, respectively. In case b) the deviation is higher: 13[2, 46]%, 13[1, 44]%, 50[17, 194]%, 20[6, 284]%, 18[8, 91]% for kidney, spleen, liver, tumour and total body without bladder activity, respectively. ***Conclusion:*** With good (i.e. the reference) starting values, it is - in principle - possible to predict the TIA values of therapy with a deviation of less than 5% when using the STP pre-treatment PET/CT fit. Subsequent tests aim to find the optimal start values to achieve a prediction TIA that is very close to the reference TIAs. ***References:*** 1. Stenvall et al., EJNMMI Res. 2022;12:75 2. Sundlöv et al., Eur J Nucl Med Mol Imag. 2022;49:3830-3840

OP-905

Accuracy of predicted kidney's absorbed doses in [177Lu]Lu-PSMA-617 therapy using single-time-point data and non-linear mixed effect modelling

D. Hardiansyah[1], *E. Yousefzadeh-Nowshahr*[2], *F. Kind*[3], *A. J. Beer*[2], *J. Ruf*[3], *G. Glatting*[2], *M. Mix*[3];
[1]*Universitas Indonesia, Depok, INDONESIA,* [2]*Ulm University, Ulm, GERMANY,* [3]*University of Freiburg, Freiburg, GERMANY.*

Aim/Introduction: In molecular radiotherapy, individual absorbed dose estimation is desirable [1]. However, this is not often performed in the clinic as it needs multiple-time-point imaging data [2]. Therefore, in this study, we investigated the accuracy of the predicted kidney's absorbed doses in [^{177}Lu]Lu-PSMA-617 therapy using single-time-point (STP) data from SPECT/CT and non-linear mixed-effects (NLME) modelling. ***Materials and Methods:*** Kidney's biokinetic data of [^{177}Lu]Lu-PSMA-617 were collected from sixty-three patients at TP1=(1.8±0.8) h, TP2=(18.7±0.9) h, TP3=(42.7±1.0) h, TP4=(66.3±0.9) h, and TP5=(160.3±24.2) h post injection using SPECT/CT. Population-based model selection with NLME (NLME-PBMS) [3] was performed to select the best function from a set of sum-of-exponential (SOE) functions. In total, nine SOE functions with four to seven parameters were included in the analysis. The best function from the NLME-PBMS analysis was selected based on the goodness-of-fit test and Akaike weight. Reference absorbed doses (rADs) were calculated using the best function and all-time-point data. STP absorbed doses (sADs) were calculated by fitting the best function parameters using STP data at different time points. The accuracy of the STP dosimetry was analysed using the absolute value of the relative deviations (RDs) and root-mean-square errors (RMSEs) between sADs and rADs. ***Results:*** A function with six adjustable parameters, i.e. $A_1e^{-(\lambda1+\lambda phys)t}+A_2e^{-(\lambda2+\lambda phys)t}-A_3e^{-(\lambda3+\lambda phys)t}-(A_1+A_2-A_3)e^{-(\lambda bc+\lambda phys)t}$, was selected as the best function with an Akaike weight of about 100%. STP dosimetry using TP3=(42.6±1.0) h showed the lowest (mean±SD) of the RDs of (6±8)% and (median [min, max]) of the RDs of (2 [0.03, 39])%. The RMSEs of the STP dosimetry at TP1, TP2, TP3, TP4 and TP5 were 23%, 16%, 10%, 20%, and 53%, respectively. Four outlier patients for STP at TP3 (outside the (mean±2SD) of the RD) were found in our study with RD values between 23% and 39%. ***Conclusion:*** STP dosimetry with SPECT/CT measurements at TP3=(42.6±1.0) h

post injection may be used to accurately determine kidney ADs using the NLME method and population-based model selection. NLME modelling allows using functions with more parameters than measured per patient. ***References:*** [1] Glatting G, Bardiès M, Lassmann M. Z Med Phys. 2013;23:262-9. [2] Hänscheid H, Lapa C, Buck AK, Lassmann M, Werner RA. J Nucl Med. 2018;59:75-81. [3] Hardiansyah D, Riana A, Eiber M, Beer A, Glatting G. Z Med Phys. 2023.

OP-906

Accuracy and Uncertainty Analysis of Reduced Time Point Imaging Effect on Time-Integrated Activity for [177Lu]Lu-DOTA-TATE PRRT in Clinical Patients and Realistic Simulations

A. Peterson[1,2], *D. M. Mirando*[3], *Y. K. Dewaraja*[1];
[1]*University of Michigan, Ann Arbor, MI, UNITED STATES OF AMERICA,* [2]*Wayne State University, Detroit, MI, UNITED STATES OF AMERICA,* [3]*MIM Software Inc, Beachwood, OH, UNITED STATES OF AMERICA.*

Aim/Introduction: Factors including scheduling can lead to undesirable imaging time points (TP) for determining time-integrated activity (TIA) and the resulting impact on [^{177}Lu]Lu-DOTA-TATE dosimetry accuracy is not well-known. We use 4TP ^{177}Lu-SPECT/CT data to perform a comprehensive analysis of the error and variability in TIA when employing reduced TP methods. ***Materials and Methods:*** The study includes 28 patients with neuroendocrine tumors who underwent SPECT/CT imaging at approximately 4, 24, 96, and 168 hours post-therapy (p.t.) following the first cycle of [^{177}Lu]Lu-DOTA-TATE. The healthy liver, kidney, spleen, and up to 5 index tumors were delineated for each patient. Time-activity curves were fit with exponentials to the 4TP data as a reference. Various combinations of 2 and 3TPs were fit to determine optimal imaging schedules and associated errors. 2 common methods of single time point (STP) TIA estimation were also evaluated. A simulation study was performed with data generated by sampling curve fit parameters from log-normal distributions and adding realistic measurement noise. In clinical and simulation studies, error and variability in TIA estimates were estimated with various sampling schedules. ***Results:*** The optimal imaging time period for STP TIA estimates was 3-5 days (71-126h) p.t. for tumor and organs (6-8 days (144-194h) p.t. for one STP method for spleen). Optimal STP estimates give mean percent errors (MPE) within ±5% and SD<9% across all structures with largest magnitude error and highest variablility for kidney (MPE=-4.1%,SD=8.4%). The optimal sampling schedule for 2TP estimates is 1-2 days (21-52h) p.t. followed by 3-5 days (71-126h) p.t. for kidney, tumor, and spleen and for 3TP estimates it is 1-2 days (21-52h) p.t. followed by 3-5 days (71-126h) p.t. and 6-8 days (144-194h) p.t. for all structures. Using the optimal schedules, the largest MPE for 2TP estimates is 1.2% for spleen and highest variability is tumor with SD=5.8% while for 3TP estimates the largest MPE is 2.5% for spleen and highest variability is tumor with SD=2.1%. Simulated results corroborate the clinical findings with similar errors and indicate many sub-optimal schedules also exhibit low error and variability. A tool has been made available online to explore error and variability associated with user-provided sampling schedules[1]. ***Conclusion:*** Reduced TP methods achieve acceptable average TIA errors over a range of sampling schedules while maintaining low uncertainty. This information can improve the feasibility of dosimetry for [^{177}Lu]Lu-DOTA-TATE and elucidate the uncertainty associated with non-ideal conditions. ***References:*** [1]Peterson AB. Reduced TP Error Checker. 2023. https://doi.org/10.5281/zenodo.7843928.

OP-907

Non-Uniqueness of Multiexponential Time-Activity Curves in Few-Timepoint Theranostic Workflows Can Increase Dosimetric Error

D. Balfour, *J. Sage, J. Willaime, D. Boukerroui;*
Mirada Medical Ltd., Oxford, UNITED KINGDOM.

Aim/Introduction: Recent literature has shown interest in reducing the number of timepoints in theranostic workflows. Many such studies use parametric, multiexponential time-activity curve (TAC) models to obtain the time-integrated activities (TIAs) required for dosimetry. Such methods then have more parameters than measurements. Mathematically, this leads to an infinity of possible curves that can solve the fitting problem, each with a different TIA. A unique curve is selected randomly by the solver or determined by some prior information, but it is not commonplace for the choice to be explicitly discussed or analysed. The non-uniqueness of the solution in situations where there are fewer timepoints than model parameters is demonstrated here and its impact on TIA estimation is assessed. ***Materials and Methods:*** A curve stripping TAC fitting method [1] was adapted and solutions analytically derived for a 3 timepoint workflow. The TAC was modelled as a 4-parameter bi-exponential decay consisting of rapid and slow washout terms since these contribute most to dosimetric accuracy. With only 3 measurements, 1 parameter remained underdetermined. A prior, $\rho \in]0,1[$, was introduced to characterise this unknown: it represented the ratio of contributions between the two washout terms at the second timepoint. The physical assumptions of the model, such as ensuring the rapid washout curve decayed faster, were analysed to obtain constraints on the range of valid values for ρ, parameterising the family of valid solutions. The equivalent range of valid TIA values was then calculated. To demonstrate on realistic data, 2 [Lu-177]-DOTATATE theranostic patients [2] were segmented and locally rigidly registered to produce a set of activity measurements for the liver at 3 timepoints. For comparison, the TIA was also estimated using trapezoidal integration extrapolated with physical-only decay. ***Results:*** The family of valid TACs was determined by identifying the upper and lower bounds on ρ. All curves between these bounds are plausible. Patient 1 had liver TIA values between 18.4 and 19.6 MBq·h/ml, (6.1% maximal underestimation) and patient 2 had TIA values between 23.9 and 24.5 MBq·h/ml (2.7% maximal underestimation). By comparison, the trapezoidal TIAs were 18.76 and 18.79 MBq·h/ml, respectively. ***Conclusion:*** Curve non-uniqueness in parametric TAC integration is a source of error not usually accounted for in uncertainty analysis. Robust means to select a unique curve is required to ensure accurate dosimetry. This can be achieved using good-quality statistical priors. ***References:*** [1] Jackson et al. (2020) https://doi.org/10.1002/mp.14243 [2] Uribe et al. (2021) https://doi.org/10.2967/jnumed.121.262748

OP-908

Estimating Biochemical PSA Dynamics after Radioligand Therapy with [177Lu]Lu-PSMA-I&T Using a Population Pharmacokinetic/Pharmacodynamic Model

H. Siebinga[1,2], *B. J. de Wit - van der Veen*[1], *D. M. V. de Vries - Huizing*[1], *J. J. M. A. Hendrikx*[1,2], *A. D. R. Huitema*[2,3,4];
[1]*Department of Nuclear Medicine, NETHERLANDS Cancer Institute, Amsterdam, NETHERLANDS,* [2]*Department of Pharmacy and Pharmacology, NETHERLANDS Cancer Institute, Amsterdam, NETHERLANDS,* [3]*Department of Clinical Pharmacy, University Medical Center Utrecht, Utrecht University, Utrecht, NETHERLANDS,* [4]*Department of Pharmacology, Princess Máxima Center for Pediatric Oncology, Utrecht, NETHERLANDS.*

Aim/Introduction: To predict response to [^{177}Lu]Lu-PSMA treatment, tumor exposure-response relationships need to be established. Pharmacokinetic/pharmacodynamic (PKPD) modelling is suitable to assess this association. Therefore, a population PK model for [^{177}Lu]Lu-PSMA-I&T using SPECT/CT was developed and related to PSA dynamics after therapy with a PKPD approach. ***Materials and Methods:*** A population PK model was developed using dosimetric SPECT/CT data of 79 patients who received multiple cycles [^{177}Lu]Lu-PSMA-I&T (7.4 GBq with 2- or 6-week interval). The PK model consisted of 5 compartments; blood, salivary glands, kidney, tumors and combined remaining tissues. Covariates were tested to explain interindividual variability. The final PK model was expanded with a PD compartment (sequential fitting approach) representing PSA dynamics. Patient PSA records were collected up to 82 weeks after the last ^{177}Lu-cycle. To explore the exposure-response relationship, individually estimated [^{177}Lu]Lu-PSMA-I&T tumor concentrations were related to PSA changes over time. ***Results:*** The population PK model adequately described observed data in all compartments. A significant declining uptake in tumors during later cycles was identified, where the average tumor uptake rate decreased to 72%, 50% and 43% in cycle 2, 3 and 4, respectively, compared to cycle 1. In addition, a cycle-to-cycle variability of 37% (RSE 20.8%) on tumor uptake was estimated and tumor volume was identified as a relevant covariate on tumor uptake, where a two-times higher volume resulted in a 2.07-fold increased tumor uptake rate.Observed PSA increase was described by an exponential growth rate (0.000118 h^{-1}). Therapy-induced PSA decrease was related to estimated tumor concentrations (MBq/L) by an E_{MAX}-model ((E_{MAX}*concentration)/(EC_{50}+concentration)) and individual PSA concentrations were adequately captured. A threshold of 116 MBq/L in tumors was determined to result in no PSA change, i.e. a minimum tumor uptake required for a PSA decrease during treatment (though this provides no information on eventual treatment response). Based on simulations of this PKPD model (n=500), 56% and 23% of the patients are expected to show no increase and >50% decrease in PSA 6 weeks after treatment (4 cycles of 7.4 GBq with 6-weeks interval), respectively. ***Conclusion:*** Our population PK model accurately described observed radioactivity in salivary glands, kidneys and tumors after [^{177}Lu]Lu-PSMA-I&T treatment and revealed a declining tumor uptake over cycles. The PKPD model adequately captured individual PSA observations and identified population response rates and tumor dose thresholds. This PKPD-approach may help to compare therapeutic regimes, individualize dosing and identify patients in whom radioligand therapy is likely to fail.

OP-909

Population-based model selection for iodine kinetics in benign thyroid disease

D. Hardiansyah[1], *A. Riana*[1], *H. Hänscheid*[2], *M. Lassmann*[2], *G. Glatting*[3];
[1]*Universitas Indonesia, Depok, INDONESIA,* [2]*University Hospital Würzburg, Würzburg, GERMANY,* [3]*Ulm University, Ulm, GERMANY.*

Aim/Introduction: Model selection is crucial in individual dosimetry of molecular radiotherapy [1,2]. Recently, we demonstrated the superiority of population-based model selection with non-linear mixed-effects model (NLME-PBMS) over conventional methods [3]. However, NLME-PBMS has not been applied to determine the optimal mathematical model for benign thyroid disease. Our study aims to utilise NLME-PBMS to accurately calculate target tissue time-integrated activity (TIAs) in ^{131}I therapy for benign thyroid disease. ***Materials and Methods:*** Biokinetic data (% administered activity) of ^{131}I-therapy in target tissue were obtained from seventy-three patients with Graves' disease/toxic nodular goitre/non-toxic goitre. Time-activity data from uptake measurements were collected at 2, 6, 24, 48, and 96 (N=53) or 120 (N=20) h after oral capsule administration of ^{131}I. Twenty-two sum-of-exponentials (SOE) functions with two to nine parameters (including the EANM SOP function [4]) were used for the model selection. The parameters of the SOE functions were fitted to the all-time-points biokinetic data in the NLME framework. The SOE function most supported by the data was selected based on the Akaike weight [2]. ***Results:*** The SOE function with five parameters, i.e. $f_{5b}=(A_1+A_2)e^{-(\lambda1+\lambda phys)t}-(A_1)e^{-(\lambda2+\lambda phys)t}-(A_2)e^{-(\lambda3+\lambda phys)t}$ was selected as the function most supported by the data. The Akaike weight of the best function was 99.99%. The estimated fixed effect ("parameter mean value in the population") of parameters A_1, A_2, λ1, λ2, and λ3 were 0.2, 0.3, 1.9×10^{-3}/h, 5.7×10^{-2}/h and 5.7×10^{-1}/h, respectively. The variances of the random effect ("width of parameter distributions in the population") of parameters A_1, A_2, λ1, λ2, and λ3 were 0.2, 0.4, 0.4/h^2, 0/h^2 and 0.2/h^2, respectively. The estimated fractional standard deviation of intra-individual variability of the function most supported by the data was 0.059. The optimal function from the model selection performed better than the function from EANM SOP based on the Akaike weight (99.99% vs 3.5×10^{-40}%). ***Conclusion:*** An optimal mathematical model (SOE with five fit parameters) was determined for calculating TIAs in ^{131}I therapy dosimetry for tumours based on NLME and model selection. The optimal mathematical model f5b has two more parameters than the EANM SOP function, which could lead to more accurate TIAs. The sum of 3 exponential terms corresponds to a compartmental model consisting of 3 compartments. ***References:*** [1]. Hardiansyah, D., et al., EJNMMI Phys, 2021. 8(1): p. 82. [2]. Kletting, P., et al., Med Phys, 2013. 40(10): p. 102504. 3. Hardiansyah, D., et al., Z Med Phys, 2023. [4]. Hänscheid, H., et al., EJNMMI, 2013. 40(7): p. 1126-34.

OP-910

131I Thyroid lesion dosimetry with quantitative imaging

E. Richetta*, C. Cutaia, A. Codegone, V. Garbaccio, R. Pellerito, M. Stasi;*
Ordine Mauriziano Hospital, Turin, ITALY.

Aim/Introduction: Post ^{131}I treatment of metastatic thyroid cancer lesion dosimetry is recommended by the Italian (DLgs 101/20) and European (EU 59/2013) laws to verify the target exposure. To this aim quantitative imaging is useful to standardize the dosimetric process. In this study the SPECT-CT quantification tool is validated and compared to the standard dosimetic method. ***Materials and Methods:*** The quantification software was installed on SPECT-CT for ^{131}I quantitative imaging (matrix 256x256, 64 views, 20s/view, attenuation-scatter corrected, 2.4 mm voxel-size). Dose were calculated both on standard iterative algorithm (IT) and quantitative (xSPECT) images for results comparisons. A ^{131}I known liquid source was employed for homogeneous phantom (22 kBq/ml) and spheres phantoms (cylinder 130 ml and 6 spheres, 7.9 MBq/ml) acquisitions to verify the activity calculation accuracy and to build recovery coefficients (RC) partial volumes effect (PVE) curves. Lesion dosimetry was performed on 10 patients and compared (23 lesions, 3 SPECT-CTs (24 h, 48h, > 96 h), biexponential fit with uptake phase, MIRD sphere model). ***Results:*** For IT images the 3.38E-5 MBq/counts absolute calibration factor was found, while for xSPECT a 0.87 volume sensitivity factor was adopted. In the homogeneous phantom activity accuracy was within -3.6% and -4.7 % for IT and xSPECT respectively. Discrepancies between the two activity calculation methods were in mean (±1dev.st) -3%

±2.9% confirming the effectiveness of the quantification tool. RC curves were significantly different for the two algorithms (IT and xSPECT respectively): 130 ml (1,1), 26.5 ml (0.93, 0.90), 11.4 ml (0.86, 0.68), 5.5 ml (0.72, 0.43), 2.6 ml (0.54, 0.25), 1.1 ml (0.33, 0.13), 0.5 ml (0.16, 0.07). For 10 patient lesion dosimetry was performed. Lesion volumes were small (100% < 35 ml, 43 % < 10 ml) and required PVE corrections. Percentage differences between IT and xSPECT were in mean (±1dev.st) -2%±26%, +3%±20% and 4.9%±22% for activity, cumulated activity and mean dose respectively. ***Conclusion:*** The quantification software is an effective tool for ^{131}I lesion dosimetry in order to standardize and simplify the dosimetric workflow. Further investigation on 3D voxel dosimetry could better explain variations founded on mean dose results with MIRD sphere model.

OP-911

Evaluation of images from patients treated with 224Ra-CaCO3-microparticles for peritoneal metastases - can 224Ra be quantified using SPECT/CT?

S. Grønningsæter[1], *L. G. Mikalsen*[1,2], *J. Blakkisrud*[1], *M. Revheim*[1,3], *S. Westrøm*[4], *S. Selboe*[1], *Ø. Bruland*[5,6], *S. Larsen*[7], *C. Stokke*[1,8]; *[1]Division of Radiology and Nuclear Medicine, Oslo University Hospital, Oslo, NORWAY, [2]Department of Life Sciences and Health, Oslo Metropolitan University, Oslo, NORWAY, [3]Faculty of Medicine, University of Oslo, Oslo, NORWAY, [4]Oncoinvent AS, Oslo, NORWAY, [5]Department of Oncology, Oslo University Hospital, Oslo, NORWAY, [6]Institute of Clinical Medicine, Oslo University Hospital, Oslo, NORWAY, [7]Department of Gastroenterological Surgey, Oslo University Hospital, Oslo, NORWAY, [8]Department of Physics, University of Oslo, Oslo, NORWAY.*

Aim/Introduction: In an ongoing Phase 1 study, SPECT-based quantification was evaluated after injecting ^{224}Ra adsorbed in calcium carbonate microparticles (^{224}Ra-$CaCO_3$-MP) to patients with peritoneal metastasis from colorectal cancer. The imaging results were compared with the estimated amount of activity in patients based on non-imaging approaches. ***Materials and Methods:*** Two days after cytoreductive surgery (CC-0) with hyperthermic intraperitoneal chemotherapy treatment (CRS-HIPEC), patients were injected intraperitoneally with approximately 7 MBq ^{224}Ra-$CaCO_3$-MP, diluted in isotonic solution. Whole body planar images and SPECT/CT scans were acquired using a Siemens Symbia Intevo Bold gamma camera at approximately 3, 24, and 120 hours after injection. Imaging was performed using a 20% energy window centred at 240 keV, with two 5% scatter windows, mainly capturing emissions from ^{212}Pb and daughters. Reconstruction of SPECT images was conducted with an OSEM Flash3d reconstruction algorithm with scatter correction, CT based attenuation correction, and 30×2 iterations×subsets. A homogenous water phantom had previously been used to find the calibration factor (176.1 counts/kBq). Whole-body probe measurements were obtained at 3, 24 and 120 hours and blood samples at 3, 6, 24, 48 and 120 hours. Kinetic modelling, based on the amounts of activity in blood and an adapted model using ICRP publication 137 models for unbound radium and lead, was used to estimate the amount of activity leaving the peritoneal cavity. The SPECT/CT images were used for quantification of activity, based on segments drawn in 3dSlicer covering the whole abdomen. The non-imaging based approach considered the injected activity, corrected for wash-out based on external probe measurements. ***Results:*** Six patients were included, with five patients completing all of the three imaging acquisitions. The kinetic model estimating that 15-25 % of the activity left the peritoneal cavity, and this was also supported by visual inspection of the images. Comparing the activity measured by SPECT to the non-imaging approaches resulted in that 74-104% of the known activity was captured at day 1, 73-137% at day 2, and 64-190% at day 6. ***Conclusion:*** Quantitative SPECT/CT imaging of ^{224}Ra, primarily based on ^{212}Pb emissions, might be adequate for quantifying ^{224}Ra, although the accuracy was found to decrease with the amount of activity. For the six patient investigated, most of the activity was contained in the peritoneal cavity, covered by a single SPECT bed position. Cavitary (or regional) treatment may represent an idealised situation for ^{224}Ra SPECT quantification compared to radiopharmaceuticals intended for distribution throughout the body.

OP-912

90Y Voxel S-Values updated Monte Carlo database including Internal Bremsstrahlung and new analytical model extending the evaluation to any voxel size

D. Pistone[1,2], *L. Auditore*[1,2], *A. Italiano*[2,3], *E. Amato*[1,2,4]; *[1]Department of Biomedical and Dental Sciences and of Morphofunctional Imaging (BIOMORF), University of Messina, Messina, ITALY, [2]INFN, National Institute for Nuclear Physics, Section of Catania, Catania, ITALY, [3]Department of Mathematical and Computer Science, Physical Sciences and Earth Sciences (MIFT), University of Messina, Messina, ITALY, [4]Health Physics Unit, University Hospital "Gaetano Martino", Messina, ITALY.*

Aim/Introduction: Voxel S-Values (VSVs) are widely employed for 3D internal dosimetry of radionuclide therapies, but databases are available for a limited set of voxel sizes. Additionally, it was recently highlighted that Internal Bremsstrahlung (IB) accompanying β-decay, up to now neglected in dosimetry, including VSVs calculation, can play a significant role in the energy deposition for some β-emitters, such as ^{90}Y. This study aimed at calculating via Monte Carlo (MC) simulation updated ^{90}Y-VSVs including IB, and developing an analytical model to extend the VSV estimation to any voxel dimension of practical interest. ***Materials and Methods:*** GATE (Geant4 Application for Tomographic Emission) MC simulations were implemented for multiple voxelized geometries of soft tissue, with cubic voxel size d from 2 to 6 mm, in steps of 0.5 mm. For each geometry, the central voxel was set as a homogeneous source of ^{90}Y decays and IB photons, and the ^{90}Y-VSVs were computed with and without the additional IB contribution. The analytical model was developed by first fitting the VSVs, including IB as a function of the "normalized radius" $R_n = R/d$ (R = distance from the central voxel), and then fitting the obtained parameters as a function of d. ***Results:*** Comparing MC-derived VSVs including and neglecting IB, differences between +25% and +30% were found for R larger than the maximum range of ^{90}Y β-particles, testifying the significant contribution of IB to the photon tails of VSVs. Comparing the VSVs from the proposed analytical model with MC ones including IB, agreement within ±5% was found in the central voxel and for the photon tails, increasing the accuracy given by the previous model by Amato et al. 2012 [1]. ***Conclusion:*** The updated ^{90}Y-VSVs proposed in this study include for the first time IB, increasing the accuracy with respect to existing databases. The new analytical model, implemented in a simple spreadsheet, constitutes a user-friendly and fast approach to calculate ^{90}Y -VSVs for non-standard voxel dimensions. ***References:*** [1] Amato E et al. Med. Phys. 2012; https://doi.org/10.1118/1.4757912

1806

Wednesday, September 13, 2023, 9:45 AM - 11:15 AM
Hall C

Clinical Oncology Track - TROP Session: Radiomics

OP-913

Texture Analysis of 68Ga-DOTATOC PET/CT Images For the Prediction of Outcome in Patients With Neuroendocrine Tumors

S. Pellegrino[1], *R. Fonti*[1], *R. Bologna*[1], *M. Panico*[1], *R. Morra*[2], *G. Palmieri*[2], *M. Giuliano*[2], *S. De Placido*[2], *S. Del Vecchio*[1];
[1]Department of Advanced Biomedical Sciences, University Federico II, Naples, ITALY, [2]Department of Clinical Medicine and Surgery, University Federico II, Naples, ITALY.

Aim/Introduction: The aim of our study was to test whether texture analysis of 68Ga-DOTATOC PET/CT images can predict clinical outcome in patients with neuroendocrine tumors (NET). ***Materials and Methods:*** Fifty patients with neuroendocrine tumors who had undergone 68Ga-DOTATOC PET/CT were included in the study. Primary tumors were localized in the gastroenteropancreatic (39), bronchopulmonary (8) and other anatomical districts (3). Patients were subjected to a mean follow-up period of 19 months (range 1-40 months). All primary lesions were segmented using an automated contouring program setting a threshold for SUV at 2.5 and then they were subjected to texture analysis using LIFEx program. Among all the extracted features, we selected CoV (SD divided by SUVmean), HISTO Skewness, HISTO Kurtosis, HISTO Entropy-log$_{10}$, GLCM Entropy-log$_{10}$, GLCM Dissimilarity and NGLDM Coarseness for further analysis. SUVmax, SUVmean, Receptor Expressing Tumor Volume (RETV) and Total Lesion Receptor Expression (TLRE) were also determined. Univariate and multivariate analyses of clinical and imaging variables were performed using Cox proportional hazards regression. Survival analysis was performed using Kaplan-Meier method and log-rank tests. ***Results:*** Fifty primary lesions were analyzed. Mean values of the conventional and volumetric parameters SUVmax, SUVmean, RETV and TLRE were 24.96±20.47, 8.42±6.58, 26.51±38.82 mL and 295.69±717.61 g, respectively. Moreover, mean values of the texture features CoV, HISTO Skewness, HISTO Kurtosis, HISTO Entropy-log$_{10}$, GLCM Entropy-log$_{10}$, GLCM Dissimilarity and NGLDM Coarseness were 0.52±0.21, 1.18±0.42, 4.04±1.30, 0.92±0.33, 1.71±0.57, 2.83±2.43 and 0.02±0.01, respectively. Survival analysis was performed including clinical variables (age, gender, grading, early or advanced stage), imaging parameters (SUVmax, SUVmean, RETV and TLRE) and texture features (CoV, HISTO Skewness, HISTO Kurtosis, HISTO Entropy-log$_{10}$, GLCM Entropy-log$_{10}$, GLCM Dissimilarity and NGLDM Coarseness). At univariate analysis, overall survival (OS) was predicted by age (p=0.0034), SUVmax (p=0.0128), SUVmean (p=0.0059), CoV (p=0.0090), HISTO Entropy-log$_{10}$ (p=0.0123), GLCM Entropy-log$_{10}$ (p=0.0126) and GLCM Dissimilarity (p=0.0086). At multivariate analysis, only the texture feature GLCM Entropy-log$_{10}$ was retained in the model for prediction of OS (χ^2=7.047, p=0.0079). Finally, survival analysis showed that patients with GLCM Entropy-log$_{10}$ >1.28 had a significantly better OS as compared to patients with GLCM Entropy-log$_{10}$ ≤1.28 (χ^2=7.1075, p=0.0077). ***Conclusion:*** Texture analysis of 68Ga-DOTATOC PET/CT images, by revealing the heterogeneity of somatostatin receptor expression, can predict the clinical outcome of NET patients.

OP-914

Association Between Absorbed Dose Heterogeneity and Metabolic Response in HCC Patients Undergoing Transarterial Radioembolization with Y-90 Resin Microspheres

N. Coskun[1], *M. Kartal*[2], *A. Erdogan*[2], *E. Ozdemir*[1];
[1]Ankara Bilkent City Hospital, Ankara Yildirim Beyazit University, Ankara, TÜRKIYE, [2]Ankara Bilkent City Hospital, Ankara, TÜRKIYE.

Aim/Introduction: Voxel-based dosimetry is known to be associated with improved response rates in the treatment of hepatocellular carcinoma (HCC) through transarterial radioembolization (TARE) using glass microspheres. However, the voxel-based dosimetric approach for resin-based microspheres has not been extensively studied and the significance of dosimetric heterogeneity remains unclear. In this study, we aimed to determine the dose thresholds associated with metabolic response and evaluate the predictive potential of intratumoral dose heterogeneity in HCC patients undergoing TARE with resin-based microspheres. ***Materials and Methods:*** We conducted a retrospective screening of patients diagnosed with HCC who underwent TARE using Y-90-loaded resin microspheres in our center between January 2021 and January 2023. Voxel-based dosimetric analysis was performed on post-treatment Y-90 PET/CT images to calculate the average absorbed tumor dose, the percentage of targetted tumor volume, and the minimum doses to consecutive volume percentages within the tumor. The metabolic response of the lesions was determined 3 months after treatment by F-18 FDG PET/CT imaging according to PERCIST criteria. Lesions with complete or partial response were deemed responsive, while lesions that remained stable or progressed were deemed non-responsive. The relationship between the calculated dosimetric parameters and the response to treatment was evaluated using independent samples T-test and ROC analysis. ***Results:*** Thirty-five lesions targeted with 22 TARE sessions in 19 patients (15 males, 4 females, mean age 60±13 years) were included in the study. Objective metabolic response was observed in 57% of the lesions (n=20). Average tumor dose, the percentage of targeted volume, and minimum absorbed doses at 20% to 95% of tumor volume were significantly higher in responsive lesions. The minimum absorbed dose at 50% of tumor volume demonstrated the most prominent difference between responsive and non-responsive lesions. The optimal cut-off values for average tumor dose, targetted tumor percentage, and minimum dose at 50% of tumor volume were 94.6 Gy (sensitivity 73%, specificity 70%, AUC 0.72), 94% (sensitivity 73%, specificity 55%, AUC 0.64), and 91 Gy (sensitivity 80%, specificity 80%, AUC 0.80), respectively. ***Conclusion:*** Our findings suggest that not only the average tumor dose but also the heterogeneous distribution of the absorbed dose within the tumor is associated with metabolic response in HCC lesions treated with resin microspheres. The use of multicompartmental, voxel-based dosimetry can provide a reliable insight into dosimetic heterogeneity. These findings, if confirmed by prospective, randomized studies, may contribute to the development of more effective treatment approaches using resin-based Y-90 microspheres.

OP-915

Development of clinical-radiomic model on baseline FDG-PET images in non-small-cell-lung cancer patients, referred to radical lung surgery

L. Travaini, *G. Zuccotti, F. Botta, S. Netti, M. Casiraghi, M. Ferrari, A. Gaeta, P. Rocca, F. Mattana, S. Fracassi, A. Barone, G. Buonsanti, G. Petralia, L. Spaggiari, F. Ceci;*
EUROPEAN INSTITUTE OF ONCOLOGY, Milano, ITALY.

Aim/Introduction: : to investigate the association of radiomic features (RFs) extracted from baseline 18F-FDG PET/CT (FDG-PET) with Overall Survival (OS) in a population of early Non-Small Cell Lung Cancer (NSCLC) patients. ***Materials and Methods:*** between 01/2015 and 12/2021 patients with stage I, II and IIIa NSCLC who underwent FDG-PET before surgery were evaluated. OS was the primary endpoint of the analysis. The dataset was randomly split into a training set and a test set consisting of 70% and 30% of the subjects, respectively. The radiomic score (RS) of each patient was determined as a linear combination of the RFs and the coefficient determined with a multivariable Cox LASSO model on the training set. Three prognostic models were evaluated: the clinical model containing only clinical information, the radiomic model containing only the radiomic score, and the clinical-radiomic model containing both clinical information and the radiomic score. The models were compared using the C-index calculated on the training and on the test cohort. Finally, Pseudo Likelihood Ratio Test (PST) was performed to explore any differences in the C-indexes of the clinical and clinical-radiomic model, respectively, on the training set. ***Results:*** three hundred ninety-six (n=396) patients met the inclusion criteria. Median follow-up was 39 months (19-59 months interquartile range IQR) on censured overall sample. The median lesion size was 40 mm (InterQuartile Range (IQR): 29-55). In the clinical model, age and pT were significantly associated with OS. However, the model showed sub-optimal fit, as the C-index was 0.60 in the training and a 0.56 in the test set. The radiomic model showed similar results, with higher performance compared with the clinical model (training C-index=0.73; validation C-index=0.59). The highest training performance was obtained by combining the clinical and radiomic model: training C-index=0.74 and validation C-index=0.58. The performance of the clinical-radiomic model was significantly higher (p≤0.001) compared to the performance of the clinical model alone in the training set. Conversely, there was no significant difference in the performance of the radiomic and clinical-radiomic models. ***Conclusion:*** our preliminary results confirm the better performance of the clinical-radiomic model compared to the others considered separately. Considering the sub-optimal performance of the model, the inclusion of CT data and the contouring of PET images with different methods is necessary to improve the performance of this radiomic approach.

OP-916

Texture Analysis of 18F-FDG PET/CT Images for the Prediction of Outcome in Patients with Multiple Myeloma

S. Pellegrino[1], *D. Origlia*[1], *C. Vallone*[1], *R. Della Pepa*[2], *S. Del Vecchio*[1], *R. Fonti*[1];
[1]*Department of Advanced Biomedical Sciences, University Federico II, Naples, ITALY,* [2]*Department of Clinical Medicine and Surgery, University Federico II, Naples, ITALY.*

Aim/Introduction: Multiple myeloma (MM) is characterized by uncontrolled growth of monoclonal plasma cells which can infiltrate the bone marrow in both focal and diffuse manner. This peculiarity makes staging and prognosis of this disease rather difficult. The aim of our study was to test whether texture analysis of 18F-FDG PET/CT images can predict survival in MM patients. ***Materials and Methods:*** Forty-six MM patients underwent 18F-FDG-PET/CT before treatment. We used an automated contouring program for segmenting the hottest focal lesion (absolute threshold for SUV at 2.5) and a lumbar vertebral body for assessment of diffuse bone marrow involvement. The conventional imaging parameters SUVmax and SUVmean and texture features such as Coefficient of variation (CoV), HISTO Skewness, HISTO Kurtosis, GLCM Entropy-log10, GLCM Dissimilarity and NGLDM Coarseness were obtained. Patients were treated and then subjected to a mean follow-up period of 51 months. ***Results:*** We examined 46 focal lesions (FL) and 46 lumbar vertebrae for assessment of diffuse involvement (DI). The mean values of all variables obtained from FL were higher than those extracted from DI, in particular SUVmax (11.05±8.30 vs 3.00±0.96), SUVmean (4.89±2.21 vs 1.80±0.57) and GLCM Dissimilarity (4.29±2.73 vs 0.96±0.31). At follow-up 24 patients died of myeloma and were compared to the 22 survivors for overall survival (OS) analysis. Univariate analysis showed that FL SUVmax (p=0.0453), FL SUVmean (p=0.0463), FL CoV (p=0.0211) and DI SUVmax (p=0.0538) predicted OS. At multivariate analysis only FL CoV and DI SUVmax were retained in the model (p=0.0154). ROC curve analysis showed that the best discriminating FL CoV and DI SUVmax values for OS prediction were 0.44 and 3.88, respectively. Kaplan-Meier method and log-rank testing showed that patients with FL CoV below the cutoff had significantly better OS than those with FL CoV above the cutoff (p=0.0003), as well as patients with DI SUVmax below the cutoff versus those with DI SUVmax above the cutoff (p=0.0006). Combining FL CoV and DI SUVmax by using their respective cutoff values, a statistically significant difference was found between the resulting four survival curves (p=0.0001). Indeed, patients with both FL CoV and DI SUVmax below their respective cutoff values had the most favorable prognosis, as opposed to those having FL CoV and DI SUVmax above their respective cutoff. ***Conclusion:*** Conventional and texture parameters derived from 18F-FDG PET/CT analysis can predict the clinical outcome of MM patients by assessing the heterogeneity and aggressiveness of both focal and diffuse infiltration.

OP-917

Inter-institutional validation of a [18F]-FDG PET radiomic signature to predict the location of tumor recurrence after re-irradiation in head and neck cancer in an independent cohort

A. Beddok[1,2], *K. Grogg*[2], *L. Rozenblum*[3,2], *C. Nioche*[1], *F. Orlhac*[1], *H. Shih*[4], *T. Marin*[2], *I. Buvat*[1], *G. El Fakhri*[2];
[1]*Institut Curie, PSL Research University, University Paris Saclay, Inserm LITO, Paris, FRANCE,* [2]*Gordon Center for Medical Imaging, Massachusetts General Hospital, Harvard Medical School, Boston, MA, UNITED STATES OF AMERICA,* [3]*Department of Nuclear Medicine, AP – HP Hôpitaux Universitaires La Pitié Salpêtrière - Charles Foix, Sorbonne Université, Paris, FRANCE,* [4]*Department of Radiation Oncology, Massachusetts General Hospital, Harvard Medical School, Boston, MA, UNITED STATES OF AMERICA.*

Aim/Introduction: A [18F]-FDG PET (PET) radiomic signature for predicting the location of locoregional recurrence (LR) after re-irradiation (reRT) was previously derived* in patients with head and neck cancer (HNC) identifying radiomic features characterizing the signal heterogeneity in the re-irradiated target volume as predictive factors. The aim of this study was to test the performance of this model in an independent cohort of patients from a separate institution. ***Materials and Methods:*** A validation cohort of 36 re-irradiated HNC patients at Massachusetts General Hospital was created ("Boston's cohort"). All patients had a PET scan before reRT, including 27 patients with a second LR. For each patient, the re-irradiated GTV (rGTV) was segmented using SUV>3 threshold extended with a 1 mm margin. Radiomic features were extracted from rGTV using LIFEX software v7.3.17 (2x2x2mm spatial resampling, fixed bin size of 0.157 SUV units). The second LR was categorized as "in-field" if 100% of its volume was in the

rGTV's 95% isodose ("outside" if < 20%). In the initial published study* using 23 HNC patients (Paris's cohort), the prediction model was created using the first principal component (PC) of a PC analysis involving four features: SUV_min, SUV_Kurtosis, GLCM_Correlation, and GLCM_Contrast. In the present work, each subject was characterized by these features, projected as a supplementary individual onto the Paris' PC, and assigned to one of the two groups using the same cut-off as the one identified in the Paris' cohort. Balance accuracy (BA) assessed the model's performance. Permutation test evaluated significance. ***Results:*** Among the 27 patients, 15 had "in-field" and 12 had "outside" second LR. The ranges of values for the four features were not significantly different between the Paris and Boston cohorts (Wilcoxon rank test: p>0.05). BA was 79% with 6 patients misclassified (one "outside" classified as "in-field", and five "in-field" classified as "outside"), corresponding to a positive predictive value (PPV) of 91%. These results were significantly higher than those from the permutation experiment (p<0.05) and close to the 84.5% BA obtained in the Paris's cohort using cross-validation. ***Conclusion:*** This study confirms in an independent cohort of patients that before reRT, a previously derived PET radiomic signature can identify patients that will relapse "in-field" after re-irradiation with a high PPV. If the robustness of the model is confirmed, PET radiomics could facilitate the identification of patients that might benefit from in-field boost in a reRT scheme. ***References:*** *Beddok et al. EJNMMI 2023 PMID: 36282298

OP-918

Multi-imaging adaptive radiotherapy for locally advanced head and neck cancer: preliminary results from the RadiomicART study

F. Gelardi[1,2], *C. Franzese*[1,3], *M. Teriaca*[3], *M. Badalamenti*[3], *M. Roghi*[3], *D. Dei*[1,3], *C. Giannitto*[4], *M. Rodari*[2], *M. Scorsetti*[1,3]; [1]*Department of Biomedical Sciences, Humanitas University, Pieve Emanuele (MI), ITALY,* [2]*Department of Nuclear Medicine, IRCCS Humanitas Research Hospital, Rozzano (MI), ITALY,* [3]*Department of Radiation Oncology, IRCCS Humanitas Research Hospital, Rozzano (MI), ITALY,* [4]*Department of Diagnostic Imaging, IRCCS Humanitas Research Hospital, Rozzano (MI), ITALY.*

Aim/Introduction: Radiation therapy, alone or in combination with chemotherapy, is the primary non-surgical treatment for locally advanced head and neck cancer (HNC). Despite the introduction of innovative modulated techniques, radiation-related toxicity is still an issue affecting patients' quality of life. Adaptive Radiotherapy (ART) can tailor the treatment plan to improve the distribution of the therapeutic dose according to radiation-induced changes from the initial simulation. We present the preliminary results from the RadiomicART study, aiming at an advanced multi-imaging-based analysis approach to predict outcome and toxicity in HNC patients treated with ART. ***Materials and Methods:*** We prospectively enrolled patients with locally advanced HNC eligible for RT in our institution. All patients underwent CT, [18F]FDG PET/CT, and MRI before RT. We delineated the target volumes on CT and adjusted them on PET/CT and MRI. The total dose delivered was 66/60/54Gy in 30 fractions, using the VMAT-simultaneous integrated boost technique. After three weeks, imaging was repeated to allow adaptive planning. We defined GTV-T and GTV-N by plotting primary tumour and lymph nodes separately. We compared disease characteristics in terms of semiquantitative parameters on PET/CT and of radiomics features on MRI between the original and adaptive plans. We assessed the correlation between imaging changes and patients' baseline characteristics. ***Results:*** We included 30 patients with HNC (median age 69 years, M:F=22:8, 50% with history of smoking). The most common site of primary tumour was oropharynx (19/30), and HPV was found in 15/30 patients. The median GTV-T and GTV-N at baseline versus at re-planning were 22 versus 20 cc, and 5.7 versus 5.5 cc, respectively. PET/CT analysis showed a significant difference in both SUVmax and SUVmean between baseline and interim scan for both primary tumour (SUVmax 18.31 vs 9.76, p<0.0001; SUVmean 9.57 vs 5.6, p<0.0001) and pathological lymph nodes (SUVmax 11.24 vs 6.85, p=0.0004; SUVmean 5.34 vs 3.74, p=0.0005). The reduction in GTV-T and GTV-N was also statistically significant (p<0.0001 and 0.04, respectively). In the primary tumour, Δ-GTV was significantly associated with gender (p=0.006), while Δ-SUVmean correlated with HPV presence (p=0.035). MRI analysis showed a significant association between the median absolute deviation of Δ-radiomics features and smoking (p<0.05), HPV presence (p<0.005), and primary tumour (p<0.005). ***Conclusion:*** Preliminary results showed significant imaging differences between the original and adaptive RT plans and specific correlations with patient characteristics. These findings suggest a potential role for advanced image analysis in treatment planning and outcome prediction in HNC patients.

OP-919

Application of an artificial intelligence-based tool in [18F]FDG PET/CT for the assessment of bone marrow involvement in multiple myeloma

C. Sachpekidis[1], *O. Enqvist*[2], *J. Ulén*[3], *A. Kopp-Schneider*[1], *L. Pan*[1], *A. Jauch*[4], *M. Hajiyianni*[5], *L. John*[5], *N. Weinhold*[5], *S. Sauer*[5], *H. Goldschmidt*[5], *L. Edenbrandt*[6], *A. Dimitrakopoulou-Strauss*[1]; [1]*German Cancer Research Center (DKFZ), Heidelberg, GERMANY,* [2]*Department of Electrical Engineering, Chalmers University of Technology, Department of Electrical Engineering, Chalmers Uni, SWEDEN,* [3]*Eigenvision AB, Eigenvision AB, SWEDEN,* [4]*Institute of Human Genetics, University of Heidelberg, Heidelberg, GERMANY,* [5]*Department of Internal Medicine V, University Hospital Heidelberg and National Center for Tumor Diseases (NCT), Heidelberg, GERMANY,* [6]*Department of Clinical Physiology, Region Västra Götaland, Sahlgrenska University Hospital, Department of Clinical Physiology, Region Västra G, SWEDEN.*

Aim/Introduction: To validate a novel three-dimensional deep learning-based tool on PET/CT images for automated assessment of the intensity of BM metabolism in multiple myeloma (MM) patients. ***Materials and Methods:*** Whole body [18F]FDG PET/CT scans of 35 consecutive, previously untreated MM patients were studied. All patients were investigated in the context of an open-label, multicentre, randomised, active-controlled, phase 3 trial (GMMG-HD7). Qualitative (visual) analysis classified the PET/CT scans in three groups based on the presence and number of focal, [18F]FDG-avid lesions as well as the degree of diffuse [18F]FDG uptake in the BM. The proposed automated method for BM metabolism assessment is based on an initial CT-based segmentation of the skeleton, its transfer to the SUV PET images, subsequent application of different SUV thresholds, and refinement of the resulting regions using postprocessing. Six different SUV thresholds were applied for definition of pathological tracer uptake in the skeleton and -using the resulting masks- subsequent calculation of the whole body metabolic tumor volume (MTV) and total lesion glycolysis (TLG) in each patient. Correlation analysis was performed between the automated PET values and the results of visual PET/CT analysis as well as histopathological, cytogenetical and clinical data of the patients. ***Results:*** BM segmentation and calculation of MTV and TLG after application of the deep learning tool was feasible in all

patients. A significant positive correlation ($p<0.05$) was observed between results of visual analysis of the PET/CT scans for the three patient groups and the MTV and TLG values after employment of all six [^{18}F]FDG uptake thresholds. Further, we could demonstrate a significant, moderate, positive correlation between bone marrow plasma cell infiltration and plasma levels of β2-microglobulin with the automated quantitative PET/CT parameters MTV and TLG, after utilization of the following four thresholds: (1) liver SUVmedian x 1.1 (axial skeleton), gluteus SUVmedian x 4 (extremities), (2) liver SUVmedian x 1.5 (axial skeleton), gluteus SUVmedian x 4 (extremities), (3) SUVmax ≥ 2.5, and (4) SUVmax ≥ 2.5 (axial skeleton), SUVmax ≥ 2.0 (extremities). ***Conclusion:*** The automated, volumetric, whole body PET/CT assessment of BM metabolic activity in MM is feasible with the herein applied method and correlates with clinically relevant parameters in the disease. This methodology offers a potentially reliable tool in the direction of optimization and standardization of PET/CT interpretation in MM. Based on the present promising findings, the deep learning-based approach will be further evaluated in future prospective studies with larger patient cohorts.

OP-920

Development and validation of 18F-PSMA PET/CT-based radiomics model to predict biochemical recurrence-free survival following radical prostatectomy

T. Li, *K. Zhao, X. Su;*
The First Affiliated Hospital, College of Medicine, Zhejiang University, Hangzhou, CHINA.

Aim/Introduction: Biochemical recurrence (BCR) following radical prostatectomy (RP) is a significant concern for patients with prostate cancer. Reliable prediction models are needed to identify patients at risk for BCR and facilitate appropriate management. This study aimed to develop and validate a radiomics model based on preoperative 18F-PSMA PET/CT for predicting BCR-free survival in patients undergoing RP for prostate cancer. ***Materials and Methods:*** A total of 236 patients with histologically confirmed prostate cancer who underwent RP were retrospectively analyzed. All patients had a preoperative 18F-PSMA PET/CT scan. Radiomics features were extracted from the primary tumor region in PET/CT images. A radiomics signature was developed using the least absolute shrinkage and selection operator (LASSO) Cox regression model. The performance of the radiomics signature in predicting BCR-free survival was assessed using Harrell's concordance index (C-index) and compared with clinicopathological variables. The model was externally validated in an independent cohort of 98 patients. ***Results:*** The radiomics signature comprised ten features and demonstrated a C-index of 0.74 (95% CI: 0.66-0.82) in the training cohort and 0.71 (95% CI: 0.61-0.81) in the validation cohort. The radiomics signature remained an independent predictor of BCR-free survival in multivariable analysis (HR: 2.48, 95% CI: 1.47-4.17, $p < 0.001$). The addition of the radiomics signature to a base model containing clinicopathological variables significantly improved the prediction performance (C-index: 0.78, 95% CI: 0.70-0.86, $p < 0.001$). ***Conclusion:*** We developed and validated a novel 18F-PSMA PET/CT-based radiomics model that can predict BCR-free survival following RP in prostate cancer patients. This model may be useful in identifying patients at a higher risk of BCR, thus enabling personalized risk stratification and tailored management strategies.

OP-921

Radiomic analysis of pre-surgery FDG-PET images in early-stage Non-Small Lung Cancer patients can improve outcome stratification

L. Travaini, *G. Zuccotti, M. Ferrari, M. Casiraghi, F. Botta, M. Colandrea, F. Mattana, C. Zanini, L. Gilardi, M. Calabrese, F. Bellerba, L. Spaggiari, G. Petralia, F. Ceci;*
European Institute Of Oncology, Milano, ITALY.

Aim/Introduction: to investigate the association of radiomic features (RFs) from baseline 18F-FDG PET/CT (FDG-PET) and diagnostic CT images with Overall Survival (OS) and Progression Free Survival (PFS) in early-stage Non-Small-Cell-Lung-Cancer (NSCLC) patients. ***Materials and Methods:*** NSCLC patients staged by baseline FDG-PET and CT before radical surgery at our Institute were retrospectively enrolled. All patients had at least 48 months of follow-up. For each patient the largest lesion was contoured manually on CT images and semiauthomatically on PET images with 2 methods (Nestle method, LifeX package; PET Tumour Segmentation PTS tool, 3DSlicer package). Ninety-three PET RFs and 137 CT RFs were extracted with Pyradiomics tool (for PET, extraction was performed for each segmentation). Feature selection was previously performed (univariate ANOVA) to exclude features significantly affected by acquisition parameters (scanner model, injected activity/weight, frame duration, injection-acquisition interval for PET; kV and reconstruction algorithm for CT). Radiomic scores for OS and PFS were created by Multivariable Cox Regression LASSO Model; clinical and clinical-radiomic models were obtained by Multivariable Cox Regression Model. The performances of the different models (radiomic, clinical and clinical-radiomic, based on CT RFs and/or PET RFs with different PET segmentations) for each endpoint were assessed (C-index, 5-fold internal cross validation) and compared (Likelihood Ratio Test (LRT) and pseudo-LRT). ***Results:*** one-hundred and twenty patients (n=120) fulfilled the inclusion criteria. In the clinical model age, neoadjuvant and adjuvant therapy were independent predictors of OS (training C-index=0.70; validation C-index=0.71). The radiomic score significantly separated high- vs. low-risk OS sub-cohorts when including CT features. The best performance was obtained with the combination of CT features and PET features with PTS method ($p=0.0015$, training C-index 0.78, validation C-index 0.80) and was significantly higher compared to the clinical model alone ($p<0.001$). Sex, pT and adjuvant therapy were independent predictors of PFS in the clinical model (training C-index=0.66; validation C-index=0.61). Significantly better results for PFS prediction were obtained when combining clinical and radiomic data, the highest performance being obtained with the PET radiomic score from PTS segmentation method: training C-index=0.74 and validation C-index=0.72 ($p<0.001$ for the comparison with clinical model alone). ***Conclusion:*** radiomic analysis applied to baseline FDG-PET and CT images in early-stage NSCLC appears to be a reliable approach for stratifying patients with more favorable vs. less favorable outcome after radical lung surgery.

1807

Wednesday, September 13, 2023, 9:45 AM - 11:15 AM
Hall F1

Inflammation & Infection Committee - TROP Session: COVID-19: Isn't it over yet?

OP-922

Noninvasive imaging of inflammatory processes by macrophage-directed PET-tracers during a SARS-CoV-2-infection in cynomolgus macaques (Macaca fascicularis)

M. Stammes[1], *G. Koopman*[1], *T. Wagner*[2], *B. Traenkle*[2], *P. Kaiser*[2], *A. Maurer*[3], *J. Schwenck*[3], *U. Rothbauer*[3], *M. Kneiling*[3], *D. Sonanini*[3]; [1]*BPRC, Rijswijk, NETHERLANDS,* [2]*University of Tübingen, Reutlingen, GERMANY,* [3]*Eberhard Karls University, Tübingen, GERMANY.*

Aim/Introduction: Monitoring the presence and dynamic distribution of distinct immune cell populations are key in understanding the impact of disease processes in the body. Macrophages are critically involved in the pathogenesis of COVID-19. In addition, it has been indicated that a SARS-CoV-2 infection leaves an inflammatory imprint in the macrophage compartment and thus alters effector functions of macrophages which subsequently might lead to the "long-COVID" syndrome. One option to monitor macrophages by noninvasive in vivo PET imaging is to target the mitochondrial translocator-protein (TSPO) which has already proven its ability to visualize SARS-CoV-2-associated pulmonary inflammation. However, imaging of ^{18}F-TSPO is limited by its low specificity and/or its preferential binding of anti-inflammatory macrophages. Recently, a specific nanobody targeting the myeloid cell population including proinflammatory macrophages was developed and radiolabeled with ^{64}Cu enabling PET imaging. The aim of this study was to validate the applicability of the newly developed tracer by visualizing the inflammation processes in non-human primates during a SARS-CoV-2 infection with immunoPET. ***Materials and Methods:*** Six female cynomolgus macaques were infected with SARS-CoV-2 and subsequently followed for two months. PET-CTs were obtained before and after infection covering the head, thorax, and abdominal region. Swabs and blood were repeatedly taken to determine the course of the infection. ***Results:*** All animals were positive for SARS-CoV-2 in the swabs on various timepoints pi. The initial development of pulmonary lesions was already detected at the first CT, performed 2 days post infection (pi). TSPO PET-CTs showed an increased uptake in both the anatomically affected and unaffected lungs tissue whereas the PET-CTs of the new nanobody tracer only revealed an increased tracer uptake in the mediastinal lymph nodes of all animals from the first scan obtained after infection. Notably, the increased nanbody tracer uptake in the spleen and bone marrow of all animals was more pronounced at three weeks pi (average $SUV_{mean,spleen}$ pre-infection 3.69 vs 5.87 pi, average $SUV_{mean,bonemarrow}$ pre-infection 2.09 vs 3.22) and even further increased for the spleen at seven weeks pi with a $SUV_{mean,spleen}$ of 7.53. ***Conclusion:*** This study illustrates that the new nanobody tracer can serve as a versatile probe for monitoring individual immune responses during the course of SARS-CoV-2 infection. In comparison to TSPO we detected individual differences in bonemarrow and spleen uptake. These studies might potentially give an insight in the inflammatory processes and the immune mechanisms involved for continuous symptoms and the onset of long-Covid.

OP-923

Role of 18F-FDG PET/CTin detecting residual or recurrent diseaseafter surgery in patients with rhino-orbito-cerebral mucormycosis: a pilot study

A. Phulia[1], *I. Singh*[1], *R. Kumar*[2]; [1]*Maulana Azad Medical College, New Delhi, INDIA,* [2]*All India Institute of Medical Sciences, New Delhi, INDIA.*

Aim/Introduction: Coronavirus disease 2019 (COVID-19) pandemic has brought an unwelcome increase in the incidence of life-threatening opportunistic infections like mucormycosis. The use of steroids in COVID-19 patients and the presence of uncontrolled diabetes as comorbidity has led to an increase in the incidence of invasive rhino-orbito-cerebral mucormycosis. Anatomical imaging modalities have limitations in detecting residual/recurrent disease in the post-surgical setting due to distortion of normal anatomy and associated post-treatment changes. The current study aims to assess the role of 18F-FDG PET/CT, to detect residual or recurrent rhino-orbito-cerebral mucormycosis in the post-surgical setting. ***Materials and Methods:*** A total of 33 COVID-19 patients with a confirmed diagnosis of rhino-orbito-cerebral mucormycosis, who have already undergone surgical debridement and now presenting with suspicion of residual or recurrent disease on clinical and/or imaging findings were included in this study. These patients underwent 18F-FDG PET/CT at least 4 weeks after the previous surgical debridement. Lesions with increased FDG uptake compared to the adjacent region and/or physiological uptake of the liver were considered positive for residual or recurrent disease. Regions of interest (ROI) were drawn around the area of abnormal uptake for measurement of semi-quantitative parameters such as standardized uptake value (SUV). All patients with positive PET/CT results underwent a KOH swab or biopsy for confirmation of the diagnosis. In cases where a KOH swab or biopsy could not be done or in cases of equivocal results, patients were assessed using clinical and/or imaging follow-up. ***Results:*** A total of 33 patients (males, 29; females 4) with a mean age of 53.27 ± 10.97 were enrolled in the study. 18F-FDG PET/CT was positive in 21 (64%) and negative in 12 (36%) patients. Based on the reference standard, 20 were true positives, 12 were true negatives, and the remaining 1 was a false positive. Four patients underwent re-operation and biopsies from all these patients were positive for residual/recurrent disease. The sensitivity, specificity, positive predictive value, negative predictive value, and accuracy were 100% (95% CI: 83% - 100%), 92% (95% CI: 64% - 100%), 95% (95CI: 75% - 99%), 100% and 97% (95% CI: 84% - 100%) respectively. ***Conclusion:*** 18F-FDG PET/CT is highly sensitive and specific for the detection of residual or recurrent disease in rhino-orbito-cerebral mucormycosis patients after surgery. It can be a valuable tool to further evaluate the effectiveness of antifungal therapy and treatment response and assess the need for further interventions.

OP-924

Covid-19. Before and after in the diagnosis of pulmonary embolism in nuclear medicine. Our experience.

C. Ruiz Corbalán, *A. Leiva Montejo, A. De Agrela Serrao, D. Cáceres Silva, M. Castellón Sanchez, L. Mohamed Salem, J. Navarro Fernadez, T. Rodriguez Locarno, A. Hernandez Martinez, L. Frutos Esteban, J. Contreras Gutierrez; Arrixaca, Murcia, SPAIN.*

Aim/Introduction: The aim of this paper is to show the changes introduced in our department in pulmonary perfusion studies for the diagnosis of pulmonary embolism (PE) after the appearance

of COVID-19 and results observed when they are complemented with SPECT-CT. ***Materials and Methods:*** This is a retrospective, descriptive, observational, retrospective study. Between 2020 and 2022, 333 patients attended our department due to suspected PE for pulmonary ventilation-perfusion scintigraphy. Given the epidemiological situation, it was not possible to perform ventilation studies. Only pulmonary perfusion studies were performed and, in case of doubts, they were complemented with SPECT-CT. Planar studies were classified as high or low probability of PE or non-diagnostic. SPECT-CT studies were classified as compatible or not compatible with PE, being compatible studies those which showed one segmental defect or two subsegmental defects without intraparenchymal alterations visualized with CT. The information obtained was analyzed in an Excel database. ***Results:*** From the total amount of cases, 14.7% of planar studies were non-diagnostic. When they were complemented with SPECT-CT, this proportion was reduced to 4.8% per year. SPECT-CT was performed in 110 studies. 85% of cases showed concordance with planar images, 1% disagreed and 14% of non-diagnostic studies were confirmed as compatible for PE. ***Conclusion:*** Due to the epidemiological situation, pulmonary ventilation studies were replaced by only-perfusion SPECT-CT to complement planar images. Thus, we observed that non-diagnostic studies were reduced. Thanks to hybrid imaging, we made more reliable diagnoses and stopped talking in terms of probability. Since June 2022, in our department, planar lung perfusion imaging and SPECT-CT have been performed in all patients with suspected PE unless the patient's baseline condition prevents it.

OP-925

Results of V/Q SPECT in the evaluation of pulmonary Long COVID - a two-year analysis of the pandemic

J. Lepej[1,2], *I. Marin*[1,2], *K. Lepejová*[3], *I. Kuglová*[1], *A. Obušeková*[1], *I. Polčová*[1], *O. Zahornacký*[4], *M. Duránik*[5];
[1]*Institut of Nuclear and Molecular Medicine, Košice, SLOVAKIA,* [2]*Clinic of Nuclear Medicine UPJŠ LF and INMM, Košice, SLOVAKIA,* [3]*Department of Clinical Biochemistry, Haematology and Immunology - Cumulus s.r.o., Košice, SLOVAKIA,* [4]*Clinic of Infectious Diseases and Travel Medicine, UPJŠ and UNLP, Košice, SLOVAKIA,* [5]*Faculty of Medicine University P.J. Šafarik, Košice, SLOVAKIA.*

Aim/Introduction: Pulmonary embolism (PE) is one of the manifestations of long COVID (LC), caused by the SARS-CoV2 virus or as a complication after vaccination. In the second year of the pandemic, V/Q scan indications due to dyspnea and pathological D-dimer (DD) levels increased by 40%. The aim of our research was to analyze these results. ***Materials and Methods:*** During the first 2 years of the pandemic, 1036 lung V/Q SPECT examinations were performed at our institution after inhalation of ^{81m}Kr and perfusion of ^{99m}Tc-MAA as a second step. Patients were divided into 3 groups: A) 281 with COVID-19 and after vaccination, as controls without COVID-19 there were two groups B) 389 (in 2021) and C) 366 (in 2020). Results were compared with medical records and available DD levels. ***Results:*** In group A) PE was present in 58/240 (24.2%) examined for LC and 12/41 (29.3%) in acute cases of PE after vaccination. The incidence of PE in the control groups was higher: B) 130/389 (33.4%) and C) 173/366 (47.3%) for a more targeted indication of examinations. DD levels increased with PE severity in all groups except PE after COVID-19. Patients from group A) had a history of cancer more often (7.9% LC and 9.8% vaccinated) than controls B) and C), only 1.2%. The proportion of chronic smokers with pulmonary embolism was lower in group A) COVID-19 (9%) than in control group C (24%). More than 38.1% of the 29.3% of smokers in the study had match V/Q defects. ***Conclusion:*** V/Q SPECT has been a useful tool for detecting PE in patients with long covid and post-vaccination. The pandemic had serious consequences for the health of the population and the level of healthcare in Slovakia, and we draw attention to some of them.

OP-926

Incidental Acute COVID-19 Infection during Radioligand Therapy

A. Mishra*, R. P. Baum, C. Müller, C. Landvogt;*
Curanosticum, Wiesbaden, GERMANY.

Aim/Introduction: Over 977 inpatient radioligand therapies (RLT) were performed between February 2020 and April 2023. As per COVID-19 pandemic regulations, indications for inpatient admission included negative rapid antigen test and absence of COVID-19 related symptoms such as fever, coughing, loss of smell and/or taste as well as contact with COVID-19 positive patient in the preceding 14 days. All patients also underwent polymerase chain reaction (PCR) test before admission. In 12 patients, PCR test was came out to be positive on the second day of admission. ***Materials and Methods:*** Upon admission, patients underwent history taking (including vaccination status), physical examination and blood tests (CBC, renal & liver panel, tumor markers). Antibody titers (BAU/ml) against SARS-CoV-2 were measured in all patients. In our hospital setting, PCR tests require between 12-24 hours to declare results (after sample collection). 14 patients, who were COVID-positive were treated without knowledge of the positive PCR test. RLT was performed under monitoring of vitals. Single-photon emission computed tomography (SPECT/CT) was performed one day after treatment. Positive patients were discharged after 24 hours (German regulations demand 48 hours stay) under appropriate radiation safety measures (the remaining radiation was < 1 mSv per year at one-meter distance from the patient). All patients were discharged in stable cardio-pulmonary conditions. Abbreviations (Patient Characteristics Table): M - male, F - female, NET - neuroendocrine tumor, PCa - prostate cancer, Lu - Lutetium, Ac - Actinium, Ct -cycle threshold. ***Results:*** RLT performed on PCR positive patients with NET, PCa, signet ring cell carcinoma and clear cell sarcoma (Ac-225 FAP-3BP-3940) were completely uneventful. Daily monitoring of vitals was unremarkable. High uptake of the radiotherapeutic in the metastases and normal physiologic biodistribution was noted in the SPECT/CT scans. ***Conclusion:*** Due to global logistics of radiopharmacy delivery, patients for RLT are planned usually weeks in advance. Our data indicate that PSMA radioligand therapy as well as radiopeptide therapy (as well as FAP PTRT) can be performed in asymptomatic COVID-positive patients - without any sequelae. Therefore, COVID-19 infection is not a limiting factor for performing RLT.

OP-927

FDG PET CT in the Neurological manifestations of COVID-19

N. Seniaray[1], *R. Verma*[1], *R. Ranjan*[2], *E. Belho*[1], *H. Mahajan*[1];
[1]*Mahajan Imaging & labs, New Delhi, INDIA,* [2]*Department of Neurology, Sir Ganga Ram Hospital, New Delhi, INDIA.*

Aim/Introduction: To determine role of 18F-FDG PET/CT in neurological manifestations of corona virus 2 (SARS- CoV-2). ***Materials and Methods:*** A retrospective analysis of 38 patients with CNS involvement attributable COVID-19 infection and who had history of COVID-19 infection within 3 months of appearance of symptoms. All the subjects were clinically and radiologically (MRI) analyzed and were further segregated into MRI positive (n=18) and negative (n=20) subjects. All the subjects underwent whole body 18F-FDG PET/CT scan with a dedicated brain sequence on

a separate day. Additional F-DOPA PET CT/ TRODAT SPECT CT was done in few patients. The FDG uptake patterns were recorded and areas of hypo/hypermetabolism that were two standard deviations from the mean were considered as abnormal. ***Results:*** Out of 18 MRI positive subjects, 12 had findings suggestive of ischemic stroke with diffusion restriction and characteristic angiographic abnormalities, 4 subjects had concurrent Rhino-cerebral Mucor mycosis with associated changes on MRI and FDG PET scan. 2 Subjects had space occupying T2 hyper intense lesions on MRI, diagnosed as focal demyelination which was non FDG and F-DOPA avid. Out of 20 subjects with non contributory MRI 12 had clusters of hypermetabolism in the pre frontal, dorso-lateral frontal, insular and cingulate cortices and 8 subjects had posterior cortical-subcortical and cerebellar hypermetabolism on FDG PET images. Antibodies to COVID-19 was found in the serum of 33 and CSF of 5 subjects. ***Conclusion:*** FDG PET CT may help in certain neurological manifestations of COVID-19, especially with non contributory MRI, thereby expediting the subsequent clinical management.

OP-928

Neuroinflammation in post-COVID individuals with and without persistent complaints 2 years after infection: a [18F]DPA-714 PET study

D. Visser[1,2], *S. S. V. Golla*[1,2], *S. C. J. Verfaillie*[3], *A. Verveen*[3], *D. W. Koch*[3], *R. M. Rikken*[1,2], *E. van de Giessen*[1,2], *M. E. den Hollander*[1], *J. Horn*[2,4], *C. M. van Heugten*[5], *M. D. de Jong*[6,7], *C. C. van den Wijngaard*[8], *T. van der Maaden*[8], *Y. M. G. van Os*[9], *M. Prins*[6,10], *J. M. A. Visser-Meilij*[11], *P. Schober*[12], *R. C. Schuit*[1,2], *A. D. Windhorst*[1,2], *S. Biere-rafi*[13], *B. Appelman*[6,14], *M. van Vugt*[6,15], *F. Barkhof*[1,16], *B. N. M. Berckel*[1,2], *R. Boellaard*[1,2], *H. Knoop*[3], *N. Tolboom*[17];
[1]*Department of Radiology & Nuclear Medicine, Amsterdam Neuroscience, Vrije Universiteit Amsterdam, Amsterdam UMC, Amsterdam, NETHERLANDS,* [2]*Amsterdam Neuroscience, Brain Imaging, Amsterdam, NETHERLANDS,* [3]*Department of Medical Psychology, University of Amsterdam, Amsterdam UMC, Amsterdam, NETHERLANDS,* [4]*Amsterdam UMC location University of Amsterdam, Intensive Care, Meibergdreef 9, Amsterdam, NETHERLANDS,* [5]*Department of Psychiatry and Neuropsychology, Maastricht University Faculty of Health Medicine and Life Sciences & department of Neuropsychology and Psychopharmacology, Faculty of Psychology and Neuroscience Maastricht University, Maastricht, NETHERLANDS,* [6]*Amsterdam Institute for Infection and Immunity, Infectious Diseases, Amsterdam, NETHERLANDS,* [7]*Amsterdam UMC location University of Amsterdam, Medical Microbiology & Infection Prevention, Meibergdreef 9, Amsterdam, NETHERLANDS,* [8]*National Institute for Public Health and the Environment (RIVM), Center for Infectious Disease Control, Bilthoven, NETHERLANDS,* [9]*Occupational Health Office, Department of Human Resources, University Medical Center Utrecht, Utrecht, NETHERLANDS,* [10]*Amsterdam UMC location University of Amsterdam, Infectious Diseases, Meibergdreef 9, Amsterdam, NETHERLANDS,* [11]*Department of Rehabilitation, Physical Therapy Science and Sports, University Medical Centre Utrecht, Utrecht, NETHERLANDS,* [12]*Department of Anaesthesiology, Location VUMC, Amsterdam UMC, Amsterdam, NETHERLANDS,* [13]*C-support, 's-Hertogenbosch, NETHERLANDS,* [14]*Amsterdam UMC location University of Amsterdam, Center for Experimental and Molecular Medicine, Meibergdreef 9, Amsterdam, NETHERLANDS,* [15]*Amsterdam UMC location University of Amsterdam, Division of Infectious Diseases, Tropical Medicine, Department of Medicine, Meibergdreef 9, Amsterdam, NETHERLANDS,* [16]*Institute of Neurology and Healthcare Engineering, University College London, London, UNITED KINGDOM,* [17]*Department of Radiology & Nuclear Medicine, University Medical Centre Utrecht, Utrecht, NETHERLANDS.*

Aim/Introduction: A considerable number of individuals suffer from long COVID or post-COVID syndrome: complaints such as debilitating fatigue and cognitive complaints persisting months to years after COVID-19 infection. Neuro-inflammation might be involved in its pathophysiology. The PET tracer [^{18}F] DPA-714 binds with high affinity to translocator protein (TSPO) that is brought to expression on activated microglia, enabling visualization of neuro-inflammation in vivo. Our main goal was to assess [^{18}F]DPA-714 binding in post-COVID individuals with and without persistent complaints compared to pre-pandemic healthy controls.[1] ***Materials and Methods:*** In this ongoing study, 20 post-COVID individuals underwent a 60-minutes dynamic [^{18}F]DPA-714 PET scan with arterial blood sampling. All individuals were high affinity binders (HABs) according to their TSPO genotype. Subjects additionally completed questionnaires, neuropsychological evaluation and MRI. Individuals reporting subjective complaints on the Checklist-Individual-Strength (CIS) concentration (≥18) and fatigue (≥35) subscales, were classified as individuals with persistent complaints. PET data were analyzed using a reversible two-tissue compartment model with additional blood volume parameter, from which binding potential (BP_{ND}; k_3/k_4) was used to assess [^{18}F]DPA-714 binding.[2] Regions-of-interest (ROIs) included brainstem, thalamus, orbitofrontal, temporal, cerebellar and global gray matter. We assessed prevalence of post-COVID individuals (with and without complaints) with elevated BP_{ND} (≥1.5SD relative to pre-pandemic controls). ANOVA adjusted for age and sex was used to assess differences in BP_{ND}. ***Results:*** Seventeen subjects with persistent complaints ([mean±SD] 26±7 months after infection, age 52±7 years, 8 female) and 3 without (16±10 months after infection, age 47±2 years, 2 female) were included. Data from 3 pre-pandemic controls (age 55±4 years, 1 female, all HAB) was available as reference. In line with our classification, CIS-concentration and -fatigue scores were higher in individuals with persistent complaints versus without (concentration: 26±6 vs 11±3, fatigue: 45±8 vs 15±6, respectively). Five out of 20 post-COVID individuals showed elevated binding relative to the pre-pandemic controls (global BP_{ND}: 2.44±0.32 versus 1.35±0.11, p=0.013), with elevated binding across all ROIs. Global elevated [^{18}F]DPA-714 binding was present in 2 out of 3 post-COVID individuals without persisting complaints, compared to 3 out of 17 individuals with persisting complaints. ***Conclusion:*** Our results so far show globally elevated [^{18}F]DPA-714 binding (>1.5SD above pre-pandemic controls) in approximately 25% of post-COVID individuals, which in this group with only limited numbers -especially of patients without persistent symptoms- does not clearly relate to reporting of persistent symptoms. ***References:*** [1]Hagens et al. J Neuroinflammation (2018), [2]Golla et al. (2015) Journal of Cerebral Blood Flow & Metabolism

OP-929

Little recovery of brain metabolic impairment in patient with persistent long COVID: a [18F]FDG PET study

T. Horowitz*, P. Dudouet, E. Kaphan, T. Radulesco, S. Gonzalez, S. Cammilleri, A. Menard, E. Guedj;*
APHM, Marseille, FRANCE.

Aim/Introduction: Imaging studies have proposed [^{18}F]FDG PET as a biomarker in neurological post COVID condition (long COVID), showing a characteristic brain hypometabolic pattern, including the limbic regions, brainstem and cerebellum. It remains unknown whether such metabolic changes may recover during follow-up of patients with prolonged symptoms. The aim of this [^{18}F]FDG PET study is to evaluate longitudinal brain metabolic changes in the follow-up of long COVID subjects with persistent

symptoms. ***Materials and Methods:*** We retrospectively included all subjects who underwent two brain [18F]FDG PET for long COVID in our department between June 2020 and November 2022 named PET1 and PET2 (56 subjects, mean age 51.1 years, range 24-71 years; 36 women). They all sustained the WHO criteria of long COVID, with a biologic prove of SARS-CoV-2 infection for 49/56. All subjects presented persistent symptoms of Long COVID at the time of the second PET,explaining its realization. The 56 long COVID subjects were compared to 51 healthy controls (mean age 51.2, range 22-78 years; 33 women). On average, PET1 and PET2 were performed respectively 7 and 16 months after acute COVID. Whole-brain voxel-based analysis compared PET1 and PET2 to healthy subjects (p-voxel <0.001 uncorrected, p-cluster <0.05 FWE-corrected); and PET1 to PET2 (first with this same threshold; and thereafter with a less constraint p-voxel < 0.005 uncorrected, p-cluster <0.05 uncorrected). ***Results:*** All subjects had persistent symptoms of long COVID, globally stable during the follow-up. Long COVID subjects at PET1 and PET2 showed significant hypometabolism in the previous reported pattern (limbic regions, brainstem and cerebellum). On the 14,068 hypometabolic voxels that were identified on PET1, 6503 voxels were found hypometabolic on PET2 (46%). On the 7,732 hypometabolic voxels that were identified on PET2, 6,094 had been found on PET1 (78%). Comparing PET1 and PET2, no findings remained significant after correction of multiple comparison for the cluster by FWE method. With a less constraint statistical threshold, two clusters presented a significant improvement at PET2 located within the pons and the right cerebellar vermis, showing respectively 8.4 and 5.2 % improvement at PET2, 9 months thereafter in average. ***Conclusion:*** Subjects with persistent symptoms of long COVID exhibit durable brain metabolic changes, even more than two years after onset of symptoms. Further studies are needed to evaluate the PET evolution in patients with clinical recovery.

OP-930

Extracerebral findings from [18F]DPA-714 PET/CT using a long axial field of view PET scanner in post-COVID

D. Visser[1,2], *X. Palard-Novello*[1,2,3], *M. Yaqub*[1,2], *E. van der Giessen*[1,2], *M. den Hollander*[1,2], *A. D. Windhorst*[1,2], *S. C. J. Verfaillie*[4], *F. Barkhof*[1,2,5], *H. Knoop*[4], *B. N. M. van Berckel*[1,2], *S. S. V. Golla*[1,2], *N. Tolboom*[6], *R. Boellaard*[1,2];
[1]*Department of Radiology & Nuclear Medicine, Amsterdam Neuroscience, Vrije Universiteit Amsterdam, Amsterdam UMC, Amsterdam, NETHERLANDS,* [2]*Amsterdam Neuroscience, Brain Imaging, Amsterdam, NETHERLANDS,* [3]*Centre Eugène Marquis, Rennes, FRANCE,* [4]*Department of Medical Psychology, University of Amsterdam, Amsterdam UMC, Amsterdam, NETHERLANDS,* [5]*Queen Square Institute of Neurology and Centre for Medical Image Computing, University College, London, UNITED KINGDOM,* [6]*Department of Radiology & Nuclear Medicine, University Medical Centre Utrecht, Utrecht, NETHERLANDS.*

Aim/Introduction: A considerable number of individuals suffer from long COVID with an unclear underlying pathophysiology. The PET tracer [18F]DPA-714 binds with high affinity to translocator protein (TSPO) that is brought to expression on inflammatory microglia. The aim of this study is to explore simplified kinetic parameters of [18F]DPA-714 uptake in various extracerebral organs in participants with persistent fatigue and cognitive complaints after COVID infection using a long axial field of view (LAFOV) PET scanner. ***Materials and Methods:*** Seventeen participants with long COVID, high-affinity binders for TSPO, were included. Questionnaire data on the Work and Social Adjustment Scale (WSAS) and pain-subscale of the RAnd-36 item Health Survey were available. Each participant received ~250 MBq [18F]DPA-714 directly followed by a 60 minutes acquisition on the Quadra PET/CT scanner. Patlak linearization was applied to estimate the net influx rate (K_i) in muscle and bone, and Logan linearization was performed to estimate the distribution volume (V_T) in adrenal gland, kidney, liver, lung, myocardium, pancreas, spleen, and thyroid. One volume of interest (VOI) was manually defined in each organ for all participants. Participants with high K_i or V_T compared to the other participants (with visual confirmation of diffuse uptake) were considered specific cases. ***Results:*** There were four participants with high diffuse [18F]DPA-714 uptake in three different organs. Two of which had a high muscle uptake with a significant increase of K_i (+213% and +112%, respectively, compared to the mean of the other participants muscles K_i), which was seen in most muscle groups throughout the body. Both participants had higher (=worse) WSAS scores (40 and 36, respectively, vs a mean of 17 (SD=11) for the other participants) and the participant with the highest muscle K_i had the lowest (=worst) RAnd36-pain score (0 vs a mean of 66 (SD=27) of the other participants). Another participant had high lung uptake with a significant increase of V_T (+219%) compared to mean lung V_T of the other participants. The CT images of this participants lungs showed diffuse ground glass opacity and dense focal opacities. One participant had a high thyroid uptake with a significant increase of V_T (+166%) compared to the mean thyroid V_T of the other participants. ***Conclusion:*** Some participants had increased diffuse uptake in certain organs. This study warrants further research regarding the clinical interpretation of these findings and exhibits the potential role of LAFOV PET scanners to extract meaningful extracerebral findings for brain studies.

1808

Wednesday, September 13, 2023, 9:45 AM - 11:15 AM
Hall F2

Bone & Joint Committee - Featured Session: Unconventional Bone & Joint: FAPI and Beyond

OP-931

Unconventional Bone & Joint

S. Annunziata*;*
Department of Radiology, Radiotherapy and Hematology, Fondazione Policlinico Universitario A.Gemelli IRCCS, Rome , ITALY.

OP-932

68Ga-FAPI PET/CT novel diagnostic tool in sarcoma.

H. Lanzafame[1,2], *R. Hamacher*[2,3], *I. A. Mavroeidi*[2,3], *K. M. Pabst*[1,2], *N. Hirmas*[1], *L. Kessler*[1,2], *T. Bartel*[1,2], *S. Leyser*[1,2], *F. Barbato*[1,2], *M. Schuler*[2,3], *S. Bauer*[2], *J. T. Siveke*[2,3,4], *K. Herrmann*[1,2], *W. P. Fendler*[1];
[1]*Department of Nuclear Medicine, West German Cancer Center, University Hospital Essen, Essen, GERMANY,* [2]*German Cancer Consortium (DKTK), Partner site University Hospital Essen, Essen, GERMANY,* [3]*Department of Medical Oncology, West German Cancer Center, University Hospital Essen, Essen, GERMANY,* [4]*Bridge Institute of Experimental Tumor Therapy, West German Cancer Center, University Hospital Essen, Essen, GERMANY.*

Aim/Introduction: Several bone sarcomas (BS) and soft-tissue sarcomas (STS) demonstrate high Fibroblast activation protein-α (FAP) expression on tumor cells and associated fibroblasts. Here we aimed to investigate the diagnostic performance of FAP-directed [68Ga]Ga-FAPI PET/CT in BS and STS and compared it to 2-[18 F]

FDG PET/CT. ***Materials and Methods:*** Patients with BS or STS undergoing [68Ga]Ga-FAPI PET/CT for staging or restaging were enrolled in a prospective observational trial. A group of patients also underwent 2-[18 F]FDG PET/CT. Number of detected lesions and uptake (SUVmax) for T, N, visceral metastases (VM) and bone metastases (BM) were recorded and analyzed. Non-parametrical t-test was employed for semiquantitative analysis. The association between [68Ga]Ga-FAPI uptake intensity and histopathologic FAP expression was analyzed with Spearman r correlation. Eligibility for FAP-directed radioligand therapy was defined as SUVmax>10 for all tumor regions. ***Results:*** We included 200 sarcoma patients (65 BS, 135 STS), of which 32(16%) were low, 141(70.5%) were high-grade sarcomas and 27(13.5%) sarcoma entities for which grading doesn't apply (N/A). [68Ga]Ga-FAPI vs. 2-[18 F]FDG detected a total of 1174 (81%) vs. 1023 (71.5%) lesions. On a per-region basis, [68Ga]Ga-FAPI vs. 2-[18 F]FDG PET demonstrated higher detection efficacy for T 144 (100%) vs. 124 (86%) lesions and M 1167(97%) vs. 1026(86%) lesions. We reported [68Ga]Ga-FAPI vs. 2-[18 F]FDG higher sensitivity (96.03% vs. 88.41%), specificity (87.8% vs. 60.0%), PPV (98.8% vs. 95.2%), NPV (67.92% vs. 38.10%) and overall accuracy (95.31% vs. 88.36%). Higher [68Ga]Ga-FAPI vs. 2-[18 F]FDG radiotracer uptake was recorded in low grade (10.36±8.5 vs. 7.08±4.5, p=0.01) and N/A (22.32±12.2 vs. 8.58±10.8, p=0.004) tumors. Higher uptake was specifically noted in patients with SFT (T SUVmax 23.49±11.9 vs. 4.45±8.7, p=0.0005; VM SUVmax 17.04±28.7 vs. 3.79±2.0, p=0.0001) and myxoid liposarcoma(T SUVmax 5.61±12.2 vs. 3.53±2.1, p=0.04). [68Ga]Ga-FAPI uptake values and histopathologic FAP expression score (n = 89) showed a moderate positive correlation (Spearman r = 0.43; p < 0.0002). 63 of 128 (49.2%) patients with metastatic sarcoma (18(45%) other, 16(76.1%) SFT, 11(36.6%) liposarcoma, 6(40%) leiomyosarcoma, 4(22.2%) chondrosarcoma, 4(13.3%) UPS, 2(25%)ewing, 1(6.25%) osteosarcoma, 1(11.1%) chordoma) were deemed eligible for FAP radioligand therapy due to intense FAP expression. ***Conclusion:*** In patients with sarcoma, [68Ga]Ga-FAPI PET demonstrated higher tumor uptake and detection rate as well as near equal accuracy when compared with 2-[18 F]FDG PET. FAP expression was sufficient for radioligand therapy in about half of sarcoma patients based on [68Ga]Ga-FAPI PET.

OP-933

Head-to-head Comparison of [68Ga]Ga-FAPI04 and [18F]-FDG PET/CT Imaging in Recurrent/Metastatic Solitary Fibrous Tumor Patients

R. Wang[1,2,3], *J. Wang*[1,2,3], *G. Wang*[1,2,3], *L. Li*[1,2,3], *Z. Zhu*[1,2,3], *X. Chen*[4,5,6], *J. Zhang*[4,5,6];
[1]*Peking Union Medical College Hospital, Chinese Academy of Medical Sciences, Peking Union Medical College, Beijing, CHINA,* [2]*State Key Laboratory of Complex Severe and Rare Diseases, Beijing, CHINA,* [3]*Beijing Key Laboratory of Molecular Targeted Diagnosis and Therapy in Nuclear Medicine, Beijing, CHINA,* [4]*Departments of Diagnostic Radiology, Yong Loo Lin School of Medicine, National University of Singapore, Singapore, SINGAPORE,* [5]*Nanomedicine Translational Research Program, NUS Center for Nanomedicine, Yong Loo Lin School of Medicine, National University of Singapore, Singapore, SINGAPORE,* [6]*Clinical Imaging Research Centre, Centre for Translational Medicine, Yong Loo Lin School of Medicine, National University of Singapore, Singapore, SINGAPORE.*

Aim/Introduction: Solitary fibrous tumours (SFTs) are rare mesenchymal origin tumors, that typically arise in the central nervous system or body cavities, such as the pleura or peritoneum. While generally benigh, SFTs pose a risk of recurrence and metastasis, with limited effective treatment options. [18F]-FDG PET/CT is widely used for evaluating systemic involvement and lesion metabolism in recurrent/metastatic tumors. The aim of this study is to compare the performance and effectiveness of conventional [18F]-FDG PET/CT and the fibroblast activating protein inhibitor [68Ga]Ga-FAPI04 PET/CT in patients with recurrent / metastatic solitary fibrous tumors. ***Materials and Methods:*** A total of 20 SFT patients with suspected recurrence/metastatic lesions were enrolled in this prospective study. Participants underwent both [18F]-FDG and [68Ga]Ga-FAPI04 PET/CT within two days using the same hybrid PET/CT scanner. The number of lesions detected by both PET/CT scans and the maximum standardized uptake value (SUVmax) of lesions were recorded. If patients had more than five lesions, five were randomly selected for further comparison. The Wilcoxon signed rank test was used for statistical analysis. ***Results:*** In the 20 SFT patients, [68Ga]Ga-FAPI04 PET/CT detected significantly more lesions than [18F]-FDG PET/CT (266 vs. 146, $p < 0.05$). In terms of lesion uptake values, [68Ga]Ga-FAPI04 PET showed a higher mean SUVmax than [18F]-FDG (11.0 ± 9.0 vs. 5.1 ± 2.5, $p < 0.001$). Due to the low expression of FAP in normal organs, [68Ga]Ga-FAPI04 PET/CT demonstrated superior tumor/background ratios in the brain and liver, which compensated for the lack of lesion masking caused by physiological [18F]-FDG uptake in these organs. ***Conclusion:*** This is the first prospective study to compare two radiotracers head-to-head in patients with SFT. Although the sample size is relatively small, [68Ga]Ga-FAPI04 showed better ability to detect recurrent/metastatic lesions in these patients. Given the current lack of effective treatments for many recurrent/metastatic SFT patients, high FAP expression in this type of tumour is expected to become a potential therapeutic target for SFT patients.

OP-934

Prognostic value of fluorodeoxyglucose positron emission tomography derived metabolic parameters and textural features in soft tissue and bone sarcomas

N. Aydin, *G. Mütevelizade, G. Gümüşer, E. Sayıt Bilgin;*
Celal Bayar University, Manisa, TÜRKIYE.

Aim/Introduction: Bone and soft tissue sarcomas are a large group of several heterogeneous tumors of mesenchymal origin that may occur at any age. The aim of this study was to evaluate the prognostic value of PET-derived metabolic features and textural parameters of primary tumors in sarcoma patients. ***Materials and Methods:*** The imaging findings of 48 patients (31 male and 17 female; age 41.1 ± 24.2 years) who underwent 18-fluorodeoxyglucose positron emission tomography (PET)/computed tomography for primary staging prior to therapy between 2017 and 2022 were retrospectively evaluated. PET metabolic data and textural features of primary tumors were obtained. Cox proportional hazards regression models were used to identify predictors for progression-free survival and overall survival. Survival curves were estimated by using the Kaplan-Meier method. ***Results:*** Distant metastases were detected in primary staging in 13 patients (27.0 %). The median follow-up duration after diagnosis was 21 months (range: 1-64 months). In the Kaplan-Meier analysis, the presence of distant metastasis, Morphological_Asphericity and Histogram_Entropy_Log10 were found as independent predictors for progression-free survival and Morphological_Compacity were found as independent predictors for overall survival. ***Conclusion:*** In addition to the presence of distant metastasis at initial diagnosis, textural features of primary tumors may be used as prognostic biomarkers to identify patients

with worse prognosis in soft tissue and bone sarcomas. ***References:*** Song H, Jiao Y, Wei W, Ren X, Shen C, Qiu Z, et al. Can pretreatment 18F- FDG PET tumor texture features predict the outcomes of osteosarcoma treated by neoadjuvant chemotherapy? Eur Radiol 2019; 29:3945-3954.Bailly C, Leforestier R, Campion L, Thebaud E, Moreau A, Kraeber- Bodere F, et al. Prognostic value of FDG-PET indices for the assessment of histological response to neoadjuvant chemotherapy and outcome in pediatric patients with Ewing sarcoma and osteosarcoma. PLoS One 2017; 12:e0183841.

OP-935

Assessing bone metabolism in chronic kidney disease-mineral bone disease (CKD-MBD) using 18F-NaF PET/CT Imaging

M. Usmani[1], *N. Ahmed*[2], *F. Marafi*[3], *G. Gnanasegaran*[4], *T. Van den Wyngaert*[5];
[1]*Sultan Qaboos Comprehensive Cancer Care and Research center (SQCCCRC), Muscat, OMAN,* [2]*Jack Brignall PET/CT Centre, Castle Hill Hospital, Cottingham, UNITED KINGDOM,* [3]*Jaber Al-Ahmad Molecular Imaging Center, Kuwait, kuwait, KUWAIT,* [4]*Royal Free Hospital NHS Trust, London, UNITED KINGDOM,* [5]*Antwerp University Hospital, Antwerp, BELGIUM.*

Aim/Introduction: Disorders of mineral metabolism and bone disease are common complications in chronic kidney disease (CKD) patients and are associated with increased morbidity and mortality. The study aims to assess regional and total bone metabolic activity in CKD patients using ^{18}F-NaF PET and correlation between semiquantitative indices of ^{18}F-NaF and blood parameters. ***Materials and Methods:*** Seventy-two subjects (mean age, 61.8±13.8 years) were included in this study. Out of 72 subjects, 24 patients had ESRD (GFR <15 mL/min/1.73 m^2), 38 had CKD (GFR between 60-15 mL/min/1.73 m^2), and the remaining 10 were control subjects with normal renal function (mean age: 65.3±11.5). All subjects underwent ^{18}F-NaF PET-CT with a dose activity of 0.06mCi/Kg. Regional and total skeletal metabolism were assessed with mean SUVs in a skeletal volume of interest (VOI), bone to soft tissue index (B/S), global SUV mean (GSUV mean) of the whole bone, and global uptake in the femoral neck. ***Results:*** There is a significant difference in femoral neck metabolism in CKD and ERSD groups 5.09±1.98 versus 6.76±2.25 in the right femur and 5.4±2.2 versus 6.86±2.47 in the left femur in comparison to control with has SUV mean of 4.66±1 in the right (p=0.003) and 4.31±0.96 in the left femur (p=0.006). Bone to soft tissue index in the femur was 3.79±1.8 in CKD and 4.6±2.48 in ESRD (p=0.016). The global SUV mean ($GSUV_5$) was 8.27±1.20 in ESRD, 7.7±0.86 in CKD, and 8.7±0.65 in healthy subjects (p=0.006). While $GSUV_2$ was measured as 5.06±0.91 in ESRD, 4.58±0.57 in CKD, and 4.92±0.41 in controls (p=0.026). There is also a significant difference in SUV mean in lumbar vertebrae (L1-L4) among CKD, ESRD, and controls. There was a moderate correlation between fluoride activity in the ^{18}F-NaF PET scan and blood parameters such as ALP and PTH. In addition, the ^{18}F-NaF uptake parameters were significantly different in low versus high bone turnover state and potentially discriminate low turnover from high turnover states of renal osteodystrophy. ***Conclusion:*** The assessment of total skeleton and regional metabolism and bone turnover in CKD patients is feasible with ^{18}F-NaF PET. The difference in NaF uptake in CKD compared to controls could be related to a change in bone turnover in CKD patients. More studies with large sample sizes are needed to confirm our findings and establish the normal range of regional and total skeletal metabolism in CKD patients and its wider clinical implications.

OP-936

99mTc-HDP-SPECT/CT in axial pain: comparison with magnetic resonance imaging and impact on image guided therapeutic intervention.

M. ROMERA[1], *Á. Bronte*[1], *V. Betech-Antar*[1], *F. Mínguez*[1], *S. Menéndez-Sánchez*[1], *J. Bastidas*[1], *E. Guillén*[2], *L. Sancho*[2], *L. García-Belaustegui*[2], *J. Arbizu*[1], *M. García Velloso*[1], *M. Rodríguez*[1], *A. Arcadi*[1], *V. Rodrigo*[1], *N. Varela*[1], *F. Pareja*[1], *J. Rosales*[1];
[1]*Clínica Universidad de Navarra, Navarra, SPAIN,*
[2]*Clínica Universidad de Navarra, Madrid, SPAIN.*

Aim/Introduction: In this study, we aimed to determine whether ^{99m}Tc-HDP-SPECT/CT (SPECT/CT) provides additional information to Magnetic Resonance Imaging (MRI) using standard sequences, in patients with axial pain. We also evaluated the response to steroid injections in facet joint arthropathy (FJA) guided by SPECT/CT findings. ***Materials and Methods:*** We retrospectively studied 193 patients with clinical history of axial pain evaluated with both SPECT/CT and MRI within a maximum interval of 180 days. Imaging reports for each technique were reviewed and pathological findings were recorded. Patients with FJA and clinical follow-up were included in the analysis. The response to targeted interventional pain treatment was classified according to the degree of pain improvement (effective: decrease >50%; partial: decrease <50%; and ineffective: no improvement). Descriptive statistical analysis was performed. ***Results:*** One-hundred-ninety-three were included (63.7% females; 36.3% male, mean age was 55.7 ± 15.3 years). Although the number of total pathological findings on MRI were higher than observed on SPECT/CT (339 vs. 268; p<0.01; t-Student) SPECT/CT was superior to MRI in FJA detection (84/268 vs 51/339), (Table 1). Fifty-five patients (28%) with FJA were treated with steroids guided by SPECT/CT. Injections were effective in 50.9% (28/55) of patients, 38.2% (21/55) reached partial response, and the injections were ineffective in 10.9% (6/55). A subset of 20 patients with previous history of partial (12/20) or ineffective (8/20) response to non-image guided steroid injection was referred to a repeated injection after SPECT/CT. In 62.5% (5/8) of subjects with previous ineffective response turned to effective, and 66.6% (8/12) of subjects with partial response reached effective response after SPECT/CT-guided repeated injection. ***Conclusion:*** While MRI shows more detailed information about anatomy and pathological processes, our preliminary findings showed a superiority of SPECT/CT in the detection of FJA. Moreover, SPECT/CT imaging can also help to guide therapeutic interventions not only in treatment naïve patients but also in those with previous non-image-guided steroid treatment.

OP-937

The value of Tc-99m-DPD bone scintigraphies in patients with alkaptonuria. A promising imaging tool for disease monitoring?

D. Schmitt[1], *S. vom Dahl*[2], *K. Mattes-György*[1], *E. Novruzov*[1], *M. Dabir*[1], *S. David*[2], *K. Jan Philipp*[1], *T. Lüdde*[2], *M. Busch*[2], *E. Mamlins*[1], *F. Giesel*[1];
[1]*Department of Nuclear Medicine, Medical Faculty and University Hospital Duesseldorf, Heinrich-Heine-University Duesseldorf, Duesseldorf, GERMANY,* [2]*Clinic for Gastroenterology, Hepatology and Infectious Diseases, Medical Faculty and University Hospital Duesseldorf, Heinrich-Heine-University Duesseldorf, Duesseldorf, GERMANY.*

Aim/Introduction: Alkaptonuria is a rare autosomal recessive disorder with a lack of the enzyme homogentisate-1,2-dioxygenase (appearance of 1:250.000-500.000). Benzochinone derivates of homogentisate accumulate inter alia in collagenous structures

such as cartilage and can lead to severe osteoarthropathy (ochronosis) and significant joint involvement which can be detected in isotope bone scans. In particular, with the EMA-approval of novel pharmaceuticals such as nitosinone, solid evidence-based data need to be generated. The diagnostic value of Tc-99m-bone scans as a response monitoring tool in the course of ochronotic disease involvement has not yet been structurally evaluated - mostly due to a lack of evidence based data. With our monocentric, retrospective study, we aimed to analyze the potential of bone scans as a monitoring tool in the course of alkaptonuria. ***Materials and Methods:*** Our medical center provides healthcare for the largest national cohort of patients with the diagnosis of alkaptonuria. We involved a total of 21 patients in our study, and analyzed the changes of tracer distribution patterns in long term follow-up bone scans (n=9, f: 4, m: 5, age at primary isotope scan: 22-68 years, median 53 years, time difference between bone scans: min. 12 months, max. 35 months). Within this group, 8 patients received nitosinone treatment at the time of the follow-up bone scan (duration of nitosinone treatment: min. 10 months, max. 24 months, daily dose 2-10 mg/dl). We investigated distribution patterns of the angiographic, blood pool and delayed phase and SPECT images in bone scintigraphies as well as the changes in the follow-up. ***Results:*** Most frequent findings were an ochronosis of the spine as well as affected large joints (especially shoulders). On nitosinone treatment most cases showed an improvement of these leading findings in the follow-up (5 out of 8 patients) or were constant (2 out of 8 patients). At the same time, a progress of not yet or slightly affected large joints was seen (4 out of 8 patients). ***Conclusion:*** Tc-99m-bone imaging appears to be an important tool to monitor the ochronotic or inflammatory/degenerative changes in the course of alkaptonuria. In particular, Tc-99m-bone scans might play a key role for the monitoring of nitosinone therapy. ***References:*** Cortes Hernandez J, Ruiz-Olivia Ruiz F, Alonso Colmeneres JI, Alvarez Ruiz S, Caton Santaren B, Alcorta Armentia MP. Ochronotic arthropathy: the value of bone scintigraphy in alkaptonuria. Rev Esp Med Nucl 2004; 23:189-192.

OP-938

^{99m}Tc-NTP15-5, proteoglycan tracer: Phase I trial (CARSPECT)

M. Chanchou[1], *P. Auzeloux*[1], *N. Sas*[1], *T. Billoux*[1], *S. Levesque*[1], *E. Thivat*[1], *E. Jouberton*[1], *E. Miot-Noirault*[2], *M. Galmier*[2], *M. Couderc*[3], *S. Mathieu*[3], *X. Durando*[1], *F. Cachin*[1];
[1]*Centre Jean Perrin/UMR1240 INSERM (IMoST)/UCA, Clermont-Ferrand, FRANCE,* [2]*UMR1240 INSERM (IMoST)/UCA, Clermont-Ferrand, FRANCE,* [3]*CHU/UCA, Clermont-Ferrand, FRANCE.*

Aim/Introduction: ^{99m}Tc-NTP 15-5, a radiotracer developed by UMR 1240 INSERM IMoST UCA, targets cartilage proteoglycans. Its affinity for healthy cartilage and its pathological variations were demonstrated in preclinical models. The main objective of this phase I study (CARPECT: NCT04481230) is to determine the injected activity of ^{99m}Tc-NTP 15-5 to obtain the best visual contrast of articular fixation on healthy cartilage, without any toxicity. The secondary objectives are quantitative analyzes of the fixation on the cartilage, biodistribution and pharmacokinetic of the tracer. ***Materials and Methods:*** Patients with unilateral knee osteoarthritis or breast cancer treated with anti-aromatase were included between November 2020 and June 2022. Three levels of activity were studied (5, 10 and 15 MBq/kg). The study design was constructed to include a maximum of six patients. A visual score measured tracer uptake in 31 joints on planar scintigraphies performed at 30 min, 2 h, 4 h and 6 h p.i: 1: uptake < diaphyseal uptake; 2: uptake = diaphyseal uptake; 3: uptake > diaphyseal uptake. A score equal to 3 at 2 h p.i for at least 80% of the joints validated the studied activity. The 3D uptake quantification, performed on SPECT-CT from the lumbosacral regions to the knees, covered 16 joint and periarticular regions. 3D Background activity was measured on bone and muscle. Pharmacokinetics, biodistribution and dosimetry of the tracer were analyzed on scintigraphic imaging and urine and blood samples. Tolerance was rated by the NCICTC 4.0 scale. ***Results:*** Five patients were finally injected with ^{99m}Tc-NTP 15-5. 15 MBq/Kg level was the best level to display at least 80% of the joint with a score 3 at 2h p.i. 2D/3D analysis showed physiological periarticular uptake, urinary and enterohepatic elimination of the tracer from the 30th minute. Cartilage/background ratio were high for five articular interfaces. No toxicity has been reported. ***Conclusion:*** These results demonstrate high accumulation of ^{99m}Tc-NTP 15-5 on articular cartilage and periarticular structures. Phase II trials will evaluate this tracer in the exploration of cartilage pathologies. Grant: I-Site CAP 20-25; ANR 15-CE18-003.

OP-939

Comparison and Clinical Significance of Hybrid Imaging and Planar Bone Scintigraphy in Patients With Oncological Lesions

P. Korol[1], *O. Shcherbina*[1], *M. Tkachenko*[2];
[1]*Shupik National University Healthcare of Ukraine, Kyiv, UKRAINE,* [2]*Bogomolets National Medical University of Ukraine, Kyiv, UKRAINE.*

Aim/Introduction: To compare and evaluate retrospectively the value of hybrid fusion single-photon emission computed tomography with (SPECT/CT) imaging versus planar scintigraphy in assessing possible bone metastases ***Materials and Methods:*** 185 cancer patients with malignant tumors of the breast, prostate, thyroid gland (123 women and 62 men) were studied. Bone scintigraphy including SPECT/CT and planar scintigraphy was performed in all patients. We first analyzed flat images, then the images merged and focused on the added value of the merged images. Diagnostic validity for each lesion was individually assessed. On planar images, we classified as sure (malignant, benign) or indeterminate lesions ***Results:*** The clinical analysis included 185 cancer patients (123 women, 62 men, mean age 57.2 ± 9.5 years). Planar images show 381 lesions: 334 were significant. (182 bone metastatic lesions and 199 benign lesions) and 48 were uncertain. After viewing the combined images: for self-confident lesions: there were six benign lesions that became suspicious based on low-dose CT. Nearly everything indeterminate became more certain of the diagnosis with 51 benign lesions and 34 metastases. In addition, the combined images also showed 39 lesions, no visualized on planar images ***Conclusion:*** The results show increased diagnostic confidence obtained with fused SPECT/CT images compared to planar images in differentiation malignant from benign bone lesions.

1809

Wednesday, September 13, 2023, 9:45 AM - 11:15 AM
Hall G2

e-Poster Presentations Session 14 - Radiopharmaceutical Sciences + Translational Molecular Imaging & Therapy - New Imaging Agents

EPS-273

Molecular PET/CT mapping of rhACE2 distribution and quantification in organs: a helper for SARS-CoV-2 targeting therapy

Z. Wang[1,2], *C. Zhao*[3], *C. Li*[4], *Q. Liu*[5], *H. Zhu*[6,5], *Y. Liu*[1];
[1]*School of Basic Medical Science, Southwest Medical University, Luzhou, CHINA,* [2]*Key Laboratory of Carcinogenesis and Translational Research (Ministry of Education/Beijing), Key Laboratory for Research Evaluation of Radiopharmaceuticals (National Medical Products Administration), Department of Nuclear Medicine, Peking University Cance, Beijing, CHINA,* [3]*Key Laboratory of Carcinogenesis and Translational Research (Ministry of Education/Beijing), Department of Biochemistry and Molecular Biology, Peking University Cancer Hospital and Institute, Beijing, Beijing, CHINA,* [4]*Department of Nuclear Medicine,First Affiliated Hospital of Hebei North University, Zhangjiakou, CHINA,* [5]*Institute of Biomedical Engineering, Peking University Shenzhen Graduate School, Shenzhen, CHINA,* [6]*Key Laboratory of Carcinogenesis and Translational Research (Ministry of Education/Beijing), Key Laboratory for Research and Evaluation of Radiopharmaceuticals (National Medical Product Administration), Department of Nuclear Medicine, Peking University Ca, Beijing, CHINA.*

Aim/Introduction: Non-invasive and repeated monitoring of rhACE2 distribution and content in organs using the ACE2-specific nuclide probe ^{68}Ga-HZ20. ***Materials and Methods:*** In this study, we optimized the labeling conditions of the probes and evaluated their safety; a mice organ in situ rhACE2 high aggregation model was constructed for the first time, and in vivo real-time PET imaging of rhACE2 was performed using ACE2-specific positron emission tomography agent ^{68}Ga-HZ20. The distribution and uptake of probes were analyzed, and the model was validated. ***Results:*** This radiotracer exhibited reliable radiochemical properties in vitro and maintained a high affinity for rhACE2 in vivo. In terms of probe uptake, ^{68}Ga-HZ20 showed a good target-to-nontarget ratio, and the correlation between the uptake value of the probe and the dose of rhACE2 was >90% in either model, which was rapidly cleared from the circulatory system and excreted by the kidneys and urinary system. No organs were damaged after the injection of high doses of probes. ***Conclusion:*** This technology non-invasively and repeatedly monitors the content and distribution of rhACE2 in vivo, which is helpful to clarify the resident capacity of rhACE2 in organs and analyze the preventive ability of rhACE2 against SARS-CoV-2 and the therapeutic ability for COVID-19.

EPS-274

Evaluating a suite of anti-FAP nanobody constructs as PET imaging agents.

J. Gallant, *Z. T. Rosenkrans, K. L. Ott, N. Y. Luo, A. S. Thickens, R. Hernandez, A. M. LeBeau;*
University of Wisconsin, School of Medicine and Public Health, Madison, WI, UNITED STATES OF AMERICA.

Aim/Introduction: Metastatic castration resistant prostate cancer (mCRPC) is a uniformly lethal disease. Underlying the challenges to generate effective therapies for mCRPC is the disease's heterogeneity and the lack of methods for monitoring disease progression that are capable across all mCRPC subtypes. Fibroblast activation protein alpha (FAP) has been identified as an antigen with ubiquitous expression across all mCRPC subtypes (1). We have developed a suite of high affinity, FAP targeting nanobodies and nanobody based constructs as useful PET imaging tracers in preclinical models of mCRPC. Here, we present a direct comparison of FAPI-46 and a lead single domain FAP nanobody (F7, K_D =9nM) as imaging agents. Further, we present a dimeric nanobody (F7HD, K_D =29pM) and nanobody-Fc fusion protein (F7Fc, K_D =38pM) characterizing their potential as additional imaging agents. ***Materials and Methods:*** Xenografts using a FAP-expressing engineered prostate cancer cell line (CWR-R1-EnzR^{FAP}) were supplanted in the hind flank of nude mice. Three anti-FAP nanobody based constructs were radiolabeled with ^{64}Cu and evaluated as PET/CT imaging agents for their ability to rapidly localize at the tumor site, the single domain nanobody was compared to ^{68}Ga-FAPI-46. Images were acquired as soon as 1h post injection and with the highest molecular weight construct imaged up until 48h post-injection. Injected dose per gram quantities were determined for non-specific and tumor-specific tissues. ***Results:*** The single domain F7 nanobody was able to rapidly localize to tumor tissues with increased uptake as compared to FAPI-46, 1.1% ID/g vs 0.5% ID/g at 1h post-injection. The F7 dimer was rapidly taken up in tumor tissue with maximal uptake at 4h, 1.43% ID/g, that was retained at 24h, 1.267% ID/g. Additionally, F7Fc demonstrated rapid uptake at 4h (7.5% ID/g) and continued to accumulate. Signal was retained in tumor tissue through 24h and 48h, 15.23% ID/g and 14.93 % ID/g respectively. Minimal on-target, off-disease accumulation was seen with expected uptake in organs suggestive of the construct's routes of excretion, blood uptake was cleared rapidly in all constructs. ***Conclusion:*** All the examined FAP nanobody based constructs show promise as PET imaging agents with uptake kinetics comparable to a small molecule approach. Additionally, the nanobody-based constructs demonstrate tunable pharmacokinetics, suggesting the possibility of using these constructs as theranostic agents. ***References:*** 1. Hintz HM, Gallant JP, Vander Griend DJ, Coleman IM, Nelson PS, LeBeau AM. Imaging Fibroblast Activation Protein Alpha Improves Diagnosis of Metastatic Prostate Cancer with Positron Emission Tomography. Clin Cancer Res. 2020;26(18):4882-91.

EPS-275

Close but no cigar? In vitro properties of small molecule PD-L1 ligands assessed by real-time radioligand binding in comparison to peptides and antibodies.

C. Donat[1], *F. Krutzek*[1], *K. Zarschler*[1], *K. Kopka*[1,2,3], *S. Stadlbauer*[1,2];
[1]*Helmholtz Centre Dresden-Rossendorf, Dresden, GERMANY,* [2]*Technical University Dresden, Dresden, GERMANY,* [3]*National Center for Tumor Diseases, Dresden, GERMANY.*

Aim/Introduction: Programmed cell death ligand 1 (PD-L1) can be overexpressed in solid cancers, exerting an immunosuppressive effect. Clinically, breakdown of immune blockade through PD-L1 specific antibodies has been employed with good success rates. However, only 30% of the patients are responders and heterogenous PD-L1 expression can render biopsies unreliable. Noninvasive molecular imaging can overcome this, given suitable radiotracers. However, the binding mode of different PD-L1 ligand classes can vary, making assessment of in vitro properties an important step in radioligand evaluation and translation. We employed real-time radioligand binding and heterogeneous interaction modelling to test different PD-L1 radiotracer candidates.

Materials and Methods: Four PD-L1 ligand classes were investigated: peptide (WL12[1]), monoclonal antibody (atezolizumab), antibody fragment (7CZD[2]) and two small molecules ([^{64}Cu]Cu-1/2), based on a biphenyl binding motif. All molecules were radiolabelled with copper-64, and PC3 cells, overexpressing human PD-L1 employed as substrate. Cells were incubated with the radioligands, and bound radioactivity measured using the LigandTracer system. Using increasing concentrations followed by buffer only, allowed to determine binding kinetics. Data were additionally analysed for heterogenous molecular interactions (InteractionMap®). ***Results:*** Real-time binding of the small molecules was best fitted using a 1:1 model , accounting for a concentration dependent bulk effect. In albumin presence, association was relatively slow and dissociation moderate, yielding a K_D in the higher nM range (1: 276; 2: 54.3 nM). Binding without albumin showed faster association, resulting in a lower K_D (1: 2.08 (±0.36); 2: 20.9 (±5.44) nM), indicating a structure-dependent interaction with albumin. Binding of peptide and antibody was best fitted using a 1:1 model. K_D was very low for [^{64}Cu]Cu-WL12: 0.79 nM (±0.42) and [^{64}Cu]Cu-atezolizumab: 0.36 nM (±0.22), without an albumin effect. [^{64}Cu]Cu-7CZD binding showed similar kinetics, best fitted using a 1:1 model, accounting for ligand depletion, yielding a K_D of 0.35 nM (±0.09). InteractionMap® analysis for small molecules reported two moderate binding interactions, one presumably caused by albumin. Without albumin, only one major binding interaction was observed, similar to peptide and antibody. [^{64}Cu]Cu-7CZD showed two moderate binding interactions, without albumin presence. ***Conclusion:*** Tested PD-L1-specific radiolabelled compounds showed suitable but variable in vitro kinetics, likely caused by reported differences in binding modes. Real-time radioligand binding provides advantages over traditional endpoint assays and together with heterogenous interaction analysis, can help define suitable structure-activity relationships for new PD-L1 radiotracers. ***References:*** 1. DeSilva et al. Mol. Pharmaceutics 2018, 15 2. Bridoux et al. Biomolecules 2020, 10

EPS-276

Al18F-DX600-BCH

J. Ding[1], *Q. Zhang*[1], *J. Jiang*[1], *N. Zhou*[1], *Z. Yu*[1], *Z. Wang*[1], *X. Meng*[1], *T. Liu*[1], *F. Wang*[1], *z. Lu*[1], *X. Yang*[2], *Z. Yang*[1], *P. Du*[1], *Z. Hua*[1];
[1]*Peking University Cancer Hospital & Institute, Beijing, CHINA,* [2]*Peking University First Hospital, Beijing, CHINA.*

Aim/Introduction: Angiotensin-converting enzyme 2 (ACE2), as a transmembrane protein, is the main entry point for certain coronaviruses including the new coronavirus SARS-CoV-2 to enter cells. ACE2 is also highly expressed in colorectal cancer, gastric cancer, and malignant proliferation of pancreatic cancer et al. By synthesizing the molecular imaging probe Al^{18}F-DX600-BCH which is high-affinity ACE2 for PET imaging, it is hoped that the expression of ACE2 in body can be detected in real time, specifically and non-invasively, and the therapeutic effect monitoring can be achieved. ***Materials and Methods:*** The radioactive probe Al^{18}F-DX600-BCH was obtained. The radiochemical purity was analyzed by radio-HPLC, and the in vitro stability was studied by incubating in each buffers. Blood samples of normal mice were collected to determine the pharmacokinetic curve of Al^{18}F-DX600-BCH in blood. The mice were sacrificed at 5 time points after injection and the organs of interest were taken out for biodistribution experiments. Normal mice and rats underwent small animal PET scans and IHC staining was obtained from rat organ sections. A total of 10 volunteers were enrolledand received PET/CT 1 hour and 2 hours after injection or dynamic PET/CT during 0-330 seconds (NCT04542863). ***Results:*** The radiochemical yield of the manually prepared Al^{18}F-DX600-BCH without attenuation correction was 20.4% ± 5.2%, the purified radiochemical purity was greater than 99%, and it was stable in vitro within 4 hours. The pharmacokinetic curve showed that the concentration of Al^{18}F-DX600-BCH in the blood decreased rapidly (the half-lives of the distribution phase and clearance phase were 2.12 min and 25.31 min, respectively). Both the biodistribution and PET imaging results of small animals showed that Al^{18}F-DX600-BCH was highly accumulated in the kidney (SUVkidney/normal > 50), and the rat image showed specific uptake of the probe in the testis (SUVtestis/normal > 10). The results of IHC staining of rats showed that kidney, gastrointestinal (++) and bronchial (+++) cells were ACE2 positive, which was consistent with the published human expression distribution of ACE2. In clinical PET imaging, strong radioactivity accumulation was observed in various organs of the genitourinary system including the kidney (SUVrenal cortex = 32.00, SUVtestis = 4.56), and moderate radioactivity accumulation was observed in several cases of conjunctiva and nasal mucosa. ***Conclusion:*** This work reported for the new probe Al^{18}F-DX600-BCH targeting ACE2, and conducted preliminary preclinical experiments and a total of 8 clinical transformations, demonstrating the potential and possibility of non-invasive mapping of ACE2.

EPS-277

Development of a dual-modality imaging probe targeting SSTR2 via a trifunctional chelate

D. Chapeau*, S. Beekman, Y. Seimbille;*
ErasmusMC, Rotterdam, NETHERLANDS.

Aim/Introduction: Surgical resection is still the mainstay of treatment for patient with localized malignant diseases. SPECT or PET/CT imaging has the potential to assess resectability, while new imaging techniques, such as fluorescence-guided surgery (FGS), can facilitate tumor visualization and margins delineation during surgery. Both imaging techniques require the use of a labeled molecule. The probe should ideally contain a radionuclide for preoperative nuclear imaging and a fluorescent dye for intraoperative image-guided surgery. Thus, a chemically identical molecule is administered to the patient for both applications. A trifunctional chelate (TFC) based on a modified DOTA-GA was synthesized and then coupled to the SSTR2-agonist octreotate and a cyanine dye.[1] Then, we studied the influence of the dual-labeling on the biochemical proprieties of the SSTR2-targeted probe. ***Materials and Methods:*** Our chelate, dubbed eTFC-01, was synthetized in 5 steps. Then, the chelate was coupled onto the protected linear peptide at the N-terminus on resin, followed by the cyclization in liquid phase. The cyanine dye (sCy5) was finally conjugated using copper-free click chemistry. In vitro competitive binding assays with [^{111}In]In-DOTA-TATE were performed using U2OS cells over-expressing human SSTR2. The fluorescent peptide was labeled with ^{111}In in sodium acetate buffer for 20 minutes at 90°C and analyzed by iTLC and radio-HPLC. $LogD_{7.4}$ and stability in PBS and serum were also determined. ***Results:*** eTFC-01 and the probe were successfully synthesized with an overall yield of 2% and 5%, respectively. The SSTR2-targeted probe was successfully labeled with $^{111}InCl_3$ with a radiochemical yield and purity exceeding 98%. It showed good stability in the labeling solution, PBS buffer (98% at 24 h) and mouse serum (98% at 1 and 4 h, and 86% at 24 h). The ^{111}In labeled probe was hydrophilic, as determined by the LogD value (-0.7 + 0.04). The probe exhibited a

two-fold higher IC_{50} value for SSTR2 than DOTA-TATE (8.8 nM vs. 4.1 nM, respectively). ***Conclusion:*** Favorable stability and binding to SSTR2 were obtained with the probe, confirming that addition of the fluorescent dye coupled to eTFC-01 did not significantly affect the binding properties. In vivo studies are underway to study the pharmacokinetics of the probe. eTFC-01 is a promising scaffold for the development of dual-labeled probes. ***References:*** 1. Ghosh, S. C. et al. Synthesis of a Fluorescently Labeled 68Ga-DOTA-TOC Analog for Somatostatin Receptor Targeting. ACS Med. Chem. Lett. 8, 720-725 (2017).

EPS-278

Conjugation of different chelators to a HER2 targeting single domain antibody for Ga-68 and Lu-177 radiolabelling

B. Altunay, *L. Obradović, F. M. Mottaghy, A. T. J. Vogg; University Hospital RWTH Aachen, Aachen, GERMANY.*

Aim/Introduction: Several single-domain antibodies (sdAbs) have been investigated as non-invasive probes for addressing HER2 receptors, since they offer the advantage of a more accurate determination of the HER2 status compared to monoclonal antibodies and have been shown to be safe and suitable in cancer diagnosis and treatment. Here, two different HER2 targeting sdAb-chelator conjugates were labelled with ^{68}Ga and ^{177}Lu and investigated with regard to their stability, cell binding capabilities and biodistribution in vivo. ***Materials and Methods:*** The activated chelators based on DTPA and DOTA-GA were mixed with the HER2 targeting sdAb, NM-02, in three different ratios each. The purified sdAb-chelator complexes were labelled with ^{68}Ga and optimized in terms of solvents, pH and temperature. The ideal chelator-sdAb ratios for DTPA and DOTAGA were determined by cell uptake studies with their labelled conjugates. The two complex conjugates labelled with ^{68}Ga and ^{177}Lu were analysed for their labelling kinetics, serum stability, shelf life and cell uptake rate. Biodistribution studies were performed in breast cancer xenografted mice. ***Results:*** Cell uptake studies indicated for both conjugates the ratio of sdAb to chelator of 1/20 to be the most appropriate. The optimized RCC was 56.1 ± 5.2 %, 71.1 ± 3.5 %, 66.4 ± 5.4% and 66.5 ± 1.5% for [^{68}Ga]Ga-DOTA-GA-NM-02, [^{68}Ga]Ga-DTPA-NM02, [^{177}Lu]Lu-DOTA-GA-NM-02, and [^{177}Lu]Lu-DTPA-NM02, respectively. While no difference was observed in the shelf-life at room temperature for the ^{68}Ga labelled sdAbchelator conjugates (RCP 76% after 5 hours), for ^{177}Lu labeled DOTA-GA complex an 11.6% higher stability was observed after 144 hours compared to the DTPA complex (RCP 80.1% vs. 68.7%). In human serum, a stability of 95% after 4 hours was detected for the ^{68}Ga labelled sdAbchelator conjugates. For the ^{177}Lu labelled conjugates, after 48 hours a RCP of 99% was observed. Since ^{68}Ga and ^{177}Lu radiolabelled DOTA-GA-NM-02 (102.6 ± 8.1 and 82.6 ± 7.3 %ID/g) showed a higher cell uptake after 4 hours compared to labelled DTPA-NM-02 (69.5 ± 3.2 and 55.5 ± 7.7 %ID/g), the DOTA-GA conjugate was further used for animal studies. Biodistribution data confirmed the specific uptake of the sdAb-chelator conjugate in the HER2-positive tumor 4 hours after the injection. ***Conclusion:*** The ^{68}Ga/^{177}Lu labelled DOTA-GA-NM-02 (1/20) conjugates showed the best radiochemical stability and highest cell uptake rate in HER2-positive cells. The in vivo images indicated that the newly synthesized tracer [^{68}Ga]Ga-DOTA-GA-NM-02 may be an effective non-invasive probe to detect the HER2 status in patients with breast cancer.

EPS-279

More than sweet: TRAP-based Sugar Trimers for Functional Liver Imaging with 68Ga

M. A. Zierke[1], *C. Rangger*[1], *K. Samadikhah*[2], *A. Schmid*[2], *R. Haubner*[1];
[1]*Nuclear Medicine, Innsbruck, AUSTRIA,* [2]*Werner Siemens Imaging Center, Tübingen, GERMANY.*

Aim/Introduction: TRAP-based multimers have shown to be efficient imaging tools for targets such as PSMA[1] and integrin $\alpha_v\beta_6$[2]. Based on this chelator, we now report the synthesis of a small library of trimeric sugar conjugates targeting the asialoglycoprotein receptor (ASGR). ASGR is a c-type lectin, which is selectively expressed on functional hepatocytes and hence, allows imaging of the functional liver reserve. Variations in sugar type and linker length generated a set of four different ligands (T0G3, T3G3, T3N3 & T3U3) that were labelled with ^{68}Ga and tested for their suitability as imaging agents for this receptor. ***Materials and Methods:*** All compounds were synthesized using CuAAC followed by demetallation of the resulting Cu-complex. Trimers featured either Galactose (T3G3), N-Acetylgalactose (T3N3) or Glucose (T3U3) with a PEG_3-Linker or Galactose without linker (T0G3). Radiolabelling was accomplished within 15 min at 95°C in a 5 M HEPES buffer (pH=5.8). In vitro evaluation included octanol/buffer distribution (logD), protein binding, and metabolic stability studies in human blood serum (incubation for 2, 30, 60, and 120 min at 37°C). For biodistribution experiments, healthy BALB/c mice were used. Animals were dissected 10, 30 and 60 min p.i. and accumulation of the tracers was measured (n=3). Additionally, the most promising candidate T3N3 was studied with PET/MR. ***Results:*** All compounds could be labelled in high yields and were obtained in high radiochemical purity (>97%). LogD values ranged from -3.8 to -4.3 indicating high hydrophilicity. Low to moderate protein binding and high stability in human blood serum was found. In biodistribution studies, T3N3 showed the highest liver accumulation, followed by T3G3. Lowest liver uptakes were found for T0G3 and T3U3. For T3N3 60 min dynamic scans allowed a clear delineation of the functional liver tissue. ***Conclusion***: Choice of the sugar is essential for target specificity. Introduction of spacers between the chelator and the sugar is required to obtain optimal binding geometries to the receptor. Multimerization of Galactose and N-Acetylgalactose on the TRAP-platform is a convenient way to access liver specific PET radiopharmaceuticals targeting the ASGR. ***References:*** [1] Wurzer et al. Mol Pharm, 2018. [2] Quigley et al. EJNMMI, 2022.

EPS-280

Novel Dual-Modality Imaging Agents Targeting the CCK2 Receptor by Chelator Scaffolding

G. GARIGLIO[1], *K. Bendová*[2], *M. Hermann*[3], *M. Petrik*[2], *E. von Guggenberg*[1], *D. Putzer*[4], *C. Decristoforo*[1];
[1]*Department of Nuclear Medicine, Medical University Innsbruck, Innsbruck, AUSTRIA,* [2]*Faculty of Medicine and Dentistry, Palacky University Olomouc, Institute of Molecular and Translational Medicine, Olomouc, CZECH REPUBLIC,* [3]*Department of Anesthesiology and Critical Care Medicine, Medical University of Innsbruck, Innsbruck, AUSTRIA,* [4]*Department of Radiology, Medical University Innsbruck, Innsbruck, AUSTRIA.*

Aim/Introduction: The outcome of cancer surgery benefits from preoperative imaging and intraoperative real-time guidance. Dual-modality probes, combining positron emission tomography (PET) with fluorescence imaging (FI) capabilities in the same molecule, can be used for both applications and therefore are

of high clinical relevance [1]. We herein present a pair of PET/FI agents addressing the tumours expressing the cholecystokinin-2 receptor (CCK2R): [^{68}Ga]Ga-SulfoCy5.5-TRAP-(PEG4MGS)$_2$ (1) and [^{68}Ga]Ga-SulfoCy5.5-FSC-(PEG4MGS)$_2$ (2). In these probes, the SulfoCy5.5 fluorophore and two units of the stabilised Minigastrin targeting peptide are individually coupled to the chelator acting as core scaffold, specifically TRAP-Pr for (1) and Fusarinine C (FSC) for (2). ***Materials and Methods:*** The synthetic strategy to both labelling precursors started with the derivatization of the chelator to enable bioconjugation of the other components by the CuAAC click reaction and concluded with the removal of coordinated metals. ^{68}Ga-labelling was accomplished within 10 min at pH 3 and 95°C for (1) and at pH 4.4 and RT for (2). In vitro characterisation included the evaluation of lipophilicity ($LogD_{7.4}$), protein binding and stability in human serum. Binding affinity (IC_{50}) and internalisation assays were performed by using AR42J and A431 cells expressing the CCK2R. Biodistribution experiments in healthy BALB/c mice were undertaken to evaluate pharmacokinetics up to 4h p.i. Biodistribution, PET and fluorescence imaging studies in A431 xenografted BALB/c mice were conducted to assess the tumour targeting in vivo. ***Results:*** ^{68}Ga-labelling resulted in > 97% radiochemical purity (radio-HPLC) for both precursors. Hydrophilic properties, rapid binding to serum proteins (> 55% after 1h) and high CCK2R affinity (IC_{50} < 1 nm) were observed. Specific receptor-mediated internalisation was found in cell uptake studies and in confocal fluorescence microscopy experiments. Biodistribution data indicated slow clearance from blood pool for both tracers. Higher accumulation in kidneys was found for (1), with (2) exhibiting a distinct liver and spleen uptake. First studies in xenografted mice with (1) showed CCK2R-positive tumour visualisation by both PET/CT (1-3h p.i.) and fluorescence imaging (24-48h p.i.); biodistribution results indicated moderate, but specific tumour uptake (6.5% ID/g 2h p.i.). ***Conclusion:*** In this study we successfully prepared a pair of analogous PET/FI agents based on TRAP-Pr or FSC scaffolds. Their comparison indicated that these chelators have distinct influences on the biodistribution. Promising in vitro and in vivo targeting properties were shown by (1). Further optimisation may improve the pharmacokinetic profiles of these tracers. ***References:*** [1] Yuen R, et al. Pharmaceutics 2022, 14(3), 645.

EPS-281

Construction and immnoPET imaging of an iodine-labeled specific antibody for targeting MMP2 detection in pan-cancer

X. Ma, *T. Liu, H. Zhu, Z. Yang;*
Peking university, Beijing, CHINA.

Aim/Introduction: A poor prognosis in cancer patients is closely related to tumor invasion and metastasis, which is affected by many factors. A prerequisite for tumor metastasis is the breakdown of the extracellular matrix (ECM), which is a natural cellular barrier. Matrix metalloproteinase-2 (MMP2) has a unique enzymatic activity with the ability to break through the ECM, which may promote tumor metastasis. The aim of this study is to provide guidance for the noninvasive detection of MMP2 in pan-cancer. ***Materials and Methods:*** Flow cytometry (FCM), Western blot (WB), and Immunofluorescence (IF) were used to verify the expression of MMP2 on the surface of human colon cancer cells LS174T, human non-small cell lung cancer cells A549, patient derived gastric cancer xenograft (PDGCX), human pharyngeal squamous cell carcinoma cells FADU, and human pancreatic cancer cells ASPC1. $^{124/125}$I-anti-MMP2 was prepared using N-bromine succinimide (NBS) as oxidant and purified by PD-10 column. The physicochemical properties, affinity, metabolic characteristics, biodistribution and immunoPET imaging of $^{124I/125}$I-anti-MMP2 were performed. ^{124}I-IgG and ^{18}F-FDG were used as controls. Finally, the correlation analysis between tumor uptake and MMP2 expression level was established. ***Results:*** LS174T, A549, PDGCX and FADU cells showed high MMP2 expression, while ASPC1 showed low expression of MMP2.The radiochemical purity was over 99% and maintained over 93% in saline or 5% Human Serum Albumin (HSA) for more than 9 d. The EC50 values of anti-MMP2 and ^{nat}I-anti-MMP2 were 4.98±0.59 ng/mL and 5.19±0.45 ng/mL, respectively.The K_d value of ^{125}I-anti-MMP2 to MMP2 protein was 3.653 nM, while that of ^{125}I-IgG was 19.54 nM.^{125}I-anti-MMP2 showed significantly higher uptake in MMP2 high-expression cells than that in MMP2 low-expression cells (P<0.001). The biological half-life of distribution and clearance phases were 1.467 h and 37.05 h, respectively. ^{125}I-anti-MMP2 showed high initial uptake in blood pool and liver, and the uptake was decreased with time.In vivo immunoPET imaging showed that the tumor-to-muscle ratio of ^{124}I-anti-MMP2 were higher than that of ^{124}I-IgG and ^{18}F-FDG (P<0.01) in MMP2 (+) tumors. The expression levels of MMP2 in cells and tumors had positive correlation with SUV_{max} values (P<0.01). ***Conclusion:*** ^{124}I-anti-MMP2 is a promising imaging technique for delineating MMP2 positive tumors. It has great potential in early diagnosis, targeted population selection of the patients.

EPS-282

Novel fluorinated Osimertinib analogue for medical nuclear imaging of EGFRm-positive non-small cell lung cancer

Y. Brief, *H. Grievink, G. Abourbeh, E. Mishani, O. Shamni;*
Cyclotron & Radiochemistry unit, Hadassah Medical Center, Faculty of Medicine, Hebrew University of Jerusalem, Jerusalem, ISRAEL.

Aim/Introduction: Non-small cell lung cancer (NSCLC) comprises the majority of lung cancer cases. Activating mutations in NSCLC patients (delE746-A750 exon 19, L858R exon 21) are found in genes coding for the tyrosine kinase (TK) domain of the epidermal growth factor receptor (EGFR), occurring in 10-30 % of NSCLC patients. Osimertinib, a third-generation EGFR TK-inhibitor (TKI) is a first-line therapy for NSCLC patients harbouring activating EGFR mutations (EGFRm). Osimertinib exhibited higher selectivity and lower toxicity than earlier EGFR-TKI's, and targets the acquired resistance mutation (T790M), often emerging in these patients. The current study aimed to develop an 18f-fluorine radiolabeled positron emission tomography probe to identify EGFRm tumors, based on Osimertinib's chemical structure. ***Materials and Methods:*** The non-radiolabeled fluorine-19 reference standard, F-OS was designed and synthesized via N'-alkylation at a region not involved in EGFR binding and was fully characterized. The potency and selectivity of F-OS were evaluated in vitro using the methylene blue IC50 assay and human NSCLC cell lines, of which three possessed different EGFRm (HCC827, NCI-H1975, and NCI-H3255), and one was the wild-type EGFR (QG56). [^{18}F]F-OS was synthesized using a fully automated 90-minute process. In vivo PET/ MRI studies were conducted using xenografts (NCI-H1975 and QG56 cell lines) and analyzed using preclinical image post-processing software. ***Results:*** F-OS was obtained at a chemical yield of 20 % (purity > 99%). F-OS binding profile toward various EGFR forms ($IC50_{F\text{-}OS}$ in cell lines: HCC827 (49), NCI-H1975 (29), NCI-H3255 (12) and QG56 (6440) nM) were comparable to that of Osimertinib ($IC50_{Osimertinib}$ in cell lines: HCC827 (2), NCI-H1975 (4), NCI-H3255

(2) and QG56 (1880) nM), and corresponded to other reported IC50 values. [^{18}F]F-OS was obtained at a low radiochemical yield (~1 %, radiochemical purity > 99 %, n=7), yet sufficient for the preclinical PET/ MRI study. [^{18}F]F-OS was evaluated in-vivo PET/ MRI study using NSCLC xenografts harboring EGFRm-(L858R/ T790M) or WT EGFR. A significant two-fold accumulation increase in the EGFRm xenografts (n=5) was observed, contrary to the WT EGFR xenografts (n=3). furthermore, a three-fold tumor/muscle [^{18}F]F-OS uptake ratio was observed for the EGFRm, compared to the WT EGFR-mice. ***Conclusion:*** This study aimed to develop a PET probe for identifying EGFRm-positive NSCLC tumors. F-OS potency and selectivity suggest a comparable binding profile to Osimertinib to different EGFR-forms expressing cell lines. [^{18}F] F-OS accumulation in the EGFRm xenografts warrants thorough PET/ MRI investigation to elucidate [^{18}F]F-OS potential as a nuclear imaging probe to identify EGFRm tumors.

EPS-283

FAPI-functionalised melanin nanoparticles for PET/MRI/ PA imaging of glioma

L. Wen, *H. Wang, S. Yang, X. Long, C. Zheng, D. Jiang; Department of Nuclear Medicine, Union Hospital, Tongji Medical College, Huazhong University of Science and Technology, Wuhan, CHINA.*

Aim/Introduction: Fibroblasts activated protein (FAP), a membrane-bound enzyme, is up-regulated in tumor-associated fibroblasts in more than 90% of epithelial tumor and low or no expression in healthy tissues. Hence, we aim to investigate the feasibility of using an ultra-small-sized, FAP specific, organic melanin nanoparticles (MNP) for photoacoustic imaging (PAI), magnetic resonance imaging (MRI), and positron emission tomography (PET) imaging of glioma. ***Materials and Methods:*** The specific nanoparticles, FMN, was constructed by ultrasonic fragmentation method and chelated with the MR contrast agent Mn^{2+} and PET radionuclide ^{64}Cu for PA/MR/PET imaging. FMNs were fully characterized for morphology and toxicity in vitro. The specificity of (^{64}Cu, Mn)-FMN was completed with U87MG and A549 cell lines to assessed via western blot, immunohistochemical staining, and cell uptake. In vivo pharmacokinetic and multimodal imaging efficacy of (^{64}Cu, Mn)-FMN were evaluated in healthy Kunming and/or subcutaneous tumor-bearing mice. ***Results:*** FMN was regular morphology with 10.47 ± 1.44 nm of hydrodynamic diameters, and exhibited excellent biocompatibility and biodegradability. The U87MG cells expressed high levels of FAP, while A549 cells expressed low levels of FAP. Additionally, (^{64}Cu, Mn)-FMN exhibited excellent high specificity and stability in vitro. In vivo pharmacokinetic test results showed that the biological half-life of distribution phase and scavenging phase were 0.086 h and 1.907 h, respectively. In U87MG tumor-bearing mice, the PA signal and T_1-weighted signal gradually increased with time, and peaked at 24 h after the nanoprobe injection. Micro-PET/ CT imaging and semi-quantitative analysis showed that the nanoprobe accumulated in the U87MG tumors, which was significantly higher than that of A549 tumors. ***Conclusion:*** We have successfully fabricated a MNP-based nanoprobe for PET, MR, and PA imaging of tumor FAP expression. The study revealed that (^{64}Cu, Mn)-FMN nanoprobe has the great potential as multimodal imaging candidate agent in U87MG tumor-bearing mice. ***References:*** [1] Garin-Chesa P, Old LJ, Rettig WJ. Cell surface glycoprotein of reactive stromal fibroblasts as a potential antibody target in human epithelial cancers. Proc Natl Acad Sci USA. 1990 Sep;87(18):7235-9.[2] Fan Q, Cheng K, Hu X, et al. Transferring Biomarker into Molecular Probe: Melanin Nanoparticle as a Naturally Active Platform for Multimodality Imaging. J Am Chem Soc, 2014, 136(43): 15185-15194.[3]Hong SH, Sun Y, Tang C, et al. Chelator-Free and Biocompatible Melanin Nanoplatform with Facile-Loading Gadolinium and Copper-64 for Bioimaging. Bioconjug Chem, 2017, 28(7): 1925-1930.[4]Ha SW, Cho HS, Yoon YI, et al. Ions doped melanin nanoparticle as a multiple imaging agent. J Nanobiotechnology, 2017, 15(1): 73.

EPS-284

Preclinical PET imaging with 89Zr-labelled oxMIF-specific antibody delineates subcutaneous tumours in colorectal murine models

F. Bachmann, *A. Puchol Tarazona, I. Mirkina, M. Thiele, A. Schinagl; OncoOne Research & Development GmbH, Vienna, AUSTRIA.*

Aim/Introduction: The oxidized isoform of the macrophage migration inhibitory factor (oxMIF) selectively occurs in tumour tissues and thus represents an attractive target to image tumours[1,2]. A bioengineered anti-oxMIF monoclonal antibody with improved pharmacokinetics, biodistribution and safety profile, compared to a previously clinically tested anti-oxMIF antibody[3] was generated. Here, the suitability of this 2nd generation anti-oxMIF antibody - ON102Ab - for positron emission tomography (PET) was evaluated. ***Materials and Methods:*** The ability of ON102Ab to trigger Fc-mediated responses was evaluated cell-based assays. The potential of ON102Ab to induce cytokine release from huPBMCs was assessed by using cytometric bead assays. Balb/c nude mice bearing subcutaneous HTC116 tumours received an i.v. injection of infrared dye-labelled ON102 and whole-body images were taken for up to 7 days. In addition, after conjugating ON102Ab with the chelator DFO* and radiolabelling with ^{89}Zr, the antibody was injected into murine colorectal cancer models, and whole-body PET images were collected 4, 7 and 10 days p.i. ***Results:*** Bioengineering extended the half-life of the antibody, enhanced tumour uptake and extended the retention in the tumour for over 10 days, overall improving the tumour-to-body AUC ratio in an HTC116 subcutaneous murine model. ON102Ab showed a favourable safety profile, as it did not induce any ADCC, ADCP, or CDC, nor triggered release of IL-6, TNF-α or MCP-1 from PBMCs in vitro. Administration of ^{89}Zr-ON102 in syngraft and xenograft murine models of colorectal cancer caused no signs of toxicity and allowed to delineate the tumours by PET. ***Conclusion:*** ON102Ab is a 2nd generation anti-oxMIF-mAb with improved biological properties. ^{89}Zr-ON102 accumulated in the tumours of murine colorectal cancer models allowing the selective imaging of the tumour tissue by PET scanning. This highlights the suitability of oxMIF as a tumour-specific target for theranostic interventions and the potential of ^{89}Zr-ON102 as a safe diagnostic tool for the detection of malignant solid tumours in humans. ***References:*** 1. Schinagl A, Thiele M, Douillard P, et al. Oxidized macrophage migration inhibitory factor is a potential new tissue marker and drug target in cancer. Oncotarget. 2016;7(45). doi:10.18632/oncotarget.11970 2. Schinagl A, Kerschbaumer RJ, Sabarth N, et al. Role of the Cysteine 81 Residue of Macrophage Migration Inhibitory Factor as a Molecular Redox Switch. Biochemistry. 2018;57(9):1523-1532. doi:10.1021/acs.biochem.7b01156 3. Mahalingam D, Patel MR, Sachdev JC, et al. Phase I study of imalumab (BAX69), a fully human recombinant antioxidized macrophage migration inhibitory factor antibody in advanced solid tumours. Br J Clin Pharmacol. 2020;86(9):1836-1848. doi:10.1111/bcp.14289

EPS-285

Preparation and preclinical evaluation of anti ROR1 labeled with 64Cu as a Radioimmunoconjugate for ROR1+ breast cancer Imaging

B. Alirezapour[1], *H. Rabbani*[2];
[1]*Nuclear Science and technology research Institute (NSTRI), Tehran, IRAN, ISLAMIC REPUBLIC OF,* [2]*Antigen and Antibody Engineering Department, Monoclonal Antibody Research Center, Avicenna Research Institute, ACECR, Tehran, IRAN, ISLAMIC REPUBLIC OF.*

Aim/Introduction: Radioimmunoscintigraphy (RIS) has attracted considerable clinical application in tumor detection. Receptor-tyrosine-kinase-like orphan receptor 1 (ROR1) is extensively expressed during embryogenesis but it is absent within most mature tissues. However, expression of ROR1 has been reported in multiple human malignancies including breast cancer. So breast cancer radioimmunoscintigraphy targeting ROR1 expression is an attractive object in molecular imaging especially nuclear medicine researches. In this study, we have developed an efficient indirect labeling method of anti-ROR1 with ^{64}Cu ($T_{1/2}$ = 12.8 h, β+ = 17%, β– = 39%, EC = 43%) through using NOTA (p-SCN-Bn-NOTA) bi-functional chelator and performed preliminary bio distribution studies in mouse bearing breast adenocarcinoma. ***Materials and Methods:*** Anti-ROR1 was conjugated with NOTA (Macrocyclics B-605), the average number of the chelator conjugated per mAb was calculated and total concentration was determined by spectrophotometrically. NOTA- anti-ROR1 was labelled with ^{64}Cu then Radiochemical purity and immunoreactivity by A549 cell line and serum stability of ^{64}Cu-NOTA-anti-ROR1 were determined. The biodistribution studies and radioimmunoscintigraphy were performed in female BALB/c mouse bearing breast adenocarcinoma tumor (^{64}Cu-NOTA- Anti-ROR1 i.v., 100 µl, 20±5 µg mAb , 6, 12, 24 and 48 h). ***Results:*** ^{64}Cu-NOTA-anti-ROR1 was prepared (RCP >98% ± 0.9, Specific activity 4.3 ± 0.7 µCi/µg). Conjugation reaction of chelator (20 molar excess ratio) to antibody resulted in a product with the average number of chelators attached to a mAb (c/a) of 2.7 ± 0.4. Labeling yield with ^{64}Cu in 400µg concentration of bioconjugate was 98.6% ± 1.1. Immunoreaction of ^{64}Cu-NOTA- anti-ROR1 complex towards ROR1 antigen was determined by RIA and the complex showed high immunoreactivity towards ROR1. In vitro and in vivo stability of radioimmunoconjugate was investigated respectively in PBS and blood serum by RTLC method. In vitro stability showed more than 92% ± 2.2 in the PBS and 81% ± 2.7 in the serum over 24 h. The Immunoreactivity of the radiolabeled anti-ROR1 towards A549 cell line was found to be 0. 82. The biodistribution of ^{64}Cu-NOTA-anti-ROR1 complex in the mice with normal and breast tumor at 6, 12, 24 and 48 h after intravenous administration, expressed as percentage of injected dose per gram of tissue (%ID/g). Biodistribution and imaging studies at 24 and 48 h post-injection revealed the specific localization of complex at the site of tumors. ***Conclusion:*** ^{64}Cu-NOTA- anti-ROR1 is a potential compound for molecular imaging of PET for diagnosis and follow up of ROR1 expression in oncology

EPS-286

Radiosynthesis and preclinical evaluation of [Zr89]mAb1 and [Zr89]mAb2 as PET tracers for B7:H3-positive tumors

B. Fernandes[1], *F. Basuli*[2], *C. P. Olkowski*[1], *D. Nambiar*[1], *S. Adler*[3], *G. L. Griffiths*[3], *F. I. Lin*[1], *P. Choyke*[1];
[1]*Molecular Imaging Branch, Center for Cancer Research, National Cancer Institute, Bethesda, MD, UNITED STATES OF AMERICA,* [2]*Chemistry and Synthesis Center, National Heart, Lung, and Blood Institute, National Institutes of Health, Rockville, MD, UNITED STATES OF AMERICA,* [3]*Clinical Research Directorate, Frederick National Laboratory for Cancer Research Frederick, Frederick, MD, UNITED STATES OF AMERICA.*

Aim/Introduction: Targeting the tumor microenvironment with antibody-based immunotherapies has emerged as an important strategy in the treatment of cancer. B7-H3 is a transmembrane protein expressed by several solid cancers with low expression by normal tissues, which makes it a suitable antigen for targeted therapies (including radioimmunotherapy). Several anti-B7-H3 antibodies exhibit high affinity for their target and have demonstrated antitumorgenic activity already in their non-radiolabeled form. This study aimed to validate the tumor-targeting potential of two radiolabeled anti-human B7-H3 monoclonal antibody candidates (MacroGenics, Inc, Rockville, MD) and to compare the in vivo biodistribution by positron emission tomography imaging in mice bearing human B7-H3-expressing tumors. ***Materials and Methods:*** [Zr^{89}]mAb1 and [Zr^{89}]mAb2 were synthesized using the desferrioxamine labeling methodology. In vitro studies determined the affinity binding of both radiotracers as well as their internalization efficiency at 37**℃**. In vivo studies evaluated the biodistribution of the radiotracers in healthy mice or mice bearing MC38 tumors expressing human B7-H3. Animals were intravenously injected with either [Zr^{89}]mAb1 or [Zr^{89}]mAb2mAb2 for biodistribution assessments at 24h, 48h, and 72h post-injection. Radiotracer uptake in the animals' organs was expressed as percent injected dose per gram (%ID/g). A Shapiro-Wilk normality test was applied to all data before analysis. Differences between groups were evaluated using a two-sided t-test (parametric data) and Mann-Whitney test (non-parametric data) and considered significant when $p<0.05$. ***Results:*** The specific activity, radiochemical yield, and radiochemical purity of [Zr^{89}]mAb1 were 122±22 MBq/nmol, 91±3%, 98±0.4%, respectively, and that for [Zr^{89}]mAb2 was 139±29 MBq/nmol, 92±1%, and 98±1%, respectively. In assays with human B7-H3 expressing cell lines, [Zr^{89}]mAb1 and [Zr^{89}]mAb2 bound with similar Kd at 4**℃** (5.6 and 3.2 nM, respectively). However, [Zr^{89}]mAb2 showed 55% internalization (p=0.004) while [Zr^{89}]mAb1 showed none (p=0.3412). In vivo biodistribution studies in healthy mice showed significantly higher excretion of [Zr^{89}]mAb1 than [Zr^{89}]mAb2 by kidneys at 48h (p=0.008), and 72h (p=0.008), while [Zr^{89}]mAb2 presented significantly higher uptake than [Zr^{89}]mAb1 in lymph organs such as spleen (p=0.016) and lymph nodes (p=0.032) at 48h. Biodistribution assessment in tumor-bearing mice showed significantly faster excretion of [Zr^{89}]mAb1 compared to [Zr^{89}]mAb2 at the three time points (24h, p=0.008; 48h, p=0.008; 72h, p=0.008). By contrast, [Zr^{89}]mAb2 uptake in tumors (36±15 %ID/g) was 119% higher (p=0.032) than that of [Zr^{89}]mAb1 (16±8 %ID/g) at 48h. ***Conclusion:*** Radiolabeled anti-human B7-H3 antibodies, [Zr^{89}]mAb1 and [Zr^{89}]mAb2, exhibited high tumor uptake in human B7-H3 tumor-bearing mice. However, [Zr^{89}]mAb2, which presented greater internalization capacity, exhibited higher tumor uptake.

EPS-287

A Zirconium Coordination Platform for Positron Emission Tomography Traceable Cargo Delivery

H. Hong, *X. Jiao, X. Li, Y. Cong, J. Hu, Y. Jiang;*
Nanjing University, Nanjing, CHINA.

Aim/Introduction: Metal coordination materials, e.g. metal-organic frameworks (MOF), can be used for delivery of many drug cargos to address their solubility issues. Our group previously established zirconium-89 containing MOFs for targeted delivery and positron emission tomography (PET) imaging of breast tumors[1,2]. The aim of this study is to produce a ^{89}Zr containing coordination platform with drug cargo as the bridging molecules instead of traditional

"drug loading" strategy, and this cargo delivery platform can be readily visualized by PET imaging. ***Materials and Methods:*** A solvothermal method was used to build a MOF platform composed by $ZrCl_4$ and hematoporphyrin monomethyl ether (HMME, used here as a model drug). Surface functionalization with polymer molecules and tumor-homing peptide ligands was conducted. The structure of ^{89}Zr-HMME was investigated by TEM, XRD, XPS etc. The in vivo pharmacokinetic behavior of ^{89}Zr-HMME was systematically studied, and the complex biological effects of ^{89}Zr-HMME against melanoma were also evaluated (such as sonodynamic therapy effect, immunological responses etc.). ***Results:*** ^{89}Zr-HMME had an isotope loading capacity of up to 50 MBq/μg with superior radiochemical stability. The ^{89}Zr-HMME conjugates had diameters of 100-160 nm by TEM and hydrodynamic diameters of 200-250 nm. Potent tumor uptake was observed for ^{89}Zr-HMME in B16F10 (~9 %ID/g at 2 h p.i.) while the blood circulation time for ^{89}Zr-HMME was ~6.5 min. In addition, ^{89}Zr-HMME could trigger strong sonodynamic effects and tumor killing in B16F10, alter the immune microenvironment in tumors (e.g. $CD4^+$, $CD8^+$ T cell infiltration etc.), and decelerate the tumor invasion. The detailed biological mechanisms were revealed. ***Conclusion:*** This ^{89}Zr-HMME coordination platform can serve as a useful tool for PET-traceable cargo delivery into different types of tumors and trigger combinational tumor therapies. ***References:*** 1. Chen et al. ACS Nano. 2017,11(4):4315-4327. 2. J Nanobiotechnology. 2022, 20(1):494.

EPS-288

Organotrifluoroborate sugar conjugates for a guided boron neutron capture therapy: radioisotopic exchange reactions for PET imaging

A. Erhard[1], *L. Confalonieri*[2], *D. Imperio*[2], *M. Balcerzyk*[1], *L. Panza*[2]; [1]*Centro Nacional de Aceleradores, Sevilla, SPAIN,* [2]*University of Eastern Piedmont Amedeo Avogadro, Novara, ITALY.*

Aim/Introduction: Sugars are a versatile tool for targeting malignant cells, using [^{18}F]FDG as a prototype. Boron neutron capture therapy (BNCT) is a cancer treatment that relies on irradiation with thermal neutrons of cancer cells previously loaded with [^{10}B]-containing compounds. The recent introduction of accelerators as a neutron source for clinical use prompts the planning of delivery compounds enriched with boron able to be traced in real time. We report the synthesis of a new class of sugar derivatives conjugated to a trifluoroborate moiety as potential theranostic agents, their stability and cytotoxicity studies, together with [^{18}F] radiolabeling optimization and in vivo preliminary microPET imaging. ***Materials and Methods:*** Synthesis of compounds with the generic structure: monosaccharide-linker-ammonium trifluoroborate group was based on a nucleophilic substitution or involving a click reaction. Toxicity was assessed on human fibroblasts by treatment with increasing concentrations (0.001-1mM) and MTT assay. Stability of the trifluoroborate group was analyzed through [^{19}F] NMR spectroscopy, using BPA as reference. Radiolabeling was performed by dissolving the compound in an acidified [^{18}F]-fluorine solution and warmed at 85ºC, 20 minutes, followed by purification with Alumina cartridge. Radiolabeling stability was analyzed in vitro by radio-TLC. The radiolabeled compound was then injected into healthy Balb/C mice for microPET/CT imaging ([^{18}F]FDG as control). ***Results:*** Compounds were synthesized and purificated (>95% purity by NMR). At a concentration of 1mM, our selected compound (Glc1) induced a reduction of cell viability at all times. Stability of Glc1 showed an hydrolisis behaviour with half-life value of 72 hours. Radiolabeling procedure provided a conversion of 49.88% and after purification, radiochemical purity was 97.2% At 37ºC we found that [^{18}F]F-Glc1 was stable for 1 hour in human plasma and for 100min in physiological solution. Preliminary results of the incorporation of [^{18}F]F-Glc1 in healthy mice by microPET/CT indicated that the radiopharmaceutical was metabolized in the liver, it did not pass the blood-brain barrier and was not metabolized in the heart, showing differences with [^{18}F] FDG biodistribution. ***Conclusion:*** Synthesis of sugars containing the -BF_3 moiety is feasible in a simple, efficient and rapid manner. Radiolabeling with [^{18}F]F was succesfully achieved on one derivative and the radiopharmaceutical was demonstrated to be enough stable both in vitro and in vivo when injected into mice for imaging. On the other hand, this compound appears to be quite toxic for BNCT applications. The discovery of a potencial theranostic candidate for BNCT remains a big challenge for researchers.

EPS-289

Preclinical characterization of novel radiolabeled and fluorescent-labeled Fibroblast Activation Protein (FAP)-targeting ligands using gamma counting, SPECT imaging and Cryo-Fluorescence Tomography (CFT)

J. Hesterman[1], *A. Novicki*[1], *K. Orcutt*[1], *S. DiMagno*[1], *S. Hillier*[1], *S. Patel*[1], *A. Amor*[1], *B. Burke*[2], *S. Archibald*[3], *J. Wright*[3], *J. Domarkas*[3], *J. Heimann*[2], *V. Yost*[2], *E. White*[4], *C. Stokes*[4], *M. Silva*[4], *A. Cordova*[4], *S. Toddes*[4], *J. Babich*[1], *J. Hoppin*[1]; [1]*Ratio Therapeutics, Boston, MA, UNITED STATES OF AMERICA,* [2]*Invicro, Needham, MA, UNITED STATES OF AMERICA,* [3]*University of Hull, Hull, UNITED KINGDOM,* [4]*Emit Imaging, Baltimore, MD, UNITED STATES OF AMERICA.*

Aim/Introduction: FAP PET followed by fluorescent-FAP guided surgical resection offers great potential in clinical practice, particularly given the lack of pan-cancer fluorescent imaging agents for surgery. This study evaluated the relative biodistribution of a ZW800-1 fluorescent-labeled and a ^{67}Cu-labeled NOTA-conjugated FAP compound of otherwise analogous structure. The biodistribution of the FAP imaging candidate compounds was captured across multiple techniques, including radiolabeled gamma counting (GC), radiolabeled whole-body SPECT (SPECT), and whole-body ex vivo cryo-fluorescence tomography (CFT). ***Materials and Methods:*** RTX-1363 and RTX-1341 are structurally similar compounds built on a trifunctional scaffold. Both exhibit sub-nanomolar enzymatic inhibition for human FAP (IC_{50}s: 50 and 85 pM, respectively) with good selectivity (FAP/PREP >50). The major structural difference is replacement of N_3O_2 NOTA chelate in RTX-1363 with optical dye ZW800-1 in RTX-1341. [^{67}Cu]RTX-1363 was prepared by adding RTX-1363 in DMSO to a solution of ^{67}Cu in 0.05M HCl and adjusting the pH to 5.5 using 3N NaOAc. Radiochemical purity was confirmed to be >95% using RP-HPLC. A 1ug mass dose of either [^{67}Cu]RTX-1363 or [ZW800-1]RTX-1341 was administered in 200 uL via tail-vain injection to U-87 MG tumor-bearing mice. Three animals were imaged using SPECT/CT at 1H and 24H post-administration. Additional animals were sacrificed at 1H or 24H post-administration for gamma counting or CFT imaging. Regions of interest were segmented from SPECT and CFT images, including tumor, knee joint, liver, and kidney. ***Results:*** Consistent biodistribution was observed across compounds through qualitative assessment and quantitative analysis. No significant differences in macro tissue distribution were noted at any time point. SPECT imaging enabled within-subject quantitative longitudinal assessment while CFT imaging provided high resolution whole-body information both anatomically and

functionally, yielding insights such as the local distribution of the ligand on the surface of the bone and heterogeneity of tumor composition and distribution. Quantitative analysis is presented, indicating strong agreement in longitudinal intensity values relative to liver in tumor, knee joint, and kidney across modalities. ***Conclusion:*** Qualitative and quantitative agreement is observed in biodistribution between ZW800-1 fluorescent labeled and ^{67}Cu radiolabeled compounds using gamma counting, whole-body SPECT and whole-body CFT. High-resolution ex vivo CFT imaging provided insights into local ligand distribution complementing low-resolution longitudinal in vivo SPECT data. Physiochemically similar characteristics between zwitterionic dye ZW800-1 and the Cu-N_3O_2 complex likely contributed to similarities in tissue biodistribution, further emphasizing the ability of CFT to complement radiolabeled techniques for compound screening in appropriately selected ligand systems.

EPS-290

68Ga-NOTA-ACN376 imaging as a non-invasive approach to diagnose CLDN18.2-positive tumors

c. yan[1,2], *Z. Hua*[3], *Z. Hua*[3], *Z. Hua*[3];
[1]*Beijing cancer hospital, Beijing, CHINA,* [2]*Guizhou University Medicine College, Guizhou, CHINA,*
[3]*Beijing Cancer Hospital, Beijing, CHINA.*

Aim/Introduction: (Claudin18.2) CLDN18.2 is highly expressed in primary malignant tumors such as gastric cancer, pancreas and esophagus,and has become another emerging target for anti-tumor since HER2. We constructed a molecular probe targeting CLDN18.2 nanobodies, performed PET/CT imaging in model animals, and evaluated its affinity and specificity for CLDN18.2-positive tumors in model animals. ***Materials and Methods:*** Nanobody ACN376 was coupled with NOTA-Mal chelating agent by site-specific modification, the ^{68}Ga-NOTA-ACN376 probe was obtained by ^{68}Ga labeling, and its quality control was carried out. The affinity of ^{68}Ga-NOTA-ACN376 to CLDN18.2 protein was determined by ELISA experiment. Cell binding experiments were performed using transfected CLDN18.2 high-expression AGS-CLDN18.2 cells and AGS cells. Blood pharmacokinetics studies were performed on ^{68}Ga-NOTA-ACN376 to explore the rate of clearance in plasma. Micro-PET imaging and biodistribution of tumor-bearing mice were used to verify the targeting and specificity of the probe. ***Results:*** The radiochemical purity of ^{68}Ga-NOTA-ACN376 was 98.56 ± 0.78% (n=5) and the specific activity was 24.7 ± 3.26 GBq/μmol. The equilibrium dissociation constant value was 27.85 nM. Cell binding experiments showed that excess ACN376 and CLDN18.2-targeted monoclonal antibody (TST001) could effectively block the uptake of probe by AGS-CLDN18.2 cells. The distribution half-life of the probe in vivo was 1.83 min, and the clearance half-life was 22.77 min, indicating that the probe had rapid in vivo distribution, metabolism and clearance rate. In Micro-PET imaging, the tumor/muscle ratio in the AGS-CLDN18.2 model 1 h after probe injection was significantly higher than that in the negative model and the blockade group (34.86 ± 4.68 vs. 15.00 ± 2.13 vs. 11.01 ± 2.09, p<0.005). Biodistribution studies showed that the uptake of 68Ga-NOTA-ACN376 in the AGS-CLDN18.2 model was significantly higher than that in the negative AGS model group (6.61 ± 0.41 %ID/g vs. 0.39 ± 0.13 %ID/g, p<0.0001). ***Conclusion:*** A series of in vitro and in vivo experimental results showed that ^{68}Ga-NOTA-ACN376 was successfully synthesized with excellent physicochemical properties and stability, fast in vivo distribution, clearance rate, and high affinity and specificity to CLDN18.2 antigen. ^{68}Ga-NOTA-ACN376 was rapidly cleared in mice, which can effectively improve the target/background ratio, thereby reducing the internal exposure to non-target organs such as blood. Preliminary preclinical studies have shown that this probe has good affinity, targeting and specificity for human CLDN18.2, providing a potentially highly sensitive and non-invasive detection method for CLDN18.2-positive tumors.

EPS-291

61Cu-PSMA PET in prostate cancer: development and selection of the first radioligand for clinical translation

T. Basaco Bernabeu[1], *R. Mansi*[1], *L. Del Pozo*[1], *S. Zanger*[1], *M. Blagoev*[2], *R. H. Gaonkar*[1], *L. McDougall*[1], *A. Johayem*[2], *L. Jaafar-Thiel*[3], *M. Fani*[1];
[1]*Division of Radiopharmaceutical Chemistry, University Hospital Basel, Basel, SWITZERLAND,* [2]*Department of Nuclear Medicine, University Hospital of Zürich, Zürich, SWITZERLAND,* [3]*Nuclidium AG, Basel, SWITZERLAND.*

Aim/Introduction: Prostate cancer is the most frequently diagnosed cancer among men in Europe. The high demand for PSMA PET tracers is likely to increase further with the broadening of PSMA PET indications. The preferred PET radioligand [^{68}Ga]Ga-PSMA-11 is facing critical supply challenges. In addition, the approved ^{18}F-labeled PSMA ligands (e.g. [^{18}F]PSMA-1007) show significant differences in biodistribution and lack of a therapeutic companion. Thus, we propose using of the cyclotron-produced Copper-61 ($t_{1/2}$=3.34h, $E_{\beta^+ max}$=1216keV) for PSMA PET imaging. ^{61}Cu can be produced in large scale, like ^{18}F, and enables delayed imaging compared to ^{68}Ga. Moreover, it forms a theranostic couple with the β$^-$-emitter ^{67}Cu. Herein, we report the development of the first ^{61}Cu-PSMA ligands and compare their performances to [^{68}Ga]Ga-PSMA-11 and [^{18}F]PSMA-1007. ***Materials and Methods:*** We developed [^{61}Cu]Cu-DOTAGA-PSMA-I&T and [^{61}Cu]Cu-NODAGA-PSMA-I&T and compared them versus [^{68}Ga]Ga-PSMA-11 and [^{18}F]PSMA-1007. In vitro (lipophilicity, affinity, cellular uptake and distribution) and in vivo (dynamic PET/CT imaging and biodistribution at 1h and 4h post-injection) studies were performed using LNCaP cells and LNCaP-xenografted nude mice. ***Results:*** [^{61}Cu]Cu-DOTAGA-PSMA-I&T and [^{61}Cu]Cu-NODAGA-PSMA-I&T were prepared at an apparent molar activity of 24 MBq/nmol and radiochemical purity ≥97%. Their PSMA-affinity was in the nanomolar range (IC_{50}=11.2±2.3 and 9.3±1.8 nM, respectively). Both were more lipophilic (logD=-2.69±0.44 and -2.95±0.08, respectively) than [^{68}Ga]Ga-PSMA-11 (-3.89±0.19) and [^{18}F]PSMA-1007 (-3.04±0.06). All radioligands showed similar cellular uptake with 50:50 distributions between surface-bound and internalization at 1h/37°C. [^{61}Cu]Cu-DOTAGA-PSMA-I&T and [^{61}Cu]Cu-NODAGA-PSMA-I&T accumulated in LNCaP tumors and PSMA-positive tissues (kidneys, adrenals, spleen and salivary glands), but to different extends. [^{61}Cu]Cu-DOTAGA-PSMA-I&T had ~10-fold higher blood values and predominant accumulation in the abdomen and the liver. At 1h p.i., [^{61}Cu]Cu-NODAGA-PSMA-I&T showed the highest tumor uptake (14.0±5.0 %IA/g), compared to [^{61}Cu]Cu-DOTAGA-PSMA-I&T (6.06±0.25, p=0.006), [^{68}Ga]Ga-PSMA-11 (10.2±1.5, p=0.097) and [^{18}F]PSMA-1007 (9.70±2.57, p=0.080). The highest tumor uptake was also seen for [^{61}Cu]Cu-NODAGA-PSMA-I&T at 4h p.i. (10.7±3.3 %IA/g), compared to [^{61}Cu]Cu-DOTAGA-PSMA-I&T (4.88±0.63, p=0.0014) and [^{18}F]PSMA-1007 (6.28±2.19, p=0.0145). Tumor-to-non tumor ratios were superior for [^{61}Cu]Cu-NODAGA-PSMA-I&T versus [^{61}Cu]Cu-DOTAGA-PSMA-I&T, and equally good or better versus [^{68}Ga]Ga-PSMA-11 and [^{18}F]PSMA-1007. Tumor-to-non tumor ratios

were further improving from 1h to 4h. PET/CT imaging of all radiotracers confirmed the biodistribution data. PET/CT images of $^{61}CuCl_2$ showed accumulation of the uncomplexed ^{61}Cu in the liver and intestine, similar to [^{61}Cu]Cu-DOTAGA-PSMA-I&T. ***Conclusion:*** [^{61}Cu]Cu-NODAGA-PSMA-I&T had seemingly better biodistribution, pharmacokinetics and imaging properties than [^{61}Cu]Cu-DOTAGA-PSMA-I&T. It showed similar distribution to [^{68}Ga]Ga-PSMA-11 and [^{18}F]PSMA-1007, while showing advantages for delayed imaging. [^{61}Cu]Cu-NODAGA-PSMA-I&T was selected for clinical translation of the first ^{61}Cu-PSMA PET.

EPS-292

Preclinical 68Ga-EMP100 PET Imaging to quantify c-Met Expression in non-small cell lung cancer (NSCLC)

A. Prignon[1,2], *T. Rusu*[2,1], *R. Anita*[2], *C. Portal*[3], *J. Cadranel*[2]; [1]*Sorbonne University, UMS28, LIMP, Paris, FRANCE,* [2]*THERANOSCAN Clinical Research Group of the Pneumology and Thoracic Oncology Department Tenon Hospital AP-HP, Paris, FRANCE,* [3]*Edinburgh Molecular Imaging, Edinburgh, UNITED KINGDOM.*

Aim/Introduction: The c-Met receptor tyrosine kinase (TK) is the cell surface receptor for hepatocyte growth factor (HGF). The c-Met/HGF axis is aberrantly activated in many cancers, particularly in NSCLC. A PET imaging agent targeting c-Met receptor could better select patients for c-Met targeted therapy compared to other routinely used techniques such as MET gene amplification by next generation sequencing (NGS) or immunohistochemistry (IHC). ***Materials and Methods:*** To non-invasively quantify c-Met levels, we developed a robust and automated radiolabelling of a c-Met targeted peptide with gallium-68, ^{68}Ga-EMP100, and evaluated its in vivo distribution, pharmacokinetics, and c-Met specificity in preclinical models of non-small cell lung cancer (NSCLC) with variable c-Met expression. MET gene amplification and IHC c-MET scoring were assessed on corresponding tumours. IHC was also conducted on tissue microarrays (TMAs) obtained from therapy naïve patients. ***Results:*** The synthesis on a fully automated system was performed successfully. The overall decay-corrected radiochemical yield was > 60% and radiochemical purity was ≥ 95% (iTLC and radioHPLC), with a sufficient specific activity in MBq/nmol for mice injection.Five different mouse models were developed using squamous (EBC-1) and adenocarcinoma (H1993, H1648, A549 and HCC827) NSCLC cell lines.^{68}Ga-EMP100 provided high-contrast PET images within 40 minutes of administration. Interestingly, ^{68}Ga-EMP100 detected variable c-Met levels according to quantitative uptake analysis in tumour performed in mean % of injected dose/g, or SUV Max in g/mL, confirmed by ex vivo analysis at 1h p.i. MET copy number was not really correlated with semiquantitative IHC measures of c-MET expression in tumours. IHC permits only to discriminate really low expression in A549 model (1+) compared to the others which were found highly positive (3+). Elements of target validation in humans were also obtained through the IHC analysis of TMAs, were 36% of adenocarcinomas, 24% of sarcomatoid carcinomas and 9% of squamous cell carcinomas were found as high c-Met overexpressing. ***Conclusion:*** The potential of PET imaging using ^{68}Ga-EMP100 was successfully demonstrated through direct comparison of its performance against currently used gold standards such as genetic tests and IHC analysis of biopsied tissues, allowing a full body quantitative assessment of the c-Met overexpression. This may represent a game changer in the clinicopathological staging of patients and their selection for c-Met targeted therapies such as antibody drug conjugate or internal systemic radiotherapy. Further studies are warranted to explore the relationship between molecular imaging and response to these specific therapies.

EPS-293

Early detection of CD38using a novel 68Ga-labeled peptidein lymphoma murine models

L. Kang[1], *Q. Yang*[1], *X. Li*[2], *L. Song*[1], *W. Huang*[1], *X. Sun*[1], *Z. Wang*[2]; [1]*Peking University First Hospital, Beijing, CHINA,* [2]*National Center for Nanoscience and Technology, Beijing, CHINA.*

Aim/Introduction: Lymphoma is a heterogeneous disease with different clinical manifestations and prognosis. Despite conventional chemotherapy and radiotherapy, many subtypes of lymphoma are highly aggressive. CD38 is highly expressed on the surface of B-derived lymphoma cell, making it a characteristic tumor biological target of lymphoma, especially in multiple myeloma. CD38 peptide can overcome limitations of antibodies and achieve precise imaging of tumor sites, providing the possibility for early diagnosis of tumors and dynamic monitoring of immunotherapy. In this study, the diagnosis role of ^{68}Ga-labeled CD38-targeted peptide was investigated for PET imaging in lymphoma murine models. ***Materials and Methods:*** After obtaining amino acid sequence through screening of combinatorial chemistry peptide library based on microchip, we synthesized CD38 peptide, PF381, by solid phase synthesis using standard Fmoc scheme. Surface plasmon resonance (SPR) method was used to detect the affinity between PF381 and human CD38 protein. PF381 was conjugated with 1,4,7,10-Tetraazacyclododecane-1,4,7,10-tetraacetic acid (DOTA) for radiolabeling with ^{68}Ga ($t_{1/2}$ = 67.7 min). ^{68}Ga-PF381 was determined using high performance liquid chromatography (HPLC). PET imaging was performed after injection of ^{68}Ga-PF381 after the lymphoma tumor-bearing murine model was established. Further, we conducted biodistribution analysis 30 minutes after injection to analyze the differences in radioactive distribution and uptake of CD38 positive tumor Ramos and negative tumor U266. ***Results:*** The SPR signal of PF381 gradually increased with the increase of protein concentration, and the KD value reached 10^{-8} M, indicating that PF381 has a strong affinity for CD38. For HPLC, the radiolabeling efficiency of ^{68}Ga-PF381 was nearly 70%. PET imaging of ^{68}Ga-PF381 showed that, significant radioactive concentration was observed 30 minutes after injection in Ramos tumor model, and lasted until 80 minutes. In U266 tumor model, no significant radioactive concentration was observed at all time points. The above results of imaging suggest the high uptake of tumors from radiolabeled PF381. The biodistribution results showed that, the uptake of Ramos tumors (0.75 ± 0.03%ID/g) is higher than that of U266 tumors (0.26±0.08%ID/g, P<0.01), which was consistent with PET imaging results. ***Conclusion:*** We developed a novel peptide targeting CD38 and proved ^{68}Ga-labeled PF381 had rapid targeting and good tumor penetration ability. Therefore, ^{68}Ga-labeled PF381 could achieve high sensitivity in vivo imaging of small lymphomas.

1811

Wednesday, September 13, 2023, 9:45 AM - 11:15 AM
Hall G1

Case Report Session 4 - TROP Session: FDG PET and Conventional Imaging: Still Surprising!

OP-943

Pre- and post-CAR-T therapy FDG PET/CT images and limitations of the Deauville Criteria: A Pictorial Essay

S. Kwon[1], *S. Ha*[1], *J. Min*[2], *J. O*[1], *Catholic University Lymphoma Group (CULG);*
[1]*Seoul St Mary's Hospital, Seoul, KOREA, REPUBLIC OF,* [2]*The Catholic University of Korea, Seoul, KOREA, REPUBLIC OF.*

Aim/Introduction: Only a few studies presenting FDG PET/CT findings in DLBCL after chimeric antigen receptor (CAR) T-cell therapy have been published to date. This study aims to describe the patterns of post-CAR-T FDG PET/CT. ***Materials and Methods:*** Patients with DLBCL with F-18 FDG PET/CT before and after CD-19 targeted CAR-T (tisagenlecleucel) infusion were reviewed. Clinical factors were collected, including demographics, initial stage, prior-treatment history, and CAR-T-related factors (use of bridging therapy, tocilizumab, adverse events including ICANS and CRS). The authors assessed PET/CT taken before, 1-month after, and 3-months after CAR-T infusion (pre, 1-mo, 3-mo PET/CT) and recorded the Deauville score (DS), SUVmax of the hottest lesion, SUVmean of non-lymphomatous organs (spleen, bone marrow, liver, and blood pool), and location of the recurrent lesions. Lesions with DS>3 were considered viable lesions. The location of new recurrent lesions in post-CAR-T PET/CT outside previous lymphoma sites was designated as unexpected recurrence sites. ***Results:*** A total of 15 patients were included (median age 61.5, range 38-83, M:F=9:6). 9 patients (60 %) were stage IV at diagnosis. Fifteen patients underwent bridging chemotherapy. Six patients underwent 1-mo, and eight patients had 6-mo PET/CT. In pre-CAR-T PET/CT, viable lymphoma lesions were seen in 12 patients (80 %), while the remaining 3 patients (20 %) showed no definite viable lesion in pre-CAR-T PET/CT. Five patients showed only nodal disease; the remaining ten had extra-nodal diseases. A total of 8 (53.3 %) patients showed progression in post-CAR-T PET/CT (2 patients in 1-mo and six patients in 3-mo PET/CT images). All three patients without viable disease in pre-CAR-T PET/CT manifested as CAR-T failure. SUVmax/liver ratio of the hottest recurrent lesion was 0.7 ~ 15.5. Most recurrent lesions showed DS 5 uptakes, except for one patient with a new DS 2 lesion in the right cheek (SUVmax/liver ratio: 0.7), which was biopsy proven to be a lymphoma lesion. The patient underwent salvage chemotherapy, but the disease progressed with unexpected extensive lymphomatosis peritoneii. The percent change of spleen-to-liver ratio (SLR) between pre- and 1-mo PET/CT ranged from -40 % to 33%. The percent change of SLR and 1-mo SLR did not show a significant difference between the patients with or without CAR-T failure. ***Conclusion:*** The unfavorable outcome following CAR-T infusion can manifest as diverse Deauville scores in pre- or post-CAR-T PET/CT images. ***References:*** Early FDG-PET response predicts CAR-T failure in large B-cell lymphoma. Blood Adv. 2022;6(1):321-326.

OP-944

Dramatic treatment response images of a metastatic lung adenocarcinoma case with Osimertinib treatment on 18F-FDG PET/CT

B. Ince, *A. Namazova, M. Bodur, S. Asa, L. Uslu-Besli, S. Sager, H. Sayman, K. Sonmezoglu;*
Istanbul University-Cerrahpasa, Istanbul, TÜRKIYE.

Aim/Introduction: We present ^{18}F-FDG PET/CT images of a patient diagnosed with metastatic lung adenocarcinoma who responded dramatically to treatment with Osimertinib. Osimertinib is a third-generation epithelial growth factor receptor-tyrosine kinase inhibitor (EGFR-TKI) and is the first treatment option for patients with lung adenocarcinoma with exon 19 deletions or exon 21 L858R mutations. It is also indicated in patients who have become resistant to other EGFR-TK inhibitors. It is known that ^{18}F-FDG PET/CT is an early predictor of outcomes and individual prognosis of patients with advanced lung adenocarcinomas receiving first-line EGFR-TKI therapy. ***Materials and Methods:*** The patient was administered 0.15 mCi/kg FDG intravenously. PET/CT imaging was obtained from the vertex and upper thigh at 60th minute after the injection. ***Results:*** A 50-year-old nonsmoker male patient was diagnosed with poorly differentiated adenocarcinoma by bronchoscopic biopsy of the upper lobe of the left lung. Initial ^{18}F-FDG PET/CT imaging showed a consolidated hypermetabolic mass lesion of the primary malignancy covering most of the parenchyma of upper lobe of the left lung, metastatic hypermetabolic peribronchial thickening in the right lung and lower lobe of the left lung, and hypermetabolic metastatic lymph nodes in the right hilar, bilateral axillary, left supraclavicular, and right lower cervical regions. Biopsy of the left supraclavicular lymph node revealed adenocarcinoma metastasis. After molecular genetic testing of the primary tumor revealed an exon 19 deletion in the EGFR gene, the patient was treated with 80 mg/day Osimertinib. ^{18}F-FDG PET/CT imaging performed after 12 weeks of treatment showed a significant morphologic and metabolic response of the primary malignant tumor in the left upper lobe and metastatic peribronchial thickening in the left lower lobe. Complete response was observed in the remaining metastatic lesions. ***Conclusion:*** We presented ^{18}F-FDG PET/CT images of the case with a dramatic response to Osimertinib treatment. ***References:*** 1. Huang, Y.-E. et al. (2022) "18F-fluorodeoxyglucose PET/CT for early prediction of outcomes in patients with advanced lung adenocarcinomas and EGFR mutations treated with first-line EGFR-Tkis," Cancers, 14(6), p. 1507. Available at: https://doi.org/10.3390/cancers14061507. 2. Kishikawa, T. et al. (2020) "Osimertinib, a third-generation EGFR tyrosine kinase inhibitor: A retrospective multicenter study of its real-world efficacy and safety in advanced/recurrent non-small cell lung carcinoma," Thoracic Cancer, 11(4), pp. 935-942. Available at: https://doi.org/10.1111/1759-7714.13378. 3. Wang, J. et al. (2022) "The predictive value of 18F-FDG PET/CT in an EGFR-mutated lung adenocarcinoma population," Translational Cancer Research, 11(7), pp. 2338-2347. Available at: https://doi.org/10.21037/tcr-22-1726.

OP-945

Imaging Plasmacytoid Dendritic Cell Neoplasm with FDG PET/CT: Atypical Presentation of a Rare Disease in a Child

M. Ben Nasr, *O. Ben Hamida, R. Belayouni, C. Mhiri, I. Slim, I. Meddeb, A. Mhiri;*
Salah Azaiez Institute of Tunis, Tunis, TUNISIA.

Aim/Introduction: Blastic plasmacytoid dendritic cell neoplasm (BPDCN), previously called "CD4/CD56 hematodermic neoplasm", is a rare hematolymphoid neoplasm with a very poor prognosis. The disease has rarely been described in the paediatric population and is characterized by cutaneous involvement in most cases with hematological dissemination. Given the low number of cases described, the role of FDG PET/CT in this disease is very little known. We herein present a case of a 14-year-old girl with BPDCN to highlight the utility of FDG PET/CT for staging and treatment follow-up in this rare entity. ***Materials and Methods:*** A 14-year-old girl with no history consulted for progressive poly-arthralgia without fever. Clinical examination revealed skin infiltrate of the left abdominal region with bilateral axillary lymphadenopathy. Initial blood count showed microcytic anemia. Skin biopsy showed massive tumour infiltration of the dermis by blastic cells and the immunohistochemical study was compatible with acute dendritic leukemia with tumour cells expressing CD4, CD56 and TCL1. Myelogram and bone marrow biopsy were performed, confirming massive blastic invasion. The computed tomography (CT) demonstrated cervical, axillary, and inguinal lymphadenopathy, hepatosplenomegaly and a multi nodular thickening of the anterolateral abdominal wall. The patient underwent FDG PET / CT for initial staging and follow up. FDG PET/CT imaging was performed 60 minutes after the intravenous injection of 148 MBq (4 mCi) of 18F-FDG with BIOGRAPH vision PET CT Siemens. ***Results:*** The exam revealed multiple hypermetabolic bilateral lymph nodes of the cervical, axillary, mediastinal, intra and retro-peritoneal regions. It showed a mild FDG-avid cutaneous lesions, osteo-medullary involvement, and unknown FDG-avid nodules in both mammary glands. The SUVmax varied between 2 and 4,6 (SUV of the liver was measured as 2.2). Treatment was initiated in collaboration with hematologists and oncologists. The patient received two cycles of induction chemotherapy combined with corticosteroid therapy. Two months later, FDG PET/ CT showed no hypermetabolic lesion with a total regression of the lymph nodes, bone marrow, cutaneous and mammary involvement. The child achieved complete remission and hematopoetic stem cell transplantation was proposed. ***Conclusion:*** FDG PET/CT has been widely used in staging, restaging and response assessment of lymphoma. Likewise, for acute leukemia patients, FDG PET/CT can also help determine the extent of the disease and assess the therapeutic response. This case demonstrates the usefulness of FDG-PET for staging and assessment of the treatment response in an extremely rare type of paediatric leukemia.

OP-946

Utility of 18F-FDG PET/CT in Rhabdomyosarcoma of Prostate

S. Jain[1], *H. Goyal*[2];
[1]*All India Institute of Medical Sciences, Bhopal, INDIA,* [2]*Jipmer, Puducherry, INDIA.*

Aim/Introduction: Rhabdomyosarcoma (RMS) of the prostate is a rare and aggressive malignancy that typically occurs in children and young adults. Literature evaluating the role of 18F-FDG PET/CT imaging in management of Prostatic RMS is scarce. FDG PET/CT imaging can help in the staging, restaging, and monitoring response to therapy. We present two cases of Prostatic RMS demonstrating the utility of 18F-FDG PET/CT in staging and treatment response, with one demonstrating complete metabolic response. ***Materials and Methods:*** In both cases, 18F-FDG was administered intravenously followed by acquisition of the whole body PET/CT from base of skull to mid thigh after 60 minutes of injection. ***Results:*** Case 1: A 19 year old man, who presented with low backache and loin pain was diagnosed with embryonal type RMS of prostate. Whole body 18F-FDG PET/CT scan revealed FDG-avid soft tissue mass lesion involving the prostate with involvement of supraclavicular, retroperitoneal and pelvic lymph nodes. Metastatic involvement of the right iliac bone was also noted. On follow-up 18F-FDG PET/CT scan after receiving 6 cycles of chemotherapy (VAC regimen - vincristine, actinomycin-D, and cyclophosphamide), complete metabolic response in these lesions was noted. Case 2: A 17 year old boy, who presented with difficulty in micturion was diagnosed with spindle cell type RMS of Prostate. 18F-FDG PET/CT was performed which revealed heterogeneously increased FDG uptake in heterogeneously enhancing soft tissue attenuation mass replacing the prostate gland, and infiltrating the urethra, posterior wall of the bladder, the seminal vesicles, and bilateral ureters. Loss of fat planes with pelvic sidewall and bilateral obturator internus muscles was also noted. Involvement of pelvic lymph nodes was seen with increased FDG uptake in right external iliac, bilateral internal iliac node, pre-sacral, and left inguinal lymph nodes. Liver (Segment VI) and skeletal (T10 vertebra, L1-L2 vertebrae, Sacrum, and neck of the right femur) metastasis were also noted with increased FDG uptake. In view of widespread metastatic involvement noted on F18-FDG PET/CT, the patient was subsequently started on chemotherapy (VAC regimen). ***Conclusion:*** 18F-FDG PET/CT imaging plays an important role in the evaluation of patients with RMS of the prostate. It is a valuable tool for the staging, restaging and treatment response assessment, and guide in effective treatment planning. ***References:*** Saltzman AF, Cost NG. Current Treatment of Pediatric Bladder and Prostate Rhabdomyosarcoma. Curr Urol Rep. 2018 Feb 22;19(1):11.

OP-947

When Histopathology is Wrong and Bone Scintigraphy is Right - an Exemplary Case of a Rare Genetic Metabolic Disease (Familial Expansile Osteolysis) Repeatedly Mistaken for Fibrous Dysplasia and Paget's Disease

D. Filipan[1], *E. Koumakis*[2,3], *V. Cormier-Daire*[4], *T. Funck-Brentano*[5], *F. Paycha*[6];
[1]*University Department of Oncology and Nuclear Medicine, Sestre Milosrdnice University Hospital Centre, Zagreb, CROATIA,* [2]*Centre de Référence des Maladies Osseuses Constitutionnelles, Service de Rhumatologie, Hôpital Cochin, Assistance Publique-Hôpitaux de Paris, Paris, FRANCE,* [3]*INSERM UMR 1163, Institut Imagine, Hôpital Necker, Paris, FRANCE,* [4]*Service de Génétique Clinique Hôpital Necker-Enfants Malades, Assistance Publique-Hôpitaux de Paris, Paris, FRANCE,* [5]*Service de Rhumatologie & BIOSCAR UMR 1132, INSERM, Université Paris Cité, Paris, FRANCE,* [6]*Service de Médecine Nucléaire, Hôpital Lariboisière, Assistance Publique-Hôpitaux de Paris, Paris, FRANCE.*

Aim/Introduction: Juvenile Paget's disease (JPD) is a rare genetic bone disease characterized by greatly increased bone turnover, skeletal pain, fractures, and deformity. There are two known somatic mutations, causing JPD1 and JPD2, the latter also known as familial expansile osteolysis (FEO). ***Materials and Methods:*** We present the case of a 45-year-old female patient with chronic knee pain. Past medical history revealed hearing loss at the age

of 5 (from bilateral aplasia of the stapes), multiple dental implants before the age of 30 for fragile and falling teeth, and resection of a bone deforming lesion of the upper jaw at the age of 15 for which histopathology report indicated fibrous dysplasia. X-ray imaging of the knees demonstrated bilateral patellofemoral arthropathy and suspicion of fibrous dysplasia of the lower end of the right femur. Dual-energy X-ray absorptiometry evidenced severe osteoporosis. Blood tests revealed elevated bone-specific alkaline phosphatase, osteocalcin and serum C-terminal telopeptide. The patient was referred for a [99mTc]bisphosphonates scintigraphy. Acquisition workflow included full body planar scan completed by SPECT/CT fields-of-view of skull, upper and lower limbs. There was an extensive polyostotic disease with increased skeletal global uptake at 1.3 times normal value, focalized on cranial vault, left maxilla, both clavicles, right humerus, distal end of both femurs and proximal 2/3 of left tibia. CT portion of hybrid imaging found expansion of the bone, bowing of long bones, scoliosis of the spine, cortico-medullary dedifferentiation of the tibiae and local Pagetic-type deformation (clavicles, humeri, right femur). There were no SPECT/CT criteria for fibrous dysplasia. Such pattern was judged consistent with an atypical polyfocal Paget's disease phase II/III with asynchronous appearance and predominance on the peripheral skeleton. ***Results:*** Elevated bone turnover markers coupled with paediatric age-onset abnormalities, Pagetic-type deformations and demineralization prompted a genetic analysis. A heterozygous mutation of TNFRSF11A gene was identified, encoding receptor activator of nuclear factor-kappa B (RANK) and thus confirmed FEO. No evidence of fractures or clinically relevant bone pain permitted an initial watch-and-wait approach, but the patient subsequently developed inflammatory thoraco-lumbar pain correlated to significant increase in bone turnover marker levels, so bisphosphonates infusion was initiated with good clinical and biological results. ***Conclusion:*** This case illustrates the complexity of a correct diagnosis in adults with rare constitutional bone diseases and shows that integrative bone SPECT/CT pattern analysis coupled with quantitative skeletal turn over may act as a problem-solver in properly diagnosing dysostoses such as JPD2.

OP-948

Delayed Onset Angiosarcoma Arising from a Femur Infarct Pictured by [99mTc]bisphosphonates SPECT/CT and [18F]FDG-PET/CT: Caution with Tumour Necrosis and Haemorrhage Phenomena in Molecular Imaging analysis!

D. Filipan[1], *N. Saleh*[2], *R. Kaci*[3], *F. Paycha*[2];
[1]*University Department of Oncology and Nuclear Medicine, Sestre Milosrdnice University Hospital Centre, Zagreb, CROATIA,* [2]*Service de Médecine Nucléaire, Hôpital Lariboisière, Assistance Publique-Hôpitaux de Paris, Paris, FRANCE,* [3]*Service d'Anatomie et de Cytologie Pathologiques, Hôpital Lariboisière, Assistance Publique-Hôpitaux de Paris, Paris, FRANCE.*

Aim/Introduction: Angiosarcoma of bone is extremely rare (less than 1% of all bone sarcomas), with rapid, aggressive progression and a very poor prognosis. It may arise within a bone infarct and is typically characterized by multifocal lesions in tubular bones (usually femur). ***Materials and Methods:*** A 70-year-old male presented with subacute painful left thigh. Past medical history revealed acute myeloid leukaemia (AML) treated 20 years prior (without total body irradiation), including long-term corticosteroid therapy with multiple bone infarcts sequelae. Radiographs detected a lytic bone lesion on a previous infarct of the left femoral diaphysis. CT scan of the left thigh confirmed an osteolytic lesion centred on the medullary cavity with permeative bone destruction of the cortex (Lodwick-Madewell type III), associated with spiculated periosteal reaction and extra-compartmental extension: two extra-osseous juxta-lesional soft-tissue masses. The patient was referred for a [99mTc]bisphosphonates scintigraphy, combining full body planar scan and additional SPECT/CT fields-of-view of the lower limbs. There was increased heterogeneous circumferential uptake (magnitude: 2xN) of the left femoral diaphysis at the site of cortical bone destruction. An [18F]FDG-PET/CT scan spotted the tissular infiltration of the vastus intermedius muscle exhibiting intense hypermetabolism (SUVmax 43, tumour metabolic volume 56 cm^3). An ultrasound-guided biopsy was performed. Immunohistochemical (IHC) analysis described tumoral proliferation in vessel-forming clusters, with intense staining by the anti-CD31/anti-ERG antibodies, and Ki67 50%. IHC stains were consistent with epithelioid angiosarcoma. Pre-operative MRI of the left thigh showed a T1 iso-signal and heterogeneous T2 hypersignal mass displaying early irregular contrast enhancement. ***Results:*** Multimodality cross-sectional imaging categorized the sarcoma as Enneking stage IIB (G2T2M0). The patient underwent en-bloc resection. Pathology report confirmed a high-grade epithelioid angiosarcoma: haemorrhagic, necrotizing (>50%), poorly delimited tumour with cortical bone destruction, medullary canal infiltration, soft tissue invasion and positive surgical margins. Follow-up [18F]FDG-PET/CT scan 2 months later elicited intensely hypermetabolic soft tissue satellite mass at surgical site (SUVmax 52), associated with hypermetabolic hepatic and bone metastases. The patient did not receive chemotherapy due to poor general condition and died 1 month later. ***Conclusion:*** Massive tumoral necrosis and haemorrhagic zones caused faint intra-osseous radiopharmaceuticals uptake, but [18F]FDG depicted soft-tissue expansion more accurately than MRI. Diagnosing bone angiosarcoma is challenging especially when competing diagnoses are bone angiosarcoma secondary to bone infarction, extra-medullary recurrence of AML, and chemotherapy-associated lymphoma of bone. Case-reporting exceptional bone sarcomas is crucial in not underestimating their incidence and gathering key imaging features to improve a dismal prognosis.

OP-949

Facial asymmetry unmasked by bone scintigraphy

L. Sobral Torres*, A. OLiveira, P. Soeiro;*
Centro Hospital Universitário de São João, Porto, PORTUGAL.

Aim/Introduction: Bone scintigraphy with single photon emission computed tomography (bone SPECT) is commonly used to diagnose condylar hyperplasia (CH). Nevertheless, facial asymmetry and mandibular malocclusion have multiple other causes also identifiable by this technique. We present an unsuspected case of fibrous dysplasia of the maxilla mimicking CH in which bone SPECT was fundamental revealing the aetiology and thus impacting the treatment approach. ***Materials and Methods:*** A 14-year-old girl presented with painless and progressive left laterognathia with malocclusion. Physical examination revealed left temporomandibular joint sounds associated with rightward deviation of the chin and a difference between the inter-incisive midlines. Routine blood tests were normal and no bone disease family history was noted. The main diagnostic hypothesis was CH. To assess the possibility of surgical treatment a 3-phase bone scintigraphy of the head with SPECT was performed using [^{99m}Tc]Tc-hydroxymethylene diphosphonate (HDP). ***Results:*** The bone scan revealed no condylar asymmetry of either perfusion or uptake of the radiopharmaceutical. Relative condylar uptake was within normal parameters, consistent with inactive growth (less than 10% difference). However, markedly increased uptake was observed in the left maxillary sinus. On transmission computed tomography (CT), the uptake matched an osteoblastic lesion occupying almost the entire left maxilla and part of the zygomatic bone. Biopsy

confirmed a benign fibro-osseous lesion consistent with fibrous dysplasia. ***Conclusion:*** A 3-phase bone scintigraphy with SPECT can identify the precise location of areas of abnormal osteoblastic activity and help diagnose the aetiology of facial asymmetry and dental malocclusion. Further improvement of this technique can be achieved by combining SPECT with transmission images.
References: Higginson JA, Bartram AC, Banks RJ, Keith DJW. Condylar hyperplasia: current thinking. Br J Oral Maxillofac Surg. 2018 Oct;56(8):655-662.doi:10.1016/j.bjoms.2018.07.017. PMID:30115459Hodder SC, Rees JI, Oliver TB, Facey PE, Sugar AW. SPECT bone scintigraphy in the diagnosis and management of mandibular condylar hyperplasia. Br J Oral Maxillofac Surg. 2000 Apr;38(2):87-93. doi:10.1054/bjom.1999.0209. PMID10864700Yang Z, Reed T, Longino BH. Bone Scintigraphy SPECT/CT Evaluation of Mandibular Condylar Hyperplasia. J Nucl Med Technol. 2016 Mar;44(1):49-51. doi:10.2967/jnmt.115.158691. PMID:26111714. Thiesen G, Gribel BF, Freitas MP. Facial asymmetry: a current review. Dental Press J Orthod. 2015 Nov-Dec;20(6):110-25. doi: 10.1590/2177-6709.20.6.110-125.sar. PMID: 26691977; PMCID: PMC4686752.

OP-950

Unexpected Finding of Myeloma in Myocardial Perfusion Imaging Study with 99mTc-sestamibi

P. Cichocki[1], *A. Płachcińska*[2], *Z. Adamczewski*[1];
[1]*Nuclear Medicine Department, Medical University of Lodz, Lodz, POLAND,* [2]*Department of Quality Control and Radiation Protection, Medical University of Lodz, Lodz, POLAND.*

Aim/Introduction: Multiple myeloma (MM) is a disease involving abnormal proliferation of plasma cells. ^{18}F-FDG PET is the primary radioisotope imaging technique used in diagnosis of MM. However, ^{99m}Tc-sestamibi is also known to accumulate in some malignant tumors (eg. breast, lung or thyroid cancers), including MM lesions. ***Materials and Methods:*** A 73-year-old man with a history of chronic coronary artery disease (CAD), myocardial infarction, myocardial dysfunction (EF=25%), atrial fibrillation, 1st degree atrioventricular block and implantation of cardioverter-defibrillator (ICD) was referred for myocardial perfusion imaging (MPI) as part of routine monitoring of CAD progression. Patient also had a history of stage G3b chronic kidney disease (CKD) and left side nephrectomy due to kidney cancer. MPI was performed using Infinia Hawkeye 4 gammacamera in a two-day REST/Regadenoson protocol after injection of 999 MBq of ^{99m}Tc-sestamibi each day. ***Results:*** MPI study revealed a post-infarction scar with moderate stress-induced ischemia. However, technologist reported abnormal uptake of ^{99m}Tc-sestamibi in bones visible in both studies during image reconstruction. Poor radiopharmaceutical quality was ruled out by quality control. Patient was referred for further diagnosis with the suspicion of MM. Follow-up investigation revealed findings typical for MM: 1) several osteolytic lesions in bones visible in skull X-ray as well as chest, abdomen and pelvis CT scans (most lesions in the chest area were corresponding to abnormal findings in ^{99m}Tc-sestamibi SPECT), 2) low hemoglobin concentration (9,7 g/dL), 3) high creatinine level (414 µmol/L; 4,68 mg/dL; eGFR (BIS1) 17 mL/min/1,73m2), 4) high calcium level (2,97 mmol/L), 5) presence of monoclonal spike on serum protein electrophoresis, 6) presence of free lambda light chains in urine sample. Patient was scheduled for further diagnosis and treatment in hematology clinic, but unfortunately contracted type A influenza before transfer and did not survive the infection. ***Conclusion:*** Non-specific accumulation of ^{99m}Tc-sestamibi in malignant tumors can lead to accidental findings with potentially high clinical significance, and should not be overlooked or dismissed as an artifact or poor radiopharmaceutical quality. In this case, symptoms of MM were masked by CAD and CKD, which could have significantly delayed the diagnosis if not for the unexpected findings in MPI. It is important for technologists to pay attention to unusual uptake patterns in the chest area during quality control and reconstruction of images in routinely performed MPI, since they are no longer visible on fully reconstructed and masked tomographic slices and polar maps used for myocardial perfusion assessment.

OP-951

Ga-68 DOTATOC PET/CT and I-123 MIBG scan in a refractory case of pediatric neuroblastoma: imaging biomarkers with complete mismatch and implications for patient management

L. Vija[1], *A. Latgé*[1], *M. Gambart*[1], *L. Guillon*[2], *S. Brillouet*[1], *D. Vallot*[1], *L. Dierickx*[1], *S. Zerdoud*[1], *F. Courbon*[1];
[1]*Institut Claudius Regaud-Oncopole, Toulouse Cedex 9, FRANCE,* [2]*CHU Toulouse, Toulouse Cedex 9, FRANCE.*

Aim/Introduction: Scintigraphy with Iodine-123 MIBG taken up by noradrenaline transporters (NAT) and Ga-68 DOTATATE with high uptake for somatostatin receptor subtype 2 (SSTR2) are used to select patients for molecular radiotherapy with Iodine-131 MIBG and Lu-177 DOTATATE. We compared the differential biodistribution of these two imaging biomarkers in a 6 year old patient with bone metastatic left adrenal neuroblastoma undergoing assessment for eligibility for molecular radiotherapy with Iodine-131 MIBG or Lu-177 DOTATATE as this patient progressed on bone metastases after three lines of chemotherapy and local irradiation of a lesion of the vertex. ***Materials and Methods:*** I-123 MIBG scintigraphy was performed on a Discovery NM/CT670 gamma camera with both planar and SPECT/CT of the whole body at 24h post injection. Ga-68 DOTATATE PET CT was performed on a Discovery Omni Legend PET/CT system (GE Healthcare) at 50 minutes after intravenous injection of 37 MBq of Ga-68 DOTATATE according to BMI and pediatric guidelines. ***Results:*** Both PET and scintigraphy scans were evaluated to assess the extent of bone marrow disease using the International Society of Pediatric Oncology European Neuroblastoma (SIOPEN) (scoring from 0-72). On I-123 MIBG scan the bone scoring was 19/72 whereas on Ga-68 DOTATOC PET the bone extent was more important, with a score of 34/72. However there was a complete mismatch between focal bone areas with intense uptake on MIBG scan versus SSTR2 expression intensity lower than the liver on Ga-68 DOTA PET, versus lesions with no uptake or faint uptake on MIBG scan and intense uptake on Ga-68 DOTA PET. Only one lesion of the vertex and another of the right femur were concordant and intense in both imaging methods. ***Conclusion:*** This case report shows biological heterogeneity in the expression of NAT and SSTR2, so that both imaging methods are complementary and useful to guide the choice of the most adequate molecular radiotherapy. Increased SSTR2 expression might be related to more aggressive lesions. Heterogeneous clonal evolution related to genomic instability might be responsible for the mismatch.

1901

Wednesday, September 13, 2023, 11:25 - 11:45

Hall A

Closing Session

OP-952

Closing Session

V. Garibotto*;*
University Hospitals and University of Geneva, Geneva, SWITZERLAND.

e-Posters

EP-01

e-Poster Area

A: Preclinical Studies -> A1 Medical Preclinical -> A11 In Vitro Studies

EP-0001

An exploratory study on the mechanism of pralatrexate killing gemcitabine-resistant pancreatic cancer cells

W. Weng, *J. Hong, D. Jiang, B. Chen, S. Zheng;*
The First Affiliated Hospital, Zhejiang University School of Medicine, Hangzhou, CHINA.

Aim/Introduction: Pancreatic cancer is one of the most lethal malignant tumors in human beings, and its low survival rate and poor prognosis have become a public health problem to be solved urgently. Although gemcitabine, a first-line treatment for pancreatic cancer, can improve the survival benefit and related clinical symptoms of patients with advanced pancreatic cancer, the drug resistance of patients to gemcitabine during treatment often leads to adverse clinical outcomes. For patients with gemcitabine-resistant pancreatic cancer, it is urgent to explore new chemotherapy drugs. In previous large-scale drug screening, we found that pralatrexate has a strong killing effect on gemcitabine-resistant pancreatic cancer cells and is safe for use in nude mice.The purpose of this study was to explore the anti-tumor mechanism of pralatrexate on gemcitabine-resistant pancreatic cancer cells, in order to provide new methods and ideas for solving the problem of gemcitabine-resistant pancreatic cancer. ***Materials and Methods:*** A new acquired gemcitabine-resistant cell line BXPC-GEM-20 was established from the parental pancreatic cancer cell line. BXPC-GEM-20 cells were treated with different concentrations of pralatrexate and the changes of related pathway proteins were detected by western blotting. ***Results:*** Western blotting showed that the expressions of AMPK,AKT,mTOR,p-mTOR were decreased, while the expressions of p-AMPK and LC3A/B were increased. ***Conclusion:*** Pralatrexate can down-regulate the expression of AKT and activate phosphorylation of AMPK, resulting in the downregulation of mTOR protein, thus increasing the expression of autophagy related protein LC3 A/B and promoting autophagy.Pralatrexate increases autophagy by down-regulating the expression of AMPK and AKT, which may be one of the mechanisms of pralatrexate killing gemcitabine-resistant pancreatic cancer cells.

EP-0002

Androgen-induced cell cycle arrest in prostate carcinoma cells as a potential risk for pseudoprogression during diagnosis with prostate-specific membrane antigen (PSMA) radiopharmaceuticals and treatment failure with PSMA radioligands. An in vitro study.

B. Meller[1], *P. Thelen*[2], *V. Unterkircher*[3], *J. Bucerius*[1], *L. Trojan*[2], *C. O. Sahlmann*[1], *F. Bremmer*[3];
[1]*University Medical Center Göttingen, Clinic of Nuclear Medicine, Göttingen, GERMANY,* [2]*University Medical Center Göttingen, Clinic of Urology, Göttingen, GERMANY,* [3]*University Medical Center Göttingen, Institute of Pathology, Göttingen, GERMANY.*

Aim/Introduction: Cell cycle arrest (CCA) is a well-known reason for radiotherapy treatment failure. It is expected that CCA might also affect the outcome of radioligand therapy. In the context of PSMA-ligand diagnostics and therapy, there is still little known about the relationship between PSMA expression and the cell cycle of prostate cancer cells (PC). Therefore, we investigated the effect of androgens (AN) on the cell cycle of prostate cancer cell lines and their uptake of PSMA radiopharmaceuticals as a model for the discontinuation of antiandrogen therapy. ***Materials and Methods:*** Two different human PC cell lines LNCaP und VCaP (ATCC) were used. In LNCaP the castration resistance (CR) bases on androgen receptor (AR)-mutations (AR-T878A) while in VCaP a wild type (WT) AR overexpression has been observed. VCaP were grown permanently with testosterone (T, revCRPC) or without T (CRPC). RevCRPC-cultures represent therefore the androgen sensitive cell type, CRPC the castration resistant VCaP (CRPC). All three cell lines were 48 h incubated with respectively 1 nmol/L T, dihydrotestosterone (DHT) and R1881 as well as 5nmol/L 3β-androstanediol (A) and 3α-A , Thereafter, the Ga-68-PSMA-11 uptake after 3 h as well as the percentage of the cells in the different phases of the cell cycle were determined. ***Results:*** In the AR-mutated LNCaP the incubation with AN did not influence the radiopharmaceutical uptake significantly. In androgen-sensitive revCRPC the uptake of Ga-68-PSMA-11 increased >30 % ($p < 0.05$) after AN withdrawal. In CRPC the incubation with testosterone doubled the uptake ($p<0.05$). The incubation with 3αA, R1881 und DHT resulted in an increase of the radiopharmaceutical uptake-of >400 % ($p<0.01$). This increase was associated with an increase of cell fraction in CCR in G0/G1 ($p<0.05$) and a significant decrease ($p<0.005$) of the cell fraction in the other phases of cell cycle. ***Conclusion:*** The expression of PSMA in WT AR-cell lines can be significantly influenced by changes in AN supplementation. The association of a higher radiopharmaceutical uptake with a cell cycle arrest point to a cell cycle dependent expression of PSMA with potential consequences for imaging and therapeutic approaches in vivo.

EP-0003

Synthesis and in vitro evaluation of a small molecule 99mTc-G2C-CBM as potential PD-L1 imaging agent

Z. Chen[1,2,3], *D. Zhu*[1,4], *C. Lu*[1,2,3];
[1]*Jiangsu Institute of Nuclear Medicine, Wuxi, CHINA,* [2]*NHC Key Laboratory of Nuclear Medicine, Wuxi, CHINA,* [3]*Jiangsu Key Laboratory of Molecular Nuclear Medicine, Wuxi, CHINA,* [4]*Department of Radiopharmaceuticals, School of Pharmacy, Nanjing Medical University, Nanjing, CHINA.*

Aim/Introduction: The checkpoint blockade immunotherapy of PD-1/PD-L1 has become a potent treatment strategy for cancers. However, the objective response rate of this immunotherapy is below 30%, which is expected to be improved. Expression level of PD-L1 play a key role in the guidance of immunotherapy, which could be quantified by noninvasive imaging with radiotracers. In this study, we develop a ^{99m}Tc labeled small molecule compound for PD-L1 imaging. ***Materials and Methods:*** The labeling precursor N - [2 - (3-cyanobenzene-1-methoxy) - 4 - (2- bromo-3-phenylbenzyloxy) - 5-chlorobenzyl] - N-sericylglycylglycylcysteine (G2C-CBM) was synthesized from 2-bromo-3-iodotoluene in a seven-step reaction sequence. Using $SnCl_2$ as reducing agent, and in the presence of sodium glucoheptonate, a series of studies were performed to optimize labeling efficiency of ^{99m}Tc-G2C-CBM. The radiolabeling yield (RLY) and radiochemical purity (RCP) of ^{99m}Tc-G2C-CBM were determined by high performance liquid

chromatography (HPLC). The in vitro stabilities of ^{99m}Tc-G2C-CBM was determined every 1h at room temperature. The partition coefficient of ^{99m}Tc-G2C-CBM was determined in n-octanol and phosphate buffer (PB) (pH 7.4) and the uptake of ^{99m}Tc-G2C-CBM was performed in PD-L1 positive cell (A375-hPD-L1) and PD-L1 negative cell (A375). ***Results:*** The chemical structures of the labeling precursor and its intermediates were verified by IR, ^{1}HNMR and MS. RLY and RCP of ^{99m}Tc-G2C-CBM were over 93% at selected condition. ^{99m}Tc-G2C-CBM was stable up to 6 h in phosphate-buffered solution (PH=7.4) and radiochemical purities was over 90% at selected condition. Partition coefficient (lgP) of ^{99m}Tc-G2C-CBM was 1.31 at pH 7.4 of the phosphate buffer. The uptake of ^{99m}Tc-G2C-CBM in A375-hPD-L1(25.84%) cell is significantly higher than that in A375(4.09%) cell after co-incubated for 4 hours. ***Conclusion:*** ^{99m}Tc-G2C-CBM is probably a potential SPECT PD-L1 imaging agent and further study is needed.

EP-0004

Robustness of radiomic features in dopamine transporter imaging with single photon emission tomography

V. Laskov[1,2], *P. Choniawko*[1,2], *D. Rotbauer*[2];
[1]*University Hospital Kralovske Vinohrady, Department of Radiology and Nuclear medicine, Prague, CZECH REPUBLIC,* [2]*Third Faculty of Medicine, Charles University, Prague, CZECH REPUBLIC.*

Aim/Introduction: In this study, we are assessing the robustness of radiomic features in dopamine transporter imaging (DaT) with single photon emission tomography (SPECT) with different reconstruction parameters using an anthropomorphic head phantom with tissue heterogeneity of our own production. ***Materials and Methods:*** We made an anthropomorphic head phantom with tissue heterogeneity, produced using a personal 3D printer. Polylactide was used as the 3D printing material for soft tissue with 82% infill. Bone was subsequently reproduced by pouring liquid plaster (plaster powder and water ratio 2:1) into the cavity of the phantom. A new cavity in the supposed region of basal ganglia was made. A cotton ball with 10 MBq of DAT SPECT radiotracer (123I-Ioflupane) was inserted. 10 MBq corresponds to the approximal brain 5% uptake after 3-4 hours from the injection. Scans were performed on the two-detector hybrid camera with acquisition parameters corresponding to international guidelines for DaT SPECT imaging. Low-dose computer tomography scan of the phantom was performed in order to calculate the attenuation correction(AC) map. SPECT reconstruction was performed on a clinical workstation using OS-EM iterative reconstruction with and without AC, and FBP algorithms. OS-EM reconstructed data had no post-filtering applied. FBP data were prefiltered using a Butterworth filter.Reconstructed data was uploaded to LifeX software, for our proposed analysis 165 radiomics features were extracted from the region of interest separately for each reconstruction and attenuation correction variant.Statistical analysis was made in RStudio software using Intraclass Correlation Coefficient(ICC) function from psych. package. Statistical significance was determined for $p<0.05$. ***Results:*** Overall radiomic features in different reconstruction parameters showed a moderate repeatability rate with ICC 0.636 ($p<0.01$, 95% CI (0,577-0,696). For each group of radiomic features, repeatability was different, with the highest repeatability rate (ICC 0.998 ($p<0.01$, 95% CI [0,997-1]) in GLRLM features, and the lowest repeatability rate (ICC 0.636 ($p<0.01$, 95% CI [0,500-0,780]) in intensity based features. ***Conclusion:*** We have identified that overall radiomics features extracted from DaT SPECT show a moderate repeatability rate within different reconstruction parameters. These results make radiomic features suitable for clinical practice and human studies, but awareness of feature selection should be held, as some groups of radiomic features are more repeatable and thus more robust than others. Descriptors of the relationships between image voxels (GLCM, RLM, SZM, NGTDM) derived textures show an excellent rate of repeatability, which gives them the highest potential for future studies in patients with Parkinsonism and clinical translation.

EP-0005

Sinomenine Hydrochloride enhances Trametinib-induced iodide-handling gene expression and radioiodine uptake

J. Zhang*, A. Yang;*
The First Affiliated Hospital of Xi'an Jiaotong University, Xi'an, CHINA.

Aim/Introduction: Radioiodine therapy is one of the main treatments after surgery for differentiated thyroid cancer (DTC). However, the downregulation of iodide-handling gene presents difficulties for radioiodine therapy in DTC cells. Thyroid cancer frequently exhibits activation of the RAS/RAF/MEK/ERK pathway. Targeted therapy has been applied in the treatment of advanced, metastatic, radioiodine-refractory thyroid cancer. Our previous study has found sinomenine hydrochloride (SH) can promote redifferentiation and radioiodine uptake in DTC. We hypothesized that addition of SH could be a rational complement to MEK inhibitor trametinib in treating thyroid cancer. ***Materials and Methods:*** The experiments focused on DTC cells, including BCPAP and TPC-1. RT-qPCR was performed to determine the expression of NIS genes after SH and trametinib addition. NIS, p-ERK, t-ERK protein were detected by Western blot after treatment with different concentrations of SH. Use γ counter to detect changes in cellular iodide uptake. ***Results:*** We observed upregulation of ERK expression with SH treatment, an effect abrogated by trametinib. SH increased the expression of NIS mRNA and protein at different concentrations. Further studies revealed that the expression of NIS mRNA and protein was significantly increased in the combination treatment group compared with the SH treatment alone or trametinib alone. Radioiodine uptake was also increased in the combination therapy group. ***Conclusion:*** Combination of SH and trametinib induces DTC cells redifferentiation and radioiodine uptake. It will lay the theoretical foundation for future clinical research and application.

EP-0006

"In house" radiolabeling of anti-PD-L1 monoclonal antibodies with 111-Indium for in vivo imaging

F. Silva[1], *R. Lopes*[1], *A. S. Capacho*[1], *M. Fortunato*[1,2], *S. Vaz*[1], *F. Oliveira*[1], *C. João*[1], *D. Costa*[1];
[1]*Champalimaud Foundation, Lisbon, PORTUGAL,* [2]*Nova School of Science and Technology, Lisbon, PORTUGAL.*

Aim/Introduction: At present, the assessment of cancer immune checkpoint inhibitors expression, such as PD-L1, is obtained via biopsy followed by immunohistochemistry. However, biopsies may be unduly aggressive due to the anatomical location of the tumor, and may not translate entire tumor burden disease heterogeneity. The combination of Immunology and Radiopharmacology has the potential for developing new diagnostic strategies aimed at improving patient selection for immunotherapy, predicting early responses and side effects. This work aims to radiolabel, in house, anti-PD-L1 monoclonal

antibodies (MPDL3280A and 6E11) with Indium-111 (^{111}In), in order to obtain their in vivo whole-body imaging distribution. Its success will provide essential knowledge and expertise for subsequent radiolabeling of other monoclonal antibodies for clinical applications. ***Materials and Methods:*** An excess (50:1) of a DTPA derivative was used to conjugate to MPDL3280A and 6E11, and radiolabeling procedures were performed by reacting the DTPA-containing antibodies with $^{111}InCl_3$. In vitro stability studies of the radiolabeled antibodies were performed in the presence of 0,9% NaCl and cell culture media, DMEM and RPMI. Assessment of the PD-L1 binding capability of the antibodies was performed through cell cytometry studies in human (MCF7 and H2444) and murine (E0771, LLC, B16F10, MOPC315, MOPC315.BM) cancer cell lines, and cellular uptake studies on high (H2444 and MOPC315) and low (MCF7 and LLC) PD-L1 expressing cells. ***Results:*** DTPA was conjugated to the antibodies and the ^{111}In-labeled MPDL3280A and 6E11 were obtained with >95% radiochemical purity. In vitro stability studies showed that after 48 h of incubation both antibodies retained >90% of the coordinated ^{111}In. Flow cytometry analysis demonstrated a higher expression of the anti-PD-L1 antibodies on the H2444 and MOPC315 cell lines, intermediate expression on the E0771, LLC, B16F10, and MOPC315.BM cells and no expression on MCF7 cell lines. For the cellular uptake studies, ^{111}In-MPDL3280A-DTPA displayed the highest uptake in H2444 cells, with 10.48% I.D./10^6 cells at 24 h post incubation, compared with low expressing PD-L1 MFC7 cells (0.45% I.D./10^6 cells). For ^{111}In-6E11-DTPA, the uptake difference was less accentuated, with 2.35% I.D./10^6 cells at 24 h for the higher PD-L1 expressing MOPC315 cells; however, it was noteworthily higher when compared with the low PD-L1 expressing LLC cell line (0.42% I.D./10^6 cells). ***Conclusion:*** ^{111}In-labeled MPDL3280A and 6E11 were successfully obtained and the resulting antibodies showed significant binding affinity towards higher PD-L1 expressing cancer cell lines, which makes them promising candidates for potential imaging of PD-L1 expression in vivo.

EP-0007

The high affinity angiotensin AT2 receptor agonist, C21, inhibits proliferation and induces cell death in prostate cancer cells by an AT2 receptor-independent mechanism

Y. Zhao, *M. Marx, U. Lützen, M. Zuhayra;*
Department of Nuclear Medicine, Molecular Imaging, Diagnostics and Therapy, UKSH, Kiel, GERMANY.

Aim/Introduction: Several studies carried out in different tumours indicate that activation of the angiotensin type 2 (AT_2) receptor inhibits cell proliferation and initiates apoptosis. In the present study, we investigated in prostate - specific membrane antigen (PSMA) positive prostate carcinoma (PCa), LNCaP cells: 1) the expression of AT_2 receptors, 2) the effect of the activation of the AT_2 receptor on proliferation and apoptosis, 3) the role of the AT_2 receptor in the PSMA-expression. The effects detected in LNCaP cells were compared with those obtained in PC3 cells, PSMA-negative PCa cells. ***Materials and Methods:*** Selective stimulation of AT_2 receptors was achieved by a 24 h exposure of cells either to angiotensin II (Ang) II (10^{-7} M) in the presence of the selective AT_1 receptor antagonist, losartan (10^{-6} M), or to the high-affinity AT_2 receptor agonist, C21 (10^{-6} M). PD 123177 (10^{-6} M) was used as the selective AT_2 receptor inhibitor. The expression of AT_2 receptors and PSMA were quantified by Western blotting. The cell growth and cell death were analysed by WST-1 assay and LDH-release into the culture medium, respectively. Histological assessment of cell proliferation was accomplished by observation of cresyl violet stained cells using an inverted light microscope. ***Results:*** Both, LNCaP and PC3 cells express the AT2 receptor. Stimulation of the membrane AT_2 receptors with Ang II + losartan in LNCaP cells did not inhibit cell proliferation nor did it induce cell death. However, the AT_2 receptor agonist, C21, which interacts with both, the membrane and intracellular AT_2 receptors, significantly reduced cell proliferation and increased LDH release, indicating that C21 induced cell death. Experiments employing cresyl violet staining confirmed the cell death-promoting effects of C21. The effects of C21 were more pronounced in PSMA-positive LNCaP cells than in PSMA-negative PC3 cells. Inhibition of AT_2 receptors in LNCaP cells by PD123177 did not affect the effects of C21. The AT_2 receptor inhibitor actually potentiated the cell death-promoting effects of the agonist as evidenced by further enhanced LDH release. In addition, C21 reduced the expression of PSMA in LNCaP cells. ***Conclusion:*** We demonstrate that the C21 induces rapid cell death in LNCaP cells most probably via activation of intracellular AT_2 receptors. The down-regulation of PSMA expression might point to a possible mechanism responsible for the observed effects of C21. Our results indicate that treatment of PCa with C21 may reduce the progression of the disease.

EP-0008

Microleakage evaluation of new composite resins for posterior teeth: bioactive resins vs bulk fill resins

A. Pires Lourenço[1,2,3], *C. M. Marto*[2,3,4], *A. Coelho*[2,3,4], *M. V. Pinto*[4], *P. Neves*[4], *I. Amaro*[2,3,4], *J. Sousa*[4], *M. Marques Ferreira*[2,3,5], *E. Carrilho*[2,3,4], *M. Laranjo*[1,2,3], *A. M. Abrantes*[1,2,3], *M. F. Botelho*[1,2,3], *A. B. Paula*[2,3,4];
[1]Univ Coimbra, Coimbra Institute for Clinical and Biomedical Research (iCBR) area of Environment Genetics and Oncobiology (CIMAGO), Institute of Biophysics, Faculty of Medicine, Coimbra, PORTUGAL, [2]Univ Coimbra, Center for Innovative Biomedicine and Biotechnology (CIBB), Coimbra, PORTUGAL, [3]Clinical Academic Center of Coimbra (CACC), Coimbra, PORTUGAL, [4]Univ Coimbra, Coimbra Institute for Clinical and Biomedical Research (iCBR) area of Environment Genetics and Oncobiology (CIMAGO); Institute of Integrated Clinical Practice and Laboratory for Evidence-Based Sciences and Precision Dentistry, Faculty of Med, Coimbra, PORTUGAL, [5]Univ Coimbra, Coimbra Institute for Clinical and Biomedical Research (iCBR) area of Environment Genetics and Oncobiology (CIMAGO); Institute of Endodontics and Laboratory for Evidence-Based Sciences and Precision Dentistry, Faculty of Medicine, Coimbra, PORTUGAL.

Aim/Introduction: Posterior tooth restorations are a sensitive technique that depends on the type of adhesive systems and composite resins used. There are some recent resins that intend to reduce the sensitivity of the technique either by using larger increments with less polymerization shrinkage (bulk fill resins) or by direct adhesion to the tooth structure without the need of the adhesive system (bioactive resins).The aim of the present study was to compare microleakage in restorations using a new bioactive resin Surefill One™, SDR®flow bulk fill resin and Spectra™ST conventional nanohybrid resin. The null hypothesis is that there are no microleakage variations between the various resins studied. ***Materials and Methods:*** An in vitro study was carried out using fifty-two premolars and molars extracted for orthodontic reasons. Identical preparations were thus performed in all of them (Class V with 4 mm mesio-distal, 3 mm occluso-gingival and 3 mm in depth) and divided into different experimental groups: 1 positive control, 1 negative control and 3 tests with bioactive composite resin (Surefill One™), bulk fill flow resin (SDR®flow), and conventional nano-hybrid composite resin (and Spectra™ST). Through quantitative techniques using Nuclear Medicine, it

was possible to evaluate microleakage using a radioactive isotope, technetium. Radioactivity emitted by the specimens was detected by a gamma camera. The different groups were compared using the ordinary one-way ANOVA and Tukey's test for multiple comparisons. ***Results:*** The results of the experimental study point to statistically significant differences between the test groups (p = 0.002), with increased microleakage in the bioactive composite resin group. The negative control group has the lowest microleakage. The positive control presents the highest microleakage with statistically significant differences compared to all other groups, Surefill (p<0.05), SDR (p<0.001) e Spectra (p<0.001). In the test groups, the conventional nanohybrid resin (p<0.001) and the bulk fill resin (p<0.001) showed statistically lower microleakage values than the bioactive resin. There were no statistically significant differences between the nanohybrid resin and the bulk fill resin, both presenting low microleakage values. ***Conclusion:*** The microleakage technique with Nuclear Medicine is validated by the results of the positive and negative control groups. The application of adhesive systems prior to the composite resin remains recommended. Bioactive resins do not have sufficient adhesiveness to perform well on posterior teeth. Bulk fill resins present similar results to conventional nano-hybrid resins, thus presenting a clinical advantage due to use in larger increments, reducing appointment times and technique sensitivity.

EP-0009

[99mTc][Tc-HYNIC-scFvD2B] vs [99mTc][Tc(CO)3(scFvD2B-HisTag)] for the imaging SPECT of prostate cancer: preliminary in vitro studies

C. Gobbi[1], *L. Melendez-Alafort*[2], *B. Spolaore*[3], *N. Salvarese*[1], *D. Carpanese*[2], *V. Rossi*[2], *A. Rosato*[2,4], *G. Fracasso*[5], *C. Bolzati*[1];
[1]*Institute of Condensed Matter Chemistry and Energy Technologies - National Research Council, Padua, ITALY,* [2]*Istituto Oncologico Veneto IOV-IRCSS, Padua, ITALY,* [3]*Department of Pharmaceutical and Pharmacological Sciences, University of Padua, Padua, ITALY,* [4]*Department of Surgery, Oncology and Gastroenterology, University of Padua, Padova, ITALY,* [5]*Department of Biomedical Sciences, University of Padua, Padua, ITALY.*

Aim/Introduction: scFvD2B is a single-chain variable fragment of the IgGD2B antibody, specific for the extracellular domain of prostate membrane antigen (PSMA), overexpressed in prostate cancer (PCa). Its small size allows a greater penetration into the tumour tissue and a faster elimination from blood than whole antibodies. With its short biological half-life, it can be coupled with short half-life radionuclide (e.g. ^{99m}Tc) to be used as imaging agent[1].In this study succinimidyl-HYNIC hydrochloride (S-HYNIC) was randomly conjugated to scFvD2B and then labelled with ^{99m}Tc; additionally the corresponding scFvD2B-HisTag, was site-specifically tagged with $[^{99m}Tc][Tc(CO)_3(OH_2)_3]^+$ thanks to the presence of the hexahistidine-tag motif on its C-terminal portion. The two radioimmunoconjugates (RIC) were characterized and their in vitro stability and affinity to the PSMA receptor in PCa cell lines were compared. ***Materials and Methods:*** 2 mg/ml of native scFvD2B was conjugated to S-HYNIC (1:10 molar ratio). Radiosynthesis was carried out at 37°C for 1 hour, adding $[^{99m}Tc][TcO_4]^-$ (500-720 MBq) to a vial containing HYNIC-scFvD2B (70-150 µg), $SnCl_2$ and EDDA/Tricine mixture as coligands.scFvD2B-HisTag (100-150 µg) was incubated with $[^{99m}Tc][Tc(CO)_3(OH_2)_3]^+$ (500-720 MBq; obtained with the IsoLink® kit) at 37°C for 2 hours.Both RICs were purified by gel filtration. Stability was evaluated by HPLC after incubation at 37°C for 24h in different media and transchelating agents. Cell studies were assed in PSMA(+) cell line (LNCaP and PC3-PIP) and PC3(-) as negative control. ***Results:*** $[^{99m}Tc]$[Tc-HYNIC-scFvD2B] was obtained with a RCY up to 50%, instead the RCY of $[^{99m}Tc][Tc(CO)_3$(scFvD2B-HisTag)] was in the range of 23-43%. After purification, RCP were higher than 95% for both RICs. They were stable in media over the investigation time.For $[^{99m}Tc]$[Tc-HYNIC-scFvD2B] cell uptake and internalization values were: 7% and 6% in LNCaP; 12% and 10% in PC3-PIP; 1,5% and 0,5% in PC3. While for $[^{99m}Tc][Tc(CO)_3$(scFvD2B-HisTag)], cell uptake and internalization were: 6% and 4% in LNCaP; 30% and 15% in PC3-PIP; and 3% and 0,7% in PC3. Blocking studies with an excess of native scFvD2B confirmed the specificity of RICs for PSMA-receptor. ***Conclusion:*** $[^{99m}Tc]$[Tc-HYNIC-scFvD2B] and $[^{99m}Tc][Tc(CO)_3$(scFvD2B-HisTag)] were stable and produced in high RCP. $[^{99m}Tc][Tc(CO)_3$(scFvD2B-HisTag)] internalization in PC3-PIP was higher than that observed for $[^{99m}Tc]$[Tc-HYNIC-scFvD2B], but in LNCaP they were comparable. In vivo studies for both RIC are now in progress. Acknowledgement to AIRC (IG-2020 ID 24528) for financial support. ***References:*** 1. Mitri et al. 2021 Adv. Nat. Sci: Nanosci. Nanotechnol. 12 035008

EP-0010

161Tb-PSMA-I&T and177Lu- PSMA-I&T treatment in T23 and ST4787 prostate cancer cell lines - a model representative of177Lu-PSMA-resistant prostate cancer phenotype

M. Kirienko*, E. Jachetti, R. Sulsenti, C. Pascali, A. Bogni, M. Colombo, E. Seregni;*
Fondazione IRCCS Istituto Nazionale dei Tumori, Milan, ITALY.

Aim/Introduction: Our objective was to evaluate the effect on cell proliferation of ^{161}Tb-PSMA-I&T and ^{177}Lu- PSMA-I&T in cell lines representative of castration resistant prostate adenocarcinoma (T23) and neuroendocrine prostate cancer (ST4787). ***Materials and Methods:*** We used two murine cell lines T23 and ST4787 transfected to overexpress human PSMA utilizing puromycin (PURO) selection based lentiviral system (T23-Folh1-PURO and ST4787-Folh1-PURO). PSMA expression was then checked by western blot. Tumor cells (7500 cells for ST4787 and 5000 cells for T23 in 1 mL medium with supplements) were seeded in plates. After adhesion and washing, the cells were incubated in 1ml medium with supplements containing ^{161}Tb-PSMA-I&T or ^{177}Lu-PSMA-I&T (0.1–10 MBq/mL), respectively, or just medium. In the first set of experiments the radiopharmaceutical-containing medium was left standing for the whole incubation time, while it was removed after 4 hours in the second set. The tumor cells were left to grow for 7 days. Tumor cell viability was assessed through cell count with Image J and it was quantified as percentage of cell count of control (untreated) cell samples. The results were analyzed for statistical significance by One-way ANOVA with Turkey's multiple comparisons test. ***Results:*** Both T23-Folh1-PURO and ST4787-Folh1-PURO, tested after infection and after at least two passages of puromycin selection, were positive for PSMA.In the first experiment, the reduction of viability of T23-Folh1-PURO and ST4787-Folh1-PURO tumor cells after exposure to ^{161}Tb-PSMA-I&T and ^{177}Lu-PSMA-I&T was observed not earlier than 7 days using 10MBq/ml. A viability reduction for T23-Folhl-PURO cells was observed also using 5 MBq/mL of ^{161}Tb-PSMA-I&T, while ^{177}Lu-PSMA-I&T did not provoke any change. In the second experiment, both cell lines resulted resistant to both radiopharmaceuticals at all the tested activities (0.5-10 MBq/ml). ***Conclusion:*** We observed that PSMA-overexpressing tumor cells

may not respond to PSMA-targeting radiopharmaceuticals and postulated that the mechanism might have similarity with the clinical observations; indeed, up to approximately 30% of patients experience disease progression (1). Our model could be useful for studying the effects of PSMA-directed radioligand treatments to identify mechanisms of resistance to ^{177}Lutetium-labelled compounds and to identify possible combination treatment strategies. ^{161}Terbium-PSMA-I&T showed promising results in overcoming resistance. ***References:*** 1- Sartor et al. Lutetium-177-PSMA-617 for Metastatic Castration-Resistant Prostate Cancer. N Engl J Med 2021; 385:1091-1103

EP-0011

αvβ3 integrin-selective RGDechi peptides labelled with [99mTc][Tc(N)(PNP)]- and [99mTc][Tc-HYNIC]- systems: an in vitro comparison

C. Bolzati[1], *C. Gobbi*[1], *N. Salvarese*[1], *A. Giorgio*[2], *D. Carpanese*[3], *V. Rossi*[3], *L. Melendez-Alafort*[3], *A. Rosato*[3,4], *M. Saviano*[5], *A. Del Gatto*[2], *L. Zaccaro*[2];
[1]*Institute of Condensed Matter Chemistry and Energy Technologies, ICMATE-CNR, PADOVA, ITALY,* [2]*Institute of Biostructures and Bioimaging, IBB-CNR, Napoli, ITALY,* [3]*Istituto Oncologico Veneto, IOV-IRCCS, PADOVA, ITALY,* [4]*Department of Surgery, Oncology and Gastroenterology, University of Padua, DiSCOG-UniPD, Padova, ITALY,* [5]*Institute of Crystallography, IC-CNR, Bari, ITALY.*

Aim/Introduction: Recently, chimeric RGD-echistatin peptides, selective for $\alpha_v\beta_3$, have been proposed as antiangiogenic agents. Radiolabelled derivatives have also been proposed for the selective imaging of $\alpha_v\beta_3$ expressing tumours. The low serum stability of the forefather peptide, named RGDechi, led to the development of the more stable truncated derivates RGDechi[1-17] and ψRGDechi. In this study, the two peptides were labelled with technetium-99m via [^{99m}Tc][Tc(N)(PNPn)]- (PNPn=diphosphinoamine) and [^{99m}Tc][Tc-HYNIC]- (Tc-organohydrazine) systems. The radiolabelled peptides were compared in their in vitro stability and affinity to $\alpha_v\beta_3$ integrin in expressing cell lines. ***Materials and Methods:*** [^{99m}Tc(N)PNPn]-labelled peptides were efficiently prepared adopting the classical two-step procedure. The first-step is required to produce a mixture of reactive $[^{99m}Tc(N)]^{2+}_{int}$ precursors. In the second-step, the reactive $[^{99m}Tc(N)]^{2+}_{int}$ was transformed into the final compound by the rapid addition of the pertinent PNPn (water-soluble PNP3OH={[$(OHCH_2)_2PCH_2CH_2]_2NCH_2CH_2OCH_3$}); more lipophilic PNP43={[$(CH_3)_2PCH_2CH_2]_2NCH_2CH_2OCH_3$}), RGDechi peptide derivative, and phosphate buffer. [^{99m}Tc-HYNIC]-tagged peptides were obtained incubating, at 70°C for 20 min, the previously HYNIC-conjugated peptides with [^{99m}Tc][TcO_4^-] in a vial containing $SnCl_2$ and EDDA/tricine as co-ligands. The stability of radiopeptides was evaluated by HPLC after incubation at 37°C in different media. Affinity to $\alpha_v\beta_3$ integrin was evaluated by cell uptake studies assed in WM-266-4 and 4T1 lines ($\alpha_v\beta_3$-positive), and HeLa ($\alpha_v\beta_3$-negative, with moderate $\alpha_v\beta_5$ expression). ***Results:*** Radiopeptides were prepared efficiently in each case. They were stable in PBS and to transchelating agents. [^{99m}Tc(N)PNPn]-labelled peptides showed good stability in cell culture medium, human and mouse sera, and mouse liver homogenate. In whole blood, [^{99m}Tc(N)PNPn(RGDechi[1-17])] were more stable than [^{99m}Tc(N)PNPn(ψRGDechi)]. In mouse kidney homogenate we observed a degradation for both compounds. Regarding [^{99m}Tc-HYNIC]-tagged peptides, their stability was low in many of the investigated milieu, including cell culture medium. Cellular studies show that only the [^{99m}Tc(N)PNPn(RGDechi[1-17])] series has a specific uptake in $\alpha_v\beta_3$-positive cells, the accumulation was significantly lower in HeLa cells, suggesting that [^{99m}Tc(N)PNPn(RGDechi[1-17])] radiopeptides are able to selectively bind $\alpha_v\beta_3$ integrin and not to cross-react with $\alpha_v\beta_5$. The amount of uptake/internalization was dependent on the nature of [^{99m}Tc(N)(PNPn)]-synthon. No specific bound was observed for [^{99m}Tc(N)PNPn(ψRGDechi)] series as well as for [^{99m}Tc-HYNIC]-tagged peptides. ***Conclusion:*** Stability and integrin affinity properties of RGDechi derivatives are strongly influenced by the adopted labelling technology. Among the tested compounds, only the [^{99m}Tc(N)PNPn(RGDechi[1-17])] series is adequately stable and has a specific uptake in $\alpha_v\beta_3$-positive cells. Thus, it was selected for further investigation. Acknowledgement to AIRC (IG-2020 ID 24528) for financial support.

EP-0012

Let's label biomolecules in mild conditions with the [99mTc][Tc(N)(PNP)]-system: the PNP3OH experience

C. Bolzati[1], *N. Salvarese*[1], *B. Spolaore*[2], *C. Gobbi*[1], *A. Vittadini*[1], *D. Forrer*[1], *S. Ghiani*[3], *A. Maiocchi*[4];
[1]*Institute of Condensed Matter Chemistry and Energy Technologies, ICMATE-CNR, PADOVA, ITALY,* [2]*Department of Pharmaceutical and Pharmacological Sciences, University of Padua, PADOVA, ITALY,* [3]*Bracco Research Centre, Bracco Imaging SpA, Torino, ITALY,* [4]*Bracco SpA, Milano, ITALY.*

Aim/Introduction: The [^{99m}Tc][Tc(N)(PNP)]-technology has long been used to label biomolecules. The most important advantage of this technology is its high chemical flexibility; nevertheless, the usage of classical, quite lipophilic PNPs leads to the need of heating over extended times to reach high radiochemical yields. This represents a limit, because these conditions are not suitable for label temperature-sensitive biomolecules. Water-soluble phosphines are an attractive class of oxidatively stable ligands that generate stable hydrophilic chelates with good pharmacokinetics. Modification of the substituents on the P atoms induces the variation of electronic and sterical properties of the ligand, which affect its reactivity for the metal ions, influencing the reaction rate, and the stereochemistry of the final complex. Hence, the water-soluble PNP3OH, {[$(OHCH_2)_2PCH_2CH_2]_2NCH_2CH_2OCH_3$}, was designed and the effect of the substituents on the corresponding ws-$[Tc(N)(PNP3OH)]^{2+}$-framework was studied in silico through a series of density functional theory calculations and compared with those of alkyl PNP ligands (PNP3 and PNP43). The reactivity was then experimentally verified using the [^{99m}Tc][Tc(N)(PNP3OH)]-framework to label different biomolecules including: RGD peptides, biotin, and apomyoglobin as model protein.[1] ***Materials and Methods:*** Computational studies aimed at predicting the molecular geometry of the intermediate complexes $TcNCl_2$PNP, and of the free ligands were performed. PNP3OH was synthesized and characterized. The biomolecules mentioned above were conjugated with a terminal cysteine residue, cys~, to allow the coordination of the [^{99m}Tc][Tc(N)(PNP3OH)]-synthon. Radiosyntheses were performed using a two-step reaction. The receptor specificity of the radiolabelled biomolecules was assessed in-vitro in pertinent cell lines. ***Results:*** Structural variation on PNP alters the coordination geometry of the $TcNCl_2$PNP precursors and ligands arrangement around the metal, affecting the strength of the metal-P and metal-Cl bonding. Data show that the Tc-Cl bonds strength are weaker in $[Tc(N)Cl_2(PNP3OH)]$ precursor than in the other $TcNCl_2$PNP. This makes the Cl atoms of $[Tc(N)Cl_2(PNP3OH)]$ more prone to substitution and thus more reactive to nucleophilic attack by cys~. Experimental results confirm this behavior; the insertion of water-soluble groups on PNP actually improves the reactivity of [^{99m}Tc][Tc(N)(PNP3OH)]-framework

towards cys~. Radiosyntheses were performed efficiently under physiological conditions at RT in 30 min, using a concentration range of 10^{-5}-10^{-6} M of cys-conjugated biomolecules. All [^{99m}Tc][Tc(N)(PNP3OH)]-tagged biomolecules preserve their receptor targeting ability. ***Conclusion:*** Data support the effective application of the [^{99m}Tc(N)(PNP3OH)]-technology to the labeling of temperature-sensitive biomolecules. Acknowledgement to Bracco Imaging and AIRC (IG-2020 ID 24528) for financial support. ***References:*** 1. Bolzati et al. Mol. Pharm., 2022, 19, 3, 876-894

EP-0013

To study uptake of 18F-AVT-011 in different cell lines expressing p-glycoprotein.

R. Thakur[1], *M. Kumar*[1], *P. chaudhari*[2], *P. Kumar*[1];
[1]*National Institute of mental health and neurosciences, Bangalore, INDIA,* [2]*Advanced Centre for Treatment, Research and Education, Mumbai, INDIA.*

Aim/Introduction: To study the uptake of 18F-AVT-011 in U87 (temozolomide sensitive) and LN18 cells (temozolomide resistant). ***Materials and Methods:*** 18F-AVT-011 was synthesized in our lab by a method published elsewhere[1]. The cell lines U87 (IC50 = 10-100μM) and LN18 (IC50 = 400-500 μM) were cultured in Dulbecco's modified eagle medium (DMEM). The MGMT levels and Pgp levels were evaluated by PCR and flow cytometry techniques respectively. The cells were detached using trypsin and then resuspended in equal proportion for the uptake study. Each test tube contained 1mL of cell suspension into which 10 μL (~ 0.74 MBq) of [18F]-AVT-011 was added and incubated for 15 min, 30 min, 60 min, and 120 min at 37ºC in a water bath. The blocking studies were performed by incubating the same cell suspension (1 mL) with 500-fold excess of Pgp blocking agent Tariquidar solution (5mM) for 30 min at 37ºC in a water bath and radioactivity was added as described above. The cell suspension was centrifuged. The pellet was washed thrice with normal saline, and the supernatant was collected separately in the other set of tubes. The radioactivity associated with cells and supernatant was counted in a gamma counter (Capnitec Inc), and the percentage of radioactivity bound to the cells was calculated. ***Results:*** ^{18}F-AVT-011 was synthesized with radiochemical purity greater than 95%. methylation was more than 90% in U87 cells and ~ 4% in LN-18 cells. The Pgp levels were distinct in both cells. The Pgp levels were higher expressed in LN18 cells. The uptake of 18F-AVT-011 was 77.9 ± 0.5 % in U87 and 74.4 ± 2.9 % in LN18 cells at 15 min but it was 72.1 ± 1.7% in U87 and 9.6 ± 1.4% in LN18 and same was observed at 2 h. The radioactivity effluxed out of LN18 cells at a faster rate which may be due to the overexpression of Pgp. The blocking study showed an increase in the uptake of radioactivity after tariquidar blocking. ***Conclusion:*** ^{18}F-AVT-011 may be a potential radiotracer for imaging Pgp activity. The validation through animal study is in progress. ***References:*** Kumar P, Thakur R, Acharya PC, Mohan HK, Pallavi UN, Maheshwari D, Mohammed K M A, Kumar A, Goud Nerella S, Joshi RK, Kumar M, Nagaraj C. Synthesis, characterization, and radiosynthesis of fluorine-18-AVT-011 as a Pgp chemoresistance imaging marker. Sci Rep. 2022 Nov 3;12(1):18584.

EP-0014

Dual-radionuclide detection for radiopharmaceutical studies

J. Campeiro, *C. D. van der Heide, J. de Swart, S. U. Dalm; Erasmus Medical Center, Rotterdam, NETHERLANDS.*

Aim/Introduction: Dual-radionuclide detection has a promising advantage for radiopharmaceutical studies. For example, research evaluating different targets expressed on prostate cancer (PCa) cells, i.e. prostate-specific membrane antigen (PSMA) and gastrin-releasing peptide receptor (GRPR), could benefit from a dual-radionuclide detection method to develop novel treatment strategies based on combined PSMA and GRPR treatment using radiopharmaceuticals labeled with different radionuclides. This is relevant as targeting both PSMA and GRPR might lead to treatment with improved efficacy and safety. However, distinguishing radionuclides, i.e. ^{111}In, ^{177}Lu and ^{161}Tb, by their energy peaks of gamma rays when combined in one solution/system is hampered by the crosstalk and overlap between the energy spectra originating from each radionuclide. To enable simultaneous dual-radionuclide detection, a detector with good energy resolution or complex scatter and crosstalk correction methods are necessary. Our objective was to develop a simple method for simultaneous detection and discrimination of gamma radiation emitted by combinations of ^{111}In, ^{177}Lu and ^{161}Tb. ***Materials and Methods:*** The radioactivity of a combined solution of ^{161}Tb&^{177}Lu or ^{111}In&^{177}Lu (1 kBq/mL per radionuclide) was measured in a HIDEX-AMG γ-counter and expressed as counts per minute (CPM). Narrow energy windows were defined to distinguish radionuclides by their energy peaks, i.e. for ^{161}Tb&^{177}Lu 20-35 keV and 187-229 keV, and for ^{111}In&^{177}Lu 400-480 keV and 102-124 keV, respectively. Moreover, the PSMA- and GRPR-expressing PCa PC3-PIP cell line was incubated with 10^{-9} M [^{111}In]In-NeoB and 10^{-9} M [^{177}Lu]Lu-PSMA-617 simultaneously or separately for 1 hour, whereafter cell uptake was determined using the above-mentioned energy windows. Data are expressed as percentage added dose (%AD). ***Results:*** Using the identified energy peaks for ^{161}Tb, ^{177}Lu and ^{111}In we were able to distinguish the CPMs per radionuclide in solutions containing ^{161}Tb&^{177}Lu or ^{111}In&^{177}Lu. The same method also enabled effective determination of the radioactivity uptake per radiopharmaceutical after incubating PC3-PIP cells simultaneously with [^{177}Lu]Lu-PSMA-617 and [^{111}In]In-NeoB. Our first results showed no significant difference in uptake after combined or separate incubation (28.6±4.3 vs 34.8±4.0 %AD for [^{177}Lu]Lu-PSMA617 and 5.6±0.9 vs 7.2±0.3 %AD for [^{111}In]In-NeoB, respectively). ***Conclusion:*** Our preliminary studies demonstrated successful simultaneous ^{161}Tb&^{177}Lu and ^{111}In&^{177}Lu gamma ray detection in a PCa cell line; by identifying narrow energy windows specific for each radionuclide, we were able to distinguish between the radionuclide source and quantify the radioactivity uptake by the cells. This method will open new venues in preclinical radiopharmaceutical research e.g. allowing the investigation of therapies combining radiopharmaceuticals labeled with different radionuclides.

EP-02

e-Poster Area

A: Preclinical Studies -> A1 Medical Preclinical -> A12 Preclinical Cardiology and Neurology

EP-0015

Age Related Changes of Cellular Contributions in FDG Uptake Correlate with Metabolic Connectivity

J. Gnörich, *L. Bartos, A. Zatcepin, R. Schäfer, S. Kunte, P. Beumers, P. Bartenstein, N. Albert, S. Ziegler, M. Brendel; LMU Munich, Munich, GERMANY.*

Aim/Introduction: 2-Fluorodesoxyglucose PET (FDG-PET) is frequently used to study glucose metabolism in mammalian brains. Alterations of glucose uptake in brain regions and brain networks occur during healthy aging. However, the cellular sources of age-related changes in FDG uptake and their impact on PET read outs during aging remain to be

elucidated. ***Materials and Methods:*** We investigated wildtype mice between 3 and 18 months of age using FDG-PET and fluorescence activated cell sorting (FACS) after in vivo tracer injection (scRadiotracing). FDG uptake per cell was quantified in isolated microglia, astrocytes and neurons. Cortical brain uptake and metabolic connectivity were determined by FDG-PET. ***Results:*** Neuronal FDG uptake strongly decreased at 18 months of age when compared to 3 and 12 months. Contrary, astrocytes and microglia showed increasing or stable FDG uptake between 12 and 18 months of age. Glucose uptake was dominated by astroglia at early (microglia predominance) and late ages (astrocyte predominance). Increases of FDG PET at late ages were explained by increasing astrocytic FDG uptake and metabolic connectivity was driven by the proportion of glucose uptake in astroglial cells. ***Conclusion:*** Trajectories of cellular glucose uptake during aging strongly differ between astroglia and neurons. Astroglial glucose uptake determines brain FDG-PET alterations and metabolic connectivity during aging.

EP-0016

Inhibition of PFKFB3 counteracts atherosclerosis via NLRP3/Casepase1/IL-1β pathway in macrophages

M. Zhao[1], *X. Wang*[2], *W. Wu*[1], *Y. Bai*[2], *X. Li*[3];
[1]The Third Xiangya Hospital of Central South University, Changsha, CHINA, [2]Xiangya Hospital of Central South University, Changsha, CHINA, [3]Division of Nuclear Medicine, Department of Biomedical Imaging and Image-guided Therapy, Medical University of Vienna, Vienna, AUSTRIA.

Aim/Introduction: Macrophages are woven into atherosclerosis occurrence and development. Inflammasome activation is a core mechanism contributing to the local high-inflammatory microenvironment in plaques. However, the trigger factor of inflammasome activation is unknown. ***Materials and Methods:*** Carotid atheroma specimens were collected from 17 patients with carotid stenosis who underwent carotid endarterectomy. High-fat western diet-treated ApoE-/- mice were selected to develop an atherosclerosis model, and a PFKFB3 inhibitor PFK158 was administered along with atherosclerosis modeling. Meanwhile, lipopolysaccharide (LPS) and TNF-γ were employed to differentiate bone marrow-derived macrophages(BMDMs) into M1-like phenotypes under either hypoxia or normoxia. The glycolytic activity was determined by in vivo 18F-FDG micro-PET/CT, ex vivo glucose uptake, and ECAR analysis; HIF-1α, PFKFB3, NLRP3, Caspase-1, and IL-1β expressions were quantified by using western-blot and real-time PCR. ***Results:*** PFKFB3 accumulations in human atherosclerotic plaques, in colocalization with NLRP3 expression and macrophages. PFK158 overruled atherosclerosis occurrence, reduced glycolytic activity, and NLRP3 inflammasome activation in murine atherosclerotic plaques. Mechanistically, hypoxia promoted glycolytic reprogramming and NLRP3 inflammasome activation in BMDMs. Blocking either HIF-1α or PFKFB3 downregulated NLRP3/Caspase-1/IL-1β pathway in hypoxic BMDMs. ***Conclusion:*** In brief, this study demonstrates that HIF-1α/PFKFB3/NLRP3 signal pathway is a crucial mechanism for inflammation activation in macrophages in atherosclerosis emergence. The targeting PFKFB3 may be a promising strategy for atheroprotection.

EP-0017

In vivo [18F]SMBT-1 imaging of reactive astrocytes in mouse models of Alzheimer's disease - temporospatial relationship with amyloid, tau and microgliosis

R. Ni[1], *Y. Kong*[2], *C. Maschio*[1], *B. Yao*[3], *J. Xiao*[2], *Q. Huang*[2], *Y. Guan*[2];
[1]University of Zurich, Zurich, SWITZERLAND, [2]PET Center, Huashan Hospital, Fudan University, Shanghai, CHINA, [3]Radiopharmacy and Molecular Imaging Center, School of Pharmacy, Fudan University, Shanghai, CHINA.

Aim/Introduction: Reactive astrocytes and microgliosis play important roles in the pathophysiology of Alzheimer's disease (AD). Here, we aim to understand the association between reactive astrocytes, microgliosis, glucose metabolism, and amyloid-β in vivo in 5×FAD transgenic mice. ***Materials and Methods:*** PET with [^{18}F]SMBT-1 (monoamine oxidase-B) [1], [^{18}F]DPA-714 (translocator protein), [^{18}F]FDG and [^{18}F]florbetapir (Aβ) and [^{18}F]PMPBB3 (tau) [2] was carried out in 3- and 6-month-old male 5×FAD mice, and aged-matched wild-type mice. The brain regional referenced standard uptake value (SUVR) was computed with the cerebellum as reference region. Immunofluorescence staining was performed with antibodies against monoamine oxidase-B, glial fibrillary acidic protein, C3d, translocator protein, Iba1, Glut1 and amyloid-β in mouse brain slices. ***Results:*** [^{18}F]SMBT-1 SUVRs were higher in the cortex and brain stem of 3 and 6-month-old 5×FAD mice than age-matched wild-type mice. [^{18}F]DPA-714 SUVRs were higher in the 6-month-old 5×FAD mice than age-matched wild-type mice. [^{18}F]florbetapir SUVRs were higher in the brain stem, cortex, hippocampus and midbrain of 6-month-old 5×FAD mice than in age-matched wild-type mice. Although an amyloidosis model, 6-month-old 5×FAD mice showed increased [^{18}F]PMPBB3 SUVRs (tau) in the cortex and hippocampus compared to 3-month-old 5×FAD mice and age-matched wild-type mice. ***Conclusion:*** The findings provide in vivo evidence for reactive astrocytes and microgliosis at early stage in 5×FAD mice. ***References:*** 1. Harada R, Hayakawa Y, Ezura M, Lerdsirisuk P, Du Y, Ishikawa Y, Iwata R, Shidahara M, Ishiki A, Kikuchi A, Arai H, Kudo Y, Yanai K, Furumoto S, Okamura N. 18F-SMBT-1: A Selective and Reversible PET Tracer for Monoamine Oxidase-B Imaging. J Nucl Med. 2021 Feb;62(2):253-258. doi: 10.2967/jnumed.120.244400. 2. Tagai K, Ono M, Kubota M, Kitamura S, Takahata K, Seki C, Takado Y, Shinotoh H, Sano Y, Yamamoto Y, Matsuoka K, Takuwa H, Shimojo M, Takahashi M, Kawamura K, Kikuchi T, Okada M, Akiyama H, Suzuki H, Onaya M, Takeda T, Arai K, Arai N, Araki N, Saito Y, Trojanowski JQ, Lee VMY, Mishra SK, Yamaguchi Y, Kimura Y, Ichise M, Tomita Y, Zhang MR, Suhara T, Shigeta M, Sahara N, Higuchi M, Shimada H. High-Contrast In Vivo Imaging of Tau Pathologies in Alzheimer's and Non-Alzheimer's Disease Tauopathies. Neuron. 2021 Jan 6;109(1):42-58.e8. doi: 10.1016/j.neuron.2020.09.042.

EP-0018

A comparison of the biodistribution and the patient dose estimation of [18F]FEPP and [18F]FEAO, potential radiotracers for PET myocardial perfusion imaging

K. Gotowicz[1,2], *U. Karczmarczyk*[3], *S. Krajewski*[1], *E. Witkowska-Patena*[4], *L. Steczek*[1], *J. Towpik*[1], *P. Kozanecki*[1], *M. Mazur*[2], *M. Dziuk*[4,5], *J. Włostowska*[1], *C. Kozanecki*[1], *P. Garnuszek*[3];
[1]Synektik SA, Research & Development Centre, Warsaw, POLAND, [2]Department of Chemistry, University of Warsaw, Warsaw, POLAND, [3]National Centre for Nuclear Researach, Radioisotope Centre POLATOM, Warsaw, POLAND, [4]Military Institute of Medicine - National Research Institute, Nuclear Medicine Department, Warsaw, POLAND, [5]Affidea Poland, Warsaw, POLAND.

Aim/Introduction: Positron emission tomography (PET) myocardial perfusion imaging (MPI) is an effective method for non-invasive evaluation of coronary obstruction in patients with suspected or established coronary artery disease. The aim of the study was to carry out a preclinical comparison of two potential PET-MPI radiotracers - [^{18}F]FEPP and [^{18}F]FEAO. ***Materials and Methods:*** The biodistribution of single intravenous administration of each ^{18}F-labelled compound was assessed on healthy, male Wistar rats. The animals were in quarantine for at least 6 days before the examination and had access to water and food ad libitum. Rats were sacrificed in groups of three at 0.25, 0.5, 1, 2, 3 and 6 hour after injection for each tracer. Dissected organs/tissues of interest were weighed and measured for their radioactivity. The obtained data was extrapolated to humans using the simplest allometric scaling model. The effective doses in mSv/MBq were calculated using software for internal dose assessment OLINDA/EXM®, version 1.1. ***Results:*** The main organ of interest for cardiac tracers is the heart and surrounding organs like the liver and the lungs. The biodistribution studies showed that [^{18}F]FEAO uptake in the cardiac muscle was high and stable (3.02 %ID/g at 15 minute and 2.79 %ID/g at 6 hour post-injection) in contrast to [^{18}F]FEPP (1.84 %ID/g and 0.05 %ID/g, respectively). Both compounds were characterized by relatively low uptake in the liver (maximum 0.89 %ID/g and 0.90 %ID/g at 15 min, respectively). The uptake in the lungs was much higher for [^{18}F]FEAO and decreased rapidly over time (from 3.02 %ID/g at 15 min to 0.55 %ID/g at 6 h). The study showed that both radiotracers were eliminated predominantly by biliary excretion. The excretion was faster for [^{18}F]FEPP, therefore the estimated effective dose for human was lower for this tracer (0.00714 mSv/MBq) compared to [^{18}F]FEAO (0.0109 mSv/MBq). ***Conclusion:*** The myocardial [^{18}F]FEAO uptake was much higher and stable in time revealing more favourable biodistribution profile in comparison to [^{18}F]FEPP. It also showed modest radiation exposure, comparable to the other ^{18}F-labelled compounds used in MPI [1]. Encouraging results merit tracer evaluation in further clinical studies. The study was funded by the National Centre for Research and Development, Poland, grant no. POIR.01.01.01-00-0089/15. ***References:*** [1] Maddahi J, et al. Phase I, first-in-human study of BMS747158, a novel ^{18}F-labeled tracer for myocardial perfusion PET: dosimetry, biodistribution, safety, and imaging characteristics after a single injection at rest. J Nucl Med. 2011;52:1490-8.

EP-0019

Early brain [18F]FDG PET imaging predicts the long-term behavioral impact of exposure to sublethal doses of organophosphates: a longitudinal study in mice exposed to NIMP, a sarin surrogate

A. Soyer[1], *A. Champault*[2], *S. Leterrier*[1], *C. Corvo*[1], *L. Breuil*[1], *B. Hosten*[1], *W. Saba*[1], *C. Leroy*[1], *A. Winkeler*[1], *G. Dal Bo*[2], *K. Thibault*[2], *N. Tournier*[1];
[1]*Laboratoire d'Imagerie Biomédicale Multimodale (BioMaps), CEA, CNRS, Inserm, Service Hospitalier Frédéric Joliot, Université Paris-Saclay, Orsay, FRANCE,* [2]*Institut de Recherche Biomédicale des Armées (IRBA), Bretigny-sur-Orge, FRANCE.*

Aim/Introduction: Organophosphate compounds (OPs) are still widely used as pesticides. Moreover, the use of OP nerve agents such as sarin as warfare neurotoxicants remains a threat. The acute and often lethal effects of high-dose exposure to OPs are widely studied. However, long-term neuro-psychiatric impairment has been reported in subjects exposed to sublethal, often asymptomatic doses of sarin. The aim of this study was to perform a longitudinal monitoring of brain function and behavior in a validated mouse model of OP exposure. We hypothesized that [^{18}F]FDG PET imaging may provide an early neuroimaging biomarker to monitor the central nervous system impact of sublethal exposure to OPs. ***Materials and Methods:*** A longitudinal brain [^{18}F]FDG microPET study was conducted in male Swiss mice. All animals were scanned at baseline, at day 1, day 7 and 1 month after administration of a single sublethal dose of 4-nitrophenyl isopropyl methylphosphonate (NIMP, 0.315 mg/kg, s.c, 50% of the LD50, n=12), a sarin surrogate, or vehicle (n=4, control). [^{18}F]FDG was injected intraperitoneally in awake mice which were then transferred in a cage for 50 min to allow for brain uptake. Mice were then anesthetized using isoflurane to provide 20 min of static PET acquisition. SUV-normalized [^{18}F]FDG PET images were co-registered to a mouse brain template. Finally, 1 month after NIMP exposure, each mouse underwent behavioral tests to assess anxiety (elevated plus maze, EPM) and cognitive performance (Y-maze). ***Results:*** Compared to baseline, a significant decrease in regional [^{18}F]FDG uptake was observed in certain brain regions of NIMP-treated mice on days 1 and 7. The decrease in [^{18}F]FDG uptake was progressive and significant in the amygdala, midbrain and cortex ($p<0.001$). Normal [^{18}F]FDG brain uptake was restored at 1 month ($p>0.05$). Such decline in [^{18}F]FDG uptake was not observed in control mice ($p>0.05$). Behavioral study at 1 month did not evidence change in cognitive performance ($p>0.05$). However, a higher level of anxiety compared with control animals was observed (decreased time spent in the open arm, $p<0.05$). Individual analysis showed that the level of anxiety was significantly correlated with the decrease in [^{18}F]FDG uptake in the amygdala at day 7 (both parameters expressed as % versus control animals, $r^2=0.906$, $p<0.001$). ***Conclusion:*** This longitudinal study shows the dynamics of altered brain glucose metabolism after sublethal exposure to OPs. Our results suggest that early [^{18}F]FDG PET data may predict the long-term behavioral impact of OP exposure, at least for anxiety.

EP-0020

Comparison of intravenous and oral administration of [18F]MC225: a feasibility study in rats

G. Salvi de Souza[1,2], *J. W. Sijbesma*[1], *J. Doorduin*[1], *A. M. Marques da Silva*[3,4], *C. R. Furini*[2,5], *A. A. Lammertsma*[1], *C. Tsoumpas*[1], *G. Luurtsema*[1];
[1]*Department of Nuclear Medicine and Molecular Imaging, University of Groningen, University Medical Center Groningen, Groningen, NETHERLANDS,* [2]*School of Medicine, PUCRS, Porto Alegre, BRAZIL,* [3]*Faculdade de Medicina, Universidade de Sao Paulo, Sao Paulo, BRAZIL,* [4]*Medical Imaging & Data Analytics, San Diego, CA, UNITED STATES OF AMERICA,* [5]*Laboratory of Cognition and Memory Neurobiology, Brain Institute, PUCRS, Porto Alegre, BRAZIL.*

Aim/Introduction: [^{18}F]MC225 is a positron emission tomography (PET) tracer to measure the P-glycoprotein (P-gp) function, which plays a dynamic role in the bioavailability of (orally) administered drugs [1]. Nearly all drugs are given orally and, therefore, oral administration of an appropriate PET tracer should be a useful method for investigating the absorption of tracers in the gut and its relation to bioavailability and uptake in other organs. This pilot study aimed to compare the brain uptake and distribution of [^{18}F]MC225 following oral and intravenous administrations in healthy rats. ***Materials and Methods:*** Six adult male Wistar rats were divided into two groups: a control group for intravenous administration of [18F]MC225 and a second group for oral administration of the tracer. The control group (n=3, 309±10 g), anaesthetised with a combination of ketamine and dexmedetomidine, received 37 MBq in a tail vein. The second

group (n=3, 324±5 g) received 10 MBq orally by gavage before being anaesthetised using the same protocol. Approximately 120 minutes post-administration, animals were euthanized and brains were dissected and blood was collected via heart punction. The brain regions evaluated were olfactory bulbs, left cerebral hemisphere, right cerebral hemisphere, midbrain, and cerebellum. Data obtained using a gamma counter were transformed into tissue to blood ratio (TBR) units. TBR values are presented as mean ± standard deviation. ***Results:*** Mean TBR values for the intravenous group were higher than those for the oral group across all regions evaluated: 2.02 ± 0.77 vs 1.30 ± 0.09 for the olfactory bulbs, 2.05 ± 0.39 vs 1.14 ± 0.02 for the left cerebral hemisphere, 2.10 ± 0.51 vs 1.16 ± 0.04 for the right cerebral hemisphere, 1.86 ± 0.34 vs 1.15 ± 0.09 for the midbrain, and 1.78 ± 0.43 vs 1.12 ± 0.07 for the cerebellum. The ratios between oral and intravenous TBR ranged from 0.54 to 0.64. ***Conclusion:*** Oral administration of [^{18}F] MC225 in healthy rats results in lower brain uptake (120 minutes after administration) compared with intravenous administration. However, oral administration still results in detectable tracer levels in the brain and, as such, it may have relevance for studying the gut-brain axis. Further dynamic imaging studies are needed to investigate the optimal oral administration protocol and the best interval for data acquisition. ***References:*** [1] Elmeliegy, Mohamed, et al. "Effect of P-glycoprotein (P-gp) inducers on exposure of P-gp substrates: review of clinical drug-drug interaction studies." Clinical pharmacokinetics 59 (2020): 699-714.

EP-0021

Short-term synaptic remodeling in a rat model of alcohol binge drinking assessed using [11C]UCB-J PET imaging

C. CORVO[1], *C. Leroy*[2], *S. Letterier*[2], *S. Goutal*[2], *F. Caille*[2], *A. Soyer*[2], *M. Goislard*[2], *S. Amargier*[2], *N. Tournier*[2], *W. Saba*[2];
[1]*Université Paris-Saclay, Inserm, CNRS, CEA, Laboratoire d'Imagerie Biomédicale Multimodale (BioMaps), ORSAY, FRANCE,* [2]*Université Paris-Saclay, Inserm, CNRS, CEA, Laboratoire d'Imagerie Biomédicale Multimodale (BioMaps), Orsay, FRANCE.*

Aim/Introduction: Binge drinking (BD) is characterized by a massive alcohol consumption in a short period of time and is mainly seen amongst teenagers, at a vulnerable period of brain development and maturation. Deleterious effects of chronic alcohol on neuronal/synaptic density and function are well known. However, preclinical studies suggest that short-term alcohol consumption is associated with synaptic remodeling in certain brain regions that may underlie addiction[1]. We hypothesized that changes in synaptic density associated with BD could be non-invasively monitored using [^{11}C]UCB-J, a specific radioligand of synaptic vesicle glycoprotein 2 isoform A (SV2A). ***Materials and Methods:*** In the BD model, male adolescent rats (33 days) were administered with ethanol (5 g/kg, orally) or water (control) every 2 days for 14 days. Dynamic brain PET imaging was performed under isoflurane anaesthesia at day 15 with [^{11}C]UCB-J (i.v, 42.6±4.9MBq, 60 min acquisition, n=5-6 per group). In additional BD and control animals (n=6 per group), [^{18}F]2-fluoro-2-desoxy-sorbitol ([^{18}F]FDS) PET imaging (i.v, 37.3±4.1MBq, 30 min acquisition) was performed as a paracellular marker of blood-brain barrier (BBB) integrity. Using a brain template, SUV-normalized time-activity curves (TACs) of [^{11}C]UCB-J and [^{18}F]FDS were generated in brain regions, and in the left heart-ventricle. Brain uptake was estimated by the regional area-under-the-TACs (AUC, SUV.min). A two-way ANOVA was performed to compare groups. ***Results:*** Significant increase in [^{11}C]UCB-J uptake in the BD group compared with control animals ($p<0.05$) was observed in several brain regions including thalamus (+21±14%), accumbens (+26±17%), ventral tegmental area (+26±18%), amygdala (+26±17%) and striatum (+21±15%), whereas radioactivity in the heart ventricle remained unchanged (+10±25%, $p>0.05$). Compared with the control group, the uptake of [^{18}F]FDS in brain regions (+6±9%; $p>0.05$) and heart ventricle (+1±13%; $p>0.05$) were not significantly increased in the BD model, suggesting preserved BBB integrity. ***Conclusion:*** The higher uptake of [^{11}C]UCB-J in certain brain regions supports an importance for a short term synaptic remodeling in an adolescent rat model of BD. This increase in brain uptake not related related to any change in the peripheral exposure of [^{11}C]UCB-J or to any BBB disruption. The dynamics and long-term impact of BD on synaptic density can be further investigated using [^{11}C]UCB-J PET imaging in this model. ***References:*** [1] Kyzar et Pandey, « Molecular Mechanisms of Synaptic Remodeling in Alcoholism ».

EP-0022

Sex differences in [18F]-FDG uptake and behavioral impairment following repetitive mild traumatic brain injury (rmTBI)

R. Moraga-Amaro*, M. Bankstahl, J. P. Bankstahl;
Hannover Medical School, Hannover, GERMANY.*

Aim/Introduction: Repetitive mild traumatic brain injuries (rmTBI) can lead to chronic traumatic encephalophaty (CTE), an early-age chronic neurodegeneration syndrome. Because of the lack of reliable biomarkers at early stages of this disease, CTE represents a significant health problem associated with disability. Using validated animal models of CTE based on rmTBI, it is possible to find prognostic biomarkers for early detection and preventive therapy of this disease. In this study, we evaluated neurological, behavioural and brain metabolic changes in animals exposed to rmTBI, focusing in the influence of sex in these differences. ***Materials and Methods:*** 20 rats aged 14-weeks (n=10 females; n=10 males) underwent 3 mTBI sessions, consisting on a free fall brass weight (450g) on the head of animals under anesthesia, with 5-days intervals between them. Sham animals without head impact were used as controls. Short- and long-term changes in weight gain, and neurological severity score (NSS) were monitored through a period of 12-weeks. Changes in anhedonic-like behaviour was measured using the Saccharin preference test (SPT) at 1-week, 2-weeks and 12-weeks after CTE induction. Open Field (OFT) and Y-maze tests to measure anxiety-like and spatial memory were performed at 12-weeks after CTE induction. [^{18}F]-FDG uptake was evaluated using regional brain VOI atlas at 1-day, 1-week, 2-weeks and 12-weeks after rmTBI. All longitudinal data was analysed using a generalized estimated equation (GEE) model, using "sex", "treatment" and "timepoint" as factors. ***Results:*** Animals exposed to rmTBI, independent from sex, showed neurological impairments compared to sham animals, present up to 12-weeks after ($p<0.01$). RmTBI exposed males showed a reduction in saccharin consumption in the SPT after 2-weeks ($p<0.01$), an effect not present in females. OFT results showed no differences in anxiety-like behaviour. However, a decrease in locomotion was found in rmTBI females only ($p<0.05$). In addition, long-term memory impairments were found in male rats exposed to rmTBI ($p<0.001$), but not in female rats. Brain regional [^{18}F]-FDG SUV_{gluc} analysis revealed an increase in brain metabolism ($p<0.05$) in the medula and frontal association cortex of rmTBI male rats at 2-weeks and 12-weeks respectively. However, a decrease of SUV_{gluc} was found instead ($p<0.01$) in the amygdala, frontal association cortex, medial prefrontal cortex, and visual cortex of female rats exposed to rmTBI. ***Conclusion:*** This study showed

sex-related short and long-term neurological, behavioural and gluco-metabolic impairments after rmTBI exposure. Correlation analysis investigating interactions between behavioural and imaging data is ongoing.

EP-0023

Longitudinal [18F]-FDG PET Characterization of Alzheimer's Disease P301S Transgenic Mice

L. García-Varela[1,2,3], *A. Custodia*[4,3], *L. Barro Rico*[1,3], *N. Gomez Lado*[1,3], *J. Codesido*[2,3,5], *A. Cuartero*[5], *A. Fernández-Ferreiro*[5], *D. Romaus Sanjurjo*[4,3], *A. Ouro*[4,3], *T. Sobrino*[4,3], *P. Aguiar*[1,2,3];
[1]*Molecular Imaging and Pharmacokinetic Modelling Group, CIMUS, USC, Santiago de Compostela, SPAIN,* [2]*Nuclear Medicine and Molecular Imaging Group, University Clinical Hospital, IDIS, Santiago de Compostela, SPAIN,* [3]*Centro de Investigación Biomédica en Red en Enfermedades Neurodegenerativas (CIBERNED), Instituto de Salud Carlos III, Madrid, SPAIN,* [4]*NeuroAging Group (NEURAL), Clinical Neurosciences Research Laboratory (LINC), IDIS, Santiago de Compostela, SPAIN,* [5]*Pharmacology Group, University Clinical Hospital of Santiago de Compostela, IDIS, Santiago de Compostela, SPAIN.*

Aim/Introduction: Although Alzheimer's Disease (AD) mouse models are valuable for studying tau accumulation throughout disease progression and testing novel treatments [1,2], conducting a thorough longitudinal characterization of these models before starting trials is crucial [3]. This study evaluated the brain glucose consumption of P301S transgenic mice throughout the development of AD pathology using [^{18}F]-FDG Positron Emission Tomography (PET). ***Materials and Methods:*** AD group consisting of P301S transgenic mice (PS19 line) (n=6) and age-matched control mice (n=3) underwent longitudinal [^{18}F]-FDG-PET/CT scans using an averaged dose of 0.23MBq/g by the tail vein. First, [^{18}F]-FDG-PET/CT scans were performed at the age of 3 months ($weight_{AD}$=18±1.05g and $weight_{control}$=21.17±0.58g), and subsequently, follow-up scans were performed at the age of 5 months ($weight_{AD}$=21.25±2.54g and $weight_{control}$=26±0.87g), 8 months ($weight_{AD}$=21.5±1.1g and $weight_{control}$=27.83±2.36g) and 11 months ($weight_{AD}$=19.3±2.08g and $weight_{control}$=30.33±2.08g). All images were processed and analyzed with PMOD v4.2 software and different Volumes of Interest (VOIs) were obtained from a mouse T2-MRI template (Ma-Benveniste-Mirrione). Standardized Uptake Values (SUV) were estimated in all the selected VOIs. Generalized Estimated Equation was used to estimate the significant changes between groups in all the PET scans and at different VOIs. ***Results:*** At 3 and 5 months of age, SUV values in the AD group were not significantly lower than the ones from the control group in any of the selected VOIs. However, at 8 months of age, SUV values of the AD group were lower than the ones of the control group in most of the selected VOIs. This decrease in the SUV was significantly different in the central gray (SUV_{AD}=1.67±0.09 vs $SUV_{control}$=2.07±0.06, p<0.001), hippocampus (SUV_{AD}=1.48±0.10 vs $SUV_{control}$=1.80±0.06, p=0.005), inferior colliculi (SUV_{AD}=1.51±0.10 vs $SUV_{control}$=1.79±0.05, p=0.017), midbrain (SUV_{AD}=1.56±0.08 vs $SUV_{control}$=1.98±0.07, p<0.001), superior colliculi (SUV_{AD}=1.58±0.10 vs $SUV_{control}$=1.90±0.05, p=0.006) and thalamus (SUV_{AD}=1.57±0.10 vs $SUV_{control}$=1.98±0.07, p=0.001). Regarding the 11 months, SUV of all selected VOIs were significantly lower in the AD compared to controls (45% reduction in whole-brain, p<0.001). Our findings are in line with the tau accumulation during AD [4], therefore decreased brain metabolism might be related to the development of AD and the gradual accumulation of tau protein in the brain. ***Conclusion:*** This study evaluates for the first time the longitudinal changes in brain glucose metabolism of P301S transgenic mice. The results showed significant differences in brain glucose metabolism in the hippocampus and thalamus already at 8 months of age, and significant differences in all the brain regions at 11 months. ***References:*** https://linkinghub.elsevier.com/retrieve/pii/S0896627316000532 https://www.frontiersin.org/articles/10.3389/fnagi.2021.761913/full https://www.mdpi.com/1422-0067/22/18/9727 https://pubs.acs.org/doi/10.1021/acschemneuro.2c00519

EP-0024

Applicability of early phase imaging with 18F-PI-2620 and 18F-Florbetaben in mouse models with Tau and Amyloid pathology

A. Englert, *L. Slemann, S. Hummel, L. Hörmann, L. Kunze, C. Palleis, K. Wind-Mark, S. Lindner, P. Bartenstein, S. Ziegler, N. Albert, J. Levin, M. Brendel, J. Gnörich;*
LMU Klinikum Campus Großhadern, Munich, GERMANY.

Aim/Introduction: Clinical studies have shown that early perfusion-weighted ^{18}F-PI-2620 scans (R1) are in no way inferior to ^{18}F-FDG-PET as a predictor of neuronal damage. This provides an immense advantage, since one single ^{18}F-PI-2620 scan can generate simultaneous information about tauburden and neuronal injury. To date however, no comparable study has yet investigated the value of tau-PET R1 in mouse models of neurodegenerative disease. Thus, we tested the applicability of early phase recordings in a PS19 tau mouse model by comparison of R1 between tracers with high (^{18}F-PI-2620) and low (^{18}F-GE-180) extraction from blood. ***Materials and Methods:*** N=16 transgenic PS19 and P301s mice with tau pathology and n=17 controls (WT mice) were investigated in this study. ^{18}F-PI-2620 (9 vs 8) and ^{18}F-GE180 (7 vs 9) scans were performed in a dynamic setting (0-60 min) with an average of 18±2 MBq using a Mediso PET/3T-MRI system. Processing of PET images was performed via PMOD. We computed R1 using simplified reference tissue modeling 2 (SRTM2) applying the striatum as a tau negative reference region. As an independent validation R1 of [^{18}F]Florbetaben-PET were correlated with striatum scaled (SUVR) quantification of [^{18}F]FDG-PET with amyloid pathology (21 vs 21). ***Results:*** R1derived from ^{18}F-PI-2620 PET indicated a significant decrease of perfusion in hindbrain regions of PS19 mice compared to wild-type mice (i.e. inferior colliculi (- 18.3%, p=0.011). Contrary, there were no relevant differences in R1 of ^{18}F-GE-180 PET between PS19 and wild-type mice. PI-2620 PET R1 showed a high agreement with [^{18}F]FDG-PET SUVR and for all brainregions obtained from Mirrione brain atlas (r=0.67, p=0.0016). ***Conclusion:*** Assessment of ^{18}F-PI-2620 delivery can be used as a surrogate of perfusion deficits in PS19 mice. Analysis of ^{18}F-GE-180 delivery in the same model served as a negative control and indicated that the use of R1 as a perfusion surrogate is specific for tracers with high blood extraction.

EP-0025

Brain Metabolic Effects of Coca-paste Acute Systemic Administration in Rats

R. Ferrando[1,2], *L. Reyes*[2], *J. Prieto*[3], *A. Paolino*[2], *A. Abin-Carriquiry*[4], *P. Oliver*[2], *E. Savio*[2], *M. Scorza*[3];
[1]*University of the Republic, Montevideo, URUGUAY,* [2]*Uruguayan Centre for Molecular Imaging (CUDIM), Montevideo, URUGUAY,* [3]*Departamento de Neurofarmacología Experimental, Instituto de Investigaciones Biológicas Clemente Estable., Montevideo, URUGUAY,* [4]*Departamento de Neuroquímica, Instituto de Investigaciones Biológicas Clemente Estable., Montevideo, URUGUAY.*

Aim/Introduction: Coca-paste (CP) is the most consumed smoked cocaine in South America and its use is mainly associated with deprived populations. In comparison with cocaine hydrochloride (CH), CP elicits a prototypical clinical profile of fast and severe dependence and impulsivity, representing a challenge for public health. In addition to the route of administration, we hypothesize that cocaine purity and the presence of active adulterants (e.g., caffeine) explain some differences between CP and CH. The aim of this study was to investigate the effect of acute CP administration on regional cerebral glucose metabolism (rCGM) in rats and compare it with that of CH. ***Materials and Methods:*** Animals were intraperitoneally injected with saline (n=9), a CP seized sample (68.9% cocaine and 15.0% caffeine) (n=8), or CH (at equivalent doses of cocaine base) (n=8). After 5 min, rats were intravenously injected with 50-74 MBq of ^{18}F-FDG, and 30 min later, they were anesthetized, and images were acquired for 60 min in a small-animal PET/CT camera. Reconstruction was performed with 3D-MLEM, and quantification was carried out using VOI analysis in PMOD and voxel-based analysis in SPM8. ***Results:*** In VOI analysis, rCGM was significantly decreased in cingulate gyrus, medial prefrontal, motor, and somatosensory cortex ($p<0.05$) of CP-treated animals compared with control and CH groups. SPM analysis showed greater cortical hypometabolism in CP administration compared to CH, as well as metabolic increases in the brain stem and cerebellum ($p<0.01$ uncorrected). ***Conclusion:*** The differences in rCGM between both treated groups can be due to an additive action of cocaine and caffeine in CP samples. Our findings can contribute to understanding the clinical profile of CP consumers.

EP-03

e-Poster Area

A: Preclinical Studies -> A1 Medical Preclinical -> A13 Preclinical Oncology

EP-0026

A study on the volume of preclinical xenograft tumours assessed by ultrasound imaging and MRI compared to calliper measurements

J. Strand[1], *C. Ceberg*[2], *M. Safi*[1], *S. Strand*[2], *F. Szczepankiewicz*[2], *D. Roth*[2];
[1]*Clinical Sciences, Oncology, Lund University, Lund, SWEDEN,*
[2]*Medical Radiation Physics, Clinical Sciences, Lund University, Lund, SWEDEN.*

Aim/Introduction: Pre-clinical models for the evaluation of response to radiotherapy include subcutaneously inoculated xenografts. The standard method for measuring the subcutaneous tumour volume is by calliper measurements directly on the skin of the animals. The length and width of the tumour are measured, the depth is assumed to be approximately the same as the width, and the volume is calculated assuming an ellipsoid geometry. However, the growth of solid tumours after radiotherapy frequently deviates from this shape. On possibility would be to use ultrasound for tumors measurement, as it enabled rapid and more accurate measurements of superficial tumor volumes. The aim of this study was to investigate the accuracy of tumour-volume measurements by calliper and ultrasound compared to MRI as standard in xenografts before and after [^{177}Lu]Lu-PSMA-617 and external radiotherapy. ***Materials and Methods:*** Seven BALB/c mice underwent treatment with 14-17 MBq of [^{177}Lu] Lu-PSMA-617. Five BALB/c mice were treated at a small-animal external-beam radiotherapy-system that delivered an absorbed dose of 10 Gy. The tumours were measured at several timepoints before and after treatment using a digital calliper, ultrasound, and MRI. For the ultrasound method, the tumour lengths, widths, and depths were measured. For the calliper method, the lengths and widths were measured, and the depths were assumed equal to the widths. For both methods, tumour-volumes were calculated assuming an ellipsoid geometry. A 9.4 T system was used for MR imaging using a RARE sequence. Volumes were calculated from manual tumour delineation. Tumour measurements by calliper and ultrasound were mostly performed separate days from MRI imaging. To compare ultrasound and calliper against MRI, linear interpolation was performed in the time-volume curves to facilitate pairwise same-day comparisons. Volume-errors were calculated for ultrasound and calliper using MRI as the reference method and assessed with Wilcoxon tests. ***Results:*** Across all ultrasound-calliper volume-pairs, the median (inter-quartile range) volume was 0.16 cm^3 (0.24 cm^3) for ultrasound, and 0.50 cm^3 (0.42 cm^3) for calliper. The median (inter-quartile range) volume-error was -0.023 cm^3 (0.087 cm^3) for ultrasound, and 0.32 cm^3 (0.26 cm^3) for calliper. Both medians were significantly different from zero, with p=0.018 (ultrasound) and p=1.1 x 10-5 (calliper), respectively. ***Conclusion:*** The present study demonstrates that measurements of subcutaneously inoculated tumour volume in mice using ultrasound exhibit significantly higher accuracy than measurements made with callipers. Accurate tumour volume estimation is important for internal radiation dosimetry, and relevant for determining the therapy effect on tumour volume.

EP-0027

Construction and Preclinical Evaluation of a 68Ga-Labeled Single-chain Fragment Variable Targeting PD-L2 in Lung Cancer

Y. Yao, *N. Li;*
Peking university cancer hospital, Beijing, CHINA.

Aim/Introduction: Programmed cell death-Ligand 1 (PD-L2), a ligand programmed cell death protein 1 (PD-1), is an immune checkpoint molecule closely related to the efficacy of immune checkpoint inhibitor therapy (ICI). The aim of this study is to design a novel tracer ^{68}Ga-NOTA-scFvE6 targeting PD-L2 and perform preclinical evaluation to dynamically monitor PD-L2 expression and screen potential beneficiaries of ICI therapy. ***Materials and Methods:*** A human single-chain fragment variable (scFv) was generated by phage display and the selected scFv was expressed by prokaryotic expression system. ^{68}Ga-labeling of NOTA-conjugated scFvE6 was carried out in NaAc-buffer at pH 4 (37°C, 10min). In vitro stability was analyzed using Radio-thin layer chromatography (Radio-TLC). The affinity of the scFvE6 were evaluated by Radio-ELISA. Pharmacokinetic experiments were used to evaluate the metabolic characteristics in vivo. Cellular uptake assays were performed using the transduced PD-L2 expressing lung cancer cell line A549 (A549-PD-L2) and wild-type A549 cells as negative control. The biodistribution experiment was used to detect the in vivo distribution of the tracer and the dosimetry estimation was conducted based on the results. Micro-PET/CT imaging was conducted with ^{68}Ga-NOTA-scFvE6 and static images were recorded at 1 h and 2 h p.i. Immunohistochemical and HE staining studies were carried out using the tumor tissue of tumor-bearing mice. ***Results:*** The radiochemical yields of ^{68}Ga-NOTA-scFvE6 were 42.76±2.37%

and the radiochemical purity (RCP) of the tracer was more than 99%. The tracer incubated in 0.01 M PBS and 5% HSA maintained relatively high stability (RCP>95%). Radio-ELISA showed that ^{68}Ga-NOTA-scFvE6 had a high affinity for the PD-L2 protein (Kd = 21.10 nM). The half-lives of the distribution phase and elimination phase were 4.136 and 43.42 min, respectively. Cellular uptake experiments confirmed that the uptake of ^{68}Ga-NOTA-scFvE6 in A549-PDL2 cells was higher than that in A549 cells at each time point. The dosimetry estimation by using Olinda software showed that the effective dose was 2.46E-02 mSv/MBq. Micro-PET/CT showed significant uptake in the tumor region of A549-PDL2 tumor-bearing mice at 1h and 2h post-injection (SUVmax = 0.75 ± 0.02 and 0.85 ± 0.06). Immunohistochemistry showed that A549-PDL2 was highly expressed in A549-PDL2 mice. ***Conclusion:*** ^{68}Ga-NOTA-scFvE6 enables easy radiosynthesis and shows excellent in vitro and in vivo PD-L2 targeting characteristics. The high tumor uptake at early imaging time points demonstrates the feasibility of ^{68}Ga-NOTA-scFvE6 for imaging of PD-L2 expression in tumors and is encouraging for further clinical applications of screening potential beneficiaries.

EP-0028

Preparation and evaluation of Evans blue modified aptamer probe targeting to EpCAM

M. Zhang, *J. Ye, Z. Xie, W. Yang, F. Kang, J. Wang;*
Department of Nuclear Medicine, Xijing Hospital, Fourth Military Medical University, Xi'an, CHINA.

Aim/Introduction: Epithelial cell adhesion molecule (EpCAM) is a potential target for early diagnosis of tumors. SYL3C, as a DNA nucleic acid aptamer, is a specific ligand for EpCAM. However, due to the fact that the nucleic acid aptamer is easy to be degraded by nuclease in vivo, which results in problems such as poor stability, short half-life of blood circulation and poor metabolism of aptamer. In order to solve the above problems, this study intends to connect the truncated Evans blue (EB) to SYL3C, through which albumin can be carried on, thus the in vivo stability and metabolism of SYL3C could be improved, and due to the enhanced permeability and retention (EPR) effect the tumor uptake could be further increased. ***Materials and Methods:*** NMEB-SYL3C and NOTA-SYL3C were synthesized and labeled with ^{68}Ga. The stability of ^{68}Ga-NMEB-SYL3C and ^{68}Ga-NOTA-SYL3C in PBS and mouse serum was investigated, respectively. Cell uptake studies of the two tracers were performed in EpCAM strongly positive cells (4T1) and negative cells (293T), respectively. PET imaging studies of the two tracers were carried out in the tumor mice bearing 4T1 at different time points. ***Results:*** The radiochemical purity of ^{68}Ga-NMEB-SYL3C and ^{68}Ga-NOTA-SYL3C was both more than 98% after purification. ^{68}Ga-NMEB-SYL3C can be stable in PBS and mouse serum for 2 hours, while only about 60% and 80% of ^{68}Ga-NOTA-SYL3C was intact in PBS and mouse serum at 1 h, respectively. The uptake of ^{68}Ga-NMEB-SYL3C in 4T1 cells was slightly lower than that of ^{68}Ga-NOTA-SYL3C, indicating that the EB modification could somewhat decrease the affinity of SYL3C to EpCAM. However, the cell uptake studies also showed that the total binding and internalization of ^{68}Ga-NMEB-SYL3C in 4T1 cells were significantly higher than those in 293T cells, which suggested that although EB modification affected the affinity of SYL3C to EpCAM, the affinity and specificity of ^{68}Ga-NMEB-SYL3C to EpCAM was still high enough. The PET imaging results showed that ^{68}Ga-NOTA-SYL3C cleared fast in mice within 5 min p.i., and there was no tumor uptake at all. Meanwhile, the results of ^{68}Ga-NMEB-SYL3C showed that the tumor could be clearly observed at 0.5 h p.i., with the uptake value gradually increased over time, and reached the highest level of 5% ID/g at 3 h p.i. ***Conclusion:*** Preliminary results showed that EB modification can effectively improve the stability and metabolic kinetics of SYL3C in vivo, and thus significantly enhance the uptake in tumor.

EP-0029

Evaluation of a Long-circulating PSMA-targeting Peptide in a Xenograft Model of Bone Metastatic Prostate Cancer.

W. Lo, *Y. Huang, M. Chen, A. Lu, S. Wang, L. Chen, S. Farn;*
Institute of Nuclear Energy Research, Taoyuan, TAIWAN.

Aim/Introduction: Prostate-specific membrane antigen (PSMA) is a target for prostate cancer given its increased expression on the surface of the prostate cancer cells. In our previous study, we synthesized a novel PSMA-targeting peptide named PSMA-INER-56, which demonstrates prolonged biological half-life, high tumor accumulation and therapeutic efficacy. The objective of this study is to assess the therapeutic efficacy and biodistribution of ^{177}Lu-PSMA-INER-56 in a xenograft model of bone metastatic prostate cancer. ***Materials and Methods:*** PSMA-INER-56 was radiolabeled with ^{177}Lu and ^{111}In, respectively, and analyzed using radio-TLC and HPLC. A xenograft model of bone metastases was established in NOD/SCID mice by intra-femoral injection of PSMA-positive prostate cancer cell line, LNCaP cells, mixed with Matrigel in a 1:1 ratio, with a total of 50,000 cells. For therapeutic efficacy assessment, the animals were treated with 29.6 MBq of ^{177}Lu-PSMA-INER-56, and the tumor volume and distribution of the radiopharmaceutical were monitored using SPECT/CT imaging. Furthermore, to confirm the therapeutic effect on day 28 post-administration, 18.5 MBq of ^{111}In-PSMA-INER-56 was utilized. ***Results:*** The labeling efficiency and radiochemical purity of both ^{177}Lu-PSMA-INER-56 and ^{111}In-PSMA-INER-56 were found to be above 95%, with retention times of 9.39 and 9.43 minutes, respectively. After 49 days of intra-femoral injection of LNCaP cells, the animal model with bone metastases was treated with a single administration of 29.6 MBq of ^{177}Lu-PSMA-INER-56. The SPECT/CT imaging of ^{177}Lu-PSMA-INER-56 revealed a tumor uptake of 18.8 %ID/g at 24 hours post-administration, and this high accumulation persisted up to 192 hours, with a remaining uptake of 19.7 %ID/g. Meanwhile, the tumor size gradually decreased from the initial measurement of 2.7 cm to 1.5 cm. At day 30 post-administration of ^{177}Lu-PSMA-INER-56, diagnostic radiolabeled ^{111}In-PSMA-INER-56 was used for therapeutic efficacy monitoring. SPECT/CT imaging revealed persistent high accumulation of the radiotracer in the tumor with a concentration of 20.0 %ID/g. Additionally, the tumor size decreased to 0.84 cm, suggesting a positive therapeutic response to the treatment with ^{177}Lu-PSMA-INER-56. ***Conclusion:*** In conclusion, the use of ^{177}Lu-PSMA-INER-56 in a xenograft model of bone metastatic prostate cancer showed promising results in terms of therapeutic efficacy. The radiopharmaceutical's high labeling efficiency, purity, and tumor accumulation, combined with its long-circulating properties, indicate its potential as an effective targeted therapy. ***References:*** Li, MH., Lo, SN., Chen, MW. et al. Molecular Imaging for Radiolabeling a PSMA-Targeted Long Circulating Peptide as a Theranostic Agent in Mice Bearing a Human Prostate Tumor. J. Med. Biol. Eng. 41, 360-368 (2021).

EP-0030

Goat milk-derived extracellular vesicle engineered for multimodal imaging of cancer stem cells

Y. Gao, *Y. Zhang, X. Lan, R. An;*
Wuhan Union Hospital, Wuhan, CHINA.

Aim/Introduction: Colon cancer is one of the most common malignant tumors, with the fourth highest number of deaths due to cancer. CD44 is a common marker expressed on cancer stem cells (CSCs) from colon cancer, which can specifically bind to

hyaluronic acid (HA). In this study, goat milk-derived extracellular vesicle (GEV) where HA was modified to target CD44 was used as a nanoprobe to trace colon cancer stem cells, hoping to carry out PET/CT imaging of colon cancer stem cells in vivo. ***Materials and Methods:*** GEV was isolated from fresh goat milk by differential centrifugation, and then DSPE-PEG-N_3 and DSPE-PEG-HA were co-incubated with GEV to form N_3-GEV-HA. The nanoprobe were characterized by transmission electron microscope and dynamic light scattering. Confocal microscopy was used to determine the ability of the probe to bind to colon cancer cells. N_3-GEV-HA was injected into the subcutaneous model of colon cancer in mice through tail vein, and near infrared fluorescence (NIRF) imaging was performed at different time points to determine the best time for pre-targeting strategy. This strategy enables the probe to circulate fully in the body and accumulate in the tumor tissue and then use short half-life radionuclides for PET/CT imaging. N_3-GEV-HA was injected into mouse colon cancer model HT29 (high expression of CD44) and DLD1 (low expression of CD44) at the best pre-targeted time points. One hour and two hours after injection of ^{68}Ga-L-NETA-DBCO, which can bind to N_3, the anesthetized mice were subjected to pre-targeting static imaging of miniature PET/CT based on "click chemistry". ***Results:*** GEV was successfully isolated from goat milk and modified. The lipid bilayer structure of the probe was confirmed by transmission electron microscope. Confocal experiment showed that the binding ability of N_3-GEV-HA to HT29 tumor cells was stronger than that of DLD1. NIRF images showed that the fluorescence signal of the tumor site in the active targeting group (HT29 with N_3-GEV-HA) was the strongest compared with the passive targeting group (HT29 with N_3-GEV) and the control group (DLD1 with N3-GEV-HA), and the fluorescence signal was the strongest at 24 hours. The PET/CT images in vivo also showed the same imaging results. No obvious signs of injury were found in the main organs of rats in each group. ***Conclusion:*** The study demonstrated that the CD44-targeted nanoprobe N_3-GEV-HA can specifically target to colon CSCs and achieve high quality PET/CT/NIRF imaging. It has a broad prospect of clinical translation.

EP-0031

Porphyrin-modified strategy contributes to aptamers' tumor targeting

S. Yang, *X. Lan, D. Jiang;*
Wuhan Union Hospital, Tongji Medical College, Huazhong University of Science and Technology, Wuhan 430022, China, Wuhan, CHINA.

Aim/Introduction: Single-stranded DNA (ssDNA) has the advantages of easy preparation and modification, high stability in vitro, and excellent biocompatibility compared with traditional drugs. It has been developed into various nucleic acid drugs, especially aptamers, which can specifically bind to corresponding tumor targets and have broad prospects for clinical translation. But the extremely rapid renal clearance greatly limits its application in tumor-targeted imaging and therapy. In this study, ssDNA was modified with a second-generation porphyrin photosensitizer (PPR), to significantly prolong its blood circulation and successfully overcome pharmacokinetic defects in tumor-targeted imaging of aptamers. ***Materials and Methods:*** All amine group modified ssDNA sequences were conjugated with PPR by amide condensation. A series of sample oligonucleotides with different base lengths were modified with PPR (including PPR-A20, PPR-A40, PPR-A60, and PPR-A80) and characterized by UV-Vis, fluorescence spectrum, mass spectrum, and high performance liquid chromatography (HPLC). By using PPR as a radiometal chelator, PPR-ssDNA were labeled with ^{68}Ga in hydrochloric acid/sodium acetate buffer. All four ^{68}Ga-PPR-ssDNAs were injected into healthy mice intravenously. Their blood circulation was calculated through microPET/CT images and was compared with unmodified ssDNA to determine the pharmacokinetic effects of the PPR modification method. Murine models of CT26 colon carcinoma were further used to test the tumor imaging capacity of PPR-ssDNA in vivo. ***Results:*** In this study, PPR was successfully modified on the amino terminal of ssDNA. UV absorption spectrum showed that the products had characteristic absorption peaks of ssDNA and PPR at 260 nm and 405 nm, respectively, and mass spectrum confirmed the successful synthesis. PET images and biodistribution studies in healthy mice showed significantly extended blood circulation of all four PPR-ssDNA when compared with unmodified counterparts, where PPR-A60 displayed the best blood retention at 29.16±1.19 %ID/g at 2 h post injection, 60 fold higher than ^{68}Ga-A20 (0.5 %ID/g). PET imaging of CT26 colon carcinoma mice showed PPR-A60 displayed 3.1± 0.72%ID/g tumor uptake at 2 h after injection. ***Conclusion:*** The one-step PPR modification strategy has greatly overcome the pharmacokinetic defects of ssDNA. Our PET imaging further confirmed excellent tumor imaging of PPR-A60 in colon tumor-bearing mice. Given PPR is a FDA-approved photosensitizer, we strongly believe that PPR-modified aptamers can improve the tumor targeting/therapeutic effect of aptamers and have excellent clinical application prospects.

EP-0032

Tumours inducing cachexia driven by Fn14 show enhanced 18F-FDG uptake in mice versus tumours that do not induce cancer cachexia: a quantitative PET analysis

I. Burvenich[1,2], *L. Osellame*[1,2,3], *A. Rigopoulos*[1], *N. Hoogenraad*[3], *A. M. Scott*[1,2,4];
[1]*Olivia Newton-John Cancer Research Institute, Heidelberg, AUSTRALIA,* [2]*School of Cancer Medicine, La Trobe University, Bundoora, AUSTRALIA,* [3]*Department of Biochemistry and Genetics, La Trobe Institute for Molecular Science, La Trobe University, Bundoora, AUSTRALIA,* [4]*Department of Molecular Imaging and Therapy, Austin Health, Heidelberg, AUSTRALIA.*

Aim/Introduction: Cachexia is a complex syndrome characterized by unintentional weight loss, progressive muscle wasting and loss of appetite. The anti-Fn14 antibody (002) targets the TWEAK receptor (Fn14) and can extend the lifespan of mice by restoring the body weight of mice[1]. Previously, we have shown that ^{18}F-FDG PET imaging demonstrates increased glucose uptake over time in syngeneic tumour models that induce cachexia versus tumours that do not induce cachexia. Here we investigate ^{18}F-FDG uptake in tumours of an Fn14 knock-out variant of the cachexia-inducing C26 tumour model (C26 Fn14 KO), and response to therapy with anti-Fn14 antibody 002 and perform quantitative PET analysis. ***Materials and Methods:*** At 1 hour after ^{18}F-FDG (14.8 MBq) tail vein injection, ^{18}F-FDG PET/MRI imaging was performed in cachexia-inducing tumour models [MEF-Fn14 and C26 tumour-bearing Nod SCID gamma (NSG) mice] versus models that do not induce cachexia (MEF, C26 tumour-bearing mice treated with 002 (10 mg/kg) and C26 FN14 KO tumour-bearing NSG mice). All animals were fasted for 3 hours prior to ^{18}F-FDG injection and kept on a heat pad during the experiment. $SUV_{average}$ was calculated for all tumours via VOI analysis of PET/MRI overlay images using PMOD software. ***Results:*** ^{18}F-FDG PET imaging demonstrated increased glucose uptake in cachectic MEF Fn14

versus non-cachectic MEF tumour-bearing mice ($SUV_{average}$ MEF Fn14, 3.3 ± 0.6; % maximum body weight, 74.06 ± 1.43 versus $SUV_{average}$ MEF, 1.0 ± 0.1; % maximum body weight, 94.91 ± 2.84, (n = 2)). Therapy with 002 was able to reduce ^{18}F-FDG uptake in C26 tumours ($SUV_{average}$ of C26 treated with vehicle control, 2.1 ± 0.3; $SUV_{average}$ of C26 treated with 002, 1.3 ± 0.3; P < 0.05, n = 3). C26 Fn14 KO tumours did not induce body weight loss and did not show an increase in ^{18}F-FDG tumour uptake over time. In non-cachectic mice bearing C26 Fn14 KO tumours, ^{18}F-FDG tumour uptake was significantly lower (P < 0.01) (SUVaverage, 0.70 ± 0.09; % maximum body weight, 96.66 ± 0.85; n = 5) than in cachectic mice bearing C26 Fn14 WT tumours (SUVaverage, 1.73 ± 0.72; % maximum body weight, 87.33 ± 6.96; n = 9). ***Conclusion:*** Our results demonstrate that the Fn14 receptor activation is linked to glucose metabolism of cachexia-inducing tumours. A clinical trial with ^{18}F-FDG PET in cachectic patients is currently ongoing. ***References:*** [1]Johnston AJ, et al. Targeting of Fn14 Prevents Cancer-Induced Cachexia and Prolongs Survival. Cell. 2015;162(6):1365-78.

EP-0033

89Zr-anti-murine CD103 PET imaging for non-invasive assessment of immune checkpoint inhibitor therapy

X. Fan, *N. P. Holland, A. Plat, H. W. Nijman, P. H. Elsinga, M. d. Bruyn;*
University of Groningen, Groningen, NETHERLANDS.

Aim/Introduction: The lack of a reliable biomarker to predict the treatment efficiency has hindered the promotion and application of Immune checkpoint inhibitors therapy. $CD103^+$ cells, as shown in multiple clinical studies, are significantly increased during successful immunotherapy across human malignancies, showing its potential to be a biomarker to predict the effect of therapy. ***Materials and Methods:*** ^{89}Zr-anti-murine tracer was developed and tested in mouse model for the feasibility of CD103 PET imaging. To further explore the behavior of the tracer in vivo, Balb/c and C57bl/6 mice were injected with various doses of ^{89}Zr-anti-murine CD103 tracer and ^{89}Zr-isotype control tracer and were scanned multiple times followed by ex vivo bio-distribution. To investigate the potential of CD103 PET-imaging for therapy monitoring MC38 tumor-bearing C57BL/6 mice were treated with a series of dual checkpoint inhibitors. CD103 PET imaging was performed after treatment to assess tumoral uptake of the tracer, and tumor volume changes were subsequently monitored to determine response. ***Results:*** A novel anti-murine CD103 mAb tracer was successfully developed and validated in a healthy mouse model. In both animal models, ^{89}Zr-anti-murine CD103 tracer shows a higher specific uptake in CD103+ cell-rich gastrointestinal tract compared to the control tracer. Ex vivo bio-distribution data further demonstrated that compared to the control tracer, there was a significantly higher tracer uptake in the small intestine, mesenteric lymph nodes, and axillary LNs. In the treatment study, all mice responded to treatment (7/7) and tumor size was significantly reduced after treatment. However, there was no difference of CD103 tracer uptake in tumors compared to isotype tracers, either with or without treatment. ***Conclusion:*** We developed and validated a novel mouse CD103 ImmunoPET tracer, providing a new tool for preclinical studies to help understand the systemic bio-distribution of the tracer and the mechanism of action of CD103+ cells in the tumor microenvironment. However, within the syngeneic mouse tumor model, there was no significant difference between the control tracer and the CD103 tracer. Due to the fact that MC38 bearing mouse model is a transplanted tumor, compared to the real human situation, tumor takes way shorter time to grow and accumulate the immune reaction. Moreover, the CD103+ tumor infiltrating cell T-cell population belongs to the tissue resident memory T-cell subpopulation, its infiltration at the tumor site may take more time. By using such syngeneic tumor model, we may not be able to observe changes in this unique subpopulation.

EP-0034

In vivo testing of a novel anti-B4GALNT1 nanobody as a potential theragnostic tool for osteosarcoma tumors.

M. Collantes[1], *N. Mendoza*[2], *J. Simón*[3], *F. Pareja*[3], *M. Ecay*[1], *G. Quincoces*[3], *M. García-Moure*[4], *A. J. Schuhmacher*[2], *I. Peñuelas*[3];
[1]*Translational Molecular Imaging Unit (UNIMTRA), Nuclear Medicine Department, Clínica Universidad de Navarra, Pamplona, SPAIN,* [2]*Instituto de Investigación Sanitaria Aragón, Zaragoza, SPAIN,* [3]*Radiopharmacy Unit, Department of Nuclear Medicine, Clinica Universidad de Navarra, Pamplona, SPAIN,* [4]*Solid TumorsProgram, CIMA-Universidad de Navarra, Pamplona, SPAIN.*

Aim/Introduction: Beta-1,4,N-acetylgalactosaminyltransferase-1 (B4GALNT1) is an enzyme involved in the biosynthesis of G(D2) glycosphingolipid and widely expressed by paediatric solid tumors, including osteosarcoma (OS). We have herein radiolabelled a nanobody designed to detect B4GALNT1+ tumors and investigated its use as a potential theragnostic tool. ***Materials and Methods:*** The nanobody (14 KDa, 80µg) was radiolabelled with 700 MBq of [99mTc][Tc(CO)3(H2O)3]+ using Isolink™ kits and the radiolabeled product purified by size exclusion chromatography. The binding specificity of the ^{99m}Tc-nanobody was tested in vitro by incubating B4GALNT1+ and B4GALNT1- cell lines and measuring the cell-bound radioactivity in a gamma counter. In vivo microSPECT/CT studies were performed in three different mouse models: 1) A xenograft model (n=6) with B4GALNT1(+) and B4GALNT1(-) tumors implanted in contralateral flanks was imaged at 0.5,2,4h after ^{99m}Tc-nanobody i.v. injection. Additionally, ex vivo measurement of radioactivity in relevant tissues was performed at 4h. 2) An orthotopic model of OS (n=4) and 3) a lung metastasis model of OS (n=4) were created injecting a patient-derived osteosarcoma cell line in tibial plateu or intravenously respectively. In both OS derived mouse models, the diagnostic performance of ^{99m}Tc-NBody as compared to ^{18}F-FDG was studied by simultaneous microSPECT/microPET/CT imaging. ***Results:*** Radiolabeling yield was> 80%, and radiochemical purity >97% after purification. In vitro studies demonstrated a specific uptake of the ^{99m}Tc-nanobody in B4GALNT1(+) cells (p<0.005, ANOVA). The in vivo images in xenograft model showed a rapid and greater uptake in B4GALNT1(+) tumors as compared to B4GALNT1(-) ones at 30m p.i. (1.7±0.34 %ID vs. 0.20±0.07; 2-way ANOVA, p<0.0001) that didn't change over time (2-way ANOVA, p=0.208). Biodistribution images showed fast renal excretion at 0.5h and minimal uptake in other organs, confirmed by ex vivo measurements at 4h (kidney:78.8±12.5% ID/g, brain:0.07±0.01%ID/g, muscle:0.26±0.03%ID/g). The diagnostic performance of the ^{99m}Tc-nanobody was clearly superior to ^{18}F-FDG in the orthotopic model of osteosarcoma with a higher SUVratio respect contralateral hindlimb (^{99m}Tc-nanobody:4,26±1,7 vs. ^{18}F-FDG:0,93±0.5; t-test p<0.05). In the lung metastasis model, ^{18}F-FDG didn't detect any tumors, while the ^{99m}Tc-nanobody was able to detect numerous metastasis confirmed by histopathological analysis. ***Conclusion:*** [99mTc][Tc(CO)3(H2O)3] radiolabeling of nanobodies is an effective technique for the quantitative study of their specificity, kinetics and biodistribution. This new designed nanobody against B4GALNT1 antigen could be a promising tool to be used in diagnosis and treatment of B4GALNT1(+) tumors like osteosarcoma.

EP-0035

Development of neurotensin analogues stabilized by Lys8-Lys9 reduction and linker modifications

C. Morgat[1,2], *S. Previti*[3], *S. Bodin*[1,2], *L. Balasse*[4], *E. Rémond*[3], *P. Garrigue*[4], *F. Debordeaux*[1], *B. Guillet*[4], *F. Lamare*[2], *D. Vimont*[2], *E. Hindié*[1,2], *F. Cavelier*[3];
[1]*Nuclear Medicine Department - University Hospital of Bordeaux, Bordeaux, FRANCE,* [2]*University of Bordeaux, CNRS, EPHE, INCIA, UMR 5287, Bordeaux, FRANCE,* [3]*Institut des Biomolecules Max Mousseron, IBMM, UMR 5247, CNRS, Université de Montpellier, ENSCM, Montpellier, FRANCE,* [4]*CERIMED, Aix-Marseille University, Marseille, FRANCE.*

Aim/Introduction: Neurotensin receptors are G-protein-coupled receptors expressed in several cancers, often so in subsets of patients with aggressive/advanced disease. We have previously developed JMV6659 (DOTA-APAC-Lys-Lys-Pro-Tyr-Ile-TMSAla-OH), a neurotensin analogue targeting neurotensin receptor-1 (NTS_1). In this work we aimed at optimizing this lead compound in terms of selectivity and stability. ***Materials and Methods:*** APAC linker was replaced with $(\beta ala)_2$ in JMV7222; Lys-Lys was reduced in JMV7259; while JMV7258 combines the two modifications. The compounds were radiolabeled with ^{68}Ga and studied in vitro. The most promising compound was subjected to µPET/CT imaging. HT-29 cells were used. ***Results:*** All analogues displayed nanomolar affinity (~5nM) towards NTS_1 and good selectivity (> 100). Internalization was high at 1h (~60% of cell-associated radioactivity) with low membrane binding (~15%). [^{68}Ga]Ga-JMV7222, [^{68}Ga]Ga-JMV7259 and [^{68}Ga]Ga-JMV7258 showed improved plasma stability compared to [^{68}Ga]Ga-JMV6659. [^{68}Ga]Ga-JMV7258 has the highest stability at 45 min (85%). All analogues were highly externalized (up to 70% at 45 min), much more than [^{68}Ga]Ga-JMV6659. Following injection of [^{68}Ga]Ga-JMV7258 in nude mice bearing HT29-tumor, kidneys showed the highest uptake (33.6±14.7%ID/g at 2h), which was significantly displaced by SR48692, a NTS_1-antagonist (14.1±4.3 %ID/g, p<0.0001). Surprisingly, HT29 xenografts showed only weak uptake (1.53±0.45 %ID/g at 2h) which was only partially displaced by SR48692 (1.11±0.29 %ID/g). We noticed that all our newly developed analogues suffered from high and fast efflux. Moreover, they displayed lower binding to neurotensin receptor-2 (NTS_2) than [^{68}Ga]Ga-JMV6659. Importantly, following NTS_2-prestimulation in vitro with 1µM levocabastine (a selective agonist of NTS2), the efflux of [^{68}Ga]Ga-JMV7258 was decreased becoming similar to [^{68}Ga]Ga-JMV6659 (~40%). Also, in vivo, uptake was 2.5-fold higher when levocabastine was added. For mechanistic studies, both NTS_1 and NTS_2 blocking was tested and uptake was not significantly decreased (p=0.095) suggesting that an NTS_1-independent pathway exists to allow the entrance of NTS_1 analogues. This is supported by the signal recorded when stimulation of NTS_2 by levocabastine was applied after NTS_1 blocking and led to a significantly higher tumor uptake than in experiment with NTS_1 blocking alone (p<0.0001). All mice injected with levocabastine had high kidney uptake and did not eliminate [^{68}Ga]Ga-JMV7258. ***Conclusion:*** This work provides new insights in neurotensin receptor physiology and targeting. First, a low efflux is needed to expect high NTS_1-uptake; second, NTS_2 stimulation increases the intracellular retention of NTS_1-selective analogues suggesting the presence of NTS_1/NTS_2 heterodimers; third: murine kidneys express NTS_2; fourth: NTS_2 binding and efflux are mandatory parameters to investigate when developing NTS_1-analogues.

EP-0036

In vivo evaluation of luteinizing hormone-releasing hormone antagonists in triple negative breast tumor-bearing model by using SPECT/CT imaging

M. Weng*, S. Farn;*
Institute of Nuclear Energy Research, Taoyuan City, TAIWAN.

Aim/Introduction: Triple negative breast cancer (TNBC) that is lack of diagnostic and effective therapeutic agents was clinically considered a subtype with low survival rate of human breast cancer patients. As we know, probes or drugs specific for receptors of luteinizing hormone-releasing hormone (LHRH-R), which is reported as potential targets for TNBC, are still under investigation as yet. In previous study, we have evaluated an peptidic abarelix-based antagonist, DOTA-LHRH, which revealed specific uptake in TNBC tumors. In this research, a cetrorelix-based antagonist, DOTA-LHRH-C, has been newly developed and also proved an effective strategy for in vivo uses by SPECT/CT imaging. ***Materials and Methods:*** The LHRH antagonist was first conjugated with a DOTA chelator; after radiolabeled with In-111, the radiochemical purity (R.C.P.) was analyzed by a radio-TLC system. The TNBC cell, HCC 1806, were incubated and subcutaneously inoculated on ASID mice. After intravenous (i.v.) injection of ^{111}In-DOTA-LHRH-C, HCC 1806-bearing mice were anesthetized and imaged at 1, 4 and 24 h by a SPECT/CT, respectively. The bio-distribution test of ^{111}In-DOTA-LHRH in HCC 1806-bearing mice was also investigated at 1, 4 and 24 h, respectively. ***Results:*** The R.C.P. of ^{111}In-DOTA-LHRH-C was determined >90% by radio-TLC. The SPECT/CT imaging data showed that ^{111}In-DOTA-LHRH-C was first collected in liver, kidney and tumors and retained in those within 24 h. In results of bio-distribution, ^{111}In-DOTA-LHRH-C was mainly collected in lung, kidney, liver and HCC 1806 tumors at 1, 4 and 24 h. The tumor-to-muscle count ratio (T/M) is calculated as 2.18 ± 0.68 and the tumor-to-brain count ratio (T/B) is 4.33 ± 1.05 at 24 h, respectively; it also demonstrates similar results in comparison with those of DOTA-LHRH. (T/M was 3.88 ± 0.34 and T/B is 17.23 ± 0.25 at 24 h, respectively.) ***Conclusion:*** This research has evaluated the characteristics of a cetrorelix-based antagonist for LHRH-R over-expressive tumors in vivo. We suggested that DOTA-LHRH-C for further diagnostic research and comparison with DOTA-LHRH in vitro and in vivo. We think they may provide innovative information for development of TNBC patient's treatment strategies in the future in Taiwan.

EP-0037

Enhancing PSMA-RLT efficacy with STING agonist in syngeneic models of prostate cancer

B. Louis[1,2], *M. Taddio*[1,2], *K. Rashid*[1,2], *E. Abt*[1,2], *E. Rosser*[1,2], *T. Le*[1,2], *K. Lueckerath*[3,4], *C. Radu*[1,2], *J. Czernin*[1,2], *C. Mona*[1,2];
[1]*University of California at Los Angeles, Department of Molecular and Medical Pharmacology, David Geffen School of Medicine, Ahmanson Translational Theranostics Division, Los Angeles, CA, UNITED STATES OF AMERICA,* [2]*Jonsson Comprehensive Cancer Center, Los Angeles, CA, UNITED STATES OF AMERICA,* [3]*Department of Nuclear Medicine, University Hospital Essen, Essen, GERMANY,* [4]*German Cancer Consortium–University Hospital Essen, Essen, GERMANY.*

Aim/Introduction: Results from the VISION phase 3 clinical trial showed that ^{177}Lu-PSMA-617 radioligand therapy (RLT) led to reduction in serum prostate specific antigen levels and improved survival in disease progression[1]. There is therefore an urgent unmet need to identify mechanisms that can enhance and prolong the efficacy of RLT. Emerging combination approaches are exploring

synergies between immunotherapy and radiation. STimulator of INterferon Genes (STING) is an interesting target for anticancer therapy because of its role in immune activation. This pathway is triggered by cytosolic dsDNA ultimately leading to type I interferon (IFN) production and immune cells activation[2]. Based on this, we tested a combination regimen consisting of PSMA-RLT and STING agonist (diABZI) in two PCa cell lines. ***Materials and Methods:*** Relative expression of IFN-related genes was assessed in vitro by qPCR in RM1-PGLS and Myc-CaP cells after exposure to vehicle, diABZI (1uM) or irradiation (8Gy). C57BL/6 or FVB mice were subcutaneously inoculated with 0.1 x 10^6 RM1-PGLS or 2 x 10^6 Myc-CaP-hPSMA cells in 100 µl PBS/Matrigel (1:1). PSMA expression was quantified in vivo by PET/CT 1h after i.v. administration of 1.1 MBq 68Ga-PSMA-617. Tumor-bearing mice were treated with 40kBq ^{225}Ac-PSMA-617 or diABZI alone (1.5 mg/kg), at a tumor volume of 75.4±34.6mm^3 for RM1-PGLS and 133.9±20.8mm^3 for Myc-Cap-hPSMA. The following day, mice in the combination group received diABZI while control and RLT mice received vehicle (PEG400, 40% in NaCl). Therapeutic efficacy (4 groups, n=12) was assessed by survival and tumor CT volumetry. ***Results:*** In vitro qPCR analysis of IFN-related genes showed that diABZI increased IFNβ expression in RM1-PGLS by 150-fold while Myc-CaP cells showed no response. In vivo, systemic diABZI combined with PSMA-RLT produced significant tumor growth control in the RM1-PGLS model and major improvement in survival. At day 20 following treatment, the mean tumor volume for control mice was 1.723±0.807cm^3 compared to 0.167±0.229cm^3 for RLT, 0.165±0.218cm^3 for diABZI, and 0.061±0.035cm^3 for the combination group. Tumor-free survival rates at day 75 were: control 0%, RLT 42%, STING agonist 67% and combination 100%. ***Conclusion:*** qPCR analysis of IFN-related genes showed a binary profile in the two PCa cell lines. Efficacy study in RM1-PGLS showed that the combination led to a better survival and highlighted the impact of such combination and value in increasing type 1 IFN production. Confirmatory results in the STING-non responsive cell line are ongoing. ***References:*** [1]Sartor et al., N Engl J. Med, 2021 [2]Deng et al., Immunity, 2014.

EP-0038

[18F](2S,4R)4-Fluoroglutamine illustrates ability to distinguish KRAS mutation in pancreatic carcinoma

S. Liu, *F. Liu, X. Xu;*
Peking University Cancer Hospital, Beijing, CHINA.

Aim/Introduction: KRAS is a crucial member of the RAS family, and plays a vital role in regulating various life processes of cell growth, such as proliferation, differentiation, apoptosis, etc. Approximately 90% of pancreatic ductal adenocarcinomas carry KRAS mutations, which are classified as driver mutations and lead to unbridled proliferative features of the cancer. Precision treatment for pancreatic cancer could improve prognosis and prolong survival for patients. As KRAS-driven cancer cells are highly dependent on glutamine, this study aims to identify the G12D and G12C mutations in KRAS using [^{18}F](2S,4R)4-Fluoroglutamine ([^{18}F]F-Gln) ***Materials and Methods:*** [^{18}F]F-Gln was radiolabeled through two-step radiosynthesis reported in a previous study. Mice model bearing tumor were establish to test its effectiveness, including PANC1 and MIA-PaCa-2 mice xenografts. Polymerase Chain Reaction was used to verify mutations in these tumors and cells. ***Results:*** The Polymerase Chain Reaction was used to detect mutations in PANC1 and MIA-PaCa-2 cells/tumors, which exhibited G12D and G12C mutations, respectively. In micro-PET/CT imaging, [$_{18}$F]F-Gln demonstrated significant uptake in PANC1 mice xenografts when compared with MIA-PaCa-2 mice xenografts. After outlining the tumor, the SUVmax value in PANC1 tumors was significantly higher than in MIA-PaCa-2 tumors (1.05 ± 0.01 vs 0.46 ± 0.06 at 30 min, 0.92 ± 0.05 vs 0.37 ±0.07 at 60 min, and 0.62 ± 0.10 vs 0.33 ± 0.05 at 120 min). Furthermore, the uptake of [^{18}F]F-Gln in tumors was highest at 30 min in both mouse models ***Conclusion:*** [^{18}F](2S,4R)4-Fluoroglutamine probe has the potential to non-invasively identify the mutation type and status of KRAS in vivo through whole-body PET imaging. This could provide precision diagnosis and prediction for pancreatic carcinoma patients, allowing for more targeted and effective treatments.

EP-0039

A novel 18F labeled TKI-PET tracer for targeting EGFR mutation

S. Liu, *F. Liu, Z. Yang;*
Peking University Cancer Hospital, Beijing, CHINA.

Aim/Introduction: The Epidermal Growth Factor Receptor (EGFR) mutation comprises approximately 30% among Asian NSCLC patients (1). The most frequent mutation in the EGFR tyrosine kinase domain (Del 19 and exon 21 L858R) occur in 30%- 50% of Asian NSCLC patients(2). EGFR tyrosine kinase inhibitors (TKIs) were regarded as a recommended first-line therapy in EGFR mutations patients(3). The development of PET probe for EGFR could monitor mutation status and predict EGFR-TKI sensitivity/resistance. ***Materials and Methods:*** ^{18}F-LF13 was radiolabeled through one-step radiosynthesis. Cell uptake and blocking assay were completed with the HCC827 and the HCC827 blocked with erlotinib to evaluate the specificity of the ^{18}F-LF13 probe. The micro-PET/CT imaging of the ^{18}F-LF13 probe were researched in HCC827 and H1975 model mice. ***Results:*** The radiolabeling yield of ^{18}F-LF13 was 1.55 ± 0.38% using manual synthesis (n=5), and radiochemical purity was over 99%. The uptake in HCC827 cell line was obvious higher than HCC827 cell line blocked with erlotinib (1.29 ± 0.08 vs 0.31 ± 0.02 at 30min, 1.24 ± 0.02 vs 0.32 ± 0.03 at 60min). In micro-PET/CT imaging, ^{18}F-LF13 showed good characteristics of targeting HCC827 tumor, which exhibited Del 19 mutation. The ^{18}F-LF13 showed better aggregation in HCC827 tumor, compared with HCC827 tumor blocked with erlotinib (SUVmax: 1.62 ± 0.02 vs 0.89 ± 0.02 at 30min) and H1975 tumor (SUVmax: 1.62 ± 0.02 vs 0.72 ± 0.03 at 30min). This probe was eliminated through intestinal tract rapidly. ***Conclusion:*** ^{18}F-LF13 probe was powerful to target EGFR del 19 mutation and potential to apply in monitoring EGFR mutation status in NSCLC patients. ***References:*** 1. T. Kawaguchi et al., Japanese ethnicity compared with Caucasian ethnicity and never-smoking status are independent favorable prognostic factors for overall survival in non-small cell lung cancer: a collaborative epidemiologic study of the National Hospital Organization Study Group for Lung Cancer (NHSGLC) in Japan and a Southern California Regional Cancer Registry databases. J Thorac Oncol 5, 1001-1010 (2010). 2. M. Ratti, G. Tomasello, Emerging combination therapies to overcome resistance in EGFR-driven tumors. Anticancer Drugs 25, 127-139 (2014). 3. M. Maemondo et al., Gefitinib or chemotherapy for non-small-cell lung cancer with mutated EGFR. The New England journal of medicine 362, 2380-2388 (2010).

EP-0040

Lenvatinib strengthened I-131-trastuzumab radioimmunotherapy in HER2 positive tumor model

I. Lim, *S. Cho;*
Korea Cancer Center Hospital, Seoul, KOREA, REPUBLIC OF.

Aim/Introduction: The purpose of this study is to investigate whether lenvatinib strengthened I-131-trastuzumab radioimmunotherapy in HER2-overexpressing tumor. ***Materials and Methods:*** Trastuzumab was radiolabeled with I-131. The specific in vitro targeting efficacy of I-131-trastuzumab was

analyzed using Lindmo assay. Cytotoxicity was evaluated via colony formation. NCI-N87 cells were implanted subcutaneously in BALB/c mice. Mice were randomized into 5 groups after tumor reaching to 200 mm3: control group, lenvatinib group, trastuzumab group, I-131-trastuzumab group, lenvatinib and I-131-trastuzumab combination group. After that, tumor sizes were evaluated. Tumors were analyzed for HER2, CD34, E-cadherin. ***Results:*** Through the serum stability test, it was confirmed that I-131-trastuzumab showed a labeling yield of 95% or more even after 48 hours to maintain stable binding. Compared with monotherapy, the combination of I-131-trastuzumab and lenvatinib inhibited the proliferation and viability of HER2-overexpressing NCI-N87 cells, resulting in almost no colony formation. In the xenograft model it also observed inhibition of tumor growth ($p< 0.001$). After tumor excision, it was detected that the HER2 level and the CD34 expression decreased, and the expression of E-cadherin increased in the combination group compared to the control group through immunofluorescence staining. ***Conclusion:*** The combination of I-131-trastuzumab and lenvatinib improved therapeutic effect in HER2-overexpressing tumor. This combination protocol might be applied to the patients in the future.

EP-0041

GRPR-antagonists based on AU-RM26-M1 and their [111In]In-radioligands: Preclinical evaluation for prostate cancer imaging

A. Abouzayed[1], *K. Obeid*[1], *P. Kanellopoulos*[1], *A. Mattsson*[1], *B. A. Nock*[2], *V. Tolmachev*[1], *T. Maina*[2], *A. Orlova*[1];
[1]*Uppsala University, Uppsala, SWEDEN,* [2]*Molecular Radiopharmacy, NCSR Demokritos, Athens, GREECE.*

Aim/Introduction: The gastrin-releasing peptide receptor (GRPR) is an important target for prostate cancer radiotheranostics, owing to its high-density expression in the majority of primary and metastatic cancer lesions. The aim of this study was to design and characterize three GRPR-antagonists based on the metabolically stable motif AU-RM26-M1 (DOTAGA-PEG_2-[Sar^{11}]RM26, [Sar^{11}]RM26: [D-Phe^6,Sar^{11},Sta^{13},Leu^{14}-NH_2]BBN(6-14), Sta: 3S,4S-4-amino-3-hydroxy-6-methyl-heptanoic acid), whereby positive charged residues were introduced in the linker, namely: AU-RM26-M2 (PEG_2-Pip, Pip: 4-amino-1-carboxymethyl-piperidine), AU-RM26-M3 (PEG_2-Arg) and AU-RM26-M4 (Arg-Arg-Pip). These analogues were labelled with In-111 and the effects of the above linker modifications on the biological profile of resulting radioligands were investigated. ***Materials and Methods:*** The three peptide-conjugates were synthesized by solid-phase peptide synthesis. They were radiolabelled with indium-111 and the resulting radioligands were evaluated for their GRPR binding specificity, cell-uptake and receptor affinity in human GRPR-positive PC-3 cells. The radioligands (30 kBq, 40 pmol) were injected in Balb/c nu/nu mice bearing PC-3 xenografts and their biodistribution compared at 4 h post-injection (pi). The metabolic stability of radiolabelled peptides was studied in mice 5 min pi. [^{111}In]In-AU-RM26-M2 was further studied in vivo at 24 h pi and SPECT/CT images were acquired. ***Results:*** All three analogues were radiolabelled with indium-111 with >95% radiochemical yields. The equilibrium dissociation constants (K_D) of the three radioligands were in the low nanomolar range (<1.8 nM). GRPR blocking resulted in significant reduction of uptake in PC-3 cells vs. controls. The percentage of internalized fractions of the radioligands during 4 h incubation at 37 °C were low (<16% of cell-associated activity), as consistent with an antagonist profile. The rank of metabolic stability in peripheral mice blood at 5 min pi was: [^{111}In]In-AU-RM26-M4 (83±2% intact) > [^{111}In]In-AU-RM26-M2 (78±2%, intact) > [^{111}In]In-AU-RM26-M3 (25±5% intact). Consistent with stability results, [^{111}In]In-AU-RM26-M4 displayed the highest tumour uptake at 4 h pi (11.8±4.9%IA/g), followed by [^{111}In]In-AU-RM26-M2 (7.1±2.4%IA/g) and [^{111}In]In-AU-RM26-M3 (2.5±0.6%IA/g). The pancreatic uptake was the highest for [^{111}In]In-AU-RM26-M4 (3.2±0.3%IA/g) followed by [^{111}In]In-AU-RM26-M2 and [^{111}In]In-AU-RM26-M3 (0.4±0.1%IA/g and 0.1±0.0%IA/g , respectively). However, the tumour-to-organ ratios at 4 h pi were the highest for [^{111}In]In-AU-RM26-M2, as it had lower uptake in most tissues than [^{111}In]In-AU-RM26-M4 and higher tumour uptake than [^{111}In]In-AU-RM26-M3. SPECT/CT images of [^{111}In]In-AU-RM26-M2 corroborated the biodistribution profile. ***Conclusion:*** This study revealed that the type and position of positively charged residues in the linker of AU-RM26-M1 can be fine-tuned to improve GRPR-affinity, cell uptake, stability, tumour uptake and overall pharmacokinetics of resulting [^{111}In]In-radioligands in mice, and potentially also in patients.

EP-0042

Using [89Zr]Zr-Oxine ex-vivo labelled macrophages and [89Zr]Zr-DFO-anti-F4/80 to investigate the effect of moderate-dose external beam radiation therapy on macrophage polarisation

V. De Santis[1], *A. Banu*[1], *S. Langdon*[1], *J. Cheng*[1], *M. Cleveland*[2], *M. Ma*[1], *S. Terry*[1];
[1]*King's College London, London, UNITED KINGDOM,* [2]*Glaxosmithkline, Stevenage, UNITED KINGDOM.*

Aim/Introduction: Tumour progression is dictated by the tumour microenvironment and its immune status among other factors. Macrophages are known to be present in tumours in large numbers and their presence is associated with metastasis, tumour progression and poor prognosis as they are co-opted by the tumour to polarise from M1-like tumoricidal macrophages to M2-like, tumour associated macrophages (TAMs). Radiotherapy is a mainstay of many cancer therapy plans. It has been suggested that targeted EBRT doses can re-program TAMs to M1-like phenotypes. Herein, differential doses of EBRT were investigated for their effect on macrophage polarisation, distribution and abundance using PET tracers [^{89}Zr]Zr-Oxine labelled macrophages and [^{89}Zr]Zr-DFO-anti-F4/80. ***Materials and Methods:*** Macrophage polarisation was assessed using flow cytometry. The pan-macrophage marker F4/80 was used to distinguish populations of macrophages from other cell populations. CD80 was used to determine M1 polarisation and CD206 was used for M2 polarisation. Female Balb/c mice were inoculated with 4T1 tumour cells orthotopically. Tumours received targeted doses of 0, 0.2, 2 and 12 Gy. After 72 hours tumours were dissected and digested for analysis. Imaged mice received doses of 0 and 2 Gy. For imaging studies, tumour bearing mice were injected intravenously with $10x10^6$ [^{89}Zr]Zr-Oxine-labelled macrophages, [^{89}Zr]Zr-DFO-anti-F4/80 or [^{89}Zr]Zr-DFO-IgG2b 48 hours after irradiation. Animals injected with [^{89}Zr]Zr-DFO-anti-F4/80 and [^{89}Zr]Zr-DFO-IgG2b were imaged at 24 post injection. Those that received [^{89}Zr]Zr-Oxine labelled macrophages were imaged at 24h and 48h post injection. ***Results:*** FACS results from irradiated tumour digests showed a dose dependent decrease in F4/80 expression with the greatest difference occurring at 2 Gy. CD80 expression decrease significantly with 0.2 and 2 Gy doses. CD206 expression decreased with a 2 Gy dose, however this effect was non-significant. Biodistribution studies with [^{89}Zr]Zr-DFO-anti-F4/80 showed a significant difference in

tumour:blood ratio between 0 and 2 Gy ($P \leq 0.0022$). Imaging studies with [^{89}Zr]Zr-oxine labelled macrophages did not show a significant difference in tumour:blood ratio between 0 and 2 Gy at 24h. Observational n=1 data at 48h shows a 126% increase in tumour:blood ratio at 2 Gy compared to 0 Gy. ***Conclusion:*** It is plausible that low to moderate doses of external beam radiation therapy cause changes in polarisation, however more studies are required elucidate whether these effects will be more visible with [^{89}Zr]Zr-PET after waiting longer periods before imaging post-injection for the tracer to clear from the lungs and blood, potentially revealing any differences.

EP-0043

[68Ga]Ga-Bedaquiline - A Potential Diagnostic Radiotracer for Overexpressed Mitochondrial ATP Synthase Composing Proteins in Lung Carcinoma

A. Chakraborty[1], *M. Tawate*[1], *A. Mitra*[2], *S. Sahu*[1], *S. Lad*[1], *S. Rakshit*[1], *G. Dhotre*[3], *M. K. Ray*[1], *A. Damle*[1], *U. Pandey*[2], *S. Kulkarni*[1];
[1]*Bhabha Atomic Research Centre, Mumbai, INDIA,* [2]*Board of Radiation & Isotope Technology, Mumbai, INDIA,* [3]*Tata Institute of Fundamental Research, Mumbai, INDIA.*

Aim/Introduction: Bedaquiline is a selective mitochondrial ATP synthase (MAS) inhibitor. The MAS plays dominant role in metabolism and progression of various cancers especially in lung metastasis. Bedaquiline inhibit the overexpression of MAS by binding to ε subunit of MAS. The present work thus envisages to establish a radiolabeling protocol for p-SCN-benzyl-DOTA conjugated bedaquiline with [^{68}Ga]$GaCl_3$. The quality control procedure was optimized. For the radioactive formulation, in-vivo bio-distribution studies in SCID mice bearing A549 xenografted tumor were carried out. The preclinical study of [^{68}Ga]Ga-DOTA-Bedaquiline, reported herein, provides confirmatory indications toward its potential for clinical translation. Potential of DOTA-benzyl-bedaquiline is being explored to radiolabel with Lutetium-177 for radionuclide therapy. ***Materials and Methods:*** After demthylation of -OCH_3 group in bedaquiline, propyl-amine derivatives of bedaquiline were synthesized using N-Boc-3-bromopropylamine and purified by column chromatography. The bedaquiline propyl-amine derivatives were conjugated with p-NCS-benzyl-DOTA at 1:10 molar ratios (pH~8.0) and purified by semi-preparative HPLC. The DOTA-benzyl-bedaquiline (50 µg) were radiolabeled with [^{68}Ga]$GaCl_3$ obtained from ^{68}Ge/^{68}Ga generator. The [^{68}Ga]$GaCl_3$ were pre-concentrated and eluted with acidified NaCl. The radiolabeling was carried out in 1M CH_3COONa buffer at 95°C for 20 minutes (pH~4.0). The reaction mixture thus purified using preconditioned C18 Sep-Pak, finally [^{68}Ga]Ga-DOTA-bedaquiline was eluted from C18 with ethanol (100%, 0.8 mL). The resultant [^{68}Ga]Ga-DOTA-bedaquiline was diluted with saline and filtered. RCP was ascertained by radio-TLC and radio-HPLC. Endotoxin limit was quantified by gel-clot BET assay. In-vitro stability was ascertained by evaluating RCP (radio-HPLC) at 2h post-radiolabeling on storage at room temperature (25°C). Human lung adenocarcinoma cell-lines A549, expressing MAS were used for in-vitro evaluation. In-vivo biodistribution and PET/CT imaging was carried out in SCID mice bearing tumor xenograft induced by A549 cell-lines. ***Results:*** Using ~0.93 GBq of [^{68}Ga]$GaCl_3$, 3-4 patients doses (~0.68 GBq) of [^{68}Ga]Ga-DOTA-bedaquiline were formulated with ~73% RCY. The pH was ~4.5, while RAC was ~50 MBq/mL. RCP (radio-TLC, R_f: 0.0-0.1) and (radio-HPLC, R_t: 14.0-15.5 minutes) were >98%. Product was sterile and endotoxin-free (EL: <25 EU/mL). Product was found to be stable upto 2h at 25°C with RCP >98%. [^{68}Ga]Ga-DOTA-bedaquiline showed rapid binding with A549 cell-lines (25%), reaching a plateau after 45m. In bio-distribution study, high retention of radioactivity were found in tumor (6.8% ID/gm), which is in corroboration with results obtained from PET/CT studies. ***Conclusion:*** Clinical doses formulation of [^{68}Ga]Ga-DOTA-Bedaquiline was successfully developed. Pre-clinical results demonstrate the promising potential of [^{68}Ga]Ga-DOTA-Bedaquiline for clinical translation in MAS overexpressed lung cancers patients.

EP-0044

Preclinical Evaluation of an Anti-Nectin-4 ImmunoPET Reagent in Tumor Bearing Mice

y. Ren[1], *Z. Yang*[2];
[1]*Guizhou University, Guiyang, CHINA,* [2]*Peking University Cancer Hospital and Institute, Beijing, CHINA.*

Aim/Introduction: Nectin-4 is selectively overexpressed in a variety of cancers and is currently under clinical investigation as a therapeutic target. A radionuclide Zr-89 labeled monoclonal antibody against Nectin-4 (9MW282) was evaluated as an Immuno-positron emission tomography (ImmunoPET) reagent. Its ability to assay nectin-4 expression was evaluated using bladder cancer mouse models. ***Materials and Methods:*** 9MW282, which is specific for nectin-4, was conjugated to desferrioxamine (DFO) and then radiolabeled with solid target nuclide Zr-89. The final product ^{89}Zr-DFO-9MW282 was identified by Radio-TLC and its stability was analyzed in vitro. A Nectin-4 positive bladder cancer model bearing SW780 tumor was established and the Nectin-4 tumor targeting of the probe was verified by PET imaging in small animals. ***Results:*** The conjugation of DFO to 9MW282 resulted in a ratio of approximately 0.87 DFO conjugates per antibody molecule. Radiolabeling with [^{89}Zr] resulted in a radiochemical purity of > 99% when purified by PD-10 column as determined by ITLC. After incubation in vitro with PBS and 5% HSA solution for 6 days, the radiochemical purity of the probe was still >90%. High binding affinity was found to bind to Nectin-4 with a dissociation constant of 9.79 nM. The specificity and target of the ^{89}Zr-DFO-9MW282 for nectin-4 was investigated using subcutaneous xenografts. The corresponding immunoPET imaging demonstrated exceptional performance in nectin-4-overexpressing diagnosis. In detail, small animals PET imaging of the probe showed high tumor targeting ability in Nectin-4 positive SW780 model mice with an increased accumulation in SW780 tumor within 72 h p.i. (SUVmax: 4.24 ± 0.03). which was significantly higher than that in ^{89}Zr-DFO-IgG control group (SUVmax: 1.13 ± 0.01, $p < 0.001$). When 500 µg cold ligand 9MW282 was injected, the uptake of ^{89}Zr-DFO-9MW282 in the tumor was significantly decreased (SUVmax: 1.67 ± 0.04, $p < 0.001$). ***Conclusion:*** A novel radionuclide labeled immunoPET probe ^{89}Zr-DFO-9MW282 has been successfully prepared, which presented good physical and biological properties. Its excellent Nectin-4 targeting ability in PET imaging provides visualization tools for the stratification and diagnosis for Nectin-4 overexpressed tumor.

EP-0045

Preclinical evaluation of 64Cu-DOTHA2-FAPI for PET Imaging of head and neck cancer

I. Ben-Salem[1], *E. Croteau*[1], *V. Dumulon-Perreault*[2], *N. Saidi*[1], *O. Sarrhini*[1], *S. Ait-Mohand*[1], *O. Bélissant*[1], *E. Turcotte*[1], *A. Oweida*[1], *B. Guérin*[1], *E. Rousseau*[1];
[1]*Département de médecine nucléaire et radiobiologie, Université de Sherbrooke, Sherbrooke, QC, CANADA,* [2]*Centre d'Imagerie Moléculaire de Sherbrooke (CIMS), Centre de Recherche du CHUS (CRCHUS), Sherbrooke, QC, CANADA.*

Aim/Introduction: Fibroblast Activation Protein (FAP) is a cell surface protein that is overexpressed in cancer-associated fibroblasts, which are cells that promote tumor growth and spread. FAP has emerged as a promising target for cancer imaging and therapy due to its high expression in various tumor types and its minimal expression in normal tissues. FAP-targeted imaging has shown promise in preclinical and clinical studies for various types of cancer, including pancreatic, ovarian and breast cancer. Its ability to distinguish between cancerous and normal tissues could potentially aid in early cancer detection, diagnosis, and monitoring of treatment response. 64Cu-labeled chelator-linked FAP inhibitors (FAPIs) have been successfully applied to PET imaging of various tumor types. To broaden the spectrum of applicable PET tracers, we herein report the radiosynthesis and preclinical evaluation of 64Cu-DOTHA2-FAPI for the imaging of head and neck cancer. ***Materials and Methods:*** Squamous cell carcinoma MOC2 cells were used to study cellular uptake and internalization of 64Cu-DOTHA2-FAPI in vitro. For in vivo study, MOC2 cells were inoculated in the buccal mucosa of mice and developed into aggressive tumors within 2 weeks of injection. Tumor-bearing mice were imaged using PET with 64Cu-DOTHA2-FAPI at 1hr, 4hr and 24hr post-injection. After PET imaging, mice biodistribution were performed. To confirm the specificity of the radiotracer to its ligand, a blocking experiment using unlabeled FAPI was conducted. ***Results:*** 64Cu-DOTHA2-FAPI was stable ex vivo in plasma and reached cellular uptake and internalization up to 69.37 ± 1.17% injected activity (IA)/10^6 cells at 24 h post-injection (p.i.). PET imaging of 64Cu-DOTHA2-FAPI allowed visualization of the tumor with uptake mostly in its periphery. Biodistribution results showed relatively low accumulation in brain (0.32±0.001 %ID/g), heart (2.21±0.009 %ID/g) and spleen (2.25±0.006 %ID/g). Tumor uptake was 7.28±0.01 with 64Cu-DOTHA2-FAPI, relatively low uptake of whole tumor could be explained by non-homogenous distribution of FAP+ cancer associated fibroblasts (FAP+ CAF) in tumor. Tumor uptake was lower in the blocked group (4.14±0.023 %ID/g, $p<0.05$) confirming the specificity of 64Cu-DOTHA2-FAPI to its FAP target. ***Conclusion:*** Our study demonstrates the potential of 64Cu-DOTHA2-FAPI for molecular imaging of oral cancer in an orthotopic mouse model. This radiotracer could be a promising tool for early detection and monitoring of head and neck cancers.

EP-0046

Evaluation of 89Zr-DFO-C23 in immuno-PET imaging of A549 xenograft models with high TIM3 expression

J. Tao[1], *Z. Zeng*[2], *H. Zhu*[3];
[1]*Peking University Cancer Hospital, Beijing, Beijing, CHINA,* [2]*Peking University Cancer Hospital, Beijing, CHINA,* [3]*Peking University Cancer Hospital and Institute, Beijing, CHINA.*

Aim/Introduction: T cell immunoglobulin and mucin domain 3 (TIM3; HAVCR2) is a transmembrane protein that plays a negative regulatory role in T cell responses and is considered a promising target in tumor immunotherapy. In this study, a monoclonal antibody probe targeting TIM3 was developed and labeled by ^{89}Zr nuclide, and the molecular probe was evaluated in vivo and in vivo by high-resolution positron emission tomography (Micro-PET/CT) technology, in order to develop a novel antibody probe targeting TIM3 to guide tumor immunotherapy targeting TIM3. ***Materials and Methods:*** The self-developed TIM3-targeting monoclonal antibody C23 was conjugated to DFO bifunctional chelating agent, and then radiolabeled with 89Zr, and purified by PD-10 desalination column to obtain ^{89}Zr-DFO-C23 probe. The A549 cell line was transfected with human TIM3 full-length plasmids to obtain an A549-TIM3 cell line with high TIM3 expression. Flow cytometry was used to detect TIM3 expression in A549-TIM3 cells. In vitro the affinity of the ^{89}Zr-DFO-C23 probe was evaluated by comparing the uptake of A549 and A549-TIM3 cells to the TIM3 target, and the stability of the probe was assessed in PBS and 5% HSA solution. The biodistribution and pharmacokinetic properties of the probe were studied by injection of ^{89}Zr-DFO-C23 in vivo, and then ^{89}Zr-DFO-C23 was injected intravenously in the tail and then subjected to static whole-body positron emission tomography (PET) scanning by Micro-PET/CT for 15 minutes at 4, 24, 48, 72 and 96 h, respectively, and the images were quantified by region of interest (ROI) to obtain the maximum uptake value (SUVmax). The targeting specificity of this molecular probe with TIM3 was studied. ***Results:*** In this study, ^{89}Zr-DFO-C23 probe was successfully prepared, and the high expression of TIM3 in A549-TIM3 cells was confirmed by flow cytometry. Compared with the blockade group or the A549-negative group, the results of cell uptake showed that the ^{89}Zr-DFO-C23 probe was significantly specific for TIM3. The results of small animal PET showed that the uptake of ^{89}Zr-DFO-C23 probe in the A549-TIM3 model reached the maximum absolute uptake value at 48 h. It was consistent with the distribution of ^{89}Zr-DFO-C23 in A549-TIM3-bearing mice. ***Conclusion:*** The ^{89}Zr-DFO-C23 probe developed in this study showed obvious targeting specificity with TIM3 in vitro and in vitro evaluation. Indicates the potential for non-invasive monitoring of TIM3 expression in tumor immunotherapy.

EP-0047

Preparation and Application of Bioorganic Nanoparticle Enhanced PDL1 Targeted Small Molecule Probe

C. He, *L. Xia;*
Beijing Institute of Cancer Prevention and Treatment, Beijing, CHINA.

Aim/Introduction: PDL1 can also be used as a specific target for the diagnosis and immunotherapy of solid tumors. A large number of drug studies show complexity and lack of evaluation criteria, a PET imaging method to non-invasively quantify PDL1 expression level would potentially help select patients for more effective treatment, and might be leveraged to study target engagement. The most reported small molecule imaging probes targeting PDL1 still have problems such as low imaging specificity, short residence time and single function. Here, we combined the biocompatible melanin nanoprobe with PD-L1-binding peptide WL12 to construct a new nanoprobe targeting PD-L1 for enhancing functionality by using nanotechnology. ***Materials and Methods:*** In this study, melanin nanoparticles were used as raw materials to couple WL12-SH onto nano carriers to obtain (WL12-PEG-MNPs-II, referred to as WPMNs). We used dynamic light scattering, transmission electron microscopy, Fourier transform infrared spectroscopy, and other methods to characterize the synthesized products; Labeling WPMNs with nuclide ^{124}I and NOTA-WL12 with ^{68}Ga was used to construct high expression PDL1 cell A549^{PDL1}. Cell uptake and kd experiments were conducted to verify the ability of ^{124}I-WPMNs to target PDL1 in vitro. Micro-PET/CT imaging studies were conducted in A549^{PDL1} bearing mice, and SUVmax was delineated at the tumor site of the two probes to compare their retention ability at the tumor site. Prove the ability of ^{124}I-WPMNs to target PD-L1 in vivo through PET/MRI studies. ***Results:*** The radiochemical purity of ^{124}I-WPMNs is more than 95%. And the uptake value of ^{124}I-WPMNs in A549^{PD-L1} cell was 1.49 ± 0.08 at 2h, which can be blocked by WL12 (0.39±0.03, $P<0.0001$). ^{124}I-WPMNs showed higher affinity to PDL1 (Kd = 18.5 nM) than

^{68}Ga-NOTA-WL12 (Kd = 24.0 nM). And the micro-PET/CT imaging demonstrated specific uptake and high signal-to-noise ratio in a A549^{PD-L1} xenograft mouse model with tumor-to-muscle ratio of 27.31±7.03 at 2 h and increased or remained for more than 72h, which significantly higher than ^{68}Ga-NOTA-WL12 in tumor uptake with 6.08±0.62 at 2 h. And the retention ability of ^{124}I-WPMNs makes it possible to conduct PET/MRI imaging for a long time and flexibly adjust the imaging with different purposes. ***Conclusion:*** A clear advance between ^{124}I-WPMNs and ^{68}Ga-NOTA-WL12 was observed for PDL1 targeting PET imaging after nanoparticle modification, supporting the application of ^{124}I-WPMNs PET as a companion diagnostic tool for optimizing treatments that target PDL1.

EP-0048

Preclinical evaluation of novel PSMA-targeting ligands labelled with gallium-68

Z. Novy[1], *K. Hajduova*[1], *M. Petrik*[1], *K. Bendova*[1], *M. Benesova*[2], *M. Hajduch*[1];
[1]*Faculty of Medicine and Dentistry, Olomouc, CZECH REPUBLIC,* [2]*German Cancer Research Center, Heidelberg, GERMANY.*

Aim/Introduction: The prostate-specific membrane antigen (PSMA) is well-known target in prostate cancer and is investigated for last 20 years. PSMA research led to clinically approved drugs like PSMA-11 or PSMA-617. Despite these great successes, research in the field is still ongoing in order to even improve target affinity or pharmacokinetics of PSMA ligands (inhibitors). In this study, we have focused in preclinical testing of three novel PSMA inhibitors. Compounds P15 and P16 possesses different binding motif compared to PSMA-617, meanwhile compound P19 is based on PSMA-617. ***Materials and Methods:*** Methods included basic stability test in PBS (0-2h), stability in human plasma (0-2h), determination of log D and evaluation of plasma protein binding for three tested compounds and for PSMA-617 as golden standard. The labelled ligands were tested in vitro to reveal their binding to LNCaP cells as well as their internalization into these cells. The ex vivo biodistribution studies were performed in LNCaP-tumor bearing mice (1, 2 h p.i.). Finally, tumor mice were injected with studied compounds and PET/CT imaging was done 1 h p.i. ***Results:*** All studied compounds reveal high stability both in PBS and in human plasma with minor decrease in radiochemical purity after 2 h. Log D values were determined to be -3 for all studied compounds. The plasma protein binding of PSMA-617 and P19 was in level of 50-60%, nevertheless P15 and P16 displayed much lower values (10-40%). Ex vivo biodistribution study showed the highest accumulation of the tracer in kidneys in case of PSMA-617, meanwhile the three tested ligands had much lower kidney uptake, but the tumor uptake was lower as well. Tumor uptake of P19 was 3,52% ID/g, compared to 5,25 %ID/g for PSMA-617. All tested compounds were able to image tumor using PET/CT. P19 showed best tumor contrast from tested compounds, but PSMA-617 had even higher contrast of tumor. Advantage of tested compounds was very low signal in kidneys compared to PSMA-617. ***Conclusion:*** In vivo experiments resulted in very favorable characteristics of all tested compounds comparable to PSMA-617. Ex vivo biodistribution revealed most remarkable difference in kidney uptake of tested, which was very low compared to PSMA-617. Nevertheless the tumor uptake was decreased as well. P19 was the only compound vere tumor/blood ratios were comparable to PSMA-617. PET/CT showed favorable tumor contrast only for P19 and PSMA-617.

EP-0049

Design of novel small molecules targeting Fibroblast activating protein and preclinical exploration of 47Sc labeling

Y. Xia;
Second Affiliated Hospital of Chengdu Medical College (China National Nuclear Corporation 416 Hospital, Chengdu, CHINA.

Aim/Introduction: Fibroblast activating protein, (FAP) is highly expressed in fibroblasts in the mesenchymal stroma of most malignancies. In this study, we used computer-aided drug design (CADD) to design and simulate several novel FAPI small molecule drugs and to evaluate the physical and therapeutic properties of the beta-emitter (^{47}Sc). ***Materials and Methods:*** A library of molecules was designed using CADD and screened for high affinity small molecules by combining different chelators, FAPI groups and albumin binding modules. The labeling conditions were refined using ^{68}Ga and ^{47}Sc to determine the LogP values, in vivo and in vitro metabolic stability, cellular uptake and specific binding of the labeled products. The products were further used for SPECT/CT imaging and therapeutic experiments in the U87MG model mouse and the MCF-7 model was used as a negative control. ***Results:*** We screened three high affinity small molecules (XY201, XY202, XY203). We selected the one with the best simulation results for the follow-up study and showed that it was well labelled with ^{68}Ga and ^{47}Sc (90°C, 15 min, pH ≈ 4) with >90% labelling and >99% radiochemical purity. SPECT/CT imaging and biodistribution studies showed high tumour accumulation, mainly 24 h after injection. Its excretion was mainly in the liver and intestine. More significant tumour suppression was found in the experimental group relative to the saline group in treatment trials. ***Conclusion:*** Using CADD as a technical premise, we have screened novel FAPI small molecule drugs that demonstrate excellent targeting and affinity. ^{47}Sc labeling shows good therapeutic potential.

EP-0050

Lead Optimisation Strategy for the Development Of New Grpr Radioantagonists

P. Paraïso[1], *C. van Deurzen*[2], *Y. Seimbille*[1,3];
[1]*Department of Radiology and Nuclear Medicine, Erasmus MC Cancer Institute, Erasmus University Medical Center, Rotterdam, NETHERLANDS,* [2]*Department of Pathology, Erasmus MC Cancer Institute, Erasmus University Medical Center, Rotterdam, NETHERLANDS,* [3]*Life Sciences Division, TRIUMF, Vancouver, BC, CANADA.*

Aim/Introduction: To improve the in vivo biodistribution and metabolic stability of the current gastrin-releasing peptide receptor (GRPR)-targeted radioligands, we investigated the substitution of amino acids within the sequence of the GRPR antagonists RM2 (DOTA-Pip^5-D-Phe^6-Gln^7-Trp^8-Ala^9-Val^{10}-Gly^{11}-His^{12}-Sta^{13}-Leu^{14}-NH_2) and NeoBOMB1 (DOTA-Pip^5-D-Phe^6-Gln^7-Trp^8-Ala^9-Val^{10}-Gly^{11}-His^{12}-NH-CH[CH_2-CH(CH_3)$_2$]$_2$) by unnatural amino acids. A library of 40 analogs was designed, synthesized and evaluated by competitive binding assay. The results of this study led to the identification of nine novel candidates for diagnosis and therapy of GRPR-positive breast tumors based on their IC_{50}, $logD_{7.4}$, cell uptake and stability. ***Materials and Methods:*** All NeoBOMB1/RM2-based compounds were synthesized by standard Fmoc-based solid-phase peptide synthesis (SPPS). Labeling with ^{111}In was carried out at 95 °C for 20 min in a solution containing ascorbic/gentisic acids (50 mM), sodium acetate (2.5 M) and L-methionine (50 mM). Affinity (IC_{50}) to GRPR was determined using T-47D cells. In addition, cell uptake

and internalization (37 °C, 60 min), lipophilicity (expressed as n-octanol/PBS partition coefficient: $logD_{7.4}$), and in vitro metabolic stability in murine serum (up to 24 h at 37 °C) have been carried out to confirm the potential of our lead candidates. ***Results:*** Similar to the synthesis of the parent compounds (NeoBOMB1 and RM2), the new GRPR-targeted derivatives were accessible by SPPS and liquid phase coupling. All compounds were obtained in 33-56% yield after HPLC purification. The GRPR affinity (IC_{50}) of the new compounds varied from 0.97 to 1428 nM compared to 1.24 nM and 1.04 nM for RM2 and NeoBOMB1, respectively. The best nine compounds were selected for further examination (pADA-RM2 2: 1.14 nM, D-Cpa^{6}-RM2 6: 1.41 nM, D-Tyr^{6}-RM2 7: 1.55 nM, D-1-Nal^{6}-RM2 8: 1.30 nM, D-2-Nal^{6}-RM2 9: 1.19 nM, D-Igl6-RM2 10: 1.33 nM, Cba^{14}-RM2 11: 0.97 nM, Thi^{14}-RM2 14: 1.89 nM, Igl^{14}-RM2 16: 1.47 nM). High radiochemical purity (RCP) was obtained for all nine radioligands (94 - 99%). Candidates 7, 8, 14 and 16 showed a slightly better stability compared to RM2 (> 16% vs. 12% for [^{111}In] In-RM2 at 24 h). ***Conclusion:*** 40 new GRPR-targeted ligands were successfully synthesized and characterized by LC-MS. Based on the cell binding assay data, nine compounds were selected for further in vitro evaluation ($logD_{7.4}$, stability). Compounds 7, 8, 14 and 16 are the most promising due to a better stability in mouse serum at 24 h. These compounds will be further evaluated to identify a lead candidate for in vivo studies in tumor bearing mice.

EP-0051

Normal organs uptake values in F 18- FDG PET/CT in relation to serum blood glucose

R. Mostafa[1], *H. Askar*[2], *M. Helbawi*[2], *H. Mahmoud*[2]; *[1]Nuclear Medicine Unit, Department of Radiation Oncology and Nuclear Medicine, South Egypt Cancer Institute, Assiut University, Assiut, EGYPT, [2]Department of Clinical Oncology and Nuclear Medicine, Faculty of Medicine, Assiut University, Assiut, Assiut, EGYPT.*

Aim/Introduction: PET/CT using F 18-FDG is widely used in oncology(1). The FDG molecule acts like glucose and accumulates at a rate proportional to glycolysis(2). The most commonly used method for quantification is the standardized uptake value (SUV). Several factors affect its measurement, including uptake period, injected dose, body mass index, and blood glucose(3). SUVmax values of healthy organs are considered as references in the evaluation of patients with different tumors. Aim: To analyze the SUVmax values of normal organs and assess their association with different factors. ***Materials and Methods:*** The Institutional Review Board approved this retrospective study which included 593 patients (276 males, 317 females; age 47 ± 20 years old; body mass index 28.31 ± 8.30). All patients underwent F 18-FDG PET/CT scans using a standardized imaging protocol. Blood glucose was measured immediately before injection. Diabetic status, BMI, uptake period and injected dose were extracted from patients records. Fixed regions of interest were drawn at cerebral hemispheres, lung, blood pool activity, liver, spleen, pancreas and muscle to extract SUVmax. Any organs with infiltration were excluded from this analysis. The study populations were divided into 2 groups depending on fasting blood glucose with a cut off value 160 mg/dl. Patients with a blood glucose less than 160 mg/dl were considered as control group. By dividing the difference in the mean SUVmax for the group with glucose ≥160 mg/dl by the mean SUVmax in the control group, effect size was calculated using pooled SDs. Multivariate linear regression analysis was used to assess the impact of important factors affecting uptake in normal organs. ***Results:*** 535 patients had fasting blood glucose level less than 160 mg/dl while 58 had blood glucose ≥ 160. Only two organs (brain and muscle) showed significant correlation with serum blood glucose. After adjustment of age, sex, body mass index, injected dose, and serum blood glucose; the brain shows significant inverse correlation with fasting blood glucose while the muscle demonstrated significant positive correlation. Age, sex, body mass index, and injected dose showed statistically significant positive correlation with uptake at different organs. ***Conclusion:*** The brain and muscle were the only two organs demonstrating a statistically significant relationship to glycemic status after adjustment for confounding potential values. ***References:*** 1. Gallamini A, Zwarthoed C, Borra A. Positron Emission Tomography (PET) in Oncology. 2014;1821-89. 2. Sarji SA. Physiological uptake in FDG PET simulating disease. 2006; 3. Fletcher JW. NIH Public Access. 2011;31(6):496-505.

EP-0052

Synthesis and preliminary assessment of 68Ga/177Lu-TATE-EB-01 for the theranostic in neuroendocrine tumor

X. Wen[1], *P. Xu*[2], *J. Liu*[1], *J. Zhang*[3], *Z. Guo*[1], *X. Chen*[3]; *[1]State Key Laboratory of Molecular Vaccinology and Molecular Diagnostics & Center for Molecular Imaging and Translational Medicine, School of Public Health, Xiamen University, Xiamen, CHINA, [2]Institute of Clinical Pharmacy & Pharmacology, Jining First People's Hospital, Jining Medical University, Jining, CHINA, [3]Department of Diagnostic Radiology, Yong Loo Lin School of Medicine and Faculty of Engineering, National University of Singapore, Singapore, SINGAPORE.*

Aim/Introduction: Somatostatin receptor (SSTR) is overexpressed in neuroendocrine tumors, TATE as an analogue of somatostatin, which could bind to SSTR with high affinity. This study aims to optimize TATE ligands through Evans blue modification to maximize the tumor uptake values and improve the therapy effect of neuroendocrine tumors. ***Materials and Methods:*** TATE-EB-01 was synthesized based on SSTR-targeting ligand (DOTA-TATE) and radiolabeled with ^{68}Ga and ^{177}Lu for radiotracer imaging and radioligand therapy. Cellular uptake assays were performed to identify the receptor binding affinity and SSTR targeting specificity. PET imaging of ^{68}Ga-TATE-EB-01 and ^{68}Ga-EB-TATE was performed to compare the tumor uptake and pharmacokinetics of the two radiotracers. In addition, SPECT/CT imaging and biodistribution studies of ^{177}Lu-TATE-EB-01 and ^{177}Lu-EB-TATE were conducted to explore the potential of theranostic in neuroendocrine tumors. ***Results:*** ^{68}Ga/^{177}Lu-TATE-EB-01 had high SSTR binding affinity and targeting specificity in vitro and in vivo. PET imaging of ^{68}Ga-TATE-EB-01 in AR42J tumor model indicated that obviously improved tumor uptake and tumor/normal tissue ratios compared to ^{68}Ga-EB-TATE. SPECT/CT imaging and biodistribution studies showed that ^{177}Lu-TATE-EB-01 had higher tumor absolute uptake, as well as longer tumor retention time than ^{177}Lu-EB-TATE and ^{177}Lu-DOTA-TATE in AR42J tumor model, which demonstrated the enormous therapeutic potential of ^{177}Lu-TATE-EB-01 in neuroendocrine tumors. ***Conclusion:*** In this study, we successfully synthesized TATE-EB-01 and radiolabeled with ^{68}Ga and ^{177}Lu. High binding affinity and SSTR targeting specificity was verified, moreover, significantly ameliorative tumor absolute uptake and retention time was observed, that makes ^{177}Lu-TATE-EB-01 has the potential to improve the therapy effect of neuroendocrine tumors with lower dosages and less cycles.

EP-0053

[18F]FDG-PET/CT and MRI to assess treatment response to anti-PD1 in an orthotopic mouse renal cancer model.

O. Bejuy, *H. Poinot, D. Colin, A. Pommier, V. Garibotto;*
University Of Geneva, Geneva, SWITZERLAND.

Aim/Introduction: Novel cancer treatments are required to improve the outcome of patients not responsive to current immunotherapies. Endogenous steroids have strong immunomodulatory functions but their role in resistance to immunotherapy in cancer is poorly understood. As a preliminary study, we evaluated the potential of multimodal Positron Emission Tomography (PET) / Computed tomography (CT) and Magnetic Resonance Imaging (MRI) in early quantification of anti-PD1 efficacy in an orthotopic mouse renal cancer model. ***Materials and Methods:*** 6-week-old balb/c female mice were orthotopically injected in the right kidney with Renca cells. Briefly, incisions of 0.5 to 0.7 cm were made into the skin of mice right flank without opening the peritoneum. Kidneys were localized and 10^5 Renca cells were slowly injected with a Hamilton syringe. The incisions were closed with surgical glue and animals were carefully monitored for 3 days. 200 µg/mouse of anti-PD-1 antibodies treatment was administrated intraperitoneally starting from day 7 after tumor cell injection followed by further administrations every 2 and 3 days, up to 35 days. Tumor growth was monitored by MRI (FSE T2 FatSat) and tumor metabolism was assessed by [^{18}F]FDG-PET/CT imaging, once a week at 2 and 3 weeks after beginning of anti-PD1 treatment. ***Results:*** MRI showed tumor growth over time and [^{18}F]FDG-PET imaging showed tumor activity evolution over time. CT imaging provided sufficient anatomical data to localize kidneys and to allow coregistering of PET data. SUV_{max} were quantified as the most relevant marker of tumor development by [^{18}F]FDG-PET/CT. During a one-week period, tumor volumes assessed by MRI showed a trend for increase. SUV_{max} assessed by [^{18}F]FDG remained stable. However, only [^{18}F]FDG-PET revealed the onset of the response modulation to anti-PD1 treatment after three weeks, although not significant. Additionally, [^{18}F]FDG-PET metabolic volumes increased over time. ***Conclusion:*** Both MRI and [^{18}F]FDG-PET modalities bring insights in the evaluation of the therapeutic effect of anti-PD1, with [^{18}F]FDG-PET possibly more sensitive to the onset of the effect of anti-PD1. Further investigations on PET quantification methods, as well as animal survival correlation studies will be conducted to fully evaluate the potential of early [^{18}F]FDG-PET compared to MRI for anti-PD1 treatment response assessment.

EP-04

e-Poster Area

A: Preclinical Studies -> A1 Medical Preclinical -> A14 Preclinical Therapy

EP-0054

FAP-targeted cancer theranostics

W. Wei*;*
Shanghai Jiao Tong University, Shanghai, CHINA.

Aim/Introduction: Fibroblast activation protein (FAP) is the most popular target in nuclear medicine imaging and cancer theranostics. Several big pharmas are developing state-of-the-art small molecule and peptide-based FAP-targeting molecular imaging and radiotherapy agents. We engineered three FAP-targeted peptide agents for molecular imaging and therapy of FAP-overexpressing tumors. There are several small molecule moieties (FAP-04 and FAP-46 etc) used for developing FAP-targeted theranostics agents. FAP-2286 is a very promising peptide under active investigation. However, the circulation time of FAP-2286 is short, resulting in rapid clearance via kidneys (associated with low tumor uptake and high kidney accumulation). For taking care of the existing drawbacks, we engineered three derivatives of FAP-2286 named as CD1, CD2, and CD3. ***Materials and Methods:*** CD1, CD2, and CD3 were synthesized using solid-phase peptide systhesis. The binding affinities of the three peptides to human and murine FAP proteins were meaused using SRP. Following this, the peptides were labeled with 68Ga and 177Lu for PET imaging and radioligand therapy, respectively. The theranostic value of the novel agents were evaluated in multiple tumor models expressing FAP. ***Results:*** All the three reported peptides bind to human and murine FAP with single digit nM affinity. After radiolabeling, CD1 has lower kidney uptake and CD2/CD3 have significantly prolonged circulation, increased tumor uptake and decreased kidney accumulation. Following thorough in vivo and in vitro studies, we found that [68Ga]Ga-DOTA-CD1 is well suited for PET imaging of FAP dynamics, [177Lu]Lu-DOTA-CD2 and [177Lu]Lu-DOTA-CD3 have impressive therapeutic effects in FAP-overexpressing tumor models. Therefore, [68Ga]Ga-DOTA-CD1/[177Lu]Lu-DOTA-CD2 and [177Lu]Lu-DOTA-CD3 are well characterized theranostic pairs. ***Conclusion:*** We developed three novel agents for . While [68Ga]Ga-DOTA-CD1 is ready for same-day PET imaging of FAP dynamics, [177Lu]Lu-DOTA-CD2 and [177Lu]Lu-DOTA-CD3 are promising radioligand therapy agents for treating FAP-overexpressing tumors. ***References:*** 1. Chen et al. J Nucl Med. 2023 Mar;64(3):386-394.2. Bastiaan M Privé et al. Eur J Nucl Med Mol Imaging . 2023 Feb 23. doi: 10.1007/s00259-023-06144-0. Online ahead of print.

EP-0055

Development ofINER-PP-F11N as the Radionuclide Theragnostics Agent against Cholecystokinin B Receptor-overexpressed Tumors

M. Chang*, C. CHEN, P. CHIANG, C. PENG;*
Institute of Nuclear Energy Research, Taipei, TAIWAN.

Aim/Introduction: We aimed to evaluate an albumin affinity structure-containing radiopharmaceutical agents INER-PP-F11N-1 and INER-PP-F11N-2 for diagnostic/therapeutic the CCK2R-overexpressed cancers ***Materials and Methods:*** We developed the radionuclide labeled In-111/Lu-177-INER-PP-F11N radiopharmaceuticals in comparison with the current PP-F11N to investigate the radiochemical purity, SPECT/CT imaging, bio-distribution, and therapeutic responses in CCK2R-expressing tumor xenograft mice. ***Results:*** The radiochemical purity of In-111/Lu-177-INER-PP-F11N radiopharmaceuticals reached more than 90% after 144 hours of labeling. Both INER-PP-F11N increased cellular uptake and internalization 27% and 11% in compared with PP-F11N, respectively. In-vivo SPECT-CT imaging confirmed INER-PP-F11N could accumulate in the tumor site of mice in 24 hours after receiving those two radiopharmaceutical agents. Bio-distribution analysis revealed a significantly greater tumor uptake and reduced accumulation of INER-PP-F11N in kidney in compared with PP-F11N. Furthermore, INER-PP-F11N could significantly inhibit growth of the CCK2R-overexpressing tumors in mice. ***Conclusion:*** The INER-PP-F11N radiopharmaceuticals was superior in comparing with the current PP-F11N as a theragnostic agent. Our study suggested INER-PP-F11N could be an innovative radiopharmaceutical agent for CCK2R-overexpress-

ing cancer patients. ***References:*** 1. Targeting of a CCK(2) receptor splice variant with (111)In-labelled cholecystokinin-8 (CCK8) and (111)In-labelled minigastrin. Eur J Nucl Med Mol Imaging. 2008;35(2):386-92. 2. Develop companion radiopharmaceutical YKL40 antibodies as potential theranostic agents for epithelial ovarian cancer. Biomed Pharmacother. 2022 Nov;155:113668

EP-0056

Local Infusion of 177Lu-Labeled Gold Nanoparticles Combined with anti-PD1 Checkpoint Immunotherapy Prolongs Survival of C57BL/6 Mice Bearing Orthotopic GL261 Murine Gliomas

C. Georgiou[1], *Z. Cai*[1], *J. T. Rutka*[2], *M. Winnik*[1], *R. M. Reilly*[1];
[1]*University of Toronto, Toronto, ON, CANADA,* [2]*The Hospital for Sick Children, Toronto, ON, CANADA.*

Aim/Introduction: Glioblastoma (GBM) is the most common and aggressive primary adult brain tumour with a poor median survival. Standard-of-care treatment does not prevent the invasive growth that leads to recurrence Previous published research showed that local infusion of ^{177}Lu-labelled gold nanoparticles as a monotherapy was impressively effective and non-toxic in controlling glioblastoma growth in an orthotopic mouse model[1]. Further improvement in therapeutic efficacy could be achieved by combining treatment modalities. We hypothesize that local infusion of ^{177}Lu-labelled gold nanoparticles by convection enhanced delivery will be synergistic when combined with anti-PD1 checkpoint immunotherapy in controlling an orthotopic murine model of GBM. ***Materials and Methods:*** AuNP (18 nm) were labeled by conjugation to a metal chelating polymer (MCP) with 8 pendant DOTA and 4 lipoic acid groups [PEG-pGlu(DOTA)$_8$-LA$_4$] complexed to ^{177}Lu. Murine GBM tumours were established by stereotaxic inoculation of GL261 cells into the right frontal lobe of C57BL6 mice. Mice were treated 10d after inoculation with either saline, anti-PD1 antibody (3×200 µg), non-radioactive AuNP, ^{177}Lu-AuNP (0.8±0.1 MBq), or combination ^{177}Lu-AuNP/anti-PD1 antibody (n=7-10). Median survival was estimated by Kaplan-Meier analysis. Novel Object Recognition (NOR) and Object-Location Task (OLT) were used to evaluate treatment effects on cognition 21d after inoculation. Flow cytometry was used to profile immune cell infiltration in the brain 21d post-inoculation of mice receiving the listed treatments. ***Results:*** Median survival of saline, non-radioactive AuNP, anti-PD1, ^{177}Lu-AuNP, ^{177}Lu-AuNP/anti-PD1 treated mice were estimated to be 24.5, 26, 32, 29, and 33d respectively with 30% of anti-PD1 treated and 43% of combination treated mice surviving long-term. NOR test and OLT revealed no differences in cognitive performance between treatment groups. Compared to saline, all treatments significantly reduced the population of CD4$^+$ T-Helper Cells (CD45$^+$,CD3$^+$,CD4$^+$,CD8$^-$) and increased the population of CD8+ Cytotoxic T-Cells (CD45$^+$,CD3$^+$,CD4$^-$,CD8$^+$). ***Conclusion:*** The novel combination of anti-PD1 checkpoint immunotherapy and local infusion of ^{177}Lu-AuNP may show synergism when used to treat orthotopic murine GBM. None of the treatments impacted cognition, indicating that the radiation dose or the checkpoint immunotherapy was safe. Analysis of infiltrating lymphocytes indicated that ^{177}Lu-AuNP/anti-PD1 combination therapy was able to modulate the immune profile of the tumours. These results may merit further advancement of the ^{177}Lu-AuNP towards human trials in combination with anti-PD1 checkpoint immunotherapy. ***References:*** Georgiou, C.J., et al., Treatment of Orthotopic U251 Human Glioblastoma Multiforme Tumors in NRG Mice by Convection-Enhanced Delivery of Gold Nanoparticles Labeled with the beta-Particle-Emitting Radionuclide, (177)Lu. Mol Pharm, 2023. 20(1): p. 582-592.

EP-0057

Compositedegradablepolymer microspheresloaded with 177Lufor Transarterial Radioembolization therapy of Rat hepatocellular carcinoma

L. Xiao, *H. Cai, L. Li;*
Department of Nuclear Medicine, West China Hospital, Sichuan University, Chengdu, CHINA.

Aim/Introduction: We developed a new biodegradable polymer microsphere that can simultaneously load ^{177}Lu and MgO (Magnesium oxide) nanoparticle (relieve tumor hypoxia). Chitosan microsphere (CS) was regarded as skeleton structure for surface modification through polydopamine (PDA) to chelate ^{177}Lu and load MgO (^{177}Lu-PDA-CS-MgO). Then, we explored TARE therapeutic efficacy and biosafety of ^{177}Lu-PDA-CS-MgO on rat HCC. ***Materials and Methods:*** 1. Microspheres preparation: CS was prepared by emulsion crosslinking method. MgO nanoparticles were loaded at PDA-CS to develop PDA-CS-MgO. Catechol group in PDA-CS was used for chelating ^{177}Lu. 2. TARE treatment efficacy evaluation in HCC rats: The HCC rats were divided into four groups: ^{177}Lu-PDA-CS-MgO group, ^{177}Lu-PDA-CS group, PDA-CS group and sham operation group. TARE was performed by laparotomy and then drug was injected through hepatic artery. SPECT/CT was performed to monitor in vivo stability of ^{177}Lu-PDA-CS-MgO and ^{177}Lu-PDA-CS. MRI scan was performed to evaluate tumor growth and gross specimens were monitored after administration. The survival duration of each rat was monitored. HE analysis, TUNEL analysis, immunohistochemical analysis, and WB (western blot) analysis were conducted on tumor tissues of each group 5 weeks after surgery. ***Results:*** CS and PDA-CS-MgO was successfully developed. The labeling rate of ^{177}Lu-PDA-CS-MgO was 87.1 ± 0.5% and loading dose was 1.11 ± 0.005 mCi/g. When ^{177}Lu-PDA-CS-MgO was placed in FBS and PBS for 11 days, radiochemical purity decreased slowly. After 216 h at FBS, radiochemical purity was 85.15 ± 0.91% , and that of PBS was 88.65 ± 0.20%. After 8 weeks of drug induction, 82 rat HCC models were successfully induced, with a success rate of 86.3% (82/95). SPECT/CT imaging after TARE operation showed that ^{177}Lu-PDA-CS-MgO was mainly distributed in the liver until 56 days post-injection. MRI scan and gross specimens indicated ^{177}Lu-PDA-CS-MgO could significantly inhibit tumor growth and spread compared with other treatment groups. HE staining and TUNEL analysis showed more tumor necrosis and apoptotic cells in ^{177}Lu-PDA-CS-MgO group. The HCC rats in this group had longer overall survival. Immunohistochemical analysis and WB results showed that ^{177}Lu-PDA-CS-MgO could reduce the expression of hypoxia inducible factor-1α (HIF-1α), CD31 and Ki-67. ***Conclusion:*** In this study, ^{177}Lu-PDA-CS-MgO was developed successfully, with high labeling rate, good degradability, blood compatibility, and good in vivo and in vitro stability. ^{177}Lu-PDA-CS-MgO can effectively inhibit tumor growth and spread, relieve hypoxia, prolong survival time in HCC rats through TARE treatment.

EP-0058

Nucleic acid nanospheres for PET imaging and antioxidant therapy of hepatic ischemia-reperfusion injury

H. Wang, *X. Lan, D. Jiang;*
Wuhan Union Hospital, Tongji Medical College, Huazhong University of Science and Technology, Wuhan, CHINA.

Aim/Introduction: Organ ischemia with inadequate oxygen supply followed by reperfusion can lead to complex inflammatory responses and oxidative stress. Liver is highly dependent on

oxygen supply and susceptible to hypoxic or anoxic conditions. Hepatic ischemia-reperfusion injury (IRI) includes the restriction and reoxygenation of blood supply to activate an immune response that may lead to cellular damage and organ dysfunction. This process is not only a pathophysiological process, but also a complex systemic process affecting multiple tissues and organs. Numerous studies have shown that oxidative stress plays a key role in IRI, and scavenging reactive oxygen species (ROS) through antioxidant supplementation can reduce oxidative stress and the ensuing organ damage. Herein, we asked whether DNA nanospheres delivered to the liver can react with ROS in the liver and alleviate the clinical symptoms of IRI. ***Materials and Methods:*** In this study, we successfully synthesized nucleic acid nanospheres (NANS) as a DNA nanoparticle with desirable ROS scavenging capacity, it can target and accumulate in the liver for antioxidant treatment of IRI. Approximately 100 μL (0.1 mCi) of ^{68}Ga-NANS or ^{64}Cu-NANS was administered intravenously to mice (n = 3) to monitor the biodistribution of NANS in vivo. PET/CT imaging was performed at three time points of 0.5, 1 and 2 h after injection of ^{68}Ga-NANS. ^{64}Cu-NANS in animals was imaged longitudinally at 0.5, 12, 24, and 48 h after injection. Tracer uptake in percentage of injected dose per gram of tissue (%ID/g) and time-activity curves were charted accordingly. At the final time point after PET/CT scanning, all mice were euthanized and dissected to collect major organs/tissues for biodistribution measurement and analysis. ***Results:*** After injection, NANS is mainly absorbed by mononuclear phagocyte system (MPS) and concentrated in Kupffer cells. NANS can effectively remove intracellular and extracellular ROS, inhibited the activation of Kupffer cells and macrophages, preventing them from releasing proinflammatory cytokines, subsequently minimizing the adhension, recruitment, and infiltration of neutrophils, and eventually inhibiting the continued inflammatory process, superoxide dismutase (SOD) levels were restored and maintain aspartate aminotransferase (AST) and alanine aminotransferase (ALT) levels in IRI mice in a relatively normal range, thereby alleviating the liver injury caused by IRI. ***Conclusion:*** NANS is mainly distributed in the liver after injection into the body, showing specific advantages in the treatment of hepatic IRI, and the increased ROS in the liver caused by IRI is consumed by NANS, which can significantly alleviate liver injury.

EP-0059

Continuous enzymatic hypoxia relief with NIR-II moderate photothermal assistance for enhanced Yttrium-90 microspheres oncotherapy

J. Li, *X. Su;*
The First Affiliated Hospital, School of Medicine, Zhejiang University, Hangzhou, CHINA.

Aim/Introduction: Radiopharmaceutical-based tumor theranostic is the representative modality in precise medicine. In situ tumor oxygenation via catalase-mimicking nanomaterials has been an attractive strategy to improve the therapeutic index of radionuclides internal radiotherapy (RIT). However, the fleeting hypoxia relief activated by the instable catalase or biodegradable nanoenzymes failed to match the days-scale therapeutic period of RIT, such as Yttrium-90 (^{90}Y) microspheres oncotherapy. ***Materials and Methods:*** A persistent RIT-enhancing method based on the NIR-II-responsive Pd-based nanoplatforms with facet-dependent catalase-like activity is proposed. Specifically, rationally designed Pd@Au nanosheets (Pd@Au NSs) enable steadily enzyme catalysis of endogenous H_2O_2 for O_2 generation to address the hypoxia-induced RIT resistance, the incompletely surface-coated Au layer can red-shift the absorption of Pd NSs to near-infrared-II (NIR-II) biowindow. With the combination of NIR-II moderate photothermal treatment, the catalase-mimicking activity of Pd@Au NSs and tumor blood perfusion are simultaneously boosted, which help building a feasible therapeutic tumor microenvironment and the inhibition of DNA damage repair for the enhanced ^{90}Y microspheres therapy. ***Results:*** The facet-dependent catalase-like activity of Pd@Au NSs with polyethylene glycol modification can efficiently accumulate in tumor by enhanced penetration and retention (EPR) effect after intravenous injection, and enable the persistently efficient hypoxia relief, which fits the days-scale therapeutic period of ^{90}Y-microshperes oncotherapy. Under the guidance of NIR-II photoacoustic imaging (PAI), the moderate NIR-II photothermal treatment was operated to further improve the enzyme activity of Pd@Au NSs and inhibit the repair of ionizing radiation-mediated DNA damage. Benefiting from this two-pronged tactic radiosensitization effect, ^{90}Y-microshperes combined with Pd@Au NSs and low power density NIR-II laser irradiation enabled efficient ablation of 4T1 subcutaneous tumors (cure rate = 80%), while the single ^{90}Y-microshperes with the same radioactivity dose could only slightly suppress tumor growth (cure rate = 0%) compared with saline-injected group. Hematoxylin-eosin and TUNEL staining analysis of treated tumors further demonstrated the enhanced therapeutic effect and good biocompatibility of this combined therapy. ***Conclusion:*** This work innovated a RIT sensitization strategy to strengthen the performance of clinically approved RIT formulations, pushing forward the incorporation of catalytic nanomedicine and nuclear medicine to improve the clinical benefits of RIT.

EP-0060

Prostate-specific membrane antigen-targeted endogenous radiotherapy of triple-negative breast cancer

A. Heesch[1], *J. Maurer*[2,3], *A. Florea*[1], *A. Morgenroth*[1], *F. M. Mottaghy*[1,4];
[1]*Department of Nuclear Medicine, University Hospital RWTH Aachen, Aachen, GERMANY,* [2]*Department of Obstetrics and Gynecology, University Hospital RWTH Aachen, Aachen, GERMANY,* [3]*Center for Integrated Oncology (CIO), Aachen, Bonn, Cologne, Düsseldorf (ABCD), GERMANY,* [4]*Department of Radiology and Nuclear Medicine, Maastricht University Medical Center (MUMC+), Maastricht, NETHERLANDS.*

Aim/Introduction: Triple-negative breast cancer (TNBC) has a very aggressive nature and affects especially young women. Current treatments include chemotherapy, radiation, and surgery, however more specialized approaches are limited. Our previous in vitro data demonstrate prostate-specific membrane antigen (PSMA) expression on TNBC associated endothelial cells. Thus we aim to develop a treatment with PSMA as a vascular target for endogenous radiotherapy with [^{177}Lu]Lu-PSMA in a TNBC xenografted mouse model. The efficacy of one high dose versus four low doses of [^{177}Lu]Lu-PSMA is analyzed concerning tumour growth inhibition. ***Materials and Methods:*** [^{177}Lu]Lu-PSMA was successfully synthesized by a routine procedure. Quality control was done with radio-HPLC. MDA-MB-231 cells were used for orthotopic tumour implantation in immunocompromised mice. For therapy, the animals were intravenously injected with [^{177}Lu]Lu-PSMA (1x for single dose or 4x for fractionated treatment) or NaCl (control). Tumour growth was monitored weekly via 2-[^{18}F]FDG microPET/CT. Ex vivo analyses included immune-, H&E, and TUNEL staining. ***Results:*** We observed significant smaller tumour

volumes in both therapy groups compared to the control group 30 days after therapy start. Tumour growth inhibition rates were 38% (1x [^{177}Lu]Lu-PSMA) and 30% (4x [^{177}Lu]Lu-PSMA). Immunolabeling with α-PSMA and α-CD31 antibodies revealed co-localization on tumour-associated vasculature. H&E staining of organ sections showed no morphological abnormalities. TUNEL staining revealed a higher amount of apoptotic cells in the tumour compared to the control. ***Conclusion:*** Treatment of TNBC xenografted mice with [^{177}Lu]Lu-PSMA successfully and significantly (single dose: $p<0.001$; fractionated dose: $p=0.02$) inhibited tumour growth. Importantly, no off-target damage to other organs was observed. More ex vivo analyses like microautoradiography and hypoxia stainings will be done and the SUV values from the PET scans will be quantified. Future studies could include a combination of [^{177}Lu]Lu-PSMA radiotherapy and cytostatics to improve treatment efficacy. ***References:*** (1) Heesch et al. Cells 2023, 12(4):551

EP-0061

Impact of injection velocity during transarterial radioembolization, an in vitro analysis

T. Snoeijink[1], *J. L. van der Hoek*[2], *H. Mirgolbabaee*[2], *E. Groot Jebbink*[2], *J. F. W. Nijsen*[1];
[1]*Radboud University Medical Centre, Nijmegen, NETHERLANDS,* [2]*University of Twente, Enschede, NETHERLANDS.*

Aim/Introduction: Transarterial radioembolization (TARE) is an established treatment method for patients with primary and secondary liver malignancies. During this treatment, radioactive microspheres are injected into the arterial vasculature of the liver via a microcatheter. Microspheres are transported through the arterial vasculature until they lodge predominantly in and around tumorous tissue. However, it is seen in clinical practice that the microsphere distribution towards tumorous tissue differs per procedure, medical practitioner and patient. The aim of the current study was to investigate the influence of injection velocity on the microsphere mixture in the blood and distribution in the blood vessels during TARE. ***Materials and Methods:*** A symmetrical right hepatic artery phantom was developed which bifurcates three times into eight outlets. A blood-mimicking fluid (BMF) was pumped through the phantom composed of water, glycerol and urea, with respective weight percentages of 55.8%, 34.2% and 10%, yielding a density of 1.1 g/ml and viscosity of 3.5 cP. To create a physiological representative blood flow waveform, a programmable piston pump (SuperPump, ViVitro labs) was used. Microsphere injections were performed with non-irradiated holmium loaded poly(L-lactic acid) microspheres (Quirem Medical B.V.) in a pulsed manner (0.2 ml per push, 24 ml/min), using a Progreat 2.7F microcatheter (Terumo). The injection solution consisted of blue dyed 0.9% saline solution with a microsphere concentration of 15 mg/ml. To monitor the microsphere stream at the catheter tip, videos were taken with a high speed camera with 500 frames/s (Fastcam SA2, Photron) during injection. BMF and microspheres were collected at each outlet. Dye concentrations were measured using a spectrophotometer (Tecan Infinite 200 PRO, Tecan Trading AG) and microspheres were extracted and weighed for comparison. ***Results:*** The first preliminary results show that the flow profile of microspheres is influenced by the injection velocity. With currently used injection velocities (24 ml/min), streamlined outflow patterns were observed at the catheter tip, implying a laminar flow. ***Conclusion:*** In TARE it is assumed that microspheres will follow the blood flow, which is favourable is case of a non-targeted injection. However, in this in vitro set-up streamlined outflow patterns were observed, having an impact on the behaviour of the microspheres in the blood and thus the microsphere distribution. Therefore, exact influence of injection velocity on the mixing and distribution should be investigated quantitatively in both phantom models and patients.

EP-0062

Sn-117m Homogeneous Colloid is a Disease-Modifying Device in the Treatment of Osteoarthritis

C. Doerr[1], *A. Bendele*[2], *J. Simon*[3], *N. Stevenson*[4], *G. Gonzales*[1];
[1]*Serene, LLC, The Woodlands, TX, UNITED STATES OF AMERICA,* [2]*Inotiv, Boulder, CO, UNITED STATES OF AMERICA,* [3]*Isotherapeutics Group, LLC, Angleton, TX, UNITED STATES OF AMERICA,* [4]*Exubrion Therapeutics, Buford, GA, UNITED STATES OF AMERICA.*

Aim/Introduction: Radionuclides have been used to treat human rheumatoid (RA) and osteoarthritis (OA) for decades outside of the United States. The procedure, radiosynoviorthesis (RSO), is the intra-articular injection of an isotope, either as a non-homogeneous microparticle (Er-169 and Y-90) or a colloid (Re-186), that is engulfed by synovial macrophages. This results in thickening of the synovium and sclerosis and fibrosis resulting in decreased joint pain. Sn-117m, used in the manufacture of a homogeneous Sn-117m colloid (HTC) for RSO procedures, is generated in nuclear reactors via 117Sn(n,n'γ)117mSn. Although radionuclide drug injections for RSO are approved in Europe, in the US the HTC device is available only for the treatment of canine elbow OA. Our aim was to investigate whether the HTC demonstrated an OA disease modifying effect, and we report here the data from cGMP/GLP rodent trials which suggest the existence of that effect. ***Materials and Methods:*** Adult rats (n=109) were studied using the surgical meniscal tear OA model. The trial consisted of rats divided into 5 arms including 2 control arms, 1 safety arm, and 2 treatment arms using RSO dosages of 2μCi (low dose) and 10μCi (high dose) HTC. Rats were sacrificed at 1, 4, 6 and 10 weeks. Sacrificed study knees received histopathology analysis. Sn-117m was produced in the BR2 nuclear reactor followed by manufacturing of HTC. ***Results:*** Generally, animals treated with 2 or 10 μCi had lesion severity that was slightly to significantly reduced compared to non-injected OA controls. Based on substantial cartilage degeneration widths with support from other cartilage degeneration parameters (scores, depth ratios, osteophyte measures), there is evidence of beneficial effects of treatment at week 1, and trends toward at 4 and 6 weeks on some parameters. ***Conclusion:*** To our knowledge, this is the first time that a medical device has provided evidence of an OA disease modifying effect. Our rat data translates to and provides validation for the Phase 1 human clinical trial of OA and RA therapy that is authorized to begin in Canada. Although OA contributors include obesity, malalignment, acute and repetitive joint injuries, generalized disease, heredity, and muscle weakness, OA ultimately progresses to include a rheumatologic component which also is well known to respond to RSO treatments. We anticipate that HTC will produce a disease modifying effect in the planned human OA/RA trials, similar to that seen in the rat trials.

EP-0063

Therapeutic potential of a Claudin 18.2 targeted alpha therapeutic [225Ac]-FPI-2474 in a pre-clinical gastric cancer tumor model

S. Almasi, *T. Kostelnik, V. Subramony, N. Robinson, W. Turnbull, B. L. Thériault, C. P. Leamon, J. Valliant;*
Fusion pharmaceuticals, Hamilton, ON, CANADA.

Aim/Introduction: Claudin 18.2 (CLDN18.2) is a tight junction protein which in healthy individuals is strictly expressed in differentiated epithelial cells of the gastric mucosa. Its high

expression has been reported on the epithelial surface of several malignant tumors such as gastric, colon, breast, and liver cancers. Its tumor-specific expression pattern points to an attractive molecular oncology target, and many therapies targeting Claudin 18.2 are currently in clinical development. To date, there is no approved targeted therapy for CLDN18.2 expressing tumors. Herein we describe the development of a Claudin 18.2 targeted alpha therapeutic (TAT), [^{225}Ac]-FPI-2474, in a pre-clinical mouse xenograft model of gastric cancer. ***Materials and Methods:*** [^{225}Ac]-FPI-2474 is a radioimmunoconjugate consisting of an anti-Claudin 18.2 monoclonal antibody conjugated to a proprietary DOTAGA-based chelate (FPI-2472) and radiolabeled with actinium-225 [^{225}Ac]. [^{177}Lu]-FPI-2473 is the Lutetium-based radiolabeled analogue. The biodistribution and therapeutic efficacy of these radioimmunoconjugates were evaluated in a gastric cancer model. MNK45 cells were engineered to stably overexpress Claudin 18.2 via lentiviral transduction (MKN45-CLDN18.2). Cell surface receptor expression was confirmed via flow cytometry, and receptor numbers quantified via radioligand binding assay. These MKN45-CLDN18.2 cells were used to generate subcutaneous tumor xenografts in athymic nude mice for in vivo evaluation. For biodistribution studies, approximately 185 MBq/kg of [^{177}Lu]-FPI-2473 was injected intravenously via the lateral tail vein, and organ radioactivity was quantified ex vivo at timepoints between 4 h and 168 h using a gamma counter by calculating the percentage of injected dose per gram of tissue (%ID/g). For therapeutic studies, a single intravenous dose of [^{225}Ac]-FPI-2474 was administered over a dose range of 92.5 to 555 kBq/kg. Tumor size and body weight were monitored for at least 30 days. Tumor volumes (V; in mm^3) were calculated as V = 0.5 x L (length) x W^2 (width). ***Results:*** A stable MKN45-CLDN18.2 overexpressing cell line was successfully generated, expressing on average 150,000 receptors/cell. Biodistribution studies of [^{177}Lu]-FPI-2473 showed robust average tumor uptake peaking at approximately 30%ID/g at 96 h post-injection, while minimal uptake (≤10%ID/g) was observed in normal organs at all time points tested. Therapeutic evaluation of [^{225}Ac]-FPI-2474 is currently underway. ***Conclusion:*** [^{177}Lu]-FPI-2473 demonstrated high tumor uptake along with minimal normal tissue uptake, suggesting a tumor specific accumulation of [^{177}Lu]-FPI-2473 in Claudin 18.2 expressing xenografts. Therapeutic evaluation of [^{225}Ac]-FPI-2474 has been initiated to ascertain whether the level of tumor uptake of the anti-Claudin 18.2 radioimmunoconjugate will translate into preclinical therapeutic efficacy.

EP-0064

Development and evaluation of fluorescent SSTR2-antagonists for intraoperative image-guided surgery of NETs

M. Handula[1], *S. Beekman*[1], *Y. Seimbille*[1,2];
[1]*Erasmus MC, Rotterdam, NETHERLANDS,*
[2]*TRIUMF, Vancouver, BC, CANADA.*

Aim/Introduction: Neuroendocrine tumors (NETs) are considered as a rare type of cancer with an incidence rate of 1-5 per 100,000 people affected yearly in Europe. Although advanced metastatic NET patients are treated with chemotherapy and peptide receptor radionuclide therapy (PRRT), surgery remains the main treatment for local neuroendocrine tumors. Considering that the somatostatin receptor subtype 2 (SSTR2) represents an optimal target for PET imaging and radionuclide therapy of NETs, it could also be exploited to design fluorescent probes that will help surgeons to visualize neoplasms and delineate surgical margins. The antagonist DOTA-JR11 showed higher tumor uptake and better biodistribution profile than the agonist DOTA-TATE during (pre)clinical evaluation. Therefore, we developed fluorescent probes based on JR11 for intraoperative image-guided surgery of NETs to reduce positive surgical margins and disease recurrence. ***Materials and Methods:*** Four fluorescent JR11 analogs were synthesized by solid-phase peptide synthesis (SPPS). The fluorescent dye, cyanine 5.5 (Cy5.5), was coupled either directly or via a 6-aminohexanoic acid, PEG_3 or PEG_6 linker at the N-terminal position of the peptide scaffold to obtain efSOMA-01, efSOMA-02, efSOMA-03 and efSOMA-04, respectively. Competitive binding assay in U2OS.SSTR2 cells was carried out to determine the affinity of the compounds to the receptor. Cell uptake assay was performed in U2OS.SSTR2 and SSTR2-negative (PC3-PIP) cells to demonstrate uptake specificity. ***Results:*** efSOMA-01-04 were obtained in 20.5, 4.4, 7.6 and 7.3% chemical yield, respectively. The four analogs were obtained in very high chemical purity (> 95%). Competitive binding assay showed that the binding affinity of the fluorescent efSOMA-01, efSOMA-02, efSOMA-03 and efSOMA-04 to SSTR2 was 4.7 to 16.3-fold lower than the binding affinity of the parent peptide DOTA-JR11 (IC_{50} values of 84.7, 58.1, 27.3 and 24.5 nM, respectively, vs. 5.2 nM for DOTA-JR11). The preliminary cell uptake assay revealed high uptake in SSTR2-overexpressing cells for all analogs, whereas no fluorescence was observed in the SSTR2-negative cells, confirming the specificity of our fluorescent JR11 analogs to the receptor. ***Conclusion:*** The four fluorescent JR11 analogs were successfully synthesized and characterized by LC/MS. They all exhibited good binding affinity to SSTR2 and showed high and specific cell uptake. In vivo studies in tumor-bearing mice are underway to confirm the applicability of our probes to fluorescence-guided surgery of NETs.

EP-0065

Preclinical studies for optimal implementation of GRPR radiotracers in clinical studies

T. S.T. Damiana[1], *P. Paraïso*[1], *C. de Ridder*[2], *D. Stuurman*[1], *L. van den Brink*[1], *Y. Seimbille*[1], *S. U. Dalm*[1];
[1]*Department of Radiology & Nuclear Medicine, Erasmus Medical Center, Rotterdam, NETHERLANDS,* [2]*Department of Experimental Urology, Erasmus Medical Center, Rotterdam, NETHERLANDS.*

Aim/Introduction: Gastrin-releasing peptide receptor (GRPR) radiotracers have successfully been studied in preclinical and/or clinical studies for imaging and treatment of breast cancer (BC), prostate cancer (PCa), and gastrointestinal stromal tumors (GIST). However, there is no clear comparison of the GRPR radiotracers available, hampering accurate selection of the most optimal radiotracer. Moreover, as GRPR expression and radiosensitivity are prerequisites for the success of GRPR-mediated interventions, it is crucial to know how these factors are affected by standard-of-care treatments for correct positioning of GRPR radiotracers in disease management. Accordingly, we performed a head-to-head comparison of the two most applied GRPR radiotracers, RM2 and NeoB, and studied the effect of standard-of-care treatments on GRPR expression and radiosensitivity of cancer cells. ***Materials and Methods:*** We compared binding of [^{111}In]In-NeoB and [^{111}In]In-RM2 to PCa, BC and GIST tissues. Tissues were incubated with 1nM [^{111}In]In-NeoB and [^{111}In]In-RM2+/-1μM Tyr^4-BBN for 1h, and analyzed using the BeaQuant. Moreover, depending on the cell line, we studied the influence of doxorubicin, docetaxel, tamoxifen and letrozole on GRPR expression and radiosensitivity of the human PCa and BC cell line PC-3 and T47D, respectively. Cells were pre-treated at the

IC50 value of the treatments, subsequently incubated with 1nM [^{111}In]In-NeoB+/- 1µM Tyr^4-BBN to determine radiopharmaceutical uptake. Additionally, GRPR mRNA levels were measured using RT-qPCR. Results are expressed relative to vehicle-treated cells set at 100%. To determine radiosensitivity, pretreated cells were exposed to 0-14 Gy external beam radiation therapy (EBRT), and cell density was determined after five days using an SRB assay. ***Results:*** The autoradiography studies revealed higher binding of [^{111}In]In-NeoB to all investigated tissues. Docetaxel decreased radiotracer uptake to 52.5±3.4%, GRPR mRNA expression to 44.7±14.5% and radiosensitivity of PC-3 cells. Regarding T47D cells, doxorubicin-pretreated cells showed an increase in GRPR mRNA expression to 242.4±53.4% and radiotracer uptake to 125.2±6.3%, and cells were less sensitive to EBRT. Tamoxifen pre-treated cells reduced radiotracer uptake to 73.8±1.8%, and both tamoxifen and and letrozole pretreatment did not influence the radiosensitivity of T47D cells. ***Conclusion:*** We demonstrated that [^{111}In]In-NeoB is superior to [^{111}In]In-RM2 in binding to human PCa, BC and GIST tissue. Furthermore, we showed that prior treatment may alter essential factors for the success of GRPR radiotracer treatment and should be considered when GRPR-mediated interventions are positioned in the clinic. In-vitro and in-vivo studies further unravelling the effects of chemotherapies and hormone therapies on GRPR expression, radiosensitivity and GRPR-targeted radionuclide therapy are ongoing.

EP-0066

Restoration of impaired portal glucose sensing by targeted manipulation of GLP-1r density in a translational model of insulin resistance

C. Malbert[1], *R. Allouche*[2], *M. Horowitz*[3], *K. L. Jones*[3];
[1]*INRAE - Aniscan, Saint-Gilles, FRANCE,* [2]*Paltech, Paris, FRANCE,* [3]*Adelaide Medical School, The University of Adelaide, Adelaide, AUSTRALIA.*

Aim/Introduction: The portal glucose sensor informs the brain of changes in glucose inflow via vagal afferents that are dependent on the glucagon-like peptide-1 (GLP-1) receptor (GLP-1r). We have shown that GLP-1r expression within the portal vein is markedly reduced in a translational model of insulin resistance (IR), associated with altered glucose signaling to the brain (1). We now investigated the potential for restoring reduced portal GLP-1r expression in IR animals using a targeted infusion of bioactive molecules, which have been demonstrated to increase GLP-1r expression in vitro. ***Materials and Methods:*** Five groups, each of five miniature Yucatan minipigs, aged three years, were used. One group was maintained lean and insulin sensitive, while the remaining four were made IR by a high fat-high sucrose diet for 4 months. The precise portal location of the low-density GLP-1r area (compared to lean animals) was initially defined using PET/CT imaging after the administration of 68Ga-DO3A- exendin-4 and a catheter, exiting in the portal connective tissue, was then fixed at this location during 3D guided laparoscopy based on PET/CT results. This catheter was used to infuse continuously either saline, dihydrotestosterone (DHT, 10 µg/kg/24H), metformin (MET, 2 mg/kg/24H), or exenatide (EX, 0.01 µg/kg/24H), i.e., molecules known to increase GLP-1r density in vitro. After 2 months continuous infusion, PET/CT imaging was repeated in all animals using the same GLP-1r radioligand. Vt/Vs coded images, were obtained from PET/CT concurrently with monitoring of the arterial input function extracted from an arteriovenous shunt and radioHPLC of the authentic ligand in the plasma. Duodenal and pancreatic Vt/Vs were also computed as references of GLP-1r expression organs. ***Results:*** In IR animals, there was a marked reduction in GLP-1r density at the portal vein ($p<0.05$), but not in the pancreas or duodenum (see table). Treatment with DHT increased GLP-1r density at the portal vein substantially to be comparable to that in lean animals. The other treatments had no effect on portal GLP-1r density. Furthermore, no treatment affected the GLP-1r density in the pancreas or duodenum. ***Conclusion:*** Localized administration of DHT normalises portal GLP-1r density in IR animals, without affecting GLP-1r density in other organs. Accordingly, it is possible to restore impaired glucose sensing in IR animals. The implications for optimal management of insulin resistance /type 2 diabetes now require evaluation in humans. ***References:*** (1) Malbert et al, Diabetes, 021 Jan;70(1):99-110. doi: 10.2337/db20-0361

EP-0067

Long-term characterization of a radiolabeled hydrogel after intrastriatal injection in rats to improve post-stroke brain repair

N. Hugues[1], *C. Pin-Barre*[2], *O. Nachar*[1], *V. Nail*[1], *L. Balasse*[1], *B. Guillet*[1], *T. Trimaille*[3], *J. Laurin*[4], *P. Garrigue*[1];
[1]*Centre Européen de Recherche en Imagerie Médicale (CERIMED), Marseille, FRANCE,* [2]*Syncrosome, Marseille, FRANCE,* [3]*Institut de Chimie Radicalaire (ICR), Marseille, FRANCE,* [4]*Insitut de Neurobiologie de la Méditerranée (INMED), Marseille, FRANCE.*

Aim/Introduction: Ischemic stroke frequently leads to functional impairments by mainly affecting the striatum area. Given that few molecules are able to reach the affected cells, it remains crucial to define a suitable method for delivering promising drugs. Injectable and biodegradable hydrogels appear as an encouraging strategy to target the lesion area, avoiding repetitive administrations by precisely and progressively releasing a drug. To do so, this hydrogel was based on an amphiphilic PNIPA-Am-b-PLA-b-PEG-b-PLA-b- PNIPAAm pentablock. Hence, we aimed to characterize the degradation and biodistribution of this hydrogel following intrastriatal injection in healthy rats. Hydrogel toxicity was evaluated in hippocampal neuronal cell cultures. Then, blood-brain barrier permeability, brain glucose metabolism, microglia activation as well as dopamine transporters concentration were investigated over a 6-month period using both SPECT/CT and PET/CT in vivo imaging. ***Materials and Methods:*** Hippocampal neurons for cell culture were obtained from Sprague-Dawley rats (E18). NODAGA-functionalized hydrogel (6µl) was added to hippocampal neuronal cells at 4 days in vitro. For in vivo measurements, 9 female Sprague Dawley rats were assigned to two conditions following unilateral intrastriatal injection of 1) gallium-67 alone (^{67}Ga-NODA-GA) and 2) gallium-67 radiolabeled, NODAGA-functionalized hydrogel. SPECT/CT acquisitions were realized over 72h after injection to follow gallium-67 spreading. Blood brain barrier permeability (^{99m}Tc-DTPA SPECT/CT; day 2, 8 and 16), brain glucose metabolism (^{18}F- FDG PET/CT; day 2, 8, 16 and 6-month), microglia activation (^{18}F-DPA-714 PET/CT; 6-month) as well as dopamine transporters concentration (^{123}I-ioflupan SPECT/CT; 6-month) were investigated. Image treatment and volumes of interest were drawn according to a rat brain atlas. Immunohistochemical measurements of microglia activation and neuronal survival were ex vivo assessed after 6 months. ***Results:*** There was no significant difference between control and hydrogel conditions in vitro. The injection of the radiolabeled hydrogel enabled a prolonged residence time of the gallium-67 SPECT signal at the site of injection, with a slower and more progressive spreading (at 1h:***P=0.001; 18h:*P=0.028; 24h:P=0.729). Both the blood-brain barrier permeability and brain glucose metabolism

were not significantly modified following hydrogel injections. Finally, neither the microglial activation nor the dopamine transporter concentrations were affected by the hydrogel at 6 months. Immunohistochemistry confirmed the imaging results. ***Conclusion:*** This study used molecular imaging to characterize the hydrogel properties at both early and later time points after intrastriatal injection in healthy rats. The use of this hydrogel thus seems suitable to assess the local effects of a loaded drug, in a rodent model of stroke.

EP-0068

miRNAs as Early Biomarkers of GEPNET Disease Progression. Evaluation of Feasibility and Preliminary Results

F. SCALORBI*, M. Gariboldi, L. Roz, G. Centonze, F. Facchinetti, G. Calareso, E. Garanzini, V. Lagano, G. Argiroffi, S. Pusceddu, M. Maccauro, E. Seregni, M. Milione;*
Istituto Nazionale Tumori Milano, MILAN, ITALY.

Aim/Introduction: Primary aim: to evaluate feasibility of miRNA expression in GEPNET (gastro-entero-pancreatic neuroendocrine tumours) paraffin samples (FFPE). Secondary aim: to early predict disease progression after RLT (radio ligand therapy) by miRNA expression. ***Materials and Methods:*** Tissue samples from G1-G2 well differentiated GEPNETs treated with RTL (177Lu-DOTATATE, 4 administrations, 7.4 GBq each) from April 2019 to December 2021 were included. FFPE collected before RLT, with at least 50% cellularity and no protein/solvent contamination were selected. Two contrast enhancement CT/MRI scans per patient were collected, performed within 3 months before and 3 months after RLT, to assess the response to treatment (progression (PD) versus non-progression), applying RECIST1.1 criteria. The expression of 13 miRNAs was quantified by qRT-PCR, after housekeeping normalisation, comparing progressive and non-progressive groups. One biological and 2 technical replicates were performed (Standard Deviation < 0,5). Delta Delta CT (DDCT) formula was applied to quantify miRNA expression. Univariate and multivariate analysis were performed to determine the power of clinical features (gender, age, Ki67 grading, primary tumor, metastatic disease) and miRNA expression to predict the disease progression. Stata v16 was applied. ***Results:*** Forty-eight FFPE samples (33/58 (68.7%) midgut, 15/58 (31.3%) foregut; 15/58 (52.1%) metastasis; whole population mean Ki67: 4.8%, SD 6.0, range 0.2-20; mean cellularity 80.3%, SD 14.1, range 50-99;) were selected. Thirty-three (68.7%) patients were females and the mean age of whole population was 56.4 years (range 33-75). No significant contaminations were observed. Results from the technical replicates were comparable for 9 out of 13 miRNAs. Eight (16.7%) cases showed progression after RLT. miRNA-21 expression and Ki67 grading were the only two significant predictive variables of PD. In details, low miRNA-21 expression has a protective role (Coefficient -0.22, 95%CI [-0.43; -0.009], p: 0.042) meanwhile high Ki67 grading (continuous values) has a negative prognostic role in terms of PD (Coefficient 1.01, 95%CI [0.30; 1.73], p: 0.010). ***Conclusion:*** Evaluation of miRNA expression is a feasible procedure in GEPNET FFPE, with good reproducibility. MiRNA-21 is a strong independent early predictor of disease progression that should be validated by clinical trials to more accurately stratify GEPNET aggressiveness and, therefore, predict the response to target therapies.

EP-0069

Implementation of a human brain tumour model in large animals, to translate holmium-166 microbrachytherapy towards the clinic.

N. Klaassen[1]*, M. Boswinkel*[1]*, N. C. Morsink*[2]*, S. A. van Nimwegen*[2]*, J. F. W. Nijsen*[1]*;*
[1]*Department of Medical Imaging, Radboud University Medical Center, Nijmegen, NETHERLANDS,* [2]*Utrecht University, Department of Clinical Sciences of Companion Animals, Faculty of Veterinary Medicine, Utrecht, NETHERLANDS.*

Aim/Introduction: Glioblastoma is an inherently aggressive tumour and the most lethal primary brain tumour in adults. Standard-of-care include surgery, radiotherapy and chemotherapy. Despite these therapy options patients often get a recurrence after a few months, with limited treatment options consequently. To improve patient survival, advances in therapy are needed. An innovative form of brachytherapy, microbrachytherapy, may lead to better treatment. Holmium-166 (^{166}Ho) is a good candidate for microbrachytherapy due to its characteristics, which allow for MRI/CT/SPECT imaging and therapy (β-irradiation). ^{166}Ho-microspheres have been injected subcutaneously in mice in vivo. However, the relatively deep penetration of ^{166}Ho β-radiation and the absence of sulci in mice, make the brain of small animals unsuitable for translational purposes. Therefore, a tumour model in a large animal with a brain anatomically comparable to human brains is needed. The aim of this study was to setup a tumour model in a pig brain to ultimately test microbrachytherapy. ***Materials and Methods:*** Immune supressed Landrace pigs (n=8) were injected with 30-70x10^6 human glioblastoma cells (U87, 50 µL) in both frontal lobes. Injection positions were confirmed using X-ray. To monitor tumour growth, animals were imaged on days 0, 7, 14, 21 and 28 post-implantation using MRI. Animal health was monitored closely and the degree of immune suppression was determined by immune suppressive drugs levels in the blood. After the last imaging session the animals were euthanised, subsequently, the brain tissue was imaged ex vivo on CT and MRI. After fixation, histology (H&E, S100, GFAP, SOX10 and Vimentin) was performed to characterize the tumour and surrounding tissue. ***Results:*** During the experiment, animals showed only minor side effects. MR imaging showed cell growth in all pig brains over time (diameter of 5 to 15 mm). The amount of tumour cells injected was optimized to 70 million cells per injection, injecting the cells very slowly into the brain and leaving the syringe for 1 min before removal. Cell growth was also seen with macroscopic and histological evaluation. Histological analysis showed the presence of tumour cells, but in several animals also a considerable amount of immune cells. In these animals levels of immune suppressive drugs in the blood turned out to be lower than anticipated. ***Conclusion:*** Implementing a human tumour model in pigs is feasible and looks promising, but the model needs further optimization to become a reliable and translatable tumour model for treatment validation.

EP-0070

Targeted Alpha Therapy Using Terbium-149 with Somatostatin Analogues: Comparison of [149Tb]Tb-DOTA-LM3 and [149Tb]Tb-DOTATATE

S. D. Busslinger[1]*, A. K. Mapanao*[1]*, C. Favaretto*[1,2]*, P. V. Grundler*[1]*, U. Köster*[3]*, K. Johnston*[4]*, R. Schibli*[1,5]*, N. P. van der Meulen*[1]*, C. Müller*[1,5]*;*
[1]*Paul Scherrer Institut, Villigen-PSI, SWITZERLAND,* [2]*University Hospital Basel, Basel, SWITZERLAND,* [3]*Institut Laue-Langevin, Grenoble, FRANCE,* [4]*ISOLDE/CERN, Geneva, SWITZERLAND,* [5]*ETH Zurich, Zurich, SWITZERLAND.*

Aim/Introduction: Terbium-149 is regarded as a particularly attractive radionuclide for targeted α-therapy. It is characterized by favorable physical decay properties ($T_{1/2}$: 4.1 h, E_α: 3.97 MeV, I:

16.7%) and the absence of α-emitting daughter nuclides [1-2]. The presence of a positron emission branch ($E_{\beta+ mean}$: 720 keV, I: 7.11%) can be exploited for PET imaging [3-5]. Stable complexation of terbium-149 by a DOTA chelator allows combination with established tumor-targeting agents. The goal of this project was to investigate terbium-149 in combination with the cell-internalizing somatostatin receptor agonist (DOTATATE) and the membrane-localizing antagonist (DOTA-LM3) for direct comparison of the therapeutic efficacy of the resultant radiopeptides. ***Materials and Methods:*** Terbium-149 was produced at ISOLDE/CERN using spallation reactions and online mass separation followed by radiochemical separation at the Paul Scherrer Institute, as previously reported [4]. [^{149}Tb]Tb-DOTATATE and [^{149}Tb]Tb-DOTA-LM3 were used to determine somatostatin receptor-positive AR42J tumor cell viability in vitro after exposure to the respective radiopeptides. In vivo, the therapeutic efficacy of the radiopeptides was directly compared in mice (n=4) bearing AR42J xenografts (initial tumor size: ⊠200 mm^3). The distribution profile of the radiopeptides was assessed using PET/CT imaging 2 h after injection of the mice. ***Results:*** [^{149}Tb]Tb-DOTATATE and [^{149}Tb]Tb-DOTA-LM3 were produced at molar activities up to 20 MBq/nmol with radiochemical purities >99%. A dose-dependent effect on the AR42J cell viability was observed for both radiopeptides. [^{149}Tb]Tb-DOTA-LM3 (EC_{50} = 0.5 kBq/mL) was somewhat more potent than [^{149}Tb]Tb-DOTATATE (EC_{50} = 1.2 kBq/mL). PET images showed high accumulation of both radiopeptides in AR42J tumor xenografts. After application of 5 MBq [^{149}Tb]Tb-DOTATATE or 5 MBq [^{149}Tb]Tb-DOTA-LM3, tumor growth was delayed, resulting in significantly prolonged median survival times of mice in the treated groups (16.5 days and 19 days, respectively) in comparison to that of untreated control mice (8 days). For both radiopeptides, a second injection of 5 MBq on the consecutive day resulted in further delay in tumor growth. ***Conclusion:*** The data of these studies demonstrated the promising potential of ^{149}Tb-based somatostatin analogues for targeted α-therapy. Only minor differences were observed between the agonist and antagonist, which indicates that the subcellular localization of the radiopeptides was not decisive to effectively treat the AR42J tumors in this study. ***References:*** [1]Beyer et al. Radiochim Acta 2002, 90:247. [2]Browne and Tuli Nucl. Data Sheets 2009, 110:507 [3]Müller et al. EJNMMI Radiopharm Chem 2016, 1:5. [4]Umbricht et al. Sci Rep 2019, 9:17800. [5]Singh and Chen Nucl. Data Sheets 2022, 185:2

EP-0071

Radiation dosimetric and biodistribution comparison of the PSMA agonists 177Lu-PSMA I&T, 99mTc-Hynic PSMA and 99Tc-PSMA I&T to the 177Lu-RM2 antagonist

G. Limouris[1,2], *M. Paphiti*[3], *A. Zafeirakis*[2];
[1]*Nuclear Medicine, Medical School, National and Kapodistrian University of Athens, Athens, GREECE,* [2]*Nucl Med Dept, Army Share Fund Hospital of Athens, Athens, GREECE,* [3]*Cyclotron Section, Pharmazac SA, Athens, GREECE.*

Aim/Introduction: Prostate cancer cells, besides PSMA, similarly over-express gastrin-releasing peptide receptor (GRPr), consisting a novel potent promising target, fulfilling the TheraGnostic concept. GRPr-antagonist RM2 with a high affinity of 3.0 to 4.7 nM, has been achieved to be labeled with beta-emitting radio-metals, as $^{177}LuCl_3$, for therapeutic purposes. We aimed to compare the absorbed doses of tumor lesions and critical organs of the agonists ^{177}Lu-PSMA I&T, ^{99m}Tc-Hynic PSMA, and ^{99}Tc-PSMA I&T, used in our Institution and compare them to the absorbed doses of the antagonist ^{177}Lu-RM2. ***Materials and Methods:*** In a tiny cohort of 9 patients (median age 73 years) suffering from hormone-resistant prostate cancer (mCRPC), candidates for n.c.a. ^{177}Lu-PSMA therapy (recently for first time implemented in our Institution), pre-therapeutic whole-body PSMA scans were performed to detect and confirm the degree of PSMA expression, using ^{177}Lu-PSMA I&T in 5, in a diagnostic activity of 444 MBq, called by us "LuteScan", ^{99m}Tc-Hynic PSMA in 2 and ^{99m}Tc-PSMA I&T in another 2 patients, in an activity of 740 MBq respectively. For dosimetry, patients underwent whole-body planar as well SPECT tomo-scintigraphy of head-neck, 4, 24 and 48h along with blood sampling, 0.5, 1, 2, 4 and 24 h p.i. Dosimetry was performed according to OLINDA/EXM 1.1 program. Individual organ masses were extracted from CT. Absorbed dose to bone marrow was calculated based on serial whole-body images and blood sampling according to the EANM guidelines. ***Results:*** The absorbed doses outcome of the three studied PSMA agonists compared to those of the antagonist RM2 showed increased uptake in tumor lesions, kidneys, lacrimal and parotid glands and not in the pancreas, observed in RM2, seen within the first p.i. 4 hrs, first-in-human reported by Kurth et al. For the latter, mean absorbed organ doses were 1.08 ± 0.44 Gy/GBq in the pancreas, 0.35 ± 0.14 Gy/GBq in the kidneys, 0.05 ± 0.02 Gy/GBq in the liver, 0.10 ± 0.06 Gy/GBq in the spleen, and 0.02 ± 0.01 Gy/GBq for the red bone marrow. The mean dose for tumor lesions was 6.20 ± 3.00 Gy/GBq. ***Conclusion:*** According to the correlative dosimetric results, the introduction and implementation of GRPr antagonist ^{177}Lu-RM2 seems to promisingly enhance the targeted radiotherapy in hormone-resistant prostate cancer patients, particularly in cases where PSMA is not overexpressed. The critical organ receiving the highest absorbed dose was the pancreas in contradistinction to the PSMA treatments performed with PSMA agonists.

EP-05

e-Poster Area

A: Preclinical Studies -> A1 Medical Preclinical -> A15 Other Medical Preclinical

EP-0072

WAY100635 and altanserin differentially modulate nigrostriatal and mesolimbic D2 receptor binding

S. Nikolaus[1], *H. J. Wittsack*[1], *M. Beu*[1], *C. Antke*[1], *B. Fazari*[2], *H. Hautzel*[3], *E. Mamlins*[1], *H. Müller*[1], *G. Antoch*[1], *F. L. Giesel*[1];
[1]*University Hospital Düsseldorf, Düsseldorf, GERMANY,* [2]*Heinrich-Heine University, Düsseldorf, GERMANY,* [3]*University Hospital Essen, Düsseldorf, GERMANY.*

Aim/Introduction: WAY100635 and altanserin (ALT) act as 5-HT1A receptor (R) agonist and 5-HT2AR antagonist, respectively. In the present study, we compared the effect of acute treatment with WAY100635 and ALT on the regional D2R binding in the rat brain. ***Materials and Methods:*** In 33 male Wistar rats, D2R binding was measured after intraperitoneal injection of WAY100635 (0.4 mg/kg), ALT (10 mg/kg) and vehicle (1 ml/kg 0.9% NaCl and 0.5 ml/kg dimethylsulfoxide, respectively). Iodine-123-IBZM (30 ± 4 MBq iv) was injected 30 and 45 min, respectively, post-challenge. Imaging data were acquired at 75 and 90 min, respectively post-challenge with the TierSPECT. For the acquisition of morphological data, rats were scanned with a dedicated small animal MRI (MRS3000

Pre-clinical MRT, 3.0 T, MR Solutions, Guildford, UK). D2R imaging data were evaluated with PMOD (version 3.5, PMOD Technologies Ltd., Zürich, Switzerland). Based on the implemented Paxinos rat brain atlas, the following regions of interest (with a diameter ≥ FWHM of the TierSPECT) were defined on SPECT-MRI overlays: nucleus accumbens (NAC), caudateputamen (CP), substantia nigra/ventral tegmental area (SN/VTA), thalamus (THAL), frontal cortex (FC), motor cortex (MC), and parietal cortex (PC), dorsal hippocampus (dHIPP) and ventral hippocampus (vHIPP), for which the presence of D2R has been confirmed (1). ***Results:*** WAY-100635 reduced D2R binding in CP (p=0.047), THAL (p=0.047), vHIPP (p=0.013), FC (p=0.015) and PC (p=0.050) relative to vehicle, whereas ALT induced an increase of D2R binding in the vHIPP (p=0.030). ***Conclusion:*** The regional reductions of D2R binding after WAY100635 reflect increases of synaptic dopamine (DA) concentrations in the nigrostriatal and mesolimbic system. Contrarily, the increase of D2R binding after ALT indicates a reduction of DA, which, however, was confined to vHIPP. From this may be concluded that DA function is modulated differentially by 5-HT1AR and 5-HT2R in the individual regions of the nigrostriatal and mesolimbic system. ***References:*** (1) Bouthenet et al., Neuroscience. 1987;20:117-55.

EP-0073

5-HT1A and 5-HT2A receptor agonists and antagonists modulate behavior and regional DAT binding in the rat brain

S. Nikolaus, *M. Beu;*
University Hospital Düsseldorf, Düsseldorf, GERMANY.

Aim/Introduction: The present study assessed the effects of the 5-HT1A receptor (R) and 5-HT2AR agonists 8-OH-DPAT and D-iodoamphetamine (DOI) and of the 5-HT1AR and 5-HT2AR antagonists WAY100635 and altanserin (ALT) on motor/exploratory behaviors and dopamine transporter (DAT) binding in the rat. ***Materials and Methods:*** The rats of the first batch (n=108) received i.p. injections of either 8-OH-DPAT (3 mg/kg), DOI (0.5 mg/kg), WAY100635 (0.4 mg/kg), altanserin (10 mg/kg) or vehicle (VEH; 1 ml/kg 0.9% NaCl and 0.5 ml/kg dimethylsulfoxide, respectively) and were placed immediately post-challenge into an open field for a 30-min assessment of motor/exploratory behaviors (duration of ambulation, rearing, sitting and explorative head-shoulder motility). The rats of the second batch (n=58) received the same treatments, but were injected 123I-FP-CIT (9±3 MBq) 30 min post-challenge into the tail vein. Specific binding of 123I-FP-CIT to the DAT was determined by subtracting unspecific binding in the cerebellar reference region from radioligand concentrations obtained 150 min post-challenge in cingulate (CING), caudateputamen (CP) and nucleus accumbens (NAC). Motor/exploratory behaviors were evaluated with Ethovision XT. ***Results:*** After 8-OH-DPAT, ambulation and head-shoulder motility were increased, while rearing and sitting were decreased relative to VEH. 8-OH-DPAT increased ambulation and head-shoulder motility, but decreased sitting relative to DOI, WAY100635 and ALT. After ALT, ambulation, rearing and head-shoulder motility were decreased, while sitting was increased relative to VEH. ALT decreased ambulation relative to DOI and explorative head-shoulder motility relative to DOI and 8-OH-DPAT. DOI decreased rearing, and WAY100635 decreased head-shoulder motility relative to VEH. WAY100635 increased rearing relative to DOI, ALT and 8-OH-DPAT. In the CING, DOI increased DAT binding relative to VEH, ALT and 8-OH-DPAT. In the CP, 8-OH-DPAT increased DAT binding relative to VEH. In the NAC, 8-OH-DPAT decreased DAT binding relative to VEH, DOI and WAY100635. Moreover, ALT decreased DAT binding relative to DOI and WAY100635. ***Conclusion:*** The 5-HT1AR agonist elevated horizontal motor activity and exploratory head-shoulder motility and reduced passive immobility relative to the other 5-HTergic compounds, while the 5-HT1AR antagonist reduced exploratory vertical motor activity relative to the other 5-HTergic compounds. Findings imply that the 5-HT1AR plays a predominant role in motor activation and inhibition as well as in the triggering of explorative behaviors. It may be inferred that the mediation of motor/exploratory behaviors is associated with 5-HTergic action on DA neurons in CING, CP and NAC.

EP-0074

Somatostatin receptor imaging in mice with different positive rate of SSTR2

Q. Xie, *X. Meng, Z. Yang, J. Yu;*
Peking University Cancer Hospital & Institute, Beijing, CHINA.

Aim/Introduction: The imaging with ^{68}Ga-DOTA-TATE, ^{68}Ga-DOTA-JR11 and Al^{18}F-NOTA-JR11 was performed to analyze the difference, and to analyze the correlation between parameters of image and pathology. ***Materials and Methods:*** The tumor bearing mouse with difference positive rate of SSTR2 was established with HEK293-SSTR2 and HEK293 cells, and the imaging was performed at the same tumor bearing mice with ^{68}Ga-DOTA-TATE, ^{68}Ga-DOTA-JR11 and Al^{18}F-NOTA-JR11 at 20, 60 and 120min. The parameters of image were obtained, including the maximum standard uptake value (SUVmax), the mean standard uptake value (SUVmean), standard deviation of SUVmean, tumor volume and coefficient of variation (CoV). Immunohistochemistry of tumor was carried out after imaging to obtain positive rate of SSTR2 and receptor expressing tumor volume (RETV). The statistics analysis was carried out to analyze the difference of three imaging and the correlation between the relative parameter of imaging and immunohistochemistry. ***Results:*** The SUVmax of Al^{18}F-NOTA-JR11 at 20min and 60min were higher than that of ^{68}Ga-DOTA-TATE (p=0.001, 0.004) and ^{68}Ga-DOTA-JR11 (p=0.033, 0.019), no significant difference was found in other groups (P>0.05). There was a significant positive correlation between positive rate and SUVmean of tumor with ^{68}Ga-DOTA-TATE, ^{68}Ga-DOTA-JR11 and Al^{18}F-NOTA-JR11 (P<0.05). And a significant positive correlation was also observed between RETV and SUVmean in all groups (P<0.05). But a significant negative correlation between positive rate and CoV was only found at the group of ^{68}Ga-DOTA-TATE at 60min and 120min (P=0.048 and 0.026). ***Conclusion:*** The uptake of tumor for Al^{18}F-NOTA-JR11 within an hour is significantly higher than that of ^{68}Ga-DOTA-TATE and ^{68}Ga-DOTA-JR11. The correlation analysis shows that the higher SUVmean of three tracers means the higher positive rate and the higher RETV. However, only does the lower CoV of ^{68}Ga-DOTA-TATE mean the higher positive rate.

EP-0075

Assessment of macrophage inflammatory activity on visceral adipose tissue in high-fat diet-induced obese mice by 18F-FDG PET/CT

K. Pahk, *H. Kwon, S. Kim;*
Korea University College of Medicine, Seoul, KOREA, REPUBLIC OF.

Aim/Introduction: Obesity induced inflamed visceral adipose tissue (VAT) secretes pro-inflammatory cytokines thereby promoting systemic inflammation and insulin resistance which further exacerbate obesity-related cardiovascular disease (CVD). Macrophages are the key players in the development of obesity-associated VAT inflammation. Extensive clinical studies

have reported that ^{18}F-fluorodeoxyglucose positron emission tomography/computed tomography (^{18}F-FDG PET/CT) can be used to evaluate the macrophage inflammatory activity on VAT in human beings. However, due to difficulty in human VAT biopsy, pathologic correlations were lacking and there was a few study on preclinical animal models. Here, we investigated whether ^{18}F-FDG PET/CT could reflect the macrophage inflammatory activity on VAT in high-fat diet-induced obese mice. ***Materials and Methods:*** Obese animal models were induced by a high-fat diet (60% fat) for 20 weeks using the male C57BL/6 mice. Insulin tolerance test was performed to evaluate the status of insulin resistance and C-reactive protein (CRP) was measured to assess the status of systemic inflammation. All animals underwent ^{18}F-FDG PET/CT before sacrifice. Macrophage inflammatory activity was evaluated using the maximum standardized uptake value (SUVmax). Flow cytometry-, histological-, and molecular analyses were performed on harvested VAT. ***Results:*** All obese animals showed insulin resistance which resembled the human metabolic syndrome, a key pathophysiological process that contributes to increase CVD risk. VAT SUVmax was increased in obese mice and significantly correlated with the levels of CRP. Furthermore, VAT from obese mice showed increased macrophage infiltration, compared to normal mice. ***Conclusion:*** ^{18}F-FDG PET/CT could visualize and evaluate the macrophage inflammatory activity on obesity-driven inflamed VAT in obese mice model. Our preclinical study strongly supports the clinical application of ^{18}F-FDG PET/CT in the assessment of VAT inflammation to patients who are vulnerable to CVD.

EP-0076

IPCEF1 serves as a novel biomarker and correlates with immune infiltration in PTC

X. Jia, *R. Gao, J. zhang, H. Xu, Y. Yang, A. Yang;*
The first hospital of Xi'an jiaotong university, Xi'an, CHINA.

Aim/Introduction: RAIR-DTC is the main reason for poor prognosis of differentiated thyroid cancer. It is widely accepted that dedifferentiation of thyroid cancer cells and loss of the ability of the iodine uptake are the primary cause. Due to the fact that this cohort of patient is generally only discovered after multiple failed iodine treatments, late-line treatment of the disease is difficult to achieve ideal results. IPCEF1 (Interaction protein for cytohesin exchange factors 1), a scaffold protein that binds to cytohesin2, has been found to be closely related to the radioiodine therapy response in DTC. However, its biological function in tumors is not clear. Its relationship with the dedifferentiation of thyroid cancer cells is also worth further exploration. ***Materials and Methods:*** The differential expression of IPCEF1 was detected in papillary thyroid carcinoma (PTC) and normal tissue using The Cancer Genome Atlas (TCGA) and Gene Expression Omnibus (GEO) databases (from the GSE3678 dataset). The relationship between IPCEF1 and tumor-infiltrating lymphocytes in the tumor microenvironment was identified using the Tumor Immune Estimation Resource (TIMER) datasets. Additionally, the biological function of IPCEF1 in PTC was evaluated using flow cytometry analysis, wound healing assays, Cell Counting Kit-8 assays, and transwell assays in vitro. The relationship between NIS and IPCEF1 was determined using clinical samples and cell lines of PTC. The diagnostic value was analyzed using receiver operating characteristic curve analysis, and the independent prognostic value of IPCEF1 was verified using Cox regression analysis in PTC patients from the TCGA cohort. ***Results:*** IPCEF1 expression were drastically downregulated and correlated with PTC grade, stage, and nodal metastasis, whereas in neighboring non-tumor thyroid tissue it was upregulated. IPCEF1 is not only involved with immune infiltration (negatively associated with dendritic cell, CD4+ central memory T cells, CD4+ effective memory T cells, Gamma delta T cell, NK cells and immunoinhibitors), but also increases apoptosis, decreases proliferation, inhibits migratory and invasive capabilities. IPCEF1 was positively associated with thyroid differentiation score and NIS expression in PTC patients in TCGA datasets. Overexpressed IPCEF1 could enhance NIS expression in vitro. Furthermore, it has the potential to provide remarkable diagnostic value in PTC (AUC = 0.966, CI = 0.952-0.980). Cox regression analysis verified IPCEF1 as an independent prognostic factor (P=0.011, HR 0.420, CI 95%: 0.215-0.815). ***Conclusion:*** IPCEF1 is a promising biomarker and may play a significant role in PTC progression, immune infiltration and differentiation.

EP-0077

Pilot study: non-invasive imaging of CD8+ T-cell infiltration during the development of type 1 diabetes in non-obese diabetic mice

S. Tokgöz[1], *C. Frielink*[1], *P. J. Wierstra*[1], *I. M. Hagemans*[2], *M. Verdoes*[2], *S. Heskamp*[1], *M. Gotthardt*[1], *M. Boss*[1];
[1]*Department of Medical Imaging, Radboud University Medical Center, Nijmegen, NETHERLANDS,* [2]*Department of Tumor Immunology, Radboud University Medical Center, Nijmegen, NETHERLANDS.*

Aim/Introduction: Type 1 diabetes (T1D) is a chronic autoimmune disease caused by immune-mediated destruction of insulin producing beta cells. Beta cell destruction is preceded by immune cell infiltration inducing inflammation of the pancreatic islets, the so-called insulitis. Although several studies suggest a potential role of autoreactive T-cells in the pathophysiology of T1D, the exact course of the T-cell infiltration during disease development is still unknown. Therefore, we have developed a non-invasive in vivo imaging technique to monitor CD8+ T-cells during the course of T1D using ^{111}In-labeled anti-CD8 SPECT/CT. The aim of this pilot study was to determine the feasibility of SPECT/CT imaging to monitor CD8+ T-cell infiltration during early immune cell infiltration, insulitis and new-onset diabetes phases of T1D in non-obese diabetic (NOD) mice. ***Materials and Methods:*** Fifteen female NOD mice aged 6, 13 and 18 weeks (n=5/group), representing early immune cell infiltration, insulitis and new-onset diabetes phases respectively, were used in this study. Mice were injected intravenously with [^{111}In]In-anti-CD8 (12.5 MBq; 8.5 µg). Three days after injection, in vivo SPECT/CT imaging was performed followed by ex vivo SPECT/CT imaging of the pancreas, ex vivo biodistribution, autoradiography, histology and immunohistochemistry (IHC) to stain for CD8+ T-cells. ***Results:*** Our results showed tracer uptake in the pancreas during the development of T1D with no significant differences in pancreatic uptake between the early immune cell infiltration (6-week-old NOD mice) and insulitis (13-week-old NOD mice) phases of T1D (1.4±0.68 vs 1.1±0.55 %ID/g, p=0.99). This was in line with IHC showing similar CD8+ T-cell infiltration in these two groups. In one mouse with new-onset T1D, we noticed lower pancreatic tracer uptake (0.34 %ID/g), which correlated well with low pancreatic CD8+ T-cell infiltration observed using IHC. In addition, we observed a clear correlation between pancreatic tracer uptake on autoradiography and CD8+ T-cell staining on IHC. ***Conclusion:*** This imaging technique allows to non-invasively follow CD8+ T-cell infiltration in the pancreas during the development of T1D. More research is required to increase our knowledge about the immunological

processes involved in the pathophysiology of T1D, which can be used to design clinical studies and thereby to possibly permit targeted therapies in T1D. This imaging technique has the potential to represent a valuable tool to monitor responses of targeted therapies. Since this imaging technique is already available in the clinics, it offers great opportunities for future clinical studies.

EP-0078

68Ga-siderophores for Klebsiella pneumoniae detection by positron emission tomography

K. Bendová[1], *M. Zappeová*[1], *P. Mlynárčik*[2], *Z. Nový*[1], *M. Popper*[1], *M. Hajdúch*[1];
[1]*Institute of Molecular and Translational Medicine, Faculty of Medicine and Dentistry, Palacký University, Olomouc, CZECH REPUBLIC,* [2]*Department of Microbiology, Faculty of Medicine and Dentistry, Palacký University, Olomouc, CZECH REPUBLIC.*

Aim/Introduction: Klebsiella pneumoniae (KP) is a bacterial pathogen that becomes increasingly more dangerous due to its growing antimicrobial resistance. Rapid and accurate diagnosis is essential to prevent the spread of this pathogen, especially in hospital setting, and to provide adequate treatment to infected patients. Here we present the use of radiolabelled siderophores, chelators produced by microorganisms, in a novel approach to diagnosis of KP infection. By replacing the iron in siderophores with radioactive gallium-68, siderophores can be detected by positron emission tomography, thereby localizing the pathogen. Based on previous testing of in vitro characteristics, we have selected several siderophores that have suitable properties and are therefore applicable candidates for in vivo imaging. ***Materials and Methods:*** Various siderophores were radiolabelled with gallium-68 and the radiochemical purity of resulting complexes was tested on radio-iTLC. In vitro uptake of radiolabelled siderophores was compared in various KP strains cultivated in different media. In vivo PET/CT imaging was performed in healthy mice and in mouse model of muscle infection with KP. Additional imaging in different animal models of KP infection was initiated. ***Results:*** All siderophores were labelled with high radiochemical purity (>95 %). Uptake in KP cultures varied depending on the KP strain and siderophore. In general, we observed very high uptake in KP cultures cultured in minimal medium in contrast to cultures cultured in rich medium. In vivo, we observed mainly renal excretion and low activity in blood 90 min p.i. in most siderophores. In addition, some of the selected siderophores showed activity in liver and intestine. In muscle infection model, we observed signal at the site of infection that varied in intensity depending on the siderophore used. ***Conclusion:*** We were able to successfully radiolabel various siderophores with high radiochemical purity and demonstrated that the resulting complexes have high in vitro uptake in KP if proper media is used. In vivo the siderophores showed accumulation at the site of infection in muscle infection model. These preliminary results indicate that siderophores might be used to diagnose KP infection, yet further testing in different infectious models is necessary and is currently being conducted. ***References:*** Acknowledgement: Funded by National Institute of virology and bacteriology (Programme EXCELES, ID Project No. LX22NPO5103) - Funded by the European Union - Next Generation EU and the Internal Grant Agency of Palacky University (project IGA_LF_2023_006)

EP-0079

Renal-clearable gambogic acid nanoparticles for PET imaging-guided acute kidney injury treatment

N. Liu*, X. Su;*
PET Center, Department of Nuclear Medicine, The First Affiliated Hospital, Zhejiang University School of Medicine, Hangzhou, CHINA.

Aim/Introduction: Acute kidney injury (AKI) is a common clinical syndrome lacking effective pharmacotherapy. Gambogic acid (GA) as an active ingredient of herbal medicines, exhibits antioxidant and anti-inflammatory effects that benefit for the treatment of AKI , but its poor aqueous solubility limits effective renal delivery. ***Materials and Methods:*** Water-soluble GA nanoparticles (GA-NPs) were prepared by PEGylating with NH2-PEG5000-NOTA. First, we characterized the physicochemical properties of GA-NPs to confirm the ultrasmall size and stability. Next, we tested its protective effects against oxidative stress damage in vitro. We further imaged the health- and AKI-mice using Al18F-labeled GA-NPs to evaluate their renal-targeting properties. Finally, the in vivo reno-protective effects and biosafety of GA-NPs were assessed by blood tests and histology analysis. ***Results:*** We had successfully constructed ultrasmall GA-NPs with preferential renal uptake for AKI theranostics. The in vitro assays confirmed that GA-NPs could protect HK-2 cells against oxidative stress damage. Besides, PET imaging of Al18F-labeled GA-NPs allowed visualization of enhanced renal uptake in murine AKI models. Importantly, the biocompatible GA-NPs efficiently ameliorated renal damage in two murine AKI models via its antioxidative, antiapoptotic, and anti-inflammatory activities. ***Conclusion:*** This work indicates that GA-NPs can be a promising therapeutic candidate for the management of AKI. ***References:*** (1) Pickkers, P.; Darmon, M.; Hoste, E.; Joannidis, M.; Legrand, M.; Ostermann, M.; Prowle, J. R.; Schneider, A.; Schetz, M., Acute kidney injury in the critically ill: an updated review on pathophysiology and management. Intensive Care Med 2021, 47 (8), 835-850. (2) Wang, L. F.; Zhang, Y. J.; Li, Y. Y.; Chen, J. H.; Lin, W. Q., Recent advances in engineered nanomaterials for acute kidney injury theranostics. Nano Research 2021, 14 (4), 920-933.(3) Hatami, E.; Jaggi, M.; Chauhan, S. C.; Yallapu, M. M., Gambogic acid: A shining natural compound to nanomedicine for cancer therapeutics. Biochim Biophys Acta Rev Cancer 2020, 1874 (1), 188381.(4) Xin, Y.; Hou, Y.; Cong, X.; Tan, H.; Wang, J.; Mao, K.; Wang, X.; Liu, F.; Yang, Y. G.; Sun, T., Kidney functional stages influence the role of PEG end-group on the renal accumulation and distribution of PEGylated nanoparticles. Nanoscale 2022, 14 (26), 9379-9391.

EP-0080

A longitudinal PET study of an open blast induced TBI model in NHP (Cynomolgus macaques) by [11C]PBR28 and [18F]FlumazenilA longitudinal PET study of an open blast induced TBI model in NHP (Cynomolgus macaques) by [11C]PBR28 and [18F]Flumazenil

P. Padmanabhan[1], *K. K. Ghosh*[1], *C. Yang*[2], *Z. Wang*[1], *K. Ng*[3], *B. Ogden*[4], *J. Lu*[3], *C. Halldin*[1], *B. Gulyás*[1];
[1]*LKC School of Medicine, NTU, Singapore, SINGAPORE,* [2]*Singapore General Hospital, Singapore, SINGAPORE,* [3]*DSO National Laboratories, Singapore, SINGAPORE,* [4]*SingHealth Experimental Medicine Centre, Singapore, SINGAPORE.*

Aim/Introduction: Traumatic brain injury (TBI) causes pervasive disability caused by impairment of consciousness and psychological disruption, which can significantly affect life quality. Extreme shifts of blastwaves cause substantial cellular disruption

in biological systems. To decrease the impact of the blast wave, it is essential to employ appropriate experimental methods. The present study includes the outcome of TBI in non-human primates (NHPs) brain due to an open blast explosion, followed by the examination of changes of neuroinflammation and neuronal density in a longitudinal manner by using PET radioligands [^{11}C] PBR28 which quantify the neuroinflamation and [^{18}F]flumazenil, measures the loss of GABAgeric neurons due to TBI consecutively. ***Materials and Methods:*** A total of six Cynomolgus macaques with ages ranging from 8-10 years were used for this evaluation. Before the radiotracers were injected by intravenously, the animals were fasted overnight and then anesthetized. The PET imaging was performed using a LFER 150 PET/CT scanner (Mediso, Hungary) at SingHealth Experimental Medicine Centre. The injected radioactivity was 74.00 to 90.00 MBq, and the maximum injected volume is capped at 5 ml for both the radiotracers. The Molar radioactivity for [^{11}C]PBR28 was 105.00 ± 24.00 GBq/umol and for [^{18}F]Flumazenil 740.00 ± 250.00 GBq/umol. All PET-CT images were analysed using PMOD. After automatic registration with CT scans, PET images were manually co-registered with the Macaca fascicularis MRI atlas. Pre-blast baseline scan. Scanning occurred 3 days, 2 weeks, and 8-9 months after the explosion ***Results:*** The longitudinal monitoring of whole-brain and regional uptake of [11C]PBR28 revealed an association between uptake and microglial activity and neuroinflammation. At 3- and 14-days post-injury, a decrease in uptake was observed. The mean regional update of [11C]PBR28, segmented by distinct brain regions, exhibited a comparable uptake pattern, with reduced uptake observed at 3 days and 2 weeks post-blast and a marked increase at 8 months. The findings indicate a delayed inflammatory response after a blast, as evidenced by the heightened uptake observed 8 months post-blast. The gradual increase in [18F]Flumazenil uptake showed an increase in receptor density between 3 days and 2 weeks after injury. At the 8-month time, the [18F]Flumazenil binding activity showed a decreasing trend in receptor density, suggesting a potential decrease in neuronal activity. ***Conclusion:*** Despite the limited availability of PET datasets, the findings of this study show the possibility of longitudinally quantifying molecular changes through PET imaging utilising [11C] PBR28 and [18F] flumazenil in a TBI NHPs model

EP-0081

GPT-MI: An automated GPT-based pipeline to meta-analyse the field of molecular imaging

P. Jané[1], *X. Xu*[2], *V. Taelman*[2], *E. Jané*[3], *K. Gariani*[1], *R. Dumont*[2], *M. Gómez*[4], *M. Walter*[2];
[1]*Hôpitaux Universitaires de Genève, Geneva, SWITZERLAND,*
[2]*University of Lucerne, Lucerne, SWITZERLAND,*
[3]*Universidad Politécnica de Madrid, Madrid, SPAIN,*
[4]*Hospital Universitario Ramón y Cajal, Madrid, SPAIN.*

Aim/Introduction: The advent of general-purpose large language models like GPT4 will revolutionize informed clinical decision-making by introducing new, fast and simple approaches to analyse big data in medicine, and allowing meta-analyses of entire clinical fields. Herein, we present an automated GPT-based approach to meta-analyse the entire field of molecular imaging. ***Materials and Methods:*** We downloaded the complete Medline dataset (courtesy of the National Library of Medicine, USA), and developed a deep learning-based hybrid human-AI pipeline with a series of different ad-hoc artificial intelligence tools and manual revision to create a database of radiopharmaceutical-gene associations as a reference standard. Then, we created a natural text query template for GPT4 to obtain the genes that need to be expressed in a cell for it to have an uptake of defined radiopharmaceuticals. We measured the precision of the GPT4 model by comparing the returned associations to our gold standard database. ***Results:*** The ad-hoc artificial intelligence tools and manual revision produced a dataset of 9'285 radiopharmaceutical-gene associations targeting 1'173 genes and their bibliographical records. We then iterated over a subset of 100 radiotracers in the gold standard dataset adapting the GPT4 template query. No fine-tuning of the model was applied to obtain these results. Overall, the GPT4 model showed a precision of 88.29%, a recall of 93.26% and an F1 Score 90.71%. When the model returned an incorrect answer, up to three correction chances were given by pointing out the mistake. Thirteen corrections were allowed to the model, producing three more true positives, and increasing the performance of the model to a precision of 88.65%, a recall of 96.63% and an F1 Score 92.47%. The whole of the false positives were initially due to errors in the abbreviation and acronym disambiguation step. In three cases the feedback of the complete chemical name helped the model identify the radiotracer and associated genes correctly. A significant amount of the false negatives was linked to molecules that were named according to their patent registration numbers. ***Conclusion:*** To the best of our knowledge, we present for the first time an automated GPT-based approach to meta-analyse the entire field of molecular imaging. This global approach will serve as a first-in-class project to automatize meta-analyses of entire clinical fields, and will allow integrating molecular imaging with other global approaches, such as genomics, proteomics and metabolomics.

EP-0082

Pilot PET study of molecular processes disturbing the electrode nerve interface in a guinea pig model of cochlear implantation

P. Deutsch[1,2], *M. Mamach*[3,2], *J. Schweiger*[4,2], *J. Bankstahl*[1], *F. M. Bengel*[1], *T. Lenarz*[4,2], *V. Scheper*[4,2], *G. Berding*[1,2];
[1]*Department of Nuclear Medicine, Hannover Medical School, Hannover, GERMANY,* [2]*Cluster of Excellence Hearing4all, German Research Foundation, GERMANY,* [3]*Department of Radiation Protection and Medical Physics, Hannover Medical School, Hannover, GERMANY,* [4]*Department of Otolaryngology, Hannover Medical School, Hannover, GERMANY.*

Aim/Introduction: There is a variety of different reasons for poor speech understanding after cochlear implantation. One type of reasons arises from disturbances of the electrode nerve interface due to molecular processes like inflammation in the cochlear caused by damaging the tissue through the insertion of the electrode or the development of fibrosis around the electrode itself. To evaluate such processes, we used PET imaging with F-18-FDG (fluorodeoxyglucose) and Ga-68-FAPI (fibroblast activation protein inhibitor) in a guinea pig model of unilateral cochlear implantation. ***Materials and Methods:*** In total 26 ears were scanned using a Siemens Inveon PET/CT, either with FDG (16) or FAPI (10) in n= 11 animals. Scans with FDG took place early after insertion of a cochlea implant (CI): CI_{early} after 7, 14 and 21 days (n = 1 animal) and late: CI_{late} after 1 year (n = 3) as well as in not implanted (NI) animals (n = 2). FAPI scans took place 1 year after insertion (n = 3) and in additional 2 NI animals (n = 2). A volume of interest (VOI) defined over the cochlea in the CT image was used to extract standardized uptake values (SUV) in the corresponding region from the PET image. SUV values were compared between groups using unpaired t-Tests. ***Results:*** The

sizes of the VOIs (in voxels) were virtually equal for all groups (FDG: NI: 2288±311, CI: 2110±241; FAPI: NI: 2342±236, CI: 2450±433). SUV values were normally distributed (Shapiro-Wilk-Test, p>0.05) in all groups. Analyses showed a significantly higher mean FDG SUV after implantation in all CI (early and late) compared to NI (CI_{all}: 878±120 vs. NI: 650±90; p=0.0035) and in CI early after insertion compared to NI (CI_{early}: 864±28 vs. NI: 650±90; p<0.001), but no significant difference when comparing CI_{early} and CI_{late} as well as CI_{late} and NI. The mean FAPI SUV for CI differed significantly from NI, with a higher activity late after implantation (CI_{late}: 656±24 vs. NI: 535±121; p=0.0393). ***Conclusion:*** The presented preliminary data suggest that early inflammatory processes and late fibroblastic activity in the cochlear after CI insertion can be measured using PET biomarkers. This pilot study is encouraging for the future use of PET after CI implantation in preclinical studies e.g. assessing new therapeutic options with locally applied anti-inflammatory drugs or its final translation into patient studies.

EP-0083

Evaluating the Relevance of Non-invasive Measurement of Protein Synthesis by Gallium-68-DOTA-puromycin PET/MRI for Imaging of Mycobacterial Infection - a Preclinical Report

J. Kleynhans[1,2], *S. Eigner*[3], *M. M. Sathekge*[4,2], *T. Ebenhan*[2,4]; *[1]Radiopharmaceutical Research, Catholic University of Leuven, Leuven, BELGIUM, [2]Nuclear Medicine Research Infrastructure NPC, Pretoria, SOUTH AFRICA, [3]Nuclear Physics Institute, Academy of Science of the Czech Republic, Rez near Prague, CZECH REPUBLIC, [4]Nuclear Medicine and Steve Biko Academic Hospital, University of Pretoria, Pretoria, SOUTH AFRICA.*

Aim/Introduction: Puromycin is a relevant scaffold for the development of a radiopharmaceutical that will allow the quantification of protein synthesis non-invasively through nuclear based imaging techniques. A significant clinical application of radiolabeled puromycin depends on the visualization of mycobacterial protein synthesis for future clinical investigations of tuberculous lesions. To date, no systematic characterization of a puromycin-based radiopharmaceuticals as potential in vivo infection imaging agents has been reported. Therefore, this study will address selectivity, sensitivity, and accuracy of [^{68}Ga]Ga-DOTA-puromycin-micro-positron emission tomography combined with magnetic resonance imaging (microPET/MRI) imaging to determine the role and value of this technique to detect mycobacterial infection in vivo. ***Materials and Methods:*** The radiopharmaceutical was produced by a previously published procedure (1). Sensitivity of [^{68}Ga]Ga-DOTA-Puromycin microPET/MRI imaging was determined using SCID mice inoculated with of 1.5 x 105 units of Mycobacterium bovis (M. Bovis). Infected mice alternatively received follow-up microPET/MRI imaging ([^{18}F] FDG and [^{68}Ga]Ga-DOTA-Puromycin) after a 12-week monitoring period. Tracer selectivity was tested using animals bearing sterile inflammation or S. aureus (reference bacteria). Imaging results were correlated to outcome from tissue immunohistochemistry for accuracy consideration. ***Results:*** MicroPET/MRI was capable of visualizing a widespread infection originating from the subdermal infection inoculum induced in the armpit. This tracer accumulation 60 min post injection resulted in good signal-to noise-ratios (2.8 ± 0.5); however acute infected lungs areas showed diffuse uptake only (ratio 0.95 - 1.49). Tracer sensitivity for chronic pulmonary infection was deemed low (range 0.07 - 0.29). Expected tracer uptake (NUV) was seen in spleen (0.33), liver (0.98), and myocardium (0.78). [68Ga]Ga-DOTA-puromycin demonstrated selectivity for infection over inflammation (ratio >2.5), however, it accumulated in both M.bovis and S.aureus, i.e., the procedure was non-selective towards imaging mycobacteria species, only. The NUVs versus infected tissue histopathology revealed a positive Spearman rank order analysis (rho = 0.735; p = 0.0012; S = 180, N=16) confirming an accurate [68Ga]Ga-DOTA-Puromycin signal to reflect protein synthesis in viable mycobacteria ***Conclusion:*** The relevance of [^{68}Ga]Ga-DOTA-puromycin-microPET/MRI for imaging of mycobacterial infection sites is presented. The results indicate that [68Ga]Ga-DOTA-puromycin has the potential to become a viable tool for the noninvasive visualization of elevated protein synthesis in infectious lesions. Tracer sensitivity may be further improved by changes to radioisotopes, radiolabeling procedures and a more tailored preclinical setting. ***References:*** (1) Eigner S, et. al. Recent Results Cancer Res., 194:269-283. (2013)

EP-06

e-Poster Area

B: Imaging Clinical Studies -> B10 Other Imaging Clinical Studies -> B101 Other Clinical Studies

EP-0084

Performance of 68Ga-FAPI PET/CT in evaluation of Erdheim-Chester disease: compared with 18F-FDG PET/CT

J. Ma*;*
Peking Union Medical College Hospital, Beijing, CHINA.

Aim/Introduction: Erdheim-Chester disease (ECD) involves multiple organs and has diverse manifestation, which causes difficulty to distinguish lesions caused by ECD from disguisers. Variable degrees of fibrosis is present in ECD. Therefore, we conducted a prospective cohort study to explore the ability of ^{68}Ga-FAPI PET/CT to detect lesion in ECD patients. ***Materials and Methods:*** 14 patients diagnosed with ECD confirmed by histology were included in this study. For every patient, ^{68}Ga-FAPI PET/CT and ^{18}F-FDG PET/CT were conducted within 1 week. The positive rate and SUVmax of lesions in the involved organs were compared between the examinations. ***Results:*** The most commonly involved organs were bones (100%), heart (57.1%), lung (57.1%), intracranial infiltration (50%), kidney (42.9%), peritoneum or omentum (35.7%) and cutaneous infiltration (35.7%). ^{68}Ga-FAPI PET/CT detected 64 of 67 lesions in 14 patients whereas ^{18}F-FDG PET/CT detected 51 of 67 lesions (p=0.004). The SUVmax on ^{68}Ga-FAPI PET/CT was significantly higher than SUVmax on ^{18}F-FDG PET/CT for heart (4.9±2.4v.s. 2.8±1.2, p=0.050), lung or pleura (6.8±4.9v.s. 3.1±1.3, p=0.025), perioneum or omentum (5.7±3.6v.s. 2.8±1.7, p=0.032) and kidney or perinephric infiltration (4.9±1.2v.s. 2.9±1.1, p=0.009). ***Conclusion:*** The detectivity of ^{68}Ga-FAPI PET/CT is superior to ^{18}F-FDG PET/CT. Besides, ^{68}Ga-FAPI PET/CT has a better image contrast and higher SUVmax for lesions in multiple organs including heart, lung, perioneum and kidney. ^{68}Ga-FAPI PET/CT is a promising tool to assess pathologic features and disease extent in ECD patients.

EP-0085

Effects of Aromatase inhibitors on bone mineral density and trabecular bone score in patients with breast cancer

V. Dabbagh[1], *F. Homaee Shandiz*[2], *A. Taghizadeh Kermani*[3], *F. Nesari Javan*[1];
[1]*Nuclear Medicine Research Center, Ghaem Hospital, Mashhad University of Medical Sciences, Mashhad, IRAN, ISLAMIC REPUBLIC OF,* [2]*Ghaem Hospital, Mashhad University of Medical Sciences, Mashhad, IRAN, ISLAMIC REPUBLIC OF,* [3]*Omid Hospital, Mashhad University of Medical Sciences, Mashhad, IRAN, ISLAMIC REPUBLIC OF.*

Aim/Introduction: One of the most important treatments in breast cancer is aromatase inhibitors (AI), which reduce bone density and increase the possibility of bone fractures. Therefore, to identify people who are at risk of fracture, bone mineral density (BMD) should be measured by bone mineral densitometry (DXA) (Dual-energy X-ray absorptiometry). In recent years, another criteria namely the trabecular bone score (TBS) has been introduced as a software to assess the bone quality of patients, which leads to changes in DXA reports and can be used to improve the assessment of bone density in patients before and after any provisional treatment. ***Materials and Methods:*** Patients with proven pathology of breast cancer, who at the discretion of the oncologist had indication for the use of aromatase inhibitors, were referred for bone mineral density before treatment. Base TBS and Bone mineral density (BMD) were registered by DXA method for the patient. After 6 months from the start of treatment, the patient's bone mineral density was repeated. BMD and TBS before and 6 months after treatment was compared. ***Results:*** A total of 50 patients (mean age of 56.33±10.67) with breast cancer were included in the study. We found that there was a significant difference between BMD in the lumbar area well as in total hip area, but no significant difference was found in TBS. Also, by comparing the 10-year risk of major osteoporosis and hip fracture (FRAX) before and after starting the drug and adjusting it to the TBS, we concluded that there is no statistically significant difference between before and after treatment.***Conclusion:*** Based on this study, bone density in the lumbar and total hip area is significantly reduced in patients treated with AIs. S it seems to be increased the risk of fracture. However, according to this study, TBS and FRAX, due to the lack of significant differences, do not help further treatment of these patients to prevent the risk of possible fractures. However duration of the 6 months for this conclusion may be a short time.

EP-0086

Bone SPECT-CT in the study of facet arthropathy

B. Martins*, A. Duarte, M. Correia, A. Figueiredo, S. Matos, N. Canto, D. Calado, C. Loewenthal;
Hospital da Luz, Lisboa, PORTUGAL.*

Aim/Introduction: Facet pain, despite being clinically recognized for decades, remains a diagnostic challenge, mainly because Revel's clinical criteria, used to select patients for therapy with infiltrations, showed a rather low sensitivity [1]. For this reason, imaging studies are essential. However, even the gold standard modality, MRI, may not be conclusive [1]. SPECT-CT can add value in the diagnostic process, detecting foci of increased osteoblastic activity, with high sensitivity and specificity [1]. Since the implementation of the SPECT-CT technique in our institution, the number of exam requests with this indication has been growing, mainly referenced by neurosurgery. In this sense, this study aims to review the series of patients already studied, analyzing the usefulness of SPECT-CT in the evaluation of facet arthropathy. ***Materials and Methods:*** The clinical records of patients referred for bone SPECT-CT due to suspected facet pain in the period between June 2020 and March 2023 were reviewed. The final sample included 169 patients, 57 men and 113 women, with a mean age of 51 years (age range 21-82). The respective SPECT-CT scans of these patients were reviewed, which were evaluated by two nuclear medicine physicians. ***Results:*** Of the 169 patients studied, 77 showed increased osteoblastic activity in at least one joint facet (45.6% of the sample). Forty-seven patients (27.8%) did not show any significant change in radiopharmaceutical uptake in the joint facets. The remaining patients (45/169) had pathological alterations other than facet arthropathy (mainly disc disease, osteophytosis and sacroiliitis). A total of 104 hypermetabolic joint facets were documented, the majority of them in the lumbar segment (n=91, 30 at the L4/L5 level and 33 at the L5/S1 level), 2 in the dorsal and 11 in the cervical segment. 100% inter-observer agreement was documented in the identification of hypermetabolic joint facets. ***Conclusion:*** The prevalence of hypermetabolic joint facets in this series overlaps with other recently published series (45.6% vs 48% in [1]), located mainly at the level of L4/L5 (28.8%) and L5/S1 (31.7%). Since the evidence of metabolic activity on SPECT-CT is predictive of treatment response, this imaging modality may contribute to reducing the number of unnecessary interventions [1]. ***References:*** [1] Perez-Roman RJ et al. Use of Single-Photon Emission Computed Tomography Imaging for Hypermetabolic Facet Identification in Diagnosis of Cervical and Axial Back Pain. World Neurosurg. 2020 May; 137:e487-e492.

EP-0087

Usefulness of bone scan in the management of Paget's disease

N. Ben Fekih[1], *W. El Ajmi*[2], *S. Cherif*[3], *A. Sellem*[2], *H. Hammami*[2];
[1]*faculty of medicine monastir, Tunis, TUNISIA,* [2]*Military Hospital of Tunis, Tunis, TUNISIA,* [3]*faculty of medicine Tunis, Tunis, TUNISIA.*

Aim/Introduction: Paget's Disease is a metabolic bone disorder that is the second most common after osteoporosis. It is primarily characterized by increased osteoclastic bone resorption and subsequent disorganized bone remodeling of poor quality. This condition affects approximately 2% of adults aged over 55 years. Bone scintigraphy with diphosphonates is a valuable tool that can be used to evaluate the osteoblastic activity associated with Paget's Disease. Through this work, we elucidate the interest of bone scintigraphy in the management of Paget's disease. ***Materials and Methods:*** This is a six-year retrospective descriptive study, from January 2017 to December 2022, including 45 patients referred for an assessment of Paget's disease. All patients underwent planar whole-body skeletal imaging using a Siemens Symbia S dual-head gamma camera, 2-3 hours after injection of a weight-adjusted activity from 370 to 740 MBq of ^{99m}Tc-hydroxymethylene diphosphonate ***Results:*** The study population consisted of 28 men (62,2%) and 17 women (37,8%), with a sex ratio of 1,64. The median age was 64 years [range: 41-80 years]. 9,1% were aged 50 years or younger. The examination was requested for a topographic assessment in 68.9% of cases. The disease was monostotic in 35.6% of cases and polyostotic in 53.3% of cases, at a mean of 3 affected bones with a maximum of 13 bones. The most commonly affected ones were the pelvis (27%), femur (17%), dorsal spine (14%), lumbar spine (15%), and skull (12%). Bone scan was required as a therapeutic evaluation assessment in 13.3% of cases (6 patients) and showed a partial

decrease of tracer uptake sometimes even restitution ad integrum. In 17.8% of cases (8 patients), bone scan was demanded to confirm a suspicious lesion on radiological examination. It did not show typical lesions of Paget's disease in 37.5% of cases and confirmed the suspicion in 62.5% of cases. ***Conclusion:*** The metabolic exploration of the whole skeleton using bone scan with diphosphonates is particularly valuable in the diagnostic and topographic assessment of active Paget's disease. Additionally, the decrease in osteoblastic activity is a reliable indicator for therapeutic monitoring. Normal bone uptake may be explained by quiescent Paget's disease.

EP-0088

Is there any added value of a DXA scan of the distal forearm to lumbar and hip DXA values in predicting osteoporotic bone fractures?

M. ROMERA[1], *Á. Bronte*[1], *V. Betech-Antar*[1], *F. Mínguez*[1], *J. Rosales*[1], *S. Menéndez-Sánchez*[1], *J. Bastidas*[1], *E. Guillén*[2], *L. Sancho*[2], *L. García-Belaustegui*[2], *J. Arbizu*[1], *M. García Velloso*[1], *F. Pareja*[1], *M. Rodríguez*[1];
[1]*Clínica Universidad de Navarra, Pamplona, SPAIN,*
[2]*Clínica Universidad de Navarra, Madrid, SPAIN.*

Aim/Introduction: To determine whether the distal forearm dual-energy X-ray absorptiometry (DXA) values allow a more accurate prediction of the probability of osteoporotic bone fracture than lumbar and hip DXA values and lumbar trabecular bone score (TBS) measures, in postmenopausal women and men >50 years. Secondarily, to determine the change that forearm values had in the final diagnosis. ***Materials and Methods:*** Patients studied between 10/2016 and 04/2023 with DXA that included distal forearm measurements were analyzed. Lumbar, hip and forearm T-Score DXA and TBS values, non-traumatic osteoporotic fractures suffered prior and after treatment, risk factors for fractures, prior diagnoses and demographic and analytic data, were gathered from medical records. Correlation between variables was studied by Pearson coefficient. To identify independent predictors for bone fractures, a logistic regression model was used. ***Results:*** Eighty-five patients were retrospectively studied. Clinical and demographic characteristics are shown in Table 1. Mean follow-up time from the DXA was 56.5 (±22.7) months. According to WHO criteria, in basal DXA, 44.7% of patients were diagnosed with osteoporosis, 48.2% osteopenia and 7.1% normal BMD. In 36/85 patients (42.4%), forearm values changed the final diagnosis (9/36 from normal to osteopenia and 27/36 from osteopenia to osteoporosis). Using TBS software, TB was classified as degraded (22.4%), partially degraded (42.4%) and normal (35.3%). Seventeen patients (20%) suffered an osteoporotic fracture after the basal densitometry. A positive correlation between forearm and lumbar T-score values and the occurrence of bone fracture was found. Patients with fractures had lower T-scores in lumbar (-2.4±1.1; p=0.005) and forearm (-2.4±1; p=0.001) than in patients who did not (-1.4±1.3; p=0.005 for lumbar and -1.2±1.3; p=0.001 for forearm). No correlation between clinical factors and bone fractures was found. Similarly, no association between TBS and fracture events was identified, except for patients with Diabetes Mellitus (p<0.001). Furthermore, and interestingly, no patients with normal baseline DXA presented osteoporotic fractures during the follow-up. On multivariate regression analysis, only baseline forearm T-score <-1.3 (OR=5.0 [95%CI:1.3-19.7, p=0.02)] significantly predicted osteoporotic bone fractures during the follow-up. ***Conclusion:*** In postmenopausal women and men >50 years, basal distal forearm T-score values were significantly lower in patients with bone breakage than in patients without fractures. A T-score value of <1.3 was a significant predictor for the risk of bone fractures. Moreover, forearm values worsen the final DXA diagnosis in 42.4% of patients. Therefore, DXA of the distal forearm provides benefit in predicting bone fractures over central DXA measurements.

EP-0089

Optimization of SPECT/CT reconstruction parameters for intrapancreatic accessory spleen imaging

D. Sfiligoj Planjsek*, S. Rep, A. Cuderman, J. Jamsek, L. Lezaic;*
UMC Ljubljana, Ljubljana, SLOVENIA.

Aim/Introduction: Intrapancreatic accessory spleen (IPAS) is a rare benign finding (representing 11-17% of all accessory spleens), that can be difficult to diagnose, especially when a pancreatic neuroendocrine tumour is suspected (1). Selective spleen scintigraphy (SSS) using Technetium-99m [^{99m}Tc]-labelled denatured erythrocytes is the preferred method for imaging accessory spleens (AS) (2), with IPAS best visualised by SPECT/CT. However, small IPAS located near the spleen can be difficult to detect due to poor sharpness and contrast in reconstructed SPECT images. Our research aimed to optimise SPECT reconstruction parameters in order to improve contrast and sharpness in SSS SPECT/CT imaging of IPAS. ***Materials and Methods:*** To evaluate the effect of different Gaussian filter FWHM (soft tissue) settings (10 mm, 8 mm, 6 mm, 4 mm and 2 mm) on contrast and sharpness, we iteratively reconstructed SPECT images with 8 iterations and 4 subsets. These parameters were used to analyse NEMA body phantoms and SPECT/CT images in a selected group of patients who had undergone SSS at our department of nuclear medicine within the last 5 years. ***Results:*** Lower values of the Gaussian filter FWHM resulted in increased contrast and sharpness of lesions, but also increased background graininess and noise. The contrast of the spheres in the NEMA body phantom was increased by narrowing FWHM from 10 mm to 8 mm, to 6 mm, to 4 mm and to 2 mm. With each narrowing of the FWHM, the contrast increased by approximately 12% for smaller (≤ 13 mm) spheres and by approximately 5% for larger (≥ 17 mm) spheres ($p < 0.05$). Likewise, in the patient group, IPAS were better defined in SPECT images at lower values of Gaussian filter FWHM. The increased noise did not affect image interpretation because the exact location of IPAS was known due to concomitant low-dose CT. The image contrast obtained using different FWHM filters was comparable to results obtained with the NEMA body phantom. ***Conclusion:*** In our opinion 2 mm of the Gaussian filter FWHM in SSS SPECT/CT images provide better contrast and sharpness especially in small IPAS positioned in close proximity to spleen. ***References:*** 1. Li B, Xu x, Guo J. Intrapancreatic accessory spleen: a diagnostic dilemma. HPB 2018; 20(11): 1004-11. 2. Ekmekçi S, Diz-Küçükkaya R, Türkmen C, Adalet I. Selective spleen scintigraphy in the evaluation of accessory spleen/splenosis in splenectomized/nonsplenectomized patients and the contribution of SPECT imaging. Mol Imaging Radionucl Ther 2015; 24(1): 1-7.

EP-0090

Identifying immunotherapy progressors by 18F-FLT PET/CT in solid tumours: a pilot study

P. Aravind[1], *M. Lythgoe*[1], *J. Evans*[2], *L. Tookman*[2], *W. E. Park*[2], *N. Sarwar*[2], *A. Sita-Lumsden*[3], *D. J. Pinato*[2], *T. D. Barwick*[1,2], *E. O. Aboagye*[1], *R. Sharma*[1,2];
[1]*Imperial College London, London, UNITED KINGDOM,*
[2]*Imperial College Hospital NHS TRUST, London, UNITED KINGDOM,* [3]*Guys and St Thomas' NHS Foundation Trust, London, UNITED KINGDOM.*

Aim/Introduction: Immunotherapy (IO) confers a survival benefit in advanced cancers. Response to IO is not adequately assessed by RECIST 1.1 due to pseudo progression and iRECIST still relies on changes in tumour size. The primary objective of this pilot study was to assess the feasibility of (^{18}F)FLT PET/CT as a marker of response to IO (modified PERCIST) and to determine PET parameters that correlate with imaging response (RECIST 1.1 and iRECIST) and progression free survival(PFS). ***Materials and Methods:*** Patients with metastatic cancer scheduled to receive IO for advanced disease underwent (^{18}F)FLT PET/CT at baseline and 12 weeks after initiating IO. All sites of disease avid above background and >10mm were outlined on PET. SUV parameters (SUV_{mean}, SUV_{max}, proliferative tumour volume (PTV), total lesion proliferation (TLP: calculated as the product of SUVmean and PTV) were calculated. (18F)FLT PET response(PERCIST, modified PERCIST: max5 lesions, unto 2 per organ, Total lesion PERCIST: all lesions outline) were compared to RECIST 1.1 and iRECIST at follow up scan at 12 weeks. PFS was calculated from baseline scan to progression. ***Results:*** Sixteen patients had evaluable PET scans. The tumour types were hepatocellular (8), non small cell lung cancer(1), Ovarian cancer (2), Renal cancer(1), endometrial cancer(1), oesophageal squamous cell cancer(3). Median age was 68yr (42-80), median cycles of IO received was 8(2-19) and the most common toxicity was fatigue. (38%, n=6) followed by liver toxicity(31%, n=5). Disease control rate after IO therapy was 74% on RECIST 1.1 response (PR: n=4, SD: n=8, PD: n=4) and 81% on iRECIST (PR: n=4, SD: n=8, immune unconfirmed PD: n=1, immune confirmed PD: n=3). For PET, 88% (14/16) were responders (PMD, SMD) on modified PERCIST and 94% (15/16) on PERCIST. Changes in tumour (^{18}F)FLT PET uptake were moderately correlated with changes in RECIST 1.1 measurements (ΔSUV_{max} p=0.049, rho -0.499, ΔSUV_{mean} p=0.009, rho-0.633). Progression was characterised by increases in ΔPTV and ΔTLP of 230 and 431, respectively (p=0.021, p=0.008) compared to non progression (-32 and -38). Median PFS was 9.3m (2m vs 10m in PD vs non-PD based on RECIST or modified PERCIST (log rank p=0.003) compared to 3.4m vs 10m based on iRECIST (p=0.005). ***Conclusion:*** Progressors on immunotherapy show increases in ΔPTV and ΔTLP at 12 weeks. (^{18}F)FLT PET/CT is a promising to detect futile immunotherapy.

EP-07

e-Poster Area

B: Imaging Clinical Studies -> B1 Oncological Imaging Clinical Study -> B11 Central Nervous System

EP-0091

Unraveling the Relationship Between Glioma Tumor Residuals from Incongruent 18F-FET PET/MR Imaging and Tumor Proliferation Utilizing Multiparametric MRI Radiomics Analysis

X. Li[1,2], *Y. Cheng*[3], *X. Han*[1], *H. Yang*[1], *B. Cui*[1,2], *J. Li*[1,2], *G. Xu*[3], *Q. Lin*[3], *X. Xiao*[3], *J. Tang*[3], *J. Lu*[1,2];
[1]*Department of Radiology and Nuclear Medicine, Xuanwu Hospital, Capital Medical University, Beijing, CHINA,* [2]*Beijing Key Laboratory of Magnetic Resonance Imaging and Brain Informatics, Capital Medical University, Beijing, CHINA,* [3]*Department of Neurosurgery, Xuanwu Hospital, Capital Medical University, Beijing, CHINA.*

Aim/Introduction: The study aimed to using multiparametric magnetic resonance imaging radiomics to predict glioma tumor residuals ($TR_{FET\ over\ MR}$) derived from incongruent O-(2-^{18}F-fluoroethyl)-L-tyrosine (^{18}F-FET) positron emission tomography/magnetic resonance (PET/MR) imaging. ***Materials and Methods:*** A total of 110 patients with gliomas who underwent preoperative hybrid ^{18}F-FET PET/MR scanning were retrospectively analyzed. The biological tumor volume (BTV) was semi-automatically segmented based on a threshold of tumor background ratio (TBR) > 1.6 on ^{18}F-FET PET images. The $TR_{FET\ over\ MR}$ was identified by the discrepancy-PET that the extent of resection (EOR) based on MRI subtracted the BTV. The expressions of molecular markers related to proliferation, including epidermal growth factor receptor (EGFR) and Ki-67, were identified by immunohistochemistry.The MRI parameters and radiomics features based on anatomical MRI, diffusion-weighted imaging, and arterial spin labeling imaging were extracted based on EOR. Subsequently, the least absolute shrinkage and selection operator (LASSO) were used to construct the radiomics score (Rad-score). Comparison of clinical features and Rad-score between $TR_{FET\ over\ MR}$ and non $TR_{FET\ over\ MR}$ groups was tested by the Mann-Whitney U test. The correlation network analysis of all features was analyzed by the Spearman's correlation tests. The methods for evaluating the accuracy of machine learning models established by logistic regression consisted of the receiver operating characteristic curve, the calibration curve, and decision curve analysis. ***Results:*** The Rad-score of the patients with the $TR_{FET\ over\ MR}$ was significantly higher than those with the non $TR_{FET\ over\ MR}$ ($p < 0.001$). The Rad-score was significantly correlated with the discrepancy-PET ($r = 0.72$, $p < 0.001$), Ki-67 level ($r = 0.76$, $p < 0.001$), and EGFR of gliomas ($r = 0.75$, $p < 0.001$), respectively. And the discrepancy-PET was also moderately correlated with the EGFR ($r = 0.64$, $p < 0.001$) and Ki-67 level ($r = 0.67$, $p < 0.001$). Moreover, there was a difference of the correlation network analysis between the $TR_{PET\ over\ MR}$ group and non $TR_{FET\ over\ MR}$ group. The nomogram combing Rad-score and clinical features had the greatest performance in predicting $TR_{FET\ over\ MR}$ (AUC = 0.90/0.87, training/testing) compared to single clinical features or Rad-score. ***Conclusion:*** Multiparametric MRI radiomics could help explain the proliferation of gliomas leading to intra-tumor heterogeneity and $TR_{FET\ over\ MR.}$ The nomogram based on MRI radiomics would predict tumor residuals caused by the absence of ^{18}F-PET PET examination and adjust EOR to improve prognosis of gliomas.

EP-0092

[18F]FDG-PET Radiomics Improves Outcome Prognostication in Patients With Primary CNS Lymphoma

S. Chen[1], *O. Yildirim*[2], *A. Mauguen*[2], *C. Grommes*[2], *H. Schöder*[2], *M. E. Mayerhoefer*[2], *S. Krebs*[2];
[1]*Weill Cornell Medical College, New York, NY, UNITED STATES OF AMERICA,* [2]*Memorial Sloan Kettering Cancer Center, New York, NY, UNITED STATES OF AMERICA.*

Aim/Introduction: Current clinical and imaging tools remain suboptimal for outcome prognostication in primary CNS lymphoma (PCNSL). This study evaluated the prognostic utility of standard metabolic parameters and radiomic features extracted from baseline [^{18}F]FDG-PET/CT in patients with newly diagnosed PCNSL and combined with clinical parameters. ***Materials and Methods:*** Ninety patients with newly diagnosed PCNSL and clearly FDG-avid lesions on [^{18}F]FDG-PET/CT of the brain before receiving standard therapy with high dose methotrexate with/without consolidation treatment (radiotherapy or chemotherapy) and with/without rituximab were included in this retrospective study. Manual segmentation of up to five [^{18}F]FDG-avid lesions per

patient was performed, and standardized uptake values (SUV_{max}), metabolic tumor volumes (MTV), total lesion glycolysis (TLG), and 158 radiomic features were extracted. ComBat harmonization of imaging features was performed to correct for potential systematic differences between PET/CT scanners, and gradient boosting was used for feature selection. Clinical and PET-based features and their combinations were tested for overall survival (OS) prognostication. ***Results:*** In 90 patients with measurable disease on PET, 195 lesions were identified, including 156 deep brain lesions. The OS was 80% at 2 years. In a multivariable analysis, age at diagnosis, KPS and treatment with rituximab were prognostic for OS. Standard metabolic parameters ($SUV_{max,}$ MTV, and TLG) and the sum thereof were not associated with outcome. Five radiomic features (three derived from the histogram, one from the co-occurrence matrix, and one from the run-length matrix) were selected from gradient boosting. Five-fold cross-validation was performed for the radiomics, the clinical, and a composite model. For 2-year OS status prediction, areas under the receiver operating characteristic curve (ROC AUC) were 0.580 for the radiomics model, 0.763 for the clinical model, and 0.863 for the composite model. ***Conclusion:*** In PCNSL, radiomic features, but not standard metabolic parameters, are prognostic of OS, and may improve clinical prognostic models.

EP-07

e-Poster Area

B: Imaging Clinical Studies -> B1 Oncological Imaging Clinical Study -> B12 Head and Neck

EP-0093

Somatostatin Receptor-Directed Theranostics in Paragangliomas of the Head and Neck

S. Serfling[1], *Y. Zhi*[2], *E. Gerhard-Hartmann*[3], *A. Weich*[4], *T. Higuchi*[5], *S. Hackenberg*[6], *R. Hagen*[2], *H. Remde*[7], *A. Scherzad*[1], *M. Fassnacht*[8], *R. A. Werner*[1];
[1]*Department of Nuclear Medicine, University Hospital Würzburg, Würzburg, GERMANY,* [2]*Department of Otorhinolaryngology, Plastic, Aesthetic and Reconstructive Head and Neck Surgery, University Hospital Würzburg, Würzburg, GERMANY,* [3]*Institute of Pathology and Comprehensive Cancer Center Mainfranken, Würzburg, GERMANY,* [4]*ENETS Center of Excellence, University Hospital Würzburg, Würzburg, GERMANY,* [5]*University Hospital Würzburg, Würzburg, GERMANY,* [6]*RWTH Aachen University, Aachen, GERMANY,* [7]*Internal Medicine II, Gastroenterology, University Hospital Würzburg, Würzburg, GERMANY,* [8]*8 Internal Medicine I, Endocrinology, University Hospital Würzburg, Würzburg, GERMANY.*

Aim/Introduction: Given their neuroendocrine origin, paragangliomas of the head and neck (HNPGL) can be imaged with somatostatin receptor (SSTR)-directed PET/CT. We aimed to determine whether the in-vivo PET signal can differentiate between varying HNPGL subtypes. In addition, we also report on feasibility of peptide receptor radionuclide therapy (PRRT) in this patient population. ***Materials and Methods:*** 14 patients with HNPGL received pretherapeutic SSTR-PET/CTs using [^{68}Ga] Ga-DOTATOC. Six (42.9%) patients had paraganglioma jugulare (PGL-J), five (35.7%) were diagnosed with paraganglioma caroticum (PGL-C) and the remaining three patients (21.4%) had a PGL-C with pathogenic SDHx germline variants (PGL-C-SDH). We performed visual and quantitative assessment of the primary on SSTR-PET, including maximum standardized uptake values (SUV_{max}) and target-to-background-ratio (TBR). Quantitative values were then compared between subgroups of patients affected with different HNPGL entities. Patients eligible for PRRT were also identified. ***Results:*** On a visual assessment, all primary HNPGL could be readily identified on SSTR-PET/CT. Quantification of HNPGL then provided substantially elevated SUV_{max} in PGL-J (101.7±58.5) when compared to PGL-C-SDH (13.4±5.6, P<0.05), but not when compared to PGL-C (66.7±27.3, P=0.4; PGL-C vs PGL-C-SDH, P=0.2). TBR of PGL-J (202.9±82.2), however, then further differentiated between PGL-C (95.7±45.4, P<0.05) and PGL-C-SDH (20.4±12.2, P<0.01; PGL-C vs PGL-C-SDH, P=0.3). Moreover, whole-body read-out revealed an M1 status in 2/3 (66.7%) PGL-C-SDH patients, with a single SSTR-expressing skeletal lesion in one subject and bipulmonary lesions in the other patient. The latter individual received 2 cycles of PRRT (cumulative activity, 14.7 GBq [^{177}Lu] Lu-DOTATOC). No acute or long-term side effects (including haemato- or nephrotoxicity) were recorded and 5 months after PRRT, mixed response was achieved. ***Conclusion:*** In patients with HNPGL, SSTR-PET identifies widespread metastatic disease and provides substantially elevated TBR, indicative for excellent image contrast. PET-based quantification can also differentiate between varying HNPGL subtypes. In a theranostic setting, PRRT might be feasible, which may achieve outcome benefits without relevant side effects.

EP-0094

Prediction of Nodal Metastasis by FDG PET/CT in Untreated Laryngeal Carcinoma; Comparison to MRI

A. Al ibraheem*, A. S. Abdlkadir, H. KHCC Group, D. Al-adhami;*
King Hussein Cancer Center, Amman, JORDAN.

Aim/Introduction: Squamous cell carcinomas account for over 95% of laryngeal tumors, necessitating accurate staging for optimal treatment and outcome. While conventional imaging, such as magnetic resonance imaging (MRI), has been used to detect primary tumors and regional nodal metastases, it lacks the ability to differentiate between metastatic and non-metastatic cervical lymph nodes. FDG PET/CT is being used to characterize metastases at local, regional, and distant levels. This study aims to determine the diagnostic accuracy of PET/CT and neck MRI in laryngeal carcinoma patients, with a focus on the prognostic value of PET/CT for survival outcomes. ***Materials and Methods:*** Data from a tertiary referral cancer center were collected and analyzed retrospectively. A cohort of patients diagnosed with laryngeal cancer between December 2014 and January 2021 was investigated. Among this group of patients, only 68 of them had undergone post-imaging neck dissection with biopsy-proven laryngeal malignancy. Sensitivity, specificity, and overall accuracy were calculated for each diagnostic test, along with 95% confidence intervals. McNemar test was used to compare data obtained separately from FDG PET/CT and neck MRI. The Kaplan-Meier method was used to plot survival curves for progression-free survival (PFS) and overall survival (OS). The log-rank test was used to assess survival differences between subgroups. ROC curve analysis was employed to determine optimal cutoff values for each continuous variable (e.g., Semiquantitative PET parameters). The Cox proportional hazards regression model was used in both univariate and multivariate analyses to assess the relationship between survival, clinicopathological factors, and several Semiquantitative PET parameters. A significant threshold of $p < 0.05$ was established. SPSS 26.0 for Windows (SPSS, Inc., Chicago, IL) was used for all analyses. ***Results:*** The sensitivity and specificity

of PET/CT, and MRI were evaluated. PET/CT had 93.8% sensitivity, 58.3% specificity, and 75% ac-curacy for nodal metastasis, while MRI had 68.8%, 61.1%, and 64.7%, respectively. At a median follow-up of 51 months, 23 patients developed disease progression, and 17 patients died. Univariate survival analysis revealed all utilized PET parameters as significant prognostic factors for OS, and PFS (p value < 0.03 each). On multivariate analysis, metabolic tumor volume (MTV) and total lesion glycolysis (TLG) predicted better PFS (p value < 0.05 each). ***Conclusion:*** PET/CT improves the accuracy of nodal staging in laryngeal carcinoma over neck MRI and adds to the prognostication of survival outcomes through the use of several PET metrics.

EP-0095

Diagnostic utility of Semiquantitative parameters on FDG PET/CT for lymph node metastases in patients with laryngeal Squamous Carcinoma

A. Al ibraheem*, A. Abdlkadir, D. Al-Adhami, King Hussein Cancer Center Head and neck cancer Group, H. KHCC Group;*
King Hussein Cancer Center, Amman, JORDAN.

Aim/Introduction: Accurate staging in laryngeal squamous carcinoma is essential for selecting the most effective treatment and achieving the best outcome. FDG PET/CT is being used to characterize metastases at locoregional, and distant levels. PET/CT can be used to assess metabolic activity in cervical lymph nodes. Hypermetabolic lymph nodes carry a high potential for metastatic processes. Therefore, it can provide concrete evidence in determining metastatic lymph nodes. Lymph nodes (LN) semiquantitative PET parameters had previously shown promising results in providing prognostic background for disease progression of respiratory tumors. This study aims to examine semiquantitative PET metrics for laryngeal cancer to determine the diagnostic value ***Materials and Methods:*** Patients diagnosed with laryngeal Squamous cell carcinoma between December 2014 and January 2021 were retrospectively enrolled. These patients had previous baseline FDG PET/CT for initial disease assessment. The PET images were reviewed visually and semi-quantitively using several metabolic PET parameters. Biopsy results were examined to determine nodal disease status and reach definitive staging results. To measure the metabolic parameters of LNs, maximum standardized uptake value (SUVmax), metabolic tumor volume (MTV), total lesion glycolysis (TLG) were examined. The diagnosis of each retrieved LN was confirmed based on histopathological examination of surgical tissue specimens. Receiver operating characteristics (ROC) curves with area under the curve (AUC) calculations and multivariate analysis by logistic regression were performed. A significant threshold of $p < 0.05$ was established. ***Results:*** Seventy-two Patients with 144 clinically diagnosed positive lymph nodes were enrolled. Of the 144 LNs, only 106 LNS were pathologically proven as positive (73.7%). The SUVmax, MTV, and TLG of LN metastasis were significantly higher than those of benign nodes. In the ROC analysis, the AUC value of LN MTV [AUC, 0.88; 95% confidence interval (CI), 0.82-0.93] was higher than that of LN TLG (AUC, 0.72; 95% CI, 0.64-0.79) or LN SUVmax (AUC, 0.69; 95% CI, 0.61-0.77). Using the optimal Cutoff value of 1.2 for LN MTV, the sensitivity, specificity, were 87.7, and 86.8%, respectively. Multivariate analysis with logistic regression showed that LN MTV was an independent predictor for LN metastasis (odds ratio, 5.19; 95% CI, 2.8-9.712; $P < 0.01$). ***Conclusion:*** Our findings suggest that LN MTV on FDG PET/CT is a useful predictor for LN metastasis in patients with laryngeal squamous carcinoma. This PET-derived metric might provide solid functional imaging evidence for future studies to pursue.

EP-0096

Role of F-18-FDG PET/CT in staging and assessment of treatment response to neoadjuvant chemotherapy in patients with extra-ocular retinoblastoma (EORB) - a single centre initial experience

S. G Ravindra*, S. Garg, A. Khurana, J. Pathak, N. Lomi, R. Seth, R. Kumar, C. S. Bal;*
All India Institute of Medical Sciences, New Delhi, INDIA.

Aim/Introduction: The most common intra-ocular malignancy of childhood is retinoblastoma. Extra-ocular dissemination, albeit rare, is the most important cause of poor prognosis and death in these children, particularly in the developing countries. The most common sites of metastasis include central nervous system, bone and lymph nodes. The systemic work-up for suspected metastatic disease includes brain and orbital MRI with or without contrast, lumbar puncture for cerebrospinal fluid cytology, bone marrow aspiration/biopsy and bone scintigraphy. Detection of distant metastasis, is important, not only to prognosticate the patient, but also to determine the appropriate dose and schedule of the chemotherapeutic regime. ***Materials and Methods:*** A total of 20 patients with a diagnosis of EORB were enrolled prospectively in this study. F-18-FDG PET/CT scan was performed at baseline, prior to initiation of chemotherapy and after 3 cycles of neoadjuvant chemotherapy. ***Results:*** A total of 20 patients of extra-ocular retinoblastoma were evaluated in the study. 14 patients had unilateral eye disease while 6 patients had bilateral eye disease. 9 patients had clinical evidence of extra-ocular extension in the form of marked proptosis. SUVmax of involved eye in patients with clinical evidence of extra-ocular extension in the form of marked proptosis was greater than 2.5 as compared to patients with only radiological evidence of extra-ocular extension. 5 patients showed evidence of bone marrow metastasis - 1 detected by bone marrow studies alone, 1 patient positive on MRI, PET/CT and bone marrow studies, 1 patient positive on PET/CT and bone marrow studies and negative on MRI, 2 patients positive only on PET/CT and negative on MRI and bone marrow studies. The reason for false negativity on bone marrow studies in these patients may be due to limited sites of bone marrow involvement. A total of 7 patients had pre-auricular lymph node metastases, of which 5 were detected only on PET/CT and not on MRI. Follow-up scan after 3 cycles of neo-adjuvant chemotherapy was done in 14 patients, who showed partial metabolic response with significant reduction in metabolic activity at sites of lymph node and distant metastases if present initially. ***Conclusion:*** F-18-FDG PET/CT may aid in identifying lymph node and distant metastases in patients with advanced extra-ocular retinoblastoma and help in accurate staging of disease and further treatment. However, more studies are required in this regard.

EP-0097

The impact of the COVID 19 pandemic on nasopharyngeal carcinoma extent at FDG PET/MR staging:the NPCOVIPET study

Y. Xu*;*
Hangzhou Universal Medical Imaging Diagnostic Center, Hangzhou, CHINA.

Aim/Introduction: To evaluate the impact of coronavirus disease 2019 (COVID-19) pandemic ondiseaseextentinnasopharyngealcarcinoma(NPC)patients using18 fuorodeoxyglucose (FDG) positron emission tomography (PET)/magnetic resonance imaging (MRI) staging as surrogate measure. ***Materials and Methods:*** Retrospective observational study including biopsy-proven, newly diagnosed NPC patients using whole-body FDG PET/MR

staging in two selected intervals: May 1, 2017 to January 31, 2020 (Group A), and February 1, 2020 to June 30, 2021 (Group B). Data regarding primary tumour, regional lymph nodal (N) status and number of involved regional lymph nodal stations, and presence and number of distant metastases (M) were collected. ***Results:*** Three hundred ninety patients were included (201 in Group A vs 189 in Group B, respectively). The median intervals to PET/MR from the initial symptom ingroup A and group B were 2.5 (0.1-60.4) and 3.4 (0.2-56.3) months, respectively (p>0.05). The median intervals to treatment from the initial symptom in group A and group B were 2.8 (0.2-60.5) and 3.6 (0.3-56.3) months, respectively (p>0.05). No significant difference was observed in terms of T classification, N classification,overall stage, N stations and M stations between the two groups (p>0.05). For the the involved neck node levels, more patients had developed level Vc metastasis in the group B (p=0.044). ***Conclusion:*** For NPC, staging by PET/MR and therapy were not significantly delayed after quarantine restrictions initiated. Although the overall stage was not affected, more NPC patients had developed level Vc metastasis in the era of COVID-19.

EP-0098

Use of 18F-FDG PET/MR as an initial staging procedure for nasopharyngeal carcinoma

Y. Xu;
Hangzhou Universal Medical Imaging Diagnostic Center, Hangzhou, CHINA.

Aim/Introduction: The purpose of this study was to determine the clinical value and cost-effectiveness of PET/MR as an initial staging procedure for nasopharyngeal carcinoma (NPC) compared with the conventional work-up (CWU). ***Materials and Methods:*** From May 2018 to March 2021, 1020 consecutive patients with biopsy-proven, newly diagnosed NPC in our center were enrolled in this study. Among them, 343 patients underwent PET/MR before treatment and the remaining 677 patients only underwent CWU. For PET/MR and CWU, charges were used as issued in 2021 by the Medical Insurance Administration Bureau of Zhejiang, China. Incremental costeffectiveness ratio (ICER) measured cost of using PET/MR per percent of patients who avoided a false-positive (FP). ***Results:*** For the whole group, the de novo metastatic disease rate was 5.2% (53/1020). A total of 187 patients with FP results were observed. More patients with FP results were observed in the CWU group (25.6% vs. 4.1%, p<0.001). The mean interval from pathological diagnosis to initiation of treatment was 13.1 days in the CWU group versus 7.9 days in the PET/MR group (p< 0.001). Mean cost per patient was $417 for CWU and $1585 for PET/MR. The ICER was $54 for each percent of patients who avoided a FP. ***Conclusion:*** Compared with CWU, PET/MR reduced FP risk and decreased workup of incidental findings, allowing for earlier treatment start. PET/MR may be cost-effective in initial staging procedure for NPC.

EP-0099

A diagnostic model of nasopharyngeal carcinoma based on PET/MRI radiomics and semi-quantitative parameters

J. Liang;
杭州通用医学影像诊断中心, 杭州, *CHINA.*

Aim/Introduction: The staging of nasopharyngeal carcinoma (NPC) is of great value in treatment and prognosis. We explored whether a positron emission tomography/ magnetic resonance imaging (PET/MRI) based comprehensive model of radiomics features and semiquantitative parameters was useful for clinical evaluation of NPC staging. ***Materials and Methods:*** A total of 200 NPC patients diagnosed with non-keratinized undifferentiated carcinoma were divided into early-stage group (I-II) and advanced-stage group (III-IV) and divided into the training set (n = 70) and the testing set (n = 30). Radiomics features (n = 382 × 2) of the primary site of NPC were extracted from MRI and PET images, respectively. Three major semiquantitative parameters of primary sites including maximum standardized uptake value (SUVmax), metabolic tumor volume (MTV), and total lesion glycolysis (TLG) in all NPC patients were measured. After feature selection, three diagnostic models including the radiomics model, the meta-bolic parameter model, and the combined model were established using logistic regression model. Finally, internal validation was performed, and a nomogram for NPC comprehensive diagnosis has been made. ***Results:*** The radiomics model and metabolic parameter model showed an area under the curve (AUC) of 0.85 and 0.82 in the testing set, respectively. The combined model based on radiomics and semiquantitative parameters showed an AUC of 0.93 in the testing set, with the best performance among the three models. ***Conclusion:*** The combined model based on PET/MRI radiomics and semiquantitative parameters is of great value in the evaluation of clinical stage (early-stage group and advanced-stage group) of NPC.

EP-0100

Detection of metastatic lymph nodes with multiparametric PET/MR in head and neck imaging

A. Harteveld, *E. H. M. Kemper, N. D. Sijtsema, P. A. Wielopolski, D. H. J. Poot, M. Segbers, F. A. Verburg;*
Erasmus MC, Rotterdam, NETHERLANDS.

Aim/Introduction: Detection of lymph node involvement has a significant negative impact on the treatment outcome for patients with head and neck squamous-cell carcinomas (SCC). Metastatic lymph nodes can be detected with high sensitivity by [18F]FDG-PET. However, false-positive metastatic lymph nodes occur relatively often. Additional information of lymph nodes which are suspected for metastasis based on the [18F]FDG-PET to improve specificity would be highly desirable. The use of physiological magnetic resonance imaging (MRI) sequences may provide this missing information. Physiological MRI sequences uses techniques that allow for the measurement of physiological processes within a tissue. Therefore, the aim of this study was to determine the added predictive value of quantitative physiological MRI in combination with [18F]FDG-PET for the detection of malignant lymph nodes in head and neck PET/MR. ***Materials and Methods:*** Between September and December 2022 25 patients with (suspected) SCC were included scheduled for a diagnostic PET/MR (Signa PET/MR, GE Healthcare), including dedicated [18F]FDG-PET and structural MR imaging of the head and neck region according to the standard clinical protocol. Physiological diffusion-weighted imaging intravoxel incoherent motion (DWI-IVIM) and dynamic contrast-enhanced (DCE) MRI sequences were acquired additionally to obtain diffusion and perfusion related quantitative parameters, respectively. Image registration was performed to align all images obtained in each patient. A region-of-interest was manually delineated in each identified lymph node to obtain quantitative parameters of DWI-IVIM (D, D*), DCE-MRI (K_{trans}, K_{ep}, V_p) and [18F]FDG-PET (SUV). Lymph node scoring was performed based on the standard PET/MR images. Pathology was obtained in a subset of lymph nodes as part of the standard clinical workup. ***Results:*** In total 10 subjects were used for analysis including 41 identified lymph nodes. Pathology

was obtained in 13 lymph nodes, three were malignant and ten non-malignant. Significant differences were found between the malignant and non-malignant lymph nodes for quantitative parameters of D, D*, K_{trans}, K_{ep} and SUV. Based on the standard PET/MR image findings, 6/10 of the non-malignant lymph nodes were scored as suspect. ***Conclusion:*** Based on these preliminary results the physiological MRI showed multiple quantitative parameters correlating to malignancy. Moreover, the relatively high number of non-malignant lymph nodes scored as suspect based on the standard PET/MR images emphasizes the potential specificity improvement additional physiological MRI may provide for head and neck PET/MR imaging. To determine this potential synergistic added value combined with [18F]FDG-PET logistic regression analysis will be performed on the entire dataset.

EP-0101

Clinical Value of [18F]FDG PET-CT In the Study of Head and Neck Carcinoma of Unknown Origin.

V. Carrero-Vásquez, *L. Rodríguez-Bel, C. Martinez-Ramos, P. Notta, L. Gracia-Sánchez, I. Sanchez-Rodriguez, A. Palomar-Muñoz, M. Cortés-Romera;*
Nuclear Medicine Department, Bellvitge University Hospital, Barcelona, SPAIN.

Aim/Introduction: Head and neck carcinoma of unknown origin (CUO) is defined as the presence of cervical adenopathies with anatomopathological (AP) confirmation of squamous cell carcinoma metastasis without evidence of primary lesion after standard diagnostic study, including physical examination and computed tomography. Our study aimed to investigate the diagnostic performance of [18F]-FDG PET-CT in identifying the primary lesion in CUO. ***Materials and Methods:*** Retrospective analysis of 20 consecutive patients (July-2018 to July-2022), 62.5 years (37-85); 12 men. 3 patients were excluded (2: diagnosis of lymphoma, 1: anaplastic carcinoma). All 17 studies included underwent full-body PET-CT and dedicated head-neck scans. Visual analysis of the primary suspect was performed through a qualitative evaluation (grouped as positive, negative or doubtful) and quantitatively with the standardized uptake value (SUVmax). The probable location of malignancy suggested by the PET-CT was confirmed by AP, additional examinations and follow-up. ***Results:*** 9 Studies were grouped as positive, with a SUVmax mean of 6.6(2-11.5); 6 had AP confirmation; in 3 patients, AP of the primary was not performed. The most frequent location was the oropharynx(4/6), most of which were HPV-related (p16+). 4 studies were grouped as doubtful: 3 had tonsillar metabolic asymmetry, with AP analysis negative or not confirmed in the follow-up; in 1 case, the supraglottic larynx was suggested to be the primary site but was located at the base of the tongue. Finally, the remaining 4 studies were grouped as negatives: in 2 patients, the primary site was not detected at follow-up; in 1 case, the post-surgical evaluation located it in the left tonsil-base of the tongue (tumour focus: 1.4mm); and in 1 case AP was not performed due to extensive lymph node and distant dissemination. Sensitivity specificity PPV and NPV were 87.5%, 50%, 77% and 66%, respectively, with an accuracy rate of 75%. Of the 17 patients included, 4 had metastatic spread at diagnosis. ***Conclusion:*** In our population, [18F]-FDG PET-CT proved to be an effective technique with high sensitivity in detecting the primary tumour in patients with CUO, also serving as a biopsy guide and remote disease detection, consistent with the published data. All of this has a clinical impact by contributing substantially to patient care, through an improvement in staging, with the consequent selection of the most appropriate treatment for each case.

EP-0102

Pretreatment PET-derived GLCM & TLG model predicts therapy outcome in patients with Head & Neck S.C.C.

M. Elahmadawy[1], *A. Ashraf*[1], *H. Moustafa*[2], *M. Kotb*[1];
[1]*Nuclear Medicine Unit, National Cancer Institute (NCI) , Cairo University, Cairo, EGYPT,* [2]*Nuclear Medicine Unit, Kasr Al-Ainy (NEMROCK Center), Cairo University, Cairo, EGYPT.*

Aim/Introduction: to assess the prognostic value of pretreatment PET-derived parameters in Head & Neck Squamous Cell Carcinoma (S.C.C). ***Materials and Methods:*** 55 adult patients with Head & Neck S.C.C. were enrolled. Semiquantitative pretherapy PET derived volumetric (SUV max & mean, TLG & MTV) and radiomics analyses (using LIFEx v7.2.0) were performed. Follow-up data were retrieved. ***Results:*** 67.3% were males and 32.7% were females with median age 57 years. 63.6% of the patients received concomitant chemo- and radio-therapies. On last follow-up 74.5% of them showed favorable response and 25.5% were non-responders. The mean value for the primary tumors SUVmax was 14.8 +/-6.3, the metabolic tumor volume (MTV) mean value was 15.4 +/-16 and the total lesion glycolysis (TLG) mean value was 153.1 +/-188.4. There were statistically significant higher MTV values reported among those who died on follow-up compared to those survived till last follow-up with mean value 26.2 +/- 24.9 compared to 13 +/- 12.5 respectively (P-value 0.045). ROC marked a cutoff value for MTV (>10.8) that was able to predict survival with AUC 0.704, sensitivity 80% and specificity 68.9% (P-value 0.048). ROC successfully marked cutoff points that predict survival for morphological_approximate volume (>10083.9), with AUC 0.736, sensitivity 90%, specificity 53.3% (P-value 0.007), morphological_integrated intensity (>97954.1), with AUC 0.702, sensitivity 80% and specificity 66.7% (P-value 0.046), intensity-based_total lesion glycolysis (>101.2), with AUC 0.762, sensitivity 90% and specificity 66.7% (P-value 0.001), GLCM_difference variance (< 81.022) ,with AUC 0.704 , sensitivity 70%, specificity 75.6% (P-value 0.014). NGTDM_coarseness (< 0.0074), with AUC 0.707, sensitivity 60%, specificity 82.2% (P-value 0.035). The synergistic performance of such significant parameters was tested to create the most accurate stable prediction model. Hence Multivariate logistic regression analysis to detect independent predictors of mortality was performed. The combination of TLG and GLCM_difference variance provided the most accurate prediction for mortality with with Sensitivity=70%, Specificity=91.1%, PPV=63.6%, NPV=93.2%, and Overall accuracy=87.3% (P-value <0.001). ***Conclusion:*** Pretreatment PET-derived radiomics, in patients with Head and Neck S.C.C., were able to predict therapy outcome with a prediction model for survival was successfully generated. ***References:*** C Nioche, F Orlhac, S Boughdad, S Reuzé, J Goya-Outi, C Robert, C Pellot-Barakat, M Soussan, F Frouin, and I Buvat. LIFEx: a freeware for radiomic feature calculation in multimodality imaging to accelerate advances in the characterization of tumor heterogeneity. Cancer Research 2018; 78(16):4786-4789

EP-0103

Application value of 18F-FDG PET/MRI in scanning for cephalic and cervical lymph node metastasis of nasopharyngeal carcinoma

J. Liang;
Hangzhou Universal Medical Imaging Diagnostic Center, Hangzhou, CHINA.

Aim/Introduction: To study the value of integrated PET/MRI scanning in the detection of cephalic and cervical lymph node metastasis in patients with nasopharyngeal carcinoma. ***Materials and Methods:*** PET/MRI imaging data of 120 patients

with pathologically confirmed nasopharyngeal carcinoma in our hospital from June 2017 to January 2023 were retrospectively analyzed. The characteristics of PET image, MRI image and PET/MRI image for lymph node detection were analyzed, and the differences of cervical lymph node metastasis diagnosis among each group were compared. ***Results:*** A total of 120 patients were found to have lesions, including 305 positive lesions and 145 negative lesions in MRI group, with sensitivity of 81.9% and specificity of 84.0%. There were 298 positive and 152 negative lesions in PET group, with sensitivity of 92.8% and specificity of 89.1%. PET/MRI group found 281 positive lesions, 169 negative lesions, sensitivity 98.5%, specificity 97.9%. ***Conclusion:*** PET/MRI scan has important application value in the diagnosis of cephalic and cervical lymph node metastasis of nasopharyngeal carcinoma, not only in the detection of lymph nodes, but also in the diagnosis of benign and malignant.

EP-0104

Application value of 18F-FDG PET/MRI in monitoring the staging and treatment effectiveness of nasopharyngeal carcinoma

J. Liang;
Hangzhou Universal Medical Imaging Diagnostic Center, Hangzhou, CHINA.

Aim/Introduction: This study was to evatuate the clinical application of ^{18}F-FDG PET/MRI to the staging, restaging, and treatment effectiveness of nasopharygeal carcinoma(NPC). ***Materials and Methods:*** The ^{18}F-FDG PET/MRI whole-body scanning data of 198 patients with NPC in our center from August 2017 to December 2022 were retrospectively analyzed. According to clinical data, pathological results and clinical follow-up results, The accuracy, specificity, sensitivity, positive predictive value and negative predictive value of ^{18}F-FDG PET/MRI and traditional imaging(including CT and MRI) were calculated. The results are compared and analyzed. ***Results:*** The total accuracy, sensitivity, specificity, positive predictive value and negative predictive value of ^{18}F-FDG PET/MRI in the diagnosis of NPC were 98.2%, 100.0%, 91.6%, 94.1% and 100.0%, respectively. Those of CT and MRI were 70.4%, 80.5%, 73.1%, 84.9% and 69.2%, respectively. The results of ^{18}F-FDG PET/MRI diagnosis changed the treatment plans of 8 patients with the staging and 28 patients with restaging, and affected the formulation of treatment plans of 4 patients with the staging and 12 patients with restaging. In the therapeutic effect monitoring group, a total of 45 cases were guided to modify the treatment plan. ^{18}F-FDG PET/MRI detected 8 secondary primary tumors, 4 of which were lung cancer, 1 laryngeal cancer, and 3 colon cancer. ***Conclusion:*** ^{18}F-FDG PET/MRI is better than CT and MRI in N and M staging and efficacy monitoring of nasopharyngeal carcinoma.

EP-0105

Deciphering Organ-Specific Interactions in Cancer-Associated Cachexia in Head and Neck Squamous Cell Carcinoma Using FDG PET/CT Imaging

J. Yu[1], *D. Ferrara*[2], *S. Gutschmayer*[2], *M. Moreira Pires*[2], *L. Shiyam Sundar*[2], *C. Spielvogel*[1], *D. Haberl*[1], *T. Beyer*[2], *M. Hacker*[1];
[1]*Medical University of Vienna, Vienna, AUSTRIA,* [2]*QIMP Team, Medical University of Vienna, Vienna, AUSTRIA.*

Aim/Introduction: Cancer-associated cachexia (CAC) is a complex syndrome characterized by unintentional weight loss, muscle wasting, and systemic inflammation. The specific patterns of organ involvement in CAC remain unclear. This study investigates the organ-specific involvement patterns in CAC among head and neck squamous cell carcinoma (HNSCC) patients. ***Materials and Methods:*** We conducted a retrospective analysis of 139 HNSCC patients, stratified by the BMI-adjusted Weight Loss Grading System (WLGS), utilizing FDG PET/CT imaging and state-of-the-art automatic segmentation software (MOOSE)[1]. Patients were classified into two cohorts based on their WLGS: WLGS0-2 (N=73, 60M/13F, mean age 58.5 years, overall survival 62 months) and WLGS3-4 (N=66, 57M/9F, mean age 56.95 years, overall survival 59 months). FDG whole-body PET/CT scans were processed using a data-centric artificial intelligence approach for automatic segmentation, and standardized uptake values (SUV) were calculated for seven distinct organ labels to assess the organ-specific involvement patterns in CAC. ***Results:*** In patients with severe cachexia (WLGS3-4), skeletal muscle (SKM) glucose uptake correlated positively with the spleen, kidneys, and liver (R=0.51, 0.31, and 0.55). Conversely, in patients with milder cachexia (WLGS0-2), SKM only correlated with the gastrointestinal tract. Our findings reveal distinct patterns of organ involvement depending on cachexia severity. Although gluconeogenesis may explain the correlation with kidney and liver, the spleen association suggests an upregulated immune response within the inflammatory setting of CAC. ***Conclusion:*** The observed organ-specific involvement patterns in CAC, particularly the association with the spleen, highlight the complex inter-organ connections in this multifactorial disease. Investigating these connections may provide insights into new treatment strategies and options for CAC patients. This preliminary finding serves as a seeding point for more in-depth analyses to elucidate the role of the immune response and explore the potential benefits of targeting specific organ systems to improve outcomes in patients with cancer-associated cachexia. ***References:*** Sundar, L. K. S., Yu, J., et al. (2022). Fully-automated, semantic segmentation of whole-body 18F-FDG PET/CT images based on data-centric artificial intelligence. Journal of Nuclear Medicine. https://doi.org/10.2967/jnumed.122.264063

EP-08

e-Poster Area

B: Imaging Clinical Studies -> B1 Oncological Imaging Clinical Study -> B13 Breast

EP-0106

Comparison of 1 day protocol and 2 day protocol of lymphoscintigraphy by subareolar injection in the detection of sentinel lymph nodes in breast cancer patients.

J. Seok;
Chung-Ang University, College of Medicine, Seoul, KOREA, REPUBLIC OF.

Aim/Introduction: Lymphoscintigraphy and sentinel node biopsy were used for the detection of axillary lymph node metastasis in breast cancer patients. We compared the results of subareolar injections on the day of surgery (1 day protocol) with injections the day before surgery (2 day protocol). ***Materials and Methods:*** This study included 1,612 breast cancer patients who underwent surgery between 2001 and 2023. For the 1 day protocol 0.8 ml of Tc-99m Tin-Colloid (37MBq) was injected in 1,200 patients in the subareolar region on the morning of the surgery. For the 2 day

protocol 0.8 ml of Tc-99m Tin-Colloid (185MBq) was injected in 412 patients on the afternoon before surgery. Lymphoscintigraphy was performed in the supine position and sentinel node identification was performed by hand-held gamma probe during surgery. ***Results:*** Among 1,200 patients with the 1 day protocol, 1,168 cases (97.3%) were identified by sentinel node lymphoscintigraphy, and 1,173 cases (97.8%) were identified by gamma probe. Among the 412 patients, in the 2 day protocol, 389 cases (94.4%) had the sentinel node identified by lymphoscintigraphy, and 379 cases (92.0%) had the sentinel node identified by the gamma probe. There was no significant difference in the identification rate of the sentinel node between the 1 day and 2 day protocol by lymphoscintigraphy and the gamma probe. ***Conclusion:*** The results of the identification of the sentinel node according to 1 day or 2 day protocols showed no significant differences. Because the 2 day protocol allows for an adequate amount of time to perform the lymphoscintigraphy, it is a more useful protocol for the identification of sentinel nodes in patients with breast cancer. ***References:*** Seok JW, Kim IJ, Heo YJ, Yang YJ, Choi YS, Kim BG, Park SJ. Comparison of subareolar injection lymphoscintigraphy with the 1-day and the 2-day protocols for the detection of sentinel lymph nodes in patients with breast cancer. Ann Nucl Med. 2009 Jul;23(5):465-9.

EP-0107

The comparative study of the validation for Tc-99m Tin-colloid and Tc-99m Phytate in sentinel node detection in breast cancer patients.

J. Seok*;*
Chung-Ang University, College of Medicine, Seoul, KOREA, REPUBLIC OF.

Aim/Introduction: Lymphoscintigraphy and sentinel node biopsy has become a standard method for detection of axillary lymph node metastasis in breast cancer patients, but the standard radiopharmaceutical was not prepared. About detection of axillary lymph node metastasis by lymphoscintigraphy and sentinel node biopsy in breast cancer patient, we compared the results of Tc-99m Tin-colloid and Tc-99m Phytate by subareolar injection. ***Materials and Methods:*** This study included 1,612 breast cancer patients who were performed operation during 2001-2023. Four hundred twelve patients were injected 0.8 ml of Tc-99m Tin-colloid (37-185 MBq) by subareolar injection. One thousand two hundred patients were injected 0.8 ml of Tc-99m Phytate (37-185 MBq). Lymphoscintigraphy was performed in supine position and sentinel node localization was performed by hand-held gamma probe in operation. ***Results:*** Among 412 patients by Tc-99m Tin-colloid, 374 cases (90.8%) were localized the sentinel node by lymphoscintigraphy and 367 cases (89.1%) were localized by gamma probe. Among 1,200 patients by Tc-99m Phytate, 1,183 cases (98.6%) were localized by lymphoscintigraphy and 1,185 cases (98.8%) were localized by gamma probe. The detection rate by lymphoscintigraphy and gamma probe was superior for Tc-99m Phytate compared to that for Tc-99m Tin-colloid, with a statistically significant difference. ($p<0.05$, $p<0.05$) ***Conclusion:*** Tc-99m Phytate is a better choice for localization of sentinel node than Tc-99m Tin-colloid in breast cancer patients. ***References:*** Seok JW, Choi YS, Chong S, Kwon GY, Chung YJ, Kim BG, Park SJ. Sentinel lymph node identification with radiopharmaceuticals in patients with breast cancer: a comparison of 99mTc-tin colloid and 99mTc-phytate efficiency. Breast Cancer Res Treat. 2010 Jul;122(2):453-7.

EP-0108

Prediction of HER2 expression status in breast cancer based on 18F-FDG PET-CT radiomics

D. Han[1,2]*, X. Duan*[1]*, N. Yu*[2]*;*
[1]the First Affiliated Hospital of Xi'an Jiaotong University, Xi'an, CHINA, [2]Affiliated Hospital of Shaanxi University of Chinese Medicine, Xianyang, CHINA.

Aim/Introduction: To evaluate the value of ^{18}F-FDG PET/CT radiomics in judging the expression status of human epidermal growth factor receptor 2 (HER2) in breast cancer. ***Materials and Methods:*** 100 patients with breast cancer were retrospectively collected, including 72 HER2 negative patients and 28 positive patients. The differences of PET/CT parameters between groups were compared, including the maximum standard uptake value (SUVmax), the average standard uptake value (SUVmean), the standard deviation (SD) of SUVmax and the metabolic tumor volume. After the PET images was standardized, the PET/CT physician manually segmented the region of interest (ROI) and radiomics features were calculated. The Radiomics risk score (RRS) was obtained by linear weighting of the dimensional-reduced radiomics features and coefficients. ROC curves were drawn and area under the curves (AUC) was calculated to evaluate the efficacy of indicators with statistically significant differences in determining HER2 status in breast cancer patients. Bootstrap 1000 repeated sampling was used for internal validation, and the corrected AUC was calculated. The corrected AUC was compared by Delong test. The net benefit of patients was evaluated by decision curve analysis. ***Results:*** SUVmax, SUVmean and SD in HER2 positive group were significantly higher than those in HER2 negative group (all $P < 0.05$). A total of 704 radiomics features were obtained. After screening, 10 non-zero coefficient features were finally obtained for calculating RRS. RRS in HER2 (+) group was greater than that in HER2 (-) group, and the difference was statistically significant ($P<0.001$). The AUC of HER2 status in patients with breast cancer judged by RRS [0.79 (95%CI: 0.70-0.86)] was greater than SUVmax, SUVmean and SD, and the difference was statistically significant (all $P<0.05$). The diagnostic sensitivity was 78.57% and the specificity was 77.78%. The results of decision curve analysis show that RRS can make the net benefit of patients higher within a larger probability threshold range. ***Conclusion:*** ^{18}F-FDG PET/CT RRS achieves medium diagnostic performance in evaluating HER2 status of breast cancer. ***References:*** CHEN Y, WANG Z, YIN G, et al. Prediction of HER2 expression in breast cancer by combining PET/CT radiomic analysis and machine learning[J]. Ann Nucl Med, 2022,36(2):172-182.

EP-0109

Detection of internal mammary lymph node chain infiltration in breast cancer patients by 18F-FDG-PET/MRI. Impact on patient management

M. Kauak Kuschel*, J. García Garzón, A. Compte, E. Valls, P. Bassa, M. Minoves, E. Llinares, L. Mont, E. Riera, M. Blanch Labrador;*
CETIR ASCIRES, Barcelona, SPAIN.

Aim/Introduction: In patients recently diagnosed with breast cancer, infiltration of the internal mammary node (IMN) chain bears a poor prognostic with impact on patient therapy. Diagnostic imaging plays a role to increase its detection rate. We aimed: 1) To assess detection rate of IMN infiltration in patients diagnosed with breast cancer, for whom 18F-FDG-PET/MRI is indicated for staging purposes 2) To assess therapy impact of IMN infiltration depending on TNM staging by 18F-FDG-PET/MRI. ***Materials and Methods:*** Prospective study including 41 women (31-89 years) with breast cancer referred for staging assessment (stage ≥IIB)

by integrated 18F-FDG-PET/MRI study in 2022. The study was dual-phase: 1) Selective prone breast PET/MRI imaging (3D-T1, T2-CUBE, DWI, 3D-VIBRANT-Gadolinium). 2) Supine whole-body PET/MRI study (T1-LAVA, T2 FAT, DWI, STIR). TNM staging was reached by consensus. Detection of an afferent vessel (AV) to IMN was assessed by Cadstream software on selective breast MRI. IMN infiltration was then correlated with patient's age, AV-IMN, T-staging, quadrant localisation, detection of axillary and distant infiltration. Multidisciplinary committee then assessed changes in therapy after TNM staging of patients with IMN involvement detected by 18F-FDG-PET/MRI. ***Results:*** The detection rate of IMN infiltration on 18F-FDG-PET/MRI was 34% (14/41), with 8 patients younger than 55 years. Node size ranged 7-20 mm. The SUVmax ranged 1.5-16.4. In all 14 patients (100%) with IMN infiltration, AV-IMN was shown, with no AV-axillary in 6 (43.9%). Among the 27 patients with no IMN infiltration, in 13 (48.1%) only AV-axillary was detected, while in the remaining 14 (51.9%) AV-axillary and AV-IMN were both shown. Regarding T staging, 57% (8/14) of cases were multicentric and 42% (6/14) were focal, in inner quadrants in 4/6 patients (66.7%). Regarding NM staging, 1/14 patient (7.1%) showed IMN infiltration only, 9/14 (64.3%) showed both axillary and IMN infiltration, while distant metastases were present in 4/14 patients (28.6%). Committee decided to carry out radiotherapy over IMN in 10/14 patients (71.4%) due to IMN only and axillary & IMN infiltration, and systemic therapy in 4/14 patients (28.6%) due to metastases. ***Conclusion:*** Detection rate of IMN infiltration by 18F-FDG-PET/MRI in staging of our breast cancer patients was 34%. Factors associated with IMN infiltration were age, multicentric tumours and when focally detected, located on the inner quadrants, AV- IMN positive, as well as IMN staging. Accurate IMN detection allowed for individualisation of therapy, thus indicating the need for thoracic radiotherapy in 71.4% of patients with IMN.

EP-0110

A pilot study of the use of positron emission tomography to evaluate early oestrogen receptor changes in patients with advanced and/or relapsed breast cancer administered endocrine therapy and CDK4/6 inhibitor combination therapy

I. Kuji[1], *K. Matsuura*[2], *A. Osaki*[2], *T. Yamane*[1], *H. Ishiguro*[2], *T. Saeki*[2];
[1]*Department of Nuclear Medicine, Saitama Medical University International Medical Center, Hidaka, Saitama, JAPAN,*
[2]*Department of Breast Oncology, Saitama Medical University International Medical Center, Hidaka, Saitama, JAPAN.*

Aim/Introduction: We performed F-18-fluoroestradiol (FES) positron emission tomography (PET)/computed tomography to observe oestrogen receptor changes in patients with advanced and/or relapsed breast cancer positive for oestrogen receptors before and after endocrine therapy and CDK4/6 inhibitor combination therapy. The efficacy of CDK4/6 inhibitor therapy for each lesion was evaluated based on changes in F-18-fluorodeoxyglucose (FDG) accumulation. ***Materials and Methods:*** Eight patients with postoperative breast cancer recurrence pathologically confirmed as oestrogen receptor-positive before pretreatment were enrolled in this study. FDG and FES PET were performed before the initiation of CDK4/6 inhibitor treatment and 2 to 3 months after treatment initiation. The FDG maximum standard uptake value (SUVmax), FDG peak standard uptake value (SUVpeak), and FES in the evaluable lesions were measured. Blood tests were performed to obtain the levels of white blood cells, red blood cells, hemoglobin, platelets, alkaline phosphatase, lactate dehydrogenase, creatinine, and estradiol. Eighteen lesions were evaluated. ***Results:*** We compared the values of the positive therapy response (RP) group (lesions with a decrease in the FDG SUVpeak >=30% after treatment) and the negative therapy response (RN) group (lesions with a decrease in the FDG SUVpeak <30%). The FES SUV was significantly different in both groups before (RPpre and RNpre) and after (RPpost and RNpost) treatment (RPpre vs. RNpre: 6.11±4.78 vs. 2.32±1.15, P=0.017; RPpost vs. RNpost: 1.65±0.49 vs. 2.42±1.21; p=0.049). The FES value was high before treatment and low after treatment. A decrease trend like FES changes was observed for the FDG SUV (RPpre vs. RNpre: 7.83±3.34 vs. 5.27±2.67, P=0.045; RPpost vs. RNpost: 1.97±0.91 vs. 4.60±1.81, p<0.001). When analysed using the receiver-operating characteristic (ROC) curve, the FES value before treatment was significant (area under the ROC curve=0.79; p=0.038). Setting the FES SUV threshold to 2.84 before treatment resulted in sensitivity of 0.84, specificity of 0.90, positive predictive value of 0.61, negative predictive value of 0.97, and accuracy of 0.89. It was again confirmed that FES accumulation and FDG accumulation decreased in the RPpost group. ***Conclusion:*** Oestrogen receptor expression was higher before treatment. Oestrogen receptor withdrawal was higher in the RP group than in the RN group after CDK4/6 inhibitor treatment. To predict the therapeutic effect of CDK4/6 inhibitor treatment, it is important to re-evaluate oestrogen receptor expression in individual tumor lesions. Different treatments could be administered for lesions with low oestrogen receptor expression even if that expression is positive at the time of initial treatment.

EP-0111

Is subcutaneous/cutaneous uptake on [18F] FDG PET/CT a prognostic marker for breast cancer patients undergoing surgery?

Y. Kitano[1], *K. Miyake*[2], *T. Nobashi*[1], *T. Ishimori*[3], *R. Nakamoto*[1], *S. Koyasu*[1], *M. Kataoka*[1], *K. Kawaguchi*[4], *Y. Takeuchi*[5], *M. Toi*[6], *Y. Nakamoto*[1];
[1]*Diagnostic Imaging and Nuclear Medicine, Kyoto University Hospital, Kyoto, JAPAN,* [2]*Department of Advanced Imaging in Medical Magnetic Resonance, Kyoto University Hospital, Kyoto, JAPAN,* [3]*Diagnostic Radiology, Medical Research Institute Kitano Hospital, PIIF Tazuke Kofukai, Osaka, JAPAN,* [4]*Department of Breast Surgery, Graduate School of Medicine, Kyoto University, Kyoto, JAPAN,* [5]*Clinical Bio Resource Center, Kyoto University Hospital, Kyoto, JAPAN,* [6]*Breast Surgery, Tokyo Metropolitan Cancer and Infectious Disease Center, Komagome Hospital, Tokyo, JAPAN.*

Aim/Introduction: To investigate the prognostic value of subcutaneous/cutaneous uptake (SCU) on pretreatment whole-body [18F] FDG PET/CT in patients with breast cancer treated with surgery. ***Materials and Methods:*** A retrospective study was performed of 171 women with M0 unilateral invasive breast cancer who underwent whole-body [18F] FDG PET/CT and were treated with surgery with or without neoadjuvant therapy (NAT) at our institution from January 2012 to March 2021. SCU was defined as abnormal FDG uptake extending along the skin apart from the tumor. The subareolar SUV ratio (sSUVr) - subareolar SUVmax of the affected side divided by the unaffected side - was used as a quantitative measure. The association of progression-free survival (PFS) and disease-specific survival (DSS) with the following 9 factors was evaluated using the log-rank test and univariate and multivariate Cox-regression analysis: age (≥60 vs. <60), visual SCU (positive vs. negative), sSUVr (>1.3 vs. ≤1.3), tumor SUVmax (>10 vs. ≤10), cT stage (T3 vs. T1-2), cN stage (N1-3 vs. N0),

histological type (ILC or others vs. IC(NST)), histological grade (G3 vs. G1-2), and subtype (triple negative vs. non-triple negative). ***Results:*** Of 171 women (median age, 56 years; range, 23-85 years), SCU was present in 27 (15.8%). After a median follow-up period of 4.4 years (range, 0.3-11.0 years), 18 (10.5%) developed recurrence and 8 (4.7%) died. The log-rank test showed that visual SCU, sSUVr, and cN stage effectively stratified patients by PFS and DSS. Univariate Cox-regression analysis showed that visual SCU-positive (PFS, hazard ratio [HR] 3.29, 95% confidence interval [CI] 1.23-8.76, p = 0.02; DSS, HR 9.89, 95% CI 2.36-41.49, p <0.01) and sSUVr >1.3 (PFS, HR 3.90, 95% CI 1.53-9.91, p <0.01; DSS, HR 9.32, 95% CI 1.87-46.39, p <0.01), and cN stage 1-3 (PFS, HR 4.45, 95% CI 1.58-12.51, p <0.01; DSS, HR 5.06, 95% CI 1.02-25.11, p = 0.05). Multivariable survival analysis revealed that sSUVr >1.3 was an independent significant prognostic factor for PFS and DSS (PFS, HR 2.75, 95% CI 1.06-7.11, p <0.01; DSS, HR 6.96, 95% CI 1.36-35.59, p <0.01). ***Conclusion:*** The sSUVr was an independent prognostic factor for recurrence and death after surgery. This study suggests that SCU is a potentially useful prognostic biomarker in patients with breast cancer treated with surgery.

EP-0112

[18F]FDG-PET/MRI in Breast Cancer

G. Argalia[1], *F. M. Fringuelli*[1], *G. Biscontini*[1], *A. Palucci*[1], *C. Romagnolo*[1], *C. Cottignoli*[1], *P. Ercolani*[2], *B. F. Simonetti*[2], *S. Borgoforte Gradassi*[2], *L. Burroni*[1];
[1]*Nuclear Medicine, Department of Radiological Sciences, University Hospital of Marche, Ancona, ITALY,*
[2]*Radiology, Department of Radiological Sciences, University Hospital of Marche, Ancona, ITALY.*

Aim/Introduction: Breast cancer is the most common malignancy and has the second highest cancer-related morbidity, in women worldwide. [18F]FDG-PET/CT has been introduced for breast cancer staging, distant-metastasis detection, prognostic prediction and evaluation of the pathological response to treatment. Contrast-enhanced-MRI, nowadays, is considered the most sensitive technique for breast cancer screening, locoregional staging and treatment monitoring. Therefore, hybrid [18F]FDG-PET/MRI exam, through which it is possible to acquire both metabolic data and high-contrast morphological images in a single exam, may be useful in the management of these patients. ***Materials and Methods:*** We enrolled all consecutive patients with breast cancer who underwent [18F]FDG-PET/MRI at our department from September 2022 to March 2023. The scans were performed with a hybrid PET/MRI tomograph permitting simultaneous acquisition of whole body PET and 3 Tesla-MRI images. MRI-contrast-agent was injected. The examination was completed with a PET/MRI bed of the breast with the patient prone and dedicated RM coils. [18F]FDG-PET/MRI was performed at different stages of the disease: staging, restaging post neoadjuvant CHT, restaging in suspected recurrence (radiological/biochemical) and follow-up. Agreement between FDG-enhancing findings and MRI contrast-enhancing findings was evaluated. ***Results:*** Overall, 17 female patients were included (9 right breast, 7 left breast, 1 bilateral neoplasm; mean age 54.4 years; range 34-83 years). 3 staging, 7 restaging post neoadjuvant CHT, 6 restaging in suspected recurrence (5 radiological and 1 biochemical) and 1 follow-up. [18F]FDG-PET/MRI and contrast-agent-MRI were concordant in the majority of cases (15/17 patients). In 2/17 cases the results were discordant: a small skin lesion and 3 axillary lymph nodes (both suspicious for recurrence) were revealed by contrast-agent-MRI, without radiotracer uptake at [18F]FDG-PET/MRI. This to underscore the importance of performing a hybrid [18F]FDG-PET/MRI examination with a synchronous MRI with contrast medium, to completely stage and restage patients with breast cancer, allowing to evaluate the metabolism of some doubtful MRI findings (without motion artifacts) and to highlight no-FDG-avid findings but still worthy of further investigation/monitoring. ***Conclusion:*** The importance of [18F]FDG-PET/CT and contrast-enhanced-MRI is already known from the literature. Based on our preliminary results, [18F]FDG-PET/MRI with contrast-agent-MRI, as a hybrid exam, results to be even more accurate in the management of breast cancer patients especially in terms of spatial resolution and metabolic activity.

EP-0113

Automated Lesion Detection for 18F-Fluoroestradiol PET/CT Images Demonstrates Lesion Heterogeneity in Patients with ER+ Metastatic Breast

M. Battle[1], *K. Wangerin*[2], *R. Miller*[1], *S. S. Houshmandi*[3], *D. T. Huff*[3], *A. J. Weisman*[3], *T. G. Perk*[3], *G. A. Ulaner*[4];
[1]*GE HealthCare, Little Chalfont, UNITED KINGDOM,*
[2]*GE HealthCare, Marlborough, MA, UNITED STATES OF AMERICA,* [3]*AIQ Solutions, Madison, WI, UNITED STATES OF AMERICA,* [4]*Hoag Family Cancer Institute, Long Beach, CA, UNITED STATES OF AMERICA.*

Aim/Introduction: Tumoral heterogeneity within individual cancer patients is increasingly recognized as a cause of therapy failure. Heterogeneity may be spatial (phenotypically diverse tumors across different disease sites) or temporal (tumour phenotype changes over time). ^{18}Ffluoroestradiol injection ([^{18}F]FES, CERIANNA) is a PET radiotracer which detects estrogen receptor (ER) available for estrogen binding. As heterogeneity of ER expression influences response to endocrine therapy, [^{18}F]FES PET can inform better treatment decisions. Utilizing an automated tool could aid lesion detection and further our understanding of image heterogeneity. ***Materials and Methods:*** Manual contouring, performed on 52 paired images from ER-positive breast cancer patients (37 [^{18}F]FES & CT, 15 [^{18}F]FES & FDG), was used for lesion identification and model training. Concordance analysis on reader-identified lesions was performed on a subset of cases for more in-depth analysis: [^{18}F]FES with [^{18}F]FDG (n=12), CT (n=12), or both (n=1), selected as a representation of the larger data set. Images were evaluated for overall lesion identification. A previously developed AI model[1] was expanded to detect and segment [^{18}F]FES -positive lesions. Model performance was assessed through lesion sensitivity and false positive rate compared to reader results. ***Results:*** For subjects with [^{18}F]FES and CT images, 2 cases showed 100% concordance. Six cases identified a proportion of lesions with CT but not [^{18}F]FES, and 3 cases included a mix of lesions identified with [^{18}F]FES only, CT only, or both modalities. Two cases identified lesions with [^{18}F]FES alone or with both [^{18}F]FES and CT. For subjects with [^{18}F]FES and [^{18}F]FDG images, 1 case showed 100% concordance. One case identified lesions only with [^{18}F]FDG. Three cases had a proportion of lesions identified with [^{18}F]FES and [^{18}F]FDG or [^{18}F]FDG only. Five cases included a mix of lesions identified with [^{18}F]FES only, [^{18}F]FDG only, or both modalities. One case reported 100% lesions identified only with [^{18}F]FES, and 2 cases identified lesions with [^{18}F]FES only or [^{18}F]FES and [^{18}F]FDG. Overall model performance gave a median sensitivity of 62%, with a median false positive rate of 0. ***Conclusion:*** Lesion heterogeneity was demonstrated between modalities ([^{18}F]FES vs CT and [^{18}F]FES vs [^{18}F]FDG), offering a useful insight into tumour composition. Understanding heterogeneity

in a subject could help inform patient management. Our model, although trained on a limited data set, performed well. With further training on a larger dataset, the model has the potential to support [18F]FES readers to quickly identify lesions for evaluation. ***References:*** Weisman et. al. JNM 63:3215, 2022

EP-0114

Potential role of 18F-FDG PET/CT in the initial staging of breast cancer.

R. Sanchez Sanchez[1], *A. González Jimenez*[2], *T. Aroui Luquin*[1], *A. Piñero Donis*[1], *J. Villa Palacios*[1];
[1]*Hospital Virgen de las Nieves, Granada, SPAIN,*
[2]*Hospital Universitario de Jaén, Granada, SPAIN.*

Aim/Introduction: Multiple studies have evaluated the usefulness of PET/CT in the initial staging of breast cancer, demonstrating an important clinical impact with a change in therapeutic management in a high percentage of these patients when compared with conventional imaging methods. However, its role in routine clinical practice is controversial and its use is still considered optional for the main guidelines. The aim of our work is to assess the usefulness of PET/CT in this context. ***Materials and Methods:*** The results of PET/CT in patients recently diagnosed with breast cancer (2021-2022) have been analyzed visually and semiquantitatively by calculating the SUVmax. Positive findings were confirmed by specific imaging procedures. ***Results:*** We prospectively evaluated 166p, mean age 59.8a ± 12.08 (SD), ductal carcinoma (81%), grade II (54%) and luminal subtype (76%). The primary tumor was detected by PET/CT in all cases, the mean SUVmax of the primary lesion was 20.7. At diagnosis, 58p (35%) presented axillary lymph node involvement by PET/CT. Lymph node involvement was detected by axillary ultrasound in 79% (46/58). In addition, in the 46p that lymph node involvement was detected by both tests, PET/CT increased the number of lymph node lesions, thus modifying the stage (N1→N2 at 13p, N1→N3 at 1p, N2→N3 at 4p).Unsuspected distant metastases were diagnosed by PET/CT in 12p (7%), ten of them had axillary lymph node involvement (17%). Distant metastasis sites: bone (n=7), liver (n=1), lung (n=1) and lymph nodes (n=3). The variables significantly associated with a higher probability of axillary or distant metastases on PET/CT were: high histological grade (2-3) (p=0.03), high Ki67 levels (p=0.002) and higher SUVmax of the primary lesion. (p=0.02). ***Conclusion:*** Our results suggest a potential utility of PET/CT in the initial staging of patients with breast cancer, particularly in those patients with metastatic axillary lymph node involvement for the detection of unsuspected distant metastases.

EP-0115

Standardized Uptake Values of Breast Cancer in Sub-millimetre 18F-FDG-PET/CT: Direct Correlation with Histopathology

L. Maris[1,2], *M. Göker*[3], *K. De Man*[4], *B. Van den Broeck*[4], *R. Van Holen*[2], *V. Keereman*[1,2], *K. Van de Vijver*[5,6], *C. Vanhove*[1,7];
[1]*Department of Electronics and Information Systems, Ghent University, Ghent, BELGIUM,* [2]*XEOS Medical, Ghent, BELGIUM,* [3]*Department of Gynaecology, Ghent University Hospital, Ghent, BELGIUM,* [4]*Department of Medical Imaging, Nuclear Medicine, Ghent University Hospital, Ghent, BELGIUM,* [5]*Department of Pathology, Ghent University Hospital, Ghent, BELGIUM,* [6]*Department of Diagnostic Sciences and Cancer Research Institute Ghent (CRIG), Ghent University, Ghent, BELGIUM,* [7]*INFINITY Lab, Ghent University, Ghent, BELGIUM.*

Aim/Introduction: The current role of PET in breast cancer (BCa) detection is limited as sensitivity depends on the lesion's size and histology. It is especially difficult to detect ductal carcinoma in situ (DCIS) and invasive lobular carcinoma (ILC), which generally show lower uptake than invasive carcinoma of no special type (NST). However, as the spatial resolution of PET scanners constantly evolves, visualization of BCa will improve in the future. Therefore, it is of great importance to improve our understanding of the distribution of radiotracers in different types of breast tissue at a previously unseen resolution. Earlier, we developed a strategy to co-register ex vivo high-resolution PET/CT images of resected cancer specimens with the corresponding histopathology. Here we present the first results of applying this technique to breast cancer specimens. ***Materials and Methods:*** We imaged BCa specimens of 9 patients who underwent breast-conserving surgery after preoperative injection with 0.8MBq/kg ^{18}F-FDG. Specimens included 8 NSTs (combined with DCIS), and 1 ILC. After resection, the specimens were sliced into ±2mm-thick lamellas. In total, 17 NST and 2 ILC lamellas were imaged using a PET/CT specimen scanner with sub-millimetre resolution. Afterwards, the tissue was further processed to obtain one H&E-stained section of every lamella. Whole-slide images (WSIs) were captured using a section scanner. To align PET/CT images and WSIs, we developed a deformable co-registration algorithm to compensate for tissue deformation. An experienced pathologist annotated the WSIs to distinguish tumour and healthy tissue, to evaluate intratumoral standardized uptake values (SUVs). ***Results:*** By acquiring PET/CT images of breast lamellas, tissue deformation was minimized and the correlation with histopathology was immediately visible. Mathematical co-registration further optimised image alignment. After transferring the histopathology annotations to the co-registered PET/CT images, the following mean tumour SUVs were found across all patients: 2.43±2.50, 1.50±1.58, and 2.70 for NST, DCIS, and ILC respectively. The SUVs for hyperplastic, inflammatory, and healthy tissue were found to be 0.55±0.41, 1.88±2.01, and 0.27±0.22 respectively. ***Conclusion:*** We collected a unique dataset of sub-millimetre ^{18}F-FDG-PET/CT images of BCa specimens, that were co-registered with annotated histopathology images. While the dataset is currently still limited, it already provides insights in breast SUVs at a sub-millimetre resolution. The preliminary results give an indication that NST and ILC generally show high SUVs compared to the background in sub-millimetre PET, while for DCIS a lower uptake is found. As expected for ^{18}F-FDG, notable uptake is detected in inflamed tissue.

EP-0116

The Role Of F-18 FDG PET/CT In The Prediction of Residual Cancer Burden After Neoadjuvant Chemotherapy In Locally Advanced Breast Cancer

E. KAYA[1], *O. VURAL TOPUZ*[1], *B. E. AKKAS*[1], *M. KAYA*[1], *T. SOYLEMEZ AKKURT*[2], *E. ACAR*[1];
[1]*University of Health Sciences, Başakşehir Cam and Sakura City Hospital, Department of Nuclear Medicine, Istanbul, Turkey., Istanbul, TÜRKIYE,* [2]*University of Health Sciences, Başakşehir Cam and Sakura City Hospital, Department of Pathology, Istanbul, Turkey., Istanbul, TÜRKIYE.*

Aim/Introduction: Presence of residual disease after neoadjuvant chemotherapy (NAC) in locally advanced breast cancer (LABC) can be measured by the pathological Residual Cancer Burden score (RCB)(1).RCB scoring system is an independent prognostic factor in survival of LABC patients. The aim of our study was to determine the value of F-18 fluorodeoxyglucose (FDG) positron

emission tomography/computed tomography (PET/CT) studies in predicting RCB scores. ***Materials and Methods:*** Patients with LABC who underwent staging (PET1) and post-NAC (PET2) PET/CT studies and subsequently operated were evaluated retrospectively. Patients were grouped according to their molecular subtypes as luminal, non-luminal HER2 positive (+) and triple negative (TN) . SUV and SUL values of breast lesions (L) and their ratio to liver SUV and SUL values (Li) were recorded (L/Li). The patients were divided into 2 groups as RCB 0-1 and RCB 2-3 according to the RCB scores in their postoperative pathology. ***Results:*** The mean age of the patients was 48.2±11,4 (27-82). 34 patients (39.1%) were luminal, 38 (43.7%) were non-luminal HER2+, and 15 (17.2%) were TN. Metabolic parameters obtained from the primary tumor in PET1 were significantly different between the groups and they were higher in the TN group (p<0.01)In PET2 scan; SUL L/Li in the TN group were significantly lower than other subtypes (0.68 vs 1.1 and 1.2, p<0.01). In postoperative pathologies, RCB scores was 0-1 in 30 patients (34.5%) and 2-3 in 57 patients (65.5%). When RCB scores were compared between the luminal and HER2 groups, no significant difference was observed, while the RCB 0-1 ratio was significantly higher in the TN group (p<0.01).While metabolic parameters in PET1 did not differ significantly between RCB groups, in PET 2, SULL and SUL L/Li differed significantly between RCB 0-1 and RCB 2-3 groups (0.6±0.1 vs 1.4 ±1.1, p<0.001). In receiver operating characteristic (ROC) analysis, PET2 SUL L/Li were found to be the highest predictor of RCB 0-1 group (AUC:0.93, 0.86-1, 95% CI). When cut-off value was determined as 0.82, the sensitivity and specificity of SULL/Li in predicting RCB 0-1 group were calculated as 88% and 80%,respectively. ***Conclusion:*** SUL L/Li and SUV L/Li obtained from post-NAC PET/CT in LABC provide a non-invasive prediction of postoperative RCB in the preoperative period. Regarding the prognostic value of RCB for LABC patients, we consider that the prediction of RCB score on preoperative PET/CT will contribute to patient management. ***References:*** 1.Yau C, et al.Lancet Oncol. 2022;23(1):149-160.

EP-0117

Therapeutic impact of [18F]FDG PET/CT for initial staging in patients with clinical stage I and IIA, HER2-positive and triple negative breast cancer

C. François[1], *A. Mailliez*[2], *S. Chrétien*[2], *L. Ceugnart*[3], *A. Oudoux*[1], *O. Cougnenc*[4], *A. Olivier*[1];
[1]*Department of Nuclear Medicine, Centre Oscar Lambret, Lille, FRANCE,* [2]*Department of Medical Oncology, Centre Oscar Lambret, Lille, FRANCE,* [3]*Department of Radiology, Centre Oscar Lambret, Lille, FRANCE,* [4]*Department of Clinical Pharmacy, Centre Oscar Lambret, Lille, FRANCE.*

Aim/Introduction: Breast cancer is a heterogeneous disease with varying treatment and prognosis according to subtype. Aggressive features like HER2+ or triple-negative increase the risk of metastases. Accurate staging is crucial for patient management. While [^{18}F]FDG-PET/CT (FDG-PET/CT) is consensual for clinical stage ≥IIB, there is lack of data regarding its actual benefit for clinical stage I or IIA HER2+ and triple-negative breast cancer patients (TNBC). These stages encompass heterogeneous population with different tumor sizes and possible axillary involvement, necessitating further study to determine which patients would benefit most from FDG-PET/CT. We propose a single-institution, retrospective study evaluating the impact of FDG-PET/CT on patient management and staging for female patients with clinical stage I or IIA HER2+ and TNBC. ***Materials and Methods:*** All patients who underwent FDG-PET/CT staging before any treatment were included. Patients with symptoms or conventional imaging suggestive of metastatic dissemination, or with prior malignancies were excluded. The initial stage was determined from mammography, ultrasound, MRI, and clinical examination. Staging and therapeutic impact based on FDG-PET/CT findings were collected, including intra- (modification of dose/site/strategy in a type of management previously indicated) and inter-modality (modification of planned treatment strategy) changes. ***Results:*** The impact of FDG-PET/CT on management and staging was evaluated in 287 female patients with clinical stage I or IIA, HER2+ or TNBC. Results showed therapeutic impact for 18% of patients (n=52), with 2.4% (n=7) undergoing an inter-modality change with omission of planned surgery. Intra-modality changes were observed for 16% of patients (n=45). The impact on patient management was higher for stage IIA patients (20%, 47/237) than stage I patients (10%, 5/50). Among patients with stage IIA disease, changes in management were more important for T2N0 patients (22%, 44/205) than T1N1 patients (9%, 3/32). While not statistically significant, this trend suggests potential usefulness of FDG-PET/CT for T2N0 patients. ***Conclusion:*** FDG-PET/CT is recommended for breast cancer patients with stage IIB or higher. However, FDG-PET/CT is often planned for patients with stage I and IIA before neoadjuvant chemotherapy, especially for those with HER2+ or TNBC. Our results support recent French National recommendations ; considering high therapeutic implications, our study suggests potential usefulness of FDG-PET/CT for patients with stage IIA, HER2-positive or TNBC with tumor size greater than 2 cm (T2N0). However, there is not enough evidence to corroborate the routine use of FDG-PET/CT for patients with stage I or IIA and tumors smaller than 2 cm (T1N1 and T1N0).

EP-0118

The Role of Primary Tumor PET/MR Quantitative Values in Predicting Pathological Complete Response after Neoadjuvant Treatment in Breast Cancer

Y. Ünlüer Ates*, U. Aydos, E. Balcı, L. Atay;*
Gazi University Medicine Faculty, Nuclear Medicine, Ankara, TÜRKIYE.

Aim/Introduction: Pathologic complete response (pCR) is a criterion for neoadjuvant therapy (NAT) success and a marker of recurrence. This study aimed to evaluate the role of primary tumor quantitative parameters obtained from 18F-FDG PET/MRI in breast cancer (BC) patients in the prediction of pCR. ***Materials and Methods:*** Female patients diagnosed with BC who underwent PET/MRI for staging and treatment response evaluation, and underwent surgical resection at the end of the treatment (EOT) were retrospectively reviewed. During the NAT period, 22 patients with interim PET/MRI (interim evaluation group, mean age: 48.8±13 years) and 34 patients with end-of-the-treatment PET/MRI (EOT evaluation group, mean age: 51.5±11.3 years) were included in the study. SUVmax, SULpeak, MTV, TLG, ADCmin, SUVmax/ADCmin values of the primary tumors were obtained from the initial, interim, and end-of treatment PET/MRI. The percentages of change of quantitative parameters according to the initial staging values were also calculated in both evaluation groups. The C4.5 algorithm was used to classify quantitative variables. The implementation of this algorithm was carried out with J48() in the Rweka package in the R software. The role of quantitative parameters in predicting pCR was evaluated by using decision tree models created as a result of classifications. ***Results:*** Ten patients (45.5%) in the interim evaluation group and 13 patients (38.2%) in the EOT evaluation group had pCR. In the model created for the interim evaluation group, patients were classified using TLG_1

(cutoff value: ≤27.6 pCR +) in the first layer and the percentage change of ADCmin (cutoff value: ≤106.4% pCR - and >106.4% pCR +) in the second layer. In the model created for the EOT evaluation group, patients were classified using triple layer with the values of SUVmax/ADCmin_2 (cutoff value: >1.86 pCR -), ADCmin_2 (cutoff value: >1.55 pCR +) and SUVmax_2 (cutoff value: ≤1.51 pCR + and >1.51 pCR -). According to the confusion matrices obtained for the two groups, the model classified 20 patients correctly (accuracy:90.9%, sensitivity:100%, specificity:86%) in the interim evaluation group, while in the EOT evaluation group, the model classified 33 patients correctly (accuracy:97.1%, sensitivity:93%, specificity:100%). ***Conclusion:*** In BC patients who received NAT, the staging TLG value and ADCmin change level in the interim evaluation group, and the EOT SUVmax/ADCmin, ADCmin, and SUVmax values in the EOT group were found as predictive factors for pCR. Assessment of tumor metabolism and cellularity together may be beneficial in the early detection of treatment response.

EP-0119

Can Tumor Heterogeneity in TNBC Obtained With FDG PET/CT Predict Survival? a Novel Method: Heterogenity index3

G. B. Babacan[1], *M. Öner Tamam*[1], *S. Saraçoğlu*[1], *M. N. Acar*[1], *M. C. Şahin*[1], *G. Kulduk*[2], *H. Özçevik*[3];
[1]*University of Health Sciences, Prof. Dr. Cemil Tascioglu City Hospital, Department of Nuclear Medicine, Istanbul, TÜRKIYE,*
[2]*University of Health Sciences, Prof. Dr. Cemil Tascioglu City Hospital, Department of Pathology, Istanbul, TÜRKIYE,*
[3]*University of Health Sciences, Hamidiye Faculty of Medicine, Department of Nuclear Medicine, Istanbul, TÜRKIYE.*

Aim/Introduction: This study aimed to investigate the potential prognostic significance of tumor heterogeneity in triple-negative breast cancer(TNBC) and compare different heterogeneity methods(the new method with HI_3). ***Materials and Methods:*** Data of the patients with histopathologically diagnosed as TNBC were analyzed. Patients in the T_1 stage, according to the 8th of TNM classification, were excluded from the study. Images of 80 patients who underwent pre-treatment ^{18}F-FDG PET/CT between January 2016 and June 2022 were evaluated. Semi-quantitative PET parameters (SUVmax, SUVmean, SUVmin, SUVpeak, MTV, TLG) were determined semi-automatically by using the auto contour tool with three-dimensional visual correction. Heterogeneity index (HI_1, HI_2, and HI_3) parameters were calculated as SUVmax minus SUVmin divided by SUVmean at a 30% threshold (HI_1), the slope of the linear regression line of the MTV with 30-40-50%($MTV_{30\text{-}40\text{-}50}$) thresholds ($HI_2$), and slope of the percentages at $MTV_{30\text{-}40\text{-}50}$ (HI_3). ***Results:*** Median age was 46.5 (range 29-88), and 18 patients (23%) died during the follow-up period. The median follow-up duration was 24(8-75) months. The PET parameters SUVmax-min-mean, SUVpeak, HI_1, and HI_3 were positively correlated with the tumor diameter (All $p<0.05$). The HI_2 was strongly correlated with tumor diameter and TLG ($p<0.001$, $r=0.906$; $p<0.001$, $r=0.817$). Among all variables, a statistically significant relationship was found between Age, T stage, M stage, HI_1, HI_2, HI_3, and survival (p=0.042, p=0.007, p<0.001, p=0.028, p=0.045, p=0.014 respectively). The predictive performances of $HI_{1\text{-}2\text{-}3}$ were measured using the area under the ROC curve, cut-off values were measured by using the Youden-index, and Odds Ratio for the cut-off values were determined by Cox regression analysis (AUC= 0.663, 0.656, 0.681; cut-off values=1.371, 1.325, 2.85; OR=2.687, 5.013 respectively). HIs were also found predictive for metastatic disease status in the initial ^{18}F-FDG PET/CT; all the HI values were statistically significantly higher in the M_1 group compared to the M_0 group (p=0.028, p=0.045, p=0.014). ***Conclusion:*** According to our results, HI variables can predict metastatic status and OS, unlike the conventional PET parameters like SUVmax-peak-mean, MTV, and TLG in this cohort group of TNBC patients. HI_2 was found strongly associated with tumor diameter and TLG meaning the results of this method may vary in the different datasets. Therefore we offered a new method in HI_3. Instead of using the MTV value itself, calculating the linear regression slope with the percentage-based measurement method may produce more standardized and size-independent values. Based on our results, this method had slightly better accuracy in predicting survival status.

EP-0120

The Role Of 68ga Dotatate Pet/Ct In Breast Cancer Imaging; A Prospective Study Compared With 18f Fdg Pet/Ct

C. Sezgin, *T. Coşkun, Y. Parlak, G. Mutevelizade, E. Sayıt, G. Gümüşer;*
Celal Bayar University, Manisa, TÜRKIYE.

Aim/Introduction: Currently, F-18 FDG PET/CT is routinely used for breast cancer staging and treatment response assessment. Most breast cancers express Estrogen Receptor (ER) and Progesterone Receptor (PR) and this subtype shows lower activity on FDG imaging. Case reports are showing 68Ga DOTATATE uptake in non-neuroendocrine tumors such as breast cancer. There are also histochemical studies showing that SSTR is a potential radiopharmaceutical target for ER+/PR+ breast cancer. In this study, we aimed to compare the uptake pattern of breast cancer lesions and HR status with 68Ga DOTATATE and 18F FDG uptake in lesions. ***Materials and Methods:*** Sixteen female patients (mean age 53±11 years) with breast cancer underwent 18F FDG and 68Ga DOTATATE PET/CT imaging at one week intervals. Images were evaluated visually and semiquantitatively. The data obtained were analyzed with SPSS 15. program ***Results:*** In 13 of 16 patients, the tumor subtype was invasive ductal carcinoma, 1 patient had lobular carcinoma, 1 patient had invasive ductal carcinoma associated with lobular carcinoma, and 1 patient had ductal carcinoma in situ. In 14 of 16 patients, the breast lesion showed activity uptake on both DOTA and FDG . In 1 patient, activity uptake was observed on FDG but not on DOTA; the subtype of breast carcinoma observed in this patient was invasive ductal carcinoma; ER and PR were negative. No significant FDG and DOTA uptake was observed in the ER+/PR+ breast lesion in the lobular carcinoma subtype. There was no statistically significant difference between the SUVmax of breast lesions in FDG and DOTA ($p>0.05$), similarly, there was no statistically significant difference between the SUVmax of the axilla ($p>0.05$) . There was no statistically significant difference between ER and PR receptor status and FDG and DOTA uptake ($p>0.05$). In 6 of 7 patients with axillary lymph node metastases, both FDG and DOTA uptake were observed, while only FDG positivity was observed in 1 patient. In 4 patients with bone metastases, bone lesions showed FDG and DOTA uptake . ***Conclusion:*** 68Ga DOTATATE PET/CT showed similar results to 18F FDG PET/CT in breast cancer imaging. Although no significant correlation was observed between HR status and both FDG and DOTA SUVmaxes in our study, further studies are needed in this area. In addition, studies with a larger number of patients suggest that 177Lu DOTATATE treatment may be considered in the treatment of metastatic breast cancer.

EP-0121

FAPI-04 uptake in healthy breast glandular tissue

Y. Zhang, *M. Su;*
Department of Nuclear Medicine, West China Hospital, Sichuan University, Chengdu, CHINA.

Aim/Introduction: Fibroblast activation protein inhibitor (FAPI) is sensitive on breast cancer staging.[1] However, its clinical utility may be limited by the high physiological FAPI uptake in normal breast tissue that can obscure primary tumors. The characteristics of breast physiological uptake on FAPI PET have been rarely reported yet.[2] The aim of this study was to elucidate the characteristics of physiological ^{68}Ga-FAPI-04 uptake in normal breast. ***Materials and Methods:*** A total of 138 consecutive women with ^{68}Ga-FAPI-04 PET between February 2022 and February 2023 were reviewed retrospectively. Maximum standardized uptake value (SUV_{max}), density and thickness of breast gland, as well as SUV_{max} of nipple, were measured. Univariate and multivariate regression analyses were used to identify factors related to the breast and nipple SUVs. ***Results:*** Twenty-four premenopausal (25.3%), 62 menopausal (65.3%) and 9 post-operative (after bilateral adnexectomy, 9.4%) women (median age, 55 years [IQR, 43-67 years]) with 98 examinations were included. All had a diffuse, symmetrical uptake in breast gland. There was no difference in FAPI uptake between bilateral breasts (P = 0.179) with a median inter-breast percentage difference (PD) of 12.1%. The median intra-breast PDs were between 52.1% to 56.7%. Breast SUVs fluctuated with the expected estrogen level throughout the menstrual cycle. Patients in menstrual status with expected high estrogen level (late follicular, ovulatory and mid luteal phases) had higher breast SUVs (median, 3.16) than those with expected moderate (early follicular, early luteal and late luteal phases; median, 1.57; P < 0.001) or low level (menopause and post-operation; median, 0.97; P < 0.001). Menstrual status was an independent predictors of breast SUV (r^2 = 0.673, P < 0.001). All the patients had a focal, symmetrical uptake in nipples with a median inter-nipple PD of 17.4%. Nipple SUV did not correlate with menstrual status (P = 0.871). ***Conclusion:*** Physiological breast FAPI uptake levels are related to menstrual status. Premenopausal patients with breast lesions should be examined ^{68}Ga-FAPI-04 PET during the perimenstrual period (five days before and during menstruation). ***References:*** 1. Ding F, Huang C, Liang C, et al. ^{68}Ga-FAPI-04 vs. 18F-FDG in a longitudinal preclinical PET imaging of metastatic breast cancer. Eur J Nucl Med Mol Imaging. 2021;49:290-300. 2. Dendl K, Koerber SA, Finck R, et al. ^{68}Ga-FAPI-PET/CT in patients with various gynecological malignancies. Eur J Nucl Med Mol Imaging. 2021;48:4089-4100.

EP-0122

Role of semi quantitative 18F-FDG PET/CT parameters in prediction of the hormone status and progression free survival of advanced stage breast carcinoma patients

S. Sarswat, *A. Singhal, K. J. Das;*
AIIMS DELHI, Delhi, INDIA.

Aim/Introduction: Role of semi-quantitative ^{18}F-FDG PET/CT parameters is coming up in prediction of histopathological features and survival. This study aimed to assess correlation of these parameters with hormone status of tumor and their role in prediction of progression free survival(PFS) of patients with invasive ductal breast carcinoma. ***Materials and Methods:*** Fifty patients who had undergone histopathological examination and had proven primary breast cancer with locally advanced/distant metastatic disease, were included in this ambispective study. All patients underwent ^{18}F-FDG PET/CT. Primary and metastatic lesions were evaluated and standardized uptake values-SUVmax, SUVmean, Tumor to background ratio (TBR), Metabolic tumor volume (MTV) and Total lesion glycolysis(TLG) were calculated. ROC analysis was done to determine cutoff of parameters to predict PFS. Kaplan Meier survival analysis & Cox proportion hazard test were performed. T test and Kruskall-Wallis tests were used to assess correlation between abovementioned PET/CT parameters and clinicopathological characteristics of patients. With data available on clinical and radiological follow up, progression free survival period was determined. ***Results:*** Among fifty (median age: 45 years) with histologically proven primary invasive ductal carcinoma breast, n= 22 had luminal type B, n=16 had luminal type A and n=12 had triple negative type carcinoma, 32 patients had de novo metastatic disease and rest had locally advanced breast cancer. SUVmax of primary lesion was 11.29. SUVmean for primary was 7.35+ 2.7, lymph node metastasis (n=50) 6.41+ 1.4, liver metastasis (n=22) 6.1+ 1.6, skeletal metastasis (n=11) 4.2+ 1.1 and for brain metastasis was (n=3 patients) 6.7+ 1.7. TBR was 2.41+ 0.67 for primary, 2.26+ 0.7 lymph nodes, 1.38+ 0.2 liver, 2.68+ 0.3 skeletal metastasis, 1.13 + 0.2 brain metastasis. average value of TLG was 285mL. The median PFS was 18 months. Cox regression analysis MTV cutoff to predict poor PFS was 31cm^3, Pvalue 0.017. AUC 0.66, Pvalue 0.022. Cutoff point of TLG was 186mL, Pvalue 0.01; with AUC 0.81, sensitivity 78% and specificity 83%. There was a moderate correlation of both MTV (r=0.6) and TLG (r=0.7) with PFS on linear regression analysis. Higher semi-quantitative parameter values (above cutoff) were associated with luminal type B or triple negative type histopathology and lower with luminal type A carcinoma. ***Conclusion:*** ^{18}F-FDG PET/CT is useful in predicting histopathology and PFS of patients with invasive ductal carcinoma breast. Further studies are required to validate this on a larger scale.

EP-0123

The Detection Value of 18F-FDG PET/MR for Breast Cancer Liver Metastasis

X. Chenjie;
Hangzhou Universal Medical Imaging Diagnostic Center, hangzhou, CHINA.

Aim/Introduction: To explore the value of 18F-FDG PET/MR systemic imaging in detecting liver metastasis of breast cancer. ***Materials and Methods:*** The PET/MR and PET/CT imaging of 78 cases of liver metastasis were analyzed retrospectively. On the same day, whole body 18F-FDG PET/CT imaging and PET/MR imaging were performed, taking pathological and clinical diagnosis as the gold standard to compare the differences in the lesions. ***Results:*** 78 patients with liver cancer, a total of 106 intrahepatic metastasis lesions, PET/MR detected all lesions, and PET/CT detected 69 lesions, with significant statistical differences (P<0.01). Among them, 25 lesions were PET-MR positive, while PET-CT was negative; and 19 other lesions were negative for both equipment PET intake. Compared with PET/CT, PET/MR changed the diagnostic results of 28 (35.9%) patients. ***Conclusion:*** The detection rate of PET/MR for breast cancer liver metastasis is significantly better than that of PET/CT.

EP-0124

Dose Reduction for 89Zr ImmunoPET Imaging Using LAFOV PET/CT: An Analysis Based on Count-Reduced Images

P. Mohr, *J. van Sluis, L. Providência, A. A. Lammertsma, A. H. Brouwers, C. Tsoumpas;*
University Medical Center Groningen, Groningen, NETHERLANDS.

Aim/Introduction: ^{89}Zr immunoPET is a valuable technique for characterising tumour lesions and supporting monoclonal antibody drug development. The long half-life of ^{89}Zr ($T_{1/2}$=78.4 h) matches the slow kinetics of monoclonal antibodies, but also leads to a relatively high radiation dose. Given the low count rates, ^{89}Zr immunoPET may benefit from the improved signal-to-noise ratio of long axial field-of-view (LAFOV) PET

systems, especially when including coincidences between all detector rings, without limiting the acceptance angle. The aim of this study was to investigate possibilities in dose reduction with full 3D reconstructions compared to the limited acceptance angle currently used. ***Materials and Methods:*** Patients with metastatic breast cancer were scanned for 30 minutes, 4 days after injection of 37 MBq [^{89}Zr]trastuzumab on a 106 cm LAFOV PET/CT acquiring data with a maximum ring difference (MRD) of 322. Image reconstructions were performed for dose reduction factors ranging from 2 to 10 by using each list-mode entry with a probability corresponding to the dose reduction factor. Two independent noise realisations were generated for each dose reduction factor. Images were reconstructed offline using E7Tools VR20 (Siemens Healthineers) with 3.3x3.3x1.65 mm^3 voxels and a 5 mm Gaussian filter for both an MRD of 85 (available on current systems) and an MRD of 322. Tumours were segmented semi-automatically using a 50% isocontour of SUV_{peak}. To indicate noise levels, the liver coefficient of variation (COV) was derived with a d=3 cm sphere. Bland-Altman analysis was used to compare repeatability coefficients (RCs) (1.96SD%) of lesion SUV_{max} and SUV_{peak} from the two noise realisations. ***Results:*** Initial results (n=8 patients) showed for a reduction factor of 2 an average liver COV of 6.5%(MRD322) compared with 8.4%(MRD85) with RCs (n=18 lesions) of 8.4%(MRD322) and 13.0%(MRD85) for SUV_{max} and 5.4%(MRD322) and 7.8%(MRD85) for SUV_{peak}. For a reduction factor of 4 liver COV was 8.7%(MRD322) compared with 11.8%(MRD85) and RCs were 16.8%(MRD322) and 23.3%(MRD85) for SUV_{max} and 7.4%(MRD322) and 11.0%(MRD85) for SUV_{peak}. Further reduction resulted in larger COV and poor repeatability coefficients: even for MRD322, liver COV was up to 14% and RCs were up to approximately 21% for SUV_{max} and 12% for SUV_{peak}. ***Conclusion:*** MRD322 reconstructed images lead to lower liver COV and to superior SUV_{max} and SUV_{peak} repeatability than MRD85. Full 3D LAFOV PET/CT makes dose reduction ^{89}Zr immunoPET by a factor of 4 feasible, if the regions of interest are not at the edges of the FOV.

EP-0125

Prone FDG PET/CT in breast cancer restaging (Response to treatment evaluation)

M. Agolti, *L. Solari;*
Centro de Medicina Nuclear Clinica Modelo, Parana, ARGENTINA.

Aim/Introduction: Supine [18F]Fluorodeoxyglucose (FDG) positron emission technology/computed tomography (PET/CT) is a commonly used modality for the restaging of breast cancer (BC). Superior sensitivity and specificity of prone FDG PET/CT image acquisition in comparison to its supine equivalent has been described in the initial staging of BC, probably due to it allows a better separation of deep breast structures from the chest wall and better relaxation of the pectoral muscles. Our aim is to determine if there is a change in restaging/response to treatment evaluation in both positions, regards local relapse, intramammary, internal mammary and axial lymph nodes. ***Materials and Methods:*** In this retrospective analysis we included 127 female patients treated with surgery and radiotherapy (when indicated), we performed conventional supine FDG PET CT images and after 1 hour we performed prone thorax images with an styrofoam device we have designed. We excluded 3 patients for involuntary movements. We compare the number of increased uptake breast lesions, the differences in Standard Uptake Value (SUV), the number of axilary lymph nodes, their SUV, the intrammammary and internal mammary lymph nodes when seen. ***Results:*** We found 54 increased uptake images in breast in prono position and 47 in supine position, we assumed as relapse, according to biopsy and follow up. One case had a seroma and adjacent to it a solid increased uptake image seen only in prono acquisition .Regards the SUV in Prono acquisition the medium SUV was 3,52 and in supine images the medium SUV was 3,27 with statistical significance (less than 0,05, in this case p=0,01) according to Wilcoxon Test. Regarding Axilary nodes we found 34 in supine position and 36 in prono. We found only three intramammary lymph nodes one of them that was less than1 cm size was not seen in supine images and one internal mammary lymph node in one patient with clear increased uptake in prone (SUV Max 2,5) regards to supine acquisition (SUV Max1,8) which allowed better visualization. ***Conclusion:*** Prono images in treated breast cancer showed relapse in 7 patients that weren't seen in conventional images , showing a change in stratification in 12,9 % of the cases. Regards lymph nodes metastasis we found no significative change in axillary nodes ; regards intramammary and internal mammary lymph nodes, it showed increased sensibility (change staging in 50%), although the number of patients (4) may not be significative.

EP-0126

Comparison of whole-body PET/CT and dedicated breast PET with F-18 Fluoroestradiol for breast cancer detection in patients with newly diagnosed ER-positive breast cancer

K. Miyake[1], *M. Takada*[2], *Y. Shimizu*[1], *S. Yuge*[1], *Y. Kitano*[1], *T. Ishimori*[3], *M. Kataoka*[1], *M. Kawashima*[2], *K. Kawaguchi*[2], *T. Oishi*[1], *K. Itagaki*[2], *Y. Yamada*[2], *Y. Takeuchi*[2], *M. Toi*[4], *Y. Nakamoto*[1];
[1]*Kyoto University Graduate School of Medicine, Kyoto, JAPAN,* [2]*Kyoto University Hospital, Kyoto, JAPAN,* [3]*Kitano Hospital, Osaka, JAPAN,* [4]*Komagome Hospital, Tokyo, JAPAN.*

Aim/Introduction: To compare the diagnostic performance of F-18 Fluoroestradiol (FES) dedicated breast PET (dbPET) with that of whole-body PET/CT in patients with newly diagnosed oestrogen-receptor (ER)-positive breast cancer. ***Materials and Methods:*** A total 27 women (age 39-80 years, median 58 years) with newly diagnosed ER-positive breast cancer who consented to an IRB-approved prospective FES PET study and underwent both whole-body PET/CT and dbPET in the absence of SERM/SERD between March 2021 and April 2023 were analyzed. Approximately 1 hour after the intravenous injection of FES, whole-body PET/CT with a PMT-based detector was obtained with a patient in the supine position (3 min/bed), and subsequently, dbPET with a ring-shaped detector was performed for each breast in the prone position (10 min/breast). After inconclusive lesions were excluded, a total of 55 lesions, including 27 index ER-positive cancers (IDC n=21, ILC n=2, mucinous carcinoma n=1, DCIS n=3) and 28 additional lesions (malignancy n=21 vs. benign and ER-negative double primary n=7), in 49 breasts were assessed. Diagnostic performance was compared between PET/CT and dbPET using McNemar`s test and Fisher's exact test. ***Results:*** On a per-breast basis, sensitivity, specificity, positive predictive value (PPV) and negative predictive value (NPV) were 89.7%, 100%, 100% and 87.0% for PET/CT and 93.1%, 95.0%, 96.4% and 90.5% for dbPET (no significant differences for all). On a per-lesion basis, sensitivity for index ER-positive tumours was 92.6% (25/27) with PET/CT and 96.3% (26/27) with dbPET (p=0.074). The sensitivity for additional malignancy was significantly greater with dbPET (81.0%, 17/21) than with PET/CT (38.1%, 8/21, p=0.016). While there were no false positives on PET/CT, dbPET showed false-positive uptake in two pathologically-proven benign lesions. PPV for additional lesions was 100% (8/8) with PET/CT and 89.5% (17/19) with dbPET (p=1.000). ***Conclusion:*** dbPET using FES was significantly superior to conventional whole-body PET/CT in detecting additional breast lesions in newly diagnosed ER-positive breast cancer patients and may be useful for preoperative surgical planning. However, we identified a few false negatives and false positives on dbPET, and further improvement in image quality and image interpretation is desired.

EP-0127

18F-FDG PET/CT for monitoring treatment response in bone-dominant metastatic breast cancer patients.

P. Portilla Merino, *C. Escabias del Pozo, Y. Abadi Sedraoui, E. López Llobet, L. Giraldo Gonzalez, S. Rizkallal Monzon, D. Monachello Araujo, C. Lancha Hernandéz, S. Rodado Marina, M. Coronado Poggio, J. Cordero García, L. Domínguez Gadea; Hospital Universitario La Paz, Madrid, SPAIN.*

Aim/Introduction: Breast cancer (BC) presents a long life expectancy and up to 70% of patients develop bone metastasic disease (BMD) at some point within the disease periode. An appropriate follow-up would allow modification and early withdrawal of ineffective or toxic treatment. ***Materials and Methods:*** We conducted a retrospective study between July 2018 to February 2023, we reviewed 158 patients (p) with BC, among them, we identify 25 p BMD, who underwent a total of 93 PET/CT. BMD are confirmed by biopsy or conventional imaging (both at initial staging and distant relapse during follow-up). We also collected morphological data on the lesions. The criteria for response evaluation by PET/CT was visual assessment, and the reports suggested: complete/partial response, stable disease and progressive disease. We categorized treatments as local or systemic, including a third category mixing both. The mean follow-up time was 51±39 months. ***Results:*** BMD was confirmed by biopsy (59%) compared to conventional imaging (41%). The average interval between PET-CT scans performed for each p was 18 months.The BMD group at initial diagnosis (n=9, age at diagnosis= 54 ± 10 years), the primary breast tumour was invasive ductal carcinoma (CDI) (67%) and invase lobular carcinoma (CLI) (33%). The lesions were mainly lytic (45%), followed by sclerotic lesions (33%). The PET/CT modified the treatment in 100%p, adding local treatment (RT or surgery) in 5p due to oligometastatic disease. During follow-up, 3p progressed (33%), the progression-free survival (PFS) was 68±73 months and one p died. In the recurrence group (n=16, mean age at diagnosis of BC: 52±11 years and BMD: 58±11 years), the primary breast tumor was CDI (81%) and CLI (19%). The lesions were predominantly lytic (75%), followed by mixed lesions (25%). All of the patients with progressive disease by PET/CT, the treatment was modified. During follow-up 8p (50%) progressed, the PFS was 44±32 months, and one p died. ***Conclusion:*** In our study, we found less progression and PFS in the group with de novo BMD. PET/CT is an effective tool for monitoring treatment in BMD, improving clinical-therapeutic decisions related to patients survival factors. ***References:*** Naghavi-Behzad, M., Vogsen, M., Vester, R.M. et al. Response monitoring in metastatic breast cancer: a comparison of survival times between FDG-PET/CT and CE-CT. Br J Cancer 126, 1271-1279 (2022). https://doi.org/10.1038/s41416-021-01654-w

EP-0128

Metabolic Parameters of FDG PET/CT to Predict Disease Progression in Breast Cancer Type

J. Park[1], *J. Choi*[1], *Z. Kim*[1], *C. Lim*[1], *J. Yoon*[2], *C. Lim*[3], *S. Park*[3], *J. Moon*[1], *S. Seo*[4], *S. Woo*[5], *J. Choi*[6];
[1]*Soonchunhyang University Bucheon Hospital, Bucehon, KOREA, REPUBLIC OF,* [2]*Ajou University Medical Center, Suwon, KOREA, REPUBLIC OF,* [3]*Soonchunhyang University Seoul Hospital, Seoul, KOREA, REPUBLIC OF,* [4]*Pai Chai University, Daejeon, KOREA, REPUBLIC OF,* [5]*Korea Institutes of Radiological and Medical Sciences, Seoul, KOREA, REPUBLIC OF,* [6]*Samsung Medical Center, Sungkyunkwan University School of Medicine, Seoul, KOREA, REPUBLIC OF.*

Aim/Introduction: Breast cancer is one of the metabolic tumors, thus we investigated whether metabolic parameters of FDG PET/CT, such as liver uptake, muscle uptake, psoas muscle volume, and psoas muscle index (PI) at L3, as well as histopathologic results, clinical and serologic metabolic profile (including neutrophil-lymphocyte ratio, total cholesterol, vitamin D level, blood glucose level, BMI and fatty liver change) with age could predict disease progression (PD) in breast cancer patients who underwent curative surgery during a 5-year follow-up period (between 2012 and 2017). ***Materials and Methods:*** A total of 176 patients with breast cancer were finally included in the analysis and exclusion criteria; 26 hepatic dysfunctions, 6 hepatic cysts, 1 portal vein thrombosis, 6 other major diseases, and 7 less than 6 mo of follow-up intervals). ***Results:*** There were the luminal type of breast cancer (N=112, 51.5 ±10.1 y.o.) and non-luminal type (N=64, 54.3±11.24 y.o.) (p=0.094): HER2 (N=22, 59.9±9.2 y.o.), triple-negative (N=22, 51.6±10.4 y.o), and luminalHER2 (N=20, 51.2±12.3 y.o.) (p=0.006), respectively. We analyzed progression-free survival (PFS), and OS using the Cox proportion hazards model with the stage of breast cancer, lymphatic invasion (LI), perineural invasion (PNI), liver-to-muscle uptake ratio at L3 (LMR), psoas muscle volume, density, psoas muscle index (PI) at L3, tumor SUVmax and total lesion glycolysis. Univariable analyses showed stage, lymphatic invasion, LMR at L3, and PI were associated with PFS. Metabolic indices which were obtained by repeatedly drawn ROIs with 2 mo. intervals showed good agreement of LMR and PI at L3 (0.74 and 0.61, respectively). The multivariable Cox hazard model, in which combined with age, stage, and PI, showed a higher predicted probability for the luminal type [C-index (SE) of 0.86 (0.05)] compared to the model with age and stage [0.74(0.06), respectively]. Meanwhile, the model that combined age, stage, and LMR for the non-luminal type showed a higher predicted probability [0.86[0.05)] than the model with age and stage [0.74 (0.07), respectively]. ***Conclusion:*** In predicting PD of patients with breast cancer who underwent curative surgery, LMR could be more effective in predicting PD in non-luminal types of breast cancer, while PI may be more suitable for the luminal type of breast cancer among the clinical and metabolic parameters using FDG PET/CT. ***References:*** Prognostic impact of skeletal muscle volume derived from cross-section computed tomography images in breast cancer. Song EJ, et al. Breast Cancer Research and Treatment 2018;172:425-436.

EP-0129

Comparative Analysis of Immunohistochemistry Markers for Breast Carcinoma (ER, PR And HER 2 NEU) With Respect to Bone Metastasis

N. Kumar Gupta, *V. K Dhingra, S. Jha, A. S.; AIIMS Rishikesh, Rishikesh, INDIA.*

Aim/Introduction: To analyze the relationship between immunohistochemistry (IHC) markers [Estrogen Receptor(ER), Progesterone Receptor (PR) and Human Epidermal Growth Factor Receptor 2 (HER2NEU)] in biopsy proven breast carcinoma patients with respect to the bone metastasis detected in 99mTc-MDP bone scintigraphy. ***Materials and Methods:*** Among the patients referred for 99m Tc-MDP bone scintigraphy to the Department of Nuclear Medicine at AIIMS, Rishikesh from 2020 to 2022, 107 biopsy proven breast carcinoma female patients with their IHC status known were analyzed retrospectively. All patients underwent 99mTc-MDP bone scintigraphy using 20mCi of 99mTc-MDP and images were then evaluated by an experienced Nuclear Medicine Physician. Patients were categorized into different IHC status groups as shown in Table 1. A comparison was made between

various IHC status groups with respect to the bone metastasis detected on the 99m-Tc MDP bone scintigraphy. ***Results:*** The mean age of the patients was 49.1 ±10.8 years. Out of the 107 female patients, 34 (31.8%) patients had skeletal metastasis and 73 (68.2%) patients had no evidence of skeletal metastasis. The most common IHC markers status combination was double positive(ER+, PR+ and Her2neu-) accounting for 37/107 patients (34.6%). In this study, 26/107 patients (24.3 %) had triple negative breast carcinoma(ER-, PR- and Her2neu-) and all of these patients had no evidence of active skeletal metastasis present.***Conclusion:*** From this study, it was concluded that skeletal metastasis was not observed in the triple negative breast carcinoma(ER-, PR- and Her2neu-) patients. Hence, the probability of skeletal metastasis is minimal in the triple negative breast carcinoma patients. This study demonstrates that the metastatic patterns in breast cancer strongly correlate with various breast cancer subtypes, mainly designated by ER, PR, and HER2. Hormone receptor-positive tumors show a predilection for bones as the first site of relapse compared to hormone-receptor-negative tumors which have a proclivity to develop as visceral metastases. ***References:*** Pareek A, Singh OP, Yogi V, Ghori HU, Tiwari V, Redhu P. Bone metastases incidence and its correlation with hormonal and human epidermal growth factor receptor 2 neu receptors in breast cancer. Journal of Cancer Research and Therapeutics. 2019 Jul 1;15(5):971-5.

EP-0130

Depth of response using total tumor volume with [18F]-Fluorodeoxyglucose PET/CT for monitoring therapy response to Cyclin Dependent 4/6 Kinase Inhibitors

O. Garcia-Perez*, P. Cabrera Galeana, I. Soldevilla Gallardo, E. Bargallo, D. Gutierrez-Cruz, A. Franco-Ardila;*
Instituto Nacional de Cancerologia, Mexico city, MEXICO.

Aim/Introduction: The most common type of breast cancer is ER positive, PR negative, and HER2 negative. A significant proportion of these patients will progress to incurable metastatic disease. CDK4/6 inhibitors as treatment have become in last years an excellent option for these patients. However, response evaluation could be a challenge due to the absence of target lesions. Currently, metrics generated with PET are capable tools for generating objective analysis for this evaluation. In recent years the estimation of the depth response has gained popularity as a predictor of overdrive. However, its estimation has only been performed with conventional imaging modalities. ***Materials and Methods:*** We retrospectively analyzed changes un values of total lesion glycolysis, total tumor volume, target lesion dimensions (RECIST 1.1), and target lesion s SUVmax (PERCIST-5) after CDK4/6 inhibitor therapy in ER-positive, PR-negative, and HER2-negative immunohistochemical profile patients with metastatic breast cancer and first-line treatment failure and compared depth of response using these molecular and anatomical metrics. ***Results:*** 15 female patients with metastatic disease were included with a median age of 54 years (range 34-71), the median baseline of TTV was 231 ml +/- 67 ml TLG 1563 mean/ml +/- 567 ml, SUVmean 5.6, SUVmax 7.1 and target lesion of 32.1 mm +/- 5.2 mm, and post-therapy TTV was 15 ml +/- 3.1 ml TLG 45 mean/ml +/- 8.1 ml, SUVmean 1.5 +/- 0.6, SUVmax 2.5 +/- 1.1 and target lesion of 25.8 mm +/- 6.8 mm. The depth of response estimated using TTV was significantly higher with a median of 89% +/- 7.1%, compared to TLG, RECIST 1.1 and PERCIST-5 with 51%, 37% and 41.6% respectively. In one case stable disease was observed (-18%), while the response rate evaluated by tumor metabolic volume was of 95%. Bone disease occurred in 100% (n=15) liver 30 % (n=3), lung 26.6% (n=4), breast 53.5 % (n=8), lymph nodes 66% n=10 . The analysis between the different response modalities showed statistical significance, especially between the VMT and the RECIST 1.1 criteria. (p=0.05) ***Conclusion:*** Metabolic information obtained with [18F]-Fluorodeoxyglucose PET/CT, especially the total tumor volume is highly efficient for estimating the depth of response in a more objective way and can avoid the information loss due to rigid criteria used in RECIST 1.1 and might provide more powerful and informative metric to understand the intensity of the response.

EP-0131

Does Body Mass Index correlate with risk of recurrence in patients with breast cancer undergoing [^{18}F]FDG PET/CT ?

N. Quartuccio*, S. Ialuna, S. Pulizzi, D. D'Oppido, M. Antoni, A. M. Moreci;*
Nuclear Medicine Unit, A.O.O.R. Villa Sofia Cervello, Palermo, ITALY.

Aim/Introduction: To investigate whether breast cancer patients with high body mass index (BMI) have increased risk of recurrence and higher glucose uptake in recurrent lesions compared to women with normal weight. ***Materials and Methods:*** The hospital database was searched to retrieve women with an histologically proven diagnosis of breast cancer, who had undergone an [^{18}F]FDG PET/CT scan before neoadjuvant chemotherapy and curative-intent surgery. At the baseline [^{18}F]FDG PET/CT scan, BMI was calculated using the following formula: weight in Kg/(height in m)^2. A median follow-up of 5 years after the baseline PET/CT scan was done by means of serial [^{18}F]FDG PET/CT scans, which were reviewed to identify recurrence in the breast (T_rec), lymph nodes (N_rec) or distant locations (M_rec); furthermore, SUVmax was measured in the sites of recurrence. A chi-square test was used to investigate any difference in the frequency of any recurrence, T_rec, N_rec, and M_rec between overweight women (BMI≥25 kg/m^2) compared to women with a BMI<25 kg/m^2 ($p<0.05$). SUVmax, measured in the sites of recurrences, was compared between the two groups using a t-test ($p<0.05$). ***Results:*** A total of 142 women (84 overweight and 58 with normal weight) were retrieved (BMI: 26.84±5.59, range: 17-44 kg/m2; age: 63.21±11.02, range: 35-86 years). There were 48 recurrence at the follow-up. The chi-square test demonstrated and increased frequency of recurrence in overweight women compared to women with a BMI<25 kg/m^2 (35 vs. 13; p=0.025). A significantly higher frequency of recurrence in the breast was found in overweight women (15 vs. 2; p=0.018). The SUVmax of the T_rec was significantly higher in overweight woman (4.74±2.90) compared to women with a BMI<25 kg/m^2 (1.85 ± 0.63; p=0.09). Only a trend for higher frequency in overweight women was found for N_rec (p=0.12) and M_rec (p=0.15) compared to women with a BMI<25 kg/m^2. ***Conclusion:*** BMI seems to correlate with an increased rate of recurrence, especially in the breast, and a higher glucose uptake in patients with recurrent breast cancer.

EP-09

e-Poster Area

B: Imaging Clinical Studies -> B1 Oncological Imaging Clinical Study -> B14 Lung (including Mesothelioma)

EP-0132

PERCIST and Beyond : revisiting 18FDG PET/CT response patterns to ICPIs for non-small cell lung cancer considering atypical response, and their long-term prognostic value.

M. Masse[1], *D. Chardin*[1,2], *P. Tricarico*[1], *N. Martin*[1], *J. Darcourt*[1], *J. Otto*[1], *O. Humbert*[1,2];
[1]*Centre Antoine Lacassagne, Nice, FRANCE,* [2]*TIRO-UMR E 4320, UCA/CEA, Nice, FRANCE.*

Aim/Introduction: Our study aimed to assess the long-term prognosis of PERCIST criteria in the context of immunotherapy and to investigate the prognostic significance of atypical response patterns, namely pseudo-progression (PsPD) and dissociated response (DR). ***Materials and Methods:*** We analyzed data of 109 patients from two prospective trials involving patients with metastatic non-small cell lung cancer (NSCLC) treated with immune checkpoint inhibitors (ICPIs). Each patient underwent ^{18}FDG PET/CT at baseline, and after 7 weeks ($PET_{interim}1$) and 3 months ($PET_{interim}2$) of treatment. Tumor response was assessed using PERCIST criteria and expanded upon them by including two new atypical response profiles: PsPD, defined by a PERCIST response or stability on $PET_{interim}2$ after initial progression and DR, characterized by the concomitance of both responding and non-responding lesions in the same exam. Long-term prognosis of each pattern was compared through overall survival (OS) and progression free survival (PFS) confirmed by a multi-disciplinary tumor board. ***Results:*** Median OS was 21 months [range 1-66] and median PFS was 8 months [range 1-60]. Using PERCIST criteria on $PET_{interim}1$, 39.5% of patients had a complete/partial metabolic response or stable disease, while 60.5% had progressive metabolic disease (PMD) (median OS : NA vs 15 months, median PFS : NA vs 5 months, $p < 0.001$). The prognosis of these four PERCIST subgroups was significantly different ($p < 0.001$). Among patients with PMD on $PET_{interim}1$ (N=66), nearly half of them had an atypical response pattern on $PET_{interim}2$: 23% subsequently showed a complete, partial, or stable metabolic response, indicated retrospectively an initial PsPD and 18.5% showed a DR. Only 58.5% showed a second homogeneous progression. There was no statistically significant difference in OS and PFS between patients with PsPD and those with DR (27 vs 29.5 months, $p = 1$; 17 vs 12 months, $p = 0.2$, respectively). Patients with PsPD or DR on $PET_{interim}2$ had significantly better median OS and PFS than those with PMD (29 vs 9 months, $p < 0.02$; 16 vs 2 months, $p < 0.001$, respectively), but worse than those who achieved a metabolic complete/partial response ($p < 0.001$). ***Conclusion:*** ^{18}FDG PET/CT is an effective tool for early prognostic stratification of NSCLC patients treated with ICPIs. By introducing new criteria that consider atypical response patterns to ICPIs (DR and PsPD) after initial metabolic progression, three distinct prognostic subgroups can be identified, allowing to refine the prognostic stratification of the usual PERCIST criteria.

EP-0133

Comparison of Diagnostic Performance Between 68Ga-FAPI-04 and 18F-FDG PET/CT in Patients with Non-Small Cell Lung Cancer

C. Li[1], *Y. Tian*[1], *Z. Xiao*[1], *J. Chen*[1], *L. Li*[1], *N. Lu*[1], *H. Li*[1], *J. Zhong*[1], *D. Zeng*[1], *B. Wen*[1], *Q. Chen*[2], *Y. He*[1];
[1]*Department of Nuclear Medicine, Zhongnan Hospital of Wuhan University, Wuhan, CHINA,* [2]*Department of Pathology, Zhongnan Hospital of Wuhan University, Wuhan, CHINA.*

Aim/Introduction: This study aimed to investigate and compare the diagnostic performance between ^{68}Ga-FAPI-04 and ^{18}F-FDG PET/CT, and to evaluate the correlation between ^{68}Ga-FAPI-04 uptake and fibroblast activation protein (FAP) expression level in the tumour stroma in non-small cell lung cancer (NSCLC). ***Materials and Methods:*** Patients with suspected or needle biopsy confirmed NSCLC who underwent both ^{68}Ga-FAPI-04 and ^{18}F-FDG PET/CT within one week for initial stage were retrospectively analyzed in this study, which was from a prospective parent study. Histopathological findings were as reference standard. The diagnostic efficiency of ^{68}Ga-FAPI-04 and ^{18}F-FDG were calculated and compared. The maximum standardized uptake value (SUVmax), mean SUV (SUVmean) of lesions were measured and recorded. The tissue sections from primary tumour were tested by hematoxylin-eosin (H&E) and FAP immunohistochemistry (IHC) staining. Spearman's correlation coefficient was used for assessing the correlation between ^{68}Ga-FAPI-04 uptake and tumour FAP expression level. ***Results:*** A total of 48 patients (34 men, age range of 44-80 years) with NSCLC confirmed by surgery or needle biopsy were finally included in this study. In lesion-based analysis, the diagnostic sensitivities were 95.83% (46/48) and 91.67% (44/48) on ^{68}Ga-FAPI-04 and ^{18}F-FDG PET/CT, respectively, for the detection of primary tumour ($p = 0.500$). There was no significant difference in the primary tumour uptake on ^{68}Ga-FAPI-04 and ^{18}F-FDG (median SUVmax: 13.40 vs. 11.84, $p = 0.486$; median SUVmean: 7.68 vs. 6.82, $p = 0.361$). For the detection of regional lymph node involvement, in patient-based analysis, ^{68}Ga-FAPI-04 showed the same sensitivity of 100% (15/15) with ^{18}F-FDG, but higher specificity (76.92% vs. 38.46%, $p = 0.063$). In lesion-based analysis, ^{68}Ga-FAPI-04 revealed much higher sensitivity (94.64% vs. 77.38%, $p < 0.001$) and specificity (95.85% vs. 80.83%, $p < 0.001$) than that of ^{18}F-FDG for the detection of regional lymph node involvement. Twenty-three patients' tissue specimens (18 surgery and 5 biopsy) from primary tumour were available for FAP IHC staining. The SUVmax and SUVmean were positively correlated with tumour FAP expression level ($r = 0.582$ and 0.562, $p = 0.004$ and 0.005, respectively). ***Conclusion:*** Our study demonstrated ^{68}Ga-FAPI-04 had superior diagnostic efficiency compared with ^{18}F-FDG in NSCLC, especially in identifying regional lymph node metastasis. ^{68}Ga-FAPI-04 uptake extent has a close association with FAP expression level in the tumour stroma of NSCLC.

EP-0134

First-in-human PET imaging of KRAS p.G12C mutation status in NSCLC and CRC patients using 18F-AMG510

J. Ye, *X. Li, M. Zhang, W. Yang, F. Kang, J. Wang;*
Xijing Hospital, Xi'an, CHINA.

Aim/Introduction: Kirsten rat sarcoma (KRAS) mutation would consecutively activate downstream oncoprotein pathway, thereby promoting tumor growth and survival. It is considered a key predictor of the efficacy of EGFR-targeted therapy in lung cancer, colorectal cancer and other tumors, and is included in guidelines such as NCCN. Therefore, accurate detection of

KRAS mutations is a significant clinical need for precision cancer diagnosis and treatment. In this study, we sought to develop a PET tracer based on newly FDA-approved KRASG12C targeted drug AMG510 (Sotorasib), and to investigate its translational potential for noninvasive screening of KRASG12C mutation in NSCLC and CRC patients. ***Materials and Methods:*** 18F-AMG510 was synthesized based on AMG510 through modifying the quinazolinone structure with polyethylene glycol chain. The binding affinity of 18F-AMG510 was assessed by molecular docking, and further verified by cell uptake (H358: KRASG12C mutation; A549: non-KRASG12C mutation) study and micro-PET/CT imaging study on tumor bearing mice. Five healthy volunteers were enrolled for investigating the safety, biodistribution and dosimetry of 18F-AMG510. Subsequently, 14 NSCLC or CRC patients with or without KRASG12C mutation underwent 18F-AMG510 and 18F-FDG PET/CT imaging. SUVmax of tumor uptake of 18F-AMG510 was quantified and compared between patients with KRASG12C mutation and non-KRASG12C mutation. ***Results:*** 18F-AMG510 was successfully prepared with high radiochemical yield and high radiochemical purity. Molecular docking assay revealed F-AMG510 bind with KRASG12C protein. 18F-AMG510 uptake in H358 was significantly higher than A549, and decreased by pretreatment with AMG510 (H358 vs. A549: 3.22 ± 0.28% vs. 2.50 ± 0.25%, $p < 0.05$, block: 2.06 ± 0.13%, $p < 0.01$). Similar results were observed in tumor bearing mice PET imaging study (H358 vs. A549: 3.93 ± 0.24 vs.2.47 ± 0.26 % ID/g, $p<0.01$; block: 2.89 ± 0.29% ID/g, $p < 0.05$). 18F-AMG510 was safe in human, and it was primarily excreted by gallbladder and intestine. The effective absorbed dose was comparable to that of 18F-FDG. The accumulation of 18F-AMG510 at KRASG12C mutated tumors was significantly higher than non- KRASG12C mutation tumors (SUVmax: 3.73 ± 0.58 vs. 2.39 ± 0.22, $p < 0.01$) in NSCLC and CRC patients. ***Conclusion:*** 18F-AMG510 is a safe and promising PET tracer for clinically non-invasive imaging of KRASG12C mutation status in NSCLC and CRC patients. This study provided a new method for accurate non-invasive screening of tumor KRASG12C mutation, be valuable in achieving precise cancer diagnosis and treatment, and provide a reference for clinical translation studies of other KRASG12C probes.

EP-0135

Qualitative Analysis of Pericardial Metastasis in Oncologic F-18 FDG PET/CT

H. Lee*;*
Dongnam Institute of Radiological and Medical Sciences, Busan, KOREA, REPUBLIC OF.

Aim/Introduction: Accurate diagnosis of the pericardial metastasis on the positron emission tomography/computed tomography with F-18 fludeoxyglucose (F-18 FDG PET/CT) in oncologic patients is challenging both in initial staging work-up on and follow-up. The aim of this study was to assess the qualitative analysis of pericardial metastasis on the F-18 FDG PET/CT in oncologic patients. ***Materials and Methods:*** Between Jan 2012 and Dec 2022, we reviewed 22,508 consecutive F-18 FDG PET/CT studies done for an oncologic indication at our institution. 43 oncologic patients (range, 37-88 y; mean age, 63.6±12.5 y), who demonstrated pericardial metastasis on F-18 FDG PET/CT enrolled in this study. A qualitative analysis was performed on the images. All pericardial metastases were scored for their extent and intensity using a 3-point scale (1 = low, 2 = moderate, 3 = high). Diffuse pericardial thickening with diffuse FDG uptake was considered as low-grade. Diffuse pericardial thickening with several hypermetabolic nodules was considered as moderate-grade. Intense hypermetabolic pericardial thickening was considered as high-grade. A final diagnosis of the pericardial metastasis was based on pericardial fluid cytology or clinical and imaging follow-up. ***Results:*** Among 43 oncologic patients with pericardial metastasis on F-18 FDG PET/CT, the most frequent primary tumor was lung cancer (21/43, 48.8%), followed by breast cancer (6/43, 14.0%), gastric cancer (5/43, 11.6%), thymic carcinoma (3/43, 7.0%), head and neck cancer (2/43, 4.7%), and six other malignancies (esophageal cancer, adenoid cystic carcinoma, pancreatic cancer, malignant B-cell lymphoma, malignant mesothelioma, and metastasis of unknown origin). Of 43 patients, the number of patients with pericardial metastasis which was diagnosed in initial staging work-up and follow-up was 14 and 29 patients, respectively. On qualitative analysis, the number of patients low-grade, moderate-grade and high-grade was 18 (41.9%), 13 (30.2%) and 12 (27.9%), respectively. In 12 patients with high-grade, the number of patients (6) who were diagnosed in initial staging was equal to that of patients (6) who in follow-up. However, in 18 patients with low-grade, the number of patients (5) who were diagnosed in initial staging was lower than that of patients (13) who in follow-up. ***Conclusion:*** In oncologic patients with F-18 FDG PET/CT, the most frequent primary tumor with pericardial metastasis was lung cancer. Patients with high-grade pericardial metastasis were observed on initial staging work-up equal to on follow-up F-18 FDG PET/CT. ***References:*** Douroukas. "Detection of metastatic involvement of the pericardium on F-18 FDG-PET/CT imaging." Clinical Nuclear Medicine 34.1 (2009): 40-41.

EP-0136

Comparison of FDG PET/CT and PET/MR Imaging for Primary Staging of Newly Diagnosed Lung Cancer

E. Erbil*, U. Aydos, Ü. Akdemir, N. Karabacak, L. Atay;*
Gazi University Faculty of Medicine, Ankara, TÜRKIYE.

Aim/Introduction: The aim of this study was to compare the diagnostic performances of FDG PET/CT and PET/MR imaging in TNM staging of newly diagnosed lung cancer patients. ***Materials and Methods:*** The images of 76 patients (59 males, 17 females, mean age: 64.1±8.5 years) diagnosed with lung cancer who underwent PET/CT and PET/MRI after a single radiopharmaceutical injection (mean activity: 214.6±55 MBq) for primary staging between 2015 and 2021 were retrospectively evaluated. The diagnostic performances of the two modalities were compared using the eighth edition of the TNM staging system of the IASLC. The imaging findings for T and N staging were compared with the histopathological results in 18 patients who underwent surgical resection after primary staging. Histological findings, follow-up imaging, and clinical management of the patients were used as reference standard in cases that did not undergo surgical resection. The diagnostic performances of two imaging methods were evaluated by using McNemars' chi-square test. Semiquantitative measurements were compared by using the Wilcoxon signed-rank test. ***Results:*** The mean time after injection was 87.7±34.8 minutes for PET/CT and 125.7±46.9 minutes for PET/MR. While PET/CT imaging was performed firstly in 60 of the patients, PET/MR imaging was performed firstly in 16 patients. Concordance between the two imaging modalities in terms of T, N, M stages and overall TNM stage was found to be 96.1%, 90.8%, 89.5%, and 90.8%, respectively. According to the histopathological results, PET/CT and PET/MR accurately determined the T stage in all patients, while the N stage was correctly detected in 58.8% of the patients. While the agreement of the reference TNM stage and

PET/CT was 81.6%, the agreement of PET/MR was 86.8%. While there was no significant difference between the two imaging modalities in T and N staging (p>0.05, each), the difference between two methods in M staging was significant (p= 0.046). The mean number of distant metastases detected in PET/MR was significantly higher than PET/CT (6.5 vs 3.2, p<0.001). There were no significant differences between the primary tumor sizes measured in the two imaging modalities (p=0.15). While SUVmax, SUVpeak and TLG values of the lesions were significantly higher in PET/MR images, MTV values were significantly higher in PET/CT images (p<0.05). ***Conclusion:*** FDG PET/CT and PET/MR have similar diagnostic performances in primary T and N staging of newly diagnosed lung cancer patients. In the M staging, the diagnostic performance of PET/MR imaging was found to be superior to PET/CT.

EP-0137

Added diagnostic sensitivity of MTV and TLG in the assessment of left adrenal gland metastasis in lung cancer with [18F]FDG PET/CT

H. Hautzel[1], *F. Özkan*[2], *C. Laschinsky*[1], *D. Kersting*[1], *M. Opitz*[3], *D. Theegarten*[4], *K. Darwiche*[2], *K. Herrmann*[1];
[1]*Department of Nuclear Medicine, University Hospital Essen, University Duisburg - Essen, Essen, GERMANY,* [2]*Department of Pneumology, Section of Interventional Pneumology, Ruhrlandklinik Essen, Universitätsmedizin Essen, Essen, GERMANY,* [3]*Institute of Diagnostic and Interventional Radiology and Neuroradiology, University Hospital Essen, University Duisburg - Essen, Essen, GERMANY,* [4]*Institute of Pathology, University Hospital Essen, University Duisburg - Essen, Essen, GERMANY.*

Aim/Introduction: Adrenal metastases account for about 20% of distant metastases in lung cancer. Therefore, it is of high relevance to correctly identify an adrenal involvement during whole body [^{18}F]FDG PET/CT staging. However, while highly sensitive specificity is apparently impaired with a false positive rate of 28% [1]. Endoscopic trans-esophageal/gastral ultrasound (EUS-B) in direct succession to endobronchial ultrasound for obtaining biopsies and hilar/mediastinal N-staging emerged as another staging tool for the left adrenal gland (LAG). By EUS-B not only the anatomical LAG configuration might be explored but also LAG biopsies can be drawn. Using EUS-B LAG results plus follow-up as reference this study aimed to test if the metabolic tumor volume (MTV) and/or the total lesion glycolysis (TLG) of the LAG might overcome the shortcoming of [^{18}F]FDG PET/CT in specificity and outperform the SUVmax estimation. ***Materials and Methods:*** 253 patients with suspected/verified lung cancer undergoing initial staging with both [^{18}F]FDG PET/CT and EUS-B were included. Using syngo.via (Siemens Healthineers, Germany) the following PET parameters were collected: SUVmax of the primary, SUVmax of LAG (SUVmaxLAG), LAG MTV and LAG TLG. Standard of reference was either EUS-B derived LAG histology or unremarkable ultrasound appearance of LAG in EUS-B plus follow-up with abdominal CT of at least 3 months. ROC analyses including area under the curve (AUC) were calculated. From these analyses cut-off values were derived for optimal sensitivities and specificities. ***Results:*** The AUC for SUVmax of the primary was highly limited with 0.543 while the AUCs of SUVmaxLAG and MTV LAG were almost the same with 0.870 and 0.873. AUC of TLG LAG was highest with 0.883. The ROC analyses translated into the following cut-off values, sensitivities and specificities: SUVmax of the primary cut-off 11.0, sensitivity 31.6%, specificity 77.3%; SUVmaxLAG cut-off 4.7, sensitivity 84.2%, specificity 75.0%; MTV LAG cut-off 2.0 ml, sensitivity 89.1%, specificity 73.2%; TLG LAG cut-off 6.6, sensitivity 89.2%, specificity 74.2%. ***Conclusion:*** The SUVmax of the primary lung tumor proved inappropriate to predict a LAG metastasis. In comparison to SUVmaxLAG MTV LAG and TLG LAG increased the sensitivity to about 90% while specificity remained almost unchanged at about 75% adding no further increase to [18F]FDG PET/CT LAG staging specificity. However, since estimation is straightforward and fast especially TLG might be implemented in clinical reading of [18F]FDG PET/CT for LAG metastasis detection in lung cancer, in particular if EUS-B is lacking. ***References:*** [1] Lang et al., World J Surg 2015;39:1902-1908

EP-0138

Value of 18F-FDGPET/CT in the Differential Diagnosis of Tuberculous Pulmonary Cavity and Lung Cancer Cavity

M. Zhao[1,2], *L. Ma*[1];
[1]*Shandong Cancer Hospital of China, Ji Nan, CHINA,* [2]*Department of Nuclear Medicine, Zibo Central Hospital, Shandong Province, Zibo City, CHINA.*

Aim/Introduction: To analyze the ^{18}F-fluorodeoxyglucose (FDG) PET/CT imaging features of lung squamous cell carcinoma cavity, lung adenocarcinoma cavity and pulmonary tuberculosis cavity, and to evaluate its value in the differential diagnosis. ***Materials and Methods:*** The ^{18}F-FDG PET/CT features of 104 patients including 38 patients with lung squamous cell carcinoma cavity, 36 patients with lung adenocarcinoma cavity and 30 patients with pulmonary tuberculosis cavity were retrospectively analyzed. The differences of lesion maximum diameter, cavity wall thickness maximum diameter, cavity maximum diameter, SUV_{max}, SUV_{avg}, SUV_{peak}, TLG and MTV values among the three groups were analyzed, and correlation analysis and ROC curve analysis were performed. ***Results:*** The ^{18}F-FDG PET/CT manifestations of pulmonary tuberculosis cavity were multiple, diverse and different activities with calcification and proliferation, and the positive rate was significantly higher than that of pulmonary squamous cell carcinoma cavity and pulmonary adenocarcinoma cavity. The SUV_{max} values of the three groups were 16.2 ± 7.8, 10.4 ± 5.5, 4.2 ± 1.8 ($P < 0.05$), the maximum lesion diameters were 6.0 ± 2.7, 3.8 ± 1.6, 3.4 ± 1.7 ($P < 0.05$), the maximum diameter of cavity wall thickness were 2.4 ± 1.7, 1.4 ± 0.8, 1.3 ± 0.8 ($P < 0.05$), the maximum cavity diameters were 3.0 ± 2.0, 2.0 ± 1.3, 2.0 ± 1.5 ($P < 0.05$). The SUV_{max} in the group of lung squamous cell carcinoma cavity was significantly higher than that of the pulmonary tuberculosis cavity ($P < 0.05$) , there were also statistical differences in lesion maximum diameter, cavity wall thickness maximum diameter, cavity maximum diameter, SUV_{avg}, SUV_{peak}, TLG and MTV between the two kinds of cavities ($P < 0.05$). The SUV_{max} of pulmonary adenocarcinoma cavity was significantly larger than that of the pulmonary tuberculosis cavity ($P < 0.05$) , the differences of SUV_{avg} and SUV_{peak} between the two groups were also statistically significant ($P < 0.05$) , however, the differences showed no statistical significace in lesion maximum diameter, cavity wall thickness maximum diameter, cavity maximum diameter ($P > 0.05$) ; The SUV_{max} of lung squamous cell carcinoma cavity was also significantly higher than that of the pulmonary adenocarcinoma cavity ($P < 0.05$) . ***Conclusion:*** Comprehensive analysis of ^{18}F-FDG PET/CT metabolic characteristics, anatomical details and quantitative indexes of lung cavities including adjacent lung tissues is of important value in differentiating lung cavities with squamous cell carcinoma, lung adenocarcinoma and pulmonary tuberculosis.

EP-0139

Contribution of 18F-FDG PET-CT in initial staging of non-small cell lung cancers

H. Noamen[1,2], *H. Charfi*[2], *I. Jardak*[1], *R. Sfar*[2], *I. Touil*[2], *K. Chatti*[2], *K. Chtourou*[1], *F. Guermazi*[1];
[1]*University hospital of Habib Bourguiba, Sfax, TUNISIA,*
[2]*University of Monastir, Monastir, TUNISIA.*

Aim/Introduction: The prognosis and choice of treatment of non-small cell lung cancers (NSCLC) depend on the TNM and stage classifications.The aim of our study is to confront the results of ^{18}F-FDG PET-CT with the data of the initial conventional imaging extension evaluation of NSCLC. ***Materials and Methods:*** Single-centre retrospective analytical transversal study performed over a period of 25 months including 75 patients referred for NSCLC extension evaluation. All patients underwent CT with enhanced contrast and then ^{18}F-FDG PET-CT. We compared the findings in TNM staging of conventional imaging (CT, bone scintigraphy), ^{18}F-FDG PET-CT, and histological data and studied the impact of the staging change in the management of these patients. ***Results:*** In (N)-staging: ^{18}F-FDG PET-CT resulted in upstaging 46% patients.The comparison of the data from PET-CT and CT to the histological findings in the evaluation of lymph node involvement showed that PET-CT reduced the number of CT false-negative cases. In (M)-staging: ^{18}F-FDG PET-CT revealed metastases in 30% of patients classified as non-metastatic by the conventional imaging, including bone, adrenal, and liver locations not detected by CT scan, as well as metastases in atypical sites poorly identified by morphological imaging. Overall, the stage of the disease was changed in 52% of the cases. The upstaging by ^{18}F-FDG PET-CT was mainly in locally advanced stages (IIIA and IIIB) and in patients classified as IIB. ^{18}F-FDG PET-CT allowed a more accurate clinical staging avoiding futile mediastinoscopy and unnecessary thoracotomy. In the 35 patients who were upstaged by PET-CT, the number of operable patients decreased, and multimodal treatment was proposed in 31 patients. The downstaging of 4 patients allowed half of them to be treated surgically. ***Conclusion:*** ^{18}F-FDG PET-CT, through its more accurate staging of the disease, allows the initial therapeutic strategy of NSCLC to be optimized, particularly for patients classified as IIIA and IIIB by conventional imaging, thus avoids invasive and unnecessary treatments. ***References:*** Schmidt-Hansen M, Baldwin DR, Hasler E, Zamora J, Abraira V, Roquéi Figuls M. PET-CT for assessing mediastinal lymph node involvement in patients with suspected resectable non-small cell lung cancer. Cochrane Database Syst Rev. 2014;2014.

EP-0140

Prediction of mediastinal node involvement in non-small lung cancer by baseline 18 F-FDG PET/CT metabolic parameters

H. Noamen[1,2], *H. Charfi*[2], *I. Jardak*[1], *R. Sfar*[2], *I. Touil*[2], *K. Chatti*[2], *K. Chtourou*[1], *F. Guermazi*[1];
[1]*University hospital of Habib Bourguiba, Sfax, TUNISIA,*
[2]*University of Monastir, Monastir, TUNISIA.*

Aim/Introduction: The aim of this study is to assess the predictive value of tumoral semi-quantitative parameters in nodal staging (N) in non-small cells lung cancer (NSCLC). ***Materials and Methods:*** Our study included 75 patients (67 M/8 F; median age 65, range 41-88) diagnosed with NSCLC who underwent pre-treatment ^{18}F-FDG PET/. We assessed whether semi-quantitative metabolic PET parameters (SUVmax, MTV and TLG) varied with the nodal status (N). ***Results:*** The median values of tumoral MTV and TLG in the group of patients with mediastinal homolateral and/or contralateral node metastasis were higher compared to the group of patients without node involvement or with only homolateral hilar node disease (MTV: M=21, IQR=[7,9-70,7] vs M=19,7, IQR=[4,6-35]; TLG: M=76,5, IQR=[16-328] vs M=185,5, IQR=[40-499]) without a statistically significant difference (p >0,05). Also, the comparison between tumoral SUVmax values in both groups didn't show a significant difference (M=11, IQR= [5,4-15,6] vs M=11,7, IQR= [8-17,3] and p>0,05). ***Conclusion:*** Despite the lack of statistical significance, this analysis suggests that ^{18}F-FDG volumetric parameters MTV and TLG would be better predictors of nodal extension than SUVmax. A further study enrolling a larger population would better demonstrate the predictive value of metabolic parameters in lymphatic node metastasis in NSCLC. ***References:*** Ouyang M li, Xia H wei, Xu M man, Lin J, Wang L li, Zheng X wu, et al. Prediction of occult lymph node metastasis using SUV, volumetric parameters and intratumoral heterogeneity of the primary tumor in T1-2N0M0 lung cancer patients staged by PET/CT. Ann Nucl Med. 2019;33(9):671-80.

EP-0141

PET attenuation correction of chest FDG PET/MRI: Deep learning-based denoising and pseudo-CT generation using fast zero-TE MRI and unpaired PET/CT data

M. Nogami[1,2], *H. Matsuo*[3], *M. Nishio*[3], *M. Tachibana*[3], *J. Inukai-Inoue*[3], *F. Zeng*[3], *K. Kubo*[1], *T. Kurimoto*[4], *T. Murakami*[3,1];
[1]*Kobe University Hospital, Kobe, JAPAN,* [2]*University of Fukui, Fukui, JAPAN,* [3]*Kobe University Graduate School of Medicine, Kobe, JAPAN,* [4]*GE Healthcare, Hino, JAPAN.*

Aim/Introduction: Zero echo-time (ZTE) is a suitable proton-density MRI for bone imaging and is used in PET/MRI for head attenuation correction (AC) of bone components. The field of view (FOV) needs to be expanded to use ZTE for chest AC, resulting in increasing the imaging time. Fast ZTE with small FOV can be used for training data of deep learning-based PET/MRI AC of the chest by expanding the data, doubling the FOV, and using deep learning to reduce noise. This study aimed to explore the feasibility of deep learning to reduce noise in fast ZTE with double FOV and to generate a pseudo-CT (pCT) for PET/MRI AC. ***Materials and Methods:*** The data of 250 patients who underwent chest FDG PET/MRI with central-frequency-adjusted ZTE were retrospectively analysed. The ZTEs, acquired in one minute with a small FOV (36 cm), were expanded and reconstructed in a FOV of 72 cm, followed by noise reduction using deep learning. Unpaired training data included bias-corrected ZTE and CT components of PET/CT. They were used for training unsupervised generative adversarial networks with a modality-independent neighbourhood descriptor (U-GAT-IT/MIND) model. Also, 20 cases with paired ZTE PET/MRI and PET/CT were used to validate the model for standardised uptake values (SUV) after AC. The mean SUV (SUVmean) of bone and liver in the chest region was measured by segmenting bone on pCT and placing a fixed region of interest in the liver, respectively. An MRI-based AC map with bone ($MRAC_{ZTE}$) was created by merging the segmented bone map onto a conventional two-point Dixon-based AC map ($MRAC_{Dixon}$) and was applied to PET reconstruction on the offline workstation. Bland-Altman plots were used to compare SUVmeans between $MRAC_{Dixon}$, $MRAC_{ZTE}$, and CT-based AC (CTAC). Wilcoxon's signed rank test was used to compare SUVmeans between AC maps. ***Results:*** Mean differences in bone SUVmeans by $MRAC_{ZTE}$ and CTAC were significantly smaller than by $MRAC_{Dixon}$ and CTAC ($p<0.05$). Bone and liver SUVmeans were significantly

larger by $MRAC_{ZTE}$ than by $MRAC_{Dixon}$ (p<0.001). The spine and liver SUVmeans were significantly larger by $MRAC_{ZTE}$ than by $MRAC_{Dixon}$. ***Conclusion:*** Deep learning-based denoising and pseudo-CT generation using fast zero-TE MRI and unpaired PET/CT data were feasible. AC maps with bone components from pCT yield smaller differences in bone SUVs with CT-based AC than $MRAC_{Dixon}$ and larger SUVs in the bone and liver than $MRAC_{Dixon}$. ***References:*** 1. arXiv:1907.10830. 2. Med Image Anal. 2012 Oct;16(7):1423-35.

EP-0142

Prediction of 131I Uptake in Lung Metastases of Differentiated Thyroid Cancer UsingDeep Learning before Radioiodine Therapy: a Pilot Study

H. Song;
Shanghai Sixth People's Hospital Affiliated to Shanghai Jiao Tong University School of Medicine, Shanghai, CHINA.

Aim/Introduction: Radioiodine therapy forms the core treatment of differentiated thyroid cancer (DTC) with lung metastases unless radioactive iodine (^{131}I) accumulation capacity is lost. Computed tomography (CT) scans can accurately detect lung metastases of DTC. Deep learning (DL) algorithms have made substantial strides in image recognition tasks and are gaining extensive attention. We attempted to develop a deep convolutional neural network (DCNN) model for the prediction of the ^{131}I uptake in lung metastases of DTC before radioiodine therapy. ***Materials and Methods:*** In this population-based cohort study, a training data set of chest CT images in DTC patients with lung metastases from our hospital (20175 imaging studies from Jan 2017 to Jan 2021, 261 patients) were collected retrospectively. According to the post-therapeutic ^{131}I whole-body scan (^{131}I-WBS), pulmonary metastases were classified as ^{131}I-avid (positive ^{131}I uptake, n_1=140) and non-^{131}I-avid (negative ^{131}I uptake, n_2=121). The anatomical structure-aware pulmonary nodule detection via parallel multi-task region-of-interest (RoI) Head was proposed. We built a predictive model from the outputs using the transfer learning techniques of a residual convolutional neural network (ResNeSt50 4s2x40d). The model's diagnostic performance was validated in an internal validation set (4530 imaging studies from Feb 2021 to Jun 2022, 59 patients). We further compared the prediction accuracy of our method with the two classic classification model architectures, Inception_V3 and ResNet50. ***Results:*** In the training and internal validation set, the accuracy of our deep learning model was 71.0%(95% CI: 70.9%-71.0%) and 62.4% (62.1%-62.6%), respectively, both higher than that of Perception_V3 and ResNet50. ResNeSt50 4s2x40d model has a good area under curve (AUC) both in the training (AUC=0.77) and internal (AUC=0.72) test sets. ***Conclusion:*** The DL model demonstrated a good performance for predicting the ^{131}I uptake in lung metastases of DTC before radioiodine therapy and may play a potential role in better screening patients who can benefit from ^{131}I therapy. Further improvement is necessary before clinical utilization.

EP-0143

The value of 18F-FDG PET/CT radiologic features and radiomics features predicting the bronchogenic carcinomas with ALK rearrangement fused gene

Y. Xu;
Hangzhou Universal Medical Imaging Diagnostic Center, Hangzhou, CHINA.

Aim/Introduction: With aim to assess whether radiologic feature and radiomics features are predictive of anapalstic lymphoma kinase(ALK) rearrangement in bronchogenic carcinomas, and to compare the differences between the two prediction models. ***Materials and Methods:*** ALK rearrangement was screened in 530 patients with pathologic proved lung cancer.Of those 48 patients detected with positive ALK fused gene were enrolled. Analyze the relationship between the positive rate of ALK and the clinical, pathological and imaging features. For radiomics features, we used AK software to extract the most relevant imageomics features for tumor classification, and randomly divided the images into training set (70%) and test set (30%). The maximum correlation and minimum redundancy (mRMR) and minimum absolute shrinkage and selection operator (LASSO) methods were used to select features from 2800 features extracted from CT and PET, and finally 12 best features were retained. ***Results:*** The prevalence of ALK positivity in bronchogenic carcinoma was 48 case,including 27 female and 21 male (p>0.05).The mean ages were 53.71±10.98 yrs and 59.94±9.75 yrs(,p<0.01).The number of non-cigarette smokers was more than that of smokers(p<0.05). There also were difference between two groups in lobuated shape and solid components within lesion(p<0.01). The mean SUVmax were 4.23±2.31 and 3.81±2.51,in positive and negative group resptectively.The area under the ROC curve of the predictive model was 0.644(95%CI:0.540-0.747). when SUVmax=3.45 was used as threshold,positive rate in ≥3.45 was much higher than less than <3.45 in diameter group(p<0.05).when multivariate factors such as age less than 50yrs, no-smoker, lobulated shape solid components and SUVmax≥3.45 in lesions used as predictive factors of ALK rearrangement, the area under the ROC curve of the predictive model was 0.809(95%CI:0.744-0.875),with sensitivity of 62.8%,and specifity of 77.6%,respectively.The established PET/CT imaging features have good prediction efficiency for the recognition of bronchogenic carcinomas with ALK rearrangement fused gene. In the radiomics prediction model, the AUC of the training group and the validation group were 0.948 (95% CI: 0.792-0.991).The results of the two prediction models have significant statistical differences(p<0.05). ***Conclusion:*** ALK fused gene showed more frequently in pulmonary adenocarcinoma,less also may detected in squamous cell and small cell lung cance. In the traditional prediction model: younger, non-cigarette, with lobulated shape, contain solid components and higher SUV value as predictor factor of ALK fused gene. Compared with the traditional prediction model combining radiologic features and clinical features, the prediction model based on radiomics has higher prediction value.

EP-0144

The value of PET/MRI radiomics features in predicting synchronous brain metastases in non-small cell lung cancer

J. Liang;
杭州通用医学影像诊断中心, 杭州, *CHINA.*

Aim/Introduction: To investigate the value of CT-based radiomics features in predicting syn-chronous brain metastases from non-small cell lung cancer (NSCLC). ***Materials and Methods:*** The clinical and imaging data of 120 patients with pathologically confirmed NSCLC in our hospital from June 2017 to June 2022 were retrospectively analyzed. According to the PET/MRI imaging features, the patients were divided into 48 patients with brain metastasis group and 72 patients without brain metastasis group. All patients were divided into the training set (84 cases) and the verification set (36 cases) in a ratio of 7:3. ITK-SNAP software was used to manually delineate the ROI of the lesions layer by layer on PET images and T2WI images respectively, and the volume ROI of the lesions was obtained by three-dimensional fusion,

and then imported into AK software to extract the texture features of each lesion. The features of PET images, T2WI images and multi-sequences (PET + T2WI) were selected by minimum redundancy maximum correlation (mRMR) and minimum absolutevalue convergence and selection operator (L.ASSO) to predict brain metastasis, the radiomics model was established by logistic regression analysis , and the radiomics score (rad-score) of each case was calculated. Through logistic regression analysis, the variables with statistically significant differences between groups in clinical and imaging data were established into a conventional model, and combined with the most effective radiomics model to establish a synthetic diagnostic model, and then nomography was drawn for evaluation the predicive rate of the model. ***Results:*** The area under curve (AUC) of PET, T2WI and combined sequences radiomics model in the training group and verification group were 0.89 and 0.86, 0.79 and 0.75, 0.91 and 0.93 respectively, and combined sequence model had the highest predictive efficiency. The AUC of the conventional model and synthetic diagnostic model in training group and validation group were 0.71 and 0.79, 0.92 and 0.95. The synthetic diagnostic model was relatively effective in predicting synchronous brain metastasis in NSCIC patients , which was significantly better than the conventional model (P=0.001), and the multi-sequences rad-score is an independent factor (OR=2.5, P<0.001). ***Conclusion:*** The prediction efficiency of all radiomics model were higher than conventional models, and the synthetic diagnostic model was significantly better than the conventional model. The radiomics is expected to become a new biological indicator to help clinically predict the risk of synchronous brain metastases.

EP-0145

The Application of Three-dimensional Ventilation/ Perfusion single photon emission tomography/ computed tomography in Asthma and COPD

H. Xie, *L. Li;*
West China Hospital of Sichuan University, Chengdu, CHINA.

Aim/Introduction: To investigate the role of ventilation/perfusion single photon emission tomography/computed tomography (V/P SPECT/CT) quantitative parameters in evaluating COPD and asthma disease severity and airway obstructivity-grade. Establish a new parameter to optimize the identification of the most affected lung lobe and to explore the value of V/P SPECT/CT in quantifying regional lung function to guide localised treatments of asthma and COPD in the future. ***Materials and Methods:*** Fifty-three subjects, including patients with COPD or asthma, and healthy controls, who underwent V/P SPECT/CT and pulmonary function tests (PFTs) were included. Preserved lung ventilation function (PLVF), preserved lung perfusion function (PLPF), airway obstructivity-grade (OG) and volume perfusion ratio (VPR) were evaluated using V/P SPECT/CT. VPR was established by combining relative lung volume from low dose CT and relative perfusion from perfusion SPECT. In addition, the difference of V/P SPECT/CT-related parameters were compared. ***Results:*** The airway OG, PLVF and PLPF differed significantly among the severe-very severe COPD and mild-moderate asthma patients (P<0.05). And the PLPF was statistically significant among the disease severity groups in asthma and COPD (P<0.05). The airway OG, PLVF and PLPF in asthma and COPD differed significantly from the control group (P<0.05). A reference range of VPR for each lung lobe in the normal population was established. In normal subjects, VPR in the right upper lobe 1.09±0.31; VPR in the middle lobe 1.15±0.43; VPR in the right lower lobe 0.91±0.22; VPR in the total right lung 0.98±0.06; VPR in the left upper lobe 1.14±0.24; VPR in the left lower lobe 0.99±0.31; VPR in the total left lung 1.02±0.07. A high VPR implies a large volume of lung lobes with correspondingly low perfusion; these lobes impede the function of the respiratory pump and are not related to the actual perfusion contribution. In the opposite case, a low VPR means that this lobe is compressed but retains perfusion function. ***Conclusion:*** Quantitative assessment of ventilation and perfusion abnormalities and the degree of pulmonary functional loss by V/P SPECT/CT shows promise as an objective measure to assess severity of disease and lung function to guide localized treatments. There are differences among the disease severity groups in asthma and COPD in SPECT/CT parameters, which may enhance, to some extent, the understanding of complex physiological mechanisms in asthma and COPD. VPR allows identifying possible target structures with much higher sensitivity than PFTs or CT alone.

EP-0146

68Ga-SSO-120 versus 18F-FDG PET in the Initial Staging of Small-Cell Lung Cancer Patients

D. Kersting[1], *P. Sandach*[1], *M. Sraieb*[1], *M. Wiesweg*[2], *M. Metzenmacher*[2], *K. Darwiche*[3], *F. Oezkan*[3], *S. Bölükbas*[4], *M. Stuschke*[5], *L. Umutlu*[6], *M. Nader*[1], *R. Hamacher*[2], *W. P. Fendler*[1], *J. Wienker*[3], *W. Eberhardt*[2], *M. Schuler*[2], *K. Herrmann*[1], *H. Hautzel*[1];
[1]*Department of Nuclear Medicine, University Hospital Essen, University of Duisburg-Essen, Essen, GERMANY,* [2]*Department of Medical Oncology, University Hospital Essen, University of Duisburg-Essen, Essen, GERMANY,* [3]*Department of Pulmonology, Section of Interventional Pulmonology, University Medicine Essen - Ruhrlandklinik, University of Duisburg-Essen, Essen, GERMANY,* [4]*Department of Thoracic Surgery and Thoracic Endoscopy, University Medicine Essen - Ruhrlandklinik, University of Duisburg-Essen, Essen, Germany, Essen, GERMANY,* [5]*Department of Radiotherapy, University Hospital Essen, University of Duisburg-Essen, Essen, GERMANY,* [6]*Institute of Diagnostic, Interventional Radiology and Neuroradiology, University Hospital Essen, University of Duisburg-Essen, Essen, GERMANY.*

Aim/Introduction: In patients with somatostatin receptor 2 (SSTR2)-expressing small cell lung cancer (SCLC), SSTR2-antagonist PET imaging using satoreotide trizoxetan (SSO-120, previously OPS-202) bears the potential for accurate tumor detection and screening for SSTR2-antagonist radionuclide therapy. Here, we evaluate tumor uptake and detection rates by ^{68}Ga-SSO-120 PET versus ^{18}F-FDG PET in the initial staging of patients with SCLC. ***Materials and Methods:*** We retrospectively included patients who underwent additional ^{68}Ga-SSO-120 PET/CT in the initial staging of SCLC. PET-positive lesions were reported in 7 anatomical regions according to the 8th-edition TNM classification for lung cancer (primary tumor, thoracic lymph nodes, and distant metastases including pleural, contralateral pulmonary, liver, bone, other) by two nuclear medicine physicians. If gold-standard ^{18}F-FDG PET/CT was available within 2 weeks prior/post ^{68}Ga-SSO-120 PET/CT and if morphologic differences in CT were absent, a comparative analysis was performed. Consensus TNM from clinical tumor board (using CT, EBUS-TBNA, PET, brain MRI) served as reference standard. ***Results:*** We included 37 patients (18 female/19 male), 13 with limited and 24 with extensive disease according to VALG classification. Mean administered activity was 140 MBq and mean uptake time was 62 min. SSO-120 positive tumor was detected in all patients (100%) and in 110 of a total of 259 evaluated regions (42.5%). Thirty-three patients (89.3 %) showed average SSO-120 tumoral uptake higher than in liver tissue (region-based mean TLR_{peak}>1) and 17 patients (45.9%) demonstrated intense

uptake (region-based mean SUV_{max}≥10). All 28 patients for whom ^{18}F-FDG PET was available had SSO-120- and FDG-positive tumor. SSO-120 versus FDG-positive thoracic lymph node metastases were detected in 25 versus 26 patients (89.3% versus 92.9%) and distant metastases in 19 versus 17 patients (67.9% versus 60.7%). In detail, ^{68}Ga-SSO-120 PET detected additional uptake in contralateral lymph nodes (N3 versus N2), cervical lymph nodes, and liver metastases in one patient each and in brain lesions in 2 patients. ^{18}F-FDG PET detected additional uptake in thoracic lymph nodes in 4 patients (3 N3 versus N2, 1 N3 versus N0) and in pancreas in one patient. Region-based detection rates were 97.6% for ^{68}Ga-SSO-120 versus 95.3% for ^{18}F-FDG PET. Lesion-based monotonical correlation between SSO-120 and FDG uptake was low (Spearman's rho 0.44 for SUV_{max}). ***Conclusion:*** ^{68}Ga-SSO-120 PET demonstrated intense tumoral uptake in nearly every second patient and offers comparable detection rates to the gold standard ^{18}F-FDG PET. Ongoing investigation aims to characterize subgroups for identification of candidates for SSTR2-directed radionuclide therapy.

EP-0147

Ongoing Trial on the Role of the Promising Oncological PET/CT Tracer [68Ga]Ga-FAPI-46 for Staging Suspected/Confirmed Lung Cancer: Preliminary Results on Patients who Underwent Radical Surgery

E. Fortunati[1], *L. Zanoni*[2], *G. Cuzzani*[1], *C. Nanni*[2], *F. Lodi*[2], *F. Antonacci*[3], *P. Solli*[3], *F. Giunchi*[4], *A. Degiovanni*[4], *M. Ferrari*[5], *F. Natali*[5], *T. Galasso*[5], *G. Bandelli*[5], *P. Candoli*[5], *A. D'Errico*[4], *S. Fanti*[1,2]; [1]*Nuclear Medicine, Alma Mater Studiorum University of Bologna, Bologna, ITALY,* [2]*Nuclear Medicine, IRCCS, Azienda Ospedaliero-Universitaria di Bologna, Bologna, ITALY,* [3]*Division of Thoracic Surgery, IRCCS, Azienda Ospedaliero-Universitaria di Bologna, Bologna, ITALY,* [4]*Pathology, IRCCS, Azienda Ospedaliero-Universitaria di Bologna, Bologna, ITALY,* [5]*Interventional Pulmunology Unit, IRCCS, Azienda Ospedaliero-Universitaria di Bologna, Bologna, ITALY.*

Aim/Introduction: To evaluate the diagnostic performance of [68Ga]Ga-FAPI-46 PET/CT in staging suspected/confirmed lung cancer (LC) patients. ***Materials and Methods:*** A prospective monocentric ongoing study (CE, AIFA approved, started April2022) is enrolling patients with suspected/confirmed LC to perform a PET/CT with the investigational tracer [68Ga]Ga-FAPI-46(FAPI), in addition to conventional-staging-flow-chart scheduled by ThoracicSurgery/InterventionalPulmonologyDepartments [within 3 (±1) weeks from standard [18F]F-FDG PET/CT (FDG)]. No changes in patient's management derive from FAPI (Thoracic physician and patient blinded to FAPI results). In pts undergoing radical surgery, histopathology represents the StandardOfTruth. Biopsy and 1-year standard follow-up are used either for patients or anatomical regions not surgically treated. For the current preliminary purpose, only patients who underwent surgery (available pathological results before March23), were included. PET/CT findings were visually defined as positive/negative for T and N, classified according to TNM-Staging_AJCC8thEdition. On a T- and N-based analysis, for both tracers: agreement to pTN,AUC,accuracy-Acc.,sensitivity-Sens.,specificity-Spec.,positive/negative-predictive-value(PPV,NPV) were evaluated; semiquantitative-parameters [SUVmax, SUVmean, SUVmax/SUVmean_ratio and Target-to-background-ratios-TBRs, calculated as TargetLesionSUVmax divided by either SUVmax or mean of healthy-backgrounds (lung/mediastinal-blood-pool,MBP/liver)] were calculated on 60min scans and ROC_AUCs applied. ***Results:*** 23 patients (among 40 to date enrolled) were included (median age:69y; M:F=16:7). Histopathology excluded malignancy in 2/23 cases (1 Actinomyces abscess, 1 fibrocalcified-necrotic lung nodule) and demonstrated: adenocarcinoma in 16, squamous-cell-carcinoma in 5; 4 pT1b, 1 pT1c, 1 pT2, 6 pT2a, 3 pT2B, 6 pT3; 1pNx, 13/23(57%) pN0 whereas 9/23(39%) LNmetastases-LNM (pN1:8/9, pN2:1/9); 100% R0; 11 PL1; 13 LV1. Median(mean±SD, range) were: n°removed LN overall=408, per patient=17(19±12, 2-53); n°LNM overall=40/408(10%) and per patient=0(2±4,0-19); dimension(max, in mm) T=25(31±18,7-68); days between FDG-FAPI 7(10±9,1-30) and between FAPI-surgery=41(46±32, 13-154). On visual analysis (FAPI vs FDG): T:TP.19vs14;FP.1vs1;TN.1vs1;FN.2vs7;AUC.0.702vs0.583;Acc.87%vs65%;Sens.90%vs67%;Spec.50%vs50%;NPV.33%vs12%;PPV.95%vs93%.N:TP.6vs7;FP.1vs3;TN.13vs11;FN.3vs2;AUC.0.798vs0.782;Acc.83%vs78%;Sens.67%vs78%;Spec.93%vs79%;NPV.81%vs85%;PPV.86%vs70%. FAPI and FDG-PET/CT equally correctly staged TN in 7/23(30%) patients. Among the discordant staging cases (16/23, 70%), PET/CT was visually classified as either in favour of FAPI in 9 (5 T; 3 N; 1TandN) or in favour of FDG in 2 (1T, 1N) or equally inferior to pathology in 5 cases (3/5 for T). ROC-AUCs of semiquantitative parameters for T evaluation were respectively (FAPI vs FDG): SUVmax.0.738vs0.595;SUVmean.0.738vs0.595;-SUVmax/SUVmean0.631vs0.786;TBRs. Varied, depending on background, between 0.619 and 0,750 (TBR_Liver_Max) vs between 0.571 and 0.667. ***Conclusion:*** Preliminary results, limited to the surgically-treated cohort, report good performance of [68Ga]Ga-FAPI-46-PET/CT for staging suspected/confirmed LC, overall slightly higher than standard tracer [18F]F-FDG, in particular when using Visual interpretation or e.g TBR_Liver_max. Enrolment and further analyses (whole population, conventional follow-up; lesion-, volume- and immunohistochemical-based analyses; collateral findings) are ongoing.

EP-0148

Can [18F] FDG PET/CT parameters Predict Pathological Response in Locally Advanced NSCLC? Findinds from NADIM Study

R. Jimeno Pernett[1], *J. Mucientes Rasilla*[1], *J. Gonzalez Larriba*[2], *A. Martinez Martí*[3], *E. Nadal*[4], *N. Viñolas*[5], *J. Bosch Barrera*[6], *A. Insa Mallá*[7], *J. Casal Rubio*[8], *M. Cobo Dols*[9], *R. Bernabe Caro*[10], *M. Mitjavila Casanovas*[1], *V. Calvo de Juan*[1], *M. Provencio Pulla*[1]; [1]*Hospital Universitario Puerta De Hierro, Madrid, SPAIN,* [2]*Hospital Univeristario Clínico San Carlos, Madrid, SPAIN,* [3]*Hospital Universitario Vall d'Hebrón, Barcelona, SPAIN,* [4]*ICO Hospitalet, Barcelona, SPAIN,* [5]*Hospital Clínic Barcelona, Barcelona, SPAIN,* [6]*Instituto Catalán de Oncología Médica de Girona, Barcelona, SPAIN,* [7]*Hospital Clínico Universitario de Valencia, Valencia, SPAIN,* [8]*Hospital Álvaro Cunqueiro, Vigo, SPAIN,* [9]*Hospital Carlos Haya, Málaga, SPAIN,* [10]*Hospital Virgen del Rocío, Sevilla, SPAIN.*

Aim/Introduction: Neoadjuvant chemo-immunotherapy in lung cancer is emerging as the treatment of choice, especially in locally advanced stages, offering high resectability rates, increased progression-free survival, and high rates of pathological complete response. There is little information on the correlation between imaging and pathological response. This aspect is crucial when planning surgery. OBJECTIVEEstablish the relationship between metabolic and pathological response, based on tumor volume parameters, MTV, TLG and SUVmax, in [^{18}F]FDG PET/CT. ***Materials and Methods:*** Analysis based on the NADIM study: Patients with locally advanced resectable non-small cell lung cancer (NSCLC) were included. Forty-two patients who received chemotherapy or chemo-immunotherapy prior to radical surgery, and who had initial and post-neoadjuvant [^{18}F]FDG PET/CTwere included. The percentage reduction of the semiquantitative parameters before and after neoadjuvant therapy and the residual metabolic

volume in post-neoadjuvant [18F]FDG PET/CT of the lung tumor and the hilar and mediastinal lymph nodes were calculated and compared with the pathological response (complete, major, and incomplete). Statistical analysis was performed using Kruskal-Wallis, Mann-Whitney U, and area under the curve (AUC) to determine the association of the described variables. ***Results:*** The percentage reduction of the quantification parameters and the residual metabolic volume of the lung tumor and the hilar lymph nodes showed statistically significant differences. In the residual metabolic volume, TLG of the lung tumor was better associated with all three classes of pathological response (Kruskal-Wallis, probability: 0.0421), and to differentiate between complete and incomplete response (Mann-Whitney U, p: 0.008239), with an AUC/ROC: 0.7454. In the hilar lymph nodes, TLG was best associated with all three classes of response (Kruskal-Wallis, probability: 0.0189) and to differentiate between complete and incomplete response (Mann-Whitney U, p: 0.00347), with an AUC/ROC: 0.7454. In the percentage reduction of the lung tumor, TLG was best associated with the pathological response (Kruskal-Wallis, probability: 0.0324; Mann-Whitney U p:0.00347; AUC/ROC: 0.7387). In the hilar lymph nodes, MTV was best associated with the response (Kruskal-Wallis, probability: 0.0338; Mann-Whitney U p: 0.01511; AUC/ROC: 0.8034). No significant differences were found in the mediastinum among the types of pathological response. ***Conclusion:*** The percentage reduction of [18F]FDG PET/CT parameters in the lung tumor and hilar region, before and after neoadjuvant chemotherapy or chemo-immunotherapy in patients with locally advanced NSCLC, is able to predict the pathological response. Mediastinal metabolic. ***References:*** Neoadjuvant chemotherapy and nivolumab in resectable non-small cell lung cancer (NADIM): an open-label, multicentre, single-arm, phase 2 trial. Lancet Oncol. 2020; 21(11): 1.413-1.422 [DOI: 10.1016/S1470-2045(20)30453-8].

EP-0149

Relationship between [18]FDG myocardial uptake and subsequent evolution towards cachexia and outcome in lung cancer patients. Assessment from the retrospective LuCaPET database.

E. Abenavoli[1], *A. Grosso*[2], *T. Beyer*[3], *S. Duke*[4], *D. Ferrara*[3], *A. Frille*[5], *S. Gruenert*[6], *M. Hacker*[6], *S. Hesse*[5], *L. Hofmann*[7], *S. Holm*[4], *O. Sabri*[7], *L. Sundar*[3], *J. Yu*[3], *R. Sciagrà*[1];
[1]*Department of Nuclear Medicine, Azienda Ospedaliero-Universitaria Careggi, Florence, ITALY,* [2]*Department of Pneumology, Azienda Ospedaliero-Universitaria Careggi, Florence, ITALY,* [3]*QIMP Team, Medical University of Vienna, Vienna, AUSTRIA,* [4]*University of Copenhagen, Copenhagen, DENMARK,* [5]*University Hospital of Leipzig, Leipgz, GERMANY,* [6]*Division of Nuclear Medicine, Medical University of Vienna, Vienna, AUSTRIA,* [7]*University Hospital of Leipzig, Leipgz, AUSTRIA.*

Aim/Introduction: Cachexia is a severe complication of lung cancer with significant prognostic implications. The purpose of the LuCaPET project (ERAPERMED2021-324) is to identify the metabolic connections that pave the way for cachexia to allow earlier therapeutic interventions. Aside from tumour characteristic aberrations of [18F]FDG uptake patterns, myocardial uptake of [18F]FDG is observed in a significant proportion of lung cancer patients. The study assessed a relationship of myocardial [18F]FDG uptake at initial PET/CT imaging and subsequent evolution towards cachexia and overall survival. ***Materials and Methods:*** 189 lung cancer patients who underwent [18F]FDG PET/CT imaging for staging were included. The presence of myocardial uptake was visually evaluated on anonymized attenuation-corrected images, taking care to avoid interference from blood pool activity. The trained observer was blinded to the clinical evolution. The cachexia diagnosis was based on the Fearon criteria [1] that were evaluated approximately six months after staging PET and first line treatment. Moreover, patient outcome was monitored, and cancer-related deaths registered. The time of the latest control or the death date was used as follow-up conclusion. The relationships between myocardial [18F]FDG uptake, cachexia diagnosis and death were analysed using the Fisher exact test. The cachexia-free survival and the overall survival curves of patients with versus without myocardial [18F]FDG uptake were compared using the Kaplan-Meier log rank test. ***Results:*** At initial PET, visible myocardial [18F]FDG uptake was registered in 72 patients. Cachexia was diagnosed in 73 subjects. During the follow-up (17 ± 4 months) 54 patients had died. There was a clear connection between cachexia and patient outcome ($p < 0.0001$). However, a significant relationship between [18F]FDG uptake and cachexia and between [18F]FDG uptake and death was observed as well ($p < 0.03$ and $p < 0.02$, respectively). Most interestingly, the Kaplan-Meier curves showed a significant difference both for cachexia-free status and for overall survival in the patients with versus those without myocardial [18F]FDG uptake: $p < 0.02$ and $p < 0.01$). ***Conclusion:*** Based on these preliminary results, the role of metabolic conditions at staging, such as in this analysis myocardial [18F]FDG uptake, for the evolution towards cachexia and even for patient outcome, can be significant and their early detection could be useful for timely therapeutic and nutritional interventions aimed at preventing cachexia and at improving prognosis. ***References:*** Fearon K, et al. Definition and classification of cancer cachexia: an international consensus. Lancet Oncol. 2011;12:489-95.

EP-10

e-Poster Area

B: Imaging Clinical Studies -> B1 Oncological Imaging Clinical Study -> B15 Gastro-Intestinal (including Liver and Non-Endocrine Pancreas)

EP-0150

Diagnostic and prognostic value of TOF-18F-FDG PET/CT in patients with malignant pancreatic tumors

S. Stanzel*, T. Nazerani-Zemann, R. M. Aigner;*
Division of Nuclear Medicine, Graz, AUSTRIA.

Aim/Introduction: The aim of this study was to evaluate whether the application of time-of-flight (TOF) in 18F-FDG PET/CT can improve the accuracy in diagnosing malignant pancreatic lesions. Furthermore, we assessed the impact of TOF on image quality and its prognostic value compared to standard PET/CT reconstruction. ***Materials and Methods:*** Eighty-six patients with a histologically proven malignant pancreatic carcinoma were included in this retrospective study and underwent a dual phase (DP) 18F-FDG PET/CT with imaging 30 and 90 min. p.i. A total of 86 pancreatic lesions were assessed by one board-certified nuclear medicine physician and a third-year resident. SUVmax, tumor volume (V), and the RI (retention index) of pancreatic lesions were compared between TOF and standard. Image quality regarding pancreatic lesion demarcation was rated according to a 6-point Likert-type scale. The median follow up was 17.2 mo. The correlation of PET-derived image features and the presence of metastases at the time of PET/CT with overall survival (OS) was assessed. ***Results:***

With TOF, 80/86 tumors were PET-positive compared to 76/86 tumors without TOF resulting in an improvement of 4.7% (4/86). With TOF, V was significantly lower than without TOF (standard, 20.4 cm^3 vs. TOF, 16.3 cm^3; P < 0.001). In TOF reconstructed images SUVmax was significantly increased (standard, 9.6; TOF, 10.4; P < 0.001), whereas RI was significantly decreased (standard, 42.5% vs. TOF, 38.3%; P = 0.024). Lesion demarcation of pancreatic lesions was excellent (standard, 2.7; TOF, 1.2; P < 0.001) in reconstructed TOF images. The RI without TOF (P = 0.041; cutoff = 38.2%), the V with TOF (P = 0.032; cutoff = 2.0 cm^3), and the presence of metastases at the time of PET/CT (P = 0.034) were strongly correlated to OS. ***Conclusion:*** TOF-PET/CT showed an improvement in the diagnosis of malignant tumors compared to imaging without TOF due to better lesion demarcation and improved image quality, which may be useful in treatment planning. In TOF-reconstructed images the lesion volume and the RI was significantly decreased due to better visualization of tumor necrosis and intratumoral heterogeneity. The RI without TOF, the V with TOF, and the presence of metastases at the time of PET/CT correlated significantly with OS. ***References:*** Hausmann D, Bittencourt LK, Attenberger U, et al. Diagnostic accuracy of 18F-choline PET/CT using time-of-flight reconstruction algorithm in prostate cancer patients with biochemical recurrence. Clin Nucl Med 2014;39:e197-e201.

EP-0151

Diagnostic and prognostic value of time-of-flight 18F-FDG PET/CT in staging of patients with pancreatic ductal adenocarcinoma using TrueX and Q.Clear reconstruction

S. Stanzel, *T. Nazerani-Zemann, R. M. Aigner;*
Medical University of Graz, Department of Nuclear Medicine, Division of Nuclear Medicine, Graz, AUSTRIA.

Aim/Introduction: The aim of the present study was to evaluate the impact of time-of-flight (TOF) reconstruction in conjunction with TrueX (=point spread function (PSF)-based algorithm) or Q.Clear (=Bayesian penalised likelihood reconstruction algorithm) on image quality (IQ), lesion detection rate, metabolic tumor volume (MTV), and SUVmax in dual-phase (DP) ^{18}F-FDG PET/CT in staging of patients with pancreatic ductal adenocarcinoma (PDAC). ***Materials and Methods:*** Seventy-two patients with a histologically proven PDAC were included in this retrospective study and underwent a dual phase (DP) ^{18}F-FDG PET/CT with imaging 30 and 90 min. p.i. Fifty-five patients had TOF reconstruction in conjunction with TrueX and 17 patients with Q.Clear on two different PET/CT scanners. Standard PET/CT imaging was performed in accordance with the EANM guidelines. A total of 72 pancreatic lesions were assessed by one board-certified nuclear medicine physician and a third-year resident. SUVmax and metabolic tumor volume (MTV) of pancreatic and metastatic lesions were compared between TOF and standard. Lesion demarcation of pancreatic tumors and overall IQ were rated according to a 6-point Likert-type scale. Interrater agreement was assessed. ***Results:*** Forty-one additional lesions in 72 patients were detected using TOF alone (SUVmax, 5.2 [2.6]; MTV, 3.1 cm^3 [1.4]). Of these two were pancreatic primary tumors, and 34 metastases (pancreas, liver, lung, adrenal glands, lymph nodes), and 5 were benign. 30/34 metastatic lesions identified with TOF alone led to therapy change in 8 patients. Lesion demarcation of PDAC was excellent (standard, 2.7; TOF, 1.2; P < 0.001) and overall IQ was excellent in reconstructed TOF images (standard, 2.7; TOF, 1.1; P < 0.001). Interrater agreement was good forcombined ratings (1 + 2, 3 + 4, 5 + 6). SUVmax was significantly increased in TOF reconstructed images (standard, 10.3 [7.7].; TOF, 11.2 [7.7]; P < 0.001), whereas there was no significant difference in MTV (standard, 16.2 [29.4] cm^3 vs. TOF, 13.0 [12.4] cm^3; P = 0.691). ***Conclusion:*** The application of TOF in conjunction with TrueX or Q.Clear seems to be of additional value in detecting pancreatic and small metastatic lesions in patients with PDAC, which has an impact on treatment planning preventing metastatic patients from surgery. TOF with TrueX or Q.Clear impacts image quality and SUVmax presenting more clearly tumor necrosis and tumor heterogeneity compared to standard imaging.

EP-0152

Evaluation of Liver Lesions with Diffusion Weighted Imaging PET/MRI in Transarterial Radioembolization Treatment Patients

A. Kibar, *F. Aghazada, L. Uslu-Besli, O. E. Sahin, S. Asa, S. Sager, K. Sonmezoglu;*
Istanbul University-Cerrahpasa, Cerrahpasa Faculty of Medicine, Department of Nuclear Medicine, Istanbul, TÜRKIYE.

Aim/Introduction: Y90 microsphere transarterial radioembolization therapy (TARE) is a well-known treatment modality for malignant liver lesions, particularly hepatocellular cancer and colon cancer metastases. Pre and post-treatment FDG PET is a useful tool for treatment planning and determination of response. Our aim in this study is to determine the relationship between MRI ADC values of liver lesions before and after Y90 treatment using FDG PET/MRI images. ***Materials and Methods:*** Forty-five patients who were treated with TARE for malignant liver lesions, had FDG PET/MR imaging before and after treatment, and had target lesion/lesions (lesion showing FDG uptake more than healthy liver tissue before treatment) were included in the study. According to PERCIST, patients divided into two groups, responders (23/45) (complete response and partial response) and non-responders (22/45) (stable disease and progressive disease). A maximum of 3 target lesions were selected for each patient. SUXmax, SUVmean, SULpeak, ADCmin , ADCmean values were determined before and after treatment for the lesions. ***Results:*** Mean ADCmean values of responders before and after treatment were 1.15+0.437x10-3 (range: 0.100-2.050x10-3) and 1.519+0.429x10-3 (range: 0.100-2.050x10-3), respectively. Mean ADCmean values of non-responders before and after treatment were 1.258+0.400x10-3 (range: 0.170-1.850x10-3) and 1.367+0.342x10-3 (range: 0.313-1.940x10-3), respectively. . While the change in ADCmean was significant in responders according to the Wilcoxon test (p=0.004), it was not significant in non-responders (p=0.108). However, when we performed the Wilcoxon test on all patients regardless of their response status, we found that ADCmin and ADCmean values increased significantly after treatment (p=0.034, p=0.001, respectively). Changes in mean SUVmax and SUVmean were not associated with change in ADCmean; (r=-0.117, p=0.445, r=-0.149, p=0.328, respectively). ***Conclusion:*** Evaluation of treatment response for Y90 is a crucial part of patient management. The MRI component of PET/MRI provides important information about the response. In our study, we found that there was an increase in ADC values after Y90 treatment, and this increase was higher in those who responded to treatment. We evaluated that ADC values can be used as a parameter in evaluating response to treatment. However SUV and ADC changes were not correlated.

EP-0153

Comparison of Tc-99m Mebrofenin Scintigraphy with Other Parameters in Prediction of Patient Status in Y-90 Patients

A. Kibar, *S. Asa, F. Aghazada, N. Yeyin, M. Abuqbeitah, K. Sahin, C. Guneren, K. Saglam, B. Ince, S. Sager, K. Sonmezoglu;*
Istanbul University-Cerrahpasa, Cerrahpasa Faculty of Medicine, Department of Nuclear Medicine, Istanbul, TÜRKIYE.

Aim/Introduction: Y90 microsphere transarterial radioembolization therapy (TARE) is an evidence-based treatment modality for malignant liver lesions, particularly hepatocellular cancer and colon cancer metastases. Child Pugh score and ALBI score can be used in patient selection and evaluation of patient status before the procedure. In our study, we aimed to investigate the correlation of liver uptake values of patients who underwent Tc99m-mebrofenin scintigraphy before Y90 with other scores, its success in predicting prognosis after treatment, and its relationship with parameters in pre-treatment function evaluation. ***Materials and Methods:*** Dynamic and SPECT/CT imaging were performed in 21 patients who were scheduled for TARE treatment due to malignant liver lesions, after 6.63+1.59 mCi Tc99m-mebrofenin injection. Liver uptake values were calculated. Spearman correlation test were applied to show the relationship of these values with ALBI score, Child-Pugh score, total bilirubin, direct bilirubin, albumin, INR, ALT and AST. In addition, t-test was performed to determine the difference in uptake between those who died and those who did not. ***Results:*** Significant correlation was found between Liver uptake of mebrofenin and total bilirubin, direct bilirubin ($p<0.001$); ALBI score ($p<0.01$) and albumin ($p<0.05$). Although the mean uptake of the patients who died were higher than the uptake of the survivors, this result was not significant (dead patients' mean: 5.3%/min/m2, median: 3.3%/min/m2, standard deviation: 4.9; survivors' mean: 6.1%/min/m2, median : 4.5%/min/m2, standard deviation: 6.5; p: 0.747). Mebrofenin uptake value correlated with other parameters measured before Y90 treatment and was lower on average in patients who died, even though it was not statistically significant in predicting the prognosis before treatment. In addition by looking at the corresponding areas in the mebrofenin scintigraphy, it can be predicted how much of the functional capacity of the liver corresponds to the area where the MAA is given. In this way, benefits can be obtained in patients who have large tumors. While the volume occupied by the MAA was approximately 70% in 3 patients in our study, we found that the function was affected less than 70% in the corresponding areas in the mebrofenin scintigraphy. ***Conclusion:*** Scintigraphic evaluation of Tc99m-mebrofenin uptake appears to be a useful method in predicting liver function, due to its capability of showing segmental function of the liver it may also provide additional information in patients who are planned to be treated with Y90. Prospective studies with large patient groups are needed.

EP-0154

Dual-tracer PET/CT protocol with [18F]FDG and [68Ga]Ga-FAPI-46 outperforms single-tracer PET/CT with [18F]FDG in gastrointestinal and head and neck cancer, due to higher tumour to background ratio and larger gross and functional tumour volume.

K. Roth[1], *S. Wegen*[2], *J. Weindler*[1], *C. Voltin*[1], *L. van Heek*[1], *K. Schomäcker*[1], *T. Fischer*[1], *S. Marnitz*[2], *C. Kobe*[1], *A. Drzezga*[1];
[1]*Department of Nuclear Medicine, Faculty of Medicine and University Hospital Cologne, Cologne, Germany, Cologne, GERMANY,* [2]*Department of Radiation Oncology, Cyberknife and Radiotherapy, Faculty of Medicine and University Hospital Cologne, Cologne, Germany, Cologne, GERMANY.*

Aim/Introduction: Fibroblast activation protein (FAP) visualized by positron-emission-tomography (PET) using fibroblast activation protein inhibitor (FAPI) appears to be a promising target for cancer imaging, staging and therapy, providing added value and strength as a complement to [^{18}F]FDG in cancer imaging. We recently introduced a combined single session/dual-tracer protocol with [^{18}F]FDG and [^{68}Ga]Ga-fibroblast activation protein inhibitor (FAPI) for cancer imaging and staging. In the present study malignant tissue visualization, target to background uptake ratios (TBR) as well as gross tumour volume (GTV) and functional tumour volume (FTV) measurement were assessed with single-tracer [^{18}F]FDG PET/CT and with dual-tracer [^{18}F]FDG&[^{68}Ga]Ga-FAPI-46 PET/CT, respectively. ***Materials and Methods:*** 19 patients with head and neck and gastrointestinal cancers received an initial [^{18}F]FDG-PET/CT followed by a dual-tracer PET/CT after additional injection of [^{68}Ga]Ga-FAPI-46 within the same medical appointment (on average 13.9±12.3 minutes after injection of [^{18}F]FDG). Two readers visually compared detection rate of malignant tissue, TBR, GTV and FTV for tumour and metastatic tissue in [^{18}F]FDG PET/CT and [^{18}F]FDG&[^{68}Ga]Ga-FAPI-46 PET/CT. ***Results:*** Diagnostic performance of dual-tracer compared to single-tracer PET/CT was superior in six patients and equal in 13 patients. Mean TBR of tumours and metastasis in [^{18}F]FDG&[^{68}Ga]Ga-FAPI-46 PET/CTs were mostly higher compared to [^{18}F]FDG PET/CT using maximal count rates (CRmax). GTV and FTV were significantly larger, when measured on dual-tracer than on single-tracer PET/CT. ***Conclusion:*** Dual tracer PET/CT with [^{18}F]FDG and [^{68}Ga]Ga-FAPI-46 showed better visualization of malignant tissue due to a generally higher TBR, larger FTV and GTV compared to [^{18}F]FDG-PET/CT in gastrointestinal and head and neck cancer, suggesting that [^{68}Ga]Ga-FAPI-46 provides added value in pretherapeutical staging.

EP-0155

Surveillance 18F-FDG PET/CT in predicting the prognosis of esophageal cancer patients

S. Chan, *C. Tseng, S. Llu;*
Hualien Tzu Chi Hospital, Hualien, TAIWAN.

Aim/Introduction: The prognostic value of performing surveillance PET/CT imaging after the conclusion of therapy in esophageal cancer is not well established. This study aimed to evaluate the predictive value of surveillance PET/CT in predicting the prognosis of esophageal cancer patients. ***Materials and Methods:*** This was a retrospective study of 202 biopsy-proven esophageal cancer patients at a single tertiary center. In total, we included 604 surveillance PET/CT scans done after the completion of treatment in this study. Median follow-up from the completion of therapy to surveillance PET scan was 23.15 months (range, 4-134.8 months). A survival benefit was measured using Kaplan-Meier plots with a Mantel-Cox log-rank test. A multivariate Cox regression model was provided with clinical covariates. ***Results:*** Of the 604 PET/CT scans, 234 had positive findings. Overall median survival from the time of the PET/ CT study was 32 months. The median survivals of PET-positive and PET-negative groups differed significantly (survival=12.4 and 55.5 months, respectively; $P < 0.0001$). The subgroup analysis demonstrated that the prognostic value of PET scans performed between 4 and 24 months after treatment ($P < 0.0001$) was more prominent than the scans after 24 months ($P = 0.0006$). However, the predictive value of surveillance PET scans was similar in early-stage patients (stage 1,2) and late-stage patients (stage 3,4). In a multivariate Cox regression model, factors associated with Overall Survival(OS) were PET/CT result ($P = 0.0012$) and chemoradiotherapy ($P=0.0024$).

Conclusion: The result of surveillance 18F-FDG PET/CT is a prognostic marker of overall survival in esophageal cancer patients, regardless of the tumor stage. The predictive power of PET/CT is better in the scans between 4 and 24 months after treatment.

EP-0156

A dose optimization study using Visual Grading Regression in [68Ga]-FAPI-46 PET imaging of patients with pancreatic lesions

T. Nilsson[1], *P. Rasinski*[1,2], *S. af Burén*[1,2], *Ö. Smedby*[3], *A. Blomgren*[1], *M. Löhr*[2,4], *E. Sparrelid*[5], *T. Tran*[6,7], *R. Axelsson*[1,8], *M. Holstensson*[1,2]; *[1]Department of Medical Radiation Physics and Nuclear Medicine, Karolinska University Hospital, Huddinge, SWEDEN, [2]Department of Clinical Science, Intervention and Technology (CLINTEC), Karolinska Institutet, Stockholm, SWEDEN, [3]Department of Biomedical Engineering and Health Systems, KTH Royal Institute of Technology, Stockholm, SWEDEN, [4]Department of Upper Gastrointestinal Diseases, Karolinska University Hospital, Huddinge, SWEDEN, [5]Division of Surgery and Oncology, Department of Clinical Science, Intervention and Technology (CLINTEC), Karolinska Institutet, Stockholm, SWEDEN, [6]Department of Oncology-Pathology, Karolinska Institutet, Stockholm, SWEDEN, [7]Department of Radiopharmacy, Karolinska University Hospital, Stockholm, SWEDEN, [8]Department of Molecular Medicine and Surgery, Karolinska Institutet, Stockholm, SWEDEN.*

Aim/Introduction: The administered activity to patients should be kept as low as reasonably achievable whilst simultaneously result in an image quality good enough to ensure a reliable diagnosis. The aim of this study is to evaluate the feasibility of reducing administered activity in ^{68}Ga-FAPI-46 imaging while maintaining a satisfactory image quality, with a certainty that it will not affect the radiologist's ability to make a clinical diagnosis. ***Materials and Methods:*** A visual grading assessment was performed on images from ongoing ^{68}Ga-FAPI-46 PET/CT studies (EudraCT 2020-002568-30; NCT05172310). Ten patients scheduled for surgery due to suspected stomach cancer or desmoplastic tumors of the pancreas were included. The patients were administered with 4.0 MBq/kg ±10% (mean 270 MBq, range 226-309 MBq). PET/CT-Imaging was performed from scull vertex to mid-thigh, 60 minutes post injection in step-and-shoot mode with list-mode enabled. The acquisition time was 4 minutes per bed position. PET-images were statistically truncated and reconstructed to represent images with an administered activity of 1, 2, 3 and 4 MBq/kg. Two radiologists performed a blinded grading of the images in Hermes (Hermes Medical Solutions AB, Stockholm, Sweden). Four image quality criteria were graded on a four-point Likert scale ranging from 1 = Completely certain that the criterion is not fulfilled to 4 = Completely certain that the criterion is fulfilled. Two criteria were defined to assess how discernible and distinct structures belonging to the thoracic cage and the heart were visualized. The other two criteria regarded the disruptive effect of noise and whether the overall image quality was good enough to make a clinical diagnosis. The gradings were analyzed with a mixed-effects ordinal logistic regression using the statistical software R. ***Results:*** Increased satisfaction of the image quality with an increase in activity was observed for all criteria. For the overall image quality, there was no significant difference between 3 MBq/kg and 4 MBq/kg images, whereas the 1 MBq/kg and 2 MBq/kg images were rated significantly ($p<0.05$) lower than the 4 MBq/kg images. For the other criteria, all images with shorter acquisition were rated significantly inferior to the 4 MBq/kg images. ***Conclusion:*** The administered activities can be reduced from 4 to 3 MBq/kg while maintaining satisfactory image quality. Reducing administered activities to 2 MBq/kg or lower is not recommended since it results in images with a low satisfaction level and a significant disruptive effect of noise on the evaluation.

EP-0157

The prognostic value of metabolic parameters and heterogeneity index of PET/CT in patients with advanced gastric adenocarcinoma

Y. Tian, *T. Zhao, W. Cai, Y. Dong, X. Ma, P. Ma, Q. Zhao; General Hospital of Ningxia Medical University, Yinchuan, CHINA.*

Aim/Introduction: Gastric cancer is one of the most common malignant cancers of digestive system. So finding effective indicators for evaluating the patients' prognosis and curative effect is key to make the best treatment strategy and improve the quality of life. The present study aimed to assess the prognostic value of PET parameters combined with clinical characteristics in patients with advanced gastric adenocarcinoma (AGA). And the prognostic value of PET parameters alone was evaluated on patients with different treatment and different Ki67 levels. ***Materials and Methods:*** 71 patients with advanced gastric adenocarcinoma and without anti-gastric-cancer therapy were included in this retrospective study. Their metabolic parameters and heterogeneity index (HI) were collected and calculated. Furthermore, clinical prognostic indicators were collected. Variables were grouped by cut-off values of Receiver operating curve and the median. Kaplan-Meier method and COX regression analysis for progression-free survival (PFS) and overall survival (OS) were used for survival analysis and evaluate the prognosis. ***Results:*** Survival analysis showed that patients in low value group have longer median PFS and median OS than corresponding high-value group. For all patients with AGA before treatment, HI-2 was the independent risk factor of PFS, while total glycolysis (TLG) was common independent risk factor for both PFS and OS. For patients in different groups, HI-2 also was the independent risk factor for PFS in patients with Ki67<70%, chemotherapy or radiotherapy and combined therapy. While in patients with Ki67≥70% and surgery, it was Maximum standardized uptake value (SUVmax) that correlated with PFS and OS. For clinicopathological factors, CEA and N staging were related to the prognosis, but only N staging was a common independent risk factor for both PFS and OS. ***Conclusion:*** HI-2, TLG and CEA, N staging played main role in the prognosis of all patients with AGA. While in different groups with the simple analysis of PET parameters, HI-2 and SUVmax correlated with PFS and OS

EP-0158

Incremental value of 18F-FDG PET-CECT over conventional imaging in evaluation of Gall Bladder Carcinoma.

P. Singh, *T. Singhal, P. Kumar, G. Parida, R. Emerson, K. Bishnoi, A. Rehman, K. Kandula, K. Agrawal, S. Patro; AIIMS Bhubaneswar, Bhubaneswar, INDIA.*

Aim/Introduction: Gallbladder carcinoma (GBCa) is one of the most common carcinomas of gastroenteric system with 5-year survival for localized, regional and distant disease being ~69, 28 & 3% respectively. Thus, making accurate staging of GBCa important. Commonly used imaging for evaluation of GBCa include ultrasonography (USG), contrast-enhanced computed-tomography (CECT), magnetic resonance imaging (MRI), and the latest addition to this armamentarium i.e., Fluo-

rine-18-fluorodeoxyglucose (18F-FDG) PET-CECT (1, 2). This study evaluated diagnostic utility of 18F-FDG PET-CECT over CECT in staging GBCa patients ***Materials and Methods:*** This was a retrospective study including patients with GBCa (initial staging, restaging and recurrence-detection) who underwent both anatomical imaging with CECT abdomen-pelvis with HRCT-thorax and 18F-FDG PET-CECT within 10 days of each-other. The difference in staging by both modalities was noted. True positive findings in case of disparities between the two modalities was considered based on follow-up or histopathological examination. ***Results:*** Fifty-seven patients (36-females) were included with median age 55 (range 35-74) years. Of these, 28 were post-cholecystectomy and 29 were treatment-naïve. In the post-cholecystectomy group, local-residual disease/recurrence was seen in 12 patients on 18F-FDG PET-CECT (11 true-positive and 1 false-positive) while CECT detected local disease only in 7 patients (6 true-positive and 1 false-positive). Thus, giving a sensitivity, specificity and diagnostic accuracy of 100%, 94.1% & 96.4% for 18F-FDG PET-CECT compared to 54.5%, 94.1% & 78.6% for CECT, respectively. In treatment-naïve group, PET-CECT increased T-stage in 4/29 (13.7%), T2-T3 in 3 patients and T3-T4 in 1 patient. For nodal-staging PET-CECT upstaged the disease in 10/57 (17.5%) patients, N0-N1 in 2 patients and N0-N2 in 8 patients. Major impact of FDG PET-CT was seen in metastatic disease detection where it upstaged 10/57 (17.5%) patients while additional metastatic lesions were identified in 21 (36.8%) patients compared to CECT alone. Based on FDG PET-CECT findings change in management was observed in 12 (21.1%) patients (table 1).

EP-0159

Prognostic value of negative FDG PET/CT in curatively treated colorectal carcinomas with rising CEA levels during surveillance

A. Suresh[1], *V. Rangarajan*[2], *N. Purandare*[2], *A. Agrawal*[2], *S. Shah*[2], *A. Puranik*[2], *A. Saklani*[2];
[1]*Tata Memorial Centre, Varanasi, INDIA,* [2]*Tata Memorial Centre, Mumbai, INDIA.*

Aim/Introduction: The purpose of this study was to determine the prognostic usefulness of negative FDG PET/CT in curatively treated non-metastatic colorectal carcinomas with growing CEA levels during surveillance. ***Materials and Methods:*** Between 2013 and 2018, a retrospective audit of 194 colorectal cancer patients (Stage I-III) with rising CEA levels during surveillance and subsequent negative FDG PET/CT (index PET/CT) was performed. Electronic medical records (EMR) were tracked for an average of 45 months (until May 2020). The following variables were audited: lesion site, baseline CEA (ng/ml), treatment (surgery, chemotherapy, and radiotherapy), time interval for CEA level to reach nadir and subsequent rise in CEA warranting PET/CT, additional investigation within 12 months (PET/CT, CECT, MRI, and staging laparoscopy), treatment started on disease detection, and final follow-up. The further investigation was used to determine if the PET/CT true negative (TN) or false negative (FN) index was the gold standard. The prognostic value of FDG PET/CT was estimated in terms of disease-free survival (DFS) and overall survival (OS). ***Results:*** Within 12 months of the initial PET/CT, only 82 of 194 (46%) patients received further investigations. Using Kaplan Meier analysis, stage 3 disease (p-value 0.046), histology of signet ring cell and poorly differentiated adenocarcinoma (p-value 0.001) were found to be poor prognostic variables. A FN index PET/CT (18 of 82, 21.9% mortality) had a median DFS of 4.21 months. Those with TN index PET/CT (64 of 82) had just 4 confirmed recurrences, one of whom was alive at the conclusion of the research period. CEA levels at the time of the index PET/CT were observed to indicate poor outcome (hazard ratios of 1.01 for OS, p-value 0.001; 1.006 for DFS, p-value 0.004). The median CEA level for FN index PET/CT was 9.7 ng/ml, while for TN index PET/CT it was 6.3 ng/ml. ***Conclusion:*** In a subset of patients with poor survival, stage 3, greater tumour grade at diagnosis and higher CEA levels during post-curative surveillance may have a falsely negative PET/CT. A prospective study should be considered to determine which additional investigation might be useful for declaring an index PET/CT true negative or positive for prognosis, as well as to identify a CEA level cut-off that could predict the false negativity of an index PET/CT in order to initiate further management.

EP-0160

Comparison of 18F-FAPI-04 and 18F-FDG PET/CT in detecting the primary tumor and metastatic lesions in patients with initial pancreatic ductal adenocarcinoma

L. Lin*, G. Wang, X. Su;*
Department of Nuclear Medicine, The First Affiliated Hospital, Zhejiang University School of Medicine, Hangzhou, CHINA.

Aim/Introduction: Gallium-68(^{68}Ga)-labeled fibroblast activation protein inhibitor (FAPI) PET/CT imaging has been widely used in the diagnosis of several malignant tumor. Compared with ^{68}Ga, ^{18}F has a great practical and economic advantage. There is very little data on the use of ^{18}F-AlF-NOTA-FAPI-04 (^{18}F-FAPI-04) for detecting pancreatic ductal adenocarcinoma (PDAC). Herein, this prospective research aimed to evaluate performance of ^{18}F-FAPI-04 in delineating the primary tumor and staging in initial pancreatic ductal adenocarcinoma, as well as to compare it with ^{18}F-FDG PET/CT. ***Materials and Methods:*** Fifty-nine patients with histologically proven PDAC via fine need biopsy were enrolled in this study for staging. Each patient underwent both ^{18}F-FAPI-04 and ^{18}F-FDG PET/CT within 3-5 days. Lesion detectability and the tracer uptake of lesions were evaluated visually and semi-quantitatively by measuring maximum standardized uptake value of tumor (SUV_{max}). Normalized SUV_{max} (the original SUV_{max} of lesion divided by the SUV_{max} of descending aorta). Histopathological findings or follow-up data such as laboratory examinations and radiographic scans were served as a standard of reference. ***Results:*** The fifty-nine enrolled patients (median age: 63 years; range: 58-70 years) included forty-one males and eighteen females. Of fifty-nine patients, twenty-one underwent Whipple surgery or pancreatoduodenectomy. For primary tumor detection, ^{18}F-FAPI-04 PET/CT has a great advantage with 100% of positive rate compared to ^{18}F-FDG PET/CT [37.3% (22/59)] due to higher both original SUV_{max} (16.0 vs. 8.1, $p<0.0001$) and normalized SUV_{max} (10.25 vs. 4.24, $p<0.0001$). For PDAC staging, ^{18}F-FAPI-04 PET/CT was superior to ^{18}F-FDG PET/CT in detecting more metastatic lesions, including portal vein tumor thrombus and metastatic lesions in lymph nodes, liver, peritoneum, and bone, particularly for lymph nodes, peritoneal and liver metastasis ($p<0.0001$, 0.0001 and $p= 0.028$, respectively), resulting in up-regulating TNM staging in seven patients compared with ^{18}F-FDG PET/CT. Furthermore, univariate and multivariate analysis showed that the maximum diameter of primary tumor and lymph nodes metastasis were independent risk factors for PDAC staging by ^{18}F-FAPI-04 PET/CT. ***Conclusion:*** ^{18}F-FAPI-04 PET/CT outperformed ^{18}F-FDG PET/CT in visualizing the primary tumor and metastatic lesions in initial PDAC and might be a promising imaging method for PDAC diagnosis and staging.

EP-0161

Comparison of Diagnostic Efficacy of 18FAl-NOTA-FAPI-04 and 18F-FDG PET/CT for recurrence and/ormetastasis in patients with gastric cancer

K. Zheng, *Y. Zhang, H. Ye, A. Xie;*
Hunan Cancer Hospital (the Affiliated Cancer Hospital of Xiangya School of Medicine, Central South University), Changsha, CHINA.

Aim/Introduction: This study aimed to compare the efficacy of ^{18}FAl-NOTA-FAPI-04 PET/CT with that of ^{18}F-FDG PET/CT for detecting tumor recurrence and/or metastases in gastric cancer. ***Materials and Methods:*** This single-center retrospective clinical study was performed at the Hunan Cancer Hospital between December 2020 and June 2022. The participants underwent both ^{18}FAl-NOTA-FAPI-04 and ^{18}F-FDG PET/CT within 14 days. Histopathologic examination, morphologic imaging, and/or follow-up imaging were used as a reference for the final diagnosis. The SUVmax and back-ground ratios (TBR) of the recurrence and metastases between ^{18}F-FDG and ^{18}FAl-NOTA-FAPI-04 PET/CT were compared using the paired-sample t test. The comparisons of sensitivity and specificity for the detection of gastric cancer between ^{18}FAl-NOTA-FAPI-04 and ^{18}F-FDG were performed with McNemar's test. ***Results:*** Forty-eight patients (27 males, aged 29 - 68 years) with gastric cancer after curative resection (27 with adenocarcinoma, 17 with signet ring cell carcinoma and 4 with mucinous adenocarcinoma) were included in the study. ^{18}FAl-NOTA-FAPI-04 accumulation was significantly higher than that of ^{18}F-FDG in cancer recurrence (SUVmax, 11.65 vs 3.48, P< 0.01; TBR, 12.93 vs 2.94,P< 0.01), lymph node metastases (SUVmax, 13.35 vs 2.75, P=0.001; TBR, 14.60 vs 2.00, P< 0.01), and distant metastases (SUVmax, 12.07 vs 2.98, P < 0.01; TBR, 13.66 vs 2.36, P < 0.01). Based on patients, ^{18}FAl-NOTA-FAPI-04 PET/CT showed a higher sensitivity (97.4% vs 71.1%, p = 0.002) in suspected cancer recurrence and/or metastases compared to ^{18}F-FDG PET/CT. ***Conclusion:*** Our findings indicate that ^{18}FAl-NOTA-FAPI-04 PET/CT outperformed ^{18}F-FDG PET/CT in the diagnosis in suspected recurrence and/or metastasis of gastric cancer.

EP-0162

Prognostic value of semiquantitative [18F]F-FDG PET/MRI parameters in patients with a newly diagnosed Pancreatic Adenocarcinoma

G. Mango[1], *P. Bartoletti*[2], *S. Serafini*[3], *R. Guastella*[4], *C. Berto*[5], *S. Da Pozzo*[6], *M. Sitara*[2], *G. Fichera*[7], *C. Giraudo*[2], *L. Evangelista*[2];
[1]*Nuclear Medicine, Department of Advanced Biomedical Sciences, University of Naples Federico II, Naples, ITALY,* [2]*Nuclear Medicine Unit, Department of Medicine DIMED, University of Padua, Padua, ITALY,* [3]*General Surgery Padua University Hospital, Padua, ITALY,* [4]*Hepato-Pancreato-Biliary Surgery and Liver Transplantation Unit, Padua University Hospital, Padua, ITALY,* [5]*Radiology Unit, Department of Medicine DIMED, University of Padua, Padua, ITALY,* [6]*Radiology Unit, Azienda Ospedaliera di Padua, Padua, ITALY,* [7]*Pediatric Radiology Unit, Padua University Hospital, Padua, ITALY.*

Aim/Introduction: To assess the prognostic value of semiquantitative [18F]F-FDG PET/MRI parameters in a cohort of patients with a newly diagnosed pancreatic adenocarcinoma ***Materials and Methods:*** From 2017 to 2022, [18F]F-FDG PET/MRI scans performed in patients with a newly diagnosed pancreatic adenocarcinoma were retrospectively collected. PET and MRI images were visually and semi-quantitatively analyzed. In particular, SUVmax, SUVmean, TLG and MTV of the primary tumor for PET images were calculated. The apparent diffusion coefficient (ADC) of the primary tumor was computed by using diffusion weighted sequences (DWI). Data about outcomes were recovered in terms of progression and overall survival (PFS and OS, respectively), by using the electronic chart. t-Student test, ROC curves and Kaplan-Meier analysis were used to test the correlation between PET/MR parameters and outcomes. ***Results:*** Data from 30 patients (median age: 70 years and male/female ratio: 22/8) were considered. Seventeen patients (57%) were treated with neoadjuvant chemotherapy, 2 (6%) were treated with neoadjuvant chemotherapy followed by surgery and 11 (37%) underwent primary surgical approach. After a median follow-up time of 29 (4-98) months, data from 28 (91%) patients were recovered. Fifteen (54%) had a progression of disease. Moreover, 12 (40%) died. Only SUVmean was significantly higher both in patients with a progressive disease and in those who died than their counterpart (4.3±1.9 vs. 3.1±1.1 and 4.4±1.9 vs. 3.2±1.2, respectively; p<0.05). At ROC analysis, the value of 3.38 for SUVmean was used as the best cut-off point (sensitivity: 75%, specificity: 75%). Indeed, at Kaplan-Meier analysis, patients with a SUVmean <3.38 in the primary tumor have a better prognosis than those with a SUVmean > 3.38 (chi-square: 5.6; log rank p<0.05). ***Conclusion:*** In pancreatic adenocarcinoma patients, our results suggest SUVmean of the primary tumor should be further investigated as a valuable prognostic factor in pancreatic ductal adenocarcinoma. ***References:*** - Diagnostics 2020; 10: 952;- Molecular Imaging and Biology 2021; 23, 456-466- Clinical Radiology 2020;75: 478.e1-478.e11- Clinical radiology 2022; 77: 436e442

EP-0163

Head-to-head comparison of 18F-FDG and 68Ga-DOTA-FAPI PET/CT for staging and therapeutic evaluation of esophageal cancer

W. Hou, *R. Tian;*
West China Hospital, Sichuan University, Chengdu, CHINA.

Aim/Introduction: Precise staging and therapeutic evaluation are essential for the management and preoperative evaluation of esophageal cancer. We aimed to compare the value of ^{68}Ga-FAPI and ^{18}F-FDG PET/CT for the detection of lesions and therapeutic evaluation of esophageal cancer. ***Materials and Methods:*** Thirty-seven patients with pathologically proven advanced esophageal cancer were enrolled from February 2022 to December 2022. ^{18}F-FDG and ^{68}Ga-FAPI PET/CT were obtained within 1 week for treatment evaluation and preoperative evaluation. Treatment strategies, SUVmax, TBR, and therapeutic evaluation were recorded. A paired Wilcoxon signed-rank test was used to compare differences between two scans. Sensitivity, specificity, PPV, NPV, and accuracy were also evaluated. ***Results:*** Among the enrolled patients, all primary lesions (100%) showed significant uptake in two scans. TBR (4.29-7.05, 5.93 vs. 14.66-23.49, 14.66, P<0.001), but not SUVmax (12.21-18.00, 15.19 vs. 13.83-19.58, 16.17, P=0.792), of FAPI was significantly higher than that of FDG in primary lesions. As for regional lymph nodes, FDG showed more lymph nodes than FAPI (0-1.5, 1 vs. 0-1,1, P=0.002). Finally, 19 (51.4%) patients underwent surgeries, and 10 patients achieved primary pathological complete response, among which 8 patients achieved pathological complete response. Compared with FDG, FAPI PET presented a higher sensitivity but a lower accuracy for residual primary tumor detection (88.89% vs. 66.67% and 56.67% vs. 38.89%, respectively). Additionally, FAPI PET showed higher sensitivity and accuracy than FDG PET (50.00% vs. 25.00% and 50.00% vs. 25.00%, respectively) for lymph node metastasis. ***Conclusion:*** Both FDG and FAPI can show the primary lesions of

esophageal cancer, but FDG can show more lymph nodes. As for therapeutic evaluation, FDG is superior to FAPI in residual primary tumor detection, but inferior to FAPI in evaluating lymph node metastasis.

EP-0164

Comparison of 3D Voxel-Based Yttrium-90 Dosimetry Quantification of using Y90 PET/CT Versus Y90 SPECT/CT

N. Kokabi[1,2], *M. Xing*[3], *D. Brandon*[2], *H. Dabbous*[2], *J. R. Galt*[4], *I. Sethi*[2], *S. Kappadath*[5], *A. Villalobos*[1], *D. M. Schuster*[2];
[1]*University of North Carolina School of Medicine, Chapel Hill, NC, UNITED STATES OF AMERICA,* [2]*Emory University School of Medicine, Atlanta, GA, UNITED STATES OF AMERICA,* [3]*University of North Carolina School of Public Health, Chapel Hill, NC, UNITED STATES OF AMERICA,* [4]*Emory University School of Medicine, Atalnta, GA, UNITED STATES OF AMERICA,* [5]*MD Anderson Cancer Center, Houston, TX, UNITED STATES OF AMERICA.*

Aim/Introduction: Post-Y90 dosimetry analysis has been used to ensure delivery of tumoricidal dose. However, there are fundamental differences in quantification of Y90 dose using positron emission tomography (PET)/computed tomography (CT) versus single-photon emission computed tomography (SPECT)/CT. The aim of this study was to further investigate these differences and identity potential correlations between these quantitative methods. ***Materials and Methods:*** In a prospective single-center clinical trial with the primary aim of evaluating the feasibility of scout activity for resin-based Y90 for treatment planning (NCT04172714) (1), patients with treatment naïve HCC were recruited. A secondary aim of the study was to evaluate dosimetry differences between Y90 PET/CT and Y90 SPECT/CT. All patients underwent both PET and SPECT after scout and therapeutic resin-based Y90. 3D voxel-based dosimetry for the targeted tumors and the perfused liver segment/lobe was performed with MIM Sureplan® (MIM Software, Cleveland, OH, USA) using cumulative scout and therapeutic activities. Paired t-tests were used compare matched dosimetry variables. Pearson linear correlations between corresponding parameters calculated by PET and SPECT were also performed. All statistical analyses were performed using SPSS v.28 (IBM, Armonk, NY, USA). ***Results:*** Overall, N=30 patients with 33 tumors were treated. Calculated mean tumor dose (TD) was significantly higher on PET compared to SPECT/CT (493 Gy vs. 366 Gy) p<0.001). Similarly, minimum TD (197 Gy vs. 179 Gy), maximum TD (966 Gy. 591 Gy), mean tumor dose to top 30% (TD-V30) (594 Gy vs. 408 Gy), and 70% (TD-V70) of tumor volume (405 Gy vs. 326 Gy) were significantly higher on PET/CT versus SPECT/CT (p-values<0.001). Moreover, there was a strong linear correlation between corresponding tumor dose variables on PET/CT and SPECT/CT (r coefficients>0.9; p-values<0.001). Conversely, mean non-tumoral liver dose (NTLD) was significantly higher on Y90 SPECT/CT vs. PET/CT (181 Gy vs. 103 Gy; p<0.001). Similarly, minimum, maximum, V-30 and V-70 NTLD were higher on SPECT versus PET, although only statistically significant for V-70 (p<0.001). There was also a strong linear correlation between mean NTLD on SPECT/CT vs. PET/ CT (r=0.9; p<0.001). ***Conclusion:*** PET/CT and SPECT/CT demonstrated significant differences in Y90 dose quantification. Specifically, tumor doses were observed to be higher on Y90 PET/CT than on Y90 SPECT/CT, while non-tumoral liver doses were observed to be lower on Y90 PET/CT than on Y90 SPECT/CT. Further investigation on post-Y90 PET/CT and SPECT/CT thresholds is warranted to ensure optimal treatment response. ***References:*** 1. Kokabi et al. JVIR. 2022.

EP-0165

2-[18F]FDG PET/CT derived semi-quantitative parameters in predicting response to chemoradiation in oesophageal squamous cell carcinoma

L. Lemos[1], *I. Lopo*[1], *P. Lapa*[1,2], *G. Costa*[1,2];
[1]*Nuclear Medicine Department, Centro Hospitalar e Universitário de Coimbra, Coimbra, PORTUGAL,* [2]*Faculdade de Medicina, Universidade de Coimbra, Coimbra, PORTUGAL.*

Aim/Introduction: Oesophageal squamous cell carcinoma has been shown to display high response rates to chemoradiation therapy (CRT), which has become a mainstay of the management of locally advanced cancers. 2-[^{18}F]FDG is extensively used in staging and response assessment of this cancer. This study aims to assess if 2-[^{18}F]FDG PET/CT derived semi-quantitative parameters at initial staging can help predict response to CRT, improving patient stratification. ***Materials and Methods:*** We retrospectively reviewed 885 studies of patients with oesophageal cancer who underwent 2-[^{18}F]FDG PET/CT in our department between January/2013-March/2023. Of these studies, we selected those with histology-proven squamous cell carcinoma who underwent neoadjuvant or definitive chemoradiation therapy and whose staging and response assessment studies were done in the same PET/CT scanner. For each staging study, semi-automatic tumour volumes of interest (VOI) were defined using an SUV threshold of 2.5g/ml, and SUVmax, SUVmean, SUVpeak, metabolically active tumour volume (MTV) and total lesion glycolysis (TLG) were extracted. Response to CRT was defined as a decrease of 30% or greater of SUVmax in the known lesions and the appearance of no new lesions in the post-therapy scans. Demographical and histological data were also collected. ***Results:*** Fifty-six patients fulfilled inclusion criteria, 87.5% of which were male, with an average age of 63.8±9.53 (39-88) years. Median FDG-PET/CT derived metrics were as follows: SUVmax 15.26 (IQR 11.28-19.63); SUVpeak 11.24 (IQR 8.78-15.55); SUVmean 5.83 (IQR 4.85-6.68); MTV 29.48 cm^3 (IQR 17.56-46.12); TLG 155.83 (IQR 89.98-318.52). The mean time between the completion of CRT and the response assessment PET/CT was 46.7±15.97 (4-90) days. Eighty-two per cent responded to CRT, whereas 18% showed no response or displayed progressive disease. Only MTV showed statistically significant differences between responders and non-responders (Mann-Whitney U, p=0.049). MTV was also the only parameter differentiating responders from non-responders (AUC 0.700, p=0.049). An MTV cut-off value of 41.1 cm^3 was able to predict the absence of response with 80% sensitivity, 76% specificity and 95% negative predictive value. However, although response in the post-chemoradiation study was associated with a higher overall survival (p=0.036), no differences in survival were found for this MTV cut-off value (p=0.070). ***Conclusion:*** In this study, 2-[^{18}F]FDG PET/CT-derived MTV at initial staging accurately predicted the response to chemoradiation therapy in squamous cell carcinoma of the oesophagus.

EP-0166

Role of whole-body FDG PET/CT in the detection of peritoneal metastases in cases of gastroesophageal junction adenocarcinoma

S. Thakur, *N. Purandare, V. Rangarajan, A. Agrawal, S. Shah, A. Puranik, C. Pramesh, G. Karimundackal, K. Prabhash, S. Jinwani, D. Niyogi, R. Kumar;*
Tata Memorial Hospital, Mumbai, INDIA.

Aim/Introduction: In this study, our aim was to evaluate the diagnostic role of 18-Flouride (18F) Flourodeoxyglucose (FDG) Positron Emission Tomography/Computed Tomography (PET/CT) for the detection of peritoneal metastases in cases of Sieverts III Gastroesophageal Junction Adenocarcinoma. To

study the relations of standardised uptake value (SUV), total lesional glycolysis (TLG), metabolic tumour volume (MTV), and FDG PET-positive nodal disease with the occurrence of peritoneal disease. And to assess the incremental value of FDG PET/CT over CT. ***Materials and Methods:*** This was a single institution, institutional review board (IRB) approved retrospective study with a study population of biopsy-proven Sieverts III gastroesophageal junction adenocarcinoma patients who were non-metastatic on initial work-up and who underwent diagnostic staging laparoscopy. There were a total of 86 cases with proven gastroesophageal junction adenocarcinomas who had undergone FDG PET CT for pretreatment initial staging. The peritoneal metastases detected on [18F]FDG-PET/CT were compared with the gold standard staging laparoscopy. Sensitivity, specificity, positive predictive value, and negative predictive value calculated using a 2x2 table were used to assess the diagnostic role of FDG PET/CT for the detection of peritoneal metastases. Logistic regression was used to identify factors related to the presence or absence of peritoneal metastases. ***Results:*** Sensitivity: 45%Specificity: 93.94%Positive Predictive value:69.23%Negative Predictive value: 84.93%Accuracy:82.56% Logistic regression showed that SUVmax Primary, TLG, MTV, and SUV Max nodes had no significant effect on the presence or absence of peritoneal metastases.Only one out of nine true positive cases showed isolated PET-positive findings, indicating no incremental benefit of PET/CT over CT. ***Conclusion:*** PET/CT has limited sensitivity but good specificity for the detection of peritoneal metastases in cases of adenocarcinoma of the gastroesophageal junction. The limited sensitivity and PPV make it a less appropriate tool for screening of peritoneal metastases and thus have a limited role in the detection of peritoneal metastases in initial staging. There is no incremental benefit of PET/CT over CT for the detection of peritoneal metastases. The metabolic parameters of PET/CT showed no relation to the occurrence of peritoneal disease.

EP-0167

18F-AlF-NOTA-FAPI PET/CT in the evaluation of gastric, liver, and pancreatic cancer and comparison with 18F-FDG PET/CT

w. xu, *J. Cai, Y. Pang, L. Sun, H. Chen;*
Department of Nuclear Medicine & Minnan PET Center, Xiamen Cancer Center, The First Affiliated Hospital of Xiamen University, School of Medicine, Xiamen University, Xiamen, China, xiamen, CHINA.

Aim/Introduction: Previous studies have reported the use of ^{68}Ga-labeled FAPIs for imaging of various types of cancer, but reports of ^{18}F-labeled FAPIs are limited. we aimed to investigate the diagnostic accuracy of ^{18}F-AlF-NOTA-FAPI PET/CT in gastric, liver, and pancreatic cancer, and compared the results with those of ^{18}F-FDG PET/CT. ***Materials and Methods:*** This study was approved by the Institutional Review Board and was registed at ClinicalTrials.gov (NCT05430841). Patients with confirmed gastric, liver, and pancreatic malignancies who underwent concurrent ^{18}F-FDG and ^{18}F-AlF-NOTA-FAPI PET/CT between July 2022 and January 2023 were retrospectively analyzed. The PET/CT findings were confirmed by histopathology or radiographic follow-up. ^{18}F-FDG and ^{18}F-AlF-NOTA-FAPI uptakes and tumor-to-background ratios were compared using the Wilcoxon signed-rank test. McNemar's test was used to compare the diagnostic accuracy between the two scans. ***Results:*** Our cohort consisted of 112 participants, including 49 patients with gastric cancer, 39 with liver cancer, and 24 with pancreatic cancer. ^{18}F-AlF-NOTA-FAPI PET/CT with a dose of 151.7-222 MBq demonstrated satisfactory image quality and lesion detectability. Regarding the lesion-based diagnostic accuracy, ^{18}F-AlF-NOTA-FAPI PET/CT showed higher sensitivity than ^{18}F-FDG in detecting primary tumor (96% [66/69] vs. 78% [54/69]), local recurrence (92% [23/25] vs. 56% [14/25]), involved lymph nodes (61% [140/230] vs. 38% [88/230]), bone and visceral metastases (98% [350/358] vs. 47% [168/358]) (all $p < 0.05$). Compared with ^{18}F-FDG, ^{18}F-AlF-NOTA-FAPI PET/CT upstaged 17 patients' TNM staging among all treatment-naïve patients (17/69, 25%). ***Conclusion:*** ^{18}F-AlF-NOTA-FAPI PET/CT is superior to ^{18}F-FDG PET/CT for detecting primary tumors, local recurrence, lymph nodes, bone and visceral metastases in gastric, pancreatic, and liver cancers, with higher uptake in most primary and metastatic lesions.

EP-0168

Diagnostic Efficiency of F-18 Fluorodeoxyglucose Positron Emission Tomography/Computed Tomography in Malignant Biliary Obstruction

Z. Koç[1], *P. Özcan*[1], *E. Reyhan*[2], *M. Yaldız*[3], *E. Üçbilek*[4];
[1]*Mersin University Hospital Nuclear Medicine Dpt., Mersin, TÜRKIYE,* [2]*Mersin University Hospital Surgical Oncology Dpt., Mersin, TÜRKIYE,* [3]*Mersin University Hospital Pathology Dpt., Mersin, TÜRKIYE,* [4]*Mersin University Hospital Gastroenterology Dpt., Mersin, TÜRKIYE.*

Aim/Introduction: Malignant Biliary Obstruction is a diagnostic challenge as it leads the patients to a process that ends up with futile surgical procedure (1). The primary lesion might most of the times be so subtle that the morphological imaging methods cannot depict (2). Thus functional cross sectional imaging by means of F-18 FDG PET/CT has clear advantage of high lesion/nonlesion contrast. However there is limited number of studies in this field (3). The aim was to determine the role of F-18 FDG PET/CT in the diagnosis of Malignant Biliary Obstruction. ***Materials and Methods:*** 45 patients (25 M, 20 F; mean: 64 years) with suspicion of malignant biliary obstruction were included in the study. Retrospective evaluation of the patients F-18 FDG PET/CT images compared to surgery and pathology results were performed. The area under curve and ROC analysis was obtained as a result. ***Results:*** The mean primary tumor lesion size was 29,8 mm and the SUVmax level was 13,7. 31 patients that had additional metastatic site with mean SUVmax level of 11,0. Pathological diagnosis was obtained in 31 patients which are malignant in 29. Five of the patients died during the disease course. The cut off level that was obtained from the ROC curves was 7.5 for SUVmax but not significant (p=0.2636) (Graph 1) (Table 1). Although the sensitivity and specificity levels were not high the imaging resulted in the clear advantage of pointing out correct diagnostic sampling site. ***Conclusion:*** F-18 FDG PET/CT guided surgical resections/interventions and management revealed high rate of successful diagnostic procedures. These results are encouraging for the determination of Malignant Biliary Obstruction by means of F-18 FDG PET/CT. ***References:*** 1. Khan SA, Davidson BR, Goldin RD, Heaton N, Karani J, Pereira SP, et al. Guidelines for the diagnosis and treatment of cholangiocarcinoma: an update. Gut 2012;61:1657-1669. 2. Schulick RD.Primary sclerosing cholangitis: detection of cancer in strictures. J Gastrointest Surg. 2008 Mar;12(3):420-2. 3. Wang SB, Wu HB, Wang QS, Zhou WL, Tian Y, Ji YH, Lv L. 18F-FDG PET/CT in differentiating malignant from benign origins of obstructive jaundice. Hepatobiliary Pancreat Dis Int. 2015 Oct;14(5):516-22.

EP-0169

Caracterization of pancreatic lessions by PETMR and evaluation of the diagnostic efficacy of this technique correlated to anatomopathological findings

C. A. Field Galán, *L. Delgado Niño, I. Plaza de las Heras, R. de Teresa Herrera, P. Recarte Ortega, L. García Cañamaque; HM Hospitales Madrid, Madrid, SPAIN.*

Aim/Introduction: Patient analysis with 18FFDG PETMR as an initial study of pancreatic lesions by comparing the findings of different image tests, morphologic and metabolic, correlating histological results of fine-needle (PAAF) puncturing of the lesion by means of echoendoscopy and/or anatomopathological analysis with SUV value. ***Materials and Methods:*** From 11-2014 until 12-2019 a retrospective analysis was carried out in 152 patients with pancreatic lesions, exclusión criteria patients with an initial study other than PET-MR and with metástasis. PETMR was required as an initial staging study for the presence of one or more pancreatic lesions detected in other diagnostic test. Studies were carried out in Siemens BiographmMR, FDG iv dose 296 +/- 37MBq. Fasting 4-6h, glucemia control levels <200mg/dl and resting 45min +/- 10 minutes prior acquisition.A localized pancreatic MR study was performed in all patients (sequences T2 sagittal, HD coronal and axial, diffusion, T1 axial, T1axial FS, T1 dynamic axial) and a complete whole body post-iv contrast study with simultaneous acquisition of 4 minute PET beds, sequences T2 HASTE and T1 VIBE. Imaging analysis was carried out jointly by a nuclear medicine specialist and a radiologist. The anatomopathological result (AP) was checked of both echo-endoscopy PAAF and the surgical piece of those patients who had undergone surgery. ***Results:*** PETMR study gave the following results and correlated the SUVmax of PET and MR findings with the presurgical hystology. Correlation SUVmax of the152 patients with presurgical histology was: 79 adenocarcinoma: media SUVmax: 6,6 (range 0-15,5)22 TNEp: media SUVmax:1,68 (0-8,39).26 TPMI media SUVmax 2,81(0-11,4). 9 atypia media SUVmax: 2,70 (0-13,5) 6cysts:media SUVmax: 0,48 (rango 0-3,8)2 cystoadenoma seroso: media SUVmax: 1,98 (0-3,96) 8 negative: media SUVmax: 1,60 (0-5,47) Results of the79 histologicaly confirmed adenocarcinomas 94% (74/79) MR suggestive of adenocarcinoma.84% (66/79) sugestive by PET(SUVmax).Of the NET 50% (11/22) sugestive by MR 59% (13/22) suggestive of G1NET by PET 100% concordancy with AP. 27% (6/22) NET G2/G3 by PET positive100% concordant with AP. 10% (2/22) not concordant with PET (highSUVmax): 2 NET low grade with avidity for FDG.2 serous cystadenomas confirmed by AP:1 suspiciousby PET and MR. 26 TMPI confirmedby AP. 42% (11/26) suggestiveby MR 54% (14/26) by PET. 6 pancreatic cysts confirmedby AP 67% (4/6) suggestive by MR.100% suggestive by PET .17 patients left were non conclusive. ***Conclusion:*** The use of PETMR increased diagnostic efficacy in caracterizing pancreatic lessions when correlating with anatomopathological findings.

EP-0170

Diagnostic Value of Integrated PET/MR in Postoperative Recurrence of Liver Cancer

X. Chenjie;
Hangzhou Universal Medical Imaging Diagnostic Center, hangzhou, CHINA.

Aim/Introduction: Compare the diagnostic value of 18F-FDG PET/MR and PET/CT in postoperative recurrence of liver cancer. ***Materials and Methods:*** Retrospective analysis of 92 patients with suspected recurrence of liver cancer, systemic 18F-FDG PET/CT examination and upper abdominal PET/MRI scan were retrospectively analyzed. Taking pathological results and clinical diagnosis as the gold standard, the image quality of PET/CT and PET/MRI was compared. Diagnostic efficiency. ***Results:*** A total of 43 patients relapsed. The sensitivity, specificity and accuracy of PET/CT are 45.15%, 90.45% and 78.38% respectively; the sensitivity, specificity and accuracy of PET/MRI are 100%, 84.61% and 94.59% respectively, and the diagnostic accuracy is significantly higher than that of PET/CT (P). <0.05). There were 15 cases of CT and PET image misalignment in PET/CT, the fusion of PET/MR images was accurate, and there were significant statistical differences between the two sides (P<0.05). A total of 25 cases of liver cancer invaded the biliary tract, 16 cases had bile duct obstruction with obstructive jaundice, 10 cases of PET/CT showed signs of obstruction, and PET/MR could clearly show that there were significant statistical differences between the two sides. In 25 cases, lymph node metastasis occurred, both of which can be clearly displayed. 20 cases of vascular invasion occurred, of which 14 invaded the portal vein or lower vena cava, which can be clearly distinguished by both devices; another 12 cases invaded abdominal trunk, superior mesenteric artery, splenic blood vessels, superior mesenteric veins, etc. PET/MR clearly diagnosed 8 cases than PET/CT, with significant statistical differences (P<0 .05). In 15 cases of invasion of lung, bone, adrenal gland, brain and other organs, PET/MR was more clearly diagnosed than PET/CT, with significant statistical differences (P<0.05). ***Conclusion:*** The sensitivity, specificity and accuracy of PET/MRI in diagnosing recurrence after liver cancer are higher than PET/CT. The image ratio is more accurate, which can better judge biliary metastasis, lymph node metastasis, peripheral structure and other organ invasion.

EP-0171

Prospective Intra-individual comparison of 68Ga-FAPI and 18F-FDG PET/CT in the diagnosis and staging of gastric malignancies

M. Jayanthi, *S. BATCHU, A. Sekaran, G. VENKAT RAO, N. Duvvur; AIG Hospitals, Hyderabad, INDIA.*

Aim/Introduction: Studies have shown a wide range of sensitivity and specificity for 18F-FDG PET/CT in gastric adenocarcinomas because of some limitations, including physiological uptake in the stomach wall, uptake due to gastritis, early gastric cancers, inherent low metabolic activity of certain histologic types like non-intestinal diffuse type, mucinous carcinoma, poorly differentiated and signet-ring cells carcinomas. In this study, we aimed to evaluate the diagnostic accuracy of 68Ga-FAPI PET/CT and 18F-FDG PET/CT in lesion based comparison for primary lesion, loco-regional disease and distant organ metastases of primary gastric adenocarcinomas ***Materials and Methods:*** We performed an intra-individual prospective comparison of 68Ga-FAPI and 18F-FDG PET/CT in 47 patients with suspected or proven gastric adenocarcinoma who presented for either diagnosis (n=9) or initial staging (n=38) of disease. Lesion detection and SUVmax were compared between the two radiotracers and are compared with the histopathologic results and/or follow up imaging, which was used as the reference standard ***Results:*** Total of 47 patients were analyzed of which 9 were referred for the purpose of diagnosis and 38 for the staging purpose. 68Ga-FAPI PET/CT showed higher SUVmax and higher sensitivity in detection / evaluation of primary tumors, particularly in early gastric malignancies. Also 68Ga-FAPI PET/CT has higher negative predictive value in the background of chronic gastritis or polypoidal disease. Absence of 68Ga-FAPI tracer uptake is consistent with absence of malignant cells in the

multiple repeated histopathology results.68Ga-FAPI PET/CT study detected lymph nodal disease, liver, peritoneal, lung and skeletal metastases with higher sensitivity and confidence intervals for the SUVmax values of two radiotracers in identifying these lesions showed that the difference is statistically significant. ***Conclusion:*** Compared with 18F-FDG PET/CT, 68Ga-FAPI PET/CT showed higher sensitivity in detection of primary lesions due to very low background uptake, absence of physiological or inflammatory uptake in the stomach. Also, 68Ga-FAPI PET/CT significantly outperformed 18F-FDG PET/CT in detection of loco-regional disease and distant organ metastases in lesion based comparison resulting in upstaging in 26% of patients

EP-0172

The value of 18F-FDG PET/MR radiomics features in predicting regenerative nodules (RN), dysplastic nodules (DN) and small hepatocellular carcinoma nodules (sHCC) in cirrhosis

Y. Xu;
Hangzhou Universal Medical Imaging Diagnostic Center, Hangzhou, CHINA.

Aim/Introduction: To explore the value of 18F-FDG PET/MR radiomics features in predicting regenerative nodules (RN), dysplastic nodules (DN) and small hepatocellular carcinoma (sHCC) in cirrhosis. ***Materials and Methods:*** The clinical data and PET/MR imaging data of 256 patients with liver cirrhosis were collected, including 88 cases of RN, 76 cases of DN and 92 cases of sHCC. Pathological and clinical diagnosis results serve as the gold standard for diagnosis. We used AK software to extract the most relevant imageomics features for tumor classification, and randomly divided the two groups of images into training set (70%) and test set (30%). The maximum correlation and minimum redundancy (mRMR) and minimum absolute shrinkage and selection operator (LASSO) methods were used to select features from 2200 features extracted from MR and PET, and finally eight best features were retained. Multivariate logistic regression analysis was performed using the radiomics features and clinical variables to establish the prediction model. The receiver operating characteristic (ROC) analysis is used to evaluate the prediction model. ***Results:*** The established PET/MR imaging features have good prediction efficiency for the recognition of RN, DN and sHCC, and there are significant differences. The AUC of the training group and the validation group were 0.898 (95% CI: 0.756-0.961), 0.872 (95% CI: 0.773 - 0.985) and 0.915 (95% CI: 0.788 - 0.979), respectively. ***Conclusion:*** The prediction model of PET/MR radiomics features can be used as an auxiliary method to predict regenerative nodules (RN), dysplastic nodules (DN) and small hepatocellular carcinoma nodules (sHCC) in cirrhosis. It can also provide objective basis for accurate clinical diagnosis and individualized treatment, and has important guiding significance for clinical treatment.

EP-0173

The Detection Value of 18F-FDG PET/MR for Small Hepatocellular Carcinoma

X. Chenjie;
Hangzhou Universal Medical Imaging Diagnostic Center, hangzhou, CHINA.

Aim/Introduction: To explore the value of 18F-FDG PET/MR systemic imaging in the detection of small hepatocellular carcinoma and the formulation of treatment plans. ***Materials and Methods:*** Retrospective analysis of PET/MR and PET/CT imaging of 89 patients with small hepatocellular carcinoma before treatment. On the same day, whole body 18F-FDG PET/CT imaging and PET/MR imaging were performed. Taking pathological and clinical diagnosis as the gold standard, the differences in detection rates and treatment plans of small hepatocellular carcinoma were compared. ***Results:*** 89 patients with small liver cancer, a total of 98 small liver cancer lesions, PET/MR detected all lesions, 90 correct diagnosis, PET/CT detected 43 lesions, 31 correct diagnosis, with significant statistical differences (P<0.01). Among them, 20 lesions were PET-MR positive, while PET-CT was negative; another 36 lesions were negative for both equipment PET intake. Compared with PET/CT, PET/MR changed the diagnosis results of 45 (50.6%) patients. ***Conclusion:*** PET/MR is of high value for the detection of small hepatocellular carcinoma, which is significantly better than PET/CT, but some small hepatocellular carcinoma still needs to enhance MR diagnosis.

EP-0174

Application value of 18F-FDG PET/MR in postoperative metastasis and restating of gastric cancer

S. Yun;
Hangzhou Panoramic Medical Imaging Diagnostic Center, Hangzhou, CHINA.

Aim/Introduction: To explore the value of 18F-FDG PET/MR systemic imaging in postoperative metastasis detection and restating of gastric cancer. ***Materials and Methods:*** The postoperative PET/MR and PET/CT imaging of 94 patients with gastric cancer were retrospectively analyzed. On the same day, whole body 18F-FDG PET/CT imaging and PET/MR imaging were performed, taking pathological and clinical diagnosis as the gold standard to compare the differences in the detection rate and restating of metastatic focal. ***Results:*** n 94 patients with gastric cancer surgery, 51 patients with distant metastases were found, with a total of 469 lesions, including 210 lymph node metastasis, 35 peritoneal implant metastasis, 30 Intrahepatic metastasis, 11 intracerebral metastasis, 5 intrapulmonary metastasis and 178 bone metastasis. The detection rate of lymph node and intestinal implant metastasis between the two devices is consistent. PET/MR found 56 more lesions than PET/CT in 28 patients, with significant statistical differences ($\chi 2=28.86$, P<0.01); 20 of them were PET-MR positive, while PET-CT was negative, including 5 brain metastasis and 15 liver metastasis; in addition There were 36 lesions and both devices with negative PET intake, but MR was diagnosed with metastasis, including 4 brain metastasis, 5 liver metastasis and 27 bone metastasis. The detection rate of PET/MR for liver, brain and bone metastasis is significantly higher than that of PET/CT ($\chi 2=30.00$, 18.33, 29.22, P<0.01). PET/CT found 20 more lesions than PET/MR, with significant statistical differences, which are lung and peritoneal implant metastasis; of the 35 lung and peritoneal implant metastasis, 10 have obvious FDG intake, 22 lesions have no intake, and 3 lung metastases are positive for PET-MR, while P ET-CT is negative. Through PET/MR examination, a total of 15 patients changed the stage of PET/CT, with significant statistical differences ($\chi 2=16.30$, P<0.01). ***Conclusion:*** PET/MR is of high value for postoperative metastasis and restating of gastric cancer. The detection rate of craniocerebral, liver and bone metastasis is higher than that of PET/CT, and CT-assisted diagnosis is still needed for lung and peritoneal lesions.

EP-0175

Comparative analysis of early and late-phase of [18F] F-Fluorocholine PET/CT adquisition in the assessment of hepatocellular carcinoma

D. Rivas-Navas, *J. Fernández-Fernández, E. Triviño-Ibáñez, J. Villa-Palacios, A. Rodríguez-Fernández;*
Hospital Universitario Virgen de las Nieves, Granada, SPAIN.

Aim/Introduction: The aim of this work is to analyze the differences observed between early and late-phase of [^{18}F]F-fluorocholine PET/CT (FCH-PET/CT) acquisition in hepatocellular carcinoma (HCC). ***Materials and Methods:*** We performed a longitudinal, retrospective observational study that included HCC patients who underwent FCH-PET/CT study with early (15 minutes) and late-phase (60 minutes) acquisitions from January 2017 to December 2022. FCH-PET/CT images were analyzed visually and semi-quantitatively, including SUL, MTB (MTVxSUVmean), and SUVratio (SUVmax/SUVliver) parameters. The intensity of uptake, signal-to-background ratio, and quantification parameters were compared between early and late acquisition. ***Results:*** Forty patients were included (mean age: 59.50±10.99 years, 90% male). FCH-PET/CT was positive in 32/40 patients (80%). All findings were visualized in both early and late-phase acquisitions. In the visual analysis, 16/32 (50%) showed higher uptake intensity and/or signal-to-background ratio in early-phase images, while the remaining 50% showed better visualization in late-phase images. The comparative analysis of quantification parameters showed significant differences between early and late-phase acquisitions: SULmax (13.70±3.09 vs. 15.39±3.20, p<0.001), SULpeak (10.19±2.44 vs. 11.17±2.48, p<0.001), SULmean (7.32±1.74 vs. 8.09±1.76, p<0.001) and SULmax of healthy liver (7.81±1.59 vs. 8.94±1.65, p<0.001). ***Conclusion:*** In the assessment of HCC, early and late-phase of FCH-PET/CT acquisition, while showing no significant differences in visual analysis, have significantly higher quantification parameters in late-phase acquisition.

EP-0176

Impact of [18F]F-Fluorocholine PET/CT in the management and prognosis of hepatocellular carcinoma.

D. Rivas-Navas, *J. Fernández-Fernández, E. Triviño-Ibáñez, J. Villa-Palacios, A. Rodríguez-Fernández;*
Hospital Universitario Virgen de las Nieves, Granada, SPAIN.

Aim/Introduction: The aim of this work is to evaluate the clinical impact of [^{18}F]F-fluorocholine PET/CT (FCH-PET/CT) in the management of hepatocellular carcinoma (HCC) and to analyze the prognostic value of quantification parameters. ***Materials and Methods:*** We performed an observational and retrospective study that included patients with HCC who underwent an FCH-PET/CT study between January 2017 and December 2022. Clinical, biochemical, imaging, and treatment parameters were collected. FCH-PET/CT images were analyzed visually and semiquantitatively, including SUL, MTV, TLG, MTB (MTVxSUVmean), and SUVratio (SUVmax/SUVliver) parameters. The impact of the results on the classification on the Barcelona Clinical Liver Cancer (BCLC) and therapeutic approach were analyzed. Finally, a regression model was adjusted to identify predictors of survival (overall survival [OS] and progression-free survival [PFS]). ***Results:*** Fourty patients were included (mean age: 59.50±10.99 years, 90% men). Ninety percent had cirrhosis, with alcoholic etiology in 45% of cases, and BCLC stage: 0 in 5%, A in 37.5%, B in 25%, and C in 30%. FCH-PET/CT was positive in 33/40 (82.5%) patients, detecting the presence of new lesions in 10/40 (25%) cases. It modified the initial therapeutic approach in 4/40 (10%) patients. 9/40 (22.5%) patients died, with BCLC stage (p=0.04) and MTV (p=0.030), TLG (p=0.014), and MTB (MTB (p=0.014) parameters being significantly associated with mortality. The median PFS was 29.0 months, and the median OS was 34.9 months. Cox regression for PFS showed that BCLC stages (HR=12.76; p<0.01) and MTV>150 (HR=6.14; p=0.032) were independently associated factors with PFS. ***Conclusion:*** FCH-PET/CT is a promising approach in identifying patients with HCC with a worse prognosis, MTV along with BCLC classification being the main factor related to the probability of tumour progression.

EP-0177

The prediction value of metabolic parameters of 18F-FDG PET/CT for risk stratification of hypermetabolic gastrointestinal stromal tumors

L. Zhang, *W. Cao, Y. Ding, Y. Liu, Y. Deng, H. Chen;*
Department of Nuclear Medicine, Union Hospital, Tongji Medical College, Huazhong University of Science and Technology, Wuhan, CHINA.

Aim/Introduction: Most high-risk gastrointestinal stromal tumors (GISTs) are positive uptake of ^{18}F-FDG. However, some of the GISTs with hypermetabolism are non-high risk based on surgical pathology after curative resection, and hypermetabolic GIST accompanying necrosis and hemorrhage tend to have significant heterogeneity. This study aimed to evaluate the value of various metabolic parameters of ^{18}F-FDG PET/CT for predicting the risk stratification for hypermetabolic GIST. ***Materials and Methods:*** We retrospectively analyzed 42 hypermetabolic GIST patients who underwent ^{18}F-FDG PET/CT before curative resection as initial treatment at two centers from 2010 to 2023. Intratumoral-metabolic heterogeneity (heterogeneity index, [HI] and heterogeneity factor, [HF]) and conventional metabolic parameters (standardized uptake value [SUV], metabolic tumor volume [MTV], and total lesion glycolysis [TLG]) of the lesions were determined. MTV and TLG were calculated based on fixed threshold of SUV_{max} at 2.5-3.5, and percentage threshold of SUVmax at 40%-60%. HI = SUVmax/SUVmean and HF was the absolute value of linear regression slope calculated by the least square method from the different thresholds of the ROI (HF1: fixed threshold of SUVmax; HF2: percentage threshold of SUVmax). GISTs were divided into non-high-risk group and high-risk group. The area under the curve (AUC) was used to evaluate the predictive ability of factors for risk stratification. ***Results:*** This study included 42 patients with GIST in hypermetabolism of the ^{18}F-FDG PET/CT (SUV_{max} > 3.5), including 20 (47.6%) patients with non-high-risk and 22 (52.4%) patients with high-risk. Location, maximum tumor diameter, mitotic count, Pathological features (necrosis or hemorrhage), MTV (2.5, 3.0, 3.5), TLG (2.5, 3.0, 3.5), HI (2.5, 3.0, 3.5), HF1, MTV (40%, 50%, 60%), TLG (40%, 50%, 60%) and HF2 in the high-risk group were significantly higher than those in the non-high-risk group (all P<0.05). To construct the preoperative prediction model, location, maximum tumor diameter, and metabolic parameters (MTV3.0, TLG2.5, HI3.0, HF1) were chosen for logistic regression analyses. In multivariate logistic regression analyses, MTV3.0 (P=0.025, OR: 17.34), location (P=0.05, OR:7.09), and maximum tumor diameter (P=0.029, OR=9.07) were independently correlated with risk stratification. The AUC of the mathematical model of MTV3.0 + location+ maximum tumor diameter was 0.926 compare to the AUC of MTV3.0 was 0.805 (P<0.05). ***Conclusion:*** Various metabolic parameters derived from ^{18}F-FDG PET/CT were higher in high-risk GIST. MTV3.0, location and maximum tumor diameter were independent risk factors for risk stratification, and the mathematical model could predict risk stratification more effectively for patients with hypermetabolic GIST preoperatively.

EP-0178

Prospective study of the diagnostic value of 68Ga-FAPI-04 PET/CT for gallbladder cancer: comparison with 18F-FDG

L. Liu, *Y. Huang, Q. Liu, D. Xu;*
The Second Affiliated Hospital of Chengdu Medical College (China National Nuclear Corporation 416 Hospital), Chengdu, CHINA.

Aim/Introduction: ^{18}F-fluorodeoxyglucose (FDG) PET/CT may sometimes not be the best choice for imaging tumors of the digestive system. In contrast, the recently developed tracer ^{68}Ga-FAPI-04, which targets fibroblast activation protein (FAP), has shown great potential in the evaluation of a wide range of tumors. Studies have indicated its promising alternative to ^{18}F-FDG in the evaluation of digestive system tumors particularly. The purpose of this study was to investigate the value of ^{68}Ga-FAPI-04 comparing with ^{18}F-FDG PET/CT in patients with gallbladder cancer (GBC), including the ability to assess primary tumors, distant metastases, lymph nodes, and peritoneal metastases in patients with GBC and the impact on clinical staging management. ***Materials and Methods:*** This prospective study included 17 patients who underwent ultrasound or MRI and were considered to have primary GBC or recurrence after treatment. All patients underwent ^{68}Ga-FAPI-04 and ^{18}F-FDG PET/CT within one week. Final histopathology, imaging, and follow-up results were used as reference standards. Shapiro-Wilk assessment of normal distribution of continuous variables. The Wilcoxon-rank test was used to compare the difference in tumor/background organ ratio (TBR) values and maximum standardized uptake values (SUVmax) between ^{68}Ga-FAPI-04 and ^{18}F-FDG in primary tumors, distant, lymph nodes, and peritoneal metastases, Pearson was used for correlation analysis. ***Results:*** A total of 17 patients were included, of whom 13 patients with primary tumors of GBC were positive for ^{68}Ga-FAPI-04 (100% detection rate), while ^{18}F-FDG detected 12 of them (92% detection rate). ^{68}Ga-FAPI-04 was more sensitive than ^{18}F-FDG in detecting distant metastases (100% VS. 81%), lymph node metastases (99% VS. 94%) and peritoneal metastases (100% VS. 19%) of GBC. ^{68}Ga-FAPI-04 had higher SUVmax for distant metastases (9.34 ± 4.45 VS. 6.65 ± 3.41, $p < 0.001$) and lymph nodes (8.97 ± 3.63 VS. 6.86 ± 4.00, $p < 0.001$) than ^{18}F-FDG. There was no significant difference in the uptake of the two tracers in the primary tumors, but the TBR values were significantly higher in ^{68}Ga-FAPI-04 than in ^{18}F-FDG (18.24 ± 8.20 VS. 5.21 ± 3.29, $p = 0.001$). ^{68}Ga-FAPI-04 identified far more peritoneal metastases than ^{18}F-FDG. Finally, the staging of four patients was revised because of the^{68}Ga-FAPI-04 results. ***Conclusion:*** ^{68}Ga-FAPI-04 is more advantageous than ^{18}F-FDG in detecting primary tumors, distant metastases, lymph node metastases, and peritoneal metastases in GBC with higher SUVmax and TBR. ^{68}Ga-FAPI-04 is more promising for staging of GBC.

EP-0179

Impact Of FDG PET CT On Management Of Patients With Treatment Naive HCC Intended For Local Surgical/ Ablative Or Embolisational Therapies

M. SARMA, *B. S T, W. Jose;*
Amrita Institute of Medical Sciences and Research, Cochin, INDIA.

Aim/Introduction: 2-deoxy-2-[fluorine-18]fluoro-D-glucose (^{18}F-FDG) PET CT has shown mixed utility in the detection of primary Hepatocellular cancer (HCC) with sensitivities of around 55-64%. FDG PET CT is more useful in detection of regional and distant extrahepatic metastases. We intended to study the impact of FDG PET CT on those patients intended for local management of treatment naïve primary HCC (local surgeries/ablative or embolisational therapies). ***Materials and Methods:*** FDG PET CT scans of 61 consecutive patients of HCC acquired between 2010 and 2020 who were intended for local surgical/ablative or embolisational therapies were retrospectively reviewed to look for change in management following the findings in FDG PET scan. Data on initial plan, findings on FDG PET CT, subsequent management, change in management if any and the reason of change in management were collected. ***Results:*** There was overall change in management in 18 out of 61 patients (29%). Most of the patients plan changed to systemic therapy because of detection of metastatic lesions (10 out of 18 patients). 2 patients plan changed to palliative therapy. In 2 patients, TACE was done instead of surgery while in another 2 patients plan was changed to extended hepatectomy. In another 2 patients, the initial plan of surgery was dropped and patient was lost to subsequent management. Detection of distant metastases (7 out of 18 patients), portal vein involvement (4 out of 18), IVC thrombus (1 out of 18), lymphnodal metastases (2 out of 18) and other lobe of liver involvement (4 out of 18 patients) on FDG PET CT were the reasons leading to management changes. ***Conclusion:*** Inspite of its low sensitivity of detecting primary HCC, FDG PET can bring about change in management in patients intended for local surgeries/ablative or embolisational therapies .

EP-0180

Diagnostic role of FAPi PET/CT in the detection of peritoneal metastases in cases of stomach and gastroesophageal junction adenocarcinoma

S. Thakur, *V. Shukla, M. Manikandan, S. Arvind;*
Mahamana Pandit Madan Mohan Malviya Cancer Centre, Varanasi, INDIA.

Aim/Introduction: In this study, our aim was to evaluate the role of 18-flouride (18F) fibroblastic protein inhibitor (FAPi) Positron Emission Tomography/Computed Tomography (PET/CT) for the detection of peritoneal metastases in cases of gastric adenocarcinoma and Sieverts III gastroesophageal junction adenocarcinoma. ***Materials and Methods:*** This was a single institution retrospective study with a study population of biopsy-proven adenocarcinomas involving the stomach and gastroesophageal junction sent to us for baseline staging scans. There were a total of 90 histopathologically proven cases who had undergone FAPi PET/CT for pretreatment baseline evaluation. A composite gold standard of visual assessment of the peritoneum, either by staging laparoscopy or during gastrectomy or CT imaging findings, was taken for comparison of peritoneal metastases found on FAPi PET imaging. Sensitivity, specificity, positive predictive value, and negative predictive value calculated using a 2x2 table were used to assess the diagnostic role of FAPi PET/CT for the detection of peritoneal metastases. ***Results:*** True positives were defined as those that demonstrated a noticeably enhanced uptake of FAPi, tested positive during staging laparoscopy or surgery, or displayed obvious peritoneal metastasis characteristics on CT imaging. 39 of these were present. True negatives were defined as those with no substantial FAPi uptake, no imaging signs of peritoneal metastases on CT, and negative staging laparoscopy or surgical results for peritoneal metastases. These 44 examples were discovered. Seven patients were classified as false negatives because staging laparoscopy or surgery revealed peritoneal metastases even though there was no appreciable increase in FAPi uptake and no imaging abnormalities on CT. No cases that were positive

on FAPi PET and negative on staging laparoscopy, surgery, or CT and could be labelled as false positives were found. Sensitivity: 84.7%, Specificity: 100%, Positive Predictive Value: 100%, Negative Predictive Value: 86.2%, Accuracy: 92% ***Conclusion:*** For the detection of peritoneal metastases in patients of stomach cancer and Sievert III gastroesophageal junction adenocarcinoma, FAPi PET/CT offers good sensitivity and great specificity. With good sensitivity and excellent positive predictive value, it can prove to be a helpful tool for the screening of peritoneal metastases and, consequently, for the detection of peritoneal metastases in the baseline evaluation of adenocarcinoma of the stomach and gastroesophageal junction.

EP-0181

Role of 99mTc-Mebrofenin SPECT/CT in preoperative determination of global and segmental liver function

A. Bakos[1], *T. Czékus*[1], *I. Farkas*[1], *L. Libor*[2], *Z. Mikó*[1], *S. Nagy*[1], *R. Német*[1], *L. Pávics*[1], *G. Sipka*[1], *S. Urbán*[1], *M. Bukva*[3], *Z. Besenyi*[1];
[1]University of Szeged Nuclear Medicine Department, Szeged, HUNGARY, [2]University of Szeged Department of Surgery, Szeged, HUNGARY, [3]University of Szeged Department of Immunology, Szeged, HUNGARY.

Aim/Introduction: The resectability of primary and metastatic liver tumors depends on sufficient functional future liver remnant (FLR) after surgery. Insufficient residual liver remnant results post-hepatectomy liver failure (PHLF), which is the major cause of liver resection mortality. ^{99m}Tc-mebrofenin hepatobiliary scintigraphy has been demonstrated to predict PHLF. The dynamic ^{99m}Tc-HBS (hepatobiliary scintigraphy) with delayed SPECT imaging have limited accuracy of the study for segmental function. The aim of our study was to determine the role of dynamic SPECT/CT. ***Materials and Methods:*** 30 patients (18 males, 12 females, mean ages: 62 years, 24-83 years) were involved into the study based on the following criteria: extended liver resection is indicated, clinically proven compensated liver function (according to MELD score and ICG-R15), surgery is not contraindicated anesthetically. Dynamic SPECT imaging was performed for 60 minutes after intravenous administration of ^{99m}Tc-mebrofenin with 3.2 minutes data collection. Low-dose CT was performed in order to delineate liver segments and for attenuation corrected post processing. Counts were measured in each segmented VOI (liver, liver lobes, blood pool, total field of view) from each SPECT set, and three time-activity curves were generated. The most commonly used cutoff value for FLR filtration for predict PHLF: 2,69 %/min/m^2. If the FLR filtration was <2.69%/min/m^2, parenchyma modulation was performed, after that a control ^{99m}Tc-mebrofenin SPECT/CT examination was done. ***Results:*** In overall 30 patients the global liver filtration (mean: 5.74 %/min/m^2±2,44) significantly correlated with clinical score: MELD (r=0,43; p<0,01) and with ICG-R15 (r=0,38; p=0,05). In 19/30 patients the measured FLR filtration was sufficient (mean: 4,12 %/min/m^2± 1,01), in 11/30 patients the FLR filtration was insufficient (mean: 1.45±0,68 %/min/m^2). In these patients the FLR filtration increased significantly (mean: 3,84±1,94%/min/m^2, p<0,005) after parenchyma modulation. Ninety day- postoperative mortality was 10% (3/30). One patient died intraoperatively, 1 patient died because of Takotsubo-cardiomyopathy and one patient died because of surgical complication. ***Conclusion:*** The use of ^{99m}Tc-mebrofenin dynamic SPECT/CT plays an important role in the preoperative planning of extended liver resections to determine global and segmental liver function.

EP-0182

Diagnostic Performance of [18F]PSMA-1007 PET/CT on Hepatocellular Carcinoma: a Prospective Clinical Study

K. Michalski[1], *F. Reiter*[2], *A. Kosmala*[1], *P. E. Hartrampf*[1], *S. E. Serfling*[1], *T. A. Bley*[3], *A. Geier*[2], *A. K. Buck*[1], *R. A. Werner*[1], *A. Weich*[2];
[1]University hospital Würzburg - Department of Nuclear Medicine, Würzburg, GERMANY, [2]University hospital Würzburg - Internal Medicine II, Würzburg, GERMANY, [3]University hospital Würzburg - Department of Diagnostic and Interventional Radiology, Würzburg, GERMANY.

Aim/Introduction: A high expression of prostate-specific membrane antigen (PSMA) is not limited to prostate cancer but can be found on other tumor entities, such as hepatocellular carcinoma (HCC), and could possibly be used for theranostic purposes. Our aim was to investigate the diagnostic potential of the hepatobiliary excreted radiotracer [^{18}F]PSMA-1007 on initial staging of HCC. ***Materials and Methods:*** This is a preliminary analysis of an ongoing prospective clinical study (NCT05547919). Five patients with treatment-naïve, histopathological proven HCC underwent [^{18}F]PSMA-1007 positron emission tomography (PET) with an unenhanced low-dose computed tomography (CT). All scans were analyzed visually and quantitatively. We assessed SUVmax of the primary tumor and SUVmean of non-affected liver parenchyma and calculated tumor-to-background-ratios (=SUVmax HCC/SUVmean liver, TBR) for each patient. In addition, we correlated local PSMA-positive tumor volume (using a lesion based 50%-threshold approach) with the tumor volume as assessed with contrast-enhanced CT. Presence of local lymph node and distant metastases was noted for [^{18}F]PSMA-1007 PET/CT and compared to the results of contrast-enhanced CT of the trunk and magnetic resonance imaging of the upper abdomen. ***Results:*** All primary tumors showed visually a high tracer uptake, which was confirmed on quantitative analysis with a mean SUVmax 37.2 ± 13 (range: 25.2 - 55.5) and a mean TBR 6.1 ± 5.5 (range: 2.6 - 17). CT-based tumor volume in the liver (294.2 ml ± 353.8 ml; range: 8.6 - 856.4 ml) correlated significantly with PSMA-positive tumor volume (132,3 ml ± 131.4 ml; range: 1.1 - 325 ml; Pearson's r = 0.94, p = 0.0188). [^{18}F]PSMA-1007 PET/CT did not reveal new distant metastatic lesions compared to contrast enhanced CT. In one patient local lymph node metastases were considered PSMA-negative. ***Conclusion:*** [^{18}F]PSMA-1007 can be used for depiction of untreated HCC and shows a high TBR compared to unaffected liver parenchyma. These preliminary results need to be confirmed in further patients of this prospective study.

EP-0183

Gallium-68 Prostate-Specific Membrane Antigen (68Ga-PSMA) PET Metabolic Metrics in Patients with Hepatocellular carcinoma with and without Hepatis B Infection

N. Nyakale[1,2], *L. M. Harry*[2], *C. Aldous*[3], *A. Maes*[4], *C. van de Wiele*[5], *M. M. Sathekge*[6,7];
[1]Department of Nuclear Medicine, Sefako Makgatho Health Sciences University and Dr George Mukhari Academic Hospital, Pretoria, SOUTH AFRICA, [2]Department of Nuclear Medicine, University of Kwa-Zulu Natal, Durban, SOUTH AFRICA, [3]Department of Genetics, College of Health Sciences, University of KwaZulu Natal, Durban, South Africa., Durban, SOUTH AFRICA, [4]Katholieke University Leuven, Kortrijk, BELGIUM, [5]Ghent University, Ghent, BELGIUM, [6]Department of Nuclear Medicine, University of Pretoria and Steve Biko Academic Hospital, Pretoria, SOUTH AFRICA, [7]Nuclear Medicine Research Infrastructure (NuMeRI), Pretoria, SOUTH AFRICA.

Aim/Introduction: Hepatitis B virus (HBV) is the most common cause of chronic liver infection, with most patients developing hepatocellular carcinoma (HCC). 68Ga-PSMA-PET/CT has recently been shown to contribute to the staging and management of HCC. The aim of the study was to investigate the value of 68Ga-PSMA-PET metabolic parameters in patients with HBV with and without HBV. ***Materials and Methods:*** Maximum standardized uptake value (SUVmax), mean standardized uptake value (SUVmean), metabolic tumor volume (MTV) and total lesion activity (TLA) were obtained on 68Ga-PSMA-PET/CT of patients with HCC. Correlation analysis and comparison between groups HBV positive versus negative patients was assessed using non-parametric tests. ***Results:*** There were 12 patients (3 men, 9 women), mean age 45.5 yrs (range 31-56 yrs) studied.The SUVmax values demonstrated a trend for higher SUVmax values in patients with HBV as opposed to HBV negative patients (p=0.070, 31.2(SD:13.2) versus 16.6(SD:10.1) respectively. We could not demonstrate a significant correlation between HBV infection and TLA (p=0.662). ***Conclusion:*** The relationship between 68Ga-PSMA-PET metabolic parameters in the differentiation of HCC patients with HBV and without HBV may warrant further exploration as a potential prognostic tool.

EP-0184

Prognostic Value of F18-FDG PET-CT in Patients With Localized Oesophageal Cancer Treated With Neoadjuvant Chemoradiation: The Use of Hopkins Criteria for Treatment Response Assessment

N. Bin Essa*, A. Alderaibi, M. Hawkins, J. Bomanji, S. Vöö;*
University College of London Hospital,
London, UNITED KINGDOM.

Aim/Introduction: Response assessment to definite neoadjuvant chemoradiotherapy (NACRT) of oesophageal cancer is centered on the role of 18F-FDG PET-CT (FDG-PET). Despite the introduction of various (semi-)quantitative measures, the differentiation between residual disease and post-therapy inflammatory change on FDG-PET remains challenging. The goal of the study was to evaluate the Hopkins criteria, a 5-point scale assessment of FDG-PET images, in assessing response to treatment in patients with oesophageal cancer following NACRT. ***Materials and Methods:*** This is a prospective, single-centre study on patients with histologically-proven, localised stage IIA-IIIA, T1-3N0-2M0 oesophageal cancer who were referred to NACRT of curative intent. FDG-PET scans were performed prior and on a 3-montly cycle up to 12 months following NACRT. Follow-up FDG-PET images were evaluated for residual disease using an assessment scale based on the Hopkins Criteria (HC): HC grade 1 (HC1), SUVmax<blood pool; HC2-3, focal uptake of SUVmax<liver or diffuse uptake >liver; HC4, focal uptake>liver and HC5, focal uptake of intense uptake. Scores of HC1-3 were considered to represent non-residual local disease, whereas scores of HC4-5 were interpreted as residual/recurrent disease. Chi-square and Fisher-Freeman-Halton exact-test were used to assess the agreement between the HC grade and gold-standard 1-year clinical follow-up endoscopy/surgery with histological confirmation. Kappa-coefficient was used to assess the interobserver variability. ***Results:*** Of a total of 20 patients, 7/20 (33.3%) were scored as HC1-3 and complete metabolic response on follow-up FDG-PETs, while 13/20 (66.6%) were scored as HC4-5 and indicative of residual or recurrent disease. All HC4-5 cases were confirmed positive for residual/recurrent disease at follow-up. Although 2 HC3 cases proved to be recurrent disease on follow-up, the site of recurrence was outside the level of the assessed primary site of disease. There has been a substantial interobserver agreement regarding the HC staging (p<0.05). Importantly, HC staging significantly outweighed SUVmax (p<0.05), as a solitary measure in assessing disease recurrence. ***Conclusion:*** HC grading proves to be a robust assessment of residual disease in patients with oesophageal cancer following curative NACRT.

EP-0185

The Evaluatiȯn Of Relationship Between F18 Fdg Pet/Ct Parameters And Sarcopenia İn Esophagus Can

M. ACAR TAYYAR[1]*, M. ÖNER TAMAM*[1]*, G. B. BABACAN*[1]*, M. ŞAHİN*[1]*, H. ÖZÇEVİK*[2]*, N. GÜRDAL*[3]*;*
[1]University of Health Sciences, Prof. Dr. Cemil Tascioğlu City Hospital of Nuclear Medicine, Istanbul, TÜRKIYE, [2]University of Health Sciences, Hamidiye Faculty of Nuclear Medicine, Istanbul, TÜRKIYE, [3]University of Health Sciences, Prof. Dr. Cemil Tascioğlu City Hospital of Radiation Oncology, Istanbul, TÜRKIYE.

Aim/Introduction: This study aimed to evaluate the relationship between semiquantitative metabolic parameters of the tumour, adipose tissue and sarcopenia in PET/CT imaging in esophageal cancers and investigate their effects on overall survival(OS). ***Materials and Methods:*** Between January 2015 and August 2022, 120 patients with esophageal carcinoma who had pre-treatment PET/CT were retrospectively analyzed. Age, gender, body mass index(BMI), primary tumour PET parameters(SUVmax , SUVmean , MTV, TLG), L3 vertebra level muscle surface area(LMA), psoas major muscle PET and CT parameters, C3 vertebra level muscle surface area(CMA), sternocleidomastoid muscle(SCM), PET and CT parameters, visceral and subcutaneous fat tissue PET and CT parameters from the retroperitoneal and abdominal regions, respectively, from the L4-L5 level, and the sarcopenia muscle index were calculated. Using Skeletal Muscle Index(L3 vertebral level muscle surface area / patient height squared; SMI)patients with lower than 45.4 cm^2/h^2 in males, 34.4 cm^2/h^2 in females were considered sarcopenic. ***Results:*** A strong correlation found between LMA and CMA(p:0.001 r:0.732). CMA was also significantly lower in sarcopenic patients (p:0.025).The surface area of psoas major and SCM muscles found correlated with both LMA and CMA(p:0.001). Subcutaneous fat tissue SUVmax values were higher in sarcopenic patients than non-sarcopenic patients. SCM MTV, SCM TLG, psoas major MTV and SMI found to be significantly lower in patients with distant metastases(p:0.024, p:0.019, p:0.045, p:0.039 respectively). Cox regression analysis performed and higher primary tumour SUVmax, TLG and MTV values found as poor prognostic factors (p=0.007, p<0.001, p<0.001). In the Kaplan-Meier survival analysis overall survival of non-sarcopenic patients found to be significantly higher than sarcopenic patients(Mantel cox log-rank method p:0.011). No correlation found between primary tumour PET parameters and sarcopenia status. ***Conclusion:*** C3 vertebra level measurements are highly correlated with L3 level and its considered it can replace L3 when calculating SMI. SCM and psoas surface area, adipose tissue SUVmax value may predict sarcopenia. According to our findings PET parameters in SCM and psoas major can predict distant metastasis status. Since low muscle index predicts distant metastases and SMI predicts OS those parameters may help clinical course of the disease, and can be measure routinely. Hence 18F-FDG PET/CT allows us to obtain data from both C3 and L3 levels in once, it is also considered superior to conventional imaging modalities on predicting sarcopenia. SMI should be evaluated in all patients since sarcopenia significantly affects overall survival in esophageal cancers.

EP-0186

[18F]F-FAPI-74 PET for initial clinical staging in patients with pancreatic cancer : a prospective pilot study

J. Gil[1,2], *W. Yun*[3], *H. Choi*[1,2], *J. Paeng*[1,2], *K. Kang*[1,2], *J. Jang*[3], *G. Cheon*[1,2];
[1]*Department of Nuclear Medicine, Seoul National University Hospital, Seoul, KOREA, REPUBLIC OF,* [2]*Department of Nuclear Medicine, College of Medicine, Seoul National University, Seoul, KOREA, REPUBLIC OF,* [3]*Department of Surgery, Seoul National University Hospital, Seoul, KOREA, REPUBLIC OF.*

Aim/Introduction: Fibroblast activation protein inhibitor (FAPI) analogs are newly introduced PET agents for cancer imaging. There is a lack of data using [^{18}F]F-FAPI-74 PET in pancreas cancer patients. We evaluated the clinical implication of FAPI PET in initial staging of pancreatic cancer. ***Materials and Methods:*** Nineteen patients who had been diagnosed with pancreatic cancer were prospectively enrolled since October 2021. Sixteen patients underwent surgery. Abdomen CT and FDG PET were taken for staging and FAPI PET was additionally performed. We assessed suspected metastatic lymph nodes (LN) on these imaging studies and compared with the pathologic results. For FAPI PET evaluation, a LN with higher activity than the background was regarded as positive finding. Measured PET parameters were SUVmax, metabolic/FAP-active tumor volume (MTV/FTV), total lesion glycolysis/FAP-activity (TLG/TLF). For measuring volumetric parameters, SUV threshold with 40% of SUVmax was used. We analyzed a relationship of PET parameters with clinical factors; carbohydrate antigen (CA) 19-9 and pathologic tumor volume. Pearson's correlation and paired t-test were used for statistical analysis. ***Results:*** FAPI PET identified metastatic LN in 6 patients while all patients showed no lymph node metastasis on conventional images including FDG PET. Among patients who had pathologically confirmed metastatic LN (n = 10), 60% (6/10) patients had positive LN findings on FAPI PET. The result of correlation between PET volume (FTV and MTV) and pathologic tumor volume was as following: FTV (r=0.14, p=0.62) and MTV (r=0.07, p=0.82). FTV were significantly larger than MTV (t=4.06, p< 0.001). FTV showed a better correlation compared to MTV, though it did not show statistical significance. CA19-9 was moderately correlated with TLF (r=0.54, p=0.02) and TLG (r=0.52, p=0.03). The other PET parameters had no statistically significant correlation with CA19-9. ***Conclusion:*** [^{18}F]F-FAPI-74 PET may detect metastatic LN in patients who did not show metastasis on conventional images. FTV tend to be larger than MTV.TLF was correlated with CA 19-9. These results suggested that [^{18}F]F-FAPI-74 PET might potentially upstage in patients with pancreatic cancer in terms of tumor extent and LN metastasis.

EP-0187

The prognostic value of 18F FDG PET/CT intra-tumoural metabolic heterogeneity in patients with esophageal squamous cell carcinoma treated with Concurrent Chemoradiotherapy or Definitive Chemoradiotherapy(dCRT)

Z. Zhu*, X. Ma, Q. Xie, X. Yao;*
The University of Science and Technology of China, Hefei, CHINA.

Aim/Introduction: Esophageal squamous cell carcinoma (ESCC) is a common gastrointestinal malignant tumor and notable for highly heterogeneous. This study aimed to quantify the intra-tumoural metabolic heterogeneity of primary tumour lesions by using ^{18}F-FDG PET/CT and evaluate the prognostic value of intra-tumoural metabolic heterogeneity in ESCC patients with definitive chemoradiotherapy (dCRT). ***Materials and Methods***: We retrospectively enrolled 194 pretreatment ESCC patients from January 2017 to December 2021 in this study. ^{18}F-FDG PET/CT images were reviewed and analyzed using Syngo. via software. The semi-quantitative metabolic parameters of primary tumour were measured, including the maximum standard uptake value (SUVmax), metabolic tumour volume (MTV), and total lesion glycolysis (TLG).Heterogeneity parameter (HI-index) were measured and calculated to quantify intra-tumoural metabolic heterogeneity. The outcome endpoint was event-free survival (EFS), including overall survival. Survival analysis was performed using Cox regression models and Kaplan Meier survival plots. Besides, the novel prognostic indices of pretherapeutic nutritional index (PTNI) were developed. ***Results:*** In all 194 newly diagnosed ESCC patients, 129 patients died. The median follow-up period of OS were 17.0 (range 3.6 - 33.6 months). The HI-INDEX (r=0.295, P<0.001) showed moderate correlation with the OS. The pretherapeutic nutritional index (PTNI) also had a weak correlation with the OS (r=0.147, P<0.05). In univariate analysis, sex (P=0.952), age(P=0.197), and clinical staging (P=0.094) were not associated with EFS.The HI-INDEX (P=0.014) and PTNI (P=0.029) remained significant in multivariate analysis.The Kaplan Meier survival analyses demonstrated that patients with higher intra-tumoural metabolic heterogeneity had worse outcomes (log-rank P=0.004). Finally, the Cox-model analysis demonstrated strong relationship between the HI INDEX and overall survival for patients with ESCC(χ2=13.217,P=0.021). ***Conclusion:*** The intra-tumoural metabolic heterogeneity of primary lesions in ESCC was an independent prognostic factor for EFS. The combined predictive effect of intra-tumoural metabolic heterogeneity provided prognostic survival information in ESCC patients.

EP-0188

Diagnostic Performances Of [18f]F-Fdg Pet, Mri And Pet/Mri In Patients With Newly Diagnosed Pancreatic Adenocarcinoma

P. Bartoletti[1], *G. Mango*[2], *S. Serafini*[3], *R. Guastella*[4], *C. Berto*[5], *S. Da Pozzo*[6], *M. Sitara*[1], *G. Fichera*[7], *C. Giraudo*[1], *L. Evangelista*[1];
[1]*Nuclear Medicine Unit, Department of Medicine DIMED, University of Padua, Padova, ITALY,* [2]*2Department of Advanced Biomedical Sciences, University of Naples Federico II, Naples, ITALY,* [3]*General Surgery, Padua University Hospital, Padova, ITALY,* [4]*General Surgery Universita' degli Studi di Padova, Padova, ITALY,* [5]*Radiology Unit, Department of Medicine DIMED, University of Padua, Padova, ITALY,* [6]*Radiology Unit, Azienda Ospedaliera di Padua, Padova, ITALY,* [7]*Pediatric Radiology Unit, Padua University Hospital, Padova, ITALY.*

Aim/Introduction: To compare diagnostic performances of [18F]F-FDG PET, MRI and [18F]F-FDG PET/MRI in patients with pancreatic adenocarcinoma. ***Materials and Methods:*** From 2017 to 2022, data about patients with suspicious or known pancreatic adenocarcinoma undergoing hybrid [18F]F-FDG PET/MRI scan were retrospectively collected. For each patient, following information was recovered for PET,enhanced MRI and PET/MRI: primary tumor (T), lymph nodes (N) and distant metastasis (M). Histopathology and clinical follow-up were used to establish the final pathological/clinical staging of disease. Diagnostic performance was expressed as sensitivity, specificity, positive and negative predictive value. ***Results:*** From a starting population of 56 patients, 30 (54%) subjects were considered. Median (range) age, CEA, Ca19.9 and bilirubin were 70 (51-85) years, 2.9 (0-54.2) ng/mL, 695.5 (0-35709) U/mL and 17.5 (4.2-345)

mg/dL. [18F]F-FDG PET was positive in 30 (100%), 9 (30%) and 9 (30%) patients, respectively for T, N and M. Conversely, MRI detected primary tumors in all patients, while it was positive for N and M in 15 (50%) and 9 (30%) patients, respectively. Nineteen (63.3%) patients were treated with neoadjuvant chemotherapy, due to the presence of borderline resectable/locally advanced disease. Totally, 13 (46.3%) subjects underwent surgery. Based on histopathological/clinical evaluation, 19 (63.3%) patients showed a lymph node involvement. Sensitivity and specificity of MRI vs. PET vs. PET/MRI regarding lymph nodes, were 52% vs. 28% vs. 60% and 60% vs. 60% vs. 60%, respectively. Moreover, positive predictive value (PPV) and negative predictive value (NPV) for the identification of lymph node involvement were equal to 88% and 23% with FDG PET/MR, therefore slightly higher when compared to PET and MRI alone (PPV: 77% and 86%; NPV: 14% and 20%, respectively). ***Conclusion:*** Our data suggest [18F]F-FDG PET/MRI outperformed MRI and PET for the evaluation of lymph nodes metastasis and could be used in the initial work up of the patients with resectable pancreatic adenocarcinoma.

EP-0189

Exploratory data on prostate-specific membrane antigen and vessels encapsulating tumour clusters in hepatocellular carcinomas: are two sides of the same coin?

R. Zanca[1,2], *R. Akpinar*[3], *L. Di Tommaso*[1,3], *F. Gelardi*[1,2], *M. Rodari*[2], *M. Sollini*[1,2];
[1]*Department of Biomedical Sciences, Humanitas University, Milan, ITALY,* [2]*Nuclear Medicine, IRCCS Humanitas Research Hospital, Rozzano, Milan, ITALY,* [3]*Pathology Unit, IRCCS Humanitas Research Hospital, Rozzano, Milan, ITALY.*

Aim/Introduction: Tumour microenvironment (TME) is an intricated dynamic framework involved in carcinogenesis and drug resistance. Recently, interest in TME as source of potential diagnostic/prognostic factors and therapeutic targets has growth. In hepatocellular carcinomas (HCCs), evidence shows that TME composition and specific vascular patterns contribute to different prognosis. Prostate-specific membrane antigen (PSMA) highlighting cancer-associated neo-vasculature in solid tumours including HCC, is negatively associated with prognosis[1]; vessels encapsulating tumour clusters (VETC) pattern is associated to metastasis, recurrence[2] and seems predict patients who benefit from sorafenib[3]. We report our experience with [18F]PSMA-1007 PET/CT in HCC staging exploring the relationship between imaging and VETC pattern. ***Materials and Methods:*** We retrospectively screened all HCC patients imaged with [18F]PSMA-1007 PET/CT in our Institution. We selected patients who underwent PET/CT for HCC staging and identified those with available HCC tissue samples. We visually scored each HCC lesion on PET/CT as positive if [18F]PSMA-1007 uptake was higher than background at the site of disease, and as negative if uptake was comparable/lower than the background. We further defined as homogenous or heterogenous [18F]PSMA-1007-avid lesions. For each case with available resection or biopsy tissue, we evaluated VETC as previously defined[2] on all available tumour blocks. We also collected clinical and follow-up data. Descriptive statistics was used to analyse data. ***Results:*** From 8/2022 to 04/2023 we identified 11/14 HCC patients (median age 76 years, range 60-80) who fulfilled the above-mentioned criteria. We analysed 32 HCC lesions (Table 1). [18F]PSMA-1007 PET/CT was positive in 9/11 patients. 11/13 [18F]PSMA-1007-avid lesions showed inhomogeneous uptake with a "cold" central area. Among negative lesions, few presented an uptake lower than the background (3/19). Tissue was available for staining in 4/11. The VECT pattern was identified in 2/4 patients and both presented inhomogeneous [18F]PSMA-1007 uptake in all lesions. Both underwent surgery: one recurred 5 months after, while the other one 1 month after surgery was disease free. The other 2/4 patients who did not exhibit the VECT pattern (one died the day after surgery for brain haemorrhage and follow-up is not yet available for the other one) presented mostly [18F]PSMA-1007 negative lesions (5/6). ***Conclusion:*** [18F]PSMA-1007 PET/CT seems promising in HCC. Although data come from exploratory and anecdotal cases, [18F]PSMA-1007 PET/CT positivity might predict the VECT pattern, possibly providing new insights into HCC evolution and prognosis. ***References:*** 1. Clin Transl Gastroenterol. Clin Transl Gastroenterol; 2019;10. 2. Hepatology . John Wiley & Sons, Ltd; 2020;71:183-95. 3. Hepatology; 2019;70:824-39.

EP-0190

Ga-68 PSMA PET/CT Imaging Findings of Cholangiocellular Carcinoma

T. Kissa, *Z. C. Balaban Genc, X. Niftaliyeva, N. Filizoglu, S. Kesim, K. Öksüzoğlu, F. Çağlıyan, S. Özgüven, F. Dede, T. Ones, H. T. Turoglu, T. Y. Erdil;*
Marmara University Pendik Research and Training Hospital, Istanbul, TÜRKIYE.

Aim/Introduction: Cholangiocellular carcinoma is the second most common primary tumor of the liver. It accounts for approximately 10% of primary liver malignancies. It is an adenocarcinoma originating from bile duct epithelium. It is more common in men and in advanced age. In this case report, we present the findings of an incidental diagnosis of cholangiocellular carcinoma on Gallium-68 (Ga-68) prostate specific membrane antigen (PSMA) positron emission tomography/computed tomography (PET/CT) in a patient followed for prostate cancer. ***Materials and Methods:*** A 69-year-old man with a history of prostate adenocarcinoma was referred to Ga-68 PSMA PET/CT for restaging due to biochemical recurrence of prostate cancer. Ga-68 PSMA PET/CT showed intense PSMA uptake in the left lobe of the liver with malignant character, which also extended to the right lobe. Subsequent biopsy of the left lobe of the liver revealed a diagnosis of cholangiocellular carcinoma. ***Results:*** Prostate specific membrane antigen is a 750 amino acid glycoprotein enzyme found in the cell membranes of prostatic acinar. It is also expressed in many other tissues such as kidney, small intestine, liver, spleen, intestine, lacrimal and salivary glands, and central and peripheral nervous system. Ga-68 PSMA PET/CT is a commonly used imaging modality for the diagnosis and follow-up of prostate cancer in routine clinical practice. PSMA expression is not specific to prostate tissue. It can also be used in the diagnosis, staging and treatment follow-up of other non-prostate malignancies. However, it has been shown to be useful in the diagnosis of various diseases, including benign and malignant neoplasms and inflammatory/infectious processes (e.g. tuberculosis). ***Conclusion:*** This case demonstrated the variable spectrum of Ga-68 PSMA uptake in prostatic and non-prostatic metastatic lesions and the usefulness of PET/CT in the evaluation of patients with concomitant malignancies for diagnosis and treatment follow-up when conventional imaging modalities fail.

EP-11

e-Poster Area

B: Imaging Clinical Studies -> B1 Oncological Imaging Clinical Study -> B16 Neuroendocrine (Pancreatic and Others)

EP-0191

68Ga-DOTA-TATE in Cervicothoracic, Coeliac and Sacral Ganglia: sites of physiological uptake in the Era of total-body PET/CT

E. Triumbari[1], *Y. Abdelhafez*[2], *D. Morland*[3], *B. A. Spencer*[2], *A. Calabrò*[4], *F. Sen*[2], *R. D. Badawi*[2], *M. Guindani*[5], *L. Nardo*[2]; *[1]Nuclear Medicine Unit, TracerGlab, Rome, ITALY, [2]Department of Radiology, UC Davis, Sacramento, CA, UNITED STATES OF AMERICA, [3]Service de médecine nucléaire, Institut Godinot, Reims, FRANCE, [4]Nuclear Medicine Department, University of Brescia and ASST Spedali Civili di Brescia, Brescia, ITALY, [5]Department of Biostatistics, University of California, Los Angeles, Los Angeles, CA, UNITED STATES OF AMERICA.*

Aim/Introduction: To characterize ^{68}Ga-DOTA-TATE uptake in sympathetic ganglia and investigate whether total-body (TB) PET/CT scanners have an impact on their detection and quantification compared to conventional scanners. ***Materials and Methods:*** Frequency of visualization, ^{68}Ga-DOTA-TATE uptake intensity and ganglion-to-background ratio (GBR) were investigated among bilateral cervicothoracic, coeliac and sacral ganglia of patients with neuroendocrine neoplasia who underwent PET/CT on both a conventional scanner and a TB system during their clinical history. Minimum two, maximum six scans per patient were collected. Comparisons between the two scanners' examinations were computed using paired T-test or two proportion Z-test when appropriate. Single predictor analyses were performed using generalized linear mixed effects models. Covariates with p-value <0.05 were included in multivariable analysis. For semiquantitative analysis, differences in SUV_{max} and GBR distribution were assessed using linear mixed effect models with random intercept. ***Results:*** Data were collected from 27 patients (8M, 19F), 102 scans: 54 (53%) on the conventional scanner and 48 (47%) on the TB scanner. The average percentage of positive scans per patient was 87.7±25.7% across all ganglion sites and exams. In only TB PET, the average number of positive scans was 95.7±12.7% compared to 79.6±32.5% for conventional PET (p=0.023), with also a statistically significant increase in detection of cervicothoracic (p=0.012) and coeliac ganglia (p=0.002) alone. In multivariable analysis, use of TB PET/CT was the only significant covariate predicting ^{68}Ga-DOTA-TATE uptake visualization on a per ganglion basis (odds ratio: 1.8, 95%CI: 1.02-3.19; p=0.042). Semiquantitative analysis showed that SUV_{max} and GBR measured on the two scanners were significantly higher in TB images. ***Conclusion:*** Sympathetic ganglia ^{68}Ga-DOTA-TATE uptake is a frequent physiologic finding. Higher sensitivity and spatial resolution of TB PET/CT increase frequency of ganglia visualization. The more accurate quantification shows higher levels of uptake of this small anatomic structure in TB PET/CT compared to conventional PET/CT. ***References:*** 1) Ng QK-T, Triumbari EKA, Omidvari N, Cherry SR, Badawi RD, Nardo L. Total-body PET/CT - First Clinical Experiences and Future Perspectives. Semin Nucl Med [Internet]. 2022 [cited 2022 Oct 11];52:330-9. Available from: https://linkinghub.elsevier.com/retrieve/pii/S0001299822000022__2) Badawi RD, Shi H, Hu P, Chen S, Xu T, Price PM, et al. First Human Imaging Studies with the EXPLORER Total-Body PET Scanner*. J Nucl Med [Internet]. 2019 [cited 2022 Apr 22];60:299-303. Available from: http://jnm.snmjournals.org/lookup/doi/10.2967/jnumed.119.226498__3) Berg Z, Koppula BR. 68Ga-DOTATATE Uptake by Cervicothoracic (Stellate) Ganglia. Clin Nucl Med [Internet]. 2019 [cited 2022 Aug 29];44:810-1. Available from: https://journals.lww.com/10.1097/RLU.0000000000002731

EP-0192

The quantification for the treatment response evaluation of Metastatic Gastroenteropancreatic Neuroendocrine Tumors in Ga-68 DOTATATE PET/CT

Z. Koç[1], *P. Özcan*[1], *E. Sezer*[2], *T. Kara*[3]; *[1]Mersin University Hospital Nuclear Medicine Dpt., Mersin, TÜRKIYE, [2]Mersin University Hospital Oncology Dpt., Mersin, TÜRKIYE, [3]Mersin University Hospital Pathology Dpt., Mersin, TÜRKIYE.*

Aim/Introduction: The treatment response evaluation by means of Ga-68 DOTATATE PET/CT in Metastatic Gastroenteropancreatic Neuroendocrine Tumors (GEPNET's) needs careful attention due to the subtle changes that might affect decision. The aim of this study is to analyze a new modified method in quantification of the Ga-68 DOTATATE PET/CT in treatment response evaluation of GEP-NET's. ***Materials and Methods:*** 37 patients with diagnosis of metastatik GEP-NET were included in the study. Comparative evaluation of Ga-68 DOTATATE PET/CT images before and after treatment were performed. Quantitative analysis as well as visual interpretation results were compared with oncology follow up. The patients were divided according to oncology follow up results as responders and nonresponders. ***Results:*** The comparative analysis results showed that the difference between mean SUVmax and index values after and before the treatment were not significant for primary lesions. However both the index values were significantly different between groups in metastatic lesions. ***Conclusion:*** Previous studies including large series for response evaluation showed that Ga-68 DOTATATE imaging significantly changed patients management in nearly half of the patients (44%) (1). Additionally the metastatic involvement (90%) and multiple lesions (35%) were determined at first staging in most of the patients included in previous series (2). The diagnostic comparison of the morphologic imaging modalities and Ga-68 DOTATATE PET/CT revealed higher detection rates in previous series; PET/CT determined 22/33 patients who were metastasis negative for liver (3). The results of this study showed that comparison of the uptake of primary tumor might not reflect the response but metastatic lesions should be prefered. SUVmax levels of the metastatic lesions sufficiently reflected the treatment response according to the statistical analysis. In case of discrapancy quantification method might be implicated. ***References:*** Skoura E, Michopoulou S, Mohmaduvesh M, et al. The impact of 68Ga-DOTATATE PET/CT imaging on management of patients with neuroendocrine tumors: experience from a national referral center in the United Kingdom. J. Nucl. Med. 2016; 57: 34-40.Norlén O, Hessman O, Stålberg P, et al. Prophylactic cholecystectomy in midgut carcinoid patients. World. J. Surg. 2010; 34: 1361-136. Albanus DR, Apitzsch J, Erdem Z, et al. Clinical value of (68)Ga-DOTATATE-PET/CT compared to stand-alone contrast enhanced CT for the detection of extra-hepatic metastases in patients with neuroendocrine tumours (NET). Eur. J. Radiol. 2015; 84: 1866-1872.

EP-0193

The additional value of SPECT/CT imaging to planar imaging in neuroendocrine tumors

***A. Tsaroucha**, N. Kapsoritakis, O. Bourogianni, G. Lamprakopoulos, M. Stathaki, E. Papadaki, S. Koukouraki;*
University Hospital of Heraklion, Heraklion,Crete, GREECE.

Aim/Introduction: To assess the benefit of SPECT/CT imaging compared to planar imaging alone in neuroendocrine tumors (NETs). ***Materials and Methods:*** A total of 83 patients with NETs (33 suspected, 15 small bowel, 13 pulmonary, 8 stomach, 1 large bowel, 2 pancreatic, 1 insulinoma, 3 medullary thyroid cancer, 2 paragangliomas, 5 metastatic NETs of unknown origin) were referred for peptide receptor imaging (33 patients for initial diagnosis, 23 for staging and 27 for follow up/recurrence). 45 patients underwent ^{111}In-pentetreotide scintigraphy. 4h and 24h whole body (WB) planar imaging was performed in all patients, as well as 24h SPECT/CT tomography in the areas of interest. 38 patients underwent ^{99m}Tc-EDDA/HYNIC-TOC scintigraphy. 1h static image of the abdomen and 4h WB planar imaging were acquired , as well as 4h SPECT/CT in the areas of interest. The planar and SPECT/CT imaging were interpreted independently and the scans were reported as negative, positive or equivocal. The number of detected lesions was calculated and the change of management due to SPECT/CT contribution was estimated. ***Results:*** 19 out of 45 WB planar ^{111}In-pentetreotide scans were reported as negative, 10 scans as positive and 16 scans as equivocal. After adding SPECT/CT imaging, the negative scans increased to 25, the positive scans increased to 19 and only 1 remained equivocal. A total of 74 lesions were depicted on planar imaging alone, and SPECT /CT added 26 new/extra lesions. 15 out of 38 WB planar ^{99m}Tc-EDDA/HYNIC-TOC scans were reported as negative, 14 as positive and 9 scans as equivocal. After adding SPECT/CT imaging, the negative scans remained 15, the positive scans increased to 18 and the equivocal scans decreased to 5, while SPECT /CT added 19 new/extra lesions to 44. Overall, the positive scans were increased from 28,9% to 44,6%, the negative ones from 41% to 48,2%, while the equivocal scans decreased from 30,1% to 7,2%. Overall, 38,1% more lesions were depicted. There was a change in management in 31 out of 83 patients or 37,3% of the patients. ***Conclusion:*** SPECT/CT remains (when PET/CT technology is not readily available) an important diagnostic tool of conventional Nuclear Medicine in evaluating NETs by increasing diagnostic confidence, reducing equivocal scans and leading to change of management in a considerable percentage of the referred patients.

EP-0194

18F-AlF-NOTA-Octreotide PET/CT: Krenning´s score and tumor burden influence by tumor volume and total lesion activity

***M. González Martínez**[1], A. Piana Bezaury[1], I. Pérez Díaz[2], M. Olarte Casas[1];*
[1]PET/CT unit, UNAM, Mexico City, MEXICO,
[2]UNAM, Mexico City, MEXICO.

Aim/Introduction: To identify and differentiate those patients who are candidates for radionuclide therapy, to obtain their percentage using 18F-AlF-NOTA-Octreotide (Fluoroctreotide) PET/CT, and to correlate tumor burden - which was obtained through the tumor volume and the total lesion activity - with the SUVmax, SUVpeak, and Krenning Score values. ***Materials and Methods:*** Adult patients diagnosed with gastroenteropancreatic neuroendocrine tumor confirmed by histopathology who were evaluated in the PET/CT unit at UNAM using the radiopharmaceutical 18F-AlF-NOTA-Octreotide (Fluoroctreotide) from January to December 2021. Tumor burden estimation by tumor volume and total lesion activity through semi-automated processing with a fixed threshold (default SUVmax of 10 and volume of 1 mL). ***Results:*** A total of 48 patients were evaluated; 31 of them showed some degree of abnormal overexpression of somatostatin receptors, 28 patients (58.33%) were considered positive for significant overexpression of somatostatin receptors (Krenning scores of 2, 3, and 4) and 27 patients (56.25%) were candidates for radionuclide therapy (Krenning scores 3 and 4). A significant directly proportional correlation was found between variables SUVmax, SUVpeak, tumor volume, and total lesion activity. ***Conclusion:*** The percentage of patients with gastroenteropancreatic neuroendocrine tumors who were candidates for radionuclide therapy was 56.25%. The tumor burden was measured by tumor volume and total lesion activity, it was adequately discriminated through semi-automated processing with a fixed threshold (default SUVmax of 10 and volume of 1 mL), and the results obtained from the aforementioned patients correlate with a high Krenning score (3 and 4). Quantifying tumor load by tumor volume and total lesion activity with fluoroctreotide correlates with the Krenning score and helps to determine which patients are candidates for radionuclide therapy.

EP-0195

Referral Patterns and Image Results of 2,249 [64Cu]Cu-DOTATATE PET/CT in a European Neuroendocrine Tumor Society Center of Excellence

***M. Loft**[1,2], E. A. Carlsen[1,2], C. B. Johnbeck[1,2], U. Knigge[2,3], M. Andreassen[2,3], S. W. Langer[2,4,5], H. H. Johannesen[1,2], J. Mortensen[1,2,5], L. H. Enevoldsen[1,2], P. Oturai[1,2], A. Kjaer[1,2];*
[1]Department of Clinical Physiology and Nuclear Medicine & Cluster for Molecular Imaging, Copenhagen University Hospital – Rigshospitalet & Department of Biomedical Sciences, University of Copenhagen, Copenhagen, DENMARK, [2]European Neuroendocrine Tumor Society Center of Excellence at Copenhagen University Hospital – Rigshospitalet, Copenhagen, DENMARK, [3]Departments of Clinical Endocrinology and Surgical Gastroenterology, Copenhagen University Hospital – Rigshospitalet, Copenhagen, DENMARK, [4]Department of Oncology, Copenhagen University Hospital – Rigshospitalet, Copenhagen, DENMARK, [5]Department of Clinical Medicine, University of Copenhagen, Copenhagen, DENMARK.

Aim/Introduction: Somatostatin receptor PET/CT, using ^{68}Ga-based tracers or [^{64}Cu]Cu-DOTATATE, is pivotal for the management of patients with neuroendocrine neoplasms (NEN) or suspicion thereof. The aim of the study was to perform a systematic analysis of the referral patterns and image results of clinical routine [^{64}Cu]Cu-DOTATATE PET/CT to support guidelines and appropriate use criteria development. ***Materials and Methods:*** We included all clinical routine [^{64}Cu]Cu-DOTATATE PET/CT performed between 10-April-2018 (start of clinical use) and 02-May-2022 at Rigshospitalet. We performed structured analyses of 1) the referral text and 2) the result report of each scan and categorised the indication and result according to clinical scenarios. The retrospective study was approved by the Directorate of Rigshospitalet (ID:22027516) and the requirement for informed consent was waived. ***Results:*** In total, 2,249 [^{64}Cu]Cu-DOTATATE PET/CT were performed in 1,290 patients. The most common indication was monitoring of patients with NEN without clinical evidence of progression accounting for 971 scans (43.2%). Initial staging after histology-verified NEN diagnosis and restaging following curative-intent surgery accounted for 222

(9.9%) and 240 (10.7%) scans, respectively. Selection of peptide receptor radionuclide therapy (PRRT) eligible patients and restaging following PRRT-completion accounted for 95 (4.2%) and 115 (5.1%) scans, respectively. Additionally, 182 (8.1%) scans were performed in the diagnostic work-up of patients with imaging suggesting NEN lesions not amenable for biopsies, and 113 (5.0%) scans in patients both without histology-verified NEN diagnosis and evidence on conventional imaging, but with biochemistry and symptoms suggestive of NEN disease. The result report analysis showed stable disease and progression (PET and/or CT) on 577 (25.7%) and 460 scans (20.4%), respectively. In 299 cases, progression was observed in patients without clinical evidence of progression (30.8% of 971 scans). In 99 cases (21.5% of all 460 progression-positive scans), progression was detected on PET but not CT. In 669 of all 2,249 scans (29.7%), no disease was detected, while confirmation of NEN disease, including primary tumour localisation, was found in 395 cases (17.6%). ***Conclusion:*** Monitoring of patients with NEN without clinical evidence of progression was the most frequent indication accounting for 971 [^{64}Cu]Cu-DOTATATE PET/CT, in which disease progression was detected in 299 cases (30.8%). In 99 (21.5%) of all 460 progression-positive cases, progression was observed on PET only. Our study provides real-life data that may contribute to further development of somatostatin receptor PET/CT guidelines for using [^{64}Cu]Cu-DOTATATE including appropriate use criteria.

EP-0196

Impact on clinical management when using [18F]AlF-NOTA-octreotide instead of [68Ga]Ga-DOTA-SSA PET/CT in neuroendocrine tumor patients: preliminary results

H. Leupe[1], *E. Pauwels*[1], *T. Vandamme*[2,3], *B. Van den Broeck*[4], *W. Lybaert*[3], *J. Dekervel*[5], *J. Jaekers*[6], *F. Cleeren*[7], *J. Hofland*[8], *A. Brouwers*[9], *M. Koole*[1], *G. Bormans*[7], *E. Van Cutsem*[5], *K. Geboes*[10], *C. Verslype*[5], *S. Stroobants*[11], *C. M. Deroose*[1];
[1]*Nuclear Medicine, University Hospitals Leuven & Nuclear Medicine and Molecular Imaging, Department of Imaging and Pathology, KU Leuven, Leuven, BELGIUM,* [2]*Center for Oncological Research (CORE), Integrated Personalized and Precision Oncology Network (IPPON), University of Antwerp, Antwerp, BELGIUM,* [3]*Oncology, NETwerk Antwerpen-Waasland CoE, Antwerp-Waasland, BELGIUM,* [4]*Nuclear Medicine, Ghent University Hospital, Ghent, BELGIUM,* [5]*Digestive Oncology, University Hospitals Leuven, Leuven, BELGIUM,* [6]*Department of Visceral Surgery, University Hospitals KU Leuven, Leuven, BELGIUM,* [7]*Radiopharmaceutical Research, Department of Pharmacy and Pharmacology, KU Leuven, Leuven, BELGIUM,* [8]*Department of Internal Medicine, Section of Endocrinology, ENETS Centre of Excellence Rotterdam, Erasmus MC Cancer Institute, Rotterdam, NETHERLANDS,* [9]*University of Groningen, University Medical Center Groningen, Department of Nuclear Medicine and Molecular Imaging, Groningen, NETHERLANDS,* [10]*Digestive Oncology, Department of Gastroenterology, Ghent University Hospital, Ghent, BELGIUM,* [11]*Nuclear Medicine, Antwerp University Hospital & Molecular Imaging and radiology, Faculty of Medicine and Health Sciences, University of Antwerp, Wilrijk, BELGIUM.*

Aim/Introduction: [^{18}F]AlF-NOTA-octreotide ([^{18}F]AlF-OC) is a promising alternative for [^{68}Ga]Ga-DOTA-SSA in PET imaging of the somatostatin receptor (SSTR). Our research consortium has recently shown in a prospective, multicenter trial that [^{18}F]AlF-OC is superior to the current gold standard in terms of lesion number detection (1). Our aim is to assess changes in TNM staging and differences in patient management when using [^{18}F]AlF-OC PET/CT instead of [^{68}Ga]Ga-DOTA-SSA PET/CT in the work-up of neuroendocrine tumor (NET) patients. ***Materials and Methods:*** Seventy-five patients from our multicenter study (1) with a NET were included for retrospective analysis. All patients underwent both [^{18}F]AlF-OC and [^{68}Ga]Ga-DOTA-TATE or -TOC PET/CT. TNM staging was determined and compared for both tracers. For each patient, the blinded [^{68}Ga]Ga-DOTA-SSA or [^{18}F]AlF-OC PET/CT images were presented in random order at a multidisciplinary tumor board-like setting to at least two clinical NET experts, a surgeon and a nuclear medicine expert. The images were presented together with clinical information and compared with previous SSTR and [^{18}F]FDG PET imaging. After a consensus decision for patient management was recorded, the board was presented with the PET/CT images from the other tracer and a decision was made for the second tracer. Differences in management were classified as major if it entailed an intermodality change and minor if it led to an intramodality change. ***Results:*** We present our preliminary analysis of the first fifty-four patients. Compared with [^{68}Ga]Ga-DOTA-SSA, the use of [^{18}F]AlF-OC led to TNM staging changes in 7/54 patients (downstaging in 1/7, upstaging in 6/7), resulting in a change in management in 3/7 patients. In total, [^{18}F]AlF-OC PET/CT impacted clinical management in 7/54 patients (13.0%), leading to a major change in 5/7 cases (4 patients switched to PRRT and 1 patient switched from SSA to everolimus) and a minor change in 2/7 cases (SSA dose escalation). All seven cases with a difference in patient management between both PET tracers were caused by additional lesion detection by [^{18}F]AlF-OC. ***Conclusion:*** In 80.7% of patients, similar TNM and therapy was observed. The use of [^{18}F]AlF-OC resulted in TNM changes in 13.0% of the patients. Differences in clinical management were seen in 13.0% of the patients, which were all cases of therapy intensification driven by higher number of lesions detected by [^{18}F]AlF-OC PET/CT. ***References:*** 1. Pauwels E, Cleeren F, Tshibangu T, et al. 18F-AlF-NOTA-Octreotide Outperforms 68Ga-DOTATATE/NOC PET in Neuroendocrine Tumor Patients: Results from a Prospective, Multicenter Study. J Nucl Med. 2023 Apr;64(4):632-638.

EP-0197

Development of a Semi-Automatic Platform for Whole Body Tumor Segmentation and Radiomic Feature Extraction From 68Ga-DOTATATE PET/CT Using TriDFusion (3DF)

S. Krebs*, D. Lafontaine, L. Bodei, M. E. Mayerhoefer, J. Humm, H. Schöder;*
Memorial Sloan Kettering Cancer Center, New York, NY, UNITED STATES OF AMERICA.

Aim/Introduction: Reliable imaging biomarkers facilitating management and outcome prognostication in patients with neuroendocrine tumors (NET) are lacking. ^{68}Ga-DOTATATE PET/CT is routinely performed to assess somatostatin receptor (SSTR) expression and stage patients with NET. However, manual segmentation of avid lesions to extract quantitative parameters for response assessment and prognostication remains time-consuming and may not be practical in widely metastatic disease. Therefore, we developed a semi-automatic software for tumor segmentation and extraction of radiomic features based on our open-source TriDFusion (3DF) platform . We tested this platform in 38 patients with SSTR-positive gastroenteropancreatic or lung NET imaged with ^{68}Ga-DOTATATE PET/CT before and after PRRT with available outcome data. ***Materials and Methods:*** Using CT images (of the PET/CT) as blue-print, the TotalSegmentor-3DF machine learning algorithm automatically computed masks for normal organs with physiologic DOTATATE uptake (e.g.; adrenal glands, kidneys), and also identified the

bone and the liver. Then, the PET was resampled based on the CT. To determine the normal liver SUVmean and standard deviation (SD), a region-of-interest was manually placed in the normal liver. For liver lesions, a threshold based on normal liver SUVmean was applied, for bone lesions a fixed SUV-threshold of 3. For the other lesions, a threshold based on average normal liver SUVmean derived from a representative patient cohort was used. Manual corrections, when necessary, were applied. Minimum lesion size was arbitrarily defined as > 0.3 cm3. Multiple output parameters including radiomic features (using 3DF-pyRadiomics) were extracted. ***Results:*** Interim analyses (7 patients, 14 scans) showed segmentation of 186 lesions (116 liver, 10 bone, 19 lung, 57 soft tissue) with mean whole body (wb) tumor volume TV (ml) of 687.45 (range, 5.18-2021.65), wb TLRE (total lesion receptor expression) 10485.74 (range, 55.39-37893.42), wb SUVmean 15.22 (range, 7.42-29.25), wb SUVmax 52.03 (range, 20.63-90.36); thereof mean liver TV of 655.04 (range, 0-1925.81), bone TV 1.33 (range, 0-5.48), soft tissue TV 31.00 (range, 0-201.75). Implementation of machine learning masks and segmentation required about 3.5-4 min per scan, and with manual adjustments, total segmentation time was 5-9 min per case. Radiomic features for individual lesions were extracted. The personalized output report provided lesion uptake metrics and an embedded image graphic facilitating lesion tracking. ***Conclusion:*** Our 3DF tool enables the rapid semi-automatic analyses of whole-body tumor burden and the extraction of radiomic features from ^{68}Ga-DOTATATE PET/CT even in widely metastatic disease. Further analyses and correlation with outcome are in progress and will be presented.

EP-0198

The risk factors of pancreatic neuroendocrine tumor predicted by 18F-FDG and 68Ga-DOTANOC PET/CT before surgery.

J. Xu*, S. Song;*
Fudan University Shanghai Cancer Center, Shanghai, CHINA.

Aim/Introduction: Operation is primary treatment of pancreatic neuroendocrine tumor (pNET). However, the indications for resection and lymph node dissection are still controversial. The purpose of our study was to evaluate the value of ^{18}F-FDG and ^{68}Ga-DOTANOC PET/CT to predict the risk factors of pNET before surgery. ***Materials and Methods:*** 109 patients with pNET were retrospectively analyzed, who underwent ^{18}F-FDG (n=44) and ^{68}Ga-DOTANOC (n=109) PET/CT for preoperative assessment and underwent surgical resection between July 2021 to December 2022. Operations were performed in two weeks after imaging and 76 patients (69.7%) received lymph nodes dissection. Patients with <3cm pNETs were separately analyzed for evaluating the value of both PET/CT to assist in the selection of lymph node dissection. Clinical characteristics, PET/CT parameters and pathological results were reviewed and compared statistically. ***Results:*** In those who underwent lymph node dissection, twenty patients (26.3%) had lymph node metastasis. The lymph nodes metastasis was missed by ^{68}Ga-DOTANOC PET/CT in 9 patients which was also missed by ^{18}F-FDG PET/CT. Tumor size is one of the most important risk factors for pNET. The tumors with vascular tumor thrombus, perineural invasion, high pathological grade, lymph node metastasis and liver metastasis are always with larger maximum diameter. It is observed that SUV_{max} of the primary tumor with vascular tumor thrombus is lower than those without vascular tumor thrombus in ^{68}Ga-DOTANOC PET/CT (26.2±17.0 vs. 41.5±26.8, P=0.007). SUV_{max} of ^{18}F-FDG PET/CT ≥ 4.5 was identified as poor prognostic predictor for lymph node metastasis (odds ratio [OR] 7.418, 95% confidence interval [CI] 0.894-61.574, P=0.036) and liver metastasis (odds ratio [OR] 5.228, 95% confidence interval [CI] 1.007-27.143, P=0.049). In the subgroup analysis, there were 78 patients with <3cm pNETs, 49 of which (62.8%) received lymph nodes dissection and only 9 patients (18.3%) had lymph node metastasis. 4 patients with positive lymph nodes were detected by ^{68}Ga-DOTANOC PET/CT. There was no statistical difference of SUV_{max} of the primary tumor in ^{18}F-FDG and ^{68}Ga-DOTANOC PET/CT between those patients with and without lymph node metastasis. In those patients with <3cm pNETs, higher upake of ^{18}F-FDG in the primary tumor was observed in NET G2 than G1 (8.41±9.99 vs. 2.16±1.12, P=0.004). ***Conclusion:*** ^{18}F-FDG and ^{68}Ga-DOTANOC PET/CT before surgery could predict the risk factors of pancreatic neuroendocrine tumor. However, it is insufficient to accurately predict the lymph node metastasis by either ^{18}F-FDG or ^{68}Ga-DOTANOC PET/CT in the patients with <3cm pNETs.

EP-0199

The use of18F-DOPA PET/CT for the diagnosis of neuroendocrine tumors suspected or confirmed from unkown origin

A. Rodríguez Pajuelo*, J. Cuenca Cuenca, M. Guerra Gómez, J. Jiménez-Hoyuela García;*
Virgen del Rocio Univsersity Hospital, Seville, SPAIN.

Aim/Introduction: The aim of the proyect was to evaluate the diagnostic efficiency of ^{18}F-fluorodihydroxyphenylalanine (^{18}F-FDOPA) PET/CT in patients with suspected neuroendocrine tumor (NET) or NET metastasis from unknown origin. ***Materials and Methods:*** From January 2013 to June 2020, we retrospectively studied ^{18}F-DOPA PET/CT scans performed in 64 patients (19 men; 45 women) with a mean age of 63 years (range:24-89), referred with the following suspicions: clinical suspicion / elevation of NET tumor markers (n=29) or with suspected/confirmed morphological image for NET. They underwent PET/CT from vertex to femur after intravenous injection of a mean 213.20 MBq (range:167-264) of ^{18}F-DOPA. The results were confirmed with pathological anatomy in 33 patients and by clinical/radiological follow-up of 81.5 months (range:1-134). Sensitivity (S), specificity (E), positive predictive value (PPV), negative predictive value (NPV) and diagnostic accuracy values were determined. ***Results:*** The prevalence of disease was 39.0%. Among the patients with ^{18}F-DOPA PET/CT-positive primary lesion, which were confirmed as NET later (true positives), the obtained mean of SUVmax was 10.8 and of size 24.6 mm. The S and E were 64% and 84.6%, with PPV and NPV of 72.7% and 78.5%. The diagnostic accuracy was 76.5%. Among the patients who were referred for suspicion/ elevated tumor markers, 2/29 had lesions that were confirmed later (in liver and lung). Another 2/29 patients with lesions (in esophagus and duodenum) were found subsequently ruling out the existence of NET. In 2/29 patients, the primary lesion confirmed was not identified by PET/CT, being located in pancreas in both cases. S=50.0% and E=92.0%, PPV=50.0% and NPV=92.0% were obtained, as well as a diagnostic accuracy of 86.2%. In patients whom a lesion suggestive of NET was detected by other morphological tests, lesions were identified by PET/CT in 17/35 patients. Some of which were confirmed pathological anatomy as metastatic NET of unknown origin. In 1/35 patients, multiple lymphatic, bone and skin metastatic lesions were located, confirmed by biopsy, without finding the primary one. S= 66.6% and E=71.4%, PPV=77.7% and NPV=58.8%, and a diagnostic accuracy of 68.5% were reached. ***Conclusion:*** Our data confirmed the good accuracy of ^{18}F-DOPA PET/CT for the evaluation of

patients with suspected NET, especially for those with symptoms/elevated markers, in whom the presence of a tumor is ruled out with high assurance. The diagnostic error was mainly associated with lesions located in the gastroenteropancreatic tract, probably secondary to the physiological activity of fluorodopa.

EP-0200

Impact of Tumor-to-Background Ratio on Training of AI for Liver Metastasis Detection in Neuroendocrine Tumors

B. Schemmer;
Uniklinik Bonn, Bonn, GERMANY.

Aim/Introduction: The accuracy and robustness of artificial intelligence (AI) in detecting liver metastasis in neuroendocrine tumors (NETs) is potentially affected by various factors, including the tumor-to-background ratio (TBR). In this study, we investigate the impact of TBR on the training of an AI for the detection of liver metastasis in NETs. ***Materials and Methods:*** We used a dataset of 50 DOTATOC-PET whole-body studies of patients with NETs with liver metastasis (mean 2 metastasis per patient) and 50 without liver metastasis to train and evaluate the AI model. The TBR was calculated by dividing the tumor SUVmax by the liver SUVmean in each image. The AI model was trained using labeled images with and without liver metastasis. The AI was specifically not trained to discern subtle metastasis with uptake values below liver uptake. Images were preprocessed and SUV values below liver SUVmean*0.5 do not appear in the training data. Detection was evaluated as successful when there was a corresponding labeled metastasis in the data. To increase the amount of training data, the whole bodies were presented as single image slices, however only images containing the liver were used (~100*100 images). ***Results:*** Our results show that the TBR has a significant impact on the training of the AI model. Training speed was higher with higher TBR, however robustness for analysis of low TBR images was also low. To alleviate this, we modified the training process so that starting with the images with the highest TBR (24.8 in our case) with each iteration more and more images with low TBR (down to 1.2) were introduced. In the test data accuracy of the model increased as the TBR increased, reaching a specificity of 98% when the TBR was greater than 2, while still generating acceptable accuracy with a TBR of 1.05 (83%). ***Conclusion:*** Our study highlights the importance of the TBR in the training of an AI for the detection of liver metastasis in NETs. A high TBR is essential for the accurate training of the AI model, and further research is needed to identify the optimal TBR for the best performance of the model. However for real world applications lower TBR images need to be introduced into the training process, as low TBR is common during therapy staging and remission control (i.e. everolimus).

EP-0201

What is the utility of combined 68Ga-DOTATOC and 18F-FDG- PET/CT in the work-up of subjects with neuroendocrine tumors of unknown origin?

I. Bloise, *S. Harsini, F. Benard, D. Wilson, J. M. Loree, P. Martineau; BC Cancer, Vancouver, BC, CANADA.*

Aim/Introduction: Neuroendocrine tumors (NETs) are epithelial neoplasms that can arise from most organs, with tumors of unknown origin accounting for 10-14% of all NETs. Identifying the site of the primary lesion and providing accurate staging in these patients can be challenging. The aim of this study was to investigate the value of performing both FDG and ^{68}Ga-DOTATOC-PET/CT in subjects with NET of unknown origin. ***Materials and Methods:*** We retrospectively reviewed ^{68}Ga-DOTATOC-PET/CTs performed under clinical trial NCT03583528 at our institution between July of 2018 and November of 2022 on subjects with "NET of unknown origin" or "unknown primary site of disease". As per clinical trial, all subjects underwent both ^{68}Ga-DOTATOC and ^{18}F-FDG-PET/CT imaging. Information regarding overall image assessment (positive or negative study), tumors grades, the interpreter's confidence in diagnosis (high, moderate, or low), number of positive lesions (1, 2, 3, 4, 5, 6-10, >10), and location of lesions (lymph nodes, liver, lung, bones) was recorded. ***Results:*** A total of 40 subjects met the inclusion criteria. For each subject, DOTATOC and FDG-PET/CTs were performed within a time interval of 2 months. Tumor grade was available for 32 subjects with 12 (38%), 16 (50%), and 4 (12%) subjects having grade 1, 2, and 3 disease, respectively. 34 (85%) subjects had DOTATOC-avid lesions, while 27 (79%) demonstrated FDG-avid disease. None of the DOTA negative subjects demonstrated FDG-avid lesions. A DOTATOC-avid primary lesion was identified in 12 (35%, high confidence) studies and possibly identified in another 5 (15%, moderate confidence). A possible primary site was identified on FDG-PET in a single (3%, moderate confidence) subject with grade 1 disease. FDG and DOTATOC revealed a similar number of lesions in 12 (30%) subjects with DOTATOC revealing a greater number of lesions in 22 (55%) cases. The single subject with an FDG-positive primary lesion demonstrated a greater number of lesions with DOTATOC. Nodal/hepatic/lung/bone metastases were detected in 48%/50%/8%/38% of patients with DOTATOC, compared to 18%/50%/5%/25% with FDG, respectively. ***Conclusion:*** DOTATOC-PET/CT identified the primary lesion in a much greater proportion of subjects than FDG-PET/CT while benefiting from greater reader confidence. DOTATOC-PET/CT also identified significantly more lesions than FDG-PET/CT and revealed a broader range of organ involvement than that seen on FDG-PET/CT. The inclusion of FDG-PET/CT provided little additional value compared to DOTATOC-PET/CT in the workup of subjects with well differentiated NETs of unknown origin.

EP-0202

[68Ga]Ga-DOTATOC PET radiomics supports lymph node metastases detection for accurate surgical planning of well-differentiated pancreatic neuroendocrine tumours patients

C. Bezzi[1,2], *P. Mapelli*[1,2], *S. Ghezzo*[1,2], *F. Muffatti*[3], *M. Schiavo Lena*[4], *V. Andreasi*[3], *C. Canevari*[2], *P. Magnani*[2], *S. Partelli*[3], *M. Falconi*[1,3], *A. Chiti*[1,2], *M. Picchio*[1,2];
[1]*Vita-Salute San Raffaele University, Milan, ITALY,* [2]*Nuclear Medicine Department, IRCCS San Raffaele Scientific Institute, Milan, ITALY,* [3]*Pancreatic Surgery Unit, Pancreas Translational & Clinical Research Centre, IRCCS San Raffaele Scientific Institute, Milan, ITALY,* [4]*Pathology Department, IRCCS San Raffaele Scientific Institute, Milan, ITALY.*

Aim/Introduction: Accurate identification of lymph node metastases (LNs) is pivotal for surgical planning of pancreatic neuroendocrine tumors (PanNETs) patients; however, imaging techniques provide poor diagnostic sensitivity [1]. Aim of this study is to investigate whether [^{68}Ga]Ga-DOTATOC PET radiomics might improve the identification of LNs in PanNET patients candidate to surgery. ***Materials and Methods:*** Retrospective study including 72 patients (31F-41M, median age: 60y) with histologically proven well-differentiated PanNET who underwent [^{68}Ga]Ga-DOTATOC PET (25 PET/MR, 47 PET/CT) at IRCCS San Raffaele (2018-2022). Inclusion criteria were: 1) preoperative [^{68}Ga]Ga-DOTATOC PET performed within 1 month from surgery

2) availability of LNs pathology. PET scans were assessed for diagnostic accuracy, sensitivity (SN), and specificity (SP) in regional LNs. Primary tumors were manually segmented on PET scans (two readers). Images were resampled, normalized, and discretized. SUV_{max}, SUV_{mean}, somatostatin receptor density (SRD), total lesion SRD (TLSRD) and IBSI-compliant radiomic features (RFs) were measured. ComBat method was used to harmonize data. Parameters were standardized and discarded if affected by inter/intra-observer segmentation variability (ICC<0.80) and if highly redundant (Spearman>0.90). Mann-Whitney U test and ROC analysis were used to select the most relevant parameters and build the radiomic signature. Different machine learning (ML) algorithms, including support vector machine (SVM), k-nearest neighbors (kNN) and linear discriminant analysis (LDA), were optimized for prediction of pathological LNs and validated using 10-times repeated 10-fold cross-validation. A control model trained with only SUV_{max} and tumor volume was generated. Average balanced accuracy (bACC), SN and SP were collected and compared (Kruskal-Wallis) among radiomic models, control model, and expert's qualitative examination. ***Results:*** LNs were present in 29/72 patients at pathological examination. [^{68}Ga] Ga-DOTATOC PET detected LNs with a diagnostic accuracy=0.64, SN=0.17 and SP=0.95, providing 5/29 true positives (TP) and 24/29 false negatives (FN). The best radiomic model was a LDA (solver="eigen", shrinkage=0.6) trained with a radiomic signature composed of SUV_{max}, Sphericity, Skewness, Kurtosis, and Strength. The model, trained on primary tumors' features, provided predictions on pathological LNs with an average bACC=0.71, SN=0.67, and SP=0.75, resulting in an average of 15/29 TP and 5/29 FN and outperforming the control model (bACC=0.61, SN=0.35, SP=0.87, p<0.05) (Table1). ***Conclusion:*** [^{68}Ga]Ga-DOTATOC PET radiomic analysis improved PanNET pathological LNs prediction, shifting the diagnostic sensitivity from 0.17 to 0.67. Furthermore, the comparison with the control model proved the role of RFs in providing pivotal, additional information on PanNET pathological LNs assessment, thus supporting surgical planning of PanNET patients. ***References:*** [1]PartelliS. et al., Ann Surg.2022, doi:10.1097/SLA.0000000000005615

EP-0203

Role of 68Ga-DOTANOC PET/CT in the assessment of Appendiceal Neuroendocrine Tumors

R. Goel, *S. A. Shamim, N. Kumar, S. Rastogi, R. Kumar, C. Bal;*
All India Institute of Medical Sciences, NEW DELHI, INDIA.

Aim/Introduction: Appendiceal neuroendocrine tumours (NETs) are rare and usually detected incidentally after appendectomy. Appendiceal NETs typically have a lesser propensity for regional and distant metastases as compared to other types of NETs Appendiceal neuroendocrine neoplasms generally express somatostatin receptors (SSTRs), thus 68Ga-DOTANOC PET/CT helps in defining disease extent and SSTR status, which further helps in their assessment and planning for peptide receptor radionuclide therapy (PRRT) [1, 2]. This study aims to evaluate the role of 68Ga-DOTANOC PET/CT in patients with NET of appendix. ***Materials and Methods:*** Data of 12 patients (mean age 37.2 ± 14.5 years, range 11-56 years, M: F = 7:5) with histologically proven Appendiceal neuroendocrine tumors who underwent 68Ga-DOTANOC PET/CT from January 2018 and March 2023 were reviewed. Two certified nuclear medicine physicians independently reviewed the 68Ga-DOTANOC PET/CT studies. The tumor SUVmax and tumor-to-liver uptake ratios (T/L) were also measured. ***Results:*** There were 12 patients who underwent a total of 24 68Ga-DOTANOC PET/CT scans. Out of the 24 scans, 2 scans were performed at diagnosis for baseline staging, 14 for response assessment, and 8 for follow up post treatment completion. Out of the 2 scans done at diagnosis for baseline staging, 1 showed SUV max = 24, T/L=1.7, and the other showed SUV max = 4.8 with T/L=1.17. One study also revealed metastases to lymph nodes and liver. Out of the 14 scans performed for response assessment, 6 showed complete remission, 6 showed stable disease, and 1 revealed partial response. Disease progression was seen in 1/14 68Ga-DOTANOC PET/CT scans that detected new hepatic subcapsular deposits, peritoneal, omental & serosal deposits, ascites and right pleural effusion. Among the 8 scans performed for follow up, none of the studies revealed any SSTR expressing residual/recurrent disease. ***Conclusion:*** 68Ga-DOTANOC PET/CT may play an important role in staging/restaging, response evaluation, and detection of suspected recurrence in patients with appendiceal NETs which would help in their overall management. However, more studies on a larger patient population are required to validate the same. ***References:*** 1.Bayhan Z, Yildiz YA, Akdeniz Y, Gonullu E, Altintoprak F, Mantoglu B, et al. Appendix neuroendocrine tumor: Retrospective analysis of 4026 appendectomy patients in a single center. Emerg Med Int 2020;2020:1-6. 2.Mizutani G, Nakanishi Y, Watanabe N, Honma T, Obana Y, Seki T, et al. Expression of somatostatin receptor (SSTR) subtypes (SSTR-1, 2A, 3, 4 and 5) in neuroendocrine tumors using real-time RT-PCR method and immunohistochemistry. Acta Histochem Cytochem 2012;45(3):167-76.

EP-0204

Clinical impact of [68Ga] Ga-DOTA-TOC PET/CT in the management of neuroendocrine tumors.

J. Villa Palacios, *T. Aroui Luquin, D. Rivas-Navas, P. Guijarro-Caba, M. Muros De Fuentes;*
Hospital Universitario Virgen de las Nieves, Granada, SPAIN.

Aim/Introduction: The aim of this study is to determine the usefulness and therapeutic impact of [68Ga] Ga-DOTA-TOC PET/CT on the management of neuroendocrine tumors. ***Materials and Methods:*** A retrospective observational study (from November 2021 to November 2022) was conducted in patients who underwent [^{68}Ga] Ga-DOTA-TOC PET/CT study for the diagnosis or suspicion of neuroendocrine tumors. The PET/CT study was performed 60 minutes after intravenous administration of 111-185 MBq of 68Ga-edotreotide. All findings in [^{68}Ga] Ga-DOTA-TOC PET/CT were confirmed histologically, by specific imaging tests (ultrasound, CT scan or MRI), and/or clinical follow-up. ***Results:*** According to this protocol 126 patients have been studied (50 men and 76 women, mean age 61 ± 14.5 years). Gastro-pancreatic tumors were the most frequent in 48/126 patients (38.1%), followed by pulmonary carcinoids in 24/126 (19.1%) and others in 19/126 (15.1%). Using WHO 2017 grading, 19.8% of patients had low grade tumor (G1), 33.3% intermediate (G2), and 8.7% high (G3). The diagnostic accuracy of [^{68}Ga] Ga-DOTA-TOC PET/CT: TP: 59, TN: 61, FP: 4, FN: 2, S: 0.97 (95% CI 0.92-1.01), E: 0.94 (95% CI 0.88-1.00), PPV: 0.94 (95% CI 0.88-1.00), and NPV: 0.97 (95% CI 0.92-1.01). There were new lesions identified on [^{68}Ga] Ga-DOTA-TOC PET/CT in 25/126 patients (19.8%). Of these patients 20 (15.8%) had a change in treatment plan. ***Conclusion:*** [^{68}Ga] Ga-DOTA-TOC PET/CT showed high sensitivity mainly due to its ability in detecting lesions unsuspected by other imaging procedures, consequently conducting to a more acurrate treatment.

EP-0205

Utility of different semiquantitative parameters of [68Ga] Ga-DOTA-TOC PET/CT and their correlation with neuroendocrine tumors differentiation grade.

J. Villa Palacios, *T. Aroui-Luquin, D. Rivas-Navas, M. Muros De Fuentes, R. Sanchez Sanchez;*
Hospital Universitario Virgen de las Nieves, Granada, SPAIN.

Aim/Introduction: To correlate the semiquantitative parameters of [^{68}Ga] Ga-DOTA-TOC PET/CT with the differentiation grade of neuroendocrine tumors. ***Materials and Methods:*** A retrospective observational study of 125 patients with neuroendocrine tumors who underwent [^{68}Ga] Ga-DOTA-TOC PET/CT for initial diagnosis and/or disease follow-up. Patient variables such as sex, age, tumor grade, index Ki67, mitotic index were analyzed. The images were analyzed visually and semiquantitatively by calculating the SUVmax, SUVmean, SULmax, SULmean, total functional volume (TFV), tumor to liver SUVmax ratio (SUV_{TLR}), tumor to spleen SUVmax ratio (SUV_{TSR}), and tumor to blood pool ratio (SUV_{TBR}). ***Results:*** 126 patients (50 men and 75 women), the mean age was 61 ± 14.5 years. Gastropancreatic tumors were the most frequent in 48/126 patients (38.1%), and 46/125 patients (36.8%) had grade 2 tumors. [^{68}Ga] Ga-DOTA-TOC PET-CT was positive in 63 patients, and the mean SUVmax of the tumor lesions was 29.1 ± 24.8, SUVmean 16.0 ± 13.3, SULmax: 19.2 ± 16.8, SULmean: 11.2 ± 10.4, TFV (cm3): 76.6 ± 71.6. The SUV_{TLR}: 2.5 ± 3.2, SUV_{TSR}: 1.02 ± 1.1, and SUV_{TBR}:34.6 ± 47.7. The values of SUV_{TSR} and SUV_{TBR} were lower in less differentiated tumors (G3) compared to more differentiated G1 and G2 tumors (P =0.03). Neuroendocrine tumors of pulmonary origin had lower SUV_{TLR} values than gastro-enteropancreatic NETs (P = 0.04). All semiquantitative parameters showed a weak negative linear correlation with Ki67 values (Pearson's r < 0.3). ***Conclusion:*** The SUV_{TLR}, SUV_{TSR}, and SUV_{TBR} may be an alternative to SUVmax in the semiquantitative evaluation of [^{68}Ga] Ga-DOTA-TOC PET-CT, allowing for better discrimination of tumor differentiation.

EP-0206

Quantification of 99mTc-EDDA/HYNIC-TOC SPECT/CT: a feasible alternative to68Ga-DOTA-PET in patients with NET disease

P. Spiridon[1], *A. Lazar*[1], *R. Maaz*[1], *J. Rabah*[1], *M. Mutuleanu*[1,2], *M. Gherghe*[1,2];
[1]*Nuclear Medicine Department, Institute of Oncology "Professor Doctor Alexandru Trestioreanu", Bucharest, ROMANIA,*
[2]*Nuclear Medicine Department, University of Medicine and Pharmacy "Carol Davila", Bucharest, ROMANIA.*

Aim/Introduction: Neuroendocrine tumors (NET) are a heterogeneous group of malignant diseases originating from neuroendocrine cells, localized mostly in the gastro-entero-pancreatic tract and lungs. The detection of somatostatin receptors (SSTR) expressed on the cellular surface of primary tumors and metastases is crucial for the diagnosis and evaluation of the prognosis in these patients. The aim of our study was to characterize the single photon emission computed tomography/computed tomography (SPECT/CT) uptake pattern of ^{99m}Tc-EDDA/HYNIC-TOC in NETs in comparison to the physiological uptake of targeted tissues, allowing for a better differentiation between physiological uptake and tumor-related SSTR expression. ***Materials and Methods:*** We performed a retrospective study, including 53 patients who underwent a total of 74 ^{99m}TcEDDA/HYNIC-TOC scans in our department, as part of their clinical management. The examination protocol included a whole-body scan acquired 2 h after radiotracer administration, and a SPECT/CT performed 4 h post-injection. Maximum standardized uptake values (SUV_{max}), normalized to lean body mass, were measured for physiological uptake in liver, spleen and bone tissue and also in hepatic, lymph node and bone metastases. Statistical tests were performed to compare normal uptake and NET disease uptake in the liver, bones and lymph nodes. ***Results:*** The main clinical indications for a SPECT/CT study in our patients were pancreatic neuroendocrine tumor in 18 patients, pulmonary NET in 7 cases, gastrointestinal NET in 13 cases and 15 patients with unknown primary tumor, whose diagnosis at presentation was the presence of liver metastases. These patients performed ^{99m}TcEDDA/HYNIC-TOC scans for diagnosis/primary staging or for the assessment of residual/recurrent disease. Mean SUV_{max} values for ^{99m}TcEDDA/HYNIC-TOC were 19.41±13.92 in 62 liver metastases, 14.86±10.11 in 39 lymph nodes and 6.63± 9.83 in 15 bone metastases. The highest normal physiological uptake was observed in the spleen with mean SUV_{max} 10.08±6.10, followed by the liver with 3.74±1.22 and bone 1.04±1.04 g/ml. The differences between malignant and non-malignant lesions were statistically significant in liver and bones, after comparing the SUV_{max} in hepatic and osseous metastases with the physiological uptake (p<0.0001). ***Conclusion:*** The quantitative analysis of ^{99m}TcEDDA/HYNIC-TOC uptake on SPECT/CT in patients diagnosed with neuroendocrine tumors could represent a good alternative to positron emission tomography (PET) with ^{68}Ga-labelled peptides for patient management. The uptake patterns in normal and tumoral tissue represents a feasible substitute to ^{68}Ga-DOTA-PET quantification for peptide receptor radionuclide therapy planning and monitoring in these patients.

EP-0207

Prognostic impact of Gallium-68 DOTANOC PET/CECT in metastatic well differentiated Gastro-entero-pancreatic Neuroendocrine Tumors (GEP NETs).

I. Dev, *V. Rangarajan, A. Puranik, A. Agrawal, N. Purandare, S. Shah, S. Shrikhande, V. Chaudhari, S. Choudhury, S. Ghosh;*
TATA MEMORIAL CENTRE, Mumbai, INDIA.

Aim/Introduction: To evaluate the prognostic value of Ga-68 DOTANOC PET/CECT (DOTA PET) based parameters in assessing progression free survival (PFS) in patients with metastatic well differentiated (WD GEP-NETs). ***Materials and Methods:*** This retrospective study included 85 patients of metastatic WD GEP NETs who underwent DOTA PET for staging/metastatic work up. Of them, 35 patients had primary site in pancreas, 40 in small bowel and remaining 10 at other sites. In 46 out of 85 patients, primary tumor was resected. Patients were stratified into two groups based on median SUVmax of target lesion (highest uptake of either primary/metastatic lesion), liver involvement on DOTA PET calculated as tumor volume measured in three planes involving more than 50% of liver, and resection of primary. PFS was calculated from the date of DOTA PET to the last date of clinical/radiological progression or death due to disease. Survival graphs were drawn using Kaplan Meier method and compared using log rank test. P value < 0.05 was considered significant. ***Results:*** Median PFS was 15 months (Range: 2-54 months). ROC analysis yielded cut-off of 35 for SUVmax of target lesion. PFS in patients with SUVmax 35 was 44 months and for those with SUVmax less than 35 was 24 months (p value 0.003). Patients with more than 50% liver involvement on DOTA PET showed lesser PFS (26 months) than in those with less than 50% involvement (49 months) (p value 0.008). PFS was higher in patients with resection of primary tumor (42 months) than in patients with unresected primary (28 months) (p value 0.039). ***Conclusion:*** Higher SUVmax of target lesion, less than 50% liver involvement on DOTA PET and resection of the primary tumor are statistically significant prognostic factors associated with improved progression free survival. ***References:***

Tsilimigras DI, Hyer JM, Paredes AZ, et al. Resection of Primary Gastrointestinal Neuroendocrine Tumor Among Patients with Non-Resected Metastases Is Associated with Improved Survival: A SEER-Medicare Analysis. J Gastrointest Surg. 2021;25:2368-2376. Cloyd JM, Ejaz A, Konda B, Makary MS, Pawlik TM. Neuroendocrine liver metastases: a contemporary review of treatment strategies. Hepatobiliary Surg Nutr. 2020 Aug;9(4):440-451.

EP-0208

Role of 68Ga-DOTANOC PET/CT in the assessment of Lung Carcinoids

S. Shamim, *R. Goel, N. Kumar, G. Arora, S. Rastogi, A. Goyal, R. Kumar, C. Bal;*
AIIMS New Delhi, Delhi, INDIA.

Aim/Introduction: Lung carcinoids (LC) are rare malignant neoplasms, accounting for a very small percentage of all lung tumors. The preoperative classification of LC into typical carcinoid and atypical carcinoid and ascertaining extent of dissemination are important factors for deciding treatment and prognosis. Majority of the LC are found to express somatostatin receptors (SSTRs), thus ^{68}Ga-DOTANOC PET/CT can help in defining disease extent and SSTR status, which further helps in their assessment and management. This study aims to evaluate the role of ^{68}Ga-DOTANOC PET/CT in patients with Lung carcinoids. ***Materials and Methods:*** We retrospectively reviewed 41 ^{68}Ga-DOTANOC PET/CT in 32 patients with Lung carcinoids at our institution between January 2017 and March 2023. ***Results:*** There were 32 patients (10 female, 22 males; age 15-63 years) who underwent ^{68}Ga-DOTANOC PET/CT scans. Out of the 41 scans, 4 scans were done for initial diagnosis of suspected lung carcinoids, 15 scans were performed for baseline staging, 13 for response assessment, 9 for suspected recurrence/surveillance.All 4 scans performed for initial diagnosis of suspected LC revealed SSTR expressing lesions in the lung/bronchus suggestive of lung carcinoids. On histopathological correlation, 2/4 patients were found to have typical carcinoids whereas a diagnoses of sclerosing pneumocytoma and mixed germ cell tumor was made for the other two patients respectively.Out of the 15 scans done at diagnosis for baseline staging, 12 were typical carcinoids whereas 3 were atypical carcinoids. Four of 15 scans also revealed metastases to lymph nodes, liver and skeletal sites.Out of the 13 scans performed for response assessment, 12 showed stable disease and 1 revealed disease progression.Among the 9 scans performed for surveillance/ suspected recurrence, 1 study revealed SSTR expressing hypodense lesions in the liver, whereas the rest showed no SSTR expressing residual/recurrent disease. ***Conclusion:*** ^{68}Ga-DOTANOC PET/CT may play an important role in staging/restaging, response evaluation and detection of suspected recurrence in patients with lung carcinoids which would help in their overall management. However, more studies on a larger cohort are still required to validate the same.

EP-0209

Assessment of glucose metabolism in skeletal muscle and adipose tissue with the use of 2-[18F]FDG PET/CT in patients with ectopic adrenocorticotropin secretion

M. Opalinska[1], *J. Kokoszka*[2], *E. Rzepka*[1], *K. Sitarz*[3], *A. Sowa-Staszczak*[1], *A. Gilis-Januszewska*[1], *A. Hubalewska-Dydejczyk*[1];
[1]*Jagiellonian University Medical College, Chair and Department of Endocrinology, Krakow, POLAND,*
[2]*Endocrinology, Oncologic Endocrinology and Nuclear Medicine Department, University Hospital in Krakow, Krakow, POLAND,* [3]*University Hospital in Krakow, Krakow, POLAND.*

Aim/Introduction: 2-[18F]FDG PET/CT, commonly used for neoplastic lesions detection, also allows assessment of the severity of the inflammatory process in muscles. Patients with Cushing's syndrome (CS) demonstrate many metabolic changes involving muscle, adipose tissue and bones, mediated by cytokines and hormones. Ectopic adrenocorticotropin secretion (EAS) accounts for 10-15% of cases of CS and is characterized by high fast-rising cortisol levels leading to deterioration of body composition including worsening of muscle quality. Some mechanisms, involving muscle steatosis leading to myopathy, are known, but their relationship to glucose metabolism is not well investigated. The aim of our study was to assess glucose metabolism with the use of 2-[18F]FDG PET/CT in skeletal muscle and adipose tissue in patients with ectopic ACTH-syndrome. ***Materials and Methods:*** Analysis of 2-[18F]FDG PET/CT scans in 12 patients with EAS in comparison to age and sex-matched control group was performed. On unenhanced CT scans the body composition on cross-sectional computed tomography images at the L3 level - skeletal muscle area (SMA), skeletal muscle index (SMI), visceral fat area (VFA), visceral fat index (VFI), subcutaneous fat area (SFA), subcutaneous fat index (SFI), intermuscular adipose tissue (IMAT), bone density in vertebrae L3 was assessed. Psoas muscle (at the L3 vertebra) and femoris muscle (medial vastus of the quadriceps femoris muscle at the mid-thigh level) metabolic volume (MV), SUV peak, lesion glycolysis (LG) in both right and left muscle groups were evaluated base on the 2-[18F]FDG-PET scan results. The results were related to the hormonal status: ACTH, midnight cortisol, cortisol after 1mg of dexamethasone concentrations. ***Results:*** The comparison of glucose metabolism muscle and fat composition assessed by 2-[18F]FDG-PET and CT respectively, showed inverse correlation between SMI and metabolic volume of femoris muscle (p=0.047). Moreover, ACTH concentration was negatively correlated with metabolic volume and SUV peak of psoas muscle (p=0.044 and p=0.033, respectively). There were no differences between study and control group regarding the prevalence of sarcopenia assessed on SMI, body composition on CT scans and skeletal muscle metabolism on PET scans. ***Conclusion:*** In our patients with EAS, at diagnosis skeletal muscle, fat and bone metabolism were not significantly deteriorated. Lower SMI with increased 2-[18F]FDG activity in femoris muscles may indicate increased inflammatory status in intramuscular adipocytes and fibrotic tissue. Negative correlation between ACTH and glucose metabolism in psoas muscle may potentially reflect better muscle state in patients in better general condition.

EP-0210

The evaluation of kidney function using the Somatostatin (SSTR)-targeting radioligands 18F-SiFA-TATE, 68Ga-DOTATATE and 68Ga-DOTATOC in a theranostic setting

M. Tiling[1], *A. Holzgreve*[1], *S. Kunte*[1], *G. Sheikh*[1], *M. Unterrainer*[2,1], *P. Bartenstein*[1], *A. Delker*[1], *L. Unterrainer*[1];
[1]*Department of Nuclear Medicine, University Hospital, LMU Munich, Munich, GERMANY,*
[2]*DIE RADIOLOGIE, Munich, GERMANY.*

Aim/Introduction: Not only tumor cells but also physiologically renal tissue expresses somatostatin receptors (SSTR), which results in a high renal uptake of SSTR-ligands. Since the application of Lu-177-DOTATATE can lead to nephrotoxicity, the renal function is often evaluated by pre- and inter-therapeutic ^{99m}Tc-MAG3 renal scintigraphy. Recently, it could be demonstrated that renal ^{18}F-PSMA-1007 uptake allowed the quantification of renal split function in prostate cancer patients. The analogue evaluation of estimating renal function in patients with neuroendocrine tumors prior, during and after Lu-177-DOTATATE therapy was evaluated. ***Materials and Methods:*** Overall, we correlated MAG3-derived renal function with kidney uptake in SSTR-PET/CT (n=30 ^{18}F-SiTATE; n=10 ^{68}Ga-DOTATATE; n=10 ^{68}Ga-DOTATOC). An obstruction in the

urinary tract system was excluded. For each of the respective PET ligands, a specific threshold of SUV_{max} (^{18}F-SiTATE: 25% of SUV_{max}; ^{68}Ga-DOTATATE: 32,5% of SUV_{max}, ^{68}Ga-DOTATOC: 25% of SUV_{max}) was applied to delineate the kidneys in correlation with their CT volume surrogate. Split renal function was calculated by two approaches. Firstly, by considering threshold-based kidney volume and SUV_{mean} (SRF_{TOTAL}), and secondly based on threshold-based SUV_{max} (SRF_{SUV}). SRF_{TOTAL} and SRF_{SUV} were correlated with the MAG3-derived split renal function (SRF_{MAG3}). Global renal function was determined by correlating the bilateral total renal tracer uptake (TRU) and MAG3 tubular excretion rate. ***Results:*** Correlation analysis of MAG3 and ^{18}F-SiTATE showed a weak, but significant correlation between SRF_{MAG3} and SRF_{TOTAL} (r=0.462; r^2=0.214; p=0.010) and no correlation between SRF_{MAG3} and SRF_{SUV} (r=-0.044; r^2=0.002; p=0.817). Bilateral ^{18}F-SiTATE uptake (TRU) was not significantly correlated with MAG3 tubular excretion rate (r=0.155; r^2=0.024; p=0.413). In the ^{68}Ga-DOTATOC and ^{68}Ga-DOTATATE cohorts, renal function evaluated by MAG3, SRF and TRU showed no significant correlation. ***Conclusion:*** Renal ^{18}F-SiTATE uptake might allow the quantification of quantify split renal function using SRF_{TOTAL} with moderate accuracy and thus might be used to predict renal function; in clinical routine, this approach might lead to early identification of patients with borderline split function even prior to further therapies. In a further step, kidney doses in the post-therapeutic SPECT/CTs should be correlated with PET-derived split renal function to additionally evaluate the impact of SSTR-targeted imaging for dose absorption in correlation with kidney function.

EP-0211

Spectrum of hyperuptake findings detected in PET/CT [68Ga]Ga-DOTA-TOC studies. Experience in our center

S. Bondia-Bescós*, J. Vercher-Conejero, J. Martin-Marcuartu, A. Rodriguez-Gasen, J. Suils-Ramón, M. Perlaza-Jiménez, M. Pudis, B. Hervás-Sanz, J. Díaz-Moreno, M. Cortés-Romera;*
Nuclear Medicine-PET (IDI) Department, Bellvitge University Hospital, Barcelona, SPAIN.

Aim/Introduction: To analyze the detection capacity of [^{68}Ga]Ga-DOTA-TOC PET/CT for neuroendocrine neoplasms (NEN) as well as other non-neuroendocrine hyper-uptake lesions and their uptake degree. ***Materials and Methods:*** Retrospective study of [^{68}Ga]Ga-DOTA-TOC PET/CT performed between April 2019 and December 2022 in patients with or suspected NENs at our center.The diagnosis of non-neuroendocrine hyper-uptake lesions was made according to biopsy, imaging semiology and/or clinical evolution.Semiquantitative analysis of non-neuroendocrine tumors using the SUV_{max} (g/ml). ***Results:*** A total of 324 studies (270 patients: 123 women, mean age 61.6 years) were evaluated. Repeated findings from the same patient were excluded.The most frequent NEN were: gastroenteropancreatic (64%), lung carcinoids (5.1%), paragangliomas/pheochromocytomas (2.6%). The most frequent degree of differentiation in GEP-NEN biopsies was G2, followed by G1 and G3.The primary tumor was detected in 38% of the examinations referred by NEN of unknown primary tumor. The study was negative at 13%. The most frequent hyper-uptake findings not related to NEN were:- Non-neoplastic (63p, 48.8%): reactive adenopathies (13/63), Multinodular goiter, BETHESDA nodules <3 (13/63), BPH/prostatitis (12/63).- Benign neoplasms (21p, 16.3%): meningioma (6/21), miomas (3/21), parathyroid/pleomorphic adenoma (2/21). The average SUV_{max} was 9.38, with a range between 0.83 (cutaneous neurofibroma) and 53.35 (meningioma).- Malignant neoplasms (12p, 9.3%): Invasive breast cancer (ductal/lobular) (3/12), Prostate adenocarcinoma (3/12), Pancreatic adenocarcinoma (2/12). The average SUV_{max} was 5.71 with a range between 1.67 (breast cancer) and 14.03 (intestinal GIST). ***Conclusion:*** [^{68}Ga]Ga-DOTA-TOC PET/CT is very useful for localizing NEN of unknown origin and assessing radiopeptide therapy.In our study, hyper-uptake non-neuroendocrine lesions were observed in 1/3 of the patients, of which 25% were of neoplastic origin. The intensity of uptake of the non-neuroendocrine neoplasms detected was variable and we found no apparent relationship with their degree of malignancy. ***References:*** Ambrosini V, Zanoni L, Filice A, et al. Radiolabeled Somatostatin Analogues for Diagnosis and Treatment of Neuroendocrine Tumors. Cancers (Basel). 2022;14(4):1055.Malan, N.; Vangu, M.D.T. Normal Variants, Pitfalls and Artifacts in Ga-68 DOTATATE PET/CT Imaging. Front. Nucl. Med. 2022, 2, 825486.

EP-0212

68Ga-DOTA peptides PET/CT radiomic parameters useful to differentiate para-physiological uptake in pancreatic uncinate process from pancreatic NET.

F. Linguanti*[1], E. M. Abenavoli[2], A. Lombardo[1], V. Briganti[2], F. Mungai[3], L. Antonuzzo[4], D. Lavacchi[4], L. Vaggelli[2], M. Matteini[2], R. Sciagrà[1], V. Berti[1];*
[1]Nuclear Medicine Unit, Department of Experimental and Clinical Biomedical Sciences 'Mario Serio', University of Florence, Florence, ITALY, [2]Department of Nuclear Medicine, Azienda Ospedaliero-Universitaria Careggi, Largo Brambilla 3, 50134, Florence, ITALY, [3]Department of Radiology, Azienda Ospedaliero-Universitaria Careggi, Largo Brambilla 3, 50134, Florence, ITALY, [4]Medical Oncology Unit, Careggi University Hospital, Largo Brambilla 3, 50134, Florence, ITALY.

Aim/Introduction: Pancreatic neuroendocrine tumors (pNET) are among the most common neuroendocrine tumors and 68Ga-DOTA peptides PET/CT (PET/CT) represents the gold standard imaging evaluation in their clinical management. However, the pancreatic uncinate process (UP) is often characterized by para-physiological uptake in PET/CT, simulating a pathological radiotracer accumulation with consequently difficulties in imaging interpretation.This study tested the diagnostic value of PET/CT radiomic parameters in the histological differentiation of pNET from para-physiological UP uptake. ***Materials and Methods:*** We retrospectively analyzed 68 patients, with pathology-proven pNET (n=34) and non-pancreatic NET (n=34) with para-physiological increased UP uptake without pancreatic alterations at morphological scans who underwent PET/CT pre-treatment.For all patients, a volume of interest (VOI) both for the pNET and the UP, was manually contoured on PET/CT images and then defined using a thresholding-based model with a cut-off of 50% of the SUVmax. Radiomic parameters were measured using LIFEx software [1].The comparison of parameters between groups was performed using ANOVA test (P<0,005). We performed factor analysis to remove redundancy of cross-correlated variables and discriminant analysis to examine the power of the potential independent predictors. ***Results:*** SUVmax, SUVmean and MTV resulted significant different between two groups and only SUVmax and SUVmean were confirmed in discriminant analysis.Based on our results, several PET textural features resulted significant predictive of tissue characterization. Among first order PET parameters, we found MORPHOLOGICAL_Maximum3Ddiameter, INTENSITY-BASED_MaximumGreyLevel and INTENSITY-BASED_Range that correctly classified more than 85% of subjects.Among second order PET parameters, GLCM_

SumAverage, GLCM_Autocorrelation; GLRLM_ShortRunHighGreyLevelEmphasis and GLRLM_HighGreyLevelRunEmphasis; GLSZM_GreyLevel Variance, GLSZM_NormalisedZoneSizeNonUniformity and GLSZM_SmallZoneHighGreyLevelEmphasis correctly classified more than 85% of subjects. ***Conclusion:*** Imaging radiomics could be useful to better characterize pancreatic tissue, differentiating pNET from para-physiological uptake of UP with an important reduction of 68Ga-DOTA peptides PET/CT pitfalls. ***References:*** [1] Nioche C, et al. Cancer Research. 2018; 78:4786-4789; www.lifexsoft.org

EP-0213

β-1600 Q.Clear Reconstruction Improves [68Ga]Ga-DOTANOC Digital PET/CT Image Quality

E. Fortunati[1], *N. Bonazzi*[1], *M. Di Franco*[1], *L. Zanoni*[2], *C. Mosconi*[3,4], *S. Civollani*[2], *D. Campana*[3,5], *C. Malizia*[6], *V. Allegri*[2], *S. Fanti*[1,2], *V. Ambrosini*[1,2];
[1]*Nuclear Medicine, Alma Mater Studiorum University of Bologna, Bologna, ITALY,* [2]*Nuclear Medicine, IRCCS, Azienda Ospedaliero-Universitaria di Bologna, Bologna, ITALY,* [3]*DIMEC, IRCCS, Azienda Ospedaliero-Universitaria di Bologna, Bologna, ITALY,* [4]*Radiology, IRCCS, Azienda Ospedaliero-Universitaria di Bologna, Bologna, ITALY,* [5]*Division of Medical Oncology, IRCCS, Azienda Ospedaliero-Universitaria di Bologna, Bologna, ITALY,* [6]*PET Radiopharmacy Unit, IRCCS, Azienda Ospedaliero-Universitaria di Bologna, Bologna, ITALY.*

Aim/Introduction: to assess the preferred Q.Clearβ-level for digital [68Ga]Ga-DOTANOC PET/CT reconstruction vs standard reconstruction (STD) for both overall scan and single lesions' visualisation (for the most-avid finding <1cm and >1cm, respectively). ***Materials and Methods:*** Inclusion criteria: (1) patients with neuroendocrine neoplasms included in a prospective observational monocentric CE-approved study between September2019/January2022; (2) [68Ga]Ga-DOTANOC digital PET/CT and contrast-enhanced-CT (ceCT) performed at our center at the same time-point. Images were reconstructed with STD and with three Q.Clearβ-levels (800, 1000, 1600). Scans were reviewed by two expert nuclear medicine readers, unaware of clinical data, who independently chose the preferred reconstruction for visual quality of both overall scan and single lesions (for the most-avid finding <1cm and >1cm, respectively). Standard of reference to validate PET/CT findings was ceCT (revised by one expert radiologist) and clinical follow-up. Semi-quantitative analysis was performed on STD and β-1600 in target lesions <1cm (t) and >1cm (T) concordant at both PET/CT and ceCT: SUVmax, SUVmean, standard deviation (SD) of the highest uptake target lesion (T and t) and liver-background (L); SUVmax-T/SUVmean-L; SUVmax-t/SUVmean-L; Signal-to-noise liver ratio (SNR-L=SUVmean/SD); Contrast-to-noise ratio (CNR=SUVmeanT-SUVmeanSurroundingBackground/SDBackground). ***Results:*** Overall, 55 patients (age: mean=60.4, median= 63 [23-87]yo) were included. Visual image quality of β-1600 was considered superior over the other reconstructions (100% agreement), for both overall scan and single lesions. PET/CT was positive in 37/55 patients: SNR-L (β-1600 vs STD: mean=9.9 vs 7.3, median=9.9 vs 7.1, range [4.7-15.7] vs [4.6-14.0]) and SD-L (β-1600 vs STD: mean and median=0.5 vs 0.7, range [0.2-1.1] vs [0.3-1.3]) were the only significantly ($p<0.001$) different parameters between β-1600 and STD. Similar results for both SNR-L and SD-L were confirmed ($p<0.001$) in the sub-group analysis of concordant lesions >1cm (T, n=18) and <1cm (t, n=10). Lesions' dependent parameters (SUVmax, SUVmean and CNR) were not significantly different for overall and subgroups (T,t) analyses. The subgroups analysis of PET/CT and ceCT discordant lesions<1cm (n=20 patients), showed that PET was TP in 11/20 (bone), VN in 4/20, FN in 4/20 (liver). ***Conclusion:*** Q.Clearβ-1600 was superior to all other reconstructions for overall image quality and lesions' visualization. Semi-quantitative analyses confirms the typical Q.Clear signal-to-noise suppression: higher SNR of the liver(reference background) was observed for β-1600 vs STD, without any significant change in lesions' dependent parameters. These preliminary results pave the way to the routine use of Q.Clearβ-1600 for image quality optimization (e.g.while SUVmax values are comparable whether Q.Clearβ-1600 or STD is used).

EP-0214

Comparison of 68Ga-DOTATATE PET/CT and 68Ga-DOTATATE PET/MR in Detection of Neuroendocrine Tumour Liver Metastasis

B. Demir[1], *C. Soydal*[1], *M. Araz*[1], *M. H. Baltacioglu*[1], *D. Kuru Oz*[2], *N. O. Kucuk*[1];
[1]*Ankara University School of Medicine Department of Nuclear Medicine, Ankara, TÜRKIYE,* [2]*Ankara University School of Medicine Department of Radiology, Ankara, TÜRKIYE.*

Aim/Introduction: ^{68}Ga-DOTATATE is a highly efficient molecular imaging agent that can be used for various malignancies like gastroenteropancreatic neuroendocrine tumours, carcinoid tumours of lung, paraganglioma, pheochromocytoma and neuroblastoma. In this study we aimed to investigate additive value of dedicated 68Ga-DOTATATE liver PET/MRI that was performed after PET/CT compared to standard whole body PET/CT. ***Materials and Methods:*** A total number of 26 patients and 30 pairs of PET/CT and dedicated respiratory gated contrast-enhanced PET/MRI acquired later in same session that was performed between November 2018-January 2023, were included in this retrospective study. Total detected lesion number, SUVmax, SUVmean, metabolic tumour volume (MTV), total lesion ^{68}Ga-DOTATATE uptake (TL-DOTATATE) and tumour to background ratio (TBR) were noted. Detected lesion numbers were grouped as no lesions, 1 lesion, 2-4 lesions, 5-10 lesions and >10 lesions for analysis. Also for each study signal/noise ratio (Liver paranchyme SUVmean/Standard Deviation) (SNR) and contrast/noise ratio ([Lesion SUVmax-Liver SUVmean]/Standard Deviation of Liver Parenchyma VOI) (CNR) values were calculated. For statistics analysis chi-square test for lesion numbers and Mann-Whitney-U test for SNR and CNR comparison were utilised. ***Results:*** In 15 studies (50%) both modalities were negative for liver metastasis. In the remaining 15 studies PET/CT detected 1 lesion in 5 patients, 5-10 lesions in 4 patients and >10 lesions 6 patients. In the same patients PET/MR detected 1 lesion in 4 patients, 2-4 lesions in 1 patient, 5-10 lesions in 2 patients and >10 lesions in 8 patients. Only in 3 patients PET/MRI detected more lesions than PET/CT. There was not any patients who was negative on PET/CT imaging with positive PET/MRI findings for liver metastasis. SNR was significantly higher in PET/MRI (median 9.45) compared to PET/CT (median 7.49) ($p=0.021$). CNR values were higher in PET/MRI (median 29.39 vs. 17.14) but did not reach significance ($p=0.202$). ***Conclusion:*** Standard whole-body ^{68}Ga-DOTATATE PET/CT is highly efficient in detection of liver metastasis of neuroendocrine neoplasms. Addition of dedicated liver PET/MRI following whole-body PET/CT imaging had a little additive value for detection of metastasis and may only be helpful in limited number of selected patients.

EP-0215

[68Ga]Ga-DOTANOC and [18F]F-FDG PET/CT Tumour Burden Across 3-Grades Functional Scoring

E. Fortunati[1], *N. Bonazzi*[1], *M. Di Franco*[1], *L. Zanoni*[2], *C. Mosconi*[3,4], *D. Campana*[3,5], *C. Malizia*[6], *E. Andrini*[5], *V. Allegri*[2], *S. Fanti*[1,2], *V. Ambrosini*[1,2];
[1]*Nuclear Medicine, Alma Mater Studiorum University of Bologna, Bologna, ITALY,* [2]*Nuclear Medicine, IRCCS, Azienda Ospedaliero-Universitaria di Bologna, Bologna, ITALY,* [3]*DIMEC, IRCCS, Azienda Ospedaliero-Universitaria di Bologna, Bologna, ITALY,* [4]*Radiology, IRCCS, Azienda Ospedaliero-Universitaria di Bologna, Bologna, ITALY,* [5]*Division of Medical Oncology, IRCCS, Azienda Ospedaliero-Universitaria di Bologna, Bologna, ITALY,* [6]*PET Radiopharmacy Unit, IRCCS, Azienda Ospedaliero-Universitaria di Bologna, Bologna, ITALY.*

Aim/Introduction: To describe [68Ga]Ga-DOTANOC and [18F]FDG-PET/CT tumour burden in patients (pts) with suspected/diagnosed neuroendocrine neoplasms (NEN) divided according to a 3-grades functional scoring. ***Materials and Methods:*** Pts prospectively enrolled in a monocentric CE-approved-prospective observational study (131/2017/O/Oss) on [68Ga]Ga-DOTANOC PET/CT, and previously also assessed with [18F]F-FDG PET/CT were included. Tumour burden parameters were: Total Receptor volume(RTV) and Total Lesion Activity(TLA=SUVmeanxRTV) on [68Ga]Ga-DOTANOC PET/CT, Metabolic Tumour Volume(MTV) and Total Lesion Glycolisis(TLG=SUVmeanxMTV) on [18F]F-FDG-PET/CT; MTV/RTV and TLG/TLA were calculated. Pts were classified into 3 categories [1]: C1=all lesions [18F]F-FDG-negative and [68Ga]Ga-DOTANOC-positive; C2= all lesions [68Ga]Ga-DOTANOC-positive, ≥1 [18F]F-FDG-positive; C3= ≥1 [18F]F-FDG-positive lesions and at least one of them [68Ga]Ga-DOTANOC-negative. Pts were also classified according to WHO-grade. ***Results:*** 60 pts were studied (median days between PET/CT scans=14[1-99]). 15/60 pts [4G1 (2pancreas, 1ileum, 1colon), 10G2 (5pancreas, 2ileum, 2atypical lung carcinoid (AC), 1CUP), 1G3 (pancreas)] were C1, with median-RTV=13,3(mean:47,4[0,9-349,5]), median-TLA=95,2(mean:462[18-3041,5]). 30/60 pts [7G1 (3pancreas, 3ileum, 1duodenum), 16G2 (5pancreas, 2AC, 4typical lung carcinoid (TC), 3ileum, 1colon, 1CUP), 6G3 (4pancreas, 1colon, 1AC), 1NEC (pancreas)] were C2 with median-RTV=52,5(mean:99,9[2,8-440,7]), median-TLA=606,2(mean:1413,3[4-7498,1]), median-MTV=25 (mean:68,8[1,4-377,6]) and median-TLG=58,3(mean261,2[3,6-1628,7]). 10/60 pts [2G1 (1TC, 1ileum), 4G2 (3AC, 1pancreas), 3G3 (1ileum, 1stomach, 1AC), 1NEC (CUP)] were C3 with median-RTV=8,3(mean:106,1[0-957,9]), median-TLA=18,3(mean:1264,6[0-11964]), median-MTV=41,9(mean:384,6[7,8-1947,6]) and median-TLG=105,3(mean:3231,3[7,5-16288,6]. In 5/60 pts [2G1 (2ileum), 2G2 (1ileum, 1TC), 1G3 (pancreas)] both scans were negative, so they were excluded from the classification. MTV and TLG were not significantly different between C2 and C3, while comparison with C1 (FDG-negative) was of course significative. TLA was significantly higher in C2 vs C3 ($p<0.03$), as a marker of increased heterogeneity, while RTV was not significantly different among groups. MTV/RTV ratio was significantly different across all groups (C2 vs C3, $p=0.002$; others: $p<0.001$). Same results were observed for the TLG/TLA ratio (C2 vs C3, $p=0.018$; others: $p<0.001$). Considering WHO-grading, MTV significantly differed between G2 and G3 ($p=0.015$) while TLG was significantly different in G1 vs G3 ($p=0.027$) and in G2 vs G3 ($p=0.01$). While no differences for RTV, MTV/RTV and TLG/TLA were observed. ***Conclusion:*** Both MTV and TLG increase, not reaching statistical significance, with functional scoring. TLA was the only parameter significantly different between C2 and C3, as a marker of increased heterogeneity. MTV/RTV ratio was significantly different across all groups. ***References:*** [1] Karfis I et al. Prognostic value of a three-scale grading system based on combining molecular imaging with 68Ga-DOTATATE and 18F-FDG PET/CT in patients with metastatic gastroenteropancreatic neuroendocrine neoplasias. Oncotarget.2020. doi:10.18632/oncotarget.27460.

EP-0216

Correlation Between Dual Tracer Imaging (68 Ga Dotanoc and 18 FDG PET) And Mib Index in WHO Grade 2 NET.

S. Kale*, A. Puranik, N. Purandare, S. Shah, A. Agrawal, V. Rangarajan, S. Shrikhande, V. Ostwal, A. Ramaswamy, M. Bhandare, V. Chaudhari;*
TATA MEMORIAL CENTRE, Mumbai, INDIA.

Aim/Introduction: Aims: To evaluate correlation between Mib index and dual tracer scores (Krenning's and FDG score) and its impact on clinical management.***Introduction: -*** Neuroendocrine tumour are heterogeneous with both intra and inter-lesional heterogeneity which can be portrayed by dual tracer imaging with DOTANOC and FDG PET CT. Well differentiated WHO Grade 2 is a large sub group with lot of tumour heterogeneity within. Here we are calculating correlation between dual tracers scores (Krenning's and FDG score) obtained from imaging and its eventual impact on clinical management. ***Materials and Methods:*** 101 patients grade 2 neuroendocrine who underwent dual tracer PET (DOTATATE PET and FDG PET CT) were chosen. They were divided into three groups as (3-5%), (6-10%) and (11-20%) according to the Mib index. Krenning's and FDG scores were calculated based on MIP images. Chi- square and Spearmen's correlation tests were used to establish correlation between dual tracer scores. Management decisions post dual tracer imaging were analyzed to assess clinical impact. ***Results:*** Chi square and Spearman's correlation tests showed no significant correlation between Krenning's score and Mib index groups. While there is positive correlation found between FDG score and Mib index groups, (r_s =.276) (p value = 0.005). Also, dual tracer imaging changed the management in 36 out of 37 patients who were previously receiving treatment. Out of the 64 patients who underwent scanning post biopsy, 33 patients turned out to be both DOTA and FDG positive (51.56%) and received PRRT + chemotherapy (22/33 patients, 66.67%) making significant impact and 26 patients turned out to be only DOTA scan positive (40.62%). PRRT is the most common treatment chosen (14/26 patients 53.84%). ***Conclusion:*** There is no significant correlation between Krenning's score (DOTA PET CT) and Mib index, while there is positive correlation between FDG score (FDG PET CT) across Mib index in grade 2 NET. Also there is significant clinical impact of dual tracer imaging in grade 2 NET.

EP-12

e-Poster Area

B: Imaging Clinical Studies -> B1 Oncological Imaging Clinical Study -> B17 Colorectal

EP-0217

Differentiating subcentimeter lung metastasis in colorectal cancer patients by radiomics and deep learning approaches: a multicenter study

D. Ma*;*
Department of Colorectal Surgery, Zhejiang Cancer Hospital, Hangzhou, CHINA.

Aim/Introduction: Preoperative evaluation of the indeterminate lung nodules is important for individual treatment of colorectal cancer (CRC). We aim to develop and validate discriminative radiomics and deep learning approaches for differentiating subcentimenter lung metastases (LMs) in CRC patients. ***Materials and Methods:*** Models were developed in a primary cohort included 1194 consecutive CRC patients with initial subcentimeter

size LMs on CT. Patients were randomly assigned (7:3) to the training or internal validation cohorts (IVC). Machine learning (ML), deep learning (DL), and the integration of radiomics and DL features were applied to classify the subcentimeter lung nodules as LMs or benign lesions. Two independent external validation cohorts (EVC) consisted of 101 (EVC1) and 40 (EVC2) patients. To verify the generalizability for nodules of smaller sizes, stepwise validations on the subgroups according to the nodule's largest diameter (10, 9, 8, 7, 6, 5, ≤4 mm) were conducted. ***Results:*** The diagnostic accuracy by radiologists was 0.705 in primary cohort. The best ML based on support vector machine (SVM) showed a 0.981 area under the curve (AUC) in IVC, a 0.961 and 0.996 AUC in EVC1 and EVC2. The best integration model showed a 0.973 AUC in the IVC and a 0.943 and 0.974 AUC in EVC1 and EVC2. The DL model showed a 0.953 AUC in the IVC and a 0.907 and 0.951 AUC in EVC1 and EVC2. Stepwise validation demonstrated that with the LM diameter decreasing, the integration model was the most stable with smaller LMs, and was the best for LM ≤5 mm. ***Conclusion:*** Our findings showed that radiomics and deep learning approaches based on CT could improve current diagnostic accuracy of subcentimeter CRC LMs. Specially, novel integration model was the best with LMs ≤5 mm. This study provided an automatic and noninvasive solution for determining subcentimeter LMs in the individual management of CRC.

EP-0218

Correlation of 18F-FDG PET/CT Parameters Such As SUVmax, MTV and TLG with Histopathological Characteristics in Colorectal Cancer Patients

B. Ural, *B. Okudan Tekin;*
Ankara Bilkent City Hospital, Ankara, TÜRKIYE.

Aim/Introduction: It has been reported that metabolic parameters such as metabolic tumor volume (MTV) and total lesion glycolysis (TLG) in 18F-Fluorodeoxyglucose (18F-FDG) PET/CT are diagnostic and prognostic biomarkers of various cancers. Microsatellite instability (MSI) is caused by mutations in DNA mismatch repair genes is found in 10-15% of sporadic colorectal cancers. The aim of this study is to investigate the relationship between metabolic parameters and histopathological features of the primary tumor obtained from 18F-FDG PET/CT for staging before treatment in patients diagnosed with colorectal cancer. ***Materials and Methods:*** Forty-nine patients who underwent 18F-FDG PET/CT for pre-treatment staging between January 2021 and December 2021 and were pathologically evaluated for MSI were included in the study. The demographic data of the cases and the histopathological features of the primary tumor in the pathology report were reviewed retrospectively. Tumor localization (right colon, left colon, and rectum), presence of perineural invasion, presence of lymphovascular invasion, T and N stage, and tumor budding were recorded from the pathology report. Areas of interest (VOI) for primary tumor areas were created from 18F-FDG PET/CT images in the LIFEx version 7.3 program. Maximum standardized uptake value of the primary tumor (SUVmax), MTV, TLG and metastasis status were recorded in PET/CT images in VOI. Statistical analysis was performed with Mann-Whitney U, Chi-square and Kendall's Tau tests using SPSS 23.0 program. ***Results:*** There was a significant difference between T stage and perineural invasion, MSI parameters. There was a significant difference between N stage and perineural and lymphovascular invasion, and differentiation parameters ($p<0.050$). There was a significant difference between the differentiation groups (good, moderate, and poor) in the parameters of perineural and lymphovascular invasion, MSI ($p<0.050$). There was a significant correlation between the degree of differentiation and perineural and lymphovascular invasion, MSI parameters ($p<0.050$). Among the histopathological parameters, only the degree of differentiation was correlated with the MTV values ($p<0.050$). No significant correlation was found between other 18F-FDG PET/CT parameters (SUVmax and TLG) and histopathological parameters. ***Conclusion:*** The expected relationship between histopathological parameters and SUVmax and TLG could not be demonstrated in this study, but there is a significant relationship between MTV and the degree of tumor differentiation. Studies with larger patient groups are needed to predict the histopathological character of colorectal cancer with the 18F-FDG/PET for staging. ***References:*** 1)Frontiers in immunology, 12, 724464.PMID: 34512653 2)Clinical nuclear medicine, 41(10),761-5.PMID: 27556789

EP-13

e-Poster Area

B: Imaging Clinical Studies -> B1 Oncological Imaging Clinical Study -> B18a Prostate Staging

EP-0219

PET/CT Imaging 2 Hours After Injection of [18F]PSMA-1007 Can Lead to Higher Staging of Prostate Cancer Than Imaging After 1 Hour

E. Hvittfeldt[1,2], *U. Bitzén*[3], *D. Minarik*[1,4], *J. Oddstig*[1,5], *B. Olsson*[2,1], *E. Trägårdh*[1,2];
[1]*Department of Translational Medicine, Wallenberg Centre for Molecular Medicine, Lund University, Malmö, SWEDEN,* [2]*Department of Clinical Physiology and Nuclear Medicine, Skåne University Hospital, Malmö, SWEDEN,* [3]*Department of Clinical Physiology and Nuclear Medicine, Skåne University Hospital, Lund, SWEDEN,* [4]*Department of Medical Physics, Skåne University Hospital, Malmö, SWEDEN,* [5]*Department of Medical Physics, Skåne University Hospital, Lund, SWEDEN.*

Aim/Introduction: [18F]PSMA-1007 is a prostate specific membrane antigen (PSMA) ligand for positron emission tomography (PET) imaging of prostate cancer. Current guidelines recommend imaging 90-120 minutes after injection but strong data about optimal timing is lacking. Our aim was to study whether imaging after 1 hour and 2 hours leads to a different number of detected lesions, with a specific focus on lesions that might lead to a change in treatment. ***Materials and Methods:*** 195 patients underwent PET imaging 1 and 2 hours after injection of [18F]PSMA-1007. Three readers assessed the status of the prostate or prostate bed and suspected metastases. We analyzed the location and number of found metastases to determine N- and M-stage of patients according to the TNM-classification (Tumor, Node, Metastasis). We also analyzed standardized uptake values (SUV) in lesions and in normal tissue. ***Results:*** Significantly more pelvic lymph nodes and bone metastases were found and higher N- and M-stages were seen after 2 hours. In twelve patients (6.1%) two or three readers agreed on a higher N- or M-stage after 2 hours. Conversely, in two patients (1.0%), two readers agreed on a higher stage at 1 hour. SUVs in suspected malignant lesions and in normal tissues were higher at 2 hours, but lower in the blood pool and urinary bladder. ***Conclusion:*** Imaging at 2 hours after injection of [18F]PSMA-1007 leads to more suspected metastases found than after 1 hour, with higher staging in some patients and possible effect on patient treatment.

EP-0220

99mTc-PSMA-SPECT/CT in primary staging of high risk prostate cancer

K. Liepe[1], *M. Baehr*[1,2], *T. M. Hoang*[3];
[1]*Klinikum Frankfurt (Oder), Frankfurt (Oder), GERMANY,*
[2]*Campus Virchow-Klinikum, Charité, Department of Diagnostic and Interventional Radiology, Berlin, GERMANY,* [3]*Statistician, Düsseldorf, GERMANY.*

Aim/Introduction: According to current data, PSMA-PET/CT is the gold standard in primary staging and biochemical recurrence of prostate cancer. Unfortunately, the worldwide availability of PSMA-PET/CT is limited by expensive radionuclides, the worldwide availability of PET/CT scanners and restricted low reimbursement rates of public health service. Hence, if PSMA-PET/CT was not available, ^{99m}Tc-PSMA SPECT/CT could be a valuable alternative. ***Materials and Methods:*** In 84 patients, SPECT/CT were performed using 689±65 MBq 99mTc-MIP-1404 (ROTOP, Dresden, Germany) or PSMA-Tc-API (DSD Pharma, Vienna, Austria). In 38 patients, additional ^{99m}Tc -MDP SPECT/CT were performed. In 32 patients MRI or contrast enhanced CT were performed additionally. ***Results:*** The patient characteristics were as followed: mean age 70 ± 9 years, mean PSA 21.4 ± 27.2 ng/ml and Gleason scores from 7 to 10. Detection rates were: prostate carcinoma 100 %, local lymph node metastases (N1) 28%, distant lymph node metastases (M1a) 13% and osseous metastases (M1b) 15%. No patient showed metastases in other organs (M1c). Correlation analysis showed a positive correlation of detection rate of extraprostatic tumour manifestations for both Gleason score and PSA level. The detection rate of metastatic disease increased significantly with an initial PSA > 20 ng/ml (n=27) from 27% to 77%. High-risk patients showed higher detection rates than low-risk and intermediate-risk patients in both initial PSA < 20 ng/ml and initial PSA > 20 ng/ml. Compared to ^{99m}Tc-MDP SPECT/CT, ^{99m}Tc -PSMA SPECT/CT showed no false negative findings. Compared with local MRI or contrast enhanced CT, ^{99m}Tc -PSMA SPECT/CT leads to an up-staging in 19% of patients and down-staging of local lymph node metastasis in 7% of patients. ***Conclusion:*** In comparison to the proPSMA study by Hofman M et al., 2021, the following results are concordant: the detection rates of extraprostatic tumour manifestations, the increased detection rates in patients with high-risk Gleason-score, the increased detection rate in patients with an initial PSA > 20 ng/ml and the superiority of PSMA imaging compared to conventional imaging, especially when local lymph nodes metastasis are of interest. ^{99m}Tc-PSMA-SPECT/CT is a valuable alternative when PSMA PET/CT is not available.

EP-0221

Clinical Utility of 68Ga-PSMA PET/CT in Initial Staging of Patients with Prostate Cancer and Importance of Intraprostatic SUVmax Values

I. Rogic, *A. Golubic, M. Zuvic, T. Smitran, N. Jukic, D. Huic;*
University Hospital Centre Zagreb, Zagreb, CROATIA.

Aim/Introduction: As it is in disease recurrence, providing clinicians with the exact extent of the disease at the time of initial diagnosis is key in the management and individual treatment of prostate cancer (PC). Under-staging, especially in men with high-risk PCa, leaves metastases untreated and may lead to poor treatment outcomes. The goal of our study was to examine the usefulness of ^{68}Ga-PSMA PET/CT in the initial staging of PC and to check out the possible correlation between prostate-specific antigen (PSA) serum values, WHO grade of the tumor and prostatic SUVmax (standardized uptake value). ***Materials and Methods:*** We retrospectively evaluated 34 studies of patients who underwent ^{68}Ga-PSMA PET/CT as part of the initial staging of prostate cancer. All our patients had a prostate cancer diagnosis on basis of histological assessment after biopsy and had Gleason score and PSA serum values obtained. ***Results:*** As expected all studies were positive with pathological 68Ga-PSMA uptake in primary prostate lesions. 19 patients had extended disease (59.37%). The mean SUVmax in prostate lesions was 19.4±12.58. WHO group 1 had a mean SUVmax of 6.25, patients with WHO group 2 had a mean SUVmax of 12.78, WHO groups 3 and 4 had the same mean SUVmax of 19.7 while WHO group 5 had a mean SUVmax of 32.27. The mean value of SUVmax of PET studies in the high-risk group was significantly higher than those of low risk (21.68±11 and 10.6±5.42). A positive correlation between gradus group and SUVmax value of prostate lesions was observed (Pearson r=0.548). ***Conclusion:*** In our study, 68Ga-PSMA PET/CT scans detected extended disease in more than half of our patients. Locating disease beyond the prostate gland allowed better-informed clinical decisions and modified initial treatment. A positive correlation was found between intraprostatic SUVmax values and gradus group of prostate cancer. High-risk patients had SUVmax values that were significantly higher than those of low-risk patients. The correlation between Gleason score and SUVmax value can be explained with increased intensity of PSMA expression as the tumor grade increases.

EP-0222

Head-to-head comparison of 68Ga-PSMA-11 with 68Ga-P137 in patients with suspected prostate cancer

T. Han, *Z. Quan, M. Wang, X. Meng, M. Zhang, J. Ye, G. Li, J. Wang, F. Kang;*
Department of Nuclear Medicine, Xijing Hospital, Fourth Military Medical University, Xi'an, CHINA.

Aim/Introduction: P137 is a novel oxalyldiaminopropionic acid-urea based prostate specific membrane antigen (PSMA) targeting agent. This study compared the uptake patterns of 68Ga-P137 and the FDA-approved PET tracer 68Ga-PSMA-11 for diagnosing prostate cancer (PCa). ***Materials and Methods:*** Twelve patients suspected of PCa were scanned respectively by 68Ga-PSMA-11 and 68Ga-P137 PET/CT, followed by prospective analysis. The tumor-to-background ratio was calculated using normal prostate tissue, blood pool, muscle, and urine as backgrounds. Pathology or follow-up results were used to analyze uptake patterns of benign/malignant lesions and various organs. ***Results:*** Nine patients were diagnosed with PCa and three with benign prostate diseases (BPD). The number and location of primary lesions, lymph nodes (n=5) and bone metastasis (n=10) detected by the two tracers were identical. Maximum standardized uptake value (SUVmax), tumor/normal prostate ratio, as well as semi-quantitative miPSMA-ES and PRIMARY diagnostic scores [1-2] (P all >0.05) showed similar uptake levels of primary lesions between 68Ga-P137 and 68Ga-PSMA-11. Compared to 68Ga-P137, the SUVmax of 68Ga-PSMA-11 was significantly higher for bone metastasis and lymph node metastasis (LNM) (17.1±3.9 vs. 13.2±2.3, 20.3±5.6 vs. 10.5±1.4, P all <0.05). One-hour post-injection, SUVmax of the duodenum (9.0±1.8 vs. 14.9±4.9), kidney (18.2±2.4 vs. 40.9±15.6), and urine (13.9±7.5 vs. 39.8±26.3) were significantly lower for 68Ga-P137 than for 68Ga-PSMA-11 (P all <0.05), whereas the radioactivity accumulation of blood pool and muscle (3.8±0.4 vs. 1.5±0.4, 1.0±0.1 vs. 0.6±0.1, P all <0.05) of 68Ga-P137 was significantly higher than 68Ga-PSMA-11.

Conclusion: The uptake level of 68Ga-P137 has no significant difference to that of 68Ga-PSMA-11 in prostate primary lesions, and their imaging performance are visually equivalent for both primary and metastatic PCa lesions, despite a higher blood pool and muscle background and a lower uptake in bone/LNM lesions. Due to lower urine excretion of 68Ga-P137, primary prostate lesions near the urine can potentially be displayed clearer with 68Ga-PSMA-11. ***References:*** 1. Eiber M, Herrmann K, Calais J, Hadaschik B, Giesel FL, Hartenbach M, et al. Prostate Cancer Molecular Imaging Standardized Evaluation (PROMISE): Proposed miTNM Classification for the Interpretation of PSMA-Ligand PET/CT. J Nucl Med. 2018;59:469-478. doi:10.2967/jnumed.117.198119.2. Emmett LM, Papa N, Buteau J, Ho B, Liu V, Roberts M, et al. The PRIMARY Score: Using intra-prostatic PSMA PET/CT patterns to optimise prostate cancer diagnosis. J Nucl Med. 2022;63:1644-1650. doi:10.2967/jnumed.121.263448.

EP-0223

Comparison of 18F-Thretide PET/CT and multiparametric MRI for the detection of intermediate and high risk prostate cancer

J. Zang[1], *Y. Yang*[1], *C. Wang*[1], *S. Chen*[1], *W. Miao*[1], *X. Chen*[2], *J. Zhang*[2];
[1]*Department of Nuclear Medicine, the First Affiliated Hospital, Fujian Medical University, Fuzhou, CHINA,* [2]*Departments of Diagnostic Radiology, Yong Loo Lin School of Medicine, National University of Singapore, Singapore, SINGAPORE.*

Aim/Introduction: The main objective of this prospective study was to assess the value of ^{18}F-Thretide (targeting PSMA) PET/CT Imaging in patients with intermediate- and high-risk prostate cancer (PCa) before planned curative-intent radical prostatectomy (RPE) and pelvic lymph node dissection (PLND), and to compare the ^{18}F-Thretide PET/CT PET/CT findings with standard of care pelvic multi-parametric magnetic resonance imaging (mpMRI) and bone scintigraphy. ***Materials and Methods:*** A total of 45 patients with biopsy proven PCa (15 intermediate and 30 high risk) were enrolled in this prospective study. All patients underwent ^{18}F-Thretide PET/CT and MRI, and 36 of them underwent bone scintigraphy. Any drug-related side effects were recorded and the vital parameters of the patients were observed for 1 week. ^{18}F-Thretide PET/CT findings were correlated with the results of mpMRI and histopathology. ***Results:*** All patients tolerated the ^{18}F-Thretide PET/CT well. Vital parameters remained stable and no patient reported any new symptoms during the observation period. In the end, a total of 38 of 45 patients underwent curative-intent radical prostatectomy and pelvic lymph node dissection. Of the 45 patients, 37 (82.2%) patients presented with a pathologic mpMRI, and 44 (97.8%) with a pathologic ^{18}F-Thretide PET/CT ($P = 0.030$). The SUVmax of the primary tumors upon ^{18}F-Thretide PET/CT was 19.3 ± 18.6. There was a low but significant correlation between SUVmax and baseline tPSA ($r = 0.371$, $P = 0.014$), but no correlation between SUVmax and risk stratification. A total of 459 LNs were removed by PLND in 38 patients. The histopathology verified 15 pelvic lymph node metastases in 21.1% (8/38) of the patients, of which 9 lymph nodes of 5 (62.5%) patients have been correctly identified on ^{18}F-Thretide PET/CT, and 1 lymph node (12.5%) of 1 patient (12.5%) on mpMRI. The sensitivity, specificity, and accuracy of ^{18}F-Thretide PET/CT in diagnosing pelvic lymph node metastasis were 60.0%, 98.7%, and 97.6%, respectively. Bone metastases and distant metastases (liver) were found in 8 (17.8%) and 1 (2.2%) of the patients on ^{18}F-Thretide PET/CT imaging, respectively. 2 of 3 patient with bone metastasis who underwent bone scintigraphy showed bone metastases, but the number of lesions displayed were less than ^{18}F-Thretide PET/CT. ***Conclusion:*** ^{18}F-Thretide PET/CT shows high diagnostic performance for patients with intermediate- and high-risk prostate cancer and is superior to mpMRI and bone scintigraphy. There is a significant correlation between SUVmax of ^{18}F-Thretide PET/CT and baseline tPSA

EP-0224

The Relationship Of Lymp Node Distance And Disease Parameters In Prostate Cancer Ga-68 PSMA PET/CT Imaging

C. Aydin[1], *B. Özdemir Günay*[2], *Ü. Korkmaz*[1], *F. Soyluoğlu*[1];
[1]*Trakya University, Edirne, TÜRKIYE,* [2]*Edirne Sultan Murat I State Hospital, Nuclear Medicine Clinic, Edirne, TÜRKIYE.*

Aim/Introduction: Metabolic staging of prostate cancer, lymph node metastases are divided into pelvic and distant lymph nodes(M1a) (1) The distance between most distant lymph nodes is an independent prognostic marker in lymphomas (2). We aimed to determine distance of lymph nodes to prostate bed and the clinical significance of PET/CT parameters of these lymph nodes. ***Materials and Methods:*** Patients who came to our clinic for staging with diagnosis of prostate cancer ; PET/CT data of patients who did not receive ADT, radiotherapy or chemotherapy were evaluated retrospectively. 67 patients with only lymph node metastasis were included. Measurements were made between middle of the lymph nodes and bladder neck .(Dmax:Measured distance, SDmax:Dmax/Body surface area) PET/CT parameters of the patients' lymph node farthest from the bladder neck (LN 1) and lymph node with the highest SUVmax (LN2); The relationship between patients' Gleason score, ISUP grade, pre-imaging PSA values, presence of PSA recurrence/persistence in patient follow-up, and patient survival were examined separately. Lymph node distance parameters were calculated and compared. The SUVmax, MTV, and activity score of the same lymph nodes were compared with the clinical findings of the patients.(1) ***Results:*** There was a correlation between survival of patients and lymph node distance parameters ($p<0.05$). These parameters were found to be significantly higher in patients who were not alive than in the patients who were alive. SDmax2 was found to be significantly higher in patients with PSA recurrence/persistence (p:0.03)In one-year PSA follow-up, the distance parameter and MTV of LN with a high SUVmax were found to be significantly higher in patients with recurrence/persistence When patients were classified (pelvic and extrapelvic), there was no significant correlation between lymph node distance (SDMax1) and clinical parameters of patients with only pelvic LN metastasis. In patients with extrapelvic LN an increase in SDMax1 was significantly correlated with PSA progression and survival ($p<0.05$) ***Conclusion:*** The lymph node distance parameters were found to be superior to Gleason score and ISUP grade in predicting the survival of patients, PSA recurrence/persistence. Gleason and ISUP scores were unsignificant. This may be due to the short follow-up times and the low number of patients .When two lymph nodes are compared; Increasing distance of lymph node with the highest metabolic activity seems to be more important than increasing distance of farthest lymph node . It can be said that this indicates the importance of metabolic imaging in prostate cancer. ***References:*** 1. DOI: 10.2967/jnumed.117.198119 2.DOI: 10.1016/j.annonc.2020.11.019

EP-0225

The Relationship of Tumor SUVmax Value in 68Ga-PSMA PET/CT with Pathological Grade Group Grading System in Patients with Prostate Cancer

F. Demir, *S. Karaçavuş, H. Gençer, A. Ozdal, Z. Erdogan, I. Ciftci, F. Cevik, N. Ozhan, H. İsci, M. Kaya;*
Kayseri City Training and Research Hospital, Kayseri, TÜRKIYE.

Aim/Introduction: In this study, we aim to investigate the role of the Prostate Gleson Group grading system, which is a relatively new grading system, in the prognosis of the disease, and to examine the relationship of this grading system between tumor parameters in PSMA PET/CT. ***Materials and Methods:*** The patients' pathology results were examined and Grade Group ratings were recorded. PET/CT images were loaded on workstations and PET parameters of the tumor (SUVmax, SUVmean, and tumor volume) were calculated. Data were analyzed in SPSS 22 program. P<0.05 was considered significant. ***Results:*** A total of 114 prostate cancer patients were included in the study. The age, SUVmax, SUvmean, tumor volume, and PSA values of the patients are summarized in Table 1. When we look at the correlation between the grade group and SUVmax, SUvmean, tumor volume, and PSA values; there was a correlation between SUVmax (p=0.010; r=0.241), SUVmean (p=0.06; r=0.258) and PSA (p<0.001; r=0.357) values. When we divided the patients into 2 groups low and medium-high risk groups according to grade group grading; Age, SUVmax SUVmean and PSA values were significantly higher among the medium-high risk group (table 2). When ROC analysis was performed for SUV max, SUVmean and PSA values in the estimation of the pathological medium-high risk group, significant cut-off values were calculated for all three values. When the cut-off value for SUVmax was taken as 9.76, the sensitivity was 69% and the specificity was 57% (AUC: 0.637, p=0.034). Taking 6.02 as the cut-off value for SUVmean, the sensitivity was 68% and the specificity was 61% (AUC:0.64; p=0.030). When a cut-off value of 1.38 was taken for PSA, the sensitivity was 66% and the specificity was 61% (AUC:0715; p=0.001). ***Conclusion:*** According to our study results, the correlation between tumor SUVmax and SUVmean values in Ga-68 PSMA PET/CT and Gleason Group was similar to the correlation between PSA and Gleason Group. SUVmax, SUVmean and PSA values were significantly higher in patients in the medium-high risk group compared to the patients in the low risk group. The cut-off value of 9.76 for SUVmax and 6.02 for SUVmean had significant predictive value in estimating the intermediate-high risk group of patients. The results show that Ga-68 PSMA PET tumor parameters can provide important information in predicting prognosis.

EP-0226

Multimodality Approach with 68Ga-PSMA-11 PET/CT in Staging High-risk Prostate Cancer Patients Candidate to Radical Prostatectomy

G. Rovera[1], *S. Grimaldi*[1], *M. Oderda*[2], *R. Passera*[1], *M. Falco*[1], *S. Dall'Armellina*[1], *P. Gontero*[2], *D. Deandreis*[1];
[1]*Nuclear Medicine, Department of Medical Sciences, AOU Città della Salute e della Scienza di Torino, Turin, ITALY,* [2]*Department of Surgical Sciences, Urology Unit, AOU Città della Salute e della Scienza di Torino, Molinette Hospital, University of Turin, Turin, ITALY.*

Aim/Introduction: Accurate primary staging of prostate cancer is essential for treatment planning in high-risk patients. Current guidelines recommend the use of conventional imaging techniques such as computed tomography (CT) and bone scintigraphy for primary staging of high-risk prostate cancer. However, molecular imaging with prostate-specific membrane antigen/positron emission tomography (PSMA-PET/CT) holds potential for improved diagnostic sensitivity compared with conventional imaging. This prospective study aimed to evaluate the ^{68}Ga-PSMA-11 PET/TC diagnostic performance in the preoperative staging of patients with high-risk prostate cancer and to compare its sensitivity with conventional imaging modalities. The secondary objective was to evaluate the diagnostic accuracy of ^{68}Ga-PSMA-11 PET/CT in pelvic nodal staging using postoperative histopathology data as reference standard. ***Materials and Methods:*** Patients were enrolled according to the following inclusion criteria: diagnosis of prostate cancer eligible for radical prostatectomy, high-risk classification according to d'Amico criteria (ISUP 4/5 and/or PSA> 20 ng/ml and/or cT3), CT and bone scintigraphy performed within three months of ^{68}Ga-PSMA-11 PET/TC. Patients with previous treatments, including androgen-deprivation therapy, were excluded. Molecular imaging was performed with standard technique by intravenous injection of 2MBq/Kg of ^{68}Ga-PSMA-11 and whole-body PET/CT acquisition after 60 minutes. CT and PET/CT detection rates were compared using McNemar's exact test. ***Results:*** Fifty patients underwent ^{68}Ga-PSMA-11 PET/TC imaging (median age 73 [IQR:67-76] years; median PSA 10.10 [IQR:6.27-19.50] ng/ml). Overall, ^{68}Ga-PSMA-11 PET/TC detected regional and/or distant metastatic localizations in 56% (28/50) of patients, while CT in 12% (6/50)(p<0.001). Compared with CT, ^{68}Ga-PSMA-11 PET/TC identified a higher number of suspected metastases in all anatomical regions: N1 46% vs 12% (p<0.001), M1a 10% vs 2% (p=0.13), M1b 22% vs 2% (p=0.002). Moreover, molecular imaging led to a TNM upstaging in 48% of cases, with no understaged patients. Compared with bone scintigraphy (BS), ^{68}Ga-PSMA-11 PET/TC identified new skeletal metastases in 16% (8/50) of patients, with no BS-only positive cases. Overall, PSMA-PET/CT would lead to a potential change of management in 30% (15/50) of patients staged with conventional imaging (CT+BS). Compared with postoperative histopathology data, ^{68}Ga-PSMA-11 PET/TC per-patient sensitivity, specificity, positive predictive value, negative predictive value and accuracy for detection of pelvic nodal metastases were 91.7%, 85.7%, 84.6%, 92.3% and 88.5%, respectively. ***Conclusion:*** ^{68}Ga-PSMA-11 PET/TC showed a high diagnostic performance in primary staging of high-risk prostate cancer: new metastatic localizations were identified in 44% and 16% of cases compared with CT and bone scintigraphy, and a high per-patient nodal staging accuracy was demonstrated at histopathology (88.5%).

EP-0227

Location-Based Detection of Low-Uptake Lymph-Node Metastasis of Prostate Cancer in the Pelvis Using PSMA-PET/CT and Artificial Intelligence

B. Schemmer;
Uniklinik Bonn, Bonn, GERMANY.

Aim/Introduction: Prostate cancer is a leading cause of cancer-related deaths worldwide, early recurrence is a major contributor to its mortality rate. Early detection of lymph node metastasis in the pelvic region in castration resistant prostate cancer with biochemical recurrence is crucial for effective treatment and improved patient outcomes. It is also a diagnostic challenge as PSMA-expression in early recurrence is significantly lower than in overt metastatic disease. Specifically in the pelvis ureter and bladder can mask or imitate metastasis. In this study, we explored the use of artificial intelligence (AI) and PSMA-PET/CT

to detect low uptake lymph node metastasis of prostate cancer in the pelvis using only the location of PSMA expressing lesions visible on PET. ***Materials and Methods:*** We included patients with histologically confirmed prostate cancer after resection who underwent PSMA-PET/CT imaging for biochemical recurrence with at least one PSMA-PET study and two PSA-values per patient (pre- and post intervention), to train and validate our AI model. We included 50 patients, median age 66 years (range, 45-85 years). The majority had intermediate-risk or high-risk disease (72%), most had a PSA-level <1.5 ng/mL (56%). No lymphnodes were surgically removed and most patients also had a probable local recurrence (67%). The AI was based on deep learning and only provided with PET-images of the pelvic region as well PSA-values. The AI was specifically not trained to find any overt metastasis with uptake above liver background. The PET-images were preprocessed, uptake values below blood pool or above liver were no longer present in the training images. Detection was evaluated as successful when there was a PSA-remission after radiation therapy that included the lymphnodes or if there was no remission when lymphnodes were not irradiated. ***Results:*** Our results showed that the AI model was able to accurately detect lymph node metastasis of prostate cancer with a high level of accuracy in cases where human observers were unsure. The model achieved a sensitivity of 96% and a specificity of 74%, indicating its potential for use in clinical settings. ***Conclusion:*** Further refinement is needed to increase specificity and validate our findings, but our results suggest that the early detection of low uptake lymph node metastasis of prostate cancer using only location on PET images as data could have significant clinical implications for the improved detection and treatment of prostate cancer.

EP-0228

Value of Ga-68 PSMA PET/CT in ISUP Grade 2 Prostate Cancer Patients

F. Aghazada, *M. Demirbilek, O. Sahin, S. Asa, B. Onal, L. Kabasakal;*
Istanbul University-Cerrahpasa, Cerrahpasa Faculty of Medicine, Istanbul, TÜRKIYE.

Aim/Introduction: The aim of our study is to evaluate the contribution of Ga-68 PSMA PET/CT in the staging of patients with ISUP grade 2 prostate cancer. ***Materials and Methods:*** 72 patients who were reported to have Gleason 3+4 prostate cancer according to TRUS biopsy results and underwent Ga-68 PSMA PET/CT imaging between June 2014 and March 2022 were retrospectively evaluated. Radical prostatectomy was performed in 46 patients after imaging. Pelvic lymph node dissection was performed in 35 patients. All patients were classified according to the PRIMARY score. Patients were divided into two groups as PRIMARY 1-2 (negative) and PRIMARY 3-4-5 (positive). The images were examined for lymph node and bone metastasis. The ability of Ga-68 PSMA PET/CT to predict upgrading in TNM and Gleason scores of patients after prostatectomy was investigated. SPSS V.22 was used. ***Results:*** Pathology results of 2 of the operated patients were reported as Gleason 3+3, 25 as Gleason 3+4, 17 as Gleason 4+3 and higher. Ductal carcinoma was detected in 2 patients. 12 patients were classified as PRIMARY 1-2 and 34 patients were classified as PRIMARY 3-4-5. Ga-68 PSMA PET detected bone metastasis in 1 (2%) patient and pelvic lymph node metastasis in 3 patients. When the 3 patients with lymph node metastasis were examined, it was determined that metastasis was false positive in 1 patient after the operation. Lymph node metastasis was not observed in any of the patients whose operative pathology result was Gleason 3+4, and bone metastasis was detected in only 1 (5%) patient. Pathology results of 35 patients who underwent pelvic lymph node dissection were compared with Ga-68 PSMA PET results. The sensitivity of Ga-68 PSMA PET in detecting lymph node metastasis was 100%, specificity was 97%, positive predictive value was 67%, and negative predictive value was 100%. Postoperative upstaging was observed in 20 patients. According to the results of the chi-square analysis, Ga-68 PSMA PET can predict the prostatectomy outcomes of the patients significantly (p=0.01). ***Conclusion:*** It is thought that Ga-68 PSMA PET does not provide additional contribution compared to conventional imaging methods in the TNM staging of ISUP grade 2 prostate cancer patients due to the low incidence of lymph node (4%) and bone (2%) metastasis detected in our study. . However, application of Ga-68 PSMA PET/CT to patients after biopsy is an acceptable approach since it can predict the outcome of prostatectomy based on the PRIMARY score.

EP-0229

Analytical performance validation of aPROMISE platform for prostate cancer tumor burden and index and dominant tumor assessment with 18F-DCFPyL PET/CT.

C. Lucas Lucas[1], *A. M. García Vicente*[2], *L. García Zoghby*[2], *J. Pérez Beteta*[3], *P. Borrelli*[4], *M. Amo Salas*[5], *A. Padilla Bermejo*[1], *M. N. Sicilia Pozo*[1], *M. Contreras Ameduri*[1], *M. Cruz Montijano*[2], *F. J. Pena Pardo*[1], *E. Noriega Álvarez*[1], *M. P. Talavera Rubio*[1], *V. M. Poblete García*[1], *Á. M. Soriano Castrejón*[2];
[1]Nuclear Medicine Department. University General Hospital of Ciudad Real, Ciudad Real, SPAIN, [2]Nuclear Medicine Department. University Hospital of Toledo, Toledo, SPAIN, [3]Mathematical Oncology Laboratory. Castilla-La Mancha University, Ciudad Real, SPAIN, [4]Department of Clinical Physiology, Sahlgrenska University Hospital, Gothenburg, SWEDEN, [5]Mathematics Department. Castilla La-Mancha University, Ciudad Real, SPAIN.

Aim/Introduction: To validate the performance of automated Prostate Cancer Molecular Imaging Standardized Evaluation (aPROMISE) software in obtaining total prostate disease burden in patients with intermediate and high-risk prostate cancer (PCa) who undergo 18F-DCFPyL-PET/CT for staging purpose and to evaluate the interobserver concordance and with the histopathologic analysis in the determination of the index (IT) and dominant tumor (DT). ***Materials and Methods:*** Patients with a recent diagnosis of intermediate/high risk PCa according to D'Amico risk classification underwent 18F-DCFPyL-PET/CT. In Positive-PSMA scans, automated prostate tumor segmentation was performed using aPROMISE software and compared with semiautomatic-manual segmentation using Matlab developed by the Mathematical Oncology group (MOLab). SUVmax, SUVpeak, SUVmean, molecular tumor volume (MTV) and total lesion activity (TLA) were compared with both software. Two observers independently assessed the laterality of DT (the highest SUVmax) and IT (the biggest metabolic volume) from the segmentation with both software. We compared the variables obtained by both software, as well as the interobserver agreement and between each one of them with the histology (DT: the highest Gleason; IT: the highest number of positive core-biopsies) using the intraclass correlation coefficient (ICC) and Kappa (k) for the concordance analysis. ***Results:*** 54 patients were included in the analysis (4 excluded due to negative PET). 85.2% high risk and 43.4% ISUP 4 or 5. In the global analysis, we observed a good correlation between MOLab and aPROMISE with respect to SUVmax followed by TLA and SUVpeak (ICC of 1, 0.950 and 0.833, respectively; p<0.001), without showing significant differences individually for the different ISUP grades and risk categories. However, there

were significant differences between both software according to the different ISUP grades and risk categories, except for TLA with the ISUP grade. DT was located in right lobe for the observers of aPROMISE and MOLab in 31 and 32 patients respectively, with a good agreement (k=0.733; p<0.001) and IT in 32 and 29 patients respectively, with a very good agreement (k=0.812; p<0.001). However, the concordance between observers using both software with histopathology was moderate (p<0.001). ***Conclusion:*** aPROMISE shows a good performance for SUVmax and TLA after segmentation of the prostate tumor compared to MOLab. However, there are significant differences between practically all the semiquantitative variables for the different ISUP groups and risk categories. The interobserver agreement in the determination of DT and IT was good, although it had a moderate agreement with the determination of these parameters in histology.

EP-0230

Contribution of 68GA-PSMA-PET/CT to Risk Classification In Prostate Cancer With Gleason Score 6

Ö. Sahin, *E. BEYHAN, Ö. E. FENERCİOĞLU, E. ARSLAN, T. F. ÇERMİK, N. ERGÜL;*
University of Health Sciences, Istanbul Training and Research Hospital, Department of Nuclear Medicine, , Turkey., Istanbul, TÜRKIYE.

Aim/Introduction: In cases of Gleason Score (GS) 3+3(6) prostate adenocarcinoma (PCa), it is frequently seen that the pathological grade is increased after prostatectomy in daily practice. The aim of the study is to investigate the contribution of 68Ga-PSMA-PET/CT to the detection of cases requiring rebiopsy that will cause a change in the risk classification of patients with GS 6 prostate cancer and to guide the treatment planning correctly. ***Materials and Methods:*** Patients with GS 6 prostate cancer were included in the study. PSMA PET/CT scans performed for "staging" or "restaging" were reviewed retrospectively. With SUVmax and SUVmean values, GS, risk class (low, medium, high), and prostate specific antigen (PSA) values obtained as a result of transrectal ultrasound guided biopsy (TRUS) or radical prostatectomy (RP) correlation was evaluated. In 68Ga-PSMA PET/CT, lesion localizations and involvement pattern in the prostate gland were compared with histopathological findings. ***Results:*** Between January 2016 and February 2023, 68Ga-PSMA PET/CT scans of 112 patients (105 patients staging, 7 patients restaging) with TRUS biopsy result GS6 (3+3) and PSA measurement were performed. Extraprostatic pathological involvement focus was detected in 11/112 (9.8%) patients. Pelvic lymph node metastasis was found in 9 of these patients, extrapelvic lymph node in 3, and bone metastasis in 6 of them. Additional focus of involvement was detected in the prostate gland in 37/112 (33%) patients on 68Ga-PSMA PET/CT.GS6 was detected in 27 of 36 patients who underwent RP. Repeated biopsy result of 1 patient was GS>6. A significant difference was found between the SUVmax and SUVmean values of 34/112 patients who were found to have GS>6 with RP or repeat biopsy and who had an increased risk class by detecting distant metastases on 68Ga-PSMA PET/CT and those whose risk class did not change (p=0.005, p= 0.009). There was a significant difference in SUVmax and SUVmean values of the primary tumor between low, intermediate and high risk groups (p=0.01, p=0.007). Lymph node and bone metastases were detected in 2 of 7 patients in the restaging group. ***Conclusion:*** 68Ga-PSMA PET/CT imaging was found to be effective in detecting the increase in risk class and degree of disease in 34/112 (30%) patients. Our findings show that 68Ga-PSMA PET/CT can be a guide in terms of biopsy repetition and treatment decision, considering the SUVmax value and the involvement pattern of the primary tumor.

EP-0231

Comparison of 68Ga-FAPI and 18F-PSMA PET/CT in the Evaluation of Ductal Adenocarcinoma of the Prostate

C. Liu, *Q. Xie, T. Liu, Z. Li, C. Guo, Z. Yang;*
Department of Nuclear Medicine, Peking University Cancer Hospital & Institute, Beijing, CHINA.

Aim/Introduction: Ductal adenocarcinoma is a rare variant of prostate cancer considered to be more aggressive than pure acinar adenocarcinoma. While PSMA-PET scans have been shown to be helpful in staging and in diagnosing sites of metastatic adenocarcinoma of the prostate, the prostatic ductal carcinoma subtype can show poor PSMA avidity. This study aims to compare ^{68}Ga-FAPI PET/CT with ^{18}F-PSMA PET/CT in evaluating prostatic ductal carcinoma. ***Materials and Methods:*** We retrospectively analyzed a cohort of 17 patients with histologically-confirmed prostatic ductal adenocarcinoma who underwent both ^{68}Ga-FAPI PET/CT and ^{18}F-PSMA PET/CT for initial staging, recurrence and patient selection for radioligand therapy. Location and number of suspicious lesions revealed by the different modalities were recorded. The tracer uptakes, quantified by maximum standardized uptake value (SUVmax) was compared for paired positive lesions between both modalities using the Wilcoxon signed-rank test. ***Results:*** 12/17 patients for ^{68}Ga-FAPI PET/CT and 11/17 patients for ^{18}F-PSMA PET/CT had focal uptake above background in tumor lesions. A total of 47 lesions were recorded. Of these, 34 (72%) were PSMA+ and 36 (76%) were FAP+. There were 13 (27%) FAP+/PSMA− lesions and 11(23%) FAP−/FDG+ lesions. Compared with ^{18}F-PSMA PET/CT, ^{68}Ga-FAPI PET/CT depicted more suspected tumor lesions in prostate (7 vs 4) and lung (6 vs 1), less lesions in lymph nodes (5 vs 10) and bone lesions (10 vs 13). The two modalities showed similar performance in the recurrent lesions and suspected metastases in liver and peritoneum. Compared to ^{18}F-PSMA PET/CT, tumor uptake was significantly lower with FAPI than with PSMA (median SUVmax was 4.0 vs 6.8, P=0.01). In a subgroup analysis, tumor uptake was higher with FAPI than with PSMA in primary prostate tumor (median SUVmax was 12.1 vs. 6.1) and lung lesions (median SUVmax was 2.1 vs. 1.4). ***Conclusion:*** The 68Ga-FAPI PET/CT with 18F-PSMA PET/CT showed heterogeneous uptake in the prostatic ductal carcinoma. We demonstrate that 68Ga-FAPI PET/CT combine with 18F-PSMA PET/CT is useful for detecting tumor lesions in patients with prostatic ductal carcinoma. ***References:*** 1.Ranasinghe W, Shapiro DD, Zhang M, et al. Optimizing the diagnosis and management of ductal prostate cancer. Nature reviews. Urology. 2021 Jun;18(6):337-358. DOI: 10.1038/s41585-021-00447-3. PMID: 33824525. 1.Qiu S, Dong A, Zhu Y, Zuo C. 68 Ga-PSMA-11 and 18 F-FDG PET/CT in a Case of Ductal Adenocarcinoma of the Prostate. Clin Nucl Med. 2022 Sep 1;47(9):836-838. doi: 10.1097/RLU.0000000000004230. Epub 2022 Apr 20. PMID: 35439204.

EP-0232

PSMA Immunohistochemistry Staining in Prostate Cancer Primary Lesion and Comparison with [68Ga]Ga-PSMA-PET/CT Findings

Z. Isik[1], *G. Güner*[2], *M. Çağlar Tuncalı*[1], *M. Karcaaltincaba*[3], *B. Akdoğan*[4], *D. Akıncı*[3], *M. Tuncel*[1];
[1]*Hacettepe University, Department of Nuclear Medicine, Ankara, TÜRKIYE,* [2]*Hacettepe University, Department of Pathology, Ankara, TÜRKIYE,* [3]*Hacettepe University, Department of Radiology, Ankara, TÜRKIYE,* [4]*Hacettepe University, Department of Urology, Ankara, TÜRKIYE.*

Aim/Introduction: PSMA over-expression is well-known in prostate cancer (PCa). Currently it is the main target for theragnostic purposes in Nuclear Medicine. F-18/Ga-68 labelled prostate-specific membrane antigen (PSMA) positron emission tomography/computed tomography PET/CT is a valuable tool for detecting PCa foci with high sensitivity and specificity. The aim of this study is to correlate primary staging (PSMA) (PET/CT) parameters with PSMA-immunochemistry (IHC) features in PCa patients. ***Materials and Methods:*** Fifty-nine patients with PCa who underwent Ga-68-PSMA-11-PET/CT and radical prostatectomy(RP) were included in this prospective study.Visual and semi-quantitative evaluation of the primary tumor was carried out by two nuclear medicine physicians based on 12 segment analyses.Index and non-index tumors in each RP specimen were correlated with PET-CT.Index lesions were defined as tumor foci with largest size and radiotracer uptake.Tumours smaller than <5mm were excluded to avoid partial volume effect.Clinical information(age, iPSA-value,grading group) and PSMA-PET/CT parameters(SUVmax,SUV mean) were compared.PSMA-IHC analysis was based on visual quantification with a four-tiered score(0 = negative,1+ = weak,2+ = moderate,3+ = strong)based on the tumoral cell staining(0:none,1:weak,2:moderate,3:strong). Specimens were also analysed divided according the percentage of IHC staining intensity in the tumor foci.Finally, the percentage of each IHC stained area was multiplied by the intensity score and added up to reach a final H-score (range 0-300). ***Results:*** All 59 patients(median age 66y, PSA 8.97 ng/mL)diagnosed with PCa were in intermediate or high-risk group.Patients ISUP grades were as follows: 2(n:24), 3(n:16), 4(n:3) and 5 in16 patients.Out of these 59 patients, 59 index and 19 non-index lesions were stained.In IHC-PSMA staining for index lesions median negative, 1+, 2+, 3+ positive area percentages and H scores were 8.59(range:0-90), 17.34(range:0-75), 24.83(range:0-100), 49.66(range:0-100) and 215.98 (range:10-300) respectively.PSMA PET detected all non-index lesions with H-score of >200. ISUP scores, pre-op serum PSA and SUVmax were correlated with PSMA 3+ area percentages(rs=0.311, 0.289 and 396 respectively n :59, p<0.05). However, there was no correlation with H scores(p=0.136). Furthermore, SUVmax was correlated with ISUP(rs=0.337, n:57, p=0.01) and preop PSA levels(rs=0.42, n:57, p=0.001).In IHC staining, PSMA PET false negative lesions' PSMA negative areas were significantly higher and high expression areas and H-score were significantly lower than ones detected by PSMA PET/CT(p=0.015). ***Conclusion:*** ISUP score and SUVmax of the primary tumour were correlated with each other and with high PSMA expression area % in IHC staining.PSMA expression parameters were predictors of detected and non-detected lesions in PSMA PET/CT.

EP-0233

Comparison of 68Ga-PSMA PET/MRI with PET and mpMRI in concise evaluation of primary prostate tumor and its prognostic value in detection of locally advanced prostate cancer

L. Uslu-Besli[1], *B. Bakir*[2], *N. Urganci*[3], *&. Gürses*[3], *S. Özel-Yıldız*[4], *C. Demirdag*[5], *K. Sönmezoglu*[1], *H. Sayman*[1];
[1]*Istanbul University-Cerrahpasa, Cerrahpasa Medical Faculty, Department of Nuclear Medicine, Istanbul, TÜRKIYE,* [2]*Istanbul University, Istanbul Medical Faculty, Department of Radiology, Istanbul, TÜRKIYE,* [3]*Istanbul University-Cerrahpasa, Cerrahpasa Medical Faculty, Department of Pathology, Istanbul, TÜRKIYE,* [4]*Istanbul University, Istanbul Medical Faculty, Department of Biostatistics, Istanbul, TÜRKIYE,* [5]*Istanbul University-Cerrahpasa, Cerrahpasa Medical Faculty, Department of Urology, Istanbul, TÜRKIYE.*

Aim/Introduction: Our aim in this study is to compare the diagnostic performance of multiparametric prostate MRI (mpMRI), ^{68}Ga-PSMA PET and PET/MRI in patients with primary prostate cancer who underwent hybrid PET/MRI. ***Materials and Methods:*** Fifty prostate cancer patients, who were planned for radical prostatectomy were included in the study. Patients underwent whole body ^{68}Ga-PSMA PET followed by regional PET/MRI with mp-MRI. The prostate gland was divided into 6 zones and peripheral zone and transitional zone were evaluated separately. All images were evaluated separately for PET, mpMRI and PET/MRI in terms of lesion location, number of prostate zones with tumor, seminal vesicle infiltration and extraprostatic extension. SUV parameters obtained from PET images and apparent diffusion coefficient (ADC) values obtained from diffusion-weighted imaging were measured for index lesion. ***Results:*** PET/MRI was more sensitive than both PET and mpMRI in detection of index lesions (92% vs 80% and 84%, respectively). Sensitivity and specificity of PET, mpMRI and PET/MRI were 60.8% and 88.2%, 62.4% and 95.8%, 71.3% and 93.3%, respectively in peripheral zone and 51.8% and 95.9%, 50.6% and 100%, 60.2% and 99.5%, respectively in transitional zone. PET/MRI had better diagnostic performance compared to mpMRI in whole prostate gland (p<0.01). While PET and PET/MRI were similar in transitional zone, PET/MRI outperforms PET in peripheral zone (p=0.019). MpMRI had higher sensitivity but lower specificity compared to ^{68}Ga-PSMA PET in detection of seminal vesicle infiltration (60% vs. 41.7% sensitivity and 86.8% vs. 91.9% specificity) and extra-prostatic extension (60% vs 55% sensitivity and 73.3% vs 83.3% specificity). Accuracy of both ^{68}Ga-PSMA PET and mpMRI were similar (79.6% and 81.3% for seminal vesicle infiltration; 72% and 68% for extra-prostatic extension). SUVmax and SUVmean values obtained from index lesions were significantly higher in patients with seminal vesicle infiltration, extraprostatic extension of lymphovascular invasion compared to those who were negative. ***Conclusion:*** PET/MRI had higher sensitivity and accuracy compared to PET or mpMRI in both peripheral zone and transitional zone of the prostate gland. Seminal vesicle infiltration, extraprostatic extension, lymphovascular invasion and lymph node metastasis were more common in cases with higher PSMA uptake. Therefore, ^{68}Ga-PSMA PET may also have prognostic value in prostate cancer patients.Note: This research was financially supported by Istanbul University-Cerrahpasa Scientific Research Projects (BAP Project number: TSA-2018- 26777) ***References:*** 1. Eiber M et al. EuroUrol. 2016;70:829-836 2. Al-Bayati et al. Urol Int 2018;100:164-171 3. Li M et al. Eur J Radiol. 2019;113:225-231

EP-0234

Preliminary Clinical Study of a Novel Small-molecule PSMA Inhibitor 68Ga-SC691: Biodistribution, Dosimetry and Prospective Comparison with 68Ga-PSMA-11

J. Cao;
416 Hospital, China National Nuclear Corporation, chengdu, CHINA.

Aim/Introduction: Prostate-specific membrane antigen (PSMA) is established as arguably emerging target for the diagnosis and treatment of prostate cancer (PCa), and small-molecule inhibitors targeting PSMA are considered to be the most valuable class of drugs. This prospective study evaluated the safety, biodistribution and effective absorbed dose of a novel Small-molecule PSMA Inhibitor ^{68}Ga-SC691 in humans and compared its efficacy and biodistribution with ^{68}Ga-PSMA-11 in PCa patients. ***Materials and Methods:*** Seven healthy subjects and twelve patients with PCa were recruited for this study after reference to inclusion/exclusion criteria. Patients' ^{68}Ga-SC691 and ^{68}Ga-PSMA-11 PET/CT images were performed during a treatment-free planning week, with scan-specific parameters kept consistent. PET/CT data were analysed for dosimetric, focal and quantitative data using Hermes Internal Radiation Dosimetry (HIRD, built-in OLINDA / EXM v2.1) and uWS-MI post-processing workstation, respectively. ***Results:*** ^{68}Ga-SC691 showed good safety in all subjects. ^{68}Ga-SC691 was mainly excreted by the urinary system. Dosimetry showed that the high absorption organs were mainly kidney (123.43±25.67 μGy/MBq) and bladder wall (171.58±39.46 μGy/MBq), and its biodistribution was similar to ^{68}Ga-PSMA-11. Compared with ^{68}Ga-PSMA-11, ^{68}Ga-SC691 showed lower non-specific organ uptake, especially lower liver uptake. In addition, ^{68}Ga-SC691 and ^{68}Ga-PSMA-11 detected the same number and location of PSMA-positive lesions in PCa primary tumor and bone/lymph nodes metastases, and the former had a higher T/NT ratio. ***Conclusion:*** As a novel small-molecule PSMA inhibitor, SC691 may be a valuable choice for PCa imaging and therapy due to its reliable safety, dose distribution and diagnostic efficacy. And Low uptake in non-specific organs makes it promising for theranostics.

EP-0235

PSMA PET/MR with parametric Patlak imaging to increase image contrast, better quantification and shorten examination times in patients with suspected prostate cancer.

M. Gammel*, I. Rauscher, M. Eiber, S. van Marwick, S. Schachoff, R. Tauber, W. A. Weber, S. Nekolla;*
TUM, Munich, GERMANY.

Aim/Introduction: In addition to multiparametric magnetic resonance imaging (mpMRI), PSMA-PET is increasingly important for detecting clinically significant prostate cancer (PCa). The aim of this study was to develop a PET/MR protocol in which PET acquisition was started with tracer injection and completed with mpMRI. ***Materials and Methods:*** PSMA PET/MR was performed on 23 patients with suspected PCa using 323±50 Mbq rhPSMA 7.3 for biopsy planning. A 20-minute dynamic PET of the prostate was started with tracer injection, while mpMRI with T2, diffusion-weighted, and contrast-enhanced sequences was simultaneously performed. A static PET/MR of the pelvis was performed after 60 minutes p.i. Parametric images of the Patlak influx constant Ki, were calculated from the dynamic PET and compared to SUV images after 20 and 60 minutes p.i. ***Results:*** PCa was histologically confirmed in all patients. The SUVmean of PCa continuously increased (3.4±2.0, 8.4±6.5, and 10.8±6.8 at 7.5, 17.5, and 62.5 minutes, respectively). Patlak plots showed irreversible uptake kinetics in the tumors. There was a strong correlation between the Ki values and SUVs (r = 0.66). The tumor-to-muscle ratio in the Ki images was 23.5±12.8, compared to 14.6±10.2 in the SUV images ($p < 0.0012$). ***Conclusion:*** The PSMA kinetics and high Ki values suggest that images can be taken after 20 minutes and achieve a good fit of the Patlak analysis. Parametric imaging potentially allows for optimizing PSMA PET-Protocols, as no waiting time between tracer injection and PET is required and no uptake spaces are needed for patients. It would also be possible to use the whole-body scanners to reduce time in whole-body staging. However, this must be evaluated in larger patient cohorts and following a broader approach, not just primary staging.

EP-0236

PSMA-PET and PCa: an exploratory analysis beyond the numerical definition of oligometastatic state

F. Mattana[1]*, L. Airò Farulla*[1,2]*, G. Marvaso*[3]*, G. Corrao*[3]*, C. Lorubbio*[3,2]*, M. G. Vincini*[3]*, M. Zaffaroni*[3]*, L. Muraglia*[1]*, M. Colandrea*[1]*, C. Fodor*[3]*, F. Ceci*[1,2]*, B. A. Jereczek-Fossa*[3,2]*;*
[1]IEO European Institute of Oncology IRCCS, Nuclear Medicine Department, Milan, ITALY, [2]Department of Oncology and Hemato-Oncology, University of Milan, ITALY, [3]IEO European Institute of Oncology IRCCS, Department of Radiation Oncology, Milan, ITALY.

Aim/Introduction: Oligorecurrent Prostate Cancer (PCa) patients are usually defined only on the number of suspected lesions on Conventional Imaging. A deeper understanding of the burden of disease is needed in order to offer the best tailored treatment. First aim of this study is to correlate clinical features with volumetric and semi-quantitative data derived from prostate-specific-membrane-antigen positron-emission-tomography (PSMA-PET). The present study is a spin-off project of the ongoing phase-II randomized clinical trial RADIOSA (NCT03940235). ***Materials and Methods:*** Oligorecurrent PCa patients enrolled within the RADIOSA trial with PSMA-PET scan at first biochemical recurrence were screened for study inclusion. Two experienced nuclear medicine physicians retrospectively reviewed PSMA-PET images blinded to all histopathological and clinical data. PSMA tumor volume(PSMA-TV) and Maximum-standardized-uptake-values (SUVmax) were collected for eligible patients. Patients were stratified according to PSA values both at the first diagnosis and at the oligorecurrence using the median values as cut-off and according to the site of metastases (bone vs lymph node). MedianPSMA-TV and SUVmax were reported for each group. Oligometastatic disease was defined by the presence of 1-3 metastatic lesions on PSMA-PET. ***Results:*** A total of 46 patients were included. Median PSA values at the first diagnosis and at the oligorecurrence were 7.62ng/mL and 1.27ng/mL respectively. Median time between first diagnosis and oligorecurrence was 46 months. A total of 29 patients had lymph nodal only localization (M1a, according to miTNM), while 17 had at least one bone localization (M1b). When stratified according to the median PSA at diagnosis, MedianSUVmax resulted higher in patients with a PSA above the median value while medianPSMA-TV and time to recurrence were comparable in both groups. When patients were stratified according to the medianPSA at recurrence, MedianSUVmax resulted higher in patients with an higher PSA(>1.27)ng/ml, while patients in the lower PSA group had a smaller PSMA-TV(1.75vs2.28cm^3). When grouping patients according to the metastatic site, those with at least one bone metastases had a shorter time interval between first diagnosis and recurrence and a lower medianSUVmax. ***Conclusion:*** both at first diagnosis and at recurrence, patients with higher PSA

showed higher medianSUVmax values on restaging PSMA-PET; patients with lower PSA at the oligorecurrence had a lower lesion volume (median PSMA-TV 1.75) and a shorter time at the recurrence. Further studies are needed to better understand the role of volumetric and semi-quantitative parameters derived from PSMA-PET in relation with the clinical outcome. Special thanks to AIRC for the support.

EP-0237

The spleen as a reference organ for PSMA expression evaluation according to PROMISE in Prostate cancer imaging with 18F-PSMA-1007 PET/CT: a critical approach

G. Arsos[1], *A. Georgiou*[2], *D. Katsampoukas*[2], *V. Mpalaris*[2], *S. Georga*[2], *E. Moralidis*[2];
[1]*3rd Department of Nuclear Medicine, Aristotle University of Thessaloniki School of Medicine, Papageorgiou Gen. Hospital, THESSALONIKI, GREECE,* [2]*3rd Department of Nuclear Medicine, Aristotle University of Thessaloniki School of Medicine, Papageorgiou Gen. Hospital, Thessaloniki, GREECE.*

Aim/Introduction: Standardized evaluation of Prostate cancer (ProCa) lesions imaged with PSMA-Ligand PET/CT has been proposed by PROMISE [1]. Scoring of lesions is based on the comparison of their uptake with that of three reference organs (blood pool, liver and parotid gland). For tracers with predominantly hepatic excretion like 18F-PSMA-1007, the spleen is proposed instead of liver. In this context, we critically comment on some concerning features of the spleen as a reference organ. ***Materials and Methods:*** Thirty four men (aged 50-87 years) with ProCa submitted to 18F-PSMA-1007 PET/CT were enrolled, one with abdominal splenosis after splenectomy, none with splenomegaly or haematologic disease. Suspect lesions were scored according to PROMISE. SUVmax, SUVav and radiodensity (RD, in Hounsfield units) of the spleen (spleniculus in one case) and liver were measured in all patients. The agreement of SUVmax, SUVav and RD between spleen and liver was assessed by Bland-Altman statistics, the mean Spleen-Liver difference denoting bias and the standard deviation imprecision. The correlation of SUVmax, SUVav and RD between spleen and liver was assessed by the Lin's Concordance Correlation Coefficient (LCCC) and the correlation of SUVmax and SUVav with age by linear regression analysis. Wilcoxon and One-sample t- tests were used for comparisons. ***Results:*** Mean±SD of SUVmax, SUVav and RD of the spleen and liver were 13.3±4.1, 11.9±3.7, 50.3±6.7 and 17.1±4.9, 14.7±3.8, 60.8±7.1, respectively ($p<0.05$ for all paired comparisons). In 10/34 cases (29.4%), the SUVmax and SUVav of the spleen were higher than the liver. The bias and imprecision of the spleen-liver differences for SUVmax, SUVav and RD were -3.2, -2.3, -10.7 and 6.6, 5.5, 9.6, respectively ($p<0.05$ for all biases). LCCC (95% confidence interval) for SUVmax, SUVav and RD was -0.041 (-0.296-0.218), -0.050 (-0.321-0,228) and -0.012 (-0.157-0.134). Both SUVmax and SUVav of the spleen were negatively correlated with age (r -0.314 and -0.349, respectively), the correlation being significant ($p<0.05$) for SUVav. ***Conclusion:*** 18F-PSMA-1007 SUVmax and SUVav and radiodensity of the spleen and liver differ significantly and are unrelated. Moreover, spleen but not liver, shows a tendency towards reduced uptake with age. Accordingly, spleen and liver must not be considered equivalent for scoring of suspect lesions. Cases with splenectomy or splenomegaly might further hamper the role of spleen as a reference organ. ***References:*** [1] Eiber M et al. Prostate Cancer Molecular Imaging Standardized Evaluation (PROMISE): Proposed miTNM Classification for the Interpretation of PSMA-Ligand PET/CT. J Nucl Med 2018

EP-0238

Evaluation of imaging, clinical and pathological factors associated with 2-year biochemical recurrence in surgical patients with intermediate- to high-risk prostate cancer: a focus on 68GaPSMA PET and pelvic 3Tesla mpMRI

M. Celli[1], *R. Gunelli*[2], *F. Ferroni*[1], *G. Feliciani*[1], *A. Sarnelli*[1], *P. Caroli*[1], *I. Marini*[1], *L. Fantini*[1], *V. Rossetti*[1], *U. De Giorgi*[1], *D. Barone*[1], *V. Di Iorio*[1], *F. Matteucci*[1];
[1]*IRCCS Istituto Romagnolo per lo Studio dei Tumori (IRST) "Dino Amadori", Meldola, ITALY,* [2]*AUSL della Romagna – Presidio Ospedaliero Morgagni-Pierantoni, Forlì, ITALY.*

Aim/Introduction: To identify staging ^{68}GaPSMA PET and pelvic mpMRI imaging-based factors, clinical and pathological features associated with 2-year biochemical recurrence in patients with intermediate- to high-risk prostate cancer (PCa) treated with radical prostatectomy ± adjuvant treatment. ***Materials and Methods:*** 26 patients (age range: 48-72 years; median: 61 years) with biopsy-proven PCa (ISUP: 1-5; PSA range: 4,1-37ng/ml; biopsy T: T2a-T2c) were prospectively staged by ^{68}GaPSMA PET and pelvic mpMRI within six weeks prior to surgery. A 12-segment prostate map was used for tumour localization and quantitation on ^{68}GaPSMA PET and pelvic mpMRI. Post-surgical adjuvant treatment and follow up were offered as per clinical practice. Non-parametric tests were used to identify imaging-based, clinical and pathological factors associated with 2-year biochemical recurrence: age, screening PSA, PSA density, percent of PCa involved cores (< 50% versus ≥ 50%), maximum PCa core length (< 50% versus ≥ 50%), biopsy ISUP (ISUP4-5 versus ISUP1-2-3), PCa ^{68}GaPSMA SUVmax (SUVmax ≤ 10 versus SUVmax > 10), intraprostatic PCa extent according to ^{68}GaPSMA PET (PCa involvement < 3 segments versus ≥ 3 segments) and to mpMRI (< 3 segments versus ≥ 3 segments), pathology ISUP (ISUP4-5 versus ISUP1-2-3), pT stage (pT2 versus pT3) and R status (R0 versus R1). ***Results:*** Pelvic mpMRI identified PCa foci in 24 patients and correctly identified PCa extraprostatic extension in 5 out of 6 patients and seminal vesicle involvement in 2 out of 4 patients. ^{68}GaPSMA PET identified PCa foci in 24 patients and correctly identified PCa extraprostatic extension in 4 out of 6 patients and seminal vesicle involvement in 3 out of 4 patients. 2-year biochemical relapse was more frequently observed in patients with more than 50% of biopsy cores involved (p: 0.0137) and in patients with PCa foci holding ^{68}GaPSMA SUVmax higher than 10 (p: 0.008). No statistically-significant difference was found between relapsed and non-relapsed patients in terms of age (p: 0.966), screening PSA (p: 0.936), PSA density (p: 0.440), biopsy ISUP (p: 0.863), maximum PCa core length (p: 0.198), intraprostatic PCa extent on ^{68}GaPSMA PET (p: 0.340) and on mpMRI (p: 0.302), pathology ISUP (p: 0.612), pT status (p: 0.863), and R status (p: 0.809). ***Conclusion:*** In this cohort of patients with intermediate-to high-risk PCa treated with radical prostatectomy ± adjuvant treatments tumour involvement in less than 50% of biopsy cores and tumour ^{68}GaPSMA SUVmax lower than 10 hold predictive potential for 2-year biochemical recurrence-free survival.

EP-0239

PSMA PET/CT and local disease: a retrospective radiomic analysis based on a single center's experience

M. Monteiro[1], *A. M. Ferreira*[1], *A. P. Moreira*[1,2], *R. Silva*[1,2], *G. Costa*[1,3];
[1]*CHUC, Coimbra, PORTUGAL,* [2]*Instituto de Ciências Nucleares Aplicadas à Saúde, Coimbra, PORTUGAL,* [3]*Faculdade de Medicina da Universidade de Coimbra, Coimbra, PORTUGAL.*

Aim/Introduction: While prostate-specific membrane antigen (PSMA) PET/CT has established itself as the preferred method for detecting metastatic prostate cancer (PCa), magnetic resonance imaging (MRI) remains the gold standard for evaluating local disease. Nevertheless, the maximum standardized uptake value (SUVmax), commonly used to assess radiopharmaceutical uptake

in the primary tumor, has been shown to correlate with key prognostic factors such as the Gleason score (GS). With advances in PET scanner technology allowing for more accurate radiomic analysis, the potential usefulness of other features in characterising primitive prostate cancer is worth exploring. This study aims to investigate the correlation between various radiomic features, including SUVmax, SUVpeak, metabolic tumor volume (MTV), and total lesion uptake (TLU), and histologic GS and International Society of Urological Pathology (ISUP) grade group obtained from prostate biopsies. ***Materials and Methods:*** A retrospective review of 368 [68Ga]Ga-PSMA PET/CT scans performed between December 2021 and March 2023 on a single digital PET/CT scanner was conducted. Patients who underwent the study in a primary staging setting and showed no evidence of metastatic disease were selected. Spheric or elliptical volumes of interest (VOIs) were manually drawn around primary lesions, taking care to avoid bladder activity. Maximum standardised uptake value (SUVmax) and SUVpeak (the average SUV of a 1 cm^3 spheric VOI centered on the region of highest uptake) were directly obtained from the VOIs. Additionally, three different metabolic tumor volumes (MTV10, MTV20, and MTV40) and total lesion uptake values (TLU10, TLU20, and TLU40) were calculated using the same VOI and three different cutoffs in relation to SUVmax (10%, 20%, and 40%). Biopsy data was then retrieved for each patient. ***Results:*** Thirty-nine patients met the inclusion criteria. SUVpeakand SUVmax showed statistically significant correlations with the Gleason score (SUVpeak Spearman's rho=0.434, p<0.05; SUVmax Spearman's rho=0.319, p<0.05) and ISUP grade group (SUVpeak Spearman's rho=0.395, p<0.05; SUVmax Spearman's rho=0.346, p<0.05), with SUVpeakcorrelating slightly better with both parameters. However, there was no statistically significant correlation between metabolic tumor volumes (MTV10, MTV20, MTV40) or total lesion uptakes (TLG10, TLG20, TLG40) and GS or ISUP. ***Conclusion:*** Our study findings suggest that SUVpeak is a more reliable radiomic feature than SUVmax for evaluating local disease in prostate cancer patients. However, no significant correlation was found between MTV and TLG with the Gleason score or ISUP grade group, indicating a need for further refinement in the segmentation of these radiomic features.

EP-0240

PSG Score of Tubarial, Submandibular and Parotid Salivary Glands Utilizing 68Ga-PSMA-PET/CT-Scans of Prostate Cancer Patients

S. Al-Sadoon, *F. Risheq, Z. Risheq, K. Faqeh;*
Nuclear Medicine PET/CT & Bone Density Center, Amman, JORDAN.

Aim/Introduction: To characterize tubarial glands; and quantify radiation hazards to tubarial, submandibular and parotid salivary glands by determining their PSG scores utilizing ^{68}Ga-PSMA-PET/CT-scans. Tubarial glands, located inside nasopharynx and throat cavity are visualized using ^{68}Ga-PSMA-PET/CT-scans [1]. PSMA receptor targets prostate cancer tissue, and also accumulates in salivary glands. This side effect results in radiation induced toxicity, manifested as xerostomia and dysphagia. Hazards can be quantified using PSG score defined as "prostate lesion Suv_{max}/salivary glands Suv_{max}" [2]. ***Materials and Methods:*** Nine patients with (Mean±SD): age (68.9±4.9) y, PSA level (16.4±32.0), and biopsy confirmed prostate cancer, underwent ^{68}Ga-PSMA-PET/CT-scan for evaluation. Tubarial right and left glands considered cylindrical, with functional length=L, diameter=D and size=Z= (π/4) LD^2. SUV_{max} of salivary glands as-well-as prostate lesions were recorded; and PSG scores determined. ***Results:*** Estimated tubarial glands' functional length=3.0±0.6cm, diameter=1.1±0.2cm, and size=2.9 ±1.3cm^3. Tubarial, submandibular and parotid glands' SUV_{max} =5.4±2.1, 14.8±2.6, and 14.7±2.8 respectively; with submandibular and parotid being identical. Tubarial glands' SUV_{max} ~1/3 submandibular or parotid. The low tubarials' SUV_{max} is due to limited blood pool. Estimated PSG score for tubarial, submandibular and parotid glands =2.4±1.4, 0.9 ±0.6, and 0.9±0.6 respectively. Most of our patients, submandibular and parotid glands' PSG-scores <1, indicating high radiation risk; while corresponding tubarial glands' PSG-scores >1; indicating lower radiation risk. Strategies reducing radiation toxicity include: keeping patients well hydrated, chewing, medication to block salivary glands, and local anesthetics/histamines [3]. ***Conclusion:*** 1- Tubarial gland considered cylindrical with: functional length-3cm, diameter-1.1cm, and size-3cm^3. SUV_{max} = 5.4 reflects low blood pool. 2- Submandibular and parotid glands have similar uptakes ~14.8, and both can be imaging marker. For most patients, corresponding PSG scores <1, and glands became radionuclide therapy dose limiting organ. 3- Screening of prostate cancer patients with ^{68}Ga-PSMA-PET/CT is recommended before radionuclide therapy. 4- Fractional dose to minimize radiation hazards is recommended for patients with PSG < 1. ***References:*** 1- Matthijs H, et al.The tubarial Salivary gland :A potential new organ at risk for Radiotherapy. Radiotherapy and Oncology 154(2021)292-298,https://doi.org/10.1016/j.radonc.2020.09.034 2- Hotta. Masatoshi, et al. PSMA -PET Tumor -to- Salivary Gland Ratio to Predict Response to ^{177}Lu- PSMA Radioligand Therapy.: An International Multicenter Retrospective Study. Journal of Nuclear Medicine, March 2023, jnumed. 122.265242, DOI: https:/doi.org/10.2967/jnumed 122.265242. 3- Nathalie Heynickx, et al. "The salivary glands as a dose limiting organ of PSMA-targeted radionuclide therapy: A review of the lessons learnt so far".Nuclear Medicine and Biology, 98-99 (2021) 30-39 0969-8051/2021, https://doi.org10.1016/j.nucmedbio.2021.04.003.

EP-14

e-Poster Area

B: Imaging Clinical Studies -> B1 Oncological Imaging Clinical Study -> B18b Prostate BC Recurrence

EP-0241

Therapeutic implications of 18F-PSMA PET/MRI in patients with prostate cancer and biochemical recurrence (PSA < 2 ng/ml) after prostatectomy

J. Garcia, *A. Compte, M. Kauak, P. Bassa, T. Blanch, J. Pastor, E. Riera;*
CETIR ASCIRES Grupo biomédico, Barcelona, SPAIN.

Aim/Introduction: To evaluate the rate of detection of recurrence and to analyse its therapeutic implications for prostate cancer patients already treated with prostatectomy and PSA <2 ng/ml on 18F-PSMA PET/MRI. ***Materials and Methods:*** Prospective study with 20 consecutive prostate cancer patients treated with prostatectomy (mean time since surgery 19 months), and PSA <2 ng/ml, PET/MRI study acquired one hour after IV administration of 185±10% MBq of 18F-PSMA, in dual-phase fashion: Prostate (multi-parametric PET/MRI emission, T1, T2, DWI, Gd). Whole-body (PET/MR emission, T1, T2, STIR, DWI). Two experts in prostate

studies (NM physician and Radiologist) analysed images visually and quantitatively. Lesions were grouped into recurrence in prostatectomy bed; (Tr), pelvic lymph nodes (N1), extrapelvic lymph nodes (M1a), bone metastases (M1b). The Oncology Committee decided the therapeutic strategy to follow upon PET/MRI findings. ***Results:*** Mean PSA was 1.1 ng/ml (0.59-1.90), with mean PSAdT of 8 months. PET/MRI with 18F-PSMA was negative in 6 patients (30%). On per-patient analysis: PET/MRI was positive in 14 (70%) classified as: TrN0M0 (n: 6); T0N1M0 (n: 4); TrN1M0 (n:1); TrN0M1b (n: 1); T0N1M1aM1b (n: 1); TrN1M1aM1b (n: 1). Regarding recurrence site: Tr (n: 9; MRI was superior in 3, and PET in 1); N1 (n: 7) infracentimetric; M1a (n: 2) infracentimetric; M1b (n: 3). As for lesion stratification: 8 were single; 4 oligoM1; 2 multiM1. As for therapeutic implications of a positive study: no change (n: 6); change in volume radiotherapy and ADT (n:4); systemic treatment implementation (n:2). ***Conclusion:*** PET/MRI with 18F-PSMA detected disease in 70% of our prostate cancer patients with PSA levels <2ng/ml after prostatectomy. Disease site detection and patient stratification allowed for a patient-tailored therapy implementation. ***References:*** Fanti S, Minozzi S, Morigi JJ, Giesel F, Ceci F, Uprimny C, et al. Development of standardized image interpretation for 68Ga-PSMA PET/CT to detect prostate cancer recurrent lesions. Eur J Nucl Med Mol Imaging. 2017;44(10):1622-35 Fanti S, Hadaschik B, Herrmann K. Proposal for Systemic-Therapy Response-Assessment Criteria at the Time of PSMA PET/CT Imaging: The PSMA PET Progression Criteria. J Nucl Med. 2020 May;61(5):678-682. doi: 10.2967/jnumed.119.233817. Epub 2019 Dec 5. PMID: 31806774; PMCID: PMC7198387

EP-0242

Clinical impact of 18F-DCFPyL PET/CT for clinical decision-making in biochemical recurrence of prostate cancer in our province.

Y. Santaella Guardiola*, J. Rodriguez-Rubio Corona, M. Piñero Fernandez-Reyes, F. Cañete Sanchez, C. Quintana Bolaño, M. Pajares Vinardell;*
Hospital Puerta del Mar, Cadiz, SPAIN.

Aim/Introduction: Since July 2021, 18F-DCFPyL PET/CT has been administered as a compassionate-use medicinal product for the diagnosis of biochemical recurrence in patients with castration-resistant prostate cancer, specifically when PSA levels are below 1 ng/mL. This imaging technique has demonstrated higher sensitivity in detecting metastatic disease compared to traditional imaging methods. Our aim was to evaluate how the integration of 18F-DCFPyL PET/CT in the province has impacted patient management. ***Materials and Methods:*** A retrospective study was carried out involving 151 patients who underwent a 18F-DCFPyL PET/CT scan between July 2021 and March 2023 at one of the five hospitals in the province of Cádiz: Hospital de Jerez, Hospital de La Línea, Hospital Puerto Real, Punta de Europa Hospital (Algeciras) and Puerta del Mar Hospital (Cádiz). The median PSA level at the time of the scan was 0.46 ng/mL (range 0.2 - 4.79 ng/mL), with a mean of 0.51 ng/mL. All PET/CT scans were evaluated by a Nuclear Medicine specialist with extensive experience. Descriptive statistics were used to analyze the impact of the scan on the clinical care of 138 patients with biochemical recurrence. For the remaining 13 patients, there was not enough information available to assess the clinical utility of the scan due to the short time elapsed since the test was performed. ***Results:*** Among the 151 patients studied, 93 (61.5%) showed an abnormal uptake of 18F-DCFPyL. These abnormalities included local recurrence in 21 patients, regional lymph node involvement in 53 patients, non-regional lymph node involvement in 10 patients, pulmonary visceral metastases in 5 patients, and bone metastases in 12 patients. Additionally, results were inconclusive in 3 patients (1.9%), and negative in 56 patients (37%). Out of the 138 patients for whom clinical information was available, 70 (50.7%) had a change in their treatment plan based on the scan results, while the treatment plan remained unchanged for 66 patients (47%). ***Conclusion:*** The incorporation of 18F-DCFPyL PET/CT in the province of Cádiz has significantly influenced clinical decision-making (50,7%) in cases of biochemical recurrence in prostate cancer. However, it is yet to be determined whether this will ultimately result in improved survival outcomes for these patients.

EP-0243

Evaluation of the Success of 18F-PSMA PET/CT in the Detection of Prostate Cancer Recurrence in Patients with Biochemical Recurrence

G. Sutcu*[1], C. Soydal[1], M. Araz[1], Y. Urun[2], E. Suer[3], S. Baltaci[3], N. O. Kucuk[1];*
[1]Ankara University Medical School Department of Nuclear Medicine, Ankara, TÜRKIYE, [2]Ankara University Medical School Department of Medical Oncology, Ankara, TÜRKIYE, [3]Ankara University Medical School Department of Urology, Ankara, TÜRKIYE.

Aim/Introduction: Prostate cancer is the most common urological cancer in men. PSMA has become an ideal molecular target for both imaging and treatment, since it is a good imaging biomarker for prostate cancer. Widely used form is ^{68}Ga-PSMA, and its sensitivity for detection of recurrent disease, in especially at low PSA levels (0.2-2.0 ng/mL), is shown to be high. However, it can assess the pelvic region difficult due to excretion from the urinary system. Although it is rarely used, ^{18}F-PSMA-1007 has been presented a potential advantage for pelvic imaging because of its minimal excretion by the urinary system. In this study, we present our first experience evaluating the success of ^{18}F-PSMA-1007 PET/CT in patients with biochemical recurrence. ***Materials and Methods:*** This study has a prospective design. After ethical committee approval, 31 patients who were being followed after primary treatment of prostate cancer and had biochemical recurrence were recruited to the study between June 2022 and February 2023. All the patients were underwent whole body PET/CT 45-60 min after iv injection of approximately 333-407 MBq ^{18}F-PSMA-1007. The images were evaluated for local recurrence, regional, distant lymph node metastases, and bone metastasis. Disease detection rates for all the regions were calculated and mean values of Gleason Scores (GS), PSA levels and PSA doubling time (PSAdt) of PET positive and negative patients were analyzed by Student's T Test. ***Results:*** The mean age of the patients participating in the study was observed at 68.26, the average Gleason score was 7.71, the average PSA at the time of imagining was 10.6, and the PSA doubling time was 139.7 days. Pathological activity in the prostate was observed in 11 (35%) of the 31 patients, and the average SUVmax was found to be 6.55. Regional lymph node recurrence was detected in 12 (38%) patients, distant lymph node metastasis in 10 (33%) patients, and bone metastasis in 9 (30%) patients. The overall detection rate was 76.7%. Median GS of PET positive and negative groups were different (p=0.03). Mean PSAdt of patients with bone metastases and without were different significantly (p=0.01). ***Conclusion:*** Although a small sample group was examined, a high detection rate was observed for ^{18}F-PSMA-1007. This suggests that ^{18}F-PSMA-1007 PET/CT may have advantages over other ^{68}Ga labelled PSMA radiopharmaceuticals, particularly in the evaluation of regional and local relapse in patients with biochemical relapse.

EP-0244

Flare phenomenon of 99mTc-bone scintigraphy is a determinant of prognosis in patients with metastatic castration-resistant prostate cancer

X. Zhang[1], *K. Nakajima*[2], *H. Horikoshi*[3], *A. Mizokami*[4], *K. Nishimoto*[5], *K. Hashine*[6], *H. Matsuyama*[7], *S. Takahashi*[8], *H. Wakabayashi*[1], *S. Kinuya*[1];
[1]*Department of Nuclear Medicine, Kanazawa University, Kanazawa, Ishikawa, JAPAN,* [2]*Department of Functional Imaging and Artificial Intelligence, Kanazawa University, Kanazawa, Ishikawa, JAPAN,* [3]*Department of Diagnostic Radiology, Gunma Prefectural Cancer Center, Ota, JAPAN,* [4]*Department of Urology, Kanazawa University, Kanazawa, Ishikawa, JAPAN,* [5]*Department of Uro-Oncology, Saitama Medical University International Medical Center, Saitama, JAPAN,* [6]*Department of Urology, National Hospital Organization Shikoku Cancer Center, Matsuyama, JAPAN,* [7]*Department of Urology, Graduate School of Medicine, Yamaguchi University, Ube, JAPAN,* [8]*Department of Urology, Nihon University School of Medicine, Tokyo, JAPAN.*

Aim/Introduction: Bone scan index (BSI) has been used in patients with prostate cancer and bone metastasis. Although flare phenomenon during chemotherapy was observed in a subset of patients with metastatic castration-resistant prostate cancer (mCRPC), clinical implications have not been clarified. The aim of this study is to determine the prognosis value of the flare phenomenon on bone scintigraphy in mCRPC patients. ***Materials and Methods:*** A cohort of patients with bone metastatic CRPC (n=72) were included from PROSTAT-BSI registry. BSI was automatically calculated with ^{99m}Tc-MDP bone scintigraphy. The flare phenomenon was defined as the increase of BSI greater than 10% in the 3rd month after the beginning of therapy, followed by an improvement in BSI three months later. Two-year all-cause death (ACD) and prostate cancer death (PCaD) were analyzed for the flare and no-flare groups. The Cox survival analysis and relationship of predictors to the final outcome were investigated. The effect of androgen receptor axis targeted agents (ARATA), such as Abirateron Abiraterone and Enzaltamide, was also examined. ***Results:*** Flare phenomenon was observed in 26/72 (36%) patients. The 2-year mortality rates were 43.5% and 26.9% in the no-flare and flare groups respectively. In the no-flare group, patients with the higher baseline BSI resulted in higher mortality while no significant difference in mortality was observed in the flare group, irrespective of ACD or PCaD. The baseline BSI>4 showed a significant higher mortality rate in the no-flare group. After accounting for flare phenomenon in addition to other factors, the survival analysis indicated that the increased PSA in 3rd month was a determinant of poor prognosis in the no-flare group especially for the patients with baseline BSI>1, while the PSA change had no impact on survival in the flare group. Regarding pharmaceutical applications, the application of ARATA lead to greater survival in the no-flare group than that in the flare group and had a strong association with the baseline BSI, but had no obvious effect in the flare group. ***Conclusion:*** Favorable prognosis was attainable in mCRPC patients who showed flare phenomenon. Other variables, such as baseline BSI, a change in PSA, and the use of ARATA, may have an impact on the survival of patients who had no flare phenomenon. A follow-up bone scintigraphy at least every three months assisted in determining prognosis for bone metastasis in mCRPC. Early use of ARATA may enable individuals with no flare phenomenon gain a better outcome.

EP-0245

Efficacy of 18-F-DCFPyL-PET/CT in the first biochemical recurrence of prostate cancer and its impact on therapeutic management

I. Obedkova*, A. Prieto Soriano, L. Santamaria Chico, S. Guzmán Ortiz, K. Velasquez Diaz, P. Soares Meneses, M. Grajeda Gallardo, I. Garrido Solesio, M. Mitjavila Casanovas;*
University Hospital Puerta de Hierro, Majadahonda, SPAIN.

Aim/Introduction: 18-F-DCFPyL (PSMA) is a radiotracer with already demonstrated results, which in our setting is only for compassionate use. The objective of this study was to evaluate the efficacy of PET-PSMA in patients with biochemical recurrence (BCR) of prostate cancer (PC), as well as its impact on therapeutic management. ***Materials and Methods:*** We prospectively recruited 63 patients (mean age 68 years) with BCR after radical prostatectomy, who underwent PET-PSMA after negative CT, bone scintigraphy and/or PET-choline. The analysis was performed on 27 patients with the first BCR. We evaluated the Gleason score, PSA levels, PSA doubling time (PSADT), PET-PSMA positivity according to EANM guidelines, and the impact of the result on therapeutic management. We used STATA for statistical analysis. ***Results:*** At diagnosis nineteen of twenty-seven patients had low/intermediate risk and eighth of twenty-seven high risk. Ten patients had PSA level of BCR <0.5, twelve patients 0.5-1.99, four patients between 1-1.99 and only one PSA≥2. The PET-PSMA positivity rate was 55.6% (40.7% oligometastatic and 14.8% multimetastatic). Patients with a positive PET-PSMA result had a lower PSADT (mean 5.6 months) than patients with a negative result (mean 6.3 months). A positive study result was obtained in 40% patient with PSA<0.5, which increased to 58.3% in patient with PSA between 0.5-0.99, 75% with PSA between 1-1.99 and 100% with PSA≥2. A change in therapeutic management was proposed in all patients (15) with positive PET-PSMA study result, in 2 of 15 it was not carried out due to patient refusal. Nine of fifteen patients received targeted radiotherapy and 4 of 15 also received hormone therapy. A decrease in a control PSA level was observed in 85% of patients with a change in treatment management. ***Conclusion:*** PET-PSMA is effective in the diagnosis of the first BCR of PC with low PSA levels, causing a change in therapeutic management with subsequent biochemical response.

EP-0246

Outcomes of [68Ga]Ga-PSMA-11 PET/CT in biochemical recurrence after brachytherapy

I. Próspero[1], *G. Ferreira*[1], *J. C. Ferro*[1], *D. Barbosa*[1], *D. G. Silva*[1], *P. Leite Silva*[2], *S. Fontão de Castro*[1], *J. P. Teixeira*[1], *H. Duarte*[1], *I. Lucena Sampaio*[1];
[1]*Department of Nuclear Medicine, Instituto Português de Oncologia do Porto, Porto, PORTUGAL,* [2]*Cancer Epidemiology Group-Research Center, Department of Epidemiology, Instituto Português de Oncologia do Porto, Porto, PORTUGAL.*

Aim/Introduction: Patients with prostate cancer (PCa) experiencing biochemical recurrence (BCR) after treatment with curative intent are at an increased risk of developing distant metastasis. Nevertheless, patients offered low-dose rate brachytherapy (LDRBT) as monotherapy are usually patients with low-risk PCa, as opposed to patients submitted to other radiotherapy modalities. The aim of this study was to describe the role of prostate-specific membrane antigen (PSMA) PET/CT in clarifying the natural history of BCR after brachytherapy. ***Materials and Methods:*** Retrospective study of 49 men who underwent [^{68}Ga]Ga-PSMA-11 PET/CT between October 2017 and December 2022 for suspected

BCR after LDRBT (Iodine-125 seeds; 145 Gy dose). Exclusion criteria included prostate-specific antigen (PSA) bounce and PSA level not in accordance with the Phoenix definition for BCR. Images were reviewed for determination of local recurrence and/or metastasis and PSMA intensity of the detected lesions, expressed as maximum standardized uptake value (SUVmax) and SUVpeak. The association between these PET/CT-parameters and PSA-related variables [PSA doubling time (PSA-DT), PSA velocity (PSAV) and PSA level at the time closest to image acquisition] was analyzed according to Spearman's correlation and Wilcoxon-Mann-Whitney test (α=0,05). The subsequent patient management decision was also registered. ***Results:*** Thirty-three patients were included (median age= 71 years; median initial PSA= 7,83 ng/mL); 64% had an initial biopsy Gleason score= 6 (ISUP grade 1). BCR occurred a median of 58,90 months after LDRBT, with a median PSA-DT of 10,5 months. Median PSA by the time of imaging was 4,89 ng/mL. [^{68}Ga]Ga-PSMA-11 PET/CT was positive in 27 patients (82%): 70% had tumor recurrence within the prostate/seminal vesicles (n=19), 33% showed regional lymph node metastasis (n=9) and 30% presented distant metastasis (n=8); 52% (n=14) had only local disease. Median SUVmax of local recurrence was 6,42. No significant association was found between PET/CT-parameters and PSA-related variables. Twenty-four patients also underwent pelvic magnetic resonance imaging (MRI), with concordance between PET/CT and MRI in 67%; in 6 patients (25%) recurrence was detected only on PET/CT. Subsequent therapeutic decision included salvage local procedures (n=10), surveillance (n=8) and hormonal therapy (n=9). ***Conclusion:*** BCR after LDRBT tended to develop locally rather than at distant sites. PSA values and kinetics were not predictive of PCa recurrence location on PSMA PET/CT, which could be explained by variability in PSA measurements and the small sample size of the study. According to PSMA PET/CT results, subsequent patient management included mostly local treatments or surveillance, delaying the introduction of hormonal therapy.

EP-0247

Impact of [18F]-DCFPyL (PSMA) PET/CT in the diagnostic and therapeutic impact in the biochemical recurrence of prostate cancer.

J. Fernández Fernández*, E. Triviño-Ibáñez, D. Rivas-Navas, J. Villa-Palacios, A. Rodríguez-Fernández;*
Virgen de las Nieves University Hospital, Granada, SPAIN.

Aim/Introduction: The aim was to evaluate the diagnostic accuracy and the impact therapeutic of [^{18}F]-DCFPyL PET/CT in the biochemical recurrence (BR) of prostate cancer (PC) treated with curative intent. ***Materials and Methods:*** An observational and prospective study was performed, including patients with PC treated with radical intent and BR criteria, who underwent an [^{18}F]-DCFPyL PET/CT study between October 2020 and August 2022. The images were analysed visually and semi-quantitatively. The results of the PET/CT study were categorised into positive or negative, using anatomical pathology, other imaging tests and/or clinical follow-up as the gold standard. We analysed the impact of the results on the therapeutic attitude and the association of quantitative parameters with PSA kinetics. The reclassification of risk and tumour volume, were was carried out according to the LATITUDE and CHAARTED criteria. ***Results:*** 101 patients were included (mean age: 63.24±6.37 years). They presented a positive [^{18}F]-DCFPyL study in 85/101 patients with a detection rate (DR) of 84.2%. Of these patients, 21.8% presented recurrence in the prostatic fossa, 29.7% had pelvic lymph node involvement, 9% had retroperitoneal lymph node involvement and 22.8% presented distant disease. DR increases in line with the increasing of PSA trigger values: PSA from 0.2 ng/ml to 0.5 ng/mL DR 78.3%; PSA from 0.5 ng/ml to 1 ng/ml DR: 89.7%; PSA from 1 ng/ml to 1.5 ng/mL DR:81.3%, PSA over 1.5 ng/mL DR: 100%. Sensitivity and specificity were 0.91 (95% CI 0.85-0.97) and 0.55 (95% CI 0.25-0.84) respectively, positive predictive value (PPV) 0.94 (95% CI 0.89-0.99), negative predictive value (NPV) 0.43 (95% CI 0.17-0.69) with a discriminatory ability (AUC) of 0.65 (95% CI 0.51-0.80, p=0.043). The result of the [^{18}F]-DCFPyL study modified the therapeutic attitude in 57/101 patients (56.4%) and reclassified 4/101 patients into high risk and tumour burden. The quantification parameters of the [^{18}F]-DCFPyL study showed a moderate-strong significant correlation with PSA kinetics. ***Conclusion:*** [^{18}F]-DCFPyL PET/CT presents good performance in the detection of disease in BR of PC even with very low PSA levels, conditioning the modification of therapeutic decisión-making in more than 50% of patients in our series.

EP-0248

Analysis of pathological findings in 18F-DCFPyL PSMA PET in recurrence of prostate cancer according to PSMA-RADS classification and E-PSMA overexpression score. Confirmation of results by pathological anatomy, biochemical response or imaging.

B. Hervás-Sanz[1]*, J. J. Robles-Barba*[1]*, J. J. Martín-Marcuartu*[1]*, S. Bondia-Bescós*[1]*, M. Pudis*[1]*, J. E. Romero-Herrera*[2]*, G. Reynés-Llompart*[3]*, F. Ferrer-González*[4]*, J. F. Suárez-Novo*[5]*, M. Cortés-Romera*[1]*;*
[1]Nuclear Medicine-PET (IDI) Department, Bellvitge University Hospital-IDIBELL, L'Hospitalet de Llobregat, SPAIN, [2]Radiopharmaceutical Department, Bellvitge University Hospital-IDIBELL, L'Hospitalet de Llobregat, SPAIN, [3]Radiophysics Department, Bellvitge University Hospital-IDIBELL, L'Hospitalet de Llobregat, SPAIN, [4]Radiation Oncology Department, Bellvitge University Hospital-IDIBELL, L'Hospitalet de Llobregat, SPAIN, [5]Urology Department, Bellvitge University Hospital-IDIBELL, L'Hospitalet de Llobregat, SPAIN.

Aim/Introduction: To validate our findings with 18F-DCFPyL PET/CT (PET/PSMA) in prostate cancer (PCa) recurrence, classified usings PSMA-RADS classification and E-PSMA score of PSMA overexpression, through subsequent confirmation by pathological anatomy (PA), biochemical response after treatment or complementary imaging techniques. To correlate the results with clinical variables related to the characteristics of the tumor and PSA kinetics. ***Materials and Methods:*** Forty-two patients with positive PET/PSMA (45-81 years old) performed because of PCa biochemical recurrence after radical therapy (PSA 0.21 to 8.5) were included. PET findings were classified according to PSMA-RADS scale and E-PSMA score of PSMA overexpression (OE). These findings were validated by: 1) PA after surgery or biopsy of the highest PSMA-RADS lesion; 2) PSA decrease after radiotherapy/SBRT of the highest PSMA-RADS lesion (patients treated with hormonal or systemic therapy were excluded) or 3) Confirmation of PET/PSMA findings by another imaging technique (MRI, CT, bone scintigraphy, another PET). Results were correlated with the most recent measure of PSA (rPSA), PSA kinetics (dobubling time, velocity, slope), ISUP, D'Amico and initial TNM classification using statistical Chi-square studies of trend and linear regression. ***Results:*** Overall confirmation rate was 88% (37/42): 6/8 by PA, 21/23 by PSA decrease and 10/11 by imaging. We found 26 patients whose highest grade lesion was classified as PSMA-RADS-5 (25/26 confirmed as PCa, although the false positive may be due

to an inadequate lymphadenectomy), 13 PSMA-RADS-4 (9/13 confirmed as PCa) and 3 PSMA-RADS-3D (3/3 confirmed as PCa). Statistically significant relationship was found between rPSA and OE (p=0.00117) and between rPSA and the presence of lesions with higher PSMA-RADS, specially when rPSA>2 (p=0.01316).A slight correlation was also found between ISUP and patients with a confirmed positive result, but no statistical correlation was found between PET/PSMA results and PSA kinetics, D'Amico or initial TNM classification. ***Conclusion:*** PET/PSMA is a fundamental technique for detection of PCa recurrence, with results that in most cases can be confirmed after treatment, biopsy, surgery or image control. PSMA-RADS and E-PSMA classifications help to intuitively categorize the findings and homogenize the reports. In our study, we frequently found lesions with higher PSMA-RADS/E-PSMA scores in those patients with higher PSA.

EP-0249

Comparison of Digital Versus Analog 68Ga-PSMA-11 PET/CT Performance in Hormone-sensitive Prostate Cancer Patients with Early Biochemical Recurrence or Persistence

G. Rovera[1], *S. Grimaldi*[1], *S. Dall'Armellina*[1], *R. Passera*[1], *M. Oderda*[2], *P. Gontero*[2], *D. Deandreis*[1];
[1]*Nuclear Medicine, Department of Medical Sciences, AOU Città della Salute e della Scienza di Torino, Turin, ITALY,* [2]*Department of Surgical Sciences, Urology Unit, AOU Città della Salute e della Scienza di Torino, Molinette Hospital, University of Turin, Turin, ITALY.*

Aim/Introduction: Recent progress in PET technology has led to the introduction of new-generation digital PET systems based on solid state detectors, which offer several technical advantages. The aim of this study was to investigate whether the favorable characteristics of digital PET (dPET) compared to previous generation analog systems (aPET) could translate into an improved disease localization in prostate cancer (PCa) patients with early biochemical recurrence/persistence (BCR/BCP) after radical treatment. ***Materials and Methods:*** A retrospective analysis was conducted on four hundred forty (n=440) consecutive ^{68}Ga-PSMA-11 PET/CT scans performed with either an analog (11/2016-11/2020, n=311) or digital (04/2021-10/2022, n=129) scanner in hormone-sensitive ADT-free PCa patients with early-BCR/BCP (PSA at PET ≤ 2.0 ng/mL), previously treated with radical intent (radical-prostatectomy/radiotherapy). Inferential statistics for continuous/categorical covariates was performed using Mann-Whitney and Fisher's exact tests. The cohorts were tested for homogeneity of baseline clinical parameters (T-stage ≥3a, ISUPgrade ≥3, radical treatment, time-to-recurrence, PSA doubling-time/velocity, adjuvant/salvage treatments). ***Results:*** dPET showed a significantly higher number of positive scans compared to aPET (49%[63/129] vs 37%[116/311], p=0.03), despite a slightly lower median PSA value in the dPET cohort (0.33[IQR:0.26-0.61] vs 0.55[IQR:0.40-0.85] ng/ml, p<0.01). dPET detection rate was significantly higher in both PSA ranges 0.2-0.5 (39%[32/82] vs 25%[34/135], p=0.03) and 0.5-1.0 ng/ml (63%[24/38] vs 41%[53/130], p=0.02), but not for PSA ≥1.0 ng/ml. Regarding lesions localization, dPET identified a higher number of cases with suspected pelvic nodal metastases (miN1, 26%[20/78] vs 14%[17/125], p=0.04) and local recurrences (miTr, 30%[14/47] vs 3%[6/176], p<0.01) in patients with PSA values ≤ 0.5 and 0.5-2.0 ng/ml, respectively. Overall, dPET showed a higher per-patient median number of pathologic findings (PSMA-RADS ≥3) (2[IQR:1-3] vs 1[IQR:1-2], p<0.01), as well as a higher number of multi-metastatic cases (>3 lesions) among N1/M1-positive scans (22%[10/46] vs 9%[9/105], p=0.03). The proportion of uncertain findings (PSMA-RADS 3) among all pathological lesions was significantly lower for dPET than aPET (24%[39/160] vs 39%[60/156], p=0.008), even when stratifying for miN1 lesions (11%[7/65] vs 41%[25/61], p<0.01). Moreover, despite the higher positivity rate of dPET, the number of patients with only uncertain findings was not significantly different (7%[9/129] vs 9%[28/311]). Finally, although the lesion/blood-pool SUVmax ratios were comparable after PSMA-RADS stratification, dPET PSMA-RADS 4 nodal metastases (miN1/M1a) showed a significantly smaller maximum diameter (5[IQR:4-7] vs 7[IQR:5-8] mm). ***Conclusion:*** ^{68}Ga-PSMA-11 dPET showed a better performance compared to aPET, resulting in a higher scan-positivity rate, a higher number of detected pathological lesion, and a lower rate of uncertain findings.

EP-0250

Whole Body Tumour Burden On PET/CT With 18F-DCFPyL Obtained By aPROMISE Platform: Associations With Tumour Biology And PSA Kinetics In Patients With Biochemical Relapse Prostate Cancer.

L. García Zoghby[1], *A. García Vicente*[1], *M. Amo-Salas*[2], *P. Borrelli*[3], *C. Lucas Lucas*[4], *A. Padilla Bermejo*[4], *N. Sicilia Pozo*[4], *M. Contreras Ameduri*[4], *M. Cruz Montijano*[1], *F. Pena Pardo*[4], *E. Noriega Álvarez*[4], *M. Talavera Rubio*[4], *V. Poblete García*[4], *Á. Soriano Castrejón*[1];
[1]*University Hospital of Toledo, Toledo, SPAIN,* [2]*Castilla-La Mancha University, Ciudad Real, SPAIN,* [3]*Sahlgrenska University Hospital, Göteborg, SWEDEN,* [4]*General University Hospital of Ciudad Real, Ciudad Real, SPAIN.*

Aim/Introduction: The objective was to analyse the associations between 18F-DCFPyL molecular variables obtained by automatic Prostate Cancer Molecular Imaging Standardized Evaluation (aPROMISE) platform with clinical characteristics and PSA kinetics in patients with biochemical relapse (BR) of prostate cancer (PCa). ***Materials and Methods:*** We analysed 275 patients with BR of PCa after radical treatment. All patients' characteristics were classified in groups before PET/CT scans: grade ISUP group (1-5), recurrence risk (low/medium/high), PSA (PSA≤1ng/ml, 1<PSA≤2 and PSA > 2 ng/ml), PSA doubling time (PSAdt) ≤ or > 6 months and PSA velocity (PSAvel) ≥ or < 0.2 ng/ml/month. All the patients underwent 18F-DCFPyL PET/CT between May 2020 and September 2022. 18F-DCFPyL PET/CT were visually assessed by two experienced nuclear medicine physicians independently. Lesions segmentation in positive 18F-DCFPyL PET/CT scans was performed using aPROMISE platform. We obtained total molecular tumour volume (total_MTV), total tumour lesion activity (total_TLA) and total aPROMISE score (total_aPROMISE), a new radiomic biomarker which is the interaction between volume and intensity by tissue type. We compared clinical characteristics in negative versus positive PET/CT scans by Mann-Whitney test. Associations between molecular variables and patients' characteristics were statistically analysed, categorical variables by ANOVA and Kruskal-Wallis test and quantitative variables by Spearman's correlation. ***Results:*** Sixty-two per cent of the patients were high-risk PCa. 18F-DCFPyL PET/CT scans were positive for PCa recurrence in 165/275 patients (60%). Mean PSA, PSAdt and PSAvel values were significantly different in positive versus negative 18F-DCFPyL PET/CTs (p<0.001; p=0.003; p< 0.001, respectively), with higher PSA level and more unfavourable PSA kinetics in positive than in negative scans. PSA and PSAvel showed significant association with total_MTV [ρ=0.500 (p<0.001); ρ=0.448 (p<0.001), respectively], total_TLA [ρ=0.465 (p<0.001); ρ=0.448 (p<0.001), respectively], and total_aPROMISE

[ρ=0.480 (p<0.001); ρ=0.470 (p<0.001), respectively]. Mean total_MTV, total_TLA and total_aPROMISE values were significantly higher in PSA > 2ng/ml group (13.05±22.34; 69.89±133.37; 24.96±44.88, respectively), PSAdt ≤ 6 months (10.76±21.68; 56.37±117.18; 20.88±43.13, respectively) and PSA ≥ 0.2ng/ml/month (16.07±27.35, 84.57±149.73; 31.38±54.74, respectively) compared to others groups. No significant association was found between grade group and recurrence risk with metabolic variables. ***Conclusion:*** Larger 18F-DCFPyL molecular tumour burden variables assessed by aPROMISE platform were associated to higher PSA values and unfavourable kinetics, defining their utility and robustness compared to other clinical variables, not only in the prediction of positive PET/CT but also in whole-body tumour burden assessment.

EP-0251

Influence of Gleason, ISUP grade, initial TNM, PSA values and kinetics on detection rate in prostate cancer recurrence by [18F]DCFPyL PSMA PET/CT

J. Martin-Marcuartu[1], *J. Robles Barba*[1], *S. Bondia Bescos*[1], *E. Romero Herrera*[2], *G. Reynes Llompart*[3], *J. Suárez Novo*[4], *F. Ferrer Gonzalez*[5], *S. Ruiz Llama*[6], *M. Cortés Romera*[1];
[1]*Department of MNU-PET/CT (IDI). Hospital Universitari de Bellvitge, Barcelona, SPAIN,* [2]*Department of Radiopharmacy. Hospital Universitari de Bellvitge, Barcelona, SPAIN,* [3]*Department of Radiophysics. ICO Duran i Reynals, Barcelona, SPAIN,* [4]*Department of Urology. Hospital Universitari de Bellvitge, Barcelona, SPAIN,* [5]*Department of Radiotherapy. ICO Duran i Reynals, Barcelona, SPAIN,* [6]*Department of Radiopharmacy. Hospital Germans Trias i Pujol, Barcelona, SPAIN.*

Aim/Introduction: To evaluate the influence of Gleason scale, ISUP grade, initial TNM, PSA values and kinetics on the detection rate (DR) of prostate cancer recurrence studied with [18F]DCFPyL ([18F]PSMA) PET/CT, as well as on the PSMA overexpression intensity (OI) of pathological findings in PET scans. ***Materials and Methods:*** We included 109 patients (45 - 82 years) with biochemical recurrence after radical therapy (PSA 0.20 to 61.4 ng/dl). We evaluated DR in different groups according to Gleason, ISUP grade and initial TNM, most recent PSA (PSAr) stratified according to 0.2-0.5ng/dl; >0.5-1ng/dl, >1-2ng/dl, >2ng/dl, and kinetics (doubling time [DT], speed and slope). The variables were also correlated with the OI of pathological findings (1: uptake between vascular pool and liver, 2: between liver and parotid, 3: >parotid). Statistical studies Chi-square and linear regression were performed to evaluate the correlation between the different variables as well as DT and OI. ***Results:*** Overall DT was 68.8% (75/109), being higher in high-risk patients by TNM (76.9% for T3b vs. 62.2% for T2) or Gleason (81.2% for Gleason 9 vs. <70% for the rest). Statistical significance was found between PSAr with DT (p=0.039) and OI (p=0.0168). Patients with PSAr >2ng/dl had DT 76.2% vs. 47.6% in PSAr 0.2-05ng/dl. OI was grade 3 in 43.5% of positive patients with PSAr >2ng/dl, while in none of the patients with PSAr between 0.2-0.5ng/dl was positive. Regarding kinetics, we did not find statistically significant results, although we did find a trend towards higher DR and OI in patients with short DT. ***Conclusion:*** PET/CT with [18F]DCFpyL is an useful technique for the detection of recurrence in prostate cancer. It has greater efficiency in high-risk patients and in recurrences with PSA from 0.5 because of greater overexpression of PSMA in patients with higher PSA. In our study we found no significant correlation between kinetics and detection rate, although there was a trend regarding doubling time.

EP-0252

Attitude and Management Change in Those Patients with Extrapelvic Findings in a PET-CT Study with PSMA

R. Bellviure-Meiro[1], *M. Simó Perdigó*[1], *S. Menendez-Sanchez*[2], *C. Franco Monterroso*[1], *I. Navales Mateu*[1], *S. Asadurova*[1], *F. Velázquez*[1], *J. Echeverri Diaz*[1], *N. Calviño*[1], *S. Aguade-Bruix*[1];
[1]*Hospital Universitari Vall d'Hebron, Barcelona, SPAIN,* [2]*Clínica Universidad de Navarra, Pamplona, SPAIN.*

Aim/Introduction: To analyze the rate of extrapelvic findings in PET-CT studies with PSMA in patients with biochemical recurrence of Prostate Cancer (PCa) and PSA <1ng/ml. We also evaluated the change in therapeutic management of these patients. ***Materials and Methods:*** We analyzed a total of 86 PET-PMSA studies carried out during 2022 and 2023. We included those patients with PCa and biochemical recurrence with potentially suspicious findings of extrapelvic tumor disease: retroperitoneal lymph nodes, supradiaphragmatic lymph nodes, bone M1 , lung M1, or others. Change in management was measured according to 3 points: follow-up, stereotactic body radiation therapy (SBRT), or systemic treatment. The confirmation of the findings was made according to biopsy, response to PSA and imaging tests. ***Results:*** The rate of extrapelvic findings in our series was 27.9% (n=24/86). 13.95% showed more than one lesion.5 patients with unique lesions were in the end considered negative in evolutionary studies (chest CT/PET-PSMA): 4 corresponded to rib bone lesions and another to a subpleural nodule. Another patient with a single lesion in the vertebral body that was initially negative by MRI was finally positive by biopsy.Thus, 19 of the 24 patients (79.17%) with extrapelvic findings by PET-PSMA were considered pathological:7 patients were candidates for SBRT: single bone lesion (n=3), pulmonary nodule (n=1), pulmonary hilar adenopathy (n=1), nodal involvement at the pelvic and retroperitoneal level (n=1) and two bone lesions (n=1). Three of these patients continue to respond and the other two show a new biochemical recurrence. The other two are too recent to assess evolution.12 patients received systemic treatment, either for multiple bone lesions, lymph nodes, or a combination of both. One patient showed a lesion on the penis' glans , confirmed by biopsy, associated with inguinal lymphadenopathy and a pelvic bone lesion. ***Conclusion:*** Extrapelvic lesions are frequent findings in PET-CT studies with PSMA with low PSA, being pathological in up to 79.17% of cases. A non-negligible number (20.83%) of the unique lesions do not have a malignant origin (especially in the ribs), so they should be evaluated with caution or a directed study should be carried out.

EP-0253

Psma PET/CT Results and Effect on Treatment in Patients with Biochemical Recurrence After Radical Prostatectomy

K. Akçay[1], *N. Selcuk*[1], *G. Beydagi*[1], *T. Toklu*[1], *E. Demirci*[1], *Ö. Sönmez*[1], *D. Karaçam*[1], *M. Yücel*[1], *E. Kaymak*[2], *O. Civi*[3], *L. Kabasakal*[4];
[1]*yeditepe university, istanbul, TÜRKIYE,* [2]*İstanbul Başakşehir Çam Sakura Hospital, istanbul, TÜRKIYE,* [3]*istanbul oncology hospital, istanbul, TÜRKIYE,* [4]*İstanbul University-Cerrahpaşa, istanbul, TÜRKIYE.*

Aim/Introduction: Ga-68 Prostate Specific Membrane Antigen (PSMA) PET/CT is recommended for restaging imaging after biochemical recurrence. Radiotherapy (RT) is applied to the prostate bed in Ga-68 PSMA negative cases if the PSA value is below 1.4 ng/ml. In cases with higher PSA levels, hormone therapy (HT) is also administered alongside RT. ***Materials and Methods:***

The aim of study investigate PSMA-PET/CT's impact on treatment planning for biochemical recurrence post-radical prostatectomy without prior treatment. In cases diagnosed with prostate cancer after radical prostatectomy and followed without treatment, 151 patients who underwent PSMA-PET/CT imaging upon biochemical recurrence development and were subsequently followed with or without treatment with PSA monitoring every 3-6 months were retrospectively included in the study. Cases with PSA levels <0.2 ng/mL undetectable were exclusion criteria for the study. ***Results:*** No distant metastases were detected before radical prostatectomy, and the preoperative mean PSA was 11.71±9.11 ng/dl. Postoperative the average rare PSA value detectable was 0.085 ng/ml. The median biochemical recurrence PSA value with persistent increase in at least two different PSA measurements or >0.2 PSA level in a single measurement was 0.45 ng/ml. PSMA-PET/CT (-) was found in 80 patients. In 17 of the 71 patients with PSMA-PET/CT (+), there was a recurrence only in the prostate bed, while 54 had PSMA-PET/CT positivity outside the prostate bed. Bone metastases were found in 24 patient, organ metastases in 7. Progression was detected in the PSA follow-ups of 10 PSMA-PET/CT (-) patients who were followed without treatment, while a significant PSA increase wasn't observed in 6 of them. In 13 of the 16 patients with PSMA-PET/CT (-) who received RT to the prostate bed (median PSA: 0.3625), PSA regression was observed (median PSA: 0.01825) (p <0.005), only 1 patient had an unmeasurable PSA level. On the other hand, PSA progression continued in 2 patients despite treatment. In the PSMA-PET/CT (-) group, PSA regression was observed in 9 of the 13 patients (median PSA: 0.3480) who started RT+HT (median PSA: 0.0060) (p <0.005), and 3 patients had an unmeasurable PSA level. ***Conclusion:*** The localization of the disease is required for salvage treatment in biochemical recurrence. How to treat PSMA-PET/CT (-) cases is a matter of debate. Local recurrence was detected in only 24% of PSMA-PET/CT (+) cases. Therefore, performing RT only to the prostate bed in PSMA-PET/CT (-) cases after biochemical recurrence appears to be a topic that needs to be discussed.

EP-0254

Serum values of prostate-specific antigen (PSA) and grade groups according to the International Society of Urological Pathology (ISUP grading), as determinants of [18F]DCFPyL PET/CT positivity in patients with biochemical recurrence of prostate cancer treated with radical prostatectomy.

A. Peñaherrera Cepeda, *L. Diaz Gonzaga, J. Villanueva Curto, J. Badell Martínez, P. García-Talavera San Miguel, F. Gómez-Caminero López, E. Campaña Diaz, S. Rama Alonso, P. Tamayo Alonso;*
Complejo asistencial universitario de Salamanca, Salamanca, SPAIN.

Aim/Introduction: To calculate [18F]DCFPyL PET/CT detection rate according to serum PSA values and ISUP grading, in patients with biochemical recurrence (RBq) of prostate cancer, treated with radical prostatectomy (RP). ***Materials and Methods:*** Were analised 145 PET/CT studies, that were performed with 333 MBq of [18F] DCFPyL from October 2020 to April 2023 (mean age: 69 ± 7 years), all with biochemical recurrence of prostate cancer treated with RP. RBq after RP was defined as a PSA elevation ≥0.2 ng/mL. The sample was subdivided into 4 groups according to the PSA value in ng/mL at the time the PET/CT was ordered into: PSA between 0.2 to 0.5, PSA between 0.51 to 1, PSA between 1.1 to 2 and PSA ≥2. Patients were also classified according to ISUP grading from 1 to 5.Descriptive statistics were used, including median and standard deviation for continuous variables and frequency and percentage for categorical variables ***Results:*** The median baseline PSA level was 0.53 ng/mL (0.20-8.26). [18F]DCFPyL PET/CT was positive in 49% of the studies performed (71 of 145 studies). In patients with PSA levels between 0.2 to 0.5 ng/mL, the detection rate was 37.5%, PSA between 0.51 to 1 was 58.1%, PSA between 1.1 to 2 was 73.3% and PSA ≥2 was 71.4%, the latter group may be underestimated due to the number of patients in this category. Patients with ISUP grading 1, the detection rate was 47.8%, ISUP grading 2 was 46.5%, ISUP grading 3 was 42.5%, ISUP grading 4 was 46.4% and ISUP grading 5 was 75%. ***Conclusion:*** [18F]DCFPyL PET/CT demonstrated an excellent detection rate in patients with biochemical recurrence of prostate cancer, with PSA values > 0.5 ng/mL. With respect to ISUP grading, PET/CT detection was similar in categories 1 to 4, with higher detection in category 5.

EP-0255

Usefulness of PET-MR with 18F-DCFPyL in the Diagnosis of Biochemical Recurrence in Prostate Cancer and its Therapeutic Implication

R. De Teresa, *I. Plaza de las Heras, C. Field, L. García Cañamaque;*
GRUPO HM HOSPITALES. UNIVERSIDAD SAN PABLO CEU, Madrid, SPAIN.

Aim/Introduction: To evaluate the usefulness of PET-MR with 18F-DCFPyL in the diagnosis of biochemical recurrence in patients with prostate cancer (PC) and its therapeutic implication. ***Materials and Methods:*** Retrospective analysis from January-22 to January-23, of patients with PC treated with curative intent by radical prostatectomy (RP) or external beam radiotherapy (RT)/brachytherapy with criteria of biochemical recurrence (RBq), being the serum PSA levels between 0.8 and 8.0 ng/ml (mean 3.25 ng/ml) after RT and PSA levels between 0.2 and 4.5 ng/ml (mean 1.68 ng/dl) after PR. Whole-body 18F-DCFPyl PET/MR (4-5 min/bed) was performed, adding multiparametric MRI of the pelvis in selected cases. PET images were acquired 120 minutes after i.v. injection. of the radiotracer and MRI with T2 HASTE, T1 VIBE and DWI sequences. ***Results:*** Thirty-five 18F-DCFPyL PET/MR were performed on 34 patients between 47-76 years of age. Of these, 19/35 (52.7%) were negative and 16/35 positive, detecting disease in 45.7% of the cases, all with negative studies using conventional techniques (CT, bone scintigraphy (OB), MRI) and 4/35 with 18F-choline PET-CT positive (11%). The sensitivity of PET to detect disease was 94%, that of MRI 55%, and that of PET-MR 100%, results similar to those described in the bibliography. Of the positives, 3/16 (18%) presented bone involvement, 1/16 (6%) liver metastasis, 7/16 (43%) lymph nodes, and 5/16 (31%) recurrence in the prostate bed. The PET/MR findings with 18F-DCFPyl modified management in 12/16 patients (33%), expanding the SBRT area in 8/12 (66%), increased bone disease in 2/12 (16%), and active surveillance 2/ 12 (16%). ***Conclusion:*** 18F-DCFPyL PET/MR has been shown to increase diagnostic safety in locoregional and distant tumor detection in patients with PCa in RBq compared to conventional diagnostic techniques (GO, CT, MR) and 18F-choline PET-CT. The findings of the PET/MR with 18F-DCFPyl modified the management of the patient.

EP-0256

To evaluate the efficacy of F-18 PSMA -1007 PET/CT to diagnose biochemically recurrent Adenocarcinoma Prostate

A. Vyas[1], *A. Tiwary Vyas*[2];
[1]*Max Superspeciality Hospital Vaishali, New Delhi, INDIA,*
[2]*Janakpuri Superspeciality Hospital, New Delhi, INDIA.*

Aim/Introduction: The aim was to evaluate the efficacy of the F 18-PSMA 1007 PET-CT to diagnose patients with recurrent adenocarcinoma prostate in India. ***Materials and Methods:*** The retrospective analysis of 120 adenocarcinoma prostate patients

with biochemical relapse (mean age 65 ± 9.6 years) and were referred for F-18 PSMA PET-CT. Whole-body PET-CT (from vertex to mid-thigh) was performed 60 min after injection of 370 ± 50 MBq F18-PSMA.85%,45% and 52 % of the patients had received prostatectomy (surgery), androgen-deprivation therapy, and radiotherapy of prostate bed respectively. Radiotherapy with surgery in 35 patients (35%). 13 patients (13%) received all three therapies. The efficacy of F-18 PSMA1007 was compared with biopsy (if available), S. PSA and 3monthly follow up. ***Results:*** Out 120 patients, 115(96 %) patients showed positive finding on F-18 PSMA1007 scan.Median PSA level was 1.1 ng/ml (range 0. 02-60.3 ng/ml).Scan positivity rates were 92%, 96% and 100% respectively with PSA levels ≤ 0.50,0.51-2.5 and >2.5 ng/ml.Overall PET positivity in these patients was 94.1 %(113/120). 02 patients showed false positive PSMA uptake in mediastinal lymphnodes. ***Conclusion:*** F-18 PSMA 1007 PET-CT can diagnose recurrent adenocarcinoma prostate in significantly high percentage of patients with early biochemical relapse, Positive predictive value was found significantly high with low PSA level ≤ 0.5 ng/ml, and may positively impact early detection.Large prospective studies are required. ***References:*** 1. Okarvi S. M. Recent developments of prostate-specific membrane antigen (PSMA)- specificradiopharmaceuticals for precise imaging and therapy of prostate cancer: an overview. Clinical and Translational Imaging . 2019;7(3):189-208. doi: 10.1007/s40336- 019-00326- [CrossRef] [Google Scholar] 2. Annunziata S., Pizzuto D. A., Treglia G. Diagnostic performance of PET imaging using different radiopharmaceuticals in prostate cancer according to published meta-analyses. Cancers . 2020;12(8):p. 2153. doi: 10.3390/cancers12082153. [PMC free article] [PubMed] [CrossRef] [Google Scholar] 3. Rovera G., Oprea-Lager D. E., Ceci F. Health technology assessment for PSMA-PET: striving towards a cost-effective management of prostate cancer. Clinical and Translational Imaging . 2021;9(5):409-412. doi: 10.1007/s40336-021-00446-9.[CrossRef] [Google Scholar] 4. Liu A., Chen L., Zhang M., et al. Impact of PSMA PET on management of biochemical recurrent prostate cancer: a systematic review and meta-analysis of prospective studies. Clinical and Translational Imaging . 2021;9(1):95-108. doi: 10.1007/s40336-020-00406-9. [CrossRef] [Google Scholar]

EP-0257

Prognostic Value of F-18 FDG PET/CT Metabolic Parameters in Prostate Cancer Patients

C. Soydal[1], *M. H. Baltacioglu*[2], *M. Araz*[1], *B. Demir*[1], *N. O. Kucuk*[1];
[1]*Ankara University Medical School, Department of Nuclear Medicine, Ankara, TÜRKIYE,* [2]*Sbu Trabzon Kanuni Training and Research Hospital Department of Nuclear Medicine, Trabzon, TÜRKIYE.*

Aim/Introduction: F-18 FDG affinity of prostate cancers is generally low due to parameters such as tumor differentiation level, androgen sensitivity and tumor hypoxia level. Therefore, its routine use in staging and restaging is not recommended. However, F-18 FDG PET/CT may have a prognostic role in castration-resistant-metastatic prostate cancer (CRPC). Therefore, in recent years, it has been recommended to be used in combination with Ga-68 PSMA PET/CT for restaging in patients with CRPC. In this study, we aimed to investigate the prognostic significance of F-18 FDG findings in patients with CRPC who underwent F-18 FDG PET/CT for restaging. ***Materials and Methods:*** The study included patients with CRPC who underwent F-18 FDG PET/CT for restaging. PET/CT findings of the patients, lesion regions with metastasis, number of lesions, standard uptake value SUVmax and SUVmean values of the most active lesion, metabolic tumor volume (MTV) and total lesion glycolysis (TLG) values were retrospectively evaluated. Survival times of patients after PET/CT imaging were calculated and the effect of PET parameters on survival was evaluated by Kaplan-Meier and Cox Regression analyses. ***Results:*** A total of 30 male patients (mean age:64.6±8.0 years) whose clinical follow-up information was available after PET/CT imaging were included in the analysis. All patients had ≥7 Gleason scores. Mean value of SUVmax were calculated as 12.1±7.9, median values of SUVmean, MTV and TLG, 5.0 (min:0 max:35.5), 164 (min:0 max:1890) cm3 and 896 (min:0 max:15777), respectively. Liver and bone metastases were detected in 8 (27%) and 19 (63%) patients, respectively. In Kaplan-Meier analysis, high MTV (p<0.001), high SUVmax (p=0.013), high TLG (p<0.001), presence of liver-bone metastases (p<0.001, p<0.001) and more than 10 lesions (p<0.001) were associated with poor survival. In Cox-regression analysis, higher SUVmax (p=0.022), TLG (p=0.013) and presence of bone metastases (p=0.005) were associated with poor survival. ***Conclusion:*** In routine clinical practice, the indication for the use of F-18 FDG PET/CT in patients with prostate cancer is very limited. However, in recent years, there are publications suggesting that F-18 FDG uptake may have prognostic value in CRPC. F-18 FDG PET/CT can be performed to predict tumor heterogeneity and treatment response, especially in patients who are planned for 177Lu PSMA treatment. The results of our study also revealed that metabolic parameters such as SUVmax and TLG may have prognostic significance. Prospective studies in larger groups will provide a clearer definition of the role of F-18 FDG PET/CT in prostate cancer patients.

EP-0258

Role of 68Ga/18F-PSMA PET/CT in the Secondary Staging of Prostate Cancer patients as a guide for clinicians

P. Mammucci*, C. Ferrari, V. Lavelli, C. Battisti, N. C. Merenda, G. Rubini;*
A.O.U. Policlinico di Bari, Bari, ITALY.

Aim/Introduction: We aim to evaluate the diagnostic performance of radiolabeled-PSMA-PET/CT in patients with recurrent (BCR) or persistent (BCP) prostate cancer (PCa) after primary treatment and to compare the results with patient features. Furthermore, we investigate the potential impact of PET findings on clinical management and therapeutic decision-making. ***Materials and Methods:*** ^{68}Ga/^{18}F-PSMA-PET/CT of 70 consecutive BCR/BCP PCa patients, performed between November 2022 and March 2023, were included. Histological, biochemical, and clinical features were collected: PSA value at time of the scan, PSA doubling time (PSAdt), Gleason Score (GS:<8 or ≥8), EAU BCR risk group, ISUP, surgical margins and ongoing hormonal therapy (HT). Clinical follow-up was performed for each patient to obtain further data, including post-PET PSA values, diagnostic investigations, and start/change treatment. Chi-square, Fisher's exact, and Mann-Whitney U tests were employed to analyze the correlation between PET/CT detection rate (DR) and patient features. ROC curve analysis defined the optimal PSA cut-off value to accurately predict PET response. In addition, sensitivity, specificity, accuracy, PPV, NPV were calculated in all sample and into PSA-subgroups defined by the PSA cut-off, considering clinical follow-up as the gold standard. A p<0.05 was considered statistically significant. ***Results:*** Mean age was 71y (range:53-85y), mean PSA 1.03 ng/mL (range:0.0-5.23), mean PSAdt 13.8 months (range:0.8-70.7), and median GS was 7 (range:6-10). Thirty-seven/70 patients (53%) had a positive PET/CT: 16/37 (43%) in prostate bed, 17/37

(46%) in lymph nodes, and 15/37 (40%) in bone. A positive PET/CT was shown in 14/36 patients with PSA≤0.7 (38.9%, p=0.016), in 16/23 with GS≥8 (69.5%, p=0.048), and in 15/17 patients with ongoing HT (88%, p=0.001), with statistically significant differences. The optimal PSA cut-off to predict a positive PET/CT was 0.74 ng/mL (AUC 0.63, 95% CI 0.49-0.76). The overall PET/CT sensitivity, specificity, PPV, NPV were 67.3%, 81.2%, 91.6%, and 44.8%, respectively, reaching an accuracy of 70.7%. Considering PSA-subgroups (≤0.7 and >0.7), sensitivity, specificity, PPV, NPV, and accuracy were: 50%, 72.7%, 78.5%, 42.1%, 57.6%, and of 84.6%, 100%, 100%, 60%, 87.5%, respectively. PET/CT results modified clinical management in 32/37 (86.5%) of positive patients, guiding specific treatments such as HT (14/32, 43.7%), nodal or prostate bed ERT/SBRT (13/32, 40.6%), both HT/RT (3/32, 9.3%), and chemotherapy (2/32, 6%). ***Conclusion:*** Radiolabeled-PSMA-PET/CT has proven to be effective in the disease detection of BCR/BCP PCa patients, especially for PSA>0.7. As confirmed by our data, nowadays radiolabeled-PSMA-PET/CT represents an essential tool to guide clinical decisions with a patient-based approach.

EP-15

e-Poster Area

B: Imaging Clinical Studies -> B1 Oncological Imaging Clinical Study -> B18c Prostate Other

EP-0259

Dual time psma pet/ct with diuretics and contrast to detect prostate cancer pelvic metastases: is there a benefit?

T. Tognoli[1], *M. R. F. Camacho*[2], *A. O. Santos*[1], *M. C. L. Lima*[1], *B. J. Amorim*[1], *U. Ferreira*[1], *E. Etchebehere*[1];
[1]*State University of Campinas (UNICAMP), CAMPINAS-SP, BRAZIL,* [2]*MND Campinas, CAMPINAS-SP, BRAZIL.*

Aim/Introduction: The renal excretion of PSMA radiotracer may render PSMA PET/CT imaging interpretation difficult to identify local recurrence and lymph node metastases in prostate cancer patients. AIM: To evaluate the best acquisition method to increase the detection rate of local recurrence and pelvic metastases on PSMA PET/CT by performing dual time-point imaging (delayed imaging) after hyperhydration, diuretics, and contrast enhancement. ***Materials and Methods:*** Patients with prior history of prostate adenocarcinoma underwent PSMA PET/CT for primary staging or due to biochemical recurrence. PSMA PET/CT acquisition consisted of delayed pelvic imaging after hyperhydration, diuretics, and excretory-phase contrast. SUV values obtained in local recurrence lesions, locoregional lymph node metastases, and bone metastases in the early and delayed PSMA PET/CT images were compared. ***Results:*** A total of 182 patients (medians: age = 66.5; Gleason score = 7.0; total PSA = 1.5) underwent PSMA PET/CT. Twenty-one patients (12%) were scanned due to primary staging, and 161 patients due to biochemical recurrence (88%). Delayed images (with only hyperhydration, without contrast or diuretics) increased diagnostic certainty in identifying local recurrence in 26.6% of patients and locoregional lymph nodes in 25%. There was a significant increase in SUV values in the delayed images compared to early images in the local recurrence (p<0.0001), locoregional lymph node metastases (p<0.0001), and bone metastases (p<0.0199). Adding excretory-phase contrast to the delayed images increased diagnostic certainty in identifying local recurrence in 9.4% of patients and locoregional lymph nodes in 8.3%. The use of diuretics only in delayed images (without excretory-phase contrast) increased diagnostic certainty in identifying local recurrence in 14% of patients; while for identifying pelvic lymph nodes increase was only mild (2.8%). The association of diuretics with excretory-phase contrast increased the diagnostic certainty in identifying local recurrence in 15.6% of patients and locoregional lymph nodes in 5.6%. ***Conclusion:*** Delayed PSMA PET/CT images increase the diagnostic certainty of identifying local recurrence and locoregional metastases in prostate cancer patients. The addition of diuretics increases diagnostic certainty and may be useful in selected cases. However, the addition of excretory-phase contrast (regardless of the use of diuretics) only mildly impacted diagnostic certainty and may be omitted. ***References:*** Freedman-Cass D et al. NCCN Guidelines Version 4.2022 Prostate Cancer. Morawitz J et al. Is there a diagnostic benefit of late-phase abdomino-pelvic PET/CT after urination as part of whole-body 68Ga-PSMA-11 PET/CT for restaging patients with biochemical recurrence after radical prostatectomy? EJNMMI Res 2022;12

EP-0260

Ultrafast & Fast F18-PSMA 1007 PET/CT Acquisition in the Era of Digital PET/CT System; Single Institution Experience

A. Sadeq[1], *Z. Alqallaf*[1], *I. Abdelrahman*[1], *M. Ibrahim*[1], *L. Ghadhanfer*[2], *F. Marafi*[1];
[1]*Jaber AlAhmad center for Molecular Imaging, Shuwaikh medical area, KUWAIT,* [2]*Faculty of Allied health sciences- Kuwait University, Jabriya, KUWAIT.*

Aim/Introduction: Recent advancement in digital PET/CT cameras adds to sensitivity of scanners with refined specifications including count statistic, time-to-flight ratio and camera resolution. ^{18}F-PSMA-1007 PET/CT is a time-consuming exam with radiation exposure concerns as it's used frequently for staging and restaging of prostate cancer. Reducing the acquisition time enhances quality by improving the patient compliance, radiation exposure, reduces costs of operating scanner personnel & cost-effectiveness. ^{18}F-PSMA-1007 PET/CT is emerging standard of care in prostate cancer used to evaluate biochemical recurrence, detection, staging and assessing therapy response. Our objective was to explore viability of reducing acquisition time of positron imaging by up to 25%. ***Materials and Methods:*** Human subjects involved in the trial were referred for ^{18}F-PSMA-1007 PET/CT to stage and restage prostate cancer by injecting 0.08mCi/Kg with average injected dose of 6.3mCi. After uptake period of 99 minutes, images of the vertex to mid-thigh were acquired on digital PET/CT scanner. A PET acquisition using institution routine imaging parameters were acquired. Images were reconstructed retrospectively from data in list mode to 15 sec./bed and 30 sec./bed using 128x128 matrix size and 2 sets, 8 subsets of OSEM iterative reconstruction. Images were interpreted by two nuclear medicine physicians. The images quality were evaluated in terms of contrast, resolution & lesions. ***Results:*** Acquired Images were retrospectively reconstructed in 15 sec/bed & 30 sec/bed in ultrafast and fast-acquisition PET with estimated total time around 2:15 minutes and 4:30 minutes, respectively. While normal routine scan would have been required in 16 minutes. Images were then reconstructed as per imposed parameters and image quality appeared consistent in the eyes of the readers. The study was done on total of 20 patients, 12 of whom were from BMI group <33.3. There were 6 patients' part of BMI group 33.4-40. The

remaining 2 patients had BMI of >40. Images of ultrafast and fast PET were noisier when compared to the routine PET; specially of BMI >40. However, all lesions were identical in obtained images, ultrafast, and fast acquisitions reconstructions. ***Conclusion:*** The successful results of this study show promising untraveled route for future of PSMA PET broadening our horizon on capability of newly acquired technological advancements. Applying ultrafast & fast PET acquisition for ^{18}F-PSMA-1007 PET/CT study in digital system allows scanning patients faster, increasing the number of studies/day. Claustrophobic and ill-patients who are reluctant to complete the lengthily procedure might benefit from such approach.

EP-0261

Multimodal Radiomics Features of periprostatic adipose tissue from 18F-PSMA-1007 PET/CT to predict Persistent Prostate-Specific Antigen

S. Bian;
the First Affiliated Hospital of Wenzhou Medical University, Wenzhou, CHINA.

Aim/Introduction: Periprostatic adipose tissue (PPAT) indexes are linked to the prognosis of prostate cancer (PCa). The serum prostate-specific antigen (PSA), as a routine indicator for monitoring PCa, indicates poor prognosis when it rises after radical prostatectomy. This study aimed to investigate the performance of predicting persistent PSA based on PPAT-related multimodal radiomics features (RFs) from ^{18}F-PSMA-1007 PET/CT. ***Materials and Methods:*** A total of 221 PCa patients who underwent ^{18}F-PSMA-1007 PET/CT were retrospectively analyzed. Patients were randomly divided into the training and testing cohort. Both PET and CT radiomics features were extracted from ^{18}F-PSMA-1007 PET/CT medical images. The robust and the most predictive 25 RFs (12 CT RFs and 13 PET RFs) were selected to calculate Rad-score after maximum relevance and minimum redundancy and the least shrinkage and selection operator analysis. The performance of different models was assessed. ***Results:*** A multimodal radiomics model was developed based on logistic analysis with an AUC of 0.79 [95% confidence interval (95% CI), 0.71 - 0.87] and 0.72 (95% CI 0.55 - 0.88) in the training and testing cohort, respectively. The combined model, which contained the Rad-score and the predictive clinical variables, achieved optimal performance with an AUC of 0.85 (95% CI 0.78 - 0.91) and 0.77 (95% CI 0.62 - 0.91) in the training and testing cohort, respectively. The calibration curves were well-calibrated both in the training and testing cohorts according to the actual and predictive rate of persistent PSA. Decision curve analysis also demonstrated the better clinical utility of the combined model against the others. ***Conclusion:*** The radiomics-clinical combined model can provide a novel tool for preoperatively individualized prediction of persistent PSA among PCa patients.

EP-0262

Association between blood-derived circulating-tumor DNA and ^{68}Ga-PSMA-HBED-CC PET/CT findings

K. Kluge[1,2], *H. Einspieler*[1], *D. Haberl*[1], *C. Spielvogel*[1,2], *S. Stoiber*[3,2], *M. Hacker*[1], *L. Kenner*[3,2], *A. Haug*[1,2];
[1]*Medical University of Vienna - Dept. of Nuclear Medicine, Vienna, AUSTRIA,* [2]*Medical University of Vienna - Christian Doppler Lab for Applied Metabolomics, Vienna, AUSTRIA,* [3]*Medical University of Vienna - Dept. of Pathology, Vienna, AUSTRIA.*

Aim/Introduction: Functional imaging with prostate-specific membrane antigen (PSMA) ligands and the analysis of circulating-tumor DNA (ctDNA) derived from liquid biopsies both have been shown to enable minimally-invasive detection and monitoring of prostate cancer (PCA). The present study aims to contextualize these methods in assessing total tumor burden (TTB) in men with PCA. ***Materials and Methods:*** 177 men (50-87 years, 184.6 MBq ± 17.9) with histological-proven prostate cancer who underwent ^{68}Ga-PSMA-HBED-CC PET/computed tomography (CT) and blood sampling between March 2018 and August 2021 at the University Hospital Vienna were prospectively recruited. We here report on the first 20 consecutive patients (57-84 years, 182.6 MBq ± 16.7) (analysis currently ongoing) who underwent cell-free DNA (cfDNA) extraction and ctDNA quantification by low-pass whole-genome sequencing (lpWGS) based on copy number variation (CNV) profiles(1,2)(Table 1). PSMA-positive tumor lesions were delineated manually on a dedicated workstation and quantitative PET parameters were extracted. Correlations between the PET-derived metabolic tumor volume (MTV) and blood-derived cf- and ctDNA concentrations and percentages were assessed using Spearman's or Pearson's coefficients according to the data distribution. The differences in mean ctDNA concentrations according to MTV quartiles were assessed with the ANOVA. The alpha risk was set for all statistical analyses to 5%. ***Results:*** A moderate positive correlation was found between cfDNA concentrations and MTV (r=0.5; p=0.024), ctDNA concentrations and MTV (r=0.52; p=0.018) as well as ctDNA percentage and MTV (r=0.5; p=0.024). Mean concentrations of ctDNA (ng/µL) were 0.054 (SD 0.015), 0.15 (SD 0.098), 0.12 (SD 0.1), 3.19 (SD 4.37) for patients in the MTV (ml) first quartile (Q1) (0 - 0.2), Q2 (0.2 - 5.4), Q3 (5.4 - 39.0) and Q4 (39.0 - 1099.1), respectively (p=0.098). ***Conclusion:*** Our preliminary findings suggest that functional PSMA imaging and blood-derived ctDNA yield associated estimates of TTB, while PSMA PET/CT provides unmatched spatial and quantitative granularity in assessing tumor burden and extent.

References: 1) Ulz P, Belic J, Graf R, et al. Whole-genome plasma sequencing reveals focal amplifications as a driving force in metastatic prostate cancer. Nat Commun. 2016;7.; 2) Adalsteinsson VA, Ha G, Freeman SS, et al. Scalable whole-exome sequencing of cell-free DNA reveals high concordance with metastatic tumors. Nat Commun. 2017;8:1324.

EP-0263

Evaluation of therapeutic response with 68Ga-prostate-specific membrane antigen (PSMA) PET/CT after androgen deprivation therapy in patients with prostate carcinoma

M. Dyankova[1,2], *T. Stoeva*[1], *Z. Dancheva*[1], *S. Chausheva*[1], *T. Yordanova*[1], *B. Chaushev*[1], *A. Klisarova*[1];
[1]*Medical University Varna "Prof. Dr. Paraskev Stoyanov", Department of Imaging Diagnostics, Interventional Radiology and Radiotherapy, Varna, BULGARIA,* [2]*St. Marina University Hospital, Department of Nuclear Medicine, Varna, BULGARIA.*

Aim/Introduction: There are insufficient reports of response assessment applying ^{68}Ga-PSMA PET/CT in androgen deprivation therapy (ADT) of naive prostate cancer (PC) patients. The aim of this study was to analyze response to ADT with ^{68}Ga-PSMA PET/CT in patients with hormone-naive PC and to confirm the assumption of a differential therapeutic response for different localizations of malignant involvement: primary tumor, regional nodal, distant nodal, as well as distant metastatic (bone and visceral) involvement. ***Materials and Methods:*** The retrospective study included 55 patients who met the following criteria: PC patients with a baseline/ staging ^{68}Ga-PSMA PETCT scan and a restaging scan to monitor treatment effect in a time range of 3-12 months after ADT. Alteration in radiopharmaceutical activity in the prostate

gland/ primary tumor, involved regional and distant nodes as well as distant metastases were semiquantitatively evaluatived on double scans applying maximum standardized uptake value (SUVmax). Treatment response was defined as complete or partial response (CR, PR) or progressive disease or stable disease (PD, SD), and correlated with well-known prognostic markers. ***Results:*** A total of 110 scans of 55 patients (of which 21 were metastatic, M+) were analyzed. After a median of 6 months of ADT, a complete response (CR) was defined for patients according to the different locations of malignant involvement as follows: for the primary tumor - 0.0%, for regional lymphadenopathy - 18 (25.0%), for distant lymphadenopathy - 13 (21.7%), for distant metastases- 3 (14.3%). Disease progression (PD) was defined for patients according to the different localizations of malignant involvement as follows: for the primary tumor- 10 (18.2%), for regional lymphadenopathy- 7 (9.7%), for distant lymphadenopathy- 8 (13.3%), for distant metastases- 8 (38.1%). Treatment response for the primary tumor was not significantly correlated with any of the prognostic markers. Therapeutic response for regional lymphadenopathy was better in M0 compared with M+ disease (CR 39.0% vs 3.4%, p = 0.003). Oligometastases showed a superior therapeutic response compared to polymetastases (CR/PR 63.4% vs. 10.2%, p = 0.05). The decrease in SUVmax of the primary tumor was positively associated with a reduction in the levels of the tumor marker/ serum prostate-specific antigen (PSA), p = 0.07. ***Conclusion:*** Nodal (regional and distant) as well as distant metastatic lesions (bone and visceral) seem more likely to respond to ADT than primary prostate tumor. Persistent increased PSMA-expression may serve as new target for a selective local therapy for appropriate patients with oligometastatic PC.

EP-0264

Comparing the Diagnostic Efficacy of 99m Tc-PSMA SPECT/CT Scanning After 75 Minutes and 4 Hours of Radiotracer Injection in Men with Prostate Cancer

A. Aghaee[1], *A. Sahebkari*[1], *S. Soltani*[2], *H. Ghorbani*[3], *K. Aryana*[1], *K. Sadri*[1];
[1]*nuclear medicine research center,Mashhad university of Medical Sciences, Mashhad, IRAN, ISLAMIC REPUBLIC OF,*
[2]*kidney translantation research center,Mashhad university of Medical Sciences, Mashhad, IRAN, ISLAMIC REPUBLIC OF,*
[3]*kidney transplantation research center,Mashhad university of Medical Sciences, Mashhad, IRAN, ISLAMIC REPUBLIC OF.*

Aim/Introduction: Prostate-Specific Membrane Antigen (PSMA) is overexpressed in primary and metastatic prostate carcinoma (PCa) and could be targeted by a Tc-99m-HYNIC-PSMA11 scan for detection of metastases. Despite extensive studies, data on the most appropriate interval between radiopharmaceutical injection and image acquisition is scarce. We compared the metastasis detection rates of the Tc-99m-HYNIC-PSMA11 scan between 75-minute and 4-hour intervals of radiopharmaceutical injection. ***Materials and Methods:*** From May 2021 to May 2022, we studied 30 consenting men with pathologically confirmed PCa who were referred to our tertiary hospital for a PSMA scan due to primary staging, biochemical recurrence, pre-177Lu-PSMA therapy, or surveillance. 75-minute and 4-hour 99mTc-PSMA SPECT-CT scan performed following injection of the radiopharmaceutical. The scan's metastasis detection rates were evaluated in 75-minute and 4-hour intervals. ***Results:*** The mean age of patients was 68.43±9.61 years, with a median PSA of 4.19 ng/ml and a median Gleason Score of 8. Nine cases had negative Tc99m-PSMA11 scans, while 21 had positive scans (8 cases with bone, 2 with lung, 4 with lymph node, and 7 with multiple organ metastases). All metastases were detected in both checkpoints, except for one patient, where 75-minute images detected three pelvic metastatic lymph nodes, while four were seen in the 4-hour scan. This small missed right external iliac lymph node did not change the patient's management. ***Conclusion:*** We found no significant difference in the detection rate of metastatic lesions in 75-minute and 4-hour intervals. These findings could help decrease crowdedness, provide efficient scheduling, and improve patient satisfaction in nuclear medicine departments.

EP-0265

Comparison of the 18F-PSMA-1007 and 18F-FAPI-42 PET/CT in the evaluation of prostate cancer and correlation between PSMA and FAPI uptake

X. Mu, *M. Li, W. Fu;*
Department of Nuclear medicine, Affiliated hospital of Guilin medical university, Guilin, CHINA.

Aim/Introduction: To compare ^{18}F-PSMA-1007 PET/CT with ^{18}F-FAPI-42 PET/CT in evaluating prostate cancer, and investigate the correlation between PSMA and FAPI uptake of lesions. ***Materials and Methods:*** In this prospective study conducted from January 2022 and October 2022, images from participants with prostate cancer who underwent both ^{18}F-PSMA-1007 with ^{18}F-FAPI-42 PET/CT examination were analyzed. The tracer uptake, quantified by maximum standardized uptake value (SUV_{max}) and target-to-background ratio (TBR), were compared for paired positive lesions between both modalities. The correlation between PSMA and FAPI uptake for positive lesions was analyzed. ***Results:*** Twenty-nine participants with prostate cancer (median age, 68 years; range: 55-83 years) were evaluated. A total of 19 prostate, 75 LN, 101 bone, and 10 lung positive lesions were detected and analyzed. From semiquantitative evaluation, the SUVmax and TBR of primary or recurrent tumors, positive lymph nodes, bone lesions, and pulmonary lesions at ^{18}F-PSMA-1007 PET/CT were all higher than those at ^{18}F-FAPI-42 PET/CT (all, $P < 0.01$). A positive correlation was observed in positive lesions ($r=0.27$, $P < 0.0001$), especially in LN lesions and bone lesions ($r=0.46$ and $r=0.44$, respectively, all $P < 0.0001$). ***Conclusion:*** ^{18}F-PSMA-1007 PET/CT showed superior ability than ^{18}F-FAPI-42 for the evaluation of prostate cancer. Nevertheless, PSMA expression may correlate positively to FAP expression for prostate cancer. ***References:*** 1. Sung H, Ferlay J, Siegel RL, Laversanne M, Soerjomataram I, Jemal A, et al. Global Cancer Statistics 2020: GLOBOCAN Estimates of Incidence and Mortality Worldwide for 36 Cancers in 185 Countries. CA Cancer J Clin. 2021;71:209-49. doi:10.3322/caac.21660. 2. Center MM, Jemal A, Lortet-Tieulent J, Ward E, Ferlay J, Brawley O, et al. International variation in prostate cancer incidence and mortality rates. Eur Urol. 2012;61:1079-92. doi:10.1016/j.eururo.2012.02.054. 3. Williams IS, McVey A, Perera S, O'Brien JS, Kostos L, Chen K, et al. Modern paradigms for prostate cancer detection and management. Med J Aust. 2022;217:424-33. doi:10.5694/mja2.51722. 4. Ng M, Guerrieri M, Wong LM, Taubman K, Sutherland T, Benson A, et al. Changes in Management After (18) F-DCFPyL PSMA PET in Patients Undergoing Postprostatectomy Radiotherapy, with Early Biochemical Response Outcomes. Journal of nuclear medicine : official publication, Society of Nuclear Medicine. 2022;63:1343-8. doi:10.2967/jnumed.121.263521. 5. Ananias HJ, van den Heuvel MC, Helfrich W, de Jong IJ. Expression of the gastrin-releasing peptide receptor, the prostate stem cell antigen and the prostate-specific membrane antigen in lymph node and bone metastases of prostate cancer. Prostate. 2009;69:1101-8. doi:10.1002/pros.20957.

EP-0266

Evaluating the diagnostic value of early static and delayed imaging of 68Ga-PSMA-11 PET/CT in detection of prostate bed recurrence and regional lymph node metastasis in prostate cancer patients

A. Aghaee, *Z. Bakhshi, V. Roshan Ravan, K. Aryana, N. Norouzbeigi;*
nuclear medicine research center,Mashhad university of Medical Sciences, Mashhad, IRAN, ISLAMIC REPUBLIC OF.

Aim/Introduction: One way to improve the accuracy of [68Ga] Ga-PSMA-11 PET/CT scans is to perform multi-time point acquisitions. The aim of this study is to evaluate the use of early and delayed imaging in PCa patients with different indications such as staging, Biochemical Recurrence (BCR), and response to treatment. We also examined the changes in pathologic lesion SUVmax among different locations and phases. ***Materials and Methods:*** 138 PCa patients were included in a single-center retrospective study for multiphasic [68Ga] Ga-PSMA-11 PET/CT. Patients underwent standard imaging, early imaging immediately after injection in 4-minute static acquisition, and delayed imaging, 2.5 to 3 hours after injection, both from the pelvic field. ***Results:*** The study evaluated 138 PCa patients, with an average age of 67.72 ± 8.70 years, a median PSA level of 7.45, and an interquartile range of (1.11-23.13), as well as Gleason scores ranging from 3+3 (3.6%) to 5+5 (4.2%). The positivity rates for PSMA-avid lesions in the early, whole-body, and delayed images were 71.5% (93/130), 73.9% (77/110), and 70% (77/110), respectively. In the early, total, and delayed phases, the total number of PSMA-avid lesions were 305, 340, and 239, respectively. The highest SUVmax (96.98) was associated with the external iliac node lymph. The detection rates for local recurrence in the early, whole-body, and delayed phases were 13.8% (18/130), 15.9% (22/138), and 17.3% (19/110), respectively, with no significant change (p=0.5). The detection rates for lymph node metastases were 23.8% (31/130), 29% (40/138), and 28% (30/110), with a significant difference observed between the early and whole-body phases (p=0.016). The detection rates for osseous lesions in the early, whole-body, and delayed images were 28.46% (37/130), 27.53% (38/138), and 21.81% (24/110), respectively, with no significant difference found (p=0.139). ***Conclusion:*** no significant differences were observed in the detection rates of bone lesions across the three phases. However, the early phase missed a focus of osseous metastasis in five patients. In two patients, the delayed images contributed to a change in disease stage during the whole-body phase, while the early phase images did not reveal any changes in disease stage. Whole-body images led to a change in the disease stage for 12 patients during the early phase, but no changes were seen during the delayed phase. The early phase was more effective in differentiating local bladder invasion but was less successful in identifying prostate bed lesions, seminal vesicle invasion, and lymph node metastases.

EP-0267

Quantitative MRI parameters adds value in PSMA PET/MR for improving diagnostic specificity of Prostate Cancer with SUVmax<12

W. Ma, *J. Wang, Z. Quan, F. Kang, J. Wang;*
Fourth Military Medical University, Xi'an, CHINA.

Aim/Introduction: MRI has been widely used but was influenced by reader experience due to the lack of objective and quantitative parameters. The adding diagnostic value of quantitative MRI parameters in PSMA PET with SUVmax<12 was investigated in this study. ***Materials and Methods:*** Between August 2021 and July 2022, patients with suspected PCa scheduled for a clinically indicated PSMA PET/MR study for initial diagnosis of prostate cancer before any therapy were retrospectively collected. All of patients underwent non-targeted ultrasound guided systematic biopsy (at least 12 cores) combining with follow-up or surgical excision. MR acquisition sequences included T1WI, axial, coronal, sagittal T2WI and diffusion-weighted imaging with b value of 1500 s/mm^2. Besides, ADC, T_1/R_1, T_2/R_2 and PD mapping value were analyzed by quantitative MRI with MAGiC sequence. Two nuclear medicine physicians reviewed the images independently. The diagnostic value of PET/MR was analyzed based on patient and lesion respectively. According to ^{68}Ga-PSMA-11 uptake in prostate, 1-2 lesions per patient was identified for the final analysis. The specificity, sensitivity, accuracy, and area under the curve of PET/MRI quantitative parameters were analyzed based on patient and lesion respectively. ***Results:*** 48 men patients (mean age, 66.8 ± 6.4 years [range: 53-83]) with 82 lesions (1-2 lesions per patient) were included finally, with SUVmax lower than 12. On patient-level analysis, 31 patients were suspected as PCa after PET imaging, including 22 patients were proved to be negative. The sensitivity of PET was 100%, a lower specificity was 68% for initial diagnosis. On lesion-level analysis, the specificity, sensitivity, and accuracy were 32.61%, 94.44%, and 59.76% when the SUVmax cutoff value was 4. The diagnostic accuracy of SUVmax (4-12) was improved with T_2/R_2 mapping by increasing specificity of PET from 59.76% to 80.49%. ***Conclusion:*** Quantitative MRI could add value for PSMA-PET to improve diagnostic accuracy of the intra-prostatic cancer with SUV<12. PSMA PET showed good agreement and has become an effective "one-stop-shop" imaging method for prostate cancer.

EP-0268

68Ga-PSMA-PETCT for the evaluation of pulmonary nodules in patients with prostate cancer

G. Mateva, *P. Bochev, N. Novoselska;*
Acibadem CityClinic Mladost, Sofia, BULGARIA.

Aim/Introduction: The purpose of this study was to investigate the incidence of reported lung nodules on 68Ga-PSMA PET/CT studies and to establish what part of the patients with reported lung nodules had metastatic lung disease. ***Materials and Methods:*** We evaluated retrospectively the reports of 68Ga-PSMA PET/CT scans of 505 prostate cancer patients available in our database for reported lung nodules. We considered all available previous and follow-up clinical information, the expression of PSMA, and also compared with the contrast-enhanced CT reports, where available. ***Results:*** We established that 73 out of 505 patients (15,5%) had one or more lung nodules reported. In 34 of them (47% of the patients with lung nodules) the findings were benign and no follow-up was recommended (including data from CT, where available). For 16 of the patients (13% of the patients with lung nodules) CT recommended follow-up to exclude metastatic disease, while 68Ga-PSMA PET/CT dismissed the suspicion. In five patients (6,9 % of the patients with lung nodules) where CT reported pulmonary metastases, 68Ga-PSMA PET/CT disagreed, and benign nodules were reported. In 10 patients (2% of the whole investigated cohort) 68Ga-PSMA PET/CT reported metastatic pulmonary disease. 6 patients (1,2%) had nodular pulmonary lesions, which were evaluated as malignant but with probable etiology different from prostate carcinoma, based on the PSMA expression and the CT features- in 5 of them primary lung carcinoma was histologically proven and in one patient there

were pulmonary metastases from rectal cancer. Only two patients from the group had PSMA-positive lung lesions that remained unclear after the 68Ga-PSMA PET/CT and additional follow up or biopsy was recommended. ***Conclusion:*** 68Ga-PSMA PET/CT is an accurate and reliable method for diagnosis of pulmonary metastases from prostate cancer and differentiating them from benign pulmonary lesions and metastases from other malignant diseases.

EP-0269

Optimizing PSMA Scintigraphy Imaging Protocols for Prostate Cancer in Resource Limited Settings

O. Kolade[1], *A. Ayeni*[1,2], *J. Holness*[3], *A. Brink*[1], *S. More*[1];
[1]*University of Cape Town / Groote Schuur Hospital, Cape Town, SOUTH AFRICA,* [2]*Klerksdorp/Tshepong Hospital Complex, Klerksdorp, SOUTH AFRICA,* [3]*Stellenbosh University, Cape Town, SOUTH AFRICA.*

Aim/Introduction: In developing countries, unfavourable Prostate Cancer (PCa) outcomes are outsized, compared to high-income countries. To bridge this disparity-gap, interest is growing in optimising PCa solutions for the less-resourced world. [^{68}Ga] Ga-PSMA PET/CT is out of reach for most low-to-lower-middle-income countries, as over 90% of them do not have PET units. [^{99m}Tc] Tc-PSMA scintigraphy (PS), though a viable alternative devoid of PET's capital demands, has largely only been evaluated within the context of multi field-of-view (FOV) SPECT/CT protocols. The practical reality is that many-to-most developing world nuclear medicine centres do not have access to SPECT/CT and only have access to planar gamma cameras or at best those with SPECT capabilities.Therefore, we aimed to explore optimisations for PS imaging protocols for resource limited settings by comparing findings from planar acquisition, with multi FOV SPECT and multi FOV SPECT/CT. Thus, exploring acquisitions that may be eliminated without significantly impacting interpretation and patient management. ***Materials and Methods:*** Patients with histologically proven PCa who also had both planar & multi-FOV SPECT/CT [^{99m}Tc]Tc-PSMA scans were included. Planar, SPECT, and SPECT/CT images were randomly interpreted individually and unanimously by three Nuclear Medicine Physicians blinded to clinical history. The prostate gland/bed, seminal vesicles, lymph nodes, skeleton, and viscera were specifically assessed. Sites were classified as positive, negative, or equivocal. Findings across modalities were then compared for each patient. Consensus SPECT/CT reporting served as the reference ***Results:*** 96 patients were included, with a head-to-head comparison of their PS planar, SPECT and SPECT/CT images. Prostatic PSMA uptake assessment was inadequate on planar imaging (14%) compared to SPECT (90%), and SPECT/CT (99%). Assessing seminal vesicle involvement was impossible on planar and SPECT imaging, compared to SPECT/CT. However, planar imaging adequately detected nodal, and skeletal lesions; SPECT though marginally better, frequently introduced diagnostic doubt via decreased specificity and false negatives- SPECT/CT satisfactorily resolved these doubts. Visceral metastasis determination was difficult on planar and SPECT, compared to SPECT/CT. No prostate-related lesions were missed on SPECT or SPECT/CT by limiting the imaged field-of-view to vertex-to-midthighs from planar whole-body acquisition ***Conclusion:*** Our findings reiterate the superiority of SPECT/CT over planar and SPECT imaging, hence the recommended single-best PS protocol should be a multi FOV SPECT/CT, if no resource limitations exist. However, in certain circumstances, if interpreted with caution, planar and SPECT PS may be adequate, especially in resource limited settings. Furthermore, limiting the FOV to exclude the distal lower limbs may provide additional time-based optimisations.

EP-0270

AI18F-PSMA-617 PET Quantitative Analysis for Prostate Cancer Diagnosis: A Comprehensive Study

B. Liu[1], *G. Hu*[2], *X. Wang*[2], *L. Huo*[2], *H. Ding*[1], *H. Zhang*[1];
[1]*Tsinghua University, Beijing, CHINA,* [2]*Peking Union Medical College Hospital, Beijing, CHINA.*

Aim/Introduction: Quantitative analysis of PET dynamic imaging can obtain tissue metabolism information derived from the kinetic modeling of the perfusion process. This provides additional diagnostic information and overcomes the limitations of semi-quantitative SUV, which is of limited clinical value. The objective of this study is to assess the potential uses of quantitative parameters obtained from AI^{18}F-PSMA-617PET imaging for detecting and characterizing prostate cancer (PCa) lesions. ***Materials and Methods:*** This study included 12 PCa patients who underwent a 60-minute dynamic AI^{18}F-PSMA-617 PET scan. Volumes of interest (VOIs) were manually defined for tumors, normal tissues, and iliac vessels for extracting image-derived blood input functions. Time-activity curves (TACs) were generated by calculating the maximum standard uptake value (SUVmax) for tumors, and the average standard uptake value (SUVmean) for iliac vessels and normal tissues. The two-tissue compartment models (2TCM) were applied to calculate kinetic parameters, such as K1, k2, k3, k4, and fractional blood volume (Vb), which were subsequently used to calculate tissue global influx (Ki), binding potential (BP), and distribution volume (Vd). The modeling effect was evaluated using the R-square (R^2) test, where higher values indicate better fitting. Statistical analysis involved using paired t-test, non-parametric Wilcoxon rank-sum test, and receiver operating characteristic (ROC) analysis. ***Results:*** The evaluations of the models are as follows. With R^2 value of 0.838±0.132 and 0.805±0.085 in tumor lesions and normal tissues, respectively, indicating 2TCM model with k4 had better fitting effect based on R^2 value than without k4. The quantitative study showed that Ki, BP, and Vd had significant differences between tumor lesions and normal tissues ($P<0.005$). ROC analysis revealed that Ki had an area under the curve (AUC) of 0.927 ($P<0.005$), BP had an AUC of 0.979 ($P<0.0001$). Especially, Vd had an AUC equals to 1 ($P<0.0001$) with cut-off value of 1.944. ***Conclusion:*** In conclusion, the best model to describe the kinetic analysis of AI^{18}F-PSMA-617 would be the reversible two-tissue compartment model. The net influx rate Ki and the distribution volume Vd show an obvious difference between tumor lesions and normal tissues, could be applied to the clinic to identify the lesion area.

EP-0271

The Effect of Folate on [68Ga]Ga-PSMA-11 Organ and Tumor Uptake: Predictions Using Physiologically Based Pharmacokinetic Modelling

H. Siebinga[1,2], *J. J. M. A. Hendrikx*[1,2], *A. D. R. Huitema*[2,3,4], *B. J. de Wit - van der Veen*[1];
[1]*Department of Nuclear Medicine, NETHERLANDS Cancer Institute, Amsterdam, NETHERLANDS,* [2]*Department of Pharmacy and Pharmacology, NETHERLANDS Cancer Institute, Amsterdam, NETHERLANDS,* [3]*Department of Clinical Pharmacy, University Medical Center Utrecht, Utrecht University, Utrecht, NETHERLANDS,* [4]*Department of Pharmacology, Princess Máxima Center for Pediatric Oncology, Utrecht, NETHERLANDS.*

Aim/Introduction: It is hypothesized that folate intake might reduce accumulation of PSMA-directed peptides due to competitive binding to the PSMA-receptor and, thus, folates could affect diagnostic imaging and radioligand therapy in prostate cancer. However, the exact relationship between folates and PSMA-ligands is not well established. Therefore, we developed a

physiologically based pharmacokinetic (PBPK) model to predict the effect of folate intake on [^{68}Ga]Ga-PSMA-11 uptake in salivary glands, kidney and tumors. ***Materials and Methods:*** A PBPK model was developed for [^{68}Ga]Ga-PSMA-11 and folate (folic acid and its metabolite 5-MTHF), with compartments added that represent salivary glands and tumor. Model evaluation for [^{68}Ga]Ga-PSMA-11 was performed with patient data from two different studies [1,2], while for folate data from literature were used [3,4]. Using the final model, the effect of varying folate doses on relative differences in [^{68}Ga]Ga-PSMA-11 accumulation in salivary glands, kidney and tumor compartments was predicted. Folate doses were selected to represent intake by means of folate-containing food (150 µg), vitamin supplements (400 µg) and folate tablets (5 and 10 mg). In addition, predictions were made for patients with different tumor volumes (10-1000 mL). ***Results:*** PBPK model predictions adequately described data for both [^{68}Ga]Ga-PSMA-11 and folates. Predictions of folate doses of 150 and 400 µg showed no clinically relevant effect (<23.5% relative difference) on salivary gland and kidney uptake. However, for 5 and 10 mg, a relevant decrease in salivary glands (34 and 36%, respectively) and kidney uptake (32 and 34%, respectively) was predicted. None of the included folate doses showed a relevant effect on tumor accumulation. Lastly, different tumor volumes did not influence the effects of folate intake on [^{68}Ga]Ga-PSMA-11 distribution. ***Conclusion:*** High folate doses (5 and 10 mg) were predicted to decrease [^{68}Ga]Ga-PSMA-11 salivary gland and kidney uptake, while intake by means of folate-containing food or vitamin supplements was predicted to show no relevant effects. [^{68}Ga]Ga-PSMA-11 tumor uptake was not affected by folate intake in the dose range studied and tumor volume differences were not expected to impact folate effects. These predictions could guide trial design aimed at using folates to reduce toxicity during PSMA-based radioligand therapy.
References: 1) Siebinga H, Heuvel JO, Rijkhorst EJ, et al. J Nucl Med.2023;64(1):63-8. 2) Olde Heuvel J, de Wit-van der Veen BJ, Sinaasappel M, et al. PLoS One.2021;16(2):e0246394. 3) Obeid R, Schön C, Pietrzik K, et al. Nutrients.2020;12(12). 4) Willems FF, Boers GH, Blom HJ, et al. Br J Pharmacol.2004;141(5):825-30.

EP-0272

PSMA PET/CT correlates with biochemical response in patients with prostate cancer undergoing High-Intensity Focused Ultrasound (HIFU) focal therapy

E. Lopci*, G. Lughezzani, V. Fasulo, D. Maffei, A. Saita, P. Colombo, R. Hurle, K. Marzo, L. Leonardi, R. Peschechera, A. Benetti, S. Zandegiacomo, L. Pasini, J. Jandric, R. Zanca, P. Casale, M. Rodari, L. Balzarini, G. Guazzoni, N. Buffi, M. Lazzeri;*
IRCCS - Humanitas Research Hospital, Rozzano MI, ITALY.

Aim/Introduction: Recent advances in PCa imaging with PSMA PET/CT offer new opportunities to detect PCa foci and monitor response to treatment. The current study is designed to evaluate the role of PSMA PET/CT for response assessment in PCa patients candidate to High-Intensity Focused Ultrasound (HIFU) focal therapy. ***Materials and Methods:*** Patients treated with HIFU FT for localized PCa and enrolled from October 2020 to April 2022 in an ongoing, prospective, single-center cohort study were considered for the analyses. Inclusion criteria: PSA <20ng/mL, radiological stage ≤T2bN0M0, ISUP grade 1-3, PSMA PET/CT at baseline and at response evaluation. Follow up included: PSA at 3, 6 and 12 months; PSMA PET/CT between 6-12 months post treatment. Biochemical response and PET response were statistically correlated: SUVmax and SUVratio to background of the target lesions were used as semi-quantitative parameters for PSMA PET/CT, together with their variations before and after HIFU FT (i.e. ΔSUVmax and ΔSUVratio). ***Results:*** Overall, 32 patients out of the 46 enrolled have completed all study procedures and met inclusion criteria for the current analysis. Median age was 67,5 years (95%CI 63-71) and median initial PSA (iPSA) was 6.3 ng/mL (95%CI 5.4-8.7). ISUP score was 1 in 20 (62.5%) patients. Median SUVmax and SUVratio before treatment resulted 4.1 (95%CI 3.3-6.9) and 1.4 (95%CI 1.3-1.9), respectively. At 3 months post-HIFU, 25% of the patients obtained a PSA response ≥50%; whereas at 6 months and 12 months, PSA responses were 32% and 45%, respectively. Median SUVmax and SUVratio post-treatment resulted 2.7 (95%CI 2.3-4.6) and 0.9 (95%CI 0.8-1.3). Median ΔSUVmax was -14.2% (95%CI -35.8 to -2.5) and ΔSUVratio resulted -25.2% (95%CI -45-4 to 3.3). Baseline SUVmax (P = 0.049) and SUVratio (P = 0.008) significantly correlated to PSA response at 6 months post-HIFU; also ΔSUVratio significantly correlated to PSA response at 12 months post-treatment (P = 0.009), while ΔSUVmax showed only a borderline correlation to response at 1 year post-HIFU (P = 0.069). ***Conclusion:*** PSMA-PET may be a useful tool for monitoring response in PCa patients undergoing HIFU Focal Therapy. Baseline SUV and its variation can predict biochemical response at 12 months post-treatment.

EP-0273

Guiding metastases-directed therapy with Prostate-Specific Membrane Antigen (PSMA) PET/CT improves the oncological outcome of oligometastatic prostate cancer patients

F. Lanfranchi*[1], L. Belgioia[1], D. Albano[2], F. Dondi[2], F. Bertagna[2], E. Mataj[3], F. Linguanti[4], E. M. Abenavoli[5], L. Vaggelli[5], B. Detti[6], L. Urso[7], N. Ortolan[7], A. Malorgio[8], M. Bartolomei[7], A. Rizzo[9], M. Racca[9], A. Guarneri[10], F. Garrou[11], S. Panareo[12], P. Ghedini[12], S. Morbelli[1], G. Sambuceti[1], M. Bauckneht[1];*
[1]Department of Health Sciences, University of Genoa and IRCCS Ospedale Policlinico San Martino, Genoa, ITALY, [2]Nuclear Medicine Department, Università degli Studi di Brescia and ASST Spedali Civili di Brescia, Brescia, ITALY, [3]Department of Radiation Oncology, Università degli Studi di Brescia and ASST Spedali Civili di Brescia, Brescia, ITALY, [4]Nuclear Medicine Unit, Department of Experimental and Clinical Biomedical Sciences "Mario Serio", University of Florence, Florence, ITALY, [5]Nuclear Medicine Division, Careggi University Hospital, Florence, ITALY, [6]Radiation Oncology Unit, Azienda Ospedaliero-Universitaria Careggi, Florence, ITALY, [7]Nuclear Medicine Unit, Oncological Medical and Specialist Department, University Hospital of Ferrara, Ferrara, ITALY, [8]Radiotherapy Unit, University Hospital of Ferrara, Ferrara, ITALY, [9]Department of Nuclear Medicine, Candiolo Cancer Institute, FPO-IRCCS, Turin, ITALY, [10]Department of Radiotherapy, Candiolo Cancer Institute, FPO-IRCCS, Turin, ITALY, [11]Nuclear Medicine Unit, Department of Medical Sciences, AOU Città della Salute e della Scienza, University of Turin, Turin, ITALY, [12]Nuclear Medicine Unit, Oncology and Haematology Department, University Hospital of Modena, Modena, ITALY.

Aim/Introduction: Oligometastatic prostate cancer (PCa) is an emerging disease state characterized by a limited number of metastatic locations. Metastases-directed therapy (MDT) with stereotactic body radiotherapy (SBRT) has been shown to decrease the tumor burden, potentially delaying systemic treatments and improving the long-term oncological outcome. In this setting, a more accurate disease staging may lead to more patients receiving the appropriate treatment, with expected better results. On these bases, we verified the impact of using next-generation compared to conventional imaging as a guide for MDT in a real-world multicentric cohort of PCa patients. ***Materials and Methods:***

We retrospectively recruited 256 de-novo oligometastatic or oligorecurrent PCa patients submitted to imaging-guided MDT in six tertiary-level cancer Centers. Inclusion criteria were: (i) histologically-confirmed diagnosis of PCa; (ii) imaging evidence of ≤5 pelvic, extra-regional nodal (M1a), or bone metastases (M1b); (iii) upfront MDT delivered through SBRT±systemic therapy guided by either bone scan+CT/MRI (conventional imaging), [18F]F-Fluorocholine, [68Ga]Ga-PSMA-11 or [18F]-PSMA-1007; (iv) availability of the subsequent clinical follow-up. Progression after MDT was defined as either biochemical recurrence (PSA raise ≥2 ng/dL and 25% above nadir), radiological or clinical progression, subsequent treatment changes, or death. Clinical, laboratory and imaging parameters were assessed as predictors of Progression-Free Survival (PFS, primary endpoint of the study). ***Results:*** At the time of MDT, 80.5% of patients presented oligorecurrent PCa, and 22.7% had Castration-Resistant PCa (CRPC). Prostate-Specific Antigen (PSA) levels before MDT were 3.76±6.22 ng/mL. MDT was guided by conventional imaging, choline PET/CT, or PSMA PET/CT in 5.1%, 63.7% and 31.2% of patients, respectively. After MDT, the PSA nadir was 2.58±8.97 ng/mL. The median follow-up was 30.8 months. At the univariate analysis, predictors of PFS were the CRPC status at the time of MDT (p=0.013), the PSA pre-MDT value (p<0.001), oligorecurrent compared to de-novo oligometastatic disease (p=0.030), the number of metastatic lesions (p=0.038), the presence of bone metastases (p=0.006), and the PSA nadir after MDT (p<0.001). Notably, the use of either conventional imaging or choline PET/CT compared to PSMA PET/CT significantly predicted PFS (p<0.001 for both). The multivariate analysis confirmed imaging modalities guiding MDT and the PSA nadir as the sole independent predictors of PFS (p<0.001 for both). Patients receiving MDT guided by conventional imaging, choline PET/CT, or PSMA PET/CT showed significantly different median PFS (5.8 vs. 13.1 vs. 34.5 months, respectively, p<0.001). ***Conclusion:*** Using next-generation imaging with PSMA PET/CT favorably impacts the oncological outcome of oligometastatic PCa patients treated with MDT.

EP-0274

Treatment response evaluation with PSMA-PET/CT imaging in patients with metastatic castration-resistant prostate cancer (mCRPC)

F. Kleiburg[1,2], *L. F. De Geus-Oei*[1,2,3], *S. A. C. Luelmo*[2], *R. Spijkerman*[1,2], *F. A. J. Toonen*[4], *F. Smit*[4], *T. van der Hulle*[2], *L. Heijmen*[2];
[1]*University of Twente, Enschede, NETHERLANDS,* [2]*Leiden University Medical Centre, Leiden, NETHERLANDS,*
[3]*Delft University of Technology, Delft, NETHERLANDS,*
[4]*Alrijne Hospital, Leiderdorp, NETHERLANDS.*

Aim/Introduction: Treatment response evaluation in mCRPC patients with serum prostate-specific antigen (PSA) levels can be insufficient and unreliable. This study aimed to assess the value of PSMA-PET/CT imaging for treatment response evaluation at set time points in patients with mCRPC, compared to PSA. ***Materials and Methods:*** 58 mCRPC patients who received treatment response evaluation with [^{18}F]-PSMA-1007-PET/CT imaging for 67 treatment lines in total were included in this retrospective study. In case of treatment with enzalutamide or abiraterone (n=33), the treatment response PSMA-PET/CT was made after three months of treatment. In case of treatment with chemotherapy (n=34), the treatment response PSMA-PET/CT was made after the last administered dose (range 6-9 cycles of chemotherapy), or when progression was suspected. PSA levels, visual response on PSMA PET/CT imaging, as well as SUV_{max}, total tumour volume (PSMA-TV, calculated with an SUV = 4 threshold) and total-lesion uptake (TL-PSMA) on the pre-treatment and treatment response evaluation PSMA-PET/CT scans were collected. Biochemical response and PSMA-PET/CT response definitions were consistent with previous literature (1,2). ***Results:*** Biochemical response and overall response on PSMA-PET/CT were discordant in 31 out of 67 cases (46%). In 28 of these cases (90%), overall response on PSMA-PET/CT was worse than the biochemical response. 19 patients showed progression of disease on PSMA-PET/CT and no PSA progression compared to PSA before therapy: in 8 patients rising PSA levels were seen around the time of the PSMA-PET/CT scan, in 4 patients biochemical progression was seen 3 to 4 months later, in 2 patients the PSMA-PET/CT scan was followed by evident clinical deterioration and in 5 patients treatment change decisions were purely based on the PSMA-PET/CT scan. In univariate Cox regression analyses, the visual overall response on PSMA-PET/CT, the response of the worst responding lesion, and the relative changes (%) in PSMA-TV and TL-PSMA were all significant predictors of biochemical progression-free survival and overall survival (p ≤ 0.01 for all). For overall survival, these PET parameters were more significant predictors than relative change in PSA (p = 0.03). ***Conclusion:*** PSMA-PET/CT imaging is more accurate in evaluating treatment response in mCRPC patients than PSA levels. In some patients, PSMA-PET/CT can detect progression of disease earlier than PSA. Also, several PET parameters are significant predictors of biochemical progression-free survival and overall survival. A follow-up study on the cost-effectiveness of response monitoring with PSMA-PET/CT imaging in these patients will follow. ***References:*** (1) https://doi.org/10.1200%2FJCO.2015.64.2702 (2) https://doi.org/10.1007/s00259-020-04934-4

EP-0275

Radium-223 response assessment and outcomes prediction using 68Ga-PSMA PET/CT: RECIP 1.0 vs PPP criteria

Q. Shagera*, P. Flamen, C. Artigas;*
Jules Bordet Institute, Université Libre de Bruxelles (ULB), Brussels, BELGIUM.

Aim/Introduction: Treatment monitoring of Radium-223 dichloride ($^{223}RaCl_2$) can be challenging. Conventional imaging techniques are limited in the setting of bone-only metastatic disease, and diagnosis of progression is frequently delayed. PSMA-PET/CT imaging has shown high accuracy in the early detection of prostate cancer lesions. Two PSMA-PET-based response criteria have been proposed and tested in ^{177}Lu-PSMA radioligand therapy and taxane-based chemotherapy, demonstrating its potential use as a prognostic biomarker. However, this has not yet been evaluated for $^{223}RaCl_2$. Therefore, we aimed to evaluate the prognostic value of PSMA-PET/CT response criteria in metastatic castration-resistant prostate cancer patients (mCRPC) receiving $^{223}RaCl_2$. ***Materials and Methods:*** This retrospective study included 28 mCRPC patients who received $^{223}RaCl_2$ and had two ^{68}Ga-PSMA-11 PET/CT scans performed: a) baseline PET within one month before treatment initiation and b) interim PET two weeks after the 3rd cycle. Visual and quantitative PET image analyses were performed, and patients were dichotomized into progressive (PD) and non-PD according to Response Evaluation Criteria in PSMAimaging (RECIP1.0)[1] and PSMA-PET Progression criteria (PPP)[2]. PSMA total tumor volume was measured using the SUV=3 threshold method, and the new lesions were recorded. The cox-regression hazard model

was used for univariate survival analysis. Survival probability was analyzed using the Kaplan-Meier method and the log-rank test. Harrell's concordance index (C-index) was evaluated for both criteria. ***Results:*** Patients were treated with a median of 5 cycles of $^{223}RaCl_2$. Sixteen (43%) and 18 (64%) patients had PD according to RECIP1.0 and PPP, respectively. Among patients with PD at interim PET, 21% presented with new sites of extraskeletal disease. After a median follow-up of 16 months, 20 (71%) patients died. Patients with PD showed a higher risk of death than non-PD according to RECIP1.0 (HR=2.9; 95%CI, 1.14-7.46; p=0.029) and to PPP (HR=2.8; 95%CI, 1.04-7.64; p=0.042). For both criteria, the median OS was shorter for PD than non-PD (36 vs. 12 months, Log-rank; p<0.05). The C-index was higher for RECIP1.0 (0.66, 95%CI, 0.56 - 0.75) compared to PPP (0.63; 95%CI, 0.53 - 0.73). ***Conclusion:*** This study shows that PSMA-PET/CT imaging is a useful tool for monitoring radium-223 treatment. Both PSMA PET/CT response criteria (RECIP1.0 and PPP) perform similarly predicting OS at interim after 3 cycles of $^{223}RaCl_2$. PSMA-PET may overcome the limitations of conventional imaging in assessing the response to $^{223}RaCl_2$. Further prospective validation in a larger population is needed. ***References:*** [1]Gafita A, J Nucl Med. 2022;63(11):1651-8. [2]Fanti S, J Nucl Med. 2020;61(5):678-82.

EP-0276

[68Ga]PSMA-11 PET/CT response in metastatic prostate cancer following systemic therapy

P. Aravind[1], *T. D. Barwick*[2,1], *S. Dubsash*[1], *M. J. Connor*[2], *H. Tam*[2], *F. A. Mauri*[1], *H. U. Ahmed*[1,2], *E. O. Aboagye*[1];
[1]*Imperial College London, London, UNITED KINGDOM,* [2]*Imperial College Hospital NHS TRUST, London, UNITED KINGDOM.*

Aim/Introduction: There is paucity of data regarding (^{68}G)-PSMA-11 PET response in metastatic prostate cancer (mPC), and as conventional imaging has limitations in this setting, we aimed to investigate ability of (^{68}G)-PSMA-11 PET/CT to detect response post-systemic therapy in mPC. We also assessed the relationship between (^{68}G)-PSMA-11 PET/CT uptake with PSMA expression by immunohistochemistry, prostate specific antigen (PSA) response and conventional imaging response. ***Materials and Methods:*** In this exploratory phase 2 imaging sub-study (of IPL2-ATLANTA[1]) newly diagnosed mPC underwent (^{68}G)-PSMA-11 PET/CT at baseline and on completion of taxane- based chemotherapy or 6 months of Enzalutamide. Lesion SUV_{max},TBR (Tumour to background ratios), PSMA expression score and Total tumour volume (50%SUV_{max} threshold) were documented. PSMA response using RECIP criteria was compared to RECIST 1.1 response at 6 months. Where available, post treatment prostatic biopsies were analysed for PSMA expression and Ki67. Biochemical response (BR) was defined as undetectable or at least 50% decrease in PSA from baseline. Concordance between PET response, RECIST 1.1 response and BR were evaluated using Kendall's coefficient. Survival data was collected. Kaplan Meier and Cox regression analysis performed. ***Results:*** 15 patients completed both scans. RECIST 1.1 responses were 2 complete response and 13 partial response. PET RECIP (and intraprostatic ΔSUV_{max}) responses were 3 complete responders (-75%), 11 partial responders (-69%) and 1 progressive disease (+16%). Of note some patients showed complete intraprostatic response but had residual extraprostatic disease. BR was, however found in all patients: median PSA decrease was 99.5% (range: 94.7-100%). Baseline total tumour volume parameters on PSMA PET/CT were predictive of RECIST 1.1 response(Wilcoxon p<0.001). Concordance between RECIP and RECIST 1.1 was 80% (n=12/15). PET RECIP response was concordant with BR in 6/15 patients (p=0.058), Kendall's concordance coefficient 0.24. Of the 5 patients with available post-treatment prostatic biopsies, 2 had PSMA and Ki67 expression that were unrelated to PSMA uptake. After follow-up of 36 months, the median OS was 18 months in complete RECIP responders, 21 months in partial RECIP responders and 17 months in progressive disease. RECIP, age, BR, RECIST 1.1, therapy type were not significant in multivariable Cox regression, while ΔTBR_{sum} was significant. ***Conclusion:*** PSMA PET response (ΔTBR_{sum}) but not BR, strongly predicted OS. Baseline total tumour volume was predictive of RECIST 1.1 response. ***References:*** 1. MJ Connor et al. Additional treatments to the local tumour for metastatic prostate cancer-assessment of novel treatment algorithms (IP2-ATLANTA): protocol for a multicenter phase II randomised controlled clinical trial.BMJOpen2021;11:e0429532

EP-0277

The use of clinical, laboratory, and imaging parameters to interpret bone focal uptakes in hormone-sensitive prostate cancer patients imaged with [18F]-PSMA-1007 PET/CT

F. D'Amico[1], *A. Signori*[1], *D. Albano*[2], *M. Riondato*[3], *F. Dondi*[2], *T. Di Raimondo*[1], *L. Sofia*[1], *F. Lanfranchi*[1], *C. Ghersi*[3], *A. Democrito*[3], *G. Fornarini*[4], *C. Marini*[5], *F. Bertagna*[2], *S. Morbelli*[1], *G. Sambuceti*[1], *M. Bauckneht*[1];
[1]*Department of Health Sciences, University of Genoa, Genova, ITALY,* [2]*Nuclear Medicine, University of Brescia and ASST Spedali Civili Brescia, Brescia, ITALY,* [3]*Nuclear Medicine Unit, IRCCS, Ospedale Policlinico San Martino, Genova, ITALY,* [4]*Medical Oncology Unit 1, IRCCS Ospedale Policlinico San Martino, Genova, ITALY,* [5]*CNR, Institute of Molecular Bioimaging and Physiology (IBFM), Genova, ITALY.*

Aim/Introduction: Improved logistics and availability led to a rapid increase in the clinical use of [18F]-PSMA-1007 for prostate cancer (PCa) PET imaging. However, clinical observations found the frequent occurrence of unspecific bone uptakes (UBU) compared to other PSMA-targeted tracers. In the clinical setting, UBUs might be erroneously interpreted as metastases, potentially leading to inadequate treatment planning of over-staged patients. We thus verified whether clinical, laboratory, and imaging parameters might predict the presence of metastases in PCa patients showing [18F]-PSMA-1007 bone focal uptakes, thus potentially guiding image interpretation. ***Materials and Methods:*** We retrospectively analyzed 329 [^{18}F]-PSMA-1007 PET/CT scans performed in histology-proven PCa patients in two tertiary-level cancer centres, looking for the presence of bone [^{18}F]-PSMA-1007 focal uptakes. The sole exclusion criterion was castration-resistant PCa. For each tracer bone uptake, the PSMA visual score was recorded. The point of maximum tracer uptake (assessed by measuring the maximum standardized uptake value, SUVmax) was selected as the centre of a volume of interest (VOI), drawn by the threshold method (40%SUVmax) to calculate SUVmean, PSMA-tumor volume (PSMA-TV), and total lesion PSMA (PSMA-TL). Relocating the same VOI on CT images, mean and maximum Hounsfield Units (HU) were also extracted. Clinical and laboratory data at the time of [^{18}F]-PSMA-1007 PET/CT were collected from the electronic medical record. Finally, a composite reference standard including follow-up histopathology, lab or imaging data was assessed to disclose PCa metastases and UBUs. ***Results:*** 362 bone [18F]-PSMA-1007 focal uptakes were identified from 195/329 PCa patients (59.2%). According to the reference standard, 146/362 (40.3%) of bone [18F]-PSMA-1007 focal uptakes corresponded to PCa metastases. At the univariate per-lesion

analysis, Prostate-Specific Antigen (PSA) at the time of PCa diagnosis (p=0.002), the administration of androgen-deprivation therapy (ADT) at the time of [18F]-PSMA-1007 PET/CT (p<0.001), the site of bone [18F]-PSMA-1007 uptake (p=0.0045), SUVmax (p<0.001), PSMA visual score (p<0.001), TL-PSMA (p=0.002), HUmean (p=0.001), and HUmax (p=0.001) were associated with the presence of PCa metastases. At the multivariate analysis, ADT at [18F]-PSMA-1007 PET/CT (p<0.001), SUVmax (p<0.001) and HUmean (p=0.001) resulted in independent predictors of bone metastases. Combining these parameters in a prognostic model, the area under the receiver-operating-characteristic curve (AUC) resulted in 0.86. ***Conclusion:*** Bone focal uptakes occur in more than half of hormone-sensitive PCa patients imaged with [18F]-PSMA-1007 PET/CT. Considering the administered treatment at the time of imaging, SUVmax, and HUmean, and combining these data in a prediction model may improve their interpretation, potentially avoiding over-staging.

EP-0278

Modified PROMISE Criteria for Standardized Interpretation of Gastrin Releasing Peptide Receptor (GRPR)-targeted PET

H. Duan, *G. A. Davidzon, F. Moradi, T. Liang, H. Song, A. Iagaru; Stanford University, Stanford, CA, UNITED STATES OF AMERICA.*

Aim/Introduction: Multiple image interpretation criteria were developed to standardize interpretation of PSMA-targeted PET. As up to 10% of prostate cancer (PC) do not express PSMA, other targets such as gastrin releasing peptide receptor (GRPR) were evaluated. GRPR-targeted imaging has been slowly increasing in usage at staging and biochemical recurrence (BCR) of PC. We therefore propose an interpretation criteria for GRPR-targeted PET using a modified Prostate Cancer Molecular Imaging Standardized Evaluation (PROMISE) (1, 2) criteria (mPROMISE). ***Materials and Methods:*** ^{68}Ga-RM2 PET data from initially prospective studies performed at our institution were retrospectively reviewed: 44 patients were imaged for staging and 100 patients for BCR PC. Two nuclear medicine physicians independently evaluated PET according to the mPROMISE criteria. A third expert reader served as standard reference. Interreader reliability was computed for GRPR expression, prostate bed (T), lymph node (N), skeleton (Mb), and organ (Mc) metastases, and final judgment of the scan. ***Results:*** The interrater reliability for GRPR PET at staging was moderate for GRPR expression (0.59; 95% confidence interval [CI] 0.40, 0.78), substantial for T-stage (0.78; 95% CI 0.63, 0.94), and almost perfect for N-stage (0.97; 95% CI 0.92, 1.00) and final judgment (0.92; 95% CI 0.82, 1.00). The interreader agreement at BCR showed substantial agreement for GRPR expression (0.70; 95% CI 0.59, 0.81) and final judgment (0.65; 95% CI 0.53, 0.78) while almost perfect agreement was seen across the major categories (T, N, Mb, Mc). Acceptable performance of the mPROMISE criteria was found for all subsets when compared to the standard reference. ***Conclusion:*** Interpreting GRPR-targeted PET using the mPROMISE criteria showed its reliability with substantial or almost perfect interrater agreement across all major categories. This proposed standardized reporting system will aid clinicians to decrease the level of uncertainty, and clinical trials to achieve uniform evaluation, reporting, and comparability of GRPR-targeted PET. ***References:*** 1. Eiber M, Herrmann K, Calais J, Hadaschik B, Giesel FL, Hartenbach M, et al. Prostate Cancer Molecular Imaging Standardized Evaluation (PROMISE): Proposed miTNM Classification for the Interpretation of PSMA-Ligand PET/CT. J Nucl Med. 2018;59:469-78. doi:10.2967/jnumed.117.198119.2. Seifert R, Emmett L, Rowe SP, Herrmann K, Hadaschik B, Calais J, et al. Second Version of the Prostate Cancer Molecular Imaging Standardized Evaluation Framework Including Response Evaluation for Clinical Trials (PROMISE V2). Eur Urol. 2023. doi:10.1016/j.eururo.2023.02.002.

EP-0279

Consensus statements on Prostate Specific Membrane Antigen (PSMA)-Targeted Surgery - outcomes from an international multidisciplinary panel

F. van Leeuwen[1], *A. Berrens*[2], *the PSMA-guided surgery panel, H. van der Poel*[2];
[1]*Leiden University Medical Center, Leiden, NETHERLANDS,*
[2]*NETHERLANDS cancer institute, Amsterdam, NETHERLANDS.*

Aim/Introduction: Prostate-specific membrane antigen (PSMA) has greatly changed the identification of prostate cancer (PCa) on imaging and is increasingly used for image-guided therapy. Surgical therapies based on PSMA are being explored in various surgical settings (open, laparoscopic, robotic), employing different technologies, and for both de novo and salvage PCa indications. We aimed to define universal clinical needs, the relationship between these needs and current/ future technological enablers, and the best way to gather evidence on the topic. To achieve this, a Delphi consensus was conducted with the current experts in the field of PSMA-targeted surgery. ***Materials and Methods:*** A steering committee (urologic end-users (46%), enabling nuclear medicine physicians (31%) and researchers (23%)) set up a questionnaire (105 statements that could be answered using a 9-point Likert scale; 1 (disagreement) - 5 (neutral) - 9 (agree), or cannot answer) and distributing it through SurveyMonkey® for anonymous answering. Following evaluation, a second round of 16 statements was distributed (89% response rate). Consensus was defined using the disagreement index (DI). DI was assessed using the research and development project (RAnd)/University of California, Los Angeles (UCLA) appropriateness method (1). ***Results:*** 86 international panel participants answered the questionnaire (62 (72.1%) clinician; 7 (8.1%) industry; 13 (15.1%) scientists and 4 (4.7%) other), most with a urological background (57.0%), followed by nuclear medicine (22.1%). Consensus was obtained on key aspects of the procedure: 1) the guiding PSMA PET/CT needs to be taken <1 month before surgery, 2) time between injection of the imaging agents used for surgical guidance and surgery is preferably 16-20 hours, 3) PSMA-targeting is most valuable for the identification of nodal metastases outside of the template, 4) Gamma- and fluorescence imaging (including signal-to-background assessments) prove to be the preferred guidance modalities, and 5) randomized controlled clinical trials with outcome and performance assessments as readout are required to gather clinical evidence. Regarding the surgical margin assessment, the view on the value of PSMA-targeted surgery was neutral or inconclusive. High "cannot answer" response rates indicated further study is necessary to address knowledge gaps in areas such as the use of Cerenkov or beta-emissions. ***Conclusion:*** Until the required clinical evidence is acquired, the present Delphi consensus helps provide guidance for clinicians and researchers that implement PSMA-targeted surgery or develop technologies for this indication. ***References:*** 1) Fitch K, Bernstein SJ, Aguilar MD, et al. The RAnd/UCLA Appropriateness Method User's Manual. Transformation. 2001;(http://www.rand.org/publications/MR/MR1269/):109

EP-0280

Evaluation of [18F]DCFPyL excretion in the saliva of patients with prostate cancer

B. Fernandes[1], *J. Roy*[1], *F. Basuli*[2], *Y. McKinney*[1], *B. M. Warner*[3], *E. Mena*[1], *L. Lindenberg*[1], *B. Turkbey*[1], *P. Choyke*[1], *F. I. Lin*[1]; *[1]Molecular Imaging Branch, Center for Cancer Research, National Cancer Institute, Bethesda, MD, UNITED STATES OF AMERICA, [2]Chemistry and Synthesis Center, National Heart, Lung, and Blood Institute, National Institutes of Health, Rockville, MD, UNITED STATES OF AMERICA, [3]National Institute of Dental and Craniofacial Research, National Institute of Health, Bethesda, MD, UNITED STATES OF AMERICA.*

Aim/Introduction: PSMA-Targeted Radionuclide Therapy (TRT) is a new exciting treatment in prostate cancer (PC) patients, especially those whose tumor overexpresses prostate-specific membrane antigen (PSMA). One concern with using PSMA-based TRT is the high uptake of the therapeutic agent in salivary glands, leading to xerostomia. Although PSMA seems to accumulate in the salivary glands, its function and fate after uptake are not well known. In this study, we investigated whether there is any excretion of the PSMA-TRT in the patient's saliva after uptake from a systemic injection, using [^{18}F]DCFPyL. ***Materials and Methods:*** Ten patients with histologically-confirmed prostate cancer and a Gleason Grande ranging from 6 to 9, received 6±0.33 mCi of [^{18}F]DCFPyL and were scanned for 60 min. Saliva samples were collected from all patients at different time points (0, 15, 30, 60, and 120 minutes) post-radiotracer injection. The [^{18}F]DCFPyL uptake was measured over 120 minutes using a gamma counter and expressed as %ID/g and mean %ID/g of [^{18}F]DCFPyL. The non-specific binding was evaluated by the percentage of [^{18}F] DCFPyL at 120 minutes time-point in the saliva supernatant and the pellet post-extraction of saliva in acetonitrile for five of the ten patients. The radiometabolites were analyzed by thin-layer chromatography (TLC) using the saliva supernatant sample and the parent tracer as a reference. Differences between groups were considered significant when $p<0.05$, and correlations were analyzed by Pearson (r, parametric data) method and were considered positive and statistically significant when $r>0.5$ and $p<0.05$. ***Results:*** All patients' scans showed high uptake of [^{18}F] DCFPyL in the salivary glands and excretion into the saliva at 120 min. A significant difference in the tracer content in the saliva was shown at 30 min ($p=0.03$), 60 min ($p<0.0001$), and 120 min ($p<0.0001$) after systemic tracer injection when compared to the baseline time point (0 min). A positive correlation ($r=0.99$, $p=0.0005$) was found between [^{18}F]DCFPyL uptake and time points. Of the [^{18}F]DCFPyL found in the saliva, 98% was in the form of the intact [^{18}F]DCFPyL found in the supernatant, while approximately 2% was found bound to various proteins in the cellular pellet after centrifugation. ***Conclusion:*** Systemically injected [^{18}F]DCFPyL shows uptake into the salivary gland, a portion of which is then secreted unbound and intact into the saliva. The amount secreted increases over time and has not peaked by 120 minutes after tracer injection.

EP-0281

Clinical Application of 18F-Thretide PET/CT and Early PET/CT Scan in Prostate Cancer

X. Cheng[1,2], *G. Hou*[1,2], *X. Wang*[1,2], *X. Chen*[3,4,5], *Y. Wang*[1,2], *V. Jakobsson*[3,4,5], *X. Shen*[1,2], *J. Zhang*[3,4,5], *R. Zheng*[1,2]; *[1]Department of Nuclear Medicine (PET-CT Center), National Cancer Center, National Clinical Research Center for Cancer, Cancer Hospital, Chinese Academy of Medical Sciences and Peking Union Medical College, Beijing, CHINA, [2]Department of Nuclear Medicine (PET-CT Center), National Cancer Center, National Clinical Research Center for Cancer, Cancer Hospital, Chinese Academy of Medical Sciences and Peking Union Medical College, Langfang, CHINA, [3]Department of Diagnostic Radiology, Yong Loo Lin School of Medicine, National University of Singapore, Singapore, SINGAPORE, [4]Nanomedicine Translational Research Program, NUS Center for Nanomedicine, Yong Loo Lin School of Medicine, National University of Singapore, Singapore, SINGAPORE, [5]Clinical Imaging Research Centre, Centre for Translational Medicine, Yong Loo Lin School of Medicine, National University of Singapore, Singapore, SINGAPORE.*

Aim/Introduction: Recent studies have demonstrated the potential of PET/CT with ^{18}F-labelled prostate-specific membrane antigen (PSMA) as a promising method for prostate cancer (PCa) diagnosis. The aim of this study is to assess the clinical value of ^{18}F-Thretide (Al^{18}F-PSMA-BCH) PET/CT and early scan with ^{18}F-Thretide PET/CT in detecting and staging PCa. ***Materials and Methods:*** From November 2022 to April 2023, a total of 62 PCa patients were referred to our department for ^{18}F-Thretide PET/CT for clinical diagnosis, staging or restaging. Whole-body PET/CT scans were conducted at a median time of 77 minutes post-injection (p.i.) (range: 59-139 min); single-bed pelvic early PET/CT scans were performed with a PET emission duration of 2 minutes, starting at a median time of 186 s p.i. (range: 165-420 s). Visual analysis of images was performed followed by semiquantitative standardized uptake value (SUV) analysis of pathologic lesions, healthy bladder, and other surrounding healthy tissues in both early PET/CT scans and routine scans. ***Results:*** As of now, 47 patients have bone scans available for analysis, of which 2 patients were diagnosed with widespread bone metastasis based on both bone scans and ^{18}F-Thretide PET/CT. For the remaining patients, PET/CT identified 134 positive bone lesions and bone scans detected 95 positive bone lesions. Of these, 79 lesions on PET/CT and 29 lesions on bone scans were determined to be indicative of bone metastasis. The target to bladder (T/BL) ratios for primary lesions increased from 0.76±0.95 in routine scans to 12.02±11.68 in early PET/CT scans ($p<0.001$), while the T/BL ratios for metastases and local recurrence increased from 0.34±0.31 in routine scans to 5.42±4.87 in early PET/CT scans ($p<0.001$). However, the SUVmax values of other surrounding tissues were found to be higher in early PET/CT scans compared to routine scans (external iliac vessels: 8.46±1.94 vs. 2.89±0.52; inferior vesical artery: 4.49±1.48 vs. 2.34±0.34; gluteus maximus muscle: 1.19±0.35 vs. 0.84±0.25). Of the 16 patients who underwent surgery prior to PET/CT scans, early PET/CT scans improved the detection rate of local recurrence from 1/16 to 4/16. ***Conclusion:*** ^{18}F-Thretide PET/CT has shown to be a valuable imaging modality in the management of patients with PCa. Early PET/CT scan can improve the detection accuracy and rate of local recurrences and provide additional information for lesions that are challenging to distinguish from urinary uptake on routine scans.

EP-0282

Dual tracer PET/CT with 68Ga-PSMA and 18F-FDG in patients with prostate cancer

***Y. Zhang**, M. Su;*
Department of Nuclear Medicine, West China Hospital, Sichuan University, Chengdu, CHINA.

Aim/Introduction: The ^{68}Ga-prostate specific membrane antigen (PSMA) positron emission tomography/computed tomography (PET/CT) is routinely used for tumor detection and staging in prostate cancer, but 5-10% of primary tumors have low PSMA ligand uptake.[1] The Gleason score is a significant predictor for PSMA-FDG+ lesions.[2] In this study, we aimed to investigate the value of dual tracer PET/CT with ^{68}Ga-PSMA and ^{18}F-FDG in prostate cancer patients. ***Materials and Methods:*** Patients with Gleason score (GS) of 8-10 were included prospectively (Trial number: ChiCTR2200066582). All patients underwent both ^{68}Ga-PSMA and ^{18}F-FDG PET/CT within one week. The patients were divided into initial staging group (Group A) and biochemical failure/recurrence group (Group B). Lesions were classified into PSMA (- or +) and FDG (- or +), and the position of the lesions was recorded. ***Results:*** Fifty-two patients were included based on inclusion and exclusion criteria. There were 21 patients (median age 67 years, IQR 61-72 years) in group A and 31 (median age 65 years, IQR 57-71 years) in group B. 16, 33, and 3 patients had GS 8, 9, and 10 respectively. Overall, 624 lesions were detected in 49 of the 52 patients, and 3 patients with GS 8 in group B were negative in both scans. The PSMA-FDG+ lesion was only found in 12 patients with GS 9-10 (11 [91.7%, 11/12] patients with GS 9, and 1 [8.3%, 1/12] patient with GS 10). For the group A patients, there were 15 (15/21, 71.4%) patients with 209 PSMA+FDG- lesions, 18 (18/21, 85.7%) patients with 88 PSMA+FDG+ lesions, and 2 (2/21, 9.5%) with 20 PSMA-FDG+ lesions (1 primary lesion and 19 parenchymatous organ lesions). For the group B patients, there were 18 (18/29, 62.1%) patients with 92 PSMA+FDG- lesions, 21 (21/29, 72.4%) patients with 111 PSMA+FDG+ lesions, and 10 (10/29, 34.5%) with 104 PSMA-FDG+ lesions (2 primary lesions, 13 regional lymph node metastases, 30 distant lymph node metastases, 11 bone metastases, and 48 parenchymatous organ lesions). ***Conclusion:*** Prostate cancer patients with Gleason score 9-10 may be detected PSMA-FDG+ lesions. It may have an impact on the therapeutic choice. ***References:*** 1. P. S. Chakraborty, M. Tripathi, K. K. Agarwal, et al. Metastatic poorly differentiated prostatic carcinoma with neuroendocrine differentiation. Clinical Nuclear Medicine. 2015;40:e163-166. 2. Chen R, Wang Y, Zhu Y, et al. The Added Value of 18F-FDG PET/CT Compared with 68Ga-PSMA PET/CT in Patients with Castration-Resistant Prostate Cancer. J Nucl Med. 2022;63:69-75.

EP-0283

Improvement of Gleason Grading prediction in Prostate Cancer Stratification for Radical Prostatectomy: a Machine Learning-based Theronostic Multi-omics Study

***J. Ning**[1], C. P. Spielvogel[1,2], D. Haberl[1], K. Trachtova[1], S. Stoiber[1], S. Rasul[1], V. Bystry[1], E. Gurnhofer[1], G. Timelthaler[1], L. Papp[1], M. Schlederer[1], M. Hacker[1], A. Haug[1], L. Kenner[1];*
[1]Christian Doppler Lab for Applied Metabolomics, Medical University of Vienna, Vienna, AUSTRIA, [2]JN and CPS shared the first authorship, Vienna, AUSTRIA.

Aim/Introduction: In this study, we aim to integrate clinical data, radiomics data, genomics data and pathomics data using high-throughput machine learning (ML) model to predict the Gleason grading of prostate cancer (PCa) for smart and precise patient stratification for radical prostatectomy (RP) and compare its predictive performance with that of needle biopsy. ***Materials and Methods:*** Study Design Totally, 146 patients with histologically confirmed PCa from the clinical trial (NCT02659527) were enrolled in this study, all of whom underwent ^{68}Ga-PSMA-11 PET/MR before RP between May 2014 to April 2020 in the nuclear medicine department of Vienna General Hospital.Radiomics Acquisition^{68}Ga-PSMA-11 PET/MR images were collected and volumes of Interest (VOIs) were delineated on Hermes, from whom radiomics features were computed using the PyRadiomics. Genomics AcquisitionDNA was isolated from FFPE samples. Whole exome sequencing analysis was performed. Functional pathways were quantified using multiple established in silico tools including EVE, CADD and PolyPhen scores. Pathway status and clinical characteristics were associated with BCR using Cox proportional hazard models. Pathomics Acquisition. We constructed TMA from RP specimens. Immunohistochemical analysis was performed using the automated staining platform DAKO Omnis. PSMA, AR, Ki-67, PSA, FASN, IL6ST, CDK2, CD3, STAT3, NKX3.1, TBb were selected as biomarkers and stained in TMA slides.ML-based Data IntegrationTo find the best ML model, 5 ML-based models including RF, XGB, KNN, SVM, IGR were used. The classification results were validated using 100-fold Monte Carlo cross-validation to ensure robustness of performance metrics. ***Results:*** The distribution of gene mutation profile with frequency of ≥10% cases are sparse. So in subsequent ML-based analysis, only pathway-level data were used considering balanced grouping standards. The AUC, ACC, SNS, SPC, PPV and NPV of 5 ML-based approaches were respectively calculated and the resulting RF classification algorithm gave the best performance with 0.87, 0.78, 0.83, 0.72, 0.80, 0.80. Compared to needle biopsy, the performance of machine learning algorithm to predict Gleason grading is better. The SPC, PPV, ACC and AUC were elevated by 18% (0.61 vs 0.72), 7% (0.75 vs 0.80),1% (0.77 vs 0.78) and 11% (0.75 vs 0.87) respectively while the SNS and NPV were decreased by 7% (0.89 vs 0.83) and 1% (0.81 vs 0.80). ***Conclusion:*** In conclusion, our findings demonstrate that our multiomics-based ML model has the better performance for the prediction of Gleason grading than the current clinical baseline, which facilitates the clinical decision-making and personalized management of PCa.

EP-0284

Assessment of Response Evaluation Criteria in PSMA PET/CT (RECIP 1.0) in Metastatic Castration-Resistant Prostate Cancer

***A. Gafita**[1], L. Djaileb[2], I. Rauscher[3], W. P. Fendler[4], B. Hadaschik[4], J. Czernin[5], K. Herrmann[4], S. P. Rowe[1], J. Calais[6], M. Rettig[6], M. Eiber[3], M. Weber[4], M. R. Benz[6], A. Farolfi[7];*
[1]Johns Hopkins University, Baltimore, MD, UNITED STATES OF AMERICA, [2]University Grenoble Alpes, Grenoble, FRANCE, [3]Technical University Munich, Munich, GERMANY, [4]University Hospital Essen, Essen, GERMANY, [5]University of California Los Angeles, Los Angeles, CA, UNITED STATES OF AMERICA, [6]University of California, Los Angeles, Los Angeles, CA, UNITED STATES OF AMERICA, [7]University of Bologna, Bologna, ITALY.

Aim/Introduction: To assess the agreement of Response Evaluation Criteria In PSMA-PET/CT (RECIP) determined using tumor segmentation software (quantitative RECIP) with RECIP determined by visual reads of nuclear medicine physicians (visual RECIP) for response evaluation in metastatic castration-resistant prostate cancer. ***Materials and Methods:*** This multicenter retrospective study at three academic centers included men who received ^{177}Lu-PSMA treatment between December 2014

and February 2019. PSMA PET/CT at baseline and 12 weeks were assessed visually by five readers for changes in total tumor volume (TTV) and for new lesions. Quantitative changes in TTV were also measured using tumor segmentation software. The status of new lesions was combined with visual changes in TTV to determine visual RECIP and with quantitative changes in TTV to determine quantitative RECIP. The primary outcome was the agreement between visual vs quantitative RECIP and interreader reliability of visual RECIP by Fleiss kappa. The secondary outcome was the association of visual RECIP with overall survival (OS) by Cox regression. ***Results:*** 124 men (median age, 73 years; IQR, 67-76 years) were included. 40/124 (32%) and 84/124 (68%) men had quantitative RECIP-progressive disease (PD) and non-PD, respectively. Agreement between visual versus quantitative RECIP was excellent (κ=0.89; 118/124 [95%]). Agreement among readers in classifying visual RECIP-PD vs non-PD was excellent (κ=0.81; 103/124 [83%]) men. RECIP-PD was associated with significantly shorter OS compared to non-PD (HR 2.55; 95%CI: 1.71, 3.81; P<0.001). ***Conclusion:*** Visually assessed Response Evaluation Criteria In PSMA PET/CT (RECIP) demonstrated excellent agreement with quantitative RECIP and excellent interreader reliability. This can be readily implemented in clinical practice for response evaluation in men with metastatic castration-resistant prostate cancer undergoing ^{177}Lu-PSMA therapy.

EP-0285

Association of Blood Count Parameters and Non-metastatic Bone Uptake at [18F]PSMA-1007 PET — Could Osteoporosis Be the Key to Unravel this Conundrum?

G. Ninatti[1], *C. Pini*[1], *R. Camedda*[2], *F. Gelardi*[3], *L. Antunovic*[4], *C. Landoni*[1,5], *P. Mapelli*[4], *M. Picchio*[6,4], *M. Sollini*[3,7], *A. Chiti*[6,4];
[1]*University of Milano Bicocca, Monza, ITALY,* [2]*University of Rome Tor Vergata, Rome, ITALY,* [3]*Humanitas University, Pieve Emanuele, ITALY,* [4]*IRCCS San Raffaele Scientific Institute, Milan, ITALY,* [5]*IRCCS-San Gerardo, Monza, ITALY,* [6]*Vita-Salute San Raffaele University, Milan, ITALY,* [7]*IRCCS Humanitas Research Hospital, Rozzano, ITALY.*

Aim/Introduction: A limitation of PET imaging with the PSMA-targeting radiopharmaceutical [^{18}F]PSMA-1007 is represented by non-metastatic bone uptake, reported in up to 72% of cases [1], possibly leading to misdiagnosis. Underlying benign bone marrow/bone disorders have been suggested as the possible cause [2,3]. Our hypothesis is that osteoporosis plays a key role in this phenomenon. Therefore, we investigated the association between blood count parameters - known markers of this condition [4] - and the occurrence of non-metastatic bone uptake. ***Materials and Methods:*** We retrospectively analysed treatment-naïve patients with a confirmed diagnosis of prostate adenocarcinoma who underwent staging [^{18}F]PSMA-1007 imaging and blood count within 3 months. All patients with confirmed metastases, synchronous malignancy and/or active inflammatory processes were excluded. Qualitative analysis of [^{18}F]PSMA-1007 images was performed independently by three experienced nuclear medicine physicians. Selected patients were divided in two groups according to the presence/absence of non-metastatic bone uptake. Clinical information (age, Gleason score, iPSA) and blood count parameters were collected. The median value of blood count parameters in the two groups was compared using the Kruskall-Wallis test. ***Results:*** We analyzed 63 patients (median age: 67). The most prevalent Gleason scores were 4+3 (33%) and 4+5 (24%); median iPSA was 7.88 ng/mL (IQR 5.4-10.5). Forty-one patients had no bone findings while 22 had non-metastatic bone uptake at [^{18}F]PSMA-1007 PET, most commonly in the ribs (64%) and pelvic bones (59%). No statistically significant difference in clinical parameters between the two groups was found. Median neutrophil count was significantly higher in patients with non-metastatic bone uptake compared to those without (4600/mm3 vs. 4000/mm3, p=0.0387). ***Conclusion:*** In our cohort, non-metastatic bone uptake at [^{18}F]PSMA-1007 PET was observed in about 1/3 of patients. Patients with non-metastatic bone uptake had a significantly higher median neutrophil count than those without any bone findings. Given the prevalence of the finding and the molecular alterations induced by osteoclastogenic processes, we may speculate that [^{18}F]PSMA-1007 non-metastatic bone uptake could be an effect of underlying osteoporosis. We will further investigate this hypothesis in a larger population and explore the role of more specific markers of osteoporosis, in a prospective setting. ***References:*** 1. Hoberück, et al. . EJNMMI Res. 2021, 11. 2. Grünig, et al. Eur. J. Nucl. Med. Mol. Imaging 2021, 48, 4483. 3. Arnfield, et al.et al. Eur. J. Nucl. Med. Mol. Imaging 2021, 48, 4495-4507. 4. Li, et al. Front. Endocrinol. (Lausanne). 2022, 13, 2163.

EP-0286

The Impact of 18F-DCFPYL Specific Activity on Organ Uptake

G. Chaussé[1], *S. Plaha*[2];
[1]*McGill University, Montreal, QC, CANADA,* [2]*University of British Columbia, Vancouver, BC, CANADA.*

Aim/Introduction: During the production 18F-DCFPYL, chemical compounds are left unlabeled, which decreases specific activity. The theoretical maximum specific activity (also called carrier-free specific activity or CFSA) when all molecules are labeled is calculated based on molecular weight of the final product, decay properties of the radioisotope and the number of attached radioisotopes per pharmaceutical. One can measure the mass of labelled compound using the ratio of its specific activity relative to the CFSA. Biodistribution of 18F-DCFPYL PET imaging can be calculated as "Total Body Uptake" (sum of the product "Volume X SUVmean" of all organs with uptake). We investigated if: 1- specific activity and mass of radiopharmaceutical of 18F-DCFPyL affect the uptake of certain organs (salivary glands, liver, kidneys) (inter-individual comparison), 2- whether the effect (or absence thereof) held true for the same individual at different times (intra-individual comparison). ***Materials and Methods:*** 111 prostate cancer patients underwent a total of 122 PET/CT scans two hours following intravenous injection of ^{18}F-DCFPyL as part of a clinical trial (NCT02899312). Informed consent was obtained prior to any procedure in conformity with local ethic committee recommendations and in accordance with the ICH E6 guidelines and Declaration of Helsinki. Images were manually segmented using tools from a commercially available software (MIM software, v.7.0). Segmented organs were the salivary glands, lacrimal glands, liver, spleen, kidneys, and bowel. The bladder is considered excreted and therefore excluded. For each scan, specific activity of the production batch, obtained in the logs of the production facility, was decay corrected for time of injection of ^{18}F-DCFPyL. The mass of radiopharmaceutical was calculated and normalized for patients' body weight, PSMA-accumulating organ volume and total body uptake. (1) A cohort of 100 PET/CTs were used for interindividual comparison. (2) 22 additional PET/CT scans with repeated PET/CT were used for intraindividual comparison. .For each normalized mass of radiopharmaceutical (by body weight, organ volume or total body uptake), patients were divided into two groups, either above or below the median. A student T test was used to compare the groups. ***Results:*** There was no statistical significance found for tracer uptake in high and low specific activity groups for both hot and cold compounds in kidneys, livers, or salivary glands. Similarly, there was no statistical significance found in organs in the repeat cohort. ***Conclusion:*** 18F-DCFPYL specific activity does not appear to impact its biodistribution.

EP-0287

Can Ga-68 PSMA PET/CT Parameters Predict Progression in Hormone-Sensitive De Novo Metastatic Prostate Cancer

S. Aksu[1], *B. B. Demirel*[1], *S. Gülbahar Ateş*[1], *Ö. Ateş*[2], *G. Uçmak*[1];
[1]*Dr. Abdurrahman Yurtaslan Ankara Oncology Training and Research Hospital, Department of Nuclear Medicine, Ankara, TÜRKIYE,* [2]*Dr. Abdurrahman Yurtaslan Ankara Oncology Training and Research Hospital, Department of Medical Oncology, Ankara, TÜRKIYE.*

Aim/Introduction: The aim of this study is to investigate the role of staging Ga68 PSMA PET/CT parameters in predicting disease progression after first-line standard treatments (androgen deprivation therapy(ADT)±docetaxel) in patients with de novo metastatic hormone-sensitive prostate cancer(mHSPC). ***Materials and Methods:*** Patients who had metastases in staging Ga68 PSMA PET/CT and were followed up after first-line standard treatments were included in this study. The patients' demographic and pathological characteristics, total PSA(tPSA) levels were recorded. The differences between the tPSA at diagnosis and the lowest tPSA achieved after treatment were calculated(delta tPSA). The standardized uptake values(SUVmax) of prostate gland, lymph nodes and distant metastasis(Table 1), liver SUVmean values were recorded. The presence and date of progression based on clinical and imaging findings were recorded. Cox regression analysis was performed to investigate factors predicting progression after treatment, and Kaplan-Meier analysis was conducted to determine progression-free survival(PFS). ***Results:*** The mean age was 67.6±8.4(48-84) years. The median tPSA at diagnosis was 103(8-6109) ng/ml. The median lowest tPSA and the delta tPSA were 0.5(0-32)ng/ml, and 102.7(7.9-6178)ng/ml, respectively. The median follow-up period was 13.0(4.0-45.0) months. Progression was observed in 21(52.5%) patients (median tPSA of 6(1-51)ng/ml). Eighteen(45%) of the patients were receiving ADT, 22(55%) were receiving ADT+docetaxel treatment. A low-to-moderate positive correlation was found between the delta tPSA and the SUVmax value of bone metastasis(p=0.042, r: 0.336). Only the lowest tPSA achieved after treatment was found to be associated with progression (p<0.001, OR:0.091, %95 CI:1.042-1.143) in univariate analysis and it was shown that it has diagnostic value in ROC analysis(AUC:0.853, %95 CI:0.740-0.962, p<0.001). When the threshold value for the lowest tPSA value was set at 0.45ng/ml, the sensitivity and specificity for predicting progression were found to be 76.2% and 73.7%, respectively. The mean PFS was 24.5 (%95 CI: 19.01-29.95) months in all patient groups, the mean PFS was 34.5(27.09-42.28) months in those with a lowest tPSA <0.45ng/ml and 15 (%95 CI: 11.08-18.90) months in those with a lowest tPSA >0.45ng/ml. ***Conclusion:*** In high-risk prostate cancer patients, although it is known that Ga68 PSMA PET/CT successfully determines disease staging and extent, our study revealed that PSMA expression intensity in de novo mHSPC patients was not significant in predicting progression. In addition, we emphasize the importance of the lowest tPSA achieved after standard primary treatments as a significant factor in predicting PFS, and the need for personalized tPSA follow-up intervals on a patient-by-patient basis.

EP-0288

Reducing the frequency of prostate cancer biopsy by F18-rhPSMA7.3 PET/MR

T. Hekimsoy[1], *S. Kleiner*[1], *M. Heck*[2], *K. Schwamborn*[3], *M. Eiber*[1], *W. Weber*[1];
[1]*Department of Nuclear Medicine, Technical University of Munich, Klinikum rechts der Isar, Munich, GERMANY,* [2]*Department of Urology, Technical University of Munich, Klinikum rechts der Isar, Munich, GERMANY,* [3]*Department of Pathology, Technical University of Munich, Klinikum rechts der Isar, Munich, GERMANY.*

Aim/Introduction: Systematic biopsy of the prostate is the current standard for the workup of patients with suspected prostate cancer. However, the procedure is associated with significant morbidity and its sensitivity for the detection of clinically significant prostate cancer (csPC) is limited by sampling errors. In the present study we evaluated whether PSMA PET/MR can potentially reduce the need for systematic biopsies in patients with suspected prostate cancer. ***Materials and Methods:*** We retrospectively analyzed F18-rhPSMA7.3 PET/MR scans of patients who were clinically suspected to have prostate cancer and underwent imaging for planning of prostate biopsy. Patients with symptoms of acute prostatitis were excluded. We analyzed multiparametric MR images using the PI-RADS score and PET images using SUVmax. In addition, we tested a score (CS) which combines information from both PET and MRI by adding the PI-RADS score to SUVmax. All patients underwent histological confirmation within 90 days following the PET/MR scan. ***Results:*** 55 consecutive patients were included, 29 of which were eventually diagnosed with csPC (ISUP ≥ 2) on histology. The diagnostic performance of the three approaches to diagnose csPC are summarized in the table. For further analysis, we defined two operational points on the ROC curve: one for the sensitivity at 100% specificity and the other for the specificity at 90% sensitivity (Table 1). When patients meet the 100% specificity criteria (where the likelihood of csPC is so high that biopsy confirmation is unnecessary before surgery) or meet the 90% sensitivity criteria (where clinically significant prostate cancer is similarly unlikely as after a negative biopsy), biopsy could potentially be avoided. Biopsy would only be considered for patients with intermediate likelihood of prostate cancer based on imaging. Following this approach biopsy could been avoided by MR, PET, and PET/MR in 18%, 45%, and 51% of the patients. ***Conclusion:*** Our analysis indicates that F18-rhPSMA7.3 PET/MR has the potential to markedly reduce the number of prostate biopsies when compared to MR alone. Such an approach could significantly decrease the discomfort and morbidity associated with unnecessary biopsies. Further prospective studies are needed to confirm these findings and validate the clinical utility of PSMA PET/MR in this setting.

EP-16

e-Poster Area

B: Imaging Clinical Studies -> B1 Oncological Imaging Clinical Study -> B19 Thyroid

EP-0289

Prediction of Lymph Node Metastasis in Differentiated Thyroid Cancer Based on Radiomics Models: A Meta-analysis and Systematic Review

J. Mu, *Y. Cao, X. Zhong, W. Diao, Z. Jia;*
West China Hospital, Sichuan University, Chengdu, CHINA.

Aim/Introduction: The accurate clinical diagnosis of lymph node metastasis plays a crucial role in the treatment of differentiated thyroid cancer (DTC). This study aims to explore and summarise a more objective approach to detect cervical malignant lymph node metastasis of DTC via radiomics models. ***Materials and Methods:*** The PubMed, Web of Science, MEDLINE, EMBASE, and Cochrane databases were searched for all eligible studies. The search period is from the beginning to August 2022. Articles that used radiomics models based on ultrasound, computed tomography

or magnetic resonance imaging to assess lymph node metastasis preoperatively were included. Characteristics and diagnostic accuracy measures were extracted. Bias and applicability judgments were evaluated using the revised QUADAS-2 tool. The estimates were pooled using a random-effects model. Additionally, a leave-one-out meta-analysis was conducted to assess the heterogeneity. ***Results:*** Twenty-nine radiomics studies with 6160 validation set patients were included in the qualitative analysis, and 11 studies with 3863 validation set patients were included in the meta-analysis. Four of them had an external independent validation set. The studies were heterogeneous, and a significant risk of bias was found in 29 studies. Meta-analysis showed that the pooled sensitivity and specificity for preoperative prediction of lymph node metastasis via US-based radiomics were 0.81 (95% CI, 0.73-0.86) and 0.87 (95% CI, 0.83-0.91), respectively. ***Conclusion:*** Although radiomics-based models for lymphatic metastasis in DTC have demonstrated moderate diagnostic capabilities, future research should focus on broader data, standardised radiomics features, robust feature selection, and model exploitation.

EP-0290

Contribution of Neck Ultrasonography to Patient Management in Patients with Differentiated Thyroid Carcinoma with Excellent Response to Therapy

I. Hekimsoy[1], *M. Guven*[2], *R. Tokac*[2], *G. Kavukcu*[3], *A. Akgun*[2];
[1]*Department of Radiology, Torbali State Hospital, Izmir, TÜRKIYE,* [2]*Department of Nuclear Medicine, Ege University, Izmir, TÜRKIYE,* [3]*Department of Radiology, Ege University, Izmir, TÜRKIYE.*

Aim/Introduction: Neck ultrasonography (US) and serum thyroglobulin (Tg)/ antithyroglobulin (anti-Tg) values are used to determine local recurrence after radioactive iodine (RAI) treatment in patients diagnosed with Differentiated Thyroid Carcinoma (DTC). US has been reported as the best method by the American Thyroid Association (ATA), even in cases with undetectable serum Tg values. In this study, we aimed to evaluate the contribution of US imaging to patient management in long-term follow-up in a group of patients with DTC with low risk and an excellent response after RAI treatment. ***Materials and Methods:*** Records of 296 patients (261 females, 35 males) who were treated with total thyroidectomy and achieved excellent response after I-131 treatment between 1996 and 2017, were analyzed retrospectively. ***Results:*** In the histopathological evaluation, 280 of the patients were diagnosed with papillary, 14 with follicular, and 2 with papillary and follicular thyroid carcinoma. Twenty three of 296 patients (7.7%) had metastatic lymph nodes at the time of diagnosis. Patients received 30-175 mCi (mean: 101 mCi) RAI and were followed for a mean of 12.5 months (range 58-312 months). An average of 9.6 (range 4-20) US examinations were performed per patient. In 62.1% (184/296) of the patients, no structural disease was detected with US during the follow-up period. Findings compatible with granulation tissue or non-functioning avascular thyroid tissue in the thyroid bed were reported in 24.6% (73/296). US examinations were repeated in our center in 2 patients with suspicion of recurrence in the thyroid bed on US performed in another center, and the findings were compatible with surgical hemostatic material. FNAB of suspicious lymph nodes identified with US was performed in 14 patients and revealed benign cytology in 12. In 2 patients with papillary thyroid cancer with metastatic lymph nodes at the time of diagnosis, suspicious lymph nodes were detected with US on the 30th and 42nd months respectively. Lymph node dissection was performed upon malignant cytology on FNAB. Suspicious lymph nodes in 5 patients were not suitable for FNAB due to the localization or small size and were stable in follow-up US examinations. ***Conclusion:*** Our findings showed that in patients with DTC who have an excellent response after RAI ablation and were low risk according to ATA criteria, US can detect metastatic lymph nodes during follow-up at a low rate. On the other hand, it leads to unnecessary investigations and interventions and does not contribute significantly to patient management.

EP-0291

Role of Thyroid Scintigraphy with pertechnetate in Congenital Hypothyroidism

A. Marques[1], *J. Carvalho*[2], *F. Abreu*[1];
[1]*Instituto de Medicina Nuclear da Faculdade de Medicina da Universidade de Lisboa, Lisboa, PORTUGAL,* [2]*Centro Hospitalar de Lisboa Ocidental, Lisboa, PORTUGAL.*

Aim/Introduction: Congenital hypothyroidism (CH) is the most preventable cause of neurodevelopmental disability with varying etiology. We analyzed our hospital´s pediatric population with CH, reviewed the different scintigraphic patterns and correlated them with TSH levels in order to assess the role of thyroid scintigraphy in the etiologic workup of CH. ***Materials and Methods:*** Children with CH referred to our Nuclear Medicine Department between January 2021 and March 2023 for thyroid scintigraphy were retrospectively included in this study. After one month thyroxine therapy withdrawal, venous samples of TSH were taken on the same day as each thyroid scan. Scintigraphic images were carried out with a pinholle or parallel collimator 20 minutes following intravenous injection of sodium pertechnetate ($Na[^{99m}Tc]TcO_4$). Average injected ativity was 111 MBq. ***Results:*** A total of 44 patients were studied (21 girls and 23 boys) with a mean age of 3 years (range 2 - 5 years). Out of all the patients, 13 (30%) were found to have a normal thyroid site and normal uptake, 1 (2%) was found to have a normal site and decreased uptake, 5 (11%) were found to have a normal site and increased uptake, 16 (36%) had no uptake and 9 (21%) had ectopic uptake. The TSH levels on the same day as scintigraphy ranged from 1,38 to 853 mU/L, with significantly higher median TSH levels seen in the no uptake and ectopic uptake groups (282 and 249 mU/L, respectively) compared with the normally sited thyroid uptake patients. ***Conclusion:*** Thyroid scintigraphy with pertechnetate gives an important diagnostic contribution in most cases of congenital hypothyroidism, especially in ectopic thyroid tissue or suspected agenesis. However, its limitations in excluding possible dyshormonogenesis or differentiating transient from permanent hypothyroidism in normally located thyroid uptake highlights the need of always having a strict correlation with ultrassound findings and laboratory results.

EP-0292

Semiquantitative analysis of 99mTc MIBI thyroid scan in patients with amiodarone induced thyrotoxicosis

L. Fischer[1,2], *N. Girotto*[1,2], *T. Bogović Crnčić*[1,2], *M. Ilić Tomaš*[1,2], *S. Grbac-Ivanković*[1,2], *M. Mavrinac*[3];
[1]*Department of Nuclear Medicine, Faculty of Medicine, University of Rijeka, Rijeka, CROATIA,* [2]*Clinical Department of Nuclear Medicine, Clinical Hospital Centre Rijeka, Rijeka, CROATIA,* [3]*Department of Medical Informatics, Faculty of Medicine, University of Rijeka, Rijeka, CROATIA.*

Aim/Introduction: ^{99m}Tc-MIBI thyroid scan has proven useful in distinguishing amiodarone induced thyrotoxicosis caused by underlying thyroid disease, AIT-1, from AIT-2 induced by thyroid cell damage. Since mixed forms are also identified (AIT-3), differentiation is not always straightforward. To increase diagnostic performance and help the choice of therapy, we introduced semi-quantitative method for MIBI uptake analysis. ***Materials and***

Methods: In 36 patients (26 men, 10 women, mean age 67 years) treated with amiodarone 2 months to 9 years (average 2.32y) with mean amiodarone therapy dose of 150 mg (25 - 400 mg), thyrotropin (TSH), free thyroxin (FT4), free triiodothyronine (FT3) and thyroid auto antibodies against peroxidase, thyroglobulin and TSH receptor (TPO-Ab, TgAb, TSI) were determined. Ultrasonography was performed with vascularization assessment (0 = normal, 1 = moderate and 2 = markedly increased). Planar scintigraphy with 99mTc-MIBI was performed 10 minutes after administration of 370 MBq 99mTc-MIBI. Semiquantitative analysis of MIBI uptake was performed by drawing two regions of interest (ROI): over the whole thyroid and single background region beneath the thyroid. Target to background ratio was calculated by subtracting the average number of counts of background ROI from the thyroid ROI, normalized with the average counts in back¬ground ROI. The results were divided by percentiles in 3 groups; ratios between 66-100 percentile were classified as AIT-1, between 0-33 percentile as AIT-2 and between 33 and 66 percentile as AIT-3. Comparisons of groups were made by one-way analysis of variance (ANOVA). Post-hoc Scheffe test was used to calculate the differences between groups. ***Results:*** TSH was suppressed in all patients (TSH mean 0,0023 mIU/L, range 0.004 - 0.336), FT4 mean was 35,35 pmol/L (range 8,2 - 100), FT3 mean was 8,57 pmol/L (range 4,3 - 44,6). Elevated TPO-Abs were detected in 7, TgAbs in 4 and TSI in 6 patients. Ultrasonographically increased vascularization was observed in 8 patients (in 6 moderately and markedly in 2), the rest had normal results. Semiquantitative analysis identified high ratio representing high MIBI accumulation (AIT-1) in 13 patients, low uptake (AIT-2) in 12 patients and intermediate (AIT-3) in 11 pts. The difference between groups was statistically significant ($p<0.05$). ***Conclusion:*** Semiquantitative interpretation of 99mTc-MIBI uptake in thyroid can improve diagnostic accuracy and helps distinction between the types of AIT. Further investigations are necessary to classify the mixed group more accurately. Supported by University of Rijeka: project (uniri-pr-biomed-19-141495).

EP-0293

The prevalence of pre-thyroidectomy thyroid function test abnormalities among patients with differentiated thyroid carcinoma: A descriptive study

A. Aghaee*, s. barashki, s. zakavi;*
nuclear medicine research center,Mashhad university of Medical Sciences, Mashhad, IRAN, ISLAMIC REPUBLIC OF.

Aim/Introduction: The present study aims to assess pre-thyroidectomy thyroid hormone disturbances among patients suffering from differentiated thyroid carcinoma (DTC). ***Materials and Methods:*** This retrospective study was performed from September 2020 to March 2021. We analyzed the hospital files of 710 patients with DTC who underwent thyroidectomy and referred to nuclear medicine department from April 2013 to September 2019. Demographics, TNM stage, pre-surgery thyroid function tests, time-interval to achieve a complete response, recurrence rate, one-year response, final response, and the need for alternative treatment modalities were extracted. Then, we analyzed the potential association of pre-surgery TSH levels with the initial disease stage and treatment response. Chi-Square, Analysis-of-variance, and Kruskal-Wallis tests were used where appropriate. ***Results:*** The mean age of participants was 40.39 ± 13.85 years. History of Hashimoto's disease was detected in 130 (18.3%) patients. Multi-focal DTC was found in 221 (31.2%) patients. Lymph node involvement was significantly higher among men ($p = 0.001$). Men also had significantly higher thyroglobulin levels ($p = 0.025$). No statistically significant association was found between pre-surgery thyroid function status and TNM stage or multifocality of the malignancy. Baseline thyroid function tests also did not show a statistically significant relationship with thyroglobulin, anti-thyroglobulin antibody, time to first excellent response, and follow-up duration. ***Conclusion:*** Baseline thyroid function status may not change the outcome of DTC. It could also be plausible that thyroid dysfunction before surgery would not increase invasiveness nor impact the treatment-response of the tumor compared to euthyroid patients.

EP-0294

Prognostic role of minimal extrathyroidal tumor extension (mETE) in the follow-up of patients with papillary carcinoma (PC) unaffected by other risk factors.

A. Marongiu*, S. Nuvoli, S. Vargiu, P. Solinas, A. Spanu, G. Madeddu;*
Unit of Nuclear Medicine, University of Sassari, viale S. Pietro 8 - 0700 Sassari, Italy, Sassari, ITALY.

Aim/Introduction: Minimal extra-thyroid tumor extension (mETE) clinical relevance is still debated, in particular in determining its role as outcome predictive factor, and a long-term follow-up is required to detect outcome differences. We further investigated whether mETE impact exists on PC prognosis during follow-up after total thyroidectomy and radioiodine ablation. ***Materials and Methods:*** Among large PC patient groups with mETE, we retrospectively enrolled 84 cases with no other risk factors, such as gross ETE, neck lymph node and distant metastases, multifocality/multicentricity, and aggressive PC variants; 65 patients were females and 19 males, and 42 were aged < 55 and 42 ≥ 55 years. Seventeen patients had tumor sizes ≤ 10 mm and 67 > 10 mm. Comparatively, we enrolled 190 matched age/sex control PC patients without both mETE and the other risk factors, as above. During long-term follow-up, all patients underwent whole body scan (WBS) and SPECT/CT after 185 MBq ^{131}I dose; radiologic procedures, serum thyroglobulin and AbTg levels were also sequentially checked. ***Results:*** During follow-up, 14/84 (16.7%) patients underwent metastases and WBS detected 7 lesions (all unclear) in 6 cases, while SPECT/CT evidenced 26 lesions (24 neck, 1 mediastinum, 1 spine) in 14 patients, characterizing all WBS unclear lesions. Thyroglobulin was undetectable in 3 cases, < 5.0 ng/ml in 7 cases, >10 in 4 cases. Among 190 controls, 13 (6.8%) cases underwent metastases, WBS evidencing 7 lesions (6 classified as unclear in the neck and one lung metastasis) in 6 cases; SPECT/CT identified 18 metastases in 13 patients (16 neck, 1 lung, 1 bone). Thyroglobulin was undetectable in 2 cases, < 5.0 ng/ml in 8 cases, between 5.0-10.0 in 2 cases, and >10 in 1 case. AbTg were under cut-off in all patient groups. The univariate analysis showed an increased risk of developing metastases in mETE patients, Odds Ratio 2.72 (95% C.I. 1.22-6.08) p=0.01; disease-free survival (DFS) in mETE cases was significantly (p=0.009) lower than in PC patients without mETE. ***Conclusion:*** PC patients with mETE and without other risk factors at surgery showed unfavorable tumor course during follow-up, with mETE as a worse outcome significant predictor on univariate analysis than PC patients without mETE, with a higher rate of recurrences and decreased DFS. Metastases were better identified by SPECT/CT than WBS in all patient groups. More careful surveillance during follow-up must be done in PC patients with mETE also when it is apparently the only identified risk factor.

EP-0295

68Ga FAPI-PET CT in patients with rising calcitonin after treatment of medullary thyroid carcinoma and negative conventional and nuclear imaging - pilot cases.

P. Bochev, *G. Mateva, N. Novoselska;*
Acibadem Cityclinic Mladost UMBAL, Sofia, BULGARIA.

Aim/Introduction: Patients with medullary thyroid cancer (MTC) who experience calcitonin elevation/biochemical recurrence after initial treatment are a serious diagnostic and treatment challenge. In this scenario workup includes neck ultrasound and CT of chest/abdomen. Although not uniformly utilized, 18F -FDG, 68Ga DOTA - somatostatin receptor imaging and 18F-DOPA could be considered a second line imaging (with F-DOPA being of very limited availability). Despite various diagnostic tests, imaging frequently fails to localize disease. Recently introduced 68Ga FAPI radiopharmaceutical showed potential in cancer imaging and seems to be positive in MTC, based on few published cases, which can be considered a background for testing feasibility in specific scenarios Aim: Pilot assessment of feasibility of 68Ga FAPI PET/CT in imaging negative MTC patients with rising calcitonin ***Materials and Methods:*** We present two cases of patients, operated for MTC and gradually elevating calcitonin levels, who failed to localize tumor recurrence on conventional imaging, as well as on FDG and 68Ga DOTA- somatostatin receptor imaging. In both patients 68Ga FAPI-04 PET/CT was performed. ***Results:*** The scans revealed a liver metastasis in one patient and lung metastases and local recurrence in the other, all FAPI positive. None of the lesions was eligible for biopsy, so diagnosis was confirmed by progression on follow-up imaging in one patient and treatment response after vandetanib treatment in the other (follow up of 12 months). ***Conclusion:*** 68Ga FAPI PET/CT appears feasible in MTC patients with rising calcitonin levels and further implementation studies seem to be justified.

EP-0296

The total volume of lung metastases from thyroid cancer based on infer artificial intelligence can predict abnormal lung function

M. Qi, *R. Huang, S. Huang;*
Department of Nuclear Medicine, West China Hospital of Sichuan University, Chengdu, CHINA.

Aim/Introduction: Lung metastasis (LMs) from differentiated thyroid cancer (DTC) is the most common distant metastasis in patients with DTC. The clinical symptoms are often not obvious when the volume of LMs is small. However, respiratory failure resulting from lung involvement may be the most common cause of death in DTC patients with LMs in advanced disease. Therefore, the main purpose of this study was to explore whether the total volume of LMs from DTC affected the lung function of DTC patients with LMs and how aspect it affected lung function. ***Materials and Methods:*** 47 DTC patients from February 2016 to February 2023 in our center for initial radioiodine therapy after thyroidectomy were reviewed retrospectively. Clinical characteristics, chest computerized tomography (CT), lung function indexes, the number and total volume of LMs were collected. The total volume of LMs from DTC was obtained by Infer Artificial Intelligence (AI). According to the indexes of lung function, the patients were divided into normal lung function group and abnormal lung function group. Abnormal lung function includes ventilatory dysfunction composed of obstructive ventilatory dysfunction (OVD) and restrictive ventilatory dysfunction (RVD),lung diffusion capacity defect (LDCD) and small-airway dysfunction (SAD). The difference of total volume of LMs was compared between normal and abnormal groups. The cut-off value of the total volume of LMs used to predict abnormal lung function was obtained according to the receiver operating characteristic (ROC) curve. ***Results:*** Among them, 17.0% (8/47) had RVD, 8.5% (4/47) had OVD, 34.0% (16/47) had SAD, and 17.0% (8/47) had LDCD. There were significant differences in the total volume of LMs between the normal and abnormal groups with OVD, SAD, and LDCD. The cut-off values of SAD, OVD and LDCD were 7860.64mm^3, 9301.85 mm^3, and 15071.59 mm^3, severally. ***Conclusion:*** The total volume of LMs can affect lung function and it was also predictive for different types of lung dysfunction including OVD, SAD and LDCD. FEV1 / FVC, MMEF%, and V50% have negative correlation with the total volume of LMs.

EP-0297

SOP for cervical ultrasound cine loops on DTC follow-up

P. Seifert, *M. P. Sopuschek, M. Freesmeyer;*
Clinic of Nuclear Medicine, Jena, GERMANY.

Aim/Introduction: DTC patients require lifelong cervical ultrasound (US) follow-up. However, no standardized procedure recommendations exist and the role of retrospective analyses of video sequences (cine loops) is not reported. The purpose of this study was to investigate the diagnostic value of a SOP for the acquisition of ultrasound cine loop in the follow-up of DTC patients. ***Materials and Methods:*** Restrospective evaluation of all US examinations of DTC patients between JAN 2010 and FEB 2018 at a university nuclear medicine clinic. Analysing the additional diagnostic benefit over conventional examination results that arose from cervical US cine loops stored on the local PACS: (A) no clinical relevance, (B) confirmation of a new finding seen on conventional live ultrasound, (C) identification of a new finding not seen on conventional live ultrasound, (D) invalidation of a new finding seen on conventional live ultrasound. ***Results:*** A total of 5.512 US examinations in 652 patients (72% female, median age of 50 years) with 67% PTC, 29% FTC and 4% other DTC were evaluated, UICC I (79%), II (12%), III+IV (6%). In 82 patients (12.6%) a clinically relevant finding was identified on the US cine loop (B=11, C=6, D=78). Additional time consumption for the acquiration of the US cine loops was approx. 1 minute per investigation. ***Conclusion:*** The introduced SOP for the acquisition of cervical cine loops in the follow-up of DTC patients was easy and fast to apply. More than every tenth patient showed a clinical benefit of the additionally applied cine loops. We recommend the SOP for applicaiton in clinical routine. ***References:*** Ultrasound Cine Loop Standard Operating Procedure for Benign Thyroid Diseases-Evaluation of Non-Physician Application.Seifert P, Maikowski I, Winkens T, Kühnel C, Gühne F, Drescher R, Freesmeyer M.Diagnostics (Basel). 2021 Jan 4;11(1):67. doi: 10.3390/diagnostics11010067.

EP-0298

[68Ga]Ga-PSMA-11 PET/CT in Thyroid Cancer - Preliminary Results

K. Zajkowska, *M. Wojewódzka-Mirocha, P. Cegła, A. Sackiewicz, P. Ochman, J. Januszkiewicz-Caulier, A. Żyłka, M. Dedecjus;*
Department of Oncological Endocrinology and Nuclear Medicine, Maria Skłodowska-Curie National Research Institute of Oncology, Warsaw, POLAND.

Aim/Introduction: Prostate-specific membrane antigen (PSMA) is expressed in prostate cancer cells and in some of the nonprostatic solid tumors including thyroid cancer. The aim of this ongoing study is to determine the utility of [68Ga]Ga-PSMA-11 PET/CT

in detecting local recurrence and distant metastases of thyroid cancer. ***Materials and Methods:*** So far 18 patients were enrolled for this single-institution prospective study: 13 patients with differentiated thyroid cancer (DTC) after total thyroidectomy and radioiodine treatment with serum thyroglobulin (Tg) elevation and negative iodine scintigraphy, and 5 patients with medullary thyroid cancer (MTC) after total thyroidectomy with serum calcitonin (Ct) elevation. In all the patients [68Ga]Ga-PSMA-11 PET/CT was performed. Patients with negative or inconclusive PSMA imaging were qualified for [18F]F-FDG PET/CT. ***Results:*** In DTC patients (Tg 0.45-2076.0 ng/mL, mean 295.92 ng/mL, median 57.57 ng/mL) [68Ga]Ga-PSMA-11 PET/CT was positive in 4/13, inconclusive in 3/13 (heterogenous radioligand uptake in lesions) an negative in 6/13 cases. Patients with negative or inconclusive PSMA imaging were qualified for [18F]F-FDG PET/CT. Up-to-date [18F]F-FDG PET/CT was performed in 5/9 patients and was positive in 1 case (pulmonary metastasis negative in PSMA), negative in 3 and inconclusive in 1 case (inconclusive also in PSMA). The lesions that shown PSMA-11 uptake were localized in thyroid bed (in 2 patients), lymph nodes (2), lungs (1) and bones (1). In MTC patients with negative imaging studies (Ct 496.7-7088.0 pg/mL, mean 2380.1 pg/mL, median 967.8 pg/mL) [68Ga]Ga-PSMA-11 PET/CT was negative in all cases (4/4), as well as [18F]F-FDG PET/CT preformed 3 months later. In MTC patient with known lesion [68Ga]Ga-PSMA-11 PET/CT was positive and revealed intense PSMA-11 uptake in superior mediastinal mass. ***Conclusion:*** In DTC [68Ga]Ga-PSMA-11 PET/CT was positive in 4/13 and not inferior to [18F]F-FDG PET/CT in 8/9 patients (4 PSMA positive, 3 PSMA and FDG negative, 1 PSMA and FDG inconclusive). The main advantage of [68Ga]Ga-PSMA-11 PET/CT in DTC patients is no need for TSH stimulation. In MTC patients with negative CT and MR imaging [68Ga]Ga-PSMA-11 PET/CT was insufficient as well as [18F]F-FDG PET/CT. In MTC patient with known lesion [68Ga]Ga-PSMA-11 PET/CT was positive. More results are needed to draw the conclusions about utility of [68Ga]Ga-PSMA-11 PET/CT in thyroid cancer.

EP-0299

Differentiated thyroid carcinoma: correlation between thyroglobulin, basal anti-thyroglobulin antibodies and post-ablative treatment study.

B. Hervás-Sanz*, A. Rodríguez-Gasén, J. Suils-Ramon, M. P. Perlaza-Jiménez, M. Pudis, S. Bondia-Bescós, J. L. Díaz-Moreno, J. L. Vercher-Conejero, M. Cortés-Romera;*
Nuclear Medicine-PET (IDI) Department, Bellvitge University Hospital-IDIBELL, L'Hospitalet de Llobregat, SPAIN.

Aim/Introduction: Differentiated thyroid carcinoma (DTC) is the most common endocrine neoplasm. It affects young patients and its mortality has been increasing in recent years. That is the reason because those patients diagnosed with DTC require close monitoring. Such monitoring is usually done with thyroglobulin values.The aim of this study is to evaluate, in patients with DTC, the relationship between baseline thyroglobulin (bTg), stimulated thyroglobulin and baseline antithyroglobulin antibodies (AbTg) with the detection of residual tumoral pathology after the first ablative treatment following total thyroidectomy. ***Materials and Methods:*** Retrospective analysis of those patients (p) who received an ablative dose (100 mCi) of radioiodine, between 2017-2020, in our center, 30-90 days after total thyroidectomy.The analyzed parameters were: bTg, baseline AbTg, stimulated thyroglobulin and presence of pathological uptake (locoregional adenopathies and/or metastases) in the planar total body scan (PTBS) at 7 days post-treatment. ***Results:*** We obtained 295p (221 women and 74 men), mean age 50 years (range 20-85), with DTC (240 papillary, 35 follicular, 10 Hürthle cell, 5 papillary + follicular and 5 poorly differentiated). Of the 295p, 261p received exogenous stimulation after two doses of TSHrh and 34p received endogenous stimulation with withdrawal of levothyroxine for 4 weeks prior.Out of the total, 74p had bTg >1ng/mL. Of these, 65% (48 out of 74) showed positive PTBS. Of the 221p with bTg values <1ng/mL, 132p had detectable stimulated thyroglobulin and, of these, 42 had positive PTBS (32%). Of those with undetectable stimulated thyroglobulin (89), 15p had positive AbTg, and of these, 6 had positive PTBS. ***Conclusion:*** In our series of over 100p, the rate of detection of metastatic disease on PTBS post-ablative treatment is higher the higher the thyroglobulin value.Positive baseline AbTg levels also play an important role, as PTBS has detected metastatic disease in 40% of these patients despite undetectable thyroglobulin levels. All these data could be taken into account in the future for precise dose adjustment in radioiodine ablative treatments.

EP-0300

Does the duplication time of thyroglobulin have any use as a predictor factor on the detection of recurrence and or metastasis in the differentiated thyroid cancer in the 2-[18F]fluoro-2-deoxy-d-glucose PET/CT.

D. Rodriguez Oviedo*, B. Manzarbeitia Arroba, M. Tagliatori Nogueira, M. Alvarez Moreno, C. Galindo, M. De La Rubia Marcos, M. Garcia Alonso, C. Paniagua Correa, C. Sandoval Moreno;*
Hospital Universitario de Getafe, Madrid, SPAIN.

Aim/Introduction: Determinate how useful the doubling time thyroglobulin (Tg-DT) is as a predictor factor in the detection of recurrence and or metastasis in the 2-[18F]fluoro-2-deoxy-d-glucose (2-[18F]FDG) PET/CT in patients with differentiated thyroid cancer (DTC), positive thyroglobulin (Tg), and negative anti-thyroglobulin antibodies (Tg-ab). ***Materials and Methods:*** The inclusion criteria were (1) patients diagnosed with DTC treated surgically and I-131 ablation therapy (2) negative Tg-ab serum levels (3) at least 3 Tg serum levels measurements during the follow-up (4) at least one [18F]FDG) PET/CT after treatment (5) pathology results of those with positive [18F]FDG) PET/CT. ***Results:*** 50 patients met the inclusion criteria, 15 of them the (2-[18F]FDG) PET/CT didn't find any signs of recurrence and or metastasis, the others 35 patients received positive results for recurrence and or metastasis. [18F]FDG) PET/CT sensitivity, specificity, positive predictive value (VPP), and negative predictive value (VPN) results were 95%, 96%, 97%, and 90% respectively. ***Conclusion:*** We found that a small Tg-DT has a higher probability of a positive [18F]FDG) PET/CT for recurrence and or metastasis. The Tg-DT area under the curve (AUC) analysis to predict the presence of recurrence or metastasis on the [18F]FDG) PET/CT of DTC was 8 months (sensibility 93%, specificity 89%, AUC= 0.90).

EP-0301

Comparative Study of [68Ga]Ga-DOTA-FAPI-04, [68Ga]Ga-DOTATATE and [18F] -DOPA in Imaging of Medullary Thyroid Carcinoma: A Case Series and 18F-DOPA in Imaging of Medullary Thyroid Carcinoma: A Case Series

G. dos Santos*[1,2], A. Quagliata[1], E. Silvera[1,2], R. Castro[1], A. Banchero[1], A. Damian[1], I. Cordero[1], K. Suanes[1], O. Alonso[1,2], E. Savio[1], P. Duarte[1], J. Gambini[1];*
[1]CUDIM, Uruguayan Center Of Molecular Imaging, Montevideo, URUGUAY, [2]Hospital de Clínicas Dr. Manuel Quintelas, Montevideo, URUGUAY.

Aim/Introduction: The management of medullary thyroid carcinoma (MTC) remains a challenge due to its heterogeneous presentation and variable clinical course. Molecular imaging has emerged as a promising tool for the diagnosis and management of MTC. Radiotracers such as [^{68}Ga]Ga-DOTA-FAPI-04, [^{68}Ga] Ga-DOTATATE and [^{18}F] -DOPA have shown potential in the imaging of neuroendocrine tumors, including MTC. However, there is limited comparative data on the performance of these radiotracers in MTC patients. The aim of our work is to compare the role of these tracers in the imaging of three MTC patients. ***Materials and Methods:*** Three patients with histologically confirmed MTC were included in this study and all patients underwent imaging with [^{68}Ga]Ga-DOTA-FAPI-04, [^{68}Ga] Ga-DOTATATE and [^{18}F] -DOPA on separate occasions. The radiotracers were administered according to established protocols. Imaging was performed using a PET/CT scanner. Images were interpreted by experienced nuclear medicine physicians and evaluated for the presence of MTC lesions, including primary tumors and metastatic lesions. The maximum standardized uptake value (SUVmax) and the SUVmax ratio (SR; defined as SUVmax/background) were measured for each lesion. Ethical approval was obtained from the institutional review board. All patients signed informed consent prior to enrollment in the study. ***Results:*** The results of our study demonstrate that [^{68}Ga] Ga-DOTA-FAPI-04 provides favorable tumour-to-background contrast compared to [^{68}Ga] Ga-DOTATATE and [^{18}F] -DOPA. In our cohort, [68Ga]Ga-DOTA-FAPI-04 detected the highest number of lesions, with 8, 6, and 1 lesions identified in each patient, respectively, compared to [^{68}Ga] Ga-DOTATATE (5,1 and 2) and to [^{18}F] -DOPA (0, 3, 0), respectively. Notably, [^{68}Ga]Ga-DOTA-FAPI-04 detected more mediastinal lymph nodes in patient one (7 lymph nodes) compared to [^{68}Ga] Ga-DOTATATE PET/CT (5 lymph nodes) and and [^{18}F] -DOPA (none identified). SR values for [^{68}Ga] Ga-DOTA-FAPI-04 had a mean SR value of 9.56, ranged from 2.68 to 30.00. In contrast, [^{68}Ga] Ga-DOTATATE had a lower mean SR of 7.97 (range: 4.80-16.67) and [^{18}F] -DOPA had the lowest mean SR of 4.3 (range: 3.67-5.11). ***Conclusion:*** Taken together, our findings suggest that [^{68}Ga]Ga-DOTA-FAPI-04 has better SR and positivity rate compared to [^{68}Ga] Ga-DOTATATE and [^{18}F] -DOPA in the detection of lesions, particularly mediastinal lymph nodes, with favorable tumour-to-background contrast. These results support the potential clinical utility of [^{68}Ga]Ga-DOTA-FAPI-04 in the management of Medullary Thyroid Carcinoma. ***References:*** Comparison of [68Ga]Ga-DOTA-FAPI-04 and [18F] FDG PET/CT for the diagnosis of primary and metastatic lesions in patients with various types of cancer. EJNMMI (2020)47:1820-1832. https://doi.org/10.1007/s00259-020-04769-z

EP-0302

Correlation Between Clinical Characteristics And Effective Washout Time In Patients Treated With High Radioiodine Activities

C. Guerrero Calatayud*, A. C. Marin, S. Prado Wohlwend, J. R. Cañón Sánchez, N. I. Orrego Castro, S. Montesinos González, A. M. Yepes Agudelo, P. Bello Arques;*
Hospital La Fe, Valencia, Valencia, SPAIN.

Aim/Introduction: Correlation between clinical variables and the delay in the effective washout time of 131I in context of differentiated thyroid cancer. ***Materials and Methods:*** Retrospective study of 754 patients treated with 131I from October 2014 to September 2022, comparing those with slow effective washout time of the radiopharmaceutical (>3 days) versus a control group with fast elimination chosen by simple randomization. The effective washout time was obtained from the exponential decay time of the radiopharmaceutical. Age, TNM, basal and stimulated maximum thyroglobulins (Tg) (Tgmax), and anti-thyroglobulin (Ab anti-Tg) were reviewed. ***Results:*** Out of 754 treated patients, 84 were those with slow effective elimination and a fast elimination control group was selected by simple randomization. Respectively, 77.8% vs 63.9% were women, with a mean age of 50 vs 56 years. The diagnosis was most frequently prompted by an incidental finding (26% vs 22%) or a cervical tumor (29.6% vs 38.8%) and the patients treated with a mean activity of 95mCi vs 107mCi. Regarding staging, 59.2% vs 44.5% were T1-T2, N+ in 25.9% vs 36% and M+ in 18.5% vs 16.6%. Median Tg were 1.94 vs 0.27 vs. Tg max 11.76 vs 3.57 and positive Ab anti-Tg in 4 vs 6 patients (these were excluded from thyroglobulin analyses). Tg and Tgmax were compared using the Mann-Whitney test, not observing statistical differences between both groups (p=0.057 and p=0.146 respectively). ***Conclusion:*** No statistically significant differences were observed between fast and slow washout to justify the excretion delay. There is a trend to a delay in 131I washout related to increased levels of thyroglobulin. Given the heterogeneity of the patients, larger series may be necessary to make a statistical inference.

EP-0303

Usefulness of 2-[18F]FDG PET/CT in indeterminate thyroid nodules (Bethesda III and IV) for risk stratification: do we still have to rely on FDG positivity? A retrospective monocentric experience

F. Serani[1]*, E. Tabacchi*[2]*, L. Calderoni*[1]*, G. Cuzzani*[1]*, S. Chillotti*[3]*, S. Damiani*[4]*, S. Fanti*[5]*;*
[1]*Nuclear Medicine, Alma Mater Studiorum -University of Bologna, Bologna, ITALY,* [2]*Nuclear Medicine Unit, IRCCS Azienda Ospedaliero-Universitaria di Bologna, Bologna, ITALY,* [3]*Pathology Unit, Alma Mater Studiorum -University of Bologna, Bologna, ITALY,* [4]*Pathology Unit, IRCCS Azienda Ospedaliero-Universitaria di Bologna-ITALY, Bologna, ITALY,* [5]*Nuclear Medicine, Alma Mater Studiorum - University of Bologna, Nuclear Medicine Unit, IRCCS Azienda Ospedaliero-Universitaria di Bologna, Bologna, ITALY.*

Aim/Introduction: Thyroid nodules are common and often incidentally discovered during imaging studies. The gold standard imaging exam is ultrasonography, followed by fine-needle aspiration biopsy (FNAB) to assess cytology and rule out malignancy. The Bethesda System for Reporting Thyroid Cytopathology provides a standardized approach for the interpretation of FNAB results, with Bethesda III and IV categories indicating indeterminate cytology. The challenge of precisely diagnosing indeterminate thyroid nodules prior to surgery has led to exploration of the introduction of molecular testing; in this context the potential utility of 2-[18F]FDG PET/CT (FDG PET) remains ambiguous and warrants further elucidation. We aimed to investigate the usefulness of FDG PET in risk stratification of indeterminate thyroid nodules (Bethesda III and IV). Specifically, we aimed to determine if there is a correlation between FDG positivity and presence of malignancy at final histology. ***Materials and Methods:*** In this retrospective descriptive monocentric experience, we selected patients who had undergone FDG PET and FNAB for thyroid nodules within 6 months (before or after) PET/CT, with subsequent thyroidectomy or hemithyroidectomy within one year of the cytology results, between January 2019 and January 2023, all performed in our institution. A lesion-based analysis was carried on using contingency tables. ***Results:*** 17 patients with 19 indeterminate thyroid nodules (15 Bethesda IV and 4 Bethesda III) were included in the analysis. 16 out of 19

nodules (84%) were positive on FDG PET, with a median SUVmax of 6.60 (IQR 4.50-8.70). Of the 19 nodules, 9 were malignant (7 follicular and 2 papillary carcinomas, with a TNM stage of pT1a in 7/9 and pT3a in 2/9 nodules) on final histology (47.4%) and 10 were found to be benign (6/10 follicular adenomas, 1/10 oncocytic adenoma and 3/10 thyroid follicular nodular disease) at final histology. FDG PET had a positive predictive value (PPV) of 44% and a negative predictive value (NPV) of 11%. Only 42.1% (8/19) of nodules had concordant PET and histology results (negative FDG PET and no malignancy or positive FDG PET and malignancy). ***Conclusion:*** Our experience confirms that FDG positivity in indeterminate thyroid nodules on cytology it is not a definitive criterion for malignancy. Ongoing and future analyses aimed at identifying predictive factors of malignancy such as ultrasonography characteristics, functional FDG PET parameters, radiomics, genetics as combination models and future prospective studies may enable better risk stratification and avoid unnecessary surgery.

EP-17

e-Poster Area

B: Imaging Clinical Studies -> B1 Oncological Imaging Clinical Study -> B20 Gynaecological

EP-0304

Vulva lesions as characterized by F-18 Fluorodeoxyglucose Positron Emission Tomography/ Computed Tomography

Z. Koç[1], *P. Özcan*[1], *T. İlhan*[2], *S. Gökulu*[2], *Y. Karabulut*[3];
[1]*Mersin University Hospital Nuclear Medicine Dpt., Mersin, TÜRKIYE,* [2]*Mersin University Hospital Gynecologic Oncology Dpt., Mersin, TÜRKIYE,* [3]*Mersin University Hospital Pathology Dpt., Mersin, TÜRKIYE.*

Aim/Introduction: Vulva malignancy (primary or metastatic lesions) has significant FDG accumulation according to previous literature. The aim of this study is to analyze the metabolic imaging characteristics of apparently malignant vulva lesions determined by F-18 FDG PET-CT. ***Materials and Methods:*** 27 female patients (mean: 56 years) with suspicious vulva lesions were retrospectively analyzed. The F-18 FDG PET-CT characteristics of the lesions, the first diagnosis of the patients and other metastatic sites were recorded and compared with pathology and or follow up and pelvic examination results. ***Results:*** The patients' first diagnoses were necessarily malignant (breast (n=5), other gynecologic tumors (n=6), lymphoma (n=5), vulva-vagen (n=4), colon (n=2), primary unknown (n=2), multiple myelom, ewing sarcoma, pancreas. The mean size of the vulva lesion in largest dimension was 15.5 and the mean SUVmax of these lesions was 16.5. The pathologic findings of the vulva lesions were obtained all of the patients. The findings were inflammatory or infectious lesions in 9 and malignant in 14 and normal in others as pathology results. The SUVmax levels of the true positive results (primary vulva lesions (n=4), metastatic lesions (n=5), local invasion (n=2), sarcoma (n=2), lymphoma (n=1)) was 19,35 and false positive results was 14,48. The accuracy of the F-18 FDG PET/CT in estimation of the vulva lesions was 48%. ***Conclusion:*** There are several case reports about these lesions in the literature (1). The results of the studies in malignant vulva tumors has shown advantages in saging and prognostification (2, 3) . There are several false positive causes in the diagnosis of vulva lesions on F-18 FDG PET-BT and this issue should be considered but pelvic examination is necessary in case of increased metabolic activity in a vulva lesion. ***References:*** 1. Shen G, Wang R, Pan L, Kuang A. Malignant Extrarenal Rhabdoid Tumor of the Vagina on FDG PET/CT. Clin Nucl Med. 2021 Dec 1;46(12):1020-1021. 2. Brar H, May T, Tau N, Langer D, MacCrostie P, Han K, Metser U. Detection of extra-regional tumour recurrence with ^{18}F-FDG-PET/CT in patients with recurrent gynaecological malignancies being considered for radical salvage surgery. Clin Radiol. 2017 Apr;72(4):302-306. 3. Rao YJ, Hassanzadeh C, Chundury A, Hui C, Siegel BA, Dehdashti F, DeWees T, Mullen D, Powell MA, Mutch DG, Schwarz JK, Grigsby PW. Association of post-treatment positron emission tomography with locoregional control and survival after radiation therapy for squamous cell carcinoma of the vulva. Radiother Oncol. 2017 Mar;122(3):445-451.

EP-0305

Comparison of the diagnostic efficacy between 68Ga-FAPI PET/CT and 18F-FDG PET/CT in gynecological malignancies: A Systemic Review and Meta-analysis

C. Zhao*, L. Li;*
West China Hospital, Sichuan University, Chengdu, CHINA.

Aim/Introduction: Gynecologic malignancies, including breast, cervical, endometrial, ovarian and fallopian tube malignancies, are critical threats to women's health. ^{68}Ga-FAPI PET/CT is a novel molecular imaging modality. Whether ^{68}Ga-FAPI PET/CT has better diagnostic efficiency than ^{18}F-FDG PET/CT on different tumors is a research hotspot. The purpose of this study is to conduct a meta-analysis to compare the diagnostic efficacy of ^{68}Ga-FAPI PET/CT and ^{18}F-FDG PET/CT on gynecologic malignancies. ***Materials and Methods:*** We searched databases including PubMed, Embase, Cochrane Library and Web of Science from inception until March 29, 2023. Subjects must be diagnosed with gynecologic malignancies by histopathology, and both ^{68}Ga-FAPI PET/CT and ^{18}F-FDG PET/CT were performed at the same period. The literature was independently screened by 2 researchers. RevMan5.3 and Stata software were used to conduct statistical analysis. ***Results:*** A total of 238 records were screened, 8 articles were reviewed and 7 articles were included in the meta-analysis. A total of 196 patients and 603 lesions were included in these 8 articles, which involving breast, ovarian, cervical, endometrial, tubal, and uterus cancers. Based on patients, the diagnostic sensitivities of ^{68}Ga-FAPI PET/CT and ^{18}F-FDG PET/CT on metastatic lymph nodes were 0.94 (95% CI: 0.68,0.99), 0.8 (95% CI: 0.8,0.8), respectively. Based on lesions, the sensitivities of ^{68}Ga-FAPI PET/CT and ^{18}F-FDG PET/CT on metastatic lymph nodes were 0.96 (95% CI: 0.83,0.99), 0.73 (95% CI: 0.59,0.84), respectively. The relative risk of ^{68}Ga-FAPI PET/CT versus ^{18}F-FDG PET/CT detecting rates was 1.30, 95% CI: 0.78,2.18 (primary, lesion-based, p=0.32); 1.12, 95% CI: 0.98,1.28 (lymph node, patient-based, p=0.1); 1.28, 95% CI: 1.04,1.57 (lymph node, lesion-based, p=0.02); 1.16, 95% CI: 1.00,1.34 (other metastases, patient-based, p=0.04); 1.61, 95% CI: 1.12,2.31 (other metastases, lesion-based, p=0.01), respectively. The tumor-to-background ratios of ^{68}Ga-FAPI PET/CT in primary tumor, metastatic lymph nodes and other metastatic lesions were significantly higher than that of ^{18}F-FDG PET/CT (p<0.05). ***Conclusion:*** ^{68}Ga-FAPI PET/CT has better diagnostic efficacy than ^{18}F-FDG PET/CT on the gynecological malignancies.

EP-0306

Prognostic value of semiquantitative parameters of18F-FDG PET/CTin the staging of cervical cancer.

L. Rodríguez Díaz, *C. Vigil Díaz, A. Laverde Mächler, J. Maraña González, S. Naranjo Sancho, M. Fernández Llana, M. Domínguez Grande, J. Suárez Fernández, N. Martín Fernández, F. González García;*
Hospital Universitario Central de Asturias, Oviedo, SPAIN.

Aim/Introduction: Cervical cancer is the fourth most common cancer among women worldwide. ^{18}F-FDG PET/CT has a relevant role in diagnosis, response evaluation and recurrence detection. The aim of this study is to evaluate the role of ^{18}F-FDG PET/CT in staging and management of cervical cancer in order to define the prognostic value of visual evaluation and semi-quantitative PET/CT parameters. ***Materials and Methods:*** Retrospective study including 26 patients (age range 30-70 years) with histological diagnosis of cervical cancer, who underwent pretreatment PET/CT between January/2021-June/2022. The variables included were tumor histology, presence of lymphovascular invasion, degree of differentiation classified into low (G1) and high-grade (G2-3), and stage defined as local (stage I) or advanced stage (II-IV), according to MRI results and following the FIGO staging system. PET/CT results were evaluated qualitatively and semi-quantitatively by calculating SUVmax, SUVmean and TLG values. Statistical analysis was performed using non-parametric Mann-Whitney U test. The area under the receiver operating characteristic (ROC) curve and cut-off values were identified. ***Results:*** 5 patients were classified as localized stages, 21 as advanced. 16 patients were classified as high grade, 9 as low grade tumors. Lymphovascular involvement was found in 11 patients. The median SUVmax, SUVmean and TLG values were 17.39 (range 4.56-65.98), 10.30 (range 2.54-41.47) and 418495.2 (35482.4-3330471.0), respectively. Statistically significant higher mean TLG values were found in patients with advanced vs. local stages (500887.0 vs. 72449.4) ($p<0.05$) nd in high-grade tumors vs. low-grade tumors (534991.8 vs. 24921.4) ($p<0.05$). ROC curve analysis revealed an AUC for TLG for stage of 0.90 ($p< 0.05$, IC 95% 0.79-1.02) and of 0.78 for grade ($p< 0.05$, IC 95% 0.60-0.96). A TLG optimal cut-off point of 102883.7 for differentiating local and advanced stage was found to have a sensitivity and specificity of 86% and 60%, respectively. The optimal determined TLG cut-off value of 123794.7 was found to have 81% sensitivity and 56% specificity for grade differentiation. No statistically significant differences were found for lymphovascular invasion. ***Conclusion:*** 18F-FDG PET/CT is an effective staging technique in cervical cancer capable of predicting tumor stage and grade prior treatment. Our series showed statistically significant differences in TLG values in patients with high-grade and advanced stage tumors compared to those with low-grade and local stage tumors.

EP-0307

Development and External Testing of Integrating PET/MR Radiomics and Clinical Characteristics to Predict Lymphovascular Space Invasion in Endometrial Carcinoma: A Dual-Center Study

X. Li[1,2], *T. Song*[1,2], *B. Cui*[1,2], *J. Li*[1,2], *J. Ma*[1,2], *H. Yang*[1,2], *Y. Wang*[3], *H. Sun*[4], *J. Lu*[1,2];
[1]*Department of Radiology and Nuclear Medicine, Xuanwu Hospital, Capital Medical University, Beijing, CHINA,* [2]*Beijing Key Laboratory of Magnetic Resonance Imaging and Brain Informatics, Capital Medical University, Beijing, CHINA,* [3]*GE Healthcare China, Shanghai, CHINA,* [4]*Department of Radiology, Shengjing Hospital of China Medical University, Shenyang, CHINA.*

Aim/Introduction: To investigate the precision and robustness of radiomics based on integrated positron emission tomography/magnetic resonance (PET/MR) imaging for predicting lymphovascular space invasion (LVSI) in endometrial carcinoma (EC) patients. ***Materials and Methods:*** Ninety-three patients with EC from two centers who underwent ^{18}F-Fluorodeoxyglucose (^{18}F-FDG) PET/MR scanning were retrospectively collected and divided into the training, validation, and testing datasets. Clinical characteristics including age, weight, height, International Federation of Gynecology and Obstetrics (FIGO) stage, CA 19-9, and carcinoembryonic antigen (CEA) were collected. The apparent diffusion coefficient (ADC) parameters and conventional PET metabolic parameters, including peak, maximum, and mean standard uptake values (SUV_{peak}, SUV_{max} and SUV_{mean}), as well as metabolic tumor volume (MTV) and total lesion glycolysis (TLG), were measured by two radiologists. The volume of interest (VOI) for tumors was semi-automatically segmented on PET images. 5106 radiomics features were extracted from VOI on anatomical MRI, ADC maps, and PET images and selected using the minimum redundancy maximum correlation (mRMR) and the the least absolute shrinkage and selection operator (LASSO) algorithms to generate multimodal Rad-scores (Rad-score_PET, Rad-score_MR, and Rad-score_PET/MR). The logistic regression algorithm established PET, MR, PET/MR, and combined machine learning models. The Mann-Whitney test was utilized to examine the differences in Rad-scores distribution between the LVSI and non-LVSI groups. The Spearman's correlation test was used to analyze the correlations between the Rad-scores and other clinicopathological characteristics. Evaluations of machine learning models were performed using receiver operating characteristic curves, calibration curves, and decision curve analysis curves. ***Results:*** Only Rad-score_PET/MR among all Rad-scores of the LVSI group was higher than those of the non-LVSI group in every dataset ($p < 0.001$). And the Rad-score_PET/MR was correlated with LVSI ($r = 0.690$, $p < 0.05$) and slightly correlated with pelvic lymph node metastasis (PLNM) ($r = 0.200$, $p < 0.05$). In the training dataset, the PET/MR model predicted LVSI well (AUC = 0.993). However, the AUC value declined significantly in the validation and testing datasets (AUC = 0.833 and 0.909, respectively). In three datasets, the combined model that integrated clinicopathological features (differentiation degree, SUV_{max}, and SUV_{peak}) with Rad-score_PET/MR had the highest precision and robustness (AUC = 0.993, 0.900, and 0.923, respectively). ***Conclusion:*** Radiomics based on integrated PET/MR could noninvasively detect LVSI in EC, which could benefit in modifying treatment regimens and predicting prognoses. Moreover, the addition of clinicopathological features can improve the reproducibility of the radiomics model.

EP-0308

Potential for time-synchronized PET/MRI with dual tracers of FDG and FES: Utility in the diagnostic capability to distinguish between benign and malignant endometrial lesions

J. Inukai-Inoue[1], *M. Nogami*[2,3], *M. Tachibana*[1], *F. Zeng*[2], *K. Kubo*[2], *T. Kurimoto*[4], *T. Tujikawa*[5], *Y. Yoshida*[6], *H. Okazawa*[3], *T. Murakami*[1,2];
[1]*Department of Radiology, Kobe University Graduate School of Medicine, Kobe, JAPAN,* [2]*Department of Radiology, Kobe University Hospital, Kobe, JAPAN,* [3]*Division of Medical Imaging, Biomedical Imaging Research Center, University of Fukui, Fukui, JAPAN,* [4]*GE Healthcare, Hino, JAPAN,* [5]*Department of Radiology, Faculty of Medical Sciences, University of Fukui, Fukui, JAPAN,* [6]*Department of Obstetrics and Gynecology, Faculty of Medical Sciences, University of Fukui, Fukui, JAPAN.*

Aim/Introduction: When using different PET scans with multiple tracers to evaluate lesions, it is difficult to establish the identical region of interest (ROI) in both images using PET information alone. In simultaneous PET/MRI, because the individual PET and MRI have different acquisition times, the MRI-based ROI of PET is inaccurate. This study aimed to generate the MRI-based ROI of PET by reconstructing PET images that perfectly match the MRI acquisition time using MRI active trigger information recorded in the PET list-mode data and evaluate the clinical utility of its quantitative values. ***Materials and Methods:*** Thirteen patients (26 examinations) with endometrial lesions who had undergone ^{18}F-fluorodeoxyglucose (FDG) and ^{18}F-fluoroestradiol (FES) PET/MRI of the pelvic region within 1 month were retrospectively evaluated. PET list-mode data obtained by simultaneous acquisition with MRI were analysed using an offline workstation. The start and end times of each MR sequence were recorded by investigating the active triggers for each MRI sequence. PET image reconstruction was performed based on the obtained start and end times to generate time-synchronised PET/MRI fusion images. The Bayesian penalised likelihood algorithm with adaptive β values was used for PET image reconstruction. The ROI was placed on the endometrial lesion on MRI, which was superimposed on the time-synchronised PET to measure the mean SUV (SUVmean) and total lesion glycolysis (TLG). For comparison, the ROI was placed based on PET/MRI fused images without time synchronisation (overlapped PET/MRI). Two radiologists/nuclear medicine physicians visually rated the fusion image accuracy of the overlapped PET/MRI and time-synchronised PET/MRI on a 7-point scale. The diagnostic performance of SUVmean and TLG measured by overlapped and time-synchronised PET/MRI was compared using the ROC analysis based on the histopathologically determined reference standard. The fusion image misregistration of overlapped and time-synchronised PET/MRI was compared using the Wilcoxon signed-rank test. ***Results:*** The FDG/FES ratio of SUVmean and TLG measured by time-synchronised PET/MRI (area under the curve [AUC] = 0.833 and 0.833, respectively) had higher diagnostic performance than that of overlapped PET/MRI (AUC = 0.750 and 0.778, respectively). The score of misregistration for synchronised PET/MRI (0.256 ± 0.568) was lower than that of overlapped PET/MRI (0.679 ± 1.179). ***Conclusion:*** Quantitative FDG and FES PET evaluation could be performed using time-synchronised PET/MRI. The FDG/FES ratio of SUVmean by time-synchronised PET/MRI had a higher diagnostic performance than that by overlapped PET/MRI in distinguishing between benign and malignant endometrial lesions.

EP-0309

Comparing CECT, 18F-FDG PET and 68Ga-FAPI PET derived peritoneal carcinomatosis index (PCI) in primary ovarian cancers.

S. Singh, *K. Verma, A. Singh;*
Globe Healthcare, Lucknow, INDIA.

Aim/Introduction: To compare peritoneal carcinomatosis index (PCI) derived from CECT, 18F-FDG PET and 68Ga-FAPI PET in patients with primary ovarian neoplasm with peritoneal metastases planned for cytoreductive surgery.To investigate the change in management due to difference in findings among these modalities. ***Materials and Methods:*** This is a single center prospective study which included 30 patients with newly diagnosed carcinoma ovary. All patients underwent staging workup by 18F-FDG PET/CT and 68Ga-FAPI PET/CT on different days. Intravenous iodinated contrast was used only in one of the CT scans. Low dose non contrast CT was done when diagnostic CECT was obtained in previous PET study. Peritoneal carcinomatosis index (PCI) was calculated by Sugarbaker PCI index method for each modality. PCI scores were compared among CECT, FDG PET and FAPI PET images, findings were reviewed to note any change in patient management due to PET findings. Imaging was performed on digital PET-CT scanner uMI550 (United Imaging). ***Results:*** Mean age of the patients was 42 years (range 30 to 55). Serous adenocarcinoma was the most common histopathological subtype (21/30) followed by mucinous and clear cell carcinomas. The median PCI scores for CECT, FDG PET and FAPI PET were 18, 24 and 29 respectively and the difference was statistically significant ($p<0.05$). 10 patients (33%) had change in management plan in form of introduction of neoadjuvant chemotherapy due to high PCI score on FDG and FAPI PET findings. FAPI PET PCI score alone changed treatment decision in 6 (20%) patient due to additional lesions. In PET studies, SUV values in peritoneal disease were higher with FAPI PET than FDG. ***Conclusion:*** 68Ga-FAPI PET results in higher PCI score than 18F-FDG PET and introduction of FDG/FAPI studies can change management in upto 33% of patients of carcinoma ovary.

EP-0310

Investigation of the Effect of Hormonal Therapy on Endometrial FDG Uptake in Postmenopausal Women

R. Nakamoto, *M. Yakami, T. Nobashi, H. Isoda, Y. Nakamoto;*
Kyoto University Hospital, Kyoto, JAPAN.

Aim/Introduction: Hormone replacement therapy (HRT) with estrogen for women suffering from menopause has been reported to be associated with a significantly increased endometrial thickness, compared with the thickness in control subjects, when assessed sonographically. However, the effect of hormonal therapy on FDG uptake in the endometrium has not been fully investigated. In this study, we examined the effect of hormone therapy, especially HRT, on FDG uptake in the endometrium of postmenopausal women. ***Materials and Methods:*** Postmenopausal women (no history of gynecological malignancies) aged 45 years and older receiving HRT or tamoxifen for breast cancer treatment (antitumoral hormonal therapy, AHT) who underwent PET/CT screening between June 2016 and April 2023 at our institution were enrolled (HT group). Menopausal status was determined by interview and/or blood data (E2<5pg/ml, FSH>40mIU/ml). As a control group, women not receiving hormonal therapy who had undergone PET/CT screening within 5 years after menopause were enrolled. The endometrial uptake (SUVmax) and 4 levels of the visual score for endometrial uptake (4: significant uptake, 3: recognizable, 2: somehow recognizable, 1: unrecognizable) in both groups were compared. The relationship between endometrial uptake and duration (months) of HRT was examined. ***Results:*** There was a significant difference in FDG uptake of the endometrium between the HT and Control groups (median SUVmax: 2.3 vs 1.9, $P = 0.0021$) (median Visual score: 2 vs 1, $P < 0.0001$). In the HT group, FDG uptake in the endometrium was higher in women receiving HRT (n=14) than in women receiving AHT (n=7) (median SUVmax: 2.45 vs 1.9, $P = 0.0362$) (median Visual score: 3 vs 1, $P = 0.0226$). A significant correlation was found between endometrial uptake and duration of HRT ($\rho = 0.55$, $P = 0.042$). Five women on HRT had high endometrial uptake (range of SUVmax, 3.7-9) (Visual score 4), one of whom was found to have endometrial thickening sonographically and no abnormality on histological examination, while another had increased endometrial

uptake on PET/CT screening the following year (SUVmax, 3.7→11.9) and subsequent endometrial histology revealed endometrial cancer. ***Conclusion:*** There was a trend toward higher FDG uptake in the endometrium of postmenopausal women on HRT for longer periods. We might be careful with the increased endometrial uptake during HRT with estrogen, which contributes to the development of endometrial cancer. ***References:*** Lerman H, et al. Normal and abnormal 18F-FDG endometrial and ovarian uptake in pre- and postmenopausal patients: assessment by PET/CT. J Nucl Med. 2004 Feb;45:266-71.

EP-0311

Treatment response evaluation using FDG-PET/CT predicts survival in women with locally advanced cervical cancer

M. Markus[1], *H. Sartor*[2], *M. Bjurberg*[3], *E. Trägårdh*[1];
[1]*Clinical Physiology and Nuclear Medicine, Malmö, SWEDEN,*
[2]*Radiology Diagnostics, Malmö, SWEDEN,* [3]*Department of Hematology, Oncology and Radiation Physics, Malmö, SWEDEN.*

Aim/Introduction: Cervical cancer is the fourth most common female malignancy worldwide. [18F]-fluorodeoxyglucose (FDG) positron emission tomography with computed tomography (PET-CT) is routinely performed in patients with advanced cervical cancer for staging and evaluation of treatment response. The maximum standardised uptake value (SUVmax) is the most used PET parameter in clinical routine but more advanced metabolic parameters (e.g metabolic tumour volume (MTV) and total lesion glycolysis (TLG)) may better predict survival. Our aim was to investigate the prognostic value of treatment response assessment for SUVmax, MTV and TLG, in women with locally advanced cervical cancer, using overall survival as outcome measure. ***Materials and Methods:*** Women with locally advanced cervical cancer referred for radiochemotherapy at the Department of Oncology at Skåne University Hospital, Sweden 2011-2019 and who underwent one PET-CT scan at baseline one at 6-month follow-up after treatment were included. Treatment response on PET-CT was assessed according to the European Organization for Research and Treatment of Cancer criteria, using SUVmax, MTV and TLG for comparison. The different treatment response outcomes were complete metabolic response (CMR), progressive metabolic disease (PMD), or either partial metabolic regression (PMR) or stable disease (SD). The response outcomes were correlated to overall survival using Cox regression analysis, with CMR as reference. Also, C-index was used to visualize the predictive potential of the different measures. ***Results:*** A total of 133 patients were included. Age- and clinical stage-adjusted analyses showed a statistically significant association ($p<0.001$) between treatment response and overall survival for SUVmax (hazard ratio (HR) for PMD 16, HR for PMR/SD 4.0), MTV (HR for PMD 16, HR for PMR/SD 2.9) and TLG (HR for PMD 16, HR for PMR/SD 2.9). Also, C-index values from adjusted Cox models were comparable between the PET-parameters (SUVmax 0.838, MTV and TLG 0.857). ***Conclusion:*** Treatment response evaluation assessed with FDG-PET/CT is predictive of overall survival. The results were similar for both SUVmax, MTV and TLG.

EP-0312

MRI and 18F-FDG PET/CT interrelationship in the postradiotherapy cervical carcinoma early response assessment

S. Lucic[1,2], *M. Spirovski*[1,2], *J. Licina*[1,2], *D. Stojanovic*[2], *A. Peter*[2], *M. A. Lucic*[1,2];
[1]*Medical Faculty, University of Novi Sad, Novi Sad, SERBIA,*
[2]*Oncology Institute of Vojvodina, Sremska Kamenica, SERBIA.*

Aim/Introduction: Adequate assessment of response and timely detection of tumour recurrence after radiotherapy (RT) treatment is of great importance. Although there is no consensus about the time interval until the first diagnostic examination after RT, MRI as a reliable diagnostic tool is usually performed in first 2-3 months after the end of treatment. Aim of this study was to determine whether 18F-FDG PET/CT could improve early post-RT diagnostic evaluation. ***Materials and Methods:*** Twenty-eight female patients (mean age 55.43±11,78; range 35-85) with locally advanced cervical cancer FIGO stage IIB-IVA treated with combined external beam radiation therapy (EBRT) and intracavitary brachytherapy with concomitant chemotherapy were included in the study. Pelvic and abdominal MRI exam were performed 2-4 months after treatment, followed by 18F-FDG PET/CT within one month after MRI in order to estimate early therapy effects. Studies results were considered as positive, negative and equivocal for rest/recurrent tumour presence, that was proven by control MRI exam done at least six months afterwards. Data sets were statistically analysed with two-tailed Pearson's correlation coefficient (r), and Spearman's rank correlation coefficient (ρ), with the level of confidence determined at $p<0.05$. Sensitivity, specificity, positive predictive value (PPV), negative predictive value (NPV) and diagnostic accuracy of both techniques were calculated. ***Results:*** Concordant results in 20/28 (71,4%) patients indicated good statistical correlation. In 10/28 (35,7%) patients PET/CT additionally revealed distant metastasis presence. Good correlation was determined for both MRI and 18F-FDG PET/CT results ($r=0.443$ p 0.018 and $\rho=0.439$ p 0.02). In comparison to the 6 months MRI control study, initial MRI results were significantly correlated ($r=0.405$; $p=0.033$ and $\rho=0.457$; $p=0.015$), but 18F-FDG PET/CT results did not demonstrate significant correlation ($r=0.122$; $p=0.537$ and $\rho=0.159$; $p=0.418$). Sensitivity, specificity, PPV, NPV, and diagnostic accuracy of MRI were determined at 66.7%, 70.6%, 54.5% and 80%, respectively, while for PET/CT the values were 60%, 55.5%, 42.6% and 71.4%, respectively. ***Conclusion:*** The ability to detect early therapy response was calculated as slightly lesser for both MRI and PET/CT than we assumed. Even though PET/CT didn't have significant impact on diagnostic confidence, by providing the additional information, it changed the treatment approach in more than one-third of the patients, allowing us to conclude that, subsidiary to MRI, 18F-FDG PET/CT can be helpful in post-RT cervical carcinoma evaluation.

EP-0313

Utility of 18F FDG PET/CT in rare gynaecological malignancies

A. Nair S, *V. Rangarajan, S. Shah, A. Agrawal, N. Purandare, A. Puranik, S. Choudhury;*
Tata Memorial Hospital, Mumbai, INDIA.

Aim/Introduction: Gynaecological malignancies are one of the most common cancers in women, with a vast majority being of adeno or squamous histopathologies, and the variations of histopathology is associated with a variation in prognosis and management. The consensus of management are well established for the more common histopathological variants, whereas the data regarding the management of infrequently encountered pathologies like uterine sarcoma, pelvic PNET (peripheral neuroectodermal tumour) are limited due to the rarity of these tumours. ***Materials and Methods:*** This is a retrospective, observational study done in 71 patients with rare gynaecological malignancies (gynaecological malignancies excluding adeno and squamous histopathologies) in whom 18-F FDG PET/CT was done at staging,

response evaluation or evaluation for suspected recurrence. A vast majority of the cases analysed were sarcomas (76%) followed by PNETs (15.5%) and neuroendocrine carcinomas (NEC) (8.5%). The sensitivity, specificity, negative predictive value, positive predictive value and accuracy of 18F FDG PET/CT was calculated for both nodal and distant metastatic lesions in these malignancies with respect to histopathological reports/clinical findings/ follow up data as the standard. ***Results:*** In the 71 patients included, indications for PET/CT were postoperative cancer staging (70.4%), suspected recurrence (15.5%) and post chemotherapy/radiation therapy response evaluation (14.1%). Histopathologically, 54 patients had sarcoma, 11 had PNET and 6 had NEC (neuroendocrine carcinoma) of the genital tract. FDG PET/CT showed 93.3% sensitivity,87.5% specificity, and 88.7% accuracy for nodal metastases. For distant metastases, the sensitivity is 95.5%, specificity is 80.8% and accuracy is 90.1%. Total percentage of extrapelvic metastases: 69.65%. ***Conclusion:*** 18F FDG has a high sensitivity, specificity and accuracy for the evaluation of rare histopathological subtypes of gynaecological malignancies. The detection of extrapelvic metastases in cases considered to be locoregional disease may result in a change of management in these patients who were previously imaged by locoregional standard imaging modalities.

EP-0314

Prognostic Role of F-18 FDG PET in Uterine Cervical Cancer Patients: 10 Years Experience

C. Soydal[1], *M. H. Baltacioglu*[2], *M. Araz*[1], *S. Taskin*[3], *N. O. Kucuk*[1], *U. F. Ortac*[3];
[1]*Ankara University Medical School, Department of Nuclear Medicine, Ankara, TÜRKIYE,* [2]*Sbu Trabzon Kanuni Training and Research Hospital Department of Nuclear Medicine, Trabzon, TÜRKIYE,* [3]*Ankara University Medical School, Department of Gynecology and Obstetrics, Ankara, TÜRKIYE.*

Aim/Introduction: The aim of this study was to investigate the role of F-18 FDG PET/CT at the time of staging in predicting the prognosis of patients with uterine cervical cancer. ***Materials and Methods:*** Thirty-two women (mean age: 52.7 ± 12.6) who underwent the F-18 FDG PET/CT for staging between January 2012 and June 2022 of uterine cervix cancer were recruited the study retrospectively. PET/CT images were re-evaluated and metabolic parameters such as SUVmax, SUVmean, metabolic tumor volume (MTV) and total lesion glycolysis (TLG) were calculated for the primary lesion, lymph nodes and distant metastases. Images were also classified according to the presence or absence of pathologic involvement of pelvic and paraaortic lymph nodes. The progression-free and overall survival times of the groups above and below the median value according to metabolic parameters and the groups with and without pelvic-paraaortic lymph node involvement were compared using Kaplan-Meier Analysis. ***Results:*** Primary tumor of 27 (84%) patients were F-18 FDG avid. Medians for SUVmax, SUVmean, MTV and TLG of primary tumors were calculated as 12.4, 6.1, 13.2 cm3 and 87.8 gr/mLxcm3 respectively. Pathological uptake was detected in pelvic 14 (44%) patients and in paraaortic lymph nodes in 3 (10%) patients. Medians for total MTV and TLG were 21.7 cm3 and 91.1 gr/mLxcm3. Disease progression was detected in 7 (22%) of patients within median 20.9 (min-max: 3-82) months follow-up period. The only significant PET parameter to predict PFS was SUVmax of primary tumor (p=0.038). During follow-up period 8 patients died. SUVmax (p=0.007), MTV (p=0.036), TLG (p=0.001) of primary tumor, presence of pathological uptake on pelvic or paraaortic lymph nodes (p=0.015), total MTV (p=0.047) and total TLG (p=0.001) were found statistically significant PET parameters to predict OS. ***Conclusion:*** F-18 FDG PET/CT has a limited role in the evaluation of the primary lesion in uterine cervical cancer staging and is especially recommended for the evaluation of lymph node metastases. Although it cannot give an idea about myometrial and parametrial invasion of the primary lesion, F-18 FDG uptake level can give an idea about the level of differentiation of the disease. There is evidence that metabolic parameters obtained from PET imaging have a prognostic value in many malignancies. However, from our analysis we conclude that metabolic parameters derived from PET imaging may have a role in predicting overall survival in patients with cervical cancer.

EP-0315

Does Peritoneal Metastasis Evaluation with 18F-FDG PET/MRI Contribute to Prognosis Prediction in Patients with Ovarian Cancer

M. Baltacioglu[1], *C. Soydal*[2], *M. Araz*[2], *D. Kuru Oz*[3], *N. O. Kucuk*[2];
[1]*Sbu Trabzon Kanuni Training and Research Hospital Department of Nuclear Medicine, Trabzon, TÜRKIYE,* [2]*Ankara University Medical School Department of Nuclear Medicine, Ankara, TÜRKIYE,* [3]*Ankara University Medical School, Department of Radiology, Ankara, TÜRKIYE.*

Aim/Introduction: The entity of peritoneal metastases in patients with ovarian cancer significantly affects the prognosis. Timely and accurate detection of ovarian cancer recurrences is important for disease survival. In this study, in patients who underwent 18F-FDG PET/CT and 18F-FDG PET/MRI for peritoneal metastasis evaluation in ovarian cancer; We aimed to compare the effects of both imaging modalities on prognosis. ***Materials and Methods:*** 45 patients (median age: 58.1 years; min-max: 33-79 years) with ovarian cancer who developed elevated serum Ca-125 during follow-up after primary surgery and underwent 18F-FDG PET/CT followed by PET/MR imaging for peritoneal disease restaging were prospectively included in this study. Peritoneal recurrences were evaluated on both imaging modalities and peritoneal carcinomatosis index (PCI) was calculated for each patient. PET/CT and PET/MR images were evaluated on a patient basis for the presence and localization of peritoneal recurrences. After peritoneal disease staging by PET/CT and PET/MRI, patients received the treatment deemed appropriate by their clinicians and were followed up for survival analysis. The date of death was noted in exitus patients. ***Results:*** In patient-based analysis; PET/MRI was positive in 33 patient (73%), while PET/CT was positive in 27 patient (60%) (p=0.03). The median PCI score was 2 (min-max:0-26) in PET/CT and 4 (min-max:0-26) in PET/MRI (p<0.001). In Kaplan Meier survival analysis, FIGO stage (p<0.001), number of peritoneal lesions detected in PET/CT (p=0.017), PCI score in PET/CT (p=0.014), abdominopelvic lymph node SUVmax value in PET/CT (p=0.007), peritoneal lesion SUVmax value in PET/MRI (p=0.035), abdominopelvic lymph node SUVmax value in PET/MRI (p=0.047) and PCI score in PET/MRI (p=0.027) were found to be parameters associated with overall survival. ***Conclusion:*** Although PET/MRI is more successful than PET/CT in showing peritoneal metastases, peritoneal uptake in PET/CT has been associated with prognosis. This suggests that PET/CT can be used for prognosis in patients with recurrent ovarian cancer.

EP-0316

Role of Radiomics Applied to Baseline 18F-FDG PET/CT in Locally Advanced Cervical Carcinoma Patients Treated with Combined Chemoradiotherapy

G. Mathoux[1], *L. Monaco*[2], *E. De Bernardi*[1], *G. Di Martino*[3], *C. Crivellaro*[2], *F. Elisei*[2], *M. Musarra*[2], *L. Bazzano*[1], *C. Landoni*[1,2,4], *L. Guerra*[1,2,4], *C. Messa*[1,4];
[1]*Università degli Studi di Milano-Bicocca, Monza, ITALY,* [2]*Nuclear Medicine Department, Fondazione IRCCS San Gerardo dei Tintori, Monza, ITALY,* [3]*UOC Gynaecology, Fondazione IRCCS San Gerardo dei Tintori, Monza, ITALY,* [4]*Tecnomed Foundation, Monza, ITALY.*

Aim/Introduction: Cervical carcinoma (CC) is one of the most common malignancies in women. Locally-advanced CC (LACC) are treated with pelvic external beam radiation (EBRT) in combination with cisplatin-based chemotherapy and subsequent brachytherapy, with a recurrence rate of 40%. The aim of this study is to evaluate whether radiomics, applied to baseline 18F-FDG-PET in LACC patients treated with chemoradiotherapy (CRT), can contribute in predicting response to therapy and in evaluating Disease-Free Survival (DFS) compared to standard clinical and radiological assessment. ***Materials and Methods:*** 56 patients with LACC, who performed 18F-FDG-PET/CT before CRT were included. Primary tumor volumes were delineated using iterative thresholds with PETVCAR™.A total of 157 radiomics features (intensity, shape, and texture) were extracted (according to IBSI recommendation) and evaluated for their prognostic value. A univariate analysis was performed to examine the association between radiomic features and response to therapy (clinical and imaging: defined as complete vs. non-complete) and DFS. In addition, Receiver Operating Characteristic (ROC) analyses were conducted.To investigate whether the addition of radiomic features could enhance the prediction of DFS compared to lymph-node invasion alone, a multivariate Cox analysis was carried out by combining radiomic features with lymph-node invasion.Kaplan-Meier curves were used to describe DFS stratified according to metabolic response, lymph-node invasion, and radiomic features. ***Results:*** In univariate analysis Szm Lzlge (p-value=0.007; AUC=0.77) and Cm Suv Avg (p-value=0.012; AUC=0.75) are strongly correlated with metabolic response. DFS is significantly correlated with metabolical response (p<0.001) and lymph-node invasion (p=0.034). No correlation was found between standard PET values (SUVmax, SUVmean, SUVpk, MTV and TLG) and these parameters. Applying Multivariate Cox Proportional Hazard Regression, the only improvement in predicting DFS without reaching statistical significance is obtained by adding the radiomic feature Szm Lzlge to lymph node invasion (p=0.077).Comparing the survival curves, patients with lymph-node metastases (N+) and Szm Lzlge<0.0198 had an oncological outcome overlapping with patients with negative lymph nodes (p<0.001). Conversely, N+ patients and Szm Lzlge >0.0198 had a 5.3 times higher probability of disease recurrence. ***Conclusion:*** Radiomics features are correlated to response to CRT in LACC and can improve the prediction of DFS, identifying high-risk patients when combined with standard prognostic factors. These results suggest that a more personalized approach to treatment planning could be achieved by identifying high-risk patients at the time of diagnosis.

EP-0317

Potential of baseline and early response FDG-PET/MRI to predict radiotherapy outcome in uterine cervical squamous cell carcinoma - a pilot study

S. Strandberg[1], *J. Jonsson*[1], *M. Zarei*[1], *K. Aglund*[1], *L. Blomqvist*[2], *K. Söderkvist*[1], *B. Zackrisson*[1];
[1]*Department of Radiation sciences, Umea University, Umea, SWEDEN,* [2]*Department of Molecular Medicine and Surgery, Karolinska Institute, Solna, SWEDEN.*

Aim/Introduction: Assessment of early response using FDG-PET/MRI might improve prediction of radiotherapy (RT) outcome in uterine cervical squamous cell carcinoma (CSCC).The aim of this study was to investigate the association between FDG-PET/MRI features and outcome in CSCC. ***Materials and Methods:*** In this pilot study, all eligible participants from the prospective clinical trial MORRIS - Multimodal Monitoring of Radiotherapy Response in Squamous Cell Cancer (MORRIS; NCT02379039), with primary CSCC and completed imaging work-up, were included. The imaging consisted of baseline FDG-PET/MRI performed one week before start of RT and early treatment response FDG-PET/MRI performed on day 8 of RT. PET/MRI was performed with an integrated PET/MRI 3.0 T scanner during 2016-2021. The imaging protocols for FDG-PET and pelvic MRI were designed according to current clinical routines. From blinded single modality assessment of T2-weighted (T2W) sequences and semi-quantitative assessment with apparent diffusion coefficent (ADC) in MRI, gross tumor volume (GTV) of the primary tumors was manually delineated at baseline and at early treatment response PET/MRI. Quantitative imaging parameters were extracted from the manual segmentations: GTV from T2W and ADC, perpendicular lesion diameters (ccxllxap) measured in T2W and ADC, SUVmax, SUVmean and functional tumor volume (FTV). Additional delta (change) parameters were calculated for early treatment response examinations. Treatment response according to RECIST 1.1 was also reported. All study participants had at least 24 months clinical follow-up. Descriptive statistics were used. ***Results:*** Of the eligible twelve CSCC study participants from the MORRIS trial, one patient was excluded due to incomplete radiology. Visual decrease in tumor size was present in 9/11 participants (range 8.2-24.6% decrease in largest diameter on T2W or ADC). Relapse occurred in 2/11, with high FTV as the most conspicuous imaging characteristic. Also 2/11, of which one relapse, had an increase in largest diameter after one week of RT. Mean change in largest tumor diameter was -9,3% (SD 9,6%), but none qualified as significant according to RECIST 1.1. ***Conclusion:*** High FDG-PET FTV at baseline as well as unfavorable response in FTV at one week after start of RT may predict non-responders to RT in CSCC. RECIST 1.1 does not seem suitable for early treatment response evaluation in CSCC treated with RT.

EP-18

e-Poster Area

B: Imaging Clinical Studies -> B1 Oncological Imaging Clinical Study -> B21 Lymphoma

EP-0318

Metabolic tumour volume in Hodgkin lymphoma - a comparison between manual and AI-based analysis

M. Sadik[1], *S. F. Barrington*[2], *J. Ulén*[3], *O. Enqvist*[4], *E. Trägårdh*[5], *B. Saboury*[6], *A. Lerberg Nielsen*[7], *A. Loft Jakobsen*[8], *J. Loaiza Gongora*[9], *J. López-Urdaneta*[1], *R. Kumar*[10], *L. Edenbrandt*[1];
[1]*Molecular and Clinical Medicine, Gothenburg, SWEDEN,* [2]*Clinical PET Centre, London, UNITED KINGDOM,* [3]*Eigenvision AB, Malmö, SWEDEN,* [4]*Eigenvision AB and Electrical Engineering, Malmö and Gothenburg, SWEDEN,* [5]*Clinical Physiology and Nuclear Medicine, Malmö, SWEDEN,* [6]*Radiology and Imaging Sciences, Bethesda, MD, UNITED STATES OF AMERICA,* [7]*Nuclear Medicine, Odense, DENMARK,* [8]*Clinical Physiology, Copenhagen, DENMARK,* [9]*Diagnostic Imaging, Oslo, NORWAY,* [10]*Nuclear Medicine, Chandigarh, INDIA.*

Aim/Introduction: Total metabolic tumour volume (tMTV) is recognised as a prognostic tool which is associated with progression-free and overall survival in Hodgkin lymphoma (HL) patients (1). Manual segmentation of tMTV however is time-consuming and subject to inter-reader variability. There is a clinical need for automated methods, which may be more objective and faster. The aim of this study was to compare tMTV, calculated using two artificial intelligence (AI)-based tools with measurements using manual segmentation by specialists as the reference. ***Materials and Methods:*** Forty-eight consecutive HL patients staged with [18F]FDG PET/CT were included. The median age was 35 years (range 7-75) and 46% of the patients were female. The tMTV was automatically measured using the AI-based tools PARS (from Siemens) and RECOMIA (recomia.org) without any manual adjustments. A group of eight nuclear medicine specialists manually segmented lesions for tMTV calculations; each of the 48 patients were independently segmented by two specialists. ***Results:*** The median of the manual tMTV was 146 cm^3 (inter quartile range (IQR) 79-568 cm^3) and the median difference between two tMTV values segmented by different specialists for the same patient was 26 cm^3 (IQR 10-86 cm^3). In 22 of the 48 patients, the manual tMTV value was closer to the RECOMIA tMTV value than to the manual tMTV value segmented by the second specialist. In 11 of the remaining 26 patients, the difference between the RECOMIA tMTV and the manual tMTV was small (<26 cm^3, which was the median difference between two manual tMTV values from the same patient). The corresponding numbers for PARS were 18 and 10 patients, respectively. ***Conclusion:*** The results of this study indicate that RECOMIA and Siemens PARS AI tools could be used without any major manual adjustments in 69% (33/48) and 58% (28/48) of patients, respectively. This demonstrates the feasibility of using AI tools to automate measurement of MTV for assessment of prognosis in clinical practice. ***References:*** 1. Barrington SF, Meignan M. Time to Prepare for Risk Adaptation in Lymphoma by Standardizing Measurement of Metabolic Tumor Burden. J Nucl Med 2019; doi:10.2967/jnumed.119.227249.

EP-0319

C-X-C Motif Chemokine Receptor 4-directed PET/CT provides improved Diagnostic Performance relative to [18F]FDG in Newly Diagnosed Patients with Marginal Zone Lymphoma

A. Kosmala[1], *S. E. Serfling*[1], *S. Schneid*[1], *T. Higuchi*[1,2], *A. Weich*[3], *C. Lapa*[4], *P. E. Hartrampf*[1], *M. Raderer*[5], *H. Einsele*[3], *A. K. Buck*[1], *M. S. Topp*[3], *J. Duell*[3], *R. A. Werner*[1,6];
[1]*Department of Nuclear Medicine, University Hospital Würzburg, Würzburg, GERMANY,* [2]*Faculty of Medicine, Dentistry and Pharmaceutical Sciences, Okayama University, Okayama, JAPAN,* [3]*Department of Internal Medicine II, University Hospital Würzburg, Würzburg, GERMANY,* [4]*Nuclear Medicine, Faculty of Medicine, University of Augsburg, Augsburg, GERMANY,* [5]*Department of Internal Medicine I, Medical University Vienna, Vienna, AUSTRIA,* [6]*Johns Hopkins School of Medicine, The Russell H Morgan Department of Radiology and Radiological Sciences, Baltimore, MD, UNITED STATES OF AMERICA.*

Aim/Introduction: C-X-C motif chemokine receptor 4 (CXCR4) is overexpressed in marginal zone lymphoma (MZL) and thus, may emerge as a theranostic target. We aimed to evaluate the diagnostic performance of CXCR4-targeting [68Ga]Ga-PentixaFor when compared to [18F]FDG PET/CT in newly diagnosed MZL. ***Materials and Methods:*** 33 MZL patients (subtypes: nodal, n=20; extranodal, n=12; splenic, n=1) received [68Ga]Ga-PentixaFor and [18F]FDG PET/CT within median 2 days, without treatment between scans. We performed a visual and quantitative analysis of the total lymphoma volume by identifying target lesions (TL). For the latter investigation, maximum/peak standardized uptake values ($SUV_{max/peak}$), and target-to-background ratio (TBR) were calculated. TBR was defined as SUV_{peak} from TL divided by SUV_{mean} from blood pool serving as reference. ***Results:*** [68Ga]Ga-PentixaFor identified MZL manifestations in 33 (100%) patients (vs. [18F]FDG, 25/33 patients [75.8%]), and substantially more MZL manifestations were evident on CXCR4-directed imaging compared to [18F]FDG (274 vs. 154). For a quantitative head-to-head comparison, we identified 143 identical TL on both scans. For concordant lesions, SUV_{peak} on [68Ga]Ga-PentixaFor was 7.1±4.0, which was significantly elevated when compared to [18F]FDG (5.3±4.3, P<0.0001). Similar results were observed for SUV_{max} ([68Ga]Ga-PentixaFor, 11.2±5.4 vs. [18F]FDG, 7.8±5.7, P<0.0001), indicative that a substantial portion of patients may be eligible for CXCR4-directed therapy. TBR was also approximately 1.7-fold higher on [68Ga]Ga-PentixaFor (median, 3.8) when compared to [18F]FDG (2.1, P<0.0001), suggestive for an improved contrast on chemokine receptor PET. ***Conclusion:*** CXCR4-directed PET/CT identifies more sites of disease in patients with newly diagnosed MZL. On a quantitative assessment, a substantial portion of patients would also be suitable for "cold" or "hot" CXCR4-targeted treatment. Last, TBR-derived image contrast was markedly higher on [68Ga]Ga-PentixaFor PET, thereby suggesting improved diagnostic read-out when compared to [18F]FDG.

EP-0320

Development of prediction models for treatment response and prognosis in patients with diffuse large B-cell lymphoma based on 18F-FDG PET radiomics

Y. Zhou*;*
West China Hospital, Chengdu, CHINA.

Aim/Introduction: Biomarkers that can accurately predict outcome in diffuse large B-cell lymphoma (DLBCL) patients are urgently needed. Radiomics features extracted from baseline [^{18}F]-FDG PET/CT scans have shown promising results. This study aims to assess the influence of lesion selection and segmentation methods on the radiomics features of DLBCL in treatment response and prognosis prediction. ***Materials and Methods:*** A total of 533 patients pathologically diagnosed with DLBCL were enrolled. 112 radiomics features (n=3 conventional PET, n=12 morphology, n=43 intensity, n=54 texture) were extracted for all individual lesions and at patient level, where all lesions were aggregated into one VOI. Three lesion selection approaches were tested (largest or hottest lesion, patient level). Manual segmentation and four semiautomatic segmentation methods were applied (SUV threshold of 2.5 [SUV2.5], SUV threshold of 4.0 [SUV4.0], 25% of SUVmax, and 41% of SUVmax). To quantify the agreement between features extracted from different segmentation methods, the intraclass correlation (ICC) agreement was calculated for each method compared with SUV4.0. The predictive value of all models was tested using a fivefold cross-validation approach with 50 repeats, yielding the mean cross-validated AUC (CV-AUC) for all lesion selection combined with segmentation methods using eXtreme gradient boosting, which were compared by Delong test. Additionally, the relative importance of individual radiomics features was determined. ***Results:*** Both in treatment response and prognosis prediction, the percentage of features yielding an ICC of at least 0.75, compared with the SUV4.0 segmentation, was lowest for 41% of SUVmax both at the patient level and for

the hottest or largest lesion, with 43%, 59%, 56% and 46%, 57%, 57% of the features yielding an ICC of at least 0.75, respectively. In treatment response prediction, CV-AUC ranged between 0.606 and 0.768 at the patient level, between 0.618 and 0.704 and between 0.616 and 0.666 at the hottest or largest lesion level, respectively. In prognosis prediction, CV-AUC ranged between 0.583 and 0.699 at the patient level, between 0.584 and 0.636 and between 0.633 and 0.705 at the hottest or largest lesion level, respectively. Texture features had the highest relative importance in most of these models. However, the prediction performance gap was not significant for each model ($p > 0.05$). ***Conclusion:*** Even though there are differences in the actual radiomics feature values derived and selected features among lesion selection and segmentation methods, there is no substantial difference in the predictive power of radiomics features among lesion selection and segmentation methods.

EP-0321

Diagnostic performance of whole-body [18F]FDGPET/MRIwith diffusion-weighted imaging for detecting bone marrow involvement in lymphomas

X. Chen, *M. Wei, T. Yuan, B. Yu, N. Zhou, Z. Hua, Z. Yang, X. Wang; Peking University Cancer Hospital & Institute, Beijing, CHINA.*

Aim/Introduction: This study aimed to investigate the diagnostic efficiency of whole-body [18F]FDG PET/MRI with diffusion-weighted imaging for detecting bone marrow involvement (BMI) in lymphomas. ***Materials and Methods:*** This single-centre prospective study recruited patients with different lymphoma pathological subtypes. Each patient underwent [18F] FDG PET/MRI and BMB. The diagnostic performance of FDG PET/MRI was assessed using visual evaluation and quantitative measurements. ***Results:*** Of the 120 patients, 39 (32.5%) had BMI (15 focal BMI and 24 diffuse BMI). PET/MRI images were divided into three groups (double-positive, double-negative and single-positive) according to visual evaluation. The accuracy of each group was 100%, 94.1% and 56.7%, respectively. The sensitivity, specificity, PPV and NPV were 66.7%, 90.1%, 76.5% and 84.9% for PET and 79.5%, 88.9%, 77.5% and 90.0% for MRI, respectively. The sensitivity and specificity of PET/MRI reached 89.7% and 100%, respectively, when compared with PET alone ($p = 0.004$) and MRI alone ($p = 0.004$). Similar results were obtained through quantitative measurements. The vertebral SUVmax, lesion-to-mediastinum ratio (LMR), lesion-to-liver ratio and ADCmean were significantly different between the lymphomas with BMI(+) and BMI(–) ($p < 0.05$). The strongest diagnostic factor of BMI was the vertebral LMR, with a cut-off value of 2.19. A moderate correlation was observed between vertebral LMR and ADCmean ($r = 0.536$, $p < 0.01$). ***Conclusion:*** WB [18F]FDG PET/MRI with DWI is a promising method for improving sensitivity and specificity by visual evaluation or quantitative parameters and stratifying the BMI risk of patients with lymphoma.

EP-0322

A focus on the impact of spleen involvement in total metabolic tumor volume measurements in Diffuse Large B-Cell Lymphoma patients.

L. Rebaud[1,2], *N. Capobianco*[3], *K. Girum*[2], *A. Cottereau*[4], *F. Morschhauser*[5], *B. Spottiswoode*[6], *I. Buvat*[2]; [1]*Siemens Healthcare SAS, Courbevoie, FRANCE,* [2]*LITO laboratory, U1288 Inserm, Institut Curie, University Paris-Saclay, Orsay, FRANCE,* [3]*Siemens Healthcare GmbH, Erlangen, GERMANY,* [4]*Cochin University Hospital, AP-HP, Department of Nuclear Medicine, Paris, FRANCE,* [5]*Service des Maladies du Sang, CHU Lille, Lille, FRANCE,* [6]*Siemens Medical Solutions UNITED STATES OF AMERICA, Inc., Knoxville, TN, UNITED STATES OF AMERICA.*

Aim/Introduction: Quantifying Total Metabolic Tumor Volume (TMTV) from FDG PET/CT in Diffuse Large B-Cell Lymphoma (DLBCL) patients has sparked a debate on the inclusion of diffuse spleen uptake in TMTV measurement. Whether the uptake is due to an immune response or to tumor cells is not always easy to determine. This study aimed to explore the impact of excluding the spleen from TMTV measurements on the prognostic value of TMTV in DLBCL patients. ***Materials and Methods:*** A cohort of 375 patients diagnosed with DLBCL from two clinical trials, NCT01122472 and NCT00498043, was investigated. Tumors were segmented by experienced physicians, and the spleen was automatically segmented using TotalSegmentator[1], with subsequent manual correction in the rare cases of incorrect segmentation. For each patient, TMTV and Total Metabolic Tumor Volume Outside the Spleen (TMTVOS) were calculated. The cohort was divided into two groups based on the presence (SI) or absence (NSI) of spleen involvement (either focal or diffuse). The correlation between TMTV and TMTVOS was assessed using Spearman's correlation coefficient. Cutoff values that maximize Youden's index for 2-year Progression-Free Survival (PFS) and 2-year Overall Survival (OS) prediction were determined, and the significance of differences in survival rates was tested (log-rank tests). ***Results:*** In the total patient cohort, 127 patients had spleen involvement, with tumor volume in the spleen accounting for 26% of TMTV on average. TMTV and TMTVOS were strongly correlated in both the entire patient cohort ($r=0.94$) and the SI group ($r=0.86$). Median TMTV and TMTVOS were significantly higher in the SI group (662 mL and 414 mL, respectively) compared to the NSI group (186 mL). SI patients demonstrated significantly lower PFS ($p=0.04$) and OS ($p=0.04$) compared to NSI patients. Optimal cutoffs for PFS were 308 mL for TMTV and 316 mL for TMTVOS. For OS, optimal cutoffs were 388 mL for TMTV and 336 mL for TMTVOS. High TMTV and low TMTV groups had significantly different survival (PFS: $p<0.01$; OS: $p=0.01$). Similarly, high TMTVOS and low TMTVOS had significantly different survival (PFS: $p<0.01$; OS: $p=0.01$). No significant differences were found in the survival of high TMTV and high TMTVOS groups (PFS: $p=0.67$; OS: $p=0.98$), nor between low TMTV and low TMTVOS groups (PFS: $p=0.83$; OS: $p>0.99$). ***Conclusion:*** While spleen involvement is predictive of PFS and OS in DLBCL patients, TMTV excluding spleen involvement remains predictive, although this exclusion impacts the optimal cut-off value. ***References:*** [1] Wasserthal, et al., arXiv, 2022;2208.05868

EP-0323

The Role Of Baseline 18F-FDG PET/CT Metrics And Radiomics Features In Predicting Primary Gastric Lymphoma Diagnosis

A. Calabro', *D. Albano, F. Dondi, P. Bellini, A. Tucci, F. Bertagna; ASST Spedali Civili of Brescia, University of Brescia, Brescia, ITALY.*

Aim/Introduction: Diffuse Large B-Cell Lymphomas (DLCBL) and mucosa-associated lymphoid tissue (MALT) are the two most common primary gastric lymphomas (PGLs), but have strongly different features. DLBCL are more aggressive, are frequently diagnosed at an advanced stage and have a poorer prognosis. The aim of this retrospective study was to investigate the usefulness of fluorine-18-fluorodeoxyglucose positron emission tomography/CT (^{18}F-FDG PET/CT) metrics and radiomics features (RFs) in predicting the final diagnosis of patients with PGLs. ***Materials and Methods:*** Patients with newly diagnosed PGLs who underwent pre-treatment ^{18}F-FDG PET/CT were included. We reviewed and analyzed the main clinical, epidemiological and PET/CT features to predict the final diagnosis. PET images were qualitatively and

semi-quantitatively analyzed by deriving maximum standardized uptake value body weight (SUVbw), maximum standardized uptake value lean body mass (SUVlbm), maximum standardized uptake value body surface area (SUVbsa), lesion to liver SUVmax ratio (L-L SUV R), lesion to blood-pool SUVmax ratio (L-BP SUV R), metabolic tumor volume (gMTV) and total lesion glycolysis of gastric lesion (gTLG), total MTV (tMTV), TLG, and first-order radiomics features (histogram-related and shape related). Student's t test, Wilcoxon's rank-sum test, and χ^2 test were used to determine the statistical difference in the main continuous and categorical variables between patients with various histological subtypes. Receiver-operating characteristic (ROC) curve analyses were performed to determine the differential diagnostic values of PET parameters. A bivariate logistic regression model was performed to derive the best combination of parameters predicting the final diagnosis. ***Results:*** 91 patients with a histological diagnosis of PGL were recruited: 54 (59%) with DLBCL and 37 (41%) with gastric MALT. PGLs were FDG avid in 83 cases (90%) with a significant difference based on the histotype: 100% in DLBCL and 78% in gastric MALT.All PET/CT metrics, such as stage of disease and tumor size, were significantly higher in DLBCL than MALT; association with H. Pylori infection was more common in MALT. At univariate analysis, all PET/CT metrics were significantly higher in DLBCL than MALT lymphomas, while among radiomics features only Shape volume_vx and Shape sphericity showed a significant difference.The combination of SUVmax with L-L SUV R and L-BP SUV R was the best predictor of the final diagnosis with a AUC value greater than 0.8. ***Conclusion:*** ^{18}F-FDG PET/CT can potentially discriminate between DLBCL and MALT lymphomas with high accuracy.SUV-related features seem to be superior to volumetric (MTV and TLG) and radiomics parameters in predicting the final diagnosis.

EP-0324

18F-FDG PET/CT radiomics features and MYC protein expression predict progression in Diffuse Large B-cell Lymphoma

C. Cui, *B. Li, X. Mu, Z. Wu;*
SXMU, Tai Yuan, CHINA.

Aim/Introduction: The prognosis of diffuse large B-cell lymphoma (DLBCL) varies greatly among patients, in part due to genetic abnormalities such as MYC oncogene rearrangement, BCL2 and/or BCL6 gene translocation. Our study aimed to analyze the relationship between high-risk molecular protein expression and DLBCL prognosis, and to investigate the additional value of radiomics features in predicting progression in DLBCL. ***Materials and Methods:*** A retrospective analysis was performed on clinical and pathological data from 91 consecutively confirmed DLBCL patients. PET and CT radiomics features were extracted, and a total of 328 radiomics features were obtained for each patient. The least absolute shrinkage and selection operator (Lasso) was used to select the radiomics features, and the radiomics score (RS) was constructed. XGBoost ensemble learning models were constructed based on clinopathological combined with PET features, RS combined with clinopathological and PET features to predict progression after 2 years. Receiver operating characteristic (ROC) curves were drawn, and the area under the curve (AUC), sensitivity, and specificity were used to evaluate the performance of the models. The Delong test was used to compare the differences in AUC between the two models. ***Results:*** A total of 91 DLBCL patients met the inclusion criteria. There were no statistically significant differences in clinical data between the two groups . 7 radiomics features were selected by Lasso. Significant intergroup differences were observed in Ann Arbor stage, IPI, MTV, TLG, and MYC (all P <0.05). The XGBoost model based on clinopathological and PET features had an AUC of 0.74 in the training set, and 0.54 in the validation set; While the XGBoost model based on RS combined with clinopathological and PET features had an AUC of 0.81 in the training set and 0.74 in the validation set. The performance of the RS combined with clinopathological-PET model was better than that of the clinopathological-PET model (P <0.05). ***Conclusion:*** MYC is a risk factor for disease progression after 2 years in DLBCL patients. Adding radiomics features to the clinopathological-PET prediction model, including IPI and MYC, improves the model's performance and positive predictive value, thereby helping to identify poor prognosis patients. ***References:*** [1]Siegel R L, Miller K D, Wagle N S. Cancer Statistics, 2023[J]. CA Cancer J Clin, 2023,73(1):17-48.[2]Feng R, Su Q, Huang X, . Cancer Situation in China: What Does the China Cancer Map Indicate From the First National Death Survey to the Latest Cancer Registration?[J]. Cancer Commun, 2023,43(1):75-86.

EP-0325

Prognostic value of baseline 18F-FDG PET/CT metabolic tumour volume and total lesion glycolysis in Diffuse Large B Cell Lymphoma patients

A. Doma[1,2], *A. Studen*[3,4], *B. Jezeršek Novaković*[1,2];
[1]Ljubljana Oncology institute, Ljubljana, SLOVENIA, [2]Faculty of Medicine, University of Ljubljana, Ljubljana, SLOVENIA, [3]Experimental Particle Physics Department, Jožef Stefan Institute, Ljubljana, SLOVENIA, [4]Faculty of Mathematics and Physics, University of Ljubljana, Ljubljana, SLOVENIA.

Aim/Introduction: To assess the prognostic value of the ^{18}F-FDG PET/CT- based pretreatment metabolic tumour volume (MTV) and total lesion glycolysis (TLG) in Diffuse Large B Cell Lymphoma (DLBCL) patients treated with standard immunochemotherapy regimen. ***Materials and Methods:*** Baseline ^{18}F-FDG PET/CT scans of 157 histologically proven stage II-IV DLBCL patients (64 female, 93 male, median age 67.0 years; range 20.0- 85.0), without a history of other malignancies, were retrospectively analysed and correlated with overall survival (OS) data (median follow up: 3.75 years ; range 0.16- 7.12). The maximum standardised uptake values (SUV_{max}), mean standardised uptake values (SUV_{mean}), MTV and TLG of all lesions were analysed. 3- dimensional segmentations with a threshold SUV>2.5 were performed by a single experienced nuclear medicine physician using Slicer 3D software. Areas of increased bone marrow activity were identified as pathological if the infiltration was not homogeneous, indicating a reactive bone marrow. Total MTV of each patient was defined as the sum of metabolic volumes of all focal lesions. A value of <0.05 was considered statistically significant. ***Results:*** The data for OS for 3 and 5 years were available for 126 (survivors n= 94) and 81 (survivors n=46) patients, respectively. Differences between groups were analysed by the Mann-Whitney U test. 3 and 5 years OS was significantly associated with lower baseline MTV (497± 706 ml and 405± 619 ml vs. 1378± 1387 ml and 1293± 1359 ml, respectively, p<0.001) and TLG (4110± 5866 g and 3571± 4913 g vs. 10852± 10598 g and 10194± 10389 g, respectively, p<0.001). No statistical correlation was found between OS and baseline SUV_{max} and SUV_{mean}.The MTV and TLG cutoff values for predicting 3 and 5 years OS were determined by ROC analysis, and the optimal thresholds found were 480 ml (AUC: 0.72), 520 ml (AUC: 0.74), 2614 g (AUC: 0.71) and 2614 g (AUC: 0.71), respectively. By Kaplan-Meier analysis, OS at follow-up was significantly better in patients with MTV and TLG lower than the cutoff compared to patients having MTV and TLG value above the cutoff (p<0.001).

Conclusion: Baseline ^{18}F-FDG PET/CT measurements of tumour burden obtained by calculating MTV and TLG may be used in the prediction of OS in DLBCL patients prior to treatment initiation.

EP-0326

PET-Based Volumetric Biomarkers for Risk Stratification in Pediatric Hodgkin's Lymphoma

M. Dunaykin, *M. Yadgarov, G. Shestopalov, K. Chaurasiya, E. Kireeva, Y. Likar;*
Dmitry Rogachev National Medical Research Center Of Pediatric Hematology, Oncology and Immunology, Moscow, RUSSIAN FEDERATION.

Aim/Introduction: The five-point Deauville score is known to be a predictive factor in Hodgkin's lymphoma (HL), identifying children with a poor prognosis. A study by Milgrom SA et al. showed an association between baseline metabolic tumor burden, as measured by pretreatment metabolic tumor volume (MTV) and the total lesion glycolysis (TLG), with event-free survival in children and adolescents with intermediate-risk HL [1]. Despite this, it is still controversial whether baseline or interim PET/CT volumetric parameters can predict survival in children with HL.The aim of our study was to assess the prognostic significance of the baseline and interim (after two cycles of chemotherapy) MTV and TLG values for prediction of progression-free survival (PFS). ***Materials and Methods:*** This single-center retrospective study included patients with newly diagnosed HL who underwent pretherapeutic and interim PET / CT scans. The examinations were reviewed and processed with commercially available software to obtain MTV and TLG using fixed absolute (SUV 2.5) and fixed relative (41% of SUVmax) thresholds. Patients were treated in accordance with EuroNet-PHL-C1. Multivariable Cox regression was performed for clinical and radiological parameters. ***Results:*** 47 patients with HL were included (30 boys, median age 14 years, range 4-17). Median follow-up was 19 months (interquartile range 12-36), 8 patients had disease progression at longest follow-up. In multivariable analysis, only baseline MTV41% (cut-off: ≥310 ml) (hazard ratio [HR] = 26.4; 95% CI 2.3-131.1; p < 0.001) and bulky disease (HR = 5.1, 95% CI 1.1-24.7; p = 0.043) were significantly associated with worse PFS when controlling for other important clinical covariates, including age and response to chemotherapy. ***Conclusion:*** Volumetric PET/CT parameters can provide prognostic value for progression-free survival in pediatric patients with HL. Patients with baseline MTV41% ≥310 ml could be classified as at high risk of unfavorable outcome. The results of this study indicate that further research is warranted, including longer follow-up periods and larger sample sizes. ***References:*** 1. Milgrom SA, Kim J, Chirindel A, Kim J, Pei Q, Chen L, Buxton A, Kessel S, Leal J, McCarten KM, Hoppe BS, Wolden SL, Schwartz CL, Friedman DL, Kelly KM, Cho SY. Prognostic value of baseline metabolic tumor volume in children and adolescents with intermediate-risk Hodgkin lymphoma treated with chemo-radiation therapy: FDG-PET parameter analysis in a subgroup from COG AHOD0031. Pediatr Blood Cancer. 2021 Sep;68(9): e29212. doi: 10.1002/pbc.29212.

EP-0327

Prognostic value of interim FDG PET/CT in Extranodal Natural Killer/T-Cell Lymphoma, nasal type : comparison of Deauville scores, deltaSUVmax and qPET

W. Hou, *R. Tian;*
West China Hospital, Sichuan University, Chengdu, CHINA.

Aim/Introduction: This retrospective study aimed to compare prognostic value of three criteria interpretating interim FDG PET/CT for patients with Extranodal natural killer/T-cell lymphoma, nasal type (ENKTL) following a full course of asparaginase-based chemotherapy: DS, deltaSUVmax and qPET. ***Materials and Methods:*** Patients admitted to our hospital between December 2013 and December 2019, and newly diagnosed with ENKTL by pathology were enrolled in this retrospective study. DS, deltaSUVmax and qPET on interim PET/CT scans were calculated for each patient. Progression-free survival (PFS) and overall survival (OS) were used as endpoints for progression evaluation. Receiver operating characteristic(ROC) curve was used to determine the best cut-off values of qPET and deltaSUVmax for predicting PFS and OS. Univariate analysis and multivariate Cox proportional hazards models were used to assess the potential independent variables for PFS and OS. ***Results:*** One hundred and sixty-two ENKTL patients with a mean follow-up time of 50.0±22.0 months (2-89 months) were enrolled in this study. ROC curve analysis showed that the best cut-off values of qPET for predicting PFS and OS were 1.95 (AUC 0.737, P<0.001, 95% CI=0.645-0.833) and 2.17 (AUC 0.668, P =0.005, 95% CI=0.562-0.815), respectively. The best cut-off value of deltaSUVmax for predicting PFS was 43.39% (AUC 0.660, P =0.002, 95% CI=0.565-0.755). deltaSUVmax (AUC 0.604, P =0.126, 95% CI=0.485-0.722) and ΔSUVpeak (AUC 0.602, P=0.131, 95% CI=0.475-0.730) were not statistically significant to predict OS. Kaplan-Meier analysis showed DS (PFS, P <0.001; OS, P =0.004), qPET (PFS, P <0.001; OS, P <0.001), and Ann Arbor stage (PFS, P <0.001; OS, P =0.004) were significant predictors for PFS and OS, while deltaSUVmax (P<0.001) and IPI (P=0.003) were the significant predictors for PFS, but not OS. Multiple analysis showed qPET (PFS, P <0.001; OS, P =0.001) and Ann Arbor stage (PFS, P =0.003; OS, P =0.047) were independent predictors for PFS and OS. ***Conclusion:*** qPET and Ann Arbor stage were independent predictors of PFS and OS. Using qPET to analyse the interim PET/CT, combined with Ann Arbor stage, may be beneficial for distincting between patients with good and poor prognosis.

EP-0328

Deep learning-based fully automatic segmentation of whole-body [18F]FDG PET/CT images from lymphoma patients: addition of CT data has poor impact on networks performance

C. S. Constantino[1,2], *F. P. M. Oliveira*[1], *S. Leocádio*[1], *M. Silva*[1], *C. Oliveira*[1], *J. C. Castanheira*[1], *Â. Silva*[1], *S. Vaz*[1], *R. Teixeira*[1], *M. Neves*[1], *P. Lúcio*[1], *C. João*[1], *S. Vinga*[2], *D. C. Costa*[1];
[1]*Champalimaud Clinical Centre, Champalimaud Foundation, Lisbon, PORTUGAL,* [2]*INESC-ID, Instituto Superior Técnico, Universidade de Lisboa, Lisbon, PORTUGAL.*

Aim/Introduction: Segmentation is paramount for the quantification of [^{18}F]FDG avid lymphoma lesions in clinical practice and research. Our aim is to investigate the added value of anatomic low-dose CT information on the performance of a fully automatic deep learning-based (DL-based) segmentation on whole-body [^{18}F]FDG PET/CT images from lymphoma patients. ***Materials and Methods:*** A training set of 144 whole-body [^{18}F]FDG PET/CT images from lymphoma patients and the corresponding lesions' manual segmentation was obtained from The Cancer Imaging Archive [1] published by autoPET MICCAI challenge [2,3]. Images were acquired on Siemens Biograph mCT PET/CT scanner. An independent set of 65 [^{18}F]FDG PET/CT images acquired on Philips Gemini TF 16 PET/CT from lymphoma patients was used for external validation. All visible lesions were identified by nuclear medicine physicians and manually segmented independently by two experienced observers (Obs1 and Obs2) [4]. Two networks were trained using the nnU-Net framework [5]: one-channel (PET) and two-channel (PET and low-dose CT). A standard 3D U-Net architecture was chosen and hyperparameters were estimated based on heuristic rules. Training was performed with five-fold cross-validation (80% train; 20% internal validation). The

proportion of overlap between segmentations was calculated using Dice coefficient (DC). Sensitivity and positive predictive values (PPV) using manual segmentations as ground truth were calculated. Wilcoxon test was used for statistical inference (significance level of 5%). Adjusted p-values were calculated using Bonferroni method. ***Results:*** Median DC, sensitivity and PPV achieved between observers' manual segmentation and one-channel U-Net was 0.82, 0.77 and 0.91 and 0.74, 0.84 and 0.83 respectively for Obs1 and Obs2. Median DC, sensitivity and PPV achieved between observers' manual segmentation and two-channel U-Net was 0.83, 0.81 and 0.92 and 0.78, 0.86 and 0.82 for Obs1 and Obs2, respectively. Median inter-observer manual segmentation DC was 0.84. The difference between the DC of manual vs one-channel segmentation and manual vs two-channel segmentation was not statistically significant: p_{adj}=0.06 (Obs1) and p_{adj}=0.22 (Obs2). Inter-observers manual segmentation DC was significantly superior to DC obtained with both DL-based approaches. ***Conclusion:*** The added value expected with the integration of the CT component in the network is not statistically proven with our data. However, a trend for better results was observed. Both DL-based networks had an outstanding performance compared to literature. Funding: LyRaCAD (Ref.:LISBOA-01-0247-FEDER-039885); OLISSIPO (H2020, No:951970); UIDB/50021/2020 (FCT) ***References:*** [1] Clark et al., https://doi.org/10.1007/s10278-013-9622-7; [2] Gatidis et al., https://doi.org/10.7937/gkr0-xv29; [3] Gatidis et al., https://doi.org/10.1038/s41597-022-01718-3; [4] Constantino et al., https://doi.org/10.1007/s10278-023-00823-y; [5] Isensee et al., https://doi.org/10.1038/s41592-020-01008-z

EP-0329

Assessment of the metabolic volume of the tumor as a marker of response to therapy with CAR-T Cells in patients with B-cell non-Hodgkin lymphoma, our experience.

M. CASALLAS CEPEDA*, J. Montalva Pastor, S. Salcedo, I. Gomez Fernandez, J. Alonso Farto;*
Hospital General Universitario Gregorio Marañón, Madrid, SPAIN.

Aim/Introduction: To assess the correlation between metabolic tumor volume (MTV), prior to infusion of therapy with CAR-T Cells, and survival (disease-free progression (PFS) and overall survival (OS)) as a prognostic marker of response in patients with refractory or relapsed non-Hodgkin lymphoma. ***Materials and Methods:*** Retrospective descriptive observational study, in which MTV and TLG were evaluated in the baseline ^{18}F-FDG-PET/CT study, prior to the infusion of CAR-T Cells therapy; with the intention of assessing disease-free progression and overall survival. Body metabolic images were quantitatively assessed manually by two nuclear medicine doctors, using GE AW Server 3.2 software. The data obtained with the subsequent ^{18}F-FDG-PET/CT and clinical history were compared, evaluating the disease-free progression and overall survival from the infusion of the therapy with cut-off until April 1, 2023. ***Results:*** 73 patients were included, of which 4 were excluded because they did not have access to the baseline ^{18}F-FDG-PET/CT for quantification (39 men and 30 women; 56.52% and 43.47% respectively) with a median age 61 years. 29 were infused with tisagenlecleucel (Kymriah®) and 40 with axicabtagene ciloleucel (Yescarta®) with a median follow-up of 447 days. Median survival data were 92 days for PFS and 447 days for OS. Therefore, we stratified the cohort according to the median MTV (114.40 cm $^{3)}$ in two groups: high tumor volume (HMTV) and low tumor volume (LMTV) (35 and 34 patients respectively), evidencing a lower number of days until PFS and OS in the HMTV group (69 and 446 days vs 94.5 and 466 days). ***Conclusion:*** A high MTV value in the ^{18}F-FDG-PET/CT prior to infusion of CAR-T Cell therapy is related to worse progression-free survival and overall survival in patients with refractory or relapse of non-Hodgkin's lymphoma. ***References:*** 1. doi: 10.1182/bloodadvances.2020001900/2. doi: 10.1182/bloodadvances.2020002394/3. doi: 10.1016/S1470-2045(18)30864-7/4. doi: 10.1016/S1470-2045(18)30864-7

EP-0330

18F-FDG PET/CT Volumetric and Radiomic Features for lesions/patients' characterization in CAR-T therapy

E. Abenavoli*[1], F. Linguanti[1], I. Cutini[2], L. Nassi[3], B. Puccini[3], M. Palazzo[3], B. Sordi[4], R. Saccardi[2], A. Vannucchi[4], R. Sciagrà[1], V. Berti[1];*
[1]Nuclear Medicine Unit, Experimental and Clinical Biomedical Sciences Department "Mario Serio", AOU Careggi, Florence, Italy, Florence, ITALY, [2]Department of Cellular Therapies and Transfusion Medicine, Careggi University Hospital, Florence, ITALY, [3]Hematology Department, Azienda Ospedaliero-Universitaria Careggi, Florence, ITALY, [4]Department of Experimental and Clinical Medicine, CRIMM, Center Research and Innovation of Myeloproliferative Neoplasms, Azienda Ospedaliera Universitaria Careggi, University of Florence, Florence, ITALY.

Aim/Introduction: 18F-FDG PET/CT(PET/CT)is currently used to assess non-Hodgkin lymphoma patients eligible to chimeric antigen receptor T cell(CAR-T)therapy.We sought to identify precocious and specific metabolic radiomic PET features measured at time of CAR-T transfusion(TT),1 month (M1) and 3 months (M3) post-CAR-T therapy,which can identify relapsed/refractory lesions(R/R). ***Materials and Methods:*** A total of 50 PET/CT (17 TT,16 M1,17 M3)from 17 patients were reviewed. Lesions were delineated using an automated preselection of 18F-FDG avid structures defined by a SUV ≥ 2.Lesions without avid uptake were drawn manually using CT as reference.Volumetric and radiomic parameters were measured on PET/CT using LIFEx software both for Reference lesion (RL) and for all lesions(nodal and extranodal).Mann-Whitney test was used to assess the difference in features between R/R and not-R/R.We performed factor analysis to remove redundancy of cross-correlated variables and discriminant analysis to examine the power of the potential independent predictors.At patient level,GLM repeated measures analysis was used to assess longitudinal changes in radiomic features derived from both global disease and RL. ***Results:*** A total of 112 lesions were segmented and analysed for radiomic features extraction.We divided lesions into 3 groups according to tissue type: nodal (18TT, 22M1, 30M3), muscle-bone (5TT, 2M1, 3M3), and soft tissue (10TT, 8M1, 14M3).R/R lesions were 72 and not-R/R lesions were 40.Biopsy has been considered gold standard to distinguish R/R from pseudoprogression. Regarding nodal lesions,SUVmax at TT,IntensityBased Local-Intensity-Peak at M1 and GLCM joint-maximum with SUVmax and TLG at M3 exhibited significant predictive power of R/R. Regarding soft tissue lesions,GLZM Small-Zone-Grey-Level-Emphasis associated with TLG,IntensityBased 25thpercentile at M1 and GLCM dissimilarity with NGTDM contrast at M3, significantly predicted R/R status. No variable exhibited significant predictive power for muscle-bone tissue lesions, probably because of small sample size. At patient level,in R/R group,the variance of SUVmean indicated a significant time effect,with reduction at TT-M1 and subsequent increase at M1-M3.Moreover,the SUVmax variance was similar to SUVmean, but with significant results only at TT-M1.No significant variance of metabolic and volumetric variables was found in not-R/R group. ***Conclusion:*** Our study demonstrated that metabolic radiomic

PET/CT parameters could provide a significant predictive power in identification of R/R status in CAR-T therapy.Interestingly,-features related to metabolic activity at all time points resulted particularly significant in nodal lesions examination.On the other hand, in soft tissue lesions,the significant predictive power was related to features evaluating heterogeneity.Longitudinal analyses demonstrated significant variation in SUVmean and SUVmax only in R/R patients. ***References:*** Nioche C,et al. Cancer Research.2018;78:4786-4789; www.lifexsoft.org

EP-0331

Is [18F]FDG PET/CT at one month of chimeric antigen receptor T-cell therapy (CAR-T) in lymphomas necessary in the early treatment response assessment?

P. Stefaneli Mormandi, *C. Soldevila-Lozano, A. Caballero-Gonzalez, S. Abouzian Senhaji, P. Torres-Quintana, A. Fernández-León, R. Valverde-Jorge, M. Velasco-Nuño, J. Duch, V. Camacho, A. Flotats;*
Hospital de la Santa Creu i Sant Pau, Barcelona, SPAIN.

Aim/Introduction: The importance of [^{18}F]FDG PET/CT in the staging and follow-up of lymphomas has been internationally accepted for several years. The new treatments force us to rethink the follow-up protocols in the response assessment in all immunotherapies. The aim of this study is to retrospectively evaluate the early metabolic response of patients with diffuse large B-cell lymphoma (DLBCL) treated with CAR-T cell therapies and to analyze current PET/CT follow-up protocols. ***Materials and Methods:*** Retrospective study of 21 patients (13 men, 8 women; mean age 50.4 years) with DLBCL, refractory to at least 2 therapeutic lines and who were treated with CD19 CAR-T therapy. A [^{18}F]FDG PET/CT was performed prior to CAR-T infusion, as well as at one (M1) and three months (M3) post-infusion. Images were assessed using the Lugano classification and the LYmphoma Response to Immunomodulatory Therapy Criteria (LYRIC). The total follow-up time was 6 months (M6). ***Results:*** The number of patients who presented complete response (CR) was 8 pts in M6, 6 pts in M3 and 4 pts in M1. A progression disease (PD) was seen in 13 pts, 12 pts and 2 pts for M6, M3 and M1 respectively. No patients presented partial response (PR) in M6, 2 pts did in M3 and 10 pts in M1 (of whom 1 pt evolved to CR in M3; 4 pts maintained PR and underwent adjuvant radio/chemotherapy; 1 pts presented an indeterminate response and the other 4 pts had a PD). Finally, indeterminate response was only seen in M3 (1 pt) and M1 (5 pts, all confirmed as PD in M3). ***Conclusion:*** The assessment made by [^{18}F]FDG PET/CT 3 months after the infusion of CAR-T cells is similar to the real evolution of the patients in the short term. In the series presented, the [^{18}F]FDG PET/CT carried out one month after CAR-T therapy was not a good predictor of response and may not be necessary.

EP-0332

Head-to-head comparison between 68Ga-Pentixafor and 18F-FDG PET/CT in diffuse large B cell lymphoma

P. Palanivelu, *H. Goyal, D. Halanaik, P. Ganesan;*
Jawaharlal Institute of Postgraduate Medical Education and Research, Pondicherry, INDIA.

Aim/Introduction: Positron emission tomography with computed tomography (PET/CT) using the standard radiotracer 18F-FDG is the most recommended method for imaging patients with diffuse large B cell lymphoma (DLBCL). However, there is significant over-expression of the CXCR4 chemokine receptor noticed in the DLBCL and marker of disease aggressiveness. Furthermore, it has the potential for theranostics and CXCR4-targeted radionuclide therapy. We evaluated in vivo expression of the CXCR4 chemokine receptor using novel tracer 68Ga-Pentixafor PET/CT in DLBCL and compared it to 18F-FDG PET/CT. ***Materials and Methods:*** Morphologically proven treatment-naive DLBCL patients were enrolled in this prospective study. The institute's ethics committee approved this study, and informed consent was obtained from all the patients. Twenty-seven patients (17 Males; 10 Females, Median age 55 years, Range 25- 73 years) underwent 18F-FDG PET/CT and 68Ga-Pentixafor PET/CT. Evaluated separately for 23 anatomic regions (12 lymph node stations and 11 organs/tissues). For lesion-to-lesion analysis, SUVmax was calculated. Concordance between 18F-FDG and 68Ga-Pentixafor PET/CT was assessed based on standard Lugano's staging. Cohen's Kappa statistics were used to analyze the agreement. ***Results:*** From the analysis of 27 patients, the mean number of nodes detected by FDG was 24.78 ± 30.56 (mean ± SD) and 23.22 ± 29.51 for Pentixafor (p-value 0.155). The mean number of extranodal sites was detected by FDG 2 ± 0.96 and 1.93 ± 1.00 for Pentixafor. A substantial agreement (Kappa 0.804) was achieved between FDG & Pentixafor in detecting the number of nodal and extranodal sites of lymphoma involvement. In visual comparison by maximum intensity projection images, 68Ga-Pentixafor shows more intense uptake than F-18 FDG in 3 (11%) patients, equal uptake in 8 (29%), and superior FDG uptake in 16 (60%) patients. The intensity of the tracer uptake in the nodal lesions was higher in 18F-FDG PET/CT, which is statistically significant. The mean SUVmax reflects this in the nodes 3.96 ± 2.44 (mean ± SD) for FDG and 2.13 ± 1.11 for Pentixafor ($p < 0.001$). Even with statistically significant differences in the SUVmax, overall Lugano staging showed a statistically significant correlation (p-value 0.001) between 68Ga-Pentixafor and 18F-FDG PET/CT. ***Conclusion:*** 68Ga-Pentixafor PET/CT showed good concordance and comparable diagnostic performance to 18F-FDG PET/CT for baseline staging in patients with DLBCL. 68G-Pentixafor PET/CT may help to select patients who might benefit from CXCR4-directed therapy.

EP-0333

18F-FDG PET/CT features as potent imaging biomarkers of efficacy and toxicity in large-B-cell lymphoma treated with CAR-T cell therapy

D. Leithner[1], *J. R. Flynn*[1], *A. Mauguen*[1], *S. M. Devlin*[1], *T. Fei*[1], *B. S. Imber*[1], *H. Hubbeling*[1], *M. E. Mayerhoefer*[1], *D. Lafontaine*[1], *L. Michaud*[2], *M. Perales*[1], *H. Schöder*[1], *R. Shouval*[1];
[1]*Memorial Sloan Kettering Cancer Center, New York, NY, UNITED STATES OF AMERICA,* [2]*Lausanne University Hospital, Lausanne, SWITZERLAND.*

Aim/Introduction: Chimeric antigen receptor T (CAR-T) cell therapy has transformed the care of patients with large B cell lymphoma (LBCL). However, toxicity and disease recurrence or progression after CAR-T remain a barrier and effective quantitative biomarkers for their outcomes represent an unmet clinical need. Our aim was to evaluate whether 18F-FDG PET/CT imaging features can inform the likelihood of response and developing immune toxicity (i.e. cytokine release syndrome [CRS] and neurotoxicity) in LBCL patients treated with CD19-directed CAR-T cell therapy. ***Materials and Methods:*** 18F-FDG PET/CT scans performed before CAR-T for LBCL were retrospectively analyzed by a board certified radiologist. Metabolic tumor volume (MTV), SUVmax, total lesion glycolysis (TLG), and presence of bulky disease were recorded using the PET-CT plugin for FIJI. Response to CAR-T cell therapy was defined according to the Lugano

criteria. CRS and neurotoxicity were graded according to ASTCT guidelines. Progression-free survival (PFS) was measured from time of CAR-T cell infusion; PFS events included death, relapse, and disease progression. Association between PET imaging features and outcomes were studied in univariable logistic regression and Cox regression models. ***Results:*** A total of 181 LBCL patients, with a median age of 65 years, treated with autologous CD19-directed CAR-T (94 axi-cel, 52 tisa-cel, 35 liso-cel) were included. We considered two time points of evaluation: 1) pre-apheresis scans (n=161; median SUVmax 19, MTV 56, TLG 427, maximum diameter 7.8 cm), and 2) latest disease evaluation before CAR-T infusion which includes post-apheresis and post-bridging scans, as well as pre-apheresis scans for patients who did not have additional imaging afterwards (n=181; median SUVmax 15, MTV 44, TLG 333, maximum diameter 7.8 cm). At the pre-apheresis point, increasing SUVmax, MTV, and TLG were associated with a higher likelihood of non-complete remission (CR) and grade 2-4 neurotoxicity (P-values 0.003, 0.021, 0.036 and 0.011, 0.04, 0.024, respectively). Similarly, the same pattern of association was observed when evaluating radiologic features measured at most recent disease assessment before CAR-T infusion. Finally, increasing SUVmax, MTV, and TLG at latest disease assessment were strongly associated with shorter PFS (HR 1.28 [95% CI 1.11-1.48], HR 1.05 [1.03-1.07], HR 1.06 [1.04-1.09], respectively, all P<0.001). ***Conclusion:*** This is the one of the largest studies demonstrating that quantitative radiologic features in LBCL may serve as biomarkers for CAR-T cell therapy toxicity and likelihood of treatment failure. These results may guide preventive interventions to increase the efficacy and safety of CAR-T cell therapy.

EP-0334

Effect of chemotherapy-related hepatic steatosis on liver 18F-FDG uptake in lymphoma patients

Y. Wang, *M. Su, L. Li;*
West China Hospital, Sichuan University, Chengdu City, CHINA.

Aim/Introduction: Nonalcoholic fatty liver disease is the most common liver disorder in the developed countries. Although typically associated with obesity and metabolic syndrome, it can also be secondary to drug toxicity. Liver uptake activity is used as a semi-quantitative reference to assess treatment response among lymphoma patients by positron emission tomography-computed tomography (PET/CT) with 2-deoxy-2-[F-18]fluoro-D-glucose (^{18}F-FDG). However, hepatic steatosis after chemotherapy may affect hepatic glucose metabolism. The aim of our study was to evaluate the impact of chemotherapy-related hepatic steatosis on liver ^{18}F-FDG uptake in lymphoma patients. ***Materials and Methods:*** We conducted a retrospective analysis of 56 lymphoma patients (23 diffuse large B cell lymphoma, 33 extranodal natural killer/T-cell lymphoma and 1 Hodgkin lymphoma) with de novo hepatic steatosis after chemotherapy. Patients with chemotherapy-related steatosis (steatosis group) were matched 1:1 to controls (non-steatosis group) by histologic type. All of them underwent a baseline whole-body PET/CT (B-PET) and interim or end-to-treatment PET/CT (I/E-PET) after chemotherapy. Patients with liver disease or steatosis on baseline PET/CT scans were excluded. Steatosis was diagnosed on the unenhanced CT part of PET/CT examinations using a cut-off value of 42 Hounsfield units (HU). The mean and maximum standardized uptake values (SUVmean and SUVmax) were recorded on the liver and the tumor target lesion. Data were analyzed by paired samples t-test and linear regression. ***Results:*** No significant differences in terms of age, gender, histologic type and Ann Arbor staging between steatosis group and non-steatosis group. In the steatosis group, liver SUVmax and SUVmean were significantly lower in I/E-PET (2.53±0.42 and 2.06±0.41, respectively) as compared with B-PET (2.84±0.35, P<0.005 and 2.32±0.32, P<0.005, respectively). But in the non-steatosis group, there were an increased liver SUVmax and SUVmean in I/E-PET(2.82±0.38 and 2.28±0.32, respectively) as compared with that of B-PET (2.62±0.37, P<0.005 and 2.12±0.35, P<0.005, respectively). CT density of liver was found to be an independent factor that correlated with liver SUVmax and SUVmean, while BMI, blood glucose level, ^{18}F-FDG dose and incubation period were not. ***Conclusion:*** PET/CT scans showed that chemotherapy-related hepatic steatosis in patients with lymphoma had decreased liver ^{18}F-FDG uptake. These alterations should be noted when a metabolic response to therapy in the interim and end-to-treatment PET/CT is determined.

EP-0335

Classical Hodgkin's Lymphoma: does baseline 18F-FDG PET/CT radiomics from the largest and hottest lesions add value to conventional prognostic models?

E. Triumbari[1,2], *D. Morland*[3], *R. Gatta*[4], *A. Collarino*[4], *E. Maiolo*[4], *A. Cuccaro*[4], *M. De Summa*[4], *S. Chiesa*[4], *L. Boldrini*[4], *M. E. Mayerhoefer*[5], *L. Nardo*[6], *S. Hohaus*[4], *S. Annunziata*[4];
[1]*1Department of Radiology, Radiotherapy and Hematology, Fondazione Policlinico Universitario A.Gemelli IRCCS, Rome, ITALY,* [2]*Radiopharmacy Research Core Facility, Fondazione Policlinico Universitario A. Gemelli IRCCS, Rome, ITALY,* [3]*Service de médecine nucléaire, Institut Godinot and CReSTIC EA 3804, Université de Reims Champagne-Ardenne, Reims, FRANCE,* [4]*Department of Radiology, Radiotherapy and Hematology, Fondazione Policlinico Universitario A.Gemelli IRCCS, Rome, ITALY,* [5]*Department of Radiology, Memorial Sloan Kettering Cancer Center, New York, NY, UNITED STATES OF AMERICA,* [6]*Department of Radiology, UC Davis, Sacramento, CA, UNITED STATES OF AMERICA.*

Aim/Introduction: Aim of this study was yo investigate the predictive role of baseline ^{18}F-FDG PET/CT (bPET/CT) radiomics from two target lesions in patients with classical Hodgkin's Lymphoma (cHL) and its value in combination with clinical and conventional PET/CT prognostic models. ***Materials and Methods:*** cHL patients with bPET/CT between 2010 and 2020 were retrospectively included and randomized into training and validation sets (60%-40%). Two target lesions were chosen: Lesion_A, with the largest axial diameter (D_{max}); Lesion_B, with the highest SUV_{max}. The total metabolic tumor volume (TMTV) was also calculated for each patient, and 212 radiomic features were extracted from each target lesion. All PET/CT features were harmonized using ComBat method across two scanners. Two outcomes were chosen: progression free survival (PFS), and Deauville Score (DS) at interim PET/CT. For each outcome, three models (and their combinations) were constructed using training data, then validated: radiomic model "R", with features selected by cross-validated LASSO regression; conventional PET/CT model "P", based on D_{max}, SUV_{max} and TMTV; and clinical model "C", based on the International Prognostic Score (IPS) and early/advanced stage. ***Results:*** 197 patients were included (training set: n=118; validation set: n=79). During a mean follow-up of 53.8±29.8 months, 38/197 (19%) patients had adverse events and 42/193 (22%) had DS≥4. Only one radiomic feature was selected for PFS prediction (F_cm.corr from Lesion_B, C-index 66.9% [56.3-77.5]) and constituted the model "R". The optimal Cox clinical model "C" was identified as a combination of stage and IPS (C-index 74.8% [66.0-83.6]), while the optimal PET/CT model "P" was composed of TMTV and D_{max} (C-index 63.3% [51.5-75.1]). At validation, models

"C", "C+R", "R+P" and "C+R+P" were significant for PFS. The best model was "C+R" (C-index 66.3% [55.9-76.7]). No model was found significant at validation for the prediction of DS. ***Conclusion:*** cHL bPET/CT radiomic features from the largest and hottest lesions may have a prognostic value in combination with clinical and conventional PET/CT data.

EP-0336

Comparison of Low dose Vs standard dose 18F-FDG PET/CT in Lymphoma Patients using Conventional PET/CT Scanner

N. Kumar, *J. Yadav, G. Arora, S. A. Shamim;*
All India Institute of Medical Sciences, New Delhi, INDIA.

Aim/Introduction: ^{18}F-FDG PET/CT plays a pivotal role in detection of lymphoma and broadly utilized in diagnosis, staging, restaging, and response evaluation of lymphoma patients. Repeated PET/CT scans are required for current disease status and response assessment. Present study aimed to develop a new protocol by using by comparing low-activity with standard ^{18}F-fluorodeoxyglucose (FDG) PET/CT in lymphoma patients using conventional PET/CT scanner without compromising the image quality and clinical information and hence decreasing the radiation exposure to the radiation worker and general public. ***Materials and Methods:*** Histopathologically confirmed lymphoma patients were prospectively included for randomized scan using low vs standard activity FDG PET/CT scan. ^{18}F-FDG PET/CT acquisition was performed after intravenous injection of low activity (group-1) 3-5mCi (111-185MBq) or standard activity (10mCi) (group-2) ^{18}F-FDG and scanning with 2-3 min. per bed at 60 minutes post-injection. Two nuclear medicine physicians with experience of more than 3 years analysed the acquired scans and suggested five-point Likert scale based on image quality. The Likert scale with score ≥ 3 was assigned as acceptable image during PET/CT reporting. The inter-reader concordance and discordance on Likert score was also evaluated. ***Results:*** A total of 30 patients, 15 in each group (16 male; 14 female) with mean age of 44.7 ± 16.4 years were enrolled prospectively and injected with mean dose of 146.76±15.92Mbq (3.96±0.43mCi) in group-1 patients while 370MBq (10mCi) in group-2 patients. Of 15 patients in each group, baseline scans were performed in only 3 patients in each group. The median SUVmax; SUVmean of lesion was 6.5 (range 1.55-23.73); 2.5 (range 1.1-6.25) and 6.8 (range 1.13-11.06); 2.1 (range 0.91-4.24) in group-1 and 2 respectively. The median TBRmax; TBRmean of lesions was 4.24 (range 1.20-20.45); 3.32 (range 0.98-6.79) and 3.84 (range 1.13-9.81); 2.28 (range 1.02-3.79), for group-1 and 2, respectively. During image analysis, all the patients of both group 1 & 2 had scores ≥3 points that fulfilled the clinical needs for diagnosis/disease status. On subjective scoring, the inter reader concordance in Likert scoring was present only in ten patient while remaining 20 were discorded. ***Conclusion:*** Whole-body PET/CT scan in both groups had comparable image quality. Thus, low-dose ^{18}F-FDG activity could maintain a satisfactory image quality with conventional PET/CT scanners and also reduces patient's as well as personnel radiation dose.

EP-0337

Do FDG PET metrics have a role for predicting the response to BeGeV therapeutic scheme in refractory Hodgkin lymphoma? A pilot study.

D. Pizzuto[1], *N. Messina*[2,3], *E. Maiolo*[2], *F. D'Alò*[2,3], *S. Hohaus*[2,3], *S. Annunziata*[1];
[1]*Nuclear Medicine Unit, GSteP Radiopharmacy, Fondazione Policlinico Universitario Agostino Gemelli IRCCS, Rome, ITALY,* [2]*Hematology Unit, Diagnostic Imaging, Radiation Oncology and Hematology Department, Fondazione Policlinico Universitario Agostino Gemelli IRCCS, Rome, ITALY,* [3]*Hematology Institute, University Department of Radiological and Hematological Sciences, Università Cattolica del Sacro Cuore, Rome, ITALY.*

Aim/Introduction: BeGeV is an effective salvage regimen with high rate of complete response in Relapsed/Refractory Hodgkin Lymphoma (R/R HL). FDG PET metrics and Deauville score (DS) represent well-established parameters for the clinical management of HL patients; however, their role should be better defined in R/R HL undergoing BeGeV scheme. The study aimed to explore if DS and semiquantitative parameters, assessed on interim 18F-FDG PET/CT after 2 BeGeV cycles (interimPET), could predict DS of BeGeV end-of-treatment PET (EOT-PET) and the patients' outcome. ***Materials and Methods:*** From a large PET dataset, patients with R/R HL completing BeGeV scheme were retrospectively included from April 2017 to October 2022. All patients underwent a 18F-FDG PET/CT before BeGeV (prePET), after two (interimPET) and four BeGeV cycles (EOT-PET). For each patient, progression-free-survival (PFS as interval from starting BeGeV scheme to the recurrence/change of therapeutic scheme) and following PET variables were collected: prePET and interimPET LesionSUV$_{max}$, deltaSUV$_{max}$ (i.e. the variation between prePET and interimPET), interimPET DS, SUV$_{peak}$, SUV$_{mean}$, MTV, TLG, LiverSUV$_{max}$, LiverSUV$_{mean}$, rPET, qPET (i.e. Lesion SUV$_{max}$/LiverSUV$_{mean}$ and LesionSUV$_{peak}$/LiverSUV$_{mean}$, respectively). Within the cohort with persistent/progression disease at interimPET (DS≥4), the patients were dichotomized into two subgroups, according to the EOT-PET DS, as follows: DS≤3 and DS≥4. Differences of PFS and interimPET metrics were assessed between the EOT-PET DS≤3 and DS≥4 subgroups. ROC analyses were performed for assessing best PET metric cut-off value, with EOT-PET DS as outcome. A p value ≤ 0.05 was considered significant. ***Results:*** 23 patients were recruited. 11/23 patients (48%) had interimPET DS≤3; among them, 10/11 (90%) showed no PFS. Conversely, 12/23 patients (52%) presented a interimPET DS≥4; among them, 6/12 patients (50%) converted to a EOT-PET DS≤3, although all of them (6/6, 100%) presented a PFS at 20 months. The remaining 6/12 patients (50%) presented PFS at 20 months in 3/6 patients (50%). Within the interimPET DS≥4 cohort, SUV$_{max}$,SUV$_{mean}$, SUV$_{peak}$, rPET, qPET were found significantly different among EOT-PET DS≤3 and DS≥4 subgroups (Mann Whitney U-Test; p=0.004, p=0.002, p=0.02, p=0.006, p=0.02, respectively). SUV$_{mean}$ cut-off value ≥ 3.50, rPET cut-off value ≥ 1.97 and qPET cut-off values ≥ 1.90 showed a sensitivity and specificity of 100% and 100% (AUC=1.00), 100% and 83.3% (AUC=0.97), 83% and 100% (AUC=0.89), respectively. ***Conclusion:*** DS and PET metrics applied on interimPET seemed to be effective to predict PFS and EOT-PET DS, respectively, so hypothesizing their usefullness for monitoring BeGeV therapeutic response in patients with R/R HL.

EP-0338

Normalization and 2-bit-quantization of FDG-PET using the Deauville Score for training an deep learning AI for lymphoma staging

B. Schemmer;
Uniklinik Bonn, Bonn, GERMANY.

Aim/Introduction: Lymphoma is a common cancer in young adults and children worldwide. Regular staging is crucial for therapy planing and patient outcome. Positron Emission Tomography (PET) is a widely used imaging modality for lymphoma staging with the standard uptake value (SUV) commonly used as a measure of tumor activity. However, SUV has limitations, and methods improve the clinical value of PET imaging have been developed. One such method is the Deauville Score, which uses a visual qualitative scoring system for the interpretation of tumor uptake before and during therapy with blood-pool(mediastinum) and liver as references. ***Materials and Methods:*** We included 25 patients (median age 26 years (range, 12-34 years)), with histologically confirmed Hodgkin/NHL cancer who underwent FDG-PET/CT imaging for primary or follow-up staging with at least two FDG-PET studies (whole body and dedicated neck), to train and validate our AI model. The majority had visible brown fatty tissue (86%) and other unspecific uptake forms of uptake from inflammation, sarcoidosis and vaccination. The AI was based on deep learning and provided with whole-body PET-images. The AI was specifically not trained to find any subtle lesions with uptake below blood-pool. The PET-images were preprocessed, uptake values below blood-pool were no longer present in the training images. Detection was evaluated as successful when there was a corresponding labeled lymph-node in the data. To increase the amount of training data, the whole bodies were presented as single image slices (~50*100 images). ***Results:*** The results of the study showed that using the Deauville Score (stage 1 and 2 combined) as quantization/normalization method for AI training a reliable detection of suspicious lesions is possible with a small dataset. We achieved a good sensitivity of 92% (mainly due to lymphnodes close to each other). However specificity was only 27% due to misinterpretation of unspecific findings such as brown fatty tissue, inflammation and vaccination, on the other hand only findings that needed human interpretation where detected. ***Conclusion:*** This study demonstrates the potential of normalization/quantization of FDG-PET using the visual Deauville Score for deep learning AIs as a method to eliminate irrelevant image findings from PET images, thus reducing the workload of the reader. The AI itself currently suffers from the detection of unspecific findings which we hope to remove from the final results by using a second post processing AI.

EP-0339

Total metabolic tumor volume (TMTV) at baseline 18F-FDG PET/CT and Laboratory Prognostic Index (LAB-PI) as outcome predictors in Large B-Cell Lymphoma (LBCL).

L. García Belaústegui, *S. Borwne, L. Sancho Rodríguez, R. Figueroa, F. Minguez, M. Canales, S. Huerga, V. Betech-Antar, E. Pena, C. Grande, M. Garcia-Velloso;*
Clínica Universidad de Navarra, Madrid, SPAIN.

Aim/Introduction: Aggressive LBCL is the most common subtype of non-Hodgkin's lymphoma and consists of a heterogeneous group of disorders with variable clinical presentation. LAB-PI is a recently validated prognostic index for LBCL that analyzes three pretreatment laboratory parameters: lactate dehydrogenase, hemoglobin and beta-2 microglobulin. This study aimed to correlate baseline PET-derived metabolic tumor volume (MTV) and LAB-PI score (LAB-PIs) with progression-free survival (PFS) and overall survival (OS) in a sample of LBCL patients to identify those with higher risk of early relapse or refractory disease. ***Materials and Methods:*** Patients with LBCL treated with R-CHOP(-like) regimens who had previously undergone a baseline ^{18}F-FDG PET/CT were retrospectively reviewed. MTVs were obtained by an experienced nuclear medicine physician using Syngo.via software, with automatic threshold equal to 1.5 times the average standardized uptake value of the liver. The extent of the disease was evaluated considering the presence of unique lymph node involvement or the existence of extranodal extension. Correlation between LAB-PIs and MTV divided into three categories - nodal, extranodal and total- was assessed. ***Results:*** 56 patients (38 male, 18 women) with a mean age of 65 years (SD:15) were selected. LAB-PIs values were divided into low (0, 1, 2) and high (3,4), with 52 patients (59.8%) in the low LAB-PIs group and 35 patients (40.2%) in the high LAB-PIs one. The median of total MTV was 144.27 cm3 (Q1=64.07 cm3, Q3=543.63 cm3). Spearman's rank test was used to study correlation between LAB-PIs and MTV groups, with the highest correlation coefficient between LAB-PIs and extranodal MTV (ρ= 0.65; p<0.001). An unexpected finding was that all patients with a total MTV higher than 100cm^3 had a greater LAB-PIs. The median follow-up was 27 months, with OS and PFS of 96.3% and 97.3% in low LAB-PIs patients and 71.5% and 68.8% in high LAB-PIs ones. A log rank test between LAB-PIs groups was performed and showed statistical significance for both OS and PFS (p=0.005 and p=0.019, respectively). Regarding the total MVT, both OS and PFS were 100% for patients with a MTV bellow the median (144.27 cm3) and 73.4% and 70.4% respectively for those patients above it. ***Conclusion:*** Despite the small sample size, this initial study proposes pretreatment MVT and LAB-PI as a set of prognostic criteria for outcome in LBCL. Further validation in larger series is needed.

EP-0340

Prognostic Value of Volumetric Parameters with 18F-FDG PET/TC in Follicular Lymphoma

P. Sarandeses[1], *M. Poza*[1], *S. Pedraza*[1], *A. Medina Benito*[2], *A. Peter Seiffert*[2], *A. Jimenez*[1], *D. Vega*[1], *P. Zaragoza*[1], *S. Angiolillo*[1], *X. Guarnizo*[1], *S. Ruiz*[1], *A. Gomez*[1], *E. Martinez*[1], *A. Saviatto*[1], *A. Galiana*[1], *S. Barrio*[1], *M. Tabuenca*[1];
[1]*HOSPITAL UNIVERSITARIO 12 DE OCTUBRE, Madrid, SPAIN,*
[2]*Universidad Politécnica Madrid, Madrid, SPAIN.*

Aim/Introduction: Follicular lymphoma (FL) is the second most common no-Hodgkin lymphoma in developed countries. It is considered an indolent disorder with a relatively favorable course. However, a subset of patients has a more aggressive course and a worse outcome. Currently, there is no established method to identify patients at risk of early disease progression at the time of diagnosis of FL.The early identification is the main purpose of moderm-day prognostic tools to consequently modulate treatment intensification and maintenance therapies in an early phase.18F-FDG PET/CT (PET/CT) provides valuable prognostic information. Specifically, Tumor Metabolic Volume (TMV) and Total Lesion Glycolysis (TLG) at diagnosis are considered an independent prognostic factor for Progression-Free Survival (PFS) and Overall Survival (OS).Our objective is to evaluate the prognostic value of TMV and TLG at diagnosis. ***Materials and Methods:*** 69 FL patients were retrospectively enrolled from

December 2012 to september 2020, who underwent PET/CT at staging before immunochemotherapy.The TMV was obtained by summing the metabolic volumes of all individual nodal and extranodal lesions, using the 41% SUVmax threshold method. The most suitable cut-off to dichotomize patients regarding outcome was determined by receiver operating characteristic (ROC) analysis. Following that, both PFS and OS were estimated with Kaplan-Meier curves based on the optimal MTV threshold. ***Results:*** 69 patients were included, 34 men and 35 women; aged 35-98 (mean 67.9). 92.7% of them with a 3-4 Ann Arbor stage. The TMV and TLG are quantitative variables with non-parametric distribution with a median of 205.75 (range 0.5-1989) and SD 1161.12 (range 2-12916) respectively.In our sample, the ROC analysis could not demonstrate an optimal cut-off point for TMV, with an area under the curve of 0.6; Furthermore, no significant relationship was observed between VMT and TLG with PFS and OS.We have observed an association between TMV and stage III-IV, the presence of a bulky mass, bone marrow infiltration, elevated LDH and increased risk (Follicular Lymphoma International Prognostic Index FLIPI). ***Conclusion:*** Although most authors reflect that TMV and TLG are independent predictors of PFS and OS in patients with FL, in our sample it has only been significantly associated with a more advanced stage of the disease and with higher risk (FLIPI). ***References:*** Tatsumi, Mitsuaki et al. "Volumetric and texture analysis on FDG PET in evaluating and predicting treatment response and recurrence after chemotherapy in follicular lymphoma." International journal of clinical oncology vol. 24,10 (2019): 1292-1300. doi:10.1007/s10147-019-01482-2

EP-19

e-Poster Area

B: Imaging Clinical Studies -> B1 Oncological Imaging Clinical Study -> B22 Other Hemato-Oncology

EP-0341

18F-FDG PET/CT maybe not so helpless in detection leptomeningeal metastasis- a case report

T. Stoeva*, M. Dyankova, S. Chausheva, T. Yordanova, Z. Dancheva, B. Chaushev, A. Klisarova;*
UMHAT "Sveta Marina" EAD- Varna, Varna, BULGARIA.

Aim/Introduction: Leptomeningeal metastasis represents secondary infiltration by neoplastic cells in meningeal space. The gold standard for diagnosing the involvement of the meninges is cerebrospinal fluid analysis and contrast enhanced-magnetic resonance imaging (MRI). Herein, we aimed to report the usefullness of 18F-FDG PET/CT for finding out leptomeningeal carcinomatosis in a patient with extraosseous plasmocytoma. ***Materials and Methods:*** We present the rare case of a 52-years-old female patient with leptomeningeal carcinomatosis from extraosseous plasmocytoma. The patient visited hospital due to complaints of severe headache and disorientation which started two weeks ago. After performing brain computed tomography (CT) a tumor lesion was found in the cerebellum. Biopsy showed involvement from a plasma cell neoplasm. Patient was referred to 18F-FDG PET/CT because of the observation for multiple myeloma. ***Results:*** Whole body 18F-FDG PET/CT was performed with a complimentary protocol for better visualization, scanning only head and neck regions. The study showed multiple metabolically active lesions on brain surface. Also a FDG-avid lesion was found in the spinal cord on S1/S2 vertebrae level. Those findings raised a great suspicion for leptomeningeal involvement from a plasma cell neoplasm. Numerous metabolically active neck and mediastinal lymph nodes were found as well. There were no evidence of bone lesions. MRI was performed and confirmed the suspicions of leptomeningeal carcinomatosis. The patient was referred for a radiotherapy. ***Conclusion:*** This case report shows that head and neck as well as whole body ^{18}F-FDG PET/CT can be used as an additional diagnostic tool for raising a suspicions of leptomeningeal carcinomatosis or as a primary diagnostic method in cases when cerebrospinal fluid analysis or contrast enhanced-magnetic resonance imaging can`t be performed.

EP-0342

18F-FDG PET/CT assessment of metabolic activity of the osteolytic lesions in patients with multiple myeloma after treatment for evaluation tumor vitality

T. Stoeva*, Z. Dancheva, M. Dyankova, S. Chausheva, T. Yordanova, B. Chaushev, A. Klisarova;*
UMHAT "Sveta Marina" EAD- Varna, Varna, BULGARIA.

Aim/Introduction: We aimed to determine the cut-off value of the glucose metabolism, assessed by value of SUVmax and 5-point scale (FPS), to evaluate the vitality of multiple myeloma (MM) after treatment. ***Materials and Methods:*** We examined 31 patients with MM with 18F-FDG PET/CT after treatment. We estimated the cut-off value of the glucose metabolism evaluated by SUVmax and FPS by ROC curve and chi-square analysis. For a reference study, we used the highest SUVmax value measured in a patient with complete response. We determined the metabolic response as: incomplete metabolic response (IMR) - a SUVmax greater than 3.12 and a score greater than 3 as assessed by FPS. Complete metabolic response from the treatment (CMR) had a SUVmax less than 3.12 and less than score 3. ***Results:*** The results of the ROC curves of the SUVmax showed that the method is reliable and have a high degree of predictability (p=0.000) with area under the curve and confidence interval as follows: AUC 91.2% and CI 0.810-1.000. The threshold value for establishing an IMR is an uptake estimated as SUVmax between the values 2.95-3.12 with a corresponding sensitivity of 0.824; 0.706 and specificity 0.071; 0.071.Most patients evaluated with score 4 and 5 have established IMR. On the other hand, all patients evaluated with score 2 and 3 fall into the group with established CR. It was observed that 1 patient with proven stable disease was evaluated with a score 3. The determined threshold value for establishing an IMR from treatment is a focal uptake evaluated as score 3 (activity above the mediastinum or equal to the liver).We determined that CMR can be predicted for a SUVmax below 2.95, and an IMR - for a SUVmax equal to or above 3.12. A CMR with a high probability can be predicted with a visual assessment score of 1-2, and an IMR - with a score 3 and higher (score 4 and 5). We advise that with a result in the gray zone of a borderline metabolic response (FPS=3 and SUVmax between 2.95-3.12) it is appropriate to repeat the test in the shortest possible time (up to 2-3 months) in correlation with laboratory tests. ***Conclusion:*** 18F-FDG PET/CT is considered as a standard technique for evaluating and monitoring the metabolic response to therapy in patients with MM. In this regard, standardization of interpretation criteria and determination of positive/negative thresholds are of great importance.

EP-0343

18F-FDG PET/CT in unknown primary suspected of multiple myeloma

***T. Stoeva**, Z. Dancheva, M. Dyankova, T. Yordanova, S. Chausheva, B. Chaushev, A. Klisarova;*
UMHAT "Sveta Marina" EAD- Varna, Varna, BULGARIA.

Aim/Introduction: In the present study, we aim to evaluate the role of 18F-FDG PET/CT in patients with osteolytic lesions of unknown origin, suspecious of multiple myeloma. ***Materials and Methods:*** We retrospectively reviewed 33 patients who underwent 18F-FDG PET/CT because of osteolytic lesions suspect to be caused by multiple myeloma (MM) detected by conventional imaging studies. We used histological verification to confirm the diagnoses. The gender distribution of patients was 57.6% (n=19) males and 42.7% (n=14) females with an average age of 62 years (44-85 years). Magnetic resonance tomography (MRT) was performed on 24.2% (n=8), 66.7% (n=22) had a computer tomography scan (CT), and 9.1% (n=3) had a bone radiography (X-ray). All of the patients had no imaging findings or medical history of malignant disease. ***Results:*** According to 18F-FDG PET/CT was found that 57.6% (n=19) were true positive with subsequent histological verification for MM, 27.3% (n=9) were true negative, and 15.2% (n= 5) were false positives. The specificity and positive predictive value of the 18F-FDG PET/CT for detecting MM in patients with osteolytic lesions were 64.29% and 79.17%, respectively. We found that 15.8% (n=3) of patients had up to 5 osteolytic lesions, 15.8% (n=3) had between 5 and 10 lesions, and in 68.4% (n=13) - more than 10 metabolically active osteolytic lesions. The average SUVmax measured in all patients was 6.8. According to the 5-point scale evaluation- 38.1% (n=8) were with score 4 (metabolic activity above the hepatic level), and 61.9% (n=13) - with 5 (metabolic activity exceeding the hepatic level). In one of the patients, the bone lesions were located in the axial skeleton, and in the remaining 18- in the axial and appendicular skeleton. In 63.2% (n=12) a soft tissue component was also found. Extramedullary spread of the disease in the pleura was found in one patient. Pathological fractures occurred in 57.9% (n=11). ***Conclusion:*** 18F-FDG PET/CT is a non-invasive and highly sensitive examination of the whole body, allowing not only the detection of the primary tumor, but also its simultaneous staging and 18F-FDG PET/CT directed biopsy. In patients with unknown primary carcinoma, it should be used as the first imaging modality of choice. In the present study, we found that 18F-FDG PET/CT helped in the diagnosis of 57.6% (n=19) of the patients and the specificity and positive predictive value of 18F-FDG PET/CT method were 64.29% and 79.17%.

EP-0344

18F-FDG PET/CT assessment of metabolic activity of the osteolytic lesions in newly diagnosed multiple myeloma patients as predictive factor for overall survival

***T. Stoeva**, Z. Dancheva, M. Dyankova, T. Yordanova, S. Chausheva, B. Chaushev, A. Klisarova;*
UMHAT "Sveta Marina" EAD- Varna, Varna, BULGARIA.

Aim/Introduction: Our aim was to assess the impact of metabolic activity of osteolytic lesions found by staging 18F-FDG PET/CT and assessed by visual scale or semiqualitative value (SUVmax) as a predictor for overall survival (OS) in newly diagnosed multiple myeloma (MM) patients. ***Materials and Methods:*** A total of 19 patients with histologically proven multiple myeloma and a staging 18F-FDG PET/CT were included in the present study. We used a qualitative assessment of the metabolic activity of bone lesions by a 5-point scale (5-PS). On the other hand a semi-qualitative evaluation was performed using the SUVmax value. As a cut-off value we accepted the average SUVmax of all the malignant osteolytic lesions in this group obtained by us - 4,20. By using Kaplan-Meier survival analysis and the Log Rank test, we compared the OS of the group. ***Results:*** After the comparison, a tendency towards a longer overall survival was found in the patients with a SUVmax value lower than 4,20 (p=0.082), as only one of the patients with higher SUVmax value survived longer- 40 months after diagnosis. The average survival time after 18-FDG-PET/CT of patients with SUVmax less than 4,20 was 27 months. The OS after 18-FDG-PET/CT of patients with SUVmax equal to or greater than 4,20 was only 13,3 months. The Kaplan Meier analysis and Log Rank test revealed a statistically significant relationship between the evaluation of metabolic activity of osteolytic lesions assessed by 5-PS and overall survival (p=0.026). A shorter survival time was observed for patients with score 5 than those with scores 3 and 4. The average survival time after 18-FDG-PET/CT of patients with scores 3 and 4 was 26,67 months and in patients with score 5 was 8,5 months. ***Conclusion:*** In our study, we found that patients evaluated with score 5 (5-PS) of osteolytic lesions had significantly lower OS than those with scores 3 and 4. Also an average value of SUVmax of 4,20 showed a trend in patient stratification, with those with a lower SUVmax cut-off having greater overall survival.

EP-0345

Impact of the Segmentation Method on the Correlation between Metabolic Tumor Volume and Total Circulating Tumor DNA

***C. D. Ramos**[1], G. Duffles[1], M. S. Takahashi[1], E. Napolitano[2], F. Lupinacci[2], L. Pereira[2], J. Maues[1], M. Chauffaille[1], I. Lorand-Metze[1];*
[1]University of Campinas, Campinas, BRAZIL,
[2]Laboratorio Fleury, Sao Paulo, BRAZIL.

Aim/Introduction: Total Metabolic Tumor Volume (TMTV) and total circulating tumor DNA (ctDNA) at baseline have been shown to be relevant prognostic factors for patients with diffuse large B-cell lymphoma (DLBCL), both positively associated with worse outcomes. Recent studies have demonstrated a strong correlation between ctDNA and TMTV [1,2]. However, there is currently no consensus on the optimal methodology for calculating TMTV. This study aimed to investigate whether the choice of the threshold used for tumor segmentation to calculate TMTV might influence its correlation with total ctDNA load in patients with DLBCL. ***Materials and Methods:*** Twelve patients (7 males, 57±17.1 years old) with DLBCL who underwent [^{18}F]FDG PET/CT imaging and ctDNA analysis before treatment were studied. TMTV was calculated using semi-automatic segmentation of attenuated corrected [^{18}F]FDG PET images, performed with the freely available Beth Israel plugin for Fiji (a distribution of ImageJ). Three different thresholds were used for tumor segmentation: absolute fixed thresholds using standardized uptake values (SUVs) of 2.5 (TMTV_2.5) and 4.0 (TMTV_4.0), and fixed relative threshold based on 41% of the maximum SUV (TMTV_41%). The representation of the tumor contour was visually analyzed for the three methods. Total ctDNA was measured by next-generation sequencing (NGS) with a panel of 11 genes and quantified in haploid genome equivalents per mL (hGE/mL). The Spearman correlation coefficient was used to assess the relationship between ctDNA and TMTV, with significance level of 5% ($p<0.05$). ***Results:*** The median (min-max) ctDNA load was 1335.1 hGE/ml (175.8 - 4862.4hGE/ml). The median (min-max) of TMTV_2.5, TMTV_4.0 and TMTV_41% were respectively 130.8mL (0-1654.5 mL), 96.8mL (0-1580.6

mL) and 164.5 mL (0-1454.9 mL). The Spearman correlation coefficient revealed a strong correlation between ctDNA and all TMTV calculation methods: TMTV_4.0 (r=0.7881; p=0.0023), TMTV_2.5 (r=0.7040; p=0.0106), and TMTV_41% (r=0.6480; p=0.0227). At visual analysis, the representation of tumor contour appeared to be more accurate for TMTV_2.5 and TMTV_4.0 than for TMTV_41%, particularly in areas with non-homogenous [^{18}F] FDG uptake. ***Conclusion:*** TMTV shows a strong correlation with ctDNA in DLBCL patients even using different thresholds for tumor segmentation. The correlation was higher for threshold of SUV=4.0 than for thresholds of SUV=2.5 or 41% of the maximum SUV. Methods that use absolute fixed threshold seems to present greater visual outline of the tumor. ***References:*** [1] Le Goff E, et al. Br J Haematol. 2023 Apr 10. doi: 10.1111/bjh.18809. Epub ahead of print.[2] Rivas-Delgado A, et al. Clin Cancer Res. 2021 Jan 15;27(2):513-521. doi: 10.1158/1078-0432.CCR-20-2558.

EP-0346

End of treatment FDG PET CT in patients with Langerhans cell histiocytosis as a predictor of disease recurrence and survival.

P. Bochev[1], *Z. Dancheva*[2];
[1]*Acibadem Cityclinic Mladost UMBAL, Sofia, BULGARIA,* [2]*Medical University "Prof.Dr Paraskev Stoyanov", Varna, BULGARIA.*

Aim/Introduction: To evaluate the value of end of treatment (EOT) FDG PET CT in patients with Langerhans cell histiocytosis (LCH) as a predictor of disease recurrence and as a prognostic factor for survival. ***Materials and Methods:*** Inclusion criteria: Histologically confirmed LCH. At least one FDG PET CT performed after any treatment completed - surgery, chemotherapy, radiotherapy or targeted therapy or after spontaneous remission. Minimum follow up after completion of treatment and a negative PET was 24 months (24 to 242 months) Exclusion criteria: Single system-skin and lung forms Criteria for PET positivity: any lesion, consistent with possible LCH involvement with above background activity (may be equalized to Deauville >2) Retrospective review of the database of the two participating centers from 2010-2020 identified 22 patients with LCH (1y10mo to 66y). Two patient with skin only and lung only disease on staging and one patient under active therapy were excluded. One patient wasa excluded due to inconsistent follow up. Of the remaining 18 patients 8 patients were with multisystem LCH (MS LCH), 5 patients with multifocal single system LCH (SS-MF) and 5 patients with single system single site (bone)- SS-SS LCH. All SS-SS were treated locally by excision. All MS and SS-MF LCH were treated by at least one line of chemotherapy ***Results:*** 16 patients achieved PET negative scan after treatment or (one) - spontaneous remission. Three of them recurred: one SS-SS recurred locally after 5 months (alive, no further data on consecutive treatment) and two patients with MS-LCH recurred 19 and 20months after chemotherapy. Furthermore the latter two achieved remission after consecutive lines of chemotherapy.Two patients with MS LCH never achieved a PET negative scan and died of the disease (both with risk organ involvement) ***Conclusion:*** The negative end of treatment FDG PET CT in patients with LCH does not necessarily guarantee durable remission, but recurrence rate is comparatively low and consecutive recurrences were eligible for successful treatment. In cases of MS-LCH, failure to achieve a PET negative scan under treatment bears a poor prognosis.

EP-0347

Unresolved Challenges in Functional Imaging of Multiple Myeloma: F-18 Fluorocholine PET/CT or F-18 FDG PET/CT? A Single Center Experience

G. KAYA[1], *S. Akın*[2], *Y. Büyükaşık*[3], *M. Tuncel*[1], *M. F. Bozkurt*[1], *P. Özgen Kıratlı*[1];
[1]*Hacettepe University Medical School Department of Nuclear Medicine, Ankara, TÜRKIYE,* [2]*Hacettepe University Medical School Department of Medical Oncology, Ankara, TÜRKIYE,* [3]*Hacettepe University Medical School Department of Hematology, Ankara, TÜRKIYE.*

Aim/Introduction: The role of FDG-PET/CT in Multiple Myeloma (MM) is well-established. In certain groups of MM, especially those with low-hexokinase enzyme expression, false negative findings are seen with FDG-PET/CT, which decreases the sensitivity of the test to 50%. In the preliminary studies, F18 Fluorocholine (FCH) PET/CT has been shown to be a good candidate in the evaluation of MM. This study aims to compare the diagnostic performance of FDG and FCH-PET/CT imaging in MM patients. ***Materials and Methods:*** FDG and FCH-PET/CT (early 10 and late 60min imaging) whole-body images of biopsy-proven MM patients performed within a 30-day period were evaluated retrospectively. IMPeTUs-criteria were used for FDG-PET/CT and also modified for FCH-PET/CT. Any focal FCH uptake higher than the physiological biodistribution was accepted as positive for MM. The sensitivity and accuracy of each imaging modality were evaluated and a ROC analysis was done. Images of both FCH and FDG-positive patients were compared with each other. Evaluation with laboratory correlation was performed as well. ***Results:*** A-total-of 75 PET-CT scans of 25 patients (F/M: 11/14; mean age: 61.4y (SD 2.4)) diagnosed with MM composed the study group. Twelve examinations were performed for newly-diagnosed patients and 13 for restaging purposes. Clinical and laboratory results showed, 24/25 patients were secretory, thus evaluated as positive for at least minimal residual disease. FCH-PET/CT scans were accepted positive in 22 of 25 patients; while 14 patients were positive on FDG-PET/CT scans. All FDG-positive patients were also FCH-positive. FDG&FCH were both positive in 14 patients; of whom 9 were FCH>FDG, but none were FDG>FCH. The sensitivity of FCH and FDG-PET/CT scans were calculated as 90% and 59%, respectively. The accuracy of FCH and FDG scans were calculated as 92% and 60%, respectively. ROC analysis showed that the AUC of FCH is higher than FDG (0.96 vs 0.79). There was no significant difference between the detection performance of early 10min and late 60min FCH scans. ***Conclusion:*** The results of this study suggest that the diagnostic performance of FCH-PET/CT is superior to FDG-PET/CT in the evaluation of patients with MM. Our data should be confirmed in larger series with different clinical scenarios.

EP-0348

Prognostic utility of baseline 18F-FDG PET/CT in relapsed and refractory Multiple myeloma patients treated with T-cell redirecting bispecific antibodies.

F. MINGUEZ[1], *V. Betech-Antar*[1], *L. Tamariz-Amador*[1], *A. Bronte Viedma*[1], *J. Rosales*[1], *J. Bastidas*[1], *C. von Gall*[2], *M. Romera*[1], *P. Echegoyen*[1], *F. Pareja del Rio*[1], *T. Cuenca*[1], *S. Menendez-Sanchez*[1], *L. García Belaustegui*[3], *L. Sancho*[3], *E. Guillen*[3], *E. Prieto*[1], *R. Ramos*[3], *J. Simon*[1], *M. Panizo*[1], *S. Huerga*[1], *J. San-Miguel*[1], *P. Rodriguez Otero*[1], *M. García-Velloso*[1];
[1]*Clínica Universidad de Navarra, Pamplona, SPAIN,* [2]*Siemens Healthineers, Molecular Imaging, Knoxville, TN, UNITED STATES OF AMERICA,* [3]*Clínica Universidad de Navarra, Madrid, SPAIN.*

Aim/Introduction: [^{18}F]FDG PET/CT is an accepted imaging technique for staging and monitoring patients with relapsed/refractory multiple myeloma (RRMM). Its prognostic value in patients treated with bispecific antibodies (BsAbs) has not been explored. We investigated the prognostic value of PET/CT before therapy with BsAbs in patients with RRMM. ***Materials and Methods:*** Forty-six patients with RRMM who had performed an FDG PET/CT before initiation of treatment with BsAbs were reviewed according to the IMPeTUS criteria with the 5-point Deauville score (DS) in bone marrow (BM) and focal lesions (FL), presence of paramedullary (PMD) and extramedullary (EMD) disease. Metabolic tumour volume (MTV) and total lesion glycolysis (TLG) were obtained using three-dimensional volume-of-interest isocontouring and bone was automatically segmented using work in progress syngo.via MI General Anatomy Segmentation software (Siemens Healthineers, Knoxville, TN). MTV and TLG for bone (BMTV and BLG), EMD (EMTV and ELG), and total (TMTV and TLG) were each calculated separately. Patients' outcome was analysed using the Kaplan-Meier method and Cox regression. ***Results:*** Median age was 64.2 years (IQR, 56 - 72 years) and 27 (58.7%) were male. PET/CT results were positive in 42 (91.3%) patients. Twenty (43.5%) patients had diffuse BM uptake with DS ≥ 4. FL were detected in 38 (82.6%) patients, with DS ≥ 4 in 35 (92.1%). PMD was present in 22 (47.8%) patients and EMD in 20 (43.5%). PET biomarkers are presented in Table 1 (PET BIOMARKERS).In the whole cohort of patients, EMD had no prognostic value. However, among patients with EMD, those with a EMTV >100 (n =7 [35%]) had shorter PFS (median 1.6 months [95% CI 0.7 - 2.7] versus 2.7 [95% CI 1.2 - 7.3] (p = 0.21); HR 3.9 [95% CI 1.2 - 12.4] (p=0.02) and shorter OS (median 2.8 months [95% CI 2.1 - 5.4] versus 6 [95% CI 2.9 - 11.9] (p = 0.16); HR 5.3 [95% CI 1.2 - 24.2] (p=0.03) than those with EMTV<100 (n = 13 [65%]). ***Conclusion:*** Baseline presence of EMTV >100 had significant impact on PFS and OS before therapy with BsAbs in patients with RRMM. In this series, neither TMTV nor TLG show prognostic impact regarding survival.

EP-0349

Comparison of C-11 Methionine and F-18 FDG PET/CT findings in evaluation of Multiple Myeloma: First Turkey Experience

*E. Özkan[1], **B. Demir**[1], G. Cengiz Seval[2], M. Araz[1], C. Soydal[1], M. Beksac[2], N. O. Kucuk[1];*
[1]Ankara University School of Medicine Department of Nuclear Medicine, Ankara, TÜRKIYE, [2]Ankara University School of Medicine Department of Hemotology, Ankara, TÜRKIYE.

Aim/Introduction: Despite advances in the treatment of Multiple Myeloma(MM), it stays as a disease that cannot be cured. The extent of the disease in diagnosis and follow-up, accurate evaluation of therapy response are important in terms of management and extending the survival. Although ^{18}F-FDG PET/CT is valuable in predicting disease prognosis, it does not have the enough sensitivity and specificity to determine disease activity. Methionine(MET), an amino acid labeled with carbon-11(C-11), performs better than ^{18}F-FDG in determining active lesions. In this study, the first ^{11}C-MET PET experience in Turkey and comparison with ^{18}F-FDG PET/CT findings was shared. ***Materials and Methods:*** Thirty-five PET images of 31 patients who underwent prospective ^{11}C-MET PET imaging with the diagnosis of multiple myeloma were evaluated. A total of 15 ^{11}C-MET and ^{18}F-FDG PET images were simultaneous in 13 of 31 patients. PET indication was for staging in 6 patients, treatment response in 2 patients, and restaging in 7 patients. For ^{11}C-MET PET, imaging was performed at 20th minute after activity injection of 6-10 MBq/kg. For ^{18}F-FDG, after 3-5 MBq/kg activity injection, imaging was performed at 60th minutes. Both methods were compared in terms of number of focal lesions, extramedullary disease, SUV and metabolic tumor burden. ***Results:*** While MET and FDG were positive in 12 examinations, more foci were detected with MET in 8 (67%) examinations. While active disease could not be detected with FDG in 1 case, it was shown to be positive with MET (MET+/FDG-). In one patient, FDG + lymph nodes suggestive of nodal disease were MET negative and myeloma involvement was also excluded histopathologically (MET-/FDG+). In 1 patient, FDG uptake in the ribs were MET negative and interpreted as false positive due to fracture. The mean SUV was 10.13 for MET and 4.83 for FDG (p=0.017). The mean metabolic tumor burdens determined by MET and FDG were 215.95 and 44.18, respectively (p=0.001). Disease foci that could not be detected by FDG in the paramedullary area in 5 examinations, in the extramedullary area in 2 examinations and in the medullary area in 4 examinations were demonstrated with MET PET. ***Conclusion:*** Although the study has significant limitations in terms of patient number and heterogeneity, it shows that MET is a more sensitive method than FDG PET in detecting myeloma lesions. The prognostic value and treatment response of MET need to be included in the assessment of a larger number of homogeneous patients.

EP-0350

Role of 18F-FDG PET/CT in patients with Castleman disease

***R. Goel**, N. Damle, Y. Dharmashaktu, C. Bal, M. Tripathi, R. Kumar, P. Kumar;*
All India Institute of Medical Sciences (AIIMS), New Delhi, INDIA.

Aim/Introduction: Castleman disease (CD) is a rare, nonclonal lymphoproliferative disorder. Due to its ability to affect lymph nodes of any part of the body, Castleman disease is a great mimic of both benign and malignant conditions. This study aims to evaluate the role of 18F FDG PET/CT in patients with clinical suspicion of Castleman disease. ***Materials and Methods:*** We retrospectively reviewed 15 18F-FDG PET/CT scans in 12 patients with clinical suspicion of Castleman disease at our institution between January 2017 and April 2023. The lesion SUVmax and lesion-to-liver uptake ratios were also measured. ***Results:*** There were 12 patients (4 females, 8 males; age 9-63 years) who underwent a total of 15 18F-FDG PET/CT scans. Out of the 15 scans, 6 were performed for diagnosis, 6 for response assessment, and 3 for surveillance/suspected recurrence. Out of the 6 scans done for diagnosis, 5/6 patients were confirmed to have Castleman disease on histopathology. Histopathology of 1/6 patients revealed a T cell lymphoma. Lymphadenopathy with increased FDG uptake was seen in 4/5 patients with CD and they had involvement of two or more nodal groups (MCD). 1/5 patients demonstrated involvement of single group of lymph nodes (UCD). The average size of lymph nodes involved was 2.1 cm (short axis dimension). Two patients with MCD also demonstrated hepatosplenomegaly. The median SUVmax and median lesion-to-liver ratios of the 5 patients with CD were 2.6 (range 1.5-14.7) and 0.87 (range 0.66-4.6) respectively. Out of the 6 scans performed for response assessment, 4 showed stable disease and 2 showed partial response. Of the three scans performed for surveillance/suspected recurrence 1 revealed metabolically active right cervical, right axillary, mesenteric and abdominopelvic lymph nodes, later confirmed to be recurrent disease. ***Conclusion:*** 18F-FDG PET/CT may play an important role in

identifying lymph nodes and lesions that are more likely to yield a definitive diagnosis on biopsy, defining extent of disease (UCD versus MCD), monitoring response to treatment, and detection of suspected recurrence in patients with Castleman disease which would help in their overall management. However, more studies on a larger patient population are required to validate the same.

EP-0351

Talquetamab, a Novel Anti-Myeloma GPRC5DxCD3 Bispecific Antibody, is Associated with Increased Oropharyngeal FDG Uptake

J. Trak, *T. Mouhieddine, G. Lancman, L. Sanchez, A. Chari, M. Ghesani;*
Mount Sinai Hospital, New York, NY, UNITED STATES OF AMERICA.

Aim/Introduction: Talquetamab (JNJ-64407564) is a first-in-class bispecific antibody that directs CD3+ T cells to G protein-coupled receptor class C group 5 member D (GPRC5D), which is highly expressed on primary multiple myeloma cells. However, up to 36% and 48% of patients receiving the recommended phase 2 dose (RP2D) (≥400 mcg/kg), reported dysgeusia. Nevertheless, the rate of talquetamab discontinuation secondary to oral toxicity remained less than 5%. While GPRC5D has limited expression in normal human tissues, RNA sequencing data has revealed GPRC5D expression in resident plasma cells of the salivary glands and tonsils. In order to better understand the potential pathophysiology underlying talquetamab-related oropharyngeal symptomatology, we characterized changes in 18F-fluorodeoxyglucose (FDG) uptake on positron emission tomography/computed tomography (PET/CT) imaging in patients enrolled in clinical trials of talquetamab. ***Materials and Methods:*** Eighty-seven patients that received talquetamab monotherapy between January 2018 and 2023 were evaluated by collecting the following parameters from PET/CTs and patient charts prior to and during/within 60 days of talquetamab discontinuation: bilateral parotid and submandibular gland SUVmax, radiotracer injected dose and circulation time, talquetamab dose(s), dysgeusia, and xerostomia. 58 patients had complete PET/CT profiles (non-I&C-adjusted). 29 patients had injected doses and FDG circulation times within a 20% margin (I&C-adjusted). Two sets of paired t-tests were performed. ***Results:*** Radiologically, paired t-test of the I&C-adjusted cohort (n=29) demonstrated a statistically significant increase in FDG uptake in the left submandibular gland in PET/CT imaging acquired during/after talquetamab therapy compared to that acquired prior to initiation of talquetamab (p=0.041). Paired t-test of the non-I&C-adjusted sample (n=58) demonstrated a statistically significant increase in FDG uptake in the right and left parotid, and left submandibular glands in PET/CT imaging acquired during/after talquetamab therapy compared to that acquired prior to talquetamab (p=0.006, 0.039, and 0.001, respectively). Clinically, in the I&C-adjusted sample, 34.5% (10/29) of patients reported grade 2 dysgeusia, 37.9% (11/29) reported grade 1, and 27.6% (8/29) did not report any dysgeusia. 17.2% (5/29) reported grade 2 xerostomia, 34.5% (10/29) reported grade 1, and 48.3% (14/29) did not report any xerostomia. ***Conclusion:*** While patients did not have clinically apparent changes in salivary glands on physical exam, the increase in FDG uptake in the bilateral parotid and left submandibular glands may suggest an ongoing inflammatory process. We hypothesize that this may reflect off tumor/on-target mediated T cell trafficking and hence a potential mediator of dysgeusia and xerostomia that warrants further detailed clinical characterization and tissue sampling.

EP-0352

A follow up of 30 patients with multiple myeloma confirmed: prognostic role of number of focal lesions and SUV max at diagnosis in 18F-FDG PET/CT

I. López Villar[1], *V. Castillo Morales*[1], *I. Hernández Pérez*[1], *A. García Noblejas*[2], *S. Hernández Muñiz*[3], *I. Salmerón Beliz*[3], *J. Alonso Farto*[4], *D. Zamudio*[4], *N. Gómez de Leon*[3];
[1]*Princesa University Hospital, Nuclear Medicine Service, Madrid, SPAIN,* [2]*Princesa University Hospital, Hematology Service, Madrid, SPAIN,* [3]*Princesa University Hospital, Radiology Service, Madrid, SPAIN,* [4]*Gregorio Marañón University Hospital. Nuclear Medicine Service, Madrid, SPAIN.*

Aim/Introduction: Flurodeoxyglucose Positron Emisión Tomography (18F-FDG-PET/CT) is a useful molecular imaging in staging and follow up of multiple myeloma patients. ***Materials and Methods:*** A baseline and follow -up study of 30 MM was carried out in University Hospital (January 2018-January 2023), Male 19 Female 11; age range:36-91 years, mean 65+/- 11.0 years). We were referred by hematologist for baseline PET/CT, after induction PET/CT and after autologous transplant PET/CT.The PET criteria for active MM were defined as focal bone lesions with visually increased 18F-FDG uptake and/or SUV max superior to 4.0 and/or diffused bone marrow metabolism superior to liver. We then correlated with number of focal lesions, SUV max and if there is extramedullary disease at baseline. ***Results:*** 30 patients with pathohistochemical examinations confirmed with MM. Of this 30 MM patients: 18F-FDG PET-CT baseline identified 20/30 p (66.7%). PET false negative was seen in 10/30 p (33,3%).Of the 20/30 patients detected by FDG tracer, the number of focal lesions were superior to 3 in 20/30, SUV max at diagnosis were superior to 4.5 in 18/20 and SUV max focal inferior or equal 4,5 in 2/20.None of the 20/30 patients had extramedullary disease at baseline. Complete FDG supresión after induction was seen in 20/30 p.Of the 20 patients detected by FDG PET, 15/20 patientsunderwent autologous transplant. Complete FDG supresión after transplant was seen in all the patientes (15) with follow up range 5 months-5 years, therefore is required longer follow-up and more studies are needed to detect the role of novel therapies (antibodies, chimeric antigen receptor (CAR) T cells etc. ***Conclusion:*** In our study: sensitivity of 18F-FDG PET-CT for detecting myeloma bone disease was 66.7% (20/30 p). False negative was seen in 10/30 (33,3%) patients with MM confirmed and could be associated with low hexokinase-2 expression.None of the 20 p (20/30) identified by PET had extramedullary disease at baseline.Complete FDG supresión after induction was seen in the 20 patients identified by PET.There is no significant associattion between SUV max and response after induction and response after transplant. Long term studies are needed.

EP-0353

[11C]-Methionine as Novel Image Biomarker of Disease Activity in Newly Diagnosed Multiple Myeloma Patients - Comparison with [18F]-FDG

S. Serfling[1], *M. Bittrich*[1], *A. K. Buck*[1], *T. Higuchi*[1], *S. Samnick*[1], *K. M. Kortüm*[1], *L. Rasche*[1], *H. Einsele*[1], *R. A. Werner*[1], *S. Knop*[2];
[1]*University Hospital Würzburg, Würzburg, GERMANY,* [2]*Klinikum Nürnberg Nord, Nürnberg, GERMANY.*

Aim/Introduction: Based on accumulation in altered immunoglobulin productions, [11C]-Methionine has demonstrated improved read-out in patients with multiple myeloma (MM) in retrospective settings. We aimed to determine the diagnostic performance of [11C]-Methionine relative to [18F]FDG in patients enrolled in a prospective Phase III trial.

Materials and Methods: 11 newly diagnosed, symptomatic multiple myeloma (MM) patients have been scanned as part of the clinical Phase III DSMM XVII trial (NCT03948035). At baseline, all subjects were scheduled for a dual-tracer approach using [11C]-Methionine and [18F]FDG. Individuals remained treatment-naïve between both scans. We then conducted a visual and quantitative assessment, determining maximum standardized uptake (SUV_{max}) values and target-to-background ratios (TBR) in sites of disease. SUV_{max} was then compared to serologic markers at time of imaging, including M component, serum free light chains (FLC), Bence-Jones-protein (BJ), lactate dehydrogenase (LDH), and Beta-2 microglobulin (B2M). Correlative analyses were performed using Spearman's Method. ***Results:*** On a visual assessment, [18F] FDG and [11C]-Methionine were rated positive in all patients (11/11 [100%], respectively). In 4/11 instances (36.4%), the latter radiotracer provided a higher detection rate on lesion-based level. On a quantitative assessment, we recorded increased SUV_{max} for [11C]-Methionine (10.0 ± 5.0 vs [18F]FDG, 6.3 ± 3.5; P=0.058). Indicative for improved image contrast, TBR were also substantially elevated for [11C]-Methionine (12.1 ± 7.9 vs [18F]FDG, 4.1 ± 2.8, P<0.01). When compared to markers of disease activity, [18F] FDG-derived SUV_{max} failed to reach significance (M component, FLC, BJ, LDH, B2M, P≥0.34). [11C]-Methionine, however, exhibited relevant associations with M component (R=0.7 [95% CI, -0.38-0.77], P<0.05), along with improved associations with other serologic markers (FLC, BJ, LDH, B2M, P≥0.2). ***Conclusion:*** [11C]-Methionine provides improved image contrast when compared to [18F]FDG in newly diagnosed MM patients and thus, allows for a more comprehensive read-out of myeloma manifestations. Future analyses of this cohort will investigate whether [11C]-Methionine also emerges as an image biomarker to monitor disease activity under novel targeted therapies.

EP-0354

Multiple Myeloma: a comparison between 18F-FDG-PET/CT and 68Ga-PSMA-PET/CT

D. Bezzi[1], *E. Zamagni*[2], *S. Fanti*[3], *L. Vetrone*[1], *M. Talarico*[2], *C. Malizia*[3], *C. Nanni*[3];
[1]*Nuclear medicine, Alma Mater Studiorum University of Bologna, Bologna, ITALY,* [2]*Seràgnoli Institute of Hematology, Bologna University, Bologna, ITALY,* [3]*Nuclear Medicine Unit, IRCCS Azienda Ospedaliero-Universitaria di Bologna, Bologna, ITALY.*

Aim/Introduction: The aim of this study was to assess the possible added value(especially in the light of theranostic approaches) and limitations of 68Ga-PSMA-PET/CT(PSMA-PET) to that of 18F-FDG PET/CT(FDG-PET) in the evaluation of myelomatous disease. ***Materials and Methods:*** We prospectively enrolled 21 consecutive patients with newly diagnosed symptomatic multiple myeloma(MM) who underwent FDG-PET and PSMA-PET, performed 0-14 days apart. The results of the two scans were compared in terms of the number of focal bone lesions(FL) and paramedullary lesions(PM), SUVmax of the hottest FL and hottest PM, and presence of diffuse pathologic bone marrow(BM) involvement. Wilcoxon rank test was used to compare SUVmax of FDG-PET and PSMA-PET. ***Results:*** A total of 245 focal lesions were detected, of which 235 were FL and 10 PM. FDG-PET detected 229/245(93%) lesions in 13 patients and PSMA-PET 61/245 (25%) lesions in 12 patients. Sixteen(7%) lesions were detected by PSMA-PET alone and 184(75%) by FDG-PET alone. FDG-PET and PSMA-PET identified 10 and 9 PM respectively, while isolated BM involvement was detected in 2 and 1 patient respectively. Seventeen patients(80%) had concordant FDG-PET and PSMA-PET scans while 4 patients(20%) had discordant scans. Regarding concordant scans, 5 patients had both negative scans while 12 patients had both positive scans. Six patients(29%) had positive FDG-PET and PSMA-PET scans identifying the same number and sites of myelomatous lesions. The remaining six patients(29%) had positive FDG-PET and PSMA-PET scans, but identified different number of lesions; indeed in 4 patients FDG PET identified more lesions (203 vs 25), while PSMA-PET did so in 2 patients (22 vs 7). Regarding discordant scans, 3 patients(14%) had a positive FDG-PET scan and a negative PSMA-PET, while 1 patient had a positive PSMA-PET and a negative FDG-PET. The highest FL-SUVmax of FDG-PET and PSMA-PET had a median(min-max) of 5,8(2,2-34,4) and 5,4(2-8,6) respectively, the highest PM-SUVmax had a median of 5,1(2,7-14,4) and 5,1(1,2-10), both with no significant difference at statistical analysis(pFL= 0,3,pPM= 0,93). Notably, the hottest SUV max in PSMA scans was higher than liver uptake in only 2/13 positive PSMA scans(SUVmax 10 and 9,1 vs liverSUVmax of 7,9 and 8,5 respectively). ***Conclusion:*** According to these preliminary data, FDG-PET appears to be more sensitive than PSMA-PET for the detection of myelomatous lesions; furthermore the PSMA uptake was low in the majority of cases (lower than the liver). These data need to be confirmed in larger series to evaluate the role of PSMA in the MM.

EP-0355

Sarcopenia and metabolic parameters of [18F]-FDG PET/CT in patients with multiple myeloma. Preliminary results.

A. Palomar-Muñoz[1], *S. Hermosa-García*[2,3], *I. Sánchez-Rodríguez*[1], *Y. Benavente*[2,3], *J. A. Jorge-Novoa*[2], *V. Carrero-Vásquez*[1], *B. Hervás-Sanz*[1], *E. Garamundi-Grimalt*[4], *G. Bustamante-Ramírez*[5], *E. Cabezudo-Pérez*[6], *M. Cortés-Romera*[1], *D. Casabonne*[2,3], *the IBERICAT/IMMAGE study collaborators;*
[1]*Nuclear Medicine Department, Hospital Universitario Bellvitge, L'Hospitalet de Llobregat (Barcelona), SPAIN,* [2]*Catalan Institute of Oncology (ICO), Bellvitge Biomedical Research Institute (IDIBELL), L'Hospitalet de Llobregat (Barcelona), SPAIN,* [3]*Consortium for Biomedical Research in Epidemiology and Public Health (CIBERESP), Madrid, SPAIN,* [4]*Pathological Anatomy Department, Hospital Universitario Bellvitge, L'Hospitalet de Llobregat (Barcelona), SPAIN,* [5]*Hematology Department, Catalan Institute of Oncology (ICO), L'Hospitalet de Llobregat (Barcelona), SPAIN,* [6]*Hematology Department, Catalan Institute of Oncology (ICO) Hospital Sant Joan Despí Moisés Broggi, Sant Joan Despí (Barcelona), SPAIN.*

Aim/Introduction: Multiple myeloma (MM) is a malignant neoplasm of plasma cells in the bone moarrow, classified as an obesity-associated cancer. Sarcopenia, defined by a reduction in muscle mass, occurs commonly with aging ad it has an overall poor clinical outcome. The aim of our work was to evaluate sarcopenia and metabolic parameters obtained in [18F]-FDG PET/CT, in patients with MM. ***Materials and Methods:*** The IMMAGE study consists of quantifying body composition in patients with MM that underwent a staging [18F]-FDG PET/CT and examine its association with prognosis factors. Skeletal muscle (SM) and musculoskeletal index (SMI defined by skeletal muscle mass area/height^2) measured at the L3 level on the CT image were coupled with glycidic quantification from PET images using the MIM Encore® software. Maximum and mean standardized uptake value (SUVmax and SUVmean), metabolic volume and total lesion glycosis (TLG) at skeletal muscle were all categorized into 2 categories based on the median (low/high). Sarcopenia was estimated using cut-off points: males BMI≥25; SMI<53 cm^2 /m^2;

males BMI<25; SMI<43 cm2 /m^2; females SMI<41 cm^2 /m^2). Odd Ratios (OR) and 95% confidence intervals (CI) were estimated using logistic regression models adjusted by age and sex using Stata v16. ***Results:*** We analysed a total of 49 patients (32 males, mean age 67 years old -SD 12 range 39 to 87 years old-), 33 (67%) of them were overweight or obese. Twenty-one patients (43%) present sarcopenia and age mean was higher among patients with sarcopenia (69 years old SD: 12) than those without sarcopenia (65 years old, SD: 12) and no differences by sex (among 47% female and 41% male). In patients with sarcopenia the mean SUVmean and metabolic volume values were 0.75 and 26.6 while in non-sarcopenic patients they were 0.64 and 37.42 respectively. Sarcopenia was associated with high SUVmean values (OR: 4.64; 95% CI, 1.29 to 16.71), high metabolic volume values (OR: 0.09; CI95% 0.01 to 0.54), while no differences were found with SUVmax (p = 0.14) and TLG (p = 0.07). ***Conclusion:*** This preliminary results show high prevalence of sarcopenia in MM patients. The [18F]-FDG PET/CT variables, SUVmean and metabolic volume, could be useful to classify patients with sarcopenia and to evaluate further the prognosis of MM patients. ***References:*** Sergentanis TN et al, Clin Lymphoma Myeloma Leuk 2015; Martin L et al, J Clin Oncol, 2013

EP-0356

[18F]- FDG PET/CT prognostic value in the assessment of multiple myeloma patients treated with CAR-T therapy

M. Tormo-Ratera[1], *I. Zugasti*[2], *A. Oliver-Caldes*[2], *V. González-Calle*[3], *V. Cabañas*[4], *P. Rodríguez-Otero*[5], *J. Reguera*[6], *M. Mateos*[7], *K. Quintero*[1], *S. Casanueva-Eliceiry*[1], *M. Cibeira*[8], *A. Niñerola-Baizan*[1], *X. Tomas*[9], *L. Rosiñol*[2], *P. Tamayo*[10], *M. García-Velloso*[11], *C. Fernández de Larrea*[2], *X. Setoain*[1];
[1]*Department of Nuclear Medicine, Hospital Clínic., Barcelona, SPAIN,* [2]*Hospital Clínic. Institut d'Investigació Biomèdica August Pi i Sunyer., Barcelona, SPAIN,* [3]*Instituto de Investigación Biomédica de Salamanca (IBSAL), Salamanca, SPAIN,* [4]*Hospital Clínico Universitario Virgen de la Arrixaca., IMIB-Arrixaca, SPAIN,* [5]*Clínica Universidad de Navarra, Centro de Investigación Médica Aplicada (CIMA), Pamplona, SPAIN,* [6]*Hospital Universitario Virgen del Rocío, Sevilla, SPAIN,* [7]*Hospital Universitario de Salamanca, Salamanca, SPAIN,* [8]*Department of Hematology, Hospital Clínic., Barcelona, SPAIN,* [9]*Department of Radiology, Hospital Clínic., Barcelona, SPAIN,* [10]*Department of Nuclear Medicine, University Hospital of Salamanca, Salamanca, SPAIN,* [11]*Nuclear Medicine Department, Clínica Universidad de Navarra, Pamplona, SPAIN.*

Aim/Introduction: The aim of this study is to describe the outcome of relapsed/refractory multiple myeloma (RRMM) patients treated with Chimeric antigen receptor T-Cell therapy (CAR-T) and to evaluate the prognostic value of baseline [18F]-FDG PET/CT visual parameters . ***Materials and Methods:*** Forty-six patients with RRMM treated with CAR-T from a multicentre study were included. Visual parameters based on the Italian Myeloma for PET use (IMPeTUs) were used for the baseline PET/CT evaluation. We assessed the presence of bone marrow (BM) diffuse uptake, more than 3 osteolytic lesions with FDG uptake (>3L) and the type of plasmacytoma (paramedullary vs. extramedullary). We analysed the contribution of baseline PET variables in the prediction of progression-free survival (PFS) and overall survival (OS) in the whole group. Statistical analysis was performed using SPSS software. Survival analysis was calculated using the log-rank test. ***Results:*** The results showed 39% of patients (18/46) with an increased diffuse BM uptake and 52% (24/46) with >3L. Plasmacytomas were present in 48% of patients (22/46), 33% (15/46) paramedullary and 15% (7/46) extramedullary. After a mean follow-up of 23 months the median PFS was 21.8 months (95%CI 14.7-29.1) and median OS was not reached with an OS rate at 18 months of 74%. An increased diffuse BM uptake or the presence of >3L did not have an impact in PFS or OS. The presence of plasmacytomas did not impact PFS (p=0.49), but median OS in patients with and without plasmacytomas was 18.8 months (95%CI 14.9-22.7) vs. not reached (NR), respectively, reflecting the difficulties in treating these subset of patients after CAR-T. In terms of the type of plasmacytoma, patients with paramedullary plasmacytomas had a similar PFS and OS compared to patients without plasmacytomas, but patients with extramedullary plasmacytomas had a shorter PFS [7.5 months (95%CI 1.6-13.3) vs. 22.3 months (95%CI 13.7-30.9); p=0.026] and OS [9.2 months (95%CI 4.8-13.6) vs. NR (95%CI NR-NR); p=0.002]. ***Conclusion:*** An increased diffuse BM uptake or the presence of >3L do not have an impact in PFS and OS in this cohort. The presence of extramedullary plasmacytomas has prognostic impact in terms of both PFS and OS. No differences were observed between patients with paramedullary vs. without plasmacytomas. These results highlight a potential value of baseline PET/CT for the evaluation of response after BCMA CAR-T therapy and the identification of high-risk patients.

EP-0357

Prognostic value of 18F-FDG PET/CT biomarkers in patients with diffuse large B-cell lymphoma treated with chimeric antigen receptor T-cell therapy Preliminary results.

J. Cañadas Salazar*, A. Martín Lopez, L. G. Díaz González, C. Montes fuentes, A. Martín García-Sancho, P. Tamayo Alonso; Sacyl, Salamanca, SPAIN.*

Aim/Introduction: Evaluate the prognostic value of PET biomarkers, such as metabolic tumor volume(MTV), total lesion glycolysis(TLG) and standard maximum uptake value(SUVmax), on the outcome of patients diagnosed with diffuse large B-cell lymphoma treated with chimeric antigen T-cell receptor (CART). ***Materials and Methods:*** We prospectively analyzed patients diagnosed with diffuse large B-cell lymphoma who received CD19-targeted CAR-T cell therapy at our center between March 2019 and January 2022. Patients underwent PET/CT studies with 18F-FDG before treatment and at 28 days post infusion. Pre-treatment serum lactate dehydrogenase (LDH) values and the presence of bulky tumor (<7cm) were defined. Treatment response was assessed by 18F-FDG PET/CT 28 days after infusion using the Deauville criteria. Two nuclear medicine specialists measured PET biomarkers with MIM(v7.0.6) software at each time point, and statistical analysis was performed with IBM_SPSS(v.25) statistical software. ***Results:*** 44 patients were selected, 25 men and 19 women, with a mean age of 60 years (range 32-76). Before treatment 36 (81%) patients had advanced stage, 26 (59%) an increased LDH level and 17 (38%) had bulky disease. The mean values of baseline PET/CT biomarkers obtained in the complete response group were MTVcr:229.6 ml, TLGcr:1903.59 and SUVmaxcr: 16.07; and of the group that did not achieve complete response MTVpr: 448.47ml, TLGpr: 4072.05 and SUVmaxpr: 24.09 demonstrating higher values in the groups that did not achieve complete response. The Mann-Whitney U test was performed on each biomarker for the presence or absence of complete metabolic response, without observing statistical significance in any of them (p>0.05) ***Conclusion:*** PET biomarkers, in this instance, do not appear to show a relationship in predicting response to CART therapy. Although they do not show a statistically significant relationship in this study, this may be due to the small sample size. Further follow-up and number of patients is required.

EP-20

e-Poster Area

B: Imaging Clinical Studies -> B1 Oncological Imaging Clinical Study -> B23 Bone and Soft Tissues

EP-0358

Dual time point [18F]FDG PET/CT can differentiate benign from malignant soft tissue tumors and outperforms the diagnostic performance of conventional PET/CT acquisition

P. D'Abadie, *O. Gheysens, R. Lhommel, T. Kirchgesner, A. De Roo, T. Schubert;*
Cliniques universitaires Saint Luc, Brussels, BELGIUM.

Aim/Introduction: ^{18}F-FDG-PET/CT can be used for the workup of soft tissue tumors (STT) but it ability for differentiating malignant from benign tumors remains controversial, with risks of false positive and negative results[1]. The aim of this study is to evaluate if dual time point PET/CT can predict with higher accuracy malignant STT. ***Materials and Methods:*** Patients with undetermined STT were prospectively enrolled in this study. ^{18}F-FDG PET/CT imaging was performed at 1h (t1) and 3h (t2) post [^{18}F]FDG injection. Delta SUV max ((SUVmax$_{t2}$ - SUVmax$_{t1}$)/ SUVmax$_{t1}$) x 100) was calculated for each tumor. Metabolic parameters were compared to histological results. The diagnostic performance of delta SUV max and SUVmax$_{t1}$ were measured using ROC curves and cutoffs defined using the Youden index. ***Results:*** 62 patients were included corresponding to 20 benign and 42 malignant tumors. Delta SUV max was significantly higher in malignant STT compared to benign STT (mean: + 16.6 % versus - 6.7 %, p <0.001). Delta SUVmax > 14% predicts tumor malignancy with a specificity (Sp) of 90% and a sensitivity (Se) of 67%. SUVmax$_{t1}$ >4.5 was less accurate with a Sp of 80% and a Se of 57%. In a subgroup of tumors with at least a slight metabolism activity at t1 (SUVmax> 2.5; n= 44), delta SUVmax significantly outperformed the diagnostic performance of SUVmax$_{t1}$ with a Sp of 100% (vs 70%) and a Area Under the ROC Curve of 0.82 (vs 0.63, p: 0.007). ***Conclusion:*** Dual time point [^{18}F]FDG PET/CT identifies malignant STT tumors with high specificity and outperforms the diagnostic performance of conventional PET/CT acquisition. ***References:*** 1- Shin et al. The clinical efficacy of ^{18}F-FDG-PET/CT in benign and malignant musculoskeletal tumors. Ann Nucl Med (2008) 22: 603-609.

EP-0359

Prognostic Value of Pre-Treatment F-18 FDG PET/CT Parameters in Soft-Tissue Sarcomas

I. Ak Sivrikoz, *H. Deveci, E. Çinçin;*
ESOGU School of Medicine Department of Nuclear Medicine, Eskisehir, TÜRKIYE.

Aim/Introduction: Soft-tissue sarcomas (STSs) are cancerous growths of mesenchymal tissues, most commonly arising from fat, muscles, and other connective tissues. Most soft tissue sarcoma (STS) has a high affinity for 18F-FDG, which is why 18F-FDG PET/CT has been proposed as a non-invasive method, useful in diagnosis and follow-up. The aim of the present study was to investigate the value of PET parameters of pre-treatment F-18 FDG PET/CT as prognostic factors in overall survival (OS) and progression-free survival (PFS) in patients with STSs. ***Materials and Methods:*** A retrospective study was conducted on 76 consecutive patients with primary locally advanced or distant metastatic STS, who underwent an F-18 FDG PET/CT before surgery or neoadjuvant treatment at our Institute between June 2014 and December 2020. A final cohort of 31 patients (mean age 61,87±17, 21 Male, 10 Female) was finally analysed. PET parameters (SUVmax, SUVmean, MTV and TLG values) were calculated according to the literature and tested as predictive factors for progression-free survival (PFS) and overall survival (OS), defined as the period starting from the date of first treatment and disease relapse or death, respectively. ***Results:*** There were 5 Liposarcoma, 4 fibrosarcoma, 7 malignant fibrous histiocytoma, 4 synovial sarcoma, 2 leiomyosarcoma, 2 rabdomyosarcoma and 7 other sarcomas. All tumors showed a significantly high and variable degree of FDG uptake, with a mean SUVmax of 12.39 ± 6.23 (range 4.3-49.4). The mean MTV and TLG were 388.61 cm3 (1.8-2115 cm3) and 1876.84 (6.82-9756), respectively. The mean follow-up time for all patients was 36 mounts. The mean PFS was 17.44 mounts. There was no significant correlation between SUVmax, SUVmean, MTV and TLG values and PFS (0.34, 0.63, 0.15 and 0.08, respectively). In total, 18 out of 31 patients died during the observation period. The mean OS was 21.6 months (95% CI: 16-not reached), with a survival rate of 58% at 1 year. There were no significant correlation between SUVmax, SUVmean, MTV, TLG values and both PFS (0.34, 0.63, 0.15 and 0.08, respectively) and OS (0.3, 0.6, 0.44, 0.26, respectively). ***Conclusion:*** In conclisuon; There were no significant association for PET parameters with PFS and OS in patients with STSs. If the prognostic value of this feature is confirmed in prospective studies with larger populations, it could be proposed to predict PFS and OS in high-risk patients with STSs.

EP-0360

Association of 'Hot Kidneys' on Bone Scintigraphy and Serum Ferritin Levels

I. Kuji[1], *K. Watanabe*[1], *E. Ryuta*[1], *Y. Matsusaka*[1], *A. Seto*[1], *I. Matsunari*[2];
[1]*Department of Nuclear Medicine, Saitama Medical University International Medical Center, Hidaka, Saitama, JAPAN,* [2]*Department of Nuclear Medicine, Saiatama Medical University Hospital, Saitama Medical University, Moroyama, Saitama, JAPAN.*

Aim/Introduction: The mechanism of 'hot kidneys' on bone scintigraphy is not well understood[1]. Renal accumulation is influenced by various factors, like renal function, nephritis, bone metabolism abnormalities, etc. We found high serum levels of ferritin in patients with autoimmune and malignant diseases who had high renal accumulation on bone scintigraphy. Therefore, we investigated the association. ***Materials and Methods:*** We retrospectively analysed data of patients who underwent bone scintigraphy and serum ferritin measurement within 1 month. Serum ferritin level was measured for anaemia scrutiny, except in cases of polyarthritis. Bilateral renal cortex counts were measured on the posterior whole-body image avoiding the ribs, and lumbar spine counts were measured avoiding degenerative changes. The renal to vertebral bone accumulation ratio of the average count per pixel was calculated as the K/V ratio, and its correlation with the blood levels of ferritin, iron, creatinine, C-reactive protein, haemoglobin, and alkaline phosphatase, as well as white and red blood cell counts was analysed using Spearman's rank correlation coefficient. Renal accumulation was also visually evaluated on a five-point scale compared to the rib and lumbar accumulation on bone scintigraphy. ***Results:*** A total of 22 patients with high renal

accumulation were included, 8 with suspected polyarthritis, 2 with amyloidosis, and 12 with malignant tumours. The mean interval between bone scintigraphy and blood collection for ferritin level measurement was 7.8±8.9 days. There was a significant correlation between the K/V ratio and ferritin level (r=0.66, p<0.001), red blood cell count (r=0.56, p=0.007), and haemoglobin level (r=0.58, p=0.005). However, there was no correlation with the following parameters, which are thought to be related to nephritis, and iron and bone metabolism: creatinine (r=0.27, p=0.22), C-reactive protein (r=-0.11, p=0.61), white blood cell count (r=-0.19, p=0.41), iron (r=0.33, p=0.21), and alkaline phosphatase (r=-0.038, p=0.88). There was also a significant correlation between the K/V ratio and the visual evaluation score (r=0.86, p<0.001). ***Conclusion:*** There was a significant correlation between serum ferritin levels and increased renal accumulation on bone scintigraphy. The detailed mechanism is unknown, but it was suspected to be related to changes in the red blood cell count caused by the red blood cell destruction unrelated to iron deficiency. ***References:*** 1. Bernard MS, Hayward M, Hayward C, et al. Evaluation of intense renal parenchymal activity ("hot kidneys") on bone scintigraphy. Clin Nucl Med. 1990; 15: 254-6.

EP-0361

Prognostic value of metabolic parameters of 18F-FDG PET-CT in the staging of adult soft tissue sarcomas

A. Berardinelli[1], *M. Meneses Navas*[1], *G. Cuesta Domingo*[1], *P. Nespral Torres*[1], *P. Romero Fernández*[1], *P. Dauden Oñate*[1], *P. Bascuñana*[1], *A. Crespo*[2], *M. Cabrera Martín*[1];
[1]*Department of Nuclear Medicine, Instituto de Investigación Sanitaria San Carlos (IdISSC), Hospital Clínico San Carlos, Universidad Complutense, Madrid, SPAIN,* [2]*Department of Radiology, Hospital Clínico San Carlos., Madrid, SPAIN.*

Aim/Introduction: Our purpose was to study the prognostic value of metabolic parameters of pre-treatment 18F-FDG PET/CT in adult patients with soft tissue sarcomas diagnosis, and their relationship with distant disease and overall survival. ***Materials and Methods:*** Seventy-six patients with pathologically confirmed soft tissues sarcomas who underwent 18F-FDG PET/CT for initial staging before treatment were retrospectively analyzed. Histological grade, percentage of necrosis, age at diagnosis, stage, and tumour recurrence were recorded as variables, as well as the maximum standardized uptake value (SUVmax), metabolic tumour volume (MTV), and total lesion glycolysis of the primary tumour (TLG). These parameters were measured using syngo.via software. The threshold at which these biomarkers correlated with the presence of distant disease was determined using ROC curves, and the relationship between these variables and overall survival (OS) was then evaluated using Kaplan-Meier analysis. Multivariate analysis was perform for survival prediction and Hazards Regression Plot. ***Results:*** Of the 76 patients, 68.4% were male with a mean age of 58.03±17.58 years; range 21-90. The maximum standardized uptake value (>12.3) and total lesion glycolysis of the primary tumour (>504) showed the best correlation with M1 (AUC 0.72). Patients with >10.5 SUVmax had worse survival, with a mean of 14 months (9-44;95% CI) compared to patients with lower SUVmax, with a mean of 89 months (95% CI). ***Conclusion:*** Initial 18F-FDG PET/CT in soft tissue sarcomas offers a more accurate TNM staging, and metabolic biomarkers appear to provide prognostic information, which could favour a more personalized treatment for each patient.

EP-0362

Utility of metabolic indices in 18F-FDG-PETCT for prediction of presence, patterns and sites of metastases in patients with osteosarcoma

N. Kundu, *S. Sagar, D. Khan, A. Roy, R. Goel, M. Y S, R. V, R. Kumar; AIIMS New Delhi, Delhi, INDIA.*

Aim/Introduction: 18F-FDG-PET/CT is widely used for staging of osteosarcoma based on increased glucose uptake by malignant cells. The degree of 18F-FDG uptake, as expressed by standardized uptake value (SUV), can be measured and quantified by 18F-FDG-PET/CT. The role of metabolic indices, such as SUVmax, MTV and TLG in predicting presence of metastases and patterns of spread of osteosarcoma is unknown. Our study aims to assess the utility of metabolic indices in 18F-FDG-PET/CT to predict the presence and pattern of metastases in osteosarcoma patients. ***Materials and Methods:*** At our center in India, we conducted a retrospective study that included 20 patients referred to our department with known osteosarcoma for baseline staging or tumour recurrence between January 2019 and December 2022. All patients underwent F^{18}FDG-PETCT according to department protocol. Imaging parameters like maximum standardized uptake value (SUV max), metabolic tumor volume (MTV) and total lesion glycolysis (TLG) of primary lesion were measured. Two experienced nuclear medicine physicians reviewed the scans, and presence of metastases was recorded such as presence of soft tissue component (STC), skip lesions(SL), lymph node (LNM), lung (LM) and distant bony metastases(DBM) and muscle deposits (MD) and the data was analysed. ***Results:*** Out of 20 patients included in the study, 13 were male and 7 were female, with average age of 18.9±12.5 years (range 7-62 years). Out of 20 patients, 10 had soft tissue component,7 had distant metastases, , 4 had skip lesions, 5 had lung metastases, 6 had lymph node metastases, 6 had muscle deposits/infiltration, 3 had bony metastases. The SUV max, MTV and TLG of patients with metastases were 63.40±40.6, 107.47±127.58 cm^3 and 30.77±20.31kBq/ml respectively. The SUV max, MTV and TLG of patients with STC were 73.06±55.13, 124.64±152.27 $cm^3$and 34.21±18.72 kBq/ml respectively. The SUV max, MTV and TLG of patients with SL were 99.91±56.16, 71.96±74.51cm^3 and 35.66±9.64kBq/ml respectively. The SUV max, MTV and TLG of patients with LM were 65.64±40.64,114.93±127.58cm^3 and 32.74±20.3kBq/ml respectively. The SUV max, MTV and TLG of patients with LNM were 64.67±50.31, 115.42±139.98cm^3 and 32.26±19.65kBq/ml respectively. The SUV max, MTV and TLG of patients with DBM were 63.34±56.16, 116.59±74.5cm^3 and 31.45±9.64kBq/ml respectively. SUV max, MTV and TLG of patients with MD were 64.16±39.59, 116.29±125.26$cm^3$and 31.81±21.05kBq/ml respectively. ***Conclusion:*** Our data concluded that TLG can be used to predict distant bony metastases and skip lesions as they showed values with compact standard deviation whereas parameters like SUVmax and MTV can show highly variable results.

EP-0363

The Relationship Between Staging F-18 FDG PET/CT Parameters and Survival in Patients Diagnosed with Soft Tissue Sarcoma

N. Aydin, *G. Mütevelizade, G. Gümüşer, E. Sayıt Bilgin; Celal Bayar University, Manisa, TÜRKIYE.*

Aim/Introduction: The aim of this study is to investigate the prognostic value of metabolic parameters obtained from staging PET/CT of patients with STS and their effects on overall survival (OS) and progression-free survival (PFS). ***Materials and***

Methods: 34 patients (49 ± 23 years) who underwent staging F-18 FDG PET/CT examination with the diagnosis of STS in our clinic between 2017-2022 were included in our study. SUVmax, SUVmean, MTV and TLG were obtained from F-18 FDG PET/CT images. The presence of lymph nodes and/or distant metastases was evaluated in PET/CT images. The relationship between the metabolic parameters of the primary tumor and clinical data was evaluated with Mann-Whitney U and Chi-square tests. Prognostic values of metabolic parameters in predicting overall survival and progression-free survival were evaluated using the Kaplan-Meier method. ROC analysis was performed ***Results:*** A total of 34 patients (13 female, 21 male) with a mean age of 49±23 were included. A statistically significant correlation was found between the presence of distant metastases and the TLG value of the primary tumor (p=0.025). However, no statistically significant correlation was found between SUVmax, SUVmean values and the presence of distant metastases at the time of diagnosis. According to Kaplan-Meier analysis, the presence of distant metastases in staging PET/CT was associated with both overall survival (p=0.019) and progression-free survival (p=0.035). No statistically significant correlation was found between SUVmax, SUVmean, MTV and TLG values of the primary lesion and OS and PFS. To predict the presence of distant metastases according to Youden index, a cut-off value of 104.2 cm3 (sensitivity: 78%, specificity: 68%) was obtained for MTV and 350 (sensitivity : 89%, specificity : 56%) was obtained for TLG. ***Conclusion:*** According to the results of our study, the presence of distant metastases at the time of diagnosis is associated with overall survival and progression-free survival was found to be the main determinant of survival. Among the metabolic parameters obtained in the staging PET/CT of patients with STS, a statistically significant correlation was observed between TLG and the presence of distant metastases. ***References:*** von Mehren M, Randall RL, Benjamin RS, et al. soft Tissue Sarcoma , Version 2.2018, NCCN Clinical practice Guidelines in Oncology . J Natl compr canc netw . 2018 May;16(5):536-563.

EP-0364

Additional diagnostic contribution of bone SPECT/CT in foot and ankle pathology

K. Bayardo*, L. F. Portugal, F. Carrera, O. Alonso, R. Ferrando;*
University of the Repubic, Montevideo, URUGUAY.

Aim/Introduction: The complex anatomy and function of the foot can make it difficult to diagnose the cause of the symptoms in patients with pathologies of the region. SPECT/CT offers considerable advantages in these cases. The objective is to evaluate the diagnostic impact of the hybrid images with respect to planar images. ***Materials and Methods:*** Retrospective study that included 63 consecutive patients (38 men, age 41 ± 13.5 years (mean ± SD), range 6-75) from 2016 to date, studied with 99mTc-MDP bone scintigraphy with whole body images, early and late sectorial planar and SPECT/CT of the feet on a GE Infinia Hawkeye 4 and a Mediso AnyScan 16 gamma cameras. All patients presented with clinical data of spontaneous or post-traumatic onset pain in the foot or ankle. ***Results:*** In 33 of the 63 patients, SPECT/CT provided additional information that allowed a diagnosis to be made compared to inconclusive planar images. The greatest impact was observed in the tarsal bones (28/33 patients). Only 3 patients had completely normal studies and in only 5 cases it was not possible to reach a final diagnosis due to nonspecific findings. Planar images revealed 164 bone lesions, while SPECT/CT detected 214 lesions. The final diagnosis was degenerative arthropathy in 12 cases, inflammatory in 8 and traumatic in 6, osteomyelitis in 16, stress fracture in 3, osteoid osteoma in 3, osteochondritis dissecans in 1, osteochondral lesion in 1, active synchondrosis in 1, coalitions tarsals 2, osteonecrosis 1 and bone viability 1. ***Conclusion:*** Bone SPECT/CT has a high impact on foot and ankle pathologies, allowing a diagnosis to be reached in 87% of cases, including 51% of patients with inconclusive planar images. Hybrid imaging should be considered in all patients presenting with foot or ankle pain whenever it is available.

EP-0365

Assessing the role of 18F-FDG PET-CT in the initial staging of soft tissue sarcomas: bone infiltration and distant metastasis

Y. Abadi Sedraoui*, J. Cordero García, E. Ortiz Cruz, I. Barrientos Ruiz, J. Pozo Kreilinger, C. Lancha Hernández, M. Coronado Poggio, S. Rizkallal Monzón, E. López LLobet, D. Monachello Araujo, L. Giraldo González, P. Portilla Merino, S. Rodado Marina, C. Escabias Del Pozo, L. Domínguez Gadea;*
Hospital Universitario La Paz, Madrid, SPAIN.

Aim/Introduction: Bone infiltration at diagnosis is one of the most important prognostic factors in diagnosing the extension of soft tissue sarcomas (STS) in adults. Likewise, the distant dissemination of STSs limits surgery, the only potentially curative treatment. We analyzed the usefulness of 18F-FDG-PET/CT in initial staging to assess the presence or absence of tumor infiltration in the adjacent bone and its value in distant staging, establishing the prognosis of the disease at diagnosis. ***Materials and Methods:*** We retrospectively reviewed STSs diagnoses between 2012 and 2021, selecting patients with an initial staging with MRI and PET/CT before surgery and assessing bone infiltration in each. We compared the findings with diagnostic CT when we suspected lung involvement with 18F-FDG. We considered positive PET/CT in case of focal deposit of the radiotracer with infiltration of the cortical bone near the lesion. We compared all the findings with the ones of surgical biopsies. Additionally, we evaluated other local anatomical structures. Any focal activity on 18F-FDG-PET/CT greater than that of the vascular pool in the mediastinum was considered suspicious of malignancy. A subsequent follow-up was carried out, with control at six months and a year. ***Results:*** We included 20 patients, ten men and ten women between the ages of 22 and 75 (mean 49), whose pathology revealed three myxofibrosarcomas, six spindle cell sarcomas, one undifferentiated synovial sarcoma, one myxoid liposarcoma, one alveolar sarcoma, two malignant fibrous histiocytomas, 1 Ewing-like tumor, one malignant tumor of the peripheral nerve, three pleomorphic sarcomas, and one fibroblastic monophasic synovial sarcoma. Among them, 15 were of high grade, 3 of intermediate grade, and 1 of low grade. We observed bone infiltration in one patient. The results were consistent with the MRI and the biopsy. None of the cases had local relapses in the first year after surgery. 2/20 patients presented pulmonary disease at diagnosis, observed by both PET/CT and diagnostic CT. We did not find other metastatic localizations. Additionally, two patients with nonspecific micronodules in diagnostic CT and negative 18F-FDG-PET/CT presented pulmonary progression at follow-up at six months (one of them with new lymph node metastasis). Finally, one patient with two synchronous malignant tumors (both spindle cells) presented bone progression in control at six months. ***Conclusion:*** 18F-FDG-PET/CT seems to show good reliability for detecting bone infiltration and metastatic involvement in our series. Our results indicate that PET/CT could be the one-stop shop for the initial staging of STS.

EP-0366

Evaluation of F-18 FDG PET-CT based parameters in prediction of histopathological response to neoadjuvant chemotherapy in patients with Osteosarcoma

S. Maitra, *N. Singh;*
P.D. Hinduja National Hospital and MRC, Mumbai, INDIA.

Aim/Introduction: To evaluate F-18 FDG PET-CT based parameters in prediction of histopathological response to neoadjuvant chemotherapy in patients with Osteosarcoma ***Materials and Methods:*** 30 patients diagnosed with osteosarcoma who underwent FDG PET-CT scan at baseline and post neoadjuvant chemotherapy(NACT), followed by surgery (between 2011 - 2016) were assessed. SUVmax, metabolic tumor volume(MTV) and total lesion glycolysis(TLG) of the primary lesion was recorded at baseline and post NACT along with post/pre NACT ratios. MTV was calculated with threshold of 45% SUVmax ; MTV(45%) and by summing the volume of voxels with SUV higher than threshold SUV 2 ; MTV(2). TLG(45%) and TLG(2) was also calculated. Histopathological reports post-surgery were obtained, necrosis fractions and response was catalogued. Histopathological necrosis fractions (HNF) were correlated with post NACT parameters and post/pre NACT ratios. Receiver operating characteristic(ROC) curve analysis was done to determine cut off, sensitivity and specificity for post/pre NACT ratios which could predict good histopathological response from poor response. Post/pre NACT ratios were compared to find out which is a better predictor of histopathological response. ***Results:*** 16 patients were good histopathological responders and 14 were poor histopathological responders. Post NACT SUVmax , MTV(2) , TLG(2) , post/pre NACT ratios of SUVmax, MTV(2), and TLG(2) showed difference between good and poor responders. Among post/pre NACT ratios, all parameters except MTV(45 %) showed correlation with HNF. TLG(2) ratio showed strong, MTV(2) ratio showed moderate and SUVmax ratio showed weak correlation. On post NACT PET-CT scan, absolute values of SUVmax and MTV(45 %) did not show correlation with HNF and MTV(2), TLG(2) and TLG(45 %) showed weak correlation. ROC curve analysis and comparing AUCs(area under curve), revealed MTV(2) ratio and TLG(2) ratio to be equally good predictors of histopathological response. MTV(2) ratio is a better predictor of histopathological response than SUVmax ratio. The sensitivity and specificity for predicting a good response was 92.8% and 75% using a MTV(2) ratio cut off of 0.17 and using a TLG(2) ratio cut off of 0.10. ***Conclusion:*** In our osteosarcoma population, the change in F-18 FDG PET-CT based parameters post NACT were useful in predicting tumor response. The change in combined metabolic/volumetric parameters like MTV and TLG (measured at threshold of SUV 2) post NACT were better predictors of histopathological response than change in the metabolic parameter, SUVmax post NACT .

EP-0367

Usefulness of SPECT/CT 99mTc MIBI for the evaluation of lesions suggestive of bone sarcomas.

F. Lemus Ramírez[1], *A. López Méndez*[2], *D. Arguelles Pérez*[1], *D. Orendain Novoa*[1];
[1]*Instituto Nacional De Rehabilitación Luis Guillermo Ibarra Ibarra, México, MEXICO,* [2]*J&J, México, MEXICO.*

Aim/Introduction: To evaluate the diagnostic utility of ^{99m}Tc-MIBI SPECT/CT, for the evaluation of lesions suggestive of bone sarcomas. ***Materials and Methods:*** Cases were retrospectively evaluated within the Instituto Nacional de Rehabilitación Luis Guillermo Ibarra Ibarra that by ^{99m}Tc-MIBI-SPECT/CT were suggestive of bone sarcoma, compared with histopathology, both primary tumor and of the metastases, in patients seen from January 2018 to March 2023. ***Results:*** A total of 24 patients were studied, of which 15/24 are men and 9/24 women, with a mean age of 24 years, the maximum age 75 years and the minimum age 8 years, all were positive results by ^{99m}Tc-MIBI-SPECT/CT and when comparing with histopathology were positive for bone sarcomas in 22 of 24 cases, giving a sensitivity of 100% for ^{99m}Tc-MIBI-SPECT/CT and a positive predictive value of 91%, pathologies that were not sarcoma are: hodgkin lymphoma and other unspecified tumors. Of these 22 positives for bone sarcoma, the most frequent primary tumor sites were the extremities in 21/22 and the sacrum in 1/22. 15/22 had positive metastases with ^{99m}Tc-MIBI-SPECT/CT at diagnosis, the most frequent sites being regional metastases 11/15, lung 3/15 and brain 1/15, 15/15 metastases were positive by histopathology, giving a sensitivity for the ^{99m}Tc-MIBI-SPECT/CT when evaluating bone sarcoma metastasis of 100% and a positive predictive value of 100%. ***Conclusion:*** ^{99m}Tc-MIBI-SPECT/CT with is a very sensitive tool to evaluate bone sarcomas as well as their regional or distant metastasis sites. Being a very useful tool for staging. Given the low incidence, it is important to carry out multicenter studies where we can correlate the prognostic role of ^{99m}Tc-MIBI-SPECT/CT, as well as expanding the already known studies where they evaluate the predictive role of ^{99m}Tc-MIBI-SPECT/CT in response to therapies. The next step is to evaluate the semi-quantitative parameters such as the uptake index (UR) and the alteration of the uptake index (AUR) and the tumor necrosis rate (TNR) (1,2), to reinforce the evidence of its usefulness as a model predictive. ***References:*** • Huang Z, Lou C. Application of the alteration uptake ratio of ^{99m}Tc-MIBI scintigraphy for evaluating the efficacy of neoadjuvant chemotherapy in osteosarcoma patients. Hell J Nucl Med. 2018;21(1):55-59.• Wu F, Huang Y, Huang X, et al. ^{99m}Tc-MIBI Scintigraphy for the Preoperative Assessment of Histological Response to Neoadjuvant Chemotherapy in Patients With Osteosarcoma: A Systematic Review and a Bivariate Meta-Analysis. Front Oncol. 2020;10:762. Published 2020 May 22. doi:10.3389/fonc.2020.00762

EP-0368

18F-NaF PET/CT in diagnosis and response assessment to Radiofrequency Ablation (RFA) in Osteoid Osteoma patients

S. Shamim, *N. Kumar, J. Pathak, G. Arora, S. Gamanagatti, S. Khan;*
AIIMS New Delhi, Delhi, INDIA.

Aim/Introduction: The CT-guided Percutaneous Radiofrequency Ablation (RFA) is the current treatment of choice for patients with osteoid osteoma. RFA is found to be a safe, minimally invasive and highly effective treatment with high success rates in these patients. Response assessment is done with clinical assessment and on Visual Analogue Scale (VAS) scores and is accepted as standard method following RFA. ^{99m}Tc-MDP (Methylene Diphosphonate) bone scan/SPECT-CT can be used for diagnosis but has disadvantage that it remains positive for long time limiting its use for post-procedure treatment assessment. With the widespread use of ^{18}F-Fluoride as bone-seeking PET radiotracer, we aimed to evaluate the role ^{18}F- NaF PET-CT for diagnosis and response assessment in post-RFA osteoid osteoma patients. ***Materials and Methods:*** Patients with clinical suspicion of osteoid osteomas were considered for the study. A total of 15 patients were prospectively included in this study. At baseline all patients were clinically evaluated for symptoms that included VAS

pain scale and other pain characteristics. All patients underwent ^{18}F-NaF PET-CT and ^{99m}Tc-MDP bone scan with SPECT-CT at baseline. All patients were followed up after RFA to evaluate for clinical recurrence. In patients with clinical suspicion of disease recurrence, ^{18}F-NaF PET-CT was done after at least 3 months of RFA. Analysis and interpretation of SPECT/CT and PET/CT images were done by two separate experienced nuclear medicine physicians. ***Results:*** Fifteen patients (11 male, 4 female) with mean age 19±1.8 years (range 11- 31 years) were recruited in this study. All 15 patients were presented with pain at baseline. Typical bone scan presentation of positivity in all the 3-phases of bone scan were noted in 66.6% (10/15) while, atypical bone scan presentation were noted in rest of the 33.3%. SPECT-CT was found to be positive in all the patients (15/15). Similarly, pre-RFA ^{18}F-NaF PET-CT were positive in all patients. Post-operative pain assessment after at least 3 months of RFA was positive in 13.33% (2/15). Thus, post-treatment PET-CT was performed in 2 symptomatic patients, both of whom showed ^{18}F-NaF uptake in which one was categorized as recurrence and one as residual disease. ^{18}F-NaF PET-CT was not done in asymptomatic patients in view of increased radiotracer uptake secondary to post-operative changes and sclerosis. ***Conclusion:*** ^{18}F-NaF PET/CT is a complementary modality to ^{99m}Tc-MDP bone scan/SPECT-CT in diagnosis and has an additional role in response assessment in post-RFA patients of osteoid osteoma.

EP-21

e-Poster Area

B: Imaging Clinical Studies -> B1 Oncological Imaging Clinical Study -> B24 Melanoma

EP-0369

The value of 18F-FDG PET/MR in the metastasis and re-stage of melanoma after operation

F. Wang*;*
Hangzhou Universal Imaging diagnostic center, Hangzhou, CHINA.

Aim/Introduction: To investigate the value of 18F-FDG PET/MR whole-body imaging in the metastasis and re-phase of melanoma after operation. ***Materials and Methods:*** The clinical data of 56 patients with melanoma after operation were retrospectively analyzed, and the PET/MR manifestations were analyzed. The PET/MR staging was compared with the traditional clinical staging based on CT and MR, and the difference between the detection rate and re-stage of metastatic lesions after operation was compared. The gold standard is clinical and pathological diagnosis. ***Results:*** Of 56 patients with melanoma after operation, 39 cases were found to have regional lymph node metastasis (N stage), a total of 128 lesions; There were 28 cases of distant metastasis (M stage), 194 lesions in total, including 35 lung metastasis, 41 liver metastasis, 17 brain metastasis, 76 bone metastasis, and 25 lymph nodes. The detection rate of regional lymph nodes by PET/MR was the same as that by conventional imaging (CT and MR) (98.4%), and the diagnostic coincidence rate of PET/MR was 97.6% higher than that of CT and MR (89.4%), with no statistical difference (P>0.05). Compared with conventional imaging (CT and MR), PET/MR found 69 more distant metastatic lesions in 28 patients, with significant statistical difference(P<0.05).Among them, 65 lesions were positive for PET-MR, negative for CT, and partial positive for MR, including 8 brain metastases, 22 liver metastases, 4 pancreas, 19 bones, 10 soft tissues, 2 lymph nodes, and 4 lesions were negative for PET uptake, but MR diagnosis was metastasis, including 1 brain metastasis, 1 liver metastasis, and 2 bone metastasis. The coincidence rate of PET/MR and MR diagnosis was 100% and 81%, respectively, with statistically significant difference (P<0.05).The detection rate and diagnostic coincidence rate of PET/MR in liver, brain, bone, muscle and soft tissue metastasis were higher than those of traditional CT and MR, with statistical significance (P<0.05). Through PET/MR examination, a total of 17 patients changed the traditional clinical stage, with significant statistical difference (P<0.05) .Among them, 8 patients increased from stage I to stage III, 3 patients increased from stage II to stage IV, and 6 patients increased from stage III to stage IV. ***Conclusion:*** 18F-FDG PET/MR is of high value for the metastasis and re-stage of melanoma after operation. The detection rate and accuracy of liver, brain, bone and soft tissue metastasis are higher than those of CT and MR, and lung lesions still need CT assistance diagnosis.

EP-22

e-Poster Area

B: Imaging Clinical Studies -> B1 Oncological Imaging Clinical Study -> B25 Any Other Malignant (including Primary of Unknown Origin)

EP-0370

Utility of 68Ga FAPI 46 PET CT scan in oncology patients with indeterminate 18 FFDG PET CT findings- A single institute study

V. Malasani*, s. dash, d. pendharkar, n. singhal, a. raj, m. mehndiratta, d. parwan, n. n. begum, a. tomar, a. javed; sarvodaya hospital and research center, faridabad, INDIA.*

Aim/Introduction: F18- FDG PET-CT is now the stranded imaging modality for tumor detection. It's not a tumor specific agent leading to false positive and false negative findings. We aim to look for the utility of Ga68 FAPI-46 (fibroblast activation protein inhibitor) PET-CT scan in these patients. Additionally, we tried to look for the utility of dual tracer study to differentiate benign from malignant pathologies. ***Materials and Methods:*** All the oncological patients who had indeterminate or negative findings in F18 FDG PET CT scan had underwent Ga 68 FAPI PET CT scan. Results were grouped based on quantification marker SUV max (maximum standard uptake value). Category 1: high likely benign (FDG positive, FAPI negative or both negative); Category 2 : Probably benign (both positive but the SUV max of FAPI is < 50% of SUV max of FDG; Category 3: indeterminate significance (both positive with SUV max of FAPI ranging from 50-70 % of SUV max of FDG), Category 4: high likely malignant (both positive with SUV max of FAPI ≥70% FDG SUV max or only FAPI positive). Histopathology or follow-up imaging served as the standard for the final diagnosis. ***Results:*** Of 40 patients with indeterminate FDG PET CT scan findings 21 were treatment naive and 19 had suspicious disease recurrence. FAPI PET CT scan alone could detect primary lesion in 5/21 (≈24%), suspicious lesions as benign in 4/21(≈19%), down staged 4/21 (≈19%) and upstaged

1/21(≈5%) patients; further dual tracer study reduced false positive rate in 4/21 (≈19%) patient. Rest 3 /21 (≈14%) patient was true positive in both the scans. In the recurrent group, FAPI PET CT scan alone detected true recurrence in 3/ 19 (≈16%) patients and prevented false positive in 5/19 (≈26%); however dual tracer study additionally prevented false positive cases in 5/19 (≈26%) patients. 2/19 (≈10.5%) patients of "indeterminate group" turned out to be tubercular in pathology. Rest 4/19 (≈21%) were true recurrence in both. ***Conclusion:*** 68 Ga FAPI PET -CT scan do have additional great advantage in reducing false negative and positive rate in various oncological scenarios pertaining to solid tumors. However, careful evaluation of benign pathologies having fibrotic sequalae may be challenging in some cases. We found that dual tracer study may help in differentiating benign vs malignant in these settings to a substantial extent. Our major limitation is the low study population; so additional studies with larger population groups are further required.

EP-0371

Comparison of Diagnostic Value between18F-FDG PET/CT and Immunohistochemistry in Lymph Node Metastatic Cancer with Unknown Primary site

Y. Yu, *S. Xu, X. Han;*
the First Affiliated Hospital,Zhengzhou, Zhengzhou, CHINA.

Aim/Introduction: To investigate the diagnostic values of ^{18}F-FDG PET/CT and immunohistochemistry of metastatic lymph nodes in patients with nodal metastatic carcinoma of unknown primary site (NCUP). ***Materials and Methods:*** A total of 190 patients (127 males,63 females, average age (57.68±11.72) years) with histological proven NCUP who underwent ^{18} F-FDG PET/CT imaging to find primary tumors from January 2011 to December 2020,133 patients who underwent preoperative lymph node immunohistochemistry were retrospectively analyzed. The histopathology of the primary lesion was taken as the gold standard for diagnosis. Calculate the sensitivity, specificity, false positive rate, false negative rate, positive predictive value, and negative predictive value of PET/CT and immunohistochemistry for exploring the primary lesion of NCUP.The correlation between gender, age, pathological classification, size (maximum diameter) of the metastatic lesion, SUVmax of the metastatic lesion, and whether the primary lesion has been found or not was analyzed using binomial classification logistic regression analysis. ***Results:*** The sensitivity, specificity, positive predictive value, and negative predictive value of PET/CT and metastatic lymph node immunohistochemistry in the diagnosis of primary lesions in NCUP patients were 88.89%/41.03%, 83.90%/69.15%, 77.11%/35.56%, and 92.52%/73.86%, respectively. Univariate logistic regression did not find any clinical factors significantly correlated with the presence or absence of the primary lesion (P<0.05). ***Conclusion:*** Although NCUP patients have early clinical staging, ^{18}F-FDG PET/CT imaging still has high sensitivity and specificity in exploring their primary lesion, and is significantly superior to tumor markers and metastatic lymph node immunohistochemistry.

EP-0372

Diagnostic Efficacy of 68Ga-NY104 PET/CT in Patients With Clear Cell Renal Cell Carcinoma

W. Zhu, *X. Li, Y. Zhang, L. Huo;*
Peking Union Medical College Hospital, Beijing, CHINA.

Aim/Introduction: Clear cell renal cell carcinoma (ccRCC) highly expresses carbonic anhydrase IX (CAIX) due to VHL mutation and upregulation of hypoxia inducible factor. CAIX-targeted PET imaging has been proved effective in REDECT trial, a prospective, phase III multicenter study describing the diagnostic performance of ^{124}I labeled cG250, a CAIX-targeting antibody, for preoperative assessment of patients with renal masses. Nevertheless, small molecule CAIX-targeting imaging probes are still needed considering the superiority of pharmacokinetics of small molecule agents compared to intact antibody. Our team has demonstrated promising preclinical data of ^{68}Ga-NY104, a small molecule CAIX-targeting PET agent, in animal models. The purpose of this study was to evaluate ^{68}Ga-NY104 in patients with ccRCC suspicion. ***Materials and Methods:*** The study was approved by the institutional review board of Peking Union Medical College Hospital (approval NO. ZS-3089). Patients were prospectively recruited in the study. They were further divided into two groups: group 1, patients with a primary renal mass who were scheduled for surgery, group 2, patients with suspected/metastatic ccRCC. All patients received an intravenous injection of ^{68}Ga-NY104 (200Mbq ± 20%) and underwent whole body PET/CT scan at 45-75 min after injection. In selective patients, comparative ^{18}F-FDG PET/CT was performed to assist clinical evaluation. The efficacy of ^{68}Ga-NY104 PET/CT scan was calculated using a final diagnosis as ground truth, which was based on pathological results or comprehensive clinical evaluation. ***Results:*** A total of 39 patients were recruited, including 16 patients in group 1 and 23 patients in group 2. The sensitivity, specificity, and accuracy of ^{68}Ga-NY104 PET scan was 69% (9/13), 33% (1/3), 62% (10/16) for group 1, 94% (17/18), 100% (5/5), 95% (22/23) for group 2, and 83% (26/31), 75% (6/8), 82% (32/39) for all patients recruited, respectively. The tumor SUVmax of ^{68}Ga-NY104 PET in patients with final diagnosis of ccRCC is 17.2 ± 11.4 for group 1, 26.1 ± 15.9 for group 2, and 22.5 ± 14.7 for all patients recruited. Of them, 22 patients (12 in group 1 and 10 in group 2) had comparative ^{18}F-FDG PET/CT scan. The tumor SUVmax is 4.4 ± 4.1 for group 1, 9.2 ± 6.7 for group 2, and 6.3 ± 5.7 for all patients recruited. ***Conclusion:*** ^{68}Ga-NY104 PET/CT scan is a powerful tool in ccRCC evaluation, especially in those with suspected/metastatic ccRCC.

EP-0373

The added values of 18F-FAPI over 18F-FDG in patients with oncologic diseases for evaluation of malignant lesions and management of incidental pathologic uptake

X. Mu, *M. Li, W. Fu;*
Department of Nuclear medicine, Affiliated hospital of Guilin medical university, Guilin, CHINA.

Aim/Introduction: The objective of our study was to compare the quantitative parameters and tumor detection rates of malignant lesions between ^{18}F-FAPI and ^{18}F-FDG PET/CT in patients diagnosed with malignancies. Additionally, we investigated the differences in uptake between ^{18}F-FAPI and ^{18}F-FDG in incidental pathological uptake of ^{18}F-FDG, and assessed whether ^{18}F-FAPI PET/CT influenced the final decision for these lesions. ***Materials and Methods:*** A total of 78 participants from December 2021 to July 2022 who underwent paired ^{18}F-FDG and ^{18}F-FAPI PET/CT within 1 week were analyzed from a prospective clinical trial. The lesion detection rates and quantitative parameters of malignant lesions were compared between two scans. For incidental pathological uptake, the uptake grade and quantitative parameters were compared between the two radiotracers. Additionally, the pitfall lesions of ^{18}F-FAPI were collected and the SUV was compared with that of the primary tumor. ***Results:*** ^{18}F-FAPI demonstrated higher lesion detection rates compared to ^{18}F-FDG, and showed similar or higher SUV_{max} values in most lesion types, except for primary tumors. Moreover, the lower normal tissue uptake distribution resulted in significantly higher TBR for ^{18}F-FAPI

compared to ^{18}F-FDG. In cases of incidental pathologic uptake of ^{18}F-FDG, ^{18}F-FAPI showed significantly lower uptake grade and SUV compared to ^{18}F-FDG in most lesion types. Therefore, the combination of ^{18}F-FAPI and ^{18}F-FDG dual radiotracers can significantly decrease the rate of further examinations by utilizing the distinct radiotracer uptake patterns of ^{18}F-FDG and ^{18}F-FAPI, reducing it from 40.2% to 8% in our cohort. ***Conclusion:*** In comparison to ^{18}F-FDG, ^{18}F-FAPI demonstrated higher detection rates of lesions and improved imaging contrast in both primary and metastatic lesions. In cases of incidental pathologic uptake of ^{18}F-FDG, the use of ^{18}F-FAPI can aid in determining the nature of these lesions, thereby influencing the diagnostic decision and avoiding unnecessary costly further examinations and false management decisions. ***References:*** 1.Riester M, Xu Q, Moreira A, Zheng J, Michor F, Downey RJ. The Warburg effect: persistence of stem-cell metabolism in cancers as a failure of differentiation. Ann Oncol. 2018;29:264-70. doi:10.1093/annonc/mdx645. 2. Pu Y, Wang C, Zhao S, Xie R, Zhao L, Li K, et al. The clinical application of (18)F-FDG PET/CT in pancreatic cancer: a narrative review. Translational cancer research. 2021;10:3560-75. doi:10.21037/tcr-21-169. 3. Hintz HM, Gallant JP, Vander Griend DJ, Coleman IM, Nelson PS, LeBeau AM. Imaging Fibroblast Activation Protein Alpha Improves Diagnosis of Metastatic Prostate Cancer with Positron Emission Tomography. Clin Cancer Res. 2020;26:4882-91. doi:10.1158/1078-0432.CCR-20-1358.

EP-0374

Using dual-time 18F-FAPI PET/CT to distinguishing the nature of lesion and avoid digestive pitfalls

X. Mu;
Department of Nuclear medicine, Affiliated hospital of Guilin medical university, Guilin, CHINA.

Aim/Introduction: The aim of this study was to evaluate the biodistribution, diagnostic performance and digestive pitfalls of dual-time 18F-FAPI PET/CT to detect the malignant and benign lesions in cancer patients, and compared the difference of uptake in malignant and benign lesions between two scans. ***Materials and Methods:*** Twelve cancer patients underwent dual-time ^{18}F-FAPI PET/ CT for initial assessment or recurrence detection. Detection rate of lesions was compared between two scans. Normal organ uptake was quantified as the mean standardized uptake value (SUVmean). Lesion uptake was quantified as the maximum standardized uptake value (SUVmax). The Wilcoxon matched pairs signed-rank test was used to compare quantitative parameters between PET modalities. ***Results:*** In most of tissues, the SUVmean was observed decreasing from early time to normal time($P<0.05$). whereas, the SUVmean was no significant difference in muscle(1.8 ±0.4 vs 1.2 ±0.3,P= 0.67) and bone(1.0 ±0.4 vs 1.0 ±0.4,P= 0.34) between early time and normal time. All lesions can be observed in early and normal time scans. For malignant lesions, no significant difference between early and normal time in SUVmax(5.9 ±2.8 vs 5.7±2.8, P=0.09). For benign lesions, SUVmax of early time scan was significant higher than that of normal time(5.6 ± 3.4 vs 3.3± 1.9, $P<0.001$). In addition, malignant lesion depicted higher SUVmax than that of benign lesion in normal time(5.7±2.8 vs 3.3± 1.9,$P<0.001$). ***Conclusion:*** Dual-time 18F-FAPI PET/CT can detect all lesions, yet benign lesions show decrease of SUVmax from early to normal time on 18F-FAPI PET/ CT that can help physicians to distinguish the nature of lesions.

References: Kratochwil C, Flechsig P, Lindner T, Abderrahim L, Altmann A, Mier W, et al. (68)Ga-FAPI PET/CT: Tracer Uptake in 28 Different Kinds of Cancer. Journal of nuclear medicine: official publication, Society of Nuclear Medicine. 2019;60:801-5. doi:10.2967/jnumed.119.227967.

EP-0375

Does Brown Adipose Tissue represent a double-edged sword with mixed effects?

W. Jalloul[1], *D. Jalloul*[1], *R. Tibu*[2], *I. Grierosu*[1,2], *T. Ionescu*[1], *C. Stolniceanu*[1,2], *V. Ghizdovat*[1,2], *M. Moscalu*[1], *C. Stefanescu*[1,2];
[1]*University of Medicine and Pharmacy U.M.F „Grigore T. Popa" Iasi, Romania, Iasi, ROMANIA,* [2]*Nuclear Medicine Laboratory, County Emergency Hospital „Sf. Spiridon", Iasi, ROMANIA.*

Aim/Introduction: Brown Adipose Tissue (BAT) has long been considered "a potential lifesaver" against metabolic pathologies, such as obesity and diabetes, however, its involvement in the development of Cancer induced Cachexia has also been reported. Through analysing the 18F-FDG BAT pattern, we aimed to study the implication of this fat on the weight status in a group of oncological patients. ***Materials and Methods:*** After investigating the total number of 18F-FDG PET/CT performed for various malignities during the period of 4 years, we selected the scans with active BAT. The patients with active brown fat were divided into non-obese (NO) (BMI≤25 kg/m^2) vs. overweight or obese (OOB) (BMI>25 kg/m^2). Moreover, SUVmax has been used to quantify this fat's activity. ***Results:*** Out of the total number of 62 patients who presented active BAT, 40 (64.5%) were NO. The mean value (mv) of patients' age showed a slight predominance among OOB with 36.1±12.9 years vs. NO with 31.5±10.6 years. We reported no significant differences between genders in the BMI groups. An important BAT expression in NO during spring, summer and autumn was recorded when compared to winter in OOB. The BMI mv was 24.62±6.12 (NO: 22.72±1.6 vs. OOB: 28.93±5.81). Our data showed that 35.5% of patients were diagnosed with Hodgkin's Lymphoma (HL), 17.7% with Non-Hodgkin's Lymphoma (NHL), 12.9% with Lung Cancer (LC), 11.3% with Cervical Cancer (CC), 11.3% with Breast Cancer (BC) and 11.3% with Gastrointestinal cancers (GCs). We noticed the predominance of each of these diagnoses in NO. 86.1% of NO presented 18F-FDG BAT uptake in multiple localisations. Brown fat was non-homogeneous in 54.9% of the scans with a greater prevalence in OOB. BAT showed a symmetric distribution of 76.6% in NO. The highest SUVmax mvs were recorded in OOB patients with 6.12±2.9 g/ml in supraclavicular, 5.1±2.82 in latero-cervical and 3.32±5.1 g/ml in paravertebral spots vs. 2.78±3.97 g/ml in mediastinal and 3.13±2.98 g/ml in latero-thoracic regions in NO group. BMI was positively correlated with latero-cervical and supraclavicular SUVmax, while this index showed a negative correlation with latero-thoracic and abdominal SUVmax. Furthermore, SUVmax decreased significantly in latero-cervical, paravertebral and abdominal spots during the increasing age of the patients. Men showed a significant lower BAT activity in the paravertebral region. ***Conclusion:*** BAT's biodistribution has an impact on the weight status of oncology patients, therefore, it is essential to consider the BAT pattern while developing treatment strategies based on this type of fat.

EP-0376

Prognostic value of volumetric and metabolic 18F-FDG indices in patients with Merkel cell carcinoma: a multicentric retrospective study

M. Ricci[1], *F. Zarrelli*[1], *B. Carabellese*[1], *A. Marzullo*[2], *M. Tudini*[3], *B. Criscuoli*[4], *G. A. Follacchio*[4], *L. Travascio*[5], *A. D. Di Nicola*[5], *E. Giovannini*[6], *F. Calabria*[7], *M. Leporace*[7], *A. Bagnato*[7], *A. Cimini*[2];
[1]*Nuclear Medicine Unit, Cardarelli Hospital, Campobasso, ITALY,* [2]*Nuclear Medicine Unit, St. Salvatore Hospital, L'Aquila, ITALY,* [3]*Medical Oncology Unit, St. Salvatore Hospital, L'Aquila, ITALY,* [4]*Nuclear Medicine Unit, Macerata Hospital, Macerata, ITALY,* [5]*Nuclear Medicine Unit, P.O. Pescara, Pescara, ITALY,* [6]*Nuclear Medicine Unit, S. Andrea Hospital, La Spezia, ITALY,* [7]*Department of Nuclear Medicine and Theragnostics, "Mariano Santo" Hospital, Cosenza, ITALY.*

Aim/Introduction: Merkel Cell Carcinoma (MCC) is a rare and aggressive skin malignancy in which positron emission tomography/computed tomography (PET/CT) with 18F-Fluorodeoxyglucose (18F-FDG) imaging is often used in the management of patients. To our knowledge, there is not a definite literature regarding the possible role of 18F-FDG volumetric and metabolic indices in prognostic stratification. The aim of this Italian multicentric study is to investigate if Metabolic Tumor Volume (MTV) and Total Lesion Glycolysis (TLG), derived from PET/CT with 18F-FDG, are correlated with overall survival (OS) and Progression Free Survival (PFS) in Patients affected by MCC. ***Materials and Methods:*** 107 consecutive scans of 61 patients with MCC (41 men and 20 women; mean age 72,09 ± 10,23) have been retrospectively examined in 6 Italian nuclear medicine units, in different stages of disease (staging, restaging or follow up). Each scan has been reviewed by 2 expert nuclear medicine physicians; MTV and TLG values have been obtained from the most active lesion in each scan (skin, lymph node, or metastatic lesion). The Shapiro test has been performed for the assessment of distribution. Then, the Mann-Whitney (U test) has been performed for the comparison of MTV and TLG values and OS and PFS indices. ***Results:*** The results reported a significant correlation between MTV and OS ($p<0.05$), between MTV and PFS ($p<0.05$), between TLG and OS ($p<0.05$), and between TLG and PFS ($p<0.05$). ***Conclusion:*** The major limitations of the present study regard the heterogeneous setting of 18F-FDG PET imaging (staging, restaging or follow up) and further prospective studies should be performed in a more homogeneous setting: however, our findings support the possible role of MTV and TLG derived from PET/CT with 18F-FDG in prognosis stratification in patients with MCC.

EP-0377

68Ga-FAPI-04 PET/CT in Renal Cell Carcinoma: A Preliminary Study

C. Civan[1], *S. Kuyumcu*[1], *D. Has Simsek*[1], *O. Sanli*[2], *Z. Ozkan*[1], *O. Hurdogan*[3], *Y. Sanli*[1];
[1]*Istanbul Faculty of Medicine, Nuclear Medicine Department, Istanbul, TÜRKIYE,* [2]*Istanbul Faculty of Medicine, Urology Department, Istanbul, TÜRKIYE,* [3]*Istanbul Faculty of Medicine, Pathology Department, Istanbul, TÜRKIYE.*

Aim/Introduction: In this study, we aimed to evaluate the role of 68Ga-FAPI-04 PET/CT (FAPI) in patients with known metastatic renal cell carcinoma (RCC) or with suspected primary renal mass and to compare our results with 18F-FDG PET/CT (FDG). ***Materials and Methods:*** Our cohort included 14 patients (7 female, 7 male, mean age: 66 years) who underwent FAPI and FDG with a median interval of 7 days (IQR=6). Indication was restaging due to metastatic disease in ten patients, while it was initial assesment in four patients who had suspicious renal mass. We compared FAPI and FDG-PET parameters including SUVmax and tumor-to-background ratio (TBR) of primary lesion, local recurrence and lymph node, lung, bone and other metastasis. ***Results:*** One patient, who had xanthogranulomatous pyelonephritis showing high uptake on both PET/CT (SUVmax; FAPI: 13.1; FDG: 14.4) was excluded from further analyses. 10 out of 13 patients had clear cell RCC, 2 patients had papillary RCC and 1 patient had chromophobe RCC. A total of 68 lesions including 4 primary lesions, 5 local recurrences and 59 metastases were analysed. Minimum and maximum FAPI-SUVmax were 1.1 and 26.1, respectively. In all lesions, FAPI-SUVmax and FAPI-TBR was higher than FDG-SUVmax (6.3 vs 5.1, $p=0.17$) and FDG-TBR (6.7 vs 2.5, $p<0.001$). In primary tumor, local recurrence, lung and bone metastases FAPI-SUVmax was higher than FDG-SUVmax, while statistically significance was present in only lung metastases (7.6 vs 2.8, $p<0.001$). FAPI-TBR was significantly higher in local recurrence, lymph node and other metastases. Contrary, FDG-SUVmax was significantly higher than FAPI-SUVmax in lymph node metastases (7.6 vs 5.7, $p=0.001$). In patient based analyses, FAPI-SUVmax was higher than FDG-SUVmax in 7 patients (54%), while FDG-SUVmax was higher in 3 patients (23%). FAPI-SUVmax was higher than 6 in 57% of all lesions and 11 patients (85%) had at least one lesion with SUVmax higher than 6. ***Conclusion:*** In this preliminary study, our first clinical experience showed that 68Ga-FAPI-PET/CT could have potential role in primary lesion and metastatic disease of RCC. Further prospective studies were needed to confirm our results.

EP-0378

68Ga-NY104 PET/CT helps discriminate metastatic clear cell renal cell carcinoma from post-surgical inflammation: compared with18F-FDG

W. Zhu, *X. Li, Y. Zhang, L. Huo;*
Peking Union Medical College Hospital, Beijing, CHINA.

Aim/Introduction: ^{68}Ga-NY104 is a novel small molecule tracer targeting carbonic anhydrase IX (CAIX), which is overexpressed in clear cell renal cell carcinoma (ccRCC) but not expressed in inflammatory process. Therefore, ^{68}Ga-NY104 PET/CT can be used to discriminate metastatic lesions from post-surgical inflammation in patients with ccRCC. ***Materials and Methods:*** A 50-year-old male had partial nephrectomy due to ccRCC of the right kidney in 2020. In Sep 2022, an avidly-enhancing right kidney mass was found on ceCT during follow-up, as well as multiple perirenal lesions. In Feb 2023, he underwent radical nephrectomy and metastasectomy. After surgery, the surgeon wanted to know if he had all lesions resected in order to help make the following treatment plan. ^{68}Ga-NY104 PET/CT, as well as a comparative ^{18}F-FDG PET/CT, was performed one month after surgery. The study was approved by the institutional review board of Peking Union Medical College Hospital (approval NO. ZS-3089). ***Results:*** A total of 14 lesions were detected on either PET, 7 of which were in the surgical area while the other 7 lesions were outside surgical area. ^{18}F-FDG PET/CT detected 10 lesions, 7 in the surgical area (considered inflammatory) and 3 outside surgical area (considered metastatic). The ^{18}F-FDG uptake is similar between inflammatory (average SUVmax 4.6) and metastatic lesions (average SUVmax 3.6). ^{68}Ga-NY104 PET/CT detected 9 lesions, 3 in the surgical area and 6 outside surgical area (all considered metastatic). The ^{68}Ga-NY104 uptake in these 9 lesions was extremely high (SUVmax, 36.8 ± 14.5, range, 13.2 - 57.8). On the contrary, the other 5 lesions that were FDG-avid

demonstrated no ^{68}Ga-NY104 accumulation (SUVmax, 1.8 ± 0.7, range, 1.0 - 2.7). Although these lesions were not confirmed by follow-up pathological results, such huge SUV difference between NY104-avid lesions and NY104-indolent lesions, meaning huge CAIX expression differences, gave us enough confidence that ^{68}Ga-NY104 PET/CT could help discriminate metastatic ccRCC lesions from post-surgical inflammatory process. Taking the results of ^{68}Ga-NY104 PET/CT as reference, the lesion-level sensitivity, specificity, and accuracy of ^{18}F-FDG were 22% (2/9), 80% (4/5), and 43% (6/14), respectively. Given the results of PET/CT, the patient was considered in metastatic status and went on lenvatinib and pembrolizumab combination therapy afterward. ***Conclusion:*** ^{68}Ga-NY104 PET/CT is better than ^{18}F-FDG PET/CT in discriminating metastatic ccRCC lesions from post-surgical inflammatory process.

EP-0379

A Rare Case of Adrenal Hemangioma with CT, MRI and Pathology Findings.

B. Karasah Erkek, *A. Akgün, Y. Ertan, M. Harman;*
Ege University, Izmir, TÜRKIYE.

Aim/Introduction: Adrenal hemangiomas (AH) are extremely rare, non-functioning benign tumors that originate from endothelial cells. They account for 0.01% of all adrenal tumors. While a small portion of these tumors can cause symptoms such as abdominal pain, nausea, and vomiting, 70-80% of them are asymptomatic. These tumors are typically incidentally detected during imaging performed for other reasons. ***Materials and Methods:*** Our patient is a 62-year-old male who was found to have a mass in the right adrenal gland during routine check-up ultrasound (US). After the US findings, the patient underwent an MRI which revealed a hyper-vascular lesion measuring 2.5 cm in the right adrenal gland, without macroscopic or microscopic fat. The findings indicated that the lesion was likely not an adenoma and suggested considering neurogenic tumors (such as pheochromocytoma) in the differential diagnosis. Additionally, it was noted that the possibility of a primary malignancy with the potential for hypervascular metastasis should not be overlooked. Subsequently, the patient underwent a FDG PET/CT scan which showed that the FDG uptake of the well-defined and cystic lesion in the right adrenal gland was similar to that of the liver parenchyma (SUV max: 3.9, liver: 4). FDG PET/CT has a sensitivity of 93% to 100% and a specificity of 90% to 94% for characterizing malignant and benign adrenal lesions. While the FDG uptake ruled out malignancy, neuroendocrine tumors could not be excluded. The patient underwent the necessary metabolic and biochemical tests, and the results ruled out neurogenic tumors. As in our case, if there is no history of malignancy, surgical resection can be performed after careful exclusion of pheochromocytoma with imaging and biochemical tests to prevent hypertensive crisis. ***Results:*** Due to the rarity of AH, there are no established treatment guidelines, and surgical resection is often the preferred method in the literature. The laparoscopic adrenalectomy performed with the patient's consent confirmed the diagnosis of AH on histopathological examination. On gross pathological examination, a yellow-brown colored tumor with distinct demarcation from the normal adrenal parenchyma was seen. The tumor measured 3 cm in diameter and was composed of multiple vascular channels lined by a single layer of endothelial cells. The tumor was well circumscribed from the adrenal gland parenchyma that was hyperplastic. ***Conclusion:*** We believe that the imaging, clinical, and pathological findings used to arrive at the definitive diagnosis for our rare case of AH will contribute to the literature.

EP-0380

Comparison of 18F-FDG and 68Ga-FAPI PET/CT in the diagnosis of lung metastasis in different malignant tumors

Z. Yang;
Fudan University Shanghai Cancer Center, Shanghai, CHINA.

Aim/Introduction: To evaluate the diagnostic value of ^{18}F-FDG and ^{68}Ga-FAPI PET/CT in lung metastasis of different malignant tumors. ***Materials and Methods:*** A retrospective analysis was performed on 20 patients with lung metastasis from May 2020 to March 2022 in Fudan University Cancer Center [13 males and 7 females, median age 58 (20-71 years old). 11 cases were confirmed as epithelial-derived malignancies and 9 cases as mesothelial-derived malignancies. The clinical, pathological and 18F-FDG and 68Ga-FAPI PET/CT images were analyzed. Wilcoxon sign rank test was used to compare the statistical difference of semi-quantitative metabolic parameters (SUVmax and TBR) between the two probes. Linear correlation was used to analyze the correlation between the semi-quantitative parameters of the two probes and the short diameter of lung metastatic lesions. ***Results:*** Among 81 lung metastases (51 cancers and 30 sarcomas), 72 were positive for 18F-FDG PET/CT, and 70 were positive for 68Ga-FAPI PET/CT. Compared with 68Ga-FAPI, lung metastatic lesions had a higher value of 18F-FDG, especially those of cancer origin ($P < 0.001$). The results of linear correlation analysis showed that the semi-quantitative metabolic parameters of the two probes were positively correlated with the short diameter of lung metastatic lesions ($P < 0.001$). ***Conclusion:*** 18F-FDG PET/CT is more advantageous than 68Ga-FAPI PET/CT in the diagnosis of lung metastasis from different types of malignant tumors.

EP-0381

Bone scan with technetium 99m-methyl diphosphonate, the missing link in the initial staging of muscle-invasive bladder carcinoma

A. Aghaee[1], *S. Soltani*[2], *H. Ghorbani*[2], *H. Ghorbani*[1], *S. Zakavi*[1], *K. Aryana*[1];
[1]*Nuclear Medicine Research Center,Mashhad University of Medical Sciences, Mashhad, IRAN, ISLAMIC REPUBLIC OF,*
[2]*Kidney Transplantation Research Center, Mashhad University of Medical Sciences, Mashhad, IRAN, ISLAMIC REPUBLIC OF.*

Aim/Introduction: Accurate staging is crucial to determine the type of treatment for patients with bladder cancer (BCa), especially in high-risk cases. We aimed to assess the role of bone scan in the initial staging of muscle-invasive bladder carcinoma (MIBC). ***Materials and Methods:*** Forty-five patients with MIBC were referred to our tertiary clinic to perform a technetium 99m-methyl diphosphonate (Tc99m-MDP) bone scan from January 2019 to March 2020. The patients underwent bone scintigraphy with pelvic SPECT/CT before radical cystectomy. Whole-body scanning was performed 4 hours after Tc99m-MDP injection in both anterior and posterior views. Since the most common bone involvement site in these patients is the pelvic bones and the spine, pelvic SPECT/CT was performed in all patients. ***Results:*** Frequency of skeletal metastasis was 26.7%. Only 19% of the metastases were detected by previous pelvic CT/MRI images performed for routine staging. All the reported skeletal metastases by previous anatomical imaging methods were detected in the bone scan. There was no statistically significant correlation between bone metastasis and the patient's age, lymph nodes metastasis (LNM), hydronephrosis, and muscle-invasive type. The mean serum calcium level was 8.7 ± 0.57 in patients with bone metastasis and 8.87 ± 0.99 in patients without bone metastasis, which was not statistically significant.

Conclusion: Bone scan has higher diagnostic performance than conventional imaging methods for detecting bone metastases. It changed the management plan in 8.8% of our patients, so we conclude that performing a whole-body bone scan in the initial staging of MIBC would be helpful.

EP-0382

The Role of Integrin αvβ6-PET/CT for Patients with Different Cancer-Preliminary Clinical Experience

L. Li, *Z. Xiao, D. Zeng, D. Xing, H. Wu, Y. Tian, C. Li, Y. He; Department of Nuclear Medicine, Zhongnan Hospital, Wuhan University, Wuhan, CHINA.*

Aim/Introduction: The αvβ6-integrin is an exclusive marker of epithelial cells and plays a critical role in the invasion and metastasis of carcinomas. The latest advancement of integrin αvβ6 tracers demonstrated promising preclinical and clinical outcomes. Specifically, ^{68}Ga-Trivehenxin, a Ga68labeled αvβ6-integrin selective PET tracer, which was synthesized by trimerization of the cyclic nonapeptide Tyr2 (c[YRGDLAYp(NMe)K]) on the triazacyclononane-triphosphinate (TRAP) chelator TRAP chelator core, has shown encouraging outcomes in accurately demarcating head-and-neck tumors and detecting primary and metastatic pancreatic cancer. Here we present an initial clinical investigation focused on ^{68}Ga-Trivehexin PET imaging in a spectrum of tumor types. ***Materials and Methods:*** A total of 17 patients (12 males and 5 females; median age, 60 years; age range, 40-80 years) with a diagnosis of 12 different cancers, including lung cancer, gastrointestinal malignancies, glioma, nasopharyngeal carcinoma, esophageal cancer, hepatobiliary and sarcoma, underwent both ^{18}F-FDG and ^{68}Ga-Trivehexin PET/CT scans. The median time interval between the two scans was 2 days (range, 1-3 days). Standardized uptake values (SUV) and tumor-to-background ratios (TBR) were generated from the contoured tumor and source organ volumes. Spherical volumes in the liver, blood pool, or normal brain were also obtained for TBR. ***Results:*** Compared to ^{18}F-FDG imaging, Trivehexin exhibited a lower uptake in normal organs including the liver and mediastinal blood pool (1.59 vs 3.32 and 1.74 vs 2.62, respectively, both $p<0.001$), rendering it rationale to enhance TBR in order to detect minute lesions. Especially when using the liver as a background, the TBR of primary lesions is significantly higher with ^{68}Ga-Trivehexin than with ^{18}F-FDG (5.18 vs 2.45, $p=0.003$). ^{68}Ga-Trivehexin has also shown a remarkable TBR advantage in detecting brain lesions, specifically in cases of gliomas and brain metastases. However, in the current solid tumor cases, ^{68}Ga-Trivehexin exhibited lower SUVmax than ^{18}F-FDG(8.97 vs 12.29, $p=0.03$), potentially due to the role of αvβ6-integrin in promoting invasive growth of malignant epithelial neoplasms. Moreover, the spillover effect of ^{18}F-FDG is not a reliable indicator of tumor malignancy level. Therefore, it is essential to collect more pathological data in the future to verify these hypotheses. ***Conclusion:*** ^{68}Ga-Trivehexin PET/CT imaging was able to demonstrate promising results and high clinical value with regard to intense tumor uptake and image contrast. We are currently conducting a large-scale cohort study and pathological analysis to further expand the applications of ^{68}Ga-Trivehexin, such as staging or non-invasive tumor characterization for patients with malignant tumors.

EP-0383

Tumor Uptake of a Bi-specific Antibody which Binds to CD137 and FAP is Shown Using 89[Zr]Zr-BI 765179 PET-imaging

M. Stavenga[1,2], *M. C. Huisman*[3,2], *G. J. C. Zwezerijnen*[3,2], *J. J. Eertink*[1,2], *K. Ridler*[4,5], *Ö. Yalkinoglu*[6], *H. Maas*[4], *D. Radonjic*[7], *J. Pasek*[8], *D. J. Vugts*[3,2], *C. W. Menke-van der Houven van Oordt*[1,2]; [1]*Amsterdam UMC location Vrije Universiteit Amsterdam, Department of Medical Oncology, Amsterdam, NETHERLANDS,* [2]*Cancer Center Amsterdam, research program, Amsterdam, NETHERLANDS,* [3]*Amsterdam UMC location Vrije Universiteit Amsterdam, Department of Radiology and Nuclear Medicine, Amsterdam, NETHERLANDS,* [4]*Boehringer Ingelheim Pharma GmbH & Co. KG, Department of Translational Medicine & Clinical Pharmacology, Biberach, GERMANY,* [5]*Invicro, A Konica Minolta Company, London, UNITED KINGDOM,* [6]*Boehringer Ingelheim International GmbH, Department of Translational Medicine & Clinical Pharmacology, Ingelheim am Rhein, GERMANY,* [7]*Boehringer Ingelheim International GmbH, TA Oncology Medicine, Ingelheim am Rhein, GERMANY,* [8]*Boehringer Ingelheim Pharmaceuticals, Early Clinical Operations, Ridgefield, CT, UNITED STATES OF AMERICA.*

Aim/Introduction: BI 765179 is a bi-specific antibody binding to CD137 on immune cells and to Fibroblast Activation Protein (FAP) frequently upregulated in the tumor environment of many cancer types. It is postulated that CD137 agonism with required concomitant binding to FAP expressed on cancer-associated fibroblasts allows for tumor-restricted T-cell activation. Knowledge regarding target availability and saturation in tumors and in healthy tissues will improve dose selection. In this study, we aim to assess the tumor accumulation and biodistribution of [^{89}Zr]Zr-BI 765179 as well as its change upon applying BI 765179 treatment doses in patients with advanced and/or metastatic solid tumors using PET imaging. ***Materials and Methods:*** This sub-study is part of the phase 1 trial (NCT04958239) and has an adaptive design. Patients undergo three PET scans (at 2/24, 48, 72 hours) after each i.v. administration of 37 MBq [^{89}Zr]Zr-BI765179 containing a low dose (selected using available PK data) at baseline and on a treatment dose two weeks later. Blood samples are drawn for PK analyses immediately after each injection and after each PET scan. Biodistribution in organs as well as tumor uptake is assessed by normalizing tissue uptake (Bq/mL) with the plasma uptake (Bq/mL), resulting in the tissue to plasma ratio (TPR). ***Results:*** The results from the 72-hour time points of the first patient are presented here. For the low mass dose, highest TPR were 0.50 (liver), 0.27 (spleen), 0.21 (kidneys), 0.13 (lungs), 0.15 (bone marrow) and 0.02 (brain). TPR slightly decreased after the high mass dose in liver (0.45) and spleen (0.24), but not in the other organs (respectively 0.20, 0.14, 0.14 and 0.02). In the lungs uptake based on the low mass dose was visually detected in two lesions, whereas in a third lesion the uptake was borderline. When comparing low dose and treatment dose the TPR_{peak} value in the largest lesion was reduced from 0.81 to 0.55, however, in the smaller lesion as well as the one with borderline uptake no difference was seen. ***Conclusion:*** Tumor uptake was variable in a patient with advanced cancer after administration of the bi-specific antibody [^{89}Zr]Zr-BI 765179. The uptake in the largest lesion could be reduced by a treatment dose, but no reduction was observed in the smaller lesions. Data analysis of subsequent participants will be presented and used to optimize the low dose, in order to capture quantitative information on lesion uptake and its change by treatment doses.

EP-0385

Diagnostic Accuracy of 18F-Flurodeoxyglucose Positron Emission Tomography-Computed Tomography in the Evaluation of Carcinoma of Unknown Primary Against Computed Tomography; Experience of Single Centre

M. Numair Younis, *U. B. Zahra, A. Shahid;*
Institute of Nuclear Medicine and Oncology-INMOL, Lahore, PAKISTAN.

Aim/Introduction: Carcinoma of unknown primary can be characterized as most heterogeneous group of cancers thus it is considered to have an extremely aggressive behaviour and has high resistance regarding therapeutic aspect. We hypothesize that if ^{18}F-FDG PET-CT is used earlier then CT, it is appropriate for the detection of primary location.Study was performed to determine the diagnostic accuracy of ^{18}F-flurodeoxyglucose positron emission tomography-computed tomography in the evaluation of carcinoma of unknown primary and compare with CT scan. ***Materials and Methods:*** The prospective study of CUP Syndrome patients was performed on those that underwent (^{18}F-FDG PET-CT) scan between October 2022 and February 2023. The primary site localized on ^{18}F-FDG PET-CT scan was proven through needle biopsy and histology which was considered as gold standard. ***Results:*** Of total 63, 57.1% men while 42.9% women with the average age of 56.27 years. The overall detection rate of ^{18}F-FDG PET/CT was 88.8% for primary sites. The positive hypermetabolic lesion indicative of primary malignancy were correctly identified in 79.36% that were true positive. The scan was false negative in 4.76% patients though malignancy was proven through other investigations. While 6.36% had true negative and 9.52% showed false positive results on the scan. The overall diagnostic accuracy was 85.7%, sensitivity 94%, specificity 40%, positive predictive value 89.2% and the negative predictive value 57.1% against CT which showed sensitivity of 67.3%, specificity of 38.1%. ***Conclusion:*** ^{18}F-FDG PET-CT is pivotal imaging modality for localization of primary site in CUP syndrome patients and may be used prior to CT alone in work up of these patients.

EP-0386

The utility of PET/CT with 18F-FDG in the localization of unknown primary tumors and its correlation with anatomopathological findings: Experience of the University Hospital of Salamanca.

J. Badell[1], *P. García-Talavera San Miguel*[2], *F. Gómez-Caminero López*[1], *A. C. Peñaherrera Cepeda*[1], *E. Campaña Díaz*[1], *S. Rama Alonso*[1], *J. G. Villanueva Curto*[1], *L. G. Díaz González*[1], *P. Tamayo Alonso*[1];
[1]*Hospital Clinico Universitario de Salamanca, Salamanca, SPAIN.*

Aim/Introduction: To determine the utility of PET/CT with ^{18}F-FDG in the detection of the primary lesion in patients studied for high suspicion of tumor of unknown origin and to establish its correlation with anatomopathologic findings. ***Materials and Methods:*** We included in the study 150 patients (81 men; 65.85 years ± 11.85 years) with suspected primary tumor of unknown origin, who were referred to our service for ^{18}F-FDG PET/CT between October 2014 to September 2017. The most frequent reasons for request were: lymph node disease 41/150 (27.33%) and the presence of pulmonary lesions 37/150 (24.66%). A full-body tomographic image was acquired 60 minutes after intravenous administration of a calculated dose of 5 MBq per kg/weight of ^{18}F-FDG. The PET/CT results were correlated with the anatomopathologic findings of pathologic hypermetabolic lesions suggestive of malignancy. The detection rate (DR) and the proportion of false positives (FP) were calculated. ***Results:*** PET/CT with ^{18}F-FDG presented at least one pathological hypermetabolic focus in 132/150 patients studied, suggestive of malignancy in 79 of them (52.66%). In 67/79 patients (84.81%) malignant etiology was confirmed by anatomopathological study and the most frequent histological subtype was low-grade adenocarcinoma. The most common primary sites of location were: lung (26/79), ENT region (9/79), ovary (6/79), thyroid (6/79), non-Hodgkin's lymphomas (6/79), breast (5/79), pancreas (3/79), urothelial (1/58), Hodgkin's lymphoma (1/79), prostate (1/79), right iliac psoas muscle (1/79) and two patients had synchronous malignancies: lung/breast (1/79) and NHL/colon (1/79). The remaining patients (12/79), with hypermetabolic lesions suggestive of malignancy, the anatomopathologic result was negative for malignancy or a benign infectious/inflammatory cause was identified, resulting in false positives: sarcoidosis (4), cryptogenic organizing pneumonia (1), cervical schwannoma (1), cervical desmoid fibromatosis (1), pulmonary hamartoma (1), pulmonary granulomas (1), pulmonary bronchiectasis (1) diverticulosis (1) and ischemic colitis (1). The detection rate obtained was 44.66% and the false positive rate was 15.18%. ***Conclusion:*** PET/CT with ^{18}F-FDG is of great value for the investigation of patients with suspected primary tumor process of unknown origin and is very useful for both localization and staging of malignant tumor disease.

EP-0387

The relevance of 18FDG-PET/CT in the therapeutic assessment of recurrent leimyosarcoma of the inferior vena cava

K. Ben Ahmed, *M. Maaloul, H. Noomen, F. Chaltout, M. Ouachem, I. Jardak, S. Charfeddine, K. Chtourou, F. Guermazi;*
Nuclear medicine department , Habib bourguiba hospital, Sfax, TUNISIA.

Aim/Introduction: Leiomyosarcoma (LMS) of the inferior vena cava (IVC) is an extremely rare malignant tumor emerging from the tunica media of the venous wall accounting for 2% of all LMSs. Since Perl and Virchow's first description in 1871, less than 400 cases have been reported in literature. ***Materials and Methods:*** Here we report the case of a 57-year-old woman with history of LMS of IVC evolving for 4 years. She was initially operated by a complete resection of the tumour which envaded the renal veins (R0) followed by reconstruction of the latter. After 3 years of control, the patient presented diffuse abdominal pain and a full body CT scan was performed revealing an enlarged mass centered on the IVC which was thrombosed with locoregional invasion associated to retroperitoneal lymph nodes and pulmonary nodules suggestive of tumour recurrence. The patient then underwent 6 courses of chemotherapy. The post-therapeutic CT scan concluded that the initial lesions were stable. Then ,18FDG-PET/CT was performed in order to evaluate the therapeutic response. ***Results:*** 18FDG-PET/CT showed a hypermetabolic mass (SUVLbm max = 4) centered on the IVC and extended to the renal hilium. There was no evidence of metabolically active lesions neither in the lungs nor in retroperitoneal lymph nodes ***Conclusion:*** IVC leiomyosarcomas are retroperitoneal neoplasms with different growing patterns : extraluminal (major proportion), intraluminal or mixed patterns.18FDG-PET/CT plays a crucial role in defining the tumor extent and assisting with appropriate treatment approach. Benz et al study of 50 patients, of which 8% had a LMS, showed that 18FDG-PET/CT was significantly more accurate than size based criteria at assessing histopathologic response to adjuvant therapy. Add to that, reduction in FDG-uptake from baseline to

end of chemotherapy by 60% were used as cutoff point to predict treatment responses in sarcoma patients. As for the prognostic impact, a recent study of Dilly et al concluded that SUVmax, MTV and TLG in baseline are predictive of overall survival, delta SUVpeak in early therapeutic evaluation is significantly correlated with progression-free survival in advanced leiomyosarcoma patients. Also it is worth mentioning the effectiveness of 18FDG-PET/CT in determining safe surgical margins for soft tissue sarcoma reported by Yokouchi et al. This is prominent for large tumors requiring extensive resection including normal tissue, accompanied by reconstruction-assisting surgery, involving high cost and long hospital days. In the present study, areas with SUV-max less than 1.0 were free of viable tumor cells.

EP-0388

PSMA Theragnostic beyond prostate cancer. A monocentric prospective observational study on the diagnostic performance of PSMA PET/CT in patients with metastatic Renal Clear Cell Carcinoma

F. Serani[1], *A. Farolfi*[2], *P. Castellucci*[2], *L. Vetrone*[1], *R. Mei*[2], *S. Fanti*[3]; *[1]Nuclear Medicine, Alma Mater Studiorum - University of Bologna, Bologna, ITALY, [2]Nuclear Medicine Unit, IRCCS Azienda Ospedaliero-Universitaria di Bologna, Bologna, ITALY, [3]Nuclear Medicine, Alma Mater Studiorum - University of Bologna, Nuclear Medicine Unit, IRCCS Azienda Ospedaliero-Universitaria di Bologna, Bologna, ITALY.*

Aim/Introduction: Prostate-specific membrane antigen positron emission tomography (PSMA PET/CT) is nowadays almost a certainty for staging and restaging of prostate cancer. However, it is well known that expression of PSMA it is not a prerogative of prostate cancer.Other malignant tumors overexpress this protein and renal clear cell carcinoma (ccRCC) has been found to be one of these.The aim of this study was to evaluate the diagnostic performance of PSMA PET/CT in patients at first evaluation of suspect metastatic ccRCC, and its potential use in a theragnostic intent. ***Materials and Methods:*** This monocentric prospective observational study included 4 patients with metastatic ccRCC who underwent PSMA PET/CT for restaging purposes within one month of the restaging contrast enhanced computed tomography (ceCT), used as a reference standard. A positive PSMA scan was defined when at least one lesion had a mean standardized uptake value (SUV mean) above the liver mean SUV. The active tumor volume (ATV) and the total lesion activity (TLA) were calculated with a semiquantitative method. ***Results:*** PSMA PET/CT was positive in all the 4 patients showing a total of 54 multiple pathological foci in all patients (median lesion number 11, IQR 8,8-15,8); in ceCT the total number of pathological foci was 39 (median 8,5, IQR 7,8-10,5). In one patient, PSMA PET/CT detected additional soft tissue uptakes, which were not detected on ceCT; however, in another patient showed less localization than ceCT (lung). In all patients, PSMA expression was highly positive at metastases, with a median SUV mean of 17,7 g/mL (IQR 16,1-19,3 g/mL) at the most avid metastases.The median ATV was 59,7 cm3 (IQR 35,9-64,7 cm3) and the TLA was 567,4 g/mL/ cm3 (IQR 830,1-306,8 g/mL/ cm3).The median SUVmean of parotid gland was 16,1 g/mL (IQR 14,3- 16,9 g/mL) and the median SUVmean of liver parenchyma was 8,1 g/mL (IQR 6,3- 9,2 g/mL).All the four patients were eligible for therapeutic treatment with PSMA considered the VISION criteria[1]. ***Conclusion:*** Our initial experience showed that PSMA PET/CT has a high diagnostic performance in detecting metastatic ccRCC and that this pathology could benefit from a theragnostic approach for PSMA targeted therapy. Further studies are needed to confirm these findings and to assess the potential use of PSMA theragnostic in other urologic cancers beside prostate cancer. ***References:*** 1. Sartor O, de Bono J, Chi KN, Fizazi K, Herrmann K, Rahbar K, et al. Lutetium-177-PSMA-617 for Metastatic Castration-Resistant Prostate Cancer. N Engl J Med. 2021;385:1091-103.

EP-23

e-Poster Area

B: Imaging Clinical Studies -> B3 Other Oncological Clinical Study -> B31 Radioguided Surgery and Radiation Therapy Planning

EP-0389

Feasibility study about the intra-operative use of a novel PET/CT Specimen Imager in Prostate Cancer and Neuroendocrine Tumors

L. Muraglia[1], *F. Mattana*[1], *L. Travaini*[1], *G. Musi*[2], *E. Bertani*[3], *G. Renne*[4], *E. Pisa*[4], *M. Ferrari*[5], *U. Fumagalli Romario*[3], *O. De Cobelli*[2], *N. Fusco*[6], *C. Francesco*[7]; *[1]Nuclear Medicine Division, European Institute of Oncology IRCCS, Milan, ITALY, [2]Urology Division, European Institute of Oncology IRCCS; Oncology and Hemato-Oncology Department, University of Milan, Milan, ITALY, [3]Digestive Surgery Division, European Institute of Oncology IRCCS, Milan, ITALY, [4]Pathology Division, European Institute of Oncology IRCCS, Milan, ITALY, [5]Medical Physics Unit, European Institute of Oncology IRCCS, Milan, ITALY, [6]Pathology Division, European Institute of Oncology IRCCS; Oncology and Hemato-Oncology Department, University of Milan, Milan, ITALY, [7]Nuclear Medicine Division, European Institute of Oncology IRCCS; Oncology and Hemato-Oncology Department, University of Milan, Milan, ITALY.*

Aim/Introduction: The aim of our study was to evaluate feasibility and clinical perspectives of the intra-operative application of a specimen PET/CT imager in Prostate Cancer and Neuroendocrine Tumors. ***Materials and Methods:*** This is a pilot analysis performed in three patients who received an intra-operative administration of 68Ga-PSMA-11 (n=2) and 68Ga-DOTA-TOC (n=1), respectively. Our patients underwent radio-guided surgery with a beta-probe detector during radical prostatectomy for prostate cancer (PCa) and salvage lymphadenectomy for recurrent neuroendocrine tumor (NET) of the ileum, respectively, within two ongoing clinical trials in our Institute (NCT05596851 and NCT05448157). A PET/CT specimen imager was used intra-operatively to scan the specimen after resection. Pathologic assessment with immunohistochemistry (PSMA-staining and SSA immunoreactivity) was considered as standard of truth. Specimen images were compared with baseline PET/CT images and histopathological analysis. ***Results:*** Patients received 1 MBq/Kg of 68Ga-PSMA-11 (PCa) and 1.2 MBq/Kg of 68Ga-DOTA-TOC (NET) prior to surgery. After surgical resection, specimens were positioned in a dedicated specimen container and scanned. In all cases the use of the PET/CT specimen imager did not significantly interfere with any procedures and the radiation exposure of the operating theater staff was lower than 40 µSv per procedure. The PET spatial resolution was sensibly higher for the specimen images compared to the baseline whole-body PET/CT images and a perfect match was observed between the findings detected by the specimen imager and histopathology. ***Conclusion:*** The image acquisition of specimens obtained by patients who received intra-surgery injection of 68Ga-PSMA-11 and 68Ga-DOTA-TOC was feasible

and reliable in a live-experience session. Since the data derived from the specimen PET/CT imager matched perfectly with the histopathological analysis, this pilot-analysis could lead to some newer research perspectives about surgical margins assessment and the evaluation of intra-lesion tumor heterogeneity.

EP-0390

Preoperative Radioisotope-guided Localization of Non-palpable Pulmonary Nodules

M. Olajos, *K. Park, Á. Ghimessy, K. Csende, M. Csaba, J. Andi, M. Téglás, L. Agócs, F. Rényi-Vámos, I. Sinkovics;*
National Institute Of Oncology, Budapest, HUNGARY.

Aim/Introduction: As a result of the development of imaging studies and the screening of high-risk groups, the detection rate of small pulmonary nodules on chest CT scans has improved. The dignity of these small nodules is questionable and therefore removal of these lesions is important both from a diagnostic and therapeutic point of view. Minimally invasive techniques, such as video-assisted thoracic surgery (VATS), are the procedures of choice nowadays. Therefore, accurate preoperative localisation of the lung nodules is essential. Several methods are available for preoperative marking of the lesion; one of them is CT-guided radioisotope marking. ***Materials and Methods:*** 75 patients (mean age 63 years) underwent minimally invasive removal of a nonpalpable lung nodule after isotopic labelling between January 2017 and March 2022 at the Thoracic Surgery Department of the National Institute of Oncology in Hungary. The size of the lung nodules ranged from 0.03 to 2 cm (mean: 0.9 cm) and their distance from the pleura averaged 0.4 cm. Under CT guidance, 10 to 15 MBq of 99mTc-labelled human serum albumin was injected into the nodule in a volume of 0.2ml. Following the administration of the radioisotope, surgery was performed within 1-3 hours. During operation a handheld gamma probe was used to identify the marked nodule, which was removed by wedge excision when possible. ***Results:*** Intraoperative localisation and removal of the nodules was successful in all cases. Primary lung tumour was confirmed in 18 patients and metastasis was found in 49 patients. In 8 patients, histological examination showed a non-malignant process (inflammation, hamartoma, tuberculosis). Isotope administration was completely uncomplicated in 43 patients, and in 32 patients the management of complications (pneumothorax, haemorrhage, bloody sputum or pleural detachment) was easily manageable during surgery. No serious complications requiring immediate intervention developed. ***Conclusion:*** Isotopic labelling of non-palpable lung nodules detected by CT scans helps to localize and remove the nodules safely using minimally invasive techniques. It allows accurate marking and correct removal of deeper lesions. During hookwire marking, breathing movements often result in wire dislodgment, making it difficult to find and remove the nodules. Conversely, with the radio-guided method this problem can be avoided. The procedure is safe, with only mild, easily treatable complications or with no complications at all. ***References:*** Marcello Carlo Ambrogi, Franca Melfi, Carmelina Zirafa, Marco Lucchi, Annalisa De Liperi, Giuliano Mariani, Olivia Fanucchi, Alfredo Mussi. „Radio-guided throracoscopic surgery (RGTS) of small pulmonary nodules." Surg endosc, 2012: 26:914-919.

EP-0391

Improving radical prostatectomy with intraoperative ex-vivo PSMA-PET/CT imaging

P. Fragoso Costa[1], *C. Darr*[2], *A. Moraitis*[1], *T. Kahl*[2], *J. Engel*[2], *M. Al-Nader*[2], *H. Henning*[3], *J. Köllermann*[3], *C. Kesch*[2], *U. Krafft*[2], *T. Maurer*[4,5], *D. Köhler*[6], *S. Klutmann*[6], *F. Falkenbach*[4], *J. Kleesiek*[7], *W. P. Fendler*[1], *K. Herrmann*[1], *B. Hadaschik*[2];
[1]Department of Nuclear Medicine, University Hospital Essen, Essen, GERMANY, [2]Department of Urology, University Hospital Essen, Essen, GERMANY, [3]Institute of Pathology, University Hospital Frankfurt, Frankfurt, GERMANY, [4]Martini-Klinik Prostate Cancer Center, University Hospital Hamburg-Eppendorf, Hamburg, GERMANY, [5]Department of Urology, University Hospital Hamburg-Eppendorf, Hamburg, GERMANY, [6]Department of Diagnostic and Interventional Radiology and Nuclear Medicine, University Medical Center Hamburg-Eppendorf, Hamburg, GERMANY, [7]Institute of Artificial Intelligence in Medicine, University Hospital Essen, Essen, GERMANY.

Aim/Introduction: In localized high-risk prostate cancer (PC) avoidance of positive resection margins improves cancer control. PSMA-PET/CT is currently used for primary staging in high-risk PC due to its higher accuracy. Here we aim to evaluate the feasibility of a novel intraoperative micro-PET/CT in radical prostatectomy (RP). ***Materials and Methods:*** In this prospective two-center feasibility study, we evaluate the diagnostic value of intraoperative ex vivo micro-PET/CT imaging of RP and lymphadenectomy specimens.Ten patients with high-risk PC underwent clinical PSMA-PET/CT preoperatively on the day of surgery. Six patients received ^{68}Ga-PSMA-11 and four ^{18}F-PSMA-1007. The resected specimen was measured using a novel micro-PET/CT device (AURA10, XEOS medical, Belgium) developed for ex-vivo intraoperative margin assessment. The resulting PET images were segmented to ascertain the extension of tracer foci, while CT was used with a soft tissue window for organ margin assessment. ***Results:*** Median Age was 66 years with a median BMI of 27. Activity concentrations in the specimens at the time of imaging were 1.0 kBq/ml (^{68}Ga) and 7.7 kBq/ml (^{18}F). All index lesions of staging multiparametric-MRI could be visualized. Overall, micro-PET/CT correlated well with conventional PET/CT regarding detection of suspicious tracer foci (pearson coefficient 0.935). In addition, micro-PET/CT demonstrated all lymph node metastases detected on conventional PET/CT (n=3), as well as three previously undetected lymph node metastases. Importantly, all positive/close (< 1mm) resection margins could be visualized in agreement with histopathology. ***Conclusion:*** In conclusion, intraoperative micro-PET/CT warrants further investigation to tailor RP, based on a good correlation with final pathology. Future trials will prospectively compare ex-vivo PET/CT to frozen section analysis for the detection of positive resection margins and bio-chemical-recurrence-free survival.

EP-0393

Preoperative CT-guided radiolabeling of lung nodules with 99mTc-MAA and Video-Assisted or Robotic-Assisted Thorascopic Surgery: experience in our center since 2017.

C. Wakfie Corieh[1,2], *E. Rodríguez Gallo*[1,2], *J. Sánchez Corral*[1,2], *N. Mimica Haasz*[1,2], *F. Moradiellos Díez*[1,2], *S. Amor Alonso*[1,2], *A. Maldonado Suarez*[1,2];
[1]Hospital Universitario Quirónsalud Madrid, Madrid, SPAIN, [2]Universidad Europea, Madrid, SPAIN.

Aim/Introduction: We evaluated our experience with preoperative CT-guided marking of lung nodules with ^{99m}Tc-MAA prior to Video-Assisted or Robotic-Assisted Thorascopic Surgery (VATS or

RATS). ***Materials and Methods:*** We retrospectively analyzed 61 patients undergoing radioguided lung nodule surgery between April 24, 2017 and February 06, 2023. Injection of ^{99m}Tc-MAA (37-296 MBq) in all cases was performed with a 25-gauge catheter, subsequently 3-4 ml of iodinated contrast was administered through the same catheter. SPECT/CT was then acquired to confirm correct nodule radiolabeling and rule out complications. After excluding 8 patients (studies with technical limitations or radiolabelling with 125-I seeds), we analyzed major diameter, attenuation, location and distance of the nodule to the pleura. We also evaluated the presence of post-puncture pneumothorax, radiolabeling, accuracy and correlation of post-radiolabeling contrast localization with that of the radiopharmaceutical. Type of surgical intervention (VATS or RATS) and histology (including surgical margins) were also collected. ***Results:*** Fifty-three patients with CT-guided radiolabeling of pulmonary nodules with ^{99m}Tc-MAA prior to surgery were included (mean age: 64±10.9 years, 34 males). Mean largest diameter of nodules was 11.7±4.8 mm; nodules were solid in 62.3% (33/53), cavitated in 7.5% (4/53), subsolid in 7.5% (4/53) and ground-glass density in the remaining 22.7% (12/53). 37.7% (20/53) were located in the right upper lobe, 25.5% (13.5/53) in the right lower lobe, 11.3% (6/53) in the left upper lobe, 24.5% (13/53) in the left lower lobe and 1% (0.5/53) in the LM. Mean distance of the nodule to the pleura was 8.5 mm (range 0-50.9). Post-puncture small pneumothorax was identified in 39.6% (21/53). The mean distance between pulmonary nodule and marking was 3.4 mm (range 0-23.4). We found concordance between contrast and radiopharmaceutical in 88.7% of the cases (47/53), discordant in 1.9% (1/53) by vascular puncture and not evaluable in the remaining 9.4% (5/53). Regarding the surgical approach, 88.7% (47/53) of the patients underwent VATS and 11.3% (6/53) underwent RATS. Most of the pulmonary nodules were malignant (84.9%, 45/53), thirty-two were primary lung tumors (60.4%), while thirteen were metastases of extrathoracic tumors (24.5%). The remaining 15.1% (8/53) were benign lesions. Complete resection of lesions was achieved in all patients. ***Conclusion:*** In our experience, preoperative CT-guided ^{99m}Tc-MAA lung nodule marking is an appropriate and safe technique that allows adequate localization and intraoperative radioguided resection by VATS and RATS approaches.

EP-0394

x2x2

E. Gromova[1], *A. Smirnova*[1], *G. Kataeva*[2], *N. Plakhotina*[1];
[1]*LDC MIBS, Saint-Petersburg, RUSSIAN FEDERATION,*
[2]*RRCRST, Saint-Petersburg, RUSSIAN FEDERATION.*

Aim/Introduction: Brain metastases occur in 20-40% of patients with various solid cancer. The problem of differential diagnosis of recurrent tumor growth and post-radiation changes is relevant. Positron emission tomography with labeled amino acids is an important method in monitoring the treatment of this patients. ***Materials and Methods:*** We performed a PET-CT examination with 18F-FET in 73 patients with brain metastasis, of whom 39.39 % were patients with lung cancer, 36.36% with breast cancer, 9.00% with melanoma, 6.06% kidney cancer and other types of cancers.62 patients were examined after radiosurgical treatment of metastases, single (50 people), double (10 people) or three times (2 people). PET-CT was performed according to the standard static protocol. All patients underwent MRI with standard sequences (T1, T2, FLAIR, T1+C). The conclusion about the progression of the disease was made on the basis of a combination of clinical and tomographic data, including data from a previous PET-CT study with 18F-FET or 11C-MET, available for 24 people ***Results:*** According to the Kaplan-Meier analysis differences of PFS in the groups of patients after single or multiple radiotherapy are significant (Cox-Mantel Test, I = 2.178374 U = 4.592147, Test statistic = 3.111355 p =0,00186). Median, lower and upper quartiles values are (12.9, 10.5;24.4) months after single RT and (7.5, 3.5;10.5) months - after repeated RT. Differences of PFS in groups of patients with a single or multiple metastases are significant (Cox-Mantel Test, I = 7.848240 U = 6.156148, Test statistic = 2.197470 p = .02799). Median, lower and upper quartiles values are (14.6, 9.8;26.7) months in group with single metastasis and (10.9, 7.2;12.8) months - in group with two and more metastases. ***Conclusion:*** 1) Median survival after single radiotherapy is comparable to treatment outcomes for primary glial tumors. This indicates the effectiveness of RT for the treatment of GM metastases.2) The presence of multiple metastases is an additional factor that reduces the value of PFS.3) To interpret PET data with TBR max in the range from 1.7 to 2.8, for a confident judgment about the genesis of increased radiopharmaceutical uptake in tumors, we cannot rely only on the value of TBR max. A search for other biomarkers of progression (beyond the appearance of new pathological foci) is required, and before their verification, a repeat PET study 2-3 months

EP-0395

Fast SPECT/CT confirmation of the preoperative location with ROLL: analysis of a 2-year single-centre real life experience

I. Lopo[1], *E. Lima*[2], *A. Bitencourt*[2], *L. Santos*[2], *A. Tavares*[2], *P. Lapa*[1,3], *G. Costa*[1,3];
[1]*Centro Hospitalar e Universitário de Coimbra, Coimbra, PORTUGAL,* [2]*A. C. Camargo Cancer Center, São Paulo, BRAZIL,* [3]*Faculdade de Medicina da Universidade de Coimbra, Coimbra, PORTUGAL.*

Aim/Introduction: ROLL (Radioguided Occult Lesion Localisation) is a simple method used for preoperative localisation of clinically-occult breast lesions, resulting in small excision volumes and little discomfort for patients. Although this technique is very precise, there can be some difficulties. To identify early and correct errors in the preoperative period, the location of the radioactive material is confirmed with SPECT/CT (single photon emission computed tomography/computed tomography) imaging by using a fast-protocol developed in the Department. When errors are identified, the surgical team is contacted or a new method of localisation is adopted, like wire-localisation. We aim to review the contribution of SPECT/CT, with a particular focus on those cases in which the ROLL method failed. ***Materials and Methods:*** We performed a retrospective study with all patients with breast lesions submitted to ROLL between September-2019 and September-2021. Patients were injected with 0.9-1mCi of 99mTc-phytate, guided either by stereotaxic-mammography or ultrasound, and surgery was performed the day after. The precision of location was analysed based on SPECT/CT findings. To evaluate the influence of incorrect location on surgical outcome, we collected all relevant clinical data available. ***Results:*** A total of 1110 ROLL were selected (mean lesion size 15.5±10.7mm). Patients (100% female) had a mean age of 52.8±12.8 years. ROLL was used for more than 1 lesion in 104 patients. There was a low prevalence of non-precise location on SPECT/CT imaging (6.4%, N=71): 55 cases (5.0%) being only reported to the surgical team and 16 (1.4%) undergoing another method of localisation, either re-injection of radiotracer (N=2) or wire-localisation

(N=14). Among these patients (2.9% invasive carcinoma, 11.4% carcinoma in situ), 11 (15.7%) had no evidence of tumour, mainly because of response to neoadjuvant chemotherapy (81.8%), and 6 lesions (8.6%) were not resected. There were involved resection-margins in 11 patients (15.7%): 3 between patients submitted to wire-localisation (21.4%) and 8 between patients in whose error was reported to the surgical team (14.5%) - 3 of these being re-operated. ***Conclusion:*** Our results show that ROLL is an effective method. Despite not being routinely used in most nuclear medicine departments, fast SPECT/CT imaging allows greater confidence in the preoperative localisation procedure, mainly in departments where the technique is starting to be implemented. Furthermore, this combined method highlights the importance of close collaboration of the different medical specialties (radiology-nuclear medicine-surgery), in the efficiency of patients' flow as well as in the optimization of surgical results.

EP-0396

Intraoperative PET/CT Specimen Imaging for the Evaluation of Surgical Margins and Nodal Metastases in Prostate Cancer Patients Undergoing Robot-assisted PSMA-radioguided Surgery

G. Rovera[1], *S. Grimaldi*[1], *M. Oderda*[2], *L. Delsedime*[3], *D. D'Agate*[2], *F. Lavagno*[2], *A. Marquis*[2], *G. Marra*[2], *L. Molinaro*[3], *P. Gontero*[2], *D. Deandreis*[1];
[1]*Nuclear Medicine, Department of Medical Sciences, AOU Città della Salute e della Scienza di Torino, Turin, ITALY,* [2]*Department of Surgical Sciences, Urology Unit, AOU Città della Salute e della Scienza di Torino, Molinette Hospital, University of Turin, Turin, ITALY,* [3]*Department of Pathology, AOU Città della Salute e della Scienza di Torino, Molinette Hospital, University of Turin, Turin, ITALY.*

Aim/Introduction: Prostate-specific membrane antigen (PSMA) is the most accurate radiopharmaceutical for detecting prostate cancer (PCa) localizations at PET/CT imaging. A high-resolution PET/CT specimen scanner recently became available, showing near five-fold higher spatial resolution compared to standard clinical PET/CTs, thus holding potential for the ex-vivo identification of PCa foci in surgically resected specimens. The aim of this feasibility study was to investigate the use of the PET/CT specimen imager in the intraoperative setting to guide robot-assisted radical prostatectomy (RARP) and pelvic lymph node dissection (PLND). ***Materials and Methods:*** Three high-risk PCa patients underwent RARP and PLND with the use of the PET/CT intraoperative specimen imager. Preoperative staging included MRI and ^{68}Ga-PSMA-11 PET/CT. In the operating room, an intravenous injection of ^{68}Ga-PSMA-11 (2 MBq/kg) was performed during trocar placement. Lymph nodes were scanned with the specimen imager after their immediate removal through the assistant trocar. After complete excision, PET/CT images of the prostate were acquired to check for positive surgical margins before performing the urethra-vesical anastomosis. Lymph nodes SUVmax, background SUVmax and nodal/background ratio (TBR) were calculated using the AMIDE(v1.0.6) software. ***Results:*** The intraoperative PET/CT scanner allowed to obtain prostatic and nodal specimen images with a mean time of 12 ± 3 minutes. The median time interval between tracer injection and PET/CT acquisitions was 98 minutes for nodal specimens and 3.8 hours for prostatatic specimens. At histopathology, the per-patient nodal yield was 17.3 ± 5.8 nodes, with only one metastatic node. At PET/CT imaging a higher focal tracer uptake was observed in the metastatic node, corresponding to a target-to-background (TBR) SUVmax ratio of 13.6. On the other hand, no uptake or diffuse, faint uptake was found in negative nodes, with a TBR range of 1-5.3. Besides correctly staging nodal metastases in all three patients, the PET/CT specimen scanner also provided intraoperative data regarding surgical margins and seminal vesicles involvement. Indeed, a significant tracer uptake in the seminal vesicles was found only in the two patients with confirmed seminal vesicles involvement at histopathology. Moreover, the intraoperative PET/CT images correctly detected negative surgical margins in two out of three patients, while only one locally advanced case presented with inconclusive findings. ***Conclusion:*** Intraoperative PSMA-PET/CT specimen imaging proved to be safe and feasible, holding potential for the improved assessment of prostate surgical margins and nodal involvement. A more precise evaluation of prostate cancer spread could allow for hyper-conservative surgical approaches while preserving oncological radicality.

EP-0397

DROP-IN robotic SPECT in sentinel lymph node prostate cancer patients

S. Azargoshasb[1], *A. Berrens*[2], *L. J. Slof*[1], *E. M. K. Wit*[2], *P. J van Leeuwen*[2], *H. G. van der Poel*[2], *M. N. van Oosterom*[1], *F. W. B. van Leeuwen*[1];
[1]*Interventional Molecular Imaging Laboratory, Department of Radiology, Leiden University Medical Cent, Leiden, NETHERLANDS,* [2]*Department of Urology, NETHERLANDS Cancer Institute-Antoni van Leeuwenhoek Hospital, Amsterdam, NETHERLANDS.*

Aim/Introduction: By allowing for robotic sentinel lymph node (SLN) resections [1] and tumor-targeted resections (PSMA salvage[2] and primary[3]), the DROP-IN gamma probe has revolutionized minimal-invasive radioguided surgery. Current DROP-IN tracing output is in the form of acoustical and numerical signals. While this output can easily be displayed in the view of the surgical console, its value is lacking a visual demarcation of the target location. The freehandSPECT technology has been poised to provide such visual target demarcations [4]. Unfortunately, this technology only works when a rigid probe is in direct line-of-sight of the tracking system. Following earlier phantom studies [5], we now present the translation of a new robotic SPECT concept that uses video-based tracking. ***Materials and Methods:*** Prostate cancer patients (n = 3) received a robot-assisted SLN procedure at a single European medical center. Following ICG-^{99m}Tc-nanoscan injection, SN locations were identified at lymphoscintigraphy and SPECT/CT. SNs were excised with a DROP-IN gamma probe that comprised clinical grade PEEK-ring tracking markers. Custom tracking and reconstruction software supported automatic segmentation of these fiducial markers from the video feeds of the Firefly (fluorescence) laparoscope, data that was used to define intraoperative probe positioning. Relating the probe output (counts/second) to its geographic location in the video feed allowed for the creation of a robotic SPECT scan that could be augmented on the laparoscopic view. ***Results:*** Patients were all clinical cT1c (2) or cT2 (1) without signs of metastases on preoperative PSMA PET/CT. In total 8 SNs were mapped on preoperative SPECT/CT and pursued with a DROP-IN gamma probe intraoperatively. During surgery, the robotic freehand data complemented the traditional DROP-IN probe output by providing a heat-map overlay that indicated which soft-tissue anatomies showed the highest count rate (average SN 600 counts/seconds). Thereby providing the surgeons with a visual que of the tissue-target location. Firefly fluorescence imaging helped confirm the target location. The total number of resected SNs was 10, of which all were detected with the DROP-IN. At pathology 2 positive

SNs were found (2 out of 3 patients). ***Conclusion:*** Integrating intraoperative SPECT imaging in robotic surgical procedures provides a means to visually enhance the surgeon's experience. Augmenting the camera view with robotically acquired nuclear medicine imaging, recorded in vivo, opens a new paradigm in radioguided surgery. ***References:*** [1] Dell'Oglio, et al., European_Urology,_(2021) [2] de Barros et al., European_Urology,_(2022) [3] Gandaglia et al., European_Urology,_(2022) [4] Wendler et al., EJNMMI,_(2010) [5] Fuerst et al., IEEE_TMI,_(2015)

EP-0398

IMPLEMENTATION OF IODINE-125 (125I) SEEDS MARKING IN NON-PALPABLE MALIGNANT BREAST LESIONS

M. Garcia Aragon*, R. Zambrano Infantino, F. Sebastian Palacid, N. Alvarez Mena, A. Sainz Esteban, M. Alonso Rodríguez, M. Moral Cano, M. Gonzalez Soto, R. Ruano Perez;*
Hospital Universitario Clínico Valladolid, Valladolid, SPAIN.

Aim/Introduction: To asses the usefulness of iodine-125I (125I) seeds in the marking of non-palpable malignant breast lesions, including cases after neoadjuvant chemotherapy (NCT), since the implantation of the technique in February-2022. ***Materials and Methods:*** The 68 patients (mean age 61.49 years) diagnosed with non-palpable breast cancer between February and January 2023 were included. The marking of the tumor was done with 125iodine seeds under ultrasound control, controlling the correct placement by mammography. The need for a second surgery due to insufficient margins was assessed. Other variables were also evaluated: seed placement time, tumor size, and previous NCT. The recovery of the seed was carried out in the Pathological Anatomy service. ***Results:*** Seeds were placed on average 5.26 days (range 1-12) before surgery. Radioguided tumorectomy was possible in all 68 cases, recovering the seed in all of them. Only 2/68 (3.03%) of the women had to undergo reoperation for affected margins. The final tumor size was 10.30mm (3-24mm), and in 4/12 cases after NCT no residual tumor was found. The sentinel node was negative in 55/68, final staging of patients without NCT (pTis: 3, pT1a:4, pT1b:18, pT1c: 29, pT2:3; pN0:48, pNmi:3, pN1:6;). ***Conclusion:*** 125iodine seed labeling of non-palpable breast cancers is a technique that involves multidisciplinary logistics. The possibility of placing the seed days before surgery facilitates the programming of the patients. The low rate of reoperations due to insufficient margins is its main potential for its healthcare implementation in breast units.

EP-0399

Minimally invasive radioguided parathyroidectomy: A descriptive report and correlation between variables of interest

M. Sanchez Torrente*, R. Nieto Serrano, A. Martin Garcia, M. Gallego Marquez, J. Venero Chaparro, D. Becerra Garcia;*
Hospital Universitario Clínico San Cecilio, Granada, SPAIN.

Aim/Introduction: The minimally invasive approach to parathyroid glands represents an important field of application in radioguided surgery. Our Aims were to perform clinical and laboratory data analysis of patients undergoing radioguided parathyroidectomy, calculate surgical success rate depending on whether sestamibi (MIBI) or macro-aggregated-albumin (MAA) is used and the variation of pre/post-surgical PTH levels regarding age and sex. ***Materials and Methods:*** A total of 78 patients who underwent radioguided parathyroidectomy with Tc99m-MIBI or Tc99m-MAA between 2016-2023 were studied. MIBI-Tc99m or MAA-Tc99m was used depending on the time-logistics from the injection to the act of surgery, uptake ratio of MIBI lesion/thyroid tissue in late phase and MIBI washout rate, performing MIBI-guided surgery whenever these parameters allowed it. We collected the variables age, sex, MIBI-Tc99m or MAA-Tc99m as surgical guide, pre/post-surgical PTH values at 5 and 10 minutes, post-surgical PTH values fall >50% compared to pre-surgical values, PTH levels normalization 2 months after surgery, parathyroid adenoma location, anatomopathological results, SPECT-CT-MIBI/Tc99m, cervical ultrasound and, if applicable, 4D-CT and 18F-Choline-PET/CT results. We performed T-Student-test to compare the mean drop in pre/post-surgical PTH values (DMPTH) depending on whether MIBI/MAA is used and the association between DMPTH and sex. We also calculated Pearson's correlation between DMPTH and age. ***Results:*** The average age was 58.9 years, female sex was the most frequent (74.36%). PTH decreased >50% 10 minutes after excision in 87.3% cases, achieving normalization of PTH after two months in 88.46% patients. The most frequent location was lower right (36.5%) followed by lower left (35.14%) and the less frequent was ectopic (5.41%). The diagnostic accuracy(DA) were 97.43% and 71.79% for SPECT-CT-MIBI-Tc99m and cervical ultrasound, respectively. 4D-CT was performed in 7 patients (DA=85.7%) and 18F-Choline-PET/CT in 4 patients (DA=100%). Anatomopathological results were: parathyroid-adenoma (92.31%), parathyroid-hyperplasia (2.56%), parathyroid-carcinoma(1.28%), normal-parathyroid-tissue (3.58%). T-Student test for DMPTH in MIBI and MAA obtained t=-1.81(p=0.037), and DMPTH and sex obtained t=-1.39(p=0.087). Pearson Correlation for DMPTH and age obtained -0.372(p=0.001). ***Conclusion:*** MIBI guided surgery and younger age showed association with DMPTH higher values. Relationship between female sex and DMPTH did not reach statistical significance, although it was very close. This suggests that with larger sample sizes we may obtain a statistically significant result. The greater DA of nuclear medicine studies and the higher success rate in MIBI-Tc99m guided surgeries stand out.

EP-0400

Lung nodule radioguided localization results.

M. Guiote Moreno[1]*, A. Lopez Cano*[1]*, S. Castejón Echevarne*[1]*, D. Tercero Garrido*[1]*, R. Zurera Pareja*[2]*, J. Vallejo Casas*[1]*;*
[1]*Hospital Universitario Reina Sofía, Cordoba, SPAIN,* [2]*IMIBIC, Cordoba, SPAIN.*

Aim/Introduction: The aim of the study is to describe our experience in lung nodule radioguided localization. ***Materials and Methods:*** 12 patients have been included in our study since January 2022 to March 2023, (5 women and 7 men) with a mean of 70,5 years old (42-80 SD 10,8). In all the cases the patients had one or multiple pulmonary nodules with suspicion of malignancy that were described in a 18F-FDG PET-CT. 6 patients had a primary lung cancer, 4 colorectal cancer, 1 chordoma, and the last one a renal cancer. The mean size of the nodules were 9 mm (21-5 mm SD 5,3 mm) with a mean of SUVmax 5,3 (42,3- 0,5 DS 11,7), which were located in left upper pulmonary lobe in 33% of the cases. Intranodular CT guided injection with 99mTc-MAA were performed in patients with a mean dose of 29.6 Mbq (37- 74 MBq SD 22.2 MBq) . A SPECT-CT was done in all patients previous to the surgery. ***Results:*** The uptake of the nodule was intralesional in 10 patients, one patient was perilesional and we found pleural efussion in two patients, (of these two patients one had the nodule radiolabeled). Only in 3 cases was a pneumothorax generated by the puncture. During surgery we found the gamma

probe-guided pulmonary nodule in 11 patients, and only in the patient who had a pleural effusion without a radiolabeled lesion, no guided nodule was found, and a lobectomy was performed. Seven of the 12 nodules were palpable by the surgeon. Finally, the pathology of the lesion was malignant in all but one case; 5 lung ADCs, one lung epidermoid carcinoma, 2 colorectal metastases, one NET tumor, and one metastatic chordoma. ***Conclusion:*** In our experience, pulmonary nodule radioguided localization has very good results, changing the clinical management of 11 of the 12 patients, with a high rate of intraoperative detection of lesions and low complications.

EP-0401

Diagnostic Value Of Salivary Gland Scintigraphy In Post-Radiation Xerostomia In Nasopharyngeal Carcinoma Patients: First Tunisian study

H. Rokbani[1], *L. Zaabar*[1,2], *S. Zarraa*[3,2], *L. Kechaou*[3], *M. El bessi*[3], *T. Ben Ghachem*[1,2], *C. Nasr*[4,2], *A. Mhiri*[1,2];
[1]*Nuclear Medicine departement, Salah Azaeiz Institute, tunis, TUNISIA,* [2]*Faculté de Médecine de Tunis, Tunis, TUNISIA,* [3]*Radiotherapy departement, Salah Azaeiz Institute, tunis, TUNISIA,* [4]*Radiotherapy departement, Salah Azaeiz Institute, Tunis, TUNISIA.*

Aim/Introduction: Post-radiation xerostomia is the most reported late post-radiation toxicity of nasopharyngeal carcinoma. Aim: Functional assessment of the main salivary glands (SG) by analyzing Technetium-99m (99mTc) clearance in patients irradiated for nasopharyngeal carcinoma. ***Materials and Methods:*** Prospective study in the Nuclear Medicine Department of the Salah Azaeiz Institute in collaboration with the Radiotherapy Department of the Salah Azaeiz Institute, on 21 patients (5 women and 16 men), aged between 30 and 60 years, who received nasopharyngeal carcinomas radiotherapy (therapeutic protocol by induction chemotherapy then concomitant radio-chemotherapy). We recorded the mean and maximum dose values for all SG and then separately. We evaluated our patients over a mean period of 11 months (extremes 6 to 22 months) by salivary scintigraphy (SS). These were dynamic acquisitions centered on the skull in anterior incidence, patient in dorsal decubitus position, immediately after intravenous injection of 148-185 MBq (4-5mCi) of 99mTc followed by Vitamin C ingestion at the 16th minute. We analyzed the images qualitatively and then semi-quantitatively (activity versus time curve). We compared our results with the doses received to the SGs and with specific radiotherapy techniques (prophylactic inclusion of submandibular IB lymph node territories). ***Results:*** N0 in 9%, N1 in 36%, N2 in 18% and N3 in 36% of cases. The mean and maximum dose values for all SG were 39 Gy and 73 Gy respectively. The mean and maximum dose values were 72 Gy and 37 Gy for the parotid glands and 58 and 70 Gy for the submaxillary glands respectively. Only 15.4% of our patients had normal overall SG function. A post-vitamin C ingestion emptying disorder was noted in 84.6% of our patients. SS showed parenchymal hypofunction in 61.5% of patients, with 38.4% involvement of the parotid glands (more important on the right side) and 69.3% of the submandibular glands bilaterally. ***Conclusion:*** The SS is an excellent tool for positive diagnosis of several degrees of radiation-induced salivary deficiency. It is a low-radiation, non-invasive exam, simple to perform, and widely available that allows reproducible quantitative analysis of SG secretory function. Our study showed high rates of hypofunction, particularly in the submandibular glands, which are more exposed in therapeutic dosimetry, which remains to be confirmed by additional studies with bigger number of patients and pre/post treatment SS.

EP-0402

Comparison of Radioactive Seed Localization and Radioguided Occult Lesion Localization in Surgical Success of Nonpalpable Breast Cancer

R. Sahin[1], *M. Baykara Ulusan*[2], *E. S. Ata*[2], *M. B. Cengiz Gökmen*[3], *N. Ergül*[1], *T. Aksoy*[1], *T. F. Çermik*[1], *E. Arslan*[1];
[1]*University of Health Sciences, Istanbul Training and Research Hospital, Department of Nuclear Medicine, Istanbul, TÜRKIYE,* [2]*University of Health Sciences, Istanbul Training and Research Hospital, Department of Radiology, Istanbul, TÜRKIYE,* [3]*University of Health Sciences, Istanbul Training and Research Hospital, Department of Surgery, Istanbul, TÜRKIYE.*

Aim/Introduction: In nonpalpable breast tumor, wire-guided localization or radionuclide-guided occult lesion localization (ROLL) is used for intraoperative tumor localization. It is an alternative method for tumor localization and surgical planning with 125-I SEED, using in many centers around the world. In this study, we aim to show the contribution of Iodine-125 SEED to surgical success compared to ROLL. ***Materials and Methods:*** A total of 24 patients with non-palpable breast tumors, with newly diagnosed or after neoadjuvant chemotherapy, were included in our prospective study. In the ROLL group (12 cases), an average of 1 mCi Tc-99m MAA (half-life: 6 hours) was marked under ultrasound guidance on the day of surgery. In the 125-I SEED group (12 cases), the 125-I SEED capsule (half-life: 59.4 days) was placed in the tumor under ultrasound guidance one day before surgery. The surgical procedure was guided by a gamma probe. The excision time and specimen weight were recorded, and differences between the groups were compared. Intraoperative frozen responses were evaluated to compare positive surgical margin and re-excision rates. ***Results:*** The 24 patients (mean age: 56.3±STD:11.89) were invasive breast cancer. The largest axial diameter of the tumor on ultrasound was 13.2±STD:5.96 mm in the ROLL group and 8.86±STD:5.32 mm in the 125-I SEED group (p=0.08). The mean operation time for excision was 11.02±STD:3.85 min for ROLL, and 9.45±STD:5.41 min for 125-I SEED (p=0.42). The specimen weight was 65±STD:15 grams in the ROLL group and 37±STD:12 grams in the 125-I SEED group (p=0.045). In the ROLL group, the lesion was correctly localized in 8/12 (66%) cases, and re-excision was required in 4 cases. In the 125-I SEED group, the lesion was correctly localized in 10/12 (83%) cases, and re-excision was performed in 2 cases (p=0.36). ***Conclusion:*** According to the preliminary findings of our study, reexcision rate was observed to be lower with 125-I SEED compared to ROLL although statistically insignificant. However, it was shown that a statistically significantly lower weight resection specimen was extracted with the 125-I SEED. The use of the 125-I SEED is an easy-to-learn, safe and effective procedure with a low incidence of positive margin. Better localization of the tumor with 125-I SEED during surgery will increase surgical success, decrease recurrence rates, and increase the psychosocial well-being of patients by preserving healthy breast tissue. In addition, due to the longer half-life of 125-I SEED, more flexible study plan will be possible.

EP-24

e-Poster Area

B: Imaging Clinical Studies -> B3 Other Oncological Clinical Study -> B32 Sentinel Node

EP-0403

SPECT/CT imaging and Sentinel lymphnode biopsy in early breast cancer in 150 patients -KMCH India experience.

K. Kamaleshwaran, *E. Ramkumar;*
Kovai Medical center and Hospital Limited (KMCH), Coimbatore, INDIA.

Aim/Introduction: Find out number of sentinel lymphnodes seen in SPECT CT imaging and sentinel probe ,identify false negative rate and recurrence rate in early Breast Cancer(EBC) Patients undergoing Sentinel Lymphnode Biopsy (SLB). ***Materials and Methods:*** Total 150 patients with EBC underwent SLB .Average age 50 -60 yrs .youngest age - 25 yrs,oldest age -83 yr old .Tc99m labelled colloid particles such as Nanocolloid or Human serum Albumin in 3 insulin syringes with each (0.5mci) was injected intra-dermally in peri-areolar region.SPECT CT of chest was done on day of surgery and identified number of nodes in three levels of axilla and informed to surgeons before surgery . Blue dye was also injected during surgery.surgeon removed hot nodes with help of hand-held gamma probe and sent to frozen section biopsy.If the nodes are negative ,no axillary lymphnode dissection (ALND) was done , if positive ,then Surgeon will Proceed with ALND. ***Results:*** Among 150 patients,overall 270 nodes were identified in all three levels of axilla in SPECT CT.In only 13 patients ,nodes were not identified in SPECT CT ,but were identified in gamma probe in surgery . Average 2-3 nodes were identified in level I and II axilla .Total 390 sentinel nodes in all 150 patients were removed . 114 patients were sentinel negative . 36 patients having sentinel positive had undergone ALND ,in those 36 ,only 6 patients showed extra nodes positive in dissection . Average nodes removed as sentinel was 1-3 and maximum 8 nodes were removed in one case.4 patients were false negative(4/150 -2.6%) .all underwent clinical breast examination every 3 months and mammogram at 1 year . There is no axillary recurrence and no arm lymphedema . 1 patient developed distant metastases after 1 year and another patient developed breast recurrence .73 patients were not completed one year followup. ***Conclusion:*** Among patients with EBC treated with breast conservation surgery, SLD provides axillary control which is equal to ALND and less false negative rate .SPECT CT helped in identifying exact location of nodes ,more number of nodes and helps surgeon in removing node confidently during surgery. ***References:*** Luan T, Li Y, Wu Q, Wang Y, Huo Z et al .Value of Quantitative SPECT/CT Lymphoscintigraphy in Improving Sentinel Lymph Node Biopsy in Breast Cancer Breast J. 2022; 28;2022:6483318.

EP-0404

Unusual lymphatic drainage pathways detected by intradermal lymphoscintigraphy for sentinel lymph node biopsy in breast cancer.

G. Tartaglione[1], *M. Pagan*[1], *F. P. Ieria*[1], *E. Covello*[2], *L. M. Marino Cosentino*[3], *S. Di Filippo*[2], *S. Ghinassi*[3], *R. Marsico*[3], *L. Leone*[3], *M. R. Limiti*[4], *P. L. Bonatti*[2,3];
[1]*Cristo Re Hospital, Nuclear Medicine, Rome, ITALY,* [2]*Santo Spirito Hospital, Breast Unit ASL Roma 1, Rome, ITALY,* [3]*San Filippo Neri Hospital, Breast Unit ASL Roma 1, Rome, ITALY,* [4]*Santo Spirito Hospital, Pathology, Breast Unit ASL Roma 1, Rome, ITALY.*

Aim/Introduction: Sentinel lymph node biopsy is the standard in staging lymphatic system for primary breast cancer. Usually, lymphoscintigraphy shows sentinel node in ipsilateral axilla. However, sometime the lymphatic drainage may occur to extraaxillary lymph nodes. This was a single centre retrospective study to evaluate the incidence and reasons of an unexpected lymphatic drainage using intradermal lymphoscintigraphy for sentinel node radio guided biopsy in breast cancer. ***Materials and Methods:*** From February 2018 to December 2022, we performed preoperative lymphoscintigraphy for sentinel node identification in 1,649 consecutive patients with breast cancer. We injected intradermally a dose of 50 MBq, 0.3 mL, 99mTc-nanocolloidal HSA in the four quadrants of the breast. Patients underwent radio guided sentinel node biopsy 3-24 hours after tracer injection. We used One Step Nucleic Acid Amplification (OSNA) method for the intraoperative analysis of sentinel lymph nodes. ***Results:*** Lymphoscintigraphy showed a sentinel node in ipsilateral axilla in 1,596 pts (96.8%), and no drainage in 19 pts (1.1%). We observed un unusual lymphatic drainage in 34 pts (2.1%), 33 f, 1 m, median age 72 y (range 51-95) with breast cancer (eighteen right, sixteen left). In thirty-three out of 34 pts the abnormal drainage was associated with recurrent breast cancer previously treated with axillary lymph nodes dissection, while 1 pt previously treated for right breast augmentation. Eighteen patients had an unusual drainage in the contralateral axilla (four of these had also a lymph drainage toward internal mammary chain). Sixteen patients had a lymph drainage toward internal mammary chain. Based on OSNA results, three patients were upstaged to pN1mi(sn) and one patient to pN2a from cN0. ***Conclusion:*** Intradermal lymphoscintigraphy may visualize aberrant lymphatic drainage pathways in recurrent breast cancer patient and ipsilateral axillary clearance, the lymph drainage pathway may across the midline of the thorax. This study shows the need of lymphoscintigraphy to find sentinel node particularly in the group of patients previously treated for breast cancer.

EP-0405

Sentinel lymph node biopsy and axillary marking after neoadjuvant treatment in node-positive breast cancer patients

P. Guardia Jimena, *A. Santos Bueno, Á. Rebollo Aguirre, E. Sánchez de Mora, A. Jiménez Heffernan;*
Hospital Universitario Juan Ramón Jiménez, Huelva, SPAIN.

Aim/Introduction: To provide our experience in sentinel lymph node biopsy (SLNB) and axillary marking in patients with breast cancer with axillary involvement at diagnosis who received neoadjuvant treatment. ***Materials and Methods:*** Retrospective observational study including 62 women, diagnosed with breast cancer with axillary involvement, confirmed with core needle biopsy, who received neoadjuvant treatment with complete radiological nodal response and subsequent surgical

intervention with SLNB between 2019 -2022. The decision to perform SLNB was made after evaluating each case individually in a multidisciplinary team. Lymphoscintigraphy with SPECT/CT was performed to determine the coincidence between the biopsied-marked node (MN), marked with clip markers (54) or magnetic seed (8), and the sentinel node. In the non-coincident ones, wire-localization marking was performed. ***Results:*** The mean age was 50.11 years (range 32 to 73). Molecular subtype: 15 Luminal-A, 14 Luminal-B, 13 Luminal-B like, 9 HER2-enriched and 11 Triple-negative. Histological type: 60 infiltrating ductal carcinoma and 2 lobular carcinoma. TNM: 8 IIA, 25 IIB, 25 IIIA, 2 IIIB, 2 IIIC. Clinical N stage: 52 N1, 8 N2, 2 N3. There was no migration of the radiotracer in 7 cases (11.3%), there were two cases in which the node was not found, and in only one case there was migration to the internal mammary arteries, in 27 the MN did not coincide with the SN (43%). 24 patients were negative in the final anatomopathological results, and 28 patients were positive (12 micrometastases and 16 macrometastases), a total of 34 lymphadenectomies were performed (14 positive); the mean number of GC identified was 1.62±0.83. Out of the 27 patients with mismatched MN and SN, in 10 patients the anatomopathologic result was different; in 7 the MN was positive and the SN negative, resulting in 4 micrometastases and 3 macrometastases, and in 3 the SN was positive and MN negative, resulting in 3 micrometastases. There was one false negative result (3.2%), in this case lymphadenectomy was performed due to the pathological aspect of the axillary nodes. ***Conclusion:*** The anatomopathologic result of MN and SN in conjunction allows us to determine with greater reliability the axillary status and avoid lymphadenectomy in patients with complete axillary response after neoadjuvant treatment.

EP-0406

Local anaesthetic improves patient experience of breast and melanoma lymphoscintigraphy

K. Jewell*, G. Kong, B. Emmerson, T. Akhurst, K. Moodie;*
Peter MacCallum Cancer Centre, Melbourne, AUSTRALIA.

Aim/Introduction: The patient experience of pain with preoperative lymphoscintigraphy is variable; techniques to minimise distress to patients during the procedure are non-standardised across Australian nuclear medicine departments. This study assesses the use of local anaesthetic to reduce pain and improve patient experience, whilst ensuring a non-inferior scintigraphic visualisation rate of target sentinel nodes. ***Materials and Methods:*** Consecutive patients undergoing preoperative lymphoscintigraphy with a single-injector at our centre from 18/08/22 to 07/02/23 were included. Patients received 1-4 injections of ~0.2ml technetium-99m antimony colloid (~10-15MBq) mixed with 0.05ml of 2% lignocaine in each syringe as intradermal injections, followed by 20-30 seconds of light massage at the injection site(s). SPECT/CT +/- dynamic imaging of the region was acquired. A series of peri-procedural audit questions evaluated patient experience:1. Time spent thinking about upcoming procedure (surrogate assessment for preprocedural anxiety).2. A pain score from 0 (none) to 10 (extreme) using the Wong-Baker FACES rating scale as reference.3. A qualitative rating of pain in relation to their diagnostic biopsy: hurt much less (1), a little less (2), same (3), a little more (4), much more (5).A sub-set of head/neck melanoma cases (n=7) did not receive local anaesthetic at the referring surgeon's request, and were used as comparator cases. ***Results:*** 99 patients were included (breast cancer n=50, melanoma n=41, penile cancer n=1), 67 female, median age 63; 92 patients received local anaesthetic. For patients with breast and melanoma, the average pain scores were 1.24 and 2.39 respectively. The solitary penile score was 2/10. The average pain score of melanoma comparator cases was 5.3 (range 0-8).Patients with breast cancer rated lymphoscintigraphy as hurting 'much less' than diagnostic biopsy (average of ratings = 1.36), while in melanoma the procedures rated as 'about the same' (2.98). The visualisation rate was 96.7% (89/92) with local anaesthetic and 85.7% (6/7) without. ***Conclusion:*** Local anaesthetic improves the patient experience of antimony colloid injections without compromising visualisation rates. Radiotracer selection and pH buffering as pain minimisation strategies are other areas of ongoing investigation.

EP-0407

Detection rates of sentinel lymph node biopsy (SLNB) in gynecological cancer. Our experience.

C. Ruiz Corbalán*, A. De Agrela Serrao, A. Leiva Montejo, D. Cáceres Silva, M. Castellón Sanchez, L. Frutos Esteban, J. Navarro Fernadez, T. Rodriguez Locarno, A. Hernandez Martinez, L. Mohamed Salem, J. Contreras Gutierrez;*
ARRIXACA, Murcia, SPAIN.

Aim/Introduction: The aim of this study is to show detection rates of SLNB in patients diagnosed with early stages of gynecological cancer who were referred to our department. ***Materials and Methods:*** This is a retrospective, observational and analytic study which included 83 patients diagnosed with endometrial (5), cervical (43) or vulvar (35) cancer who underwent SLNB between 2014 and 2022. The mean age was 60±16.6 years old. The technique performed in all patients lied in administering a perilesional dose of 6mCi of 99mTc-nanocolloid divided in 3 or 4 injections the previous day to surgery and performing a lymphoscintigraphy with early and late planar images with or without SPECT-CT for a more specific localization. Besides SLNB, in 75% of patients a unilateral or bilateral lymphadenectomy was performed. ***Results:*** The presence of lymphatic drainage was observed in 87% of patients. Of the remaining 13% whose drainage was not visualized, just in 4 of the cases the sentinel lymph node (SNL) was found during surgery. On the other hand, from those patients who showed drainage in the images, it was not possible to find the SNL with gamma probe in 3 of them. This means that among the 72 patients who showed lymphatic drainage, in 69 of them it was possible to find SLN during surgery, what gave our department a global detection rate of 95,8% for this technique (91,9% for cervical cancer, 100% for endometrial cancer and 97,1% for vulvar cancer), showing a positive significant correlation between visualization of lymphatic drainage in molecular imaging techniques and SNL detection in surgery (p-value under 0.001). ***Conclusion:*** SLNB is a reliable technique that guarantees a less invasive surgery and a correct lymph node staging in gynecological cancer, with a great correlation between lymphatic drainage visualized in molecular imaging techniques and SLN detection during surgery.

EP-0408

Radiation-free bimodal sentinel node procedure combining fluorescence and magnetic guidance and pre-operative resonance imaging in prostate cancer - A first in-human study

B. Michalik*[1], S. Engels[1], M. C. Otterbach[2], M. N. van Oosterom[3], M. Maurer[2], F. Wawroschek[1], A. Winter[1];*
[1]University Hospital for Urology, Klinikum Oldenburg, Carl von Ossietzky University Oldenburg, Oldenburg, GERMANY, [2]University Institute for Diagnostic and Interventional Radiology, Klinikum Oldenburg, Carl von Ossietzky University Oldenburg, Oldenburg, GERMANY, [3]Interventional Molecular Imaging Laboratory, Department of Radiology, Leiden University Medical Center, Leiden, NETHERLANDS.

Aim/Introduction: In prostate cancer (PCa), pelvic sentinel lymph node dissection (sLND) using a bimodal fluorescent-radioactive hybrid tracer significantly improves staging ability due to pre-operative lymphoscintigraphy and intra-operative lymph node (LN) visualisation through fluorescence imaging (FI). Based on our pre-clinical proof of concept [1], here, we introduce the clinical translation of a radiation-free bimodal sentinel node procedure combining pre-operative magnetic resonance imaging (MRI), intra-operative FI and magnetic guidance. ***Materials and Methods:*** In March 2023, six PCa patients at an individual risk for LN involvement of 8-58% (Winter nomogram [2]) received magnetometer- and FI-guided pelvic sLND during radical prostatectomy at our centre. The day before surgery, patients were intraprostatically injected with a mixture of indocyanine green (ICG) and superparamagnetic iron oxide nanoparticles (SPION; 0.5 mg ICG in 2 ml SPION) under transrectal ultrasound guidance. Approximately five hours after injection, pelvic sentinel LNs with SPION uptake were visualised by MRI to define a lymphatic road map for surgical planning. During surgery, all fluorescent LN samples visualised by FI and/or magnetically active LN samples detected by a handheld magnetometer were dissected. Each resected sample was checked for ex situ fluorescence and magnetic activity, respectively, and was analysed for LN as well as for metastatic yield by an experienced uropathologist. ***Results:*** Pre-operative MRI identified 80 (median 12, range 6-21) LNs with SPION uptake in the external and internal iliac and obturator fossa regions. From these regions, we dissected 83 (median 13, range 8-21) LNs, of which 45 (median 6, range 3-13) were magnetically active and 49 (median 7, range 5-13) were fluorescent, respectively. During surgery, fluorescence as well as magnetic signal could be detected in each patient. Ex situ, each magnetically active LN showed also fluorescence signal, which could not be detected during surgery in four samples due to anatomical location. None of the dissected LNs contained metastasis. ***Conclusion:*** These are the first promising in-human results combining MRI and intra-operative FI presenting a radiation-free alternative to the conventional fluorescent-radioactive hybrid tracer for pelvic sLND in PCa patients particularly during robotic surgery. ***References:*** [1] Azargoshasb et al. (2022) IJCARS 17:211-218, doi: 10.1007/s11548-021-02458-2; [2] Winter et al. (2017) J Cancer 8:2692-2698, doi: 10.7150/jca.20409

EP-0409

Validation of sentinel node biopsy in head and neck tumors at one single center. Our experience.

D. Rivas-Navas*, J. Fernández-Fernández, E. Triviño-Ibáñez, C. Ramos-Font, R. Sánchez-Sánchez;*
Hospital Universitario Virgen de las Nieves, Granada, SPAIN.

Aim/Introduction: The aim of this work is to validate the sentinel lymph node biopsy (SLNB) in head and neck tumors at the Virgen de las Nieves University Hospital (Granada, Spain) and to statistically analyze the collected data. ***Materials and Methods:*** We performed an observational and prospective study that included patients with early-stage (T1 and T2) head and neck tumors who underwent SLNB between February 2021 and October 2022. Statistical, technical, clinical parameters, image and pathological anatomy results were collected. Following SLNB, bilateral cervical lymphadenectomy was performed in all patients to assess the effectiveness of the technique by comparing both techniques. ***Results:*** A total of 31 patients (mean age: 64.39 ± 13.02 years, 54.8% men) were included. The primary tumor was most commonly located on the lateral border of the tongue (61.3%) followed by the floor of the mouth (29%), while the most common affected side was the left (48.4%). 58.1% had well-differentiated squamous cell carcinoma, with cT2 being the most common stage (54.8%). In all cases, tracer migration to the SLN was observed in both early and late images and SPECT/CT (100% identification of the SLN), bilateral in 11/31 (35.5%) cases. The mean number of identified SLN was 3, and the most frequent location was cervical levels II and III (65.4%). 32.3% had a positive result in the anatomopathological study. In 9/10 cases, the SLN was the only node affected in the lymphadenectomy. The mean number of removed nodes in lymphadenectomy was 31.6. The false negative rate was 10%. The only factor associated with a higher probability of a positive result in the SLNB, in the binary logistic regression model, was the female sex (OR: 14.63, p=0.019). ***Conclusion:*** SLNB is a feasible technique in patients with head and neck cancer, being able to avoid unnecessary lymphadenectomies.

EP-0410

Nodal staging in patients with penile cancer. Correlation between [18F]FDG-PET/CT and sentinel node biopsy.

A. Piñeiro Donis*, J. Fernández Fernández, E. Triviño Ibáñez, C. Ramos Font, R. Sánchez Sánchez;*
Hospital Universitario Virgen de las Nieves, Granada, SPAIN.

Aim/Introduction: The aim of this work is to evaluate and correlate the use of positron tomography with [^{18}F]FDG in the staging of patients with penile cancer, with the result of sentinel lymph node biopsy (SLNB). ***Materials and Methods:*** We performed an observational retrospective study. All patients underwent preoperative [^{18}F]FDG-PET/CT study and SLNB with [^{99m}Tc]-nanocolloid. The histologic result of sentinel lymph node (SLN) is correlated with the findings of imaging techniques. Statistical analysis was performed. ***Results:*** 10 males were included (mean age: 73±11.72 years). The most frequent location of the primary tumor was the glans (40%), followed by the foreskin (30%). Fifty percent presented well-differentiated squamous cell carcinoma. In 6/10 (60%) of the cases the radiopharmaceutical was injected pericicatricially, in 2/10 (20%) perilesionally and in 2/10 (20%) in the balanopreputial sulcus. In all cases tracer migration to the sentinel lymph nodes were observed in both early and late images, being 70% bilateral inguinal and unilateral in the remaining 30%. SPECT-CT was performed in 80% of the patients. The anatomical pathology (AP) of the SLN result was negative in 9/10 (90%) of the patients. The result of the [^{18}F]F-FDG PET/CT study was negative at the lymph node level in 90% of the cases, showing 100% concordance with the SLN AP results. Comparative analysis of quantification parameters (SUVmax, SUVpeak, SUVmed, MTV and TLG) between the moderate-undifferentiated and well-differentiated histological subgroups showed higher values for the moderate-undifferentiated group, although statistical significance was not reached. ***Conclusion:*** [^{18}F]FDG-PET/CT and SLNB are accurate techniques in the nodal staging of penile cancers, obtaining an excellent correlation of their results with respect to pathological anatomy.

EP-0411

Investigation into the frequency of systemic tracer uptake when performing sentinel lymph node examinations

A. Carradus[1,2]*, M. Bradnam*[1,3]*, J. Foster*[1,3]*, A. Bolster*[1,2,3]*;*
[1]Department of Clinical Physics and Bioengineering, NHS Greater Glasgow and Clyde, Glasgow, UNITED KINGDOM, [2]Nuclear Medicine, North East Sector Glasgow, NHS Greater Glasgow and Clyde, Glasgow, UNITED KINGDOM, [3]College of Medical, Veterinary and Life Sciences, University of Glasgow, Glasgow, UNITED KINGDOM.

Aim/Introduction: In sentinel lymph-node (SLN) procedures, 99mTc-Nanocolloid is injected intradermally to find the first lymph-node in the drainage pathway. A gamma probe is used in theatre to locate the sentinel node for biopsy. While the procedure is thought to be the optimal method for detecting the SLN[1], the false-negative rate is relatively high, with one study reporting a false-negative rate of 5.7% over a 15-year period[2], although this was 29.4% in the first year. However, during routine imaging of breast and melanoma patients at Glasgow Royal Infirmary and Stobhill Ambulatory Care Centre, we have occasionally seen tracer uptake in the liver, suggesting that some 99mTc-Nanocoll has travelled systemically through the bloodstream, which would potentially reduce the amount of tracer travelling to the SLN. The aim of this study was to audit SLN imaging procedures performed at Glasgow Royal Infirmary and Stobhill Ambulatory Care Hospital over the previous six years, to determine the proportion of procedures which had resulted in ^{99m}Tc-nanocolloid travelling systemically through the circulatory system. ***Materials and Methods:*** 1627 ^{99m}Tc-nanocolloid SLN patients (2017-2022) were audited through visual inspection. Injection sites were masked automatically and images were automatically windowed and displayed using Python. If the liver was visible on the images, this was determined to be an administration which has moved into the circulatory system. Quantification was performed on a sample of 25 positive scans by comparing the uptake in the liver to the uptake in the injection site. ***Results:*** Systemic tracer uptake could be seen in 85 SLN patients (5.22%). When considering only breast cancer patients, some systemic tracer uptake could be seen in 15 of 1372 patients (1.09%), and for melanoma patients some systemic tracer uptake could be seen in 70 of 255 patients (27.5%). Median liver uptake was 1.7% when comparing to the injection site, and the maximum uptake seen was 16.2%. ***Conclusion:*** It is important to note that systemic uptake does not mean that the procedure has been unsuccessful, rather that the signal from the gamma probe may be reduced compared to other patients. These results may also have wider implications for the use of other tracers where the effects of systemic uptake may be unknown. ***References:*** [1]Sadkin, Vladimir, et al. "99mTc-labeled nanocolloid drugs: development methods." Scientific Reports 10.1 (2020). [2]Veenstra, Hidde J., et al. "Less false-negative sentinel node procedures in melanoma patients with experience and proper collaboration." Journal of surgical oncology 104.5 (2011).

EP-0412

Single Institution Study of Sentinel Lymph Node Detection in Cervical Cancer: Validating an Alternative to Pelvic Lymphadenectomy

D. Rombo[1], *D. Fraga*[1], *M. Bernardino*[2], *I. Vitorino*[1], *E. Sousa*[1], *J. Aço*[1], *I. P. Carvalho*[1], *R. Sousa*[1], *A. F. Jorge*[2], *L. Salgado*[1]; [1]*Serviço de Medicina Nuclear, Instituto Português de Oncologia de Lisboa Francisco Gentil E.P.E., Lisboa, PORTUGAL,* [2]*Serviço de Ginecologia, Instituto Português de Oncologia de Lisboa Francisco Gentil E.P.E., Lisboa, PORTUGAL.*

Aim/Introduction: Cervical cancer (CC) is the fifth most common cancer among women in Portugal with an estimated prevalence of 10.7 per 100,000 women. Lymph node status is a key prognostic factor in CC, with nodal metastasis indicating a poorer prognosis and the need for more aggressive treatment. Sentinel lymph node (SLN) detection has emerged as a promising alternative to traditional lymphadenectomy in CC, allowing for accurate staging with reduced morbidity. This study aims to validate SLN detection in women with early-stage CC, as an alternative to pelvic lymphadenectomy, in our institution. ***Materials and Methods:*** We retrospectively reviewed 46 women with early-stage CC (stages IA to IIA1, FIGO 2018) who underwent SLN detection followed by complete pelvic lymphadenectomy from 05/2021 to 04/2023. Lymphatic mapping was conducted preoperatively with [^{99m}Tc] Tc-nanocolloidal albumin (111 MBq) injections in four cardinal points of the cervix, followed by planar and SPECT/CT imaging, as well as intraoperatively with patent blue injections. SLNs were identified as blue and/or radioactive by visual inspection and using a gamma probe, respectively. Pathological evaluation of the SLNs was performed separately from the remaining pelvic lymph nodes. ***Results:*** At least one SLN was identified in 40 patients (87.0%) and bilateral SLNs were identified in 33 patients (71.7%). The median number of SLNs identified per patient was two (range, 1 to 5). The locations of SLNs included external iliac (41.4%), obturator (25.3%), common iliac (21.8%), internal iliac (10.3%) and parametrium (1.15%) regions. There was no difference in detection rates between patients with body mass index <30kg/m^2 versus ≥30kg/m^2, tumor size ≤2cm versus >2cm or between patients with/without conization. The detection rate was significantly lower in women aged >60 years (OR 9.43, 95% CI 1.70-53.3). Metastatic disease was detected in SLNs of eight patients (20.0%). Two patients had a false-negative result. In both cases, metastatic involvement was detected in the contralateral lymph nodes, where no SLN was identified. The technique yielded a sensitivity of 80.0% (95% CI 49.0%-96.5%) and a negative predictive value of 93.8% (95% CI 79.9%-98.9%). The follow-up median time was 7 months (range, 1 to 23) with only one patient experiencing a local relapse 5 months after surgery. ***Conclusion:*** Our study confirms that SLN procedure is a reliable alternative to pelvic lymphadenectomy, with comparable sensitivity and negative predictive value to those reported in the literature. This supports the adoption, in our institution, of isolated SLN mapping, without lymphadenectomy, in future procedures.

EP-0413

Prospective evaluation of SPECT/CT & intra-operative Gamma probe techniques for identification of sentinel lymph node (SLN) in early stage oral cancer

M. L Narayan[1], *P. Kaul*[2], *P. Singh*[3], *T. Singhal*[3], *M. Negi*[1], *P. K. Garg*[2]; [1]*All India Institute of Medical Sciences (A.I.I.M.S), Rishikesh,India, INDIA,* [2]*SGRR Institute of Medical Sciences and SMI Hospital, Dehradun, Uttarakhand, India, INDIA,* [3]*All India Institute of Medical Sciences (A.I.I.M.S), Bhubneshwar , Orissa, INDIA.*

Aim/Introduction: The aim of this prospective study was to assess the feasibility of SLNB and compare SPECT-CT, with gamma probe techniques, for identifying SLN in early stage oral cavity cancer (T1/2) at a newly established tertiary care Institute of North India ***Materials and Methods:*** A total of 17 patients could be recruited for this study with a median age of 49 years(41-54 years),including14(82%) male & 3 were females. 15/17(88.2%) Tongue was the most common sub-site involved by the tumor 12(70.6%), followed by buccal mucosa and floor of mouth in four(23.5%) and one(5.9%) patients respectively. On clinical assessment, 47%(n=8) of tumors were staged as T1 while remaining 53%(n=9) were staged as T2.All patients underwent Lymphoscintigraphy (LSG), using either one or two day protocol with 250-500 microCi(in 0.4-0.5ml) of 99mTc-Sulphur colloid (filtered), that was injected superficially (either submucosally or intradermally) in the four cardinal points around the tumor. Planar, SPECT-CT images were acquired upto 90min post injection, followed by methylene blue injection (peritumour) &

intraoperative localization of SLN using Gamma probe. ***Results:*** The sentinel lymph node identification rate was 94.1% with SPECT-CT. Additional draining lymph nodes were identified in 14/17(82.35%) patients. Bilateral drainage was seen in two(11.7%) patients on SPECT-CT. Neck dissection was either a SND I-III (n=11, 64.7%) or SND I-IV (n=3. 17.6%) and MND I-V (n=3. 17.6%). Contralateral neck dissection- SND I-III was done in one(5.9%) patient with primary located in floor of mouth.SLN identification rates for SPECT-CT, gamma probe, blue dye and dual technique localization (gamma probe+blue dye) were 94.1%, 88.2%, 76.4% & 94.1% respectively. The sensitivity, specificity, PPV, NPV and diagnostic accuracy of various techniques namely, SPECT-CT, gamma probe and dual technique (gamma probe + blue dye), against the current standard i.e., END was 100 %All patients were alive and disease free during the last follow up visit, except one patient with oral tongue primary (pT2N1), who developed regional recurrence during 6th month of follow-up, denied any further treatment and died two months later. ***Conclusion:*** The SLNB is feasible technique for neck staging in early stage oral cancer and has a high sensitivity, specificity, positive and negative predictive value. A high concordance was noted between the findings of SPECT-CT and intraoperative gamma probe for identification of SLN. Thus, use of this technique should be encouraged to reduce morbidity associated with extensive surgery and achieve a comparable survival outcome, to elective neck dissection.

EP-0414

DROP-INradioguidanceduring robotic sentinel nodeprocedures in bladder cancer

D. Rietbergen[1], *M. N. van Oosterom*[1], *E. van Gennep*[1], *B. van Rhijn*[2], *H. G. van der Poel*[2], *F. W. B. van Leeuwen*[1];
[1]*Leids Universitair Medisch Centrum (LUMC), Leiden, NETHERLANDS,* [2]*NKI, Amsterdam, NETHERLANDS.*

Aim/Introduction: In the management of bladder cancer, lymph node invasion has proven to be an independent predictor and prognostic factor for recurrence and cancer-specific survival. We recently demonstrated the feasibility of using the hybrid tracer ICG-99mTc-nanocolloid for sentinel node (SN) procedures in bladder cancer, all be it with a high degree of non-visualizations [1]. As bladder surgery is increasingly being conducted robotically, radioguidance modalities must adapt accordingly. Based on initial technological validations during prostate cancer SN procedures [2], we have now studied the use of the DROP-IN gamma probe technology during robot-assistedbladder SN surgery. ***Materials and Methods:*** This study group included a bladder cancer patient population of n= 11, treated at a single European center. All patients had histologically confirmed muscle-invasive bladder cancer (cN0M0), but no suspected nodal disease on diagnostic imaging (i.e., CT and 18F-FDG). Given the investigative nature of this setup, patients not only received a SN biopsy, but also benefitted from an extended pelvic lymph node dissection(ePLND). Following transurethral injection of the hybrid tracer ICG-99mTc-nano-colloid, SN mapping was performed using lymphoscintigraphy and SPECT/CT. Intraoperative localization was guided by both DROP-IN gamma probe and Firefly fluorescence imaging. ***Results:*** After hybrid tracer injection (mean injected activity of 213 MBq), 3 out of 11 patients had non-visualization on preoperative imaging. Excluding these 3, on average 1.4 SNs were mapped per patient. During surgery, the sterilizable DROP-IN could successfully be used repeatedly. After insertion in to the abdominal cavity by the bedside assistant (either through or next to a trocar), the surgeon could autonomously pick up and maneuver the probe with thesteerable Prograsp-forceps instrument. Intraoperative DROP-IN guidance proved effective, directing the surgeon to SNs located in the various anatomies found in this patient cohort (i.e., iliac communis, iliac externa and the obturator area).Once the SNs were localized in situ, fluorescence imaging provided confirmation and helped guide the resection in real-time. On average 1.6 SNs were dissected per patient, and on average a total of 18.6 lymph nodes were harvested per patient. Interestingly, in 1 patient with non-visualization at preoperative imaging, still 2 active SNs were found during surgery. Histopathology showed lymph node metastases in 2/11 patients. ***Conclusion:*** The DROP-IN gamma probe also proves valuable during robotic SN procedures of bladder cancer. Thereby helping to advance this technically challenging SN indication. ***References:*** 1. Rietbergen et al., Clin Nucl Med, 20222. Dell'Oglio et al., Eur Urol, 2021

EP-0415

Lymphoscintigraphy patterns in recurrent breast cancer. Can they predict the outcome?

B. Pereira*, P. Soeiro, A. Fernandes, A. Oliveira;*
Centro Hospitalar Universitário de São João, Porto, PORTUGAL.

Aim/Introduction: Breast cancer is the most common malignancy in women and is associated with high morbidity and mortality. Identifying the individual lymph node drainage pattern with lymphoscintigraphy allows better staging of each tumour and helps to determine treatment and follow-up plans. This study aims to evaluate lymph node drainage patterns in women with recurrent breast cancer and to assess its association with subsequent lymph node spread of the disease. ***Materials and Methods:*** A retrospective, longitudinal, single-centre observational study was conducted, enlisting patients whose breast cancer recurrence had previously been treated surgically and who had undergone sentinel node lymphoscintigraphy in our department between November 2009 and December 2022. Statistical analyses were performed using SPSS Statistics 28® software. Statistical significance was set at $p \leq 0.05$. ***Results:*** From 677 patients, 108 met our inclusion criteria. All patients were female; 86.5% had invasive tumours, 13.5% had ductal carcinoma in situ. Most patients (62%) had at least one lymphatic drainage pathway identified: 75% had ipsilateral axillary lymph nodes (24% from multiple pathways), 25% had contralateral axillary lymph nodes, 24% had ipsilateral internal mammary lymph nodes and 3% had contralateral internal mammary lymph nodes; 25% had drainage to more than one lymphatic chain. From these patients, 24% had previous axillary lymph node dissection;during follow-up 7% were diagnosed with metastatic axillar lymph node disease. From the patients without identifiable lymphatic drainage (38%), 39% had previous axillary lymph node dissection; during follow-up, 15% were diagnosed with metastatic axillar lymph node disease. We found no statistically significant association was found between a specific drainage pattern and a higher risk of recurrence of lymph node disease during follow-up. ***Conclusion:*** In recurrent breast cancer previously operated on, lymph node drainage patterns are diverse and cannot predict the recurrence of lymph node disease. Nevertheless, secondary metastatic lymph node disease is more common in patients whose lymphoscintigraphy found no drainage. ***References:*** Donohoe KJ, et al. Summary: Appropriate Use Criteria for Lymphoscintigraphy in Sentinel Node Mapping and Lymphedema/Lipedema. J Nucl Med. 2023 Apr;64(4):525-528. doi: 10.2967/jnumed.123.265560.

EP-0416

Lymphoscintigraphy in Breast Cancer. Is there a difference in primary versus recurrent disease?

***B. Pereira**, P. Soeiro, P. Dias, A. Oliveira, A. Fernandes;*
Centro Hospitalar Universitário de São João, Porto, PORTUGAL.

Aim/Introduction: Breast cancer that spreads through the lymph nodes is relatively common. For accurate staging, it is therefore essential to assess the involvement of the lymph nodes. There are several techniques for this purpose, with lymphoscintigraphy being one of the most common for sentinel lymph node biopsy. Lymphoscintigraphy is an accessible and straightforward technique, which is why it is often used. Nevertheless, there are different scenarios that can alter the sensitivity and accuracy of this technique. Therefore, we aim to evaluate the differences in outcomes obtained with this technique in patients with primary breast cancer compared with patients with cancer recurrence and previous treatments. ***Materials and Methods:*** A retrospective, longitudinal, single-centre observational study was conducted involving patients ≥ 18 years who underwent sentinel node lymphoscintigraphy for breast cancer in our department from January 2014 to December 2021. Clinical and histological data were obtained from medical records. Statistical analysis was performed using SPSS Statistics 28® software. Statistical significance was set at p≤0.05. ***Results:*** 194/209 patients met the inclusion criteria (100% female, mean age: 54.75±13.11 years). The left breast was affected in 49% of patients, the right breast in 48% and 3% of patients had bilateral disease. Most tumours were invasive (82%), only 18% were ductal carcinoma in situ (DCIS). 45% of patients had recurrent previous treated breast cancer. Sensitivity, specificity, accuracy, PPV and NPV were 77.3%, 95.9%, 91.6%, 85.9% and 93.4% for all groups, respectively, 93.1%, 93.6%, 93.5%, 84.4% and 97.3% in the treatment-naïve group, and 46.7%, 98.6%, 89.7%, 87.5% and 89.9% in the group with recurrent previously treated disease. Axillary secondary lymph node disease occurred more frequently during follow-up in the groups with invasive breast cancer (9.4% vs. 5.5%), prior breast surgery (11.4% vs. 6.5%), prior lymph node dissection (15.6% vs. 7.4%) and chemotherapy prior to lymphoscintigraphy (13.2% vs. 7.0%). However, no statistically significant difference was found for any of the variables between the two groups. The prevalence of secondary axillary lymph node disease was similar during follow-up in patients with or without prior sentinel node biopsy, with or without prior radiotherapy to the breast, axilla or both, regardless of the number or location of sentinel lymph nodes identified by lymphoscintigraphy. ***Conclusion:*** Lymphoscintigraphy is a very accurate and specific technique with a very high negative predictive value for identifying sentinel lymph nodes, even in patients with pre-treated and recurrent breast cancer.

EP-0417

Concordance between portable SPECT and conventional scintigraphy for detection of sentinel node in breast cancer

***J. Orozco Cortés**[1], Á. Esteban Hurtado[2], C. Siscar Gelo[2], M. Navas de la Cruz[2], L. Casas Calabuig[2], Á. Badenes Romero[3], T. Mut Dolera[2], D. Reyes Ojeda[1], D. Balaguer Muñoz[2], P. Abreu Sánchez[2], P. Carcamo Ibarra[1], C. Plancha Mansanet[2], E. Caballero Calabuig[2];*
[1]Hospital Clínico Universitario de Valencia, Valencia, SPAIN,
[2]Hospital Universitario Doctor Peset Valencia, Valencia, SPAIN,
[3]Hospital Universitario Joan XXIII Tarragona, Tarragona, SPAIN.

Aim/Introduction: Introduction: Portable SPECT can be a useful imaging technique for preoperative planning of selective sentinel lymph node biopsy (SLNB) as it allows localization of the sentinel node (SN) by 3D and real-time tomographic imaging and determines its depth after a few minutes of scanning. ***Materials and Methods:*** 100 patients with a diagnosis of invasive breast cancer and no clinical evidence of lymph node involvement prospectively underwent selective sentinel node biopsy. The preoperative study included portable SPECT imaging at 15 minutes after injection and LG imaging at 25 and 60 minutes (early and late). The observed agreement was analyzed and a concordance study was performed between the number of SNs detected with portable SPECT and LG. ***Results:*** The observed agreement in the detection of CG between portable SPECT and early LG was 72%; between portable SPECT and late LG was 85%; and between early and late LG was 87%. In the concordance study, there was moderate concordance between portable SPECT and early LG (kappa coefficient: 0.42); moderate-high concordance between portable SPECT and late LG (kappa coefficient: 0.60); and moderate-high concordance between early and late LG (kappa coefficient: 0.70), with no significant differences between them (p-value=0.16). ***Conclusion:*** Portable SPECT presented a moderate-high concordance with conventional imaging studies and could be a valid alternative for the pre-surgical study of BSGC in breast cancer. ***References:*** Orozco Cortes, J. Badenes Romero, Á. Garrigos, G. Estellés, N. Implementación del uso del SPECT portátil para valoración de márgenes quirúrgicos en cáncer de mama con indicación de ROLL. Primeros resultados. Revista Española de Medicina Nuclear e Imagen Molecular. (2022). doi:10.1016/j.remn.2022.09.004 Badenes Romero, Á. (2020). Detección radioguiada de lesión oculta no palpable (ROLL) en un caso de metástasis abdominal de tumor neuroendocrino. Revista Española de Enfermedades Digestivas. Vol. 112, Nº. 10, 2020, págs. 768-771 Federica Orsini, Federica Guidoccio, Sergi Vidal-Sicart, Renato A. Valdés Olmos, and Giuliano Mariani. General Concepts on Radioguided Sentinel Lymph Node Biopsy: Preoperative Imaging, Intraoperative Gamma-Probe Guidance, Intraoperative Imaging, and Multimodality Imaging. En Mariani, G., Manca, G., Orsini, F., Vidal-Sicart, S., & Valdés Olmos, R. A. (Eds.). (2013). Atlas of Lymphoscintigraphy and Sentinel Node Mapping.

EP-0418

Is SPECT/CT useful in selective sentinel lymph node biopsy in melanoma in all primary lesion location?

***P. Zaragoza Ballester**, X. T. Guarnizo Poma, S. Angiolillo Grau, D. Vega Pérez, P. Sarandeses Fernández, Á. Galiana Morón, A. Saviatto Nardi, E. Martínez Albero, S. Ruiz Solís, M. Marín Ferrer, V. Godino Gulloteu, A. Gómez Grande, M. Tabuenca Mateo;*
Hospital Universitario 12 De Octubre, Madrid, SPAIN.

Aim/Introduction: SPECT/CT added to planar imaging can increase sensitivity of melanoma sentinel node (MSN) detection and improve anatomical localisation at the time of surgery. However, increased scanning time may have controversial implications on delays to surgery and scanner availability. In this study, we want to evaluate our experience in selective sentinel lymph node biopsy (SLNB) in melanoma and SPECT/CT contribution. ***Materials and Methods:*** We perform a retrospective study (January 2018 - December 2022) collecting all melanoma sentinel node studies performed at our institution. Cases were stratified by tumour site (head/neck, trunk, upper limbs and lower limbs). Clinical and histological data, number and localisation of nodes detected in planar images and additional nodes and localisation on SPECT/CT were recorded. We analyzed whether SPECT/CT modified the surgical approach (new MSN, location and/or depth) compared to planar images. ***Results:*** 93 patients were collected (15 without SPECT/CT due to technical failure).

54.8% male (n=51), mean age 61.79 years (range: 29-87 years). Initial lesion location: head/neck (n=13), trunk (n=47), upper limbs (UL) (n=15), lower limbs (LL) (n=17) and vulva (n=1). Lesions in head/neck, UL, LL and vulva, always drained to their ipsilateral and most proximal lymphatic region (laterocervical, axillary and inguinal, respectively). 57.5% (27/47) of truncal lesions showed a single lymphatic region. Cases with SPECT/CT: head/neck (n=11), trunk (n=41), UL (n=11), LL (n=13), vulva (n=1). SPECT/CT modified surgical approach in 3/11 patients (27.7%) of head/neck and 3/41 (7.3%) of trunk, locating nodes not observed in the planar images. Also, it modified the surgical approach in all cases of head/neck, 8/41 (19.5%) of trunk and in 2/13 (15.38%) of LL. We observed no differences between planar imaging and SPECT-CT in the UL and vulvar lesion groups. ***Conclusion:*** SPECT/CT improves accuracy in the localisation of sentinel nodes, specially in lesions of the head/neck, trunk and lower limbs. According to the experience in our center, where we have multidisciplinary teams experienced in axillary surgery, we have observed that we could save tomographic studies in melanomas of the upper limbs. However, further studies are needed to assess their optimal indication. ***References:*** 1. Bluemel, C., Herrmann, K., Giammarile, F., Nieweg, O. E., Dubreuil, J., Testori, A., Audisio, R. A., Zoras, O., Lassmann, M., Chakera, A. H., Uren, R., Chondrogiannis, S., Colletti, P. M., & Rubello, D. (2015). EANM practice guidelines for lymphoscintigraphy and sentinel lymph node biopsy in melanoma. European Journal of Nuclear Medicine and Molecular Imaging, 42(11), 1750-1766. https://doi.org/10.1007/s00259-015-3135-1

EP-0419

Selective sentinel lymph node biopsy (SLNB) in early stages oral cavity cancer: a single center study

A. De Agrela Serrao*, C. Ruiz Corbalan, A. M. Leiva Montejo, J. L. Navarro Fernández, M. Castellón Sanchez, T. E. Rodríguez Locarno, L. Frutos Esteban, A. C. Hernández Martínez, L. Mohamed Salem, D. R. Cáceres Silva, J. F. Contreras Gutierrez; Hospital Clinico Universitario Virgen de Arrixaca, Murcia, SPAIN.*

Aim/Introduction: To determine the detection rate of SLNs in the operating room previously visualized on lymphoscintigraphy as well as to determine the impact on final TNM staging after performing selective sentinel node biopsy. ***Materials and Methods:*** Retrospective, descriptive single center study of 25 patients with squamous cell carcinoma of the oral cavity in stages T1-T2N0M0 from January 2019 to December 2022. All of them underwent lymphoscintigraphy after perilesional injection of 3 mCi of ^{99m}Tc-albumin nanocolloid, performing a dynamic study, delayed images and SPECT/CT. The following day, intraoperative detection of the sentinel node was carried out using an intraoperative gamma probe, with subsequent clinical and/or imaging follow-up (CT or ultrasound). ***Results:*** 25 patients (18 men), with a mean age of 64.04±13.21 years, mean follow-up of 11.3±9.66 months. The lesions were located on the tongue in 80% of the cases, 12% on the oral mucosa, and 8% on the floor of the mouth. 72% of the patients presented unilateral drainage, 28% bilateral. The most frequent histology was squamous cell carcinoma with 88%, followed by verrucous carcinoma with 12%. The number of nodes visualized in the image ranges from 1 to 4 per patient (mean of 2.36±1.03), we detected intraoperative an average of 2.20±0.86 SLN, corresponding to 93.2% of the total visualized, detecting at least 1 SLN in 100% of patients. The reported pathology was non-malignant in 22 of the patients (88%) and nodal metastases or micrometastases were identified in 3 patients (12%) that the clinical and radiological assessment was unable to detect, which allowed early identification for more aggressive treatment. The estimated mean time to relapse/progression was identified is 7.5 months (CI: 95% 2.65-12.3 months). Twenty-one patients were followed up with 1 local recurrence and 3 lymph node recurrences (13.6%). The overall survival was 27.48 months (95% CI: 21.19-33.68 months), without finding significant differences between both sexes. ***Conclusion:*** SLNB is a safe, effective, and well tolerated method for staging cN0 oral cancer, modifying the final TNM staging of patients in 12% of the cases. SLNB shows a high intraoperative detection rate of 93.2%, Patients with negative SLNB have greater overall disease-free survival than those with initially positive biopsies.

EP-0420

Sentinel Lymph Node Mapping For Endometrial Cancer: Results of the First Tunisian, Arab and African study.

L. Zaabar[1,2]*, H. Bouaziz*[3,2]*, S. Sghaier*[4]*, G. Sahraoui*[5,2]*, M. Slimane*[4,2]*, M. Hechiche*[4,2]*, K. Mrad*[5,2]*, K. Rahal*[4,2]*, A. Mhiri*[1,2]*;*
[1]Salah Azaeiz Institute, Nuclear Medicine departement, Tunis, TUNISIA, [2]Faculté de Médecine de Tunis, Tunis, TUNISIA, [3]Salah Azaeiz Institute,Surgical Department of Oncology, Tunis, TUNISIA, [4]Salah Azaeiz Institute, Surgical Department of Oncology, Tunis, TUNISIA, [5]Salah Azaeiz Institute, Pathological Anatomy Department, Tunis, TUNISIA.

Aim/Introduction: Endometrial cancer represents the most common gynecological cancer mostly diagnosed at stage I (90%). Sentinel lymph node (SLN) arised as a valuable option to lymph node dissection.Our aim was to determine negative predictive value, positive predictive value, overall and bilateral detection rates of SLN in endometrial cancer stage I. ***Materials and Methods:*** This was a cross-sectional prospective study including 38 patients with endometrial cancer stage I treated at Salah Azaiz Institute over a period of 34 months from March 2018 to January 2021 with descriptive and analytical parts. ***Results:*** The median age was 59.79. The histologicc type was mostly represented by endometrioid adenocarcinoma in 89% of cases. A pelvic magnetic resonance imaging showed a stage IA in 58% of tumors and IB in 42% of cases. The detection techniques were combined (48%), colorimetric (34%) and radioisotope (18%). Lymphoscintigraphy was conducted in 66% of women demonstrating overall and bilateral detection rates of 92% et 24%, respectively and a detection failure in 8% of cases. The SLNs were mainly localized in the right internal iliac in 36% of cases. The overall and bilateral intra-operative detection rates were of 76% and 37%, respectively. Intra-operative detection failed in 24% of cases. The blue SLNs were mostly in the right internal iliac (46%). The «hot-spot» SLNs were also mainly localized in the right internal iliac (37%). A micrometastasis (1%) was noted in one case among a total of 87 SLNs. False negative rate and negative predictive value were of 0% and 100%. Positive predictive value was 0%. Specificity was of 98.85%. Factors that affected overall detection were initial histologic grade (p=0.01) and tumor size (p=0.04) on magnetic resonance imaging. Final histologic grade 1 (p=0.005), 2 (p=0.002) and myometrial invasion (p=0.04) were also significant factors. A final IA stage (p=0.03) as well as low risk (p=0.03) and high-intermediate risk (p=0.04) groups represented significant contributors. No significant factors affecting bilateral detection were set. ***Conclusion:*** False negative rate and negative predictive value were of 0% and 100% similarly to previous results through literature. We aim to continue this promising protocol toward including more patients that may helps us improve our overall and bilateral detection rates.

EP-0421

Performance of99mTc-albumin nanocolloid and indocyanine green as tracers in sentinel lymph node detection in cervical and endometrial cancer.

M. Grajeda Gallardo, *A. Prieto Soriano, P. Meneses Soares, K. Velasquez Díaz, I. Garrido Solesio, L. Santamaria Chico, I. Obedkova, S. Guzmán Ortiz, M. Mitjavila Casanovas;*
Hospital Universitario Puerta de Hierro, Madrid, SPAIN.

Aim/Introduction: To evaluate the detection rate (DR) of the sentinel lymph node (SLN) in cervical and endometrial cancer with lymphoscintigraphy (LS) and with indocyanine green (ICG), both combined and separately. ***Materials and Methods:*** Sixty patients (62.4± 13.4 years) were prospectively included in the period between 2020 and 2023, diagnosed with cervical cancer (16) and endometrial cancer (44). LS was performed the day before surgery and ICG, on the day of the surgery. The intraoperative detection and biopsy of SLNs was performed. We compared the findings of both techniques separately and jointly. The level of agreement between both techniques was determined by measuring Cohen's Kappa index. A statistical software was used to perform the data analysis. ***Results:*** In patients with endometrial cancer, the SLN DR with LS was 56.8% (25/44) and with ICG 84.0% (37/44). The DR with both techniques was 86.3% (38/44). In one patient, the SLN was detected exclusively with LS, while with ICG it was detected in 13. No migration was observed in 6 patients. Bilateral migration with LS was detected in 34.1% patients (15/44) and with ICG in 75% (33/44). With the combined technique, bilateral detection of 75% (33/44) was obtained. Lymph node metastasis rate was 9.1% (4/44). Comparing both techniques, statistically significant differences were observed in nodal mapping and concordance was obtained in 68.2% of the patients (30/40), with a Cohen´s Kappa index of 0.298 (fair agreement). In patients with cervical cancer, the DR was 81.3% (13/16) with LS and 75% (12/16) with ICG. The DR with both techniques was 93.7% (15/16). In one patient, no SLN was located with either technique. Bilateral SLN detection was achieved in 50% (8/16) with LS and 56.3% (9/16) with ICG. Bilateral detection with both techniques was achieved in 80% of the patients (12/16). Lymph node metastasis rate was 6.25% (1/16). Comparing both techniques, no statistically significant differences were observed in nodal mapping, and concordance was obtained in 68.8% of the patients (11/16), with a Cohen´s Kappa index of 0.0909 (insignificant agreement). ***Conclusion:*** In patients with endometrial cancer, ICG has a higher SLN detection rate compared to LS. In patients with cervical carcinoma, the detection rate was higher with LS. In both cases, the use of radiotracer and dye techniques is complementary and together they improve the overall detection rate in these patients.

EP-25

e-Poster Area

B: Imaging Clinical Studies -> B4 Cardiovascular Imaging Clinical Study -> B41 Perfusion

EP-0422

C-reactive protein and myocardial perfusion imaging

C. Sioka, *A. Kekiopoulou, P. Kekiopoulos, A. Bechlioulis, A. Rammos, A. Papadopoulos, J. Al-Boucharali, S. Tsiouris, X. Xourgia, D. Dristiliaris, C. Katsouras;*
University Hospital of Ioannina, Ioannina, GREECE.

Aim/Introduction: Inflammation induced by a cytokine cascade is an important mechanism leading to the formation of an atherosclerotic plaque. C-reactive protein (CRP) is the most widely used biomarker in daily clinical practice to detect inflammation and has also been associated with various structural heart diseases. The present study investigated the correlation of myocardial perfusion scintigraphy (SPECT) findings with the corresponding CRP values, in clinically stable patients. ***Materials and Methods:*** The study included consecutive patients (n=102, mean age 71 years, 68% males) who underwent myocardial perfusion imaging (MPI) SPECT due to clinical indication. Patients were required to have a recent CRP measurement available (within one month). None of the subjects had signs and symptoms of recent infection or acute coronary syndrome, and those with a history of autoimmune disease were clinically stable, to rule out other common causes of elevated CRP. ***Results:*** The increased value of CRP (>6mg/L) was related to a pathological cumulative stress score [summed stress score (SSS) >3] and an increased cumulative score during rest [summed stress score (SRS) (p=0.006 and p=0.001 respectively), however this correlation was applicable only to patients over 70 years old (p=0.027 and p=0.005 respectively. ***Conclusion:*** CRP is a useful biomarker for the evaluation of ischemia in MPI. Further studies are needed to show whether it could be used to the selection of patients referred for MPI, considering clinical indications and other risk factors.

EP-0423

Atrial fibrillation is an independent predictor of the extent and severity of myocardial ischemia in myocardial perfusion imaging

C. Sioka, *A. Bechlioulis, P. Zotou, S. Alexiou, A. Kekiopoulou, E. Gkika, P. Kekiopoulos, D. Dristiliaris, A. Rammos, L. Lakkas, K. Naka, L. Michalis, C. Katsouras;*
University Hospital of Ioannina, Ioannina, GREECE.

Aim/Introduction: Atrial fibrillation (AF) and coronary artery disease (CAD) are highly prevalent cardiovascular conditions. The importance of AF history in the detection of ischemia in patients undergoing myocardial perfusion imaging (MPI) is unknown. This study investigated the association of extent and severity of perfusion abnormalities in MPI with AF in patients with suspected stable CAD. ***Materials and Methods:*** A total of 251 consecutive patients (mean age 64 years) without a prior history of CAD who had a 99mTc MPI with single photon emission computed tomography (SPECT) due to suspected stable CAD were included in the study retrospectively. Semi-quantitative assessment of the extent and severity of perfusion abnormalities with summed stress score (SSS) and summed difference score (SDS) were evaluated. ***Results:*** Patients with a history of AF (n=85) were older (p<0.001) and had a higher prevalence of male gender, dyslipidemia and smoking (p<0.05 for all) compared to patients without AF history. History of AF was associated with increased SSS ≥4 (OR 5.12, p<0.001) and SDS ≥2 (OR 2.66, p<0.001). After adjustment for other risk factors, history of AF remained an independent predictor of increased SSS ≥4 (OR 4.54, p<0.001) and SDS ≥2 (OR 2.77, p<0.001). ***Conclusion:*** Medical history of AF was shown to be an independent predictor of the extent and severity of perfusion abnormalities in high risk patients with suspected stable CAD. Whether AF constitutes a risk factor or merely a risk marker of perfusion defects in SPECT imaging needs to be clarified in future studies.

EP-0424

How did the COVID-19 pandemic affect SPECT myocardial perfusion scans? A single center experience

A. Aghaee, *s. ataei nakhaei, e. askari, h. mohammadzadeh, h. roustaee, f. karamian;*
nuclear medicine research center,Mashhad university of Medical Sciences, Mashhad, IRAN, ISLAMIC REPUBLIC OF.

Aim/Introduction: The aim of this study is to evaluate the effects of the COVID-19 pandemic on characteristics of myocardial perfusion scans (MPS) during the COVID-19 pandemic

period. ***Materials and Methods:*** We respectively reviewed SPECT-myocardial perfusion scans performed between June and September 2020 (n = 423) during the COVID-19 pandemic in our center and compared them with findings of studies acquired in the same months before the pandemic (2019; n = 619) . ***Results:*** The number of patients with non-anginal or typical chest pain significantly decreased during the COVID-19 pandemic, while atypical chest pain cases increased significantly. Cases with high pretest probability decreased significantly and patients with intermediate pretest probability increased non-significantly. No statistically significant difference was observed on the rate of myocardial ischemia for COVID-19 era versus non-COVID-19 era .However, the number of stress SPECT-MPS studies performed during the COVID-19 pandemic (n = 423) was significantly lower (p = 0.014) compared with the number of studies carried out in the dedicated months of the year 2020 (n= 619). ***Conclusion:*** Our survey demonstrated significantly reduction in the number of SPECT-MPS studies during the COVID-19 pandemic and patients in the two ends of anginal chest pain spectrum (i.e., non-anginal & typical chest pain) were referred less frequently for MPS. However, patients in the middle of the spectrum (i.e., the atypical chest pain) underwent MPS more often. No change in the rate of myocardial ischemia or cardiomyopathy was observed in the COVID-19 period.

EP-0425

Stress Myocardial Perfusion Imaging (MPI) for Predicting Major Cardiac Events in Diabetic Women and Men

N. Fatima[1,2], *S. Zaman*[3], *A. Zaman*[4], *J. Bano*[2], *M. u. Zaman*[5,2];
[1]*Dept of Radiology Aga Khan University, Karachi, PAKISTAN,* [2]*Dept of Nuclear Cardiology, Karachi Institute of Heart Diseases (KIHD), Karachi, PAKISTAN,* [3]*Dr Ruth Pfau (CHK), Karachi, PAKISTAN,* [4]*Dept of Medicine, Sunny Downstate Medical Centre, New York, NY, UNITED STATES OF AMERICA,* [5]*Dept of Radiology Aga Khan University, KARACHI, PAKISTAN.*

Aim/Introduction: The major adverse cardiac events (MACEs) between men and women in diabetic patients stratified by CAD (previous MI and/or coronary revascularization, CR) were analyzed. ***Materials and Methods:*** A cohort of 1135 consecutive diabetic patients (age 61.5±9 years) underwent gated SPECT (single-photon emission computed tomography) myocardial perfusion imaging (MPI). In 281 individuals (40 females, 55 ± 12 Yr and 241 males, 56 ± 10 Yr), MPI was positive for CAD. Risk factor in female and male participants were hypertension (68 Vs 78%), dyslipidemia (43 Vs 27%) and positive family history (25 Vs 30%). Female diabetics were found to have significantly higher body mass index (37.43 ± 4.20 Vs 24.27 ± 2.98). ***Results:*** The cohort was followed for a mean period up of 12-60 month for MACEs (fatal and non-fatal MI). Female diabetics were found to have fixed defect in 12% and reversible defect in 88% on MPI. Male diabetics were found to have fixed defect in 45% and reversible defect in 55% on MPI. During follow-up period, fatal events in female were significantly higher (3 events; survival 92.5%) as compared to males (0 event; 100% survival) [Log Rank = 27.166, p <0.5]. During follow-up period, non-fatal events in female were significantly higher (05 events; survival 87.5%) as compared to males (02 event; 99.2% survival) [Log Rank = 16.419, p <0.5]. ***Conclusion:*** The prognosis of diabetic patients for MACEs is different in men and women stratified by CAD. The worst prognosis for MACEs occurs in women with known CAD.

EP-0426

Prognostic Value of Rest SPECT MPI Derived Left Ventricular Shape Indexes in Patients with Prediabetes

Y. Hu, *Y. Zhao, R. Wang, L. Yang, Y. Li, Y. Wang, X. Diao, S. Li;*
Department of Nuclear Medicine, First Hospital of Shanxi Medical University, Taiyuan, CHINA.

Aim/Introduction: Prevalence of prediabetes is rising worldwide and prediabetes is associated with increased cardiovascular risk. The prognostic value of left ventricular (LV) remodeling has been well validated in cardiovascular diseases including myocardial infarction (MI). LV shape index (SI) by single photon emission computed tomography (SPECT) myocardial perfusion imaging (MPI) has clinical implications in patients with diabetes. However, the prognostic value of LVSI in patients with prediabetes remains unknown. We aimed to elucidate the prognostic value of LVSI in individuals with prediabetes. ***Materials and Methods:*** We retrospectively recruited a total of 171 patients (mean age 61.64 ± 11.64 years, 67 women) with prediabetes(5.6 mmol/L ≤ fasting plasma glucose < 7 mmol/L and/ or 5.7 ≤ HbA1c < 6.5%) and known or suspected CAD who underwent rest SPECT MPI. The major exclusion criteria were structural heart disease and a history of myocardial infarction. All the patients were followed up and categorized for the occurrence of major adverse cardiac events. The clinical characteristics and MPI findings processed by Quantitative perfusion SPECT (QPS) and Quantitative gated SPECT (QGS) software programs were collected. All variables were first assessed by univariate Cox proportional hazards regression analysis. Receiver operator characteristic (ROC) curve analyses were applied to determine the optimal cutoff value of variables showing univariate relationships with outcome. Multivariate Cox regression and Kaplan-Meier survival analysis were conducted for prognostic prediction and risk stratification. ***Results:*** During a median follow-up of 44.2 (3.0 -79.8) months, 86 (38.6%) MACE occurred. Patients who occurred MACE had higher SI (0.62 ± 0.09 vs. 0.58 ± 0.07, P = 0.001), end diastolic (ED) SI (0.65 ± 0.08 vs. 0.62 ± 0.07, P = 0.016) and end systolic(ES) SI (0.54 ± 0.10 vs. 0.50 ± 0.08; P = 0.001) compared to those without MACE. Multivariate Cox regression analysis showed an abnormal ESSI (> 0.5) was the only independent predictor for MACE (HR: 2.580, 95% CI: 1.115-5.970, P < 0.05) after adjustment for clinical and imaging risk predictors as determined by preliminary univariate analysis. MACE-event-free survival in patients with abnormal ESSI was significantly lower than that in patients with normal ESSI (χ^2 = 12.785, log-rank P < 0.001). ***Conclusion:*** LV remodeling conveys prognostic value in individuals with prediabetes. ESSI assessed by rest SPECT MPI is the novel independent predictor of MACE and might improve the risk stratification in prediabetes patients.

EP-0427

The Correlation Study between MPI and CAG in Risk Stratification of CAD Patients with Different Uric Acid Levels

Y. Chen[1], *X. Liu*[1], *X. Li*[1], *M. Cai*[2], *S. Li*[3];
[1]*Shanxi Medical University, Tai Yuan, CHINA,* [2]*Shanxi provincial People's Hospital & Fifth Clinical College of Shanxi Medical University Medicine, Tai Yuan, CHINA,* [3]*The first hospital of Shanxi Medical University, Tai Yuan, CHINA.*

Aim/Introduction: To study the correlation between myocardial perfusion imaging (MPI) and coronary angiography (CAG) in risk stratification of coronary heart disease (CAD) patients with different uric acid levels. ***Materials and Methods:*** We collected patients with coronary artery disease who were admitted to

our hospital from July 2021 to December 2022, and all patients underwent both stress myocardial perfusion imaging and coronary angiography and completed uric acid, blood lipid and serum creatinine tests after admission. The patients were then divided into a group of CAD patients with hyperuricemia (HUA) and a group of CAD patients with normal uric acid levels based on their uric acid levels. Subsequently, the patients were stratified according to the summed stress score(SSS)of myocardial perfusion imaging and the coronary stenosis score shown by angiography. And the correlation between the two for the stratification results was evaluated. ***Results:*** A total of 106 CAD patients were collected, including 46 patients with hyperuricemia and 60 patients with normal uric acid. There was a moderate correlation between MPI and CAG in the risk stratification of all CAD patients (r=0.527, P<0.001), especially in the medium-risk group and high-risk group showed a strong correlation (r=0.772, P<0.001). The stratification results of patients in the low-risk group were significantly different, showing no correlation (r=0.131, P>0.05).In CAD patients with normal uric acid, MPI was weakly correlated with CAG in the stratification of risk (r=0.277, P<0.05), with moderate correlation in the medium-risk group and high-risk group (r=0.401, P<0.05), and no correlation in the low-risk group (r=0.279, P>0.05).In CAD patients with hyperuricemia, MPI and CAG showed a strong correlation in the stratification of risk (r=0.787, P<0.001), the medium-risk group and high-risk group showed a very strong correlation (r=0.846, P<0.001), and the low-risk group showed a very weak correlation (r=0.144, P<0.05). ***Conclusion:*** For this study, in the risk stratification results of MPI and CAG for CAD patients, the correlation between hyperuricemia patients was strong, which was extremely weak in the low-risk group, and extremely strong in the medium-risk group and high-risk group. The correlation was higher than that of the whole patient group and the normal uric acid level group. For coronary heart disease patients with hyperuricemia, MPI can provide accurate and effective risk assessment information. For such patients, MPI can be given priority as a reliable means to evaluate the severity and progression of the disease.

EP-0428

Prognostic Value of Gated SPECT MPI Varied by Atherosclerotic Cardivascular Disease Risk: A Retrospective Study

Y. Li, *Y. Zhao, R. Wang, Y. Hu, Y. Wang, X. Diao, J. Zhang, S. Li;*
First Hospital of Shanxi Medical University, Taiyuan, CHINA.

Aim/Introduction: Patients with atherosclerotic cardiovascular disease (ASCVD) have a significantly different risk of occurrence of adverse cardiovascular events and clinical management for patients with very-high and extreme risk for ASCVD is still suboptimal. While single photon emission computed tomography (SPECT) myocardial perfusion imaging (MPI) parameters are increasingly used to guide management in patients with stable chest pain, information on whether prognostic value of MPI parameters varies across ASCVD risk is missing. This study aimed to validate the incremental prognostic value of MPI parameters beyond ASCVD very-high and extreme risk. ***Materials and Methods:*** We retrospectively recruited a total of 1584 patients with known or suspected coronary artery disease (CAD) who underwent rest SPECT MPI and followed up for major adverse cardiac events (MACE). According to the risk stratification scheme of ASCVD in the Chinese Guidelines for Lipid Management 2023, all patients were assigned into primary and secondary prevention group (G1 and G2) based on whether they had ASCVD or not, and then further divided into very-high and extreme risk with the pooled cohorts equation in G2. The clinical characteristics and MPI parameters were collected. Multivariable Cox regression analyses were used to determine independent predictors. The Youden index was used to select optimal thresholds for predictors. Kaplan-Meier survival analyses were conducted for prognostic prediction and risk stratification. ***Results:*** Among 1,584 patients (61±13 years, 66.5% men, median follow-up of 3.05 years), 167 were in G1 (16.8% MACE), and 1,417 in G2 (42.8% MACE). In multivariate analysis after adjustments for clinical and imaging risk factors, left ventricular shape index obtained by QPS (SI_{QPS}) >0.625, end systolic volume (ESV) >67.5ml, and peak filling rate (PFR) <1.415ml/s all emerged as independent predictors of MACE (HR=1.522,1.482, and 0.694 respectively, all $P < 0.001$) in G2; however, they didn't show significant correlation with MACE in G1. MACE-event-free survival analyses displayed significant differences for SI_{QPS}, ESV and PFR ($\chi 2 = 20.087$, 29.438 and 21.110 respectively, all log-rank $P < 0.001$). ***Conclusion:*** Prognostic values of MPI parameters differ by ASCVD risk categories. SI_{QPS}, ESV and PFR predicted MACE solely in patients with very-high and extreme risk of ASCVD. These findings suggest that SPECT may improve lipid management and treatment goals through further risk stratification.

EP-0429

Improving multi-pinhole cadmium zinc telluride myocardial perfusion imaging specificity without changing sensibility by using adapted prefilter parameters

F. Vauchot, *A. Bourdon, M. Benkiran, J. Dubois;*
CHU Gui de Chauliac, Montpellier, FRANCE.

Aim/Introduction: Meta-analysis show the diagnostic performance of cardiac dedicated multi-pinhole cadmium zinc telluride (CZT) myocardial perfusion imaging (MPI) with a sensibility and a specificity around 0.9 and 0.7 respectively. The aim of the present study is to explore a simple method in order to generate less artefact on MPI using single photon emission computed tomography (SPECT) and to enhance specificity without altering sensibility. ***Materials and Methods:*** From October 2018 to March 2019, 200 patients who underwent single photon-emission tomography (SPECT) with ^{99m}Tc-tetrofosmin using cardiac dedicated multi-pinhole CZT were prospectively recruited: 100 patients with ischemia or necrosis diagnosis (first arm), and 100 patients with myocardial reversible SPECT artefact (second arm). Each SPECT was explored using two image processes based on a Butterworth prefilter: the original image processing (treatment A) with a cut-off frequency equals to 37% of the Nyquist frequency and order equals to 7, and a second image processing (treatment B) with a cut-off frequency equals to 25% of the Nyquist frequency and order equals to 5. For each patient, sum stress or rest score with and without septum (SSRS and SSRSws respectively) were calculated with the two treatments leading to four absolute parameters (SSRSa, SSRSwsa, SSRSb, SSRSwsb). Absolute variations between the two treatments (Δ = SSRSa-SSRSb and Δws = SSRSwsa-SSRSwsb) and relative variations (Δr = Δ/SSRSa and Δrws = Δws/SSRSwsa) were calculated. We used a two-tailed Student's t-test to compare different scores for the two treatments. ***Results:*** No significant statistical difference between SSRSa and SSRSb was identified for the first arm (p=0.54) and the relative variation Δr was -0.5 ± 11.1 % (IC95 -2.6-1.8). We found a significant statistical difference between SSRSa and SSRSb for the second arm ($p < 0.0001$) with a relative variation

Δrws of 86.5 ± 14.6 % (IC95 83.6-89.4). ***Conclusion:*** In conclusion, using a prefilter cut-off frequency equals to 25% of the Nyquist frequency and a five order before iterative reconstruction generates less artefact and improves myocardial SPECT specificity without altering sensibility when compared to the conventional treatment using a prefilter cut-off frequency equals to 37% of the Nyquist frequency and a seven order. ***References:*** Cantoni and al. Diagnostic performance of myocardial perfusion imaging with conventional and CZT single-photon emission computed tomography in detecting coronary artery disease: A meta-analysis. J Nucl Cardiol. 2019.

EP-0430

Spherization Indexes by Rest SPECT Improves Risk Stratification in Patients with Non-obstructive Coronary Artery Disease

Y. Zhao, *Y. Hu, P. Wu, Y. Li, S. Li;*
Department of Nuclear Medicine, First Hospital of Shanxi Medical University, Taiyuan, CHINA.

Aim/Introduction: The prevalence of non-obstructive coronary artery disease (CAD) is substantial, and its risk-stratification remains suboptimal. The prognostic role of left ventricular remodeling (LVR) has been extensively investigated in various populations, including patients with myocardial infarction. However, there is a paucity of data to inform the prognostic value of spherization indexes assessed by single photon emission computed tomography (SPECT) myocardial perfusion imaging (MPI) for non-obstructive CAD. Therefore, we aimed to evaluate the prognostic value of spherization indexes in individuals with non-obstructive CAD. ***Materials and Methods:*** 285 patients (mean age 56.60 ± 12.28 years, 129 women) with non-obstructive CAD who underwent resting SPECT MPI were retrospectively enrolled. The clinical characteristics and MPI findings including spherization indexes (shape index (SI) and eccentricity index (EI)) by Quantitative perfusion SPECT (QPS) and Quantitative gated SPECT (QGS) were collected. Patients were followed up for major adverse cardiovascular events (MACE) and categorized into groups by MACE occurrence. Receiver operating characteristic (ROC) curve analyses were applied to find optimal cutoff value as appropriate. All variables were first assessed by univariate analyses. Multivariate Cox regression and Kaplan-Meier survival analyses were conducted for prognostic prediction. ***Results:*** There were 66 (23.2%) patients occurred MACE during a median follow-up of 47.2 ± 20.8 months, and they had higher SI_{QPS} (0.60 ± 0.07 vs. 0.58 ± 0.06; P = 0.013), lower EI_{QPS} (0.812 ± 0.044 vs. 0.829 ± 0.041; P = 0.004) and EI_{QGS} (0.832 ± 0.044 vs. 0.845 ± 0.046; P = 0.034) compared to those without MACE. The other spherization indexes did not differ between groups (P > 0.05). MACE-event-free survival analysis displayed significant differences for $SI_{QPS,}$ EI_{QPS} and EI_{QGS} in all patients (χ^2= 7.840, 6.598 and 6.706, respectively, all Log-rank P < 0.05). Multivariate analysis showed abnormal SI_{QPS} (HR: 2.141, 95% CI: 1.158-3.958, P = 0.015) and EI_{QPS} (HR: 1.818, 95% CI: 1.064-3.108, P = 0.029) were both independent predictors for MACE when they were put into the same model respectively, after adjustment with age, diabetes and number of vessels diseased. ***Conclusion:*** For patients with non-obstructive CAD, spherization indexes, especially SI_{QPS} and EI_{QPS}, were associated with long-term MACE, may be a more preferable indicator for risk stratification and prognostic prediction.

EP-0431

Long-term Outcome of Patients after Radionuclide Myocardial Perfusion Imaging

J. Huang[1], *K. Chien*[2], *Y. Wu*[3];
[1]*Department of Nuclear Medicine, National Taiwan University Hospital and National Taiwan University College of Medicine, Taipei, TAIWAN,* [2]*Institute of Epidemiology and Preventive Medicine, College of Public Health, National Taiwan University, Taipei, TAIWAN,* [3]*Division of Cardiology, Cardiovascular Medical Center, Far Eastern Memorial Hospital, New Taipei City, TAIWAN.*

Aim/Introduction: Prognostic implications of myocardial perfusion imaging (MPI) are imperative to provide proper management of coronary artery disease. Few studies have investigated the impact of computed tomography attenuation correction (CTAC) on the prognostic value of MPI and revealed discordant results. The purpose of this study was to investigate the long-term prognostic value of MPI using a large cohort from a stable agricultural county. ***Materials and Methods:*** From 2008 to 2010, 4,687 patients who underwent CTAC and non-AC (NC) Tl-201 MPI were followed for all-cause mortality, hospitalization of all cardiovascular (CV) reasons including coronary intervention and heart failure (HF) till December 2018. Medical records were reviewed, and missing information was completed by telephone contact. The prognostic significance was evaluated by Kaplan-Meier (KM) analysis, univariable and multivariable Cox proportional hazards models. We also analyzed the effect of coronary interventions on survival with KM analysis and Cox model. Sensitivity analysis was done after excluding patients who received intervention to check the robustness of our result. ***Results:*** A total of 2278 patients (893 women, 64.22 ± 10.37 years of age) were included. After a mean follow-up period of 8.17 ± 2.17 years, 516 (22.7%) patients died, 645 (28.3%) had been hospitalized for CV events, 382 (16.8%) received coronary interventions, and 140 (6.1%) had been admitted for HF. KM curves for all-cause mortality by previously reported cutoffs of summed stress score (SSS) and summed rest score (SRS) showed significant differences between 4 curves in SSS, SRS and both in CTAC and NC MPI (p<0.0001). In the multivariable model, SRS was the independent predictor for all-cause mortality and SSS was the independent predictor for all secondary endpoints. Coronary intervention after MPI was a significant protecting factor for all-cause mortality (HR: 0.42-0.44, p<0.001). Also, the independent predictive effect of scores derived from MPI remained after adding intervention as an explanatory variable. In sensitivity analysis, KM curves for all-cause mortality by conventional cutoffs of SSS and SRS also showed significant differences in patients without coronary intervention. In addition, the prognostic values of MPI persisted in the 2-, 5- and 10-year survival models. ***Conclusion:*** Both CTAC and NC MPI had good long-term prognostic values for risk stratification for future cardiac events. SRS showed superior risk stratification than SSS or SDS for all-cause mortality and SSS was a good predictor for all measured future CV events. Also, coronary intervention seems a strong protective predictor against all-cause mortality.

EP-0432

Comparison of Myocardial Perfusion Imaging Studies of Patients with Confirmed Coronary Artery Disease Performed on Traditional SPECT Gamma Camera and Dedicated Semiconductor Cardiac Gamma Camera

P. Cichocki[1], *M. Blaszczyk*[1], *A. Aulich*[1], *Z. Adamczewski*[1], *A. Plachcinska*[2];
[1]*Nuclear Medicine Department, Medical University of Lodz, Lodz, POLAND,* [2]*Department of Quality Control and Radiological Protection of the Medical University of Lodz, Lodz, POLAND.*

Aim/Introduction: Discovery 530c (DIS) is a semiconductor gamma camera dedicated for myocardial perfusion imaging (MPI). It uses pinhole collimators and different image reconstruction

than traditional cameras. This is known to affect final reconstructed images (eg. by eliminating breast attenuation artifacts commonly seen on traditional cameras in women). The aim of this study was to assess differences in perfusion defects found in MPI preformed using DIS and traditional SPECT gamma camera in a group of patients with confirmed coronary artery disease (CAD). ***Materials and Methods:*** 90 patients (59 male, 31 female) with a history of CAD were included in the study. Each patient underwent MPI on two cameras - Discovery 530c and Optima 630NM/CT (OPT) in a 2-day stress-rest protocol in supine position using 10MBq/kgbw of ^{99m}Tc-Sestamibi. Studies were assessed using a semiquantitative scale (0 - normal perfusion, 4 - complete absence of perfusion) in 17 segments, resulting in summed stress, rest and difference scores (SSS, SRS and SDS, respectively) for whole myocardium (TOT) and 3 main vascular territories. ***Results:*** SSS, SRS and SDS>3 for TOT or >1 for vascular territories were considered abnormal. In TOT, in following number of cases assessed scores were normal on DIS vs abnormal on OPT: SSS-17, SRS-10, SDS-21, and abnormal on DIS vs normal on OPT: SSS-7, SRS-11, SDS-10. According to McNemar's test, differences in assessment were statistically insignificant for SRS (p=1,0), while for SSS and SDS they were at the borderline of statistical significance (p=0,07). In vascular territories, statistically significant differences were observed in LAD for SSS (p=0,0001, men p=0,0009, women p=0,08) and SRS (p=0,046, men p=0,75, women p=0,039), and in RCA for SRS (p=0,02, men p=0,02, women p=0,39). In these territories, in the following number of cases assessed scores were normal on DIS vs abnormal on OPT: LAD SSS-24, LAD SRS-18, RCA SRS-4, and abnormal on DIS vs normal on OPT: LAD SSS-3, LAD SRS-7, RCA SRS-15. This did not cause statistically significant differences for SDS. ***Conclusion:*** Our study focused on patients with confirmed CAD, almost all of whom had perfusion defects in MPI. Comparison of MPI results showed a general trend of fewer abnormal results in rest and stress studies acquired using Discovery 530c camera, especially in LAD territory. Opposite trend was observed only for SRS in RCA territory. In our material, these differences were at the borderline of statistical significance in case of whole myocardium SSS and SDS.

EP-0433

Coronary Reserve assessement by means of routine standard perfusion SPECT (no first-pass): easy method to evaluate macro-angiopathy and microvascular lesions.

L. Philippe, *C. Prunier-Aesch, Y. El Yaagoubi;*
Medecine Nucleaire Tourangelle, Chambray-les-Tours, FRANCE.

Aim/Introduction: Coronary Flow Reserve (CFR) assessment is important to understand myocardial perfusion. Analysis of epicardial coronary flow, is not sufficient when a micro-angiopathy dysfunction is present, as for diabetes. However, methods evaluating CFR are not everywhere available. We have developed an easy and reliable method to quantify CFR, by means of a Coronary Reserve Index (CRI), using routine SPECT 99mTc-tetrofosmin (1 day Stress-Rest protocol) with no need of 1st pass acquisition. ***Materials and Methods:*** Myocardial tetrofosmin uptake is related to myocardial perfusion. CFR is defined by the myocardial counts ratio Stress/Rest. To use this ratio, we apply 5 successive corrections allowing to get the CRI and functional images representing CFR. This processing was applied to a series of 60 patients addressed to our institution for routine myocardial Stress/Rest, with suspicion of CAD. CRI was computed for each patients. Previous study indicated a CRI value of 3 for the threshold normal/abnormal. Patients with previous revascularization were not included. Invasive Coronary Angiography (ICA), performed for the 60 patients, was considered as the gold standard for ischemia diagnosis. ***Results:*** Among the 60 patients, we studied the group of 16 patients with normal ICA (no significant Coronary Artery Disease (CAD)) for 16 patients: CRI < 3 for 9/16 patients (mean CRI = 1.62), and CRI >3 for 7/16 patients (mean CRI = 3.86). For the16 normal ICA, according to risk factors, mean CRI was 2.9 for patients with Hypertension, 2.39 for patients with Hypertension + Diabetes, and 3.16 with no risk factor. CRI performances (60 patients) for CAD diagnosis are good for Sensitivity (0.82) and Positive Predictive Value (0.80), but specificity was only 0.40 . This result is the consequence of considering ICA, as "gold standard", since ICA does not analyze micro-circulation. If micro-circulation is impaired, without epicardial coronary lesions, ICA considers CRI <3 as False Positive, decreasing Specificity and Positive Predictive Value. We propose the following global perfusion analysis: Normal perfusion SPECT and CRI> 3 : Normal / Normal perfusion SPECT and CRI< 3 : microvascular lesions / Abnormal perfusion SPECT and CRI> 3 : Epicardial lesions and preserved microcirculation / Abnormal perfusion SPECT and CRI< 3 : Epicardial coronary lesions + microvascular lesions. ***Conclusion:*** Gated SPECT with CRI calculation allows evaluation of macro- and microvascularization. The CRI calculation is fully automatic and can be performed with every routine standard perfusion SPECT, or retroactively.

EP-0434

Clinical value of Tc-99m MIBI Myocardial Gated SPECT in children and adolescents presenting with exercise related chest pain

A. Alakbarli[1], *M. A. Karacan*[1], *Y. Ozananar Sevinc*[2], *Y. Ceylan*[3], *A. M. Argon*[1], *Z. Ozcan*[1];
[1]*Ege University Hospital Nuclear Medicine, Izmir, TÜRKIYE,* [2]*Bakircay University Cigli Regional Education Hospital, Izmir, TÜRKIYE,* [3]*Usak University Hospital, Usak, TÜRKIYE.*

Aim/Introduction: Chest pain on exertion or syncope attack is a common complaint in paediatric cardiology practice. While it is rarely associated with cardiac ischemia, chest pain due to cardiac reasons may lead to life-threatening situations. Therefore, it is critical to detect or to exclude the presence of ischemia for differential diagnosis and patient management. Although MPS is frequently used in adult population, it is less commonly used in paediatric ages for cardiac evaluation. This study aims to retrospectively examine MPS findings to reveal the presence of ischemia in children presenting with effort-induced chest pain or syncope. The value of MPS in the evaluation of ischemia and also in the clinical management has been reviewed in relation to clinical and other imaging findings. ***Materials and Methods:*** The study group included 10 cases with chest pain or syncope attacks after exertion. They were clinically examined according to paediatric guidelines including detailed physical evaluation and ECG. Transthoracic echocardiography was performed to evaluate common heart diseases in children. Those cases with abnormal ECG findings, T wave inversion, ST changes, and suspected ischemia in the exercise test referred for cardiac perfusion and functional evaluation with Tc-99m MIBI. MPS was performed as SPECT Gated study with a single-day Tc-99m MIBI protocol. Cardiac CT imaging was also performed in all cases except for one. ***Results:*** Cardiological assessment and TTE excluded possible heart diseases that might induce chest pain such as congenital heart disease, cardiomyopathy, myocarditis, and Kawasaki disease. MPS gated SPECT study detected reversible perfusion defects related to anterior wall ischemia in 2 of 10 cases. Left ventricular wall motion and stress EF were normal. Cardiac CT showed myocardial bridging in these cases which was compatible with the ischemic area observed in MPS. No evidence of coronary abnormality was noted in other cases in agreement with MPS. Those cases with ischemia due to MB were followed up closely under medication

and competitive sports were restricted accordingly. ***Conclusion:*** MPS, is a safe and non-invasive method for the evaluation of ischemia in adolescents and children with exercise-related chest pain. Though MB is a rare entity in paediatric practice, the results of this very selected and limited case series indicate that it should be considered in cases with perfusion defects on stress MPS. Also, MPS provides complementary information for patient management and clinical follow-up such as limiting intensive sports activity in these cases due to possible myocardial risks.

EP-0435

Long-term prognostic value of semi-quantitative myocardial perfusion imaging in patients with homozygous familial hypercholesterolemia

J. Jiao, *W. Dong, T. Mou, H. Mi, Y. Zhang;*
Department of Nuclear Medicine, Beijing Anzhen Hospital, Capital Medical University, Beijing, CHINA.

Aim/Introduction: To evaluate the long-term prognostic value of myocardial perfusion imaging (MPI) in patients with homozygous familial hypercholesterolemia (HoFH). ***Materials and Methods:*** Patients who were confirmed HoFH by clinical diagnosis and chromosome genetic tests and underwent stress/rest MPI were retrospectively enrolled from June 2010 to March 2022. Patients were followed up for 5.9 ± 3.0 years. Major adverse cardiac events (MACE) included all-cause death and unplanned revascularization. MPI images were analyzed using AHA 17-segment 5-point method. The severity of the MPI defect was semi-quantitated using the summed stress score (SSS) and summed difference score (SDS). SDS 0-1 was normal and ≥2 was abnormal. The functional parameters such as stress end-diastolic volume (SEDV), rest end-diastolic volume (REDV), stress end-systolic volume (SESV), rest end-systolic volume (RESV), stress ejection fraction (SEF) and rest ejection fraction (REF) were calculated automatically. Cox univariate and multivariate regression analysis were used to determine the risk factors and independent predictors for MACE. Patients were grouped according to independent predictors. Receiver operating characteristic curve (ROC) analysis was used to identify the best cutoff point. The Kaplan Meier survival curve together with log rank test was used to analyze the incidence of MACE in different groups. ***Results:*** 45 HoFH patients (22 males, mean age: 19.00 ± 10.20 years) were enrolled. During follow-up, 12 patients (12/45, 26.7%) occurred MACE. In the Univariate Cox regression analysis, SSS, SDS, SEDV, REDV, SESV, RESV, SEF and REF were risk factors for MACE (P<0.05). After corrected for age, low density lipoprotein cholesterol (LDLC), SEDV, SESV and SEF, multivariate Cox regression analysis showed SDS and SESV were independent predictors for MACE. The SDS abnormal group (n=21) exhibited higher risk of MACE. The adjusted hazard risk ratio was 8.623 (95% CI: 1.799~41.333, P=0.007). In Kaplan-Meier analysis, the incidence of MACE in SDS abnormal group was significantly higher than that in SDS normal group (47.6% vs. 8.3%, Log Rank χ^2=12.402, P <0.05). In ROC analysis of SESV, the area under the curve was 0.7. The optimal cut-off value was 35.5 mL. In Kaplan-Meier analysis, the incidence of MACE in SESV≥35.5 mL group (n=22) was higher than that in SESV<35.5 mL group (n=23) (40.9% vs. 13.0%, P=0.035). ***Conclusion:*** MPI has important prognostic value in HoFH patients. SDS and SESV of MPI are independent predictors of MACE. Patients with normal SDS and SESV<35.5mL had an excellent prognosis. Abnormal SDS or SESV≥35.5mL increased the risk of MACE.

EP-0436

The relationships between apolipoproteins and myocardial blood flow in patients with non-obstructive coronary artery disease

K. Zavadovsky, *A. Maltseva, K. Kopeva, A. Mochula, O. Trubacheva, E. Grakova;*
Cardiology Research Institute, branch of the Federal State Budgetary Scientific Institution «Tomsk National Research Medical Center of the Russian Academy of Sciences», Tomsk, RUSSIAN FEDERATION.

Aim/Introduction: Dyslipidemia can be a reason for the development of microvascular dysfunction (MD) in patients with non-obstructive coronary artery disease (NOCAD). Over the past few years, scientific data have demonstrated that NOCAD patients could have high risk for adverse cardiovascular events. From this point of view, new opportunities for the risk stratification in NOCAD population may be considered as a field of future investigations. The aim of the study is to assess the relationships between apolipoproteins and myocardial blood flow and reserve impairment in NOCAD patients. ***Materials and Methods:*** Based on CCTA results, patients with NOCAD (stenosis <50%) were included in the study. All patients underwent dynamic SPECT CZT with the assessment of myocardial perfusion: SSS, SRS, SDS, stress and rest myocardial blood flow (MBF), myocardial flow reserve (MFR), flow difference (FD) [1]. The Net Retention with attenuation correction flow model was used for quantitative analysis. Furthermore, the blood lipid levels were assessed: low-density lipoprotein cholesterol (LDL-C), apolipoprotein B (ApoB), apolipoprotein A1 (ApoA1) and index of apolipoprotein B/apolipoprotein A1 (ApoB/ApoA1). Based on the LDL-C level was divided into two groups: 1. High level of LDL-C, 3.33(3.0;3.95), n=29; 2. Normal level of LDL-C, 1.7(1.4;2.3), n=15. ***Results:*** The study included 44 patients (27 men, age 56.4±9.5 years). Lipid profile was differed significantly in two groups: apoB 3.38(2.91;3.59) vs 2.61(2.27;2.81) mg/ml, apoA1 10.66(8.29;12.71) vs 11.41(8.41;12.04) mg/ml, ApoB/ApoA1 0.33(0.26;0.37) vs 0.24(0.19;0.3), respectively. SPECT CZT parameters did not differ significantly in two groups: SSS 0.0(0.0;2.0) vs 2.0(0.0;2.0), SDS 0.0(0.0;2.0) vs 2.0(0.0;2.0), stress MBF 1.33(1.05;1,63) vs 1.4(1.01;1.71) ml/min/g, MFR 2.51(1.57;3.31) vs 2.53(1.56;2.84), DFR 0.75(0.36;1.3) vs 0.73(0.38;1.27) ml/min/g, respectively. The Spearman correlation showed that ApoB/ApoA1 had negative relationships with MFR (ρ=-0.64, p=0.01) and FD (ρ=-0.63, p=0.03), meanwhile ApoA1 had positive relationships with MFR (ρ=0.63, p=0.02) and FD (ρ=0.58, p=0.01) in normal LDL-C patients. Based on ROC analysis, ApoB/ApoA1 value of 0.27 (AUC=0.85, 95%CI 0.564-0.98, p=0.008) had a sensitivity of 75% and specificity of 90%, in prediction of reduced MFR (<2.0). ApoA1 value of 7.77 (AUC=0.88, 95%CI 0.593-0.988, p=0.004) allowed to predict decreased MFR with sensitivity and specificity of 75% and 100%, respectively. ***Conclusion:*** Myocardial flow reserve and flow difference had strong relationships with ApoA1 and index of ApoB/ApoA1 in NOCAD patients. ***References:*** 1. Mochula AV, et al. The myocardial flow reserve in patients with heart failure with preserved ejection fraction. Heart Vessels. 2023;38(3):348-360. DOI:10.1007/s00380-022-02161-5.

EP-0437

Predictive Factors of Myocardial Perfusion SPECT Positivity using a CZT D SPECT Camera in 3594 Patients Referred For Myocardial Perfusion Imaging In one year.

M. Esnault[1], *D. Legallois*[2], *P. Richard*[3], *D. Agostini*[2], *M. Alain*[2];
[1]*Caen University, Caen, FRANCE,* [2]*Caen University Hospital, Caen, FRANCE,* [3]*Hospital privé Saint Martin, Caen, FRANCE.*

Aim/Introduction: The number of normal myocardial perfusion SPECT significantly increased over the last decades. Given the widespread use of dedicated cardiac CZT cameras, the aim of this study was to analyze the predictive factors of positive myocardial

SPECT results using a CZT camera. ***Materials and Methods:*** This retrospective study evaluated the results of myocardial SPECT using a D-SPECT camera (Spectrum dynamics, Caesarea, Il) with the use of 99mTc-labeled radiopharmaceutical in our department during 2019 and a one-day stress/rest protocol. A myocardial perfusion SPECT was considered positive in case of (i) a reversible perfusion defect in at least 2 myocardial segments and/or (ii) a nonreversible perfusion defect with a matched segmental wall motion abnormality. ***Results:*** The cohort consisted of consecutive 3594 patients (3028 performed a pharmacological stress, 196 exercise, and 370 a combined pharmacological and exercise stress test). Patients were referred for diagnostic of suspected coronary artery disease (n=2167, 60%), risk assessment of documentedcoronary artery disease (n=1194, 33%), or preoperative assessment before noncardiac surgery (n=233, 7%). There were a total of 594 (16.5%) positive myocardial SPECT. In univariate analysis, among all clinical variables, predictors of positive CZT SPECT were male gender ($p < 0.0001$), age ($p < 0.0001$), BMI ($p < 0.0001$), obesity ($p < 0.005$), hypertension ($p = 0.0015$), diabetes ($p < 0.0001$), smoking ($p = 0.0005$), dilated cardiomyopathy ($p = 0.0004$), peripheral arterial disease ($p < 0.005$), and the clinical indication for SPECT examination ($p < 0.005$). Using multivariate analysis, the independent predictors of myocardial CZT SPECT positivity were male gender (OR: 1.45, $p <0.001$), age (OR: 0.98, $p < 0.0001$), diabetes (OR: 1.43, $p < 0.001$), smoking (OR: 1.33, $p < 0.01$), and preoperative assessment (OR: 1.7, $p < 0.01$). ***Conclusion:*** In this single-center study, the rate of negative perfusion SPECT was high (83.5%). Positive myocardial SPECT was higher in men, older patients, diabetics, smokers and patients referred for preoperative assessment before non-cardiac surgery.

EP-0438

Shorten Acquisition of Dynamic 11C-Acetate Cardiac PET/CT in Quantifying Pharmacokinetic Parameters

T. Gong[1], *F. Shang*[1], *X. Tang*[1], *L. Huo*[2], *S. Liu*[1];
[1]*School of Life Science, Beijing Institute of Technology, Beijing, CHINA,* [2]*Department of Nuclear Medicine, Peking Union Medical College Hospital, Beijing, CHINA.*

Aim/Introduction: Shorten acquisition of dynamic 18F-FDG PET/CT could achieve a strongly correlated pharmacokinetic parameters with long-time acquisition[1,2]. This study investigated (K_1 and k_2). ***Materials and Methods:*** This retrospective study analyzed 55 subjects with dynamic ^{11}C-acetate cardiac PET/CT imaging. Each subject was injected with about 740MBq ^{11}C-acetate before a 40 minutes' PET/CT scan. Arterial input function was image-derived from blood pool in left ventricle. All pharmacokinetic parameters were obtained by a one-tissue compartment model. Linear regression was performed on pharmacokinetic parameters between shortened and 40 minutes' acquisitions. Relative differences (RD) between shortened and 40 minutes' acquisitions were obtained, and evaluated at global left ventricle, the left anterior descending (LAD), right coronary artery (RCA), and left circumflex artery (LCX). ***Results:*** The regression coefficient of K_1 and k_2 between shortened and 40 minutes' acquisitions summarized in Table 1. K_1 and k_2 from acquisition time over 16 min (≥ 36 frames) exhibited a strong correlation with those obtained from 40 minutes' acquisition (all $R^2 > 0.9$). Meanwhile, the regression coefficients of K_1 ranged from 0.962 to 1.000, while k_2 ranged from 0.975 to 1.032. When the scan time was set to 16 min (36 frames), the regression coefficients of K_1 and k_2 were 0.962 and 0.975, respectively, and the relative difference (RD) of pharmacokinetic parameters were [K_1: (3.87 ± 2.40) %, k_2: (13.14 ± 8.17) %] at global, [K_1: (3.87 ± 2.40) %, k_2: (13.14 ± 8.17) %] at LAD, [K_1: (2.99 ± 2.20) %, k_2: (10.20 ± 7.29) %] at RCA, and [K_1: 3.71 ± 2.52, k_2:12.33 ± 8.32] at LCX. ***Conclusion:*** Shorten acquisition of cardiac ^{11}C-acetate PET/CT with a time of 16 min (36 frames) were strongly correlated with 40 minutes' acquisition in quantifying the pharmacokinetic parameters. This study demonstrated the feasibility of dynamic cardiac ^{11}C-acetate PET/CT with shorten acquisition.

References: [1] Liu G, Yu H, Shi D, et al. Short-time total-body dynamic PET imaging performance in quantifying the kinetic metrics of 18F-FDG in healthy volunteers. Eur J Nucl Med Mol Imaging. 2022 Jul; 49(8):2493-2503. [2] Sari H, Eriksson L, Mingels C, et al. Feasibility of using abbreviated scan protocols with population-based input functions for accurate kinetic modeling of [18F]-FDG datasets from a long axial FOV PET scanner. Eur J Nucl Med Mol Imaging. 2023 Jan; 50(2):257-265.

EP-0439

Evaluation and related influencing factors of left ventricular systolic dyssynchrony after PCI in patients with acute myocardial infarction by gated myocardial perfusion imaging

J. Wang[1,2], *Y. Wang*[1,2];
[1]*The Third Affiliated Hospital of Soochow University, Changzhou, CHINA,* [2]*Institute of Clinical Translation of Nuclear Medicine and Molecular Imaging, Soochow University, Changzhou, CHINA.*

Aim/Introduction: To clarify whether left ventricular systolic dyssynchrony(LVSD) occurs after percutaneous coronary intervention (PCI) in patients with acute myocardial infarction(AMI) and its associated factors by gated myocardial perfusion imaging (GMPI) . ***Materials and Methods:*** The patients with AMI who underwent PCI in the third affiliated Hospital of Soochow University from January 2020 to December 2021 were prospectively enrolled (registration number: ChiCTR2000038729). All patients underwent rest + stress GMPI, electrocardiogram and echocardiography within 1-2 months after PCI. After GMPI image reconstruction, Cedars-Sinai QGS quantitative analysis was used to obtain the LVSD parameters of resting GMPI: phase histogram bandwidth (BW) and phase standard deviation (SD). QPS quantitative analysis was used to obtain the quantitative index of resting GMPI to evaluate myocardial infarction size: myocardial perfusion defect size (Extent, %). The abnormal critical threshold (BW: 60.6°; SD: 22.62°) was taken as the mean ± 2 standard deviations of the BW and SD values of the normal population, and any index greater than the threshold was defined as LVSD. ***Results:*** A total of 175 AMI patients undergoing PCI were included. There was no significant difference in sex, age, body mass index, previous drinking and smoking history, hypertension, diabetes and hyperlipidemia between the Non-LVSD group (n = 91) and the LVSD group (n = 84) (all $P > 0.05$). Compared with the Non-LVSD group, the ECG QTc interval of the LVSD group was significantly prolonged (416.26ms ± 49.74ms vs. 402.37ms ± 25.76ms), and left ventricular ejection fraction (LVEF) is significantly lower (56.89% ± 6.84% vs. 59.71% ± 5.08%) (all $P < 0.05$). The proportion of multi-vessel coronary artery disease, the proportion of MPI residual myocardial ischemia and Extent in the LVSD group were significantly higher than those in the Non-LVSD group (76.19% vs. 59.34%; 52.38% vs. 28.57%; 11% vs. 3%). Multivariate Logistic regression analysis showed that coronary multi-vessel disease (OR=3.526, 95%CI:1.346~9.238, P=0.010) and Extent (OR=1.144, 95%CI:1.070~1.222, P=0.000) were independent risk factors for LVSD after PCI in patients with AMI. ***Conclusion:*** LVSD still exists in about half of the patients with AMI after PCI, and multi-vessel coronary artery disease and myocardial perfusion defect extent (Extent) are independent risk factors for LVSD after PCI in AMI patients, indicating that the higher the probability of LVSD after PCI is in AMI patients with multi-vessel coronary artery disease and / or higher myocardial perfusion defect extent.

EP-0440

The Characteristics of Perfusion in Cardiac SPECT/CT of Suspected INOCA and Obstructive Coronary Artery Disease Patients.

M. Kalnina[1,2], *B. Vitola*[3,4], *J. Kedrova*[1], *I. Mintale*[3,5], *A. Erglis*[3,2]; [1]*Department of Radiology, Pauls Stradins Clinical University Hospital, Riga, LATVIA,* [2]*Faculty of Medicine, University of Latvia, Riga, LATVIA,* [3]*Latvian Centre of Cardiology, Pauls Stradins Clinical University Hospital, Riga, LATVIA,* [4]*Faculty of Medicine, Riga Stradins University, Riga, LATVIA,* [5]*University of Latvia, Faculty of Medicine, Riga, LATVIA.*

Aim/Introduction: Ischemia with non-obstructive coronary artery disease (INOCA) is highly prevalent in symptomatic patients with a female predominance diagnosed by cardiac SPECT/CT. As the cardiovascular risk is high and quality of life is reduced in INOCA patients, the confirmed functional disorders in patients with no obstruction in coronary arteries is of high importance. The aim of the study was to find out if there is a difference in myocardial perfusion in patients with suspected INOCA and in obstructive (CAD) patients. ***Materials and Methods:*** In total 726 [99mTc] SPECT/CT in women with suspected CAD was performed from 2018 to 2021 at university hospital. True myocardial perfusion defect was detected in 125 patients (17.2%). Further analysis included 121 patients in whom coronary angiography or CT coronorography was performed. The patients were divided into 2 groups: suspected INOCA and obstructive CAD. The perfusion defects were characterized by localization and segments involved. The prevalence of CVD risk factors was assessed. ***Results:*** In the suspected INOCA group were 93 patients, but in the obstructive CAD group - 28 patients. The mean age in both groups was 70,5 years. The prevalence of dyslipidemia and elevated body mass index (BMI) were similar. In the INOCA group previous myocardial infarction (7,5% vs 42,9%), percutaneous coronary intervention (15% vs 64.3%) and arterial hypertension (58.0% vs 96.0%) were less common. Although the established diagnosis of depression was more frequent into the INOCA group (4.3% vs 0%). The localization of perfusion defects differed between both groups. In patients with obstructive CAD, defects were more present in one coronary artery region. In patients with suspected INOCA the defect was more diffuse (36.0% vs 18.0%). In both groups perfusion defects were found mostly in apex and apical segments - 47% in obstructive CAD and 44% in suspected INOCA group. ***Conclusion:*** The localization and severity of myocardial perfusion defects in suspected INOCA patients did not differ from the obstructive CAD group. Suspected INOCA group had more diffuse pattern of the disease. Further analysis performing intracoronary physiological measurements is necessary to detect INOCA and its endotype to start early treatment of the disease.

EP-0441

Comparison of Ejection Fraction Measurements with Novel Multi-pinhole Collimator on Triple-NaI-Detector SPECT and Conventional Dual-NaI-Detector Parallel-hole Collimator Technique

Á. Krizsán[1], *K. Kukuts*[1], *L. Balazs*[2], *J. Kiss*[3], *M. Alamin*[1], *V. Linczerne Bencze*[1], *S. Barna*[1], *I. Garai*[1], *J. Mester*[4], *A. Forgacs*[1]; [1]*ScanoMed Nuclear Medicine Centers, Debrecen, HUNGARY,* [2]*Mediso Ltd., Budapest, HUNGARY,* [3]*Medical Imaging Clinic Radiology, Clinical Center, University of Debrecen, Debrecen, HUNGARY,* [4]Universitäsklinikum *Hamburg-Eppendorf, Hamburg, GERMANY.*

Aim/Introduction: In this study we evaluated the Left Ventricle Ejection Fraction (LVEF) measurement accuracy of a novel Multi-pinhole collimator (MPH-Cardiac) on a Triple-NaI-Detector SPECT/CT system with patient scans and 3D printed phantom scans evaluated with three commercially available cardiac software suites. ***Materials and Methods:*** Resin based 3D printing of three LV models (20 ml, 60 ml and 140 ml with 10 mm fillable wall thickness) were performed on an Elegoo Mars II Pro 3D printer. The phantom set was filled from a stock solution of 41.71 ± 6.42 kBq/ml ^{99m}Tc-sestamibi at the start of the SPECT acquisitions. Image acquisitions were performed with LEHR collimators on a dual head SPECT system AnyScan SC in 90° detector configuration, 64 views covering 180° scan arc, and the MPH-Cardiac collimators on a triple head SPECT system AnyScan TRIO in 75° detector configuration, 125° scan arc. Ecg-triggered gated SPECT acquisitions were performed with scan duration of 16 minutes. Image reconstructions were performed with Tera-Tomo 3D SPECT using 5 iterations 8 subsets 3.6 mm voxel size for the MPH-Cardiac, and OSEM with Butterworth pre-filter 6.5 mm voxel size in case of the LEHR. End Diastole Volume (EDV) was determined from the image sets using Cedars-Sinai QGS, Invia 4DM and Emory Toolbox. Gated SPECT scans of 42 patients with suspected coronary artery disease (CAD) were performed on both the LEHR and MPH-Cardiac systems. EDV, End Systole Volume (ESV) and LVEF were determined for both techniques with all three cardiac software suites. ***Results:*** In case of dual-head LEHR measurements EDV values were found to be 12 ml, 54 ml, 123 ml with QGS, 11 ml, 49 ml, 125 ml with Corridor 4DM and 11 ml, 47 ml, 117 ml with Emory Toolbox. In case of triple-head MPH-Cardiac measurements EDV values were found to be 19 ml, 59 ml, 139 ml with QGS, 19 ml, 58 ml, 138 ml with Invia 4DM and 18 ml, 55 ml, 133 ml with Emory Toolbox. Median values of the distribution of LVEF values for all patients were found to be lower due to significantly higher ESV values in case of MPH-Cardiac compared to the LEHR technique. ***Conclusion:*** The MPH-Cardiac collimator on a Triple-NaI-Detector SPECT/CT system provides more precise volume measurements and consequently more reliable LVEF results compared to dual head LEHR SPECT.

EP-0442

Prognostic Value of Myocardial Blood Flow and Coronary Flow Reserve on Dynamic Myocardial SPECT

M. Havel*, M. Kaminek, A. Klegova, L. Quinn, L. Henzlova, P. Koranda, V. Icova, G. Havlova; Department of Nuclear Medicine, University Hospital and Faculty of Medicine and Dentistry Palacký University, Olomouc, CZECH REPUBLIC.*

Aim/Introduction: Dynamic SPECT on a CZT dedicated camera enables absolute quantification of myocardial blood flow (MBF) and coronary flow reserve (CFR). The aim of the work is to assess the prognostic significance of CFR detected using dynamic SPECT on a CZT camera. ***Materials and Methods:*** Retrospective analysis of 44 patients examined with dynamic myocardial SPECT. The adverse cardiac events (CE) defined as sudden cardiac death, myocardial infarction, situations requiring coronary revascularization, and hospitalization for heart failure with reduced ejection fraction, were recorded. ***Results:*** Patients with CE (n = 11) had comparable rest MBF (1.24 vs 1.23 ml/min/g) but significantly lower stress MBF (1.82 vs 2.73 ml/min/g ; a cut-off value for the prediction of CE was 2.35 ml/min/g with a sensitivity of 91% and a specificity of 67%) and a lower CFR (1.48 vs 2.40). In the group with a reduced CFR <2 (n = 18), a significantly higher incidence of CE (50% vs. 7.7%, p = 0.003) and a significantly shorter time to CE were observed (p = 0.001). ***Conclusion:*** Lower stress MBF and lower CFR detected by dynamic myocardial SPECT on a CZT camera represents an increased risk for the occurrence of adverse cardiac events. ***References:*** Crea F, Camici PG, Bairey

Merz CN. Coronary microvascular dysfunction: an update. Eur Heart J. 2014;35(17):1101-1111.Herzog BA, Husmann L, Valenta I, et al. Long-term prognostic value of 13N-ammonia myocardial perfusion positron emission tomography added value of coronary flow reserve. J Am Coll Cardiol. 2009;54(2):150-156.Johnson NP, Gould KL, Di Carli MF, Taqueti VR. Invasive FFR and Noninvasive CFR in the Evaluation of Ischemia: What Is the Future?. J Am Coll Cardiol. 2016;67(23):2772-2788. Garcia D, Harbaoui B, van de Hoef TP, et al. Relationship between FFR, CFR and coronary microvascular resistance - Practical implications for FFR-guided percutaneous coronary intervention. PLoS One. 2019;14(1):e0208612. Published 2019 Jan 7.

EP-0443

Role of Myocardial Scintigraphy in Evaluating Patients in the Emergency Department

I. Gotuzzo[1], *P. Ferro*[1], *R. Boni*[1], *P. Vai*[1], *R. H. J. A. Slart*[2], *P. A. Erba*[3]; *[1]Nuclear Medicine Department ASST Ospedale Papa Giovanni XXIII, Bergamo, ITALY, [2]Medical Imaging Center, University Medical Center Groningen, Groningen, NETHERLANDS, [3]Department of Medicine and Surgery, University of Milan Bicocca and Nuclear Medicine Department ASST Ospedale Papa Giovanni XXIII Bergamo, Bergamo, ITALY.*

Aim/Introduction: Chest pain (CP) accounts for a significant number of attendances at emergency departments (ED). Although history, physical examination, electrocardiogram (ECG), echocardiography, and serial troponins can rule out acute coronary syndrome (ACS) and aid prompt discharge of patients, additional testing might still be warranted to decide whether to safely discharge or hospitalize patients. Myocardial scintigraphy (MS) has emerged as an important diagnostic modality for evaluation of CP in the ED for patients at low to intermediate risk for ACS. Several clinical trials have shown it has an excellent negative predictive value in the detection of coronary artery disease. We examined the utility of performing stress myocardial perfusion imaging for stratification of low-risk patients presenting with CP in the emergency department for safe and rapid discharge. ***Materials and Methods:*** From July 2017 to September 2022, 100 low-intermediate risk non-critical patients accessing the ED with CP underwent MS; 51 were included. Data on risk factors, ECG, echocardiography, troponin values and previous cardiac events were collected. One-day protocol stress (pharmacological or physical according to the patients 'needs) and rest MS with 99mTc-tetrofosmin or 99mTc-sestamibi on a CZT tomograph was performed according to EANM guidelines. MS results, the decision of ED physicians and follow-up data were also analyzed. ***Results:*** 5.8% of patients presented with troponin elevation, 1.9% with ECG suggestive for STEMI and 37.2% with either akinesia or hypokinesia at echocardiography. 63.8% of MS were negative, 21.3% showed ischemia, 4.2% myocardial necrosis and 10.7% both ischemia and necrosis. No complications after MS ensued. 23.9% were hospitalized and 10.9% underwent coronography, which only in 4 patients was not concordant with MS results. 73.9% of patients, including all those with negative MS, were discharged: 41.3% without undergoing further invasive examinations, and 19.6% with medical therapy adjustments. None of those patients experienced further cardiac events during the time of follow-up. Only 2.2% of MS were inconclusive. ***Conclusion:*** Our study demonstrated that positive MS and coronography showed concordance in identifying the myocardial territory affected by CAD in most cases. Conversely, negative MS guided ED clinicians towards discharging patients without further examinations. Follow-up proved the decision to be safe, as no other cardiac events were observed, and avoided unnecessary hospitalization. Studies on a larger cohort with longer follow-ups are needed to assess the actual clinical impact of MS performed in the emergency setting and the benefits of early discharge rather than unnecessary hospitalization in terms of cost-effectiveness.

EP-0444

myocardial injury Assessment of SPECT MPI in fulminant and suspected myocarditis compared with CMR

J. Cui, *S. Wang, Y. Ge;*
Henan Provincial People's Hospital Heart Center, Zhengzhou, CHINA.

Aim/Introduction: The aim of our study was to access the SPECT Myocardial perfusion imaging (MPI) findings in fulminant myocarditis (FM) and clinically suspected myocarditis (CSM) of left ventricle compared with cardiac magnetic resonance (CMR). ***Materials and Methods:*** 30 FM patients and 21 CSM patients with both MPI and CMR examinations were included in this retrospective study, with interval time less than 5 days. CMR were performed in 1 week after weaned from Mechanical Circulatory Support (including IABP, Impella & ECMO) for FM patients. Additionally to the routine CMR protocol, T2-mapping and late gadolinium enhancement (LGE) data were acquired and segmented according to the 16-segments AHA-model, as well as the segmental pixel-standard deviation (SD) were analyzed, MPI applies a 17-segment model and the total summed rest score (SRS) of the left ventricle. Compared the abnormal findings of MPI toT2-mapping and LGE. ***Results:*** There were 5 diffuse lesions, 18 multiple focal lesions, 6 single focal lesions and 1 normal in FM. There were 2 diffuse lesions, 9 multiple focal lesions, 7 single focal lesions and 3 normal in CSM. The total SRS has high co-relation with total T2-mapping and LGE, with an AUC of 0.82 and 0.79 in ROC-analysis. The location of lesions from visual and 16-segments has high co-relation too. There has significant difference between FM and GSM on SRS, T2-mapping value and LGE±5SD. ***Conclusion:*** MPI was in good agreement with CMR in evaluating the location and degree of myocarditis, and its radioactivity distribution was high correlated with edema on T2 mapping and injury on LGE.

EP-0445

Psychology of attendants/caregivers during the myocardial perfusion imaging of patients

C. Sioka, *A. Bechlioulis, P. Giantsouli, Z. Panagiotou, S. Alexiou, P. Kekiopoulos, A. Kekiopoulou, A. Papadopoulos, L. Astrakas, P. Zotou, J. Zika, A. Arseniou, K. Pappas, C. Katsouras, P. Petrikis; University Hospital of Ioannina, Ioannina, GREECE.*

Aim/Introduction: Examinations performed in a Nuclear Medicine Department may provoke or exacerbate the appearance of anxiety of the patient and his or her companion for the course and the outcome of the disease. Usually, family is the one who takes the burden of care, and the caregiver develops negative emotions, depression, stress, chronic fatigue, health problems and doubt about the care. The aim of this study was the assessment of anxiety and depression of companions (relatives/caregivers) of patients, who came to the Nuclear Medicine department for a myocardial perfusion scintigram (MPI). ***Materials and Methods:*** The existence of anxiety and depression was assessed in 98 companions of patients who underwent MPI in the context of suspected coronary artery disease. Demographic data questionnaires, the Hamilton Anxiety Rating Scale (HAM-A) and the Zung Self-Rating Depression Scale (SDS) were used to collect

the data. ***Results:*** Of the 98 attendants who completed the questionnaires, 27 were men (28%, mean age 54 years) and 72 were women (72%, mean age 51 years). Seventy-two attendants (74%) reported a feeling of anxiety, while based on the questionnaires 78 attendants indicated mild anxiety (HAM-A <17) and 20 people more than mild anxiety (HAM-A ≥18). Based on the SDS scale, 4 people were diagnosed with depression, while 10 people were already on treatment with antidepressants. The results of the two scales HAM-A and SDS presented a positive correlation (r 0.615, p<0.001). Women presented higher values in the HAM-A scale (r 0.352, p<0.001) and SDS (r 0.414, p<0.001). Companions who reported anxiety also had higher values on the HAM-A scale (r 0.222, p=0.028). ***Conclusion:*** About 3 in 10 caregivers experience stress during a Nuclear Medicine examination of a patient. Anxiety is mainly experienced by female attendants regardless of the patient's history. These feelings are probably related to the examination and its findings as well as the course of the patients' disease.

EP-0446

The effect of Attenuation correction on myocardial blood flow and reserve measured by dynamic SPECT

A. Mochula*, A. Maltseva, A. Cygikalo, O. Mochula, K. Zavadovsky;*
Cardiology Research Institute, Tomsk NRMC,
Tomsk, RUSSIAN FEDERATION.

Aim/Introduction: Myocardial blood flow (MBF) and reserve (MFR) are the most informative indices for myocardial perfusion evaluation, at this moment. Currently, the dynamic SPECT by on CZT-detectors gamma-camera allows obtaining the MBF and MFR values. Nevertheless, the influence of attenuation correction [1] on a value quantitative dynamic SPECT data has been studied not enough.Aim of the study to assess, the Influence of attenuation correction on a value quantitative dynamic SPECT data ***Materials and Methods:*** In the study was enrolled 245 stable patients with various cardiac pathologies. The comprehensive clinical and instrumental examination for all patients was performed. Additionally, dynamic SPECT on the two days rest-stress protocol was provided. Dynamic SPECT protocol with evaluating MBF and MFR described in previously study. ATF in 160 mcg/kg/min as a stress-agent was used [2]. Net retention and one-compartment tissue with and without attenuation (NRAC, NRNC, 1CAC, 1CNC) were used for post-processing. Stress and rest MBF, difference flow and MFR were assessed. ***Results:*** Pairwise comparison (Durbin-Conover test) showed significant difference between four models in all indices, except stress and rest MBF for NRAC vs NRNC pair - 1.17 (0.73; 1.59) vs 1.33 (0.75; 1.82) for stress MBF and (0.55 (0.41; 0.81) vs 0.56 (0.37; 0.83) for rest MBF, respectively . Moreover, the use of attenuation correction increased of values MFR: for one-compartment 1.74 (1.21; 2.61) vs 1.82 (1.40; 2.51) and for net retention 1.93 (1.31; 2.61) vs 2.13 (1.56; 2.76) - for AC and NC measurement, respectively. Bland-Altman analysis showed that models were not agreement for stress and rest MBF, except NRAC and NRNC pair for rest MBF. However, MFR values showed were agreement (-0.09 (-0.19/0.02), p=0.11) for AC models - 1.74 (1.21; 2.61) vs 1.93 (1.31; 2.61); that does not apply to NC models (-0.24 (-0.34/-0.2), p<0.0001), 1.82 (1.40; 2.51) vs 2.13 (1.56; 2.76) - for 1-compartment and Net Retention models respectively. ***Conclusion:*** The use of attenuation correction for evaluating quantitative perfusion indices by dynamic SPECT increases of agreement for the most used models. ***References:*** 1. Wells RG, Marvin B, Poirier M, Renaud J, deKemp RA, Ruddy TD. Optimization of SPECT Measurement of Myocardial Blood Flow with Corrections for Attenuation, Motion, and Blood Binding Compared with PET. J Nucl Med. 2017;58(12):2013-2019. doi:10.2967/jnumed.117.1910492. Mochula A, Zavadovsky K, Andreev S, Lishmanov Y. Dynamic Single-Photon Emission Computed Tomography Data Analysis: Capabilities for Determining Functional Significance of Coronary Artery Atherosclerosis. MATEC Web Conf. 2016;79. https://doi.org/10.1051/matecconf/20167901080

EP-0447

Transient ischemic dilatation and heart rate at stress and rest: Searching for a threshold of significance in patients with normal perfusion.

A. Alomar*, A. Camarero, I. Blanco, N. Rudic, I. Saura, J. Cruz, A. Barrera, M. Ribelles, E. Goñi;*
Hospital Universitario de Navarra (HUN), Pamplona, SPAIN.

Aim/Introduction: The existence of Transient Ischemic Dilatation (TID) during the stress is a scintigraphic sign that has been associated with worse prognosis in patients with positive findings for myocardial ischemia. However, it has also been detected in patients without scintigraphic evidence of myocardial ischemia, and the possible cause is considered to be heart rate variability. The aim of this study is to assess the influence of heart rate (HR) variability on TID in patients who have undergone myocardial perfusion imaging at stress and rest, with an additional objective of searching for a possible threshold from which HR variability will result in the appearance of transient dilatation in non-ischemic patients. ***Materials and Methods:*** A total of 296 consecutive patients who underwent two-day protocol gated myocardial perfusion imaging with 99mTc-Sestamibi (Siemens Symbia Intevo T6/IQ-SPECT) were analyzed. Heart rate was recorded during the acquisition of both studies, and the difference in heartbeats was calculated as a percentage, along with the TID in studies without attenuation correction. ***Results:*** Patients (mean age of 63.8 between 37 and 87 y.o being men 62.3%) were classified into three groups according to the test results: negative for ischemia (n=181; ΔHR=12.0%±1.0; TID=1.00 [1.19-0.81]), positive (n=103; ΔHR=13.5%±1.5; TID=1.03[1.25-0.82]), and non-conclusive (n=12; ΔHR=12.0%±2.2; TID=0.99±0.05). A strong correlation (r=-0.615, p=0.00) was observed between the percentage difference in HR and TID. This correlation was maintained in non-ischemic patients (r=-0.667, p=0.000), but was lower in patients with ischemia (r=-0.547, p=0.000), and not significantly correlated in the non-conclusive group (p=0.084). In non-ischemic patients, the threshold from which HR variability was significantly associated with alteration of TID was 15.97%. ***Conclusion:*** Heart rate variability between stress and rest may result in an alteration of TID due to the strong correlation between these variables, which is stronger in the group with normal perfusion than in the ischemic group. In patients with ischemia, who have lower HR variability, the alteration of TID could be due to the influence of ischemia itself, which needs to be evaluated in future studies. No correlation was found in non-conclusive group possibly due to a low number of patients.

EP-0448

The prognostic value of complex CMR and dynamic SPECT assessment in patient with acute myocardial infarction

A. Mochula*, O. Mochula, E. Nalesnik, A. Maltseva, A. Sulejmanova, V. Ryabov, K. Zavadovsky;*
Cardiology Research Institute, Tomsk NRMC,
Tomsk, RUSSIAN FEDERATION.

Aim/Introduction: Acute myocardial infraction (AMI) is one of the major cause of mortality and morbidity in the developed world. If a diagnostic algorithms of detection and treatment of this acute condition is clear and developed enough, predictors of adverse course of the disease have not been sufficiently identified. Aim of this study to reveal of a complex diagnostic accuracy of dynamic SPECT and cardiac MRI in predicting of adverse course of the disease. ***Materials and Methods:*** Ninety patient with first identified AMI average age 62.5±10.5 years (61% male) were included. Complete clinical and instrumental examination according to ESC guide-lines was provided. Additionally, CMR with gadolinium enhancement due to 2-7 days and dynamic rest-stress SPECT within 7-10 day after admission were provided. Rates of incident MACE following 12 months after acute coronary event was assessed. ***Results:*** MACE were identified in 11 patients: nonfatal stroke in 5 patients, 5 cases of cardiovascular death and nonfatal MI in one patient. MACE group of patients characterized significant increase of myocardial mass, end systolic and diastolic volumes of LV; end systolic volume of RV compare to group without MACE: 285 (198;450.6)g vs 182 (157.9;225.5)g, 98 (65; 317) ml vs 41.3 (32.7;55.5) ml; 160 (152;385.6)ml vs 120 (102;137.4)ml, 54 (47;85)ml vs 41 (32;56)ml, respectively. Ejection fraction of LV and RV as well as myocardial salvage index were lower in patients with MACE: 39.2 (16;55)ml vs 63.5 (54.9;70)ml and 35 (28;43) ml vs 51 (46;56)ml; 11.62 (0.51;13.5) vs 30.95 (10.5;44.4) - against non-MACE patients, respectively. Other CMR indices were not significant difference. Compare of dynamic SPECT indices showed that MACE group of patient against non-MACE characterized increase of summed stress score and summed rest score 6.5 (6;30) vs 5 (3;12) and 6 (4.5;26) vs 3 (0;7), respectively. Moreover, stress and rest myocardial blood flow decreased in MACE patients: 0.86 (0.44;1.12)ml/min/g vs 1.09 (0.81;1.67) ml/min/g and 0.48 (0.28;0.48) ml/min/g vs 0.67 (0.40;1.04) ml/min/g. However myocardial flow reserve did not differ between enrolled groups of patients. Multivariate logistic regression analysis revealed that ESV LV (1,04 [1,02-1,06]), EF RV (0,84 [0,76-0,98]) and rest MBF (0,85 [0,77-0,94]) were independed predictors of MACE in patients with AMI (sensitivity 0.85, specificity 0.67, accuracy 0.79 and AUC 0.91). ***Conclusion:*** The complex evaluation of cardiac MRI and dynamic SPECT performed in subacute period of AMI is an informative approach and can be used in the prognosis of MACE. These results require further investigation.

EP-0449

Attenuation correction in SPECT-Myocardial perfusion imaging:It can be corrected, but is it really useful?

S. Abhilash*, S. Jeevan, P. Pradeep, S. Sarath, L. N. Manishi;*
All India Institute of Medical Sciences, Rishikesh, INDIA.

Aim/Introduction: SPECT myocardial perfusion imaging (MPI) is a non-invasive diagnostic method for assessing myocardial perfusion in patients with coronary artery disease (CAD). Soft tissue attenuation can affect its accuracy, but attenuation correction (AC) compensates for this by correcting for photon absorption. With the advent of hybrid SPECT/CT cameras, CT-based AC is now widely used. This study evaluated the benefits of AC in three major vascular territories and compared it to coronary angiography (CAG) and echocardiography (ECHO). ***Materials and Methods:*** We retrospectively analysed 42 patients who were referred by the cardiologist for assessment of myocardial perfusion (SPECT-MPI). CAG done within 5 months of MPI along with recent ECHO findings were taken as the reference standard. A coronary artery stenosis >75% and wall motion abnormality on ECHO were considered the reference standards. For all patients, cardiac SPECT with low-dose CT was acquired 1 hour after i.v. injection of 10-15 mCi of 99mTc Sestamibi at rest. Images were reconstructed and CT-based attenuation correction was applied. Images were processed using Emory Cardiac Toolbox software V:3.2 (ECT box; Emory University, Atlanta, GA) on a Xeleris 4.0 Nuclear Medicine workstation. Both AC and NAC images were compared. ***Results:*** 42 patients (39 males and 3 females) with a mean age of 57 years were studied. Using a standard 17-segment polar map, a total of 126 major coronary artery territories (42 LAD, 42 RCA, and 42 LCX) were analysed.On visual and semiquantitative analysis, 23/126 (RCA = 9, LCX = 1) vascular territories showed normalisation of perfusion defects after AC. 1/126 new perfusion defects were observed after AC in apparently normal territories (LAD = 1). On comparing MPI findings with reference standards, LAD territory defects that were observed (34/126) on MPI remained unchanged after AC and correlated well with reference standards. 13/21 RCA and 11/17 LCX territory defects had significant stenosis and RWMA, which were persistent even after AC, were considered true positives. However, 8/21 RCA and 2/17 LCX defects normalised after AC, thus being considered false negatives. ***Conclusion:*** In our study, though fallacious inferior wall defects involving RCA in non-AC MPI images resolved with AC, few apparent perfusion defects were underestimated with AC. It is important to understand that CT-based AC can overcorrect perfusion defects and introduce new artefacts. It should be used with caution; both non-corrected and corrected image datasets should be reviewed before integrating them into the final report.

EP-26

e-Poster Area

B: Imaging Clinical Studies -> B4 Cardiovascular Imaging Clinical Study -> B42 Metabolism and Innervation

EP-0450

Automated absolute quantitation of cardiac sympathetic activity using convolutional neural network and 123I-MIBG SPECT/CT

S. Saito[1]*, K. Nakajima*[2]*, L. Edenbrandt*[3,4]*, M. Larsson*[5]*, O. Enqvist*[5]*, J. Ulén*[5]*, S. Kinuya*[1]*;*
[1]Department of Nuclear Medicine, Kanazawa University, Kanazawa, JAPAN, [2]Department of Functional Imaging and Artificial Intelligence, Kanazawa University, Kanazawa, JAPAN, [3]Sahlgrenska University Hospital, Gothenburg, SWEDEN, [4]University of Gothenburg, Gothenburg, SWEDEN, [5]Eigenvision, Malmö, SWEDEN.

Aim/Introduction: We have already created algorithm for segmentation of cardiac region in ^{123}I-MIBG SPECT images without X-ray CT using convolutional neural networks (CNN). We have also attempted to use ^{123}I-MIBG SPECT/CT images and successfully conducted automatic heart segmentation based on CNN. Since CNN-based automatic absolute quantitation in ^{123}I-MIBG SPECT/CT has not been evaluated, the purpose of this study was to quantify CNN-based absolute heart counts and standardized uptake value (SUV) using ^{123}I-MIBG SPECT combined with low-dose CT for attenuation correction purposes and compare these values with conventional planar image-based quantitation. ***Materials and Methods:*** A total of 70 patients (46% men, mean

age 66.7 years) with cardiac and neurological diseases, including Parkinson's disease, Lewy body disease, and chronic heart failure, were assessed by ^{123}I-MIBG early and delayed planar and SPECT/CT images. The heart was automatically segmented on SPECT/CT images by using a CNN with 3D U-Net architecture, in which analysis and synthesis paths have multiple resolution stages. The CNN was trained to segment the heart on 50 manually annotated images (40 for training and 10 for validation) using cross entropy loss and the Adam optimizer with the CT image as input. The CNN-based heart segmentation in 20 cases of early and delayed ^{123}I-MIBG SPECT/CT images was tested. The standardized uptake value (SUV) was then determined by dividing the ^{123}I-MIBG activity in the heart (Bq/cm^3) by the injected dose (Bq)/body weight (g). Further, we calculated CNN-based SPECT/CT washout rates (WR) based on early and delayed SUV values. Ultimately, we examined correlations between CNN-based SPECT/CT SUV and planar HMR, as well as CNN-based SPECT/CT WR and planar WR. We also classified WR into normal and abnormal categories based on linear regression lines derived from the relationship between CNN-based SPECT/CT WR and planar WR, and then analyzed their agreement. ***Results:*** CNN-based early and delayed SUV, which were calculated using ^{123}I-MIBG SPECT/CT, correlated significantly with the planar HMR ($R^2 = 0.51$ and 0.69, $p < 0.0001$, respectively). There were also statistically significant correlations between CNN-based SPECT/CT WR and planar WR ($R^2 = 0.87$, $p<0.0001$). The contingency table results for high and low WR (cutoffs: 33% and 34% for SPECT/CT and planar studies, respectively) demonstrated 90.0% agreement between CNN-based and planar methodologies. ***Conclusion:*** The CNN-based method can effectively quantify cardiac counts and calculate SUV using ^{123}I-MIBG SPECT/CT images. Automatic three-dimensional absolute quantification of sympathetic innervation was significantly correlated with conventional planar image quantification.

EP-0451

Long-term cardiac risk in recovered Covid-19 patients evaluated by 123I-mIBG

A. Liebich[1], *G. Sheikh*[2], *B. Nittbaur*[1], *R. A. Bundschuh*[1], *M. Kircher*[1], *A. Dierks*[1], *P. Raake*[3], *M. Rieger*[3], *T. Higuchi*[4], *C. Lapa*[1], *C. H. Pfob*[1]; [1]*Nuclear Medicine, Faculty of Medicine, University of Augsburg, Augsburg, GERMANY,* [2]*Department of Nuclear Medicine, LMU Munich, Munich, GERMANY,* [3]*Cardiology, Faculty of Medicine, University of Augsburg, Augsburg, GERMANY,* [4]*Department of Nuclear Medicine, University Hospital Wuerzburg, Wuerzburg, GERMANY.*

Aim/Introduction: COVID-19 patients without underlying heart disease can develop heart failure, myocarditis or cardiac arrhythmias. Significant cardiac involvement seems to occur independent from the severity of the initial disease pattern and may persist during the long-term recovery period. To evaluate the presence of cardiac sympathetic nervous dysfunction in such patients, non-invasive imaging using the radiotracer ^{123}I-metaiodobenzylguanidine (mIBG), a norepinephrine analogue, was performed in COVID-19 patients without pre-existing cardiac conditions. ***Materials and Methods:*** 33 recovered COVID-19 patients (14 men and 19 women; aged 21 - 66 years) without any known severe cardiac, renal, neurological or metabolic diseases underwent ^{123}I-mIBG -SPECT/CT and echocardiography as well as serum measurement of cardiac enzymes, renal retention parameters and electrolytes 0 to 3 months after recovery. In 82% of these patients (27/33), follow-up was performed 6 to 8 months after diagnosis, nine patients (27%) underwent additional imaging after 12 to 15 months. SPECT/CT scans were acquired 15 minutes and 4 hours post-injection of 370 MBq ^{123}I-mIBG. For quantification of results, a circular region of interest (ROI) was placed over the heart and mediastinum to calculate late (4-hour) heart-to-mediastinum ratios (HMR), a method commonly employed in clinical settings. ***Results:*** Increased cardiac sympathetic activity as indicated by decreased late HMR (mean HMR 1.8±0.22), was observed in 67.7% of the patients (23/33, 95% CI 0.54 - 0.854). At 6-8 months follow-up, cardiac sympathetic innervation abnormalities were still present in 70.4% of the patients (19/27, 95% CI 0.532 - 0.876), with a mean late HMR of 1.74±0.27. Additionally, 9 of the patients showing an initial abnormal sympathetic innervation underwent follow up 12 - 15 months post-diagnosis. All were found to have persistently abnormal HMRs. Left ventricular ejection fraction (LVEF) and cardiac enzyme levels remained normal in all cases during both the initial diagnosis and follow-up periods, with no significant correlation identified between LVEF, nt-pro-BNP or troponin levels and HMR. ***Conclusion:*** Persistent increased cardiac sympathetic activity is observed in COVID-19 patients without any prior cardiac disease. Further follow-up is necessary to investigate potential long-term consequences, such as COVID-induced heart failure.

EP-0452

The characteristic myocardial accumulation pattern in oncologic FDGPET/CT under long-term fasting is likely indicative of ischemic lesions

Y. Yashima[1], *K. Takanami*[2], *K. Kiso*[2], *A. Masuda*[2], *M. Saito*[2], *Y. Toyama*[2], *Y. Maekawa*[2], *K. Takase*[2], *Y. Taniyama*[1], *T. Kamei*[1]; [1]*Department of Surgery,Tohoku University Hospital, 1-1, Seiryo-cho, Aoba-Ku,Sendai, Miyagi, JAPAN,* [2]*Department of Diagnostic Radiology,Tohoku University Hospital, 1-1, Seiryo-cho, Aoba-Ku,Sendai, Miyagi, JAPAN.*

Aim/Introduction: The purpose of this study was to retrospectively examine the association between myocardial accumulation patterns and ischemic heart disease in the oncologic FDGPET under prolonged fasting. ***Materials and Methods:*** Forty-six patients who underwent FDGPET performed for tumor diagnostic purposes and stress myocardial perfusion imaging performed for ischemic lesion scrutiny within 3 months between March 2019 and July 2022 were selected through chart review. Then, 36 cases with blood glucose <150 mg/dl before FDGPET and a fasting duration of at least 12 hours were included in the study. FDG accumulation patterns in the left ventricular myocardium on tumor FDG PET were classified as "none" "basal ring" "diffuse high" "focal high" and "focal defect on diffuse high" with the latter two patterns defined as positive, suggesting ischemia. Fasting duration and blood glucose level at the time of examination were also investigated. Stress MPI was scored using a 17-segment model, and Summed Stress Score (SSS) of 4 to 8 was defined as low risk and 9 or more points as moderate or high risk. ***Results:*** The mean duration of fasting during FDG PET was 17.3±1.6 hours (range,14-21). There was no difference in fasting duration between the diabetic and insulin-using groups. 14 of the 36 patients had "focal high" or "focal defect on diffuse high," and 12 (85.7%) of the 14 patients also had abnormal findings on stress MPI. Six patients had an SSS score of 9 or higher, indicating moderate risk or higher for cardiac events, and five patients had a "focal high" myocardial accumulation pattern on FDG PET, while the rest had "none".The sensitivity, specificity, and accuracy of ischemia findings on FDG PET were 66.7 %, 88.9 %, and 77.8 %, respectively, when patients with abnormal findings of 9 or more SSS points on stress MPI were defined as sick. There was no difference in HbA1c and blood

glucose at the examination between the positive and negative groups of stress MPI and myocardial FDG accumulation patterns. ***Conclusion:*** The characteristic myocardial accumulation pattern on oncologic FDG PET under sufficiently prolonged fasting duration and at appropriate blood glucose levels is likely to suggest ischemic heart disease.

EP-0453

Combined Assessment of PET and CMR for Decision Making in patients with Coronary Artery Disease

X. Han, *L. Wang, S. Song, W. Fang;*
Fuwai Hospital, National Center for Cardiovascular Diseases, Chinese Academy of Medical Sciences and Peking Union Medical College, Beijing, CHINA.

Aim/Introduction: The aim of this study is to explored whether combined application of myocardial viability and scar could provide potential incremental value. ***Materials and Methods:*** All patients with CAD and LVEF<50% underwent myocardial viability assessment with 18F-FDG PET metabolic imaging, as well as CMR examinations. The total extent of mismatch on FDG PET and the transmural extent on LGE CMR were calculated for each patient. Primary endpoint of the study was all-cause mortality and secondary endpoint was a composite clinical outcome. Event rates over time in groups across mismatch and LGE categories were estimated. The HRs with 95% CIs were compared using univariate and multivariable Cox proportional hazards regression models. ***Results:*** The patients were divided into four groups: group-A: mismatch>10% and LGE≤26% (n=168, 33.14%); group-B: mismatch≤10% and LGE≤26% (n=108, 21.30%); group-C: mismatch>10% and LGE>26% (n=133, 26.23%); and group-D: mismatch≤10% and LGE>26% (n=98, 19.33%).Patients who underwent CABG had lower overall rates of death than those who received medical therapy in group-A, group-B and group-C. When individually adjustment for significant baseline prognostic variables in multivariate model, the risk for primary endpoint remained higher among patients without CABG in group-A (HR=10.595, 95%CI 3.407-32.952, P<0.001). Patients who received medical therapy were also associated with an increased rates of secondary endpoint compared with those who underwent CAB in group-A and group-B. The composite endpoint rates in patients received medical therapy were remain significantly higher compared with those underwent CABG in group-A and group-B (group-A: HR=4.938, 95%CI 2.284-10.679, P<0.001; group-B: HR=3.059, 95%CI 1.294-7.229, P=0.011). ***Conclusion:*** CABG plus medical therapy is associated with significantly lower events rates compared with medical therapy alone in patients with large mismatch and small LGE. The combined assessment of mismatch and LGE has independent and incremental value in predicting whether patients likely to benefit from CABG.

EP-0454

Comparing the heart-to-mediastinum ratio of 123I-mIBG myocardial scintigraphy between a 2D image and a pseudo planar image converted from a 3D image acquired with a conventional and a ring CZT gamma camera

J. Hagerman[1], *D. Minarik*[2], *R. Smith*[3,4], *E. Stormrud*[3,4], *S. Hall*[3,4], *A. Nahimi*[3,4], *O. Hansson*[3,4], *F. Hedeer*[1,5];
[1]*Clinical Physiology and Nuclear Medicine, Skåne University Hospital, Lund/Malmö, SWEDEN,* [2]*Radiation Physics, Skåne University Hospital, Lund/Malmö, SWEDEN,* [3]*Clinical Memory Research Unit, Lund University, Malmö, SWEDEN,* [4]*Memory Clinic, Skåne University Hospital, Malmö, SWEDEN,* [5]*Clinical Physiology and Nuclear Medicine, Department of Clinical Sciences, Lund University, Lund, SWEDEN.*

Aim/Introduction: Myocardial sympathetic innervation can be visualized and quantified (heart-to-mediastinum ratio, H/M) with ^{123}I-mIBG myocardial scintigraphy. The calculation of H/M traditionally requires a static planar scintigraphic (2D) image of the thorax. Recently, a new generation of gamma cameras (ring CZT) has been introduced utilizing multiple digital solid-state detectors (CZT) in a ring design, featuring SPECT (3D) imaging only and the possibility to convert a SPECT image to a pseudo-planar image. We aimed to explore ^{123}I-mIBG myocardial scintigraphy H/M quantification of 2D imaging on a conventional gamma camera compared to a pseudo-planar image converted from 3D SPECT imaging on a ring CZT gamma camera. ***Materials and Methods:*** ^{123}I-mIBG scintigraphy images from 37 subjects (controls n=7, suspected Parkinson´s Disease n=5, suspected idiopathic rapid eye movement sleep behavior disorder n=25) participating in an ongoing research study (The Swedish Sleep Study) were analyzed. A static planar image was acquired 226 (220-229) minutes (mean (range)) post injection of 116 (108-130) MBq ^{123}I-mIBG with a conventional gamma camera, followed by a SPECT/CT acquired with a ring CZT gamma camera 20 (16-29) minutes after the static image. A regularized expectation maximization reconstruction using a relative difference prior, with attenuation and resolution correction but no scatter correction, was used for the SPECT images. SPECT images were converted to pseudo-planar images using software from the manufacturer. Region-of-interest was drawn over the heart and mediastinum, and the H/M was calculated for the static planar and the pseudo-planar image, respectively. Data were analyzed with a paired two-sample t-test (significance level p<0.05). ***Results:*** A significant difference in the H/M was observed comparing the two imaging methods (conventional 1.59 (1.01-2.74), ring CZT 1.52 (0.98-2.46), p=0.02). Stratifying by a H/M cutoff value of 1.8, there was a significant difference among subjects with a H/M >1.8 (conventional 2.25 (1.95-2.74), ring CZT 2.09 (1.75-2.46), n=13, p=0.02), but not among subjects with a H/M <1.8 (conventional 1.23 (1.01-1.76), ring CZT 1.21 (0.98-1.68), n=24, p=0.56). H/M was <1.8 for 24 subjects and >1.8 for 12 subjects on both gamma cameras. In one subject, H/M was >1.8 for the conventional (1.95) and <1.8 for the ring CZT gamma camera (1.75). ***Conclusion:*** ^{123}I-miBG myocardial scintigraphy H/M quantification on a pseudo-planar image (ring CZT gamma camera) is feasible and identified subjects with impaired sympathetic innervation of the heart at a similar rate as conventional 2D planar imaging.

EP-0455

Prognostic Role of 123i-Mibg Cardiac Scintigraphy in Patients With Cardiac Transthyretin Amyloidosis (Attr)

F. Sebastián Palacid, *B. Pérez López, R. Zambrano Infantino, M. García Aragón, N. Álvarez Mena, M. Alonso Rodríguez, J. Gómez Hidalgo, C. Gamazo Laherrán, R. Ruano Pérez;*
Hospital Clínico Universitario Valladolid, Valladolid, SPAIN.

Aim/Introduction: To determine the prognostic role of ^{123}I-MIBG cardiac scintigraphy in patients diagnosed with cardiac transthyretin amyloidosis (ATTR). ***Materials and Methods:*** Comparative study of 26 patients (18 men and 8 women) with a suspected diagnosis of ATTR due to heart failure and ventricular hypertrophy, who were previously evaluated with cardiac scintigraphy with ^{99m}Tc-DPD. All underwent cardiac scintigraphy with ^{123}I-MIBG, using a chest-centred planar imaging protocol at 15 minutes and 4 hours post-administration. The heart-to-mediastinum ratios (HMR) and washout index (WI) were evaluated

in both groups and the results were correlated with the clinical evolution of these patients in the 6 months after the scan. ***Results:*** 13 patients (50%) had a positive ^{99m}Tc-DPD scan (84.6% male; 84.6% Perugini grade 3). In all patients with a negative ^{99m}Tc-DPD scan, ATTR or other types of amyloidosis were ruled out. The mean WI in both patient groups were above the normal range, being slightly higher in the ATTR group (WI 39.8% vs. 37%; p=ns).There were no significant differences in both groups in terms of early or late HMR: Early HMR 1.52 ± 0.17 (ATTR) vs. 1.57 ± 0.32 (non ATTR); late HMR 1.4 ± 0.12 (ATTR) vs, 1.46 ± 0.27 (non ATTR). 4 patients in the ATTR group had fatal cardiac events within 6 months of the scan, while no patient in the non-ATTR group suffered serious cardiac events (p=0.0081). When looking for differences within the group with TTR amyloidosis, it was shown that deceased patients had an average higher WI than the rest (WI 52.75 vs 39.95; p=0.0224). ***Conclusion:*** ^{123}I-MIBG cardiac scintigraphy could be an useful tool in patients with TTR cardiac amyloidosis.The increment of the washout index might be a parameter to be considered in the prognosis of these patients.

EP-27

e-Poster Area

B: Imaging Clinical Studies -> B4 Cardiovascular Imaging Clinical Study -> B43 Heart Failure (including Sarcoidosis and Amyloidosis)

EP-0456

The proportion of hibernating myocardium in total perfusion defect predicts the reversal of ventricular remodeling and clinical outcomes in patients with HFrEF after CABG

Y. Lu*, X. Zhang;*
Department of Nuclear Medicine, Beijing Anzhen Hospital, Capital Medical University, Beijing, CHINA.

Aim/Introduction: To evaluate the predictive value of the proportion of hibernating myocardium (HM) in total perfusion defect (TPD) on reversing ventricular remodeling (RR) and outcomes after coronary artery bypass graft (CABG) in patients with heart failure with reduced ejection fraction (HFrEF) by myocardial perfusion imaging (MPI) and ^{18}F-FDG gated PET(GPET). ***Materials and Methods:*** Patients diagnosed with HFrEF at Beijing Anzhen Hospital of Capital Medical University were prospectively recruited. MPI combined with GPET was performed before surgery and the patients received follow-up MPI and GPET at different stages (3~12m) after surgery. Δ indicated changes (post-pre). ESV reduced at least 10% was defined as RR, patients were divided into reverse remodeling (RR+) group and the non-reverse group (RR-). Binary logistic regression analysis was used to identify predictors of RR. ROC curve analysis was performed to assess the cut-off value for predicting RR. Additionally, we retrospectively enrolled patients with HFrEF as the validation group, who underwent MPI and GPET before surgery. Echocardiography was performed before and after CABG. In the validation group, the reliability of obtaining the cut-off value for the ROC curve was verified. The endpoints included heart failure, coronary revascularization and cardiac death. The survival curves were obtained by the Kaplan-Meier (K-M) method. ***Results:*** A total of 28 patients with HFrEF (26 males; 56.9±8.7 years) were included in the prospective cohort. HM/TPD was significantly higher in the RR + group than in the RR – group (P = 0.016). Binary logistic regression analysis revealed that HM/TPD was an independent predictor of RR [Odds ratio=1.073, 95% Confidence interval: 1.005-1.145, P=0.035]. ROC curve analysis revealed that HM/TPD=38.3% yielded the highest sensitivity, specificity, and accuracy (all 75%) for predicting RR and the AUC was 0.786 (P=0.011). Meanwhile, a total of 100 patients with HFrEF (90 males; 59.7±9.6 years) were included in the validation group. In the validation group, HM/TPD=38.3% predicted RR in HFrEF patients with the highest sensitivity, specificity and accuracy (82%, 60% and 73% respectively). Compared with the HFrEF patients in the HM/TPD<38.3% group (n=36), RR and cardiac function improved significantly in the HM/TPD≥38.3% group (n=64) (P < 0.05).K-M analysis showed that the cumulative cardiovascular event-free survival rate of patients in the HM/TPD≥38.3% group was significantly higher than that in the HM/TPD<38.3% group (P=0.024). ***Conclusion:*** HM/TPD is an independent factor for predicting RR in patients with HFrEF after CABG, and HM/TPD ≥ 38.3% can accurately predict RR and outcome after CABG.

EP-0457

Dynamic SPECT in heart failure with preserved ejection fraction: tips and tricks

K. Kopeva*, A. Maltseva, A. Mochula, V. Shipulin, A. Gusakova, E. Grakova, K. Zavadovsky;*
Cardiology Research Institute, branch of the Federal State Budgetary Scientific Institution «Tomsk National Research Medical Center of the Russian Academy of Sciences», Tomsk, RUSSIAN FEDERATION.

Aim/Introduction: To evaluate the prognostic role of dynamic SPECT parameters in adverse events (AEs) in patients with heart failure with preserved ejection fraction (HFpEF) during 12-month follow-up period and to assess their relationship with biomarkers and echocardiographic parameter. ***Materials and Methods:*** Totals of 58 patients (age of 64 [54; 65] years) with non-obstructive CAD and HFpEF of NYHA class I-III (LVEF of 63 [59; 64]%) were enrolled. Dynamic CZT SPECT and echocardiography were performed baseline. Serum levels of NT-proBNP, fibroblast growth factor-23, tissue inhibitor of metalloproteinase-1 (TIMP-1), soluble ST2, matrix metalloproteinase-9 and tetranectin, hsC-reactive protein, interleukin-1β, 6 and 10 were measured using ELISA. ***Results:*** After 12 months of observation, the patients were divided into 2 groups: group 1 (n=11) included patients with AEs, group 2 (n=47) comprised those withou it. MFR and rest-MBF significantly correlated with NT-proBNP levels (r=-0.763 and r=0.401, respectively). MFR correlated with sST2 (r=-0.337), global longitudinal strain (GLS, r=0.721), left atrial volume index (r=-0.464) and septal e' (r=0.375), and rest-MFR with E/e' (r=0.424). Interleukin 10 levels correlated with MFR (r=0.511, p=0.005), rest-MBF (r=-0.432, p=0.045), and stress-MBF (r=0.317; p=0.012) values, while interleukin 1β levels significantly only correlated with MFR values (r=-0.371; p=0.046). In group 1, the level of NT-proBNP was 3,8-hold higher than in group 2 (284.5 [183.42; 716.73] and 1071.4 [272.4; 2168.1] pg/ml, respectively). In group 1, soluble ST2 levels were higher by 17.1% (p<0.001), TIMP-1 by 31.1% (p=0.012), MMP-9 by 23.4% (p=0.049), hsC-reactive protein by 1.9 times (p=0.004), and interleukin-1β by 2 times p=0.048) compared to group 2. MFR values were lower in group 1 by 45.4% (p<0.001) than in group 2 (1.19 [0.86; 1.55] vs. 2.18 [1.7; 2.55], respectively). Rest-MBF levels were higher by 23.6% (p=0.046) and stress-MBF lower by 28.2% (p=0.046) in group 1 than in group 2. In multivariate regression analysis, NT-proBNP levels (OR 3.23; p=0.008), GLS (OR 2.27; p=0.012), and MFR (OR 8.09; 95% CI p<0.001) were independent predictors of AEs. Based on ROC-analysis, MFR levels ≤1.62 (AUC=0.827; p<0.001), GLS ≤-18 (AUC=0.756; p=0.002) and NT-proBNP ≥760.5 pg/ml (AUC=0.708; p=0.040) may be considered as markers of AEs. However, the combined determination of NT-proBNP with MFR had a greater significance (AUC 0.935; p<0.001) in risk stratification. ***Conclusion:*** Dynamic SPECT parameters were associated with biomarkers

of fibrosis and inflammation, and LV remodeling. Levels of NT-proBNP, GLS and MFR may be used as non-invasive markers of AEs in HFpEF patients with non-obstructive CAD. ***References:*** Funding: MK-4257.2022.3

EP-0458

Left ventricle myocardial remodeling and coronary flow reserve in heart failure patients with non-obstructive coronary artery disease

K. Kopeva*, A. Maltseva, A. Smogon, A. Mochula, V. Shipulin, K. Zavadovsky;*
Cardiology Research Institute, branch of the Federal State Budgetary Scientific Institution «Tomsk National Research Medical Center of the Russian Academy of Sciences», Tomsk, RUSSIAN FEDERATION.

Aim/Introduction: To evaluate the relationships between the miocardial (MFR) flow reserve and myocardial blood flow (MBF) indicators, obtained by dynamic SPECT, and the left ventricle (LV) myocardial remodeling parameters and cardiac biomarkers in heart failure patients with preserved ejection fraction (HFpEF) and non-obstructive coronary artery disease (CAD). ***Materials and Methods:*** A total of 27 patients (44.4% men, median age of 64 [54; 65] years) with HFpEF of NYHA class I-III and baseline LVEF of 63% [59; 64]% were enrolled. Dynamic CZT SPECT, echocardiography and coronary computed tomography angiography studies were performed baseline. Serum levels of NT-proBNP were measured using ELISA. ***Results:*** Depending on MFR value, all patients were divided into 2 groups: group 1 included patients with MFR >2 (n=13), group 2 included those with MFR ≤2 (n=14). The median values of NT-proBNP (p<0.0001) were 743.75 (261.1; 1987.2) pg/mL in group 1 and 125.81 (87.2; 531.4) ng/mL in group 2. The values of myocardial systolic and diastolic stresses parameters were higher by 6.9% (p=0.043) and by 7.8% (p = 0.043), respectively, in group 1 than in group 2. Myocardial-arterial stiffness was significantly higher among group 1 patients in comparison to group 2 patients (0.65 [0.57, 0.95] and 0.54 [0.52, 0.64], respectively). The global longitudinal strain of LV were lower by 25.1% (p<0.001) in group 1 than in group 2 (-14.9 [-13.7; -18.6] vs. -19.9 [-17.8; -20.9]%, respectively). The lateral e' values were lower in group 1 (p=0.006) by 32% than in group 2. The peak rate of tricuspid regurgitation was higher by 11.7% (p=0.043), the E/e' ratio by 21.4% (p=0.041) and indexed left atrial volume by 22.1% (p=0.036) in group 1 than group 2. The values of MFR significantly correlated with global longitudinal strain (r =0.508; p=0.007), end-systolic elasticity (r=0.347; p=0.008), integral systolic remodeling index (r=0.532; p=0.004), E/e'(r =0.769; p<0.001), lateral e' (r=-0.680; p=0.001), and E/A (r=0.416; p=0.038). MFR and rest-MBF significantly correlated with NT-proBNP levels (r=-0.763 and r=0.401, respectively). MFR also correlated with sST2 (r=-0.565), interleukin-10 (r=0.645; p=0,008), interleukin 1β (r=-0.371; p=0.042). ***Conclusion:*** Our data suggest that MFR is associated with LV remodeling and fibrosis and inflamation biomarkers in patients with HFpEF and non-obstructive CAD. HFpEF patients with CMD had more severe LV remodeling then those without it. ***References:*** Funding: MK-4257.2022.3

EP-0459

Diagnostic Value of Semi-Quantitative Parameters Obtained from [99mTc]Tc-PYP Bone Scintigraphy and SPECT/CT in Cardiac Amyloidosis

K. Kucuker*, A. Aksu, B. Turgut;*
Izmir Katip Celebi University, Ataturk Training and Research Hospital, Nuclear Medicine Department, Izmir, TÜRKIYE.

Aim/Introduction: Scintigraphy with bone-seeking agents has a diagnostic role in cardiac amyloidosis. It is aimed to evaluate [^{99m}Tc]Tc-pyrophosphate(PYP) bone scintigraphy in the diagnosis of cardiac transthyretin amyloidosis using semi-quantitative data obtained from both planar and Single Photon Emission Computerized Tomography/Computerized Tomography (SPECT/CT) images. ***Materials and Methods:*** Patients referred to our department with the suspicion of cardiac transthyretin amyloidosis were included. Anterior-posterior chest and whole-body images were taken 90 minutes after [^{99m}Tc]Tc-PYP administration. Afterwards, SPECT/CT was performed on the thoracic region of all patients. Myocardial involvement of [^{99m}Tc]Tc-PYP was assessed visually on planar images according to the Perugini Grading Scale (Grade 0:negative, 1:equivocal, 2-3:positive). H/Cl_{Ant} was calculated by dividing the counts from Region of Interests (ROI) plotted over the heart(H) and contralateral hemithorax(CL) region in anterior planar images only. The $H/Cl_{GeoMean}$ was calculated as the ratio of the geometric mean of the heart and contralateral hemithorax obtained from ROIs of both anterior and posterior images. In addition, Voxel of Interests (VOI) were drawn on the areas compatible with the heart and corpus sterni(S) on axial SPECT images with CT correlation. H/S_{SPECT} was obtained by dividing the mean voxel counts of VOI areas. The semi-quantitative data were compared statistically between positive and equivocal/negative patients. Patients with sternotomy or trauma to thorax history were excluded from study group. ***Results:*** Thirty-two patients (18 male, 56.2%) with a mean age of 59±12 (37-80) were included in the study. Sixteen patients were Grade 0 (50%), 11 were Grade 1 (34.4%), two were Grade 2 (6.3%) and three were Grade 3 (9.4%). A total of five patients were evaluated positive for cardiac transthyretin amyloidosis. Median H/S_{SPECT} was 1.43 (1.13-1.9) and 0.8 (0.35-1.18), median $H/Cl_{GeoMean}$ was 1.26 (1.07-1.46) and 1.05 (0.89-1.79) and median H/Cl_{Ant} 1.37 (1.11-1.48) and 1.08 (0.85-1.99) in positive and equivocal/negative groups respectively. Statistically significant differences were found in H/S_{SPECT}, $H/Cl_{GeoMean}$ and H/Cl_{Ant} between groups. Best cutoffs according to Youden index were found 1.11 (AUC: 0.993, 0.969-1.000, 95% CI, 100% sensitivity, 96.3% specificity) for H/S_{SPECT}, 1.165 (AUC: 0.900, 0.763-1.000, 95% CI, 80% sensitivity, 96.3% specificity) for $H/Cl_{GeoMean}$ and 1.105 (AUC: 0.878, 0.745-1.000, 95% CI, 100% sensitivity, 66.7% specificity) for H/Cl_{Ant}. ***Conclusion:*** Our results show that semi-quantitative data obtained from SPECT images are more successful in detecting cardiac transthyretin amyloidosis than those obtained from planar scintigraphic imaging. Analyzing SPECT images may enable us to detect patients with cardiac transthyretin amyloidosis with higher sensitivity and specificity.

EP-0460

Prognostic value of right ventricular involvement in Transthyretin Cardiac amyloidosis: a quantitative 99mTc-DPD SPECT/CT study

M. Zhao[1]*, R. Calabretta*[2]*, P. Binder*[2]*, J. Yu*[2]*, Z. Jiang*[2]*, M. Hacker*[2]*, X. Li*[2]*;*
[1]*The Thrid Xiangya Hospital of Central South University, Changsha, CHINA,* [2]*Division of Nuclear Medicine, Department of Biomedical Imaging and Image-guided Therapy, Medical University of Vienna, Vienna, AUSTRIA.*

Aim/Introduction: To evaluate the prognostic value of right ventricular (RV) bone tracer uptake in patients with transthyretin cardiac amyloidosis (TTR-CA) by using quantitative (SPECT/CT. ***Materials and Methods:*** We enrolled 53 patients with scintigraphy-confirmed TTR-CA based on Perugini's uptake(grade 2-3) and exclusion of monoclonal gammopathy. All patients underwent ^{99m}Tc-DPD scintigraphy with both planar and SPECT/CT acquisitions. Left ventricle (LV), RV free wall, adjacent vertebra, and ascending aorta SUVmax were calculated. Myocardial SUVmax was also normalized to bone activity (nSUVmax) or blood pool (wSUVmax), respectively. The primary outcome was the occurrence of major adverse cardiac events (MACEs), defined as

all-cause deaths, hospitalization due to heart failure, complete atrioventricular block, recurrence or onset of sustained ventricular tachycardia, atrial fibrillation/flutter, mitral regurgitation, and coronary revascularization. ***Results:*** Thirty-five (66%) patients had RV uptake visible on planar scintigraphy. Patients with RV uptake had significantly greater serum NT-proBNP($p<0.05$), troponin T($p<0.05$), and interventricular septum(IVS) thickness($p<0.01$) than those without. During a median follow-up of 16.1 months, 19 events were recorded. On univariate Cox regression analysis, NT-proBNP, TnT, 6-MWT, NYHA class, amyloid type, LV wSUVmax , and RV wSUVmax were associated with MACEs ($P<0.10$ for all). RV wSUVmax were the independent predictors associated with MACEs at univariable Cox analysis (HR:1.12, 95%CI:1.02-1.22; $p<0.05$). ***Conclusion:*** RV uptake appears to represent a more advanced stage of disease burden in TTR-CA and could serve as a new prognostic marker in TTR-CA patients with worse outcomes.

EP-0461

Evaluation of left ventricular contractile function in patients with large perfusion defects: is gated MPI applicable?

V. Shipulin, *S. Andreev, T. Shelkovnikova, V. M. Shipulin, A. Maslova, K. Zavadovsky;*
Cardiology Research Institute, branch of the Federal State Budgetary Scientific Institution «Tomsk National Research Medical Center of the Russian Academy of Sciences», Tomsk, RUSSIAN FEDERATION.

Aim/Introduction: Gated myocardial perfusion imaging (gMPI) is a widely used technique to evaluate left ventricular (LV) function along with perfusion. However, in patients with extent perfusion defects relevance of such approach is controversial. The aim of the present study was to assess the applicability of gMPI in evaluation of LV contractile function in presence of large perfusion defects. ***Materials and Methods:*** Sixty-four patients with ischemic cardiomyopathy were included in the study. All of them underwent gMPI and gated blood pool SPECT (gBPS), as well as cardiac magnetic resonance (CMR). All investigations were performed at rest. Then patients were divided into two groups according to gMPI data (summed rest score, SRS): with large (≥20% of LV, LPD) and medium (<20% of LV, MPD) perfusion defect. The following parameters of LV contractile function were estimated by nuclear modalities: ejection fraction (EF, %), end-systolic (ESV, ml) and end diastolic (EDV, ml) volumes, as well as mechanical dyssynchrony (MD) parameters (phase histogram standard deviation (PSD, degree) and bandwidth (HBW, degree)). With cardiac magnetic resonance LVEF, EDV and ESV were evaluated. ***Results:*** MPD group comprised 21 patients (SRS 11.7 (IQR 5.8; 16.1) %), LPD group - 43 (SRS 30.8 (25; 41.1) %). In the MPD, no intermodal differences in evaluated parameters were found. In the LPD group all evaluated parameters differed between gMPI and gBPS (EF: 25 (23; 29)% and 30 (22; 35)%, p=.03; EDV: 348 (300; 405) ml and 292 (248; 343) ml, p=.005; ESV: 294 (221; 322) ml and 208 (176; 254) ml, p=.005; PSD: 61 (59; 73) deg. and 52 (43; 66) deg., p=.04; HBW: 288 (237; 309) deg. and 205 (170; 260) deg., p=.0001, respectively). According to Bland-Altman analysis, all parameters were comparable in the MPD group, whereas in the LPD group volumes and MD were significantly overestimated by gMPI (mean differences: EDV 52.5 ml, ESV 35.9 ml, PSD 7.9°, HBW 67.2°) and EF was underestimated (-3.4%). According to Friedman ANOVA in the LPD group significant differences were found between gMPI and both gBPS and CMR, while no difference was found between gBPS and CMR. ***Conclusion:*** In patients with extend perfusion defect the use of gMPI may lead to errors in evaluation of LV volumes and contractile function, including mechanical dyssynchrony parameters.

EP-0462

Prediction value of left ventricular mechanical dyssynchrony indicators associated with super response to cardiac resynchronization therapy

T. Atabekov, *A. Mishkina, R. Batalov, S. Sazonova, S. Krivolapov, V. Saushkin, M. Khlynin, Y. Varlamova, K. Zavadovsky, S. Popov;*
Cardiology Research Institute, branch of the Federal State Budgetary Scientific Institution "Tomsk National Research Medical Center of the Russian Academy of Sciences", Tomsk, RUSSIAN FEDERATION.

Aim/Introduction: The cardiac resynchronization therapy (CRT) has been shown to improve heart failure (HF) morbidity, quality of life, and survival in those with the reduced left ventricular ejection fraction (LVEF). Patients (pts) with CRT who exhibit above the expected improvement are known as super responders. The left bundle branch block (LBBB) with wide QRS duration, nonischemic HF, and female gender are most powerful predictors for CRT super response (SR). We aimed to evaluate the value of left ventricular (LV) mechanical dyssynchrony parameters detected by the cardiac scintigraphy in CRT SR predicting in chronic HF (CHF) pts. ***Materials and Methods:*** 49 sinus rhythm pts (male - 34 [69.4%], age 58.3 ± 11.4 years) with QRS duration ≥ 150 ms, permanent LBBB and New York Heart Association (NYHA) II-III functional class (FC) of CHF were included to the study. In all cases CRT devices with the defibrillation function (CRT-D) were implanted. Before and 6 month after CRT-D implantation myocardial perfusion scintigraphy (MPS) and gated blood pool single-photon emission computed tomography (gBPS) were performed. Pts were considered as super responders to CRT if they fulfilled after 6 month follow-up the following combined criteria: NYHA FC improvement ≥ 1 class + LV end systolic volume (LVESV) decrease > 30% or NYHA FC improvement ≥ 1 class + LVEF improvement > 15%. ***Results:*** The 1st group included 28 (57.1%) pts with SR to CRT, the 2nd group - 21 (42.9%) pts without it. Groups were comparable in terms of pre CRT-D implantation clinical and instrumental parameters, with the exception of MPS and gBPS parameters. The multivariate logistic regression with the inclusion factors such as baseline QRS duration, ΔQRS, female gender, non-ischemic CHF, baseline LVEF and right ventricular systolic pressure, LV lead lateral position, quadripolar LV lead, biventricular pacing percentage, MPS and gBPS indicators had shown that only Δphase standard deviation (PSD) (adjusted odds ratio [OR] 1.0508; 95% confidence interval [CI] 1.0021-1.1018; p=0.04), LV septal PSD (OR 1.0837; 95% CI 1.0235-1.1475; p=0.005) and interventricular dyssynchrony (IVD) (OR 1.0374; 95% CI 1.0114-1.0640; p=0.004) were CRT SR independent predictors. The univariate ROC-analysis showed that ΔPSD increase > 6.22° (AUC=0.758; p=0.0002), LV septal PSD increase > 23° (AUC=0.704; p=0.007) and IVD increase > 71.8 ms (AUC=0.770; p=0.0001) were predictors of the SR. ***Conclusion:*** LV mechanical dyssynchrony indicators (ΔPSD, IVD and LV septal PSD) assessed by MPS and gBPS were independently associated with CRT SR.

EP-0463

Potential utility of SPECT/CT with 99mTc-Tektrotyd for imaging of post myocardial infarction inflammation

J. Ilyushenkova, *S. Sazonova, A. Syrkina, A. Trusov, O. Mochula, A. Mishkina, V. Ryabov;*
RI Cardiology, Tomsk, RUSSIAN FEDERATION.

Aim/Introduction: There is a need to develop methods for post myocardial infarction (MI) inflammation monitoring. Scintigraphy with somatostatin receptor targeted radiotracers has prospects in this regard [1]. The purpose was to study the association of ^{99m}Tc-Tektrotyd uptake intensity in myocardial infarction MI area with heart contractility indices in 6 months period. ***Materials and Methods:*** Fourteen patients with acute ST-segment elevation

anterior MI (STEMI) were examined with ^{99m}Tc-Tektrotyd SPECT/CT, myocardial perfusion scintigraphy (MPS) at rest, cardiac magnetic resonance imaging (cMRI) and transthoracic echocardiography (TTE). Initial scintigraphic results were compared with 6-month TTE indices ***Results:*** On the 7th day after MI onset cardiac ^{99m}Tc-Tektrotyd uptake was found in 7 of 14 patients. Median of ^{99m}Tc-Tektrotyd SUVmax was 1.59 (1.38; 2.83), summed rest score (SRS) - 11 (5; 18), infarct size (by cMRI) - 13.15 (3.3; 32.2) %. ^{99m}Tc-Tektrotyd SUVmax strongly correlated with 6-month heart contractility indices (r=0.81, p<0.05 for end diastolic volume; r=0.61 p<0.05 for Δ end diastolic volume), with SRS (r=0.85, p<0.05) and infarct size (by cMRI) (r=0.79, p<0.05). ***Conclusion:*** The intensity (SUVmax) of ^{99m}Tc-Tektrotyd uptake in the area of recent MI directly depends on a size of ischemic myocardial injury and correlates with changes of heart contractility indexes within 6 months follow-up.This work is supported by Russian Science Foundation, grant № 22-25-00234
References: 1. Sazonova SI, Syrkina AG, Mochula OV, Anashbaev ZZ, Popov EV, Ryabov VV. Subacute myocardial infarction detected by technetium-99m-labeled somatostatin analog scintigraphy. J Nucl Cardiol. 2022;29(6):3586-3589. doi:10.1007/s12350-021-02644-4

EP-0464

99mTc-PYP Quantification Through SPECT/CT-Based Parameters in the Assessment of Cardiac Transthyretin Amyloidosis: Feasibility and Correlation with Semiquantitative Planar Indices

A. Lazar[1], *M. Mutuleanu*[1,2], *A. Jercan*[3], *S. Badelita*[3], *D. Coriu*[3,2], *M. Gherghe*[1,2];
[1]*Institute of Oncology "Professor Doctor Alexandru Trestioreanu", Bucharest, ROMANIA,* [2]*University of Medicine and Pharmacy "Carol Davila", Bucharest, ROMANIA,*
[3]*Fundeni Clinical Institute, Bucharest, ROMANIA.*

Aim/Introduction: Bone scintigraphy using ^{99m}Tc-labelled bone-seeking radiopharmaceuticals is currently used in standard practice for the imaging assessment of patients suspected for transthyretin-related cardiac amyloidosis (ATTR). Currently diagnosis is primarily based on visual scoring and semiquantitative indices, but the introduction of new, potential life-prolonging medication for ATTR has underlined the necessity for a better evaluation of the cardiac amyloid burden, thus raising the opportunity for its estimation through single photon emission computed tomography/computed tomography (SPECT/CT) quantification. The present study assesses if quantitative SPECT/CT measurements of absolute ^{99m}Tc-pyrophosphate (^{99m}Tc-PYP) uptake can accurately diagnose patients suspected for ATTR. ***Materials and Methods:*** This study prospectively evaluated 18 patients, mean age 47.44±8.15 years old, suspected for cardiac ATTR, who underwent ^{99m}Tc-PYP scintigraphy in our department between June 2022 to February 2023, both planar acquisition 1 hour post ^{99m}Tc-PYP administration and SPECT/CT imaging of the thoracic region 3 hours post-injection. All patients had also either serum or urine immunofixation performed. Obtained images were independently analysed by two physicians and semiquantitative planar indices and body-weight adjusted standardized uptake values (SUV), SUV_{max} and SUV_{peak}, were measured. A cardiac SUV retention index (CRI) was also calculated by normalizing the SUV_{max} value of the myocardium to the SUV_{mean} of bone tissue and paraspinal muscle. Obtained results were statistically correlated. ***Results:*** Out of the 18 patients we evaluated, 14 had myocardial uptake positive for ATTR on the planar scans, presenting a visual Perugini score over grade 2, which was then confirmed on the SPECT/CT examination. All three measured SPECT-based parameters, SUV_{max}, SUV_{peak} and CRI, correlated with the Perugini score and heart-to-contralateral lung ratio (p<0.05 for all). A receiver operating curve analysis was performed for all the measured quantitative parameters and it revealed that CRI had the best area under curve (AUC=0.964), obtaining a diagnostic CRI threshold of 0.681. Both SUV_{max} and SUV_{peak} exhibited good diagnostic performances as well, presenting AUC of 0.857, respectively, of 0.847. The patients with positive myocardial uptake underwent genetic testing, all of them having the Glu54Gln mutation. ***Conclusion:*** Quantitative SPECT/CT parameters can be used to assess patients suspected for cardiac ATTR, for a more accurate evaluation of myocardial uptake, this method offering good prospects in the appraisal of cardiac amyloid burden and treatment monitoring. CRI is the most feasible parameter for evaluating the cardiac amyloid burden, but both SUV_{max} and SUV_{peak} can be used with good diagnostic accuracy.

EP-0465

Utility of SPECT/CT in 99mTc-PYP scan in patients with suspected ATTR cardiac amyloidosis

B. Bardessi, *P. Canales, J. Quintana, I. Díaz, C. Waeger, F. Aguila, A. Hiplan, D. Jordan, N. Covarrubias, R. Jaimovich, K. Colorado;*
Pontificia Universidad Catolica de Chile, Santiago de Chile, CHILE.

Aim/Introduction: Myocardial scintigraphy labeled with Tc99m-pyrophosphate (PYP) has a high sensitivity and specificity in the diagnosis of ATTR-type cardiac amyloidosis. In static images qualitative - Perugini score (PS)- and semiquantitative -heart/contralateral thorax index- measurements are made . The main limitation in the interpretation of these images is the differentiation between the uptake of the radiopharmaceutical in the vascular pool vs myocardium. The objective of our study was to compare the values assigned in static images PS with visual interpretation in SPECT/CT images in order to see the correlation between PS assigned to each patient and the outcome of the visual analysis in SPECT/CT images. ***Materials and Methods:*** We reviewed all pyrophosphate myocardial scintigrams performed in our center (50 exams). Static images and SPECT/CT were evaluated after an hour of injection of the radiotracer.The PS in the static image of all the patients was compared with the result of SPECT/CT image (positive qualitative evaluation for uptake of the radiotracer in myocardium that exceeds rib uptake or negative for uptake in myocardium) ***Results:*** Of 50 patients evaluated, 8 were reported with Perugini Score 0 and 33 with PS 1, all of them presented vascular pool uptake on SPECT/CT images (true negatives). 6 patients had PS 3, of which 5 presented uptake in myocardium in SPECT/CT images (true positives) and 1 presented uptake in vascular pool. When evaluating with Perugini 2 (3 patients), only 1 of them presented myocardial uptake in the SPECT/CT, the other 2 presented activity in the vascular pool, this coincides with what has been reported in the literature (up to 2/3 of exams with grade 2 PS are false positive or equivocal findings when performing SPECT/CT). ***Conclusion:*** The utility of SPECT/CT in patients with suspected ATTR amyloidosis is greater in PS grade 2, since the tomographic image improves diagnostic accuracy by allowing a more precise visualization of the distribution of the radiotracer. For this reason, routine SPECT/CT is recommended for all PYP myocardial scintigrams. ***References:*** Avalon JC, Fuqua J, Deskins S, Miller T, Conte J, Martin D, Marano G, Yanamala N, Mills J, Bianco C, Patel B, Seetharam K, Raylman R, Sengupta PP, Hamirani YS. Quantitative single photon emission computed tomography derived standardized uptake values on 99mTc-PYP scan in patients with suspected ATTR cardiac amyloidosis. JNucl _ heart 2023 Feb;30(1):127-139 doi : 10.1007/s12350-022-02988-5. Epub 2022 Jun 2. PMID: 35655113

EP-0466

Potential of glucose metabolic rate obtained from dynamic18F-FDG PET/CT scan in differentiating cardiac sarcoidosis from physiological accumulation

M. Nagao[1], *Y. Shirai*[1], *A. Yamamoto*[1], *K. Kaneko*[1], *A. Sakai*[1], *N. Komura*[2], *S. Sakai*[1];
[1]*Tokyo Women's Medical University, Tokyo, JAPAN,*
[2]*Siemens Health Care, Tokyo, JAPAN.*

Aim/Introduction: ^{18}F-Fludeoxyglucose PET (FDG-PET) is a useful tool in the diagnosis and therapeutic monitoring of cardiac sarcoidosis (CS). In order to suppress physiological glucose metabolism in the myocardium, patients are forced to prolonged fasting and restriction of glucose intake. Nevertheless, physiological accumulation is often difficult to distinguish from active CS. The glucose metabolic rate (MRglu mg/min/100ml) is a new quantification of glucose metabolic kinetics derived from dynamic FDG-PET scan with a silicon photomultiplier. We investigate the potential of MRglu in differentiating active CS from physiological accumulation. ***Materials and Methods:*** One hundred CS patients and sixty-three cancer-bearing patients who underwent four sets of dynamic FDG-PET scan with a silicon photomultiplier from 30 minutes after FDG administration were enrolled. Preparation included 18 hours of fasting and restricted glucose intake for the former and 6 hours of fasting for the latter. Myocardial uptake of SUVmax 2.7 or greater was defined as active CS in the former (Ref. 1) and physiological accumulation in the latter. Parametric analysis of dynamic FDG-PET data was performed on these lesions, and SUV and MRglu were calculated. ***Results:*** Thirty-four of 100 CS patients (34%) had active CS, with SUV and MRglu of 4.1±1.5 and 1.9±1.1 mg/min/100ml. Twenty-eight of 63 cancer-bearing patients (44%) had physiological accumulation, with SUV and MRglu of 4.9±2.1 and 2.9±1.6 mg/min/100ml. Both SUV and MRglu were significantly greater for physiological accumulation than active CS ($p<0.005$). MRglu and SUV showed a significant positive correlation in both groups [CS: Pearson r, 0.841 (95%CI 0.775-0.889), $p<0.0001$; Physiological accumulation: Pearson r, 0.916 (95%CI 0.881-0.942), $p<0.0001$]. The correlation coefficient was significantly greater for physiological accumulation than active CS ($p=0.0072$). Receiver-operating-characteristic analysis revealed that the area under the curve for active CS diagnosis was 0.626 for SUV, 0.721 for MRglu, and 0.741 for the ratio of MRglu to SUV, respectively. ***Conclusion:*** For both active CS and physiological accumulation, MRglu was significantly positively correlated with SUV. However, the correlation coefficient was greater for physiological accumulation than active CS. The use of MRglu improved the discrimination between active CS and physiological accumulation compared to SUV alone. ***References:*** 1. Kaneko K, Nagao M, Yamamoto Y, et al. FDG uptake patterns in isolated and systemic sarcoidosis. J Nucl Cardil 2022. DOI: 10.1007/s12350-022-03106-1.

EP-0467

Relationship between the distribution of diphosphonate uptake and changes in cardiac MRI in patients with transthyretin cardiac amyloidosis

L. Santamaría-Chico, *K. Velásquez-Díaz, M. Mitjavila-Casanovas, P. Soares-Meneses, I. Obedkova, M. Grajeda-Gallardo, I. Garrido-Solesio, M. Pastrana-Ledesma, F. de Haro-del Moral;*
Hospital Universitario Puerta de Hierro, Madrid, SPAIN.

Aim/Introduction: Transthyretin cardiac amyloidosis (ATTR) is a myocardial disease caused by the deposition of altered transthyretin fibrils, either naturally or hereditary. In recent decades, it has been seen that 99mTc-diphosphonates bind to these protein deposits in such a way that scintigraphy allows us to diagnose them. However, we do not yet know the role of diphosphonate uptake in the quantification of myocardial amyloid burden. This study aims to assess the distribution of the deposit in the different segments and its relationship with changes in cardiac MRI. ***Materials and Methods:*** We studied 24 patients (22 men and 2 women) aged between 60 and 92 years (mean 77.58), diagnosed with ATTR, who presented a grade 3 of Perugini in cardiac scintigraphy. Taking advantage of the intense myocardial uptake, a G-SPECT was performed to obtain a polar map of the distribution of uptake in the 17 segments in which the myocardium is divided, and were compared with the phenomenon of altered kinetics in the delayed enhancement sequences of cardiac MRI. ***Results:*** The maximum uptake in the G-SPECT was observed in segments 3 (basal inferoseptal) (92-100%) and 9 (medial inferoseptal) (79-100%). Intense uptake was also observed in segments 2 (basal anteroseptal) and 8 (medial anteroseptal). The segment with the lowest uptake was 12 (medial anterolateral) (0 -75%) and in some patients segments 1, 5, 6, 7, 10, 11 and 12 did not show uptake. Regarding the phenomenon of altered kinetics in the late enhancement sequences of the cardiac MRI, the least affected segments were the apical ones, being very variable in the rest of them. On the contrary, the deposit in the apex was very variable (between 6 and 87%). After gadolinium administration, global myocardial enhancement, typical of cardiac amyloidosis, was observed in all patients. ***Conclusion:*** Most patients had greater uptake of diphosphonate on the septal side, and the degree of uptake does not correlate with the phenomenon of altered kinetics in late enhancement sequences of cardiac MRI. ***References:*** 1. Castillo E, Bluemke DA. Cardiac MR imaging. Radiol Clin N Am. 2003;41:17-28. 2. Dembo LG, Shifrin RY, Wolff SD. MR imaging in ischemic heart disease. Radiol Clin N Am. 2004;42:651-73. 3. Fathala AL. Cardiac magnetic resonance imaging. A teaching atlas with emphasizing curent clinical indications. J Saudi Heart Association. 2011;23:255-66.

EP-0468

Using reprojected planar images from 99mTc-labelled diphosphonate scintigraphy for visual scoring of transthyretin amyloidosis: validating a novel ring-configured cadmium zinc telluride gamma camera

I. Ceric Andelius[1,2], *D. Minarik*[1,2], *R. Fridriksdóttir*[3], *F. Hedeer*[3,4], *A. Stenvall*[1,4], *E. Trägårdh*[2,3], *J. Oddstig*[1,2];
[1]*Radiation Physics, Skånes University Hospital, Lund/Malmö, SWEDEN,* [2]*Department of Translational Medicine and Wallenberg Centre of Molecular Medicine, Lund University, Malmö, SWEDEN,* [3]*Department of Clinical Physiology and Nuclear Medicine, Lund/Malmö, SWEDEN,* [4]*Department of Clinical Sciences, Lund University, Lund, SWEDEN.*

Aim/Introduction: Myocardial uptake due to cardiac amyloidosis in planar ^{99m}Tc-labelled diphosphonate (^{99m}Tc-DPD) scintigraphy is widely accepted as a diagnostic tool for detecting transthyretin amyloidosis (ATTR-amyloidosis) with high sensitivity and specificity. Recently ring-configurated cadmium zinc telluride (CZT) single-photon emission computed tomography-computed tomography (SPECT/CT) systems have been introduced. These systems only enable reprojected anterior and posterior planar images generated from reconstructed SPECT-data. When scoring amyloidosis planar imaging and SPECT/CT are recommended by American Society of Nuclear Medicine and European Association of Nuclear Medicine. We aimed to compare planar versus reprojected planar images to validate the reprojected images into

clinical practice. ***Materials and Methods:*** 30 patients referred to clinically indicated amyloidosis scintigraphy were scanned on both a conventional gamma camera and a ring-configurated CZT gamma camera. Planar imaging from the conventional gamma camera was compared to reprojected planar images (reconstructed using block-sequential regularized expectation maximization (BSREM) with 10 iterations, 10 subsets, RDP regularisation with beta 0.2, 0.3, 0.4, 0.6 and 0.8 and gamma 4). SPECT/CT from the ring-configurated CZT system (reconstructed with BSREM 10 iteration 10 subsets beta 0.4 and gamma 2) was used for anatomical correlation when planar scintigraphy was positive. The images were evaluated regarding image quality and Perugini score in a blinded fashion by three nuclear medicine physicians. The contrast to noise ratio ($CNR=ROI_{rib,mean}-ROI_{background,mean}/sqrt(SD_{ROI,rib,mean}^{2}+SD_{ROI,background,mean}^{2})$) was analysed quantitatively by placing a ROI in the rib and the background. ***Results:*** There was no significant difference between the planar and reprojected images regarding image quality and inter observer variability (p= 0.6 and 0.4) and Perugini score and inter observer variability (p= 1 and 0.7) which enables a clinical reconstruction within the beta range 0.2-0.8. The highest image quality scores were given for beta 0.2 and 0.4. Higher CNR was observed for reprojected planar images compared to planar scintigraphy. Reprojected images reconstructed using beta 0.4 yielded slightly higher CNR compared to other beta factors. ***Conclusion:*** Reprojected planar images reconstructed with BSREM can be used to score ATTR-amyloidosis. The 3D data generated from the ring configurated CZT system is sufficient for the assessment of ATTR-amyloidosis.

EP-0469

Different extracardiac uptake, evidenced on 99mTc-HDP scintigraphy, in various types of cardiac amyloidosis

M. Starace[1], *F. Cappelli*[2], *F. Perfetto*[3], *E. Costanzo*[4], *R. Sciagrà*[5], *V. Berti*[1];
[1]*Nuclear Medicine Unit, Department of Experimental and Clinical Biomedical Sciences "Mario Serio", University of Florence, 50134 Florence, Italy., florence, ITALY,* [2]*Tuscan Regional Amyloid Centre, Careggi University Hospital, Florence, Italy, florence, ITALY,* [3]*Tuscan Regional Amyloidosis Centre, Careggi University Hospital, Florence, Italy., florence, ITALY,* [4]*Department of Nuclear Medicine, Azienda Ospedaliero-Universitaria Careggi, Largo Brambilla 3, 50134, Florence, Italy., florence, ITALY,* [5]*Nuclear Medicine Unit, Department of Experimental and Clinical Biomedical Sciences "Mario Serio", University of Florence, 50134 Florence, Italy, florence, ITALY.*

Aim/Introduction: Cardiac amyloidosis is a rare form of restrictive cardiomyopathy caused by the deposition of amyloid fibrils at the cardiac level. The causative amyloid fibril deposits are of monoclonal light chain (AL) or transthyretin (ATTR) types. ATTR amyloidosis may be wild-type or associated with variants in the transthyretin gene. Increased cardiac uptake on ^{99m}Tc-HDP scintigraphy has showed diagnostic values in cardiac amyloidosis but extracardiac uptake has been poorly studied. We evaluated if extracardiac uptake was observed in ^{99m}Tc-HDP scintigraphy in different amyloidosis types. ***Materials and Methods:*** Results of bone scintigraphy were analyzed from 115 patients with cardiac amyloidosis. Of these, 90 patients had cardiac amyloidosis ATTR wild-type (wt), 13 had cardiac amyloidosis ATTR mutated (m) and 12 had amyloidosis AL. In these three groups, we considered the Perugini score and then we observed if ^{99m}Tc-HDP uptake was present at the level of the soft tissues (particularly the limbs), lungs, liver, abdominal wall, and right ventricle. For each parameter we created continhgency tables and applied a chi-square test. Statistical significance was set at p<0,05. ***Results:*** Extracardiac uptake in ^{99m}Tc-HDP scintigraphy was differently distributed in the 3 groups. In particular, soft tissues and liver uptake is more evident in amyloidosis AL (41,7% and 16,7% respectively), compared with ATTRwt (soft tissue uptake 36,7%, hepatic 0%) and ATTRm (soft tissue uptake 38,5%, hepatic 7,7%). Accumulation in the abdominal wall and right ventricle is more represented in amyloidosis ATTRm (69,2% and 61,5% respectively) compared with amyloidosis ATTRwt (adbominal wall uptake 64,4%, right ventricle 51,1%) and amyloidosis AL (abdominal wall uptake 25%, right ventricle 16,7%). Finally, pulmonary uptake is more pronounced in amyloidosis ATTRwt (67,8%) than in amyloidosis ATTRm (61,5%) and amyloidosis AL (25%). ***Conclusion:*** ^{99m}Tc-HDP scintigraphy can be used for visualization of extracardiac uptake in the various types of amyloidosis and could help direct the diagnosis toward a specific type of the disease.

EP-0470

The Relationship of Tc-99m Pyp Scıntıgraphy Parameters wıth Prognosis and Life Expectation ın Cardiac Amiloidosis

Ü. Aksu[1], *E. Akgün*[1], *S. G. Yaran*[1], *M. Ayer*[2], *A. Güler*[3], *G. B. Güler*[3], *A. Türkvatan*[4], *M. Kaya*[1], *B. E. Akkas*[1];
[1]*Başakşehir Çam and Sakura Hospital Clinic of Nuclear Medicine, Istanbul, TÜRKIYE,* [2]*Başakşehir Çam and Sakura Hospital Clinic of Hematology, Istanbul, TÜRKIYE,* [3]*Mehmet Akif Ersoy Thoracic and Cardiovascular Surgery Hospital Clinic of Cardiology, Istanbul, TÜRKIYE,* [4]*Mehmet Akif Ersoy Thoracic and Cardiovascular Surgery Hospital Clinic of Radiology, Istanbul, TÜRKIYE.*

Aim/Introduction: The aim of the study is to determine cardiac amyloidosis involvement with 99mTc-PYP scintigraphy and to investigate the relationship between scintigraphic parameters and survivals in patients investigated for transtiretin cardiac amyloidosis (TTR CA). ***Materials and Methods:*** A total of 127 patients (64 M, 63 F mean age: 60.5) who were referred to our clinic for 99mTc-PYP scintigraphy with suspected CA were included in the study. Clinical and laboratory data, ECG, ECHO, MR findings were noted. Serum Kappa/Lambda ratio, immunofixation test results, and biopsy results were noted for light chain (AL) amyloidosis. Counts were taken from the heart (H) and from the contralateral side of the heart (CL) with the same size ROI(Region of interest) on planar images. Patients were categorized in 3 groups according to H/CL ratio (≤1: Group 1, n=18; 1-1.5: Group 2, n=104; >1.5: Group 3, n=5). Those with heart/CL ratio > 1.5 and/or Perugini score GRADE 2-3 and negative hematological tests for AL amyloidosis were accepted as TTR CA. The PYP scintigraphy results of the patients were compared with clinical data, and survivals. ***Results:*** Group 1 patients were considered negative for CA either ATTR and AL, In group 2, 13 patients (17%) were diagnosed with AL CA. There was no TTR CA. The diagnosis was confirmed with biopsy in 4 of them. During follow-up 4 of these patients dead because of AL CA. In Group 3, all of 5 patients were accepted as TTR CA. One of them dead because of TTR cardiac involvement. Other six patients dead from cardiac causes other than CA (Group 1 n= 0 Group 2 n=6). When H/CL ratio cut-off was chosen as 1.3, mortality rates increased significantly along with H/CL ratios (21% 7/33 vs 4.2% 4/94; p=<0,05). Mortality rates were 30.7% in AL CA cases, 20% in TTR CA cases, and 5.5% in cases without cardiac amyloidosis involvement. ***Conclusion:*** Our findings support that AL CA has a worse prognosis than TTR-CA. It shows that mortality rate increases significantly myocardial radiopharmaceutical uptake on PYP scintigraphy. Scintigraphy findings are prognostic as well as diagnostic in CA. ***References:*** Poterucha TJ et al. Diagnosing Transthyretin Cardiac

Amyloidosis by Technetium Tc 99m Pyrophosphate: A Test in Evolution. JACC Cardiovasc Imaging. 2021 Jun;14(6):1221-1231. Connors LH et al. Cardiac amyloidosis in African Americans: comparison of clinical and laboratory features of transthyretin V122I amyloidosis and immunoglobulin light chain amyloidosis. Am Heart J. 2009 Oct;158(4):607-14.

EP-0471

Is there any relation between "Red flags" for cardiac amyloidosis, extracardiac uptake and the type of cardiac amyloidosis?

A. Roteta Unceta Barrenechea[1,2], *F. Asensio Pérez*[3], *G. Martínez Arias*[1], *D. Nogueira Souto*[1], *M. Parra Rina*[1], *T. Escalera Temprado*[1], *Y. Saker Diffalah*[1], *M. Delgado Castro*[1], *G. Guzmán Prudencio*[1], *L. Tardin Cardoso*[1], *P. Razola Alba*[1], *A. Andrés Gracia*[1,2];
[1]*UCMHMNA - Clinic Hospital "Lozano Blesa", Zaragoza, SPAIN,* [2]*IIS-Aragon, Zaragoza, SPAIN,* [3]*Universidad de Zaragoza, Zaragoza, SPAIN.*

Aim/Introduction: To identify the number and location of extracardiac uptake in patients undergoing bone scintigraphy for suspected cardiac amyloidosis (CA). In addition, we will study possible statistical associations between the "Red Flags" for cardiac amyloidosis and the different types of extracardiac uptake. ***Materials and Methods:*** Bone scans for suspected cardiac amyloidosis with extracardiac uptake (regardless of the final diagnosis made by noninvasive diagnosis by clinicians -table 1-) between 2014 and 2022 were included. Clinical "Red Flags" (carpal tunnel syndrome, atraumatic rupture of the biceps brachii tendon and lumbar canal stenosis) have been collected from the electronic medical history. A descriptive and an analytical study will be carried out, in which the possible association between the type of uptake and the "Red Flag" type will be determined by calculating the Habermann's corrected typed residuals. ***Results:*** A total of 280 patients were reviewed, 31 of whom met the inclusion criteria. According to the descriptive study, the prevalence of extracardiac uptake was 11.1% (31); 9 patients had pulmonary, 6 hepatic and 21 soft tissue uptake. In respect of the 9 pulmonary uptakes (3 unknown-origin CA, 4 ATTR and 2 non-CA), 2 presented carpal tunnel syndrome and were classified as unknown-origin CA and ATTR. None of the 6 hepatic uptakes presented "Red Flag" and all patients were classified as non-CA. Regarding to the 21 soft-tissue uptakes (8 unknown-origin CA, 10 ATTR, 1 AL and 2 non-AC), 7 presented carpal tunnel syndrome (2 unknown-origin CA and 5 ATTR) and 1 atraumatic rupture of the biceps brachii tendon that was diagnosed as ATTR. In the analytical study, there was statistical association between the presence of carpal tunnel syndrome and unknown-origin CA, the presence of carpal tunnel syndrome and ATTR, the absence of carpal tunnel syndrome and no CA. We also found a statistical association between the presence of pulmonary uptake in bone scintigraphy and ATTR and its absence with non-CA. Finally, we detected a statistical association between the presence of soft tissue uptake in bone scintigraphy and unknown-origin CA or ATTR, and the absence with non-CA. ***Conclusion:*** The association between the different clinical Red Flags and the type of extracardiac uptake cannot be concluded. However, in our study the presence of carpal tunnel syndrome, soft tissue and pulmonary uptake pointed to CA (ATTR or unknown CA), whereas hepatic uptake was not related to CA and might be caused by other etiologies.

EP-0472

Is T-DM1 cardiotoxicity close monitoring relevant in palliative breast cancer patients? A single center experience using equilibrium radionuclide ventriculography (ERNV)

D. Silva*, H. Duarte, P. Leite-Silva, J. F. Ferro, I. Próspero, D. Barbosa, S. F. Castro, G. Ferreira, J. P. Teixeira, I. L. Sampaio;*
Instituto Português de Oncologia do Porto Francisco Gentil, Porto, PORTUGAL.

Aim/Introduction: Ado-trastuzumab emtansine (T-DM1) is a standard of care option for patients with advanced breast cancer with positive human epidermal growth factor receptor 2 (HER2). Due to its association with cardiotoxicity, left ventricle ejection fraction (LVEF) is evaluated before and during the treatment period using either equilibrium radionuclide ventriculography (ERNV) or echocardiogram (ECHO). Besides this recommendation, published "real life studies" with palliative patients showed low levels of cardiac toxicity with none/very few cases of treatment interruption for that reason, and disease progression being the number one cause of T-DM1 discontinuation. The aim of this study was to evaluate systolic and diastolic dysfunction (which is thought to be an earlier predictor of cardiac malfunction) over T-DM1 treatment time in our center. ***Materials and Methods:*** We included all patients (n= 40) who started palliative treatment with T-DM1 from 1/1/2018 to 31/12/2022 whose cardiotoxicity was assessed by ERNV during the treatment period. Patients' sequential ERNV tests (from baseline until 12 months of treatment or discontinuation) were re-analysed using Xeleris™-4-DR GE workstation and LVEF, peak filling rate (PFR) and time to peak filling rate (TPFR) values were collected. Patients' demographic and clinical data were recorded and analysed. Wilcoxon signed-rank test was performed in R version 4.0.5 to access any statistically significant variation over time. ***Results:*** Patients group presented a median age of 55 years old (20-80), ECOG PS 0-1, and a median treatment period of 10 months (3-43). Median baseline LVEF value was 61% (50-72%) and none of the patients presented a decrease of LVEF value equal/superior to 10 percentage points plus LVEF<50%. Four patients (10%) discontinued T-DM1 due to other toxic side effects (hematologic, hepatic, and cutaneous), and the other 90% thanks to disease progression (namely progression of bone, brain, and liver disease). Regarding diastolic parameters there weren't significant differences over time, all patients demonstrated normal PFR and TPFR values during the treatment period. ***Conclusion:*** The present study has some limitations due to small sample size. Nevertheless, our results endorse T-DM1's satisfactory safety profile of published studies. The vast majority of patients discontinued treatment due to disease progression before evidence of drug-induced cardiotoxicity. Pertinence of close cardiotoxicity monitoring must be questioned in the setting of breast cancer palliative treatment with T-DM1.

EP-0473

Diagnostic Performance of Cardiac Magnetic Resonance and Cardiac Scintigraphy in patients with clinical suspicion of Transthyretin Cardiac Amyloidosis

M. Pudis[1], *P. C. Notta*[1], *L. Gràcia-Sánchez*[1], *I. E. Sánchez-Rodríguez*[1], *E. Claver-Garrido*[2], *C. Diez-López*[2], *J. González-Costello*[2], *V. Carrero-Vasquez*[1], *C. Martínez-Ramos*[1], *S. Bondia-Bescós*[1], *B. Hervás-Sanz*[1], *J. Diaz-Moreno*[1], *M. Cortés-Romera*[1];
[1]*Nuclear Medicine - PET (IDI), Bellvitge University Hospital, L'Hospitalet de Llobregat, Barcelona, SPAIN,* [2]*Cardiology Department, Bellvitge University Hospital, L'Hospitalet de Llobregat, Barcelona, SPAIN.*

Aim/Introduction: The aim of this study was to evaluate and compare the diagnostic efficacy of two imaging techniques - Cardiac Scintigraphy (CS) with ^{99m}Tc-HMDP and Cardiac MRI (CMRI) - in the diagnosis of cardiac amyloidosis due to transthyretin (CA-ATTR) using statistical parameters. ***Materials and Methods:*** This study retrospectively analyzed patients (p) who were clinically suspected of having cardiac amyloidosis caused by transthyretin (CA-ATTR) and underwent both cardiac scintigraphy (CS) and cardiac magnetic resonance imaging (CMRI) as part of their diagnostic workup between 2016 and 2022. Patients with a final clinical diagnosis of CA-ATTR were included in the analysis. The study calculated the sensitivity (S), specificity (Sp), positive predictive value (PPV), and negative predictive value (NPV) of both diagnostic techniques. These metrics were used to evaluate the diagnostic performance of CS and CMRI in identifying CA-ATTR in this patient population. ***Results:*** A total of 103p with suspected CA-ATTR underwent both imaging techniques. Among them, 17p were found to be positive for CA-ATTR by either one or both imaging techniques. However, five of the 17p who were diagnosed with CA-ATTR by MRI were later found to have other types of CA-AL (n=3) or CA-AA (n=2) upon further evaluation and were excluded from the analysis. Out of the remaining 12p who had a final clinical diagnosis of CA-ATTR, 6p were diagnosed concordantly by both imaging techniques. 3p were diagnosed with CA-ATTR only by cardiac scintigraphy, while MRI revealed alternative diagnoses of hypertrophic cardiomyopathy or Fabry disease. The remaining 3p were diagnosed only by MRI, all of whom were recipients of domino liver transplant DLT from patients with familial amyloid polyneuropathy (FAP) and in the early stage of the disease. There were no differences between the S=75% and Sp=100% or PPV=100% and NPV=96.8% of both imaging techniques when considering the same number of false negatives (n=3) and false positives (n=0). ***Conclusion:*** CS and CMRI have proven to be useful techniques in the diagnostic workup of CA-ATTR. Both techniques have high sensitivity and high positive predictive value. CS seems to be more reliable in most of the patients with an exception of receivers of DLT from FAP patients, where CMRI was able to detect depositions in an early stage.

EP-0474

Usefulness of semi-quantitative analysis in cardiac amyloidosis.

J. Venero Chaparro, *M. Gallego Márquez, M. Sánchez Torrente, F. Garí Martínez, D. Guirado Llorente, M. Martínez-Valle Torres; Hospital Clínico San Cecilio, Granada, SPAIN.*

Aim/Introduction: This study was designed to evaluate the quantification of myocardial uptake of 99mTc-HDP in patients with suspected amyloidosis and to establish an optimal threshold to differentiate between transthyretin (ATTR) and light chain (AL) deposition. ***Materials and Methods:*** An observational, descriptive, cross-sectional analysis was performed in which, retrospectively, 75 patients with suspected cardiac amyloidosis were selected between 2022 and 2023, with an anteroposterior planar scintigraphic study 2 hours after radiopharmaceutical injection. Patients were classified according to the Perugini scale into 3 uptake grades. The quantification test result, R, is defined as the ratio between the number of counts obtained in the ROI corresponding to the heart (H) and the number of counts in the ROI corresponding to the contralateral thorax (CL). The test is considered positive for ATTR if R=H/CL > TH. The paper analyses the effect of the choice of TH on the diagnostic ability of the test, determining the values of sensitivity, specificity, positive predictive value, negative predictive value and diagnostic accuracy using Monte Carlo methods. Furthermore, in order to characterise the uncertainties, a study of the dependence of the results on the observer is carried out in the semi-quantitative analysis. For this purpose, 5 patients are randomly taken from the sample and analysed by 4 different nuclear medicine physicians, who follow the process of defining the ROIs and determining R from them. An average uncertainty for the R value is established from the standard deviations calculated from the four R values for each patient. ***Results:*** For the determination of ATTR of grade ≥1, the optimal threshold, obtained from the point where sensitivity and specificity are equal, is found to be TH=1.3. For this threshold value, a sensitivity and specificity of 0.875 ± 0.003 are obtained; whereas, for the commonly used threshold, TH=1.5, a sensitivity of 0.657 ± 0.006 and a specificity of 0.973 ± 0.001 are obtained. All uncertainties correspond to a coverage factor k=2. The average inter-observer variability (standard deviation) in the calculation of R is 6.9%, with a range between 1.5% and 16%. ***Conclusion:*** The semi-quantitative planar imaging analysis used in the study is a reliable method with high sensitivity and specificity to differentiate transthyretin (ATTR) from light chain (AL) deposition, with an optimal threshold of 1.3 in the H/CL ratio for the sample studied.

EP-0475

Ventricular Function Patterns In Ttr Cardiac Amyloidosis: Can We Select Patients For Resynchronization Therapies Using ^{99m}TC-DPD Gspect?

F. Sebastián Palacid, *B. Pérez López, M. García Aragón, R. Zambrano Infantino, N. Álvarez Mena, M. Alonso Rodríguez, J. Gómez Hidalgo, C. Gamazo Laherrán, R. Ruano Pérez; Hospital Clínico Universitario Valladolid, Valladolid, SPAIN.*

Aim/Introduction: To evaluate amyloid deposition and ventricular function patterns in ATTR using ^{99m}Tc-DPD gated-SPECT-CT. ***Materials and Methods:*** Analysis of 34 patients with a gammagraphic diagnosis of TTR amyloidosis (24 males and 10 females; mean age: 83.5 ± 6.28 years; 85.3% Perugini grade 3) who underwent a GATED SPECT-CT study focused on the thoracic region. Images were processed and quantified with Myovation Evolution GE® and Emory Cardiac Tool Box GE® softwares. Demographic variables, left ventricular function variables and myocardial uptake of 99mTcDPD were analyzed by SPSS.We use normal phase values (peak, bandwidth and kurtosis) established by Chen et al in perfusion studies[1]. ***Results:*** GATED SPECT-CT study was performed in all patients. 85.3% were classified as Grade 3 according to Perugini grade. Mean SUV_{max} was 9,65±2,87, being grade 3 Perugini the group with higher SUV_{max} (p=0.004).Left ventricular ejection fraction (EF) and volumes were obtained, being mean EF of 51.3±15.5%. 16 patients (47%) had an EF <50%.13 patients (38.2%; 6 females and 7 males) presented abnormal phase peak, kurtosis and bandwidth values (mean phase peaks were 122.1 ± 24º in men and 151.4 ± 26.8º in women), indicating dyssynchrony.When looking for differences within sex, women showed worse peak phase values than men (p=0.004). In addition, in this group a negative correlation was found between EF and bandwidth (p=0.002).In the male group, a negative correlation between phase peak and kurtosis (p=0.004) and a positive correlation between the degree of Perugini and age (p=0.001) were demonstrated. Indeed, males with pathological peak phase (7/24) showed a positive correlation between the degree of Perugini and age (p=0.001) ***Conclusion:*** According to our data, using ^{99m}Tc-DPD GATED SPECT-CT is a feasible technique that allows us a quantitative assessment of amyloid deposition as

well as left ventricular function in the same study. This technique might allow the identification of patients with impaired EF and ventricular synchrony susceptible to cardiac resynchronization therapy, 38.2% of patients in our study. However, further studies are needed to confirm the results. ***References:*** [1] Chen J, García EV, Bax JJ, Iskandrian AE, Borges-Novo S, Soman P. SPECT myocardial perfusion imaging for the assessment of left ventricular mechanical dyssinchrony. J Nucl Cardiol 2011;18:685-94.

EP-28

e-Poster Area

B: Imaging Clinical Studies -> B4 Cardiovascular Imaging Clinical Study -> B44 Other Cardiovascular Imaging (including Plaque)

EP-0476

The Utility of Right Ventricular Myocardial Strain Ratio Estimated by Ammonia Positron Emission Tomography to Stratify the Risk for Coronary Artery Disease

A. Yamamoto[1], *M. Nagao*[1], *M. Kawakubo*[2], *R. Nakao*[1], *Y. Matsuo*[1], *A. Sakai*[1], *M. Momose*[1], *K. Kaneko*[1], *K. Fukushima*[3], *J. Yamaguchi*[1], *S. Sakai*[1];
[1]*Tokyo Women's Medical University Hospital, Tokyo, JAPAN,* [2]*Kyushu University, Fukuoka, JAPAN,* [3]*Fukushima Medical University, Fukushima, JAPAN.*

Aim/Introduction: We have made it possible to measure right ventricular myocardial strain (RVMS), adapting a feature–tracking technique to electrocardiography–gated high–resolution ^{13}N–ammonia positron emission tomography (NH_3–PET). We indicated that RVMS identified right coronary artery territory ischemia in patients with ischemic heart disease (IHD). Previous studies showed that RV function was a prognostic factor of cardiovascular events. The aim of this study was to investigate the potential of RVMS estimated by NH_3–PET as a prognostic factor in patients with IHD. ***Materials and Methods:*** Between January 2017 to January 2021, 577 consecutive patients performed resting and stressed myocardial NH_3–PET because of known or suspected IHD were enrolled. Patients with congenital heart disease, a transplanted heart, adenosine ineffectiveness, or poor imaging that could not be analyzed were excluded.RVMS in the free wall was measured by a feature–tracking technique on the NH_3–PET images of horizontal long–axis slices, and the RVMS ratio (RVMSR) was defined as RVMS at stress divided by that at rest. The endpoint was major adverse cardiac events (MACEs) comprising cardiac death or hospitalization due to heart failure. The patients were divided into two groups using the RVMSR cutoff value obtained by receiver–operating characteristic (ROC) analysis, and event–free survival was analyzed by Kaplan–Meier and log–rank test. For imaging parameters, hazard ratios (HR) and 95% confidence intervals (CI) were calculated using the Cox proportional hazards regression model. ***Results:*** 480 patients were retrospectively analyzed. The ROC analysis demonstrated a cutoff of 1.006 for MACE with RVMSR, and showed that area under the curve, sensitivity, and specificity were 0.84, 84% and 82%. Patients with RVMSR <1.006 had a significantly higher MACE rate than those with RVMSR ≥1.006 (p<0.0001). Multivariate analysis indicated that RVMSR was an independent marker that could predict MACE in imaging parameters (HR: 454, 95% CI: 40–6727, p <0.0001). ***Conclusion:*** RVMSR is a prognostic factor for MACE in patients with IHD.It is possible to predict cardiovascular events from the RV function assessed by routine NH_3–PET without additional imaging or radiation exposure.

EP-0477

The relationships between quantitative CCTA and dynamic CZT SPECT in patients with non-obstructive coronary artery disease

K. Zavadovsky[1], *A. Maltseva*[1], *R. Dorzhieva*[2], *A. Mochula*[1], *K. Kopeva*[1], *E. Grakova*[1];
[1]*Cardiology Research Institute, branch of the Federal State Budgetary Scientific Institution «Tomsk National Research Medical Center of the Russian Academy of Sciences», Tomsk, RUSSIAN FEDERATION,* [2]*Siberian State Medical University of the Ministry of Health of the Russian Federation, Tomsk, RUSSIAN FEDERATION.*

Aim/Introduction: Nowadays, CCTA is a well-established method for identification of coronary artery disease in patients with low pre-test probability. Most of these patients have non-obstructive coronary artery disease (NOCAD) and microvascular dysfunction. However, the data about the relationships between coronary plaque composition and the values of myocardial blood flow and reserve is lacking. The aim of the study is to assess the relationships between quantitative CCTA variables and dynamic CZT SPECT in NOCAD patients. ***Materials and Methods:*** Based on CCTA results, patients with NOCAD (stenosis <50%) were included in the study. In addition to stenosis severity, quantitative analysis of coronary atherosclerosis was performed by estimation of the following variables (in mm3 and in %): general plaque volume (GPV), soft tissue plaque volume (STPV), fibrous plaque volume (FPV), calcified plaque volume (CPV). All patients underwent dynamic SPECT CZT with the assessment of stress and rest myocardial blood flow (MBF), myocardial flow reserve (MFR) [1]. The 1-tissue-compartment model with attenuation correction was used for quantitative analysis. ***Results:*** The study included 55 patients (31 men, age 57.0±8.8 years). Quantitative CCTA parameters were the following: GPV 42.4 (0.0;138.1) mm3, 2.5 (0.0;7.2)%; STPV 0.1 (0.0;9.5) mm3, 0.006 (0.0;0.4)%; FPV 34.0 (0.0;113.5) mm3, 1.9 (0.0;5.2)%; CPV 3.5 (0.0;20.5) mm3, 0.2 (0.0;0.98)%. Based on SPECT CZT results, stress MBF was 1.59 (1.27;1.93) ml/min/g, rest MBF - 0.7 (0.5;0.94) ml/min/g and MFR - 2.26 (1.61;3.01). The Spearman correlation showed that stress MBF had negative relationships with GPVmm3 (ρ=-0.38, p=0.008), GPV% (ρ=-0.35, p=0.01), STPVmm3 (ρ=-0.33, p=0.02), STPV% (ρ=-0.32, p=0.03), FPVmm3 (ρ=-0.35, p=0.02), FPV% (ρ=-0.34, p=0.02). Meanwhile, rest MBF had negative relationships with GPVmm3 (ρ=-0.48, p=0.0005), GPV% (ρ=-0.41, p=0.003), STPVmm3(ρ=-0.5, p=0.0002), STPV% (ρ=-0.52, p=0.0002), FPVmm3 (ρ=-0.47, p=0.0007), FPV% (ρ=-0.41, p=0.003), CPVmm3 (ρ=-0.33, p=0.02), CPV% (ρ=-0.31, p=0.03). Myocardial flow reserve did not have significant association with quantitative CCTA parameters. ***Conclusion:*** Based on dynamic quantitative CCTA data, the structure of atherosclerosis plaques has strong relationships with stress and rest myocardial blood flow in NOCAD patients. ***References:*** 1. Mochula AV, et al. The myocardial flow reserve in patients with heart failure with preserved ejection fraction. Heart Vessels. 2023;38(3):348-360. DOI:10.1007/s00380-022-02161-5.

EP-0478

Prognostic value of coronary artery calcifications (CAC) applying a dedicated ECG-gated CT protocol using a hybrid gamma camera in combination with cardiac SPECT performed with a CZT scanner in patients during primary diagnosis of ischemic heart disease.

M. Chojnowska, *A. Giżewska, A. Mazurek, M. Dziuk;*
Military Institute of Medicine - National Research Institute, Warsaw, POLAND.

Aim/Introduction: In diagnosis of primary coronary artery disease (CAD) both ECG-gated CT with evaluation of coronary artery calcifications (CAC) and cardiac single-photon emission computed tomography (SPECT) are used. However diagnostic value of correlating these two methods is yet to be established. In this study we aim to perform a head-to-head comparison and examine the relationship between those two methods in diagnosis of primary coronary artery disease. ***Materials and Methods:*** We included 50 subjects without previous cardiovascular disease diagnosis who had been referred to our Nuclear Medicine Department for primary CAD diagnostics using cardiac SPECT performed with a CZT scanner. During the day of admission an additional ECG-gated CT with CAC score evaluation was performed. The acquired results were then analyzed based on a number of criteria, including, but not limited to comorbidities, symptoms and demographical data. ***Results:*** During statistical analysis. ***Conclusion:*** According to the current state of knowledge the CAC score and cardiac SPECT results have positive combined diagnostic value, increasing the interpretative certainty. However in our study we focus specifically on the CZT scanner, which combined diagnostic value with the CAC score is yet to be well established. During statistical analysis we also hope to find additional factors (or lack thereof) influencing the correlation. In the future we are planning to rise the number of subjects to 100.

EP-0479

Myocardial Extracellular Volume Fraction from Late Iodine Enhancement for Risk Stratification in Non-ischemic Heart Failure

J. Deng, *D. Li*;*
Sun Yat-sen Memorial Hospital, Sun Yat-sen University, Guangzhou, CHINA.

Aim/Introduction: Our previous study demonstrated that CT-ECV derived from LIE can serve as an excellent alternative to CMR-ECV in noninvasively quantifying diffused myocardial fibrosis. We will further explore the potential of CT-ECV derived from late iodine enhancement (LIE) via using dual-layer spectral detector computed tomography (SDCT) for disease risk stratification in patients with non-ischemic heart failure(NIHF). ***Materials and Methods:*** Eighty-two NIHF patients (52±13 years, 21 female) underwent SDCT. CT-ECV was calculated based on LIE images according to AHA's 16-segmentation. Clinical data of NIHF patients were reviewed and patients were followed up for primary clinical endpoints, the primary clinical endpoint was the first occurrence of a major adverse cardiovascular event (MACE), which included hospital admission for heart failure and all-cause mortality. Receiver operating curve (ROC curve) and area under curve (AUC) were used to evaluate the prediction model. ROC curve and Yoden index determine the optimal cut-off value of CT-ECV. Kaplan-Meier curve and log-rank test were used to analyze the relationship between MACE and CT-ECV of patients with NIHF. ***Results:*** Clinical outcome data were collected from 82 patients with NIHF after a median follow up of 10 months. Final status check was performed during March 2023, and 7 patients lost follow-up. 31 (41.3%) of the 75 patients with MACE, including 28 (37.3%) patients were hospitalized for heart failure, and all-cause mortality occurred in 3 (4%) patients. The ROC curves demonstrated CT-ECV ≥ 31.28 % to be the optimal cut-off point for MACE with 83.9% sensitivity, 75% specificity and the area under the ROC curve = 0.863 (95% CI 0.782 to 0.944). Kaplan-Meier survival curves and Log-rank test demonstrate that NIHF patients with CT-ECV ≥ 31.28% had higher probability of MACE than NIHF patients with CT-ECV < 31.28%. ***Conclusion:*** CT-ECV derived from Late Iodine enhancement can assist in risk stratification in patients with non-ischemic heart failure.

EP-0480

First-pass determination of thoracic aortic blood flow rate

V. Saushkin, *Y. Varlamova, N. Ryumshina, A. Vrublevsky, D. Panfilov, B. Kozlov, S. Sazonova;*
Cardiology Research Institute, Tomsk NRMC, Tomsk, RUSSIAN FEDERATION.

Aim/Introduction: Aneurysm is a common pathology of the aorta and is the 13th leading cause of death in developed countries. The pathological enlargement is located in the ascending aorta (AA) and the aortic arch in more than 60% of cases. Until now, the only criterion for surgical treatment has been the diameter of the ascending aorta (55 mm). Recent studies have shown that an aortic diameter of less than 45 mm is associated with life-threatening complications such as aortic dissection and rupture. The search for new criteria for the assessment of the adverse effects of aortic dilatation is an urgent task. The aim of this work was to calculate the blood flow (BF) rate in the thoracic aorta and compare with the AA diameter, wall elasticity in patients with AA dilatation. ***Materials and Methods:*** We studied 16 patients with AA dilatation. All patients underwent ECG-gated CT angiography and first pass (FP). Experimental evaluation of the mechanical strength of the aortic wall was carried out on a testing machine. The AA wall specimens were stretched to failure. Circular strain (CS), longitudinal deformation (LS), compliance, distensibility aortic wall were calculated by CT. Thoracic aortic BF rate was calculated by FP. Tensile strength index, strain and area under the curve were determined by experimental evaluation. ***Results:*** Decrease of an AA deformation was noted in patients with AA dilatation (CS: 2.78[1.81;6.17] %; LS: 1.23[-2.99;8.30] %). Compensatory increased compliance (2.88[1.45;5.12] mm^2/mmHg) and decreased distensibility (0.12[0.03;0.22] %/mmHg) of the AA were also noted in patients with AA dilatation. We revealed a negative correlation (r=-0.59) between tensile strength of the aneurysm wall and patient's age. A moderate positive correlation was found between the mechanical strength of the aorta and its diameter (r=0,65). In addition, there was a moderate decrease in BF rate in the thoracic aorta (455 [445; 618] mm/sec. Strong correlations between BF rate and tensile strength index (r=-0.84) as well as BF rate and AA LS (r=-0.83) were found. Diameter AA and BF rate were not correlated. ***Conclusion:*** The BF rate of the thoracic aorta calculated using the first pass can be used as an additional criterion to assess the negative effects of AA dilatation. Increasing the length and mechanical stiffness of the AA results in a decrease in aortic BF rate. To establish detailed relationships, further research is needed. Acknowledgment: This study was supported by Russian Science Foundation, grant № 21-15-00160

EP-0481

Unusual discovery of a lipomatous hypertrophy of interatrial septum causing hot spot on 18 fluorodeoxyglucose positron emission tomography: a case report

T. Ben Ghachem, *M. Somai, I. Yeddes, I. Slim, A. Mhiri; Salah Azaiez Institute, Tunis, TUNISIA.*

Aim/Introduction: Lipomatous hypertrophy of the interatrial septum (LHIS) is a benign but less recognized pathology of the heart. It is caused by benign fatty infiltration of the interatrial septum which most often spares the fossa ovalis. The importance of this pathology is that there is increased incidence of atrial arrhythmias and sudden cardiac death. ***Materials and Methods:*** We share a case report of A 70-year-old men with no significant past medical history who originally presented with left thigh melanoma with lymph node metastasis. He was treated with surgery: extended excision with inguinal lymph node dissection and immunotherapy. In a short-term follow-up computed tomography (CT) scan showed 3 suspicious pulmonary micronodules. A reassessment whole-body PET-CT was then performed 60 minutes after the injection of 210.9 Megabecquerel (MBq) of 18F-FDG. ***Results:*** 18F-FDG PET/CT revealed intense 18F-FDG uptake, maximum standardized uptake value (SUVmax): 13.3,of the interatrial septum with no suspicious hypermetabolic focus on the rest of the explored volume and in particular within the pulmonary micronodules.Magnetic resonance imaging (MRI) and transoesophageal echocardiography confirmed typical LHIS. ***Conclusion:*** Recognizing LHIS is important to avoid misdiagnosis of cardiac metastases which may lead to unnecessary cardiac surgery or given suboptimal treatment.

EP-29

e-Poster Area

B: Imaging Clinical Studies -> B5 Neurological Imaging Clinical Study -> B51 Neurodegeneration

EP-0482

Neuroimagen. Enfoque multimodal para la evaluación de pacientes con enfermedad de Alzheimer leve y terapia neuroprotectora.

Y. Peña Quián[1], *L. Pérez*[2], *J. Batista*[1], *L. Torres*[1], *L. Rodríguez*[3], *T. Rodríguez*[2];
[1]*Centro de Isotopos, La Habana, CUBA,* [2]*Center for Molecular Immunology., La Habana, CUBA,* [3]*Hermanos Ameijeiras Hospital, La Habana, CUBA.*

Aim/Introduction: Introduction: Alzheimer's disease (AD) represents a growing health problem. In clinical practice, it is difficult to obtain an early diagnosis and determine the therapeutic stages of this disease.Objective: To evaluate the integration of neuroimaging in a multimodal approach for the early diagnosis and follow-up of patients with AD who received neuroprotective therapy. ***Materials and Methods:*** Multicenter, controlled and randomized clinical trial. 200 patients with possible AD (NIA-AA 2018) were evaluated before and one year after treatment neuroprotective (recombinant human erythropoietin with low sialic acid content) versus placebo. Clinical evaluation, electroencephalogram (EEG), single photon emission computed tomography (SPECT) and magnetic resonance imaging (MRI) were performed. Bilateral posterior temporal-parietal hypoperfusion and the volume of the hippocampus was determined. SPECT/MRI co-registrations were performed. Changes in cerebral perfusion, clinical response, and the results of the techniques were compared. ***Results:*** Early and differential diagnosis: SPECT: Sensitivity 78,2%; specificity 82.8%. Established the differential diagnosis with other neurodegenerative entities. MRI: Sensitivity 71%; specificity 65%. The intensity of cortical atrophy was more precisely determined. SPECT/MRI: Sensitivity 80.8%; specificity of 85.7%. Treatment evaluation: Clinical Evaluation:54% of patients showed significant clinical improvement (FDA criteria). There was a significant difference between treated patients versus placebo(p=0.001).EEG:56,2% of the treated patients stabilized or decreased the EEG alterations versus placebo(p=0.003). SPECT:Neuroprotective group: 61.3% of patients showed increased brain perfusion in previously affected regions. 31.2% presented no perfusion changes and 7.5% had a slight decrease in perfusion. Control group: 0.8% of the patients showed increased brain perfusion in the frontal regions. 33% showed no perfusion changes and the rest had decreased perfusion. Increased brain perfusion was associated with clinical improvement(r=0.98). MRI:42% of the treated patients showed volume increase in the hippocampus. 6% had a decrease in volume. 52% showed no changes. ***Conclusion:*** The integration of neuroimaging in a multimodal approach was useful for early diagnosis and follow-up of patients with AD who received neuroprotective therapy. The increase in cerebral perfusion in the treated patients was associated with clinical improvement. SPECT/MRI improved diagnostic accuracy. The multimodal approach is an important instrument for the identification of AD and its treatments.

EP-30

e-Poster Area

B: Imaging Clinical Studies -> B6 Endocrinological Imaging Clinical Study -> B61 Endocrinology (including Thyroid Benign)

EP-0483

Screening of risk factors influencing the responsiveness of lung metastatic forci of differentiated thyroid cancer under 131I radiotherapies

W. Muyu[1], *X. Liu*[2], *C. Liu*[3], *S. Qin*[4], *X. Lin*[1], *W. Shi*[5], *Q. Ding*[3], *X. Zhang*[3], *P. Li*[1];
[1]*Department of Nuclear Medicine, Ruijin Hospital, School of Medicine, Shanghai Jiao Tong University, Shanghai, CHINA,* [2]*Department of General Surgery, Xinqiao Hospital, Army Medical University, Chongqing, CHINA,* [3]*School of Mathematical Sciences, Shanghai Jiao Tong University, Shanghai, CHINA,* [4]*Department of Nuclear Medicine, Shanghai Tenth People's Hospital, Tongji University School of MedicineUniversity, Shanghai, CHINA,* [5]*Department of Nuclear Medicine, Tianjin Medical University General Hospital, Shanghai, CHINA.*

Aim/Introduction: Clinically, patients diagnosed with metastatic differentiated thyroid cancer (mDTC), especially with diffuse metastatic pulmonary forci, are commonly suggested for iodine-131 (^{131}I) radiotherapy. However, the therapeutic efficacies

are always challenging to predict due to individual distinctions of different patients. Thereafter, seeking factors influencing the ^{131}I radiotherapeutic responsiveness of mDTC has always been a pivotal but ambiguous issue in clinical practice. ***Materials and Methods:*** In order to screen the possible key factors influencing the responsiveness of metastatic pulmonary forci of mDTC under iodine-131 radiotherapies, 66 patients with at least 3 continuous ^{131}I radiotherapies were enrolled from two centers, and 24 features of whom were considered. The feature_importances function in Scikit-Learn Library of Decision Tree and Random Forest (RF) algorithms was employed to achieve the pivotal features with significant influences in responsiveness. Furthermore, receiver operating curves (ROC) and their corresponding area under the curve (AUC values) were illustrated to evaluate the classification efficacies of these two models. Finally, the predict_proba function in Scikit-Learn was utilized to give some detailed predictions and reclassifications of our patients. ***Results:*** We firstly screened 6 and secondly screened 8 crucial factors which mainly dertermine the therapeutic responsiveness of metastatic pulmonary forci of mDTC and their corresponding weighting factors were obtained. The AUC values of RF and Decision Tree algorithms could reach 0.9 and 0.7, respectively and the accuracy, sensitivity and specificity of RF algorithm in testing set was 0.833, 0.800 and 0.833 (with first screened 6 factors); 0.802, 0.963 and 0.483 (with second screened 8 factors). Furthermore, the decision surface verified the accuracy of our models as well. Finally, the programs and softwares were fabricated to give some responsive probability predictions as well as detailed reclassifications of the responsiveness to ^{131}I radiotherapies. ***Conclusion:*** Our present study results indicate that the screened pivotal features were capable of classifying the responders and nonresponders under ^{131}I radiotherapies with Decision Tree & RF algorithms and feature_importances function. Meanwhile, further responsive probabilities and reclassification details could be presented via predict_proba function as well. ***References:*** [1] J. Maciel, D. Cavaco, C. Silvestre, J. Simões Pereira, H. Vilar, V. Leite, Clinical outcomes of a cohort of 271 patients with lung metastases from differentiated thyroid carcinoma, Clinical endocrinology, 97 (2022) 814-821.[2] B. Charbuty, A.J.J.o.A.S. Abdulazeez, T. Trends, Classification based on decision tree algorithm for machine learning, 2 (2021) 20-28.

EP-0484

An exploratory study on pathologic molecular characteristics of sestamibi single positron emission computed tomography/computed tomography in predicting primary hyperparathyroidism

J. Yang, *X. Su, J. Zhang, W. Weng, P. Zhou;*
the First Affiliated Hospital, Zhejiang University School of Medicine, Hangzhou, CHINA.

Aim/Introduction: Dual-phase ^{99}Tc^{m}-MIBI SPECT/CT imaging has become a commonly used preoperative diagnostic imaging method for PHPT patients. However, there are many clinicopathological factors that affect the accurate localization of ^{99}Tc^{m}-MIBI SPECT/CT, and the mechanism of ^{99}Tc^{m}-MIBI uptake in lesions is not completely clear at the histopathological and immunohistochemical levels. ***Materials and Methods:*** Single parathyroid pathological specimens of PHPT patients who underwent ^{99}Tc^{m}-MIBI SPECT/CT imaging and surgery in our institution from August 2017 to December 2020 were retrospectively analyzed. Correlation analysis and multivariate regression analysis were performed for the length and diameter of the lesion, the ratio of eosinophils, the expression of proliferating cell nuclear antigen (PCAN) and P-glycoprotein (P-gp) in the nucleus and cell membrane of the lesion and the $ROI_{T/NT}$ value of the lesion in dual-phase ^{99}Tc^{m}-MIBI SPECT/CT imaging. ***Results:*** A total of 146 PHPT patients with complete clinicopathological data and a single lesion were included in this study, with an average age of 55±12 years, 69.2% of whom were female. The average length of the lesions was 20.5±10.4 mm. Oxyphil cells were scattered, localized and diffused in the lesions, accounting for different proportions of oxyphil cells, ranging from 0 to 99.6%, among which no oxyphil cells were found in 27.4%. PCNA and P-gp were expressed in the nucleus and cell membrane of parathyroid tissues to different degrees. The average IOD/area value (IOD, Intergrated Optical Density) of PCNA was 0.25 (range: 0.04-0.48), and the median IOD/area value of P-gp was 111.12 (range: 0.82-2362.67). 129 lesions of 146 patients in ^{99}Tc^{m}-MIBI SPECT/CT, which was consistent with the intraoperative results, the average $ROI_{T/NT}$ was 6.99 (range: 1.32-26.15). The length diameter of the parathyroid gland (r=0.041, p=0.014) and the proportion of eosinophils (r=0.119, p=0.0) were positively correlated with the $ROI_{T/NT}$ value, and there was no correlation between PCNA (p=0.233) and P-gp (p=0.979) expression and the $ROI_{T/NT}$ value. Multivariate regression analysis showed that IOD/area values of the long diameter (p=0.047, OR=3.93) and P-gp expression levels (p=0.0, OR= 9.50) were independent factors to predict negative imaging. ***Conclusion:*** This study was found that the size of the parathyroid gland and eosinophil ratio of lesions were positively correlated with the $ROI_{T/NT}$ value of ^{99}Tc^{m}-MIBI SPECT/CT, while the size of lesions and P-gp expression were risk factors for negative ^{99}Tc^{m}-MIBI SPECT/CT imaging. ^{99}Tc^{m}-MIBI SPECT/CT can provide an important basis for clinicians to predict the pathological molecular features of lesions.

EP-0485

Graves' disease: do TRAb measurement help predicting thyroid radioiodine uptake?

I. Casimiro, *G. Costa, R. Silva;*
Centro Hospitalar e Universitário de Coimbra, Coimbra, PORTUGAL.

Aim/Introduction: Graves' disease (GD) is an autoimmune disorder clinically characterized by thyrotoxicosis due to the production of autoantibodies against thyrotropin-receptor (TRAb), which continuously activate the TSH receptor (TSH-R). This condition can be successfully treated with radioactive iodine-131 (RAI), administered as Na[^{131}I]I. A theranostic approach can help to personalize this treatment modality, being the 24-hour thyroid RAI uptake (24h%RAIU) a valuable functional parameter for therapeutic activity estimation (easily obtained from a diagnostic test with Na[^{131}I]I). Knowing that the RAI thyroid follicular cell uptake depends on the activation of the TSH-R, is reasonable to expect a positive correlation between TRAb and 24h%RAIU. This study aims to verify, in our population of GD patients submitted to RAI thyroid test in the last decade in our department, if there is a relationship between TRAb titer and 24h%RAIU. The relationship between TRAb titer and the TSH levels and the thyroid mass was also evaluated. ***Materials and Methods:*** We retrospectively reviewed the clinical file of all GD patients referred to our department for treatment with Na[^{131}I]I, between January-2012 and December-2021. We selected the 250 patients who had blood measurements of TSH and TRAb within 6 months before RAI therapy was planned with a diagnostic test using Na[^{131}I]I. The 24h%RAIU and the thyroid mass estimation based on scintigraphic imaging were recorded. Conducting a non-parametric test, we calculated the Spearman's

Rank correlation coefficient between TRAb values and 24h%RAIU, TSH levels and gland mass of the corresponding patients. ***Results:*** We found a statistically significative (p<0.001) moderate negative correlation between TRAb and TSH values (ρ=-0,454). Also, there was a statistically significative (p<0.001) weak positive correlation between TRAbs levels and thyroid gland mass (ρ=0,240). Concerning the RAI thyroid uptake, we observed that 82% of patients had a 24h%RAIU>50%. Besides that, we found a very weak positive correlation between TRAbs levels and 24h%RAIU (ρ=0,144) that was statistically significative (p=0,023). ***Conclusion:*** Our study showed that even though elevated TRAbs are frequently used to diagnose GD, the elevation of these antibodies is a poor predictor of the gland mass or its iodine uptake at 24h, as the correlation with these variables is weak and very weak, respectively. Concerning TSH levels, we found a moderate negative correlation with TRABs, confirming the commonly observed low TSH level in hyperthyroidism patients.

EP-0486

Does the hypothalamus-pituitary-adrenal axis play a role in the difference in treatment response to GLP-1 receptor agonists in type 2 diabetes?

S. Tokgöz[1], *T. J. P. Jansen*[1], *R. Meijer*[2], *C. Frielink*[1], *C. J. Tack*[2], *B. E. de Galan*[2,3], *M. Gotthardt*[1], *M. Boss*[1];
[1]*Department of Medical Imaging, Radboud University Medical Center, Nijmegen, NETHERLANDS,* [2]*Department of Internal Medicine, Radboud University Medical Center, Nijmegen, NETHERLANDS,* [3]*Department of Internal Medicine, Maastricht University Medical Center, CARIM School for cardiovascular diseases, Maastricht, NETHERLANDS.*

Aim/Introduction: Glucagon-like peptide-1 receptor agonists (GLP-1RA) are potent antidiabetic drugs for treatment of type 2 diabetes (T2D), but up to 20% of all individuals with T2D are partly or completely unresponsive to treatment with GLP-1RAs. Besides the insulinotropic effects on pancreatic beta cells, GLP-1RAs can stimulate the hypothalamic-pituitary-adrenal (HPA) axis, inducing cortisol secretion. Cortisol is pro-diabetogenic, which is associated with weight gain and insulin resistance. We thus hypothesized that this effect could be at the root of unresponsiveness to GLP-1RA treatment. To investigate this, we used PET/CT imaging with a radiolabeled stable GLP-1 analogue ([^{68}Ga]Ga-NODAGA-exendin-4) to quantify GLP-1R expression in the pituitary of individuals with T2D with (responders) and without (non-responders) an adequate response to GLP-1RA treatment and assessed the downstream effects on the HPA axis. ***Materials and Methods:*** The responder and non-responder groups were defined based on the level of HbA1c and weight loss after a maximum of one year of GLP-1RA treatment. Both responders (n=10) and non-responders (n=8) underwent an oral glucose tolerance test, HPA axis stimulation test, 24h urine collection to assess baseline cortisol levels and a 60 min dynamic PET/CT scan of the brain after infusion with 100±5 MBq of [^{68}Ga]Ga-NODAGA-exendin-4. The maximum standardised uptake value (SUV_{max}) between 45 and 60 min was used to quantify GLP-1R expression. ***Results:*** Our data showed tracer uptake in the pituitary in all individuals with T2D, which did not significantly differ between responders and non-responders (SUV_{max} 2.7±1.0 vs 3.2±1.3, p=0.41). However, when analysing the entire study population (n=18), we found significant interindividual differences in pituitary GLP-1R expression (25th vs 75th percentile of SUV_{max}: 1.8±0.19 vs 4.5±0.75, p<0.001). No significant differences were observed in beta cell function ($AUC_{C\text{-}peptide}$ p=0.44; $AUC_{C\text{-}peptide}$:$AUC_{glucose}$ ratio p=0.26) and hormones related to HPA axis stimulation (AUC_{ACTH} p=0.47; $AUC_{cortisol}$ p=0.18) between responders and non-responders. Pituitary tracer uptake did not correlate to BMI (R^2=0.00053, p=0.93), beta cell function ($AUC_{C\text{-}peptide}$ R^2=0.074, p=0.32; $AUC_{C\text{-}peptide}$:$AUC_{glucose}$ ratio R^2=0.051, p=0.42) and hormones related to the HPA axis (AUC_{ACTH} R^2=0.10, p=0.23; $AUC_{cortisol}$ R^2=0.010, p=0.71). ***Conclusion:*** Our data do not indicate a role of pituitary GLP-1R expression and HPA axis stimulation in the difference in treatment response to GLP-1RA among individuals with T2D. The origin of these differences in treatment response thus remains unclear. The substantial tracer uptake with significant interindividual differences that we observe does point to a potential role of GLP-1R in the pituitary, which requires further elucidation.

EP-0487

68Ga-NODAGA-exendin4 PET-CT Imaging of Pancreatic Beta Cells: Preliminary Data in Type 1 Diabetic Patients and in Obese People

L. Ruffini[1], *M. Scarlattei*[1], *G. Ladisa*[1], *S. Migliari*[1], *G. Baldari*[1], *V. Spigoni*[2], *R. Aldigeri*[2], *G. Cinquegrani*[2], *A. Dei Cas*[2], *R. Bonadonna*[2];
[1]*Nuclear Medicine Division, University Hospital of Parma, Parma, ITALY,* [2]*Dept of Medicine & Surgery, University of Parma, Parma, ITALY.*

Aim/Introduction: PET scans of radioactive exendin-4, a ligand of the GLP-1 receptor (GLP1R) expressed on the β-cell surface, have been proposed to provide a tentative quantitative in vivo biomarker of pancreatic β-cell mass. Throughout 2020-2022 we developed and validated a fully automated radiosynthesis of 68Ga-NODAGA-exendin4 (68Ga-Ex4) with high specific activity, and subsequently, we optimized a PET-CT scan method to assess 68Ga-Ex4 uptake by pancreatic endocrine cells. Aim of this work was to assess the performance of 68Ga-Ex4 PET-CT in a clinical study of patients with long standing type 1 diabetes (T1DM) and of obese people (OB). ***Materials and Methods:*** The synthesis of 68Ga-Ex4 was performed using an automated synthesis module (Scintomics GRP®) connected to a GMP-certified 68Ge/68Ga generator (GalliaPharm®) as previously described [Migliari et al. Molecules 2022].The radiopharmaceutical was administered i.v. over 5 minutes after an overnight fast. Blood pressure, heart rate, blood glucose were measured before tracer injection and at each image time point. Soon after tracer injection dynamic images were acquired over 20 minutes (one bed on pancreatic/cardiac region). Whole body PET/CT was performed 60' post injection. Semiquantitative analysis of tracer uptake was performed using spherical volumes of interest (VOIs) semi-automatically drawn on the pancreatic head, body and tail to measure SUVmax and SUVmean at each time point. ***Results:*** Eight patients (age 50±4 yrs; BMI 26.6±1.9 kg/m2) with long standing (34±3 yrs) T1DM (HbA1c: 58±4 mmol/mol) and 8 OB subjects (age 49±2 yrs; BMI 37.4±2.1 kg/m2) were injected with 68Ga-Ex4 (mean dose 117.44 MBq). Mean RCP%, RCY% and Am of the produced radiopharmaceutical were 97.50%, 49.29%, and 259.05 GBq/umol respectively; mean peptide amount was 2.66 ug. Average SUVmean of the whole pancreas at 20' (grouped dynamic images) was 3.4±0.8 in T1DM and 5.0±0.5 in OB (p=0.0115); 1.9±0.8 in T1DM and 3.7±1.1 in OB at 60' (p=0.0025). Average SUVmax was 4.7±1.3 in T1DM and 7.5±1.0 in OB at 20' (p=0.0008); 3.1±1.1 in T1DM and 5.8+1.4 in OB at 60' (p=0.0011). Renal uptake was intense at both time points (average SUVmax and SUVmean 88.5±20, 55.2±13.8). No side effects were registered. ***Conclusion:*** 68Ga-Ex4 allows to visualize pancreatic GLP1R expression capturing quantitatively different pattern of receptor engagement. The fully automated production of high specific activity 68Ga-Ex4 remains reproducibile and accurate for routine use. Next steps to improve 68Ga-Ex4 imaging

will be correction of quantitative measures for renal excretion. ***References:*** Migliari S. Molecules 2022 PMID:35056858; Migliari S. Curr Radiopharm. 2022 PMID:33687908

EP-0488

Role of 68Ga DOTANOC PET/CT In Localisation of Culprit Ectopic ACTH Secreting Tumors

R. Kumar, *S. Sagar, D. Khan, R. Khadgawat;*
All India Institute of Medical Sciences, New Delhi, INDIA.

Aim/Introduction: Ectopic Cushing's syndrome (ECS) or ectopic ACTH syndrome, accounts for 10-15% of the cases of Cushing's syndrome. We aim to evaluate the role of ^{68}Ga DOTANOC PET/CT in localisation of culprit ectopic ACTH secreting tumors. ***Materials and Methods:*** All consecutive patients with clinical evaluation suggestive of EAS, referred to our department for ^{68}Ga DOTANOC PET/CT from 2017 to 2022, were evaluated retrospectively. All patients were injected 3-4mCi of ^{68}Ga DOTANOC intravenously and underwent whole body PET/CT 40-60 minutes post-injection, on either Biograph mCT PET/CT, Siemens or Discovery 710 PET/CT, GE. Scanned images were interpreted by two nuclear physicians independently with an experience of 3-20 years. ^{68}Ga DOTANOC PET/CT findings were corroborated with clinical details. ***Results:*** Over the study period, 50 (29 females (58%) and 21 males (42%) patients having mean age of 32.41(range-13 to 69 years) with ECS underwent ^{68}GaDOTANOC PET/CT .^{68}GaDOTANOC identified the suspected primary ECS in 14 out of 50 patients (28%). Of these, six patients had increased SSTR expression in lungs with another four patients having increased SSTR expression in different lymph nodes. Other two patients had adrenal lesion causing ECS. Out of the remaining two out of 14, one had increased SSTR expression at fourth inter costal space and other had at third part of duodenum. These fourteen patients had a mean SUVmax of 10.97(95%CI= 5.30-16.64) compared to background mean SUVmax of 0.80 (95%CI= 0.35-1.25). ***Conclusion:*** Our study reinforces the role of ^{68}Ga-DONANOC PET/CT to localise ectopic ACTH secreting tumors in appropriate clinical settings. In the future, advances in imaging techniques will improve the identification of small occult NETs and thus allow their removal, thereby further limiting the time bound complications of hypercortisolism.

EP-0489

Short 4D 18F-Fluorocholine PET/CT for hyperparathyroidism: A new tool for hyper-functional parathyroid finding ?

A. CALLAUD[1], *M. Bailly*[2], *G. Metrard*[2];
[1]*CHR, Orléans, FRANCE,* [2]*CHRU Orléans, Orléans, FRANCE.*

Aim/Introduction: In primary hyperparathyroidism, preoperative imaging is essential for diagnosing hyper-functional parathyroid(s), and 18F-Fluorocholine (FCH) PET can be used in addition to ultrasound and scintigraphy. However, 18F-FCH PET protocol lacks standardization. An alternative modality is 4D-CT, but it appears to be less sensitive. Combining the two modalities has succinctly been tried, with discordant result and seems to be irradiating and complex. In this preliminary work we propose a simplified approach using a "short 18F-FCH 4D PET/CT" with 2 CT acquisitions and an early 18F-FCH PET acquisition only (at 5 minutes) for detection of hyper-functional parathyroid, and evaluate its performance compared to full dual time point 18F-FCH PET/CT. ***Materials and Methods:*** Dual time point 18F-FCH PET exams with 2 low-dose CT (non-enhanced and contrast-enhanced) were retrospectively collected and blindly analyzed. For each patient, operative and histopathological analysis reports were fully available and used as a reference. Exams were read separately by two nuclear medicine physicians. Patients were classified into four diagnosis categories: adenoma, multi-glandular disease, negative, or non-conclusive. Each exam was read twice, first with the early PET acquisition and non-enhanced CT (and immediately after with the late PET acquisition) and 2 weeks after with the early PET acquisition alone and contrast enhanced CT ("4D-CT"). ***Results:*** Between May and October 2022, 25 patients were included, 18 women, 7 men, mean age 68.2 Y (41-81), mean BMI 27.4 kg/m2 (18-69). 18F-FCH PET accuracy rates for diagnosis were respectively: 78%, 80% and 88% for early acquisition only, dual-time PET, and short 4D-PET/CT. Adding contrast-enhanced CT seemed to reduce false positive foci detection, without reducing the excellent sensibility of 18F-FCH PET for foci detection that were almost identical for the 3 readings. ***Conclusion:*** Thus, short 4D 18F-FCH PET/CT not only saved time for the patient and the system, but also appears to have better global performance than dual time point FCH PET. Our preliminary results indicate that short 4D PET/CT might be a relevant "all-in-one" pre-surgical imaging modality, fitting perfectly in the hybrid imaging era. Further analysis (such as reproducibility and more patients) are needed. It should also be compared directly to other imaging modalities to compare its performances.

EP-0490

Detection of hyperfunctioning parathyroid glands using 18F-choline PET/CT in patients with negative or equivocal results of the complex 99mTcO4/99mTc-MIBI scintigraphy (including SPECT/CT)

P. Koranda[1], *L. Quinn*[1], *M. Jenčo*[1], *J. Klacanek*[1], *M. Halenka*[2], *M. Mocňáková*[3], *M. Kamínek*[1];
[1]*Dept. of Nuclear Medicine, Univ. Hospital and Palacký University, Olomouc, Olomouc, CZECH REPUBLIC,* [2]*Dept. of Internal Medicine III, Univ. Hospital and Palacký University, Olomouc, Olomouc, CZECH REPUBLIC,* [3]*Dept. of Surgery II, Univ. Hospital and Palacký University, Olomouc, Olomouc, CZECH REPUBLIC.*

Aim/Introduction: To assess the diagnostic value of ^{18}F-choline PET/CT in cases where complex scintigraphy (combining ^{99m}TcO4/^{99m}Tc-MIBI subtraction including ^{99m}TcO4 washout using perchlorate - to eliminate patient´s displacement between scans, ^{99m}Tc-MIBI SPECT/CT, and two-phase evaluation of ^{99m}Tc-MIBI scintigraphy) yields negative or equivocal results. ***Materials and Methods:*** A retrospective analysis was performed on a cohort of 35 patients (pts.) who underwent ^{18}F-choline PET/CT. Previous complex scintigraphy results were negative in 18 cases, equivocal in 9 cases. Scintigraphic findings were highly suspicious and required verification in 6 cases, and 2 cases were not evaluated with ^{99m}Tc-MIBI due to claustrophobia. The ^{18}F-choline PET/CT findings were classified as positive (21 pts.), negative (7 pts.), or equivocal (7 pts.), ***Results:*** ^{18}F-choline PET/CT detected enlarged parathyroid tissue in 8 out of 18 scintigraphically negative patients (44%), 5 out of 9 cases with equivocal scintigraphy findings, and in both claustrophobic patients. Among the subset of patients from these three groups who could not be indicated for targeted surgical intervention based on scintigraphy, 15 out of 29 cases (52%) had successful localization of parathyroid tissue using ^{18}F-choline PET/CT. All 6 cases referred for verification of highly suspicious scintigraphy findings were confirmed by ^{18}F-choline PET/CT. In 7 cases, ^{18}F-choline PET/CT findings were classified as equivocal, and 3 surgeries were performed (2 false positives, 1 true positive). Seven times the PET/CT finding was interpreted as negative. ***Conclusion:*** Although the detection rate in our cohort of patients is lower than in published studies [1], it is evident that

^{18}F-choline PET/CT is beneficial in cases of suspected primary or tertiary hyperparathyroidism when ^{99m}TcO4/^{99m}Tc-MIBI SPECT/CT findings are negative or equivocal. The reason for relatively lower ^{18}F-choline PET/CT yield in our group of patients may be related to the very complex performance of previous ^{99m}TcO4/^{99m}Tc-MIBI scintigraphy (including CT as a part of SPECT/CT). This complexity could be a prerequisite for efficient detection of enlarged parathyroid tissue using scintigraphies (in accordance with the article [2]). In cases of equivocal ^{18}F-choline PET/CT findings, there is an increased risk of false positive results. ***References:*** [1], Quak E, et al. Detection, resection and cure: a systematic review and meta-analysis od 18F-choline PET in primary hyperparathyroidism. Q J Nucl Med Mol Imaging. 2023. doi: 10.23736/S1824-4785.23.03512-4.[2] Tlili G, et al. Dual-tracer 99mTc-sestamibi/123I imaging in primary hyperparathyreoidsm. Q J Nucl Med Mol Imaging. 2023. doi: 10.23736/S1824-4785.23.03509-4.

EP-0491

[^{18}F]Fluorocholine PET-CT in Preoperative Localization of Hyperfunctioning Parathyroid Glands: Continuing to Strengthen the Evidence

S. Casanueva Eliceiry[1,2], *N. Sánchez Izquierdo*[2,1], *A. Niñerola-Baizán*[2,1], *M. Manyalich-Blasi*[1,3], *P. Domínguez-Garijo*[1,3], *M. Mora-Porta*[1,3], *F. Hanzu*[1,3], *M. Rodrigo-Calvo*[1,4], *S. Vidal-Sicart*[2,1], *O. Vidal-Pérez*[1,3], *D. Fuster-Pelfort*[2,1];
[1]*Hospital Clínic Barcelona, Barcelona, SPAIN,* [2]*Instituto de diagnótico por la imagen CDI, Barcelona, SPAIN,* [3]*Instituto Clínic de Enfermedades Digestivas y Metabólicas (ICMDM), Barcelona, SPAIN,* [4]*Centro de Diagnóstico Biomédico (CDB), Barcelona, SPAIN.*

Aim/Introduction: Primary hyperparathyroidism (pHPT) is a relatively common endocrine disorder in which one or more parathyroid glands (PTG) secrete excess amounts of parathyroid hormone (PTH), with surgery being the only curative treatment. Minimally invasive parathyroidectomy (MIP) is the preferred approach, wherein preoperative localization of hyperfunctioning parathyroid tissue (HFPT) is crucial. In this regard, ^{99m}Tc-MIBI parathyroid scintigraphy has already proven to be useful and is currently established as the standard preoperative imaging modality in many centers worldwide. However, there has been a steadily increasing interest in using [^{18}F]Fluorocholine, a positron emission tomography (PET) radiotracer, for preoperative localization of HFPT, particularly in situations where conventional techniques had failed. The aim of this study was to determine the efficacy of [^{18}F]Fluorcholine PET-CT (FCH) in locating HFPT and to compare it with that of ^{99m}Tc-MIBI SPECT-CT (MIBI). ***Materials and Methods:*** Retrospective observational study. A total of 90 consecutive pHPT patients who underwent MIP were included. Both MIBI and FCH imaging modalities were used for preoperative evaluation. MIBI images were acquired 90 minutes post-injection of 24 mCi (888 MBq) ^{99m}Tc-MIBI. FCH images were obtained 60 minutes after the injection of 5.4-10 mCi (200-370 MBq) [^{18}F]-Fluorocholine. Regional focal uptake not associated with thyroid disease was considered positive for HFPT. Images were analyzed by a Nuclear Medicine specialist and a resident in training. Pathology reports from resected PTG were compared to findings from both imaging modalities and served as the gold-standard. The diagnostic performance of both imaging modalities was calculated and compared using McNemar's test, with statistical significance set at P<0.05. The cure of pHPT was defined as a reduction of 50% or greater in postoperative serum PTH. ***Results:*** A total of 92 PTG were resected, comprising 86 adenomas, 5 hyperplasias and 1 lipo-adenoma. On a gland-based analysis, FCH presented higher diagnostic performance compared to MIBI; with sensitivity, positive predictive value and accuracy rate of 96.7%, 100% and 95.7% vs. 69.5%, 100% and 70.2%, respectively (P<0.001). 84 patients had follow-up data on PTH. Biochemical criteria for cure was met in 76.1%(64/84) and was correctly located by FCH and MIBI in 100%(64/64) and 71.8%(46/64), respectively. ***Conclusion:*** FCH demonstrated superior diagnostic performance compared to MIBI, and was able to accurately characterize all patients that met the cure criteria. These findings support the promising role of FCH in the preoperative setting of pHPT.

EP-0493

Diagnostic and Prognostic Value of [18F]F-DOPA PET/CT for Medullary Thyroid Cancer

S. Li, *E. Rainer, S. Rasul, L. Hargitai, P. Riss, C. Scheuba, M. Hacker; Medical University of Vienna, Vienna, AUSTRIA.*

Aim/Introduction: Correct diagnosis and prognostic evaluation of medullary thyroid cancer (MTC) are crucial for the therapy of MTC. The purpose of this study was to evaluate the diagnostic and prognostic value of [^{18}F]F-DOPA PET/CT in patients with MTC. ***Materials and Methods:*** [^{18}F]F-DOPA PET/CT examinations of 60 patients with histologically verified MTC were analysed. Serum basal calcitonin (bCt) and stimulated calcitonin (sCt) as well as CEA were determined. The diagnostic value of PET/CT for detection of tumour lesions were calculated. Overall survival (OS) was estimated using the Kaplan-Meier method. ***Results:*** 53 of 60 patients had positive [^{18}F]F-DOPA PET scans with a sensitivity of 88 % and specificity of 100 %. The lesion-related sensitivity of [^{18}F]-F-DOPA PET was 96 % (308 of 320 lesions). Significant correlations were found between bCt, sCt and CEA with [^{18}F]F-DOPA-uptake (SUVmax, $p < 0.01$). Patients with negative [^{18}F]F-DOPA PET had longer survival than patients with positive [^{18}F]-F-DOPA-PET results. ***Conclusion:*** High sensitivity and specificity of [^{18}F]F-DOPA PET were shown for evaluation of MTC. The uptake of [^{18}F]-F-DOPA in tumour lesions correlates significantly with bCt, sCt and CEA. [^{18}F]F-DOPA PET/CT may be of great value for diagnosis and prognostic assessment in patients with MTC.

EP-0494

Correlation between SUVmax and analytical values in patients with primary hyperparathyroidism undergoing 18F-choline PET/CT

E. Rodriguez Gallo[1,2], *C. Wakfie Corieh*[1,2], *A. Fernandez Alfonso*[1,2], *A. Álvarez Vázquez*[1,2], *E. Jodar Gimeno*[1,2], *B. Pérez-Arroyo*[1,2], *J. Martín Gil*[3], *A. Maldonado*[1,2];
[1]*Hospital Universitario QuironSalud Madrid, Madrid, SPAIN,* [2]*Universidad Europea, Madrid, SPAIN,* [3]*Hospital Quirónsalud San José, Madrid, SPAIN.*

Aim/Introduction: To establish the correlation between the standard uptake value (SUV) and the parathyroid hormone (PTH), serum calcium and ionic calcium in patients diagnosed with primary hyperparathyroidism undergoing ^{18}F-choline PET/CT as an adenoma localisation test. ***Materials and Methods:*** A retrospective analysis of 111 patients with primary hyperparathyroidism undergoing 18F-choline PET/CT between October 2015 and March 2023 was performed; PTH, serum calcium and ionic values were obtained for the month prior to PET/CT. Patients with no blood tests and in absence of parathyroid adenoma were excluded. On the day of the scan, 150 µCi/kg of ^{18}F-choline was injected, images were acquired at 20 (with intravenous contrast administration) and 60 minutes; a visual and semi-quantitative analysis with SUVmax measurement was

performed once the adenoma was located on both images. The Statistical Package for the Social Sciences (SPSS) 25.0 was used for the statistical analysis. Not all variables showed a normal distribution, so non-parametric statistics were used. Statistical significance was defined as $p < 0,05$. It was decided to use the SUVmax of the late image as the reference value. Non-parametric bivariate analysis was performed to detect influential factors on SUVmax. Spearman's correlation coefficient and scatterplot were used as graphical representation. A linear regression was carried out to analyse the relationships between variables, using the r-squared coefficient and the equation of the model. ***Results:*** Assessing the results of the Spearman's correlation between SUVmax and PTH values, it is observed that there is a direct correlation between both variables, statistically significant ($p< 0.05$). With respect to serum calcium and ionic calcium values, these correlations are also direct, but not statistically significant. An indirect correlation was observed between SUVmax and age, which, although not statistically significant, may be a variable to consider in future studies. ***Conclusion:*** There is a positive correlation between the SUV value of parathyroid adenoma on ^{18}F-choline PET/CT and the analytical value of PTH. These data may be useful in further studies to evaluate their relationship with pathological anatomy in patients undergoing parathyroidectomy.

EP-0495

Impact of digital [18F] Fluorocholine (FCH) PET/CT reconstruction technique on detection rate, reader confidence and agreement in localisation of parathyroid adenomas in persistent/ recurrent primary hyperparathyroidism

M. Naik, *C. Ferguson, S. Lazic, A. Eccles, S. Khan, S. Khan, F. Palazzo, K. Houghton, T. D. Barwick;*
Imperial College Healthcare NHS Trust, London, UNITED KINGDOM.

Aim/Introduction: In persistent or recurrent primary hyperparathyroidism, (PHPT) parathyroidectomy remains the only cure. However, redo-surgery is has higher complication and failure rates; thus accurate localisation is essential. Reported detection rates of [18F] Fluorocholine (FCH) PET/CT for persistent and recurrent pHPT are 58-65% using previous-generation PET/CT scanners. Digital silicon-photomultiplier (SiPM) PET/CT scanners offer higher spatial resolution and coincidence time resolution. Post-reconstruction smoothing filters reduce noise and improve image quality, but may decrease lesion contrast and reduce conspicuity of small lesions. (1,2)We aimed to assess differences in detection rates, diagnostic confidence and level of lesion uptake using three reconstructions (Gaussian 6.0, Gaussian 4.5 and unfiltered All Pass) on a digital PET/CT scanner. We also assessed inter-observer agreement. ***Materials and Methods:*** Single-centre retrospective observational study of consecutive persistent/recurrent pHPT (n=29) patients undergoing FCH PET/CT on a digital scanner.Two expert, two moderately experienced, and two inexperienced readers independently reviewed randomised anonymised reconstructions with at least one week washout between each set of reads.Three expert reviewers agreed a consensus for detection rates for each reconstruction. ***Results:*** Detection rates were 51%, 72%, and 86% for Gaussian 6.0, Gaussian 4.5, and All Pass reconstructions respectively. Diagnostic confidence for positive lesion detection was highest with the All Pass reconstruction. Median SUVmax for detected lesions was 3.5, 4.1, and 6.1 for Gaussian 6.0, Gaussian 4.5, and All Pass reconstructions respectively. Inter-observer agreement was high between expert ($\kappa \geq 0.65$) and moderate readers ($\kappa \geq 0.67$) across all reconstructions. For inexperienced readers, highest agreement was observed when using the unfiltered All Pass reconstruction ($\kappa=0.93$) compared to traditional Gaussian filtering. ***Conclusion:*** Digital smoothing reconstructions impact detection rate, diagnostic confidence and SUVmax in localisation of parathyroid adenomas using FCH PET/CT. Detection rates and diagnostic confidence are highest with the All Pass reconstruction, outperforming previously reported rates utilising previous-generation PET/CT scanners. ***References:*** (1) Performance Characteristics of the Digital Biograph Vision PET/CT System. van Sluis J, de Jong J, Schaar J, Noordzij W, van Snick P, Dierckx R, Borra R, Willemsen A, Boellaard R. J Nucl Med. 2019; 60(7):1031-1036. (2) Comparison of image quality and lesion detection between digital and analog PET/CT. López-Mora DA, Flotats A, Fuentes-Ocampo F, Camacho V, Fernández A, Ruiz A, Duch J, Sizova M, Domènech A, Estorch M, Carrió I. Eur J Nucl Med Mol Imaging. 2019; 46(6):1383-1390.

EP-0496

Utility of 18F-fluorocholine PET/CT in the management of primary hyperparathyroidism: our experience.

M. Sicilia Pozo[1], *V. Poblete García*[1], *A. Padilla Bermejo*[1], *C. Lucas Lucas*[1], *M. Contreras Ameduri*[1], *L. García Zoghby*[2], *M. Cruz Montijano*[2], *F. J. Pena Pardo*[1], *M. P. Talavera Rubio*[1], *E. Noriega Álvarez*[1], *A. M. García Vicente*[2], *Á. Soriano Castrejón*[2];
[1]*Nuclear Medicine Department, University General Hospital of Ciudad Real, Ciudad Real, SPAIN,* [2]*Nuclear Medicine Department, University General Hospital of Toledo, Toledo, SPAIN.*

Aim/Introduction: To assess the utility of 18F-fluorocholine PET/CT in the management of primary hyperparathyroidism with negative parathyroid scintigraphy and its association with parathyroid hormone (PTH) level. ***Materials and Methods:*** Retrospective study including successively patients who underwent a 18F-fluorocholine (FCH) PET/CT scan, from June 2019 to November 2022, for diagnostic suspicion of primary hyperparathyroidism, with prior negative localization imaging techniques, including at least a negative parathyroid scintigraphy. We collected clinical variables and PTH level, to evaluate their association with the result of FCH PET/CT scans using Pearson's chi-square test and Spearman's rank correlation coefficient. Additionally, we evaluated the association between FCH PET/CT and surgery results by Fisher's exact test, in those patients that underwent parathyroid surgical intervention in the follow-up. ***Results:*** The cohort included 122 patients (86 women), with a mean age of 60 ± 13.7 years. FCH PET/CT scans were positive for hyperfunctioning parathyroid tissue in 53/122 patients. The median PTH level was 119 pg/ml (41-1899). In the follow up, 28 patients went under surgery, 22 of them with positive result in the FHC PET/TC scan. In 2/6 patients operated with negative FHC PET/CT, no parathyroid adenoma was found. PTH level and FCH PET/CT positivity showed a statistically significant correlation (0.385, $p < 0.001$), with stronger association in the patients that underwent surgery, with a Spearman's coefficient of 0.507 ($p = 0.006$). We found better results in patients with FCH PET-guided surgery, with a statistically significant association between histopathological confirmation and FCH PET/CT positivity ($p = 0.04$). No other significant association was found. ***Conclusion:*** FCH PET-guided surgery shows utility in patients with suspected primary hyperparathyroidism and previous negative imaging techniques, with better results in those patients with higher PTH level.

EP-0497

Role of 18F-DOPA PET/CT imaging in patients with Hyperinsulinemic Hypoglycemia(HI)

S. Sagar, *N. A. Damle, D. Khan, P. Kumar, C. Bal, M. Tripathi, R. Sharma, V. Jain, M. Jana, N. Tandon;*
AIIMS, Delhi, INDIA.

Aim/Introduction: Hyperinsulinemic hypoglycaemia(HI) is a rare but life threatening disease. ^{18}F-DOPA, is known to be useful modality in the localization of focal pancreatic lesions in these patients. We aimed to assess the role of ^{18}F-DOPA in this disease at our institution. ***Materials and Methods:*** ^{18}F-DOPA scans and clinical details of 10 adults and 22 children with clinical diagnosis of HI were reviewed. Scans were acquired 30-45 min post-injection of 2-3 mCi of ^{18}F-DOPA (without carbidopa premedication). The scans were acquired on dedicated PET/CT scanners (Biograph mCT, Siemens Inc and Discovery PET/CT, GE). Only abdominal spot images over 1-2 bed positions were acquired for ^{18}F-DOPA. Additional early images were acquired for adult patients at 5min post injection. ***Results:*** A total of 10 adults and 22 children were included in the study. Out of 22 children (9 female and 13 male), 14 were infants. The age of the children ranged from 1 month to 8 years. Sixteen children had undergone genetic analysis, 13 were positive for ABCC8, 1 for GLUD-1, 1 for GCK mutations and 1 had not showed any mutation. ^{18}F-DOPA PET/CT scan showed 5 focal pancreatic lesions in 5 children (1 in each), two focal lesions in 1 child and diffuse pancreatic uptake in 16 children. Of the 13 ABCC8 mutation positive children, ^{18}F-DOPA PET scan showed focal pancreatic lesion in 5 (38.4%) and diffuse uptake in 8. Of the 7 children who inherited ABCC8 paternal monoallelic recessive mutation, 5 (71.4%) were having focal pancreatic lesions on ^{18}F-DOPA PET scan. One child with GLUD-1 mutation showed multifocal pancreatic uptake, 1 with GCK mutation showed diffuse pancreatic uptake and one child with no mutation on gene analysis showed mild diffuse uptake on PET scan. However, in 6 children with unknown mutation status, ^{18}F-DOPA scan showed diffuse uptake. Out of 10 adults underwent ^{18}F-DOPA PET/CT scan between 2017 to 2023 at our institution. Our results showed diffuse uptake in all 10 patients. Of these 10 patients only one underwent surgery with HPE corroboration of scan findings, other 9 patients on follow up were undergoing medical management. ***Conclusion:*** In children with persistent hyperinsulinemic hypoglycemia, 18F-DOPA PET/CT is an effective method for identifying focal pancreatic lesions but in adults without Carbidopa premedication it doesn't appear useful, and early imaging doesn't substitute for this deficiency. The detection rate is particularly high in paediatric patients with a paternal monoallelic recessive gene mutation in ABCC8.

EP-0498

Efficacy of F-18 Fluorocholine PET/CT in detection of culprit lesions in normocalcemic & hypercalcemic primary hyperparathyroidism: Does it differ?

R. Wakankar, *N. A. Damle, Y. Dharmashaktu, A. Khurana, P. Kumar, C. Bal, M. Tripathi, S. Agarwal, N. Tandon, R. Khadgawat;*
AIIMS, New Delhi, INDIA.

Aim/Introduction: Some patients with primary hyperparathyroidism (pHPT) remain normocalcemic, however, they are susceptible to the adverse effects of pHPT. There is paucity of literature in assessing the role of F-18 Fluorocholine (FCH) PET/CT in this subgroup of patients. We aim to compare the efficacy of FCH PET/CT in localization of culprit lesions in patients of normocalcemic pHPT as compared to hypercalcemic pHPT. ***Materials and Methods:*** Data of 101 patients with clinical and biochemical evidence of pHPT, who underwent an FCH PET/CT in our department from November 2017 to February 2020 were retrospectively analyzed. The scans were acquired 45-60 minutes post-injection of 3-5mCi of FCH from the floor of the orbit to the diaphragm on dedicated PET/CT scanners (Biograph mCT, Siemens Inc and 710 Discovery PET/CT, GE) and the images were reconstructed using OSEM algorithm (iterations=3; subsets=21). FCH PET/CT scan findings were reviewed by two experienced nuclear medicine physicians and the findings were correlated with the biochemical and clinical details of said patients. Histopathology results were considered as the gold standard. ***Results:*** In total 101 patients (61 females; 40 males) were recruited for the study. Surgery was performed in 34 patients (22 with hypercalcemic pHPT; 12 with normocalcemic pHPT), 33 of which were reported positive on FCH scan. FCH scan had a sensitivity and positive predictive value (PPV) of 100% and 95.4%, respectively for hypercalcemic pHPT and a sensitivity and PPV of 91.7% and 100%, respectively for normocalcemic pHPT. ***Conclusion:*** Within the limited subgroup of patients who underwent surgery, these were the findings. The sensitivity of FCH PET/CT was higher in the hypercalcemic pHPT, with a higher PPV being present in the normocalcemic pHPT. The two groups did not differ significantly from each other in terms of their biochemical parameters with the singular exception of their serum Calcium levels.

EP-0499

Does myocardium and liver fractional uptake of circulating fatty acids change after consuming a meal in people with prediabetes?

J. Fernández Fernández[1], *G. Sánchez-Delgado*[2,3,4], *S. Hogan-Lamarre*[4,5], *G. Richard*[4], *F. Frisch*[4], *S. Phoenix*[4,6], *M. Fortin*[3,4], *L. Bouffard*[4], *C. Noll*[4], *W. Mampuya*[4], *B. Guérin*[4,6], *É. E. Turcotte*[4,6], *J. Hoeks*[7], *P. Schrauwen*[7], *A. C. Carpentier*[3,4], *D. P. Blondin*[4,8];
[1]*Department of Nuclear Medicine, Virgen de las Nieves University Hospital, Granada, SPAIN,* [2]*Institute of Nutrition and Food Technology "Jose Mataix" and University Institute of Sports and Health, University of Granada, Granada, SPAIN,* [3]*Department of Medicine, Division of Endocrinology, Université de Sherbrooke, Sherbrooke, QC, CANADA,* [4]*Centre de recherche du Centre hospitalier universitaire de Sherbrooke, Sherbrooke, QC, CANADA,* [5]*Department of Pharmacology-Physiology, Université de Sherbrooke, Sherbrooke, QC, CANADA,* [6]*Department of Nuclear Medicine and Radiobiology, Université de Sherbrooke, Sherbrooke, QC, CANADA,* [7]*Department of Nutrition and Movement Sciences, NUTRIM School of Nutrition and Translational Research in Metabolism, Maastricht University Medical Center, Maastricht, NETHERLANDS,* [8]*Department of Medicine, Division of Neurology, Université de Sherbrooke, Sherbrooke, QC, CANADA.*

Aim/Introduction: The increased uptake and accumulation of fatty acids in lean tissues is a causal factor in the development of insulin resistance and type 2 diabetes mellitus. The uptake rate of non-esterified fatty acids (NEFA) by lean tissues depends on NEFA plasma concentrations and the fractional extraction by the tissue. Because NEFA concentration is regulated by insulin action, it is largely modified during the postprandial period. However, whether the fractional uptake of NEFA in key organs such as the liver and the heart vary between fasted and postprandial periods has never been assessed. Here, we aim to compare the heart and liver fractional NEFA uptake of individuals with prediabetes between the fasting and postprandial states. ***Materials and Methods:*** Twelve people with prediabetes have already participated in this ongoing study. Of them, four have available

data at the time of submitting this abstract (2 men / 2 women; 53-70 years old; Body mass index: 28.6-30.9 kg/m^2). Participants arrived at the research center early in the morning after an overnight fast, and consumed a standardized liquid meal (400 mL, 854 Kcal, 33.1% fat, 17.2% protein and 49.8% carbohydrates) after a ~3-hour resting period. Before and after consuming the meal, a 30-minute dynamic [^{11}C]-palmitate positron emission tomography scan, combined with a computerized tomography of the thoraco-abdominal area, was performed. The liver NEFA fractional uptake was calculated following the model proposed by Iozzo et al.(1), whereas the calculation of the heart´s fractional uptake rate was performed following de Jong et al.'s model(2). ***Results:*** The study is ongoing, but we observed a trend towards an increase in both the liver (0.35±0.06 vs 0.40±0.11 min^{-1}, increased in 3 out of 4 participants) and heart (0.24±0.02 vs 0.30±0.05 min^{-1}, increased in all 4 participants) NEFA fractional uptake rate in the first 4 participants. ***Conclusion:*** This study will unravel whether the fractional NEFA uptake of key lean organs varies along the fasting and feeding cycle. These findings will contribute to a better understanding of the pathophysiology of type 2 diabetes and will be very informative for the design of future studies investigating fatty acid metabolism in humans. ***References:*** 1. Iozzo, P. et al. Fatty acid metabolism in the liver, measured by positron emission tomography, is increased in obese individuals. Gastroenterology 139, 846-56, 856.e1-6(2010). 2. de Jong, H. W. A. M. et al. Kinetic models for analysing myocardial [(11)C]palmitate data. Eur. J. Nucl. Med. Mol. Imaging 36, 966-78(2009).

EP-0500

Incremental value of Tc-99m-sestamibi SPECT/CT in patients with positive planar scintigraphy in the detection of additional lesions in patients with Secondary/Tertiary hyperparathyroidism

R. Goel, *N. A. Damle, Y. Dharmashaktu, C. Bal, P. Kumar, A. Kumar, Y. Gupta, R. Aphale, G. Puri, S. Chumber;*
All India Institute of Medical Sciences (AIIMS), New Delhi, INDIA.

Aim/Introduction: Tc-99m-sestamibi scintigraphy is of value in non-invasively localizing abnormal parathyroid glands before surgical exploration as well as for ruling out ectopic glands in patients with secondary/tertiary hyperparathyroidism. However, most centres in India restrict to planar scintigraphy rather than SPECT/CT. In this retrospective analysis, we aim to demonstrate the incremental value of Tc-99m-sestamibi SPECT/CT over planar scintigraphy in detecting additional culprit lesions in patients with secondary/tertiary hyperparathyroidism. ***Materials and Methods:*** We retrospectively reviewed data of 313 patients (205 female, 108 males; age 2.5-80 years) with biochemical evidence of hyperparathyroidism referred from Endocrinologists(mainly from our institute) between January 2021 to December 2022. All patients were injected with 20mCi of Tc-99m-sestamibi intravenously. Planar images were acquired at 15-minute, 50-minute, and 2-hour intervals. SPECT/CT images were acquired at 50 minutes. The imaging findings were correlated with histopathology. ***Results:*** Out of the total 313 patients, 94(61-female, 33-male; age 2.5-72years) had secondary/tertiary hyperparathyroidism with a mean iPTH of 1351.2 pg/mL. In patients with tertiary hyperparathyroidism, planar scintigraphy was positive for presence of hyperfunctioning parathyroid in 30/94 patients(31.9%), while SPECT/CT detected lesions over and above planar imaging in 21/30 patients(70%). In these 21 patients, planar imaging detected a total of 33 lesions, of which 3 were in right superior location, 14 in right inferior, 5 in left superior and 11 in left inferior.SPECT/CT of these 21 patients revealed 27 additional lesions of which 8 were in right superior location, 6 in right inferior, 9 in left superior and 4 in left inferior location. Of the 27 additional lesions on SPECT/CT, 5 were considered positive, 16 suspicious and 6 indeterminate for a parathyroid adenoma. 16/27 of these lesions were less than 1cm in longest axis dimension and therefore likely to be missed on planar imaging.4/21 patients underwent surgery and 14 supposed lesions were excised in total. On a per patient analysis, SPECT/CT correctly identified lesions over and above planar imaging in 4/4 patients. On a lesion-based analysis, 14/14 lesions resected during surgery were positive on histopathology for adenoma/hyperplasia. 7/14 lesions were described in planar and SPECT/CT imaging. 5/14 were described only in SPECT/CT images. 1/5 lesions were given as positive and 4/5 as suspicious for a parathyroid adenoma/hyperplasia. 2/14 lesions were not described on either. ***Conclusion:*** Tc-99m-sestamibi SPECT/CT provides incremental value over planar scintigraphy in the detection of additional lesions thus reducing the possibility of failed parathyroidectomy in patients with secondary/tertiary hyperparathyroidism.

EP-0501

Predictive value of preoperative 18F-Flurocholine PET/CT in bone mineral density improvement after parathyroidectomy in primary hyperparathyroidism.

S. Seyedinia[1], *S. Mirshahvalad*[2,1], *T. Kiener*[1], *H. Kässmann*[1], *M. Beheshti*[1], *C. Pirich*[1];
[1]*Division of Molecular Imaging & Theranostics, Department of Nuclear Medicine, University Hospital Salzburg, Paracelsus Medical University, Salzburg, AUSTRIA,* [2]*Joint Department of Medical Imaging, University Health Network, University of Toronto, Toronto, ON, CANADA.*

Aim/Introduction: To evaluate the predictive value of semi-quantitative metabolic parameters derived by 18F-Flurocholine PET/CT (FCH PET/CT) in bone mineral density (BMD) changes after parathyroidectomy in patients with clinical diagnosis of primary hyperparathyroidism (PHP). ***Materials and Methods:*** Imaging and clinical findings of 71 Patients (62 female, 9 male, mean age: 65.80± 13.3) with clinical diagnosis of PHP and histopathologically proven parathyroid adenoma were analysed in this retrospective study. Inclusion criteria were FCH PET/CT imaging prior to the parathyroidectomy as well as pre-and postoperative follow-up dual energy X-ray absorptiometry (DXA). Semi-quantitative FCH-PET parameters (SUVmax, SUVmean, SULpeak, and SULmean) and metabolic short-axis diameter (mSAD) of the detected parathyroid lesions were extracted. Successful surgery was assessed by histopathological and follow-up laboratory data. The patients were divide into two groups of responder and non-responder according to the BMD changes between pre and postoperative follow-up DXA scans. Main outcome measure was percentage of BMD-change on lumbar spine (LS). Predictors were dichotomised via the receiver operating characteristics curve to find the best coordinate point. ***Results:*** On the post-operative follow-up BMD examinations, the distal radius region showed the lowest improvement (p-value = 0.01), while the lumbar spine and neck of femur had a comparable significant improvement (p-value>0.05).On univariate analysis, SULmean and mSAD were significantly associated with improvement of bone mineral density on follow-up LS-BMD (p<0.05). On multivariate analysis, SULmean was the most sensitive (72%) and specific (70%) predictor of BMD-response to surgery. Moreover, a cutoff SULmean value of >2.95 of the resected lesions were highly predictive of LS-BMD improvement

showing responder in 92% of cases. ***Conclusion:*** FCH PET/CT not only appears to be a promising functional imaging modality for accurate detection and localization of parathyroid adenomas (1), but also may independently predict BMD improvement after surgery. SULmean of parathyroid adenomas detected by FCH PET/CT was the most sensitive and specific semi-quantitative metabolic parameter for predicting treatment response. Quantitative metabolic FCH-PET imaging parameters could potentially be incorporated into clinical prediction models to identify PHP patients, who could benefit from active surveillance and prophylactic treatment approaches after parathyroidectomy. ***References:*** 1.Beheshti et al. 18F-Fluorocholine PET/CT in the assessment of primary hyperparathyroidism compared with 99mTc-MIBI or 99mTc-tetrofosmin SPECT/CT: a prospective dual-centre study in 100 patients. Eur J Nucl Med Mol Imaging. 2018 Sep;45(10):1762-1771.

EP-0502

18F-Choline PET/CT in the detection of parathyroid adenomas hidden from conventional imaging techniques

E. López Llobet*, C. Lancha Hernandez, L. Domínguez Gadea, J. Cordero García, S. Rizkallal Monzon, D. Monachello Araujo, Y. Abadi Sedraoui, L. Giraldo Gonzalez, P. Portilla Merino; Hospital Universitario La Paz, Madrid, SPAIN.*

Aim/Introduction: Preoperative detection of pathological parathyroid glands in primary hyperparathyroidism(PPH) currently plays an essential role in surgical planning, increasing success rates, simplifying surgical approach and associated comorbidities. However, a small percentage of patients (around 20-30%) present false negatives in conventional imaging techniques (neck ultrasonogrohpy, 99mTc-sestamibi SPECT-CT). The objective of our study was to analyze the usefulness of 18F-CholinePET-CT in the detection of parathyroid adenomas in patients with previous negative localization techniques. ***Materials and Methods:*** Sixty-five patients diagnosed of PPH, with surgical criteria and negative conventional tests, were retrospectively reviewed.In all of them a PET/CT was performed in a Siemens Biograph system, 30 min after the intravenous injection of 4MBq/Kg of 18F-Fluorocholine. PET/CT acquisitions were performed from the skull base to the diaphragm.All focal 18F-fluorocholine uptakes more intense than the background tissue with correlation in the CT (nodular lesion located in the cervical o mediastinal area), were considered positive.When a low intensity focal uptake with no clear morphological correlation was detected, the PET/CT was considered doubtful.Every finding location was described according to its position regarding the thyroid gland (left/right, superior/inferior or ectopic)All patients underwent surgery.Sensitivity and positive predictive value (PPV) of PET/CT were calculated. Demographic variables, clinical and biochemical parameters, as well as surgical procedure were analyzed. ***Results:*** A total of 65 patients were included, mean age of 61 years and female predominance (92%). The mean levels of preoperative biochemical parameters were: PTH 134pg/mL, Ca 10.67mg/dL, VitD 38.76ng/mL, and a mean post-operative PTH level of 29.95pg/mL. 62 patients had single adenomas and the remaining 3 had double adenomas, a total of 68 adenomas were analyzed.PET/CT detected 62/68(91%) parathyroid adenomas, 60 of them were single adenomas and in one patient 1 double adenoma was detected.There were 5/68(7%) false negatives. Three of them were single adenomas and the remaining two had a second contralateral adenoma not detected by the PET/CT.In 1/68(2%) PET/CT was considered doubtful and was subsequently confirmed histologically as a single parathyroid adenoma. Sensitivity was 92% and PPV 98%. Minimally invasive techniques were used in 55(85%) patients, and in the remaining 10(15%) bilateral cervical exploration was performed: 3 patients without preoperative localization, 3 with double adenoma and 4 by surgeon's decision. ***Conclusion:*** PET/CT with 18F-Fluorocholine is a technique with high sensitivity and PPV for the detection of parathyroid adenomas in patients with negative conventional imaging.This could reduce the frecuency of extensive surgeries and therefore their associated comorbidities.

EP-0503

PET/CT with 18F-choline in the study of primary hyperparathyroidism: evaluation of the technique, and correlation with histopathological and biochemical findings

E. Campaña Díaz*, P. García-Talavera San Miguel, J. Alvarez Pérez, F. Gómez-Caminero López, C. Montes Fuentes, A. Peñaherrera Cepeda, J. Badell Martinez, S. Rama Alonso, M. Tamayo Alonso; Hospital Universitario de Salamanca, Salamanca, SPAIN.*

Aim/Introduction: Assess the efficacy of 18F-Choline in the localization of primary hyperparathyroidism (pHPT) with negative or doubtful imaging techniques, analyzing the dual point imaging protocol. To correlate fluorocholine uptake with biochemical parameters and glandular weight. ***Materials and Methods:*** We included 20 patients (14 females; 56.3 ± 14.4 years) in whom 18F-Choline PET/CT was performed for pre-surgical localization of pHPT in cases with negative or doubtful imaging techniques. Standard 18F-Choline images were acquired 5 and 60 minutes after 185 MBq intravenous administration. PET/CT results were correlated with intraoperative histopathological findings and biochemical parameters. Calcium and iPTH were collected after surgery to ensure success. Initial and delayed images were assessed visually and semiquantitatively with pathological parathyroid SUVmax (P-SUVmax), thyroid gland SUVpeak (T-SUVpeak) and mediastinum SUVpeak (M-SUVpeak). Pearson's chi-squared test was used to calculate the correlation between P-SUVmax with calcium, PTH and adenoma size. Mann-Whitney U test was used to evaluate the differences between initial vs delayed P-SUVmax, T-SUVpeak, P-SUVmax/T-SUVpeak index and P-SUVmax/M-SUVpeak index. ***Results:*** In surgery the pathological gland was located in 19 cases (18 solitary adenomas, 1 double adenoma). PET/CT was positive in 17/19, one of them with multiglandular disease was not detected by PET/CT. 2/19 had negative PET/CT (one with multiglandular disease, not localized in any imaging technique).The patient in whom parathyroid adenoma was not found during surgery was a false positive because of papillary thyroid carcinoma on PET/CT.The detection rate per patient is 89.5%, and per lesion 81%. In the visual analysis of the 17 positive cases: in 7 delayed images offer relevant information, in 4 initial images, in 6 cases both images provide the same information.In the semiquantitative analysis the initial P-SUVmax (5.0 ±2.26) did not increase in the delayed images (4.65 ± 2.71). The initial (3.19± 1.5) vs delayed (2.64 ± 1.2) T-SUVpeak showed statistical significance (p=0.03); P-SUVmax/T-SUVpeak index did not show significant differences initial vs delayed (1.61±0.57 vs 1.83±0.82); P-SUVmax/M-SUVpeak index initial vs delayed (3.43±2.14 vs 5.17±2.45) had statistical significance (p=0.014).There was correlation between P-SUVmax and adenoma weight (initial: p=0.93; delayed: p=0.94), and with pre-surgical PTH (initial: p=0.67; delayed: p=0.79). No correlation was observed

with pre-surgical calcium. ***Conclusion:*** 18F-Choline PET/CT is a recommended preoperative localization technique in patients with hyperparathyroidism with negative or doubtful imaging techniques, showing good correlation with histopathological and biochemical findings. Dual time point imaging is necessary for localization of pathological parathyroid gland in more than half of the cases (65%).

EP-0504

Role of [18F]F-choline PET/TC for presurgical identification of hyperfunctioning parathyroid glands in patients with primary hyperparathyroidism and inconclusive conventional imaging

P. Azpeitia Hernández, *O. Ajuria Illarramendi, A. Martínez Lorca, P. Paredes Rodríguez, T. Navarro Martínez, U. Vera Schmülling, M. Gutiérrez Guerrero, M. Orduña Díez;*
Hospital Universitario Ramón Y Cajal, Madrid, SPAIN.

Aim/Introduction: Primary hyperparathyroidism (HPT) is an endocrine disorder caused by hyperfunctioning parathyroid, and for those patients with surgical criteria, localization is essential. Therefore, when ultrasound and/or [99Tc]Tc-MIBI parathyroid scintigraphy (conventional imaging) are negative or inconclusive, more accurate images are required. We evaluate [18F]F-choline PET/TC role in the presurgical identification of hyperfunctioning parathyroid glands in patients with primary hyperparathyroidism and inconclusive conventional imaging. Check if there is a correlation between preoperative PTH versus [18F]F-choline PET/TC findings. ***Materials and Methods:*** A retrospective study between September 2020 and December 2022 of patients with primary HPT presenting previous negative or inconclusive ultrasound and/or parathyroid scintigraphy, performing [18F]F-Choline-PET/CT (two phases), assessed visually and semiquantitatively. Histopathological correlation was the standard reference technique. In addition, laboratory values (PTH and calcemia) prior to diagnostic tests and their correlation with [18F]F-Choline-PET/CT results were analyzed. ***Results:*** Fifty-six patients (mean age 61.5 (±10.7) years; 73.2% women) with primary HPT and surgical criteria (51.8% osteoporosis) were included. In addition, 83.9% had cervical ultrasound (83.9% negative, 16.1% doubtful) and all [99mTc]Tc-MIBI scintigraphy-SPECT/CT (78.6% negative, 21.4% doubtful). [18F]F-Choline-PET/CT (Dose 191.41±19.9MBq) detected 64.3% positive, 32.1% negative, and 3.6% doubtful. Positive parathyroid lesions: mean size 7.4mm(r3-17), early SUVmax 3.8±1, and late SUVmax 3.7±1. Location rate: posterior lower right (31.6%) and left (26.3%), posterior upper right (7.9%) and left (7.9%), and right tracheoesophageal groove (7.9%).25% (14/56) underwent surgery with [18F]F-Choline-PET/CT positive, surgically removed with pathological confirmation of adenomas (sensitivity 100%). PTH: pre-surgical 103.5pg/ml(71.4-218, 7pg/ml) with post-surgical normalization: 42.9pg/ml (10.4-70pg/ml). The remaining 73.2% (41/56): 13 who did not undergo surgery (3 rejected surgery with positive [18F]F-Choline-PET/CT and 10 due to negative [18F]F-Choline-PET/CT), .28 pending reassessment (75%[18F]F-Choline-PET/CT positive).Laboratory data prior to ultrasound PTH 119.6pg/ml(70.9-196pg/ml), Ca 10.1mg/dL(±0.6mg/dL); scintigraphy PTH 122pg/ml(70.9-214.4pg/ml), Ca 10.2mg/dL(±0.7mg/dL); [18F]F-Choline-PET/CT PTH 117.4pg/ml (64.6-233.7pg/ml), Ca 10.2mg/dL(±0.7mg/dL).Despite the small sample size, statistical significance ($p<0.05$) was observed between PTH prior to [18F]F-Choline-PET/CT with size (Spearman=0.4; p=0.016), early SUVmax (Spearman=0 .45;p=0.005) and result [18F]F-Choline-PET/CT (Spearman=0.3;p=0.039). ***Conclusion:*** [18F]F-Choline PET/CT is a very sensitive hybrid technique for localizing parathyroid adenomas in primary HPT with inconclusive ultrasound and/or [99mTc]Tc-MIBI scintigraphy-SPECT/CT, facilitating surgical treatment and therefore PTH normalization. In addition, there is a significant correlation between PTH with size, early SUVmax, and [18F]F-Choline PET/CT positivity.

EP-0505

Role of 99mTechnetium Sestamibi SPECT/CT in patients with negative planar scintigraphy in lesion localization in patients with hyperparathyroidism

Y. Dharmashaktu, *N. A. Damle, R. Goel, C. Bal, P. Kumar, S. Chumber, G. Puri, R. Aphale;*
All India Institute of Medical Sciences, Delhi, INDIA.

Aim/Introduction: ^{99m}Tc-SestaMIBI scintigraphy is a widely used first line non-invasive imaging modality for detection of culprit lesions in patients with hyperparathyroidism. Although SPECT/CT has higher sensitivity and specificity over planar imaging, many facilities only perform planar scintigraphy. Here we demonstrate the role of SEPCT/CT in lesion detection in patients with hyperparathyroidism. ***Materials and Methods:*** 318 patients with hyperparathyroidism (HPT) were retrospectively evaluated who underwent ^{99m}Tc Sestamibi scintigraphy from January 2021 to January 2023. Patients were injected with 20 mCi of ^{99m}Tc Sestamibi intravenously and planar images were taken at 15 mins, 50 mins and 2 hours post injection along with early SPECT/CT at 50 min interval. Lesions were graded as positive, suspicious and indeterminate by a Nuclear Medicine physician. ***Results:*** 136/318 patients were negative on planar scintigraphy. Of those 136 patients (84 were females and 52 were males), 75 patients (46 primary HPT and 29 secondary/ tertiary HPT patients) were negative on both planar scintigraphy and SPECT/CT and rest 61 patients had atleast one lesion on SPECT/CT (27 primary HPT and 34 secondary/tertiary HPT patients). In 27 primary HPT patients, mean iPTH was 197.8 pg/ml and mean age was 45.6 years. SPECT/CT detected 38 lesions (3 ectopic, 10 in right superior, 11 in right inferior, 7 in left superior and 7 in left inferior location). 2 lesions were graded as positive, 24 were suspicious and 12 were indeterminate. 3 ectopic lesions were located in superior mediastinum and right cervical level III & IV (1 in each location). In 34 secondary/ tertiary HPT patients, mean iPTH was 1160 pg/ml and mean age was 37.5 years. SPECT/CT showed 62 lesions (19 in right superior, 17 in right inferior, 16 in left superior and 10 in left inferior location). 5 lesions were graded as positive, 22 were suspicious and 35 were indeterminate. 7/61 patients underwent surgery and 11 supposed lesions were excised. Histopathology of excised glands revealed, 8 adenomas, 2 hyperplasia, and 1 normal gland.On a lesion-based analysis, of these 11 lesions, 1 was given as positive, 6 as suspicious, and 3 as indeterminate on SPECT/CT for a parathyroid adenoma. 1 lesion was not described in SPECT/CT images. ***Conclusion:*** Combined interpretation of ^{99m}Tc Sestamibi planar scintigraphy and SPECT/CT helps in better localization and identification of additional suspicious lesions needing correlation with other modalities so as to define the exact kind of surgery required potentially reducing chances of persistent/recurrent HPT.

EP-0506

[18F]fluorocholine positron emission tomography/computed tomography characterization of benign thyroid nodules

K. Bajuk Studen[1,2], *S. Rep*[1], *S. Gaberscek*[1,2], *K. Zaletel*[1,2], *E. Skorjanec Armic*[1], *L. Lezaic*[1,2];
[1]*University Medical Centre Ljubljana, Ljubljana, SLOVENIA,*
[2]*Medical Faculty, University of Ljubljana, Ljubljana, SLOVENIA.*

Aim/Introduction: [^{18}F]fluorocholine (FCH) positron emission tomography/computed tomography (PET/CT) has gained an important role in the preoperative diagnosis of patients with primary hyperparathyroidism (pPHP). In these patients, thyroid nodules are frequently found on preoperative ultrasound. FCH PET/CT provides a high negative predictive value to reliably

exclude cancer in thyroid nodules with low uptake[1]. However, more than half of benign thyroid nodules have been reported to have high uptake of FCH. The aim of our study was to evaluate the characteristics of FCH PET/CT uptake in benign thyroid nodules. ***Materials and Methods:*** A retrospective study was performed in patients with pPHP who were investigated by FCH PET/CT and concomitantly diagnosed with thyroid nodules larger than 1 cm on neck ultrasound. [^{99m}Tc]pertechnetate scan was performed in all patients, and benign nature of the nodules was confirmed by either high uptake or by fine-needle aspiration biopsy in patients with low uptake. Neck PET/CT acquisitions were performed 10 (early) and 60 (late) minutes after injection of 1.3 MBq/kg FCH, and maximum standardized uptake value (SUV max) of the nodules was measured. ***Results:*** Thirty-four patients (30/88.2% female, mean age 66.9±9.3 years) with 34 (15/44% hypofunctioning, 19/56% hyperfunctioning) thyroid nodules were included. A trend towards positive but non-significant correlation (r=0.3, p=0.09) of thyroglobulin level (mean 37.5±38.3 µg/L) with early SUVmax was observed, but no further statistically significant correlation of early or late SUVmax with TSH (mean 1.3±0.8 mIU/L), free T_4 (mean 15.3±2.0 pmol/L), free T_3 (mean 4.9±0.7 pmol/L), thyroid peroxidase antibodies level (median 30.0±253.5 kU/L) or nodule volume (mean 4.5±4.9 mL) was observed. Mean early SUVmax was 5.2±1.8; no difference in SUVmax was detected between hyperfunctioning and hypofunctioning thyroid nodules (mean, 4.9±1.8 and 5.6±1.7, respectively, p=0.28). The mean late SUVmax was 4.3±1.8; no difference in SUVmax was found between hyperfunctioning and hypofunctioning thyroid nodules (mean, 4.3±2.1 and 4.4±1.3, respectively, p=0.42). ***Conclusion:*** Biochemical parameters of thyroid function and autoimmunity do not correlate with FCH uptake in benign thyroid nodules. Hypofunctioning and hyperfunctioning thyroid nodules do not differ significantly in FCH uptake. Further studies should identify those characteristics of benign thyroid nodules that contribute to high uptake on FCH PET/CT scans to increase the specificity of FCH PET/CT in detecting malignant thyroid nodules. ***References:*** 1. Ciappuccini R, et al. [18]F-flurocholine positron emission tomography/computed tomograhy is a highly sensitive but poorly specific tool for identifying malignancy in thyroid nodules with indeterminate cytology: The Chocolate Study. Thyroid 2021; 31 (5): 800-809.

EP-0507

Diagnostic Performance of C-X-C Motif Chemokine Receptor 4-directed PET/CT in Patients with Advanced Adrenocortical Carcinoma

W. Schlötelburg[1], *A. Kosmala*[1], *P. E. Hartrampf*[1], *S. E. Serfling*[1], *A. Schirbel*[1], *M. Fassnacht*[2], *A. K. Buck*[1], *S. Hahner*[2], *R. A. Werner*[1,3]; *[1]Department of Nuclear Medicine, University Hospital Würzburg, Würzburg, GERMANY, [2]Division of Endocrinology and Diabetes, Department of Medicine I, University Hospital Würzburg, Würzburg, GERMANY, [3]The Russel H Morgan Department of Radiology and Radiological Science, Johns Hopkins University School of Medicine, Baltimore, MD, UNITED STATES OF AMERICA.*

Aim/Introduction: C-X-C motif chemokine receptor 4 (CXCR4) is highly expressed in adrenocortical cancer (ACC) tumor lesions and thus, may emerge as a theranostic target in those difficult-to-treat patient population (1). Therefore, we aimed to determine the diagnostic performance of CXCR4-directed [^{68}Ga]Ga-PentixaFor relative to [^{18}F]FDG PET/CT in patients with metastatic ACC and to identify individuals eligible for CXCR4-directed radioligand therapy (RLT) in a theranostic approach. ***Materials and Methods:*** 33 patients with advanced ACC which had exhausted previous treatment options underwent [^{68}Ga]Ga-PentixaFor PET/CT to determine eligibility for RLT. In all subjects, concurrent [^{18}F]FDG PET/CT were also available. We then compared staging results and tumor-to-background ratios (TBR, to evaluate image contrast) between [^{68}Ga]Ga-PentixaFor and [^{18}F]FDG PET. For TBR assessment, the entire tumor burden was investigated. Moreover, patients eligible for CXCR4-RLT were also determined based on molecular imaging. ***Results:*** When compared with [^{18}F]FDG PET/CT, staging changes were recorded in 12/33 (36.4%) instances based on [^{68}Ga]Ga-PentixaFor PET/CT. Among those subjects, upstaging was seen in 5/33 (15.2%), and downstaging in 7/33 (21.2%). In those five patients with upstaging, the following additional lesions were observed on CXCR-directed imaging: multiple liver metastases in 3/5 (60.0%), cerebral metastasis in 1/5 (20.0%) and vascular infiltration in the remaining subject (20.0%). In the 7 downstaged patients, [^{68}Ga]Ga-PentixaFor missed lesions in the following organ compartments: lung in 4/7 (57.1%), soft tissue in 2/7 (28.6%) and lymph nodes and liver in 3/7 (42.9%), respectively. TBR were higher on [^{68}Ga]Ga-PentixaFor PET (8.43 ± 4.88) when compared to [^{18}F]FDG (4.39 ± 2.94, P<0.001), indicative for better contrast in sites of disease accumulating [^{68}Ga]Ga-PentixaFor. In addition, 18/33 (54.5%) patients were considered eligible for CXCR4-targeted RLT based on molecular imaging. ***Conclusion:*** Despite improved image contrast with intense radiotracer accumulation in sites of disease, CXCR4-directed PET/CT led to inappropriate downstaging due to missed lesions in a substantial number of subjects when compared to [^{18}F]FDG. Nonetheless, over half of patients were considered eligible for RLT using ß-emitting therapeutic equivalents in a theranostic setting. Funding: IZKF Z-2/91 ***References:*** (1) ClinNuclMed. 2017 Jan;42(1):e29-e34. doi: 10.1097/RLU.0000000000001435. Investigating the Chemokine Receptor 4 as Potential Theranostic Target in Adrenocortical Cancer Patients Christina Bluemel, Stefanie Hahner, Britta Heinze, Martin Fassnacht, Matthias Kroiss, Thorsten A Bley, Hans-Juergen Wester, Saskia Kropf, Constantin Lapa, Andreas Schirbel, Andreas K Buck, Ken Herrmann

EP-0508

Minimally Invasive Radio-Guided Parathyroidectomy in Patients with Hyperparathyroidism: Experience at Our Center

N. Calviño, *D. Villasboas-Rosciolesi, M. De Bonilla-Candau, A. Ciscar, A. Martin del Rey, J. Echeverri-Díaz, S. Asadurova, F. Velazquez, R. Bellviure-Meiro, A. García-Burillo; Hospital Universitario Vall de Hebron, Barcelona, SPAIN.*

Aim/Introduction: This study aimed to retrospectively analyze the results of the ROLL technique in our center, including the injection site, intraoperative detection rate of parathyroid glands, postoperative complications, and re-operation. ***Materials and Methods:*** Between January 2021 and August 2022, 89 patients (66 female) with hyperparathyroidism were included in the study. All patients underwent preoperative detection tests (neck ultrasound, [99mTc]Tc-MIBI scintigraphy, [18F]fluorocholine PET/CT) to detect affected glands. Of the 89 patients, 47 (52.8%) underwent the ROLL technique. Patients were administered between 14-185 MBq of [99mTc]Tc-MAA intralesional or perilesional, guided by ultrasound, and subsequently SPECT/CT (GE Discovery 670) was performed to confirm the location. On the day of surgery, a gamma probe (EuroProbe3.2) was used to detect the marked lesion, and intraoperative PTH monitoring was performed to assess the success of the extraction. The final diagnosis was confirmed by histopathological analysis, and clinical and analytical follow-up

of the patients was conducted. ***Results:*** Forty-seven patients (35 women, mean age 59.8 years [range 22-80]) underwent ROLL. Conventional ultrasound and, [99mTc]Tc-MIBI scintigraphy detected the affected gland in 15 (32%) patients, while ultrasound and [18F]fluorocholine PET/CT detected it in 7 (15%) patients. [18F]fluorocholine PET/CT alone detected the affected gland in 7 (15%) patients (6 of whom had negative ultrasound and [99mTc]Tc-MIBI scintigraphy, and 1 of whom had negative ultrasound). [99mTc]Tc-MIBI and [18F]fluorocholine detected the affected gland in 6 (13%) patients, [99mTc]Tc-MIBI alone in 6 (13%) patients, all three methods in 5 (10%) patients, and ultrasound alone in 1 patient. Based on SPECT-CT images, the radiopharmaceutical was administered intralesionally in 28 patients (59%) and perilesionally in 9 patients (19%). A total of 52 glands were surgically removed, with a 100% detection rate. Histopathological analysis identified 36 adenomas, 13 hyperplasias, and 3 non-pathological parathyroid tissues. Only 3 patients (6%) experienced surgical complications, all of which were dysphonia. Only one patient required surgical reintervention. ***Conclusion:*** Our results showed a high rate of lesion detection using the ROLL technique, allowing for a minimally invasive procedure with a low percentage of complications and need for reintervention.

EP-0509

Diagnostic performance of 18FCH-PET/CT in Primary Hyperparathyroidism: semiquantitative analysis and correlation with biochemical data

C. Ferrari, *F. Iuele, M. Frugis, P. Mammucci, C. Palumbo, A. Di Palo, G. Rubini;*
Nuclear Medicine Department, University of Bari "Aldo Moro", Bari, Italy, Bari, ITALY.

Aim/Introduction: The detection of hyperfunctioning parathyroid gland(s) (HPTG) in patients with primary hyperparathyroidism (PHPT) with negative/inconclusive first-line imaging is a significant challenge. In this setting, ^{18}FCH-PET/CT has shown promising results, suggesting superiority over ^{99m}Tc-MIBI parathyroid scintigraphy (MIBI-scintigraphy). We aim to assess the diagnostic performance of ^{18}FCH-PET/CT in the detection of HPTG in patients with PHPT, considering both visual and semiquantitative analysis, and its comparison with MIBI-scintigraphy. ***Materials and Methods:*** We prospectively enrolled 42 PHPT patients (6 men, 45 women; mean age 62y) who performed ^{18}FCH-PET/CT preoperatively. Thirty/42 patients had a previous negative/inconclusive MIBI-scintigraphy. SUVmax and MTV were recorded for positive ^{18}FCH-PET/CT findings. PTH and serum calcium levels were also collected together with histopathology, if available. Correlation between ^{18}FCH-PET/CT detection rate and PTH was assessed using Mann-Whitney U test. PET semiquantitative parameters and laboratory values were correlated using the Spearman coefficient. ROC curve analysis was used to find: 1)a PTH cut-off predictive of a positive scan and 2)semiquantitative parameters predictive of positive histopathology. The agreement between ^{18}FCH-PET/CT and MIBI-scintigraphy results as well as between ^{18}FCH-PET/CT and histological findings was assessed using Cohen's K test. A p>0.05 was considered statistically significant. ***Results:*** ^{18}FCH-PET/CT was positive in 34/42 (81%) PHPT patients. SUVmax and MTV mean values were 7.13 (±4.33; range:2.4-18.8) and 1.78 cm^3 (±2.41; range:0.1-13.4) respectively. PTH and serum calcium mean values were 169.59 pg/ml (±16.97; range:26.9-958.9) and 10.78 mg/dl (±1.31; range:7.7-13.4) respectively. A strong positive correlation between ^{18}FCH-PET/CT detection rate and preoperative PTH (p<0.00001) was observed. A significant correlation was found between preoperative calcium levels and both SUVmax (p=0.00005) and MTV (p=0.00084). Applying ROC curves, a PTH of 90.15 pg/ml was predictive of a positive PET (AUC 0.78, 95%CI 0.57-0.99, sensitivity 73.5%, specificity 75%), while a SUVmax of 4.5 (AUC 0.88, 95% CI 0.70-1, sensitivity 75%, specificity 100%) and MTV of 1.5 cm^3 (AUC 0.63, 95%CI 0.29-0.96, sensitivity 42%, specificity 100%) significantly predicted a positive histopathology. MIBI-scintigraphy was positive in 12/30 (40%). Compared with ^{18}FCH-PET/CT results, 12/30 were positive-concordant, 4/30 negative concordant, 14/30 discordant, with a slight agreement (k=0.18). Histopathology was available in 26/34 patients: 24/26 positive-concordant and 2/26 discordant. A strong agreement was observed between ^{18}FCH-PET/CT and histological findings (k=0.85) ***Conclusion:*** Our preliminary results supported the use of ^{18}FCH-PET/CT for the diagnosis of HPTG, showing better performance over MIBI-scintigraphy. Choline metabolism correlated with both PTH and calcium level. Semiquantitative analysis could help in imaging interpretation and histopathology prediction.

EP-0510

Usefulness of 18F-Choline PET/CT in localizing hyperfunctioning parathyroid glands with negative 99mTc-MIBI scintigraphy and its correlation with pathological findings

I. Garrido Solesio, *K. Velásquez Díaz, P. Meneses Soares, A. Grajeda Gallardo, I. Obedkova, L. Santamaría Chico, M. Mitjavila Casanovas, A. Prieto Soriano;*
Hospital Universitario Puerta de Hierro, Madrid, SPAIN.

Aim/Introduction: Primary hyperparathyroidism (HPT) is an endocrine disorder with an alteration of the parathyroid hormone (PTH) secretion that affects the regulation of calcium and phosphorus metabolism. It is usually caused by single adenomas (80%), hyperplasia (10-15%), multiple adenomas (5%), or parathyroid cancer (<1%).The only curative treatment is surgery, therefore, pre-surgical detection of hyperfunctioning glands is a crucial step. The objective of this study is to correlate the ^{18}F-Choline PET/CT findings with the pathological findings after surgery in patients with negative MIBI scan. ***Materials and Methods:*** Retrospective analysis of patients with primary hyperparathyroidism diagnosis who had surgical criteria, a negative ^{99m}Tc-MIBI scintigraphy and ^{18}F-Choline PET/CT study at our center from January 2018 to December 2021.Healing criteria were established by the normalization of calcium levels 2-3 months after surgery according to the latest consensus. ***Results:*** Of the 64 patients with HPT and ^{18}F-Choline PET/CT study, 42 patients who underwent surgery were included. Of which 29 (69%) were considered PET positive, 9 (21%) PET negative and 4 (10%) uncertain.All patients with a positive result underwent directed resection and had pathology of adenoma/hyperplasia.Of the negative results, 1 (11.1%) had an ultrasound scan that was considered sufficient to perform a directed resection (pathology: adenoma/hyperplasia). The other 8 (88.8%) underwent bilateral cervical exploration and parathyroidectomy +/- hemithyroidectomy depending on intraoperative findings (pathology: 6 adenomas/ hyperplasia and 2 negatives).All 4 (100%) patients with uncertain results underwent bilateral cervical exploration presenting pathology of adenoma/hyperplasia.From all 42 MIBI negative patients that would have gone to invasive surgery only 12 did go after PET results (those considered uncertain and 8/9 negative).Calcemia evaluation showed that 38 (90%) patients presented normal values. The other 4 (10%) persisted with elevated values after

surgery. To sum up, from a total of 30 patients with minamally invasive surgery, 27 (90%) were considered cured (the 3 patients with persistent HPT had a positive PET scan). On the other hand, 12 patients that underwent bilateral cervical exploration and 11 ended with calcium within healthy levels (the odd one out had an uncertain PET result). ***Conclusion:*** ^{18}F-Choline PET/CT is a sensitive and specific technique for locating hyperfunctioning parathyroid glands. As a result, it allows to perform minimally invasive surgeries with the advantages for the patient that this entails and a decent curative rate.

EP-31

e-Poster Area

B: Imaging Clinical Studies -> B7 Infection and Inflammation -> B71 Bone Infection and Inflammation

EP-0511

The study of non-infectious inflammatory diseases in paediatric patients: morpho-functional methods compared (18FDG-PET and 99mTc-WB Bone Scintigraphy vs STIR-MRI).

A. Monaci[1], *A. Perrone*[2], *A. Tondo*[2], *F. Carra*[2], *T. Giani*[2], *C. Olianti*[1];
[1]*University of Florence, Firenze, ITALY,* [2]*University Hospital Meyer, Firenze, ITALY.*

Aim/Introduction: There is not much literature on the use of nuclear medicine imaging for the study of paediatric patients with inflammatory disease of a non-infectious nature, as in most cases its usefulness is not established and the use of radiation-free techniques such as MRI is favoured. The aim of this study is to compare the different morpho-functional methods (^{18}FDG-PET and ^{99m}Tc-WB Bone Scintigraphy vs STIR-MRI) in the therapeutic diagnostic procedure of these patients. ***Materials and Methods:*** 9 patients (5 males and 4 females) scheduled between 2014 and 2021, who were between 18 months and 18 years old at the time of the investigations, were selected ($\mu = 9.27 \pm 5.47$ age). The time interval between the performance of the MRI and the ^{18}FDG-PET/^{99m}Tc-WB Bone Scintigraphy ranged between 1 and 20 days, except in the case of two patients, for whom approximately 3 and approximately 18 months elapsed, respectively ($\mu = 8 \pm 5.96$ days). Most of the patients came to the physicians' attention with signs and symptoms such as bone and/or joint pain, fever, difficulty in walking (lameness) and elevation of inflammatory indices (Erythrocyte Sedimentation Rate - ESR); although bone biopsy was not always available, patients with a definite diagnosis in the majority of cases were suffering from Chronic Recurrent Multifocal Osteomyelitis (CRMO) (33%), followed by 1 patient with scurvy, 1 with osteomyelitis, while the remainder appeared without a clear diagnosis (44%). ***Results:*** When comparing radiological and nuclear medical imaging, in most cases the changes visible on MRI images coincided with areas of radiopharmaceutical (^{18}FDG or ^{99m}Tc MDP) uptake. In some cases, especially among patients investigated with ^{18}FDG-PET, the latter appeared to show additional localisations of metabolically active tissue compared to the findings on MRI. Accuracy, PPV, NPV, sensitivity and specificity are summarized for the two metabolic tools in the tables. Comparison MRI as gold standard vs 18FDG-PET considering 12 bone segments: ***Conclusion***: This result appears to confirm the high sensitivity of medical-nuclear imaging and semiquantitative parameters (Maximum Standardised Uptake Value - SUVmax) are still being evaluated, to obtain a cut-off value between positive and negative and thus to define positive and negative predictive values to better assess the role that these methods could have in the diagnosis and management of patients with non-infectious inflammatory pathology.

EP-32

e-Poster Area

B: Imaging Clinical Studies -> B7 Infection and Inflammation -> B72 Vasculitis and Endocarditis

EP-0512

Role of 18 Fluorodeoxyglucose positron emission tomography - computed tomography in the diagnosis of infective endocarditis : A report of 19 cases

O. Ben Elkilani*, S. Mensi, G. Baazoug, Z. Missaoui, A. Ezzine, T. Dardouri, R. Sfar, K. Chatti;*
University Hospital Sahloul, Sousse, TUNISIA.

Aim/Introduction: Infective endocarditis is a relatively rare infectious disease, but with a significant morbidity and mortality, the diagnosis is often difficult and is based on clinical, biological and radiological features (Duke's Criteria), nevertheless, in a significant number of patients, the results are inconclusive leading to a sort of therapeutic problem. The goal of this study is to clarify the utility of 18FDG PET CT in diagnosing IE. ***Materials and Methods:*** We have studied 19 cases of suspected IE that benefited from a 18FDG PET CT, these cases spanned between January 2020 and March 2023. All patients were studied on local level (the cardiac region) and on a global level (whole body PET-CT). ***Results:*** In the 19 cases studied, the mean age was 45 (6-78), 12 (63%) were males and 7 (37%) were females, 6 had valvular prothesis, 3 had endoaortic prothesis, 1 had RV-PA conduit and 4 had implanted pacemakers. 2 had a history of anterior episodes of IE, 4 had persistent fever, 6 had a biological inflammatory syndrome, 3 had positive blood cultures, 7 patients had cardiac ultrasound suggestive of IE. Overall, 7 exams were positive (36.8%) and 2 exams were excluded because of inadequate regimen, the rest were inconsistent with endocarditis. In patients with valvular prothesis, PET-CT revealed valvular hypermetabolism that was diffuse in 3 cases, heterogenous in 1 case and focal in 2 cases that were consistent with IE (mean SUV=6.6 : 2-11). Of the patients with endoaortic prothesis, 2 revealed diffuse hypermetabolism, Of the 4 patients with pacemaker, 1 was positive and revealed a focal hypermetabolism regarding pacemaker probe. On the global level, the exams revealed septic emboli in splenic (1case), internal iliac (1 case) and in the femoral (2cases) arteries, the results were highly suggestive of suspected secondary localizations in the spine (2cases), in the hip bone (2cases) and in the sternum (2cases). Moreover, one revealed pneumopathy, one acute cholecystitis and one revealed lytic lesions of the hip bone. ***Conclusion:*** 18FDG PET-CT may play an important role in diagnosing IE when traditional tools are inconclusive. The suggestive findings are especially focal hypermetabolism regarding valves/prothesis. It's also a powerful tool in diagnosing distant complications.

EP-0513

Takayasu's Disease - A Pathway To Diagnosis: Clinical Case Solved Using 18F-FDG PET/CT

P. Ilieva-Gabarska[1,2,3], *Z. Dancheva*[3], *R. Pencheva*[4], *M. Slavova*[1], *L. Petrakiev*[1], *A. Antonov*[5], *M. Dyankova*[6,3], *I. Vasilev*[7], *T. Baltova*[7], *Y. Todorova-Doneva*[8];
[1]*Nuclear medicine laboratory, Medical center "St. Marina - diagnostics and therapy", Pleven, BULGARIA,* [2]*Department of Radiology and Radiotherapy, Medical university Pleven, Pleven, BULGARIA,* [3]*Department of Imaging diagnostics, Interventional radiology and Radiotherapy, Medical university "Prof. Dr. Paraskev Stoyanov", Varna, BULGARIA,* [4]*Rheumatology department, UMHAT "Dr Georgi Stranski", Pleven, BULGARIA,* [5]*Department of haematology, University hospital "St. Marina - Pleven", Pleven, BULGARIA,* [6]*Department of nuclear medicine and radionuclide therapy, UMHAT "St. Marina", Varna, BULGARIA,* [7]*MBAL Avis Medica, Department of Radiology, Pleven, BULGARIA,* [8]*ENT department, UMHAT "Dr Georgi Stranski", Pleven, BULGARIA.*

Aim/Introduction: Takayasu's disease is a type of autoimmune vasculitis causing inflammation of the arterial walls of medium and large vessels, including the aorta. Its pathogenesis is based on systemic granulomatous inflammation chain reaction. Our aim was to describe a case of Takayasu's arteritis (TAK) with unusual presentation and delayed diagnosis -extravascular manifestation with infection of the middle ear and TAK-associated polychondritis (of nose and ear) and polyserositis. ***Materials and Methods:*** To present a case of a 44 y.o. caucasian woman with acute inflammation in right middle ear with swelling and redness in right auricle dating 2 weeks without any effect to antibiotic treatment. Additional symptoms were present - dizziness, fatigue, subfebrile temperature, arthralgia in small hand and feet joints, night sweats and weight reduction. After otolaryngology consultation and treatment, according to rheumatologist's recommendations a panel of laboratory tests, including antibody tests, was conducted, which showed high levels of leukocytes, C-reactive protein, thrombocytes, rheumatoid factor, erythrocyte sedimentation rate, and iron deficiency anaemia. Based on these results, the diagnosis of relapsing polychondritis was accepted. After haematology consultation there was a haematological disorder still suspected. A CT study of the head was performed with imaging findings suspecting tumor involvement of left piriform sinus and carcinosis in left carotid space. The patient was referred for a 18F-FDG PET/CT study and a total body protocol with low-dose CT for attenuation correction was conducted. ***Results:*** The PET/CT findings included: diffusely increased uptake of the radiopharmaceutical into the vessels' walls of the thoracic and abdominal aorta, bilateral carotid and femoral arteries including perivascular reaction with moderate wall thickening and inflammatory changes (endarteritis); area with high uptake in the nose cartilage and diffusely activated bone marrow. A focal area of pathological FDG accumulation was found in the area of right carotid artery, which was further examined with MRT and was proven to be kinking of the right internal carotid artery with endarteritis. A bone marrow trephine biopsy and genetic molecular testing excluded myeloproliferative disorder. The diagnosis of TAK was accepted and a treatment with cyclophosphamide, methylprednisolone and methotrexate was initiated. ***Conclusion:*** 18F-FDG PET/CT acted as a valuable method in detecting an active inflammatory process of the arterial blood vessels' walls and carotid abnormality leading to the diagnosis of Takayasu's arteritis. This case adds to the literature, expands knowledge of the spectrum of changes in TAK and addresses the need of multidisciplinary approach to difficult diagnostic cases.

EP-0514

Role of FDG PET-CT in Takayasu arteritis

Z. Missaoui*, M. Nouira, G. Baazoug, O. Ben Elkilani, K. Ayed, S. Raja, K. Chatti;*
University Hospital Center Sahloul, Sousse, TUNISIA.

Aim/Introduction: Takayasu's vasculitis is an inflammatory arteritis of large and medium-sized vessels . It is characterised by clinical polymorphism , the absence of biological or histological markers. The aim of this study is to determine the indications and to assess the impact of FDG PET-CT in the exploration of Takayasu arteritis . ***Materials and Methods:*** We identified all patients who underwent FDG PET-CT in our department for the investigation of Takayasu's vasculitis from September 2020 to February 2023. In total nine patients were included. The protocol for FDG PET-CT examinations was standard. Exames were interpreted with visual analysis comparing the degree of an arterial FDG uptake to that of the liver. 3 grades are distinguished . PET-CT was considered positive for grades 2 or 3. ***Results:*** In our study, we identified two indications for FDG PET-CT in the investigation of Takayasu arteritis: Firstly, two patients were referred to our departmentfor suspicion of Takayasu's vasculitis. The two corresponding PET scans were negative andthe subsequent evolution of the patients' state of health was good with no need for treatment with corticosteroids. Suspicion of relapse was the second indication. The PET scan results were positive in two cases showing a vascular hypermetabolismconfirming therelapse of the disease and negative in the other five cases. The rapid attenuation of vascular fixation under treatment of Takayasu disease is known. Four of our patients were on corticosteroids. Two of them had a negative PET-CT scan. The risk of false-negative results on steroids cannot be assessed in our study due to the small number of patients included. ***Conclusion:*** FDG PET-CT is a useful imaging modality for the diagnosis of Takayasu Arteritis because of the early detection of inflammatory activity. It contributes also todiagnose relapsesand to obtain a therapeutic assessment. A study of a larger number of patients is needed to determine the sensitivity and specificity of the examination and to establish a correlation between the intensity of vascular uptake and disease activity. ***References:*** -Lillian Barra and al : imaging modalities for the diagnosis and desease activity assessment of takayasu's arteritis .-Berit Nielsen et al : Three days of high-dose glucocorticoid treatment attenuates large-vessel 18F-FDG uptake in large-vessel giant cell arteritis but with a limited impact on diagnostic accuracy .-Martin a walter and al : The value of [18F]FDG-PET in the diagnosis of large-vessel vasculitis and the assessment of activity and extent of disease.

EP-33

e-Poster Area

B: Imaging Clinical Studies -> B7 Infection and Inflammation -> B73 Other Infections and Inflammatory Diseases

EP-0515

FDG PET/CT response criteria in assessment of post Anti Koch's Treatment evaluation.

H. Rathore*, N. R. Thaker, Bombay Hospital, Mumbai;*
Bombay Hospital And Medical Research Centre, Mumbai, INDIA.

Aim/Introduction: Tuberculosis(TB) is a highly infectious disease with a record global incidence of high morbidity and mortality. Monitoring disease activity and evaluating treatment response with conventional methods such as culture or chest x-ray is time-consuming and non-specific. Active TB-lesions are typically highly FDG-avid and may be assessed on whole-body

18-fuorine-fuorodeoxyglucose positron emission tomography/computed tomography scan(FDG-PET/CTscan). We hypothesized that FDG-PET/CTscan is highly efficacious for evaluation of disease extent, treatment response and outcome in TB-infected patients undergoing anti-koch's therapy(ATT). ***Materials and Methods:*** Pre and post-ATT FDG-PET/CT scan done for various sign symptoms like pyrexia of unknown origin, weight loss, lymphadenopathy etc which were diagnosed as TB included in the study, to look for the extent of disease before initiation of Anti-Tubercular or Anti-Koch's therapy(ATT or AKT), for the identification of other sites, completely cured patients, non-responders, recurrence of disease, and drug-resistance. FDG-PET/CTscan is also very helpful tool in identification of right biopsy site, to rule out the possibilities of other mimicking granulomatous-infection, lymphoproliferative-disorder or malignancy, and to avoid empirical use of AKT. ***Results:*** A total of 60 biopsy proven patients were included with pulmonary and extrapulmonary-involvement, out of them 35% patients had multiorgan-disease. 23.33% have only nodal-disease, 18.33% have isolated pulmonary-disease with or without mediastinal-nodes, 10% have osseous involvement, 5% have ovarian and 1.6 % of each has testes, prostate, uterus, transplanted kidney, and diffuse peritoneal involvement respectively. 16.66% patients were studied with follow up FDG-PET/CTscan out of them 5 has shown the complete morphological and anatomical response with AKT, 3 were having residual morphological disease with complete metabolic-response and 2 patients were identified as non responders with metabolically active disease which on re-biopsy confirms the drug resistance. ***Conclusion:*** Despite high heterogeneity there was a trend towards the usefulness of FDG-PET/CTscan for evaluation of disease extent prior to treatment and ATT response. Impending research with large-number of patients is needed to further clarify the predictive value of FDG-PET/CTscan with formulation of new guidelines in tuberculosis. ***References:*** 1. Stephanus T. Malherbe et al. Quantitative 18F-FDG PET-CT scan characteristics correlate with tuberculosis treatment response. Malherbe et al. EJNMMI Research (2020) 10:8 https://doi.org/10.1186/s13550-020-0591-9. 2. 2. Hannes Sjölander et al. Value of FDGPET/CT for treatment response in tuberculosis: a systematic review and metaanalysis. Clinical and Translational Imaging (2018) 6:19-29 https://doi.org/10.1007/s40336-017-0259-2. 3. 3. Wei-Ye Yu et al. Updates on 18F-FDG-PET/CT as a clinical tool for tuberculosis evaluation and therapeutic monitoring. Quant Imaging Med Surg 2019;9(6):1132-1146 | http://dx.doi.org/10.21037/qims.2019.05.24.

EP-0516

Osteoarticular Inflammatory Activity Response To Tocilizumab In Patients With Refractory Polymyalgia Rheumatica: Contribution Of Semiquantitative Analysis Of [18F]FDG-PET/CT

I. Martínez-Rodríguez[1], *D. Prieto-Peña*[2], *Á. Gutiérrez-González*[3], *M. De Arcocha-Torres*[3], *F. J. Gómez-de la Fuente*[1], *N. Martínez-Amador*[3], *A. Sánchez-Salmón*[3], *J. Jiménez-Bonilla*[3], *V. Mendi-Barcina*[3], *A. Bota-Bota*[4], *M. Pombo-López*[4], *M. A. González-Gay*[2], *R. Quirce*[3];
[1]*Nuclear Medicine Service. Marqués de Valdecilla University Hospital. Molecular Imaging Group (IDIVAL). University of Cantabria, Santander, SPAIN,* [2]*Rheumatology Service. Marqués de Valdecilla University Hospital. Genetics and atherosclerosis research group on systemic inflammatory diseases (IDIVAL), Santander, SPAIN,* [3]*Nuclear Medicine Service. Marqués de Valdecilla University Hospital. Molecular Imaging Group (IDIVAL). University of Cantabria, Santander, SPAIN,* [4]*Nuclear Medicine Service. Marqués de Valdecilla University Hospital. Molecular Imaging Group (IDIVAL). University of Cantabria, Santander (España), SPAIN.*

Aim/Introduction: To evaluate if a semiquantitative analysis would improve the ability of the visual analysis of [18F]FDG-PET/CT in the assessment of the osteoarticular inflammatory activity response to tocilizumab (TCZ) therapy in patients with refractory polymyalgia rheumatica (PMR). ***Materials and Methods:*** A deep study of 12 consecutive patients with symptomatic PMR and giant cell arteritis (10 women, 67.0±8.6 years-old) refractory to corticosteroids/methotrexate and treated with TCZ was performed. A baseline and follow-up PET/CT after TCZ were performed (interval: 15.1±6.0 months). Eleven patients were on therapy at the time of baseline PET/CT. PET/CT were obtained 180' after [18F]FDG administration. A semiquantitative analysis of images, based on the SUVmax target-to-liver ratio (TLR), was performed. The results were compared with a previous visual evaluation (score 0-3 compared to liver uptake). Fourteen osteoarticular regions were evaluated per patient: shoulders, sternoclavicular joints, ischial tuberosities, hips, greater trochanters, knees, cervical and lumbar interspinous bursae. ***Results:*** Previous visual analysis had shown uptake >0 in 72/168 (42.9%) regions evaluated at the baseline PET/CT (grade 1=28, grade 2=16, grade 3=28) and in 65 regions (38.7%) after TCZ therapy (grade 1=32, grade 2=18, grade 3=15). TLR decreased from 0.88±0.57 at the baseline PET/CT to 0.78±0.36 at the follow-up (non-significant, p=0.5169). In the 86 regions showing visual score >0 at the baseline and/or follow-up PET/CT, TLR decreased from 1.10±0.70 to 0.93±0.42 (non-significant, p=0.3424). After TCZ therapy, 7/12 patients showed complete clinical response (CR). In the 51 regions with visual score >0 TLR decreased from 0.83±0.31 to 0.79±0.30 (non-significant, p=0.3219). Five patients showed partial response (PR). TLR in the 35 regions with visual score >0 decreased from 1.48±0.93 to 1.13±0.46 (non-significant, p=0.4278). Patients with PR showed higher baseline and follow-up TLR compared to those with CP (baseline: 1.48±0.93 vs. 0.83±0.31, follow-up: 1.13±0.46 vs. 0.79±0.30, p<0.005). TLR decreased in 54.1% and 48.6% of regions in patients with CR and PR, respectively. Discrepancies in individual behaviour of TLR and the visual score were more frequent in patients with PR (18/35 (51.4%) vs. 19/51 (37.3%) regions). ***Conclusion:*** The semiquantitative analysis of [18F]FDG-PET/CT showed a decrease in the TLR after TCZ therapy, globally and in patients with CR and PR, although the differences were not significant. A higher TLR, both at baseline and at the follow-up, was associated with a lower clinical response to TCZ. Discrepancies in individual behaviour of the visual score and TLR were more frequent in patients with PR.

EP-0517

Comparative study of body fat distribution in naive people living with HIV (PLHIV) and after 48 weeks of antiretroviral therapies (ART) with Dolutegravir/lamivudine vs TAF/FTC/Bictegravir.

A. Piñeiro*, C. Hidalgo Tenorio, E. Triviño Ibáñez, C. Ramos Font, R. Sánchez Sánchez;*
Hospital Universitario Virgen de las Nieves, Granada, SPAIN.

Aim/Introduction: The aim of this work is to analyze after 48 weeks of treatment with these antiretroviral therapies (ARTs) whether changes in body fat distribution occur, and whether these predominate in any regimen. ***Materials and Methods:*** This work is a substudy of two clinical trials (DOLAVI ClinicalTrials.gov Identifier: NCT04002323 and BIC-NOW The EudraCT number: 2019-003251-11) of a single arm, in naive patients, performing dual energy X-ray absorptiometry (DEXA) of body fat before and after 48 weeks of ART. ***Results:*** 13 PLHIV were included. 46.2% with T/F/BIC and 53.8% DTG/LMV, comparable in variables: mean age 31.5 vs 31 (p=0.91); gender 83.3% vs 100%, (p=0.46), AIDS stage 33.3 vs 28.6% (p=1), immediate ART initiation 100% vs 100%, CD4 285.7 vs 411.7 cells/uL (p=0.32), CD4/CD8 ratio 0.34 vs 0.22 (p=0.62) and viral load 5.86 vs 4.94 (log10) (p=0.25); median weight 75 vs 69 kg

(p=0.27), waist 81 vs 77 cm (p=0.48) and Body Mass Index (BMI) 24 vs 23 (p=0.28) and distribution of lean mass and total fat mass and in percentage of upper limbs, lower limbs, and trunk, and the type of distribution gynecoid or android. After 48 weeks we found no differences between both ART (T/F/BIC vs DTG/LMV) in weight 76 vs 68.5 kg (p=0.47); waist 83.5 vs 80 cm (p=0.7) or BMI 25.1 vs 24.6 (p=0.57); nor comparing each patient with each other according to ART (T/F/BIC weight 0.59; waist p=0.34; BMI 0.4 vs DTG/LMV, weight p=0.15; waist p=0.14; BMI p=0.11). Regarding body fat at DEXA we found that DTG/LMV treated patients experienced a post-treatment increase in upper limb fat mass (Left: 1225 basal vs 1576; Right 1221 vs 1443, p=0.018) and lean mass (Left 2550 vs 2927; p=0.018) and total fat percentage (Left 32.3% vs 38.4% p=0.018; Right 32.3% vs 34.4% p=0.018). ***Conclusion:*** DTG/LMV produces an increase in total fat in arms after 48 weeks. This effect needs to be analyzed in larger cohorts to see the possible impact on the occurrence of future cardiovascular events.

EP-0518

18F-FDG PET/CT Imaging in Infectious Mononucleosis: Mimicking Lymphoma and Clinical Implications

N. Damle, *J. Jaleel, S. Jain, A. Rasheed, V. Goenka, K. Gyanraj Sa, A. Khurana;*
All India Institute of Medical Sciences, New Delhi, INDIA.

Aim/Introduction: Infectious mononucleosis caused by the Epstein-Barr virus is a common infectious disease in young adults that presents with fever, lymphadenopathy and hepatosplenomegaly and usually follows a self-limiting course. Persistence of symptoms, significant atypical lymphocytosis and disproportionate weight loss can sometimes cause IMN to closely mimic a lymphoreticular malignancy. We present 18F-FDG PET/CT findings in a case of a young adult male who presented with findings closely resembling a lymphoma but was finally diagnosed to have infectious mononucleosis after a detailed diagnostic evaluation. ***Materials and Methods:*** A 31-year-old male presented to the ER with a 6-day history of high-grade fever. His investigations showed mild thrombocytopenia, deranged liver function and probable myocarditis. He was empirically started on antibiotics for a suspected tropical fever (?severe scrub typhus). CT chest-abdomen was unremarkable except for mild hepatosplenomegaly. The microbiological workup returned negative, and despite the antibiotics, the patient continued to have persistent symptoms into the third week of illness. Patient was referred for 18F-FDG PET/CT with a clinical diagnosis of undifferentiated pyrexia under evaluation. Serological workup for EBV and other viral infections were sent and reports were awaited at the time of the PET/CT. ***Results:*** 18F-FDG PET/CT revealed intense bilaterally symmetrical FDG uptake in nasopharynx and bulky bilateral tonsils. FDG avid bilateral preauricular, right intraparotid, bilateral parapharyngeal, bilateral cervical level IB, bilateral level II, III, IV and V lymph nodes were noted. Hepatosplenomegaly was noted with diffusely increased FDG uptake but no focal lesions. A few FDG avid peripancreatic, portocaval, paraaortic, aortocaval, mesenteric, bilateral common iliac, bilateral external iliac and inguinal lymph nodes were noted. There was a diffusely increased FDG uptake in bone marrow with no focal lesions. Based on the above findings, we gave differentials of lymphoma, infectious mononucleosis and post viral lymphoid activation, The diagnosis of EBV-associated infectious mononucleosis was clinched after a positive EBV VCA IgM. Antibiotics were stopped. The patient became afebrile after three weeks of illness and was discharged in a hemodynamically stable state with no subsequent recurrence of symptoms on follow-up. ***Conclusion:*** Infectious mononucleosis can be a close mimicker of lymphoma both clinically and on imaging. This case highlights the importance of considering infectious mononucleosis as a possible differential in young patients with prolonged fever, B-symptoms, lymphadenopathy and hepatosplenomegaly, even when the imaging findings are similar to lymphoma. An accurate diagnosis in such a setting is crucial to avoid unnecessary invasive procedures and patient panic.

EP-0519

Real world comparison of radiopharmaceutical parameters and clinical utility in kit based and in house labelled 99m Tc Ubiquicidin as a infection imaging agent

D. Khan, *S. Katala, N. A. Damle, C. Bal, S. Sagar, G. Arora, P. Kumar, M. Ansari, R. Kumar, H. Verma;*
AIIMS Delhi, Delhi, INDIA.

Aim/Introduction: ^{99m}Tc Ubiquicidin (UBI) 29-41 is used as an infection imaging agent. Ubiquicidin is a cationic synthetic antimicrobial peptide fragment that binds specifically to the anionic microbial cell membrane at the infection site. Though commercial kits are available, in house synthesis is also possible. The aim of this study was to compare the radiopharmaceutical and clinical aspects of the in house labelling technique with the kit based method of tracer synthesis. ***Materials and Methods:*** We retrospectively analysed forty ^{99m}Tc-Ubiquicidin patient scans done using radiopharmaceutical synthesised by both in-house (n=20) and commercially available kits (n=20) performed during a period of two years. After intravenous injection of 10 mCi (555-740MBq) of 99mTc-UBI, dynamic images were taken for 15 minutes (with a 15-second frame per frame), followed by serial static (spot) images at 15, 30, 45, 60, and 120 minutes (atleast three sets of images per patient). A dual head SPECT/CT gamma camera with low energy higher resolution (LEHR) collimator was used to acquire the scans. At 45- 60 minutes after injection, whole-body anterior and posterior images were taken to confirm the biodistribution. A SPECT/CT scan was taken at the time of peak uptake in the suspected pathological lesion. ***Results:*** Both methods were evaluated for radiochemical purity through paper chromatography, and in-house labelling was found to be comparable with the kit-based labelling technique with a mean radiochemical purity of >90%. Biodistribution to liver, kidney and bladder was comparable in most of the scans by both techniques. However splenic uptake was noted more frequently in the kit based technique. Kit based method was approximately 10 times costlier than in house labelling method. Kits were available at periodic intervals while in house technique could be used daily thus serving to the patient requirements on time basis. ***Conclusion:*** Based on its cost effectiveness and easy, immediate availability, the in-house prepared 99mTc-UBI appears to be a more practically useful option than the kit-based preparation with comparable lesion uptake and biodistribution. Thus, the in-house method may be practised for labelling of UBI 29-41 with ^{99m}Tc, especially in resource constrained settings.

EP-34

e-Poster Area

B: Imaging Clinical Studies -> B8 Nephro-Urological Imaging Study -> B81 Nephro-Urology

EP-0520

Heterogeneity of PSMA Expression Assessed by 68Ga-PSMA-11 PET/CT in Patients with clear-cell renal cell carcinoma

M. Zhang;
Department of Nuclear Medicine, Xijing Hospital, Xi'an, CHINA.

Aim/Introduction: Used 68Ga-PSMA-11 PET/CT to observe intra-tumoral and extra-tumoral heterogeneity of PSMA uptake in primary lesion and metastatic of clear-cell renal cell carcinoma (ccRCC). And analyzed the impact of primary lesions on metastatic lesions. ***Materials and Methods:*** Seventy-five ccRCC patients with preoperative 68Ga-PSMA-11 PET/CT scans and complete surgical specimens were retrospectively enrolled in this study. Radiographic parameters were obtained from PET/CT images, including SUVmax and VP (volume proportion of lesion in VOI: SUV higher than 50% SUVmax). Immunohistochemistry was used to measure the expression of PSMA. The Mann-Whitney U test analyzed continuous variables, and Chi-square test analyzed categorical variables respectively. Used ANOVA and t-test to compare the subtype groups, and used correlation analysis to assess the impact of primary lesions on metastatic lesions. Using Correlation Analysis to Analyze the Relationship between primary and metastatic. ***Results:*** Of the 75 primary lesions, 100% (75/75) PSMA uptake were positive. The average of SUVmax was 14.8±8.2 (CV=72.0%), TBR was 3.14±1.84 (CV=58.6%), and VP was 0.31±0.23 (CV=74.2%). Four patients with 21 bone metastases, 100% (21/21), PSMA uptake were positive. The average of SUVmax was 18.4±10.5 (CV=57.1%), TBR was 3.14±1.51 (CV=48.1%), and VP was 0.48±0.18 (CV=37.5%). Five patients detected tumor thrombus, 60% (3/5) was positive. The average of SUVmax was 7.1±6.0 (CV=84.5%), TBR was 2.14±2.11 (CV=98.6%), and VP was 0.79±0.15 (CV=19.0%). There were significant differences in PSMA SUVmax uptake (P=0.027) and high uptake area volume proportion (VP) (P=0.000) among the primary and metastatic lesions of ccRCC. There was no significant difference in PSMA SUVmax and VP of the primary lesion between local and advanced/metastatic ccRCC. However, the PSMA uptake avid and intra-tumoral heterogeneity of the primary lesion affected the attributes of metastatic lesions, especially the tumor thrombus (SUVmax: r=0.892; P=0.042; VP: r=0.954; P=0.193). ***Conclusion:*** The uptake of PSMA in the primary lesion and metastases of ccRCC had intra-tumoral and extra-tumoral heterogeneity. Heterogeneity of primary tumor, bone metastasis and tumor thrombus were different. The uptake characteristics of the primary lesion may impact on the metastatic lesion.

EP-0521

Dynamic characteristics of ureteral cancer with [11C]-choline total-body PET/CT

C. Liu[1], *S. Wang*[2], *R. Wu*[3], *Q. Xie*[1], *Y. Yang*[2], *Z. Yang*[1];
[1]*Department of Nuclear Medicine, Peking University Cancer Hospital & Institute, Beijing, CHINA,* [2]*Department of Urology, Peking University Cancer Hospital & Institute, Beijing, CHINA,* [3]*Beijing United Imaging Research Institute of Intelligent Imaging, Beijing, CHINA.*

Aim/Introduction: The aim of this preliminary study was to investigate the value of dynamic [11C]-choline PET scans on the ureteral cancer. ***Materials and Methods:*** Nine patients with ureteral cancer were enrolled who were referred to [11C]-choline PET/CT before starting treatment. The patients underwent PET/CT scans with a United Imaging uEXPLORER PET/CT immediately after received an injection of [11C]-choline. The PET data were acquired using a list-mode for 30 minutes and dynamic image series in 1 minute per frame were reconstructed, resulting total 30 frames per patient. Volume-of-interests (VOIs) were placed on the primary tumor, descending aorta, posas major muscle and bladder by an experienced nuclear radiologist. The VOIs were carefully placed and adjusted on all dynamic image frames to keep the target tissue in the VOIs. The maximal standard uptake value (SUVmax) in the VOI was measured on each frame and time-activity-curve (TAC) of SUVmax was plotted. The tumor-to-muscle ratio (TMR) was calculated. ***Results:*** The patient cohort included 5 women and 4 men with an average age of 61±16 years, a height of 163±11 cm, a weight of 60±11 kg, and an injection dose of 250±25 MBq. All patients underwent the dynamic scans successfully without significant motions and the image quality of 1-minute frame was satisfactory for tumor delineation. The TMR reached 90% of the maximal level in 1 to 5 minutes after the injection. Normalized TAC of the tumors showed 3 dynamic patterns: plateau, ascent, and descent after a quick upward phase at the beginning frame. The activity in the aorta returned to the background level after 2 minutes post injection. We also found high bladder activity in 3 patients. ***Conclusion:*** Our result suggested static PET imaging between 2nd to 5th minute post injection provide optimal tumor-to-background contrast for ureteral cancer and minimize the interference of the blood pool or bladder. The TAC analysis demonstrated ureteral tumors have 3 dynamic patterns, although the physiological meaning of these patterns requires further study.

EP-0522

Role of Tc99m SestaMIBI SPECT/CT in characterization of renal lesions - A prospective study

K. Agrawal, *R. Emerson P, P. Nayak, S. Purkait, P. S. Patro, G. K. Parida;*
All India Institute of Medical Sciences (AIIMS), Bhubaneswar, INDIA.

Aim/Introduction: Many benign renal masses are overtreated as a result of conventional imaging overlap between benign and malignant imaging features. Even with biopsy, 10-20% of biopsy results are ambiguous, and biopsy of smaller lesions is difficult. Tc-99m SestaMIBI is a lipophilic cationic molecule taken up by cells that are rich in mitochondria. Clear cell and papillary renal cell carcinoma (RCC) have microvilli but no mitochondria. Therefore, we evaluated role of Tc-99m SestaMIBI in differentiation of malignant and benign renal masses. ***Materials and Methods:*** We prospectively included patients with the solid renal mass, who have not undergone biopsy or surgery, age >18 years and patients who will be willing to give a written informed consent form. The exclusion criteria were patients who have undergone previous biopsy or treatment for RCC, critically ill or hemodynamically unstable patients and pregnant and lactating mothers. The study was approved by institute ethics committee. 15 mCi of Tc-99m sestaMIBI was administered intravenously. SPECT-CT images of the abdomen was acquired at 1 hr. The image counts in 1 cm2 ROI was calculated in the renal mass and liver. ***Results:*** We included 16 patients in the study (male 11, female 5) with mean age 50.9

years (age range: 32 -77 years). Of 16 renal masses, 9 were clear cell RCC, 2 were papillary RCC, 1 undifferentiated malignant spindle cell tumour, 1 poorly differentiated malignancy, 1 granulomatous pyelonephritis and 1 angiomyolipoma. Renal mass to liver (R/L) count ratio was less than 1 in 13/16 patients (all 13 were malignant histopathology). R/L ratio was more than 1 in 3 patients (one clear cell RCC, one granulomatous pyelonephritis and one angiomyolipoma). Sensitivity of R/L ratio in diagnosis of malignant pathology is 92.8% and specificity is 100%. ***Conclusion:*** Although the number of patients studied in the study is less, early result shows that renal count to liver count ratio in the Tc-99m SestaMIBI SPECT-CT is highly sensitive and specific method to distinguish malignant and benign renal lesion.

EP-35

e-Poster Area

B: Imaging Clinical Studies -> B81 Nephro-Urology & B101 Other Clinical Studies

EP-0523

Are non-sampling methods useful for assessing GFR in a potential living kidney donor? A comparative study with the 3-sample method

M. A. Hernández Fructuoso, *C. G. Franco Monterroso, B. Santos Montero, L. Garcia Lama, L. Rey Sánchez, V. Pascual Pascual, A. Garcia Burillo;*
Hospital Universitari Vall d'Hebron, Barcelona, SPAIN.

Aim/Introduction: The glomerular filtration rate (GFR) is the best overall indicator for the evaluation of renal function and its accurate determination is required in donor candidates for renal transplantation. Estimated GFR (eGFR) calculations can be performed using different methods. We have previously validated a three-blood sample method with [^{99m}Tc]Tc-DTPA (SM) that was used as a reference in this study (1). Our aim was to assess the agreement between in vitro blood sampling method (SM) with other commonly used method in clinical practice: in vivo GFR measurement using [^{99m}Tc]Tc-DTPA scintigraphy (Gate's method), and two different GFR estimation equations based in creatinine clearance (Chronic Kidney Disease Epidemiology Collaboration, CKD-EPI, and Modification of Diet in Renal Disease, MDRD-4). ***Materials and Methods:*** GFR was measured in 57 potential kidney donors (aged 55; range 71-26 years, female 35) by bolus i.v. injection of 18.5MBq of [^{99m}Tc]Tc-DTPA and plasma clearance analysis using 3 extractions at 120', 180' and 240' and Chandler's correction was applied. After, 185MBq were administered i.v. and immediately dynamic study was performed in gammacamera for twenty minutes, and GFR was estimated by Gate's method. GFR was also calculated according to the CKD-EPI and MDRD-4 equations based on creatinine clearance. The correlation and agreement of SM, Gate's method, CKD-EPI and MDRD- 4 were assessed by linear regression and the absolute errors (Ea= SM GFR- non-sampling methods GFR) were calculated. ***Results:*** Mean measured GFR by MS method was 105.39±20.55 ml/min/1.73m^2 and median was 106.66 ml/min/1.73m^2. Means estimated by Gate's methods, by CKD-EPI and by MDRD-4 were 72.08±16.79 ml/min/1.73m^2, 93.45 ±12.35 ml/min/1.73m^2, and 92.08± 14.71 ml/min/1.73m^2 respectively. The Pearson's correlations between MS and Gate's method, MS and CKD-EPI and MS and MDRD were r=0.51, r=0.61 and r=0.59 p< 0.01, respectively. All methods underestimated GFR, and the mean absolute error was 32.82, 12.72 and 15.06 ml/min/1.73m^2 for Gate's, CKD-EPI and MDRD-4 methods. ***Conclusion:*** Gate's GFR estimation showed a weak positive correlation with MS and equations based on creatinine clearance showed a moderate correlation with MS, but all methods systematically underestimated the GFR obtained by the three-sample method. Furthermore, the Gate's method seems to be unacceptable to estimate GFR in potential kidney donors due to their wide range of error. ***References:*** 1) Eur J Nucl Med Mol Imaging (2020) 47 (Suppl 1): S1-S753

EP-0524

Assessing the Reliability of GFR Estimation with Lateral Kidney Centroid Depth of 99mTc-DTPA and 99mTc-MAG3 Renography

K. Thawinprawat;
Siriraj Hospital, Bangkok, THAILAND.

Aim/Introduction: Camera-based Glomerular filtration rate (cGFR) from ^{99m}Tc-diethylene triamine pentaacetic acid (^{99m}Tc-DTPA) and mercaptoacetyltriglycine (MAG3) clearance methods from ^{99m}Tc-MAG3 are commonly used in clinical practice due to their non-invasiveness and simplicity. However, cGFR and derived GFR (dGFR) from MAG3 clearance can be affected by the depth of the kidney. Hence, we proposed the lateral kidney centroid depth (L-depth) method to improve the estimated GFR (eGFR) and evaluated its performance with commercially available methods. ***Materials and Methods:*** The study population comprised 69 patients (6 ^{99m}Tc-DTPA, 63 ^{99m}Tc-MAG3). Scintigraphy was performed after injecting 370 MBq of two radiopharmaceuticals (^{99m}Tc-DTPA and ^{99m}Tc-MAG3), followed by dynamic acquisition for 30 minutes and bilateral static scans for 1 minute. Kidney depth was measured using commercially available methods (Taylor's method and Tonnensen's method) and L-depth. Subsequently, cGFR and dGFR were compared with eGFR. ***Results:*** Based on the type of radiopharmaceutical administered, the data were sorted into two groups. In the ^{99m}Tc-DTPA group, cGFR from Tonnensen's method and L-depth show weak correlation with eGFR (r^2 = 0.193 and r^2 = 0.199, respectively). In contrast, in the ^{99m}Tc-MAG3 group, dGFR from Taylor's method and L-depth show moderate correlation with eGFR (r^2 = 0.412 and r^2 = 0.452, respectively). The weighted r-square of commercially available methods and L-depth to eGFR are 0.346 and 0.364, respectively. ***Conclusion:*** Lateral scanning is a more reliable approach in determining GFR for both radiopharmaceuticals.

EP-0525

Reproducibility of normal Gallbladder Ejection Fraction at 30 min by Biliary Scintigraphy for Diagnosis of Biliary Dyskinesia

M. A. Olarte, *D. Cardosa-Cisneros, I. Soldevilla-Gallardo;*
American British Cowdray Medical Center, Mexico City, MEXICO.

Aim/Introduction: The diagnosis of gallbladder dyskinesia is usually made by calculating the gallbladder ejection fraction via cholescintigraphy. Ziessman et al. evaluated the use of a commercially available lactose-free fatty-meal food supplement, as an alternative to CCK analog cholescintigraphy, to develop a standard methodology, and to determine normal gallbladder ejection fractions (GBEFs) for this supplement at 1 h later. Being a dynamic and time-consuming scan, it is necessary to determine the gallbladder ejection fraction at 30 minutes in order to reduce the image acquisition time, improve patient comfort, and increase the availability of the gamma camera to be able to carry out other

scans. ***Materials and Methods:*** Thirty-four patients (19 women, 15 men) were studied. They ranged in age from 40.4 to 43.4y. Conventional cholescintigraphy was performed. After voiding, the patient ingested 240-mL (8 oz) can of the supplement while sitting. Patients again lay supine, and images were acquired for 60 min (60 s/frame, 128 x 128). Image processing was performed at the Infinia Hawkeye 4.0 equipment workstation, obtaining the gallbladder ejection fraction at 30 and 60 min after oral stimulation with standardized food, following the recommendations proposed in the guide: Guideline for Hepatobiliary Scintigraphy 4.0 (SNMMI) published in 2010. ***Results:*** Gallbladder ejection fractions (GBEFs) ranged from 1% to 95% at 30 min. The activity-time curves were variable for each patient. Most of the patients presented a time-activity curve with a linear pattern and only one subject showed delayed phase to contractile stimulus at 30 minutes (1% emptying at 30 minutes). The lowest GBEF of the other 33 subjects was 21%. However, the results obtained at 30 min depend on the contractile response of the gallbladder of each patient. ***Conclusion:*** In special situations in which it is not possible to perform a conventional cholescintigraphy, either due to the prolonged inability of the patient to remain lying down or due to insufficient time, we recommend a 30 min phase of vesicular contraction instead of 60 min using a commercially available lactose-free fatty flour food supplement standardized. Normal GBEF values with this short protocol is established with a lower limit of normality of 21% at 30 min. If GBEF is above that value, the patient can be considered not to have a functional disorder of the gallbladder. ***References:*** Ziessman Harvey A. et al. Cholecystokinin Cholescintigraphy: Methodology and normal values using a lactose-free fatty-meal food supplement. J Nucl Med. 2003;44:1263-1266.

EP-0526

75Se- Taurocholic acid in the study of Chronic Diarrhea. Our Experience

C. Paniagua Correa*, L. Castillejos Rodríguez, A. Herrero Muñoz, D. Rodriguez Oviedo, C. Galindo Fernández, B. Manzarbeitia Arroba, M. Alvarez Moreno, A. Ortega Valle, C. Sandoval Moreno, M. De la Rubia Marcos, M. Tagliatori Nogueira, P. García Alonso; Hospital De Getafe, Getafe, SPAIN.*

Aim/Introduction: To assess our experience with ^{75}SeHCAT scintigraphy in the diagnosis of bile acid malabsorption (BAM) as a cause of chronic diarrhea. ***Materials and Methods:*** We studied 168 patients with diarrhea (119 women and 49 men, mean age 53.9 years), from April/2015 to December/2022. After oral administration of 0.01 mCi (0.37 MBq) capsule of ^{75}Se-taurocholic acid, abdominal scintigraphic images were acquired (at 3 h and on the 7th day), and pre/post-acquisition fundus measurements, to calculate its percentage retention (positive study due to retention of the tracer on the 7th day < 10%). ***Results:*** • Of the 168 patients, the test was positive in 74 (43.45%). • According to the reason for the request: o 40/168 (23.8%) had undergone cholecystectomy: 25 (62.5%) were positive; o 20/168 (11.9%) had a history of ileal and/or colonic surgery: 14 cases (70%) positive; o 2/168 (1.19%) had Crohn's disease, both positive (100%); o 80/168 (47.6%) had mainly diarrhea: 31 cases were positive (38.75%); o 26/168 (15.47%) were associated with other clinical-analytical data: 2 positive (7.69%) had vitamin B12 deficiency. • We observed a notable increase in requests for the test in the last 2 years, as it was included in the diagnostic algorithm for chronic diarrhea (because it is a simple, objective and cost-effective method), representing 57.14% of the studies performed (96/168), and 47.3% of the positives (35/74). In the previous 6 years (72 studies/168 = 42.86%), the percentage of positives (39/74 = 52.7%) corresponded mainly to patients with a surgical history, including 42 of the 60 operated patients in the sample (70%), with 64.28% (27/ 42) being positive. ***Conclusion:*** The ^{75}SeHCAT test is a non-invasive, objective, easy-to-perform and relatively inexpensive test of high diagnostic value in chronic diarrhea, being considered a gold standard method for BAM. Especially useful in patients with digestive surgery.

EP-0527

99米Tc-DTPA肾脏动态成像评估成人患者双功肾功能

X. Yan[1]*, Y. Ning*[1]*, Y. Chen*[1]*, M. Cai*[2]*, S. Li*[3]*;*
[1]Shanxi Medical University, Tai Yuan, CHINA, [2]Shanxi provincial People's Hospital & Fifth Clinical College of Shanxi Medical University, Tai Yuan, CHINA, [3]The first hospital of Shanxi Medical University, Tai Yuan, CHINA.

Aim/Introduction: To explore technetium-99m-diethylene-triaminepentaacetic acid (^{99m}Tc-DTPA) renal dynamic imaging in evaluating the function of duplex kidneys in adult patients. ***Materials and Methods:*** A retrospective study was conducted on 19 patients with duplex kidney who were subjected to ^{99m}Tc-DTPA renal dynamic imaging. Patients were divided into normal and abnormal group according to the imaging data. Additionally, 19 normal patients were selected as the control group. After imaging, the region of interest (ROI) of the kidneys were delineated, and the renography were obtained, which could provide renal function parameters, including glomerular filtration rate (GFR), T_{max}, $T_{1/2}$, renal clearance, and the uptake rate of duplex renal segment (upper renal moiety). ***Results:*** Compared to the control group, the serum creatinine in the duplex kidney group was higher (P=0.026), and the GFR was lower (P=0.008); the patients with impaired renal function were mainly in the abnormal renography group (P=0.008). In the duplex kidney group, the renal clearance of the affected kidney was lower than contralateral kidney (P=0.009), but no significant differences in other indicators. There were no differences in renal function indicators between different uptake rate in upper renal moiety; however, there was a trend that when the uptake rate was higher than 50%, the renal function was worse. ***Conclusion:*** This study showed that ^{99m}Tc-DTPA renal dynamic imaging could be used to evaluate total and split renal function, and even upper urinary tract patency in patients with duplex kidney. The patients with abnormal renography had worse renal function, and the patients with poor renal clearance in affected renal moiety should receive surgical treatment.

EP-0528

V/P-SPECT detection of pulmonary thromboembolism in patients with respiratory infections: a diagnostic challenge?

I. C. Ferreira*, R. T. Ferreira, J. G. Santos, A. I. Santos; Hospital Garcia de Orta, E.P.E., Almada, PORTUGAL.*

Aim/Introduction: Infectious conditions, particularly viral infections, have been associated with increased risk of venous thromboembolism. The association between respiratory infections (RI) and pulmonary thromboembolism (PTE) has not been well established, however, pneumonia is a common cause of hospitalisation that can be complicated by PTE, especially in patients with risk factors such as immobility. PTE diagnosis in these patients can be challenging because of overlapping features. Clinical suspicion, D-Dimer values (DD) and CT pulmonary angiogram are often first line diagnostic measures for PTE, but ventilation/perfusion single photon emission

computed tomography (V/P-SPECT) may also be used. We aimed to evaluate the prevalence of PTE in hospitalised patients with RI in whom V/P-SPECT was performed due to either persistent respiratory symptoms despite adequate treatment or appearance of other signs or symptoms. ***Materials and Methods:*** We retrospectively analysed hospitalised patients with a diagnosis of RI who underwent V/P-SPECT in our department, referred for suspicion of PTE, and classified them according to V/P-SPECT results (positive or negative for PTE). DD (µg/mL), age, gender, RI aetiology, reason for referral, and hospitalisation time in days (HT) were also recorded. Descriptive statistics and nonparametric tests were applied using IBM SPSS Statistics for Macintosh, Version 26.0. ***Results:*** Between January and December 2022, 35 patients (60% female) were selected, 27(77%) with negative and 8(23%) with positive V/P-SPECT, median ages being, respectively, 73[P25:65;P75:83] and 56[P25:39;P75:72] years; and median DD being 0,99[P25:0,48;P75:2,58] and 3,65[P25:1,96;P75:14,52] µg/mL, respectively. Mann-Whitney Test (MWT) showed a statistically significant difference in age and DD, between the two groups (p=0.017 and p=0.027, respectively). However, no statistically significant difference was found for hospitalisation time between the two groups (p=0.923; MWT). Of those with positive V/P-SPECT, 6(75%) had viral RI (3 with SARS-CoV-2 infection), with the remaining having bacterial RI. Within the negative V/P-SPECT sample, 11% had viral RI and 89% had bacterial RI. Pulmonary hypertension was present in 1 positive V/P-SPECT and in 3 of the negative group. ***Conclusion:*** Our results suggest an increased possibility of PTE in the presence of viral RI, younger age, and higher D-Dimer levels, as expected. Surprisingly, hospitalisation time (often linked to immobilisation and higher PTE risk) was not longer in our PTE group. However, small sample size limited our study. Further research is needed to validate these findings and establish the optimal clinical and analytical standards for requesting V/P-SPECT.

EP-0529

Diagnostic Contribution of Volumetric Analysis of Lung Perfusion SPECT/CT in Location of Pulmonary Thromboembolism

N. Alvarez Mena, *F. Sebastián Palacid, M. García Aragón, R. Zambrano Infantino, B. Pérez López, R. Ruano Pérez;*
Hospital Clínico Universitario de Valladolid, Valladolid, SPAIN.

Aim/Introduction: To assess the diagnostic accuracy of volumetric analysis of pulmonary perfusion SPECT/CT for the localisation of pulmonary thromboembolism and to compare these results with those observed with visual analysis. ***Materials and Methods:*** Retrospective series of 100 consecutive patients diagnosed with pulmonary thromboembolism (PTE) after a positive result in lung perfusion SPECT/CT (> 50% segment involvement and visualised in all three planes). Variables such as age, sex, acute or chronic PTE, laterality (uni- or bilateral), location and extent of perfusion defects were analysed. To evaluate the location and extent of perfusion defects, quantification analysis was performed using SPECT/CT segmentation (Q.Volumetrix software, GE). Subsequently, these results were compared with those observed in the visual analysis and the concordance between the two methods was assessed ($\chi 2$ test). ***Results:*** Mean age 73 ± 16 years (26-98 years). 59% female. When comparing the results obtained in the volumetric analysis with the visual analysis, a discordance of up to 41% of the patients evaluated was observed ($p < 0.05$). In this group, up to 68% (28/41) had chronic PTE. Regarding laterality, no significant differences were noted (23 bilateral and 18 unilateral). In the assessment of perfusion defect, overestimation of perfusion defects with visual analysis was more frequent (23 patients actually with less extension: 15 patients with involvement of fewer lobes and 8 patients with involvement of fewer segments). In addition, discordance in the location of the perfusion defect was observed in up to 9 patients (involvement of a different lobe in 4 patients and of a different segment in 5 patients). Of the 41 patients with discordance between the two analyses, 80% (33/41) had involvement in 2 or more lobes (55% of these were associated with involvement of 2 or more segments). Of the 59 patients with concordance between volumetric and visual analysis, up to 60% with single lobe involvement (97% of these with single segment involvement). ***Conclusion:*** Volumetric analysis of lung perfusion SPECT/CT is superior to visual analysis for more accurate localisation of perfusion defects in the clinical setting of pulmonary thromboembolism. Furthermore, it has a special interest in patients with chronic pulmonary thromboembolism or with multilobar or multisegmental involvement, where perfusion defects can often be difficult to evaluate. Finally, since volumetric analysis shows a better estimation of perfusion defects compared with visual analysis, its clinical application could modify the therapeutic approach.

EP-0530

The prevalence of pulmonary thrombo-embolism in pregnancy guided clinically by maternal tachycardia

A. Alnabulsi[1], *A. Ayeni*[2], *S. More*[1];
[1]*Division of Nuclear Medicine, Department of Radiation Medicine, University of cape Town, Cape Town, SOUTH AFRICA,*
[2]*Division of Nuclear Medicine, Department of Radiation Medicine, University of cape Town, Capetown, SOUTH AFRICA.*

Aim/Introduction: Pulmonary embolism (PE) is a life-threatening complication in pregnant and postnatal patients. Clinical suspicion of PE on the basis of clinical presentation varies particularly in pregnant patients. The challenge is still growing, especially in the absence of sensitive pretest clinical probability for PE in pregnancy utilizing VQ studies. The purpose of this retrospective study was to evaluate the accuracy of the clinical index in predicting PE in pregnant and postnatal patients and to determine the rate of false suspicion based on maternal tachycardia as a presenting symptom. ***Materials and Methods:*** A retrospective study of SPECT VQ scans of all female patients with clinical suspicion of PE was undertaken in the Department of NM. Studies were performed between 2016 and 2023. The study included all pregnant patients and those 6 weeks postpartum. Patients also had to have tachycardia that was defined by >100 beats/minutes with sign and symptoms of possible PE. The EANM criteria was used to define positive PE as a Ventilation/Perfusion mismatch of at least one segment or two sub-segments in keeping with the pulmonary vascular anatomy. ***Results:*** A total of 73 patients were included as part of the study. Thirteen (13) patients out of 73 were positive for PE (18%) with only one patient during pregnancy, in the age range of 16 to 39 years old, with a median age of 26 years old. The positive PE cases (10 patients) representing 14% of total positive PE cases presented from two days post caesarean section. While there were only 2 positive cases after the 2nd week of normal vaginal delivery. In total there were 58 (82%) negative scans for PEs. On the other hand, there were two positive scans for PEs during pregnancy with normal heart rate and known comorbidity. There was no significant association with clinical symptoms and maternal tachycardia in the patients who had negative scans for PE. ***Conclusion:*** The study suggests that the clinical index with

guidance of maternal tachycardia was of limited value during pregnancy and could not be accurate enough to predict PE during pregnancy. While during postnatal period, especially after C-section the prevalence of positive PE was the highest out of all, representing roughly 77% of all positive PE cases. The unnecessary exposure to radiation during pregnancy is highly concerning. This study is intended to encourage further development of the clinical suspicion criteria and algorithm during pregnancy for PE.

EP-0531

Are Planar Images In Pulmonary Perfusion Scintigraphy Sufficient For Positive Diagnosis Of Pulmonary Embolism In Pregnant Women?

L. Zaabar[1,2], *K. Ben Amara*[3], *T. Ben Ghachem*[1,2], *D. Ben Sellem*[1,2], *B. Letaief*[1,2], *A. Mhiri*[1,2];
[1]*Salah Azaeiz Institute, Tunis, TUNISIA,* [2]*Faculté de Médecine de Tunis, Tunis, TUNISIA,* [3]*Health Ministery, Tunis, TUNISIA.*

Aim/Introduction: Pulmonary embolism (PE) in pregnant women (PW) remains a major cause of maternal morbidity and mortality. Its positive diagnosis is difficult due to non-specificity of clinical and para-clinical signs (excluding imaging). Our study's aim was to describe the contribution of pulmonary perfusion scintigraphy (PPS) with basic scanning protocol in PW with suspected PE, and thus the risks of irradiation incurred for the fetus. ***Materials and Methods:*** Descriptive retrospective study conducted from January 2019 to December 2021, including 184 PW with suspicion of PE, referred to nuclear medicine department at Salah Azaiez Institute in Tunis for PPS. PPS were performed in planar mode (4 views at least). We did not perform ventilation imaging (not available) neither tomography . Patient results were classified into three groups according to PIOPED criteria (G1:High probability of PE. G2: Normal PPS, no PE. G3: inconclusive result: Low probability and intermediate probability of PE). ***Results:*** Median age to patients was 30.3 years. Mean age of pregnancy was 30 week of amenorrhea with a median of 31. Diagnostic yield of PPS was 84% (contribution in 155 PW): G1 with 18 PW (10%) and G2 with 137 PW (74%). It was inconclusive in 29 PW (16%): intermediate probability of PE (16 patients, 9%) and low probability of PE (13 patients, 7%). The statistically significant correlation between clinical symptoms and a positive PPS result was found for the triple association "palpitation, chest pain and dyspnea" noted in three patients (p=0.03), with a sensitivity of 16.67%, a specificity of 96.84%, positive predictive value (PPV) of 37.5% and negative predictive value (NPV) of 91.07%. PPS performances were as comparable as PPS associated to ventilation scanning reported in the litterature.Fetal radiation exposure from chest CT angiography and PPS was poor, lower than natural radiation exposure. ***Conclusion:*** Diagnostic approach orientation in PE depends crucially on clinical probability, but the different clinical scores are not validated in PW and need to be reviewed and adapted as well as the safety and PPV and NPV of imaging means. Technically, the indication of PPS in hybrid mode (SPECT/CT) remains to be enlarged more and more routinely, even in the situation of high clinical probability in PW.

EP-0532

Hepatic [18F]FDG uptake in patients with obesity: a study on the effect of NAFLD

U. Ustsinau*, O. Kulterer, M. Krssak, I. Rausch, F. Kiefer, C. Philippe; Medical University of Vienna, Vienna, AUSTRIA.*

Aim/Introduction: Excessive hepatic fat accumulation characterizes Non-alcoholic Fatty Liver Disease (NAFLD), which is prevalent in more than 80% of people with obesity. The potential limitations of hepatic [^{18}F]FDG-PET imaging for patients with NAFLD are being investigated. The study aimed to determine the reliability of standardized uptake values (SUVs) obtained from [^{18}F]FDG-PET in obese subjects, focusing on correction for liver fat content and the effects of whole-body normalizations. ***Materials and Methods:*** Twenty-one lean (M: 10, F: 11, BMI: 19-26kg/m^2) and eleven volunteers with obesity (M: 8, F: 3, BMI: 30-39kg/m^2) underwent [^{18}F]FDG-PET/MR scanning. Dixon images were used to estimate liver fat content and to correct SUV_{aver} for fat[1]. The liver SUVs (aver and max) were normalized to body weight (BW), lean body mass (LBM) and body surface area (BSA) for comparison. Blood samples were analyzed for glucose, GPT, GOT, gGT, insulin, triglycerides, cholesterol, HDL and LDL levels. ***Results:*** Under all normalizations, the median hepatic [^{18}F]FDG uptake (SUV_{aver}) of the obese group was insignificantly lower compared to the lean group having similar glucose levels. Dixon images confirmed the presence of NAFLD (>5.6% fat[2]) in nine out of eleven volunteers with obesity. Correction of SUV_{aver} for liver fat resulted in increased uptake values in all subjects, with a significant increase in SUV_{aver}(BW) in the obese group, likewise observed in SUV_{max}(BW). Looking at the individual values using BW and LBM normalizations, with a rise of BMI, SUVs of lean volunteers decreased (SUV_{aver}) or remained steady (SUV_{max}), whereas the obese group always increased. With BSA normalization, slope of both groups is high, and the extreme minimum lies in BMI of 23-32kg/m^2. Additionally, SUVs were independent of levels of GPT, GOT, gGT, insulin, triglycerides, cholesterol and LDL, but low HDL levels (<35 mg/dL) could be associated with an increased hepatic [^{18}F]FDG uptake in the obese group. ***Conclusion:*** Hepatic [^{18}F]FDG uptake is a result of a combination of hepatocyte function, effects of fat dilution and whole-body metabolic state, including blood glucose and insulin resistance. Therefore, to achieve accurate results for patients with obesity, raw SUV should be combined with correction for the liver fat, corresponding normalization (LBM) and careful consideration of blood glucose and HDL levels. The findings provide insights for clinicians and researchers working in the field of obesity and NAFLD and may help to improve the reliability of hepatic [^{18}F]FDG-PET imaging. ***References:*** [1] Keramida G et al. doi:10.2214/AJR.13.12147 [2] Sheka AC et al. doi:10.1001/jama.2020.2298

EP-0533

Pre-treatment pituitary gland [18F]FDG uptake in oncological patients

C. A. Ruiz-Bedoya[1,2], *S. F. Barrington*[1,3], *M. Yakubu*[1], *A. Hammers*[1], *G. J. R. Cook*[1,3], *M. Subesinghe*[1,3];
[1]*King's College London & Guy's and St. Thomas' PET Centre, London, UNITED KINGDOM,* [2]*Department of Imaging Chemistry & Biology, School of Biomedical Engineering and Imaging Sciences, King's College London, London, UNITED KINGDOM,* [3]*Department of Cancer Imaging, School of Biomedical Engineering and Imaging Sciences, London, UNITED KINGDOM.*

Aim/Introduction: Research exploring the variability of physiological pituitary uptake on [^{18}F]FDG PET-CT is scarce although sex and age-related differences in pituitary size on MRI have been described. Knowledge of the range of physiological pituitary uptake will help identify pituitary abnormalities, which is of importance in the era of immunotherapy and immune-related adverse events, which include hypophysitis. The aim of this study was to quantify normal ranges for pre-treatment pituitary [^{18}F]FDG uptake and explore any sex and age-related variation in oncological patients. ***Materials and Methods:*** Retrospective analysis on pre-treatment [^{18}F]FDG PET-CT scans obtained between April and December 2022 in adult patients (≥ 18 years) with either myeloma

or head and neck cancer (HNC), where scan coverage included the pituitary. Patient demographics and scan acquisition parameters were collated. SUV_{max}/SUV_{mean} for the pituitary and mediastinal blood pool (MBP) were obtained using a $1cm^3$ volume of interest centred on the sella turcica and aortic arch, respectively; this enabled calculation of pituitary-to-mediastinal blood pool ratios, i.e. target-to-background ratios (TBRs). ***Results:*** 256 FDG PET-CTs were reviewed with a higher proportion of males (171 patients = 66.8%), particularly in patients with HNC. There were no significant differences between the sexes with respect to age 64.7 ± 12.7 years; BMI 25.4 ± 5.4 kg/m^2; injected [^{18}F]FDG dose 337.0 ± 24.5 MBq; uptake period 64.2 ± 5.9 min and capillary blood glucose level 5.9 ± 1.2 mmol/l (Table 1). The median pituitary SUV_{max} in our cohort was 2.9 (interquartile range (IQR): 2.6-3.4), SUV_{mean} 2.5 (IQR:2.1-2.8), TBR_{max} 1.6 (IQR: 1.3-1.8) and TBR_{mean} 1.5 (IQR: 1.3-1.7). There was no correlation between age and $SUV_{max/mean}$ and $TBR_{max/mean}$ parameters ($r< 0.001$, $p > 0.1$). The median pituitary SUV_{max} in females (3.2; IQR: 2.6-3.6), was significantly higher ($p = 0.001$) than in males (2.9; IQR: 2.5-3.2); the median pituitary SUV_{mean} was also significantly higher in females (2.7 vs. 2.2, $p = 0.0002$). There was no significant difference in TBR_{max} between females (1.6; IQR 1.4-1.9) and males (1.6; IQR: 1.3-1.8) nor TBR_{mean} (1.6 vs. 1.5, $p > 0.5$). ***Conclusion:*** Our study quantifies the variation in normal physiological pituitary uptake on [^{18}F]FDG PET-CT in oncological patients, prior to treatment, and is the first to highlight differences in pituitary uptake between males and females. Although further research is required to understand the reasons underpinning this, these data will assist PET-CT reporters to differentiate normal from abnormal pituitary uptake.

EP-0534

Relationship between the severity of vesicoureteral reflux and renal scarring in children. About 162 patients.

M. Habbache, *Q. Naili, M. Abdi;*
Nuclear medicine Center or Blida, Algier, ALGERIA.

Aim/Introduction: Vesicoureteral reflux (VUR) is associated with an increased risk of renal scarring, which can lead to long-term complications such as hypertension and renal failure. The aim of this retrospective study was to evaluate the relationship between the severity of VUR and renal scarring in children. ***Materials and Methods:*** We retrospectively studied 162 children under 14 years old with VUR who presented to our department between 2013 and March 2023. Children who were more than 6 months after their last urinary tract infection episode were included. Static renal scintigraphy with Tc-99m dimercaptosuccinic acid (DMSA) was used to evaluate renal scarring. The severity of VUR was graded according to the International Reflux Study, and Pearson correlation coefficient was used for statistical analysis ***Results:*** Of the 240 kidneys with reflux evaluated, 58.7% had renal scars on DMSA scans. The percentage of scarring kidneys increased with the severity of VUR: 13% in grade I , 27% in grade II , 45% in grade III , 81% in grade IV , and 92% in grade V . There was a strong correlation between the severity of VUR and the formation of renal scarring ($r = 0.985$, $p < 0.01$). High-grade VUR (grades 3-5) was responsible for 95 (39%) of scarring, while low-grade VUR (grades 1-2) was only responsible for 13 (5%) of scarring. Five patients with high-grade bilateral reflux were at the stage of renal failure ***Conclusion:*** The severity of VUR is strongly associated with renal parenchymal damage and the formation of renal scarring. High-grade VUR is particularly associated with a higher risk of renal scarring and potential long-term complications. Early detection and management of VUR in children is crucial in preventing the development of renal scarring and long-term sequelae

EP-36

e-Poster Area

C: Therapy Clinical Study -> C1 Oncological Therapy Clinical Study -> C11 Neuroendocrine Therapy

EP-0535

Actinium225 -DOTATATE peptide receptor radionuclidetherapy(PRRT) as first line treatment in two cases of bowel Neuroendocrine tumors

K. Kamaleshwaran, *E. Ramkumar;*
Kovai Medical center and Hospital limited (KMCH), Coimbatore, INDIA.

Aim/Introduction: we report first clinical experience of two cases of rectal and ileal NET treated with Actinium225(Ac225)-DOTATATE as first line treatment . ***Materials and Methods:*** First patient is 65 year old male presented with rectal pain ,on evaluation found to have rectal lesion and biospy showed grade 1 NET(Ki67-4%).Ga68 DOTANOC PET CT showed intense avid pararectal lesion, retroperiotneal lymphnodes ,liver lesions and right rib metastases.He underwent Ac225 DOTATATE . Posttherapy images were acquired at 24 hours. High energy general purpose collimators were used for both whole body and SPECT/CT using 218.keV and 440keV photon energies with 20% window width. Repeat PET CT at 2 months showed partial response in all lesions and CgA showed decreasing trend. He underwent 2nd cycle and on followup with no side effects and complete pain relief. ***Results:*** Second patient is 70 year old male on diagnostic laparascopy showed multiple small bowel lesions ,on biopsy showed grade 1 NET .Ga68 DOTANOC PET CT images showed atleast 5 lesions in ileum with mesentric nodes .Patient prefered for Ac225 DOTATATE as first line treatment .After 2 months ,Interim PET CT showed partial response and without any side effects . ***Conclusion:*** We present here our first clinical experience on Ac225- DOTATATE therapy in 2 NET patients, a promising first line treatment option extending new dimension to treatment of NET.Post therapy Ac225 DOTATATE SPECT CT and whole body images were acquired at 218 and 440 Kev .Both patients showed partial response with no side effects and is on followup . ***References:*** Ian Selçuk N, Demirci E, Ocak M, Toklu T, Ergen S, Kabasakal L.Almost Complete Response with a Single Administration ^{225}Ac-DOTATATE in a Patient with a Metastatic Neuroendocrine Tumor of Unknown Primary.Mol Imaging Radionucl Ther. 2022 27;31(2):139-141

EP-0536

Discovery of blood transcriptomic markers for response to [177Lu]Lu-DOTATATE in locally advanced or metastatic neuroendocrine neoplasms

S. Bae[1], *H. Sung*[2], *H. Choi*[2], *H. Im*[3], *M. Suh*[2], *J. Paeng*[2], *G. Cheon*[2], *K. Kang*[2];
[1]*Institute of Radiation Medicine, Medical Research Center, Seoul National University, Seoul, KOREA, REPUBLIC OF,* [2]*Department of Nuclear Medicine, Seoul National University Hospital, Seoul, KOREA, REPUBLIC OF,* [3]*Department of Applied Bioengineering, Graduate School of Convergence Science and Technology, Seoul National University, Seoul, KOREA, REPUBLIC OF.*

Aim/Introduction: [^{177}Lu]Lu-DOTATATE is a treatment of choice for advanced or metastatic well-differentiated neuroendocrine neoplasms (NENs) that highly express the somatostatin receptor (SSTR). Imaging modalities including CT and SSRT PET have limitation in predicting response to radioligand therapy (RLT).

A few blood biomarkers such as NETest and PPQ have been suggested for assessing and predicting response, but might not completely explain dynamic changes during RLT. The study aims to identify early transcriptomic alterations in blood during RLT in relation to treatment responses. ***Materials and Methods:*** Locally advanced or metastatic NEN patients receiving [^{177}Lu]Lu-DOTATATE and with no prior RLT were prospectively enrolled from June 2021 to May 2022. Response to RLT was evaluated after the fourth cycle using contrast-enhanced CT and RECIST 1.1. Blood samples were collected before the first cycle and within one day of the second cycle for bulk RNA sequencing and differential gene expression analysis. Genes exhibiting larger absolute time differences in PD compared to PR or SD, with increased or decreased expression relative to baseline, were classified as 'PD:pos' or 'PD:neg'. Similarly, for comparison between PR and SD or PD, genes were grouped as 'PR:pos' or 'PR:neg'. The expression of the selected genes in primary or metastatic NEN tissues and in normal tissues was compared using publicly available datasets. The proportion and alteration of immune cells in blood across time were examined. ***Results:*** In the study, 16 patients were enrolled, consisting of 10 men and 6 women ranging in age from 26 to 78 years old. The tumor volume measured by SSTR PET was not significantly different between the response groups. Among PD:pos, PD:neg, PR:pos, and PR:neg gene groups, PR:pos group was significantly associated with Gene Ontology (GO) such as the G protein-coupled receptor signaling pathway and regulation of calcium ion. Additionally, 10 out of 15 genes in the PR:pos group showed lower average expression in NENs compared to normal tissues. PR:pos genes did not overlap with the NETest genes, and the NETest genes did not show significant transcriptomic alteration during the first cycle of PRRT. Finally, among the cell types, proportion of CD4+ T cells demonstrated a decreasing pattern over time in the PD group, whereas changes were irregular in other response groups. ***Conclusion:*** The response to RLT was associated with early upregulation of GPCR-related calcium pathways after the first treatment. The proposed dynamic blood biomarkers are expected to represent early biological events after RLT.

EP-0537

Long-term effects of peptide receptor radionuclide therapy (PRRT) used as a first-line treatment of GEP-NET - a single centre experience

M. Opalinska, *K. Morawiec-Slawek, A. Kurzynska, A. Sowa-Staszczak, A. Hubalewska-Dydejczyk;*
Department of Endocrinology, Jagiellonian University Medical College, Krakow, Poland, Krakow, POLAND.

Aim/Introduction: Peptide receptor radionuclide therapy (PRRT) is a well-recognized treatment option for inoperable/metastatic somatostatin receptor-positive neuroendocrine tumours (NET). According to the current guidelines it is recommended as a second or a third line of the treatment. Aim: Retrospective analysis of the outcomes and adverse effects of PRRT in patients treated with ([90Y]Y-DOTA-TATE or [90Y]Y/[177Lu]Lu-DOTA-TATE or [177Lu]Lu-DOTA-TATE) as a first line treatment due to metastatic GEP-NET in comparison to PRRT used as a standard 2. line treatment after progression on long-acting somatostatin analogues. ***Materials and Methods:*** Thirteen patients (7 men and 6 women) treated with PRRT as a first line treatment due to metastatic well differentiated GEP-NET (G1 or G2) in 2007-2013 were eligible to analysis. There were 6 patients with pancreatic, 5 with small intestine, 2 with large intestine NET and 1 subject with unknown primary site. As a comparison the group of 13 patients (primary site and WHO grade matched to first group, 6 men, 7 women) treated with PRRT as a second line treatment were analysed. In the first group all patients had liver, 9 lymph node, and 5 bone metastases, while in the second group metastases to the liver were present in all cases, in 11 cases were seen in the lymph nodes, and in 5 cases in bones. ***Results:*** Group in which PRRT was used as first-line therapy: -Median time of follow-up 125 months (range 84-204) -Median progression-free survival (PFS) 66 months (range 18 - 132 months) -Worsening of renal function during follow-up time in 10 of 13 patients (grade IV renal toxicity, required haemodialysis in 3 cases) -No significant long-term hematologic toxicity Group in which PRRT was used as second-line therapy: -Median time of follow-up 37 months (range 5-66) -Median progression-free survival (PFS) 24 months (range 2 - 53 months) -Worsening of renal function during follow-up time in 3 of 15 patients (grade IV renal toxicity, required haemodialysis in 0 cases) ***Conclusion:*** The long-term results of PRRT used as first-line treatment are very encouraging and appear to be much better than in case of PRRT used as a second line therapy. The risk of renal function impairment associated with PRRT increases over time, especially after a period of 5 years after the end of PRRT. Prospective studies are warranted to confirm this observation.

EP-0538

Visual and Whole-Body Quantitative Analysis of 68-Ga-DOTATATE PET/CT to Predict Outcomes after 177Lu-DOTATATE

I. Sonni[1,2], *M. Hotta*[1,3], *P. Thin*[1], *K. Nguyen*[1], *L. Gardner*[1], *L. Ciuca*[1], *A. Hayrapetian*[1,4], *M. P. Lewis*[1,5], *D. J. Lubin*[1,6], *M. Allen-Auerbach*[1];
[1]*University of California, Los Angeles, Los Angeles, CA, UNITED STATES OF AMERICA,* [2]*Università Magna Graecia, Catanzaro, ITALY,* [3]*National Center for Global Health and Medicine, Tokyo, JAPAN,* [4]*University of South Alabama, Mobile, AL, UNITED STATES OF AMERICA,* [5]*Kaiser Permanente Los Angeles Medical Center, Los Angeles, CA, UNITED STATES OF AMERICA,* [6]*SUNY Upstate, Syracuse, NY, UNITED STATES OF AMERICA.*

Aim/Introduction: Somatostatin receptors (SSTR) represent an ideal target for nuclear theranostics applications in neuroendocrine tumors (NET). Studies suggest that a high uptake on SSTR PET is associated with response to SSTR peptide receptor radionuclide therapy (PRRT). However, the prognostic value of whole-body SSTR PET in patients undergoing PRRT is unknown. The purpose of this study was to evaluate the role of baseline whole-body (WB) ^{68}Ga-DOTATATE PET/CT (DOTA-PET) quantitative parameters, and the presence of NET lesions without DOTA uptake on DOTA-PET, as predictors of outcome in patients with NET treated with ^{177}Lu-DOTATATE PRRT. ***Materials and Methods:*** All patients with NET who underwent at least 4 cycles of 177Lu-DOTATATE PRRT in our institution between 07/2016 and 03/2021 were included in this retrospective analysis if they fulfilled the following inclusion criteria: available DOTA-PET within 6 months of 1st PRRT cycle, available follow-up CT and/or MRI performed >6 months after the 4th cycle of PRRT. The DOTA-PET analysis consisted in a visual analysis, conducted by one physician with dual board certification (nuclear medicine and radiology), and a quantitative analysis done by a nuclear medicine physician. The visual analysis assessed the presence of NET lesions visible on the DOTA-PET co-registered CT showing DOTA uptake ≤ liver uptake. The quantitative analysis consisted in contouring all DOTA-avid lesions on DOTA-PET and extracting WB quantitative parameters: SUVmean (WB-SUVmean), SUVmax of the lesion with highest uptake (H-SUVmax), and tumor volume (WB-TV). Quantitative DOTA-PET parameters and the presence of DOTA-negative lesions

were correlated to overall survival (OS), progression-free survival (PFS) and radiologic response (assessed by RECIST 1.1 criteria). Fisher's exact test, Mann-Whitney's U-test and Kaplan-Meier curves with Cox-regression analysis were used for the statistical analysis. ***Results:*** Forty patients (F/M: 21/19; 34/40 with GEP NET, 6/40 with non-GEP NET) were included in the analysis. The median follow-up period after the 4th PRRT cycle was 25.7 months (range: 15.2 - 59.1). Fourteen/40 (35%) patients showed radiologic response (RECIST PR). PFS and OS events were 17/40 (42.5%) and 6/40 (15%), respectively. Thirteen/40 (32.5%) patients had DOTA-PET negative lesions at baseline. Higher WB-SUVmean and H-SUVmax were associated with better response (p= 0.015 and 0.005, respectively). The presence of DOTA-PET negative lesions and higher WB-SUVmean were associated with shorter PFS (p=0.026 and 0.008, respectively). Higher WB-TV was associated with poorer OS (p=0.006). ***Conclusion:*** Visual and quantitative analysis of baseline DOTA-PET can be valuable measures to predict outcome after 177Lu-DOTATATE PRRT.

EP-0539

Therapy in Advanced Small Cell Lung Carcinoma - Investigating Outcome, Toxicity Profile and Prognostic Determinants

P. Hartrampf[1], *A. Weich*[2], *F. Lutz*[1], *A. K. Buck*[1], *T. Higuchi*[1], *S. E. Serfling*[1], *Y. Zhi*[3], *R. A. Werner*[1];
[1]*Klinik und Poliklinik für Nuklearmedizin, Würzburg, GERMANY,*
[2]*Medizinische Klinik und Poliklinik II, Würzburg, GERMANY,*
[3]*Klinik und Poliklinik für Hals-, Nasen- und Ohrenkrankheiten, plastische und ästhetische Operationen, Würzburg, GERMANY.*

Aim/Introduction: In advanced small cell lung carcinoma (SCLC), treatment options are limited. We aimed to evaluate the therapeutic efficacy and toxicity profile of SSTR-directed PRRT in advanced disease, along with determinants of outcome. ***Materials and Methods:*** 24 patients with advanced SCLC, which had exhausted previous treatment options, were scheduled for PRRT. Disease control (DC, partial response [PR] or stable disease [SD]), was evaluated investigating follow-up CTs. Progression-free (PFS) and overall survival (OS) were also recorded. Prior to PRRT and upon last available follow-up (n=15), we also investigated hematotoxicity (including leukocytes, thrombocytes, and hemoglobin), nephrotoxicity (glomerular filtration rate [GFR], serum creatinine) and serum chemistry (lactate dehydrogenase [LDH], aspartate aminotransferase [AST], alkaline phosphatase [AP] and C-reactive protein). For assessing factors associated with survival, univariable cox regression was applied. ***Results:*** 1/24 (4%) patient died due to infection independent from treatment, leaving 23/24 (96%) for outcome analysis. The majority received one cycle 15/24 (63%; two cycles in 5/24 [21%], three cycles in 2/24 [8%], five and six cycles in 1/24 [4%], respectively). DC was observed in 3/24 (13%; with PR in 1/3 [33%] and SD in 2/3 [67%]). Median PFS was 56 days and median OS was 89 days. Directly after administration of the radiotherapeutic agent, no acute toxicity was recorded in any of the subjects. During follow-up, we observed the following grade III/IV toxicities: anemia grade III in 5/15 (33%), and thrombopenia grade III in 1/15 (7%; grade IV in 2/15 [13%]). No leukopenia or nephrotoxicity higher than grade II occurred. Pretherapeutic elevated LDH (HR 1.001 [95%CI, 1.000-1.002], p<0.02), AST (HR 1.013 [95%CI, 1.003-1.022], p<0.01) and AP (HR 1.007 [95% CI, 1.000-1.013], p<0.03) were associated with shorter OS in univariable analysis. ***Conclusion:*** In the present cohort of end-stage disease patients affected with advanced SCLC, PRRT is feasible, along with grade III/IV toxicities in selected cases. As such, PRRT may be incorporated earlier in the disease course, preferably in patients with improved general conditions or by applying dosimetry-based individualized activity concepts.

EP-0540

Impact of kidneys absorbed dose assessment during177Lu-PRRT (peptide receptor radionuclide therapy) on patient management: examples from clinical experience

M. Ferrari, F. Botta, ***C. Grana****, D. Alio, A. Barone, G. Castiglione Minischetti, S. Papi, I. Clerici, F. Ceci;*
Istituto Europeo di Oncologia, Milano, ITALY.

Aim/Introduction: ^{177}Lu-PRRT is an established treatment for patients affected by neuroendocrine tumours. Kidneys are the major organ at risk, with late toxicity absorbed dose thresholds around 28Gy. In this study dosimetry results are reported, and examples from clinical experience are presented to support the contribution of dosimetry in patient management during ^{177}Lu-PRRT. ***Materials and Methods:*** Simplified dosimetry based on 24h post-injection SPECT-CT analysis was performed for all patients at each cycle. Whenever possible, multiple points dosimetry was performed during at least one cycle for each patient. Dosimetry results were discussed on patient basis to tailor the subsequent cycles or to implement dose modifying strategies. ***Results:*** Thirty-eight patients were treated for a total of 111 cycles (14 patients 4 cycles, 11 patients 3 cycles, 9 patients 2 cycles, 4 patients 1 cycle). The mean (range) kidneys absorbed dose/activity was 0.7 (0.3-1.5) Gy/GBq. Intra-patient variability (mean ± standard deviation) among different cycles was 13%±12%. The average (range) ratio of absorbed dose obtained with simplified versus multi-points dosimetry, for a same cycle, was 1.01 (0.8-1.2); the variability range reduced to (0.9-1.1) when considering only cases for which the last image was acquired later than 100 hours post-injection. During 31/111 cycles (28%), the kidneys absorbed dose was higher than 0.8 Gy/GBq, a value that projected over 4 cycles with full activity potentially lead to cumulative dose higher than the 28Gy threshold, assuming 20% uncertainty associated to absorbed dose evaluation. The management of these cases was discussed on case-by-case basis, considering different tailoring strategies (including treatment completion or reduction of activity/cycle or number of cycles) to balance treatment outcome and risk of complications. Two patients, affected by urinary infection during two cycles each, exhibited significantly higher doses than the average population, ranging from 0.9 to 1.3Gy/GBq; during subsequent cycles, they both underwent an additional amino acids infusion the day after activity administration. ***Conclusion:*** Kidneys dosimetry during ^{177}Lu-PRRT is an important tool for treatment optimization. If performed at each cycle, it allows to monitor the therapy effect on kidneys, and to undertake adjustment strategies if deemed necessary after a risk-to-benefit balance. Urinary infection might lead to significantly high absorbed doses and it should be accurately monitored. Multiple time-point dosimetry is desirable, with late time point preferably acquired later than 5 days post-injection. Simplified, single-point dosimetry is feasible and can still provide useful information despite affected by higher uncertainty, to be properly taken into account.

EP-0541

Factors Predicting Response and Survival in Lutetium-177 DOTATATE Treatment of Neuroendocrine Tumours: Preliminary Results

Z. MAMMADKHANLI[1], *F. SOYLUOGLU*[1], *B. OZDEMIR GUNAY*[2], *C. AYDIN*[1], *U. KORKMAZ*[1];
[1]*Trakya University, School of Medicine, Department of Nuclear Medicine, Edirne, TÜRKIYE,* [2]*Sultan 1. Murat State Hospital, Clinic of Nuclear Medicine, Edirne, TÜRKIYE.*

Aim/Introduction: Neuroendocrine tumors (NETs) are a heterogeneous group of tumors expressing somatostatin receptors (SSTR).177Lu-DOTATATE, a radioactively labelled SSRT analogue, is an approved treatment for SSRT receptor positive advanced metastatic or inoperable NETs.In this study, we aimed to evaluate the results and overall survival of patients treated with 177Lu-DOTATATE in our clinic in the light of factors such as haematological parameters and tumour heterogeneity ***Materials and Methods:*** Patients diagnosed with NET and admitted to our clinic for Lu-177 DOTATE treatment between 2016 and 2021 were retrospectively reviewed.The primary lesion SUVmax value,Krenning score(KS),visual tumour heterogeneity and metastatic involvement sites obtained from Ga68 PET/CT were recorded.Overall survival analyses were performed ***Results:*** 28 patients (mean age: 56±17 years) were included in the study. Tumour sites: 10 patients with pancreas,stomach-5, lung-3,small bowel-3,liver-2,colorectal NET-2, medullary thyroid cancer-1,neuroblastoma-1 and 1 patient with paraganglioma. Median Ki-67 was 10%. Four patients had Grade 1, 19 patients had Grade 2, and 5 patients had Grade 3 NETs.On PET/CT, 8 patients were evaluated as KS 2, 11 patients as KS 3, and 9 patients as KS 4. In visual evaluation,SSRT expression was heterogeneous in 15 patients. A total of 106 cycles of Lu-177 treatment were administered at intervals of 8-12 weeks with an average of 4 cycles per patient. After treatment, partial response was observed in 7 patients, stable disease in 8 patients and progression in 13 patients. There was a significant correlation between treatment response and bone metastasis andtreatment initiation time (p=0.016 and 0.008, respectively). Other organ metastases, platelet/lymphocyte, neutrophil/lymphocyte and monocyte/lymphocyte ratios were not correlated with treatment response. During the follow-up period (median 55.2±38.7 months), 14 patients died. Median survival time was 114.7±26.6 months and 2-year and 5-year survival times were 89% and 68%, respectively. The mortality rate was 21.4% in patients who received RNT within 16 months after diagnosis, while this rate was 78.6% in patients who received RNT later.Grade and heterogeneity (p=0.027 and 0.015, respectively) were found to be the determining factorsin survival analyses. In multivariate analysis, tumour heterogeneity (HR=0.2, 95%CI 0.060-0.843,p=0.027) was the only independent predictor of overall survival. ***Conclusion:*** In patients with advanced NET, Lu-177 DOTATATE treatment provides disease control in more than half of patients. Although tumor heterogeneity is the only independent factor affecting overall survival, tumor grade and time from diagnosis to treatment also seem to be effective factors in survival and prospective studies with a larger number of patients are needed.

EP-0542

Impact of the SBVR 177Lu activity quantification method on organ and tumor dosimetry results after PRRT and on patient management

A. Chicheportiche*, S. Raskin, Y. Krausz, J. Godefroy, S. Grozinsky-Glasberg, S. Ben-Haim;*
Hadassah Ein Kerem Hospital, Jerusalem, ISRAEL.

Aim/Introduction: Conventional calibration of gamma cameras involves calculating calibration factors (CFs) as a function of volume. However, this method yields inconsistent results when the background activity varies. We have recently proposed a new quantification method for ^{177}Lu that aims to correct for background effects by considering the sphere-to-background counts/voxel ratio (SBVR) in addition to volume [1]. The SBVR method was validated on anthropomorphic phantoms and has been shown to be more accurate, improving the quantification of tumors and organs by 60% (from 14% error in quantification to 6%) and 80% (from 20% to 3%) in average, respectively. The aim of this study is to quantify the impact of SVBR on the dosimetry calculations and to evaluate its potential impact on patient management. ***Materials and Methods:*** ^{177}Lu-DOTA-TATE SPECT/CT data after PRRT of 10 consecutive patients with metastatic neuroendocrine tumors (10 treatments, 4 therapy cycles per treatment, total of 40 therapy cycles) were retrospectively analyzed. Absorbed doses (ADs) were calculated for 40 kidneys, 40 livers, 32 spleens and 92 tumors using both the conventional and SBVR quantification methods and cumulative ADs were compared. The impact of the SBVR method on the decision of whether to stop PRRT because of "expected" kidney AD exceeding the 25 Gy safety threshold was evaluated. ***Results:*** Mean cumulative ADs of 146.4 ± 106.4 Gy, 13.9 ± 3.8 Gy, 5.9 ± 2.3 Gy, and 22.6 ± 12.3 Gy were respectively obtained for tumors, kidneys, liver, and spleen using the conventional quantification method, compared to 140.9 ± 103.4 Gy, 17.8 ± 4.7 Gy, 6.6 ± 2.3 Gy, and 28.1 ± 15.6 Gy with SBVR. The decision to administer the fourth treatment cycle was similar with the two methods for all patients. However, the maximum number of treatment cycles that a patient could receive without exceeding the kidney safety threshold was higher with the conventional method at 8 ± 1 cycles, compared to 6 ± 1 cycles with the SBVR method. ***Conclusion:*** These preliminary results show that the SBVR methodology has an impact on the cumulative absorbed dose calculations, with relative differences ranging between 10% and 20%. Furthermore, in the context of personalized dosimetry-based treatments, the SBVR method may improve patient management, enabling more accurate determination of the maximum number of treatments that can be administered safely. ***References:*** [1] Raskin, S. et al. Towards accurate 177Lu SPECT activity quantification and standardization using lesion-to-background voxel ratio. EJNMMI Phys 10, 5 (2023).

EP-0543

Neoadjuvant PRRT with 90Y-DOTATOC: preliminary results from a monocentric prospective study

A. Barone[1], *F. Mattana*[2], *L. L. Travaini*[2], *P. Rocca*[2], *M. Colandrea*[2], *L. Gilardi*[2], *S. Fracassi*[2], *S. Papi*[3], *I. Clerici*[3], *M. E. Ferrari*[4], *F. Botta*[4], *E. Bertani*[5], *F. Spada*[6], *N. Fazio*[6], *F. Ceci*[2], *C. M. Grana*[2];
[1]*Division of Nuclear Medicine, Istituto Europeo di Oncologia IRCCS, Milan, Italy, Milan, ITALY,* [2]*Division of Nuclear Medicine, Istituto Europeo di Oncologia IRCCS, Milan, ITALY,* [3]*Division of Pharmacy, Istituto Europeo di Oncologia IRCCS, Milan, ITALY,* [4]*Medical Physics Unit, Istituto Europeo di Oncologia IRCCS, Milan, ITALY,* [5]*Division of Digestive Surgery, Istituto Europeo di Oncologia IRCCS, Milan, ITALY,* [6]*Division of Gastrointestinal Medical Oncology and Neuroendocrine Tumors, Istituto Europeo di Oncologia IRCCS, Milan, ITALY.*

Aim/Introduction: Surgery is considered the only curative treatment for pancreatic neuroendocrine tumors (pNETs), but it is feasible only in a few patients. A new possible therapeutical strategy in pNETs is preoperative peptide Receptor Radionuclide Therapy (PRRT), as its cytoreductive effect could increase the efficacy of surgery. The aim of this prospective study is to evaluate the response and rate of R0 surgery in patients with unresectable or borderline resectable G1/G2 pNET eligible to PRRT with ^{90}Y-DOTATOC and associate the response to circulating NET transcripts measured before and after PRRT. ***Materials and Methods:*** This study included patients with histopathologic diagnosis of unresectable or borderline resectable G1/G2 pNET, with limited liver disease based on pre-treatment ^{68}Ga- DOTATOC PET/CT. To date, 8 out 30 patients (2 females and 6 males) were enrolled. All the patients received at least one cycle of 1.85 GBq/cycle of ^{90}Y-DOTATOC; the protocol foresaw a cumulative activity of 9.25-11.1 GBq in 5-6 cycles. At first cycle, each patient received also ^{111}In-OctreoScan activity in order to perform a dosimetric study on kidneys; moreover, a dosimetric study was also performed during the subsequent cycles on ^{90}Y-DOTATOC SPECT/CT imaging for comparison. ***Results:*** PRRT was well tolerated by all the patients, without any toxicity. Four patients completed all scheduled 6 cycles of therapy, obtaining a SD (1), a CR (1), and a PR with resecability criteria (1); the fourth patient is scheduled to receive the imaging during the next month. One patient received only 4 cycles, because of elevated dose to the kidneys, obtaining a partial response but was not considered operable. One patient received only one cycle due to the worsening of clinical conditions. Two patients are still in treatment. ***Conclusion:*** These preliminary data of neoadjuvant PRRT with ^{90}Y-DOTATOC confirm the good tolerability of ^{90}Y-DOTATOC PRRT in a group of patients where surgery could be challenging. Based on literature reports, the objective response rates expected exceed the 35%[1]. ***References:*** [1] Imhof A, Brunner P, Marincek N, Briel M, Schindler C, Rasch H, Mäcke HR, Rochlitz C, Müller-Brand J, Walter MA. Response, survival, and long-term toxicity after therapy with the radiolabeled somatostatin analogue [90Y-DOTA]-TOC in metastasized neuroendocrine cancers. J Clin Oncol. 2011 Jun 10;29(17):2416-23.

EP-0544

Inflammatory markers as prognostic factor inTNE treated with 177Lu-DOTATATE

J. Villa Palacios*, E. Triviño-Ibáñez, M. Muros de Fuentes, T. Aroui-Luquin, R. Sanchez-Sanchez;*
Hospital Universitario Virgen de las Nieves, Granada, SPAIN.

Aim/Introduction: AIM: To assess the utility of different inflammatory markers as predictors of survival in patients with NETs treated with 177Lu-DOTATATE. Background: Neutrophil-to-Lymphocyte ratio (NLR) and Platelet-to-Lymphocyte ratio (PLR) are useful markers in assessment of inflammatory response and are prognostic markers in cancer patients. N-terminal pro-brain natriuretic peptide (NT-proBNP) is produced by cancer cells without cardiac faillure. These markers, when elevated, may be a poor prognostic factor in GEP-NETS. ***Materials and Methods:*** 28 patients with metastatic NETs of different origins (21GEP, 3 TOD, 2 pulmonary, 2 other origins) treated with four cycles of 177Lu-DOTATATE. The tumor variables analyzed were grade, Ki67, mitotic index, number of treatments received (surgery, somatostatin analogues, chemotherapy, everolimus QUETA) and inflammatory markers such as Neutrophil-to-Lymphocyte ratio (NLR), and Platelet-to-Lymphocyte ratio (PLR) and pro-brain natriuretic peptide (NT-proBNP). Survival results were recorded by Kaplan-Meier analysis. The functional status of the patient was also assessed (Karnofsky and ECOG scales). ***Results:*** The mean age at diagnosis was 56.14 years in our patients, with an average of 5.68 years of evolution (1-25 years) and 2 lines of previous treatment (1-4). Overall survival was assessed with a median of 36.75 months (12-55 months). The relationship between their overall survival and the above variables was analyzed. We have analyzed the predictive role of survival of the NLR and PLR. The NLR does come out significantly associated with survival, the higher the NLR, the worse survival. Using the ROC curve analysis, I have selected the point with the best discriminative capacity (cut-off) of 3 . An NLR >3 increases the probability/risk of dying by 4.43 (HR: 4.43, p=0.035). The PLR analysis does not reach statistical significance. ***Conclusion:*** NLR >3 increases the probability/risk of dying by 4.43 (HR: 4.43, p=0.035) and NT-proBNP greater than 300 pg/ml implies an increased risk of death of 7.76 in these patients. Inflamation markers may be useful to asses the usefulness and prognosis of therapy with177Lu-DOTATATE.

EP-0545

Kidneys functional volumes changes of patients undergoing 177Lu-DOTATATE treatment and the uncertainties measures in kidney dosimetry

J. Khan*[1], T. Rydèn[2], J. Svensson[3], M. Van Essen[4], P. Bernhardt[5];*
[1]Department of Medical Radiation Sciences, Institute of Clinical Sciences, Gothenburg, SWEDEN, [2]Department of Medical Physics and Biomedical Engineering (MFT), Sahlgrenska University Hospital, Gothenburg, SWEDEN, [3]Department of Oncology, Institution of Clinical Sciences, Sahlgrenska Academy at University of Gothenburg, Gothenburg, SWEDEN, [4]Department of Clinical Physiology, Sahlgrenska University Hospital, Gothenburg, SWEDEN, [5]Department of Medical Radiation Sciences, Institute of Clinical Sciences, Sahlgrenska Academy at University of Gothenburg, Gothenburg, SWEDEN.

Aim/Introduction: Kidney dosimetry procedure after peptide receptor therapy using ^{177}Lu-DOTATATE consist of multiple steps. The aim of this study was to determine the dosimetry uncertainties associated with manual segmentation of kidney parenchymal volume (KPV) in CT images. ***Materials and Methods:*** SPECT/CT images of 18 patients were acquired over the abdomen at ~ 4 hours (h) (D0), 24 h (D1), 48 h (D2) and 168 h (D7) after ^{177}Lu-DOTATATE treatment. The reference kidney volumes were estimated by using the KPVs that correspond to the acquired SPECT acquisition for kidney activity measurements. For obtaining the uncertainties that depends on the accuracy of KPV based on all possible combinations of the four individual KPVs was used to determine the activity distributions in kidney at each time-point. Bi-exponential curve fit was used for determining the time-integrated activity. ***Results:*** For a single cycle of 7.4 GBq, the segmented kidney volumes were between 31 and 243 ml. The KPV was statistically significant at D1 compared to D7. With KPV acquired at D7 CT images as reference, the Bland-Altman analyse resulted in bias of 8.74%, 10.73%, 2.92% for D0, D1, D2, and the corresponding uncertainties were 12.4%, 16.32% and 8.31%, respectively. The absorbed dose uncertainties when using only one KPV and a constant RCs of 0.85 were 6.29%, 3.85%, 6.13%, and 3.91%, whereas, with patient-specific RCs 5.55%, 4.40%, 4.73%, and 3.43%, respectively. ***Conclusion:*** The kidneys volumes varied significantly from D0 to D7, which will influence the absorbed dose estimation. However, kidney dosimetry with only one delineated KPV can be performed with satisfying accuracy using either a constant RCs of 0.85 or patient-specific RCs.

EP-0546

Evaluation of RadioLigand Therapy response in GEP-NETs: the role of 177Lu-Dotatate imaging

S. Valente[1], *F. Linguanti*[1], *M. E. Abenavoli*[1], *L. Antonuzzo*[2], *V. Briganti*[3], *D. Lavacchi*[4], *M. Matteini*[3], *F. Mungai*[5], *R. Sciagrà*[1], *G. Simontacchi*[6], *L. Vaggelli*[3], *V. Berti*[1];
[1]*Nuclear Medicine Unit, Department of Experimental and Clinical Biomedical Sciences "Mario Serio", University of Florence, 50134, Florence, ITALY,* [2]*Clinical Oncology Unit, Careggi University Hospital, Florence, Italy; Department of Experimental and Clinical Medicine, University of Florence, Florence, Italy, Florence, ITALY,* [3]*Department of Nuclear Medicine, Azienda Ospedaliero-Universitaria Careggi, Largo Brambilla 3, 50134, Florence, Italy, Florence, ITALY,* [4]*Clinical Oncology Unit, Careggi University Hospital, Florence, Italy, Florence, ITALY,* [5]*Department of Radiology, Azienda Ospedaliero-Universitaria Careggi, Largo Brambilla 3, 50134, Florence, Italy, Florence, ITALY,* [6]*Radiation Oncology, Azienda Universitaria Ospedaliera Careggi, Florence, ITALY.*

Aim/Introduction: Theranostic approach using 177Lutetium-Dotatate (Lutate) is approved in gastroenteropancreatic neuroendocrine tumors (GEP-NET). Imaging at 24 hours after Lutate treatment is used to evaluate radiotracer distribution and for dosimetry purposes. The aim of our study is to assess the potential value of Lutate imaging in evaluating treatment response and predicting 6 months clinical outcome. ***Materials and Methods:*** We enrolled 15 GEP-NET patients, eligible for radioligand therapy and treated with Lutate. Each Lutate scan (1, 2, 3, 4) has been analyzed drawing regions of interest (ROIs) on each lesion, which were classified according to the organ to which it belongs (hepatic, nodal, GEP tract, bone). Mean count values were extracted from each ROI, normalized to lumbar mean activity, and percentage differences between Lutate cycles were calculated (Δ%). Patients were divided according to 6 months follow-up into 3 groups (partial response -PR, stable disease -SD and progressive disease -PD). Differences between groups was analyzed using ANOVA, and statistical significance has been set at $p<0.05$). ***Results:*** At a lesion level, hepatic lesions demonstrated Δ% between 4th and 1st Lutate scans of -14,06 +- 29,46 %, nodal lesions of -18,26 +- 19,46 %, GEP tract lesions of 3,17 +- 26,99 %, and bone lesions of 21,44 +- 54,05 %. At a patient level, the Δ% between 4th and 1st Lutate scans of the "least responsive lesion" was the most significantly different variable between groups. At post-hoc analyses, the differences resulted particularly significant in differentiation of PR patients from both SD and PD patients. Also mean Δ% of each patients resulted different between groups at the limits of significance, but the difference was observed only between PR and the other 2 groups. ***Conclusion:*** Percentage differences of lesion activities between Lutate cycles measured at Lutate imaging may provide useful parameters to predict 6 months clinical outcome of GEP-NET patients treated with radioligand therapy. The most significant parameter resulted the percentage difference between 4th and 1st Lutate scans of the "least responsive lesion", which was able to successfully differentiate outcome of patients.

EP-0547

Efficacy of [177Lu]Lu-DOTA-TATE in metastatic neuroendocrine neoplasms of different locations: our experience.

M. Pudis[1], *J. L. Vercher-Conejero*[1], *J. J. Martín-Marcuartu*[1], *A. Teule-Vega*[2], *S. Bondia-Bescós*[1], *B. Hervás-Sanz*[1], *A. Rodríguez-Gasén*[1], *J. Diaz-Moreno*[1], *M. Cortés-Romera*[1];
[1]*Nuclear Medicine - PET (IDI), Bellvitge University Hospital, L'Hospitalet de Llobregat, Barcelona, SPAIN,* [2]*Medical Oncology, Institut Català d'Oncologia (ICO), L'Hospitalet de Llobregat, Barcelona, SPAIN.*

Aim/Introduction: The aim of the study is to present our experience with [^{177}Lu]Lu-DOTA-TATE therapy and to assess the tolerability and efficacy of this treatment in patients with tumors expressing somatostatin receptors. ***Materials and Methods:*** We retrospectively reviewed all the patients treated with [^{177}Lu]Lu-DOTA-TATE in our center (Bellvitge University Hospital, Barcelona, Spain) with at least 3 month follow-up after the last cycle. All of these patients had SSTR-overexpressing, histologically confirmed neoplasm. [^{177}Lu]Lu-DOTA-TATE was administered at a dose of 7.4 GBq iv per cycle, in 4 cycles with an interval of 8-10 weeks together with an amino acid solution to protect the kidneys. The data evaluated included demographic information (age, sex), the origin and primary tumor site, location of metastases, histopathological grade and Ki67, prior treatments, assessment of toxicity, clinical, immunohistochemical and radiological response to [^{177}Lu]Lu-DOTA-TATE. All patients were re-evaluated by post-therapy CT scans at the end of treatment (generally on the 3rd month) using RECIST 1.1 criteria. ***Results:*** In total, we treated 60 patients (27 women; mean age 58.7 years [38-82]) with a mean follow-up of 22,5 months [3-117 months] during the study. The origin of the tumor was gastroenteropancreatic in 54p (90%), paraganglioma in 3p (5%), pheochromocytoma, bronchopulmonary and urogenital tract (renal) with 1p each. The primary gastroenteropancreatic tumor site was ileal in 28p (52%), followed by pancreatic in 16p (30%), intestinal in 6p (11%) and colorectal in 4p (7%). 2 cervical and 1 pelvic paragangliomas. Hepatic (92%), nodal (80%), osseous (30%) and peritoneal (30%) were the most common metastatic sites. All the patients had well differentiated NEN, 25p (42%) Ki67<3% (grade 1), 33p (55%) Ki67 3-20% and 2p with Ki67>20%. 29p (48%) received lutetium as a 2nd line, 14p (23%) as a 3rd line and 10p (17%) as 4th line of treatment. The most common adverse effects were gastrointestinal (27%), hematological (25%): grade 3-4 in 7% and nephrotoxicity (5%). 13p did not complete the treatment, 8p because of progression and 5p because of the toxicity. 47p completed the therapy, 33p (55%) with stable disease, 19p (32%) with partial response and 8p (13%) with progression on the post-therapy CT scans. Median progression-free survival (PFS) was 23.2 months [6-ongoing]. ***Conclusion:*** Our experience confirms the efficacy and safety of [^{177}Lu]Lu-DOTA-TATE in a wide range of metastatic SSTR-expressing NENs. 87% of patients presented favorable responses (stable/partial). This treatment has been well tolerated, with scant adverse events that were generally mild.

EP-0548

Evaluation of the quality of life of patients with neuroendocrine tumors treated with Lutetium-177-DOTATATE

S. Asadurova, *D. Villasboas, J. Hernando, F. Velazquez, R. Bellviure, J. Echeverri-Diaz, N. Calviño, A. García-Burillo; Hospital Universitari Vall d´Hebron, Barcelona, SPAIN.*

Aim/Introduction: To evaluate the changes in the quality of life of patients with NETs treated with Lutetium-177-DOTATATE. ***Materials and Methods:*** a single center prospective study including 38 patients with NETs treated with Lutetium-177-DOTATATE. The patients filled out the QLQ-GINET21 quality of life questionnaire before each treatment cycle (4 questionnaires per patient). It was determined that each patient had to answer at least 2 questionnaires. Two patients were excluded for filling out just one questionnaire. The questionnaire includes 21 questions, grouped into 5 categories (endocrine symptoms, gastrointestinal symptoms, treatment-related, disease-related worries, social

functioning) and 5 individual questions - weight loss, weight gain, muscle and/or bone pain, information and sexual functioning. The response is on a scale from 1 (least symptomatology/problem) to 4 (greater symptomatology/problem) and some questions have the option of "not applicable". We analyze one hundred twenty one questionnaires in total. The responses were transformed into a score on a scale from 0 to 100 through a linear transformation, using the EORTC guidelines. A change by 5 to 10 points on the 0-100 scale is considered "a little" better (or worse), a change of 10 to 20 was described as a "moderate" change and a change greater than 20 is considered "very much" better (or worse). A statistical analysis was performed. ***Results:*** We observed a moderate improvement in the problem of weight loss. There is little improvement in the area of social functioning, especially in terms of the possibility of travelling (moderate improvement), which we associate with the reduction of the symptoms. Also, there is a little improvement in receiving information and a little improvement in the concerns related with the results of the tests. Surprisingly, we observed a little worsening of endocrine symptoms, especially of the night sweats. ***Conclusion:*** Treatment with Lutetium-177-DOTATATE in patients with NETs is related to an improvement in quality of life, especially in terms of symptoms.

EP-0549

Radiomics analysis in 177Lu-DOTATATE therapy: Extracting new information from theranostic images

H. Abdollahi[1], *X. Hou*[2], *J. Beauregard*[3], *C. Uribe*[1], *A. Rahmim*[1]; [1]*BC Cancer Research Institute, Vancouver, BC, CANADA,* [2]*Department of Radiology, University of British Columbia, Vancouver, BC, CANADA,* [3]*Cancer Research Centre and Department of Radiology and Nuclear Medicine, Université Laval, Quebec City, QC, CANADA.*

Aim/Introduction: Radiopharmaceutical therapy using 177Lu-DOTATATE has shown promise for neuroendocrine tumor (NET) patients. Quantitative analysis of diagnosis and therapeutic images can aid in improving the therapy's effectiveness. In this study, we extracted quantitative measures from theranostic images, including SPECT and CT images, to investigate changes in SPECT features within therapy cycles, changes in CT radiomic features between the first and last cycles, and correlations between therapeutic activity and SPECT features. ***Materials and Methods:*** We enrolled four NETs patients undergoing 177Lu-DOTATATE therapy who underwent QSPECT/CT after each cycle. Radiomics features were extracted from the liver lesions segmented on all CT and QSPECT images. Changes in features were assessed between T0, T1, and T3, as well as between the first and last injection. Percentage changes were calculated and reported. Correlations between SPECT feature values and therapeutic activity were measured using the Pearson method and the correlation coefficient (CC) reported. ***Results:*** In total, 103 features were extracted from each lesion or kidney from the QSPECT images. Results showed that 34 radiomics features mimicked time activity curves, increasing from T0 to T1 and decreasing from T1 to T3. Intensity-based and intensity histograms had the highest changes (77%-91%), with Kurtosis, Variance, Energy, Mean, and 75thPercentile as the most varying features. In total, 108 radiomics features were extracted from each lesion in liver CT images. Several radiomic features changed due to 177Lu therapy, including 10th Percentile and Large Zone High Grey Level Emphasis as the most decreasing, and Strength and Minimum Grey Level as the most increasing radiomics feature changes. For correlation analysis, the range of therapeutic activity was found to be 108-543 millicuries. The CC ranged from -0.77-0.76 for lesions and -0.53-0.49 for kidneys. Three GLSZM features were found to be the most negatively correlated in lesions, and Kurtosis (Intensity Histogram), Normalised Inverse Difference (GLCM), Strength (NGTDM), and Normalised Grey Level Non-Uniformity (GLRLM) with CC; 0.75-0.77 were the most positively correlated features. ***Conclusion:*** Quantitative radiomics features analysis during RPTs can depict heterogeneities within uptake and aid in dosimetric measures. Changes in radiomics features inter-cycle of therapy may show the biological properties of tissue, correlating with receptor density and the success of therapy. Radiomics features can be a good marker for patient response to RPT, and several lesion radiomics features are highly correlated to therapeutic activity, which can be used as uptake measures for further clinical outcome modeling.

EP-0550

Assessment of response to therapy and safety of177Lu-DOTATATE in GEP-NET patients

M. Raddi*, F. Di Gennaro, F. De Lauro, V. Porfidia, C. Maisto, G. Ventanieri, S. Melone, P. Gaballo, L. D'Ambrosio, S. Lastoria; National Cancer Institute IRCCS Pascale, Naples, ITALY.*

Aim/Introduction: Peptide receptor radionuclide therapy (PRRT) is a radionuclide treatment used for gastroenteropancreatic neuroendocrine (GEP-NET) tumors that express somatostatin receptors (SSTRs). Aim of this study is to assess the short-time efficacy of PRRT with [^{177}Lu]Lu-DOTATATE in patients with progressive metastatic gastroenteropancreatic NETs. ***Materials and Methods:*** We evaluated 41 patients (20 females and 21 males; median age 61 years) who received all 4 cycles of [^{177}Lu]Lu-DOTATATE (7.4 GBq each infusion) between 2019-2023. Interval between each administration was 8 weeks. Primary tumor site was pancreas in 22 (54%) patients, midgut in 9 (22%) patients, foregut in 3 (7%) patients, hindgut in 1 (2%) patient and unknown primary site with gastrointestinal profile in 6 (15%) patients. 17 of 41 patients had a partial or total resection of the primary tumor. Before each infusion and during the follow-up, patients were monitored with laboratory tests (hematological, renal and liver panel). SPECT/CT acquisitions were performed for dosimetric estimations at 3, 20 and over 90 hours after each cycle. Morphological imaging (CT and/or MRI) and [^{68}Ga]Ga-DOTATATE PET/CT were performed before starting the treatment and 3-4 months after the last therapy administration to assess the effects on primary tumor and on metastatic lesions. Median follow-up was 12 months. ***Results:*** Partial response (PR) was documented in 12 (29%) patients, stable disease (SD) in 23 (56%) patients and progressive disease (PD) in 6 (15%) patients. Of the 22 patients with the pancreatic primary site 10 showed PR, 9 SD and 3 PD; of the 9 patients with the midgut primary site 8 had SD and 1 had PD; of the 3 patients with foregut primary site 1 had PR and 2 SD; the patient with hindgut primary site had SD; and of the 6 patients with unknown primary site 1 had PR, 2 PD and 3 SD. Renal cumulative dose did not reach the threshold value (23 Gy) in any patient. In 3 patients, with high hepatic metastatic burden, bone marrow cumulative dose was higher than 2 Gy, however, no hematological toxicity was observed. Target lesions received an absorbed dose between 23 and 423 Gy. ***Conclusion:*** Our results confirm that [^{177}Lu]Lu-DOTATATE is an effective and well tolerated, therapeutic option in patients with GEP-NETs, obtaining PR or SD in 85% of patients without hematological and renal acute or chronic toxicity.

EP-0551

Evaluation of different infusion protocols and dosimetry assessment in patients undergoing peptide receptor radionuclide therapy with 177Lu-DOTATATE

A. Varallo[1], *L. Piscopo*[1], *V. Gaudieri*[1], *S. Grasso*[1], *E. Zampella*[1], *C. Nappi*[1], *C. Oliviero*[2], *M. Italiano*[1], *F. Volpe*[1], *M. Falzarano*[1], *S. Clemente*[2], *A. Cuocolo*[1], *M. Klain*[1];
[1]*Department of Advanced Biomedical Sciences, University of Naples "Federico II", Naples, ITALY,* [2]*Unit of Medical Physics and Radioprotection, University of Naples "Federico II", Naples, ITALY.*

Aim/Introduction: Peptide receptor radionuclide therapy (PRRT) is a radionuclide treatment used for gastroenteropancreatic tumors. The efficacy of the therapy depends on many factors, including the infusion procedure and the imposed flow rates also have impact on the injected and residual activity. Aim of this study is to analyze the impact of different flow rates used for the administration of ^{177}Lu-DOTATATE and the preliminary results of personalized internal dosimetry. ***Materials and Methods:*** We evaluated 17 consecutive patients underwent PRRT with ^{177}Lu-DOTATATE. 7.4 GBq were injected every eight weeks for four cycles. SPECT/CT imaging acquisitions were at 4 hours (h), 24 h, 48 h and 168 h for dosimetric estimations after each cycle. Differences between three different flow rate protocols were assessed: a) a constant flow rate throughout the treatment; b) one increase in flow rate at T_1=10 min and T_2=20 min; c) two increases in flow rate at T_1=10 min, T_2=20 min and T_3=30 min. The residual activity was measured using each protocol. Absorbed dose (AD) to organs and lesions was analyzed using the software MIM SurePlan MRT (MIM, Cleveland). ***Results:*** We treated 3 women and 14 men (median 61 years), for a total of 56 infusions. No extravasation of radiopharmaceutical was observed. The administrated and residual mean activity was 7.3 ± 0.2 GBq and 0.1 ± 0.1 GBq, respectively. The mean treatment time was 44.8 ± 5.9 min. 86% of infusions had a residual activity below the threshold (set at 2% of the initial average activity). The threshold was achieved in 55% of the cycles at T_{treat}= 30 min, in 73% of the cycles at T_{treat}= 40 min and in 86% of the cycles at T_{treat}= 45 min. The constant flow rate throughout the treatment protocol reached the threshold at the end of the treatment in a lower percentage of cases than the other protocols. For liver, kidneys and lungs the mean AD was 2.09 ± 3.80 Gy, 1.33 ± 0.44 Gy and 0.22 ± 0.18 Gy respectively. Mean AD to normal tissue was 0.21 ± 0.28 Gy. AD to lesions ranged from 5.08 ± 0.91 Gy to 16.39 ± 4.61 Gy. ***Conclusion:*** Infusion protocols that adapt flow rate have a significant impact on residual activity. The infusion protocol used should be taken into account in order to have a more accurate estimate of the absorbed dose.

EP-37

e-Poster Area

C: Therapy Clinical Study -> C1 Oncological Therapy Clinical Study -> C12 Prostate Cancer Therapy

EP-0552

TheraP-based Selection Criteria Do Not result in a Survival Benefit When Compared With VISION Trial Criteria in Prostate Cancer Patients Scheduled for PSMA-targeted Radioligand Therapy

K. Michalski[1], *A. Kosmala*[1], *R. A. Werner*[1], *S. Serfling*[1], *A. K. Seitz*[1], *C. Lapa*[2], *A. K. Buck*[1], *P. E. Hartrampf*[1];
[1]*Universitätsklinikum Würzburg, Würzburg, GERMANY,* [2]*Universitätsklinikum Augsburg, Augsburg, GERMANY.*

Aim/Introduction: Two randomized clinical trials demonstrated the efficacy of prostate-specific membrane antigen (PSMA) radioligand therapy (PSMA RLT) in metastatic castration-resistant prostate cancer (mCRPC). While the VISION trial used criteria within PSMA PET/CT for inclusion, the TheraP trial used dual tracer imaging including [^{18}F]FDG PET/CT. Therefore, we investigated whether the application of the TheraP trial criteria compared to the VISION criteria lead to a survival benefit for patients with mCRPC after PSMA RLT. ***Materials and Methods:*** Thirty-five patients with mCRPC who had received PSMA RLT and pretherapeutic imaging with [^{18}F]FDG and [^{68}Ga]Ga-PSMA I&T or [18F]F-PSMA-1007 were studied. Therapeutic eligibility was retrospectively evaluated using the VISION and TheraP study criteria. ***Results:*** 26 of 35 (74%) treated patients fulfilled the VISION criteria (=VISION+) and only 17 of 35 (49%) fulfilled the TheraP criteria (=TheraP+). Significantly reduced overall survival after PSMA RLT was observed in patients rated VISION- with 3 months compared to VISION+ with 12 months (hazard ratio (HR) 3.1, 95% confidence interval (CI) 1.0-9.1, p<0.01). For patients rated TheraP-, no significant difference in survival after PSMA RLT was observed compared to TheraP+ patients (TheraP-: 5.5 vs. TheraP+: 11 months, HR 1.6, 95% CI 0.8-3.3, p=0.2). Within patients rated TheraP-, patients with discordant FDG-positive/PSMA-negative (=FDG+/PSMA-) tumor lesions (n=12) showed a significantly reduced OS of 4.5 months (HR 2.8, 95% CI 1.1-6.8, p<0.01) after PSMA RLT, whereas low PSMA expression alone (n=6) was not a significant prognosticator with a median OS of 15 months (HR 0.8, 95% CI 0.3-2.1, p=0.6). ***Conclusion:*** Retrospective application of the inclusion criteria of the TheraP study did not lead to a survival benefit after PSMA RLT compared to the criteria of the VISION study, even though FDG+/PSMA- lesions are a negative prognostic marker. This could be due to the definition of low PSMA expression used in the TheraP trial.

EP-0553

The efficacy of prognostic factors derived from Ga68-PSMA PET-CT images in predicting treatment response and survival in patients with metastatic castration-resistant prostate cancer treated with Lu-177PSMA

M. Oflas[1], *D. Has Simsek*[1], *Y. Sanli*[1], *S. Kuyumcu*[1], *E. Isik*[1], *S. Karadogan*[1], *M. Basaran*[2], *M. Ekenel*[2], *A. Mudun*[1], *Z. G. Ozkan*[1];
[1]*Istanbul Faculty Of Medicine Department Of Nuclear Medicine, Istanbul, Türkiye,* [2]*Istanbul University Institute Of Oncology, Department Of Medical Oncology, Istanbul, TÜRKIYE.*

Aim/Introduction: We aimed to determine the efficacy of metabolic parameters obtained from Ga68-PSMA PET/CT images performed in the early period after 2 cycles of Lu177-PSMA therapy to evaluate the therapy response and prognosis in patients with metastatic castration-resistant prostate cancer (mCRPC). ***Materials and Methods:*** Patients diagnosed with mCRPC, who were treated ≥2 cycles of Lu177-PSMA treatment in our department were retrospectively examined. Metabolic tumour volume (MTV) and total lesion PSMA (TLP) values were calculated on Ga68-PSMA PET/CT images performed before and after second Lu-177 PSMA treatment. In the evaluation of treatment response, ≥30% decrease in basal MTV and TLP values was accepted as consistent with partial responsive disease (PR), ≥30% increase with progressive disease (PD), and <30% increase/decrease with stable disease (SD),respectively. ≥ 50% reduction in basal PSA value was evaluated as PR ; ≥25 % increase as PD; the remaining group evaluated as SD, respectively. In addition, information about overall survival (OS) was obtained through medical records. ***Results:*** 89 male patients were included in

the study (mean age: 72 years). Pre- / post-treatment median serum PSA, MTV and TLP values are indicated in Table 1.OS was calculated as 17 months (4-55 months) from the start of Lu-177 PSMA treatment. When survival analysis is evaluated according to PSA change after 2 cycles; OS was calculated as 27 months in PR (n:40), 16 months in SD (n:20) and 10 months in PD (n:29), respectively. The differences in OS were statistically significant (p <0.001).When survival analysis is performed according to MTV values after 2 cycles; OS was calculated as 27 months in PR (n:30), 18 months in SD (n:23) and 12 months in PD (n:36), respectively. The OS differences were statistically significant (p:0.002).When survival analysis is evaluated according to TLP after 2 cycles ; OS was calculated as 20 months in PR (n:41), 13 months in SD (n:23), and 14 months in PD (n:25), respectively .The OS differences between these groups were not statistically significant (p=0.088). ***Conclusion:*** It was determined that change of MTV value obtained from Ga68-PSMA PET/CT images before and after the first 2 cycles of Lu-177 PSMA treatment was correlated with overall survival in mCRPC patients .However, change of TLP values was not correlated with overall survival .Therefore, MTV value has been found as a favorable parameter in addition to PSA in order to help the clinician for earlier evaluation of treatment response and providing prognostic information.

EP-0554

Dosimetric evaluation of 177Lu-PSMA-617 therapy: Feasibility of Single Time Point Imaging Protocol

S. Rezaei, *E. Gharepapagh;*
Department of Nuclear Medicine, Medical School, Tabriz University of Medical Sciences, Tabriz, IRAN, ISLAMIC REPUBLIC OF.

Aim/Introduction: Radiopharmaceutical therapies with Lutetium-177 prostate-specific membrane antigen (PSMA) ligands have shown promising results in metastatic castration-resistant prostate cancer (mCRPC). Patient-specific activity personalization is currently impossible due to the lack of absorbed dose-effect relationships. Dosimetry needs to be incorporated into the routine clinical workflow of radiopharmaceutical therapies using simplified methods such as single time point (STP) imaging protocols rather than multiple time point (MTP). This study aims to assess differences between image-based dosimetry for ^{177}Lu-PSMA-617 therapy on lacrimal glands, salivary glands, and tumors using STP versus MTP. ***Materials and Methods:*** There were 40 patients with mCRPC with ^{177}Lu-SPECT imaging data (24h, and 72h post-drug administration) available on the first and second ^{177}Lu-PSMA-617 treatment cycles. We employed two different dosimetry methods: the MTP method, which incorporated images from both imaging time points, and the STP method. A method based on the difference between Gaussian curves was used to delineate tumors, while salivary glands and lacrimal glands were drawn manually. Support vector machines were used to classify tumors based on their mean density and coefficient of variation. ***Results:*** There were a few exceptions to the pattern of decreasing absorbed doses and the number of tumors with each therapy cycle. The 2-point method seemed to correlate well with the second imaging interval. Furthermore, the mean absorbed dose per time-integrated activity for lacrimal glands was 0.61 ± 0.11 (MTP method), 0.65 ± 0.13 (STP method 24h-image), and 0.52 ± 0.12(STP method 72h-image) Gy/GBq, to submandibular glands it was 0.41 ± 0.11(MTP method), 0.37 ± 0.15 (STP method 24h-image), 0.23 ± 0.12 (STP method 72 h-image) Gy/GBq, and for parotid glands 0.35 ± 0.10 (MTP method), 0.37 ± 0.11 (STP method 24h-image) and 0.24 ± 0.16 (MTP method 72h-image) Gy/GBq. ***Conclusion:*** Based on the low mean difference in absorbed dose compared to MTP, STP dosimetry for ^{177}Lu-PSMA-617 therapy at 24 h was found to be sufficiently accurate for ^{177}Lu-PSMA-617 therapy.

EP-0555

Safety and Efficacy of re-treatment with Lutetium-177 PSMA Beyond Six Cycles in Patients with Castration-Resistant Prostate Cancer

E. Medhurst[1], *R. Alipour*[2], *T. Akhurst*[2], *A. Azad*[3], *J. P. Buteau*[1], *A. Cardin*[2], *B. Emmerson*[1], *M. B. Haskali*[4], *G. Kong*[2], *L. Kostos*[3], *P. Jackson*[1], *K. Raghava*[2], *A. Ravi Kumar*[2], *J. Saghebi*[2], *S. Sandhu*[3], *L. Spain*[3], *B. Tran*[3], *M. S. Hofman*[1];
[1]*Prostate Cancer Theranostics and Imaging Centre of Excellence; Molecular Imaging and Therapeutic Nuclear Medicine, Cancer Imaging,Peter MacCallum Cancer Centre, Melbourne, AUSTRALIA,* [2]*Department of Nuclear Medicine, Peter MacCallum Cancer Centre, Melbourne, AUSTRALIA,* [3]*Department of Medical Oncology, Peter MacCallum Cancer Centre, Melbourne, AUSTRALIA,* [4]*RadiopharmaceuticalProduction and Research Laboratory, Peter MacCallum Cancer Centre, Melbourne, AUSTRALIA.*

Aim/Introduction: Lutetium-177 PSMA radioligand therapy (LuPSMA) is a life-prolonging treatment for patients with metastatic castration-resistant prostate cancer (mCRPC). Landmark studies reported the outcomes of up to 6 cycles of LuPSMA. This study aimed to evaluate the safety and efficacy of re-treatment with LuPSMA in patients beyond the initial 6 cycles of LuPSMA. ***Materials and Methods:*** We conducted a retrospective analysis of patients with mCRPC who received over 6 cycles of LuPSMA therapy at a single centre. Patients were initially treated on clinical trials or registry with PSMA-617 (N=287) or compassionate access with PSMA-I&T (N=46). Administered radioactivity for additional (re-treatment) cycles was 6.0 GBq/cycle. The primary outcome was PSA response rate (PSA-RR). Secondary outcomes included treatment-emergent adverse events (AEs) and overall survival (OS). AEs were restricted to G2-4 xerostomia, haematological and renal toxicity, or any G3-4 toxicity attributed to Lu-PSMA (CTCAE v5). OS defined from date of PSMA PET prior to the first cycle. Data cut-off; 28Feb2023. ***Results:*** From 9/2015 to 2/2023, 36/333 (10%) patients (median age 76, IQR 71-80) received >6 cycles of LuPSMA. The median total number of LuPSMA cycles received was 8 (range 7-17, IQR 8-9). Prior to LuPSMA, 36/36 (100%) of patients received androgen-receptor pathway inhibitor (16% receiving >1), 91% docetaxel, 19% cabazitaxel and 3% carboplatin. During first 6 cycles, PSA50-RR and PSA90-RR occurred in 36/36 (100%) and 33/36 (91%), respectively. Median time between cycle 6 and cycle 7 was 7 months (range 2.7-34.9 months, IQR 5.7-10.7). A median of 2 (range 1-6) cycles were administered before pausing and waiting for progression with each re-treatment. Median cumulative administered radioactivity was 56.2 GBq (IQR 54.9-62.2). Following additional treatments beyond cycle 6, PSA50-RR and PSA90-RR occurred in 12/36 (33%, 95%CI 20-50%), and 5/36 (14%, 95%CI 6-29%), respectively. AEs were xerostomia (G2: 8.3%), anemia (G2: 13.8%, G3: 5.5%), thrombocytopenia (G2: 2.7%, G4: 2.7%), kidney dysfunction (G2: 13.8%, G3: 5.5%). Myelodysplastic syndrome occurred in 2/36 (5.5%) both with PSMA-I&T and causality uncertain. No treatment-related deaths. Median OS 38.1 months (95%CI 19.1-57.2). 11/36 (30%) continue to receive LuPSMA. ***Conclusion:*** This retrospective study indicates that administering LuPSMA beyond 6 cycles is feasible for a selected group of patients with mCRPC who initially responded to treatment.

EP-0556

Can a cutoff be set for pre-treatment 68Ga-PSMA-11 PET/CT parameters to predict 177Lu-PSMA-I&T response and patient survival?

S. Mirshahvalad[1,2], *R. Eisazadeh*[1], *G. Rendl*[1], *S. Gampenrieder*[3], *G. Schweighofer-Zwink*[1], *H. Griessner*[4], *C. Pirich*[1], *M. Beheshti*[1];
[1]*Division of Molecular Imaging & Theranostics, Department of Nuclear Medicine, University Hospital, Paracelsus Medical University, Salzburg, AUSTRIA,* [2]*Joint Department of Medical Imaging, University Health Network, University of Toronto, Toronto, ON, CANADA,* [3]*Division of Molecular Imaging & Theranostics, Department of Oncology, University Hospital, Paracelsus Medical University, Salzburg, AUSTRIA,* [4]*Division of Molecular Imaging & Theranostics, Department of Urology, University Hospital, Paracelsus Medical University, Salzburg, AUSTRIA.*

Aim/Introduction: To evaluate the prognostic value of pre-treatment ^{68}Ga-PSMA-11 PET/CT in prostate cancer (PCa) patients receiving ^{177}Lu-PSMA-I&T, considering the treatment response and patient survival. ***Materials and Methods:*** Sixty PCa patients (age:73±8, baseline PSA:185±371) who received ^{177}Lu-PSMA-I&T therapy between October 2018 and January 2023 were included. Eligible patients had metastatic castration-resistant prostate cancer, underwent ^{68}Ga-PSMA-11 PET/CT before treatment, and had serum PSA levels available at baseline and after each treatment cycle. All patients underwent pre-treatment ^{68}Ga-PSMA-11 PET/CT, and clinical follow-up data were recorded. SUVmax, SULmax, SUVpeak, and SULpeak of the most-avid tumoral lesion in each patient and SUVmean of the normal parotid and liver tissues (backgrounds) were measured. ^{177}Lu-PSMA-I&T was administered based on a multidisciplinary recommendation. The standard approach of 4-6 therapy cycles was considered unless patients revealed a major adverse event or showed a significant progression, resulting in therapy termination. We considered clinical (PSA level; PCWG3 criteria) and imaging (^{68}Ga-PSMA-11 PET/CT; RECIP1.0 criteria) composite for the response assessment. The outcomes were dichotomised as "responder" (partial response) vs "non-responder" (stable and progressive disease). ***Results:*** Overall, 26/60 (43%) and 30/60 (50%) patients were responders and progressive in the final assessment, respectively. Regarding the baseline clinical or imaging differences, pre-treatment SUVmax, SULmax, SUVmax-to-backgrounds, and SULmax-to-backgrounds significantly differed between responders and non-responders. Notably, no baseline clinical characteristic was significantly different. To predict response outcome, SUVmax, SULmax, SUVmax-to-liver background, SULmax-to-liver background, SUVmax-to-parotid background and SULmax-to-parotid background were significant factors in the univariate regression. In the multivariate analysis, only the SULmax-to-liver background was significant (p-value=0.028). To find a cutoff, the SULmax-to-liver SUVmean of 8 was the optimal coordinate point, showing sensitivity and specificity of 69% and 72% for predicting response to ^{177}Lu-PSMA-I&T. Regarding survival analysis, in a median follow-up of 360 (91-1114) days, 11/60 (18%) mortal events were documented. In univariate Cox analysis, SUVpeak (hazard ratio [HR]=3.8; 95%CI=1.1-14.2), SULmax (HR=3.5; 95%CI=1.0-13.2), SUVmax-to-parotid background (HR=3.6; 95%CI=1.0-13.5) and SULmax-to-parotid background (HR=4.0; 95%CI=1.1-15.0) were significant. In the multivariate analysis, only the highest SULmax-to-parotid background was significant (p-value=0.043; HR=4.0), having a cutoff of 2.4. ***Conclusion:*** Pre-treatment ^{68}Ga-PSMA-11 PET/CT could potentially predict response to ^{177}Lu-PSMA-I&T therapy and overall survival. The most prominent factors in this regard were the SULmax-to-background ratios. In searching for cutoffs, the SULmax-to-liver SUVmean of 8 and SULmax-to-parotid SUVmean of 2.4 were the best for predicting response outcome and overall survival, respectively. Our findings may help clinicians stratify patients at ^{177}Lu-PSMA-I&T therapy initiation to enhance patient management.

EP-0557

Clinical outcomes after treatment following the use of 18F-PSMA PET/CT scans in patients with recurrent prostate cancer

J. Rodriguez-Rubio Corona, *F. Cañete Sánchez, Y. Santaella Guardiola, M. Piñero Fernandez-Reyes, C. Quintana Bolaño, M. Pajares Vinardell;*
Hospital Universitario Puerta del Mar, Cádiz, SPAIN.

Aim/Introduction: The optimal treatment for recurrent biochemically recurrent prostate cancer (BCR) is still unknown. Positron emission tomography/computed tomography (PET/CT) with prostate-specific membrane antigen (PSMA) can visualize micrometastatic disease, thus expanding treatment options for BCR ranging from observation to androgen deprivation therapy (ADT), radiation therapy (RT/SBRT), chemotherapy (CT), and new generation hormonal agents (NHA). Our objective was to describe how BCR patients were managed after positive PSMA PET/CT with ^{18}F-DCFPyL (^{18}F-piflufolastat), taking into account that a high percentage of patients had a PSA<1. ***Materials and Methods:*** We conducted a retrospective review of 151 patients from the province of Cadiz who underwent a ^{18}F-DCFPyL PET/CT between July 2021 and March 2023. 93 of these 151 patients had a positive result (61.5%) and 77 met inclusion criteria: information on the type of treatment and follow-up with PSA determination 3 months after completion of treatment. Additionally, trigger-PSA levels were collected at the time of ^{18}F-DCFPyL PET/CT, which was in the range of biochemical recurrence, considered as PSA>0.2. ***Results:*** Of the 77 positive PSMA patients who met inclusion criteria, in 38/77 (49.3%) had trigger-PSA levels below 0.49; in 27/77 (35.06%), it was between 0.5-0.99 and only in 12/77 (15.5%) was trigger-PSA greater than 1. Regarding the treatment received, 51.9% of cases underwent RT/SBRT, of which 90% had disease control at 3 months with a decrease in PSA levels below 0.2. CT treatment was given to 2 patients, both of whom had a PSA decrease of 100%. 13 patients were treated with NHA, and in 12/13, the PSA decreased after therapy, except for one patient who had poor adherence to treatment. ADT was performed in 6 patients with a good response except for one patient. There were 4 patients who received combined therapy (RT+ADT, RT+NHA) who were included in the above-mentioned groups. ***Conclusion:*** Despite low PSA levels, ^{18}F-DCFPyL PET/CT can detect disease recurrence, allowing for personalized treatment planning and achieving disease control in a short period of time. The impact on patient survival will be assessed in the future.

EP-0558

The Tyr Phenomena: Hypo-calcemic Response in High Volume Treatment Responders to 177Lutetium PSMA Therapy

M. Swiha[1,2], *S. Kumar*[3], *M. Crumbaker*[1], *C. Harvey*[1], *S. Pathmanandavel*[1], *N. John*[1,4], *M. M. McDonald*[5,6], *R. Clifton-Bligh*[3,6], *A. Lee*[3,7,8], *P. Bastick*[9], *W. Counter*[1], *A. Nguyen*[1,4], *L. Emmett*[1,4,5];
[1]*St Vincent's Hospital, Sydney, AUSTRALIA,* [2]*Schulich School of Medicine and Dentistry, University of Western Ontario, London, ON, CANADA,* [3]*Royal North Shore Hospital, Sydney, AUSTRALIA,* [4]*St Vincent's Clinical School, University of New South Wales, Sydney, AUSTRALIA,* [5]*Garvan Institute of Medical Research, Sydney, AUSTRALIA,* [6]*School of Medical Science, Faculty of Medicine and Health, University of Sydney, Sydney, AUSTRALIA,* [7]*Northern Clinical School, Faculty of Medicine and Health, University of Sydney, Sydney, AUSTRALIA,* [8]*Genesis Care, Sydney, AUSTRALIA,* [9]*St George Hospital, Sydney, AUSTRALIA.*

Aim/Introduction: ^{177}Lutetium PSMA (^{177}Lu-PSMA) is an effective treatment for metastatic castrate-resistant prostate cancer (mCRPC). Rarer treatment-related adverse events, such as treatment response related hypo-calcemia have not yet been described. ***Materials and Methods:*** We present case reviews of two men with marked hypocalcemic osteosclerotic response following ^{177}Lu-PSMA I&T therapy. Additionally, a clinical dataset of ^{177}Lu-PSMA I&T therapy was evaluated to estimate incidence and clinical association with hypocalcemia. This dataset included 127 men with mCRPC who had disease progression after at least one androgen receptor axis-targeted agent (ARAT) and either failed or were ineligible for taxane-based chemotherapy. All patients were treated with ^{177}Lu-PSMA I&T in a clinical treatment program (2022/ETH00924) and received a minimum of 2 doses at six-weekly intervals. A median of 8.0 GBq (IQR 8.0-8.5 GBq) was administered at each dose via slow intravenous injection. Blood samples were collected prior to each dose and at 3 weekly intervals for biomarkers including hemoglobin, platelets, lactate dehydrogenase (LDH), calcium, alkaline phosphatase (ALP), albumin and prostate specific antigen (PSA). ***Results:*** Of 127 patients treated, 41 (32%) had a fall in serum calcium of any magnitude at any point between starting treatment and dose 3 of ^{177}Lu-PSMA (12 weeks). Two patients developed severe hypocalcemia (corrected serum calcium < 1.7 mmol/L (NR 2.15 - 2.55mmol/L)) requiring high dose steroid treatment. Both patients (cases 1&2) had high volume bone metastatic disease with marked PSA response (>90% reduction) to ^{177}Lu-PSMA I&T. Overall, 6/127 (5%) developed clinical hypocalcemia despite denosumab cessation after commencing ^{177}Lu-PSMA therapy. Mean PSA response in those with hypocalcemia was 78% (SD 24%) with one patient showing no PSA response (hypocalcemia due to progressive disease). Baseline ^{177}Lu-SPECT total tumour volume in bone was higher in those who had a reduced calcium compared to those with normal calcium levels (median 1017mL (IQR 331-1831mL) vs 369mL (IQR 96-1035mL) (p= 0.01)) and in those who developed hypocalcemia compared to those who did not (median 3249mL (IQR 1856-3852mL) vs 465mL (IQR 135- 1172mL) (p= 0.002)). Patients with hypocalcemia following treatment developed marked osteosclerosis subsequently, despite excellent biochemical and imaging treatment response. ***Conclusion:*** Hypocalcemia may occur in response to ^{177}Lu-PSMA I&T, particularly with both high-volume bone metastases and significant PSA response. Importantly, calcium and calcitriol supplementation were insufficient in managing severe hypocalcemia and glucocorticoid therapy was required. Further evaluation of ^{177}Lu-PSMA I&T induced hypocalcaemia is required to better understand mechanisms, optimal treatments, and repercussions from subsequent osteosclerotic response.

EP-0559

Evaluation of Radium-223 Dichloride in the Treatment of Castration-Resistant Prostate Adenocarcinoma with Symptomatic Bone Metastases

R. Maestre-Cutillas[1], *A. M. Sanchez-Tornero*[2], *L. Baz-Sanz*[1], *G. Rubio-Fernández*[1], *L. Casas-Fernandez*[2], *M. Romero-Otero*[2], *J. A. Pérez-Iruela*[1];
[1]*Hospital Universitario Ramon y Cajal, Madrid, SPAIN,*
[2]*Hospital Clínico Universitario de Valencia, Valencia, SPAIN.*

Aim/Introduction: To evaluate our experience with the use of Radium-223 Dichloride for the treatment of castration-resistant prostate adenocarcinoma in patients with symptomatic bone metastases and without visceral metastases. ***Materials and Methods:*** 50 patients from two different centres who received treatment with Radium-223 (6 doses of 55 kBq/kg at 4-week intervals) between March 2014 and January 2022 were included in the study. The variables studied were overall survival (OS), time to disease progression (TDP), time to bone progression (TBP), total alkaline phosphatase (AP) response, prostate-specific antigen (PSA) progression and blood haemoglobin levels. In OS, patients were stratified according to PSA levels at baseline. Treatment-related adverse events have also been reported. ***Results:*** The mean age of the patients was 75.54 ± 8.40 years. Radium-223 treatment was used as first (4%), second (32%), third (40%), fourth (16%) or fifth line (8%). Previous treatments used were antiandrogens (mainly abiraterone) (82%), enzalutamide (36%), docetaxel (48%), cabazitaxel (16%) and pembrolizumab (2%). The time taken between detection of bone metastases and initiation of treatment with Radium-223 was 31.04 ± 21.75 months, with a median of 24.5 months. Median OS was 15.5 months, with significant differences ($p < 0.05$) according to PSA level (10 months with PSA > 100ng/ml and 19.5 months with PSA < 100ng/ml). The medians for TBP and TDP were 9.5 and 8 months, respectively. Reduction of PSA levels was observed in 21% of cases and AP in 58%. Pain was reduced or controlled in 69% of patients. 18/50 (36%) patients experienced some type of treatment-related adverse reaction, including haematological toxicity and asthenia. Haemoglobin decreased in 43% of patients and ten patients (20%) required blood transfusions. Sixteen patients (32%) did not complete treatment, five of them (10%) due to haematological toxicity, implying a 68% compliance rate. ***Conclusion:*** In our experience, Radium-223 Dichloride is an effective treatment in reducing bone pain, well tolerated and with high compliance. Patients with less advanced disease (PSA<100ng/ml) benefit more from treatment, with higher OS, which implies great importance of early diagnosis and speed of action. The results (OS, TBP and TDP) are consistent with published literature.

EP-0560

Personalized [177Lu] Lutetium-PSMA therapy for patients with pre-treated castration-resistant prostate cancer: a single institution experience

J. Friedrich[1], *W. Thaiss*[1,2,3], *F. Zengerling*[4,3], *V. Hechler*[4], *M. Grunert*[5,1], *C. Bolenz*[4,3], *T. Wiegel*[6], *A. J. Beer*[1,3], *V. Prasad*[1,3];
[1]*Department of Nuclear Medicine, University Hospital Ulm, Ulm, GERMANY,* [2]*Department of Diagnostic and Interventional Radiology, University Hospital Ulm, Ulm, GERMANY,* [3]*Surgical Oncology Ulm, i2SOUL Consortium, Ulm, GERMANY,* [4]*Department of Urology and Pediatric Urology, University Hospital Ulm, Ulm, GERMANY,* [5]*Department of Nuclear Medicine, German Armed Forces Hospital, Ulm, GERMANY,* [6]*Department of Radiation Oncology, University Hospital Ulm, Ulm, GERMANY.*

Aim/Introduction: Castration resistant prostate cancer (CRPC) patients have in general shorter overall survival. [177Lu]-Lutetium-PSMA (Lu-PSMA) treatment has proven efficacy in these patients. However, little is known about the success of Lu-PSMA if offered in personalised approach based on laboratory, clinical and PSMA PET features. ***Materials and Methods:*** For this retrospective study 86 CRPC patient charts were evaluated. Overall survival (OS), PSMA PET/CT response, PSA-response, safety, and tolerability (CTCAE adverse event reporting) in all patients was assessed. PSMA expression profile was taken into consideration: patients with high PSMA heterogeneity, assessed visually, PSMA negative suspicious lesions on CT/MRI were either not offered the treatment or the lesions were biopsied prior to the therapy. Interim PSMA PET/CT was performed after 2nd or 3rd cycle. Efficacy endpoints were

calculated using stratified Kaplan Meier methods, univariate and Cox regression models. ***Results:*** Patients received an average of 3.6 (range 1-8) therapy cycles with total median applied dose of 17.7 GBq (median 5.3 ± 1.1 GBq per cycle) Patients were followed up for a median of 12.4 months (range 1-39). The median OS was found to be 15 months (95% CI 12.8-17.2). The best overall response rate in patients assessed with PSA response and PSMA PET/CT was 27.9% whereas 50.0% had at least stable disease. Twenty-three patients had a ≥ grade 3 adverse event with anaemia being the most frequent adverse event. Positive predictors for a prolonged OS were number of cycles > 3, pre-treatment haemoglobin level of ≥ 10 g/dL, a >50% best overall PSA response and time to PSA progression >60 days of Lu-PSMA therapy. Patients achieving partial response or disease stabilisation on PET/CT were also found to have favourable OS. Interestingly OS in patients with visceral metastases was not worse however, liver metastases was found to be negative prognostic marker in univariate analyses. ***Conclusion:*** Individualized Lu-PSMA treatment approach appears to be feasible. Patients with dose-limiting factors or intensely PSMA avid visceral metastases can still be treated with good efficacy without negatively influencing the safety profile.

EP-0561

No substantial subacute nephrotoxicity in patients with mCRPC treated with Lu-177 PSMA I&T regardless of mean absorbed kidney dose

M. Dotinga[1,2], *E. C. Owers*[1], *E. J. Rijkhorst*[1], *D. M. V. de Vries-Huizing*[1];
[1]*NETHERLANDS Cancer Institute, Amsterdam, NETHERLANDS,* [2]*Leiden University Medical Center, Leiden, NETHERLANDS.*

Aim/Introduction: Nephrotoxicity is a rare adverse event in patients treated with peptide radioligand therapy (PRLT). The aim of this study was to assess changes in kidney function in relation to the mean absorbed dose (MAD) of the kidneys in patients with metastatic Castration-Resistant Prostate Cancer (mCRPC). ***Materials and Methods:*** A total of 22 patients with mCRCP with a baseline estimated glomerular filtration rate (eGFR) >30 ml/min/1.73m² were included in this retrospective study. PRLT consisted of two cycles of 7.4 GBq [^{177}Lu]Lu-PSMA-I&T, administered two weeks apart. This sequence was repeated in a subset of 5 patients after 12±1 weeks after the first administration. Post-therapy SPECT/CT scans were performed 24 hours and 5-7 days after each administration. The kidney cortex was segmented in PLANET Onco and the dose rate (convolution with CT density correction) was assessed in PLANET Dose (DOSIsoft SA). The MAD was accordingly calculated using a mono-exponential curve. Creatinine levels and eGFR were evaluated at baseline and 8 weeks after cycle 2 and 4 after which nephrotoxicity (eGFR and increase in creatinine levels) was scored according to CTCAE 5.0. Subsequently, absolute changes in eGFR and creatinine levels (%) were analyzed and related to the average MAD of both kidneys. ***Results:*** After two cycles, changes of -5.1±7.6% (range: -20.6-19.0%) were observed in creatinine levels and the eGFR changed 4.7±6.3% (-10.8-21.4%) with a MAD of 8.4±2.9 Gy (3.5-15.1 Gy). For this group, no relation was found between MAD and absolute changes in creatinine levels and eGFR (p>0.6). For the 5 patients receiving four cycles, the MAD was 13.8±4.4 Gy (6.3-23.1 Gy), creatinine level changes were 15.5±21.9% (-29.3-70.0%), and the eGFR changed with -6.7±12.2% (-27.8-17.7%). Subacute nephrotoxicity after therapy was limited to grade 2, regardless of the number of cycles and average MAD. ***Conclusion:*** No substantial subacute nephrotoxicity was observed in mCRPC patients undergoing two to four cycles of Lu-177 PSMA I&T therapy. Currently, retrospective analyses are ongoing for a larger population and other organs-at-risk. Long-term effects of [^{177}Lu] Lu-PSMA therapy on kidney function in relation to the MAD are yet to be assessed and analyzed.

EP-0562

Prognostic Role Of 18F-Choline PET/CT Vs Bone Scintigraphy In Prostate Cancer Patients Treated With 223Ra-Dichloride.

L. García Zoghby[1], *M. Cruz Montijano*[1], *A. García Vicente*[1], *M. Amo Salas*[2], *A. Padilla Bermejo*[3], *C. Lucas Lucas*[3], *N. Sicilia Pozo*[3], *M. Contreras Ameduri*[3], *F. Pena Pardo*[3], *E. Noriega Álvarez*[3], *M. Talavera Rubio*[3], *V. Poblete García*[3], *Á. Soriano Castrejón*[1];
[1]*University Hospital of Toledo, Toledo, SPAIN,* [2]*Castilla-La Mancha University, Ciudad Real, SPAIN,* [3]*University General Hospital of Ciudad Real, Ciudad Real, SPAIN.*

Aim/Introduction: To determine the prognostic capacity of bone scintigraphy (BS) and 18F-Choline PET-CT (FC-PET/CT) in castration resistant prostate cancer patients treated with ^{223}Ra; as well as to establish advantages that FC-PET/CT can provide in therapeutic failure prediction. ***Materials and Methods:*** Multicentre, prospective, and non-randomized study (ChoPET-Rad) where all patients treated with ^{223}Ra from November/2015 to March/2022 were studied. Those who fulfilled all inclusion criteria and no exclusion criteria were selected, previous BS and FC-PET/CT evaluation (basal). Both clinical and imaging variables were collected: Gleason score, previous Docetaxel treatment, metabolic vs osteoblastic activity, superscan pattern, location, and bone metastasis (BM) number, among others. Progression free survival (PFS) and overall survival (OS) were assessed performing Kaplan-Meier curves and Cox regression. Concordance analysis between techniques (Kappa=k) for homonymous variables and relationship of all variables with therapeutic failure (non-completion of ^{223}Ra entire regimen) were evaluated using Pearson's chi-squared test. ***Results:*** 77 patients were included with a median age of 72.73 years (±8.76). Gleason score was ≥8 in 48%. 59.7% did not complete entire regimen and 90.9% died during the follow up. Median PFS and OS were 3 and 16 months, respectively. Concordance degree between techniques regarding BM number and location was good/moderate, k= 0.701 and k=0.703 respectively (p<0.001). Variables statistically associated with a lower PFS and OS were: good concordance degree between techniques (p=0.048, $\chi2$=6.07 and p=0.028, $\chi2$=7.16, respectively), superscan pattern (p=0.018, $\chi2$=5.60 and p<0.001, $\chi2$=37.15, respectively) and BM SUVmax higher than liver pool (p=0.035, $\chi2$=4.45 p=0.008, $\chi2$=7.15, respectively). BM number showed in both, BS and FC-PET/CT, was statistically associated with PFS (p=0.005, $\chi2$=12.82) and OS (p=0.006, $\chi2$=12.30). Dose number and basal PSA were inversely and directly associated, respectively, with OS (HR=0.729, p>0.001 and HR=1.025, p=0.019; respectively). PSA rise ($\chi2$=16.52 p<0.001), BM location and number showed in FC-PET/CT ($\chi2$=4.90; p=0.027 and $\chi2$=9.948; p=0.002, respectively), BM types (osteoblastic vs osteolytic) ($\chi2$=7.02 p=0.031), superscan pattern on FC-PET/CT ($\chi2$=5.61; p=0.018) and BM SUVmax higher than liver pool ($\chi2$=6.57; p=0.01), were all statistically associated with therapeutic failure. ***Conclusion:*** Higher disease spread showed in FC-PET/TC and major extension of disease in both techniques were statistically significant prognostic factors in patients who received ^{223}Ra. Metabolic pattern of BM showed with FC-PET/TC the most reliable marker of therapeutic failure.

EP-0563

Evaluation of the clinical significance of parametric data of PSMA uptake in the prostate bed and its contribution to prognosis.

Z. Mammadkhanli[1], *B. Ozdemir Gunay*[2], *E. Gokdemir*[1], *F. Ustun*[1]; *[1]Trakya University, Faculty of Medicine, Department of Nuclear Medicine, Edirne, TÜRKIYE, [2]Sultan 1. Murat State Hospital, Clinic of Nuclear Medicine, Edirne, TÜRKIYE.*

Aim/Introduction: Prostate cancer is a common malignancy in men worldwide. 68 Ga-PSMA PET/CT is a non-invasive imaging technique used to diagnose, stage, and evaluate response to treatment in patients with prostate cancer. 177 Lu-PSMA treatment is a targeted therapy for patients with resistant prostate cancer. However, the relationship between PSMA expression and tumor biology is still not well understood. Our aim in this study was to investigate the clinical significance of PSMA receptor affinity in the prostate bed, its effect on prognosis, and whether it affects normal physiological uptake in patients with prostate cancer who underwent 68 Ga-PSMA PET/CT imaging. ***Materials and Methods:*** We retrospectively analyzed preoperative 68 Ga-PSMA PET/CT images of 82 patients with histopathological diagnosis of prostate cancer and available follow-up data. Two groups were formed based on the presence or absence of pathological radiopharmaceutical uptake in the prostate bed. We compared metabolic parameters of the primary lesion, PSA values, SUVmax values of organs with physiological receptor affinity, presence of metastasis, and their SUV values between the two groups. ***Results:*** 39 of the 82 patients had physiological PSMA receptor affinity in the prostate lumen (group 1), while 43 patients had pathological and focal PSMA receptor affinity in the prostate lumen (group 2). Patients without pathological PSMA uptake in the prostate lodge had a longer survival time compared to group 2 (p=0.015).Statistically significant PSA elevation was found in the group with prostatic involvement compared to the group without (p=0.034).The mean value of metastasis was found to be higher in group 2 compared to group 1 (p=0.008).There was no statistically significant difference between the groups in terms of SUVmax values of liver (p=0.156), spleen (p=0.145), kidney (p=0.958), submandibular and parotid glands (p=0.311). ***Conclusion:*** In conclusion, our study demonstrates the clinical significance of PSMA receptor affinity in the prostate bed and its impact on prognosis in patients with prostate cancer. The results of this study provide important insights into the use of 68 Ga-PSMA PET/CT imaging for the diagnosis and management of prostate cancer.

EP-0564

Health-related quality of life in mCRPC patients receiving treatment with[177Lutetium] prostate specific membrane antigen targeted radioligand therapy

A. Karimzadeh[1], *B. Feuerecker*[2], *K. Knorr*[2], *M. Heck*[3], *R. Tauber*[3], *C. D`Alessandria*[2], *W. Weber*[2], *M. Eiber*[2], *I. Rauscher*[2]; *[1]Department of Diagnostic and Interventional Radiology and Nuclear Medicine, University Medical Center Hamburg-Eppendorf, Hamburg, GERMANY, [2]Department of Nuclear Medicine, School of Medicine, Technical University of Munich, Munich, GERMANY, [3]Department of Urology, School of Medicine, Technical University of Munich, Munich, GERMANY.*

Aim/Introduction: In patients with metastatic castration resistant prostate cancer (mCRPC), prostate-specific membrane antigen (PSMA) targeted radioligand therapy (RLT) has emerged as a promising treatment option. The most common metastatic site in mCRPC patients are bone metastases, often causing pain and impaired mobility with a concordant decline in health-related quality of life (HRQoL). Therefore, the aim of this retrospective analysis was to assess changes in HRQoL in mCRPC patients during treatment with ^{177}Lu-PSMA RLT. In addition, we analyzed differences in HRQoL in patients dichotomized according to Eastern Cooperative Oncology Group 0 (no functional impairment) and 1/2 (moderate functional impairment). Moreover, the impact of early treatment discontinuation was analyzed. ***Materials and Methods:*** A total of 60 mCRPC patients were included in this analysis. EORTC QLQ C-30 questionnaires were analyzed prior each treatment cycle up to the 5th treatment cycle. A mixed effects model was performed to analyze repeated measures data of HRQoL in the total patient cohort and in patients stratified according to their ECOG performance status at baseline (ECOG 0 and ECOG 1/2). DFS curves were estimated using the Kaplan-Meier method for estimation of event time distributions and logrank tests were used for group comparisons. ***Results:*** HRQoL was significantly improved revealing an improved global health status at the 2nd and 4th cycle of ^{177}Lu-PSMA RLT (p=0.014 and p=0.039, respectively). Concordantly, functional scales such as emotional functioning showed significant improvements (at 2nd and 4th treatment cycle: p=0.035 and p=0.007, respectively). In addition, disease-related symptoms were significantly alleviated at 2nd and 4th treatment cycle as well (e.g. pain: p=0.035 and p=0.034, respectively). Patient stratification according to the ECOG performance status was clearly associated with an impact on HRQoL (e.g. mean physical functioning at baseline in ECOG 0 vs. ECOG 1/2, p<0.0001). Additionally, patients who discontinued treatment after two treatment cycles due to disease progression presented with a concordant decline in HRQoL (e.g. mean physical functioning at baseline vs. after 2nd treatment cycle: 61.7 vs. 53.9, p=0.0495) and had a higher risk of deterioration in quality of life compared to patients who responded after the initial two cycles (e.g. physical functioning: HR=2.2, 95% CI, 1.1-4.8; p=0.013). ***Conclusion:*** MCRPC patients presented with significant improvements in HRQoL during treatment with ^{177}Lu-PSMA RLT. Furthermore, patients with an early discontinuation of treatment presented with an analogue decline in HRQoL and had a higher risk of quality of life deterioration.

EP-0565

Safety and Efficacy of [177Lu]Lu-rhPSMA-10.1 Re-Challenge Therapy in Progressive mCRPC after [177Lu] Lu-PSMA I&T Therapy: Preliminary Results

A. Gäble[1], *J. Enke*[1], *A. Amerein*[1], *O. Viering*[1], *A. Rinscheid*[2], *M. Kircher*[1], *G. Wienand*[1], *C. Pfob*[1], *C. Lapa*[1], *A. Dierks*[1], *R. Bundschuh*[1]; *[1]Nuclear Medicine, Faculty of Medicine, University of Augsburg, Augsburg, GERMANY, [2]Medical Physics and Radiation Protection, University Hospital Augsburg, Augsburg, GERMANY.*

Aim/Introduction: [^{177}Lu]Lu-rhPSMA-10.1 is a new PSMA derivative that has shown promising results in dosimetric studies for the treatment of metastatic castration-resistant prostate cancer (mCRPC) with a higher therapeutic index as compared to [^{177}Lu]Lu-PSMA I&T. Therefore therapy re-challenge with [^{177}Lu]Lu-rhPSMA-10.1 is a viable therapeutic option after initial disease progression under treatment with [^{177}Lu]Lu-PSMA I&T. This study aims to determine the feasibility, efficacy, and safety of [^{177}Lu]Lu-rhPSMA-10.1 re-challenge therapy. ***Materials and Methods:*** Eight patients (age, 73±7 years) with progressive mCRPC after previous 2-6 cycles of standard [^{177}Lu]Lu-PSMA I&T were subsequently treated with up to two cycles of [^{177}Lu] Lu-rhPSMA-10.1 every 6 weeks. Response assessment with

[^{68}Ga]Ga-PSMA-I&T-PET/CT using RECIP 1.0 criteria was done after 2 cycles or if disease progression was clinically suspected. PSA response was assessed according to the PCWG3 criteria 8-12 weeks after the first [^{177}Lu]Lu-rhPSMA-10.1 cycle. Safety was evaluated according to Common Terminology Criteria for Adverse Events (CTCAE) v5.0 criteria. ***Results:*** Mean per cycle and cumulative administered activities were 7.4 ± 0.04 GBq and 13.9 ± 2.3 GBq, respectively. Generally, therapy was well tolerated with no acute adverse events. According to CTCAE v5, grade 4 thrombocytopenia and grade 3 anemia occurred in one patient, in the remaining subjects, no relevant toxicity (> grade 2) was observed. Regarding serum PSA values, biochemical partial response, stable disease, and progressive disease were seen in 1/8 (12.5%), 4/8 (50%), 3/8 (37.5%) patients. RECIP 1.0 criteria revealed disease stabilization in 4/8 (50 %) subjects with partial remission in one individual (12.5 %) and stable disease in 3/8 (37.5%) cases. Outcome data in terms of PFS and OS are still pending at the time present. ***Conclusion:*** Despite very limited numbers, the results of this study suggest that [^{177}Lu]Lu-rhPSMA-10.1 may induce therapeutic effects in mCRPC patients who have experienced progressive disease under [^{177}Lu]Lu-PSMA I&T. Further studies to corroborate these preliminary findings are highly warranted.

EP-0566

PSMA avidity-based recurrent patterns after 177Lu-PSMA I&T in metastatic castration-resistant prostate cancer

S. Kwon[1,2], *I. Rauscher*[1], *C. D'Alessandria*[1], *M. Eiber*[1], *W. Weber*[1]; *[1]Rechts der Isar Medical Center, Technical University of Munich, Munich, GERMANY, [2]Chonnam National University Medical School and Hwasun Hospital, Jeonnam, KOREA, REPUBLIC OF.*

Aim/Introduction: PSMA targeted radioligand therapy (PSMA-RLT) can be highly effective for treatment of metastatic castration resistant prostate cancer (mCRPC) but virtually all patients develop recurrent disease eventually. The mechanisms for resistance to PSMA RLT are not well understood. In this study we evaluated whether loss of PSMA expression is a resistance mechanism. ***Materials and Methods:*** Thirteen consecutive patients, who had an exceptional response to PSMA RLT (≥ 90% PSA decline) after ^{177}Lu-PSMA I&T and developed recurrent disease during follow-up were analyzed. Recurrent lesions were classified into three groups: 1) recurrent group (RG, recurrence from complete response), 2) progressive group (PG, progression from partial response (≥ 50% decrease in SUVmax)), or 3) newly developed group (NG, no lesion on initial PET/CT). SUVmax of all lesions were measured from both pretherapeutic (preSUV) and follow-up (postSUV) ^{18}F-rhPSMA-7 PET/CT. We compared postSUV among three groups and investigated whether there was a difference between preSUV and postSUV in RG and PG. ***Results:*** Among 49 metastatic lesions out of 13 patients, there were 20 lesions in RG, 13 lesions in PG, and 16 lesions in NG, respectively. There was no significant difference of preSUV between RG and PG (28.99 ± 21.10 vs. 40.56 ± 39.70, P = 0.283) and postSUV between PG and NG (36.26 ± 23.23 vs. 37.12 ± 18.60, P = 0.912). postSUV in RG (19.56 ± 13.09) was significantly lower than that in PG (P = 0.013) or NG (P = 0.004). There was no statistically significant difference between preSUV and postSUV in RG (P = 0.075) and PG (P = 0.563), respectively. ***Conclusion:*** PSMA expression was not significantly reduced in patients recurring after PSMA-RLT. This suggests that loss of PSMA is not a common resistance mechanism. Further research is warranted why PSMA expression is not reduced despite the selective pressure of effective PSMA-RLT.

EP-0567

Effect of [223Ra]Radium dichloride on bone health

K. Krieger*, A. Afshar-Oromieh, A. Rominger, S. Weidner; Inselspital Bern, Bern, SWITZERLAND.*

Aim/Introduction: [223Ra]Radium chloride is approved for the treatment of painful osseous metastases in prostate cancer. In 2018, the ERA223 trial found increased risks of fractures and premature deaths from [223Ra]$RaCl_2$ when combined with abiraterone and prednisolone [1]. In response, we instated a standard monitoring of serologic markers of bone metabolism in patients undergoing [223Ra]$RaCl_2$ treatment. In this case series we offer evidence that bone health is grossly unaffected by [223Ra]$RaCl_2$ and the adverse effects observed in ERA223 were likely due to the combination regimen used. ***Materials and Methods:*** Available records were screened for patients who underwent at least two cylces of [223Ra]$RaCl_2$ treatment while the aforementioned policy was in effect. Levels of beta-Crosslaps (β-CTx), intact N-terminal procollagen type 1 (P1NP) and alkaline phosphatase activity (AP) were obtained from the laboratory database. Demographical information was extracted from patient files. Statistical analysis was performed in IBM SPSS Version 28. ***Results:*** 40 patients met eligibility criteria, of which 18 patients had undergone six or more cycles. Median age at the start of treatment was 73.4 years. β-CTx levels did not change significantly under treatment (median +8 pg/ml, 95% CI -2.3 to 18.3), neither did P1NP (median -0.3 µg/l, 95% CI -5.9 to 5.3). AP activity significantly declined (median -27 U/l, 95% CI -34.7 to -19.3, p<0.0001). At the time of writing, 30 patients had expired at a median age of 74.5 years (median survival 296 days after the last cycle). ***Conclusion:*** Markers of osteoblastic and osteolytic activity did not change under treatment with [223Ra]$RaCl_2$, while AP activity significantly declined. This suggests overall bone turnover is not affected by [223Ra]$RaCl_2$ and the excess of adverse events observed in ERA223 was due to the combination regimen, with prednisolone being a likely culprit. Lowering AP levels may reflect lessening osseous tumor burden. These results encourage efforts to broaden the use of [223Ra]$RaCl_2$ to other entities and diseases. ***References:*** 1. Smith M, Parker C, Saad F, Miller K, Tombal B, Ng QS, Boegemann M, Matveev V, Piulats JM, Zucca LE, Karyakin O, Kimura G, Matsubara N, Nahas WC, Nolè F, Rosenbaum E, Heidenreich A, Kakehi Y, Zhang A, Krissel H, Teufel M, Shen J, Wagner V, Higano C. Addition of radium-223 to abiraterone acetate and prednisone or prednisolone in patients with castration-resistant prostate cancer and bone metastases (ERA 223): a randomised, double-blind, placebo-controlled, phase 3 trial. Lancet Oncol. 2019 Mar;20(3):408-419.

EP-0568

First preliminary results on safety and efficacy of non carrier added (n.c.a.) 177Lutetium PSMA-I&T radioligand therapy, in a Single Institute

G. Limouris[1,2], *M. Paphiti*[3], *A. Manetou*[2], *A. Zafeirakis*[2]; *[1]Nuclear Medicine, Medical School, National and Kapodistrian University of Athens, Athens, GREECE, [2]Nucl Med Dept, Army Share Fund Hospital of Athens, Athens, GREECE, [3]Cyclotron Section, Pharmazac SA, Athens, GREECE.*

Aim/Introduction: Radioligand therapy with 177Lutetium labeled peptides gained popularity and has been increasingly implemented in the treatment of patients with metastatic castration-resistant prostate cancer (mCRPC). By the present, we aimed to assess the safety and efficacy of n.c.a. 177Lutetium-PSMA-I&T in metastatic castration-resistant prostate cancer (mCRPC) patients for further routine settle in our Institution.

Materials and Methods: In nine men (median age 73 years, range 73-81 years) with progressive mCRPC, n.c.a. 177Lutetium-PSMA-I&T was i.v. infused. The non-carrier added 177LuCl3 is predilected due to its exceptionally high specific activity (since almost every single atom is radioactive) and radionuclidic purity (absence of the long-lived high-spin Isomer Lutetium -177m). To reduce myelotoxicity, 75 mg of DTPA in trip-trop diluted in about 200 ml normal saline water was infused 30 min before the initialization of the radiopeptide therapy, lasting for about 4 hrs. Whole-body scintigraphy was performed immediately, 24 h and 48 hrs post-infusion. Absorbed doses delivered to metastases, kidneys, and red marrow were calculated according to OLINDA/EXM 1.1 program. Toxicity (World Health Organization criteria) was measured using blood and urine tests of renal and bone marrow function. ***Results:*** A mediocre PSA response [≥ 28% PSA decline 16 weeks after the first (initial) 177Lutetium-PSMA-I&T cycle] was observed in 4/9 (44.4%) patients whereas in the rest 5/9 (55.6%) a ≥ 40% PSA decline was noticed. Median imaging-based progression-free survival (PFS) was 8 months and median overall survival (OS) was 13 months. Grade ≥ 3 hematological toxicity was observed in 2/9 (22.3%) a temporary slight xerophthalmia in 1/9 (11.1%) and temporary mediocre xerostomia in 7/9 (77.8%). In a median of 6 sessions with a mean treatment activity of 6.8 ± 1.2 GBq per session, a mean cumulative activity of 40.8 ± 14.3 GBq was reached. The median absorbed dose for the lacrimal and parotid glands was 2.6 ± 1.4 and 2.1 ± 1.2 Gy/GBq respectively, for kidneys 0.81 ± 0.28 Gy/GBq, for liver 0.14 ± 0.36 Gy/GBq, for spleen 0.18 ± 0.24 Gy/GBq, for osseous metastatic lesions in a range of 2.20 -12.38 Gy/GBq and for bone marrow 0.038 ± 0.009 Gy/GBq. ***Conclusion:*** In mCRPC patients, the introduction of n.c.a. 177Lutetium-PSMA-I&T is well tolerated and effective with an acceptable toxicity profile. Dosimetry of kidneys, lacrimal and salivary glands, considered dose-limiting organs and exhibiting high physiological 177Lu-PSMA uptake, should be a necessary appendage.

EP-0569

Radium-223 dichloride ([223Ra]RaCl2) for metastatic Castration-Resistant Prostate Cancer (mCRPC): results of a real-world experience from a seven-year clinical practice

D. Barbosa*, H. Duarte, J. Ferro, I. Próspero, D. Silva, S. Fontão de Castro, G. Ferreira, L. Violante, F. Lopes, I. Lucena Sampaio; Portuguese Institute of Oncology, Oporto, PORTUGAL.*

Aim/Introduction: Radium-223 dichloride ([223Ra]RaCl2) is an alpha-emitter therapeutic agent indicated for metastatic castration-resistant prostate cancer (mCRPC), with symptomatic bone metastases but no visceral metastases. Despite the promising results of ALSYMPCA trial, real-world experience appears to be less positive. The aim of this study is to report our Cinical experience with [223Ra]RaCl2 in patients with mCRPC. ***Materials and Methods:*** Retrospective analysis of demographic, clinical and laboratory data from all patients with bone mCRPC who received [223Ra]RaCl2 in our institute over a 7-year period. T-test and Kaplan-Meier method were used for statistical purposes (p-value/Logrank-test <0,05 were considered statistically significant). ***Results:*** Twenty-four men, mean age 74 years-old (SD = 9) at the time of [223Ra]RaCl2 first treatment; total of 109 cycles, between 2016 and 2023. Median activity of 4,30MBq (range 3,90-4,60). Median Gleason-score, Prostate-Specific Antigen, Alkaline Phosphatase and Lactate Dehydrogenase were, respectively, 8 (range, 7-9), 86ng/mL (range, 43-345), 287U/L (range, 132-504) and 264U/L (range, 228-312).Mean Hemoglobin, Neutrophils and Platelets counts were, respectively, 12,4g/dl (SD=1,38), 5,56x10^9/L (SD=2,58) and 220x10^9/L (SD=58,7) at the beginning of treatment.All patients had symptomatic bone pain, a positive bone scan (10 or more uptake foci) and no visceral metastases.Eleven patients (46%) were previously treated with chemotherapy and new androgen receptor pathway inhibitors (ARPis); the others were treated after one therapeutic line (6 after chemotherapy; 7 after ARPis).Eleven patients (46%) completed all 6 [223Ra]RaCl2 cycles and 14 (58%) underwent at least 5.Thirteen patients discontinued treatment due to clinical deterioration or hematological toxicity.Hematological toxicity (G2/G3) was seen in 14 patients, with anemia being the most common (12 events). Most common adverse effects were nausea/vomiting (42%) and diarrhea (30%). Eight patients (33%) reported pain improvement with an impact on quality of life: 7 completed all 6 [223Ra]RaCl2 cycles and 1 patient completed 5.Median overall survival (OS) since [223Ra]RaCl2 first infusion was 10 months (17 months in patients that received at least 5 cycles). There was no significant difference in OS whether [223Ra]RaCl2 was used as 2nd or 3rd line therapy (12 vs 9,5 months; p-value 0,425). ***Conclusion:*** Despite the limitations of this study (small sample size and retrospective analysis), our results appeared to be unfavorable in terms of OS, number of treatments completed, hematological toxicity and/or clinical progression, compared to those reported in studies under ideal conditions, even when [223Ra]RaCl2 was used as a second-line therapy, possibly due to advanced stage disease with extensive bone involvement of our patients.

EP-0570

The Relationship Between F-18 FDG Avidity and Response to Lu-177 PSMA Therapy in Prostate Cancer Metastases

N. Coskun*[1], M. Kartal[2], A. Erdogan[2], E. Ozdemir[1]; [1]Ankara Bilkent City Hospital, Ankara Yildirim Beyazit University, Ankara, TÜRKIYE, [2]Ankara Bilkent City Hospital, Ankara, TÜRKIYE.*

Aim/Introduction: The development of appropriate patient selection criteria for lutetium-177 prostate-specific membrane antigen (Lu-177 PSMA) therapy is crucial, given the variability of treatment outcomes among different patients and among different lesions within the same patient. Increased F-18 FDG uptake in metastatic prostate cancer lesions is thought to be associated with tumor aggressiveness, poor treatment response, and decreased survival. In this study, we aimed to investigate the possible role of F-18 FDG PET/CT in patient selection by evaluating the relationship between pre-treatment F-18 FDG uptake and response to treatment in metastatic lesions of mCRPC patients receiving two cycles of Lu-177 PSMA therapy. ***Materials and Methods:*** Patients who received at least two cycles of Lu-177 PSMA therapy and underwent both Ga-68 PSMA PET/CT and F-18 FDG PET/CT before the first cycle between January 2021 and July 2022 at our center were included. Lesions with SUVmax value higher than the liver SUVmean in the baseline F-18 FDG PET/CT study were deemed FDG-avid. Patients with a second primary malignancy and patients with clinical, imaging, and/or laboratory findings consistent with neuroendocrine differentiation were excluded from the study. Response levels achieved after two cycles of Lu-177 PSMA therapy were categorized as responsive (≥30% increase) or unresponsive (≥30% decrease) according to the SUVmax values on Ga-68 PSMA PET/CT imaging performed three weeks after the second cycle. Independent T-test and logistic regression analysis were used to evaluate the relationship

between treatment response and baseline glucose metabolism. ***Results:*** A total of 227 metastatic lesions (188 bone metastases, 35 lymphatic metastases, and 4 visceral metastases) from 11 patients (mean age 72±7) were included in the study. The median (min-max) time difference between Ga-68 PSMA PET/CT and F-18 FDG PET/CT was 20 (3-57) days. The lesion-based response rate to two cycles of Lu-177 PSMA therapy was 46.7% (n=106). Increased F-18 FDG uptake was observed in 80 lesions (35.24%). The rate of FDG avidity was significantly higher in unresponsive lesions compared to responsive lesions (43.4% vs 28.1%, p=0.016). Logistic regression analysis revealed a significant relationship between lesion-based FDG avidity and unresponsiveness to two cycles of Lu-177 PSMA therapy (odds ratio: 1.96; 95% confidence interval: 1.13-3.41, p=0.017). ***Conclusion:*** Our results suggest that insufficient response to two cycles of Lu-177 PSMA therapy is associated with lesion-based FDG avidity. If confirmed with future prospective cohorts, this phenomenon can contribute to the development of optimal patient selection criteria and effective patient management strategies.

EP-38

e-Poster Area

C: Therapy Clinical Study -> C1 Oncological Therapy Clinical Study -> C13 Local Radionuclide Therapy (including Spheres)

EP-0571

Correlation Of Y90-Absorbed Radiation Dose To Albi Scores In Liver Malignancies: Is It Safe Over 500 Gy Tumor Absorbed Dose With Voxel Based Dosimetric Approach?

E. Akgun*;*
University of Health Science Turkey, Basaksehir Cam and Sakura City Hospital, Istanbul, TÜRKIYE.

Aim/Introduction: We planned this retrospective study to assess the correlation between the absorbed doses using Y90 radioembolization and liver function tests results in liver malignancies. ***Materials and Methods:*** Thirty-five patients treated with Y90 embedded glass microsphere included the study. Twenty-two patients were diagnosed with hepatocellular carcinoma (HCC). In all patients absorbed doses were calculated with voxel-based dosimetric approach. Pretreatment, posttreatment 2. Week and 4. Week liver function test results were recorded and albumin-bilirubin (ALBI) scores were calculated. Associations between dose and ALBI scores were studied. Response to treatment were assess according to modified Response Evaluation Criteria in Solid Tumors and Positron Emission Tomography Response Criteria in Solid Tumors after 2 months of treatment. ***Results:*** Thirty-one (89%) patients underwent selective treatment, and 4 (11%) patients underwent lobar treatment. Only 5 (14%) patients had progressive disease after the treatment. Median radiation doses were 618 Gy (min-max: 500-1000) for tumor, 497 Gy (min-max: 270-843) for total perfuse liver, 281 Gy (min-max: 97-764) for perfuse normal liver, 8.5 Gy (min-max: 1-49) for normal liver, 52.5 Gy (min-max: 11-204) for total liver. Twenty-eight (80%) patients' ALBI scores were Grade 1, and rest of all were Grade 2 before the treatment. In 2 HCC patients, ALBI scores were increased up to 2 in second week of the treatment. Their treatment response was consistent with partial regression. Tumor, perfused normal, and normal liver absorbed doses ere 618/550 Gy, 116/97 Gy, 12/8 Gy, respectively. Perfused normal liver to whole liver ratios were only 0.2/0.7%. When compared with all cases, it was concluded that the absorbed doses were not significantly higher in these cases. However, tumor/whole liver ratios were significantly higher than rest of cases (27-35%). In 1 metastatic patient, score increased to Grade 2 in 4. week of the treatment. However, in this patient, liver function failure attributed progressive disease after the treatment. None of Grade 2 patients' scores increased to Grade 3. ***Conclusion:*** It was concluded that; with voxel based dosimetry, and selective approach higher tumor doses with low whole liver normal absorbed doses were safe.

EP-0572

Differences in PET/MRI and PET/CT post-therapy dosimetry in hepatocellular carcinoma (HCC) treated with yttrium-90 microspheres

K. Knesaurek*, A. Abdelrahman, M. Ghesani;*
Icahn School of Medicine at Mount Sinai, New York, NY, UNITED STATES OF AMERICA.

Aim/Introduction: The aim of our study was to investigate the relationships between tumor (T) and normal tissue (N) absorbed dose obtained from PET/CT and PET/MRI post-therapy studies in hepatocellular carcinoma (HCC) treated with yttrium-90 microspheres (1). ***Materials and Methods:*** After treatment with Y-90 microspheres, 12 patients (1 female and 11 males, mean age 69.0± 7.8y), underwent PET/MRI and PET/CT imaging. For a PET/MRI study, the acquisition time was 20 min, and attenuation correction was done using the scanner standard 4 segment (air, soft tissue, lung, and fat) MR based attenuation map. The reconstruction matrix size was 172x172x127 and voxel size 4.17x4.17x2.03 mm^3. The acquisition time for a PET/CT study was 15 min. The reconstruction matrix size was 200x200x75 and voxel size 4.07x4.07x3.00 mm^3. The low dose, non-diagnostic CT images were used for attenuation correction for the PET/CT studies. PET/MRI and PET/CT reconstructed images were transferred to a common platform and used to calculate Y-90 dosimetry using MIM 7.1 software (MIM Software Inc., Cleveland, Ohio). Local deposition method was used to calculate dosimetry. For each patient, regions-of-interest (ROIs) for whole liver and tumor(s) were manually created; the normal tissue ROI was created automatically. ***Results:*** For 12 patients, the mean liver, tumor and normal tissue doses (mean ± SD) were, 48.10±23.21 Gy, 806.66±1010.57 Gy and 41.50±15.28 Gy, respectively from PET/CT studies, and 40.84±22.53 Gy, 689.00±871.60 Gy and 35.87±16.59 Gy, respectively from PET/MRI studies. Although, the mean dose to the tumor can be significantly different, up to 38% difference, mean dose from both modalities for liver and normal tissue were relatively close, with less than 17% difference. ***Conclusion:*** PET/MRI usually provides better delineated of liver and tumor contours due to superior MRI soft tissue contrast. On the other side, PET/CT provides better quantification of PET images due to better attenuation correction. In addition to these factors, different voxels and matrix sizes also contribute to relatively small and clinically acceptable differences in between PET/MRI or PET/CT Y-90 dosimetry results. ***References:*** 1.Knešaurek K, Tuli A, Kim E, Heiba S, Kostakoglu L. Comparison of PET/CT and PET/MR imaging and dosimetry of yttrium-90 (^{90}Y) in patients with unresectable hepatic tumors who have received intra-arterial radioembolization therapy with ^{90}Y microspheres. EJNMMI Phys 5: 23, 2018 https://doi.org/10.1186/s40658-018-0222-y

EP-0573

Predicting response in HCC selective internal radiation therapy with Y-90 microspheres using advanced PET/CT based dosimetry; LATAM and USA centers experience

D. Mena[1], *I. Hume*[2], *R. García Monaco*[2], *C. Collaud*[2], *O. Peralta*[2], *A. Mollerach*[2], *P. Rodriguez*[2], *V. Jager*[2], *I. Arma*[2], *C. Cianciarelli*[2], *M. Chacon*[2], *V. Gonzalez*[2], *S. Sunagua*[2], *N. Pabstleben*[2], *K. Knešaurek*[3]; [1]*Nuclear Medicine World, CDMX, MEXICO,* [2]*Hospital Italiano de Buenos Aires, Buenos Aires, ARGENTINA,* [3]*Mount Sinai, NY, NY, UNITED STATES OF AMERICA.*

Aim/Introduction: The aim of our work is to evaluate the role of advanced PET/CT based dosimetry for predicting response in patients undergoing locoregional therapy to the liver with Y-90 microspheres. ***Materials and Methods:*** To assess response to Y-90 treatment, mRECIST criteria done on contrast enhanced MRI and/or CT were used at a month post treatment and subsequently every three months after it. Due to the limited number of partial response and stable disease cases, only 60 patients (11 female:49 male, mean age 66.2±8.4y) with complete response (CR) and progression of disease (PD) were selected. PET/CT images were acquired for 15 min. The low dose, non-diagnostic CT images from PET/CT were used for localization of the Y-90 microspheres and attenuation correction. The reconstruction matrix size was 200x200x75 mm and voxel size 4.07x4.07x3.00 mm. Local deposition method was used for dosimetry calculations. For each patient, volume-of-interest (VOI) for whole liver and tumor(s) was manually created and a program automatically created normal tissue VOI. ***Results:*** 60 patients (11 female:49 male, mean age 66.2±8.4y) are the subject of the study. The mean liver, tumor, and normal tissue doses (mean ± SD) were 49.22±24.69 Gy, 830.71±764.09 Gy and 40.12 ±20.90 Gy respectively. Among these patients, 50 (83%) showed CR and 10 (17%) showed PD. For CR patients the mean tumor dose was 943.53±781.40 Gy and for patients with PD, the mean tumor dose was significantly lower 266.61±280.64 Gy. The mean liver and normal tissue doses were similar; for CR patients, liver and normal tissue doses were 49.43±22.64 Gy and 40.55±21.23 Gy, respectively and for PD patients the same values were 48.17±34.71 Gy and 38.01±20.13 Gy, respectively. ***Conclusion:*** Although the number of PD cases was limited and partial volume effect was not considered, our data shows that patients with complete response have a statistically higher (P = 0.0001) tumor dose than those with progression of disease.

EP-0574

Correlation of 90y Microsphere Dose Planned with Voxel-Based Dosimetry with Actual Absorbed Tumor Dose

A. Dere*, E. Akgun, K. Bozkurt, B. Armutlu, B. E. Akkas, M. Kaya; University of Health Sciences,Basaksehir Cam ve Sakura City Hospital, ISTANBUL, TÜRKIYE.*

Aim/Introduction: We aimed to retrospectively compare voxel-based dosimetric calculations obtained from Tc99mMAA SPECT/CT images with the absorbed doses and volumes applied on treatment. ***Materials and Methods:*** MAA SPECT/CT images and PET/CT images after 90Y treatment of 40 liver lesions treated with intra-arterial 90Y glass microsphere were analyzed. Volumes of tumor, perfused tissue, normal liver and whole liver were plotted and absorbed doses were recorded both for MAA SPECT/CT and for Y90 treatment PET/CT images. The volumes and planned doses using MAA SPECT/CT data were compared with the real absorbed doses and volumes on Y90 treatment PET/CT images. From the histogram curves, the planned and received doses of 50-70-95% of the tumor volume were compared. ***Results:*** Tumor volumes measured from SPECT and PET images of 40 lesions (r=0.97, p<0.001), perfused area (r=97,p<0.001), total liver (r=0.96,p<0.001), normal liver tissue volumes (r=0.78,p<0.001) were highly correlated. Tumor (r=0.81,p<0.001), perfused tissue (r=0.81,p<0.001), normal perfused (r=0.37,p<0.002), normal liver (r=0.73, p<0.001) and whole liver (r=0.99 p<0.001) absorbed doses were also highly correlated. When absorbed doses of 50%, 70% and 95% of the perfused volumes were compared in MAA and 90Y dosimetric analysis, statistically strong correlation was observed (r=0.77 p<0.001, r=0.67 p<0.001, r=0.61 p <0.001).When the same comparison was performed for the tumor absorbed doses, the doses absorbed by 50% and 70% of the tumor volume were correlated (r=0.75 p<0.001, r=0.61 p<0.01), while the doses received by 95% of the tumor volume were not (r=0.026 p>0.05). On head- to- head correlation, treatment absorbed doses did not differ from the planned doses in 27 of 40 lesions. However, in 13 lesions, we observed that the applied doses were significantly higher within a range of 25%- 87% from the scheduled doses (mean: 51%).When evaluated the effect of temporary embolization of hepatic arterioles, split dosage delivery, pre/post calibrated dosage use, and the interval between MAA and 90Y treatment on this dosimetric difference, we observed that the rate of split dosing was slightly higher in these 13 lesions (p:ns , % 38 vs. 22%). ***Conclusion:*** Absorbed doses and volumes planned with voxel-based dosimetry were significantly correlated with the absorbed doses and volumes achieved in the majority of patients. However, significant deviations were seen in some tumor absorbed doses. In addition, Tc99m MAA and 90Y distribution may differ when 95% of the tumor volume is compared. This situation may be explained by the different nature of MAA and Y90 particles.

EP-0575

Development of a Topical Application Device for Non Melanoma Skin Cancer Therapy

M. Buonanno*, M. Aurilio, A. Esposito, A. Morisco, R. De Marino, L. D'ambrosio, C. Maisto, V. Porfidia, S. Lastoria; IRCCS TUMORI FONDAZIONE G. PASCALE, Napoli, ITALY.*

Aim/Introduction: Non-melanoma skin cancers (NMSC) can usually be eradicated by surgery and local radiation treatment. A new method using topical application of radionuclides, as an effective alternative, has been proposed. The aim of this research is to produce radioactive skin patches; fully individualized preparations designed considering the effective shape of the lesion/s to treat. ***Materials and Methods:*** We have focused our interest in producing "therapeutic" using the radionuclide [^{223}Ra]-Ra, as RaCl solution, that was impregnated in a scaffold, or mixed with a resin material to form a uniform layer. A homogeneous distribution of radioactivity was determinated by phosphorescence imaging using Cyclone, to create a standard that allows us to calculate the activity present in each prepared device.As a basic material to form the scaffold or device we used polymeric type mixtures with cornstarch dispersions at concentrations between 10-30%, polyvinylpyrrolidone solution at 15%, gelatin solutions at concentrations between 20-30% and hydroxypropyl methylcellulose (HPMC) dispersions at different concentrations 2-30% with the inclusion of 10% glycerol in all case, as a plasticizing agent. In each case, rheological characteristics were observed at the time of making the patch, and the distributions of the Ra-223 activity were determined using the elaborated calibration curve ***Results:*** The scaffold made by gelatin and polyvinylpyrrolidone solutions,

showed an insufficient viscosity, that was unable to maintain the radioactive dispersion on the polymeric base. Such limit makes impossible to avoid the contamination of the patient. The scaffold made by cornstarch did not guarantee a uniform distribution of radioactivity. Conversely, HPMC dispersion at 30% with glycerin at 10% showed the best characteristics for viscosity and a uniform distribution of the radioactivity. The efficacy of patches containing up to 4 MBq of ^{223}Ra-Cl is currently being tested on cell culture of NMSC OF different thickness in order to define the proper timing to obtain the most effective therapeutic results. ***Conclusion:*** HPMC dispersion showed the best results in terms of future clinical applicability. The production of lesion-shaped patches, by 3D printers is the optimization of the manufacturing process. ***References:*** Pashazadeh A et al., Conceptual design of a personalized radiation therapy patch for skin cancer. Current Directions in Biomedical Engineering, 2018, 4,1.Li, Y., Sun, X., Liang, Y. et al. Monte Carlo simulation of linac using PRIMO. Radiat Oncol (2022) 17, 185.

EP-0576

Is There Any Affect Of Tumor Location On Radioembolisation Treatment Response In Hepatocellular Carcinoma?

E. Akgun*;*
University of Health Science Turkey, Basaksehir Cam and Sakura City Hospital, Istanbul, TÜRKIYE.

Aim/Introduction: We planned this retrospective study to compare 90Y glass radioembolization treatment response between central and peripheral located hepatocellular carcinoma (HCC). ***Materials and Methods:*** Thirty-nine patients treated with Y90 embedded glass microsphere included the study. Absorbed doses were calculated with voxel-based dosimetric approach.The location being central (Group 1, n=19) versus peripheral (Group 2, n=20) was defined by the coefficient of the HCC, which is ratio of the distance from the hilum of the liver at the portal vein bifurcation to the central of the HCC divided by the diameter of the whole liver on the same line.Treatment response according to AFP value, modified Response Evaluation Criteria in Solid Tumors (mRECIST, n=30), and Positron Emission Tomography Response Criteria in Solid Tumors (PERCIST, n=31) criteria's were analyzed after 2 months of treatment. ***Results:*** In Group 1; mean age was 65.6. In 5 cases split infusion, in 11 cases tumor selective treatment approach were applied. According to PERCİST/mRECIST criteria treatment responses categories: complete response in 2/1 cases, partial response in 7/7 cases, stable disease in 2/2 cases, progressive diseases in 3/4 cases; respectively. AFP value decreased in 3 cases, increased in 6 cases, and was stable in 1 case. Median (min-max) absorbed doses were 325 Gy (115-600) for tumor, 114 Gy (35-304) for perfused normal tissue, and 12 Gy (3-70) for normal liver. Ratio of perfuse tissue volume to tumor volume ranged between 1.1 to 19.8 (median 1.90).In Group 2; mean age was 65.2. In 4 cases split infusion, in only 1 case non-selective treatment approach were applied. According to PERCİST/mRECIST criteria treatment responses categories: complete response in 6/4 cases, partial response in 6/9 cases, stable disease in 2/0 cases, progressive diseases in 3/3 cases; respectively. AFP value decreased in 9 cases, increased in 2 cases, and was stable in 1 case. Median (min-max) absorbed doses were 475 Gy (150-800) for tumor, 157 Gy (35-652) for perfused normal tissue, and 14 Gy (1-69) for normal liver. There is no statistically significant difference in gender, treatment responses, tumor volumes, perfuse tissue volumes, perfuse tissue to tumor ratios between 2 groups. However, tumor selective approach, and perfuse tissue absorbed doses were significantly higher in Group 2 (p=0.007, and p=0.004; respectively). ***Conclusion:*** Contrary to expectation, centrally located HCC cases could be treated as successfully as peripherally located HCC cases.

EP-0577

Factors Affecting Outcome in Hepatocellular Cancer Patients Treated with Selective Intra-arterial Radiomicrosphere Therapy

B. Soydas Turan[1]*, B. Volkan-Salancı*[2]*, M. F. Bozkurt*[2]*, G. Eldem*[3]*, E. Karabulut*[4]*, S. Yalcin*[5]*, F. Çay*[3]*, B. Peynircioğlu*[3]*, O. Ugur*[2]*;*
[1]Etlik City Hospital, Department of Nuclear Medicine, Ankara, TÜRKIYE, [2]Hacettepe University Faculty of Medicine, Department of Nuclear Medicine, Ankara, TÜRKIYE, [3]Hacettepe University Faculty of Medicine, Department of Interventional Radiology, Ankara, TÜRKIYE, [4]Hacettepe University Faculty of Medicine, Department of Biostatistics, Ankara, TÜRKIYE, [5]Hacettepe University Faculty of Medicine, Department of Medical Oncology, Ankara, TÜRKIYE.

Aim/Introduction: To explore which factors may influence outcome of hepatocellular cancer (HCC) patients after selective intra-arterial radiomicrosphere therapy (SIRT). ***Materials and Methods:*** HCC patients treated with SIRT between 2008 and 2018 were retrospectively enrolled. Previous therapies, baseline liver function tests and alfa-fetoprotein (AFP) levels, Barcelona Clinic Liver Cancer (BCLC) stage and Child-Pugh score were noted. Baseline CT/MRI were re-assessed for tumor size and number, presence of portal vein invasion and extrahepatic metastases. SIRT was applied using either resin or glass microspheres. Treatment dose of glass microspheres was calculated by non-compartmental partition model whereas dose of resin treatments was calculated by using the body surface area method. Univariate analysis was carried out using Kaplan-Meier survival curves and for statistical comparison log rank test was used. The effect of microsphere type, BCLC stage, Child-Pugh score, prior liver resection, baseline liver functions and AFP levels were assessed using multivariate Cox regression model. ***Results:*** 106 HCC patients treated with SIRT (49 resin, 57 glass) were included. The median overall survival (OS) was 13.9 months (range: 10.1-17.7). In univariate analysis, survival was significantly longer in patients with prior liver resection (33.8 vs 11.9 months, p: 0.01). Patients with portal vein invasion (5.9 vs 15.3 months, p: 0.016), BCLC class C (5.9 vs 15.5 months, p: 0.007), Child-Pugh score B (7.9 vs 15.3 months, p:0.012) and progressive disease after SIRT (9.7 vs 17.6 months, p: 0.003) had significantly low survival, as expected. Although baseline characteristics of two microsphere groups were similar with regard to demographics, BCLC stage, Child-Pugh score, liver function tests and AFP levels (Table 1), patients treated with glass microspheres had lower median OS when compared to resin (10.1 vs 23.1 months, p: 0.012). Multivariate analyses showed treatment with glass microspheres (Hazard Ratio [HR]: 2.537, p: 0.001), BCLC class C (HR: 1.706, p: 0.058), lower baseline albumin (HR: 0.501, p: 0.017) and higher baseline aspartate aminotransferase level (HR: 1.01, p<0.001) were associated with worse survival. Gender (p: 0.306), prior trans-arterial chemotherapy (p: 0.792), prior radiofrequency ablation (p: 0.465), presence of extrahepatic disease (p: 0.146), bi-lobar involvement (p: 0.079) and number of lesions (p: 0.190) did not have impact on OS. ***Conclusion:*** Treatment with glass microspheres, BCLC class C, lower baseline albumin and higher baseline aspartate aminotransferase level had a negative effect on OS of HCC patients who received SIRT. Further larger prospective dosimetric studies are warranted to confirm these findings.

EP-0578

A Case of Meningioma Applied İntraarterial Lu-177 DOTATATE

K. Mammadli, *B. Karaşah Erkek, M. Parıldar, Ö. Şanlı; Ege University Faculty Of Medicine, Department Of Nuclear Medicine, Bornova, TÜRKIYE.*

Aim/Introduction: Peptide receptor radionuclide therapy (PRRT) has been used for over 20 years as a systemic treatment for advanced neuroendocrine tumors (NENs) and is a continuously evolving treatment modality. The basic mechanism of action of PRRT is based on the principle of using a beta or alpha particle-emitting radionuclide to deliver somatostatin analogues to the interior or surface of tumor cells. The treatment of meningiomas that are resistant to surgery and radiotherapy is challenging, and the effects of various systemic treatments are often limited with low rates of progression-free survival. Somatostatin receptors are overexpressed in meningiomas and are one of the most specific immunohistochemical markers. The number of studies on PRRT in meningioma patients is limited and much less compared to NENs . ***Materials and Methods:*** A 67-year-old male patient presented to our clinic with symptoms of headache, numbness on the face, and nausea. The patient had previously undergone surgery and postoperative radiotherapy for a left temporal mass. Subsequent follow-up revealed recurrence, and the patient was symptomatic with no option for reoperation or radiotherapy. Prior to treatment, MRI and Ga68 DOTATATE PET/CT were performed for evaluation. MRI showed a mass consistent with meningioma at the sphenoid wing on the left, and Ga68 DOTATATE PET/CT showed increased DOTATATE uptake in this area. Diagnostic angiogram was performed to identify the arterial structure perfusing the tumor, and then intra-arterial selective method was used to demonstrate tumor uptake by injecting 2.5 mCi of Ga68-DOTATATE from the internal maxillary artery-A. meningea junction. After this procedure, intense Ga68 DOTATATE uptake was observed in the recurrent meningeal lesion located caudal to the craniectomy defect on Ga68 DOTA PET/CT imaging. Subsequently, the patient received a total of 4 doses of intra-arterial Lu-177 DOTATATE treatment, totaling 650 mCi. No adverse effects were observed with the treatments. After treatment, partial regression was observed in the lesion on Ga68 DOTA PET/CT, while MRI images showed complete regression of the intracerebral extension of the lesion and partial dimensional regression with cystic necrotic features in the component adjacent to the sphenoid bone. ***Results:*** Intra-arterial PRRT can significantly increase tumor radiotherapeutic accumulation due to the first-pass effect and may provide safe and promising improvement in symptomatic and inoperable meningioma patients resistant to conventional treatments. In addition patient symptoms decreased after treatment. ***Conclusion:*** Futher studies are nedeed to better understand the effectivesess and safety of intraarterial PRRT in meningioma patients.

EP-0579

Hepatic transarterial radioembolization (TARE) with 90Yttrium glass microspheres for treatment of liver tumours: safety and survival outcomes.

A. De Agrela Serrao, *A. M. Leiva Montejo, C. Ruiz Corbalan, M. Castellón Sanchez, J. L. Navarro Fernandez, T. E. Rodriguez Locarno, A. C. Hernández Martínez, L. Frutos Esteban, D. R. Cáceres Silva, L. Mohamed Salem, J. F. Contreras Gutierrez; Hospital Clinico Universitario Virgen de Arrixaca, Murcia, SPAIN.*

Aim/Introduction: The aim of this study was to analyse the overall survival (OS) outcomes of hepatic transarterial radioembolization with ^{90}Yttrium glass microspheres (TARE) for patients diagnosed with hepatocellular carcinoma (HCC), liver metastasis of neuroendocrine tumours (NETs), intrahepatic cholangiocarcinoma (ICC) or liver metastasis of colorectal adenocarcinoma (CRC). ***Materials and Methods:*** Retrospective, monocentric study which included 39 patients that underwent TARE treatment for liver tumours between January 2019 and January 2023. (2 patients were excluded due to lack of follow up). previous chemotherapy and local treatments to TARE were noted, radiation dosimetry and immediate complications were recorded. The therapeutic response was categorised as complete response, partial response or progressive disease. Survival outcomes and clinical or biochemical adverse events were analysed. ***Results:*** 52 TARE were performed in 39 patients (age 66.85±10.34 years, 89.7% men, mean follow-up 17.38±12.66months). Thirty patients (76.9%) had localized HCC, five patients (12.8%) had liver metastases from NETs, two patients (5.1%) had ICC and two patients had liver metastases from CRC. Sixteen patients (41%) had received at least one previous systemic treatment and fourteen patients (35.9%) had received at least one previous local treatment. Fourteen (35.9%) cases presented bilobar liver involvement. In unilobar cases (64.1%) the most frequent involvement was in the right hepatic lobe (82.1%). The mean of perfused volume and Yttrium-90 activity was 777.18±410.96 cm3 and 2.63±1.25 Gbq respectively with an absorbed dose in the tumour tissue of 153.27±50.61 Gy in a monocompartment dosimetry system, lung absorbed dose was 13.76±9.33 Gy. In the follow up a complete response to treatment was observed in six patients (15.4%), partial response in eight patients (20.5%), stable disease in ten patients (25.6%), and progressive disease in 15 patients (38.5%). The estimated time until progression was 22,48±3,56 months. There were acute complications in 4 patients (10.3%), 50% fever and 50% abdominal pain. Eighteen (46.2%) patients died, six (15.4%) of which died from unrelated causes to the cancer. Mean OS was 32.58±3.32 months (95% CI 26.07-39.106) from TARE to death. None of the patients with NETs died during the follow-up and 80% had a complete response. Histology of HCC was associated with a better OS (34.3±3.21 months) than CRC and ICC (20±11 and 7.5±4.5 months) ($p<0.0001$). ***Conclusion:*** TARE is an effective am safe treatment for liver tumours specially HCC an NETs, but more data is needed to properly assess the OS in ICC and CRC.

EP-0580

Efficacy and safety of Y-90 radioembolization for colorectal cancer liver metastases.

J. Villa Palacios, *E. Triviño-Ibáñez, E. González-Flores, P. Pardo-Moreno, A. Rodríguez-Fernández; Hospital Universitario Virgen de las Nieves, Granada, SPAIN.*

Aim/Introduction: To analyze the efficacy, toxicity, and survival outcomes of transarterial hepatic radioembolization with yttrium-90 (TARE) for colorectal cancer (CRC) liver metastases. ***Materials and Methods:*** We performed an observational and prospective study that patients with CRC liver metastases treated by TARE, between November 2015 and August 2022. Data on previous treatments, biochemical parameters before and after treatment, dosimetry, and complications were recorded. Therapeutic response was evaluated at 3 and 6 months after TARE (using RECIST1.1 criteria). Clinical and/or biochemical adverse events were also recorded. ***Results:*** 42 TARE were performed in 33 patients (mean age 61.730±8.31 years, 63.6% male, mean follow-up 41.84±23.12 months). Of these patients, 90.1% (30/33) had received at least one line of systemic chemotherapy. Bilobar liver involvement was present in 51.5% (17/33) cases, with tumour burden greater than 25% in 51.5% of cases. The administered yttrium-90 activity was 3.11 ± 2.02 Gbq, with a mean absorbed

dose in tumour tissue of 193.15 ± 111.21 Gy and a mean tumour-to-normal liver ratio of 27.76 ± 44.47. At 3 months, one patient (3.1%) had a complete response (CR), 7 (21.2%) had a partial response (PR), 11 (33.3%) had stable disease (SD), and 13 (39.4%) had disease progression (PD). At 6 months, one patient remained in CR, 5 had SD, and 18 had PD. Twelve patients experienced acute or delayed toxicity, with hyperbilirubinemia being the most frequent adverse event (grade 3 or 4 in 5 patients). ***Conclusion:*** In our study, TARE was a safe and effective treatment for unresectable CRC liver metastases.

EP-0581

Factors impacting survival in colorectal liver metastases treated with Y-90 radioembolization.

J. Villa Palacios, *E. Triviño-Ibáñez, J. Ciampi-Dopazo, E. González-Flores, A. Rodríguez-Fernández;*
Hospital Universitario Virgen de las Nieves, Granada, SPAIN.

Aim/Introduction: To investigate factors associated with survival in colorectal carcinoma (CRC) with liver metastases treated with yttrium-90 (Y-90) radioembolization (TARE). ***Materials and Methods:*** Observational and prospective study that included 33 patients with CRC liver metastases treated by TARE between November 2015 and August 2022. Data related to previous treatments, biochemical parameters, dosimetry, and complications were collected. Therapeutic response was evaluated at 3 and 6 months after TARE using RECIST 1.1 criteria. Survival probabilities (overall survival [OS] and progression-free survival [PFS)]) were generated using the Kaplan-Meier method, and a Cox regression model was used to study the association of different predictive biomarkers. ***Results:*** Forty-two TARE procedures were performed in 33 patients (mean age 61.730±8.31 years, 63.6% male, mean follow-up 41.84±23.12 months). Ninety-one percent (30/33) of the patients had received at least one line of systemic chemotherapy. Bilobar hepatic involvement was present in 51.5% (17/33) of cases, with a tumour burden greater than 25% in 51.5% of cases. The administered yttrium-90 activity was 3.11 ± 2.02 GBq, with an absorbed dose in the tumour tissue of 193.15 ± 111.21 Gy. Seventy-eight-point eight percent (26/33) of patients died during follow-up. The median OS was 36.35 months from the diagnosis of liver metastases and 11 months from TARE. Factors associated with lower OS were: extrahepatic metastases (HR: 2.72, p=0.044), aspartate aminotransferase (HR: 1.03, p=0.044), neutrophil-to-lymphocyte ratio (HR: 1.40, p=0.013), and platelet-to-lymphocyte ratio (HR: 1.01, p<0.01) pre-TARE, injected activity (HR: 1.21, p=0.037), perfused volume (HR: 1.01, p=0.029), absorbed tumour dose <120 Gy (HR: 2.5, p=0.042), and toxicity after TARE (HR: 2.33, p=0.049). ***Conclusion:*** Predictive factors for survival in colorectal liver metastases treated by TARE include biochemical, dosimetry and toxicity parameters.

EP-0582

Tumoricidal dosing approach with parenchymal sparing using voxel-based dosimetry in the Y90 glass microspheres treatment of liver lesions

C. Sin, *B. E. Akkas, M. Kaya, E. Akgun;*
University of Health Sciences,Basaksehir Cam ve Sakura City Hospital, İSTANBUL, TÜRKIYE.

Aim/Introduction: Investigate the effect of absorbed doses and tumor volume on ALBI scores in patients treated with 90Y glass microspheres. ***Materials and Methods:*** 81 patients (HCC n:46, cholangiocellular cancer (ICC) n:6, metastatic tumor n: 29) were included (49 M, 32 F, mean age: 62.4 (13-91). ECOG and Child Pugh scores, laboratory values and ALBI scores were recorded. Patients were grouped as ALBI-1 (≤-2.60), ALBI-2 (-2.60< ALBI≤-1.39) and ALBI-3 (>-1.39). Follow-up PET/CT was performed for treatment response evaluation 6 weeks after therapy. ***Results:*** Child Pugh scores were A in 40 patients and B in 6 patients. Baseline ALBI scores were 1 in 55 cases, 2 in 25 cases and 3 in 1 case. Tumor absorbed dose (TAD) averaged 427.2 Gy (120-1000 Gy); average tumor volume was 192.3cc (21-2871 cc). Total liver absorbed dose was 31.1 Gy (1.1- 68.9 Gy); perfused normal parenchyma dose was calculated as 210 Gy (22.1-602.4 Gy). On follow-up PET/CT, complete metabolic response (CR) was observed in 8 patients and partial response (PR) was observed in 30 patients with the absence of non-target progression. In 7 patients, PR was observed in the target lesion, with non-target hepatic and/or systemic progression. Progression of the target lesion (PD) was observed in 10 patients. 11 patients died in the first 6 months on follow-up. PET/CT examination could not be performed in 15 patients. We observed a gradual significant increase in objective treatment response with increasing TAD; 575 Gy in CR, 417.6 in PR, 308.3 in PD and 233.6 Gy in exitus patients; (p<0.001). After treatment, ALBI score groups 72/81 (89%) patients (Group1) did not change. However, 9/81 (11%) patients ALBI score was impaired (Group2). There was no statistically significant difference between absorbed doses of non-tumoral parenchyma (140 Gy vs. 130 Gy) and the total liver absorbed doses (72 Gy vs 79 Gy) between groups. TAD was significantly higher in Group1 (402 Gy vs 253 Gy, p=0.01). Tumor volumes were significantly lower in Group1 (320 cc vs 525 cc, p=0.02). Five of the 9 patients whose ALBI scores deteriorated, died on follow-up. ***Conclusion:*** The lower TAD and higher tumor volumes in patients with impaired ALBI scores compared to the other group showed that developing hepatic dysfunction was due to high tumor burden and/or tumor-related causes other than radiotoxicity. Tumoricidal ablative doses can be achieved with sparing future liver functions using voxel-based dosimetric approach in 90Y glass microspheres treatment.

EP-0583

PET/CT-based Y-90 microsphere dosimetry to predict contralateral lobe hypertrophy after unilobar radioembolization in treatment-naive hepatocellular carcinoma

Y. Kang, *J. Paeng;*
Seoul National University Hospital, Seoul, KOREA, REPUBLIC OF.

Aim/Introduction: Radioembolization is a treatment option for hepatic tumors that can lead to the control of tumor growth, and cause hypertrophy of the future remnant liver for surgical resection. Despite the increasing use of PET-based dosimetry in radioembolization, its effectiveness for predicting contralateral lobe hypertrophy has not been fully evaluated in solid patient groups. This study aimed to identify potential predictors of contralateral lobe hypertrophy after radioembolization in treatment-naive hepatocellular carcinoma (HCC) patients, based on Y-90 microsphere PET/CT dosimetry and clinical factors. ***Materials and Methods:*** Twenty patients that underwent unilobar radioembolization for right lobar treatment-naive HCCs were retrospectively enrolled. In all patients, contrast-enhanced CT scans were performed before treatment (within a month), and two to four months after treatment. Post-treatment Y-90 PET/CT scans were performed in 16 to 24 hours after Y-90 microsphere injection. PET/CT images were realigned to match the pre-treatment CT images, and voxel-based absorbed dose was calculated from PET/CT images using a dedicated analysis

software. Dose histograms were obtained for each region, including the tumor, target liver (right lobe), target non-tumor liver, and future remnant liver (FRL, left lobe). To evaluate the degree of contralateral lobe hypertrophy, the volume of the FRL was calculated based on manually defined volumes of interest (VOIs) on both pre-treatment and post-treatment CT images. Relative increase in FRL volume was calculated as the difference between post-treatment and pre-treatment volumes, divided by the pre-treatment volume. PET dosimetry factors were tested with pre-treatment clinical factors, including tumor size, portal vein thrombosis, ascites, splenomegaly, and laboratory test results, for prediction of FRL volume increase by multivariate regression analyses. ***Results:*** The mean relative FRL volume increase was 12.4% (95% CI 4.6-20.1%). In univariate Pearson correlation analyses using dosimetry factors, the mean absorbed dose of target non-tumor liver was the most significant predictors for relative FRL volume change (r=0.660; p=0.002). Among clinical factors, platelet count exhibited significant positive correlation (r=0.667; p=0.001). In multivariate regression analysis, both the mean absorbed dose of target non-tumor liver, and platelet count were demonstrated as independent predictors for FRL volume increase (r = 0.595 and 0.604, respectively; overall model p<0.001). ***Conclusion:*** This study suggests that the mean absorbed dose of target non-tumor liver, and platelet count have the potential to predict contralateral lobe hypertrophy after radioembolization for treatment-naive HCCs. Further studies with large cohorts are needed to validate the results and establish the clinical significance of these predictors.

EP-0584

The Role of Tumor FDG Metabolism and AFP Level in Predicting Treatment Response In HCC Patients Treated with 90Y Microspheres

G. Yilmaz, *B. E. Akkaş, M. Kaya, E. Akgün, Ö. Vural Topuz; University of Health Sciences Basaksehir Cam and Sakura City Hospital, İstanbul, TÜRKIYE.*

Aim/Introduction: Tumor FDG uptake and serum AFP levels are inversely correlated with tumor differentiation in hepatocellular carcinomas (HCC). The aim of this study is to compare the Y90 microsphere treatment response with the differentiation features of the tumor predicted by pretreatment serum AFP value and FDG uptake. ***Materials and Methods:*** 32 HCC patients who were treated with selective intra-arterial 90Y glass microspheres were included. Barcelona Clinic Liver Cancer (BCLC) stages were as follows; Stage A: 18 patients, Stage B :13 patients, Stage C: 1 patient. Child Pugh scores were A in 26 patients, B in 6 patients. Pretreatment 18F-FDG PET/CT examination was performed and SUVmax/mean/peak of the lesions and normal liver parenchyma were measured. Tumor-to-normal liver SUV ratios (T/Li) were recorded. Absorbed tumor and normal liver doses were calculated by voxel-based multi-compartment dosimetric analysis on hepatic artery 99mTc-MAA SPECT/CT images. Treatment response was evaluated by 6th week PET/CT and 8th week MR images according to PERCIST and mRECIST criteria. ***Results:*** 32 HCC cases (25 M, 7 F, mean age: 66.8± 9.5 years) were included. The tumor-absorbed dose range was 116-800 Gy (mean 387±165). On follow up PET/CT, treatment responses for target lesions were as follows; Complete response (CR) in 5 patients, partial response (PR) in 15 patients, stable disease (SD) in 4 patients, and progression (PD) in 8 patients. Non-target intrahepatic progression (NTP) and/or extrahepatic disease were observed in 9 of 20 patients with complete and partial response. Tumor absorbed doses were significantly higher in CR compared to PR, SD and PD (564.6 Gy vs.381.4 vs 401.5 and 281.2 Gy, respectively, p:0.01). There was no significant correlation between the T/Li SUV and AFP values with regard to treatment responses. Follow-up PET/CT detected NTP and systemic progression in 17 of 32 patients. Progression was not correlated to BCLC stages. T/Li SUV ratios did not differ in these patients compared to others. However, serum AFP levels were significantly higher in patients with NTP compared to others (median: 3.9 min-max:1.59-3170 ng/dl vs median:47.5 min-max:2.77-50864, p <0.001). ***Conclusion:*** In this study, there was no significant correlation between tumor FDG metabolism and serum AFP values and the response of the target lesion to 90Y therapy. In 90Y microsphere treatment, the most important parameter determining the early treatment response is the tumor absorbed dose. We observed that even in poorly differentiated HCC, successful treatment response can be achieved when tumoricidal doses were administered.

EP-0585

Hepatic transarterial radioembolization with three different compounds: are there any survival-related biomarkers?

L. Asensio Valero, *H. Rodriguez Parra, J. Orozco Cortes, C. Castillo Arias, L. Blanco Verdejo, A. Sanchez Tornero, M. Redal Peña, R. Díaz Expósito;*
Hospital Clínico de Valencia, Valencia, SPAIN.

Aim/Introduction: The main objective of this study was to assess the survival of patients with liver lesions treated with radioembolization using Y90 and Ho166 loaded microspheres in relation to their clinical and paraclinical context. ***Materials and Methods:*** A total of 100 patients were evaluated, of which 96 were treated and four were dropped due to contraindications. The sample included 70 men (67.2%) and 26 women (32.8%), with an age range between 22 and 87 years old (mean±SE: 67.1±1.2). Overall, 78 patients were treated with 90Y-resin, 13 with Y90-glass and five with 166Ho loaded microspheres. Among them, there were 70 cases of hepatocarcinoma (67,3%), 19 colorectal cancer (18,3%), nine cholangiocarcinoma (8,8%), one gastrointestinal stromal tumor (0,9%), one intraductal papillary mucinous neoplasm (0,9%), one carcinoma of unknown primary (0,9%), and one gastric cancer (0,9%). Mean tumor volumes (TV) ranged from 3cc to 1433cc (220.48±27.7cc), and tumor burden (TB) ranged from 0.13% to 88.23% (12.2±1.5%). Of the 96 subjects, 80 died at the time of analysis, with overall survival (OS) ranging from one to 82 months (m) (17.25±1.5m). Statistical analysis was performed using SPSS STATISTICS v28. ***Results:*** Multi-segmental involvement was observed in 65% of cases, with two-segment or three-segment implication predominating, accounting for 26% and 20%, respectively. Amidst the different compounds, no statistical difference in OS was detected between yttrium-resin and yttrium-glass microspheres, while data from holmium-treated patients were insufficient for proper assessment. A total of 124 procedures were performed. OS in the single treatment group (72 patients, 75%) was significantly lower than in the two (20 patients, 20,8%) or three (four patients, 4,2%) treatment groups (14.5±1.4m vs 25.2±4.7m vs 26.7±5.2m; Kruskal-Wallis p:0.027). Re-treatment was considered in subsequent controls with tumor viability or in two-stage procedures. Parametric analysis showed that non-cirrhotic patients (23.00±3.04m) survived longer than cirrhotic patients (14.14±1.44m) (T p: 0.002). Furthermore, the enolic habit group had also a significantly lower OS than nondrinkers (3.54±2.4m vs 19.62±1.9m; T p:0.03). Among all pre-treatment liver function parameters studied, those subjects with higher levels of GOT (Kruskal-Wallis p:0.02) and GPT (Kruskal-Wallis p:0.07)

showed lower OS. No other differences were found between survival and lesion characteristics (TV, TB). ***Conclusion:*** The data suggests that it is possible to consider cirrhosis, alcoholism, and elevated pretreatment GOT and GPT values as biomarkers of poor prognosis.

EP-0586

Quantification of 99mTc-MAA for lung shunt estimation before 90Y radioembolization: comparison of three methods

E. Milan, *D. Barbisan, G. Zambon, C. La Verde, P. Barzi, M. Sutto, S. Barbiero, F. Nistri, L. Vendramin;*
Ospedale Cà Foncello ULSS2, Treviso, ITALY.

Aim/Introduction: In order to avoid radiation pneumonitis, planning for 90Y microspheres SIRT requires estimation of liver-lung shunt fraction (LSF) by using 99mTc-MAA procedure. Currently, regions of interest over liver and lungs in 2D planar imaging of 99mTc-MAA are manually drawn. This method, although mandatory, has some limits: it's time-consuming, observer dependent, limited by absence of both attenuation and scatter correction. Aim of the study was to compare the performances for LSF quantification of the manual method versus a nearly automatic one based on the use of a commercially available software analysing both 2D and 3D SPECT/CT images. ***Materials and Methods:*** 54 planar and SPECT/CT scans acquired after injection of 99mTc-MAA were evaluated using three approaches: 1) manual 2D (m2D), 2) semiautomatic 2D (s2D) and 3) SPECT/CT with attenuation (AC) and scatter correction (SC) (3D) ***Results:*** the mean LSF from m2D was 5.34 % (range from 0.8 % to 24.5 %) and was not significantly different from s2D 5.39 % (from 1,7% to 27.4 %) (p=NS). The mean LSF from 3D was 3.63 % (range from 0.5 % to 14.7 %) and was significantly different from m2D (p<0.0005) and from s2D (p<0.0005), respectively. The quantification of LSF was not significanly different by using m2D or s2D (R= 0,87). There was a substantial overestimation of LSF using planar imaging compared to SPECT/CT with AC and SC: m2D vs 3D (R=0.69) and s2D vs 3D (R= 0.60). Only 4 patients showed lesions localized in the dome of the liver and in all of them the LSF was higher using both m2D and s2D in comparison to 3D method ***Conclusion:*** semiautomatic evaluation of LSF is a reliable tool that helps reducing processing time. Our results confirm that planar imaging overestimates LSF in comparison to SPECT/CT especially in presence of lesions in the dome of the liver.

EP-0587

Dose-response relationship for yttrium-90 resin microspheres in patients with liver metastases from colorectal carcinoma.

L. Sancho Rodriguez[1], *C. Carballo Menayo*[2], *J. González-Martín*[2], *J. Bastidas Tamayo*[3], *E. Guillén Valderrama*[1], *M. Rodríguez-Fraile*[3];
[1]*CLINICA UNIVERSIDAD DE NAVARRA, MADRID, SPAIN,* [2]*Complejo Hospitalario Universitario Insular Materno Infantil de Las Palmas de Gran Canaria, Las Palmas de Gran Canaria, SPAIN,* [3]*CLINICA UNIVERSIDAD DE NAVARRA, PAMPLONA, SPAIN.*

Aim/Introduction: To analyze which voxel-based dosimetry parameters obtained from post-radioembolization ^{90}Y-PET/CT study are able to predict the relationship between the dose absorbed by the tumor and its radiological response in patients with liver metastases of colorectal carcinoma(mCCR). ***Materials and Methods:*** Retrospective review of prospectively collected data (May/2012-September/2019) that included patients with mCRC treated with radioembolization using ^{90}Y-resin microspheres(SIR-Spheres) who underwent a ^{90}Y-PET/CT study(Siemens Biograph_mCT) and had at least 3 months of follow-up. Dosimetric parameters were obtained using a 3D voxel dosimetry software(Planet Dose; Dosisoft). The total liver, target healthy liver tissue and tumors were segmented. Tumors selected for the dosimetric analysis were the five largest or most representative for each patient. From the dose-volume histograms, the parameters that quantify the heterogeneity of the absorbed dose by the tumor were obtained: minimum dose received by 98% of the volume (D98), D95, D90, D70, D50, D40 and D20, or the percentage of lesion that received ≥120 Gy(V120), 100, 70, 50, 40, and 30 Gy. Tumor response was evaluated at least three months after treatment, quantified according to RECIST1.1 criteria. In the analysis, response was considered when there was partial response (PR)(≥30% decrease in lesion diameter on CT/MR images) or stable disease (SD)(neither PR no PD) and non-response when there was progression disease (PD)(≥20% increase in lesion diameter). ROC analysis was performed to determine the area under the curve(AUC) and the cut-off point of the dosimetric parameters to assess their diagnostic accuracy. ***Results:*** Twenty-six patients with mCRC(105 lesions) were analysed. Thirteen were bilobar treatments(50%), 11 unilobar(42.3%) and 2 segmentectomies(7.7%). Most patients(96%) were progressions to second line chemotherapy. Ninety lesions (85.7 %) responded, 16(15.2%) showed PR and 74(70.5%) SD, and 15 lesions(14.3%) did not response (PD). In the analysis per patients, 22 patients(84.6 %) were responders (3 (13.6%) showed PR and 19 (86.4%) SD) and 4 patients(15.4 %) had PD. The parameters most related to radiological response were D98(cut-off-point =23.83 Gy showed an AUC=0.82; and an accuracy=86%) and V30(cut-off-point=90.69% showed an AUC=0.79; and an accuracy =79%). Therefore, a dose >23.83Gy received by 98% of the tumor volume, and a tumor volume >90.69% receiving at least 30Gy are related to a tumor response (≥30% reduction in tumor diameter). ***Conclusion:*** This study, despite its small sample size, identifies two dosimetric parameters (D98 and V30) obtained by 3D voxel dosimetry related to tumor response in patients with mCRC treated with radioembolization. ***References:*** JClinOncol.2021. Dec10;39(35):3897-3907. LancetOncol2017Sep;18(9):1159-1171.

EP-0588

Assessment of Similarity Between the Distributions of Tc-99m MAA Particles and Y-90 Resin Microspheres in Patients Receiving Transarterial Radioembolization for Liver Tumors

N. Coskun[1], *A. Erdogan*[2], *M. Kartal*[2], *E. Ozdemir*[1];
[1]*Ankara Bilkent City Hospital, Ankara Yildirim Beyazit University, Ankara, TÜRKIYE,* [2]*Ankara Bilkent City Hospital, Ankara, TÜRKIYE.*

Aim/Introduction: Transarterial radioembolization (TARE) for the treatment of liver tumors is based on the injection of Y-90-loaded microspheres into the hepatic arteries. Precise prediction of microsphere distribution is crucial for an effective dosimetric approach. However, the reliability of macroaggregated albumin (MAA) particles for predicting microsphere distribution remains a subject of ongoing debate. The aim of this study was to evaluate the level of similarity between the distributions of MAA particles and resin microspheres, and to evaluate the agreement between the absorbed doses according to the two procedures. ***Materials and Methods:*** Patients who underwent hepatic perfusion scintigraphy with Tc-99m MAA and TARE with Y-90 loaded resin microspheres in our center between January 2021 and January 2023 were included in the study. Whole liver volume, total perfused volume,

tumoral foci, and healthy liver parenchyma were segmented in both modalities by overlapping Tc-99m MAA SPECT/CT and Y-90 PET/CT images of each patient. The similarity of distributions was evaluated using the Jaccard similarity index and the Szymkiewicz-Simpson overlap coefficient. Spearman correlation coefficient and Bland-Altman analysis were used to evaluate the level of agreement between the doses determined by the two modalities. ***Results:*** Sixty-one patients were included in the final analyses (74% male, mean age 61±12 years). The mean Jaccard similarity index between Tc-99m MAA and Y-90 microsphere distributions was 56%, and the mean Szymkiewicz-Simpson overlap coefficient was 83%. The median tumor doses according to Tc-99m MAA and Y-90 resin microspheres were 143 and 171 Gy, respectively, while the median doses to healthy parenchyma were 80 and 75 Gy, respectively. There was a strong correlation between the median tumor doses (Spearman's rho=0.847, p<0.001) and between the parenchymal doses (Spearman's rho=0.768, p<0.001). Bland-Altman analysis showed that the absorbed tumor doses determined with both modalities were mostly within the 95% agreement interval, and there was no systematic bias between the two modalities. ***Conclusion:*** These results suggest a distribution similarity between Tc-99m MAA particles and resin microspheres ranging from 56% to 83% according to the adopted similarity approach. Variations of distribution can occur due to possible differences between the position of the angiographic catheter and the physical characteristics of the beads. Nevertheless, a comparison of predicted and achieved doses revealed a strong positive correlation. No systematic error was observed between the two procedures. This finding emphasizes the predictive value of Tc-99m MAA SPECT dosimetry for resin-based microspheres.

EP-39

e-Poster Area

C: Therapy Clinical Study -> C1 Oncological Therapy Clinical Study -> C14 Thyroid Therapy

EP-0589

Association between successful adjuvant therapy and quantitative evaluation of radioactive iodine accumulation in the thyroid bed in patients with differentiated thyroid cancer

Y. Iizuka[1,2], *T. Katagiri*[1], *R. Nakashima*[1], *M. Inoue*[1], *K. Nakamura*[1], *T. Mizowaki*[1];
[1]*Kyoto University, Kyoto, JAPAN,* [2]*Shizuoka City Shizuoka Hospital, Shizoka, JAPAN.*

Aim/Introduction: Adjuvant therapy (AT), which involves administration of radioactive iodine (iodine-131 [I-131]) is widely accepted to reduce the risk of recurrence and prolong survival in patients with differentiated thyroid cancer (DTC) without metastases. Using I-131 scintigraphy, we investigated the association between the outcomes of AT and quantitative parameters of iodine uptake at the thyroid bed. ***Materials and Methods:*** We retrospectively analysed 25 sets of images obtained from patients with DTC, who received I-131 as AT at our hospital between February 2017 and December 2018. All patients were treated with I-131 (3.70 GBq [100 mCi]) after total thyroidectomy without metastasis. We performed an I-131 whole-body scan and single-photon emission computed tomography/computed tomography 3 days after I-131 administration using a reference I-131 capsule in the same field of view. The radioactivity of the capsule was able to be calculated from its test date. Using our quantitative method [1] for estimation of the dose based on regression lines derived from reference capsule doses, we calculated radioactivity (MBq) levels at the thyroid bed. Initial successful AT was defined as absence of I-131 accumulation in the thyroid bed confirmed on diagnostic I-131 scintigraphy and a serum thyroglobulin concentration of <2.0 ng/mL without thyroid-stimulating hormone stimulation, 6-12 months after AT. We investigated the association between quantitative I-131 values measured at the thyroid bed and successful and failed AT. ***Results:*** Among 25 patients, AT was successful in 16 (64.0%). The mean and median activities of I-131 at the thyroid bed in all patients were 3.9 and 2.6 (range 0.2-14.0) MBq, respectively. The mean and median activities of I-131 were 3.2 and 2.5 MBq and 3.9 and 1.5 MBq in the successful and failed groups, respectively. Although, the median radioactivity of I-131 tended to be higher in the successful group, we observed no statistically significant intergroup differences in the association between radioactivity levels measured at the thyroid bed and AT outcomes (p=0.34). ***Conclusion:*** We observed no significant association between AT outcomes and I-131 accumulation in the thyroid bed in patients with DTC. ***References:*** [1] Iizuka Y, Katagiri T, Inoue M, et al. Comparison between planar and single-photon computed tomography images for radiation intensity quantification in iodine-131 scintigraphy, Sci Rep. 2021 11.21858

EP-0590

H. Wang*, R. Tian;*
West China Hospital, Sichuan University, Chengdu, CHINA.

Aim/Introduction: To evaluate the performance of the 2015 American Thyroid Association (ATA) recurrence risk stratification system (RSS) in predicting the response to treatment one year after the initial treatment in Chinese population diagnosed with differentiated thyroid cancer (DTC). ***Materials and Methods:*** Retrospective analysis of thyroid cancer patients from the thyroid cancer Electronic Medical Records (EMR)-based database of West China Hospital, Sichuan University was performed. We reviewed all records in the database and selected consecutive cases that satisfied the following criteria: (1) patients underwent thyroid surgery from January 1, 2009, to November 1, 2019 and diagnosed with DTC; (2) available data for RSS evaluation; (3) data of the one-year follow-up visit were available (carried out 6-18 months after the initial treatment) to classify response to treatment. Initial treatment was categorized into three groups: (1) thyroid lobectomy (TL); (2) total/near-total thyroidectomy (TT/near-TT); (3) TT/near-TT plus RAI treatment. The performance of the RSS in predicting the response was evaluated using the ordinal logistic regression analysis. ***Results:*** Out of 12452 case records in the database at data lock, a total of 6959 patients were included in the final study cohort, 1260 (18.1%) patients underwent TT/near-TT as initial treatment, 5190 patients (74.6%) underwent TT/near-TT plus RAI treatment, and other 509 patients (7.3%) underwent TL. The RSS was classified as low-risk in 2226 (32.0%), intermediate-risk in 3177 (45.7%), and high-risk in 1556 (22.4%) patients. At the 1-year follow up visit, excellent response, indeterminate, biochemical incomplete, and structural incomplete responses were documented in 3885 (56 %), 2123 (31%), 545 (8%), and 406 (6%) patients, respectively. The RSS was able to predict the response to treatment (intermediate-risk: OR=1.42, 95%CI=1.27-1.58, P<0.001; high-risk: OR=2.76, 95%CI=2.42-3.15, p<0.001). Among patients who underwent different initial treatments, intermediate- and

high-risk patients had a significantly increased chance of having less than excellent response as well (OR for TL: 6.12, 38.72; OR for TT/near-TT: 3.23, 5.67; OR for TT/near-TT plus RAI treatment: 1.61, 3.33). ***Conclusion:*** The RSS is a reliable system for predicting the short-term response in patients with DTC treated with TL, TT/near-TT, and TT/near-TT plus RAI treatment in a real-world clinical setting in China.

EP-0591

Follow-up Findings in the Group of Patients with Tall Cell Papillary Thyroid Cancer

B. Karasah Erkek*, H. Sarıyıldız Gümüşgöz, R. Halit Tokaç, B. Sarıkaya, Y. Ertan, A. Akgün;*
Ege University, Izmir, TÜRKIYE.

Aim/Introduction: The tall cell variant of papillary thyroid carcinoma (TCVPC) is the most common aggressive variant of papillary thyroid cancer (PTC). In our study, we aimed to evaluate the clinical status, outcomes of I-131 treatment, and follow-up findings of patients with histopathologically confirmed TCVPC. ***Materials and Methods:*** For this purpose, the clinical data of 37 patients diagnosed with TCVPC in our clinic were retrospectively analyzed. During follow-up, I-131 whole-body scanning (WBS), stimulated thyroglobulin (sTg) and anti-Tg values, ultrasound (US), and chest CT findings were evaluated. ***Results:*** The patient age range at diagnosis was 24-77 years, with 33 females and 4 males. The tumor sizes of patients who underwent total thyroidectomy were between 0.1-5 cm (mean: 1.45 ± 0.97), and central compartment and lateral cervical lymph node dissection were performed in 9 and 3 patients, respectively. Histopathological evaluation revealed lymphovascular invasion in 20/37 patients, parancimal invasion in 1/37 patients, extrathyroidal extension in 5/37 patients, and lymph node metastasis in 5/37 patients. At initial staging, none of the patients had findings consistent with distant metastasis. Cumulative doses of I-131 treatment ranging from 30-350 mCi (mean: 111.8 ± 55.96) were administered to the patients. The follow-up period ranged from 11-240 months (mean:37.7 ± 40.63). According to the ATA criteria, in the group of patients diagnosed with TCVPC, considering the 9th month sTg level, I-131 WBS and US findings, complete response was detected in 89% (33/37), indeterminate response in 2.7% (1/37), biochemical incomplete response in 2.7% (1/37), and anatomical incomplete response in 5.4% (2/37). In one patient who achieved complete response, a metastatic nodule in the lung, confirmed histopathologically as PTC metastasis, developed in the 17th postoperative year. After high-dose I-131 treatment, I-131 WBS was negative, sTg was <0.1 ng/mL, and normal US and chest CT findings were observed during follow-up. In a patient with anatomical incomplete response, metastatic lymph nodes were detected on US in the first postoperative year, confirmed histopathologically. The patient progressed after metastatic I-131 treatment and was evaluated as iodine-refractory. During oncology follow-up, the patient died (2.7%). ***Conclusion:*** Although TCVPC is defined as an aggressive variant according to the ATA criteria, our findings indicate a high rate of complete response with high-dose I-131 ablation treatment and a low rate of local recurrence, distant metastasis, and mortality during follow-up. According to the literature, a high response rate is due to early diagnosis and developing surgical techniques.

EP-0592

Effectiveness of Empirical High-Dose I-131 Therapy in Patients with Differential Thyroid Cancer with Biochemical Incomplete Response

B. Kocabeyoglu[1]*, M. Guven*[1]*, G. Kavukcu*[2]*, A. Akgun*[1]*;*
[1]*Department of Nuclear Medicine, Ege University, Izmir, TÜRKIYE,*
[2]*Department of Radiology, Ege University, Izmir, TÜRKIYE.*

Aim/Introduction: In this study, we aimed to evaluate the benefit of empirical high-dose I-131 treatment in patients with differentiated thyroid cancer (DTC) with biochemical incomplete response after RAI ablation according to the American Thyroid Association (ATA) classification. ***Materials and Methods:*** Records of 24 patients with DTC who were treated with total thyroidectomy and RAI ablation between 1994-2022 and were given empirical high-dose I-131 treatment due to biochemical incomplete response were retrospectively analyzed. Patients were followed with risk-appropriate follow-up studies and imaging modalities. Treatment success was defined as a 25% decrease in Tg level. ***Results:*** There were 17 women and 7 men, 21 to 71 years of age (mean: 50.6±13.59 years) at the time of diagnosis. Tumor sizes ranged from 0.5 to 9 cm (mean: 4.06±2,41cm). Eleven patients underwent cervical lymph node dissection in addition to total thyroidectomy. The types of primary thyroid cancer were as follows: Papillary carcinoma (n=20), poorly differentiated carcinoma (n=1), Hurle cell carcinoma (n=1), and follicular carcinoma (n=1). Lymphovascular invasion was observed in 16/24, parenchymal invasion in 15/24, extrathyroidal spread in 7/24, and lymph node metastasis in 8/24 of the patients histopathologically. None of the patients had distant metastasis at initial staging. FDG PET/CT imaging performed before empirical high-dose I-131 treatment in 18 patients revealed no findings consistent with metastasis/relapse. The patients received I-131 treatment as a cumulative dose ranging between 300-1275 mCi (mean: 619.5±270.14). The follow-up period was between 24-240 months (mean 103.6 months). The fTg values ranged from 9.7 to 300+ (mean: 73.9±100.41) ng/dl , and from 0.42 to 300+ (mean: 51±96.7) ng/dl respectively before and after the empirical high-dose I-131 treatment. There was a significant decrease in 41.6% (10/24) of the patients . During the follow-up, metastatic lesions (5 lungs, 6 lymph nodes) were detected in 11 (45.8%) patients with imaging studies on the 6th to 120th months. Currently, 58.3% (14/24) of the patients are followed up with an incomplete biochemical response, while 37.5% (9/24) were referred to tyrosine kinase inhibitor therapy due to metastases without I-131 uptake on imaging. One patient died not related to thyroid cancer. ***Conclusion:*** Although there was a significant decrease in fTg level in nearly half of the patients after the empirical high-dose I-131 treatment, the development of structural disease could not be prevented. Therefore, we concluded that its clinical benefit was limited in long-term in patients with differentiated thyroid cancer with biochemical incomplete response.

EP-0593

The evaluation of the value of human recombinant thyrotropin administration for the patients with differentiated thyroid cancer during thyroid hormone withdrawal preparation for high dose radioiodine treatment.

J. Cha*, W. Kang1;*
Department of Nuclear Medicine, Severance Hospital, Yonsei University College of Medicine, Seoul, Republic of Korea, Seoul, KOREA, REPUBLIC OF.

Aim/Introduction: Among the patients with differentiated thyroid cancer (DTC) preparing radioiodine treatment (RIT) with thyroid hormone withdrawal, there were patients whose pre-ablative thyrotropin (TSH) was ≤ 30 μIU/mL. Our purpose was to evaluate the relationship between administration of human recombinant TSH (rhTSH) with excellent response (ER) for these patients. ***Materials and Methods:*** Among the patients who had received initial high dose RIT (100-150 mCi), 218 patients had pre-admission TSH level of ≤ 30 μIU/mL which was done at 2-5 days before RIT. Treatment response was classified according to 2015 ATA guideline. ***Results:*** A total of 218 patients were enrolled. Among them, 145 patients had been received rhTSH administration. The pre-admission TSH level was significantly lower in the rhTSH administration group (15.58 ± 8.12 vs. 26.56 ± 4.42, p<0.001). A total of 129 (59.2%) of patients showed ER. In the logistic regression model analysis, administration of rhTSH (HR 1.86 [CI, 1.04-3.32]; p=0.037) and dose of RIT (HR 1.92 [CI, 1.09-3.37]; p=0.023) were significant independent factors associated with ER. Among the patients who proceed with RIT without administration of rhTSH or postponement of a schedule, TSH level of >35.67 μIU/mL at the day of RIT was significant factor predicting ER (HR 3.23[1.19-8.19]; p=0.022). ***Conclusion:*** Administration of rhTSH was associated with higher rate of ER for the patient who received high dose RIT. For the patients who proceed with RIT without administration of rhTSH or postponement of a schedule, TSH level of >35.67 at the day of RIT was related to higher rate of ER.

EP-0594

Effectiveness of Iodine-131 therapy in patients with hyperthyroidism: The experience in the Nuclear Medicine Department of "Saints Anargyri" Cancer Hospital

S. Saranti*, C. Altani, T. Karianos, K. Kouvelis, M. Bella, E. Taktikou;*
"Agioi Anargyroi" Cancer Hospital, Athens, GREECE.

Aim/Introduction: Iodine-131 (I-131) therapy is a safe treatment for hyperthyroidism concerning either aged patients or younger patients with recurrence after ATD therapy . Dosimetric and fixed I-131 doses have been used. The goal of the I-131 therapy is to cure the patients by a single dose. The aim of this study is the evaluation of the effectiveness of I-131 therapy with a variable iodine dose based on the degree of hyperthyroidism as expressed mainly by the I-131 uptake (4 and 24 hours) in patients with Graves disease and thyroid toxic adenoma. ***Materials and Methods:*** A total of 93 patients were included in the study : Group 1 with 76 patients (11 men, 65 women) with Graves disease and Group 2 with 17 patients (5 men, 12 women) with toxic adenoma. Among the patients with Graves disease, 13 presented with ophthalmopathy (inactive for 8/13 and low to moderate active for 5/13 patients). All patients underwent a Tc99m thyroid scintigraphy during the last 6 months and a recent 4 and 24 hours I-131 uptake 5-7 days after the discontinuation of ATD treatment and with desirable TSH levels <0.1 μIU/ml while I-131 therapy took place under identical conditions . All patients also had a thyroid ultrasonography. The 5/13 patients with active ophthalmopathy underwent prophylactic corticosteroid treatment. The efficacy of I-131 treatment -meaning euthyroid or hypothyroid status- was estimated 1 year after therapy (low term efficacy) and for a 3-10 years period (long term efficacy) for both groups. ***Results:*** For Group 1 the thyroid uptake was 39.44±23.78% at 4 hours and 59.66±24.38% at 24 hours while for Group 2 it was 13.56±9.13% and 31.05±21.61% respectively. The given I-131 dose was inversely proportional to thyroid uptake. Therefore for Group 1 patients (Graves disease) the I-131 therapeutic dose was 14.31±5.69 mCi while for Group 2 patients (toxic adenoma) it was 17.84±2.55 mCi. All patients became euthyroid or hypothyroid within a year. In particular 25/76 (32.89%) patients of Group 1 and 11/17 patients of Group 2 (64.71%) became euthyroid while 51/76(67.11%) patients of Group 1 and 6/17(35.29) patients of Group 2 became hypothyroid . None of the patients demonstrated relapse the following 3-10 years. ***Conclusion:*** I-131 therapy for Graves disease and thyroid toxic adenoma is very effective. According to our study, the calculation of I-131 therapeutic dose on the basis of I-131 uptake is a very determining factor for achievement of a successful therapy.

EP-0595

Prognosis of Differentiated Thyroid Cancer after Reoperation

J. Cha*, W. Kang, H. Cho;*
Department of Nuclear Medicine, Severance Hospital, Yonsei University College of Medicine, Seoul, Republic of Korea, Seoul, KOREA, REPUBLIC OF.

Aim/Introduction: Despite patients with differentiated thyroid cancer (DTC) have excellent survival, recurrence is common. We examined the outcome in patients with DTC after reoperation due to recurrence and assessed the role of radioactive iodine therapy (RIT). ***Materials and Methods:*** We retrospectively reviewed patients who underwent reoperation due to recurrence, and initially received bilateral total thyroidectomy and RIT from March 2006 to March 2020. Clinicopathological characteristics including age, sex, AJCC stage, time to recurrence (the time interval from initial surgery to reoperation), presence of soft-tissue recurrence, ratio of positive to resected lymph nodes, size of recurred lesion, presence of perilesional extension, and the dose of RIT after reoperation were assessed for the risks of recurrence. Hazard ratios (HRs) were estimated from Cox proportional hazards regressions. ***Results:*** During the median follow-up of 28.45 months, 30/150 (20.0%) patients had recurrence. Older age (years, 50.47±12.63 vs. 41.05±13.92; p=0.001), male sex than female (17/30 vs. 34/120; p=0.003), AJCC stage II-IV than stage I (10/30 vs. 16/120; p=0.010), presence of soft-tissue recurrence than absence (6/30 vs. 8/120, p=0.025), and shorter time to recurrence (years, 3.64±2.71 vs. 5.08±2.83; p=0.003) were related to recurrence. In the multivariate Cox-regression analysis, male sex (HR 2.23 [confidence interval (CI), 1.04-4.77]; p=0.039), time to recurrence ≤3.61 (HR 2.85 [CI, 1.28-6.32]; p=0.010), presence of soft-tissue recurrence (HR 3.44 [CI, 1.36-8.70]; p=0.009) were significant independent factors predicting recurrence. The dose of RIT (GBq, <3.7 vs. ≥3.7) after reoperation did not predict recurrence. ***Conclusion:*** Male sex, time to recurrence, and presence of soft-tissue recurrence were associated with recurrence in DTC patients after reoperation. In recurrent disease, the addition of RIT to reoperation does not appear to improve outcome.

EP-0596

Aggressiveness and efficacy of 131I therapy in papillary thyroid carcer with peripheral nerve invasion: a propensity score matching study

X. Xiong*;*
Zhujiang Hospital, Southern Medical University, Guangzhou, CHINA.

Aim/Introduction: To analyze the invasiveness of papillary thyroid cancer with peripheral nerve invasion and the influence of papillary thyroid cancer with peripheral nerve invasion on the short-term curative effect and the long-term curative effect.

Materials and Methods: Logistic regression analysis was used to determine the relationship between clinicopathological factors and short-term efficacy. Survival analysis and Cox regression analysis the relationship between clinicopathological factors and long-term efficacy. Propensity scorematching method was used to equalize the data bias, then the above steps were repeated to further clarify the impact of PNI on the efficacy of PTC. ***Results:*** Efficacy was assessed in 842 patients with a median follow-up of 57 months. According to propensity score matching method, 63 cases were matched in PNI group and nPNI group respectively. It was found that there was no difference in persistence/progression survival between PNI and nPNI group (P =0.88), which was still not an independent factor of short-term and long-term efficacy, while male patients were significantly associated with worse short-term and long-term efficacy. ***Conclusion:*** Peripheral nerve invasion was a predictor of more aggressive disease status at the time of assessment, but was not independent influencing factor of short-term or long-term outcome.

EP-0597

Quantitative analysis of residual thyroid gland radioactive counts and peripheral lymphocyte subsets before and after first radioactive iodine therapy in papillary thyroid carcinoma with Braf mutation

J. Zhang, *H. Liu;*
First Hospital of Shanxi Medical University, Taiyuan, CHINA.

Aim/Introduction: The aim of the study was to investigate the differences of residual thyroid gland I^{131} uptake and changes in peripheral lymphocyte subsets before and after the first radioiodine treatment(RAIT) after total thyroidectomy for PTC patients with Braf mutation. ***Materials and Methods:*** The residual thyroid gland was outlined as region of interest (ROI) on I^{131} Whole-body Scan (WBS) getting the maximum value of the unit pixel. Tumor and serum samples were collected from 37 patients with papillary thyroid carcinoma (PTC). The Braf gene of these patients was assessed by direct DNA sequencing of PTC specimens using quantitative real-time polymerase chain reaction (qPCR). The absolute number and percentage of peripheral lymphocyte subsets (T, B, $CD4^+$ T, $CD8^+$ T, NK, Th1, Th2, Th17, and Treg cells) were measured by flow cytometry. ***Results:*** We found there were no significant difference between $Braf^{V600E}$-mutant and $Braf^{WT}$-mutant PTC patients in residual thyroid gland radioactive counts (P=0.065). More types of lymphocyte subsets (T(P<0.001), B(P<0.001), CD4+T(P<0.001), NK(P<0.05), Th1(P<0.05), Th2(P<0.05), Th17(P<0.05), and Treg (P<0.01) cells) of $Braf^{V600E}$-mutant PTC patients were decreased by RAIT compared to $Braf^{WT}$-mutant PTC patients. In addition, the number of multiple lymphocyte subsets (T(P<0.05), NK(P<0.05), Th1(P<0.05) and Th17 cells(P<0.05)) in the peripheral circulation of $Braf^{WT}$-mutant PTC patients were higher than $Braf^{V600E}$-mutant PTC patients before RAIT and the similar result was also observed after RAIT (T(P<0.01) and Th17(P<0.05)). RAIT inhibited the number of Th1(P<0.01) cells in $Braf^{WT}$-mutant PTC patients to a greater extent. ***Conclusion:*** RAIT inhibited more Th1 cells of $Braf^{WT}$-mutant PTC patients than that for $Braf^{V600E}$-mutant PTC patients, whereas lymphocyte subsets of $Braf^{V600E}$-mutant PTC patients were more broadly inhibited. For PTC patients with different Braf genes, their peripheral blood immune cell subsets respond differently to RAIT and the peripheral blood immune cell subsets of $Braf^{WT}$-mutant PTC patients are more tolerant to RAIT. There might be no differences between the two groups in I^{131} uptake of residual thyroid gland.

EP-0598

Development and validation of a lung metastasis-predicting Nomogram for intermediate- to high-risk differentiated thyroid carcinoma patients

F. Yu, *J. Wang, W. Yang, Z. Yang, W. Ma;*
Xijing Hospital, Fourth Military Medical University, Xi'an, CHINA.

Aim/Introduction: Differentiated thyroid carcinoma (DTC) with distant metastasis led to worse prognosis than those without metastasis. Therefore, early diagnosis of lung metastasis is essential for adequate therapy and better response. This study aimed to develop a clinically predictive nomogram model to predict the lung metastasis probability from DTC with intermediate- to high-risk. ***Materials and Methods:*** 375 DTC patients with intermediate- to high-risk were enrolled in the present study. For the established model's accuracy and clinical application efficiency, patients were randomly separated into training set (70%) and validation set (30%). The univariate and multivariate analysis were conducted to investigate the influence of age, gender, histological type, multifocality, tumor size, T status, N status, AJCC stage, $BRAF^{V600E}$ mutation, postoperative stimulated TSH (ps-TSH) and postoperative stimulated thyroglobulin (ps-Tg) levels before ^{131}I therapy on DTC with lung metastasis. The nomogram was developed based on the training cohort to explore lung metastasis rates for intermediate- to high-risk DTC patients. Finally, the reliability and accuracy of the constructed nomogram was verified in the validation cohort via the calibration, receiver operating characteristic (ROC) curve, and decision curve analysis (DCA). ***Results:*** Univariate analysis showed that histological type, multifocality, tumor size, T status, N status, AJCC stages, $BRAF^{V600E}$ mutation, and ps-Tg levels were significantly associated with lung metastasis from DTC. Multivariate analysis indicated that histological type, multifocality, tumor size, $BRAF^{V600E}$ mutation, and ps-Tg levels were independent predictors of lung metastasis from DTC. The nomogram had a high C-index 0.86 (95% CI: 0.818-0.911), for predicting lung metastasis, which indicated that the models had a high accuracy prediction. The calibration curves demonstrated excellent consistency between the predicted result and the actual probability of lung metastasis in intermediate- to high-risk DTC patients. ROC analysis showed that the AUC for lung metastasis rate in the training cohort was 0.865 and 0.845 in the validation cohort. Also, the DCA curve indicated that this nomogram had better clinical utility in predicting lung metastasis rate in intermediate- to high-risk DTC patients. ***Conclusion:*** Follicular, multifocality, bigger tumor size, BRAFV600E mutation-positive, and higher ps-Tg levels might predict higher rate of lung metastasis from DTC. In addition, a novel nomogram was constructed to comprehensively estimate the lung metastasis probability of DTC patients with intermediate- to high-risk. The model might be able to predict the lung metastasis probability visually and accurately with a higher net benefit.

EP-0599

Second Neoplasms in Patients with Differentiated Thyroid Carcinomas (CDT) Treated With 131I (RAIT).

A. Peña, *I. Vinagre Perez, M. Astudillo Sarmiento, R. Nuñez Muñoz, Y. Carreres Ortega, M. Muñoz del Diego, T. Ruiz Juan, S. Perez Fernandez, E. Rodeño Ortiz de Zarate;*
Hospital Universitario de Cruces, Barakaldo, SPAIN.

Aim/Introduction: To investigate the association of second neoplasms (SN) with RAIT in a cohort of patients with CDT treated at a single tertiary medical center. We have compared these patients with a group of CDT not treated with 131I.

Materials and Methods: We have performed a retrospective study of 505 patients (398 women, 107 men; median age: 48.0 years, 25th: 36.0, 75th: 60.0) with CDT (83.2% papillary, 16.8% follicular). 450 patients received RAIT and 55 patients did not. Patients treated with 131I were divided into 5 groups according to the activity received: 1.110 MBq (55), from 1.147-7.363 (268), 7.400-14.763 (61), 14.800-22.163 (32) and >22.200 (33). For the statistical analysis, the statistical software R Core Team version 4.0.1 was used. ***Results:*** In the total group, the median follow-up was 12.9 years (25th: 8.83, 75th: 20.6). The median time to onset of the second neoplasm was 10.7 years (25th: 4.49, 75th: 18.2) since first doses. Median age at second tumor diagnosis was 68 years (25th: 57.0, 75th: 75.2). In the whole group 76 (15%) SN was diagnosed. RAIT group showed 64 SN (14.2%), distributed as follows: 9 breast cancers, 6 bladder, 3 hematologic, 3 gastric and 43 solid tumors. In the group that did not receive 131I 12 SN was observed (21.8%): 3 breast cancers, 2 bladder, 1 hematologic and 6 solid tumors. We did not find significant differences between the ages of both groups (p: 0.210). When SN were considered, we did not find statistical significant differences between patients treated with RAI and the other group (p: 0.198). We also did not observe differences when comparing the different RAIT groups (p: 0.109). However, when we compare the group of patients treated with less than 22,200 MBq with those treated with more, we did find statistically significant differences (p: 0.042). ***Conclusion:*** RAIT appears not to be associated with an increased risk of SN compared with subjects receiving no RAI treatment (p: 0198). However, the risk appears to be higher in patients treated with more than 22,220 MBq. ***References:*** 1-Edmons CJ, Smith T. The long-term hazards of the treatment of thyroid cancer with radioiodine. Br J Radiol, 59 (1986), pp. 45-512-Hall P, Holm LE, Lundell G, Ruden B. Cancer risk in thyroid cancer patients. Br J Cancer, 64 (1991), pp. 159-1633-Schhumberger M, Vathaire F. Iode 131: utilisation médicale. Effects cancérigènes et génétiques. Annales d'Endocrinologie, 57 (1996), pp. 166-176

EP-0600

Radioiodine Avidity and Prognosis of Diffuse Sclerosing Subtype of Papillary Thyroid Cancer

C. Turkan[1], *G. Güler*[2], *M. Tuncel*[1];
[1]*Hacettepe University Department of Nuclear Medicine, Ankara, TÜRKIYE,* [2]*Hacettepe University Department of Pathology, Ankara, TÜRKIYE.*

Aim/Introduction: Diffuse sclerosing subtype of papillary thyroid cancer(DSS-PTC) is a rare subtype of PTC.It is well known for its aggressive behavior at presentation,but its response to surgery&radioiodine(RAI)therapy and overall prognosis are not well studied.Therefore we aimed to describe its RAI avidity and clinical outcomes. ***Materials and Methods:*** We have retrospectively analyzed the clinical and imaging data of 1751 patients with thyroid cancer.All patients were followed at the Nuclear Medicine Department between 2008-2023. Out of 1751 patients, we had 30 patients diagnosed with DSS-PTC.These patients' clinical and pathological data were recorded from the hospital's database. RAI avidity of these tumours was also analysed in patients with biopsy-proved residual disease during RAI therapy. Patients were followed,and treatment response was evaluated by ATA response criteria. ***Results:*** Out of 30 patients,20(%66) were females.The median-age at the presentation was 27.5(range 15-65).The median follow-up time was 48 months(range:7-154). Seven patients had total thyroidectomy(TT),23 had TT+lymph node dissection(LND) as an initial treatment.Seven patients had additional surgery for persistent disease before RAI-therapy.Histologically,bilateral tumors were present in 53.3%(16/30) of patients, 40%(12/30) had an extrathyroidal extension and 20%(6/30) showed lymphovascular invasion.Patients most frequently staged with pT1b(33.3%,10/30) disease.Twenty-four patients(80%, 24/30) had lymph node(LN) metastasis, extra-capsular extension was documented in 11/24 patients (45.8%) with LN metastasis.One patient presented with lung metastasis,and none developed distant metastasis during the follow-up.All of the patients were treated with RAI at least once with a median activity of 5.55 GBq(3.7-7.4GBq).Five patients(16.7%) had treated with multiple RAIs and median cumulated activity was 11.1 GBq(range 11.1-22.2GBq). During the first RAI-therapy 21 patients(70%) had no evidence of persistent disease other than RAI uptake in remnant thyroid tissue. One patient(3.3%) had RAI non-avid LN metastases,7(23.3%) had RAI avid LN, and 1(3.3%) had RAI avid LN and lung metastases.After the first RAI treatment, two patients(one RAI negative and one RAI positive) underwent LND without additional RAI. Three patients underwent LND and treated with additional RAI. Two patients with LN met and 1 patient with LN and lung met received additional RAI without surgery.Two RAI-positive patients did not receive other therapies during their follow-up.None of the patients died during the follow-up.At the last appointment, 25 patients(83.3%) had excellent response, one patient(3.3%) had a structural incomplete response and 4 patients(13.3%) had indeterminate response. ***Conclusion:*** DSS-PTC may present with advanced disease,mainly with LN metastases, and requires extensive surgical treatment. Despite this presentation, considerable amount of these patients showed RAI avidity, supporting patients' good overall survival.

EP-0601

Analysis of hematological complications in patients with differentiated thyroid cancer

A. Savchenko*;*
V. N. Karazin Kharkiv National University, Kharkiv, UKRAINE.

Aim/Introduction: ***The aim*** of this retrospective case-control study was to analyze and search for predictors of hematological complications of therapy in patients with differentiated thyroid cancer. ***Introduction***. Differentiated thyroid cancer (DTC) is the most common endocrine tumor. The standard of care for DTC is surgery, radioiodine therapy and hormone therapy. Theoretically, each component of the treatment process can cause adverse somatic consequences in future, the study of which can help to prevent and correct them. One of the possible complications arising upon therapy thyroid cancer treatment is anaemia. ***Materials and Methods:*** The study was based on follow-up data of 120 individuals who were undergoing treatment of DTC at the Institute clinic from 2013 to 2017, and underwent regular screening examinations after treatment. The database created for the study contained, digitized arrays of the medical records and its consequences in patients with a follow-up period exceeding 1 year after special treatment. The database contained information on the levels of calcium, the levels of parathyroid hormone, the indicators of a complete blood cell count(after surgery, before and after radioiodine therapy and every next 2 months in the post-treatment monitoring phase, as well as information on age, weight, somatic complications, surgical complications, etc. WizWhy packages (Data Mining category) and the general purpose software package STATISTICA were used to make hypotheses and test them. ***Results:*** The anaemia was observed in 15.8 ± 3.3% of patients (19 individuals). The onset of secondary anaemia was shown to be inducible by post-operative hypoparathyroidism (p

< 0.01, chi-squared Pearson test). Indeed, 15 (30 ± 6.5%) of the 50 patients with hypoparathyroidism (HPT) developed anaemia. On the other hand, only four (5.7 ± 2.8%) of the 70 patients without HPT developed anaemia. The relation between onset of secondary anaemia as an early treatment complication, and reduced blood calcium prior to radioiodine therapy, was also statistically significant (p < 0.01, Mann-Whitney test). Patients who developed anaemia over the course of treatment presented a median calcium level under 2.05 mmol/L prior to radioiodine therapy. Patients that were nonanaemic after radioiodine therapy presented a median calcium level of 2.4 mmol/L beforehand. ***Conclusion:*** These results suggest an association between hypocalcaemia, and onset of secondary anaemia in patients with hypoparathyroidism. Given the probability of asymptomatic hypocalcaemia and post-operative hypoparathyroidism, these observations call for monitoring and therapeutic correction of blood calcium prior to radioiodine therapy.

EP-0602

Comparison of Malignities Accompanying Thyroid Cancer According to RAI Treatment

D. Yüksel, *M. Yücel, O. Yaylalı, T. Şengöz, A. Gültekin, F. S. Şimşek; Pamukkale Universitesi Tip Fakültesi, Denizli, TÜRKIYE.*

Aim/Introduction: It is the view of the relationship between thyroid cancer and other cancer types that are seen together. ***Materials and Methods:*** Data of 2282 patients sent to RAI treatment was reviewed. Among these patients, patients with thyroid cancer and another type of cancer were identified. These patients were examined in two groups; Group1: first non-thyroid cancer-second thyroid cancer; Group2: first thyroid cancer-second non-thyroid cancer. Demographic data, the time between the two cancers, the other cancer type and the RAI treatment, the size of the tumor (<1cm;>1cm), and the presence of metastases were recorded. ***Results:*** In 116 of 2282 patients, another tumor with thyroid cancer was detected. Group 1: 40 patients (15M, 25F) with a mean age of 62±13 years (range: 40-91 years). The interval between two cancers was 37±51 months (range: 0-216 months). 20 of the patients received RAI treatment. While two of those receiving RAI died, 18 were still alive. Metastasis was observed in only one of 20 patients who did not receive RAI treatment, while metastasis of DTC was not observed in 19 patients. While 6 died, 14 are still alive. Group 2: 76 patients (19M, 57F) with a mean age of 61±12 years (range:31-88 years). The time between two cancers was 67±61 months (range: 0-396 months). 70% of the patients (53 patients) received RAI treatment. Of the 7 patients with metastases, 5 were papillary cancer and 2 were follicular cancer. While 13 of the patients who received RAI treatment died, 40 are still alive. Metastasis was observed in 2 of 23 patients who did not receive RAI treatment, and no metastasis of DTC was observed in 21 patients. While 7 patients died of papillary cancer, 16 are still alive. While age (p=0.001) and time between two cancers (p=0.037) were associated with survival, no significant correlation was observed with whether the patient received RAI, the dose of RAI and the number of RAI, the order of occurrence of tumors, the type and size of thyroid cancer, and the metastasis. ***Conclusion:*** Among the cases with secondary cancer after thyroid cancer and the cases with primary non-thyroid cancer, and then secondary thyroid cancer, taking RAI has no effect on survival in gender, thyroidal tumor type, tumor size, order of tumor occurrence and metastasis. This suggests that RAI treatment may not have an additional contribution in terms of secondary cancer development and survival.

EP-0603

Prognostic Associations and Oncological Outcomes Regarding Intermediate Risk Differentiated Thyroid Cancer in Latin-American Population: A 13 Years Follow Up Retrospective Cohort

S. Gonzalez Rueda[1], *A. Calderon Avila*[2], *J. Vargas Ahumada*[1], *P. Casanova Triviño*[1], *F. Garcia Perez*[1], *E. Gomez Argumosa*[1]; [1]*Instituto Nacional de Cancerología, Tlalpan, Ciudad de México, MEXICO,* [2]*Centro Medico Nacional S. XXI, Cuahutemoc, Ciudad de México, MEXICO.*

Aim/Introduction: American Thyroid Association's(ATA) intermediate-risk for well-differentiated thyroid carcinoma(DTC) comprises a wide variety of patients with different risk factors and disease's behaviour;in Latin-American population, it often displays a much darker spectrum of the disease.The main objective of this study was to identify prognostic factors between intermediate risk DTC and American Joint Committee on Cancer(AJCC)prognostic groups,impact of first radioiodine therapy(RAIT),histopathological risk factors and locoregional and distant metastases.Secondary objectives were to determine disease persistency, as well as mean overall survival(OS),disease-free survival(DFS),progression-free survival(PFS) and mortality ratio. ***Materials and Methods:*** We performed a single centre(National Cancer Institute, México), non-randomized,retrospective cohort study, where thirty-two patients with intermediate-risk DTC were recruited from January 2007-2010 and followed-up through 13-years since diagnosis. SPSS V24.0 was used for statistical analysis, linear trend X^2 test was used for differences between frequencies and Kaplan Meier curves were used for OS,DFS and PFS,statistically significant data was consider with a p value of<0.05. ***Results:*** Thirty-two patients who were diagnosed at our centre with DTC, underwent total thyroidectomy and adjuvant RAIT with 3.7-5.5 GBq,after which a post-therapy whole-body-scan was performed,leading to a change in TNM(AJCC groups)staging in 21.9%(6.3%upstaging N1+, 15.6%upstaging M1+).Regarding RAIT effects on thyroglobulin(Tg) behaviour;Tg diminished in 75%, stayed stable in 12.5% and increased in 12.5%. AJCC prognostic groups were associated in both 6° and 8° editions(previously effective vs. currently in use) as follows: I(40.6%), II(12.5%), III(25%),IVA(6.3%),IVC(15.6%)and I(53.1%),II(34.4%),III(3.1%),IVB(9.4%)for 6° and 8° editions, respectively(p=0.019,p= 0.016).Histopathological risk factors evaluated were multifocality, extrathyroid extension(ETE) and surgical margins(R1 and R2) which also were positively associated with locoregional(32.1%) and distant metastases(42.9%).Within time, 25%of patients did not present any type of metastases,while 31.3%developed locoregional lymph-node metastases and 43.8%progressed to distant metastases(p=0.038), the latter distributed as: lungs 9.4%,non-neck lymph-nodes 15.6%,other sites 18.8%(bone, central nervous system, skin)(p=0.05).Disease was persistent in 71.9% of patients.Furthermore,mean OS,DFS and PFS in months were 136,38.21 and 96.59.Mortality ratio was 21.8%. ***Conclusion:*** Intermediate-risk DTC is a broad scope category,nevertheless,regarding Latin-American population,it appears to be a more aggressive entity than historically stated in European and north American populations.First radioiodine dose administered can lead to a change in AJCC staging and diminishes post-surgical Tg importantly.AJCC prognostic groups have a statistically significant association with intermediate-risk patients.Multifocality,ETE and surgical margins were associated with locoregional and distant metastases. Intermediate-risk DTC in Latin-American population has still a good overall prognosis when compared to other neoplasms,yet it does have an elevated persistency percentage,worst oncological outcomes(OS,DFS and PFS) and a higher mortality rate compared to those currently reported worldwide.

EP-0604

Evaluation of the efficacy of treating Graves Disease with low doses of 131-iodine compared to high doses

B. Manzarbeitia Arroba, *G. Guijarro de Armas, D. Rodriguez Oviedo, M. Alvarez Moreno, A. Ortega Valle, L. Castillejos Rodriguez, P. García Alonso, C. Sandoval Moreno;*
Hospital Universitario de Getafe, Getafe, SPAIN.

Aim/Introduction: To compare the efficacy of treating Graves Disease (GD) with low doses of 131-iodine (9mCi) to that of the treatment with high doses (20 mCi) reflected in literature. ***Materials and Methods:*** 107 patients were followed up for 18 months following the administration of 131-I treatment (keeping track of TSH, T4 and T3).Every patient underwent a thyroid scintigraphy using 5 mCi (185 MBq) of 99mTc, with a pattern compatible with GD. 5 days after, a dose of 9 mCi (185 MBq) of 131-I was administered orally.For our study, we considered therapeutic success when patients achieve euthyroidism or hypothyroidism within a year of the treatment. ***Results:*** 75 patients completed follow-up: 21.3% achieved euthyroidism (16 patients), 64% hypothyroidism (48 patients) and 14.7% hyperthyroidism (11 patients), translating a success rate of 85.3%. This result is similar to that described using high doses in literature (with a success rate of up to 86% and a hypothyroidism rate of 64%). ***Conclusion:*** Even though 131-I treatment for GD has been used for a long time, there is no international consensus or clinical guidelines regarding the doses that should be used. In some countries, particularly in America, the doses used tend to be higher than those used in Europe. In our experience, treating GD with low doses of 131-I has a similar success rate than that described in literature with high doses (20 mCi-740 MBq), with a comparable hypothyroidism rate. These findings support the use of low dose therapy in comparison to high doses given the similar efficacy and the superior radioprotection profile.

EP-0605

Evaluation of the efficacy of treating Graves Disease with fixed doses of 131-iodine compared to calculated doses

B. Manzarbeitia Arroba, *G. Guijarro de Armas, M. Alvarez Moreno, D. Rodriguez Oviedo, M. de la Rubia Marcos, A. Herrero Muñoz, C. Paniagua Correa, P. Garcia Alonso, C. Sandoval Moreno;*
Hospital Universitario de Getafe, Getafe, SPAIN.

Aim/Introduction: To compare the efficacy of treating Graves Disease (GD) with empiric fixed doses of 131-iodine to that of the treatment with calculated doses using Marinelli's formula in literature. ***Materials and Methods:*** 107 patients were followed up for 18 months following the administration of 131-I treatment (keeping track of TSH, T4 and T3).Every patient underwent a thyroid scintigraphy using 5 mCi (185 MBq) of 99mTc, with a pattern compatible with GD. 5 days after, a dose of 9 mCi (185 MBq) of 131-I was administered orally.For our study, we considered therapeutic success when patients achieve euthyroidism or hypothyroidism within a year of the treatment. ***Results:*** 75 patients completed follow-up, succeeding in 85.3% of cases (16 patients achieved euthyroidism and 48 hypothyroidism). These results translate a higher success rate than that described in literature using calculated doses (77% success rate in the series described by Zhao et al.), but at the expense of a greater number of hypothyroidism cases (16.6% against our 64%). ***Conclusion:*** These findings support the use of empiric fixed doses of 131-I given that the success percentage is higher than using calculated doses. However, calculated doses might be better to avoid iatrogenic side effects, with a lower rate of hypothyroidism.

EP-0606

Efficacy of empirical radioiodine therapy in patients with differentiated thyroid cancer and elevated serum thyroglobulin without evidence of structural disease

L. Piscopo[1], *E. Zampella*[1], *C. Nappi*[1], *F. Volpe*[1], *V. Gaudieri*[1], *D. Bianco*[2], *F. Volpicelli*[1], *M. Falzarano*[1], *L. Pace*[3], *A. Cuocolo*[1], *M. Klain*[1];
[1]*Department of Advanced Biomedical Sciences, University Federico II, Napoli, ITALY,* [2]*CIRA-Centro Italiano Ricerche Aerospaziali, Capua (CE), ITALY,* [3]*Department of Medicine, Surgery and Dentistry, University of Salerno, Salerno, ITALY.*

Aim/Introduction: In patients with differentiated thyroid cancer (DTC) the treatment of choice consists of surgery followed by radioactive iodine (RAI) therapy. In patients with raising serum thyroglobulin (Tg) during follow-up, empiric RAI therapy may be considered also without evidence of structural disease. However, the survival benefit of this approach remains controversial. We assessed the outcome of patients with DTC according to the administration of empiric ^{131}I therapy. ***Materials and Methods:*** We retrospectively evaluated 1112 patients with DTC submitted to total thyroidectomy followed by remnant ablation with ^{131}I and without distant metastases after the first treatment. Response to initial treatment was assessed 12 months later and 225 patients with detectable Tg (>1 ng/dl) but without evidence of structural disease were enrolled. Patients were categorized according to the administration of empiric RAI therapy. Follow-up was then performed every 6-12 months with serum Tg determination and imaging procedures: the need of additional therapy and the occurrence of structural disease were considered as end-point. Hazard ratios were obtained by Cox regression analyses. Disease free survival analysis was performed by Kaplan-Meier method. ***Results:*** Among 225 patients, 127 (56%) received empiric treatment and 98 (44%) did not. The post-therapy whole-body scan performed at 7 days was positive in 49 (39%) patients; of those, neck uptake was found in 30 (24%) patients, lung uptake in 7 (6%) and bone disease in 2 (2%). During a mean time of 64±53 months, 75 structural events occurred (33% cumulative event rate). The patients with events were older (49±17 vs. 41±18 years, $p<0.01$) and showed higher 12-months Tg values (56±23 vs. 16±34 ng/dl, $p<0.05$) as compared to those without. The rate of events was lower in patients who received empiric therapy (n=34) as compared to those without (n=93) (45% vs. 62%, $p<0.05$). At COX regression analysis 12-months Tg ($p<0.001$) and the administration of empiric therapy ($p<0.01$) resulted independent predictors of events. At Kaplan-Meyer analysis, the worst prognosis was observed in patients who did not receive empiric therapy ($p<0.001$). ***Conclusion:*** In patients with DTC treated with surgery with detectable Tg values at 12-months evaluation but without evidence of structural disease, prognosis seems to be affected by Tg values and empiric treatment. The identification of candidates to this approach may improve prognosis.

EP-40

e-Poster Area

C: Therapy Clinical Study -> C1 Oncological Therapy Clinical Study -> C15 Other Oncological Treatments

EP-0607

Occurence of hematotoxic side effects during 90Y-FAPI-46 radioligand therapy (RLT) in patients with advanced metastatic tumor diseases

K. Pabst[1], *R. Hamacher*[2], *H. Lanzafame*[1], *I. A. Mavroeidi*[2], *T. Bartel*[1], *M. Nader*[1], *S. Bauer*[2], *J. T. Siveke*[2,3,4], *M. Weber*[1], *D. Kersting*[1], *W. Jentzen*[1], *M. Ahrens*[5], *K. Herrmann*[1], *W. P. Fendler*[1], *P. Fragoso-Costa*[1];
[1]*Department of Nuclear Medicine, West German Cancer Center, University Hospital Essen, Essen, GERMANY,* [2]*Department of Medical Oncology, West German Cancer Center, University Hospital Essen, Essen, Germany, Essen, GERMANY,* [3]*Bridge Institute of Experimental Tumor Therapy, West German Cancer Center, University Hospital Essen, Essen, GERMANY,* [4]*Division of Solid Tumor Translational Oncology, German Cancer Consortium (DKTK, Partner Site Essen) and German Cancer Research Center, DKFZ, Heidelberg, GERMANY,* [5]*Medical Clinic II, University Hospital Frankfurt, Frankfurt am Main, Germany, Frankfurt am Main, GERMANY.*

Aim/Introduction: Repeat treatment with 90Y-based FAP inhibitor (FAPI) RLT may lead to disease stabilization in patients with advanced, metastatic tumor diseases. However, some patients demonstrated therapy continuation-limiting hematoxicity. Thus for optimal treatment planning radiotoxicity of the bone marrow needs to be defined. ***Materials and Methods:*** 20 patients that received one ore more cycles of 90Y-FAPI-46 RLT at intervals of 4-7 weeks with available bone marrow dosimetry were included. Hematologic parameters including white blood cells (WBC), neutrophils, lymphocytes, hemoglobin and platelets were assessed (CTCAE criteria) at different time points (at each cycle/between two cycles). Kaplan-Meier curves for occurrence of an adverse event, subdivided by each blood count parameter, were shown. The impact of bone marrow absorbed dose (BMAD) on hematological parameters was investigated using Pearson correlation. Multivariate Cox regression analysis was performed to evaluate the influence of additional factors (hematotoxic therapy within the last month prior to 90Y-FAPI-46 RLT, presence of bone metastases, MTV (metabolic tumor volume) of bone metastases, baseline toxicity, and ≥4 hematotoxic therapies) on occurring hematologic AEs. MTV of bone metastases was measured in the performed 68Ga-FAPI-46 PET/CT prior to RLT with a predefined VOI (volume of interest) consisting of 41% threshold from SUVmax. ***Results:*** Under and/or after treatment n=13/20 patients (65%)/n=6/20 (30%) demonstrated at least one hematological AE/SAE (CTCAE ≥ grade 3: thrombocytopenia: n=3/20 (15%), lymphocytopenia: n=3/20 (15%), neutropenia: n=1/20 (5%), leucopenia: n=1/20 (5%)). N=16/20 (80%) showed baseline hematotoxicity. Bone metastases were present in n=10/20 (50%) patients with an MTV spanning from 0.6 to 485.54 cm^3. N=8/20 (40%) patients received ≥4 prior hematotoxic therapies, n=11/20 (55%) received hematotoxic therapy within the last month prior to 90Y-FAPI-46 RLT. Pre-treatment with hematotoxic therapy within the last month prior to RLT showed a significant association with the occurrence of hematologic AE (p=0.011). The cumulative median BMAD was 0.46 Gy (± 0.29 Gy, range: 0.11-0.98 Gy). No significant correlation was observed between BMAD and changes in the aforementioned hematological parameters (WBC: p=0.49, hemoglobin: p=0.26, platelets: p=0.98, neutrophils: p=0.51, lymphocytes: p=0.72). ***Conclusion:*** Administration of 90Y-FAPI-46 RLT in patients with advanced, metastatic tumor diseases was associated with a low rate of new hematotoxic events. Previous hematotoxic therapy was associated with occuring hematological AE. Under dosimetry guidance, BMAD was not associated with hematotoxicity.

EP-0608

Feasibility of high-dose targeted radiation with I131-apamistamab in patients with relapsed/refractory AML: Dosimetry and radiation safety experience from the phase 3 SIERRA trial

N. Pandit-Taskar[1], *K. Prasad*[2], *L. Chen*[3], *T. Senglaub*[4], *M. Zgaljardic*[5], *P. Brodin*[6], *B. Serencsits*[7];
[1]*Molecular Imaging and Therapy, Memorial Sloan Kettering Cancer Center, New York, NY, UNITED STATES OF AMERICA,* [2]*University of Pennsylvania Health System, Philadelphia, PA, UNITED STATES OF AMERICA,* [3]*Banner MD Anderson Cancer Center, Gilbert, AZ, UNITED STATES OF AMERICA,* [4]*Medical College of Wisconsin, Milwaukee, WI, UNITED STATES OF AMERICA,* [5]*Weill Cornell Medical Center, New York, NY, UNITED STATES OF AMERICA,* [6]*Actinium Pharmaceuticals, Inc., New York, NY, UNITED STATES OF AMERICA,* [7]*Memorial Sloan Kettering Cancer Center, New York, NY, UNITED STATES OF AMERICA.*

Aim/Introduction: High-dose targeted radiation as induction and conditioning prior to allogeneic hematopoietic cell transplant (aHCT) was investigated using I131-apamistamab delivered with a personalized prescribed activity ranging from 11.1 GBq to 38.1 GBq. Strategies were devised in collaboration with nuclear medicine and radiation safety staff at treating institutions for dosimetry, safe administration, patient isolation and minimizing exposure. Here, we present our experience related to dosimetry and radiation safety, demonstrating the feasibility of delivering this treatment in various settings. ***Materials and Methods:*** Patients with active relapsed/refractory AML were randomized to receive either I131-apamistamab or conventional care (CC). Patients on the I131-apamistamab arm received study drug in combination with fludarabine and total body irradiation (2 Gy) followed by aHCT. Patients on the CC arm not achieving disease control were eligible to cross over to I131-apamistamab. Personalized dosimetry was performed based on gamma camera imaging (0h, 24h, 72-96h) following tracer dose administration and the therapeutic dose was administered intravenously over a median of 5h. Patients remained in radiation isolation for 3-7 days after treatment, with training for infusion procedures, room preparation, safety precautions and site-specific evaluations conducted at each participating site, including the use of mobile shielding. ***Results:*** Of 153 patients enrolled in the SIERRA trial, a total of 106 patients received the therapeutic dose of I131-apamistamab, 40 of which were crossover patients. All patients that received the therapeutic dose went on to receive aHCT. Patients were treated at 22 participating sites, 38% with lead-lined rooms, 33% with partially shielded rooms and 29% with non-shielded rooms. Median administered activity was 24.6 GBq in the I131-apamistamab arm and 22.7 GBq for the crossover patients, with respective absorbed bone marrow doses of 16 Gy (range: 5 to 45 Gy) and 16 Gy (range: 6 to 40 Gy). From dosimetry analyses, I131-apamistamab cleared from the body with a median effective half-life of 42.5h (IQR: 39.2h to 51.3h). Radiation exposure to staff caring for these patients measured at 5 participating sites

demonstrated average exposure of 0.09 mSv, well below the 50 mSv/yr limit for radiation workers, and adjacent public areas were successfully below regulatory limits of 0.02 mSv/hr. ***Conclusion:*** Safe administration and delivery of high-dose targeted radiation using I131-apamistamab was demonstrated with minimal exposure to staff caring for these patients, despite high activities of I-131. Furthermore, the feasibility of delivering this treatment was demonstrated in a variety of clinical settings, with or without lead-lined rooms.

EP-0610

SSTR-directed Peptide Receptor Radionuclide Therapy in recurrent Meningioma

P. Hartrampf[1], *M. Müller*[1], *S. E. Serfling*[1], *A. K. Buck*[1], *B. Polat*[2], *R. A. Werner*[1];
[1]*Klinik und Poliklinik für Nuklearmedizin, Würzburg, GERMANY,*
[2]*Klinik und Poliklinik für Strahlentherapie, Würzburg, GERMANY.*

Aim/Introduction: Given high levels of SSTR expression in meningioma in an ex-vivo setting, SSTR-targeting peptide receptor radionuclide therapy (PRRT) may emerge as a suitable therapeutic option for patients after surgery or radiotherapy. We aimed to determine prognosticators for overall survival (OS) in patients with recurrent meningioma under PRRT and to characterize treatment-related toxicity. ***Materials and Methods:*** We identified 35 patients with recurrent meningioma treated with PRRT. We investigated SSTR-PET positive tumour burden at baseline, along with aspartate aminotransferase (AST), alkaline phosphatase (AP), lactate dehydrogenase (LDH) and C-reactive protein (CRP). To determine haemato- and nephrotoxicity, haemoglobin, leukocytes, platelet counts (n=33) and eGFR (n=32) at baseline and after therapy were also recorded. Adverse events were classified according to the Common Terminology Criteria for Adverse Events (CTC) v5.0. We performed univariable cox regression analysis, followed by Kaplan Meier analyses. ***Results:*** Median age of patients was 63 years (30-84). Most patients were diagnosed with WHO grade II (15/35, 43%), followed by WHO I (12/35, 34%; WHO III, 6/35 [17%]; unknown, 2/35 [6%]). A median of two (1-8) cycles of PRRT were administered (cumulative activity: 15.6 GBq (6.9-60.3)). Median SSTR-positive volume was 14.7 (0.42-217.5) ml (median SUVmax, 24.3 [5.3-297.1]). Median decreases of 26%, 21% and 5% were seen in leukocytes, platelets and haemoglobin, while eGFR increased by 2%. CTC grade III/IV toxicity for leukocytopenia, thrombocytopenia and anaemia occurred in 6%, 3% and 3%, respectively. No CTC grade III/IV nephrotoxicity was recorded. Radiographic progression was documented in 4/12 (33.3%) patients with WHO I (median after 17 months), in 10/15 (66.7%) patients with WHO II (after 17 months) and 6/6 (100%) patients with WHO III (after 4.5 months). Median OS was 49 months, while 14/35 (40%) patients died. Univariable analysis provided only LDH (per U/l, HR, 1.008, 95% CI 1.000-1.015; P=0.03) and WHO grade (per grade, HR, 2.3, 95% CI 1.03-5.6; P<0.05) as prognosticators for OS. WHO grade III patients (17 months) exhibited shorter median OS relative to WHO grade I (56 months, HR 0.25, 95% CI 0.04-1.40; P=0.02) and II (47 months, HR 0.3, 95% CI 0.06-1.57; P=0.04), while no difference was seen between WHO grade I and II (P=0.6). ***Conclusion:*** PRRT in patients with recurrent meningioma achieves considerable anti-tumour effects with an acceptable safety profile. Baseline LDH and WHO grade showed prognostic ability for survival, while PET-based quantification failed.

EP-0611

Sequential treatment of High-risk Neuroblastoma combining I-131 MIBG high-dose and Topotecan. First experience

N. Orrego, *S. Prado-Wohlwend, J. Balaguer-Guill, I. Torres-Espallardo, M. Part-Lopez, C. Guerrero-Calatayud, J. Cañón-Sanchez, S. Montesinos-Gonzalez, P. Bello-Arques;*
Hospital Universitari i Politecnic La Fe, Valencia, SPAIN.

Aim/Introduction: Neuroblastoma is the most common extracranial tumor in childhood. High risk neuroblastoma (HR-NB) is related to those patients older than 1 year, with a metastatic debut, stage 2, 3, or with N-Myc amplification. 5-year survival rate in this group does not exceed 50 %. Current treatment includes an induction therapy before surgery, conditioning chemotherapy followed by haematopoietic progenitor rescue and treatment of minimal residual disease. The response rate is between 60-80% of all patients, but many patients relapse. The aim of this study is to describe our experience by treating children with HR-NB combining high-dose I-131 MIBG and topotecan followed by autologous progenitor cell transplant, as an intensification phase after induction therapy with busulfan and melphalan. ***Materials and Methods:*** Retrospective analysis of patients treated with high-dose 131-I-MIBG and topotecan, from 2017 to date. 85% of cases were male, with metastatic disease at diagnosis, none had amplified N-myc. 57.14% of primary tumor were abdominal/adrenal, 28.57% paravertebral and 14.29% pelvic. The average age at diagnosis was 6 years (2.6-15.6) and at treatment administration was 10 years (4.7-18.8). Statistical analyses were performed using IBM SSPS Statics version 29. ***Results:*** From 2017 to 2023, 7 patients with HR-NB underwent sequential treatment with high-dose I-131 MIBG and Topotecan as an intensification phase of their treatment. Administered average activity was 10.07 MBq (7.42-11.99), with a whole-body absorbed dose of 1.476 Gy (0.74-2.323) after first treatment and 8.84 MBq (4.22-12.99), with a whole-body absorbed dose of 1.145Gy (0.603-1.711) after the second. After completion of 2 cycles, the average whole-body absorbed dose was 2.65 Gy (1.463-3.990). With an average follow-up of 31.28 months (0-74), the disease-free survival time was 16.7 months. No treatment-related deaths were observed. The most frequent toxicity was gastrointestinal and the highest grade toxicity (3-4) was haematological (20% and 28% after first and second treatment respectively) and one case of neurological toxicity (autoimmune encephalitis). We have no reported cases of treatment-associated hypothyroidism. ***Conclusion:*** Sequential administration of high-dose 131I-mIBG and topotecan followed by autologous progenitor cell transplant after induction therapy is safe, complex but feasible, and improve the disease-free survival in patients with advanced neuroblastoma. More studies are necessary, especially compared to other myeloablative treatments.

EP-0612

New development Paradigm for Rare CNS cancers: Real World Data (RWD) Compared to Ongoing Safety and Feasibility Results from a Phase 1/2 Clinical Trial of 186RNL (Rhenium-186 Nanoliposome) (186Re) Obisbemeda in Recurrent Glioma: The ReSPECT-GBM Trial

N. LaFrance[1], *A. Brenner*[2], *J. Michalek*[2], *T. Patel*[3], *A. Bao*[4], *W. Phillips*[2], *M. Hedrick*[5], *M. Moore*[5], *J. Weinberg*[6], *M. Youssef*[3], *J. Floyd*[2];
[1]*Norman LaFrance, Austin, TX, UNITED STATES OF AMERICA,* [2]*UT Health San Antonio, San Antonio, TX, UNITED STATES OF AMERICA,* [3]*UT Southwestern Medical Center, Dallas, TX, UNITED STATES OF AMERICA,* [4]*Case Western Reserve University, Cleveland, OH, UNITED STATES OF AMERICA,* [5]*PLUS Therapeutics, Austin, TX, UNITED STATES OF AMERICA,* [6]*MD Anderson Cancer Center, Houston, TX, UNITED STATES OF AMERICA.*

Aim/Introduction: ^{186}RNL is a BMEDA-chelated ^{186}Re encapsulated in nanoliposomes delivered via convection enhanced delivery (CED) with ongoing Phase 1 dose escalation and Phase 2 study. Unique ^{186}Re properties (1-MeV β-decay and simultaneous γ-decay of 137 keV, allows therapy and imaging and has achieved durable, localized tumor retention, and high absorbed radiation doses[ARD]. We present updated results from ongoing trial ReSPECT-GBM (NCT01906385) with comparison to RWD in ^{186}RNL in recurrent glioma patients. ***Materials and Methods:*** An analysis [data sourced from the Medidata Enterprise Data Store (MEDS)] was performed to determine if bevacizumab patients is an appropriate external control group for evaluating the treatment effect in current and upcoming CED trials. Deidentified patient-level historical clinical trial data, study and patient-level data from historical rGBM CED studies [D'Amico, J Neurooncol 2021] and an on-going Plus Therapeutics CED study were analyzed. Aggregate summary statistics were based on combined study- and patient-level data using weighted (by sample size) means, median of medians, incidence and OS rates (completed studies). Statistical analyses by log rank, proportional hazards and accelerated failure time (AFT) models were performed on the Phase 1 cohorts leading to the Phase 2 dose selection and trial initiation. ***Results:*** Twenty-one adult recurrent glioma patients across the first six dose-cohorts were analyzed. Single ^{186}RNL dose ranged from 1.0-22.3 mCi in a volume of 0.6-8.8 mL, CED administration rate was 5-20 µl/min using 1-4 catheters and was well-tolerated. For the Phase 1 cohorts[6] leading to the ongoing Phase 2, three patients remain alive and 18 have died. The median overall survival (N=21) by log-rank analysis for patients receiving AARD of >100 Gy was 30 months. Proportional hazards and AFT modeling demonstrated AD and %tumor treated significantly correlated with OS. For RWD control analysis, all cohorts reported similar characteristics over a broad set of demographics, disease characteristics and medical history [age, race, gender, recurrence, grade and prior treatment]. While the baseline composition of rGBM study patients world-wide has changed over time to enroll healthier patients (ECOG=0) with smaller tumors, median OS has remained constant (bevacizumab:7.9 months; CED studies:8.4 months). ***Conclusion:*** Single-dose ^{186}RNL by CED in adult patients with rGBM achieves high absorbed doses without significant toxicity, is well tolerated, with favorable overall survival compared to RWD controls. We are enrolling two studies in rGBM: larger tumors in the Phase 1 dose- escalation [>20 cm^3]; Phase 2 [tumor ≤20 cm^3]. Developing and Current results will be presented.

EP-0613

Peptide Receptor Radionuclide Therapy In Advanced Refractory Meningiomas: Tocicixy And Efficacy In A Long Therm Follow Up

S. Severi[1], *I. Grassi*[2], *A. Bongiovanni*[2], *A. Sarnelli*[2], *V. Di Iorio*[2], *N. Ranallo*[2], *F. Matteucci*[2], *I. Marini*[2], *E. Amadori*[2], *I. Azzali*[2], *N. Riva*[2], *L. Gurrieri*[2], *S. Nicolini*[2], *P. Caroli*[2], *M. Sansovini*[1];
[1]*IRST IRCCS, Meldola, ITALY,* [2]*IRST IRCCS, Forlì-Cesena, ITALY.*

Aim/Introduction: Recurrence of meningiomas deserve specific attention for the lack of active therapies after surgery and radiotherapy. The high frequency of somatostatin receptors (SSTr2) overexpression onto the cell membrane of these tumors open the way for a peptide receptor radionuclide therapy (PRRT). Diagnosis with 68Ga-Dota octreotide and therapy with 90Y/177Lu Dota-octreotide is currently possible within experimental protocols or as compassionate use. ***Materials and Methods:*** From October 2009 to October 2021 we enrolled meningioma patients highly positive to 68Ga-dotatoc PET and in radiological recurrence after standard therapies. They were treated with 90Y-dotatoc (dosage of 1.1 or 5.5GBq) or with 177Lu-dotatate (dosage of 3.7 or 5.5GBq) according to clinical status, in a mean 4 cycles. ***Results:*** Of 42 patients treated, 5 received 90Y-Dotatoc with a cumulative activity of 11.1GBq and 37 patients 177Lu Dotatate with a cumulative activity of 22GBq. Overall disease control rate (DCR) was 57% with better outcomes for younger age and moderate disease burden. In a median follow up of 63 months, mPFS was 16 months and mOS was 36 months. A re-challenge 177Lu-dotatate was carried out in 6 patients with a median injected activity of 13 GBq in mean 5 cycles. In a 75.8 months follow up we demonstrated a mPFS of 6.5 months and a mOS 17 months. PRRT was well tollerated as favored by personalized radiopharmaceutical dosages; only one patient discontinuing treatment due to G3 platelet toxicity. In the 6 re-challenged patients we had a rapidly transient G2 toxicity on neutrophils in one patient. ***Conclusion:*** PRRT in patients with advanced meningiomas overexpressing SSTr2 receptor was well tolerated, showed a 57% DCR and has a potential re-challenge option. The therapy efficacy can improve if applied at earlier stage. Due to the very low toxicity, further studies to explore possible association with other treatment are warranted.

EP-0614

64CuCl2treatment: preliminary data on recurrent glioblastoma patients

D. Stanimirovic[1], *D. Milakovic*[1], *J. Mijatovic*[1], *I. Rakita*[1], *G. Vuleta*[1], *M. Basile*[2], *S. Valentini*[2];
[1]*University Clinical Center of the Republic of Srpska, Banja Luka, BOSNIA AND HERZEGOVINA,* [2]*A.C.O.M.-Advanced Center Oncology Macerata-S.R.L., Montecosaro (MC), ITALY.*

Aim/Introduction: Glioblastoma (GBM) is one of the most prevalent and aggressive malignant brain tumors in adult patients, usually with poor prognosis and low survival rates. Despite multimodality treatment efforts in the past two decades, the overall survival has not significantly increased and the disease relapse is inevitable. $^{64}CuCl_2$ is an innovative theragnostic agent and this study aimed to determine the maximum tolerated dose (MTD) based on dose-limiting toxicity (DLT) and the preliminary efficacy of $^{64}CuCl_2$ treatment. ***Materials and Methods:*** Adult patients belonging to the class of recurrent/progressive GBM after standard treatments (surgery, radiotherapy, chemotherapy) have been recruited. All patients performed a $^{64}CuCl_2$ PET/CT scan for treatment selection. The therapy consisted of 7 doses administered once a week. Six patients received escalated doses in stage 1 (3+3 scheme), according to smoothed modified Fibonacci sequence, and were evaluated to determine the DLT/MTD and biodistribution by analysing PET/CT scans at different time points (1h, 4h, 24h, 48h). Patients included in stage 2 have received fixed doses and 5 patients were evaluated for response to treatment by MRI assessment according to RANO criteria. ***Results:*** Stage 1 evaluation has shown that $^{64}CuCl_2$ uptake increases up to 4h post-injection and decreases thereafter in the liver, followed by kidney and L2-L4 regions. However, no treatment related toxicities were registered associated to liver/kidney and red marrow distribution. 20 Adverse Events were detected and 4 SAE occurred not correlated to drug administration. No DLT occurred and the positive safety profile allowed to select the highest dose tested in stage 1 to proceed with the stage 2. Data cut-off was performed after 5 patients have been included in stage 2. Treatment response evaluation, in term of anti-tumor activity of $^{64}CuCl_2$ measured by MRI, showed that more than 50% of patients resulted as responders (stable disease,

partial or complete response) to $^{64}CuCl_2$ treatment. ***Conclusion:*** These preliminary data have demonstrated a favourable dosage scheme for $^{64}CuCl_2$ treatment of recurrent GBM patients both from a safety and an efficacy point of view, encouraging the development of this radiopharmaceutical.

EP-0615

Substantiation of an individual therapeutic dose of 153Sm-oxabiphor for the treatment of bone metastases

G. Grushka[1], *L. Stadnyk*[2], *V. Bobrova*[2];
[1]*Kharkiv National Medical University, Kharkiv, UKRAINE,* [2]*Grigorev Institute for Medical Radiology and Oncology, Kharkiv, UKRAINE.*

Aim/Introduction: The majority of recommendations for the management of radionuclide therapy pain bone metastases do not provide individual dosimetric planning for patients. Individualized activity allows to optimize the radionuclide bone therapy (RBT) and prevents hematological toxicity. Aim of the investigation was optimization of the intravenous dose of ^{153}Sm-oxabiphor for limitation of the red bone marrow absorbed dose (RBMAD) up to about 2 Gy. ***Materials and Methods:*** 26 patients with painful bone metastases received 39 courses of RBT. The average value of administered activities of ^{153}Sm was 2630.0 ± 970.0 MBq. Using the external body radiometry the coefficient of retention of ^{153}Sm in bone tissues (K_{ret}) for all patients was determined using the external body dosimetry which was carried out not less than 3 times during three-four days: the first - 0,5 hour after the first injection. Coefficients of variability of the volume of trabecular bone of the L_2-L_4 vertebra (K_{L2-L4}) for each patient were calculated using CT-exams. Estimation of cumulative activity in bone tissues and RBMAD and their correlation with the values of individual K_{ret} and K_{L2-L4} was performed. ***Results:*** RBMAD is associated with the individual pharmacokinetics of ^{153}Sm-oxabiphor and the anatomical features of patients. The obtained data during the first course of RBT allowed to take into account the peculiarities of the distribution of radiopharmaceutical in the skeleton and red bone marrow for each patient separately and analysed the dependence of the RBMAD from the product of the assigned optimal specific activity (A_{spec}), K_{ret} and K_{L2-L4} for each patient. The correlation coefficient between these parameters was R2 = 0.96. The RBMAD was determined with the calculation of the values of the individual K_{ret} and K_{L2-L4} during the first course of the radionuclide therapy. The RBMAD ranged from 0.45 to 3.56 Gy and averaged (1.49 ± 0.89) Gy. In most cases (83%), the RBMAD did not exceed the allowable limit of 2 Gy. This was found the analytical correlation for the estimation of the value of optimal specific activity (A_{spec}) by ^{153}Sm for the following RBT courses with the value of the limit of RBMAD - 2000 mGy. ***Conclusion:*** The prognostic assessment of the RBMAD at the first course of the radionuclide bone therapy allows optimize the individual activity of ^{153}Sm-oxabiphor for next courses of the RBT and prevents hematological toxicity. This can make the significant contribution to improving the effectiveness of bone metastases treatment.

EP-41

e-Poster Area

C: Therapy Clinical Study -> C2 Non-Oncological Treatments -> C21 Non-Oncological Treatments (including Thyroid Benign)

EP-0616

Radiosynoviorthesis of debilitating joints in haemophilia and rheumatoid arthritis : a local South East Asian hospital experience

K. Loke[1], *W. Tay*[1], *L. T. Cheng*[2], *C. Ng*[1], *H. Low*[1];
[1]*Singapore General Hospital, Singapore, SINGAPORE,* [2]*National University Hospital Singapore, Singapore, SINGAPORE.*

Aim/Introduction: Aim/Introduction: RSO is an efficacious treatment in symptomatic haemophilia and rheumatoid arthritis patients who are not well controlled with systemic or local targeted treatments. RSO is well tolerated and effective especially in patients who are treated in the early disease course with mild to moderate joint destruction[1,2]. ***Materials and Methods:***The Department of Nuclear Medicine and Molecular Imaging, Singapore General Hospital has been treating patients with RSO since 2013. To assess treatment response, clinical assessment of joint swelling, synovial thickening and symptomatology by way of pain score using VAS was used. ***Results:***Steadily increasing procedure numbers are possibly due to increased clinician and patient awareness. Since then, an annual average of 3-4 RSO procedures are performed. From 2018 to 2023, 24 RSO have been performed (11 knee, 11 ankles, 1 elbow and 1 wrist joint).Almost all patients reported an improvement of joint swelling/stiffness and/or pain reduction as early as 2-4 weeks following RSO of target joint. The duration of symptom control was from 6 to 20 months. Several patients reported symptom improvement allowing resumption of daily activities or work. Interestingly, it was noted that 2 patients experienced good response to initial target joint injections and returned to the clinic requesting for RSO of other affected joints. ***Conclusion:*** RSO is an uncommon well-tolerated and effective intraarticular nuclear medicine procedure for haemophilia and rheumatoid arthritis patients with debilitating joint symptoms[3]. An increasing number of patients with debilitating joints were treated within our department especially within the last 5 years from 2018 to 2022. RSO in these patients has been noted to improve patients' symptoms and in some patients, allowed them to return to previous functional status and regain employment. ***References:*** References:1. Deutsch E, Brodack JW, Deutsch KF. Radiation synovectomy revisited. Eur J Nucl Med. 1993;20(11):1113-27.2. Van Vulpen LFD, Thomas S, Keny SA, Mohanty SS. Synovitis and synovectomy in haemophilia. Haemophilia. 20203. W.U. Kampen, B. BoddenbergPätzold, M. Fischer, M. Gabriel, R. Klett, M. Konijnenberg, E. Kresnik, H. Lellouche, F. Paycha, L. Terslev, C. Turkmen, F. van der Zant, L. Antunovic, E. Panagiotidis, G. Gnanasegaran, T. Kuwert, T. Van den Wyngaert. The EANM guideline for radiosynoviorthesis. European Journal of Nuclear Medicine and Molecular Imaging (2021) 49:681-708

EP-0617

The Impact Role of High Specific activity of Radioactive Iodine 131I in Hyperthyroidism Response Rate

M. Al Rowaily[1], *M. Al-Qahtani*[2];
[1]*KFSHRC & Alfaisal University, Riyadh, SAUDI ARABIA,* [2]*KFSHRC, Riyadh, SAUDI ARABIA.*

Aim/Introduction: The mechanism of action of RAI is physiological. Iodine is the precursor of thyroxine. The radioactive form of iodine is taken up by iodide transporter of the thyroid the same way as natural iodine and is similarly processed. The beta particle destroys the follicular cell, gradually leading to volume reduction and control of the thyrotoxicosis however high specific activity is mandatory to achieve high response rate. ***Materials and Methods:*** In our study the choice made to use high dose of Iodine-131in purpose to achieve high cure rate. during year 2002-2010 (538) patients were treated with a response rate range from 70%-80% and 20%-30% needed a second dose of 131I-RAI who achieved a cure after second dose. in 2010-2011 response rate was low about 50%, more than 20 patients (40-50%) needed second dose of therapy. ***Results:*** After investigating and searching for the causes to this drop, we found that all these patients have been received high dose of Iodine-131 post calibration in other ward low specific activity. Shelf life usually 3 weeks 5 days before calibration and Two-weeks post calibration. A new role was stablished in our department after that no 131-Iodine should be given post calibration for Graves patient. A year after only one patient didn't respond to the therapy and after investigation found that the patient prescribed dose was 15 mCi who has received16.2 mCi using a 25 mCi capsule 5 days post calibration administered by new employee. Since that time more than 90% the response rate. ***Conclusion:*** High specific activity of I-131 is very crucial therefore always use pre-calibration Doses. Patient preparation ensures efficacy of RAI and reduces the potential complications. Important issues like the consent procedure, pregnancy and timing of medication.

EP-0618

Plasma Volume Deficit estimation using Cr-51 labelled RBC in Acute Pancreatitis Patients

N. Kumar, *S. Ballal, M. P. Yadav, M. Tripathi, C. Bal;*
All India Institute of Medical Sciences, New Delhi, India, New Delhi, INDIA.

Aim/Introduction: Acute pancreatitis (AP) is the glandular parenchymatous inflammation of retroperitoneal organ that may involve multiple organ dysfunction if not treated, which may lead to death. Hypovolemia is the major complication that that may occur secondary to vomiting, reduced oral intake, third space extravasation, respiratory losses and diaphoresis. Therefore, patient's hydration is required to resolve the hypovolemia. Thus, early fluid therapy is the cornerstone of the treatment of acute pancreatitis and is universally recommended. There is a lack of consensus and proper guidance regarding the amount of fluid deficit in AP patients. The present work was aimed to estimate plasma volume (PV) deficit using Cr-51 labelled RBC in acute pancreatitis (AP) patients thereby establishing its clinical utility and also enabling institution of definitive therapeutic regimens early on, as treatment protocols differ widely depending on etiology of the abdominal pain and fever. ***Materials and Methods:*** Approximately 15-20 ml of blood was withdrawn from the patient and added to a sterile multi-injection bottle containing 4-5 ml of ACD solution. In-vitro labelling of RBC's was performed with approx. 100µCi of Cr-51 sodium chromate at room temperature. 10mL of tagged red blood cell (RBC) suspension mixture was reinjected intravenously as such and the remaining tagged RBC suspension was used to determine standard samples such as A, B and C. All counting samples were made in total volume of 4mL. Again, approx. 20 mL of blood was withdrawn from a different vein at 20-25min post-injection that was used to make other standard samples such as D, E and F. Counting was done with well counter (Biodex Atomlab 950 thyroid uptake system with optional well counter) in Cr-51 window. Background subtracted counting values were used to determine red cell volume. ***Results:*** Twenty six (17 men; 9 women) AP patients with mean age 41.23±15.38 years were screened and admitted within 72 hours of the onset of AP. The median ideal PV at equilibrium was 2905 mL, range (1883-3916 mL). The median intravascular PV deficit was 1568 ml. There was significant reduction in median ideal PV of 2905 mL to estimated median PV of 1587 mL with P value = 0.0002. ***Conclusion:*** All patients were revived by replacing the deficit volume with fluids and were recovered. Hence, the recovery of the patient validated our PV estimation results.

EP-0619

Urinary Excretion Rate of I-131 During Treatment of Benign Thyroid Disease

U. Beguš[1], *P. Tomše*[2], *K. Bajuk Studen*[2], *E. Pirnat*[2], *S. Gaberšček*[2], *K. Zaletel*[2];
[1]*Faculty of Mathematics and Physics, University of Ljubljana, Ljubljana, SLOVENIA,* [2]*Department of Nuclear Medicine, University Medical Centre Ljubljana, Ljubljana, SLOVENIA.*

Aim/Introduction: The use of radioactive iodine (I-131) is an effective treatment for benign thyroid disease. It selectively destroys hyperfunctioning thyroid tissue by emission of beta radiation, and simultaneously emits gamma radiation. However, during treatment, the significant excretion of the administered activity in the urine poses a radiation risk to personnel and the environment. Therefore, appropriate radiation safety protocols must be followed when treating patients, especially those wearing diapers. Since there is little literature on the urinary excretion rate of I-131 in patients treated for benign thyroid disease, we aimed to investigate this issue. ***Materials and Methods:*** We performed a study in hospitalized patients with hyperthyroidism due to thyroid autonomy or Graves' disease. Urine samples were collected 2 and 4 hours after oral administration of the I-131 capsule and at the time of patient discharge from the hospital (24, 48, or 72 hours after administration). The time and volume of urine collection were recorded, and 0.05 ml of each urine sample was diluted with 0.95 ml of saline. We measured the count rate (cps) in the diluted samples with a gamma counter, and the accuracy of the sample activity (MBq) was obtained by calibrating the gamma counter beforehand, namely by measuring 6 samples of an I-131 solution with known activity. Linear fitting provided a calibration factor to calculate the percentage of excreted activity in each urine sample. ***Results:*** We collected urine samples from 34 patients (8 men, 26 women) aged 26 to 82 years (mean age, 62.5±13.2 years) who were administered a median dose of 890 MBq (730-1095 MBq). The median volume of urine samples collected was 200 ml (20-540 ml). A linear fit across gamma count measurements yielded a relation of activity = 2.46 * counts with 41% efficiency. Urine samples collected 2 and 4 hours after therapy showed substantial excretion of administered I-131 (7.9±3.6% (1.9-16.5%) and 7.3±4.6% (0.2-16.4%), respectively), whereas excretion 24, 48 and 72 hours after administration was low (1.08±0.51%, 0.85±0.90%, and 0.18±0.14%, respectively). Paired t-test showed significant

differences between samples collected 2 or 4 hours after therapy and at discharge (p<0.001), but not between the first two samples collected (p=0.46). ***Conclusion:*** Our finding that urinary I-131 excretion is high immediately after administration and decreases significantly after only 24 hours may improve patient care by providing more accurate radiation safety guidelines. These will contribute to lower radiation exposure to themselves and those around them.

EP-0620

Quality of life after radioisotope synoviorthesis in patients with chronic inflammatory diseases refractory to conventional treatments.

J. Venero Chaparro, *M. Sánchez Torrente, M. Gallego Márquez, F. Garí Martínez, D. Becerra García, M. Martínez-Valle Torres; Hospital Clínico San Cecilio, Granada, SPAIN.*

Aim/Introduction: The objective is to describe our experience after radioisotope synoviorthesis (RSO) as the local treatment of choice in patients with chronic arthritis and synovitis of large and medium-sized joints, who have not responded to first-line treatments. In addition, to analyse the effectiveness of the treatment at one year and to assess its impact on quality of life. ***Materials and Methods:*** This is an observational, descriptive, cross-sectional study in which 22 RSOs performed in our centre between 2017 and 2023 were assessed. Twenty knees were injected with 185MBq of Ytrium Citrate (Y-90) and two elbows with 111MBq of Rhenium (Re-186). In both procedures the injection was performed inside the joint space and was guided by sonography, after administration of intra-articular anaesthetic in order to avoid movements during the injection that could interfere with the correct procedure. Finally, corticosteroids were administered to reduce post-therapy inflammation.Once the radioisotope is injected, the beta emission generated will irradiate the inflamed synovium, causing fibrosis and obliteration of the pain receptors of the synovial membrane, resulting in clinical improvement. To evaluate the clinical response, all patients were given a questionnaire before the procedure, 3 months and 1 year after treatment. The three variables analysed were: 1. Reduction of pain through the visual analogue scale (VAS), considering an adequate response if it decreased more than 25% in relation to the initial VAS; 2. Improvement of the activity of the disease, determined by increased joint mobility and decreased inflammation; 3. Improvement of the quality of life with decreased first-line analgesics. ***Results:*** All patients showed improvement in all three variables analysed. 1. Pain intensity was reduced by 63.7% at 3 months and by 65.3% at 1 year after treatment. 2. The decrease in disease activity was 73.7% at 3 months and 77.2% at 1 year after the procedure. 3. At one year post procedure, 72.1% of patients showed significant improvement in their quality of life. ***Conclusion:*** Radiosynoviorthesis is a useful and safe therapeutic alternative in patients with chronic arthritis and synovitis, resulting in a significant improvement in quality of life and reduction of inflammation parameters.

EP-0621

The most important problems of supervision over a patient qualified for knee synovectomy based on 10 years single-centre experience

M. Wlodarczyk, *Z. Adamczewski; Nuclear Medicine Department, Central Clinical Hospital, Medical University of Lodz, Lodz, POLAND.*

Aim/Introduction: Radioisotope synovectomy (RS) is a recognized method used in the treatment of joint effusions in the course of diseases such as rheumatoid arthritis (RA), psoriatic arthritis, juvenile idiopathic arthritis, pigmented villonodular synovitis or degenerative joint disease. Exudative changes in the course of these diseases are often accompanied by secondary synovial hyperplasia. Radioactive colloid particles administered intra-articularly during RS are phagocytosed by synoviocytes leading to coagulative necrosis, fibrosis and involution of synovial hyperplasia. The effectiveness of this type of therapy depends to a large extent on the initial diagnosis. In the case of RA, it can be up to 80%. ***Materials and Methods:*** The Nuclear Medicine Department of the Medical University of Łódź (NMD) has extensive experience in performing radiosynovectomy of the knee joints. Over the last 10 years, 885 procedures of this type have been performed in 643 patients, mainly (36%) with RA. In most patients (N=465, 53%), the procedure was performed once. The rest of patients received the isotope 2-6 times over several years (N=420, 47%). The group treated multiple times was diverse. It included both patients in whom the procedure was repeated due to the ineffectiveness of the previous attempt, as well as those in whom the repetition was due to the desire to prolong the positive effect of the therapy. ***Results:*** In the majority of single-treated patients, there was no feedback on the effectiveness of therapy. Post-treatment follow-up was conducted by clinicians and rarely reported to NMD. In returning patients this assessment was mainly based on indicators such as pain reduction, swelling reduction or improvement in joint mobility. The most important was the overall improvement subjectively felt by the patient. Finally, among all procedures with information about the effectiveness, improvement was noted in about 80% of cases. ***Conclusion:*** In order to objectively assess the effectiveness of isotopic treatment, the procedure is now extended to include ultrasonographic measurements of the thickness of synovial folds and the amount of effusion in the joint during the qualification visit for the synovectomy. The control of clinical and ultrasound effects is scheduled 3-6 months after the RS, during an additional follow-up visits in NMD. This way of proceeding will ensure an objective evaluation of treatment effects, it will make it independent of the influx of information from clinicians, and in the case of qualifying new patients, it will enable the introduction of personalized rules of conduct.

EP-0622

Treatment of Hidradenitis suppurativa (HS) - A pilot study : Can Nuclear Medicine therapy be the answer?

P. Gupta, *K. K. Verma, R. Kumar; AIIMS, New Delhi, INDIA.*

Aim/Introduction: Hidradenitis suppurativa (HS) is a dermatological condition characterized by inflamed and swollen lumps which are purulent and painful. As it usually occurs in underarms and groin region, it significantly affects the everyday activities. It is believed to be caused by hair follicles being obstructed, with the nearby apocrine sweat glands being strongly implicated in this obstruction. Antibiotics, immunosuppressive medication, laser therapy or surgery may help in partial improvement of symptoms. However, no definite cure is known and the present available options offer partial help with chances of recurrence. In this pilot study, we tried to explore if Nuclear Medicine therapy beholds the answer to the treatment of HS.The aim of the study was to determine if Nuclear Medicine therapy with radioactive patches can be used for treatment of Hidradenitis suppurativa (HS). ***Materials and Methods:*** A prospective pilot study was conducted with two patients (M/F:1/1) aged 32 yrs and 48 yrs. Written informed consent was obtained from both patients. Both patients had clinically confirmed HS lesions on underarms. The lesions were characterized by swelling, pus discharge and

severe pain at the lesion site affecting the daily activities of both the patients. Antibiotics of anti-infective tetracyclines class were started in both patients to reduce purulence and suppuration. After the initial baseline laboratory investigations were done, radioactive patches of Rhenium-188 were custom made according to shape of the lesions, sealed and applied locally over the lesions. A total of 45-50 Gy radiation dose was superficially delivered to the lesions in five fractions. Patients were followed up at 2 weeks, 6 weeks and 12 weeks. ***Results:*** Initial radiation induced dermatitis and inflammation was noted at the lesion site at 2 weeks in both the patients which gradually healed. At 6 weeks, inflammation was absent and there was partial improvement at the lesion sites with decreased swelling and pain. There was no pus discharge at the lesion sites. At 12 weeks, all the symptoms had subsided. Swelling, pain and pus discharge had completely subsided with significant improvement in the quality of life of patients. There was complete flattening of the lesions though some hypopigmentation was noted at the treated lesion sites. Routine laboratory examinations at the follow ups did not reveal any toxicity. ***Conclusion:*** Nuclear Medicine therapy using radioactive patches can be an effective option for treatment of Hidradenitis suppurativa (HS).

EP-0623

Percutaneous Microwave thermoablation (PMWT) for dominant benign thyroid nodules(BTN): a two years single centre experience

B. Criscuoli[1], *C. Manni*[1], *G. Follacchio*[1], *F. Salvatori*[2], *C. Mincarelli*[2], *S. Alborino*[2], *F. Capoccetti*[1];
[1]*Nuclear Medicine Unit, Macerata General Hospital, AST Macerata, ITALY,* [2]*Interventional Radiology Unit, Macerata General Hospital, AST Macerata, ITALY.*

Aim/Introduction: Image-guided thermal-ablation(LTA; RFA) are well established therapy options in selected BTN.PMWT is a mini-invasive technique recently applied in thyroid disease;purpose is to demonstrate effectiveness of PMWT in treatment of BTN,and its application inside a thyroid pathways in a nuclear medicine unit. ***Materials and Methods:*** From May 2021,95 patients (66F,29 M, Aged 29-84,Mean 59,2)with BTN symptomatic/in growing,non eligible to surgery were enrolled. Inclusion criteria:solid nodule≥ 20%,diameter ≥ 2 cm,2 FNA cytology confirmed as benign(TIR2 sec ITCCS 2014).Baseline were performed ECG,ENT consults,where necessary anesthesiologic too,laboratory assessment(fT3,fT4,TSH,TPOAb,TgAb, calcitonin,blood count,clotting indexes).Additionally 52/95 pts done Thyroid-scintiscan with ^{99}mTc-Pertecnetate(35 cold;11hot;6 non focal findings).Single-session of US-guided PMWTA was carry-out under local anesthesia through microwave-antenna,delivering 10-15 W in 10-15 minutes,depends on the BTN volume;in 2 cases,due to the high baseline volume,procedure was repeated in 6 months. Nuclear medicine physician effects anamnestic/thyroid physical examination,rating symptomatology with a Compressive Score(CS on a 10 cm visual-analog scale),Aesthetic Score (AS from 1-no palpable-to4 palpable-visible in all positions).US thyroid was performed to record Volume of BTN-target (VnT),baseline and scheduled after procedure at 1, 6, 12 months,in selected patients also at 18 months. Additionally volume reduction rate %(VRR) was calculated. Considering the baseline VnT,we divided in 2Groups: Group A >10 mL n°43 pts;Group B < 10 mL n°52 pts).Success rate fixed in a volume reduction ≥ 50%. ***Results:*** No peri-procedural major complications were observed. 4/95 with hot-nodules after procedure showed laboratoristic transient increase of thyroid hormone levels,1/4 develop 10 days after PMWT atrial fibrillation pharmacologically reverted;2/95 skin burn;1/95 transient lowering of voice. Clinically was registered CS mean score from 3,9 (baseline) to 1,8 and 0,95 (6 and 12 months respectively),AS from 3,2 (baseline) to 2 (6 and 12 months). Baseline mean VnT of 14,8 mL(range 77-1,2 mL) and 12 months post-procedure mean VnT of 5,8 mL (range 32,9-0,39 mL). In Group A the mean VRR at 1,6,12 months was respectively 45,5 %, 58,8 %, 63,8 %. In Group B the mean VRR at 1,6,12 months was respectively 49,3 %, 55,4 %, 61,9 %.The success rate was in Group A 89%,and 83 % in Group B.Neither a significant re-growth occurred in this middle-term evaluation, confirmed at 18 months control. ***Conclusion:*** From our results,PMWT is an effective option in selected BTN, demonstrated an high-successful rate as nodule shrinking,safe,well-tollerated and low complication rate,with a satisfactory clinical-response. No significant difference dividing patients by volume in 2 groups,assuming a spread potential inside decision making into thyroid pathways.

EP-42

e-Poster Area

D: Technical Studies -> D1 Instrumentation -> D11 SPECT and SPECT/CT

EP-0624

SPECT Imaging Predictors of Social Anxiety Disorder Treatment Response: A New Way Forward

S. Rezaei*, E. Gharepapagh;*
Department of Nuclear Medicine, Medical School, Tabriz University of Medical Sciences, Tabriz, IRAN, ISLAMIC REPUBLIC OF.

Aim/Introduction: Precision psychiatry aims is to accurately predict treatment response. Here, we tested pre-treatment patient characteristics and functional imaging markers to predict treatment response accuracy in patients with social anxiety disorders (SAD). ***Materials and Methods:*** The selective serotonin reuptake inhibitor (SSRI) escitalopram or placebo was administered for 9 weeks to 40 SAD patients (mean SD age 32.1 ± 8.2 years, 20 women). The Clinical Global Impression Improvement scale was used to define treatment responders (CGI-I ≤ 2). Imaging with single photon emission computed tomography (SPECT) was conducted before and after treatment. Based on pre-treatment neuroimages, support vector machines (SVMs) were used to separate responders from non-responders. SVM models were tested using leave-one-subject-out cross-validation. ***Results:*** High accuracy was achieved by classifying treatment responders from non-responders using a linear SVM. Higher post-treatment perfusion was observed in responders compared to non-responders, particularly in those treated with SSRIs. ***Conclusion:*** Based on these results, psychiatric symptoms of clinical recovery are consistent with functional brain perfusion imaging findings on an individual basis.

EP-0625

Feasibility of an 123I-Ioflupane single photon emission tomography attenuation correction method with a deep convolutional neural network

Y. Sayawaki[1], *T. Ueda*[1], *T. Tomimatsu*[1], *R. Nagaoka*[1], *K. Yamasita*[1], *S. Ito*[2];
[1]*Graduate school of Health Sciences, Kumamoto University, 4-24-1 Kuhonji Chuo-ku,Kumamoto-shi, Kumamoto-ken, JAPAN,* [2]*Faculty of Life Sciences, Kumamoto University, 4-24-1 Kuhonji Chuo-ku,Kumamoto-shi, Kumamoto-ken, JAPAN.*

Aim/Introduction: An attenuation correction (AC) is essential for 123I-FP-CIT single photon emission computed tomography (SPECT) for analysis and quantification of striatal. The CT based attenuation correction (CTAC) method have been used for 123I-FP-CIT SPECT. However, the use of CT scans increases radiation exposure to patients. Therefore, an AC method without radiation exposure and CT scan is required for clinical study. We developed a direct attenuation correction method (DAC) for brain positron emission tomography images without using MR images or CT images by using a deep convolutional neural network (DCNN). This method can be applied to 123I-FP-CIT SPECT without radiation exposure.The purpose of this study was to confirm the feasibility of the 123I-FP-CIT SPECT DAC by using DCCNN. ***Materials and Methods:*** Thirty patients who underwent 123I-FP-CIT SPECT/CT were used for training and testing for DCNN. A U-net architecture was used for generating DAC images and both CT attenuation correction (CTAC) and non-AC images were trained to predict DAC images. Images of 15 patients were used as training images, the images of remaining 15 patients data were used as examination set for accuracy evaluation of DAC images. The accuracy of DAC image was compared with the original CTAC image. ***Results:*** The normalized mean absolute error (NMSE) and structural similarity (SSIM) between the DAC and CTAC images were 0.31%±0.13%, and 0.96±0.0014, respectively. The DAC images were approximately equal to CTAC images. The SSIM with the DAC method was 0.96, suggestive of almost no differences between the DAC and CTAC images. Based on these results, the precision of NMSE and SSIM with the direct method is considered to have been very high, with good consistency between the two methods, encouraging their application in attenuation correction. ***Conclusion:*** Using a DNN, the 123I-FP-CIT DAC method that do not involve radiation exposure, were developed. The DAC images were similar to images corrected by CTAC, suggesting the clinical usefulness of this method. ***References:*** Development of attenuation correction methods using deep learning in brain-perfusion single-photon emission computed tomography:Taisuke Murata et al.MR-based synthetic CT generation using a deep convolutional neural network method:Xiao Han

EP-0626

Prognostic value of right ventricular dysfunction in chronic heart failure patients

A. Mishkina*, T. Atabekov, S. Sazonova, S. Popov, K. Zavadovsky;*
Cardiology Research Institute, branch of the Federal State Budgetary Scientific Institution «Tomsk National Research Medical Center of the Russian Academy of Sciences», Tomsk, RUSSIAN FEDERATION.

Aim/Introduction: Gated blood pool SPECT(GBPS) is a well-established method for the assessment of right ventricle (RV) function due to its high accuracy and reproducibility[1]. Although recent studies proved that RV dysfunction is a predictor of adverse cardiac events in chronic heart failure (CHF) patients, the data regarding the role of RV dysfunction in cardiac resynchronization therapy (CRT) candidates is limited. The aim of this study was to evaluated RV function dynamic after CRT and prognostic value of RV dysfunction in CRT response. ***Materials and Methods:*** Patients with CHF eligible for CRT were included in this study. All patients underwent GBPS before and 6 months after CRT. The following RV indices were analyzed: end diastolic (EDV), end systolic (ESV) volumes, ejection fraction (EF), global and RV free wall phase standard deviation,degree(deg.) (PSD), phase entropy,% (PE), RV phase histogram bandwidth,deg. (PHBW), interventricular dyssynchrony, deg. (IVD), peak ejection rate (PER), peak filling rate (PFR), mean filling rate for one-third of diastole (MFR/3). Moreover before and six months after CRT implantation all patients underwent transthoracic echocardiography for assessment of left ventricle(LV) ESV, LV EDV, LV EF. ***Results:*** This study included 73 patients with CHF referred for CRT (males - 65%; mean age - 57±11 years; 38% - ischemic HF). Thirty patients had baseline RV dysfunction (RV ejection fraction<45% assessed by GBPS). Patients with RV dysfunction more common had atrial fibrillation, higher RV systolic pressure, higher RV_EDV, lower RV_PFR and higher RV dyssynchrony. RV contractility decreased from baseline to 6-month follow-up in all group of patients: RV_EF 54(IQR 41-56)% to 41(33-50)%, p=0.02; RV_SV 86(70.5 - 113)ml to 71.5(58.5 - 88) ml, and IVD 25(15.5 - 37.5)deg. to 21.5(11 - 26.5)deg, p=0.047. RV_EF changes after 6-month follow-up correlated suboptimal with baseline indices: QRS duration (r=-0.43,p=0.0019), RV systolic pressure (r=0.53,p=0.012), RV_ESV (r=0.48,p=0.0009), RV_PE (r=0.3,p=0.04), RV_MFR3 (r=-0.42,p=0.005), IVD (r=0.53,p=0.0002). According to the linear multivariate regression analysis (R2=0.82, p=0.004), significant predictors of LV_ESV changes after CRT implantation were: atrial fibrillation (p=0.0008), age (p=0.0005), RV_SV (p=0.001), RV_MFR/3 (p=0.0016), RV_PER (p=0.008), RV_PE (p=0.029). ***Conclusion:*** GBPS is useful for RV dysfunction assessment in patients with CHF. CRT implantation associated with the decreasing of RV_EF, RV_SV, IVD. The improvement of LV_ESV at 6 months after CRT is associated with atrial fibrillation, age, baseline RV_SV, RV_MFR/3, RV_PER, RV_PE. ***References:*** 1. Lebedev DI, Popov SV, Mishkina AI et al. Effect of right ventricular myocardial contractility on the response to cardiac resynchronization therapy. Kardiologiia. 2018;58(2).P:19-24. DOI:10.18087/cardio.2436

EP-0627

Comparing myocardium perfusion imaging features between 3D and 2D general-purpose SPECT/CT systems

T. Noponen[1]*, L. Kääriä*[2]*, R. Hirvilammi*[2]*, M. Hakulinen*[3]*, M. Seppänen*[2]*;*
[1]Department of Clinical Physiology and Nuclear Medicine and Department of Medical Physics, Turku University Hospital, Turku, FINLAND, [2]Department of Clinical Physiology and Nuclear Medicine, Turku University Hospital, Turku, FINLAND, [3]Diagnostic Imaging Center, Kuopio University Hospital, Kuopio, FINLAND.

Aim/Introduction: In SPECT/CT myocardium perfusion imaging (MPI), a high contrast for ischemic defects and uniformity in normally perfused myocardium are desired features. A novel 3D digital SPECT/CT system may provide an increased contrast for a defect detection with respect to traditional 2D SPECT/CT systems. Capabilities of 3D digital SPECT/CT system for MPI were compared with the 2D SPECT/CT systems employing left ventricle phantoms. ***Materials and Methods:*** Two custom-designed 3D-printed left-ventricle phantoms were utilized. Both phantoms had realistic dimensions of human male anatomy, other modeling uniform myocardial perfusion without defects and other having three defects. Two cube-shaped defects had 10x10x10 mm dimensions, one located in an anterior cardiac wall and other on the lateral side of the apex. A large 20-mm height defect was located in an inferior cardiac wall. The phantoms having ^{99m}Tc activity concentration (c_A) of 0,080 MBq/ml were inserted in a plastic container (20x35x45 cm, c_A = 0,002 MBq/ml) modelling upper torso. The phantoms were imaged using three modern general-purpose SPECT/CT systems: 2D analog NaI, 2D digital CZT and novel 3D digital CZT system. Standard clinical acquisition and reconstruction protocols were used with 2D systems having 22-min SPECT imaging time and with 3D digital system 9-min. The acquisition was repeated with 3D system using 16-min imaging

time. The images of 2D systems were reconstructed using CT attenuation (CTAC) and resolution recovery corrections and 3D system using a Bayesian penalized-likelihood iterative algorithm with CTAC and median root prior regularization. Background regions and three defects were segmented in CT guidance using a modern commercial nuclear medicine analysing software. Defect contrast ((background-defect)/background) and uniformity (sd/mean) of background activity distribution were calculated. The defects were also visually interpreted using a polar plot. ***Results:*** 3D digital system had 77.4% contrast for large and 23.0-26.5% for small defects. The background uniformity ranged between 14.8-16.1% for the images of 3D system. 2D systems had 57.7-61.7% contrast for large and 8.6-15.2% for small defects and uniformity ranging between 10.3-11.0%. With the 16-min imaging time the background uniformity in 3D system decreased to 14.1%. With 3D system the small defects could be visually detected in a polar plot whereas with 2D systems they were not reliable detectable. ***Conclusion:*** 3D digital SPECT/CT system detects myocardial defects with clearly better contrast than 2D systems in MPI. However, also image non-uniformities are larger with 3D compared to 2D systems. Non-uniformities could be decreased by increasing an acquisition time.

EP-0628

Use of SPECT-CT In The Combined SLNB Technique and Node Labeling with 125i Seeds in Breast Cancer Patients Treated with Neoadjuvant Chemotherapy.

M. Pérez Avila[1], *M. Caballero Vivanco*[1], *F. González Asid*[1], *E. Córdoba Cañete*[1], *R. Sánchez Sánchez*[2];
[1]*Hospital Universitario Virgen de las Nieves, Granada, SPAIN,* [2]*Hospital Universitario Virgen de las Nieves, Maracena, Granada, SPAIN.*

Aim/Introduction: Selective sentinel lymph node biopsy (SLNB) is the procedure of choice for axillary staging of breast cancer, and allows the selection of patients in whom axillary lymphadenectomy does not provide any additional benefit. Currently, the performance of SLNB after neoadjuvant chemotherapy is accepted in patients with negative axilla at diagnosis, but in patients with positive axilla its application has limitations. Different lymph node markers have been proposed to guarantee their intraoperative identification and removal in axillary surgery. I125 seed labeling is a suitable procedure for intraoperative localization of biopsied positive lymph nodes in combination with SLNB and improves post-treatment axillary staging. The aim of our job is to present our protocol for carrying out the combined technique of SLNB and lymph node labeling with 125I seeds. ***Materials and Methods:*** 125I seed labeling of the biopsied positive axillary node is performed before starting neoadjuvant chemotherapy treatment. After treatment, the day before surgery, 74-111 MBq of 99mTc-albumin nanocolloid were injected periareolarly and then lymphoscintigraphy was performed until the sentinel node was visualized. The visualized node(s) was identified as sentinel node(s), especially if they are connected to a lymphatic channel, and once confirmed, their location on the skin was marked with the gamma radiation detector probe (99mTc energy window: 140 ± 10% keV). Next, SPECT/CT fusion images were acquired, which provide anatomical correlation of the SLNs and make it possible to check whether they coincide with the seed-labelled node, so this information helped to plan the surgery. ***Results:*** Of the 50 N1 patients with SRI-125 (GM) marking, 44 pre-QtNeo and 6 post-QtNeo, GM was identified in 97.2%: 23 negative, 26 positive. SLNB was performed in 45 and was identified in 93.3%: 26 negative, 16 positive. In 1 case the SRI-125 was not placed correctly and SLN was not located due to non-migration. In 61.9% of the patients, the GM was among the SLN(s) identified at surgery. In 5 patients, with non-coincident SLN and GM, the pathological result of the SLN was negative and the LM was positive. Axillary lymphadenectomy was performed in 53.8% of the patients. ***Conclusion:*** The addition of the SPECT/CT study to the lymphoscintigraphy is of special interest in patients with axillary labeling with I125 seeds, it allows to see coincidence with sentinel node and improves the surgical approach.

EP-0629

PSF correction and Tc-99m quantitative performance of a disruptive CZT multiple-head SPECT-CT

A. Seret[1], *C. Bernard*[2];
[1]*UNIVERSITY OF LIEGE, Liege, BELGIUM,*
[2]*CHU of LIEGE, Liege, BELGIUM.*

Aim/Introduction: A methodology developed for a comparison of NaI SPECT-CT [1] was used to analyze the quantitative potentialities of a CZT multiple-head SPECT-CT. ***Materials and Methods:*** Phantoms: NEMA NU-2 1994 scatter, 9.4-cm (L) and 20-cm (XL) diameter cylinder. The last one was also converted in a contrast phantom (TOM) with two cold and hot rods inserts while leaving a uniform compartment. They were filled with 730-860 (360 for L) MBq of Tc99m and concentration was identical in all radioactive part. Acquisitions: Veriton 200, Focus mode, 4 orbits, 100 (800 for L) Mcounts, 2.46-mm pixels, WEHS collimator, factory default energy windows. Reconstructions: OSEM, CT-based attenuation, resolution recovery, optional scatter correction (SC) with dual-energy window, additional PSF recovery so-called quantitative (PSFRq) or display (PSFRd), OSEM iterations x subset number (ITER) from 40 to 240. Processing: NEMA NU-2 1994 methodology was followed to get the residual fraction (RF) in air, water and Teflon inserts of NEMA phantom. Cylindrical ROIs of about 35% rod height and rod full (FROI) or half (HROI) physical diameter (d) were drawn on the CT images of TOM together with a large cylindrical ROI in the uniform part. Mean ROI count per pixel (C) was computed and also standard deviation (SD) in the large ROI. Recovery coefficient (RC) was computed as $C_{rod}/C_{uniform}$ for hot rods and $1-C_{rod}/C_{uniform}$ for cold rods. Coefficient of variation (COV) in the uniform part was $SD/C_{uniform}$. Calibration factor (CF) were obtained from L and XL phantom using large cylindrical ROIs and applied to C of TOM uniform part and NEMA radioactive area. ***Results:*** RF decreased when ITER increased, was 5.5-10% without SC and 0-2% with SC. RC increased with ITER and rod diameter. For cold rods, a plateau was reached for d≥20mm at (FROI/HROI): 56/68%, 79/95% (SC), 57/70% (PSFRq), 80/97% (PSFRq+SC), 79/89% (PSFRd). Up to 10mm hot rods, RC increase was steep and then RC fluctuated with a maximum at d=20mm (FROI/HROI): 47/74%, 51/88% (SC), 49/77% (PSFRq), 52/88% (PSFRq+SC), 91/209% (PSFRd). COV increased almost linearly with ITER: 4.7-6.8%, 5.9-8.6% (SC), 5.1-7.3% (PSFRq), 6.3-9.3% (SC+PSFRq), 11.6-16.1% (PSFRd). Quantification error (SC and SC+PSFRq) depended moderately on the phantom and ROI size used to obtain CF and was in the range [-2.5,3.4]% for TOM and [-5.4,2.9]% for NEMA. ***Conclusion:*** SC or PSFRq increased contrasts but moderately for hot rods. SC or PSFR increased COV. PSFd should be restricted to visualization purpose. ***References:*** [1] EJNMMI Research 2012, 2:45.

EP-0630

Energy window narrowing or classical dual-energy window substraction for scatter correction in a CZT multiple-head SPECT-CT

A. Seret[1], *C. Bernard*[2];
[1]*UNIVERSITY OF LIEGE, Liege, BELGIUM,*
[2]*CHU of LIEGE, Liege, BELGIUM.*

Aim/Introduction: A methodology developed for a previous comparison of SPECT-CT [1] was used to analyze scatter removal in a CZT multiple-head SPECT-CT. ***Materials and Methods:*** Phantoms: NEMA NU-2 1994 scatter (770 MBq) and 20-cm diameter cylinder (950 MBq) with cold and hot rods inserts and a uniform compartment (identical concentration in all radioactive part). Acquisitions: StarGuide, focus mode, 4 orbits, 100 Mcounts, 2.46-mm pixels, standard tungsten collimator, list-mode files. Reconstructions: OSEM, CT-based attenuation, resolution recovery, 6, 10, 15, 20% wide main peak energy window (EW), optional dual-energy window scatter correction (DEW) with 20% main and 10% secondary scatter energy windows, OSEM iterations x subset number (ITER) from 40 to 200. Processing: NEMA NU-2 1994 methodology was followed to get the residual fraction (RF) in air (A), water (W) and Teflon (T) inserts of NEMA phantom. Cylindrical ROIs of about 35% rod height and rod full (FROI) or half (HROI) physical diameter (d) were drawn on the CT images of contrast phantom together with a large cylindrical ROI in the uniform part. Mean ROI count per pixel (C) was computed and also standard deviation (SD) in the large ROI. Recovery coefficient (RC) was computed as $C_{rod}/C_{uniform}$ for hot rods and $1-C_{rod}/C_{uniform}$ for cold rods. Coefficient of variation (COV) in the uniform part was $SD/C_{uniform}$. ***Results:*** Reported values are for ITER200 and for d=20mm in contrast phantom. RF decreased when ITER increased down to (A/W/T) 1/9/2.2% (EW20) and 1.8/0.6/0.001 (DEW). Additional RF results for the other energy window will be added. RC increased with ITER. For cold rods, RC increased with d reaching a plateau for d≥20mm at (FROI/HROI): 68/87% (EW20), 70/85% (EW15), 73/87% (EW10), 74/89% (EW6),81/93% (DEW). Smallest hot rods were not visible for d≤13mm with DEW. RC was below 10% for d=4mm and all EW and fluctuated for the other rods (6-20mm) with a maximum (FROI/HROI) at d=20mm: 51/74% (EW20), 52/77% (EW15), 54/81% (EW10), 55/84% (EW6), 8/31% (DEW). $C_{uniform}$ was 89% (EW15), 76% (EW10), 59% (EW6), 63% (DEW) of its value for EW20. COV increased almost linearly with ITER and reached 10.3% (EM20), 10.8% (EM15), 11.7% (EM10), 13.5% (EM6), 12.9% (DEW) at ITER200. ***Conclusion:*** This study questions the use of the classical wide energy windows and scatter correction methods for this SPECT systems fitted with CZT detectors.

References: [1] EJNMMI Research 2012, 2:45.

EP-0631

Small feature quantification in SPECT/CT - a focus on mandibular condyles

S. De Schepper[1,2], *O. Lenssen*[3], *G. Gnanasegaran*[4], *T. Van den Wyngaert*[1,2], *J. C. Dickson*[5];
[1]*Department of Nuclear Medicine, Antwerp University Hospital, Edegem, BELGIUM,* [2]*Faculty of Medicine and Health Sciences (MICA—IPPON), University of Antwerp, Wilrijk, BELGIUM,* [3]*Department of Oral and Maxillofacial Surgery, ZNA Middelheim, Antwerp, BELGIUM,* [4]*Department of Nuclear Medicine, Royal Free London NHS, London, UNITED KINGDOM,* [5]*Institute of Nuclear Medicine, University College of London Hospitals NHS Foundation Trust, London, UNITED KINGDOM.*

Aim/Introduction: Unicondylar hyperplasia (UCH) causes facial asymmetry, and bone scintigraphy is the standard to assess growth and guide treatment. However, reconstruction and analysis techniques are heterogeneous, producing conflicting results. Absolute quantification using SPECT/CT may offer a solution, yet, concerns exist regarding its limited spatial resolution and associated partial volume effects (PVE), hampering its use in smaller features below 2cm, such as the condyles. Partial volume correction (PVC) may overcome these limitations using recovery coefficients (RC), typically derived from a NEMA IQ phantom. We aimed to determine the impact of PVE in UCH using the NEMA IQ phantom and hypothesized that disease-specific anthropomorphic phantoms could provide superior results. ***Materials and Methods:*** Anthropomorphic phantoms were created using patient CT data and consisted of two spheres enclosed within a background volume simulating bone (with an HK_2O_4P solution to mimic trabecular bone density). One phantom modeled normal anatomy (both spheres: Ø 8mm) and one UCH (left: Ø 8mm, right: Ø 13mm). Phantoms were filled with a clinically relevant spheres-to-background ratio of 120kBq/mL:40kBq/mL of activity (^{99m}Tc). The impact of the PVE was assessed using clinically relevant acquisition protocols of the phantoms with/without resolution modeling (RM) reconstructions. Next, we compared RCs derived from NEMA phantom data and our anthropomorphic phantom to perform PVC and assess the quantitative accuracy. ***Results:*** The PVE was significant for the anthropomorphic phantom's 8mm and 13mm spheres, with a recovery of 47% and 71% of the true activity, respectively. Without the application of RM recovery significantly worsened to 29% and 44%, respectively. However, using RM leads to an overestimated recovered activity in the background volume from 86% to 126%. Using the NEMA phantom-derived RC of 26% for the 8mm spheres and 48% for 13mm resulted in an overestimation of true activity by 81% and 61% for the 8mm and 13mm spheres, respectively. The dependency of RCs on sphere position in the NEMA phantom could explain this observation, as we observed varying RCs for 8mm between 26% to 46% depending on sphere positions. Interestingly, using our anthropomorphic phantoms, applying the RC derived from the UCH phantom to the symmetric phantom, showed significant improvements in the deviations from the true activity concentration in left and right condyle: -2.6% and +2.5% (with RM) and +1.1% and -11.7% (without RM), respectively. ***Conclusion:*** Absolute quantification on SPECT/CT of small features benefits from anthropomorphic phantoms to improve the recovered activity, with potential clinical relevance in UCH.

EP-0632

Reduction of the acquisition time and improvement of the dopaminergic imaging quality with CZT gamma camera. Comparison with conventional gamma cameras.

S. Asadurova, *C. Lorenzo-Bosquet, S. Aguade, A. García-Burillo;*
Hospital Universitari Vall d´Hebron, Barcelona, SPAIN.

Aim/Introduction: Validate a 50% reduction in dopaminergic imaging acquisition time without affecting the visual or semiquantitative analysis of the studies. Comparison with conventional gamma cameras. ***Materials and Methods:*** 25 consecutive studies performed with each gamma camera are compared, analyzing parameters of: acquisition (matrix, zoom, pixel size, total counts, maximum counts/pixel), visual analysis (definition, contrast, resolution) and quantitative using DaTQUANT™ (SBR: Striatal Binding Ratio). All patients were injected with 185 MBq 123I-FP-CIT, with image acquisition 3 hours post injection. The conventional acquisition protocol uses LEHR collimators, 128x128 matrix, with 1.45 zoom and 3.3 mm pixel for G2, and 1.5 and 2.95 mm for G3. The G1 consists of 12 CZT detectors (CZT crystal thickness 7.25 mm, energy range 40-279 keV) in a circular arrangement, ME/LEHR collimator, 2.46 mm pixel size, with

adjustable zoom and matrix.The acquisition time is 30 minutes for G2 and G3, and 15 minutes for G1. It has been reconstructed with FBP and Metz 0.3/15 for the conventional ones, and Q.Clear, Butterworth 0.9/5 for the CZT, all without attenuation correction. The visual analysis was performed by a resident physician and two experts. ***Results:*** The average number of total counts in the entire detection field was 2,522,556 for G3, 2,152,531 for G2, and 1,124,763 for G1. The average number of maximum counts/pixel was 41 for G3, 73 for G2 and 85 for G1. Visual analysis shows greater contrast, definition and resolution in G1 images compared to conventional ones. No inter-observer differences have been found in the assessment of definition, contrast and resolution between the images from all the gamma cameras. In quantification, no significant differences in SBR values were observed between the different gamma cameras. ***Conclusion:*** The CZT gamma camera allows a significant reduction in acquisition time and better image quality, without affecting visual interpretation or quantification.

EP-0633

The Art of Juggling: On the Influence of Sphere Positioning on Recovery Coefficients Determined Using an IEC-NEMA Phantom

J. Leube[1], *J. Gustafsson*[2], *M. Lassmann*[1], *M. Salas Ramirez*[1], *J. Tran-Gia*[1];
[1]*University Hospital Würzburg, Würzburg, GERMANY,* [2]*Lund University, Lund, SWEDEN.*

Aim/Introduction: The NEMA IEC PET Body Phantom ("NEMA Phantom") with sphere inserts represents the go-to method for recovery assessment and partial volume correction in PET/CT and SPECT/CT imaging. Aiming at a reliable harmonization between imaging sites, this work investigates the influence of the sphere positioning on sphere-based recovery coefficients (RC). ***Materials and Methods:*** An in silico model of a NEMA Phantom was created based on sphere centers, attenuation map and detector trajectory of a clinical SPECT/CT measurement. Simulations for all 720 possible permutations of the sphere positioning were performed for two sets of spheres (standard NEMA Phantom with diameters 10-37 mm ["NEMA_PET"] and adapted SPECT NEMA Phantom with diameters 13-60 mm ["NEMA_SPECT"]) using the SIMIND [1] Monte Carlo program. Reconstructions were performed using OSEM without (CASToR [2], AC, SC, 5 iterations, 10 subsets, "OSEM") and with PSF modelling (STIR [3], AC, SC, 20 iterations, 10 subsets, "OSEM_PSF"). Recovery Coefficients (RC) were calculated as the ratio of SPECT-based activity (nominal contour) to known sphere activity. A fit of the recovery curve as function of the volume V was performed: $f_RC(V)=1/(1+(\beta/V)^{\gamma})$. ***Results:*** In general, OSEM resulted in lower RCs than OSEM_PSF (NEMA_PET: 0.09/0.41 [10mm] - 0.60/0.89 [37mm], NEMA_SPECT: 0.10/0.57 [13mm] - 0.72/1.00 [60mm] for OSEM/OSEM_PSF). Furthermore, a strong dependence of the sphere positioning on RC was found, where again, OSEM_PSF outperform OSEM (maximum RC variation with respect to the mean [(maximum-minimum)/mean], NEMA_PET: 97%/48% [10mm] - 15%/7% [37mm], NEMA_SPECT: 110%/60% [13mm] - 10%/7% [60mm] for OSEM/OSEM_PSF). For OSEM, a strong dependence of RC on the distance between sphere and detector was found, with the largest RCs when positioning the sphere at the top of the phantom (smallest possible distance between sphere and detector). For OSEM_PSF, RC mainly depends on the volumes of the two adjacent spheres. Thus, the adjacency of the largest spheres resulted in smaller RCs. The sphere positioning also influenced the fit parameters and thus also a potential partial volume correction (mean±standard deviation; NEMA_PET: β=(12.6±0.9)ml, γ=0.66±0.05/ β=(0.67±0.12)ml, γ=0.82±0.13; NEMA_SPECT: β=(15.2±0.6)ml, γ=0.59±0.04/ β=(0.70±0.22) ml, γ=0.71±0.12). ***Conclusion:*** Our study shows that sphere positioning has a considerable influence on recovery coefficients obtained in NEMA Phantom measurements. This applies to both the standard NEMA Phantom (diameters 10-37 mm) and a NEMA phantom adapted for SPECT imaging (diameters 13-60 mm). ***References:*** [1] Ljungberg et al., Comput Meth Prog Bio, 1989(29) [2] Merlin et al., Phys Med Biol, 2018(63) [3] Thielemans et al., Phys Med Biol, 2012(57)

EP-0634

Objective Assessment of Gamma Camera's Intrinsic Resolution

P. Trindev[1], *M. Dimcheva*[2];
[1]*Retired, 1233 Sofia, BULGARIA,* [2]*Department of Nuclear Medicine, Sofia Cancer Center, Sofia, BULGARIA.*

Aim/Introduction: This study aimed to design a new test pattern that would provide a more accurate estimate of intrinsic resolution.There are three main parameters of the detector field of the gamma camera - sensitivity, linearity, and intrinsic resolution. Sensitivity and linearity are software supported online in acceptable limits across the entire detector field. In time, methods have been developed for a sufficiently accurate assessment of sensitivity and linearity to objectively verify the values declared by the manufacturer in a datasheet. The situation is different in the third parameter - intrinsic resolution. The problem lies in the fact that intrinsic resolution varies across the entire detector field. Therefore, the recommended objective method (1) for assessing intrinsic resolution is based on the average estimate of many 30 mm bins, with the assessment result greater than the value declared in the datasheet. ***Materials and Methods:*** We have developed a new phantom, further referred to as TP-phantom, which consists of 2 parts - a slit phantom and an irradiation source. The slit phantom consists of 2 lead plates 33x110x5 mm each, which are fixed stationary with 2 additional aluminum tiles. The slit width between the two lead plates can be adjusted down to a size 10 пъти по-малък от измерваната стойност. The desired slit width is established with a gamma radiation transparent insert - for example, cardboard with corresponding thickness. The irradiation source is a vial with Tc-99m solution encapsulated in a lead container. At the bottom of the container, a hole with a diameter of 25 mm is cut to irradiate the slit. ***Results:*** Easy access to any point of the detector field allows us to determine exactly the extreme points of the intrinsic resolution - on a PMT and between 2 PMTs, respectively. A method of evaluating intrinsic resolution by measurement at constant support points is proposed. This approach allows us to objectively verify the value of intrinsic resolution in the datasheet during acceptance testing as well as to track the status in subsequent testing. ***Conclusion:*** The TP-phantom provides the following advantages: access literally to any point of the UFOV; adjustable slit width; adjustable count rate (below 20 kcps); short time to collect reliable information; zero radiation hazard for staff. ***References:*** 1. National Electrical Manufacturers Association. NEMA NU 1. (2018) Performance measurement of scintillation cameras. Rosslyn,VA: NEMA. 6-10

EP-0635

Calibration Factor and Recovery Coefficients for Lu-177 in a ring-shaped CZT gammacamera

A. Garcia, *A. Seoane;*
Vall d'Hebron Hospital Campus, Barcelona, SPAIN.

Aim/Introduction: Targeted radionuclide therapies with Lu-177 isotope have experienced a great increase during last years due to well-established treatments in neuroendocrine tumours, and new prostate-specific membrane antigen labelled with Lu-177. The possibility to calculate the absorbed dose to tumour and organs for every patient based on imaging, allows to make individual dose prescriptions.The recently developed family of gammacameras based on cadmium-zinc-telluride (CZT) detectors arranged in a ring reduce the time needed to acquire SPECT.We determined the Calibration Factor (CF) and Recovery Coefficients (RCs) for the General Electric Starguide gammacamera (CZT), and compared to values obtained in the Anger-type camera GE Discovery NM670 (NaI crystal based detectors, MEGP collimator). ***Materials and Methods:*** The CF was determined by acquiring a SPECT of a cylindrical phantom filled with Lu-177. Images were acquired for the 208 keV emission peak, with an energy window of ±6% for the Starguide during 600 s, and ±10% for the Discovery during 1125 s (90 projections, 45 s/projection). CFs were obtained by measuring the counts per second divided by the activity within a spherical volume of diameter 15 cm.To measure the RCs, a NEMA/IEC Body Phantom was filled with a sphere-to-background activity ratio of 27:1. RCs were obtained by measuring the cps divided by the activity in the spheres defined by a threshold. SPECTs were corrected for scatter, attenuation and detector resolution. The algorithms used for reconstruction were Q.Clear for the Starguide and OSEM for the Discovery, both with 10 subsets and 4 to 50 iterations, with and without a Butterworth Filter (BWF) (critical frequency = 0.4; power = 10) applied. ***Results:*** Mean CFs with BWF were 79.4 and 21.6 cps/MBq for the Starguide and Discovery respectively. No differences were found without BWF applied. CFs were stable with the number of iterations, with maximum deviations of 1.9% for Starguide and 0.8% for Discovery. The RCs increased with iterations from 4 to 20, remaining stable after this value. Table shows the RCs for 20 iterations. Values for Starguide camera compared to Discovery for diameters > 2 cm were on average 9% and 14% lower with and without BWF applied respectively. ***Conclusion:*** Lu-177 Calibration Factor for the Starguide CZT camera was almost 4 times greater than for the Discovery. This allows a considerable reduction in the clinical imaging time.The Recovery Coefficients were found to be slightly lower in the Starguide camera and remained stable for N≥20 iterations.

EP-0636

Reducing scan time for post-therapy [131I]NaI SPECT/CT scans and [99mTc]Tc-HDP bone scintigraphy SPECT

T. Ball, *K. Sabanayagam, H. McMeekin, A. Haroon, M. Vadrucci, J. Buscombe, E. Nowosinska, M. Krishnamurthy;*
Barts Health NHS Trust, London, UNITED KINGDOM.

Aim/Introduction: SPECT/CT scans post [^{131}I]NaI administration for thyroid ablation therapy are performed to assess radiopharmaceutical uptake and guide future treatment. Two- or three-bed SPECT images are often acquired with unacceptably long scan durations for patient comfort and departmental throughput. It was aimed to assess whether scan times could be reduced using third-party SPECT reconstruction software while maintaining acceptable image quality. [^{99m}Tc]Tc-HDP is administered to patients in order to visualise bone uptake. A reduction in scan time would allow for improved departmental throughput and patient comfort, or a reduced injected activity. These scans will be assessed using the same method as per the [^{131}I]NaI scans. ***Materials and Methods:*** Poisson resampling was used to simulate scan durations 30% and 50% that of the original. OSEM reconstruction was applied with 5i15ss, CTAC, MC scatter correction, Gaussian resolution recovery, and a 0.9cm FWHM Gaussian post-filter. Another reconstruction applied advanced MC collimator modelling for I-131. These reconstructions and the current reconstruction performed on the acquisition station were presented, randomised and de-identified, to three NM consultants for scoring on a scale of 1-5 for diagnostic confidence. At the time of presenting this method will also have been applied to [^{99m}Tc]Tc-HDP bone scintigraphy SPECT scans using a reconstruction with identical parameters but 16 subsets. 10 patient studies were included for the [131I]NaI post-therapy scans and by the time of publication a further 10 will be included for [^{99m}Tc]Tc-HDP acquisitions. ***Results:*** Two-tailed T-tests of the average score for each reconstruction compared with the current reconstruction showed no statistically significant differences ($p > 0.05$) apart from one ($p = 0.003$), where MC collimator modelling was applied to full count data. The average scores for the current reconstruction, third-party 30%, third-party 50%, and third-party 100% were 3.19 (SD 0.48), 3.22 (SD 0.52), 3.42 (SD 0.48), and 3.55 (SD 0.39). The MC collimator modelling offered no significant benefits in diagnostic confidence for the reduced count data. Early results of the same type for reconstructed [^{99m}Tc]Tc-HDP scans indicate similarly that reducing acquisition time by 50% would not reduce clinical confidence in patient scans, for the final report further data will be acquired. ***Conclusion:*** These data support scanning at 50% or even 30% of the current acquisition time using the third-party reconstruction software for [^{131}I]NaI scans. ***References:*** Sohlberg, A. O., & Kajaste, M. T. (2011). Fast Monte Carlo-simulator with full collimator and detector response modelling for SPECT. Annals of Nuclear Medicine.

EP-43

e-Poster Area

D: Technical Studies -> D1 Instrumentation -> D12 PET/CT

EP-0637

The earlier 18F-FDG and 68Ga-DOTA-FAPI-04 dual-tracer total-body PET/CT scan timing: a feasibility study

Z. Zheng, *Y. He, W. Mao, H. Yu, H. Wu, P. Hu, H. Shi;*
Zhongshan hospital, fudan university, Shanghai, CHINA.

Aim/Introduction: To investigate the feasibility of 2-[^{18}F]-fluoro-2-deoxy-D-glucose-fibroblast activation protein inhibitors (FDG-FAPI) dual-tracer positron emission tomography/computed tomography (PET/CT) earlier imaging. ***Materials and Methods:*** Thirty-seven patients who underwent FDG-FAPI dual tracer imaging with ^{18}F-FDG (0.37MBq/kg) and ^{68}Ga-FAPI-04 (0.925MBq/kg) were enrolled retrospectively; among them, 11 patients were confirmed by pathological examination. Another 11 patients who underwent 60-min dynamic ^{68}Ga-FAPI-04 scans were selected accordingly for matching with the pathological results. The image of the FDG-FAPI group was reconstructed at 34-39min and 50-60min, named PET_{G34-39} and PET_{G50-60}, respectively. The image of the ^{68}Ga-FAPI-04 group was reconstructed at 34-39min and named PET_{FAPI}. The image quality was evaluated by objective analysis. Objective analysis indicators of PET image quality included the mean of standardized uptake value (SUVmean) of the liver, standard deviation (SD) and

signal-to-noise ratio (SNR). The background SUVmean, lesion SUVmean and lesion-to-background ratios (LBRs) were compared between PET_{G34-39}, PET_{G50-60} and PET_{FAPI}. To determine the lesions detectability at PET_{G34-39}, PET_{G50-60} served as the reference. ***Results:*** Most normal organs were significantly higher on PET_{G34-39} than on PET_{FAPI}. Liver SNR on PET_{G34-39} (18.36±7.43) was lower than that on PET_{G50-60} (21.64±8.74) and PET_{FAPI} (21.65±5.18), but the differences were not significant (P=0.07, P=0.06, respectively). Liver SUVmean on PET_{G34-39} was significantly higher than that on PET_{FAPI} (1.97±0.82 vs 1.32±0.54, P=0.03), but was similar with PET_{G50-60} (1.97±0.82 vs 1.93±0.88, P=0.95). Although the LBRs on PET_{G34-39} were higher than that on PET_{G50-60} and PET_{FAPI}, there were no statistically difference among them (all P>0.05). The SUVmean of metastases on PET_{G34-39} were higher than that on PET_{G50-60} (lymph nodes metastases: 7.05±2.36 vs 6.05±2.11, P<0.001; distant metastases: 8.10±3.32 vs 7.12±2.89, P=0.005). PET_{G34-39} and PET_{G50-60} were comparable with lesions detectability. The SUVmean of distant metastases on PET_{G34-39} was significantly higher than that on PET_{FAPI} (8.10±3.32 vs 4.14±2.80, P=0.008), but there was no statistically significant difference in LBRs. The SUVmean and LBRs of primary tumours and metastatic lymph nodes were not statistically different between that on PET_{G34-39} and PET_{FAPI}. ***Conclusion:*** Dual-tracer (FDG-FAPI) PET at 34-min could provide sufficient information to meet the needs of clinical diagnosis and demonstrate better compatibility and feasibility with clinical practice.

EP-0638

Clinical evaluation of a head motion correction algorithm on PET/CT system

W. Yang[1], *F. Kang*[1], *Z. Xie*[1], *G. Li*[1], *K. Guo*[1], *C. Xi*[2], *H. Liu*[2], *Y. Li*[2], *C. Sun*[2], *E. M. Revilla*[2], *Y. Zhao*[2], *D. Zhang*[2], *L. Shi*[2], *H. Yi*[2], *Y. Zhao*[2], *Y. Lu*[2], *J. Wang*[1];
[1]*Department of Nuclear Medicine, Xijing hospital, Xi'an, CHINA,* [2]*United Imaging Healthcare, Shanghai, CHINA.*

Aim/Introduction: In brain PET imaging, head motion (HM) is a major limitation that reduces image resolution and generates artefacts. In clinical settings, accurate quantification is crucial in treatment planning, diagnosis and response evaluation. Thus, modern PET scanners with higher spatial resolution are now being developed, e.g., sub 3-mm in full-width-half-maximum and even minor HM may cause resolution loss. Recently, a data-driven head motion correction (HMC) algorithm, which is a statistics-based HMC method that automatically detects HM using centroid-of-distribution (COD) without parameter tuning, is provided for the PET/CT system. The aim of this work is to evaluate this vendor-provided HMC algorithm and to reveal the head motion prevalence among short clinical ^{18}F-FDG scans. To the best of our knowledge, this is the first study that applied an HMC algorithm to a relatively large clinical cohort. ***Materials and Methods:*** Single-bed, 3-min brain ^{18}F-FDG scans (N=392) were retrospectively analyzed. CT scan was conducted prior to PET for attenuation correction. For each study, an in-house CT segmentation algorithm was used to segment the brain into 116 regions of interests (ROIs). A binary gray-matter (GM) mask was also generated. The intersection between the GM mask and 116 ROIs were used to generate the refined 116 ROIs. By merging all the refined ROIs into 11 regions based on the AAL definition, final 11 GM ROIs were generated. Furthermore, results were divided into two categories: small and large motion, where SUV change smaller/larger than 5% at frontal lobe after HMC was used as the criteria for grouping. ***Results:*** Quantitative results of SUV change at different GM ROIs showed that 38 of the participants experienced large HM and yielded 10.9±8.9% SUV increase after HMC while the rest showed insignificant uptake increase (0.1±1.3%). For large GM regions, SUV increase in frontal and temporal regions were 12.9±8.3% and 10.0±8.1%, respectively. Conversely, small GM regions like caudate and amygdala yielded 22.9±13.7% and 19.9±20.8% increase in uptake, respectively. Overall, the magnitude of motion in the large motion category (5.6±3.7 mm, 2-3 min post injection) was greater than it in the small motion (1.3±1 mm). ***Conclusion:*** We evaluated the efficacy of a vendor-provided HMC algorithm using short clinical ^{18}F-FDG studies for a PET/CT system. The evaluation study revealed that approximately 12% of the clinical brain studies experienced large magnitude head motion that require correction. The HMC algorithm effectively corrected for HM and regarded sufficient for clinical brain ^{18}F-FDG studies.

EP-0639

18F-FDG PET/CT for evaluation of metastases in non-small cell lung cancer on the efficacy of immunotherapy

Y. Feng*, P. Wang, Y. Chen, W. Dai;*
Department of Nuclear Medicine, The First College of Clinical Medical Science, China Three Gorges University, Yichang city, CHINA.

Aim/Introduction: Aim This study aimed to investigate the relationship between metabolic parameters and metastases and the efficacy of ICIs treatment for advanced non-small cell lung cancer (NSCLC). ***Materials and Methods:*** 34 advanced NSCLC patients who received ^{18}F-fluorodeoxyglucose positron emission tomography/computed tomography (^{18}F-FDG PET/CT) before ICIs treatment were retrospectively included in this study. All patients were divided into two groups, the clinical benefit (CB) group and the no-clinical benefit (no-CB) group and the clinical information, survival, and glucose metabolic parameters were evaluated. ***Results:*** 24 patients were in the CB group, and 10 patients were in the no-CB group. There was a significant difference between the CB group and the no-CB group in TNM stages, metabolic tumor volume of primary lesion (MTV-P, P=0.003), metabolic tumor volume of lymph node metastasis (MTV-LN, P=0.023), total lesion glycolysis of lymph node metastasis (TLG-LN, P=0.023), metabolic tumor volume of whole-body (MTVwb, P=0.005) and total lesion glycolysis of whole-body (TLGwb, P=0.015). For patient outcomes, the independent prognostic factor associated with PFS were TNM IV stage (HR=0.14, 95%CI 0.04 ~0.53, P=0.00), TLG-P>7.512 (HR=0.11, 95% CI 0.03 ~0.50, P=0.11), TLG-LN>61.06 (HR=0.12, 95% CI 0.03 ~0.45, P=0.00). But there was not any independent prognostic factor associated with OS. ***Conclusion:*** High MTV and TLG predicted poor clinical benefit and a large burden of metastatic lymph nodes predicted short PFS in advanced NSCLC with ICI treatment in advanced NSCLC patients.

EP-0640

PET imaging and quantification of small animals using a clinical SiPM-based camera

C. Desmonts[1,2], *C. Lasnon*[3,2], *C. Jaudet*[3], *N. Aide*[2];
[1]*Caen University Hospital, Caen, FRANCE,* [2]*Normandy University, UNICAEN, INSERM 1086 ANTICIPE, Caen, FRANCE,* [3]*Comprehensive Cancer Centre F. Baclesse, Caen, FRANCE.*

Aim/Introduction: Small-animal PET imaging is an important tool in preclinical oncology. This study evaluated the ability of a clinical SiPM-PET camera to image several rats simultaneously and to perform quantification data analysis. ***Materials and Methods:*** Intrinsic spatial resolution was measured using 18F

line sources, and image quality was assessed using a NEMA NU 4-2018 phantom. Quantification was evaluated using a fillable micro-hollow sphere phantom containing 4 spheres of different sizes (ranging from 3.95 to 7.86 mm). Recovery coefficients were computed for the maximum (Amax) and the mean (A50) pixel values measured on a 50% isocontour drawn on each sphere. Measurements were performed first with the phantom placed in the centre of the field of view and then in the off-centre position with the presence of three scattering sources to simulate the acquisition of four animals simultaneously. Quantification accuracy was finally validated using four 3D-printed phantoms mimicking rats with four subcutaneous tumours each. All experiments were performed for both 18F and 68Ga radionuclides. ***Results:*** Radial spatial resolutions measured using the PSF reconstruction algorithm were 1.95 mm and 1.75 mm for centred and off-centred acquisitions, respectively. Spill-overs in air and water and uniformity computed with the NEMA phantom centred in the FOV were 0.05, 0.1 and 5.55% for 18F and 0.08, 0.12 and 2.81% for 68Ga, respectively. Recovery coefficients calculated with the 18F-filled micro-hollow sphere phantom for each sphere varied from 0.51 to 1.43 for Amax and from 0.40 to 1.01 for A50. These values decreased from 0.28 to 0.92 for Amax and from 0.22 to 0.66 for A50 for 68Ga acquisition. The results were not significantly different when imaging phantoms in the off-centre position with 3 scattering sources. Measurements performed with the four 3D-printed phantoms showed a good correlation between theoretical and measured activity in simulated tumours, with r^2 values of 0.99 and 0.97 obtained for 18F and 68Ga, respectively. ***Conclusion:*** We found that the clinical SiPM-based PET system was close to that obtained with a dedicated small-animal PET device. This study showed the ability of such a system to image four rats simultaneously and to perform quantification analysis for radionuclides commonly used in oncology.

EP-0641

Value of 2-[18F]FDG-PET/CT in detecting immune-related adverse events in patients with malignant melanoma or non-small cell lung cancer: a systematic scoping review

S. Nadaraja[1], *J. Helsing*[1], *M. Bezhad*[1], *L. H. Land*[2], *C. H. B. Ruhlmann*[2], *O. Gerke*[1,3], *M. G. Hildebrandt*[1,3,4];
[1]*Department of Nuclear Medicine, Odense University Hospital, Odense C, DENMARK,* [2]*Department of Oncology, Odense University Hospital, Odense C, DENMARK,* [3]*Department of Clinical Research, University of Southern Denmark, Odense C, DENMARK,* [4]*Centre for Personalized Response Monitoring in Oncology (PREMIO), Odense University Hospital, Odense C, DENMARK.*

Aim/Introduction: The aim of this systematic scoping review was to outline 2-[18F]FDG-PET/CT-reported prevalence of immune-related adverse events (irAEs) and evaluate the diagnostic accuracy of 2-[18F]FDG-PET/CT in identifying irAEs in patients with metastatic malignant melanoma or non-small cell lung cancer (NSCLC), receiving treatment with immune checkpoint inhibitors (ICIs). ***Materials and Methods:*** A comprehensive literature search was performed on April 11, 2023, using Medline (PubMed), Embase, and Scopus databases without time restriction. After applying inclusion/exclusion criteria and abstract/full-text review, seven articles with 478 patients with malignant melanoma and two articles with 155 patients with NSCLC were included in the analysis. The reference standard was irAE, corroborated clinically, biochemically, histologically, or on other imaging modalities. This work was conducted according to PRISMA guidelines for scoping reviews. ***Results:*** Malignant melanoma: Five studies reported the sensitivity of 2-[18F]FDG-PET/CT, while two reported the prevalence of irAEs detected only by 2-[18F]FDG-PET/CT (without other verification of irAEs).[1-7] The clinically reported prevalence of irAEs was 14-18% for thyroiditis and 29% for colitis. The sensitivity of FDG-PET/CT was 100% for thyroiditis and 49% for colitis, and the sensitivity for a sarcoid reaction in mediastinal lymph nodes, lungs, and skin was 100%, 43%, and 29%, respectively. In another study, sensitivity and specificity were 100% and 49% for irAEs relating to bowel, 100% and 96% for lung, and 89% and 81% for thyroid. [7] Lung cancer: The prevalence of 2-[18F]FDG-PET/CT detected irAEs included midgut/hindgut inflammation (36%), gastritis (21%), pneumonitis (18%), and thyroiditis (15%).[8] A sensitivity of 60% has been demonstrated for thyroiditis.[9] ***Conclusion:*** Studies suggest that 2-[18F]FDG-PET/CT is a valuable, non-invasive tool for detection of adverse events to anticancer treatment with ICIs. This allows for swift and relevant clinical management of irAEs for the benefit of patients. Prospective studies exploring the clinical impact are needed to determine the role and optimal timing of FDG-PET/CT in identifying irAEs. ***References:*** 1.Melin A, et al.Cancers.2022. 2.Lang N, et al.Immunotherapy.2019. 3.Frelau A, et al.Cancer Immunol Immunther.2021. 4.de Filette J, et al.J Clin Endocrinol Metab.2016. 5.Tirumani SH, et al.Cancer Immunol Res.2015. 6.Iravani A, et al.Eur J Nucl Med Mol Imaging.2020.7.Hribernik N, et al.Eur J Nucl Med Mol Imaging.2022 8.Humbert O, et al.Eur J Nucl Med Mol Imaging.2022. 8.Eshghi N, et al.J Nucl Med Technol.2018.

EP-0642

Quantitative consistency assessment along the axial field of view of a total-body PET scanner

X. Meng[1], *Y. Wu*[2], *F. Wang*[1], *Y. Song*[1], *R. Wu*[2], *N. Li*[1], *Z. Yang*[1];
[1]*Peking University Cancer Hospital & Institute, Beijing, CHINA,* [2]*Shanghai United Imaging Healthcare, Shanghai, CHINA.*

Aim/Introduction: Total-body PET scanners (TB-PET) extend the axial field of view (AFOV) and add a new dimension to the detector structure. Obvious image quality inconsistency has been noticed between the central and peripheral parts of the scanner. This study aims to assess the quantitative consistency along the AFOV of a TB-PET. ***Materials and Methods:*** The TB-PET studied contains 8 detector units that span 1.94 m. The quantification process was conducted based on the EARL recommendation. However, the phantoms were placed across the AFOV, including the 8 centers of each unit and the 8 joints between adjecent units. The NEMA IQ phantoms was acquired at each position for 10 min, and the relative change of the activity during the acquisition period was contorlled within ±10%. Three positron emitters including ^{18}F, ^{68}Gas and ^{89}Zr was used in this study. The image was reconstructed using 3 iterations, 20 subsets, point spread function (PSF) enabled, and no Gaussain filter. The results were quantified with a custom software called BCH_EARL, and the recovery coefficients (RC) including RC_{mean}, RC_{max}, and RC_{peak}, were obtained for each hot sphere at each position with each positron emitter. ***Results:*** The RC_{mean} and RC_{max} for the larger spheres fluctuated very little along the axial direction, while those for the smaller spheres fluctuated obviously. Take ^{18}F for example, the RC_{mean} for the 37 mm large sphere fell into the narrow range between 0.88 and 0.93, while the RC_{mean} for the 10 mm small sphere fell from 1.13 by the edge of the detector to 0.71 around the center of the AFOV. RC_{max} demonstrated a similar trend. The quantitative discrepancy is due to the elevated noise level at the edge of the detector, which excerts a stronger effect on the smaller spheres. However, the trend for RC_{peak} was somewhat different, and the larger spheres were more prone to fluctuation. The minimum RC_{peak} of the 37

mm sphere was 0.78 which is around the edge of the detector. This is due to the fact that the edge of the larger spheres are more affected by the PSF effect compared to the smaller spheres. ^{68}Gas and ^{89}Zr showed the similar trends. ***Conclusion:*** Although the quantitative performance along the axial direction of the AFOV of TB-PET is consistent, fluctuations exist, especially on the peripheral part of the AFOV. Precuations should be taken in the imaging of the head and the feet in clinical applications.

EP-0643

68Ga-Pentixafor in Squamous Cell Carcinoma of the head and neck, a pilot study

B. Hadebe[1], *L. Harry*[1], *L. Gabela*[1], *S. Masikane*[1], *M. Patel*[1], *P. Bipath*[1], *N. Cebekhulu*[1], *N. E. Nyakale*[2], *C. Aldous*[1], *M. M. Sathekge*[3], *M. Voster*[1];
[1]*University of KwaZulu Natal, Durban, SOUTH AFRICA,* [2]*Sefako Makgatho Health Sciences University, Pretoria, SOUTH AFRICA,* [3]*University of Pretoria, Durban, SOUTH AFRICA.*

Aim/Introduction: Head and neck squamous cell carcinoma (HNSCC) is common [1] and its incidence is increasing, particularly in HIV-infected individuals who present with more aggressive disease [2]. Despite aggressive treatment, the prognosis remains poor due to resistance to chemoradiation therapy [3]. So far, studies report very low tracer avidity in HNSCC [4]. This study investigated the diagnostic performance of CXCR4-directed imaging of squamous cell carcinoma of the head and neck with PET/CT using the radiolabelled chemokine ligand ^{68}Ga-Pentixafor. ***Materials and Methods:*** Twenty-one (21) patients with head and neck SCC underwent [^{68}Ga]-Pentixafor-PET/CT. In 14/21 patients, 2-[^{18}F]fluoro-2-deoxy-D-glucose (^{18}F-FDG), performed within 1 month of the [^{68}Ga]-Pentixafor-PET/CT and immunohistochemistry served as standard of reference. All primary lesions were visually rated as Pentixafor and FDG positive or negative, qualitative assessment of the images was performed using the 5 point Likert scale. For both tracers, SUVmax, SUVmean of the primary lesions as well as tumor to muscle ratio (TMR), tumor to liver (TBR), was documented and correlated with HIV, HPV and survival. ***Results:*** Twenty one (21) patients, 16 males and 5 females aged 35 - 73 years (mean 52 ± 10)with primarily diagnosed (n=16) or pre-treated (n=5) SCC of the oral cavity (n=10), oropharynx (n=8), nasopharynx (n=2) and unknown primary (n=1) underwent ^{68}Ga-Pentixafor-PET/CT. [^{68}Ga] Pentixafor-PET/CT was visually positive in 18/21 patients cases with a sensitivity of 86%, however [^{18}F]FDG PET demonstrated higher SUV_{max} in all patients compared to [^{68}Ga]Pentixafor PET. The SUV_{max} and SUV_{mean} were 5,8 ± 2.6 and 3± 1.6 and TBR_{max} was 2,36 ± 1.4 for [^{68}Ga]Pentixafor. The SUV_{max} and SUV_{mean} were 16 ± 6.7 and 9.3 ± 4.1 and TBR_{max} 4.9 ± 2.3 for [^{18}F]FDG. Fourteen percent (14%) 3/21 of the patients were HIV positive, there was higher accumulation of both ^{68}Ga]Pentixafor and FDG in HIV positive patients. Also, nasopharyngeal cancer demonstrated more intense tracer accumulation than oropharyngeal and oral cavity malignancies. ***Conclusion:*** Our data shows that PET/CT imaging the CXCR4 chemokine receptor with [^{68}Ga]Pentixafor is in SCC of the oral cavity, oropharynx and nasopharynyx is feasible but less avid than [^{18}F]FDG and can be considered complementary to [^{18}F]FDG-PET/CT. Of note, CXCR4 expression seems to be higher in nasopharyngeal SCC, followed by oropharynx and low in oral cavity SCC, however this should be confirmed in a larger sample. ^{68}Ga-Pentixafor is limited by accumulation in the tonsils and reactive nodes in the neck which may complicate image interpretation in head and neck malignancies.

EP-0644

The asymmetry of tau deposition and its correlation with cerebral metabolic asymmetry in Alzheimer's disease

H. Lin*, p. wu, c. zuo;*
Deparment of Nuclear Medicine / PET Center, Huashan Hospital, Fudan University, Shanghai, CHINA.

Aim/Introduction: The correlation between tau deposition and metabolism has been observed in Alzheimer's disease (AD), but the asymmetry of tau deposition and its correlation with metabolic asymmetry have not been roundly studied in AD. To analyze the asymmetry of tau deposition in AD and investigate its correlation with cerebral metabolic asymmetry. ***Materials and Methods:*** 142 patients with AD who underwent ^{18}F-FDG PET and ^{18}F-Florzolotau PET imaging at the same period were retrospectively enrolled. Standardized uptake value ratios (SUVRs) were obtained from ^{18}F-FDG and ^{18}F-Florzolotau positron emission tomography (PET) images of all participants, and the asymmetry indices (AIs) of metabolism and tau deposition were calculated according to the SUVRs. AD group was divided into left/right-dominant or bilateral symmetric hypometabolism (AD-L/AD-R or AD-BI), or left/right-dominant or bilateral symmetric tau deposition (tau-L/tau-R or tau-BI) when more than half of the AIs of the 20 pairs of regions of interest (ROIs) closely related to AD were < -2SD, > 2SD, or between ± 1SD. Clinical differences among metabolic or tau deposition subgroups in AD were compared, and the correlation between asymmetry of tau deposition and metabolic asymmetry in bilateral cerebral hemispheres of 20 pairs of ROIs were analyzed. ***Results:*** In 142 AD patients, the proportion of AD-L, AD-R and AD-BI were 26.1%, 14.8% and 16.2%, and tau-L, tau-R and tau-BI were 22.5%, 23.9% and 4.9% respectively. In clinical, asymmetric hypometabolic patients had younger age of onset, and poorer cognitive function than symmetric hypometabolic patients, but theses was no significant difference in tau subgroups. The asymmetry of tau deposition was negatively correlated with the metabolic asymmetry in the following 16 pairs of ROIs: Frontal_Sup, Frontal_Sup_Orb, Frontal_Mid, Frontal_Mid_Orb, Frontal_Inf_Oper, Frontal_Inf_Tri, Frontal_Inf_Orb, Frontal_Sup_Medial, Frontal_Mid_Orb, Parietal_Sup, Angular, Precuneus, Temporal_Sup, Temporal_Mid, Temporal_Pole_Mid, Temporal_Inf ($r=-0.639\sim-0.192$, $P < 0.05$). That is, with the tau deposition in bilateral hemispheres increased, the reduction of metabolism became more significant in AD. But there was no significant correlation between ^{18}F-FDG and tau deposition in the other 4 ROIs: Parietal_Inf, Temporal_Pole_Sup, Hippocampus and Cingulum_Post ($P > 0.05$). ***Conclusion:*** There is a negative correlation of asymmetry between tau deposition and cerebral glucose metabolism AD, but the metabolic asymmetry may also be influenced by other factors.

EP-0645

Characterizing the 5-Ring GE Discovery MI PET/CT Scanner Using AAPM TG-126 and Compare these Results with the NEMA NU 2-2012 Results

R. Almazrou[1], *S. Alanazi*[1], *M. Alrabiah*[2], *R. Al-Fakhranee*[1], *O. Mawlawi*[3];
[1]*King Faisal Specialist Hospital and Research center, Riyadh, SAUDI ARABIA,* [2]*GE HealthCare, Riyadh, SAUDI ARABIA,* [3]*University of Texas MD Anderson Cancer Center, Houston, TX, UNITED STATES OF AMERICA.*

Aim/Introduction: To report on the performance characteristics of two 5-ring GE Discovery MI PET/CT systems using the AAPM TG-126 report (1) and compare these results to NEMA NU 2-2012

(2) where applicable. ***Materials and Methods:*** TG-126 testing and NEMA NU 2-2012 were performed on two GE discovery MI 5-Rings. Tests performed included spatial resolution, PET/CT image-registration accuracy, sensitivity, count rate performance, accuracy of corrections, image contrast, scatter/attenuation correction and image uniformity. All acquired data was analysed using scanner console or free software tools as described by TG-126 and NU 2-2012. ***Results:*** Both scanners gave similar TG-126 and NEMA results. The FWHM of radial/tangential/axial spatial resolution measurements using the filtered back projection algorithm were 5.1/5.0/5.8 mm, 5.7/5.7/8.4 mm and 7.4/5.2/8.0 mm at 1, 10, and 20 cm from the centre of the FOV, respectively. For NEMA testing, these values were 4.5/4.2/5.2 mm, 5.5/4.5/6.9 mm, and 7.5/4.9/7.0 mm. Image-registration accuracy between PET and CT using clinical protocol showed excellent results with values < 1 mm. Sensitivity using TG-126 was 18.4 cps/kBq while for NEMA the value was 19.7 cps/kBq. The peak noise-equivalent counting rate is not comparable between TG-126 and NEMA NU-2 due to differences in phantoms and methods used to measure and calculate this parameter. TG-126 results were 2174 kcps at 63.1 kBq/ml while NEMA results were 273 kcps at 22.7 kBq/ml. The accuracy of corrections for count losses for TG-126 were expressed in SUV values for the range of activity concentration between 0.26 KBq/cc and 76.5 KBq/cc and found to be 1.1 g/ml and 0.9 g/ml, respectively. Image contrast and scatter/attenuation correction using the TG-126 method gave acceptable results. Image uniformity assessment resulted in values within the recommended + 5% limits. ***Conclusion:*** To our knowledge this is the first study that reports on PET system characterization using the AAPM TG-126 report. These results show that PET scanner testing using TG-126 is reproducible and has similar results to NEMA NU 2-2012 tests where applicable. Due to the lack of manufacturer PET scanner performance characterization using TG-126, we hope these results start to form the basis by which these systems can be compared to one another. ***References:*** (1) Mawlawi OR, Jordan DW, Halama JR, Schmidtlein CR, Wooten WW. PET/CT Acceptance Testing and Quality Assurance: The Report of AAPM Task Group 126, 2019.(2) National Electrical Manufacturers Association. "NEMA Standards Publication NU 2-2012: Performance Measurements of Positron Emission Tomographs," Rosslyn, Virginia, USA, 2013.

EP-0646

Clinical solution to minimize mis-registration artifacts in PET/CT

T. Pan*;*
The University of Texas, Houston, TX, UNITED STATES OF AMERICA.

Aim/Introduction: Misregistration between CT and PET can impact PET/CT image quality and is due to mismatch of temporal resolution between CT (< 1 second) and PET (averaged over many cycles of respiration). Most misregistration issues occur in the chest and/or abdomen regions. We implemented a measure to minimize misregistration on a network of 9 PET/CT scanners from two vendors including a total body (TB) PET/CT scanner by fusing a repeat short CT scan not bounded by the fixed PET bed positions over the misregistration area to a whole body (WB) CT for attenuation correction (AC) of the PET data and for minimum CT radiation to the patient. ***Materials and Methods:*** The minimum coverage of repeat CT, set by the vendors, ranges from 21.6 to 104 cm for one bed of PET scan in our 9 PET/CT scanners, and is much larger than the misregistration area ~14 cm observed over the lower lungs and upper abdomen in our patient population. A decision to repeat a limited CT only on the misregistration area is made at the last bed of PET acquisition when a misregistration between CT and PET is observed. The repeat CT, which can overlay in part with two beds, and the WB CT are sent to a server shared by the 9 PET/CT scanners to fuse the repeat CT with the WB CT to the requesting PET/CT scanner for AC of the WB or TB PET. This step is to ensure the fused CT can be used for AC. The turn-around time between sending and receiving data for AC is < 2 min, shorter than the time between patients for PET/CT. ***Results:*** The proposed measure is effective for reduction of misregistration but at a cost of a limited repeat CT over the misregistered area to the patient, which is about 5% of PET/CT radiation dose. The scan coverage of this approach can be prescribed on the scout or topogram rather than by pencil and paper for a scan coverage tied to the starting and ending positions of the PET beds set by the vendors. ***Conclusion:*** We have developed an effective solution to minimize misregistration between CT and PET on our 9 PET/CT scanners of two vendors including a TB PET/CT scanner.

EP-0647

Physical and Clinical Optimization of Acquisition Durations on a Digital BGO High Sensitivity PET-CT System

Q. Maronnier*, M. Terroir, T. Cassou-Mounat, A. Latgé, J. S. Texier, L. Vija, F. Courbon, O. Caselles;*
Oncopole Claudius Regaud, Toulouse, FRANCE.

Aim/Introduction: During the past decade, new PET-CT systems emerged with performances that could change clinical practice. A system coupling a significantly increased sensitivity and an extended field of view (FOV) was evaluated. Its characteristics could allow optimized acquisition protocol to reduce exam duration while maintaining equivalent image quality with no impact on the quantitation of PET images. In this study, we evaluated the impact of reduced acquisition times on phantom and on patient. ***Materials and Methods:*** The study was performed on the Omni Legend PET-CT system (General Electric Healthcare, Waukesha, WI USA) using Bayesian penalized likelihood reconstruction algorithm, optimized according to the image statistics. First, we evaluated the quantitative impact of reduced acquisition durations (2-min/FOV, 1.5-min/FOV, 1-min/FOV, 0.5-min/FOV) based on the EARL optimization procedure, its acceptance criteria and our clinical practice (2MBq/kg and protocol). Secondly, we applied the same parameters to four clinical cases of 18F-FDG PET-CT to assess the impact of acquisition times reduction on patient data. The images obtained were blindly analyzed by four nuclear medicine physicians using 5-levels scale for four clinical criteria (Likert scale). The images were judged clinically acceptable if the score was strictly above 2 for each criterion, this threshold corresponding to a non-degradation of clinical information. Additionally, based on clinical results, we applied Precision Deep Learning (PDL), a deep learning software simulating Time-Of-Flight information on PET images, and evaluated its impact on the clinical criteria. ***Results:*** Physical analysis performed on phantoms showed that the EARL2 criteria were fulfilled for all acquisition durations studied except 0.5-min/FOV. The analysis of clinical data was consistent with phantom results, as only the shortest acquisition time failed to meet the criteria. However, based on the differences in scoring, we opted for 1.5-min/FOV in order to maintain the quality of clinical images. Finally, by applying PDL on the 1-min/FOV duration, we observed Likert scale scoring on par with 1.5-min/FOV without PDL. ***Conclusion:*** It is possible to reduce acquisition duration to 1.5-min/FOV for 18F-FDG PET-CT exams without affecting the overall quality of images. Furthermore, the results obtained with PDL suggest that a reduction to 1-min/FOV would be acceptable. Currently, in our center, all 18F-FDG PET-CT acquisitions are performed using 1.5-min/FOV. Regarding these results, we are now considering reducing the acquisition time even further to 1-min/FOV once we ensured PDL doesn't alter images.

EP-0648

Quantitative Evaluation of Low-dose Whole-body Indirect Patlak Parametric Imaging with Deep Progressive Reconstruction

Q. Ye[1], *C. Xi*[1], *H. Dai*[1], *H. Zeng*[1], *Y. Zhao*[1], *G. Li*[2], *F. Kang*[2], *J. Wang*[2], *Y. Lv*[1], *Y. Lu*[1];
[1]*United Imaging Healthcare, Shanghai, CHINA,* [2]*Xijing Hospital, Xi'an, CHINA.*

Aim/Introduction: For PET scanners with short axial field of view (AFOV), whole-body Patlak parametric imaging requires multi-pass multi-bed acquisition protocols. This practice leads to discontinuous data collection with relatively short-time acquisition for each bed position within one pass, which results in high image noise in the subsequent parametric images via post-reconstruction Patlak fitting. Direct Patlak parametric imaging directly reconstructs the kinetic parameters from PET raw data, which helps to reduce the image noise but requires higher computation burden and more complex algorithm design than the indirect method, i.e., post-reconstruction fitting. Here, we proposed a whole-body indirect Patlak method with an aid of a deep learning-based reconstruction algorithm, i.e., deep progressive reconstruction (DPR), to provide denoised parametric images without introducing extra computation cost. We compared the proposed method with the indirect Patlak method using PMOD. ***Materials and Methods:*** Whole-body dynamic ^{18}F-FDG (6.4-9.5 mCi) scans were performed on four participants (3/1 M/F, 57-67 yrs, 53-75 kg) from Xijing Hospital (Xi'an, China). Each 0-60 min post-injection scan was composed of a 10-min single-bed acquisition centered at the cardiac region, followed by a multi-pass acquisition (5 pass×4 bed×90 sec and 1 pass×4 bed×300 sec). Image-derived input function was generated from the descending aorta. Low-dose data were simulated by down-sampling the listmode data of the multi-pass acquisition. The proposed method was applied to generate parametric images at full, 1/2, and 1/3 dose levels. Indirect Patlak fitting with PMOD at full dose was used as the reference. Regions of interest (ROI) including thalamus, cerebellum, myocardium, liver, and lesions (N = 32) were drawn manually. Coefficient of variance (CoV) at liver and contrast-to-noise ratio (CNR) of lesions were calculated. ***Results:*** Correlation analysis of K_i values for all the ROIs and all the participants was performed. Comparing to the PMOD results, the proposed method showed high correlation with R^2 of 0.9943, 0.9913, and 0.9909 at full, 1/2, and 1/3 dose levels, respectively. The liver K_i CoV increased with the dose decreased and showed comparable results at 1/3 dose with the PMOD results at full dose. The lesion K_i CNR values were 25.4±19.3, 22.2±15.1, and 19.8±12.3 at full, 1/2, and 1/3 dose, respectively, while the full-dose PMOD yielded 18.8±13.1 in lesion CNR. ***Conclusion:*** Without extra computation cost, the proposed method was demonstrated quantitatively accurate and showed similar performance in noise reduction and contrast recovery at 1/3 dose as compared with the conventional indirect method at full dose.

EP-0649

Deep learning-based method for the reconstruction of high-quality 3D PET image from low-dose data

R. Guo[1,2], *J. Wang*[3], *Y. Miao*[1,2], *S. Xue*[4], *Y. Zhang*[1,2], *K. Shi*[4], *B. Li*[1,2], *G. Zheng*[3];
[1]*Ruijin Hospital, Shanghai Jiao Tong University School of Medicine, Shanghai, CHINA,* [2]*Collaborative Innovation Center for Molecular Imaging of Precision Medicine, Ruijin Center, Shanghai, CHINA,* [3]*Institute of Medical Robotics, School of Biomedical Engineering, Shanghai Jiao Tong University, Shanghai, China, Shanghai, CHINA,* [4]*Department of Nuclear Medicine, University of Bern, Switzerland, Bern, SWITZERLAND.*

Aim/Introduction: Deep learning models have shown great potential in reconstruction of full-dose PET image from low-dose ones. However, most methods only focus on the reconstruction of a single view and ignore the 3D characteristics of PET image. We aim to reconstruct the high-quality 3D PET image on three views by a deep learning-based spatial fusion method and evaluate the generalization of this method on different scanners and traces. ***Materials and Methods:*** The study was performed on 456 participants scanned on 3 different PET scanners with 2 different tracers. We proposed a spatial fusion model to reconstruct the high-quality 3D PET image based on three views and compared the qualitative and quantitative results with the state-of-the-art methods of 2D and 3D. The quantitative metrics were NRMSE, PSNR, SSIM. The qualitative results were assessed by two nuclear medicine physicians independently and they were asked to use a 5-point grading scheme for visual image quality assessment. Furthermore, we also evaluated the generalization of this method on different PET scanners and tracers. ***Results:*** The results reconstructed by our method showed the significant NRMSE improvement of low-dose PET image, compared with 2D C-Gan and 3D-Unet (Table1). All pair-wise tests had P values <0.0001. Additional results of PSNR and SSIM showed the same tendency as the NRMSE results. The clinical evaluation scores of two nuclear medicine physicians had high agreement that our method perform the best results on three views (Axial: 4.2 from our method vs. 3.8 from C-Gan and 3.7 from 3D-Unet; Sagittal: 4.2 from our method vs. 2.9 from C-Gan and 4.0 from 3D-Unet; Coronal: 4.1 from our method vs. 3.0 from C-Gan and 3.8 from 3D-Unet). For the generalization evaluation, the performance of our method also exhibited the NRMSE improvement of low-dose PET image on different PET scanners and tracers with different dose reduction factors (DRF) from 4 to 100 (Table2). ***Conclusion:*** The method we proposed can reconstruct the high-quality 3D PET image on three views and have great generalization on different scanners and traces.

EP-0650

Diffuse high uptake of 68Ga-FAPI in both kidneys helps with diagnosis of kidney diseases

X. Zhong[1], *J. Cheng*[2], *M. Su*[2], *W. Zhang*[3];
[1]*Nuclear Medicine Department and Biomedical Big Data Center, West China Hospital of Sichuan University, Chengdu, CHINA,* [2]*Nuclear Medicine Department, West China Hospital of Sichuan University, Chengdu, CHINA,* [3]*Biomedical Big Data Center, West China Hospital of Sichuan University, Chengdu, CHINA.*

Aim/Introduction: Gallium-68 labeled fibroblast activation protein inhibitor (^{68}Ga-FAPI) is a promising novel imaging agent beyond tumor disease. The aim of this study is to investigate the relationship between diffuse increased uptake of ^{68}Ga-FAPI in kidneys and glomerular filtration rate (GFR), and its diagnostic ability for kidney diseases. ***Materials and Methods:*** We conducted a retrospective study from February 2022 to September 2022, analyzing images from participants who underwent whole-body or abdominal ^{68}Ga-FAPI PET/CT examinations. The relationship between tracer uptakes, quantified by maximum standardized uptake value (SUVmax) and mean standardized uptake value (SUVmean), and GFR was analyzed using Pearson correlation analysis. The diagnostic performance of ^{68}Ga-FAPI PET/CT for renal diseases was evaluated by receiver operating characteristic (ROC) curve and the area under the curve (AUC). Optimal SUVmax threshold for diagnosing kidney disease was determined using the percentile method recommended by the American Clinical

and Laboratory Standardization Institute (CLSI). ***Results:*** A total of 121 images of 99 patients (median age, 59 years [interquartile range: 23 - 83 years]; 82 men) were included. Pearson correlation analysis showed an inverse association between renal SUVmax and SUVmean with GFR, with R^2 values of 0.233 and 0.226, respectively. The AUC of SUVmax for diagnosing renal disease was 0.961. The sensitivity, specificity, and accuracy of SUVmax > 2.15 for diagnosing kidney disease were 90.48% (19/21), 73.91% (17/23), and 81.82% (36/44), respectively. ***Conclusion:*** The concentration of ^{68}Ga-FAPI in renal parenchyma is inversely associated with GFR and shows great potential for the diagnosis of kidney diseases.

EP-0651

Designing a 1-mm Resolution Brain-Dedicated PET System with a Hemispherical Detector Arrangement

T. Yamaya[1], *E. Yoshida*[1], *G. Akamatsu*[1], *K. Narita*[2,1], *H. Tashima*[1], *Y. Iwao*[1], *M. Takahashi*[1];
[1]*National Institutes for Quantum Science and Technology (QST), Chiba, JAPAN,* [2]*Chiba University, Chiba, JAPAN.*

Aim/Introduction: Due to the strong demand for PET diagnosis of dementia, the development of brain-dedicated PET systems is drawing attention worldwide. Even for amyloid PET, high spatial resolution is needed for quantitative diagnosis by separating cortical amyloid from non-specific accumulations in white matter. For brain tumour treatment, higher spatial resolution is required for more accurate identification of a tumour invasion area. In practice, not only high spatial resolution but also high sensitivity and low cost are desired, and we have proven that a hemispherical detector arrangement can achieve higher sensitivity with a smaller number of detectors than a conventional cylindrical geometry [1]. In addition, a smaller detector ring leads to better spatial resolution by eliminating a photon non-collinearly effect, which determines the theoretical resolution limit of about 2 mm for whole-body PET and of about 1 mm for brain-dedicated PET. Therefore, our aim in this work was to design a practical brain-dedicated PET system that will achieve the theoretical limit of 1-mm resolution. ***Materials and Methods:*** The proposed 1-mm resolution brain PET consists of two component technologies. The first one is the hemispherical detector arrangement, which can balance the sensitivity and the costs and minimize the photon non-collinearly effect. The second one is our original crosshair light-sharing (CLS) detector, which enables both time-of-flight (TOF) and depth-of-interaction (DOI) measurements. The hemispherical arrangement of the CLS detectors, on a ring diameter of 28 cm, was simulated by Geant4, and spatial resolution to be expected was assessed. ***Results:*** Using a module detector with 4.2 mm pitch lutetium fine silicate (LFS) crystals (10 mm long) and 229 ps TOF resolution, we developed the first prototype system, which demonstrated 2.2 mm rod separation. For better spatial resolution, the CLS detector with 1.5 mm pitch and 15 mm long lutetium-gadolinium orthosilicate (LGSO) crystals was developed, and 3-layer DOI discrimination and 293 ps TOF resolution were achieved. The simulation in which the CLS detectors formed the hemispherical geometry showed that 0.75 mm rods were separated with a valley-to-peak ratio of 0.684. In addition, reconstructed images of a simulated Hoffman phantom and a BigBrain phantom showed high contrast between the gray and white matters. ***Conclusion:*** A feasibility of the 1-mm resolution brain-dedicated PET system was numerically shown with the combination of the CLS detector and its hemispherical arrangement, both of which have been experimentally proven. ***References:*** [1] Takahashi M et al EJNMMI Phys 9 69 (2022)

EP-0652

68Ga -FAPI PET/CT Improves Detection Rates of Gastrointestinal Mucinous Adenocarcinoma or Signet Ring Cell Carcinoma: A Comparative Study with 18F-FDG

Y. Sun*;*
Fudan University, Shanghai Cancer center, Shanghai, CHINA.

Aim/Introduction: Purpose: The aim of this study was to investigate the diagnostic value of Gallium 68 (^{68}Ga) labeled fibroblast activation protein inhibitor (FAPI) PET/CT in gastric and colorectal mucinous adenocarcinoma (MAC) and signet ring cell carcinoma (SRCC) by comparing it with ^{18}F-FDG PET/CT. ***Materials and Methods:*** ^{68}Ga-FAPI PET/CT was performed in patients with inconclusive findings by conventional imaging. The detection rate, the SUVmax and tumor-to-background ratio (TBR) of ^{18}F-FDG and ^{68}Ga-FAPI PET/CT were evaluated and compared. ***Results:*** Fifty-seven patients were enrolled. When compared with ^{18}F-FDG, ^{68}Ga-FAPI showed a superior detection rate for primary tumors (100% vs 80%) and the SUVmax was significantly higher (8.9 ± 3.7 vs 5.3 ± 3.3, $p = 0.035$). In the patient-based analysis, all patients with metastatic peritoneum were FAPI-positive (40/40, 100% detection rate), whereas only fourteen were also FDG-positive (14/40, 35%). In the lesion-based analysis, ^{68}Ga-FAPI showed better sensitivity and specificity in peritoneal metastases than ^{18}F-FDG (sensitivity 89.16% vs 53.61%, $p < 0.001$; specificity 82.30% vs 59.29%, $p = 0.001$). Additionally, peritoneal lesions showed intense ^{68}Ga-FAPI uptake (6.8 ± 2.4 vs 3.6 ± 2.5, $p < 0.001$). The TBRs were higher for ^{68}Ga-FAPI in all the recurrent anastomotic stoma, involved lymph nodes, bone and visceral metastases ($p < 0.001$). Additionally, immunofluorescence staining demonstrated that metastatic lesions had high FAP expression and low Glut-1 expression, corresponding with paired PET/CT. ***Conclusion:*** ^{68}Ga-FAPI PET/CT was superior to ^{18}F-FDG in the detection of both primary and metastatic tumors in patients with gastrointestinal MAC/SRCC, particularly in patients with peritoneal metastases.

EP-0653

Effect of Radiopharmaceutical Extravasation on the Accuracy of SUV Estimation in PET/CT

I. Znamenskiy[1,2,3], *V. Volkov*[2,3], *A. Kondakov*[1,2], *M. Beregov*[3], *D. Mosin*[1,2];
[1]*Petrovsky National Research Centre of Surgery, Moscow, RUSSIAN FEDERATION,* [2]*Pirogov Russian National Research Medical University, Moscow, RUSSIAN FEDERATION,* [3]*Federal center of brain research and neurotechnologies, Moscow, RUSSIAN FEDERATION.*

Aim/Introduction: The evaluation of a patient's clinical case and staging in PET studies partially relies on the calculation of standardized uptake value (SUV). This value can be altered by an incomplete injection of the prescribed dose or its leakage into soft tissues (also known as extravasation) [1]. Extravasation should also be monitored in myocardial blood flow quantification, i.e. with Rb-82 chloride. Our goal was to estimate the importance of extravasation for SUV quantification in the choice of further treatment tactics. ***Materials and Methods:*** This is an ongoing study. To date, 7 patients with visible extravasation were retrospectively enrolled. Extravasation radioactivity was calculated in VOI by multiplying scanner-measured activity by its volume defined by an isocontour with a 5% cut-off of maximum value. As a reference, we used the mean intact liver parenchyma SUV measured in a 50 ml VOI. For the patients with metastatic lesions, the most active lesion was included in analysis. ***Results:*** Of the 7 PET/CT studies 6 had extravasation radioactivity of 1% or less of

the total injected dose. One patient had the measured activity at the extravasation site equal to 5% of the injected dose. Normal tissue and lesions demonstrated extravasation corrected SUVmax, SUVmean, and SUVpeak values that were inversely proportional to the % change in injected dose. This naturally follows from the SUV calculation procedure, which allows us to establish the following relation: SUV increases in 1(1-x) times for x % extravasation of the injected dose. Percent change in SUV ranged from 0 to 5%. ***Conclusion:*** In the majority of patients even visible extravasation usually accounts for less than 1% of the injected dose and therefore leads to SUV alterations of approximately less than 1%, which is consistent with previously published data [2]. However, a non-linear relationship between extravasation activity and SUV results in a disproportionate increase of SUV on higher degrees of extravasation, which could be of critical importance for both diagnostic PET and evaluation of response to therapy. Automated methods for dose correction would be simple and clinically valuable. ***References:*** 1. H. Nathan, Z. Jun, R. Robert, H. Deborah, K. Michael, Impact of FDG extravasation on SUV measurements in clinical PET/CT. Should we routinely scan the injection site? Journal of Nuclear Medicine 47, 115P (2006) 2. Kiser JW. The decision to reimage following extravasation in diagnostic nuclear medicine. Front. Nucl. Med. 3:1171918. (2023)

EP-0654

Last generation digital PET: comparison of the performances of 5 vs. 6 rings systems and optimization of the overlap value

M. Bernardini[1], *T. Mbaye*[1], *M. Alqabandi*[2], *F. Hyafil*[1]; [1]*Hôpital Européen Georges Pompidou (HEGP), Paris, FRANCE,* [2]*Nuclear Medicine Department, Faculty of Medicine, Kuwait University, Kuwait City, KUWAIT.*

Aim/Introduction: Novel 5-rings (5R) and 6-rings (6R) PET systems offer longer detector coverages and increased sensitivity. The objectives of this study were: 1. to evaluate the impact of extending the field-of-view (FOV) from 25cm to 30cm on performance tests; 2. to identify the best overlap value for the 6R-system. ***Materials and Methods:*** A digital PET system of 25cm-FOV was installed initially and then upgraded to 30cm-FOV. Performance tests were realized on both systems following the NEMA-NU-2-2018 procedures. The impact of overlap on image quality and quantification was tested for 0.9%, 28%, 35%, 42% and 50% overlap values and compared to a single FOV acquisition. For analysis of image quality, hot contrast recovery coefficient (HCRC), recovery coefficient (RC) and background variability (BV) were measured on the NEMA-IQ phantom acquired with clinical parameters. For measurement of spatial resolution (SR), FWHM were assessed using the triple-line phantom. ***Results:*** On NEMA-NU-2-2018 tests, SR values were found similar for 5R and 6R systems (3.80mm and 3.77mm for 1cm radial FWHM, respectively). NEMA-NU-2-2018 HCRC and BV values were similar on both systems (mean difference of 1.9 and -1 points of %, respectively). Average sensitivity and equivalent noise count rate (NECR) were, however, much higher on the 6R system (62 % and 67%, respectively). In clinical conditions, HCRC and RC coefficients for 28%, 35%, 42% and 50% overlap values were similar but lower than 1FOV (up to -10.2 and -4.0 points of %, respectively), except for the smallest sphere for which overlaps did improve results, and with the same extent for 35% and 42% overlaps (12.5 and 9 points of % respectively). For all overlaps, the improvement in BV compared to 1FOV was small (< 3 points of %). SR values with Q.Clear reconstructions were similar to 1FOV (2.2 mm) for all overlaps, except for 0.9% (3.5 mm). With VPFX-S reconstructions, SR values were similar to 1FOV, but significantly higher than with Q.Clear (7.0 mm). ***Conclusion:*** Our study demonstrates that image quality and quantification are similar with the 6R and 5R-PET systems. Yet, in addition to the longer FOV, the percentage of overlap on the 6R-PET may be reduced from 42% to 35% without significant loss in detectability, noise, spatial resolution or absolute quantification translating into faster whole-body PET acquisitions. The dramatic increase in sensitivity observed on the 6R-system paves the way for improved image quality and quantification for low-count or short-time-frame PET acquisitions.

EP-0655

Influence of the CT-Energy on the Attenuation Correction of the PET/CT and the Impact on Small Bone Lesions

A. Haslauer*, E. Solari, J. Brosch-Lenz, W. Weber, S. G. Nekolla; Klinikum rechts der Isar, Technical University Munich, Munich, GERMANY.*

Aim/Introduction: For the reconstruction of PET data in multimodal PET/CT systems, an attenuation map (μ-Map) is created from CT images. Therefore, the photon energy from the 120kV CT is extrapolated into 511keV. Photons with lower energy are attenuated stronger in dense material (e.g. cortical bones) than higher energy photons, which leads to our assumption that bones will have a higher HU-value and thickness in the CT. This higher bone thickness will presumably have an impact on the activity measured in small bone lesions. ***Materials and Methods:*** To evaluate the effect of the CT energy, pig bones and a reference abdomen phantom (QRM) were measured in a clinical PET/CT (Vision, Siemens) and a high-energy industrial CT (Fraunhofer Institut, Inline CT, HEITEC PTS). Additionally, the bones were scanned with tubes of 7mm diameter filled with FDG (4.4MBq/mL +/- 0.4 MBq/mL activity). The PET was performed with the e7 tools (Siemens, Knoxville), the PET data was evaluated with Siemens TrueD. This measurement setup was positioned in a larger, water filled container, with 6 tubes in bones and 5 tubes in water. ***Results:*** A measurement of the bones in the clinical CT at 120kV compared with the industrial CT of 450kV gives a difference in the thickness of the bones of 1.7mm as mean value, which is a deviation of 6%. Extrapolated to the μ-Map, the thickness difference changes to 25% (SD = 20%) compared to the HE-CT. A line integral through the bones showed that the industrial CT is on average 13% thinner than the clinical CT and 11% thinner than the μ-Map. The energy extrapolation was performed with the bilinear conversion [1]. The maximum activity in the tubes in water showed an average of 3.0MBq/mL (SD = 0.3MBq/mL). This is 9.5% smaller than the average maximum activity in the tubes in bone (mean = 3.3MBq/mL, SD = 0.2MBq/mL). ***Conclusion:*** The results of the bone thickness and associated line profile proof our assumption that the conversion of CT images to μ-Map contain an error that stems not only from linear attenuation coefficients but also from cortical bone thickness. These measurements showed that lesions around cortical bones are overcorrected. ***References:*** [1] Carney, J.P.J., Townsend, D.W. Method for transforming CT images for attenuation correction in PET/CT imaging. Medical Physics 33,4 (2006)

EP-0656

PET digitization chain for Monte Carlo simulation in GATE

J. Salvadori[1], *A. Merlet*[2], *B. Presles*[3], *A. Etxebeste*[4], *J. Vrigneaud*[3], *D. Sarrut*[4];
[1]*Institut de cancérologie Strasbourg Europe (ICANS), Strasbourg, FRANCE,* [2]*Imagerie et Vision artificielle, ImViA EA 7535, Dijon, FRANCE,* [3]*Institut de Chimie Moléculaire de l'Université de Bourgogne (ICMUB), UMR CNRS 6302, University of Burgundy, Dijon, FRANCE,* [4]*Universitée de Lyon, CREATIS; CNRS UMR5220; Inserm U1044; INSA-Lyon; Universitée Lyon 1; Centre Leon Bérard., Lyon, FRANCE.*

Aim/Introduction: We proposed a comprehensive method for accurately modeling a PET imaging system using Monte Carlo simulation. Accurate Monte Carlo modeling involves implementing a complex analytical signal processing chain, called Digitizer, to closely reproduce the different counts rates of the real system. The Digitizer shapes the signal, determines the timestamp and the position of the interactions, models the timing resolution, the energy resolution, the saturation effects of the detectors, and implements the pulse-processing logic for selecting and coupling single events into coincidences. ***Materials and Methods:*** The proposed method includes 1) modeling the Digitizer as closely as possible to the detection chain of a real system and incorporating all freely available or manufacturer-provided parameters, 2) estimating of remaining parameters (such as background noise level, detection efficiency, dead time, and pile-up) through a two-steps optimization process and 3) validating the estimated parameters with experimental data. The method was applied and validated using experimental data from the NEMA protocol count rates test for three state-of-the-art SiPM TOF-PET : Philips Vereos (digital SiPM), GE Discovery MI 4-ring and Siemens Biograph Vision 600 (analog SiPM). ***Results:*** For all three PET systems, results showed that the relative absolute differences between simulated and experimental data for Single, Prompt, True, Scatter, Random and NEC rates were less than 2 %, 3 %, 5.1 %, 6.7 %, 2.5 % and 10.8 % on clinical activity range (< 10 kBq/mL) and less than 2 %, 3 %, 12 %, 13 %, 2.5 % and 23 % up to the activity of the $NECR_{peak}$. ***Conclusion:*** Overall, the proposed Digitizer optimization method was able to accurately reproduce the counts and NEC rates of three of the latest generation SiPM-based TOF-PET imaging systems.

EP-0657

Sensitivity comparison of non-TOF and TOF PET/CT

L. Carnegie-Peake*, J. Dickson, S. McQuaid;*
University College London Hospital, London, UNITED KINGDOM.

Aim/Introduction: Commercial scanners are available using detectors both with and without time-of-flight (TOF) capabilities. To compensate for the lack of TOF information, non-TOF PET scanners must be more sensitive. The aim of this work was therefore to determine the fundamental sensitivity requirements of a non-TOF system to obtain equivalent contrast and noise properties to that obtained with a TOF system. ***Materials and Methods:*** The NEMA image quality phantom with 6 fillable spherical inserts (volume range: 0.6 - 32 ml) containing F-18 with a sphere to background activity concentration ratio of 12 was scanned on a Siemens Vision 600 (TOF resolution 240 ps) and list mode data were acquired. The data were reconstructed using TOF and non-TOF image reconstruction algorithms. First, reconstruction parameters were selected such that the degree of convergence between the contrast recovery curves (CRC) of the TOF and non-TOF reconstruction methods were matched. The RMSE was evaluated between the CRCs of a standard OSEM TOF reconstruction (4 iterations, 5 subsets) and multiple non-TOF image reconstructions (Iteration number range: 4 to 30). The reconstruction with the minimum RMSE was used as the reference non-TOF reconstruction in the remainder of the work. Second, to obtain equivalent noise in the datasets, the list mode data used in the TOF reconstruction were downsampled. The SNR was evaluated for the six spheres using these downsampled TOF datasets and for the previously determined reference non-TOF reconstruction. The RMSE was evaluated between the TOF and non-TOF SNR curves. The relative sensitivity increase required by a non-TOF system to match the SNR performance of a TOF reconstruction was determined based on the downsampled dataset with the minimum RMSE. ***Results:*** The CRC of a non-TOF image reconstruction with 15 iterations matched the CRC of a standard TOF image reconstruction with 4 iterations (both with 5 subsets). Good agreement of the SNR properties between this non-TOF reference reconstruction was identified when the TOF data was downsampled to 35%. This corresponds to a relative sensitivity increase requirement of 2.9 for a non-TOF system, compared to a TOF system with a timing resolution of 240 ps. ***Conclusion:*** Non-TOF scanners are required to be significantly more sensitive to compete with the good SNR provided by TOF systems. However, non-TOF systems have the ability to match both the contrast and SNR of images obtained from a TOF system if the PET detector sensitivity is sufficiently high.

EP-0658

Development and Validation of a Monte Carlo Simulation Workflow for a Total-Body PET Scanner

C. Pommranz[1,2], *E. Elmoujarkach*[3], *J. Cabello*[4], *W. Lan*[5], *M. Rafecas*[3], *J. Mannheim*[1,6], *P. Linder*[5], *A. Santangelo*[2], *C. la Fougère*[5,6], *B. Pichler*[1,6], *F. Schmidt*[1,5];
[1]*Werner Siemens Imaging Center, Department of Preclinical Imaging and Radiopharmacy, Eberhard Karls University Tuebingen, Tuebingen, GERMANY,* [2]*Institute for Astronomy and Astrophysics, Eberhard Karls University Tuebingen, Tuebingen, GERMANY,* [3]*Institute of Medical Engineering, University of Lübeck, Lübeck, GERMANY,* [4]*Siemens Medical Solutions UNITED STATES OF AMERICA, Inc., Knoxville, TN, UNITED STATES OF AMERICA,* [5]*Department of Nuclear Medicine and Clinical Molecular Imaging, University hospital Tuebingen, Tuebingen, GERMANY,* [6]*Cluster of Excellence iFIT (EXC 2180) "Image Guided and Functionally Instructed Tumor Therapies", University of Tuebingen, Tuebingen, GERMANY.*

Aim/Introduction: The latest generation of total-body PET scanners feature high sensitivity and a long axial field of view that enable novel clinical applications. Monte Carlo simulation studies potentially help understanding and characterizing these scanners as well as to optimizing scan protocols due to repeatability and known ground truth information. The purpose of this study was to develop and validate an end-to-end Monte Carlo simulation workflow for a total-body PET scanner, ranging from modeling physical properties of events and their detection to producing tomographic images. ***Materials and Methods:*** The Geant4 Application for Emission Tomography (GATE) was used together with a proprietary scanner-specific digitizer and coincidence sorter to determine list-mode event data. Image reconstruction was performed using the same vendor proprietary software that is used for the emission data of the real scanner. Normalization correction was performed using a normalization matrix from the real scanner with a calibration factor adapted for simulation. Phantom simulation studies including image quality,

quantification and sensitivity assessment were performed and validated against measurements. Patient-like simulations with the XCAT phantom were enabled by implementing voxelized synthetic μ-maps in the workflow. ***Results:*** Activity concentrations determined for three different phantoms were found to agree with the simulation ground truth with differences below 1%. For a simulation of the image quality phantom (4:1 sphere to background ratio, 5.5 kBq/ml background activity), contrast recovery coefficients were found to be 87.3% and 85.5% (37 mm sphere), 83.5% and 82.4% (28 mm sphere), 79.0% and 77.7% (22 mm sphere), 74.4% and 74.6% (17 mm sphere), 69.2% and 67.9% (13 mm sphere), and 55.5% and 64.3% (10 mm sphere) for the simulation and measurement [1], respectively. The lung residual error was 4.7% for the simulation and 4.8% for the measurement. Sensitivity profiles for different acceptance angles showed a good correlation with experimental data. Preliminary results from a 20s short simulation of the XCAT phantom indicate its potential as a surrogate for real patient scans. ***Conclusion:*** A workflow based on GATE and proprietary image reconstruction software is proposed for precise Monte Carlo simulations of a total-body PET scanner. Future work will include a full NEMA based validation of the simulation workflow. The simulation workflow can be used to generate training and validation datasets, including simulation of ground truth information for machine learning algorithms (e.g., validation of motion correction algorithms), and to investigate scenarios impractical for patients (e.g., varying applied dose). ***References:*** [1] Prenosil et al., 2022

EP-0659

Can SUVmax be used to predict the development of anatomical correspondence in bone uptakes detected by 18F-PSMA-1007-PET/CT?

L. Eklund*, M. Anttinen, J. Vanhatalo, S. Malaspina, T. Noponen, J. Kemppainen, P. Boström, M. Seppänen, O. Ettala;*
University of Turku, Turku, FINLAND.

Aim/Introduction: To improve the diagnostic accuracy in detecting local and metastatic prostate cancer (PCa), various radioligands have been developed. Unlike the FDA approved ^{Ga}68-PSMA-11 and ^{18}F-PSMA-DCFPyl, ^{18}F-PSMA-1007 is eliminated via the hepatobiliary route, which represents an advantage in local staging and restaging of PCa. However, a limitation of ^{18}F-PSMA-1007 is the higher incidence of non-specific bone uptakes. The objective of this study was to describe how many bone uptakes without anatomical correspondence detected by ^{18}F-PSMA-1007-PET/CT developed correspondence during follow-up and investigate if baseline SUVmax values can predict this development. ***Materials and Methods:*** This retrospective study analyzed data from two prospective, registered trials, the PROSTAGE study (NCT03537391) and the ADTPSMA2 study (NCT03876912), which recruited treatment-naïve high-risk or metastatic PCa subjects. Subjects with at least one uptake without correspondence in the baseline ^{18}F-PSMA-1007 PET/CT were included. To determine the development of anatomical correspondence during follow-up, either whole body contrast-enhanced CT or ^{18}F-PSMA-1007 PET/CT were used. Baseline SUVmax values in bone uptakes were compared between those that developed correspondence and those that didn't. AUC, sensitivity, and specificity were calculated for SUVmax in predicting the development of anatomical correspondence. ***Results:*** At baseline in 70 subjects, ^{18}F-PSMA-1007 PET/CT identified a total of 714 bone uptakes. Of these, 470 (65.8%) were with anatomical correspondence, and 244 (34.2%) were without. Out of the uptakes without correspondence, 219 had at least one follow-up image. Median (IQR) follow-up time was 13 (12; 35) months, during which 82 (37.4%) uptakes developed anatomical correspondence. The median (IQR) SUVmax in the baseline ^{18}F-PSMA-1007-PET/CT were 10.3 (6.18; 14.63) and 5.6 (4.2; 8.5) for lesions that did and did not develop anatomical correspondence, respectively. Wilcoxon two-sample test showed a statistically significant difference between groups ($p<0.0001$). In predicting the development of correspondence, baseline SUVmax ROC analysis achieved AUC of 0.725. The highest sum for sensitivity and specificity was achieved at SUVmax 7.5, where sensitivity and specificity reached 0.71 and 0.69, respectively. At SUVmax 4.0 sensitivity and specificity were 0.96 and 0.18, respectively. ***Conclusion:*** This study showed that a notable number of the PSMA uptakes without anatomical correspondence developed correspondence, suggesting a metastatic nature. Baseline SUVmax values in those lesions were significantly higher compared to those that did not develop correspondence. However, due to its unsatisfactory performance in terms of sensitivity and specificity, baseline SUVmax in ^{18}F-PSMA-1007-PET/CT bone uptakes seems to be of limited clinical utility in predicting the development of correspondence.

EP-0660

Measurement of NECR in a Long Axial Field of View Scanner using a Custom Humanoid Phantom covering the Full Axial Field

S. Holm*, J. V. *Henriksen, T. L. Andersen, F. L. Andersen;*
Rigshospitalet, Copenhagen University Hospital, Copenhagen, DENMARK.

Aim/Introduction: Recent developments in PET provided scanners with large axial field of view (LAFOV) >1 meter, having markedly increased sensitivity over systems with 15-25cm AFOV. We examined a LAFOV system with length 106cm. Assessment using NEMA NU-2-2018 standard showed peak noise equivalent countrate (NECR) value 1.92 Mcps@25 kBq/mL for full ring acceptance. However, the NEMA phantom (70cm) is too short to reflect clinical use. Here we aim to characterize the system NECR using a humanoid phantom, covering the full FOV and reaching from activity beyond system electronic capacity down to background by intrinsic radiation from LSO-detectors. This information is relevant for decisions on system use both for fast studies with high activity and studies with ultralow activity/dose over prolonged time. ***Materials and Methods:*** A phantom was composed of independent compartments with varying concentrations of FDG and a total volume of 37 liters (total weight 53 kg). Brain: Hoffman phantom. Heart, lungs and liver: home-made thorax phantom. Abdomen: two NEMA IQ phantoms (with hot/cold spheres). Bladder: small bottle included in the lower NEMA IQ. Legs: 2L bottles. With background in thorax and abdomen phantoms =1.00, concentrations were: brain, myocardium, "hot spheres" (4.0), liver (2.0), heart ventricle (1.0), legs (0.5) and bladder (~50). The phantom contained a total of 2244 MBq at scan start. Five minute scans were performed for 30 h, at intervals 20 min until 8 hours, 30 min until 12 hours, then 60 min. Global NECR was calculated from measured prompts and delayed randoms. ***Results:*** Peak NECR for the body phantom was 1.02 Mcps@17.3 kBq/mL. This value (like in NEMA measurements) seems determined by a coincidence bottleneck rather than detector deadtime or (random) correction effects. At the break point, the NECR curve is already very flat, but clinical use with standard activity (3 MBq/kg) is not compromised. However, the slope of the NECR curve is

reduced to 47% of maximum and radiation protection concerns may warrant the use of lower activity. In this phantom, reduction from 3 MBq/kg to 0.3 MBq/kg is compensated by an increase in time by a factor 7. Only below 0.01 kBq/mL, random corrections from background will influence quality. The peak point likely will shift with patient size; a phantom extension to mimic obesity is considered. ***Conclusion:*** The 106 cm LAFOV system is well suited to patient studies in the normal range of injected activities with wide possibilities for balancing activity versus time.

EP-0661

Feasibility study of Sub-minute acquisition with deep-learning reconstruction using 18F-FAPI Total-body PET/CT

E. Liu, *L. Jiang;*
Guangdong Provincial People's Hospital, Guangdong Academy of Medical Sciences, Guangzhou, CHINA.

Aim/Introduction: FAPI PET/CT has demonstrated promising outcomes in the detection and restaging of various cancer types, showcasing superior image contrast and tumor-background ratio.This is beneficial for reducing the tracer injection doses and shortening the acquisition time, especially with the long axial field-of-view (LAFOV) PET/CT scanners and deep-learning-based reconstruction algorithms. This study aimed to evaluate the feasibility of ^{18}F-FAPI-04 total-body PET/CT sub-minute acquisition combined with deep-learning reconstruction (DLR). ***Materials and Methods:*** Fourteen restaging patients (2 females, 12 males; mean age, 59.0 years; range, 34 - 78 years) with different types of malignant tumors were included in the study. All patients underwent a 300-second list-mode ^{18}F-FAPI-04 total-body PET/CT (1.85 MBq/kg). The entire dataset was divided into groups of durations of 10, 20, 30, 60, 120, and 180-second. PET images were reconstructed using ordered subset expectation maximization (OSEM) with a Gaussian smoothing filter (3 mm) and DLR. A region of interest (ROI) with a round circle (2D mode) and a diameter of 1 cm was selected in the right posterior lobe of the liver , ascending aorta (bronchial bifurcation), and bilaterally in the gluteal muscle (the upper edge of the acetabulum). The SUVmax, SUVmean, and standard deviation (SD) were recorded for each ROI. Considering the 300-second OSEM reconstruction image as a standard, a 5-point Likert scale and semi-quantitative analysis were used to compare the effects of OSEM and DLR on image quality, detection rate, and uptake value of primary and metastatic lesions at different acquisition durations. ***Results:*** Fourteen patients with recurrence were identified, with nine primary and eleven metastatic lesions. The signal-to-noise ratio (SNR) of the liver, ascending aorta, and gluteal muscle in images acquired for 10, 20, and 30 seconds of OSEM reconstruction were lower compared to images reconstructed with 300-second OSEM reconstruction ($P<0.01$). The visual image quality scores of images and SNR acquired for 10, 20, 30, and 60 seconds were significantly improved with DLR compared to OSEM reconstruction ($P < 0.01$). No significant difference was observed in the SNR of the liver, the ascending aorta, and the gluteal muscle, SUVmax of primary and metastatic lesions between the 20 and 30-second DLR and 300-second OSEM reconstruction images ($P>0.05$). ***Conclusion:*** DLR can significantly improve the image quality of ^{18}F-FAPI-04 total-body PET/CT with ultrafast acquisition. Compared with 300-second OSEM reconstruction, the 20 and 30-second DLR image quality and tumor (primary and metastatic lesions) quantitative evaluation are comparable.

EP-0662

Effect of time-of-flight capabilities on noise in clinical PET-CT

S. McQuaid, *L. Carnegie-Peake, J. C. Dickson;*
Institute of Nuclear Medicine, London, UNITED KINGDOM.

Aim/Introduction: PET systems with different time-of-flight (ToF) capabilities and crystal sensitivities are commercially available. The aim of this work was to assess the impact of ToF on noise in a variety of patient study types, and therefore to determine the relative gain in crystal sensitivity needed to overcome a lack of ToF capabilities in each study type. ***Materials and Methods:*** Ten datasets acquired in listmode on a Siemens Vision 600 (ToF resolution: 240ps) were used for this study: 3 paediatric FDG studies, 4 brain FDG studies and 3 Rb-82 cardiac studies. Each dataset was reconstructed with and without ToF, and reduced-count ToF datasets were reconstructed by using 80, 60, 40 and 20 % of the original listmode data. All ToF reconstructions used OSEM with PSF modelling, with 4 iterations and 5 subsets. The non-ToF dataset reconstructions used 15 iterations to produce equivalent convergence (as previously determined from phantom data), but all other parameters were matched. Noise was compared between reconstructions for each patient through evaluation of the standard deviation (SD) of counts within volumes-of-interest (VOIs). The downsampled ToF dataset with matched noise to the non-ToF data was determined and used as an estimate of the effective sensitivity gain introduced by the ToF capabilities. ***Results:*** Liver VOIs in FDG wholebody data demonstrated higher noise in non-ToF datasets, with VOI SDs on average 60% higher (47-82%) compared to the non-ToF datasets. Noise was matched when the ToF datasets were downsampled to on average 29% (range 22-32%) of the full counts, indicating a factor effective sensitivity increase of over 3 produced by the ToF capability. Other VOIs exhibited similar results: small FDG hotspot VOIs in the wholebody data required ToF downsampling to 31% on average (range 27-34%) to match non-ToF SDs, brain VOIs matched at 24% (range 20-33%) downsampling and Rb-82 myocardial VOIs matched at 38% (range 27-44%) downsampling. These are equivalent to factor increases in effective sensitivity of 3.5, 3.3, 4.1 and 2.6 for each of the VOIs/scan types respectively. ***Conclusion:*** Although variations between patients and between study types were seen, the use of ToF produced substantial gains in effective sensitivity for all study types, with noise being matched to non-ToF reconstructions with 20-40% of the counts. Systems without ToF capabilities therefore need at least a 3-fold increase in sensitivity to produce images with equivalent noise to that of a 240-ps resolution ToF system with the same axial field-of-view.

EP-44

e-Poster Area

D: Technical Studies -> D1 Instrumentation -> D13 PET/MR

EP-0663

Development of a low-cost protocol using standard equipment for the constant infusion administration of [18F]FDG in PET-MR

A. Cripps[1], *J. Taylor*[1,2], *M. Singleton*[1], *D. Selvarajah*[1,2], *G. Armitage*[1], *A. Scott*[1];
[1]*Sheffield Teaching Hospitals NHS Foundation Trust, Sheffield, UNITED KINGDOM,* [2]*University of Sheffield, Sheffield, UNITED KINGDOM.*

Aim/Introduction: PET-MR research study required the constant infusion of [^{18}F]FDG at a slow rate (36mL/hr) for 1 hour to a patient on the PET-MR scan bed. The administered activity was patient weight-dependent, expected to be an average of 300MBq/patient. There was no appropriate method in the literature, and no pieces of equipment available to us that could meet the needs of the study, so we have developed a low-cost protocol using a standard infusion pump to perform constant infusion of PET tracers in the MR environment. This method aimed to keep the radiation dose to staff and the patient as low as reasonably practicable, to minimise radiation contamination risk, and to maintain MR safety. ***Materials and Methods:*** It was decided to eliminate the need for MR-shielding of equipment, by hosting much of the set-up in an adjacent room that contained a hatch into the scan room. A drip stand was used to hold a burette with two inputs, one of which was attached to a saline bag, and the other was used as a port to inject [^{18}F]FDG into. The [^{18}F]FDG and saline were mixed in the burette. The burette output port was connected to a volumetric infusion pump, which was attached to 6.75m of extension lines, passing through the hatch into the scan room, and terminating at the patient bed, where they could be connected to a cannula. The only significant cost was attributed to custom lead shielding that clamped onto the drip stand to surround the burette. Radiation doses were calculated manually and using computed dose simulation software. Doses were considered for the whole body, skin/extremity, and eye dose for all aspects of the routine work, as well as several reasonably foreseeable incidents. ***Results:*** The developed protocol met the specification, with radiation and MR safety accounted for. The total cost of the project was less than £400, which is significantly less than the cost of an MR-compatible infusion pump. The projected radiation doses to staff were 0.036mSv/procedure for routine external whole-body and eye dose, and 6.3mSv/procedure for external skin/extremity dose. The greatest reasonably foreseeable incident dose was 28.5mSv to the skin/extremities, if [^{18}F]FDG was ejected from the line. These results added justification to the ongoing classification of the staff concerned. ***Conclusion:*** We have successfully developed a low-cost protocol for the slow infusion of [^{18}F]FDG in the PET-MR environment, that considers both radiation and MR safety.

EP-0664

Addressing PET Attenuation Correction Challenges for the ACR Accreditation of a Simultaneous PET/MR Scanner

H. Kulkarni[1], *A. Samuels*[1], *T. Faasse*[1], *V. Sridhar*[2], *L. Hu*[2], *J. Botti*[1]; [1]*BAMF Health, Grand Rapids, MI, UNITED STATES OF AMERICA,* [2]*UIH America, Houston, TX, UNITED STATES OF AMERICA.*

Aim/Introduction: Integrating both PET and MRI modalities into a single scanner with simultaneous acquisition has several advantages in various clinical applications but is met with unique challenges for implementation with the highest quality standards. The uPMR 790 PET/MR combines the SiPM-based HD TOF 32-cm-axial-field-of-view PET with a 3T MRI. This advanced technology needs standardized quality assurance. The American College of Radiology (ACR) accreditation ensures clinically relevant and standardized image quality measurement using phantom testing. Although PET/CT imaging utilizes CT-based PET-attenuation correction, the MR-generated maps cannot be used for accurate attenuation correction in PET/MR, causing potential bias of molecular imaging parameters like SUV. We describe the quality assurance of the PET/MR scanner based on ACR testing guidelines for MRI and PET, along with unique solutions to intrinsic imaging-related challenges. ***Materials and Methods:*** The ACR-PET-Phantom was used to perform adequate F-18-PET testing. The phantom was filled with F-18, and SUVs in the background, and the radioactivity-filled regions were assayed. Best practices included measurement of the residual syringe activity, scanner cross-calibration, and clock synchronization. Specific μ-maps registering ACR phantom images for attenuation and scatter correction were generated and used. Standardized phantom fixation and positioning ensured the correct alignment of μ-maps in relation to PET. PET images were reconstructed per ACR parameters. The ACR-MRI-Phantom was scanned using recommended MRI sequences. Axial T1W images were obtained as follows: TR= 4500, 5.0mm-slice-thickness with 5.00mm-gap, 480x480-matrix. Axial T2W images were obtained as follows: TR=2000, 5.0-mm-slice-thickness with 5.00mm-gap, 384x 384-matrix. Additionally, all site coils (Body, Integrated Spine, Large and Medium Flex, Knee, Shoulder, Breast, and Head Coils) were tested with T1W acquisitions as follows: TR=300, TE=20, 5.0mm-slice-thickness with 5.00mm-gap, and 384x384-matrix. ***Results:*** PET imaging of the ACR phantom registered with the specific μ-maps showed the background SUVmean of 0.93 and SUVmax of 1.91-2.75, both within the recommended ACR limits. Uniformity and noise were evaluated qualitatively through inspection of reconstructed tomographic sections by a certified medical physicist and were found to be within acceptable limits. All ACR MRI phantom sequences produced a relative SNR of 1.0 (100%), acceptable according to ACR guidelines on all coils and sequences. ***Conclusion:*** The performance measurements of the uPMR 790 PET/MR system are comparable with other state-of-the-art PET/CT systems using unique solutions created to address challenges pertaining intrinsically to the imaging modality, and these can be extended for use in other clinical systems. ***References:*** ACR guidance documents for nuclear medicine/PET and MRI accreditation.

EP-45

e-Poster Area

D: Technical Studies -> D1 Instrumentation -> D15 Quality Control, Performance and Standardization

EP-0666

Coincidence distribution in 2-layer hemispheric PET geometries

K. Scheiff*, A. Pashazadeh, C. Hoeschen; Otto-von-Guericke-University Magdeburg, Magdeburg, GERMANY.*

Aim/Introduction: Positron Emission Tomography (PET) is used for diagnostic and research purposes of a wide range of brain diseases, requiring high resolution of about 1mm. To achieve such resolution, brain-dedicated geometries have been proposed and prototyped in recent years.[1] Many of these PET-systems use (hemi-)spherical geometries to minimize the scanner's radius and reach a desired resolution.[2] Like most PET-systems, brain-dedicated geometries commonly utilize detectors with pixelated crystals. However, over the last decade, detectors using monolithic crystals have achieved intrinsic resolutions comparable to pixelated ones.[3] Since the intrinsic resolution of monolithic crystals is related to their thickness, a second layer of detectors can be added to achieve the same total-crystal-depth as that

used in pixelated detectors and to close gaps in the positioning of the first layer. By having pixelated crystals on the inner layer and monolithic detectors on the outer layer, time-of-flight resolution and depth-of-interaction resolution can be achieved, respectively. The ratio of coincidences on each layer and interlayer-coincidences provides information on the impact of the abilities on the image quality. ***Materials and Methods:*** The simulation study was conducted using GATE. We simulated 2-layer hemispheric PET-geometries with detectors, employing pixelated crystals on the inner and monolithic crystals on the outer layer. The geometries were simulated for BGO, LSO and LYSO crystals and activities between 0.1MBq and 100MBq. An in-house coincidence sorter provides the number of coincidences, with singles either on the inner layer, outer layer or one on each layer. ***Results:*** The coincidence distribution regarding the layers is presented. For all materials, interlayer-coincidences dominate, with an average percentage between 55.2% (BGO) and 58.9% (LSO). The second highest fraction of coincidences were inner-layer-coincidences, with an average between 36.3% (BGO) and 29.4% (LYSO). The smallest contribution to total coincidences was observed for outer-layer-coincidences, ranging from 8.4% (BGO) and 16.6% (LYSO) in average. ***Conclusion:*** More than 50% of the coincidences in 2-layer geometries are interlayer-coincidences. Outer-layer-coincidences contribution is highly material dependent. The impact of special abilities of different detector types is therefore limited. The interlayer-coincidences effect on the resolution needs further investigation. ***References:*** [1] Ciprian Catana, Development of Dedicated Brain PET Imaging Devices: Recent Advances and Future Perspectives,J.Nucl.Med.2019Aug.;60(8):1044-1052. [2] Hideaki Tashima et al 2019, First prototyping of a dedicated PET system with the hemisphere detector arrangement,2019Phys. Med.Biol.64 065004 [3] Andrea Gonzalez-Montoro et al, Evolution of PET Detectors and Event Positioning Algorithms Using Monolithic Scintillation Crystals, IEEE Transaction on radiation and plasma medical sciences,Vol.5,No.3,May2021

EP-0667

MC Simulator Framework for Monolithic Scintillator Based PET and SPECT

J. Peter*, L. P. Clemens;*
German Cancer Research Center, Heidelberg, GERMANY.

Aim/Introduction: A fully integrated Monte Carlo (MC) simulation (and reconstruction) framework tailored for monolithic scintillator-based PET and SPECT imaging systems is proposed in order to investigate particular aspects of system design and imaging realization. ***Materials and Methods:*** The framework integrates dedicated simulators for positron and high-energy photon propagation within heterogeneous phantoms as represented by arbitrary integration of multi-parametric polygonal surface meshes (PSMs) and point/cell clouds. Phantom, source and parameter management for all involved physical entities is compatible with the multimodal simulation and reconstruction framework Musiré, [1], it is however extended by time/space probabilistic parameter modeling. Scintillation crystals can be defined either as arbitrary PSMs in free space or constrained to (cylindrical, orbital) scanner geometry, including phoswich capabilities, and can be fitted with digital sensors, e.g. Silicon photomultiplers, that include diverse primary and correlated noise models. Low energy scintillation light distributions within the crystals are modeled using an integrated dedicated simulator yielding light fluences on the crystal surfaces. From those, photoelectric interaction sites are estimated employing various approaches from inline statistical fluence moment estimation to unsupervised machine learning approaches using Gaussian mixture models. For subsequent image reconstruction, estimated interaction sites can be preserved as point clouds to enable novel image reconstruction strategies or, to be compatible with existing reconstruction software, can be discretized into virtual binning planes. This new framework, when integrated into the Musiré ecosystem, supports automatic distribution and parallel execution of simulation requests in a multimodal context. It also extends that ecosystem by adding simulator and reconstructor pipelines. ***Results:*** The monolithic scintillator kernel allows for the investigation of detection, energy, timing, and position information for a variety of crystal and sensor arrangements. One exemplary field of application is the study of extended axial field-of-view (total body) PET systems. A simulation study was executed to assess and to improve spatial resolution and partial volume homogeneity, which can be impaired by parallax effects of oblique lines-of-responses in conventional voxelized block detector systems (e.g. Siemens Biograph Quadra Vision), through modified monolithic detector implementation. ***Conclusion:*** Physically exact MC simulation in nuclear imaging not only remains, but increasingly becomes a more and more prolific research tool helping to advance the current state-of-the-art. ***References:*** [1] Peter, J. "Musiré: multimodal simulation and reconstruction framework for the radiological imaging sciences" RSTA, 379(2021).

EP-0668

The Situation of Nuclear Medicine in China: A Report of the First Official Nationwide Survey in 2021

H. Zhang*[1], J. Zheng[2], N. Hu[1], Y. Liu[1], H. Jing[1], L. Huo[1];*
[1]Peking Union Medical College Hospital, Beijing, CHINA, [2]Department of Radiology, University of Cambridge, Cambridge, UNITED KINGDOM.

Aim/Introduction: National Nuclear Medicine Quality Control Center of China conducted the first official survey to investigate the nationwide situation of nuclear medicine in 2021. The survey aimed to unveil the current nuclear medicine situation and its quality control in China. These results are the foundation for the establishment of the quality control management system. ***Materials and Methods:*** The web-based survey was conducted and the data was collected via the National Clinical Improvement System of China from June 31 to August 31, 2021. Significant deviations from the reported data were checked and corrected with phone confirmation. ***Results:*** A total of 808 institutes across 30 provinces responded to the national survey. For human resources, there are 4460 nuclear medicine physicians (1.6 to 10.3 per million population among provinces), 3077 technicians (0.8 to 7.7), and 339 physicists (0.1 to 0.9). There are 887 single-photon imaging instruments, including 354 (40%) SPECT, and 365 PET instruments, including 314 (86%) PET/CT. There are on average 1.0 SPECT and 0.4 PET per million population. 600 (74%) institutes perform SPECT examinations and 302 (37%) perform PET examinations. 60% of SPECT scans are bone scintigraphy. 97% of PET scans use an ^{18}F-FDG tracer. Furthermore, 551 (68%) institutes provide radionuclide therapy services but only 280 (35%) have admission rooms. Among the 808 institutes, the top three radionuclide therapies are ^{131}I-targeted therapy for hyperthyroidism with 546 (68%) institutes, ^{89}Sr-targeted therapy for bone metastasis with 400 (50%) institutes and ^{131}I-targeted therapy for differentiated thyroid cancer with 286 (35%) institutes. Finally, for the frequency

of equipment quality control per year, there are about 67 times (ranging from 7 to 172) self-inspections within the department for SPECT instruments and 111 times (ranging from 9 to 278) for PET instruments on average in each province. There are about 4 failures (ranging from 2 to 6) of SPECT and 5 failures (ranging from 2 to 12) of PET on average per year in each province. There are 408 institutes (of 600 SPECT institutes) performing quality control of SPECT radiopharmaceuticals, 216 (of 302) for PET and 373 (of 551) for radionuclide therapy. ***Conclusion:*** There are high heterogeneities in geographical distributions of human resources and equipment, and in common types of SPECT scintigraphy, PET tracer usage and radionuclide therapy. The average quality control frequency of SPECT complies with the government regulation with a lack of government regulations for quality control of PET and radionuclide therapy.

EP-0669

Monte Carlo performance with impact of different crystal materials on sensitivity characteristic of preclinical PET scanner

Z. Karimi[1], *P. Sheikhzadeh*[2], *M. Ay*[3];
[1]*Faculty of Physics, University of Isfahan, Isfahan, IRAN, ISLAMIC REPUBLIC OF,* [2]*Department of Nuclear Medicine, Imam Khomeini Hospital Complex, Tehran, IRAN, ISLAMIC REPUBLIC OF,* [3]*Research Center for Molecular and Cellular Imaging (RCMCI), Advanced Medical Technologies and Equipment Institute (AMTEI), Tehran University of Medical Sciences (TUMS), Tehran, IRAN, ISLAMIC REPUBLIC OF.*

Aim/Introduction: Nowadays, significant technological advances have been made in design of small animal PET scanners that improved image quality and quantitative accuracy such as development of new scintillation materials. New our developed dedicated small animal scanner was manufactured based on Silicon Photomultipliers (SiPMs) with LYSO crystals. However, it is necessary to choose the appropriate crystal that can improve the scanner's performance or provide a cost-effective scanner. The aim of this research is to develop an accurate Monte Carlo simulation model of this scanner, and outcome simulating an impact of scintillation material on absolute sensitivity characteristic to find the optimum material. ***Materials and Methods:*** The animal PET scanner was simulated via (GATE), the Geant4 Application for Tomographic Emission with eight different scintillation materials (CeBr3, GLuGAG, LaBr3, LFS, LSO, LYSO, LuAP, LuYAP). The Absolute sensitivity was calculated following the guidelines of National Electrical Manufactures Association (NEMA) NU-4 2008 standard, therefore a point source with activity of 11.1 kBq was simulated at center of FOV. It emitted mono-energetic back-to-back 511 keV photons with time running of 70 seconds then replace it via step of 5 mm along the axial FOV (50.3 mm). Two classes of energy window (250-650 keV and 400-700 keV) were also selected. The obtained results were compared together to find optimum crystal for the animal PET configuration. ***Results:*** The highest absolute sensitivity at CFOV was 3.35% for LuAP material at energy window of 250-650 keV and 2.53% at energy window of 400-700 keV. LFS, LYSO and LuYAP had absolute sensitivity of 2.96%, 2.80% and 2.55% respectively after LuAP with energy window of 250-650 keV and also 2.24%, 2.06% and 1.80% at energy window of 400-700 keV. These values are appropriate for manufacturing preclinical PET scanner with high sensitivity in comparison to other materials such as LSO, GLuGAG, LaBr3 and CeBr3. ***Conclusion:*** After our analysis, we determined that the sensitivity could be enhanced by utilizing LuAP scintillator material. This choice would result in high-performance capabilities and is well-suited for preclinical molecular imaging-based research. Additionally, utilizing GLuGAG as a low-cost design further supports this conclusion. ***References:*** Ghabrial, A., Franklin, D., & Zaidi, H. . A Monte Carlo simulation study of the impact of novel scintillation crystals on performance characteristics of PET scanners. Physica Medica, 2018. 50, 37-45.

EP-0670

Determination of the Kernel with which to Smooth the CT for Air Fraction Correction in Lung PET/CT Studies

F. Leek[1,2], *C. Anderson*[3], *A. P. Robinson*[2,4,5], *R. M. Moss*[1], *B. F. Hutton*[1], *K. Thielemans*[1];
[1]*University College London, London, UNITED KINGDOM,* [2]*National Physical Laboratory, Teddington, UNITED KINGDOM,* [3]*University College London Hospital NHS Foundation Trust, London, UNITED KINGDOM,* [4]*The Christie NHS Foundation Trust, Manchester, UNITED KINGDOM,* [5]*University of Manchester, Manchester, UNITED KINGDOM.*

Aim/Introduction: Voxel-wise air fractions (AF) determined from the CT can be used to correct for variable air content in lung PET/CT [1]. However, resolution mismatch between PET and CT can cause artefacts in the AF-corrected image. We compare methodologies for determining the optimal kernel to smooth the CT when PET images are reconstructed with iterative reconstruction methods. ***Materials and Methods:*** Noiseless simulations and non-TOF MLEM reconstructions were performed. An idiopathic pulmonary fibrosis (IPF) patient-realistic digital phantom was constructed. The optimal smoothing was determined in six VOIs within the lungs via i) the point-source insertion-and-subtraction method, h_{pts}; ii) AF-correction with varyingly smoothed CT to achieve the lowest RMSE with respect to the ground truth AF-corrected VOI, h_{AFC}; iii) smoothing a ground truth image to match the reconstruction within the VOI, h_{PVC}. Optimal kernels were used for AFC and VOI RMSE was calculated. A non-uniform AF-corrected lung (cold sphere walls) prohibits the application of h_{AFC} to measured data; only the h_{PVC} method was considered. A modified thorax phantom (spherical inserts in each lung) was acquired on two clinical scanners. Ground truth images were constructed from CT and known activity concentrations. The WMSE in a single VOI, the physical diameter of the spheres (0-4 voxel dilations), determined the optimal kernel. The largest VOI was used to determine the RMSE. ***Results:*** Simulations: for iterative reconstruction, optimal kernel FWHM was dependent on iteration number (i) and VOI position. At 1000i, a kernel FWHM range still existed (7.01-10.6mm), depending on method and VOI position. Despite this, the range of the RMSE of the AF-corrected reconstructed VOIs was 4.46-10.3%. Measured: the range of h_{PVC} FWHMs for varying VOI diameters was 8.75-9.55mm. VOI RMSE ranged between 5.61-9.10% of the unAF-corrected ground truth. ***Conclusion:*** All three kernel determination methods on simulated data produce roughly equivalent AF-corrected RMSE, suggesting that AF-corrected quantification is not very sensitive to the smoothing applied to the CT. This provides confidence in the h_{PVC} method and a single VOI approach to determining a global kernel for AFC on measured data. The small range of h_{PVC} FWHMs obtained for varying VOI sizes on the measured data suggests that kernel width is not very dependent on VOI size. The low RMSE indicates that h_{PVC} has the potential to be utilised to determine the appropriate kernel for AFC on clinical scanners for application to patient PET/CT lung scans. ***References:*** [1] Lambrou et al., EJNMMI, 38, 2011.

EP-0671

Is It Reliable to Use NMQC-Toolkit as a Self-QC Software for Nuclear Medicine Departments?

N. KODALOGLU[1], *G. Vural*[2], *N. C. Gülaldi*[3];
[1]*University of Health Sciences, Dr. Abdurrahman Yurtaslan Oncology Training and Research Hospital, Department of Radiation Oncology, ANKARA, TÜRKIYE,* [2]*University of Health Sciences, Dr. Abdurrahman Yurtaslan Oncology Training and Research Hospital, Department of Nuclear Medicine, ANKARA, TÜRKIYE,* [3]*University of Health Sciences, Ankara Bilkent City Hospital, Department of Nuclear Medicine, ANKARA, TÜRKIYE.*

Aim/Introduction: IAEA (International Atomic Energy Agency) (1), NEMA (National Electrical Manufacturers Association)(2), EANM (European Association of Nuclear Medicine)(3), have different guidelines for analysing routine quality control and quality assurance testing of gamma camera and SPECT systems. However, since many countries lack experienced personnel, independent analysis software is needed to evaluate the QC test images to take action. Nuclear Medicine Quality Control (NMQC) Toolkit (4) is a QC image processing and analysis software developed under the auspices of IAEA. We want to investigate whether this program is feasible and reliable for those nuclear medicine departments that have independent evidence of the quality control decision of their gamma camera units. ***Materials and Methods:*** In this study, we analyzed the images of the planar (intrinsic flood field) uniformity, tomographic resolution etc. tests of the SPECT-CT system (Mediso AnyScan SC, SPECT/CT Hungary) in 2 different time period and compared them to the vendor's results. The results of the analysis of the software are presented in Table 1. The pass criterion for NEMA NU-1 (2) or IAEA HHS-6 (1) testing is between 3.5-5% (upper limit: 5%). Ultra-high-performance threshold levels for differential Central Field of Volume (CFOV), differential Useful Field of Volume (UFOV), integral CFOV, integral UFOV are 1.4%, 1.9%, 1.9%, 2.4%, respectively.) ***Results:*** As can be seen from Table 1, all QC test results after the calibrations were within acceptable limits or below the threshold defined by NEMA and IAEA guidelines. ***Conclusion:*** The NMQC-toolkit is a user-friendly tool to adapt to the daily routine. It doesn't take time to install the software, get used to the interface, and access the software's results to decide when to take action to respond to an unacceptable result. It can be used as a self-QC software for the nuclear medicine departments who owe different kind of SPECT devices and want to collect and store their QC data with the same and independent software. ***References:*** 1. IAEA Human Health Series No. 6. Quality Assurance for SPECT Systems. Vienna: International Atomic Energy Agency, 2009.2. NEMA Standards Publication NU 1-2007. Performance Measurements of Gamma Cameras. S.l.: National Electrical Manufacturers Association, 2007.3. EANM Quality Control of Nuclear Medicine Instrumentation and Protocol Standardisation (2017).4. IAEA NMQC-toolkit manual.

EP-0672

The Role of SPECT/CT NEMA NU2 Calibration in Quantitative Imaging

I. Irimescu[1,2], *R. Maaz*[1], *A. Lazar*[1], *M. Mutuleanu*[1,3], *C. Petroiu*[1], *M. Mihailescu*[2], *M. Gherghe*[1,3];
[1]*Institute of Oncology „Professor Doctor Alexandru Trestioreanu", Bucharest, ROMANIA,* [2]*Applied Sciences Doctoral School, Politehnica University, Bucharest, ROMANIA,* [3]*„Carol Davila" University of Medicine and Pharmacy, Bucharest, ROMANIA.*

Aim/Introduction: Quantification is one of the major benefits of molecular imaging. Compared to PET/CT, the "gold standard" for absolute quantification, quantitative SPECT/CT imaging allows the usage of a wider range of radiopharmaceuticals and applications. Performing acquisitions using SPECT/CT systems that meet the requirements of periodic quality control tests and are properly calibrated according to NEMA/IAEA/AAPM international guidelines is essential for obtaining accurate quantitative results. ***Materials and Methods:*** In our study, we used SPECT/CT acquisitions of a cylindrical homogeneous phantom and a NEMA NU2 phantom on two Discovery 670 DR SPECT/CT systems (GE Healthcare), equipped with low energy - high resolution collimators, to evaluate the operational mode and the quality of the obtained images. Six spherical inserts (10, 13, 17, 22, 28, and 37 mm in diameter) were filled with Tc99m-pertechnetate, with an activity concentration 8.5 times higher than the concentration of the phantom background. The following tests were performed: volumetric sensitivity of the SPECT/CT system (according to NEMA No. 1: 2018), accuracy of activity recovery, image noise evaluation and deviation from the total activity. For these tests, we used a cylindrical phantom of known volume, containing radioactive solution, performing acquisitions according to the NEMA protocol, with 120 projections per 360 degrees (60 degrees per detector). Quantitative SPECT reconstructions for the obtained test images were done with the dedicated software module, using the Ordered Subset Expectation Maximization (OSEM) algorithm. ***Results:*** Our results showed that the best quantitative reconstruction algorithm can be obtained for 10 iterations with 4 subsets, because this algorithm conveys into less noise, and its accuracy is higher than 95%, finding a balance between quantitative accuracy and visual analysis of the obtained images. The activity concentration recovery in the insert with diameter > 24 mm was satisfactory (variation of less than 5%). Following the tests, no results were obtained for one of the equipment according to the acceptance criteria recommended by the manufacturer and the international guidelines, and corrective actions and recalibrations were required. ***Conclusion:*** The set of images used for diagnostic purposes is made with a limited number of iterations and with post-filtering. For quantitative accuracy, the reconstruction includes correction for patient motion, attenuation, scatter, and collimator blur. For more accurate quantitative results, the number of iterations should be increased and post-filtering avoided. The resulting image is quantitatively more accurate, but also noisier and less suitable for viewing.

EP-0673

Stability of Brain PET/CT Image Quantification for Imaging with a VR Headset

L. Raes[1,2], *S. Bourgeois*[1], *A. Bracke*[1], *T. De Haan*[1], *H. Everaert*[1,2];
[1]*Universitair Ziekenhuis Brussel, Brussels, BELGIUM,*
[2]*Vrije Universiteit Brussel, Brussels, BELGIUM.*

Aim/Introduction: Acquiring SPECT/CT or PET/CT images in patients suffering from claustrophobia can be challenging due to long acquisition times and camera design. This often results in degradation of imaging quality. Virtual Reality (VR) headsets have been successfully used in the emergency department to reduce anxiety and could potentially offer a solution to address this issue in nuclear medicine, hereby obliterating the need for pharmacological sedation. ***Materials and Methods:*** A clinical PET/CT system (FOV 16.2 cm) was used to acquire a 720s PET scan of a Hoffman 3D brain phantom filled with ~23kBq/mL [^{18}F]-FDG. Scan data were reconstructed using various reconstruction settings and were compared to baseline (clinically used reconstruction settings). Recovery Coefficient (RC) and Grey Matter (GM) to White Matter (WM) ratio (GMWMr) were calculated for the whole brain, as well as for the Frontal- (FL), Parietal- (PL) and Occipital Lobes (OL). Contours were delineated on the phantoms without VR headset mounted, to which the phantoms with VR

headset were registered using rigid transformations. ***Results:*** No significant systematic discrepancies in the RC of multiple regions and GMWMr were observed between images with and without VR headset. RCs of the regions as reconstructed without Point Spread Function (PSF), resp. without and with VR headset mounted, were as follows: RC_{GM}=[0.73-0.75], RC_{GM-FL}=[0.81-0.82], RC_{GM-OL}=[0.78-0.79], RC_{GM-PL}=[0.73-0.72], RC_{WM}=[0.38-0.39], RC_{WM-FL}=[0.45-0.47], RC_{WM-OL}=[0.42-0.44], RC_{WM-PL}=[0.42-0.41], leading to a GMWMr between [1.73-1.93]. For reconstructions with PSF, the following RCs were obtained: RC_{GM}=[0.77-0.78], RC_{GM-FL}=[0.84-0.86], RC_{GM-OL}=[0.82-0.82], RC_{GM-PL}=[0.75-0.74], RC_{WM}=[0.36-0.37], RC_{WM-FL}=[0.42-0.44], RC_{WM-OL}=[0.40-0.42], RC_{WM-PL}=[0.41-0.40], leading to a GMWMr between [1.85-2.13]. No visual differences were present in the PET image, although some streak artefacts were present in the CT image at the level of the battery pack. The attenuation map of that image was less subject to artefacts: [0.02-0.02]/mm vs [134-176] HU_{Avg} for a sphere VOI close to the battery pack within the plastic discs, respectively without and with VR headset mounted. ***Conclusion:*** The impact on PET imaging is limited. We conclude that a VR headset can be used during PET/CT imaging. ***References:*** Rousseaux F, Panda R, Toussaint C, Bicego A, Niimi M, Faymonville ME, Nyssen AS, Laureys S, Gosseries O, Vanhaudenhuyse A. Virtual reality hypnosis in the management of pain: Self-reported and neurophysiological measures in healthy subjects. Eur J Pain. 2023 Jan;27(1):148-162. doi: 10.1002/ejp.2045. Epub 2022 Oct 24. PMID: 36196745; PMCID: PMC10091709.

EP-46

e-Poster Area

D: Technical Studies -> D2 Data Analysis -> D21 Data Analysis in Neuro and Cardio

EP-0674

Parametric imaging of P-glycoprotein function at the blood-brain barrier using KE,brain-maps generated from dynamic [11C]metoclopramide PET data in rodents, monkeys, and humans

L. Breuil[1,2], *M. El Bialil*[3], *D. Vodovar*[1], *S. Marie*[1], *S. Auvity*[1,2], *S. Goutal*[1], *S. Rodrigo*[1], *M. Bauer*[3], *O. Langer*[3,4], *N. Tournier*[1];
[1]*1.BioMaps, Laboratoire d'Imagerie Biomédicale Multimodale Paris-Saclay,Inserm, CNRS, CEA, Université Paris-Saclay, Orsay, France, Orsay, FRANCE,* [2]*2. Inserm UMR-S1144, University of Paris Cité, 75006 Paris, France., Paris, FRANCE,* [3]*3.Department of Clinical Pharmacology, Medical University of Vienna, 1090 Vienna, Austria., Vienna, AUSTRIA,* [4]*4.Department of Biomedical Imaging and Image-guided Therapy, Medical University of Vienna, Austria., Vienna, AUSTRIA.*

Aim/Introduction: The P-glycoprotein (P-gp) is the most studied efflux transporter expressed at the blood-brain barrier (BBB). Kinetic modeling of PET imaging data using the radiolabeled substrate [^{11}C]metoclopramide showed the importance of P-gp-mediated brain-to-blood efflux ("k_2-effect") in promoting the elimination of solutes from the brain. Taking advantage of this property, the elimination slope from the brain ($K_{E,brain}$, min^{-1}), which can be directly calculated from dynamic PET images without arterial blood sampling, was evaluated as an outcome parameter to describe P-gp-mediated efflux function at the BBB in several species. ***Materials and Methods:*** The $K_{E,brain}$ parameter was obtained from linear regression of Log-transformed time-activity curves (TACs) obtained in rats, monkeys, and humans. The $K_{E,brain}$ values obtained in the baseline situation were compared with values obtained after complete P-gp inhibition using tariquidar in rats (n=4) and monkeys (n=4) and after partial inhibition using cyclosporin A in humans (n=10), (unpaired Student's t-test). Full kinetic modeling using the 1-tissue compartment model in monkeys enabled a comparison of the sensitivity of $K_{E,brain}$ versus the total volume of distribution (V_T), influx (K_1), and efflux (k_2) rate constants obtained in the same individuals. Finally, $K_{E,brain}$-maps were generated in each species using the PXMOD module of the PMOD software. ***Results:*** The linear part of the Log-transformed brain TACs used to calculate $K_{E,brain}$ was 10-30 min in rats, 15-60 min in baboons, and 20-60 min in humans. P-gp inhibition significantly decreased $K_{E,brain}$ values rats by 39±12% in rats, 32±6% in monkeys, and 37±22% in humans. In monkeys, complete P-gp inhibition was associated 101±12% increase in V_T, a 28±14% increase in K_1 and a 36±9% decrease in k_2. Visual analysis of $K_{E,brain}$-maps displayed an evident decrease in $K_{E,brain}$ in brain of all tested species, although the calculation of parametric images was associated with a loss in spatial resolution. ***Conclusion:*** The $K_{E,brain}$ of [^{11}C]metoclopramide provides a simple outcome parameter to describe the P-gp function in the brain. This method takes advantage of the particular pharmacokinetic properties of [^{11}C]metoclopramide (absence of brain radiometabolites and fast plasma clearance). The sensitivity of $K_{E,brain}$ to detect change in P-gp function reflects the "k_2-effect" but is not as sensitive as V_T, which estimation requires arterial blood sampling. $K_{E,brain}$ decreases when P-gp function decreases whereas K_1 and V_T increase. $K_{E,brain}$-maps therefore provide an intuitive representation of the P-gp activity. $K_{E,brain}$-mapping may not be suitable in rodents but may be useful for voxel-wise analysis in monkeys and humans.

EP-0675

Coupling between Cortical Thickness and Glucose Metabolism in the Human Brain: a PET/MRI study

Q. Huang[1], *Y. Yang*[2], *N. Qi*[2], *S. Ren*[1], *J. Wang*[1], *Y. Guan*[1], *J. Zhao*[2], *F. Xie*[1];
[1]*Department of Nuclear Medicine & PET center Huashan Hospital Fudan University, Shanghai, CHINA,* [2]*Department of Nuclear Medicine, Shanghai East Hospital, Tongji University School of Medicine, Shanghai, CHINA.*

Aim/Introduction: The human brain is an intricately organized system where structure and function of different regions work together to accomplish complex tasks. Disruption of this balance has been implicated in neurological and psychiatric disorders. This study investigated the coupling between cortical thickness (CTh) and glucose metabolism using ^{18}F-FDG PET/MRI. ***Materials and Methods:*** 138 subjects who performed brain 18F-FDG PET/MRI were retrospectively recruited. The subjects were divided into two age groups: middle adult (MA, 41 male and 28 female, mean age: 42.33±5.25 years) and old adult (OA, 41 male and 28 female, mean age: 60.19±4.88 years) group. All subjects were clinically evaluated and confirmed by whole-body PET/MRI with no brain disorders. The CTh and FDG uptake values were calculated using SPM12 (http://www.fil.ion.ucl.ac.uk/spm) and CAT12 (http://www.neuro.uni-jena.de/cat/). The Spearman-rank correlation coefficient was calculated between the FDG uptakes and CTh values of the series of regions for each subject to explore the structural and functional coupling (S-F coupling) at regional level. And the association between S-F coupling and age was calculated to explore the physiological effects of the S-F coupling. The structural connectivity (SC) based on CTh and functional connectivity (FC) based on glucose metabolism were constructed by calculating

Spearman-rank correlation coefficients between CTh or FDG uptake values of each pair of brain regions in an inter-subject manner. To explore the structural and functional connective coupling (SC-FC coupling), the correlations between the SC and FC matrix were calculated for each group, that is, each row in SC matrix was correlated via Spearman-rank with the same region's row in the FC matrix. ***Results:*** In regional level, 97.83% of subjects exhibited significant negative correlation between regional CTh and FDG uptake across the whole brain ($p<0.05$ with FDR correction), and the S-F coupling was negatively associated with age ($r = -0.35$, $p<0.001$), suggesting a larger discordancy between brain structure and function with aging. While in connective level, SC-FC coupling was almost entirely positive, with more regions in OA exhibiting significant FC-FC coupling than in MA group. SC-FC coupled regions in MA mainly related to visual and sensorimotor functions, while SC-FC coupled regions in OA covered the whole range of functions from primary to high level. ***Conclusion:*** The human brain CTh and glucose metabolism were coupled from regional to connective level, and this coupling could reflect the aging progress. These findings may have implications for the diagnosis and treatment of neurological and psychiatric disorders.

EP-0676

Spinal Cord imaging by [11C]PIB PET/MRI: evaluation of drawing methods and reference region use in myelin uptake quantification of Healthy Volunteers and Multiple Sclerosis Patients

L. Zorante de Lucena, *M. Sales Pitombeira, K. Repiso Campanholo, C. Alberto Buchpiguel, D. de Paula Faria; Centro de Medicina Nuclear do Hospital da Clínicas da Faculdade de Medicina da USP (CMN-HC-FMUSP), São Paulo, BRAZIL.*

Aim/Introduction: Multiple sclerosis (MS) is a neurodegenerative disease subdivided in Progressive MS (PMS) and Relapsing-Remitting MS (RRMS), affecting Spinal Cord (SC) in 90% of patients, mainly at the cervical level. PET imaging studies of SC are scarce and challenging, due to the low dimensions, movement's artefacts, and lack of methods to define the Volume of Interests (VOIs) and myelin content. PET/MRI enables the interplay between pathophysiology and morphology of the SC in vivo, contributing to understanding MS pathology. This study aims to evaluate different VOI drawing methods and quantification of cervical SC [^{11}C]PIB PET/MRI images in patients with MS. ***Materials and Methods:*** The [^{11}C]PIB PET and T1-weighted 3T-MRI of 10 healthy volunteers (HV) were evaluated using four VOIs drawing methods, in a semiautomatic and automatic form on sagittal and axial plane. Hence, [^{11}C]PIB PET and T1-weighted 3T MRI of 49 MS and 19 HV were assessed using semiautomatic VOI on axial plane and sphere VOI on a neck muscle. The Cervical SC VOIs were based on the anatomical level of the C1/C2, C3 and C4 vertebrae. The results are presented in SUV (Standardized Uptake Value) and SUVr (SUV ratio), with the muscle as reference tissue. The variables evaluated were the [^{11}C]PIB PET uptake of the last 20 minutes, considering p-value < 0.05. ***Results:*** No differences were found between the VOI drawings, therefore, the drawing choice can be based on the analyst preference and the time-consuming, considering that VOIs drawing on axial plane takes 1/4 hours, whereas on sagittal plane 30/60 minutes, using automatic and semiautomatic methods respectively. [^{11}C]PIB SUV was significantly lower in PMS SC at: C3 level, compared to HV (p=0.02); C4 level, compared to HV (p=0.04) and RRMS (p=0.03). The [^{11}C]PIB SUVr in patients with PMS was significantly lower compared to: HV and RRMS at C1/C2 (p=0.24; p=0.028); C3 (p=0.31; p=0.033) and C4 levels (p=0.01; p=0.005). Our results demonstrate that SUVr, using a neck muscle as reference, was more sensitive to differentiate SC myelin content in the PMS group. ***Conclusion:*** We got similar results in the four VOIs drawings strategies, allowing the analyst to choose based on preference and time availability. Regarding the myelin uptake, the SUVr was more sensitive to show Cervical SC myelin content differences in the PMS group in all spinal cord segments evaluated. Thus, SUV ratio using the neck muscle as reference region can be suited to evaluate cervical SC myelin uptake.

EP-0677

Quantification of Neuroinflammation using [18F]DPA714 PET in individuals with Long COVID

S. Golla[1], *D. Visser*[1], *S. C. J. Verfaillie*[2], *E. M. Coomans*[1], *R. M. Rikken*[1], *E. van de Giessen*[1], *M. E. den Hollander*[1], *M. Yaqub*[1], *A. Verveen*[2], *F. Barkhof*[1,3], *J. Horn*[4], *B. Koopman*[5], *P. Schober*[6], *D. W. Koch*[2], *R. C. Schuit*[1], *A. D. Windhorst*[1], *M. Kassiou*[7], *M. van Vugt*[8], *H. Knoop*[2], *B. N. M. van Berckel*[1], *N. Tolboom*[9], *R. Boellaard*[1]; [1]*Department of Radiology & Nuclear Medicine, Amsterdam Neuroscience, Vrije Universiteit Amsterdam, Amsterdam, NETHERLANDS,* [2]*Department of Medical Psychology, Amsterdam University Medical Centers, University of Amsterdam, Amsterdam Public Health Research Institute, Amsterdam, NETHERLANDS,* [3]*Institute of Neurology and Healthcare Engineering, University College London, London, UNITED KINGDOM,* [4]*Department of Intensive Care & Laboratory of Experimental Intensive Care and Anesthesiology (L·E·I·C·A), University of Amsterdam, Amsterdam UMC, Amsterdam, NETHERLANDS,* [5]*Pulmonary Medicine, OLVG, Amsterdam, NETHERLANDS,* [6]*Department of Anaesthesiology, Amsterdam Neuroscience, Vrije Universiteit Amsterdam, Amsterdam UMC, Amsterdam, NETHERLANDS,* [7]*School of Chemistry, The University of Sydney, Sydney, AUSTRALIA,* [8]*Department of Internal Medicine, University of Amsterdam, Amsterdam UMC, Amsterdam, NETHERLANDS,* [9]*Department of Radiology & Nuclear Medicine, University Medical Centre Utrecht, Utrecht, NETHERLANDS.*

Aim/Introduction: 'Long COVID', occurs in a significant number of individuals after a COVID-19 virus infection. Previous histopathology studies have indicated severe neuroinflammatory responses in COVID-19 patients. Positron emission tomography with [^{18}F]DPA714 can be used to study in vivo neuroinflammation. Quantification of in vivo kinetics of [^{18}F]DPA714, however, requires identification of optimal kinetic parameter(s). Earlier studies showed that distribution volume (V_T) is affected by the rate of influx of the tracer from blood (K_1), suggesting V_T to be unreliable. Moreover, K_1 appears to be highly variable, possibly due to inter-region/subject variations in the extraction fraction, maybe due to the binding to endothelium of blood vessels in the brain observed with [^{18}F]DPA714. The aim of the current study was to identify a suitable kinetic parameter to assess the (specific) signal in post-COVID individuals. ***Materials and Methods:*** For this study, 23 post-COVID individuals (18 high affinity binders (HAB), 5 mixed-affinity binders (MAB)) with persistent and severe complaints and, 3 post-COVID individuals (3 HABs) without substantial complaints were included. All subjects underwent a 60 min dynamic PET acquisition using [^{18}F] DPA714 with arterial sampling. Regions of interests were defined using PVElab and Hammers template. A plasma input reversible two tissue compartmental model with blood volume correction was applied to obtain micro/macro-parameters. Associations of V_T and binding potential ($BP_{ND} = k_3/k_4$) with K_1 were evaluated. Inter-region/subject non-displaceable distribution volume ($V_{ND} = K_1/k_2$) were assessed. Pseudo distribution volume ratio (DVR_{WhBr}) was estimated by correcting V_T with V_{ND} of whole brain grey

matter. Additionally, differences between the HABs and MABs using different micro/macro-parameters for different regions of interest were explored. Linear regression and t-tests were performed to evaluate the associations and significance ($p<0.01$) between different parameters. ***Results:*** Significant association between V_T and K_1 ($r = 0.57$) was observed for all subjects (even when segregated into different subject groups). Inter-region/subject differences for V_{ND} were observed, though, inter-regional differences seem to be minimal compared to inter-subject differences. No significant differences between MABs and HABs was observed for V_{ND} of whole brain grey matter. Significant differences for whole brain grey matter between MABs and HABs with K_1, k_3, V_T, BP_{ND} and DVR_{WhBr} were observed. ***Conclusion:*** V_T does not seem to be a suitable parameter for quantification of [^{18}F]DPA714 binding due to its strong association with K_1. We propose either the use of BP_{ND} or DVR_{WhBr} for quantification of [^{18}F]DPA714 in individuals with (Long)COVID.

EP-0678

Florbetaben PET quantification strongly agrees with histopathological confirmation of amyloid-beta load and visual reads.

S. Bullich[1], *J. Koikkalainen*[2], *A. Jovalekic*[1], *N. Roé-Vellvé*[1], *G. D. Kolinger*[1], *N. Koglin*[1], *A. W. Stephens*[1], *L. Thurfjell*[2];
[1]*Life Molecular Imaging GmbH, Berlin, GERMANY,*
[2]*Combinostics Oy, Tampere, FINLAND.*

Aim/Introduction: Positron emission tomography (PET) with florbetaben is an established tool for detecting amyloid-beta deposition in the brain either by visual inspection or quantitation. Several software packages have been developed allowing continuous measurement of amyloid-beta burden. This work assessed the performance of florbetaben PET quantification using cPET against post-mortem histopathological confirmation, the comparison against visual examination, and its capacity to detect subtle longitudinal amyloid-beta deposition. ***Materials and Methods:*** This analysis used florbetaben PET images from previous clinical trials (n=673). PET scans were quantified with cPET (Combinostics Oy) using either the PET-only pipeline (PET-pipeline) or structural MRI (MRI-pipeline) to obtain standardized uptake value ratios (SUVR) with the whole cerebellum as reference region and centiloids (CL). The optimum cutoffs for amyloid-beta load classification were derived using receiver operator characteristic curve analysis using histopathology as the standard of truth (Bielschowsky silver staining in combination with immunohistochemistry) (n=90). The percentage of agreement between quantification and majority visual assessment from 5 independent blinded readers was also compared using the derived cutoffs (n=386). Amyloid-beta deposition over time was assessed in a group of mild cognitively impaired subjects (n=41) that underwent at least a one-year follow-up scan. ***Results:*** The optimal SUVR cutoffs to classify amyloid-beta positive and negative scans were 1.13 (26.9 CL) (MRI-pipeline), 1.11 (35.5 CL) (PET-pipeline). The mean sensitivity, specificity, and accuracy were 96.3%, 96.2%, and 96.3% (MRI-pipeline), and 90.7%, 100.0%, and 94.4% (PET-pipeline). The percentage of agreement between binary quantitative assessment and visual read was 92.8% (MRI-pipeline) and 94.8% (PET-pipeline). In those subjects where the five independent blinded readers assessed the scans by consensus, the agreement was 98.2% (MRI-pipeline) and 98.8% (PET-pipeline). In a subset of amyloid-beta negative elderly cognitively normal subjects, 95% of the subjects had SUVR values below 1.1 (22.9 CL)(MRI-pipeline) and 1.0 (17.1 CL) (PET-pipeline). Both pipelines detected statistically significant differences in amyloid-beta deposition over time between negative and positive subjects at baseline. ***Conclusion:*** cPET quantification exhibits a high sensitivity and specificity to detect amyloid-beta load and excellent agreement with visual assessment. The results suggest that quantification obtained from cPET can be used for continuous measurement of amyloid-beta burden and to assess amyloid-beta change over time.

EP-0679

Attenuation correction of cardiac PET with end-expiratory CT and average CT

K. Sander[1], *T. Pan*[2], *A. Roby*[1];
[1]*University of Texas Medical School, Houston, TX, UNITED STATES OF AMERICA,* [2]*University of Texas at M. D. Anderson Cancer Center, Houston, TX, UNITED STATES OF AMERICA.*

Aim/Introduction: Misregistration between PET and CT data can compromise attenuation correction (AC) and quantification of cardiac perfusion on ^{82}Rb PET scan. Although average CT (ACT) is effective for AC of cardiac PET, it can suffer from irregular respiration (IR) due to acquisitions of 1 to 2 breathing cycles of cine CT data. New end-expiratory (EE) CT can be extracted from the same cine CT data for ACT via data-driven gating. The aim is to compare ACT and EECT in AC of cardiac perfusion ^{82}Rb PET. ***Materials and Methods:*** 35 patients were scanned for cardiac perfusion at rest and stress with ^{82}Rb on a GE DMI-20cm PET/CT scanner totaling 70 acquisitions. The protocol consists of 5.7s free-breathing low-dose cine CT scans every 2cm followed by PET rest and stress. ACT was averaged from cine CT images and EECT was derived from cine CT images with the largest CT numbers in the lung regions or the largest expansion of the body contour outside the lung regions. Both ACT and EECT were derived from the same cine CT data. Registration between PET and ACT or EECT were performed manually. Comparisons were made between ACT and EECT maximum activity (μCi/cc), myocardial blood flow (MBF) (cc/min/gm), and the size of relative perfusion defect, defined as percent of the left ventricle less than 60% of the maximum activity. ***Results:*** IR impacted ACT in 14 patients (28 acquisitions) and EECT in 4 patients (8 acquisitions). The maximum activities in the myocardium for ACT and EECT were 4.42±1.10 and 4.52±1.13 μCi/cc, respectively, and statistically different ($p < 0.0001$). The difference of quartile MBF was not significantly different by paired t-test at rest (septal p=0.55, anterior p=0.14, lateral p=0.15, inferior p=0.18) or stress (septal p=0.53, anterior p=0.13, lateral p=0.46, inferior p=0.14), respectively. Of the ACT acquisitions impacted by IR, EECT decreased the relative perfusion defect in 16 of 28 (57%). ***Conclusion:*** Overall, EECT was less impacted by IR than ACT. EECT renders higher maximum activity than ACT in the myocardium. Switching from ACT to EECT did not impact quartile MBF. Relative defect size was decreased for acquisitions impacted by IR. For IR compromised ACT, EECT is an additional option for cardiac PET AC. ***References:*** Pan T, Thomas MA, Luo D. Data-driven gated (DDG) CT: An automated respiratory gating method to enable DDG PET/CT. Med Phys, 3/2022. e-Pub 3/2022. PMID: 35324002.

EP-0680

"Enhancing Quantitative and Qualitative Analysis in Transthyretin Amyloid Cardiomyopathy Imaging: Preliminary Results from the iTAC IAEA Project"

P. Knoll[1], *L. Torres Aroche*[2], *F. Mut*[3], *G. Grossmann*[4], *S. Orbala*[5], *G. Agu*[6], *S. Mirzaei*[6], *I. de Souza Baptista*[4], *D. Paez*[1], *A. Brink*[1], *M. Ljungberg*[7];
[1]*IAEA, Vienna, AUSTRIA,* [2]*Nuclear medicine department, Centis, La Habana, CUBA,* [3]*Servicio Medicina Nuclear, Hospital Italiano, Montevideo, URUGUAY,* [4]*Hospital Moinhos de Vento, Porto Alegre, BRAZIL,* [5]*Brigham and Women's Hospital, Harvard Medical School, Boston, MA, UNITED STATES OF AMERICA,* [6]*Department of Nuclear Medicine, Klinik Ottakring, Vienna, AUSTRIA,* [7]*Lund University Skane University Hospital, Lund, SWEDEN.*

Aim/Introduction: The growing significance of 99mTc-PYP SPECT and SPECT/CT imaging in assessing the severity of transthyretin (TTR) cardiac amyloidosis necessitates accurate quantification and high-quality images. This study aims to establish and evaluate procedures to ensure accurate clinical evaluation metrics, such as, activity concentration and SUV and to attain optimal image quality for detection. These preliminary evaluations are part of the newly started iTAC IAEA coordinated research project. ***Materials and Methods:*** We utilized a cardiac insert within a cylindrical Jaszczak phantom to simulate realistic clinical examination conditions. A comprehensive assessment of image processing parameters (iterations and subsets) was conducted to optimize activity uptake recovery in the heart wall. The Activity Calibration Factor (ACF) was assessed following well-established procedures using a homogenous activity in a cylinder phantom. Image quality parameters, such as Signal-to-Noise Ratio (SNR), image-noise levels (RMS) together with an estimate of the wall thickness were computed and analyzed. We employed clinical OS-EM reconstruction method together with a Monte-Carlo-based software for image reconstruction and activity quantification; 3D image segmentation, curve fitting and complementary image/data processing techniques were used. ***Results:*** Our optimization approach identified 100 updates (10 iterations, 10 subsets) as the optimal parameter set for OS-EM reconstruction and from this recovering over 97% of the maximum uptake under clinical conditions. The ACF for the evaluated system was approximately 78.6 cps/MBq. Relative differences between estimated and measured activity in the myocardial wall were 7.9% and 11.3% in air and water environments, respectively. SNR values met the Rose criteria (SNR > 5) for adequate detectability when using 100 updates. Initial SPECT and SPECT-CT studies of patient revealed activity concentration values and cavity-to-myocardium ratios that varied depending on disease severity. Qualitative image quality assessment deemed the patient data-sets acceptable. ***Conclusion:*** We propose and implemented a novel methodology for optimizing quantitative and qualitative analyses in transthyretin amyloid cardiomyopathy studies. Initial evaluations with phantoms and real patients show good results in terms of accuracy and feasibility. Further evaluations are warranted to assess the methodology's performance across a broader range of clinical conditions. ***References:*** Ren C., Ren J., Tian Z., et al. Assessment of cardiac amyloidosis with 99mTc-pyrophosphate (PYP) quantitative SPECT. EJNMMI Physics (2021) 8:3. Dorbala D., Park MA, Cuddy S. et al. Absolute Quantitation of Cardiac 99mTc-Pyrophosphate Using Cadmium-Zinc-Telluride-Based SPECT/CT. J Nucl Med 2021; 62:716-722

EP-0681

A novel assisted workflow created to obtain cardiac semiquantitative indexes from 99mTc-DPD-scintigraphy and to correlate them with different etiologies of transthyretin-related cardiac amyloidosis.

S. E. Prisco[1], *S. Mattoni*[1], *A. Paccagnella*[2], *F. Mattana*[3], *M. F. Morrone*[4,5], *G. Della Gala*[4], *M. Sguazzotti*[6], *S. Longhi*[6], *G. Saturi*[6], *S. Fanti*[1,7], *N. Galiè*[6], *L. Strigari*[4], *R. Bonfiglioli*[7];
[1]*Nuclear Medicine, Alma Mater Studiorum University of Bologna, Bologna, ITALY,* [2]*Nuclear Medicine Unit, AUSL Romagna, Cesena, ITALY,* [3]*, IEO European Institute of Oncology IRCSS, Milano, ITALY,* [4]*Department of Medical Physics, IRCCS Azienda Ospedaliero-Universitaria di Bologna, Bologna, ITALY,* [5]*Specialization School in Medical Physics, University of Bologna, Bologna, ITALY,* [6]*Cardiovascular Department, IRCCS Azienda Ospedaliero-Universitaria di Bologna, Bologna, ITALY,* [7]*Nuclear Medicine, IRCCS, Azienda Ospedaliero-Universitaria di Bologna, Bologna, ITALY.*

Aim/Introduction: Semi-quantitative analysis of Technetium-99metastable-3,3-diphospono-1,2-propanodicarboxylic acid (99mTc-DPD) bone scintigraphy is promising in diagnosing cardiac amyloidosis but prone to processing errors and time consuming. As previously demonstrated in another study, the Geometric Mean image (GMi) can be used to perform a more efficient semi-quantitative analysis than standard method (reported as Classic Method (CM)). Based on these results, we implemented a novel assisted workflow (referred to AW) designed to further enhance the evaluation of semi-quantitative indexes, such as Heart Whole Body ratio (H/WBr), Heart retention (Hr) and Whole Body retention (WBr) on the GMi, and compared it to CM. In addition, we investigated the capability of the indexes thus obtained to differentiate the etiology (mutated vs wild-type) in cardiac transthyretin-related amyloidosis (cATTR) patients. ***Materials and Methods:*** 154 patients with cATTR confirmed diagnosis were retrospectively enrolled. Firstly, a random subset of 30 patients were extracted to compare CM and AW. The H/WBr, Hr and WBr, were calculated extracting counts by WB, kidneys, bladder and heart on early and late planar image scans and applying the background, scan-time and decay corrections, using GMi both with CM and AW. The comparison between CM and AW was executed with Pearson's correlation and Bland Altman analysis. Subsequently, the selected semi-quantitative indexes were measured with AW in the entire enrolled patients cohort. H/WBr, Hr and WBr and several clinical variables (age, sex, interventricular septum, left ventricular ejection fraction) were used to implement three different models, Least Absolute Shrinkage and Selection Operator (LASSO), Random Forest (RF) and Neural Network (NN) to predict two etiologies, ATTR mutated (ATTRm) and ATTR wild-type (ATTRwt). Receiver operating characteristic (ROC) curves and area under the curve (AUC) were calculated. ***Results:*** The AW and CM resulted highly correlated for Hr, WBr and H/WBr, (Pearson's linear correlation coefficient= 0.98, R=1). The Bland-Altman analysis between CM and AW within the assisted workflow showed the H/WBr bias of 0.12% [CI: 0.04%;0.19%], the Hr bias of 0.07% [CI: 0.01%;0.13%] and the WBr bias of -0.50% [CI: -1.22%;0.22%]. The three models, LASSO and NN had good performance in predicting different etiologies with AUC values of 87.3% and 73.6%, respectively. The RF model showed a performance with AUC of 55.8%. ***Conclusion:*** The GMi developed in the assisted workflow (AW) was both highly correlated and more efficient than CM. The use of Hr calculated with AW in LASSO, RF and NN allowed to obtain good prediction performances for cATTR etiology.

EP-0682

Long-term prognostic value of automated measurements in nuclear cardiology: Comparisons with the expert reading scoring

G. Angelidis*, V. Valotassiou, I. Tsougos, C. Tzavara, S. Giannakou, D. Psimadas, E. Theodorou, A. Ziaka, C. Ziangas, J. Skoularigis, F. Triposkiadis, P. Georgoulias;*
University of Thessaly, Larissa, GREECE.

Aim/Introduction: Automated methods for the analysis of myocardial perfusion studies have been incorporated into the clinical practice, given their advantage to exclude the subjective character of interpretation. However, computer-based assessment is currently used only as an adjunct to visual interpretation, and there is only scarce data regarding the incremental value of the corresponding automated measurements. In the present study, using three widely available software packages [Emory Cardiac Toolbox (ECTb), Myovation (MYO), Quantitative Perfusion SPECT (QPS)], we aim to evaluate the role of automated measurements of summed stress score (SSS), summed rest score (SRS), and summed difference score (SDS) as long-term prognostic markers

of morbidity and mortality, in comparison to the prognostic value of expert reading. ***Materials and Methods:*** The study was conducted at the Nuclear Medicine Laboratory of the University of Thessaly, Larissa, Greece. 378 consecutive patients with known or suspected coronary artery disease were enrolled in the study, as they did not meet any of the exclusion criteria. All participants were referred to our laboratory for the performance of stress/rest myocardial perfusion single photon emission computed tomography. Stress testing was performed according to the Bruce protocol, while patients with contraindication or inability to achieve a satisfactory exercise level underwent pharmacologic testing, with or without low-level exercise. Scintigraphic studies were carried out using a dual-headed camera, without attenuation-scatter correction. Follow-up data was recorded after phone contacts, as well as through review of the patients' hospital records. All-cause death, cardiovascular death and non-fatal myocardial infarction were considered as hard events, while stroke, revascularization and hospitalization (due to unstable angina, heart failure or resuscitated cardiac arrest) as soft events. ***Results:*** The prognostic ability of SSS, SRS, and SDS was compared between the three software packages and the expert reading. It was found that ECTb-derived SSS had significantly lower prognostic ability in comparison to expert scoring ($p<0.001$), while expert scoring of SSS had also significantly greater prognostic ability in comparison to MYO- and QPS-derived measurements ($p<0.001$ for both comparisons). Moreover, expert scoring of SDS was associated with greater prognostic ability compared to all software packages ($p<0.001$ for all comparisons). Similarly, automated SRS values were associated with lower prognostic ability in comparison to expert scoring. ***Conclusion:*** Despite the useful contribution of automated analyses in the interpretation of myocardial perfusion studies, expert reading should continue to have a crucial role, not only in clinical decision making, but also in the assessment of prognosis.

EP-0683

Centiloid Calibration of a Commercial Amyloid Quantitation Software for different Fluorine-18 Radiotracers

R. Fahmi;
Siemens Healthineers, Knoxville, TN, UNITED STATES OF AMERICA.

Aim/Introduction: Variability in amyloid-beta (Aβ) PET quantification using standardized-uptake-value-ratio (SUVr) makes it challenging to compare amyloid-PET acquired with different tracers and/or processed using different methods. The centiloid (CL) method was proposed by Klunk et al. [1] to standardize measures of Aβ burden from PET images using a standard processing method. Our aim is to calibrate a commercial PET-only amyloid quantification method, henceforth referred to as 'syngo-Aβ', to the centiloid scale for florbetapir (FBP), florbetaben (FBB), and flutemetamol (FLUTE) radiotracers. ***Materials and Methods:*** Calibration PET images and their corresponding SUVr and CL reference data were obtained from the GAAIN website. For each tracer, level-2 calibration analysis prescribed in [1] was performed to generate direct syngo-Aβ SUVr-to-CL transformations. A global cortical SUVr value was calculated using six tracer-specific cortical regions in reference to the whole cerebellum, as implemented in syngo-Aβ software. Results corresponding to other reference regions and to standard cortical regions from the GAAIN project were also generated but are not reported here. For validation purposes, we downloaded two independent datasets (N=162 florbetapir and N=118 florbetaben) from the ADNI study and compared the generated CL values against the ones calculated using ADNI CL pipeline [2]. ***Results:*** The transformation equations derived using the calibration images, from GAAIN, fulfilled the acceptance criteria, with strong agreement and little bias between syngo-Aβ CL values and those computed and published using the standard method [1], with R^2=0.97 (FBP), R^2=0.98 (FBB), and R^2=0.95 (FLUTE). The syngo-Aβ SUVr-to-CL transformations were: CL=173.26×SUVr - 174.63 (FBP); CL=181.31×SUVr - 175.90 (FBB); and CL=120.73×SUVr - 116.81 (FLUTE). The independent validation demonstrated strong agreements between syngo-Aβ and ADNI CL values with the following regressions and R^2 values: $^{syngo}CL=1.044\times {}^{ADNI}CL - 0.712$; R^2 = 0.97 (FBP) and $^{syngo}CL=1.095\times {}^{ADNI}CL - 7.241$; R^2 = 0.98 (FBB). ***Conclusion:*** We have successfully calibrated a commercially available amyloid quantification software to the centiloid scale for the three commercially available amyloid tracers. Validation on two independent datasets showed strong agreement with the ADNI calibration pipeline for FBP and FBB. Validation results for FLUTE will be added.***References:*** [1] Klunk W et al. Alzheimer's & Dementia (2015) [2] S. Kolibash et al., 'Centiloid Level-2 Analysis of [18F]Florbetaben (FBB) and [18F]Florbetapir (FBP) PET Image Data using the ADNI Pipeline', https://ida.loni.usc.edu/.

EP-0684

Comparison of MR arterial spin labelling regional Cerebral Blood Flood estimates to early amyloid PET measurements

J. Anton Rodriguez[1,2], *J. C. Matthews*[3], *L. A. Scott*[3], *J. J. McFadden*[3], *B. R. Dickie*[2], *K. Herholz*[3], *L. M. Parkes*[3];
[1]*The Christie NHS Foundation Trust and University of Manchester, Manchester, UNITED KINGDOM,* [2]*Division of Informatics, Imaging and Data Sciences, MAHSC, University of Manchester, Manchester, UNITED KINGDOM,* [3]*Division of Psychology, Communication and Human Neuroscience , Faculty of Biology, Medicine and Health-University of Manchester, Manchester, UNITED KINGDOM.*

Aim/Introduction: [^{15}O]water PET is the gold standard measurement of regional cerebral blood flow, $rCBF_{water}$ (mL/min/dL). However, it is only available in a few sites as it requires on-site [^{15}O]water production and full-kinetic analysis. Early amyloid-PET has been proposed as a surrogate for relative rCBF [1], $rCBF_{Amy}$(kBq/ml). The non-invasive MRI technique arterial-spin-labelling (ASL) can also measure $rCBF_{ASL}$(mL/min/dL). Previous reports show that although there is a good correlation between $rCBF_{ASL}$ and $rCBF_{water}$, there are quantitative differences resulting in underestimations within subcortical regions with ASL [2]. We compare $rCBF_{ASL}$ and $rCBF_{Amy}$ measurements in a cohort of cognitively normal and MCI elderly participants. ***Materials and Methods:*** Twenty-two participants, 70(60-80) years old (mean(range)), 13 cognitively normal/9 mild cognitive impairment, were scanned using a GE SIGNA PET/MR. $rCBF_{Amy}$ corresponded to summed images 20s-80s post-arrival of tracer in the brain following the injection of ~185MBq of [18F]flutemetamol. Enhanced-ASL with pCASL labelling and 3D spiral FSE acquisition was acquired with six post-labelling delays and processed to obtain voxel-wise CBF_{ASL} and arterial-transit-time (ATT) maps using a single-blood compartmental model [3]. Voxel-wise M_0 calibration was employed. For each patient, tissue T_1 and T_2^* maps were available. FreeSurfer brain segmentation on each participant's T1wMPRAGE was used to estimate median values for 13 brain regions in all available maps ($rCBF_{ASL}$, $rCBF_{Amy}$, ATT, T_1 and T_2^*). Regression models were used to compare $rCBF_{ASL}$ and $rCBF_{Amy}$ to assess the dependency of the gradient and intercept on the region and the covariates ATT, T_1 and T_2^*.

Parameters to scale the $rCBF_{Amy}$ values across all participants were included in the model. Statistical testing (F-tests) was conducted to assess the significance of model parameters. ***Results:*** There was a statistically significant positive intercept (p=0.016; range 24-40 mL/min/dL), also dependent on T_2^* (p=0.003). The gradient was statistically different from zero (p=0.000) and was dependent on both T_2^* (p=0.003) and region (p=0.012). There was no dependency of the intercept or gradient on T_1 or ATT. The relative differences in the gradients between regions and the relative mean values of $rCBF_{ASL}$ and $rCBF_{Amy}$ across regions agreed well with values previously reported using $rCBF_{water}$ [2]. ***Conclusion:*** This work supports the previous findings of quantitative regionally dependent differences between ASL and PET measurements of $rCBF_{water}$[2]. It also suggests that these differences are partially due to T_2/T_2^* differences between tissues, with further corrections required to make ASL rCBF measurements accurate. ***References:*** [1]Anton-Rodriguez et al., EANM2020-meeting-Vienna,OP-1001; [2]Fahlström et al., Diagnostic,11(5):821-2020 [3]Parkes and Tofts, MRM,48(1):27-2002

EP-0685

A ROI-based Quantitative Pipeline for [18]F-FDG PET Metabolism and pCASL Perfusion Joint Analysis: Validation on [18]F-FDG PET Data

V. Cerina[1], *E. De Bernardi*[2], *C. Crivellaro*[3], *S. Morzenti*[4], *F. E. Pozzi*[1], *L. Jonghi Lavarini*[2], *V. Bigiogera*[2], *R. M. Moresco*[2], *G. Basso*[2,5]; [1]*PhD program in Neuroscience, Department of Medicine and Surgery, University of Milano Bicocca, Milano, ITALY,* [2]*Department of Medicine and Surgery, University of Milano Bicocca, Milano, ITALY,* [3]*Nuclear Medicine, Fondazione IRCCS San Gerardo dei Tintori, Monza, ITALY,* [4]*Medical Physics, Fondazione IRCCS San Gerardo dei Tintori, Monza, ITALY,* [5]*Neuroradiology, Fondazione IRCCS San Gerardo dei Tintori, Monza, ITALY.*

Aim/Introduction: In neurodegenerative dementias the study of brain metabolism, provided by [18]F-FDG PET, can be integrated with brain perfusion by means of pseudo-Continuous Arterial Spin Labelling MR sequences (pCASL). Aim of this study is to validate, on PET images relying on normative data, a region-based pipeline constructed to be independently applied to PET and pCASL data to jointly analyse metabolism and perfusion. ***Materials and Methods:*** Thirty-six MCI patients and 107 healthy-controls PET images were considered. Pre-processing included MNI normalization, Grey Matter segmentation through mean Tissue Probability Map, partial volume error (PVE) correction and smoothing. Sixteen ROIs were derived from AAL3 atlas and SUV ratios (SUVr) normalized on cerebellum activity were extracted. For each ROI, SUVr mean and standard deviation in healthy controls were computed. Patient SUVr values falling outside (σ, 1.5σ, 2σ) normality range were considered hypometabolic. Results were compared to: 1) visual analysis (supported by CortexID-Suite); 2) two different SPM statistical analyses (SPM-A: voxel-size 2x2x2 mm^3, smoothing Gaussian Kernel FWHM 8x8x8 mm^3; SPM-B: voxel-size 1x1x1 mm^3, PVE correction). This analysis was conducted for each ROI separately. Agreement among methods was assessed with accuracy, sensitivity, specificity and Cohen's κ. ***Results:*** By using visual analysis as reference, the (σ, 1.5σ, 2σ) normality ranges obtained, on average on the 16 ROIs, accuracy (76, 78, 76)%, sensitivity (84, 67, 47)%, specificity (69, 85, 94)%, and κ (49, 60, 60) %, respectively. With SPM-A as reference, accuracy (71, 79, 83) %, sensitivity (89, 75, 59)%, specificity (63, 80, 93)%, and κ (42, 58, 67)% were obtained. With SPB-B as reference, accuracy (76, 77, 73)%, sensitivity (79, 64, 46) %, specificity (71, 88, 97)%, and κ (51, 54, 47)% were obtained. SPM-A (SPM-B) compared to visual analysis obtained 79(75)% accuracy, 60(76)% sensitivity, 92(75)% specificity, 57(51)% κ. SPM-B compared to SPM-A obtained 79% accuracy, 94% sensitivity, 72% specificity, 58% κ. ***Conclusion:*** The proposed region-based analysis pipeline with the 1.5σ normality range showed a good agreement with reference methods, in line with intra reference methods agreement levels. It can be therefore considered as a promising tool for future PET-pCASL joint analyses. ***References:*** Festari C. et al., Alzheimer's Dement, 2022; Yan L. et al., NeuroImage Clin, 2017; Musiek E.S. et al., Alzheimer's Dement., 2013; Guedj E. et al., J. Nucl. Med. Mol. Imaging, 2022; Perani D. et al., NeuroImage Clin, 2014; Caminiti S. P. et al., Eur. J. Nucl. Med. Mol. Imaging, 2021

EP-0686

Method evaluation for quantification of cerebral blood flow for [15O]-water PET/CT, a segmentation comparison between using ASPECTS method for simplified quantification to a 3D-volume based arterial atlas

A. Eriksson*, J. Patrick Connelly, A. Gul Sherwani, L. Gridset, K. Angell, L. Gyland Mikalsen, C. Stokke, M. Stavrinou; Oslo Universityhospital, Oslo, NORWAY.*

Aim/Introduction: [15O]-water PET/CT is the gold standard to quantify cerebral blood flow (CBF). In order to extract the vascular brain areas an anatomical arterial atlas and dedicated software is needed. However, if a subject cannot undergo MRI, or is in an acute situations a fast method for simplified quantification would be preferable. In this study a CT-based semi-manual segmentation method based on pc-ASPECTS (Alberta Stroke Programme Early CT Score) including posterior circulation has been used for quantification, and compared to an arterial atlas. ***Materials and Methods:*** Six subjects with suspected Moyamoya disease were included for a cross-evaluation of the two methods. Each subject underwent two dynamic [15O]-water PET/CT acquisition with a continuous arterial sampling, pre- and post-vasodilator (acetazolamide 1g IV). For the ASPECTS, segmentations were performed in four axial levels from base to vertex on CT or T1-weighted MRI, divided into 20 bilateral territories [1]. The arterial method is a 3D atlas, which include 32 territories [2]. The arterial atlas was then used for automatic segmentation based of an isometric T1-weighted MRI. To obtain quantitative CBF values, kinetic modelling with the same set of parameters was performed for both methods of segmentations using a commercial software. Relative differences were calculated between the pre- and post-vasodilator acquisitions, and results for corresponding regions for the two segmentation methods compared. ***Results:*** For smaller regions such as the lentiform nucleus, thalamus and caudate there is good agreement the values from ASPECTS and the arterial atlas. For larger territories such as frontal or parietal portions of the MCA (middle cerebral artery) the majority of values from the ASPECTS method shows greater variability from the arterial atlas values. ***Conclusion:*** In this study only the relative difference for CBF between pre- and post-vasodialator was used as a control parameter, since the segmentations were in focus. Since the ASPECTS model is only based on slices at four levels it is therefore sensitive to local variations due to noise or pathology. In contrast, the arterial atlas is volume based and will often contain both normal and pathological regions, yielding an averaged CBF. In conclusion, the results from this small subject sample supports that the ASPECTS based segmentation method may be more representative for smaller pathological regions and could potentially be expanded for more CT or MRI slices for better brain coverage. ***References:*** [1] Barber et al.,Lancet 2000; 355: 1670-74 [2] Liu, CF. et al., Scientific Data 2023; 10:74

EP-47

e-Poster Area

D: Technical Studies -> D2 Data Analysis -> D22 Other Data Analysis

EP-0687

Comparison of Results Analysis for Isotopic Determination of Plasma Volume: a Prospective Study

M. Ragot, *R. Charmelot, P. Orhon, B. Berton, A. Revy, M. Tempier, S. Levesque;*
Centre Jean Perrin, Clermont-Ferrand, FRANCE.

Aim/Introduction: Determination of blood volumes, including plasma volume (PV), is central for the diagnosis of polycythaemia. According to the 1980 ICSH recommendation, the gold standard (GS) for PV is the use of ^{125}I labelled human serum albumin (^{125}I-HSA), with 3 plasma samples (10-20-30 min after injection) and extrapolation of results to the time of injection (t_0). There is however no consensus in clinical practice. This study was conducted to compare various methods, to determine the optimum method: minimum samples for equivalent results to GS. ***Materials and Methods:*** Patients with suspected polycythaemia were enrolled from September 2021 until December 2022. Patients were injected with 1.8 kBq/kg of ^{125}I-HSA. Based on the dilution technique, PV is calculated from the quotient of the administered dose and the ^{125}I-HSA concentration (average or linear extrapolation at t_0), deducted from the amount of activity present in the plasma samples taken 10, 20, 30 and 40 minutes after injection. The data was analysed on Excel and R. Five methods (2, 3 or 4 samples, with or without extrapolation) were compared to the GS, with Student test (paired measures, $\alpha = 0.05$) to conclude on statistical difference and Bland-Altman plots to analyse agreement. ***Results:*** 75 patients were included: 63 men and 12 women, with an average age and BMI of 59 years and 28 kg/m^2. Although extrapolation is described in GS, it has limitations: it can overestimate PV if the last samples show higher concentrations than the first one, leading to the exclusion of five patients from our analysis. When results are extrapolated to t_0, there is no statistically significant difference when adding a sample at 40 min. However, extrapolating from only two samples (10-20 min) leads to substantial unpredictable random error. The alternative is to use average values, which overestimates the PV by neglecting the loss of ^{125}I-HSA from the plasma. The method M2, based on average concentrations of only 2 samples (10-20 min), leads to an average systemic error of +0.08L (+3%). Using a fixed correction factor instead of extrapolation will prevent this phenomenon and remove the systemic error. When a correction factor of 3% is applied to the PV obtained with M2, results are not statistically different from GS. ***Conclusion:*** Switching from a 3 dots extrapolation to an average 2 dots analysis integrating a corrective factor concluded to statistically equivalent results, allowing for a less time-consuming procedure for patients and personal.

EP-0688

Discordance between 90Y PET/CT(MR)-estimated activity and dose calibrator measured administered activity: an international patient study in SIRT with resin and glass microspheres

T. Carlier[1], *S. Gnesin*[2], *J. Mikell*[3], *M. Conti*[4], *J. Prior*[5], *C. Bailly*[1], *M. Pérez Lago*[6], *Y. Dewaraja*[7], *T. Lima*[6];
[1]*University Hospital of Nantes, Nantes, FRANCE,* [2]*Institute of Radiation Physics, Lausanne University Hospital and University of Lausanne, Lausanne, SWITZERLAND,* [3]*Department of Radiation Oncology, University of Michigan, Saint Louis, MI, UNITED STATES OF AMERICA,* [4]*Siemens Medical Solutions UNITED STATES OF AMERICA, Inc, Knoxville, TN, UNITED STATES OF AMERICA,* [5]*Department of Nuclear Medicine and Molecular Imaging, Lausanne University Hospital and University of Lausanne, Lausanne, SWITZERLAND,* [6]*Department of Radiology and Nuclear Medicine, Luzerner Kantonsspital and Faculty of Health Sciences and Medicine, University of Lucerne, Luzern, SWITZERLAND,* [7]*Division of Nuclear Medicine, Department of Radiology, University of Michigan, Ann Arbor, MI, UNITED STATES OF AMERICA.*

Aim/Introduction: Permanent implantation of ^{90}Y-loaded microspheres is routinely applied in selective internal radiotherapy of primary and secondary liver tumours. ^{90}Y-PET is the reference post-therapy imaging modality that is used to evaluate absorbed dose for efficacy and toxicity assessment. A recent study showed that manufacturer-declared vial activities were substantially overestimated/underestimated for glass (Gm) and resin microspheres (Rm) respectively. The main aim of this work is to confirm the above discrepancies observed for vials, using patient data. We also evaluate how the discrepancies are impacted by using two different background scaling (BS) methods for the single scatter simulation (SSS) with different PET systems. ***Materials and Methods:*** Patients (Gm: 60, Rm: 11) were enrolled retrospectively from 4 different institutions (CHUV Lausanne, Switzerland; University of Michigan, USA; Luzern Kantonsspital, Switzerland and Nantes Hospital, France). ^{90}Y-PET images were acquired and reconstructed using 4 different systems (Vision 600 and 450, Biograph mCT and mMR), following the local procedures. Residuals after therapeutic injection were measured using either a survey-meter or by PET imaging. Sixty patients were imaged using a PET/CT (with time-of-flight, TOF) and 11 (all Gm) with the PET/MR (without TOF). The PET measured activity (A_{PET}) was assessed in a volume encompassing the liver (CT/MR-based segmentation) expanded by 1cm to account for resolution and motion spill-out effects. The ratio A_{PET}/A_M was subsequently calculated for each patient where A_M was the injected activity as measured by the dose calibrator corrected for residual and lung shunt. Two different methods of SSS BS were considered: tail fitting (TFBS) and absolute (ABS). Comparison used a Wilcoxon signed-ranked test. ***Results:*** The mean $A_{PET/CT}/A_M$ (respectively, $A_{PET/MR}/A_M$) for Gm was significantly different using TFBS (0.84±0.07 resp. 0.69±0.12) vs ABS (0.91±0.06 resp. 0.80±0.07). The mean $A_{PET/CT}/A_M$ for Rm was also significantly different using TFBS (1.15±0.09) vs ABS (1.29±0.12). While unpaired, a significant difference between PET/CT and PET/MR was highlighted. The mean LSF was 1.8±1.1% and the mean residual fraction was 2.5±3.4% for Gm and 5.6±3.0% for Rm, hence the expected uncertainty in these values is unlikely to substantially impact the observed discrepancies. ***Conclusion:*** We confirmed in patients the discrepancies previously reported with vials. TFBS BS should be avoided when estimating the scatter component. A significant difference between PET/CT and PET/MR was also reported highlighting the importance of the field-of-view diameter and the potential benefit of TOF availability.

EP-0689

Using Different Dichotomisation Methods for Lesion Dissemination to Predict Survival Outcomes in Lymphoma Patients

X. Wong[1], *L. Yong*[1], *Y. Chen*[2,3], *S. Liu*[1,3], *K. Lue*[1];
[1]*Tzu Chi University of Science and Technology, Hualien, TAIWAN,* [2]*Tzu Chi University, Hualien, TAIWAN,* [3]*Hualien Tzu Chi Hospital, Hualien, TAIWAN.*

Aim/Introduction: The lesion dissemination feature, the largest distance between two lesions (Dmax), measured using ^{18}F-FDG PET, can be useful in determining the prognosis of patients with lymphoma. A cut-off point for Dmax is commonly used to stratify patients into good or poor prognoses. However, the cut-off may vary depending on the dichotomisation method used. This study investigated whether various methods of dichotomising Dmax influenced survival prediction in patients with lymphoma. ***Materials and Methods:*** Ninety patients diagnosed with lymphoma who underwent baseline ^{18}F-FDG PET were retrospectively enrolled. All the patients had at least two detectable lesions. ^{18}F-FDG-avid lesions were contoured using a standardised uptake value threshold above 4.0. The centroid of each lesion was identified, and the distances between all pairs of lesions were computed in three-dimensional coordinates. The maximum distance (Dmax) was calculated for each patient. The standardised Dmax (SDmax) was normalised to the body surface area of the patient. The cut-off points for the dissemination features (Dmax and SDmax) were determined using the Youden index of receiver operating characteristic analysis, X-tile bioinformatics software (Yale University, New Haven, USA), and the Cut-off Finder web application (Charite, Berlin, Germany). The respective prognostic effects on survival outcome prediction were compared using the Cox hazard regression, Kaplan-Meier analysis, and log-rank tests. All images were analysed using the LIFEx software (LITO, Orsay, France) and the ACCURATE tool (VUmc, Amsterdam, Netherlands). ***Results:*** The median (interquartile range) Dmax and SDmax values were 0.269 m (0.155-0.526 m) and 0.169 m^{-1} (0.089-0.327 m^{-1}), respectively. The cut-off values for Dmax in predicting progression-free survival (PFS) and overall survival (OS) ranged from 0.191 m to 0.587 m and 0.227 to 0.590 m, respectively. The cut-off values for SDmax in predicting PFS and OS ranged from 0.116 m^{-1} to 0.183 m^{-1} and 0.156 m^{-1} to 0.327 m^{-1}, respectively. All dichotomisations significantly predicted PFS and OS, except for one that was based on a mixture of two Gaussian distributions in the OS. Patients were stratified into distinct prognostic groups based on survival curves. The Harrell's concordance index for predictive performance ranged from 0.588 to 0.631 (hazard ratio, 1.924-4.066) and 0.603 to 0.623 (hazard ratio, 2.648-2.778) for PFS and OS, respectively. ***Conclusion:*** Although the cut-off points varied using different dichotomisation methods, Dmax and SDmax could remain predictive values for survival in lymphoma patients. A consistent method to determine dissemination feature cut-off should be considered when defining the threshold.

EP-0690

Evaluation of Image Quality and Quantification with Various Scan Times on 64 Copper PET/CT Imaging: Phantom and Clinical study

F. Sadeghi[1], *A. Monsef*[2], *P. Sheikhzadeh*[1,3];
[1]*Department of Medical Physics and Biomedical Engineering ,Tehran University of Medical Sciences, Tehran, IRAN, ISLAMIC REPUBLIC OF,* [2]*Department of Radiation Oncology, University of Minnesota Medical School, Minneapolis, MN, UNITED STATES OF AMERICA,* [3]*Department of Nuclear Medicine, Imam Khomeini Hospital Complex, Tehran University of Medical Sciences, Tehran, IRAN, ISLAMIC REPUBLIC OF.*

Aim/Introduction: Recently, there is a growing trend in utilizing copper isotopes as radiopharmaceuticals for positron emission tomography (PET) imaging. The aim of this work was to evaluate 64-copper PET/CT image quality and quantitative parameters using ordered subset expectation maximization (OSEM) method with reduced scan times for different activity concentrations and lesion sizes. ***Materials and Methods:*** NEMA phantom with lesion to background ratios of 4:1 and 8:1, as well as patients who were administered with 64-copper. We conducted OSEM reconstruction using varying time intervals, ranging from 1⁄2 to 1⁄32 of the original duration in the phantom study and 30s, 60s, 90s ,120s and original scan time (180s) in clinical study. We evaluated images in the terms of signal-to-noise ratio (SNR), contrast-to-noise ratio (CNR), recovery coefficient (CR) and background variability. In clinical data, we measured the noise and SNR in the liver. ***Results:*** As the acquisition time was decreased, there was an increase in BV, as well as, a reduction in quantitative parameters. The BV for OSEM with 1⁄2 and 1⁄4 of original time at LBR 4:1 and only 1⁄2 of original time at LBR 8:1 were within the acceptable noise range(<5%). In this acceptable noise level, for all lesions and both LBRs, CNR satisfied the Rose criteria in image detectability (CNR>5). The CNR decreased by 3.6% at LBR 4:1, when the scan time was reduced to half, while at LBR 8:1, the reduction was 21.2%. The decrease of SNR for smallest sphere in 1⁄2 of standard acquisition time was 33.2% at LBR 4:1 and 42.2% at LBR 8:1 compared to full acquisition time. There is no specific relationship between changes in scan time and the RC. The RC of a sphere with diameters of 22 mm on 1⁄2, 1⁄4 and 1⁄8 of the original scan time were reduced by 0.7%, 0.4% and 1.6% compare to original scan time, respectively. In clinical study, only images at 120s and 180s had noise in acceptable level. We reported 7.1% decrease in SNR in liver when the scan time was reduced to 120 seconds. ***Conclusion:*** In larger lesions, it is possible to further reduction of the scan time with preserving the lesion detectability, while the SNR and CNR in smaller lesions are more susceptible to degradation with reduced time. Whole-body PET/CT scan used 64-copper can reduce the acquisition duration to 120s for each bed position without compromising the image quality.

EP-0691

Cluster Analysis in Binary Classification of Amyloid PET/MR Imaging with/without-Partial Volume Effect Correction

E. Balci[1], *U. O. Akdemir*[1], *M. A. Topcuoglu*[2], *E. Saka*[2], *L. O. Atay*[1];
[1]*Gazi University Medical Faculty Department of Nuclear Medicine, ANKARA, TÜRKIYE,* [2]*Hacettepe University, Faculty of Medicine, Department of Neurology, ANKARA, TÜRKIYE.*

Aim/Introduction: The aim of this study is to investigate the binary classification (positive or negative) of amyloid PET images using unsupervised clustering algorithms: k-means, partitioning around medoids (PAM), and agglomerative nesting (AGNES), and the contribution of partial volume effect correction (PVEC) to the discriminative power of the classification. ***Materials and Methods:*** PET/MR imaging (3D T1-MR, [18F]-Flutemetamol) was performed on a total of forty-nine patients diagnosed with subjective cognitive decline (SCD, n=11), amnestic mild cognitive impairment (aMCI, n=17), and Alzheimer's disease (AD, n=21). Volume of interest (VOI) of the sixty-eight cortical regions of the brain were determined by performing parcellation on T1-MR images using FreeSurfer. The PET images were applied the extended Müller-Gärtner PVEC method with PetSurfer. The standardized uptake value ratio (SUVr) values of the regions were obtained for with/without-PVEC. SUVr

values of the VOIs in sixty-eight cortical regions were used as inputs in cluster algorithms. k-means, PAM, and AGNES cluster algorithms were performed using R software. PET images were classified as positive or negative by two experienced nuclear medicine experts, and this classification was used as a reference to compare the results of clustering algorithms. ***Results:*** In the visual evaluation of [18F]-Flutemetamol PET images, the SCD group was found to be negative, except for one patient in the MCI group, which was positive, and the AD group was positive. In the classification performed without applying PVEC, similar results were obtained with k-means (accuracy: 82%, sensitivity: 100%, specificity: 57%), PAM (accuracy: 88%, sensitivity: 100%, specificity: 67%), and AGNES (accuracy: 78%, sensitivity: 100%, specificity: 52%) algorithms. However, after applying PVEC, the results of the k-means (accuracy: 90%, sensitivity: 100%, specificity: 71%), PAM (accuracy: 90%, sensitivity: 100%, specificity: 71%), and AGNES (accuracy: 98%, sensitivity: 100%, specificity: 92%) algorithms increased positively. ***Conclusion:*** The k-means, PAM, and AGNES cluster algorithms used in the study are valuable tools for classifying [18F]-Flutemetamol PET images due to their ability to classify without the need for a training set and their repeatability using standard packages in R software. Sensitivity was 100% for all algorithms with/without- PVEC. Applying PVEC to the images improves specificity and classification accuracy but accuracy and specificity values were not at the desired level except for AGNES. The AGNES algorithm provides highly accurate results in classifying [18F]-Flutemetamol PET images with-PVEC.

EP-0692

Improving Efficiency of Simultaneous Dual-Tracer PET Imaging

Z. Li[1], *V. Shah*[2], *S. L. M. Viol*[3], *P. van Snick*[1], *G. Luurtsema*[1], *R. H. J. A. Slart*[1], *A. Lammertsma*[1], *C. Tsoumpas*[1];
[1]*Department of Nuclear Medicine and Molecular Imaging, University of Groningen, University Medical Center Groningen, Groningen, NETHERLANDS,* [2]*Molecular Imaging, Siemens Medical Solutions UNITED STATES OF AMERICA, Inc., Knoxville, TN, UNITED STATES OF AMERICA,* [3]*Department of Radiology and Nuclear medicine, Amsterdam University Medical Center, Amsterdam, NETHERLANDS.*

Aim/Introduction: Simultaneous imaging of two PET tracers would reduce overall scanning time and provide molecular information in exactly the same physiological condition. However, separating signals from different PET tracers is difficult as all coincidence photons have the same energy. One possibility of separating signals is to utilise differences in half-life between two tracers. The purpose of this study was to explore the feasibility of pre-processing techniques, in combination with differences in half-life, to achieve rapid separation without compromising image quality, as well as to evaluate the impact of both acquisition time and frame duration on image quality. ***Materials and Methods:*** A NEMA IQ phantom filled with [^{18}F]fluorodeoxyglucose ([^{18}F]FDG) in the spheres and [^{15}O]water in the background compartment was scanned at the centre of the FOV for 20min using an LAFOV PET/CT scanner. A 4D extended cardiac-torso (XCAT) phantom was generated by selecting six organs, containing [^{11}C]choline and [^{18}F]FDG and simulating a 20min acquisition. In addition, to evaluate the possibility to reduce scan duration, image data were reprocessed for different acquisition times (120, 300, 450, 600 and 1200s) and frame durations (10 and 5s) for both phantoms. A linearization method was applied to the conventional half-life method [1]. Subsequently, several estimators and optimization methods were adjusted and implemented for separation of individual tracer concentrations. Resulting images were evaluated using the pixel-wise normalized root mean square error (NRMSE) and the pixel-wise multiscale structural similarity (MS-SSIM). ***Results:*** Application of the pre-processing linearization method resulted in a reduction in computation time by a factor of 3 to 13 compared with the conventional half-life method. For both phantoms, the image quality did not significantly improve for acquisition times above 600s. (MS-SSIM: 1 and 0.998, NRMSE: 0 and 0.025 for NEMA IQ and XCAT phantoms, respectively, when comparing 600 and 1200s images). Frame duration had a negligible effect on separation performance, with both phantoms exhibiting MS-SSIM higher than 0.9994 and NRMSE lower than 0.015 when comparing frame durations of 5 and 10s. ***Conclusion:*** This preliminary study demonstrates that using a pre-processing linearization method significantly improves computation time without loss of image quality. Furthermore, both overall acquisition times longer than 600s and shorter frame durations may not be necessary to obtain optimal image quality for both phantoms. The pre-processing linearization method should now be tested in real dual tracer patient studies. ***References:*** [1] Figueiras et al. Mol Imaging Biol. 2011;13(3):500-510.

EP-0693

Patlak graphical analysis: Net Influx Rate (Ki) obtained with a fully-automated Multiparametric PET Suite versus traditional Regional Plot

A. Capotosti[1], *R. Moretti*[1], *M. De Summa*[2], *S. Taralli*[1], *E. Perrone*[1,3], *M. L. Calcagni*[1,3], *L. Indovina*[1];
[1]*Fondazione Policlinico Universitario Agostino Gemelli IRCCS, Rome, ITALY,* [2]*Medipass S.p.a. Servizio Integrativo PET/CT - Radiofarmacia, TracerGLab, Fondazione Policlinico Universitario A.Gemelli IRCCS, Rome, ITALY,* [3]*Università Cattolica del Sacro Cuore, Rome, ITALY.*

Aim/Introduction: Patlak model is a graphical analysis technique that can be applied to PET images to estimate dynamic processes. This type of analysis is usually performed offline using the mean values of the signal present in the volumes of interest (VOIs) by setting up a'regional'Patlak. Today, with the introduction of the fully automated Multiparametric PET Suite feature, all the information required for Patlak analysis is included in the PET acquisition protocol, allowing image series to be expressed in terms of glucose consumption. The aim of this study is to compare the net influx rate (K_i) derived from a fully-automated multiparametric PET suite to the one obtained with the traditional Patlak regional plot. ***Materials and Methods:*** Four patients with small-cell lung cancer who underwent dynamic 18F-FDG PET were evaluated. Patients were injected on the bed at the same time as the PET acquisition started (entire exam lasting about 71 minutes). First 6 minutes were acquired as a static single-bed over the cardiac region, while remaining 65 minutes were acquired over whole-body in continuos bed motion. These two acquisitions were used to generate parametric images of the K_i. VOIs were defined over the descending thoracic aorta of each patient and over target lesions (n=19) on the full dynamic PET reconstructions. Regional K_i on the full dynamic PET reconstructions by standard regional Patlak plot analysis using Image Derived Input Function (0-70min) and tissue response (40-70min) curves from VOIs was obtained. The same VOIs were placed on parametric images derived from the dedicated suite and net Ki values were obtained. Net K_i values obtained with the traditional Patlak regional plot were compared to the ones obtained from multiparametric PET suite. ***Results:*** Mean percentage difference between K_is obtained with regional Patlak and voxel-based ones was found to be -7% ± 13%. Linear

regression plot showed a slope of 0.75 and intercept value of 0.004 with a good correlation (R^2=0.95). The Passing-Bablok regression for comparison between regional K_i and K_i from parametric imaging showed a slope of 0.78 and intercept value of 0.0001 (R^2=0.98). ***Conclusion:*** The introduction of the fully-automated Multiparametric PET Suite guaranties an accurate measurement of the K_i related to the metabolic rate of glucose in tissue and to local glucose consumption. This preliminary work showed a good correlation between K_i from regional Patlak analysis and K_i obtained from multiparametric imaging.

EP-0694

PET imaging with somatostatin analogue (SomaKitTOC®) for assessment of neuroendocrine tumors: unknown physiological uptake, patient in/dependent? Experience feedback

C. Provost[1], *C. Schmitt*[1], *J. Fouque*[1], *O. Madar*[1], *L. Champion*[2];
[1]*Institut Curie, Radiopharmacology department, Saint Cloud, FRANCE,* [2]*Institut Curie, Nuclear Medicine departement, Saint Cloud, FRANCE.*

Aim/Introduction: Radiopharmaceuticals somatostatin analogues are used for neuroendocrine tumours, which are characterized by an overexpression of somatostatin receptors in more than 80% of subtypes 2 and 5. In our institute, we have used [^{68}Ga]Ga-edotreotide (SomaKit TOC®) for positron emission tomography (PET) imaging since 4 years. Physicians have described some misunderstood physiological uptakes in the stomach, pancreas and liver. The purpose of this study is to find some explanation of these uncommon physiological uptakes. For this, we investigate on quality control of the radiopharmaceutical and ^{68}Ge/^{68}Ga generator used. ***Materials and Methods:*** Fifty-seven radiopharmaceutical preparations were analysed, from 2019 to 2021. Quality control consisted in two radio-thin-layer chromatographies to determine the percentage of free ^{68}Ga and ^{68}Ga colloids. Respectively 41 and 16 preparations were carried out with, GalliaPharm®/E&Z and Galliad®/ Ire ELiT generators. The final activities were ranging from 426 to 1090 MBq. One hundred and five patients were injected for PET imaging, 78 patients had 1 PET-scan, 17 had 2 scans, 6 had 3 scans and 4 had 4 scans. ***Results:*** Radiochemical purity (RCP) mean was 98 ± 1.33 %, with the percentage of free ^{68}Ga ranging from 0.05 to 1.92% and the percentage of ^{68}Ga colloids ranging from 0.03 to 3.41%. No significate difference was observed between percentage of free ^{68}Ga and ^{68}Ga colloids and between RCP and brand of generator. Uptake evaluation of stomach, liver and pancreas on patients PET scans do not show difference when preparations had a percentage of ^{68}Ga colloids > 2% or/and free ^{68}Ga > 1%. ***Conclusion:*** No matter which generator was used, there was no difference for the quality control of the preparation. The percentage of free ^{68}Ga and ^{68}Ga colloids do not seem to have an impact on the physiological uptakes in stomach, liver or pancreas. Regardless of the generator used, there is no difference in the quality control of the preparation and the interpretation of images. Physiological uptakes could be explain by patient treatments or hormone levels. Regarding our cohort of patients, those parameters need to be investigate. ***References:*** 1. Johnbeck CB, et al. PET tracers for somatostatin receptor imaging of neuroendocrine tumors: current status and review of the literature. Future Oncol. 2014 Nov;10(14):2259-77. 2. Al-Ibraheem A, et al. Focal uptake of 68Ga-DOTATOC in the pancreas: pathological or physiological correlate in patients with neuroendocrine tumours? Eur J Nucl Med Mol Imaging. 2011 Nov;38(11):2005-13.

EP-0695

A fuzzy C-mean segmentation technique to estimate methodological uncertainties on time-activity curves in dynamic quantitative positron emission tomography studies

P. Laporte[1], *J. Carrier*[1,2,3];
[1]*Département de Physique, Faculté des Arts et Sciences, Université de Montréal, Montréal, QC, CANADA,* [2]*Institut de Génie Biomédical, Faculté de Médecine, Université de Montréal, Montréal, QC, CANADA,* [3]*Département de radiologie, radio-oncologie et médecine nucléaire, Faculté de Médecine, Université de Montréal, Montréal, QC, CANADA.*

Aim/Introduction: Dynamic positron emission tomography (PET) acquisitions can be used to compute time-activity curves (TACs) for an imaged subject, from a selected region of interest (ROI). These curves can then be used to extract pharmacokinetic parameters. To obtain a relevant ROI, a segmentation technique must be used. The obtained ROI depends on the segmentation scheme, as well as the timeframe(s) used as reference. This latter part introduces a significant variation in the ROI, which can then lead to varying values for the pharmacokinetic parameters. Since many clinical trials use a small number of test subjects, it is relevant to assess the methodological impacts pertaining to the selection of the ROI. ***Materials and Methods:*** Using a home-made dynamic phantom, PET acquisitions have been obtained, using FDG. This phantom is a simple three-compartment device, for which the analytical model can be derived. Using a Fuzzy C-mean (FCM) segmentation technique, more specifically the SpectaQle algorithm [1], a rough ROI can be obtained. Using statistical sampling on the voxels' probability of belonging to the ROI, an uncertainty has been estimated for the TAC. From there, using a nested sampling algorithm, the pharmacokinetic parameters of the analytical model are obtained. All the numerical analysis were conducted using Python3.8. ***Results:*** The obtained TACs with error bars show a higher degree of statistical overlap compared to TACs obtained from a segmentation on a single timeframe. The obtained pharmacokinetic parameters show a larger range of values, but are more reproducible. ***Conclusion:*** The advantage of this whole process is to allow the analysis of TACs from a single patient, as would be the case in the context of clinical care. With the emergence of new radiopharmaceutical compounds, this will yield greater medical confidence in the administration of specific drugs to patients. :This segmentation method with the proposed methodology to obtain a time-activity curve with error bars lead to safer statistical analyses of dynamic quantitative PET acquisitions. This helps in making the scientific endeavour more reproducible, transparent, and honest. ***References:*** Lapuyade-Lahorgue, J. et al. SPEQTACLE : An automated generalized fuzzy C-means algorithm for tumor delineation in PET. Med. Phys. 42 (10).

EP-0696

Influence of normal database sample size on the development of new statistical image analysis software for bone SPECT imaging

Y. Yakushiji[1], *K. Miwa*[2], *K. Wagatsuma*[1,3], *S. Fukuda*[1], *T. Yamao*[2], *Y. Kamitaka*[3], *N. Miyaji*[2], *T. Hasegawa*[1];
[1]*Kitasato University Graduate School of Medical Sciences, Kanagawa-ken, JAPAN,* [2]*Fukushima Medical University, Fukushima-ken, JAPAN,* [3]*Tokyo Metropolitan Institute of Gerontology, Tokyo-to, JAPAN.*

Aim/Introduction: Bone metastasis is currently diagnosed based on standardized uptake values (SUV) derived from bone single photon emission computed tomography (SPECT) images; however, they vary according to patient size or lesion location.

We focused on Z-scores calculated using an anatomical statistical method as a new quantitative index for bone SPECT images. We developed a new statistical image analysis software for bone SPECT imaging that inputs projection data and CT images, automatically reconstructs and corrects scatter and attenuation, normalizes and anatomically standardizes between reconstructed SPECT and CT images, and analyzes anatomical statistics. Z-scores were substantially affected by the size of the normal database (NBD). The statistical image analysis software for brain SPECT required data from at least 15 normal persons to create the NDB. The amount of data in the NDB required to calculate Z-scores for bone SPECT imaging is unclear. The present study aimed to validate the impact of NDB size on bone SPECT imaging. ***Materials and Methods:*** Twenty-two patients with (n = 3) and without (n = 19) bone metastasis were assessed by 99mTc-MDP pelvic SPECT imaging using a Symbia Intevo (Siemens Healthineers) under clinical conditions. We created NDB-16 (n = 16) and NDB-8 (n = 8) comprising persons without bone metastasis and compared them. We quantified the means and standard deviations (SD) of pixels at five points in the pelvis, then calculated the SD/mean to determine the accuracy of the NDB. We calculated Z-scores from the ilium and lumbar regions in three persons each with and without bone metastasis, and from lesions in three patients with bone metastasis. ***Results:*** The median SD/mean values were 17.2 and 13.8 for NDB-16 and NDB-8, respectively and did not significantly differ (p = 0.31, Mann-Whitney tests). The median Z-scores were 1.92 and 1.86 for NDB-16 and NDB-8, respectively, and 1.05 and 1.39 for NDB-16 and NDB-8 in patients with and without metastasis, respectively. The median Z-scores in metastatic lesions were 17.81 and 30.67 for NDB-16 and NDB-8, respectively. ***Conclusion:*** We created a small NDB (n < 10) using statistical image analysis software for bone SPECT imaging. The Z-scores were < 2.0 and > 2.0 in normal regions and metastatic lesions. Z-scores might be a novel quantitative index for bone SPECT imaging.

EP-0697

The Management of Diabetic Patients During the Positron Emission Tomography Examination: the Experience of Sahloul University Hospital

A. Ben Naceur, *A. Toumi, N. Ayachi, K. Chatti;*
Sahloul University Hospital, Sousse, TUNISIA.

Aim/Introduction: Positron Emission Tomography (PET) marked with ^{18}F-2-fluoro-2-deoxy-D- glucose (^{18}F-FDG) is a functional imaging technique of notable sensitivity and specificity. However, high blood glucose levels might decrease the sensitivity of PET due to a low absorbance of ^{18}FDG. Our goal is to study the follow-up of the preparation of diabetic patients for the PET examination to establish a management protocol for them. ***Materials and Methods:*** This is a descriptive prospective study consisting of monitoring the preparation of diabetic patients for the PET scan taking into account antidiabetic treatments, blood sugar levels, tolerance to fasting, risk of hypoglycemia and/or hyperglycemia, glycemic profile in previous PET scans, weight, etc. Then, we analyzed the feasibility of the examination in order to establish a common protocol to guarantee the minimum number of canceled examinations. Our study has been underway for two months now in the nuclear medicine department of Sahloul university hospital in Tunisia. ***Results:*** The study has been conducted on 33 diabetic patients, 27 with non-insulin-dependent diabetes and 6 with insulin-dependent diabetes. As part of the optimization of FDG doses in PET aiming to scan the maximum number of patients, we injected 4 patients at a time between 10:30 a.m. and 12:00 p.m. These patients have been fasting since 5 a.m, while 29 patients have been fasting since the night before the examination, and they were injected at a time between 7:45 a.m. and 9:30 a.m. On the examination day, 27 patients (81.8%) had a fasting blood sugar inferior to 2 g/dl, and 6 patients (18.2%) had a fasting blood sugar superior to 2 g/dl which counter-indicates the performance of the examination. These patients were injected with 4 IU of regular insulin and their blood sugar levels were monitored every hour for 4 hours. 2 of the 6 patients had a blood sugar level inferior to 2 g/dl 4 hours post-injection, while 4 patients (66.66%) did not experience an improvement in their blood glucose levels leading to the cancellation of their appointments. In conclusion, 4 examinations among the 33 (12.12%) were postponed due to uncontrolled diabetes. ***Conclusion:*** According to our study, a rigorous preparation of the patient is essential to limit the glycemic imbalances leading to the delay of the examination. The percentage of patients whose examination was postponed (12.12%) could be reduced with further management. The study continues to determine the most effective mode of preparation.

EP-0698

Towards AI application with automatic subtraction to improve parathyroid adenomas detection

O. Boukhennoufa[1], *L. Comas*[2,3], *E. Lajeune*[1], *C. Ungureanu*[2], *M. Soualhi*[1], *J. Nicod*[1], *N. Zerhouni*[1], *H. Boulahdour*[2,3];
[1]*Université de Franche-Comté, SUPMICROTECH, CNRS, institut FEMTO-ST, Besançon, FRANCE,* [2]*Service de Médecine Nucléaire, CHU Besançon, Besançon, FRANCE,* [3]*Université de Franche-Comté, LNIT, F-25000, Besançon, FRANCE.*

Aim/Introduction: Nuclear medicine parathyroid imaging is an efficient diagnostic procedure to detect parathyroid adenomas. With dual tracer imaging system, addition of a processing layer of collected images can lead to efficient detection and localization of hyperfunctioning parathyroids. The processing is a subtraction between normalized ^{99m}Tc-MIBI and the ^{123}I images after defining the best factor of subtraction which is actually performed fastidiously. Also, the normalization is calculated after determining the region of interest (ROI), automatically or manually by physicians. This study aims to automatically find an adaptive optimal subtraction image for physicians towards AI applications. ***Materials and Methods:*** A total of 42 patients (5 men; mean age 63.8 years, range 28-91 years) were retrospectively included. After two injections of radioactive products, ^{99m}Tc-MIBI and ^{123}I, static LEHR and PINHOLE images were collected. In these acquisitions, three examinations were excluded from the study due to the absence of thyroid uptake preventing the determination of the ROI which is a crucial step for the normalization of ^{99m}Tc-MIBI and ^{123}I images. The proposed methodology starts by determining the thyroid ROI with an optimal threshold, which is 50% of the maximum pixel value in the thyroid area (40 lines in the center of the image). Then, the ROIs obtained from each patient of the ^{99m}Tc-MIBI and ^{123}I images are normalized so that the thyroid activity is comparable on the two images, allowing an optimal adaptive subtraction image for each patient. After simulation of subtraction with weight factors ranging from 0 to 2, the sum of pixels inside ROI is stored. Thus, optimal weight is obtained by the first positive derivative. Finally, the subtraction activity is the difference between the normalized ^{99m}Tc-MIBI and ^{123}I images with the adaptive normalization factor multiplied by the optimal threshold. ***Results:*** First, the 39 pinhole images were subtracted manually by the physician. Then, the manual subtraction was

compared to the proposed automatic one. The performance comparison between these two approaches was by calculating the correlation coefficient in the thyroid ROI of each subtracted image. The obtained correlation coefficients are promising with a mean value of 0.935. ***Conclusion:*** The developed algorithm allows automatic generation of an adaptive optimal subtraction of the static images. This method is fast and can be used for diagnostics by physicians and towards AI applications. ***References:*** Petranović Ovčariček, Petra, et al. "The EANM practice guidelines for parathyroid imaging." European journal of nuclear medicine and molecular imaging 48 (2021): 2801-2822.

EP-0699

Evaluation of PaIRe PET/CT segmentation software as cancerous lesion contouring tool in fully-automated annotation workflows for image-based research studies

D. Abler[1], *M. Jreige*[2], *O. Michielin*[1,3], *N. Schaefer*[2], *J. O. Prior*[2], *A. Depeursinge*[4,2], *M. A. Cuendet*[1,5,6], *P. Blanc Durand*[7];
[1]*Department of Oncology, Precision Oncology Center, Lausanne University Hospital and University of Lausanne, Lausanne, SWITZERLAND,* [2]*Nuclear Medicine and Molecular Imaging Department, Lausanne University Hospital and University of Lausanne, Lausanne, SWITZERLAND,* [3]*Department of Oncology, Geneva University Hospital and University of Geneva, Geneva, SWITZERLAND,* [4]*Institute of Informatics, School of Management, University of Applied Sciences Western Switzerland, Sierre, SWITZERLAND,* [5]*Swiss Institute of Bioinformatics, University of Lausanne, Lausanne, SWITZERLAND,* [6]*Department of Physiology and Biophysics, Weill Cornell Medicine, New York, NY, UNITED STATES OF AMERICA,* [7]*Nuclear Medicine Department, Henri-Mondor University Hospital, Créteil, FRANCE.*

Aim/Introduction: Assistive automatic segmentation tools for clinical applications frequently prioritize detection of 'suspicious' regions of interest (ROIs), thereby accepting many false positives. While these can be discarded by expert review, fully-automated annotation is important for large-scale retrospective research[1]. This study assesses the PaIRe PET/CT segmentation software[2] and its potential role in such settings. ***Materials and Methods:*** Tumour ROIs in 20 whole-body PET/CT images of 10 metastatic melanoma patients at baseline and after treatment with Immune-Checkpoint-Inhibitors were contoured by a nuclear medicine expert aware of all clinical and follow-up information to obtain a ground-truth (GT) segmentation. For these images, PaIRe (version 0.2.1) yielded: (a) contours of suspicious ROIs, and (b) maps indicating each voxel's likelihood of being pathological. Agreement between GT and PaIRe contours was investigated at the voxel and lesion level. For each ROI, the number of True Positive (TP), False Positive (FP) and False Negative (FN) voxels was established. PaIRe ROIs sharing at least one voxel with GT were considered TP lesions. To investigate alternative operating points, PaIRe's sensitivity-recall curve was computed by assessing contours resulting from varying decision thresholds. ***Results:*** The GT dataset contained 98 malignant lesions across 19 PET/CT scans with average total metabolic tumour volume (TMTV) of 33.9cm^3 per patient (1 scan not evaluable). PAIRE, using default settings, identified an average TMTV of 125.1cm^3 and 399 ROIs. Of these, 92 TP and 307 FP (6 FN), corresponding to a (precision, recall) by lesion (PRL) of (0.23, 0.94) and by voxel (PRV) of (0.23, 0.84). Decision thresholds between 0.01 and 0.99 yielded PRLs between (0.06, 1.00) and (0.69, 0.70), and PRVs between (0.08, 0.98) and (0.88, 0.22), respectively. The highest average dice index (0.75) for corresponding ROIs was achieved at a decision threshold of 0.6 with PRL of (0.53, 0.85) and PRV of (0.70, 0.67). ***Conclusion:*** While PaIRe achieved almost perfect recall for cancerous lesion detection, any alternative operating point with acceptable recall (e.g., >0.8) resulted in large FP/TP ratios, possibly exacerbated by the presence of immunotherapy-induced pseudo-progression in this cohort. Further processing steps for removing FP (non-pathological, pathological but non-cancerous) lesions/voxels are thus required for automated workflows. Overall, PaIRe's voxel precision exceeded lesion detection precision, while the opposite applied to recall. Consequently, the optimal choice will depend on the specific research use case. ***References:*** [1] D. Abler et al. JCO Clinical Cancer Informatics. 2023; in-press. [2] A. Van Der Gucht et al. Médecine Nucléaire. 2021;45(4):192.

EP-0700

Pituitary Gland: Do We Really See It?

A. Macula[1,2], *L. Airo*[3], *S. Colombo Serra*[2], *M. Ali*[4], *S. Papa*[4], *G. Valbusa*[2], *A. Bifone*[1], *P. Gandolfo*[4];
[1]*Università di Torino, Torino, ITALY,* [2]*Bracco Imaging S.p.a., Milano, ITALY,* [3]*Università di Milano, Milano, ITALY,* [4]*Centro Diagnostico Italiano, Milano, ITALY.*

Aim/Introduction: The pituitary gland is an endocrine organ that releases several hormones, including prolactin and growth hormones, along with pituitary hormones such as follicle-stimulating hormone, luteinizing hormone, thyroid-stimulating hormone, and adrenocorticotropic hormone. Oncological evaluation of cerebral parenchyma is not usually investigated by [18F]FDG-PET/CT imaging. However, during clinical practice, an anomalous uptake has been noticed on the hypophysis of many patients without sellar symptoms. The aim of this work is to analyze this phenomenon and its possible correlation with some clinical parameters. ***Materials and Methods:*** Scans from eighty-one patients who underwent [18F]FDG-PET/CT from 03/2018 to 01/2023 at our center (Centro Diagnostico Italiano, Milan, Italy) were selected by a qualitative analysis which compares the pituitary uptake with the mediastinal uptake. Inclusion criteria were: (a) cancer patients, (b) patients with at least two acquisitions, (c) [18F]FDG-PET/CT performed according to standard execution modalities, (d) whole body acquisitions starting from vertex, (e) patients without any pituitary biochemical examination or radiological evidence of pituitary adenoma. For each patient, clinical attributes of interest were automatically extracted from the clinical reports, by filtering reason for study, conclusions, and findings fields through keywords. An incidence count analysis was conducted by linking the presence/absence of hypophysis uptake with the type of therapy (chemio, radio, immuno, none), primary tumor (breast, lungs, others), setting (staging, follow up), result of the investigation (positive or not), status of the disease (progression or not). ***Results:*** The qualitative analysis showed focal uptake (> mediastinal) of the pituitary gland on forty-four patients (54%) while thirty-seven patients (46%) were considered negative. The preliminary incident count analysis did not show any evident connection between anomalous hypophysis uptake and any of the considered parameters. ***Conclusion:*** The finding of pituitary uptake in [18F]FDG-PET/CT is a very rare occurrence (0.07-0.8% [1]). However, in patients with a known tumor, especially in those with lung or breast cancer, the incidental pituitary uptake should be furthered investigated, although it could have functional or flogistic significance. For this reason, we designed a more structured retrospective study to: - Expand the dataset to investigate the possible correlation between the positive hypophysis cases and the primary tumor or the secondary lesions; - Perform a semi-quantitative analysis by eventually establishing a cut-off

to systematically classify the positive/negative cases; - Exclude any concomitant pathology of endocrine/non-endocrine nature which can have an impact on hypophysis uptake. ***References:*** 1. Iglesias, P., https://doi.org/10.1016/j.ejim.2019.08.008

EP-0701

A statistical method to adapt a normal range for thyroid uptake measurements following replacement of a gamma camera

A. Gemmell[1,2,3], *C. Brown*[1,2], *S. Ray*[3], *S. Small*[1,2];
[1]*Nuclear Medicine, Gartnavel General Hospital, Glasgow, UNITED KINGDOM,* [2]*Department of Clinical Physics & Bioengineering, Glasgow, UNITED KINGDOM,* [3]*School of Mathematics & Statistics, University of Glasgow, Glasgow, UNITED KINGDOM.*

Aim/Introduction: Semi-quantitative ^{99m}Tc-Pertechnetate thyroid uptake measurements on a gamma camera provide useful diagnostic information for patients with hyperthyroidism. Guidelines suggest that centres should determine a local normal range due to geographical variations in normal thyroid measurements [1]. When a camera is replaced, previously established normal ranges may no longer be valid due to variations in camera performance [2]. This study uses a statistical batch harmonisation approach [3] to adapt an existing normal range to a new camera. ***Materials and Methods:*** Thyroid uptake measurements were gathered retrospectively for camera A (112 cases) and its replacement camera B (287 cases). The full dataset were harmonised using Location-Scale harmonisation [4]. The normal range for camera A (0.5% - 3.5%) was adjusted based on the resultant model to create a normal range for camera B. Repeated testing using random samples of the dataset was performed to determine minimum required sample size for accurate harmonisation. ***Results:*** Harmonisation of the full dataset improved distribution of the measurements between the two cameras from p=0.052 to p=0.988. Normal range was adjusted from 0.5% - 3.5% to a new range of 0.44% - 4.49%. Variations in potential normal ranges reduced with increasing sample size. Improvements were minimal with sample sizes > 100, where mean p=0.926 and mean adjusted normal range was 0.45% - 4.46%. ***Conclusion:*** The batch harmonisation method adjusts the distributions of thyroid uptake measurements from two gamma cameras, making them statistically more alike. Applying the adjustment to an existing normal range can correct for differences in camera performance. A downside is harmonisation can only be applied after sufficient data has been acquired on the new camera. Facilitating earlier harmonisation, smaller sample sizes may be used but with greater uncertainties - an iterative process of adaptation as more data is acquired may be appropriate. ***References:*** 1. L. Giovanella et al., "EANM practice guideline/SNMMI procedure standard for RAIU and thyroid scintigraphy," Eur. J. Nucl. Med. Mol. Imaging, vol. 46:12, pp. 2514-2525, 2019, doi: 10.1007/s00259-019-04472-8. 2. S. C. Kappadath, W. D. Erwin, and R. E. Wendt, "Observed Inter-Camera Variability of Clinically Relevant Performance Characteristics for SIEMENS Symbia Gamma Cameras," Med. Phys., vol. 33:6, p. 2014, 2006, doi: 10.1118/1.2240756. 3. W. E. Johnson, C. Li, and A. Rabinovic, "Adjusting batch effects in microarray expression data using empirical Bayes methods," Biostatistics, vol. 8:1, pp. 118-127, 2007, doi: 10.1093/biostatistics/kxj037. 4. J.-P. Fortin, "neuroCombat:Harmonization of multi-site imaging data with ComBat." 2021, https://github.com/Jfortin1/neuroCombat_Rpackage.

EP-0702

EImpact of using different SUV thresholds for delineating human brown adipose tissue volume with 18F-FDG PET-CT

Y. Garcia-Rivero, *E. Rodríguez García, S. Beltrán Arenas, M. Pérez Gómez, C. Rodríguez García, Á. García Rodriguez, M. Ruiz Molina, G. Sánchez-Delgado;*
Hospital Virgen De Las Nieves, Granada, SPAIN.

Aim/Introduction: Brown adipose tissue (BAT) has emerged as a promising target for treating obesity and metabolic diseases since its discovery in human adults in the early 21st century. Despite extensive research, many fundamental questions about BAT remain unanswered. One of the main knowledge gaps concerns the uncertainty surrounding the amount of BAT that adult humans possess. Various SUV thresholds have been employed in 18F-FDG PET-CT scans to evaluate BAT volume, which is the most commonly used technique. This study aims to determine the impact of different SUV thresholds on BAT volume quantification. ***Materials and Methods:*** The ACTIBATE study recruited 135 young, healthy adults (45 men, 90 women; 22.0±2.1 years old; 24.9±4.7 kg/m2) to assess their BAT using a static 18F-FDG PET-CT scan. Participants were exposed to a 2-hour personalized cold exposure while wearing cooling vests connected to a temperature-controlled water circulation system. The individual shivering threshold was considered to individualize the cold exposure. A bolus of ~185 MBq 18F-FDG was administered 1 hour after starting the cold (1 hour before the PET-CT). PET-CT images were acquired from the atlas vertebrae to the mid-chest. A range of radiodensity (-190 / -10 Hounsfield Units) was first applied to focus on adipose tissue, followed by three different SUV thresholds (1.5, 2, and individualized: 1.2*(lean body mass/body mass)). BAT volume, SUVmean, and SUVpeak were then calculated for each SUV threshold. ***Results:*** The mean BAT volume was 70.5±58.8 ml when using the individualized SUV threshold, 73.7±63.7 ml when using the 1.5 SUV threshold, and 99.5±79.7 ml when using the 2 SUV threshold, with all values differing significantly (all P<0.003). SUVmean was also impacted by the SUV threshold (Individualized SUV threshold: 3.8±2.0; 2 SUV threshold: 3.7±2.0; 1.5 SUV threshold: 3.3±1.5; all P<0.15). In contrast, SUVpeak was similar when using the Individualized SUV threshold (11.4±8.3) and 2 SUV threshold (11.4±8.4) (P=0.594) but differed when using the 1.5 SUV threshold (11.5±8.2) (all P<0.01). ***Conclusion:*** The use of different SUV thresholds significantly affects the quantification of BAT volume and activity in humans. Therefore, determining the most appropriate SUV threshold and standardizing it across studies is urgently needed.

EP-0703

Parametric Images And KEi Index In A Small Kidneys Clearance Function Assessment

K. Filipczak, *P. Cichocki, J. Kusmierek, A. Plachcinska, Z. Adamczewski;*
Medical University of Lodz, Lodz, POLAND.

Aim/Introduction: Parametric images of clearance function are the result of processing data from Dynamic Renal Scintigraphy (DRS). Visualized clearance parameter can be presented also in the form of clearance efficiency classes, which allows visual assessment of the clearance function. This study presents a method for visual assessing of kidney function, which allows to compare results between patients, compare studies of the same patient, as well as assess clearance function of small kidney. ***Materials and Methods:*** Results of DRS of healthy volunteers (26

- 66 y/o, average 50 y/o, without urinary tract diseases or other diseases that could impair kidney function) were processed to define clearance function classes. Subsequently, 15 patients, whose one kidney appears relatively small and for which a standard way of assessment of the clearance function was problematic, was examined with a new method. Scintigraphy data were obtained using the standard DRS protocol, (60 images 20s, 128x128 matrix, 111MBq ^{99m}Tc-EC). The gamma camera detector was in a position that includes the heart area. Clearance parametric images were generated and KEi (kidney efficiency index) was determined. KEi index and its standard deviations were used to define ranges of values characterizing the clearance function as: normal (very high, high), impaired (reduced or trace) and lack of active renal parenchyma. According to defined ranges, a color map was created for the parametric images. ***Results:*** Small kidney clearance was assessed using parametric images and a dedicated clearance color map. ***Conclusion:*** Parametric images with colormap of classified clearance function allows an easy visual assessment of a single kidney clearance function. The method appears very useful in assessment of small kidney function and also in comparison of results within the same patient and between patients. ***References:*** DOI 10.5603/NMR.2020.0025

EP-0704

Standardized Uptake Values for SPECT-CT in Normal Lumbar Spine, using xSPECT Quant Bone Reconstruction

A. Duarte, *D. Calado, N. do Canto, M. Correia, A. Figueiredo, S. Matos, B. Martins, C. Pinto, V. Sousa;*
Hospital da Luz, Lisboa, PORTUGAL.

Aim/Introduction: Diphosphonates, such as HMDP (hydroxymethylene diphosphonate) labeled with ^{99m}Tc are used to perform bone scintigraphy. The hybrid techniques such as SPECT-CT are helpful in diagnosis of bone pathology. Hybrid images of SPECT and CT create attenuation correction maps that are used for quantitative analyses through the standardized uptake value (SUV). In clinical practice, the use of SPECT-CT can significantly increase the diagnostic value of bone scintigraphy, by displaying sites of higher osteoblastic activity and perhaps sites warranting directed treatment. xSPECT Bone® is a new reconstruction algorithm for hybrid bone imaging. CT-based tissue segmentation is incorporated into the reconstruction to provide SPECT images with better bone definition.In this study, we aimed to determine standard SUV values of [99mTc] Tc-HMDP uptake in normal lumbar vertebrae, using SPECT-CT images reconstructed with xSPECT Bone®. ***Materials and Methods:*** We conducted a retrospective study between June 2020 and March 2023, with 173 patients undergoing SPECT-CT using [99mTc] Tc-HMDP. From those, only 31 patients (11 men and 20 women) complied with the inclusion criteria: adults (21 at 66 years) and have all the measures required for quantification (height; weight; dose activity; time of injection; residual dose). The median: age 40 years, weight 70 kg, and height 167 cm. We analyzed 140 normal lumbar vertebrae and obtained the maximum SUV Body Weight (SUV_{BWmax}) for each one. We studied the relationship of SUV_{BWmax} values with age, height and weight of the patients. ***Results:*** Mean $SUV_{BW\ max}$ values were calculated for each of the lumbar vertebrae: L1 (12,10 ± 2,36), L2 (12,13 ± 2,43), L3 (12,08 ± 2,33), L4 (12,02 ± 2,33) e L5 (11,87 ± 2.04). There was no significant correlation of the mean $SUV_{BW\ max}$ value for the lumbar spine, with age, weight and height ($p = 0.160$; $p = 0.871$; $p = 0.453$). ***Conclusion:*** Using the new reconstruction algorithm xSPECT Bone®, it was possible to quantify standard SUV values for the lumbar spine. In this study there was no significant association of SUV_{BWmax} values with age, weight and height, although it is necessary to carry out future studies with larger samples to study the impact of biometric parameters and age in SUV_{BWmax} values. ***References:*** Qi, N., Meng, Q., You, Z., Chen, H., et al. Standardized uptake values of 99mTc-MDP in normal vertebrae assessed using quantitative SPECT/CT for differentiation diagnosis of benign and malignant bone lesions. BMC Med Imaging. 2021 Feb 27;21(1):39. PMID: 33639

EP-0705

Relationship of 18F-FDG PET/CT metabolic parameters reduction during neoadjuvant chemotherapy to complete cytoreduction and pathologic response in primarily inoperable high-grade serous ovarian cancer.

L. Sancho Rodriguez[1], *L. Sánchez Lorenzo*[1], *F. Boria Alegre*[1], *T. Iscar Galán*[1], *L. García Belaustegui*[1], *V. Carrasco Rubio*[1], *C. Beorlegui Arteta*[2], *M. Romera Caballo*[3], *V. Betech Anta*[3], *M. García Velloso*[3];
[1]*Clinica Universidad De Navarra, Madrid, SPAIN,* [2]*Departamento de Salud. Gobierno de Navarra. Pamplona., Pamplona, SPAIN,* [3]*Clinica Universidad De Navarra, Pamplona, SPAIN.*

Aim/Introduction: To evaluate the usefulness of reduction of ^{18}F-FDG-PET/CT metabolic parameters after neoadjuvant chemotherapy(NACT) as predictors of complete cytoreduction and NACT response, in patients with advanced FIGO stage(III/IV) high-grade serous ovarian cancer(HGSC). ***Materials and Methods:*** Retrospective review of prospectively collected data from primarily inoperable HGSC patients who underwent ^{18}F-FDG-PET/CT before(PETpre) and after NACT(PETpost). Reduction of CA-125 levels after NACT, pathological chemotherapy response score(CRS1-no response, CRS2-partial response and CRS3-complete response) and cytoreduction(R0-complete vs. R1-incomplete) were used to evaluate NACT response. ^{18}F-FDG-PET/CT parameters were obtained by means of the segmentation of the supradiaphragmatic disease and the different abdominal areas (primary tumor, peritoneal carcinomatosis and infradiaphragmatic lymph nodes) using Syngo. via (Version VB60A Siemens), with automatic thresholding at 30% of SUVmax. The metabolic parameters studied were: metabolically active tumor volume (MTV) and total lesion glycolysis (TLG), for each segmented region and for the entire disease. The variation for all these parameters between PETpre and PETpost were calculated. The presence of ascites with pathological uptake of ^{18}F-FDG (SUVmax ascites > SUVmean blood pool) was evaluated. Variables were described by mean (SD) or median (IQR) depending if data followed normal distribution. The relationship between quantitative variables were assessed by Spearman correlation coefficient (rho), and between quantitative and binary variables by logistic regression and ROC analysis. ***Results:*** Seventeen patients were included, with a mean age of 63.6 years (range: 37-78); most patients (94.1%) received three cycles of NACT. Only two patients (11.8%) presented R1, eight (47.1%) complete response (CRS 3) and only one did none response (CRS1). All patients associating pathological uptake in ascites on PETpre (n=13, 76.5%) normalized on PETpost. The reduction of CA-125 was moderately correlated to the reduction of the total TLG value (rho: 0.535; p=0,027), the total infradiaphragmatic disease MTV (rho: 0.577; p=0,015) and TLG (rho: 0.597; p=0,011) values and the total peritoneal disease MTV (rho: 0.609; p=0,012) and TLG (rho: 0.609; p=0,014) values. No significant relationship was detected among metabolic variables and cytoreduction; only variation of peritoneal MTV and total

infradiaphragmatic disease showed a p-value <0.200. No variables were found to be associated to CRS. ***Conclusion:*** Despite the small sample size, this study identifies some metabolic parameters of ^{18}F-FDG-PET/CT whose variations could predict cytoreduction and NACT response in patients with FIGO stage III-IV HGSC. ***References:*** Eur J Nucl Med Mol Imaging (2018) 45:1224-1232. Annals of Nuclear Medicine (2020) 34:128-135. CJ Gynecol Oncol. 2022 May;33(3):e28. Cancer Res Treat. 2020:52(4):1211-1218. Gynecologic Oncology 140 (2016) 29-35.

EP-0706

Is there any metabolic parameter of staging 18F-FDG-PET/CT related to the therapeutic strategy performed (primary cytoreduction vs. neoadjuvant chemotherapy and interval cytoreduction) in patients with high-grade serous ovarian cancer?

L. Sancho Rodriguez[1], *L. Sánchez Lorenzo*[1], *F. Boria Alegre*[1], *T. Iscar Galán*[1], *L. García Belaustegui*[1], *E. eguillenv@unav.es*[1], *V. Carrasco Rubio*[1], *C. Beorlegui Arteta*[2], *M. Romera Caballo*[3], *V. Betech Anta*[3], *M. García Velloso*[3];
[1]*Clinica Universidad De Navarra, Madrid, SPAIN,* [2]*Departamento De Salud. Gobierno De Navarra, Madrid, SPAIN,* [3]*Clinica Universidad De Navarra, Pamplona, SPAIN.*

Aim/Introduction: To analyze if there is any metabolic parameter of the staging ^{18}F-FDG-PET/CT related to the therapeutic strategy performed [primary cytoreduction vs. neoadjuvant chemotherapy(NACT) and interval cytoreduction] in patients with high-grade serous ovarian cancer(HGSC). ***Materials and Methods:*** Retrospective review of prospectively collected data from patients with HGSC who underwent a staging ^{18}F-FDG-PET/CT before defining the therapeutic strategy to be performed: A(primary cytoreduction) or B(NACT and interval cytoreduction). ^{18}F-FDG-PET/CT parameters were obtained by means of the segmentation of the supradiaphragmatic disease and the different abdominal areas (primary tumor, peritoneal carcinomatosis and infradiaphragmatic lymph nodes) using Syngo.via(Version_VB60A_Siemens), with automatic thresholding at 30% of SUVmax. The metabolic parameters studied were: metabolically active tumor volume(MTV) and total lesion glycolysis(TLG), for each segmented region and for the entire disease. The presence of ascites with pathological uptake of ^{18}F-FDG (SUVmax ascites>SUVmean blood pool) was evaluated. Clinical data as age, basal CA-125(U/mL), complete or incomplete cytoreduction were also collected. The dependent variable was the therapeutic strategy performed. Data were described by median(IQR) and frequency(%). Chi-square and Mann-Whitney U tests were used to compare groups and ROC analysis to dichotomize continuous variables. The predictors of the therapeutic strategy performed were analyzed using multiple logistic regression analysis. ***Results:*** 42 patients were included, 25 in group A (primary cytoreduction) and 17 in group B (NACT and interval cytoreduction). Both groups were similar in relation to age (61 years (56-66) in group A vs. 65 years (58-71) in group B; p = 0,155), median basal CA-125 (667 U/mL (143-1113) vs 840 U/mL (299-1778); p =0.289), and frequency of complete cytoreduction (68 vs 87.5%; p=0.102). Group A display significantly less ascites with pathological uptake (32 vs 76.5%; p=0.005), smaller MTV and TLG values for supradiaphragmatic disease (0 (0-0) vs 8.7 (3.9-55.0)) and (0 (0-0) vs 25.5 (11.4-132.0)), respectively, both p<0.001) and smaller MTV and TLG values for infradiaphragmatic disease, (208.2 (35.04-411.56) vs 455.9 (152.9-683.9) p=0.028) and (502.2 (194.3-1460.8) vs 2082 (999.3-2935.2) p=0.032), respectively, than group B. Both, ascites with pathological uptake (OR=0.197 (0.045-0.865); p=0.031) and MTV value >286 for infradiaphragmatic disease (OR=0.225 (0.052-0.954); p=0.044) were independent predictors of the therapeutic strategy (Sensitivity=64.7% and specificity=92%). ***Conclusion:*** This study, despite its small sample size, identifies very useful 18F-FDG PET/CT biomarkers for deciding the therapeutic strategy in patients with HGSC. ***References:*** Eur J Nucl Med Mol Imaging(2018)45:1224-1232. Annals of Nuclear Medicine(2020 34:128-135. J Gynecol Oncol. 2022 May;33(3):e28. Cancer Res Treat. 2020:52(4):1211-1218.

EP-0707

Quantification parameters of 99mTc-MDP single-photon emission computed tomography/computed tomography in the diagnosis of active condylar hyperplasia.

M. Umar, *D. Khan, S. Sagar, S. Ahmad Shamim, R. Kumar; Aiims, Delhi, INDIA.*

Aim/Introduction: 99mTc-MDP SPECT/CT has a significant role in the identification of active condylar hyperplasia. The aim of our study is to assess the quantification parameters of 99mTc-MDP single-photon emission computed tomography/computed tomography (SPECT/CT) for the diagnosis of active condylar hyperplasia (CH) and studies based on this concept is scarce in the literature. ***Materials and Methods:*** 30 patients who underwent 99mTc-MDP bone scan (with regional SPECT/CT) were retrospectively enrolled in the diagnosis of active CH. Images were evaluated by 2 nuclear medicine physicians in consensus.ROI was drawn around the bilateral condyles, radioactive counts were measured per region of interest, and the respective percentages were calculated. The anteroposterior and transverse dimensions of the normal and abnormal sides were measured on CT. A cutoff difference percentage score above which can be confidently reported as active CH was also calculated. The DPS was calculated by taking the abnormal and normal side counts, and then calculating extra percentage uptake on the abnormal side. ***Results:*** The mean age of the patients was 20.84 ± 5.15 years, with 22 males and 8 females. SPECT/CT was positive in 56% (17/30), while the rest of the 13 patients had negative scans. We calculated the uptake percentage of the positive scans (abnormal side counts/total counts x100) and found mean uptake as 58% on the abnormal side. Also calculated quantitative parameter for the differentiation of disease from the normal side: difference percentage score (DPS) (abnormal side counts-normal side counts/normal side counts x100). Average difference percentage of the 17 patients was found to be 63 %. Size of the condyles as measured on the CT showed, a mean AP of 0.945 ± 0.36cm and TR of 1.785± 0.18 cm at the abnormal side compared to the normal side mean AP of 0.705 ± 0.14cm and TR of 1.745± 0.27 cm respectively. A significant difference in anteroposterior CT measurements (p=0.05) of the abnormal and normal sides of the condylar hyperplasia was noted. Both groups had no significant difference (p=1.00) in transverse measurements. ***Conclusion:*** Quantitative parameters of 99m Tc-MDP SPECT /CT like percentage counts and DPS give an insight into the correct prediction and diagnosis of active CH. Also, abnormal anteroposterior CT measurement of active CH is the best CT parameter for differentiation. Larger studies are needed to establish absolute values for the same and will therefore help as an objective tool to assess condylar hyperplasia in 99m Tc-MDP SPECT /CT. ***References:*** doi: 10.1097/MNM.0000000000000607.

EP-0708

Normalizing SUV values by lean body mass effectively reflect patient weigt and body composition variations improving SUVmax values determination in 18F-FDG PET-CT imaging.

A. Hurtado de Mendoza, *M. Yaryes, C. Soza-Ried, H. Amaral; Positronmed, Santiago, CHILE.*

Aim/Introduction: This study aims to compare the SUV max, signal-to-noise ratio (SNR) and tumour-to-background ratio (TBR) values between SUV normalized by body weight and lean body mass in patients undergoing F^{18}-FDG PET/CT imaging and to determine whether body mass index (BMI) affects SNR. This parameter is particularly relevant in oncologic patients since their body weight suffers significant fluctuations during treatment. ***Materials and Methods:*** A total of 45 patients who underwent F^{18}-FDG PET/CT imaging were included in this retrospective study. Nuclear medicine physicians with over ten years of experience determined and evaluated SUV values. The tumoral lesion with the highest uptake was chosen in each patient to compare SUV max, SNR and TBR values using SUV normalize by weight and SUV normalize by lean body mass. We categorized the sample into normal weight (BMI ≤ 24.9), overweight (BMI 25-29.9), and obese (BMI ≥ 30) to analyze the effect of BMI on SUVmax, TBR and SNR. The results were analyzed by non-parametric statistical tests and considered significant when p-values < 0.05. ***Results:*** Comparison analysis between SUV normalization by body weight and LBM showed that normalization by LBM reduced variability and decreased overestimation of SUVmax values compared to SUV normalization by body weight. There were no statistically significant differences in SUVmax and TBR values between the three BMI categories. In contrast, BMI significantly affected SNR values, showing less noise in the normal BMI group. ***Conclusion:*** Our findings suggest that LBM normalization is the preferable approach to normalizing SUV values in PET/CT imaging due to less variability and overestimation of SUVmax values than body weight normalization. An appropriate SUV normalization method can effectively account for patient weight and body composition variations, less impacting SUV values determination and interpretation. However, the study did not identify an optimal SUV normalization method for each BMI category, emphasizing the necessity for additional research in this area.

EP-0709

Current status and new trends in technetium-99m described through a patent analysis (2000-2022)

M. Riondato[1], *D. Rigamonti*[2], *P. Martini*[3], *C. Cittanti*[3], *A. Boschi*[3], *L. Uccelli*[3];
[1]*University Policlinic Hospital of Genoa, Genoa, ITALY,* [2]*European and Italian Patent Attorney, Milan, ITALY,* [3]*University of Ferrara, Ferrara, ITALY.*

Aim/Introduction: During the last 60 years, Nuclear Medicine has undergone many changes, but the discipline demonstrated to evolve rapidly following the considerable advances in several scientific fields, such as molecular biology, chemistry and radiochemistry. PET seems to better take the advantage of this opportunity and the recent achievements in the use of radiopharmaceuticals labelled with positron emitters hardly affected the field of SPECT. in this context there are some uncertainties as to what will be the role of technetium-99m in the next future. The main goal of the study was to identify key areas of development by examining patent data from the past 20 years, highlighting innovation trends and market predictions for the coming years. ***Materials and Methods:*** QUESTEL's ORBIT Intelligence® system was used for the collection of technetium inventions disclosed in patents and patent applications in more than 96 countries, in the period 2000-2022. Patent documents underwent to cleaning processes using the software and manually by the authors, addressing the required information and identifying trends and topics of interest. ***Results:*** The keywords "+99MTC+" or "TECHNETIUM" were identified as the search query that best retrieves technetium-related patents. 2768 patent documents were analyzed. Each item was referred to a single patent family, filed in various countries to protect a single invention. After several cleaning processes a total of 221 patent documents, regularly granted and pertinent to technetium, were retrospectively analyzed to identify the major areas of discovery and developments in the last 20 years. The criteria were based on the current major lines of innovation, including novel modalities for supporting technetium-99m availability (39 patents), labelling methods (21), expanded use or reformulation of established radiopharmaceuticals (19), new radiotracers (65, as candidates with the ambition to become radiopharmaceuticals) and molecular carrier which might be used as the building block for developing new probes (41). Other patents (36) were not matching with the previous groups. In eastern economies, such as China and other emerging markets, patent applications are on the rise, while those in developed western countries are stagnating, with some exceptions for the USA. ***Conclusion:*** The place of SPECT imaging using ^{99m}Tc-radiopharmaceuticals is still solid. The result of this study is an impulse that fuels the rediscovery of technetium-99m, an unique radionuclide within the scenario of Nuclear Medical imaging for its ideal nuclear properties, availability and the easy preparation radiopharmaceuticals.

EP-0710

Building a Normative Database for [18F]-FDG imaging: Insights from a Japanese Screening Cohort

S. Gutschmayer[1], *T. Beyer*[1], *Z. Chen*[2], *T. Junichi*[3], *S. Kinuya*[2], *L. Shiyam Sundar*[1], *S. Takeda*[3], *H. Wakabayashi*[2];
[1]*Quantitative Imaging and Medical Physics (QIMP) Team, Medical University of Vienna, Vienna, AUSTRIA,* [2]*Department of Nuclear Medicine, Kanazawa University Hospital, Kanazawa, JAPAN,* [3]*PET Center, Kanazawa Advanced Medical Center, Kanazawa, JAPAN.*

Aim/Introduction: Whole-body and total-body [^{18}F]-FDG-PET enable insights into the global physiology of the human body by assessing glucose metabolism. However, to interpret metabolic aberrations across organs, a normative inter-organ mapping of tracer uptake is needed. A key confounder of glucose uptake resembles subject ethnicity. This study aims to report the first insights from two healthy control groups of different ethnicity used to establish normative [^{18}F]-FDG-PET template images. ***Materials and Methods:*** To date, 15 healthy subjects of Japanese ethnicity (13M/2F, 71±11 kg, 2 scans with 1-y apart) and 19 healthy subjects of European ethnicity (10M/9F, 76±17 kg, 1 scan) underwent whole-body [^{18}F]-FDG -PET/CT imaging. A normative template PET/CT image pair was first established for each scan/cohort by a process that starts by overlapping and averaging all CT images within a cohort to an initial template image. Using diffeomorphic co-registration, all CT images are aligned iteratively to the initial template. The resulting warp fields are applied to the corresponding PET images. The aligned CT and PET images are averaged in each iteration, acting as the following iteration template. Once the template CT image is deemed sharp enough (determined within the frequency domain), the

process is stopped, resulting in a cohort-specific, normative PET/CT template image. A normative SUV and an SUV variance image are also created for each cohort. This study ascertains voxel- and organ-wise intensity and SUV differences between the Japanese and European cohorts for five automatically delineated [1] organs, the skeleton, subcutaneous fat and muscle. ***Results:*** The volume, maximum and mean SUV change of selected tissues between the two scans of the Japanese cohort was below 8.5%, 15%, and 2.2%, respectively. Subcutaneous fat and liver showed the highest volume change of 6% and 8%. Volume and mean SUV were up to 90% and 93% higher in the European cohort, with a noticeably higher peak SUV in the liver, muscle and subcutaneous fat. Maximum voxel SUV variance was also significantly higher in the European cohort (45) than in both Japanese (10, 13). ***Conclusion:*** This study presents a viable approach to building a normative [^{18}F]-FDG-PET/CT template for assessing voxel-based aberrations of incoming study subjects. The significant voxel-wise intensity and SUV differences found between the Japanese and European cohorts suggest that additional high-quality, healthy control studies are needed to investigate further key confounders.
References: [1] Sundar LKS, Yu J, Muzik O, et al. J Nucl Med. 2022; doi:10.2967/jnumed.122.264063. Online ahead of print.

EP-48

e-Poster Area

D: Technical Studies -> D2 Data Analysis -> D23 Image Reconstruction

EP-0711

Validation for dual-gate motion correction techniques using ECG gating and data-driven respiratory motion correction for cardiac PET: A pilot study

K. Takanami[1], *H. Odagiri*[2], *H. Watabe*[3], *H. Kodama*[4], *H. Kawakami*[5], *A. Katsuki*[5], *N. Uetake*[5], *K. Takase*[1];
[1]*Tohoku University Hospital, Sendai, JAPAN,* [2]*Department of Diagnostic Image Analysis, Tohoku University Graduate School of Medicine, Sendai, JAPAN,* [3]*Division of Radiation Protection and Safety Control, Cyclotron and Radioisotope Center, Sendai, JAPAN,* [4]*Department of Radiology, Tohoku University Hospital, Sendai, JAPAN,* [5]*GE Healthcare Japan, Tokyo, JAPAN.*

Aim/Introduction: We aim to validate the clinical feasibility of the dual motion correction techniques using ECG gating and data-driven respiratory motion correction for cardiac PET. ***Materials and Methods:*** This study included the five patients who underwent cardiac PET under overnight fasting condition using F18-FDG for the evaluation of cardiac sarcoidosis. One hour after the intravenous injection of 3.7 MBq/kg BW of FDG, 30-minute emission scans were acquired using Discovery MI PET/CT scanner (GE HealthCare) while ECG was acquired with body surface electrodes. All PET data were reconstructed under 4 conditions: "without motion correction", "with 3-segment ECG-gating", "with data-driven respiratory motion correction (DDMC)", and "with both gating (DDMC+ECG-gating)". Especially, "DDMC" and "DDMC+ECG-gating" were performed using PET reconstruction software (PET toolbox, GE HealthCare). A boundary box was set at lower chest and upper abdomen including the whole heart. A 2-second ultra-fast frame reconstruction was executed from a list data, and respiratory motion was estimated using a volume inside the boundary box by 3D image-based registration. The reference for registration was set to the frame at 30 seconds. The ratio of the accumulation of FDG in the left ventricular (LV) wall compared to those in the liver or blood pool, and the metabolic tumor volume (MTV) of the accumulation in the whole left ventricular wall with the threshold of SUV of the blood pool (MTV-LV) were compared among the 4 conditions using Wilcoxson's signed rank test. $P<0.05$ was set at statistical significance. ***Results:*** The average and range of the MTV-LV for "without motion correction", "ECG-gating", "DDMC", and "DDMC+ECG-gating" were 173.1 ml(48.5-264.0), 162.8 ml (39.9-236.0), 156.2 ml (45.8-229.0), and 120.4 ml (29.9-210.0) ,respectively. There was statistically significant difference in MTV-LV only between "DDMC+ECG-gating" and "without motion correction"($p < 0.05$). Meanwhile, there was no statistically difference among the ratio of the accumulation of the LV wall compared to the liver or blood pool. ***Conclusion:*** The dual motion correction techniques using ECG gating and DDMC for cardiac PET may reduce blurring of myocardial accumulation associated with respiration and heartbeat, allowing more accurate assessment of the distribution of myocardial accumulation.

EP-0712

Determining the optimal reconstruction algorithm for FDG brain PET/CT images in BGO-based Whole body PET scanner

M. Asami[1], *M. Ay*[1], *S. Farzanehfar*[2], *P. Ghafarian*[3], *P. Sheikhzadeh*[2];
[1]*Department of Medical Physics and Biomedical Engineering ,Tehran University of Medical Sciences, Iran, Tehran, IRAN, ISLAMIC REPUBLIC OF,* [2]*Department of Nuclear Medicine, Imam Khomeini Hospital Complex, Tehran University of Medical Sciences, Tehran, Iran, Tehran, IRAN, ISLAMIC REPUBLIC OF,* [3]*PET/CT and Cyclotron Center, Masih Daneshvari Hospital, Shahid Beheshti University of Medical Sciences, Tehran, Iran, Tehran, IRAN, ISLAMIC REPUBLIC OF.*

Aim/Introduction: In this study, we aimed to evaluate and compare image quality parameters in order to obtain the optimal reconstruction algorithm for PET brain imaging. To achieve this goal, we optimized the number of iterations and subsets in the OSEM algorithm, as well as the amount of noise control factor (beta parameter) in the BPL algorithm. ***Materials and Methods:*** A Carlson phantom, a two-slice Hoffman phantom and a point source were used and scanned by a five ring BGO-based PET/CT scanner. The obtained images were reconstructed with iterations"2-4-8-14-20" and subset "1-6-12" and beta "50 to 500" by steps of 50 and in addition a reconstruction with the default scanner algorithm (12 iterations and 12 subsets) were done. Then, the spillover ratio, Recovery coefficient (RC), point source FWHM and peak-to-valley ratio were measured. also 10 clinicaly Brain FDG PET/CT study were reconstructed with the same algorithms and the ratio of putamen and caudate to the background(BG) was calculated to validate the phantom results. ***Results:*** The highest RC in the largest sphere (22.3 mm) corresponds to beta "50 to 150" and iteration-subset 12/20, which is 3% more than iteration-subset 12/12 which is the recommended value by scanner manufacturer in the best case. The lowest spillover ratio in the largest sphere (17.9 mm) is related to beta "50 and 100" and iteration-subset 12/20, which is 17% less than the recommended value as well. The lowest FWHM value obtained is related to beta "50 to 500" (3.36-3.41 mm), versus 4.1 mm for 12/12. The highest value of peak-to-valley ratio in the line profile drawn in the Hoffmann phantom is related to beta (50 to 150) and iteration-subset of 12/20 . Also, the evaluation of clinical images shows that the highest ratio of putamen/BG and caudate/BG is in beta "50 and 100" and It/sb of 12/20. ***Conclusion:*** On average, BPL produces better resolution and RC than OSEM. The best resolution is related to beta 50. Gibbs artifacts can be

seen in the reconstructed images with beta 50 and 100, since the difference in the values obtained between betas 50 and 150 is minor, therefore BPL reconstruction with beta 150 can be considered as the optimal reconstruction algorithm in brain PET images in five ring BGO-based PET/CT scanners.

EP-0713

Faster time-of-flight performance reduces effect of misregistration on myocardial uptake scores in cardiac PET-CT

M. Hylle[1], *N. A. Bebbington*[2], *M. R. Pedersen*[3], *H. D. Zacho*[1];
[1]*Aalborg University Hospital, Aalborg, DENMARK,*
[2]*Siemens Healthcare A/S, Aarhus, DENMARK,*
[3]*Lillebaelt Hospital, Vejle, DENMARK.*

Aim/Introduction: PET-CT misregistration is common in cardiac examinations, due to differences in respiratory position between PET and CT acquisitions. However, misregistration artifacts are reduced with time-of-flight (TOF) reconstruction, as described by Conti (2011) with a study using a lutetium-oxyorthosilicate/photomultiplier (LSO/PMT)-based system (1). Yet, development of silicon photomultiplier (SiPM)/LSO-based systems has since dramatically advanced TOF performance. The aim of this study was to assess the impact of PET-CT misregistration on myocardial uptake scores, and to determine whether improved TOF performance reduces the effect of misregistration on myocardial uptake scores. ***Materials and Methods:*** An air-filled cylindrical phantom with water-filled cardiac insert was scanned with surrounding fat layers to simulate a patient chest. The insert was filled with ~75MBq [F-18]FDG, and scanned for 30 minutes on LSO/PMT-based (540ps timing resolution) and LSO/SiPM-based (249ps timing resolution) PET-CT systems. Four new registration matrices were created with CT offsets of 5 and 10 pixels in inferior and posterior directions. PET reconstructions were made for the original registration matrix and the four misregistered matrices, using TOF together with point-spread-function (PSF) modelling, and with PSF-only (without TOF). Total uptake scores were calculated in Corridor 4DM. Percentage myocardial uptake values for misregistered reconstructions were subtracted from corresponding values without misregistration, providing the Percentage Reduction in Uptake through Misregistration (PRUM) value. The absolute percentage reduction in PRUM with TOF was determined by calculating $PRUM_{PSF}$ - $PRUM_{PSF+TOF}$, and values for PRUM reduction with TOF were compared between PET-CT systems. ***Results:*** For the LSO/PMT system, PRUM values for PSF-only reconstructions were 5.7%, 4.5%, 9.6% and 13.7%, for 5 pixels inferior, 5 pixels posterior, 10 pixels inferior and 10 pixels posterior, respectively. Reductions in PRUM with the addition of TOF were 0.4%, 3.2%, 0.0% and 7.0%. For the LSO/SiPM system, PRUM values for PSF-only reconstructions were 5.5%, 7.8%, 10.2% and 15.2%. Corresponding reductions in PRUM with TOF were 3.1%, 3.4%, 4.2% and 5.5%. This demonstrated a greater mean reduction in PRUM with TOF for the LSO/SiPM system (4.1%) compared with the LSO/PMT system (2.7%). ***Conclusion:*** Cardiac PET-CT misregistration provides images with apparently reduced tracer intensity in affected walls, thereby artefactually reducing myocardial uptake scores. However, this effect is reduced with TOF reconstruction, and the faster timing resolution associated with LSO-SiPM systems reduces this effect even further. ***References:***
Conti M (2011) Why is TOF PET reconstruction a more robust method in the presence of inconsistent data? Phys Med Biol 56:155-168

EP-0714

Optimizing the Block Sequential Regularized Expectation Maximization (BSREM) Algorithm for 68Ga-PSMA PET-CT Imaging: Phantom and Clinical Study

F. Sadeghi[1,2], *P. Sheikhzadeh*[1,3], *N. Kasraie*[4], *S. Farzanehfar*[3], *M. Abbasi*[3], *Y. Salehi*[3], *M. Ay*[1,2];
[1]*Department of Medical Physics and Biomedical Engineering ,Tehran University of Medical Sciences, Tehran, IRAN, ISLAMIC REPUBLIC OF,* [2]*Research Center for Molecular and Cellular Imaging, Tehran University of Medical Sciences, Tehran, IRAN, ISLAMIC REPUBLIC OF,* [3]*Department of Nuclear Medicine, Imam Khomeini Hospital Complex, Tehran University of Medical Sciences, Tehran, IRAN, ISLAMIC REPUBLIC OF,* [4]*Department of Radiology, UT Southwestern Medical Center, Dallas, TX, UNITED STATES OF AMERICA.*

Aim/Introduction: The Block sequential regularized expectation maximization (BSREM) algorithm was created as a solution to address the issue of excessive noise. It involves a point spread function and noise penalization factor. This study aimed to identify the most effective noise penalization factor on 68Ga-PSMA imaging. ***Materials and Methods:*** We examined NEMA IQ phantom and 15 prostate cancer patients with injections of 68Ga-PSMA. Images were reconstructed using Ordered Subset Expectation Maximization (OSEM) and BSREM, with various β-values. Clinical lesions were classified into small and large size groups. We evaluated background variability (BV), contrast recovery (CR), signal-to-noise ratio (SNR), and lung residual error (LE) using phantom data, as well as Signal-to-Background Ratio (SBR) and contrast using clinical data. ***Results:*** There is not a significant difference on BV and SUVmax behavior in higher β-values. As the β increased from 100 to 200, BV decreased by 29.4%, while from 900 to 1000, BV decreased by 3.4%. there was a negative correlation between β-value and CR. Highest CR was attributable to BSREM with β-value of 100.RC of small lesions, resulting from BSREM with all β-values was less than 1. In contrast, in large lesions, RC from lower β-values was greater than 1. The relative differences of SNR was dependent on sphere size. As the β-value increased from 100 to 1000, the SNR also increased by 140.5%, 37.6% and 29.0% in the smallest, mid and largest spheres respectively. BSREM using all examined β-values, resulted in lower LE compared to OSEM. in clinical study, The mean SUVmax of small and large lesion size groups for $BSREM_{500}$ was 12.1 ± 2.4 and 25.0 ± 8.1 and the mean SUVmax for OSEM was 7.9 ± 3.2 and 21.8 ± 8.6 , respectively. The SBR and contrast increase with decreasing β-value, whereas an increase on β-value translates into an increase in SNR. The lowest SBR and contrast was related to the OSEM, irrespective of lesion size and β-value. When β-values decreased from 500 to 100, the SBR and contrast rose by 69.7% and 71.8% in small lesions and 35.6% and 33.0% in large lesions respectively. ***Conclusion:*** When the size of the lesion decreased, the ideal β-value also decreased. The findings of both studies indicated that a β-value of 400 was most suitable for reconstructing small lesions. However, for larger lesions, a β-value of 600 and 500 were recommended for the phantom and clinical studies, respectively.

EP-0715

Evaluation of advanced artificial intelligence-based PET image reconstruction (HYPER DPR) on brain PET/CT imaging

K. Miwa[1], *M. Watanabe*[2], *M. Ishiguro*[2], *T. Yamao*[1], *N. Miyaji*[1], *K. Hasegawa*[1], *A. Takenaka*[3], *Y. Inui*[3], *H. Toyama*[3];
[1]*Fukushima Medical University, Fukushima, JAPAN,*
[2]*Fujita Health University Hospital, Aichi, JAPAN,* [3]*Fujita Health University School of Medicine, Aichi, JAPAN.*

Aim/Introduction: HYPER DPR (Deep Progressive Reconstruction) represents a cutting-edge artificial intelligence (AI) PET image reconstruction algorithm, recently introduced by United Imaging Healthcare for their PET scanners[1]. The present study aimed to validate the impact of HYPER DPR on the ability of brain [18F] F-FDG PET imaging. ***Materials and Methods:*** We used a uMI550 PET/CT system (United Imaging Healthcare) to acquire 30-min PET scans of Hoffman 3D Brain and cylindrical phantoms each containing 20 MBq of [18F]F-FDG at the starting acquisition. We reconstructed using OSEM+TOF, and HYPER DPR (postfilter; combined non-local means; Gaussian and Metz filters), and a 256 × 256 matrix. Gray-white contrast (%contrast) and recovery coefficients (RC) for grey and white matter were calculated from images generated by the Hoffman 3D Brain phantom, and image noise (CV) and uniformity (SD) were calculated from those generated by the cylindrical phantom according to the Japanese Society of Nuclear Medicine (JSNM) and the European Association of Nuclear Medicine (EANM) phantom test criteria. ***Results:*** The %contrast exhibited significant improvement when reconstructed using HYPER DPR (range of 72.9%-90.5%) compared to OSEM (63.1%). The RCs for grey (RC_{GM}) and white (RC_{WM}) matter were 0.79 and 0.27, respectively, for OSEM, and 0.82-0.88 and 0.24-0.26 for HYPER DPR. The %contrast, CV and SD of HYPER DPR for all conditions met the JSNM criteria (%contrast ≥ 55%, CV ≤15%, SD ≤ 0.0249). The HYPER DPR with Enhance2, which contains non-local mean and Metz filters as a postfiltering option, outperformed other evaluated reconstruction methods. ***Conclusion:*** Overall, our findings demonstrate that the HYPER DPR enhances image quality and quantitative accuracy when compared to OSEM-based reconstruction methods for diagnosing Alzheimer's disease using brain [18F]F-FDG PET images. HYPER DPR reduced noise, improved image contrast, and augmented PET image quantitation. ***References:*** 1) Lv Y, et al. Phys Med Biol. 2021;66(10):105016.

EP-0716

Impact of the 68Ga Source Model on Positron Range Simulations and 68Ga-specific PET Reconstructions

P. Gavriilidis[1,2,3], *A. Marinus*[4,1], *F. M. Mottaghy*[5,1,2], *T. W. Deller*[6], *F. P. Jansen*[6], *M. Koole*[3], *R. Wierts*[1,2];
[1]*Maastricht University Medical Center, Maastricht, NETHERLANDS,* [2]*Maastricht University, Maastricht, NETHERLANDS,* [3]*Katholieke Universiteit Leuven, Leuven, BELGIUM,* [4]*Eindhoven University of Technology, Eindhoven, NETHERLANDS,* [5]*RWTH University Hospital, Aachen, GERMANY,* [6]*GE HealthCare, Waukesha, WI, UNITED STATES OF AMERICA.*

Aim/Introduction: The positron range (PR) distribution profile of a radionuclide can be obtained from Monte Carlo simulations. For those simulations, a point source is usually employed. However, in positron emission tomography (PET), the point source assumption is not accurate, as voxelated PET images are reconstructed. We investigate whether positron range correction (PRC) based on a cubic source, having the same size as the reconstructed PET voxels, is superior compared to a point source approach. ***Materials and Methods:*** Monte Carlo simulations were performed for both ^{18}F and ^{68}Ga. A point source (diameter=0.001 mm) or cubic source (2.73x2.73x2.8 mm^3) of ^{18}F or ^{68}Ga was placed in the center a water based uniform phantom (20x20x20 cm^3). Each simulation generated 8.88 million positron emissions from which the PR distribution profile of the corresponding radionuclide was generated. Each profile was modeled as a spatially invariant Gaussian function of which the full width at half maximum (FWHM) was calculated. For each type of source, ^{68}Ga-specific PRC was performed by adding/subtracting the respective $^{68}Ga/^{18}F$ FWHM to the Gaussian filter applied in the image space of the Hybrid-Space PET Point Spread Function (Hybrid PSF) [1]. ^{68}Ga-specific Hybrid PSF (^{68}Ga-specific PSF) was applied to OSEM+PSF (2 iterations, 34 subsets) and Q.Clear (β=700) reconstructions which were compared to the non-corrected reconstructions. A line source and NEMA IQ phantom were imaged using ^{68}Ga-PSMA. Spatial resolution (FWHM), average recovery coefficient (RC) and background coefficient of variation (COV) measurements were performed. ***Results:*** Although cubic sources showed wider PR distribution profiles than point sources for both ^{68}Ga (3.99 vs 3.53 mm) and ^{18}F (1.99 vs 0.71 mm), the calculated FWHM of the Gaussian filter applied in the ^{68}Ga-specific PSF reconstruction was identical for both source types (difference < 0.01%). For the line phantom, ^{68}Ga-specific PSF resulted in improvements in the transaxial and axial FWHM for both OSEM (14.7%, 12.7%) and Q.Clear (16.7%, 16.6%). Furthermore, RC values were improved by 10.6% for OSEM and 6.2% for Q.Clear. For OSEM the COV was reduced by 21.7% and for Q.Clear it was slightly increased by 1.5%. ***Conclusion:*** Although the source size was shown to affect the PR distribution profiles of ^{68}Ga and ^{18}F, it did not affect the FWHM of the Gaussian filter used in ^{68}Ga-specific PSF reconstruction. ^{68}Ga-specific PSF improved the spatial resolution and RC as measured in phantoms. ***References:*** [1] T. W. Deller et al., IEEE Nucl Sci Symp Conf Rec, 2021, pp. 1-5.

EP-0717

Transforming a low-count nuclear medicine image into a high-count image using Dynamic Stochastic Resonance

A. Pandey*, S. Kumar, P. D. Sharma, C. Patel, R. Kumar;*
All India Institute of Medical Sciences, New Delhi, INDIA.

Aim/Introduction: Low-count nuclear medicine images are observed in routine nuclear medicine practice. However, it is always desired to have a high-count image because of better signal to noise ratio. Various methods are continuously being developed for further improvement of nuclear medicine images. In this study, we investigated the dynamic stochastic resonance (DSR) technique for transforming a low-count nuclear medicine image into a high-count image. DSR is a type of stochastic resonance in which a controlled amount of noise (in this case internal noise of the image) is added to the image itself, to improve the signal-to-noise ratio. DSR may be explained using motion dynamics of a particle oscillating in a bistable double-well system, in the presence of a weak periodic signal, and noise, the double well gets tilted back and forth asymmetrically following the equation: $x_{n+1} = x_n + \Delta t[ax_n - bx_n^3 + Signal + Noise]$. ***Materials and Methods:*** A phantom was filled with 99mTc, and a dynamic acquisition (256 X 256 image matrix, 30 seconds per frame for 10 minutes) was performed. The first frame of the study was considered as a low count image and the high-count image (of 10 minutes duration) was formed by summing all the frames of the study. At each value of Δt low-count image was transformed into 30 different high-count images (creating one image at each iteration). Twelve different values of Δt were used. The low-count image, DSR-transformed-high-count image and high-count image (of 10 minutes duration) were compared. ***Results:*** The DSR transformed image looks identical to the high-count image (of 10 minutes duration). At value of Δt =0.1,0.2,0.3, 0.5 and 2.5, after 30 iterations, although the DSR-transformed image looked equivalent to high-count image, the total counts in the DSR-transformed-high-count image was less than the high-count image. At value of Δt= 5.5, 7.0, 9.0, 10.5, 15.5, and 25.5, with increase in

number of iterations the DSR-transformed image (until the total counts reached was up to 18 million counts) progressively became equivalent to high-count image, with further increase in iteration the DSR-transformed image became very high contrast image and at 30th iterations all pixels got equally bright. ***Conclusion:*** A low-count nuclear medicine image can be transformed into a high-count image using DSR by adding a controlled amount of noise till the image counts becomes 18 million in 256 X 256 image.

EP-0718

Role of dynamic stochastic resonance in enhancing the contrast between the abnormal and no-abnormal tau uptake on reconstructed tau (F-18 ML-104) PET images

A. Pandey[1], *J. Yadav*[2], *M. Tripathi*[1];
[1]*All India Institute of Medical Sciences, New Delhi, INDIA,*
[2]*All India Institute of Medical Sciences, Faridabad, INDIA.*

Aim/Introduction: Nuclear medicine physicians look for the intensity difference between the abnormal and no-abnormal uptake of tau in cortex of brain tau PET images. Usually, the signal to noise ratio in PET images is very good. However, in many instances, the signal to noise ratio (here in this case, the contrast difference between the abnormal and no-abnormal uptake of tau) is not very obvious, and hence might lead to incorrect interpretation of tau PET images in patients with cognitive impairment. Thus, there is need for a post processing method that can improve the contrast for better interpretation of topography on F-18 ML-104 tau PET images. In this study we have investigated the role of dynamic stochastic resonance (DSR) in enhancing the contrast between the abnormal and no-abnormal tau uptake on reconstructed tau PET images. . ***Materials and Methods:*** Each image slice of Ten tau PET studies was processed using DSR technique. The number of iterations used were 2,5,10 and 20, these four enhanced images were visually compared with its input image. During the image review, nuclear medicine physician looked for contrast difference between abnormal and no-abnormal tau uptake region. The number of iterations at which enhanced image had better contrast between abnormal and no-abnormal uptake was labelled as the best image. ***Results:*** NM Physician labelled the DSR-enhanced image obtained at number of iterations = 2 as the best image. In DSR-enhanced image obtained at number of iterations = 2, NM Physician found two important characteristics: 1) difference between abnormal and no-abnormal tau uptake regions were obvious compared to its input image, and 2) size of the abnormal and no-abnormal tau uptake regions were comparable to its input image. In the remaining three sets of DSR-enhanced images, the difference between abnormal and no-abnormal tau uptake region was slightly less obvious and their size (abnormal and no-abnormal tau uptake region) was not so comparable to that of its input image. ***Conclusion:*** Application of DSR (number of iterations = 2) enhances the contrast between the abnormal and no-abnormal tau uptake on reconstructed tau (F-18 ML-104) PET images.

EP-0719

Comparative study of respiratory gating techniques on pulmonary 18F-FDG PET lesions

A. BORGES TAVARES[1], *R. Amblard*[1], *F. Hugonnet*[2], *B. Paulmier*[2], *N. Garnier*[1], *R. Villeneuve*[1], *V. Natal*[2], *F. Mocquot*[2], *M. Faraggi*[2], *B. Serrano*[1];
[1]*Centre Hospitalier Princesse Grace - Medical Physics Department, Monaco, MONACO,* [2]*Centre Hospitalier Princesse Grace - Nuclear Medicine Department, Monaco, MONACO.*

Aim/Introduction: Pulmonary lesions affected by respiratory motion are commonly studied in PET/CT images with respiratory gating correction. Actually, several standard gating correction techniques are available as phase-based-gating (PBG), amplitude-based-gating (ABG) and elastic-motion-based-gating with (EMBG) and without device (EMBGWD). We aimed to compare these four gating methods on maximum standardized uptake value (SUVmax) and uptake volume (UV) measurements in a series of 28 patients with pulmonary lesions. ***Materials and Methods:*** This study was performed on a PET/CT, fitted with 26cm axial field of view and time of flight (TOF) with motion flow table option. We study 28 patients with 40 18F-FDG PET/CT pulmonary lesions classified by amplitude movement: 11 nodules with amplitude movement ≥ 0.7cm and 29 < 0.7cm. The nodules sizes varied between 0.4 to 89cc. The 18F-FDG activity injected to the patients was 2.5±0.9 MBq/kg, and a fixed table speed of 1.3mm/s was chosen in the thoracic region. Gated acquisitions were monitored with pressure sensor device (Anzai Medical Corporation). Parameters reconstructions were: 3 iterations, 5 subsets, gaussian filter (FWHM=3mm), matrix size 400x400 pixels, TrueX+TOF algorithm (ultraHD-PET). We studied 5 different PET reconstructions: standard acquisition without gating correction (WG) and respectively PBG, ABG, EMBG and EMBGWD corrections. The pulmonary nodules SUVmax of each gating correction was compared to the WG. UV for the five reconstructions was determined with a 30% threshold of SUVmax and compared to the WG acquisition. ***Results:*** In comparison to the SUVmax value obtained with WG, SUVmax increased significantly in all 40 lesions with PBG acquisitions (Δ_{SUVmax}=17±22%, $p<10^{-6}$) and ABG acquisitions (Δ_{SUVmax}=14±14%, $p<10^{-6}$), while average gain on SUVmax were moderate with EMBG acquisitions (Δ_{SUVmax}=8±6%, $p<10^{-6}$) and EMBGWD (Δ_{SUVmax}=8±5 %, $p<10^{-6}$). Compared to the UV obtained with WG, Δ_{UV} for nodules with amplitude movement ≥ 0.7cm decrease notably with PBG (Δ_{UV}=-29±22%, $p<10^{-3}$) and ABG (Δ_{UV}=-24±19%, $p<10^{-3}$) acquisitions and slightly with EMBGWD (Δ_{UV}=-16±12%, $p<10^{-3}$) and EMBG (Δ_{UV}=-16±13%, $p<10^{-3}$) acquisitions. For nodules with amplitude movement < 0.7cm, the Δ_{UV} difference was smaller for all acquisitions, respectively for EMBG (Δ_{UV}=-9±26%, $p<10^{-3}$), ABG (Δ_{UV}=-10±22%, $p<10^{-3}$), PBG (Δ_{UV}=-10±23%, $p<10^{-3}$) and EMBGWD (Δ_{UV}=-12±14%, $p<10^{-3}$). ***Conclusion:*** For all pulmonary nodules the gating acquisition corrections allows to increase the SUVmax measurement especially for the PBG (17%) and ABG (14%). The uptake volume decreases with all gating corrections and the major impact was for amplitude movement ≥ 0.7cm: Δ_{UV} up to -29, -24 and -16% for respectively PBG, ABG and EMBG with or without device.

EP-0720

Assessment of a new PET event-by-event image-based motion correction for brain imaging in amyloid and epilepsy on a multimodality PET-MR scanner

J. Anton Rodriguez[1,2], *K. Herholz*[3], *C. Oldfield*[1], *M. G. Spangler-Bickell*[4], *T. W. Deller*[4], *L. M. Parkes*[3], *J. C. Matthews*[3];
[1]*The Christie NHS Foundation Trust, Manchester, UNITED KINGDOM,* [2]*Division of Informatics, Imaging and Data Sciences, MAHSC, University of Manchester, Manchester, UNITED KINGDOM,* [3]*Division of Psychology, Communication and Human Neuroscience , Faculty of Biology, Medicine and Health-University of Manchester, Manchester, UNITED KINGDOM,* [4]*GE HealthCare, Waukesha, WI, UNITED STATES OF AMERICA.*

Aim/Introduction: We used phantom and clinical brain datasets to assess a new image-based motion correction approach for brain imaging that corrects event-by-event

acquired list mode (LM) to obtain motion-free images using rigid-body transformations calculated from registrations of consecutive 2-sec framed reconstructions [1]. ***Materials and Methods:*** A Flangeless Esser-PET-phantom™ (contrast ratio of 4-1 hot-cylinders-inserts to background), taped to a wooden board, was scanned three times (10min, 6min, 6min), with the phantom moved in a heterogeneous manner (discrete, continuous, rotations and translations) during each session and with increasing magnitude of motion. Full-length and 2-minute frames were reconstructed. Quantitative analysis was performed using background image roughness (IR), background variability (BV) and contrast recovery of the inserts (CRC). Clinical data: 43 participants were injected with [^{18}F]flutemetamol (41/43) or [^{18}F]florbetaben (2/43), and three paediatric epilepsy [^{18}F] FDG scans were analysed (20 min scans). MR T_1-weighted 1-mm isotropic MPRAGE images, the MNI-Hammers' brain atlas and the PET data were co-registered to extract SUVs for different brain regions. Additionally, for amyloid scans, centiloid ROIs, both non-refined and grey-matter-refined, were used to calculate SUVR. All data were acquired on a GE SIGNA PET/MR (GE HealthCare, Waukesha, WI). Reconstructions were performed using GE-ListMode-of-fline-reconstruction (ImDuetto_v02.18) for non-motion-correction (noMC) and motion-correction (MC) with Q.Clear using β=250/250/100 (phantoms/amyloid/FDG). ***Results:*** Phantom acquisitions: MC images showed visual and CRC improvements for all inserts without any increase in the noise (BV and IR). For example, CRC-12mm full-scan length (acq1-acq2-acq3): 70.0% (motion-free); 51.4%-42.9%-32.8% (noMC); and 69.6%-66.7%-67.3% (MC). For the 2-min frame reconstructions, 5+3+3=11 overall, CRC-12mm was (68.8±2.5)% (average±std) (MC). Clinical data: Visual image quality improvements were observed for 5 amyloid and 2 FDG scans. The main observed difference with MC was the alignment of the PET and the MR-derived attenuation correction map (MRAC) for 29 scans with medium to high motion, including all three FDGs. Despite these differences, changes in SUVR for the amyloid scans were at most small (4-6% observed). For FDG scans, improvements in GM/WM ratio of up to 5% were observed within the temporal lobes. ***Conclusion:*** This deviceless brain motion correction approach retains precision and accuracy over the three independent phantom acquisitions with heterogeneous motion. Such corrections could be very valuable in patient groups that are likely to move during scan acquisition, such as patients with dementia and children. Despite a large number of scans with PET-MRAC mismatches, quantification improvements were modest for the particular applications we investigated. ***References:*** [1]Spangler-Bickell et al., JNM, 63(10):1604-1610,2022

EP-0721

Analysis of segmented single-photon emission computedtomography images acquired with and without a copper filter

S. Kheruka, *N. Al Maymani, N. Al Makhmari, K. Al Riyami, R. Al Sukaiti, A. Jain, S. Usmani;*
Department of Radiology & Nuclear Medicine, Sultan Qaboos Comprehensive Cancer Care and Research Center, Muscat, OMAN.

Aim/Introduction: Reliable measurement of photon flux attenuation in tissue is crucial for single-photon emission computed tomography (SPECT) to produce reconstructed images. Computed tomography (CT) scanners give attenuation correction data for SPECT as well as anatomical data for diagnostic reasons.As part of the segmentation process, an image is divided into regions with similar brightness, contrast, color, texture, and grey level. The use of image segmentation may be advantageous for analyzing medical images. We used a copper filter to remove the low-energy X-rays in the poly-energetic X-ray beam used in CT scans in order to calculate the appropriate attenuation factor. Images collected with and without filters were statistically evaluated using the segmentation technique to reduce human error. ***Materials and Methods:*** Axial images of the AAPM CT phantom with a 3 mm copper filter (low intensity) and without a copper filter (high intensity) were obtained using low-dose CT (140 kvp and 2.5 mA) of a SPECT/CT system (Hawkeye, GE Healthcare). Segmentation is accomplished using the Simulated Annealing Based Fuzzy C-means technique. For quantitative quality assessment, we employ the universal image quality index. The attenuation correction map of the filtered CT images was validated using a SPECT scan after the Jaszczak SPECT phantom was filled with 500 MBq of 99m Tc. Low-dose CT images were collected in order to account for attenuation during SPECT image reconstruction. Another set of CT images was collected after a 3 mm additional copper filter was added. Two sets of axial SPECT images were reconstructed using an attenuation map generated from the CT images collected both with and without a filter. ***Results:*** When we applied Simulated Annealing Based Fuzzy c-means segmentation to both CT images, the CT images with the filter improved significantly, and all six sections of the spheres in the Jaszczak SPECT phantom were clearly visible after using CT images with a 3 mm copper filter for attenuation correction. ***Conclusion:*** We found that hardening the X-ray beam with a 3 mm copper filter removes artifacts without reducing photon flow. Image quality increased with nearly no artifact, a frequent issue with poorly filtered X-ray beams. The 3.00 mm copper filter produces high-quality photos without bloom artifact. This research also indicated that image segmentation reduces human error in image analysis.

EP-0722

Advantages and opportunities of using an open-source reconstruction platform for SPECT quantification

S. Varzakis[1], *A. Denis-Bacelar*[2], *D. Deidda*[2], *J. Dickson*[3], *S. McQuaid*[3], *K. Thielemans*[1];
[1]*University College London, London, UNITED KINGDOM,*
[2]*National Physical Laboratory, London, UNITED KINGDOM,*
[3]*University College London Hospital, London, UNITED KINGDOM.*

Aim/Introduction: Molecular radiotherapy has grown significantly in the past decade. Dosimetry for these treatments has made absolute quantification for SPECT systems necessary. The proposed EARL Lu-177 quantitative SPECT accreditation scheme provides a method of assessing the quality of quantitation by characterizing the recovery of activity concentration in different sized volumes, which can be heavily affected by the reconstruction method, collimator design and detector positioning [1]. Most sites are limited by manufacturers' image reconstruction options. The aim of this project is to demonstrate the advantages of a "non-black box" open-source reconstruction platform (STIR [2]) allowing a variety of reconstruction options in SPECT quantification and image optimisation applicable to any system. ***Materials and Methods:*** Two Lu-177 phantoms were prepared according to EARL [3] requirements: a cylindrical uniform phantom and a NEMA IQ phantom. The projections were reconstructed in STIR with 2 subset OSEM, saving every 5 sub-iterations, correcting for attenuation and scatter. Permutations with and without PSF modelling (in 2D)

were investigated with and without incorporating a log-cosh prior and two different penalty strengths. Recovery coefficients (RC) were estimated for the 60mm sphere for all the tested algorithms, while noise was estimated by the standard deviation in a 40 mm region within the largest sphere. The algorithms were compared for noise and quality of convergence at 100 sub-iterations. ***Results:*** In the PSF reconstructions, ringing artefacts were visible within the two largest spheres. Application of the prior eliminated the artefact after 100 sub-iterations. Compared to OSEM applying PSF decreased the standard deviation from 6.22 to 3.54, while RC (60mm) was improved from 0.814±0.035 to 0.880±0.037. Applying the prior without PSF for penalty weightings of 0.1 (resp. 0.01), standard deviation was 1.07 (resp. 2.71) with the RC (60mm) hardly affected at 0.803±0.034 (resp. 0.812±0.034). The combination of PSF and prior provided the best results with standard deviation at 1.02 (resp. 3.16) while preserving the RC (60mm) at 0.871±0.037 (resp. 0.878±0.037) for a penalty strength of 0.1 (resp. 0.01). ***Conclusion:*** Appropriate use of priors allows noise suppression without compromising accuracy in SPECT quantification. STIR as an open-source reconstruction platform provides the benefit of customising and testing a variety of reconstruction techniques to optimise quantification in SPECT. ***References:*** [1] J. Dickson et al, EARL SPECT accreditation (DOI:10.1007/s00259-022-05924-4), [2] Fuster et al. Integration of advanced 3D SPECT modelling into the open-source STIR framework (https://doi.org/10.1118/1.4816676), [3] https://earl.eanm.org/wp-content/uploads/2022/04/EARL_QSPECT_15Mar22.pdf

EP-49

e-Poster Area

D: Technical Studies -> D2 Data Analysis -> D24 Radiomics

EP-0723

Utility of delta radiomics for response evaluation in primary mediastinal large B-cell lymphoma

F. Yousefirizi[1], *C. Gowdy*[2], *I. Klyuzhin*[3], *K. Savage*[1], *C. Uribe*[1], *A. Rahmim*[3];
[1]Bc Cancer, Vancouver, BC, CANADA, [2]BC Children's Hospital, Vancouver, BC, CANADA, [3]BC Cancer Research Institute, Vancouver, BC, CANADA.

Aim/Introduction: Delta-radiomics is the analysis of alterations in radiomics features before and after an intervention. In this study, a cohort of patients with primary mediastinal large B-cell lymphoma (PMBCL) was examined to predict response to treatment. ***Materials and Methods:*** Baseline ^{18}F-FDG PET scan and post-therapy scan after 6 cycles of R-CHOP chemotherapy were obtained for each of 30 patients. Patients were dichotomized as responders or non-responders depending on the Deauville criteria. Lesions were segmented using the PET-Edge algorithm in MIM. Radiomics features were extracted using the Pyradiomics package (3.0.1) from primary tumors on pre- and post-PET scans. Maximum and mean standardized uptake values (SUVmax and SUV mean), metabolic tumor volume (MTV), total lesion glycolysis (TLG), and the maximum diameter of the primary tumors were also calculated. After feature normalization (z-scores), we used the individual coefficient approximation for risk estimation (ICARE) model) [1]. ICARE mitigates the risk of biased estimation of feature importance in the case of limited training data. and reduces the risk of overfitting using a minimal learning approach, achieved by dropping highly correlated features (Pearson r>0.8). It evaluates each feature sign using an univariate approach (Cmin threshold) . Features are also normalized and multiplied by their sign. For precise classification, the ensemble (aggregated with median) of 1000 binary-weighted models with a random number of selected features (F) was trained, and each model was trained on a random sample of size of the training data drawn with replacement. The hyperparameters of the model (r, Cmin, and F) were optimized by random search and the best-selected sets were used for the ensemble model. To evaluate the model, we applied 10-fold cross-validation on 85% of the dataset and 15% of the dataset was used as test data. ***Results:*** Mean accuracy of the classifiers was (0.72±0.2) for sole ICARE and (0.77±0.19) for ensemble ICARE. Mean accuracy of the best model on the unseen test data was 0.68 for the sole ICARE and 0.75 for the ensemble of best ICARE models. The order of the predictive power of the radiomics features are Delta-Entropy, Delta-NGTDM strength, Delta-NGTDM coarseness, Delta-TLG, Delta-NGTDM contrast, Delta-NGTDM busyness, Delta-GLRLM RLN, Delta-GLRLM GLN, Delta-MTV, Delta-SUVmax, Delta-SUVmean and Delta-NGTDM complexity. ***Conclusion:*** We found that delta-radiomics enable the development of predictive biomarkers for disease response prediction in PMBCL. The ensemble ICARE binary-weighted model was found to perform well in classifying responder vs non-responder. ***References:*** [1] Rebaud et al. 2023. Springer Nature Switzerland.

EP-0724

Noninvasive diagnostic models based on CT scans for differentiating solitary pulmonary metastasis in colorectal cancer patients by artificial intelligence : a multicenter study

D. Ma;
Department of Colorectal Surgery, Zhejiang Cancer Hospital, Hangzhou, CHINA.

Aim/Introduction: Indeterminate solitary pulmonary nodules are often encountered on CT scans, and diagnosis of solitary pulmonary metastasis (PM) is important for patients with colorectal cancer (CRC). We aim to build and validate proper noninvasive artificial intelligence diagnostic models based on routine chest CT for solitary PM in CRC patients. ***Materials and Methods:*** All patients (n=212) with pretreated solitary CRC PM on chest CT were reviewed in the local database in Zhejiang Cancer Hospital between 2012 and 2022, and randomly divided into the training or internal validation groups on 7: 3. A total of 185 patients with pretreated T1 stage primary lung cancer and 256 patients with benign solitary pulmonary nodules were randomly selected. Artificial intelligence models based on machine learning (Decision Tree, Extra Trees, Light GBM, Radom Forest, Support Vector Machine, XGBoost) and deep learning were built to classify the solitary pulmonary nodules as PM, benign lesion or primary lung cancer. External validation group included 44 CRC patients with solitary PM from two independent hospitals. ***Results:*** For classification between PM and benign solitary pulmonary nodule, the machine learning model based on support vector machine showed the best diagnostic ability, with a 0.995 area under the curve (AUC) in the internal validation, a 0.977 AUC in external validation. The deep learning model showed a 0.966 AUC in the internal validation, and 0.893 AUC in external validation. For classification between PM and lung cancer, the best machine learning model based on support vector machine showed a 0.991 AUC in internal validation and the deep learning model showed a 0.949 AUC. ***Conclusion:*** Non-contrast CT based radiomic analyses can be useful for noninvasively differentiating solitary PM and benign pulmonary nodule or primary T1 stage lung cancer which can aid clinical decision in CRC patients with indeterminate solitary pulmonary nodules detected by CT.

EP-0725

Bio-functional radiomics based machine learning for improving the accuracy of hypermetabolic lymph node metastasis in lung cancer

C. Ren;
Shanghai Proton and Heavy Ion Center, Shanghai, CHINA.

Aim/Introduction: ^{18}F-FDG PET/CT is one of the best methods for the staging of lung cancer, but there is still a problem of high false positive rates (FPR) in the diagnosis of high metabolic lymph node (LN) metastasis. Therefore, the aim of this study is to develop and validate a bio-functional radiomics based machine learning model to reduce the FPR of hypermetabolic LNs in lung cancer and improve the accuracy of LN staging. ***Materials and Methods:*** A total of 260 patients with lung cancer who underwent radical surgery from January 2019 to June 2022 were retrospectively analyzed, and randomly divided into the training (n=182) and validation (n=78) sets. The preoperative PET/CT images showed that the patients' mediastinum and hilar LNs were all positive (SUVmax≥2.5 or higher than the mediastinal background). Preoperative clinical factors, serum tumor markers, and PET, CT radiomic features were analyzed. Prediction models were developed using the least absolute shrinkage and selection operator (LASSO) regression analysis. The performance of the models was evaluated and compared by the area under receiver-operator characteristic curve (AUC), accuracy, FPR and DeLong test. Then, a nomogram was developed based on the model with the best predictive efficiency and clinical utility and was validated using the calibration plots. ***Results:*** In total, 151 LN positive (LN+) and 109 LN negative (LN-) patients with lung cancer were enrolled in this study. 3 independent prediction models were separately developed to differentiate LN+ from LN- using clinical factors-tumor markers, PET/CT radiomics, and their combination. The AUC of PET/CT for the diagnosis of LN metastasis in the training set was 0.83 (0.77-0.89), the accuracy was 75.27%, and the FPR was 14.10%. The DeLong test showed that the Combined Model composed of patient age, serum CEA, LN SUVmax and size, and radiomics signature had the highest efficiency in diagnosing LN metastasis, with AUCs of 0.90 (0.86-0.95) and 0.89 (0.82-0.96) in the training and validation sets, respectively, with an accuracy of 84.07% and 82.05%, and FPRs of 12.82% and 6.45%, respectively. Compared with PET/CT, the FPR of Combined Model decreased by 9.08%, and the AUC and accuracy increased by 8.43% and 11.69% ($p<0.05$), respectively. ***Conclusion:*** In this study, a machine learning model integrating clinical features, serum tumor marker levels, and PET/CT radiomics was constructed, which could reduce the FPR of hypermetabolic LNs, greatly improve the accuracy of mediastinal and hilar LN staging, assist clinical treatment decisions, and achieve precise treatment.

EP-0726

Multimodal Radiomic Analyses Allow IDH-Prediction in Glioma Patients at Initial Diagnosis

L. Kaiser[1], *S. Quach*[2], *A. J. Zounek*[1], *A. Zatcepin*[1], *A. Holzgreve*[1], *A. Bollenbacher*[1], *L. Bartos*[1], *V. Ruf*[3], *G. Böning*[1], *L. von Baumgarten*[2], *N. Thon*[2], *J. Herms*[3], *M. J. Riemenschneider*[4], *S. Stöcklein*[5], *M. Brendel*[1], *R. Rupprecht*[6], *J. Tonn*[2], *P. Bartenstein*[1], *S. Ziegler*[1], *N. L. Albert*[1];
[1]*Department of Nuclear Medicine, University Hospital, LMU Munich, Munich, GERMANY,* [2]*Department of Neurosurgery, University Hospital, LMU Munich, Munich, GERMANY,* [3]*Center for Neuropathology and Prion Research, LMU Munich, Munich, GERMANY,* [4]*Department of Neuropathology, University Hospital Regensburg, Regensburg, GERMANY,* [5]*Department of Radiology, University Hospital, LMU Munich, Munich, GERMANY,* [6]*Department of Psychiatry and Psychotherapy, University of Regensburg, Regensburg, GERMANY.*

Aim/Introduction: Gliomas are classified according to the new WHO classification based on their IDH mutation status. To predict this non-invasively at the time of initial diagnosis prior to any therapeutic intervention, we assessed the diagnostic value of multimodal radiomic analyses (FET-PET, TSPO-PET, and MRI) for identifying an IDH-wildtype glioma. ***Materials and Methods:*** 87 glioma patients who received TSPO-PET by [^{18}F]GE180, dynamic [^{18}F]FET-PET, and MRI examination at initial diagnosis were included. The following images were analyzed: 5-15 and 20-40 min p.i. FET-PET, 60-80 min p.i. TSPO-PET, T1-weighted MRI with contrast agent, and T2-weighted MRI. Static PET and MRI images were normalized to the background signal of the contralesional side (TBR). In addition, time-to-peak (TTP) and late slope ($Slope_{FET,15-40}$) images were extracted from dynamic FET-PET data. First, T2 volumes were applied to extract VOI-based radiomics from each modality. Furthermore, the tumor volumes segmented on each original modality were used to extract radiomic features. Multivariate analysis was performed with logistic regression and L1 regularization using nested cross-validation with 5 folds and 50 repeats in the outer loop to report reliable AUC values. ***Results:*** When T2 volumes were used for the extraction of radiomics in all modalities, only radiomics derived from TTP and $Slope_{FET,15-40}$ images showed high performance. The performance of all PET images was higher when radiomics were extracted from the tumor volumes segmented in each original modality, reaching AUC values above 0.8. Multimodal analyses further improved the performance reaching AUC values above 0.9. Parameters from TBR_{GE180}, $Slope_{FET,15-40}$ and TTP images showed the highest average LR-coefficients. ***Conclusion:*** Multimodal analyses of FET-PET, TSPO-PET and MRI showed a high performance for non-invasive IDH-prediction in newly diagnosed gliomas. Notably, the tumor segmentation method used for the extraction of radiomics seems to have a high impact on the performance of each modality, which needs to be considered in future studies.

EP-0727

Non-Invasive Pathological Gleason Score Prediction in Prostate Cancer Patients Using Machine Learning and 68Ga-PSMA PET/CT Radiomic Features

Z. Vosoughi[1], *N. Hamzian*[2], *P. Geramifar*[3], *H. Vosoughi*[4], *F. Emami*[5], *S. Faraji*[6], *G. Hajianfar*[7], *I. Shiri*[7], *H. Zaidi*[7];
[1]*Department of Medical Physics, School of Medicine, Shahid Sadoughi University of Medical Sciences, Yazd, IRAN, ISLAMIC REPUBLIC OF,* [2]*Department of Medical Physics, School of Medicine, Medical Physics department of Shahid Sadoughi University of Medical Sciences, Yazd, IRAN, ISLAMIC REPUBLIC OF,* [3]*Research Center for Nuclear Medicine, Shariati Hospital, Tehran University of Medical Science, Tehran, IRAN, ISLAMIC REPUBLIC OF,* [4]*Nuclear Medicine Department, Razavi Hospital, Imam Reza International University, Mashhad, IRAN, ISLAMIC REPUBLIC OF,* [5]*Nuclear Medicine Department, Razavi Hospital, Imam Reza International University, Mashhad, IRAN, ISLAMIC REPUBLIC OF,* [6]*Department of Medical Physics, Mashhad University of Medical Science, Mashhad, IRAN, ISLAMIC REPUBLIC OF,* [7]*Division of Nuclear Medicine and Molecular Imaging, Geneva University Hospital, Geneva, SWITZERLAND.*

Aim/Introduction: This study aimed to evaluate the performance of radiomics and machine learning algorithms for Gleason Score (GS) prediction of primary prostate cancer (PCa) from ^{68}Ga-PSMA-PET/CT images. ***Materials and Methods:*** Altogether,138 patients with PCa referred to the nuclear medicine department from December 2018 to March 2023, and undergoing ^{68}Ga-PSMA-PET/CT for staging before giving any

medical treatment, were enrolled. All patients are grouped into two groups based on GS; above 4+3 as malignant and under 3+4 as benign. The tumor in the prostate bed was diagnosed and segmented from PET and CT images by an experienced nuclear medicine physician. Subsequently, 27 radiomic features including shape, first-order, GLCM, GLRLM, GLSZM, and GLDM were extracted from the volume of interest (VOI) of a local tumor on PET and CT images, separately. The features selected by mRMR and Recursive Feature Elimination (RFECV) with Cross-Validation. Nested cross-validation was applied with 3-fold cross-validation for the outer and inner loops. Five models were assessed, including support vector machine (SVM), Logistic regression, Random Forest, Decision Tree, and K-Neighbors. The best model of each outer loop was determined using the area under the curve (AUC) of the receiver operating characteristic (ROC curve. The performance of the models was evaluated based on the outer loop results. ***Results:*** The results of this study were split into two parts, CT alone and PET alone. All five models that were applied to predict Gleason grade were compared to each other using AUC Score. Firstly, logistic regression achieved the best results on CT images, in which mean AUC, sensitivity, and specificity were 0.80, 0.87, and 0.61, respectively. Secondly, K-Neighbors reached the best predictive performance on PET images, achieving a mean AUC Decision Tree 0.75, sensitivity of 0.72, and specificity of 0.76. ***Conclusion:*** The results of the present study demonstrate that radiomic models based on PET/CT images could be a promising non-invasive approach to predict pathological indices, such as GS in primary PCa.

EP-0728

The value of 18F-FDG PET/MR radiomics features in predicting the pathological classification of rhabdomyosarcoma in children

Y. Xu*;*
Hangzhou Universal Medical Imaging Diagnostic Center, Hangzhou, CHINA.

Aim/Introduction: To explore the value of 18F-FDG PET/MR radiomics features in predicting the pathological classification of rhabdomyosarcoma in children. ***Materials and Methods:*** The clinical data and PET/MR imaging data of 125 children with pathologically confirmed rhabdomyosarcoma were collected. They were divided into two groups: embryonal rhabdomyosarcoma (ERMS) (n=75) and acinar rhabdomyosarcoma (ARMS) (n=50). Pathological and clinical diagnosis results serve as the gold standard for diagnosis. We used AK software to extract the most relevant imageomics features for tumor classification, and randomly divided the two groups of images into training set (70%) and test set (30%). The maximum correlation and minimum redundancy (mRMR) and minimum absolute shrinkage and selection operator (LASSO) methods were used to select features from 1800 features extracted from MR and PET, and finally eight best features were retained. Multivariate logistic regression analysis was performed using the radiomics characteristics and clinical variables to establish the prediction model. The receiver operating characteristic (ROC) analysis is used to evaluate the prediction model. ***Results:*** The established PET/MR radiomics features have good prediction efficiency for the recognition of ERMS and ARMS classification, and there are significant differences. The AUC of the training group and the validation group were 0.918 (95% CI: 0.783-0.979) and 0.856 (95% CI: 0.775 - 0.996), respectively. ***Conclusion:*** The prediction model of PET/MR radiomics features can be used as a promising and practical auxiliary method to predict the pathological classification of rhabdomyosarcoma in children. It can also provide objective basis for accurate clinical diagnosis and individualized treatment, and has important guiding significance for clinical treatment.

EP-0729

Correlating 68Ga-PSMA PET/CT Imaging Features with PSA Variation for Castration-Resistant Prostate Cancer Patients

R. Eduardo[1,2]*, J. Badel*[3]*, D. Sarrut*[1]*, E. Paquet*[3]*, A. Giraudet*[3]*;*
[1]Creatis, Lyon, FRANCE, [2]Siemens Healthcare SAS, Paris, FRANCE, [3]Centre Léon Berard, Lyon, FRANCE.

Aim/Introduction: Prostate cancer is a major health concern worldwide, and the treatment of advanced prostate cancer is still challenging. Radiopharmaceutical therapy with ^{177}Lu-PSMA has emerged as a promising approach to address this issue. PET/CT imaging is commonly used to determine the extent of disease and the correlation between PET/CT imaging features and serum PSA levels has been shown to predict treatment outcomes [1]. In this work, we analyzed some correlations between imaging features and PSA levels to highlight the importance of PET/CT imaging in predicting the response to ^{177}Lu-PSMA therapy. ***Materials and Methods:*** We conducted a retrospective analysis of 45 male patients who received ^{177}Lu-PSMA treatment, all patients had a 68Ga-PSMA PET/CT imaging. The images were pre-processed using a deep learning automatic segmentation (TotalSegmentator [2]); the physiological organs uptake, obtained by expanding ^{68}Ga-PSMA-avid known OARs (liver, kidneys, spleen, stomach, pancreas ⋯), was set to zero to obtain one single whole-body tumor region (WBTR) encompassing all potential tumors without physiological uptake. For each patient, the biological PSA (initial and final) was retrieved, and we studied the correlation between the PET radiomics and the PSA values using Spearman's rank correlation, a Multi-Layer Perceptron with three hidden layers, and a Random Forest. We compared the results to a standard approach where the $WBTR_{standard}$ is obtained by a threshold set as the kidney's mean SUV. ***Results:*** A significant but weak correlation was found between the WBTR volume and the PSA variation. The correlation coefficient was -0.41 (p-value: 0.01), while for the standard approach it was -0.34 (p-value: 0.02). Moreover, we evaluated the predictive performance of MLP and Random Forest models for PSA variation. We obtained a mean absolute error of 163% for MLP and 563% for Random Forest. The standard approach had an error of 149% for MLP and 558% for Random Forest. ***Conclusion:*** This preliminary study only showed the presence of a weak correlation between the WBTR volume and the PSA variation. The use of simple statistics is not enough to establish a significant improvement. Further research through advanced machine learning techniques is necessary to explore the potential of this method. ***References:*** [1] Moazemi, May 2021, Annals of Translational Medicine[2] Wasserthal, 2022, arXiv

EP-0730

Prediction of pathological complete response in T-stage III rectal cancer using 18F-FDG PET texture features

S. Woo*, J. Yang, H. Ju, K. Kim, A. Muath, S. Cho, U. Shin;*
KIRAMS, Seoul, KOREA, REPUBLIC OF.

Aim/Introduction: Rectal cancer is is known to have low chance to have pCR with combined multimodal therapy. Therefore, it is important to predict pCR to avoid treating insensitive patients. Several studies on the prediction of ractal cancer has been conducted based on the machine learning (ML) model using

radiomics feature extracted from anatomical image modality including MRI, and CT. In this study, the rectal cancer pCR prediction ML model was developed based using multimodal radiomics feature extracted from ^{18}F-FDG PET/CT image. ***Materials and Methods:*** ^{18}F-FDG PET/CT images were acquired from ractal cancer patients. Internal dataset (n=105) consisted of 21 pCR and 84 non-pCR patients. External dataset (n=30) comprised of 6 pCR and 24 non-pCR patients obtained from different institution. Total patients were diagnosed pathologic T-stage III rectal cancer. Textural analysis was conducted with extracted 23 of intensity and 32 of texture feature using LIFEx software. As a ML prediction model, RF was used, which were implemented by the Scikit-learn library in Python. To evaluate the performance of the prediction model, k-fold cross validation was applied. For quantitative evaluation of the model, the accuracy and ROC-AUC was calculated. ***Results:*** The estimation of pCR prediction model with extracted intensity and texture image features from PET/CT was proceeded. The internal validation of RF model accuracy and ROC-AUC were 0.916 and 0.969 with PET feature, 0.883 and 0.946 with CT features 0.898 and 0.961 with PET/CT feature. The internal test of RF model accuracy and ROC AUC were 0.720 and 0.720 using PET features, 0.600 and 0.600 using CT features, 0.600 and 0.600 using PET/CT features. The external test of RF model accuracy and ROC AUC were 0.492 and 0.492 with using PET features. The external test of RF model accuracy, precision, and ROC-AUC were 0.640 and 0.640 with using PET texture features. ***Conclusion:*** RF model estimation result using ^{18}F-FDG PET image features was higher than using CT image features for predicting pCR in rectal cancer. RF model with ^{18}F-FDG PET/CT image feature showed lower performance than RF model using ^{18}F-FDG PET and CT separately. RF model to predict pCR with 32 of texture feature shows higher evaluation value than model construction with total of intensity and texture features from ^{18}F-FDG PET. In order to improve external test results, it is necessary to consider the bacth effect in using multicenter data.

EP-0731

Reproducibility of CT radiomic features extracted from resampled images using various interpolation methods.

G. Mehta[1], *A. Tripathi*[1], *S. Panchal*[1,2], *U. B. Sherkhane*[1,3], *N. Purandare*[1,2], *S. Mithun*[1,2,3], *A. K. Jha*[1,2], *V. Rangarajan*[1,2];
[1]*Department of Nuclear Medicine and Molecular Imaging, Tata Memorial Hospital, Mumbai, INDIA,* [2]*Homi Bhabha National Institute (HBNI), Deemed University, Mumbai, INDIA,* [3]*Department of Radiation Oncology (Maastro), GROW School for Oncology and Reproduction, Maastricht University Medical Centre+, 6229 ET Maastricht, NETHERLANDS.*

Aim/Introduction: Role of radiomics based prediction models is increasing in oncology. However, the stability of radiomic features needs to be assessed before its utilization in prediction model development. There are mainly two causes of instability of these features i.e. 1) variability in imaging and image reconstruction and 2) variability in pre-processing steps. The aim of this study is to assess the stability of radiomic features due to variability in image pre-processing i.e. image interpolation. ***Materials and Methods:*** CT images of NSCLC case (n=35) were selected for this retrospective study and loaded onto the Philips IntelliSpace Discovery workstation. The delineation of tumour volume was performed by an experienced nuclear medicine physicist. The volume was contoured, named as GTVand saved as an RTSTRUCT file. The input CT had slice thickness of 2mm and pixel size -0.9707,0.9707. These files were loaded on the 3-D slicer image computing software for further processing. Here, the images were resampled to 1*1*1mm3 using three methods of interpolation, namely, linear, nearest neighbour, and bspline. For the original and resampled images, 1129 radiomic features were extracted. The features were analysed using the Intra class correlation (ICC3) method and the percentage of highly correlating features were obtained. We categorise the features based on the ICC values as, excellent: ICC ≥0.9, good: 0.9>ICC ≥0.75, moderate: 0.75>ICC≥0.5, and poor: ICC<0.5. ***Results:*** When all four sets were correlated, a total of 323/1129(28.6%) presented excellent reproducibility. 154/1129 (13.6%) features presented good reproducibility.281/1129 (24.8%) features showed moderate and 371/1129 (32.8%) showed poor reproducibility. On correlating just the resampled images ie., bspline, linear and nearest neighbour interpolation methods, the excellent features increased to 51%. 586/1129(51.9%) presented excellent reproducibility. 190/1129 (16.8%) features presented good reproducibility.171/1129 (15.1%) features showed moderate and 182/1129 (16.1%) showed poor reproducibility. On correlating two sets extracted by bspline and linear interpolation, 861/1129(76.2%)features presented excellent reproducibility. 183/1129 (16.2%) features presented good reproducibility.73/1129 (6.4%) features showed moderate and 85/1129 (7.5%) showed poor reproducibility. ***Conclusion:*** The reproducibility of CT radiomic features is highly influenced by the image resampling and methods of interpolation applied while image pre-processing. When the correlation is performed with original and resampled images the reproducibility is shown by 28% features only. In our study, the 3 methods applied show high reproducibility ie., >50% of features showed excellent correlation. The percentage increases to 76% when reproducibility of 2 methods is analysed (bspline and linear).

EP-0732

A Comparative Study on Radiomics Pipelines for Histological Classification of Non-Small Cell Lung Cancer through [18F]FDG PET/CT

L. Wichert-Ana*, L. Alexandre-Santos, A. C. Trevisan, L. R. Suzuki, F. A. Pitella, O. Y. Fukumori, M. Kato, P. M. Azevedo-Marques, M. Koenigkam-Santos;*
Ribeirão Preto Medical School - University of São Paulo, Ribeirao Preto, BRAZIL.

Aim/Introduction: In clinical oncology, a biopsy of neoplastic tissue and histopathological investigation are valuable diagnostic tools for investigating non-small cell lung cancer (NSCLC) cases. However, the gold standard analysis is limited by the possibility that the sample may not be representative of the entire tumour volume to be treated due to the spatial and temporal heterogeneity of the tumour. The number of times a biopsy can be performed, or the inability to perform the procedure depending on the patient's clinical condition due to the high risk of complications are other limitations observed that make this diagnostic evaluation unfeasible for identifying the histological features. Radiomics techniques can complement the therapy approach by highlighting portions of more significant histological heterogeneity, mainly when identification is made through increased local metabolic activity imaged with the [18F]FDG-PET-CT. This study aimed to assess the performance of different machine learning pipelines in classifying NSCLC cases through [18F]FDG-PET-CT images. ***Materials and Methods:*** We investigated 81 PET images of patients diagnosed with NSCLC of type adenocarcinoma (Adc) and squamous cell carcinoma (SCC), confirmed through histopathological assessment. A nuclear medicine physician manually segmented the images to extract

2082 radiomic features that could contribute to histological classification. We used three feature selection and dimensionality reduction methods (high correlation Spearman, ANOVA F-Score (ANOVA), Mutual Information (MI), and Principal Component Analysis (PCA)) along with six classification methods (Random Forest, Support Vector Machine, k-Nearest Neighbors, Gaussian Naïve Bayes, Decision Tree, and XGBoost) to build machine learning pipelines capable of differentiating between the two types of NSCLC. The model complexity and area under the curve (AUC) were used as metrics to assess the performance of the methods. ***Results:*** The eighteen classification pipelines assessed evidenced good performance through AUC values for XGBoost+ANOVA and MI (AUC > 0.9 for the test) and increased performance for the pipeline with PCA for dimensional reduction. ***Conclusion:*** The radiomic machine learning methods for classifying NSCLC cases have demonstrated accurate performance in distinguishing [18F]FDG-PET/CT images of Adc and SCC when implemented with feature selection methods ANOVA and MI. However, the performance was compromised for the PCA method.

EP-0733

Assessing PET andCMR radiomic featuresfor detectionof cardiac sarcoidosis

N. Mushari[1], *G. Soultanidis*[2], *L. Duff*[3], *M. G. Trivieri*[2,4], *Z. A. Fayad*[2], *P. M. Robson*[2], *C. Tsoumpas*[1,2,5];
[1]*Leeds Institute of Cardiovascular and Metabolic Medicine, University of Leeds, Leeds, UNITED KINGDOM,* [2]*BioMedical Engineering and Imaging Institute, Icahn School of Medicine at Mount Sinai, New York, NY, UNITED STATES OF AMERICA,* [3]*Beatson Institute for Cancer Research, Glasgow, UNITED KINGDOM,* [4]*Cardiovascular Institute, Icahn School of Medicine at Mount Sinai, New York, NY, UNITED STATES OF AMERICA,* [5]*Department of Nuclear Medicine and Molecular Imaging, University Medical Centre Groningen, University of Groningen, Groningen, NETHERLANDS.*

Aim/Introduction: Cardiac sarcoidosis (CS) is a granulomatous inflammatory disease which can be diagnosed with [^{18}F]-FDG PET. However, myocardium signal suppression, which is needed to improve the diagnostic accuracy of PET, does not work effectively for around 25% of patients and therefore it may result in false-positive findings. On the other hand, cardiovascular magnetic resonance (CMR) imaging is a non-specific tool for diagnosing CS but can detect scarring tissue that may indicate inactive CS. The independent use of visual data of PET and CMR imaging may fail to identify CS with high specificity. This study aimed to evaluate the specificity of PET and CMR radiomic features in differentiating CS from other diseases and in this particular case, post-covid (PC) patients. ***Materials and Methods:*** PET and CMR were treated separately in this work. For PET analysis, subjects were classified into PC (36 patients) and CS (40 patients). Two different regions of interests (ROI) were drawn manually; a hot region (segmentation A) and the entire left ventricle (segmentation B). Segmentation B is unlikely to be influenced by the experience of observers. For CMR analysis, there were 25 PC patients and 30 CS patients. The ROI was drawn manually in the entire left ventricle. The radiomic features were then extracted. To achieve the purpose of the study, two major methods were followed: one with the individual features by applying Mann-Whitney U tests and the other by testing machine learning (ML) classifiers for separating CS from PC patients. ***Results:*** The Mann-Whitney U tests and logistic regression were trained with individual features to build a collection of features. For PET analysis, maximum target-to-background ratio (TBR_{max}) showed very high area under the curve (AUC) and accuracy with small p-value (< 0.00053) among different segmentations (segmentation A: accuracy and AUC 1.00; segmentation B: accuracy 0.89 and AUC 0.95). Also, Energy showed promising results in segmentation B only. For MR analysis, Gray Level Run Length Matrix (glrlm)_Run Length Non-Uniformity showed good results with smallest error bars (accuracy 0.78 and AUC 91). Principal Component Analysis was used as another way to collect the best group of features with cumulative variance higher than 90%. ***Conclusion:*** Using of radiomic features may prove useful in identifying individuals without the disease. Some features showed promising results to differentiate between PC and CS. By automating the analysis of joint radiomic features, the patient management process can be accelerated and improved.

EP-0734

Role of Textural and Radiomic Analysis Parameters in Predicting Histopathological Parameters of the Tumour in Breast Cancer Patients.

M. Ravina*, R. Kote, T. Lukose, R. K. Gupta, Y. Kashyap, D. Mohanty; All India Institute of Medical Sciences, Raipur, Raipur, INDIA.*

Aim/Introduction: Texture and Radiomic analysis characterises the tumor!s phenotype and evaluates its microenvironment in quantitative terms. In case of breast cancer, histopathological parameters of the tumor are important prognostic factors. This study aims to investigate the role of textural and radiomic analysis parameters in predicting these prognostic factors. ***Materials and Methods:*** 156 Primary breast cancer patients underwent 18F FDG PET/CT on GE DISCOVERY MIDR PET/CT scanner for staging. The images were processed in commercially available textural analysis software. ROI (Region of interest) was drawn over the primary tumor with a 40% threshold and was processed further to derive 42 textural and radiomic parameters. These parameters were then compared with Histopathological factors like the type of tumor (Ductal vs Mucinous), molecular subtype (Triple-negative, Luminal A, Luminal B, HER 2 enriched, Luminal HER 2 positive), Modified Bloom Richardson Grade, Nuclear grade, Tubule differentiation and Mitotic rate of the tumor. ROC analysis was performed with a p value<0.05 for statistical significance using statistical analysis software. ***Results:*** A retrospective study of 156 primary breast cancer patients was done. In the case of histological type, seven patients had mucinous carcinoma, and 149 patients had ductal carcinoma. Fourteen textural analysis parameters turned out to be significant (AUC>0.7) in predicting the histological type. Among them, six parameters had AUC > 0.8, suggesting a better correlation. The cut off were also calculated for them -GLRLM_LGRE(0.0029), GLRLM_SRLGE(0.0027), GLRLM_LRLGE(0.004), GLZLM_LGZE(0.0027), GLZLM_SZLGE(0.0015), GLZLM_LZLGE(0.714). None of the textural and radiomic parameters were found to be significant for predicting molecular subtypes or hormone receptor status. 60 patients had Modified Bloom Richardson grade III tumors. Nine textural analysis parameters turned out to be significant for the grade of the tumor. They were SUVmin, SUVmean, SUVmax, SUVstd, GLRLM_HGRE, GLRLM_SRHGE, GLRLM_LRHGE, GLZLM_SZE, GLZLM_HGZE. The statistical analysis was also performed for the nuclear grade, tubule differentiation, and mitotic rate of the tumor. Three textural analysis parameters - GLCM_Contrast, NGLDM_Contrast, and GLZLM_SZE- were significant for predicting a higher grade of tubule differentiation, and only one parameter, GLZLM_SZE, was significant in predicting a higher mitotic rate in the tumor. However, the textural parameters could not predict the nuclear grade. ***Conclusion:*** Though textural analysis could not predict the

hormonal status and molecular subtype of the tumor, it could predict the tumor!s histologic type and grade noninvasively. A PET-based machine learning method can be made in the future, which may help predict various histopathological prognostic factors.

EP-0735

The Impact of Bayesian Penalized Likelihood (BPL) Reconstruction Algorithm With Various β-values on Radiomic Features Reproducibility: An [18F]FDG PET Phantom Study

Z. Valibeiglou[1], *J. Pirayesh Islamian*[1], *Y. Soleymani*[2], *P. Sheikhzadeh*[3,4];
[1]*Department of Medical Physics, Faculty of Medicine, Tabriz University of Medical Sciences, Tabriz, IRAN, ISLAMIC REPUBLIC OF,* [2]*Department of Neuroscience and Addiction Studies, School of Advanced Technologies in Medicine, Tehran University of Medical Sciences, Tehran, IRAN, ISLAMIC REPUBLIC OF,* [3]*Department of Medical Physics and Biomedical Engineering, Faculty of Medicine, Tehran University of Medical Sciences, Tehran, IRAN, ISLAMIC REPUBLIC OF,* [4]*Department of Nuclear Medicine, Imam Khomeini Hospital Complex, Tehran University of Medical Sciences, Tehran, IRAN, ISLAMIC REPUBLIC OF.*

Aim/Introduction: The tumor heterogeneity assessment using various radiomics features has recently been considered increasingly in the PET imaging community. It is unclear how radiomics features are impacted by the PET imaging reconstruction focusing on noise correction. The purpose of this study was to determine the impact of different noise-controlling variables (β-values) on the robustness of various PET-derived radiomic characteristics using Bayesian penalized likelihood (BPL) image reconstruction algorithm. ***Materials and Methods:*** Six spheres with inner diameters of 37, 28, 22, 17, 13, and 10 mm that were filled with 18F-FDG solution, as the standard National Electrical Manufacturers Association (NEMA) image quality phantom, with a lesion-to-background ratio (LBR) of 4:1 were scanned and reconstructed using the BPL reconstruction algorithm with β-values of 50, 100, 150, 200, 250, 300, 350, 400, 450, 500, 600, and 700. Considering the LIFEx software default preprocessing settings, following segmentation, 130 radiomic characteristics (14 morphological, 60 intensity-histogram, and 56 textural features) were obtained from each of the spheres. The coefficient of variation (COV) was used for categorizing all the radiomics characteristics. The measures of COV<5%, 5%<COV<10%, 10%<COV<20%, and COV>20% were considered as very small, small, intermediate, and large variations, respectively. ***Results:*** Out of the total analyzed morphological features, 78.57% (11 features) exhibited very small variations, 14.28% (2 features) had small variations, and 7.14% (one feature) showed intermediate variations. No morphological feature was found to have a large variation by changing β-values. On the other hand, among intensity-histogram features, 26 (43.33%), 17 (28.33%), 11 (18.33%), and 6 (10%) had very small, small, intermediate, and large variations across different β-values, respectively. Furthermore, very small, small, intermediate, and large variations were seen for 12 (21.42%), 15 (26.78%), 16 (28.57%), and 13 (23.21%) textural features, respectively. No statistically significant differences in COV values were found by changing the inner diameter of spheres. ***Conclusion:*** It seems that PET-derived radiomics feature values are affected by changing noise-controlling variables. Considering the β-values, different groups of radiomic features showed differently with morphological and textural features the most and least robust features. Therefore, according to the PET multi-center research, radiomic features should be extracted and selected with more caution. Features that exhibit a very small or low COV may be considered as promising candidates for accurate tumor quantification.

EP-0736

Can We Predict Future Relapsed Lymph Nodes on Staging PET/CT for Pediatric Hodgkin's Lymphoma?

N. C. M. Gülaldi[1], *M. O. Kartal*[2];
[1]*University of Health Sciences, Ankara Bilkent City Hospital, Department of Nuclear Medicine, Ankara, TÜRKIYE,* [2]*Health Ministry of Türkiye Republic, Ankara Bilkent City Hospital, Department of Nuclear Medicine, Ankara, TÜRKIYE.*

Aim/Introduction: Our goal is to distinguish lymph nodes that may recur in the future within the staging phase PET/CT scans of pediatric lymphoma patients. We used textural features of the lymph nodes and compared them to those that later resurfaced. ***Materials and Methods:*** Staging phase PET/CT scans of 23 pediatric Hodgkin's lymphoma patients who had relapsed lymph node/nodes in their follow-up PET/CT scans were included into the study. Lymph nodes with complete metabolic response and preserve their state in their follow-up scans were segmented and analyzed with LifeX 7.3.1 texture analyzing software [1]. 97 lymph nodes which recurred and showed increased metabolic activity after chemotherapy in 23 patients on follow-up scans were also noted and retrospectively analyzed within the same PET/CT images to see any textural differences within these nodes to predict future failure to treatment response. VOI-based calculations were segmented over diseased lymph nodes and software applied a gray-level co-occurrence matrix (GLCM) to those images. ***Results:*** 23 variants of GLCM measurements were made through images. Most of the parameters did not fit into normal distributions. Hence, we used non-parametric Wilcoxon signed-rank test to compare lymph nodes with complete metabolic response and recurred ones. GLCM_joint maximum and GLCM_joint average (p=0.021), GLCM_Joint entropy Log2 and Log10 (p=0.04), GLCM_difference entropy (p=0.04) showed significant difference between the groups. However, other parameters related to GLCM values did not show any statistically significant difference. ***Conclusion:*** Entropy is a kind of texture feature to measure of the randomness or unpredictability of the distribution of pixel intensities in an image [2]. A higher entropy value indicates a more random and unpredictable texture. It suggests tumor heterogeneity and the presence of necrosis and hypoxia. We found entropy-related textural parameters of future-recuring lymph nodes were significantly differ from the lymph nodes with complete metabolic response. We believe if clinicians aware of these lymphatic groups with heterogeneous features at the beginning, it can be taken into consideration to implement more aggressive treatment at the very early phase of the disease. ***References:*** 1. Nioche C, Orlhac F, Boughdad S, Reuzé S, Goya-Outi J, Robert C, et al. LIFEx: A Freeware for Radiomic Feature Calculation in Multimodality Imaging to Accelerate Advances in the Characterization of Tumor Heterogeneity. Cancer Research. 2018;78:4786-9.2. Wagner MW, Bilbily A, Beheshti M, Shammas A, Vali R. Artificial intelligence and radiomics in pediatric molecular imaging. Methods. 2021;188:37-43.

EP-50

e-Poster Area

D: Technical Studies -> D2 Data Analysis -> D25 Artificial Intelligence

EP-0737

The XGBoost algorithm combined with 18F-FDG PET/CT imaging in the differentiation between benign and malignant thyroid incidentalomas

J. Di[1], *X. Ma*[1], *Z. Ge*[1], *Q. Xie*[1], *D. Kong*[1], *S. Liu*[1], *S. Lin*[2], *J. Ma*[3], *H. Pei*[3], *Y. Zhong*[4], *W. Qu*[1], *X. Zheng*[1];
[1]*Department of Nuclear Medicine Department, The Second Affiliated Hospital of Xi'an Jiaotong University, Xi'an, CHINA,* [2]*School of Computer Science and Engineering, Sun Yat-sen University, Guangzhou, CHINA,* [3]*The MOE Key Laboratory for Intelligent Networks and Network Security, Xi'an, CHINA,* [4]*Department of Clinical Laboratory, The Second Affiliated Hospital of Xi'an Jiaotong University, Xi'an, CHINA.*

Aim/Introduction: The detection rate of thyroid incidentalomas (TIs) based on ^{18}F-FDG PET/CT has increased significantly, of which approximately 33.3% have been confirmed as malignant by the pathologist. However, it is still controversial in the differentiation between benign and malignant TIs by ^{18}F-FDG PET/CT imaging with SUVmax greater than 2.5, which contributes to the reliance on ultrasonography to guide the follow-up treatment. We aimed to utilize the XGBoost algorithm to establish a new model for improving the ability of ^{18}F-FDG PET/CT imaging in the differentiation between benign and malignant TIs. ***Materials and Methods:*** A total of 377 patients examined by ^{18}F-FDG PET/CT in our institution from November 2022 to March 2023 were reviewed. There were 264 patients who were diagnosed or suspected of having non-thyroid cancer, of whom 45 had thyroid abnormalities detected by ultrasonography and pathological examinations. The semiautomatic segmentation of 3D-Slicer software (version 5.3.0) was used for the accurate contouring of the thyroid glands and TIs. The datasets were saved in CSV files and were used to train the XGBoost model. The sensitivity, specificity, F1-score, and AUC (area under the curve) of ROC charts were evaluated. ***Results:*** There were 39 patients (14.77%) who detected TIs in 264 patients diagnosed with or suspected of non-thyroid cancer. 13 male and 26 female cases with an average age of 62.51±13.36 were observed among TIs patients. The average SUV_{max} in TIs patients (5.71±1.23) was significantly higher than those without TIs (1.08±0.77, $p<0.01$). It was noticed that 33 were benign and 6 were malignant (18.18%) in all TIs patients according to the pathological examination. All TIs patients obtained ultrasound and the XGBoost algorithm combined with ^{18}F-FDG PET/CT imaging. For the ultrasound tests combined with ^{18}F-FDG PET/CT imaging of TIs individuals, the sensitivity, specificity, and accuracy were 66.67%, 81.82%, and 79.49%, respectively. For the XGBoost algorithm combined with ^{18}F-FDG PET/CT imaging of TIs individuals, we found that the AUC and F1-score were 0.94 and 0.48, respectively, as well as 100.00% and 35.29% sensitivity and specificity. The XGBoost algorithm combined with ^{18}F-FDG PET/CT imaging significantly improved the sensitivity ($p<0.05$) and maximized the identification of all TIs, but the specificity of the algorithm model should be adjusted. ***Conclusion:*** The XGBoost algorithm combined with ^{18}F-FDG PET/CT imaging will effectively improve the differentiation ability between benign and malignant TIs, which provides a new foundation for clinical diagnosis and therapy.

EP-0738

Image quantitative parameters using deep learning-based denoising of ultra-fast whole-body [18F]FDG PET/CT are comparable to standard acquisitions

L. C. Silva[1], *C. S. Constantino*[1], *M. Silva*[1], *F. P. M. Oliveira*[1], *R. Vigário*[2], *D. C. Costa*[1];
[1]*Champalimaud Foundation, Lisbon, PORTUGAL,* [2]*NOVA School of Science and Technology, Lisbon, PORTUGAL.*

Aim/Introduction: This study aims to assess the feasibility of reducing the acquisition time of whole-body [^{18}F]FDG PET scans to 15s/AFOV through deep-learning-based denoising. ***Materials and Methods:*** 82 whole-body [^{18}F]FDG PET/CT scans of oncological patients were included in the training (57+10) and testing (15) of a 2.5D U-Net convolutional neural network. Mean squared error (MSE) was employed as the loss function for training. Images were acquired on the Philips Vereos Digital PET/CT. From the standard-duration (70s/AFOV) raw data, ultra-fast scans were simulated by cropping the data to 15s/AFOV and 30s/AFOV. Reconstruction was performed on-site using the manufacturer's OSEM algorithm and following EARL1 standards. MSE, intraclass correlation coefficient (ICC) and structural similarity index measure (SSIM) were used for a voxel-wise standardized uptake value (SUV) comparison between deep-learning-denoised images (DL) and reference images (70s/AFOV). Further quantitative analysis was performed in terms of signal-to-noise ratio (SNR = mean SUV/standard deviation) on the regions with "expected" uptake uniformity (liver and lungs). On a lesion basis, SUV_{max} discrepancy was quantified. For benchmarking, Gaussian filter (GF) denoising was implemented and its width optimized through MSE minimization relatively to the reference images. ***Results:*** Voxel-wise ICC, SSIM and MSE between reference and DL-denoised images showed a statistically significant improvement relatively to the original (not denoised) 15s/AFOV and 30s/AFOV images and the GF-denoised images ($p<0.001$). Average ICC, SSIM and MSE for 15s/AFOV-based sets were of, respectively, 0.987, 0.950 and 0.009 [DL], against 0.980, 0.939 and 0.014 [GF] and 0.972, 0.923 and 0.019 [original]. For 30s/AFOV-based sets: 0.991, 0.967 and 0.006 [DL], against 0.989, 0.965 and 0.007 [GF] and 0.987, 0.959 and 0.009 [original]. Concerning SNR, the relative difference to 70s/AFOV was promising for DL denoising, displaying an improvement even regarding the reference images: +79.8±30.1% [DL] against -20.6±16.9% [GF] and -49.1±9.2% [original] for 15s/AFOV-based images in the liver, and +27.3±26.3% [DL] against -6.8±16.8% [GF] and -29.7±11.7% [original] for 30s/AFOV-based images in the liver. Similarly improved results were obtained for SNR in the lungs. For 55 identified lesions, SUV_{max} relative difference to 70s/AFOV was of -14.8±17.9% [DL], -21.9±10.4% [GF] and -0.2±11.6% [original] for 15s/AFOV-based images and -6.8±11.7% [DL], -14.1±8.7% [GF] and -0.4±9.6% [original] for 30s/AFOV-based images. ***Conclusion:*** The implemented DL algorithm proved to be a viable denoising method for ultra-fast (15s/AFOV) whole-body [^{18}F]FDG PET scans, having achieved comparable quantitative parameters with 70s/AFOV. In addition, it outperformed optimized Gaussian filtering.

EP-0739

A pilot of study: Development of AI model to automatically segment the metastatic lesions on FDG-PET/CT in patients with differentiated thyroid carcer

Y. Li[1], *K. Hirata*[1,2,3], *J. Takenaka*[1,2], *H. Endo*[1], *M. Tang*[1], *S. Watanabe*[1,2], *R. Kimura*[1,4], *K. Kudo*[1,3,4];
[1]*Department of Diagnostic Imaging, Graduate School of Medicine, Hokkaido University, Sapporo, JAPAN,* [2]*Department of Nuclear Medicine, Hokkaido University Hospital, Sapporo, JAPAN,* [3]*Global Center for Biomedical Science and Engineering, Faculty of Medicine, Hokkaido University, Sapporo, JAPAN,* [4]*Department of Diagnostic and Interventional Radiology, Hokkaido University Hospital, Sapporo, JAPAN.*

Aim/Introduction: Thyroid cancer is one of the most common malignant tumors of the endocrine system. In recent years, the number of patients with differentiated thyroid cancer (DTC) has increased rapidly. Patients with poor prognosis are identified by measuring metabolic tumor volume with FDG-PET/CT. In order to solve the time-consuming and low reproducibility task of tumor segmentation by hand, the aim of this study was to create an AI model that can automatically segment metastatic lesions of DTC from FDG-PET/CT images. ***Materials and Methods:*** We retrospectively analyzed FDG PET/CT images of 112 patients who had DTC and showed FDG-avid before undergoing I-131 treatment at Hokkaido University Hospital from 2014 to 2022. In our study, a researcher segmented FDG-avidity metastatic lesion (SUV>3) on FDG-PET/CT using Metavol software, and the segmentation was confirmed by a nuclear medicine physician. Each case included 180 maximum intensity projection (MIP) images by projecting in 1° step. After taking the logarithm of the SUV, the images were resized to the resolution at 512x512, saved as PNG format. The PNG was augmented by using image rotation from -170° to 180° in 10° step. The 80 of 112 patients were selected, and of each patients, a total of 180 images were randomly picked up for training : validation : test-1 (internal test group) datasets = 7:1:1. The rest of 32 patients were used as test-2 (external test group) dataset. We trained a ResNet-50 model via Matlab. The training parameters were as follows: optimizer stochastic gradient descent with momentum (Momentum SGD), maximum training epochs 4, mini-batch size 192, initial learning rate 0.001, momentum 0.9, L2 regulation 0.05. ***Results:*** The mean Dice similarity coefficient (DSC) of the test-1 and test-2 were 0.54±0.17 (standard deviation) and 0.53±0.18, respectively. The AI-predicted tumor areas showed a significant correlation with the areas of annotation in test-1 (R=0.98) but a lower correlation with that in test-2 (R=0.68). For sub-analysis, we classified the patients into four groups according to the areas of tumor lesions: <100, 100-200, 200-1000, and >1000 pixels. DSC tended to be higher for larger tumors (The mean DSC of <100 pixels and >1000 pixels were 0.40±0.14 and 0.73±0.08). ***Conclusion:*** The results indicated that AI model could automatically segment the lesions of DTC in FDG-PET/CT images, although more data also necessary to improve the accuracy of AI model. The performance of segmentation was affected by the tumor size.

EP-0740

Predicting Sentinel Lymph Node Status by Using FDG-PET Imaging-Based Texture Analysis in Breast Cancer

K. Saglam*, S. ASA, A. KİBAR, M. SAĞER, K. SÖNMEZOĞLU;*
Istanbul Univercity-Cerrahpasa Cerrahpasa Medical Faculty, Istanbul, TÜRKIYE.

Aim/Introduction: Breast cancer is the most frequently diagnosed malignancy globally, with more than two million cases yearly [1]. FDG-PET imaging is performed to evaluate the extent of disease and tumor burden in the preoperative period. In many cases lymph node metastasis cannot be detected in FDG-PET imaging or axillary node biopsies; lymph node metastases are seen as a result of intraoperative sampling, and this guides the course of the operation(2). In this retrospective study, we aimed to evaluate FDG-PET imaging-based texture analysis applications in predicting the sentinel lymph node outcome and create machine learning models to predict sentinel node outcome using obtained parameters. ***Materials and Methods:*** FDG-PET scintigraphies of patients diagnosed with breast cancer were scanned. FDG-PET images of 412 patients who underwent intraoperative sentinel axillary node sampling were analyzed. Patients with no clinical node metastasis detected by preoperative USG and sentinel node biopsy and who weren't treated with chemotherapy or radiotherapy were selected. Patients with multiple lesions and lesion size >5 cm were excluded. According to the pathology results of intraoperative sentinel lymph node sampling, FDG-PET imaging of 58 patients, 27 positives and 31 negatives, was studied with LIFEX(https://www.lifexsoft.org/ index.php) imaging analysis. Parameters obtained from LifeX program were evaluated with WEKA. Parameters for decision tree algorithms in WEKA program were determined with WEKA-Attribute Evaluator. Predictability values were tested by decision tree algorithms such as RandomForest. Machine learning models evaluated prediction accuracy. In addition, SUVMax, SUVMean , lesion sizes, 5 other parameters detected by OneR, and 3 other parameters detected by attribute evaluator with WEKA were evaluated separately with T-test. ***Results:*** Intensity-Based_Minimum_Grey_Level is the most significant parameter among the studied parameters. (p-Value:0,0006913). Satisfactory results (75%-85% accuracy) were obtained on the efficiency of machine learning applications in predicting the data in the pool. ***Conclusion:*** Texture analysis-based machine learning methods may reduce the dependence on invasive interventions in the initial evaluation of breast cancer cases. In addition, it is thought that the accuracy values predicted by the machine will be more successful with the inclusion of data obtained with the standard imaging protocols and large patient groups in the study. ***References:*** 1. GLOBOCAN 2020: New global cancer data. https://www.uicc.org/news/globocan-2020-new-global-cancer-data 2. Chagpar,A.B.; Horowitz, Does lymph node status influence adjuvant therapy decision-making in women 70 years of age or older with clinically node negative hormone receptor positive breast cancer?

EP-0741

Construction of a prognostic risk score model with multimodal features of18F-FDG PET/CT images of non-small cell lung cancer byfeatures fusing

X. Wang[1,2]*, X. Li*[1,2]*, C. Cui*[1,2]*, Z. Wu*[1]*, Z. Wu*[3]*;*
[1]Department of Nuclear Medicine, First Hospital of Shanxi Medical University, Taiyuan, Shanxi, CHINA, [2]Collaborative Innovation Center for Molecular Imaging of Precision Medicine Shanxi Medical University, Taiyuan, Shanxi, CHINA, [3]Collaborative Innovation Center for Molecular Imaging of Precision Medicine Shanxi Medical University, Taiyuan,Shanxi, CHINA.

Aim/Introduction: Through a small multicenter dataset, we extracted radiomics features and deep learning features from PET/CT images of different modalities to construct machine learning models for feature fusion, obtained their prediction scores as input features, combined them with clinical information, and constructed a Cox proportional risk regression model as the prediction model for the risk of death scores of patients with non-small cell lung cancer, to provide support for clinical decisions such as early detection of patients and improvement of patient prognosis. ***Materials and Methods:*** In this study, we used the ^{18}F-FDG PET/CT public dataset (98 cases) as the training set and our data as the validation set (41 cases). The 3D lesions were first outlined to extract the radiomics features, and then the ResNet50 and VGG16 networks were constructed by transfer learning to extract the deep learning features at the largest lesions of 2D PET and CT images. After feature selection by the Lasso method, RSF, XGBoost, GBM, Coxboost, SSVM, and Deepsurv survival analysis machine learning models were constructed to fuse high-dimensional features, respectively. The best performance

models were selected to output predictive values combined with clinical data (gender, age, smoking history, pathological staging, and TNM stage) to construct risk score prediction models by univariate and multifactor Cox analysis. ***Results:*** 139 patients were included in this study. Outcome events occurred in 43 (28 in the training set and 15 in the test set.) ROC analysis showed that the GBM model constructed using CT and PET radiomics features and deep learning features performed best. It was selected to fuse various types of features and output predictive values, and after univariate and multifactor Cox analysis by combining clinical features to select T-stage (HR=1.680), CT-radiomic-GBM predictive score (HR=2.759), PET-radiomic-GBM predictive score (HR=2.539), CT-ResNet50-GBM predictive score (HR=7.778), and PET-VGG16-GBM predictive score (HR=3.317) were selected as predictors to construct the Cox proportional risk model. The model performed well in the test set (AUC=0.738±0.072) and could bring more benefits for clinical decision-making compared with the traditional TNM staging model. ***Conclusion:*** By fusing high-dimensional features through machine learning models, deep learning features can effectively complement radiomics features to combine anatomical and metabolic information from PET/CT images with clinical data to predict the prognosis of patients with non-small cell lung cancer. The risk score model constructed in this study showed strong predictive ability compared to conventional TNM staging.

EP-0742

Section-Based Regional Recognition of FDG PET/CT Images with Machine Learning

S. Asa, *A. Kibar, S. E. Biyiklioglu, M. T. Bodur, S. Sager, K. Sonmezoglu;*
Istanbul University Cerrahpasa, Istanbul, TÜRKIYE.

Aim/Introduction: The use of machine learning algorithms in medical imaging is increasing daily. Machine learning applications can make it easier for physicians to make the right decisions by evaluating the images and reducing the workload. In our study, we aimed to assess the success of machine learning in determining which region the slice belongs to by using axial PET, CT, and PET/CT fusion images of patients who underwent FDG PET/CT. ***Materials and Methods:*** A total of 4672 cross-sections whole-body FDG PET/CT images of 6 patients in whom FDG had physiological distribution were included in the study. Axial PET, CT, and PET/CT fusion sections of the patients' whole-body PET/CT images were converted from DICOM to JPEG format. Areas were classified in separate folders: head, neck, thorax, abdomen, and pelvis. The orange program was used for image analysis(VGG-16) and classification. While the images of 3 of the six patients were used in training, the remaining three were used for testing. Random forest, linear regression, and Suppor vector machine algorithms were used for machine learning. ***Results:*** When PET, CT, and PET/CT fusion sections of patients with physiological distribution were evaluated with random forest, logistic regression, and Suppor vector machine models, the highest correct classification ratio (90.1%) was found in the logistic regression model of CT images (table 1). PET/CT and CT correct classification ratios were similar. However, PET correct classification ratios were lower than PET/CT and CT sections(Table 1). In addition, the highest specificity (97.3%) among the models was found in the logistic regression model of CT(Table 2). ***Conclusion:*** In our study, machine learning algorithms seem successfully detect the region on cross-section in fusion PET/CT and CT images. Studies in which large patient groups will be evaluated with fully automatic models are required.

EP-0743

Assessing the Feasibility of Deep Learning-Based Attenuation Correction using Photon Emission Information in 18F-FDG PET Images for Dedicated Head and Neck PET Scanners

M. Shahrbabaki Mofrad[1], *A. Ghafari*[1], *A. Amiri Tehranizadeh*[2], *M. Ay*[1], *S. Farzenefar*[1], *P. Sheikhzadeh*[1];
[1]*Tehran University of Medical Sciences, Tehran, IRAN, ISLAMIC REPUBLIC OF,* [2]*Mashhad University of Medical Science, Mashhad, IRAN, ISLAMIC REPUBLIC OF.*

Aim/Introduction: In this study, we investigated the feasibility of directly predicting measured attenuated corrected (MAC) images from non-attenuated corrected (NAC) in the head and neck ^{18}F-FDG PET images using only head and neck based training deep learning method. ***Materials and Methods:*** A neural network with ResNet architecture was used to train the data through 2D head and neck PET images of 114 patients without any pathology and artifacts, 21 patients' images were used for validation during training, 24 patients' images without pathology and artifacts, and 12 patients' images with pathology were used for testing. The neural network's performance in the test images was evaluated using RMSE, SSIM, PSNR, and MSE parameters by considering the MAC images obtained from the scanner as a reference. To quantitatively examine the images and evaluate the effect of the data used in the training, we obtained contrast and PSNR for the tumoral/hot areas and evaluated it with Paired-t-test. ***Results:*** Head and neck MAC images predicted by the neural network were very similar to the reference images. The findings for PSNR, SSIM, RMSE, and MSE in the normal test group were 44.02 ± 1.77, 0.99 ± 0.002, 0.007 ± 0.0019, 0/000053 ± 0/000030, and in the pathological test group were 43.14 ± 2.10, 0.99 ± 0.005, 0.0078 ± 0.0015 and 0.000063± 0/000026. In the Paired-t-test, there was no significant difference between SNR and Contrast of the test images without pathology (p value>0.05), but in the pathologic case, the differences were significant (p value<0.05). ***Conclusion:*** The deep learning network was able to directly generate head and neck MAC images similar to the reference head and neck images. The trained model with training on more data can be used in dedicated head and neck PET scanners without need for CT.

EP-0744

A cascade AI-threshold system for volume segmentation and characterization of lung masses on 18F-FDG PET/CT

G. Savelli[1], *E. Schiavon*[2], *M. Interlenghi*[2], *C. Bnà*[1], *C. Ferrari*[1], *M. Bonacina*[1], *C. Salvatore*[2,3], *I. Castiglioni*[4];
[1]*Fondazione Poliambulanza Istituto Ospedaliero, Brescia, ITALY,* [2]*DeepTrace Technologies, Milan, ITALY,* [3]*Department of Science, Technology and Society, Scuola Universitaria IUSS, Pavia, ITALY,* [4]*Department of Physics, Università degli Studi di Milano-Bicocca, Milan, ITALY.*

Aim/Introduction: Manual segmentation methods of lung masses on 18F-FDG PET/CT studies are affected by inter and intra-observer variability, long annotation times, missed and false edge detection, in particular in low signal-to-noise or multifocal masses. Lack of objective efficient tools for 18F-FDG PET/CT lung mass analysis hinder their quantitative evaluation and characterization. Aim of this study was to provide 18F-FDG PET/CT physicians with a tool for lung mass segmentation that can be helpful in the clinical workflow improving objective quantitation and characterization and reducing segmentation time. ***Materials and Methods:*** Whole body 18F-FDG PET/CT studies were retrospectively collected from 152 patients with lung masses including a retrospective fully-anonymized dataset of Fondazione

Poliambulanza Hospital (Brescia, Italy). Lung masses were manually segmented by an experienced operator in both PET and CT to extract the reference standard for Metabolic-Tumor-Volume (MTV) and Gross-Tumor-Volume (mean MTV=36.6cm^3±48.2, mean GTV=42.4cm^3±70.6). Manual segmentation time was measured. An AI system, based on a combination of 2 cascade convolutional-neural-networks and a threshold algorithm for mass raw segmentation plus refinement, was developed on fused CT and PET images. Specifically, U-Net++ neural networks were trained from scratch in a cascade approach, first in 3D then in 2D, using binary cross-entropy as loss function (image augmentation was performed by rotation <15%). Quantitation performances were evaluated in terms of Dice coefficient for both MTV and GTV. Radiomics metrics were extracted characterizing the segmented masses. System segmentation time was measured. ***Results:*** The system segmented the lung mass in less than 1 minute in both PET and CT studies compared to 5-32 minutes of manual segmentation. The majority of lung masses (80%) showed Dice >0.80. Dice >0.85 and >0.90 were found for MTV and GTV, respectively. Very low signal-to-noise ratio or multifocal lung mass showed Dice >0.60 but <0.80 and needed human correction to achieve Dice>0.80. A total of 8 radiomic features for PET and 4 for CT were extracted for all masses for objective quantitative characterization. ***Conclusion:*** The developed cascade AI-threshold system showed promising results in segmenting lung masses on 18F-FDG PET/CT, and could have a positive impact on clinical practice, reducing the time required for lung mass segmentation and improving their objective assessment.

EP-0745

A New Thoracic CT and Lung Perfusion SPECT Dataset for Developing Analysis of the Lobar Lung Function Assessment

E. Amini[1,2], *R. Klein*[1,3,4];
[1]*Ottawa Hospital Research Institute, Ottawa, ON, CANADA,* [2]*Carleton University, Ottawa, ON, CANADA,* [3]*The Ottawa Hospital Department of Nuclear Medicine, Ottawa, ON, CANADA,* [4]*University of Ottawa Department of Medicine, Ottawa, ON, CANADA.*

Aim/Introduction: Quantitative lobar lung function has valuable information for tailoring treatment plans, including surgical planning. However, application has been limited due to tedious manual segmentation by expert operators. In recent years, deep learning-based segmentation and registration methods have been introduced in an attempt to address this limitation. However, development and validation of solutions is hampered by a lack of openly available dataset representing the wide range of diseases. We present a new thoracic computed tomography (CT)/lung perfusion single-photon emission computed tomography (SPECT) dataset with accurate segmentation of the lung lobes and trachea. ***Materials and Methods:*** In this REB approved study, we collated diagnostic and low-dose CT scans of the thorax with an associated (on average, within 58 days) lung perfusion SPECT. CT scans were acquired using a variety of imaging protocols with CT slice thickness ranging from 0.8 to 3 mm, while SPECT acquisition was standardized according to our local clinical practice (74-185 MBq ^{99m}Tc-MAA, 128 step, 8 seconds per step, OSEM reconstruction, 128x128 pixels, 4.8^3 mm pixels). For each CT scan, the lobes were semi-automatically segmented on sagittal slices using clinically validated software and postprocessed to fix inaccuracies. In addition, the trachea was segmented using a fully automated region-growing algorithm. SPECT data includes raw projection data (with lower scatter window) and CT rigid co-registered reconstructed volumes. Metadata includes patient demographics, imaging parameters, relevant clinical history, excerpts of physician reports, and qualitative fissures information. CT scans were visually scored (3 levels) for lung lobe segmentation difficulty based on overall fissure perceptibility, missing fissures, incomplete fissures, and disease patterns resembling fissures (e.g., emphysema). ***Results:*** The dataset consisted of 150 patients (53% male, ages 18-85) and represents various diseases such as different subtypes of lung carcinoma, lung infiltration, bronchiectasis, interstitial lung disease, and hypersensitivity pneumonitis. The number of lobes on average was 4.8 ranging 3-5. ***Conclusion:*** The presented dataset provides a valuable resource for developing and/or testing fully automated lung lobar function assessment workflow. Another potential use of this dataset is to investigate the relationship between lung structure and function in patients with pulmonary diseases to identify patterns of structural and functional abnormalities that could guide the development of new diagnostic and therapeutic strategies. We plan to make a portion of this dataset openly available.

EP-0746

Deep-learning Model for Differentiation of Pediatric Bone Diseases by Bone Scintigraphy: A Feasibility Study

P. Yang[1], *L. Jiang*[1], *Y. Xiang*[1], *J. Wei*[2], *Z. Zhao*[1], *H. Cai*[1], *Z. Yi*[2], *L. Li*[1];
[1]*West China Hospital, Chengdu, CHINA,*
[2]*Sichuan Universtiy, Chengdu, CHINA.*

Aim/Introduction: Technetium-99m methylene diphosphonate (^{99m}Tc-MDP) Bone scintigraphy (BS) plays a prominent role in pediatric bone disease. We aimed to explore the feasibility of a convolutional neural network (CNN) based deep-learning model for distinguishing benign and malignant pediatric bone disease from bone scintigraphic images. ***Materials and Methods:*** We retrospectively collected 933 bone scintigraphic images from pediatric patients (age 12.91±4.28 years) with benign or malignant bone diseases. The CNN models were constructed and trained based on 745 cases and then validated with the rest 188 cases. The performance of models in differentiating bone diseases was evaluated by diagnostic accuracy, sensitivity, specificity, and receiver operating characteristic (ROC) curves. ***Results:*** CNN-based AI model achieved considerable performance with accuracy of 86.17% (162/188), specificity of 91.67% (110/120) and the sensitivity of 76.47% (52/68) in this test. Furthermore, in the subset analysis of primary bone tumours, CNN model indicated slightly higher AUC value of 0.891 than that of full group (0.851). ***Conclusion:*** The CNN-based approach holds promising feasibility in differentiating benign and malignant pediatric bone disease based on bone scintigraphy.

EP-0747

Reliable and Precise Assessment of Liver Function with a Deep Learning Model-Based Workflow Using Hepatobiliary Scan

H. Sung[1], *K. Cho*[1], *K. Kim*[1], *H. Choi*[1,2], *G. Cheon*[1,2];
[1]*Department of Nuclear Medicine, Seoul National University Hospital, Seoul, KOREA, REPUBLIC OF,*
[2]*Department of Nuclear Medicine, Seoul National University College of Medicine, Seoul, KOREA, REPUBLIC OF.*

Aim/Introduction: Accurate assessment of liver function is crucial for patients who are undergoing major hepatectomy surgery. Dynamic hepatobiliary scanning using [^{99m}Tc]Tc-Mebrofenin enables the calculation of liver clearance rate, an indicator of liver

function. This study aims to develop a novel machine learning model that can provide dependable and precise results. ***Materials and Methods:*** We collected forty dynamic hepatobiliary scan using [^{99m}Tc]Tc-Mebrofenin for our study. Of these, 30 scans were utilized to train the deep learning model for placing ROIs in planar images to determine liver clearance rate. The ROIs for the training were manually drawn by experienced nuclear medicine physicians in the left ventricle, liver, and the entire field of view. The remaining 10 scans were analyzed automatically to calculate liver clearance rate as a validation study. The trained deep learning model and two nuclear physicians estimated liver clearance rate using independently drawn ROIs for the same 10 hepatobiliary scans. The interclass correlation coefficient was employed to compare the results obtained from the machine learning model and physicians, as well as between the two physicians. ***Results:*** Our findings indicate that there was a strong correlation between the deep learning model and the two nuclear medicine physicians, with ICC (2,1) values of 0.88 and 0.85, respectively. Additionally, the ICC (2,1) value between the two nuclear physicians was 0.89, suggesting similar agreement between nuclear medicine physicians and the model. ***Conclusion:*** The deep learning model-based automatic calculation of liver clearance rate was well correlated with those estimated by nuclear medicine physicians. This automatic workflow can provide a reliable and precise result of liver clearance rate using hepatobiliary scan. ***References:*** Ekman M, Fjälling M, Friman S, Carlson S, Volkmann R. Liver uptake function measured by IODIDA clearance rate in liver transplant patients and healthy volunteers. Nucl Med Commun. 1996 Mar;17(3):235-42. doi: 10.1097/00006231-199603000-00011. PMID: 8692492.

EP-0748

ORCA - Optimized Registration through Conditional Adversarial networks for improved PET/CT co-registration using synthetic CT

Z. Chalampalakis*, D. Iommi, I. Rausch, B. Geist, M. Hacker, T. Beyer, L. K. S. Sundar;*
Medizinische Universität Wien, Vienna, AUSTRIA.

Aim/Introduction: PET/CT is a hybrid imaging modality providing functional and anatomical imaging information. However, during acquisition, PET and CT data are acquired sequentially, which may result in a regional spatial mismatch from involuntary subject motion. In these cases, a post-acquisition correction is needed to co-register the PET and CT image data. Specifically in whole-body and total-body imaging scenarios, this correction needs to account for complex elastic motion between the PET and CT images. For this problem, we propose ORCA, a generative tool for PET/CT co-registration which utilizes generated synthetic data and diffeomorphic non-rigid image registration. ***Materials and Methods:*** We facilitate the co-registration of complementary PET and CT image data by generating a synthetic CT (sCT) from an FDG PET image. We do so by making use of our prior efforts based on conditional Generative Adversarial Networks (cGAN) [1]. The generated sCT is used for co-registering CT image data to their respective PET data using a recently introduced, fully-automated, whole-body diffeomorphic registration tool (FALCON) [2]. The cGAN was trained with a ResNet-based generative model using 19 FDG-PET/CT datasets of healthy volunteers imaged on a Siemens Vision PET/CT system. Two datasets from the same cohort were used for qualitative assessment of PET/CT co-registration. Both scans included visible arm mismatch between PET and CT, which in one case included PET intra-frame motion. ***Results:*** The application of ORCA on the two test cases resulted in realistic sCT datasets, which visually matched their respective PET data. Visual inspection of the CT co-registrations to their respective PET images showed improved PET-CT alignment in both cases, without the prior seen mismatch. In the test case with PET intra-frame motion the result sCT and subsequent CT registration resulted in a noticeable artifact in the form of additional tissue beyond the expected arm contour. ***Conclusion:*** The proposed tool provides a simple and reliable framework for post-acquisition co-registration of whole-body PET/CT data. In the future, this tool will be retrained with more data, expanded to include PET data from additional frequently used tracers, and finally be distributed as open-source software for the scientific community. ***References:*** 1. Sundar, Lalith Kumar Shiyam, et al. "Conditional generative adversarial networks aided motion correction of dynamic 18F-FDG PET brain studies." Journal of Nuclear Medicine 62.6 (2021): 871-879.2. 2. Sundar, Lalith Kumar Shiyam, et al. "Fully Automated, Fast Motion Correction of Dynamic Whole-Body and Total-Body PET/CT Imaging Studies." Journal of Nuclear Medicine, in press.

EP-0749

May Automated PET Lesion Detection Be Improved Focusing "AI-Brain" On Single Organs?

A. Macula*[1,2], L. Airo[3], S. Colombo Serra[2], M. Alì[4], S. Papa[4], G. Valbusa[2], A. Bifone[1], P. Gandolfo[4];*
[1]Università di Torino, Torino, ITALY, [2]Bracco Imaging S.p.a., Milano, ITALY, [3]Università di Milano, Milano, ITALY, [4]Centro Diagnostico Italiano, Milano, ITALY.

Aim/Introduction: Automated lesion segmentation in [18F] FDG-PET/CT images is a huge challenge currently addressed by different AI-based strategies, the most common being deep neural network. The aim of this work is assessing whether the performance of nnUNET [1] as PET lesion detection and segmentation tool can be improved using as input single organ rather than whole body images. As a proof of concept, we applied the here proposed strategy on liver. ***Materials and Methods:*** AutoPET challenge [2] database (composed by 900 [18F]FDG-PET/CT exams) was used for this study. Eligibility criterion was the presence of at least one lesion within the hepatic tissue, resulting in a final database of 116 patients (further divided in training/test set with ratio 80/20). The pre-trained AI segmentation model TotalSegmentator [3] was applied to CT images to get the liver mask for each patient. Then, nnUNET architecture was trained using three different versions of the input images: 1) whole-body [18F]FDG-PET/CT images with windowing centred on typical abdominal HU values; 2) a subset of 90 slices centred over the abdominal region with windowing centred on typical abdominal HU values; 3) a subset of 90 slices centred over the abdominal region with windowing centred on typical abdominal HU values and masked with the liver segmentation previously obtained. Predicted masks of hepatic lesions were compared with ground truth segmentation by measuring Dice coefficient, number of false positive and false negative, volume of false positive and false negative. ***Results:*** Among the three tested strategies, the first one showed the best results both in terms of Dice coefficient and in terms of number/volume of false positive/negative (see Table below). When the network was allowed to look at the whole anatomical context, rather than on liver only, its performance in detecting hepatic lesion resulted improved both in segmentation and in lesion detection accuracy. ***Conclusion:*** On the base of this preliminary

results obtained on the hepatic tissue, there is no advantage in applying organ segmentation before feeding a neural network aimed at detecting lesions in [18F]FDG-PET/CT images. Further studies are needed to deeper investigate the topic, either applying the tested method to other organs (e.g. bones, lungs) or optimizing the AI-method employed. ***References:*** 1. Isensee F., https://doi.org/10.1038/s41592-020-01008-z 2. Gatidis S., https://doi.org/10.1038/s41597-022-01718-3.3. Wasserthal J., https://doi.org/10.48550/arXiv.2208.05868.

EP-0750

CT-free Total-body PET segmentation

C. Clement[1], *S. Xue*[1], *Y. Mao*[2], *R. Guo*[2], *M. Viscione*[1], *A. Rominger*[1], *B. Li*[2], *K. Shi*[1];
[1]*Inselspital Bern, Bern, SWITZERLAND,*
[2]*Ruijin Hospital, Shanghai, CHINA.*

Aim/Introduction: Low-dose positron emission tomography (PET) imaging has become feasible with high-sensitivity, long axial field-of-view PET/computed tomography (CT) scanners. However, the incorporation of CT introduces a significant radiation burden. Deep learning (DL)-based methods have been proposed as alternatives for CT-based PET attenuation and scatter correction [1], yet the anatomical localization ability of CT is still needed. This study aims to achieve total-body PET multi-organ segmentation on non-corrected PET images using a DL approach, moving toward completely CT-free PET imaging. Our method uses automatically generated segmentation labels for training and physician-delineated labels for validation, effectively addressing the label scarcity problem in medical image segmentation. ***Materials and Methods:*** We developed a DL-based multi-organ segmentation pipeline for total-body ^{18}F-FDG PET imaging using a dataset of 114 patients scanned with a Siemens Biograph Vision Quadra. For 108 patients, multi-organ segmentation labels were generated using CT images as input to the Multi-Organ Objective Segmentation (MOOSE) software [2], which served as the ground truth for training. For six patients, board-certified nuclear medicine physicians manually segmented organs, which served as the test set. A 3D U-Net-like model was trained on non-attenuation and non-scatter corrected PET images for 1,000 epochs using the sum of cross-entropy and Dice score as the loss function. The segmentation pipeline was implemented using nnU-Net [3]. ***Results:*** Our preliminary results demonstrate an accurate overlap between physician-delineated labels and our predicted organ segmentations: 40% of targeted organs had Dice similarity coefficients (DSCs) of greater than 0.80, 80% of greater than 0.6, while two organs exhibited lower scores, namely pancreas with 0.58 and adrenal glands with 0.34. ***Conclusion:*** We investigated total-body PET multi-organ segmentation using a DL-based method that does not require anatomical information from CT. Our method shows good quantitative performance, with a high overlap between physician-generated labels and predicted segmentations. This is a significant step toward CT-free PET imaging, with the potential to enhance the efficiency and safety of PET scans. Future work will focus on developing models fine-tuned on manually delineated segmentation labels and expanding the dataset to include data from various scanner types. ***References:*** [1] Guo, R. et al., Nat Communications 13, 5882 (2022). [2] Sundar, L.K.S. et al., Journal of Nuclear Medicine Jun (2022). [3] Isensee, F. et al., Nat Methods 18, 203-211 (2021).

EP-0751

Convolutional neural networks for the prediction of changes in brain metabolism

E. Doering[1,2], *T. Deusser*[3], *M. C. Hönig*[1,4], *G. N. Bischof*[1,4], *T. van Eimeren*[1], *A. Drzezga*[1,4], *L. M. Ellingsen*[5,6];
[1]*University of Cologne, Faculty of Medicine and University Hospital Cologne, Department of Nuclear Medicine, Cologne, GERMANY,* [2]*German Center for Neurodegenerative Diseases (DZNE), Bonn, GERMANY,* [3]*Fraunhofer IAIS, Bonn, GERMANY,* [4]*Research Center Jülich, Institute of Neuroscience and Medicine - Molecular Organization of the Brain (INM-2), Jülich, GERMANY,* [5]*Department of Electrical and Computer Engineering, University of Iceland, Reykjavík, ICELAND,* [6]*Department of Electrical and Computer Engineering, The Johns Hopkins University, Baltimore, MD, UNITED STATES OF AMERICA.*

Aim/Introduction: Brain [^{18}F]Fluorodeoxyglucose PET (FDG-PET) allows differentiating various neurological abnormalities. Follow-up FDG-PET scans can help monitor disease progression, or evaluate treatment efficacy. However, the time frame and the amount of radiation exposure hence involved are unfavorable for the patient. In recent years, convolutional neural networks (CNNs) have proven beneficial in various medical imaging tasks, yet their value in medical imaging time series prediction remains unexplored. Here, as a proof-of-principle study, we use CNNs to predict a person's FDG-PET scan in year two from the FDG-PET at baseline and year one. ***Materials and Methods:*** We identified all participants from the Alzheimer's Disease Neuroimaging Initiative who were amyloid-beta positive and who received FDG-PET scans in three consecutive years (n=83). A supervised CNN was implemented and trained on spatially and intensity-normalized scans from baseline and year one, which were subsequently fused to generate a prediction for the year-two scan. The performance of the CNN was evaluated by means of mean absolute error (MAE) and structural similarity (SSIM) using five-fold cross-validation. To demonstrate the necessity of deep learning methodology in this task, the performance of the model was compared to a naïve voxel-wise linear regression model, referred to as "pseudo predictions", using a paired t-test. Finally, to assess the clinical validity of our predictions, we performed voxel-wise t-tests comparing year-two scans of CN with year-two, predicted, and pseudo-predicted scans of Alzheimer's disease (AD) patients. ***Results:*** Our model showed an excellent MAE of 0.040 and SSIM of 0.945, which was significantly better than the MAE (0.052, lower is better, $t = -3.64$, $p = 0.02$) and SSIM (0.935, higher is better, $t = 6.06$, $p = 0.04$) of pseudo predictions. In year-two scans, as well as in predicted and pseudo-predicted scans, significant hypometabolism in the precuneal and inferior temporal parts of the brain, typical of AD, was observed, thus confirming the clinical validity of the predicted scans. ***Conclusion:*** Changes in brain metabolism observed over the period of one year (baseline to year one) enable precise prediction of brain metabolism in year two, thereby motivating further research of prediction in more extended time frames. If successful on a larger scale, our model may be relevant for data augmentation in scientific longitudinal studies, or to document deviations from expected longitudinal brain metabolic degradation in individual subjects (e.g. under therapy).

EP-0752

A Feasibility Study of Attenuation and Scatter Correction in Whole-Body PET Imaging with 68Ga-Dotatate using Deep Learning: A Dual-Center Investigation

M. Sobhi[1], *J. Pirayesh Islamian*[1], *N. Seyedi*[2], *M. Shahrebabaki Mofrad*[3], *R. Samimi*[4], *P. Sheikhzadeh*[5];
[1]*Department of Medical Physics Tabriz University of medical sci, Tabriz, IRAN, ISLAMIC REPUBLIC OF,* [2]*Nursing and Midwifery Care Research Center, Iran University of Medical Sciences, Tehran, IRAN, ISLAMIC REPUBLIC OF,* [3]*Medical Physics and Biomedical Engineering Department,Medical Faculty,Tehran University of Medical Sciences, Tehran, IRAN, ISLAMIC REPUBLIC OF,* [4]*Department of Medical Radiation Engineering, Shahid Beheshti University, Tehran, IRAN, ISLAMIC REPUBLIC OF,* [5]*Department of Nuclear Medicine, Imam Khomeini Hospital Complex, Tehran University of Medical Sciences, Tehran, IRAN, ISLAMIC REPUBLIC OF.*

Aim/Introduction: Normal 0 false false false EN-US X-NONE AR-SA /* Style Definitions */ table.MsoNormalTable {mso-style-name:"Table Normal"; mso-tstyle-rowband-size:0; mso-tstyle-colband-size:0; mso-style-noshow:yes; mso-style-priority:99; mso-style-parent:""; mso-padding-alt:0cm 5.4pt 0cm 5.4pt; mso-para-margin-top:0cm; mso-para-margin-right:0cm; mso-para-margin-bottom:8.0pt; mso-para-margin-left:0cm; text-align:right; line-height:107%; mso-pagination:widow-orphan; font-size:11.0pt; font-family:"Calibri",sans-serif; mso-bidi-language:AR-SA;} Since attenuation correction is one of the critical phenomena in quantitative imaging, especially with PET/CT, and considering that in the PET/CT imaging, CT applies a higher dose to the patient than the radiopharmaceutical. the feasibility of direct scatter and attenuation correction of whole-body 68Ga-Dotatate PET images from uncorrected images (PET-nonASC) was evaluated using deep residual networks. ***Materials and Methods:*** Normal 0 false false false EN-US X-NONE AR-SA /* Style Definitions */ table.MsoNormalTable {mso-style-name:"Table Normal"; mso-tstyle-rowband-size:0; mso-tstyle-colband-size:0; mso-style-noshow:yes; mso-style-priority:99; mso-style-parent:""; mso-padding-alt:0cm 5.4pt 0cm 5.4pt; mso-para-margin-top:0cm; mso-para-margin-right:0cm; mso-para-margin-bottom:8.0pt; mso-para-margin-left:0cm; text-align:right; line-height:107%; mso-pagination:widow-orphan; font-size:11.0pt; font-family:"Calibri",sans-serif; mso-bidi-language:AR-SA;} Non-attenuation/ scatter corrected (NAC) and CT-based attenuation/ scatter corrected(CT_ASC) Whole-body 68Ga-Dotatate PET images of 150 patients from two different centers were used in this study, 15% of data from each center were considered for validation and 15% for the test, a residual deep learning model which uses NiftyNet framework where a highres3dnet model was implemented was used for the train. Image data were compared with the CT-ASC images using different evaluation parameters such as peak signal-to-noise ratio(PSNR), structural similarity index(SSIM), mean square error (MSE), root mean square error(RMSE), and Imaging was also done with the same radiopharmaceutical by a NEMA phantom, and performance of the model was also evaluated. ***Results:*** Normal 0 false false false EN-US X-NONE AR-SA /* Style Definitions */ table.MsoNormalTable {mso-style-name:"Table Normal"; mso-tstyle-rowband-size:0; mso-tstyle-colband-size:0; mso-style-noshow:yes; mso-style-priority:99; mso-style-parent:""; mso-padding-alt:0cm 5.4pt 0cm 5.4pt; mso-para-margin-top:0cm; mso-para-margin-right:0cm; mso-para-margin-bottom:8.0pt; mso-para-margin-left:0cm; text-align:right; line-height:107%; mso-pagination:widow-orphan; font-size:11.0pt; font-family:"Calibri",sans-serif; mso-bidi-language:AR-SA;} Quantitative analysis demonstrated PSNR of 51.12 ± 6.86, SSIM of 0.994 ± 0.003, MSE of 0.00014 ± 0.0001, RMSE of 0.011 ± 0.004 in the test set of images, and PSNR of 32.41, SSIM of 0.902, MSE of 0.0038, RMSE of 0.062 in phantom images. Bias map analysis showed that in all images of the test set, the largest errors were observed in the lung and while the smallest errors were observed in the liver and bladder, and no errors were found in the phantom images. ***Conclusion:*** The results indicate that direct attenuation and scatter correction of whole-body 68Ga-Dotatate PET images using the proposed deep learning model can achieve high and significant accuracy without necessitating the use of CT images or subjecting the patient to high doses.

EP-0753

Assessment of CNN Performance in Cases of Breast Cancer, Staging and Restaging- A Tumour Type Not Included in Algorithm Training

A. Nawwar[1,2,3], *D. Darian*[4], *J. Searle*[5,2], *T. Shimizu*[6], *I. D. Lyburn*[7,2,8];
[1]*University Hospitals Bristol and Weston, NHS Foundation Trust, Bristol, UNITED KINGDOM,* [2]*Cobalt Medical Charity, Cheltenham, UNITED KINGDOM,* [3]*Faculty of Medicine, Cairo University, Cairo, EGYPT,* [4]*Siemens Healthcare Ltd., Camberley, UNITED KINGDOM,* [5]*Gloucestershire Hospitals NHS Foundation Trust, Gloucestershire, UNITED KINGDOM, Cheltenham, UNITED KINGDOM,* [6]*Siemens Medical Solutions UNITED STATES OF AMERICA, Inc., Chicago, IL, UNITED STATES OF AMERICA,* [7]*Gloucestershire Hospitals NHS Foundation Trust, Gloucestershire, UNITED KINGDOM, CHELTENHAM, UNITED KINGDOM,* [8]*Cranfield Forensic Institute, Cranfield University, Wiltshire, UNITED KINGDOM.*

Aim/Introduction: To quantitatively assess the lesion classification performance of a convolutional neural network (CNN), using semi-automated segmentation, on metastatic breast cancer which is outside the data training set. The CNN was designed with the aim of supporting a reading physician to calculate total disease burden. ***Materials and Methods:*** 30 staging and restaging metastatic breast cancer F18 FDG PET/CT scans were analysed by 3 expert PET/CT readers and subsequently using a CNN algorithm. PERCIST criteria with a cut off of 41% was used in both readings to segment foci and measure metabolic tumour volume (MTV); the initial human read involved manual segmentation using an isocontour tool whereas the CNN algorithm classified foci based on an automated segmentation algorithm. Foci agreement on both reads was recorded for sensitivity/specificity analysis; MTV agreement was assessed with Spearman's rank correlation and Bland-Altman plots. Foci classification was verified by further correlation with other imaging modalities and clinical follow-up. ***Results:*** PERCIST segmentation criteria identified 1191 foci. CNN classification sensitivity, specificity, accuracy and precision for these foci were 72%, 97%, 93% and 81%. This agrees with previous testing on unseen datasets. Good correlation was observed between the ranked MTV as measured by the CNN and the expert readers (Spearman's $\rho = 0.85$, $p>0.001$), however a positive bias was observed in the CNN measured MTV relative to the manual measurement. This additional MTV was likely due to inclusion of physiological false positives (predominantly brown fat and bowel). The CNN classified 21 false positive (FP) and 14 false negative (FN) foci. The tendency to classify FP foci results in a precision score of 81%, however these FP findings are common and were easily identified by users.In total, 89 corrections (7% of total foci) were required by the expert readers when using the CNN (30 FP, 50 FN, 9 not segmented); 3 edits per patient on average using the current segmentation criteria. This demonstrates the robustness of the CNN to data from outside the training set. ***Conclusion:*** The automated segmentation plus CNN classification algorithm requires minimal human interaction for assessment of foci and calculation of MTV in a metastatic breast cancer cohort; minor

discrepancies were clinically insignificant and would not change patient management. This confirms the value of the software in assisting clinical reads and the potential of improving diagnostic confidence and ongoing management.

EP-0754

Performance analysis of deep progressive learning denoising method vs conventional methods on low dose 18F-FDG whole body PET/CT scans with low counts/ reduced time protocol

S. Singh, *S. Nigam, R. Vajpayee;*
Globe healthcare, Lucknow, INDIA.

Aim/Introduction: PET images greatly suffer from noise and for accurate diagnosis, good PET image quality is important. With the introduction of deep learning (DL) denoising techniques, image quality has been shown to improve even with low injected dose of radiotracer. This study evaluates the performance of deep progressive learning denoising algorithm on image quality and semi quantitative parameters with data having low counts and acquired over shorter time protocols. ***Materials and Methods:*** The study retrospectively included 110 patients undergoing an F-18 FDG PET/CT imaging on digital PET-CT scanner (uMI550 United Imaging) with acquisition of 120 seconds per bed position. The list-mode data was rebinned into five datasets: 120 (reference), 90, 60, 45 and 30 seconds corresponding to 100%, 75%, 50%, 37.5% and 25% of the total counts respectively. All images were reconstructed by OSEM algorithm and post-processed with the DL and Gaussian filter (GS). 110 FDG avid lesions more than 1 cm on CT images were selected to determine lesion detectability. Lesions were deemed detectable if focal uptake with SUVmax more than 2 times the surrounding background**.** Standardized uptake values (SUVs) in liver, mediastinum, liver and mediastinal signal-to-noise ratio (SNR) were compared among different subsets. The background noise and lesion contrast was assessed using a 5-point Likert scale along with contrast to noise ratio (CNR) for representative lesions. ***Results:*** Average injected 18F-FDG dose was 3±0.5 MBq/kg body weight. Mean Uptake time was 60±10 minutes. All lesions >1 cm were detectable by both sets of images. Overall, there was significant difference between SUVmax of liver and mediastinum between all subsets of DL based and GS based denoising methods, however difference in SUVmean was non significant. SNR of liver was significantly higher in DL group compared to GS cohort. Image noise was significantly less in the DL group than the GS group ($p<0.05$) in all the subsets. However, significant difference in lesion contrast was only observed in 45s and 30s image cohorts. In DL group, SUV values, SNR, background noise and lesion contrast were showed no significant difference between reference (120s) and 90s cohort. ***Conclusion:*** Deep learning based denoising method results in better reduction in image noise and signal to noise ratio compared to GS method at low dose FDG PET scans. Image acquisition time per bed position can be reduced to 90 seconds without compromising with lesion detectability, image quality and semi-quantitative data.

EP-0755

Effects of CNN-based PET image denoising on image quality and lesion detectability

S. Gnesin[1], *S. Medici*[1], *M. Jreige*[2], *M. Conti*[3], *J. Schaefferkoetter*[3], *J. O. Prior*[2];
[1]*Institute of Radiation Physics, Lausanne University Hospital and University of Lausanne, Lausanne, SWITZERLAND,* [2]*Department of Nuclear Medicine and Molecular Imaging, Lausanne University Hospital and University of Lausanne, Lausanne, SWITZERLAND,* [3]*Siemens Medical Solutions UNITED STATES OF AMERICA, Knoxville, TN, UNITED STATES OF AMERICA.*

Aim/Introduction: Positron emission tomography (PET) is inherently noisy, usually reconstructed images are smoothed to reduce image noise before clinical interpretation. Recently AI-based methods including deep learning and convolutional neural networks (CNNs) showed their potential over standard post-reconstruction smoothing. We investigated the impact of AI image denoising on signal detectability of lung nodules in ^{18}F-FDG PET patient data at different noise levels simulating lower injected activity in lung cancer screening conditions. ***Materials and Methods:*** A CNN with a nested residual architecture was trained for denoising PET images, training data were generated through patient decimated list-mode data. The network learned generate images which resembled full count reconstructions, from noisy input images reconstructed from a subset of the original data simulating decreasing injected activity. We assessed 20 whole-body ^{18}F-FDG PET whose acquired on a Biograph Vision (Siemens Medical Solutions, Knoxville TN) and reconstructed with the full acquired statistic, 10% and 5% of events respectively with and without additional CNN denoising - yielding 6 total images per subject. The tracer uptake detectability in the lung nodules was assessed by visual analysis by two physicians. We segmented a total of 24 lung lesions in 10 whole-body PET/CT surrounding background and liver background. Lesion detectability was assessed by CNR. We computed liver SNR to assess image quality. ***Results:*** A total of 43 lung nodules were visually assessed. Visual detectability was preserved in 93% (40/43) vs 91% (39/43) and 84% (36/43) vs 77% (33/43) and of lesions in 10% and 5% CNN-denoised vs. non-denoised PET reconstructions. CNN denoised PET images had higher liver SNR compared to the non-denoised counterparts, average SNR increased by a factor 1.4, 5.2 and 5.9 in the full statistics, 10% and 5% reconstructions respectively. CNN-denoised images yielded on average higher lesion CNR in decimated reconstructions. CNR improved by a factor 1.5 and 1.8 in 10% and 5% reconstructions respectively, whereas 10% and 5% CNN-denoised images preserved on average 96% and 89% of the original lesion CNR respectively. CNN denoising decreased the CNR in only 1/24 lesions. ***Conclusion:*** The reduced-count, CNN-denoised images demonstrated visual improvements over the non-denoised counterparts, with an average higher lesion CNR and increased liver SNR. A more robust analysis including the inclusion of a higher number of PET patients and lesions with a structured observer detection task to better reflect the actual clinical significance of CNN denoising for lesion detectability is currently under investigation.

EP-0756

Comparison of two artificial intelligence tools for anomaly detection and segmentation in 18F-FDG-PET/CT in a monocentric lung and breast cancers patient cohorts

M. Mechti, *P. Blanc-Durand, E. Itti;*
CHU Henri Mondor, PARIS, FRANCE.

Aim/Introduction: In cancer care, 18F-FDG-PET/CT evaluates disease and monitors treatment. To enhance scan analysis, auto-segmentation software are developed. This study compares two of them, PAIRE and AUTOID in lung and breast cancer lesion detection and segmentation, assessing anomaly detection and total lesion volume (TLV) estimation. ***Materials and Methods:*** Between September 1, 2019 and September 1, 2022, 131 patients having performed FDG PET-CT for the initial extension assessment of lung and breast cancers, in CHU Henri Mondor (Créteil, France) were retrospectively collected. They were all analyzed using PAIRE v0.2.1(Paris, FRANCE) and AUTOID (Siemens, Erlangen, Germany).

AUTOID failed for 7 patients. Manual corrections of AUTOID predictions in Syngo.via interface (VB60) established the ground truth, including all hypermetabolic, inflammatory, or tumoral lesions. The concordance between AUTOID and PAIRE contours was examined by calculating the True Positive (TP), False Positive (FP), and False Negative (FN) lesion counts for each individual and were secondly manually reviewed and reclassified. A predicted Region of Interest (ROI) that had a minimum of one overlapping voxel with the Ground Truth (GT) was classified as a TP lesion. In contrast, predicted ROIs without any overlapping voxels with the GT were categorized as FP lesions. Lastly, GT ROIs that did not have any common voxels with the predicted ROIs were identified as FN lesions. TLV was performed at 41% SUVmax thresholding. ***Results:*** 131 patients (64 with lung cancer, 67 with breast cancer, average age : 65 years old, 86 women) were included. The sensitivities of PAIRE and AUTOID to detect FDG-avid lesions were 93.0 ± 1.5% (1027 / 1104) and 60.1 ± 2.9% (664/1104), respectively. The false positive rate was 1.6 for PAIRE and 0.5 for AUTOID. Mean TLV were 55 ± 117 and 54 ± 96 mL for PAIRE and AUTOID, respectively, versus 45 ± 90 mL for GT ($p<0.01$ and $p<0.01$). These volumes were correlated with the ground truth, ro=0.82 and 0.70 for PAIRE and AUTOID respectively ($p<0.01$). AUTOID's FP (n=307) were mostly digestive (19%) ; articular (17%); vascular (16%) or muscular (16%) structures. PAIRE's FP (n=1631) were surprisingly mostly tumoral non annotaded lesions (27%) ; inflammatory lesions (22%) ; muscular (8%) or vascular structures (8%). ***Conclusion:*** PAIRE demonstrates superior sensitivity compared to AUTOID, albeit with an elevated false-positive rate. Utilizing artificial intelligence facilitates expedited scan interpretation and offers crucial metrics, including metabolic burden quantification. Perfect ground truth are complex to obtained, multiple review must be performed.

EP-0757

Deep Learning for Automatic Prostate Segmentation On 18F-DCFPyL PET/CT In Prostate Cancer.

M. Cysouw, *W. I. Luining, B. M. de Vries, D. E. Oprea-Lager, A. N. Vis, R. Boellaard;*
Amsterdam UMC, Amsterdam, NETHERLANDS.

Aim/Introduction: Quantitative data on PSMA-expression on PSMA PET may be useful for tumor phenotyping and initial staging. To quantify intra-prostatic PSMA-expression, pre-segmentation of the prostate is often necessary to exclude background activity (e.g. bladder or rectum) from tumor-specific activity. We aimed to develop a 3D convolutional neural network (CNN) for automated prostate volume segmentation on ^{18}F-DCFPyL PET. ***Materials and Methods:*** ^{18}F-DCFPyL PET/CT images from 100 patients with intermediate- to -high risk prostate cancer were analyzed. A fully 3D CNN with U-net architecture was constructed and trained (with and without data-augmentation) in 5-fold cross-validation using manual prostate segmentations as ground truth. Both PET-only and concatenated PET/CT images were used as model input (64x64x64 voxel bounding boxes placed around the prostate). The Sørensen-Dice coefficient (DSC) was used to evaluate prostate volume segmentation accuracy. Next, intra-prostatic tumor volumes were segmented using i) commonly used isocontour-based delineation (VOI_{ISO}) and ii) a previously published[1] 3D CNN requiring a predefined prostate volume (VOI_{CNN}). Whole prostate and intra-prostatic tumor PET metrics (volume, SUVs, total PSMA) and radiomics features were extracted from the segmentations. Intraclass-correlation coefficients (ICC) were used to assess agreement between data from CNN-based versus manual prostate segmentations. ***Results:*** We observed mean DSC of 0.86 (0.04 SD) and 0.83 (0.06 SD) for the PET model without and with data augmentation, respectively, and 0.87 (0.04 SD) and 0.85 (0.05 SD) for the PET/CT model without and with data augmentation, respectively. In three patients (with urinal catheters) segmentation failed. Spatially shifting the manually placed bounding boxes reduced DSC by a mean -0.11 (0.08 SD) and 0.00 (0.01 SD) for the models trained without and with data augmentation, respectively. Between PET-metrics derived from manual versus CNN-based prostate segmentations, ICCs for the prostate mask, VOI_{ISO} and VOI_{CNN} were 0.95 (0.06 SD), 0.94 (0.12 SD) and 0.99 (0.01 SD), respectively). Between radiomics features derived from the manual versus CNN-based prostate segmentations, ICCs for the prostate mask, VOI_{ISO} and VOI_{CNN} were 0.91 (0.16 SD), 0.89 (0.14 SD), and 0.91 (0.12 SD), respectively). ***Conclusion:*** We developed a 3D CNN that automatically segments prostate volumes on ^{18}F-DCFPyL PET images and can be used to quantify intra-prostatic PSMA-expression with high accuracy compared to manual segmentations. ***References:*** 1. Kostyszyn D et al. Intraprostatic Tumor Segmentation on PSMA PET Images in Patients with Primary Prostate Cancer with a Convolutional Neural Network. J Nucl Med. 2021 Jun 1;62(6):823-828

EP-0758

Assessment of a Deep Learning-Based Noise Reduction Algorithm on the Ultra-Fast Whole-Body Bone Tomoscintigraphies Recorded by a 360° CZT Camera

A. Bahloul[1,2], *Y. Lamash*[3], *N. Roth*[3], *A. Dari*[1], *P. Marie*[1,2], *L. Imbert*[1,2];
[1]*CHRU-Nancy, Department of Nuclear Medicine, Nancy, FRANCE,* [2]*Université de Lorraine, INSERM U1254, IADI, Nancy, FRANCE,* [3]*Spectrum Dynamics Medical, Caesarea, ISRAEL.*

Aim/Introduction: High-sensitivity 360° CZT-cameras provide high-quality images with marked reductions in injected activities or recording times. This study aimed to determine whether these parameters could be further reduced with the addition of a deep learning-based noise reduction filter for whole-body bone tomoscintigraphy. ***Materials and Methods:*** We selected the list-mode files of whole-body tomoscintigraphies recorded: (i) almost 3 hours after the injection of 550±32 MBq 99mTc HDP, (ii) in 15 patients (8 women, 65±10 years-old, 28±5 kg.m-2 body mass index) for an oncologic indication (10 with bone metastasis and 5 without) and (iii) with a 360° CZT-SPECT camera providing whole-body SPECT recordings of only 9 minutes. SPECT datasets were reconstructed with the noise reduction algorithm (NR+) and without (NR-), for different recording times (RT): 100% (≈ 9 min), 80% (≈ 7 min), 70% (≈ 6 min), 60% (≈ 5 min), 50% (≈ 4,5 min) and 30% (≈ 3 min). All reconstructed images were corrected for scatter and partial volume and analyzed: (i) visually by a blinded experienced observer through a 4-grade quality score (3: excellent, 2: good, 1: suboptimal with a decreased diagnostic confidence, and 0: impossible analysis), and (ii) quantitatively, with the determined maximal Standardized Uptake Values (SUVmax) from each bone lesion and contrast-to-noise ratios from normal femoral shafts. ***Results:*** At 100% RT, mean quality scores (MQS) were 2.8±0.4 for NR- and 2.9±0.3 for NR+. For NR+, MQS remained unchanged with shorter RT down to 60% (2.9±0.4), then decreased starting from 50% RT (2.2±0.7). For NR-, MQS was already decreased at 80% RT (2.1±0.5). Contrast-to-noise ratios decreased according to RT shortening but remained higher for NR+ than NR- whatever the RT level - i.e., at 100% RT, 2.3±0.3 vs. 2.1±0.3 ($p<0.001$), and at 50% RT, 2.1±0.2 vs. 1.9±0.3 ($p<0.001$). Finally, SUVmax from bone lesions were slightly lower for NR+ than NR- (respective mean SUVmax at 100% RT: 11.7±8.5 vs. 12.6±8.7 ($p<0.001$)) but

remained unchanged between different RT levels. ***Conclusion:*** When applying a deep learning-based noise reduction algorithm to ultra-fast (9 min) whole-body bone SPECT recordings currently provided by the 360° CZT-camera, a further decrease to only 60% of original recording counts is possible, without any significant loss in image quality. This decrease could support (i) shortening whole-body SPECT recordings further (down to 5 min RT) or (ii) decreasing the injected activity to 330 MBq, thus combining a low dose protocol with the 9 min whole-body SPECT recordings.

EP-0759

Automatically acquired tumour staging (T) in FDG-avid lung tumours aided by artificial intelligence.

P. Borrelli[1], *M. Milà López*[2], *P. Fierro Alanis*[2], *M. Larsson*[3], *R. Rossi Norrlund*[1], *R. Kaboteh*[1], *L. Edenbrandt*[1,4], *E. Trägårdh*[5,6];
[1]*Department of Clinical Physiology, Region Västra Götaland, Sahlgrenska University Hospital, Gothenburg, SWEDEN,* [2]*Servicio Medicina Nuclear Hospital Universitari Joan XXIII de Tarragona, Tarragona, SPAIN,* [3]*Eigenvision AB, Malmö, SWEDEN,* [4]*Department of Molecular and Clinical Medicine, Institute of Medicine, Sahlgrenska Academy, University of Gothenburg, Gothenburg, SWEDEN,* [5]*Department of Translational Medicine and Wallenberg Center for Molecular Medicine, Lund University, Lund, SWEDEN,* [6]*Department of Clinical Physiology and Nuclear Medicine, Skåne University Hospital, Malmö, SWEDEN.*

Aim/Introduction: Lung-cancer is the most prevalent/deadly cancer worldwide. Correctly staging patients is fundamental. Developing an AI-based-tool to automatically identify TNM status is part of an ongoing effort by our research group. The first natural step and aim in this study is to identify FDG-avid tumours in PET-images and correlate them to the morphological finding in CT-images in patients with suspected/known lung-cancer and get the measurements for Tumour staging (T). ***Materials and Methods:*** 58 patients from two hospitals were evaluated Initially, a convolutional neural network (CNN) is employed to identify/segment the lung-tumour in the PET-image. The input to this CNN includes the CT and PET images, as well as an organ mask produced by a separate method. Subsequently, another CNN is applied to the area around the main lung tumour (highest TLG if more than one was detected). The segmentation output by the second CNN aligns with the tumour tissue visible in the CT image, which usually differs slightly to the high uptake region in the PET images, primarily due to breathing artifacts. The second CNN utilizes the output of the first CNN in addition to the PET/CT images. After the tumour CT-segmentation, the largest diameter is automatically calculated in the three planes. Manual measurements were obtained in the three planes and were compared to those automatically obtained. T-stage was assigned to each patient based on the manual and automatically obtained tumour dimensions. ***Results:*** FDG-avid tumours were present in 46/58 patients. The AI-based tool was able to identify 40 of those (sensitivity-87.0%). In 12 patients neither a specialist nor the AI-tool identified FDG-avid tumours (specificity 100%). Manual median diameter 3.4 cm (IQR 2.3 to 4.3), AI-based median diameter 3.0 cm (IQR 2.0 to 3.9). Difference median diameter -0.4 cm (IQR -0.8 to -0.1). Difference between Manual and AI-based Diameter was on average 0.4cm in 25 patients with a manual diameter <4cm. For larger diameters the average difference was larger. These measurements lead to agreement between manual and AI-based T stage in 30/40 patients (75%), one stage difference in nine patients and two stages difference in one patient. ***Conclusion:*** A completely automated AI-based analysis can detect FDG avid lung tumours with high sensitivity and specificity, measure tumour dimension in CT, and assign a T stage comparable to a manual analysis. These results show feasibility of an automated T-staging. The AI method is available for research purposes on request at www.recomia.org.

EP-0760

Unsupervised and explainable phenotying on multiparametric contrast enhanced MRI and dynamic 18F-FDOPA PET images of patients with glioma at initial diagnosis

T. Zaragori[1,2], *A. Zinsz*[2], *M. Doyen*[1,2], *L. Imbert*[1,2], *J. Oster*[1,3], *A. Verger*[1,2];
[1]*Université de Lorraine, IADI, INSERM, UMR 1254, Vandoeuvre-lès-Nancy, FRANCE,* [2]*Department of Nuclear Medicine & Nancyclotep Imaging Platform, CHRU-Nancy, Université de Lorraine, Vandoeuvre-lès-Nancy, FRANCE,* [3]*CHRU Nancy, INSERM, CIC, Innovation Technologique, Université de Lorraine, Vandoeuvre-lès-Nancy, FRANCE.*

Aim/Introduction: Investigating associations between multiple type of images at the voxel level implies to identify groups of similarly behaving voxels and to explain the construction of these groups by possibly linking them to an underlying physiological process or a specific pathology subphenotype. The objective is to develop an explainable clustering of a multimodal imaging depiction of a glioma for characterization at initial diagnosis. ***Materials and Methods:*** Fifty-six patients having undergone a contrast enhanced (CE) MRI and a ^{18}F-FDOPA dynamic PET with positive uptake for glioma assessment at initial diagnosis were retrospectively included. After co-registration and semi-automated segmentation, CE MRI images, static tumor-to-background ratio (TBR), parametric TTP_{ratio} and $slope_{ratio}$ dynamic ^{18}F-FDOPA PET images were analyzed at the voxel level. Unsupervised clustering of 1,481,146 voxels data was performed using an Hierarchical Density-Based Spatial Clustering algorithm after non-linearly projecting the data in a 2D space using the Uniform Manifold Approximation and Projection algorithm. SHAP values were used for the introspection of the unsupervised analysis to understand the mechanism behind the group construction. The percentage of voxels with each cluster label in each lesion was extracted and fed as features for a survival task predicting time-to-treatment failure (TTF). ***Results:*** Four clusters were identified by our proposed method. The two main clusters consisted of voxels mostly without CE, TBR uptake and either low TTP_{ratio}/negative $slope_{ratio}$ (C1) or high TTP_{ratio}/positive $slope_{ratio}$ (C2). TTP_{ratio} was the most contributive feature to identify C1 along with CE for C2. The two remaining clusters exhibited voxels with CE, high TTP_{ratio}/positive $slope_{ratio}$ and were discriminated by their TBR uptake (high uptake C3 and low/no uptake C4) with the model relying more on TBR for C3, while relying on CE and TTP_{ratio} for C4. Regarding TTF prediction, fraction of C1 was the third most important feature (18%) after the total volume (23.9%) and having undergone a surgery (23.5%). Moreover, higher fraction of C1 in a tumor was associated with lower TTF. ***Conclusion:*** We developed a completely unsupervised method that was able to identify groups of similar behaving voxels on multimodal imaging. SHAP values analysis identified mechanisms behind the group construction and its associations with an important clinical endpoint: gliomas at initial diagnosis in which a high percentage of voxels had low TTP_{ratio}/negative $slope_{ratio}$ values were correlated to lower TTF.

EP-0761

Artificial intelligence Respiratory Gating in PET/CT Imaging: changes on MTV, TLG and SUVmax

P. Meneses Soares, *A. Grajeda Gallardo, J. Mucientes Rasilla, R. Jimeno Pernett, M. Mitjavila Casanovas;
HOSPITAL PUERTA DE HIERRO, MAJADAHONDA, SPAIN.*

Aim/Introduction: The Metabolic Tumor Volume (MTV) and Total Lesion Glycolysis (TLG) are parameters of increasing interest in lesion evaluation using 18F-FDG PET/CT. Respiratory gating during PET/CT reduces artifacts caused by respiratory movements. In the

past, this technique was dependent on gating devices, which led to longer exploration and preparation times. However, with the advent of artificial intelligence (AI), it is now possible to benefit from respiratory gating without the need for a device, avoiding many of the problems associated with its use.The objective of this study is to assess differences between MTV and TLG with and without respiratory gating, as well SUVmax increase in respiratory gating. ***Materials and Methods:*** This is a retrospective study and involved the selection of patients with lung or mediastinal lesions who underwent PET/CT imaging using our newly acquired equipment that integrates AI respiratory gating. Fifty patients met the inclusion criteria and were included in the final analysis. The maximum standardized uptake value (SUVmax), metabolic tumor volume (MTV), and total lesion glycolysis (TLG) were measured for each lesion, and the mean difference between the results obtained with and without AI respiratory gating was calculated. ***Results:*** The study revealed a mean difference of 13.89% in MTV and 11.52% in TLG between patients undergoing PET/CT imaging with and without AI respiratory gating. Furthermore, the difference in values for the lower pulmonary lobes was significantly higher than for the upper pulmonary lobes, with a difference of 23.7% in MTV and 20.78% in TLG (upper lobes: MTV 7,8% and TLG 5,5%). The global SUVmax increased by 9.3%, while lesions on the inferior pulmonary lobes had an increase of 15.7%, and lesions on other locations had an increase of only 7.47%. Indirectly the changes on the images facilitated lesion delimitation and characterization, particularly in paradiafragmatic lesions. ***Conclusion:*** The use of AI respiratory gating during PET/CT imaging can lead to changes in MTV, TLG and SUVmax. Is important to take that into account. AI respiratory gating leads to improved image quality, well-defined images, less respiratory artifacts and more contrast between normal and pathologic lung metabolic activity. These findings can lead to improved lesion delimitation and characterization resulting in better patient outcomes. ***References:*** Kesner AL, et al. On transcending the impasse of respiratory motion correction applications in routine clinical imaging - a consideration of a fully automated data driven motion control framework. EJNMMI Physics

EP-51

e-Poster Area

D: Technical Studies -> D3 Radiation Protection -> D31 Radiation Exposure and Protection

EP-0762

Potential airborne releases of 68Ga and 177Lu: a method of preventive assessment

M. Marengo[1], *S. Rubow*[2];
[1]*University of Bologna, Bologna, ITALY,* [2]*University of Stellenbosch, Stellenbosch, SOUTH AFRICA.*

Aim/Introduction: The handling of radioactive solutions can lead to the production of airborne radioactivity which can potentially be released into the environment. To reduce this risk to a minimum, containment and protection systems are adopted. However, during processing, unwanted situations may occur, releasing some radioactivity. Given the high activity concentration levels of the products, even a small volume can contain significant radionuclide activity. In this work we present a method for preventive risk assessment, evaluating the potential release of radioactive gases in the case of two important radionuclides, ^{68}Ga and ^{177}Lu. ***Materials and Methods:*** The source term, the amount of radioactivity released to air, can be evaluated according to the method introduced by the US Department of Energy. For a liquid to be made airborne, in realistic situations, the bulk liquid must be subdivided into droplets small enough to be entrained in the local airflow. Not considering explosions or fires, this may have different causes, like heating the solution, fall and rupture of the container or resuspension due to the aerodynamic action of ventilation. The key point is the evaluation of the airborne release factor (ARF), the fraction of activity that is released to air. For all the following calculations we assumed a single, conservative ARF value of $3 \cdot 10^{-5}$, according to DOE Handbook 3010 for heating of aqueous solutions.To assess the effective dose to the population living in the area surrounding the facility, the use of 1850 MBq of ^{68}Ga solution for 2 procedures for 200 days/year, and of 7400 MBq of ^{177}Lu solutions for 100 procedures/year were considered. A total release of 22.2 MBq/year for each radionuclide was input in the well-known code HotSpot, modelling a gaussian plume emission and different meterological conditions. ***Results:*** The maximum effective dose values calculated for the close proximity of the facility were 0.1 uSv/y for ^{177}Lu and 0.06 uSv/y for ^{68}Ga. These values represent the worst case scenario and can be further reduced considering the role of specific containment and filtration systems. ***Conclusion:*** This preventive evaluation method demonstrates that the potential airborne release of ^{68}Ga and ^{177}Lu is not radiologically relevant. It can generally also be applied to other radionuclides in aqueous solution, in order to demonstrate compliance during authorization processes. ***References:*** DOE-HDBK-3010-94 Volume I (Reaffirmed 2013), Airborne Release Fractions/Rates and Respirable Fractions for Nonreactor Nuclear Facilities, Volume I

EP-0763

CT dose reduction in hybrid PET/CT imaging

C. Pettinato, *M. Schiavini, A. Castello, L. Florimonte, C. Canzi, F. Bardo, F. Buffoni, C. Colombo, V. Longari, E. Orunesu, M. Campoleoni, M. Castellani;*
Fondazione IRCCS Ca' Granda Ospedale Maggiore Policlinico, Milano, ITALY.

Aim/Introduction: PET/CT imaging is a high dose diagnostic procedure (ACR criteria: ED > 10 mSv). While PET dose reduction can be achieved by reducing the injected activity, CT dose can be controlled using automatic mA modulation algorithms and reducing the applied KVs. Moreover, the introduction of iterative algorithms for CT images reconstruction allows to obtain good image quality while containing patient dose. Dose reduction is particularly important in young patients and in patients enrolled in tight follow-up protocols which include WB PET/CT imaging. The aim of this work was to minimize CT dose in PET/CT imaging personalized on patient weight. ***Materials and Methods:*** All patients underwent a whole-body PET/CT study after the administration of about 3.5-4MBq/Kg of 18F-FDG, using a Biograph Vision 450 PET/CT scanner in flow motion acquisition mode. The CT protocol involved a modulating mA automatic system with constant 120 KV. CT images were reconstructed using the SAFIRE (Sinogram Affirmed Iterative Reconstruction) algorithm. Before each scan, CTDI values shown on the workstation screen were recorded using both 120 and 100 KV and for smaller patients also 80 KV (patient weight < 55 Kg). Evaluation of CT dose optimization was done by calculating the percentage change in the theoretical CTDI values by varying the applied KVs. ***Results:***

25 consecutive patients were enrolled in this study. Mean patient weight and height were respectively 69.4 Kg (range: 41-123 Kg) and 166 cm (range: 150-186 cm) and the mean injected activity was 273.3 MBq (range: 164-400 MBq). The mean CTDI values at 120 KV and 100 KV were respectively 7.2 mGy (range: 2-16 mGy) and 4.6 mGy (range: 1-11 mGy). The mean dose reduction in terms of CTDI values when using 100 KV versus 120 KV was 38.4% (range: 32.4-42.5%). For smaller patients the mean CTDI reduction changing from 120 KV to 80 KV was 71.9% (range: 68.8-75.5%). ***Conclusion:*** CT dose in PET/CT imaging can be easily reduced of about 40% in standard patients and even more, about 70%, for smaller patients by lowering the KV applied and using iterative reconstruction algorithms. In our clinical routine we started using 80 KV for smaller patients (<55 Kg), 100 KV for standard patients (55-80 Kg) and 120 KV for larger patients (>80 Kg). An evaluation of image quality is still ongoing as well as the opportunity to use patient BMI instead of weight to personalize the applied KVs

EP-0764

Ambient Dose Equivalent and Occupational Exposure for 177Lu-PSMA-I&T Radionuclide Therapy

Z. Hu[1], *C. Liu*[2], *J. Liu*[2], *Z. Yang*[2], *R. Qiu*[1];
[1]*Tsinghua University, Beijing, CHINA,* [2]*Beijing Cancer Hospital, Beijing, CHINA.*

Aim/Introduction: ^{177}Lu-PSMA-I&T is a commonly used agent for radioligand therapy in patients with advanced metastatic castration-resistant prostate cancer. However, there have been no reports on radiation exposure measurements for this agent. The objective of this study is to assess occupational exposure and ambient dose equivalent for ^{177}Lu-PSMA-I&T radionuclide therapy and to measure blood clearance. ***Materials and Methods:*** A total of 17 treatments for 9 patients treated with 7.4 GBq ^{177}Lu-PSMA-I&T at Beijing Cancer Hospital between July 2022 and March 2023 were included in the study. A handheld radiation dosimeter was used to measure the ambient dose equivalent rate at various distances from the patients and at different time points from 0 to 24 hours after infusion. Occupational exposure doses for medical staff were measured using electronic personal dosimeters, while ring thermoluminescence dosimeters were used to measure finger doses for pharmacists and nurses. Blood activity was measured using a gamma counter from 0 to 24 hours after infusion. ***Results:*** The ambient dose equivalent rates at a distance of 1m from the patients were 12.7±1.9 μSv/h and 10.8±1.6 μSv/h at 4 and 6 hours after infusion, respectively, while those at a distance of 3m were 2.2±0.3 μSv/h and 1.8±0.3 μSv/h. The mean effective doses for pharmacists, nurses, and physicians were 0.19±0.08 μSv, 2.64±0.84 μSv, and 1.54±0.39 μSv per patient, respectively. The finger doses for pharmacists and nurses were 200.4±46.1 μSv and 184.1±42.3 μSv per patient, respectively. ***Conclusion:*** Our findings suggest that ^{177}Lu-PSMA-I&T is a reasonably safe option for outpatient treatment, but attention should be paid to radiation protection for the hands of medical staff.

EP-0765

Evaluation of staff exposure to ionising radiation in a PET/CT department

P. Archontakis[1,2,3], *K. Silivridou*[2], *K. Mainta*[2,3], *D. Maintas*[2,3];
[1]*National and Kapodistrian University of Athens, Athens, GREECE,* [2]*Iatriko Athinon, Athens, GREECE,* [3]*Institute for Isotopic Studies, Athens, GREECE.*

Aim/Introduction: The aim of this study is to evaluate the staff exposure to ionising radiation in a PET/CT department and categorise the magnitude of each exposure-related task. According to the literature[1], the manual dispensing of radiopharmaceuticals can result in high equivalent dose in extremities, which could be 5-6 times greater compared to what the ring dosimeter detects. ***Materials and Methods:*** The operation chain consists of ^{18}F radiopharmaceutical vial measurement, dose dispensing, dose injection, patient positioning and discharge. The personnel involved in exposure-related tasks in our department is the medical physicist responsible for vial measurement and dose dispension and two radiology technologists responsible for injecting, positioning and discharging the patients. Thermoluminescent (TLD) and optically stimulated luminescent (OSLD) dosimeters are used to evaluate the effective dose of the staff and ring dosimeters were used to measure and compare the equivalent dose to the fingers for both dominant and secondary hand. In addition, wrist dosimeters were used to create a correlation factor between finger and wrist equivalent dose. So far, the collected data represent a 6-month period, from October 2022 until March 2023 and the corresponding number of patients is 987 with injected activity of 340 ± 68 MBq (±1sd) per patient. ***Results:*** The procedure associated with the highest exposure is found to be the manual dispensing (288 ± 56 μSv/GBq) followed by the manual injection (104± 24 μSv/GBq). The vial measurement equivalent dose is evaluated at 5.1 ± 1.1 μSv/GBq and the correlation factor between wrist and finger equivalent dose is estimated equal to 16. Additionally, the exposure of the dominant hand was around 10% lower than that of the secondary. Finally, the effective dose in μSv/patient is found to be 1.18 ± 0.12 for the medical physicist and 2.00 ± 0.59 for each radiology technologist. ***Conclusion:*** Using an average workload of 12 patients per day divided equally to three operators, the annual equivalent dose from the whole operation chain sums up to 137mSv/operator and the corresponding effective dose to 3mSv/operator. It is evident that the biggest contribution of staff exposure to ionizing radiation comes from manual dispension and injection of the radiopharmaceutical. The most effective way to minimize these contributions is by introducing an automated dispension and injection system. ***References:*** [1]Robert Kollaard et al 2021, Journal of Radiological Protection 41 R60

EP-0766

Beta radiation protection in Phosphorous-32 microparticles therapy. Tungsten or methacrylate shielding?

C. G. Franco Monterroso, *B. Santos Montero, L. Rey Sánchez, L. García Lama, V. Pascual Pascual, M. A. Hernández Fructuoso; Hospital Universitari Vall d'Hebron, Barcelona, SPAIN.*

Aim/Introduction: Phosphorous-32 (^{32}P) microparticles are used in radionuclide therapy as a novel brachytherapy device for the treatment of unresectable locally advanced pancreatic cancer in combination with chemotherapy. Radiation protection requirements related to the preparation and administration of radionuclides in therapy are very important. ^{32}P is a pure beta-emitter radioisotope with a physical half-life of 14.27 days. Beta particles interact with matter by collision with atomic electrons, and the radioactive process resulting in photons is known as bremsstrahlung. The maximum range of ^{32}P beta particles in methacrylate and tungsten is 0.7 cm and 0.04 cm respectively. Thus, shielding thicker than the range has no added effect on beta radiation penetrating the shield but will attenuate the bremsstrahlung radiation produced. The aim of this study is to evaluate which shield is better to attenuate the bremsstrahlung radiation during dose preparation in order to reduce personal dosimetry. ***Materials and Methods:*** Four samples of ^{32}P microparticles (13.4, 25.5, 45.7 and 68.2 MBq) were drawn into a 5

ml plastic syringe and placed into two different syringe shieldings: a tungsten syringe shielding (8 mm tungsten and 15 mm lead glass window) and a 10 mm methacrylate syringe shielding. Each sample equivalent dose rate was measured three times with a commercially dose rate meter (E0111280 series MiniTrace Gamma) in close contact to the shielding and at a distance of 30 cm. For each measurement, background was recorded and the results were corrected for background. ***Results:*** For the methacrylate syringe shielding, the average dose rates obtained for 13.4, 25.5, 45.7 and 68.2 MBq syringes were 0.0, 0.1, 0.1 and 0.3 µSv/h at 30 cm and 5.9, 10.7, 18.3, 30.6 µSv/h in close contact. For the tungsten syringe shield, the average dose rates obtained for 13.4, 25.5, 45.7 and 68.2 MBq syringes at 30 cm were similar to background and 0.1, 1.1, 2.0 and 3.0µSv/h in close contact. Under these conditions, tungsten shielding is 10 times more effective than methacrylate reducing dose rate in close contact for activities greater than 25.5 MBq. ***Conclusion:*** Choosing an appropriate syringe shielding is relevant during the preparation and administration of radionuclides in therapy. Compared to methacrylate shielding, our results suggest a significant reduction of radiation exposure when using tungsten shielding.

EP-0767

Study of yttrium-90 radiation attenuation using different types of shielding

L. Rey Sánchez*, C. G. Franco Monterroso, B. Santos Montero, V. Pascual Pascual, L. García Lama, M. A. Hernández Fructuoso; Hospital Universitario Vall d'hebron, Barcelona, SPAIN.*

Aim/Introduction: Yttrium-90 is used in hepatic radioembolization treatments at high doses, which carries a risk of irradiation for the operator during dose preparation. As a high-energy beta emitter, the use of shields with a low atomic number, plastic/aluminium, is recommended to attenuate the braking radiation (Bremsstrahlung) produced by the radionuclide. The aim of our work was to evaluate which shield is most suitable for attenuating Yttrium-90 radiation. ***Materials and Methods:*** 10 samples with increasing yttrium-90 activities were prepared in 5 ml syringe: 688.2 MBq (Syringe 1,S1), 743.7 MBq (Syringe 2, S2), 791.8 MBq (Syringe 3,S3), 1287.6 MBq (Syringe, S4), 1491.1 MBq (Syringe 5, S5), 2201.5 MBq (Syringe 6, S6), 3052.5 MBq (Syringe 7, S7), 3984.9 MBq (Syringe 8, S8), 4016.35 MBq (Syringe 9, S9) and 4306.8 MBq (Syringe 10, S10). Each sample was placed into a 13 mm thick methacrylate shielding and an 8 mm tungsten shielding with a 15 mm leaded glass window and the equivalent dose rate (µSv/h) in contact and at 30 cm with a Geiger-Müller detector (MiniTrace Gamma E0111280 series) was determined. 3 measurements were performed by syringe. ***Results:*** The mean dose rate in contact of methacrylate shielding syringes S1, S2, S3, S4, S5, S6, S7, S8, S9 and S10 was 421.1 µSv/h, 488.8 µSv/h, 713.63 µSv/h, 1042.9 µSv/h, 1076.5 µSv/h, 1594.2 µSv/h, 2324.2 µSv/h, 3066.5 µSv/h, 3202.9 µSv/h and 3642.4 µSv/h respectively while with tungsten shielding syringes was 157.8µSv/h, 175.0 µSv/h, 217.6 µSv/h, 290.4 µSv/h, 348.3 µSv/h, 483.5 µSv/h, 597.6 µSv/h, 668.8 µSv/h, 743.4 µSv/h and 778.5 µSv/h.The mean dose rate for methacrylate shielding syringes S1, S2, S3, S4, S5, S6, S7, S8, S9 and S10 to 30 cm was 10.8 µSv/h, 13.0 µSv/h, 13.99 µSv/h, 21.3 µSv/h, 25.1 µSv/h, 35.9 µSv/h, 53.8 µSv/h, 68.5 µSv/h, 71.6 µSv/h and 71.9 µSv/h respectively; versus 2.5 µSv/h, 2.8 µSv/h, 3.8 µSv/h, 4.8 µSv/h, 5.0 µSv/h, 7.6 µSv/h, 9.8 µSv/h, 13.6 µSv/h, 13.7 µSv/h and 15.4 µSv/h in tungsten shielding syringes. ***Conclusion:*** In all cases, the dose rate values were lower for tungsten-shielded syringes. Therefore, tungsten shields seem to be more suitable because they offer better radiological protection to the operator; however, methacrylate shields are more ergonomics (greater visibility and lower weight).

EP-0768

Evaluating the effectiveness of lead apron in a Nuclear Medicine (PET-CT) facility

A. Shaikh*[1], R. Vatsa[1], V. Sawant[1], V. Rangarajan[2]; [1]Advanced Centre for Treatment, Research, and Education in Cancer, Navi Mumbai, INDIA, [2]Tata Memorial Centre, Mumbai, INDIA.*

Aim/Introduction: Positron emission tomography-computed tomography (PET-CT) using ^{18}F-FDG is an essential imaging modality used for staging, re-staging, disease, and response evaluation in cancer patients. A PET-CT technologist is involved in ^{18}F-FDG dose dispensing followed by patient positioning and image acquisition which involves substantial radiation exposure. The present study aims to assess the radiation exposure of a PET-CT technologist with and without wearing lead apron while handling both ^{18}F-FDG radiopharmaceutical and patients. ***Materials and Methods:*** A lead apron of 0.5 mm thickness, tested for leakage was used. The absorbed dose was measured by a semiconductor based calibrated electronic pocket dosimeter (dose range 1µSv-10 Sv). The average number of patient intake in the department for PET-CT imaging was 15. To measure the absorbed dose, pocket dosimeter was clipped at chest level while routinely working without lead apron and was placed inside of lead apron at same chest level while wearing lead apron. The absorbed dose readings were recorded simultaneously while dispensing ^{18}F-FDG, monitoring injection, patient positioning, contrast administration, patient acquisition with contrast and non-contrast study. ***Results:*** A cumulative radioactivity of 294.16 mCi vs 309.92 mCi of ^{18}F-FDG was dispensed with and without lead apron respectively. The absorbed dose of 20 µSv vs 25 µSv was observed when the ^{18}F-FDG was dispensed with and without lead apron. was used and these exposure values were higher while working without lead apron as per the recorded data. During the contrast patient acquisition with and without lead apron, the absorbed dose observed was 28 µSv and 45 µSv respectively. The absorbed dose in case of non-contrast patient acquisition with and without lead apron was 8 µSv and 7 µSv respectively. ***Conclusion:*** The present study suggested that the use of lead apron while dispensing ^{18}F-FDG and patient acquisition reduces the exposure. The study indicated that the use of lead apron will be beneficial in reducing the exposure to the radiation professional with maximum advantage for centres where either the patient work load in very high or the radiation professional staff is limited.

EP-0769

A radiation exposure comparison between manual and automated setups during GALLIUM-68 peptide labelling

M. Costa*[1,2], R. Parafita[1,2], A. Canudo[1,2,2], A. Capacho[1], F. Silva[1], H. Delgado[1,2], J. Correia[1,2], M. Correia[1,2], M. Silva[1,2], M. Andrade[1,2], M. Machado[1], P. Ferreira[1], P. H. Ferreira[1,2], R. Oliveira[1,2], S. Batanete[1,2], S. Teixeira[1,2], V. Vieira[1,2], F. Oliveira[1], D. Costa[1]; [1]Champalimaud Foundation, Lisbon, PORTUGAL, [2]Mercurius Health, Lisbon, PORTUGAL.*

Aim/Introduction: In-house production of radiopharmaceuticals with Ga-68 is a concern for radiation exposed professionals. Our aim is to compare the radiation exposure of the operator during radiopharmaceutical synthesis/production of peptides

labelled with Ga-68 using manual versus automated procedures. ***Materials and Methods:*** Two setups were evaluated: manual and automated. The manual setup used an ITM synthesis module with 36-50 mm thick lead walls containing a 50 mm lead barrier Ge-68/Ga-68 generator. Between the operator and the module, there was an "L" shaped lead barrier (60 mm thick, 360 mm wide and 470 mm tall). The automated setup had an IRE Ge-68/Ga-68 generator with an equivalent 50 mm lead barrier, installed inside a 50 mm lead hot cell. In both setups, lead containers (17 mm thick) were used to accommodate the product and waste. During the production period, the operator wore an EPD Mk2 electronic dosimeter in the chest (centered above the rib cage) to measure the effective dose received in the whole body. The effective dose was then normalized for the amount of eluted activity for each Ga-68 production, thus obtaining the exposure per MBq eluted (μSv/MBq). ***Results:*** Taking into consideration all manual and automated setups, a total of 425 and 93 measurements were registered, respectively. The median (quartiles Q1; Q3) eluted activities were 932 (733; 1158) (manual) and 611 (572; 666) MBq (automated), and the median normalized effective dose was 1.9×10^(-3) (1.1×10^(-3); 2.9 ×10^(-3)) (manual) and 1.7×10^(-3) (1.5×10^(-3); 2.4× 10^(-3)) μSv/MBq (automated). Assuming 3 daily productions and 22 days during 12 months, if all productions were performed by the same operator (worst-case scenario), then the median annual effective dose due to this task would have been 1.48 (0.83; 2.33) (manual) and 1.34 (1.19; 1.89) μSv/MBq (automated). For instance, considering 1 GBq of eluted activity, and the referred worst-case scenario, a median annual effective dose of 1.48 (manual) and 1.34 mSv (automated) is to be expected. ***Conclusion:*** Our data is quite reassuring in terms of professional exposure during radiopharmaceutical Ga-68 peptide labelling "in-house". Considering the worst-case scenario, the median annual exposure when using the manual setup and 1 GBq of eluted activity is approximately 7% of the annual effective dose limit for nuclear medicine professionals (20 mSv). Annual exposure is further reduced by using automated setup, in line with the ALARA principle. Both evaluated setups are safe, as long as, rigorous protocols are implemented and followed.

EP-0770

Typical values of quantities related to the patient dose from PET/CT in Bulgaria: first results

M. Sibinova[1], *T. K. Todorova*[2], *A. R. Zagorska*[3];
[1]*Sofia University "St Kliment Ohridski", Sofia, BULGARIA,*
[2]*National center of radiobiology and radiation protection, Sofia, BULGARIA,* [3]*Acibadem City Clinic University Hospital Tokuda, Sofia, BULGARIA.*

Aim/Introduction: Positron emission tomography (PET), used in combination with computed tomography (CT) in all modern PET/CT devices is an important part of the oncologic clinical practice. These hybrid systems lead to a significant patient exposure, due to both PET and CT components. The aim of this study is to present the typical values of the quantities related to the patient dose for both imaging modalities independently and to analyze the potential of optimization. ***Materials and Methods:*** A retrospective study of typical radiation metrics for 2021[1] was carried out for nine out of ten Nuclear medicine departments in Bulgaria. Data was collected about the equipment manufacturer and model of the PET/CT device, type of examination, patient age, weight and height, and administered activity per body weight (for the PET part), $CTDI_{vol}$ and DLP (for the CT part) for at least 20 patients per modality for oncology PET/CT examinations. ***Results:*** The typical values for radiation metrics are as it follows: administered activity per body weight: 2.6 (2-3.95), 0.5 MBq.kg-1, CTDIvol: 2.7 (2.5-14.1), 3.8 mGy and DLP: 278 (235-1578), 436 mGy.cm. Median, minimum and maximum in parenthesis, standard deviation values are presented. The highest presented value for the administered activity is for the oldest PET/CT scanner. The results show that the typical CTDIvol values are five-fold higher than the median values. ***Conclusion:*** This study is the first to present and to analyze typical doses from different PET/CT imaging modalities in Bulgaria. The typical values for the administered activity per weight seem to be very well optimized in all Nuclear medicine departments that participated in the current study. Unlike the nuclear medicine part of the examination, there is a significant variation in the typical CT radiation exposure. There is a potential of optimization and an effort must be done in order to optimize the used CT protocols.

EP-0771

Radiation Dose Reduction Strategy for SPECT/CT Bone Scan

M. Alezzi[1], *O. Kotbi*[1], *G. Hammid*[1], *A. Fouda*[1], *Y. Zabarmawi*[2];
[1]*KING ABDULLAH MEDICAL CITY, Makkah, SAUDI ARABIA,*
[2]*Umm Al-qura University, Makkah, SAUDI ARABIA.*

Aim/Introduction: The aim of this study is to introduce the optimization method of CT parameters to reduce patient radiation exposure in bone SPECT/CT while maintaining image quality. The results of the new protocol were then compared to the results of the standard protocol saved in the nuclear medicine department`s data at King Abdullah Medical City. ***Materials and Methods:*** First part: Using Deluxe Jaszczak Phantom. The cylindrical phantom consisted of six bottles in a pie arrangement. These bottles were placed in the source tank. SPECT/CT scans were carried out with different x-ray tube current values at three different slices of thicknesses (2.5, 3.75, and 5mm). The contrast ratio (CR) and coefficients of variation (COV) in the SPECT images as well as the signal-to-noise ratio (SNR) and CTDIvol were all measured. Second part: The study was done on patients who required a SPECT/CT bone scan of the spine area (thoracic spine (T1-T12) and lumbar spine (L1-L5)). Some patients were excluded from this study because of the image quality that was affected by several factors. Different parameters obtained from the new reduced protocol were compared to old historical data saved in the system for patients who did the same image using the old standard protocol. The difference between the two systems was only in the current of the X-ray tube (the old 60 mA versus the new 40 mA). ***Results:*** The optimal set of parameters for bone SPECT/CT was determined based on a phantom part that has been implemented in clinical practice. Two groups of patients were examined according to the baseline and optimized protocols, respectively. The new SPECT/CT protocol substantially reduced patients' radiation exposure as compared to the old protocol, while also maintaining the required diagnostic quality of SPECT and CT images. ***Conclusion:*** The newly established bone scan SPECT/CT protocol was implemented into clinical practice. It has significantly reduced patients' exposure dose as compared to the old protocol while maintaining the required diagnostic quality of SPECT and CT images. ***References:*** 1. ADDIN Mendeley Bibliography CSL_BIBLIOGRAPHY Bartel, T. B., Kuruva, M., Gnanasegaran, G., Beheshti, M., Cohen, E. J., Weissman, A. F., & Yarbrough, T. L. (2018). SNMMI procedure standard for bone scintigraphy 4.0. Journal of Nuclear Medicine Technology, 46(4), 398-404. 2. Chen, E. J., Tan, T. H., & Chew, M. T. (2021). Superscan: Superiority of xSPECT/CT over OSEM SPECT/CT in bone scans of prostate cancer patients. Radiation Physics and Chemistry, 178(March), 108998. https://doi.org/10.1016/j.radphyschem.2020.108998

EP-0772

Radiation safety during 177-Lu labellingand therapy: experience in Bulgaria

A. Zagorska;
Acibadem City Clinic University Hospital Tokuda, Sofia, BULGARIA.

Aim/Introduction: The application of 177-Lu for radioligand therapy is growing worldwide. Special attention must be paid during treatment center design to radiation protection due to the physical characteristics of 177-Lu. The aim of this study is to present our experience and lessons learned in the field of radiation protection in 177-Lu labelling and treatment of patients with 177-Lu. ***Materials and Methods:*** Relevant published national and international recommendations were reviewed. The efficacy of available lead aprons (0.5 mm Pb), four types of vial shielding, and 2 mm lead equivalent screen was investigated regarding radiation protection when handling 177-Lu. Measurements were performed with an Atomtex AT 1123, calibrated in ambient dose equivalent, H*(10), mSv. ***Results:*** For educational purposes and with the support of the IAEA, online training on radiation protection for patients, staff and the public during Lu-177-based radiopharmaceutical therapy was organized. National legislation and the ALARA concept require the preparation of detailed radiation safety protocols. 1) Public: Kurt at al [1] method was used and a patient release criterion of 30 µSv/h at 1 m. Restrictions were proposed to limit radiation exposure to household members of patients and the public. 2) Staff: Nurses and radiochemists were identified as having a higher potential of contamination and external exposure. To avoid unnecessary staff exposure and to facilitate communication with the patient during treatment, 2 mm transparent lead equivalent screen was installed in the patient room. The patient dose rate was attenuated approximately 90% by the lead screen. The attenuation coefficients for 177-Lu of vial shielings were calculated to be between 100 and 1000 times depending on the composition and thickness of the material. The attenuation of available lead aprons was approximately 50 %. In addition to the regular radiation protection training, a dedicated training was organised to cover physical properties of 177-Lu, the effectiveness of shielding and special cases in radionuclide therapy such as extravasation and actions in case of extravasation. 3) Patient: to ensure patient safety, video monitoring was provided. ***Conclusion:*** Two of the available vial shieldings do not provide the required level of protection. The available aprons can be used during 177-Lu treatment. Team training and teamwork are very important to ensure radiation protection of patient and staff. ***References:*** Kurth J, Krause BJ, Schwarzenbock SM, et al. External radiation exposure, excretion, and effective half-life in 177Lu-PSMA-targeted therapies. EJNMMI Res. 2018 Apr 12;8(1):32. doi: 10.1186/s13550-018-0386-4.

EP-52

e-Poster Area

D: Technical Studies -> D4 Dosimetry and Radiobiology -> D41 Preclinical Dosimetry and Radiobiology

EP-0773

Monte Carlo quantification damage by 64Cu incorporate in DNA

J. Carrasco, *E. Padilla;*
Instituto de Ciencias Nucleares, CDMX, MEXICO.

Aim/Introduction: Topas-nBio was used to calculate DNA damage (Double Strand Breaks) for Auger emitters (AEs) including Cu-64 of interest in Targeted Radionuclide Therapy, when are incorporated in DNA genome of a mammalian cell nucleus. ***Materials and Methods:*** Calculations of DSBs for five AEs ^{125}I, ^{123}I, ^{111}In, ^{99m}Tc and ^{64}Cu have been performed by incorporating the AE in DNA genoma of a nucleus of 9.3 um diameter, density 14 Mbp/mm^3 and 6.08 Gbp. The Topas-nBio Monte Carlo tool was employed for simulating collision-by-collision the complete trajectories of electron tracks in liquid water when the AE was placed in two configurations off the central axis of DNA: 0.25 nm and 1.15 nm. For all the considered radionuclides, with exception of ^{99m}Tc, the physical decay process was explicitly simulated with the G4RadiactiveDecay module from Geant4, whereas for ^{99m}Tc the energies and yields of the Auger electron spectrum were obtained from published data. The DSB yields per decay incorporated in DNA for ^{64}Cu are firstly reported in this work. ***Results:*** Monte Carlo simulations of DNA damage with Topas-nBio reveal that, the calculated DBS yields for ^{64}Cu incorporated in genome are 0.171 and 0.190 per decay for 0.25 and 1.15 nm off the DNA central axis, respectively. DSB Yields per decay for ^{111}In, ^{125}I, ^{123}I, ^{99m}Tc were compared with reported calculated or measured data for validation purposes. ***Conclusion:*** Our results show that ^{64}Cu may have therapeutic effects in tumor cells when combined with Targeted Radionuclide Therapy. ***References:*** Schuemann, J., McNamara, A. L., Ramos-Méndez, J., Perl, J., Held, K. D., Paganetti, H., .. & Faddegon, B. (2019). TOPAS-nBio: an extension to the TOPAS simulation toolkit for cellular and sub-cellular radiobiology. Radiation research, 191(2), 125-138.Zhu, H., McNamara, A. L., McMahon, S. J., Ramos-Mendez, J., Henthorn, N. T., Faddegon, B., .. & Schuemann, J. (2020). Cellular response to proton irradiation: a simulation study with TOPAS-nBio. Radiation research, 194(1), 9-21.

EP-0774

Evaluation of Repeatability of 177Lu Quantitative Imaging Using Monte Carlo Simulation

K. Ishikawa[1], *C. Kubota*[1], *Y. Yasumoto*[1], *T. Sakashita*[2], *H. Daisaki*[1];
[1]*Gunma Prefectural College of Health Sciences, Gunma, JAPAN,* [2]*National Institutes for Quantum Science and Technology, Gunma, JAPAN.*

Aim/Introduction: Good repeatability of quantitative values is necessary for accurate dosimetry using ^{177}Lu imaging. While there are research papers on quantitative accuracy, there have been no reports to date on the repeatability of quantitative values. The purpose of this study is to identify optimal imaging conditions for achieving good repeatability in ^{177}Lu imaging. ***Materials and Methods:*** A NEMA body phantom was digitally created to mimic imaging of tumors in the liver at 6 hours after 7.4 GBq of ^{177}Lu (Hot=1.85, BG=0.201 MBq/mL) [1]. Pseudo-projection data (30 projections per condition) assuming a GE Discovery NM/CT 670 scanner were generated under several imaging conditions using the SIMIND program (Lund University) and the digital phantom. Acquisition conditions were as follows: 1) MEGP or ELEGP collimator, 2) main window with 113 keV±10% or 208 keV±10%, 3) upper and lower sub-energy window with 10 keV width, and 4) scan duration with 2.5 min, 5.0, and 7.5 min/60 projection. SPECT images were reconstructed by ordered subset expectation maximization (OSEM) method (3 iterations, 10 subset) after scatter correction (Triple Energy Window method), attenuation correction (Chang method), and noise reduction by Butterworth filter (cut-off frequency; 0.50 cycles/cm) using Prominence Processor Ver3.1 [2]. The SPECT images were converted to Bq/

mL units by applying the Bq calibration factor calculated from simulated Pool phantom images using RAVAT (Nihon-Medi Physics). The repeatability was evaluated by the coefficient of variation (CV: %) of VOIs placed in the BG region (n=12) and each hot sphere. For comparison of CVs in the BG region, one-way ANOVA test was used to confirm the significance, and then the Tukey's test was used for multiple comparisons. A $p<0.05$ was considered statistically significant. ***Results:*** The repeatability of the quantitative values decreased as the hot spheres became smaller. The CV of the BG region in the ELEGP+208 keV condition was significantly lower than the other three conditions ($p<0.05$). The CV can be improved by increasing the scan duration. The scan duration to achieve CV<5% were 2.5 min for ELEGP+208 keV, 5.0 min for MEGP+208 keV, 7.5 min for ELEGP+113 keV, and not achieved for MEGP+113 keV. ***Conclusion:*** The repeatability of quantitative values depends on the combination of collimator, energy window setting, and scan duration. Superior repeatability of quantitative values can be obtained by using ELEGP+208 keV imaging conditions. ***References:*** [1] Annals of Nuclear Medicine (2021) 35:823-833. [2] http://nm.jsrt.or.jp/blog.html

EP-0775

Preclinical in vivo tumour dosimetry of a Lu-177-labelled ligand using a gamma probe

A. Klotsotyra[1], *D. Arbuznikova*[1,2,3], *N. Steinacker*[1,2], *L. Domogalla*[1,2], *A. Eder*[1,2], *M. Mix*[1];
[1]*Department of Nuclear Medicine, Medical Center – University of Freiburg, Faculty of Medicine, University of Freiburg, Freiburg, GERMANY,* [2]*Division of Radiopharmaceutical Development, German Cancer Consortium (DKTK), partner site Freiburg, Freiburg, Germany and German Cancer Research Center, Heidelberg, GERMANY,* [3]*Department of Radiation Oncology, Medical Center – University of Freiburg, Faculty of Medicine, University of Freiburg, Freiburg, GERMANY.*

Aim/Introduction: Lu-177-PSMA-617 is widely used in prostate cancer (PCa) therapy and has recently been approved by FDA and EMA. In this study we established a workflow for tumour absorbed dose (TAD) determination in cancer xenografts of nude mice using a gamma probe. ***Materials and Methods:*** 17 mice with implanted LNCaP xenograft tumours were treated with Lu-177-PSMA-617 (G1: n=8, 21.0 ± 7.0 MBq and G2: n=9, 44.7 ± 4.5 MBq). A gamma probe was used to measure tumour and body background (BG) counts per second (CPS), for two weeks p.i. A monoexponential fit was used to determine the BG corrected time-activity curves. Effective half-life ($T_{1/2,eff}$) was computed for each mouse. Tumour size was measured 3 times with a caliper (beginning, middle and end of experiment). For the tumour volume (TV) calculation, tumours were considered as ellipsoids. To determine the calibration factor (CF) for the gamma probe (kBq/CPS), tumours from 4 sacrificed mice were measured with the gamma probe and then in the gamma counter. The CF was derived from the average of all measurements. The tumour absorbed dose rate was tallied according to MIRD formalism using S values for spherical tumours, as an approximation of the ellipsoidal tumours. Correction for time dependent TV was done with absorbed fraction of the full Lu-177 beta-spectrum. TAD for each mouse was computed by integrating the dose rate curve until the end of experiment. Mann-Whitney U-test was used for the statistical analysis of the results at significance level of 5%. ***Results:*** Average TV 3 h p.i. and $T_{1/2,eff}$ were 0.12 ± 0.03 mL and 93.8 ± 13.5 h for G1 and 0.08 ± 0.03 mL and 86.7 ± 8.8 h for G2 respectively. The error of the dose rate curves fitting parameter (λ) was 7.8%. CF for the gamma probe was 0.6 kBq/CPS with 23% standard deviation. The average TAD during the experiments was for G1 0.12 ± 0.02 Gy/MBq and for G2 0.42 ± 0.18 Gy/MBq. Our study revealed a statistically significant difference for TV and TAD in the two groups, although for the $T_{1/2,eff}$ there is no significant difference. ***Conclusion:*** Simple gamma probe measurements can be reliable for TAD estimation in preclinical experiments with Lu-177-labelled ligands. Main error sources are the CF for the gamma probe and the caliper-based TV measurements. Overall accuracy of the method will be increased with ongoing optimization of gamma probe measurements and CF determination.

EP-0776

Evaluation of the quantitative accuracy using Monte Carlo simulations in 177Lu imaging

C. Kubota[1], *K. Ishikawa*[1], *Y. Yasumoto*[1], *T. Sakashita*[2], *H. Daisaki*[1];
[1]*Gunma Prefectural College of Health Sciences, Gunma, JAPAN,* [2]*National Institutes for Quantum Science and Technology, Gunma, JAPAN.*

Aim/Introduction: High quantitative accuracy in ^{177}Lu imaging is necessary for accurate dosimetry. Appropriate correction and quantification methods in ^{177}Lu imaging have not been established. The purpose of this study was to validate the accuracy of the ^{177}Lu imaging quantification process using Monte Carlo (MC) simulations. ***Materials and Methods:*** Noiseless pseudo-projection data were generated using the SIMIND and two types of digital phantoms (cylindrical and NEMA body phantom). Cylindrical phantoms were used to confirm the accuracy of scatter and attenuation corrections (AC) and to calculate the Bq calibration factor (BCF), while NEMA body phantoms were used to validate the accuracy of activity quantification. Imaging conditions of cylindrical phantom were as follows: 1) MEGP or ELEGP collimator, 2) 113 keV ± 10% or 208 keV ± 10% main window, 3) upper and lower sub-windows with 10 keV width, 4) scan durations with 5.0 min / 60 projections. Projection data were corrected for scattered radiation using TEW method after Butterworth filtering (0.22 cycles/cm) for projection data of sub-windows. Image reconstructions were performed by OSEM with Chang's AC after Butterworth filtering (0.50 cycle/cm). The μ value for Chang's AC was determined to be the value that minimizes the coefficient of variation of the profile curve between 0.10 and 0.20 cm^{-1}. BCFs were calculated using the cylindrical phantom. SPECT images of the NEMA body phantom simulating ^{177}Lu activity with Hot=1.85 and BG=0.20 MBq/mL were reconstructed using appropriate corrections (this simulates tumors in the liver imaged 6 hours after administration of 7.4 GBq of ^{177}Lu). VOIs were placed in the BG region and Hot sphere to measure the activity and evaluate the accuracy. ***Results:*** Uniform profile curves were obtained by 0.22 cycles/cm for Butterworth filtering of the sub-window and μ values of 0.16-0.17 cm^{-1} at 113 keV and 0.14 cm^{-1} at 208 keV for Chang's AC. The quantification accuracy of BG was within ±5%, and quantification was possible using appropriate imaging conditions and BCFs. The activity of Hot spheres was underestimated by -34 to -28% at 37 mm, -43 to -36% at 28 mm, -52 to -44% at 22 mm, -70 to -64% at 17 mm, -76 to -70% at 13 mm, and -81 to -79% at 10 mm. ***Conclusion:*** MC simulations are useful for validating appropriate imaging conditions and can estimate the accuracy of quantitative values. The agreement between phantom experiments and MC simulations using ^{177}Lu should be carefully verified in the future.

EP-53

e-Poster Area

D: Technical Studies -> D4 Dosimetry and Radiobiology -> D42 Clinical Dosimetry

EP-0777

IDAC-Dose 2.2. An internal dosimetry software for diagnostic nuclear medicine using the ICRP computational framework and calculation of the absorbed dose and effective dose to all 12 ICRP reference individuals

M. Andersson[1,2], *K. Eckerman*[3], *S. Mattsson*[2];
[1]*Department of Medical Radiation Sciences,Institute of Clinical Sciences, Sahlgrenska Cancer Center, Gothenburg, SWEDEN,* [2]*Medical Radiation Physics, Malmö, Malmö, SWEDEN,* [3]*Center for Radiation Protection Knowledge, Oak Ridge National Laboratory, Oak Ridge, TN, UNITED STATES OF AMERICA.*

Aim/Introduction: Estimations of the radiation-absorbed dose to organs and tissues for patients investigated with radiopharmaceuticals are derived via calculations based on models of the human body and the biokinetic behaviour of the radionuclide. The ICRP estimates of absorbed dose in organs and tissue and the effective dose to patients from various radiopharmaceuticals were in ICRP Publ.128 derived using the computer program Internal Dose Assessed by Computer (IDAC)1.0. To improve the accuracy of the calculations, ICRP has adopted a new computational framework using more realistic voxel phantoms to incorporate in Monte Carlo simulating the energy transport and absorption of photons,electrons and alphas. Together with the new computational framework, ICRP has also updated the effective dose methodology. Therefore, has the internal dosimetry computer program, IDAC-Dose, now been substantially upgraded (IDAC-Dose2.2) and incorporates now absorbed dose and effective dose calculations for all the ICRP reference individuals (male and female of adults,15-yrs,10-yrs,5-yrs,1-yr and 100 days old). ***Materials and Methods:*** With IDAC-Dose2.2 it is possible to calculate the dose from 1252 different radionuclides. The software uses the latest biokinetic models and assumptions of the ICRP TG-36, and includes also the latest tissue weighting factors from ICRP Publ.103. The IDAC-Dose2.2 has 83 source regions where activity can be placed and calculates the mean absorbed dose to 43 different organs and tissues. It is also possible to interpolate the organ doses by weight and age interpolations between the ICRP adult and newborn reference phantoms. IDAC-Dose2.2 was applied on two frequently used radiopharmaceuticals: 2-[18F]FDG and ^{99m}Tc-pertechnetate. ***Results:*** The absorbed doses and effective dose of ^{99m}Tc-pertechnetate determined by IDAC-Dose2.2 were compared with the results of the dosimetry program DCAL,showing identical results. IDAC-Dose2.2 was used to calculate absorbed doses for 2-[^{18}F]FDG and ^{99m}Tc-pertechnetate. The effective dose per administered activity was estimated for the adult phantoms to be 0.016mSv/MBq for 2-[^{18}F]FDG and 0.014mSv/MBq for ^{99m}Tc-pertechnetate. ***Conclusion:*** IDAC-Dose2.2 is the main ICRP software for effective dose in diagnostic nuclear medicine. The results from other software, using the same primary data (e.g. ICRP SAF-values and decay data) may differ from the results of IDAC-Dose2.2 if the former do not follow the ICRP computational framework for the absorbed dose calculations. The IDAC-Dose2.2 software is a free software for research and available at www.idac-dose.org. The online version can be operated directly through a web browser and the standalone version is an executable file, which is downloaded and installed directly on the local computer.

EP-0778

IDAC-ALPHA: AN online ALPHA DOSIMETRY SOFTWARE FOR NORMAL ORGANS And TISSUES

M. Andersson[1,2], *S. Mattsson*[2];
[1]*Department of Medical Radiation Sciences, Institute of Clinical Sciences, Sahlgrenska Cancer Center, Göteborg, SWEDEN,* [2]*Medical Radiation Physics, Malmö, Malmö, SWEDEN.*

Aim/Introduction: Radiopharmaceuticals are used for the treatment of various cancers since the 1940s. In recent years, the benefit of alpha-emitting radionuclides has emerged as a favourable treatment option. However, most alpha-emitting radionuclides have long decay chains with long-lived daughter radionuclides. This leads to uncertainties in the dosimetry for both tumour tissue and healthy organs and tissues when established dosimetry models are used. Since it is not always possible to image or measure organ- and patient-specific activities of all daughter products to radionuclides used for alpha radiation therapy, one solution might be to also consider generic reference values for dosimetry to improve the accuracy of the dosimetry. ***Materials and Methods:*** IDAC-Alpha [1] has been updated with a new curve fitter, to more accurately predict uptake in organs and tissues and incorporate the biokinetic transfer of daughter elements with regard to the parent uptake. The software now includes ^{227}Th, ^{225}Ac, ^{224}Ra ^{223}Ra, ^{212}Bi, ^{213}Bi, ^{212}Pb and ^{149}Tb, and consider also the individual biokinetics of all daughter radionuclides The dosimetry software was applied to a dataset of patients treated with ^{223}Ra-dichloride [2]. In this dosimetry model, individual biokinetics for each daughter radionuclide was considered. The results were compared with those of a dosimetry model in which the daughter radonuclides are assumed to follow the biokinetics of the parent radionuclide. ***Results:*** Inclusion of element-specific transfer of daughter radonuclides in the biokinetic model for $^{223}RaCl_2$ results in a decrease in absorbed dose of 14% for bone surfaces and 18% for bone marrow, compared with assuming that all daughter radionuclides decay in the same position as the parent nuclide. The decrease is due to a lower activity uptake of the daughter radionuclides in bone compared to the parent nuclide radium. ***Conclusion:*** The software includes separate transfer of the various progenies. Inclusion of the biokinetics of the progeny elements allows better estimation of the absorbed dose and better prediction of radiotoxicity in normal tissue. The IDAC-Alpha software is a software for research and available at www.idac-dose.org. The online software can be operated directly through a web browser. ***References:*** 1)Andersson, M. et al, IDAC-Alpha: An alpha dosimetry software for normal organs and tissues, Radiat.Prot. Dosim.195(3-4), 2021. 2)Taprogge, J. et al. Compartmental model for 223Ra-dichloride in patients with metastatic bone disease from castration-resistant prostate cancer. Int.J.Radiat.Oncol.Biol. Phys.105(4),2019.

EP-0779

Dosimetric model for patients with renal failure undergoing dialysis during I-131 therapy for thyroid cancer

V. Nuttens, *O. De Winter;*
OLVZ, Aalst, BELGIUM.

Aim/Introduction: Adapted dosing for renally cleared medicine is commonly used for hemodialysis patients. This study aims to create an easy-to-use dosimetric model that can estimate the

to-be-administered activity to a patient for I-131 therapy who has almost to no renal clearance. ***Materials and Methods:*** Based on literature values [1] [2] renal clearance estimates were used to determine time activity curves. Dialysis in the simulation takes place 42h and 90h after administration of the I-131 capsule and gives rise to a stepwise decrease in activity on the dialysis moments. The time-integrated activity (TIA-ratio) is defined as $\tilde{A}_{dialysis}/\tilde{A}_{normal}$ and gives a measurement of the dose for the patient with dialysis compared to a patient with healthy kidneys [3] with recombinant human thyroid-stimulating hormone stimulation or thyroid hormone withdrawal. ***Results:*** A 50% reduction of administered activity corresponds to a TIA-ratio of 1.2 [1.124, 1.305]. 100% of the activity for normal patients results in a TIA-ratio of 2.4 [2.248, 2.611. Therefore, a 50% dose reduction is recommended for the chosen dialysis scheme. ***Conclusion:*** The dosimetric model can compare the radiation dose for a hemodialysis patient to a normal patient. Furthermore, it can be seen that careful consideration of the administered activity and dialysis scheme is needed when considering I-131 therapy for patients with almost to no renal clearance; the blood pool activity stays high for a longer time and can therefore result in a high dose to the bone marrow.Further work will include validation of the model with blood sample and whole body dose rate measurements. ***References:*** [1] Holst JP, Burman KD, Atkins F, Umans JG, Jonklaas J. Radioiodine therapy for thyroid cancer and hyperthyroidism in patients with end-stage renal disease on hemodialysis. Thyroid. 2005 Dec;15(12):1321-31. doi: 10.1089/thy.2005.15.1321. PMID: 16405403. [2] Vermandel M, Debruyne P, Beron A, Devos L, Talbot A, Legrand JF, Provôt F, Lion G. Management of Patients with Renal Failure Undergoing Dialysis During 131I Therapy for Thyroid Cancer. J Nucl Med. 2020 Aug;61(8):1161-1170. doi: 10.2967/jnumed.119.232017. Epub 2020 Jan 10. PMID: 31924716. [3] Remy H, Borget I, Leboulleux S, Guilabert N, Lavielle F, Garsi J, Bournaud C, Gupta S, Schlumberger M, Ricard M. 131I effective half-life and dosimetry in thyroid cancer patients. J Nucl Med. 2008 Sep;49(9):1445-50. doi: 10.2967/jnumed.108.052464. Epub 2008 Aug 14. PMID: 18703593.

EP-0780

Comparative analysis of positron-emitters for theranostic applications based on small bioconjugates

C. Morgat[1,2], *U. Köster*[3], *C. Champion*[4], *P. Zanotti-Fregonara*[5], *E. Hindié*[1,2,6];
[1]*Nuclear Medicine Department - University Hospital of Bordeaux, Bordeaux, FRANCE,* [2]*University of Bordeaux, UMR CNRS 5287, INCIA, Bordeaux, FRANCE,* [3]*Institut Laue Langevin, Grenoble, FRANCE,* [4]*University of Bordeaux, CNRS, CEA, CELIA, UMR 5107, Talance, FRANCE,* [5]*Molecular Imaging Branch, National Institute of Mental Health, Bethesda, MD, UNITED STATES OF AMERICA,* [6]*Institut Universitaire de France, Paris, FRANCE.*

Aim/Introduction: Targeted radionuclide therapy (TRT) with ^{177}Lu-labelled small conjugates is expanding rapidly. Appropriate patient selection conditions the success of TRT. Companion diagnostic conjugates are usually labelled with ^{68}Ga offering good imaging up to ≈2h post-injection with conventional Positron Emission Tomography (PET) scanners. However, the optimal tumor-to-background ratio is often reached later. This work examines some promising positron-emitting radiometals with half-lives between 3h to 24h and β^+ intensity ($I_{\beta+}$) ≥ 15%: ^{43}Sc, ^{44}Sc, ^{45}Ti, ^{55}Co, ^{61}Cu, ^{64}Cu, ^{66}Ga, ^{85m}Y, ^{86}Y, ^{90}Nb, ^{132}La, ^{150}Tb and ^{152}Tb. Also, ^{133}La (7.2% $I_{\beta+}$) has been added because it has been discussed recently, together with ^{132}La, as a possible diagnostic match for ^{225}Ac. Comparisons with ^{68}Ga were made. ***Materials and Methods:*** We compared total electron and photon doses per decay and per positron, possibly interfering prompt γ-ray emission, typical activities to be injected for imaging for same day or next day measurement, positron range, as well as available production routes ***Results:*** For each annihilation process useful for PET imaging, the total energy released (MeV) is: ^{45}Ti (1.5), ^{43}Sc (1.6), ^{61}Cu and ^{64}Cu (1.8), ^{68}Ga (1.9), ^{44}Sc and ^{133}La (2.9), ^{55}Co (3.2), ^{85m}Y (3.3), ^{132}La (4.8), ^{152}Tb (6.5), ^{150}Tb (7.1), ^{90}Nb (8.6) and ^{86}Y (13.6). Significant amounts (≥10%) of ≈0.5 MeV photons that may fall into the acceptance range of PET scanners are emitted by ^{55}Co, ^{66}Ga, ^{85m}Y, ^{86}Y, ^{132}La and ^{152}Tb. Compton background from more energetic photons is expected for ^{44}Sc, ^{55}Co, ^{66}Ga, ^{86}Y, ^{90}Nb, ^{132}La,^{150}Tb and ^{152}Tb. The mean positron range (mm) of ^{64}Cu (0.6), ^{85m}Y (1.0), ^{45}Ti (1.5), ^{133}La (1.6), ^{43}Sc and ^{61}Cu (1.7), ^{55}Co (2.1), ^{44}Sc and ^{86}Y (2.5) and ^{90}Nb (2.6) are lower than ^{68}Ga (3.6). DOTA chelation is applicable for most discussed radiometals, though not ideal for ^{61}Cu/^{64}Cu, while ^{45}Ti and ^{90}Nb require different complexing agents (e.g. DFO). Overall ^{43}Sc, ^{45}Ti and ^{61}Cu have excellent properties and can be economically produced by proton-induced reactions at medical cyclotrons. ***Conclusion:*** In particular ^{43}Sc, ^{45}Ti and ^{61}Cu have overall excellent β^+ decay-characteristics for theranostic applications complementing ^{177}Lu-labelled small conjugates and can be sustainably produced. ^{43}Sc and can be labelled with DOTA just as Lu, but ^{45}Ti requires different chelates and for ^{61}Cu this is preferable too.

EP-0781

Dosimetry and External Radiation Exposure in 177Lu-PSMA-617 Radioligand Therapy. The INT Pascale Experience

L. D'Ambrosio*, V. Pirozzi Palmese, C. Maisto, R. de Marino, M. Aurilio, A. Morisco, V. Porfidia, C. Traino, R. De Migno, M. Raddi, F. De Lauro, F. Di Gennaro, S. Lastoria;*
National Cancer Institute IRCCS Pascale, Naples, ITALY.

Aim/Introduction: ^{177}Lu-PSMA-617 radioligand therapy is a promising treatment for patients with metastatic castration resistant prostate cancer (mCRPC). A standard activity of 7.4 GBq at six weeks intervals for a total of four to six cycles is the standard regimen. We present our dosimetric protocol to measure organs at risk absorbed dose and relevant parameters to define radiation protection and safety necessities. In 23 patients dose evaluation of kidneys, parotid and submandibular glands was performed. ***Materials and Methods:*** The protocol includes the infusion of a 10% mannitol solution as protector agent and an external ice pack cooling strategy was used to reduce blood flow supply to salivary glands before therapy. SPECT-TC images were acquired at different times post injection (2.5 h, 20 h, > 90 h pi). The activity concentration in kidneys, parotid glands (PGs) and submandibular glands (SMs) was determined by a commercial software and the absorbed dose was obtained using residence time and personalized organ masses as input data for the OLINDA/EXM® software. Measurements with external probe at different time points (before any excretion, after first voiding bladder and at 1, 1.5, 4, 20, > 90 h pi) were performed to collect the radiation contribution of the entire body and to estimate the activity within the body of the patient. The retention of ^{177}Lu-PSMA was modelled on a bi-exponential decay process with As and Al the constants of the short and long components and λs and λl the effective decay constants. Dose rates at 1 m at discharge (20 h pi) were measured to determine appropriate radiation precautions to be followed in order to comply with national law. ***Results:*** The mean absorbed dose was 0,11-0,58 Gy/GBq (mean 0,31 Gy/GBq)

for kidneys, 0,16-1,8 Gy/GBq (mean 0,62 Gy/ GBq) for PGs and 0,09-2,2 Gy/GBq (mean 0,58 Gy/GBq) for SM. Our data showed that absorbed dose (Gy/GBq) in OARs appeared to decrease in the next cycles. The mean retention constants As and Al and mean effective half-lives of the short and long component were 0.46, 0.53 and 5.9 h, 74.9 h respectevely. Mean exposure rate at 1 m at discharge was 9.6 microSv/h (4.0-18.5 microSv/h). ***Conclusion:*** Our experience indicates that dosimetry can be easily realized in routine practice if the patients are compliances and the results are similar to previously published papers. We are evaluating absorbed dose to lesions in order to correlate it with the clinical response.

EP-0782

Partial volume correction on Lu-177 PSMA-617 parotid gland dosimetry

G. Mok[1], *Z. Lu*[1], *G. Chen*[1], *Y. Liu*[1], *A. Afshar-Oromieh*[2], *A. Rominger*[2], *K. Shi*[2];
[1]*University of Macau, Taipa, MACAO,* [2]*University of Bern, Bern, SWITZERLAND.*

Aim/Introduction: Parotid gland (PG) highly affects patient's life quality, and thus is a dose-limiting organ in ^{177}Lu-PSMA-617 therapy. Its activity quantification and subsequent dosimetry are subjected to large errors particularly due to partial volume effect (PVE), which manifests when the object size is about 2-3 times of the system resolution as in the case of ^{177}Lu-SPECT imaging (8-10 mm) of PG (mean 3.4 cm). This study aims to apply partial volume correction (PVC) on post-therapeutic sequential ^{177}Lu-PSMA images for personalized PG dosimetry. ***Materials and Methods:*** Sequential quantitative SPECT/CT images at 2, 20, 40 and 60 (n=5)/200 (n=5) h after 6.0-8.0 GBq ^{177}Lu-PSMA-617 injection with full corrections were analyzed retrospectively for 10 patients in 10 treatment cycles (first:forth:fifth cycle=8:1:1). CT images at latter time points were rigidly registered to those at the first time point [1] focusing on the head. PVC was performed on SPECT images using the reblurred van-cittert deconvolution method [2] based on the reported system resolution [3]. The resultant deformed vectors were then used to align the corresponding SPECT images. The voxel-S-value for soft tissues with density correction was applied on the registered SPECT images to generate dose rate maps. Segmentations of PG were based on the exact CT and expanded CT maps with 1 cm extra margin separately [4]. Median and D_{50} PG absorbed dose was obtained using bi-exponential voxel-based curving fitting and integration. ***Results:*** PG was clearly visualized and separated from the adjacent high uptake regions after PVC on SPECT images at all time points. The median PG absorbed dose was 0.34 and 0.22 Gy/GBq after and before PVC for the exact segmentation, and 1.05 and 0.89 Gy/GBq for the expanded segmentation respectively. The median D_{50} absorbed dose was 2.61 and 1.65 Gy after and before PVC for the exact segmentation, and 1.16 and 0.97 Gy for the expanded segmentation respectively. ***Conclusion:*** PG absorbed dose is generally underestimated by PVE in ^{177}Lu-PSMA-617 therapy, and can be effectively restored by PVC. Segmentation on the expanded map is suggested even PVC is applied to fully cover the PG activity. The median PG absorbed dose is increased by ~60% after PVC. PVC is important for PG dosimetry in ^{177}Lu-PSMA-617 therapy. ***References:*** [1] Klein et al., IEEE TMI 29.1 (2009): 196-205.[2] Thomas et al., PMB 61.22 (2016): 7975.[3] Huizing et al., J. Appl. Clin. Med. Phys. 21.9 (2020): 272-277.[4] Violet et al., JNM 60.4 (2019): 517-523. Research support: FDCT 0099/2021/A

EP-0783

A new approach for individual dose monitoring in Molecular Radionuclide Therapy

R. Mirabelli[1], *L. Campana*[1], *B. Cassano*[2], *F. Collamati*[3], *R. Faccini*[1], *G. Iaccarino*[2], *C. Mancini Terracciano*[1], *S. Morganti*[3], *F. Nicolanti*[1], *M. Pacilio*[4], *A. Soriani*[2], *E. Solfaroli-Camillocci*[5];
[1]*"Sapienza" - Università di Roma, Rome, ITALY,* [2]*IRCCS Regina Elena National Cancer Institute, Rome, ITALY,* [3]*National Institute of Nuclear Physics, Rome, ITALY,* [4]*Azienda Ospedaliera-Universitaria Policlinico Umberto I, Rome, ITALY,* [5]*Bambino Gesu` Children's Hospital, Rome, ITALY.*

Aim/Introduction: A systematic measurement of the activity distribution in the body for patients undergoing Molecular Radionuclide Therapy (MRT) would enable treatment improvements and individualization of the activity to be administered. A treatment personalization could increase the local control, while sparing healthy tissues and lowering toxicity. Furthermore, current European regulation (EU Directive 59/2013) considers mandatory the treatment planning and verification in all patients undergoing radiotherapy procedures, including MRT. However, it is not an easy task, since the dose absorbed to tissues depends on several interconnected key factors and the uptake and excretion largely fluctuate from patient to patient. ***Materials and Methods:*** A new approach for individual radioagent biokinetics determination is proposed with the Wearable Individual Dose Monitoring Apparatus (WIDMApp). The WIDMApp system is conceived as a wearable multi-channel detector system for in-vivo radiation detection, a MC simulation for particle interaction and a data analysis tool to deconvolve the activity distribution and its evolution over time in different organs (i.e., time- activity data) [1]. This system could provide an effective tool to characterize more accurately the radiopharmaceutical biokinetics in MRT patients, reducing the need of resources of nuclear medicine departments, such as technologist and scanner time, to perform individualized biokinetics studies. Different studies have been carried out as proof-of-principles of the system. In the first Monte Carlo feasibility studies simulating a MIRD anthropomorphic phantom and in the first experimental feasibility study with an anthropomorphic phantom, combining the simulated results with the data acquired, the unfolding algorithm deconvolved the detected signals and it has been able to assess the decay half-lives that best reproduce the observed exponential decays. ***Results:*** The WIDMApp system has been resulted effective in deconvolving the cumulative detected signal into contributions from different emitting volumes. The results obtained from the first phantom feasibility study and from a Monte Carlo simulation of the system justify the development of an actual prototype to characterize this technique under realistic clinical conditions. ***Conclusion:*** The proof-of-principle of WIDMApp showed that reconstruction of the individual biokinetics using small portable detectors is in principle possible. The relatively simple hardware for the approach proposed would allow its application to large numbers of patients. Taking advantage of the data sampling more frequent than conventional biokinetics studies, the WIDMApp system can be an effective tool for the time-activity trend determination in lesion and organs at risk of toxicity, fully characterizing the accumulation, the uptake and the retention. ***References:*** [1] 10.1002/mp.15311

EP-0784

131I and 177Lu Voxel Dosimetry: characterization, verification and preliminary patient results

E. Richetta, *C. Valero, B. Elia, V. Pirro, M. Manfredi, R. Pellerito, M. Stasi;*
Ordine Mauriziano Hospital, Turin, ITALY.

Aim/Introduction: Voxel dosimetry software are effective tools for exposure verification after radionuclide therapies, as required by radiation protection regulations, still rarely used in the clinical practice. Aim of this work is to investigate calibration methods, in order to define the best dosimetric protocol. ***Materials and Methods:*** A commercial voxel dosimetry software (^{131}I and ^{177}Lu) was installed for SPECT-CT imaging calculations (3 time-points, 10IT-8SUB, attenuation and scatter corrected) performed with two equipment (NaI detector I:3/8', B:5/8'). The quantitative calibration was performed with a homogeneous phantom (9355 ml) filled with high activity ^{131}I (2940 MBq - ^{177}Lu 3681 MBq). Calibration factors (cps/MBq) were obtained and dead time effects investigated. Doses were calculated with different voxel kernels (^{177}LuLanconelli 3mm7x7x7, ^{177}LuGraves 2.3mm353x353x353, ^{177}LuMCNP 3mm7x7x7 and ^{131}ILanconelli 3mm11x11x11, ^{131}IGraves 3mm279x279x279) for different voxel size (2.4mm, 4.8mm) and number of views (128, 64) and compared to MIRD sphere model. Verification and partial volumes curves were performed on NEMA phantom (cylinder 130 ml, 6 spheres) filled with activity (^{131}I 7.1 MBq/ml, ^{177}Lu 15.4 MBq/ml). The dosimetric protocols waere applied (2 SPECT-CT 24h, > 96 h) on patients (^{131}I 9 thyroid metastases and ^{177}Lu Dotatate NET 13 organ at risk or metastases). ***Results:*** ^{177}Lu absolute calibration factors (I 19.7 cps/MBq, B 35.7 cps/MBq) showed small variations for acquisitions, matrix size, numbers of views (< 5 %) and phantoms (< 1.5%) while for ^{131}I (I 54.6 cps/MBq, B 98.9 cps/MBq) variations (~15 %) between homogeneous phantom and cylinder insert were found as well dead time effects (up to 30 % from the first to the last acquisitions) requiring corrections. Recovery coefficient curves were applied for small volumes (< 30-50 ml) (130ml 0.95, 11.7ml 0.69, 5.8ml 0.58, 2.7ml 0.41, 1.2ml 0.2, 0.7ml 0.1) up to a 3 ml volume limit for accurate dosimetry. High voxel kernels dose variations were found (^{177}LuLanconelli/^{177}LuGraves -18.5%, ^{177}LuLanconelli/^{177}LuMCNP -11%, ^{177}LuMCNP/^{177}LuGraves -6.6%, ^{177}LuGraves/^{177}LuMIRD +1.7% and ^{131}ILanconelli/^{131}IGraves -49%, ^{131}IGraves/^{131}IMIRD +28%). For the clinical protocol Graves voxel kernel was chosen. ^{177}Lu patient doses showed a good agreement (< 5%) for larger volumes compared to MIRD mean doses, while for small targets variations up to 40 %. Higher discrepancies (up to 55%) were found for ^{131}I. ***Conclusion:*** Voxel dosimetry for radionuclide treatments in an effective tool for ^{131}I and ^{177}Lu post for accurate and standardized dose calculations. Many aspects pointed out in this work (voxel kernels, corrections factors) need further investigations.

EP-0785

True Single Time Point Dosimetry for [177Lu]Lu-PSMA targeted therapy - Is Haenscheid's method applicable?

J. Kurth, *M. Heuschkel, B. Krause, S. M. Schwarzenböck;*
Rostock University Medical Center, Rostock, GERMANY.

Aim/Introduction: PSMA-targeted therapy has become an essential pillar of therapy for mCRPC. Studies are underway to apply PSMA therapy also in earlier stages of the disease and in this context, individualized dosimetry of organs at risk and tumors will be an important tool for optimization [1]. However, the resources of the departments and the clinical condition of the patient often do not allow for elaborate imaging. Therefore, single-time-point protocols have been in focus for some time [3]. Hänscheid et al. have elegantly shown for other nuclear medicine therapies [4, 5] that a reliable organ and tumor dosimetry is possible by using single imaging. Our study aimed to investigate whether this relatively simple approach is also applicable to [^{177}Lu]Lu-PSMA therapies. ***Materials and Methods:*** Retrospectively, data from 58 consecutive treatment cycles of [^{177}Lu]Lu-PSMA-617 therapy have been evaluated (28 patients, mean age 73y, mean activity 6.2 GBq) were included. Imaging was performed by quant. SPECT/CT of the abdomen (2h, 24h, 48, 72h p.i.). The dosimetric calculations for kidneys and tumors followed the MIRD scheme on the one hand and the method of Haenscheid on the other hand [5], whereby 24h, 48h, and 72h, respectively, were assumed as the time of measurement. The calculated absorbed doses were compared using the Bland-Altman method and statistically evaluated. ***Results:*** The absorbed dose for the kidneys and the tumors according to the MIRD scheme averaged 2.34Gy and 15.63Gy, respectively. When using the Haenscheid-method, the doses were underestimated. For the kidneys, the mean error was -20.5%, -7.6%, and -16.2% for 24h, 48h, and 72h, respectively, with significant differences only for the 24-hour measurement. For the tumors, the mean error was -51.8%, -26.6%, and -14.4%, respectively, again with significant differences only for 24-hour imaging. ***Conclusion:*** In principle, Haenscheid's method also seems suitable for estimating organ and tumor doses in PSMA therapy. However, the imaging times must be adjusted depending on the organ/tissue under consideration. Variations in the time of measurement in each cycle to assess the absorbed doses of different organs and tumor lesions with extrapolation of the accumulated doses would be an alternative. ***References:*** [1] Violet J et al. J Nucl Med. 2019. 60(4):517-523.[2] Jackson PA et al. J Nucl Med. 2020. 61(7):1030-1036 [3] Brosch-Lenz J Nucl Med. 2023 Jan 19;jnumed.122.264594. [4] Hanscheid H et al. Z Med Phys 2011, 21(4):250-257. [5] Hanscheid H et al. J Nucl Med 2018, 59(1):75-81.

EP-0786

Accuracy of Few-Time-Point Dosimetry Using Non-Linear Mixed-Effects Modelling in Peptide-Receptor Radionuclide Therapy

R. Subangun[1], *D. Hardiansyah*[1], *R. Ibrahim*[1], *B. Patrianesha*[1], *A. Beer*[2], *G. Glatting*[2];
[1]*Universitas Indonesia, Depok, INDONESIA,*
[2]*Ulm University, Ulm, GERMANY.*

Aim/Introduction: Personalized dosimetry is recommended in radionuclide therapy [1]. However, dosimetry with a high number of biokinetic data, e.g. five data, is time-consuming, corresponds to an increased workload for the patient and the staff, and is expensive for the healthcare system. Therefore, a few-time-point (FTP) dosimetry approach, which uses fewer biokinetic data for dosimetry, is highly desirable. The aim of this study was to investigate the accuracy of FTP dosimetry using non-linear mixed-effects (NLME) modelling in peptide-receptor radionuclide therapy (PRRT). ***Materials and Methods:*** Biokinetic data of [^{111}In]In-DOTATATE in kidneys at T1= (2.9±0.6) h, T2= (4.6±0.4) h, T3= (22.8±1.6) h, T4= (46.7±1.7) h, and T5= (70.9±1.0) h post injection were obtained from eight patients using planar imaging. The Sum-of-exponential (SOE) function $A_1/\{((1-\alpha)/(\lambda1+\lambda phys))-(\alpha/(\lambda2+\lambda phys))-((1-2\alpha)/(\lambda bc+\lambda phys))\}\ e^{-\lambda phys(t)}\ \{(1-\alpha)\ e^{-\lambda1(t)}-\alpha e^{-\lambda2(t)}-(1-2\alpha)e^{-\lambda bc(t)}\}$ which was selected as the best model for the kidney's biokinetics data of [^{111}In]In-DOTATATE in the literature [2] was used in this study. The parameters of the SOE functions were fitted to the all-time-point data in the NLME framework to

derive reference time-integrated activity (rTIAs). The fittings were repeated with FTP data which contain different combinations of single-, two-, three-, four-time point data to derive the predicted time-integrated activity (pTIAs). The accuracy of the different FTP schedules was assessed by calculation the relative deviations (RDs) and root-mean-square errors (RMSE) between the pTIAs and rTIAs. ***Results:*** The lowest RDs and RMSEs were found for those FTDs, which included the T3 measurement. The lowest (mean±SD) of RDs for the single-, two-, three-, four-time point FTDs were (0±8) % (T3), (1±6) % (T3 & T4), (3±5) % (T2, T3 and T4), and (0±2) % (T2, T3, T4, and T5), respectively. The lowest RMSE for the single-, two-, three-, four-time point FTD were 8% (T3), 6% (T3 & T4), 5% (T2, T3 and T4), and 2% (T2, T3, T4, and T5), respectively. ***Conclusion:*** In this study, we showed the accuracy of FTP dosimetry in PRRT. The knowledge of the accuracy of all FTP dosimetry schedules could provide valuable information for physicians to optimise patient care while reducing costs and improving the overall efficiency of the treatment. ***References:*** [1]. Glatting, G., M. Bardiès, and M. Lassmann. Z Med Phys, 2013. 23(4): p. 262-9.[2]. Hardiansyah, D., et al.,. EJNMMI Phys, 2023. 10(1) : p.12.

EP-0787

Validation of Pretherapeutic Dosimetry in Metastatic Thyroid Cancer Patient with Chronic Kidney Disease for I-131 Treatment

A. Al Jabri[1,2], *J. Cooke*[3], *S. Cournane*[4], *S. Ludgate*[5], *M. Healy*[5];
[1]*Sultan Qaboos University, Muscat, OMAN,* [2]*Trinity College Dublin, Dublin, IRELAND,* [3]*Children's Health Ireland at Crumlin, Dublin, IRELAND,* [4]*St Vincent's University Hospital, Dublin, IRELAND,* [5]*St James's Hospital, Dublin, IRELAND.*

Aim/Introduction: Radioactive iodine (I-131) therapy for remnant ablation post thyroidectomy is standard practice for thyroid cancer treatment. Personalised I-131 has become a legal requirement under Euratom 2013/59. To avoid changing tumour biokinetics leading to cancer cells becoming radioresistant, maximising the administered activity of the first therapeutic attempt is advantageous. There is limited literature investigating the predictability of pretherapeutic (PT) dosimetric assessment in patients with chronic kidney disease (CKD). This case study implemented an adaptation of the European Association of Nuclear Medicine (EANM) blood and bone dosimetry protocol in a patient with papillary thyroid cancer (PTC) with distal metastasis and CKD, to compare I-131 biokinetics before and during treatment (DT). ***Materials and Methods:*** A 67 year old male with history of advanced CKD was diagnosed with metastatic PTC in May 2020 at St James's Hospital, Ireland. He also had secondary Anti-Neutrophilic Cytoplasmic Autoantibody (ANCA) associated vasculitis and pre-existing Glomerulonephritis. He underwent total thyroidectomy and manubriumectomy, then referred for I-131 ablative therapy in November 2020. A dosimetric evaluation was requested to assess the safe administration of a fixed activity of 3.7 GBq. A two-week EANM dosimetry protocol was conducted PT and a similar dosimetric protocol was conducted DT, with the results between PT and DT compared. ***Results:*** The patients data varied between the PT and DT dosimetry assessment in the range: eGFR=22-26 ml/min/1.73m^2, Creatinine=210-257 umol/L and Urea=12.8-15.1 mmol/L. Kidney function changed due to compliance with a special renal diet after the PT assessment, as advised by the renal medicine consultant. This led to a large difference in calculated maximum tolerable activities, where the PT dosimetry underestimated the DT dosimetry by 36% difference in the EANM model. He had slower clearance in the PT assessment with a 22% and 41% difference between blood and whole-body residence times, respectively. The estimated absorbed dose per administered activity was 0.30 Gy/GBq in the PT dosimetry, which would have resulted in a 1.1 Gy absorbed dose to the bone-marrow if a 3.7 GBq therapeutic capsule was administered. However, the patient administered activity was 2.64 GBq, which resulted in a bone marrow absorbed dose of 0.51 Gy. ***Conclusion:*** Fluctuation in kidney function resulted in a significant difference in I-131 retention. Implementing dosimetry in patients with CKD requires continuous monitoring of eGFR and creatinine level, as changes in kidney function will alter the accuracy of the estimated results.

EP-0788

A phantom study on I-124 digital PET/CT quantification performance for lesion dosimetry in (re)differentiated thyroid cancer

M. Dotinga[1,2], *D. Vriens*[1], *L. F. de Geus-Oei*[1,3,4], *P. Dibbets-Schneider*[1], *M. K. Stam*[1], *M. Pool*[1], *F. Smit*[1,5], *E. Kapiteijn*[1], *F. H. P. van Velden*[1];
[1]*Leiden University Medical Center, Leiden, NETHERLANDS,* [2]*NETHERLANDS Cancer Institute, Amsterdam, NETHERLANDS,* [3]*University of Twente, Enschede, NETHERLANDS,* [4]*Technical University of Delft, Delft, NETHERLANDS,* [5]*Alrijne Hospital, Leiderdorp, NETHERLANDS.*

Aim/Introduction: Accurate I-124 PET/CT quantification is needed for lesion dosimetry in studies investigating renewed radioiodine uptake after tyrosine kinase treatment to warrant subsequent I-131 therapy in patients with radioiodine-refractory thyroid cancer. In this phantom study, we compare the quantification performance of I-124 and F-18 FDG and determine the I-124 quantification performance for different background-to-lesion ratios and acquisition times for protocol optimization and recovery correction on a digital PET/CT system (Vereos, Philips). ***Materials and Methods:*** A phantom study was performed using a cylindrical phantom and the NEMA image quality phantom with six fillable spheres. Phantom acquisitions were performed according to EARL protocol. For I-124, acquisition duration was varied (1, 2, 4 and 20 min. per bed position). F-18 FDG and I-124 calibration accuracy, coefficient of variation (CoV) and recovery coefficients (RCs) for background-to-lesion ratio 1:10 were assessed and compared to F-18 FDG EARL specifications. For I-124, clinically relevant background-to-lesion ratios were simulated including 1:infinity, 1:500, 1:250 and 1:125. For each ratio, scans were repeated four times and acquisition time duration was adjusted accordingly to obtain similar count statistics and. Sphere RCs obtained within background-adaptive 50% isocontours (A50) were compared between ratios and fitted to obtain a recovery correction curve. ***Results:*** Calibration accuracy and CoV were comparable between phantoms for both F-18 FDG (mean 0.95 and 4.9%, respectively) and I-124 (0.94 and 8.0%). All values were within F-18 FDG EARL specifications. F-18 FDG RCs complied with EARL in contrast to I-124, reaching a RC_{A50} of 0.79 and 0.69 for the biggest sphere, respectively. Increasing acquisition duration did not improve I-124 RCs for all sphere sizes, while CoV was decreased from 17% to 4.4% for 1 to 20 minutes per bed position. An acquisition time duration of 4 minutes per bed position was selected to keep the CoV <10% and total scan time clinically feasible. In the varying background-to-lesion ratios, fit parameters were comparable for RC_{A50} ($p>0.3$) suggesting a single fit can be used in clinical practice for recovery correction. For all sphere sizes, the final fit deviated 0.9±2.9% (range: -6.1-8.1%) from mean measured RC_{A50}.

Deviations were <5% for all sphere sizes except 13 and 17 mm. ***Conclusion:*** In contrast to F-18 FDG measurements, I-124 RCs did not comply with F-18 FDG EARL specifications. A single fit can be obtained for I-124 RC_{A50} with background-to-lesion ratios ranging from 1:125 to 1:infinity for recovery correction in pre-therapeutic I-124 lesion dosimetry.

EP-0789

Comparison of bone marrow absorbed dose estimated using blood sampling and gamma camera methods for 177Lu labelled radiopharmaceuticals

G. Katre[1,2], *T. Srichandan*[1,2], *A. Konuparamban*[1], *S. Ghag*[1], *A. Puranik*[1], *A. Agarwal*[1], *S. Mithun*[1,2,3], *A. Jha*[1,2], *V. Rangarajan*[1,2];
[1]Department of Nuclear Medicine and Molecular Imaging, Tata Memorial Hospital, Mumbai, INDIA, [2]Homi Bhabha National Institute (HBNI), Deemed University, Mumbai, INDIA, [3]Department of Radiation Oncology (Maastro), GROW School for Oncology and Reproduction, Maastricht University Medical Centre+, Maastricht, NETHERLANDS.

Aim/Introduction: Internal Dosimetry is a process to estimate the absorbed dose to the organ and tumor, helping in patient selection and treatment planning for radionuclide therapy.^{177}Lu-Trastuzumab, ^{177}Lu-DOTATATE and ^{177}Lu-PSMA are the choices of radiopharmaceuticals for treatment of HER2 positive (HER2+) metastatic breast cancer, Neuroendocrine Tumours and Prostate cancer respectively. Being one of the dose limiting organ, estimation of absorbed dose to bone marrow is necessary. Therefore, our study aims to calculate and compare absorbed dose to the bone marrow by blood sampling and imaging method. ***Materials and Methods:*** A total of 13 patients (Age 61 ± 11 years) among which 4 patients with histologically proven HER2+ metastatic breast cancer,2 patients with metastatic prostate cancer,7 patients with NETs were included in this study. The sequential whole-body planar acquisition was performed at 4h,24h,72h/96h ,160h post administration for ^{177}Lu-Trastuzumab and 4h,24h,72h for ^{177}Lu-PSMA &^{177}Lu-DOTATATE along with one SPECT/CT at 72/96 hrs and at 24 hrs for ^{177}Lu-Trastuzumab and ^{177}Lu-PSMA &^{177}Lu-DOTATATE respectively. The normalized cumulated activity (NCA) for imaging method was obtained by mono-exponential curve fitting in dosimetry toolkit software, Xeleris workstation,GE Healthcare and mean absorbed dose per unit activity (DpA) was estimated using OLINDA/EXM 2.0 software. For blood sampling method the blood samples were collected at 1h ,4h,,8h, 24h &72h post administration for ^{177}Lu-PSMA &^{177}Lu-DOTATATE and at 4h ,24h,72h/96h,160h for ^{177}Lu-Trastuzumab.Blood cumulated activity concentration were determined by counting blood samples of different time points in calibrated gamma well counter and $T_{eff1/2}$ of radiopharmaceutical was obtained from time activity curve. NCA is calculated using bone marrow mass, blood mass,$T_{eff1/2}$ of RP in blood. DpA values for bone marrow were estimated by using OLINDA/EXM 2.0 Software. ***Results:*** The administered dosage for ^{177}Lu-Trastuzumab pretherapy, ^{177}Lu-Trastuzumab therapy, ^{177}Lu-DOTATATE and ^{177}Lu-PSMA therapy were 407±44 MBq, 3885±37MBq and 6839±399MBq 7400±209MBq respectively. The DpA for bone marrow calculated by blood sampling method for Lu177-Trastuzumab, Lu177-DOTATATE, Lu177-PSMA were 0.274±0.05mGy/MBq,0.121±0.12mGy/MBq,0.11±0.03mGy/MBq respectively. The DpA for bone marrow calculated by imaging method for ^{177}Lu-Trastuzumab, ^{177}Lu -DOTATATE, Lu177-PSMA were 0.273±0.19mGy/MBq, 0.115±0.074mGy/MBq,0.15±0.06mGy/MBq respectively. Paired t test (two-tailed) was applied on the above data and p value of 0.42 was obtained. ***Conclusion:*** Our study shows no significant difference between the two methods used for estimation of bone marrow absorbed dose for 177Lu based radiopharmaceuticals.

EP-0790

Lu-177-PSMA Infusion vs Injection: No Difference in Dose Rates of Patients at the Time of Outpatient Discharge

V. Reijonen[1], *K. Kiviluoto*[2,1], *V. Ahtiainen*[1];
[1]Comprehensive Cancer Center, Helsinki University Hospital, Helsinki, FINLAND, [2]HUS Pharmacy, Helsinki University Hospital, Helsinki, FINLAND.

Aim/Introduction: We aimed to study whether there is a pharmacokinetic difference between intravenous (IV) infusion vs injection administration of Lu-177-PSMA (lutetium-177 labelled prostate-specific membrane antigen) that reflects to the dose rates measured from patients treated for metastatic castration-resistant prostate cancer (mCRPC). Patients received small molecule PSMA-targeted radioligand that has well-known pharmacokinetic, safety and efficacy profiles; however, the treatment could be further optimised (1). ***Materials and Methods:*** We analysed 20 patients who received their first cycle of peptide Lu-177-PSMA therapy for mCRPC: ten patients as a 30 min IV infusion (mean activity 7.1±0.3 GBq diluted in extra 100 ml isotonic saline) and ten patients as a 1-5 min manual IV injection (activity 7.3±0.2 GBq). The patients were treated on an outpatient basis and were measured with a dose rate meter at a one meter (1 m) distance before their hospital discharge. The patients received IV isotonic saline solution initiated approximately 30 min before administering Lu-177-PSMA at a continuous rate between 250-300 ml/h. The patients were encouraged to drink fluids regularly and empty their bladder just before measuring the dose rate for discharge. ***Results:*** Dose rates at 1 m distance from patients with infusion administration (21.6 ± 5.3 µSv/h, range 15.1-29.9 µSv/h) were not significantly different from dose rates of patients with injection administration (20.5 ± 4.6 µSv/h, range 15.0-28.5 µSv/h), t(18)=0.491, p=0.630. Reasons such as IV fluid administration and cooling of the salivary glands affected the time of the dose rate measurement, and when measured from the end of Lu-177-PSMA administration, there was no difference between the groups: 2.8 ± 0.6 h (1.7-3.8 h) after the end of infusion, and 2.8 ± 0.5 h (2.1-3.5 h) after the end of injection, t(18)=0.183, p=0.857. ***Conclusion:*** We did not observe a statistically significant difference between the dose rates measured from patients treated with Lu-177-PSMA infusion vs injection. After less than four hours from the end of Lu-177-PSMA administration, the dose rate at 1 m was below 30 µSv/h for all the patients. ***References:*** 1. van der Gaag S, Bartelink IH, Vis AN, Burchell GL, Oprea-Lager DE, Hendrikse H. Pharmacological Optimization of PSMA-Based Radioligand Therapy. Biomedicines. 2022 Nov 23;10(12):3020.

EP-0791

Simplified Organ and Tumor Dosimetry for Lu-177-PSMA-I&T Radionuclide Therapy

W. Lehnert, *L. Schatz, A. Karimzadeh, I. Apostolova, R. Buchert, S. Klutmann;*
University Medical Center Hamburg-Eppendorf, Hamburg, GERMANY.

Aim/Introduction: Multiple time point imaging for accurate internal dosimetry is time consuming and hence can be demanding for nuclear medicine departments as well as patients. The aim of this study was to investigate a possible simplified dosimetry protocol to reduce this burden. ***Materials and Methods:*** This study included 16 patients each treated with 4 cycles of [^{177}Lu]Lu-PSMA-I&T. They underwent whole body SPECT/CT imaging (3 bed positions) at four time points at 2h, 24h, 48h and 72h or 120h post-injection (p.i.). Full 3D dosimetry

(reference method) was performed for all patients and dose cycles for organs at risk (kidneys, parotid and submaxillary glands) and up to ten tumor lesions per patient (resulting in 91 lesions overall). For dosimetry calculation time integrated activities were estimated using analytical integration based on a mono- or biexponential curve fit applied to the time activity curves. Trapezoidal integration was used where a fit to all data points was not possible due to long uptake phases with an extrapolation to infinity using a monoexponential function fitted to the last 2 or 3 time points. The simplified dosimetry method generated time activity curves for cycles 2 to 4 using a single time point of imaging assuming the same kinetics as in dose cycle 1. ***Results:*** Compared to the full dosimetry approach the simplified method using the third imaging time point at 48h p.i. resulted in the lowest mean differences and standard deviations for all organs at risk with mean percent deviations of 2.10% ± 16.25% for the kidneys, -2.54% ± 20.11% for the parotid glands and -2.43 % ± 17.35% for the submaxillary glands, respectively, averaged over all dose cycles. For lesions better results were achieved using the fourth time point at 72h or 120h with a mean difference and standard deviation of -3.46% ± 14.14% compared to the reference method. ***Conclusion:*** Simplification of dosimetry protocols is possible for [^{177}Lu]Lu-PSMA-I&T therapy. If tumor dosimetry is of interest in addition to safety dosimetry a later (≥ 72h) or second imaging time point should be used to account for the slower kinetics of tumors compared to organs at risk.

EP-0792

Single time point tumour dosimetry after 177Lu-DOTATATE therapy

S. Ballout;
Cambridge University Hospital NHSFT, Cambridge, UNITED KINGDOM.

Aim/Introduction: A fixed administered activity of 7.4 GBq for 4 cycles remains the standard dosing regimen for ^{177}Lu-DOTATATE therapy of neuroendocrine tumours. Simplified methods to determine tumour absorbed dose may allow us to implement patient specific dosing regimens which may result in improved efficacy of treatment. Single time point (STP) dosimetry methods using the Hänscheid approximation, Madsen approximation and a cycle 1 effective half-life were evaluated in comparison to multiple time point (MTP) dosimetry using SPECT and SPECT/CT acquisitions on days 0, 4 and 7 after therapy. ***Materials and Methods:*** 17 patients having 62 cycles of therapy at our centre were included in the study. The largest lesion for each patient was analysed across all cycles of treatment. Lesion segmentation was performed via thresholding using 3D Slicer. Recovery coefficients based on phantom work using a NEMA IEC body phantom were used to recover the true activity concentration. S-values based on tumour mass were used to estimate the dose to a lesion, assuming the composition of a tumour was 100% soft tissue. ***Results:*** The mean tumour dose across all therapy cycles using MTP dosimetry was 36 Gy, with doses ranging from 6-75 Gy. The mean dose decreased over four cycles from 44 Gy (n=16) in cycle 1 to 26 Gy (n=15) in cycle 4. Using a cycle 1 effective half-life and a single SPECT/CT on day 4 and day 7 of subsequent cycles, 63% and 93% of results respectively were within + 10% of MTP dosimetry. Using the Hänscheid approximation with a day 4 and day 7 SPECT/CT resulted in 57% and 95% of lesion doses within + 10% of MTP dosimetry. Using the Madsen approximation with a population effective half-life of 130 hours and a single SPECT/CT on day 4 and day 7 after therapy resulted in 34% and 85% of lesion doses within + 10% of the MTP method respectively. ***Conclusion:*** STP dosimetry for tumour lesions is more accurate when using a day 7 SPECT/CT in comparison to a day 4 SPECT/CT. The use of a cycle 1 effective half-life scaled with a day 7 SPECT/CT is most accurate, however the Hänscheid approximation using only a day 7 SPECT/CT was also suitable. Previous research showed that a day 4 SPECT/CT was most suitable for STP kidney dosimetry, so a compromise is needed if both kidney and tumour dosimetry are required.

EP-0793

Role of lung density in voxel-based dosimetry of90Y-TARE evaluated with Voxel S-Value (VSV) method and fast Monte Carlo simulation

R. Moretti[1], *A. Capotosti*[1], *M. Vaccaro*[2], *C. d. Ribeiro*[2], *M. Nardini*[1], *G. Meffe*[1], *L. Placidi*[1], *L. Zagaria*[1], *M. De Risi*[1], *G. Perotti*[1], *L. Leccisotti*[1], *R. Iezzi*[1], *L. Indovina*[1];
[1]*Fondazione Policlinico Universitario Agostino Gemelli, Rome, ITALY,* [2]*Università Cattolica del Sacro Cuore, Rome, ITALY.*

Aim/Introduction: In ^{90}Y-TARE treatments, lung-absorbed dose should be calculated according to the manufacturer's instructions, using the MIRD-scheme.This scheme is derived from the assumption that ^{90}Y-microspheres deliver the dose in a water-equivalent medium. Since the density of the lung is quite different from that of the liver, the absorbed dose to the lung could vary considerably, especially at the liver/lung interface. The aim of this work is to compare the dosimetric results obtained by two dedicated software packages, implementing a water-equivalent dose calculation and a Monte Carlo (MC) simulation, respectively. ***Materials and Methods:*** An anthropomorphic IEC phantom and a retrospective selection of 24 patients with a diagnosis of hepatocellular carcinoma were taken into account. In the phantom study, the liver cavity was manually fixed at 1.3 MBq/mL on PET series using a dedicated software, while the lung compartment was manually expanded to simulate a realistic situation in which liver and lung are adjacent on CT series. A first simulation was performed with only the liver compartment manually filled with the aforementioned concentration; a second simulation was performed with the lung compartment also manually filled, simulating a 10% lung shunt fraction. Dose values derived by Voxel S-Value (VSV) and MC approach, for both phantoms and patients, were calculated with two different softwares. ***Results:*** In the phantom simulations, the percentage mean dose differences (ΔD%) between VSV and MC in the first and second simulations were found to be respectively: 1.2 and 0.5% (absolute dose variation, ΔD, of 0.7 and 0.3 Gy) for the liver, -56 and 70% (ΔD of -0.3 and -16. 2 Gy) for the lung, -48 and -60% (ΔD of -4.3 and -16.5 Gy) for the liver/lung interface region. The patient study reported similar results with ΔD% between VSV and MC of 7.0%, 4.1% and 6.7% for the whole liver, healthy liver and tumor, respectively, while -61.2% for the left lung and -61.1% for both right lung and lungs. ***Conclusion:*** Both VSV and MC allowed accurate radiation dose estimation with small differences (<7%) in regions of uniform water equivalent density (i.e. within the liver). Larger differences (>50%) were observed for air-equivalent regions in both the phantom simulation study and the patients.

EP-0794

A Dosimetric Comparison of Radioembolization and External Beam Radiation Treatment For Liver Cancer

K. Wysoczynski, *B. Mehadji, P. Park, S. Benedict, E. Roncali;*
University of California, Davis, Davis, CA, UNITED STATES OF AMERICA.

Aim/Introduction: Liver cancer is a high-impact area in clinical practice with rising mortality [1]. The most common treatment is resection, but the number of tumors, position, and complex

vasculature often prevent surgery. Stereotactic Body Radiation Therapy (SBRT) can provide a localized radiation dose with photons produced by a linear accelerator. Yttrium-90 (Y-90) radioembolization is delivered through microspheres injected into the hepatic artery. We are comparing the dose distribution and conformity of a treatment performed with Y-90 microspheres and a simulated plan for SBRT for a patient. ***Materials and Methods:*** In this study, one patient with hepatocellular carcinoma (single 155 cc lesion) was treated using Y-90 microspheres with an injected activity of 2.27 GBq. We performed radioembolization dosimetry based on a PET scan acquired 24h post-treatment to measure Y-90 activity, using multiple organ and tumor contours delineated on whole-body CT. We also simulated a treatment plan using an SBRT conventional linac with 5 mm leaf width. We compared dose distributions of the two modalities for several organs based on dose-volume histograms. ***Results:*** The microsphere treatment delivered a mean dose of 390 Gy to the gross tumor volume and an average of 47 Gy to the liver volume. The SBRT plan resulted in a mean tumor dose of 51 Gy and mean liver dose of 11 Gy. It is important to note that 2% of the tumor (D2) received at least 54 Gy in the plan, while Y-90 microspheres delivered 908 Gy at D2 of gross tumor volume. The patient received a 5 Gy lung dose with Y-90, but the SBRT plan predicted 0.36 Gy. This large dose with Y-90 is due to the lung shunt fraction of 14.6% for this patient. ***Conclusion:*** While microspheres can deliver extremely high radiation doses to the tumor in just one administration, SBRT is performed over 6-10 fractions. However, Y-90 microspheres deliver more radiation to surrounding tissue. Well-vascularized small tumors benefit the most from radioembolization, but dosage to surrounding organs requires analysis with more patients. To better gauge side effects from these very different radiation modalities, biological effective dose calculation will be performed. Other modalities, such as HDR Ir-192 and proton therapy, will be included in further studies. ***References:*** [1] A.Taebi, C. Vu, and E. Roncali. "Multiscale Computational Fluid Dynamics Modeling for Personalized Liver Cancer Radioembolization Dosimetry." ASME. J Biomech Eng. January 2021.

EP-0795

Impact of SPECT acquisition and reconstruction parameters in dosimetry of [177Lu]Lu-PSMA-617 and analogues

T. Lima*, M. Gravinatti, A. Zander, H. Grünig, U. Bhure, M. Pérez Lago, K. Strobel;*
Luzerner Kantonsspital, Luzern, SWITZERLAND.

Aim/Introduction: Prostate-specific membrane antigen (PSMA) is a transmembrane protein that is overexpressed in prostate cancer cells. Single-photon emission computed tomography/computed tomography (SPECT/CT) is a widely used imaging modality for ^{177}Lu-PSMA post-therapy imaging, but the impact of SPECT acquisition and reconstruction parameters on dosimetry accuracy and harmonization is not fully characterised. The aim of this work is to understand and characterise the impact of acquisition and reconstruction parameters in ^{177}Lu-PSMA dosimetry. ***Materials and Methods:*** A standardised phantom with known sphere sizes was used. Lesions and background were filled with ^{177}Lu and the activity concentration was set to mimic the ones found in patients. The phantom was then imaged in a clinical device with varying acquisition time (5, 10, 15 and 20 seconds per projection), matrix size (128x128 or 256x256), reconstruction iterations (5, 10, 15, 20, 25, 30, 35, 40, 45 and 50) and the use of post-processing Gaussian filter (0, 5 or 10mm). All other parameters were kept as per the manufacturer's recommendation (reconstruction method, subsets, angular trajectory and angular steps). The quantification was evaluated based on the sphere recovery coefficient for different sizes. The lung insert and the background were evaluated based on the residual lung error and coefficient of variance, respectively. Lastly, dosimetry based on the single time-point dosimetry implemented clinically was calculated for each generated dataset. Comparisons were made based on their spheres' absorbed doses both with respect to the mean values and dose volume histograms. ***Results:*** The results demonstrated that acquisition statistics and reconstruction parameters significantly affected dosimetry measurements. Higher count statistics led to more accurate and precise dosimetry estimates, while shorter acquisition times led to higher variability in dose estimates. Smaller voxel sizes improved the accuracy of dosimetry estimates but increase variability. Standardization of acquisition and reconstruction protocols across different institutions may be necessary to ensure consistent dosimetry estimates and improve patient outcomes. ***Conclusion:*** The findings of this study highlight the importance of SPECT acquisition and reconstruction parameters in dosimetry of [^{177}Lu]Lu-PSMA-617 and analogues and their impact on accuracy and harmonization. The results suggest that acquisition statistics and reconstruction parameters should be carefully considered and optimized to improve the accuracy and consistency of dosimetry calculations. Standardization of acquisition and reconstruction protocols may be necessary to ensure consistent dosimetry estimates and improve patient outcomes.

EP-0796

Commissioning and planning of treatment planning systems for Selective Internal Radiation Therapy

M. Santoro*[1], G. Della Gala[1], G. Paolani[1], G. Rasoatsaratanany[2], S. Strolin[1], L. Strigari[1];*
[1]IRCCS Azienda Ospedaliero-Universitaria di Bologna, Bologna, ITALY, [2]International Centre for Theoretical Physics, Trieste, ITALY.

Aim/Introduction: Treatment Planning Systems (TPSs) have been recently introduced to personalize ^{90}Y-selective internal radiation therapy (SIRT). Unfortunately, there are no harmonization or guidelines on commissioning these tools. The aim of this study is to assess the discrepancies among four clinical TPSs for ^{90}Y-SIRT in terms of volumes of interest (VOIs), mean absorbed doses, and Dose Volume Histograms (DVHs). ***Materials and Methods:*** Two experimental (NEMA homogeneous and abdominal anthropomorphic) phantoms were acquired with a SPECT/CT scanner and filled with ^{99m}Tc-pertechnetate to mimic ^{99m}Tc-MAA distribution. Three virtual phantoms were generated in DICOM format by an in-house MATLAB script, two reproducing the experimental ones and assuming to be homogeneously filled. The kernel phantom was generated focusing the activity inside a voxel at the center of the NEMA phantom. VOIs were created within a TPS for each phantom. Images and VOI were imported into four clinical TPSs for ^{90}Y-SIRT dosimetry. Two methods were used for voxel-based dosimetry calculations within the TPSs: the local deposition method and the dose kernel convolution assuming a known injected activity. The descriptive statistics and differences in calculated volumes and dose metrics were determined and compared with the Bland-Altman analysis using R software. ***Results:*** Differences up to 5% between NEMA homogeneous virtual and experimental phantom were found while trivial differences between anthropomorphic virtual and experimental one were observed. The mean absorbed dose for

the homogenous phantom ranged from 3 to 5.1 Gy. Concerning the two anthropomorphic phantoms, the dose difference was up to 10 times for the cold sphere, where the absorbed dose range of the virtual phantom was shifted 100 Gy higher than the experimental one. Bland-Altman plots showed discrepancies for each VOI volume up to 25% and 10% for homogeneous and anthropomorphic phantoms, respectively. In addition, the Bland-Altman plots comparing the mean absorbed doses of VOIs showed discrepancies of up to 20% for the virtual phantoms and up to 10% for the experimental phantoms. The difference in the mean absorbed dose of smaller volume of kernel phantom obtained from different TPSs largely varied based on the implemented kernels and calculation methods. The DVHs were different for homogeneous and anthropomorphic (virtual and experimental) phantoms due to the image noise and likely the low resolution of the experimental images. ***Conclusion:*** Significant discrepancies in calculated dose metrics were found due to the adopted kernels and calculation methods adopted in the investigated TPSs demanding an appropriate harmonization.

EP-0797

Effect of segmentation uncertainty on pre-therapeutic dosimetry of selective internal radiation therapy using Yttrium-90 Microsphere for hepatocellular carcinoma

A. Nautiyal*, T. Melhuish, G. Lewis, S. Michopoulou;*
University Hospital Southampton, Southampton, UNITED KINGDOM.

Aim/Introduction: Precise segmentation of perfused liver volume (PLV), tumour volume (TV) and whole liver (WLV) is the basis and prerequisite for the treatment planning of selective internal radiation therapy (SIRT) using Yttrium-90 (^{90}Y)-microsphere. As per EANM practical guidance on dosimetry, uncertainty in the delineation of volume of interest (VOI) is the major factor of variation in the counts and dosimetry calculations in molecular radiotherapy. Our aim was to investigate the impact of PLV, TV and WLV delineation on the estimation of required administered activity and absorbed dose in the tumour and normal liver tissue. ***Materials and Methods:*** Three patients having single hepatic lesions and referred for ^{90}Y-SIRT were analysed retrospectively. For each patient, three different experiments were performed to estimate the tumour dose (TD), normal liver tissue dose (LD) and required administered activity of ^{90}Y-microsphere. In the first experiment, TV and WLV VOIs were kept fixed while PLV threshold on SPECT/CT images was changed for each unit (5-28%). In second experiment, PLV and WLV VOIs were fixed while threshold-based TV VOIs (24-50%) were changed for each unit. In final experiment, the VOIs of PLV and TV were fixed while different CT-based WLV VOIs (1-1.74l) were drawn. A standard fixed dose of 120Gy to the PLV was used for all experiments. A commercial dosimetry planning software was used for all volumetric segmentation and dosimetric calculations. ***Results:*** As expected, the parameters i.e., TD, LD and required administered activity of ^{90}Y microsphere change linearly (r=1) with the diameter of PLV VOI. A strong negative association was noted between TV VOI vs TD (r=-0.97) and TV VOI vs LTD (r=-0.99). Similarly, a strong negative correlation was noted between WLV VOI and LD (r=-0.99). In experiment one, each unit of threshold VOI change around PLV generates an approximate error of 3.5 % in TD estimation, 10 % in LD and 8% in the required administered activity of the 90Y-microsphere. In experiment two, each unit of threshold VOI change around TV generates an approximate error of 2% in TD and 2% in LD. In experiment three, changes in VOI around the liver generate an error of 2% in LD. ***Conclusion:*** The VOI delineation around the perfused liver site substantially changes the tumour dose and required administered activity in the ^{90}Y-SIRT treatment. To optimise dosimetry, accurate VOI delineation by an experienced operator is required, using high-resolution SPECT combined with diagnostic contrast-enhanced CT or MRI images.

EP-0798

Clinical dosimetry of patients treated with Capecitabine, Temozolomide and [177Lu]Lu-DOTA-TOC combined therapy.

A. Cichonski*[1], J. B. Ćwikła[2], A. Kolasińska-Ćwikła[3], M. Kempińska-Wróbel[2];*
[1]National Centre for Nuclear Research, Warsaw, POLAND, [2]Medical School, University of Warmia and Mazury, Olsztyn, POLAND, [3]The Maria Skłodowska-Curie National Institute of Oncology, Warsaw, POLAND.

Aim/Introduction: Accurate and reliable dosimetry evaluation of [^{177}Lu]Lu-DOTA-TOC therapy in clinical routine is crucial to ensuring the safety and effectiveness of treatment. The aim of this study was to perform a dosimetry assessment of both organs and lesions using widely-used tools. ***Materials and Methods:*** The study group consisted of 17 patients who were treated for neuroendocrine tumors. The somatostatin receptor-targeted therapy using [^{177}Lu]Lu-DOTA-TOC included 3 cycles for 3 subjects, while the rest of the patients had 4 cycles with 2-months intervals. In each cycle, an average dose of 6243 MBq of [^{177}Lu]Lu-DOTA-TOC was administered and post-therapy SPECT was performed to follow the tracer concentration in volume of interest at certain time points: 6 hours, 27 hours, 84 hours, and 127 hours average. The TAC curve fitting was performed using a mono-exponential method based on SPECT/CT acquisitions at no less than three time points. In 8 patients also the pre-treatment diagnostic somatostatin receptor scintigraphy with [^{99m}Tc]Tc-EDDA/HYNIC-TOC was performed. The uptake of ^{99m}Tc in SRS and the subsequent therapy with ^{177}Lu were compared for those patients. Dosimetry evaluation was carried out based on informations obtained from quantitative analysis of SPECT images performed in the workstation application and direct dose calculations were carried out in external software. ***Results:*** The mean cumulated absorbed dose for the liver was 6.1 Gy (SD = 6.5 Gy, N = 17), for kidneys 9.5 Gy (SD = 5.8 Gy, N=17), for the spleen 5.9 Gy (SD = 4.7 Gy, N=12) and heart 0.07 Gy (SD = 0.07 Gy, N = 17). Bone marrow dosimetry results of cumulated absorbed dose were average of 32 mGy (SD = 30 mGy, N = 17). The target lesions dosimetry results was mean absorbed dose 52.4 Gy (SD = 33.5 Gy, N = 44). The contribution of the beta component of 177Lu radiation in the total dose was 95.2% for the liver, 97.2% for the kidneys, 97.2% for the spleen, and 0.48% for the heart. ***Conclusion:*** Dosimetry can be performed in a convenient manner mainly using tools available on clinical workstation to obtain required data and calculations easy to perform in available external software. The heart is an organ out of risk and can be excluded from dosimetry evaluation if needed. The only image-based dosimetry for bone marrow is insufficient and should be completed with blood-based methods.

EP-0799

Voxel-level comparison of99mTc-MAA SIRT planning SPECT-CT with90Y-Microspheres post-therapy PET-CT

S. Heard, *D. Gillett, R. Crawford, I. Harper, T. C. See, N. Shaida, L. Aloj;*
Cambridge University Hospitals NHS FT, Cambridge, UNITED KINGDOM.

Aim/Introduction: Selective internal radiation therapy (SIRT) with ^{90}Y-Microspheres for liver cancer is typically preceded by ^{99m}Tc-MAA imaging to assess whether shunting to the lungs will be within safe limits. Increasingly ^{99m}Tc-MAA SPECT CT is also used to predict the therapeutic activity distribution and hence plan radiation doses to tumours and healthy tissue. The importance of individualised planning taking into consideration overall liver function, volume of affected liver and volume of normal liver likely to receive a significant radiation dose is increasingly recognised. Comparisons between planning and therapeutic activity distribution have been investigated in the literature. We present a detailed voxel-level comparison of predicted and actual perfused volume as well as planned and delivered absorbed dose in both healthy and tumoural tissues. ***Materials and Methods:*** The planning ^{99m}Tc-MAA SPECT-CTs for ten patients were registered to their respective post-treatment ^{90}Y-Microspheres PET-CTs. Using dosimetry software package Simplicit90y actual doses to tumour volumes were compared with the planned doses. In addition, 3D Slicer was used to compute dose images (predicted and delivered) and to perform voxel-wise subtraction, generating a difference image for each pair. Furthermore, the total perfused volumes (planned and delivered) were segmented and compared using their Dice coefficient to assess the similarity of the volumes. ***Results:*** The mean doses delivered to tumour and total perfused volume were 120% (range: 65% - 189%) and 107% (range: 81% - 189%) respectively of the planned doses. The mean perfused volume obtained in the post treatment PET CT images was 86% (range: 39% - 114%) of the planned perfused volume. The similarity of the volumes (size, shape and extent) was high with an average Dice coefficient of 0.77 (range: 0.43 - 0.91). Despite a mean difference of only +0.6 Gy the differences seen between the predicted and actual doses at a voxel level varied considerably, beyond the contribution of image noise, with a standard deviation of 44 Gy and a range of -244 to +339 Gy. ***Conclusion:*** ^{99m}Tc-MAA SPECT/CT is a reliable method to determine perfused volume and predict average absorbed dose when delivering ^{90}Y-Microspheres. This method, however, is a poor proxy for relative activity distribution within the target volume. Importantly, delivered tumour doses were generally found to be higher than predicted on the ^{99m}Tc-MAA SPECT-CT. Underdosing tumour lesions is unlikely to occur when this simple approach is used for treatment planning of SIRT.

EP-0800

Clinical experience of whole body and tumour dosimetry of 131-I-mIBG treatment for pediatric patients

I. Torres Espallardo[1,2], *N. Orrego*[1], *M. Gandia-Ferrero*[2], *V. Cotanda*[3], *C. Olivas*[1], *L. Martí-Bonmatí*[1,2], *P. Bello-Arques*[1], *J. Balaguer*[1], *S. Prado-Wohlwend*[1];
[1]*Clinical Area of Medical Imaging, Valencia, SPAIN,* [2]*Health Research Institute La Fe, Valencia, SPAIN,* [3]*Fundacion IVO, Valencia, SPAIN.*

Aim/Introduction: ^{131}I-metaiodobenzylguanidine (^{131}I-mIBG) is a targeted radiopharmaceutical mostly used for paediatric patients with refractory or relapsed neuroblastoma. Recent research suggests that numerous infusions of high-dose ^{131}I-mIBG result in a better response. Our therapy approach consists of two injections spaced 3-4 weeks apart. The treatment goal is to deliver a 4 Gy whole-body dose. WB and tumour dosimetry were used in this investigation to assess the connection with clinical outcomes. ***Materials and Methods:*** Six patients were included, each of whom received two administrations. The WB absorbed dose for all individuals and administrations were computed. WB-dosimetry was estimated using the MIRD schema and was based on external dose rate data. Tumor dosimetry was performed using SPECT/CT scans taken at three separate time intervals (72, 96, and 144 hours after treatment). Tumor S-values have been calculated using the uniform and unit density sphere models and the MIRD formalism. ***Results:*** For the entire treatment, the WB-doses were 2.6±1.1 Gy. When the ratio of absorbed dose (D) to given activity (A) is compared between the first (R1=D1/A1) and second (R2=D2/A2) infusions, R1 > R2 results in exitus (2 patients). Two of the four remaining patients have progressed. Interestingly, the dose of the relevant lesions rose significantly from the first to the second cycle (from 0.01 to 0.26 mGy; and from 0.20 to 0.55 mGy). ***Conclusion:*** WB and tumour dosimetry aid in our comprehension of therapy response. These studies are viable in clinical practice, but require a well-established process and a multidisciplinary team. We detected interindividual and intercycle variability in radiation exposure and consequently individual susceptibility to this sort of treatment in our investigation. Further research with larger population is needed to assess the correlation between radiation dose and clinical outcomes in order to predict individual response to ^{131}I-mIBG therapy. This should be done at multicenter level given small patients sample.

EP-0801

DosePredict: An Open-source Software to Support Treatment Planning for Personalised Radiopharmaceutical Therapy

C. Gomes Ferreira[1], *V. R. Warschun*[2], *J. Hu*[1], *S. Xue*[1], *L. Mercolli*[3], *T. W. Vidal*[2], *N. Navab*[2], *A. Afshar-Oromieh*[3], *A. Rominger*[3], *K. Shi*[1];
[1]*University of Bern, Bern, SWITZERLAND,* [2]*Technical University of Munich, Munich, GERMANY,* [3]*Inselspital, Bern University Hospital, Bern, SWITZERLAND.*

Aim/Introduction: Radiopharmaceutical therapy (RPT) has been successful in the systematic treatment of multiple metastatic cancers. However, despite the European Council Directive (2013/59 Euratom) requiring personalized or tailored treatment, the current approach still relies on fixed dosages. One of the reasons for this limitation is the lack of tools for pre-therapy dose prediction. To address this issue, we have developed an academic software tool, called "DosePredict" that integrates an AI-based pre-therapy dose prediction algorithm to assist with treatment planning for personalized RPT. ***Materials and Methods:*** "DosePredict" is an open-source client-side software developed in Python, encompassing simplified dose prediction and verification tasks during the general RLT workflow. The current version is restricted for PSMA-directed RPT for prostate cancer. Four main modules are being developed independently and integrated in a Qt- and VTK-based interface to provide separate functionalities: "Pre-therapy Prediction", "Segmentation", "Post-therapy Dosimetry", and "Evaluation". ***Results:*** A deep learning based voxel-wise pre-therapy dosimetry prediction algorithm based on static PET/CT was implemented in the "Pre-therapy Prediction" module[1]. A semi-automatic segmentation algorithm using first deep learning for pre-segmentation followed by optional manual refinement

was implemented for the "Segmentation" module[2]. A voxel-wise multi-time point dosimetry estimation was implemented for SPECT/CT images in the "Post-therapy Dosimetry" model[1]. The "Evaluation" module allows the users to assess the dose volume histogram and evaluate the dose prediction accuracy based on post-therapy dosimetry measurements. ***Conclusion:*** This simple open-source software provides a tool to support the users to implement dose prediction for the investigation of dosimetry-guided RPT treatment, which may accelerate the development for personalized treatment planning. ***References:*** 1. Xue, Song, et al. "Voxel-wise prediction of post-therapy dosimetry for 177Lu-PSMA I&T therapy using deep learning." (2020): 1424-1424.2. Parhi, Subhadarshini, et al. "Semi-automatic Segmentation of Metastatic Tumor Load for 177Lu-PSMA Therapy." (2022): 3074-3074.

EP-54

e-Poster Area

D: Technical Studies -> D4 Dosimetry and Radiobiology -> D43 Clinical Radiobiology

EP-0802

Comparison of Administered Lu-177 and Ac-225 Activities of PSMA Treatments Against Metastatic Prostate Cancer: Radiobiological Factors

V. Ahtiainen[1,2], *V. Reijonen*[1], *M. Tenhunen*[1];
[1]*Helsinki University Hospital Comprehensive Cancer Centre, Helsinki, FINLAND,* [2]*Helsinki University, Helsinki, FINLAND.*

Aim/Introduction: Potential benefits of alpha emitters are better microscopic dose distribution and radiobiological factors: independence from dose rate and oxygen effect. Experimental models have been presented to define safe and efficient protocols for therapeutical applications being confirmed in the clinical safety trials first. So far, there are no clinical trials comparing alpha and beta emitting radiopharmaceuticals in the same group of patients. We have compared the published results of Lu-177 and Ac-225 labelled PSMA-617 trials (1, 2). ***Materials and Methods:*** Trial (1) consists of 200 patients, n=99 of them treated with up to six Lu-177-PSMA-617 administrations. Meta-analysis (2) collects data from 6 trials with 201 patients treated with 1-8 (median = 3) Ac-225-PSMA-617 administrations. The analysis was performed using calculated average values for administered activities. Consistent and surprisingly similar end-point indicators could be found from both datasets for tumour response (PSA decline>50%) in (1): 66% and (2): 66%, hematological toxicity (anemia>G3) in (1): 8% and (2): 12%, and xerostomia in (1): 60% and (2): 77% of cases, respectively. ***Results:*** Firstly, providing similar biodistribution and kinetics of all data sets (difference in the physical half-life omitted due to the shorter biological clearance), it is possible to compare the ratio of administered activities directly: (1) Lu-177: 37.5 GBq (2) Ac-225: 21.0 MBq. Secondly, if photon radiation is omitted, the locally absorbed energy per decay is (1) Lu-177: 148 keV, (2) Ac-225: 28.2 MeV (alphas) and 675 keV (electrons) [ICRP 107]. Assuming that electron radiation's relative biological effectiveness (RBE) is close to one, the effective RBE of Ac-225 decay chain alphas thus becomes 9.35. This is higher by a factor of ≈1.6 which could be expected based on the alpha energies. Again, this may be due to microscopic dose distribution, underestimation of current RBE for alphas, or low dose-rate effect of beta radiation. ***Conclusion:*** With two patient sets of equivalent dose responses, comparing simple physical/radiobiological factors of alpha and beta emitters is possible. ***References:*** 1. Hofman M et al. ^{177}Lu-PSMA-617 versus Cabazitacel in patients with metastatic castration-resistant prostate cancer (TheraP): a randomised, open-label, phase 2 trial. Lancet 397:797-804, 2021. 2. Ma et al. Efficacy and Safety of ^{225}Ac-PSMA-617-targeted Alpha Therapy in Metastatic Castration-Resistant Prostate Cancer: A Systematic Review and Meta-Analysis. Front.Oncol: 12: Article 796657, 2022.

EP-55

e-Poster Area

D: Technical Studies -> D5 Radiopharmacy/ Radiochemistry -> D51 New Radiopharmaceuticals - SPECT

EP-0803

Preparation of a 99mTc-labeled Bromobenzyl Ether Derivative Targeting PD-L1

W. Hongyong*, C. Lu, Y. Liu, J. Wu, H. Wu, G. Han, P. Zou;*
Jiangsu Institute of Nuclear Medicine, Wuxi, Jiangsu, CHINA.

Aim/Introduction: The expression level of PD-L1 on tumor surfaces is an important indicator for guiding the use of PD-1/PD-L1 checkpoint inhibitors. Currently, the tumor surface PD-L1 expression level is mainly determined by immunohistochemistry, which has certain invasiveness and cannot reflect the overall immune status of the tumor. In theory, a radiolabeled molecular probe targeting PD-L1 can quantitatively reflect the tumor's PD-L1 level in real-time and comprehensively, providing a basis for immune therapy. Due to the strong affinity between 2-cyanobenzyl bromide derivative and PD-L1, we designed a small molecule bromobenzyl ether derivative suitable for 99mTc labeling to develop a molecular probe targeting PD-L1. ***Materials and Methods:*** Starting from 2-bromo-3-iodotoluene, we synthesized 2-hydroxy-4-(2-bromo-3-phenylbutoxy)-5-chlorobenzaldehyde through a reaction with phenylboronic acid, followed by a reaction with 2,4-dihydroxy-5-chlorobenzaldehyde, and a reaction with 3-cyanobenzyl bromide to generate 2-(3-cyanobenzyl methoxy)-4-(2-bromo-3-phenylbutoxy)-5-chlorobenzaldehyde. The reaction with N-[2-(2-(S-(4-methoxyphenyl) mercapto) ethylamino) ethyl] -S-(4-methoxyphenyl)-2-aminoethylthiol (N2S2) generated the labeling precursor N-[2-(3-cyanobenzyl methoxy) -4-(2-bromo-3-phenylbutoxy)-5-chlorobenzyl]-N-[2-(2-mercapto) ethylamino) ethyl] -2-aminoethylthiol (abbreviated as N2S2-CBMBC). The labeling precursor N2S2-CBMBC was dissolved in ethanol, and then sodium gluconate, stannous chloride, and pertechnetate solution were added. After shaking and heating at 90-100℃ for 30 minutes, the cooled solution was obtained as the desired ^{99m}Tc-N2S2-CBMBC. The labeling rate, radiochemical purity, and stability were examined by isotope HPLC. Furthermore, the oil-water partition coefficient of ^{99m}Tc-N2S2-CBMBC was measured, and the cell uptake experiment of 99mTc-N2S2-CBMBC was performed. ***Results:*** The total synthesis yield of the labeling precursor N2S2-CBMBC was 12.96%. The labeling rate of ^{99m}Tc-N2S2-CBMBC was above 94%. After being placed at room temperature for 6 hours, the radiochemical purity remained above 90%. The oil-water partition coefficient was 0.91. The cell uptake experiment showed that the cell uptake of ^{99m}Tc-labeled 3-cyanobenzyl N2S2 bromobenzyl

ether derivative (8.55%) was 171 times that of ^{99m}Tc-blank (without labeling precursor) in MDA-MB-231 breast cancer cells, which was consistent with the high expression of PD-L1 on the surface of MDA-MB-231 breast cancer cells reported in the literature. ***Conclusion:*** ^{99m}Tc-N2S2-CBMBC is a small molecule bromobenzyl ether derivative that is stable at room temperature in vitro and suitable for clinical application, with the potential for targeting PD-L1. It is worthy of further research and development.

EP-0804

[113mIn]In-FAPI-46 radiolabeled complex: a new agent for SPECT imaging of FAP-expressing tumors

f. Bolourinovin[1], *F. Badipa*[1], *s. zolghadri*[2], *h. yousefnia*[3]; *[1]PARS-ISOTOPE, karaj, IRAN, ISLAMIC REPUBLIC OF, [2]Radiation Applications Research School, Nuclear Science and Technology Research Institute, P.O.Box: 11365-8486, Tehran-Iran, Tehran, IRAN, ISLAMIC REPUBLIC OF, [3]Radiation Applications Research School, Nuclear Science and Technology Research Institute, P.O.Box: 11365-8486, Tehran-Iran, tehran, IRAN, ISLAMIC REPUBLIC OF.*

Aim/Introduction: Nowadays, targeting of cancer-associated fibroblasts by fibroblast activation protein (FAP) inhibitor (FAPI) is well-proven. FAPI-46 is a quinoline-based FAP-targeted tracer used for imaging of a multitude of different cancers showing has higher tumor accumulation and prolonged tumor retention. In this study, [^{113m}In]In-FAPI-46 radiotracer was prepared at optimal conditions using a domestically produced ^{113}Sn/^{113m}In generator as a new agent for single positron emission computed tomography (SPECT) imaging of FAP-expressing tumors. ***Materials and Methods:*** ^{113m}In was prepared by milking the recently developed ^{113}Sn/^{113m}In generator in the form of [^{113m}In] $InCl_3$. Several experiments were performed by changing the amounts of FAPI-46, time, pH and the temperature of the reaction, to obtain the optimal labelling conditions of the FAPI-64 with ^{113m}In. The radiochemical purity of the final complex was checked by radio thin layer chromatography (RTLC) and high performance liquid chromatography (HPLC). The stability of the radiolabelled complex was checked in PBS buffer (4 ºC) and human serum (37 ºC). Biodistribution of [^{113m}In]In-FAPI-46 was studied in normal mice using scarification and SPECT imaging. ***Results:*** [^{113m}In]In-FAPI-46 radiolabeled complex was obtained with a radiochemical purity of >99% (RTLC and HPLC) at optimized conditions. The investigation of the stability of the labeled compound showed a radiochemical purity of more than 96% for at least three hours in PBS buffer and in human blood serum. The results of investigating the biodistribution and the images of the indium-m113-FAPI-46 in healthy mice showed that the major portion of the activity excrete via urinary tract and other organs did not demonstrate significant accumulation. ***Conclusion:*** According to the results, [^{113m}In] In-FAPI-46 radiolabeled complex can be considered as a new agent for SPECT imaging of the FAP-expressing tumors, however more biological data are still needed.

EP-0805

First Experience with [195mPt]Cisplatin Imaging in Lung Cancer Patients

D. Hoogenkamp[1], *E. A. Aalbersberg*[1], *K. van der Schilden*[2], *H. N. Hendrikse*[3], *M. P. J. Mooijer*[3], *U. Funke*[3], *B. D. Windhorst*[3], *L. J. de Wit-van der Veen*[1], *M. M. G. Rossi*[1], *J. S. A. Belderbos*[1], *W. V. Vogel*[1]; *[1]NETHERLANDS Cancer Institute (NKI-AVL), Amsterdam, NETHERLANDS, [2]Nuclear Research and Consultancy Group (NRG), Petten, NETHERLANDS, [3]Amsterdamumc (location VUmc), Amsterdam, NETHERLANDS.*

Aim/Introduction: Platinum-based chemotherapy reveals heterogeneous responses and the development of nephrotoxicity is common. Patient selection before therapy could aid in increasing effectiveness and decreasing toxicity. Radiolabeled [^{195m}Pt] Cisplatin is hypothesized to provide useful in vivo information on its distribution and aid in this process of patient selection. This imaging study evaluates the absorbed dose of [^{195m}Pt]Cisplatin SPECT/CT in lung cancer patients. ***Materials and Methods:*** Five patients with locally advanced non-small-cell lung cancer (NSCLC) who received concurrent chemoradiation (66 Gy/24 fractions) with low-dose cisplatin were included. Patients received a single dose of 100 MBq [^{195m}Pt]Cisplatin in their second or third week of treatment. For the synthesis of [^{195m}Pt]Cisplatin a known procedure was modified [2]. ^{195m}Pt was supplied by the Nuclear Research & Consultancy Group (Petten, Netherlands) and produced under GMP at the Amsterdam UMC (location Vumc, Netherlands) with a radiochemical purity of ≥95% at a radioactivity concentration of 11.1 ± 4.9 MBq/ml. Up to six SPECT/CTs (Intevo Bold Siemens, Germany) were acquired between 1 and 168 hours after injection. Time-activity curves were generated by mono-exponential fitting of organ specific activities acquired using automated full organ segmentations in 3DSlicer (TotalSegmentator). S-values for ^{195m}Pt were obtained from IDAC-Dose 2.1. ***Results:*** Tracer elimination depended on renal clearance and bladder voiding, with a half-life of 32 ± 18 hours. Blood clearance was relatively slow, with $T_{50\%}$ at 29,6 ± 15 hours. The liver received the highest [^{195m}Pt]Cisplatin amounts; 7.6% ± 1.1% of the total administered [^{195m}Pt]Cisplatin at T = 1.5 hours. Also, highest absorbed radiationdose was found in the liver (62.6 mGy ± 11.1 mGy), followed by bladder wall (48.5 mGy ±22.5) and kidneys (42.3mGy ± 9.6mGy). Patients received a mean effective dose of 15.6 ± 2.5 mSv per 100 MBq [^{195m}Pt]Cisplatin. Effective dose estimates were highly influenced by estimates of the bladder dose. ***Conclusion:*** [^{195m}Pt]Cisplatin as a diagnostic tool is safe to use in patients with NSCLC, with a mean effective dose of 15.6±2.5 mSv (0.16±0.025 mSv/MBq). In following studies, tumor accumulation and imaging quality will be further assessed. ***References:*** [1] E.A. Aalbersberg, B.J. de Wit - van der Veen, O. Zwaagstra, et al. Preclinical imaging characteristics and quantification of Platinum-195m SPECT. Eur J Nucl Med Mol Imaging (2017) 44:1347-1354 [2] J.D. Hoeschele, T.A. Butler, J.A. Roberts, C.E. Guyer. Analysis and refinement of the microscale synthesis of the ^{195m}Pt-labeled antitumor drug, cis-Dichlorodiammineplatinum(II), cis-DDP. Radiochimica Acta (1982), 31, 27-36.

EP-0806

Preparation and quality control of [113mIn]In-PEG4-BBN(7-14) as a new agent for SPECT imaging of GRPR-expressing tumors

s. zolghadri, *F. Badipa, H. Yousefnia, B. Alirezapour, A. Bahrami-Samani, S. Shirvani-Arani, F. Bolouri-Novin; Nuclear Science and Technology Research Institute (NSTRI), Tehran, IRAN, ISLAMIC REPUBLIC OF.*

Aim/Introduction: Nowadays, due to the suitable characteristics of peptides, peptide-based radiopharmaceuticals have found an important role in the development of diagnostic and therapeutic radiopharmaceuticals. Gastrin-releasing peptide receptors (GRPRs) are overexpressed in many cancers such as prostate, breast, pancreatic, and small cell lung carcinoma. Bombesin (BBN) analogs radiolabeled with different diagnostic radionuclides have indicated excellent efficacy for imaging of tumors with GRPRs. This study aimed to produce [^{113m}In]In-PEG4-BBN(7-14) as a new agent for single positron emission computed tomography (SPECT) imaging of GRPR-expressing tumors. ***Materials and Methods:***

^{113m}In was eluted from the in-house developed ^{113}Sn/^{113m}In generator in the form of [^{113m}In]$InCl_3$. While several experiments were performed to determine the optimal conditions for radiolabeling of DOTA-PEG4-BBN(7-14) with ^{113m}In, the radiochemical purity of the final complex was checked by radio thin layer chromatography (RTLC) and high performance liquid chromatography (HPLC). The stability of the radiolabelled complex was checked in PBS buffer (4 ºC) and human serum (37 ºC). Cellular studies (binding affinity and internalization) were carried out in PC3 and CHO cell lines, as the GRPRs positive and negative cell lines, respectively. Biodistribution of [^{113m}In]In-PEG4-BBN(7-14) was studied in normal mice using organ %ID/g calculation and SPECT imaging. Biodistribution studies in GRPR-expressing animal tumor model are ongoing. ***Results:*** The radiolabeled complex was obtained with a radiochemical purity of >99% (RTLC and HPLC) at the optimized conditions. The radiochemical purity of the complex was higher than 98% for at least four hours in PBS buffer and human blood serum. Cellular studies of [^{113m}In]In-PEG4-BBN(7-14) showed the high affinity of the complex to the GRPR-expressing cell line and no affinity to CHO cell line. Also, the radiolabeled complex was rapidly internalized into the PC3 cell lines whereas the internalization into CHO cells was negligible. The biodistribution studies in normal mice demonstrated the renal excretion of the radioactivity and significant accumulation of the radiolabeled compound in GRPR-expressing organs. ***Conclusion:*** The initial results demonstrated that [^{113m}In]In-PEG4-BBN(7-14) radiolabeled complex has a high potential for SPECT imaging of the GRPR-expressing tumors.

EP-0807

Preclinical evaluation of a novel PSMA-targeting radioligand [99mTc]Tc-BQ0413

E. Bezverkhniaia[1], *P. Kanellopoulos*[1], *A. Abouzayed*[1], *M. Oroujeni*[1], *A. Vorobyeva*[2], *U. Rosenström*[1], *V. Tolmachev*[1], *A. Orlova*[1];
[1]*Uppsala university, Uppsala, SWEDEN.*

Aim/Introduction: Several types of radiolabelled PSMA inhibitors have been investigated for imaging of prostate cancer. The most extensively investigated type of high-affinity inhibitors are urea-based ligands. Clinical practice demonstrated good specificity of such tracers labelled with positron emitters. However, current progress in development of SPECT/CT cameras creates a potential of using this modality for detection and staging of prostate cancer. BQ0413 is a PSMA inhibitor, which was optimized using structure modelling. To enable labelling with ^{99m}Tc, a EEEC chelator was incorporated in BQ0413. The aim of this study was to perform initial preclinical evaluation of [^{99m}Tc]Tc-BQ0413. ***Materials and Methods:*** BQ0413 was radiolabelled with ^{99m}Tc using transchelation from gluconate. Labelling stability of [^{99m}Tc]Tc-BQ0413 was evaluated in vitro. In vitro PSMA-binding specificity, cellular processing and binding kinetics of [^{99m}Tc]Tc-BQ0413 was evaluated using PSMA-transfected PC-3.pip cells. Biodistribution of [^{99m}Tc]Tc-BQ0413 was measured in NMRI mice, and data were used for dosimetry upscaling to humans. ***Results:*** BQ0413 was radiolabelled with radiochemical yield above 95% according to iTLC and radio-HPLC analysis. The label was stable (no measurable release) during 1 h in 300 molar excess of L-cysteine and PBS at room temperature and in human serum at 37° C. The binding of [^{99m}Tc]Tc-BQ0413 to PC-3.pip cells was saturable by a commonly used PSMA-11 ligand. Binding to non-transfected PC-3 cells was much lower than the binding to PC-3,pip. These data suggest that the binding was PSMA-specific. The internalized fraction was approximately 40% after 4 h. Real-time binding kinetics of [^{99m}Tc]Tc-BQ0413 demonstrated extremely slow dissociation rate. The quilibrium dissociation constant (KD) value was 33±14 pM. The biodistribution profile demonstrated rapid clearance from all of organs and tissues (excluding kidneys). Major clearance was through glomerular filtration. The highest uptake was in kidneys, 80% of injected activity 1 hour past injection. Retention in kidneys was stable between 1 and 6 h and but decreased 7-fold by 24 hours. According to dosimetry estimation, the organ with the highest absorbed dose should be kidneys (0.1170 mGy/MBq). Doses to other organs and tissues are expected below 10^{-2} mGy/MBq. The estimated effective dose for humans is 0.0018 mSv/MBq. ***Conclusion:*** PSMA-inhibitor BQ0413 that can be easily radiolabelled with technetium-99m using techniques permitting development of a single-vial kit. BQ0413 demonstrated specific binding to PSMAS-transfected cells. [^{99m}Tc]Tc-BQ0413 cleared rapidly from normal organs via kidneys, but the renal uptake and retention were high. The data suggest that evaluation of [^{99m}Tc]Tc-BQ0413 in tumor-bearing mice is justified.

EP-56

e-Poster Area

D: Technical Studies -> D5 Radiopharmacy/ Radiochemistry -> D52 New Radiopharmaceuticals - PET

EP-0808

Expanding the Versatility of F-18 Indirect Labeling: Optimizing the Synthesis of TDBFB Boronic Acid Derivatives for Indirect Labeling via Suzuki Coupling

Y. Yagi[1,2,3], *H. Kimura*[2], *M. Ando*[1], *K. Kawaguchi*[1], *A. Sato*[1], *A. Shimizu*[1], *M. Fujimura*[1], *T. Higuchi*[3,4];
[1]*Kyoto college of Medical Science, Nantan, JAPAN,*
[2]*Kyoto Pharmaceutical University, Kyoto, JAPAN,*
[3]*University Hospital Würzburg, Würzburg, GERMANY,*
[4]*Okayama University, Okayama, JAPAN.*

Aim/Introduction: Positron emission tomography (PET) utilizes bioactive compounds labeled with F-18 radioisotopes as probes. While nucleophilic substitution reactions with the [^{18}F]fluoride ion are commonly used for introducing F-18, it remains challenging to introduce it into electron-rich aromatic rings. To overcome this challenge, we previously reported a new F-18 labeling method that employs the Suzuki coupling reaction with an indirect labeling reagent, the boronic acid derivative 4-(4,4,5,5-Tetramethyl-1,3,2-dioxaborolan-2-yl)-[^{18}F]fluorobenzene (4-[^{18}F]TDBFB). In this study, we further enhanced the versatility of TDBFB by improving the synthesis of 4-[^{18}F]TDBFB. Additionally, we investigated the synthesis of 3-[^{18}F]TDBFB and 2-[^{18}F]TDBFB. ***Materials and Methods:*** Initially, we investigated various F-18 sources, solvents, reaction temperatures, and additives to synthesize 4-[^{18}F]TDBFB from 1,4-benzenediboronic acid bis(pinacol)ester instead of using the diaryliodonium precursor. To evaluate the labeling rate of F-18 fluorination, we used Radio-Thin Layer Chromatography (Radio-TLC) and Radio-HPLC. Subsequently, we utilized the Suzuki coupling reaction to synthesize [^{18}F]fluorobiphenyls and a pitavastatin derivative, [^{18}F]pitavastatin-OMe, as applications of [^{18}F]TDBFB. We monitored the reaction progress using the same method. ***Results:*** At first, the [^{18}F]fluoride ion was eluted from the cation

exchange resin using DMAP/OTf, and subsequently heated at 120ºC for 20 min in dimethylacetamide, in the presence of 4-TDBFB precursor and copper catalyst, leading to the confirmation of the target product on Radio-TLC. This reaction condition resulted in a 2-fold increase in yield compared to previously reported conditions[1]. While microwave heating conditions[2] yielded 4-[^{18}F]TDBFB in a similar yield to conventional heating conditions, they enabled a shorter reaction time. The reaction progress was also evaluated using 3-[^{18}F]TDBFB and 2-[^{18}F]TDBFB precursors, yielding similar results. To synthesize [^{18}F]fluorobiphenyls and [^{18}F]pitavastatin, we employed [^{18}F]TDBFB with iodo or triflate precursors for [^{18}F]fluorobiphenyls, and a bromine-labeled precursor for pitavastatin. These coupling reactions proceeded successfully. ***Conclusion:*** The study supports the idea that [^{18}F]TDBFB could be utilized as a more versatile indirect labeling reagent. ***References:*** 1. Tetrahedron Letters, 107, 154010 (2022), 2. J. Labelled Compd. Radiopharm. 57(12), 680-6. (2014)

EP-0809

Automated One-Pot Synthesis of [18F]AlF-NOTA-Ubiquicidin[29-41] in Aqueous Solution with Preparative HPLC for Clinical PET/CT imaging

A. Meyer, *C. Fischer, D. Hellwig;*
University Hospital, Regensburg, GERMANY.

Aim/Introduction: Ubiquicidin[29-41], a cationic-rich peptide fragment, exhibits affinity towards bacterial cell membranes. [^{99m}Tc] or [^{68}Ga] have been used to label the peptide fragment for imaging infection sites. However, the radiolabeling of the NOTA-conjugated Ubiquicidin[29-41] with ^{18}F, an ideal radionuclide for PET, remains unexplored. Thus, we aimed to develop and optimize a GMP-compliant radiolabeling method for the synthesis of [^{18}F]AlF-NOTA-Ubiquicidin[29-41] in aqueous solution suitable for clinical PET imaging. ***Materials and Methods:*** The synthesis process involves a protic reaction solution that enables the formation of the intermediate transition metal [^{18}F]AlF^{2+}. We utilize a Raytest SynChrom R&D platform for the radiosynthesis of [^{18}F]AlF-NOTA-Ubiquicidin[29-41]. A cyclotron-produced activity of 40 GBq ^{18}F is fixed on a Sep-Pak Accell Plus QMA light and eluted with 0.9% saline. After addition of 500 µL sodium acetate buffer 0.5 M (pH 4.0) and 35 µL $AlCl_3 \cdot 6\ H_2O$ 10 mM, [^{18}F]AlF^{2+} is formed within two minutes at room temperature. After addition of 1 mL precursor solution (1 mg/mL NOTA-Ubiquicidin[29-41] in EtOH 10%), [^{18}F]AlF-NOTA-Ubiquicidin[29-41] is built at 105 °C within 15 minutes. Purification is performed on a preparative Nucleodur C18 Pyramid column using two mobile phases, one phosphate buffer/EtOH 98:2 (pH 7.0) for elution of ionic impurities (e.g. [^{18}F]F^-) and the other phosphate buffer/EtOH 90:10 (pH 7.0) for elution of the product at 16.7 minutes (flow rate of 5 mL/min). The product peak is collected in 10 mL Wfl by switching the valve triggered by in-process monitoring. The formulation is sterilized by sterile filtration while being filled into a vial in the dispenser under validated type A clean room conditions. Quality control is carried out according to predefined specifications. ***Results:*** The synthesis of [^{18}F]AlF-NOTA-Ubiquicidin[29-41] is carried out within 45 minutes with a radiochemical yield of 15 % and a radiochemical purity (RCP) of 96.5% using 40 GBq [^{18}F], 350 nmol $AlCl_3 \cdot 6\ H_2O$ and 1 mg NOTA-Ubiquicidin[29-41] in aqueous acetate buffer (pH 4.0) (n=3 replicates) with a final ethanol concentration of 3.0%. Product activity can be adjusted to meet individual needs by varying the amounts of [^{18}F], $AlCl_3 \cdot 6\ H_2O$ and precursor. The formulation is stable with an RCP ≥90% after 10 hours. Bioburden and media fill confirm GMP-compliance. ***Conclusion:*** Our developed GMP-compliant radiolabelling procedure provides reproducible results with sufficient yield to use PET/CT imaging with [^{18}F]AlF-NOTA-Ubiquicidin[29-41] for studies to localize and characterize infection sites. The synthesized radiopharmaceutical can potentially improve clinical diagnosis and treatment of bacterial infections.

EP-0810

Development of a 18F-PD-L1 radiotracer for cancer patient response to immunotherapy

M. Goodman, *L. Chavan, W. Seo, H. Zecca, R. Voll, L. Birnbaum, J. Kelvin, E. Dreaden, N. Jui;*
Emory University, Atlanta, GA, UNITED STATES OF AMERICA.

Aim/Introduction: Introduction: Immunotherapies represent new weapons in the fight against cancer. Monoclonal antibodies are at the forefront of these therapies that target the PD-1/PD L1 axis. Several anti-PD-L1 antibodies have recently received FDA approval for treating recurrent/metastatic disease in melanoma, kidney, bladder, gastric, lung and head and neck cancers. Accurate PD-L1 diagnostic tools are critical to predict which patients are likely to respond to anti-PD-L1 therapies. Here we report the synthesis, radiolabeling and characterization of a new ^{18}F-PD L1 small molecule, as a radioligand for imaging PD L1 expression in cancer with PET. ***Materials and Methods:*** (2S,4S)-1-(2-cyano-3-(2,3-dihydrobenzo[b][1,4]dioxin-6-yl)phenyl)-4-fluoropyrrolidine-2-carboxylic acid, PD-L1 A2, was designed based on therapeutics by Incyte[1] . PD-L1 A2 was synthesized in five linear steps starting from commercially available 2-bromo-6-fluoro-benzonitrile. Binding affinity for PD L1 was determined by surface plasmon resonance measurement. Radiolabeling of ^{18}F-PD-L1 A2 was accomplished with an GE TracerLab FX2 N by treatment of a tosylate precursor (3R,5R)-1-(2-cyano-3-(2,3-dihydrobenzo[b][1,4]dioxin-6-yl)phenyl)-5-methylpyrrolidin-3-yl 4-methylbenzenesulfonate with $K_{222}/K^{18}F/K_2CO_3$ in CH_3CN at 100 °C followed by deprotection with 1:1 1N NaOH:CH_3OH v/v, neutralization with CH_3CO_2H and HPLC purification. ***Results:*** PD-L1 A2 exhibited moderate affinity for PD-L1 (Ki = 50 µmole) and good physiochemical properties log $D_{7.4}$ = 1.0. ^{18}F-PD-L1 A2 was obtained in 66 min in 12.5% decay-corrected radiochemical yield with specific activity >1 Ci/µmole, radiochemical and chemical purities of >99%. ***Conclusion:*** Tosylate precursor 1 is an effective precursor for ^{18}F-PD-L1 A2. Additionally, the moderate binding affinity and Log D7.4 suggest that ^{18}F-PD-L1 A2 could be a potential agent for quantitating PD-L1 by PET. Research supported by the Emory Biological Discoveries Through Chemical Innovations (BDCI) program. ***References:*** 1. Heterocyclic compounds as immunomodulators. WO2017/205464 A1.2017

EP-0811

rhTATE: A Radiohybrid Approach for 18F or177LuLabelled Somatostatin Analogues Generating Chemically Identical Compounds

S. Deiser, *V. König, S. Fenzl, T. Günther, N. Urtz-Urban, S. Inoue, A. Casini;*
Technical University Munich (TUM),
Garching by Munich, GERMANY.

Aim/Introduction: We recently successfully established the radiohybrid (rh) concept within our group for PSMA-targeted compounds[1], which enables the use of chemically identical compounds for PET imaging, and radioligand therapy, irrespective wether fluorine-18 or lutetium-177 is applied. Hence, we developed rh-based somatostatin analogues, which contain

a novel silicon-based fluoride acceptor (SiFA) building block ("SiFA-SeFe") for ^{18}F-labelling and a DOTA moiety for ^{177}Lu-labelling. For a preclinical proof-of-concept study, we used the binding motif of DOTATATE and introduced a novel linker disign to optimize pharmacokinetics of [^{18}F]F-[^{nat}Lu]Lu-rhTATE. All compounds were evaluated by state-of-the-art experiments and compared with [^{18}F]F-SiFAlin-TATE and [^{177}Lu]Lu-DOTATATE. ***Materials and Methods:*** All peptides were synthesized by standard solid-phase peptide synthesis (SPPS). ^{18}F-labelling was conducted via isotopic exchange reaction at room temperature within 10 min (ammonium formate in anhydrous DMSO) using previously dried [^{18}F]fluoride with subsequent purification by catridge. Sst2r affinity (expressed as IC_{50}) was determined on CHO_{sst2} cells. Lipophilicity (expressed as n-octanol/phsphate buffered saline solution distribution coefficient, $logD_{7.4}$) was determined. Human serum albumin (HSA) binding was determined by high-performance affinity chromatography (HPAC). Biodistribution studies were carried out at 1 h post-injection (p.i.) in AR42J tumour-bearing CD1-nu/nu mice. ***Results:*** Labelling of [^{18}F]F-[^{nat}Lu]Lu-rhTATE analogues was completed within <30 min and resulted in radiochemical yields (RCY) and purities (RCP) >35% and >95%, respectively. Labelling of [^{nat}F]F-[^{177}Lu]Lu-rhTATE derivatives was completed within 5 min and resultad in RCY >95% and RCP >95%. All [^{18}F]F-[^{nat}Lu]Lu-rhTATE analogues showed low nanomolecular affinity (5.2-9.3 nM), elevated lipophilicity ($logD_{7.4}$: -1.68 to -0.18) and high HSA binding as compared with the reference radiopharmaceuticals [^{18}F]F-SiFAlin-TATE and [^{177}Lu]Lu-DOTATATE (>95% versus 92% and 51%, respectively). In vivo at 1 h p.i., the most promising [^{18}F]F-[^{177}Lu]Lu-rhTATE derivative revealed high tumour and low liver uptake (27.3±9.0 and 4.5±0.5 %ID/g, respectively), but high kidney accumulation (99.8±8.0 %ID/g), while acivity levels in the blood and the bone were low (<2 %ID/g). ***Conclusion:*** In summary, we have developed a new generation of radiohybrid-based somatostatin ligands that enable the use of chemically identical ligands, irrespective wether fluorine-18 or lutetium-177 is applied. The most promising [^{18}F]F-[^{nat}Lu]Lu-rhTATE analogue revealed similar pharmacokinetics to the established [^{18}F]F-SiFAlin-TATE and [^{177}Lu]Lu-DOTATATE and might terefore, be beneficial for future applications as a theranostic platform. ***References:*** [1] A.Wurzer, D. Di Carlo, A. Schmidt, R. Beck, M. Eiber, M. Schwaiger, H.-J. Wester J.Nucl.Med 2020, 61 (5), 735-742.

EP-0812

Phenolate-containing AAZTA-like chelators for 68Ga labelling. An in vitro and in vivo study.

L. Tei[1], *J. Martinelli*[1], *M. Boccalon*[2], *A. Vagner*[3], *D. Szikra*[4], *G. Trencsenyi*[4], *Z. Baranyai*[2];
[1]*Department of Science and Technological Innovation, University of Piemonte Orientale, Alessandria, ITALY,* [2]*Bracco Research Centre, Bracco Imaging S.p.A., Colleretto Giacosa, Via Ribes 5, ITALY, ITALY,* [3]*Scanomed Ltd., Debrecen, Nagyerdei krt. 98, HUNGARY,* [4]*Division of Nuclear Medicine and Translational Imaging, Department of Medical Imaging, Faculty of Medicine, University of Debrecen, Debrecen, Nagyerdei krt. 98, HUNGARY.*

Aim/Introduction: In the search for chelators with high affinity and selectivity for Ga(III), the heptadentate chelator AAZTA and its derivatives have been recently selected because of their characteristics in between the linear and macrocyclic structure allowing both fast complexation kinetics and high inertness of the Ga(III) complexes.[1] However, this success is weakened by the formation of a hydroxo ternary species characterized by lower inertness and lower radiolabelling performance at neutral pH. The introduction of phenolate donors was shown to increase contemporaneously both the basicity and the rigidity of the ligand and both the stability and the kinetic inertness of the corresponding metal complexes.[2] ***Materials and Methods:*** The ligands AAZ2A-exoHB and AAZ3A-endoHB with the hydroxybenzyl pendant arm on the exocyclic or endocyclic amine were synthesized and a study on the thermodynamic and kinetic properties of the Ga(III) was undertaken. Then, the labelling efficiency of the chelators with ^{68}Ga was examined at different temperatures, pH and ligand concentration to determine the optimal labelling conditions. Subsequently, the chelator with the best performance was chosen and a bifunctional derivative bearing an isothiocyanate group was synthesized for the conjugation to a cyclo(RGD) peptide for $\alpha_v\beta_3$ integrin targeting. Finally, the tracer was labelled with ^{68}Ga isotope, and the resulting radiotracer tested for its stability in human serum and then in vivo for targeting B16-F10 tumours with miniPET imaging. ***Results:*** The ligands AAZ2A-exoHB and AAZ3A-endoHB with the hydroxybenzyl pendant arm on the exo- or endocyclic amino groups were synthesized and a study on the thermodynamic and kinetic properties of the Ga(III) was undertaken. The labelling efficiency with ^{68}Ga was examined at different temperatures, pH and ligand concentration to determine the optimal conditions. Subsequently, the chelator with the best performance was chosen and a bifunctional derivative was synthesized and conjugated to a cyclo(RGD) peptide for $\alpha_v\beta_3$ integrin targeting. Finally, the tracer was labelled with ^{68}Ga, and the resulting radiotracer tested for its stability in human serum and in vivo for targeting B16-F10 tumours with miniPET imaging. ***Conclusion:*** More basic phenolate O-donor atoms have better coordination abilities than carboxylates to Ga(III), forming complexes with higher thermodynamic stability and improved kinetic inertness. Thus, the conjugates of AAZ3A-endoHB with different targeting vectors can be suitable examples for the development of ^{68}Ga-based PET imaging tracers with improved chemical properties in vivo. ***References:*** [1] C. Fersing et al. Pharmaceuticals 2022, 15, 234; [2] J. Martinelli et al. Inorg. Chem. Front. 2022, 9, 2271

EP-0813

Automated Synthesis Method To Produce The Pet Tracer [68ga]Ga-Fapi-46 For Clinical Applications: Development, Optimization And Validation

S. Migliari*, G. Ladisa, M. Scarlattei, G. Baldari, L. Ruffini;*
Nuclear Medicine Division, Azienda Ospedaliero-Universitaria of Parma, Parma, ITALY.

Aim/Introduction: Fibroblast activation protein (FAP) is a serine protease selectively expressed in many disorders associated with fibrotic dysregulation.FAP expression in healthy tissues is low, but significantly elevated in sites of tissue remodelling and repair. This specific pattern of expression makes FAP an ideal target for imaging and therapy and then FAP-specific small-molecule inhibitors (FAPIs) have been developed. The most promising molecule has been found FAPI-46, functionalized with DOTA to obtain a PET probe. Our goal was to develop, optimize and validate a new automated synthesis method to label DOTA-FAPI-46 with Ga-68 and a new quality control system to make the radiopharmaceutical available. ***Materials and Methods:*** Synthesis and quality assessment of 68Ga-FAPI-46 radiotracer was done using the automated synthesis module Scintomics GRP® connected to the GMP certified 68Ge/68Ga generator (GalliaPharma®, Eckert and Ziegler). The radiopharmaceutical production process has been conducted by a scale down method from 50 µg of peptide precursor to 10 µg (50-40-30-20-10 µg). Synthesis efficiency and release criteria have

been assessed for all the final products evaluating radiochemical yield (RY%), radiochemical purity (RCP%) with both Radio-TLC and Radio-UV-HPLC, specific activity (As) or molar activity (Am), chemical purity, pH and LAL test. ***Results:*** Best results were yielded with 20 µg DOTA-FAPI-46 and three different batches of validation were obtained with optimal RY% (67.75%) as well RCP% (99.76%) and Am (26.23 GBq/µmol). ***Conclusion:*** The excellent synthesis and QCs results ensure that our developed production process is very efficient and safe for a multi-dose application of 68Ga-FAPI-46 in clinical settings. ***References:*** [1] Lindner T et al. J Nucl Med. (2018). [2] Loktev A et al. J Nucl Med. (2019

EP-0814

Synthesis and Biological Evaluation of 18F-labelled Deuterated Tropane Derivatives as Dopamine Transporter Probes

Q. Hu[1], *Z. Chen*[1,2,3], *Q. Li*[2,3], *J. Tang*[2], *Y. Fang*[2], *C. Liu*[2], *J. Liu*[1,2], *M. Qi*[2,4]; [1]*Department of Radiopharmaceuticals, School of Pharmacy, Nanjing Medical University, Nanjing, CHINA,* [2]*NHC Key Laboratory of Nuclear Medicine, Jiangsu Key Laboratory of Molecular Nuclear Medicine, Jiangsu Institute of Nuclear Medicine, Wuxi, CHINA,* [3]*Jiangsu Key Laboratory of New Drug Research and Clinical Pharmacy, School of Pharmacy, Xuzhou Medical University, Xuzhou, CHINA,* [4]*School of Pharmaceutical Science, Inner Mongolia Medical University, Hohhot, CHINA.*

Aim/Introduction: Dopamine transporter (DAT) is a promising target for positron emission tomography (PET) imaging of many neuropsychiatric diseases. ^{18}F-labelled N-alkyl tropane analogues were reported to be useful PET radioligands for DAT. However, the drawback of ^{18}F-labelled tropane analogues is that N-alkyl on tropane is easily metabolized in vivo, which interferes with brain imaging. To develop a more in vivo stable DAT-targeted PET radioligand with high DAT affinity and specificity, in this study, we synthesized and compared a series of ^{18}F-labelled novel deuterated N-fluoropropyl tropane derivatives ([^{18}F]FP-CPT-d_6, [^{18}F]FP-CFT-d_6, [^{18}F]FP-CCT-d_6, [^{18}F]FP-CMT-d_6, [^{18}F]FP-CIT-d_6) for DAT tracing. ***Materials and Methods:*** Five deuterated N-fluoropropyl-d_6 tropane derivatives (FP-CPT-d_6, FP-CFT-d_6, FP-CCT-d_6, FP-CMT-d_6, FP-CIT-d_6) and corresponding non-deuterated compounds (FP-CPT, FP-CFT, FP-CCT, FP-CMT, FP-CIT) were synthesized, and their semi-inhibitory concentrations (IC_{50}) were measured by competitive binding assay. These radioligands were obtained by two-step one-pot radio-labelling reactions. The selectivity and specificity of these radioligands were evaluated by cellular uptake and microPET in normal rats. [^{18}F]FP-CIT-d_6 was selected for further investigation with autoradiography, biodistribution experiments, and microPET of the PD model and compared with its non-deuterated structure [^{18}F]FP-CIT. Finally, in vivo metabolic stability was analyzed by radio-HPLC. ***Results:*** Five deuterated N-fluoropropyl tropane analogs and corresponding nondeuterated structure were synthesized. All these compounds had high DAT affinity (IC_{50} = 2 - 21 nM), in which FP-CIT-d_6 had the lowest IC_{50} of 2.7 nM. ^{18}F-labelled deuterated and non-deuterated probes were obtained with radiochemical yields ranging from 10.6 ± 2.8% to 35.1 ± 5.4% with molar activities > 20 GBq/µmol and the radiochemical purities > 99%. [^{18}F]FP-CIT-d_6 showed the highest cell uptake (12%) and CFT inhibition efficacy (~ 72%) among deuterated probes. MicroPET results showed [^{18}F] FP-CIT-d_6 has the highest target to non-target ratio (striatum/cerebellum) from 30 to 120 min. Therefore, [^{18}F]FP-CIT-d_6 was then selected for further biological evaluation. Ex vivo autoradiography experiment confirmed high specific binding of [^{18}F]FP-CIT-d_6 towards DAT. Biodistribution results indicated that [^{18}F]FP-CIT-d_6 has a higher striatum/cerebellum value than [^{18}F]FP-CIT at 30 - 120 min. Furthermore, in vivo metabolism studies in rats revealed improved stability of [^{18}F]FP-CIT-d_6 as compared with that of [^{18}F] FP-CIT. ***Conclusion:*** The new probe [^{18}F]FP-CIT-d_6 is a promising candidate with good DAT affinity, specificity and metabolic stability for PET imaging, and might provide reliable diagnosis and prognostic detection of DAT-related neuropsychiatric diseases. Acknowledgements: This work was supported by the National Natural Science Foundation of China (82172054), the Natural Science Foundation of Jiangsu Province (BK20201133, BK20210062).

EP-0815

18F-labeled TTCO-PSMA Conjugate as a novel PET agent for prostate cancer imaging

T. Zhang*, Z. Zhang, G. Dong, L. Le, X. Ji, C. Peng, K. Li, X. Chen; Nanjing Medical University, Nanjing, CHINA.*

Aim/Introduction: In order to achieve more effective prostate-specific membrane antigen (PSMA)-targeted agents for the diagnosis of prostate cancer, a novel ^{18}F-labeled PSMA-targeting agent (^{18}F-TTCO-PSMA) was developed based on the high-affinity Glu-urea-Lys scaffold and biorthogonal linker. ***Materials and Methods:*** ^{18}F-TTCO-PSMA was obtained by three steps of acylation, reduced by 10% palladium/carbon and bioorthogonal conjugation. Micro PET/CT and biodistribution studies were performed in the LNCaP tumor-bearing mice. ***Results:*** The radiochemical purity of ^{18}F-TTCO-PSMA was over 97%, which met the quality control standard. The PET/CT imaging results showed that the tumor uptake of ^{18}F-TTCO-PSMA was 8.8 ± 3.3, 9.1 ± 2.1 and 8.2 ± 2.2% ID/g at 0.5 h, 1.5 h and 3 h, respectively, indicating that the uptake of the probe in the tumor was obvious and did not decrease significantly with time. Although ^{18}F-TTCO-PSMA had obvious uptake in the kidney, it had an obvious downward trend with time. Compared with ^{68}Ga-PSMA-11, which has been approved by FDA (2020), the probe had a lower kidney uptake and a significant downward trend over time, while maintaining a high tumor uptake and a low liver and muscle uptake. ***Conclusion:*** The introduction of the linker TTCO improves the stability, pharmacodynamics, and pharmacokinetics properties of the probe due to its biorthogonal structure and improved biocompatibility in function. ^{18}F-TTCO-PSMA has significant tumor uptake and low non-target uptake, making it a promising PET probe worth further evaluation for its clinical value in patients with prostate cancer.

EP-0816

A novel 68Ga-labeled spermine derivative probe for tumor imaging

K. Qin[1], *D. Shi*[1], *H. Wang*[1,2,3], *S. Li*[1,2,3]; [1]*Shanxi Medical University, Taiyuan, Shanxi, CHINA,* [2]*Shanxi Key Laboratory of Molecular Imaging, Taiyuan, Shanxi, CHINA,* [3]*Collaborative Innovation Center for Molecular Imaging of Precision Medicine Shanxi Medical University, Taiyuan, Shanxi, CHINA.*

Aim/Introduction: Polyamine transporter system (PTS) mediates the transmembrane transport of polyamines. The expression of PTS was upregulated in most tumors, making it a promising target for tumor imaging and therapy. It has been reported that radionuclide-labeled spermine can characterize the expression of PTS in cancer cells and image PTS-positive tumors in vivo, such as ^{99m}Tc-HYNIC-spermine and ^{99m}Tc -spermine. Persisted uptake in the liver is the main limitation of the currently reported probes targeting

PTS. Developing stable PTS-targeting probes with lower liver uptake is highly desirable, particularly in the context of precise therapy. Given this, we developed a novel gallium-68-labeled spermine derivative for tumor imaging targeting PTS in this study. ***Materials and Methods:*** Herein, the precursor NOTA-Spermine was obtained by the modification of spermine with the bifunctional chelating agent NOTA. Then, the [^{68}Ga]Ga-NOTA-Spermine was prepared by labeling the precursor with gallium-68. The biodistribution and stability of [^{68}Ga]Ga-NOTA-Spermine were determined in healthy mice, and the cell uptake assays was conducted with A549 (PTS+) cell lines to determine the PTS specific binding. The tumor imaging potential of [^{68}Ga]Ga-NOTA-Spermine were explored using micro-PET/CT imaging in DU145 tumor-bearing mice. ***Results:*** [^{68}Ga]Ga-NOTA-Spermine were successfully obtained with high radiochemical yields (50-55%) and purity (>98%), and had good stability in serum. Cell uptake showed that [^{68}Ga]Ga-NOTA-Spermine could be taken up by A549 tumor cell with the peak uptake at about 90 min (15.4% ±0.68%). Biodistribution showed that there was a low tracer uptake in liver for [^{68}Ga]Ga-NOTA-Spermine, which differs from other reported probes. The improvement might facilitate the visualization of abdominal lesions. Static micro-PET/CT scan showed a clear DU145 tumor uptake, and the radioactivity mainly accumulated in kidney with a rapid blood clearance (>60% within 30 min postinjection) and a low uptake in the majority of organs, which facilitated a good tumor-to-no tumor contrast. ***Conclusion:*** We have successfully synthesized a novel ^{68}Ga-labeled spermine derivative, and the evaluated results suggested that it might be a promising probe in tumor imaging targeted PTS. Further studies of [^{68}Ga]Ga-NOTA-Spermine will assess its application in tumors with different expression levels of PTS, as an effective technique for monitoring PTS expression in solid tumors.

EP-0817

Micro-PET Imaging Study of the Novel 68Ga-labeled PET Probe 68Ga-NOTAGA-Nap-Gal

Y. Xu[1], *P. Zhou*[2], *Y. Wu*[2], *H. Wu*[1], *Y. Liu*[1], *H. Wang*[1], *P. Zou*[1];
[1]*Jiangsu institute of Nuclear Medicine, WuXi, CHINA,*
[2]*Nanjing Medical University, Nanjing, CHINA.*

Aim/Introduction: Synthesize a novel PET probe ^{68}Ga-NOTAGA-Nap-Gal,which targets tumors with high expression of beta-galactosidase.Perform Micro-PET imaging of the probe and study its uptake in tumors and liver based on imaging results. ***Materials and Methods:*** The precursor NOTAGA-Nap-Gal was labeled with ^{68}Ga to obtain the target probe ^{68}Ga-NOTAGA-Nap-Gal, and the radiochemical purity of the probe was detected by radioactive HPLC. Ovarian cancer cells OVCAR-3 and breast cancer cells MDA-MB-468 were cultured and implanted into the armpits of nude mice to establish tumor-bearing nude mouse models. After the tumors grew to an appropriate size, the probe ^{68}Ga-NOTAGA-Nap-Gal was injected into the tail vein, and 10 min of Micro-PET static imaging was performed at 1 and 2 h after injection. The tumors and livers in the Micro-PET images were delineated in three consecutive layers, and the percentage of injected dose per gram of tissue (%ID/g) was calculated to study the uptake performance of the probe in tumors and livers. ***Results:*** Radiolabeled HPLC showed that the radiochemical purity of ^{68}Ga-NOTAGA-Nap-Gal probe was greater than 95%, and no further purification was required for subsequent experiments. The Micro-PET imaging of the probe in the xenograft OVCAR-3 and MDA-MB-468 models showed clear visibility of the tumors. The tumor uptake values at 1 and 2 h in the OVCAR-3 model were 3.57±0.48 and 2.68±0.19 %ID/g, respectively, and the liver uptake rates at 1 and 2 h were 4.56±0.73 and 3.58±0.39 %ID/g, respectively. In the MDA-MB-468 model, the tumor uptake values at 1 and 2 h were 2.71±0.44 and 2.12±0.29 %ID/g, respectively, and the liver uptake rates at 1 and 2 h were 4.25±0.53 and 2.95±0.47 %ID/g, respectively. ***Conclusion:*** This probe is easy to prepare and has good imaging effects in high-expressing beta-galactosidase tumor models. Further tissue distribution experiments are needed for validation of in vivo tissue distribution.

EP-0818

Atlas-Based Simulation for Pre-Estimation of Absorbed Dose in Critical Target Organs: A Study Using Monte Carlo Simulations with XCAT Phantoms and Real Patient Data in 68Ga-PSMA PET/CT

N. Vahidfar*, M. Fallahpoor, S. Farzanefar;*
Tehran University of Medical Sciences,
Tehran, IRAN, ISLAMIC REPUBLIC OF.

Aim/Introduction: The pre-estimation of absorbed radiation dose in critical target organs can be calculated in advance using atlas-based simulations, utilizing advanced anthropomorphic phantoms and Monte Carlo codes, to minimize side effects of radiopharmaceuticals and achieve accurate estimations. In this study, we aimed to calculate S-values (a measure of absorbed dose) of 68Ga-PSMA in different body mass indices (BMIs) using XCAT male phantoms through Monte Carlo simulations, and then compare the results with real patient data. ***Materials and Methods:*** Seven BMIs of XCAT male phantoms were generated, with the spine, prostate, kidneys, and salivary glands chosen as the source organs, and the kidneys, spleen, liver, salivary glands, prostate, spine, small intestine, and lung as the target organs. Dosimetry calculations were performed using the GATE Monte Carlo code for an activity of 20 MBq of both agents. For the patient-based study, six patients with castrate-resistant prostate cancer (CRPC) underwent 68Ga-PSMA-11 PET/CT scans, and the PET images as activity maps and CT as attenuation maps were used for dosimetry calculations with the GATE Monte Carlo code. S-values were reported for critical organs relevant to diagnostic and therapeutic PSMA-based tracers, and standard uptake value (SUV)max measurements were also performed in the same organs for comparative analysis. ***Conclusion:*** The results of this study demonstrated a reasonable correlation between the S-value results obtained from the XCAT phantoms and the patient study, indicating the potential of atlas-based dosimetry applications.

EP-0819

Evaluation of Different Ranges of [18F]Fluoride for Production of [18F]F-FAPI-74

A. MORISCO*, C. Maisto, R. de Marino, L. D'Ambrosio, E. Squame, M. Buonanno Recchimuzzo, A. Esposito, M. Aurilio, P. Gaballo, S. Lastoria;*
ISTITUTO NAZIONALE TUMORI - IRCCS - Fondazione G. Pascale, Napoli, ITALY.

Aim/Introduction: Fibroblasts activation protein (FAP) plays a pivotal role in tumors, being involved in remodeling of extracellular matrix and facilitating growth and cellular invasion. Radiolabeled FAP inhibitors (FAPI) are becaming successful pantumoral PET agents. In order to set up reliable conditions for in-house production of the FAP inhibitor [^{18}F]F-FAPI-74, we investigated the optimal conditions of synthesis to gain the best

radiochemical yield (RCY). We report the results of [^{18}F]F-FAPI-74 production, starting from different ranges (Low and High) of [^{18}F] Fluoride. ***Materials and Methods:*** [^{18}F]F-FAPI-74 was produced on the TRASIS AllinOne platform in according to the manufacturer's procedure: [^{18}F]Fluoride was trapped on QMA, then eluted to the reactor with 72 µg of precursor; the reaction was conducted via $(Al^{18}F)^{2+}$ complex, time reaction was 20 min and the final product was purified trough solid phase (SPE) cartridge. Radiochemical purity (RCP) was evaluated by radio-HPLC. RCP was tested also by iTLC using 1 M ammonium acetate/acetonitrile (1:1) as mobile phase and iTLC-SG as stationary phase. The final products were also tested for pH, radionuclidic purity, Limulus Amebocyte Lysate test (LAL), residual solvents. Radiochemical stability was conducted by radio-HPLC in the time (1h, 3h and 6h). ***Results:*** The low range (L) was performed with a starting [^{18}F]Fluoride activity of 21 GBq, the high (H) was performed with a higher activity, 98.7 GBq. The RCY values at end of synthesis (EOS), not corrected for decay, were ≥41% (L) and ≥45% (H) . RCP evaluated on the final product resulted ≥99% in both cases. The identity of [^{18}F] F-FAPI-74 was confirmed using the validated radio HPLC method by determining the relative retention of the principal peak with the reference solution using the UV/VIS detector. Stability test performed at 1h, 3h and 6h after EOS revealed a RCP ≥99%, showing no evidence of radiolysis or detectable, increasing, amounts of free [^{18}F]Fluoride. The synthesis resulted successful and reliable. ***Conclusion:*** Methodological aspects for an optimal production of [^{18}F]F-FAPI-74 have been evaluated to define the best operating procedures. Preliminary observed data suggest a good reliability of used methods, although further evidences are needed. In particular, the medium range of [^{18}F]Fluoride should be investigated to confirm the same percentage of RCY (40%) as obtained for ranges L and H. The choice of the optimal range of [^{18}F]Fluoride is mainly correlated to the number of performed exams (25/day), being the costs per production of [^{18}F]F-FAPI-74 the same for each condition.

EP-0820

Peptidic heterodimer-based radiotracer targetingfibroblast activation protein and integrin αvβ3

K. Liu;
Department of Nuclear Medicine, Xiangya Hospital, Central South University, Changsha, CHINA.

Aim/Introduction: Fibroblast activation protein (FAP) and integrin αvβ3 are both considered suitable targets for radionuclide theranostics due to their over-expression in the tumor microenvironment or tumor cells. Continuous efforts are being made to optimize the in vivo kinetics and tumor retention of radiopharmaceuticals, while the theranostic efficacy of monospecific tracers can be hampered by tumor heterogeneity. To meet this challenge, we aimed to design and synthesize a bispecific peptide heterodimer targeting FAP and integrin αvβ3 for superior diagnostic sensitivity and prolonged tumor retention. sensitivity and prolonged tumor retention. ***Materials and Methods:*** Hetero-dimer DOTA-FAP-RGD was synthesized and labeled with gallium-68, denoted as ^{68}Ga-FAP-RGD. The cell uptake and competitive binding assays were assessed in HT1080-FAP (FAP**+/**$\alpha_v\beta_3$**-**) and U87MG (FAP**+/**$\alpha_v\beta_3$**+**) cells. Small animal PET/CT imaging and ex vivo biodistribution studies were performed to compare the pharmacokinetic characteristics of ^{68}Ga-FAP-RGD with its monomeric counterpart ^{68}Ga-FAP-2286 or ^{68}Ga-RGDfK. ***Results:*** ^{68}Ga-FAP-RGD possessed high stability in phosphate-buffered saline or fetal bovine serum up to 4 h. Cell uptake and blocking experiments demonstrated the specific binding of ^{68}Ga-FAP-RGD to FAP and integrin $\alpha_v\beta_3$ in vitro. The heterodimer ^{68}Ga-FAP-RGD has a nanomolar binding affinity (IC50 = 32.1 nM towards FAP and IC50 = 115.9 nM towards integrin $\alpha_v\beta_3$) that comparable to corresponding monomers ^{68}Ga-FAP-2286 (28.5 nM) and ^{68}Ga-RGDfK (98.7 nM). Micro-PET/CT scans in HT1080-FAP tumor models revealed improved diagnostic efficiency of ^{68}Ga-FAP-RGD compared to ^{68}Ga-labeled FAP-2286 and FAPI-04 with higher tumor to non-tumor (T/NT) ratios. The U87MG tumor accumulation for ^{68}Ga-FAP-RGD (5.86 ± 0.37 %ID/g) was more stable than that for ^{68}Ga-FAP-2286 (3.36 ± 3.36 %ID/g) or ^{68}Ga-RGDfK (0.49 ± 0.10 %ID/g) up to 4 h ($P < 0.001$). The results were further confirmed by ex vivo biodistribution and immunohistochemistry studies. ***Conclusion:*** The peptidic heterodimer-based radiotracer ^{68}Ga-FAP-RGD showed improved diagnostic efficiency and tumor retention compared to the corresponding monomer ^{68}Ga-FAP-2286 or ^{68}Ga-RGDfK, making it a promising strategy for cancer theranostics.

EP-0821

Initial clinical experience with 18F-JK-PSMA-7 PET-CT in evaluation of staging and biochemical recurrence of prostate carcinoma.

P. Chandra, *S. Chinnappan, G. Chandran, C. L. Abraham; Zydus Hospital, Vadodara, INDIA.*

Aim/Introduction: ^{18}F-JK-PSMA-7, developed at Research center Julich and University Hospital Cologne, has been shown to have better acutance and higher resolution compared to ^{68}Ga PSMA 11 and ^{18}F-DCFPyL (1). Studies related to this promising novel tracer in prostate carcinoma (PCa) imaging are limited. ***Materials and Methods:*** Consecutive patients of PCa from Aug 2022 to March 2023 referred for staging and evaluation of biochemical recurrence (BCR) were included . Vertex to mid-thigh static scans were acquired after 60-90min of injection of 180-300MBq of 18F-JK-PSMA-7. Additional early dynamic PET acquisition for 10-min post injection and delayed PET imaging (at 120 min) were done in few patients to assess the pharmacokinetics. Imaging findings were correlated with biopsy/histopathology findings. ***Results:*** 34 patients were included in this study, mean age 68 years. 27/34 patients were evaluated for staging and 7/34 were for BCR evaluation . Of staging patients, 59.2% were high risk, 18% were intermediate risk and 22% were low risk. Early dynamic imaging showed fast blood clearance, no significant urinary activity with high tumor to urinary activity ratio, especially in higher grade tumors. Of 16 patients with high-risk biopsy, 81% patients had positive nodal metastasis and 43% had both nodal and metastatic disease on PSMA PET-CT. Organ confined disease was noted in all low risk and intermediate risk staging patients. Mean primary tumor SUVmax of patients with high-risk histology was significantly higher compared to intermediate-low risk group (30.85 vs 11.1, p-0.01). Detection rate was 100 % in all 7 patients with BCR even with PSA as low as 0.3ng/ml. All 7 patients of BCR had salvageable disease on PET/CT with operated bed recurrence with locoregional disease in 3 patients. Delayed imaging at 120 min showed 30% higher mean primary tumor SUVmax compared to 60-90min images irrespective of the tumor grade. Non-specific bone lesions showing low grade PSMA uptake was seen in 8% (3/34 patients). No adverse reactions were reported. ***Conclusion:*** ^{18}F-JK-PSMA-7 PET-CT offers high sensitivity and high-resolution PCa imaging for staging high risk cancers and evaluation of biochemical recurrence. Scan quality is comparable to, if not better than other commercially available PSMA ligands.

As with other urinary excreted PSMA tracers, early dynamic and 2 hr delayed post-diuretic imaging may further improve lesion detectability. ***References:*** 1. Hohberg M et al. Biodistribution and radiation dosimetry of [^{18}F]-JK-PSMA-7 as a novel prostate-specific membrane antigen-specific ligand for PET/CT imaging of prostate cancer. EJNMMI Res. 2019 Jul 25;9(1):66.

EP-0822

Synthesis and Characterization of Zr/Mannose-Conjugated Indocyanine Green-Loaded Liposomes as Sentinel Lymph Node Multimodal Diagnostic Agents for PET/NIR Fluorescence Imaging

G. Kim[1], *D. Jeong*[1,2], *H. Lee*[1];
[1]*Dongnam Institute of Radiological and Medical Sciences (DIRAMS), Busan, KOREA, REPUBLIC OF,* [2]*Dongguk University, Gyeongju, KOREA, REPUBLIC OF.*

Aim/Introduction: The development of multimodal diagnostic agents using radioisotope and near-infrared (NIR) fluorescence molecules is highlighted for improved preoperative positron emission tomography (PET) imaging and intraoperative mapping of sentinel lymph nodes (SLN). We synthesized a nano-sized liposome containing indocyanine green (ICG) inside and bonded non-radiative zirconium to the surface to confirm the labeling potential of zirconium-89. Mannose analogs were introduced to improve the SLN target effect, and the physicochemical properties of the final compound were evaluated. ***Materials and Methods:*** Phospholipids and cholesterol were synthesized into nano-sized liposomes by self-assembly method, and ICG was loaded in the process of redispersing liposomes. To target SLN, mannose analogs were bound to the liposome surface and a chelator, desferrioxamine (DFO), was also introduced. Non-radioactive zirconium was used to confirm the introduction of zirconium-89 and chemically bound to DFO on the liposome surface. ***Results:*** Observations with a scanning electron microscope (SEM) confirmed that the diameter of the liposomes was about 60 nm, and the average hydrodynamic size of the liposome measured using dynamic light scattering (DLS) analysis was confirmed to 233.4 nm. The loading amount of ICG measured using UV/Visible spectroscopy was 33.16 μmol/mg. The binding of DFO and mannose analogs was confirmed using fourier transform-infrared spectroscopy (FT-IR), and the binding of zirconium was confirmed by inductively coupled plasma-mass spectrometry (ICP-MS) analysis. ***Conclusion:*** We successfully synthesized Zr/mannose-conjugated indocyanine green-loaded liposomes. It is expected that effective diagnostic agents for PET/NIR fluorescence imaging targeting SLN will be developed in the future by performing various biological evaluations through zirconium-89 labeling. ***References:*** Ji Youn Lee et al., Naphthol Blue Black and 99mTc-Labeled Mannosylated Human Serum Albumin (99mTc-MSA) Conjugate as a Multimodal Lymph Node Mapping Nanocarrier, Scientific Reports, (2018) 8:13636, DOI:10.1038/s41598-018-31933-1

EP-0823

Biological Evaluation of Escherichia Coli Labeled with Zirconium-89 for the Development of Radiopharmaceuticals for Positron Emission Tomography

D. Jeong[1,2], *G. Kim*[1], *E. Choi*[2], *S. Park*[2], *H. Lee*[1], *S. Kim*[2];
[1]*Dongnam Institute of Radiological and Medical Sciences (DIRAMS), Busan, KOREA, REPUBLIC OF,* [2]*Dongguk University, Gyeongju, KOREA, REPUBLIC OF.*

Aim/Introduction: In this study, the surface of E. coli, which is self-motile and shows high accumulation in tumor tissues, is stably introduced with the diagnostic radioisotope zirconium-89 through chemical modification, and the possibility of bacterial-based radiopharmaceuticals for positron emission tomography (PET) is confirmed through biological evaluation. ***Materials and Methods:*** The primary amine group expressed on the surface of E. coli was reacted with the fluorescein isothiocyanate (FITC) to quantitatively analyze the primary amine group. After chemically binding the chelator desferoxamine (DFO), the stable isotope zirconium was chelated to confirm the possibility of zirconium-89 binding. The in vitro stability of E. coli labeled with zirconium-89 was evaluated using human serum. The cell uptake of zirconium-89 labeled E. coli for CT-26 and A549 cancer cell lines was evaluated. ***Results:*** As a result of measurement with a fluorescent spectrophotometer, it was confirmed that there were 0.88 pmol (5.29 x 10^{11} molecules). Binding of the stable isotope zirconium was confirmed by inductive coupled plasma mass spectrometry (ICP-MS) analysis. The labeling studies of E. coli labeled with zirconium-89 was confirmed through radio-thin layer chromatography (radio-TLC). The labeling rate of zirconium-89 was 99.9%, and it was confirmed to be more than about 95% when the stability was evaluated at human serum and PBS. The cell uptake of zirconium-89 labeled E. coli showed higher uptake of A549 than CT-26 at 24 hours. ***Conclusion:*** Through this study, we labeled the diagnostic radioisotope zirconium-89 on the surface of E. coli and confirmed the in vitro stability of E. coli through biological evaluation. It is expected to contribute to tumor targeting research using PET through various biological evaluation. ***References:*** Kang SR, Jo EJ, Nguyen VH, Zhang Y, Yoon HS, Pyo A, Kim DY, Hong Y, Bom HS, Min JJ. Imaging of tumor colonization by Escherichia coli using ^{18}F-FDS PET. Theranostics. 2020 Apr 1;10(11):4958-4966. doi: 10.7150/thno.42121. PMID: 32308761; PMCID: PMC7163454.

EP-0824

It's Twins!? 68Ga &18F-labelled TriGalactan for Functional Liver Imaging

M. A. Zierke[1], *K. Samadikhah*[2], *C. Rangger*[1], *M. Panzer*[3], *A. Schmid*[2], *R. Haubner*[1];
[1]*Nuclear Medicine, Innsbruck, AUSTRIA,* [2]*Werner Siemens Imaging Center, Tübingen, GERMANY,* [3]*Internal Medicine I, Innsbruck, AUSTRIA.*

Aim/Introduction: Non-invasive liver imaging is of great interest in a variety of clinical settings including liver surgery and transplantation. Therefore, functional hepatocytes are addressed via the asialoglycoprotein receptor (ASGR), which is almost exclusively found in liver tissue. Here we present [^{68}Ga]Ga-NODA-GA-TriGalactan (1) & [^{18}F]AlF-NOTA-TriGalactan (2), a diagnostic pair of galactose trimers for PET imaging. ***Materials and Methods:*** Following structural data from Khorev et al. indicating high affinity of trimeric galactose conjugates, Tris(hydroxymethyl) aminomethane was chosen as a synthetic scaffold. Ligands were synthesized in solution using peptide chemistry techniques and CuAAC. To allow for labelling with either ^{68}Ga or ^{18}F, NODAGA or NOTA were introduced as chelators, respectively. Radiolabelling of 1 with ^{68}Ga was accomplished within 10 min in a 1 M acetate buffer (pH=5) at 56°C. Fluorination of 2 via the aluminium-fluoride method occurred within 15 min at 95°C in a 0.1 M acetate buffer (pH=4). In vitro evaluation included octanol/buffer distribution (logD), protein binding, and metabolic stability studies in human blood serum (incubation for 2, 30, 60, and 120 min at 37°C). For biodistribution experiments with 1, healthy BALB/c mice were used. Animals were dissected 10, 30 and 60 min p.i. and accumulation of the tracer was measured (n=3). Additional pharmacologic studies with both compounds were carried out

in healthy C57Bl/6 male mice using PET/MR (n=3). For analysis, PET and MRI images were fused, corresponding ROIs were drawn based on the MRI scan and TACs were generated for selected organs. ***Results:*** Synthesis of the precursors could be achieved in seven steps and radiolabelling resulted in high (>95%) radiochemical purity. LogD values indicated high hydrophilicity of both tracers. Compound 1 showed high metabolic stability in human blood serum (between 99% and 93% intact tracer up to 2 hours incubation) and low plasma protein binding (approx. 6% protein bound fraction after 30 min incubation). Biodistribution data of 1 revealed high liver uptake (32% iD/g) and excellent target-to-background ratios. Small animal imaging data demonstrated that TACs of liver and heart are well separated. Liver uptake peaked between 5-10 min p.i., followed by a slight washout during the rest of the scan. In contrast, imaging with 2 resulted in both high liver and bone uptake indicating partial complex decomposition in vivo. ***Conclusion:*** [^{68}Ga]Ga-NODA-GA-TriGalactan showed promising in vitro and in vivo results demonstrating the successful development of a small molecular weight PET radiopharmaceutical targeting the ASGR. ***References:*** Khorev et al. Bioorg Med Chem, 2008.

EP-0825

Model of Pharmacokinetic Based on Copper-64 Labeled DNA Bipyramid Nanostructure

P. Li*, J. Li;*
Inner Mongolia Medical University, Hohhot, CHINA.

Aim/Introduction: DNA is well-known as genetic information carrier with a double-helix structure. From a nanomaterials point of view, DNA is also a kind of material as material to become a molecular probe. DNA nanomaterials can be constructed by self-assembly protocols that exploit the Watson-Crick principle. This nanomaterial is essentially non-toxic and has excellent biological compatibility. DNA nanomaterials of various sizes and shapes have been designed. DNA nanostructures have attracted attention in many fields, such as biosensing, drug delivery, and in vivo imaging due to their excellent properties. However, the pharmacokinetics of DNA nanomaterials is poorly understood. In this study, PET imaging was used to visualize the DNA Bipyramid Nanostructure (DBN) distribution in vivo and to model the DNA pharmacokinetics. ***Materials and Methods:*** DBN was annealed and assembled in TM buffer by rapidly cooling from 95°C to 4°C within 30 minutes. Size exclusion chromatography was used to purify DBN. The amine-functionalized Single-stranded DNA was first conjugated with NOTA in carbonate buffer, and HPLC was used to purify NOTA-ssDNA. NOTA-ssDNA solution was added to 2 mCi of $^{64}CuCl_2$ in NaAc buffer for 1 h at 37 °C, under constant shaking. ^{64}Cu-ssDNA was purified with a PD-10 column, the highly radioactive component was used for hybridization to produce ^{64}Cu-DBN. ^{64}Cu-DBN was administered to the mice, and a 1h dynamic PET imaging was then carried out to monitor the biodistribution process of DBN in vivo. The pharmacokinetic model was established by analyzing Region-of-interest (ROI). ***Results:*** We use the Polyacrylamide gel electrophoresis to characterize the DBN self-assembly process. Dynamic light scattering analysis showed that the average diameter for DBN was 26.91 ± 2.45 nm. Cell Counting Kit-8 test and hematoxylin and eosin proved that DBN was not biotoxic. PET imaging showed that DBN was mainly excreted through the kidneys. ***Conclusion:*** In this study, a simple and fast method for the preparation of ^{64}Cu-DBN was developed. PET imaging allows us to make a dose assessment of ROI. This approach was used to model the pharmacokinetics of DBN. The model we have developed using nuclear medicine techniques will guide further optimization of DNA nanomaterials. ***References:*** 1. Jiang D, Ge Z, Im HJ, et al. DNA origami nanostructures can exhibit preferential renal uptake and alleviate acute kidney injury. Nat Biomed Eng. 2018;2(11):865-877.

EP-0827

Radionuclide cisternography with PET/CT using Cu-64-DOTA

J. Greiser*[1], S. Groeber[1], T. Weisheit[1], T. Niksch[1], C. Kuehnel[1], M. Schwab[2], R. Drescher[1], M. Freesmeyer[1];*
[1]Clinic of Nuclear Medicine, University Hospital, Jena, GERMANY,
[2]University Hospital, Clinic of Neurology, Jena, GERMANY.

Aim/Introduction: The imaging of the cerebrospinal system (cisternography) may help diagnose abnormalities and pathologies of the intracranial cerebrospinal fluid (CSF)-filled cavities, particularly in cases of suspected CSF leaks. Radionuclide cisternography can help to identify and localize CSF leaks, when established CT or MRI procedures fail or cannot be applied. However, SPECT radionuclide cisternography with In-111-DTPA or Tc-99m-DTPA provides lower image resolution compared to PET. Therefore, we have investigated the potential of the PET tracer Cu-64-DOTA as intrathecal agent for PET radionuclide cisternography. ***Materials and Methods:*** Manual Cu-64-DOTA preparation was validated in accordance to GMP guidelines. Quality control included radio HPLC and radio TLC for RCP determination, gamma spectrometry, osmolality and pH testing as well as sterility testing and testing for endotoxins in accordance with Ph. Eur. and USP requirements on agents intended for intrathecal administration, whenever applicable. Cu-64-DOTA and In-111-DTPA were administered on separate days into the CSF cavity of a patient and PET/CT image acquisition was performed. Urine samples were collected for excretion profiling. ***Results:*** Cu-64-DOTA can be prepared from Cu-64-chloride and DOTA in PBS buffer, resulting in high RCY and RCPs ≥ 95.0 %. The formulation was in accordance to Ph. Eur. and USP requirements on agents intended for intrathecal administration, particularly in regard to endotoxin content, pH and osmolality. Additionally, Cu-64-DOTA exhibits very low concentrations of excipients compared to established CT and MRI contrast agents, thus decisively lowering the probability of adverse events in comparison. A CSF leak was detected successfully with Cu-64-DOTA PET, while radionuclide cisternography with In-111-DTPA gave a false negative. Cu-64-DOTA is mainly excreted renally. ***Conclusion:*** Radionuclide cisternography using PET can be performed with Cu-64-DOTA, providing an alternative to established procedures in cases of inconclusive results. Due to the higher image resolution, CSF leak detection with Cu-64-DOTA may be superior to established agents In-111-DTPA or Tc-99m-DTPA.

EP-0828

11C-Labeled histamine derivatives for PET imaging

X. Shao*, K. Mhanna, A. Brooks, J. Witek, D. Raffel, P. Scott;*
University of Michigan, Ann Arbor, MI,
UNITED STATES OF AMERICA.

Aim/Introduction: Histamine is a heterocycle that exhibits a range of biological activities in various pathological and physiological conditions. Based on our success in the imaging of cardiac sympathetic nerves and neuroendocrine tumors using $^{11}C/^{18}F$-guanidines,[1] we have designed and radiosynthesized ^{11}C-N-[2-(1H-imidazolyl-4-yl)ethyl]guanidine (IEG), a ^{11}C-guanylated derivative of histamine. The automated radiosynthesis of [^{11}C]IEG and PET

imaging studies of rats and non-human primates is reported here. ***Materials and Methods:*** Production of [^{11}C]IEG was carried out using a GETracerLab FX$_m$. Briefly, [^{11}C]cyanogen bromide was formed from hydrogen [^{11}C]cyanide[2] and bubbled into a reactor containing the histamine precursor in sodium borate buffer (pH 8.0). The produced [^{11}C]cyanamide intermediate was treated with a 35% ammonium chloride in ammonium hydroxide solution to yield [^{11}C]IEG. Ammonium acetate buffer (pH 5.0) was added and the product was purified using semi-preparative HPLC (Luna SCX 250x10mm; 10mM NH_4OAc and 400mM NaCl in H_2O; 5 mL/min). The peak around 10 min was collected and diluted with USP water for injection. Whole body imaging was performed by dynamic animal PET scanning for 60 minutes in rats and myocardial imaging was performed in a non-human primate (rhesus). ***Results:*** 18.5 ± 5.8 mCi of [^{11}C]IEG was synthesized with a radiochemical yield (RCY) of 13.2 ± 8.4% (n = 5) and radiochemical purity (RCP) greater than 95% based on analytic HPLC (Luna SCX column 250x4.6mm, 10mM NH_4OAc and 400mM NaCl in H_2O; 2 mL/min; UV 212nm and Rad). The rodent imaging of rats showed uptake and rapid washout in the heart, high uptake and retention in kidney, and no brain uptake was observed. The preliminary monkey imaging showed no myocardial uptake and high uptake and retention in the kidney. ***Conclusion:*** We have successfully synthesized [^{11}C] IEG and have developed an effective purification method without any organic solvent. The final injectable doses are qualified for periclinal use and potentially for clinical application. The animal studies showed low myocardial uptake and retention. Further exploration of this finding, as well as structural modifications and PET imaging focusing on the kidney, are currently under investigation and will be reported in due course. ***References:*** [1] Raffel, D. M.; Jung, Y.; Koeppe, R. A.; Jang, K. S.; Gu, G.; Scott, P. J. H.; Murthy, V. L.; Rothley, J.; Frey, K. A. First-in-Human Studies of [18F] Fluorohydroxyphenethylguanidines. Circ.: Cardiovasc. Imaging 2018. [2] Westerberg, G.; Kärger, W.; Onoe, H.; Långström, B. [11C]Cyanogen Bromide in the Synthesis of 1,3-Di(2-tolyl)-[11C] guanidine. J. Labelled Compds. Radiopharm. 1994, 34, 691-696.

EP-0829

Synthesis and Preclinical Evaluation of two novel 68Ga-labeled (R)-pyrrolidin-2-yl-boronic acid-based FAP-targeted tracers for Cancer Imaging with Positron Emission Tomography

S. Bendre, *H. Kuo, H. Merkens, Z. Zhang, J. Zeisler, N. Coplo, F. Bénard, K. Lin;*
BC Cancer Research Center, Vancouver, BC, CANADA.

Aim/Introduction: Fibroblast activation protein (FAP) is a membrane-anchored serine protease overexpressed in the reactive stromal fibroblasts of >90% human carcinomas. Its restricted normal tissue distribution and involvement in tumorigenesis makes it a promising target for developing radiopharmaceuticals for imaging and therapy of carcinomas. Here we synthesized two novel (R)-pyrrolidin-2-yl-boronic acid-based FAP-targeted ligands; SB02055 (DOTA-conjugated (R)-(1-((6-(3-(piperazin-1-yl)propoxy) quinoline-4-carbonyl)glycyl)pyrrolidin-2-yl)boronic acid) and SB04028 (DOTA-conjugated ((R)-1-((6-(3-(piperazin-1-yl)propoxy) quinoline-4-carbonyl)-D-alanyl)pyrrolidin-2-yl)boronic acid). ^{nat}Ga- and ^{68}Ga-complexes of both ligands were evaluated in preclinical studies and compared with previously reported ^{nat}Ga/^{68}Ga-complexed PNT6555 [1]. ***Materials and Methods:*** Complexation of ^{nat}Ga and ^{68}Ga was conducted in acetate buffer (0.1M, pH 4.5) and HEPES buffer (2M, pH 5.0), respectively. All ^{nat}Ga complexes were subjected to in vitro FAP binding assays. PET/CT imaging and ex vivo biodistribution studies were performed in HEK293T:hFAP tumor-bearing mice at 1 h post-injection. [^{68}Ga]Ga-SB02055 and [^{68}Ga]Ga-SB04028 were also subjected to in vivo stability testing at 15 min post-injection. ***Results:*** ^{nat}Ga complexes were obtained in 36-98% yields. IC_{50}(FAP) values for ^{nat}Ga-SB02055, ^{nat}Ga-SB04028 and ^{nat}Ga-PNT6555 were 0.41±0.06, 13.9±1.29 and 78.1±4.59 nM, respectively. ^{68}Ga-labeled analogues were obtained in 19-58% decay-corrected radiochemical yields with >92% radiochemical purity. PET/CT images showed clear tumor visualization with good contrast by [^{68}Ga]Ga-SB04028 and [^{68}Ga]Ga-PNT6555, but not [^{68}Ga]Ga-SB02055. Biodistribution data showed that while [^{68}Ga]Ga-SB02055 exhibited nominal tumor uptake (1.08±0.37 %ID/g), [^{68}Ga]Ga-SB04028 demonstrated ~1.5-fold higher tumor uptake (10.1±0.42 %ID/g) than [^{68}Ga]Ga-PNT6555 (6.38±0.45 %ID/g). High accumulation in the bladder indicated renal excretion of all three tracers. [^{68}Ga]Ga-SB04028 displayed background level uptake in most normal organs/tissues,and comparable to those of [^{68}Ga]Ga-PNT6555. However, since the tumor uptake of [^{68}Ga]Ga-SB04028 was considerably greater than [^{68}Ga]Ga-PNT6555, the corresponding tumor/organ uptake ratios for [^{68}Ga]Ga-SB04028 were significantly higher than those of [^{68}Ga]Ga-PNT6555. In vivo stability testing revealed no intact [^{68}Ga]Ga-SB02055 in the mouse plasma, with ~94% remaining intact in the urine, indicative of its rapid washout. The intact fractions for [^{68}Ga]Ga-SB04028 in plasma and urine were ~ 47% and ~ 55%, respectively. ***Conclusion:*** We successfully synthesized and evaluated two novel (R)-pyrrolidin-2-yl-boronic acid-based FAP-targeted PET tracers. While the P2-glycine bearing [^{68}Ga]Ga-SB02055 displayed nominal tumor uptake, its P2-D-alanine congener [^{68}Ga]Ga-SB04028 demonstrated higher tumor uptake and superior imaging contrast compared to [^{68}Ga]Ga-PNT6555. [^{68}Ga]Ga-SB04028 is a promising tracer for clinical translation to detect cancer lesions with PET. Efforts are currently underway to replace DOTA with a suitable chelator that would allow labeling with the most widely used isotope ^{99m}Tc to enable SPECT imaging. ***References:*** [1] Bachovchin et al., JNM, volume 63 (supplement 2) 4028

EP-0830

[89Zr]Zr-desferrioxamine-B: A novel agent for PET imaging of Vibrio cholerae infection

H. Yousefnia, *F. Mohammadpour-Ghazi, S. Zolghadri;*
Nuclear Science and Technology Research Institute (NSRTI), Tehran, IRAN, ISLAMIC REPUBLIC OF.

Aim/Introduction: Precise and timely diagnosis of infectious diseases is a crucial step for effective patient care and epidemic prevention. Cholera is an epidemic and acute diarrheal disease caused by the toxigenic Vibrio cholerae. Some bacteria are able to produce siderophores, which can act as small iron chelators to provide this essential metal nutrient. In this study, [^{89}Zr]Zr-desferrioxamine-B ([^{89}Zr]Zr-DFO-B) was prepared at optimized condition and evaluated as a new PET tracer for detection of Vibrio cholera infection. ***Materials and Methods:*** ^{89}Zr was produced by ^{89}Y(p,n)^{89}Zr nuclear reaction via 30 MeV IBA cyclotron and separated from Y target and other possible impurities using ZR resin. [^{89}Zr]Zr-DFO-B was prepared at optimized condition and its stability, partition coefficient and protein binding was studied in vitro. Finally, the biodistribution of the complex was investigated in normal and cholera mice models using organs %ID/g calculation and imaging. ***Results:*** [^{89}Zr]Zr-DFO-B was prepared with high radiochemical purity > 98% (RTLC). The complex was stable in PBS buffer (4 °C) and human blood serum (37 °C) at least for 72 h (> 95%). The radiolabeled complex showed the fast blood clearance

and renal excretion which is related to the hydrophilic nature of [89Zr]Zr-DFO-B. The tracer also demonstrated high uptake of Vibrio cholera strain in vitro and in vivo that could be blocked with an excess of iron-DFO-B. ***Conclusion:*** According to the results, [89Zr]Zr-DFO-B radiolabeled complex can be considered as a high potential agent for PET imaging of Vibrio cholerae infection, however more biological data are still needed.

EP-0831

Preclinical evaluation of [18F]FEAO, a novel radiotracer for myocardial perfusion imaging in PET

M. Dziuk[1], *E. Witkowska-Patena*[1], *S. Krajewski*[2], *J. Towpik*[2], *L. Steczek*[2], *K. Gotowicz*[2], *P. B. Kozanecki*[2], *J. Wlostowska*[2], *C. Kozanecki*[2];
[1]*Military Institute of Medicine National Research Institute, Warsaw, POLAND,* [2]*Synektik Research, Warsaw, POLAND.*

Aim/Introduction: Positron emission tomography (PET) is now an established method for myocardial perfusion imaging (MPI). The available tracers show a number of limitations, therefore the 18F-labelled tracer is in high demand now. In this study, we present the preclinical characterisation of [18F]FEAO, a novel MPI radiotracer for PET. ***Materials and Methods:*** The [18F]FEAO biodistribution and pharmacokinetics were analysed by 45-minute dynamic microPET imaging in Wistar rats (n=4). The pharmacodynamics was assessed in vitro in radioligand binding assays for 68 receptors, ion channels and transporters. The tracer metabolism was studied by FEAO incubation in rat, dog and human hepatocytes. The absorption (n=18) and potential toxicity (n=30) of FEAO were assessed in male and female Wistar rats after a bolus intravenous administration of 2 mg/kg of the tracer. The compound concentration in plasma was measured in samples (n=3) collected at 4, 15, 30, 60 minute, 4, and 24 hour time-points after injection. The test item effects on clinical, haematological, biochemical, enzymatic parameters, gross and histopathological lesions in tissues and internal organs were evaluated at 24 hour and 14 day after injection. ***Results:*** The time activity curves yielded from microPET images showed rapid, high and stable myocardial [18F]FEAO uptake with an average standardized uptake value of about 4 throughout the scan time. The scans also confirmed hepatic and renal elimination of the tracer. Radioligand binding assays showed significant responses in 3/68 assays: muscarinic acetylcholine M1 and M2 receptors and potassium channel hERG. The FEAO showed rapid plasma clearance within 1 hour post injection (2.59 L/h/kg) with elimination half-life of 0.26 hour. The compound was mostly metabolised via an oxidative N-dealkylation, while the fluor substituent was not separated from the molecule. The tested level of 2 mg/kg was considered to be the No Observed Adverse Effect Level (NOAEL). ***Conclusion:*** The study revealed a favourable pharmacokinetic and pharmacodynamic profile of [18F]FEAO. The dynamic microPET images clearly visualised the myocardium. In conclusion, the imaging procedure is expected to be safe for the human subjects. Promising study results prompt further tracer evaluation in a clinical trial.

EP-0832

LANTana: A phase Ib study nvestigating epigenetic modification of somatostatin receptor-2 with ASTX727 to improve therapeutic outcome with [177Lu]-DOTA-TATE in patients with metastatic neuroendocrine tumours

R. Sharma[1], *S. R. Khan*[2], *M. Naik*[2], *T. D. Barwick*[3], *E. O. Aboagye*[4];
[1]*imperial college london, London, UNITED KINGDOM,* [2]*Imperial college NHS Heatlhcare Trust, London, UNITED KINGDOM,* [3]*Imperial College Healthcare NHS Trust London, London, UNITED KINGDOM,* [4]*Imperial College London, London, UNITED KINGDOM.*

Aim/Introduction: Suitability for peptide receptor radionuclide therapy (PRRT) for neuroendocrine neoplasia (NENs) depends on presence of SSTR2 determined by [68Ga]-DOTA-peptide-PET. A significant number of patients will have low or no uptake on [68Ga]-DOTA-peptide-PET, precluding PRRT. The upstream promoter region of SSRT2 is methylated, with percentage of methylation correlating with SSTR2 expression. Demethylating agents increase uptake on PET imaging in vivo such that tumours previously negative on PET imaging become positive, correlating with a dose dependent increase in tumoural SSTR2 expression. LANTana aims to determine whether treatment with the demethylating agent, ASTX727, results in re-expression of SSTR2 using [68Ga]-DOTA-peptide-PET to image epigenetic modification of the SSTR2 locus, allowing subsequent treatment with [177Lu]-DOTA-TATE. ***Materials and Methods:*** 27 participants with a histologic diagnosis of NEN (Ki67<55%) with no or low uptake on baseline [68Ga]-DOTA-TATE-PET/CT will be recruited. Patients will receive 5 days of ASTX727 (fixed dose 35mg decitabine + 100mg cedazuridine). [68Ga]-DOTA-TATE-PET/CT will be repeated day 8+2; where there is significant uptake, [177Lu]-DOTA-TATE will be administered. ***Results:*** Primary objective is to determine re-expression of SSTR2 on PET imaging. Tolerability, progression free survival, overall response and quality of life will be assessed. LINE-1 methylation in peripheral blood mononuclear cells and tumoral methylation will be evaluate.Results from the first 5 patients enrolled will be presented ***Conclusion:*** LANtana is the first human study to investigate epigenetic modification to re-sensitize tumours to SSTR2-targeting radiotheranostic drugs. · This trial will provide prospective evidence on the efficacy of a demethylation strategy to re-express SSTR2 allowing subsequent treatment with [177Lu]-DOTATATE in patients who otherwise would be excluded. · Novel manipulation of receptor expression through the use of demethylation agents may be applicable to other tumour types ***References:*** Torrisani, J., et al., Identification of an upstream promoter of the human somatostatin receptor, hSSTR2, which is controlled by epigenetic modifications. Endocrinology, 2008. 149(6): p. 3137-47. Taelman, V.F., et al., Upregulation of Key Molecules for Targeted Imaging and Therapy. J Nucl Med, 2016. 57(11): p. 1805-1810. Veenstra, M.J., et al., Epidrug-induced upregulation of functional somatostatin type 2 receptors in human pancreatic neuroendocrine tumor cells. Oncotarget, 2018. 9(19): p. 14791-14802.Evans, J.S., et al., Epigenetic potentiation of somatostatin-2 by guadecitabine in neuroendocrine neoplasias as a novel method to allow delivery of peptide receptor radiotherapy. Eur J Cancer, 2022. 176: p. 110-120.

EP-0833

Comparison of [68Ga]Ga-FAPI-46 PET/CT and [18F] FDG PET/CT hepatic tumors

F. Novruzov[1], *E. Mehdi*[1], *N. Orucova*[2], *N. Aliyeva*[1], *R. Shukurov*[3], *Z. Dadashov*[2], *F. Valla*[4], *J. Aliyev*[5];
[1]*Azerbaijan National Centre of Oncology, Department of Nuclear Medicine, Baku, AZERBAIJAN,* [2]*Azerbaijan National Centre of Oncology, Department of Nuclear Medicine, Baku, Azerbaijan, Baku, AZERBAIJAN,* [3]*Azerbaijan National Centre of Oncology, Department of Nuclear Medicine, Baku, Azerbaijan, Baku, Azerbaijan, Baku, AZERBAIJAN,* [4]*Sofie, Totowa, NJ, UNITED STATES OF AMERICA,* [5]*Azerbaijan National Centre of Oncology, Department of General Surgery, Baku, Azerbaijan, Baku, AZERBAIJAN.*

Aim/Introduction: Fibroblast activation protein (FAP) is commonly expressed in activated stromal fibroblasts found in various types of epithelial tumours. Its ability to detect primary liver tumours is notably higher than other imaging modalities. The objective of this study was to evaluate and compare the

imaging performance of 68Ga-FAPI PET and 18F-FDG PET in hepatic tumours. ***Materials and Methods:*** Two male patients with liver lesions underwent whole-body PET/CT scans using [18F] FDG and 68Ga-FAPI tracers at least one week apart for staging and metastasis evaluation. The tracer accumulation intensity was evaluated using the maximum standardized uptake value (SUVmax) and the tumor-to-background ratio (TBR) methods. ***Results:*** The first case was a 54-year-old male patient with a cirrotic liver who presented to our department with a suspicious lesion. We performed both an 18F-FDG scan and a 68Ga-FAPI scan on the patient. The FDG scan revealed multiple hypermetabolic lesions in the liver with an SUVmax of 9.9. Similarly, the 68Ga-FAPI scan showed lesions with high 68Ga-FAPI concentration and an SUVmax of 11.5. 68Ga-FAPI scan also identified an additional lesion measuring 1.5 cm on the right 8th rib, which displayed high 68Ga-FAPI concentration with an SUVmax of 12.7. The highest tumor-to-background ratio of both scans was 5 and 10 respectively. The second patient, a 60-year-old male, was admitted to our department upon discovering a liver tumor. The FDG scan revealed lesions with moderate FDG uptake (SUVmax=3.2). The patient also presented with portal lymph nodes, which showed no FDG accumulation. Moreover, we observed an infiltrative lesion left lung, which did not show any FDG accumulation. On the 68Ga-FAPI scan, we noticed high 68Ga-FAPI uptake in the liver lesions (SUVmax=13.0). The portal lymph nodes also did not show any accumulation of 68Ga-FAPI. The lesion in the upper lobe of the left lung showed mild 68Ga-FAPI accumulation (SUVmax=2.8). The tumor-to-background ratio of greatest liver lesions was 1,5 and 13 respectively. ***Conclusion:*** In both of our patients, we observed an higher tumor-to-background ratio with higher uptake of tumors on the FAPI scan, indicating its superiority over FDG in liver cancers. As FDG has limited effectiveness in the evaluation of liver cancers, the use of FAPI scans may offer clear advantages.

EP-57

e-Poster Area

D: Technical Studies -> D5 Radiopharmacy/ Radiochemistry -> D53 New Radiopharmaceuticals - Therapy

EP-0834

Radioimmunotherapy of experimental systemic mucormycosis in a murine model

J. Carvalho, *M. E. Malo, K. J. H. Allen, C. Frank, Z. Xiao, R. Jiao, E. Dadachova;*
University of Saskatchewan, Saskatoon, SK, CANADA.

Aim/Introduction: Opportunistic fungal infections such as aspergillosis, cryptococcosis, candidiasis, and mucormycosis are causing devastating morbidity and mortality in immunocompromised patients as anti-fungal agents do not work in the setting of immunosuppression. For example, species of Rhizopus lead to high incidence and high mortality from fungal pneumonias in patients with hematologic malignancies and hematologic stem cells transplants. The COVID-19 pandemic has created a novel landscape for opportunistic fungal infections. COVID patients suffer from severe immune dysfunction due to the disease, use of steroids for reducing inflammation, and high incidence of comorbidities (with diabetes being the most prominent). Thus, it is imperative to develop novel diagnostic and treatments tools that would work in the setting of severe immunosuppression and comorbidities, and that would have acceptable risk profiles. Radioimmunotherapy (RIT) uses monoclonal antibodies (mAbs) to target radiation to cancerous or infectious cells, and is not dependent on the immune status of a patient.The aim of this study was to investigate the application of RIT against mucormycosis-causing fungus Rhizopus oryzae in a murine model of systemic infection using mAbs to the pigment melanin or to 1,3-β-glucan - two prominent fungal antigens. ***Materials and Methods:*** Female C57Bl6 mice were infected intravenously with 10^4 R. oryzae spores. The infection was imaged in mice using microSPECT/CT. Targeting of ^{111}In-labeled anti-melanin mAb c8C3 and anti-1,3-β-glucan mAb was compared to MOPC21, an irrelevant control mAb. Imaging mAb were administerd 24 hours post-infection with R. oryzae and imaged 48-120 hrs post-infection. For RIT, infected mice were treated with 1.85 or 3.7 MBq of ^{177}Lu-labeled c8C3 mAb, ^{177}Lu-labeled 400-2 mAb, or with 3.7 MBq irrelevant control MOPC21 mAb. The mice were sacrificed 48 hrs post-treatment and the fungal burden in their major organs was measured by colony forming units. ***Results:*** microSPECT/CT imaging showed very different patterns of biodistribution in infected mice between mAbs to fungal antigens melanin and 1,3-β-glucan and the control mAb with much slower clearance of the latter from the circulation. RIT of infected mice with ^{177}Lu-labeled mAbs to melanin and 1,3-β-glucan resulted in dose dependent and statistically significant ($p<0.05$) clearance of the fungal burden from the major fungal dissemination organs, such as brain, lungs, spleen and liver in comparison with ^{177}Lu-labeled control mAb and untreated mice. ***Conclusion:*** RIT of experimental systemic mucormycosis proved to be effective in immunocompetent mice and its evaluation in immunosuppressed mice is currently underway.

EP-0835

[123I]CC1: a Radiotheranostic Agent for PARP-expressing Cancer Imaging and Therapy

C. Chan, *Z. Chen, M. Veal, G. Dias, G. Destro, M. Mosley, F. Guibbal, V. Gouverneur, B. Cornelissen;*
University of Oxford, Oxford, UNITED KINGDOM.

Aim/Introduction: Fighting cancer has been a worldwide priority for many years. The global increases in cancer diagnoses and deaths have led to a huge demand on the development of cancer research for diagnostic and therapeutic applications. Furthermore, despite the significant improvement in the prognosis for patients over the past decades, the emergence of treatment resistance after the standard of care such as radiotherapy and chemotherapy is frequently observed, and some hard-to-treat cancers such as those of pancreas and brain still remain low survival rates, hence the need for new selective, mechanism-based therapeutics to tackle this life-threatening disease. Targeting DNA damage repair (DDR) signalling is a fast-expanding field for cancer therapy. Among all DDR proteins, poly(ADP-ribose)polymerase (PARP) family is one of the main players in regulating of various DDR pathways to help with DNA damage repair, and its aberrant expressions in many cancers makes it become a potential therapeutic strategy for cancer carrying DDR gene mutations or high PARP expressions. Our on-going efforts has developed and identified a PARP-targeting radiotheranostic agent, [^{123}I]CC1, which emits different type of radiations that allows visualisation of the lesion site and precise delivery of ionising radiation to tumour cells for lethal effects, hence enabling clinicians to achieve "see what you treat & treat what you see". Such development may potentially create new directions for personalised therapeutic strategies for cancers. Here, we investigated the therapeutic potential of [^{123}I]CC1

in human cancer models: PSN1 (pancreatic adenocarcinoma) and U87MG (glioblastoma). ***Materials and Methods:*** Cu-mediated ^{123}I-iododeboronation of a boronic pinacol ester precursor afforded [^{123}I]CC1. The level and specificity of cell uptake and therapeutic efficacy of [^{123}I]CC1 were determined in PSN1 and U87MG cells. Tumour uptake and tumour growth inhibition of [^{123}I]CC1 was assessed in mice bearing human cancer xenografts. ***Results:*** In vitro and in vivo studies showed selective uptake of [^{123}I]CC1 in both models. Significantly reduced clonogenicity, a proxy for tumour growth inhibition by ionising radiation in vivo, was observed in vitro after treatment with as low as 10 Bq [^{123}I]CC1. Biodistribution at 1 h after intravenous administration showed PSN1 tumour xenograft uptake of 0.9±0.06%ID/g. Intravenous administration of a relatively low amount of [^{123}I]CC1 (3 MBq) was able to significantly inhibit PSN1 and U87MG xenografts tumour growth, without significant toxicity to normal tissues. ***Conclusion:*** Taken together, these results show the potential of [^{123}I]CC1 as a targeted radiotheranostic agent for PARP-expressing cancer imaging and therapy.

EP-0836

Theranostics approach to imaging and treating experimental melanoma with 203/212Pb-labeled antibodies to melanin

R. Jiao[1], *K. J. H. Allen*[1], *M. Malokja782@mail.usask.ca*[1], *J. Wilson*[2], *B. J. B. Nelson*[2], *F. Wuest*[2], *E. Dadachova*[1];
[1]*University of Saskatchewan, Saskatoon, SK, CANADA,*
[2]*University of Alberta, Edmonton, AB, CANADA.*

Aim/Introduction: Metastatic melanoma continues to be a deadly disease claiming thousands of lives each year in spite of several immunotherapeutic agents introduced into the clinic in the past decade. This leaves a great potential for the development of novel diagnostic approaches as well as the exploration of combination therapies for the treatment of metastatic melanoma. One such approach is targeting melanin pigment with radionuclide therapy. We have been investigating targeting melanin with melanin-specific radiolabeled antibodies as a strategy to treat metastatic melanoma. ***Materials and Methods:*** Female C57Bl6 mice were injected with 0.5M B16F10 murine melanoma cells. Chimeric antibody (c8C3) was used in this study to target the melanin. To image the tumor uptake, c8C3 antibody was labeled with ^{203}Pb-TCMC, followed by microSPECT/CT for 3h, 24h, 48h, and 120h. The tumor bearing mice were followed by radioimmunotherapy with a c8C3 antibody radiolabeled with an "in vivo generator" ^{212}Pb/^{212}Bi, which emits alpha particles. 5μCi, 10 μCi, or 17 μCi of ^{212}Pb labeled antibodies were IV injected into the mice. Tumor size and health conditions were monitored 3 times a week; blood was collected at the end of the study for further analysis. ***Results:*** microSPECT/CT produced distinctive tumor imaging of B16F10 tumors. The ^{212}Pb/^{212}Bi-labeled c8C3 antibody demonstrated a significant dose response in slowing down the tumor growth when compared to the untreated and radiolabeled control antibody. No liver or kidney dysfunction were noticed. ***Conclusion:*** We conclude that the $^{203/212}$Pb-labeled antibody to melanin is a promising theranostic modality for metastatic melanoma which warrants further investigation.

EP-0837

Co-treatment with Trastuzumab Improved Therapy of HER2 expressing Xenograftswith [177Lu]Lu-ABY-027 Affibody Molecule

Y. Liu[1], *T. Xu*[1], *A. Vorobyeva*[1], *A. Loftenius*[2], *V. Bodenko*[3], *A. Orlova*[1], *F. Y. Frejd*[2], *V. Tolmachev*[1];
[1]*Uppsala University, Uppsala, SWEDEN,* [2]*Affibody AB, Solna, SWEDEN,* [3]*Tomsk Polytechnic University, Tomsk, RUSSIAN FEDERATION.*

Aim/Introduction: Human epidermal growth factor receptor 2 (HER2) is overexpressed in several cancers. Affibody molecules are small (7 kDa) scaffold proteins with excellent targeting of HER2, but high renal uptake limits their application for radionuclide therapy. ABY-027 is an Affibody molecule, fused with albumin binding domain to prevent glomerular filtration and therefore reduce renal uptake. Biodistribution of [^{177}Lu]Lu-ABY-027 suggests potential for radionuclide therapy of HER2-expressing tumours. Anti-HER2 monoclonal antibody trastuzumab and ABY-027 bind to different epitopes of HER2, which enables possible combination therapy. The aim of this study was to evaluate therapeutic efficacy of [^{177}Lu]Lu-ABY-027 alone and in combination with trastuzumab in an animal model. ***Materials and Methods:*** HER2-expressing xenografts were obtained by implantation SKOV3 cells to Balb/c nu/nu mice. Treatment was initiated one week later. Mice were randomized into 5 groups, 10 animals per group. Animals in therapy group were intravenously injected with 20 MBq (20 μg) of [^{177}Lu]Lu-ABY-027. Animals in another group were treated with 6 injections of trastuzumab, according to clinical protocol. Mice in combination group were treated with both [^{177}Lu]Lu-ABY-027 and trastuzumab, with the same dose as in mono-treatment groups. One control group was treated with 1% BSA in PBS as vehicle and another with 20 μg of unlabelled ABY-027. The animals were euthanized when tumours reached a size of 1000 mm^3 or became ulcerated. Survival data were analysed using log-rank Mantel-Cox test. ***Results:*** The treatment with trastuzumab resulted in the median survival of 55.5 days, which is significantly ($p<0.05$) longer than the median survival of mice in the control groups treated with vehicle (33 days) or unlabelled ABY-027 (42 days). Treatment with [^{177}Lu]Lu-ABY-027 prolonged median survival till 77 days, which is significantly longer than that of group treated with trastuzumab. In the combination group, eight mice were alive at the study termination (day 90) and tumors in two animals had disappeared completely. Thus, the median survival was not reached and the survival was significantly longer compared to mice treated with trastuzumab or [^{177}Lu]Lu-ABY-027 alone. No pathologic change was observed in kidneys and livers for all mice. ***Conclusion:*** The radionuclide therapy using [^{177}Lu]Lu-ABY-027 increases survival of mice with HER2-expressing xenografts. It is more efficient than the treatment with trastuzumab alone. Co-treatment with [^{177}Lu]Lu-ABY-027 and trastuzumab improved the therapy outcome even further and provided some tumor remissions. This makes the combination of trastuzumab and [^{177}Lu]Lu-ABY-027 radionuclide therapy a promising candidate for clinical translation.

EP-0838

Organotrifluoroborate Enhances Tumor Targeting of Fibroblast Activation Protein Inhibitors for Targeted Radionuclide Therapy

Y. Liu, *M. Xu, J. Chen, X. Cui, Z. Liu;*
Peking University, Beijing, CHINA.

Aim/Introduction: Fibroblast activation protein (FAP) is a pan-cancer target and now the state-of-the-art to develop radiopharmaceuticals. FAP inhibitors have been of great success in developing imaging tracers. Yet, the overly rapid clearance cannot match with the long half-lives of regular therapeutic radionuclides. Though strategies that aim to elongate the

circulation of FAPIs are being developed, here we describe an innovation that uses α-emitters of short half-lives to pair the rapid pharmacokinetics of FAPIs. ***Materials and Methods:*** An organotrifluoroborate linker is engineered to FAPIs to give two advantages: 1) selectively increases tumor uptake and retention; 2) facile ^{18}F-radiolabeling for positron emission tomography to guide radiotherapy of α-emitters, which can hardly be traced in general. The obtained ligands are labeled with F-18 and radiometals. The labeling yield, purity, and stability are tested using HPLC. The binding affinity is measured in HT-1080-FAP cells. PET imaging and biodistribution experiments are performed to evaluate the pharmacokinetics. Finally, [^{213}Bi]Bi-FT-FAPI is used for the targeted radionuclide therapy. ***Results:*** A series of FAP inhibitors named FT-FAPIs are synthesized. The F-18 radiolabeling yield is > 30%, the radiochemical purity is > 99%, and the labeling process is < 25 minutes. The IC_{50} of four screened [^{18}F]F-FT-FAPIs are 22.35, 10.87, 5.34, and 8.03 nM, respectively. PET imaging shows that [^{18}F]F-FT-FAPIs have high tumor uptake and tumor-to-background ratios. Among them, the tumor SUV_{mean} of [^{18}F]F-FT-FAPI-02 is 1.30 ± 0.49, 1.35 ± 0.66, and 1.26 ± 0.22 at 0.5, 1, and 4 hours post-injection (n = 4), which are significantly higher than [^{68}Ga]Ga-FAPI-04 (0.91 ± 0.16, 1 h p.i.) and [^{18}F]F-AMBF$_3$-FAPI without DOTA (0.36 ± 0.07, 1 h p.i.). In the head-to-head comparison, the tumor uptake of [^{68}Ga]Ga-FT-FAPI-02 is also significantly higher than that of [^{68}Ga]Ga-FAPI-04 (1.56 ± 0.23 vs 0.91 ± 0.16, 1 h p.i.). A cumulative dose of 13.2 MBq of [^{213}Bi]Bi-FT-FAPI-02 significantly inhibits tumor growth, while the same dose of [^{213}Bi]Bi-FAPI-04 shows no efficacy. Besides, FT-FAPI is successfully labeled by F-18 and Bi/Pb/Tb to mimic the in vivo pharmacokinetics of these difficult-to-trace α-emitters. ***Conclusion:*** Organotrifluoroborate optimizes tumor targeting of FAPI. The high-quality PET imaging of [^{18}F]F/[^{68}Ga]Ga-FT-FAPI make it promising for cancer diagnosis. A cumulative dose of 13.32 MBq of [^{213}Bi]Bi-FT-FAPI suppresses tumor growth. Besides, FT-FAPI owns the ability to address the issue that therapeutic radiometals are not compatible with PET. These results taken together make FT-FAPI a favorable theranostic agent for FAP-targeted cancer diagnosis and therapy.

EP-0839

Development of anti-cancer radioimmunotherapy method targeting angiogenesis.

B. Park*, J. Yoon, Y. An, S. Kim;*
Ajou University Hospital, Suwon, Gyeonggi-Do, KOREA, REPUBLIC OF.

Aim/Introduction: In order to develop and verify anti-angiogenic therapeutics targeting ectopic ATP synthase, a β-emitting isotope (Lu-177) was labeled with an anti-ATP synthase mAb to develop a radiopharmaceutical for radioimmunotherapy and its usefulness to cells and animal experiments. ***Materials and Methods:*** Anti-ATP synthase mAb were labeled to Lu-177 through the conjugation with DOTA. Labeling yield was measured for tracer. The expression of Anti-ATP synthase mAb in various tumor cells was evaluate by western blot analysis. The cellular uptake was tested in various cells at 1, 4, and 24 hours. ^{177}Lu-DOTA-mAb is injected intravenously in tumor animal models, and organs are harvested on days 1, 2, 4, and 7 to obtain biodistribution. Treatment was performed for 4 weeks to evaluate the effect of combination therapy of ^{177}Lu-DOTA-mAb and sunitinib in tumor animal models. ***Results:*** The average labeling yield is 95±3%. Among 5 cancer cells tested, MKN-45 (human gastric adenocarcinoma) showed the highest cellular binding at 24 hr (0.010688% ±0.00051%), FTC-133 cell (follicular thyroid carcinoma) showed the lowest cellular binding at 24 hr (0.004720%±0.00025%). ^{177}Lu-DOTA-mAb was injected intravenously in a tumor model, and biodistribution was observed on the 1st, 2nd, 4th, and 7th days. The tumor uptake increased over time, and the MKN-45 model (15.96 ±2.59 %ID/g, @7D) showed higher uptake than in the FTC-133 model (7.65 ± 1.93 %ID/g, @7D). In order to evaluate the effects of single and combined treatment of ^{177}Lu-DOTA-mAb and sunitinib in tumor models, 4 weeks of treatment showed that the treatment effect of the combined treatment group (MKN-45: 639.54 ± 638 mm^3, FTC-133: 2815.76 ± 2341 mm^3) was higher than that of single treatment (MKN-45: 1188.92 ± 846 mm^3, FTC-133: 4099.96 ± 597 mm^3), and in the case of FTC-133 cell, the growth rate was very high. ***Conclusion:*** Lu-177 was labeled to anti-ATP synthase mAb with a sufficient labeling efficiency and its specific binding was confirmed in tumor cells. ^{177}Lu- anti-ATP synthase mAb showed therapeutic effects in various tumor cells and could be valuable as a target for theragnostic angiogenesis imaging. ***References:*** Park BN (2017) Molecular Imaging. 16:1-10 Lee KH (2003) European Journal of Nuclear Medicine and Molecular Imaging. 30:1032-1037. Jurgen Grunberg (2005) Clin Cancer Res. 11(14):5112-5120 Rhona Stein (2001) J Nucl Med. 42:967-974 Lars R. Perk (2005) J Nucl Med. 46:1898-1906 Argyros O (2017) Oncotarget. 8(23): 37250-37262

EP-0840

Antimony-119, a promising Auger emitter for targeted radionuclide therapy to eradicate single tumor cells and tumor clusters

A. Larouze[1]*, M. Alcocer-Avila*[2]*, C. Morgat*[1]*, C. Champion*[1]*, E. Hindié*[1]*;*
[1]*Université de Bordeaux, Bordeaux, FRANCE,*
[2]*Université de Lyon, Lyon, FRANCE.*

Aim/Introduction: Early use of targeted radionuclide therapy (TRT) to eradicate tumor cell clusters and micrometastases might offer cure. However, it is essential to assign appropriate radionuclides and assess the potential impact of non-uniform targeting. Here, we investigated absorbed radiation doses from antimony-119 (^{119}Sb), a promising Auger emitters [1], in comparison with lutetium-177 (^{177}Lu). ***Materials and Methods:*** The Monte Carlo code CELLDOSE was used to assess nuclear and membrane absorbed doses from ^{119}Sb and ^{177}Lu in single cells (14 µm diameter, 10 µm nucleus) and in a cluster of 19 cells. The radionuclide distributions considered here were: cell surface, intracytoplasmic, or intranuclear, with 1436 MeV released per labeled cell. For non-uniform targeting, four cells were stochastically unlabeled. ***Results:*** In the case of single cell, ^{119}Sb delivered 17- to 22-fold higher nuclear absorbed dose, and 18- to 48-fold higher membrane absorbed dose, than ^{177}Lu. In the cell cluster, when all 19 cells were targeted, ^{119}Sb delivered 7- to 18-fold higher absorbed doses than ^{177}Lu to cell nuclei and 10- to 44-fold higher absorbed doses than ^{177}Lu to cell membranes. Nuclear and membrane absorbed doses were mainly dependent upon the location of the radionuclide. With cell surface distribution in particular, membrane absorbed doses were substantially higher than nuclear absorbed doses, both with ^{119}Sb (1686-1710 Gy vs 40-50 Gy) and ^{177}Lu (38-41 Gy vs 4.7-7.2 Gy). However, in case of non-uniform targeting, with four unlabeled cells within the cluster, absorbed doses from ^{119}Sb to unlabeled cells dropped dramatically. For example, with ^{119}Sb on the cell surface, the membranes of unlabeled cells received on average only 0.9% of the expected absorbed doses, and the nuclei of unlabeled cells received only 14% of the absorbed doses, as compared to a cluster with uniform targeting. With ^{177}Lu, the

impact of non-uniform targeting was lower. The membranes of unlabeled cells received on average 10% of the absorbed doses, and the nuclei of unlabeled cells received 60% of the absorbed doses, as compared to a cluster with uniform targeting. ***Conclusion:*** To eradicate single cells and small tumor clusters, ^{119}Sb may be a better candidate than ^{177}Lu. However, non-uniform cell targeting can result in substantial heterogeneity in absorbed dose distribution. Dual-targeting could be of interest to counter this heterogeneity, which needs to be investigated. ***References:*** [1] Bennett KT et al., Large-Scale Production of ^{119m}Te and ^{119}Sb for Radiopharmaceutical Applications, ACS Cent. Sci, 2019, 5, 494-505

EP-0841

A Nanodepot Incorporating 177Lu-Labeled Gold Nanoparticles is Ineffective for Treatment of 4T1 Tumours in Balb/c Mice Due to Low β-Particle Energy and Spatially Lower Doses and Shorter Dose Penetration

R. Liu[1], *Z. Cai*[1], *E. Wong*[2], *Y. Lu*[2], *M. A. Winnik*[2], *R. M. Reilly*[1,3,4];
[1]*Department of Pharmaceutical Sciences, Leslie Dan Faculty of Pharmacy, University of Toronto, Toronto, ON, CANADA,* [2]*Department of Chemistry, University of Toronto, Toronto, ON, CANADA,* [3]*Department of Medical Imaging, Temerty Faculty of Medicine, University of Toronto, Toronto, ON, CANADA,* [4]*Joint Department of Medical Imaging and Princess Margaret Cancer Centre, University Health Network, Toronto, ON, CANADA.*

Aim/Introduction: We previously reported that intratumoural (i.t.) implantation of a calcium alginate seed (nanodepot) incorporating 3.5 MBq of ^{90}Y-labeled gold nanoparticles ([^{90}Y]Y-AuNPs) emitting moderate energy (2.28 MeV) and maximum 12 mm range β-particles strongly inhibited the growth of 4T1 tumours in Balb/c mice [1]. Our aim here was to study the effectiveness and normal tissue toxicity of a nanodepot incorporating [^{177}Lu]Lu-AuNPs emitting lower energy (0.5 MeV) and shorter range (maximum 2 mm) β-particles for treatment of 4T1 tumours. ***Materials and Methods:*** Tumour and normal tissue uptake in Balb/c mice with s.c. 4T1 tumours (0.8 × 0.5 cm) was determined up to 14 d post-implantation (p.i.) of a nanodepot incorporating 5.3 ± 3.0 MBq of [^{177}Lu]Lu-AuNPs (1 × 10^{14} AuNPs). SPECT/CT images were used to construct a radiation absorbed dose map around the nanodepot and calculate dose volume histograms (DVH) for [^{177}Lu]Lu-AuNPs and [^{90}Y]Y-AuNPs. Treatment was performed in Balb/c mice with s.c. 4T1 tumours implanted i.t. with a nanodepot incorporating 8.5 ± 2.3 MBq of [^{177}Lu]Lu-AuNPs (1 × 10^{14} AuNPs). Control mice were implanted with a nanodepot incorporating unlabeled AuNPs or received no treatment. Tumour growth was assessed by a tumour growth index (TGI) up to 14 d p.i. Normal tissue toxicity was evaluated by monitoring body weight and hematology and blood biochemistry analyses. ***Results:*** Tumour retention was 89.9% implanted dose/g (%ID/g) at 14 d p.i. but normal tissue uptake was low (<4.5 %ID/g). In contrast to a nanodepot with [^{90}Y]Y-AuNPs [1], there was no significant effect on TGI for mice treated with a nanodepot incorporating [^{177}Lu]Lu-AuNPs. No normal tissue toxicity was observed for [^{177}Lu]Lu-AuNPs. Radiation dose maps estimated 9,000 Gy at the nanodepot surface and 200 Gy at 0.3 cm for [^{90}Y]Y-AuNPs, while for [^{177}Lu]Lu-AuNPs, doses were 12,000 Gy at the nanodepot surface but 2 Gy at 0.3 cm. DVH indicated that 60% of the tumour volume received 2,000 Gy for a nanodepot incorporating [^{90}Y]Y-AuNPs but only 30 Gy for [^{177}Lu]Lu-AuNPs. ***Conclusion:*** The low energy and short range of the β-particles emitted by ^{177}Lu resulted in spatially lower doses and shorter dose penetration than ^{90}Y which may explain the ineffectiveness of a nanodepot incorporating [^{177}Lu]Lu-AuNPs for treatment of 4T1 tumours in mice. ***References:*** 1. Cai Z et al. ^{90}Y-Labeled Gold Nanoparticle Depot (NPD) Combined with Anti-PD-L1 Antibodies Strongly Inhibits the Growth of 4T1 Tumors in Immunocompetent Mice and Induces an Abscopal Effect on a Distant Non-Irradiated Tumor. Mol Pharm. 2022;19:4199-211.

EP-0842

Radiation Nanomedicines for Local Treatment of Glioblastoma Multiforme - Epidermal Growth Factor Receptor-Targeted and Non-Targeted Gold Nanoparticles Labeled with the Auger Electron-Emitter, 197Hg

M. Brown[1], *Z. Cai*[1], *S. Chen*[2], *V. Radchenko*[2], *W. Chung*[3], *M. Winnik*[3], *J. T. Rutka*[4], *R. M. Reilly*[1,5];
[1]*Department of Pharmaceutical Sciences, Leslie Dan Faculty of Pharmacy, University of Toronto, Toronto, ON, CANADA,* [2]*Life Sciences Division, TRIUMF, University of British Columbia, Vancouver, BC, CANADA,* [3]*Department of Chemistry, University of Toronto, Toronto, ON, CANADA,* [4]*Division of Neurosurgery, Hospital for Sick Children and Division of Neurosurgery, Department of Surgery, Temerty Faculty of Medicine, University of Toronto, Toronto, ON, CANADA,* [5]*Joint Department of Medical Imaging and Princess Margaret Cancer Centre, University Health Network, Toronto, ON, CANADA.*

Aim/Introduction: Glioblastoma Multiforme (GBM) is the most lethal form of brain cancer. Despite treatment, GBM recurs in 90% of patients possibly due to residual disease at the surgical margins. Our aim was to synthesize an EGFR-targeted or non-targeted radiation nanomedicine composed of gold nanoparticles (AuNPs) labeled with the Auger electron (AE)-emitter, ^{197}Hg that may be infused into the surgical cavity to eradicate residual tumour and improve patient outcome. ***Materials and Methods:*** [^{197}Hg]Hg-AuNPs were synthesized by the Turkevitch method by trisodium citrate reduction of tetrachloroauric acid (25 mM) at pH 4.0 refluxed at 100°C for 10 mins, and incorporated ^{197}Hg into the reaction. [^{197}Hg]Hg-AuNPs were stabilized with 0.5% Tween-20 or by surface coating with lipoic acid-polyethylene glycol (LA-PEG2K). Labeling efficiency (LE) was evaluated by ultracentrifugation at 15,000xg for 15 mins and measured ^{197}Hg bound to AuNPs using a radioisotope dose calibrator. Particle size and morphology were evaluated by transmission electron microscopy, dynamic light scattering, and UV-visible spectroscopy. Stability of [^{197}Hg]Hg-AuNPs was determined in DMEM/10% FBS at 37°C for up to 2 d. EGFR-targeted [^{197}Hg]Hg-AuNPs were constructed by direct binding of 2 µg of panitumumab (0.2 mg/mL in ddH_2O) to 8.0x10^{11} AuNPs. The uptake of EGFR-targeted and non-targeted [^{197}Hg]Hg-AuNPs by U251-Luc human GBM cells in vitro was measured. The clonogenic survival of U251-Luc cells treated with targeted and non-targeted [^{197}Hg]Hg-AuNPs for 13 h at 37°C then cultured for 10 d was determined. ***Results:*** The LE for [^{197}Hg]Hg-AuNPs was 99.0 ± 0.1%. Spherical [^{197}Hg]Hg-AuNPs were synthesized in a similar size (25.1 ± 5.3 nm) as unlabeled AuNPs (18.2 ± 2.7 nm) and exhibited similar spectroscopic properties. Approximately 70% of ^{197}Hg remained bound to AuNPs after incubation for 2 d in DMEM/10% FBS at 37°C. The uptake of Tween-20 stabilized and LA-PEG2K stabilized [^{197}Hg]Hg-AuNPs by U251-Luc cells was 12.3 ± 0.1% vs. 2.0 ± 0.0%, respectively. Panitumumab conjugation increased cellular uptake of Tween-20 stabilized [^{197}Hg]Hg-AuNPs to 39.7 ± 0.2%. The clonogenic survival of U251-Luc cells decreased 33-fold to 0.03 ± 0.02 by treatment of 500-600 cells with 0.2 MBq (1 MBq/mL) of [^{197}Hg]Hg-AuNPs. Further clonogenic survival assays with EGFR-targeted [^{197}Hg]Hg-AuNPs are in progress. ***Conclusion:*** EGFR-targeted and non-targeted [^{197}Hg]Hg-AuNPs were accumulated by human GBM cells in vitro and potently killed

these cells by emission of AEs. Future studies will evaluate their effectiveness for treatment of human GBM tumours in the brain of mice and their normal tissue toxicity.

EP-0843

Modification and Evaluation of EGFRvIII-Targeting Peptides for the Targeted Radiotherapy of Glioblastoma Multiforme

F. Schuderer[1,2], *D. Werner*[2], *M. Rassner*[3], *C. Braun*[3], *J. Galamba Correia*[4], *A. Casini*[1,2];
[1]*Chair of Medicinal and Bioinorganic Chemistry, Department of Chemistry, Technical Unversity of Munich, Garching, GERMANY,* [2]*Chair of Pharmaceutical Radiochemistry, Department of Chemistry, Technical University of Munich, Garching, GERMANY,* [3]*Department of Pediatrics, Dr. von Hauner Children's Hospital, University Hospital, Ludwig Maximilians University of Munich (LMU), Munich, GERMANY,* [4]*Centro de Ciências e Tecnologias Nucleares and Departamento de Engenharia e Ciências Nucleares, Instituto Superior Têcnico, Universidade de Lisboa, Lisbon, PORTUGAL.*

Aim/Introduction: Glioblastoma multiforme (GBM) is the most aggressive form of malignant brain tumours. As there is no cure, but only palliative treatment, the median overall survival is as short as 12-14 months from diagnosis. This demonstrates the pressing need for new treatment options.[1,2] This need is addressed here, by the development of peptide-conjugates designed for the targeted radiotherapy of GBM. The cancer specific mutant of the epidermal growth factor receptor (EGFRvIII) was chosen as a target structure since it is expressed in 25-64% of GBM patients and is absent in healthy adult tissue, presenting the potential for high tumour to brain ratios.[3] ***Materials and Methods:*** All peptides are synthesized by automated or manual solid phase peptide synthesis (SPPS) and purified via reversed phase - high performance liquid chromatography (RPHPLC). Radiolabelling with [^{177}Lu]Lu is performed with no-carrier-added [^{177}Lu]$LuCl_3$ in 0.04 m HCl with sodium acetate buffer (pH=5.5), at elevated temperatures (80-90°C). Iodination with [^{125}I]I using the iodogen-method is carried out at room temperature (15 min), with subsequent RPHPLC purification. For the cell assays two glioblastoma cell lines, stably transduced with EGFRvIII are used, namely DKMGvIII and U87vIII. The rabbit monoclonal antibody RM419, with specific affinity to EGFRvIII is utilized in the process of evaluating the receptor expression of both cell lines and designing the cell assays. ***Results:*** All synthesized peptides were obtained in high purity (> 95% by RPHPLC). Stability issues in one published EGFRvIIItargeting peptide (PEPHC1) were identified and successfully overcome by exchanging the cysteine in the sequence with other amino acids.[4] PEPHC1 and two other published EGFRvIII-targeting peptides - namely, FALGEA by Denholt 2008[5] and VLGREEWSTSYW by Mansour 2022[6] - were successfully modified and labelled with either [^{177}Lu]Lu or [^{125}I]I. The design of the affinity cell assays and subsequent evaluation of the synthesized peptide structures is ongoing. ***Conclusion:*** Several derivatives of EGFRvIII-targeting peptides, modified for radioactive labelling are currently under investigation for their affinity to that receptor. A combination with a peptide blood-brain barrier (BBB) shuttle is planned, once derivatives with satisfying affinity for the receptor are identified. ***References:*** [1] Bolcaen, J., et al., Theranostics, 2021, 11, 7911-7947.[2] Shergalis, A., et al., Pharmacol. Rev., 2018, 70, 412-445.[3] Gan, H. K., et al. FEBS J, 2013, 280, 5350-5370.[4] Campa, M. J., et al., Biochem Biophys Res Commun 2000, 275, 631-636.[5] Denholt, C. L., et al., Biopolymers, 2008, 91, 201-206.[6] Mansour, S., et al., Sci Rep, 2022, 12, 20725.

EP-0844

Novel cMet Targeted Radiotheragnostics: Preclinical Development and Optimisation for Clinical Use

C. Portal[1], *N. Swanwick*[1], *A. Prignon*[2], *A. Gibson*[1];
[1]*Edinburgh Molecular Imaging Ltd., Edinburgh, UNITED KINGDOM,* [2]*Laboratoire d'Imagerie Moleculaire Positonique (LIMP) UMS28 Small Animal Phenotyping, Sorbonne University, Paris, FRANCE.*

Aim/Introduction: Upregulation of the cMet receptor tyrosin kinase present in many solid cancers is heavily correlated with invasiveness and poor prognosis. A significant number of cMet targeted drugs have however failed in the clinic or are hindered in their development by the current patient selection methods. cMet is therefore an attractive target for the development of (radio)theragnostic approaches where the PET imaging agent would yield a full body assessment of cMet overexpression and allow for selection of patients for the therapeutic counterpart, delivering of a cytotoxic payload to the cancer cell by only relying on the increased presence of the receptor and not its function. ***Materials and Methods:*** The radiopharmaceutical candidate precursors based on a common cMet targeted peptide were screened in vitro for target affinity and radiolabelled with either ^{68}Ga or ^{177}Lu to afford the imaging and therapy candidates, respectively, which were tested for in vitro efficacy with cell based affinity assays, cellular toxicity and clonogenic survival assays) with the use of suitable controls. Pharmacokinetics, biodistribution of the optimal candidates alongside in vivo tumour uptake and residence time were assessed in rodent animal models. Further in vivo efficacy experiments were performed on some therapeutic candidates such as in vivo tumour growth assessment. ***Results:*** Several cMet targeted radiotheragnostic ligands were designed, synthesised and assessed. [^{68}Ga]EMP-100 emerged as a suitable imaging agent for the assessment of cMet expression in patients: the radiotracer displayed ideal fast tumour accumulation (~5% ID/g @ 1h post injection) and clearance from background tissues and other key organs with excretion via the kidneys, with no signs of toxicity. In parallel, lead optimisation of the therapeutic compound has yielded an increase in target affinity and a longer tumour residence time in animal models (~3% ID/g remaining in tumour @ 72h). ***Conclusion:*** [^{68}Ga]EMP-100 was successfully developed and is now ready for clinical development for the whole body determination of cMet expression and subsequent eligibility for treatment with cMet targeted therapies. Ongoing optimisation of the therapeutic candidate should allow its clinical translation in the future. ***References:*** Burggraaf, J et al., Nature Medecine, 2015 Unterrainer, L et al., European Journal of Nuclear Medicine and Molecular Imaging, 2023 Mittlmeier, L et al., European Journal of Nuclear Medicine and Molecular Imaging, 2021

EP-0845

Analysis of the effectiveness of 177Lu-Oxodotreotide in the treatment of neuroendocrine tumors sensitive to somatostatin receptors

Á. Alonso García[1], *M. L. Bravo-Ferrer Moreno*[1], *A. Blesa Jiménez*[1], *M. A. Asensio Ruiz*[1,2], *M. T. Martínez Martínez*[1,2];
[1]*Radiopharmacy Service, Virgen de la Arrixaca Hospital, Murcia, SPAIN,* [2]*Instituto Murciano de Investigación Biosanitaria (IMIB)-Arrixaca, Murcia, SPAIN.*

Aim/Introduction: ^{177}Lu-Oxodotreotide is a radiopharmaceutical indicated for the treatment of somatostatin receptor (G1 and G2) positive gastroenteropancreatic neuroendocrine tumors in adults. The dosage of this treatment consists of 4 doses of 7400 MBq with an interval of 8 weeks. Since its authorization in 2017, its

prescription has been increasing significantly. The objective of this work is to determine the effectiveness of this treatment in clinical practice. ***Materials and Methods:*** A retrospective observational study of patients treated with ^{177}Lu-Oxodotreotide from April 2016 to June 2022 in our hospital. Demographic, diagnostic, therapeutic and clinical variables were collected. The effectiveness was assessed through the progression-free survival (PSF) and overall survival (OS). The PSF was calculated as the difference between the date of disease progression and the start of treatment of patients who complete the 4 cycles. OS was calculated as the difference between the date of death and the start of treatment of deceased patients who completed treatment. PSF and OS were compared with the efficacy results of the NETTER-1 trial that gave authorization to this radiopharmaceutical. ***Results:*** The study included 32 patients (18 men and 14 women) with a mean age of 59.65 years ± 10.31, with ECOG 0-1, 74.07% and ECOG 2-3, 25.93%, treated with at least one dose of 7400 MBq of ^{177}Lu -Oxodotreotide. The primary tumor was pancreatic in 59.39% of patients, digestive 9.37%, small intestine 15.63%, paraganglioma 6.24%, and other 9.37%. Treatment was administered as first line in 9.37% of patients, second line 53.13%, third line 31.15% and fourth line 6.25%. Of the patients studied, 24 complete the treatment and of these, 15 developed disease progression and 6 died. The PSF were of 22.9 months (95%CI 14.6-31.2) and an OS 33.3 months (95% CI 16.2-50.4). The PSF values are consistent with the NETTER-1 trial but OS are significantly lower. ***Conclusion:*** Results obtained from PSF have been those expected for the treatment of patients with neuroendocrine tumors sensitive to somatostatin receptors with ^{177}Lu-Oxodotreotide. However, OS values are lower than expected, probably due to the small sample size of deceased patients, so the study would have to be prolonged over time.

EP-58

e-Poster Area

D: Technical Studies -> D5 Radiopharmacy/ Radiochemistry -> D54 New Biological Targets and Ligands

EP-0846

Targeting Regulatory T cells in experimental colon cancer with radioimmunotherapy.

Z. Xiao, *R. Jiao, K. J. H. Allen, M. E. Malo, C. Frank, S. Giri, J. L. C. Carvalho, E. Dadachova;*
University of Saskatchewan, Saskatoon, SK, CANADA.

Aim/Introduction: Colorectal cancer remains a formidable threat to human health around the world. Immunotherapy with immune checkpoint inhibitors while becoming a game changer for various types of cancer, produces mixed results in colorectal cancer with only a small number of patients experiencing long term progression-free survival. Regulatory T cells (Tregs) are an immunosuppressive subset of T lymphocytes, and a particular subset of Tregs, so called tumor infiltrating Tregs (ti-Tregs) can interfere with immunotherapy. Radioimmunotherapy (RIT) can precisely deliver highly cytotoxic radionuclides to localized or systemic cancer deposits. In this study we tested the hypothesis that RIT targeting ti-Tregs can eliminate these cells in colon tumors thus potentially increasing the success of immunotherapy. ***Materials and Methods:*** Two syngeneic murine models of colorectal cancers - CT26 in balb/c mice and MC38 in C57Bl6 mice were used. Tumor-bearing mice were imaged with SPECT/CT using 111In labeled anti-ti-Tregs antibody to establish the presence of ti-Tregs in the tumors. The numbers of ti-Tregs in the tumors and in the spleen were analyzed by flow cytometry. Simultaneous RIT of CT26 and MC38 tumor-bearing mice and mechanistic study to evaluate the effects of RIT on tumor progression and on the numbers of ti-Tregs were performed with 225Ac-labeled anti-ti-Tregs antibody. At the completion of the study the tumors were harvested and analyzed for ti-Tregs by immunohistochemistry (IHC). ***Results:*** SPECT/CT imaging demonstrated anti-ti-Tregs antibody binding to ti-Tregs within the tumors while flow cytometry analysis revealed 10 times more ti-Tregs in the tumors than in the spleen. RIT with 225Ac-anti-ti-Tregs antibody had a significant retardation effect on the CT26 and MC38 tumors in mice in comparison with the unlabeled antibody and untreated controls with 400 nCi dose being more effective than 200 nCi dose. There was a decrease of ti-Tregs in RIT treated tumors in both models according to IHC. ***Conclusion:*** RIT with 225Ac-anti-ti-Treg antibody proved to be effective in reducing the numbers of ti-Tregs in both CT26 and MC38 colorectal tumor mouse models. RIT also had a profound effect on the tumor size. The experiments combining RIT and immunotherapy with anti-CTLA-4 antibody are currently in progress.

EP-0847

177Lu-PSMA treatment impacts on the full transcriptome of prostate cancer cells.

F. Amoroso[1], *E. O'Neill*[1], *B. Cornelissen*[2,1];
[1]*MRC Oxford Institute for Radiation Oncology, Department of Oncology, University of Oxford, Oxford, UNITED KINGDOM,* [2]*Nuclear Medicine and Molecular Imaging, University Medical Center Groningen, University of Groningen, Groningen, NETHERLANDS.*

Aim/Introduction: Radiotherapy is an effective therapeutic option for locally advanced prostate cancer (PCa). However, when PCa progresses, metastatic disease is incurable. Despite the promising results of the clinical trials with ^{177}Lu-labelled PSMA (1), and the ever-mounting interest and investment by the pharmaceutical industry, we are far from curing locally advanced and advance prostate cancer (PCa). Improving our understanding of the (radio)biology of the damage induced by ^{177}Lu-PSMA will aid in designing new targeted and more effective treatments for PCa patients. ***Materials and Methods:*** We performed a comprehensive analysis on the full transcriptome of a prostate cancer cells (22Rv1), treated with ^{177}Lu-PSMA, over a period of 10 days, with RNA-Seq. ***Results:*** We recorded a progressive enrichment of genes that are differentially expressed over time as a consequence of ^{177}Lu-PSMA treatment. Performing pathway analysis, we confirmed the activation of pathways that relate to the induction of genomic reorganization (e.g., of DNA and RNA synthesis-related processes), DNA damage repair (such as Nucleotide Excision Repair) and autophagic processes that are known to correlate with cellular responses to ionizing radiation (2). We also identified new biologies that are impacted by the treatment with this radiolabelled peptide. ***Conclusion:*** With this study we aimed to improve our understanding of the radiobiological effects that beta and gamma emitter ^{177}Lu-PSMA has on prostate cancer cell lines. We shed the light on new pathways that are not strictly related to the induction of the DNA damage and can represent new therapeutic avenues for prostate cancer patients. ***References:*** (1) Novartis. Phase III VISION study. 2021 (2) Chaurasia M, et al., Free Radic Res. 2016;50(3):273-90. doi: 10.3109/10715762.2015.1129534. Epub 2016 Jan 14. PMID: 26764568.

EP-0848

Molecular imaging based response monitoring of non-contact induction heating therapy on infected prosthetic joints

***T. Buckle**, M. M. Welling, D. D. D. Rietbergen, F. W. van Leeuwen, B. G. Pijls;*
Leiden University Medical Center, Leiden, NETHERLANDS.

Aim/Introduction: Prosthetic joint infection (PJI) is a devastating and frequent complication following total joint arthroplasty. In PJI bacteria form a biofilm on the implants that protects them from antibiotics, the immune system and treatments such as debridement surgery, resulting in failure of initial treatment of 20-40%. Non-contact induction heating (NCIH) of metal implants is an emerging treatment for PJI that uses heat to kill and weaken bacteria [1, 2]. It is, however, unclear how NCIH performs on implants with complex geometry and how its performance compares to classical cleaning approaches. We therefore used a previously developed method that allows quantification and visualization of the bacterial load on femur prosthesis [3] to determine the possible beneficial effect of NCIH. ***Materials and Methods:*** S. aureus infected femur prosthesis of different materials (cobalt-chromium, titanium alloy or stainless steel) were used as a model system. The infection was topically stained with the bacteria specific bimodal tracer ^{99m}Tc-UBI$_{29-41}$-Cy5 (8 µM, 1hr). Prior to and after NCIH (40 sec, 20V, 2Ah) and/or cleaning (2 min, with CHD, BET or 3% NaCl) the bacterial load and biofilm was determined using fluorescence and gamma imaging (including freehandSPECT; N=3 per condition). The temperature distribution over the infected area and obtained temperature maximum (Temp$_{max}$) was recorded using 6 thermocouples, complemented with thermal infrared imaging. Microbiological culturing (1-6 days) was used to correlate the imaging findings with the residual bacterial load (CFU at day 1) and re-infection (CFU at day 6). ***Results:*** The effect of debridement could be effectively visualized using both fluorescence- and radioactivity-based assessments. A significant correlation was found between the number of residual viable bacteria and the radioactive signal ($R = 0.445$, $p<0.001$). Classical cleaning methods were prone to residual bacteria in 22.2% of samples on e.g., surface irregulates, transition of prosthesis head and neck and screw hole. CHD yielded the lowest incidence of residual bacteria and subsequent reinfection. For NCIH this number was 33%. Combined therapy using NCIH and CHD yielded effective prosthetic debridement. The effect of NCIH was shown to be temperature/alloy dependent and supported treatment of surfaces that were hard to clean mechanically. ***Conclusion:*** During bacterial debridement of femur prosthesis, combined fluorescent and nuclear assessment confirmed the beneficial effect of non-contact induction heating in combined therapy. ***References:*** 1. Pijls BG, et al., Bone Joint Res. 2017;6:323-30. 2. Pijls BG, et al., Bone Joint Res. 2018;7:609-19. 3. Welling MM, et al., Bone Joint Res. 2023;12:72-9.

EP-0849

Association Constant Determination of Macropa as Chelator for the Stable Complexation of Barium-131, Lanthanum-133 and Luthetium-177

***M. Blei**[1,2], B. Drobot[3], J. Kretzschmar[3], H. J. Pietzsch[1], K. Kopka[1,2], F. Reissig[1], C. Mamat[1,2];*
[1]Helmholtz-Zentrum Dresden-Rossendorf, Department of Radiopharmaceutical Cancer Research, Dresden, GERMANY, [2]TU Dresden, Dresden, GERMANY, [3]Helmholtz-Zentrum Dresden-Rossendorf, Department of Resource Ecology, Dresden, GERMANY.

Aim/Introduction: Due to its excellent complexation properties, the macrocyclic chelator macropa (mcp)[1,2] was reported to be an excellent complexing agent for ^{225}Ac[3] and a very promising starting point for the development of $^{223/224}$Ra radioconjugates. To follow theranostic concept, ^{131}Ba[4] (SPECT) and ^{133}La[5] (PET) are available as diagnostic radionuclides, due to their chemical similarities with these alpha emitters. We aim to establish a new workflow to evaluate and predict the complex stability of new chelating systems based on the macropa skeleton by obtaining both protonation constants for respective ligands and association constants for their metal complexes starting with mcp. ***Materials and Methods:*** The protonation constants (pKa) of mcp were determined by pH dependent ^{1}H NMR studies as a prerequisite for the calculation of stability constants (log(K)). Based on this data, the Eu-mcp-complex was examined by time-resolved laser-induced luminescence spectroscopy (Eu-TRLFS) to determine the speciation of the ion and pH-dependency of the complexation. Finally, the association constants of Pb-, La-, Eu-, Tb-, Ba- and Lu-mcp-complexes were determined by isothermal titration calorimetry (ITC) and the log(K) values were evaluated using parallel factor analysis. ***Results:*** Depending on the protonation ability of the functional groups found in mcp (two amines and two carboxylates), four pKa values were obtained (2.45, 3.09, 6.77 and 7.64) as well as the log(K) values for the respective mcp complexes (Table). ***Conclusion:*** The combination of ^{1}H NMR, Eu-TRLFS and ITC allows us to fully characterize the ligand by determining the pKa values, metal ion speciation, and log(K) values of the resulting complexes, which agrees with previously published data. This method can be easily transferred to other functionalized chelators and their complexes with a wide variety of metal ions which contain radionuclides of radiopharmaceutical interest. Additionally, a reliable comparison of the individual affinities of the different chelators to the metal ions and thus a predictability of the complex stabilities for future radiopharmaceuticals is possible. ***References:*** [1] Roca-Sabio et al., J. Am. Chem. Soc. 2009, 131, 3331. [2] Thiele et al., J. Am. Chem. Soc. 2018, 140, 17071. [3] Reissig et al., Cancers 2021, 13, 1974. [4] Reissig et al., Pharmaceuticals 2020, 13, 272. [5] Brühlmann et al., Pharmaceuticals 2022, 15, 1167. [6] Ferreirós-Martínez et al., Inorg. Chem. 2011, 50, 3772.

EP-0850

Development and Characterization of Novel Peptide-Based Apelin Theranostic Probes for Glioblastoma

***E. Besserer-Offroy**[1,2], P. Jeanjean[1], F. Al Banaa[1], S. Kwock[1], E. Breault[3], J. Fournier[3], P. Sarret[3,4], D. A. Nathanson[1,5], J. Czernin[1,5], G. Carlucci[1,5], C. E. Mona[1,5];*
[1]David Geffen School of Medicine, University of California, Los Angeles, Los Angeles, CA, UNITED STATES OF AMERICA, [2]Inserm U1086 - François Baclesse Comprehensive Cancer Centre, Caen, FRANCE, [3]Faculty of Medicine and Health Sciences, Université de Sherbrooke, Sherbrooke, QC, CANADA, [4]Sherbrooke University Hospital - Research Centre, Sherbrooke, QC, CANADA, [5]UCLA Jonsson Comprehensive Cancer Center, Los Angeles, CA, UNITED STATES OF AMERICA.

Aim/Introduction: Glioblastoma (GBM) is the most aggressive and life-threatening form of brain cancer, with a 5- year survival rate of 4%. Despite numerous advances in research, a cure has remained elusive. Nonetheless, recent research efforts have identified the apelin receptor (APJ) as a promising therapeutic target for GBM. APJ is a class A G-protein coupled receptor that is highly expressed at the surface of GBM tumor cells and endothelial cells irrigating the tumor. Apelin, APJ's natural ligand, has been shown to promote

GBM proliferation and increase tumor vascularization. The apelin/APJ axis plays a critical role in GBM progression, invasion, and tumor angiogenesis. Hence, APJ represents a potential target for targeted radioligand therapy (RLT) and precision oncology. In this study, we designed, synthesized, and characterized new peptide-derived probes based on apelin-13 for imaging and therapy. ***Materials and Methods:*** RNA-Seq was used to quantify expression of APJ in purified GBM patient samples from UCLA Health, as well as matching Patient-Direct Orthotopic Xenograft (PDOX) and derived gliomaspheres. Peptide-derived probes were synthesized using standard Fmoc-based solid-phase peptide synthesis. A DOTA was conjugated to the peptide sequence at its N-terminus using a PEG linker. Different probes were developed, incorporating amino-acid substitutions in the apelin sequence. To increase probe retention into the blood stream, we also integrated an albumin-binder moiety based on Evan's blue into the probe sequence. Probes were then radiolabeled using ^{68}Ga, ^{64}Cu, or ^{225}Ac. NSG mice were implanted with U87MG, a human GBM cell line, engineered to overexpress APJ, for Apelin receptor PET imaging. Apelin probes labelled with 64Cu were used for biodistribution studies. When tumors reached around 100 mm^3, mice were randomized into three groups: (1) vehicle, (2) 60 kBq ^{225}Ac-Apelin13, and (3) 60 kBq ^{225}Ac-AB-Apelin13. Tumor growth and overall survival were evaluated. Additionally, DNA-damage and APJ expression were assessed by immunohistochemistry (IHC) on resected tumors. ***Results:*** We found that our newly synthesized PET probes showed promise in PET imaging. 30 min after injection, the reported SUVmax is 2.2 with a tumor to background ratio of 56. Apelin probes with an albumin-binding moiety showed an SUVmax of 2.5 after 30 min and 5.2 after 2 hours. Mice treated with ^{225}Ac-Apelin and ^{225}Ac-AB-Apelin-13 showed significant tumor growth delay and increased survival. ***Conclusion:*** These results suggest that apelin probes have the potential to image GBM tumors and deliver RLT; however, orthotopic models will be required to evaluate brain penetration.

EP-0851

PATO-Cy5, a bi-modal tracer for image-guided hepatobillary surgery

D. Rietbergen, *T. Buckle, M. P. van Meerbeek, L. J. Slof, M. van Oosterom, F. W. B. van Leeuwen;*
Leids Universitair Medisch Centrum (LUMC), Leiden, NETHERLANDS.

Aim/Introduction: Liver cancer (primary and metastases) is a leading cause of cancer deaths worldwide. Surgical resection of these lesions is increasingly guided by the disrupted bile excretion of the near-infrared fluorescent dye indocyanine green (ICG) [1]. Fluorescence imaging unfortunately only supports the identification of superficial lesions. By exploiting the synergy of in-depth radio- and fluorescence-guidance, bi-modal (radioactive and fluorescent) tracers can help advance the precision of hepatobiliary surgery. ***Materials and Methods:*** A library of tracers containing Cyanine 5 (Cy5) infrared fluorescent dyes with varying end-groups (e.g. -SO3-, Ar) and chelates (e.g., DTPA, Mas_3, Mag_3) was synthesized and evaluated for (photo)physical properties. Bile excretion was initially evaluated in 2D hepatocyte mono-layer cultures, using cholyl-glycylamido-fluorescein and non-functionalized dye as a control. These results were further substantiated via flow cytometry. Lead selection was based on (photo)photophysical and bile excretion properties. Following radiolabeling with ^{99m}Tc, the selected lead compound had its pharmacokinetics assessed in mice (%ID/g, SPECT/CT imaging and fluorescence imaging. The ability to provide real-time surgical guidance at 4 hrs p.i. was studied in a porcine model using ICG as control. Ex vivo assessment of excised lesions was performed to validate the location of the fluorescence signal. ***Results:*** The dye-chelate combination in hHEPATO-Cy5 (serum binding: 94%, LogP: 0.80 ± 0.03, Absorption/emission: 640/665 nm, brightness: 3445) helped to provide a molecular signature that promotes bile excretion. In vitro hHEPATO-Cy5 showed fast clearance (within 10') in a manner that is similar to that of (fluorescent) bile salts. Biodistribution of hHEPATO-Cy5 in mice confirmed hepatobiliary clearance; uptake levels decreased over time (11 ± 3 %ID, 238 ± 108 %ID/g and 22 ± 9 %ID/g at 2hr vs. 2.0 ± 0.3 %ID, 2 ± 0.6 %ID/g and 0.1 ± 0.1 %ID/g at 24hr for liver, gallbladder, and intestines), respectively, yielding negligible background in the liver at 4hr post injection. During robot-assisted hepatobillary surgery in a porcine model, hHEPATO-Cy5 supported fluorescence-based lesion identification, comparable to the guidance provided by ICG. ***Conclusion:*** The unique molecular composition of hHEPATO-Cy5 promotes hepatobiliary excretion, hereby allowing the use of the agent for the surgical identification of lesion margins. ***References:***

Verbeek FP, van der Vorst JR, Schaafsma BE, Hutteman M, Bonsing BA, van Leeuwen FWB, et al. Image-guided hepatopancreatobiliary surgery using near-infrared fluorescent light. J Hepatobiliary Pancreat Sci. 2012;19:626-37.

EP-59

e-Poster Area

D: Technical Studies -> D5 Radiopharmacy/ Radiochemistry -> D55 Radiopharmacokinetics and Drug Development

EP-0852

Modifying Biodistribution of EpCAM-targeting DARPin Ec1 by Fusion with Albumin Binding Domain (ABD): Effect of ABD Position

M. Oroujeni[1], *A. Vorobyeva*[1], *A. Hani Binti Rosly*[1], *J. Garousi*[2], *Y. Liu*[1], *A. Schulga*[3], *E. Konovalova*[4], *A. Orlova*[1], *S. Deyev*[3], *V. Tolmachev*[1];
[1]*Uppsala University, Uppsala, SWEDEN,* [2]*Royal Institute of Technology (KTH), Stockholm, SWEDEN,* [3]*Tomsk Polytechnic University, Tomsk, RUSSIAN FEDERATION,* [4]*Russian Academy of Sciences, Moscow, RUSSIAN FEDERATION.*

Aim/Introduction: The epithelial cell adhesion molecule (EpCAM) is overexpressed in several types of cancer and can be used as a target for the delivery of drugs and toxins. Designed ankyrin repeat protein (DARPin) Ec1 is a scaffold protein, which has a high affinity to EpCAM (68 pM) and small size (18 kDa). A rapid renal excretion of Ec1 provides an excellent imaging of EpCAM-expressing xenografts in mice. However, the use of DARPins for targeted delivery of cytotoxic payload would require increased bioavailability and longer residence in circulation and decreased accumulation in kidneys. We have tested a hypothesis that a fusion of albumin binding domain ABD to DARPin Ec1 and ABD position could influence renal uptake and the biodistribution of DARPin Ec1. ***Materials and Methods:*** ABD was fused to Ec1 either at N- or at C-terminus. The constructs were designated as ABD-Ec1 and Ec1-ABD, respectively. DOTA chelator was conjugated at C-termini of both variants for labelling with ^{111}In. In vitro characterisation was performed using EpCAM-expressing

cell lines, SKOV-3 and OVKAR3. Biodistribution was measured in mice bearing SKOV-3 xenografts at 48 h after injection. To check in vivo specificity, EpCAM-negative Ramos xenografts were used. To evaluate the effect of ABD fusion, biodistribution of ABD-fused Ec1 variants was compared with a non-ABD-fused Ec1. ***Results:*** Radiolabelling with ^{111}In was resulted in radiochemical purity >98%. Both constructs bound specifically to EpCAM in vitro. K_D values for both variants were in subnanomolar range (0.523±0.212 and 0.368±0.086 nM for Ec1-ABD and ABD-Ec1, respectively), but affinity was significantly reduced in the presence of human albumin serum for Ec1-ABD (2.6±1.9 nM). Uptake of both radioconjugates in SKOV-3 xenografts was significantly ($p < 0.05$) higher than in Ramos xenografts at 48 h after injection, confirming EpCAM-specific accumulation in vivo. Significantly ($p < 0.0001$) higher blood concentration was observed for both ABD-fused Ec1variants compared with non-ABD-fused Ec1. The blood half-life of ABD-Ec1 ($T_{1/2}$=12 h) was longer than for Ec1-ABD ($T_{1/2}$=10.3 h). The renal uptake was significantly ($p<0.0001$) lower for [^{111}In]In ABD-Ec1 and [^{111}In]In Ec1-ABD (12.1±1.1 %ID/g and 9.6±1.2 %ID/g, respectively) compared with [^{111}In]In-Ec1 (168±28 %ID/g). Tumor uptake was significantly ($p < 0.005$) higher for [^{111}In]In-ABD-Ec1 (13.2±1.5 %ID/g) than for [^{111}In]In Ec1-ABD (6.6±1.2 %ID/g) and [^{111}In]In-Ec1 (2.7±0.5 %ID/g). ***Conclusion:*** ABD fusion prolonged the blood residence resulting in higher accumulation in tumour and reduced renal uptake. Position of ABD influenced the overall biodistribution and tumour targeting using DARPin Ec1-ABD fusion.

EP-0853

Development of new bone-seeking radiolabeled compounds

K. Ogawa*, K. Nishizawa, K. Mishiro, N. Effendi, T. Fuchigami, M. Munekane, H. Wakabayashi, S. Kinuya;*
Kanazawa University, Kanazawa, JAPAN.

Aim/Introduction: Previously, we evaluated oligo-aspartic acid derivatives as carriers for developing bone-seeking radiopharmaceuticals (1, 2). In this study, we hypothesized that the density of carboxy groups is important for higher bone affinity, and thus γ-carboxy glutamic acid peptides [$(Gla)_n$] could be a superior carrier to bone. N,N′-Bis-[2-hydroxy-5-(carboxyethyl)benzyl]ethylenediamine-N,N′-diacetic acid (HBED-CC) was selected as a chelator for radiogallium. [^{67}Ga]Ga-HBED-CC-$(Gla)_n$ (n = 2, 5, 8, 11, and 14) were synthesized and evaluated in vitro and in vivo by comparison with [^{67}Ga]Ga-HBED-CC-$(Glu)_n$. In this fundamental study, the radiogallium complexes were prepared using the easy-to-handle radioisotope, ^{67}Ga rather than ^{68}Ga. ***Materials and Methods:*** After HBED-CC-$(Gla)_n$ was synthesized using Fmoc-based solid-phase methodology, [^{67}Ga]Ga-HBED-CC-$(Gla)_n$ was prepared by complexing ^{67}Ga with HBED-CC-$(Gla)_n$. Hydroxyapatite binding assays, biodistribution experiments, and SPECT/CT imaging were performed. ***Results:*** [^{67}Ga]Ga-HBED-CC-$(Gla)_n$ were prepared with radiochemical purities of over 95% without any purification. In the hydroxyapatite binding assay, binding of [^{67}Ga]Ga-HBED-CC-$(Gla)_n$ tended to increase with the length of the amino acid chain. As a whole, the binding affinity of [^{67}Ga]Ga-HBED-CC-$(Gla)_n$ was higher than that of [^{67}Ga]Ga-HBED-CC-$(Glu)_n$. In biodistribution experiments, [^{67}Ga]Ga-HBED-CC-$(Gla)_n$ showed higher accumulation in the bone than [^{67}Ga]Ga-HBED-CC-$(Glu)_n$. In particular, [^{67}Ga]Ga-HBED-CC-$(Gla)_5$, [^{67}Ga]Ga-HBED-CC-$(Gla)_8$, and [^{67}Ga]Ga-HBED-CC-$(Gla)_{11}$ showed higher accumulation in bone and rapid clearance from the blood. SPECT/CT images of [^{67}Ga]Ga-HBED-CC-$(Gla)_n$ showed high accumulation in bone. ***Conclusion:*** [^{67}Ga]Ga-HBED-CC-$(Gla)_n$ showed superior characteristics as bone imaging agents. Therefore, oligo Gla peptides could be more suitable as a carrier to the bone. ***References:*** 1. K. Ogawa et al. PLoS One. 8(12):e84335. (2013) 2. K. Ogawa et al. Sci Rep. 7(1):13971. (2017)

EP-0854

Development of fluorinated α-methyl-3BPA derivatives for BNCT/PET theranostics

F. Hirano*[1], N. Kondo[1], Y. Murata[2], A. Sudani[2], T. Temma[1];*
[1]Osaka Medical and Pharmaceutical University, Osaka, JAPAN, [2]Stella Pharma Corporation, Osaka, JAPAN.

Aim/Introduction: Since BNCT achieves an anti-cancer effect by nuclear reaction of ^{10}B with thermal neutrons, it is required to selectively deliver ^{10}B into the tumor and estimate the ^{10}B accumulations in advance. 4-Boronophenylalanine (BPA), the only marketed BNCT agent accumulating in the tumor via L-type amino acid transporter 1 (LAT1), has insufficient selectivity over LAT2 and poor water solubility, necessitating solubilizers. We have recently demonstrated that 3BPA, a meta-isomer of BPA, exhibits extremely high water solubility with sustaining similar tumor targetability without solubilizer addition [1]. In this study, we designed fluorinated α-methyl-3BPA derivatives with the expectations of improving LAT1/LAT2 selectivity and future BNCT/PET theranostics application and evaluated the efficacy as BNCT agents. ***Materials and Methods:*** We designed and synthesized α-methyl-3BPA (αMe-3BPA), fluorinated 3BPAs (F-3BPAs), and fluorinated αMe-3BPAs (F-αMe-3BPAs). Water solubility was determined by measuring boron concentration in the saturated aqueous solution of compounds using ICP-MS. The compounds were incubated with HEK293 cells of forced expressing LAT1 or LAT2 (HEK-LAT1, 2), followed by boron measurement. After intravenous injection of α-methylated derivatives into LAT1-positive T3M4-xenograft mice, tissues were excised and weighed, followed by boron measurement. ***Results:*** All compounds had more than ten times higher water solubility than BPA. While F-3BPAs showed similar accumulation ratios (HEK-LAT1/LAT2) to BPA, α-methylated derivatives exhibited more than five times higher ratios than BPA due to reduced accumulation in HEK-LAT2 cells, suggesting that α-methylation improved LAT1/LAT2 selectivity. Similarly, biodistribution studies revealed that α-methylated derivatives enabled comparable tumor accumulations to BPA with reduced accumulations in muscle and plasma, leading to more than four times higher tumor-to-muscle ratios and more than 1.5 times higher tumor-to-plasma ratios, respectively, of α-methylated derivatives than BPA. It is suggested that the improved LAT1/LAT2 selectivity of α-methylated derivatives successfully contributed to lessening accumulations in non-target tissues. αMe-3BPA and F-αMe-3BPAs showed comparable biodistributions, which indicated a minimal effect of fluorination on the chemical properties of compounds. ***Conclusion:*** α-Methylated 3BPA derivatives improved LAT1/LAT2 selectivity in vitro and tumor-to-muscle and tumor-to-plasma ratios in vivo with sustaining high tumor accumulations. The fluorinated α-methyl-3BPA derivatives (F-αMe-[^{10}B]3BPA/[^{18}F]F-αMe-3BPA) could be promising candidates for future BNCT/PET theranostics. ***References:*** [1] Kondo N, Hirano F, Temma T., Pharmaceutics, 14(5), 1106 (2022).

EP-0855

In Vivo Stability Evaluation of Astatobenzene Derivatives Having Neighboring Substituents

S. Hirata[1], *K. Mishiro*[1], *K. Washiyama*[2], *T. Fuchigami*[1], *M. Munekane*[1], *K. Takahashi*[2], *Y. Arano*[3], *S. Kinuya*[1], *K. Ogawa*[1]; [1]*Kanazawa University, Kanazawa, JAPAN,* [2]*Fukushima Medical University, Fukushima, JAPAN,* [3]*Chiba University, Chiba, JAPAN.*

Aim/Introduction: Astatine-211 (^{211}At) is a promising α-particle emitting radionuclide for targeted alpha therapy (TAT). In basic research on the radioiodinated and astatinated compounds, radiohalogens are generally introduced into an aromatic ring. However, for some astatinated compounds, a release of free astatine from the aromatic ring is observed. The deastatination reaction could attenuate therapeutic effects and induce adverse effects by accumulating free astatine in non-targeted tissues. Until now, a reliable way to improve in vivo stability of the aromatic carbon-astatine bond has not been established. Therefore, we aimed to improve the in vivo stability of the astato group in astatobenzene derivatives by modifying substituents on the aromatic ring. A hippuric acid derivative, (4-astatobenzoyl)glycine, was reported to undergo considerable in vivo deastatination while its radioiodinated variant has high in vivo stability[1]. We designed and evaluated some (4-astatobenzoyl)glycine derivatives having two identical neighboring substituents next to the astato group. To compare the in vivo stability, we also synthesized the corresponding radioiodinated derivatives. ***Materials and Methods:*** For the synthesis of the radiolabeled compounds, corresponding precursors having tributylstannyl group were prepared. Astatinated or radioiodinated compounds were synthesized by oxidative trialkyltin-halogen exchange reaction using oxidant and [^{211}At]At$^-$ or [^{125}I]NaI and purified by HPLC. The in vitro stability in murine plasma and biodistribution in normal mice of the radiolabeled compounds were evaluated. ***Results:*** After HPLC purification, each radiohalogenated compound was obtained with >95% radiochemical purity. In in vitro stability experiments in murine plasma, all radiolabeled compounds remained >80% intact. In in vivo biodistribution experiments in normal mice, each compound showed a different biodistribution. One astatinated compound showed high in vivo stability comparable to the corresponding iodinated compound, although deastatination occurred in other astatinated compounds, as indicated by an increase of the radioactivity level over time in the stomach and thyroid. ***Conclusion:*** Our study suggested that structural modification of the aromatic ring can improve the in vivo stability of astatobenzene derivatives. These results would contribute to developing more effective ^{211}At-labeled radiopharmaceuticals for TAT. ***References:*** [1]S. Wilbur et al. Bioconjug Chem. (2004)

EP-0856

Development of FAP-Targeted Inhibitors with Extended Blood Circulation

L. Feng[1], *X. Zeng*[2], *J. Fang*[2], *H. Liu*[2], *X. Zhang*[3], *D. Jiang*[1], *R. Zhuang*[2];
[1]*Department of Nuclear Medicine, Union Hospital, Tongji Medical College, Huazhong University of Science and Technology, Wuhan, CHINA,* [2]*Center for Molecular Imaging and Translational Medicine, State Key Laboratory of Molecular Vaccinology and Molecular Diagnostics, School of Public Health, Xiamen University, Xiamen, CHINA,* [3]*Department of Nuclear Medicine & Department of Medical Research Center, Peking Union Medical College Hospital, Chinese Academy of Medical Sciences & Peking Union Medical College, Beijing, CHINA.*

Aim/Introduction: Fibroblast activation protein inhibitors (FAPI)-based nuclear imaging tracers have garnered significant interest for cancer imaging in clinical settings. However, their limited blood circulation and tumor retention have posed great challenges for targeted radionuclide therapy. Our aim is to modify FAPI-04 to extend its blood circulation and increase its tumor uptake. ***Materials and Methods:*** FM, as modified based on clinically used FAPI-04, was synthesized and labeled with ^{68}Ga and ^{177}Lu, followed by radiochemical characterization using high-performance liquid chromatography (HPLC). Subsequent in vivo PET imaging and ^{177}Lu treatment were carried out in both 4T1 tumor-bearing mice and ovarian cancer patient-derived xenograft models. ***Results:*** HPLC analysis showed that the radiochemical purity (RCP) and radiochemical yield (RCY) of FM labeled with ^{68}Ga/^{177}Lu were both above 99%, and the resulting products exhibited excellent stability within 2 h. FM exhibits a higher retention capability in circulation compared to FAPI-04, with a blood circulation half-life of 7.11 ± 0.34 h. Imaging results demonstrated that the tumor-to-muscle ratio of probe [^{68}Ga]Ga-FM reached 9.21, while probe [^{177}Lu]Lu-FM primarily accumulated in the liver and kidneys, with tumor uptake reaching a level higher than that of kidneys at 24 h post-injection, and further increasing in subsequent time points. ***Conclusion:*** The ^{68}Ga- and ^{177}Lu-labeled probes targeted to FAP were successfully prepared. These probes demonstrated high retention in blood circulation, exhibiting promising properties for potential applications in tumor diagnosis and therapy.

EP-0858

Method development for the analysis of 14C-acetaminophen by HPLC-MS

P. Chang, *S. Farn;*
Institute of Nuclear Energy Research, Tao-Yuan, TAIWAN.

Aim/Introduction: Carbon-14 (^{14}C) is commonly employed for the study of drug pharmacokinetics and metabolism. The laboratory of drug metabolism at the Institute of Nuclear Energy Research (INER) in Taiwan has developed a systemic platform that has been certificated by OECD GLP for evaluation of drug safety, efficacy, pharmaceutical kinetics, properties, and potential metabolism by using ^{14}C-labeled molecules. In the study, ^{14}C-labeled acetaminophen was used as a radiolabeled drug to validate the developed method for the quality and quantitative analysis of ^{14}C-labeled compounds. ***Materials and Methods:*** ^{14}C-labeled acetaminophen was provided by a commercial company. HPLC-MS was conducted on an Agilent 1100 HPLC system interfaced with a Sciex 4000 QTRAP triple-quadrupole mass spectrometer. ^{14}C-acetaminophen was analyzed by an MS detector monitored in positive ionization mode for compound structure identification. The HPLC also connects to a UV detector and a liquid scintillation analyzer (LSA) for compound quantification. The compound structures of various peaks in LC-LSA chromatography can be deduced with the assistance of the peaks of LC-MS chromatography at their respective retention time in LSA spectra. ***Results:*** The stability and homogeneity of the C-14-APAP solution were assessed by comparing the quantity of C-14-APAP in the solutions under different tested conditions. The variation of the concentration within 4 and 24 hours was below 2%, indicating good stability. The RSD value of the concentrations in the upper, middle, and down layers is below 2%, indicating significant homogeneity. The mass-to-charge ratio (m/z) of ^{14}C-acetaminophen and acetaminophen precursors were 154 and 152, separately, indicating single-charged [M+1] ions were predominant in the MS spectra. The m/z of ^{14}C-acetaminophen

and acetaminophen precursor has a mass difference of 2 Dalton. Two most high-abundance fragment ions at m/z of 112 and 95 in MS/MS spectra of ^{14}C-acetaminophen were observed. In the spectra of acetaminophen, they were 110 and 93. ***Conclusion:*** The developed method is capable of qualitative and quantitative determination of ^{14}C-acetaminophen. Although the current study aimed to identify ^{14}C-labeled acetaminophen, these results will allow us to elucidate the relevant metabolic profiles of the drug candidates using ^{14}C-radiolabeled drugs during the drug discovery and development process.

EP-0859

Radiolabeling and biodistribution evaluation of orally administered nanovaccines against enterotoxigenic Escherichia coli formed by vesicles of their outer membrane encapsulated in Gantrez®-mannosamine nanoparticles

G. Quincoces[1], *M. Berzosa*[2], *F. Pareja*[1], *M. Collantes*[3], *M. Ecay*[3], *R. Ramos-Membrive*[1], *J. Simón*[1], *V. Betech-Antar*[4], *J. Rosales*[4], *I. Peñuelas*[1];
[1]*Radiopharmacy Unit. Nuclear Medicine Department. University Clinic of Navarra, Pamplona, SPAIN,* [2]*Microbiology Department. University of Navarra, Pamplona, SPAIN,* [3]*UNIMTRA. Nuclear Medicine Department. University Clinic of Navarra, Pamplona, SPAIN,* [4]*Nuclear Medicine Department. University Clinic of Navarra, Pamplona, SPAIN.*

Aim/Introduction: Enterotoxigenic Escherichia coli (ETEC) represents a major cause of mortality in children in developing countries. Since there is no effective vaccine against this pathogen, the development of nanovaccines formed by ETEC outer membrane vesicles (OMV) in zein nanoparticles coated with Gantrez®-mannosamine (NPZ-GM) is being investigated. The biodistribution of the vaccine complex and its components was evaluated by means of radiolabeling and molecular imaging in vivo and ex vivo. ***Materials and Methods:*** Radiolabeling of OMV and NPZ-OMV-GM was performed by reduction of technetium-99m with $SnCl_2$ [40µl $SnCl_2$ $2H_2O$ (0.50mg/ml for OMV and 0.25mg/ml for NPZ-OMV-GM). OMV was radiolabelled [40µl $SnCl_2$ $2H_2O$ (1 mg/ml)] and encapsulated in the nanoparticles using the coacervation/desolvation method.The particle size was determined by DLS and the radiochemical purity by radioTLC. ^{99m}Tc-OMV (26.2±1.1MBq), ^{99m}Tc-NPZ-OMV-GM (96.2±0.5MBq) and NPZ-OMV-^{99m}Tc-GM (4.70±0.5 MBq) were oral administered to BALB/c mice and MicroSPECT/CT images were acquired 1, 4, 7 and 10 h later, then the animals were euthanized and the radioactivity of the digestive and lymphatic systems was quantified in a gamma counter. ***Results:*** The Radiochemical Purity of the radiolabeling was greater than 98 %. The particle size of the nanovaccines was 200 nm (PDI<0.2). In vivo and ex vivo biodistribution studies demonstrated slower transit of encapsulated OMVs through the intestine than free OMVs. The ex vivo study detected a significantly higher signal in the lymph nodes of mice treated with encapsulated OMVs compared to the other groups ($p<0.01$ ANOVA). ***Conclusion:*** The encapsulation of OMV increase their residence time in the intestine when they are administered orally in the murine model increasing their exposure to the immune system and therefore their potential effectiveness as a vaccine.

EP-0860

Effects of DOTATATE on plasma protein-binding and tumour cell-uptake of 68Ga- and 177Lu-DOTATATE

L. Schneider*, Y. Zhao, M. Zuhayra, U. Lützen;*
Department of Nuclear Medicin, Molecular Imaging, Diagnostics and Therapy UKSH, Kiel, GERMANY.

Aim/Introduction: Peptide-Radio-Receptor-Therapy (PRRT) with ^{177}Lu-DOTATATE has shown encouraging results in treatment of neuro-endocrine malignant tumours (NET). ^{68}Ga-DOTATATE-PET/CT with its high-quality imaging is in great demand for diagnosis. Previous study has reported that modified DOTATATE with albumin binding motif increases tumour uptake of ^{177}Lu-DOTATATE through prolonged blood retention. On the other hand, elevated blood maintenance of ^{68}Ga-DOTATATE extends the "washout time" thereby reducing the specificity and sensitivity of PET imaging. In the present study, we investigated different concentrations of the precursor, DOTATATE, on plasma binding and tumour cell uptake of ^{68}Ga- or ^{177}Lu-DOTATATE to provide the optimal concentration for the synthesis of the radiotracer. ***Materials and Methods:*** ^{68}Ga-DOTATATE or ^{177}Lu-DOTATATE in the presence of different amounts of DOTATATE (0.5 to 1000 µg/ml) were added to plasma or cultured SH-SY5Y cells, human neuroblastoma cells highly expressing SSTR2, and incubated for 30 min. The plasma-bound fraction was separated using ammonium sulfate as a protein precipitation agent. After washing out the unbound tracer, cell fractions bound to the tracers were collected with 0.1N NaOH and neutralized with 0.1 N HCl. The radioactivity of the plasma and cell fractions were measured in a γ-counter. Protein levels in the fractions were measured with the protein analysis kit. The data are expressed as cpm/mg protein. ***Results:*** According to standard protocol ^{68}Ga-DOTATATE was prepared using 2.5 µg/ml and ^{177}Lu-DOTATATE using 10 µg/ml of DOTATATE. The plasma binding for ^{68}Ga- and ^{177}Lu-DOTATATE was significantly enhanced when DOTATATE was increased to 40/400 µg/ml in the final product ($p<0.05$). A reduction of the ^{68}Ga-DOTATATE- and ^{177}Lu-DOTATATE plasma binding was detected when DOTATATE was used at concentration of 5 or 10 µg/ml ($p<0.01$). Interestingly, the cell-uptake of ^{68}Ga-DOTATATE significant decreased when the concentration of cold DOTATATE was up to 20 µg/ml ($p<0.01$). The cell-uptake of ^{177}Lu-DOTATATE decreased at 400 µg/ml of DOTATATE without statistical significance ($p = 0.8889$). ***Conclusion:*** Our results demonstrate that high concentrations of DOTATATE diminishes the tumor cell-uptake of ^{68}Ga-DOTATATE, while lower concentration of DOTATATE reduces the plasma binding and leads to an increase of the sensibility and specificity of PET scan. Concomitant addition of DOTATATE, which increases blood retention of ^{177}Lu-DOTATATE without affecting tumour cell uptake, may be beneficial for PRRT treatment. These findings require further confirmation in order to test the potential of the simultaneous treatment with ^{177}Lu-DOTATATE and DOTATATE in chemo-or radio-resistance NET models.

EP-0861

Evaluation of influence of albumin binding domain position on biodistribution of HER2-targeting DARPin-DM1 drug conjugates using radiolabeling

A. Vorobyeva[1], *T. Xu*[1], *Y. Liu*[1], *M. Oroujeni*[1], *A. Schulga*[2,3], *J. Garousi*[4], *E. Konovalova*[2], *Y. Liao*[1], *A. Zikrileh*[1], *P. Kanellopoulos*[1], *O. Bragina*[5,3], *T. Gräslund*[4], *A. Orlova*[1], *S. M. Deyev*[2,3], *V. Tolmachev*[1];
[1]*Uppsala University, Uppsala, SWEDEN,* [2]*ShemyakinOvchinnikov Institute of Bioorganic Chemistry, Moscow, RUSSIAN FEDERATION,* [3]*Tomsk Polytechnic University, Tomsk, RUSSIAN FEDERATION,* [4]*Royal Institute of Technology (KTH), Stockholm, SWEDEN,* [5]*Tomsk National Research Medical Center, Tomsk, RUSSIAN FEDERATION.*

Aim/Introduction: Designed ankyrin repeat protein (DARPin) G3 has the potential for tumor-targeted delivery of cytotoxic drugs due to selective and high-affinity binding to human epidermal growth factor receptor 2 (HER2). Fusion with albumin-binding domain (ABD) might extend its half-life in vivo. By introducing a

single cysteine for conjugation, the drug number and position can be well-controlled. We developed two drug conjugates based on G3 carrying maytansinoid DM1 and having ABD at the N or C terminus of G3 (G3-ABD-DM1 and ABD-G3-DM1). The aim of this study was to investigate the impact of ABD position on HER2 targeting and biodistribution. ***Materials and Methods:*** The drug conjugates were radiolabeled site-specifically at N-terminal $(HE)_3$-tag using technetium-99m tricarbonyl, and studied for binding specificity, affinity, and cellular processing using HER2-overexpressing cell lines. Cytotoxicity in cell lines with high and low HER2 expression was investigated. Biodistribution of $^{99m}Tc(CO)_3$-labeled drug conjugates was performed in Balb/c nu/nu mice bearing SKOV3 xenografts at 4, 24 and 48 h post-injection (pi). The biodistribution at 48 h pi was compared with DARPin G3 (without ABD fusion). Tumor targeting specificity was evaluated using mice bearing HER2-negative Ramos xenografts. ***Results:*** The drug conjugates were labeled with 50-80% radiochemical yield and purified with radiochemical purity over 95%. Binding to HER2-overexpressing cancer cells was specific and preserved in the presence of albumin. The internalized fraction was between 20-30% at 24 h. Both constructs had a more substantial cytotoxic effect in the presence of albumin, with lower IC50 values for G3-ABD-DM1 (1.4-6 nM) in cell lines with high HER2 expression. The biodistribution of $^{99m}Tc(CO)_3$-labeled drug conjugates was characterized by an extended half-life in blood and renal clearance. G3-ABD-DM1 had a longer half-life than ABD-G3-DM1, which resulted in a larger area under the curve (AUC) for the tumor. The highest tumor uptake was at 24 h pi for both conjugates, 6±1 %ID/g for G3-ABD-DM1 and 5±1 %ID/g for ABD-G3-DM1. The uptake was significantly lower in HER2-negative Ramos xenografts. The AUC for hepatic uptake of G3-ABD-DM1 was smaller than for ABD-G3-DM1. The combination of more potent cytotoxicity and favorable biodistribution profile suggests G3-ABD-DM1 as a preferable candidate for therapy. ***Conclusion:*** Radiolabeling using residualizing $^{99m}Tc(CO)_3$ label enabled quantitative characterization and comparison of DARPin-drug conjugates in vitro and in vivo. Placing ABD at the C terminus of G3 provided a conjugate with more favorable HER2 targeting properties and biodistribution.

EP-0862

Preparation, double radiolabeling of Albumin Nanoparticles (HSA-NPs) with technetium-99m and gallium-67 and in vivo biodistribution studies using microSPECT/CT to accelerate their pharmaceutical development as nanovaccines

F. Pareja del Rio[1], *E. van Brandwijk*[1], *J. A. Simon*[1], *A. Bronte*[1], *V. Betech-Antar*[1], *F. Minguez*[1], *M. Romera*[1], *J. J. Rosales*[1], *M. Collantes*[1], *R. Ramos*[2], *G. Quincoces*[1], *I. Peñuelas*[1];
[1]*Nuclear Medicine Department. Clínica Universidad de Navarra., Pamplona, SPAIN,* [2]*Nuclear Medicine Department. Clínica Universidad de Navarra, Madrid, SPAIN.*

Aim/Introduction: Developing new vaccines is essential to fight against emerging infectious diseases such as COVID-19 or Shigelosis. The use of antigen protein-loaded nanosystems for subcutaneous administration as vaccines has very many advantages, and the study of their biodistribution using molecular imaging of radiolabeled nanoparticles (NP) can help accelerate their pharmaceutical development. With this purpose, we have optimized the preparation and simultaneous double radiolabeling procedures of antibody-loaded human serum albumin (HSA) NP with technetium-99m and gallium-67 for in vivo biodistribution studies by microSPECT/CT molecular imaging. ***Materials and Methods:*** As a model antigenic protein, we used a widely available IgG1: bevacizumab (BVZ). After tagging it with a chelator (p-NCS-benzyl-NODA-GA) and purifying it by size exclusion chromatography, 4.5mg of BVZ-NODAGA were added to 37MBq of $[^{67}Ga]GaCl_3$ (obtained from [^{67}Ga]Ga-Citrate) at pH=4. After 30' at 37ºC, the radiochemical purity was analyzed by RadioTLC (ITLC-SG with 1M Na-Citrate and AcNH4:methanol (50:50)). PEG coated HSA-NPs loaded with [^{67}Ga]Ga-NODAGA-BVZ were prepared by desolvation/coacervation by adding 1mL (4mg) of the labeled antibody to 100mg of HSA in 7.84mL of water, 8mL of ethanol and 500µL of PEG35,000 (100mg/mL). Ethanol was removed by using a rotary evaporator, and the nanoparticles obtained in 6 mL. Particle size was determined by Dynamic Light Scattering (DLS). Finally, 1 mL of PEG-HSA-[^{67}Ga]Ga-NODAGA-BVZ NPs were directly radiolabeled with 74 MBq of $[^{99m}Tc]NaTcO_4$ using 40µL of 0.07mg/mL $SnCl_2$ as reducing agent. For biodistribution studies, 150µL of the double-radiolabeled NPs (5.55MBq of gallium-67 and 11.1MBq of technetium-99m) were administered subcutaneously to healthy balb/C mice and MicroSPECT/CT images obtained 1,18 and 42h post-administration. Images were reconstructed by using the photopeaks of technetium-99m and gallium-67 and analysed in PMOD. Control mice received either $[^{99m}Tc]TcO_4^-$ and $[^{67}Ga]GaCl_3$ subcutaneously. ***Results:*** The radiochemical purity of the double radiolabeling procedure was bigger than 95%. The particle size was 250 nm (PDI <0.2) before and after radiolabeling, showing no significant modifications of the NP. At 18h and 42h post-administration, activity was observed in axillary and inguinal lymph nodes, suggesting stimulation of the immune system. In comparison with the controls of $[^{99m}Tc]TcO_4^-$ and $[^{67}Ga]GaCl_3$, no activity was observed in stomach, intestine, salivary glands and bone marrow. ***Conclusion:*** We have stablished a procedure for preparation and double radiolabeling of BVZ-loaded HSA-NPs and made MicroSPECT/CT studies showing accumulation of the radioactivity in lymph nodes. These studies could be used as a role model to accelerate the pharmaceutical development of new nanovaccines for subcutaneous administration.

EP-0863

Pharmacological implications of molar activity of 225Ac-labeled PSMA targeting agents in prostate cancer tumor models.

R. Hernandez*, A. Thickens, H. Comas Rojas, N. Clemons, A. Carston, Y. Medina Guevara, L. Lambert Lepesevich, A. Pinchuk; University of Wisconsin-Madison, Madison, WI, UNITED STATES OF AMERICA.*

Aim/Introduction: The pharmacological implications of administering high molar activity (MA) ^{225}Ac-PSMA targeted alpha therapy (TAT) agents remain relatively unexplored. Here, we studied the impact of MA and injected mass dose on the biodistribution of two PSMA-targeting TAT agents in murine models of prostate cancer. ***Materials and Methods:*** Subcutaneous PSMA-expressing PC3-PIP tumors were generated in male immunocompromised nude mice. Two urea-based PSMA ligands, ART1 and PSMA-617, with different pharmacokinetics, were labeled with ^{225}Ac at a MA of 0.04, 0.4, or 4.0 GBq/µmol. Radiolabeled compounds were purified via solid-phase extraction and formulated in an injectable solution. PC3-PIP-bearing mice (100 mm^3) were administered low, medium, or high MA ^{225}Ac-ART1 or ^{225}Ac-PSMA-617 (n=3-5) 4-40 KBq (~0.1-1.0 µCi) intravenously, and serial ex-vivo biodistribution was performed at days 0, 1, 2, 5, and 7 post-injection (p.i.). Tumor and normal tissue distribution were quantified as injected activity per gram of tissue (%IA/g). PSMA blocking studies were carried out by co-injecting ^{225}Ac-ART1 with PMPA (40 nmol). ***Results:*** High

MA ^{225}Ac-ART1 showed markedly different biodistribution with significantly higher (P < 0.01) liver (21.8± 0.9 %IA/g at 48 h p.i.) and spleen uptake (6.2 ± 1.2 %IA/g at 48 h p.i.) compared to medium and low MA, across all timepoints. Notably, ^{225}Ac-ART1 tumor uptake increased with lowering MAs with peak values at 48 h p.i. of 3.0 ± 0.7, 5.4 ± 0.2, and 8.0 ± 2.1 %IA/g in the high, medium, and low groups, respectively. At 3 h p.i., high MA ^{225}Ac-PSMA-617 uptake was higher for liver and spleen (2.6 ± 0.07, 1.3 ± 0.5, respectively) and lower for tumor (13.9 ± 2.4) compared to medium and low MA. At 24 h p.i., this trend continued for liver and spleen uptake, but the tumor uptake was not significantly different across the MA range for ^{225}Ac-PSMA-617. Low MA had the best tumor-to-normal tissue ratios for both TAT agents. Notably, co-injecting high MA ^{225}Ac-ART1 with PMPA had a similar biodistribution as low MA administration. ***Conclusion:*** Our results showed the significant impact of administered MA on the biodistribution and clearance of PSMA-based TATs agents. High accumulation in normal tissues was largely PSMA-driven and negatively affected tumor uptake in the high MA administrations, which demonstrates the importance of MA and mass dose optimization in developing effective TAT agents.

EP-0864

In vitro stability of 99mTc-FITC-SFN for Oral Drug Delivery System

M. Asensio Ruiz[1,2], *Á. Alonso García*[1], *M. Bravo-Ferrer Moreno*[1], *A. Blesa Jiménez*[1], *A. A. Lozano-Pérez*[2,3], *M. T. Martínez Martínez*[1,2];
[1]*Radiopharmacy Service, Virgen de la Arrixaca Hospital, Murcia, SPAIN,* [2]*Instituto Murciano de Investigación Biosanitaria (IMIB)-Arrixaca, Murcia, SPAIN,* [3]*Departamento de Biotecnología Genómica y Mejora Vegetal, Instituto Murciano de Investigación y Desarrollo Agrario y Medioambiental, Murcia, SPAIN.*

Aim/Introduction: Silk Fibroin Nanoparticles (SFN) are a promising tool as a Drug Delivery System (DDS) for anti-inflammatory purposes (1). The objective of this work is to characterize in vitro the stability in gastric and intestinal media of SFNs labeled with FITC and ^{99m}Tc for oral biodistribution studies. ***Materials and Methods:*** 1 mg of FITC-SFN (4×10^{11} nanoparticles/mg; Zaverage=161.5±1.95nm; PdI=0.152±0.009; Zpot= -31±1.57mV) were labeled by incubation with 20 µg of $SnCl_2$ and 37 MBq of sodium pertechnetate, as described previously (2). The radiolabeled nanoparticles were recovered by centrifugation, and subsequently SFN were incubated during 4 hours at 37ºC under gentle stirring in artificial gastric and intestinal media prepared according to the Royal Spanish Pharmacopoeia. Radiolabeling efficiency (RLE%) was determined as percentage of added radiactivity linked to nanoparticles. Radiochemical Purity (RCP%) was analyzed by iTLC with SG/methyl ethyl ketone. The in vitro stability of the radiolabeling was evaluated by measuring the RCP% for 4 hours. Dynamic Light Scattering (DLS) was performed after a decay period of 12 τ½. ***Results:*** RLE% was of 98.92±0.15 % (n=3) and the Radiochemical Purity (RCP%) was >98% (n=3). When incubating the ^{99m}Tc-FITC-SFN in gastric medium (n=3), 5.35 ± 2.34% of ^{99m}Tc eluted at t=0, maintaining this value after 4 hours of incubation. Regarding the hydrodynamic characteristics, there was an increase in Z average and Zpotential (Zaverage=4828±1467nm;PdI=0.311±0.086;Zpot.=12± 0.404mV). When incubating in intestinal medium (n= 3), <1% of ^{99m}Tc was eluted at t=0 and after 4 hours of incubation. No significant variations in the hydrodynamic characteristics were seen (Zaverage=156.8±2.12nm; PdI=0.201±0.012; Zpot.= -30.7±2.1mV). ***Conclusion:*** The changes in the hydrodynamic characteristics and the percentage of eluted ^{99m}Tc are expected due to the acid pH. ^{99m}Tc-FITC-SFN remains stable in gastric and intestinal medium after 4 hours of incubation, optimal for oral biodistribution studies.

References: (1)Ruiz-Alcaraz, AJ;Núñez-Sánchez, MÁ; AsensioRuiz, MA; Martínez-Sánchez, MA; Oliva-Bolarín, A; MartínezMartínez,T; PérezCuadrado,JJ; Ramos-Molina,B; Lozano-Pérez,AA. Optimizing the Preparation of Silk Fibroin Nanoparticles and Their Loading with Polyphenols: Towards a More Efficient Anti-Inflammatory Effect on Macrophages. Pharmaceutics. 2023;15(1):263. (2)Asensio Ruiz,M.A.; Alonso García,Á.; Bravo-Ferrer Moreno, M.d.l.L.; Cebreiros-López,I.; Noguera-Velasco,J.A.; LozanoPérez,A.A.; Martínez Martínez,T. In Vitro Hemocompatibility and Genotoxicity Evaluation of Dual-Labeled[99mTc]Tc-FITC-Silk Fibroin Nanoparticles for Biomedical Applications. Pharmaceuticals. 2023;16: 248

EP-0865

Development of new molecular drug delivery tools based on PET imaging : in vivo performance research of nucleic acid nanomaterials

Q. Xia*;*
Department of Nuclear Medicine ,School of Medicine, Shanghai Jiao Tong University, Shanghai, CHINA.

Aim/Introduction: For developing new molecular drug delivery tools, Three typical three dimensional (3D) DNA origami frameworks with distinguished structural properties were subjected to mice intravenous injection to systematically investigate their in-vivo behaviors. ***Materials and Methods:*** Tracing the radioisotope ^{89}Zr trapped at the inner space of the frameworks, positron emission tomography (PET) imaging was employed to record the real time bio-distribution of the structures and acquire their pharmacokinetic parameters in the major metabolic organs, e.g. kidney and liver. ***Results:*** The 43 nm diameter icosahedral framework(DIF) outstand in liver accumulation and retention. The DIF structure which showed the longest mean residence time(MRT) with pretty high local concentration. The calculated drug clearance rate (CL) of each sample in different organs further demonstrated the lowest CL of DIF in liver (1.21E-3 mbq/min*ID/g). And the surface modifications (e.g. ssDNA and PEG) could further regulate its performance. Decorated by a specific liver-targeting-agent, triantennary N-acetylgalactosamine (GalNAc), the significantly enhanced icosahedral framework uptake in liver cells, especially in hepatocytes, was discovered through flow cytometry analysis. ***Conclusion:*** To summarize, 3D DNA origami frameworks performed differently in pharmacokinetics and bio-distributions compared with the reported sister structures (tFNA, 2D sheets and 1D rod).The icosahedra framework (DIF) with the smallest size and most rigid construction resulted as the most liver preferred structure, and the ssDNA extensions on DIF remarkably enhanced its liver targeting efficiency. With the modification of GalNAc, a specific hepatocyte targeting agent, DIF was further improved in liver cell uptake, especially in hepatocyte.Compared wiht the other origami frameworks and the dsDNA-G, the better performance of DIF-os and especially DIF-G indicated that a qualified and powerful liver-delivery vehicle/strategy could be developed upon the DNA icosahedral framework.Therefore, as the 2D DNA origami sheets have been successfully applied to treat kidney disease, the 3D DOFs possess the potential in dealing with hepatopathies.

EP-0866

Preparation and in vitro evaluation of an anti-HER2 Affibody radiolabelled with Zr-89

D. Niculae[1,2], *R. Leonte*[1], *R. Cornoiu*[1], *D. Cocioaba*[1], *L. Chilug*[1], *S. Baruta*[1], *B. Burghelea*[1], *L. Craciun*[1], *A. Popa*[1], *A. Necsoiu*[1], *D. Draganescu*[2];
[1]*Horia Hulubei National Institute for Physics and Nuclear Engineering, Bucharest (Magurele), ROMANIA,* [2]*University of Medicine and Pharmacy Carol Davila, Bucharest, ROMANIA.*

Aim/Introduction: ^{89}Zr, a positron-emitting radionuclide with a half-life of 78.41 hours has opened possibilities of positron emission tomography (PET) imaging and visualization of in-vivo processes with favorable pharmacokinetics of emerging biovectors such as affibodies. A combination of small size, ease of engineering, high affinity, and specificity vectors, they proved to be a suitable alternative to monoclonal antibodies for molecular imaging of receptor-overexpressing tumors. ***Materials and Methods:*** ^{89}Zr was produced with high yield and high specific activity on a TR-19 cyclotron via ^{89}Y(p,n)^{89}Zr nuclear reaction, by irradiation of 250 µm nat-yttrium foils on the fully automated Solid Target Irradiation System installed on the extension line. The optimal parameters were set based on the SRIM/TRIM simulations of the particular geometry, at 15.2± 0.3 MeV extracted proton energy degraded to 12.9 MeV (± 0.78MeV straggling) by an aluminum foil and irradiated for 4 hours at a 20 µA beam current. An Affibody molecule was synthesized, consisting of three alpha helices, with 63 amino acids. The affibody binds selectively to HER2 receptors with picomolar affinity. Its molar mass of about 7 kDa (7260.14), theoretical pI: 5.37, and Kd: 60 pM resulted from post-synthesis characterization.^{89}Zr radiolabelling was performed after the conjugation of affibody with DFO, using zirconium oxalate solution, purified on ZR cartridges, pH 4.5-5.5, 500±25 MBq/ml. ***Results:*** ^{89}Zr-oxalate as a labelling precursor was successfully optimized on a customized target and beam geometry and standardized post-purification, radiolabelling, and evaluation procedures were implemented. The irradiation process yielded an activity of 2.95 ± 0.25 GBq/batch EOB, [^{89}Zr]Zr-oxalate complies with technical specifications. antiHER2 affibody was conjugated with DFO (DFO to affibody molar ratio 3:1) at 37ºC for 30 min, at pH = 8.9 - 9.1, and purified on PD10. Radiolabelling of DFO-affibody resulted in PRC > 95%. Preclinical evaluation of ^{89}Zr-DFO-antiHER2 affibody, performed in vivo on HER2+ models (BT 474 and MCF7 breast cancers, and SKOV3 ovarian cancer) against HER2- line (A431 epidermoid carcinoma), shows a stable uptake in cancer cells. Specific binding and fast uptake were observed for BT 474 and MCF7 breast cancers, while a higher initial uptake on SKOV3 ovarian cancer resulted in medium retention after 2 h of incubation. The uptake profiles of the 89Zr radiolabelled affibody were compared with those of a full antibody anti-mErb2/HER2. ***Conclusion:*** 89Zr-DFO-antiHER2 affibody in vitro preclinical evaluation shows positive results, therefore it will be further evaluated in vivo as PET imaging agent of HER2 positive cancers.

EP-0867

The Impact of Renal Uptake on 18F-DCFPyL Biodistribution

G. Chaussé[1], *S. Plaha*[2];
[1]*McGill University, Montreal, QC, CANADA,* [2]*University of British Columbia, Vancouver, BC, CANADA.*

Aim/Introduction: ^{18}F-DCFPyL (PSMA) has intense renal uptake. Given that a standardized dose is administered to all patients, large kidneys may drain more of the radiopharmaceutical and thereby decrease uptake to the remainder of the organs. Biodistribution of 18F-DCFPYL PET imaging can be calculated as "Total Body Uptake" (sum of the product "Volume X SUVmean" of all organs with uptake). We investigated if: 1-the change in the volume of high-uptake organs (the kidneys) affected uptake to other organs, and 2-if 18F-DCFPyL renal uptake correlated with renal function. ***Materials and Methods:*** 11 patients with history of surgically treated renal cell carcinoma underwent PET/CT scans two hours following intravenous injection of ^{18}F-DCFPyL as part of a clinical trial (NCT02899312). Informed consent was obtained prior to any procedure in conformity with local ethic committee recommendations and in accordance with the ICH E6 guidelines and Declaration of Helsinki. Some patients were treated with partial nephrectomy, others with complete nephrectomy, resulting in variable renal uptake. Images were manually segmented using tools from a commercially available software (MIM software, v.7.0). Segmented organs were the salivary glands, lacrimal glands, liver, spleen, kidneys, and bowel. The bladder is considered excreted and therefore excluded. SUV_{mean} and volumes were collected for each organ. We compared the renal volume against the renal total uptake (Volume x SUV_{mean}) and correlated that with the renal function (creatinine level at the time of the scan). The 11 patients were sorted by renal volume or renal total uptake, divided into above or below the median and tested with a student T test. ***Results:*** There is a statistically significant inverse correlation between renal volume and ^{18}F-DCFPyL biodistribution to other organs and a statistically significant correlation between renal function and ^{18}F-DCFPyL renal uptake. ***Conclusion:*** Renal function and volume appear to impact overall radiopharmaceutical biodistribution. ^{18}F-DCFPyL may be able to measure renal function, however larger cohorts with highly variable renal volumes would be needed to confirm these findings.

EP-60

e-Poster Area

D: Technical Studies -> D5 Radiopharmacy/ Radiochemistry -> D56 Radionuclide Production

EP-0868

Preparation of Ga/Ni Solid Target for Cyclotron-produced 68Ge by Electrodeposition

Y. Shen;
China Institute of Atomic Energy, Beijing, CHINA.

Aim/Introduction: The main applications of ^{68}Ge are its use as a long-lived positron source for attenuation corrections and calibration of PET/CT , and its role as mother radionuclide for the preparation of ^{68}Ge/^{68}Ga radionuclide generators. The ^{68}Ge/^{68}Ga radionuclide generator systems attracted interest in nuclear medicine because of its significant potential for PET/CT imaging using ^{68}Ga labelled radiopharmaceuticals. The low melting point of the target material in the production reaction ^{69}Ga (p, 2n) ^{68}Ge has limited the availability of ^{68}Ge. In order to use the existing industrial cyclotron hardware to produce ^{68}Ge, a method of electrodepositing gallium-nickel alloy was set up in this study. ***Materials and Methods:*** The Ga/Ni solid target was prepared by electric deposition method for cyclotron producing ^{68}Ge. Acidic requirements were met through the preparation of the gallium-nickel alloy targets and by optimizing the plating bath

composition and electrodepositing conditions, the influences of current density, temperature, pH value, Ga/Ni concentration on the target quality were investigated. ***Results:*** The gallium-nickel solid targets with a gallium content of 75% was prepared by electric deposition method. After three irradiation tests, the process was certified to produce targets of Germanium 68. ***Conclusion:*** This process is user-friendly, the preparation of the targets is of stable quality, and it can be applied to the cyclotron production of Germanium 68. ***References:*** 1.G.-J-Meyer, Macke, H., Schuhmacher, J. , & Knapp, W. H. . (2004). ^{68}Ga-labelled dota-derivatised peptide ligands. European journal of nuclear medicine(8), 31,1097-1104. 2. Breeman, W. , MD Jong, Blois, E. D. , Bernard, B. F. , Konijnenberg, M. , & Krenning, E. P. . (2005). Radiolabelling dota-peptides with ^{68}Ga. European journal of nuclear medicine and molecular imaging, 32(4), 478-485.3. Mäkinen, T. J. , Lankinen, P. , Pöyhönen, T. , Jalava, J. , Aro, H. T. , & Roivainen, A. . (2005). Comparison of ^{18}F-FDG and ^{68}Ga pet imaging in the assessment of experimental osteomyelitis due to staphylococcus aureus. European Journal of Nuclear Medicine & Molecular Imaging, 32(11), 1259-12684. Cheng, W. L. , Yun, J. , & Lo, L. . (2000). Preparation of ^{68}Ge/^{68}Ga generator with a binary ga/ag electrodepositions as solid target. Journal of Radioanalytical&Nuclear Chemistry,245(1),25-30.

EP-0869

Developing Actinium-225 large-scale supply

S. Bertrand[1], *S. Van den Berghe*[1], *W. Leysen*[2], *J. Mermans*[2], *S. Heinitz*[2], *D. Maertens*[1], *G. Scheveneels*[2], *C. Gameiro*[3], *A. Cea*[2], *P. Vanwolleghem*[1], *M. Sprangers*[2];
[1]*Pantera, Mol, BELGIUM,* [2]*Belgian Nuclear Research Centre (SCK CEN), Mol, BELGIUM,* [3]*Ion beam applications, Louvain-la-Neuve, BELGIUM.*

Aim/Introduction: Within the field of theranostic, one of the most promising therapeutic radioisotope is the alpha-emitting Actinium-225 (225Ac). Alpha emitters present high LET (linear energy transfer- about 100 KeV/µm) and short path length in (50-100 µm) which results in high cytotoxic potency limited to few cancerous cells while sparing surrounding healthy tissues[1]. In addition, 225Ac has apropriate half-life (10 days) which facilitate smooth logistics process and a centralized industrial distribution scheme. One of the main challenges for worldwide patient access is to ensure the availability of high-quality -225Ac in large quantities. The project aims at establishing a new factory that will be able to produce large-scale quantitiesof 225Ac for patient use. ***Materials and Methods:*** Given the objective to supply large scale amounts of Actinium, the "gamma route" 226Ra(g,n) 225Ra -> 225Ac was selected.To enable the large-scale and high-quality production via the gamma route, several challenges must be tackled:- The source material 226Ra has very limited availability. - The overall process efficiency must be high to allow long-term operation and avoid Radium losses- The cross-section of the gamma route reaction is low, so the gamma flux on the Radium target and Radium quantity in the target must be high to enable commercial production of 225Ac.- Handling of 226Ra target material which is radioactive and releases radioactive Radon- The end-product quality must respond to pharmaceutical drug quality standards. ***Results:*** The commercial production facility aims at producing, with an electron beam accelerator, large quantities of purified ^{225}Ac enabling commercial distribution. The process described should lead to the cumulated production of more than 100 Ci of ^{225}Ac per year and per accelerator. Several production lines could be added to supply a growing demand. ***Conclusion:*** As clinical trials are progressing, the demand for ^{225}Ac is continuously increasing. It has been estimated that the worldwide demand could easily reach several hundreds of Ci per year as soon as the first commercial products reach the market (around 2027). It is essential that the radioisotope supply community provides confidence to the pharmaceutical companies that a high quantity, high quality and reliable ^{225}Ac supply chain will be achieved. This joint effort and other ongoing initiatives are a clear sign of the commitment to make this supply chain a reality. ***References:*** [1] R.Eychenne, M. Chérel,, F. Haddad, F. Guérard, J-F Gestin, Pharmaceutics 2021, 13, 906

EP-0870

CERAD, Center of Design and Synthesis of Radiopharmaceuticals for Molecular Targeting and 30 MeV cyclotron for medical isotope production in Poland

R. Mikolajczak, *D. Pawlak, W. Wojdowska, I. Cieszykowska, T. Szyszko, P. Garnuszek;
National Centre for Nuclear research- POLATOM, Otwock, Poland, POLAND.*

Aim/Introduction: In order to meet the high demand for radiometals with potential for medical applications, with a particular focus on their theranostic value, the new research facility is being built at NCBJ/POLATOM: Center of Design and Synthesis of Radiopharmaceuticals for Molecular Targeting, CERAD. It's main component is the 30 MeV cyclotron which accelerates protons and alpha particles to 30 MeV and deuterons to 15 MeV. It will be a powerful tool for production of novel radioisotopes for medical use, which were not available in Poland up today. Among them the radioisotopes such as ^{18}F, $^{44/43}$Sc, ^{64}Cu, ^{67}Cu, Ge^{68}, ^{89}Zr, ^{123}I and ^{211}At will be produced. Installation of a new high-current cyclotron at NCBJ, with an equipment and infrastructure, combined with already existing scientific base, creates the unique and pro-development research capabilities. ***Materials and Methods:*** The cyclotron of CERAD, Cyclone 30XP, provided by Ion Beam Applications, Belgium, next to protons and deuterons also accelerates alpha particles, it is equipped with the alpha ion source. The new building not only hosts the cyclotron but also a number of dedicated labs with hot-cells for radioisotope processing, with the QC and research laboratories. The entire facility offers a space of 2500 m^2. The upcoming infrastructure will be open to PRISMAP, SECURE and other users projects. ***Results:*** The infrastructure of CERAD can be used for both research and commercial activities, it creates the platform for comprehensive studies oriented at research and design of new medicinal products, in particular radiopharmaceuticals, and at implementing diagnostic and therapeutic procedures for diseases, which are currently treated ineffectively. ***Conclusion:*** The CERAD project has found its place on the Polish Roadmap of Large Research Infrastructure because it will not only offer new radioisotopes but also a possibility to design innovative radiopharmaceuticals. The research potential of NCBJ as consortium leader is supported by partner institutions: University of Warsaw, Warsaw Medical University, Institute of Nuclear Chemistry and Technology, Jagiellonian University Medical College and Medical University of Bialystok. ***References:*** CERAD project is co-financed under Smart Growth Operational Programme 2014-2020, Priority IV: INCREASING THE RESEARCH POTENTIAL, Measure 4.2. Development of modern research infrastructure of the science sector.

EP-0871

Cyclotron production of 68Ga with in-target dissolution

D. Szikra, *V. Forgács;*
University of Debrecen, Debrecen, HUNGARY.

Aim/Introduction: ^{68}Ga was produced from ^{68}Zn metal with proton irradiation. The irradiated target material was dissolved in the target system and transferred to the hotcell for purification and labeling. ***Materials and Methods:*** The d.o.t.s. solid target system from Syniq Ltd was installed on a GE PETtrace cyclotron and used for isotope production. ***Results:*** 40 mg ^{68}Zn target material was irradiated with 50 uA proton beam for 10-180 min, yielding 7-60 GBq ^{68}Ga at the end of bombardment. The irradiated target material was dissolved with 7 M HNO3 and transferred to the hotcell via capillary line. The target solution was purified on a Trasis mini AiO module. The target solution was neutralized with ammonium formate and trapped on TK230 resin. After rinsing with 0.01 M HCl the gallium was eluted with 0.75M HCl and concentrated on CUBCX resin. The final elution was done with 0.5 ml 1 M HCl and 4.5 M 0.01 M HCl. The purified gallium was mixed with 1M NaOAc pH 4.5 buffer and reacted with 20 ug PSMA-11 for 5 minutes at 100 °C. Overall decay corrected yield was approx. 70-75%. 20-21 GBq ^{68}GaPSMA-11 was produced from 2h irradiation. ***Conclusion:*** The produced ^{68}GaPSMA-11 met the requirements of PhEUR and thus suitable for human application.

EP-0872

Development of New Automated Methods for [18F]-NaF Productions using FDG synthesizer.

S. NGOKPOL, *S. Kijprayoon, T. Saonam;*
Bangkok hospital, Bangkok, THAILAND.

Aim/Introduction: The shortage of technetium-99m has caused an urgent need for [^{18}F]sodium fluoride for PET imaging of bone metastasis. We modified a fully automated method for [^{18}F]NaF synthesis by re-configuring a commercial FDG synthesizer. ***Materials and Methods:*** The Lookout program was used to sequence the steps for automated synthesis using an Excel spreadsheet. The [^{18}F]fluoride solution is transferred to the synthesis module. The [^{18}F]fluoride ions are trapped in the QMA-light Sep-Pak cartridge. The QMA cartridge is then washed with sterile water for injection and eluted with 0.9% NaCl. The final product was passed through a 0.22 µm sterile filter to a sterile product vial. ***Results:*** [^{18}F]NaF was successfully produced consistently with a high yield. The non-decay corrected yield after synthesis is at least 85%. Module cleaning and preparation before synthesis takes 25 minutes. The total synthesis time is 7 minutes. Quality control of [^{18}F]NaF is performed according to USP and EP requirements. The QC results are passed. ***Conclusion:*** This design of fully automated synthesis showed reproducible, user-friendly, and very good radiochemical yields. This module could be used for [^{18}F]NaF production in our department. ***References:*** 1. F. Dehghan, S. Jaloo, H. Afarideh*, DEVELOPMENT OF NEW COMBINED SYSTEM FOR PRODUCTION OF FDG And NaF RADIOPHARMACEUTICALS, Proceedings of Cyclotrons2013, Vancouver, BC, Canada, 390-392.2. C. Collet et al., [2015], Applied Radiation and Isotopes 102:87-92.

EP-0873

How Can Nuclear Physicians Mitigate the Patient's Fear of Medical Radiation Exposure? -Lessons Learned from Fukushima Dai-ichi Nuclear Power Plant Accident -

K. Ohno[1], *M. Kajisako*[2];
[1]*Kyoto Collage of Medical Science, Kyoto Nantan, JAPAN,* [2]*Kyoto University Hospital, Kyoto, JAPAN.*

Aim/Introduction: On March 2011 Fukushima Daiichi Nuclear Power Plant (FNP-1) accident has occurred. All over the world, people were anxious about the effects of ionizing radiation, especially about internal exposure. At the same year we had a medical accident of nuclear medicine at a small municipal hospital in Japan. Forty-nine pediatric patients had received larger-than-standard dose of radiopharmaceuticals. This sensational news confused the local community. The municipality established an accident investigation committee. This party was able to gain the trust of the media and patients' families by using risk communication method lessons learned from FNP-1 accident. We will publish the results with the aim of providing nuclear medicine professionals around the world with useful materials for risk communication in the event of an accident. ***Materials and Methods:*** The committee decided to obtain the consent of the parties concerned for the following 1 The hospital's administrative staff will fully cooperate with the disclosure of the hospital's internal documents. 2.The hospital will release the full text of the investigation report on the web. 3.The academic societies concerned will accept the recommendations in the report. The committee also decided that they would brief the media representatives after each meeting and respond to questions and answers. In addition, a member who is a nuclear medicine specialist, will meet all family members to directly hear the actual situation. After that, the committee will conduct individual interviews. ***Results:*** All the committee's decision-making policies were approved. The media was briefed in detail on the progress of the investigation. They gradually became more interested in the internal system that caused the accident than in the effects of radiation. The patient's family blamed themselves because they had chosen this hospital for their child. During the individual interviews, they wished to know the disclosure of accurate exposure doses and the effects and impact on the future growth of their children. The anxiety of the patients' families and its change over time was remarkably similar to that of the parents of pediatric patients who were concerned about radiation exposure. ***Conclusion:*** In a serious medical radiation accident, it is effective for experts to continue to provide carefully explanations that are acceptable to the media and for family members to respond in a manner similar to that used to deal with patients who are concerned about radiation. The law changed to require doctors to chart the actual dosage to the patient.

EP-0874

A low energy cyclotron, as an enabler for cancer diagnosis in emerging countries

J. Geets, *E. Kral, J. Harray, V. Petry;*
Ion Beam Applications SA, Louvain-La-Neuve, BELGIUM.

Aim/Introduction: A new low energy cyclotron was released with the aim of providing access to cancer diagnosis with modern nuclear medicine PET/CT for the largest number of patients across the globe, hence bridging healthcare disparities and democratizing advanced treatment for all. ***Materials and Methods:*** Installation requirements are set to their minimum. Unlike all the other accelerators, this new cyclotron does not request compressed air, dry nitrogen nor expensive helium cooling and democratizes the set-up of a new production center with its independence from resource scarcity. The choice of a low energy proton beam was driven as tradeoff of sufficient for ^{18}F production but also easier to shield and reducing infrastructure cost as well as long term activation for future decommissioning. Reliability is a key success factor of this cyclotron. For the first time,

the ease of the maintenance has been pushed a step further by removing the needs for adjustments and jigs for each task like ion source maintenance or target maintenance. Thanks to its unique design, energy consumption and its impact on operating cost has been reduced to the minimum. The power consumption of subsystems such as magnetic power supply or ion source power supply, have been further reduced by at least a factor two compared to other accelerators. The use of turbomolecular pumps for vacuum system is more efficient than conventional resistor driven oil diffusion pumps while being tolerant to mains network outage. The guidance for safe and reliable operation has been specifically addressed through the entire redesign of its software. Production workflow has never been that intuitive. The full center can run with no specific requirement on staff education. Dedicated training can turn any hospital technician into a site operator. Besides the cyclotron as source of ^{18}F, the system is packaged with synthesis unit for FDG & other tracers, dispensing unit, and integrated quality control system in shielded compartment. ***Results:*** This new cyclotron has been successfully qualified in factory. Waiting for the building completion of the first customers for shipment. Work is currently in progress. ***Conclusion:*** From first results and practical implementation, the system clearly addresses the need of emerging countries to access to modern nuclear medicine modalities for cancer diagnosis. This solution paves the way to reliable and safe FDG production bridging healthcare disparities across the globe.

EP-61

e-Poster Area

D: Technical Studies -> D5 Radiopharmacy/ Radiochemistry -> D57 Radiopharmaceutical Preparation and Quality Control

EP-0875

Radiosynthesis and Formulation of [18F]mFBG : The challenge of a clinical use radiopharmaceutical for a pediatric population

J. Fouque, *L. Trump, B. Irumva, M. Steffann, E. Da Costa Branquinho, Q. Bruyer, C. Provost, O. Madar;*
Institut Curie, Saint-Cloud, FRANCE.

Aim/Introduction: Neuroblastoma is the most common childhood cancer in France and is still diagnosed/followed by a SPECT radiopharmaceutical, the [^{123}I]meta-iodobenzylguanidine ([^{123}I]mIBG). This radiopharmaceutical requires thyroid blockade, leads to poor resolution image and needs at least 24h of biodistribution to have a sufficient ratio signal/noise. In this context, the development of PET radiopharmaceutical, the [^{18}F] meta-fluorobenzylguanidine ([^{18}F]mFBG), is relevant to simplify the scan procedure, to improve resolution and detection of neuroblastoma. We focused on the development of a performant radiosynthesis while offering a well-tolerated formulation for children. ***Materials and Methods:*** The radiosynthesis of [^{18}F]mFBG was previously developed on an All-in-one synthesizer (Trasis) using a boronate ester precursor (BEp). A new development was designed using a spirocyclic iodonium(III) ylide precursor (SIYp). In both cases, the multi-steps radiosynthesis starts with a radiofluorination followed by a deprotection. For the BE precursor, the formulation consisted in a cationic exchange on a cartridge after the HPLC purification. For the SIYpj, the formulation was combined with the HPLC purification by using an injectable eluent. Using BEp, sodium ascorbate (NaAsc) was inserted to mix the bulk, while using SIYp, NaAsc was inserted since the deprotection step. ***Results:*** The optimal conditions with BEp allowed to obtain a RCY of 14 ± 4% with 240 ± 27 GBq of starting activity (n=4) and 10 ± 2% with 384 ± 42GBq (n=3). For the SIYp, RCY of 27% with 13 GBq of starting activity (n=1), 14% with 130 GBq (n=2) and 13% with 240 GBq (n=1) were obtained. The RCY drastically decreases with the rise of starting activity indicating a sensitivity towards radiolysis. Even if the NaAsc was inserted earlier in SIYp radiosynthesis no improvement of the RCY was observed. We suppose that the radiolysis already occurs during the radiofluorination. Consequently, the two radiosynthesis are close in term of RCY but the sequence with SIYp is simpler and faster, 45 vs 53 min, and thus activity yield is more interesting for clinical production. ***Conclusion:*** [^{123}I]mIBG scintigraphy will eventually be replaced by [^{18}F]mFBG in few years. Offering a PET imaging in the management of neuroblastoma for pediatric population is highly valuable. The radiosynthesis based on BEp or SIYp seems to be very sensitive to radiolysis. To conclude, two robust processes were developed on the AIO for the radiosynthesis of MFBG with moderate yields, sufficient for clinical trials. ***References:*** Matthew Tredwell et al.; Angew. Chem. 2014 ; Benjamin H.Rotstein et al.; Chem. Sci. 2016

EP-0876

Automated Production of 177Lu-Labelled Radiotracers Using Microfluidic Approach

S. Lahdenpohja[1], *C. Piatkowski*[2], *L. Tanguy*[2], *B. Kuhnast*[1];
[1]*Université Paris-Saclay, CEA, CNRS, Inserm, BioMaps, Orsay, FRANCE,* [2]*PMB Alcen, Peynier, FRANCE.*

Aim/Introduction: Lutetium-177 ($T_{½}$=6.76d, $E_{β\text{-max}}$=0.497MeV, maximum range in tissue 2.5mm) is one of the most important theranostic radionuclides as it has favourable nuclear characteristics for cancer therapy.[1,2] Production of therapeutic doses (typically >5GBq) of ^{177}Lu-radiopharmaceuticals demands automated manufacturing process from the safety and quality point of view. In this study, our goal was to show the usability of an automated microfluidics based radiosynthesiser in dose-on-demand type of production of ^{177}Lu-radiotracers. In addition, we aimed to develop a solid phase extraction (SPE) based method for $^{177}LuCl_3$ concentration to adjust the volume in which $^{177}LuCl_3$ can be delivered for subsequent labelling reactions. ***Materials and Methods:*** Two different labelling approaches were studied; in the first approach aqueous $^{177}LuCl_3$ (0.04M HCl) solution was mixed directly with precursor in 0.1M ammonium acetate in a microfluidic cassette. Three different peptides were labelled with 10 min reaction time at 37°C. Manual reaction was conducted in parallel to verify the effectiveness of the microfluidic process. For proof-of-concept, full labelling synthesis with formulation step was conducted in the microfluidic cassette. Radiolabelled compounds were analysed with radioHPLC. In the second approach, acidified $^{177}LuCl_3$ solution (approx. 4M HCl) was trapped on a lanthanide dedicated SPE resin and eluted with only 200µL of diluted HCl before mixing with precursor in 0.5M ammonium acetate. Different methods for washing the resin after trapping step were studied to increase the pH of the eluant without compromising the elution efficiency. ***Results:*** Direct mixing of ^{177}Lu-solution and precursors in a microfluidic cassette yielded ^{177}Lu-DOTA-PSMA with 55±6% (manual 59%) radiochemical conversion (RCC), ^{177}Lu-DOTA-cRGD with 30±8% RCC and ^{177}Lu-DOTA-octreotide with 23% RCC. As a proof-of-concept, formulated

^{177}Lu-DOTA-PSMA was produced with 100% radiochemical purity. In the second approach, trapping efficiency of ^{177}Lu was >95% and elution efficiency with 200µL 0.04M HCl was 66±2% (manual 87%). ***Conclusion:*** Novel fully automated microfluidic approach can be used for ^{177}Lu-labelling of peptides. Trapping and elution of $^{177}LuCl_3$ from an SPE resin using a microfluidic cassette is a method to control and standardise the volume of $^{177}LuCl_3$ before its use in subsequent labelling reactions. Further studies are needed to adjust the pH of the eluant for suitable buffering of subsequent labelling reactions. ***References:*** [1]Am.J.Nucl.Med. Mol.Imaging;2021;11(6):443 [2]Oncologist;2022;27(6):e957

EP-0877

Comprehensive analysis of environmental monitoring data from the GMP radiopharmaceutical facility of the UMCG obtained between 2010-2022

H. Boersma[1], *L. B. S. Bekhof*[2], *T. W. T. Poiesz*[2], *M. M. Woerdenbag*[1], *D. Giesen*[1], *H. T. Tholen*[1], *G. Luurtsema*[1], *M. N. Lub-de Hooge*[1], *H. J. Woerdenbag*[2];
[1]*University Medical Center Groningen, Groningen, NETHERLANDS,* [2]*University of Groningen, Groningen, NETHERLANDS.*

Aim/Introduction: In this study, the quality of manufacturing conditions at the GMP radiopharmaceutical facility of the UMCG was evaluated. Hereto, data obtained from environmental monitoring over the period 2010-2022 were analysed. ***Materials and Methods:*** The data were sorted according to the GMP classification of the respective premises with their corresponding limits, and frequencies were determined per location. The analysed environmental monitoring techniques included active air sampling, passive air sampling, contact prints, and particle counting. The data were compared and statistically evaluated using a 2-sided Fisher's exact test ($p < 0.05$ was considered significant). In addition, the Contamination Recovery Rate (CRR) over time was calculated and analysed. ***Results:*** The frequencies of conducted measurements gradually increased between the start and end of the assessed period. There was a trend of increased action limit excursions observed between 2010-2022 for active air sampling and contact prints. Interestingly, environmental monitoring in grade A areas significantly less complied to GMP specifications than the combined data from all sampled premises at the facility ($p < 0.00001$), which could not be explained by seasonal conditions. Furthermore, the Glovebox A cabinet revealed more microbiological excursions than other grade A areas($p < 0.0001$), which may be explained by the higher number and complexity of manual activities performed in this cabinet during radiopharmaceutical production. The CRR found for cleanroom conditions was sufficient. A trend was also found for reduced action limit excursions for passive air sampling and particle counting, suggesting improved GMP compliance over time for this specific type of environmental monitoring. ***Conclusion:*** From this comprehensive data analysis we learn that, in order to be fully compliant to requirements set in the upcoming GMP Annex 1 revision (in force as of August 2023), strategies to further improve microbiology and thereby the product, are advised. For example, improved cleaning procedures, efficient working methods as well as optimization of the conditions under which aseptic manufacturing is performed. The evaluation of a recent optimisation of our cleaning procedure is now work in progress.

EP-0878

Fully Automated Radiosynthesis Quality Control and GMP Validation of [68Ga]Ga-PentixaFor for CXCR4 PET Imaging: First Taiwan Experience

M. Li[1], *L. Hung*[1], *S. Yang*[1], *T. Lin*[1], *Y. Huang*[1], *W. Pai*[2];
[1]*Koo foundation Sun Yat-Sen Cancer Center, Taipei, TAIWAN,* [2]*Advancharis Science and Research Co., Ltd, New Taipei City, TAIWAN.*

Aim/Introduction: PentixaFor is a promising radiopharmaceutical for PET in the detection of lymphoproliferative diseases. [^{68}Ga]Ga-PentixaFor has shown high-affinity specific binding to the binding pocket of CXCR4 lymphomas. The preparation process of [^{68}Ga]Ga-PentixaFor was fully automated for clinical use to meet the radiation safety and GMP PET drug guidance requirements in Taiwan. Base on risk-based QMS, our strategy was to evaluate the automated synthesis of [^{68}Ga]Ga-PentixaFor on Part 11 compliant systems and sterilized reagent kit/labelling cassette for clinical application. ***Materials and Methods:*** GMP grade PentixaFor and [^{69}Ga]Ga-PentixaFor were obtained from PentixaPharm (Germany). Radiosynthesis parameters were set up by specific labelling conditions (95 °C, 5 min) with the MLPT(EZ, Germany) module. The automated synthesis platform (MLPT), reagent kit (EZ-102, GMP for APIs), disposable cassettes (C4-GA-PEP, plastic reaction vial) for ^{68}Ga-labelling, and pharmaceutical-grade ^{68}Ge/^{68}Ga generator (GalliaPharm®) used in the process validation tests were purchased from EZ (Germany). The parameters such as temperature, precursor concentration, reaction time, buffer concentration with volume used, bubble point test for 0.22 um filter integrity, and pH, as well as product purification step (C18 Cartridges), were optimized and set up in control program. Process optimization was conducted regarding product quality (Radio-HPLC, GC, MCA, TLC, Bacterial Endotoxin Test) and quantity (>5 mCi/dose, 1 MBq~60MBq/nmol), as well as process reproducibility. ***Results:*** The reproducible and GMP-compliant automated production of [^{68}Ga]Ga-PentixaFor with on-line documentation was developed. The decay-corrected radiochemical yield was >83% (n = 3, process validation test) at the end of the synthesis with a labeling synthesis duration of 20 min and a quality control including release procedure of 20 min. The average radiochemical purity of the products was >95% (n = 3) with the total amount of the peptide in the preparation of 50µg (n = 3, GMP grade, ABX). Radionuclide purity (>99.9%), radiochemical purity (>95%), sterility, endotoxin content, residual solvent content (EtOH < 10%), and sterile filter integrity tests met the acceptance criteria. The product was stable at room temperature for 2 hrs. ***Conclusion:*** The fully automated GMP-compliant manufacturing process was developed and thoroughly validated. The resulting [^{68}Ga]Ga-PentixaFor will be using in a clinical study for accurate evaluation of several lymphomas for noninvasive detection of CXCR4 receptor relative disease at Koo Foundation Hospital. This process validation and quality control methodology could be compliant with GMP regulations for future clinical application in Taiwan. ***References:*** Cancers 2022, 14, 3814. EJNMMI Radiopharmacy and Chemistry 2023, 8:4.

EP-0879

Radiosynthesis of Theranostic FAP-2286: This Is the Way

M. Aurilio, *C. Maisto, A. Esposito, V. Porfidia, M. Buonanno, R. de Marino, A. Morisco, E. Squame, S. Lastoria;
National Cancer Institute G. Pascale, Napoli, ITALY.*

Aim/Introduction: FAP targeting using FAP-based radiolabelled tracers is a promising tool for diagnosis and therapy of numerous malignant tumors. One of the most promising compounds

with the highest reported FAP affinity is FAP-2286. FAP-2286 is a FAP-targeted peptidomimetic functionalized with a DOTA chelator that can therefore bind theranostic pairs, such ^{68}Ga and ^{177}Lu. The aim of this work was to optimize the synthesis of the radiopharmaceutical, in diagnostic and therapeutic form, using a single synthesis module and standardized quality controls, in order to have an easy and reliable procedure optimizing economic resources. ***Materials and Methods:*** The radiolabelling with ^{68}Ga/^{177}Lu was performed using a cassette-based automatic module. $^{68}GaCl_3$, eluted from generator with starting activity of 1220 ±74 MBq, is used without purification and added to a solution of 50 microgram FAP-2286 dissolved in 1 ml of 0,7 M sodium acetate buffer. The reaction mixture was heated to 90 °C for 10 minutes and after was loaded for purification with the preactivated C18 cartridge and eluted with ethanol. For preparation of [^{177}Lu] Lu-DOTAFAP-2286, the same automatic module was used. A solution of 7400 MBq of ^{177}Lu, in 300 microliter 0.05 M HCl, was added to a peptide dissolved in 2 ml of ascorbic buffer pH 4,5 (40 MBq/microgram peptide). The labelling reaction was carried out at 120°C for 4 minutes and then at 100°C for 26 minutes. No purification step was applied. Both radiopharmaceuticals were formulated in 0,9% saline solution after sterile filtration. Quality controls were performed according to regulatory guidelines to establish a clinical routine production. ***Results:*** Radiochemical, chemical and radionuclide purity, pH, half-life, residual organic solvents were assessed for both the radiolabelled preparations. FAP-2286 showed good radiochemical yield (RCY) when radiolabelled with ^{68}Ga, in the range of 70-80%, and a RCP > 99 % without significant amount of both free ^{68}Ga and colloidal ^{68}Ga. For the radiosynthesis of [^{177}Lu]Lu-DOTAFAP-2286, we obtained high molar activities, about 60 GBq/mmol, with high RCP > 99.8% that was stable for 24 hours. ***Conclusion:*** ^{68}Ga/^{177}Lu-FAP-2286 was successfully synthesized fully-automated. All quality control parameters were in accordance with the EuPh and the stability was > 24h for [^{177}Lu]Lu-DOTAFAP-2286.The automatic synthesis therefore test making FAP-2286 a very convenient theranostic agent and will facilitate the implementation of this radiopharmaceutical pair in clinical practice.

EP-0880

The Optimization of the Current ININ Method of Lu-177 DOTA-HYNIC-iPSMA

Y. Omar[1], *Y. Atteya*[1], *N. Taha*[2], *M. AbdelKawi*[1];
[1]*Misr Radiology Center, Cairo, EGYPT,* [2]*Ain Shams University, Cairo, EGYPT.*

Aim/Introduction: PSMA (Prostate-Specific Membrane Antigen) is an overexpressed cell surface protein in prostate cancer cells, making it an attractive target for cancer diagnosis and treatment. One way to target PSMA is through radiolabeled small molecules that bind specifically to the protein.The chelators can be conjugated to PSMA-targeting small molecules for radiolabeling with therapeutic isotopes like Lutetium-177 (Lu-177). The chelators DOTA (1,4,7,10-tetraazacyclododecane-1,4,7,10-tetraacetic acid) attached to HYNIC (6-hydrazinonicotinic acid) generates a rigid chemical structure that minimizes the number of intramolecular hydrogen bonds, producing a favorable spatial orientation of the active site (Lys {Nal) - NH-CO ~ NH-Glu) in the molecule for biological re-comforting by the PSMA protein. ***Materials and Methods:*** The labelling process was improved by using softer conditions, lower temperatures, and less time. In the optimized method, the DOTA-HYNIC-iPSMA molecules shows reduced degradation and a higher radiolabeling efficiency. It also shows better stability of molecules and robust post-labeling compared to the current method of labeling from ININ (Instituto Nacional De Investigaciones Nucleares). The current labelling process from ININ Kits includes 50 mg of mannitol and 100 mg of ascorbic acid, after being reconstituted with 1.1 ml of 1 M sodium acetate buffer at pH 5.0 and heated up to 95° C for 30 min incubation. This method showed degradation in the compound due to long reaction times and higher temperatures. The optimized method for labelling required a lower temperature of 85° C, a shorter reaction time of 10 min, and a lower quantity of ascorbic acid. ***Results:*** The optimized method shows a better purity on the HPLC system, radiolabeling efficiency above 98%, and reproducibility. ***Conclusion:*** Lu-177 DOTA-HYNIC-iPSMA molecule radioligand is a promising approach for the treatment of prostate cancer. The optimization of the labelling method from the current kits produced by ININ shows better purity, shorter labelling time and lower temperature compared to the current condition. ***References:*** 1-Luna-Gutiérrez, M., Hernández-Jiménez, T., Serrano-Espinoza, L. et al. Freeze-dried multi-dose kits for the fast preparation of 177Lu-Tyr3-octreotide and 177Lu-PSMA(inhibitor) under GMP conditions. J Radioanal Nucl Chem 314, 2181-2188 (2017).

EP-0881

Automated cassette-based synthesis of [18F]Fluoro-L-DOPA via Cu-mediated process for routine production in a GMP environment

N. Emmanuel, *D. Goblet, G. Decoux, C. Gameiro;*
IBA, Louvain-la-Neuve, BELGIUM.

Aim/Introduction: The continuously growing success of [^{18}F] fluoride for PET imaging has resulted, in the recent years, in a need of diversity of radiotracers. For this purpose, specific methodologies have been explored for the labelling of a variety of chemical structures. Cu-mediated ^{18}F-fluorination is an efficient method for the labelling of aromatic and heteroatomic compounds such as arylstannanes[1]. [^{18}F]Fluoro-L-DOPA, a tracer used for the detection of neuroendocrine tumors and diagnosis of Parkinson's disease, was successfully obtained using this method. Robust automated synthesis in a GMP environment is crucial to ensure a reliable routine production of this radiopharmaceutical. In this abstract, optimized and fully automated synthesis of [^{18}F] Fluoror-L-DOPA in a disposable, cassette-based module and its quality control results (according to the European pharmacopoeia) will be described. ***Materials and Methods:*** Fully automated synthesis has been established on a cassette-based platform. The [^{18}F]fluoride was trapped on a QMA cartridge and eluted with 900 µL of TEA into the reactor. After a thorough drying of the [^{18}F] fluoride, the precursor solution (BBTE 20 mg, an arylstannane, in 1 mL dimetylacetamide containing the Cu-catalyst) is added to the same reactor. The fluorination was performed at 100 ☒ for 10 minutes. The reaction mixture was then diluted with EtOH 30% (8 mL) and purified from its metallic component (Sn, Cu) with a tC18 cartridge. [^{18}F]Fluoro-L-DOPA was eluted from tC18 to the reactor with 2 mL of acetonitrile and 2 mL of HBr 48% were added for hydrolysis. The hydrolysis was performed at 150°C for 10 min. Subsequently, NaOH was added to neutralize the pH before purification on HPLC column (Synergi Hydro-RP). The overall synthesis time was 60 minutes, including the purification step. Quality control tests were performed including appearance, pH, radionuclidic purity, radiochemical purity, chemical purity, chiral purity, ICP-MS and residual solvents, according to the European pharmacopoeia (04/2019:2481), where possible. ***Results:*** In this

present study, automated radiosynthesis of [18F]Fluoro-L-DOPA has been achieved with radiochemical yields of 25-30% non-decay corrected (n.d.c) for incoming activity up to 74 GBq. In all runs (n=3), radiochemical purity was >95% and residual solvents below ICH Q3 limits. [18F]Fluoro-L-DOPA enantiomeric purity was confirmed by chiral HPLC analysis. ***Conclusion:*** Fully automated, optimized and simplified synthesis of [18F]Fluoro-L-DOPA has been obtained on cassette-based module with high radiochemical and chemical purity. Ready-to use consumables are available to help streamline routine clinical production in a GMP setting. ***References:*** [1]F. Zarrad,B.D. Zlatopolskiy,P. Krapf,J. Zischler and B.Neumaier,Molecules 22;2231, 2017.

EP-0882

The Use of a Mobile Clean Room for (Re)loading of a More Durable Sr-82/Rb-82 Generator

R. Claessens[1], *J. C. Vink*[2], *K. Baggerman*[2];
[1]*Rubigen b.v, 's-Hertogenbosch, NETHERLANDS,*
[2]*Baggerman Farma Consult, Eindhoven, NETHERLANDS.*

Aim/Introduction: We developed a Sr-82/Rb-82 generator to be (re)loaded every 4 weeks under aseptic conditions in a mobile clean room with a usability period of 12-13 weeks. ***Materials and Methods:*** The design of the generator is based on the 'Ottawa generator' [1] with a few changes. The generator is loaded with Sr-82 up to 3 times every 4 weeks (3700 MBq Sr-82 for first loadings, 2600 MBq for reloadings). After 12 weeks the generator is replaced by a fresh one. PEEK (polyether ether ketone) is used as column material to allow disinfection with a hypochlorite solution once a week. (Re)loading at a central facility is a logistic challenge. Instead, after inspectorate approval a mobile clean room at the client's premises is used to load and test the generators. ***Results:*** Between 2012 and 2021 79 generators were produced and 205 generator loadings were performed. All samples taken met the specifications from the US Pharmacopeia (USP). The maximum elution volume over 12 weeks was 50 l. Between 2017 and 2021 the average value per year for the Sr-82 break-through in a generator after 4 weeks of clinical use declined from 14,5 to 2,5 percent of the limit value (USP). In 2019 a marketing authorization for The Netherlands was obtained from the Dutch Medicines Evaluation Board. The mobile clean room was equipped with a GMP class A biohazard bench used for assembly of the generator system. The heavy (900 kg) generator wagon can't be placed in a biohazard bench. Instead, loading of the generator is performed in a GMP class C environment under a screen of air filtered by a high efficiency particulate air (HEPA) filter, thus simulating the conditions in a biohazard bench. The mobile clean room is equipped with all instruments needed for analysis of the generator eluate, including an electrically cooled high purity Germanium gamma detector. ***Conclusion:*** By introducing the concept of reloading every 4 weeks a Sr-82/Rb-82 generator is developed that has less decline of activity than a conventional generator, using the same activity of Sr-82. The concept requires the use of a mobile clean room for loading and quality control. The generator is delivered ready for use meeting all specifications from the USP. ***References:*** T.M. Alvarez-Diez et al. Manufacture of Sr-82/Rb-82 generators and quality control of Rb-82 chloride for myocardial perfusion imaging in patients using positron emission tomography. Applied Radiation and Isotopes 1999; 50: 1015-1023.

EP-0883

[68Ga]Ga-Pentixafor automatized synthesis using a new module: development and quality control before use in routine for CXCR4 PET imaging

T. Daniel, *C. Balouzet Ravinet, J. Clerc, R. Batista, Y. Mouraeff;*
Hôpital Cochin, Assistance publique - Hôpitaux de Paris, Paris, FRANCE.

Aim/Introduction: We have recently acquired a new radiopharmaceutical drug synthesis module and drug control equipment, allowing the development of radiosyntheses for clinical research. As Pentixafor labeled with Gallium 68 is a promising radiopharmaceutical drug in several indications such as hematological malignancies and solid cancers, we aimed at setting up its synthesis process with our equipment. Existing methods do not use this type of module, so the synthesis is not yet described. We present here the method to develop an optimized and automatized radiosynthesis in order to submit an Investigational Medicinal Product Dossier (IMPD) to the French National Agency for the Safety of Medicines and Health Product (ANSM). ***Materials and Methods:*** Quality controls were performed in accordance with the European Pharmacopoeia (EP) and the International Council for Harmonization (ICH) Q2 standards. The radiochemical purity (RP) was assessed by Instant Thin Layer Chromatography (ITLC) and radio-High Pressure Liquid Chromatography (HPLC). We adjusted the elution of the C18 cartridge and optimized the synthesis and heating times to achieve the highest labeling yield with a RP above 95%. The optimized method was validated by performing 3 syntheses under Good Manufacturing Practices (GMP) conditions. ***Results:*** Among 22 syntheses carried out in 3 months, 2 were removed due to the detection of a cassette leak. Temperatures ranging from 90°C to 98°C with heating time ranging from 4 to 7 minutes were evaluated with 50 µg of peptide. The labeling yields ranged from 60% to 95% while the RP assessed by ITLC ranged from 83% to 98%, and from 97% to 100% by HPLC. Performing the synthesis at 97°C for 4 min was determined to be the best compromise between RP and yield. With these settings, the mean radiolabeling efficiency under GMP-conditions was 87.0% (Standard deviation (SD) 6.67%). The average RP was 99.1% (SD 0.25%) assessed by ITLC and 99.8% (SD 0.09%) by HPLC. Endotoxin levels were <5 EU/mL, and pH was 6.5. We assessed the stability of the radiotracer for up to 4 hours at room temperature. ***Conclusion:*** The [68Ga]Ga-Pentixafor synthesis method we described here complements the other existing methods in the literature. However, any comparison should be approached with caution given the differences in settings. This development of an optimized and robust synthesis process, and the validation of the quality controls with respect to the EP, allowed us to support the IMPD's request. It could be suitable for multidose application in clinical settings.

EP-0884

Formulation of a Kit for Preparing 89Zr-DFO-Pembrolizumab Injection Under Good Manufacturing Practices for Imaging the Uptake of Pembrolizumab into Brain Metastases in Patients with Lung Cancer by PET

S. Borlase[1], *C. Chan*[1], *R. Reilly*[1,2];
[1]*Leslie Dan Faculty of Pharmacy, University of Toronto, Toronto, ON, CANADA,* [2]*Joint Department of Medical Imaging and Princess Margaret Cancer Centre, University Health Network, Toronto, ON, CANADA.*

Aim/Introduction: Pembrolizumab is a checkpoint immunotherapy that binds to programmed cell-death protein-1 (PD1) on T-cells and inhibits its interaction with PDL-1 on tumour cells which enables a cytotoxic T-cell response. Pembrolizumab is used to treat metastatic lung cancer. However, delivery across the blood-brain-barrier for the treatment of brain metastases is limited. Imaging pembrolizumab uptake into brain metastases by PET is crucial to predict its effectiveness for treating brain metastases. I will formulate a kit under Good Manufacturing Practice (GMP) conditions to prepare ^{89}Zr-DFO-pembrolizumab injection for imaging its uptake into brain metastases by PET in patients with metastatic lung cancer in a planned clinical trial. ***Materials and Methods:*** Pembrolizumab was reacted with p-isothiocyanate desferrioxamine (p-SCN-DFO). DFO-pembrolizumab was purified by ultrafiltration on an Amicon Ultra-0.5 device, repeated 6 times. The purity and homogeneity of DFO-pembrolizumab was assessed by SDS-PAGE. MALDI-TOF mass spectrometry was used to determine the number of DFO/pembrolizumab. Preliminary studies were conducted to determine the optimal conditions for conjugating pembrolizumab with DFO and labeling with ^{89}Zr. The labeling efficiency at increasing specific activities was determined. Radiochemical purity was measured by instant thin layer-silica gel chromatography (ITLC-SG). Kits were formulated by dispensing DFO-pembrolizumab through a 0.22 µm sterilizing filter into unit-dose vials. Quality control testing included labeling efficiency with ^{89}Zr (ITLC-SG), purity (SDS-PAGE), pH (5.2-5.7), PD1-binding (surface plasmon resonance), sterility and endotoxins (USP). ***Results:*** Pembrolizumab (1 mg) was reacted with a 5, 10, 15 or 20-fold molar excess of p-SCN-DFO which introduced 1.2±0.5, 1.9±1.0, 2.5±0.8 and 3.3±0.7 DFO/pembrolizumab, respectively. SDS-PAGE revealed a pure and homogenous immunoconjugate with a single band at 150 kDa. The labeling efficiency of DFO-pembrolizumab with ^{89}Zr at specific activities of 10, 18, 26, 46 and 100 MBq/mg was 97.3%, 98.6%, 98.8%, 99.2%, and 99.1%, respectively for pembrolizumab conjugated with 2.5±0.8 DFO. Kits were formulated by reacting pembrolizumab (30 mg) with a 20-fold molar excess of p-SCN-DFO resulting in 6.4 DFO/pembrolizumab. DFO-pembrolizumab (1mg/vial) was dispensed into unit-dose glass vials. The pH was 5.5. Kits were labeled with ^{89}Zr at a specific activity of 18.5 MBq/mg which achieved a labeling efficiency >95%. Sterility and endotoxin results are pending. A commercial surface plasmon resonance assay for assessing PD1 binding is being adapted and results will be reported. ***Conclusion:*** We report here for the first time, a kit formulated under GMP conditions for preparing ^{89}Zr-DFO-pembrolizumab injection in high radiochemical purity suitable for patient administration.

EP-0885

Investigation of the Radiolabelling Potential of the Aurora A Kinase Inhibitor Alisertib with Iodine-123 [123I]

E. Uygur[1], *C. Sezgin*[1], *B. Y. Akdağ*[2], *T. Özbey*[2], *Y. Parlak*[1], *K. B. Karatay*[3], *F. G. Gümüşer*[1], *F. Z. Biber Müftüler*[3];
[1]*Manisa Celal Bayar University, Manisa, TÜRKIYE,* [2]*TENMAK, Ankara, TÜRKIYE,* [3]*Ege University, İzmir, TÜRKIYE.*

Aim/Introduction: Alisertib (ALS) is an Aurora kinase inhibitor of interest for cancer therapy [1]. Overexpression of Aurora kinase can cause chromosomal instability and cell transformation. Since Aurora kinase overexpression is frequently shown in tumor cell lines, it is thought to have a causal relationship with tumor formation. Many studies have reported that Aurora Kinase A expression is increased in many malignancies such as prostate cancer, colorectal cancer, and T-cell lymphomas. Many studies on the imaging of Aurora Kinase A (AURK-A) expression are in the literature [5-6]. In this study, ALS was radiolabelled with Iodine-123 [^{123}I]I ($t_{1/2}$: 13.2 hours, γ: 159 keV) using the iodogen method and quality control studies of the [^{123}I]I-ALS was performed by Thin Layer Radio Chromatography (TLRC) method. ***Materials and Methods:*** The [^{123}I]I radionuclide was produced at the TENMAK Nuclear Energy Research Institute according to [^{124}Xe]Xe (p,2n), [^{123}Cs]Cs, [^{123}Xe]Xe, [^{123}I]I the nuclear reaction. The radioiodination ([^{123}I]I-ALS) reaction was carried out by the iodogen method. The radiochemical yields of [^{123}I]I-ALS and the stability of the compound were determined by TLRC. The ALS compound was labelled with inactive iodine (K[^{127}I]I) and the molecular structure analysis of the K[^{127}I]I-ALS was determined by High-Performance Liquid Chromatography (HPLC) and Nuclear Magnetic Resonance (^{1}H-NMR) methods. ***Results:*** [^{123}I]-NaI was obtained at a concentration of 890 MBq/mL. The radiochemical yield of [^{123}I] I-ALS was found to be 95.1 ± 0.98% (n=3. The radiochemical yield of [^{123}I]I-ALS was over 90% at the end of 24 h. The retention times of ALS and K[^{127}I]I-ALS were found to be 2.54 and 2.21 minutes, respectively at HPLC. To obtain the experimental ^{1}H-NMR, ALS/Iodine/Iodogen ratios were prepared stoichiometrically as 1/2/1, the pH value was adjusted to 8 with 1N NH_4OH and incubated for 12 hours and the reaction was completed with 0.1-N Na_2SO_3. According to the ^{1}H-NMR results, the ppm values of hydrogens attached to carbons to which [^{123}I]I is likely to bind are expected to be 7.85 and 7.79, respectively. ***Conclusion:*** The ALS compound was radiolabeled with [^{123}I]I with high purity. The iodine molecule of ALS is thought to be bound at the ortho or para position in the aromatic benzene ring. However, more comprehensive structural analyses may be needed using ^{1}H-NMR, ^{13}C-NMR and X-ray crystallography methods. It is thought that this study, which is a preliminary study for the imaging of AURK-A expression, should be supported by in vitro and in vivo preclinical studies.

EP-0886

Radiolabeling of [225Ac]Ac-PSMA-617 vs [225Ac]Ac-DOTATATE: What Analogies? What Differences?

A. Esposito*, M. Aurilio, M. Buonanno, A. Morisco, C. Maisto, L. D'Ambrosio, D. Di Martino, S. Lastoria;*
IRCCS INT "Fondazione Pascale", Naples, ITALY.

Aim/Introduction: Alpha-emitters have gained a great interest as novel cytotoxic agents for Targeted Alpha-Therapy (TAT). They enable the release of α-particles with a short path length in tissue and high linear energy transfer, leading to a higher double strain breaks probability in DNA. Thus, they are currently investigated as candidates in cancer treatment, especially in micrometastasis. Actinium-225 (^{225}Ac) is an α-emitter that with its decay chain, generates 4 α-particles contributing to increase its cytotoxicity if compared with other α-emitters. One of the most suitable chelating agents for complexation of this isotope is DOTA. Our goal was to standardize a method for the radiolabeling of more DOTA-peptides. For this purpose, the DOTA-peptides most commonly used, PSMA-617 and DOTATATE, were radiolabeled with ^{225}Ac. ***Materials and Methods:*** [^{225}Ac]Ac-PSMA-617 and [^{225}Ac]Ac-DOTATATE were synthetized at the same conditions: 100 micrograms of peptide was added to 350 microliters of gentisic buffer (acid 0,25M and sodium acetate 0,35M) pH 5.5. This solution was added to 100 microliters of $AcCl_3$ (8±0,3 MBq) and heated at 97±2°C for 30 minutes. ^{225}Ac-DOTA-peptides were monitored via iTLC using Silica gel as stationary phase and, Sodium Acetate 0,1M pH 5 and Acetonitrile/Water 1:1 as mobile phases. The iTLC strips were acquired at time 0 and reacquired

at 3 hours, when ^{221}Fr and ^{213}Bi were in Secular Equilibrium with ^{225}Ac[1], to establish with accuracy the radiochemical purity (RCP) of radiopharmaceuticals. The stability was evaluated via iTLC at 24 hours. ***Results:*** The mean RCP of [^{225}Ac]Ac-PSMA-617 and [^{225}Ac]Ac-DOTATATE post-synthesis were 97,05±1,34 and 94,43±4,91 respectively, while at 3 hours were 96,55±0,07 and 93,18±0,95. The mean stability at 24 hours was 90,7±0,14 for [^{225}Ac]Ac-PSMA-617 and 81,03±2,09 for [^{225}Ac]Ac-DOTATATE. ***Conclusion:*** The RCP of [^{225}Ac]Ac-DOTATATE and [^{225}Ac]Ac-PSMA-617 was acceptable, demonstrating that our in-house radiolabeling method was suitable for both peptides.The different stability at 24 hours of [^{225}Ac]Ac-PSMA-617 and [^{225}Ac]Ac-DOTATATE, probably, was the result of the respective structures of the peptides. DOTATATE is an octapeptide, whereas PSMA-617 is a peptidomimetic inhibitor that demonstrated high radiolytic stability for at least 72 hours[2]. Therefore, it is necessary to identify a stabilizing system for [^{225}Ac]Ac-DOTATATE that is not essential for [^{225}Ac]Ac-PSMA-617. ***References:*** [1]Kelly JM, et all. A suitable time point for quantifying the radiochemical purity of ^{225}Ac-labeled radiopharmaceuticals. EJNMMI Radiopharm Chem. 2021 Dec 20;6(1):38.[2]Benešová M, et all. Preclinical Evaluation of a Tailor-Made DOTA-Conjugated PSMA Inhibitor with Optimized Linker Moiety for Imaging and Endoradiotherapy of Prostate Cancer. J Nucl Med. 2015 Jun;56(6):914-20.

EP-0887

Comparison of 111In and201Tl Radiopharmaceutical Adsorption on Acrylic Phantoms

T. Inagaki[1], *N. Fujita*[2], *R. Isobe*[1], *T. Nagahara*[1], *S. Abe*[2], *K. Kato*[1];
[1]*Nagoya University Graduate School of Medicine, Nagoya, JAPAN,* [2]*Department of Radiological Technology, Nagoya University Hospital, Nagoya, JAPAN.*

Aim/Introduction: Radiopharmaceuticals are known to adsorb onto phantoms during phantom experiments. When adsorption occurs in phantom experiments, it hinders the analysis, e.g., making it difficult to set the region of interest. In addition, adsorption affects clinical imaging conditions because the imaging conditions used in clinical practice are determined from such experiments. In a previous study, ^{111}In radiopharmaceuticals were found to adsorb on the inner wall of the phantom during phantom experiments. Therefore, adsorption should be observed over time even for ^{111}In and ^{201}Tl radiopharmaceuticals, which are long half-life nuclides in nuclear medicine examinations. In this study, we evaluated the adsorption of ^{111}In and ^{201}Tl radiopharmaceuticals on acrylic phantoms and examined the changes in adsorption by different nuclides. ***Materials and Methods:*** The phantom was an acrylic container (75 × 75 × 60 mm). Four radiopharmaceuticals (^{111}In-pentetreotide, ^{111}In-DTPA, $^{111}InCl_3$, and ^{201}TlCl) were used. The solutions of ^{111}In-pentetreotide, ^{111}In-DTPA, $^{111}InCl_3$, and ^{201}TlCl were sealed in the phantoms, respectively, and the liquid volume was 50 mL. Counts were collected by planar imaging of the prepared phantom using a SPECT/CT system. The radiopharmaceutical solution was drained from the phantom and lightly rinsed with water. Then, the counts were collected by planar imaging again. Finally, the adsorption rate was determined. The adsorption rate was calculated as the counts of the phantom after the removal of the solution relative to the counts of the phantom filled with the solution. ***Results:*** The adsorption rates for ^{111}In-pentetreotide, ^{111}In-DTPA, $^{111}InCl_3$, and ^{201}TlCl were 0.54%, 0.15%, 29.2%, and 0.17%, respectively. $^{111}InCl_3$ planar images showed a large amount of radiopharmaceuticals remaining in the phantom. The images of ^{111}In-pentetreotide showed radiopharmaceutical adsorption along the inner wall of the phantom, while no adsorption was observed in the images of ^{111}In-DTPA and ^{201}TlCl. ***Conclusion:*** Among the four radiopharmaceuticals, $^{111}InCl_3$ showed the highest adsorption rate, and little adsorption occurred with ^{111}In-DTPA and ^{201}TlCl.

EP-0888

Cassette-Based Sterility Testing of Radiopharmaceuticals: A Novel Approach to Ensuring Quality and Safety

M. Nousch[1], *G. Reischl*[2], *R. Schulze*[3], *K. Tautz*[4], *D. Freitag-Stechl*[1];
[1]*CUP Laboratorien Dr. Freitag GmbH, Radeberg, GERMANY,* [2]*Universitätsklinikum Tübingen, Tübingen, GERMANY,* [3]*Sächsisches Staatsministerium für Soziales und Gesellschaftlichen Zusammenhalt, Dresden, GERMANY,* [4]*Eckert & Ziegler GmbH, Berlin, GERMANY.*

Aim/Introduction: Sterility testing is an essential part for the manufacturing process of all pharmaceutical products that are used to treat human diseases. These tests assess the presence or absence of microorganisms and ensure patient safety. Although sterility testing of most pharmaceutical products is part of the production routine, these tests can be challenging for radiopharmaceuticals. The safety precautions accompanying the work with radioactive substances often requires the use of specialized laboratories. Only few laboratories world-wide are equally authorized to handle radioactivity, and are also equipped to carry out sterility tests. Hence, the aim of this project was to develop a concept and for a half-automated system which facilitates sterility testing of radiopharmaceuticals. ***Materials and Methods:*** A system was designed which utilizes a sterile, single-use cassette that contains all the necessary components for conducting the sterility test, including the filtration membrane and culture media. It was tested whether this setup in general is sterile and can be used for the analysis of radiopharmaceuticals such as ^{68}Ga, ^{177}Lu and ^{64}Cu containing substances. Additionally, we tested whether aerobic and anaerobic growth is possible in our system. To this end, a defined number of microorganisms was introduced into the filter units, various amounts of specific growth media were added in the last filter step and general growth was analyzed. For assessing aerobe growth, Bacillus subtilis, Candida albicans or Aspergillus brasiliensis were incubated in tryptone soya broth (TSB) at 25°C. For assessing anaerobic growth Staphylococcus aureus, Pseudomonas aeruginosa or Clostridium sporogenes were incubated in Thioglycolate broth at 32°C. ***Results:*** By establishing a closed system in which the individual parts can be sterilized, we were able to minimize the risk of introducing microbial contamination. The different sterile parts were connected in a clean bench. The process itself can run on a normal lab bench. Growth was only detected in filter units that have been deliberately exposed to solutions containing microorganisms. All tested bacterial, yeast and fungi strains were able to display significant growth within five days of incubation. ***Conclusion:*** Our system is designed to be easily integrated with existing automated radiopharmaceutical production systems, streamlining the process and minimizing human intervention. The overall setup allows microbial growth if microbes are present. This innovative proof of concept study has the potential to revolutionize the quality control of radiopharmaceuticals by providing a base for standardized sterility testing which could be introduced into many routine production processes.

EP-0889

Determination of Extractables and Leachables in Radiopharmaceuticals

M. Nousch[1], *M. Janich*[1], *S. Becker*[2], *T. Otten*[2], *M. Zurbruegg*[2], *R. Schulze*[3];
[1]*CUP Laboratorien Dr. Freitag GmbH, Radeberg, GERMANY,* [2]*Intertek (Schweiz) AG, Reinach, SWITZERLAND,* [3]*Sächsisches Staatsministerium für Soziales und Gesellschaftlichen Zusammenhalt, Dresden, GERMANY.*

Aim/Introduction: The presence of extractables and leachables in pharmaceutical products can have a significant impact on product quality, safety, and efficacy; and ultimately the success of life-saving treatments. During production and storage of (radio) pharmaceuticals, polymeric materials are directly exposed to the formulation and therefore small molecules can be release from the polymers into the drug formulation. These phenomena could be particularly pronounced for radiopharmaceuticals because radiation is known to have an impact on the polymer structures, leaching behavior and degradation of polymer additives. Hence, this study aims to develop robust and reliable analytical methods for the identification and quantification of extractables and leachables in radioactive pharmaceutical products. ***Materials and Methods:*** To simulate worst case conditions and real-world scenarios, storage vials used in ^{68}Ga tracer preparations were subjected to accelerated aging and various storage conditions using a range of solvents (e.g. water, ethanol, and dimethyl sulfoxide) with varying polarities and pH values. Analyses of extractables and leachables were performed by headspace (HS)/direct injection gas chromatography-mass spectrometry (GC-MS), liquid chromatography-mass spectrometry (LC-MS), or inductively coupled plasma mass spectrometry (ICP-MS). For all identified critical substances a risk assessment was conducted based on established toxicological thresholds. ***Results:*** The developed analytical methods demonstrated excellent specificity, linearity and recovery, meeting the ICH guidelines' requirements. A total of 38 extractables and 3 leachables were identified and quantified in the investigated ^{68}Ga-containing radiopharmaceutical. Most of these compounds were plasticizers, antioxidants, lubricants, and their degradation products or elemental impurities, which are commonly found in pharmaceutical packaging materials. The risk assessment indicated that many of the extractables and most of the leachables in these ^{68}Ga preparations were present at levels below the established toxicological thresholds. ***Conclusion:*** Results of the study demonstrate the successful development of a robust and reliable analytical methodology for the determination of extractables and leachables in radioactive pharmaceutical products. By combining (HS)GC-MS, LC-MS, and ICP-MS a wide range of chemicals were identified and quantified that can be released from polymeric materials by the exposure to radioactive substances. The study indicates that all detectable chemicals released from container closure vials through the exposure to ^{68}Ga, were below the established toxicological threshold. Hence, our developed methodology can contribute to the ongoing efforts to develop safer, more effective, and regulatory-compliant radioactive pharmaceuticals for the treatment of various diseases.

EP-0890

Comparative analytical methods for testing residual solvents in quality control of PET radiopharmaceuticals

V. Mendi Barcina[1], *M. De Arcocha Torres*[1], *Á. Gutiérrez González*[2], *I. Martínez Rodríguez*[2], *N. Martínez Amador*[2], *F. Gómez de la Fuente*[2], *A. Sánchez Salmón*[2], *J. Jiménez Bonilla*[2], *M. Pombo López*[2], *A. Bota Bota*[2], *R. Quirce Pisano*[2];
[1]*Radiopharmacy Unit. Nuclear Medicine Service Marqués de Valdecilla University Hospital. Molecular Imaging Group (IDIVAL). University of Cantabria, Santander, SPAIN,* [2]*Nuclear Medicine Service Marqués de Valdecilla University Hospital. Molecular Imaging Group (IDIVAL). University of Cantabria, Santander, SPAIN.*

Aim/Introduction: The manufacture of PET radiopharmaceuticals produced according to Good Manufacturing Practices (GMP), calls for compliance with a set of quality controls, published in the European Pharmacopoeia and the ICH guidelines. These include residual solvent testing.Depending on the number of standards used, there are several options for performing a calibration: with a single concentration of the chemical standard, the "single point calibration" or using three or more concentrations of chemical standard, the "multi-point calibration". The aim of this study was to assess the correlation between results obtained with "single point calibration" and "multi-point calibration" models to carry out Gas Chromatography (GC) method of analysis for the routine quality control (QC) of L-[methil-11C]- methionine to secure the quality of the finished product. ***Materials and Methods:*** A calibration curve is elaborated following the internal standard (IS) method (isopropanol 0.8 mg/ml), with decreasing concentrations of ethanol (12.5;2.5;0.5;0.1;0.02 mg/ml), ratio (1:1). On the other hand, 10 standard samples with known concentration of ethanol (12.5;11;10;9;8;7;6;5;4;3 mg/ml) are prepared with IS, ratio (1:1). The analytical response from the different standard samples are interpolated in the calibration curve, to know the concentration. The samples were injected three times.Furthermore, using the standard sample with the highest concentration (12.5 mg/ml), the calibration factor (area/concentration) is obtained, necessary to calculate the concentration of each standard. Data analysis was performed through the Paired t-test as statistical analysis. ***Results:*** Excellent linearity was found between 0.02 and 12.5 mg/ml, with a correlation coeficient for calibration curves (r^2) equal to 0.9999. The standard deviation (SD) between average different concentrations (n=10) obtained by two methods was 0.02 to 0.03. The Paired t-test did not show statistical significant differences between the different calibration methods: single point calibration with IS vs. multi-point calibration with IS ($p = 0.97$). ***Conclusion:*** According to the results obtained in our study, the single-point method with internal standard is an alternative to carry out in the residual solvent test, when looking for faster, easier and more adaptable methods to specific samples and analytes, with the advantage of the quickness and simplicity of the assay compared to the multiple injection method with internal standard.

EP-0891

Highly efficient, biocompatible radiolabeling method for in vivo cell tracking

R. Hernandez, *A. Thickens, Z. Rosenkrans, L. Lambert-Lepesevich, J. Kink, E. Aluicio-Sarduy, A. Pinchuk, J. Engle;*
University of Wisconsin-Madison, Madison, WI, UNITED STATES OF AMERICA.

Aim/Introduction: Current cell labeling methods for in vivo cell tracking using PET/CT suffer from low activity incorporation yields and poor radiolabel stability. We addressed these limitations by directly conjugating the chelator Deferoxamine (DFO) to ubiquitous cell surface glycans, which enabled efficient and stable ^{89}Zr-radiolabeling of live cells under biocompatible conditions. ***Materials and Methods:*** DFO was derivatized with aminooxy acetic acid, and the resulting aminooxy-DFO (AOD) was purified by flash chromatography and identified by NMR and mass spectrometry. Reactive aldehydes were generated in the cell surface of the monocytic cell line U937 through sialic acid oxidation with $NaIO_4$ (5-1000 µM) at four or 37 °C for 15 min to 2 h. Subsequently, cells were incubated with AOD (100-500 µM) at room temperature for up to 1h in the presence of aniline, and cells were washed and resuspended in PBS. Next, AOD-conjugated ($5\text{-}7 \times 10^6$) cells were radiolabeled with ^{89}Zr (37-74 MBq) at room

temperature for 1h, then washed thrice to eliminate unlabeled ^{89}Zr, and the radiochemical yield was measured. Cell viability was assessed at each step via trypan blue staining. For in vivo PET/CT imaging, male NSG mice (N=3) were administered ^{89}Zr-U937 cells (3-5 x 10^5 5.6 MBq) via tail vein injection and static PET/CT scans acquired at 3, 24, 72, 164, and 192 h post-injection (p.i.). Region-of-interest analysis and biodistribution studies were performed to quantify the longitudinal in vivo distribution of the labeled cells. ***Results:*** The glycan-reactive AOD was generated with excellent chemical purity (>95%). Glycan oxidation with $NaIO_4$ had minimal effect on cell viability at the tested temperature and reaction times. Similarly, AOD conjugation and ^{89}Zr-labeling did not affect viability, which remained over 93% post-radiolabeling. The exceptional radiochemical yields observed, ranging from 6.1-10.2 MBq per 10^6 live cells, a 100-fold improvement over other methods, enabled tracking fewer cells (~300,000) with improved detectability. PET/CT images showed initial accretion of injected cells in the lungs (19.9±0.3 %IA/g) and the liver (23.7±0.7 %IA/g) at 3 h p.i., and their subsequent redistribution to the liver (31.5 ± 0.8 %IA/g) and spleen (13.5±2.0 %IA/g) at later time points. The low bone uptake and minimal whole-body radioactivity excretion were indicative of the excellent stability of the label in vivo. ***Conclusion:*** Our results showed unprecedented ^{89}Zr radiolabeling efficiencies and negligible impact on cell viability, affording improved imaging performance and hinting at the potential clinical value of this method for in vivo cell tracking.

EP-0892

Comparative methods of labeling red blood cells

M. Crespí Busquets[1], *J. Romero Herrera*[1], *S. Maymó Garrido*[1], *D. Rodriguez Puig*[1], *C. Munuera Sañudo*[1], *E. Pineda Fernández*[1], *M. Bueno Raspall*[1], *M. Cortés Romera*[2];
[1]*Radiopharmacy Department, Bellvitge University Hospital-IDIBELL, L'Hospitalet de Llobregat, Barcelona, SPAIN,*
[2]*Nuclear Medicine-PET (IDI) Department, Bellvitge University Hospital, L'Hospitalet de Llobregat, Barcelona, SPAIN.*

Aim/Introduction: To compare two methods of red blood cells labeling; the first one by following the Guidelines of the Spanish Agency for Medicines and Health Products (AEMPS) (Reference method: MR) and the second method by labeling red blood cells with ethylenediaminetetraacetic acid (EDTA) as a chelator for the extracellular stannous pyrophosphate (Alternative method: MA). ***Materials and Methods:*** These comparatives methods were applied in samples of 17 patients. Two samples of 4,4 mL of blood were obtained from every patient by adding 0.6 ml of ACD-A anticoagulant in each syringe. The RM sample was transferred to a Falcon™ tube with 2,5 µg Sn^{2+}. It was incubated at 37 ºC for 10'. Subsequently, washing was performed by adding 40 ml of physiological saline (SF), centrifuging for 10' at 1000 G and finally the cell button was separated from the plasma manually by using a sterile Pasteur pippete. Later around 28 - 35 mCi of [99mTc]$NaTcO_4$ were added into the cell button and incubated for 10' at 37ºC. Afterwards, a second wash was carried out the same as the previous one to obtain the final blood button and the supernatant. In that moment it is measured the activity obtained in both parts to calculate the yield of the radiolabeling. For the MA, the sample was incorporated into a Falcon™ tube with 22.34 µg of Sn^{2+}. After it was centrifuged at 1000 G for 5' and the plasma was removed, obtaining the blood button. Later than, the sample was homogenized by adding 0,5 ml of 2,2 % EDTA, 5 ml of SF and around 28 - 32 mCi of [99mTc]$NaTcO_4$. It was incubated at 37 ºC for 5' and centrifuged for 3' at 1000 G. Finally, the supernatant was removed. After that the activity of the final button and the supernatant was measured to be able to calculate the yield of the radiolabeling. The labelings were made in parallel by measuring the time invested. ***Results:*** The mean labeling yield was 81,1 ± 5,8 % for the MR and 97,1 ± 1,5 % for the MA. The time invested for the MR and MA was 68 ± 5 min and 25 ± 4 min respectively. ***Conclusion:*** The MA simplifies the technique by decreasing the labeling time and improving the reproducibility and the yield of the radiolabeling. We would recommend MA in daily clinical practice.

EP-0893

Automated Production Of [18F]UCB-J Using A Dibenzothiophenium Salt Precursor For Labelling

D. Pritchard, *F. Sirindil, M. Glaser, R. Awais, F. Twyman, E. Eedan, K. Sander, E. Arstad;*
University College London, London, UNITED KINGDOM.

Aim/Introduction: [^{11}C]UCB-J is a leading PET tracer for imaging of the synaptic vesical glycoprotein 2A (SV2A), but practical applications are limited by the challenging radiosynthesis and the short half-life of carbon-11 (20 min).[1] Although the tracer contains a 1,2,3-trifluorophenyl moiety, labelling of UCB-J with fluorine-18 (half-life 110 min) has proven exceedingly difficult. Potential precursors for labelling have either been found to be synthetically inaccessible, or have shown low reactivity, giving low radiochemical yields (<5%) and requiring harsh reaction conditions which cause racemization.[1] We recently reported that racemic UCB-J can be labelled with fluorine-18 under mild conditions using a dibenzothiophenium salt precursor.[2] With the aim to enable large scale production and distribution of [^{18}F]UCB-J, we have automated the labelling of this tracer using a Good Manufacturing Practice (GMP) compatible synthesis module. ***Materials and Methods:*** Automated labelling of [^{18}F]UCB-J was established on a GMP compatible synthesis module using a disposable cassette. We investigated the impact of the reaction temperature, reaction time and precursor load on the activity yields and the amount of non-radioactive UCB-J formed in the reaction to assess the molar activity that potentially can be achieved when the method is scaled up to high activity levels. ***Results:*** Direct labelling of [^{18}F]UCB-J proceeded under mild conditions (100 °C) and with a short reaction time (<10 min). Activity yields in excess of 20% (n=3) were obtained with <45 min total production time (excluding formulation). When using an enantiomerically pure precursor, no racemization of the tracer was observed with chiral HPLC. There was a clear trend of increased formation of non-radioactive UCB-J with increased reaction time. Although the molar activity is likely to be moderate even when scaled up to high activity levels, our preliminary results suggest that the method readily can allow production of multiple patient doses of [^{18}F]UCB-J and meet the release specifications that have been established for [^{11}C]UCB-J. ***Conclusion:*** Translating the labelling of [^{18}F]UCB-J from manual labelling to automated production was straightforward and gave comparable activity yields. The results are encouraging and suggest that the method can allow GMP compatible production of this tracer. We are currently developing a formulation step and investigating scale-up of the method for multidose production. ***References:*** (1) G Becker, S Dammicco, M.A. Bahri and E Salmon, Molecules, 25(10), 2303.(2) F Sirindil, S Maher, M Scholl, K Sander and E Årstad. Int. J. Mol. Sci., 2022, 23, 15481.

EP-0894

Ga68-PSMA-11 : push it to the limit with prepurification

M. Debarge[1], *A. Lombard*[1], *S. Journo*[1], *N. Veran*[1], *Q. Citerne*[1], *B. Demore*[2,1];
[1]*Nancy University Hospital, Vandoeuvre-lès-Nancy, FRANCE,*
[2]*Lorraine University, EA 4360 APEMAC, Nancy, FRANCE.*

Aim/Introduction: Awaiting Pharmaceutical companies are able to provide enough radiolabelled 18F-PSMA to serve the growing needs of nuclear medicine, in particular for monitoring of radionuclide therapy , Gallium 68 (68Ga) is still essential for peptide labelling in PET imaging, especially 68Ga-PSMA-11. The highest market authorized generator calibration available is 1.85 GBq of Ge-68, so 1.3 GBq of Ga-68 at start of synthesis (SOS). These characteristics led us to develop a dual generator fractionate elution to meet our needs, method used since 2022 January, which provide around 2 GBq SOS. A new Ga-68 pre-purification method provided by a synthesizer manufacturer allow theorically the simultaneous use of not only two generators, but maybe three, or more, with a significant increase of PSMA PET imaging by synthesis. ***Materials and Methods:*** Using manufacturer synthesis kits and synthesizer and some programming changes, from one to four 68Ga generator's elutions are injected through an ion exchange (SCX) cartridge, followed by elution to the reactor with a mixture of sodium and hydrogen chloride, where PSMA-11 precursor in sodium acetate buffer is waiting for labelling. After 95°C heating for 7 minutes, bulk is purified on HLB cartridge, eluted with ethanol and reformulated in 10 ml of sodium chloride. Final product, residual cartridges and waste activities are measured and decay corrected to end of synthesis time (EOS). European pharmacopeia compliant quality control is performed. ***Results:*** First tests were failures with multiple peaks in hplc and a low radiochemical purity. Ascorbic acid addition (1mg) lead to a good final quality product. One, two, three and four generator synthesis provided a radiochemical purity higher than 97% in HPLC and higher than 99% in TLC. Corrected yield of all synthesis are closed to 85% (82% to 88%). 7% of activity is found in waste (free 68Ga identified by HPLC), 4% in ion exchange cardridge and 4% in purification cartridge. All synthesis complies with clinical quality control specifications. The highest final product activity obtained is 1.94 GBq EOS (more than 3.2GBq SOS) which mean around 30% increase over staged routine elution way. ***Conclusion:*** Generators number not affect the final product quality with this prepurification method and can be used to increase the final 68Ga-PSMA-11 activity and serve the growing demand. However, the high concentration sodium chloride eluent for SCX can lead to radiolysis and has to be neutralised by ascorbic acid addition, which is not present in all market available precursor.

EP-0895

Initial experience on the cassette-based synthesis of 11C-Pittsburgh Compound-B

H. Gama Romero, *F. Trejo-Ballado, E. Zamora-Romo, M. Mendoza-Figueroa, G. Tecuapetla-Chantes, U. Rabadán-Domínguez, G. Contreras-Castañón, A. Zárate-Morales, A. Flores-Moreno, M. Ávila-Rodríguez;*
Unidad Radiofarmacia-Ciclotrón, Facultad de Medicina, Universidad Nacional Autónoma de México, MEXICO.

Aim/Introduction: The compound 2-(4'-N-[^{11}C]methylamino-phenyl)-6-hydroxybenzothiazole, also know as [^{11}C]Pittsburgh Compound B ([^{11}C]PIB), is a radiotracer extensively used to target beta-amyloid plaques in the brain, one of the hallmarks of Alzheimer's disease. The aim of this work is to report our initial experience on the production of this radiotracer using a single-use cassette and kit of reagents in a commercially available synthesizer. ***Materials and Methods:*** The disposable cassette consist in four manifolds with 6 three-way valves, and together with the reagent kit (excluding the chemical precursor) can be obtained from the manufacturer of the synthesizer [1]. The synthesis of [^{11}C]PIB was accomplished by using the so-called "wet" method. Briefly, carbon-11 was produced in an 11 MeV cyclotron in the chemical form of CO_2, trapped on a molecular sieve, desorbed at 200°C, and flushed through a solution of $LiAlH_4$ in tetrahydrofuran to form [^{11}C]methanolate by reduction of [^{11}C]CO_2. Then hydriodic acid is added to the reactor obtaining [^{11}C]methy iodine, wich is carried as a gas in a steam of nitrogen through a silver triflate reactor at 190°C to make the conversion to [^{11}C]methyl triflate. The compound [^{11}C]CH_3OTf is flush through a tC-18 cartridge pre-load with the chemical precursor (1 Mg, 6-OH-BTA-0), were the chemical synthesis takes place at 65°C to obtain [^{11}C]PIB. The product is purified by reverse phase semipreparative HPLC using MeCN:H_2O (60:40, v/v) as mobile phase. The colected fraction is reformulated by SPE using a tC18 cartridge, eluted with EtOH, and diluted with saline. ***Results:*** [^{11}C]PIB was obtained in a radiochemical of 12.7±0.9 % n.d.c. (n=5) with a radiochemical purity >98%. The total duration of the process from start of synthesis to the transfer of final product is approximately 20 min, however the preparation of the synthesis module, which includes the placement and test of the cassette, conditioning of the triflate reactor and the molecular sieve trap, takes about 2 h. In addition to the cassette, only a molecular sieve module needs to be connected to the synthesizer. ***Conclusion:*** The synthesis of [^{11}C]PIB in a multipurpose synthesizer using a disposable single-use cassette and a reagent kit is very convenient, reliable, and facilitates reproducible production conditions. The final product complaints to all the quality control requirements obtaining [^{11}C]PIB in enough quantity and quality to be used in clinical applications. Project supported by UNAM-DGAPA PAPIIT-IT200221, SECTEI/226/2021 and CONACYT-PRONACES 322512. ***References:*** [1] Trasis manual, AllinOne 11C PiB Specific Application V.1.0, Doc. Ref 003895

EP-0896

GMP Production of 89Zr-DFO-Pembrolizumab for Immuno-PET: predicting response in non-small lung cancer

I. Hrynchak[1], *M. Silva*[1], *S. Silva*[2], *A. Fonseca*[1], *A. Falcão*[3], *A. J. Abrunhosa*[1,3];
[1]*ICNAS Pharma Unipessoal, Lda, Coimbra, PORTUGAL,*
[2]*Pulmonology, Leiria Hospital Center, Leiria, PORTUGAL,*
[3]*CIBIT/ICNAS, Institute for Nuclear Science Applied to Health – University of Coimbra, Coimbra, PORTUGAL.*

Aim/Introduction: Programmed cell death protein 1 (PD-1) antibody - Pembrolizumab - is the standard first line treatment for non-small cell lung cancer (NSCLC) in patients with programmed cell death ligand 1 (PDL-1) expression ≥ 50%. However, non-responders to this treatment exist in a higher-than-expected percentage which raises concerns and requires special attention. The accurate evaluation by immuno-PET, using [^{89}Zr]Zr-DFO-Pembrolizumab, seems to represent a valid and clinically useful strategy to predict response to immune checkpoint inhibitors and improve global NSCLC treatment strategy [1,2]. Such radiopharmaceutical availability, nevertheless, requires substantial process development and validation.Therefore, the current work addresses practical considerations on the GMP-compliant, production of [^{89}Zr]Zr-DFO-Pembrolizumab from a medical cyclotron using a liquid target, with clinically proven

results and ready to be distributed outside the production center. ***Materials and Methods:*** Zirconium-89 (^{89}Zr) has been produced by our group through the bombardment of $Y(NO_3)_3.6H_2O$ in nitric acid solution (HNO_3) via the $^{89}Y(p,n)^{89}Zr$ nuclear reaction at 14 MeV, in a liquid target setup. After purification on hydroxamate resin, the [^{89}Zr]Zr-oxalate has been directly used for radiolabeling the DFO-Pembrolizumab [conjugation via random lysine using p-Bn-SCN-DFO (1:10)]. The product was isolated by size exclusion chromatography using a PD10 column and formulated to arrive at an injection dose of 37 MBq (2.5 mg of [^{89}Zr]Zr-DFO-Pembrolizumab + 2.5 mg Pembrolizumab). ***Results:*** Until now, several clinical doses (i.e., 37 MBq) of [^{89}Zr]Zr-DFO-Pembrolizumab were successfully produced with high radiochemical purity (98.68 ± 2.12 % by HPLC), in compliance with the current GMP, and injected in patients with NSCLC. The [^{89}Zr]Zr-DFO-Pembrolizumab injection was shown to be safe and feasible. Whole-body [^{89}Zr]Zr-DFO-Pembrolizumab images which were obtained on day 7 show selective accumulation at tumor sites. ***Conclusion:*** The automated labeling is GMP-compliant and results in acceptable product quantities (~37 MBq/patient) with excellent quality. This work also highlights the feasibility of [^{89}Zr]Zr-DFO-Pembrolizumab production using the widely installed base of medical cyclotrons that are already optimized to produce and distribute ^{18}F-labeled radiopharmaceuticals produced routinely from liquid targets. ***References:*** [1] Kok IC, et al. Ann Oncol. 2022 Jan;33(1):80-88. doi:10.1016/j.annonc.2021.10.213.[2] Neimeijer ALN, et al. J Nuc Med. 2021 Jul. doi: 10.2967/jnumed.121.261926.

EP-0897

Optimizing of automated production of Gallium-68 radiolabeled clinical agents by cyclotron liquid target system

Y. Shimizu[1], *K. Miyake*[2], *Y. Nakamoto*[2];
[1]*Kyoto University Hospital, Kyoto, JAPAN,* [2]*Kyoto University Graduate School of Medicine, Kyoto, JAPAN.*

Aim/Introduction: In recent years, Gallium-68 radiolabeled agents such as ^{68}Ga-DOTATOC (a somatostatin receptor-targeting PET imaging agent) and ^{68}Ga-gozetotide (a PSMA-targeting PET imaging agent) have been developed and used clinically. Those ^{68}Ga-radiolabeled agents are produced with $^{68}GaCl_3$, which is usually obtained from a ^{68}Ge/^{68}Ga generator. There have been problems with the stable supply of $^{68}GaCl_3$ due to the rising cost of ^{68}Ge/^{68}Ga generators and supply delays. Recently, a novel production method of $^{68}GaCl_3$ based on a cyclotron liquid target system has been developed. In this study, we optimized the production method of ^{68}Ga-radiolabeled agents and evaluated the routine production of ^{68}Ga-DOTATOC and ^{68}Ga-gozetotide using a cyclotron liquid target system and following a multipurpose automated synthesizer. ***Materials and Methods:*** ^{68}ZnO was dissolved in 0.6 M HNO_3 and then irradiated with protons at 40 µA for 60 min on a PETrace860 ^{68}Ga liquid target system (GE Healthcare). After the irradiation, the target solution was transferred to FASTlab multipurpose synthesizer (GE Healthcare) and then purified on hydroxamate-based resin and trioctylphosphine oxide (TOPO)-based resin columns. The obtained $^{68}GaCl_3$ was then reacted with DOTATOC or PSMA-11 (^{68}Ga-gozetotide precursor) dissolved in 1.2 M sodium acetate solvent at 95°C for 10 min. Those reactants were purified on a C18 Sep-Pak column to obtain ^{68}Ga-DOTATOC or ^{68}Ga-gozetotide, and quality tests (radiochemical purity, pH, endotoxin, sterility test, etc.) were performed. ***Results:*** $^{68}GaCl_3$ was obtained with a radioactivity of 2.0 ± 0.6 GBq (0.5 ~ 2.8 GBq) (n=29). ^{68}Ga-DOTATOC and ^{68}Ga-gozetotide were acquired with a radioactivity of 1.4 ± 0.3 GBq (0.6 ~ 1.9 GBq) (n=24) and 0.8 ± 0.2 GBq (0.5 ~ 1.0 GBq) (n=3) respectively, and passed all quality tests. As for the routine production, sudden decreased yield (lower than 1.5 GBq) of $^{68}GaCl_3$ production was observed 8 out of 29 times, and in 2 of them, ^{68}Ga-radiolabeled agents could not be acquired. It is predicted to be owing to some trouble with metal contamination and was able to be improved by replacing the transfer line from the cyclotron. ***Conclusion:*** Our results suggest that the optimized production method with the cyclotron liquid target system can provide enough radioactivity and quality of ^{68}Ga-radiolabeled agents for clinical use.

EP-0898

Single center experience in the [18F]DPA-714 production using commercial disposable cassettes on AllinOne synthesizer

M. Riondato[1], *A. Democrito*[1], *C. Ghersi*[1], *S. Grugni*[2], *M. Bauckneht*[1], *S. D. Morbelli*[1], *C. Marini*[3], *G. Sambuceti*[1];
[1]*University Policlinic Hospital of Genoa, Genoa, ITALY,* [2]*Gamma Servizi srl, Borgherello Pavia, ITALY,* [3]*CNR Institute of Molecular Bioimaging and Physiology (IBFM), Milan, ITALY.*

Aim/Introduction: The translocator protein 18 kDa (TSPO) is a validated diagnostic/imaging biomarker for the evaluation of inflammatory related-disease state and progression, as well as a recognized target for the development of new therapeutic agents for neurological, psychiatric disorders and oncological applications.Labelled ligands based on pyrazolo[1,5-a]pyrimidine acetamide core constitute a unique class with high affinity and selectivity for TSPO. Among several radiotracers [^{18}F]DPA-714 is nowadays widely used as a PET imaging probe in Clinical Trials. In this work we present our experience in the production and quality controls for the preparation of the IMPD for a Clinical Trial application. ***Materials and Methods:*** The synthetic process is fully automated on a Trasis AllInOne 36 synthesizer implemented with a HPLC semipreparative purification module, using an in-house designed cassette based on FDOPA and a dedicated sequence adapted from the Cybulska et al. method [1]. [^{18}F]DPA-714 was synthesized by a one-step labelling process using 25-40 GBq of [^{18}F]Fluorine and 4.5-5.5 mg of Tos-DPA-714 as precursor in 1 mL of ACN at 95°C (nucleophilic aliphatic substitution) for 10 min, followed by semi-preparative high-performance liquid chromatography (HPLC). The purified product was trapped on C18 cartridge and then removed with 1,8 mL ethanol 70%, reformulated with NaCl 0.9% to 15 mL and finally sterilized by filtration. All tests have been designed and performed according to the European Pharmacopeia specification if available and literature. ***Results:*** [^{18}F]DPA-714 production process was easily implemented for its simplicity and robustness, enabling rapid training of radiopharmacy personnel. Radiochemical yields were in the range 17,4-22,6 % (ndc) with molar activities of 364-613 GBq/µmol. The final volume was 15 ±0,5 mL and the radiochemical purity was 98,6-99,0 % at EoS. A full set of quality control tests were on three consecutive production batches for [^{18}F]FDPA-714 in order to prepare the dossier relative to the manufacturing qualification of clinical production, including stability studies (6h EoS). The results of quality controls such as chemical/radiochemical purity, radionuclide purity, sterility and content of bacterial endotoxin complied with the requirements of the European Pharmacopoeia and other designed specification. ***Conclusion:*** The developed [^{18}F]DPA-714 synthetic process is reliable and robust using an automated module with modified

disposable cassettes, thus being implementable for routinary productions. The process and quality control complied with the standards required for human use Clinical Trials. ***References:*** Cybulska, K.A. et al., Optimised GMP-compliant production of [^{18}F] DPA-714 on the Trasis AllinOne module. EJNMMI Radiopharmacy and Chemistry, 2021, 6 (1), 20

EP-62

e-Poster Area

E: Other Studies -> E1 Case Reports

EP-0899

18F-FDG- PET/CT guided biopsy has an essential role in the diagnosis of primary extranodal diffuse large B-cell lymphoma of bone- a clinical case.

Z. Dancheva, *S. Spasova, T. Stoeva, I. Kobakova, M. Dyankova, S. Chausheva, T. Yordanova, B. Chaushev, A. Klisarova, B. Balev;*
St Marina University Hospital, Varna, BULGARIA.

Aim/Introduction: Primary bone lymphoma exclusively affects skeletal tissue. It is a rare disease, estimated to be 3-7% amongst primary bone tumors and less than 2% amongst all lymphomas in adults. [1] We present a case demonstrating the clinical impact of 18F-FDG PET/CT in the multimodality approach to the diagnosis of primary extranodal diffuse large B-cell lymphoma of the left hemipelvis. ***Materials and Methods:*** We present a 50 years old male patient with an anamnesis of trauma 7 months before final diagnosis. He complained of a growing pain in his left pelvis and hip, weight loss and subfebrile temperature. After an examination by an orthopedic surgeon and a normal bone radiography, a treatment with antibiotics and analgesics was started. A non-contrast enhanced MRT of the hip was performed after 5 months of unsuccessful treatment, concluding it was a tumor mass- chondrosarcoma or fibrosarcoma of the left pelvis. A new radiography was performed, showing diffuse osteosclerotic and osteopenic changes of the left hemipelvis with small areas of bone destruction, suspicious of osteomyelitis or lymphoproliferative disease. Controversies persisted also after the bone biopsy, revealing only osteomyelitis of the bone. ***Results:*** 18-F FDG PET/CT was performed in order to characterize the metabolic aspect of the lesion, to exclude another primary tumor, and choose a proper biopsy place. Our findings were diffuse cortical changes- osteosclerosis and cortical thickening, affecting the left hemipelvis, corresponding to diffuse high glucose metabolism- characteristics close to osteomyelitis. There were also four soft tissue masses found, causing cortical destruction, where the biopsy was proposed. After the PET- directed biopsy a thorough pathological and immunochistochemical analysis were performed revealing an intense membrane expression of CD20 in 100% of tumor cells and positive CD79a, proving the lymphogenic origin of the tumor. On the second round high proliferation activity- Ki67 - nuclear expression in >50% of tumor cells and positive Bcl6 were found, confirming the final diagnosis- large B-cell lymphoma of the bone. ***Conclusion:*** As it was stated in the literature, the diagnosis of primary bone lymphoma was delayed due to unspecific clinical signs and equivocal imaging findings. 18F-FDG PET/CT acted as a key imaging method in the multidisciplinary management, guiding the biopsy, which finally led to the correct diagnosis. ***References:*** Dubey P, Ha CS, Besa PC, Fuller L, Cabanillas F, Murray J, et al, Localized primary malignant lymphoma of bone. Int J Radiat Oncol Biol Phys. 1997 Mar 15;37(5):1087-93. doi: 10.1016/s0360-3016(97)00106-5. PMID: 9169817.

EP-0900

A rare finding in 18F-FDG PET/CT restaging - unilateral diaphragmatic crura increased uptake in patient with pneumonectomy - a Case report

T. Stoeva, *T. Yordanova, M. Dyankova, S. Chausheva, Z. Dancheva, B. Chaushev, A. Klisarova;*
UMHAT "Sveta Marina" EAD- Varna, Varna, BULGARIA.

Aim/Introduction: The knowledge of normal and pathological uptake of F-18 fluoro-2-deoxy-glucose (^{18}F-FDG) whole-body positron emission tomography (PET) with computed tomography (CT) is essential for identification of the presence and extent of malignant disease. The advantages of combining functional and anatomical information can help us to precisely localize and stage primary non-small-cell lung cancer, find a proper biopsy place, evaluate the tumor response after treatment and help in radiotherapy planning. However, there are some artefacts and pitfalls which can easily misguide the ^{18}F-FDG-PET/CT interpretation. ***Materials and Methods:*** We present a case of a 74-years-old male with lung carcinoma. Baseline ^{18}F-FDG-PET/CT was positive in the upper part of the left lung without nodal or distant metastases. Histopathology confirmed non-small-cell lung cancer. The patient's symptoms were alleviated after left pneumonectomy and chemotherapy. Stable disease was reported after postoperative computed tomography. Due to generalized pain syndrome, another ^{18}F-FDG-PET/CT was performed after two and a half years. ***Results:*** The follow-up ^{18}F-FDG-PET/CT revealed increased uptake in the contralateral, right diaphragmatic crura. This was an unusual finding, because diaphragmatic crus uptake is usually bilateral. Hyperventilation and increased compensatory work of the right lung was thought to be the potential underlying mechanism of this condition. ***Conclusion:*** This rare and unusual case report of unilateral diaphragmatic crus increased uptake after pneumonectomy enriches the knowledge of possible artifacts and pitfalls. It gives us the opportunity to be more precise in ^{18}F-FDG- PET/CT post treatment restaging, which is always a challenge.

EP-0901

Osteomyelitis in patient with multiple myeloma- the invisible threat seen in 18F-FDG PET/CT

T. Stoeva, *M. Dyankova, Z. Dancheva, T. Yordanova, S. Chausheva, B. Chaushev, A. Klisarova;*
UMHAT "Sveta Marina" EAD- Varna, Varna, BULGARIA.

Aim/Introduction: Herein, we aim to present a rare PET/CT finding in a patient with multiple myeloma (MM)- osteomyelitis of the sternum. ***Materials and Methods:*** We present a male patient with complaints of pain in the left hip joint area, initially only during exercise and at a later stage in a relaxed state due to multiple myeloma. The patient underwent staging 18F-FDG PET/CT, which revealed a single osteolytic lesion in the left acetabulum and high metabolic activity in the seventh left rib. Due to acute aortic dissection (Stanford type A, DeBakey type I), aortic valve reconstruction was performed with intervascular prosthetics of the ascending aorta and aortic wall, with a complicated postoperative period due to osteomyelitis of the sternum. Sequestrectomy, surgical revision of the graft and long-term antibiotic treatment were implemented. After 9 courses of chemotherapy, a remission of the disease was registered. ***Results:*** A post-treatment 18F-FDG

PET/CT scan revealed a prevascular soft tissue mass in the anterior mediastinum with high metabolic activity, propagating through the sternum, with a well-defined fistula course to the skin surface. The sternum itself had a highly altered structure, in places, especially around the metal osteosynthetic elements with destruction and pronounced sclerotic transformation. In addition, when osteomyelitis develops against the background of an osteolytic lesion, the clinical outcome is often poor. In severe cases, the infection leads to life-threatening complications. Although bone infections are manageable in most reported cases with broad-spectrum antibiotics, prolonged hospitalization, antibiotic treatment, and additional surgeries can significantly increase disease burden and seriously affect prognosis with increased mortality. Drug-resistant bacterial infection could potentially be a major threat to MM patients in the future. ***Conclusion:*** Patients with MM who are immunocompromised by chemotherapy, transplantation, or steroid drugs may be susceptible to infections. Vertebral osteomyelitis of bacterial or fungal origin is particularly specific in immunocompromised patients [1]. Medical literature rarely highlights the risks of bone infection associated with myeloma bone disease. Although the literature to date consists mainly of individual case reports rather than rigorous prospective studies, it is suggested that this may be an area that merits further investigation. ***References:*** Yu S.F., Lui C.C., Pei S.N., Liu J.W., Cheng T.T. Unsuspected multiple myeloma presenting as Escherichia coli infectious spondylitis: a case report. Int J Rheum Dis. 2010;13(4):e55-e58

EP-0902

18F-FDG PET/CT in a patient with two metachronous tumors and the possible diagnostic pitfalls

T. Stoeva, *Z. Dancheva, M. Dyankova, S. Chausheva, T. Yordanova, B. Chaushev, A. Klisarova;*
UMHAT "Sveta Marina" EAD- Varna, Varna, BULGARIA.

Aim/Introduction: We aim to present a case of a patient with two metachronous malignancies and the possible diagnostic pitfalls in the interpretation of 18F-FDG PET/CT images. ***Materials and Methods:*** We present a patient with two metachronous malignancies- carcinoma of the right kidney and multiple myeloma (MM). In June 2018 a laparoscopic partial kidney resection was performed. In 2019 was established progression of the disease- single metastatic lesions in the left lung. A one-month treatment with Pazopanib was conducted and a complete response was reported. MM was diagnosed in October 2020. After conducted chemotherapy, partial response was reported. The patient was referred to 18F-FDG PET/CT due to CT findings of enlarged abdominal lymph nodes. ***Results:*** The performed restaging 18F-FDG PET/CT revealed generalized malignant lymphadenopathy, represented by multiple lymph nodes- bilaterally paraaortic, retrocrural, in the mediastinum and in the right supraclavicular space. Multiple scattered metabolically active osteolytic bone lesions were found as well, possibly associated with the known multiple myeloma. The absence of pre-therapeutic 18F-FDG PET/CT made it difficult to assess the response to the treatment of multiple myeloma. Persistence of high metabolic activity in the osteolytic lesions, exceeding that of the liver, can be considered in two ways - as a poor response to treatment for myeloma disease or as secondary lesions related to progression of renal carcinoma. Given the less common generalized lymphadenopathy in multiple myeloma, it was likely a progression of the renal carcinoma. After conducting laboratory tests and histological verification of the findings, MM progression was established and treatment was started. ***Conclusion:*** The combination of these two types of carcinoma in one patient is rare. Usually, the second neoplasia is caused by immunosuppression as a result of treatment (chemotherapy, radiotherapy) of the first. Multiple myeloma and renal cell carcinoma have similar risk factors (obesity, smoking, hypertension). Pathophysiological mechanisms are common to both renal carcinoma and multiple myeloma—in particular, the role of interleukin-6, which is produced by renal cells and stimulates the proliferation of myeloma cells. This should direct the clinicians attention to the possibility of recurrence of one malignant disease, even though progression of the other metachronous tumor is subsequently proven.

EP-0903

A case report of abnormal bone imaging caused by bevacizumab

T. Yi, *C. Yu;*
The Second Affiliated Hospital of Guilin Medical University, Guilin, CHINA.

Aim/Introduction: Bevacizumab has osteoarthritis records in its adverse drug reaction instructions, but the corresponding literature is very few, and its related adverse reaction meta-analysis has not been clearly reported. ***Materials and Methods:*** A 43-year-old female with stage IVA of cervical poorly differentiated squamous cell carcinoma treated with docetaxel plus nidaplatin plus bevacizumab for 6 sessions and radiotherapy. She did not have clinical symptoms related to osteoarthritis, such as morning stiffness, and no corresponding positive serological indicators. Then SPECT/CT whole-body-scan(WBS) examination was performed to evaluate the bone metastasis of the tumor. ***Results:*** WBS showed radioactivity concentration was symmetrically distributed in bilateral shoulder, elbow, wrist, knee, ankle, interphalangeal joint, and interphalangeal joints, but no signs of metastasis in the whole body bone . SPECT/CT fusion images showed abnormal radioactivity increase in those joints listed above, but no obvious bone destruction was seen on fusion CT . The arthritis caused by bevacizumab should be considered because of the recent history of Bevacizumab. ***Conclusion:*** SPECT/CT WB scan is a highly sensitive examination method for bone related lesions. From this case, it may be concluded that SPECT/CT WB scan is a sensitive method for clinical diagnosis of suspected osteoarthritis adverse reactions caused by drugs. ***References:*** 1.Alqahtani MM, Fulton R, Constable C, et al. Diagnostic performance of whole-body SPECT/CT in bone metastasis detection using 99mTc-labelled diphosphate: a systematic review and meta-analysis. Clin Radiol. 2020;75(12):961.e11-961.e24. 2.Smith R. Nuclear Medicine Bone Imaging. Radiol Technol. 2020;91(3):249-263.3.Wu S, Pan Y, Mao Y, et al. Current progress and mechanisms of bone metastasis in lung cancer: a narrative review. Transl Lung Cancer Res. 2021;10(1):439-451.4.Gu H, Sun L, Dou Z, et al. Analysis of lung adenocarcinoma with bone metastasis: a case report. Transl Lung Cancer Res. 2020;9(2):389-392.5.Kim JY, Choi YY, Kim CW, et al. Bone Scintigraphy in the Diagnosis of Rheumatoid Arthritis: Is There Additional Value of Bone Scintigraphy with Blood Pool Phase over Conventional Bone Scintigraphy? J Korean Med Sci. 2016;31(4):502-9.6.Aletaha D, Neogi T, Silman AJ, et al. 2010 Rheumatoid arthritis classification criteria: an American College of Rheumatology/European League Against Rheumatism collaborative initiative. Arthritis Rheum. 2010;62(9):2569-81.7.Vadalà G, Ambrosio L, Cattani C, et al. Bevacizumab Arrests Osteoarthritis Progression in a Rabbit Model: A Dose-Escalation Study. J Clin Med. 2021;10(13):2825.8.Xun X, Ai J, Feng F, et al. Adverse events of bevacizumab for triple negative breast cancer and HER-2 negative metastatic breast cancer: A meta-analysis. Front Pharmacol. 2023;14:1108772.

EP-0904

Primary colorectal cancer with increased 68Ga-PSMA expression on PET/CT: incidental second malignancy in primary staging for prostate cancer (PC)

M. Dyankova[1,2], *S. Chausheva*[1], *Z. Dancheva*[1], *T. Stoeva*[1], *T. Yordanova*[1], *B. Chaushev*[1], *A. Klisarova*[1];
[1]*Medical University Varna "Prof. Dr. Paraskev Stoyanov", Department of Imaging Diagnostics, Interventional Radiology and Radiotherapy, Varna, BULGARIA,* [2]*St. Marina University Hospital, Department of Nuclear Medicine, Varna, BULGARIA.*

Aim/Introduction: ^{68}Ga-prostate-specific membrane antigen (PSMA) PET/CT has shown superb results in imaging of Prostate Cancer (PC). PSMA has been found in tumor-associated neovasculature endothelial cells in various nonprostatic malignant diseases, including colorectal cancer and multiple other types of solid tumor. Nevertheless, synchronous malignancies with increased PSMA expression are not common (0.7%) in PC patients. ***Materials and Methods:*** We present a case of a 71-year-old male, in whom a second primary metastatic rectal cancer was detected with a PSMA PET/CT imaging performed for PC staging. The male was recently diagnosed with prostate adenocarcinoma, Gleason score 6 (3 + 3) with high initial serum prostate-specific antigen levels (PSA) 75.0 ng/ml. He was referred for staging with 68Ga-PSMA PET/CT prior to treatment. ***Results:*** PSMA-PET was performed and fusion PET/CT images revealed a larger focus of intense pathologic PSMA activity, which correlated to widely thickened rectal wall-presacral tumor and one pelvic lymph node with increased tracer uptake (with SUVmax-values up to 8.9), which were subsequently histologically proven as moderately differentiated primary rectal adenocarcinoma with associated pelvic lymph node metastasis and inflammatory ascites. PSMA expression has also been reported in known primary PC. ***Conclusion:*** In present case report we demonstrate the significance of histological confirmation of lesions with increased 68Ga-PSMA expression, but atypical for PC involvement. This case with considerable nonprostatic PSMA activity highlights the need for careful interpretation of PSMA PET/CT results and also provides premise to study the possible role of PSMA-targeted radiopharmaceutical therapy in progressive/ advanced colorectal cancer. Keywords: 68Ga-PSMA PET/CT, synchronous primary colorectal cancer, adenocarcinoma

References: 1. Medhat M. Osman, Amir Iravani, Rodney J. Hicks and Michael S. Hofman. Detection of Synchronous Primary Malignancies with 68Ga-Labeled Prostate-Specific Membrane Antigen PET/CT in Patients with Prostate Cancer: Frequency in 764 Patients. Journal of Nuclear Medicine December 2017, 58 (12) 1938-1942; DOI: https://doi.org/10.2967/jnumed.117.190215 2. Salas Fragomeni, R. A., Amir, T., Sheikhbahaei, S., Harvey, S. C., Javadi, M. S., Solnes, L. B. et al. Imaging of Nonprostate Cancers Using PSMA-TargetedRadiotracers: Rationale, Current State of the Field, and a Call to Arms.J Nucl Med 2018; 59:871-877 DOI: 10.2967/jnumed.117.203570.

EP-0905

Unusual recurrence of secondary renal hyperparathyroidism caused by a ectopic undescended parathyroid adenoma:a case report

w. Weng*;*
The First Affiliated Hospital, Zhejiang University School of Medicine, Hangzhou, CHINA.

Aim/Introduction: Recurrence of secondary renal hyperparathyroidism is not uncommon after parathyroidectomy. However, recurrence caused by ectopic undescended parathyroid adenoma is rare. ***Materials and Methods:*** Here, we report a case of 59-year-old female with progressively elevated serum intact parathyroid hormone after underwent parathyroidectomy for secondary hyperparathyroidism. A suspected abnormal nodule near the bifurcation of carotid artery was found by ^{99m}Tc-sestamibi scintigraphy with single positron emission tomography / computed tomography (SPECT/CT). ***Results:*** After excision of the suspected nodule near the bifurcation of carotid artery, the intact parathyroid hormone value of the patient decreased. The nodule was pathologically confirmed as a parathyroid adenoma. ***Conclusion:*** Ectopic undescended parathyroid adenoma is an exceptional cause of Secondary hyperparathyroidism, intense pre-operative localization diagnostic is necessary.

References: 1. Fraser WD. Hyperparathyroidism. Lancet. 2009;374(9684):145-158. 2. Pasnicu C, Radu PA, Garofil D, et al. Clinical Aspects of Parathyroid Hyperplasia in Secondary Renal Hyperparathyroidism. Chirurgia (Bucur). 2019;114(5):594-601. 3. Li JG, Xiao ZS, Hu XJ, et al. Total parathyroidectomy with forearm auto-transplantation improves the quality of life and reduces the recurrence of secondary hyperparathyroidism in chronic kidney disease patients. Medicine (Baltimore). 2017;96(49): e9050. 4. Agha A, Loss M, Schlitt HJ, Scherer MN. Recurrence of secondary hyperparathyroidism in patients after total parathyroidectomy with autotransplantation: technical and therapeutic aspects. Eur Arch Otorhinolaryngol. 2012;269(5):1519-1525.5. Tominaga Y, Uchida K, Haba T, et al. More than 1,000 cases of total parathyroidectomy with forearm autograft for renal hyperparathyroidism. Am J Kidney Dis. 2001;38 Suppl 1: S168-171. 5. Agha A, Loss M, Schlitt HJ, et al. Recurrence of secondary hyperparathyroidism in patients after total parathyroidectomy with auto- transplantation: technical and therapeutic aspects. Eur Arch Otorhino-laryngol. 2012;269(5):1519-1525. 6. Ohe MN, Santos RO, Neves MC, et al. Autotransplant tissue selection criteria with or without stereomicroscopy in parathyroidectomy for treatment of renal hyperparathyroidism. Braz J Otorhinolaryngol. 2014;80(4):318-324. 7. Abruzzo A, Gioviale MC, Damiano G, et al. Reoperation for persistent or recurrent secondary hyperparathyroidism. Acta Biomed. 2017;88(3):325-328. 8. Abruzzo A, Gioviale MC, Damiano G, et al. Reoperation for persistent or recurrent secondary hyperparathyroidism. Acta Biomed. 2017;88(3):325-328. 9. Kanack MD, Maawy AA, Oh DK, Bouvet M. Undescended parathyroid adenoma. BMJ Case Rep. 2015;2015: bcr2014208277. 10. Strambu V, Bratucu M, Garofil D, et al. The Value of Imaging of the Parathyroid Glands in Secondary Hyperparathyroidism. Chirurgia (Bucur). 2019;114(5):541-549.

EP-0906

Incidental Paget bone disease as a potential pitfall in 18-F FDG PET/CT in melanoma patient

S. Moustafa*;*
Assiut university hospital, Assiut university, EGYPT.

Aim/Introduction: Paget bone disease is a chronic progressive bone disease of uncertain etiology charchetrized by excessive bone remodeling along three stages (resorption, mixed and finally burnout or sclerotic phase). Scintigraphic features of this disease depend on its stages. It can be misdiagnosed as a metastatic bone lesions, so accurate diagnosis is mandatory to guide for the right management. I have reported the case of incidental only pagetiod bone disease in patient with newly diagnosed left foot melanoma yet no osseous metastases. It was diagnosed by the typical CT feature as well as the specific scintigraphic feature of the complementary of the bone scan. ***Results:*** Figure 1: A 64 years old presented to our oncology department after tumoral excision

from sole of left foot, pathologically proven as superficial spreading melanoma. The patient is requested to do F-18 FDG PET/CT for as post-operative staging imaging modality. PET/CT showed diffuse FDG activity within the left hemiplevis appreciated at the left acetabulum and ischium mimicking metastases corresponding to heterogeneous sclerosis and ground glass appearance at CT image. Complementary bone scan and added SPECT/CT images for the pelvis, showed the characteristic scintigraphic intense uptake at a right hemiplevis. ***Conclusion:*** Benign etiologies should be on our mind while assessing and interpretatating bone lesions showing 18-F FDG and/or 99mTc-MDP uptake during staging and follow-up, both due to changing the treatment plan and its effect on survival by proper management. ***References:*** 1. Engur CO, Turoglu HT, Ozguven S, Tanidir Y, Erdil TY. 68Ga-Prostate-Specific Membrane Antigen PET-Positive Paget Bone Disease With Metastatic Prostatic Carcinoma. Clinical Nuclear Medicine. 2020;45(9):e425-e6. 2. Browne C, Mutsaers A, Fisher B. A Case of Mistaken Identity: Paget's Disease of the Bone Causing Cord Compression—Case Report and Review of the Literature. Practical radiation oncology. 2019;9(6):e613-e9. 3. Shankar YU, Misra SR, Vineet DA, Baskaran P. Paget disease of bone: a classic case report. Contemporary clinical dentistry. 2013;4(2):227.

EP-0907

Pitfall In Tumor Assessment FDG-PET/CT Imaging In Hodgkin Lymphoma Due To Cocaine-Induced Nasal Inflammation

A. Jougla[1], *J. Alberini*[1,2,3], *B. Durand-Bailloud*[1], *R. Ahond-Vionnet*[1]; *[1]Department of Nuclear Medicine, Hôpital Pierre Beregovoy, Nevers, FRANCE, [2]Department of Nuclear Medicine, Centre Georges-François Leclerc, Dijon, FRANCE, [3]ICMUB Laboratory, UMR CNRS 6302, University of Burgundy, Dijon, FRANCE.*

Aim/Introduction: Chronic inflammation can accumulate 18F-FDG and mimic tumor involvement. We present a case of cocaine-induced chronic inflammation of the nasal cavity, found by serendipity in a patient referred for FDG-PET/CT scan in staging and tumor response assessment for a Hodgkin lymphoma. ***Materials and Methods:*** A 25-year-old male patient presented a gradually growing cervical lymph node on the right side. Diagnosis of Hodgkin Lymphoma was established on the lymph node biopsy. In this context, the patient was referred to our department to perform sequential three FDG-PET/CT scans at baseline, then three months later after two cures of chemotherapy and finally four months later at the end of chemotherapy and radiotherapy. ***Results:*** At baseline, PET/CT scan revealed increased FDG uptake in cervical lymph nodes (SUVmax = 22.6) and in retropharyngeal region, both on the right side. Moreover an intense FDG uptake was found in the right nasal cavity. This FDG uptake involved the nasal septum and the middle and inferior nasal concha (SUVmax = 11.6). No FDG uptake was observed in the left nasal cavity, nor in the sinuses. The thickness of nasal mucosa was increased on CT scan. The patient reported regular cocaine intake, twice a month, snorting exclusively through the right nostril. The second PET/CT scan performed after two cures of chemotherapy showed a complete disappearance of the FDG uptake in cervical lymph nodes and in retropharyngeal region, in favour of a metabolic complete response. However, intense FDG uptake described in the right nasal cavity (SUVmax = 10.8) was still observed with a morpho-metabolic stability. Then the patient underwent a clinical examination by an otorhinolaryngologist who confirmed chronic inflammation of the nasal mucosa with synechiae unrelated to the Hodgkin lymphoma. At the end of treatment (chemotherapy and irradiation of the cervical lymph nodes), FDG-PET/CT confirmed the metabolic complete response. A slight decrease of the FDG uptake in the right nasal cavity (SUVmax = 7.5) was observed and could be explained by the reduction of cocaine intake reported by the patient. ***Conclusion:*** To our knowledge, this is the first report of nasal FDG findings due to cocaine-intake. This case illustrated a setting of cocaine-snorting which induced chronic inflammation in the nasal cavity, which can mimic malignancy and could be misinterpreted as active residual lymphoma lesions.

EP-0908

Suspected Central Pontine Myelinolysis detected by 18F-FDG PET/CT in a patient with septic shock

L. Locantore*, M. Cucca, E. Biggi, R. J. Egoue Mongoue, I. Ravelli, D. Riolo, M. Zuffante;*
Nuclear Medicine Unit, AOUI, Verona, ITALY.

Aim/Introduction: We describe the case of a 59-year-old Caucasian male with a known history of alcohol abuse who was admitted in Intensive Care Unit (ICU) due to coma in sepsis. ***Materials and Methods:*** Emogas data analysis showed metabolic acidosis with severe hypoglycaemia, treated by initial 500 ml of 20% glucosate solution. Patients had also renal impairment with serum Creatinine of 2.53 mg/dl and increased CRP (263 mg/L) Not significant abnormal sodium or potassium levels were found; anyway patient was treated with 1500 cc of elettrolitic solution. Antibacterial therapy with Pip/Tazo was also administered, prior to blood colture results (finally showed S.hominis positivity). Patient underwent brain MRI to value septic cerebral embolism and/or vascular injuries. Patients was also scheduled for 18F-FDG-PET/CT (PET/CT) to value the origin of sepsi and/or the presence of septic embolism localizations. ***Results:*** MRI found some small vascular chronic lesions and diffusion restriction in the pons, thus suggesting central pons myelinolysis (CPM). PET/CT found bilateral lung consolidations and peripheral ground glass opacities characterized by increased metabolism likely due to septic pneumonia. An intense and diffuse FDG uptake was also found in pancreas due to probably chronic pancreatitis. Brain evaluation showed intense increased uptake of the pons, together with right periventricular white matter inhomogeneous increased uptake. These finding, according to MRI results and to other case reports, was suspected for central pontine myelinolysis with possible extrapontine foci of demielinization. After 7 days from PET/CT patient had negative perypheral blood colture, inflammatory index decreasing and negative lactates, with renal function improvement. Patient remained apiretic but ventilated by ETT ; infectivologists decided to withrawal antibacterial therapy. Patiens is still today hospitalized in ICU. ***Conclusion:*** CPM is a demyelinating lesion of the pons, resulting in several neurological symptoms. The exact cause of CPM is not clear, but a relation between loss of myelin and osmotic stress was suggested, together with rapid correction of hyponatremia. In our case, this last evidence was not so clear, while we could hypotize CPM due to chronic alcohol abuse. PET/TC could be useful to detect CPM when clinically or radiologically suspected. ***References:*** 1.Rønne F, Tfelt-Hansen PC, Rørdam L. Central Pontine Myelinolysis and Localized Fluorodeoxyglucose Uptake Seen on 18F-FDG PET/CT. World J Nucl Med. 2017 Jan-Mar;16(1):56-582.Uchino A, Yuzuriha T, Murakami M, Endoh K, Hiejima S, Koga H, Kudo S. Magnetic resonance imaging of sequelae of central pontine myelinolysis in chronic alcohol abusers. Neuroradiology. 2003 Dec;45(12):877-80.

EP-0909

FDG PET/CT in the Evaluation of Multi-systemic Involvement in Erdheim Chester Disease

M. Guven[1], *M. Eroglu*[2], *A. Oral*[1], *C. Eraslan*[2], *Z. Ozcan*[1];
[1]*Department of Nuclear Medicine, Ege University, Izmir, TÜRKIYE,*
[2]*Department of Radiology, Ege University, Izmir, TÜRKIYE.*

Aim/Introduction: Erdheim-Chester disease (ECD) is a rare non-Langerhans cell histiocytosis that presents with different clinical findings due to involvement of mainly bone and extra-bone organs. It may produce a multi systemic clinical picture involving the skeletal system, central nervous system (NS), respiratory system, skin, cardiovascular system, kidneys, retroperitoneal area, and eyes, or it may be asymptomatic as well. This presentation will highlight the multimodality imaging findings in a case of ECD, a relatively rare condition in nuclear medicine practice that is notable for involvement of the brain and paranasal sinuses in addition to typical multiple bone/bone marrow lesions on FDG PET imaging. ***Materials and Methods:*** A 49-year-old female patient who presented with diabetes insipidus, progressive weakness, and balance disorders was diagnosed with ECD after bone marrow biopsy. Whole body FDG PET/CT imaging was performed to assess the extent of the disease using non-contrast enhanced low dose CT protocol. ***Results:*** FDG PET/CT showed multifocal hypermetabolic findings in bone marrow regions in addition to lytic sclerotic findings in the bone structures. Additionally, hypermetabolic activity were noted at the level of the pons in the brainstem and focal FDG uptake in the pituitary infundibular portion. There were hypermetabolic inflammatory changes in the bilateral maxillary sinuses and sclerotic changes in the para-sinusoidal bone surfaces. MRI performed to examine the central nervous system (CNS) in detail revealed diffuse infiltrative foci consistent with the disease in the pituitary-infundibulum and bilateral cerebral hemispheres. At the level of the pons in the brainstem, MRI showed no significant specific contrast enhancement consistent with the metabolic activity on PET/CT, but pathologic signal enhancements were noted in these areas. ***Conclusion:*** ECD is easily recognized on metabolic imaging with its typical features of bone and bone marrow involvement. CNS findings are less common and are considered a sign of poor prognosis. In this case, hypermetabolic findings in the pons and pituitary gland were notable even over the physiological cerebral FDG uptake. Moreover, FDG uptake indicated additional areas with abnormal signal enhancement on cerebral MRI. Additionally, the increase in hypermetabolic thickness in the maxillary sinus, which is less common, showed that the disease involved the respiratory system. This case report aims to raise awareness among nuclear medicine physicians of ECD, which elicits a wide range of imaging findings and underlines the contribution of FDG PET/CT imaging in the assessment of disease extent.

EP-0910

Accidently Detected Lung Masses as Carcinoma in 99mTc (V)-DMSA SPECT Imaging

E. Gharehpapagh[1], *S. Rezaei*[1], *L. Namvar*[2];
[1]*Department of Nuclear Medicine, Medical School, Tabriz University of Medical Sciences, Tabriz, IRAN, ISLAMIC REPUBLIC OF,* [2]*Tuberculosis and Lung Disease Research Center, Tabriz University of Medical Sciences, Tabriz, IRAN, ISLAMIC REPUBLIC OF.*

Aim/Introduction: A 74-year-old woman with a previous history of asthma, diabetes mellitus, hypertension, and cervical vessel stenting after falling recently underwent CT scan. Several pulmonary masses were randomly identified in the chest CT report, including one with a diameter of 30 mm in the upper lobe of the right lung. There was a possibility of carcinomatosis lymphangitis due to the RUL lesion and interstitial edema, and further evaluation was recommended. ***Materials and Methods:*** On the control CT performed 10 days later, the same masses were found without changes, also several enlarged lymph nodes in the mediastinum and lungs' hilum, and no evidence of thrombosis or pulmonary artery stenosis on both sides. ^{99m}Tc (V)-DMSA imaging was requested by the attending physician for further evaluation of pulmonary masses. The whole body scan, as well as thoracic SPECT images, were taken two hours after the intravenous injection of 590 MBq of ^{99m}Tc (V)-DMSA. ***Results:*** The scan showed two lesions with increased radiotracer uptakes, one in the lower region of upper lobe and the other in the superior segment of Rt. and Lt. lungs respectively. The lesions had posterior locations in both lungs best detected by SPECT projections. In semi-quantitative analysis, the lesion to background ratio was 1.52 on the right side and 1.61 on the left side. As well, there were some patchy lesions with slightly increased uptake in the upper and middle parts of both lungs. The possibility of malignancy in two obvious lesions in the right and left lungs based on the ^{99m}Tc (V)-DMSA scan report. ***Conclusion:*** Consequently, the patient underwent lung transbronchial biopsy and bronchial washing cytology which showed the result of lung cancer, adenocarcinoma poorly differentiated. The chemotherapy was started for this patient.

EP-0911

Unusual uptake of bone metastases in 99mTc-MAG3 dynamic renal scintigraphy

K. Aslaner, *B. Arca, D. Has Simsek, F. Buyukkaya, Y. Sanli, S. Kuyumcu;*
Istanbul University, Istanbul, TÜRKIYE.

Aim/Introduction: Neuroendocrine tumors (NET) are a heterogeneous group of tumors originating from neuroendocrine cells that can arise from different organs. In metastatic NETs, peptide radionuclide therapy (PRRT) makes significant contributions to disease survival. Kidney is one of the critical organs in PRRT, and renal function is evaluated with dynamic renal scintigraphy before the treatment to determine obstructive pathologies or renal disfunction. In this case report, unusual uptake of bone metastases were demonstrated in ^{99m}Tc-MAG3 dynamic renal scintigraphy of a patient who was planned ^{177}Lu-DOTATATE therapy for metastatic NET. ***Materials and Methods:*** An 18 years old female patient with a diagnosis of paraganglioma was referred to our clinic for PRRT due to progression under systemic chemotherapy and sandostatin treatment. ^{68}Ga-DOTATATE PET/CT images of the patient showed intense somatostatin receptor expression in metastatic lymph nodes in bilateral retrocrural areas and multiple metastatic lesions in the vertebral column, calvarium,pelvis and extremities, most prominently in the L1-L3 vertebrae. The patient was eligible for ^{177}Lu-DOTATATE therapy, and ^{99m}Tc-MAG3 dynamic renal scintigraphy was planned before the treatment. ***Results:*** ^{99m}Tc-MAG3 dynamic renal scintigraphy showed unusual increased activity in metastatic bone lesions in lumbosacral vertebrae. In presentcase, increased activity in bone metastases was prominent in early images and decreased in late images, suggesting that may be related to increased blood flow secondary to malignancy. The stomach was not visualized in all images which ruled out the possibility of free ^{99m}Tc-pertechnetate. In literature, similar few case reports were published and emphasized that detection of skeletal involvement on dynamic renal scintigraphy is frequently associated with malignancy[1-3]. ***Conclusion:*** Increased activity of metastatic bone lesions on ^{99m}Tc-MAG3 dynamic renal scintigraphy is a rare finding. Extrarenal

involvement on dynamic renal scintigraphy has been reported to be associated with malignancy due to increased vascularity, and incidental bone uptake in dynamic renal scintigraphy needs further investigation due to the malignancy risk. ***References:*** 1) Wang T, Zhao J, Xing Y. Uptake of ^{99m}Tc-DTPA in bone metastases from renal cancer. Clin Nucl Med 2015;40:840-12) Peng Xie, Huan-Li Li. Incidental bone metastases identified by renal dynamic scintigraphy. Medicine (2018) 97:323) Sebastian Hoberücks, Enrico Michler. Unexpected Bone Metastases in ^{99m}Tc-Pertechnetate Scan of Recurrent Goiter. Clin Nucl Med 2019 Jan;44(1):72-74.

EP-0912

Contribution of SPECT-CT in the Differentiation of Ectopic Thyroid Tissue and Thyroglossal Duct Cyst

G. Deniz[1], *E. G. Isik*[2], *D. Has Simsek*[2], *Y. Sanli*[2], *B. Arca*[2], *S. Kuyumcu*[2];
[1]*Istanbul University Istanbul Faculty of Medicine Nuclear Medicine Department, Istanbul, TÜRKIYE., Istanbul, TÜRKIYE,* [2]*Istanbul University Istanbul Faculty of Medicine Nuclear Medicine Department, Istanbul, TÜRKIYE.*

Aim/Introduction: The thyroid gland forms between the first and second pharyngeal sacs, near the base of the tongue. During migration, the thyroid tissue may remain attached anywhere along the thyroglossal duct. However, thyroglossal duct cysts and ectopic thyroid tissue can be difficult to detect using methods such as USG and planar scintigraphy. To detect the presence of ectopic/pyramidal thyroid tissue in the thyroglossal duct and to determine the anatomical localization of the thyroid tissue, Tc99m-pertechnetate SPECT/CT can be used. In this case, we aimed to detect ectopic/pyramidal thyroid tissue with SPECT/CT. ***Materials and Methods:*** A 41-year-old female patient, who had a subtotal thyroidectomy 20 years ago, was referred to us with a complaint of swelling in the neck. In previous thyroid ultrasound (USG) imaging, it was not possible to distinguish between ectopic thyroid tissue and thyroglossal duct cyst in the anterior region of the neck, located superior to the thyroid gland. Thyroid scintigraphy and SPECT/CT imaging were performed. Uptake was observed in the thyroid bed, consistent with residual thyroid tissue on the right. Additionally, in SPECT/CT, the patient exhibited activity involvement due to lobulated ectopic/pyramidal thyroid tissue starting from the infrahyoid region and extending to the lower level of the thyroid cartilage with no thyroglossal cyst. ***Conclusion:*** Thyroid tissue can also be found in other parts of the descending tract, where thyroglossal duct cysts can be observed. However, the probability of ectopic thyroid in the cyst wall is less than 5%. While it does produce thyroid hormones, its concentrations are often below normal.[1 2] In our case report, tracer involvement was observed in the anterior midline of the neck in the planar thyroid scintigraphy. However, it did not provide information about the anatomical localization of the ectopic thyroid tissue. On the other hand, ultrasonography did not provide many benefits in the differentiation of thyroglossal duct cysts and ectopic thyroid tissue. In SPECT/CT, on the other hand, the localization of the lesion, whether it is located within the cyst and its relationship with the surrounding tissue can be clearly understood. ***References:*** 1. Noussios G, Anagnostis P, Goulis DG, Lappas D, Natsis K. Ectopic thyroid tissue: anatomical, clinical, and surgical implications of a rare entity. European journal of endocrinology. 2011;165(3):375-382. 2. Rao PN, Pandit N, Kumar R, Upadhya IV, Sagar MSV. Ectopic functioning thyroid tissue in the thyroglossal duct detected by radionuclide imaging. Clinical nuclear medicine. 2005;30(9):630.

EP-0913

Case report: Pulmonary Langerhans cell histiocytosis (PLCH) - is it a challenge for 18F-FDG PET/CT?

M. Dyankova[1,2], *T. Stoeva*[1], *Z. Dancheva*[1], *S. Chausheva*[1], *T. Yordanova*[1], *B. Chaushev*[1], *A. Klisarova*[1];
[1]*Medical University Varna "Prof. Dr. Paraskev Stoyanov", Department of Imaging Diagnostics, Interventional Radiology and Radiotherapy, Varna, BULGARIA,* [2]*St. Marina University Hospital, Department of Nuclear Medicine, Varna, BULGARIA.*

Aim/Introduction: Pulmonary Langerhans cell histiocytosis (PLCH) is a rare disease presenting with nonspecific symptoms. Initial 18F-FDG PE/CT assessment of PLCH and therapeutic response evaluation in this form of malignant involvement is a complex challenge and requires a diverse approach. ***Materials and Methods:*** A 18-year-old man with an acute onset of progressive shortness of breath, hospitalized urgently in a clinic with evidence of spontaneous left-sided pneumothorax. A left thoracocentesis and pleural drainage were performed. A month later pneumothorax recurred contralaterally on the right side. From the performed conventional imaging studies were found diffuse advanced changes, involving both lungs. A lung and pleural biopsy was performed with histological and immune histochemical analysis result - LCH. ***Results:*** FDG- PET/CT revealed multiple bilateral pulmonary thin-walled cavitating lesions with a diffuse distribution- "honey-comb" type, thickened interlobular septa, reticulonodular changes with inhomogeneous mild to moderately increased uptake, corresponding with lung involvement from the LCH. Pneumothorax and small pleural effusion on the left side were found as well. Moreover malignant involvement by LCH of left costal pleura was suspected. Restaging PET/CT two month later after chemotherapy and corticosteroid therapy showed significantly enlarged emphysematous bullae compared to the previous scan. Significantly increased pneumothorax on the right with a small -onset pleural effusion. Metabolically active changes, newly emerged on the right costal pleura with appearance of malignant involvement from LCH. There was no sign of previously found left pleural effusion and metabolically active changes on the costal pleura. The newly appeared metabolically active changes on the right costal pleura and pleural effusion couldn't define progression of LCH, given the peculiarities of the course of the disease- migrating nature of the lesions. Restaging PET/CT was defined as stable disease (SD). ***Conclusion:*** In the early stage of the PLCH, the small-sized nodules develop from cavitating lesions into initially thick-walled, then thin-walled cysts, which finally confluence and form the lung parenchyma mainly apically with relative preservation of the lung parenchyma basally. The described findings are difficult to distinguish from emphysema and lead to a delay in the diagnosis of the disease and initiation of appropriate treatment. Deep knowledge of the nature of PLCH is the basis for timely diagnosis, correct treatment and appropriate assessment of the therapeutic response. Keywords: : Pulmonary Langerhans cell histiocytosis, 18F-FDG PET/CT

EP-0914

Diagnostic pitfall in a PET/CT case of thyroid cancer with 18F-FDG multi-uptake

T. Yi, *C. Yu;*
The Second Affiliated Hospital of Guilin Medical University, Guilin, CHINA.

Aim/Introduction: Thyroid tuberculosis is a rare disease, even in areas of high prevalence such as India, and thyroid tuberculosis combined with thyroid cancer is even more rare. ***Materials and Methods:*** A 59-year-old female with low back pain was hospitalized, and before the hospitalization her MR of thoracolumbar spine showed that the bone destruction of T3 vertebral body and accessories, considering metastasis,

abnormal signal of T11 vertebral body, considering the possibility of hemangioma and multiple intervertebral disc herniation considered multiple metastases of malignant tumors. The patient had chronic renal insufficiency with regular hemodialysis for more than 4 years. The right pleura was considered to be tuberculous pleurisy before this hospitalization and had never been treated with anti-tuberculosis drugs. There were no clinical symptoms related to tuberculosis in this case. Meanwhile, PET / CT found that there were abnormal metabolic increases in many organs including thyroid. MRI and CT found that bone destruction also considered the source of malignant tumor, which was considered to be caused by the metastasis of thyroid cancer. ***Results:*** However, the final surgical pathology found that the thyroid tuberculosis and neck lymph nodes were also tuberculosis, while the focus of thyroid cancer was only 0.2cm, which is micro papillary carcinoma. No signs of metastasis were found. ***Conclusion:*** This case emphasizes the importance of comprehensive analysis of medical history. The history of dialysis for more than 4 years was ignored, of which induced tuberculosis was not uncommon. Therefore, dialysis leads to systemic blood circulation transmission, which increases the probability of thyroid and axillary lymph node infection with tuberculosis. At the same time, although PET / CT is sensitive, its specificity is relatively low. As to multiple abnormal 18F-FDG metabolisms, it cannot be simply diagnosed as tumor and secondary metastasis through by the "monism". ***References:*** 1.Abrantes AM, Pires AS, Monteiro L, et al. Tumour functional imaging by PET. Biochim Biophys Acta Mol Basis Dis. 2020;1866(6):165717. doi:10.1016/j.bbadis.2020.1657172. Kinoshita I, Higashino M, Omura S, et al. Thyroid tuberculosis diagnosed as papillary thyroid carcinoma with fever of unknown origin. Auris Nasus Larynx. 2022 ;49(6):1093-1097.3.Stefanova DI, Bose A, Ullmann TM, et al. Does the ATA Risk Stratification Apply to Patients with Papillary Thyroid Microcarcinoma?. World J Surg. 2020;44(2):452-460. 4Yu J, Deng Y, Liu T, et al. Lymph node metastasis prediction of papillary thyroid carcinoma based on transfer learning radiomics. Nat Commun. 2020;11(1):4807.

EP-0915

Persistent bone focal uptake of 18F-PSMA-1007 in patient with prostate cancer and undetectable levels of PSA under hormone therapy

G. Bellettati[1], *S. Pacella*[2], *A. Castello*[2], *E. Lopci*[3], *L. Florimonte*[2], *M. Castellani*[2];
[1]*University of Milan, Milano, ITALY,* [2]*Fondazione IRCCS Ca'Granda, Ospedale Maggiore Policlinico, Milano, ITALY,* [3]*Humanitas Clinical and Research Hospital, Rozzano, ITALY.*

Aim/Introduction: Prostate cancer (PCa) is the second most common malignancy in men. Serum prostate-specific antigen (PSA) is a well-established biomarker for PCa screening and a reliable marker for disease monitoring. PET/CT whole body with radioligands for PSMA proved to be important for evaluation of treatment response. Our case report presents the role of ^{18}F-prostate-specific membrane antigen (PSMA)-1007 PET/CT in detecting persistent bone focal uptake in a patient with biochemical response (BR) to androgen deprivation therapy. ***Materials and Methods:*** PSMA is a transmembrane protein overexpressed in the PCa cells and its metastases. PET/CT imaging with different radioligand of PSMA is increasingly used in staging, in assessment of biochemical recurrence and treatment response of PCa. ^{68}Ga-PSMA-11 is the most widely used radiopharmaceutical, even though ^{18}F-PSMA-1007 has been recently registered for the detection of PCa and its metastases. ***Results:*** A 75-years-old man with PCa (Gleason score 4+3) and PSA of 11 ng/mL at the time of diagnosis underwent staging ^{18}F-PSMA PET/CT in July 2022. Along with increased uptake on the prostate gland, PET/CT also showed two areas of intense uptake on the 6th right rib and on the left iliac bone highly suspicious for BM. Patient started hormonal therapy with initial BR (PSA 2.5 ng/ml) confirmed by the reduction of uptake on prostatic gland and disappearance of bone uptake areas at PET/CT with ^{68}Ga-PSMA performed in September 2022. Another ^{18}F-PSMA PET/CT performed two months later showed again intense uptake on the same skeletal sites. PSA decreased (PSA <0.03 ng/ml). A subsequent MRI confirmed the metastatic nature of the left iliac bone; latest ^{18}F-PSMA PET/CT performed in April 2023 confirmed the same skeletal foci. ***Conclusion:*** The findings of our case report suggest some interesting topics to focus on: -the different sensitivity of ^{68}Ga-PSMA and ^{18}F-PSMA in the detection of bone metastases and the risk of false positive imaging of fluorinated radioligand; -the role of MRI in the interpretation of nuclear medicine imaging. Taking into account all these aspects, our clinical report could underline the importance of ^{18}F-PSMA PET/CT for early detection of suspected bone metastasis, as well as suggesting an interesting topic of discussion for oncologists regarding the timing for changing the treatment. ***References:*** 1. Pianou NK, Stavrou PZ, Vlontzou E, Rondogianni P, Exarhos DN, Datseris IE. More advantages in detecting bone and soft tissue metastases from prostate cancer using ^{18}F-PSMA PET/CT. Hell J Nucl Med. 2019 Jan-Apr;22(1):6-9. doi: 10.1967/s002449910952. Epub 2019 Mar 7.

EP-0916

Isolated limb perfusion (ILP) in a patient with myxoid liposarcoma (MLPS) of the lower extremity - case report

J. Peric*, I. Žagar;*
Institute of Oncology Ljubljana, Ljubljana, SLOVENIA.

Aim/Introduction: Myxoid liposarcoma accounts for 30% of all cases of liposarcoma and 10% of all soft tissue sarcomas. Management of the locally advanced extremity soft tissue sarcoma is demanding, especially in cases of tumor recurrence or tumor adjacent to the neurovascular structures and joints. Hypertermic ILP with TNF-α and Melphalan is indicated in patients with limb sarcomas where amputation would be the only radical treatment. ***Materials and Methods:*** We present the case of a 44 years old male, in whom MRI and CT imaging revealed a 12 x 15 x 25,5 cm large tumor in the left soleus muscle, with no signs of distant metastatic spread, histologically proven to be a grade 2 myxoid liposarcoma. During the ILP procedure, the major vessels of the tumor bearing left lower limb were exposed and cannulated, limb was separated from the systemic circuit by a tourniquet, its circuit maintained by extracorporeal perfusor (heart/lung machine) and gradually heated up to a tissue temperature of 40^{0}C. For continual leakage measurements a conventional scintilation detector with a 3x3 inch NaI (Tl) crystal, connected to a dedicated analyzer with acquisiton, processing and display software was positioned above the heart ROI at a minimal distance. After stabilisation of the limb circuit, 15 MBq activity of Tc-99m-labeled human serum albumin (99mTc-HSA) was injected into sistemic circuit and a homogenous radiopharmaceutical distribution was reached in 5 - 10 minutes. A ten-fold higher activity of the radiopharmaceutical was then injected into isolated limb circuit. As no leakage was shown, a TNF-α injection folowed into isolated limb circuit 20 minutes after and a cytostatic Melphalan (phenilalanin mustard, 1,2 - 1,5 mg/Kg body weight) injection at 45 minutes. One-minute activity measurements were continually repeated during one-hour

isolated limb perfusion, at the end of which the limb was washed-out and the vessels were repaired. Mild erythema of the limb was present after procedure, with no other complications. Left lower limb MRI imaging 2 months after ILP revealed stable disease. ILP was followed by external beam radiotherapy of the left lower limb (50 Gy in 25 fractions). ***Results:*** A follow-MRI revealed tumor shirinkage, necrosis and pseudocapsule formation; a follow-up CT revealed no distant metastatic disease. Extensive trumor resection and reconstruction with free latissimus dorsi flap coverage followed. ***Conclusion:*** ILP proves to be an effective limb sparing treatment in patients with advanced sarcomas, in whom otherwise amputation would be the only radical treatment.

EP-0917

Phase analysis using CZT-SPECT for evaluating mechanical synchronization: a case report on Left bundle branch-optimized cardiac resynchronization therapy(LOT-CRT)

Q. Sun[1,2], *S. Li*[2,3];
[1]*Department of Nuclear medicine, Shanxi Cardiovascular Hospital, Tai yuan, CHINA,* [2]*Department of Nuclear Medicine, First Hospital of Shanxi Medical University, Tai yuan, CHINA,* [3]*Collaborative Innovation Center for Molecular Imaging of Precision Medicine, Tai yuan, CHINA.*

Aim/Introduction: LOT-CRT is an innovative technique which combining left bundle branch area pacing (LBBP) and conventional CRT implanting coronary venous (CV) electrode . Currently, limited large sample follow-up studies suggest that LOT-CRT could improve the long-term prognosis for patients with HF. Accordingly, it is necessary to confirm which implantation technique can accurately improve LV synchrony and the outcome for individual patients. ***Materials and Methods:*** A patient with dilated cardiomyopathy underwent LOT-CRT enrolled in this study. Mechanical systolic synchronization parameters included PSD and PHB were evaluated by CZT-SPECT GMPI phase analysis technique before LOT-CRT. Moreover, resting GMPI was performed three times on day three after implantation. First time: unclosed electrode (LOT-CRT); Second time: LBBP means closed CV electrode; Third time: CV pacing means closed left bundle branch electrode. We analyzed which locations during pacing lead implantation played an important role in improving mechanical synchronization for patient response.The patient were followed for 6 months after LOT-CRT. ***Results:*** Mechanical synchronization parameters were analyzed. The results suggested that there were a few differences in mechanical synchronization between LBBP and LOT-CRT and the parameters between CV pacing and the preoperative parameters were not significantly different. At 6-month follow-up, This is a responder to LOT-CRT implantation. There were significant improvement between baseline parameters and 6 months parameters . In addition, his heart failure symptoms have significantly improved from NYHA class IV toll. ***Conclusion:*** The pacing effect of LBBP is similar to LOT-CRT . Moreover, CV pacing was ineffective in improving the mechanical synchronization for the patient. ***References:*** [1] Keping Chen, Yuqiu Li, Yan Dai, Qi Sun, Bin Luo, Chao Li, Shu Zhang. Comparison of electrocardiogram characteristics and pacing parameters between left bundle branch pacing and right ventricular pacing in patients receiving pacemaker therapy[J].Europace:European pacing, arrhythmias, and cardiac electrophysiology : journal of the working groups on cardiac pacing, arrhythmias, and cardiac cellular electrophysiology of the European Society of Cardiology 2019 Apr 01;21(4):673-680 doi:10.1093/europace/euy252.[2] Xiaofei Li, Hui Li, Wentao Ma, Xiaohui Ning, Erpeng Liang, Kunjing Pang, Yan Yao, Wei Hua, Shu Zhang, Xiaohan Fan. Permanent left bundle branch area pacing for atrioventricular block: Feasibility, safety, and acute effect[J].Heart rhythm 2019 12;16(12):1766-1773 doi:10.1016/j.hrthm.2019.04.043[3] Marek Jastrzębski, Paweł Moskal, Wim Huybrechts, Karol Curila, Praveen Sreekumar, Leonard M Rademakers, Shunmuga Sundaram Ponnusamy, Bengt Herweg, Parikshit S Sharma, Agnieszka Bednarek, Marek Rajzer, Pugazhendhi Vijayaraman. Left bundle branch-optimized cardiac resynchronization therapy (LOT-CRT): Results from an international LBBAP collaborative study group[J]. Heart rhythm 2022 01;19(1):13-21 doi:10.1016/j.hrthm.2021.07.057.

EP-0918

Study of joint infection in a Jehovah's Witness patient with 99mTc-Besilesomab

P. Guardia Jimena*, A. Santos Bueno, E. Sánchez de Mora, C. Salgado Garcia, A. Jiménez Heffernan;*
Hospital Universitario Juan Ramón Jiménez, Huelva, SPAIN.

Aim/Introduction: Jehovah's Witnesses refuse transfusions of blood components, including their own, what is not known is that their religion allows fractions of primary components such as albumin or immunoglobulins and it is individual to accept them. Besilesomab is a murine immunoglobulin of the IgG1 isotype indicated for the diagnosis of inflammation/infection in peripheral bones in patients with suspected osteomyelitis. ***Materials and Methods:*** We present a 53-year-old Jehovah's Witness patient who underwent total left knee arthroplasty. One month after the operation he suffered a traumatism in the left knee, associated with cellulitis and great inflammation, so he was followed in consultation due to intense pain, functional limitation and joint effusion that required arthrocentesis of serohematic fluid with negative cultures. Low-grade fever was confirmed, so three-phase bone scintigraphy and labeled leukocyte scintigraphy were indicated before a new intervention. ***Results:*** The patient comes to our service reluctant to undergo tests due to his religious background, the indicated tests were explained, and initially, a three-phase bone scintigraphy with 99mTc-hydroxyphosphonate (740 MBq) was performed, showing increased uptake in early phases, compatible with an active inflammatory process, uptake at tibial level in the late phase, unable to confirm mobilization due to the short time since the intervention (6 months). Scintigraphy with labeled leukocytes was indicated, it is exposed to the patient who completely rejects its performance. Immunoscintigraphy with antigranulocytes antobodies is proposed and explained. The patient understands, asks his family for advice and accepts the test signing the informed consent. After the administration of 555 MBq of 99mTc-Besilesomab, images were acquired at 4 and 24 hours postinjection, showing increased periprosthetic uptake which decreases in the delayed images, confirming the inflammatory process and ruling out underlying infection. Finally, the patient underwent a new surgery finding correctly cemented components, negative tissue cultures and generalized fibrosis that was removed significantly improving the pain. ***Conclusion:*** The scintigraphy with 99mTc -Besilesomab allowed us to rule out infection in a patient who refused other tests due to his religious beliefs, which allowed surgery that improved his quality of life. ***References:*** Sniecinski R, Levy JH. What is blood and what is not? Caring for the Jehovah's Witness patient undergoing cardiac surgery. Anesth Analg. 2007 Apr;104(4):753-4. doi: 10.1213/01.ane.0000255644.73211.f2. PMID: 17377074.

EP-0919

Perineural Spread Into Cerebello Pontine Angle, High Grade Salivary Duct Carcinoma Mimicking as Vestibular Schwannoma diagnosed on F18 FDG PET/CT - A Case report

A. Dixit;
Rajiv Gandhi Cancer Institute And Research Centre, North West Delhi, INDIA.

Aim/Introduction: Salivary duct carcinoma (SDC) is a rare malignant epithelial tumor mostly involving the parotid gland representing 1-3 % of salivary gland neoplasm. Histologically similar to ductal carcinoma of female breast with aggressive clinical course. Perineural invasion by SDC mimicking vestibular swannoma has rarely been reported on F18 FDG PET /CT scan. MRI head and neck has low to intermediate sensitivity for diagnosis of parotid gland tumor. ***Materials and Methods:*** 60 year old lady, presented with complaints of facial paralysis since 4 years, she was on alternative medicines. On MRI brain- a well defined extra axial lobulated enhancing lesion is seen at the right cerebello pontine angle diagnosed as Acoustic Schwannoma. She received stereotactic radiotherapy 1800 cGy (3 cycle) to the lesion. Follow up MRI brain with clinical symptoms suggested progressive disease. She underwent F18 FDG PET/ CT scan showing the right cerebello pontine angle lesion, and right parotid gland lesion, cervical lymphadenopathy with bony lesions. ***Results:*** Biopsy from the right parotid gland lesion suggested high grade SDC. She received 5 cycles of paclitaxel based chemotherapy and on follow up F18 FDG PET/ CT scan suggested partial response to treatment. ***Conclusion:*** SDC is a rare, aggressive salivary malignancy often diagnosed at an advanced stage. MRI has low-to intermediate-signaling intensity on T2-weighted images with ill-defined borders, and invasion into surrounding structures. However, F18 FDG PET /CT with few limitations appears to be a better non-invasive tool for tumor staging and guiding biopsy sites for diagnosis in cases of salivary duct carcinoma mimicking vestibular Swannoma and early treatment response assessment. ***References:*** 1. O. Kleinsasser, et al , "Salivary duct carcinoma, a group of salivary gland tumors analogous to mammary duct carcinoma," Arch Klin Exp Ohren Nasen Kehlkopfheilkd, vol. 192, no. 1, pp. 100-105, 1968. 2. A. Etges, et.al , "Salivary duct carcinoma: immunohistochemical profile of an aggressive salivary gland tumour," Journal of Clinical Pathology, vol. 56, no. 12, pp. 914-918, 2003.

EP-0920

SAPHO syndrome - a rare and challenging diagnosis on FDG PET/MRI

J. Foukal, *T. Koprivova, H. Kašpárková;*
Fakultni nemocnice Brno, Brno, CZECH REPUBLIC.

Aim/Introduction: The SAPHO syndrome encompasses a variety of osteoarticular disorders that are frequently accompanied by dermatoses but can also occur in isolation. It is rare, although probably underrecognized because its diagnosis may be challenging due to the wide variability in its musculoskeletal and cutaneous manifestations. The pathogenesis is unknown, but a genetic predisposition to an atypical immune response to bacterial infection is suspected. ***Materials and Methods:*** A 41-year-old man was referred for a FDG PET/MRI with a year long history of persisting osteomyelitis of mandible, recurrent spondylodiscitis of thoracic and lumbar spine and persistent joint pain. Although no causative pathogen was identified, the patient has undergone long-term treatment with antibiotics with little to no clinical effect. Paraneoplastic or haemato-oncological etiology was considered therefore, a PET/MRI was performed. ***Results:*** On PET/MRI multiple foci of markedly increased activity surrounding many bones and joints were present, but no pathological activity was present inside the bones themselves. Affected regions included mandible, scapulae, acromio-clavicular and sterno-clavicular joints, ribs, thoracic and lumbar vertebrae, iliac bones. As the presentation was not suggestive of malignancy, atypically extensive image of inflammatory process was considered. Biopsy of the infiltrates around the pelvis and clavicle was performed with findings of inflammatory changes. The clinical presentation, results of PET/MRI and biopsies together led to a diagnosis from the group of autoinflammatory bone lesions of the SAPHO syndrome type or recurrent nonbacterial chronic osteomyelitis. Specific therapy was started, it included corticosteroids, chemotherapy and biological therapy followed by immunosuppressive therapy. ***Conclusion:*** SAPHO is a rare and probably underdiagnosed disease and the path to a correct diagnosis can be long and complex. Even histology alone cannot accurately diagnose the disease; clinical symptoms, imaging and histological findings must be correlated. In the presented case it took more than a year from the first symptoms to the correct diagnosis and therapy. ***References:*** Nguyen MT, Borchers A, Selmi C, Naguwa SM, Cheema G, Gershwin ME. The SAPHO syndrome. Semin Arthritis Rheum. 2012 Dec;42(3):254-65. Duan N., Chen X., Liu Y, Wang J.,Wang Z. Multimodal imaging findings of SAPHO syndrome with no skin lesions: a report of three cases and review of the literature. Experimental and Therapeutic Medicine, (2016); 12(4), 2665-2670.

EP-0921

Isolated splenic metastasis from colon cancer

S. Pacella[1], *E. Farè*[2], *E. Collovà*[2], *L. Roncoroni*[2], *C. Migliorisi*[2], *A. Calcagno*[2], *M. Carletto*[2], *L. Maffioli*[3];
[1]*IRCCS Fondazione Cà Granda Ospedale Maggiore Policlinico, Milano, ITALY,* [2]*ASST Ovest Milanese-Ospedale Civile di Legnano, Legnano, ITALY,* [3]*ASST Sette Laghi, Varese, ITALY.*

Aim/Introduction: Isolated splenic metastases from solid tumors occurs rarely, accounting for less than 1% of all metastases . Isolated solitary splenic metastasis from colorectal carcinoma is exceptional. ***Materials and Methods:*** In this case report we evidenced the importance of ^{18F}FDG PET/CT in a woman with an isolated splenic lesion detected 7 months after right emicolectomy that it finally revealed to be a metastasis from colon cancer. ***Results:*** A 92-year-woman referred to our Nuclear Medicine Unit because she had an ultrasound suspected lesion of the spleen of unknown origin. 7 months before she underwent a right emicolectomy for a colon adenocarcinoma locally advanced with lymphangioinvasion and neuroinvasion (TNM stage pT4N0), without the expression of MLH1 and of PMS2, but with a BRAF mutation (V600E). So we decided to perform a ^{18F}FDG PET/CT study in order to characterize this splenic lesion. ^{18F}FDG PET/CT study showed focal intense area of FDG uptake in the spleen, with no other abnormal findings. After 2 months a splenectomy was performed and histopathologic examination confirmed the lesion as a metastasis from colon adenocarcinoma. ***Conclusion:*** ^{18F}FDG PET/CT proved to be an important diagnostic tool for characterization of lesions and for early evaluation of treatment response to therapy in colorectal cancer. In this case report ^{18F}FDG PET/CT guided to the best therapeutic option for this patient that was the surgical approach (splenectomy) in order to find out the nature of this splenic lesion. ***References:*** -Gilardi, Laura MD; Vadrucci, Manuela MD "Isolated

Metachronous Splenic Metastasis From Colon Cancer Found by 18F-FDG PET/CT", Clinical Nuclear Medicine: January 2017 - Volume 42 - Issue 1 - p 79-80 doi: 10.1097/RLU.0000000000001437. -Abi-Saad GS, Hussein M, El-Saghir NS, Termos S, Sharara AI, Shamseddine A. "Isolated splenic metastasis from colorectal cancer". Int J Clin Oncol. 2011 Aug;16(4):306-13. doi: 10.1007/s10147-010-0182-2. Epub 2011 Jan 22. PMID: 21258837. -Vriens D, de Geus-Oei LF, van der Graaf WT, Oyen WJ. "Tailoring therapy in colorectal cancer by PET-CT". Q J Nucl Med Mol Imaging. 2009 Apr;53(2):224-44. PMID: 19293770.

EP-0922

The role of 2-[18F]FDG-PET/CT in a rare case of Nasal Cavity Melanoma

I. C. Ferreira[1], *R. T. Ferreira*[1], *A. T. Xavier*[2], *S. Carmona*[1], *A. I. Santos*[1];
[1]*Hospital Garcia de Orta, E.P.E., Almada, PORTUGAL,* [2]*Centro Hospitalar Barreiro Montijo, E.P.E., Barreiro, PORTUGAL.*

Aim/Introduction: Malignant Melanoma of the nasal cavity mucosa (MMNCM) is extremely rare, has no established risk factors and is more aggressive than its cutaneous counterpart, with worse prognosis and overall survival. Due to its rarity and nonspecific symptoms, diagnosis and management can be difficult. PET/CT with 2-[^{18}F]FDG (FDG-PET/CT) has become important for the diagnosis, staging, and monitoring of various malignancies, including aggressive types of melanoma. We present a case of MMNCM in which FDG-PET/CT was used to detect tumour recurrence, and aided in assessing the extent of disease and guiding treatment decisions. ***Materials and Methods:*** A 69 year-old woman with a history of MMNCM, excised and submitted to local radiotherapy in other institutions with complete response, presented to our hospital two years later with complaints of unilateral epistaxis. Clinical examination was normal. An FDG-PET/CT scan was performed and showed intense focal radiotracer uptake in the posterior right nasal fossa, sphenoid sinus and several deep cervical lymph nodes, without distant metastasis. Ipilimumab was started. Due to clinical worsening with progressive bilateral amaurosis and headache, the patient was admitted to the hospital and underwent cranial CT and MRI scans. These demonstrated an expansive mass in the right nasal fossa causing bone destruction of the sphenoid, erosion of the posterior ethmoid plate and involvement of both optic channels. ***Results:*** Despite the inexistence of distant metastasis and given the complexity of the lesion's location with its ensuing difficulty of surgical approach, a multidisciplinary team was assembled and transnasaltranssphenoidal total macroscopic excision of the mass was performed, although with positive margins on histologic evaluation, confirming melanoma recurrence. Decompression of neurological structures was achieved, with immediate benefit on quality of life, namely vision improvement and headache control. Seven months later, disease progression was detected and the patient died. ***Conclusion:*** MMNCM is a rare entity with aggressive behaviour and overall poor prognosis, despite adequate local control. Local recurrence and distant metastasis are common. For early and localized tumours, first line treatment is surgery and eventually radiotherapy. Early detection and quality of resection with negative surgical margins are the most important prognostic factors, however, they remain challenging due to nonspecific symptoms and complexity of surrounding anatomical structures. As shown in this case FDG-PET/CT can be a valuable resource for the management of these patients, helping in early diagnosis of local recurrence and at the same time providing accurate whole-body staging, essential for successful therapeutic decisions.

EP-0923

A Rare Coexistence of Rectal Adenocarcinoma and Primary Squamous Cell Carcinoma of the Thyroid: Emphasizing the Importance of FDG PET/CT Whole-Body Imaging

J. Yu, *X. Cao, Y. Wang;*
The Fifth Affiliated Hospital of Sun Yat-sen University Department of Nuclear Medicine, Zhuhai, CHINA.

Aim/Introduction: This case report aims to emphasize the importance of FDG PET/CT whole-body imaging in the early diagnosis and differentiation of a rare coexistence of rectal adenocarcinoma and primary squamous cell carcinoma of the thyroid (PSCCT). PSCCT accounts for less than 1% of all thyroid tumors and has an aggressive nature and poor prognosis. This case highlights the significance of comprehensive diagnostic tools in detecting and managing patients with such unusual tumor combinations. ***Materials and Methods:*** A 40-year-old male with a 6-month history of bloody stools underwent tumor marker tests, revealing a CEA level of 32.80 ng/mL. The patient then underwent 18F-FDG PET/CT imaging, which showed a thickened right intestinal wall at the rectosigmoid junction and an enlarged right thyroid lobe with a hypodense nodule, indicating the need for differentiation between thyroid adenoma and thyroid cancer. ***Results:*** Colonoscopy biopsy revealed tubular adenoma in the descending colon and adenocarcinoma 9cm from the anal verge. Fine-needle aspiration biopsy of the thyroid nodule indicated non-keratinizing squamous cell carcinoma. Immunohistochemical staining demonstrated cancer cells positive for CK-P, p40, CK5/6, p63, weakly positive for CK7, and negative for Tg, TTF-1, CK20, and Villin, confirming the rare co-occurrence of rectal adenocarcinoma and thyroid squamous cell carcinoma. ***Conclusion:*** This case report underscores the advantage of 18F-FDG PET/CT whole-body imaging in early tumor diagnosis and the importance of considering multiple primary malignancies in patients presenting with unusual tumor combinations. Comprehensive diagnostic approaches, including PET/CT imaging and immunohistochemical staining, are crucial for accurately identifying rare cases and guiding appropriate patient care.

EP-0924

Gallbladder visualization, a false positive finding on 99mTc-labeled red blood cell

A. Leiva Montejo, *A. De Agrela Serrao, D. Cáceres Silva, C. Ruiz Corbalán, T. Rodriguez Lorcano, J. Contreras Gutierrez, J. Navarro Fernández, L. Frutos Esteban, A. Hernandez Martinez, L. Mohamed Salem, M. Castellon Sánchez;*
Hospital Virgen de la Arrixaca, Murcia, SPAIN.

Aim/Introduction: 99mTc-labeled red blood cell (RBC) scan is a used nuclear medicine procedure that can detect gastrointestinal bleeding, which could be a common finding after an abdominal surgery. Gastrointestinal bleeding scintigraphy (GIBS) is performed in this patients to determine the exact anatomical location of bleeding. GIBS allow us a continuous monitoring of the gastrointestinal tract up to 24 hrs whether the suspicion persists. The importance of this study is based on performing sequential images that increases the possibility of detection of intermittent bleeding. ***Materials and Methods:*** A 38-year-old man, known case of type 1 diabetic with nephropathy underwent pancreatic transplantation in October 2022, followed by blood loss within 2 months. In December 2022, during a hemodialysis session, he presented an hypotension episode with a hemoglobin level of 5.6 mg/dl and received multiple blood transfusions. He urderwent

a surgical reintervention due to the suspicion of bleeding in the graft anastomosis. An abdominal CT with contrast was normal. As a result, the Transplant Committee decided to complete the study with a 99mTc-labeled RBC scan. ***Results:*** 99mTc-labeled RBC scintigraphy was performed, it consisted in a dynamic fase that didn't show alterations, but static images at 1 hr and 2 hr revealed an abnormal focal tracer uptake in the right hypochondrium. Single-photon emission computed tomography/ computed tomography (SPECT/CT) images of the abdomen at 2 hr determined the location of the radiotracer concentration which was the gallbladder. Imaging was continued until 24 hr, where this tracer uptake persisted, without any evidence about its displacement along the intestine. ***Conclusion:*** Gall bladder visualization during 99mTc-labeled RBC scan for occult gastrointestinal blood leak is a rare finding. Anemia, multiple blood transfusions and hemodyalisis could explained the uptake tracer in the gallbladder because of the bile labeling, originated by the breakdown of hemoglobin into bilirrubin. Labeled heme part is introduced to the biliary system because heme is the biochemical precursor of bilirrubin. In addition, another possible explanation is the prior multiple blood transfusions which accelerates the breakdown of theses RBCs with unusual concentration of labeled bilirrubin in the bile. Finally, SPECT-CT is an important image tool that provide better anatomical localization of tracer distribution, like in this case, where the 99mTc-labeled RBC showed an uptake in the right hypochondrial region that could have been taken wrong as a positive result for active bleeding, without the SPECT-CT.

EP-0925

18F-FDG PET/CT identifying breast and pancreas metastases of Nasal Mucosal Melanoma

A. Leiva Montejo*, C. Ruiz Corbalán, A. De Agrela Serrao, D. Cáceres Silva, J. Contreras Gutierrez, T. Rodriguez Lorcano, J. Navarro Fernández, L. Frutos Esteban, A. Hernandez Martinez, L. Mohamed Salem, M. Castellon Sánchez;*
Hospital Virgen de la Arrixaca, Murcia, SPAIN.

Aim/Introduction: Mucosal melanoma is a rare variant of melanoma representing around 1% of total cases of melanoma diagnosed. Sinus melanomas represent only 20% of nasal mucosa melanomas but are aggressive with less 5-year survival compared to nonsinus type.18F-FDG PET/CT is a useful modality for regional and distant staging of high-risk melanoma at initial diagnosis. ***Materials and Methods:*** A 60-year-old woman presented with nasal respiratory failure and left periocular pain, of 2-month evolution and weight loss (15 kg) in June 2018. No epistaxis, no hyposmia, nor neurological focus. The neck was masses free. Nasal endoscopy revealed a friable and bleeding tumor in the left nostril that respected nasal cavity's floor. Magnetic resonance imaging (MRI) of face and sinuses revealed a lesion in the left nostril which occupied the frontal sinus until the middle turbinate, with fine peripheral contrast uptake. There was no apparent bone destruction. Biopsy from the mass was taken which revealed nasal mucosa melanoma with tumor cells positive for HMB-45 and Melan A, Ki 67 index 80%. ***Results:*** 18F-FDG PET/CT showed increased uptake in the left nostril (SUVmax 14.6) with probable ethmoid cells left anterior involvement (SUVmax 4.2). No other disease location was found. In June 2021, she felt a node in her right breast. Mammography and an ultrasound with biopsy of the lesion was taken which revealed compatible cells with malignant melanoma. After 2 months, other 18F-FDG PET/CT showed a new subcutaneous nodular formation adjacent to the right anterolateral 5th costal arch (SUVmax 17.8). Increased FDG uptake was located in pancreas (SUVmax 7.4), nonspecific, and further diagnostic imaging procedures were recommended in order to study it. The last 18F-FDG PET/CT was performed in December 2021 that showed pathological uptake of the radiotracer in pancreas (SUVmax 11.8) with more extension than previous study and with adjacent lymphadenopathies. The patient died after one year. ***Conclusion:*** Nuclear medicine imaging with 18F-FDG PET/CT could represent an important tool for the evaluation of malignant melanoma, especially in staging, restaging and assessing response to treatment. Besides, a precise delimitation of the tumor provided by 18F-FDG PET/CT is necessary since sinonasal melanoma definitive's treatment is surgical, but if it detects additional disease, surgery could be obviated. On the other hand, 18F-FDG PET/CT is less accurate in melanomas involving skull base and brain, where MRI is superior.

EP-0926

99mTc-labelled heat-Damaged Red Blood Cell scintigraphy in the study of unspecific nodular foci on CT - a case report

R. Silva*, M. Silva, H. Martins, D. Leiro, A. Barbosa, L. Costa;*
Centro Hospitalar Universitário de Santo António, Porto, PORTUGAL.

Aim/Introduction: Splenosis refers to implants of splenic tissue at any site of the body resulting from spillage of cells, usually after traumatic injury or surgery. The splenic tissue can implant on various organs, and form nodules. Splenosis can present as unspecific symptoms and mimic other conditions. Diagnosis can be challenging, but functional and anatomical imaging techniques, such as ^{99m}Tc-labelled heat-Damaged Red Blood Cell(***^{99m}***Tc-DRBC) with Single Photon Emission Computed Tomography (SPECT) and Computed Tomography (CT) images can be valuable tools. ***Materials and Methods:*** Clinical diaries and diagnostic exams were reviewed in the hospital's informatic system. ***Results:*** A 51-year-old male patient was experiencing unspecific abdominal discomfort, early satiety, and 19.8% weight loss over 11 months. Past medical history was significant for multiple cardiovascular risk factors, and right-sided heart failure with signs of mild pulmonary hypertension in a previous echocardiography. He had a history of abdominal trauma that resulted in splenectomy, and a moderate restrictive lung disorder due to post-traumatic hemidiaphragm paralysis. An abdominal ultrasound showed moderate abdominal ascites, that was later characterized by an abdominal CT, showing hepatic congestion, massive ascites, and a heterogeneous aspect of the mesenteric fat in the anterior portion of the abdomen, with multiple nodular, unspecific foci, with no evidence of primary source of a tumor. A diagnostic hypothesis of peritoneal carcinomatosis was made. He was later electively admitted to a surgery ward to determine the site of possible primary cancer. Blood tests, a diagnostic paracentesis, upper endoscopy with biopsy, colonoscopy, head&neck CT, and a 2-[^{18}F]FDG PET/CT were negative for malignancy. A CT was again performed showing nodular foci on the abdomen, which maintained stable dimensions. Considering the history of abdominal trauma and surgery, the hypothesis of splenosis was considered. ^{99m}Tc-DRBC were administered, and SPECT-CT images were acquired. The exam showed multiple foci with increased radiotracer uptake that corresponded to the morphological changes on CT, confirming the diagnosis. Further evaluation concluded that the ascites was due to decompensated right-sided heart failure due to venous pulmonary hypertension in the context of his restrictive lung disease. Pharmacological treatment was optimized. ***Conclusion:*** The case highlights the importance of considering splenosis in

the differential diagnosis of unspecific, nodular abdominal masses. Despite inconclusive results from various diagnostic tests, the use of 99mTc-DRBC SPECT-CT images was crucial for its non-invasive diagnosis. This underscores the value of combining functional and anatomical imaging techniques, playing a crucial role in the diagnosis of certain conditions.

EP-0927

Why Should We Look at the Thyroid Gland in Myocardial Perfusion Scintigraphy?

B. Pereira, *P. Soeiro, A. Fernandes, A. Oliveira;*
Centro Hospitalar Universitário de São João, Porto, PORTUGAL.

Aim/Introduction: Hyperthyroidism's effect on cardiac function is well known. [^{99m}Tc]Tc-Tetrofosmin (tetrofosmin) is a radiopharmaceutical frequently used for myocardial perfusion imaging (MPI), for assessing the location of parathyroid adenomas, and less commonly for evaluating amiodarone-induced thyrotoxicosis. ***Materials and Methods:*** A 59-year-old Caucasian male with several high-risk factors for cardiovascular disease (including diabetes mellitus, hypertension and dyslipidemia), underwent an MPI with tetrofosmin after having a myocardial infarction and being treated with a percutaneous coronary intervention of the right coronary artery. The patient's chronic medication included a β-blocker, an ACE inhibitor, a statin, and anti-platelet therapy. ***Results:*** MPI revealed a reversible perfusion defect on the anterior wall and apex and a partially reversible perfusion defect on the inferior wall (SSS - 5; SRS - 1; SDS - 4). Ejection fraction, cardiac volumes, transient ischemic dilation index and motility were normal. Additionally, the thyroid gland revealed intense and homogeneous uptake, which can be associated to an hyperfunctioning thyroid gland or with amiodarone-induced thyrotoxicosis. Previous amiodarone therapy was excluded and the patient was referred to the endocrinology department. Thyroid blood tests and a thyroid ultrasound revealed TRABs-positive hyperthyroidism, compatible with a Graves disease diagnosis. To control the disease, chronic anti-thyroid medication was started. ***Conclusion:*** Hyperthyroidism's impact on the heart is well known and, above all, patients with cardiovascular disease should have it controlled. A watchful eye on the thyroid on myocardial perfusion imaging can add vital information and improve the management of these patients. ***References:*** Elshimy G, Alsayed M, Targovnik J, Sidarous G, Milas KM. The Use of 99mTc-Methoxy-isobutyl-isonitrile (sestaMIBI) Uptake on Scintigraphy (99m-STS) in Amiodarone-Induced Thyrotoxicosis: Case Series and Review of the Literature. Case Rep Endocrinol. 2020 Aug 1;2020:2493460. doi: 10.1155/2020/2493460. PMID: 32832167; PMCID: PMC7421811.

EP-0928

Hyperparathyroidism Jaw Tumor Syndrome: A Case Report

E. Gharehpapagh, *S. Rezaei;*
Department of Nuclear Medicine, Medical School, Tabriz University of Medical Sciences, Tabriz, IRAN, ISLAMIC REPUBLIC OF.

Aim/Introduction: A 37-year-old female with complication of a large mass in her right mandible, which may have originated from the parathyroid gland. According to her CT scan, there was an expansible lesion in her mandible body, measuring 80x55 mm, extended to the lower ramus, resulting in the displacement of her inferior alveolar nerve canal to the superior and medial sides. Two possible diagnoses were considered: intraosseous atypical form of neurofibroma, and ossifying fibroma. ***Materials and Methods:*** Biopsy results of this mass showed a vascular myxoid spindle cell lesion, and it was recommended to repeat it due to the incompleteness of the biopsy sample. During the blood test on the patient, Ca=9.2, P=2.5, and PTH=629 were detected. A repeat test after an interval of eight days showed Ca=9.8, iPTH= 738, and VitD3=8. Testing results led to a request for parotid scanning by SPECT method using ^{99m}Tc-MIBI. Following intravenous injection of 15 mci of the radiotracer, the patient's neck and mandible were scanned in planar and SPECT modes at 15 and 120 min intervals (early and delayed phases). ***Results:*** According to the parathyroid scan, the lower part of the Left thyroid's lobe showed focally increased uptake, which also retention of the radiotracer in delayed images. The right mandible mass also displayed irregular increased uptake with deformity. According to the scan findings, highly probability of parathyroid adenoma in the left lower lobe, as well as, expansible tumoral involvement in the right mandible with MIBI avid pattern was highly supposed. The probable final diagnosis was hyperparathyroidism jaw tumor syndrome. ***Conclusion:*** Afterward, the patient underwent parathyroidectomy and jaw mass resection. As a result of the pathology report, parathyroid carcinoma was diagnosed.

EP-0929

PET/CT [18F]FDG Findings in Post-COVID-19 Syndrome with Cognitive Sequelae: A Case Report

L. Wichert-Ana, *L. E. Lopes-Santos, D. L. Ferreira, A. C. Trevisan, L. Alexandre-Santos, M. P. Foss, M. Kato, F. B. Rodrigues, F. A. Pitella, O. Y. Fukumori, V. Tumas;*
Ribeirão Preto Medical School - University of São Paulo, Ribeirao Preto, BRAZIL.

Aim/Introduction: The long COVID syndrome presents physical symptoms and neurocognitive damage when SARS-CoV-2 infection exceeds 12 weeks. Positron Emission Tomography/Computed Tomography (PET/CT) highlights metabolic changes associated with cognitive dysfunction in critically ill patients, mainly the older, in the post-COVID period. However, there are few studies on cerebral glucose metabolism in patients with cognitive complaints after mild COVID-19 without hospitalisation. This case report aims to describe the findings of [18F]FDG PET/CT and neuropsychological evaluation in a patient with persistent cognitive complaints after mild COVID-19. ***Materials and Methods:*** A female, white, 33-year-old patient without psychotropic drugs presented a positive Polymerase Chain Reaction (PCR) test for SARS-CoV-2. She had symptoms of ageusia, fatigue, intense sore throat, anosmia and myalgia. Two months after the acute phase, the patient reported frequent forgetfulness, difficulty concentrating, slow thinking and difficulty absorbing new information, both in the work and academic environment. Nine months after the onset of symptoms, she underwent a neurological PET/CT scan with 5mCi of [18F]FDG. ***Results:*** PET/CT demonstrated glycolytic hypermetabolism in the posterior cingulate gyrus (PCG) and hypometabolism in the bilateral anterior mesial temporal lobes. The neuropsychological evaluation showed average intellectual efficiency but indicated difficulty in cognitive control—the short-term recall of verbal content and significant impairment in auditory-verbal operational memory. Our findings agree with literature studies on brain regions involved in the performance of neuropsychological tests. GCP hypermetabolism is associated with greater deconcentration and impaired information processing during attentional tasks. In addition, the perisylvian areas of the dominant hemisphere are implicated in components of operational memory, especially the phonological loop, which plays an essential role in the maintenance and

operation of auditory-verbal content. ***Conclusion:*** The metabolic abnormality areas were compatible with the areas involved in the neuropsychological performance of the patient; therefore, the neurological PET/CT findings contributed significantly to the clinical management of the case.

EP-0930

A Rare Case of Bone Epithelioid Angiosarcoma In a Patient with History of Acute Myeloid Leukemia andSteroid-induced Osteonecrosis

D. Bucur, *F. Paycha;*
Hopital Lariboisiere, Paris, FRANCE.

Aim/Introduction: Angiosarcoma of bone is a very rare malignant neoplasm in which the tumor cells exhibit endothelial differentiation, accounting for less than 1% of all primary bone sarcomas. Typically, it is observed in adults, with the highest incidence between 50 and 70 years of age, and it can affect any part of the skeleton, although the axial skeleton and long tubular bones of the extremities are most commonly involved. Epithelioid angiosarcoma is a rare variant that mimics poorly differentiated carcinoma through its epithelial appearance. ***Materials and Methods:*** A 70-years-old male presents with pain in the anterior part of the left thigh for about 3-4 months, progressively worsening, with functional impotence of the left lower limb and without notion of trauma, accompanied by weight loss (~4 kg). The patient has a medical history of Acute Myeloid Leukemia treated 20 years prior with an allogeneic bone marrow transplant, chemotherapy, corticosteroids, and immunosuppressants. It is notable that he did not receive radiotherapy. However, the patient experienced complications from the corticosteroid therapy, including multifocal osteo-medullary infarctions in several bones, involving the humeral heads, femoral heads (requiring bilateral total hip replacement treatment), diaphysis and distal metaphysis of the femurs. ***Results:*** Plain radiographs and a CT scan reveal centromedullary osteolysis of the lower diaphysis of the left femur, corresponding to a Lodwick II lytic bone lesion, destroying the cortical bone, with a moth-eaten aspect and a small spiculated periosteal reaction in its supero-dorsal portion. Two small soft tissue masses accompany the lesion in its antero-superior portion. A bone scan is performed with the SPECT CT configuration showing unique osteoblastic hyperactivity of the distal third of the left femoral diaphysis. FDG PET/CT is subsequently performed to characterize the lesion and assess the extra-osseous condition, revealing increased FDG uptake, particularly of the dissemination to the soft tissue (SUVmax of 43), without abnormal uptake otherwise. The patient undergoes ultrasound-guided biopsy and the diagnosis of epithelioid angiosarcoma is established. ***Conclusion:*** Although most primary malignant bone tumors develop de novo in normal bone, they can arise from pre-existing benign bone conditions or from iatrogenic causes such as chemotherapy. The association of bone infarct with an epithelioid angiosarcoma is very rare, the most common sarcomas being malignant fibrous histiocytoma, osteosarcoma, fibrosarcoma and mixed sarcomas. However, being very aggressive in nature, it should be included in the differential diagnosis, especially taking into account the context and the imaging aspect.

EP-0931

18F-FDG PET-CT in Merkel cell carcinoma: case report

A. Ciocan[1], *L. Mititelu*[2,3], *C. Mazilu*[4], *T. Mititelu*[2,3], *A. Mazilu*[5], *D. Cuzino*[6], *M. Oancea*[6], *D. Zob*[7], *D. Costache*[8], *R. Mititelu*[2,4];
[1]*Oncologic Institute "Prof. Dr. Alexandru Trestioreanu", Bucharest, ROMANIA,* [2]*University of Medicine and Pharmacy "Dr Carol Davila", Bucharest, ROMANIA,* [3]*Institute of Military Medicine, Bucharest, ROMANIA,* [4]*Clinic of Nuclear Medicine, Central University Emergency Militari Hospital Bucharest, Bucharest, ROMANIA,* [5]*Clinic of Endocrinology, Central University Emergency Militari Hospital Bucharest, Bucharest, ROMANIA,* [6]*Clinic of Radiology, Central University Emergency Militari Hospital Bucharest, Bucharest, ROMANIA,* [7]*Oncologic Institute "Prof. Dr. Alexandru Trestioreanu", Oncology department, Bucharest, ROMANIA,* [8]*Clinic of Dermatology, Central University Emergency Militari Hospital Bucharest, Bucharest, ROMANIA.*

Aim/Introduction: Merkel cell carcinoma (MCC) is a rare but highly aggressive skin cancer with neuroendocrine features that usually presents as a solitary cutaneous or subcutaneous nodule in the areas most exposed to the sun. Staging and degree of extension can be assessed by FDG PET CT, which provides valuable images and quantification tools. ***Materials and Methods:*** We present the case of an 89-year-old man who presented with a laterocervical tumor. The patient's personal pathologic history, biochemical values, and physical examination did not reveal any unusual features. The laterocervical tumor was excised and was found to be a lymph node with the histopathologic features of MCC. Positive immunohistochemical markers AE1/AE3, CK20, chromogranin, and neurofilament confirmed the diagnosis. The patient was then referred to FDG-PET-CT for staging, in part because the primary MCC lesion was not found on physical examination. ***Results:*** The PET-CT scan shown intense uptake of 18F-FDG in the lymph nodes in the left laterocervical region, mediastinum, and lung hilum with a SULmax of up to 15.81 (subcarinal); no other foci of pathologic uptake were detected in other organs. As far as we know, this is the first reported case of MCC that initially presented as carcinoma of unknown primary, with no evidence of the primary lesion and with later reccurence with distant disease. Usually, spontaneous regression of MCC has a good prognosis compared to other skin cancers, such as malignant melanoma. In 1986, the first case of spontaneous regression of MCC was described in the literature by O'Rourke and Bell. To date, less than 60 cases of spontaneous regression have been reported. Two cases have been published so far in which spontaneous regression was followed by recurrence, one distant at the level of the vertex, and one regional, with the primary tumor atypically located on the foot. Our case, as shown by histopathology and PET-CT, can be established as a spontaneous regression of an MCC that presented atypically as carcinoma unknown primary with distant metastatic recurrence. ***Conclusion:*** Even if the spontaneous regression in MCC is usually associated with a good prognosis, there can be situations, such as the case of our patient, that can be followed by distant recurrence. FDG PET CT can be a valuable tool for managing MCC patients and help identify the real extent of highly aggressive variants.

EP-0932

Pitfall in 68Ga PSMA PET/CT interpretation - Pathological Uptake in a Patient with Prostate Carcinoma and Pulmonary Tuberculosis

S. Fares[1], *I. Rogić*[2], *D. Huić*[2];
[1]*General Hospital Varazdin, Varazdin, CROATIA,*
[2]*University Hospital Centre Zagreb, Zagreb, CROATIA.*

Aim/Introduction: Prostate-specific membrane antigen (PSMA) is a transmembrane glycoprotein found on the surface of prostate cells. It is typically overexpressed in prostate cancer cells but is also found in small amounts in other tissues such as kidneys,

liver and salivary glands. PSMA expression in non-prostatic lesions can be explained with increased PSMA expression in capillary endothelial cells in non-prostatic tissue (non-prostatic neoplasms, regenerative and inflammatory tissue). Another cause of PSMA uptake in non-prostatic lesions could be increased blood flow in hyperemia, usually present in inflammation. With increasing number of PSMA positron-emission tomography/computed tomography (PET/CT) scans performed in initial staging, biochemical recurrence of disease and in PSMA-targeted prostate cancer therapy it is important to point out a possible pitfall and a false positive finding on Ga-68 PSMA PET/CT scans. ***Results:*** A 74-year-old male patient with known prostate carcinoma (Gleason score 4+4=8, initial prostate-specific antigen - PSA 87.67 ng/mL) and biochemical recurrence of disease (PSA 5,65 ng/mL) was referred to our department in December of 2021 for Ga-68 PSMA PET/CT scan. Since diagnosis of prostate carcinoma in 2014 the patient underwent radical prostate radiotherapy, hormonal therapy and stereotactic ablative body radiotherapy (SABRT). PET/CT scan revealed pathological uptake of Ga-68 PSMA in a soft tissue node in the pelvis indicating prostate cancer metastasis but also revealed pathological uptake in several lesions in both lungs. The patient was referred to an oncologist and hormonal therapy was initiated, but he also underwent extensive pulmonary evaluation including fibreoptic bronchoscopy (FOB), endobronchial ultrasound transbronchial needle aspiration (EBUS-TBNA) and transthoracic puncture (TTP). In February of 2022 the patient was diagnosed with pulmonary tuberculosis after isolation of Mycobacterium tuberculosis in bronchoalveolar lavage culture. Combined anti-tuberculosis antibiotic therapy was applied for 6 months and a follow-up CT scan performed 3 months after the completion of antibiotic therapy showed significant regression of pulmonary infiltrates. ***Conclusion:*** Differentiating metastatic pathological PSMA uptake from a false positive finding is key to proper patient management and recognizing the variety of conditions with increased PSMA expression in non-prostatic tissue is necessary to improve specificity of PET/CT reports. With this case report we would like to point out a possible false positive finding in Ga-68 PSMA PET/CT scan and sensitize practitioners for active tuberculosis cases. ***References:*** 1. DA Silver, I Pellicer, WR Fair, WD Heston, C Cordon-Cardo. Prostate-specific membrane antigen expression in normal and malignant human tissues. Clin Cancer Res. 1997 Jan; 3(1):81-5.

EP-0933

Papillar Thyroid Carcinoma discovered on peritoneal carcinosis nodes : A case report of a 37-year-old woman

A. Bauduer, *M. Krim, A. Latge, S. Zerdoud;*
Oncopole, Toulouse, FRANCE.

Aim/Introduction: Papillary thyroid carcinoma (PTC) is the most frequent histological type of thyroid cancer (90%), originating from follicular cells. Distant metastases from PTC are rare and usually occur in lungs or bones. Peritoneal carcinomatosis is defined as an advanced stage of abdominal neoplastic disease ; an extraabdominal primary cancer causing it is rare. A 2018 study interrogating the National Cancer Registry of Ireland identified 5791 patients diagnosed with peritoneal metastasis during the period 1994-2012. Of these, only 9% had an extra-abdominal primary malignancy. We report the case of a Papillar Thyroid Carcinoma discovered on peritoneal carcinomatosis, in which iodine therapy secondly reavealed bone metastasis. ***Materials and Methods:*** A 37-year-old woman in a context of endometriosis underwent a pelvic MRI showing latero-rectal and retro-uterine nodes. Surgical excision was performed and pathological analysis revealed nodes were not endometriosis but secondary lesions from a PTC. PET-CT with 18FDG imaging did not find any significant uptake neither in the thyroid nor in the ovaries and peritoneum. Total thyroidectomy was then performed; however, histological analysis did not find any primary thyroid cancer. 3700 Mbq of ^{131}iodine were given to the patient. Thyroglobulin level was 71.48 ug/L after stimulation by rhTSH, with no anti-thyroglobulin antibody. The post-therapeutic SPECT/CT revealed mutiple bone uptakes suggestive of metastases. There was no other iodine fixation (nothing in the thyroid area or in the peritoneum). ***Results:*** Patient was seen 2 and 3 months after iodine therapy, thyroglobulin levels were respectively 2.4 ug/L with TSH 0.16 mUI/L and 0.58 ug/L with TSH 0.29 mUI/L, without anti-thyroglobulin antibody each time. Spine MRI confirmed bone metastasis in the vertebrae. Gynaecologic follow-up did not show any abnormality. Multidisciplinary consultation meeting decided to go for 2 new treatments by 5550 Mbq of radioiodine under hormone withdrawal, respectively 6 months and 1 year after the first iratherapy. ***Conclusion:*** This case report kills two birds with one stone : it presents an unusual discovery mode of thyroid carcinoma, and highlights the importance of the iodine in the treatment and staging of these cancers. The originality of our presentation is also the absence of primitive tumour in the thyroid. One hypothesis could be a stroma ovarii but the lack of iodine uptake in the ovaries, the normality of the pelvic MRI and the rarety of these tumours do not strenghten this assumption. ***References:*** M. Flanagan and al. Peritoneal metastases from extra-abdominal cancer - A population-based study. EJSO 2018;44;1811-1817.

EP-0934

Recurrent Pituitary Adenoma ACTH-Secretant Detected Using 99mTc-EDDA/HYNIC-TOC - A Case Report

A. Bajenaru[1], *C. Mazilu*[2], *M. Mititelu*[2,3];
[1]*Nuclear Medicine Departament, Oncology Institute „Prof. Dr. Alexandru Trestioreanu", Bucharest, ROMANIA,* [2]*Clinic of Nuclear Medicine, Central Emergency Military University Hospital "Dr. Carol Davila", Bucharest, ROMANIA,* [3]*University of Medicine and Pharmacy "Dr. Carol Davila", Bucharest, ROMANIA.*

Aim/Introduction: Recently, 99mTc-labeled peptides have emerged as an option for scintigraphic imaging of neuroendocrine tumors in clinical practice. They have advantages over 111In-pentetreotide, including better image quality on gamma cameras and lower radiation exposure to patients, thus allowing higher doses of radiotracer. ***Materials and Methods:*** We present the case of a 54-year-old woman with a history of HBV infection, obesity, and hypertension. After an endocrinological examination, she was diagnosed with Cushing's syndrome following clinical symptoms and features of hypercortisolism. An IRM examination confirmed the presence of a pituitary adenoma (PA), which was likely responsible for the patient's symptoms. Therefore, she underwent transsphenoidal neurosurgery, and it was confirmed histopathologically to be an ACTH-secreting PA. An increase in ACTH levels 6 months later prompted another IRM examination, which revealed a residual tissue that extended to the cavernous sinus and retrosellar on the right side. The subsequent indication was to perform somatostatin receptor scintigraphy. We performed whole-body and SPECT-CT acquisition after intravenous administration of 740 MBq of 99mTc-EDDA/HYNIC-TOC. SPECT-CT showed residual activity in the sella corresponding to the residual PA detected by IRM; the scan also showed diffuse uptake in the adrenal glands, possibly due to prolonged exposure to high levels of ACTH secretion. ***Results:*** Most neuroendocrine tumors express somatostatin receptors, so they can be visualized by scintigraphy

after intravenous injection of a radiolabeled somatostatin analog. The sensitivity of 99mTc-EDDA/HYNIC-TOC in detecting PA has been reported to be as high as 90.91%. We were able to confirm radiotracer uptake in our patient's residual PA tissue, demonstrating the existence of SSTR at this level. Furthermore, we did not find any other abnormal uptake in the rest of the body, so we ruled out the possibility of ectopic ACTH secretion. Although some previous studies state that ACTH-secreting PA's do not express somatostatin receptors, other studies show their presence in these tumors, and our case confirms their findings. ***Conclusion:*** 99mTc-EDDA/HYNIC-TOC can be used in investigations of well-differentiated PA for assessing the uptake in the sellar region as well as to exclude an ectopic lesion.

EP-0935

Two examples of how 18F-FES-PET may assist oncologists in clinical dilemmas in breast cancer patients

S. Nogueira, *F. A. B. Da luz, V. Iacone, A. M. S. Petinatti, S. C. Lima, A. Osawa, L. Y. I. Yamaga;*
Hospital Israelita Albert Einstein, São Paulo, BRAZIL.

Aim/Introduction: The radiotracer 16-18F-fluoro-17-estradiol (^{18}F-FES), which is selective for detecting tumors positive for estrogen receptors (ER), is crucial for monitoring and choosing patients with breast cancer who are eligible for hormone therapy. This report highlights two cases in which ^{18}F-FES-PET was essential for selecting the best therapy. ***Materials and Methods:*** Case 1: An 81-year-old patient with a left breast mastectomy. In 2022, she underwent a CT scan that identified multiple pulmonary nodules, probably secondary to the underlying disease. After this result, the patient underwent a mammography, ultrasound, and magnetic resonance (MRI) imaging, identifying a nodule in the right breast, Birads 5. Breast and bone scintigraphy exams confirmed the nodule in the right breast and indicated a low probability of bone involvement. The core biopsy anatomopathological evaluation identified the lesion as invasive ductal carcinoma of the right breast, CA 125, 49.78 U/ml. The patient was referred for ^{18}F-FES-PET/CT to verify if the pulmonary nodules were metastases from ductal carcinoma. The PET/CT images showed a slight increase in radiotracer uptake in the right breast, indicating the presence of ER, but the pulmonary nodules were ER-negative. These finds may suggest a neoplastic lesion of another nature, indicating the need for a change in treatment. ***Results:*** Case 2: Patient 66 years old, with right mastectomy and lymph node dissection in 2003 due to an "in-situ" carcinoma, Human epidermal growth factor receptor-2 (HER2) positive, Ki67 18%, treated with Tamoxifen. In 2021, a control mammogram identified a new nodule in the left breast, Birads 3; in 2022, the ultrasound showed the presence of enlarged axillary lymph nodes (Birads 6); a core-biopsy classified the nodule as multifocal lobular invasive carcinoma, HER2 negative, KI67 30%. After it, she performed a left mastectomy with lymph node dissection. Post-surgical MRI and ^{18}F-FDG-PET/CT revealed suspected metastasis areas and a slight increase in glucose metabolism strictly in the left breast with unspecific bone tracer uptake. Considering the high risk for systemic disease, the oncologist prescribed an ^{18}F-FES-PET/MRI, which confirmed the multiple lesions throughout the body. For this result, letrozole and ribociclib were chosen to treat the patient. In PET/MRI performed seven months after the treatment introduction, the ^{18}F-FES uptake was significantly reduced. ***Conclusion:*** In these reports, it was feasible to demonstrate cases in which the positive or negative result of ^{18}F-FES in PET/CT or PET/MR might assist the physician in solving clinical dilemmas, allowing for improved therapy targeting.

EP-0936

A rare case of bilateral seminal vesicle metastasis in carcinoid tumor of caecum

A. Kumar[1], *G. Gunasekaran*[1], *N. Pandit*[2];
[1]*JIPMER, Puducherry, INDIA,* [2]*JIPMER, Pondicherry, INDIA.*

Aim/Introduction: Neuroendocrine tumors (NET) are a rare variegated group of neoplasm that derives their origin from neural crest cells with an incidence of about 4 in 100,000 people. Rare sites of metastasis include the heart, breast, retro-orbital, uterus, skin, brain, spleen, testes, and seminal vesicles. Well-differentiated NETs express Somatostatin receptors (SSTR) and they can be imaged using radiotracers labeled with somatostatin agonists like 68Ga-DOTATOC. Patients showing good SSTR expression can be treated with a novel treatment modality called peptide receptor radionuclide therapy (PRRT) using 177Lu-DOTATATE, the localization of which can be imaged using a gamma camera. ***Materials and Methods:*** We are reporting an interesting case of a 35 years old gentleman with two children, who has been diagnosed with a well-differentiated neuroendocrine tumor of the caecum with multiple metastases to the liver 8 years ago. He underwent a right hemicolectomy with wedge resection of the liver lesion in September 2013. Postoperative Histopathological examination of the specimen revealed a carcinoid tumor of the caecum with a metastatic lesion to the liver. He then underwent transarterial chemoembolization of the left hepatic artery in November 2013 followed by a left lobectomy of the liver in May 2014. The patient lost follow-up following surgery. He then presented with exertional dyspnea in November 2017. On evaluation, he was diagnosed with carcinoid heart syndrome. He was managed symptomatically for the past 3 years. He was then referred to our department for PRRT. He underwent both 18F-FDG PET/CT and 68Ga-DOTATOC PET/CT as a part of the pre-therapeutic evaluation. 68Ga-DOTATOC PET showed increased SSTR expression in the multiple liver lesions and bilateral seminal vesicles. He underwent PRRT with 177Lu-DOTATATE. Post therapy scan following 177Lutetium DOTATATE therapy revealed the same findings as that of 68Ga-DOTATATE PET confirming the seminal vesicle metastasis. ***Results:*** Not applicable ***Conclusion:*** So far in literature, only a single case of unilateral seminal vesicle metastasis is reported in neuroendocrine tumours. The case reported by us is the first case of bilateral seminal vesicle metastasis in literature. We should actively screen the pelvic region for seminal vesicle lesions in neuroendocrine tumours as it may be misinterpreted as nodal metastasis. ***References:*** Carreras C, Kulkarni HR, Baum RP. Rare metastases detected by (68)Ga-somatostatin receptor PET/CT in patients with neuroendocrine tumors. Recent Results Cancer Res. 2013;194:379-84. PMID: 22918770.

EP-0937

Different Pattern of Brain Metabolic Changes on 18F-FDG Brain PET in a Patient with Fronto-Temporal Lobar Degeneration: Case Report

A. Bajenaru[1], *L. Mititelu*[2,3], *C. Mazilu*[4], *D. Cuzino*[5,3], *C. Sirbu*[6,3], *M. Mititelu*[4,3];
[1]*Nuclear Medicine Departament, Oncology Institute „Prof. Dr. Alexandru Trestioreanu", Bucharest, ROMANIA,* [2]*Institute of Military Medicine, Bucharest, ROMANIA,* [3]*University of Medicine and Pharmacy "Dr. Carol Davila", Bucharest, ROMANIA,* [4]*Clinic of Nuclear Medicine, Central Emergency Military University Hospital "Dr. Carol Davila", Bucharest, ROMANIA,* [5]*Clinic of Radiology, Central Emergency Military University Hospital "Dr. Carol Davila", Bucharest, ROMANIA,* [6]*Clinic of Neurology, Central Emergency Military University Hospital "Dr. Carol Davila", Bucharest, ROMANIA.*

Aim/Introduction: Fronto-temporal lobar degeneration (FTLD) is a heterogenous syndrome associated with the degeneration of the frontal and anterior temporal lobes, being responsible for 5% of all cases of dementia based on autopsy studies. The condition is usually underdiagnosed. ***Materials and Methods:*** We present the case of a 55-year-old patient suffering from severe cognitive impairment with delirium that occurred in 2020 in a context of negative emotional stress. The cognitive decline was progressive, consistent with a possible frontal lobe disorder manifested by abulia, dromomania, apraxia, disinhibition, pregnancy ideation, impoverished speech, decreased appetite, decreased self-care, sleep disturbances and sphincter incontinence, without sensorimotor or coordination deficits. An electroencephalogram showed brief, sharp and non-sustained discharges of slow waves, particularly in the left temporal region. A subsequent MRI scan showed brain atrophy without signal abnormalities in the brain parenchyma. We performed cerebral PET/CT with 18F-FDG. We used CortexID Suite software to assess regional cerebral metabolism compared to a normal database. Z-scores below -2 were considered pathologic. ***Results:*** Brain PET revealed hypometabolic changes in the lateral and medial prefrontal cortical areas and in the anterior cingulate cortex, bilaterally. We also found increased metabolic activity in the temporal and parietal cortex (especially on the right side) and in the occipital area. In most cases, patients with FTLD are characterized by hypometabolism occurring mainly in the frontal, anterior temporal, and anterior cingulate cortex, which is helpful in the differential diagnosis with Alzheimer's disease (AD). Interestingly, we also found brain areas with hypermetabolic activity in our patient. Although the presence of hypometabolism in FTLD is well documented, hypermetabolic areas are mentioned in only a small number of studies. The presence of hypermetabolic areas is atypical of dementia but has been previously documented in FTLD in association with mutations of the C9orf72 gene. Some studies also suggest that neurodegenerative diseases may in some cases show hypermetabolism in the temporal lobes and hyperactivation on fMRI scans and predict a worse prognosis. ***Conclusion:*** PET/CT with 18F-FDG is a useful investigation to evaluate brain metabolism and determine both hypo- and hypermetabolic areas in the brain responsible for a variety of behavioral changes, as well as to differentiate between AD and FTLD. Although no treatment is available for FTLD, differential diagnosis with AD is important because of differences in treatment management; cholinesterase inhibitors should be avoided because of exacerbation of symptoms.

EP-0938

Diagnosis of Erdheim-Chester disease by bone scintigraphy

A. Doumas[1], *D. Boundas*[2], *P. Exadaktylou*[1], *E. Giannoula*[1], *A. Tsangaridi*[1], *G. Gerasimou*[1], *E. Papanastasiou*[1], *I. Iakovou*[1];
[1]*Aristotle University, Thessaloniki, GREECE,* [2]*Private Nuclear Medicine Centre, Ippokratis, Thessaloniki, GREECE.*

Aim/Introduction: Erdheim-Chester disease (ECD) is a rare histiocytosis, with less than 1500 cases reported worldwide. Recently, it has been identified as a neoplastic disorder due to the discovery of MAPK mutations (RAS-RAF-MEK-ERK). The typical findings of ECD include central diabetes insipidus, renal fibrosis, and sclerotic bone lesions. However, histopathological diagnosis can be challenging due to non-specific inflammatory and fibrotic findings in tissue samples. Most patients with ECD require treatment, except for a small minority with minimally symptomatic single-organ disease. The first guidelines for ECD were published in 2014. Given recent molecular discoveries and the approval of the first targeted monoclonal antibody (vemurafenib) therapy for BRAF-V600-mutated ECD, it is essential to inform nuclear physicians about this disease which presents a characteristic scintigraphic and radiological picture. ***Materials and Methods:*** We present the case of a 54-year-old woman, referred to her orthopedic, complaining of persistent, deep pain in the knee joints. Initially treated with non-steroidal anti-inflammatory drugs for suspected degenerative arthropathy, she was later found to have symmetrical sclerotic lesions in the epiphyses of the tibia and femur on x-ray. Bone scintigraphy demonstrated the typical picture of ECD. The patient was diagnosed with BRAF-V600 mutation in an Academic hospital, which is the hallmark of ECD disease ***Conclusion:*** Although a case of possible ECD has already been described in the Greek literature, we announce this patient's case for the vigilance of nuclear physicians regarding a rare disease, with a characteristic scintigraphic image that can safely establish the diagnosis.

EP-0939

Radiation-Associated Angiosarcoma After Breast Cancer detected on [18F]FDG PET/CT

M. Pudis[1], *J. Suils-Ramón*[1], *I. Blazquez-Muñoz*[2], *F. X. Sanjuan-Garriga*[2], *A. Palomar-Muñoz*[1], *M. Cortés-Romera*[1];
[1]*Nuclear Medicine - PET (IDI), Bellvitge University Hospital - IDIBELL, L'Hospitalet de Llobregat, Barcelona, SPAIN,* [2]*Anatomical Pathology Department, Bellvitge University Hospital - IDIBELL, L'Hospitalet de Llobregat, Barcelona, SPAIN.*

Aim/Introduction: Radiation-induced angiosarcomas (RIAS) of the breast are rare but serious complications of radiation therapy. Angiosarcomas are aggressive malignant tumors that develop from the endothelial cells lining blood vessels. They can occur spontaneously or as a result of exposure to ionizing radiation. RIAS of the breast typically occur years after radiation therapy for breast cancer. They can present as a breast mass, skin changes, or both. The diagnosis is often challenging, and biopsy is required for confirmation. ***Materials and Methods:*** A 73-years-old woman diagnosed with breast cancer in her 50's, treated with neoadjuvant chemotherapy, lumpectomy with axillary lymph node dissection (ALND). Pathology revealed infiltrating ductal carcinoma ypT1a ypN1/15 (AJCC 8th ed). According to the protocol, local radiotherapy was performed and the patient has been treated with letrozole ever since. In successive controls, the patient detected a small lump in the irradiated breast. On physical examination, she presented significant induration in the left breast with purpuric areas (Figure A). An [18F]FDG PET/CT showed an FDG avid heterogenous fibrosis (arrows) and nodules (circles) in the subcutaneous adipose tissue of the previously irradiated breast (Figure B), suggestive of RIAS. ***Results:*** Biopsy findings revealed characteristic histological features of angiosarcoma (irregularly shaped blood vessels with atypical endothelial cells and areas of hemorrhage and necrosis), as well as immunohistochemical markers (CD31, CD34, ERG, and c-myc) that confirmed the diagnosis (Figure C). The treatment involved mastectomy, removing the cancerous tissue, followed by radiation therapy and chemotherapy. ***Conclusion:*** It is important for breast cancer survivors who have undergone radiation therapy to be aware of the risk of radiation-associated angiosarcoma and to monitor their breast health regularly. This may involve self-examinations, regular check-ups with a doctor, and breast imaging studies, such as mammography or ultrasound. ***References:***

Monroe AT, Feigenberg SJ, Mendenhall NP. Angiosarcoma after breast-conserving therapy. Cancer. 2003 Apr 15;97(8):1832-40. doi: 10.1002/cncr.11277. PMID: 12673708. Alves I, Marques JC. Radiation-induced angiosarcoma of the breast: a retrospective analysis of 15 years' experience at an oncology center. Radiol Bras. 2018 Sep-Oct;51(5):281-286. doi: 10.1590/0100-3984.2017.0129. PMID: 30369653; PMCID: PMC6198847.

EP-0940

A rare manifestation of multiple solitary extramedullary plasmacytomas

M. Dobrenic[1,2], *J. Batinic*[1];
[1]*Clinical Hospital Centre Zagreb, Zagreb, CROATIA,* [2]*School of Medicine University of Zagreb, Zagreb, CROATIA.*

Aim/Introduction: Extramedullary plasmacytomas are an uncommon type of monoclonal plasma cell tumours that arise outside the bone marrow, usually involving soft tissues in the head and neck region. Multiple solitary extramedullary plasmacytomas are characterised by multiple soft tissue lesions. They differ from multiple myeloma by the lack of systematic abnormalities typical of multiple myeloma (hypercalcaemia, anaemia, renal insuficiency). Very rarely, extramedullary plasmacytoma can involve trachea, causing significant respiratory distress. ***Materials and Methods:*** Case presentation:We herain report a rare presentation of multiple solitary extramedullary plasmacytomas in a 49 year old male patient who sufffered from acute chest pain and dyspnea. A chest X ray showed a whole left lung atelectasis, while a high resolution CT scan of thorax region revealed endoluminal soft tissue mass obstructing left main bronchus, with associated mediastinal precarinal and subcarinal soft tissue lesions. During bronhoscopy, additional soft tissue lesions in oropharynx and larynx were found. Diagnosis of extramedullary plasmacytomas was established following the biopsies of the oropharyngeal and left main bronchus lesions. To evaluate the extent of disease, whole body 18F FDG PET CT was performed, and intense 18F FDG uptake in soft tissue lesions in oropharynx, larynx, mediastinum, and left main bronchus was found. ***Conclusion:*** Ability of 18F FDG PET CT to distinguish between metabolically active and inactive lesions makes it a preferred functional imaging modality for staging of monoclonal plasma cell disorders. Furthermore, the importance of accurate staging of the disease lies with the potential of the plasmacytomas to progress to multiple myeloma.

EP-0941

PRRT for symptomatic paragangliomas and bilateral pheochromocytomas in an adult patient with a cyanotic heart condition

C. Burger[1], *T. Moalosi*[1], *M. Mix*[2], *M. Conradie*[1];
[1]*Stellenbosch University and Tygerberg Hospital, Cape Town, SOUTH AFRICA,* [2]*Medical Center – University of Freiburg, Freiburg, GERMANY.*

Aim/Introduction: A 46-year-old female with an unrepaired tetralogy of Fallot (TOF), was incidentally diagnosed with bilateral pheochromocytomas and multicentric extra-adrenal paragangliomas during cardiac assessment. She was centrally cyanosed (but comfortable at rest), clubbed and polycythaemic and reported episodes of flushing, palpitations, sweating and headaches. Blood pressures were fluctuating with episodes of hypertension. Raised urinary normetanephrines [24 743 nmol/24hrs (normal range 650-2462)] and metanephrines [928 nmol/24hrs (normal range 152-913)] confirmed functionality of the tumours. Genetic tests did not identify a significant associated variant. She was not considered a surgical candidate for the repair of the TOF or for adrenalectomy. ***Materials and Methods:*** Iodine-123 Metaiodobenzylguanidine ([^{123}I]I-MIBG) scintigraphy, Fluorine-18 Fluorodihydroxyphenylalanine ([^{18}F]F-DOPA) Positron emission tomography with computed tomography (PET/CT) and Gallium-68 [DOTA0,Tyr3]-octreotide ([^{68}Ga]Ga-DOTANOC) PET/CT were performed. Bilateral pheochromocytomas, four cervical paragangliomas and an aortocaval paraganglioma were identified. Discordant uptake was seen between the different radiopharmaceuticals. The measured glomerular filtration rate (GFR) corrected for body surface area was 56 ml/min/1.73m^2. Normal left ventricular systolic function was documented with cardiac echocardiography. A multidisciplinary team discussion identified Peptide Receptor Radionuclide Therapy (PRRT) with Lutetium-177 [DOTA0,Tyr3]-octreotate ([^{177}Lu]Lu-DOTA-TATE) as the most suitable treatment modality. [^{131}I]I-MIBG therapy was deemed impractical due to the need for continuous monitoring in a high care facility. Three cycles of [^{177}Lu]Lu-DOTA-TATE were administered, over a period of 7 months. ***Results:*** Chronic hypoxia activates hypoxia inducible factors responsible for development of the multiple paragangliomas and bilateral pheochromocytomas in this patient.[1] As the underlying cause cannot be eliminated, the therapeutic intent was palliation and symptom/blood pressure control by reducing tumor burden and functionality. Blood pressure fluctuated during and immediately after therapy and invasive (arterial) blood pressure monitoring proved essential to improve control. Slow pretreatment hydration, careful titration of alpha blockade while avoiding beta blockade (due to cardiac capacity concerns) and adjusted rate of the amino acid and [^{177}Lu] Lu-DOTA-TATE infusions were required. No haematological or renal toxicity two months after the last therapy were noted. Symptoms, general well-being and exercise tolerance improved. Lowering of metanephrine and normetanephrine values were documented. Further treatment with PRRT may be considered. Voxel-based dosimetry results will be presented. ***Conclusion:*** PRRT is possible and may be beneficial in patients with cyanotic heart disease and multiple paragangliomas and pheochromocytomas, but special attention needs to be paid to blood pressure control during and after therapy. ***References: 1*** Wcislak SM et al. Multifocal pheochromocytoma-paraganglioma in a 29-year-old woman with cyanotic congenital heart disease. Surgery. 2019 Jan;165(1):228-231.

EP-0942

Nodal Migration of ruptured implant contents detected on [18F]FDG-PET/CT

M. Pudis, *J. Suils-Ramón, A. Palomar-Muñoz, V. Carrero-Vasquez, C. Martínez-Ramos, S. Bondia-Bescós, B. Hervás-Sanz, J. Diaz-Moreno, M. Cortés-Romera;*
Nuclear Medicine - PET (IDI), Bellvitge University Hospital, L'Hospitalet de Llobregat, Barcelona, SPAIN.

Aim/Introduction: Extracapsular breast implant rupture refers to a situation where the contents of a breast implant leak out of the fibrous capsule that forms around the implant and migrate outside the breast tissue. This can occur due to a number of reasons, including trauma, normal wear and tear of the implant, or a defect in the implant itself. When the contents of an extracapsular ruptured implant migrate outside the breast tissue, they can potentially enter the lymphatic system and migrate to the lymph nodes. This is referred to as nodal migration of implant contents. ***Materials and Methods:*** A 44-year-old woman with a history of bilateral breast cancer at ages 27 and 35 treated with mastectomy, selective sentinel node biopsy, and reconstruction with breast implants. The genetic study detected the c.291delA mutation of the BRCA2 gene and prophylactic bilateral adnexectomy was

performed at 40 years of age. During clinical follow-up, the patient reported pain in the left sternal region, adjacent to the treated breast. [18F]FDG PET/CT was requested to rule out locoregional recurrence or distant metastasis. ***Results:*** A maximum intensity projection of [18F]FDG PET (Figure 1a) shows heterogeneous FDG uptake around the left breast implant. An axial plane of CT and PET/CT (Figure 1b) shows signs of extracapsular breast implant rupture with an enlarged FDG avid internal mammary lymph node, related to nodal migration of implant contents. ***Conclusion:*** Nodal migration of implant contents can cause a number of health concerns, including inflammation, pain, and infection in the lymph nodes. In some cases, the migrated contents may also interfere with the accuracy of breast cancer screening tests such as mammograms and ultrasounds. PET/CT imaging can be a valuable tool in detecting and evaluating the extent of extracapsular breast implant rupture. ***References:*** Khakbaz E, Lang C, Lelkaitis G, Grønhøj C. Late migration of silicon as a complication to breast transplant rupture: Case report and literature review. Int J Surg Case Rep. 2021 Aug;85:106241. doi: 10.1016/j.ijscr.2021.106241. Epub 2021 Jul 27. PMID: 34333256; PMCID: PMC8346674.

EP-0943

Tumoral thrombosis of the inferior vena cava in a patient with multiple-relapsed adrenal cortical carcinoma

A. Mitoi[1], *C. Mazilu*[1], *M. Oancea*[1], *M. Alexa*[1], *S. Serbanescu*[1], *A. Militaru*[1], *D. Craciun*[1], *A. Zaharia*[1], *M. Matei*[1], *R. Mititelu*[2,1]; [1]*Central Universitary Emergency Military Hospital, Bucharest, ROMANIA,* [2]*University of Medicine and Pharmacy "Carol Davila", Bucharest, ROMANIA.*

Aim/Introduction: Adrenal cortical carcinoma (ACC) is a rare and highly aggressive malignancy, with a very poor prognosis, that affects mostly females. ACC can extend in the inferior vena cava (IVC) to form a tumor thrombus. Due to its aggressiveness, ACC usually express high proliferation rate, being therefore suitable for follow up with 18F-FDG PET/CT in the follow-up of ACC patients. ***Materials and Methods:*** We present a unique case of a 67-year-old female who underwent right adrenalectomy for ACC, received adjuvant mitotane therapy, and experienced multiple recurrences over a 10-year period, with the latest recurrence involving invasion of the IVC. In March 2022, MRI demonstrated a gadolinium enhanced lesion located behind the retro-hepatic segment of the IVC and expansion to the IVC. In January 2023, a CT showed the same lesion described on MRI, with dimensional growth and with invasion of IVC. The PET/CT scan performed in March 2023 showed low distribution of 18F-FDG in the hepatic right lobe and a lesion near the right crus of the diaphragm with high metabolic activity, without clear demarcation from the hepatic parenchyma, and with invasion of IVC, the lesion extended from the renal veins level to the diaphragm. ***Results:*** Most of the ACC are nonfunctional and they tend to manifest late during the course of disease. ACC are frequently found incidentally and are often unresectable due to of the extent of the tumor. There are several studies showing that patients with recurrent disease have a poor prognosis, with estimated 5-year survival of 15% and overall survival to about 14 months. PET/CT can make the difference between a benign and malignant tumor thrombus because the tumor thrombus has an intense uptake of 18F-FDG as a result of its hypervascularity and high metabolic neoplastic activity with a cut-off value of 3.63.[1] Previous studies have shown that PET/CT has superior diagnostic accuracy compared to CT for initial staging and restaging of ACC patients. ***Conclusion:*** To our knowledge, this is the first case report of a multiple relapsed ACC, with the last recurrence showing tumor invasion of IVC and PET/CT scans for 10 years. We suggest that FDG PET/CT becomes part of the post-operative follow-up protocol of ACC patients due to the high diagnostic ability of recurrence and metastasis prior to conventional imaging techniques. ***References:*** 1 Sharma P, Kumar R, Jeph S, et al. 18F-FDG PET-CT in the diagnosis of tumor thrombus. Nucl Med Commun. 2011;32(9):782-788. doi:10.1097/MNM.0b013e32834774c8

EP-0944

Aneurysmal Bone Cyst in a patient with McCune-Albright Syndrome

N. Aydin*, G. Mütevelizade, G. Gümüşer, E. Sayıt Bilgin; Celal Bayar University, Manisa, TÜRKIYE.*

Aim/Introduction: Fibrous dysplasia of bone (FD) is a rare bone disease that causes pain, fracture and deformity in the bone. This disease shows a wide spectrum from benign monostotic FD to FD-associated McCune-Albright Syndrome (MAS). McCune-Albright Syndrome (MAS) is characterized by the triad of fibrous dysplasia, cafe´-au-lait spots and precocious puberty, but other endocrinopathies may also be present. ***Materials and Methods:*** A 12-year-old girl who was followed up with the diagnosis of McCune-Albright Syndrome was admitted to our hospital with a painless swelling of 4x3 cm in the frontal region 10 days after her history of sinusitis. In the MRI imaging, lesions with an expanded appearance in the cranial bones, hypointensity in T1 and T2 sequences and heterogeneous contrast brightening were observed. In addition, in the left part of the frontal bone, the T2 signal was high and the T1 signal was isointense cystic lesion, measuring 50x50 mm in size, showing peripheral contrast brightening was evaluated in favor of aneurysmal bone cyst. Increased blood flow and hyperemia in the left femur in 3-phase bone scintigraphy performed by selecting the femur area of interest in order to determine the extent of bone lesions; In the late static images, intense increased Tc-99m methylene diphosphonate (MDP) uptake was observed in the left femur, left tibia, posterior parts of the left 9th and 11th ribs and cranial bones. In the left part of the frontal bone, a well-circumscribed photopenic area was detected in the localization, which was evaluated as an aneurysmal bone cyst on MRI. After pre-operative endovascular embolization, the lesion in the frontal bone was surgically excised. ***Results:*** Secondary aneurysmal bone cysts may develop in the ribs and craniofacial bones due to bone enlargement. Aneurysmal bone cyst formation is common in areas of fibrous dysplasia due to the increased vascularity of the lesion, and these enlarged cysts can rapidly lead to intracranial symptoms. Bone scintigraphy is used to determine the extent of the disease. ***Conclusion:*** Bone scintigraphy is used to determine the extent of the disease. Paget's disease, which may be characterized by similar scintigraphic findings, should be considered in the differential diagnosis; findings should be evaluated together with radiological imaging methods, clinical and laboratory results. ***References:*** Sundaram, Murali. Imaging of Paget's disease and fibrous dysplasia of bone. Journal of Bone and Mineral Research, (2007), 22 (SUPPL. 2).

EP-0945

Disseminated infection complicating acupuncture revealed by Gallium-67 scintigraphy

T. Chow;
Tuen Mun Hospital, Hong Kong, HONG KONG.

Aim/Introduction: Acupuncture is a traditional Chinese medicine treatment by inserting needles in the body for therapeutic purposes. It is generally considered to be safe and major complications are uncommon. Previous systemic review based on published case reports revealed that the main complication of acupuncture was injury of internal organ, tissue or nerve (63%)[1]. Acupuncture infection was uncommon (9%), and most cases were due to tetanus[1]. This is a rare case showing disseminated methicillin-sensitive staphylococcus aureus (MSSA) septic foci after acupuncture revealed by Gallium-67 (Ga-67) scintigraphy. ***Materials and Methods:*** A 20-year-old woman with chronic back pain and otherwise good past health had acupuncture at the back and thighs. One week later, she presented with fever and worsening low back pain and soon developed septic shock requiring admission to intensive care unit. Blood culture showed growth of MSSA. ***Results:*** Contrast CT demonstrated multiple small consolidation scattered in both lungs with basal predominance and patchy hypoenhancement in bilateral kidneys, suggestive of septic pulmonary emboli and pyelonephritis respectively. Ga-67 scintigraphy was also arranged to delineate the extent of infection. Whole body planar images demonstrated numerous septic foci in the pelvis and four limbs. Fused transaxial SPECT/CT images further revealed septic arthritis of right sacroiliac joint and multiple intramuscular septic foci. Echocardiogram showed no evidence of vegetation. The patient received a prolonged 6-week course of antibiotics and recovered uneventfully. ***Conclusion:*** Disseminated MSSA infection complicating acupuncture revealed by Ga-67 scintigraphy was extremely rare. ***References:*** 1. Wu J, Hu Y, Zhu Y, et al. Systematic Review of Adverse Effects: A Further Step towards Modernization of Acupuncture in China. Evid Based Complement Alternat Med. 2015;2015:432467.

EP-0946

Mitral annular calcification as a potential false positive for cardiac amyloidosis in [99mTc]Tc-DPD] scintigraphy accurately identified by SPECT/CT - a case report

R. Nunes, *V. Alves;*
Centro Hospitalar Universitário de São João, Porto, PORTUGAL.

Aim/Introduction: Cardiac amyloidosis is defined by the deposition of amyloid fibrils in the myocardium, which is mostly caused by the deposition of misfolded transthyretin (ATTR) or monoclonal immunoglobulin light chains (AL). [^{99m}Tc]Tc-PYP/DPD/HDMP cardiac scintigraphy has a pivotal role in the diagnosis of ATTR cardiac amyloidosis. The combined findings of a Perugini visual score of 2 or 3 in the scan and the absence of monoclonal proteins in blood and urine are highly specific for ATTR cardiac amyloidosis and, thus, sufficient for diagnosis of this condition without a tissue biopsy. However, scintigraphy (or SPECT) alone has a lower specificity and, besides AL amyloidosis, other causes for a false positive result may occur. We report a case of mitral annular and valve calcification accurately identified in the SPECT/CT, but which could be misinterpreted as ATTR cardiac amyloidosis if only acquiring planar and SPECT images. ***Materials and Methods:*** We present a case of a 71-year-old female with a history of pulmonary interstitial disease, atrial fibrillation, a mechanical aortic valve, anemia, and hyperthyroidism who was hospitalized in the context of acute hypoxemic respiratory failure after vaccination against Sars-CoV-2. The thoracic CT showed extensive areas of consolidation in both lungs. The transthoracic aspiration biopsy demonstrated areas of fibrosis and a lymphoid infiltrate as well as amyloid deposition in the wall of a vessel of uncertain clinical significance. The transthoracic echocardiography showed concentric left ventricular hypertrophy and mitral insufficiency owing to an extensive calcification of the mitral valve and annulus, but the biventricular systolic function was normal. No infectious agent was detected. The patient progressed favorably with antibiotic and support treatment and was discharged. Subsequently, the hypothesis of systemic and/or cardiac amyloidosis was investigated, which included monoclonal protein testing and [^{99m}Tc]Tc-DPD scintigraphy and SPECT/CT. ***Results:*** Monoclonal protein testing was negative. The planar images showed mild diffuse increased tracer uptake in the projection of the heart and raised the hypothesis of cardiac amyloidosis (preferably ATTR amyloidosis). However, the SPECT/CT images accurately located the tracer uptake in the calcifications of the mitral valve and annulus, which is consistent with the previous echocardiogram, and excluded the diagnosis of cardiac amyloidosis. ***Conclusion:*** In our case report, the acquisition of SPECT/CT images changed the most likely diagnosis of cardiac amyloidosis given by the planar imaging, and accurately located the tracer uptake in the mitral annulus and valve calcifications, thus preventing a false positive result.

EP-0947

Increased 68Ga-PSMA uptake in avascular necrosis of the hip

B. Okudan Tekin[1], *B. Seven*[2];
[1]*Department of Nuclear Medicine, Ankara City Hospital, University of Health Sciences, Ankara, TÜRKIYE,*
[2]*Department of Nuclear Medicine, Sabuncuoğlu Şerefeddin Training and Research Hospital, Amasya, TÜRKIYE.*

Aim/Introduction: Avascular necrosis (AVN) or ischemic bone necrosis or osteonecrosis results from disruption of the bone vasculature and can lead to significant morbidity and impairment of patient function. The authors describe the findings of AVN on ^{68}Ga-PSMA PET/CT imaging of a patient with prostate cancer. ***Materials and Methods:*** ^{68}Ga-PSMA uptake in the prostate bed suggestive of local recurrence was detected in the images of a 71-year-old male patient who had undergone radical prostatectomy for adenocarcinoma, who underwent ^{68}Ga-PSMA PET/CT imaging for biochemical recurrence. In addition, increased ^{68}Ga-PSMA uptake with suspected metastasis was observed in the right femoral head and neck. Then, MRI scan of the patient revealed stage 2/stage 3 AVN findings accompanied by diffuse bone marrow edema in the right femoral head and neck. Stage 2 AVN findings were also reported in the left femoral head and neck. ***Results:*** This case shows the incidentally detected AVN findings on ^{68}Ga-PSMA PET/CT imaging. ***Conclusion:*** The importance of ^{68}Ga-PSMA in prostate cancer management is well understood. PSMA expression is not restricted to prostate cells, and benign processes such as inflammation or infection found in atelectasis/pneumonia have been reported to exhibit a diverse, usually mild uptake of ^{68}Ga-PSMA. The increased availability of PSMA ligands at the site of inflammation/infection as a result of increased regional blood flow and vascular permeability is considered a process of PSMA expression by immune cells. The presented case shows that AVN-related inflammation may cause increased ^{68}Ga-PSMA uptake.

EP-0948

Pseudosarcomatous Periosteal Metastases of Lower Limbs Initially Misdiagnosed for Secondary Hypertrophic Osteoarthropathy then Properly Identified by [68Ga]Ga-PSMA PET/CT in a Patient Treated for Prostate Carcinoma

D. Filipan[1], *P. Moreau*[2], *C. Thibault*[3], *F. Montravers*[2], *F. Paycha*[4]; [1]*University Department of Oncology and Nuclear Medicine, Sestre Milosrdnice University Hospital Centre, Zagreb, CROATIA,* [2]*Service de Médecine Nucléaire, Hôpital Tenon, Assistance Publique-Hôpitaux de Paris, Paris, FRANCE,* [3]*Service d'Oncologie Médicale, Hôpital Européen Georges Pompidou, Assistance Publique-Hôpitaux de Paris, Paris, FRANCE,* [4]*Service de Médecine Nucléaire, Hôpital Lariboisière, Assistance Publique-Hôpitaux de Paris, Paris, FRANCE.*

Aim/Introduction: Sunburst periosteal reaction of bone metastases is rare (less than 5% of cases) and only associated with osteoblastic metastases. It is most reported in malignant primary bone tumours such as osteosarcoma, but it can also be found in solid neoplasms (prostatic carcinoma (30%)). ***Materials and Methods:*** A 73-year-old male presented with oligometastatic prostate cancer, Gleason score 9 (4+5), resistant to castration, with osteoblastic phenotype bone and lymph-node metastases. The patient has been treated by radical prostatectomy and taxanes. Painful bone metastases of the right hemi-pelvis and left tibia received external beam radiotherapy. Baseline [99mTc] bisphosphonates bone scan, performed in initial post-surgical assessment, disclosed solitary increased uptake of the right acetabulum. Four years later, the patient's ECOG2 performance status and prostate specific antigen (PSA) rising from PSA nadir 0.09 ng/mL to 2.9 ng/mL, prompted a new bone scan. Acquisition workflow combined planar whole-body scan and additional SPECT/CT field-of-view of tibias. There was high-intensity increased uptake of the right ilium, left femoral diaphysis in partial and along the cortico-periosteal layer of the left tibial diaphysis. These bone turnover disturbances were congruent with divergent spiculated periosteal reaction on CT portion of hybrid imaging. Upper half-skeleton, spine included, exhibited normal uptake. A [68Ga]Ga-PSMA PET/CT study was subsequently performed as a theranostic tool for internal radioligand therapy by [177Lu]Lu-PSMA with palliative intent in this patient bearing a high-volume bone metastatic burden. Diffuse and intense ligand uptake was distributed throughout both hematopoietic axial skeleton and (non-hematopoietic) tubular bones of lower limbs. Most intensive uptake was concentrated at the site of florid aggressive periosteal reaction encompassing the pelvis and lower limbs. No lung metastases were evidenced. ***Results:*** Linear increased uptake of [99mTc]bisphosphonates along cortico-periosteal layer (railroad-track pattern) was initially interpreted as a classical picture of hypertrophic osteoarthropathy, where periosteal new bone formation (typically symmetric and widely distributed) is present primarily in tubular long bones of the extremities. Hence, the divergent spiculated pattern of the periosteal reaction and the production of osteoid was elicited by [99mTc]bisphosphonates, while [68Ga]Ga-PSMA evidenced subperiosteal prostate cancer metastases, properly diagnosing the lesions as pseudosarcomatous periosteal metastases of prostatic cancer. Given the patient's poor clinical condition, no bone biopsy was attempted. ***Conclusion:*** This case exemplifies the importance of hybrid bone-seeking and prostate cancer-targeted molecular imaging both as a key to finding the right diagnosis of an infrequent painful and aggressive bone metastatic disease, and as a theranostic selector for radionuclide PSMA-based therapy.

EP-0949

Retroperitoneal Fat-Containing Tumor. Tiptoeing between malignant and benign: A Case Report

M. Matei[1], *A. Mitoi*[1], *S. Serbanescu*[1], *C. Mazilu*[1], *R. Mititelu*[1,2]; [1]*Nuclear Medicine Department, Central Universitary Emergency Military Hospital, Bucharest, ROMANIA,* [2]*University of Medicine and Pharmacy Dr Carol Davila, Bucharest, ROMANIA.*

Aim/Introduction: Retroperitoneal lipomas are extremely rare, benign tumors of mature adipocytes, usually asymptomatic until they start displacing the adjacent abdominal structures. The aim of this report is to emphasize the importance of metabolic imaging in the differential diagnosis of fat containing retroperitoneal tumors, including benign pathologies - lipoma, renal angiomyolipoma with exophytic expansion or malignant - liposarcoma. ***Materials and Methods:*** We present a case of a 43-year-old female with no prior medical history (menopause onset in January 2021) presented with diffuse and dull abdominal pain with a normal physical examination and normal laboratory tests. Radiological abdominal studies showed a well-defined, retroperitoneal mass of ~14/9/9 cm in the left renal space, which presented with scattered areas of internal soft-tissue density (fine septa and blood vessels) and shifting the upper left abdominal structures (spleen, stomach and the body and tail of the pancreas) anterior and medial. The MRI showed areas with persistent high T2 signal on the FAT-SAT T2 sequence with signs of local invasion - densification of the apical perirenal fat, thus raising the suspicion of a low-grade well differentiated liposarcoma. 18F-FDG PET/CT was recommended. ***Results:*** The patient underwent a PET/CT scan with 18F-FDG that revealed minimal uptake of FDG of the left retroperitoneal mass, probably due to the presence of the fibrous septa and the vascular network. Due to the presence of multiple smaller angiomyolipomas on both kidneys, the mass appeared as if it was bursting from the left renal cortex ("claw sign") with the feeding artery of the tumor originated from the renal cortex ("prominent feeding artery"); these findings were highly evocative for renal angiomyolipoma with exophytic growth. A biopsy was taken from the primary mass; interestingly, histopathological examination and immunohistochemical staining were performed, confirming the diagnosis of lipoma. ***Conclusion:*** This case highlights the importance of PET/CT in assessing retroperitoneal slow growing fat-predominant tumors. The accuracy of the initial radiological diagnosis is important for the design of the operative plan, because of the radical approach in case of liposarcoma and the more conservative path in benign cases. Even though the PET/CT findings were suggestive for renal angiomyolipoma and the histopathological result was indicative of lipoma, the PET/CT was successful in differentiating a benign tumor (lipoma/angiomyolipoma) from a potentially more aggressive malignant tumor, thus changing the further planning of the case.

EP-0950

Can PSMA based PET/CT scan be used in management of salivary gland neoplasms?

N. Ghesani, *M. Posner, r. Kulkarni, M. Ghesani; Icahn School of Medicine at Mount Sinai, New York, NY, UNITED STATES OF AMERICA.*

Aim/Introduction: The Prostate-specific membrane antigen (PSMA) is a transmembrane glycoprotein of the prostate secretory acinar epithelium that is upregulated in prostate cancer (PC). PSMA-based diagnostics and targeted therapy(theranostics) are utilized in metastatic PC. PSMA PET/CT depicts physiological uptake in the salivary and lacrimal glands, liver, and kidneys,

and in benign and malignant neoplasms, mostly adenomas and adenocarcinomas, of glandular or epithelial origin. Value of PSMA-based theranostics in the neoplasms of non-prostatic origin has been explored. In this report, we demonstrate absence of PSMA uptake in salivary duct carcinoma(SDC) and discrepancy between Fluorodeoxyglucose (FDG) and PSMA uptake in metastases on PET/CT scans. ***Materials and Methods:*** An 85-year-old man with newly diagnosed prostate cancer, Gleason score 7, PSA level - 2 ng/mL, underwent ^{18}F piflufolastat (PSMA) PET/CT scan. Primary prostate neoplasm was non-PSMA-avid. Minimal radiotracer uptake in the sclerotic lesions in the right iliac bone (SUVmax 1.5) and 10th thoracic vertebra. No PSMA uptake in right submandibular gland and enlarged right neck lymph nodes. Simultaneously, patient was also undergoing work-up for enlarging right neck mass. CT scan demonstrated 1.6 x 1.2 cm mass in enlarged right submandibular gland and right neck lymphadenopathy. Biopsy suspicious for epithelial carcinoma. ***Results:*** Patient underwent right submandibular mass resection and right neck lymph nodes(LN) dissection. Pathology demonstrated high-grade SDC and metastases in all 15 resected LNs, the largest tumor deposit, 4.5 cm. Subsequent ^{18}F FDG PET/CT scan after surgery demonstrated metastatic lesions in left lobe of the liver, 10th thoracic vertebra, the sternum, left and right iliac wings (SUVmax 24.7). Rt iliac bone biopsy confirmed metastatic SDC. ***Conclusion:*** To our knowledge, this is the first study demonstrating absence of PSMA uptake in the SDC, both at the primary site and in metastases. The metastatic lesions had minimal PSMA uptake but robust FDG uptake. While reporting PET/CT scan, lack of PSMA uptake in the salivary glands should be mentioned since it can represent several entities such has atrophy from prior radiation therapy, sialolith, including primary neoplasm. Variable degrees of immunohistochemical reactivity of PSMA are observed in the salivary gland tumors but most studies demonstrated lower reactivity with SDC[1]. Further prospective studies are needed to explore PSMA positivity in different varieties of salivary gland neoplasms to explore PSMA theranostics in these neoplasms. ***References:*** 1. Nishida H, Kondo Y, Kusaba T, Kadowaki H, Daa T. Immunohistochemical Reactivity of Prostate-Specific Membrane Antigen in Salivary Gland Tumors. Head Neck Pathol. 2022 Jun;16(2):427-433.

EP-0951

A rare case of atypical lung carcinoid metastasis detected in the breast on 68Ga-DOTATATE PET/CT

B. Okudan Tekin[1], *B. Seven*[2], *A. Albayrak*[3], *A. Yıldırım*[1]; *[1]Department of Nuclear Medicine, Ankara City Hospital, University of Health Sciences, Ankara, TÜRKIYE, [2]Department of Nuclear Medicine, Sabuncuoğlu Şerefeddin Training and Research Hospital, Amasya, TÜRKIYE, [3]Department of Pathology, Ankara City Hospital, University of Health Sciences, Ankara, TÜRKIYE.*

Aim/Introduction: Lung carcinoid tumors are rare tumors that rarely metastasize. The authors report an unusual case of metastasis to the breast from an atypical lung carcinoid. ***Materials and Methods:*** 68Ga-DOTATATE PET/CT imaging was performed on a 73-year-old female patient, whose mammography scan revealed a nodule in her right breast, which was reported as a metastatic neuroendocrine tumor on histopathological examination. In the obtained sections, mild 68Ga-DOTATATE uptake in the right breast nodule and a nodular lesion with moderate 68Ga-DOTATATE uptake in the right lung middle lobe was detected. Final histopathological findings of the subsequently resected lung lesion confirmed the presence of atypical carcinoids in the setting of diffuse idiopathic pulmonary neuroendocrine cell hyperplasia. ***Results:*** This case shows an unusual metastasis to the breast from an atypical lung carcinoid detected on 68Ga-DOTATATE PET/CT. ***Conclusion:*** Concomitant diffuse idiopathic pulmonary neuroendocrine cell hyperplasia and atypical carcinoid are uncommon. Also, breast metastases are extremely rare and there are only a few cases reported in the literature. PET/CT with 68Ga-labeled somatostatin analogs stands out as a tool in the diagnostic evaluation of lung carcinoids, tumors characterized by high expression of somatostatin receptors.

EP-0952

F18-FDG PET-CT in Diagnosis and Staging of Lacrimal Gland Carcinoma: a Case Report

A. Militaru[1], *A. C. Rosu*[2], *C. V. Mazilu*[1], *M. M. Matei*[1], *S. I. Serbanescu*[1], *M. G. Alexa*[1], *A. Mitoi*[1], *A. M. Zaharia*[1], *R. M. Mititelu*[1,3]; *[1]Central Universitary Emergency Military Hospital, Bucharest, Bucuresti, ROMANIA, [2]Elias Emergency University Hospital, Bucuresti, ROMANIA, [3]University of Medicine and Pharmacy "Carol Davila" Bucharest, Bucuresti, ROMANIA.*

Aim/Introduction: Lacrimal gland tumors account for 10% of intraorbital masses, making them among the rarest tumors with an incidence of < 1/1,000,000 cases. Epithelial tumors of the lacrimal gland include a number of rare pathologies, among which adenoid cystic carcinoma (ACC), which accounts for approximately 60% of cases of lacrimal gland malignancy. Adenoid-cystic carcinoma is an aggressive tumor that usually develops in the salivary glands, although involvement of the lacrimal gland is very rare. To date, fewer than 100 cases of ACC with lacrimal gland involvement have been described in the literature. ***Materials and Methods:*** We describe the case of a 70-year-old man suffering from left exophthalmos, headache, diplopia, decreased visual acuity, limitation of the left visual field, and progressive limitation of eye movements. A biopsy of the lesion was performed, with histopathologic examination and immunohistochemical staining confirmed the presence of cystic adenoid carcinoma with a Ki67 cell proliferation index of 25%. MRI examination revealed an orbital lesion with optic neuritis likely due to compression. A PET-CT examination with 18F-FDG is performed after preparation of the patient preparation and using dedicated equipment. ***Results:*** PET-CT revealed a solid lesion in the left orbit showing increased and inhomogeneous FDG uptake. Thinning of the bony cortex in the adjacent bony structures is observed. PET-CT also showed high uptake in some laterocervical lymph nodes, bilaterally. High uptake was also noted in a lymph node corresponding to the right pulmonary hillium. No other distant hypermetabolic lesions were noted. Previous studies have shown that FDG PET-CT can detect lesions not observed with other imaging modalities in these rare cases of patients with lacrimal carcinoma, making a very important contribution to the visualisation of distant metastases and locoregional recurrences.[4] Other studies have shown greater sensitivity than an MRI exam at initial stage and bring additional information to the who-body examination. ***Conclusion:*** 18F-FDG PET-CT is important in the management of lacrimal gland tumors because it provides useful information in the initial staging and evaluation of relapse. In our case, FDG PET-CT revealed regional lymph node involvement, not previously diagnosed with conventional imaging and MRI. ***References:*** K. H. Hui et al "Value of positron emission tomography/computed tomography in diagnosis and staging of primary ocular and orbital tumors," Saudi Journal of Ophthalmology, vol. 26, no. 4, pp. 365-371, Oct. 2012, doi: 10.1016/j.sjopt.2012.08.008.

EP-0953

18F-FDG uptake in portal vein thrombosis: the upshot of IIIB-stage pulmonary adenocarcinoma and liver cirrhosis

M. Alexa[1], *S. Serbanescu*[1], *A. Mitoi*[1], *C. Mazilu*[1], *M. Matei*[1], *M. Oancea*[1], *D. Craciun*[1], *R. Mititelu*[1,2];
[1]*Central Universitary Emergency Military Hospital, Bucharest, ROMANIA,* [2]*University of Medicine and Pharmacy Carol Davila, Bucharest, ROMANIA.*

Aim/Introduction: 18F-FDG PET-CT is an essential tool in oncologic diagnosis for the assessment of liver involvement - liver metastases and, to a lesser extent, hepatocellular carcinoma. Portal vein thrombosis is a relatively frequent complication of hepatocellular carcinoma and liver cirrhosis. We present the case of a patient with pulmonary adenocarcinoma who underwent surgical treatment and adjuvant radiotherapy; the patient also had liver cirrhosis and portal vein thrombosis. 18F-FDG PET-CT examination revealed portal vein uptake suggestive of neoplastic thrombosis. No other pathologic changes suggestive of liver metastasis or hepatocellular carcinoma were noted. ***Materials and Methods:*** Our patient is a 55-year-old man, heavy smoker (35 packs per year), who was occupationally exposed to toxic substances in the respiratory tract (for 24 years), with stage IIIB lung adenocarcinoma that underwent surgery (left pneumectomy) and adjuvant radiotherapy; the patient also suffered from chronic hepatitis B infection (currently treated with entecavir), liver cirrhosis, and pulmonary tuberculosis. Initially, the CT and PET-CT showed no local tumor relapse or distant metastases. Six months later, an MRI scan was performed for the follow-up of an incidental hepatic nodule originally discovered during a routine US scan; this revealed extensive thrombosis in the portal vein and both hepatic branches, for which the patient was treated accordingly. Further ultrasonography revealed ascites in small quantity. We performed 18F-FDG PET-CT. ***Results:*** In February 2023, the PET-CT scan showed no ascites; the liver nodule showed no FDG uptake. However, the PET-CT showed dilated portal and splenic veins with hyperdense content and increased 18F-FDG uptake (SULmax up to 6,99). Portal vein thrombosis is a considerably common complication of hepatocellular carcinoma and liver cirrhosis; some previous studies have shown that portal vein thrombosis with tumoral thrombi can occur in patients with hepatocellular carcinoma. A metabolically active portal vein thrombosis detected on PET-CT examination is suggestive of a tumoral thrombus, as the enlarged caliber of the portal vein with linear uptake of F18-FDG underscores its neoplastic origin. Some previous studies have shown that the SULmax value is capable of distinguishing a benign thrombus from a malignant one with high sensitivity, specificity, and accuracy. In this case, no other active liver lesions were detected, probably due to either their small size or the low degree of differentiation in hepatocellular carcinoma. ***Conclusion:*** In short, the PET-CT exam is useful in differentiating tumoral from benign thrombi, facilitating the thorough management of an oncologic patient with multiple comorbidities.

EP-0954

Additional value of PET/MRI in diagnostic workflow of cognitive impairment

M. Pudis[1], *M. Suarez-Piñera*[1], *S. Flores-Casaperalta*[2], *N. Vidal-Sarro*[3], *L. Rodríguez-Bel*[1], *C. Martínez-Ramos*[1], *S. Bondia-Bescós*[1], *B. Hervás-Sanz*[4], *M. Cortés-Romera*[1];
[1]*Nuclear Medicine - PET (IDI), Bellvitge University Hospital, L'Hospitalet de Llobregat, Barcelona, SPAIN,* [2]*Radiodiagnostics (IDI), Hospital Duran i Reynals, L'Hospitalet de Llobregat, Barcelona, SPAIN,* [3]*Anatomical Pathology Department, Bellvitge University Hospital, L'Hospitalet de Llobregat, Barcelona, SPAIN,* [4]*Nuclear Medicine - PET (IDI), Bellvitge University Hospital, Barcelona, SPAIN.*

Aim/Introduction: Hybrid imaging techniques such as PET/CT and PET/MRI combine anatomical and functional imaging modalities to provide more comprehensive information about the disease process. The anatomical component of hybrid imaging (CT or MRI) provides detailed structural information, while the functional component (PET) provides information about metabolic and physiological processes. By combining these two imaging modalities, hybrid imaging can provide more accurate and precise information than either modality alone. ***Materials and Methods:*** A 74-year-old male, presented to his neurologist with complaints of cognitive impairment, including memory loss and difficulty with orientation. His symptoms had been gradually worsening over the past several months, and he had become increasingly concerned about his ability to function independently. Due to the rapid worsening, the neurologist has requested a brain [^{18}F]FDG PET/CT scan followed by Amyloid Brain PET/MRI. ***Results:*** An [18F]FDG PET/CT scan (Figure 1) was performed to investigate the cause of his symptoms, but it did not show any typical neurodegenerative pattern. However, it did reveal a mild hypometabolic area in the right parietal lobe, not considered clinically significant. Due to continued cognitive impairment, an amyloid PET/MRI was ordered to rule out incipient Alzheimer's disease. [^{18}F]Flutemetamol PET/MRI scan (Figure 2) revealed a focal area of decreased amyloid uptake in the right parietal lobe which corresponded to a lesion visualized on the MRI. Further MRI sequences were performed and a diagnosis of glioblastoma was suggested. Further investigation, including a biopsy of the lesion (Figure 3), confirmed the diagnosis of grade 4, IDH-mutated glioblastoma. An excision was performed to remove as much of the tumor as possible, followed by radiation therapy and chemotherapy. ***Conclusion:*** We presented a rare case of grade 4 glioblastoma (GM) with low FDG uptake. Usually, these kinds of GM are known to exhibit high FDG uptake on PET imaging due to their highly metabolically active nature. This study points out the importance of performing functional and morphological images in a single study in patients with cognitive impairment, being PET/MR the most adequate technique.

EP-0955

Pericardial mesothelioma: a case report.

B. Hervás-Sanz[1], *P. C. Notta*[1], *L. M. Gràcia-Sánchez*[1], *L. Rodríguez-Bel*[1], *S. A. Bolívar-Cuevas*[2], *D. Castellón-Plaza*[2], *I. E. Sánchez-Rodríguez*[1], *M. Pudis*[1], *M. Cortés-Romera*[1];
[1]*Nuclear Medicine-PET (IDI) Department, Bellvitge University Hospital-IDIBELL, L'Hospitalet de Llobregat, SPAIN,* [2]*Diagnostic Radiology Department, Bellvitge University Hospital-IDIBELL, L'Hospitalet de Llobregat, SPAIN.*

Aim/Introduction: Pericardium primary mesothelioma (PPM) is an extremely rare neoplasm that originates in the mesothelial cells.It is frequently limited to the pericardium, causing pericardial effusion and restrictive symptoms such as dyspnea, although it also has the capability to infiltrate adjacent structures.It is more common in males, with a mean age of 46 years.Its etiology is still unknown although it seems to be related to asbestos as is the case with pleural mesothelioma.The diagnosis of this neoplastic process is a challenge and often requires different imaging techniques. The final diagnosis is obtained by biopsy and frequently this occurs directly in post-mortem analysis.The aim of this study is to recognize the features visualized in [18F]FDG-PET/CT, in a patient diagnosed with MPP. ***Materials and Methods:*** A 48-year-old man attended the emergency department presenting chest tightness and dry cough of one month's evolution, for

which a chest X-ray was performed, showing cardiomegaly with suspected pericardial effusion, hence he was admitted for study.Several imaging tests were performed, including [18F] FDG-PET/CT, which showed a hypermetabolic mass in the anterior mediastinum surrounding the great vessels, with cardiac extension and associated with severe pericardial effusion.The patient also had hypermetabolic pulmonary nodules and lymph nodes, all suggestive of tumor dissemination. In the biopsies and subsequent anatomopathological analysis, mesenchymal cells were visualized, finally leading to the diagnosis of metastatic MPP. ***Results:*** Figure 1: A) MIP showing a large uptake in the mediastinum as well as small thoracic deposits and visualization of the bone marrow, suggesting underlying infiltration.B) Axial fusion images show the primary tumor, with cardiac extension, as well as severe pericardial effusion.C) Multiple metastatic hypermetabolic pulmonary nodules associated with small hypermetabolic nodules corresponding to suspicious adenopathy. These findings raise the differential diagnosis between lymphoproliferative process and pericardial tumor. Figure 2: Pleural fluid histological study showing abundant mesothelial cellularity as well as lymphocytes and macrophages. The immunohistochemical study ruled out an underlying lymphoproliferative process, leading to a final diagnosis of PM. ***Conclusion:*** MPP is a very infrequent process, with unfavorable prognosis. The [18F]FDG-PET/CT allows us to obtain a global vision, being able to study its metabolism and extension as well as a differential diagnosis between the different aetiological possibilities.

EP-0956

Molecular Imaging Findings in Erdheim-Chester Disease-An Extremly Rare Multisystemic Disorder

A. Marcuseanu[1], *A. Budau*[2], *D. Vasile*[1], *A. Lazar*[3], *C. Sterea*[3], *M. Gherghe*[3,4];
[1]*National Institute of Infectious Diseases "Prof. Dr. Matei Bals", Bucharest, ROMANIA,* [2]*Central Military Emergency Hospital "Dr. Carol Davila", Bucharest, ROMANIA,* [3]*Institute of Oncology "Prof. Dr. Alexandru Trestioreanu", Bucharest, ROMANIA,* [4]*"Carol Davila" University of Medicine and Pharmacy, Bucharest, ROMANIA.*

Aim/Introduction: Erdheim-Chester disease (ECD) is a very rare non-Langerhans cell histiocytosis, defined by overproduction and multisystemic accumulation of histocytes, leading to diverse manifestations. The most common involvement sites are represented by the skeleton, central nervous system, lungs, cardiovascular system, kidneys and skin. Due to its complicated and various symptomatology, this disease can be easily misdiagnosed. ***Materials and Methods:*** We report the case of a 53-year-old HIV-positive male patient with a history of progressive pericardial effusion, diagnosed with Erdheim-Chester disease in 2023. Prior to coming into our clinic, the patient had a history of severe weight loss and bilateral exophthalmia since 2021, which led to performing a computed tomography (CT) displaying large pericardial effusion and abdominal fat stranding, as well as blood tests. A CT scan was repeated one year later, describing additional bilateral orbital masses. A bone biopsy was performed and histopathological examination confirmed the diagnosis of non-Langerhans histiocytosis. The patient was recommended a "whole-body" ^{18}F-Fluorodeoxyglucose (^{18}F-FDG) PET/CT to assess the extension of the disease. ***Results:*** The ^{18}F-FDG PET/CT scan revealed bilateral hypermetabolic intraorbital masses (SUV_{max} 6.63 g/ml in the right eye and 6.78 g/ml in the left eye), circumferential pericardial thickening with increased metabolic activity (SUV_{max} 6.97 g/ml), large areas of hypermetabolic retroperitoneal and perirenal fat (SUV_{max} 4.58g/ml) infiltrating vascular, renal and muscular structures, and appendicular bones involvement (SUV_{max} of 3.15 g/ml in the left humeral diaphysis and, respectively, of 2.87 g/ml in the left proximal femoral epiphysis). The described hypermetabolic findings were consistent with the morphological components found on the previous CT scans. Complementary to the ^{18}F-FDG PET/CT scan, a ^{99m}Tc-hydroxydiphosphonate (HDP) "whole-body" bone scintigraphy was achieved, which showed increased radiotracer uptake in all long bones, including the distal femur and tibia, symmetrically and bilaterally. Treatment with Cladribine was established. A future ^{18}F-FDG PET/CT follow-up scan is scheduled in order to evaluate the therapeutic response. ***Conclusion:*** The diagnosis is usually delayed, because ECD is a rare disease with various onset presentations and multi-organ involvement. The ^{18}F-FDG PET/CT findings have an essential role in the diagnosis, especially for disease extension assessment, detecting visceral and vascular infiltrations. Furthermore, because the treatment depends on the metabolic activity of the disease, ^{18}F-FDG/PET CT is of great value for patient follow-up and treatment response.

EP-0957

Assessment of False Positive PET/CT Pulmonary Lesions in Gastric Adenocarcinoma Staging

D. Craciun[1], *C. Mazilu*[1], *A. Zaharia*[1], *A. Mitoi*[1], *R. Mititelu*[1,2];
[1]*Nuclear Medicine Department, Central Universitary Emergency Military Hospital, Bucharest, ROMANIA,* [2]*University of Medicine and Pharmacy Dr Carol Davila, Bucharest, ROMANIA.*

Aim/Introduction: 18F-Fluorodeoxyglucose (18F-FDG) PET/CT scan is a well-established method for staging in oncologic patients so that appropriate treatment can be assigned. Multiple pathologies can mimic a similar pulmonary uptake of 18F-FDG such as tuberculosis, anthracosis or parenchymal metastasis. Anthracosis occurs due to the deposition of small particles during chronic smoke exposure and is diagnosed with a biopsy in order to differentiate from tuberculosis since on a CT scan both have similar characteristics and they can occur simultaneously. ***Materials and Methods:*** A 57-year-old man with a history of tuberculosis, smoking, and occupational exposure to multiple toxic alloys presented with vomiting and severe weight loss. The diagnosis of gastric adenocarcinoma (Lauren diffuse type) was confirmed by gastric biopsy; multiple pulmonary lesions were seen on the CT scan. The patient fasted for 6 hours before the examination, and the images were acquired with a special PET /CT scanner. ***Results:*** The pulmonary fibrous scar lesions and calcifications showed no metabolic activity, but the nodules exhibited intense 18F-FDG uptake with a SULmax of up to 4.71. These lesions raised suspicion of metastasis or reactivated pulmonary tuberculosis, so accurate differentiation between these conditions is crucial because it significantly impact the treatment strategy. A CT -guided biopsy of the pulmonary nodules was performed, which revealed pulmonary anthracosis. After completion of all essential investigations, the oncologists were able to start neoadjuvant therapy for gastric adenocarcinoma with fluorouracil (5- FU), leucovorin, oxaliplatin, and docetaxel, followed by imaging follow-up, planned surgery, and hyperthermic intraperitoneal chemotherapy (HIPEC). Accurate staging of gastric adenocarcinoma was made possible by interdisciplinary collaboration between the departments of oncology, pathology, and nuclear medicine, which allowed comprehensive correlation of case information. ***Conclusion:*** This case illustrates how a false positive 18F- FDG PET /CT finding

can alter the course of treatment for an oncologic patient when similar pulmonary lesions could have multiple etiologies. It also illustrates how complementary investigations are needed to gain a more complete understanding of the case so that the patient can receive the best treatment.

EP-0958

Incidental detection of hydatid cyst on 18F-FDG PET/CT imaging

B. Okudan Tekin[1], *B. Seven*[2];
[1]*Department of Nuclear Medicine, Ankara City Hospital, University of Health Sciences, Ankara, TÜRKIYE,*
[2]*Department of Nuclear Medicine, Sabuncuoğlu Şerefeddin Training and Research Hospital, Amasya, TÜRKIYE.*

Aim/Introduction: Hydatid cyst is a parasitic infestation caused by Echinococcus granulosus. Most of its symptoms result from a mass effect associated with cyst volume. The main complications caused by cysts are cyst rupture causing cough, chest pain and hemoptysis. The authors present a case with hydatid cyst in the liver on 18F-FDG PET/CT imaging. ***Materials and Methods:*** In an 82-year-old female patient who underwent 18F-FDG PET/CT imaging to evaluate the metabolic activities of nodular lesions located in the upper lobe of the right lung, multiple hypometabolic cystic lesions were detected in the liver, the largest of which was approximately 63x61 mm in size, some of which had intense calcification. Subsequently, in the abdominal US performed on the patient, many cysts were detected that were considered to be compatible with hydatid cyst corresponding to the lesions described in PET/CT. ***Results:*** This case shows the incidentally detected hydatid cyst in the liver on 18F-FDG PET/CT imaging. ***Conclusion:*** Hepatic hydatid disease causes highly variable symptoms and signs and can be found incidentally in an asymptomatic patient. Early diagnosis and appropriate treatment will help reduce the complication rate and prevent recurrence. With the presented case, it is aimed to remind that 18F-FDG PET/CT can contribute to the diagnosis of non-malignant processes such as hydatid cyst.

EP-0959

18F-FDG PET/CT findings in a patient with systemic lupus erythematosus

B. Okudan Tekin[1], *B. Seven*[2];
[1]*Department of Nuclear Medicine, Ankara City Hospital, University of Health Sciences, Ankara, TÜRKIYE,*
[2]*Department of Nuclear Medicine, Sabuncuoğlu Şerefeddin Training and Research Hospital, Amasya, TÜRKIYE.*

Aim/Introduction: Systemic lupus erythematosus (SLE) is an immune complex disease of unknown etiology that causes excessive production of autoantibodies against components of the cell nucleus. The authors present a case of SLE with diffuse bone marrow involvement on 18F-FDG PET/CT imaging. ***Materials and Methods:*** It was determined that the nodular lesion described in the obtained sections of a 61-year-old male patient who underwent 18F-FDG PET/CT imaging to evaluate the metabolic activity of the nodular lesion located in the lower lobe of the left lung did not show significant 18F-FDG uptake. However, diffuse bone marrow involvement was observed in the axial and appendicular skeleton. ***Results:*** This case shows 18F-FDG PET/CT findings in a patient with SLE. ***Conclusion:*** In conclusion, with the presented case of known SLE, it is desired to reemphasize that 18F-FDG PET/CT is a valuable tool in the evaluation of patients with SLE, as it can visualize not only the degree of disease activity or inflammatory burden, but also the distribution of the disease throughout the body.

EP-0960

The importance of metabolic activity imaging in the evaluation of Central Nervous System Rosai-Dorfman Disease: A Case Report

M. Matei[1], *C. Mateescu*[1], *A. Rosu*[2], *C. Mazilu*[1], *R. Mititelu*[1,3];
[1]*Nuclear Medicine Department, Central Universitary Emergency Military Hospital, Bucharest, ROMANIA,* [2]*University Hospital ELIAS, Bucharest, ROMANIA,* [3]*University of Medicine and Pharmacy Dr Carol Davila, Bucharest, ROMANIA.*

Aim/Introduction: Rosai-Dorfman disease (RDD), otherwise recognized as sinus histiocytosis with massive lymphadenopathy, is a rare, benign lymphoproliferative disorder of the histiocytes that most commonly involves the lymph nodes. Extranodal disease is relatively frequent and may include skin/subcutaneous soft tissue, nasal cavity/sinus, bone, central nervous system, kidney; other infrequent sites were described in the literature. The involvement of the central nervous system is rare, manifesting more often as dural-based masses, intraparenchymal involvement being less common. ***Materials and Methods:*** We present a case of a 25-year-old woman, with a recent history of RDD affecting the spinal cord, manifested as a dural based mass, located in the right S2 nerve root. Surgery was performed and after the removal of the mass, histopathological studies and immunohistochemical staining were performed, showing S-100, CD68 positive large histiocytes with focal emperipolesis, thus confirming the diagnosis of RDD. One month later following the surgery, the MRI of the cervical and thoracic spine revealed two bone lesions, one of them located at the posterior arch of the tenth right rib, with low T1 signal intensity, isointense T2 signal and hyperintense STIR signal, without cortical bone interruption or expansive changes. The second lesion was located at the left scapula, close to the scapulohumeral joint, being small and focal, showing high STIR signal intensity. A ^{18}F-FDG-PET/CT scan was recommended for assessing the disease extension. ***Results:*** The PET/CT scan with ^{18}F-FDG revealed no metabolic activity in the bone lesions, previously described at the MRI, but showed an increased uptake compared to the physiological metabolic activity in the cervical and lower thoracic spinal cord. Incidentally, the cerebellum cortex showed a diffuse hypometabolism of ^{18}F-FDG without any other changes in the brain metabolism. The CT revealed multiple hyperdense lesions, some of which calcified, located bilaterally in the parieto-temporo-occipital cerebral cortex. These findings may indicate parenchymal involvement of the central nervous system, thus a close follow-up being recommended. ***Conclusion:*** Given the multiple systems that can be affected, this case emphasizes the value of FDG PET/CT in the evaluation of the Rosai-Dorfman disease.

EP-0961

Functional change in a patient with neurological symptoms post-exercise disclosed by rest and stress cerebral blood flow perfusion imaging (99m)Tc-ECD SPECT

R. Moreira[1], *R. Castro*[2], *D. S. Lobo*[1], *L. R. Sabioni*[1], *H. A. Guenka*[1], *I. Gottlieb*[1];
[1]*Casa De Saude Sao Jose, Rio De Janeiro, BRAZIL,*
[2]*Ipanema Health Club, Rio De Janeiro, BRAZIL.*

Aim/Introduction: 46-year-old man, healthy, with sporadic neurological symptoms post-exercise, characterized by altered state of consciousness, visual clouding, muscle hypertonia in upper limbs and muscle hypotonia in lower limbs, with spontaneous improvement of symptoms, normal cerebral angiotomography and normal magnetic resonance imaging. ***Materials and Methods:*** Single photon emission tomography (SPECT) was performed 60

minutes after the intravenous injection of 30 mCi of 99mTc-ECD in two phases (rest and stress), on differents days. Administration of the radiopharmaceutical in the stress phase occurred after the onset of symptoms, stimulated by cardiopulmonary exercise testing. ***Results:*** Rest phase showed usual distribution pattern of the radiopharmaceutical in the analyzed structures. Stress phase showed focal decrease in radiopharmaceutical concentration in the left occipital lobe and the other cortical regions of the cerebral and cerebellar hemispheres, basal ganglia and thalamus present preserved concentration of the radiopharmaceutical. ***Conclusion:*** Rest and stress cerebral blood flow perfusion imaging (99m) Tc-ECD SPECT identified symptom onset zone.

EP-0962

Radioguided occult lesion localization (ROLL) method in metastatic colorectal cancer - a case report

D. Silva*, H. Duarte, I. Sousa, J. C. Ferro, I. Próspero, D. Barbosa, S. F. Castro, G. Ferreira, J. P. Teixeira, M. J. Sousa, P. Martins, I. L. Sampaio;*
Instituto Português de Oncologia do Porto Francisco Gentil, Porto, PORTUGAL.

Aim/Introduction: Radioguided surgery (RGS) is one of the fields of Nuclear Medicine (NM) with more significant development in the last few years. It comprises a large number of procedures that are carried out through a multidisciplinary collaboration between surgeons, pathologists, and radiologists, thus, enabling short and long-term benefits to the patient, such as the reduction of iatrogenic lesions, shortening of the surgical time, and the potential improvement of local-regional control of the malignant disease. ***Materials and Methods:*** We present a case of a 58-year-old man diagnosed in 2018 with a transverse colon adenocarcinoma with hepatic metastasis and submitted to surgery. Four years later, a follow-up 18F-FDG PET/CT scan showed a suspicious nodular lesion with intense 18F-FDG uptake in the vicinity of the right internal iliac vessels. One month later, the patient was submitted to a right iliac lymphadenectomy for which histopathology revealed no metastatic involvement in the collected samples. Five months afterward, the patient was reassessed with a new 18F-FDG PET/CT scan, showing a persistent hypermetabolic lesion in the same location. It was then decided to repeat the surgery performing Radioguided Occult Lesion Localization (ROLL) and excision. Two hours before surgery the lesion was CT-guided labelled with 179.5 MBq (4.9 mCi) of ^{99m}Tc Albumine Macroagregates (MAA). A SPECT-CT was executed immediately before surgery to confirm the proper location of MAA (images were also confronted with those of the PET scan) and to rule out any extralesional spillage that would compromise the correct localization. ***Results:*** During the procedure, surgeons were quickly able to identify the metastatic deposit using the gamma probe and after resection the sample was sent to histological analysis, which later confirmed the malignant involvement. ***Conclusion:*** This case report demonstrates the importance of multidisciplinary teamwork between Surgery, Interventional Radiology and Nuclear Medicine in order to provide the most effective treatment to patients, confirming NM as an important ally to surgeons when patients present non-palpable lesions. RGS has been an ever-evolving part of NM and ROLL has been recognized as a technique that allows an efficient and reliable way to surgically remove occult lesions by making it easier to localize them and to better estimate disease extension.

EP-0963

Brown tumours: an unmet need

B. Pereira*, P. Soeiro, A. Fernandes, A. Oliveira;*
Centro Hospitalar Universitário de São João, Porto, PORTUGAL.

Aim/Introduction: End-stage renal disease with tertiary hyperparathyroidism, and thus the number of brown tumours, is increasing worldwide. Abnormal parathyroid glands may be identified with [^{99m}Tc]Tc-MIBI scan (MIBI). Brown tumours however can prove difficult to diagnose with much debate about the best imaging technique. Some studies advocate X-rays, and others advocate MRI or CT, but there is always some uncertainty with these tests. Histopathological findings are also not specific, sometimes requiring, genetic profiling. The outcome and evolution of these tumours are also unclear, with some regressing after parathyroidectomy. ***Materials and Methods:*** We present the case of a 28-year-old man with end-stage renal disease admitted to our hospital because of bilateral swelling in the oral cavity, mainly on the left side. He also reported feeling tired and having generalized bone pain for the last few months. In the biochemical tests, the main finding was a very high parathyroid hormone (> 5000 pg/mL). Ultrasonography of the neck and head, neck and chest CT revealed three nodules behind the thyroid gland, several small lytic bone lesions (extending from the skull to the sternum, vertebrae, and scapulae) as well as two larger bone lesions on the mandible, interpreted as either ossifying fibromas or brown tumours. A dual-phase and dual tracer MIBI scan with SPECT/CT was requested to localise the hyperplastic parathyroid glands. ***Results:*** The scan showed MIBI uptake in the three nodules located posteriorly to the thyroid gland and in only one of the two known mandibular tumours. A biopsy revealed that both bone lesions were compatible with brown tumours. ***Conclusion:*** This case highlights the utility of MIBI scans detecting brown tumours and their different patterns of uptake, depending on their different metabolic phase. Understanding the significance of these patterns could help determine the best non-invasive method to diagnose them. ***References:*** Vilanilam G K, Nikpanah M, Vo C D, Kearns C. Osteitis Fibrosa Cystica: Brown Tumors of Hyperparathyroidism and End-Stage Renal Disease. Radiographics, 43(5). https://doi.org/10.1148/rg.220211

EP-0964

The role of radio-guided surgery in choosing vascularized lymph nodes transfer microsurgery flap after breast cancer surgical treatment.

D. Rodriguez Oviedo*, A. Maldonado Morillo, B. Manzarbeitia Arroba, M. Alvarez Moreno, M. Tagliatori Nogueira, M. De La Rubia Marcos, C. Sandoval Moreno, C. Galindo, M. Garcia Alonso, M. Castillejos Rodriguez;*
Hospital Universitario de Getafe, Madrid, SPAIN.

Aim/Introduction: Lymphedema is a chronic disease with a high incidence that affects more than 200 million people around the world after surgical treatment for breast cancer. It has a medical treatment that is complex, long, and requires a lot of effort from the patient and that's why vascularized lymph nodes transfer (VLNT) microsurgery has become one of the best alternatives for these patients, being a key subject finding the best donor lymph nodes. A common place is the groin, that's why using radio-guided surgery we try to reduce the incidence of iatrogenic lymphedema. ***Materials and Methods:*** Case 1 A 46-year-old woman treated with mastectomy and lymphadenectomy developed lymphedema in the left arm without response to medical treatment. Using 99mTc lymphoscintigraphy technique, administrated one hour prior to

the surgery we can locate lower extremities lymph nodes using a radioactive detection probe during the procedure (Fig1). Fig 1. Using a radioactive probe (white arrow) to identify the groin lymph nodes carrying 99mTc (green arrow) surgeons can safely exclude them from the VLNT flap (blue arrow) leaving intact the leg lymphatic drain avoiding iatrogenic lymphedema. Case 2 A 52-year-old woman developed lymphedema in the right arm after breast cancer surgery treatment with lymphadenectomy. Using a radioactive probe to clear the VLNT flap of any 99mTc lymphoscintigraphy marked lymph nodes (Fig 2.) surgeons can proceed harvesting the other lymph nodes without including the legs nodes. Fig 2. Radioactive probe (white arrow) checking the VLNT flap (blue arrow) for any 99mTc lymph nodes (green arrow) belonging to the leg lymphatic drain system. ***Results:*** After eight weeks of the procedures, none of the patients had developed iatrogenic lymphedema in the donor side of the VLNT flap, making radio-guided surgery one safe option for treating lymphedema with great results in experts' hands. ***Conclusion:*** Radioguided surgery represents an excellent option for surgical treatment of lymphedema, helping to reduce the chances of generating adverse effects. It still requires more studies to make it a first-line treatment. ***References:*** Maldonado AA, Ramos E, García-Alonso P, Jover JJ, Holguín P, Fernández-Cañamaque JL, Cristóbal L. Abordaje multidisciplinar en el paciente con linfedema: de la rehabilitación a la microcirugía [Multidisciplinary approach in the lymphedema patient: From rehabilitation to microsurgery]. Rehabilitacion (Madr). 2022 Apr-Jun;56(2):150-158. Spanish. doi: 10.1016/j.rh.2021.06.003. Epub 2021 Sep 17. PMID: 34538653.

EP-0965

Incidentaloma on [18F]FDG PET-CT breast cancer staging - a rare case of Schwannoma

B. Martins*, P. Lopes, R. Veiga, C. Loewhental, J. L. Passos-Coelho;*
Hospital da Luz, Lisboa, PORTUGAL.

Aim/Introduction: We report the clinical case of a 65-year-old woman, without past medical personal history other than a non-recent surgical intervention on the left knee, who was referred to an oncology appointment after a mammogram and breast ultrasound in January 2023, which documented a 28mm nodule in the upper outer quadrant of the right breast with suspicious homolateral axillary lymph nodes (BIRADS 5). The biopsy of the nodule documented an invasive carcinoma (NOS) with positive hormone receptors (ER 100%, PR 90%), HER2 negative and a Ki-67 of 50%) with axillary lymph node involvement. An [^{18}F]FDG PET-CT was requested for staging. ***Materials and Methods:*** A whole body study was performed with 3D mode acquisition, approximately one hour after intravenous administration of the radiopharmaceutical. Low-dose CT was obtained for attenuation correction and anatomical referencing. ***Results:*** The breast lesion was observed in the external quadrants of the right breast (31x11mm in the axial planes with SUVmax 3.58), as well as homolateral axillary adenopathies, the largest measuring 18x12mm with SUVmax 3.6. No other suspicious lymph nodes were seen. A previously unknown tumor was seen in the right iliac fossa, between the psoas and iliac muscles, with 54x49x60mm (ApxTxL) and SUVmax 7.6 On further questioning the patient referred a shooting-type pain in the right leg for the previous three years, which had been worsening. A biopsy of the iliac lesion documented a peripheral nerve neoplasm, compatible with Schwannoma. ***Conclusion:*** The patient underwent surgical treatment. A lumpectomy of the right breast, right axillary lymphadenectomy and, in the same operative time, removal of the iliac fossa tumor, were performed. Histology of the latter confirmed the diagnosis of Schwannoma. Although benign, Schwannomas usually present high SUV values. This feature, especially in some territories, can lead to false positives [1]. Schwannomas result from abnormal proliferation of Schwann cells, are usually single lesions, mostlyindolent. They involve more commonly the brachial and lombar plexus, origin of the limb nerves. [1]. Since it is not possible to distinguish a Schwannoma from a malignant lesion on [^{18}F]FDG PET-CT, biopsy is mandatory before treatment, to avoid misdiagnosis [1]. ***References:*** [1] Boré P et al. (2018). False positive 18F-FDG Positron Emission Tomography Findings in Schwannoma - A caution for reporting Physicians. Front. Med. 5:275

EP-0966

Hepatic Artery Vasculitis: A rare presentation of single-organ vasculitis documented by 2-[18F]FDG PET/CT

R. T. Ferreira*, I. C. Ferreira, F. Vinagre, S. Carmona, A. Prata, A. I. Santos;*
Hospital Garcia de Orta, E. P. E., Almada, PORTUGAL.

Aim/Introduction: Vasculitis are a group of diseases characterized by inflammation and damage to blood vessels, often with systemic involvement. Single-organ vasculitis (SOV) is a rare condition that affects blood vessels in a specific organ. Gastrointestinal SOV, with exclusive involvement of the hepatic artery, is particularly rare, to the best of our knowledge with only 5 cases described in the literature and none of them submitted to Nuclear Medicine techniques. We present a case of vasculitis that exclusively involves the hepatic artery, documented by 2-[^{18}F]FDG PET/CT. ***Materials and Methods:*** A 53-year-old man, without prior medical history, presented to the emergency department with recurring epigastric pain, vomiting, non-selective anorexia and constipation for the last 5 days. There was no fever, weight loss, joint pain, or other systemic symptoms reported. ***Results:*** Physical examination revealed only elevated blood pressure. Laboratory tests showed a slightly elevated C-reactive protein level, normal levels of haemoglobin, white blood cells, liver enzymes and amylase, and negative ANA, ENA, ANCA, anti-dsDNA and cryoglobulins. Abdominal X-ray was normal. CT scan showed an unspecific adipose tissue oedema surrounding the celiac trunk. CT angiography revealed narrowing of the common hepatic artery lumen, due to thickening of the vessel, possibly indicative of vasculitis. A 2-[^{18}F]FDG PET/CT scan was performed to evaluate other vascular regions and showed intense diffuse hypermetabolism along the common hepatic artery, with no changes in other vascular territories. Blood cultures, viral and bacterial serologies were also conducted, and no changes were detected, ruling out infectious causes. Based on the most likely diagnosis of single-organ vasculitis, corticosteroid therapy was initiated and the patient was discharged. On 3 months follow-up, C-reactive protein values normalized and there was a complete regression of the clinical symptoms. ***Conclusion:*** Vasculitis diagnosis is often challenging and when we face a specific rare subtype as SOV, which affects a specific organ or tissue such as the skin, gastrointestinal tract, or genitourinary system, this challenge rises significantly due to its isolated nature. 2-[^{18}F]FDG PET/CT, as an all-body non-invasive exam, can be valuable to assess the extent of involvement, as shown in this case. Although corticosteroid therapy has a favourable prognosis for SOV, long-term follow-up is recommended due to the possibility of progression to systemic disease and, as shown in other types of vasculitis, 2-[^{18}F]FDG PET/CT might also have a potential role to monitor therapy and to evaluate the future progression of this disease.

EP-0967

18F-FDG PET/CT findings in a patient with renal angiomyolipoma

B. Okudan Tekin[1], *A. S. Erdoğan*[1], *B. Seven*[2];
[1]*Department of Nuclear Medicine, Ankara City Hospital, University of Health Sciences, Ankara, TÜRKIYE,*
[2]*Department of Nuclear Medicine, Sabuncuoğlu Şerefeddin Training and Research Hospital, Amasya, TÜRKIYE.*

Aim/Introduction: Renal angiomyolipoma (AML) is a common benign tumor of the kidney. It may occur sporadically, as well as with tuberous sclerosis complex (TSC) or pulmonary lymphangiomyomatosis. Although renal AMLs are benign formations, they can sometimes undergo malignant transformation. It undergoes malignant transformations similar to renal cell carcinoma, especially as a result of various mutations of atypical epithelioid cells. Renal AMLs are usually silent on 18F-FDG PET/CT. However, it may be useful in detecting malignant transformations or malignant masses containing fat. ***Materials and Methods:*** A 22-year-old female patient, who was followed up with tuberous sclerosis and epilepsy, had multiple masses in both kidneys in the tomography taken due to flank pain, and in the abdominal MRI performed both a few suppressed in fat-suppressed sequences and a few AMLs thought to be poor in fat component were consistent with nodular and mass lesions were observed. Minimally increased 18F-FDG uptake, which can be distinguished from physiological urinary activity, in multiple heterogeneous nodular lesions in both kidneys, 40x34 mm in size, the largest in the left kidney upper pole, in 18F-FDG PET/CT imaging performed because the patient was diagnosed with tuberous sclerosis (SUVmax: 2.67) has drawn attention. Trucut biopsy of the left kidney upper pole lesion was consistent with renal AML. ***Results:*** This presentation demonstrates the 18F-FDG PET/CT findings in a patient with renal AML. ***Conclusion:*** Renal AMLs are benign formations with low FDG affinity. When a tumoral tissue containing a fat component is detected on CT, it is important to distinguish AML from a malignant tumor with a fat component. It should be kept in mind that the low FDG affinity of AML in PET/CT can be found in the differential diagnosis of malignant kidney masses containing the fat component.

EP-0968

Rare complication in the cholangiocarcinoma treatment - biliary bronchial fistula - localized with cholescintigraphy with SPECT/CT

P. Gadzicki, *M. Nowak, A. Dyla, Z. Adamczewski;*
Medical University of Lodz, Lodz, POLAND.

Aim/Introduction: Biliary bronchial fistula is a rare condition characterized by abnormal communication between the biliary tract and the bronchial trees. This case demonstrates the usefulness of cholescintigraphy with SPECT/CT in the localization of biliary bronchial fistula. ***Materials and Methods:*** Previously intensively treated 61 year-old woman with cholangiocarcionoma developed symptoms such as cough, bilioptysis and weakness. The patient was treated oncologically for over four years; the therapeutic process consisted of radiotherapy, chemotherapy, left-sided hemihepatectomy extended to the resection of the segment V and VIII with lymphadenectomy of the hepatoduodenal ligament and cholecystectomy as well as multiple bile ducts stent implementation. Three months before the cholescintigraphy, a biliary-bronchial fistula was diagnosed and excised. Due to persistent symptoms such as expectoration of sputum with bile and progressive weakness, a number of diagnostic tests were performed and the patient was admitted to hospital to check the effects of the treatment. ***Results:*** The persistent biliary bronchial fistula was visualized with the use of cholescintigraphy with SPECT/CT. ***Conclusion:*** The persistent biliary bronchial fistula was visualized with the use of cholescintigraphy with SPECT/CT.

EP-0969

SPECT/CT Diagnosis of single adrenal metastasis of differentiated thyroid cancer

K. Bayardo, *J. Naula, O. Alonso, R. Ferrando;*
University of the Repubic, Montevideo, URUGUAY.

Aim/Introduction: Differentiated thyroid carcinoma (DTC) is the main endocrine neoplasia, and its incidence has increased in recent decades. Distant CDT metastases are not common, but when they are present, 5-year survival drops to 54.9% compared to 98.3% for regional metastases and 99.9% for localized disease. Most common sites are lymph nodes, lungs, and bone. Rare sites include brain, liver, kidneys, adrenal glands, skin, and muscles. They represent less than 1% of the total, making diagnosis difficult. We present a case of a single metastasis of CDT in the adrenal gland diagnosed by SPECT/CT. ***Materials and Methods:*** 64-year-old female patient diagnosed with a 48 mm follicular thyroid carcinoma in the left lobe with vascular invasion. After total thyroidectomy, she was administered 150 mCi of radioactive iodine (RAI). Post operative RAI scanning showed concentration in bilateral thyroid remnants, without abnormal uptake in the rest of the body. RAI scanning performed 1 year later was negative. During next years, Tg values increased and remained in a range of 45-50 ng/ml under hormonal suppression. Twelve years after diagnosis Tg values reached 500 ng/ml without hormonal suppression and RAI scanning detected an area of intense uptake in the lower mediastinum or epigastrium lateralized to the right, which could not be accurately localized on planar images. ***Results:*** Non-contrast CT reported a right adrenal adenoma. Four months later, a new RAI scan with SPECT/CT showed intense uptake in the right adrenal gland, correlated with a nodular lesion on CT images, consistent with adrenal metastasis. Right adrenalectomy was performed with posterior histopathology confirmation and decrease in Tg values. ***Conclusion:*** CDT metastases in rare locations such as adrenal glands are exceptional events that can imply a great diagnostic challenge. SPECT/CT images can be a fundamental tool for the accurate diagnosis and correct management of this type of lesions.

EP-0970

Role of [18F]FDG PET/CT in the detection and differential diagnosis of peritoneal tuberculosis

S. Bondia-Bescós[1], *V. Carrero-Vasquez*[1], *I. Sánchez-Rodriguez*[1], *A. Palomar-Muñoz*[1], *L. Gràcia-Sánchez*[1], *M. Pudis*[1], *B. Hervás-Sanz*[1], *J. Díaz-Moreno*[1], *M. Santin-Cerezales*[2], *X. Solanich-Moreno*[1], *M. Cortés-Romera*[1];
[1]*Nuclear Medicine-PET (IDI) Department, Bellvitge University Hospital, Barcelona, SPAIN,* [2]*Infeccious Diseases Department, Bellvitge University Hospital, Barcelona, SPAIN.*

Aim/Introduction: Peritoneal carcinomatosis (PC) is a relatively common extension for tumors, particularly from abdomen and pelvis origin, however, there are other conditions that may involve the peritoneum like tuberculous peritonitis (TBP), which are often complicated to differentiate since there are clinical and analytical manifestations that can overlap. Various differential characteristics have been described for each of these entities. The mechanisms by which the peritoneum can be involved in TBP are mostly through hematogenous dissemination, by direct propagation or

through the lymphatic route. On the other hand, most frequent routes for dissemination in PC are by direct pelvic invasion and via transceoelomic. Making this affectation clear with imaging tests is crucial in their differentiation.The aim of this study is to evaluate the role of PET/CT in the detection and differential diagnosis of PTB in patients whose initial suspicion was occult neoplasia with PC. ***Materials and Methods:*** Retrospective study of a 3 case series with presence of peritoneal disease showed on [^{18}F] FDG PET/CT, and clinical suspicion of occult neoplasia in which the definitive diagnosis was PTB.Selection of 3 cases with [^{18}F]FDG PET/CT and confirmed peritoneal carcinomatosis from different primary neoplasms (ovary, endometrium, gallbladder).Analysis of the morphometabolic characteristics, pattern of the peritoneal involvement and presence of extraperitoneal involvement from these two entities. ***Results:*** In PTB patients (2 women, mean age 42.67 years) the form of presentation was similar in the three cases, highlighting en extensive and uniform parietal peritoneal involvement with slight associated glucose activity, mild uniform hypermetabolic thickening of the greater omentum, and ascites without FDG avidity. Active extraperitoneal involvement was detected in all patients, without clinical suspicion.Among PC patients (2 women, mean age 76.33 years), the involvement distribution was heterogeneous, but the pattern had common findings including focal thickening and major nodularity of the implants. ***Conclusion:*** In our case series the involvement observed in PET/CT had a fundamental role in the diagnosis of TBP, evaluating its extension and detecting other foci of active infection not visualized in conventional imaging techniques.The recognition of these morphometabolic patterns is very useful since it allows guiding the clinical diagnosis and assessing the extension, facilitates biopsy guidance, and reduces treatment initiation time. ***References:*** Ahmed Khan FY. Peritoneal tuberculosis: Advances and controversies. Libyan J Med Sci 2018;2:3-7 Wang SB, He H, Xv DD, et al. Visual PET/CT scoring of mesenteric fdg uptake to differentiate between tuberculous peritonitis and peritoneal carcinomatosis. Diagn Interv Radiol. 2020;26(6):523-530.

EP-0971

Dual-tracer PET/CT imaging to determine tumor heterogeneity in a patient with liver metastatic neuroendocrine neoplasm: A case report.

R. Moreira, *I. Gottlieb, D. S. Lobo, H. A. Guenka;*
Casa De Saude Sao Jose, Rio De Janeiro, BRAZIL.

Aim/Introduction: We present a case of a patient with neuroendocrine neoplasm with biologic heterogeneity between a primary tumor and hepatic metastases.The diagnosis was obtained and multidisciplinary management was conducted with magnetic resonance imaging (MRI) and a positron emission tomography/computed tomography (PET/CT) scan with Fluor-18 [18F]-AlF-NOTA-octreotide ([18F]-OC) and Fluor-18 [18F]-fluorodeoxyglucose ([18F]-FDG). ***Materials and Methods:*** An MRI showed a primary lesion in the terminal ileum with adjacente lymphadenopathy and six suspicious hepatic lesions. A biopsy of the largest hepatic lesion revealed neuroendocrine carcinoma and then PET/CT was performed. A PET/CT scan revealed a difference between [18F]-OC and [18F]-FDG uptake in primary tumor and liver metastases. PET/CT showed lack [18F]-FDG uptake and high [18F]-OC uptake in the primary tumor and adjacente lymphadenopathy, whereas no [18F]-FDG uptake and lack [18F]-OC uptake were identified in the hepatic metastases. ***Results:*** PET/CT imaging with two tracers demonstrated a biologic heterogeneity between a primary tumor and metastases. By providing a noninvasive means of evaluating tumor biology, dual tracer PET/CT offered a practical alternative to multiple biopsies, facilitating clinical decision-making and improving patiente outcomes. ***Conclusion:*** Tumor heterogeneity is a known predictor of aggressive disease and dual tracer PET/CT is a noninvasive imaging technique that enables the evaluation of tumor biological status and impacts patient management strategies.

EP-0972

18 FDG PET/CT imaging in anaplastic thyroid carcinoma : a case report

F. Chaltout, *K. Ben Ahmed, M. Ouachem, T. Bint Mohamed, M. Maaloul, S. Charfeddine, K. Chtourou, F. Guermazi;*
Department of Nuclear Medicine, Habib Bourguiba University Hospital of Sfax, Tunisia, Sfax, TUNISIA.

Aim/Introduction: Anaplastic thyroid carcinoma (ATC) is an aggressive form of thyroid cancer characterized by uncontrolled growth of cells in the thyroid gland. It shows a rapid growth and local invasion. This form of cancer carries the worst prognosis among all thyroid cancers due to its relenless progression and resistance to cancer treatments. ***Materials and Methods:*** We present a case of 65 year old patient having anaplastic thyroid carcinoma not yet treated. As part of the initial evaluation, a whole body scan was done, which showed a huge thyroid mass with signs of skin invasion reaching the cervical spine . this mass engages the primary carotid artery and compresses the internal jugular vein which remains permeable. The scan showed also some bilateral jugulocarotid nodes and a hepatic nodule which can be an atypical angioma or a metastasis. Consequentely, FDG PET/CT was requested to disocver the metabolic behavior of these lesions. ***Results:*** 18 FDG PET / CT showed an intense hypermetabolic cervical mass (SUVLbm max =28.38) centrered by an hypometabolic necrosis, associated to bilatreal hypermetabolic jugulocarotid and left supraclavicular lymph nodes . There was no evidence of metabolically active lesion elsewhere in the body. Therfore, this tumor was classified IVB . ***Conclusion:*** Anaplastic thyroid carcinoma (ATC) accounts for 1% - 2% of all thyroid malignancies .It's ahighly agressive and results in over 50% of deaths from thyroid cancer with a median estimated survival of 6-8 months. Its managing is challenging and includes rapid diagnosis, adequate staging and multimodal treatments. FDG PET/CT has been useful at many steps in the therapeutic care process. In fact, it's recommended in the primary staging in order to evaluate the lesion resectability and to unveil unkown metastasis. Add to that, it has an important role in the follow up of ATC after primary surgery for detection of residual, recurrent, or metastatic disease. In a series reported by Poisson et al, it was also found that SUVmax and metabolic tumor volume had a prognostic significance . they suggested that SUVmax >18 and a 18F-FDG uptake volume >300 mL had a significantly worse 6 month survival.

EP-0973

Sacrococcygeal metastasis revealing a papillary carcinoma of the thyroid . A Case report

M. Bourouba;
Nuclear Medicine Clinique Fatema Al Azhar, Algiers, ALGERIA.

Aim/Introduction: A 24-year-old girl who underwent neurosurgery with an invasive osteolytic tumor lesion (108x94x66 mm), located at the level of the sacrum , suggestive of a schwanoma, which led to severe pain with right sciatalgy without motor deficit or sphincter disorders. CT examination shows an extension to the

sacroiliac joints and a lysis of the right iliac bone, extending to the posterior L5 process in contact with the L5 roots, infiltrating the pre-vertebral muscles, and reaching anterior to the contact of the internal iliac artery ***Materials and Methods:*** Partial exeresis performed by posterior route was performed. The pathological study revealed a metastasis of papillary carcinoma of the thyroid in its vesicular form. (Immunohistochimestery : Anti CK7, Anti TTF1 and Anti Tg positive) .The exploration of the thyroid gland shows a cystic lesion of 13 mm diameter lying in the left lobe. A total thyroidectomy was performed, as well as a bilateral dissection of the lymph nodes, revealing a lack of malignancy of the samplings.For the purpose of therapeutic complement the patient is addressed to us for iratherapy. Bone scintigraphy shows an intense uptake (sacrum and coccyx) without evidence of other localizations.The thyroglobulin level is greater than 5000ug/l without replacement therapy since the intervention, greater than one month.The patient receives 6,30 GBq of Iodine 131 capsule (CAPSION CURIUM), ***Results:*** The post-therapeutic scan confirms the uptake of the pelvic focus which appears intense and of large volume.The level of thyroglobulin remains high 3 months after the first iratherapy (> 5000 ug / l) The patient is followed for a second course of iratherapy and surgery are planned, after noting the reduction of the tumor volume ***Conclusion:*** The presence of such a location is quite rare. Its fortuitous discovery, evokes most of the time a neurological problem (schwanome) or tumoral type teratoma of the ovary with bone extension. Moreover, the analysis of the thyroidectomy specimen can evoke a papillary microcarcinoma of the thyroid. Indeed, a replay of the blades could be desirable.

EP-0974

Gastric Empty and Esophagus Transit Scintigraphy Imaging of Long Term Tip 1 Diabetic Patient accidentally consuming Formic Acid

D. Yüksel*, U. Moran, M. Yücel, S. Demirezen, A. Çelik;*
Pamukkale Universitesi Tip Fakültesi, Denizli, TÜRKIYE.

Aim/Introduction: Gastroparesis can result from autonomic (vagal) neuropathy, intrinsic neuropathy affecting xcitatory and inhibitory intrinsic nerves or interstitial cells of Cajal, or a combination of extrinsic and intrinsic neuropathic or myopathic disorders(1). In some cases, GES is ordered in patients with known GERD to determine whether some component of gastric stasis may contribute to GERD. Gastric distention may induce GER by triggering lower esphageal sphincter (LES) relaxation (2). In this case report, we present a type 1 Diabetus Mellitus patient and a case who drank formic acid because there are two pathologies that can cause esophageal and stomach motility disorders together. ***Materials and Methods:*** Solid and liquid gastric emptying scintigraphy(4) and esophageal passage scintigraphy(5) were performed according to the consensus report and guidelines. ***Results:*** The patient had type 1 diabetus mellitus for 30 years and drank half a glass of 50% formic acid 3 years ago and vomited. He has hypoglycemia and hyperglycemia attacks because dysphagia and insulin blood sugar regulation could not be achieved. Although the patient has epigastric pain, he does not have any complaints of burning in the throat or retrosternal. On the esophagus scintigraphy, when the esophagus transit time is normal in examinations with liquid, the passage speed of the esophagus lower 1/3 segment slowed. In our examinations made for gastric empty, it was found to be delayed as 964 minutes for liquid. For the solid, it was extended to 422 minutes. ***Conclusion:*** In this patient with type 1 diabetes and a history of drinking formic acid, a delay in esophageal passage and a significant prolongation in gastric emptying were detected. ***References:*** 1.Triadafilopoulos G, Nguyen L, Clarke JO. Patients with symptoms of delayed gastric emptying have a high prevalence of oesophageal dysmotility, irrespective of scintigraphic evidence of gastroparesis. BMJ Open Gastroenterology 2017;4:e000169. doi: 10.1136/bmjgast-2017-000169 2.Holloway R, Hongo M, Berger K, et al: Gastric distention: A mechanism for post-prandial gastroesophageal reflux. Gastroenterology 1985;89:779-784 3.Donohoe KJ, Maurer AH, Ziessman HA, Urbain JL, Royal HD, Momin J; Society for Nuclear Medicine; American Neurogastroenterology and Motility Society. Procedure guideline for adult solid-meal gastric-emptying study 3.0. J Nucl Med Technol 2009;36:196-200. 4.Maurer AH. Gastrointestinal Motility, Part 1: Esophageal Transit and Gastric Emptying. J Nucl Med 2015;56:1229-1238

EP-0975

FDG PET/CT imaging in intra-abdominal round cell desmoplastic tumors: a case report

N. Abaouz*, A. Guensi;*
Department of Nuclear Medicine, University Hospital Ibn Rochd, Casablanca, MOROCCO.

Aim/Introduction: Desmoplastic small round cell tumor, according to the International Classification of Diseases for Oncology (2020), is classified as malignant tumor of uncertain differentiation. This tumor usually develops in the abdominal cavity. It is a very uncommon soft tissue tumor in children and young adults. It has an aggressive evolution and its survival is usually poor. In general, the assessment of tumor burden and response is based on CT or MRI. However, these tumors are often metabolically active and can be assessed by FDG PET/CT. In this case, we present the potential usefulness of PET/CT in the evaluation of distant metastases at the time of staging. ***Materials and Methods:*** The patient was 15 years old and was diagnosed with a histologically confirmed intra-abdominal round cell desmoplastic tumor. The patient was admitted to the department of nuclear medicine, CHU IBN ROCHD Casablanca, for a PET/CT scan prior to induction chemotherapy for staging. ***Results:*** Diagnostic abdominal and pelvic CT showed peritoneal masses, the largest one was at the pelvic level (19x13mm) and associated with a right pelvic cystic formation and secondary hepatic and splenic lesions suggesting peritoneal carcinosis.The FDG PET/CT scan revealed, in addition to abundant ascites associated with intensely hypermetabolic thickening of the peritoneal sheets, hypermetabolic liver lesions as well as a hypodense pelvic mass without a metabolism and a hypometabolic splenic lesion. On the same examination, supra-diaphragmatic adenopathies uptake (cervical, mediastinal, and axillary) were identified as secondary lymph node extensions. At the bone level, the uptake was heterogeneous with hypermetabolic foci (C2, right humeral head) suspected of secondary extension. ***Conclusion:*** Although FDG PET/CT is rarely indicated in intra-abdominal round cell desmoplastic tumors, it has its place as an initial extensional examination to determine distant extensions for appropriate treatment.

EP-0976

Interest of FDG PET/CT Compared to Bone Scan in the Detection of Lytic Bone Metastasis in Breast Cancer

N. Abaouz*, A. Guensi;*
Department Of Nuclear Medicine, University Hospital Ibn Rochd, Casablanca, MOROCCO.

Aim/Introduction: Breast cancer is one of the most osteophilic cancers and bone is the most frequent distant location in this pathology. In fact, PET-CT can be used to identify lymph node invasion and distant metastasis in a single examination. In addition, PET-CT is more sensitive and specific than CT or bone

scans in the detection of lytic or mixed bone metastasis, or osteomedullary invasion. Our purpose, in this case, is to compare the accuracy of PET/CT with bone scintigraphy for the detection of lytic bone metastasis in a patient followed for breast cancer. ***Materials and Methods:*** The patient was 55 years old and was followed up for a lobular carcinoma of the right breast classified as Luminal B associated with homolateral lymph node extension. She was admitted to the nuclear medicine department of the CHU IBN ROCHD of Casablanca for the initial assessment of extension, firstly for a bone scan, and then for FDG PET/CT. ***Results:*** The planar bone scan performed showed 3 hours after injection of 17 mCi of 99mTc-labelled HMDP a homogeneous and symmetrical distribution of the radiotracer over the entire skeleton explored without any clearly identifiable hyperfixing lesion. On the other hand, FDG PET/CT showed 60 minutes after injection of 250 MBq 18FDG, in addition to the hypermetabolic right breast process and homolateral axillary adenopathies, a hypermetabolic lytic bone lesion of the left sacroiliac, which is consistent with a single bone metastasis. ***Conclusion:*** This case illustrates the superiority of FDG PET/CT over planar bone scans in the detection of lytic bone metastasis in breast cancer.

EP-0977

Unexpected 131I iodine scintigraphy finding

A. Aulich*, B. Stefański, Z. Adamczewski;*
Nuclear Medicine Department, Medical University of Lodz, Lodz, POLAND.

Aim/Introduction: Radioactive iodine 131I is the oldest radiopharmaceutical used in the theranostics concept. It allows the application of the same vector in diagnostics as well as therapy of both benign and malignant thyroid conditions. Radioiodine (RAI) scintigraphy is an invaluable tool for assessment of thyroid diseases including the detection of thyroid cancer metastases. Although extrathyroidal foci of abnormal 131I uptake are highly suggestive of disseminated thyroid cancer, other infrequent causes should be taken into consideration. Warthin's tumor (cystadenoma lymphomatosum) may be one of them, possibly on account of unsatisfactory excretory mechanism in comparison with physiological function of salivary glands and sodium/iodide symporter (NIS) expression in the tumor. ***Materials and Methods:*** An 81-year old woman with toxic nodular goiter was referred for 131I iodine scintigraphy in order to measure thyroid iodine uptake before planned radioiodine treatment. The radiotracer was given orally in a standard protocol, using 4 MBq sodium iodide 131I. The value of thyroid uptake was 22%, which was measured 24h after administration. ***Results:*** Radioiodine scan revealed unexpected accumulation of the radiotracer in the right parotid gland, significantly exceeding physiological level of salivary glands' uptake. The patient had no history of thyroid malignancy. Upon further inquiry she admitted having been diagnosed with Warthin's tumor, confirmed previously by fine needle aspiration biopsy. Surgical treatment was excluded due to significant comorbidities. Radioiodine uptake within the tumor was 4%. Ultrasound scan of the right parotid salivary gland showed an ovoid, hypoechoic, heterogeneous lesion, which measured 26x36x45mm. The image of a solid lesion can be observed in multiple conditions, including Warthin's tumor, although it is not specific. In addition, 99mTc-pertechnetate salivary gland scintigraphy was performed and showed an increased uptake of the radiotracer within the tumor, which is typical for Warthin's tumor. ***Conclusion:*** Although extrathyroidal foci of abnormal 131I uptake are highly suggestive of disseminated thyroid cancer, other infrequent causes should be taken into consideration. Warthin's tumor may be one of them due to NIS overexpression.

EP-0978

Incidental finding of pulmonary tumour in lung ventilation and perfusion SPECT: the importanceof a combined low-dose CT scan

J. Carvalho*, J. R. Duarte, A. Marques, F. Abreu, S. Pintão;*
Centro Hospitalar de Lisboa Ocidental, Carnaxide, PORTUGAL.

Aim/Introduction: Lung imaging with SPECT is commonly indicated in patients with suspected pulmonary embolism. The introduction of integrated multimodality SPECT/CT cameras has enabled the simultaneous acquisition of lung ventilation and perfusion SPECT (V/P_{SPECT}) with a combined low-dose CT scan, which confers slightly improved specificity for pulmonary embolism, as it may be helpful in identifying nonthromboembolic parenchymal abnormalities. ***Materials and Methods:*** We report a case of a 64-year-old woman with suspected pulmonary embolism with findings suggestive of infarction on chest radiography. The patient underwent lung ventilation and perfusion SPECT in order to quantify the infarcted lung area. ***Results:*** $V/P_{SPECT/CT}$ demonstrated a matched V/P defect in the lower lobe of the left lung, with an associated peripheral opacification in the low-dose CT scan. Due to the suspicion of malignancy, a high resolution CT scan of the thorax was promptly performed, which showed a peripheral spiculated nodule not present in previous exams, highly suggestive of a primary malignant lesion. PET/CT scan with 2-[^{18}F]FDG confirmed the presence of a metabolically active lesion in the left lower lobe. A transthoracic biopsy was performed in order to histologically characterize the nodule. ***Conclusion:*** The added value of a low-dose CT scan in lung scintigraphy has been validated in patients with COPD, but not in other subgroups of patients. Despite the additional radiation dose, it can be useful in patients with suspected pulmonary embolism with other concomitant parenchymal abnormalities, not only by increasing diagnostic accuracy, but also by detecting incidental findings that require urgent care, such as pulmonary neoplasms.

EP-0979

An adrenal nodule with very high 18F-FDG uptake

S. Fontão de Castro*, J. Ferro, I. Próspero, D. Barbosa, D. Silva, L. Violante, G. Ferreira, I. Lucena e Sampaio;*
Portuguese Institute of Oncology - Porto, Porto, PORTUGAL.

Aim/Introduction: Benign adrenal adenoma with high metabolic uptake is rare. We present a case of a 40-year-old-women, succinate dehydrogenase subunit B (SDHB) mutation carrier, with a previous adrenalectomy due to a paraganglioma, presented with a fast growing adrenal node. Computed tomography (CT) and magnetic resonance imaging (MRI) scans were suggestive of benign adenoma, however, 2-[^{18}F]FDG positron emission tomography / computed tomography (PET/CT) showed a very high metabolic uptake (SUVmax 15.5; tumor-to-liver (T/L) SUVmax ratio: 4.9). The adrenal node was resected and pathology revealed a benign adenoma. ***Materials and Methods:*** A forty-year-old woman, asymptomatic, SDHB mutation carrier, with history of a previously treated metanephrine-producer paravertebral paraganglioma (left adrenalectomy and radiotherapy), presented with new node in the right adrenal gland. The patient underwent a CT scan that showed a growing low density lesion (10*15mm to 25*19mm in 20months; Hounsfield Units <10). MRI demonstrated a homogeneous signal drop on opposed-phase images, suggesting a fat lipid-rich adenoma. Notwithstanding, it was a fast growing lesion in a patient with history of paraganglioma, and further investigation was conducted. In order to exclude a new pheochromacytoma, the patient underwent [^{68}Ga] Ga-DOTANOC-PET/CT however the adrenal node did not show

significantly increased somatostatin receptor expression. Patient also underwent a 2-[^{18}F]FDG-PET/CT scan, demonstrating a very high uptake in the adrenal node: SUVmax 15.5 and T/L SUVmax ratio: 4.9. Fine needle biopsy aspiration was inconclusive. The case was discussed in a multidisciplinary group meeting and based on the continuous growth, very high 2-[^{18}F]FDG uptake and patient preference, it was decided to performed a right adrenalectomy. ***Results:*** Histology revealed an encapsulated lesion compatible with an adenoma (Weiss score: 0). 2-[^{18}F]FDG PET/CT has been pointed as a tool to distinguish adrenal adenomas from malignant lesions. Among the several papers, it is concordant that tumor-to-liver ratio is a more accurate and reliable parameter than SUVmax to predict malignancy. Kunikowsska analyzed 102 nonsecreting adrenal tumor and concluded that T/L SUVmax ratio of 3.7 has a 95% sensibility (CI 85-96%) and a 90% specificity (CI 84-96). In another study a best diagnosis accuracy cut-off point was 2.5 T/L SUVmax ratio. About 5% of adrenal adenomas have a 2-[^{18}F]FDG uptake greater than the liver, and the reason for this is unknown. ***Conclusion:*** To best of our knowledge, a benign adrenal adenoma with such high uptake and T/L SUVmax ratio has never been described and it is important to have in mind this possible pitfall.

EP-0980

Detection of a right ventricle cardiac metastasis from lung adenocarcinoma in a 18F-FDG PET/CT study

S. Pacella[1], *M. Mangano*[2], *L. Venegoni*[3], *M. Cergnul*[3], *A. Calcagno*[3], *R. Ferrara*[4], *C. Migliorisi*[3], *M. Carletto*[3], *L. Maffioli*[5]; [1]*IRCCS Fondazione Cà Granda Ospedale Maggiore Policlinico, Milano, ITALY,* [2]*ASST Valle Olona, Saronno, ITALY,* [3]*ASST Ovest Milanese-Ospedale Civile di Legnano, Legnano, ITALY,* [4]*ASST Ovest Milanese-Ospedale di Magenta, Magenta, ITALY,* [5]*ASST Sette Laghi, Varese, ITALY.*

Aim/Introduction: Primary cardiac tumours are extremely uncommon, while secondary tumours or cardiac metastasis are not. The incidence of cardiac metastasis is of 1.5%- 20% of autopsies of cancer patients. Primary lung cancer represents about one third of cardiac metastasis followed by breast cancer and haematologic malignancies. $^{18\,F-}$fluorodeoxyglucose positron emission tomography/computed tomography ($^{18\,F-}$FDG PET/CT) is a very important imaging tool in oncology for tumor staging, restaging, detection of recurrence and monitoring treatment response. Due to the high physiological FDG uptake in the myocardium , it's very challenging the detection of a suspected focal cardiac uptake. ***Materials and Methods:*** $^{18F-}$FDG PET/CT for the detection of a right heart metastasis in a patient with a non small-cell lung cancer. ***Results:*** A 78-year-old male underwent $^{18F-}$FDG PET/CT for staging his lung tumor. Whole-body $^{18F-}$FDG PET/CT demonstrated an increased uptake in the lung mass located in the upper left lobe and showed intense uptake in an enlarged lymph node in the aortopulmonary window. Another intense focal uptake was in the right ventricle. A contrast-enhanced MRI performed after our FDG PET/CT study showed late Gadolinium enhancement in the antero-basal wall of the right ventricle, suspected for a secondary localization ***Conclusion:*** $^{18F-}$FDG PET/CT was an important tool in the diagnostic setting of a patient with a lung adenocarcinoma for the detection of metastatic sites, like the cardiac involvement, that is a rare phenomenon. ***References:*** 1) Jiang JY, Lee M, Kang C, Wong VCK, Mansberg R. Atypical metastatic lung cancer of the right ventricle on FDG PET/CT. Radiol Case Rep. 2021 Sep 16;16(11):3569-3573. doi: 10.1016/j.radcr.2021.07.092. PMID: 34567334; PMCID: PMC8449183. 2) Orcurto MV, Delaloye AB, Letovanec I, Martins Favre M, Prior JO. Detection of an asymptomatic right-ventricle cardiac metastasis from a small-cell lung cancer by F-18-FDG PET/CT. J Thorac Oncol. 2009 Jan;4(1):127-30. doi: 10.1097/JTO.0b013e318189f60e. PMID: 19096320.3)Tagliabue L, Manfrinato G, Luciani A. An Unusual Case of Myocardial Localization of Non-Small Cell Lung Cancer Metastasis: A Case Report and Review of Literature. Indian J Nucl Med. 2017 Jul-Sep;32(3):208-210. doi: 10.4103/ijnm.IJNM_153_16. PMID: 28680205; PMCID: PMC5482017.

EP-0981

Expect the unexpected- a rare case of incidentally detected recurrent bone invasive giant meningioma on F-18 FDG PET/CT, in a patient with stomach neoplasm

S. Chausheva, *B. Chaushev, T. Stoeva, M. Dyankova, T. Yordanova, Z. Dancheva;*
University Hospital St Marina Varna, Varna, BULGARIA.

Aim/Introduction: Meningioma is a primary neoplasm of the central nervous system. Up to 3% of people over 60 are thought to be at risk for asymptomatic meningioma. However, even after perfect resection, there is between 9% and 32% risk or recurrency in the 15 years post-surgery. Still, the extent of bone involvement, caifications and the giant size of the reccurent meningioma reported in this paper are of much lower incidence. ***Materials and Methods:*** A 53-year-old male patient was diagnosed with gastric carcinoma and underwent subtotal gastrectomy. He presented at the Department of Nuclear medicine for a scheduled staging F-18 FDG PET/CT and did not report any symptoms regarding his nervous system. According to the clinical history the patient had a meningioma 24 years earlier which was completely removed. Whole-body PET/CT was performed using i.v. F-18 FDG at a dose of 3.5 mCi, where the images were obtained 65 minutes after injection. ***Results:*** The scan showed a large calcified mass with the characteristics of a meningioma, parasagittally, in the left parieto-occipital region. The mass was extra-axial, with lobulated sharp margins and large dimensions - 56/57/64mm. It had low 18F-FDG uptake, probably because of the massive calcifications or the histological type of the tumor. The structure of the mass was inhomogeneous due to predominantly calcium-dense components with a density of around 800HU. There were also several oval, relatively low-dense areas with soft-tissue density. The finding was located mainly along the left surface of the cerebral falx with a small contralateral component at its most parietal point with bone invasion of the parietal bone in the left. Dorsally, the mass expands into the inner cortical layer of the parietal bone as well as partially into the outer cortical layer. There was evident mass-effect with contralateral shift of the ventricular system, approximately 7mm from the mid-line. Ventral dislocation of the posterior horn of the left lateral ventricle was noticed, but no evidence of ventricular dilatation. ***Conclusion:*** Unexpected findings, often without increased uptake, are not infrequently encountered in PET/CT imaging. However, the dimensions and complicity of the meningioma described here are quite rare. Although this is a "can't miss finding" it comes to remind us that underneath any oncological condition there could be additional lesions which are sufficient enough to prompt a systematic review of the CT images obtained during the PET/CT study. Check your CT imiges twice, print your report once!

EP-0982

99mTc-antigranulocite antibody scintigraphy in mycosis fungoides

A. Velidaki, *S. Episkopopoulou, I. Sevaslidou, N. Prosotsianiotis, E. Dagrakis, A. Kolindou;*
Laiko General Hospital of Athens, Athens, GREECE.

Aim/Introduction: Mycosis fungoides (MF) is a non-Hodgkin's lymphoma of T-cell origin, primarily involving the skin. ^{99m}Tc anti-granulocyte monoclonal antibody is used by Nuclear Medicine Physicians mainly for the detection of bone infection but it has also the ability to reveal infection in soft tissues and internal organs. In our study, we present a case of highlighting multiple foci throughout the skin during whole-body ^{99m}Tc anti-granulocyte monoclonal antibody scintigraphy in a woman with MF. ***Materials and Methods:*** A 34-year-old woman was hospitalized due to fever. She had a history of MF with patches and plaques all over her skin. Her blood culture was positive for MRSA. She presented to our Nuclear Medicine Department for investigation of suspected osteomyelitis after surgical debridement of a tibial ulcer. She underwent a ^{99m}Tc anti-granulocyte monoclonal antibody scintigraphy. ***Results:*** The study ruled out any discrete focus of infection in tibia or other bones and internal organs, but it revealed multiple skin foci throughout the body. Skin radiopharmaceutical uptake seen on scintigraphy, seemed to correspond to the patient's skin lesions. ***Conclusion:*** Skin manifestations of mycosis fungoides are patches, plaques and tumors. The diagnosis of MF can be difficult. Obtaining adequate tissue for biopsy can often be a problem. Literature shows FDG PET-CT may be inferior to clinical examination in mapping the extent of cutaneous lesions, especially when there are macules or thin plaques, but it offers the advantage of characterizing the metabolic activity in the lesions and guide for biopsies. F-18 FDG uptake in disease-involved lesions due to co-existing inflammation is something that limits its specificity. When skin lesions ulcerate, they accumulate inflammation cells and they can be imaged by labeled WBCs scintigraphy. This is the first-to our knowledge- case of MF imaging with 99mTc anti-granulocyte antibody. The demonstration of multiple uptake foci of the radiopharmaceutical, probably implies the presence of another uptake mechanism beyond the presence of inflammation. ^{99m}Tc anti-granulocyte monoclonal antibody scintigraphy may be an easy and effective way to assess the extent, activity and severity of the disease and may also contribute to disease monitoring.

EP-0983

Incidental increased Ga-68 FAPI Uptake in Calcified Meningioma

A. Namazova, *A. Kibar, L. U. Beşli, O. E. Sahin, K. Sönmezoğlu;*
Istanbul University-Cerrahpasa, Cerrahpaşa Faculty of Medicine, Department of Nuclear Medicine, ISTANBUL, TÜRKIYE.

Aim/Introduction: Meningioma is the most common type of primary brain tumor, accounting for approximately 30 percent of all brain tumors. Most meningiomas are benign, slow-growing lesions. They are typically found incidentally. The aim of our study is to present 68Ga -fibroblast activation protein inhibitor (FAPI) PET/CT findings of primary meningioma in a 74-year-old woman. ***Materials and Methods:*** After the patients were injected with 37MBq (0.1 mci)/kg intravenous of 68Ga FAPI, PET/CT images were taken of the vertex-upper thigh were taken at the 45th minute. ***Results:*** We would like to present a 74-year-old patient with ovarian cancer who underwent 18F-FDG PET/CT and FAPI PET/CT. A high 68Ga-FAPI (SUV MAX, 5,5) uptake was observed in the calcified lesion in the anterior of the falx cerebri. According to the location and radiological and clinical characteristics, the diagnosis of meningioma was defined. ***Conclusion:*** Many studies suggested that meningioma can cause increased uptake of various radiotracers, including 18F-FDG, 68Ga-DOTATATE, 68Ga-PSMA, 18F-FLT, 18F-florapronol and 68Ga FAPI. 68Ga-labeled FAPI has recently been introduced as a promising tumor imaging agent, which has shown promising results in the diagnosis of cancer and inflammatory diseases. In this case, we show a case with calcified benign meningioma which showed increased FAPI activity, which may be mistaken for metastasis in oncological imaging.

EP-0984

Bilateral Warthin tumour with coexisting metastatic lung cancer: a rare case demonstrated by 2-[18F]FDG-PET/CT

I. C. Ferreira, *R. T. Ferreira, I. Oliveira, A. I. Santos;*
Hospital Garcia de Orta, E.P.E, Almada, PORTUGAL.

Aim/Introduction: Warthin tumour (WT) is the second most common benign salivary gland tumour, typically originating in the parotid and affecting males aged 50-70. It grows slowly and has low malignant potential. Bilateral and multifocal lesions are uncommon. Lung cancer (LC) frequently metastasizes to other organs. Several benign aetiologies can cause false positive results on PET/CT with 2-[18F]FDG (FDG-PET/CT). Avidity of WT for 2-[^{18}F]FDG is variable, but high uptake has been described. Studies show smokers have an increased risk of developing both WT and LC. While coexistence of LC and WT is rare, it is of diagnostic importance because multifocal WT may mimic metastasis. Our aim was to review the role FDG-PET/CT had in managing such an infrequent case. ***Materials and Methods:*** A 69 year-old man with a history of arterial hypertension, dyslipidemia, heavy smoking and bilateral Warthin tumours (awaiting surgery in another hospital), presented to our institution with sudden onset of dysarthria, dysphagia, involuntary movements of the neck and right amaurosis, resolving after 30 minutes. He also reported weight loss and hemoptoic sputum in the previous week. Neurological exam was normal except for right central facial paresis. Cranio-encephalic (CE), cervical and thoracic CT angiography scans showed a lesion in the left frontal region and a suspicious nodule in the right lung. The patient was admitted for investigation and started therapy with Tacosamide and corticosteroids for suspected focal epileptic seizure due to CE metastasis. ***Results:*** CE RM scan confirmed two brain lesions in the left frontal, temporal and parietal lobes. FDG-PET/CT showed intense radiotracer uptake in a bulky lesion of the upper lobe of the right lung, in a small cerebral lesion and in several large nodules in both parotid glands. Transthoracic needle aspiration biopsy revealed extensively necrotic squamous cell carcinoma. Stereotactic radiosurgery was performed on the brain lesions. Lung surgery was proposed, but the subject was readmitted a month after discharge due to recurrence of neurological symptoms and died two days later from complications of acute infarction of the right middle cerebellar peduncle. ***Conclusion:*** Our case highlights the importance of including WT in the differential diagnosis of salivary gland lesions and recognizing them as potential causes of false-positive findings in FDG-PET/CT studies used for tumour staging. Although rarely reported, coexistence of bilateral WT and lung cancer is noteworthy due to their shared association with smoking as a risk factor.

EP-0985

Brown tumors mimicking bone metastasis in a woman with a Parathyroid carcinoma. A Case report.

A. Genova[1], *F. Porcaro*[1], *I. Annarumma*[1], *M. Prisco*[1], *L. Turchetta*[1], *A. Biasiucci*[2], *M. Catalano*[1];
[1]*Nuclear Medicine Unit, AORN A. Cardarelli, Naples, NAPLES, ITALY,*
[2]*Histopathology Unit, AORN A. Cardarelli, Naples, NAPLES, ITALY.*

Aim/Introduction: Brown tumors are rare skeletal manifestation of hyperparathyroidism. Persistence of high levels of Parathyroid hormon (PTH) causes increase osteoclasts activity with bone demineralization and microhemorrages creating an excess of cortical bone resorption that produces cysts. Parathyroid Carcinoma (PC) is a very rare cause of multiple brown tumors, in about <1% of hyperparathyroidism cases, its clinical, radiological and Nuclear Medicine findings can create a challenging differential diagnosis. ***Materials and Methods:*** A 47-year old female was admitted for a severe anemia (Haemoglobin 4gr/dl), Hypercalcemia(12.6 mg/dl) and severe bone pelvis pain. Patient had no history of cancer. Chest and abdomen computed tomography (CT) revealed multiple osteolytic lesions on the ribs, scapula and the major on pelvis (6x3 cm), with no findings suggestive of a primary tumor. Tc-99m methylene diphosphonate (MDP) bone scintigraphy confirmed the osteolytic lesions showing multiple foci of reducted MDP uptake, whereas the other bone districts presented a global increased pathological uptake. Consequently, extended blood tests and tumor Markers were investigated. Alphafetoprotein (AFP), CEA, CA19-9, CA125 and Bence-Jones protein levels were normal, however Calcium and PTH are severely increased (14.4mg/dl , 1936.7pg/ml, respectively). ***Results:*** Neck ultrasonography showed a 3.5cm solide nodule in right lobe region; parathyroid scan after injection of technetium 99m-methoxyisobutylisonitrile (MIBI) revealed a large area of increased uptake in corrispondence of right lobe nodule, in both early and delayed phases. Meanwhile patient underwent bone biopsy of the pelvis to reach a definitive diagnosis, that showed a framework of giant osteoclast cells with reactive modifications of the bone tissue, in accordance with Brown tumor diagnosis. Resultantly parathyroid tumor was suspected and inferior right parathyroid gland was surgical resected. Pathological examination, with immunohistochemistry analysis that showed positivity for Pancytokeratin, Chromogranin, GATA3 and negativity for TTF1, Synaptophysin. Over-expressed cyclin D1, Proliferation index 5%. The prevailing reports (infiltration of the fibrous capsule, size, presence of some mitoses) oriented for a low-grade PC. After 5 days from surgery, Sierum Calcium levels dropped from 13.5 mg/dl to 11 mg/dl and PTH levels dropped from 1870 mg/dl to 700 mg/dl. ***Conclusion:*** Osteolytic lesions are common in advanced stages of malignant neoplams. However, it is important not to neglect the hypothesis that they may be signs of brown tumors. In differential diagnosis it should be considered that brown tumors, although rare, may have radiological and nuclear medicine aspects similar to metastatic lesions. An accurate global clinical evaluation should be performed in these complex scenarios.

EP-0986

An atypical aspect of bone scintigraphy in AL Amyloidosis

M. Bel lakhdar, *H. Guerrouj, J. Rahali, I. Ghfir, N. Ben Raïs;*
University mohamed V, Faculty of Medicine and Pharmacy, RABAT, MOROCCO.

Aim/Introduction: Bone scintigraphy is actually a tool with a diagnostic and prognostic good value in amyloid transthyretin cardiac amyloidosis. Cardiac uptake is the most frequently studied extraosseous uptake in this disease.We present a rare pattern of altered bone tracer accumulation, which is consistent with AL amyloidosis in a myeloma patient. ***Materials and Methods:*** The patient was a 36-year-old female with a history of bilateral carpal tunnel syndrome who was admitted to the internal medicine department with symptoms of dyspnea, lower limb edema, macroglossia, and polyarthralgia. Echocardiography and CMR imaging indicated a high suspicion of cardiac amyloidosis. Planar bone scintigraphy was performed two hours after the injection of 740MBq of 99mTc- HMDP. ***Results:*** Bone scintigraphy revealed increased uptake around the joints and in the oro-cervical region without skeletal uptake. Serum protein electrophoresis showed hyper alpha 1 and hyper alpha 2 globulin, and the immunofixation demonstrated a band of light chains type Lambda with L/K ratio of 264. The diagnosis of AL amyloidosis was confirmed by a minor salivary gland biopsy. 30% of clonal plasma cells found on myelogram and the presence of related organ or tissue impairment (CRAB) were consistent with the diagnosis of myeloma. ***Conclusion:*** Our case report presents rare findings of altered bone tracer accumulation, indicative of amyloidosis associated with multiple myeloma. The report sheds light on the underlying mechanisms that may cause the altered tracer distribution in such cases. The findings may have significant implications for the diagnosis and treatment of patients with this condition.

EP-0987

Uncommon presentation of an aggressive tumor- FDG PET/CT clinching the diagnosis.

S. Sagar, *D. Khan, N. A. Damle, M. Tripathi, M. Bhatt, Y. Gupta, N. Tandon;*
AIIMS, Delhi, INDIA.

Aim/Introduction: SIADH is a common paraneoplastic syndrome that occurs in patients with lung cancer, particularly SCLC (1). It is characterized by excessive release of antidiuretic hormone (ADH) from the pituitary gland or other ectopic sources, leading to hyponatremia and low serum osmolality (2).PET/CT is a valuable diagnostic tool for the detection of SCLC and other malignancies, with a reported sensitivity and specificity of 90-95% and 80-85%, respectively (3). In our case, PET/CT not only confirmed the presence of a lung mass but also showed hypermetabolic activity, which is suggestive of a malignant process. The patient presented to endocrinologist despite having widespread metastases and a large lung mass, the patient neither presented with chest symptoms nor with pain at metastatic site. ***Materials and Methods:*** the scan was acquired on dedicated PET/CT scanners (Biograph mCT, Siemens Inc and Discovery PET/CT, GE). ***Results:*** We report the case of a 62-year-old female patient who presented with a 6-month history of fatigue, weight loss, and hyponatremia. The patient's medical history was significant for hypertension and hyperlipidemia. Upon admission, laboratory tests showed a serum sodium level of 124 mmol/L and a serum osmolality of 252 mOsm/kg. Her urine osmolality was elevated at 440 mOsm/kg, and her urine sodium was 85 mmol/L. The patient was diagnosed with the syndrome of inappropriate antidiuretic hormone secretion (SIADH) and was referred for FDG PET/CT. PET/CT scan confirmed the presence of a lung mass with hypermetabolic activity in the left pulmonary region with metastases to multiple skeletal sites. Biopsy of the lung mass revealed small-cell lung carcinoma (SCLC).The patient was started on fluid restriction, and her serum sodium levels gradually improved to 135 mmol/L. However, due to the aggressive nature of SCLC, the patient was started on chemotherapy with cisplatin and etoposide. ***Conclusion:*** This case highlights that PET/CT is a useful tool for the detection of SCLC and can also provide valuable

information regarding the metabolic activity of the tumor. FDG PET/CT can help in diagnosis, staging and excluding alternate diagnosis. ***References:*** 1.Grimaldi C, Pasqualetti P, Tognetti F, et al. Small cell lung cancer and hyponatremia: a retrospective study. Intern Emerg Med. 2011;6(6):503-508. 2.Ellison DH, Berl T. Clinical practice. The syndrome of inappropriate antidiuresis. N Engl J Med. 2007;356(20):2064-2072. 3.Lardinois D, Weder W, Hany TF, et al. Staging of non-small-cell lung cancer with integrated positron-emission tomography and computed tomography. N Engl J Med. 2003;348(25):2500-2507.

EP-0988

Basal Cell Carcinoma Transformation to Squamous Cell Carcinoma Following Systemic Treatment: Impressive PET/CT Images and Clinical Implications.

M. Pudis[1], *P. C. Notta*[1], *B. Hervás-Sanz*[1], *J. R. Ferreras-Riera*[2], *M. Cortés-Romera*[1];
[1]*Nuclear Medicine - PET (IDI), Bellvitge University Hospital, L'Hospitalet de Llobregat, Barcelona, SPAIN,*
[2]*Department of Dermatology, Bellvitge University Hospital, L'Hospitalet de Llobregat, Barcelona, SPAIN.*

Aim/Introduction: Basal cell carcinoma (BCC) is the most common type of skin cancer, usually characterized by slow growth and local invasion. However, in some rare cases, BCC may undergo transformation into a more aggressive form of skin cancer, such as squamous cell carcinoma (SCC), which is associated with a higher risk of metastasis and mortality. ***Materials and Methods:*** We present a case of a 66-year-old woman with a more than 20-year-old ulcerative lesion in the right hemiabdomen (Figure 1) that was diagnosed as an infiltrating basal cell carcinoma. An [^{18}F] FDG PET/CT (Figure 2) staging scan revealed cutaneous, muscular, and bone involvement with destruction of the right iliac crest (Figure 3). The patient received two lines of systemic treatment with disease progression, as confirmed by follow-up PET/CT scans revealing lung and bone metastasis. Due to the patient's poor condition and disease progression, a new biopsy was performed, which revealed transformation to squamous cell carcinoma. ***Results:*** Due to the patient's general condition, frailty, and tumor-related bleeding and infection, she was not eligible for clinical trials. Furthermore, radiation therapy was ruled out due to the extensive and deep involvement of the lesion, affecting even the subcutaneous fat. The patient is currently under palliative care follow-up. ***Conclusion:*** This case highlights the importance of early diagnosis and prompt intervention in preventing disease progression and improving patient outcomes. In addition, PET/CT imaging can provide valuable information on disease extent and response to treatment, as evidenced by the impressive images obtained in this case. However, the limited treatment options for advanced cases underscore the need for better understanding of the pathogenesis of BCC transformation to SCC and the development of more effective therapies.

EP-0989

Case report: Soft Tissue Metastasis in Lung Cancer - The impact of 2-[18F]FDG PET/CT

R. T. Ferreira, *I. C. Ferreira, I. Oliveira, D. Canário, S. Carmona, J. G. Santos, J. A. Sequeira, A. I. Santos;*
Hospital Garcia de Orta, E. P. E., Almada, PORTUGAL.

Aim/Introduction: Lung cancer is the second most common cancer worldwide, with a high incidence of distant metastasis. Soft tissue metastases (STM) are rare, particularly when compared to cancer spread sites, such as the brain, bones, liver, and adrenal glands. We present two lung cancer cases, in which a correct M1 staging diagnosis was possible due to 2-[^{18}F]FDG PET/CT (FDG-PET/CT) visualization of a single STM - in one case detected in the initial staging and in the other after thoracic disease progression. ***Materials and Methods:*** Case 1 was a 54-year-old male smoker (60 pack/year), with history of nephrectomy for renal cell carcinoma and co-infection with HIV/HCV. The patient was asymptomatic and was referred for assessment of a solitary lung nodule detected during a chest CT. Subsequent staging using FDG-PET/CT revealed not only a mild increase in metabolic activity in the nodule located in the left upper lobe of the lung and in a homolateral hilar lymph node, but also an intense focal uptake in a suspicious lesion located in the right thigh. Case 2 was a 62-year-old female smoker (1,5 packs/year) who had previously been diagnosed with lung adenocarcinoma staged T1b N0 M0. The patient underwent left upper lobectomy and mediastinal lymph node dissection and was subsequently put under surveillance. Approximately six months later, thoracic disease progression was detected on chest CT, revealing a large lesion invading soft tissue and ribs within the chest wall. The subsequent restaging using FDG-PET/CT revealed increased metabolic activity within the thoracic lesion, and identified a new suspicious lesion located in subcutaneous soft tissue in the right thigh. ***Results:*** Biopsy of the lesions identified through FDG-PET/CT confirmed the suspicion of STM from lung adenocarcinoma, confirming ineligibility for surgery and thus, modifying the therapeutic approach in both cases. ***Conclusion:*** Approximately 50% of lung cancer cases are metastatic at the time of diagnosis and most patients do progress from the initial stage to a more advanced disease. Distant metastases to soft tissue, defined as metastases to skeletal muscle, skin and subcutaneous tissues, are rarely reported in the literature. Early detection of STMs is challenging due to their nonspecific clinical and radiological manifestations. FDG-PET/CT is a non-invasive whole-body imaging modality that, as shown in these cases, very efficiently identifies previously unknown metastatic sites, including STMs, thereby making it an essential tool for both initial staging and subsequent monitoring of patients, allowing prompt treatment and possible better prognosis.

EP-0990

Evaluation of metabolic response with18F-FDG PET-CT in advanced thymic adenocarcinoma

H. Noamen, *K. Ben Ahmed, W. Amouri, T. Mohamed, I. Jardak, M. Maaloul, S. Charfeddine, K. Chtourou, F. Guermazi;*
University hospital of Habib Bourguiba, Sfax, TUNISIA.

Aim/Introduction: Thymic adenocarcinomas of the mediastinum are extremely rare and aggressive tumors. Patients with advanced or recurrent thymic carcinomas often need several consecutive lines of chemotherapy and radiotherapy. The aim of this case report is to show the utility of ^{18}F-FDG PET/CT in assessing the metabolic response in a recurrent advanced thymic adenocarcinoma. ***Materials and Methods:*** A 45-year-old male patient was diagnosed three years ago with poorly differentiated thymic adenocarcinoma initially unresectable with lymphatic mediastinal and hilar invasion on both CT scan and ^{18}F-FDG PET/CT. The patient was treated with neoadjuvant chemotherapy and radiotherapy. CT findings showed one year after treatment progressive cervical, mediastinal, and abdominal lymphatic disease with lymphangitic pulmonary lesions therefore second-line chemotherapy was indicated. After treatment, the disease was considered stable on morphological response criteria. ^{18}F-FDG PET/CT was requested to assess metabolic response and to better plan radiotherapy of the residual lesions. ***Results:*** ^{18}F-FDG PET/CT showed high metabolic activity in multiple cervical, mediastinal, and abdominal lymph nodes, high FDG uptake in pulmonary nodules, and unilateral adrenal gland. These findings were suggestive of recurrent advanced disease. Salvage-intensive chemotherapy

Conclusion: Thymic adenocarcinomas are rarely reported and have usually a poor prognosis. As a promising metabolic imaging method in terms of patient management, ^{18}F-FDG PET/CT makes important contributions to a therapeutical evaluation in routine clinical practice of thymic carcinomas. Further studies need to be done in order to assess the role of ^{18}F-FDG PET/CT in thymic epithelial tumors. ***References:*** Kaira K, Murakami H, Miura S, Kaira R, Akamatsu H, Kimura M and al. 18F-FDG uptake on PET helps predict outcome and response after treatment inunresectable thymic epithelial tumors. Ann Nucl Med. 2011;25:247-53.

EP-0991

DLBCL mimicking infection on FDG PET/CT - resolving the conundrum

D. Khan*, N. A. Damle, M. Tripathi, B. Pridhivi, P. Sethi, N. Wig, S. Sagar, A. Narayan;*
AIIMS Delhi, Delhi, INDIA.

Aim/Introduction: Diffuse large B cell lymphoma (DLBCL) is most common type of non-Hodgkin's lymphoma. It primarily presents as generalized lymphadenopathy. Bone involvement in DLBCL is relatively rare, while osteonecrosis is rarer. Here we present a clinically challenging case of DLBCL with unusual presentation. ***Materials and Methods:*** A 46-year-old male presented to medicine OPD with low back ache and bilateral thigh & leg pain since 5 months, progressively worsening in severity. Physical examination, blood tests, ultrasonography, bone marrow biopsy, muscle biopsy, and two FDG PET/CT were performed to investigate cause of symptoms. Finally, guided bone biopsy of left hip performed based on intensely avid lesion as noted in FDG PET/CT and it revealed diagnosis. ***Results:*** Lab investigation of patient revealed pancytopenia and raised inflammatory markers. Also MRI of patient revealed red marrow re conversion changes in visualised vertebrae. Subsequently patient underwent bone marrow biopsy which showed necrotic/infarcted marrow. Bone marrow culture revealed pseudomonas aeruginosa. As cytopenias improved, patient was discharged and advised to continue antibiotics for 2 weeks . However one month later patient was readmitted with aggravated symptoms and physical examination showing splenomegaly and tenderness in lower back region. Repeat MRI revealed multiple vertebral lesions, left psoas collection and multiple muscular hyperintensities. As the muscle biopsy was inconclusive and psoas collection appeared sterile, to solve diagnostic dilemma FDG PET/CT was performed .It showed diffuse marrow uptake with few focal marrow lesions along with increased tracer avid lytic lesions in the bilateral pelvic bones with hypodensities in few lower limb muscles and significant splenomegaly. CT guided biopsy from left iliacus and left iliac bone revealed extensive coagulative necrosis. Patient was treated as a case of infection related myonecrosis, myositis and sacroiliitis and was started on analgesics with significant improvement of symptoms. Repeat FDG PET/CT was advised to look for resolution of symptoms after one month. It demonstrated progression with extensive marrow lesions and few lytic lesions predominantly in bilateral pelvic along with subcentimetric lymph nodes and persistent splenomegaly. We advised biopsy from intensely FDG avid lesion marrow lesion in left anterior superior iliac spine which was ultimately revealed as case of DLBCL. ***Conclusion:*** This clinically challenging case sheds light on unusual presentation of DLBCL, which is typically characterized by generalized lymphadenopathy. Bone involvement in DLBCL is rare. This case highlights importance of considering lymphoma as a potential diagnosis in patients with unexplained back pain and bone lesions.

EP-0992

Osteoblastoma like osteosarcoma - diagnostic challenge - a case report

N. Manevska*[1], T. Makazlieva[1], S. Kostadinova Kunovska[2], S. Stojanoski[1], A. Gavrilovski[3];*
[1]Institute of Pathophysiology and Nuclear medicine, Medical Faculty, University of Ss Cyril and Methodius, Skopje, NORTH MACEDONIA, [2]Institute of Pathology, Medical Faculty, University of Ss Cyril and Methodius, Skopje, NORTH MACEDONIA, [3]University Clinic for Orthopedic Surgery, Medical Faculty, University of Ss Cyril and Methodius, Skopje, NORTH MACEDONIA.

Aim/Introduction: Osteoblastoma like osteosarcoma is a rare variety of osteosarcoma (1.1%). Although literature presents these tumors as low-grade malignant tumors, the World Health Organization (WHO) Classification classifies these tumors in the group of conventional (high-grade) osteosarcomas. Differential diagnosis between these kind of tumors from aggressive osteoblastoma as well as osteosarcoma is quite challenging and controversial. ***Materials and Methods:*** 20 year-old girl complained of a pain and limited movement in the right shoulder over a year. The pain was especially strong in the evening, there is tingling and shaking in the hand. ***Results:*** Rtg showed on the proximal metaphysis of the neck of the right humerus, an oval lytic defect medially with a sclerotic rim about 15 mm long. On the CT scan in the proximal meta-epiphysis of the right humerus, localized posteriorly, a lytic change was observed affecting the cortex of the bone with cortical swelling and thinning, expansively related to the environment and measuring 19 x 21 mm on axial scans, 24 mm on coronal scans. A discrete, slightly irregular periosteal reaction was observed. Perilesional soft tissue edema was present. Differential diagnosis included osteoblastoma, chondromyxoid fibroma, and an aggressive aneurysmal bone cyst. MRI presented a tumor mass relatively with a homogeneous signal, with a weak hypersignal in relation to the muscles in T1, and with a hypersignal in T2. Significantly larger part of this tumor mass as an exophytic soft tissue component is outside the bone and around it there is a collection of liquid. Differential diagnosis were paraosteal ostesarcoma or chondroblastoma. Bone scan (99mTc-MDP) was also performed with findings of a high vascularity in the pool phase and intensive pathologic accumulation of the tracer in the meta-diaphysis of the right humerus (tumor mass) on the WBS and the SPECT/CT. She was admitted at the Clinic of Orthopedics and after surgical operation the histopathology revealed osteoblastoma like osteosarcoma. ***Conclusion:*** The right diagnosis is of importance in the treatment protocol of patients with a diagnosis of osteoblastoma like osteosarcoma. Wide surgical margins have to be achieved to prevent future recurrence.

EP-0993

Contribution of whole-body bone scan coupled with SPECT/CT in the diagnosis of SAPHO syndrome: case report.

j. Charfi*, S. Marwa, O. Ben Hamida, C. Mhiri, I. Slim, A. Mhiri;*
salah azaiez institute, tunis, TUNISIA.

Aim/Introduction: SAPHO syndrome (acronym for Synovitis, Acne, Pustulosis, Hyperostosis and Osteitis) is characterized by neutrophilic skin involvement associated with chronic osteomyelitis. It is an autoimmune disease that most often affects young people without sparing older patients. Tc99m bone scintigraphy is very valuable for diagnosis insofar as the fixation of the isotope may precede the clinical and even radiological manifestations, especially since a link between SAPHO and spondylarthropathies has been established. The aim of our report is to present a case of SAPHO syndrome associated with a vertebral expectation discovered by bone scan. ***Materials and Methods:*** We report the case of a 57-year-old patient admitted

to the orthopedic department for chronic anterior thoracic bone pain. ***Results:*** Clinical ecamination revealed a slight deformation of the right sternoclavicular joint. Biological tests showed an inflammatory syndrome.A standard chest X-ray showed a hypertrophic and condensing aspect of the right sternoclavicular junction. A whole-body scan coupled with SPECT/CT showed at the early stage a moderate hypercaptation of the right sternoclavicular joint and the pubic symphisis. At the late stage, the examination showed intense and diffuse hyperfixation of the right sternoclavicular joint and the manubrium-sternal body junction. Moderate fixation of the left hemi-body of L5 was found associated with condensation and erosion of the vertebral body and hyperfixation of the pubic symphysis with condensation of the left pubis. The whole-body bone scan coupled with SPECT/CT has confirmed the diagnosis of SAPHO in the sternoclavicular junction and has showed also a subclinical localization in the 5th lumbar vertebra. ***Conclusion:*** SAPHO syndrome remains a non-disabling condition and its treatment is essentially symptomatic. Early diagnosis is associated with a better prognosis. This confirms the value of bone scintigraphy which is sensitive even before the onset of clinical manifestations.

EP-0994

Place of peritoneal scintigraphy in the diagnosis of pleuro-peritoneal communication: A case report.

K. Ayed, *H. Charfi, M. Nouira, R. Sfar, K. Chatti;*
Nuclear Medicine Department, Sahloul Hospital, Sousse, TUNISIA.

Aim/Introduction: Pleuro-peritoneal communication is a rare complication of peritoneal dialysis, affecting 1.6 to 2% of patients. Its diagnosis is suspected in the presence of suggestive clinical symptoms, and currently, there is no consensus on complementary tests that should be performed to confirm it. Through this case report, we emphasize the role of peritoneal scintigraphy using 99mTc-labeled nanocolloids in the diagnostic approach of this complication. ***Materials and Methods:*** We report the case of a 56-year-old patient with a history of chronic kidney failure at the stage of peritoneal dialysis, who presented to the nephrology consultation with recent-onset dyspnea and progressive worsening. Chest X-ray showed a moderate amount of right pleural effusion. Pleural fluid analysis revealed a transudative fluid, low in LDH and high in glucose, suggesting a passage of peritoneal dialysis fluid into the pleural cavity. Based on these findings, the diagnosis of pleuro-peritoneal leak was considered to be the most probable. ***Results:*** A peritoneal scintigraphy was performed for diagnostic and localizing purposes. Immediate dynamic images and SPECT/CT were obtained, showing a positive examination: passage of the radiotracer injected into the dialysate bag (5mCi of 99mTc-labeled nanocolloid) to a moderate amount of right pleural effusion, with the maximum uptake seen in the right posterior-inferior part of the diaphragm. ***Conclusion:*** Peritoneal scintigraphy is a very effective imaging technique in the diagnostic approach of pleuro-peritoneal communications as a sensitive, low-irradiating, and non-invasive imaging modality that can be used for diagnostic and localizing purposes.

EP-0995

Is Captopril renography with 99mTc-DTPA still of merit in renovascular hypertension? a case report

R. Belayouni, *O. Ben Hamida, M. Ben Nasr, M. Somai, I. Slim, i. meddeb, I. Yeddes, A. Mhiri;*
Salah Azaiez Institute, Tunis, TUNISIA.

Aim/Introduction: We present a case of unilateral renovascular hypertension (RVH) confirmed by Captopril renography (CRS) with 99mTc-DTPA. ***Materials and Methods:*** A 5-year-old child, with no particular medical history was admitted to a pediatric ward for confirmed hypertension. Blood pressure (BP) ranged from 150-135 mmHg systolic and 70- 95 mmHg diastolic in the setting position. He had a kidney function decline with a glomerular filtration rate at 70 ml/min. Abdominal auscultation and renal ultrasound showed no abnormalities. The patient was then referred to us for CRS with 99mTc-DTPA. This exam was performed according to two-time one-day protocol. At first, a baseline study was fulfilled. Then, renography was repeated 1 hour after the oral administration of captopril (50 mg) with cheking BP every 15 minutes. sequential renal images were acquired by means of a gamma camera at the rate of one frame every 10 sec for 30 minutes in the supine position after a bolus injection of 162 MBq of 99mTc-DTPA. This scintigraphic protocol was the same in all studies. A background-subtracted renogram was obtained after image treatment. ***Results:*** 99mTc-DTPA sequential images and renogram in the baseline study demonstrate a normal pattern of tracer uptake and excretion in the two kidneys with a symetrical renal functions in both sides. Sequential images and the renogram in captopril study showed a dramatic change in the left kidney as is clearly shown by the shift of the nephrogram to the right, the appearance of a left renal stasis and the increase in peak time (16 minutes Versus 3 minutes) and residual activity which argues in favor of hemodynamically significant renovascular disease in the left kidney.There are no significant changes in the renogram of the right kidney. A medical treatment has been prescribed while waiting for renal artery revascularization. ***Conclusion:*** RVH is a potentially curable etiology. CRS with 99mTc-DTPA is a non-invasive, low-radiation procedure which still being an excellent technique tu use in the exploration of patients with renal artery stenoses. it allows the selection of patients who can successfully benefit from a surgical or endoscopic revascularization procedure.

EP-63

e-Poster Area

E: Other Studies -> E3 Other Study (including Training, Projects)

EP-0996

Implementation of 3D digital SPECT/CT device for clinical workflow in myocardial perfusion imaging - a multidisciplinary collaborative project approach

J. Kaunisto, *A. Keinänen, H. Gröhn, T. M. Laitinen, M. Hakulinen, S. Koponen, S. Halttunen, T. P. Laitinen;*
Kuopio University hospital, Kuopio, FINLAND.

Aim/Introduction: New 3D digital SPECT/CT enables dynamic 3D myocardial perfusion imaging (MPI) which allowed us to include dynamic scans in clinical rest/stress MPI protocol. Efficient implementation of the new protocol to clinical use is a challenging task. Utilization of continuous improvement (Kaizen) is one of the strategic principles in our hospital. Our aim was to use the LEAN methods to recognize the most critical aspects contributing to successful implementation of the new technology and make corresponding actions as a part of clinical workflow. ***Materials and Methods:*** LEAN A3 report was used to summarize the challenges, status and aim of the dynamic

MPI implementation. Ishikawa diagram was utilized for detailed analysis of critical factors affecting the implementation. To follow PDCA (plan-do-check-act) principle, above analyses were updated based on gained experience from first patient studies, in several brainstorming sessions, by multidisciplinary team. To identify wasted time during the MPI protocol, duration of different phases and waiting time was recorded. ***Results:*** By utilizing Ishikawa diagram, Personnel, Methods and Materials were found to be the most critical factors contributing to the development process. To achieve required expertise level of Personnel, two technologists were named as superusers. They received extensive training from manufacturer and made site visit to other hospital which uses the same equipment and performs similar studies. Multidisciplinary team developed orientation plan for all professional groups which included for example schedule and detailed checklists for required knowledge and skills for each profession. As Methods, imaging protocol and data analysis are continuously developed. Imaging protocol from literature was used as a starting point and modified in iterative process. Imaging protocol and data analysis were further improved with help of manufacturer and analysis software company. As Materials, in addition to orientation plan related material, patient information sheets and operation procedures were updated accordingly.As an overall result, our clinical workflow and patient scheduling has been improved compared to both the starting point of the process with the new device and previous MPI protocol. ***Conclusion:*** Using LEAN methods, we were able to focus our efforts to the essential aspects of implementing the new technology including dynamic MPI protocol as part of the clinical workflow. The well-planned, correctly focused training of the personnel was found to be one of the most important aspects for successful implementation. Process required multidisciplinary team committed to continuous development. The next phase is to concentrate on optimizing study protocol.

EP-0997

Annual DXA Operator Audit - A single site experience

D. Teixeira Macarico, *C. Reilly, A. Nicol;*
Nuclear Medicine Department, Queen Elizabeth University Hospital, Department of Physics and Bioengineering, NHS Greater Glasgow and Clyde, Glasgow, UNITED KINGDOM.

Aim/Introduction: Dual X-Ray Absorptiometry (DXA) is the gold standard method for diagnosis of Osteoporosis. Due to the high levels of precision needed for this technique it is important that routine audits are performed for the operators in order to ensure the accuracy and reproducibility for diagnosis and treatment monitoring. Nuclear Medicine at the South of Glasgow offers DXA scans. In 2022 following review of scanning protocols and implementation of new techniques, a new audit tool was created for quarterly operator checks as per international recommendations. The aim of this study is use the audit tool to perform a review per quarter and per operator, adopting a learning from excellence and training needs approach. ***Materials and Methods:*** Quarterly audits were performed by a senior operator in 10 randomly selected patients per DXA operator (n=5) at the Queen Elizabeth University Hospital in Glasgow. Scanning and analysis parameters (e.g anatomical area centred and straight, femoral box adjusted, vertebral exclusion correctly performed) were scored between 1 (lowest) to 5 (highest) for all scans (Anterior-Posterior Lumbar Spine, Proximal Femur, Vertebral Fracture Assessment and 33% Radius). The average score per parameter was calculated per each operator as well as the score per anatomical area and the overall department scores. These were used through the year to identify training needs and adjust practice. A final yearly overview was created to assess progression using this audit tool. ***Results:*** A total of 200 patients were included in this audit (5 operators x 4 scan sites x 4 quarters) - AP Spine (n=197), Proximal Femur (n=187), 33% Radius (n=125) and Vertebral Fracture Assessment (n=198). The operator scores were Q1: average 4.7 (4.4 - 5.0); Q2: average 4.8 (4.6-5.0); Q3: average 4.8 (4.6-5.0); Q4: average 4.8 (4.5-5.0). The minimum operator score (33% radius, 3.6) was in Q1 and the minimum thereafter was 4.1 (33% radius). The target score of 4.5 was achieved in Q1: 17/20; Q2: 18/20; Q3: 17/19; Q4: 17/19 datasets. ***Conclusion:*** This was a useful local audit tool undertaken throughout the year. Good practice was celebrated and follow up actions focused on the radius scans which had recent protocol changes, resulting in improving practice. It is also noted that radius scans are less frequently indicated. There were a few limitations including the disparity of the amount of patients each operator scanned.

EP-64

e-Poster Area

E: Other Studies -> E3 Other Study (including Training, Projects) -> Organisation and optimisation in nuclear medicine worldwide

EP-0998

University of Tor Vergata, Rome, Italy, contributes to the EU Horizon-2020 INCISIVE project for the development of Artificial Intelligence in Health Imaging

E. Triumbari[1], *A. Kosvyra*[2], *T. Loncar-Turukalo*[3], *A. Tzelepakis*[4], *C. Barelle*[5], *C. Symvoulidis*[6], *S. Nabhani*[7], *L. Zacharias*[7], *G. Tsakou*[8], *A. Chiaravalloti*[1];
[1]*Nuclear Medicine Unit, Department of Biomedicine and Prevention, University of Rome Tor Vergata, Rome, ITALY,* [2]*Aristotle University of Thessaloniki, Thessaloniki, GREECE,* [3]*Faculty of Technical Sciences, University of Novi Sad, Novi Sad, SERBIA,* [4]*Centre for Research & Technology Hellas, Hellas, GREECE,* [5]*European Dynamics Luxembourg SA, Luxembourg, LUXEMBOURG,* [6]*Telesto IOT solutions limited, Athens, GREECE,* [7]*School of Life Sciences, Pharmacy and Chemistry, Kingston University London, Kingston, UNITED KINGDOM,* [8]*Maggioli SPA, Greek site, Athens, GREECE.*

Aim/Introduction: INCISIVE is an EU-Horizon 2020 project, part of the Artificial Intelligence (AI) for Health Imaging (AI4HI) network, that aims to develop and validate a multimodal AI-based toolbox for the empowerment of imaging analysis related to the diagnosis, prediction, and follow-up of cancer, while also contributing to the development of an open, standard-based, interoperable Federated European Cancer Imaging repository. ***Materials and Methods:*** The project's consortium comprises 27 partners from 9 countries, each covering different expertise. The Italian University of Tor Vergata (UNITOV) acts as one of the major data providers for nuclear medicine (18F-FDG PET/CT) imaging cases of lung, breast, and colorectal cancer. Collection of clinical and imaging data is carried out in both retrospective and prospective settings. Once the patients are identified, an automated data curation and annotation workflow must be followed, ensuring good quality and integrity of the data. Next, aggregation and segmentation through a Machine Learning-aided annotation tool take place. Data are finally uploaded in the Imaging repository for AI training, validation, and feasibility testing and for AI models implementation. The delivery of all services to the healthcare professionals is foreseen through the development of a hybrid infrastructure with intuitive interactive user interfaces. ***Results:*** For the retrospective phase of the study, UNITOV collected,

anonymized, annotated and uploaded 80 lung cancer PET/CT imaging cases, 40 breast cancer cases and 20 colorectal cancer cases. For the currently ongoing prospective phase of INCISIVE, the number of PET/CT exams collected by UNITOV are 135 for lung cancer, 97 for breast cancer, and 127 for colorectal cancer. Data curation and imaging annotation currently are the most time-consuming phases of the process. Performance of the quality check for collected data demonstrated no major issues, with only limited effort needed for tool debugging. A first prototype of the INCISIVE federated repository has been implemented, integrated and delivered. Further training and validation with INCISIVE data is ongoing. ***Conclusion:*** INCISIVE moves towards the exploration of the full potential of AI solutions in cancer imaging, with preliminary results being expected at the beginning of 2024. The AI-based toolbox will improve the accuracy of PET/CT examinations for the detection of primitive cancers and recurrences.

EP-1000

NOAR COST Action: Advancing Targeted Alpha Therapy with Astatine-211 for Cancer Treatment

E. Janevik-Ivanovska[1], *J. Gestin*[2], *E. Aneheim*[3], *S. Lindegren*[3], *J. Gaschet*[4], *S. Palm*[5], *D. Niculae*[6], *P. Bouziotis*[7], *M. Pruzynski*[8], *P. Kolenc*[9], *A. I. Jensen*[10], *A. Abrunhosa*[11], *L. Navarro*[12], *H. Jensen*[13], *R. Mikolajczak*[14], *M. M. Herth*[15], *M. Konijnenberg*[16], *F. Guerard*[17];
[1]*University Goce Delcev Stip, Faculty of Medical Sciences, Stip, NORTH MACEDONIA,* [2]*Université de Nantes, Inserm, CNRS, Centre de Recherche en Cancérologie et Immunologie Intégrée Nantes—Angers (CRCIINA)—UMR 1307, UMR 6075, *Action Chair of the COST Action CA19114, Network for Optimized Astatine labeled Radiopharmaceuticals (NOAR), 44007 Nantes Cedex 1, FRANCE,* [3]*Department of Medical Radiation Sciences, Institute of Clinical Sciences, the Sahlgrenska Academy, University of Gothenburg;, 413 45 Gothenburg, SWEDEN,* [4]*Université de Nantes, CNRS, Inserm, CRCINA, 44000, Nantes, FRANCE,* [5]*Department of Medical Radiation Sciences, Institute of Clinical Sciences, the Sahlgrenska Academy, University of Gothenburg;, 413 45 Gothenburg, SWEDEN,* [6]*Radiopharmaceutical Research Centre, Horia Hulubei National Institute for Physics and Nuclear Engineering, 30 Reactorului Street, Măgurele, 077125 Ilfov, ROMANIA,* [7]*Radiochemical Studies Laboratory, INRASTES, National Center for Scientific Research Demokritos, Aghia Paraskevi, 15341 Athens, GREECE,* [8]*Institute of Nuclear Chemistry and Technology, Dorodna 16, 03-195 Warsaw, POLAND,* [9]*Department of Nuclear Medicine, University Medical Centre Ljubljana, 1000 Ljubljana, SLOVENIA,* [10]*Center for Nanomedicine and Theranostics (The Hevesy Laboratory), DTU Health Technology, Technical University of Denmark (DTU), Ørsteds Plads 345C, 2800 Lyngby, DENMARK,* [11]*ICNAS/CIBIT, Institute for Nuclear Sciences Applied to Health, University of Coimbra, Coimbra, PORTUGAL,* [12]*Precirix, Brussels, BELGIUM,* [13]*Cyclotron and PET unit KF-3982, Copenhagen University Hospital, Copenhagen, DENMARK,* [14]*National Centre for Nuclear Research, Radioisotope Centre POLATOM, 05-400 Otwock-Swierk, POLAND,* [15]*Department of Drug Design and Pharmacology, Faculty of Health and Medical Sciences, University of Copenhagen, Universitetsparken 2, 2100 Copenhagen, DENMARK,* [16]*Department of Radiology and Nuclear Medicine, Erasmus MC, 3000 CA Rotterdam, NETHERLANDS,* [17]*Université de Nantes, Inserm, CNRS, Centre de Recherche en Cancérologie et Immunologie Intégrée Nantes—Angers (CRCIINA)—UMR 1307, UMR 6075, 44007 Nantes, FRANCE.*

Aim/Introduction: The aim of the NOAR COST Action CA19114 is to demonstrate the feasibility and efficacy of using Astatine-211 Targeted Alpha Therapy (TAT) as the European standard for treating certain cancerous pathologies. This will be achieved through efficient knowledge exchange and networking among all European stakeholders and partners outside of Europe. ***Materials and Methods:*** The NOAR COST Action will address the following points: Astatine-211 targetry, production, and logistics; correct speciation of At-211 for pharmaceutical production; optimization of vectors for At-211 labeling and development of validated radiolabeling protocols; automation in production of At-211 and At-211 radiopharmaceuticals; development of dosimetry techniques for At-211 TAT; identification of the regulatory environment for TAT using At-211 radiolabeled vectors; investigation of pharmacoeconomics of TAT with At-211; education and communication aspects. ***Results:*** The NOAR COST Action CA19114 is expected to yield the following outputs: a strong capacity to produce At-211 radiopharmaceuticals by bringing together European skills in radiochemistry, chemistry, biology, dosimetry, and preclinical and clinical research; robust partnerships among participants, leading to increased collaboration; training of Early Career Investigators (ECIs) and PhD students through Short Term Scientific Missions (STSMs); establishment of a network that permits innovative technology on At-211 TAT. ***Conclusion:*** The NOAR COST Action will facilitate efficient knowledge exchange and networking among all European stakeholders interested in promoting At-211 for medical applications and will allow association with partners outside of Europe (USA, South Africa, Japan). By joining European and international research efforts, fundamental and applied knowledge on At-211 will be significantly increased, and Europe will take a technology lead in the field of At-211 TAT.

References: Guérard F, Gestin JF, Brechbiel MW. Production of [(211)At]-astatinated radiopharmaceuticals and applications in targeted α-particle therapy. Cancer Biother Radiopharm. 2013 Feb;28(1):1-20. doi: 10.1089/cbr.2012.1292. Epub 2012 Oct 17. PMID: 23075373; PMCID: PMC3545490.

EP-1001

Appropriation of hybrid practices in oncological imaging: the situation of PET-CT in France from a management perspective.

R. Guignard[1,2], *B. Geffroy*[2], *V. Fernandez*[3];
[1]*Clinique de Genolier, Genolier, SWITZERLAND,* [2]*IMT Atlantique - LEMNA, Nantes, FRANCE,* [3]*TELECOM Paris, Paris, FRANCE.*

Aim/Introduction: As a hybrid technological device, PET-CT changes the practice of nuclear medicine (NM) physicians while introducing professional practices coming from radiology. The management issues of the adoption of health technologies and the appropriation of innovation in hybrid NM practices (hNMp) have never been addressed in qualitative research. ***Materials and Methods:*** Between 1st January 2022 and 30th June 2022, we conducted a series of 24 semi-structured interviews (average interview length: 70.2±17.7 minutes) among French healthcare professionals working in 6 different NM departments. The aim of these interviews was to find out how NM physicians use PET-CT as a hybrid technology in their daily practice. Interview data were collected, coded, analyzed and triangulated by 3 researchers. ***Results:*** 22 NM physicians and 2 chief NM technologists were interviewed (m/f sex ratio: 1.4; 41.3±8.5 years old). 77.3% of professionals reported an initial training in radiology (6 months minimum) and 14.7±6.7 years of experience in NM.In PET-CT imaging, hNMp was divided into 2 continuous parts, in which different types of professional behaviour were observed: the operational part (ie. imaging protocol, mostly managed by technologists) and the intellectual part (ie. medical interpretation). For each part, we actually identified a number of variables that may have an impact on appropriation process of hNMp.The

fundamentals of hNMp can be supported by several parameters, such as the intrinsic features of the technology (i.e. benefit-risk ratio), a complete expertise of the NM teams in radiological practices, or a standardisation of the procedure with a normalised framework that is understandable for all stakeholders. Dynamic of hNMp appropriation can be explained by the intrinsic dynamic of NM itself, by individual levers and barriers, or by the substitution of CTscans for oncological purposes. The legitimisation of hNMp is first of all part of the legitimisation strategies of PET imaging itself. Among adopters of hNMp, acquisition of transversal skills through a specific training leading to functional autonomy and external influences (demand pressure from oncologists) are important levers. ***Conclusion:*** Our study highlights the heterogeneity of PET-CT imaging practices among French NM physicians, who own PET-CT as a capital resource, and then provides some insights into innovative technology adoption.Socio-organisational boundaries between 2 independent medical specialties, defined by their medical competencies and responsibilities, lead to inequalities in the multimodality approach to PET-CT. Our results support the necessity of different organisational approaches for the management of multimodal imaging.

EP-1002

Novel approach for the technical implementation of radiowater studies for a pet/ct- scanner in hospital environment

M. Hakulinen[1], *P. Poutiainen*[2];
[1]*Diagnostic Imaging Centre, Kuopio University Hospital, Kuopio, FINLAND,* [2]*Cyclotron and radiopharmacy unit, Kuopio University Hospital, Kuopio, FINLAND.*

Aim/Introduction: Oxygen-15 labelled water, i.e. radiowater, is used as a radioactive tracer for perfusion of heart, brain, and tumors. There are several clear benefits for the use of radiowater in particular, such as low effective dose for the patient, it is metabolically inert and passes freely across cell membranes and thus, the distribution and clearance of radiowater depends completely on the rate of blood flow. However, the use of radiowater is limited since it requires on-site cyclotron and technical implementation can be very challenging. E.g. short half-life of oxygen-15 as well as optimization for the oxygen and radiowater flows in long tubing. Good manufacturing practice (GMP) requirements needs to be carefully designed to full fill the quality demands for drug production. In this study, we will introduce a novel approach for setting up oxygen-15 studies in PET facilities at Kuopio University Hospital. ***Materials and Methods:*** The technical plan for the use of oxygen-15 in clinical PET/CT- studies included several different aspects 1) radiation safety 2) reliability of operation, 3) GMP and quality control requirements 4) maintenance/fault repair and 4) practical work considerations while maintaining the transfer line as short as possible. There were several engineers involved in the project related to electric, HPAC, building automation planning as well as construction experts. This project was part of larger relocation project of our nuclear medicine department. ***Results:*** As a results of this project, we developed a novel floor gutter to scanned rooms enabling reliable connections to the transfer lines especially considering practicality and radiation safety. The system allows several endpoints where the radiowater is used. Easy to operate automated system to control the selection of production lines and waste gas lines were build including simple light system to notify users in different areas where the radioactive gas flows. The safety system was designed to notice and control the flow of possible leaked activities and system design allows at least 300meters long transfer lines. The system was designed to fulfill the GMP requirements and make it possible to build the system outside the cleanroom area. ***Conclusion:*** Novel plan for technical implementation of radiowater studies was achieved. The system was especially designed to enable use of radiowater in multiple endpoints while considering radiation safety, practicability and easy to access characteristics of the system. The system was also designed to fulfill GMP requirements.

EP-1003

Identifying the unique needs of transgender, non-binary and gender diverse patients in the nuclear medicine department

A. Cripps[1], *J. Taylor*[1,2], *R. Salmon*[1];
[1]*Sheffield Teaching Hospitals NHS Foundation Trust, Sheffield, UNITED KINGDOM,* [2]*University of Sheffield, Sheffield, UNITED KINGDOM.*

Aim/Introduction: Transgender and non-binary people face significant barriers to healthcare, exacerbated by a widespread lack of knowledge of their unique healthcare needs amongst healthcare providers[1]. In this study, a literature review, staff interviews and surveys were used to identify the aspects of the nuclear medicine patient pathway where transgender, non-binary and gender diverse (TGD) patients have unique needs. After identifying these needs, a training presentation was developed and delivered to nuclear medicine staff, to increase their understanding of how best to care for these patients. ***Materials and Methods:*** A literature review was conducted of TGD experiences in healthcare, focussing on staff-patient interaction, policy and procedures, and radiology-specific experiences. A focus group with senior staff members in a nuclear medicine department was conducted to understand the background and context surrounding TGD patients in the department and identify knowledge-deficient areas. Patient-facing clinical staff were surveyed to identify any situations in which they would struggle to give high-quality care to a TGD patient, or situations that they felt a TGD patient might find uncomfortable. This data was thematically analysed to identify nuclear medicine-specific issues. These issues arose from aspects of the patient experience where gender is used to determine an aspect of care, or where TGD people are especially vulnerable to discomfort. Training on these key issues was written and delivered, then staff were surveyed post-training to provide feedback. ***Results:*** Four key aspects of the nuclear medicine patient experience were identified: pregnancy enquiries; pregnancy and breastfeeding advice post-therapy; genital, chest or breast injection sites; and gendered normal ranges. Each of these has the capability to either cause discomfort for a TGD patient or result in them receiving substandard care due to lack of knowledge amongst staff. The training described these issues and suggested solutions from the literature. This was overarchingly well-received by staff, with the survey results showing that the modal rating was 'very informative', 'very useful', and 'very relevant'. Thematic analysis revealed a strong sense of increased understanding and empathy for TGD patients post-training. ***Conclusion:*** To conclude, a training presentation was created to identify the unique needs of TGD patients in the nuclear medicine department, and present these to staff, alongside suggestions to ameliorate these patients' experiences. This is a step towards removing barriers to healthcare for a marginalised group and was well-received by staff. ***References:*** (1) Hobster K, McLuskey J. Transgender patients' experiences of health care. British Journal of Nursing. 2020;29(22):1348-53.

EP-1004

Illuminating actionable practice to improve recall of medical information in nuclear medicine department

S. Ibba[1], *P. Gandolfo*[1], *L. Airò Farulla*[2], *D. Zago*[1], *G. Fosci*[1], *S. Papa*[1];
[1]*CDI Centro Diagnostico Italiano S.p.A., Milan, ITALY,* [2]*University of Milan, Milan, ITALY.*

Aim/Introduction: To prepare patients for nuclear medicine examinations, they are usually provided with a written information note at the time of booking, explaining how the examination is conducted and how they should prepare for it (e.g., interruption of medications). However, nuclear medicine patients are often debilitated, anxious or elderly which causes some of them to fail to understand the complex instructions they receive. This results in some patients arriving on the day of the examination unprepared and thus unable to undergo the procedure. Therefore, we aim to increase the recall of information for nuclear medicine exam preparation to improve patient compliance. ***Materials and Methods:*** In addition to written instructions, in 2019 we introduced a telephone structured interview with the patient carried out by a trained operator of our centre able to explain step by step the preparation for PET and DaTSCAN SPECT and how they are conducted. The interview, which is performed a week before the procedure, is tailor-made and based on a structured checklist. ***Results:*** Before introducing the interview, occasionally patients did not fully understand the written instructions given at the time of booking. If the patient was unprepared for examination, he was dismissed causing delayed diagnosis, a sense of frustration for the patient, and a negative impact on the department's productivity. Implementation of the tailor-made interview, in addition to the written information note, has enabled us to significantly reduce the number of patients who did not follow the correct exam preparation protocol, decreasing the drop-out rate from ~30% to ~2%. The second advantage is that we can intercept any potential issue (e.g., claustrophobia, acute bronchitis..) and implement strategies to counteract them without losing the quality of the examination. This allowed us to greatly improve the patient's physical and psychological compliance during procedures. ***Conclusion:*** Our project allowed us to considerably reduce the number of patients who showed up unprepared for examinations confirming that specific information is better recalled than generally formulated information [1] and accurate knowledge improves patient compliance and satisfaction and decreases anxiety [2]. Finally, this activity contributed to improve the quality of the service provided and the productivity of the department. ***References:*** [1] Kessels, R. (2003). Patients' memory for medical information. Journal of the Royal Society of Medicine, 96(5), 219-222.[2] van der Meulen N., et al. (2008). Interventions to improve recall of medical information in cancer patients: a systematic review of the literature. Psychooncology, 17(9), 857-68.

EP-1005

Religion, beliefs and needs in thyroid cancer patients

E. Olariu*, D. Piciu;*
The Oncology Institute Cluj-Napoca, Cluj-Napoca, ROMANIA.

Aim/Introduction: There is limited research specifically addressing the impact of religion and beliefs on quality of life in thyroid cancer patients. However, studies examining the influence of religion and spirituality on quality of life in cancer patients more broadly suggest that these factors can have a significant impact on patients' well-being. Patients who have strong religious or spiritual beliefs may have a greater sense of purpose, meaning, and hope, which can contribute to better mental health and a more positive outlook. ***Materials and Methods:*** We underwent a questionnaire based-study on 72 differentiated thyroid cancer patients who were admitted in the nuclear medicine department for radioiodine therapy between November 2022 and February 2023. For assessing the needs, we used Spiritual Needs Questionnaire (Sp NQ) a reliable and valid questionnaire for research and clinical application and for the religious assessing tool we used the System of Belief Inventory questionnaire (SBI-15R). ***Results:*** 72 patients completed the questionnaires (48 female and 24 male) with a medium age of 52 years old. 58/72 pts were married, 31/72 pts employee and 31/72 pts retired, with most of them with university degree (58/72 pts). The most frequent religion declared was orthodoxy (54/72 pts) followed by catholic (6/72 pts) and other (9/72 pts). Patients reported in more than 90% that religion is a very important issue in their life, with a need for praying/meditation, giving them a strong support in copping with the oncological disease, a real need for recovering the inner spiritual health and to strengthen the relationship with their family. ***Conclusion:*** It's important to note that the impact of religion and beliefs on quality of life can vary depending on the individual patient and their specific circumstances. It's important for healthcare providers to recognize and respect the role that religion and beliefs can play in a patient's experience with cancer, and to provide support that is sensitive to each patient's individual needs and preferences. ***References:*** 1. Jim HS, Pustejovsky JE, Park CL, Danhauer SC, Sherman AC, Fitchett G, Merluzzi TV, Munoz AR, George L, Snyder MA, Salsman JM. Religion, spirituality, and physical health in cancer patients: A meta-analysis. Cancer. 2015 Nov 1;121(21):3760-8. doi: 10.1002/cncr.29353. Epub 2015 Aug 10. PMID: 26258868; PMCID: PMC4618080. 2. Kristeller JL, Zumbrun CS, Schilling RF: 'I would if I could': how oncologists and oncology nurses address spiritual distress in cancer patients. Psychooncology 8 (5): 451-8, 1999 Sep-Oct.

EP-1006

Performance Evaluation of the Incorporation of PET/CT Procedures in the SUS

B. Prates*, L. Pozzo;*
Nuclear and Energy Research Institute, IPEN–CNEN/SP, São Paulo, BRAZIL.

Aim/Introduction: High-complexity technologies, such as PET/CT, should have their incorporation constantly analyzed and enhanced to support their consolidation. The evaluation of the performance of these equipment commits to the understanding of subjects such as the clinical application effectiveness, the usage of these devices in the patient's real life, and the impact of this technology in the different regions where they are applied. Therefore, this work aimed to evaluate the performance incorporation PET/CT equipments and procedures by the Brazilian National Health System (SUS) according to admissibility, economic, innovation, and technical criteria, accordant to the Methodological Guideline for the Elaboration of Studies for the Evaluation of EMA (medical-assistance equipment). Furthermore, the demand for the application of this technology was also considered. ***Materials and Methods:*** The data collection methodology was based on an active search for information, such as the consultation of bibliographies and websites that presented data of interest, such as ANVISA, DATASUS, CNEN, and RHC. ***Results:*** Thirteen records of equipment from seven distinct manufacturers were identified within the validity period. Moreover, there are 110 registrations with at least one PET/CT equipment in the National Registration of Health Facilities (CNES) and 160 registrations of facilities authorized by the National Commission of Nuclear Energy (CNEN). Published by the National Health Fund (FNS), the

value proposed for such equipment in 2022 is BRL 6,405,000.00. Regarding approved financing proposals, seven are registered and distributed in the records of five facilities. The applied taxes observed are IPI, PIS, and COFINS. Per procedure, according to the SUS table records, the amount paid was BRL 2,107.22, and the total amount paid since the incorporation of the technology is BRL 348,446,738.37. ***Conclusion:*** The development of the work led to the perception that, although there was some difficulty in obtaining some data that permeate the PET/CT technology, the incorporation of this technology took place in a satisfactory manner. There was divergence in results such as the number of devices. This fact was due to the way in which information was made available, as many data are self-declared by interested parties. Because it is the incorporation of a high-complexity technology in full use, few studies evaluating its performance were observed. Based on Consolidation Ordinance No. 1/2017 - which adopts the recommendation of one PET/CT unit per 1.5 million inhabitants, it was found that few Brazilian states have available the number of devices to meet the needs of demand.

EP-1007

Patient experience at the heart of the implementation of a PET/MRI system in our centre

J. Vercher-Conejero, *M. Cortés-Romera, J. Martín Marcuartu, S. Millat Servent, I. Feliu Perez, C. Martínez Ramos, V. Carrero Vasquez, M. Pudis, S. Santamaria Lopez, I. Bonilla Aguilar, M. Fernandez Yuste;*
Bellvitge University Hospital, L'Hospitalet de Llobregat (Barcelona), SPAIN.

Aim/Introduction: Our strategy, as an organization, is focused on improving the patient experience. Our hospital wants to take a step forward to incorporate the patient experience into the organization's culture. Our objective was to create a new culture at the service of the patient as a central axis in the project to set up a PET/MR system in our department, incorporating the patients' point of view (expectations and needs) to improve their experience. ***Materials and Methods:*** The methodology used is known as Design Thinking, which starts from an objective (a better future situation), instead of a problem to be solved. This is based on:1.-Identify the most common patient profile, creating "person maps".2.-Identify the Patient Journey Map from the touch points and pain points. This step involves patients and professionals.3.-Transform the pain points into insights (answer to the question of why the pain point occurs) and from this answer, propose an improvement project.4.-Prioritise improvement projects and develop a prototype.5.-Discuss the prototype with a group of patients, patient relatives and professionals.6.-Define the implementation strategy.7.-To measure patient experience through quality indicators. Quality indicators based on patient experience are needed. The average duration of a patient experience project is estimated to be 2-3 months. This generates a report listing the projects derived from the "pain points" reported by patients, with the aim of incorporating these recommendations into the development process to improve the patient experience.This method, which incorporates small group of patients and the interview as techniques, allows to know the needs and expectations of the patients (and their caregivers). ***Results:*** The results were highly satisfactory with the participation of 13 patients/10 healthcare professions.28 improvement projects were generated, with 2 projects prototyped based on patient impact and feasibility.Satisfaction surveys were conducted with the professionals involved:78% gave an overall satisfaction score of 9 to 10 when participating in a project, and 100% considered that patient experience should be considered in projects for the creation of new hospitals or medical services.Finally, participating patients expressed a high level of satisfaction. ***Conclusion:*** This project is applicable to all medical centres and institutions, taking into account the differences and characteristics of each centre.It is easy to implement and allows to know the needs and expectations of the patient, and to measure their participation in the process.Changing the culture of a healthcare organization to improve patient care requires prior collaboration with the different professionals involved.

EP-1008

Knowledge, Attitude and Practice towards the Utility of Medical Radioisotopes for Diagnosis and Therapy of Disease used in Nepal

A. Gupta, *P. Sah, S. Prasad, D. Baral;*
B.P. Koirala Institute of Health Sciences (BPKIHS), Dharan, NEPAL.

Aim/Introduction: In the last few years, medical use of radioisotopes has been increased dramatically in Nepal for both diagnosis and therapy of various diseases including many cancers. Radioisotopes such as Technetium-99m has been used for gamma imaging in Nepal since very long for the diagnosis of many diseases. Recently, PET imaging has been started in Nepal that uses Flourine-18 (F-18) radioisotope for the diagnosis of many cancers at their early stage. This study was conducted to assess the knowledge, attitude and practice (KAP) among the radiation oncology and nuclear medicine personnel towards the utility of medical radioisotopes used in Nepal for the diagnosis and therapy of disease including cancers. ***Materials and Methods:*** This study was conducted after the approval from Institutional Review Committee (IRC) of B.P. Koirala Institute of Health Sciences (BPKIHS), Dharan, Nepal. Data were collected through the questionnaire from thirty-two radiation oncology and nuclear medicine personnel working at different cancer hospitals and nuclear medicine centers in Nepal where radioisotopes are currently being used. The questionnaire included 38 questions (11 questions for knowledge, 11 questions for attitude and 16 questions for practice) to assess the KAP of the participants. The data collected were entered in the MS excel 2013 and analyzed using statistical analysis software package SPSS 11.5. For descriptive statistics, frequency, percentage, mean and standard deviation (SD) were used along with graphical and tabular presentation. Analyses tests used in this study was independent samples t-test and the Chi-squared test. A p-value <0.05 were considered statistically significant. ***Results:*** Thirty-two participants (n=32) of age 22-51 years were included in this study for the interview through the questionnaire. Of the total 32 respondent, 26 (82.25%) were man and 6 (18.75%) were female. Results obtained showed that the knowledge regarding the usage of radioisotopes among the participants is inadequate. The overall knowledge among the participants found to be 40.6% only. Similarly, the attitude of the participants toward the application of medical radioisotopes was found to not satisfactory. The overall attitude of the participants was assessed to be 43.75% only. It was also found that the practice of radioisotopes among the participants are very unsatisfactory (18.75%). ***Conclusion:*** The overall knowledge, attitude and practices of the participants towards the utility of medical radioisotopes found to be 40.6%, 43.75% and 18.75% respectively. From this study, it can be concluded that the awareness regarding the application of medical radioisotopes should be improved.

EP-1009

Cyclotron production of ultra-pure indium-111 radionuclide using gold-plated capsules in Iran

P. Ashtari[1,2], *Y. Fazaeli*[2], *G. Aslani*[1], *S. Feizi*[2];
[1]*Pars Isotope Co., Tehran, IRAN, ISLAMIC REPUBLIC OF,* [2]*Nuclear Science & Technology Research Institute, Tehran, IRAN, ISLAMIC REPUBLIC OF.*

Aim/Introduction: The aim of this study is to introduce a new, rapid, simple, low cost, and innovative method for the production and purification of Indium-111 for use in nuclear medicine. The main advantage is the elimination of chemical electrolysis, as well as the complex chemical dissolution of the metallic target and its copper substrate. ***Materials and Methods:*** Due to the proper selection of the target isotope, cadmium -112 and optimal bombardment energy, only the Zn-65 impurity is observed in the sample solution. After the separation process, the amount of zinc-65 decreased to less than its standard level in the Indium-111 solution. The cadmium content of the In-111 is determined by polarography method. ***Results:*** The cadmium content of the product is less than 0.1 ppm. Due to the chemical and radiochemical purity, it can be used for labeling of the peptides. ***Conclusion:*** Product efficiency is evaluated using it in the project entitled "production and quality control of the Indium octreotide". The labelling efficiency is more than 97%. ***References:*** [1] S. Lahiri, M. Maiti, K. Ghosh, Production and separation of 111In: An important radionuclide in life sciences: A mini review, J. Radioanal. Nucl. Chem., 297(2013) 309-318.[2] M. Roca, E.F. de Vries, F. Jamar, O. Israel, A. Signore, Guidelines for the labelling of leucocytes with 111In-oxine, Eur. J. Nucl. Med. Mol. Imaging, 37 (2010) 835-841. [3] C.T. Thomas, P.T. Bradshaw, B.H. Pollock, J.E. Montie, J.M. Taylor, H.D. Thames, P.W. McLaughlin, D.A. DeBiose, D.H. Hussey, R.L. Wahl, Indium-111-Capromab Pendetide Radio-immunoscintigraphy and Prognosis for Durable Biochemical Response to Salvage Radiation Therapy in Men After Failed Prostatectomy, J. Clin. Oncol., 21 (2003) 1715-1721. [4] N. Pandit-Taskar, J.A. O'Donoghue, C.R. Divgi, E.A. Wills, L. Schwartz, M. Gönen, P. Smith-Jones, N.H. Bander, H.I. Scher, S.M. Larson, M.J. Morris, Indium 111-labeled J591 anti-PSMA antibody for vascular targeted imaging in progressive solid tumors, EJNMMI Research (2015) 5:28 (Open Access). [5] CH. Bedel-Cloutour, L. Maneta-Peyret, M. pereyre, Synthesis of monoclonal antibody-indium-111 porphyrin conjugate, J. Immunol. Methods, 144 (1991) 35-41. [6] Y. Fazaeli, S. Shanehsazzadeh, A. Lahooti, S. Feizi, A.R. Jalilian, Preclinical dosimetric estimation of [^{111}In] 5, 10, 15, 20-tetra phenyl porphyrin complex as a possible imaging/PDT agent, Radiochimica Acta, 104 (2016) 327-336. [7] Y. Fazaeli1, A.R. Jalilian, M.M. Amini, M. Mirzai, A. Majdabadi, G.R. Aslani, A. Rahiminejad, F. Bolourinovin, S. Moradkhani, Radiosynthesis and biological evaluation of 111In-tris [8-Hydroxy-2-methylquinoline] complex as a possible imaging agent, Iran. J. Nucl. Med., 19 (2011) 20-27.

EP-1010

New method for synthesis of HMPAO compound and a novel method for purification of final product for Triple usage

M. Alizadeh*, v. ghasemi, e. maleki, h. m. mehrabani, f. farajbakhsh, m. ghapanvari;*
parsisotope, Tehran, IRAN, ISLAMIC REPUBLIC OF.

Aim/Introduction: The main goal of the present research is a new method for the synthesis and purification of the HMPAO compound to produce a radiopharmaceutical kit for the imaging of the tissue involved in the infection, brain scanning and pelacet labeling considering the structure of the desired compound and paying attention to the fact that the desired product in the carbons (3 and 9 positions) is symmetrical. The main purpose of this project is not only synthesis of API but also finding a new method for separation of isomers. l, d HMPAO is synthesized in 2 steps, each step checked by FT-IR and NMR. After purifying the structure and reaching the desired isomers, the final product was used to prepare the kit. ***Materials and Methods:*** 2,3-Butanedione monoxime, 2,2-dimethyl-1,3-diaminopropane, and PTSA refluxed in anhydrous ethanol. The final solution was checked by TLC sheets after finding the new point of intermediate on TLC sheets the reaction continued by adding sodium borohydride to a cooled solution of the reaction mixture. For the separation of isomers, we used green solvent recrystallization process. The final products were utilized for kit preparation, and the radiochemistry check was used to understand the presence of labeled synthesized API with technetium. ***Results:*** synthesis of HMPAO was done in 2 step reaction and many steps of the purification process. The final pure product was checked by FT-IR peaks at the range of 1626 cm^{-1} and 1636 cm^{-1} are related to C=N-OH and N=C, the ^{13}C-NMR spectrum of pure d, l-hexamethyl propylene amine oxime shows peaks at 159.00, 57.79, 56.23,34.93, 25.06, 24.86, 19.73 and 8.74. and the bio distribution was checked in 2 steps. the first step was done on rat, and the second one, was checked on the human body. ***Conclusion:*** This study provides valuable data showing beneficial results that the labeled HMPAO with Technetium-99m can use for labeling of white blood cells, and monitoring the place of body tissue involved in the infection, and the final product can use for brain scan. The infection and the final product can use for brain scan. Also, one of the interesting results of this research is the unique ability of the HMPAO to mark blood platelets in order to detect the location of internal bleeding.

EP-1011

Comparison of diagnostic efficacy of 99mTc-MIBI SPECT/CT and ultrasonography for primary and secondary renal hyperparathyroidism

M. Jiang*, W. Mei;*
Ningbo No.2 Hospital, Ningbo, CHINA.

Aim/Introduction: This study aimed to compare the efficacy of ^{99m}Tc-MIBI double-phase scintigraphy (DPS), SPECT/CT, and ultrasound (US) in the preoperative diagnosis of PHPT and SHPT. ***Materials and Methods:*** From September 2018 to February 2023, the imaging and clinical data of 113 patients with HPT (including 95 cases of PHPT and 18 cases of SHPT) who underwent ^{99m}Tc-MIBI SPECT/CT and US before surgery in Ningbo No.2 Hospital were retrospectively analyzed. The postoperative pathological diagnosis of parathyroid hyperplasia, adenoma, and cancer was considered as positive, while the other results were negative. Fisher's exact test was used to compare the diagnostic efficacy of different tests in PHPT and SHPT. ***Results:*** Of the 95 patients with PHPT, 90 were pathologically confirmed as positive and 18 as negative. In 18 patients with SHPT, there were 44 positive lesions and 2 negative lesions. The accuracy of DPS, SPECT/CT, US, DPS + US, and SPECT/CT + US in the diagnosis of PHPT patients was 88.0% (95/108), 92.6% (100/108), 79.6% (86/108), 86.1% (93/108), and 88.0% (95/108), respectively. For patients with SHPT, the rates were 58.7% (27/46), 87.0% (40/46), 71.7% (33/46), 78.3% (36/46), and 84.8% (39/46), respectively. The diagnostic accuracy of DPS in patients with PHPT was significantly higher than that of SHPT ($P < 0.001$), while there was no statistically significant difference in the diagnostic accuracy of SPECT/CT and US in the two types of HPT ($P = 0.357$ and $P = 0.299$). For SHPT patients, the accuracy of SPECT/CT was significantly higher than that of DPS ($P = 0.004$), but

there was no statistically significant difference between SPECT/CT and US, as well as between US and DPS (P = 0.121 and P = 0.274). ***Conclusion:*** The use of DPS, SPECT/CT, and US has high efficiency in the localization diagnosis of HPT, but the diagnostic accuracy of DPS in PHPT is superior to that of SPHT. For patients with SHPT, ^{99m}Tc-MIBI SPECT/CT is preferred to obtain higher accuracy.
References: [1] Pappachan JM, Lahart IM, Viswanath AK, et al. Parathyroidectomy for adults with primary hyperparathyroidism [J], Cochrane Database Syst Rev, 2023;3(3):CD013035. [2] Bandeira F, de Moura Nobrega J, de Oliveira LB, et al. Medical management of primary hyperparathyroidism [J], Arch Endocrinol Metab, 2022;66(5):689-693. [3] Huang Y, Wang J, Zeng M, et al. Predictive value of characteristics of resected parathyroid glands for persistent secondary hyperparathyroidism during parathyroidectomy [J], BMC Surg, 2023;23(1):36.

EP-1012

ATTR Cardiac Amyloidosis and Carpal tunnel syndrome

S. Giourgouli*, A. Kokkini-Paschou, V. Pantzou, M. Stathopoulou, J. Koutsikos;*
Henry Dunant Hospital Center, Athens, GREECE.

Aim/Introduction: The "carpal tunnel" is a narrow passageway that runs from the base of the hand through the wrist. Several tendons and the median nerve, the main nerve of the front forearm, pass through the carpal tunnel. When any of those tendons become irritated from repetitive or strenuous hand motions and overuse, the median nerve gets compressed. Carpal tunnel syndrome (CTS) occurs from excessive pressure on the median nerve. This may cause a variety of symptoms, which typically are mild to start and gradually grow more intense — especially if left undiagnosed. The association between CTS and systemic amyloidosis has been widely described with a high prevalence of CTS in ATTR Cardiac Amyloidosis (ATTR-CA), ranging from 15% to 60%. The aim of our case is to highlight this association and raise awareness of non-specific findings in bone scintigraphy. ***Materials and Methods:*** We present a case of a 78 y.o. male, presenting to our department for bone scintigraphy because of prostate cancer. As to his medical history, he mentioned hypothyroidism and diabetes. His main symptom was transient pain followed by swelling, mainly in dominant hand. Non-steroidal anti-inflammatory drugs (NSAIDs) helped relieve the pain. 20 mci Tc-99m DPD was injected i.v. and 3 hrs later a whole body scintigraphy was performed. ***Results:*** There was no evidence of metastatic disease and the only finding from the skeletal was the unilateral radiopharmaceutical accumulation in the wrists. An unexpected finding was the diffuse accumulation in the left hemithorax. A SPECT study was followed immediately for better evaluation. The study was indicative of ATTR-CA. Further investigation of the patient, revealed increased LV wall thickness in echocardiography, with EF 55%, while CTS was considered as the cause of the symptoms in both hands. ***Conclusion:*** Bone scintigraphy isn't a method of choice for evaluating CTS. Of imaging methods, magnetic resonance imaging (MRI) has shown the greatest sensitivity and specificity. One relatively new finding is that people with bilateral CTS, may be at increased risk for CA. The awareness of this association offers the possibility of an early pre-clinical ATTR-CA diagnosis. Non-specific findings in bone scintigraphy or findings of the WBS in scintigraphy provide further prognostic information.

EP-1013

Monitoring Of Adverse Reactions Caused By [99m Tc] Tc-Mibi

G. Rubio-Fernández*, R. Maestre-Cutillas, L. Baz-Sanz, L. Cebollada-Cameo, R. Castro-Velasco, C. Juan-Piriz, J. Pérez Iruela;*
Hospital Ramón y Cajal, Madrid, SPAIN.

Aim/Introduction: To evaluate the adverse drug reactions (ADR) observed when administering and reported by the Radiopharmacy Unit, looking in depth at the incidence and possible causes. ***Materials and Methods:*** An observational and retrospective analysis of ADR was produced by [^{99m}Tc]Tc-MIBI reported through the Spanish Pharmacovigilance System for Medicines for Human Use, from 2020 to March 2023. The ADR, the indication of the radiopharmaceutical, and the development of the ADR were collected. It was checked whether it was indicated in the technical data sheet, its frequency and whether it was related to any excipient of the reagent kit or to the radiopharmaceutical itself. ***Results:*** Between 2020 and March 2023, 4042 doses of [^{99m}Tc] Tc-MIBI were administered. Among these, 23 (0.57%) ADR have been reported, 18/23 (78.26%) are women. 22/23 (95.65%) ADR were indicated for parathyroid scintigraphy (PS), although only 766/4042 doses were used for this indication, implying 2.87% ADR in PS. The predominant ADR was dysgeusia and its development was the onset within seconds of administration which disappeared spontaneously without intervention. ***Conclusion:*** Dysgeusia is the most frequent ADR observed, mainly caused by the radiopharmaceutical [^{99m}Tc] Tc-MIBI for PS. This may be due to the reagent kit binder [Tetrakis(2-methoxy-2-methylpropyl-1-isocyanide) copper(I) tetrafluoroborate], which contains copper and often produces a bitter taste. Other factors that can be affected are high levels of the radiopharmaceutical in the bloodstream or speed of injection. It is striking that 766/4042 of the doses of [^{99m}Tc]Tc-MIBI produced 22/23 ADR; this may be due to the fact that most of the remaining doses were used for cardiac stress scintigraphy, in which the patient, while running on a treadmill, can ignore the reaction. In our population, a higher incidence of ADR was observed in women. The percentage of ADR is low and inconsequential, but it is important that they are reported in order to control them.

EP-1014

Assessment of agreement between three creatinine-based GFR predicting equations and 99mTc-DTPA plasma clearance GFR in adult Caucasian patients : a single-center study

G. Arsos[1]*, D. Katsampoukas*[1]*, A. Kalaitzoglou*[1]*, E. Manou*[2]*, E. Moralidis*[1]*;*
[1]*3rd Department of Nuclear Medicine, Aristotle University of Thessaloniki School of Medicine, Papageorgiou Gen. Hospital, Thessaloniki, GREECE,* [2]*Nephrology Clinic, Papageorgiou Gen. Hospital, Thessaloniki, GREECE.*

Aim/Introduction: Serum/plasma Creatinine (SCr) and/or Cystatin C-based equations incorporating age, sex and race variables, are widely used for clinical GFR estimation (eGFR). The CKD-EPI Creatinine Equation 2009 (CKD-EPI 2009), applicable to both black and non-black adults, has been followed by the unifying, race variable-free CKD-EPI Creatinine Equation (CKD-EPI 2021) and the European Kidney Function Consortium equation (EKFC) has been introduced in 2021 for full age spectrum non-black patients. Recently, 99mTc-DTPA has emerged as the dominant radiotracer for plasma clearance GFR measurement (mGFR-DTPA) in Europe. We explore the agreement between the three above equations and mGFR-DTPA in adult Caucasian

patients. ***Materials and Methods:*** GFR was measured for clinical purposes in 515 adult Caucasian patients (age 18-88 years, 42.3% females, 9.7% prospective kidney donors) by the 99mTc-DTPA plasma clearance (bolus i.v. injection, 3 blood samples at 2, 3 and 4 hours post-injection and monoexponential modeling according to BSNM). SCr was measured (mg/dL) with an ID-LC/MS calibrated Jaffe method. eGFR-CKD-EPI 2009, eGFR-CKD-EPI 2021 and eGFR-EKFC were estimated by the CKD-EPI 2009, CKD-EPI 2021 and EKFC equations, respectively. All GFR values were expressed in ml/min/1.73 m2. Agreement between each eGFR and mGFR-DTPA was assessed by the Bland-Altman statistics, with the mean of eGFR-mGFR differences showing the bias and their standard deviation the imprecission). Accuracy was expressed as the percentage of eGFR within ±10% (A10) and ±30% (A30) of mGFR-DTPA values. The correlation between each eGFR and mGFR-DTPA was assessed by the Lin's Concordance Correlation Coefficient (LCCC). One-sample and Paired t-tests, Repeated-measures ANOVA with Bonferroni correction for multiple comparisons, Cochrane Q test and Levene's test for equality of variance were applied as appropriate. ***Results:*** SCr and mGFR-DTPA (mean±SD) were 1.8±1.0 mg/dL and 54.8±27.0. The differences between eGFR-CKD-EPI 2009, eGFR-CKD-EPI 2021, eGFR-EKFC and mGFR-DTPA (mean±SD) were 5.0±12.4, 8.0±12.9 and 2.3±11.2, respectively. All the means differed significantly in comparison to 0 ($p<0.001$) and to each other in all pairwise comparisons ($p<0.001$) as did their variances ($p<0.05$). A10 was 33.0%, 31.3% and 37.1% and A30 77.7%, 73.6% and 83.7% ($p<0.001$ for both) and LCCC was 0.895 (poor agreement), 0.872 (poor agreement) and 0.916 (moderate agreement) for eGFR-CKD-EPI 2009, eGFR-CKD-EPI 2021 and eGFR-EKFC, respectively. ***Conclusion:*** Among the GFR prediction equations CKD-EPI 2009, CKD-EPI 2021 and EKFC, the later shows the best agreement with GFR measured by 99mTc-DTPA plasma clearance in adult Caucasian patients.

EP-1015

Development of a boronic acid targeting fluorescent sensor for evaluation of intracellular localization and quantification of blood concentration of boronoagents for BNCT

S. Takada[1,2], *N. Kondo*[2], *T. Temma*[2], *M. Hagimori*[1]; *[1]Laboratory of Analytical Chemistry, Faculty of Pharmaceutical Sciences, Mukogawa Women's University, 11-68 Koshien Kyubancho, Nishinomiya, Hyogo, JAPAN, [2]Department of Biofunctional Analysis, Graduate School of Pharmaceutical Sciences, Osaka Medical and Pharmaceutical University, 4-20-1 Nasahara, Takatsuki, Osaka, JAPAN.*

Aim/Introduction: In BNCT, the intratumor concentration and intracellular localization of [^{10}B]boron are strongly related to therapeutic efficacy. In general, boron concentration in tumors is calculated from blood boron concentration measured by ICP analysis, but it has problems in simplicity. Intracellular boron localization is observed by fluorescence microscopy using the boronic acid targeting fluorescence sensor "DAHMI", but the reaction is slow and the fluorescence produced is weak. Therefore, developing a boronic acid targeting fluorescence sensor with excellent fluorescence properties would enable not only to visualize the boron localization in cells but also to quantify the blood boron concentration. We here designed a novel boronic acid targeting sensor BITQ and evaluated its effectiveness. ***Materials and Methods:*** Emission spectra of BITQ (1 μM) were measured in 0.5% DMSO-H_2O before and after adding p-boronophenylalanine (BPA, 100 μM). Temporal change in fluorescence intensity of BITQ after the addition of BPA was examined for 30 min. The relative quantum yields were measured in EtOH before and after mixing with phenylboronic acid.The results were compared with DAHMI. A microscopic fluorescence observation using BITQ (10 μM) was performed on T3M-4 cells treated or untreated with BPA-Fructose (1 mM) beforehand. BPA-fructose solution (0-900 μM) was added to blood collected from mice, and after deproteinization, BITQ (5 μM) was added, and fluorescence intensity was measured after 15 minutes. The results were compared with the ICP-MS method. ***Results:*** BITQ showed strong fluorescence at 480 nm for the maximum emission wavelength after the addition of BPA. The fluorescence intensity of BITQ stabilized within 1 minute after BPA addition, while DHAMI did not plateau until 30 min after BPA addition. The quantum yield of BITQ after adding phenylboronic acid was 0.53, which was ten-fold larger than that of DAHMI (0.053). The microscopic observation revealed a higher fluorescence in the BPA-treated T3M-4 cells compared to the BPA-untreated group. Boron concentrations measured from BITQ fluorescence method was linearly correlated with those evaluated from ICP-MS analysis with a slope of 1 ($r=0.99$). ***Conclusion:*** In this study, we developed a boronic acid targeting fluorescence sensor, BITQ, showing high quantum yield, rapid reactivity, and high quantitative scope for BPA. BITQ had excellent fluorescence properties, visualized intracellular BPA, and quantified BPA in the blood samples. Therefore, BITQ is an excellent fluorescence sensor for analyzing boronoagent for BNCT.

EP-1016

Introducing a method for increasing yield and removing the harmful and toxic solvents during the synthesis process of Sestamibi and labeling it by 99mTc to investigate its applications in vascular imaging.

V. Ghasemi*, m. alizadeh, h. m. mehrabani, e. maleki, m. ghapanvari, f. farajbakhsh, E. Lohrasbi, J. Aghamohammadi; parsisotope, Tehran, IRAN, ISLAMIC REPUBLIC OF.*

Aim/Introduction: ^{99m}Tc-Sestamibi (MIBI) is an agent increasingly used for vascular tissue imaging. Yet, toxic and harmful solvents are usually used extensively to synthesize Sestamibi. Therefore, this paper aims to introduce an approach for removing these harmful solvents during the synthesis process of Sestamibi and labeling it by ^{99m}Tc to investigate its applications in vascular imaging. ***Materials and Methods:*** The synthesis of Sestamibi began with 2-Methylallylamine hydrochloride salt as the starting material and after 3 steps, the 2-Methoxyisobutylisonitrile was successfully obtained. Each step was monitored by TLC sheets and FT-IR spectroscopy. The final crude was synthesized by reacting Tetrakis (acetonitrile) copper (i) tetrafluoroborate with 2-Methoxyisobutylisonitrile. The synthesized API agent was characterized through FT-IR, HPLC, NMR, CHNX, and mass spectrometer. Additionally, the radiochemical purity of ^{99m}Tc-Sestamibi was confirmed by Gamma-ray spectrometry. ***Results:*** The yield of the product was optimized and improved by up to 80%. The main purpose of this study was to remove toxic solvents such as Benzene and Pyridine and also to produce a pure product. To determine the pure product HPLC was used and accordingly, a single sharp peak in the HPLC diagram was observed proving that the product was pure. To confirm the structure of the product FT-IR, NMR, and Mass spectrometer were utilized. The results confirmed the structure of Sestamibi. The radiochemical study showed that the synthesized API had been properly labeled. Eventually, the biodistribution of the prepared kit was checked on the rat and the results showed high cellular uptake in the coronary tissues.

Conclusion: This method proves that Sestamibi can be synthesized with high yield and purity. The preclinical studies of the prepared kit show high cellular uptake in the Coronary tissues. Considering the wide diagnostic applications of ^{99m}Tc-Sestamibi and its complex production process in which harmful solvents are usually used, this approach not only has removed the said toxic solvents but also has proved a high yield.

EP-65

e-Poster Area

Technologists e-Posters

EP-1017

Implementation of the new national directive to reduce radioactive waste disposal costs in nuclear medicine and radiometabolic therapy departments

M. Anelli[1], *M. Nicoletto*[2], *A. Zambelli*[3], *A. Di Nicola*[1];
[1]*Azienda Sanitaria Locale di Pescara, Pescara, ITALY,*
[2]*Policlinico di Abano Terme, Abano Terme (PD), ITALY,* [3]*Azienda Ospedaliera Universitaria di Padova, Padova, ITALY.*

Aim/Introduction: This study concerns the compliance of nuclear medicine departments with the new ministerial directives provided for by Legislative Decree No. 101 dated July 31st, 2020 (Directive 2013/59/EURATOM). This act aims to explain and regulate proper management of radioactive waste that is generated in nuclear medicine and radiometabolic therapy departments, also according to national standards. The regulation adjustment provided a new internal protocol concerning radioactive waste management, which was edited on 31st January 2023 in collaboration with the medical physics department. In the relevant case, new storage areas have been identified and new tools for residual radiation counting have been acquired. ***Materials and Methods:*** Nuclear medicine and metabolic therapy use unsealed radioactive substances for diagnostic and therapeutic purposes, thus producing:- solid waste consisting of vials with residual solutions, needles, syringes, disposable gloves, absorbent cotton, paper towel, patient disposal items and belongings that have been in contact with contaminated excretions;- Tc99m generators;- solid waste consisting of protecting equipment used by the staff for radiation protection purposes such as gloves and shoe covers. Generally, radioactive isotopes found in waste are F18, Tc99m, I131, I123, In111, Ga67, Tl201, characterized by a half-life (T/2) lower than 60 days. ***Results:*** The new ministerial directive has brought to significant improvements in the management of radioactive waste. As a result, radioactive waste must go through three steps before being disposed of:1. First, the waste is placed in shielded containers and maintained in temporary storage areas with shielded walls until the containers are filled.2. Once the containers are filled, they are placed in biohazard containers, then sealed, labelled and transported to a new storage area where waste will be listed and divided depending on the isotope. 3. Finally, when it is no longer radioactive (less than 1 kBq/kg), it will be delivered to hospital waste management operators. ***Conclusion:*** Management of radioactive waste has been simplified through the identification of a storage area (see point 3) which is located outside the department, allowing waste to lose radioactivity far from operators and patients. Once radioactivity has decreased enough, the waste can be disposed of, as it is done with ordinary hospital waste. According to first estimates, this method will allow savings of 36% in disposal costs on an annual basis. Furthermore, a first CME course was held by a qualified expert in March 2023, with the purpose of updating all department members. ***References:*** Legislative Decree No. 101/2020, Directive 2013/59/EURATOM

EP-1018

Usefulness of simplified respiratory motion freeze devise (IKI-TOMEHIRO-KUN) in myocardial perfusion SPECT

H. Ichikawa[1,2], *T. Kato*[1], *H. Kondo*[3], *T. Shibutani*[2], *H. Shimada*[1], *M. Onoguchi*[2];
[1]*Toyohashi Municipal Hospital, Toyohashi, JAPAN,*
[2]*Kanazawa university, Kanazawa, JAPAN,* [3]*Nagoya University Hospital Department of Cardiology, Nagoya, JAPAN.*

Aim/Introduction: Patient and organ motion occurs in 25-36% of cases in myocardial perfusion SPECT and contributes to artifact generation, and artifact can lead to an inaccurate diagnosis [1, 2]. The purpose of this study was to assess a usefulness of a simplified respiratory motion freeze (RMF) devise (IKI-TOMEHIRO-KUN, ITK). ***Materials and Methods:*** ITK is a pentagonal shape with a length of 20 cm, a width of 20 cm, and a thickness of 10 cm, constructed of Styrofoam. ITK was wrapped around the patient's abdomen during deep exhalation with a gamma camera belt to effectively suppress cardiac motion associated with respiratory motion. We retrospectively evaluated 91 patients who underwent 1-day load/rest or early rest/delayed MPS with ^{99m}Tc-labeled agents for suspected or known CAD at our institution. SPECT of all patients were scanned on one day in two phases; early (stress or rest) and delayed (rest). All projected data were classified into four levels of degree of cardiac motion: absent (0), mild (1), moderate (2), and severe (3), based on observation of cinematic displays, sinograms, and linograms. The degree of artifacts in SPECT images was visually assessed by motion artifact and overlapping hot spots due to activity in the gastrointestinal tract. ***Results:*** The degree of motion in the control group was absent 10.3%, mild 51.7%, moderate 34.5%, and severe 3.4%, and in the RMF group 39.7%, 38.1%, 19.0%, and 3.2%, respectively, in the same order. In the projection data, the degree of heart motion in RMF group was significantly smaller than that in the control group. The frequency of cardiac bounce in RMF and control groups was identical, whereas the frequency of cardiac shift and creep in RMF group was markedly lower than that in the control group. The degree of motion artifact in SPECT images of RMF group was significantly smaller than that of the control group. ***Conclusion:*** ITK may be a useful device in myocardial perfusion SPECT to reduce patient and organ motion and prevent artifact generation. ***References:*** Germano G. Technical aspects of myocardial SPECT imaging. J Nucl Med. 2001;42(10):1499-507.Wheat JM, Currie GM. Incidence and characterization of patient motion in myocardial perfusion SPECT: Part 1. J Nucl Med Technol. 2004;32(2):60-5.

EP-1019

Does high Radiochemical purity obviate the need for a biodistribution whole body image in 68Ga-NOTA-UBI PET/CT?

S. Maurya, *N. Damle, S. Ballal, A. Singhal, V. Tiwari, C. Bal, N. Singh, Y. Dharmashaktu, D. Khan, S. Sagar, A. Gawande;*
All India Institute of Medical Sciences, New Delhi, INDIA.

Aim/Introduction: ^{68}Ga-NOTA-UBI is a PET based infection imaging agent with evolving interest. Biodistribution of the tracer is in liver, kidneys and bladder and sometimes spleen. Abnormal biodistribution however can lead to false results. Since it is a relatively new tracer synthesized in house each time, we acquire

a wholebody image to confirm appropriate biodistribution before attempting to interpret the scans. We aimed to study if the whole-body image can be done away with and only a regional spot view taken when normal biodistribution is repeated. ***Materials and Methods:*** NOTA-UBI was procured from ABX, Germany. 300ug of peptide was used in each synthesis. ^{68}Ga-Cl3 was eluted from the generator and sodium acetate buffer was added followed by addition of the peptide The contents were heated at 95degrees C for 10 minutes. After cooling, it was passed through a C18 Sep Pak cartridge. The product was eluted with 50% ethanol. Quality control was performed by paper chromatography with sodium citrate as the solvent. ***Results:*** We synthesized the tracer a total number of 12 times. Time for synthesis after elution of ^{68}GaCl3 was 16±2 minutes (range 14-20min). Starting activity of ^{68}Ga was 13.8±1.5 mCi (range 8-17.9mCi). Final tracer synthesized was 7.05 ± 0.95 mCi (range 4-11mCi). Quality control revealed Radiochemical purity of 98.28 ± 2.25 % (range 96.26-99.45). Images were analysed qualitatively by three independent Nuclear Medicine physicians. Biodistribution was satisfactory in all 23 patients and images were considered interpretable. Delayed imaging of region of interest revealed similar uptake in suspicious lesions with no qualitative difference as assessed by visual analysis. ***Conclusion:*** In the setting of high radiochemical purity, it is adequate to perform only a limited imaging over the region of interest and get satisfactory images. A whole body image to confirm biodistribution seems unnecessary and may be omitted to decrease the radiation exposure to the patient as well as time for completion of the scan. This is especially important in a busy department with high patient volumes.

EP-1020

Evaluation of 68Ga-NOTA-Ubiquicidin (29-41) PET/CT with early and delayed imaging through qualitative and quantitative analysis.

N. Singh, *N. Damle, S. Maurya, A. Singhal, S. Ballal, V. Tiwari, A. Gawande, P. Kumar, C. Bal, S. Sagar, J. Jaleel;*
All India Institute of Medical Sciences, New Delhi, INDIA.

Aim/Introduction: Radiolabelled Ubiquicidin (UBI) 29-41 shows preferential binding of cationic peptide with the anionic microbial cell membrane at the site of infection. This peptide can be chelated with a bifunctional chelating agent (BFCA) NOTA to allow complexation with 68Ga to form 68Ga-NOTA-UBI [1]. We aimed to evaluate whether delayed imaging is better for interpretation as compared to routine imaging performed at 45-60 min [2]. ***Materials and Methods:*** Seventeen patients with suspected periprosthetic, soft tissue, and lung infections were included in the study.148 MBq of 68Ga-NOTA-UBI-29-41 were administered intravenously to the patients. PET imaging (whole body) was performed at 45-60 min (early) and repeated at 1.5 h (delayed) only at the region of interest. A qualitative and semi-quantitative evaluation was performed. Qualitative analysis was performed by three independent nuclear medicine physicians who evaluated the image quality and their scan interpretation was noted. Image quality was classified as excellent, good, and acceptable. The semi-quantitative analysis was performed by comparing the target-to-background ratio (TBR) in early and delayed imaging. The target-to-background ratio (TBR) was calculated by dividing the maximum standardized uptake value (SUVmax) of a positive lesion by its contralateral side. ***Results:*** Out of 17 patients (mean age, 46.1 years; range, 23-67 years), 14 were males and 3 were females. In qualitative analysis, out of 17 scans, 14 were graded excellent, 2 were good and 1 was satisfactory in image quality. Delayed imaging was better in 2/17 cases by one of the physicians. On the visual score, the target-to-background contrast (T/B) of the lesion was perceived to be almost similar in both sets of images. In semi-quantitative analysis, the mean value of TBR of the region of interest in the early image was 3.12 ± 1.54 & in the delayed image it was 3.948 ± 1.91. There was no statistically significant difference between the TBR of early and delayed images (p=0.2). ***Conclusion:*** We conclude that single time point imaging at 60 min is sufficient to achieve acceptable diagnostic confidence & delayed imaging may not have an additional benefit. ***References:***
1. Akhtar MS, Qaisar A, Irfanullah J, Iqbal J, Khan B, Jehangir M, et al. Antimicrobial Peptide 99mTc-Ubiquicidin 29-41 as Human Infection-Imaging Agent: Clinical Trial. Journal of Nuclear Medicine. 2005 Apr 1;46(4):567-73. 2. Nishiyama Y, Yamamoto Y, Monden T, Sasakawa Y, Tsutsui K, Wakabayashi H, et al. Evaluation of delayed additional FDG PET imaging in patients with pancreatic tumour. Nuclear Medicine Communications. 2005 Oct;26(10):895.

EP-1021

The impact of multi-bed SPECT-CT misregistration on routine clinical service delivery

L. Wason, *R. Williamson, J. Dixon, C. Reilly, A. Nicol;*
NHS Greater Glasgow and Clyde, Glasgow, UNITED KINGDOM.

Aim/Introduction: Many centres perform multi-bed SPECT-CT to localise areas of radiopharmaceutical uptake indicative of disease. Commissioning of a new SPECT-CT gamma camera identified misregistration of the SPECT and CT data for multi-bed acquisitions that did not occur for single bed acquisitions. Further investigations confirmed the artefact on another system in the department. Modifications are required to our acquisition and reconstruction techniques for both systems utilising multi-bed acquisition mode. Precise SPECT-CT registration is necessary for localisation of radiopharmaceutical uptake and accurate reconstruction (e.g. attenuation correction, scatter correction), this work outlines the practical solutions implemented across two different systems within our department. ***Materials and Methods:*** New image reconstruction workflows were developed for multi-bed SPECT-CT acquisitions. Hardware and software differences between each system required implementation of different image reconstruction workflows. Upgraded software options available on the new system allows reconstruction of the multi-bed SPECT data as one dataset, with minimal misregistration, to be viewed fused with the single CT acquisition, covering the whole field of view. Technologist staff review this registered image, comparing high intensity landmarks (e.g. liver/kidneys on ^{99m}Tc-Tektrotyd scans) to relevant CT anatomy to check for misregistration. On the older system, where this upgraded software is not available, the SPECT data from each bed position must be reconstructed and checked individually, to prevent significant misregistration occurring. This means the benefit of multi-bed acquisitions is lost from a reporting perspective, but there is still a benefit from the acquisition viewpoint in that there is a dose saving from not overlapping CT between each SPECT bed position. ***Results:*** The detection of this fault prevents misregistration of the SPECT and CT data occurring on a patient acquisition. Collaboration with the manufacturer confirmed the existence of the fault in other systems, improving understanding of the cause leading to development of new image reconstruction workflows across all affected systems that included a registration quality check. Implementation of these workflows has enabled multi-bed acquisition, resulting in a time saving for the patient and staff, as well as a dose saving from not overlapping CT exposures. ***Conclusion:*** This investigation demonstrates there may be technical challenges associated with reconstructing

multi-bed SPECT-CT acquisitions. The technique increases patient throughput, reduces waiting times, and through use of a single CT acquisition, helps to reduce the patient's CT exposure to as low as reasonably practicable. Further work on this will include raising operator awareness and developing an ongoing quality assurance programme.

EP-1022

Image evaluation of different 99mTc/123I ratios for simultaneous dual-isotope myocardial SPECT using D-SPECT cardiac camera

T. Shibutani[1], *M. Onoguchi*[1], *H. Yoneyama*[2], *T. Konishi*[2], *K. Nakajima*[3];
[1]*Department of Quantum Medical Technology, Institute of Medical, Pharmaceutical and Health Sciences, Kanazawa University, Kanazawa, Ishikawa, JAPAN,* [2]*Department of Radiological Technology, Kanazawa University Hospital, Kanazawa, Ishikawa, JAPAN,* [3]*Department of Functional Imaging and Artificial Intelligence, Kanazawa University, Kanazawa, Ishikawa, JAPAN.*

Aim/Introduction: The ^{99m}Tc images for ^{99m}Tc/^{123}I simultaneous dual-isotope myocardial SPECT with cadmium-zinc-telluride cardiac camera are affected by scattered radiation and crosstalk from ^{123}I, and scatter correction (SC) is expected for quantitation. However, the image characteristics of the ^{99m}Tc SC image was influenced by various ^{99m}Tc and ^{123}I injection dose settings as experienced in clinical studies. We demonstrated the image quality and correction effect of the ^{99m}Tc images for different ^{99m}Tc/^{123}I ratios. ***Materials and Methods:*** Three types of myocardial models of normal, anterior, and inferior wall defective myocardium were created using an anthropomorphic myocardial phantom. The ^{99m}Tc/^{123}I ratio was set to 1.0, 3.5, 5 and 6.5, which were determined by possible clinical settings of ^{123}I-MIBG and ^{123}I-BMIPP imaging. Energy settings were 105-130 keV for ^{99m}Tc scatter window, 133-145 keV for ^{99m}Tc main window, 145-152 keV for ^{123}I scatter window and 152-168 keV for ^{123}I main window. SPECT images were acquired by D-SPECT (Spectrum Dynamics Medical), and the scan time was adjusted with a left ventricular count of 1.5 million counts for ^{123}I. Reconstructed images with no correction (NC) and SC were obtained using Spectrum Dynamics (SD) reconstruction. The parameters of Gaussian filter were set to 1, 3 and 5 as a kernel setting, and 0.25 to 1 as Gaussian standard. The percent coefficient of variance (%CV) was calculated from a 17-segment polar map. Cavity contrast and circumferential profile were analyzed using normal and defect myocardial images. ***Results:*** ^{99m}Tc SC images in a normal model showed a lower %uptake in the inferior wall compared with ^{99m}Tc NC images. The %uptake of the inferior wall for the ^{99m}Tc SC images decreased approximately 5% with decreasing ^{99m}Tc/^{123}I ratio. However, the decrease of %uptake in the inferior wall was improved by adjusting the kernel of the Gaussian filter. The minimum %uptake on the short-axis circumferential profile for ^{99m}Tc/^{123}I ratio of 1.0, 3.5, 5.0 and 6.5 in ^{99m}Tc SC image was 34.8%, 24.7%, 26.1% and 26.6% for the anterior wall, and 30.5%, 32.3%, 34.3% and 34.5% for the inferior wall, respectively. The %uptake of defect region was independent of ^{99m}Tc/^{123}I ratio. ***Conclusion:*** The normal myocardial distribution of the ^{99m}Tc SC images was affected by ^{99m}Tc/^{123}I ratio and reduced inferior activity with relatively low ^{99m}Tc/^{123}I ratio could be corrected by appropriate Gaussian filter setting. The dependency of accuracy on ^{99m}Tc/^{123}I ratio needs to be considered when ^{99m}Tc/^{123}I mismatch is relatively small.

EP-1023

Assessing glomerular filtration rate through blood sampling via port and arm vein.

C. H. Led[1], *L. J. Jeppesen*[1], *O. Gerke*[1,2], *S. Hvidsten*[1], *J. A. Simonsen*[1,2];
[1]*Department of Nuclear Medicine, Odense C, DENMARK,* [2]*Department of Clinical Research, University of Southern Denmark, Odense, DENMARK.*

Aim/Introduction: Glomerular filtration rate (GFR) can be determined accurately from plasma clearance of Tc-99m-DTPA. To avoid recurrent venous punctures in cancer patients, who often have fragile vessels, a subcutaneous port with a catheter extending into a central vein can be installed. The port has a silicone membrane through which drugs can be injected and blood samples drawn. However, the membrane may retain part of the injected tracer biasing calculations and hence GFR. Furthermore, the port has a reservoir in which the tracer may accumulate and eventually be withdrawn by blood sampling. We have previously demonstrated the feasibility of injection of the GFR tracer and blood sampling by port. In the present study, we set out to investigate whether GFR based on blood samples from the port differed from those obtained from a peripheral vein. ***Materials and Methods:*** Patients referred to our department for GFR examination, who already had a port installed, were invited to participate in the trial. Eight patients consented. We administered the tracer into the port through a single-lumen catheter with only one access point. We injected 8 MBq of Tc-99m-DTPA through a three-way stopcock and flushed it with isotonic saline. After three hours we draw two blood samples from an arm vein and four blood samples from the port, the first two portal samples were discarded. The blood samples were processed as in the clinical routine; hence, after centrifugation and pipetting, plasma activity was counted in a well counter (Wizard 2470 gamma counter) and GFR was calculated according to Groth & Aasted. ***Results:*** The mean (range) GFR calculated from peripheral venous blood samples was 59.9 (29-101) ml/min compared to 63.8 (31-108) ml/min for the portal samples. The difference between GFR from the peripheral and portal samples ranged from -7 to -1, and GFR from the arm vein was statistically lower (mean difference: -3.81, 95% CI: -5.86 to -1.77; p-value 0.008, Wilcoxon matched-pairs signed-rank test). ***Conclusion:*** Our concern regarding contamination of the portal samples and thus a falsely reduced GFR was belied since there was consistently lower activity in the portal than in peripheral venous samples. We speculate that this surprising difference stems from a mixture of the central venous blood with filtered blood from the renal veins combined with the longer return time of the peripheral blood. Further, venous stasis from tourniquet placement during venipuncture may delay the return of the peripheral venous blood.

EP-1024

Examination of optimum conditions for 99mTc brain perfusion SPECT using a new SZHRX collimator

T. Nishiyama[1], *M. Onoguchi*[1], *T. Shibutani*[1], *A. H. Vija*[2], *F. Massanes*[2], *T. Shimizu*[2], *H. Yoneyama*[3], *T. Konishi*[3], *H. Mori*[4], *K. Nakajima*[5];
[1]*Department of Quantum Medical Technology, Graduate School of Medical Sciences, Kanazawa University, Kanazawa, JAPAN,* [2]*Siemens Medical Solutions UNITED STATES OF AMERICA, Inc., Hoffman Estates, IL, UNITED STATES OF AMERICA,* [3]*Department of Radiological Technology, Kanazawa University Hospital, Kanazawa, JAPAN,* [4]*Department of Nuclear Medicine, Kanazawa University Hospital, Kanazawa, JAPAN,* [5]*Department of Functional Imaging and Artificial Intelligence, Kanazawa University, Kanazawa, JAPAN.*

Aim/Introduction: A new multi-focal SMARTZoom class collimator with a suitable high resolution and extended magnification volume (SZHRX) is applied to nuclear cardiology and neurology applications. The goal of this study is to investigate optimal counts and reconstruction conditions for brain perfusion SPECT using the SZHRX collimator. ***Materials and Methods:*** The Symbia Intevo 16 (Siemens Healthineers) SPECT/CT scanner was equipped with prototype SZHRX collimators. A Hoffman phantom was filled with ^{99m}Tc solution. The SPECT data were acquired with 256× 256 matrices, 2.4mm pixel size with a circular brain centered orbit radius of 26cm, and 3 deg./angular step, and the average count in the anterior view of the brain planner image is 2-24 counts/pixel. The SPECT image were reconstructed with a prototype quantitative xSPECT using the ordered subset conjugated gradient method (OSCGM) including system modeling, attenuation, and scatter corrections. The reconstruction parameters were varied from 24 to 60 for the number of updates and from 4.8 to 12mm for a full width at half-maximum (FWHM) of Gaussian filter. For physical analysis, each condition was evaluated by percent-coefficient of variation (%CV), percent contrast (%contrast), normalized mean square error (NMSE). In addition, image uniformity and separation of thalamus were evaluated by visual evaluation. ***Results:*** %contrast was nearly constant for 8 counts or more regardless of Gaussian filter FWHM and the number of updates. On the other hands %contrast varied significantly at lower counts. Similarly, %CV and NMSE showed almost constant values up to approximately 8 counts, while their values were higher at lower counts. %contrast was higher for increasing number of updates and decreasing Gaussian filter FWHM, whereas the %CV was worse. The optimal reconstruction conditions were determined from the physical and visual assessment. ***Conclusion:*** We determined that the optimal reconstruction parameter for brain perfusion SPECT imaging of the SZHRX collimator were Gaussian filter FWHM 7.2mm and number of updates 48 for more than 8 counts, Gaussian filter FWHM 9.6mm and number of updates 48 or more for less than 8 counts.

EP-1025

Inter- and intraobserver and the test-retest variability in bone density measurement in vertebral fracture assessment on DXA

S. Wongjarern*, A. Willemsen, R. Slart;*
UMCG, Groningen, NETHERLANDS.

Aim/Introduction: During an audit of the Dual-energy X-ray absorptiometry (DXA) at our department of Nuclear Medicine the variability in bone density measurement (BDM) and vertebral fracture assessment (VFA) was lacking and it was advised to evaluate this. Therefore, the aim of this project was to evaluate the variability in BDM and VFA. ***Materials and Methods:*** In total thirty patients were scanned twice by three technologists. The BDM of the left hip and the mean of the four lumbar spine (L1-L4) was determined. In addition, the VFA (Th4-L4) was scored as normal, crush, wedge or biconcave. The first scans, test (T), were processed by each technologist to determine the interobserver variability. In addition, each technologist processed ten of these scans for the second time, to determine the intraobserver variability. Similarly, each technologist also processed ten of the second scans, retest (RT). The results were compared with the first scan to determine the test-retest variability. For each comparison the mean and standard deviation (SD) were calculated and reported as percentages. As for the BDM, the same approach was used to determine the inter- and intraobserver variability. For the VFA we calculated the concordance as match, mismatch or missing, when a vertebrae could not be evaluated. ***Results:*** The interobserver variability between the three technologists ranged on average for the hip from -0,47% to 0,09% and for the lumbar spine -0,51% to 0,24%, respectively. The intraobserver variability ranged on average for the hip from -0,06% to 0,5% and for the lumbar spine -0,01% to -0,08%, respectively. As expected the mean error was very small indicating there is no bias. The SD were similar for all three observers. On average the intraobserver variability was lower than the interobserver variability. The test-retest variability was somewhat higher than the inter- and intraobserver variability indicating that the scan itself is the major source of variability. For the VFA a concordance 90% was found for both the inter- and intraobserver comparison. The remaining 10% was approximately equally divided between mismatch and missing. ***Conclusion:*** The inter-and intraobserver variability on DXA was lower than the test-retest variability for BDM with an excellent agreement for VFA. For therapy evaluation, taking a difference of two SD as significant, we found a threshold slightly less than 4%.

EP-1026

The Advantages of using Nitrogen-13 Ammonia PET Imaging in Flow Quantification of Microvascular Diseases

G. Daigneault*, M. Balu, M. Menelas;*
CHUM, Montreal, QC, CANADA.

Aim/Introduction: Clinical PET myocardial perfusion imaging provides significant improvement in diagnostic performance of myocardial perfusion, in comparison to SPECT imaging. Particularly, it allows assesment of microvascular diseases and accurate blood flow quantification, and other potential applications. ***Materials and Methods:*** 1300 PET N-13-Ammonia myocardial perfusion imaging quantification were performed in our hospital since 2018. All patients were recruited through our open label research protocol. The onsite cyclotron generates from 620 to 800 mCi per beam, so 4 patients can be imaged per batch. In our facility, with the involvement of our technologists, nuclear medecine physicians and cyclotron team, we have established a rigorous onsite protocol, to have an effective way of executing the N-13-Ammonia perfusion imaging. ***Results:*** Considering the limitations of this particular exam (availability of the radionuclide, selective criterias for patient selection in the study, department resources), the contribution in the diagnosis of microvascular diseases has a high specificity and accuracy for cardiologists, especially in hemodynamics. It has been integrated in our Women's Cardiovascular Health Clinic, with a high success rate in diagnosis and prognosis in cases of equivocal SPECT imaging or suspect microvascular diseases. ***Conclusion:*** Quantification of myocardial perfusion using PET N-13-Ammonia provides a high performance level myocardial perfusion imaging, both in accuracy and specificity, and is minimally invasive. It is also a good exam to consider in advanced atherosclerosis, in nonatherosclerosis microvascular diseases, defining prognosis, and evaluation of therapies. ***References:*** Clinical PET Myocardial Perfusion Imaging and Flow Quantification, Daniel Juneau et al., 2016; Assessment of Diagnostic Performance of Quantitative Flow Measurements in Normal Subjects and Patients With Angiographically Documented Coronary Artery Disease by Means of Nitrogen-13 Ammonia and Positron Emission Tomography, Otto Muzik et al., Journal of the American College of Cardiology, Volume 31, Issue 3, March 1998, Pages 534-540; In-house protocol chart.

EP-1027

Investigation of volumetric measurements from gated myocardial perfusion Multi-Pinhole SPECT with shortening acquisition time

M. Alamin[1], *S. Barna*[2], *V. Bencze Linczerné*[3], *K. Kukuts*[3], *A. Oszlanszki*[3], *J. Varga*[4], *Á. Krizsán*[3], *A. Forgács*[3], *I. Garai*[2];
[1]*University of Debrecen, Debrecen, HUNGARY,* [2]*University of Debrecen, Faculty of Medicine, Department of Medical Imaging, Division of Nuclear Medicine; Scanomed Nuclear Medicine Centres, Debrecen, HUNGARY,* [3]*Scanomed Nuclear Medicine Centres, Debrecen, HUNGARY,* [4]*University of Debrecen, Faculty of Medicine, Department of Medical Imaging, Division of Nuclear Medicine, Debrecen, HUNGARY.*

Aim/Introduction: Triple-headed system equipped with multi-pinhole collimator (MPH-Cardiac) has significantly improved system volumetric sensitivity for cardiac imaging, making possible to reduce acquisition time. The aim of this study was to evaluate how volumetric parameters of gated myocardial perfusion SPECT are reproducible with shorter time. In addition, we have extracted and compared the same parameters from parallel-hole SPECT imaging. ***Materials and Methods:*** 34 patients (median age: 61 years) underwent 46 cardiac gated ^{99m}Tc- MIBI MPI scans (17 rest, 29 stress). Using 2-days protocol. 40 ± 20 min after the administration of 350 MBq ^{99m}Tc-MIBI each patient were examined on two systems in randomized order. Image acquisitions were performed with LEHR collimators on a dual-headed SPECT system (AnyScan-SC) in 90° detector configuration, 64 views covering 180° scan arc, and the MPH-Cardiac collimators on a triple head SPECT system (AnyScan-SC-TRIO) in 75° detector configuration, 125° scan arc. Projection images with shorter acquisition time (10, 8, 6, 4, and 2 minutes) were generated from the MPH-Cardiac SPECT list mode. Image reconstructions were performed with Tera-Tomo 3D SPECT using 128 resolution, iterations 8 subsets 3.6 mm voxel size for the MPH-Cardiac, and OSEM with Butterworth pre-filter 6.5 mm voxel size in case of the LEHR. Attenuation and scatter correction was not applied. Ejection fraction (EF), end diastolic volume (EDV) and end systolic volume (ESV) were evaluated by two experienced nuclear medicine experts using dedicated cardiac software (INVIA-Corridor-4DM, 2017). Observer variability were investigated with the calculation of Interclass Correlation Coefficient (ICC) for each parameter (EDV, ESV, EF) and for both acquisitions and for each acquisition time regarding MPH-cardiac SPECT. The presence of differences between the measured volumetric parameters were evaluated with nonparametric paired-sample test (Wilcoxon signed rank test). The statistical calculation was carried out using IBM SPSS, 28. ***Results:*** Observer variability indicates good reliability for parallel hole images (worst ICC = 0.766 for EF) and excellent reliability for MPH cardiac images (ICC > 0.9), even for 4 and 2 minute scans. There was no significant difference between the measured ESV (mean 36.6 ml for MPH and 30.2 ml LEHR, p=0.857) and EF (p=0.065, for MPH 69.9 ml vs 68.6 ml LEHR). The EDV values were significantly bigger for MPH-Cardiac images (p<0.001, mean 110.2 ml for MPH and 90.4 ml for LEHR). ***Conclusion:*** Triple-headed SPECT system equipped with dedicated cardiac multi-pinhole collimator provide reliable volumetric measurements during significantly shorter acquisition time with excellent reader agreement.

EP-1028

Overall survival of patients undergoing transarterial radioembolization (TARE) and the influence of additional treatments, injected activity and mean dose to the tumor

S. Ialuna[1], *N. Quartuccio*[1], *D. Scalisi*[2], *F. D'Amato*[3], *M. R. Barcellona*[4], *M. G. Bavetta*[4], *G. Fusco*[4], *E. Bronte*[5], *E. Musso*[5], *F. Bronte*[6], *V. Picciotto*[4], *A. Carroccio*[4], *F. Verderame*[5], *G. Malizia*[6], *F. La Gattuta*[7], *A. M. Moreci*[1];
[1]*Nuclear Medicine Unit, A.O.O.R. Villa Sofia Cervello, Palermo, ITALY,* [2]*Health Physics Unit, A.O.O.R. Villa Sofia Cervello, Palermo, ITALY,* [3]*Unit of Interventional radiology, A.O.O.R. Villa Sofia Cervello, Palermo, ITALY,* [4]*Internal Medicine Unit, A.O.O.R. Villa Sofia Cervello, Palermo, ITALY,* [5]*Clinical Oncology Unit, A.O.O.R. Villa Sofia Cervello, Palermo, ITALY,* [6]*Gastroenterology Unit, A.O.O.R. Villa Sofia Cervello, Palermo, ITALY,* [7]*Interventional Radiology Unit, A.O.O.R. Villa Sofia Cervello, Palermo, ITALY.*

Aim/Introduction: To present the preliminary experience of our center with transarterial radioembolization (TARE) with Yttrium-90, with regards to overall survival (OS) in different pathologies. The secondary goals of the study included the influence of additional treatments, injected activity, mean dose to the tumor on OS. ***Materials and Methods:*** The database of our center was interrogated to retrieve patients who had undergone TARE with Yttrium-90 glass or resin microspheres. The following information were searched for the inclusion to the study: 1) type of pathology; 2) sex; 3) age; 4) administered activity; 5) mean dose to the tumor; 6) additional treatments; 7) OS. The OS of the different groups of patients, based on pathology and additional treatment were compared (p<0.05). A bivariate correlation (p<0.05) was used to investigate the association between injected activity and OS, and between mean dose to the tumor on OS. ***Results:*** From a total of 150 patients who had undergone TARE, 39 patients with complete datasets were retrieved (Sex: 27 M, 12 F; mean age: 61.26 ± 14.95 years). The pathologies treated with TARE were hepatocellular carcinoma (HCC; n=23) and liver metastasis from colon cancer (n=16). The median follow-up from TARE to the last available record (April 2023) was 69 months (range: 39-91 months). Mean administered activity was 2.2 ± 0.9 GBq; mean dose to the tumor was 282.68 Gy. Additional treatments included Sorafenib (n=7), Regorafenib (n=2) or both (1). Patients with HCC demonstrated a significantly longer OS than those with liver metastasis (22.66±19.11 vs. 10.41±8.75 months; p=0.022). Patients with liver metastases from colon receiving additional treatment demonstrated a longer OS than patients receiving only TARE (23.50±19.76 months vs. 8.54±5.31; p=0.018); there was a direct correlation between injected activity and OS (R=0.55, p=0.034) and between mean activity reaching the tumor and OS (R=0.812; p=0.008). Patients with HCC receiving additional treatment (n=8) demonstrated a trend for longer OS than patients receiving only TARE (n=15; 31.07±18.20 months vs. 18.20±18.66; p=0.13); there was a trend towards a direct correlation between mean dose to the tumor and OS (R=0.45, p=0.118). ***Conclusion:*** In our experience, patients with HCC receiving TARE achieve a longer OS than those with liver metastases from colon cancer. Additional treatments and increasing injected activity and mean dose to the tumor are beneficial for outcome, especially in patients with liver metastases from colon cancer.

EP-1029

Quantitative Parameters of 99mTc-PYP SPECT/CT Correlates with Left Ventricle Diastolic Dysfunction in Transthyretin Amyloid Cardiomyopathy, Not Myocardial Perfusion Reserve

Y. Chen[1], *C. Ko*[1], *J. Cheng*[1], *A. Yu*[2], *C. Tsai*[2], *P. Tseng*[3], *C. Chao*[4], *M. Cheng*[1], *Y. Lin*[2];
[1]*Department of Nuclear Medicine, National Taiwan University Hospital and National Taiwan University College of Medicine, Taipei City, TAIWAN,* [2]*Department of Internal Medicine, Division of Cardiology, National Taiwan University Hospital and National Taiwan University College of Medicine, Taipei City, TAIWAN,* [3]*Department of Internal Medicine, Division of Gastroenterology, National Taiwan University Hospital and National Taiwan University College of Medicine, Taipei City, TAIWAN,* [4]*Department of Neurology, National Taiwan University Hospital and National Taiwan University College of Medicine, Taipei City, TAIWAN.*

Aim/Introduction: Coronary microvascular dysfunction has been previously documented in cardiac amyloidosis even in the absence of obstructive epicardial coronary artery disease (CAD). ^{99m}Tc-pyrophosphate (PYP) scintigraphy is used to support the diagnosis of transthyretin amyloid cardiomyopathy (ATTR-CM) when unexplained increased left ventricle (LV) wall thickness is observed on echocardiography. However, the relationship between PYP accumulation, LV morphology, and myocardial blood flow (MBF) remains unexplored. Consequently, our study aims to assess the roles of ^{99m}Tc-PYP scans, echocardiography, and quantitative ^{201}Tl myocardial perfusion imaging (MPI)-derived parameters in patients with ATTR-CM. ***Materials and Methods:*** We retrospectively analyzed 34 patients (mean age 65.6±6.8 years, 71% women) diagnosed with ATTR-CM without CAD. All patients underwent quantitative ^{201}Tl MPI, ^{99m}Tc-PYP scan, and echocardiography within a 3-month period. Quantitative global stress/rest MBF and myocardial perfusion reserve (MPR) were computed using in-house software. PYP images were analyzed using both planar heart-to-contralateral lung (H/CL) ratio and volumetric heart-to-lung (H/L) ratio from SPECT/CT. These parameters were compared with indices derived from echocardiography (including interventricular septal diameter (IVSd), left ventricular posterior wall diameter (LVPWd), left ventricular end-diastolic diameter (LVEDd), left ventricular ejection fraction (LVEF), and stroke volume) and serum N-terminal pro-B-type natriuretic peptide (NTproBNP) levels through Pearson correlation analysis. ***Results:*** The median serum NTproBNP level and LVEF were 733.8 pg/mL(range, 31.1-3269) and 62.7%(range, 33.3-81.3%). NTproBNP showed a negative correlation with stress MBF (r=-0.667, p<0.0001), MPR (r =-0.532, p<0.005), and LVEF (r =-0.526, p<0.005), but a positive correlation with LVPWd (r=0.644, p<0.0001). Both stress MBF and MPR demonstrated negative correlations with wall thickness (IVSd, LVPWd, r=-0.401, -0.554, and -0.352, -0.339, respectively, all p<0.05). The volumetric H/L ratio was the only parameter that displayed a negative correlation with LVEDd (r=-0.352, p<0.05) and stroke volume (r=-0.447, p<0.01). No significant correlation was found between the volumetric H/L ratio and LV wall thickness or dynamic MPI indices. ***Conclusion:*** The results of our study suggest that a reduced myocardial reserve, as seen in dynamic MPI, has a relationship with elevated cardiac biomarkers and increased LV wall thickness identified in echocardiography. In contrast, the volumetric H/L ratio, obtained from PYP scans, displays a negative correlation with end-diastolic diameter and stroke volume. These findings underline the potential value of PYP imaging in assessing the degree of diastolic dysfunction in ATTR-CM, a condition often first detected in patients with preserved ejection fraction.

EP-1030

Optimization of Classical Pulmonary SPECT on a Revolutionary Camera

S. Hirsi[1,2], *A. E. Pedersen*[3,2], *H. Precht*[3,4,5], *S. Hess*[6,7,8], *R. Horvat*[6,7], *M. H. Vilstrup*[6,7], *P. L. Hansen*[2,4], *T. Q. Christensen*[7,9];
[1]*Department of Nuclear Medicine and PET Centre, Aarhus University Hospital, Aarhus, DENMARK,* [2]*Education of Radiography, UCL University College, Odense, DENMARK,* [3]*Department of Radiology, Lillebaelt Hospital, University Hospitals of Southern Denmark, Kolding, DENMARK,* [4]*Health Sciences Research Centre, UCL University College, Odense, DENMARK,* [5]*Department of Regional Health, University of Southern Denmark, Odense, DENMARK,* [6]*Department of Radiology and Nuclear Medicine, Hospital South West Jutland, Esbjerg, DENMARK,* [7]*IRIS - Imaging Research Initiative Southwest, Esbjerg, DENMARK,* [8]*Department of Regional Health Research, Faculty of Health Sciences, University of Southern Denmark, Odense, DENMARK,* [9]*Department of Clinical Engineering, Region of Southern Denmark, Esbjerg, DENMARK.*

Aim/Introduction: Shorter acquisition times improve throughput and patient comfort. We investigated if a new 12-detector cadmium-zinc-telluride (CZT) SPECT enabled shorter acquisition times for pulmonary ventilation/perfusion (V/Q) SPECT while maintaining image quality. Further, we investigated the potential of utilizing a Block Sequential Regularized Expectation Maximization (BSREM) reconstruction algorithm, which recently became commercially available in SPECT. ***Materials and Methods:*** Eight patients with suspicion of pulmonary embolism were scanned on both a 12-detector CZT SPECT and a 2-detector NaI SPECT. All had Q-SPECT with an acquisition time of 17 minutes after injection of 200 MBq +/-10% Tc-99m macro-aggregated albumin. Four patients further underwent 12 minutes of V-SPECT after inhaling approximately 25 MBq of Tc-99m-technegas. Images from the 12-detector SPECT were reconstructed with list-mode files at reduced times of 33%, 42%, 50%, and 67% using Ordered Subset Expectation Maximization (OSEM) with 5 iterations (i), 8 subsets (s) and 3mm Gaussian post-filter. The BSREM algorithm was investigated at 50% acquisition time with 20i10s using the relative differences for maximum regularization method with gamma of 1 and varying regularization strength factors (beta) of 0.02, 0.05 and 0.08. Three nuclear medicine physicians evaluated image quality through absolute Visual Grading Analysis with regards to visibility of interlobar fissures (VIF), visibility of lung boundaries (VLB), and diagnostic confidence (DQ); the former two and VLB were assessed using a four-point forced-choice scale, whereas VIF was done binarily. Visual grading characteristics curves (VGC) were generated and area under the curve (AUC_{VGC}) were calculated. Fleiss' Kappa and Cohen's Weighted Kappa were used to assess interrater/intrarater reliability. ***Results:*** AUC_{VGC} curves on OSEM reconstructions were below 0.5 for all acquisition times for most parameters on the 12-detector SPECT compared to 2-detector SPECT, except for VIF, which had an AUC_{VGC} of 0.507 (CI: 0.375-0.670) when using 100% acquisition time on OSEM. However, when BSREM was used on 50% acquisition time and beta-value of 0.08, AUC_{VGC} increased from 0.037, 0.070, 0.436 and 0.170 to 0.440, 0.473, 0.559 and 0.480 for IQ, DC, VIF and VLB, respectively. ***Conclusion:*** Our study indicates the possibility of reducing acquisition time by 50% for V/Q SPECT without compromising image quality on the 12-detector SPECT when using BSREM 20i10s with beta-value of 0.08. Image quality was lower across all OSEM reconstructions for the 12-detector SPECT compared to the 2-detector SPECT, possibly due to the use of smaller voxel volumes (2.46 mm). These results warrant further investigation.

EP-1031

Quantitative (FDG)PET/CT - How huge a small error can be

I. Pestean, *A. Sabo, M. Cecan, M. Crisan, E. Barbus, D. Piciu;*
Institute of Oncology, Cluj, ROMANIA.

Aim/Introduction: The SUV (Standardized Uptake Value) in PET-CT is the one of the greatest achievements of PET-CT technique, having impact on the primary tumor evaluation, disease progression evaluation and treatment response assessment. It is necessary to optimally choose the right SUV normalization type, calculated by the body weight, body surface area, or, as recommended by most specialists, by lean body mass (SUVlbm). The SUV SUVlbm formula depends on the administrated radiopharmaceutical activity, disintegration time, patient weight and height. We evaluated the SUVlbm variation when input data errors occurred due to misregistration. ***Materials and Methods:*** We evaluated three types of malignant lesions findings, 10 with low, 10 with medium and 10 with high SUVlbm values (the median SUVlbm value being 3.78, 6.66 and 20.21). We calculated the SUVlbm of the lesions having an error of 10%, 20%, 30% and 50% in the input data, respectively administrated activity, patient height and weight, named as SUVlbm10, SUVlbm20, SUVlbm30 and respectively, SUVlbm50. We expressed the changings of SUVlbm as percentage of the correct SUVlbm to correlate the impact of the SUVlbm changings with the errors of the input data. ***Results:*** The SUVlbm variations in the case of height errors ranged between 6.08% and 27.63%, the highest error occurring in lesions with medium SUVlbm. The SUVlbm variations when weight errors were simulated ranged between 4.35% and 24.87%, the highest impact being noticed in lesions with low SUVlbm. The SUVlbm variations ranged between -9.16% and -33.48% in the case of administrated activity error simulations, with highest impact in lesions with medium uptake. ***Conclusion:*** The SUVlbm is changed when input data are misregistrated, the changes occur at any type of uptake and at any level of error and the variations are significant in SUVlbm evaluations.SUV is a predictable parameter highly correlated with tumor aggressiveness, commonly used in comparative studies, a specific indicator for treatment response and its standardizations and accuracy is mandatory

EP-1032

Description amyloid PET (18F-Florbetaben) imaging protocol in patients with suspected Alzheimer's disease

M. Caballero Vivancos[1], *M. Pérez Ávila*[1], *F. González Asid*[1], *E. Córdoba Cañete*[1], *R. Sánchez Sánchez*[2];
[1]*Hospital Universitario Virgen de las Nieves, Granada, SPAIN,* [2]*Hospital Universitario Virgen de las Nieves, Maracena, Granada, SPAIN.*

Aim/Introduction: Alzheimer's disease (AD) is a neurodegenerative condition characterized by progressive cognitive decline and memory loss, and is the most common form of dementia. Amyloid plaques with neurofibrillary tangles are a neuropathological hallmark of AD that produces synaptic dysfunction and culminates later in neuronal loss. Amyloid PET is a useful, available and non-invasive technique that provides in vivo information about the cortical amyloid burden. ***Materials and Methods:*** These are studies that do not require special preparation, do not require fasting or withdrawal of the usual medication. The dose is administered as a slow bolus and washing the line with approximately 5-15ml of sterile 0.9% sodium chloride. After a rest period of 45-130 minutes, the images are acquired. It is recommended that the patient empty the bladder to obtain maximum comfort and avoid movement during image acquisition, in addition to reducing local irradiation. The patient, in the supine position, must have adequate and fixed support for the head, avoiding extreme extension or flexion of the neck, including the entire brain in the study. Images should be acquired in three-dimensional mode with appropriate corrections and reconstructed using attenuation correction with a transaxial pixel size of 2-3mm and a slice thickness of 2-4mm. ***Results:*** The application of this protocol in our institution allows the correct interpretation of amyloid PET studies.Nuclear physicians have been able to interpret the study in a binary, positive or negative way for the presence of cortical amyloid plaques. ***Conclusion:*** Amyloid PET is a useful and available technique that provides us with in vivo information on amyloid deposits.

EP-1033

Evaluation of image quality according to the difference in acquisition methods(SS and CBM) between PET/CT manufacturers in the 68Ga study

E. Seo, *J. Ryu;*
Asan Medical Center, Seoul, KOREA, REPUBLIC OF.

Aim/Introduction: Each manufacturer has different spatial resolution and image quality as a result of different image acquisition methods (Step-and-shoot method; SS and Continuous Bed Motion; CBM) which can influence diagnostics information in Nuclear Medicine. This study investigated the image quality of each PET/CT scanner using an ACR phantom with ^{68}Ga. ***Materials and Methods:*** GE and Siemens PET/CT scanners were used. SS method was performed for 1~5 min per bed. CBM (only Siemens) was performed at a speed of 0.9~2.9mm/s). Reconstructed Images were applied with Gaussian 2mm Iteration 2, subset 6, TOF, PSF and then analyzed as spatial resolution, recovery coefficients, contrast-noise ratio (CNR), and signal-noise ratio (SNR). ***Results:*** For the SS method, spatial resolution was improved in proportion to acquisition time, while CNR and SNR did not differ significantly more than 3 minutes for GE and 3.5 minutes for Siemens. For the CBM of Siemens, the spatial resolution decreased by 1 step as the speed increased by 0.4 mm/s, and the CNR and SNR did not have significant values when the speed was 2.1mm/s or faster. ***Conclusion:*** Considering that the patient's movement and breathing artifacts increase as the scan time increases, especially when we perform the ^{68}Ga study, the maximum level of the scan speed in the CBM method is 1.7 mm/s, and in the SS method, the maximum acquisition time for obtaining adequate image quality is 3 ~3.5 min. ***References:*** - Comparison of image quality and spatial resolution between 18F, 68Ga, and 64Cu phantom measurements using a digital Biograph Vision PET/CT- Continuous bed motion in a silicon photomultiplier-based scanner provides equivalent spatial resolution and image quality in whole body PET images at similar acquisition times using the step-and-shoot method

EP-1034

99mTc Radiopharmaceuticals: Evaluation of Radiochemical Purities in the Last Two Years of Use

D. Di Martino, *A. Prisco, F. Rescigno, M. Buonanno, V. Porfidia, A. Esposito, M. Aurilio, S. Lastoria;*
Istituto Tumori G.Pascale, Napoli, ITALY.

Aim/Introduction: ^{99m}Tc radiopharmaceuticals are the most frequently used products in the nuclear medicine and they prepared in the hospital, start from colds kit. The most important quality test, before the administration, is radiochemical purity (RCP) that indicates the ratio of radionuclide contained in the

radiopharmaceutical in the desired chemical form and is expressed in percentage. This parameter aims to determine the produced radiopharmaceutical is in accordance with the summary of product characteristics (SPC). ***Materials and Methods:*** In the hospital radiopharmacy the applicable quality control method is radio-thin layer chromatography (radioTLC). With this technique, the components of the radiopharmaceutical are separated according to the solubility in the solvent and adsorption to the support medium. Moreover, in order to separate and quantify two or more impurity, two or more paper strip can be used with different eluents. A digital autoradiography system was used for the identification and quantification of radioactivity distribution along the chromatographic strips.The time taken for each control range from 5 (1 strip) to 7 minutes (2 strip). ***Results:*** The study was performed over a period of two years (January 1 2021- December 31 2022) and included a total of 1186 radiopharmaceutical preparations and their quality control. The radiopharmaceutical preparations were the following: ^{99m}Tc-albumin colloid (N=451), ^{99m}Tc-oxidronate (N=494), ^{99m}Tc-diethylene triamine-pentacetic acid (N=209) and ^{99m}Tc-sestamibi (n=32). The mean results of RCP determination are: ^{99m}Tc-albumin 99,7 % (Min 95%); ^{99m}Tc-oxidronate 99,08% (Min 96,5%) for strip A and 99,1% (Min 97,9%) for strip B; ^{99m}Tc-diethylene triamine pentacetic acid 98,9 % (Min 97,5%) for strip A and 98,8% (Min 97,4%) for strip B and 97,8 % (Min 97%) for ^{99m}Tc-sestamibi. Zero out of the 1186 preparations were non-conforming for clinical use with the RCP limits indicated by manufacturer acceptance. ***Conclusion:*** QC regarding the determination of RCP is mandatory for all ^{99m}Tc radiopharmaceuticals. Radiochemical impurities actually may cause difficulty in evaluating images and even inaccurate clinical diagnosis. For most radiopharmaceuticals, the lower limit of RCP is 95 percent; that is, at least 95 percent of the radioactive isotope must be attached to the ligand. Correctly following the manufacturer's instructions that can be found in the package insert, all prepared radiopharmaceuticals found to comply with the quality specifications.

EP-1035

How to optimize the synthesis of [177Lu]Lu-DOTATOC, from a simple manual operation

P. Christensen*;*
Aarhus University Hospital, Aarhus, DENMARK.

Aim/Introduction: Peptide Receptor Radionuclide Therapy (PRRT) with [^{177}Lu]Lu-DOTATOC is used in therapy of neuroendocrine tumours. The Department of Nuclear Medicine & PET-Centre, Aarhus University Hospital, have offered this treatment since 2016. For patients participating in a clinical trial and those not covered by the Lutathera authorization, we have an in-house production of [^{177}Lu]Lu-DOTATOC, with an annually average of 66 treatments. ***Materials and Methods:*** All syntheses were carried out using the Eckert & Ziegler Modular-Lab PharmTracer automated synthesis system. Materials and methods were used according to the instructions given by the manufacturer of the system. For all the synthesis, we have used no-carrier added lutetium chloride supplied from ITG. The [^{177}Lu]Cl_3 have a half-life of 6.7 days and were delivered in a 2 mL v-vial. In 2018 we introduced a manual operation, to optimise the total yield, since much of the [^{177}Lu]Cl_3 still remains in the delivered v-vial at the end of synthesis. After transfer of the v-vial content, acetate labelling buffer is added to the v-vial, and the v-vial washed by simply turning the vial upside down. This ensures that as much as possible of the radioactivity is transferred to the reaction vial. We have measured the radioactivity in the delivered v-vial before start of the synthesis and the radioactivity in the product vial after synthesis. We have also measured the remaining activity in the v-vial after synthesis and the activity in the bottle containing the waste of the synthesis. By non-decay corrected calculations, we determined the yield and identified where the free [^{177}Lu]Cl_3 was located. ***Results:*** This poster will show, how this manual operation has some positive effects on overall yield of the synthesis of [^{177}Lu]Lu-DOTATOC, thus a more efficient usage of the delivered [^{177}Lu]Cl_3 radioactivity and hereby cost reduction.

EP-1036

Impact of images reconstructed using Bayesian penalized likelihood on ability of [11C]MET-PET to differentiate malignant grades in brain gliomas

Y. Kamitaka*[1,2], K. Wagatsuma[1,3], M. Inaji[4], K. Ikemoto[3], K. Miwa[5], K. Ishii[1], M. Kobayashi[2];*
[1]Research Team for Neuroimaging, Tokyo Metropolitan Institute of Gerontology, Tokyo, JAPAN, [2]Division of Health Sciences, Graduate School of Medical Sciences, Kanazawa University, Ishikawa, JAPAN, [3]Radiological Technology, Medical Engineering and Technology, School of Allied Health Sciences, Kitasato University, Kanagawa, JAPAN, [4]Department of Neurosurgery, Tokyo Medical and Dental University, Tokyo, JAPAN, [5]Department of Radiological Sciences, School of Health Sciences, Fukushima Medical University, Fukushima, JAPAN.

Aim/Introduction: The role of amino acid positron emission tomography (PET) imaging using [^{11}C]methionine ([^{11}C]MET) is to differentiate between malignant glioma grades. Quantitative parameters such as standardized uptake values (SUVs) are increased when images are reconstructed using the Bayesian penalized likelihood (BPL) compared with conventional ordered subset-expectation maximization (OSEM). The present study aimed to determine whether [^{11}C]MET-PET images reconstructed using BPL can differentiate malignant grades in brain gliomas. ***Materials and Methods:*** Thirty-six primary glioma lesions that were assessed in 32 patients by [^{11}C]MET-PET imaging were classified as grades 2 and 3 (n = 14) and 4 (n = 18) based on the WHO 2021 classification. We then measured the SUV_{mean} in normal tissues and the SUV_{max} and SUV_{peak} in gliomas from PET images reconstructed using OSEM with time-of-flight (TOF) and BPL with TOF (β200). Tumor-to-normal tissue ratios (T/N) were calculated as T/N_{max} and T/N_{peak}. Mean Ki-67 and quantitative values (SUV_{max}, SUV_{peak}, T/N_{max}, and T/N_{peak}) were compared between malignant grades (2 and 3 vs. 4) using OSEM and BPL. Relationships between Ki-67 and quantitative values were assessed using Pearson correlations. We then calculated the area under receiver operating characteristic (ROC) curves (AUC) for Ki-67 and the quantitative values. ***Results:*** The means of Ki-67, SUV_{max} in BPL, and SUV_{peak} in OSEM and BPL were statistically higher in grade 4 than grades 2 and 3. Quantitative values increased under BPL reconstruction regardless of the malignant status of gliomas. The correlation coefficients derived using OSEM and BPL were respectively: SUV_{max}, 0.344 and 0.392; SUV_{peak}, 0.346 and 0.352; T/N_{max}, 0.221 and 0.269; T/N_{peak}, 0.250 and 0.252. The AUCs derived using OSEM and BPL were respectively Ki-67, 0.97; SUV_{max}, 0.69 and 0.72; SUV_{peak}, 0.68 and 0.70; T/N_{max},0.63 and 0.66; T/N_{peak}, 0.64 and 0.65. ***Conclusion:*** The reconstruction of [^{11}C]MET-PET images using BPL differentiated between malignant grades in gliomas using SUV_{max} and SUV_{peak} and led to increased quantitative values regardless of the malignant status of gliomas. The BPL improved the ability to discriminate malignant from benign gliomas on [^{11}C]MET-PET images.

EP-1037

Nuclear Medicine

A. Alshehri, *T. Wright, K. M Prise, A. Cole;*
Queens University Belfast, Belfast, UNITED KINGDOM.

Aim/Introduction: Despite continued advancements into the treatment of PCa, it continues to represent a major burden in men worldwide. This is particularly problematic upon progression to MCRPC which has metastasised to bone. Of the current therapeutics available two agents targeting the androgen receptor pathway: Abiraterone and Enzalutamide are now routinely used as standard of care. These agents have been shown to result in significant increases to OS in MCRPC patients, however, questions still remain to their optimisation and effects when combined with radiation. ***Materials and Methods:*** Colony assays-Cells were pre-treated with 10μM Abiraterone or Enzalutamide one-hour before irradiation and irradiated at dose 0-8Gy.Western Blot and cell cycle.Samples were pre-treated with 10μM Abiraterone/Enzalutamide one or 24hours before irradiation at 2Gy. Samples were harvested 1,24, 48hours post-radiation for western blot and CellCycle analysis. ***Results:*** Radiosensitising effects of Abiraterone and Enzalutamide: Having previously established the cytotoxic potential of Abiraterone and Enzalutamide as single agents and their significant additive impact when combined with 2Gy.The radiosensitising potential of these hormonal agents was investigated.LNCaPs showed increased radiosensitivity when pre-treated 24hours before radiation for both Abiraterone(SER=1.23) and Enzalutamide(SER=1.23).No radiosensitising effects were observed with Enzalutamide across both PC3s(SER=0.96) and SJSA-1s(SER=1.01).However, Abiraterone displayed synergy with radiation regardless of AR status, with PC3s(SER=1.19) and SJSA-1s(SER=1.17).Abiraterone and Enzalutamide inhibit DNA repair through RAD51 suppression:The AR has been linked to the upregulation of key DNA repair genes.Therefore, the impact of AR suppression on DNA repair pathways such as homologous recombination was investigated through investigation of RAD51 expression.AR suppression with Abiraterone and Enzalutamide resulted in total visible reduction in or RAD51 expression, correlated with PSA expression.Importantly, these effects were shown to be conserved with 2Gy co-treatment when Abiraterone and Enzalutamide was administered 24hours before radiation.Cell cycle distribution was also investigated to determine if these impacts were direct or result of cell cycle distribution change.Abiraterone and Enzalutamide results in cell cycle distribution changes. ***Conclusion:*** Results suggest radiosensitisation effect with Abiraterone and Enzalutamide in AR sensitive prostate models, while Abiraterone seems to induce radiosensitisation regardless of AR status. Hinting at alternative mechanism of action.The underlying mechanisms for AR suppression based sensitation involves the reduction of key DNA DSB repair pathways such as HR and NHEJ.With reductions in HR at least partially the result of cell cycle distribution changes. Comparison of Abiraterone against Enzalutamide suggest Abiraterone to be more effective across all in vitro metrics measured, providing a rationale for selection of Abiraterone over Enzalutamide. ***References:*** 1.SgourosG,RoeskeJCM,MichaelR,etal. Radiobiologyanddosimetryofalpha-particleemittersfortargetedradionuclidetherapy.JNuclMed(201051:311-28.2.SollazzoA,BrzozowskaB,ScherthanH,WojcikA.Livedynamicsof53BP1focifollowingsimultaneousinductionofclustered.IntJMolSci(2018)19:1-16.

Aalbersberg, E. A. EP-0805, OP-451
Abadi Sedraoui, Y. EP-0127, **EP-0365**, EP-0502
Abaouz, N. **EP-0975**, **EP-0976**
Abayazid, M. OP-627
Abbas, A. OP-100
Abbasi, M. EP-0714, OP-248
Abdallah, N. **EPS-184**, **OP-092**
Abdlkadir, A. EP-0094, EP-0095
Abdayem, P. EPS-260
Abdelhafez, Y. EP-0191, OP-775
AbdelKawi, M. EP-0880
Abdelrahman, A. EP-0572, **OP-657**
Abdelrahman, I. EP-0260
Abdelrazek, S. **EPS-071**
Abdi, M. EP-0534, **OP-630**
Abdlkadir, A. EP-0095, EP-0094, EPS-082
Abdollahi, H. **EP-0549**, OP-091
Abduli, L. OP-897
Abdul Razak, H. TEPS-002
Abe, S. EP-0887
Abe, T. EPS-012
Abenavoli, E. **EP-0149**, **EP-0330**, EPS-174, EP-0212, EP-0273, EP-0546
Abhilash, S. **EP-0449**
Abin-Carriquiry, A. EP-0025
Abler, D. **EP-0699**
Aboagye, E. O. EP-0090, EP-0276, EP-0832, OP-590
Abourbeh, G. EPS-282
Abouzayed, A. **EP-0041**, EP-0807, EPS-217, EPS-218, EPS-220
Abouzian Senhaji, S. EP-0331
Abraham, C. L. EP-0821
Abrantes, A. M. EP-0008, EPS-211
Abreu, F. EP-0291, EP-0978
Abreu Sánchez, P. EP-0417
Abrunhosa, A. EP-1000, EPS-094, EP-0896
Abt, E. EP-0037
Abuqbeitah, M. EP-0153
Abusamra, M. OP-802
Acampa, W. OP-382, OP-383
Acar, E. EP-0116
Acar, M. N. EP-0119
Acar Tayyar, M. **EP-0185**
Aço, J. EP-0412
Adamczewski, Z. EP-0432, EP-0621, EP-0703, EP-0968, EP-0977, EPS-097, OP-950
Adilbay, D. OP-896
Adler, S. EPS-286
Aebersold, D. M. OP-337
Aeschbach, D. OP-798
af Burén, S. EP-0156
Afshar-Oromieh, A. EP-0567, EP-0782, EP-0801, EPS-106, EPS-244, OP-058, OP-666, OP-716
Aftimos, P. OP-573
Agarwal, A. EP-0789
Agarwal, M. OP-783
Agarwal, S. EP-0498, EPS-079
Aggarwal, P. **EPS-190**, OP-651
Aghaee, A. **EP-0264**, **EP-0266**, **EP-0293**, **EP-0381**, **EP-0424**, **OP-650**, **OP-803**
Aghaei, A. OP-523
Aghahosseini, F. **OP-248**
Aghamohammadi, J. EP-1016
Aghazada, F. EP-0152, EP-0153, **EP-0228**
Aglund, K. EP-0317
Agócs, L. EP-0390
Agolti, M. **EP-0125**
AGOSTINI, D. EP-0437, EPS-137, OP-389
Agostini, S. OP-585
Agrawal, A. EP-0159, EP-0166, EP-0207, EP-0216, EP-0313
Agrawal, K. EP-0158, EPS-044, **EP-0522**, OP-649
Agrawal, S. EPS-120
Ågren, H. OP-562
Agu, G. EP-0680
Aguade, S. EP-0632
Aguade-Bruix, S. EP-0252
Aguiar, P. EP-0023
Aguila, F. EP-0465
Ahamed, S. **OP-711**
A. Hernández Fructuoso, M. **EP-0523**
Ahlawat, P. OP-783
Ahmad Saad, F. TEPS-002
Ahmad Shamim, S. EP-0707
Ahmed, A. EPS-252
Ahmed, H. U. EP-0276, OP-511
Ahmed, N. OP-935
Ahond-Vionnet, R. EP-0907
Ahrari, S. OP-586
Ahrens, M. EP-0607
Ahtiainen, V. EP-0790, **EP-0802**, TEPS-007
Ahuja, P. OP-034, OP-036
Ai, Z. OP-288
Aide, N. EP-0640
Aigner, R. M. EP-0150, EP-0151
Airo, L. EP-0700, EP-0749, EP-0236, EP-1004
Aita, Y. OP-631
Ait-Mohand, S. OP-557, EP-0045
Ajdinovic, B. EPS-024
Ajuria Illarramendi, O. EP-0504, **OP-849**
Akamatsu, G. EP-0651
Akbari, A. OP-499
Akcay, K. OP-163, OP-375, **EP-0253**
Akdağ, B. Y. EP-0885
Akdemir, U. O. EP-0691
Akdemir, Ü. EP-0136, OP-510
Akdoğan, B. EP-0232
Akgün, A. EP-0379, EP-0591, EP-0290, EP-0592
Akgün, E. EP-0470, **EP-0571**, EP-0574, **EP-0576**, EP-0582, EP-0584
Akhurst, T. EP-0406, EP-0555, EPS-010, OP-437, EPS-172
Akinlusi, R. OP-657
Akkaş, B. E. EP-0584, EPS-047, EP-0116, EP-0470, EP-0574, EP-0582
Akın, S. EP-0347
Akıncı, D. EP-0232
Akpinar, R. EP-0189
Ak Sivrikoz, I. **EP-0359**
Aksoy, T. EP-0402, OP-194
Aksu, A. EP-0459
Aksu, F. OP-712
Aksu, S. **EP-0287**
Aksu, Ü. **EP-0470**
Al-Adhami, D. EP-0094, EPS-082, EP-0095
Alain, M. EP-0437, EPS-137
Alakbarli, A. **EP-0434**
Alamin, M. EP-0441, **EP-1027**
Alanazi, S. EP-0645
Alano, R. OP-440, OP-509, EPS-122
Alan-Selcuk, N. OP-163, OP-375
Al-Awar, A. EPS-215
Al-Balooshi, B. EPS-159
Al Banaa, F. EP-0850
Albano, D. EP-0273, EP-0277, EP-0323, OP-166
Albattat, K. **OP-089**
Albayrak, A. EP-0951
Albeaini, S. OP-664
Alberini, J.-L. EP-0907, EPS-015
Albert, N. L. EP-0024, EP-0015, EP-0726, EPS-092, OP-082, OP-110, OP-467, OP-538, OP-584, OP-588
Alberti, G. EP-0999
Alberto Buchpiguel, C. EP-0676
Alberts, I. OP-246, EPS-106
Alborino, S. EP-0623
Al-Boucharali, J. EP-0422
Albring, J. C. OP-099
Alcaide Corral, C. OP-289
Alcocer-Avila, M. EP-0840
Aldea, M. EPS-260
Aldehlaui, A. **EPS-133**
Alderaibi, A. EP-0184
Aldigeri, R. EP-0487
Aldous, C. EP-0183, EP-0643
Alduraibi, A. **OP-514**
Alejandre Lafont, M. **OP-491**
Alevroudis, E. OP-339
Alexa, M. EP-0943, EP-0952, **EP-0953**

Alexandre-Santos, L. EP-0732, EP-0929, EPS-061
Alexiou, S. EP-0423, EP-0445
Alezzi, M. **EP-0771**
Alfake, H. TEPS-005
Al-Fakhranee, R. EP-0645
Ålgars, A. OP-529
Alghazo, O. OP-338
Alhuseinalkhudhur, A. OP-579
Alì, M. EP-0700, EP-0749
Ali, N. EPS-036
Ali Abobaker Hassan, W. OP-897
Aliberti, G. OP-674
Al-Ibraheem, A. **EP-0094**, **EP-0095**, **EPS-082,** EPS-159
Alibrandi, A. OP-524
Alic, L. OP-088
Alio, D. EP-0540
Alipour, R. EP-0555, EPS-010, OP-437
Alirezapour, B. EP-0806, **EPS-285**
Aliyev, J. EP-0833
Aliyeva, N. EP-0833
Alizadeh, M. **EP-1010**, EP-1016
Al Jabri, A. **EP-0787**
Allam, N. OP-155
Allegri, V. EP-0213, EP-0215
Allegrini, O. EPS-090
Allen, K. J. EPS-212, EP-0834, EP-0836, EP-0846, OP-698
Allen-Auerbach, M. EP-0538
Allman, P. OP-194
Allmann, J. OP-497
Allouche, R. EP-0066
Al Makhmari, N. EP-0721
Al-Mansour, L. EPS-080
Almasi, S. **EP-0063**
Al Maymani, N. EP-0721
Almazrou, R. **EP-0645**
Almeida, L. **EPS-078**
Almendros-Riaza, Á. EPS-096
Alnabulsi, A. **EP-0530,** OP-884
Al-Nader, M. EP-0391
Aloj, L. EP-0799
Alomar, A. **EP-0447**, **EPS-070**, **EPS-203**, EPS-063
Alonso, O. EP-0301, EP-0364, EP-0969, OP-665
Alonso Echarte, A. EPS-063
Alonso Farto, J. EP-0329, EP-0352
Alonso García, Á. **EP-0845**, EP-0864
Alonso Rodríguez, M. EP-0398, EP-0455, EP-0475, EPS-043
Alqabandi, M. EP-0654
Al-Qahtani, M. EP-0617
Alqallaf, Z. EP-0260, **TEPS-005**
Alrabiah, M. EP-0645
Al-Rasheed, U. EPS-082
Al Riyami, K. EP-0721
Al Rowaily, M. **EP-0617**
Al-Sadoon, S. **EP-0240**
Alshehri, A. **EP-1037**
Al Sukaiti, R. EP-0721
Altaf, N. OP-642
Altani, C. EP-0594
Altini, C. **EPS-037**
Altunay, B. **EPS-278**
Aluicio Sarduy, E. OP-903, EP-0891
Álvarez, A. EPS-143
Alvarez Mena, N. EP-0398, EP-0455, EP-0475, **EP-0529**, EPS-043, **OP-168**
Alvarez Moreno, M. EP-0300, EP-0526, EP-0604, EP-0605, EP-0964
Álvarez-Nadal, M. EPS-023
Alvarez Pérez, J. EP-0503
Álvarez Vázquez, A. EP-0494
Alves, V. EP-0946
Amadori, E. EP-0613
Amara, W. OP-858
Amaral, H. EP-0708, OP-327
Amareller, D. OP-713
Amarelli, C. OP-383
Amargier, S. EP-0021
Amaro, I. EP-0008
Amato, E. EPS-093, OP-912
Amblard, R. EP-0719
Ambrogio, A. OP-171
Ambrosini, V. EP-0213, EP-0215
Amelio, D. OP-585
Amerein, A. EP-0565, **OP-856**
Amghar, M. **OP-719**
Amico, J. TEPS-021
Amini, E. **EP-0745**, **OP-223**
Amiri Tehranizadeh, A. EP-0743
Amor, A. EPS-289
Amor Alonso, S. EP-0393
Amor Coarasa, A. **OP-494**
Amorim, B. J. EP-0259
Amoroso, F. **EP-0847**
Amoroso, L. OP-315
Amo Salas, M. EP-0229, EP-0562, EPS-050, EP-0250, EPS-259, OP-638
Amouri, W. EP-0990
Amso, Z. OP-137
An, R. EP-0030, OP-143, OP-216, OP-700
An, Y. S. EP-0839
Anagnostopoulos, C. D. EPS-178
Ananth Kumar, S. **OP-651**
Anda, E. EPS-070, EPS-203, EPS-063
Andersen, F. L. EP-0660
Andersen, T. L. EP-0660
Anderson, C. EP-0670
Andersson, M. **EP-0777**, **EP-0778, OP-148**, **OP-148**
Andersson, U. OP-360
Andi, J. EP-0390
Ando, M. EP-0808
Andrade, M. EP-0769
Andrassy, G. OP-107
Andreas, S. OP-785
Andreasi, V. EP-0202
Andreassen, M. EP-0195
Andreev, S. EP-0461, EPS-139
Andrés Gracia, A. EP-0471
Andrini, E. EP-0215
Aneheim, E. EP-1000, OP-615
Anelli, M. **EP-1017**, **OP-323**
Angelidis, G. **EP-0682**
Angelis, G. D. EPS-061
Angell, K. EP-0686
Angelucci, E. OP-050
Angiolillo, S. EP-0340
Angiolillo Grau, S. EP-0418
Anita, R. EPS-292
Annarumma, I. EP-0985
Annovazzi, A. OP-447, OP-581
Annunziata, S. EP-0335, EP-0337
Anousakis Vlachichristou, N. EPS-178
Ansari, M. EP-0519, EPS-060
Antke, C. EP-0072, OP-560
Antoch, G. EP-0072
Antonacci, F. EP-0147
Antoni, G. OP-458
Antoni, M. EP-0131
Antonopoulos, A. EPS-178
Antonov, A. EP-0513
Anton Rodriguez, J. **EP-0684**, **EP-0720**
Antonuzzo, L. EP-0212, EP-0546
Anttinen, M. EP-0659
Antunovic, L. EP-0285, EPS-161
Anzai, Y. EPS-152
Aphale, R. EP-0500, EP-0505, EPS-073
Apostolova, I. EP-0791
Appel, L. OP-458, OP-459
Appelman, B. OP-928
April, G. OP-236
Arabi, H. EPS-159, OP-535
Arakawa, R. OP-563
Arano, Y. EP-0855
Araújo, M. EPS-078
Aravind, P. **EP-0090**, **EP-0276**
Araz, M. EP-0214, EP-0243, EP-0257, EP-0314,

EP-0315, EP-0349, EPS-116, OP-158
Arbizu, J. EP-0088, EPS-011, OP-460, OP-507, OP-936
Arbuznikova, D. EP-0775
Arca, B. EP-0911, EP-0912
Arcadi, A. OP-936
Archambault, L. OP-848
Archibald, S. EPS-289
Archontakis, P. **EP-0765**
Arcidiacono, A. OP-289
Arends, B. EPS-087
Argalia, G. **EP-0112**, **EPS-053**
Argiroffi, G. EP-0068, OP-234, OP-674
Argon, A. M. EP-0434
Arguelles Pérez, D. EP-0367
Ariano, S. OP-653
Arico, D. OP-447
Aridhasan Meenakshi, L. **OP-097**, OP-161
Arlicot, N. OP-799
Arma, I. EP-0573
Armitage, G. EP-0663
Armstrong, A. OP-898, OP-340
Armstrong, W. OP-192, OP-509, OP-040
Armutlu, B. EP-0574
Arnaldi, D. OP-455
Arnaud, E. EPS-017
Arndt, C. OP-357
Arnone, A. OP-106
Arntz, M. J. EPS-205
Arora, G. EP-0208, EP-0336, EP-0368, EP-0519, OP-251
Aroui Luquin, T. EP-0114, EP-0204, EP-0205, EP-0544
Arruda Matheos de Lima, B. **EPS-007**
Arsenault, F. OP-236
Arseniou, A. EP-0445
Arslan, E. EP-0230, EP-0402
Arsos, G. **EP-0237**, **EP-1014**
Arstad, E. EP-0893
Artigas, C. EP-0275, **EPS-112**, OP-232, OP-238, OP-664
Artiko, V. **EPS-002**
Arulananda, S. OP-230
Arumugam, P. OP-382
Arvind, S. EP-0180
Aryana, K. EP-0264, EP-0266, EP-0381, OP-650, OP-803
Arzberger, T. OP-562
Asa, S. EP-0152, EP-0153, EP-0228, **EP-0742**, OP-035, OP-658, OP-944, EP-0740
Asadurova, S. EP-0252, EP-0508, **EP-0548**, **EP-0632**
Asami, M. **EP-0712**
Aschele, C. EPS-183
Asensio Pérez, F. EP-0471
Asensio Ruiz, M. **EP-0864**, EP-0845
Asensio Valero, L. **EP-0585**
Ashraf, A. EP-0102
Ashtari, P. **EP-1009**
Ashton, N. OP-104
Askar, H. EP-0051
Askari, E. EP-0424, OP-523, OP-803
Askling, F. OP-808
Aslaner, K. **EP-0911**
Aslani, G. EP-1009
Aslanidis, I. EPS-128, EPS-129, EPS-130
Asma, E. OP-025
Assadi, M. EPS-159, **OP-169**
Assante, R. OP-382, OP-383
Assumpção, L. EPS-078
Astiazaran-Rascon, I. **OP-142**
Astrakas, L. EP-0445
Astudillo Sarmiento, M. EP-0599
Ata, E. S. EP-0402
Atabekov, T. **EP-0462**, EP-0626, **OP-864**
Ataei Nakhaei, S. EP-0424
Atay, L. O. EP-0691, EP-0118, EP-0136, OP-510
Ateş, Ö. EP-0287
Atteya, Y. EP-0880
Attinger, A. OP-360
Auclin, E. EPS-263
Auditore, L. **EPS-093**, OP-912
Auerbach, M. OP-192
Auernhammer, C. J. OP-656
Auffray, E. OP-368
Auge, A. OP-897
Aulich, A. EP-0432, **EP-0977**
Auriac, J. **OP-637**
Aurilio, M. EP-0575, EP-0781, EP-0819, **EP-0879**, EP-0886, EP-1034
Auvity, S. EP-0674
Auzeloux, P. OP-938
Aveline, C. OP-805
Ávila-Rodríguez, M. EP-0895
Awais, R. EP-0893
Axelsson, R. EP-0156
Ay, M. EP-0669, EP-0712, EP-0743, EPS-177, EP-0714
Ayachi, N. EP-0697
Ayati, N. OP-523
Aydin, C. **EP-0224**, EP-0541
Aydin, N. **EP-0363**, **EP-0944**, **OP-934**
Aydın, B. OP-053, OP-055
Aydos, U. EP-0118, EP-0136, OP-510
Ayed, K. EP-0514, **EP-0994**
Ayeni, A. EP-0269, EP-0530
Ayer, M. EP-0470
Aygun, A. OP-658
Azad, A. EP-0555, OP-437, OP-338
Azar, M. EPS-165
Azarbar, K. EPS-140, OP-388
Azargoshasb, S. **EP-0397**, EPS-270, OP-298, OP-300
Azevedo-Marques, P. M. EP-0732
Azhdarinia, A. OP-769
Azpeitia Hernández, P. **EP-0504**, OP-849
Azzali, I. EP-0613

Baazoug, G. EP-0512, EP-0514
Babacan, G. B. **EP-0119**, EP-0185
Babich, J. EPS-289, OP-494
Baccini, M. OP-234
Bachmann, F. **EPS-284**
Bachmann, H. OP-297
Bachmann, M. OP-357
Backhaus, P. **OP-356**, **OP-802**
Badalamenti, M. OP-918
Badawi, R. OP-776, EP-0191, OP-567, OP-775
Badel, J. EP-0729, EPS-247
Badelita, S. EP-0464
Badell, J. **EP-0386**, **EPS-052**
Badell Martínez, J. EP-0254, EP-0503, OP-170, OP-787
Badenes Romero, Á. EP-0417
Badipa, F. EP-0804, EP-0806
Bae, S. **EP-0536**, OP-362
Baehr, M. EP-0220
Baete, K. OP-366, OP-667
Baggerman, K. EP-0882
Bagheri, S. OP-562
Bagieński, M. OP-641
Bagnalasta, M. OP-674
Bagnara, C. OP-051
Bagnato, A. EP-0376
Bahce, I. EPS-195
Bahloul, A. **EP-0758**, OP-250
Bahrami-Samani, A. EP-0806
Bahri, H. OP-056
Bahtouee, M. OP-169
Bai, C. EPS-006
Bai, Y. EP-0016. **EPS-145**
Bailly, C. EP-0688, OP-194
Bailly, M. EP-0489
Bajenaru, A. **EP-0934**, **EP-0937**
Bajén-Lázaro, M. T. EPS-265
Bajuk Studen, K. **EP-0506**, EP-0619
Baker, A. H. OP-289
Bakhshi, Z. EP-0266
Bakir, B. EP-0233
Bakker, J. OP-253
Bakos, A. **EP-0181**
Bakos, G. OP-719

Bakr, H. **EPS-215**, EPS-230
Bal, C. EP-0497, EPS-055, EPS-076, EP-0519, EP-0096, EPS-027 EP-0208, EP-0498, EP-0505, EP-0618, EP-1019, EP-1020, EPS-060, EPS-079, EPS-204, OP-307, OP-316, EP-0203, EP-0350, EP-0500, EPS-054, EPS-073
Balaban Genc, Z. C. EP-0190
Balaguer, D. OP-233
Balaguer, J. EP-0800, EP-0611
Balaguer Muñoz, D. EP-0417
Balajan, G. TEPS-021
Balasse, L. EP-0035, EP-0067
Balazs, L. EP-0441
Balcı, E. EP-0118, OP-510, **EP-0691**
Balcerzyk, M. EPS-288
Baldari, G. EP-0487, EP-0813
Baldari, S. OP-392, OP-524, OP-801
Balev, B. EP-0899
Balfour, D. **OP-907**
Ball, T. **EP-0636**
Ballal, S. EP-0618, EP-1019, EP-1020, EPS-060, OP-307
Ballout, S. **EP-0792**
Balma, M. OP-447
Balogh, V. OP-289
Balogova, S. OP-805
Balouzet Ravinet, C. EP-0883
Baltaci, S. EP-0243
Baltacioglu, M. H. EP-0214, EP-0257, EP-0314, **EP-0315**
Baltova, T. EP-0513
Balu, M. EP-1026
Balzarini, L. EP-0272, OP-039
Ban, D. OP-036
Banchero, A. EP-0301
Bandelli, G. EP-0147, OP-879
Bang, J. I. OP-049
Bankstahl, J. EP-0082, EP-0022
Bankstahl, M. EP-0022
Bano, J. EP-0425
Banu, A. EP-0042
Bao, A. EP-0612, OP-857
Bao, W. **EPS-057**
Baral, D. EP-1008
Baraldi, C. OP-474
Barantin, L. OP-799
Baranyai, Z. EP-0812
Barashki, S. EP-0293
Barata Coelho, P. OP-528
Barbato, F. OP-508, OP-580, OP-932
Barbé, E. EPS-019
Barbiero, S. EP-0586
Barbisan, D. EP-0586
Barbosa, A. EP-0926
Barbosa, D. EP-0246, EP-0472, **EP-0569**, EP-0962, EP-0979, OP-469, **OP-472**, OP-473, OP-539
Barbus, E. EP-1031
Barcellona, M. R. EP-1028
Barceló, B. EPS-143
Barci, E. OP-082
Bard, J. A. OP-556
Bardessi, B. **EP-0465**
Bardet, S. OP-806
Bardin, T. OP-858
Bardo, F. EP-0763
Bardo, M. OP-328
Bareggi, C. EPS-183
Barelle, C. EP-0998
Barentsz, M. W. OP-670
Bargallo, E. EP-0130
Barkhof, F. EP-0677, EPS-150, OP-109, OP-566, OP-928, OP-930
Barlatey, S. OP-047
Barlesi, F. EPS-260
Barlow, J. **OP-764**
Barna, S. EP-0441, EP-1027, OP-369
Barnhart, T. E. OP-903
Baron, T. OP-240
Barone, A. EP-0540, **EP-0543**, EPS-107, OP-668, OP-669, OP-854, OP-915
Barone, D. EP-0238
Barraco, E. OP-664
Barrera, A. EP-0447, EPS-070, EPS-203
Barrera Cerpa, A. EPS-063
Barrientos Ruiz, I. EP-0365
Barrington, S. OP-102, EP-0318, EP-0533
Barrio, S. EP-0340
Barro Rico, L. EP-0023
Barroso, N. OP-034, OP-036
Barry, I. OP-642
Barski, D. OP-468
Bartek, J. OP-555
Bartel, T. EP-0607, **OP-190**, OP-932
Bartenstein, P. EP-0015, EP-0024, EP-0210, EP-0726, EPS-003, EPS-092, EPS-148, EPS-237, OP-082, OP-110, OP-467, OP-538, OP-588, OP-656, OP-717, OP-838, OP-839
Barthel, H. EPS-148, EPS-156, **OP-108**
Bartholomeusz, D. OP-140
Bartoletti, P. EP-0162, **EP-0188**, EPS-074
Bartolomei, M. EP-0273, OP-447
Barton, S. OP-852
Bartos, L. EP-0015, EP-0726, OP-769, OP-082, OP-110, OP-588
Bartuś, S. OP-641
Baruta, S. EP-0866
Barwick, T. D. EP-0090, EP-0276, EP-0495, EP-0832, OP-511
Barzi, P. EP-0586
Basaco Bernabeu, T. **EPS-291**, OP-430, OP-491
Basaran, M. EP-0553, OP-333
Bascuñana, P. EP-0361, EPS-020, EPS-167, EPS-081
Basile, L. OP-647
Basile, M. EP-0614
Basi Massanes, F. OP-838
Bassa, P. EP-0109, EP-0241
Bassermann, F. OP-769
Bassetti, C. OP-710
Basso, G. EP-0685
Bastiaannet, R. **OP-147**, OP-149
Bastick, P. EP-0558
Bastidas, J. EP-0348, EPS-011, OP-507, EP-0088, OP-098, OP-936, EP-0587
Bastit, V. OP-806
Basuli, F. EP-0280, EPS-286
Batalov, R. EP-0462, OP-864
Batanete, S. EP-0769
Batchu, S. EP-0171
Bateman, T. OP-389
Batinic, J. EP-0940
Batista, J. EP-0482
Batista, R. EP-0883
Battisti, C. EP-0258
Battisti, U. **OP-615**
Battle, M. **EP-0113**
Bauckneht, M. EP-0273, EP-0277, EP-0898, EPS-260, OP-050, OP-455
Baud, M. OP-047
Bauder Wüst, U. EPS-210, OP-719
Baudier, T. EPS-247
Bauduer, A. **EP-0933**
Bauer, A. OP-107, OP-798
Bauer, M. EP-0674
Bauer, S. EP-0607, OP-190, OP-932
Baues, C. OP-101
Baujat, B. OP-805
Baum, R. OP-620, OP-188, OP-237, OP-302, OP-468, OP-617, OP-926
Bauman, A. OP-191, OP-716
Baumgartner, P. OP-187
Baun, C. **EPS-228**, OP-659
Bavelaar-Croon, C. D. OP-183
Bavetta, M. G. EP-1028
Bax, J. J. OP-389
Bayardo, K. **EP-0364**, **EP-0969**
Bayat, Z. **EPS-239**
Baykara Ulusan, M. EP-0402
Bayne, M. OP-511
Baz-Sanz, L. EP-0559, EP-1013, **EPS-023**, **EPS-025**, EPS-026
Bazzano, L. EP-0316
Beanlands, R. OP-389
Beaulieu, A. OP-236
Beaumont, T. EPS-246

Beauregard, J. M. EP-0549, EPS-251,OP-236
Bebbington, N. A. EP-0713, OP-181, OP-500, **OP-501**, **OP-502**
Becerra Garcia, D. EP-0399, EP-0620
Bechlioulis, A. EP-0422, EP-0423, EP-0445
Beck, R. OP-141, OP-617, OP-767
Becker, S. OP-151, EP-0889
Beckmann, L. OP-099
Beddok, A. **OP-917**
Beekman, S. EP-0064, EPS-224, EPS-277
Beer, A. EPS-248, OP-904, EP-0560, OP-905, EP-0786
Beer, L. OP-648
Beer, S. OP-798
Beguš, U. **EP-0619**
Begum, N. N. EP-0370
Behe, M. OP-139, OP-765, OP-897
Behera, A. OP-299
Beheshti, M. EP-0501, EP-0556, OP-446
Bejuy, O. **EP-0053**
Bekhof, L. B. S. EP-0877
Beksac, M. EP-0349
Belakroum, R. **EPS-039**
Belayouni, R. **EP-0995**, OP-945
Belderbos, J. S. A. EP-0805
Belgioia, L. EP-0273
Belho, E. OP-927
Beşli, L. U. EP-0983
Bélissant, O. EP-0045, OP-805
Belka, C. OP-082, OP-588
Bella, M. EP-0594
Bel lakhdar, M. **EP-0986**
Bellaye, P. S. EPS-219
Bellerba, F. OP-921
Bellettati, G. **EP-0915**
Bellinge, J. **OP-642**
Bellini, P. EP-0323
Belló, P. OP-233, EP-0302, EP-0611, EP-0800, EPS-096
Bellviure, R. EP-0548, **EP-0252**, EP-0508
Beltrán Arenas, S. EP-0702
Ben Ahmed, K. **EP-0387**, EP-0972, EP-0990
Ben Ali, K. OP-513
Ben Amara, K. EP-0531
Bénard, F. EPS-115, OP-084, OP-715, EP-0201, EP-0829, EPS-223 EPS-242, EPS-251, OP-091, OP-142, OP-431
Benavente, Y. EP-0355
Bencze Linczerné, V. EP-1027
Bendele, A. EP-0062
Bendová, K. EPS-280, EP-0048, **EP-0078**
Bendre, S. **EP-0829**
Beneš, V. OP-719
Benedict, S. EP-0794
Ben Elkilani, O. **EP-0512**, EP-0514
Benesova, M. EPS-210, OP-719, EP-0048
Benetti, A. EP-0272, OP-039
Ben Fekih, N. **EP-0087**
Bengel, F. M. EP-0082, OP-779
Ben Ghachem, T. EP-0401, **EP-0481**, EP-0531, EPS-038, **EPS-042**
Bengrine, L. OP-160
Ben-Haim, S. EP-0542
Ben Hamida, O. EP-0993, EP-0995, OP-945
Benítez-Segura, A. M. EPS-265
Benkiran, M. EP-0429
Bennacef, I. OP-703
Ben Naceur, A. **EP-0697**
Ben Nasr, M. EP-0995, **OP-945**
Benner, K. OP-499
Bennis, M. OP-805
Ben Raïs, N. EP-0986
Ben-Salem, I. **EP-0045**
Ben Sellem, D. EP-0531, EPS-038
Benson, T. OP-340
Benz, M. OP-192, EP-0284, OP-509
Beorlegui, C. OP-507, EP-0705, EP-0706
Berardinelli, A. **EP-0361**, EPS-081, EPS-020
Berckel, B. N. M. OP-928
Berdal, M. EPS-227
Berding, G. EP-0082, OP-779
Beregov, M. EP-0653
Berehova, N. **OP-298**
Berenbaum, A. EPS-017
Berenji, G. OP-041
Berger, P. OP-765
Berglund, H. EPS-067, **OP-766**
Bergsten, J. OP-240
Berlis, A. OP-856
Berman, D. OP-389
Bermejo-Segú, J. O. EPS-265, OP-784
Bernabe Caro, R. EP-0148
Bernard, C. EP-0629, EP-0630
Bernardini, M. **EP-0654**
Bernardino, M. EP-0412
Bernhard, J.-C. OP-194
Bernhardt, P. EP-0545, EPS-009, EPS-067, OP-080, OP-191, OP-836
Berntsen, E. M. EPS-160
Berrani, S.-A. OP-630
Berrens, A.-C. EP-0279, EP-0397, EPS-113, EPS-270
Berry, O. OP-030
Bertagna, F. EP-0273, EP-0277, EP-0323, OP-166
Bertani, E. EP-0389, EP-0543, OP-294, OP-668, OP-854
Bertaut, A. EPS-015, OP-160
Berti, V. EP-0212, EP-0330, EP-0469, EP-0546
Berto, C. EP-0162, EP-0188
Bertoglio, D. **OP-556**
Bertolini, M. EP-0999
Berton, B. EP-0687
Bertrand, S. **EP-0869**
Berzosa, M. EP-0859
Bes, A. L. OP-102
Besenyi, Z. EP-0181
Beshiri, K. **EPS-260**
Besse, B. EPS-260, EPS-263
Besserer-Offroy, E. **EP-0850**, OP-434
Besson, F. **OP-845**
Besson, I. OP-056
Besson, V. **OP-160**
Besutti, G. EPS-014
Betech, V. OP-460, EP-0705, EP-0706, EP-0339, EP-0348, EP-0088, EP-0862, EPS-011, **OP-098**, OP-507, OP-936, EP-0859
Betts, B. C. OP-616
Beu, M. EP-0072, EP-0073, OP-560
Beumers, P. EP-0015
Beydagi, G. EP-0253, **OP-163**, **OP-375**
Beyer, D. OP-492
Beyer, L. OP-110
Beyer, T. EP-0105, EP-0149, EP-0710, EP-0748, EPS-126, EPS-174, OP-567, OP-775, OP-776
Beyhan, E. EP-0230
Beykan, S. **OP-833**
Bezak, E. OP-140, OP-441
Bezhad, M. EP-0641
Bezverkhniaia, E. **EP-0807**, EPS-220, OP-704
Bezzi, C. **EP-0202**, OP-505
Bezzi, D. **EP-0354**, OP-534
Bezzina, P. OP-660
Bhandare, M. EP-0216
Bharkhada, D. EPS-126
Bhat, A. OP-137, OP-138
Bhatt, M. EP-0987
Bhure, U. EP-0795
Bian, S. **EP-0261**
Bianchi, A. OP-447
Bianchi, M. OP-052
Bianco, D. EP-0606, EPS-065
Biasiucci, A. EP-0985
Biassoni, L. OP-496
Biber Müftüler, F. Z. EP-0885
Biczok, A. OP-584
Bidard, F.-C. EPS-017
Biechele, G. OP-110
Biere-rafi, S. OP-928
Bifone, A. EP-0700, EP-0749
Biggi, E. EP-0908
Bigiogera, V. EP-0685

Bilgic, M. S. EPS-200
Bilgic, S. OP-035, **OP-391**
Bilinska, A. OP-432
Billoux, T. OP-938
Binder, P. EP-0460, OP-648
Bin Essa, N. **EP-0184**
Bint Mohamed, T. EP-0972
Bipath, P. EP-0643
Birindelli, G. OP-368
Birnbaum, L. EP-0810
Bischof, G. **EPS-147**, OP-105, OP-107, EP-0751
Bischoff, E. OP-137
Biscontini, G. EP-0112, EPS-053
Bishnoi, K. EP-0158, EPS-044, OP-649
Bispo, A. C. EPS-007, OP-489
Bitencourt, A. EP-0395
Bittrich, M. EP-0353
Bitzén, U. EP-0219, TEPS-012
Biyiklioglu, S. E. EP-0742
Bjurberg, M. EP-0311
Blackham, K. A. OP-191
Blagoev, M. EPS-291, OP-491
Blakkisrud, J. EPS-188, OP-436, **OP-439**, **OP-831**, OP-832, OP-911
Blanc, A. OP-139, OP-765, OP-897
Blanc, F. OP-855, OP-160
Blanc Durand, P. EP-0699, EP-0756
Blanch, T. EP-0241
Blanchardon, E. OP-495
Blanch Labrador, M. EP-0109
Blanco, I. EP-0447, EPS-070, EPS-203, EPS-063
Blanco Verdejo, L. EP-0585
Blasco, A. EPS-048
Blaszczyk, M. EP-0432
Blautzik, J. OP-716
Blazquez-Muñoz, I. EP-0939
Blei, M. **EP-0849**
Blennow, K. OP-104
Blesa Jiménez, A. EP-0845, EP-0864, EPS-269
Bley, T. A. EP-0182, OP-517
Blin, N. OP-100
Bloise, I. **EP-0201**, EPS-115, **EPS-223**, EPS-242, EPS-251, OP-715
Blomgren, A. EP-0156
Blomqvist, L. EP-0317
Blondin, D. P. EP-0499
Blonski, M. OP-586
Blumenberg, V. OP-099
Blunschi, J. OP-897
Bnà, C. EP-0744
Boada, M. OP-103
Bobek-Bilewicz, B. OP-589
Bobrova, V. EP-0615
Boccalini, C. OP-104, OP-106, OP-455
Boccalon, M. EP-0812
Boccato, T. EPS-018, OP-590
Bocci, M. OP-355, OP-356
Bochev, P. EP-0268, **EP-0295**, **EP-0346**
Bodar, Y. J. L. OP-506
Bode, J. W. OP-492
Bodei, L. EP-0197, OP-309
Bodenko, V. EP-0837, EPS-218
Bodensohn, R. OP-584
Bodet-Milin, C. OP-100
Bodin, S. EP-0035, OP-150, **OP-895**
Bodur, M. T. EP-0742, OP-944
Boehm, E. EPS-010
Boellaard, R. OP-102EP-0677, EP-0757, EPS-019, OP-027, OP-109, OP-364, OP-451, OP-566, OP-928, OP-930
Boer, J. **OP-381**, OP-042
Boersma, H. **EP-0877**
Bogni, A. EP-0010
Bogos, R. EPS-040
Bogović Crnčić, T. EP-0292
Boldrini, L. EP-0335
Bolenz, C. EP-0560
Bolin, M. **OP-563**
Bolívar-Cuevas, S. A. EP-0955
Bolland, G. EPS-206
Bollenbacher, A. EP-0726, EPS-092
Bolm, C. EPS-229
Bologna, R. OP-913
Bolouri-Novin, F. EP-0806
Bolourinovin, f. **EP-0804**
Bolster, A. EP-0411
Bölükbas, S. EP-0146
Bolzati, C. EP-0009, **EP-0011**, **EP-0012**
Bomanji, J. EP-0184
Bombaci, M. OP-447
Bombay Hospital, Mumbai, EP-0515
Bonacina, M. EP-0744
Bonadonna, R. EP-0487
Bonanni, L. OP-455
Bonatti, P. L. EP-0404
Bonatto, E. EPS-183
Bonazzi, N. EP-0213, EP-0215
Bondia Bescos, S. EP-0251, **EP-0211**, EP-0248, EP-0299, EP-0473, EP-0547, EP-0942, EP-0954, **EP-0970**, **EPS-031**, EPS-048, EPS-049, EPS-154, EPS-265
Bonet, J. **EPS-212**
Bonfiglioli, R. EP-0681
Bongiovanni, A. EP-0613
Boni, R. EP-0443
Bonilla Aguilar, I. EP-1007
Böning, G. EP-0726, EPS-092, EPS-237, OP-838, OP-839
Bonneau, C. EPS-017
Bonnet-Brilhault, F. OP-799
Bono, B. EPS-161
Bono, F. OP-537
Bonomi, A. M. OP-854
Booker, K. OP-440
Boonkawin, N. EPS-109
Boonsingma, N. EPS-109
Borchmann, P. OP-099, OP-101
Boreel, D. OP-358
Borges Tavares, A. **EP-0719**
Borgoforte Gradassi, S. EP-0112
Boria Alegre, F. EP-0705, EP-0706
Borkowska, A. OP-675
Borlase, S. **EP-0884**
Bormans, G. EP-0196, OP-558
Borrelli, P. EP-0229, EP-0250, **EP-0759**
Borsatti, E. OP-052
Borwne, S. EP-0339
Borysenko, A. OP-140
Bosch, M. EPS-143
Bosch Barrera, J. EP-0148
Boschi, A. EP-0709
Bosque, J. J. EPS-259, OP-638
Boss, M. EP-0077, EP-0486
Bosshart, A. OP-897
Bossis, T. **EPS-246**
Boström, P. EP-0659
Bosveld, B. **OP-183**
Boswinkel, M. EP-0069, OP-220, **OP-488**
Bot, P. OP-381
Bota Bota, A. EP-0890, EP-0516
Botelho, M. F. EP-0008, EPS-211
Botta, F. EP-0540, EP-0543, OP-669, OP-915, OP-921
Botti, J. EP-0664
Botticella, A. EPS-260
Bottoni, G. OP-315
Bouaziz, H. EP-0420
Bouchelouche, K. EPS-106, OP-730
Bouffard, L. EP-0499
Boukerroui, D. OP-907
Boukhennoufa, O. **EP-0698**
Boulahdour, H. EP-0698
Boundas, D. EP-0938, EPS-136, OP-542
Bouquillon, B. OP-858
Bourbonne, V. OP-855
Bourdon, A. EP-0429
Bourgeois, M. OP-155
Bourgeois, S. EP-0673

Bourhis, D. OP-855
Bourien, H. OP-160
Bourogianni, O. EP-0193, **EPS-083**, OP-859
Bourouba, M. **EP-0973**, OP-630
Boursier, C. **EPS-008**, EPS-240
Boursier, M. OP-764
Bouvet, F. EPS-246
Bouvet, G. OP-236
Bouwman, F. EPS-150
Bouziotis, P. EP-1000
Bozkurt, K. EP-0574
Bozkurt, M. F. EP-0577, EP-0347, EPS-202
Braat, A. **OP-852**, EPS-198, OP-295, OP-670, OP-850
Brabander, T. EPS-103, OP-670
Braca, D. EPS-085
Bracke, A. EP-0673
Brackman, M. OP-340
Bradley, K. EPS-176, OP-227
Bradnam, M. EP-0411
Brady, K. OP-490
Bragina, O. EP-0861, OP-578
Brahmi, M. OP-056
Brandon, D. EP-0164
Brandsma, D. EPS-158
Braun, C. EP-0843
Bravo, Y. OP-359
Bravo-Ferrer Moreno, M. L. EP-0845, EP-0864
Brayton, C. OP-149
Breault, E. EP-0850
Bregenzer, C. **OP-058**, OP-246, OP-516, **OP-521**, **OP-636**, OP-666
Brembilla, G. OP-505
Bremmer, F. EP-0002
Brendel, M. EP-0015, EP-0024, EP-0726, EPS-148, OP-082, OP-108, OP-110, OP-467, OP-588, OP-710, OP-769
Brenner, A. EP-0612, OP-857
Bressel, M. OP-338
Breuil, L. EP-0019, **EP-0674**, OP-559
Breyer, L. EPS-102
Brief, Y. **EPS-282**
Briganti, A. EPS-107, OP-505
Briganti, V. EP-0212, EP-0546
Brighi, N. OP-723
Brillouet, S. OP-804, OP-951
Brink, A. EP-0269, EP-0680, **EPS-087**, OP-318, OP-884
Brisse, H. OP-311
Brocchi, S. OP-534
Brodin, P. EP-0608, OP-193
Broeckaert, C. OP-664
Broersen, A. EPS-178
Broggio, D. EPS-246
Bronowicki, J.-P. OP-160
Bronte, Á. EP-0088, EP-0862, EPS-011, EPS-148, OP-098, OP-507, OP-936
Bronte, E. EP-1028
Bronte, F. EP-1028
Bronte Viedma, A. EP-0348
Brooks, A. EP-0828
Brooks, J. D. OP-504
Brorson, J. OP-386
Brosch-Lenz, J. EP-0655, **EPS-115**, EPS-242, EPS-251, OP-154, OP-309, OP-442, **OP-497**, **OP-715**
Brouwer, E. OP-515
Brouwers, A. EP-0196, EP-0124, OP-573
Brown, C. EP-0701, EPS-179
Brown, M. **EP-0842**
Brown, T. EPS-206, OP-718
Bruchertseifer, F. OP-335, OP-719
Brühlmann, S. **OP-020**
Bruijnen, R. C. G. EPS-198, OP-295, OP-850
Bruland, Ø. OP-911
Brunotte, F. OP-078
Brusaferri, L. OP-846
Bruscoli, M. OP-462
Brust, P. OP-558
Bruyer, Q. EP-0875
Bruyere, A. EPS-099
Bruyn, M. d. EP-0033
Brynolfsson, J. OP-041
Bucerius, J. EP-0002
Buchert, R. EP-0791, OP-710
Buchpiguel, C. OP-843
Buck, A. K. EP-0182, EP-0319, EP-0353, EP-0507, EP-0539, EP-0552, EP-0610, EPS-117, EPS-235, OP-152, OP-291, OP-305, OP-332, OP-517, OP-785, OP-866
Buckle, T. **EP-0848**, EP-0851, EPS-113, OP-298
Bucur, D. **EP-0930**
Budau, A.-M. EP-0956
Budzynska, A. OP-675
Buechel, R. R. OP-239
Bueno Raspall, M. EP-0892
Buffardi, S. OP-052
Buffi, N. EP-0272, OP-039
Buffoni, F. EP-0763, OP-328
Buhl, C. S. OP-730
Buhl, E. M. EPS-229
Bujanow, A. EPS-156
Bukva, M. EP-0181
Bullich, S. **EP-0678**, EPS-085, OP-103
Bulten, B. F. OP-183
Bulzico, D. A. EPS-007, OP-471
Bundschuh, R. A. EP-0451, OP-655, EP-0565, OP-856
Buonanno, M. **EP-0575**, EP-0879, EP-0886, EP-1034, EP-0819
Buongiorno, P. OP-382, OP-383
Buonsanti, G. OP-915
Burger, C. **EP-0941**
Bürger, K. EPS-148
Burghelea, B. EP-0866
Burke, B. EPS-289
Burnazi, E. OP-802
Burniston, M. OP-496
Burroni, L. EP-0112, EPS-053
Burvenich, I. **EP-0032**
Busch, M. OP-937
Buschiazzo, A. OP-447
Buscombe, J. EP-0636
Busslinger, S. D. **EP-0070**
Bustamante-Ramírez, G. EP-0355
Buteau, F.-A. A. OP-236
Buteau, J. P. EP-0555, EPS-172, OP-037, OP-338, OP-437
Büther, F. OP-356, OP-779
Buvat, I. EP-0322, EPS-017, EPS-185, OP-311, OP-567, OP-637, OP-709, OP-917
Büyükaşık, Y. EP-0347
Buyukkaya, F. EP-0911
Bystry, V. EP-0283
Byun, J. **OP-285**
Bzowski, P. OP-589

Caballero Calabuig, E. EP-0417
Caballero-Gonzalez, A. EP-0331
Caballero Vivanco, M. EP-0628, **EP-1032**, TEPS-001
Cabañas, V. EP-0356
Cabaret, A.-L. **EPS-263**
Cabel, L. EPS-017
Cabello, J. EP-0658, OP-025, OP-774
Cabezudo-Pérez, E. EP-0355
Cabrera Galeana, P. EP-0130
Cabrera Martín, M. EP-0361, EPS-020, EPS-081, EPS-167
Cacciatore, F. OP-383
Cáceres Silva, D. R. EP-0419, EP-0579, EP-0407, EP-0924, EP-0925, EPS-269, OP-924
Cachin, F. OP-938
Cadranel, J. EPS-292
Cagle, B. S. OP-144
Cagnin, A. EPS-149
Cai, H. EP-0057, EP-0746
Cai, J. EP-0167, OP-427
Cai, M. EP-0427, EP-0527
Cai, W. EP-0157
Cai, Z. EP-0056, EP-0841, EP-0842, **OP-898**
Caille, F. EP-0021
Calabrese, M. OP-921

Calabretta, R. EP-0460, **OP-648**, OP-713
Calabria, F. EP-0376
Calabrò, A. EP-0191, OP-166, **EP-0323**
Calado, D. EP-0086, EP-0704
Calais, J. EP-0284, EPS-110, EPS-122, OP-034, OP-036, OP-040, OP-192, OP-434, OP-440, OP-508, OP-509
Calareso, G. EP-0068, OP-234
Çağlar Tuncalı, M. EP-0232
Calcagni, M. L. EP-0693, EPS-153, EPS-196, OP-634
Calcagno, A. EP-0921, EP-0980
Caldarella, C. **EPS-196**
Calderón, E. **OP-572**
Calderon Avila, A. EP-0603
Calderoni, L. EP-0303
Calegaro, J. **EPS-045**
Calheiros, R. OP-472
Callahan, J. OP-567
Callaud, A. **EP-0489**
Calviño, N. EP-0252, EP-0548, **EP-0508**
Calvo de Juan, V. EP-0148
Çağlıyan, F. EP-0190
Camacaro, J. F. OP-018
Camacho, M. R. F. EP-0259
Camacho, V. EP-0331
Camardese, G. OP-456
Camarero, A. EP-0447, EPS-070, EPS-203
Camarero Salazar, A. EPS-063
Camedda, R. EP-0285
Caminiti, S. **OP-045**
Cammilleri, S. OP-929
Camozzi, V. EPS-074
Campana, D. EP-0213, EP-0215
Campana, L. EP-0783
Campaña Diaz, E. EP-0254, EP-0386, **EP-0503**, EPS-052, OP-170, OP-787
Campdelacreu-Fumado, J. EPS-154
Campeiro, J. **EP-0014**
Campenni', A. **OP-392**, **OP-524**, OP-525, **OP-801**
Campion, L. OP-155
Campoleoni, M. EP-0763
Cañadas Salazar, J. C. EPS-052, **EP-0357**
Canales, M. EP-0339
Canales, P. EP-0465
Canali, G. OP-858
Canário, D. EP-0989
Cancelinha, D. EPS-211
Candoli, P. EP-0147, OP-879
Cañete Sanchez, F. EP-0242, EP-0557
Canevari, C. EP-0202
Cannatà, V. EPS-037
Cano, J. OP-233
Cano Carrizal, R. EPS-020, EPS-081
Cañón Sánchez, J. R. EP-0302, EP-0611
Canora, A. EPS-167
Canto, N. EP-0086
Cantoni, V. OP-647
Cantuarias, L. OP-489
Canudo, A. EP-0769
Canzi, C. EP-0763
Cao, C. OP-635
Cao, J. **EP-0234**
Cao, W. EP-0177
Cao, X. EP-0923
Cao, Y. EP-0289
Cao, Z. OP-490
Caobelli, F. **OP-246**, OP-516, OP-521
Capacho, A. EP-0769, EP-0006
Caplin, H. OP-495
Capobianco, N. EP-0322
Capoccetti, F. EP-0623, OP-395
Capolongo, D. OP-328
Caponnetto, D. OP-447
Capotosti, A. **EP-0693**, EP-0793
Cappelli, f. EP-0469
Capponi, M. OP-395
Cappuzzo, F. OP-581
Captier, N. OP-637
Carabellese, B. EP-0376
Carballo Menayo, C. EP-0587
Carcamo Ibarra, P. EP-0417
Cardaci, J. OP-230
Cardile, D. OP-392, OP-524, OP-801
Cardillo, G. OP-634
Cardin, A. EP-0555, EPS-010, OP-437
Cardinale, J. OP-512, OP-772
Cardosa-Cisneros, D. EP-0525
Cardoso, A. OP-058, **OP-666**
Cardoso, M. A. S. EPS-007
Carletto, M. EP-0921, EP-0980
Carli, G. OP-462
Carlier, T. **EP-0688**, EPS-184, OP-092
Carlsen, E. A. EP-0195
Carlucci, G. EP-0850, OP-434
Carmona, S. EP-0922, EP-0966, EP-0989
Carmona-Bayonas, A. OP-233
Carnegie-Peake, L. **EP-0657**, EP-0662
Carneiro, M. P. EPS-007
Caroli, P. EP-0238, EP-0613, OP-723
Carpanese, D. EP-0009, EP-0011
Carpentier, A. C. EP-0499
Carra, F. EP-0511
Carradus, A. **EP-0411**
Carrasco, J. **EP-0773**
Carrasco Rubio, V. EP-0705, EP-0706
Carrasquillo, J. OP-304, OP-310
Carrera, F. EP-0364
Carreras-Delgado, J. EPS-167
Carreres Ortega, Y. EP-0599
Carrero Vasquez, V. EP-1007, **EP-0101**, EP-0355, EP-0473, EP-0942, EP-0970, **EPS-048**, **OP-784**, EPS-049
Carrier, J. F. OP-225, EP-0695, OP-848
Carriere, C. OP-447
Carrilho, E. EP-0008
Carroccio, A. EP-1028
Carroll, P. OP-040
Carston, A. EP-0863
Carvalho, I. P. EP-0412
Carvalho, J. **EP-0834,** EP-0291, **EP-0978**, EP-0846
Casabonne, D. EP-0355
Casadei, B. OP-099
Casale, P. EP-0272, OP-039
Casallas Cepeda, M. **EP-0329**
Casal Rubio, J. EP-0148
Casanova, E. OP-081
Casanova Triviño, P. EP-0603
Casanueva Eliceiry, S. **EP-0491**, EP-0356
Casas Calabuig, L. EP-0417
Casas-Fernandez, L. EP-0559
Casasnovas, O. EPS-185
Caselles, O. EP-0647, EPS-089, EPS-246
Casillas Sagrado, E. EPS-052, OP-787
Casimiro, I. **EP-0485**
Casini, A. EP-0811, EP-0843, OP-141
Casiraghi, M. OP-915, OP-921
Cassano, B. EP-0783, EPS-232
Cassou Mounat, T. OP-804, EP-0647
Castanheira, J. OP-221, EP-0328
Castejón Echevarne, S. EP-0400
Castellani, M. EP-0763, EP-0915, EPS-183, EPS-272, OP-328, OP-540
Castellano, A. EPS-037
Castello, A. EP-0763, EP-0915, EPS-183, **EPS-272**, OP-540
Castellon, M. OP-233
Castellón-Plaza, D. EP-0955
Castellón Sanchez, M. EP-0407, EP-0419, EP-0579, EP-0924, EP-0925, EPS-269, OP-924
Castellucci, P. EP-0388, EPS-107, OP-474, OP-879, OP-881, OP-882
Castiglione Minischetti, G. EP-0540
Castiglioni, I. EP-0744
Castillejos Rodríguez, L. EP-0526, EP-0604
Castillejos Rodriguez, M. EP-0964
Castillo Arias, C. EP-0585
Castillo Morales, V. EP-0352

Castro, I. EPS-094
Castro, R. EP-0301, EP-0961
Castro, S. F. EP-0472, EP-0962
Castro-Velasco, R.-M. EP-1013, EPS-023
Casuscelli, J. OP-717
Catafau, A. M. OP-340
Catalano, M. EP-0985
Catapano, A. OP-639
Cattabriga, A. OP-534
Cattaneo, M. EPS-272
Cavarec, M.-B. OP-806
Cavelier, F. EP-0035, OP-150, OP-895
Cavinato, L. **EPS-180**, OP-362
Cavuto, S. EP-0999, EPS-014
Çay, F. EP-0577
Cazzamalli, S. OP-355, OP-356
Cazzola, E. **TEPS-021**
C Costa, D. EPS-173
Cea, A. EP-0869
Cebekhulu, N. EP-0643
Ceberg, C. EP-0026
Cebollada-Cameo, L. EP-1013, EPS-023, EPS-025, EPS-026
Cecan, M. EP-1031
Cecchin, D. **EPS-149**
Ceci, F. EP-0236, EP-0540, EP-0543, EPS-107, **OP-038**, OP-294, OP-337, OP-668, OP-669, OP-854, OP-915, OP-921
Cegła, P. EP-0298
Celebioglu, E. C. EPS-200
Célier, D. OP-495
Celik, S. OP-163, OP-375
Çelik, A. EP-0974
Celli, M. **EP-0238**, OP-723
Cengiz Gökmen, M. B. EP-0402
Cengiz Seval, G. EP-0349
Centonze, G. EP-0068
Cergnul, M. EP-0980
Ceriani, L. OP-102, OP-525
Ceric Andelius, I. **EP-0468**
Cerina, V. **EP-0685**
Çermik, T. F. EP-0402, EP-0230
Cerna, L. EPS-041
Cernov, V. EPS-040
Ceugnart, L. EP-0117
Cevik, F. EP-0225
Ceylan, Y. EP-0434
C. Ferreira, I. EP-0966
C. Ferro, J. **OP-539**
Cha, J. **EP-0593**, **EP-0595**
Chaban, A. **OP-309**
Chabiron, M. EPS-243
Chacon, M. EP-0573
Chaib, S. **OP-470**
Chakraborty, A. **EP-0043**
Chalampalakis, Z. **EP-0748**
Chalewska, W. OP-675
Chalopin, T. OP-100
Chaltout, F. EP-0387, **EP-0972**
Chaman Baz, A. **EPS-075**
Chamberlain, R. EPS-175
Champault, A. EP-0019
Champion, C. EP-0780, EP-0840
Champion, L. EP-0694, EPS-017
Chamuleau, M. OP-102
Chan, C. **EP-0835**, EP-0884, OP-898
Chan, H.-P. OP-397
Chan, S. C. **EP-0155**
Chanchou, M. **OP-938**
Chandekar, K. EPS-054
Chandra, P. **EP-0821**
Chandran, G. EP-0821
Chang, C. C. OP-180
Chang, M. C. **EP-0055**
Chang, P.-C. **EP-0858**
Chang, W. T. EPS-162
Chang, Y. T. OP-180
Chao, C. C. EP-1029
Chapeau, D. **EPS-277**
Chardin, D. EP-0132
Charfeddine, S. EP-0387, EP-0972, EP-0990
Charfi, H. EP-0139, EP-0140, EP-0994
Charfi, j. **EP-0993**
Chari, A. EP-0351
Charles, K. OP-304, OP-310
Charmelot, R. EP-0687
Chary-Valckenaere, I. OP-250
Chatterjee, S. OP-018
Chatti, K. EP-0139, EP-0140, EP-0697, EP-0512, EP-0994, EP-0514
Chaudhari, P. EP-0013
Chaudhari, V. EP-0207, EP-0216
Chauffaille, M. EP-0345
Chaurasiya, K. EP-0326
Chaushev, B. EP-0263, EP-0341, EP-0342, EP-0343, EP-0344, EP-0899, EP-0900, EP-0901, EP-0902, EP-0904, EP-0913, EP-0981, EPS-267
Chausheva, S. EP-0263, EP-0899, EP-0904, EP-0913, **EP-0981**, EPS-121, EPS-267, EP-0341, EP-0342, EP-0343, EP-0344, EP-0900, EP-0901, EP-0902
Chaussé, G. **EP-0286**, **EP-0867**
Chauvet, P. EPS-184, OP-092
Chavan, L. EP-0810
Cheewadhanaraks, S. **EPS-109**
Chen, A. P. OP-304, OP-310
Chen, B. EPS-164, EPS-207, EP-0001, OP-644
Chen, C. Y. OP-561
Chen, C. T. EP-0055
Chen, C. C. OP-304, OP-310
Chen, D. **EPS-056**
Chen, G. EP-0782, OP-359
Chen, H. EP-0167, OP-374, OP-398, OP-427, OP-790, EP-0177
Chen, J. EP-0133, EPS-209, OP-096, OP-376, EP-0838
Chen, K. T. OP-228
Chen, K. OP-111
Chen, L. C. EP-0029
Chen, L. EP-0608, EPS-108
Chen, M. K. OP-193
Chen, M.-W. EP-0029
Chen, N. OP-448
Chen, Q. EP-0133
Chen, S. EP-0842, EP-0223, OP-378, OP-791, **EP-0092**, EPS-114, EPS-191, **OP-095**, **OP-159**
Chen, X. OP-448, EP-0052, EP-0223, EP-0281, OP-237, OP-378, OP-576, OP-721, OP-933, EP-0815, EPS-091, **EP-0321**, EPS-197, **OP-377**
Chen, Y. **EP-0427**, EP-0527
Chen, Y. C. **EP-1029**, EPS-162
Chen, Y. H. EP-0689, EPS-182, EPS-258, OP-090
Chen, Y. EPS-056, EP-0639
Chen, Z. EPS-028, OP-622, OP-902, EP-0814, **EP-0003**, EP-0710, **OP-284**, OP-290, OP-776, EP-0835
Cheng, J. OP-082, EP-0042, EP-0650
Cheng, J. S. EP-1029
Cheng, K. EPS-191, OP-159
Cheng, L. T. EP-0616
Cheng, M. F. EP-1029, EPS-162, OP-319
Cheng, R. **OP-714**
Cheng, X. **EP-0281**
Cheng, Y. EP-0091, OP-048, EPS-006
Chenjie, X. **EP-0123**, **EP-0170**, **EP-0173**
Cheon, G. EP-0186, EP-0536, OP-285, EP-0747
Cheon, S. M. EPS-168
Cherbuin, N. OP-331
Cherel, M. OP-153, OP-155
Cherif, S. EP-0087
Chernov, V. OP-578
Cherry, S. OP-776, OP-567, OP-775
Cheung, S. OP-159, **EPS-114**
Chevalier, E. EPS-008, EPS-240, OP-160
Chhabra, S. OP-802
Chi, K. EPS-115, OP-340, OP-715
Chiang, C. EPS-010
CHIANG, P. F. EP-0055
Chiappetti, R. OP-383

Chiaravalloti, A. EP-0998
Chicheportiche, A. **EP-0542**
Chien, K.-L. EP-0431
Chierichetti, F. OP-585
Chiesa, C. OP-674
Chiesa, S. EP-0335
Chillotti, S. EP-0303
Chilug, L. EP-0866
Chim, J. C. OP-095
Chincarini, A. EPS-149, OP-051
Chinnappan, S. EP-0821
Chiola, S. OP-455
Chiorazzo, T. OP-765, OP-897, OP-139
Chirindel, A. **OP-716**
Chiti, A. EP-0202, EP-0285, EPS-161, OP-505, OP-653, OP-712
Chiu, P. Y. OP-180
Chiu, Y. L. OP-397
Chmielik, E. OP-589
Cho, H. EP-0595, TEPS-014
Cho, K. EP-0747, OP-049
Cho, S. EP-0040, EP-0730
Choi, E. EP-0823
Choi, H. EP-0186, EP-0536, EP-0747, OP-049, OP-362
Choi, J. OP-179, EP-0128, OP-049, EP-0128
Choi, S. OP-049
Chojnowska, M. **EP-0478**
Cholewiński, W. OP-157
Chong, A. OP-049
Chongjiao, L. OP-782
Choniawko, P. EP-0004
Choo, K. EPS-169
Chopitea, A. EPS-011
Chotipanich, C. EPS-109, OP-662
Choudhury, P. OP-783
Choudhury, S. EP-0207, EP-0313
Chouin, N. OP-153
Chow, T. **EP-0945**
Choyke, P. EP-0280, EPS-286
Chrétien, S. EP-0117
Christensen, K. **OP-181**, OP-500, OP-501, OP-502
Christensen, N. **OP-730**
Christensen, P. **EP-1035**
Christensen, T. Q. EP-1030
Christin-Maître, S. OP-805
Christos, F. OP-676
Chroustova, D. **EPS-041**
Chtourou, K. EP-0139, EP-0140, EP-0387, EP-0972, EP-0990
Chuang, P. J. **EPS-162**, OP-319
Chumber, S. EP-0500, EP-0505, EPS-073, EPS-079
Chung, I. OP-044
Chung, W. EP-0842
Ciampi-Dopazo, J. EP-0581
Cianchetti, M. OP-585
Cianciarelli, C. EP-0573
Cianni, L. OP-429
Ciappuccini, R. OP-806
Ciarmiello, A. EPS-183
Cibeira, M. EP-0356
Ciccioli, G. OP-395
Cicconi, A. OP-764
Cichocki, P. **EP-0432**, EP-0703, EPS-097, **OP-950**
Cichonski, A. **EP-0798**
Cieniewicz, A. OP-359
Cieszykowska, I. EP-0870
Ciftci, I. EP-0225
Ciglar-Hlasc, M. EPS-264
Cimini, A. EP-0376, EPS-159, **OP-535**
Çinçin, E. EP-0359
Cinquegrani, G. EP-0487
Ciocan, A. **EP-0931**
Cirone, A. OP-315
Ciscar, A. EP-0508
Cistaro, A. OP-052
Cisternino, S. TEPS-021
Citerne, Q. EP-0894
Cittanti, C. EP-0709
Ciuca, L. EP-0538
Ciucci, D. EPS-037
Civan, C. **EP-0377**, OP-333
Civelek, A. C. OP-304, OP-310
Civi, O. EP-0253
Civollani, S. EP-0213
Claesener, M. OP-356
Claessens, R. **EP-0882**
Claeys, W. **OP-366**
Clarisse, B. OP-806
Classen, J. OP-108
Clausen, A. S. OP-615
Claver-Garrido, E. EP-0473
Cleeren, F. EP-0196
Cleland, J. L. OP-793
Clemens, L. P. EP-0667
Clement, C. **EP-0750**, **OP-368**, OP-710
Clemente, S. EP-0551
Clemons, N. EP-0863
Clerc, J. EP-0883, EPS-185
Clerici, I. EP-0540, EP-0543, OP-669
Cleveland, M. EP-0042, EPS-195
Cliatt-Brown, C. J. EPS-152
Clift, R. OP-137, OP-138, OP-359
Clifton-Bligh, R. EP-0558
Clotagatide, A. EPS-080
Cloughesy, T. OP-434
Cobo Dols, M. EP-0148
Cocciolillo, F. EPS-153, EPS-196, OP-456
Cochet, A. EPS-015, EPS-123, EPS-219, OP-078, OP-160
Cocioaba, D. EP-0866
Codegone, A. OP-910
Codesido, J. EP-0023
Coelho, A. EP-0008
Coelho, M. OP-330
Coerts, H. **OP-800**
Cohalan, C. OP-225, OP-848
Coşkun, T. EP-0120
Colandrea, M. EP-0236, EP-0543, OP-921
Colarinha, P. OP-185, OP-663
Cole, A. EP-1037
Cole, D. OP-137
Colin, D. EP-0053
Collamati, F. EP-0783, OP-038, **OP-294**, OP-854
Collantes, M. **EP-0034**, EP-0859, EP-0862, EPS-095
Collarino, A. EP-0335
Collaud, C. EP-0573
Collij, L. E. OP-109, **EPS-150**
Collin, B. EPS-219
Collovà, E. EP-0921
Colombié, M. OP-155
Colombo, C. EP-0763
Colombo, M. EP-0010
Colombo, P. EP-0272, OP-039
Colombo Serra, S. EP-0700, EP-0749
Colorado, K. EP-0465
Colpo, N. EPS-115, EPS-223, OP-142, OP-431, OP-715
Comas, L. EP-0698
Comas Rojas, H. EP-0863
Compte, A. EP-0109, EP-0241
Confalonieri, L. EPS-288
Cong, Y. EPS-287, OP-212
Connor, M. J. EP-0276, OP-511
Conradie, M. EP-0941
Consigny, M. OP-855
Constantinescu, A. OP-897
Constantino, C. EPS-173, **OP-087,** OP-221, **EP-0328,** EP-0738
Conte, M. OP-315
Conti, M. EP-0688, EP-0755
Contreras Ameduri, M. EP-0229, EP-0250, EP-0496, EP-0562, EPS-050,**EPS-268**
Contreras-Castañón, G. EP-0895
Contreras Gutierrez, J. F. EP-0419, EP-0579, EP-0407, EP-0924, EP-0925, EPS-269, OP-924
Cook, G. J. R. EP-0533
Cook, M. J. OP-025

Cooke, J. EP-0787
Coomans, E. M. EP-0677, OP-109
Cooperberg, M. OP-040
Coplo, N. EP-0829
Cordero, I. EP-0301, **OP-665**
Cordero García, J. EP-0127, EP-0365, EP-0502
Cordier, D. OP-191
Córdoba Cañete, E. EP-0628, EP-1032, **TEPS-001**
Cordova, A. EPS-289
Corela, D. OP-859
Coretti, B. G. EPS-061
Coriu, D. EP-0464
Cormier-Daire, V. OP-947
Cornelissen, B. EP-0835, EP-0847, OP-493
Cornoiu, R. EP-0866
Coronado Poggio, M. EP-0127, EP-0365
Corradini, N. OP-056
Corrao, G. EP-0236
Correia, J. EP-0769
Correia, M. EP-0086, EP-0704, EP-0769
Correia, P. EPS-094
Cortes Gonzalez, M. OP-555
Cortés Romera, M. EP-0251, EP-0892, EP-0101, EP-0211, EP-0248, EP-0299, EP-0355, EP-0473, EP-0547, EP-0939, EP-0942, EP-0954,EP-0955, EP-0970, EP-0988, EP-1007, EPS-031, EPS-048, EPS-049, EPS-154, EPS-265, OP-784
Coruzzi, C. EP-0999, EPS-014
Corvo, C. EP-0019, **EP-0021**
Coskun, N. **EP-0570**, **EP-0588**, **OP-914**
Costa, C. H. F. EPS-007
Costa, D. EP-0006, EP-0769, EP-0328, EP-0738, OP-087 OP-221
Costa, G. EP-0165, EP-0239, EP-0395, EP-0485, EPS-211
Costa, L. EP-0926
Costa, M. **EP-0769**
Costa, P. **OP-660**
Costa, T. O. EPS-078
Costa, V. OP-455
Costache, D. EP-0931
Costanzo, E. EP-0469
Cosulich, S. OP-555
Cotanda, V. EP-0800
Cotar, U. TEPS-006
Cottereau, A. S. EP-0322, EPS-185
Cottignoli, C. EP-0112, EPS-053
Cottu, P. EPS-017
Couderc, M. OP-938
Cougnenc, O. EP-0117
Counter, W. EP-0558, EPS-120
Courbon, F. EP-0647, EPS-089, OP-654, OP-804, OP-951
Cournane, S. EP-0787
Courteau, A. **OP-078**
Coutant, C. EPS-015
Covarrubias, N. EP-0465
Covello, E. EP-0404
Cox, C. P. W. **EPS-103**
Craciun, D. EP-0943, EP-0953, **EP-0957**
Craciun, L. EP-0866
Crawford, R. EP-0799
Cremonesi, M. EPS-249
Crespí Busquets, M. **EP-0892**, EPS-265
Crespo, A. EP-0361
Cripps, A. **EP-0663**, **EP-1003**
Crisan, M. EP-1031
Criscuoli, B. EP-0376, **EP-0623**
Crivellaro, C. EP-0316, EP-0685, OP-537
Croci, G. A. EPS-272
Croes, G. **EPS-233**
Croset, A. OP-897
Crosta, G. **OP-540**
Croteau, E. EP-0045
Crouy-Chanel, O. OP-806
Crumbaker, M. EP-0558, OP-230, OP-335
Cruz, J. EP-0447, EPS-070, EPS-203
Cruz Montijano, M. EP-0229, EP-0250, EP-0496, EP-0562, EPS-050, EPS-268
Cruz Vasquez, J. **EPS-063**
Csaba, M. EP-0390
Cselényi, Z. OP-555
Csende, K. EP-0390
Cuartero, A. EP-0023
Cucca, M. EP-0908
Cuccaro, A. EP-0335
Cucchiara, V. OP-505
Cuderman, A. EP-0089
Cuenca, T. EP-0348, EPS-011
Cuenca Bandín, T. EPS-095
Cuenca Cuenca, J. EP-0199, EPS-072
Cuendet, M. A. EP-0699
Cuesta Domingo, G. EP-0361, **EPS-020**, EPS-081, EPS-167
Cufe, J. OP-356
Cui, B. EP-0091, EP-0307, EPS-166
Cui, C. **EP-0324**, EP-0741, OP-633
Cui, J. **EP-0444**
Cui, X. EP-0838, **OP-435**
Cui, Y. EPS-146, **OP-863**, TEPS-020
Cuocolo, A. EP-0551, EP-0606, EPS-065, OP-382, OP-383, OP-647
Cuomo, M. OP-234, **OP-674**
Currie, G. EPS-206
Custodia, A. EP-0023
Custodio, A. OP-233
Cutaia, C. OP-910
Cutini, I. EP-0330
Cuzino, D. EP-0931, EP-0937
Cuzzani, G. EP-0147, EP-0303, OP-879, **OP-881**, **OP-882**
Cwikla, J. EP-0798, **OP-231**
Cwojdzinski, T. OP-141
Cygikalo, A. EP-0446
Cysouw, M. **EP-0757**
Czékus, T. EP-0181
Czernin, J. EP-0037, EP-0284, EP-0850, EPS-122, OP-040, OP-192, OP-434, OP-440, OP-508, OP-509
Czibor, S. OP-102

D'Abadie, P. **EP-0358**
Dabbagh, V. **EP-0085**
Dabbous, H. EP-0164
Dabir, M. OP-937
Dabiri Oskue, S. EPS-271
Da Costa Branquinho, E. EP-0875, OP-360
Dadachova, E. EP-0834, EP-0836, EP-0846, EPS-212, OP-698
Dadashov, Z. EP-0833
Dadgar, H. **EPS-159**, OP-535
D'Agate, D. EP-0396
Dagrakis, E. EP-0982
Dahl, J. OP-808
Dahl, K. OP-555
Dahlbeck, M.-L. OP-623
Dahlbom, M. OP-296, OP-440
Dai, H. OP-652, EP-0648
Dai, W. EP-0639
Dai, Z. OP-144
Daigneault, G. **EP-1026**
Daisaki, H. EP-0774, EP-0776, EPS-088
Dal Bo, G. EP-0019
Dalen, N. OP-660
D'Alessandria, C. EP-0566, OP-145, OP-487, EP-0564, OP-154
Daley, A. OP-440
Dall'Armellina, S. EP-0226, EP-0249
Dall'Olio, F. G. EPS-260, EPS-263
Dalm, S. U. EP-0014, EP-0065, EPS-213, OP-083, OP-433
D'Alò, F. EP-0337
Da luz, F. A. B. EP-0935
Dam, J. H. EPS-228
D'Amato, F. EP-1028
D'Ambrosio, L. EP-0550, EP-0575, **EP-0781**, EP-0819, EP-0886
Damian, A. EP-0301
Damiana, T. **EP-0065**
Damiani, S. EP-0303
D'Amico, F. **EP-0277**, OP-050, OP-051

D'Amico, A. OP-589
Damle, A. EP-0043
Damle, N. EP-0350, **EP-0518**, EP-1019, EP-1020, **EPS-060**, EPS-073 EP-0497, EP-0498, EP-0500, EP-0505, EP-0519, EP-0987, EP-0991, EPS-054, EPS-055, EPS-076, EPS-079, OP-316
Damy, T. OP-858
Danad, I. OP-241
Dancheva, Z. EP-0263, EP-0341, EP-0342, EP-0343, EP-0344, EP-0346, EP-0513, **EP-0899**, EP-0900, EP-0901, EP-0902, EP-0904, EP-0913, EP-0981, EPS-121, **EPS-267**
D'Andrea, M. EPS-232
Danfors, T. OP-458, OP-459
Daniel, T. **EP-0883**
Danieli, R. OP-232, OP-238, **OP-367**, **OP-444**, **OP-629**
D'Antonio, A. OP-383, **OP-382**
Dantuma, M. OP-086
Da Pieve, C. OP-589
Da Pozzo, S. EP-0162, EP-0188
Dar, D. OP-589
Darcourt, J. EP-0132
Dardouri, T. EP-0512
Dari, A. EP-0758
Darian, D. EP-0753
Da Ros, V. OP-780
Darr, C. EP-0391, OP-301
Darwiche, K. EP-0137, EP-0146
Das, C. K. EPS-190
Das, K. J. EP-0122, EPS-027
Das, S. OP-673, **OP-786**
Dasgupta, S. OP-299
Dash, S. EP-0370
D'Asseler, Y. EPS-231
Date, H. EPS-262
Datta, P. OP-563
Dauden Oñate, P. EP-0361, **EPS-081**
Daum, J. OP-189
Davì, V. OP-524, OP-801
Davicioni, E. EPS-118
David, S. OP-937
Davidse, M. EPS-098
Davidzon, G. A. EP-0278, OP-504
Davies, B. OP-555
Davies, R. H. OP-713
Davis, C. OP-574
Dawicki, W. OP-698
Daza-Cajigal, V. EPS-143
De Agrela Serrao, A. EP-0407, **EP-0419**, **EP-0579**, EP-0924, EP-0925, EPS-269, OP-924
De Almeida Carrapiço, C. OP-024
Deandreis, D. EP-0226, EP-0249, EP-0396, EPS-260
De Arcocha Torres, M. EP-0890, EP-0516
Deatsch, A. OP-676
de Bakker, M. OP-029
Debarge, M. **EP-0894**
De Bernardi, E. EP-0316, EP-0685
De Bie, K. **OP-506**
De Bondt, P. OP-443
De Bonilla-Candau, M. EP-0508
de Bono, J. OP-340
Debordeaux, F. EP-0035
Deckers, W. OP-366, OP-667
De Cobelli, F. OP-505
De Cobelli, O. EP-0389, OP-038
Deconinck, L. OP-513
Decotte, A. OP-654
Decoux, G. EP-0881, OP-489
Decristoforo, C. EPS-280, OP-254, OP-306
Dede, F. EP-0190
Dedecjus, M. EP-0298, OP-675
Dedja, M. **OP-227**
Defreyne, L. EPS-231
de Galan, B. E. EP-0486
de Geus-Oei, L. F. EP-0274, OP-167, OP-086, EP-0788
De Giorgi, U. EP-0238, OP-723
Degiovanni, A. EP-0147
de Groot, M. OP-339
De Haan, T. EP-0673
de Haro-del Moral, F. EP-0467
Dei, D. OP-918
Dei Cas, A. EP-0487
Deidda, D. EP-0722
Deinum, J. EPS-075
De Ioris, M. EPS-037
Deiser, S. **EP-0811**
de Jong, H. W. A. M. EPS-198, OP-295
de Jong, I. J. OP-339
de Jong, M. D. OP-928
de Jong, R. OP-852
de Jongh, C. OP-086
de Keizer, B. EPS-075, OP-295, OP-800
DeKemp, R. EPS-126
Dekempeneer, Y. **EPS-227**
Dekervel, J. EP-0196
Dekkers, I. A. OP-167
Dekorsy, F. J. OP-584
Delage, J. **OP-153**
De Langen, A. J. EPS-195
De La Rubia Marcos, M. EP-0300, EP-0526, EP-0605, EP-0964
De Lauro, F. EP-0550, EP-0781
De Leon, J. EPS-120
Deleporte, A. OP-232, OP-238
Deleu, A.-L. OP-573
Delgado, H. EP-0769
Delgado-Cano, A. EPS-167
Delgado Castro, M. EP-0471
Delgado Niño, L. EP-0169
Del Gatto, A. EP-0011
Delie, T. OP-672
Delker, A. EP-0210, EPS-092, EPS-237, OP-467, OP-838, OP-839
Della Gala, G. EP-0681, EP-0796
Della Pepa, R. OP-916
Dellar, C. EPS-115, OP-715
Dellavedova, L. EPS-183
Deller, T. W. EP-0716, EP-0720, EPS-100
Delpassand, E. OP-213
Del Pozo, L. EPS-291
del Rivero, J. OP-304, OP-310
Delsedime, L. EP-0396
del Sol Pérez Lago, M. OP-716
Delva, A. OP-457
Del Vecchio, S. OP-639, OP-913, OP-916
De Man, K. EP-0115
De Marino, R. EP-0575, EP-0781, EP-0819, EP-0879
De Meester, I. OP-429
de Meijer, V. E. EPS-201
Demenaga, K. M. OP-252
Demetrio De Souza Franca, P. OP-896
De Migno, R. EP-0781
Demir, B. EPS-245, **EP-0214**, EP-0257, **EP-0349**, **EPS-116**, **EPS-200**, **OP-158**
Demir, F. **EP-0225**
Demirbilek, M. EP-0228, OP-035
Demirci, E. EP-0253, OP-163, OP-375
Demirdag, C. EP-0233
Demirel, B. B. EP-0287
Demirezen, S. EP-0974
Democrito, A. EP-0277, EP-0898
Demore, B. EP-0894
den Braber, A. OP-109
Deng, J. **EP-0479**
Deng, Y. EP-0177
den Hollander, M. OP-027, OP-566, OP-930, EP-0677, OP-928
Denis-Bacelar, A. EP-0722
Deniz, G. **EP-0912**
Denizmen, D. **EPS-189**
Dennis, J. TEPS-013
Deol, M. OP-036
de Paula Faria, D. EP-0676, OP-843
Depeursinge, A. EP-0699
De Placido, S. OP-639, OP-913
De Re, V. OP-052
Dere, A. **EP-0574**

de Ridder, C. EP-0065, EPS-213
De Rimini, M. L. OP-447
De Risi, M. EP-0793
Derkyi, A. OP-304, OP-310
De Roo, A. K. EP-0358
de Roode, K. E. **OP-220**
Deroose, C. OP-366, EP-0196
De Rose, F. OP-430, OP-491
D'Errico, A. EP-0147
Desai, A. OP-193
De Santis, V. **EP-0042**
De Schepper, S. **EP-0631**
Desmonts, C. **EP-0640**
de Souza Baptista, I. EP-0680
De Stefano, V. EPS-196
de Steur, W. O. OP-086
Destro, G. EP-0835
De Summa, M. EP-0335, EP-0693
de Swart, J. EP-0014
Desy, A. OP-236
De Teresa, R. **EP-0255**, EP-0169
Detti, B. EP-0273
Deuschl, C. OP-580
Deusser, T. EP-0751
Deuther-Conrad, W. OP-558
Deutsch, P. **EP-0082**
Dev, I. **EP-0207**
Deveci, H. EP-0359
Devillers, A. OP-155, OP-806
Devlin, S. M. EP-0333
Devoogdt, N. EPS-227
de Vries, B. M. EP-0757
de Vries, E. G. OP-573
de Vries - Huizing, D. M. V. EPS-250, OP-908, OP-852, EP-0561, OP-628, OP-670
Dewaraja, Y. EP-0688, OP-436, OP-439, OP-906
De Winter, O. EP-0779, OP-443
de Wit - van der Veen, B. J. EP-0271, OP-908, OP-628
de Wit-van der Veen, L. EPS-158, EP-0805, EPS-250
de Wolf, T. OP-146
Deyev, S. M. EP-0861, EP-0852
Dhadamus, M. **OP-457**
Dharmashaktu, Y. EP-0350, EP-0498, EP-0500, **EP-0505**, EP-1019, EPS-054, EPS-060, EPS-073, **EPS-079**
Dhingra, V. EP-0129
Dhiantravan, N. OP-338
Dhondt, E. EPS-231
Dhotre, G. EP-0043
D'Huyvetter, M. EPS-227
Di, J. **EP-0737**
Diamand, R. EPS-112
Diao, W. EP-0289
Diao, X. EP-0426, EP-0428
Dias, A. M. M. EPS-219
Dias, G. EP-0835
Dias, P. EP-0416
Díaz, I. EP-0465
Díaz Expósito, R. EP-0585
Diaz Gonzaga, L. EP-0254
Díaz González, L. G. EP-0357, EP-0386, OP-787
Diaz-Moreno, J. EP-0473, EP-0547, EP-0942, EPS-154, EP-0299, EPS-049, EPS-265, EP-0211, EP-0970, EPS-031
Di Battista, M. OP-171
Dibbets-Schneider, P. EP-0788, OP-628
Di Benedetto, L. OP-456
Di Carlo, D. OP-617, OP-620
Dickie, B. R. EP-0684
Dickson, J. EP-0657, EP-0722, EP-0631, EP-0662
Dierckx, R. A. J. O. OP-326, OP-364
Dierickx, L. OP-951, OP-804
Dierks, A. EP-0451, EP-0565, OP-655
Dietlein, M. OP-101
Dietz, M. EPS-080
Dietze, M. **OP-295**
Dieudonne, A. **OP-151**
Diez-López, C. EP-0473, EPS-049
Di Filippo, S. EP-0404
Di Franco, M. EP-0213, EP-0215, **OP-534**
Di Gennaro, F. EP-0550, EP-0781
Di Giuda, D. OP-456
Di Giuliano, F. OP-780
Di Iorio, V. EP-0238, EP-0613, OP-723
Di Magno, S. EPS-289, OP-494
Di Martino, D. EP-0886, **EP-1034**
Di Martino, G. EP-0316
Dimcheva, M. EP-0634, EPS-029
Dimitrakopoulou-Strauss, A. EPS-266, OP-449, OP-450, OP-564, OP-919
Ding, H. EP-0270, OP-847
Ding, J. **EPS-276**, OP-215, OP-218, OP-377
Ding, Q. EP-0483
Ding, S. OP-032
Ding, Y. EP-0177
Di Nicola, A. D. EP-0376, EP-1017, OP-323
Dinkel, V. OP-309
DiNunzio, E. OP-703
Di Palo, A. EP-0509
Di Pietro, M. OP-535
Di Raimondo, T. EP-0277, **OP-050**, OP-051
Di Rocco, G. OP-234
di Santo, G. OP-306
Disconzi, L. OP-039
Di Stasio, F. OP-535
Di Tommaso, L. EP-0189, OP-653
Di Treglia, S. OP-447
Dittmann, H. OP-314, OP-572
Dixit, A. **EP-0919**
Dixon, J. EP-1021
Djaileb, L. EP-0284, **OP-040**, OP-192
Djerroudi, L. EPS-017
Dobrenic, M. **EP-0940**
Dobrolinska, M. **OP-241**
do Canto, N. EP-0704
Doddipalli, S. OP-036
Doering, E. **EP-0751**, OP-105, **OP-107**
Doerr, C. **EP-0062**
Doi, T. OP-245
Dolci, S. OP-780
Doma, A. **EP-0325**, OP-452
Domarkas, J. EPS-289
Domenici, F. OP-780
Dominguez, C. OP-556
Domínguez Gadea, L. EP-0127, EP-0365, EP-0502
Domínguez-Garijo, P. EP-0491
Domínguez Grande, M. EP-0306
Domínguez Serrano, I. EPS-081
Domling, A. OP-493
Domogalla, L.-C. EP-0775, OP-621, OP-771
Donat, C. **EPS-275**
Donati, D. M. OP-881
Doncic, N. **OP-297**
Dondi, F. EP-0273, EP-0277, EP-0323, **OP-166**
Dondi, M. EPS-087
Donegani, M. OP-051
Dong, G. EP-0815
Dong, P. OP-526
Dong, W. EP-0435, **EPS-141**, **OP-287**
Dong, Y. EP-0157
Dong, Z. OP-644
Donner, D. **OP-585**
Donniaquio, A. OP-051
D'Onofrio, A. OP-456
Donswijk, M. OP-506
Doorduin, J. EP-0020
D'Oppido, D. EP-0131
Dorbala, S. OP-389
Dore, F. EPS-149
Dörrler, A.-L. OP-866
Dorten, P. OP-356
Dorzhieva, R. EP-0477
dos Santos, G. **EP-0301**
Dotinga, M. **EP-0561**, **EP-0788**, EPS-250

Dottorini, M. EPS-149
Doubravova, D. EPS-084
Doucet, L. OP-155
Doughty, P. OP-078
Douglas, A. OP-254
Doumas, A. **EP-0938**, **EPS-136**, **OP-542**
Dovhyi, I. OP-022
Doyen, M. EP-0760, **EPS-099**, OP-454
Draganescu, D. EP-0866
Drakaki, A. EPS-122
Dreaden, E. EP-0810
Dreher, N. OP-291
Drescher, R. EP-0827, OP-488
Dresel, S. OP-575
Drexler, W. OP-706
Driest, F. V. EPS-178
Dristiliaris, D. EP-0422, EP-0423
Driver, C. H. S. OP-076
Drobot, B. EP-0849
Droogers, E. **EPS-253**
Drzezga, A. OP-108, EP-0154, EP-0751, EPS-147, OP-099, OP-105, OP-107, OP-798
Du, P. EPS-276
Du, X. OP-379
Duan, H. **EP-0278**, **OP-504**
Duan, X. EP-0108
Duarte, A. EP-0086, **EP-0704**
Duarte, H. EP-0246, EP-0472, EP-0569, EP-0962, OP-469, OP-472, OP-473, OP-539
Duarte, J. R. EP-0978
Duarte, P. EP-0301, OP-665
Dubashi, B. OP-097
Dubegny, C. OP-100
Dubois, J. EP-0429
Dubois, M. OP-858
Dubsash, S. EP-0276
Duch, J. EP-0331
Dudek, D. OP-641
Dudouet, P. OP-929
Duell, J. EP-0319
Duff, L. EP-0733
Duffles, G. EP-0345
Dührsen, U. OP-102
Duke, S. EP-0149, EPS-174
Dumont, R. EP-0081
Dumulon-Perreault, V. EP-0045, OP-557
Dunaykin, M. **EP-0326**
Dunckley, C. P. OP-018
Dunn, S. M. OP-153
Dupont, A.-C. **OP-799**
Dupont, F. EPS-134, OP-624
Durand-Bailloud, B. EP-0907
Durando, X. OP-938
Duránik, M. OP-925
Duriseti, S. **OP-041**
Durmo, R. EP-0999, EPS-014
Dursun, B. EPS-116
Dursun, E. OP-158
Duval, X. OP-513
Duvenhage, J. EPS-046
Duvivier, K. M. EPS-019
Duvvur, N. EP-0171
Dwivedi, P. **OP-178**
Dyankova, M. **EP-0263**, EP-0341, EP-0342, EP-0343, EP-0344, EP-0513, EP-0899, EP-0900, EP-0901, EP-0902, **EP-0904**, **EP-0913**, EP-0981, **EPS-121**, EPS-267
Dyla, A. EP-0968
Dzialas, V. OP-107
Dziedzic, T. OP-587
Dziewierz, A. OP-641
Dziuk, M. EP-0018, EP-0478, **EP-0831**, OP-807

Eapen, R. OP-338
Easty, M. OP-496
Ebbers, S. **OP-670**, OP-850
Ebenhan, T. EP-0083, **EPS-046**, **OP-076**
Eberhardt, W. EP-0146
Eberlein, U. EPS-235, EPS-236, OP-152
Ebine, K. TEPS-009
Ecay, M. EP-0859, EP-0034, EPS-095
Eccles, A. EP-0495
Echegoyen, P. EP-0348, EPS-011, **EPS-095**
Echeverri Diaz, J. EP-0252, EP-0508, EP-0548
Ecke, T. H. OP-468
Eckenweber, F. OP-110
Eckerman, K. EP-0777
Ecsedi, B. **OP-093**
Edenbrandt, L. EP-0318, EP-0450, EP-0759, OP-708, OP-919
Eder, A. C. EP-0775, OP-771, OP-621
Eder, M. OP-615, OP-621, OP-771
Eduardo, R. **EP-0729**
Eedan, E. EP-0893
Eertink, J. OP-102, EP-0383, EPS-195
Effendi, N. EP-0853
Eggers, K. OP-387
Eggerstedt, R. OP-520
Eglseder, B. OP-520
Egoue Mongoue, R.J. EP-0908
Ehara, T. OP-137, OP-138
Eiber, M. EP-0235, EP-0284, EP-0288, EP-0564, EP-0566, EPS-110, EPS-124, OP-192, OP-334, OP-497, OP-520, OP-707, OP-722
Eibler, L. OP-702
Eich, H.-T. OP-101
Eichhorn, F. OP-189
Eichler, R. OP-016
Eidt, S. OP-468
Eigler, C. **OP-191**
Eigner, S. EP-0083
Eikenes, L. EPS-160
Einsele, H. EP-0319, EP-0353
Einspieler, H. EP-0262, EPS-125
Eisazadeh, R. EP-0556
Eismant, A. OP-188
Ekaeva, I. EPS-128, EPS-129, EPS-130
Ekenel, M. EP-0553
Ekkelenkamp, E. OP-852
Eklund, L. **EP-0659**
Elahmadawy, M. **EP-0102**
El Ajmi, W. EP-0087
El Bessi, M. EP-0401
El Biali, M. EP-0674
Eldem, G. EPS-202, EP-0577
El Fakhri, G. OP-917
El Fakiri, M. OP-615, **OP-621**
Elg, L. TEPS-007
Elia, B. EP-0784
Elia, C. OP-052
Elisei, F. EP-0316
El Jari, B. EPS-134
Ellingsen, L. M. EP-0751
Ells, Z. OP-296, **OP-440**
Elmenhorst, D. OP-107, OP-798
Elmenhorst, E. M. OP-798
Elmoujarkach, E. EP-0658
El Ouni, M. EPS-038
Elsayed, W. EPS-036
Elsinga, P. OP-493, EP-0033, TEPS-019
Elvas, F. **OP-429**
Elwakeel, M. EPS-036
El Yaagoubi, Y. EP-0433
Emami, F. EP-0727
Emerson, R. EP-0158, EPS-044, OP-649, EP-0522
Emineni, S. OP-335
Emmanuel, N. **EP-0881**, OP-489
Emmerson, B. EP-0406, EP-0555, OP-338, **OP-437**
Emmett, L. EP-0558, EPS-110, EPS-120, **OP-230**, OP-337, OP-335
Endo, H. EP-0739
Encarnação, P. EPS-094
Enevoldsen, L. H. EP-0195
Eng, W. EPS-119
Engbers, P. OP-146

Engel, J. EP-0391
Engelbrecht, G. OP-249
Engels, S. EP-0408
Engle, J. EP-0891, OP-903
Englert, A. **EP-0024**
Şengöz, T. EP-0602
Enke, J. EP-0565
Enqvist, O. EP-0318, EP-0450, OP-708, OP-919
Episkopopoulou, S. EP-0982
Eraslan, C. EP-0909
Erba, P. A. EP-0443
Erbil, E. **EP-0136**
Ercolani, P. EP-0112
Erdil, T. Y. EP-0190
Erdoğan, A. EP-0967, EP-0570, EP-0588, OP-914
Erdogan, Z. EP-0225
Erglis, A. EP-0440
Ergül, N. EP-0230, EP-0402
Erhard, A. **EPS-288**
Eriksson, A. **EP-0686**
Erkens-Schulze, S. OP-083
Eroglu, M. EP-0909
Ertan, Y. EP-0379, EP-0591
Escabias del Pozo, C. EP-0127, EP-0365
Escalera Temprado, T. EP-0471
Escano, L. EPS-223
Escrihuela-Vidal, F. EPS-049, EPS-048
Eskola, M. TEPS-007
Esmatinia, M. OP-650
Esnault, M. **EP-0437**, **EPS-137**
Espinoza-Vinces, C. OP-460
Esposito, A. OP-505, EP-0575, EP-0819, EP-0879, **EP-0886**, EP-1034
Esposito, E. OP-171
Esposito, J. TEPS-021
Esposito, T. **OP-770**, OP-896
Esposto Pirani, P. EPS-053
Esteban Hurtado, Á. EP-0417
Estienne, A. OP-806
Esvant, A. OP-806
Etchebehere, E. EP-0259, EPS-078
Ettala, O. EP-0659
Etxebeste, A. EP-0656
Evangelista, L. EP-0162, EP-0188, EPS-074, **OP-447**
Evans, J. EP-0090
Evbuomwan, O. **OP-249**
Everaert, H. EP-0673
Evetovic, E. OP-499
Ewald, J. D. EPS-228
Ewald, J. T. OP-144
Exadaktylou, P. EP-0938, EPS-136, OP-542
Extebeste, A. OP-370
Ezzine, A. EP-0512

Faasse, T. EP-0664
Facchinetti, F. EP-0068
Faccini, R. EP-0783, OP-294
Fagin, J. A. OP-802
Fahmi, R. **EP-0683**, OP-710, **OP-774**
Faivre-Chauvet, A. OP-153
Falcão, A. EP-0896
Falco, M. EP-0226
Falconi, M. EP-0202
Falkenbach, F. EP-0391
Falkenhorst, J. OP-190
Fallahpoor, M. EP-0818
Falzarano, M. EP-0551, EP-0606, EPS-065, OP-382, OP-383
Fan, A. C. OP-194
Fan, X. **EP-0033**, **OP-237**
Fan, Y. EPS-028
Fanello, S. EPS-014
Fang, B. OP-340
Fang, J. EP-0856
Fang, P. EPS-119
Fang, W. EP-0453
Fang, Y. EP-0814

Fani, M. EPS-291, OP-191, OP-306, OP-430, OP-491, OP-614, OP-716
Fanti, S. OP-102, EP-0147, EP-0213, EP-0215, EP-0303, EP-0354, EP-0388, EP-0681, EPS-107, EPS-110, OP-099, OP-337, OP-474, OP-534, OP-879, OP-881, OP-882
Fantini, L. EP-0238
Faqeh, K. EP-0240
Faraggi, M. EP-0719
Farahani, M. EPS-177
Farahati, J. OP-575
Farajbakhsh, F. EP-1010, EP-1016
Faraji, S. EP-0727
Farde, L. OP-555, OP-563
Farè, E. EP-0921
Fares, S. **EP-0932**
Farkas, I. EP-0181
Farn, S.-S. EP-0029, EP-0036, EP-0858
Farolfi, A. EP-0284, EP-0388, EPS-107, OP-040, OP-099, **OP-192**, OP-440, OP-879, OP-881, OP-882
Farrar, G. EPS-150
Farruggia, P. OP-052
Farsad, M. EPS-149
Farzanefar, S. EP-0818, EPS-239, OP-248, EP-0712, EP-0714, EP-0743
Fassnacht, M. EP-0093, EP-0507, OP-305
Fasulo, V. EP-0272, OP-039
Fatima, N. **EP-0425**, EPS-252
Faudemer, Z. OP-770
Faure, S. OP-845
Favaretto, C. EP-0070, OP-016
Fayad, Z. A. EP-0733
Fazaeli, Y. EP-1009
Fazari, B. EP-0072, OP-560
Fazel, M. OP-056
Fazio, N. EP-0543, OP-668, OP-669
Fedrigo, R. **EPS-242**, **EPS-251**
Fei, A. OP-256
Fei, T. EP-0333
Feizi, S. EP-1009
Feldman, J. OP-389
Feldmann, A. OP-357
Feldwisch, J. OP-579
Fele Paranj, A. **OP-084**
Feliciani, G. EP-0238
Feliu Perez, I. EP-1007
Felix, C. OP-440
Felix, R. C. M. EPS-007, OP-471
Femenias, J. EPS-143
Fendler, W. EPS-118, OP-041, OP-334, EP-0146, EP-0284, EP-0391, EP-0607, EPS-110, OP-190, OP-192, OP-301, OP-308 OP-380, OP-508, OP-580, OP-932
Fenercioğlu, Ö. E. EP-0230
Feng, H. OP-522
Feng, L. **EP-0856**
Feng, Y. **EP-0639**, OP-143, OP-901
Fenzl, S. EP-0811
Ferdinandus, J. **OP-101**
Ferguson, C. EP-0495
Fernandes, A. **OP-528**, EP-0415, EP-0416, EP-0927, EP-0963
Fernandes, B. **EP-0280**, **EPS-286**
Fernandez, S. OP-895
Fernandez, V. EP-1001
Fernandez Alfonso, A. EP-0494
Fernández de Larrea, C. EP-0356
Fernández Fernández, J. **EP-0247**, EP-0410, **EP-0499**, EP-0175, EP-0176, EP-0409
Fernández-Ferreiro, A. EP-0023
Fernández-León, A. EP-0331
Fernández Llana, M. EP-0306
Fernandez Yuste, M. EP-1007
Ferraioli, C. OP-647
Ferrando, R. **EP-0025**, EP-0364, EP-0969
Ferrante, M. EPS-018, OP-590, **OP-846**
Ferrara, D. EP-0105, EP-0149, **EPS-174**, OP-567, **OP-776**
Ferrara, G. OP-395
Ferrara, R. EP-0980

Ferrari, C. EP-0744, EP-0258, **EP-0509**, OP-447
Ferrari, M. EP-0540, OP-854, OP-915, OP-921, EP-0543 EP-0389, OP-669, EP-0147, OP-879
Ferreira, A. M. EP-0239
Ferreira, D. OP-672, EP-0929, EPS-061
Ferreira, G. EP-0246, EP-0472, EP-0569, EP-0962, EP-0979, OP-469, OP-472, OP-473, OP-539
Ferreira, I. C. **EP-0528**, **EP-0922**, **EP-0984**, EP-0989
Ferreira, P. EP-0769, EP-0769
Ferreira, R. EP-0528, EP-0922, **EP-0966,** EP-0984, , **EP-0989**
Ferreira, U. EP-0259
Ferrer, L. **EPS-243**, OP-155, OP-187
Ferreras-Riera, J. R. EP-0988
Ferrer Gonzalez, F. EP-0251, EP-0248
Ferrero, S. EPS-272
Ferretti, G. OP-581
Ferri, V. OP-793
Ferro, J. EP-0569, EP-0979, OP-472
Ferro, J. C. EP-0246, EP-0962, OP-469, OP-473
Ferro, J. F. EP-0472
Ferro, P. EP-0443
Ferroni, F. EP-0238
Feuerecker, B. EP-0564
Fic, N. OP-897
Fichera, G. EP-0162, EP-0188
Field, C. EP-0255
Field Galán, C. A. **EP-0169**
Fierro Alanis, P. EP-0759
Figueiredo, A. EP-0086, EP-0704
Figueiredo, S. OP-331
Figueroa, R. EP-0339
Filice, A. **EP-0999**, **EPS-014**
Filipan, D. **EP-0948**, **OP-947**, **OP-948**
Filipczak, K. **EP-0703**
Filipczuk, A. **OP-157**
Filippi, N. OP-429
Filizoglu, N. EP-0190
Finze, A. OP-110
Fioroni, F. EPS-014
Fischer, B. M. OP-640
Fischer, C. EP-0809
Fischer, L. **EP-0292**
Fischer, S. OP-767
Fischer, T. EP-0154
Fitzgerald, H. A. OP-018
Fiz, F. **OP-315**
Fizazi, K. OP-340
Flachskampf, F. A. OP-240
Flagg, M. OP-021
Flamen, P. EP-0275, EPS-112, OP-232, OP-238, OP-367, OP-444, OP-573, OP-629, OP-664
Flaus, A. EPS-080
Fleischmann, D. F. OP-588
Florea, A. EP-0060
Flores, L. OP-213
Flores-Casaperalta, S. EP-0954
Flores-Moreno, A. EP-0895
Florimonte, L. EP-0763, EP-0915, EPS-183, EPS-272, OP-540
Floris, R. OP-780
Flossdorf, S. OP-099
Flotats, A. EP-0331
Floyd, J. EP-0612, OP-857
Flux, G. OP-031
Flynn, J. R. EP-0333
Foca, F. OP-723
Focaccia, M. OP-881
Fodor, C. EP-0236, OP-669
Foerges, A. OP-798
Fogante, M. EPS-053
Fois, G. EPS-236
Fokem-Fosso, H. OP-311
Follacchio, G. A. EP-0376, EP-0623, OP-395
Fonseca, A. EP-0896
Fonseca Cabrera, G. O. OP-903
Fontão de Castro, S. EP-0246, EP-0569, **EP-0979**, OP-469, OP-472, OP-473, OP-539
Fonti, R. OP-639, OP-913, OP-916
Forbrig, R. OP-538, OP-584
Forgacs, A. EP-0441, EP-1027
Forgács, V. EP-0871
Fornarini, G. EP-0277
Forrer, D. EP-0012
Forrer, F. OP-716
Forsberg Morén, A. OP-563
Forssell-Aronsson, E. EPS-215, **EPS-230**
Forster, J. C. OP-441
Fortin, M. EP-0499
Fortunati, E. **EP-0147**, **EP-0213**, **EP-0215**, **OP-879**, OP-881, OP-882
Fortunato, M. EP-0006
Fortuny, E. EPS-143
Foschi, N. EPS-022
Fosci, G. EP-1004
Foss, M. P. EP-0929, EPS-061
Foster, J. EP-0411
Fouda, A. EP-0771
Fougner, L. EPS-251
Foukal, J. **EP-0920**
Foukarakis, E. OP-859
Fouque, J. EP-0694, **EP-0875**
Fouquier, A. OP-160
Fournier, J. EP-0850
Fournier, P. OP-858
Fowler, C. EPS-133
Foxton, C. OP-145
Fracassi, S. EP-0543, OP-915, OP-669
Fracasso, G. EP-0009
Fraga, D. EP-0412
Fragoso Costa, P. **EP-0391**, EPS-238, OP-301, OP-330, OP-580, EP-0607
França Velo, A. **OP-834**
Francesco, C. EP-0389
Francis, R. OP-037, OP-642
Francken, T. OP-676
Franco-Ardila, A. EP-0130
François, C. **EP-0117**, **OP-100**
Franco Monterroso, C. EP-0523, EP-0767, EP-0252, **EP-0766**
Frank, C. EP-0834, EP-0846, EPS-212, **EP-698**
Frank, S. OP-765
Franssen, G. EPS-225, OP-358
Frantellizzi, V. OP-245
Franzese, C. OP-918
Franzmeier, N. EPS-148, OP-110
Frasoldati, A. EPS-014
Fraticelli, P. EPS-053
Freesmeyer, M. EP-0297, EP-0827
Freitag-Stechl, D. EP-0888
Frejd, F. EPS-067, OP-578, EP-0837, OP-579, OP-704
Frelaut, M. EPS-260
Fremer, C. EPS-156
Frenay, J. EPS-219
Frensch, S. OP-107
Frey, E. OP-672
Frey, K. A. OP-436, OP-439
Fridriksdóttir, R. EP-0468
Friebe, M. OP-494
Friedersdorff, F. OP-468
Friedrich, J. **EP-0560**
Friedrichs-Maeder, C. OP-047
Frielink, C. EP-0077, EP-0486
Frille, A. EP-0149, EPS-174
Frings, M. EPS-229
Fringuelli, F. M. EP-0112, EPS-053
Frisch, F. EP-0499
Friske, J. EPS-102
Frismand, S. OP-454
Frisoni, G. OP-455, OP-106, OP-104
Frisoni, T. OP-881
Fröhlich, M. OP-291, **OP-517**
Frugis, M. EP-0509
Frutos Esteban, L. EP-0407, EP-0419, EP-0579, EP-0924, EP-0925, EPS-269, OP-924
Frydenberg, M. OP-037

Fu, H. EPS-119, OP-374, **OP-398**
Fu, W. EP-0265, EP-0373
Fuchigami, T. EP-0853, EP-0855
Fuentes Gago., M. OP-170
Fuglsang, J. K. OP-324
Fuglsang, S. EPS-163, OP-384, OP-385
Fujimura, M. EP-0808
Fujisawa, T. OP-289
Fujita, N. EP-0887
Fukami, M. TEPS-015
Fukase, K. OP-772
Fukuda, S. EP-0696, **OP-325**
Fukumori, O. Y. EP-0732, EP-0929, EPS-061
Fukushima, K. EP-0476
Fumagalli Romario, U. EP-0389, OP-668, OP-854
Funck-Brentano, T. OP-947
Funke, U. EP-0805
Furini, C. R. EP-0020
Furtuna, P. OP-166
Fusco, G. EP-1028
Fusco, N. EP-0389, OP-038, OP-854
Fuster-Pelfort, D. EP-0491
Fütterer, C. EPS-124
Fütterer, J. J. OP-853

Gaballo, P. EP-0550, EP-0819
Gabela, L. EP-0643
Gaberšček, S. EP-0619, EP-0506
Gäble, A. **EP-0565**, OP-856
Gabrielson, K. OP-149
Gadzicki, P. **EP-0968**
Gaeta, A. OP-915
Gafita, A. **EP-0284**, EPS-122, OP-040, OP-192, **OP-509**, OP-722
Gagliani, C. **EPS-074**, EPS-149
Gai, Y. OP-143, OP-216, OP-700
Gairola, M. OP-783
Gajecki, L. **OP-702**
Galamba Correia, J. EP-0843
Galasso, T. EP-0147, OP-879
Galbiati, A. OP-764, **OP-355**, OP-356
Galette, P. EPS-206
Galiana, A. EP-0340
Galiana Morón, Á. EP-0418
Galiè, N. EP-0681
Galindo, C. EP-0300, EP-0964
Galindo Fernández, C. EP-0526
Gallant, J. **EPS-274**, OP-616
Gallego Marquez, M. EP-0399, EP-0474, EP-0620
Galli, A. OP-045
Gallicchio, R. OP-447
Galmier, M.-J. OP-938
Galt, J. R. EP-0164
Gamanagatti, S. EP-0368, EPS-204
Gama Romero, H. **EP-0895**
Gamazo Laherrán, C. EP-0455, EP-0475, EPS-043
Gambaro, M. OP-315
Gambart, M. OP-951
Gambella, M. OP-050
Gambini, J. EP-0301
Gameiro, C. EP-0869, EP-0881
Gammel, M. **EP-0235**
Gampenrieder, S. EP-0556
Gandaglia, G. EPS-107
Gandia-Ferrero, M. EP-0800, **EPS-096**
Gandolfo, P. EP-0700, EP-0749, EP-1004
Ganesan, P. EP-0332
Ganga, R. OP-299
Gao, H. EPS-091
Gao, M. **OP-646**
Gao, R. EP-0076, EPS-064, OP-878
Gao, X. **EPS-068**, **OP-527**
Gao, Y. **EP-0030**
Gaonkar, R. **OP-614**, EPS-291, OP-430
Garaci, F. OP-780
Garai, I. EP-0441, EP-1027, OP-369
Garamundi-Grimalt, E. EP-0355
Garanzini, E. EP-0068, OP-234
Garavand, H. EPS-135
Garaventa, A. OP-052, OP-315
Garbaccio, V. OP-910
Garcia, A. **EP-0635**
Garcia, C. EPS-260, EPS-263
Garcia, E. V. OP-389
Garcia, J. **EP-0241**
Garcia Alonso, M. EP-0300, EP-0964
García Alonso, P. EP-0526, EP-0604, EP-0605
Garcia Aragon, M. **EP-0398**, EP-0455, EP-0475, EP-0529, EPS-043, OP-168
García Belaustegui, L. EP-0348, **EP-0339**, EP-0705, EP-0706 EP-0088, EPS-011, OP-936
Garcia Burillo, A. EP-0523, EP-0508, EP-0548, EP-0632, OP-233
García Cañamaque, L. EP-0169, EP-0255, OP-233
García Garzón, J. EP-0109
Garcia Lama, L. EP-0523, EP-0766, EP-0767
García Monaco, R. EP-0573
García-Moure, M. EP-0034
García Noblejas, A. EP-0352
Garcia Perez, F. EP-0603
Garcia-Perez, O. **EP-0130**
García Poblete, V. EPS-268
Garcia Quinto, V. EPS-206
Garcia-Rivero, Y. **EP-0702**
García Rodriguez, Á. EP-0702
García-Sánchez, A. OP-103
García Talavera, P. OP-170, EP-0254, EP-0386, EP-0503, EPS-052, OP-787
García-Varela, L. **EP-0023**
García Velloso, M. EP-0088, EP-0705, EP-0706, OP-936, EP-0339 EP-0348, OP-098, EP-0356
García Vicente, A. M. EP-0229, EP-0496, EPS-050, EPS-259, OP-638, EP-0250, EP-0562, EPS-268
García Zoghby, L. EP-0229, **EP-0250**, EP-0496, **EP-0562**, EPS-050, EPS-268
Gardner, L. EP-0538
Garg, P. K. EP-0413
Garg, S. EP-0096, **EPS-027**
Garganese, M. EPS-037
Gariani, K. EP-0081, EPS-077
Gariboldi, M. EP-0068
Garibotto, V. EP-0053, EPS-077, OP-104, OP-106, OP-455
Gariglio, G. **EPS-280**
Garí Martínez, F. EP-0474, EP-0620
Garipov, R. OP-078
Garnier, N. EP-0719
Garnuszek, P. EP-0018, OP-306, OP-675, EP-0870
Garo, M. OP-392
Garousi, J. EP-0852, EP-0861
Garpered, S. TEPS-012
Garrido Solesio, I. EP-0245, EP-0421, **EP-0510**, EP-0467
Garrigue, P. EP-0035, EP-0067, OP-895
Garrou, F. EP-0273
Gaschet, J. EP-1000
Gascón-Bayarri, J. EPS-154
Gasior-Perczak, D. OP-675
Gatta, R. EP-0335
Gauden, D. OP-145
Gaudiano, C. OP-534
Gaudieri, V. EP-0551, EP-0606, OP-382, OP-383
Gaujoux, S. OP-805
Gavane, S. OP-657
Gavriilidis, P. **EP-0716**, **EPS-100**
Gavrilovski, A. EP-0992
Gawande, A. EP-1019, EP-1020, EPS-060
Gawlik, T. EPS-013
Ge, J. EPS-155, **OP-792**, **OP-794**
Ge, Q. EPS-146
Ge, Y. EP-0444
Ge, Z. EP-0737
Gear, J. OP-031
Gebhart, G. OP-573
Geboes, K. EP-0196
Geets, J.-M. **EP-0874**

Geffroy, B. EP-1001
Geibl, F. OP-562
Geier, A. EP-0182
Geis, N. M. **OP-771**
Geist, B. EP-0748, OP-776
Gelardi, F. EP-0189, EP-0285, EPS-161, OP-653, **OP-712**, **OP-918**
Geleijnse, P. **OP-667**
Gemmell, A. **EP-0701**, **EPS-179**
Gençer, H. EP-0225
Genova, A. **EP-0985**
Genova, C. EPS-260
Genung, N. OP-563
Geo, L. OP-764
Georga, S. EP-0237
Georgiou, A. EP-0237
Georgiou, C. **EP-0056**
Georgiou, C. J. OP-898
Georgoulias, P. EP-0682
Geramifar, P. EP-0727
Gerasimou, G. EP-0938, EPS-136, OP-542
Geraths, C. **OP-139**
Gerhard-Hartmann, E. EP-0093, OP-785
Gerke, O. EP-0641, EP-1023
Gernert, M. OP-517
Geronazzo, R. EPS-171
Gerritsen, W. R. OP-339
Gertsen, E. C. OP-086
Gervasi, E. EP-0999
Gestin, J. F. EP-1000
Gesuelli, G. OP-395
Getty, K. OP-703
Ghadhanfer, L. EP-0260, TEPS-005
Ghadjar, P. OP-337
Ghafari, A. EP-0743, EPS-177
Ghafarian, P. EP-0712
Ghag, S. EP-0789
Ghaly, M. OP-672
Ghapanvari, M. EP-1010, EP-1016
Gharehpapagh, E. **EP-0910**, **EP-0928**, EP-0554, EP-0624, EPS-271
Ghasemi, V. EP-1010, **EP-1016**
Ghazal, A. EPS-055
Ghebremariam, S. OP-340
Ghedini, P. EP-0273
Gherghe, M. EP-0206, EP-0464, EP-0672, EP-0956, OP-292
Ghersi, C. EP-0277, EP-0898
Ghesani, M. EP-0351, EP-0572, EP-0950, EPS-257
Ghesani, N. **EP-0950**, EPS-257, OP-788
Gheysens, O. EP-0358, EPS-046, EPS-134
Ghezzo, S. EP-0202, **OP-505**
Ghfir, I. EP-0986
Ghiani, S. EP-0012
Ghiggi, C. OP-050
Ghimessy, Á. EP-0390
Ghinassi, S. EP-0404
Ghizdovat, V. EP-0375
Ghodhbane, R. EPS-042
Ghodsirad, M. EPS-135
Ghorbani, H. EP-0264, EP-0381, EP-0381
Ghosh, A. OP-555
Ghosh, K. K. EP-0080
Ghosh, S. EP-0207, OP-769
Ghossein, R. A. OP-802
Gianeri, R. OP-051
Giani, T. EP-0511
Giannakou, S. EP-0682
Giannitto, C. OP-918
Giannoula, E. EP-0938, EPS-136, OP-542
Giantini Larsen, A. OP-834
Giantsouli, P. EP-0445
Giavarini, M. OP-328
Gibson, A. EP-0844
Gibson, J. OP-718
Giehl, K. OP-107
Gierse, F. OP-356
Giesel, F. L. EP-0072, OP-560, OP-772, OP-512, OP-937
Giesen, D. EP-0877
Gietema, J. A. OP-339
Giżewska, A. EP-0478
Gil, J. **EP-0186**
Gilardi, L. EP-0543, OP-921
Gilardoni, E. OP-355, OP-356
Gildehaus, F. OP-839, EPS-092
Gilis-Januszewska, A. EP-0209
Gillett, D. EP-0799
Gil-Santos, S. OP-472
Ginés-Cárdenas, S. EPS-096
Giorgio, A. EP-0011
Giourgouli, S. **EP-1012**
Giovacchini, G. **EPS-183**
Giovanella, L. OP-392, OP-524, **OP-525**, OP-801
Giovannini, E. EP-0376, EPS-183
Giraldo Gonzalez, L. EP-0127, EP-0365, EP-0502
Girard, N. OP-637
Giraudet, A. EP-0729, EPS-247
Giraudo, C. EP-0162, EP-0188
Giri, S. EP-0846
Girotto, N. EP-0292
Girum, K. EP-0322, **EPS-185**
Gissot, V. OP-799
Giuliano, M. OP-913
Giunchi, F. EP-0147
Giunta, E. F. OP-723
Gjertsson, P. EPS-009
Gkika, E. EP-0423
Gkotsoulias, D. EPS-156
Glas, M. OP-580
Glaser, M. EP-0893
Glass, R. OP-082
Glatting, G. EP-0786, EPS-248, EPS-249, OP-904, OP-905, OP-909
Glaudemans, A. W. J. M. EPS-059, OP-252, OP-326, OP-364, OP-519, OP-570
Gloudemans, M. OP-358
Glowa, B. OP-306
Gnanasegaran, G. EP-0631, OP-935
Gnesin, S. EP-0688, **EP-0755**, EPS-093, OP-153
Gnörich, J. **EP-0015**, EP-0024, **EPS-148**, OP-110
Goasduff, G. OP-855
Gobbi, C. **EP-0009**, EP-0011, EP-0012
Goblet, D. EP-0881
Godefroy, J. EP-0542
Gödel, P. OP-099
Godino Gulloteu, V. EP-0418
Goehringer, F. EPS-099
Goel, R. **EP-0203**, EP-0208, **EP-0350**, EP-0362, **EP-0500**, EP-0505, **EPS-054**, EPS-060, **EPS-073**, EPS-079
Goellner, A. OP-713
Goenka, V. EP-0518
Goerges, R. OP-525
Goffin, K. OP-366, OP-667
Goislard, M. EP-0021, OP-559
Gokdemir, E. EP-0563
Göker, M. EP-0115
Gökulu, S. EP-0304
Gold, L. **OP-082**
Goldschmidt, H. OP-919
G. Oliveira, R. EPS-094
Golla, S. OP-928, OP-930, OP-109, **EP-0677**
Golubic, A. EP-0221
Golukhova, E. EPS-129, EPS-130, EPS-128
Golvet, M.-F. **TEPS-004**
Gomes, M. L. EPS-007
Gomes Ferreira, C. **EP-0801**
Gomez, A. EP-0340
Gomez, C. OP-489
Gómez, M. EP-0081
Gomez Argumosa, E. EP-0603
Gómez Caminero, F. OP-170
Gómez-Caminero López, F. EP-0254, EP-0386, EP-0503, EPS-052, OP-787
Gómez de la Fuente, F. EP-0890, EP-0516
Gómez de Leon, N. EP-0352
Gomez Fernandez, I. EP-0329

Gómez Grande, A. EP-0418
Gómez Hidalgo, J. EP-0455, EP-0475
Gomez Lado, N. EP-0023
Goncalves Gameiro, C. OP-489
Gong, T. **EP-0438**
Goñi, E. EP-0447, EPS-070, EPS-203
Goñi Gironés, E. EPS-063
Gontero, P. EP-0226, EP-0249, EP-0396
Gonzales, G. EP-0062
Gonzalez, S. OP-929
Gonzalez, V. EP-0573
González Asid, F. EP-0628, EP-1032
González-Calle, V. EP-0356
González Corredera, N. TEPS-001
González-Costello, J. EP-0473, EPS-049
González-Flores, E. EP-0580, EP-0581
González García, F. EP-0306
González-Gay, M. A. EP-0516
González Jimenez, A. EP-0114
Gonzalez Larriba, J. EP-0148
González-Martín, J. EP-0587
González Martínez, M. **EP-0194**
Gonzalez Rueda, S. **EP-0603**
Gonzalez Soto, M. EP-0398, EPS-043
Goodman, M. **EP-0810**
Gorczewska, I. OP-589
Gorgoni, G. TEPS-021
Gormsen, L. C. OP-386, OP-862
Gorsi, U. EPS-190
Gossili, F. **EPS-106**
Gotowicz, K. **EP-0018**, EP-0831
Gotthardt, M. EP-0077, EP-0486, EPS-075, OP-339
Gottlieb, I. EP-0961, EP-0971
Gotuzzo, I. **EP-0443**
Götze, K. OP-769
Goubier, A. OP-897
Goudin, N. OP-148
Gourand, F. OP-100
Gourni, E. OP-432
Goutal, S. EP-0021, EP-0674, OP-559
Gouverneur, V. EP-0835
Govender, T. EPS-046
Gowdy, C. EP-0723
Goyal, A. EP-0208, EPS-073
Goyal, H. EP-0332, OP-946
Goyal, S. OP-783
Gözlügöl, N. OP-058, OP-246, OP-516, OP-521, OP-666
Gracia-Sánchez, L. EP-0101, EP-0473, EPS-048, EP-0955, EPS-049, EP-0970
Grafe, H. OP-380
Grajeda Gallardo, A. EP-0510, EP-0761
Grajeda Gallardo, M. EP-0245, **EP-0421**, EPS-051, EP-0467
Grakova, E. EP-0436, EP-0457, EP-0477, OP-645, OP-724
Gram Kjærulff, M. **OP-862**
Grana, C. M. EP-0543, OP-668, **EP-0540**, **OP-669**
Grande, C. EP-0339
Grande, D. OP-764
Grangeret, J. EPS-008
Gräni, C. OP-239
Gräslund, T. EP-0861
Grassi, E. EPS-014
Grassi, I. EP-0613, OP-723
Grasso, S. EP-0551
Gravina, G. L. OP-535
Gravinatti, M. EP-0795
Gray, G. A. OP-289
Grbac-Ivanković, S. EP-0292
Green, R. OP-647
Greenblatt, E. **OP-222**
Greifenstein, L. OP-188, OP-302, OP-468, OP-617, OP-620
Greiser, J. **EP-0827**
Grellard, J.-M. OP-806
Grendele, S. OP-882
Greuter, M. OP-241, OP-503
Grewal, R. K. OP-802
Grey, J. OP-030
Gridset, L.-E. EP-0686
Grierosu, I. EP-0375, **EPS-040**
Griessner, H. EP-0556
Grievink, H. EPS-282
Griffiths, G. L. EPS-286
Grimaldi, S. EP-0226, EP-0249, EP-0396
Grings, A. OP-080
Grintsevich, S. OP-429
Grochowska, A. OP-641
Groeber, S. EP-0827
Grogan, T. EPS-122, OP-034, OP-036, OP-509, OP-040
Grogg, K. OP-917
Gröhn, H. EP-0996, **EPS-241**
Grommes, C. EP-0092
Gromova, E. **EP-0394**
Grønningsæter, S. **OP-911**
Groothof, D. OP-860
Groot Jebbink, E. EP-0061
Grosch, M. OP-110
Groß, M. EPS-148
Grossmann, G. EP-0680
Grosso, A. EP-0149
Grosso, M. OP-171
Grosu, A. L. OP-337
Grouws, C. A. EPS-046
Grozinsky-Glasberg, S. EP-0542
Gruber, L. EPS-225
Gruenert, S. EP-0149, EPS-174
Grugni, S. EP-0898
Grundler, P. V. EP-0070, OP-016, OP-141
Grunenwald, S. OP-654, OP-804
Grunert, M. EP-0560
Grünert, S. OP-081, OP-648
Grünig, H. EP-0795
Grushka, G. **EP-0615**
Grzmil, M. **OP-765**
Gu, B. **OP-379**
Gu, S. OP-863
Guan, Y. EP-0017, EP-0675, EPS-057, EPS-151, OP-111, OP-256, OP-792, OP-794
Guardia Jimena, P. **EP-0405**, **EP-0918**
Guarneri, A. EP-0273
Guarnizo, X. EP-0340
Guarnizo Poma, X. T. EP-0418
Guastella, R. EP-0162, EP-0188
Guazzoni, G. EP-0272, OP-039
Guckian, K. OP-563
Guedj, E. EPS-099, OP-929
Guendel, D. **OP-558**
Guenka, H. A. EP-0961, EP-0971
Guensi, A. EP-0975, EP-0976
Guerard, F. EP-1000
Guérin, B. EP-0045, EP-0499, **OP-557**
Guermazi, F. EP-0139, EP-0140, EP-0387, EP-0972, EP-0990
Guerra, L. EP-0316, OP-537
Guerra Gómez, M. EP-0199, **EPS-072**
Guerrero Calatayud, C. **EP-0302**, EP-0611
Guerrouj, H. EP-0986
Guery, C. OP-806
Guest, M. OP-137, OP-138
Guggenberger, K. V. OP-517
Guibbal, F. EP-0835
Guichard, L. **EPS-015**
Guida, E. OP-780
Guignard, R. **EP-1001**
Guignard, S. OP-858
Guijarro-Caba, P. EP-0204
Guijarro de Armas, G. EP-0604, EP-0605
Guillemin, M. EPS-219
Guillen, E. EP-0348, EP-0088, EPS-011, OP-507, OP-936, EP-0587, EP-0706
Guillet, B. EP-0035, EP-0067, OP-895
Guillon, L. OP-951
Guillouet, S. OP-100
Guimarães, T. T. EPS-007
Guindani, M. EP-0191

Guinot, A. OP-056
Guiot, T. OP-573, OP-664
Guiote Moreno, M. **EP-0400**
Guirado Llorente, D. EP-0474
Gülaldi, N. C. EP-0671, **EP-0736**
Gülbahar Ateş, S. EP-0287
Guldbrandsen, K. **OP-640**
Güler, A. EP-0470
Güler, G. B. EP-0470, EP-0600
Gul Sherwani, A. EP-0686
Gültekin, A. EP-0602
Gulya, M. EPS-142
Gulyás, B. EP-0080
Gümüşer, F. G. EP-0885, EP-0120, EP-0363, EP-0944, OP-934
Gunasekaran, G. EP-0936
Gundacker, S. OP-773
Gunelli, R. EP-0238
Güner, G. EP-0232
Guneren, C. EP-0153
Günther, T. EP-0811, **OP-141**, **OP-617**, OP-620, OP-655, OP-767
Guo, C. EP-0231
Guo, H. OP-164
Guo, J. OP-461
Guo, K. EP-0638
Guo, L. OP-635
Guo, N. OP-490
Guo, Q. OP-048
Guo, R. **EP-0649**, EP-0750, EPS-101, EPS-192, OP-226
Guo, W. **OP-374**, OP-398
Guo, Z. EP-0052, OP-576
Gupta, A. **EP-1008**
Gupta, M. **OP-783**
Gupta, P. **EP-0622**, EPS-170, EPS-181, EPS-204
Gupta, R. EPS-073, EP-0734
Gupta, Y. EP-0500, EP-0987, EPS-073, EPS-076, EPS-079
Gürdal, N. EP-0185
Gurnhofer, E. EP-0283
Gurrieri, L. EP-0613
Gürses, &. EP-0233
Gurunath Bharathi, P. OP-026, **OP-778**
Gusakova, A. EP-0457, OP-645
Gusella, S. OP-447
Gustafsson, J. EP-0633, EPS-248, OP-371, OP-904
Gutierrez-Cruz, D. EP-0130
Gutiérrez González, Á. EP-0890, EP-0516
Gutiérrez Guerrero, M. EP-0504, OP-849
Gutjahr, E. OP-162, OP-189
Gutschmayer, S. EP-0105, **EP-0710**, EPS-125, OP-567, **OP-775**, OP-776
Guven, M. EP-0290, EP-0592, **EP-0909**
Guzmán Ortiz, S. EP-0245, EP-0421, **EPS-051**
Guzmán Prudencio, G. EP-0471
G. van der Poel, H. EP-0397
Gyanraj Sa, K. EP-0518
Gyland Mikalsen, L. EP-0686
Györke, T. OP-102

Ha, J. M. OP-049
Ha, S. **OP-044**, OP-049, OP-943
Haanen, J. B. A. G. OP-451
Haas, H. OP-254
Haas, M. EPS-102
Haass, C. OP-110
Haba, H. OP-772
Habbache, M. **EP-0534**, OP-630
Haberkorn, U. OP-162, OP-189, OP-512, OP-518
Haberl, D. EP-0105, EP-0262, EP-0283, EPS-125, OP-093, **OP-709**, OP-713
Hackebeil, M. OP-139
Hackenberg, S. EP-0093, OP-785
Hacker, M. EP-0105, EP-0149, EP-0262, EP-0283, EP-0460, EP-0493, EP-0748, EPS-102, EPS-125, EPS-174, OP-081, OP-093, OP-286, OP-648, OP-706, OP-713, OP-776
Hacısahinogulları, H. EPS-189
Hadaschik, B. EP-0284, EP-0391, EPS-110, EPS-118, OP-192, OP-301
Haddad, F. OP-155
Hadebe, B. **EP-0643**
Haeuber, E. OP-193
Hagemans, I. M. EP-0077
Hagen, R. EP-0093, OP-785
Hagenbuchner, J. EPS-225
Hagens, M. J. EPS-105, OP-042
Hagerman, J. **EP-0454**, **EPS-033**
Hagimori, M. EP-1015
Hagmarker, L. **EPS-009**
Hahn, J. OP-152
Hahner, S. EP-0507, OP-305
Hajduch, M. EP-0048, EP-0078
Hajduova, K. EP-0048
Hajianfar, G. EP-0727
Hajiyianni, M. OP-919
Hakansson, A. EPS-118
Hake, R. OP-468
Hakulinen, M. EP-0627, EP-0996, **EP-1002**, EPS-241
Halanaik, D. EP-0332, OP-097, **OP-161**
Halenka, M. EP-0490
Halit Tokaç, R. EP-0591
Hall, S. EP-0454
Hallberg, B. EPS-230
Halldin, C. EP-0080, OP-555, OP-563
Halttunen, S. EP-0996
Hamacher, R. EP-0146, EP-0607, OP-190, OP-380, OP-932
Hamaji, M. EPS-262
Hamdan, B. EPS-082
Hamerlik, P. OP-555
Hammami, H. EP-0087
Hammar, M. **OP-499**
Hammers, A. EP-0533
Hammersen, N. **EPS-238**
Hammid, G. EP-0771
Hamya, M. OP-855
Hamzian, N. EP-0727
Han, D. **EP-0108**
Han, G. OP-137, OP-138, EP-0803
Han, T. **EP-0222**, EPS-021
Han, X. EP-0091, EP-0371, **EP-0453**
Hanaoka, K. **TEPS-008**
Hancock, S. L. OP-504
Handke, A. **EPS-118**
Handkiewicz-Junak, D. **EPS-013**
Handula, M. **EP-0064**, **EPS-224**
Hani Binti Rosly, A. EP-0852
Hanoun, C. OP-102, OP-099
Hänscheid, H. OP-909
Hansen, K. **EPS-124**, OP-722
Hansen, M. OP-025
Hansen, P. L. EP-1030
Hansson, E. OP-615
Hansson, O. EP-0454
Hanzu, F. EP-0491
Happel, S. OP-022
Hara, T. OP-781
Hardiansyah, D. EP-0786, OP-835, **OP-905**, **OP-909**
Harding, R. OP-030
Hargitai, L. EP-0493
Harman, E. OP-018
Harman, M. EP-0379
Harms, H. J. OP-240, OP-387
Harms, M. OP-614
Haroon, A. EP-0636
Harper, I. EP-0799
Harray, J. EP-0874
Harris, K. OP-336
Harry, L. EP-0643, EP-0183
Harsini, S. EP-0201, EPS-242, EPS-251, OP-091
Harter, P. OP-467, OP-538
Harteveld, A. **EP-0100**, EPS-253
Hartikainen, J. E. K. OP-728
Hartikainen, S. **EPS-127**
Hartman, J. OP-579
Hartrampf, P. **EP-0539**, **EP-0610**, **EPS-117**, EPS-235, EP-0182, EP-0319, EP-0507, EP-0552, OP-291, OP-305,

OP-332, OP-866
Hartung, K. EPS-156
Harvey, C. EP-0558
Hasan, M. OP-147
Hasbak, P. EPS-126
Hasegawa, K. EP-0715, TEPS-010
Hasegawa, T. EP-0696, OP-325
Hasenauer, N. **OP-291**, OP-866
Hashine, K. EP-0244
Haskali, M. OP-254, P-0555, OP-338, OP-437
Haslauer, A. **EP-0655**
Hassan, H. **TEPS-002**
Hassel, J. OP-450, EPS-266, OP-449
Has Simsek, D. EP-0377, EP-0553, EP-0911, EP-0912, EPS-189, OP-333
Hassse-Lazar, K. EPS-013
Hatt, M. EPS-184, OP-092
Haubner, R. EP-0824, EPS-279
Haug, A. EP-0262, EP-0283, EPS-125, OP-709, OP-713
Hautzel, H. EP-0072, **EP-0137**, EP-0146, OP-330, OP-580
Havel, M. **EP-0442**
Havlova, G. EP-0442
Hawkins, C. OP-718
Hawkins, M. OP-336, EP-0184
Hayden, C. OP-242, OP-731, OP-732
Haymann, J.-P. OP-805
Hayoz, S. OP-337
Hayrapetian, A. EP-0538
Hayward, C. EPS-206, OP-194, OP-718
Hazenberg, B. P. C. OP-860
He, B. OP-393, OP-530, OP-672
He, C. **EP-0047**
He, H. **EPS-119**
he, k. **OP-111**
He, Q. **OP-256**
He, S. OP-286
He, Y. EP-0637, EPS-091, OP-492, EP-0133, EP-0382, EPS-209, EPS-255, OP-096, OP-164, OP-373, OP-376
Heald, R. A. OP-764
Healy, M.-L. EP-0787
Heard, S. **EP-0799**
Hechiche, M. EP-0420
Hechler, V. EP-0560
Heck, M. EP-0288, EP-0564, EPS-124
Hedeer, F. EP-0454, EP-0468
Hedrick, M. EP-0612, OP-857
Heesch, A. **EP-0060**
Heger, J.-M. OP-099
Hehenwarter, L. OP-446
Heidenreich, A. OP-468
Heijmen, L. EP-0274
Heikkinen, J. OP-184
Heimann, J. EPS-289
Heine, D. EPS-143
Heinitz, S. EP-0869
Hekimsoy, I. **EP-0290**
Hekimsoy, T. **EP-0288**, OP-334
Helbawi, M. EP-0051
Helbich, T. EPS-102
Helbling, A. EPS-219
Heller, G. V. OP-389
Hellwig, D. EP-0809
Helou, K. EPS-230
Helsing, J. EP-0641
Hemmingsson, J. OP-836
Hendlisz, A. OP-232, OP-238
Hendrikse, E. **TEPS-019**
Hendrikse, H. N. EP-0805
Hendrikx, J. J. M. A.. EP-0271, OP-908
Henke, J. OP-560
Hennebicq, S. OP-855
Henning, H. EP-0391
Henrard, E. EPS-229
Henrich, M. OP-562
Henriksen, J. V. EP-0660
Henriksen, A. C. EPS-163, OP-385
Henry, E. C. EPS-234, OP-851
Hentschel, M. OP-191
Henzlova, L. EP-0442
Herceg, D. EPS-264
Herholz, K. EP-0684, EP-0720
Hering, H. OP-563
Hermann, M. EPS-280
Hermann, S. OP-356
Hermie, L. EPS-231
Hermosa-García, S. EP-0355
Herms, J. EP-0726, OP-588
Hernandez, R. **EP-0863**, **EP-0891**, EPS-274
Hernández Fructuoso, M. A. EP-0766, EP-0767
Hernández Martínez, A. C. EP-0419, EP-0579, EP-0407, EP-0924, EP-0925, EPS-269, OP-924
Hernández Muñiz, S. EP-0352
Hernández Pérez, I. EP-0352
Hernando, J. EP-0548
Herrador-Galindo, L. EPS-049
Herrero Muñoz, A. EP-0526, EP-0605
Herrmann, K. EP-0137, EP-0146, EP-0284, EP-0391, EP-0607, EPS-110, EPS-118, EPS-238, OP-099, OP-190, OP-192, OP-301, OP-308, OP-330, OP-334, OP-340, OP-380, OP-508, OP-580, OP-932
Herscovitch, P. OP-304, OP-310
Herth, M. M. OP-615
Hervás Sanz, B. **EPS-049**, EP-0211, **EP-0248**, **EP-0299**, EP-0355, EP-0473, EP-0547, EP-0942, EP-0954, **EP-0955**, EP-0970, EP-0988, EPS-031
Hervas-Sanz, B. EPS-048, EPS-154, **EPS-265**, OP-784
Herweg, K. OP-773
Hescot, S. EPS-017
Heskamp, S. EP-0077, OP-220, OP-358
Hess, S. EP-1030
Hesse, M. **EPS-134**, **OP-624**, OP-629
Hesse, S. EP-0149, EPS-174
Hesterman, J. **EPS-289**, OP-340, **OP-837**
Heurgue, A. OP-160
Heuschkel, M. EP-0785
Hey-Hawkins, E. OP-558
Heymann, M.-F. OP-155
Heymans, M. W. OP-102
Hicks, R. OP-567
Hickson, K. OP-441
Hidalgo Tenorio, C. EP-0517
Hielscher, T. OP-719
Higgins, G. S. OP-764
Higuchi, T. EP-0093, EP-0319, EP-0353, EP-0451, EP-0539, EP-0808, EPS-117, OP-291, OP-517, OP-866
Hildebrandt, M. EP-0641, EPS-228, OP-659
Hillhouse, C. C. OP-016, OP-141
Hillier, S. EPS-289
Hindié, E. EP-0035, EP-0780, EP-0840, OP-150, OP-654, OP-895
Hiplan, A. EP-0465
Hippeläinen, E. EPS-249, TEPS-007
Hirano, F. **EP-0854**
Hirata, K. EP-0739, EPS-012, **OP-777**
Hirata, S. **EP-0855**
Hirato, T. OP-561
Hirayama, K. EPS-131
Hiret, S. OP-155
Hirmas, N. OP-380, OP-932
Hiromasa, T. OP-284, OP-290
Hirsi, S. **EP-1030**
Hirvilammi, R. EP-0627
Hitzl, W. OP-446
H. Led, C. **EP-1023**, **OP-659**
Hlongwa, K. **OP-318**, **OP-884**, OP-574
Ho, A. L. OP-802
Ho, C. EPS-114, EPS-191, OP-095, OP-159
Ho, I. **EPS-191**
Hoang, T. M. EP-0220
Hobbs, R. OP-837, OP-147, **OP-149**, **OP-530**, OP-393
Hobbs, T. OP-556
Hocevar, M. TEPS-011
Hochmuth, D. **OP-450**

Hoeben, F. J. M. OP-220
Hoeks, J. EP-0499
Hoekstra, O. S. OP-451
Hoenig, M. **OP-105**
Hoermann, A. A. EPS-225, OP-306
Hoeschen, C. EP-0666, EPS-086
Hoffmann, L. OP-357
Hofland, H. OP-670
Hofland, J. EP-0196, EPS-213
Hofman, M. EPS-010, **OP-037**, OP-192, OP-254, **OP-338**, EP-0555, EPS-110, EPS-172, OP-437
Hofman, S. OP-253
Hofmann, L. EP-0149, EPS-174
Hogan-Lamarre, S. EP-0499
Hogg, L. TEPS-013
Höglinger, G. U. OP-110
Högnäsbacka, A. OP-555
Hohaus, S. EP-0335, EP-0337
Hojski, A. OP-297
Holdgaard, P. OP-181, OP-501, OP-502, **OP-500**
Höljer, E. OP-499
Holland, N. P. EP-0033
Holm, S. **EP-0660**, EP-0149, EPS-174
Holness, J. EP-0269
Holstensson, M. EP-0156
Holzgreve, A. EP-0210, EP-0726, EPS-003, OP-082, **OP-467**, **OP-538**, **OP-588**, OP-656, OP-717
Holzleitner, N. OP-141, OP-617, **OP-620**, OP-655, **OP-767**
Homaee Shandiz, F. EP-0085
Homolya, M. OP-081
Hong, H. **EPS-287**, **OP-212**
Hong, I. OP-049
Hong, J. EP-0001, EPS-180, **OP-362**, OP-710, **OP-844**
Honguero-Martinez, A. F. EPS-259, OP-638
Hongyong, W. **EP-0803**
Hönig, M. OP-107, EP-0751
Honkanen, A.-P. TEPS-007
Hoogenkamp, D. **EP-0805**
Hoogenraad, N. EP-0032
Hooshyar Yousefi, B. **OP-562**
Hope, T. A. EPS-110, OP-508
Hopes, L. OP-454
Hoppin, J. EPS-289
Hoppner, J. OP-189, OP-518
Horal, R. EPS-047
Horcas-Villaverde, S.-G. EPS-025, EPS-026
Horikoshi, H. EP-0244
Hörmann, L. EP-0024
Horn, J. EP-0677, OP-928
Horne, C. **OP-021**
Horowitz, M. EP-0066
Horowitz, T. EPS-099, **OP-929**
Horton, S. OP-138
Horvat, R. EP-1030
Horvatic Herceg, G. **EPS-264**
Hosseini, S. EPS-187
Hosseinzadeh, E. **EPS-135**
Hosten, B. EP-0019, **OP-559**
Hostetler, E. OP-703
Hotta, M. EP-0538, OP-192
Hou, G. EP-0281
Hou, J. EPS-164, EPS-207, **OP-797**
Hou, M. OP-633
Hou, W. **EP-0163**, **EP-0327**
Hou, X. EP-0549, EPS-115, OP-442, OP-715
Houghton, K. EP-0495
Houshmandi, S. S. EP-0113
Houwerzijl, E. J. OP-860
Houwing, K. EPS-270
Hovind, P. OP-384, OP-385, OP-729
Hribernik, N. OP-452
Hruby, G. EPS-120
Hrynchak, I. **EP-0896**
Hsiao, E. OP-037
Hsiao, I. T. OP-180
Hsieh, W. OP-140
Hu, F. EPS-157
Hu, G. EP-0270, OP-847
Hu, J. OP-714, EPS-287, OP-212, EP-0801, **EPS-244**
Hu, L. EP-0664
Hu, N. EP-0668
Hu, P. EP-0637, EPS-091
Hu, Q. **EP-0814**
Hu, S. EPS-164, EPS-207, OP-448, OP-461, OP-795, OP-796, OP-797, OP-885
Hu, Y. **EP-0426**, EP-0428, EP-0430, EPS-138
Hu, Z. **EP-0764**
Hua, F. EPS-057
Hua, Z. EP-0321, EPS-276, EPS-290, EPS-290, EPS-290, OP-214
Huang, B. OP-363
Huang, J. **EP-0431**, OP-398, OP-461
Huang, M. OP-336
Huang, Q. EP-0017, **EP-0675**, EPS-057, OP-111
Huang, R. EP-0296, EPS-066, EPS-069, OP-652
Huang, S. **OP-635**, EP-0296
Huang, W. EPS-293, OP-622, OP-902
Huang, Y. H. EPS-162
Huang, Y. EP-0178, OP-111
Huang, Y. Y. EP-0878
Huang, Y.-R. EP-0029
Huang, Z. OP-303
Hubalewska-Dydejczyk, A. EP-0209, EP-0537, OP-306, OP-675
Hubbeling, H. EP-0333
Huchet, V. EPS-017
Hudson, A. OP-359
Huerga, S. EP-0339, EP-0348, OP-098
Huff, D. T. EP-0113, EPS-165
Huffman, C. OP-672
Hugenberg, V. OP-023
Hughes, J. EPS-118
Hugonnet, F. EP-0719
Hugues, N. **EP-0067**
Huhtanen, J. T. OP-660
Hui, J. EPS-064
Huić, D. EP-0932, EP-0221
Huisman, M. C. EP-0383, EPS-195
Huisman, W. TEPS-019
Huitema, A. D. R. EP-0271, OP-908
Huizing, M. OP-573
Hull, A. **OP-140**
Humbert, O. EP-0132
Hume, I. EP-0573
Humm, J. EP-0197, OP-834
Hummel, S. EP-0024
Hung, G.-U. OP-180
Hung, I. OP-137
Hung, L.-M. EP-0878
Huo, L. EP-0270, EP-0372, EP-0378, EP-0438, EP-0668, EPS-004, EPS-006, EPS-193, OP-303, OP-701, OP-847, OP-883
Hurdogan, O. EP-0377
Hurle, R. EP-0272, OP-039
Hurstel, M. EPS-058
Hurtado de Mendoza, A. **EP-0708**, **OP-327**
Hurtado Romero, A. OP-168
Husevåg, T. **EPS-188**
Husztik, B. OP-369
Hüttmann, A. OP-102
Hüttmann, T. EPS-117
Hutton, B. F. EP-0670
Huxley, P. OP-621
Huyck, L. EPS-231
Huynh, T. **OP-901**
Hvass, L. OP-615
Hvidsten, S. EP-1023
Hvittfeldt, E. **EP-0219**
Hyafil, F. EP-0654, **OP-858**
Hylle, M. **EP-0713**

Iaccarino, G. EP-0783, EPS-232
Iacoban, A. EPS-040
Iacobone, M. EPS-074

Iacone, V. EP-0935
Iagaru, A. EP-0278, OP-504
Iakovou, I. EP-0938, EPS-136, OP-542
Ialuna, S. EP-0131, **EP-1028**
Ibba, S. **EP-1004**
Ibrahim, M. EP-0260
Ibrahim, R. EP-0786
Ichikawa, H. **EP-1018**
Icova, V. EP-0442
Ieria, F. P. EP-0404, EPS-022
Ieva, F. EPS-180
Iezzi, R. EP-0793
Iida, H. **OP-247**, OP-365
Iizuka, Y. **EP-0589**
Ijpma, F. F. A. EPS-059
Işık, E. EPS-245
Ikeda, K. OP-561
Ikemoto, K. EP-1036
Ikoma, Y. OP-079
Ilieva-Gabarska, P. **EP-0513**
Ilić Tomaš, M. EP-0292
Ilyushenkova, J. **EP-0463**
Im, H. J. EP-0536
Imber, B. S. EP-0333
Imbert, L. EP-0758, EP-0760, EPS-008, **EPS-240**, OP-250, OP-454, OP-586
Imbriaco, M. OP-647
Imlimthan, S. OP-432
Imobersteg, S. OP-139, OP-897
Imperio, D. EPS-288
Inagaki, T. **EP-0887**, OP-182
Inaji, M. EP-1036
Ince, B. EP-0153, OP-165, **OP-944**
Indovina, L. EP-0693, EP-0793
Inglese, M. **EPS-018**, OP-045, **OP-590**, OP-846, OP-050, OP-051
Inoue, M. EP-0589
Inoue, S. EP-0811
Insa Mallá, A. EP-0148
Interlenghi, M. EP-0744
Inui, Y. EP-0715
Inukai-Inoue, J. EP-0141, **EP-0308**, EPS-104
Iommi, D. EP-0748, OP-709
Ionescu, T. EP-0375, EPS-040
Iqbal, R. EPS-019
Iravani, A. OP-037
Irigaray, A. EPS-070
Irimescu, I. **EP-0672**, OP-292
Irrizari, M. EPS-147
Irumva, B. EP-0875
Isa, K. OP-561
Isa, T. OP-561
Isal, S. EPS-080
Isambert, A. OP-495
Iscar Galán, T. EP-0705, EP-0706
İsci, H. EP-0225
Isgum, I. OP-241
Ishiguro, H. EP-0110
Ishiguro, M. EP-0715
Ishii, K. TEPS-008, EP-1036
Ishikawa, K. **EP-0774**, EP-0776
Ishikawa-Morimoto, D. TEPS-008
Ishimori, T. EP-0111, EP-0126
Isik, E. EP-0912, EP-0553, EPS-189
Isik, Z. **EP-0232**
Islam, S. OP-590
Ismail, A. OP-385
Ismail, R. OP-324
Isnardi, V. **OP-056**
Isobe, R. EP-0887, OP-182
Isoda, H. EP-0310
Istatieh, F. EPS-082
Itagaki, K. EP-0126
Italiano, A. EPS-093, OP-912
Italiano, M. EP-0551
Ito, H. OP-177
Ito, S. EP-0625
Ito, T. TEPS-008
Itti, E. EP-0756
Iuele, F. EP-0509
Iung, B. OP-513
Ivashchenko, O. EPS-233, **EPS-249**
Iwao, Y. EP-0651
Iyer, V. OP-579

Jaafar-Thiel, L. EPS-291, OP-430, OP-491
Jabbour, T. EPS-112
Jachetti, E. EP-0010
Jackson, P. EP-0555, EPS-172, OP-338, OP-437
Jacquet-Francillon, N. **EPS-080**
Jaekers, J. EP-0196
Jafari, E. OP-169
Jäger, E. OP-107
Jager, V. EP-0573
Jaimovich, R. EP-0465, EPS-087
Jain, A. EP-0721
Jain, S. **OP-946**, EP-0518
Jain, V. EP-0497
Jaiswal, V. EPS-027
Jajcisinova, E. OP-024
Jajodia, A. OP-783
Jakobsson, V. EP-0281, OP-188, OP-237, OP-302
Jaleel, J. EP-0518, EP-1020, EPS-060, EPS-170, EPS-181
Jalloul, D. EP-0375
JallouL, W. **EP-0375**, EPS-040
James, M. L. OP-793
Jamet, B. OP-100
Jamsek, J. EP-0089
Jana, M. EP-0497
Jandric, J. EP-0272, OP-039
Jané, E. EP-0081, EPS-077
Jané, P. **EP-0081**, **EPS-077**
Janevik-Ivanovska, E. **EP-1000**
Jang, A. OP-336
Jang, J. Y. EP-0186
Jang, S. OP-049
Janich, M. EP-0889
Jankowski, C. EPS-015
Janota, B. OP-306
Jan Philipp, K. OP-937
Jansen, F. EPS-176, EP-0716, EPS-100
Jansen, M. A. OP-289
Jansen, T. J. P. EP-0486
Janssen, M. J. R. EPS-205, OP-339, OP-853
Jantarato, A. EPS-109, OP-662
Januszkiewicz-Caulier, J. EP-0298
Jardak, I. EP-0139, EP-0140, EP-0387, EP-0990
Jaronen, M. OP-660
Jauch, A. OP-919
Jaudet, C. EP-0640
Javed, a. EP-0370
Jawa, Z. EPS-087
Jayanthi, M. **EP-0171**
Jean Jean, P. OP-296, EP-0850, **OP-434**
Jeba Selvaraj, A. OP-161
Jeevan, S. EP-0449
Jegoux, F. OP-806
Jehanno, N. EPS-017, OP-311, TEPS-004
Jenniskens, S. F. M. OP-853
Jenčo, M. EP-0490
Jensen, A. EP-1000, OP-615
Jensen, H. EP-1000, OP-615
Jentjens, S. OP-667
Jentzen, W. EP-0607, EPS-238, OP-301
Jeon, K. EPS-168
Jeong, D. EP-0822, **EP-0823**
Jeong, J. OP-574, OP-049
Jeong, S. OP-049
Jeong, Y. **EPS-168**
Jeppesen, L. EP-1023
Jeraj, R. EPS-165, OP-676
Jercan, A. EP-0464
Jereczek-Fossa, B. A. EP-0236

Jessen, F. OP-107
Jewell, K. **EP-0406**
Jezeršek Novaković, B. EP-0325
Jha, A. **OP-304**, **OP-310**, EP-0731, OP-178, EP-0789
Jha, P. EPS-067
Jha, S. EP-0129
Ji, X. EP-0815
Jia, B. OP-219, OP-288, OP-361, OP-878
Jia, F. OP-490
Jia, J. **TEPS-020**
Jia, R. EPS-006
Jia, X. **EP-0076**, EPS-064, **OP-878**
Jia, Z. EP-0289
Jiang, D. EP-0031, EP-0058, EP-0856, EPS-283, OP-216
EP-0001,OP-256
Jiang, J. EPS-276
Jiang, L. EP-0661, EPS-132, OP-565, OP-571, EP-0746
Jiang, M. **EP-1011**
Jiang, T. **EPS-186**
Jiang, X. **OP-900**
Jiang, Y. EPS-287, OP-373, OP-376
Jiang, Z. EP-0460
Jiao, H. **EPS-028**
Jiao, J. **EP-0435**, EPS-141, OP-287
Jiao, R. EP-0834, **EP-0836**, EP-0846, EPS-212
Jiao, X. EPS-287
Jie, W. **EPS-151**
Jie, Z. **EPS-108**
Jimenez, A. EP-0340
Jiménez Bonilla, J. EP-0890, EP-0516
Jimenez-Fonseca, P. OP-233
Jiménez Heffernan, A. EP-0405, EP-0918
Jiménez-Hoyuela García, J. EP-0199, EPS-072
Jimenez Londoño, G. **EPS-259**, **OP-638**
Jimeno Pernett, R. EP-0761, **EP-0148**
Jin, X. OP-377
Jing, H. EP-0668, OP-312, OP-671
Jinwani, S. EP-0166
Jo, I. OP-049
João, C. EP-0006, EP-0328
Jochumsen, M. **OP-386**
Jodar Gimeno, E. EP-0494
Johannes, J. OP-555
Johannesen, H. H. EP-0195, EPS-160
Johayem, A. EPS-291, OP-491
John, L. OP-919
John, N. EPS-120, EP-0558
Johnbeck, C. B. EP-0195
Johnsen, R. EPS-176, OP-227
Johnson, F. L. OP-144
Johnston, K. EP-0070, OP-016
Johnström, P. OP-555
Jonasson, M. **OP-458**, **OP-459**
Jones, J. OP-025
Jones, K. OP-770, EP-0066
Jonghi Lavarini, L. EP-0685, **OP-537**
Jonker, M. A. OP-339
Jonsson, J. EP-0317
Joosten, L. EPS-225
Jordan, D. EP-0465
Jorge, A. F. EP-0412
Jorge-Novoa, J. A. EP-0355
Jose, W. EP-0179
Joshua, A. M. EPS-120, OP-335
Jotic, A. EPS-254
Jouberton, E. OP-938
Jougla, A. **EP-0907**
Journo, S. EP-0894
Jovalekic, A. EP-0678
Jovin, M. OP-793
Jreige, M. EP-0699, EP-0755
Ju, H. EP-0730
Juan-Piriz, C. EP-1013, EPS-023
Juarez Orozco, L. E. EPS-171
Jucaite, A. OP-555
Juhlin, C. EPS-067
Jui, N. EP-0810
Jukema, R. OP-241
Jukic, N. EP-0221
Jundi, A. OP-835
Juneau, D. OP-848
Jungels, C. OP-232, OP-238
Junichi, T. EP-0710
Jurecka-Lubieniecka, B. EPS-013
Jurkschat, K. OP-656
Juweid, M. E. EPS-082
Juzeniene, A. EPS-222

K, D. EPS-079
Kääriä, L. EP-0627, **OP-529**
Kabasakal, L. EP-0228, EP-0253, OP-035, OP-163, OP-375
Kaboteh, R. EP-0759
Kaci, R. OP-948
Kacperski, K. OP-675
Kaderabek, R. EPS-084
Kadonaga, Y. OP-772
Kadumberi, A. OP-222
Kahl, T. EP-0391, OP-301
Kaida, H. TEPS-008
Kaiser, L. **EP-0726**, EPS-092, OP-082, OP-588
Kaiser, P. OP-922
Kajisako, M. EP-0873
Kakkar, N. EPS-190
Kalaitzoglou, A. EP-1014
Kalantari, F. **OP-446**
Kale, S. **EP-0216**
Škalič, K. OP-452
Kalidindi, T. OP-770, **OP-896**
Kälin, R. OP-082
Kalinovsky, A. EPS-142
Kalisvaart, G. M. OP-086
Kaliszczak, M. OP-563
Kalnina, M. **EP-0440**
Kalykakis, G. **EPS-178**
Kamaleshwaran, K. **EP-0535**, **EP-0403**
Kamei, T. EP-0452
Kamenshikov, N. EPS-142
Kaminek, M. EP-0442, EP-0490
Kaminska, O. OP-807
Kaminski, G. OP-675, OP-807
Kamitaka, Y. EP-0696, **EP-1036**, OP-325
Kamp, C. OP-660
Kan, K. Y. EPS-182
Kandolf Sekulovic, L. OP-453
Kandula, K. EP-0158, EPS-044
Kane, N. OP-041
Kaneda-Nakashima, K. OP-772
Kanekiyo, M. EPS-147
Kaneko, K. EP-0466, EP-0476
Kaneko, Y. OP-177
Kanellopoulos, P. EP-0041, EP-0807, EP-0861, **EPS-217**, **EPS-220**
Kang, F. EP-0028, EP-0134, EP-0222, EP-0267, EP-0638,
EP-0648, EPS-021, EPS-194, OP-428
Kang, K. EP-0186, EP-0536, OP-285
Kang, L. EPS-028, **EPS-293**, **OP-622**, **OP-902**
Kang, S. OP-049
Kang, W. EP-0595
Kang, Y.-K. **EP-0583**, OP-049
Kang, W. EP-0593
Kanno, I. OP-079
Kanoun, S. OP-804
Kašpárková, H. EP-0920
Kaphan, E. OP-929
Kapiteijn, E. EP-0788
Kaplin, D. OP-393, OP-530
Kappadath, S. EP-0164, **EPS-234**, **OP-851**
Kaprélian, T. **OP-370**
Kapsoritakis, N. EP-0193, EPS-083, OP-859
Kara, T. EP-0192
Karaşah Erkek, B. EP-0578
Karabacak, N. EP-0136
Karabulut, E. EP-0577

Karabulut, Y. EP-0304
Karaçam, D. EP-0253
Karacan, M. A. EP-0434
Karaçavuş, S. EP-0225
Karadogan, S. EP-0553
Karak, P. OP-541
Karakatsanis, N. A. OP-025
Karamian, F. EP-0424
Karasah Erkek, B. **EP-0379**, **EP-0591**
Karatay, K. B. EP-0885
KarayeL, E. OP-658
Karcaaltincaba, M. EP-0232
Karcher, G. EPS-008
Karczmarczyk, U. EP-0018
Karfis, I. OP-232, OP-238, OP-664
Karianos, T. EP-0594
Karimi, Z. **EP-0669**, **EPS-177**
Karimundackal, G. EP-0166
Karimzadeh, A. **EP-0564**, EP-0791
Karindotter-Borgendahl, N. OP-623
Karlberg, A. EPS-160
Karlberg, I. OP-704
Kärpijoki, H. OP-842
Karri, R. **EPS-172**
Kartal, M. EP-0736, EP-0570, EP-0588, OP-914
Kashyap, R. OP-437
Kashyap, Y. EP-0734
Kasivisvanathan, V. EPS-107, OP-037
Kaspera, W. OP-589
Kasraie, N. EP-0714
Kassar, M. OP-844
Kassiou, M. EP-0677
Kässmann, H. EP-0501
Kastner, L. OP-468
Kataeva, G. EP-0394
Katafuchi, T. OP-182
Katagiri, T. EP-0589
Katala, S. EP-0519
Kataoka, M. EP-0111, EP-0126
Kaths-Lundie, M. EPS-046
Kato, K. EP-0887, OP-182
Kato, M. EP-0732, EP-0929, EPS-061
Kato, T. EP-1018
Katre, G. **EP-0789**
Katsampoukas, D. EP-0237, EP-1014
Katsouras, C. EP-0422, EP-0423, EP-0445
Katsuki, A. EP-0711
Kauak, M. EP-0241
Kauak Kuschel, M. **EP-0109**
Kaufmann, P. A. OP-239
Kaul, P. EP-0413
Kaunisto, J. **EP-0996**
Kaviani, S. **OP-225**, OP-848
Kavukcu, G. EP-0290, EP-0592
Kawada, M. TEPS-009
Kawaguchi, K. EP-0808, EP-0111, EP-0126
Kawakami, H. EP-0711
Kawakubo, M. EP-0476
Kawashima, M. EP-0126
Kaya, E. **EP-0116**
Kaya, G. **EP-0347**, **OP-053**
Kaya, M. EP-0225, EP-0116, EP-0470, EP-0574, EP-0582, EP-0584
Kayembe, M. T. OP-451
Kaymak, E. EP-0253
Kibar, A. EP-0740
Kebir, S. OP-580
Kechaou, L. EP-0401
Kedrova, J. EP-0440
Keereman, V. EP-0115
Keidar, Z. OP-033
Keigley, Q. OP-676
Keinänen, A. EP-0996
Kekiopoulos, P. EP-0422, EP-0423, EP-0445
Kekiopoulou, A. EP-0422, EP-0423, EP-0445
Kellberg, A. O. EPS-163
Kellerbauer, A. **OP-024**
Kelley, B. M. EPS-234
Kelvin, J. EP-0810
Kemper, E. H. M. EP-0100
Kempińska-Wróbel, M. EP-0798
Kemppainen, J. EP-0659
Kendi, A. T. OP-340
Keniza, T. OP-470
Kennedy, J. **OP-033**
Kenner, L. EP-0262, EP-0283, EPS-125
Kerleguer, K. OP-855
Kero, T. EPS-140, OP-240, OP-387, OP-388
Keromnes, N. OP-806
Kersting, D. EP-0137, **EP-0146**, EP-0607, EPS-238, OP-301, OP-308, **OP-580**
Kertesz, H. EPS-126
Kesch, C. EP-0391, EPS-118
Kesim, S. EP-0190
Keskimäki, S. TEPS-007
Kesner, A. L. OP-025
Kessler, L. OP-932
Khadgawat, R. EP-0488, EP-0498
Khairwa, H. OP-251
Khalighi, M. OP-026, OP-778
Khamwan, K. **OP-841**
Khan, D. EP-0362, EP-0488, EP-0497, **EP-0519**, EP-0707, EP-0987, **EP-0991**, EP-1019, **EPS-055**, EPS-076, OP-251
Khan, J. **EP-0545**
Khan, S. EP-0495, EP-0832, EP-0495, EP-0368
Khangembam, B. **EPS-170**, EPS-181
Khani Meynaq, Y. OP-563
Khatib, M. OP-895, OP-150
Khazaei, M. OP-169
Kheetan, R. EPS-082
Kheruka, S. **EP-0721**
Khetarpal, V. OP-556
Khlynin, M. EP-0462, OP-864
Khoshhosn, H. **OP-720**
Khurana, A. EP-0096, EP-0498, EP-0518, EPS-027
Kiatkittikul, P. EPS-109, OP-662
Kibar, A. **EP-0152**, **EP-0153**, EP-0742, EP-0983, **OP-035**
Kiefer, F. EP-0532
Kiefer, L. S. OP-572
Kiener, T. EP-0501
Kifjak, D. OP-648
Kijprayoon, S. EP-0872
Kilicaslan, A. **OP-172**
Kim, B. EPS-030, OP-049
Kim, D. EPS-030, **EPS-169**, OP-034, EPS-169
Kim, G. OP-049, **EP-0822**, EP-0823
Kim, H. OP-036
Kim, J. OP-049, EPS-030, TEPS-003
Kim, K. EP-0730, EP-0747
Kim, S. EP-0823, EP-0839, EP-0075, EPS-144
Kim, Y. OP-285, OP-049
Kim, Z. EP-0128
Kimura, H. EP-0808
Kimura, R. EP-0739, EPS-012, OP-777
Kind, F. OP-905
Kingkiner, G. OP-439
Kingpetch, K. OP-841
Kink, J. EP-0891
Kinuya, S. EP-0244, EP-0450, EP-0710, EP-0853, EP-0855, OP-284, OP-290, OP-776, OP-781
Kir, K. M. EPS-200
Kircher, M. EP-0451, EP-0565, OP-655
Kirchgesner, T. EP-0358
Kirchleitner, S. V. OP-082
Kireeva, E. EP-0326
Kirienko, M. **EP-0010**, OP-653, OP-674
Kirkwood, I. OP-037
Kishan, A. OP-440
Kiso, K. EP-0452
Kiss, J. EP-0441
Kissa, T. **EP-0190**
Kitano, Y. **EP-0111**, EP-0126
Kiviluoto, K. EP-0790, TEPS-007

Kjaer, A. EP-0195, EPS-126, OP-615
Kjoel Tornes, A. **EPS-222**
Klaassen, N. **EP-0069**, OP-627
Klacanek, J. EP-0490
Klages, C. EPS-156
Klain, M. EP-0551, EP-0606, EPS-065
Kleesiek, J. EP-0391
Klega, A. OP-188
Klegova, A. EP-0442
Kleiburg, F. **EP-0274**
Kleijn, L. H. J. OP-220
Klein, R. EP-0745, OP-223
Kleinendorst, S. **OP-358**
Kleiner, S. EP-0288, OP-520
Kleinová, M. OP-022
Kleinschnitz, C. OP-580
Klemm, N. OP-621
Klén, R. OP-842
Kleynhans, J. **EP-0083**
Klingler, M. EPS-225
Klisarova, A. EP-0263, EP-0341, EP-0342, EP-0343, EP-0344, EP-0899, EP-0900, EP-0901, EP-0902, EP-0904, EP-0913, EPS-121, EPS-267
Klomp, M. J. OP-083, **EPS-213**
Klompenhouwer, L. G. OP-670
Klotsotyra, A. **EP-0775**
Kluge, K. **EP-0262**, **EPS-125**, OP-713
Klutmann, S. EP-0391, EP-0791
Klyuzhin, I. EP-0723
Knaapen, P. OP-241
Knappe, L. OP-246, **OP-516**, OP-521
Knešaurek, K. EP-0573
Kneiling, M. OP-922
Knesaurek, K. **EP-0572**
Knigge, U. EP-0195
Knip, J. J. **EPS-019**
Knol, R. J. J. OP-243, EPS-105, OP-242, OP-731, OP-732
Knoll, P. **EP-0680**
Knoop, H. EP-0677, OP-928, OP-930
Knop, S. EP-0353
Knorr, K. EP-0564
Knuuti, J. EPS-178, OP-247, OP-365, **OP-389**, OP-842
Ko, C. L. EP-1029, OP-228
Ko, H. **OP-179**
Ko, K. Y. **OP-244**
Kobakova, I. EP-0899
Kobayashi, M. EP-1036
Kobayashi, T. TEPS-008
Kobe, C. EP-0154, OP-099, OP-101
Koç, Z. **EP-0168**, **EP-0192**, **EP-0304**, **OP-317**
Kocabeyoglu, B. **EP-0592**
Koch, D. W. EP-0677, OP-928
Koch, S. OP-468
Kocvara, R. EPS-041
Koczyk, K. OP-587
Kodaloglu, N. **EP-0671**
Kodama, H. EP-0711
Koelblinger, P. OP-446
Koenigkam-Santos, M. EP-0732
Koerber, S. OP-337
Koester, U. OP-016
Koglin, N. EP-0678, OP-103
Köhler, D. EP-0391
Koikkalainen, J. EP-0678
Kokabi, N. **EP-0164**
Kokkini-Paschou, A. EP-1012
Kokoszka, J. EP-0209
Kolade, O. **EP-0269**, OP-884
Kolasińska-Ćwikła, A. EP-0798, OP-231
Kolenc, P. EP-1000, OP-306
Kolindou, A. EP-0982
Kolinger, G. EP-0678, **EPS-085**, **OP-103**
Köllermann, J. EP-0391
Kolodziej, M. OP-675, **OP-807**
Kominia, M. OP-493
Komoike, Y. TEPS-008
Komura, N. EP-0466
Kon, Y. OP-772
Kondakov, A. EP-0653
Kondo, H. EP-1018
Kondo, M. OP-898
Kondo, N. EP-0854, EP-1015
Kong, D. EP-0737
Kong, G. EP-0406, EP-0555, EPS-010, EPS-172, OP-437
Kong, Y. EP-0017
König, V. EP-0811
Konijnenberg, M. EP-1000, OP-146, OP-358, EPS-225, OP-029, OP-627
Konishi, T. EP-1022, EP-1024, TEPS-016, TEPS-017
Konnerup, T. C. EPS-106
Kono, T. TEPS-015
Konovalova, E. EP-0852, EP-0861
Konuparamban, A. EP-0789
Koole, M. EP-0196, EP-0716, EPS-100, OP-366, OP-443
Koopman, B. EP-0677
Koopman, G. OP-922
Koperski, L. OP-587
Kopeva, K. EP-0436, **EP-0457**, **EP-0458**, EP-0477, **OP-645**, **OP-724**
Kopka, K. EP-0849, EPS-275, OP-020, OP-558
Koponen, S. EP-0996
Koppes, J. C. C. EPS-105
Kopp-Schneider, A. EPS-266, OP-449, OP-919
Koprivova, T. EP-0920
Kopyeva, K. EPS-142
Koranda, P. EP-0442, **EP-0490**
Korkmaz, Ü. EP-0224
Korkmaz, U. EP-0541
Korn, M. OP-335
Korol, P. **OP-939**
Kortüm, K. M. EP-0353
Koshino, K. OP-631
Kosmala, A. EP-0182, **EP-0319**, EP-0507, EP-0552, OP-291, OP-305, OP-785, **OP-866**
Kossatz, S. **OP-769**
Kostadinova Kunovska, S. EP-0992
Kostelnik, T. EP-0063
Köster, U. EP-0070, EP-0780
Kostos, L. EP-0555, OP-437
Kosvyra, A. EP-0998
Kotb, M. EP-0102
Kotbi, O. EP-0771
Kote, R. EP-0734, OP-299
Kotiah, S. OP-672
Kotipalli, G. B. OP-562
Koukouraki, S. EP-0193, EPS-083, **OP-859**
Koumakis, E. OP-947
Koutsikos, J. EP-1012
Kouvelis, K. EP-0594
Kovacs, A. OP-369, EPS-230
Kovalski, G. OP-229
Kovan, B. **EPS-245**, OP-333
Kowalska, A. OP-675
Koyasu, S. EP-0111, EPS-262
Kozaka, T. OP-284, OP-290
Kozanecki, C. EP-0018, EP-0831
Kozanecki, P. EP-0018, EP-0831
Kozempel, J. OP-017
Kozlov, B. EP-0480
Kracmerova, T. EPS-084
Kraeber-Bodéré, F. OP-100, OP-155
Krafft, U. EP-0391
Krajewski, S. EP-0018, EP-0831
Krakauer, M. OP-384, OP-385, OP-729
Kral, E. EP-0874
Kramer, C. OP-188, OP-302
Kramer, V. **OP-489**
Kramer-Marek, G. **OP-589**
Krapf, P. OP-107
Kratochwil, C. OP-512, OP-719
Kraus, N. OP-866
Kraus-Deuringer, J. OP-520
Krause, B. OP-340, **OP-575**, EP-0785

Krausz, Y. EP-0542
Krebold, A. OP-856
Krebs, S. EP-0092, **EP-0197**, OP-702
Krebs-Fleischmann, H. W. A. OP-520
Kreisl, T. OP-335
Kreissl, M. OP-525
Kreller, M. OP-020
Kretzschmar, J. EP-0849
Krieger, K. **EP-0567**, OP-047, OP-058, OP-666, OP-710
Krim, M. EP-0933
Krishna, S. OP-299
Krishnamurthy, M. EP-0636
Kristensen, B. W. EPS-228
Krivolapov, S. EP-0462, OP-864
Krizsán, Á. **EP-0441**, EP-1027
Kroeze, S. G. C. OP-337
Królicki, L. OP-587
Kroll, T. OP-107
Kroon, D. OP-358
Kropinska, A. EPS-013
Kroselj, M. OP-306
Krotov, M. OP-512
Krssak, M. EP-0532
Krueger, M. A. OP-077
Kruger, H. G. EPS-046
Kruithof-De Julio, M. OP-368
Krutzek, F. EPS-275
Kubeil, M. OP-357
Kubik, A. OP-675
Kübler, H. EPS-117, OP-332
Kubo, K. EP-0141, EP-0308, EPS-104
Kubota, C. EP-0774, **EP-0776**
Kuchenbauer, F. EPS-223
Kucuk, N. O. EP-0214, EP-0243, EP-0257, EP-0314, EP-0315, EP-0349, EPS-116, EPS-200, OP-158
Küçükali, S. **OP-510**
Kucuker, K. **EP-0459**
Kudo, K. EP-0739, EPS-012, OP-777
Kudomi, N. OP-247
Kuehnel, C. EP-0827
Kuglová, I. OP-925
Kuhnast, B. EP-0876
Kuikka, P. OP-728
Kuji, I. **EP-0110**, **EP-0360**
Kukuts, K. EP-0441, EP-1027
Kulduk, G. EP-0119
Kulkarni, H. **EP-0664**
Kulkarni, R. EP-0950, **EPS-257**, **OP-788**
Kulkarni, S. EP-0043
Kulterer, O. EP-0532
Kumakawa, S. TEPS-008
Kumar, A. EP-0500, **EP-0936**
Kumar, C. EPS-079
Kumar, M. EP-0013
Kumar, N. EP-0203, EP-0208, **EP-0336**, EP-0368, **EP-0618**, **EPS-204**, OP-251
Kumar, P. EP-0013, EP-0158, EPS-044, OP-649, EP-0350, EP-0497, EP-0498, EP-0500, EP-0505, EP-0519, EP-1020, EPS-054, EPS-055, EPS-073, EPS-076, EPS-079, **OP-316**
Kumar, R. EP-0519, EP-0318, EPS-111, EPS-190, OP-651, EP-0166, EP-0096, EP-0203, EP-0208, EP-0350, EP-0362, **EP-0488**, EP-0622, EP-0707, EP-0717, EPS-054, OP-251, OP-923
Kumar, S. EP-0717, EP-0558, **EPS-111**, OP-861
Kumar, V. EPS-060
Kumar Gupta, N. **EP-0129**
Kümmel, S. OP-580
Kunawudhi, A. EPS-109, OP-662
Kundu, N. **EP-0362**, OP-251
Kunert, P. OP-587
Kunikowska, J. OP-587
Kunte, S. EP-0015, OP-110, EP-0210, EPS-003, OP-717, **OP-656**
Kuntner, C. **EPS-102**
Kunz, W. OP-717, OP-099
Kunze, L. EP-0024
Kuo, H. T. EP-0829, EPS-223, OP-142, OP-431
Kuo, M. OP-310, OP-304
Kuo, P. OP-222, **OP-340**
Kuo, S.-Y. **OP-228**
Kurch, L. OP-102
Kurimoto, T. EP-0141, EP-0308, EPS-104
Kurth, J. **EP-0785**, OP-575
Kurtz, K. OP-702
Kuru Oz, D. EP-0214, EP-0315, EPS-200, OP-158
Kurzynska, A. EP-0537
Kusacic-Kuna, S. EPS-264
Kusmierek, J. EP-0703
Kutsch, N. OP-099
Kuyumcu, S. EP-0377, EP-0553, EP-0911, EP-0912, EPS-189, EPS-245
Kvacskay, P. OP-518
Kvassheim, M. **OP-832**
Kvernby, S. **EPS-140**, OP-388
Kwock, S. EP-0850, OP-434
Kwon, D. EPS-223
Kwon, H. EP-0075, EPS-144
Kwon, S. **EP-0566**, OP-044, OP-049, **OP-943**
Kwon, W. **TEPS-003**

Labeyrie, C. OP-858
Lacerda, K. J. C. C. EPS-062
Lachachi, B. OP-852
Lachachi, C. OP-470
Lacombe, M. OP-155
Lad, S. EP-0043
Ladenson, P. OP-393, OP-530
Ladev, M. TEPS-007
Ladisa, G. EP-0487, EP-0813
Ladoire, S. EPS-015
Lafontaine, D. EP-0197, EP-0333
La Fougère, C. EP-0658, OP-077, OP-314, OP-572
La France, N. **EP-0612**, OP-857
La Frenière, N. OP-236
Lagano, V. EP-0068
La Gattuta, F. EP-1028
Lahdenpohja, S. **EP-0876**
Lahner, H. OP-308, OP-852
Lahoutte, T. EPS-227
Lai, A. OP-359
Lai, Y. OP-377
Laitinen, T. M. EP-0996, EPS-127, EPS-241, OP-728
Laitinen, T. P. EP-0996, OP-728
Lajeune, E. EP-0698
Lak, A. OP-433
Lakes, A. L. OP-018
Lakkas, L. EP-0423
Lal, A. EPS-190
Lalire, P. OP-187
Lam, M. OP-852, EPS-198, OP-295, OP-670, OP-850
Lamare, F. EP-0035
Lamart, S. EPS-246
Lamash, Y. EP-0758
Lambert, B. **EPS-231**
Lambert Lepesevich, L. EP-0863, EP-0891
Lammers, T. EPS-229
Lammertsma, A. EP-0020, EP-0124, EP-0692, OP-503
Lamprakopoulos, G. EP-0193, EPS-083
Lan, W. EP-0658, OP-077, OP-572
Lan, X. EP-0030, EP-0031, EP-0058, EPS-157, OP-143, OP-216, OP-700
Lancha Hernandéz, C. EP-0127, EP-0365, EP-0502
Lancman, G. EP-0351
Land, L. H. EP-0641
Landoni, C. EP-0285, EP-0316, EPS-161, OP-537, OP-653
Landvogt, C. OP-188, OP-302, OP-926
Lane, D. P. OP-766
Lanfranchi, F. **EP-0273**, EP-0277, OP-050, **OP-455**
Lang, M. OP-162
Lang, P. OP-314
Langbein, T. EPS-124
Langdon, S. EP-0042
Langenhuijsen, J. F. EPS-075
Langer, J. EPS-041

Langer, O. EP-0674
Langer, S. W. EP-0195
Langermans, J. OP-253
Langsteger, W. OP-648
Lania, A. G. OP-653
Lanka, S. OP-336
Lanzafame, H. OP-852, EP-0607, OP-190, OP-308, OP-380, **OP-932**
Lapa, C. EP-0319, EP-0451, EP-0552, EP-0565, OP-334, OP-620, OP-655, OP-767, OP-856
Lapa, P. EP-0165, EP-0395
Lapela, M. OP-529
Laporte, P. **EP-0695**
Läppchen, T. **OP-432**
Lapucci, C. OP-050
Laranjo, M. EP-0008
Lardinois, D. OP-297
Larkina, M. OP-578
Laroni, A. OP-051
Larouze, A. **EP-0840**
Larsen, A. OP-384
Larsen, M. E. EPS-163
Larsen, R. H. EPS-222
Larsen, S. OP-911
Larson, S. OP-702, OP-802
Larsson, M. EP-0450, EP-0759, OP-708
Lasalle, S. TEPS-004
Laschinsky, C. EP-0137
Laskov, V. **EP-0004**
Lasne-Cardon, A. OP-806
Lasnon, C. EP-0640, OP-806
Lassen, M. OP-567, **EPS-126**
Lassmann, M. EP-0633, EPS-235, EPS-236, OP-152, OP-371, OP-833, OP-909
Lastoria, S. EP-0550, EP-0575, EP-0781, EP-0819, EP-0879, EP-0886, EP-1034
Latgé, A. EP-0647, EP-0933, EPS-089, OP-804, OP-951
Lattuada, F. **EPS-158**
Laubscher, L. OP-239
Laurin, J. EP-0067
Laurins, C. TEPS-013
Laursen, V. S. EPS-228
Lavacchi, D. EP-0212, EP-0546
Lavagno, F. EP-0396
Lavaud, P. EPS-260, EPS-263
Lavelli, V. EP-0258
La Verde, C. EP-0586
Laverde Mächler, A. EP-0306
Laverman, P. EPS-225, OP-488
Lawal, I. O. OP-574
Lawrence, R. OP-555
Lawrentschuk, N. OP-037, OP-338
Lay, I. EPS-202
Layton, J. OP-336
Lazar, A. EP-0206, **EP-0464**, EP-0672, EP-0956, **OP-292**
Lazarenko, S. **OP-242**, OP-243, OP-731, OP-732
Lazaridis, L. OP-580
Lazaruc, T. EPS-040
Lazic, S. EP-0495, OP-511
Lazzeri, M. EP-0272, OP-039
Le, L. EP-0815
Le, T. EP-0037
Le, W. OP-490
Leamon, C. P. EP-0063
Le Beau, A. M. EPS-274, OP-616
Lebeda, O. **OP-022**
Leccisotti, L. EP-0793
Lecorche, P. OP-213
Ledet, E. OP-336
Ledwon, A. EPS-013
Lee, A. EP-0558
Lee, E. OP-049
Lee, H. **EP-0135**, EP-0822, EP-0823
Lee, J. TEPS-014, OP-703, **OP-019**
Lee, M. EPS-010
Lee, M.-Y. OP-228
Lee, R. OP-049
Lee, S. OP-102, OP-037, OP-194
Lee, W. TEPS-014
Lee, Y.-S. OP-285
Leek, F. **EP-0670**
Lefebvre, Y. OP-573
Le Gal, G. OP-855
Legallois, D. EP-0437, EPS-137, OP-858
Legenne, P. OP-897
Legrand, B. OP-806
Lehnert, W. **EP-0791**
Lehto, J. TEPS-007
Lei, P. OP-216
Leide-Svegborn, S. TEPS-012
Leiro, D. EP-0926
Leite Silva, P. EP-0246, EP-0472
Leithner, D. **EP-0333**
Leiva Montejo, A. EP-0407, **EP-0924**, **EP-0925**, **EPS-269**, OP-924, EP-0419, EP-0579
Lemos, J. OP-660
Lemos, L. **EP-0165**
Lemus Ramírez, F. **EP-0367**
Lenarz, T. EP-0082, OP-779
Lenda-Tracz, W. OP-675
Lengyelova, E. EPS-120
Lennen, R. J. OP-289
Lenssen, O. EP-0631
Lenzo, N. OP-230, OP-718
Leo, A. OP-171
Leo, E. OP-555
Leo, R. OP-328
Leocádio, S. EP-0328
Leonardi, L. EP-0272, OP-039
Leone, L. EP-0404
Leonte, R. EP-0866
Le Pechoux, C. EPS-260
Lepej, J. **OP-925**
Lepejová, K. OP-925
Leplat, C. EPS-112
Leporace, M. EP-0376
Lepre, R. OP-382, OP-383, OP-647
Lerberg Nielsen, A. EP-0318
Lerche, C. OP-107
Lerdsirisuk, P. OP-662
Le Roux, P.-Y. **OP-855**
Leroy, C. EP-0019, EP-0021
Leskinen, H. OP-184
Lesourd, S. OP-155
Letaief, B. EP-0531, EPS-038
Leterrier, S. EP-0019, OP-559, EP-0021
Le Thiec, M. **OP-155**, OP-187
Leube, J. **EP-0633**, OP-367, **OP-371**, OP-629
Leung, E. K. OP-025
Leung, E. OP-193
Leung, W. OP-159
Leupe, H. **EP-0196**
Levänen, K. **OP-184**
Levesque, S. EP-0687, OP-938
Levigoureux, E. OP-470
Levillain, H. OP-148, OP-232, OP-238, OP-367, OP-444, OP-629
Levin, J. EP-0024, EPS-148
Levin, M. C. OP-698
Levy, A. EPS-260
Levy, S. M. **OP-254**
Lewandowska, A. OP-157
Lewis, B. OP-336
Lewis, D. OP-567
Lewis, G. EP-0797
Lewis, J. S. EPS-016
Lewis, M. P. EP-0538
Leysen, W. EP-0869
Leyser, S. **OP-308**, OP-932
Lezaic, L. EP-0089, EP-0506, OP-306, TEPS-011
İlhan, T. EP-0304
Lhommel, R. EP-0358, EPS-134, OP-624
Li, B. EP-0649, EP-0750, EPS-101, EPS-192, OP-226, OP-714, OP-791, EP-0324, OP-111

Li, C. EPS-242, OP-635, OP-288, **EP-0133**, EP-0382, EPS-209, EPS-255, OP-096, OP-164, OP-373, OP-376, EPS-273, EPS-157
Li, D. OP-697, OP-215
Li, F. OP-312, OP-671
Li, G. **OP-137**, **OP-138**, OP-359, EP-0222, EP-0638, EP-0648, EPS-194, OP-428
Li, H. OP-646, EP-0133, **EPS-209**
Li, J. **OP-461**, EP-0825, EP-0091, EP-0307, **EP-0059**, OP-672, OP-562
Li, K. EP-0815
Li, L. EP-0145, EP-0057, EP-0305, EP-0334, EP-0746, OP-526 EP-0133, **EP-0382**, OP-376, OP-933, OP-215, **OP-219**, **OP-361**
Li, M. EP-0265, EP-0373, OP-144, **EP-0878**
Li, N. EP-0027, EP-0642
Li, P. EP-0483, **EP-0825**
Li, Q. EP-0814
Li, S. **EPS-120**, **EP-0493**, EP-0426, EP-0427, EP-0428, EP-0430, EP-0527, EP-0816, EP-0917, EPS-138, OP-286, OP-397
Li, T. EPS-056, **OP-920**, OP-312
Li, W. EPS-237, OP-164
Li, X. EP-0016, EP-0134, EP-0460, **EPS-021**, EPS-146, OP-286, OP-648, OP-713, EP-0741, **OP-633**, **EP-0091**, **EP-0307** EPS-287, OP-212, EP-0372, EP-0378, EPS-193, OP-701, OP-883, OP-878, EP-0427, EPS-293
Li, Y. OP-883, **EP-0739**, EP-0426, **EP-0428**, EP-0430, EP-0638
Li, Z. **EP-0692**, EPS-069, EP-0231, OP-903
Li, D. EP-0479
Liang, J. **EP-0099**, **EP-0103**, **EP-0104**, **EP-0144**, **EPS-035**, **OP-313**
Liang, T. EP-0278, OP-504
Liang, T.-J. OP-397
Liang, Y. OP-635
Liao, Y. EP-0861
Liao, Z. OP-018
Liatsou, I. OP-147, OP-149
Libor, L. EP-0181
Librizzi, D. OP-562
Licina, J. EP-0312
Lidberg, K. OP-359
Lieberman, A. OP-336
Liebich, A. **EP-0451**
Liedberg, F. EPS-208
Liepe, K. **EP-0220**
Liga, R. EPS-178
Light, A. **OP-511**
Liguore, W. OP-556
Likar, Y. EP-0326
Lilley, L. M. OP-018
Lim, C. EP-0128
Lim, H. EPS-169
Lim, I. **EP-0040**
Lima, B. A. M. **OP-471**
Lima, E. EP-0395
Lima, M. EPS-078, EP-0259
Lima, S. C. EP-0935
Lima, T. EP-0688, **EP-0795**
Limiti, M. R. EP-0404
Limouris, G. **EP-0071**, **EP-0568**
Lin, C. Y. OP-244, **OP-319**
Lin, E. OP-563
Lin, F. OP-138, EP-0280, EPS-286, OP-304, OP-310
Lin, H. EPS-182, EPS-258, OP-090, **EP-0644**, OP-794
Lin, K. J. OP-180
Lin, K. S. EP-0829, EPS-223, OP-142, OP-431
Lin, L. **EP-0160**
Lin, Q. OP-790, EP-0091
Lin, R. **OP-378**
Lin, S. EP-0737
Lin, T.-C. EP-0878
Lin, W. **OP-903**
Lin, X. EP-0483, OP-219
Lin, Y. H. EP-1029
Lin, Y. EPS-091
Lin, Z.-K. OP-180
Linares-Galiana, I. EPS-265
Linczerne Bencze, V. EP-0441
Lind, D. EPS-230
Lindegren, S. EP-1000, OP-615
Linden, F. OP-468
Lindenberg, L. EP-0280
Linder, P. EP-0658
Lindman, H. OP-579
Lindner, S. EP-0024, EPS-237, OP-656
Ling, A. OP-304, OP-310
Ling, X. OP-048
Linguanti, F. **EP-0212**, EP-0273, EP-0330, EP-0546
Link, E. OP-037
Link, J. OP-556
Lira, S. EPS-122
Lireux, B. OP-806
Lirola, S. EPS-143
Liss, P. OP-579
Liu, B. **EP-0270**, **OP-847**
Liu, C. **EP-0231**, **EP-0521**, EP-0764, EP-0483 OP-244, EP-0814
Liu, D. **OP-144**
Liu, E.-T. **EP-0661**, **OP-571**
Liu, F. EPS-157, OP-226, EPS-155, EP-0038, EP-0039, OP-219, OP-361, **OP-705**
Liu, H. EP-0597, EP-0638, EP-0856
Liu, J. EP-0052, OP-059, OP-217, EPS-069, EP-0764, EP-0814
Liu, K. EPS-056, **EP-0820**
Liu, L. **EP-0178**, OP-556
Liu, M. EPS-004, EPS-006, **OP-303**, TEPS-020
Liu, N. **EP-0079**
Liu, Q. EPS-273, EP-0178, **OP-899**
Liu, R. **EP-0841**, OP-898
Liu, S. OP-509, EP-0737, EP-0155, EP-0689, EPS-182, EPS-258, OP-090, EP-0438, EPS-021, **EP-0038**, **EP-0039**
Liu, T. EP-0231, EPS-276, EPS-281, OP-618
Liu, V. EPS-120
Liu, X. OP-286, EP-0427, EP-0483
Liu, Y. EP-0803, EP-0817, EPS-118, EP-0782, **EP-0837**, EP-0852, EP-0861, OP-704, EPS-273, EP-0177, EP-0668, **EP-0838**
Liu, Z. EP-0838, OP-435
Liubchenko, G. EPS-237, **OP-839**
Lizak, C. **OP-897**
Lizarraga, A. OP-046
Ljungberg, M. EP-0680, OP-296, OP-623
Llabrés, M. EPS-143
Llinares, E. EP-0109
Lo, T. OP-359
Lo, W.-L. **EP-0029**
Loaiza Gongora, J. EP-0318
Loap, P. EPS-017
Lobeek, D. OP-029, OP-628
Lobo, D. S. EP-0961, EP-0971
Lo Bue, R. EPS-206
Locantore, L. **EP-0908**
Lococo, F. EPS-272
Lodi, F. EP-0147
Loening, A. OP-504
Loeuille, D. OP-250
Loewenthal, C. EP-0086, OP-536, EP-0965
Loft, M. **EP-0195**
Loftenius, A. EP-0837, OP-578
Loft Jakobsen, A. EP-0318
Loggia, M. L. OP-846
Löhr, M. EP-0156
Lohrasbi, E. EP-1016
Loirat, D. EPS-017
Loke, K. **EP-0616**
Lolli, C. OP-723
Lombard, A. EP-0894
Lombardo, A. EP-0212
Lomi, N. EP-0096
Loncar-Turukalo, T. EP-0998
Løndalen, A. OP-831, EPS-188
Long, X. EPS-283

Long, Y. OP-143, OP-700
Longari, V. EP-0763, OP-540
Longhi, S. EP-0681
Lonsdale, M. EPS-163, OP-385, **OP-384**
Lööw, T. OP-808
Lopci, E. **EP-0272**, EP-0915, **OP-039**, **OP-052**
Lopes, F. EP-0569, OP-539
Lopes, L. **OP-710**
Lopes, P. EP-0965
Lopes, R. EP-0006
Lopes-Martin, V. EPS-025, EPS-026
Lopes-Santos, L. E. EP-0929, EPS-061, EPS-062
Lopez, B. P. EPS-234, OP-851
Lopez Cano, A. EP-0400
López Llobet, E. EP-0127, EP-0365, **EP-0502**
Lopez Martinez, C. TEPS-018
Lopez Medina, A. OP-498
López Méndez, A. EP-0367
Lopez Perez, R. EPS-210
López Puche, S. EPS-052, **OP-787**
López-Urdaneta, J. EP-0318
López Villar, I. **EP-0352**
Lopo, I. EP-0165, **EP-0395**
Lorand-Metze, I. EP-0345
Loree, J. M. EP-0201
Lorenzo-Bosquet, C. EP-0632
Lorenzoni, A. OP-674
Lorubbio, C. EP-0236
Losa, M. OP-455
Lothmann, J. OP-107
Lotsholm Persson, H. EPS-067
Louis, B. **EP-0037**
Loureiro, L. OP-357
Lourenco, J. OP-768
Lovibond, S. OP-702
Low, H. EP-0616
Lowe, K. OP-393, OP-530
Lozada, F. EPS-070, EPS-203
Lozano-Borbalas, A. OP-784
Lozano-Pérez, A. A. EP-0864
Lu, A. C. EP-0029
Lu, C. EP-0003, EP-0803
Lu, J. EP-0080, OP-710, EP-0091, EP-0307, EPS-146, EPS-166, OP-643, OP-863
Lu, N. EP-0133, EPS-209, **OP-164**
Lu, X. OP-697
Lu, Y. **EP-0456**, EP-0638, EP-0648, EP-0841
Lu, Z. EPS-276, EP-0782
Lubas, A. OP-807
Lubberink, M. EPS-140, OP-240, OP-387, **OP-388**, OP-458, OP-459, OP-579
Lub-de Hooge, M. N. EP-0877
Lubin, D. J. EP-0538
Lucas Lucas, C. **EP-0229**, EP-0250, EP-0496, EP-0562, EPS-050, EPS-259, EPS-268, OP-638
Lucena Sampaio, I. EP-0979, OP-539, EP-0246, EP-0569, OP-469, OP-472, OP-473
Lucero, M. M. EPS-227
Lucia, F. OP-855
Lucic, M. A. EP-0312
Lucic, S. **EP-0312**
Lucidi Pressanti, G. EPS-085
Lúcio, P. EP-0328
Lücke, J. OP-779
Lückerath, K. EPS-118
Lüdde, T. OP-937
Ludgate, S. EP-0787
Ludwig, R. C. OP-018
Ludwiga, D. OP-514
Lue, K.-H. EP-0689, **EPS-182**, **EPS-258**, OP-090
Lueckerath, K. EP-0037
Luelmo, S. A. C. EP-0274
Lughezzani, G. EP-0272, OP-039
Lugtenburg, P. OP-102
Luining, W. **EPS-105**, EP-0757
Lukose, T. EP-0734, OP-299
Lundmark, F. EPS-218
Lundsten Salomonsson, S. OP-766
Luo, N. Y. EPS-274
Luo, W. OP-164
Luo, X. **OP-396**
Luo, Y. OP-789
Luo, Z. OP-156
Luong, T. V. OP-862
Lupinacci, F. EP-0345
Luporsi, M. **OP-311**, OP-637, TEPS-004
Luquin, M. OP-460
Lusque, A. OP-654
Luster, M. OP-562
Lutz, F. EP-0539
Lützen, U. EP-0007, EP-0860
Luurtsema, G. EP-0020, EP-0692, EP-0877
Luzzago, S. OP-038
Lv, X. OP-143, **OP-216**
Lv, Y. EP-0648
Lyashchenko, S. K. EPS-016, OP-802
Lybaert, W. EP-0196
Lyburn, I. D. EP-0753
Lyer, R. OP-676
Lythgoe, M. EP-0090
Lyu, Z. OP-571

Ma, D. **EP-0217**, **EP-0724**
Ma, J. **EP-0084**, EP-0307, EP-0737
Ma, K. OP-672
Ma, L. EP-0138
Ma, M. EP-0042
Ma, P. EP-0157
Ma, T. EPS-194
Ma, W. **EP-0267**, EP-0598
Ma, X. EP-0737, **EPS-281**, **OP-618**, OP-219, OP-361, EP-0157, OP-713, EP-0187
Ma, Y. EPS-166
Maaloul, M. EP-0387, EP-0972, EP-0990
Maas, H. EP-0383
Maaz, R. EP-0206, EP-0672, OP-292
MacAskill, M. G. OP-289
Maccauro, M. EP-0068, OP-234, OP-674
Maccora, D. EPS-232, **OP-581**
Machado, M. EP-0769
Mackenzie, J. EP-0836
Macula, A. **EP-0700**, **EP-0749**
Madar, O. EP-0694, EP-0875
Maddahi, J. OP-389
Madeddu, G. EP-0294
Madra, W. EPS-071
Madru, R. **OP-623**
Madsen, M. A. OP-730
Madsen, S. OP-862
Maebe, J. OP-568
Maekawa, Y. EP-0452
Maertens, D. EP-0869
Maes, A. EP-0183, OP-574
Maestre-Cutillas, R. **EP-0559**, EP-1013, EPS-023, EPS-025, EPS-026
Maffei, D. EP-0272, OP-039
Maffioli, L. EP-0921, EP-0980
Magalhães, A. EPS-094
Magnani, F. OP-585
Magnani, P. EP-0202
Mahajan, H. OP-927
Mahapane, J. OP-574
Mahida, B. **OP-513**
Mahmoud, H. EP-0051
Mahvash, A. EPS-234, OP-851
Maiello, C. OP-383
Maier, M. OP-557
Maigne, L. EPS-236
Mailliez, A. EP-0117
Maina, T. EP-0041, EPS-217
Mainolfi, C. OP-647
Mainta, K. EP-0765
Maintas, D. EP-0765

Maiocchi, A. EP-0012
Maiolo, E. EP-0335, EP-0337
Maisto, C. EP-0550, EP-0575, EP-0781, EP-0819, EP-0879, EP-0886
Maitra, S. **EP-0366**
Majithiya, J. OP-764
Mak, Y. X. OP-627
Makazlieva, T. EP-0992
Maker, M. OP-222
Malasani, V. **EP-0370**
Malaspina, S. EP-0659
Malbert, C. H. **EP-0066**
Maldonado, A. EP-0494
Maldonado Morillo, A. EP-0964
Maldonado Suarez, A. EP-0393
Maleki, E. EP-1010, EP-1016
Malicet, C. OP-213
Malik, D. **OP-673**, OP-786
Malik, N. OP-793
Malinowski, K. OP-641
Malizia, C. EP-0213, EP-0215, EP-0354
Malizia, G. EP-1028
Mallaev, M. OP-297
Malmbeck, R. OP-024
Malo, M. E. EP-0834, EP-0846, EPS-212
Malorgio, A. EP-0273
Malpetti, M. OP-110
Maltseva, A. EP-0436, EP-0446, EP-0448, EP-0457, EP-0458, EP-0477, OP-645, OP-724
Mamach, M. EP-0082, OP-779
Mamat, C. EP-0849, OP-020
Mamlins, E. EP-0072, **OP-512**, OP-560, OP-937
Mammadkhanli, Z. **EP-0541**, **EP-0563**
Mammadli, K. **EP-0578**
Mammatas, L. H. EPS-019
Mammucci, P. **EP-0258**, EP-0509
Mampuya, W. EP-0499
Mancini Terracciano, C. EP-0783
Manetou, A. EP-0568
Manevska, N. **EP-0992**
Manfredi, M. EP-0784
Manfredi, S. OP-160
Mangano, M. EP-0980
Mango, G. **EP-0162**, EP-0188
Manhas, V. EPS-055
Manikandan, M. EP-0180
Manishi, L. N. EP-0449
Maniyankerikalam, I. OP-617
Mannarino, T. OP-382, **OP-383**
Mannheim, J. EP-0658, **OP-077**, OP-567
Manni, C. EP-0623, **OP-395**
Manou, E. EP-1014
Manser, S. OP-239
Mansi, R. EPS-291, OP-430, OP-614
Mansour, A. EPS-082
Mantovani, D. B. A. **OP-843**
Manyalich-Blasi, M. EP-0491
Manz, N. OP-239
Manzarbeitia Arroba, B. EP-0300, EP-0526, **EP-0604**, **EP-0605**, EP-0964
Mao, W. EP-0637, EPS-091
Mao, Y. EP-0750
Mapanao, A. K. EP-0070
Mapelli, P. EP-0202, EP-0285, OP-505
Marañ, F. EP-0260, OP-935, TEPS-005
Maraña González, J. EP-0306
Marchal, E. OP-845
Marchetti, G. EPS-037
Marchianò, A. OP-234
Marciano, A. **OP-171**
Marcoval-Caus, J. EPS-265
Marcuseanu, A. **EP-0956**
Marec-Berard, P. OP-056
Marek, K. OP-108
Marengo, M. **EP-0762**, EPS-087
Margaritora, S. EPS-272
Marí, R. EPS-143
Maricich, S. OP-793
Marie, P.-Y. EP-0758, EPS-008, EPS-240, OP-250
Marie, S. EP-0674
Marin, A. C. EP-0302
Marin, C. OP-232, OP-238, OP-367, OP-444, OP-629
Marin, G. OP-232, OP-238
Marin, I. OP-925
Marin, T. OP-917
Marín Ferrer, M. EP-0418
Marini, C. EP-0277, EP-0898
Marini, I. EP-0238, EP-0613, **OP-723**
Mariniello, P. OP-764
Marino Cosentino, L. M. EP-0404
Mariño Méndez, A. OP-233
Marinus, A. EP-0716, EPS-100
Marion, J.-M. EPS-184, OP-092
Maris, L. **EP-0115**
Marizzoni, M. OP-104
Mark, P. **OP-729**
Marketou, M. OP-859
Markiewicz, P. OP-025
Markus, M. **EP-0311**, **EPS-208**
Marner, L. EPS-163, **EPS-163**, OP-385, **OP-385**, OP-729
Marnitz, S. EP-0154
Marongiu, A. **EP-0294**
Maronnier, Q. **EP-0647**, **EPS-089**
Marques, A. **EP-0291**, EP-0978
Marques, I. A. EPS-211
Marques da Silva, A. EP-0020, OP-843
Marques Ferreira, M. EP-0008
Marquié, M. OP-103
Marquis, A. EP-0396
Marra, C. EPS-153
Marra, G. EP-0396
Marsh, I. OP-149, **OP-393**, OP-530
Marshall, C. OP-089
Marsico, R. EP-0404
Martarello, L. OP-563
Martí-Andrés, G. **OP-460**
Martí-Bonmatí, L. EP-0800, EPS-096
Martí-Climent, J. EPS-011, EPS-095
Martin, C. OP-437
Martin, J. M. OP-037
Martin, L. D. OP-556
Martin, M. OP-307
Martin, N. EP-0132
Martina, S. **EPS-206**, **OP-194**, **OP-718**
Martin del Rey, A. EP-0508
Martineau, P. EP-0201
Martinelli, J. EP-0812, OP-487
Martinez, E. EP-0340
Martínez Albero, E. EP-0418
Martínez Amador, N. EP-0890, EP-0516
Martínez Arias, G. EP-0471
Martinez-Clark, P. OP-389
Martínez Lorca, A. EP-0504, OP-849
Martinez Lucio, T. S. OP-731, OP-732, OP-242, **OP-243**
Martinez Martí, A. EP-0148
Martínez Martínez, M. T. EP-0845, EP-0864
Martínez Ramos, C. EP-1007, EP-0101, EP-0473, EP-0942, EP-0954, EPS-048, EPS-049, EPS-154, OP-784
Martínez Rodríguez, I. EP-0890, **EP-0516**
Martínez-Sanchis, B. EPS-096
Martínez-Valle Torres, M. EP-0474, EP-0620
Martín Fernández, N. EP-0306
Martin Garcia, A. EP-0399, EP-0357
Martín Gil, J. EP-0494
Martín Gómez, E. OP-170
Martini, A. **OP-462**
Martini, P. EP-0709, TEPS-021
Martín-Liberal, J. J. EPS-265
Martín Lopez, A. EP-0357
Martín Marcuartu, J. EP-1007, EP-0248, EP-0547, EP-0211, **EP-0251**
Martins, B. **EP-0086**, EP-0704, **EP-0965**, **OP-536**
Martins, H. EP-0926
Martins, P. EP-0962

Martin-Vaello, R. OP-784
Marto, C. M. EP-0008
Maruszak, N. OP-641
Marvaso, G. EP-0236
Marwa, S. EP-0993
Marx, M. EP-0007
Marzi, C. OP-234
Marzo, K. EP-0272, OP-039
Marzullo, A. EP-0376, OP-535
Mascarin, M. OP-052
Maschio, C. EP-0017
Mascitti, L. OP-234
Maserumule, L. C. OP-574
Mashhadani, N. EPS-082
Masikane, S. EP-0643
Maslova, A. EP-0461
Masmejean, F. OP-895
Massa, F. OP-455
Massa, S. EPS-227
Massanes, F. EP-1024, TEPS-016, TEPS-017
Masse, M. **EP-0132**
Massollo, M. OP-315
Massone, F. OP-315
Master, V. OP-194
Masuda, A. EP-0452
Mataj, E. EP-0273
Mateescu, C. EP-0960
Matei, M. **EP-0949**, **EP-0960**, EP-0943, EP-0953, EP-0952
Matela, N. EPS-173
Mateos, M. EP-0356
Mateva, G. **EP-0268**, EP-0295
Mathieu, A. OP-495
Mathieu, S. OP-938
Mathoux, G. **EP-0316**, **OP-106**
Mathur, Y. EPS-111
Matías-Guiu, J. EPS-167
Matos, S. EP-0086, EP-0704
Matsubara, K. OP-631
Matsumoto, K. **EPS-088**
Matsunari, I. EP-0360
Matsuo, H. EP-0141, EPS-104
Matsuo, Y. EP-0476
Matsusaka, Y. EP-0360
Matsutomo, N. TEPS-015
Matsuura, K. EP-0110
Matsuyama, H. EP-0244
Mattana, F. **EP-0236**, EP-0389, EP-0543, EP-0681, EPS-107, **OP-668**, OP-669, **OP-854**, OP-915, OP-921
Matteini, M. EP-0212, EP-0546
Mattes-György, K. OP-937
Matteucci, F. EP-0238, EP-0613, OP-723
Matthews, J. C. EP-0684, EP-0720
Matthews, K. OP-660
Mattoli, M. V. OP-455
Mattoni, S. EP-0681
Mattsson, A. EP-0041, EPS-217
Mattsson, S. EP-0777, EP-0778
Mattucci, I. OP-383
Matusch, A. OP-107
Matzner, M. OP-897
Maucherat, B. OP-187
Maues, J. EP-0345
Mauguen, A. EP-0092, EP-0333, OP-802
Mauguen, M. OP-855
Maurer, A. OP-922
Maurer, C. OP-856
Maurer, J. EP-0060
Maurer, M. EP-0408
Maurer, T. EP-0391
Mauri, F. A. EP-0276
Maurya, S. **EP-1019**, EPS-060, EP-1020
Mauz-Koeholz, C. OP-052
Mavi, M. **EPS-202**
Mavrinac, M. EP-0292
Mavroeidi, I. A. EP-0607, OP-190, OP-932
Mavuduru, R. S. EPS-190
Mawlawi, O. EP-0645, OP-032
Mayerhoefer, M. E. EP-0092, EP-0197, EP-0333, EP-0335
Maymó Garrido, S. EP-0892, EPS-265
Mayr, Y. **OP-046**
Mazarei, R. OP-169
Mazilu, A. EP-0931
Mazilu, C. EP-0931, EP-0934, EP-0937, EP-0943, EP-0949, EP-0953, EP-0957, EP-0960
Mazilu, C. V. EP-0952
Mazur, M. EP-0018
Mazurek, A. EP-0478, OP-807
Mazza, R. EPS-085
Mazzaglia, S. OP-234
Mazzei, M. EPS-153
Mazzeo, C. OP-462
Mazziotti, G. OP-653
Mbaye, T. EP-0654
McBride, J. L. OP-556
McBride, K. M. OP-018
McDonald, A. OP-490
McDonald, M. M. EP-0558
McDonnell, K. OP-621
McDougall, L. EPS-291, OP-191
McFadden, J. J. EP-0684
McGowan, D. EPS-176, OP-227
McGrath, J. OP-078
McInstosh, L. EPS-172, OP-338, OP-437
McKinley, L. OP-030
McKinney, Y. EP-0280
McMeekin, H. EP-0636
McMorrow, R. OP-433
McQuaid, S. EP-0657, **EP-0662**, EP-0722
McVey, A. OP-338
M. Davarpanah OP-720
Mdlophane, A. H. EPS-046
Mechti, M. **EP-0756**
Meddeb, I. EP-0995, OP-945
Meddens, M. B. M. OP-295
Medema, J. TEPS-019
Medhurst, E. **EP-0555**, OP-437
Medici, S. EP-0755, OP-331
Medina Benito, A. EP-0340
Medina Guevara, Y. EP-0863
Meeker, R. OP-676
Meffe, G. EP-0793
Mehadji, B. EP-0794
Mehdi, E. EP-0833
Mehesen, M. **EPS-036**
Mehndiratta, M. EP-0370
Mehra, N. OP-339
Mehrabani, H. M. EP-1010, EP-1016
Mehranian, A. **EPS-176**, OP-227
Mehta, G. **EP-0731**
Mei, R. EP-0388, EPS-107, OP-534
Mei, W. EP-1011
Meijer, D. EPS-105, OP-339, OP-506
Meijer, R. EP-0486
Melendez-Alafort, L. EP-0009, EP-0011
Melhuish, T. EP-0797
Melki, S. **EPS-058**
Meller, B. **EP-0002**
Melone, S. EP-0550
Mena, D. **EP-0573**
Mena, E. EP-0280
Menard, A. OP-929
Ménard, L. EPS-246
Mendes, A. OP-058, OP-666
Mendi Barcina, V. **EP-0890**, EP-0516
Mendogni, P. EPS-272
Mendoza, N. EP-0034
Mendoza-Figueroa, M. EP-0895
Mendoza-Ibañez, O. I. OP-242, OP-243, **OP-731**, **OP-732**
Ménégaux, F. OP-805
Menelas, M. EP-1026
Menéndez, E. OP-432
Menendez-Sanchez, S. EP-0348, EP-0088, EP-0252, **EPS-011**,

OP-098, OP-507, OP-936
Meneses Navas, M. EP-0361, EPS-020, EPS-081
Meneses Soares, P. EP-0510, EP-0421, **EP-0761**
Menezes, L. OP-713, TEPS-018
Meng, H. OP-791
Meng, J. OP-646
Meng, X. OP-703, EP-0074, **EP-0642**, EPS-276, EP-0222
Meng, Z. OP-164
Menichini, M. OP-535
Menke - van der Houven van Oordt, C. W. EPS-195, OP-573, EP-0383, EPS-019
Mensi, S. EP-0512
Mera Carreiro, S. EPS-081
Meral, R. C. OP-391
Mercante, G. OP-653
Mercolli, L. EP-0801, EPS-244
Merenda, N. C. EP-0258
Merisaari, H. OP-247, **OP-365**
Merkens, H. EP-0829, EPS-223, OP-142, OP-431
Merkt, W. OP-518
Merkx, R. OP-194
Merlet, A. EP-0656
Mermans, J. EP-0869
Meshaw, R. OP-901
Messa, C. EP-0316
Messerschmidt, K. EPS-156
Messina, N. EP-0337
Mester, J. EP-0441
Meszaros, N. OP-369
Metrard, G. EP-0489
Metzenmacher, M. EP-0146
Meyer, A. **EP-0809**
Meyer, P. T. OP-771
Mezzanotte, L. OP-433
Mhanna, K. EP-0828
M. Herth, M. EP-1000
Mhiri, A. EP-0401, EP-0420, EP-0481, EP-0531, EP-0993, EP-0995, EPS-038, EPS-042, OP-945
Mhiri, C. EP-0993, OP-945
Mi, H. EP-0435, EPS-141, OP-287
Mi, Y. EPS-119
Miao, W. EP-0223, OP-378, OP-721
Miao, Y. EP-0649, EPS-192
Michael, M. EPS-010
Michalek, J. EP-0612, OP-857
Michalik, B. **EP-0408**
Michalis, L. EP-0423
Michalski, K. **EP-0182**, **EP-0552**, EPS-117, OP-291
Michaud, L. EP-0333
Michel, C. **OP-495**
Michel, E. EPS-015
Michielin, O. EP-0699
Michno, M. OP-798
Michopoulou, S. EP-0797
Midthun, R. OP-831
Miedema, I. H. C. EPS-195
Miet, S. **OP-187**
Miettinen, N. OP-184
Migliari, S. EP-0487, **EP-0813**
Migliorisi, C. EP-0921, EP-0980
Miguel, B. OP-233
Mihailescu, M. EP-0672
Mijatovic, D. EPS-264
Mijatovic, J. EP-0614
Mikalsen, L. G. OP-911
Mikell, J. EP-0688
Mikhaeel, N. OP-102
Mikó, Z. EP-0181
Mikolajczak, R. **EP-0870**, EP-1000, OP-306, OP-675
Milakovic, D. EP-0614
Milà López, M. EP-0759
Milan, E. **EP-0586**
Milan, L. OP-525
Milano, A. EPS-183
Mileva, M. **OP-232**, **OP-238**, **OP-573**
Milione, M. EP-0068, OP-234
Militaru, A. EP-0943, **EP-0952**
Miljuš, B. EPS-024
Millat Servent, S. EP-1007
Miller, C. **OP-442**
Miller, R. EP-0113
Millo, C. OP-304, OP-310
Mills, N. L. OP-289
Millul, J. **OP-430**, OP-614
Milosevic, A. OP-190, OP-580
Milot, L. OP-852
Milovanovic, J. EPS-254
Mimica Haasz, N. EP-0393
Min, J. OP-044, OP-943
Min, Y. OP-769
Minarik, D. EP-0219, EP-0454, EP-0468, EPS-033
Mincarelli, C. EP-0623
Mingels, C. OP-246, OP-516, OP-521, OP-636
Minguez, F. EP-0339, EP-0088, **EP-0348**, EP-0862, OP-098, OP-507, OP-936
Minoshima, S. EPS-152
Minosse, S. OP-780
Minoves, M. EP-0109
Minsky, D. M. EPS-171
Mintale, I. EP-0440
Miot-Noirault, E. OP-938
Mirabelli, R. **EP-0783**, OP-038, OP-294, OP-854
Mirando, D. M. OP-906
Mirgolbabaee, H. EP-0061
Mirkina, I. EPS-214, EPS-284
Mirshahvalad, S. EP-0501, **EP-0556**
Mirzaei, S. EP-0680
Miseo, L. **EPS-232**
Mishani, E. EPS-282
Mishiro, K. EP-0853, EP-0855
Mishkina, A. EP-0462, EP-0463, **EP-0626**, OP-864
Mishra, A. OP-188, **OP-926**
Missaoui, Z. EP-0512, **EP-0514**
Mistretta, F. A. OP-038
Miszczyk, M. EPS-107
Mitchell, C. OP-338
Mithun, S. EP-0731, EP-0789
Mititelu, L. EP-0931, EP-0937
Mititelu, M. EP-0934, EP-0937
Mititelu, R. EP-0931, EP-0943, EP-0949, EP-0953, EP-0957, EP-0960, EP-0952
Mititelu, T. EP-0931
Mitjavila Casanovas, M. EP-0148, EP-0245, EP-0421, EP-0510, EP-0761, **OP-233**, EP-0467
Mitoi, A. **EP-0943**, EP-0949, EP-0952, EP-0953, EP-0957
Mitra, A. EP-0043
Mitschke, J. OP-621
Mittal, B. EPS-190, OP-861, EPS-111
Mitterhauser, M. OP-648
Miwa, K. EP-0696, **EP-0715**, EP-1036, OP-177, OP-325, TEPS-010
Mix, M. EP-0775, EP-0941, OP-905
Miyaji, N. EP-0696, EP-0715, OP-177, **TEPS-010**
Miyake, K. **EP-0126**, EP-0897, EP-0111
Mizokami, A. EP-0244
Mizowaki, T. EP-0589
Mlynárčik, P. EP-0078
Moalosi, T. EP-0941
Mocňáková, M. EP-0490
Mocanu, A. EPS-040
Mochula, A. EP-0436, **EP-0446**, **EP-0448**, EP-0457, EP-0458, EP-0477, OP-645, OP-724
Mochula, O. EP-0446, EP-0448, EP-0463
Mock, J. OP-355, OP-356
Mocquot, F. EP-0719
Moelker, A. OP-670
Mogensen, A. W. EPS-106
Mohajer Shojai, T. EPS-067, OP-766
Mohamad, I. EPS-082
Mohamed, T. EP-0990
Mohamed Salem, L. EP-0407, EP-0419, EP-0579, EP-0924, EP-0925, EPS-269, OP-924
Mohammadi, A. OP-079

Mohammadpour-Ghazi, F. EP-0830
Mohammadzadeh, H. EP-0424
Mohanty, D. EP-0734
Mohnike, K. OP-575
Mohnike, W. OP-575
Mohr, P. **EP-0124**
Mok, G. **EP-0782**
Mokoala, K. **OP-574**
Mokri, M. OP-225, **OP-848**
Moldovan, R.-P. OP-558
Molinaro, L. EP-0396
Molkenboer-Kuenen, J. OP-358
Möller, H. EPS-156
Mollerach, A. EP-0573
Momose, M. EP-0476
Mona, C. EP-0037, OP-296, OP-434, EP-0850
Monachello Araujo, D. EP-0127, EP-0365, EP-0502
Monaci, A. **EP-0511**
Monaco, L. EP-0316
Mondala, P. OP-359
Monsef, A. EP-0690
Mont, L. EP-0109
Montalva Pastor, J. EP-0329
Monteiro, M. **EP-0239**
Monterrat, M. EPS-219
Montes fuentes, C. EP-0357, EP-0503
Montesinos González, S. EP-0302, EP-0611
Monti, M. OP-723
Montravers, F. EP-0948, OP-805
Moodie, K. EP-0406
Mooijer, M. P. J. EP-0805
Moon, D. OP-338
Moon, E. S. OP-432
Moon, J. EP-0128
Moore, M. EP-0612, OP-857
Mora, N. EPS-143
Moradi, F. EP-0278, **OP-026**, OP-504, OP-778, **OP-793**
Moradi, S. OP-706
Moradiellos Díez, F. EP-0393
Moraga-Amaro, R. **EP-0022**
Moraitis, A. EP-0391, EPS-238, **OP-301**, OP-330
Moral Cano, M. EP-0398
Moralidis, E. EP-0237, EP-1014
Moran, M. OP-898
Moran, S. OP-672
Moran, U. EP-0974
Mora-Porta, M. EP-0491
Mora-Ramirez, E. OP-438
Morawiec-Slawek, K. EP-0537
Morbelli, S. EP-0273, EP-0277, EPS-149, OP-050, OP-051, OP-455, EP-0898
More, S. EP-0269, EP-0530, OP-318, OP-884
Moreau, M. EPS-219
Moreau, P.-L. EP-0948
Moreci, A. M. EP-0131, EP-1028
Moreira, A. P. EP-0239
Moreira, R. **EP-0961**, **EP-0971**
Moreira Pires, M. EP-0105
Morelec, I. EPS-080
Morel-Thierry, A. OP-187
Morera, C. EPS-096
Moresco, R. M. EP-0685
Moretti, R. EP-0693, **EP-0793**
Morgan, T. E. F. OP-289
Morganti, S. EP-0783, OP-038, OP-294
Morgat, C. **EP-0035**, **EP-0780**, EP-0840, **OP-150**, OP-895
Morgenroth, A. EP-0060, EPS-229
Morgenstern, A. OP-719, OP-335
Mori, H. EP-1024, OP-284, OP-290
Morin, M.-A. **OP-236**
Morisco, A. EP-0575, EP-0781, **EP-0819**, EP-0879, EP-0886
Morizot, C. OP-250
Morland, D. EP-0191, EP-0335
Morley, N. OP-089
Mörnsjö Centofanti, F. OP-499
Morra, R. OP-639, OP-913
Morré, C. J. W. M. **OP-042**
Morris, E. **OP-496**
Morris, M. OP-340, **OP-672**
Morris, M. A. OP-194
Morrisa, V. OP-514
Morrone, M. F. EP-0681
Morschhauser, F. EP-0322, EPS-185
Morsink, N. C. EP-0069
Mortada, A. OP-586
Mortensen, A. **EPS-067**
Mortensen, J. EP-0195
Morzenti, S. EP-0685
Moscalu, M. EP-0375
Mosconi, C. EP-0213, EP-0215, OP-534
Mosin, D. EP-0653
Mosley, M. EP-0835
Moss, R. M. EP-0670
Mostafa, R. **EP-0051**
Mostafapour, S. **OP-503**
Mottaghy, F. M. EP-0060, EP-0716, EPS-100, EPS-229, EPS-278
Mou, L. TEPS-021
Mou, T. EP-0435, EPS-141, OP-287
Mouhieddine, T. EP-0351
Mouraeff, Y. EP-0883
Mousavi, H. OP-779
Moussa, E. EPS-036
Moustafa, H. EP-0102
Moustafa, S. **EP-0906**
Mozzetta, S. EPS-149
Mpalaris, V. EP-0237
M Prise, K. EP-1037
Mrad, K. EP-0420
M. Ribeiro, F. **EPS-094**
Mu, J. **EP-0289**
Mu, L. OP-492
Mu, W. OP-635
Mu, X. **EP-0265**, **EP-0373**, **EP-0374**, EP-0324
Muath, A. EP-0730
Mucientes Rasilla, J. EP-0148, EP-0761
Mudd, G. E. OP-621
Mudun, A. EP-0553
Mueller, C. OP-188, OP-302, OP-016
Mueller, F. OP-773
Mueller, N. OP-555
Muffatti, F. EP-0202
Muhlebner, A. OP-583
Muhsin Al-Alawi, H. EPS-159
Muin, D. EPS-125
Mulders, P. OP-194
Müller, C. OP-926, EP-0070, OP-080, **OP-492**
Muller, F. **OP-568**
Müller, F. H. H. OP-575
Müller, H.-W. EP-0072
Müller, J. OP-152
Müller, M. OP-615, EP-0610
Müller-Vahl, K. EPS-156
Multhoff, G. OP-487
Münch, J. OP-614
Munekane, M. EP-0853, EP-0855
Mungai, F. EP-0212, EP-0546
Muñoz, E. EPS-096
Muñoz del Diego, M. EP-0599
Muñoz Iglesias, J. OP-498
Munoz-Sanjuan, I. OP-556
Muntinghe, F. L. H. OP-860
Munuera Sañudo, C. EP-0892
Muraglia, L. EP-0236, **EP-0389**, EPS-107, OP-038
Murakami, T. EP-0141, EP-0308, EPS-104
Murat, T. OP-525
Murata, Y. EP-0854
Murialdo, A. OP-051
Muros De Fuentes, M. EP-0204, EP-0205, EP-0544
Murphy, D. OP-037, EPS-172, OP-338
Murray, I. OP-031
Murtas, F. EPS-232
Musarra, M. EP-0316

Muselaers, C. H. J. OP-339
Mushari, N. **EP-0733**
Musi, G. EP-0389, OP-038, OP-294
Mussalo, H. OP-728
Musso, E. EP-1028
Mussolin, L. OP-052
Mut, F. EP-0680
Mut Dolera, T. EP-0417
Mutevelizade, G. EP-0120, EP-0363, EP-0944, OP-934
Mutuleanu, M. EP-0206, EP-0672, EP-0464, OP-292
Muyu, W. **EP-0483**
Muzik, O. OP-567
Mysliwiec, J. EPS-071

Nabhani, S. EP-0998
Nachar, O. EP-0067
Nadal, C. EPS-143
Nadal, E. EP-0148
Nadaraja, S. **EP-0641**
Nader, M. EP-0146, EP-0607, OP-190, OP-380, OP-580
Nadig, V. **OP-773**
Nag, S. OP-563
Nagahara, T. EP-0887, **OP-182**
Nagai, T. OP-777
Nagao, M. **EP-0466**, EP-0476
Nagaoka, R. EP-0625
Nagarajah, J. OP-220, OP-339
Nagy, F. OP-369
Nagy, S. EP-0181
Nahar, A. OP-193
Nahimi, A. EP-0454
Naicker, T. EPS-046
Naik, M. **EP-0495**, EP-0832
Nail, V. EP-0067
Naili, Q. EP-0534, OP-630
Nair S, A. **EP-0313**
Naka, K. EP-0423
Nakajima, K. EP-0244, EP-0450, EP-1022, EP-1024, **OP-245**, OP-781, TEPS-016, TEPS-017
Nakako, T. OP-561
Nakamoto, R. EP-0111, **EP-0310**
Nakamoto, Y. EP-0111, EP-0126, EP-0310, EP-0897, EPS-262
Nakamura, K. EP-0589
Nakamura, M. OP-561
Nakao, R. EP-0476
Nakashima, R. EP-0589
Nakata, T. OP-245
Nakayama, T. OP-561
Nakuz, T. OP-713
Nalesnik, E. EP-0448
Nam, K. **TEPS-014**
Namazova, A. **EP-0983**, **OP-165**, OP-944
Nambiar, D. EPS-286
Namer, I. EPS-090
Namías, M. **EPS-165**, **EPS-171**, **OP-224**
Namvar, L. EP-0910
Nan, N. EPS-141
Nanni, C. EP-0147, EP-0354, OP-534, OP-879, OP-881, OP-882
Napolitano, E. EP-0345
Nappi, A. G. OP-447
Nappi, C. EP-0551, EP-0606, EPS-065, OP-647
Naqiyyun, M. OP-835
Naranjo Sancho, S. EP-0306
Narayan, A. EP-0991
Narayan, M. **EP-0413**
Nardini, M. EP-0793
Nardo, L. EP-0191, EP-0335
Narita, K. EP-0651
Nasisi, E. OP-562
Nasr, C. EP-0401
Nassi, L. EP-0330
Nataf, V. EP-0719
Natali, F. EP-0147, OP-879
Nathanson, D. OP-434, EP-0850
Natwa, M. OP-193
Naula, J. EP-0969
Nautiyal, A. **EP-0797**
Navab, N. EP-0801, OP-707
Navaei Lavasani, S. OP-298, OP-300
Navales Mateu, I. EP-0252
Navarro, L. EP-1000, EPS-227
Navarro Fernadez, J. EP-0407, OP-924, EP-0419, EP-0579, EP-0925, EP-0924, EPS-269
Navarro Martínez, T. EP-0504, OP-849
Navas de la Cruz, M. EP-0417
Nawwar, A. **EP-0753**
Nayak, P. EP-0522
Nayak, T. **OP-703**
Nazari, A. OP-165
Nazari, M. A. OP-304, OP-310
Nazerani-Zemann, T. EP-0150, EP-0151
Ndlovu, H. OP-508, OP-574
Necsoiu, A. EP-0866
Neeson, L. **EPS-010**
Neeson, P. OP-338
Negi, M. EP-0413
Neglia, D. EPS-178
Nekolla, S. EP-0235, OP-497, EP-0655, OP-520, OP-707
Nelson, B. J. B. EP-0836
Nelwan, D. V. OP-588
Német, R. EP-0181
Neri, D. OP-355, OP-356
Nesari Javan, F. EP-0085, OP-523
Nespral, P. EPS-020, **EPS-167**, EP-0361, EPS-081
Nesterov, S. OP-842
Nestor, M. EPS-067, OP-766
Netti, S. OP-915
Neuber, C. **OP-357**
Neumaier, B. OP-107, OP-798
Neves, M. EP-0328
Neves, P. EP-0008
Newby, D. E. OP-289
Ng, C. EP-0616
Ng, K. EP-0080
Ng, P. EPS-223, OP-142, OP-431
NgokpoL, S. **EP-0872**
Nguyen, A. EP-0558, EPS-120
Nguyen, D. EPS-058
Nguyen, K. EP-0538
Nguyen, N. T. OP-769
Ni, R. **EP-0017**
Ni, Y. C. **OP-180**
Nicastro, N. OP-455
Nickols, N. OP-041
Nicocia, A. OP-392, OP-524, OP-801
Nicod, J.-M. EP-0698
Nicol, A. EP-0997, EP-1021, TEPS-013
Nicolai, E. EPS-065
Nicolanti, F. EP-0783
Nicolas, G. OP-191, OP-716
Nicolas, V. OP-187
Nicoletto, M. EP-1017, OP-323
Nicolini, S. EP-0613, OP-723
Nicoloso, V. EPS-037
Niculae, D. **EP-0866**, EP-1000
Niedbala, M. OP-589
Nielsen, R. OP-862
Niemczyk, S. OP-807
Nienhuis, H. L. A. OP-860
Nienhuis, P. OP-088, **OP-515**
Nieto Serrano, R. EP-0399
Niftaliyeva, X. EP-0190
Nigam, S. EP-0754
Niimi, T. **EPS-131**
Nijman, H. W. EP-0033
Nijsen, J. F. W. EP-0069, EPS-201, EPS-205, OP-029, OP-488, OP-627, EP-0061, OP-853
Nijsten, M. W. N. OP-252
Nikolaus, S. **EP-0072**, **EP-0073**, **OP-560**
Niksch, T. EP-0827
Nilsson, T. **EP-0156**
Nilubol, N. OP-304, OP-310

Ninatti, G. **EP-0285**, **EPS-161**
Niñerola-Baizan, A. EP-0356, EP-0491
Ning, J. **EP-0283**, OP-713
Ning, Y. EP-0527
Nioche, C. OP-311, OP-637, OP-917
Nishida, K. EPS-088
Nishimoto, K. EP-0244
Nishio, M. EP-0141, EPS-104
Nishiyama, T. **EP-1024**
Nishizawa, K. EP-0853
Nistri, F. EP-0586
Nitsche, C. OP-713
Nitta, N. OP-079
Nittbaur, B. EP-0451
Nitzsche, E. OP-716
Niyazi, M. OP-082, OP-467, OP-538, OP-584, OP-588
Niyogi, D. EP-0166
Noamen, H. **EP-0139**, **EP-0140**, **EP-0990**
Nobashi, T. EP-0111, EP-0310
Nock, B. A. EP-0041, EPS-217
Nogami, M. **EP-0141**, EP-0308, EPS-104
Nogueira, S. **EP-0935**
Nogueiras Alonso, J. M. OP-498
Nogueira Souto, D. EP-0471
Noll, C. EP-0499
Noncovich, A. OP-138
Nonne, G. OP-171
Nonnekens, J. OP-146
Noomen, H. EP-0387
Noordzij, M. A. OP-042
Noordzij, W. EPS-233, OP-339
Noortman, W. A. **OP-086**
Noponen, T. **EP-0627**, EP-0659, OP-529
Noppeney, R. OP-099
Norberg, P. OP-808
Noriega Álvarez, E. EP-0229, EP-0250, EP-0496, EP-0562, EPS-050, EPS-259, OP-638, EPS-268
Norman, E. OP-030
Norouzbeigi, N. EP-0266, EPS-159
Nosotti, M. EPS-272
Notohamiprodjo, S. **OP-520**
Notta, P. EP-0101, EPS-048, EP-0473, EP-0955, EP-0988, EPS-049, EPS-031
Nottage, M. OP-037
Nouira, M. EP-0514, EP-0994
Nousch, M. **EP-0888**, **EP-0889**
Novi, G. OP-051
Novicki, A. EPS-289
Novoselska, N. EP-0268, EP-0295
Novruzov, E. OP-937
Novruzov, F. **EP-0833**
Nový, Z. EP-0078, **EP-0048**
Nowak, A. OP-587
Nowak, M. EP-0968
Nowicka, E. OP-589
Nowicka, G. OP-231
Nowosinska, E. EP-0636
Numair Younis, M. **EP-0385**
Nummenmaa, L. OP-247, OP-365, OP-842
Nunes, P. EPS-015
Nunes, R. **EP-0946**
Nuñez Muñoz, R. EP-0599
Nuttens, V. **EP-0779**, OP-366, **OP-443**
Nuutila, P. OP-247, OP-365
Nuvoli, S. EP-0294
Nyakale, N. **EP-0183**, EP-0643
Nyholm, D. OP-458, OP-459
Nyiranshuti, L. OP-359

O, J. OP-044, OP-943
Oancea, M. EP-0931, EP-0943, EP-0953
Obedkova, I. **EP-0245**, EP-0421, EP-0467, EP-0510, EPS-051
Obeid, K. EP-0041, EPS-217
Obradović, L. EPS-278
O'Brien, J. OP-037, OP-338
Obušeková, A. OP-925
O'Byrne, K. OP-230
Ocak, M. OP-163, OP-375
Ochagavía Cámara, S. EPS-081
Ochman, P. EP-0298
Ochoa Figueroa, M. **OP-808**
Odagiri, H. EP-0711
Oddo, L. OP-780
Oddstig, J. EP-0219, EP-0468, EPS-033, OP-499
Oderda, M. EP-0226, EP-0249, EP-0396
O'Doherty, J. EPS-249
O'Donoghue, J. OP-802
Oezkan, F. EP-0146
Oflas, M. **EP-0553**
Ogawa, K. **EP-0853**, EP-0855, OP-284, OP-290
Ogawa, T. OP-777
Ogden, B. EP-0080
Oghina, S. OP-858
Ohno, K. **EP-0873**
Ohnona, J. OP-805
Ohshima, S. **OP-725**
Ohtani, A. TEPS-008
Oikonen, V. OP-842
Oishi, T. EP-0126
Okar, y. **EPS-047**
Okazawa, H. EP-0308
Öksüzoğlu, K. EP-0190
Okuda, K. **OP-781**
Okudan Tekin, B. EP-0218, **EP-0947**, **EP-0951**, **EP-0958**, **EP-0959**, **EP-0967**, OP-172
Okura, Y. OP-625
Olajos, M. **EP-0390**
Olariu, E. **EP-1005**
Olarte, M. A. **EP-0525**, EP-0194
Olczyk, T. EPS-013
Oldfield, C. EP-0720
Olianti, C. EP-0511
Oliinichenko, O. **EPS-032**
Olivas, C. EP-0800
Oliveira, A. EP-0415, EP-0416, EP-0927, EP-0963, OP-949
Oliveira, C. EP-0328
Oliveira, E. R. EPS-007
Oliveira, F. EP-0006, EP-0769, EPS-173, **OP-221**, EP-0328, EP-0738, OP-087
Oliveira, I. EP-0984, EP-0989
Oliveira, M. EPS-173
Oliveira, R. EP-0769
Oliver, P. EP-0025
Oliver-Caldes, A. EP-0356
Olivier, A. EP-0117
Oliviero, C. EP-0551
Olkowski, C. P. EPS-286
Ollero, M. EPS-070
Olsen, B. B. EPS-228
Olsson, B. EP-0219, OP-499, **TEPS-012**
Omar, Y. **EP-0880**, EPS-159, EPS-206
Onal, B. EP-0228, OP-035, OP-194
Ondrák, L. OP-017, OP-022
Ondrák Fialová, K. OP-017, OP-022
O'Neill, K. OP-590
O'Neill, E. EP-0847
Öner Tamam, M. EP-0119, EP-0185
Ones, T. EP-0190
Ong, C. OP-142
Ono, N. OP-247, OP-365
Onoe, H. **OP-561**
Onoguchi, M. EP-1018, EP-1022, EP-1024, TEPS-016, TEPS-017
Onur, Ö. OP-107
Ooe, K. OP-772
Oon, S. OP-338
Oosterwijk, E. OP-358
Opalinska, M. **EP-0209**, **EP-0537**, **OP-306**, **OP-641**, **OP-675**
Opar, P. OP-437
Opitz, M. EP-0137
Oprea-Lager, D. E. EP-0757, EPS-019, EPS-105, OP-339
Oral, A. EP-0909
Orbala, S. EP-0680

Orcutt, K. EPS-289
Orduña, M. OP-233, EP-0504, OP-849
Orendain Novoa, D. EP-0367
Orengo, S. OP-315
Orhon, P. EP-0687
Origlia, D. OP-916
Oriuchi, N. TEPS-010
Orlhac, F. OP-311, OP-637, OP-917
Orlova, A. EP-0041, EP-0807, EP-0837, EP-0852, EP-0861, EPS-217, **EPS-218**, EPS-220, OP-578, OP-704
Ormanci, A. **EPS-256**
Oroujeni, M. EP-0807, **EP-0852**, EP-0861, EPS-218, OP-578, **OP-704**
Orozco Cortés, J. **EP-0417**, EP-0585
Orrego, N. **EP-0611**, EP-0800, EP-0302
Orta, N. **EPS-143**
Ortac, U. F. EP-0314
Ortega Candil, A. EPS-020, EPS-081
Ortega Valle, A. EP-0526, EP-0604
Orth, M. OP-082
Ortiz-Berbel, D. EPS-049
Ortiz Cruz, E. EP-0365
Ortolan, N. EP-0273
Orucova, N. EP-0833
Orunesu, E. EP-0763
Orvieto, F. OP-703
Osaki, A. EP-0110
Osawa, A. EP-0935
Osele, A. EPS-149
Osellame, L. EP-0032
Osorio-Higa, K. EPS-049
Ossenkoppele, R. EPS-150, OP-109
Oster, C. OP-580
Oster, J. EP-0760
Østergård, L. L. OP-181, OP-500, OP-501, OP-502
Ostwal, V. EP-0216
O'Sullivan Coyne, G. OP-304
Oszlanszki, A. EP-1027
Othman, M. TEPS-002
Ott, K. **OP-616**, EPS-274
Otten, T. EP-0889
Otterbach, M. C. EP-0408
Otto, J. EP-0132
Otto, T. OP-468
Oturai, P. EP-0195
Ouachem, M. EP-0387, EP-0972
Oudot, A. EPS-219, OP-078
Oudoux, A. EP-0117
Ouro, A. EP-0023
Ouyang, W. OP-396
Oven, B. OP-375, OP-163
Owczarek, A. **EPS-097**
Oweida, A. EP-0045
Owers, E. **EPS-250**, EP-0561
Oyen, W. OP-573
Ozananar Sevinc, Y. EP-0434
Özbey, T. EP-0885
Özcan, P. EP-0168, EP-0192, EP-0304, OP-317
Ozcan, Z. EP-0434, EP-0909
Özçevik, H. EP-0119, EP-0185
Ozdal, A. EP-0225
Ozdemir, E. EP-0570, EP-0588, OP-914
Özdemir Günay, B. EP-0224, EP-0541, EP-0563
Özel-Yıldız, S. EP-0233
Özgen Kıratlı, P. EP-0347, OP-053, OP-055
Ozgur, H. OP-719
Özgüven, S. EP-0190
Ozhan, N. EP-0225
Özkan, E. EP-0349, EPS-116
Özkan, F. EP-0137
Ozkan, Z. EP-0553, EP-0377
Ozturk, M. EPS-116

Pabst, K. **EP-0607**, OP-525, OP-190, OP-380, OP-932
Pabstleben, N. EP-0573
Pacak, K. OP-304, OP-310
Paccagnella, A. EP-0681, OP-099
Pace, L. EP-0606, EPS-065
Pacella, S. EP-0915, **EP-0921**, **EP-0980**, EPS-272, OP-540
Płachcińska, A. OP-950
Pacheco, C. TEPS-018
Pacilio, M. EP-0783, EPS-232
Padilla, E. EP-0773
Padilla Bermejo, A. EP-0229, EP-0250, EP-0496, EP-0562, **EPS-050**, EPS-268
Padmanabhan, P. **EP-0080**
Padovan-Neto, F. E. EPS-062
Padovano, F. EPS-085
Paeng, J. EP-0186, EP-0536, EP-0583, OP-285
Paesmans, M. OP-573
Paez, D. EP-0680, EPS-087
Pafundi, P. C. OP-634
Pagan, M. EP-0404
Paganelli, G. OP-723
Pagano, F. OP-368
Pagano, M. EP-0999
Pahk, K. **EP-0075**, **EPS-144**
Pai, M. C. OP-180
Pai, W.-C. EP-0878
Pais, B. OP-230
Pajares Vinardell, M. EP-0242, EP-0557
Palanivelu, P. **EP-0332**
Palard, X. OP-160
Palard-Novello, X. **OP-566**, OP-930
Palau San Pedro, A. EPS-171
Palazzo, F. EP-0495
Palazzo, M. EP-0330
Palchan-Hazan, T. OP-033
Palermo, A. OP-585
Paliczka-Cieślik, E. EPS-013
Palleis, C. EP-0024
Palm, S. EP-1000
Palmedo, H. OP-575
Palmer, R. EPS-230
Palmieri, G. OP-913
Palmisano, A. OP-505
Palomar-Muñoz, A. EP-0101, **EP-0355**, EP-0939, EP-0942, EP-0970, EPS-031, EPS-049
Palonen, S. **OP-842**
Palucci, A. EP-0112, EPS-053
Palumbo, C. EP-0509
Pan, L. OP-450, **OP-564**, OP-919
Pan, T. **EP-0646**, EP-0679, **OP-032**
Panagiotou, Z. EP-0445
Panareo, S. EP-0273, OP-447
Panchal, S. EP-0731
Pandey, A. **EP-0717**, **EP-0718**
Pandey, U. EP-0043
Pandit, N. EP-0936, **EP-0608**, **OP-193**, OP-194, OP-834
Pandya, K. OP-289
Panfilov, D. EP-0480
Pang, H. OP-899
Pang, Y. EP-0167, OP-374, **OP-427**
Paniagua Correa, C. EP-0300, **EP-0526**, EP-0605
Panico, M. OP-382, OP-383, OP-913
Panin, V. EPS-126, **OP-569**
Panizo, M. EP-0348, OP-098
Panperee, P. OP-662
Pantuck, A. J. OP-194
Pantzou, V. EP-1012
Panza, L. EPS-288
Panzer, M. EP-0824
Paolani, G. EP-0796, **OP-780**
Paolino, A. EP-0025
Papa, S. EP-0700, EP-0749, EP-1004
Papadaki, E. EP-0193, EPS-083
Papadopoulos, A. EP-0445, EP-0422
Papadopoulos, N. EPS-136, OP-542
Papanastasiou, E. EP-0938, EPS-136, OP-542
Papathanassiou, D. OP-160
Papavramidis, T. OP-542
Paphiti, M. EP-0071, EP-0568
Papi, S. EP-0540, EP-0543, OP-669

Papo, N. OP-901
Papp, L. EP-0283, OP-093, **OP-706**, OP-709
Pappas, K. EP-0445
Paquet, E. EP-0729, EPS-247, OP-056
Para, M. OP-513
Paradossi, G. OP-780
Parafita, R. EP-0769
Paraïso, P. **EP-0050**, EP-0065
Pardini, M. OP-051, OP-455
Pardo-Moreno, P. EP-0580
Paredes Rodríguez, P. EP-0504, OP-849
Pareja, F. EP-0034, EP-0088, EP-0859, EPS-095, OP-507, OP-936
Pareja del Rio, F. EP-0348, **EP-0862**
Parhizkar, S. OP-110
Parida, G. EP-0158, EPS-044, **OP-649**, EP-0522
Park, B.-N. **EP-0839**
Park, E. **EPS-152**
Park, H. EPS-168
Park, J. OP-019, OP-793, **EP-0128**, OP-049
Park, K. OP-049, EP-0390
Park, P. EP-0794
Park, S. EP-0128, OP-179, EP-0823
Park, W.-H. E. EP-0090
Parkes, L. M. EP-0684, EP-0720
Parlak, Y. EP-0120, EP-0885
Parıldar, M. EP-0578
Parra Rina, M. EP-0471
Partelli, S. EP-0202
Part-Lopez, M. EP-0611
Parulekar, W. R. EPS-115, OP-715
parwan, d. EP-0370
Pascal, P. OP-804
Pascali, C. EP-0010
Pascual, T. EPS-087
Pascual Pascual, V. EP-0523, EP-0766, EP-0767
Pasek, J. EP-0383
Pashazadeh, A. EP-0666, EPS-086
Pasini, L. EP-0272, OP-039
Paslawski, W. OP-562
Passera, R. EP-0226, EP-0249
Passos-Coelho, J. L. EP-0965
Pastor, J. EP-0241
Pastrana-Ledesma, M. EP-0467
Patel, C. EP-0717, EPS-170, **EPS-181**
Patel, K. OP-713
Patel, M. EP-0643, OP-304, OP-310
Patel, N. EPS-206, OP-718
Patel, S. **OP-880**, EPS-289
Patel, T. EP-0612, OP-857
Pathak, J. EP-0096, EP-0368
Pathmanandavel, S. EP-0558
Pathmaraj, K. EPS-087
Patrianakos, A. OP-859
Patrianesha, B. EP-0786, **OP-835**
Patrick Connelly, J. EP-0686
Patro, P. S. EP-0522
Patro, S. EP-0158, EPS-044, OP-649
Patsch, T. OP-081
Patt, M. EPS-156, OP-108
Patteson, J. OP-703
Pałucki, J. OP-231
Paula, A. B. EP-0008
Paula Santos, A. OP-472
Paulmier, B. EP-0719
Pauwels, E. EP-0196
Pawlak, D. EP-0870
Pávics, L. EP-0181
Payan, N. **EPS-123**
Paycha, F. EP-0930, EP-0948, OP-947, OP-948
Payne, R. OP-770, OP-896
Pedersen, A. E. EP-1030
Pedersen, L. K. EPS-160
Pedersen, M. R. EP-0713
Pedraza, S. EP-0340
Peeken, J. C. OP-337
Pehlivanoglu, H. OP-658
Pei, H. EP-0737
Pelka, K. **OP-587**
Pellegrino, S. **OP-639**, **OP-913**, **OP-916**
Pellerito, R. EP-0784, OP-910
Pelletier-Galarneau, M. OP-389
Peña, A. **EP-0599**
Peña, C. EPS-143
Pena, E. EP-0339
Peña, Q. EPS-229
Peñaherrera Cepeda, A. C. EP-0386, **EP-0254**, EP-0503, **OP-170**
Pena Pardo, F. EP-0250, EP-0229, EP-0496, EPS-050, EP-0562, EPS-268
Peña Quián, Y. **EP-0482**
Pencheva, R. EP-0513
pendharkar, d. EP-0370
Peng, C. EP-0815, EP-0055
Peng, X. OP-789
Peng, Y. OP-714
Penín-Mosquera, R. M. EPS-265
Pentlow, K. OP-802
Peñuelas, I. EP-0034, EP-0859, EP-0862, EPS-095
Perales, M.-A. EP-0333
Peralta, O. EP-0573
Perani, D. OP-045, OP-462
Pereira, B. **EP-0415**, **EP-0416**, **EP-0927**, **EP-0963**
Pereira, L. EP-0345
Pereira-Cubillo, J. **OP-438**
Peretti, D. **OP-104**, OP-106
Pérez, A. EPS-143
Pérez, L. EP-0482
Perez, T. EPS-249
Pérez-Arroyo, B. EP-0494
Pérez Avila, M. **EP-0628**, EP-1032
Pérez Beteta, J. EP-0229, EPS-259, OP-638
Pérez Díaz, I. EP-0194
Perez Fernandez, S. EP-0599
Perez-Garcia, V. M. EPS-259, OP-638
Pérez Gómez, M. EP-0702
Peréz Gracia, J. OP-507
Pérez Iruela, J.-A. EP-1013, EP-0559, EPS-023, EPS-025, EPS-026
Pérez Lago, M. EP-0795, EP-0688
Pérez López, B. EP-0455, EP-0475, EP-0529, EPS-043
Pérez-Martínez, E. OP-103
Perfetto, F. EP-0469
Peric, J. **EP-0916**, TEPS-006
Périé, S. OP-805
Perk, T. G. EP-0113
Perlaza-Jiménez, M. EP-0299, EP-0211
Perlaza-Jiménez, P. EPS-048, OP-784
Perlman, S. OP-676
Perneczky, R. EPS-148
Perotti, G. EP-0793
Perovnik, M. EPS-165
Perrio, C. OP-100
Perrone, A. EP-0511
Perrone, E. EP-0693, **EPS-153**, OP-456, OP-634
Pesaresi, F. OP-456
Peschechera, R. EP-0272, OP-039
Pessina, F. EPS-161
Pestean, I. **EP-1031**
Peter, A. EP-0312
Peter, J. **EP-0667**
Peters, S. M. OP-318
Peter Seiffert, A. EP-0340
Peterson, A. **OP-436**, **OP-906**, OP-439
Petinatti, A. M. S. EP-0935
Petitot, C. **EPS-219**
Petrakiev, L. EP-0513
Petralia, G. OP-915, OP-921
Petranović Ovčariček, P. OP-392, OP-525
Petretta, M. OP-647
Petric, P. EPS-251
Petrik, M. EP-0048, EPS-280
Petrikis, P. EP-0445
Petroiu, C. EP-0672, OP-292

Petrov, N. OP-453
Petrovic, J. EPS-002, **EPS-254**
Petrovic, N. EPS-002
Petry, V. EP-0874
Pettersson, D. EPS-230
Pettinato, C. **EP-0763**
Peynircioğlu, B. EP-0577, EPS-202
Pfob, C. EP-0565, OP-334, EP-0451, OP-655, OP-856
Phannajit, J. OP-841
Philippe, C. EP-0532, OP-081
Philippe, L. **EP-0433**
Phillips, E. **OP-541**
Phillips, W. EP-0612, **OP-857**
Phoenix, S. EP-0499
Phromphao, B. OP-841
Phulia, A. **OP-923**
Piacenti, V. OP-703
Piana Bezaury, A. EP-0194
Piatkova, Y. **OP-454**
Piatkowski, C. EP-0876
Picazo-Pineda, F. OP-642
Piccardo, A. OP-052, OP-315
Piccart-Gebhart, M. OP-573
Picchio, M. EP-0202, EP-0285, OP-505
Picciotto, V. EP-1028
Pichler, B. EP-0658, OP-314
Piciu, D. EP-1005, EP-1031
Picori, L. OP-585
Picot-Dilly, E. OP-187
Pierce, I. OP-713
Pietrzak, A. OP-157
Pietzsch, H. J. EP-0849, OP-020
Pihl, V. EPS-208
Pijls, B. G. EP-0848
Pijnenburg, Y. EPS-150, OP-109
Pike, A. OP-555
Pilatis, E. OP-432
Pillarsetty, N. V. K. OP-802, OP-770, OP-896
Pillay, J. OP-252
Pinaquy, J.-B. OP-160
Piñar, A. EPS-143
Pinato, D. J. EP-0090
Pin-Barre, C. EP-0067
Pinchuk, A. EP-0863, EP-0891
Pineda, J. EPS-070
Pineda Fernández, E. EP-0892
Piñeiro, A. **EP-0517**, OP-233, **EP-0410**, EP-0114
Piñero Fernandez-Reyes, M. EP-0242, EP-0557
Piñerúa-Gonsálves, J. EPS-043
Pini, C. EP-0285, **OP-653**
Pinot, F. OP-855
Pinot, L. EPS-246
Pintão, S. EP-0978
Pinto, A. EPS-094
Pinto, C. EP-0999, EP-0704
Pinto, M. V. EP-0008
Piraccini, B. OP-474
Pirayesh Islamian, J. EP-0735, EP-0752
Pirazzo Teixeira, E. EPS-077
Pires, M. OP-567
Pires Lourenço, A. **EP-0008**, **EPS-211**
Pirich, C. EP-0501, EP-0556, OP-446
Piriou, N. OP-858
Pirnat, E. EP-0619
Pirozzi Palmese, V. EP-0781
Pirro, V. EP-0784
Pisa, E. EP-0389, OP-668, OP-854
Piscitello, D. OP-764
Piscopo, L. EP-0551, **EP-0606**, EPS-065
Pistone, D. EPS-093, **OP-912**
Pitella, F. A. EP-0732, EP-0929, EPS-061
Pitombeira, M. S. OP-843
Pizzichemi, M. OP-368
Pizzoferro, M. EPS-037
Pizzuti, L. OP-581
Pizzuto, D. **EP-0337**, **OP-456**
Plachcinska, A. EP-0432, EP-0703, EPS-097
Placidi, L. EP-0793
Plaha, S. EP-0286, EP-0867
Plakhotina, N. EP-0394
Plancha Mansanet, C. EP-0417
Planchard, D. EPS-260
Plat, A. EP-0033
Platsch, G. OP-774, OP-838
Plaza de las Heras, I. EP-0169, EP-0255
Plenteda, C. OP-881
Plevritaki, A. OP-859
Pliakos, I. OP-542
Plotnikov, E. OP-704
Poblete García, V. EP-0229, EPS-050, EP-0250, EP-0496, EP-0562
Pocha, O. OP-336
Poiesz, T. W. T. EP-0877
Poinot, H. EP-0053
Polat, B. EP-0610
Polikarpov, S. EPS-139
Polito, C. EPS-037
Polčová, I. OP-925
Polson, L. EPS-242, **OP-626**
Pombo Antunes, A. EPS-227
Pombo López, M. EP-0890, EP-0516
Pommier, A. EP-0053
Pommranz, C. **EP-0658**
Ponce-Aix, S. EPS-260
Poniger, S. OP-490
Ponnala, S. OP-494
Pons, J. EPS-143
Ponsard, B. OP-141
Ponsiglione, A. OP-647
Pontoglio, M. OP-148
Pool, M. EP-0788
Poot, D. H. J. EP-0100
Popa, A. EP-0866
Popov, S. EP-0462, EP-0626, OP-864
Popper, M. EP-0078
Porcaro, F. EP-0985
Porcelli, C. OP-491
Porfidia, V. EP-0550, EP-0575, EP-0781, EP-0879, EP-1034
Poriz, V. EPS-084
Port, M. EPS-235, OP-152
Portal, C. **EP-0844**, EPS-292
Portilla Merino, P. EP-0365, **EP-0127**, EP-0502
Portugal, L. F. EP-0364
Posner, M. EP-0950, EPS-257, OP-788
Potard, G. OP-806
Pottakkat, B. OP-161
Poulie, C. B. M. OP-615
Poutiainen, P. EP-1002
Poza, M. EP-0340
Pozo Kreilinger, J. EP-0365
Pozzi, F. E. EP-0685
Pozzo, L. EP-1006
Prabhash, K. EP-0166
Pradeep, P. EP-0449
Pradier, O. OP-855
Prado Wohlwend, S. EP-0302, EP-0611, EP-0800, EPS-096
Prakken, N. OP-241
Pramesh, C. EP-0166
Prasad, K. EP-0608
Prasad, S. EP-1008
Prasad, V. EP-0560
Prata, A. EP-0966
Prates, B. **EP-1006**
Prawira, A. OP-230
Precht, H. EP-1030
Prescott, E. OP-385, OP-729
Presles, B. EP-0656
Presotto, L. OP-045, OP-462
Preussig, M. **OP-162**
Previti, S. EP-0035, OP-895
Prevo, R. OP-764
Prevrhal, S. OP-025
Pridhivi, B. EP-0991

Prieto, E. EP-0348, EPS-011, EPS-095, OP-460
Prieto, J. EP-0025
Prieto Canalejo, M. A. EPS-171
Prieto-Peña, D. EP-0516
Prieto Soriano, A. EP-0245, EP-0421, EP-0510
Prignon, A. EP-0844, **EPS-292**
Prins, M. OP-928
Prior, J. EP-0688, EP-0699, EP-0755, OP-153, OP-331
Prisco, A. EP-1034
Prisco, M. EP-0985
Prisco, S. E. **EP-0681**
Pritchard, D. **EP-0893**
Privé, B. **OP-339**
Prodanov, T. OP-304, OP-310
Promteangtrong, C. EPS-109, OP-662
Prosch, H. OP-648
Prosotsianiotis, N. EP-0982
Próspero, I. **EP-0246**, EP-0472, EP-0569, EP-0962, EP-0979, **OP-469**, OP-472, **OP-473**, OP-539
Provencio Pulla, M. EP-0148
Providência, L. EP-0124, OP-364
Provost, C. **EP-0694**, EP-0875
Pruis, I. J. EPS-253
Prunier-Aesch, C. EP-0433
Pruzynski, M. EP-1000
Pryds, K. OP-862
Psimadas, D. EP-0682
Pubul, V. OP-233
Pucci, N. OP-780
Puccini, B. EP-0330
Puchol Tarazona, A. **EPS-214**, EPS-284
Pudis, M. EP-0211, EP-0248, EP-0299, **EP-0473**, **EP-0547**, **EP-0939**, **EP-0942**, **EP-0954**, EP-0955, EP-0970, **EP-0988**, EP-1007, EPS-031, EPS-048, EPS-049, **EPS-154**, EPS-265
Pujatti, P. B. EPS-007, OP-471
Pulizzi, S. EP-0131
Pullen, L. C. E. OP-086
Püllen, L. OP-301
Purandare, N. EP-0159, EP-0166, EP-0207, EP-0216, EP-0313, EP-0731
Puranik, A. EP-0159, EP-0166, EP-0207, EP-0216, EP-0313, EP-0789
Puri, G. EP-0500, EP-0505, EPS-073
Purkait, S. EP-0522
Pusceddu, S. EP-0068, OP-234
Putzer, D. EPS-280
Pyka, T. **OP-047**, OP-636, OP-710

Qi, J. **OP-363**
Qi, M. EP-0814, **EP-0296**
Qi, N. EP-0675
Qin, K. **EP-0816**
Qin, S. EP-0483, EPS-216, EPS-221
Qin, Y. OP-765
Qiu, R. EP-0764
Qiu, Y. EPS-028, OP-622, OP-902
Qu, W. EP-0737
Qu, X. OP-213
Quach, S. EP-0726, OP-538, OP-584, OP-588
Quagliata, A. EP-0301
Quak, E. **OP-806**
Quan, M. OP-714
Quan, Z. EP-0222, EP-0267, EPS-194
Quaranta, D. EPS-153
Quartuccio, N. **EP-0131**, EP-1028
Querellou, S. OP-100
Quincoces, G. EP-0034, **EP-0859**, EP-0862
Quinn, L. EP-0490, EP-0442
Quintana, J. EP-0465
Quintana Bolaño, C. EP-0242, EP-0557
Quintero, K. EP-0356
Quirce, R. EP-0516
Quirce Pisano, R. EP-0890
Quirt, J. OP-021
Quon, H. OP-393, OP-530

Raake, P. EP-0451
Rabadán-Domínguez, U. EP-0895
Rabah, J. EP-0206
Rabbani, H. EPS-285
Rabbitts, T. OP-768
Racca, M. EP-0273
Radchenko, V. EP-0842
Raddi, M. **EP-0550**, EP-0781
Rademaker, F. J. OP-086
Raderer, M. EP-0319
Radermacher, H. OP-773
Radonjic, D. EP-0383
Radosavcev, L. EPS-024, **OP-453**
Radu, C. EP-0037
Radulesco, T. OP-929
Radulovic, M. **EPS-024**, OP-453
Raes, L. **EP-0673**
Rafecas, M. EP-0658
Raffa, A. OP-392
Raffa, S. OP-455
Raffel, D. EP-0828
Raghava, K. EP-0555
Ragot, M. **EP-0687**
Rahal, K. EP-0420
Rahali, J. EP-0986
Rahbar, K. OP-334, OP-340
Rahmim, A. EP-0549, EP-0723, EPS-115, EPS-187, EPS-242, EPS-251, OP-025, OP-084, OP-091, OP-442, OP-711, OP-715
Raijmakers, P. OP-241
Raileanu, D.-A. EPS-040
Raimbourg, J. OP-155
Rai Mittal, B. OP-651
Rainer, E. EP-0493
Rainford, L. OP-660
Raiola, A. OP-050
Raithel, J. L. F. OP-800
Raj, A. EP-0370
Raja, S. EP-0514
Rajadhas, F. **OP-250**
Rajala, S. **TEPS-007**
Rajaraman, V. OP-097, OP-161
Rajendra, E. OP-764
Rajovic, M. OP-453
Rajwa, P. EPS-107
Rakita, I. EP-0614
Rakshit, S. EP-0043
Ralea, R. EPS-251
Ráliš, J. OP-022
Rama Alonso, S. EP-0254, EP-0386, EP-0503, EPS-052, OP-170, OP-787
Ramaekers, S. OP-141
Raman, S. OP-034, OP-036
Ramaswamy, A. EP-0216
Ramdhani, K. **OP-850**
Ramirez, A. OP-107
Ramkumar, E. EP-0403, EP-0535
Rammos, A. EP-0422, EP-0423
Ramos, C. D. **EP-0345**
Ramos, R. EP-0348, EP-0862
Ramos Font, C. EP-0410, EP-0517, EP-0409
Ramos-Membrive, R. EP-0859
Ranallo, N. EP-0613
Rangarajan, V. EP-0159, EP-0166, EP-0207, EP-0216, EP-0313, EP-0731, EP-0768, EP-0789, OP-178
Rangger, C. EP-0824, EPS-279, OP-306
Ranjan, P. EPS-055
Ranjan, R. OP-927
Ranjit, N. EPS-219
Rantala, I. TEPS-007
Ranzani, M. OP-764
Rappazzo, A. OP-392, OP-524, OP-801
Rasche, L. EP-0353
Rasheed, A. EP-0518
Rashid, K. EP-0037
Rasinski, P. EP-0156
Raskin, S. EP-0542

Rasmussen, I. OP-385, OP-384
Rasmussen, T. R. OP-640
Rasoatsaratanany, G. EP-0796
Rassner, M. EP-0843
Rastogi, R. OP-144
Rastogi, S. EP-0203, EP-0208
Rasul, S. EP-0283, EP-0493
Rath, A. OP-299
Rathke, H. OP-512
Rathore, H. **EP-0515**
Rau, L.-E. EPS-040
Rauchmann, B. S. OP-110
Rausch, I. EP-0532, EP-0748, EPS-102, EPS-126
Rausch, T. OP-719
Rauscher, I. EP-0235, EP-0284, EP-0564, EP-0566, EPS-124, OP-707, **OP-722**
Ravelli, I. EP-0908
Ravi, R. OP-437
Ravi Kumar, A. EP-0555, EPS-010, EPS-172, OP-437
Ravina, M. **EP-0734**, **OP-299**
Ravindra, S. EPS-027, **EP-0096**
Ray, M. K. EP-0043
Ray, S. EP-0701, EPS-179
Razola Alba, P. EP-0471
Rea, S. OP-581
Rearden, J. OP-672
Rebaud, L. **EP-0322**
Reberšek, M. OP-452
Rebollo Aguirre, Á. EP-0405
Recarte Ortega, P. EP-0169
Rech, F. OP-586
Redal Peña, M. EP-0585
Reed, J. D. OP-574
Regis, C. OP-513
Reguera, J. EP-0356
Regula, N. OP-387
Regupathy, A. R. OP-621
Rehaman, A. OP-649
Rehman, A. EP-0158, EPS-044
Reichen, C. OP-897
Reid, V. **OP-289**
Reijonen, V. **EP-0790**, EP-0802, **OP-028**, TEPS-007
Reilly, C. EP-0997, EP-1021
Reilly, R. EP-0884, EP-0056, EP-0841, EP-0842, OP-898
Reina, F. OP-382, OP-383
Reinertsen, I. EPS-160
Reinhard, S. EPS-180
Reinhardt, H. C. OP-099
Reinheckel, T. OP-621
Reischl, G. EP-0888, OP-314
Reissig, F. EP-0849, OP-020
Reiter, F. EP-0182
Reiter, R. OP-036, OP-040
Reiter, T. OP-291, OP-866
Remde, H. EP-0093
Remde, Y. OP-719
Rémond, E. OP-895, EP-0035
Remon Masip, J. EPS-260
Ren, C. **EP-0725**, OP-303
Ren, S. EP-0675, EPS-057
Ren, y. **EP-0044**
Renaud, C. OP-804
Rendl, G. EP-0556, OP-446
Renne, G. EP-0389, OP-038
Rényi-Vámos, F. EP-0390
Rep, S. EP-0089, EP-0506, OP-306, **TEPS-011**
Repetto-Llamazares, A. EPS-222
Repiso Campanholo, K. EP-0676
Resch, S. EPS-237, **OP-838**, OP-839
Rescigno, F. EP-1034
Resende Geao, A. **OP-663**
Reshtebar, N. **EPS-187**
Ressner, M. OP-808
Restuccia, G. OP-392
Rettig, M. EP-0284, OP-041, OP-192, OP-509, EPS-122
Reuvers, T. OP-146
Revheim, M. E. OP-832, OP-911
Revilla, E. M. EP-0638
Revy, A. EP-0687
Reyes, E. TEPS-018
Reyes, L. EP-0025
Reyes-Junca, J. G. EPS-265
Reyes Ojeda, D. EP-0417
Reyhan, E. EP-0168
Reymann, M. OP-838
Reynaert, N. OP-148, OP-367, OP-444, OP-629
Reynes Llompart, G. EP-0251, EP-0248, OP-784
Rey Sánchez, L. EP-0523, EP-0766, **EP-0767**
Rezaei, S. **EP-0554**, **EP-0624**, EP-0910, EP-0928, **EPS-271**
Riana, A. OP-909
Ribaldi, F. OP-104
Ribeiro, B. **TEPS-018**
Ribeiro, C. d. EP-0793
Ribelles, M. EP-0447, EPS-070, EPS-203, EPS-063
Ribizzi, G. OP-051
Ricci, M. **EP-0376**, EPS-159, OP-535
Ricciardi, S. OP-634
Richard, G. EP-0499
Richard, P. EP-0437, EPS-137
Richardson, S. OP-137, OP-138, OP-359
Richetta, E. **EP-0784**, **OP-910**
Richter, N. OP-107
Ridler, K. EP-0383
Rieger, C. OP-468
Rieger, M. EP-0451
Riemann, B. OP-525
Riemenschneider, M. J. EP-0726, OP-082, OP-588
Riera, E. EP-0109, EP-0241
Rietbergen, D. **EP-0414**, **EP-0851**, EP-0848
Rigamonti, D. EP-0709
Righi, S. OP-315
Rigopoulos, A. EP-0032
Rijkhorst, E. J. OP-628, EPS-250, EP-0561
Rijpkema, M. OP-220
Rikken, R. M. EP-0677, OP-109, OP-928
Riley, L. M. OP-289
Rinscheid, A. EP-0565, OP-856
Rio, E. OP-155
Riolo, D. EP-0908
Riondato, M. EP-0277, **EP-0709**, **EP-0898**, OP-051
Ripoll, T. EPS-143
Rischpler, C. EPS-140, OP-388
Risheq, F. EP-0240
Risheq, Z. EP-0240
Riss, P. EP-0493
Ritt, P. OP-080
Riva, N. EP-0613
Rivas-Navas, D. EP-0204, EP-0205, **EP-0175**, **EP-0176**, EP-0247, **EP-0409**
Riveira-Martin, M. **OP-498**
Riverol, M. OP-460
Rivière, J. OP-769
Rizkallal Monzon, S. EP-0127, EP-0365, EP-0502
Rizzo, A. EP-0273
Robe, P. A. J. T. OP-583
Robels-Plannels, C. OP-144
Roberts, M. OP-037
Robertson, A. J. OP-616
Robev, B. EPS-029
Robillard, M. S. OP-220
Robinson, A. P. EP-0670
Robinson, H. OP-764
Robinson, J. **OP-031**
Robinson, N. EP-0063
Robles Barba, J. EP-0251, EP-0248, EPS-031
Robson, P. M. EP-0733
Roby, A. EP-0679
Rocca, P. EP-0543, OP-915, OP-669
Roccatagliata, L. OP-051
Roch, V. EPS-240, OP-250
Rodado Marina, S. EP-0127, EP-0365
Rodak, M. OP-589

Rodari, M. EP-0189, EP-0272, EPS-161, OP-039, OP-918
Rodeño, E. OP-233, EP-0599
Rodman III, S. N. OP-144
Rodrigo, S. EP-0674
Rodrigo, V. OP-936
Rodrigo-Calvo, M. EP-0491
Rodrigues, F. B. EP-0929, EPS-061
Rodríguez, L. EP-0482
Rodríguez, M. EP-0088, OP-936
Rodriguez, P. EP-0573
Rodríguez, T. EP-0482
Rodriguez Alfonso, B. EPS-051
Rodríguez-Bel, L. EP-0101, EP-0954, EP-0955, EPS-154, OP-784
Rodriguez-Berriguete, G. OP-764
Rodríguez Díaz, L. **EP-0306**
Rodríguez-Fernández, A. EP-0175, EP-0176, EP-0247, EP-0580, EP-0581
Rodríguez-Fraile, M. EP-0587, OP-507
Rodríguez Gallo, E. EP-0393, **EP-0494**
Rodríguez García, C. EP-0702
Rodríguez García, E. EP-0702
Rodriguez-Gasen, A. EP-0211, EP-0299, EP-0547, EPS-031
Rodríguez Locarno, T. E. EP-0419, EP-0579, EP-0407, OP-924, EP-0924, EP-0925, EPS-269
Rodriguez Otero, P. EP-0348, EP-0356, OP-098
Rodriguez Oviedo, D. **EP-0300**, EP-0604, EP-0605, **EP-0964** EP-0526
Rodríguez Pajuelo, A. **EP-0199**, EPS-072
Rodriguez Parra, H. EP-0585
Rodriguez Puig, D. EP-0892
Rodríguez Rey, C. EPS-020, EPS-081
Rodriguez-Rubio Corona, J. EP-0242, **EP-0557**
Roehrich, M. **OP-189**
Roelants, V. EPS-134
Roesch, F. OP-307
Roé-Vellvé, N. EP-0678, OP-103
Roggisch, J. OP-468
Roghi, M. OP-918
Rogić, I. EP-0932, **EP-0221**
Rognoni, M. OP-328
Röhrich, M. OP-162, OP-518
Rokbani, H. **EP-0401**
Roll, W. OP-525
Rolland, F. OP-187
Romagnolo, C. EP-0112, EPS-053
Romaus Sanjurjo, D. EP-0023
Rombo, D. **EP-0412**
Romera, M. EP-0348, **EP-0088**, EP-0862, OP-098, OP-507, **OP-936**
Romera Caballo, M. EP-0705, EP-0706
Romero Fernández, P. EP-0361, EPS-020, EPS-081
Romero Herrera, E. EP-0251
Romero Herrera, J. EP-0892, EP-0248
Romero-Otero, M. EP-0559
Romiani, A. EPS-230
Rominger, A. EP-0750, EP-0782, EP-0801, EPS-101, EPS-192, EPS-244, OP-047, OP-058, OP-059, OP-226, OP-246, OP-362, OP-368, OP-432, OP-516, OP-521, OP-636, OP-666, OP-710, OP-844
Rominger, A. EP-0567
Roncali, E. EP-0794
Roncoroni, L. EP-0921
Rönnlund, C. OP-579
Roof, S. EPS-257, OP-788
Roosen, J. EPS-201, EPS-205, OP-029, OP-627
Ros, M. OP-381
Rosales, J. EP-0862, EP-0348, EPS-011, EP-0088, EP-0859, OP-098, **OP-507**, **OP-518**, OP-936
Rosarno, H. OP-392
Rosato, A. EP-0009, EP-0011
Rösch, F. OP-432
Roscher, M. EPS-210, OP-719
Rosenfeld, L. OP-901
Rosenkrans, Z. EP-0891, EPS-274
Rosenström, U. EP-0807, EPS-218
Roshanravan, V. EP-0266, OP-650, OP-523
Rosini, D. OP-882
Rosiñol, L. EP-0356
Roslin, S. OP-458, OP-459
Rosser, E. EP-0037
Rossetti, V. EP-0238
Rossi, M. M. G. EP-0805
Rossi, V. EP-0009, EP-0011
Rossin, R. OP-220
Rossi Norrlund, R. EP-0759
Rosso, L. EPS-272
Rosu, A. EP-0960, EP-0952
Rotbauer, D. EP-0004
Roteta Unceta Barrenechea, A. **EP-0471**
Roth, D. EP-0026, **OP-296**
Roth, K. **EP-0154**, OP-099, OP-101
Roth, N. EP-0758
Rothbauer, U. OP-922
Rotstein Habarnau, Y. V. OP-224
Roudaut, N. OP-806
Rousseau, C. EPS-243, OP-155, OP-187
Rousseau, E. EP-0045
Rousseau, F. OP-139
Rousseau, J. OP-557
Roustaee, H. EP-0424
Rouzet, F. OP-513
Rovera, G. **EP-0226**, **EP-0249**, **EP-0396**
Rowe, S. P. EP-0284
Roy, A. EP-0362, EPS-170, EPS-181
Roy, J. EP-0280
Roya, M. **OP-570**
Roz, L. EP-0068
Rozemuller, A. EPS-150
Rozenblum, L. OP-917
Ruan, W. EPS-157
Ruano Perez, R. EP-0398, EP-0455, EP-0475, EP-0529, EPS-043, OP-168
Rübenthaler, J. OP-656
Rubí, S. EPS-143
Rubini, G. EP-0258, EP-0509, OP-447
Rubino, M. OP-669
Rubio-Fernández, G. EP-0559, **EP-1013**, EPS-023, EPS-025, **EPS-026**
Rubow, S. EP-0762, EPS-087
Rudic, N. EP-0447, EPS-070, EPS-203
Rudic Chipe, N. EPS-063
Rudolf, H. OP-575
Ruf, J. OP-905
Ruf, V. EP-0726, OP-588
Ruffini, L. **EP-0487**, EP-0813, EPS-149
Ruggeri, R. OP-392, OP-524, OP-801
Ruhlmann, C. H. B. EP-0641
Ruiter, S. J. S. EPS-201
Ruiz, A. OP-103
Ruiz, S. EP-0340
Ruiz-Bedoya, C. A. **EP-0533**
Ruiz Corbalán, C. **EP-0407**, EP-0419, EP-0579, EP-0924, EP-0925, EPS-269, **OP-924**
Ruiz Juan, T. EP-0599
Ruiz Llama, S. EP-0251
Ruiz Molina, M. EP-0702
Ruiz Solís, S. EP-0418
Rullmann, M. **EPS-156**, EPS-174, OP-108
Rumeau, C. EPS-058
Rumiantcev, M. **EPS-237**, OP-839
Rumyantseva, M. EPS-128, EPS-129, EPS-130
Ruohola, J. OP-529
Rupprecht, R. EP-0726, OP-110, OP-588
Rushforth, D. OP-031
Russelli, L. OP-487
Russo, S. OP-524
Rusu, D. OP-187
Rusu, T. EPS-292
Rutherford, N. OP-037
Rutka, J. T. EP-0056, EP-0842
Ruurda, J. P. OP-086
Ruzzeh, S. EPS-082
Ryabov, V. EP-0448, EP-0463
Rybina, A. OP-578

Rydèn, T. EP-0545, EPS-009, OP-836
Ryer, E. OP-704
Ryhiner, M. OP-362
Rynja, S. P. OP-042
Ryoo, H. **OP-049**
Ryoo, W. OP-044
Ryser, M. **OP-331**
Ryu, J. EP-1033
Ryumshina, N. EP-0480
Ryuta, E. EP-0360
Rzepka, E. EP-0209

S., A. EP-0129
Sá, V. R. EPS-062
Saad, F. EPS-115, OP-715
Saadani, H. **OP-451**
Saba, W. EP-0019, EP-0021
Sabanayagam, K. EP-0636
Sabé-Fernández, N. EPS-049
Sabioni, L. R. EP-0961
Sabo, A. EP-1031
Sabo, K. EPS-251
Saboktakin, F. OP-248
Sabouret, P. OP-858
Saboury, B. EP-0318, EPS-242, OP-025, OP-084, OP-304
Sabri, O. EP-0149, EPS-148, EPS-156, EPS-174, OP-108
Sabunchi, S. OP-583
Saccardi, R. EP-0330
Sachithanandan, N. EPS-010
Sachpekidis, C. **EPS-266**, **OP-449**, OP-450, OP-564, **OP-919**
Sachs, J. OP-229
Sackiewicz, A. EP-0298
Sadeghi, F. **EP-0690**, **EP-0714**
Sadeghi, M. EPS-239
Sadeq, A. **EP-0260**, TEPS-005
Sadic, M. **OP-726**
Sadik, M. **EP-0318**
Sadri, K. EP-0264
Saeedzadeh, E. EPS-239
Saeki, T. EP-0110
Sağer, M. S. OP-391, EP-0740
Sağer, S. OP-165
Safari, M. OP-848
Safi, M. EP-0026
Sagar, S. EP-0362, EP-0488, **EP-0497**, EP-0519, EP-0707, **EP-0987**, EP-0991, EP-1019, EP-1020, EPS-055, EPS-060, **EPS-076**, OP-251
Sagastume, E. OP-144
Sage, J. OP-907
Sager, D. F. **OP-239**
Sager, S. EP-0152, EP-0153, EP-0742, OP-944
Saghebi, J. EP-0555, EPS-010, OP-437
Saglam, K. EP-0153, **EP-0740**, **OP-658**
Sah, P. EP-1008
Sahebkari, A. EP-0264
Şahin, M. EP-0185, EP-0119
Sahin, K. EP-0153
Sahin, Ö. **EP-0230**
Sahin, O. EP-0152, EP-0983, OP-035, EP-0228, OP-658
Sahin, R. **EP-0402**
Sahlmann, C. O. EP-0002
Sahlstedt, H. OP-041
Sahoo, R. OP-307
Sahraoui, G. EP-0420
Sahu, S. EP-0043
Saidi, N. EP-0045
Saila, T. OP-660
Sainz Esteban, A. EP-0398
Saita, A. EP-0272, OP-039
Saito, M. EP-0452
Saito, S. **EP-0450**
Saju, F. OP-880
Saka, E. EP-0691
Sakai, A. EP-0466, EP-0476
Sakai, S. EP-0466, EP-0476
Sakamoto, J. S. EPS-061
Sakashita, T. EP-0774, EP-0776
Saker Diffalah, Y. EP-0471
Saklani, A. EP-0159
Sala, A. OP-052, OP-045, OP-046
Salapa, H. E. OP-698
Salas Ramirez, M. EP-0633, **EPS-236**, OP-371, OP-438
Salaün, P.-Y. OP-155, OP-806, OP-855
Salcedo, S. EP-0329
Saldanha, A. OP-703
Saldarriaga Vargas, C. OP-148
Saleh, N. OP-948
Salehi, Y. EP-0714, OP-248
Sales Pitombeira, M. EP-0676
Salgado, L. EP-0412
Salgado Garcia, C. EP-0918
Sali-Dauda, M. OP-806
Salmerón Beliz, I. EP-0352
Salmon, R. EP-1003
Salomaa, M. TEPS-007
Salvà, G. EPS-143
Salvador, K. OP-137, OP-138
Salvador, P. EPS-203
Salvador Gomez, F. J. OP-498
Salvadori, J. **EP-0656**, **EPS-090**
Salvarese, N. EP-0009, EP-0011, EP-0012
Salvatore, C. EP-0744
Salvatori, F. EP-0623
Salvi de Souza, G. **EP-0020**
Salwig, S. OP-779
Salzmann, M. OP-557
Samadikhah, K. EP-0824, EPS-279
Samanes Gajate, A. OP-505
Sambuceti, G. EP-0273, EP-0277, EP-0898, OP-050, OP-455
Samimi, R. EP-0752
Samnick, S. EP-0353, OP-517
Sampaio, I. L. EP-0472, EP-0962
Sampunta, T. OP-772
Samuels, A. EP-0664
Sanaat, A. OP-225
Sanabria, Á. OP-103
Sanchez, L. EP-0351
Sanchez Bertomeu, N. TEPS-004
Sánchez Corral, J. EP-0393
Sánchez-Delgado, G. EP-0499, EP-0702
Sánchez de Mora, E. EP-0405, EP-0918
Sánchez Izquierdo, N. EP-0491
Sánchez Lorenzo, L. EP-0705, EP-0706
Sanchez-Rodriguez, I. EP-0101, EP-0355, EPS-048, EP-0970
Sánchez-Rodríguez, I. E. EP-0473, EP-0955, EPS-049, EPS-265
Sanchez-Rodriguez, V. OP-808
Sánchez Salmón, A. EP-0890, EP-0516
Sanchez Sanchez, R. **EP-0114**, EP-0205, EP-0410, EP-0517, EP-0628, EP-1032, TEPS-001, EP-0409, EP-0544
Sanchez Tornero, A. EP-0585, EP-0559
Sanchez Torrente, M. **EP-0399**, EP-0474, EP-0620
Sancho, L. EP-0088, EP-0348, OP-936, EP-0339, **EP-0587**, **EP-0705**, **EP-0706**
Sand, F. OP-107
Sandach, P. EP-0146
Sander, K. **EP-0679**, EP-0893
Sandhu, S. EP-0555, EPS-172, OP-338, OP-437
Sandoval Moreno, C. EP-0300, EP-0526, EP-0604, EP-0605, EP-0964
Sandström, M. EPS-249
Sanjuan-Garriga, F. X. EP-0939
Sanli, M. OP-333
Sanli, O. EP-0377, EP-0578
Sanli, Y. EP-0377, EP-0553, EP-0911, EP-0912, OP-333, EPS-245
San-Miguel, J. EP-0348, OP-098
Sanoesan, V. OP-841
Sansovini, M. EP-0613, OP-723
Sansum, F. OP-496
Santaella Guardiola, Y. **EP-0242**, EP-0557
Santamaría Chico, L. EP-0510, EP-0245, EP-0421, **EP-0467**
Santamaria Lopez, S. EP-1007
Santangelo, A. EP-0658
Santens, F. EPS-227

Santhanam, P. OP-393, OP-530
Santiago-Ribeiro, M.-J. OP-100, OP-799
Santin-Cerezales, M. EP-0970
Santoni, D. EPS-153
Santoro, M. **EP-0796**, OP-780
Santoro-Fernandes, V. **OP-676**
Santos, A. EPS-078, EP-0966, **OP-185**, OP-663
Santos, A. O. EP-0259
Santos, A. I. EP-0528, EP-0922, EP-0984, EP-0989
Santos, J. G. EP-0528, EP-0989
Santos, L. EP-0395
Santos Bueno, A. EP-0405, EP-0918
Santos Montero, B. EP-0523, EP-0766, EP-0767
Santus, R. OP-151
Saonam, T. EP-0872
Saraçoğlu, S. EP-0119
Saracyn, M. OP-675, OP-807
Sarandeses, P. **EP-0340**, EP-0418
Saranti, S. **EP-0594**
Sarath, S. EP-0449
Sari, H. OP-058, OP-636, OP-666, OP-247
Sarini, J. OP-654
Sarıkaya, B. EP-0591
Sarma, M. **EP-0179**
Sarnelli, A. EP-0238, EP-0613, OP-723
Sarret, P. EP-0850
Sarrhini, O. EP-0045, OP-557
Sarrut, D. EP-0656, EP-0729, EPS-247, OP-370
Sarswat, S. **EP-0122**
Sartor, H. EP-0311
Sartor, O. **OP-336**, OP-340
Sarwar, N. EP-0090
Sarıyıldız Gümüşgöz, H. EP-0591
Sas, N. OP-938
Sathekge, M. **OP-335**, EPS-206, OP-508, EP-0083, EP-0183, EP-0643, EPS-046, OP-574
Sato, A. EP-0808
Sato, T. **TEPS-015**
Saturi, G. EP-0681
Sauer, S. OP-919
Saunavaara, V. OP-247, OP-365
Saur, D. OP-108
Saura, I. EP-0447, EPS-070, EPS-203
Saura Lopez, I. EPS-063
Saushkin, V. EP-0462, OP-864, **EP-0480**
Sauvage, C. OP-858
Savage, K. EP-0723
Savchenko, A. **EP-0601**
Savelli, G. **EP-0744**
Saviano, M. EP-0011
Saviatto, A. EP-0340
Saviatto Nardi, A. EP-0418
Savio, E. EP-0025, EP-0301
Savoldi, L. EP-0999, EPS-014
Sawakuchi, G. OP-764
Sawamura, M. OP-561
Sawant, V. EP-0768, OP-178
Sawatnatee, T. OP-841
Sayawaki, Y. **EP-0625**
Sayman, H. EP-0233, OP-944
Sayıt, E. EP-0120, EP-0363, EP-0944, OP-934
Sazonova, S. EP-0462, EP-0463, EP-0480, EP-0626, OP-864
İsbir, C. OP-317
Scalisi, D. EP-1028
Scalorbi, F. **EP-0068**, **OP-234**, OP-674
Scarlattei, M. EP-0487, EP-0813
Scarpuzza, M. OP-171
Scartoni, D. OP-585
Schachoff, S. EP-0235, OP-707
Schaefer, J. OP-314
Schaefer, N. EP-0699, OP-153, OP-716
Schaefferkoetter, J. EP-0755
Schäfer, L. **EPS-229**
Schäfer, M. EPS-210, OP-719
Schäfer, R. EP-0015
Schäfers, K. OP-356
Schäfers, M. OP-356
Schatz, L. EP-0791
Scheffler, B. OP-580
Scheffler, M. OP-106
Scheidhauer, K. OP-520
Scheifele, M. EPS-148
Scheiff, K. **EP-0666**, **EPS-086**
Scheinberg, D. OP-702
Scheltes, J. OP-300
Schemmer, B. **EP-0200**, **EP-0227**, **EP-0338**, **EPS-005**, **OP-394**
Schenke, S. OP-525
Scheper, V. EP-0082
Schepisi, G. OP-723
Scherthan, H. EPS-235, EPS-236, OP-152
Scherzad, A. EP-0093
Scherzag, A. OP-785
Scheuba, C. EP-0493
Scheuermann, S. OP-314
Scheveneels, G. EP-0869
Schiavini, M. EP-0763, **OP-328**
Schiavo Lena, M. EP-0202
Schiavon, E. EP-0744
Schibli, R. EP-0070, OP-016, OP-492, OP-765, OP-897
Schicchi, N. EPS-053
Schichor, C. OP-538, OP-584
Schick, M. OP-719
Schick, U. OP-855
Schinagl, A. EPS-214, EPS-284
Schindler, K. OP-047
Schirbel, A. EP-0507, OP-305
Schirrmacher, R. OP-656
Schlamp, K. OP-189
Schlederer, M. EP-0283
Schleiermacher, G. OP-311
Schlögl, S. OP-833
Schlötelburg, W. **EP-0507**, EPS-117, **OP-305**
Schmalzing, M. OP-517
Schmid, A. EP-0824, EPS-279
Schmid, H. **EPS-003**
Schmidt, F. EP-0658
Schmidt, F. P. OP-077, OP-572
Schmidt, K. OP-194
Schmidt, T. OP-580
Schmidt Hegemann, N. S. OP-337
Schmitt, C. EP-0694
Schmitt, D. **OP-937**
Schmitt, S. EPS-156
Schmitz, J. OP-798
Schneid, S. EP-0319
Schneider, L. **EP-0860**
Schober, P. EP-0677, OP-928
Schöder, H. EP-0092, EP-0197, EP-0333, OP-802
Scholte, A. EPS-178
Schomäcker, K. EP-0154
Schoof, S. EPS-235
Schoonjans, W. OP-498
Schott, B. OP-676
Schou, M. **OP-555**
Schrauwen, P. EP-0499
Schröder, C. OP-573
Schroeter, C. OP-162
Schroeter, M. OP-108
Schubert, J. OP-703
Schubert, T. EP-0358
Schuck, P. N. OP-843
Schuderer, F. **EP-0843**
Schuetze, J. OP-239
Schug, D. OP-773
Schuhmacher, A. J. EP-0034
Schuit, R. C. EP-0677, OP-928
Schuler, M. EP-0146, OP-580, OP-932
Schulga, A. EP-0852, EP-0861
Schultz, C. OP-642
Schultz, M. OP-673, OP-144
Schulz, V. OP-773
Schulze, R. EP-0888, EP-0889

Schumann, S. **EPS-235**, OP-152
Schuster, D. M. EP-0164, OP-194
Schütz, S. OP-897
Schwab, M. EP-0827
Schwamborn, K. EP-0288
Schwandt, M. OP-468
Schwartz, J. OP-336
Schwarzenböck, S. M. EP-0785, OP-575
Schweiger, J. EP-0082
Schweighofer-Zwink, G. EP-0556, OP-446
Schwenck, J. OP-314, OP-922
Schwenkenbecher, K. OP-300
Schymkowitz, J. OP-139
Sciacca, G. TEPS-021
Sciagrà, R. EP-0149, EP-0212, EP-0330, EP-0469, EP-0546, EPS-174
Scibè, R. OP-395
Scifo, P. OP-505
Sciuto, R. EPS-232, OP-447, OP-581
Scorsetti, M. OP-918
Scorza, M. EP-0025
Scott, A. OP-672, EP-0663, OP-194, OP-490, EP-0032
Scott, F. OP-490
Scott, L. A. EP-0684
Scott, P. EP-0828
Sdraiati, C. OP-328
Searle, J. EP-0753
Seban, R.-D. **EPS-017**
Sebastian Palacid, F. EP-0398, **EP-0455**, **EP-0475**, EP-0529, EPS-043, OP-168
Sebus, H. J. **EPS-195**
See, T. C. EP-0799
Segbers, M. EP-0100, EPS-103
Seibyl, J. OP-108
Seifert, P. **EP-0297**
Seifert, R. **EPS-110**, EPS-118, OP-099, OP-308, OP-334
Seimbille, Y. EP-0050, EP-0064, EP-0065, EPS-224, EPS-277
Seitova, K. EPS-218
Seitz, A. EP-0552, EPS-117, OP-332
Seitz, C. OP-314
Sekaran, A. EP-0171
Seki, C. OP-079
Seklecka, N. OP-231
Selboe, S. OP-911
Selcuk, N. EP-0253
Selhane, F. EPS-260
Sellem, A. EP-0087
Selvarajah, D. EP-0663
Sembele, L. OP-328
Semino Bruzzone, G. OP-315
Sen, F. EP-0191
Sen, I. OP-673, OP-786
Senglaub, T. EP-0608
Seniaray, N. **OP-927**
Sennung, D. OP-440
Sensi, F. OP-051
Seo, E. **EP-1033**
Seo, S. EP-0128
Seo, W. EP-0810
Seoane, A. EP-0635
Seok, J. **EP-0106**, **EP-0107**, OP-049
Seppänen, M. EP-0627, EP-0659, OP-529
Sequeira, J. A. EP-0989
Serafini, S. EP-0162, EP-0188
Serani, F. **EP-0303**, **EP-0388**
Serbanescu, S. EP-0943, EP-0953, EP-0952, EP-0949
Sercic, D. **TEPS-006**
Sereeborwornthanasak, K. EPS-109
Sereesongsaeng, N. OP-768
Seregni, E. EP-0010, EP-0068, OP-234, OP-674
Serencsits, B. EP-0608
Sereno, J. EPS-094
Seret, A. **EP-0629**, **EP-0630**
Serfling, S. **EP-0093**, **EP-0353**, EP-0552, **OP-785**, EP-0182, EP-0319, EP-0507, EP-0539, EP-0610, EPS-117, OP-291, OP-305, OP-517, OP-866
Sergieva, S. EPS-029
Serra, A. EPS-037
Serrano, B. EP-0719
Sestini, S. EPS-149, OP-462
Seth, R. EP-0096
Sethi, I. EP-0164
Sethi, P. EP-0991
Seto, A. EP-0360
Setoain, X. EP-0356
Sevaslidou, I. EP-0982
Seven, B. EP-0947, EP-0951, EP-0958, EP-0959, EP-0967
Severi, S. **EP-0613**, OP-723
Seyedi, N. EP-0752
Seyedinia, S. **EP-0501**
Sezer, E. EP-0192
Sezgin, C. **EP-0120**, EP-0885
Sezgin, I. EPS-047
Sfar, R. EP-0139, EP-0140, EP-0512, EP-0994
Sfiligoj Planjsek, D. **EP-0089**
Sghaier, S. EP-0420
Sgouros, G. OP-147, OP-393, OP-530, OP-672, OP-837
Sguazzotti, M. EP-0681
Shafiee, S. OP-523
shafiei, s. OP-803
Shagera, Q. **EP-0275**, EPS-112, **OP-664**
Shah, R. OP-304
Shah, S. EP-0159, EP-0166, EP-0207, EP-0216, EP-0313
Shah, T. T. OP-511
Shah, V. EP-0692
Shahid, A. EP-0385
Shahrbabaki Mofrad, M. **EP-0743**, EP-0752
Shaida, N. EP-0799
Shaikh, A. **EP-0768**
Shakher, R. OP-037
Shakhova, A. **EPS-128**, **EPS-129**, **EPS-130**
Shalgunov, V. OP-615
Shalimar, S. EPS-204
Shamim, S. A. EP-0203, EP-0336, EPS-204, **EP-0208**, **EP-0368**, **OP-251**
Shamni, O. EPS-282
Shan, L. **OP-865**
Shang, F. EP-0438
Shang, J. OP-048
Shao, X. **EP-0828**
Shariat, S. EPS-107
Sharma, A. EPS-143
Sharma, G. OP-338, OP-589
Sharma, P. D. EP-0717
Sharma, R. EP-0497, EP-0090, **EP-0832**
Shcherbina, O. OP-939
She, Y. Y. OP-397
Sheikh, G. EP-0210, EP-0451, EPS-003, **OP-717**, OP-656
Sheikhzadeh, P. EP-0669, EP-0690, EP-0712, EP-0714, EP-0735, EP-0743, EP-0752, EPS-177, EPS-187, OP-248
Shelkovnikova, T. EP-0461
Shen, D. Y. **OP-397**
Shen, J. EPS-122, OP-509
Shen, X. EP-0281, OP-838
Shen, Y. **EP-0868**
Sheng, X. OP-215
Sheokand, P. OP-307
Shepple, B. OP-389
Sherkhane, U. B. EP-0731
Shestopalov, G. EP-0326
Shi, D. EP-0816
Shi, H. EP-0637, EPS-091
Shi, K. EP-0649, EP-0750, EP-0782, EP-0801, EPS-101, EPS-180, EPS-192, EPS-244, OP-059, OP-154, OP-226, OP-362, OP-368, OP-636, OP-710, OP-844
Shi, L. EP-0638
Shi, W. EP-0483
Shi, Y. OP-110, OP-377
Shibutani, T. EP-1018, **EP-1022**, EP-1024, TEPS-016, **TEPS-017**
Shih, H. OP-917
Shih, I. L. EPS-182
Shimada, H. EP-1018
Shimizu, A. EP-0808
Shimizu, T. EP-0753, EP-1024, TEPS-016, TEPS-017

Shimizu, Y. EP-0126, **EP-0897**
Shin, U. EP-0730
Shinohara, N. EPS-012
Shipulin, V. EP-0457, EP-0458, EP-0461, EPS-139, **EP-0461**, **EPS-139**
Shirai, Y. EP-0466
Shirakami, Y. OP-772
Shirakawa, Y. **TEPS-009**
Shiri, I. EP-0727
Shirvani-Arani, S. EP-0806
Shiyam Sundar, L. EP-0105, EP-0710, EPS-125, EPS-174, **OP-567**, OP-775, OP-776
Shouval, R. EP-0333
Shrikhande, S. EP-0207, EP-0216
Shuch, B. M. OP-194
Shukla, J. OP-651
Shukla, V. EP-0180
Shukurov, R. EP-0833
Shurupova, I. EPS-128, EPS-129, EPS-130
Sibille, L. **EPS-175**
Sibinova, M. **EP-0770**
Sicilia Pozo, M. N. EP-0229, EPS-050, **EP-0496**, EPS-268, EP-0250, EP-0562
Siebinga, H. **EP-0271**, **OP-908**
Siefried, G. OP-150
Siersema, P. D. OP-086
Sigfridsson, J. **OP-240**, OP-387
Signori, A. EP-0277
Sijbesma, J. W. EP-0020
Sijtsema, N. D. EP-0100
Sikdar, S. EPS-055
Silivridou, K. EP-0765
Silva, A. EP-0328, OP-221, EPS-094
Silva, D. **EP-0472**, EP-0569, **EP-0962**, EP-0979, OP-472, EP-0246, OP-469, OP-473, OP-539
Silva, F. **EP-0006**, EP-0769
Silva, J. W. E. EPS-007
Silva, L. **EP-0738**
Silva, M. EP-0896, EP-0328, EP-0738, EP-0769, OP-087, OP-221, EPS-289, EP-0926
Silva, R. **EP-0926,** EP-0239, EP-0485, EPS-007
Silva, S. EP-0896
Silvera, E. EP-0301
Sim, B. Z. OP-254
Simetic, L. EPS-264
Simon, J. EP-0348, EP-0062, EP-0034, EP-0859, EP-0862
Simoncic, U. OP-306
Simonetti, B. F. EP-0112
Simón Martínez, J. EPS-095
Simons, M. OP-110
Simonsen, J. EP-1023
Simonsson, K. EPS-230
Simontacchi, G. EP-0546
Simó Perdigó, M. EP-0252
Şimşek, F. S. EP-0602
Sin, C. **EP-0582**
Sinaii, N. OP-304
Singh, A. EP-0309
Singh, H. EPS-111, EPS-190
Singh, I. OP-923
Singh, N. EP-0366, EP-1019, **EP-1020**
Singh, P. **EP-0158**, EP-0413, EPS-044, OP-649, OP-494
Singh, S. **EP-0309**, **EP-0754**
Singhal, A. EP-0122, EP-1019, EP-1020, EPS-027, EPS-060
Singhal, N. EP-0370
Singhal, T. EP-0158, EP-0413, **EPS-044**, OP-649
Singleton, M. EP-0663
Sinha, B. OP-519
Sinigaglia, M. OP-804
Sinkovics, I. EP-0390
Sioka, C. **EP-0422**, **EP-0423**, **EP-0445**
Sipka, G. EP-0181
Siracusa, M. OP-392, OP-524, OP-801
Sirbu, C. EP-0937
Sirca, K. TEPS-011
Sirindil, F. EP-0893
Siripongsatian, D. EPS-109, OP-662
Siscar Gelo, C. EP-0417
Sisic, M. EPS-024
Sisk, A. OP-034, OP-036
Sita-Lumsden, A. EP-0090
Sitara, M. EP-0162, EP-0188
Sitarz, K. EP-0209
Sivashankar, K. OP-251
Siveke, J. T. EP-0607, OP-190, OP-380, OP-932
Siyanbola, R. **OP-330**
Sjögreen Gleisner, K. EPS-009, EPS-248, OP-904
Skálová, M. **OP-017**
Skjulsvik, A. J. EPS-160
Skorjanec Armic, E. EP-0506
Skorkiewicz, K. OP-306
Skoularigis, J. EP-0682
Skvortsova, I. I. EPS-225
Slart, R. EP-1025, OP-088, OP-241, EP-0443, EP-0692, EPS-098, OP-086, OP-243, OP-252, OP-364, OP-515, OP-519, OP-731, OP-732, OP-860
Slavin, M. OP-254
Slavova, M. EP-0513
Slemann, L. EP-0024
Slim, I. EP-0481, EP-0993, EP-0995, EPS-042, OP-945
Slimane, M. EP-0420
Slodnjak, I. TEPS-011
Slof, I. EPS-113
Slof, L. J. EP-0397, EP-0851, EPS-270, OP-298, OP-300
Small, S. EP-0701, EPS-179
Smedby, Ö. EP-0156
Smirnova, A. EP-0394
Smit, E. F. EPS-195
Smit, F. EP-0274, EP-0788, OP-167
Smith, C. OP-566, **OP-027**
Smith, G. OP-764
Smith, N. **OP-359**
Smith, R. OP-089, EP-0454
Smitran, T. EP-0221
Smits, K. **OP-836**
Smits, M. L. J. EPS-198, OP-295, OP-850
Smorgon, A. OP-645, EP-0458
Smoszna, J. OP-807
Sneeden, E. OP-672
Snijders, T. J. OP-583
Snoeijink, T. **EP-0061**, EPS-201
Soares, R. OP-528
Soares Meneses, P. EP-0245, EP-0467
Sobhi, M. **EP-0752**
Sobic Saranovic, D. EPS-002, EPS-254
Sobral, M. **EPS-173**
Sobral Torres, L. **OP-949**
Sobrino, T. EP-0023
Soda, P. OP-712
Söderkvist, K. EP-0317
Soeiro, P. EP-0415, EP-0416, EP-0927, EP-0963, OP-949
Sofia, L. EP-0277, OP-050, **OP-051**
Sofiyanski, T. **EPS-029**
Solanich-Moreno, X. EP-0970
Solanki, R. **OP-861**
Solari, E. EP-0655, **OP-707**
Solari, L. EP-0125
Soldevila-Lozano, C. EP-0331
Soldevilla Gallardo, I. EP-0130, EP-0525
Solem, R. OP-499
Soleymani, Y. EP-0735
Solfaroli Camillocci, E. EPS-037, EP-0783
Solheim, O. EPS-160
Soliman, A. OP-710
Solinas, P. EP-0294
Solli, P. EP-0147
Sollini, M. EP-0189, EP-0285, EPS-161, OP-653
Soltani, S. EP-0264, EP-0381
Somai, M. EP-0481, EP-0995
Sombon, S. OP-662
Sombroek, C. OP-253

Sonanini, D. OP-922
Song, H.-C. OP-049
Song, H. EP-0278, EPS-118, OP-504, **EP-0142**
Song, J. **OP-577**
Song, L. EPS-293, OP-622, OP-902, **OP-255**
Song, S. EP-0198, OP-379, EP-0453
Song, T. EP-0307
Song, X. OP-143, OP-216, EPS-141
Song, Y. **OP-154**, OP-309, EP-0642
Sönmez, Ö. EP-0253, OP-163, OP-375
Sonmezoglu, K. EP-0152, EP-0153, EP-0233, EP-0742, OP-658, OP-944, EP-0740, EP-0983, OP-165, OP-391
Sonni, I. **EP-0538**, **EPS-122**, **OP-034**, **OP-036**
Sood, A. OP-651, OP-861
Sopina, L. OP-640
Sopuschek, M. P. EP-0297
Sordi, B. EP-0330
Sörensen, J. EPS-140, OP-240, OP-387, OP-388, OP-578, **OP-579**, OP-730
Soriani, A. EP-0783, EPS-232
Soriano Castrejón, Á. EP-0250, EP-0496, EP-0562, EPS-050, EPS-268 EP-0229, EPS-259, OP-638
Sorrentino, S. OP-315
Sorysz, D. OP-641
Sotolongo-Grau, O. OP-103
Soualhi, M. EP-0698
Soultanidis, G. EP-0733
Sousa, E. EP-0412
Sousa, I. EP-0962
Sousa, J. EP-0008
Sousa, M. J. EP-0962
Sousa, R. EP-0412
Sousa, V. EP-0704
Sousa, V. OP-555
Souweidane, M. OP-834
Souza, T. EPS-078
Sowa-Staszczak, A. EP-0209, EP-0537, OP-306, OP-641, OP-675
Soydal, C. EP-0214, EP-0243, **EP-0257**, **EP-0314**, EP-0315, EP-0349, EPS-116, EPS-200, OP-158
Soydas Turan, B. **EP-0577**, **OP-055**
Soyer, A. **EP-0019**, EP-0021
Soylemez Akkurt, T. EP-0116
Soyluoglu, F. EP-0541
Soyluoğlu, F. EP-0224
Soza-Ried, C. EP-0708, OP-327, OP-489
Spada, F. EP-0543, OP-669
Spaggiari, L. OP-915, OP-921
Spain, L. EP-0555
Spangler-Bickell, M. OP-026, EP-0720
Spanu, A. EP-0294
Sparrelid, E. EP-0156
Spasova, S. EP-0899
Spazzoli, B. OP-881
Spencer, B. OP-776, EP-0191, OP-567, OP-775
Sperti, S. EPS-074
Spetz, J. EPS-230
Spielvogel, C. EP-0105, EP-0262, EP-0283, OP-093, OP-706, OP-709, **OP-713**
Spiering, W. EPS-075
Spigoni, V. EP-0487
Spijkerman, R. EP-0274, OP-086
Spimpolo, A. OP-447
Spiridon, P. **EP-0206**
Spirovski, M. EP-0312
Spitilli, M. EPS-085
Spittler, A. OP-081
Spitzweg, C. OP-656
Spolaore, B. EP-0009, EP-0012
Spottiswoode, B. EP-0322, OP-242, OP-710, OP-774
Sprangers, M. EP-0869
Squame, E. EP-0819, EP-0879
Squatrito, M. OP-555
Sraieb, M. EP-0146
Srbljin, S. EPS-105
Srichandan, T. EP-0789
Sridhar, V. EP-0664
Srinivas, S. OP-504
Srinivasan, S. OP-556
S T, B. EP-0179
Stadlbauer, S. EPS-275
Stadnyk, L. EP-0615
Staelens, S. OP-556
Stairs, J. OP-025
Stam, M. K. EP-0788, OP-628
Stamate, R. EPS-040
Stammes, M. **OP-253**, **OP-922**
Stanimirovic, D. **EP-0614**
Staniszewska, A. OP-555
Stanzel, S. **EP-0150**, **EP-0151**
Stapleton, A. M. **OP-030**
Starace, M. **EP-0469**
Starcea, I. EPS-040
Stark, A. W. OP-239
Stasi, M. EP-0784, OP-910
Statescu, A.M. EPS-040
Stathaki, M. EP-0193, EPS-083, OP-859
Stathopoulou, M. EP-1012
Staus, P. OP-337
Stavenga, M. **EP-0383**
Stavrinou, M. EP-0686
Stawitzki, F. EPS-238
Steczek, L. EP-0018, EP-0831
Stefaneli Mormandi, P. **EP-0331**
Stefanescu, C. EP-0375, EPS-040
Stefański, B. EP-0977
Steffann, M. EP-0875
Steinacker, N. EP-0775, OP-771
Steiner, D. OP-897
Stein-Thoeringer, C. K. EPS-266
Stella, M. OP-367, OP-444, OP-628, OP-629
Stelljes, M. OP-099
Stenberg, V. Y. EPS-222
Stenkrona, P. OP-555, OP-563
Stenman, A. EPS-067
Stenslik, M. OP-703
Stenvall, A. EP-0468, TEPS-012
Stephens, A. EPS-147, OP-103
Stephens, A. W. EP-0678
Sterea, C. EP-0956
Stessl, A. EPS-102
Stevens, D. OP-145
Stevenson, N. EP-0062
Stief, C. OP-717
Stöcklein, S. EP-0726
Stockley, M. OP-764
Stoeva, T. EP-0263, **EP-0341**, **EP-0342**, **EP-0343**, **EP-0344**, EP-0899, **EP-0900**, **EP-0901**, **EP-0902**, EP-0904, EP-0913, EP-0981, EPS-121, EPS-267
Stoiber, S. EP-0262, EP-0283
Stojanoski, S. EP-0992
Stojanovic, D. EP-0312
Stokes, C. EPS-289
Stokke, C. EP-0686, EPS-188, EPS-249, OP-831, OP-832, OP-911
Stokkel, M. EPS-158, OP-451, OP-670
Stolniceanu, C. EP-0375, EPS-040
Stommel, M. W. J. OP-853
Stormrud, E. EP-0454
Storto, G. OP-447
Strašek, K. OP-452
Stragliotto, G. OP-555
Strand, J. **EP-0026**, OP-296
Strand, S. EP-0026, OP-296
Strandberg, S. **EP-0317**
Stricker, P. EPS-120
Strigari, L. EP-0681, EP-0796, OP-474, OP-780
Strobel, I. **OP-152**
Strobel, K. EP-0795
Strolin, S. EP-0796, OP-780
Stroobants, S. EP-0196, OP-573
Strudwick, R. OP-660
Struelens, L. OP-498
Studen, A. EP-0325, OP-306, OP-452

Stuschke, M. EP-0146, OP-580
Stute, S. OP-025
Stuurman, D. EP-0065, EPS-213
Su, J. OP-448
Su, K. EPS-176, EPS-089, OP-026
Su, M. EP-0121, EP-0282, EP-0334, EP-0650, EPS-199, OP-789
Su, X. EP-0059, EP-0079, EP-0160, EP-0484, EPS-056, OP-920
Suanes, K. EP-0301, OP-665
Suardi, N. OP-505
Suárez Fernández, J. EP-0306
Suárez Novo, J. EP-0251, EP-0248
Suarez-Piñera, M. EP-0954, EPS-154
Subangun, R. **EP-0786**
Subesinghe, M. EP-0533
Subklewe, M. OP-099
Subramony, V. EP-0063
Sudani, A. EP-0854
Suer, E. EP-0243
Suh, M. EP-0536
Suils-Ramón, J. EP-0211, EP-0299, EP-0939, EP-0942
Sukprakhun, C. OP-841
Sulejmanova, A. EP-0448
Sulsenti, R. EP-0010
Sun, C. EP-0638
Sun, H. EP-0307
Sun, L. EP-0167, OP-374, OP-398, OP-427
Sun, Q. **EP-0917**
Sun, X. EPS-293, OP-902
Sun, Y. **EP-0652**
Sunagua, S. EP-0573
Sundar, L. K. S. EP-0748, EP-0149
Sundaram, P. OP-880, OP-880
Sundin, T. OP-579
Sundlöv, A. EPS-009
Sung, H. EP-0536, **EP-0747**
Sure, U. OP-580
Suresh, A. **EP-0159**
Surkova, N. EPS-128, EPS-129, EPS-130
Susantitaphong, P. OP-841
Sutcu, G. **EP-0243**
Sutherland, A. OP-289
Sutto, M. EP-0586
Suyama, J. TEPS-009
Suzuki, L. R. EP-0732
Svanström, P. **OP-387**
Svenningsson, P. OP-562
Svensson, J. EP-0545, EPS-009, OP-836
Swales, J. OP-555
Swanepoel, C. OP-076
Swanwick, N. EP-0844
Swiha, M. **EP-0558**
Sygula, A. EPS-013
Symvoulidis, C. EP-0998
Syrkina, A. EP-0463
Szczepankiewicz, F. EP-0026
Szikra, D. EP-0812, **EP-0871**
Szolikova, M. **OP-369**
Szubstarska, P. OP-675
Szumowski, P. EPS-071
Szyszko, T. EP-0870

Tabacchi, E. EP-0303
Tabouret-Viaud, C. OP-160
Tabuenca, M. EP-0340
Tabuenca, O. OP-498
Tabuenca Mateo, M. EP-0418
Tachibana, M. EP-0141, EP-0308, **EPS-104**
Tack, C. J. EP-0486
Tada, H. OP-245
Taddio, M. EP-0037
Taelman, V. EP-0081
Taffurelli, M. OP-882
Tagawa, S. T. OP-340
Taghizadeh Kermani, A. EP-0085
Tagliatori Nogueira, M. EP-0526, EP-0300, EP-0964
Taha, N. EP-0880
Tahirovic, S. OP-110
Tahseen, R. EPS-252
Taïeb, D. OP-304, OP-310, OP-654
Taillandier, L. OP-586
Tajra, J. EPS-045, EPS-045
Takada, M. EP-0126
Takada, S. **EP-1015**
Takahashi, K. EP-0855
Takahashi, M. S. EP-0345, EP-0651
Takahashi, N. OP-177
Takahashi, R. OP-561
Takahashi, S. EP-0244
Takahiro, H. OP-785
Takami, K. **TEPS-016**
Takanami, K. EP-0452, **EP-0711**
Takase, K. EP-0452, EP-0711
Takeda, S. EP-0710, OP-776
Takenaka, A. EP-0715
Takenaka, J. EP-0739, **EPS-012**, OP-777
Takes, M. T. L. OP-297
Takeuchi, S. EPS-012
Takeuchi, Y. EP-0111, EP-0126
Taki, J. OP-284, OP-290, OP-776
Taktikou, E. EP-0594
Talarico, M. EP-0354, OP-534
Talavera Rubio, M. P. EP-0229, EP-0496, EPS-050, EP-0250, EP-0562, EPS-268
Talbot, J.-N. **OP-805**
Talin, A. OP-166
Talip, Z. OP-016, OP-141
Talleruphuus, U. OP-384, OP-385
Talvacchio, S. OP-304, OP-310
Tam, H. EP-0276, OP-511
Tamaki, N. EPS-088, OP-389
Tamariz, L. OP-098, EP-0348
Tamayo, P. EP-0356
Tamayo Alonso, M. EP-0503
Tamayo Alonso, P. EP-0254, EP-0357, EP-0386, EPS-052, OP-170, OP-787
Tamborino, G. **OP-146**
Tan, Z. OP-048
Tandon, N. EP-0497, EP-0498, EP-0987, EPS-076
Tang, C. OP-037
Tang, J. EP-0091, EP-0814
Tang, L.-H. OP-244
Tang, M. EP-0739
Tang, P. **EPS-199**
Tang, S. **OP-096**, TEPS-020
Tang, X. EP-0438
Tang, Y. OP-048, **EPS-164**, **EPS-207**, OP-795, **OP-885**
Tanguy, L. EP-0876
Taniyama, Y. EP-0452
Tank, J. OP-798
Tao, J. **EP-0046**
Tao, R. OP-878
Tapani, K. T. EPS-241
Taraji, L. OP-664
Taralli, S. EP-0693, EPS-153, EPS-196, **OP-634**
Tardin Cardoso, L. EP-0471
Tarnawski, R. OP-589
Tárraga, L. OP-103
Tartaglione, G. **EP-0404**, **EPS-022**
Tartari, J. OP-103
Tashima, H. EP-0651, OP-025
Taskin, S. EP-0314
Tassorelli, C. OP-045
Tauber, C. EPS-184, OP-092, OP-799
Tauber, R. EP-0235, EP-0564
Taubman, K. OP-037
Tauchmanova, L. OP-194
Tautz, K. EP-0888
Tavares, A. OP-289, EP-0395
Tawate, M. EP-0043
Tay, W. EP-0616
Taylor, J. EP-0663, EP-1003
Tecuapetla-Chantes, G. EP-0895

Téglás, M. EP-0390
Tei, L. **EP-0812**, **OP-487**
Teixeira, J. P. EP-0246, EP-0472, EP-0962, OP-469, OP-473, OP-539
Teixeira, R. EP-0328
Teixeira, S. EP-0769
Teixeira Macarico, D. **EP-0997**, **TEPS-013**
Telli, T. EPS-118, **OP-334**
Tellmann, L. OP-107
Telo, S. OP-879, OP-881, OP-882
Temma, T. EP-0854, EP-1015
Tempier, M. EP-0687
Templon, J. OP-556
Temsamani, J. OP-213
ten Hove, D. **OP-519**
Tenhunen, M. EP-0802, OP-028
Teodoro, R. OP-558
Terauchi, T. TEPS-010
Tercero Garrido, D. EP-0400
Terentes-Printzios, D. EPS-178
Teriaca, M. OP-918
Ter-Pogosyan, A. OP-034
Terroir, M. EP-0647, **OP-654**, OP-804
Terry, S. EP-0042
Tervonen, J. TEPS-007
Terzic, J. **OP-324**
Teske, N. **OP-584**, OP-588
Tesselaar, M. OP-852, OP-670
Teule-Vega, A. EP-0547
Teunissen, C. E. OP-109
Teunissen, J. J. M. EPS-019
Texier, J. S. EP-0647
Thaiss, W. EP-0560
Thaker, N. R. EP-0515
Thakral, P. OP-673, OP-786
Thakur, R. **EP-0013**
Thakur, S. **EP-0166**, **EP-0180**
Thawinprawat, K. **EP-0524**
Theegarten, D. EP-0137
Theis, H. OP-107
Thelen, P. EP-0002
Theodorou, E. EP-0682
Thériault, B. L. EP-0063
Theysohn, J. OP-852
Thibault, C. EP-0948
Thibault, K. EP-0019
Thickens, A. EP-0863, EP-0891, EPS-274
Thieblemont, C. EPS-185
Thiele, M. EPS-214, EPS-284
Thielemans, K. EP-0670, EP-0722, **OP-025**
Thin, P. EP-0538
Thisgaard, H. EPS-228
Thivat, E. OP-938
Tholen, H. T. EP-0877
Thomas, H. OP-040
Thomas, L. **OP-661**
Thomas, P. OP-037
Thompson, D. OP-040
Thon, N. EP-0726, OP-467, OP-588
Thurfjell, L. EP-0678
Tian, M. EPS-155
Tian, R. EP-0163, EP-0327, EP-0590, EPS-199
Tian, T. **EPS-066**, **OP-652**
Tian, Y. **EP-0157**, EP-0133, EP-0382, EPS-209, **EPS-255**, OP-096, OP-164, OP-373, OP-376
Tibu, R. EP-0375, EPS-040
Tietz, O. OP-768
Tieu, W. OP-140
Tijms, B. OP-109
Tiling, M. **EP-0210**
Timelthaler, G. EP-0283
Timmermans, B. OP-339
Timóteo, T. OP-536
Tinetti, C. EPS-165
Tingen, H. **OP-860**
Tiraboschi, L. EPS-085
Tirado Hospital, J. EPS-072
Tischendorf, L. OP-497
Tiwari, V. EP-1019, EP-1020, EPS-055, EPS-060
Tiwary Vyas, A. EP-0256, **OP-057**
Tkachenko, M. OP-939, EPS-032
Toddes, S. EPS-289
Todorova, T. K. EP-0770
Todorova-Doneva, Y. EP-0513
Tognoli, T. **EP-0259**
Toi, M. EP-0111, EP-0126
Tokac, R. EP-0290
Tokgöz, S. **EP-0077**, **EP-0486**
Toklu, T. EP-0253, OP-163, OP-375
Tol, J. OP-573
Tolbod, L. P. OP-386, OP-730, OP-862
Tolboom, N. EP-0677, OP-086, OP-566, **OP-583**, OP-928, OP-930
Tolmachev, V. EP-0041, EP-0807, EP-0837, EP-0852, EP-0861, EPS-217, EPS-218, EPS-220, **OP-578**, OP-579, OP-704
Tolvanen, T. OP-247, OP-365
tomar, a. EP-0370
Tomas, X. EP-0356
Tomše, P. EP-0619
Tomimatsu, T. EP-0625
Tomiyama, N. OP-772
Tompuri, T. EPS-127
Toms, J. OP-656
Tondo, A. EP-0511
Tönjes, A. EPS-174
Tonn, J.-C. OP-082, OP-538, OP-588, EP-0726, OP-584
Tookman, L. EP-0090
Toompong, P. **OP-662**
Toonen, F. A. J. EP-0274
Toosi, A. **OP-091**
Topal, E. **OP-333**
Topcuoglu, M. A. EP-0691
Topp, M. S. EP-0319
Toramatsu, C. **OP-079**
Tordo, J. EPS-080
Tormo-Ratera, M. **EP-0356**
Toroi, P. OP-028
Torralba, I. EPS-143
Torres, L. EP-0482, EPS-087
Torresan, F. EPS-074
Torres Aroche, L. EP-0680
Torres Espallardo, I. **EP-0800**, EP-0611, EPS-096
Torres-Quintana, P. EP-0331
Toschi, N. EPS-018, OP-590, OP-846
Touil, I. EP-0139, EP-0140
Toulza, O. OP-858
Toumi, A. EP-0697
Toumia, Y. OP-780
Tournier, N. EP-0019, EP-0021, EP-0674, OP-559
Toussaint, M. OP-558
Touzeau, C. OP-100
Townrow, S. TEPS-018
Towpik, J. EP-0018, EP-0831
Toyama, H. EP-0715
Toyama, Y. EP-0452
Toyoshima, A. OP-772
Trachtova, K. EP-0283
Trädgårdh, E. EPS-033
Traenkle, B. OP-922
Trägårdh, E. EP-0219, EP-0311, EP-0318, EP-0468, EP-0759, EPS-208, **OP-708**
Traino, C. EP-0781
Trak, J. **EP-0351**
Tran, B. EP-0555, OP-437
Tran, J. OP-359
Tran, T. EP-0156
Tran Gia, J. OP-367, OP-629, EP-0633, EPS-249, EPS-251, OP-371
Tranquart, F. OP-389
Traub-Weidinger, T. OP-093, OP-713
Trautwein, N. **OP-314**
Travaini, L. **OP-915**, **OP-921**, EP-0543, OP-854, EP-0389
Travascio, L. EP-0376
Treibel, T. A. OP-713
Trejo-Ballado, F. EP-0895

Tremblay, S. OP-557
Tremolières, P. OP-155
Trencsenyi, G. EP-0812
Tresorier, R. OP-858
Trevisan, A. C. EP-0732, EP-0929, EPS-061
Tricarico, P. EP-0132, **OP-632**
Triemstra, L. OP-086
Trifirò, G. EPS-149
Trimaille, T. EP-0067
Trindev, P. **EP-0634**
Tripathi, A. EP-0731
Tripathi, M. EP-0350, EP-0497, EP-0498, EP-0618, EP-0718, EP-0987, EP-0991, EPS-054, EPS-055, EPS-076, EPS-079, OP-307
Triposkiadis, F. EP-0682
Triumbari, E. **EP-0191**, **EP-0335**, **EP-0998**
Trivieri, M. G. EP-0733
Triviño Ibañez, E. TEPS-001, EP-0410, EP-0517, EP-0175, EP-0176, EP-0247, EP-0409, EP-0580, EP-0581, EP-0544
Trnka, J. EPS-041
Trofimiuk-Muldner, M. OP-306
Trojan, L. EP-0002
Trojanova, E. **EPS-084**
Tronchin, S. **OP-441**
Trubacheva, O. EP-0436
Truillet, C. OP-559
Trump, L. EP-0875
Trusov, A. EP-0463
Tsai, C. H. EP-1029
Tsai, F. J. OP-397
Tsai, I. J. OP-319
Tsai, S. OP-041
Tsakou, G. EP-0998
Tsangaridi, A. EP-0938, EPS-136, OP-542
Tsaroucha, A. **EP-0193**, EPS-083
Tsen, S.-P. OP-180
Tseng, C.-S. EP-0155
Tseng, P.-H. EP-1029
Tsiouris, S. EP-0422
Tsitoura, E. EPS-083
Tsougos, I. EP-0682
Tsoumpas, C. EP-0020, EP-0124, EP-0692, EP-0733, OP-243, OP-364, OP-503, OP-570
Tsuchikawa, T. EPS-012
Tsukada, H. OP-561
Tsukamoto, S. **EPS-262**
Tsvetkov, N. OP-297
Tually, P. EPS-206
Tubben, A. OP-860
Tucci, A. EP-0323
Tudini, M. EP-0376
Tuisku, J. OP-842
Tujikawa, T. EP-0308
Tulipan, A. J. OP-832
Tumas, V. EP-0929, EPS-061
Tuncel, F. OP-317
Tuncel, M. EP-0232, EP-0347, EP-0600, EPS-256
Tuoro, A. OP-537
Turchetta, L. EP-0985
Turcotte, É. E. EP-0499
Turcotte, E. EP-0045
Turgut, B. EP-0459
Turk, L. EPS-149
Turkan, C. **EP-0600**
Turkbey, B. EP-0280
Türkvatan, A. EP-0470
Turnbull, W. EP-0063
Turoglu, H. T. EP-0190
Tutino, F. EPS-183
Tworowska, I. **OP-213**
Twumasi-Boateng, K. OP-358
Twyman, F. EP-0893
Tylski, P. OP-470
Tzavara, C. EP-0682
Tzelepakis, A. EP-0998

Üçbilek, E. EP-0168
Uccelli, A. OP-051
Uccelli, L. EP-0709
Uçmak, G. EP-0287
Udelson, J. E. OP-389
Ueberham, L. OP-558
Ueberschaer, M. OP-584
Ueda, T. EP-0625
Uetake, N. EP-0711
Ugur, O. EP-0577
Uhlending, A. **OP-023**
Ulaner, G. OP-672, EP-0113, EPS-016
Ulén, J. EP-0318, EP-0450, OP-708, OP-919
Umar, M. **EP-0707**
Umutlu, L. EP-0146, OP-580
Ungania, S. EPS-232
Unger, N. OP-308
Ungureanu, C. EP-0698
Ünlüer Ates, Y. **EP-0118**
Untch, M. OP-575
Unterkircher, V. EP-0002
Unterrainer, L. EP-0210, EPS-122, OP-192, OP-440, **OP-508,** EPS-003, OP-082, OP-467, OP-588, OP-656, OP-717
Unterrainer, M. EP-0210, OP-082, OP-588, OP-656, OP-717
Ural, B. **EP-0218**
Urbán, S. EP-0181
Urbanova, I. EPS-041
Urganci, N. EP-0233
Urhan, M. EPS-047
Uribe, C. EP-0549, EP-0723, EPS-115, EPS-242, EPS-251, OP-084, OP-442, OP-715, OP-091, OP-711
Uribe-Munoz, C. OP-629
Urso, L. EP-0273, OP-447
Urtz-Urban, N. EP-0811, OP-141, OP-620
Urun, Y. EP-0243, EPS-116
Uslu Besli, R. OP-658
Uslu-Besli, L. EP-0152, **EP-0233**, OP-944
Usmani, M. **OP-935**
Usmani, S. EP-0721, EPS-159
Usta, Y. OP-317
Ustsinau, U. **EP-0532**
Ustun, F. EP-0563
Uğur, Ö. EPS-202
Uygur, E. **EP-0885**
Uzuegbunam, B. OP-562

V, R. EP-0362, **OP-307**
Vaccarin, C. OP-492
Vaccaro, M. EP-0793
Vadali, K. OP-194
Vadrucci, M. EP-0636
Vaduva, P. OP-806
Vaggelli, L. EP-0212, EP-0273, EP-0546
Vagner, A. EP-0812
Vahidfar, N. **EP-0818**, EPS-239, OP-248
Vai, P. EP-0443
Vajpayee, R. EP-0754
Valbusa, G. EP-0700, EP-0749
Valdés Olmos, R. A. OP-183
Valente, S. **EP-0546**
Valentini, S. EP-0614
Valerdiz Menéndez, N. EPS-072
Valero, C. EP-0784
Valevich, A. OP-171
Valibeiglou, Z. **EP-0735**
Valkema, R. EPS-253
Valla, F. EP-0833
Vallati, G. E. EPS-232
Vallejo Casas, J. EP-0400
Valliant, J. EP-0063
Vallis, K. **OP-768**
Vallone, C. EPS-065, OP-639, **OP-647**, OP-916
Vallot, D. OP-951
Valls, E. EP-0109
Valotassiou, V. EP-0682
Valverde-Jorge, R. EP-0331

van Berckel, B. N. M. EP-0677, OP-109, OP-566, OP-930
Van Bogaert, C. OP-232, OP-238
van Brandwijk, E. EP-0862
Van Cutsem, E. EP-0196
Vandamme, T. EP-0196
van de Burgt, A. **OP-167**
van de Giessen, E. EP-0677, **OP-109**, OP-928, EPS-150
Van den Berghe, S. EP-0869
Vandenberghe, S. OP-568
Vandenberghe, W. OP-457
van den Brekel, A. **EPS-201**
van den Brink, L. EP-0065, EPS-213, **OP-083**
Van den Broeck, B. EP-0115, EP-0196
van den Wijngaard, C. C. OP-928
Van den Wyngaert, T. EP-0631, OP-935
van der Bruggen, W. OP-183
van der Eerden, A. W. A. EPS-253
Van der Flier, W. M. EPS-150, OP-109
van der Garde, M. OP-769
van der Giessen, E. OP-566, OP-930
Van der Graaf, W. OP-573
van der Heide, C. D. EP-0014, **OP-433**
van der Hoek, J. L. EP-0061
van der Hulle, T. EP-0274
van der Kant, R. OP-139
Vanderlinden, B. OP-232, OP-238, OP-367, OP-444, OP-629
van der Maaden, T. OP-928
van der Meer, P. OP-860
van der Meulen, N. **OP-016**, EP-0070, OP-080, OP-141
van der Poel, H. EP-0279, EPS-113, EP-0414, EPS-270, OP-506
van der Schilden, K. EP-0805
van der Vegt, M. **OP-326**
Van der Veken, P. OP-429
van der Velde, S. EPS-019
van der Werf, N. OP-241
van der Zant, F. OP-731, OP-242, OP-243
van Deurzen, C. EP-0050
Van de Vijver, K. EP-0115
Van de Voorde, M. OP-141
van de Wiele, C. EP-0183, OP-574
van Diemen, P. OP-241
van Eimeren, T. EP-0751, EPS-147, OP-105, OP-107, OP-108
Van Essen, M. EP-0545, EPS-009
Van Gemert, W. A. OP-339
van Gennep, E. EP-0414
Van Ginderachter, J. A. EPS-227
van Ginhoven, T. M. OP-800
van Golen, L. OP-852
Vanhatalo, J. EP-0659
van Heek, L. EP-0154, OP-101
van Heugten, C. M. OP-928
van Hillegersberg, R. OP-086
Van Holen, R. EP-0115
Vanhove, C. EP-0115
van Kemenade, F. J. OP-800
van Koetsveld, P. M. EPS-213
van Laarhoven, K. J. H. M.. OP-853
Van Laere, K. OP-457
van Leer, B. **OP-252**
van Leeuwen, F. **EP-0279**, **EPS-113**, OP-294, EP-0848, EP-0414, EP-0851, EPS-270, OP-298, OP-300, EP-0397
van Leeuwen, P. EPS-113, EPS-105, OP-506, EP-0397
van Leeuwen, S. I. EPS-270
van Marwick, S. EP-0235
van Meerbeek, M. P. EP-0851, OP-298
van Nimwegen, S. A. EP-0069
Vannucchi, A. EP-0330
van Oort, I. M. OP-339
van Oosterom, M. EP-0851, EPS-113, **EPS-270**, **OP-300**, EP-0397, EP-0408, EP-0414, OP-294, OP-298
van Os, Y. M. G. OP-928
van Praagh, G. **EPS-098**, OP-088
van Praet, C. OP-194
van Rhijn, B. EP-0414
van Rijsewijk, N. D. **EPS-059**
van Rooij, R. EPS-198, OP-295, OP-628
Van Rymenant, Y. OP-429
Van Sleen, Y. OP-515
van Sluis, J. EP-0124, EPS-059, EPS-233, OP-326, **OP-364**, OP-503, OP-570
van Snick, J. H. EPS-059, OP-252, OP-364, OP-570
van Snick, P. EP-0692, OP-503, OP-519
van Speybroeck, C. D. E. OP-628
van Velden, F. H. P. EP-0788, OP-086, OP-167, OP-628
van Velzen, S. OP-241
Van Vlierberghe, H. EPS-231
van Vugt, M. EP-0677, OP-928
van Weerden, W. M. OP-083
van Wijk, M. W. M. **EPS-205**, OP-627
van Wolfswinkel, G. EPS-205
Vanwolleghem, P. EP-0869
van Wunnik, L. OP-243, OP-242
van Zweeden, A. EPS-019
Vaquero-Palomo, M. EPS-025, EPS-026
Varallo, A. **EP-0551**
Varela, N. OP-936
Varga, J. EP-1027
Vargas Ahumada, J. EP-0603
Vargiu, S. EP-0294
Varlamova, Y. EP-0462, EP-0480, OP-864
Varmenot, N. EPS-243, OP-155
Vartiainen, N. **OP-728**
Varzakis, S. **EP-0722**
Vasanawala, S. OP-504
Vasic, V. **EPS-248**, **OP-904**
Vasile, D.-E. EP-0956
Vasilev, I. EP-0513
Vasseur, A. EPS-058
Vassileva, V. OP-145
Vatsa, R. EP-0768
Vauchot, F. **EP-0429**
Vaz, S. EP-0006, EP-0328
Vázquez-Martínez, M. EPS-096
Veach, D. OP-702
Veal, M. EP-0835
Veerman, H. OP-506
Vega, D. EP-0340
Vega Pérez, D. EP-0418
Veggerby Grønlund, R. OP-145
Vegt, E. OP-086
Veiga, R. EP-0965
Vela, I. OP-037
Velasco-Nuño, M. EP-0331
Velásquez Díaz, K. EP-0510, EPS-051, EP-0421, EP-0245, EP-0467
Velázquez, F. EP-0252, EP-0508, EP-0548
Veldhuijzen van Zanten, S. E. M. EPS-253
Veldhuis, W. OP-852
Velidaki, A. **EP-0982**
Velikyan, I. EPS-140, OP-388, OP-579
Veloso, J. EPS-094
Veltrup, E. OP-468
Vendramin, L. EP-0586
Venegoni, L. EP-0980
Venero Chaparro, J. EP-0399, **EP-0474**, **EP-0620**
Venkat Rao, G. EP-0171
Ventanieri, G. EP-0550
Vera, P. OP-151
Veran, N. EP-0894
Vera Schmülling, U. EP-0504, OP-849
Verberne, H. J. OP-245
Verburg, F. A. EP-0100, EPS-103, OP-800
Vercellino, L. EPS-185
Vercher-Conejero, J. **EP-1007**, EP-0299, EP-0547, EP-0211
Vercouillie, J. OP-799
Verderame, F. EP-1028
Verdier, M.-A. EPS-246
Verdoes, M. EP-0077
Verduin, J. J. OP-850
Verena, A. **OP-431**
Verfaillie, S. C. J. EP-0677, OP-928, OP-930
Verger, A. EP-0760, EPS-058, EPS-099, OP-454, OP-586
Vergnaud, L. **EPS-247**

Verhaeghe, J. OP-556
Verma, H. EP-0519
Verma, K. EP-0309, EP-0622
Verma, R. OP-927
Verreck, F. OP-253
Versari, A. EP-0999, EPS-014
Verschure, D. O. OP-245
Versleijen, M. W. J. OP-670
Verslype, C. EP-0196
Verveen, A. EP-0677, OP-928
Vervenne, R. OP-253
Vetrone, L. EP-0354, EP-0388, **OP-474**, OP-534
Vichi, S. OP-474
Vici, P. OP-581
Vidal, A. OP-155
Vidal, T. W. EP-0801
Vidal-Pérez, O. EP-0491
Vidal-Sarro, N. EP-0954
Vidal-Sicart, S. EP-0491
Vieira, V. EP-0769
Vierboom, M. OP-253
Viering, O. EP-0565, **OP-655**, OP-856
Vigário, R. EP-0738
Vigil Díaz, C. EP-0306
Vija, A. EP-1024, TEPS-016, TEPS-017, OP-838
Vija, L. EP-0647, OP-654, **OP-804**, **OP-951**
Vijverberg, J. OP-109
Villa, A. OP-897
Villagran Asiares, A. G. OP-520
Villalobos, A. EP-0164
Villani, M. EPS-037
Villanucci, E. EPS-037
Villanueva Curto, J. EP-0386, EP-0254, OP-170
Villa Palacios, J. EP-0114, **EP-0204**, **EP-0205**, **EP-0544**, **EP-0580**, **EP-0581**, EP-0175, EP-0176, EP-0247
Villar, M. EPS-143
Villasboas, D. EP-0548
Villasboas-Rosciolesi, D. EP-0508
Villemagne, V. OP-108
Villeneuve, R. EP-0719
Vilstrup, M. H. EP-1030
Vimont, D. EP-0035, OP-895
Vinagre, F. EP-0966
Vinagre Perez, I. EP-0599
Vincini, M. G. EP-0236
Vindstad, B. **EPS-160**
Vinga, S. EP-0328
Vinicius Gomes Ferreira, C. EPS-244
Vinjamuri, S. EPS-087
Vink, J. C. EP-0882
Viñolas, N. EP-0148
Vinti, L. OP-052
Viol, S. L. M. EP-0692
Violante, L. EP-0569, EP-0979, OP-539
Violas, X. OP-151
Virgolini, I. OP-306
Vis, A. N. EP-0757, EPS-105, OP-339, OP-506
Viscione, M. EP-0750, EPS-101, EPS-192, OP-226, OP-636
Visser, D. EP-0677, OP-109, OP-566, **OP-928**, **OP-930**
Visser, J. OP-076
Visser, P. J. OP-109
Visser-Meilij, J. M. A. OP-928
Visvikis, D. EPS-178
Vitola, B. EP-0440
Vitorino, I. EP-0412
Vittadini, A. EP-0012
Vlastara, M. OP-220
Vlk, M. OP-017
Vocaturo, F. OP-634
Vodovar, D. EP-0674
Vogel, W. V. EP-0805
Vogg, A. T. J. EPS-278
Volkan Salancı, B. EPS-202, OP-053, EP-0577, OP-055
Volkov, V. EP-0653
Voll, R. EP-0810
Volpe, F. EP-0551, EP-0606, **EPS-065**
Volpe, M. T. OP-166
Volpicelli, F. EP-0606, EPS-065
Volterrani, D. OP-171
Voltin, C.-A. EP-0154, **OP-099**
vom Dahl, S. OP-937
von Baumgarten, L. EP-0726, OP-082, OP-467, OP-538, OP-588
von Beschwitz, S. OP-314
von Gall, C. EP-0348
von Guggenberg, E. EPS-225, EPS-280
von Rohr, K. OP-588
von Tresckow, B. OP-099
Vöö, S. EP-0184, OP-514
Vorobyeva, A. EP-0807, EP-0837, EP-0852, **EP-0861**
Vorster, M. OP-574
Voskamp, M. **OP-779**
Vosoughi, H. EP-0727
Vosoughi, Z. **EP-0727**
Voß, P. C. OP-468
Voster, M. EP-0643
Vrachimis, A. OP-337, OP-339, OP-525
Vraka, C. **OP-081**
Vriens, D. EP-0788
vries, h. **OP-088**
Vrigneaud, J. M. EPS-123, OP-078, EP-0656
Vromen, E. OP-109
Vrublevsky, A. EP-0480
Vugts, D. EP-0383, EPS-195, OP-573
Vuleta, G. EP-0614
Vural, G. EP-0671
Vural Topuz, Ö. EP-0116, EP-0584
Vyas, A. **EP-0256**, OP-057

Waeger, C. EP-0465
Wagatsuma, K. EP-0696, EP-1036, OP-325
Wagemaker, S. EPS-158
Wagemans, M. **EPS-198**
Wagner, I. OP-805
Wagner, T. OP-922
Wahl, R. L. OP-193
Wail, S. OP-222
Wakabayashi, H. EP-0244, EP-0710, EP-0853, OP-284, OP-290, OP-776
Wakabayashi, N. EPS-012, OP-777
Wakankar, R. **EP-0498**, EPS-079
Wakfie Corieh, C. **EP-0393**, EP-0494
Waldman, A. D. OP-590
Waldner, M. OP-468
Waldron, B. OP-145
Walji, A. OP-703
Walker, M. EPS-176, OP-227
Walle, M. OP-858
Walter, M. EP-0081
Walter, T. OP-852
Walther, M. OP-020
Walton, K. K. OP-616
Wan, H. OP-703
Wanek, T. EPS-102
Wang, A. EPS-229
Wang, C. EP-0223, OP-378
Wang, C.-H. EPS-162
Wang, D.-S. OP-244
Wang, D. OP-156
Wang, F. **EPS-132**, **EP-0369**, EP-0642, EPS-276, OP-377
Wang, G. EP-0160, OP-377, OP-721, OP-933, EPS-056
Wang, H. EPS-192, OP-226, **EP-0058**, EPS-283, OP-393, OP-530, EP-0816, OP-286, **EP-0590**, EP-0817
Wang, J. EP-0649, EPS-155, **EP-0439**, OP-727, OP-933, EP-0675, OP-111, EP-0028, EP-0134, EP-0222, EP-0267, EP-0598, EP-0638, EP-0648, EPS-021, **EPS-155**, EPS-194, OP-428, OP-792, OP-492, OP-644, EP-0267, EPS-194
Wang, L. EP-0453, **OP-644**
Wang, M. EP-0222
Wang, P. OP-705, **OP-312**, **OP-671**, EP-0639
Wang, R. **OP-576**, **OP-933**, EP-0426, EP-0428
Wang, S. EP-0029, OP-705, OP-377, EP-0521, EP-0444

Wang, X. EPS-004, OP-156, **EP-0741**, OP-633, EP-0016 EP-0281, EP-0321, EPS-197, OP-377, EP-0270, OP-847
Wang, Y. OP-143, EP-0426, EP-0428, EPS-119, EP-0307 EP-0281, OP-096, OP-644, EP-0923OP-878, OP-212,**EP-0334**, EP-0439, OP-727, OP-142
Wang, Z. EPS-056, EP-0080, EPS-293, **EPS-273**, EPS-276, **OP-218**
Wangerin, K. EP-0113
Wängler, B. OP-656
Wängler, C. OP-656
Warner, B. M. EP-0280
Warschun, V. R. EP-0801
Wartenberg, M. EPS-180
Washington, S. OP-040
Washiyama, K. EP-0855
Wason, L. **EP-1021**
Watabe, H. EP-0711, OP-631
Watabe, T. **OP-772**
Watanabe, K. EP-0360
Watanabe, M. EP-0715, **OP-380**
Watanabe, S. EP-0739, EPS-012, OP-777, TEPS-008
Wawroschek, F. EP-0408
Weber, M. EP-0284, EP-0607, OP-380, OP-525, OP-308, OP-713
Weber, S. **OP-332**
Weber, W. EP-0288, EP-0564, EP-0566, EP-0655, OP-154, OP-309, OP-334, OP-497, OP-562, OP-707, OP-802
Weber, W. A. EP-0235, EPS-124, OP-520, OP-722, OP-769
Wegen, S. EP-0154
Wehbe, J. OP-335
Wei, J. EP-0746
Wei, M. EP-0321, EPS-197, OP-377
Wei, N. OP-700
Wei, W. **EP-0054**, OP-216, OP-217, **OP-619**
Wei, X. X. OP-340
Weich, A. EP-0093, EP-0182, EP-0319, EP-0539, OP-291
Weidner, L. OP-082
Weidner, S. EP-0567
Weijland, J. OP-027
Weinberg, J. EP-0612
Weindel, K. OP-773
Weindler, J. EP-0154
Weinhold, N. OP-919
Weis, H. **OP-798**
Weisheit, T. EP-0827, OP-488
Weisman, A. J. EP-0113
Weiss, A. R. OP-556
Weissler, B. OP-773
Weller, A. OP-105
Welling, M. M. EP-0848
Wellingta, L. S. C. EPS-062
Wells, G. OP-025
Welt, A. OP-580
Wen, B. EP-0133, OP-376
Wen, L. **EPS-283**
Wen, N. OP-714
Wen, W. OP-646
Wen, X. **EP-0052**, OP-576
Weng, M.-C. **EP-0036**
Weng, W. **EP-0001**, EP-0484, **EP-0905**
Wenker, S. OP-358
Wenter, V. OP-467, OP-656, OP-717
Werner, D. EP-0843
Werner, R. A. EP-0093, EP-0182, EP-0319, EP-0353, EP-0507 EP-0539, EP-0552, EP-0610, EPS-117, OP-291, OP-305, OP-517, OP-866, OP-785, OP-332
Weru, V. EPS-266, OP-449
Wester, H.-J. OP-617, OP-620, OP-655, OP-767
Westerbergh, F. **OP-080**, OP-836
Westlund Gotby, L. E. L. **OP-029**, **OP-627**, **OP-628**
Westrøm, S. OP-911
Wetzel, C. OP-588
Wheatcroft, M. OP-358
White, E. EPS-289
Whitehead, A. C. OP-846
Wichert-Ana, L. **EP-0732**, **EP-0929**, **EPS-061**, **EPS-062**
Wichmann, C. **OP-490**
Wiedemann, N. **OP-360**
Wiegel, T. EP-0560, OP-337
Wiegers, S. OP-102
Wielopolski, P. A. EP-0100
Wienand, G. EP-0565, OP-655
Wienker, J. EP-0146
Wierstra, P. J. EP-0077
Wierts, R. EP-0716, EPS-100, OP-628
Wiesweg, M. EP-0146
Wig, N. EP-0991
Wijngaarden, J. E. EPS-195
Wikke Hallund, M. OP-145
Wild, D. OP-191, OP-297, OP-716
Wilderman, S. J. OP-436, OP-439
Willaime, J. OP-907
Willemsen, A. EP-1025, EPS-233, TEPS-019
Williams, M. OP-590
Williams, S. OP-037, OP-338
Williamson, R. EP-1021, TEPS-013
Willink, C. Y. **OP-853**
Wilson, D. EP-0201, EPS-115, OP-715
Wilson, J. EP-0836
Wimana, Z. OP-232, OP-238, OP-573
Windhorst, A. OP-253, EP-0677, EPS-019, OP-928, OP-930
Windhorst, B. OP-566, EP-0805
Wind-Mark, K. EP-0024, OP-110
Winkeler, A. EP-0019, OP-559
Winkelmann, M. OP-099
Winkler, D. OP-139
Winnik, M. EP-0056, EP-0842, EP-0841
Winter, A. EP-0408
Winter, E. OP-512
Winter, H. OP-189
Winter, R. **EPS-210**
Wirtz, H. EPS-174
Wirtz, R. **OP-468**
Wiseman, G. OP-193
Wit, E. EP-0397
Witek, J. EP-0828
Withofs, N. OP-568
Witjes, A. J. OP-339
Witkowska-Patena, E. EP-0018, EP-0831
Wittmann, D. EPS-078
Wittsack, H. J. EP-0072
Wlodarczyk, M. **EP-0621**
Wlostowska, J. EP-0831
Woerdenbag, H. J. EP-0877
Woerdenbag, M. M. EP-0877
Woff, E. OP-637
Wojewódzka-Mirocha, M. EP-0298
Wolkewitz, M. OP-337
Wollenweber, S. D. OP-227, EPS-176
Wolter, J. OP-897
Wolterink, J. M. EPS-098
Wong, C. OP-340
Wong, E. EP-0841
Wong, H. L. EPS-010
Wong, K. OP-436, OP-439, EPS-120
Wong, L. M. OP-037
Wong, X. **EP-0689**, EPS-258, OP-090
Wong, Y. EPS-114, OP-095
Wongjarern, S. **EP-1025**
Woo, K. J. EPS-030
Woo, S. K. EP-0128, **EP-0730**
Woodrow, E. EPS-087
Włostowska, J. EP-0018
Wojdowska , W. EP-0870
Wouthuyzen-Bakker, M. EPS-059
Wright, J. EPS-289
Wright, T. EP-1037
Wu, H. EP-0637, EPS-091, EP-0803, EP-0817, OP-398 OP-048, EP-0382, **OP-373**
Wu, J. EP-0803
Wu, K. EPS-191, OP-095
Wu, P. EP-0430, EP-0644, **OP-286**, OP-710, OP-792, OP-794
Wu, R. EP-0521, EP-0642
Wu, W. EP-0016, EPS-004

Wu, Y.-W. EP-0431, EPS-162
Wu, Y. EP-0642, EP-0817
Wu, Z. OP-903, EP-0324, EP-0741, EP-0741, OP-255, OP-286, OP-633
Wuest, F. EP-0836
Wullschleger, S. OP-897
Wurzer, A. OP-145
Wysoczynski, K. **EP-0794**

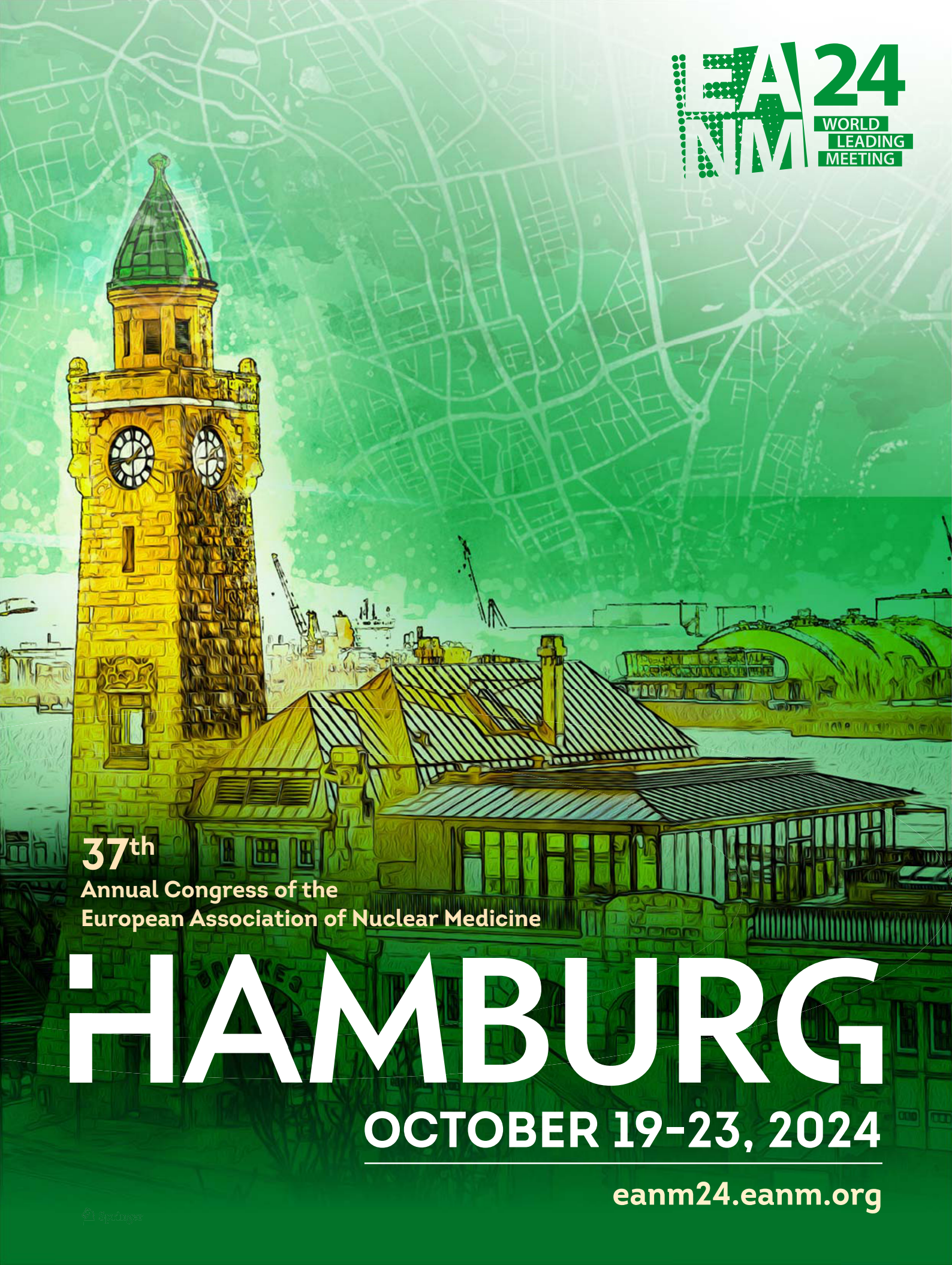
Xavier, A. T. EP-0922
Xi, C. EP-0638, EP-0648
Xi, X. OP-644
Xia, L. EP-0047
Xia, Q. **EP-0865**, OP-059, OP-217
Xia, Y. **EP-0049**
Xiang, X. OP-110
Xiang, Y. EP-0746
Xiang, Z. OP-286
Xiao, J. EP-0017, OP-156
Xiao, L. EPS-164, EPS-207, **OP-795**, OP-797, OP-885, **EP-0057**, OP-526
Xiao, Q. OP-797
Xiao, S. **OP-493**
Xiao, X. EP-0091
Xiao, Z. EP-0133, EP-0382, EPS-209, OP-096, OP-164, OP-373, OP-376, EP-0834, **EP-0846**
Xie, A. EP-0161
Xie, F. EP-0675, EPS-057, EPS-151, OP-111, OP-256
Xie, H. **EP-0145**
Xie, Q. EP-0187, **EP-0074**, EP-0231, EP-0521, EP-0737
Xie, Z. EP-0028, EP-0638
Xing, D. EP-0382, EPS-209, OP-164, OP-376
Xing, M. EP-0164
Xing, T. EPS-194
Xiong, X. **EP-0596**
Xourgia, X. EP-0422
Xu, D. EP-0178, **OP-697**
Xu, F. OP-378
Xu, G. EP-0091
Xu, H. OP-048, EP-0076
Xu, J. **EP-0198**
Xu, K. **OP-376**
Xu, L. OP-286
Xu, M. EP-0838
Xu, P. EP-0052, OP-576
Xu, Q. OP-794, EPS-004
Xu, S. EP-0371, OP-710
Xu, T. EP-0837, EP-0861, OP-704
Xu, W. **EP-0167**, OP-374, OP-427
Xu, X. EP-0038, EP-0081
Xu, Y. **EP-0817**, **EP-0097**, **EP-0098**, **EP-0143**, **EP-0172**, **EP-0728**, **EPS-034**, **EPS-157**
Xu, Z. OP-216
Xue, S. EP-0649, EP-0750, EP-0801, **EPS-101**, **EPS-192**, EPS-244, OP-059, **OP-226**

Yabe, A. OP-631
Yacub, M. OP-566
Yadav, J. EP-0336, EP-0718
Yadav, M. P. EP-0618, OP-307
Yadgarov, M. EP-0326
Yagi, Y. **EP-0808**
Yakami, M. EP-0310
Yakubu, M. EP-0533
Yakushev, I. OP-046, OP-520
Yakushiji, Y. **EP-0696**, OP-325
Yalcin, S. EP-0577
Yalcintas Bethune, E. **OP-018**
Yalçın, S. EPS-202
Yaldız, M. EP-0168
Yalkinoglu, Ö. EP-0383
Yamada, Y. EP-0126
Yamaga, L. Y. I. EP-0935
Yamaguchi, J. EP-0476
Yamakawa, Y. TEPS-008
Yamakuni, R. OP-177
Yamamoto, A. EP-0466, **EP-0476**
Yamamoto, M. OP-625
Yamamoto, T. TEPS-015
Yamane, T. EP-0110
Yamao, T. EP-0696, EP-0715, **OP-177**, OP-325, TEPS-010
Yamashita, K. TEPS-010, EP-0625
Yamaya, T. **EP-0651**, OP-079
Yan, C. EPS-119, **EPS-290**
Yan, M. OP-286
Yan, X. **EP-0527**, OP-215
Yanagida, H. OP-137, OP-138
Yang, A. EP-0005, EP-0076, EPS-064
Yang, B. **OP-143**
Yang, C. T. EP-0080
Yang, F. OP-697
Yang, H. EP-0091, EP-0307, EPS-166
Yang, J. EP-0730, EPS-164, EPS-207, OP-795, OP-885, **EP-0484**
Yang, L. EP-0426, **EPS-138**, **OP-526**
Yang, M. EPS-216, EPS-221, OP-288, OP-644
Yang, P. **EP-0746**
Yang, Q. EPS-293, OP-622, OP-902
Yang, R. EPS-091
Yang, S. **EP-0031**, EPS-283, EP-0878, EPS-056
Yang, W. EP-0028, EP-0134, EP-0598, **EP-0638**, EPS-194
Yang, X. EPS-276
Yang, Y. EPS-146, **EPS-064**, OP-878, **OP-448**, EP-0675 EP-0076, EP-0521, EP-0223, OP-378, OP-721
Yang, Z. EP-0039, EP-0044, EP-0074, EP-0231, EP-0321, EP-0521, EP-0642, EP-0764, EPS-197, EPS-276, EPS-281, OP-214, OP-215, OP-219, OP-361, OP-377, OP-618, OP-705, **OP-727**, EP-0598, OP-379 **EP-0380**, OP-379, **OP-699**
Yano, R. **OP-625**
Yao, B. EP-0017
Yao, X. EP-0187
Yao, Y. **EP-0027**
Yap, W. OP-193
Yaqub, M. EP-0677, OP-027, OP-930
Yaqun, J. **OP-782**
Yaran, S. G. EP-0470
Yaryes, M. EP-0708, OP-327
Yashima, Y. **EP-0452**
Yasumoto, Y. EP-0774, EP-0776
Yaylalı, O. EP-0602
Ye, H. EP-0161
Ye, J. EP-0028, **EP-0134**, EP-0222
Ye, Q. **EP-0648**
Yeddes, I. EP-0481, EP-0995
Yeh, R. **EPS-016**
Yepes Agudelo, A. M. EP-0302
Yeyin, N. EP-0153
Yi, H. EP-0638
Yi, T. **EP-0903**, **EP-0914**
Yi, Z. EP-0746
Yildirim, O. EP-0092
Yilmaz, G. **EP-0584**
Yin, B. EPS-004
Yin, X. OP-772
Yip, Y. EPS-114, OP-159
Yıldırım, A. EP-0951
Yoneyama, H. EP-1022, EP-1024, OP-781, TEPS-016, TEPS-017
Yong, H. OP-782
Yong, L. EP-0689, EPS-258, **OP-090**
Yoo, M. OP-049
Yoon, H. J. **EPS-030**, OP-049
Yoon, J.-K. EP-0128, EP-0839
Yordanova, T. EP-0263, EP-0341, EP-0342, EP-0343, EP-0344, EP-0899, EP-0900, EP-0901, EP-0902, EP-0904, EP-0913, EP-0981, EPS-121, EPS-267
Yoshida, E. EP-0651
Yoshida, S. EPS-088, EPS-131
Yoshida, Y. EP-0308
Yost, V. EPS-289
Younes, A. OP-018
Yousefirizi, F. **EP-0723**
Yousefnia, H. EP-0804, EP-0806, **EP-0830**
Yousefzadeh-Nowshahr, E. EPS-248, OP-904, OP-905

Youssef, M. EP-0612, OP-857
Y S, M. EP-0362
Yu, A. L. EP-1029
Yu, B. EP-0321
Yu, C. EP-0903, EP-0914, EPS-119
Yu, F. **OP-643**, **EPS-216**, **EPS-221**, **EP-0598**
Yu, H. EP-0637, EPS-091
Yu, H. OP-794
Yu, J. EP-0074, **EP-0923**, **EP-0105**, EP-0149, EP-0460, EPS-174, OP-567
Yu, N. EP-0108
Yu, Q. EPS-220
Yu, Y. OP-646, **EP-0371**
Yu, Z. EPS-276
Yuan, H. EPS-132, **OP-565**
Yuan, K. TEPS-020
Yuan, P. **OP-700**
Yuan, T. EP-0321, **EPS-197**
Yuasa, T. OP-631
Yücel, M. EP-0253, EP-0602, EP-0974
Yudistiro, R. EPS-206
Yuge, S. EP-0126
Yüksel, D. **EP-0602**, **EP-0974**
Yun, M. EPS-169, EPS-145, OP-646
Yun, S. **EP-0174**, **OP-054**
Yun, W. G. EP-0186
Yusufaly, T. OP-149
Yuzefovich, B. OP-229

Za, T. EPS-196
Zaabar, L. EP-0401, **EP-0420**, **EP-0531**, **EPS-038**, EPS-042
Zabarmawi, Y. EP-0771
Zaccaro, L. EP-0011
Zacharias, L. EP-0998
Zacherl, M. EPS-003, OP-839, OP-467, OP-717
Zacho, H. D. EP-0713, EPS-106
Zackrisson, B. EP-0317
Zafeirakis, A. EP-0071, EP-0568
Zaffaroni, M. EP-0236
Zaganas, I. OP-859
Zaganjori, M. EPS-148
Žagar, I. EP-0916
Zagaria, L. EP-0793
Zaghloul, M. S. EPS-036
Zagni, F. OP-474
Zago, D. EP-1004
Zagorska, A. **EP-0772**, EP-0770
Zaharia, A. EP-0943, EP-0957, EP-0952
Zahornacký, O. OP-925
Zahra, U. B. EP-0385
Zaidi, H. EP-0727, EPS-159
Zajkowska, K. **EP-0298**
Zakaria, Z. TEPS-002
Zakavi, S. **OP-523**, EP-0293, EP-0381
Zaletel, K. EP-0506, EP-0619, TEPS-011
Zalutsky, M. OP-901
Zamagni, E. EP-0354, OP-534
Zaman, A. EP-0425, EPS-252
Zaman, M. EP-0425, **EPS-252**
Zaman, S. EP-0425, EPS-252
Zaman, U. EPS-252
Zambelli, A. EP-1017, OP-323
Zamboglou, C. **OP-337**
Zambon, G. EP-0586
Zambrano Infantino, R. **EPS-043**, EP-0398, EP-0455, EP-0475, EP-0529, OP-168
Zamora-Romo, E. EP-0895
Zampella, E. EP-0551, EP-0606, EPS-065, OP-382, OP-383
Zamudio, D. EP-0352
Zan, C. OP-255
Zana, A. OP-356
Zanca, R. **EP-0189**, EP-0272, OP-039
Zandegiacomo, S. EP-0272, OP-039
Zander, A. EP-0795
Zanelli, F. EP-0999
Zang, J. **EP-0223**, OP-378, **OP-721**
Zanger, S. EPS-291
Zanini, C. OP-921
Zanoni, L. EP-0147, EP-0213, EP-0215, OP-879
Zanotti, S. OP-882
Zanotti-Fregonara, P. EP-0780
Zanzonico, P. OP-834
Zappeová, M. EP-0078
Zaragori, T. **EP-0760**, **OP-586**
Zaragoza, P. EP-0340, **EP-0418**
Zárate-Morales, A. EP-0895
Zarei, M. EP-0317
Zarraa, S. EP-0401
Zarrad, F. OP-308
Zarrelli, F. EP-0376
Zarschler, K. EPS-275
Zatcepin, A. EP-0015, EP-0726, EPS-092, **OP-110**
Zattoni, F. EPS-107
Zavadovsky, K. **EP-0436**, EP-0446, EP-0448, EP-0457, EP-0458, EP-0461, EP-0462, **EP-0477**, EP-0626, EPS-139, **EPS-142**, OP-645, OP-724, OP-864
Zavvar, T. **EPS-225**
Zecca, H. EP-0810
Zech, C. J. OP-297
Zedenius, J. EPS-067
Zeevaart, J. EPS-046
Zeglis, B. M. EPS-016
Zeimpekis, K. OP-058, OP-666
Zeisler, J. EP-0829
Zelchan, R. OP-578
Zeng, C. **OP-048**
Zeng, D. EP-0133, EP-0382, OP-164
Zeng, F. EP-0141, EP-0308, EPS-104
Zeng, H. EP-0648
Zeng, X. EP-0856
Zeng, Z. EP-0046, **OP-215**, OP-361
Zengerling, F. EP-0560
Zeniya, T. **OP-631**
Zepeda-Orozco, D. OP-144
Zerdoud, S. EP-0933, EPS-246, OP-654, OP-804, OP-951
Zerhouni, N. EP-0698
Zetterberg, H. OP-104
Zevnik, K. **OP-452**
Zeyen, P. OP-107
Zgaljardic, M. EP-0608
Zhang, D. EP-0638
Zhang, H. **EP-0668**, OP-303, OP-312, EP-0270, OP-847
Zhang, J. EPS-216, EPS-221, OP-378, **EP-0005**, EP-0076 EP-0052, EP-0223, EP-0281, **OP-188**, OP-237, **OP-302**, OP-312, OP-378, OP-576, OP-671, OP-721, OP-933, EP-0428, EP-0484, **EP-0597**
Zhang, L. **EP-0177**
Zhang, M. **OP-791**, **EP-0520**, **EP-0028**, EP-0134, EP-0222, **EPS-194**
Zhang, Q. EPS-276, **OP-214**
Zhang, T. **EP-0815**, EPS-056
Zhang, W. EP-0650, OP-789, TEPS-020
Zhang, X. EP-0856, OP-576, EP-0456, EPS-145, OP-646, OP-865 EP-0483, **OP-288**, **OP-522**, **EPS-069**, EPS-057 **EP-0244**, OP-284, **OP-290**
Zhang, Y. OP-377, EP-0161, EP-0435, OP-287, EP-0030, OP-216, OP-700, EP-0649, OP-644, **EP-0121**, **EP-0282**, **EPS-166**, OP-643, EPS-255, EPS-197, EP-0372, EP-0378, EPS-193, OP-701, OP-883, OP-303, OP-312, OP-671
Zhang, Z. EP-0829, EP-0815
Zhang-Ying, J. OP-805
Zhao, C. EPS-273, OP-218, **EP-0305**
Zhao, J. EP-0675
Zhao, K. EPS-056, OP-920
Zhao, L. OP-374, OP-427, **OP-790**
Zhao, M. OP-526, **EP-0016**, **EP-0138**, **EP-0460**, OP-713
Zhao, Q. EP-0157
Zhao, S. OP-644
Zhao, T. OP-237, OP-721, EP-0157
Zhao, X. G. OP-901
Zhao, Y. **EP-0007**, EP-0860, EP-0638, EP-0648, EP-0638, EP-0426, EP-0428, **EP-0430**, OP-286

Zhao, Z. EP-0746, **OP-156**
Zheng, C. EPS-283, **EPS-146**, OP-863
Zheng, G. EP-0649
Zheng, J. EP-0668
Zheng, K. **EP-0161**
Zheng, R. EP-0281
Zheng, S. EP-0001
Zheng, X. EP-0737
Zheng, Z. **EP-0637**, **EPS-091**
Zhi, Y. EPS-108, EP-0093, EP-0539, OP-785
Zhong, J. **OP-796**, EP-0133, OP-164
Zhong, X. EP-0289, **EP-0650**, **OP-789**
Zhong, Y. EP-0737
Zhou, C. TEPS-020, **OP-428**
Zhou, E. OP-796
Zhou, H. OP-048, EPS-101
Zhou, M. OP-448
Zhou, N. EP-0321, EPS-276
Zhou, P. EP-0817, EP-0484
Zhou, X. **OP-059**, **OP-217**
Zhou, Y. **EP-0320**
Zhou, Z. OP-703
Zhu, D. EP-0003
Zhu, H. EP-0046, EPS-197, EPS-273, EPS-281, OP-215, OP-218, OP-377, OP-618
Zhu, W. **EP-0372**, **EP-0378**, **EPS-004**, **EPS-006**, **EPS-193**, OP-303, **OP-701**, **OP-883**
Zhu, Z. **EP-0187**, OP-576, OP-721, OP-933
Zhuang, R. EP-0856
Ziaka, A. EP-0682
Ziangas, C. EP-0682
Ziauddin Siddiqui, Z. OP-897
Ziegler, S. EP-0015, EP-0024, EP-0726, EPS-092, EPS-237, OP-082, OP-368, OP-839, OP-110
Zielinski, R. OP-213
Zientek, F. EPS-156
Zierke, M. A. **EP-0824**, **EPS-279**
Zijlstra, J. OP-102
Zika, J. EP-0445
Zikrileh, A. EP-0861
Zinsz, A. EP-0760, OP-586
Zinzani, P. L. OP-099
Ziv, O. **OP-229**
Znamenskiy, I. **EP-0653**
Zob, D. EP-0931
Zokian, H. OP-703
Zolghadri, S. EP-0804, **EP-0806**, EP-0830
Zong, Y. OP-036
Zorante de Lucena, L. **EP-0676**
Zotou, P. EP-0423, EP-0445
Zou, P. EP-0803, EP-0817
Zouain, D. OP-489, EPS-007
Zounek, A. **EPS-092**, EP-0726
Zrajkowska, A. OP-231
Zucca, E. OP-102
Zucchetta, P. OP-052
Zuccotti, G. OP-915, OP-921, OP-668, **EPS-107**
Zuffante, M. EP-0908
Zugasti, I. EP-0356
Zuhayra, M. EP-0007, EP-0860
Zukowski, L. EPS-071
Zuo, C. EP-0644, EPS-057, EPS-155, OP-792, OP-794
Zurbruegg, M. EP-0889
Zurera Pareja, R. EP-0400
Zuvic, M. EP-0221
Zwan, M. EPS-150
Zwezerijnen, G. **OP-102**, OP-566, EP-0383, EPS-195, OP-027
Żyłka, A. EP-0298


EANM 24
WORLD LEADING MEETING
37th
Annual Congress of the
European Association of Nuclear Medicine
HAMBURG
OCTOBER 19-23, 2024
eanm24.eanm.org

12 SEPTEMBER, 2023

DOORS OPEN AT 19:00



FEATURING:
THE BAD POWELLS

LOCATION: PALAIS WERTHEIM
CANOVAGASSE 1-5, 1010, VIENNA